



---

DAVID SUTTON · JEREMY W. R. YOUNG (Eds.)

# A SHORT TEXTBOOK OF CLINICAL IMAGING

---

With 1769 Figures

Springer-Verlag  
London Berlin Heidelberg New York  
Paris Tokyo Hong Kong

David Sutton MD, FRCP, FRCR, DMRD  
Consulting Radiologist, St. Mary's Hospital, Praed Street, London W2 and The National Hospital for Nervous Diseases, London WC1, UK

Jeremy W. R. Young, MA, BM, BCh, FRCR  
Chief of Diagnosis, Diagnostic Radiology Department, University of Maryland Hospital, 22 South Greene Street, Baltimore, Maryland 21201, USA

*Front cover illustration:*

DSA selective right coronary arteriogram using 2 ml contrast medium showing proximal stenosis.

CT scan unenhanced. Large right pheochromocytoma with cystic areas. The mass is displacing liver.

Early intrauterine gestation: 9–10 weeks. A transabdominal sonogram through the gravid uterus at 9–10 weeks shows fetal features such as head, lower extremity and spine.

Partial agenesis of the corpus callosum shown by MRI midline sagittal section (T<sub>1</sub>-weighted).

ISBN-13: 978-1-4471-1757-5      e-ISBN-13: 978-1-4471-1755-1  
DOI: 10.1007/978-1-4471-1755-1

**British Library Cataloguing in Publication Data**

A short textbook of clinical imaging.

1. Medicine. Diagnosis. Imaging

I. Sutton, David, 1917–      II. Young, Jeremy W. R., 1948–  
616.0754

**Library of Congress Cataloging-in-Publication Data**

A short textbook of clinical imaging / David Sutton and Jeremy W. R. Young, eds.

p. cm.

1. Diagnostic imaging. I. Sutton, David, 1917– . II. Young, Jeremy W. R.

RC78.7.D53S48 1990

616.07'57—dc20

90-9608

CIP

Apart from any fair dealing for the purposes of research or private study, or criticism or review, as permitted under the Copyright, Designs and Patents Act, 1988, this publication may only be reproduced, stored or transmitted, in any form or by any means, with the prior permission in writing of the publishers, or in the case of reprographic reproduction in accordance with the terms of licences issued by the Copyright Licensing Agency. Enquiries concerning reproduction outside those terms should be sent to the publishers.

© Springer-Verlag London Limited 1990

Softcover reprint of the hardcover 1st edition 1990

The use of registered names, trademarks etc, in this publication does not imply, even in the absence of a specific statement, that such names are exempt from the relevant laws and regulations and therefore free for general use.

**Product liability:** The publisher can give no guarantees for information about drug dosage and application thereof contained in this book. In every individual case the respective user must check its accuracy by consulting other pharmaceutical literature.

Filmset and printed by BAS Printers Limited, Over Wallop, Hampshire

2128/3916–543210 (Printed on acid-free paper)

# PREFACE

---

In recent decades imaging has proved one of the most rapidly expanding areas of medicine. The present day trainees entering radiology are no longer trained by radiologists who cover and are well informed on most aspects of their specialty as was the case with previous generations. Instead they encounter a confusing array of subspecialists divided both by systems and by techniques.

The system specialists include neuroradiologists, vascular radiologists, gastrointestinal radiologists, chest radiologists, and skeletal radiologists. Technique specialists include experts in nuclear medicine, ultrasound, computed tomography and magnetic resonance, and there are subspecialists in both groups, not to mention others like pediatric radiologists who fit into neither classification.

It is our experience that this plethora of experts each with his own individual approach is bewildering and intimidating to the novice radiologist. The numerous monographs on individual subjects and techniques and the large textbooks so valuable to the more advanced radiologist are also confusing and unhelpful to the new recruit.

It was for these reasons that we decided to embark on this new *Short Textbook*. The aim was to produce a concise and integrated volume which could provide the beginner with a balanced and realistic view of the true place of different imaging techniques in current practice. Details of technique are generally excluded; most will be inevitably absorbed with increasing practical experience. The emphasis throughout is on clinical usage, and the relative and often changing importance of different methods in specific clinical contexts.

Apart from the junior radiological trainee in his first or second year at whom the book is primarily aimed, we hope this new work will also prove useful to those physicians and surgeons requiring an up-to-date outline of the scope of modern imaging either for personal education or as an aid for higher medical and surgical examinations both in America and Britain.

January 1990

David Sutton, London  
Jeremy Young, Baltimore

# CONTENTS

---

List of Contributors .....	x
----------------------------	---

## 1 RESPIRATORY SYSTEM

1 Methods of Investigation and Interpretation of the Chest Radiograph <i>M. Rubens</i> .....	3
2 The Chest Wall, Diaphragm and Pleura <i>M. Rubens</i> .....	27
3 Diseases of the Airways: Pulmonary Collapse and Consolidation <i>M. Rubens</i> .....	45
4 Pulmonary Infections <i>M. Rubens</i> .....	61
5 Pulmonary Neoplasms <i>M. Rubens</i> .....	77
6 Diffuse Lung Disease <i>M. Rubens</i> .....	93
7 The Mediastinum <i>M. Rubens</i> .....	107
8 Chest Trauma, the Post-operative Chest and Intensive Care <i>M. Rubens</i> .....	123

## 2 CARDIOVASCULAR SYSTEM

9 Cardiac Imaging <i>P. Wilde and G.G. Hartnell</i> .....	139
10 Acquired Heart Disease <i>P. Wilde and G.G. Hartnell</i> .....	157
11 Congenital Heart Disease <i>P. Wilde and G.G. Hartnell</i> .....	183
12 Cardiac Tumors: Implants: Pericardium: Interventional Techniques <i>P. Wilde and G.G. Hartnell</i> .....	217
13 Angiography <i>D. Sutton</i> .....	235

**3 SKELETAL SYSTEM AND SOFT TISSUES**

<b>14</b>	Congenital Abnormalities of Bone	
<i>J.W.R. Young</i>	.....	257
<b>15</b>	Trauma	
<i>J.W.R. Young</i>	.....	273
<b>16</b>	Tumors and Tumor-like Lesions of Bone	
<i>J.W.R. Young</i>	.....	295
<b>17</b>	Metabolic and Endocrine Disorders Affecting Bone	
<i>J.W.R. Young</i>	.....	323
<b>18</b>	Hemopoietic Disorders	
<i>J.W.R. Young</i>	.....	337
<b>19</b>	Bone Infections	
<i>D. Nelson</i>	.....	347
<b>20</b>	Osteonecroses, Osteochondroses, Paget's Disease and Miscellaneous Disorders	
<i>D. Nelson</i>	.....	359
<b>21</b>	Articular Disorders	
<i>C.S. Resnik</i>	.....	377
<b>22</b>	Simple Radiography of the Soft Tissues	
<i>F. Starer</i>	.....	399
<b>23</b>	Mammography	
<i>R. McLelland</i>	.....	411

**4 ABDOMEN**

<b>24</b>	The Acute Abdomen	
<i>Janet Murfitt</i>	.....	431
<b>25</b>	The Biliary Tract	
<i>Janet Murfitt</i>	.....	447
<b>26</b>	Liver and Spleen	
<i>Janet Murfitt</i>	.....	463
<b>27</b>	The Pancreas	
<i>Janet Murfitt</i>	.....	485
<b>28</b>	The Adrenal Glands	
<i>Janet Murfitt</i>	.....	497
<b>29</b>	Salivary Glands, Oropharynx and Esophagus	
<i>D.J. Ott</i>	.....	507
<b>30</b>	The Stomach and Duodenum	
<i>D.W. Gelfand</i>	.....	529
<b>31</b>	The Small Intestine	
<i>Dina F. Caroline and D.D.T. Maglinte</i>	.....	545
<b>32</b>	The Colon	
<i>Dina F. Caroline</i>	.....	573

**5 GENITOURINARY SYSTEM**

<b>33</b> Renal Imaging: Congenital Lesions <i>Nancy S. Curry</i> . . . . .	601
<b>34</b> Cysts and Neoplasms <i>Nancy S. Curry</i> . . . . .	617
<b>35</b> Calculi: Infection: Miscellaneous <i>Nancy S. Curry</i> . . . . .	633
<b>36</b> The Lower Urinary Tract <i>D. Rickards and S. Jones</i> . . . . .	657
<b>37</b> Gynecology <i>Kathryn Grumbach</i> . . . . .	671
<b>38</b> Obstetric Ultrasound <i>Kathryn Grumbach</i> . . . . .	687

**6 CNS AND SKULL**

<b>39</b> The Central Nervous System: Methods, Congenital Lesions <i>D. Sutton</i> . . . . .	715
<b>40</b> Neoplasms <i>D. Sutton</i> . . . . .	727
<b>41</b> Vascular Lesions <i>D. Sutton</i> . . . . .	751
<b>42</b> Infection: Trauma <i>D. Sutton</i> . . . . .	767
<b>43</b> White Matter, Degenerative and Metabolic Disorders <i>D. Sutton</i> . . . . .	783
<b>44</b> The Spine and Spinal Cord <i>J.M. Stevens</i> . . . . .	791
<b>45</b> Orbital Imaging <i>G. Lloyd</i> . . . . .	813
<b>46</b> Radiology of the Teeth and Jaws <i>P. Renton</i> . . . . .	825
<b>47</b> The Paranasal Sinuses <i>S.I. Schabel</i> . . . . .	839
<b>Subject Index</b> . . . . .	845

# CONTRIBUTORS

---

**Dina F. Caroline, MD**

Associate Professor of Diagnostic Imaging, Department of Diagnostic Imaging, Temple University Hospital, Philadelphia PA, USA

**Nancy S. Curry, MD**

Director of Uroradiology, Department of Radiology, Medical University of South Carolina, Charleston, South Carolina, USA

**D.W. Gelfand, BSc, MD**

Professor and Chief of Gastrointestinal Radiology, Department of Radiology, Bowman Gray School of Medicine, Winston Salem, North Carolina, USA

**Kathryn Grumbach, MD**

Assistant Professor of Radiology, Department of Radiology, Hospital of the University of Pennsylvania, Philadelphia PA, USA

**G.G. Hartnell, MRCP, FRCR**

Consultant Radiologist, Department of Radiodiagnosis, Bristol Royal Infirmary, University of Bristol, Marlborough Street, Bristol, UK

**S.N. Jones, MB, BS, MRCP, FRCR**

Consultant Radiologist, Poole General Hospital, Longfleet Road, Poole, Dorset, UK

**G.A.S. Lloyd, MA, DM, FRCR**

Consulting Radiologist, Department of Radiology, Royal National Throat, Nose and Ear Hospital, Gray's Inn Road, London, UK

**R. McLelland, MD**

Professor of Radiology, Department of Radiology, University of North Carolina School of Medicine, Chapel Hill, North Carolina, USA

**D.D.T. Maglinte, MD, FACR**

Gastrointestinal Radiologist, Section of Abdominal Radiology (GI), Department of Radiology, Methodist Hospital of Indiana, Clinical Professor of Radiology, Indiana University School of Medicine, Indianapolis, IN, USA

**Janet Murfitt, MRCP, FRCR**

Consultant Radiologist, The London Hospital, Whitechapel Road, London, UK

**D.W. Nelson, MD**

Head, Division of Musculoskeletal Radiology, Assistant Professor, Oregon Health Sciences University, Department of Radiology, Portland, Oregon, USA

**D.J. Ott, MD**

Professor of Radiology, Bowman Gray School of Medicine, Winston Salem, North Carolina, USA

**P. Renton, FRCR, DMRD**

Consultant Radiologist, University College Hospital Dental Hospital, Mortimer Market, London, UK

**C.S. Resnik, MD**

Associate Professor of Radiology, Department of Radiology, University of Maryland Hospital, Baltimore, Maryland, USA

**D. Rickards, FRCR, FFR(D)SA**

Consultant Radiologist, Department of Radiology, The Middlesex Hospital, London, UK

**M.B. Rubens, MB, BS, DMRD, FRCR**

Consultant Radiologist, National Heart, Brompton and London Chest Hospitals, London, UK

**S.I. Schabel, MD**

Professor of Radiology, Department of Radiology, Medical University of South Carolina, Charleston, South Carolina, USA

**F. Starer, FRCPEd, FRCR**

Consultant Radiologist, Westminster Hospital, Dean Ryle Street, London, UK

**J.M. Stevens, FRCR**

Consultant Radiologist, St Mary's Hospital, Praed Street, London, UK and The National Hospitals for Nervous Diseases, London, UK

**D. Sutton, MD, FRCP, FRCR, DMRD**

Consulting Radiologist, St. Mary's Hospital, University of London and The National Hospitals for Nervous Diseases, London, UK

**P. Wilde, BSc, MRCP, FRCR**

Consultant Cardiac Radiologist, Department of Radiodiagnosis, Bristol Royal Infirmary, Marlborough Street, Bristol, UK

**J.W.R. Young, MA, BM, BCh, FRCR**

Chief of Diagnosis, University of Maryland Hospital, Baltimore, Maryland, USA

---

**PART 1**  
**Respiratory System**

---

## CHAPTER 1

# METHODS OF INVESTIGATION AND INTERPRETATION OF THE CHEST RADIOGRAPH

*M. Rubens*

---

## METHODS OF INVESTIGATION

---

Various methods of imaging the chest are listed in Table 1.1. Radiologists should also be aware of other techniques important in the diagnosis of chest disease and these are listed in Table 1.2.

### PLAIN FILMS

#### Standard Views

The PA View. The patient is positioned erect with his anterior chest wall against the film, and scapulae rotated forwards so that they are clear of the lungs. A short exposure time minimizes blur due to cardiac pulsation. A voltage of about 70 kVp will produce good bony detail and demonstrate abnormal calcification. However, mediastinal detail and the lung posterior to the heart are not well demonstrated. On films taken at higher voltage (125–150 kVp) the bones and abnormal calcification are poorly demonstrated, but the pulmonary and mediastinal detail is improved (Fig. 1.1). Although the chest film is a fundamental investigation in suspected pulmonary or mediastinal disease it is important to remember that a normal chest radiograph does not exclude significant disease. For example, most cases of chronic bronchitis have a normal chest radiograph; small pleural effusions may not be visible on the standard film; CT

**Table 1.1.** Techniques for imaging the chest

Plain films
standard views: PA and lateral
other views: AP, supine, expiratory, apical, lordotic, decubitus, oblique
Linear tomography
Fluoroscopy
Bronchography
Barium studies
Angiography
pulmonary arteriography, aortography, bronchial arteriography, venography, lymphangiography
Computerized tomography
Radionuclide imaging
Ultrasound
MRI
Percutaneous biopsy

**Table 1.2.** Non-imaging techniques for investigating the chest

Respiratory function tests
Sputum examination for organisms and abnormal cells
Skin tests and serology
Bronchoscopy
transbronchial biopsy
bronchoalveolar lavage
Thoracoscopy
Mediastinoscopy and mediastinotomy
Thoracotomy and open lung biopsy

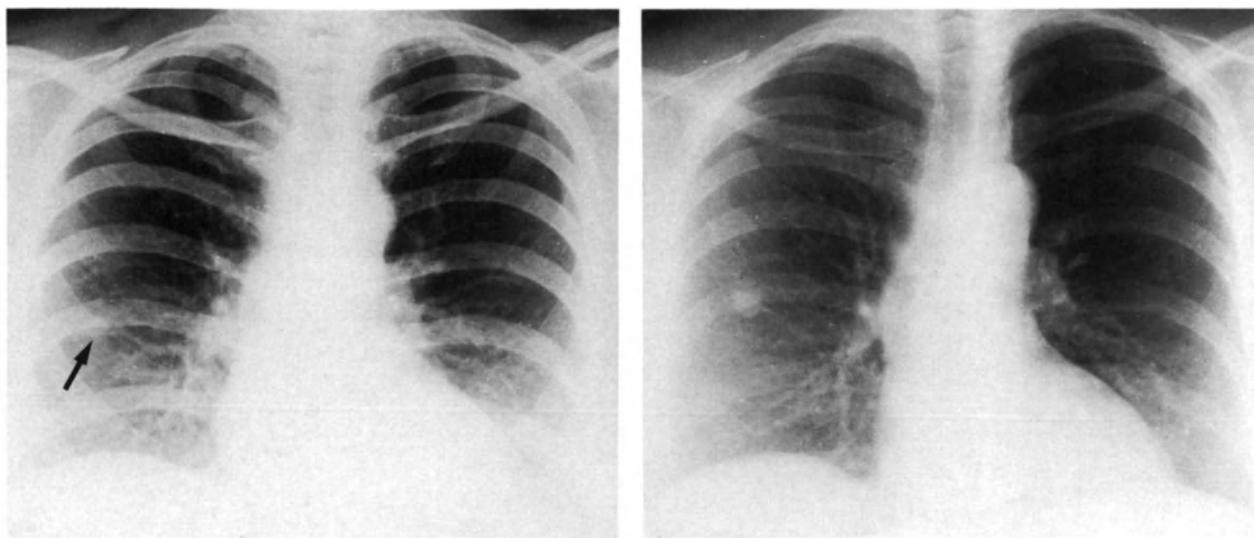


**Fig. 1.1.** A Low kVp film. Bone detail is well shown but a right mid-zone opacity (arrow) is barely visible. B High kVp film 7 days later. The right mid-zone nodule is clearly demonstrated – it was a carcinoid tumor. Compared to A the trachea is more clearly seen, but the ribs are not.

often shows small pulmonary nodules or evidence of pulmonary fibrosis not apparent on the chest film; patients with severe bronchiectasis, significant chronic obstructive airways disease or pulmonary emboli may have a normal chest radiograph.

Many manufacturers of X-ray equipment are currently developing digital chest radiography units. These units will not only provide easier storage, retrieval and transmission of images but will also improve image quality. Theoretically, all images will be of good technical quality, and the observer will be able to manipulate the data to produce the sort of image that is required.

**The Lateral View.** The lateral view may provide further information on the location, size and morphology of abnormalities seen on the PA view. Occasionally the lateral film will reveal an abnormality not visible on the other view, especially in the retrosternal and retrocardiac areas.

#### Other Views

**The AP View.** Most chest films taken with mobile equipment are AP views; compared to the PA view the heart is magnified. On occasion, a PA film shows a nodule that is completely overlaid by a rib. In these instances an AP film, by altering the projection of lungs and ribs, will determine if the nodule is within rib or lung.

**Supine Film.** In patients not fit enough for an erect film, a supine film may be taken. In this position, compared to an erect film, the upper zone vessels appear enlarged and may mimic pulmonary venous hypertension. Free pleural fluid, if present, may settle posteriorly and cause extensive opacification (Chap. 2, Fig. 2.24C).

**Expiratory Film.** A standard PA film should be taken at end-inspiration. However, a PA film at end-expiration may be useful to demonstrate air trapping or a small pneumothorax (Chap. 2, Fig. 2.28; Chap. 3, Figs 3.10, 3.11).

**Apical and Lordotic Views.** These views may demonstrate the lung apices more clearly than the standard PA view by

projecting the clavicles above the lung. The lordotic view may on rare occasions be used to demonstrate right middle lobe collapse (Chap. 3, Fig. 3.24).

**Decubitus Views.** Decubitus films may be used to demonstrate small pleural effusions, and to differentiate between elevation of the diaphragm and subpulmonic pleural effusion, and between free fluid and other pleural shadowing (Chap. 2, Fig. 2.19).

**Oblique Views.** Oblique films are useful to demonstrate or confirm the presence of pleural plaques. They are best produced with fluoroscopy so that the optimum degree of obliquity may be selected (Chap. 2, Fig. 2.37).

#### LINEAR TOMOGRAPHY

Where CT is available linear tomography of the chest is now rarely performed. If CT is not available it may be used in the following situations:

- Pulmonary Nodules and Masses.** Tomography may provide morphological data that are not apparent on the plain film, and which may aid diagnosis (Fig. 1.2). These include the absence or presence of calcification, cavitation or an air bronchogram and the characteristics of the edge of the lesion and involvement of adjacent structures. Whole lung tomography may be used to search for metastases or other lesions. Tomography may also be used to locate a lesion visible on only one of the standard views of the chest.
- Pulmonary Apices.** Tomography demonstrates the lung apices more clearly than apical and lordotic views.
- Hila.** In cases of hilar enlargement tomography may differentiate between enlargement of vessels and lymphadenopathy or other masses. Some authorities advocate the use of the 55° posterior oblique position for this purpose.

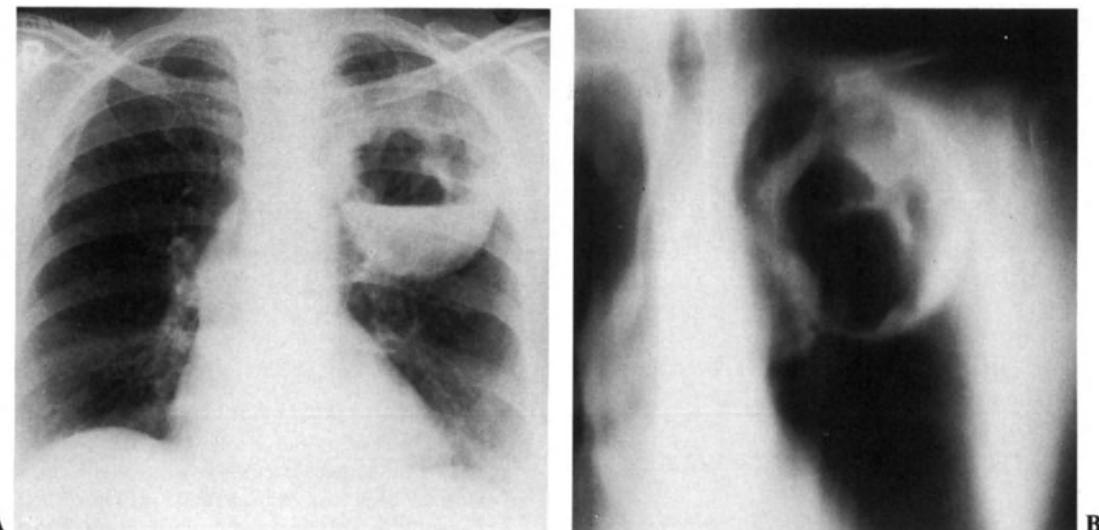


**Fig. 1.2.** A A fluid level is clearly visible in the left mid-zone, but the upper zone shadowing is not clearly seen. B Linear tomography clearly demonstrates a cavity with an irregular wall. Squamous cell carcinoma.

4. *The Mediastinum.* Mediastinal masses and abnormalities of the major airways may be shown more clearly than on plain films (Chap. 3, Figs 3.2, 3.4).

#### FLUOROSCOPY

Fluoroscopy is useful in assessing movement of the diaphragm in suspected phrenic paresis or paralysis. It may be used to assess movement of the mediastinum, especially in children, where there is suspected obstructive emphysema. It is also useful in helping to locate abnormalities that are visible on only one of the standard views of the chest. It is a poor method of differentiating between transmitted and true pulsation of a mass.



**Fig. 1.3.** Barium swallow demonstrates compression of mid-esophagus by enlarged subcarinal lymph nodes in patient with carcinoma of lung.

#### BARIUM STUDIES

Barium swallow may be used in neonates to diagnose esophago-tracheal fistulae. In adults it may demonstrate esophageal causes of lung disease e.g., aspiration pneumonia secondary to pharyngeal pouch, hiatus hernia, achalasia, scleroderma or broncho-esophageal fistula.

Vascular rings may produce characteristic indentation of the barium-filled esophagus, and mediastinal lymphadenopathy or other masses may displace, narrow or invade the esophagus (Fig. 1.3).

#### BRONCHOGRAPHY (Fig. 1.4)

The segmental and subsegmental bronchi are best assessed by fibre-optic bronchoscopy, so that bronchography is now only used to any extent in the diagnosis of bronchiectasis (Chapt. 3, Figs 3.15, 3.16), and even here there is increasing use of narrow section CT.

Bronchography may be performed by passing a tube through the mouth or nose, by cricothyroid membrane puncture or via a fibre-optic bronchoscope.

#### ANGIOGRAPHY

*Pulmonary Arteriography.* The main use of pulmonary arteriography is in the diagnosis of pulmonary embolism. Other indications are the evaluation of pulmonary arterial hypertension, and the assessment of congenital pulmonary vascular abnormalities (e.g., arteriovenous malformation (Fig. 1.5), pulmonary valve stenosis, pulmonary artery hypoplasia, anomalous pulmonary venous return).

*Aortography.* Arch aortography is used to assess widening of the mediastinum following acute trauma. Aortography is also used to investigate pulmonary sequestration.

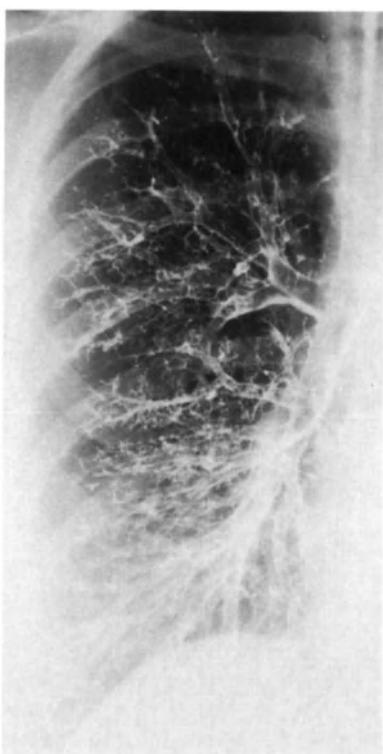


Fig. 1.4. Bronchogram showing normal right lung.

**Bronchial Arteriography.** Bronchial arteriography may be used to investigate the source of recurrent or severe hemoptysis in cases of bronchiectasis or mycetoma, and may be combined with therapeutic bronchial artery embolisation.

**Venography.** Superior vena cavography may be indicated in superior vena caval obstruction. Leg venography may be performed in cases of pulmonary embolism.

**Lymphangiography.** Lymphangiography may be indicated in the evaluation of chylothorax.

#### COMPUTERIZED TOMOGRAPHY (CT)

CT provides excellent anatomic detail of the chest wall, pleura, lungs and mediastinum (Fig. 1.6), and with contrast enhancement the great vessels are well demonstrated (Fig. 1.7). The main indications for chest CT are as follows:

1. *Staging Lung Cancer.* This is discussed in Chapter 5.
2. *Staging Other Malignant Tumors.* In patients with known malignant disease, CT is much more sensitive in detecting small pulmonary metastases than the chest film. Nodules as small as 3 mm in diameter may be identified. However, this may present a problem where a solitary nodule is discovered, since it is often impossible to differentiate a granuloma from a metastasis.
3. *Diffuse Lung Disease* (Fig. 1.8). Narrow section CT is more sensitive than the chest film in detecting pulmonary fibrosis, emphysema and bronchiectasis. Areas of air trapping may be demonstrated on expiratory scans.
4. *Pleural Disease.* Small pleural effusions and plaques are more easily seen than on plain films. It is possible to distinguish between pleural fluid and pleural thickening, and the extent of pleural tumors can be shown (Fig. 1.7). CT is also useful in differentiating empyema from lung abscess in difficult cases.
5. *Mediastinal Disease.* CT may be used to assess mediastinal widening. It is used to stage lymphomas and other mediastinal tumors. With rapid sequential scanning CT provides accurate assessment of aortic aneurysms and aortic dissection.

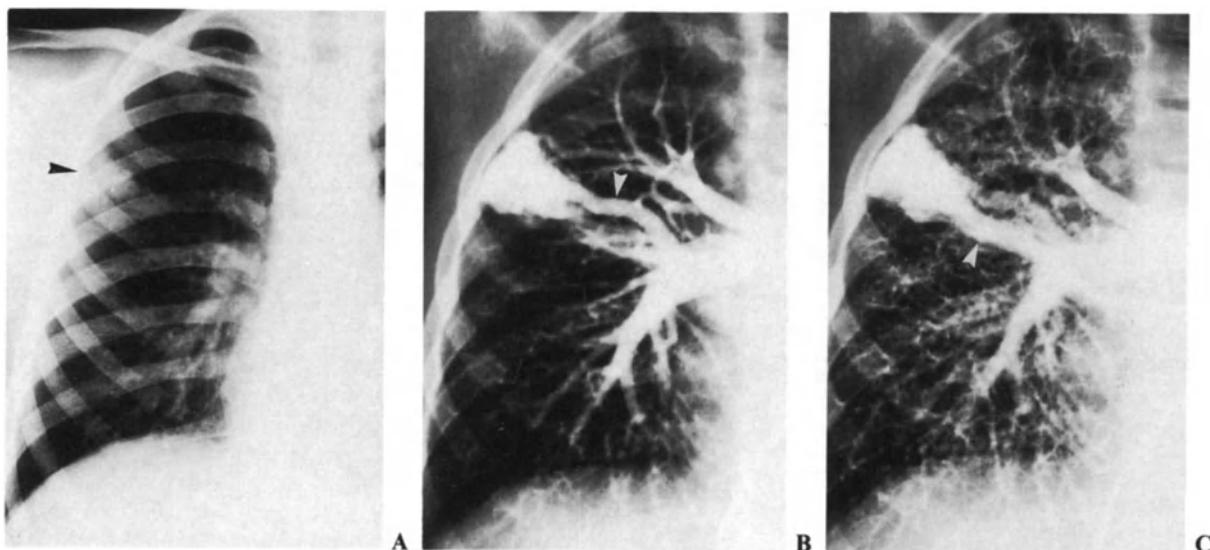
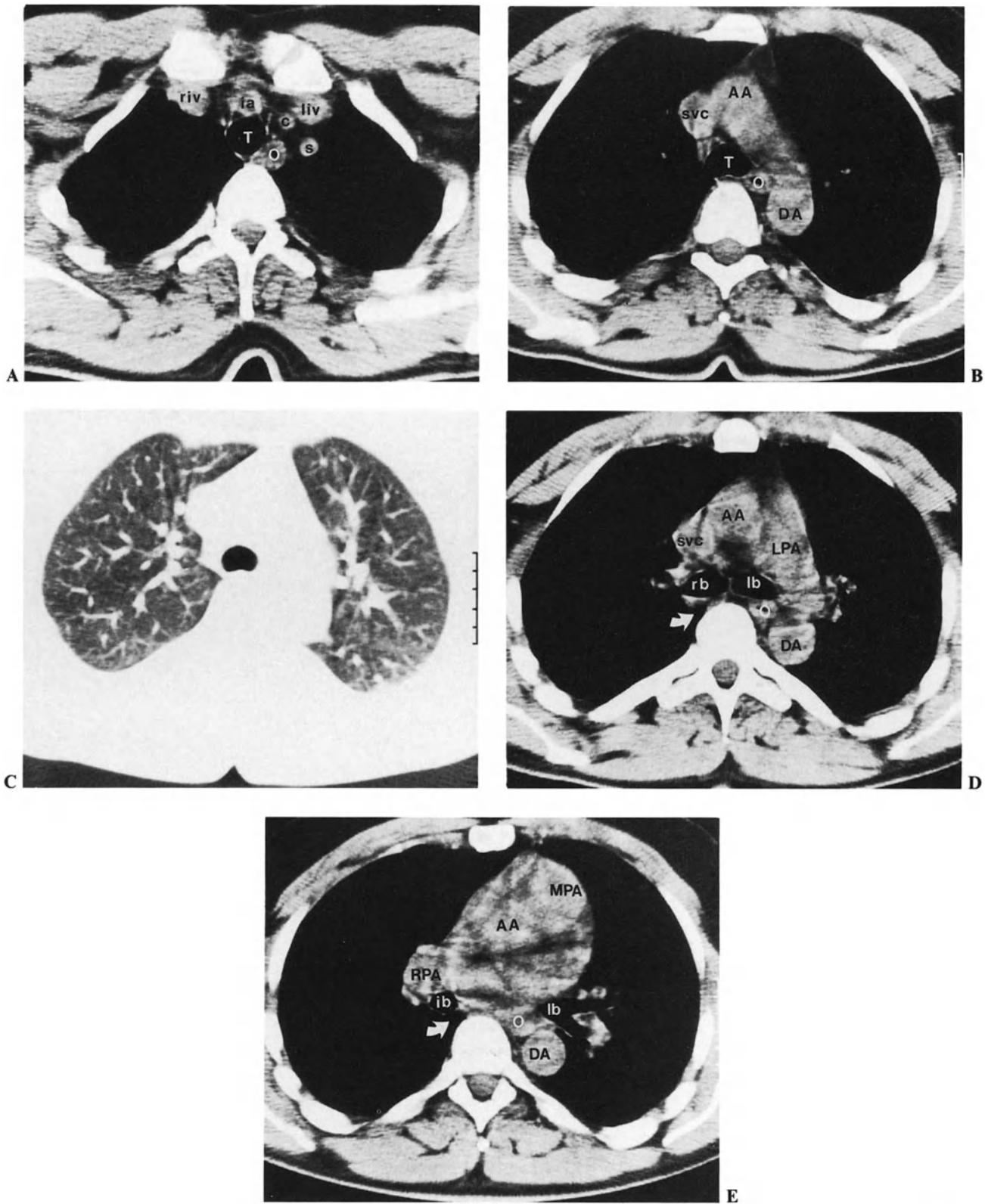


Fig. 1.5.A Peripheral opacity (arrowhead) can be seen in periphery of right upper zone. B Pulmonary arteriogram: early arterial phase shows opacification of the opacity by large feeding artery (arrowhead). C Late arterial phase shows early filling of draining vein (arrowhead). Pulmonary arteriovenous malformation.



**Fig. 1.6A–E.** Normal unenhanced CT scans. A Above level of aortic arch. B Just below aortic arch, through aorticopulmonary window. C Same level as B on lung settings. D At level of carina. E Below carina. AA, ascending aorta; DA, descending aorta; C, left common carotid artery; S, left subclavian artery; ia, innominate artery; riv, right innominate vein; liv, left innominate vein; SVC, superior vena cava; MPA, main pulmonary artery; LPA, left pulmonary artery; RPA, right pulmonary artery; T, trachea; O, esophagus; lb, left bronchus; rb, right bronchus; ib, intermediate bronchus. Curved arrow indicates azygo-esophageal recess.

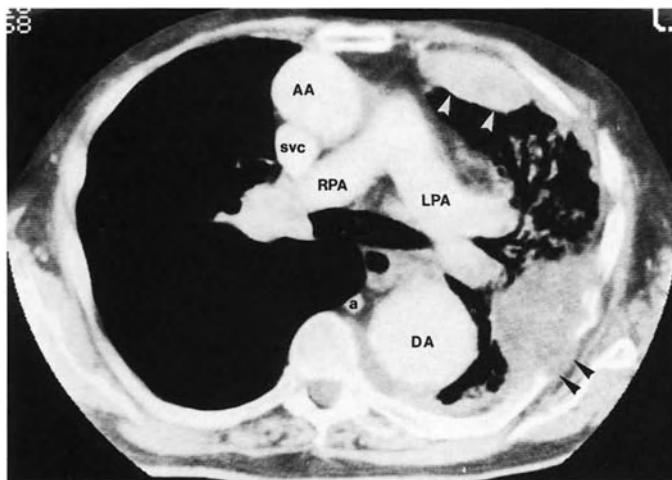
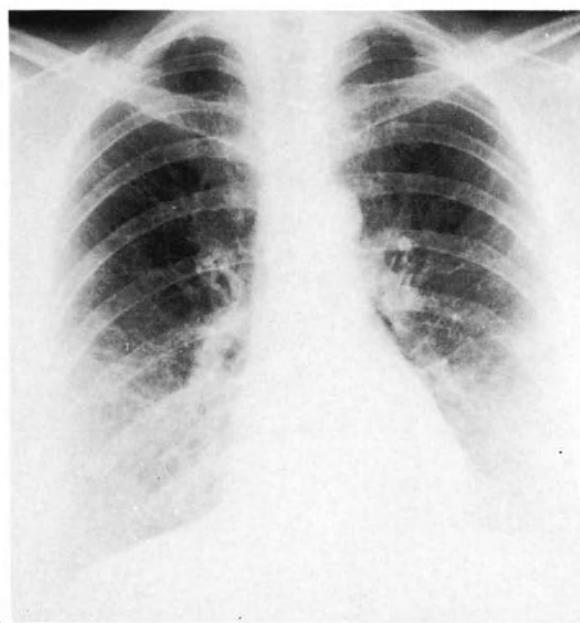


Fig. 1.7. Enhanced CT scan at level of bifurcation of main pulmonary artery. The left lung is surrounded by pleural masses (arrowheads); the posterior mass is invading the chest wall. The vascular anatomy of the mediastinum is well shown. a, azygos vein. Other abbreviations as in Fig. 1.6. The descending aorta is dilated.

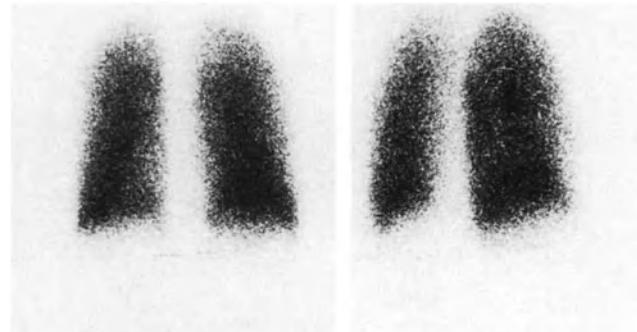


A



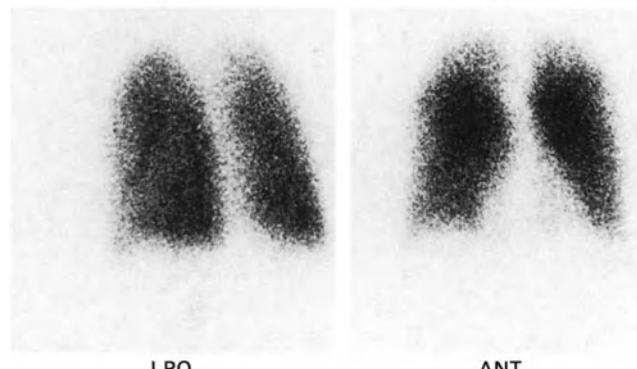
B

Fig. 1.8A,B. Diffuse lung disease. A The chest radiograph appears normal. B Narrow section (3 mm) CT scan shows diffuse honeycomb shadowing.



POST

RPO



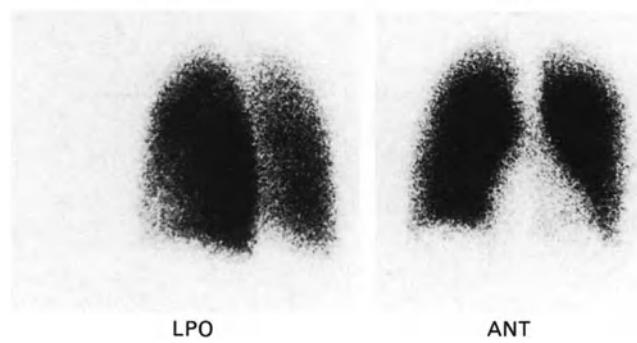
LPO

ANT



POST

RPO



LPO

ANT

B

Fig. 1.9.A Normal istope ventilation scan.  $^{99}\text{Tc}$ -DTPA aerosol. B Normal isotope perfusion scan.  $^{99}\text{Tc}$ -labelled microaggregate.

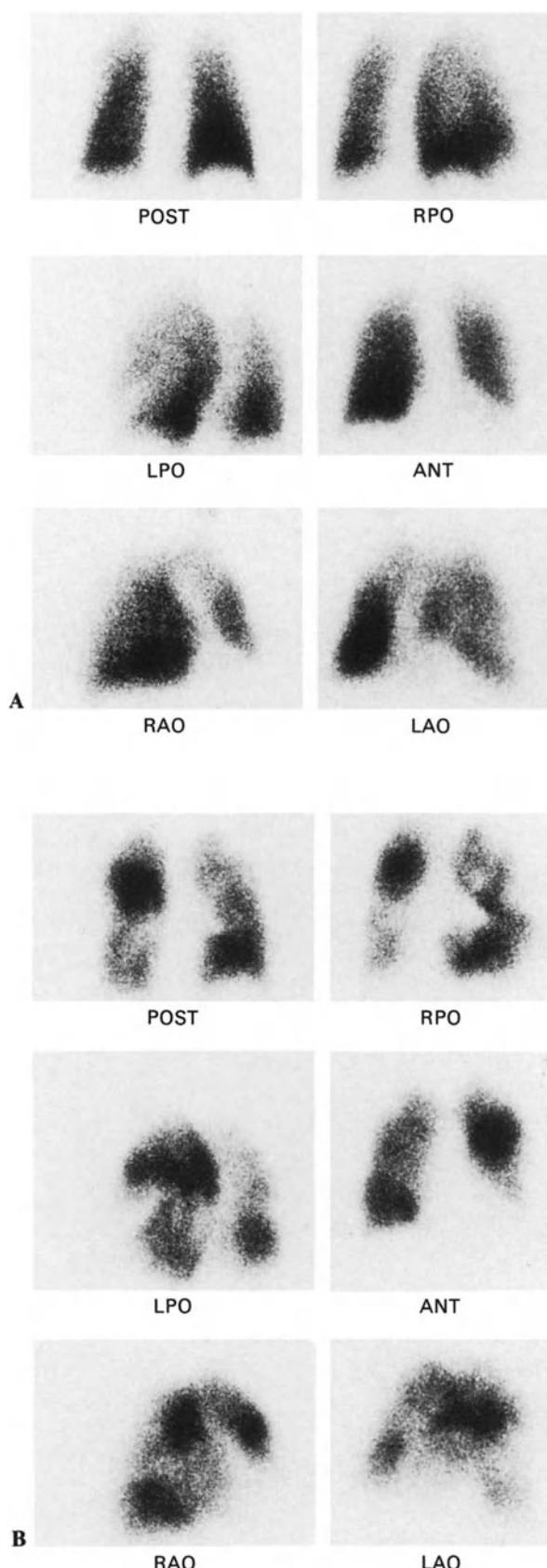


**Fig. 1.10A,B.** Multiple pulmonary emboli. A Normal ventilation scan. B Multiple pleural-based, segmental perfusion defects.

## RADIONUCLIDE SCANNING

**Ventilation and Perfusion Scanning** (Fig. 1.9). Pulmonary ventilation scanning is usually performed with xenon, krypton or a technetium aerosol.  $^{133}\text{Xe}$  is most commonly used; its half-life of 5.7 days allows it to be used to assess not only which areas of lung are ventilated, but also areas of air trapping.  $^{81}\text{Kr}^m$  has a half-life of 13 seconds. It is derived from rubidium-81 which is produced by a cyclotron and has a half-life of 4.5 hours. Its use, therefore, depends on a nearby source, and is limited to defining areas of ventilation.

$^{99}\text{Tc}$ -DTPA aerosol is a convenient alternative to the above gases; it is readily available and inexpensive, but tends to be deposited in the major airways in patients with obstructive airways disease. However, in other patients it works well.

Perfusion scanning is usually performed with  $^{99}\text{Tc}$ -labelled human serum albumin microspheres or microaggregates, injected intravenously. The patient is scanned in the anterior, posterior and both oblique positions and distribution of isotopes reflects the perfusion of the lungs. The main indication for ventilation/perfusion scanning is the diagnosis of *pulmonary embolism*. Relative contraindications to perfusion scanning are pulmonary arterial hypertension and right-to-left intracardiac shunts.

Multiple segmental perfusion defects with a normal ventilation scan and chest radiograph are diagnostic of pulmonary emboli (Fig. 1.10). Matching ventilation and perfusion defects may be seen with a variety of parenchymal pulmonary abnormalities.

**Gallium Scanning.** Gallium-67 has been used to identify areas of infection, inflammation and neoplasia in the chest, and areas of abnormal uptake may be present without radiographic abnormality. It has been used to assess activity of sarcoidosis and fibrosing alveolitis.

## ULTRASOUND

Ultrasound is useful in assessing pleural, mediastinal and subphrenic disease. It is possible to localize pleural fluid collections accurately. Moreover, it will differentiate between pleural fluid and pleural thickening or masses (Fig. 1.11).

## MAGNETIC RESONANCE IMAGING (MRI)

The place of MRI in the investigation of pulmonary and pleural disease has yet to be established. There is no doubt that it is a useful method in examining the heart and great vessels, where it provides both morphological (Fig. 1.12) and hemodynamic information. It is more sensitive than CT in detecting hilar and mediastinal lymphadenopathy. However, in the lungs it has not yet been shown to have any advantage over CT, other than its non-use of ionizing radiation, and the greater ease of reconstructing images in any chosen plane.

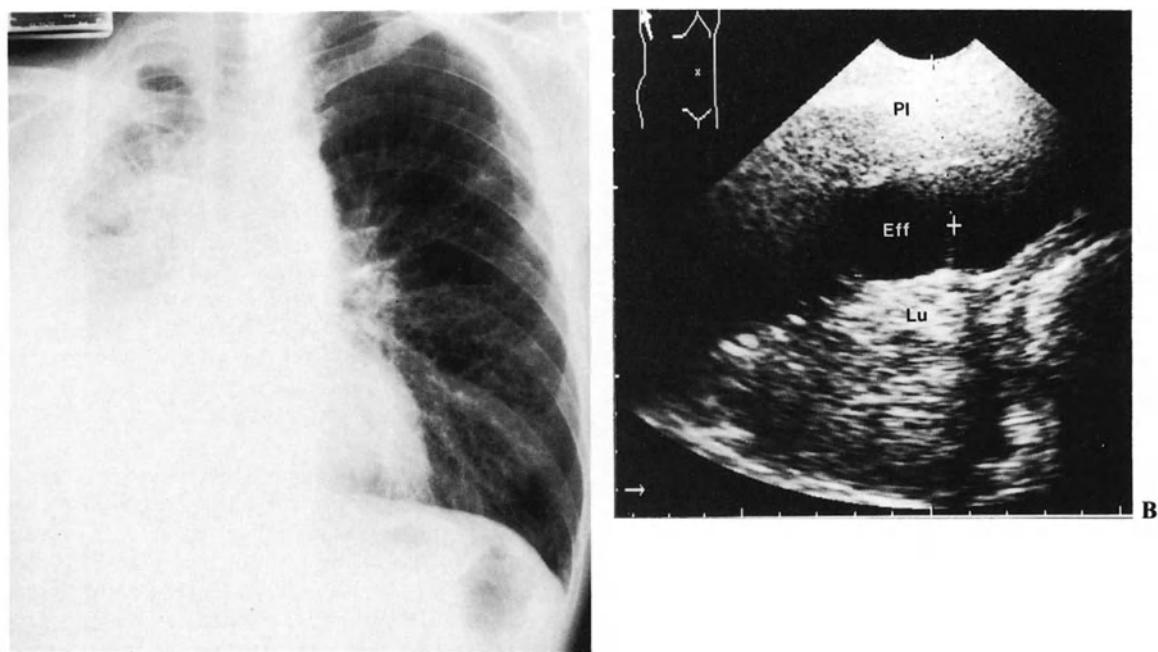


**Fig. 1.11.** A Chest radiograph shows extensive right pleural shadowing. B Ultrasound scan shows that the pleural abnormality is due to gross pleural thickening (pl) and pleural effusion (Eff), and that the underlying lung (Lu) is consolidated.

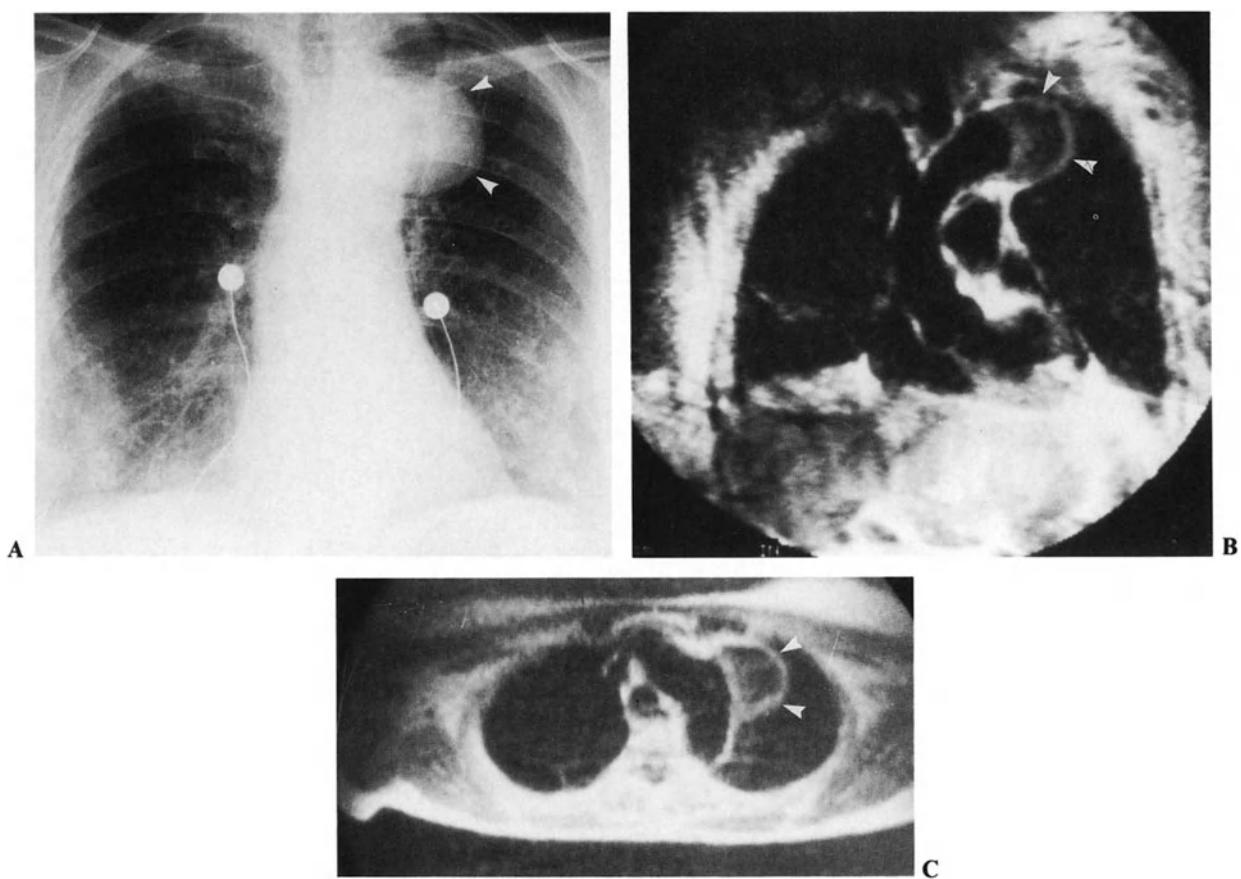


**Fig. 1.12.** A Chest radiograph shows a rounded opacity (arrowheads) contiguous with the aortic knuckle. B, C Coronal and transverse MRI scans show that the mass is an aneurysm of the arch of the aorta and that it is filled with thrombus.

## PERCUTANEOUS BIOPSY

Percutaneous needle biopsy of pulmonary and pleural lesions may be performed with fluoroscopic, ultrasound or CT con-

trol. For intrapulmonary lesions a narrow gauge needle (22 to 18 s.w.g.) is usually used. For pleural-based masses a larger, cutting needle may be used. Complications include pneumothorax and hemoptysis.

## INTERPRETATION OF THE CHEST RADIOGRAPH

Correct analysis of the chest radiograph requires an orderly approach to the film, and a knowledge of normal criteria. A suggested routine is outlined in Table 1.3.

**Table 1.3.** Analysis of the chest radiograph

Clinical data	
name	
age	
gender	
clinical problem	
Technical data	
right/left marker	
centering	
penetration	
depth of inspiration	
Bones and soft tissues	
bone texture	
skeletal deformity	
evidence of previous surgery, trauma or bone destruction	
Diaphragm	
clarity	
shape	
position	
Upper abdomen	
abnormal gas shadows or calcification	
Lungs	
relative density of lungs	
vascular pattern	
size, shape, density and position of hilae	
position of fissures	
clarity of costophrenic angles	
abnormal opacities	
Mediastinum	
trachea	
position	
subcarinal angle	
azygos vein: size	
aorta: size, position	
heart: size, shape, position	

### Clinical Data

It is essential to check the film for the name of the patient and the date of the examination. It is important to know the age and sex of the patient and other clinical data which will make various diagnoses more or less likely.

### Quality of the Film

1. Look for the right or left marker. Abnormal situs is of greater importance in congenital heart disease than in pulmonary disease, but there is an association between bronchiectasis and situs inversus.

2. Is the film properly centered? The medial ends of the clavicles should be equidistant from the mid-line (Fig. 1.13). Rotation of the patient may distort the mediastinum and the side to which the patient is rotated may appear hypertransradiant.

3. Is the film properly penetrated? An overpenetrated film may need examination with a bright light to reveal low density shadows, while an underpenetrated film may conceal overlapping structures.

4. Has the patient taken a full inspiration? The mid-point of the right hemidiaphragm should lie between the anterior ends of the 5th and 7th ribs. An expiratory film may give a false impression of cardiomegaly and abnormal basal pulmonary shadowing (Fig. 1.13).

### Bones and Soft Tissues

The bones and soft tissues should be carefully examined for abnormalities (see Chap. 2).

Normal features that may mimic pulmonary disease are nipple shadows, companion shadows related to the ribs and clavicles, clavicular rhomboid fossae and costal cartilage calcification.

### Diaphragm

The right hemidiaphragm is usually 1–2 cm higher than the left, but a large amount of air in the stomach or splenic flexure may alter this relationship. The curve of the diaphragm may be assessed by measuring the distance between the highest point of the diaphragm and a line joining the costophrenic and cardiophrenic angles (Fig. 1.13). This should normally be at least 1.5 cm.

### Upper Abdomen

Look below the diaphragm for any abnormal gas shadows. An occasional normal variant is interposition of bowel between the liver and diaphragm – Chilaiditi's syndrome (Fig. 1.14). The position of the stomach, liver and spleen should be checked if abnormal situs is suspected. Calcified hepatic and splenic granulomas and gallstones are occasionally visible on the chest radiograph.

### Lungs

The lungs should be equally transradiant. Pulmonary vessels and interlobar fissures are responsible for the normal lung markings. All other opacities overlying the lungs require explanation, and should be regarded as pathological until proved otherwise. Overlying soft tissues and skeletal opacities, combination shadows and artefacts are a frequent explanation. The costophrenic angles should be clearly defined.

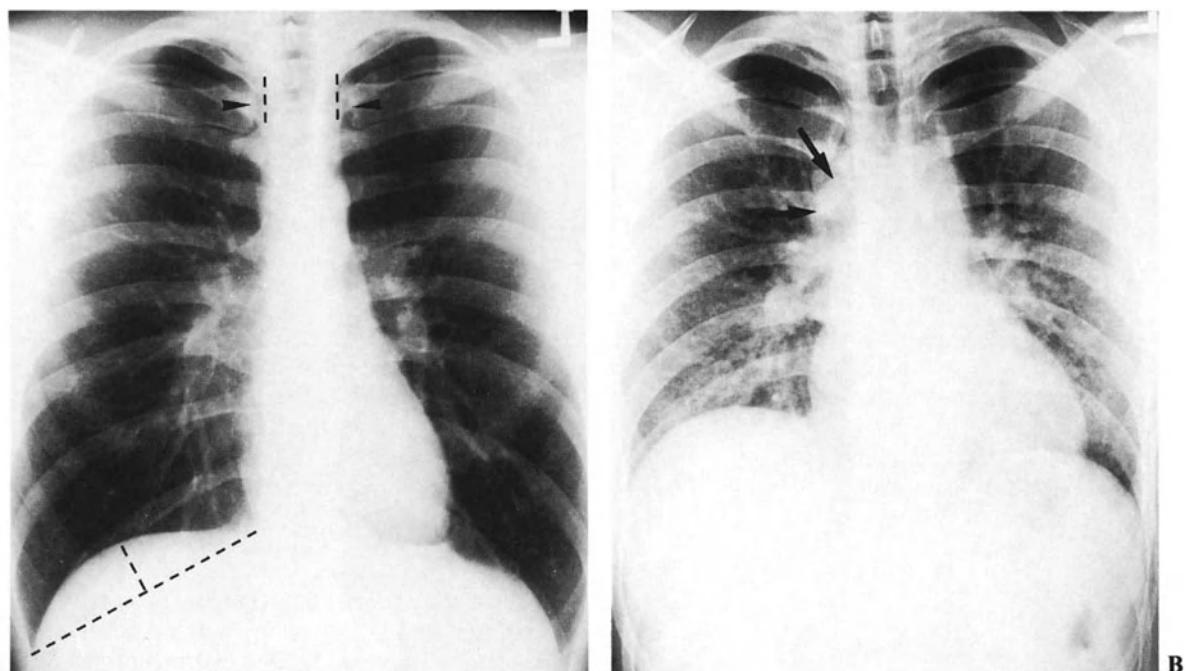


**Fig. 1.13.** A Normal PA film at end-inspiration. The level of the diaphragm is below the anterior end of the 6th rib. This film is well-centered and the curvature of the diaphragm is normal – see text. B Same patient. PA film at end-expiration. Compared to A the heart appears larger, the density of the lungs has increased, the hila are prominent and the azygous vein (arrows) has enlarged.

There are certain areas where abnormalities are easily overlooked and they require careful scrutiny. These are the apices, the retrosternal space, the retrocardiac area, the perihilar regions and the posterior costophrenic recesses. The lateral film is often helpful in assessing these areas.

**Pulmonary Vessels.** On an erect film the lower zone vessels are larger than the upper zone vessels. Comparison of the lower, mid and upper zones on either side should show symmetry in both size and number of vessels in each lung (Fig. 1.15). The diameter of the normal right basal artery is 9–

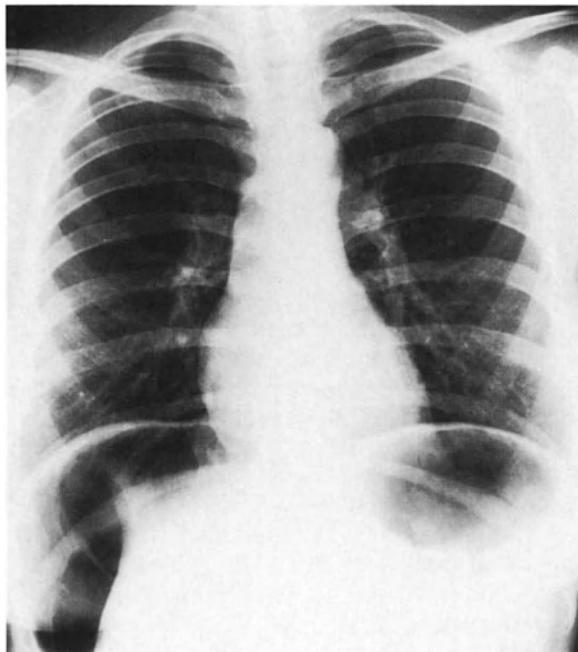


**Fig. 1.14.** Colon is interposed between the liver and right hemidiaphragm.

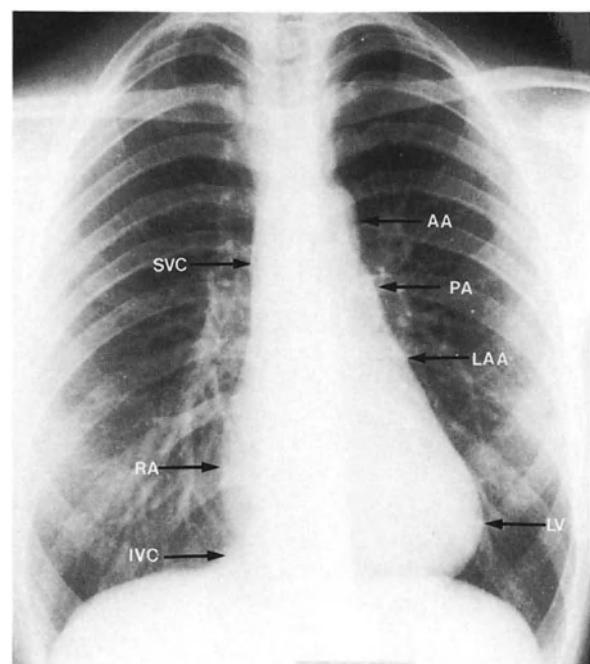


**Fig. 1.15.** Normal chest radiograph. The lungs are equally transradiant and the pulmonary vascular pattern is symmetrical. AA, aortic arch; SVC, superior vena cava; PA, pulmonary artery; LAA, left atrial appendage; RA, right atrium; LV, left ventricle; IVC, inferior vena cava.

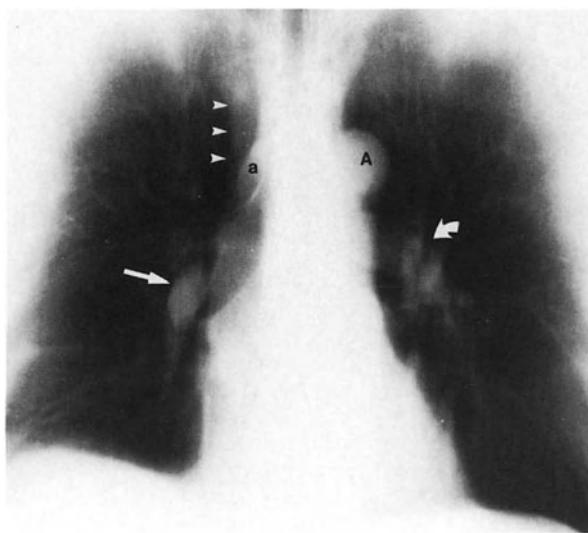


**Fig. 1.16.** Tomogram shows that right hilum (straight arrow) is lower than the left (curved arrow). Superior vena cava (arrowheads), azygos vein (a) and aortic knuckle (A) are well seen.

16 mm. Disturbance of the pulmonary vascular pattern may be due to pulmonary or cardiovascular disease.

**The Hila.** On the chest radiograph the normal hilar shadows are formed by the pulmonary arteries and upper lobe veins. Normal lymph nodes are not visible. The left hilum is 0.5–1.5 cm higher than the right (Fig. 1.16). They

should be of similar radiodensity. Hilar enlargement may be due to enlargement of the hilar vessels or lymph nodes, or to a mass. Vascular enlargement tends to produce a smooth convex outline, but masses and lymphadenopathy often appear lobulated.

**Interlobar Fissures (Fig. 1.17).** The horizontal fissure separates the right upper and right middle lobes. It is visible on approximately 50% of chest radiographs. The oblique fissure separates the lower lobe from the rest of the lung, and is often visible on the lateral film. An azygos fissure is present in approximately 1% of the population. It encloses the azygos vein and separates an azygos lobe from the rest of the right upper lobe. A superior accessory fissure is rarely seen. It separates the apical segment of the lower lobe from the basal segments.

### Mediastinum

**Trachea and Main Bronchi.** The trachea lies in the mid-line proximally, but distally it is deviated to the right by the aortic arch. The lumen appears as a translucent band of uniform width. In adults it is normally 1.5–2 cm wide. The right paratracheal stripe is a band of tissue outlined by air in the tracheal lumen and right lung; it is normally less than 5 mm wide. The subcarinal angle, subtended by the main bronchi, is normally 60–70°. This angle may be increased by left atrial enlargement and subcarinal lymphadenopathy (Fig. 1.18).

**Azygos Vein (Figs 1.13, 1.16).** The termination of the azygos vein may be seen as it arches anteriorly in the angle between the trachea and right main bronchus. It is normally less than 7 mm in diameter on an erect film.

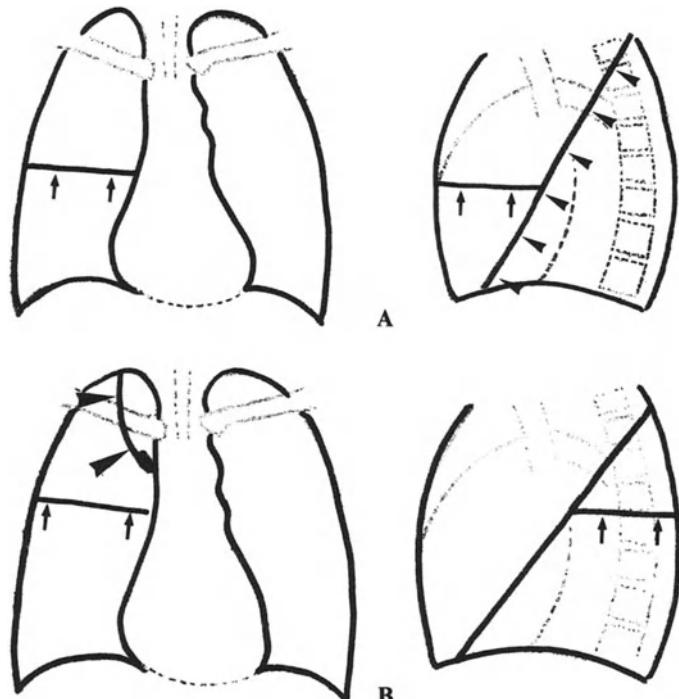


**Fig. 1.17.** A Normal fissures. Horizontal fissure (arrows). Oblique fissure (arrowheads). B Accessory fissures. Azygos fissure (arrowheads). Superior accessory fissure (arrows).

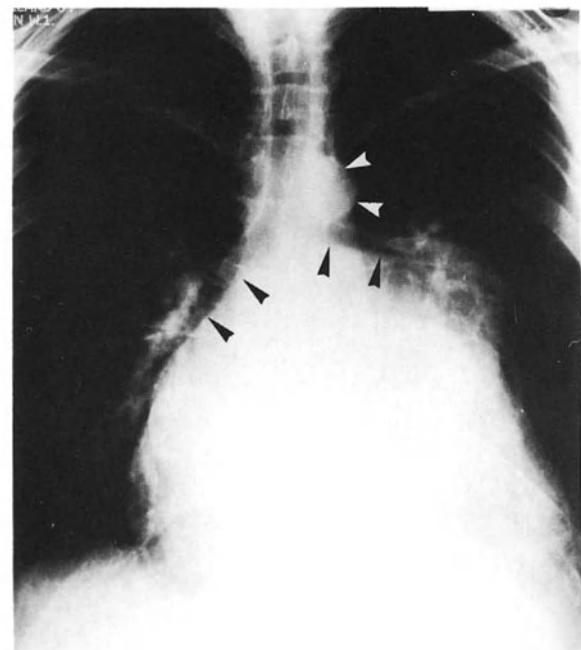


**Fig. 1.18.** Increased subcarinal angle. The angle between the right and left bronchi (black arrowheads) is increased, the left bronchus being elevated by a grossly enlarged left atrium. The aortic arch (white arrowheads) is left-sided.

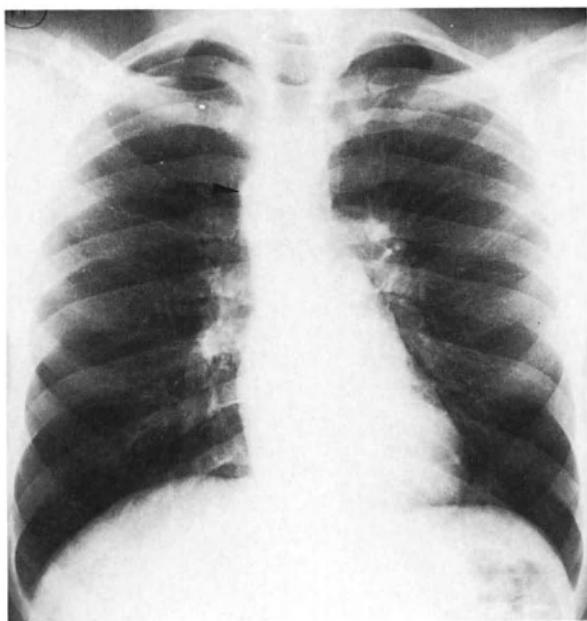


**Fig. 1.19.** Right aortic arch (arrowhead). This should not be mistaken for a right paratracheal mass.

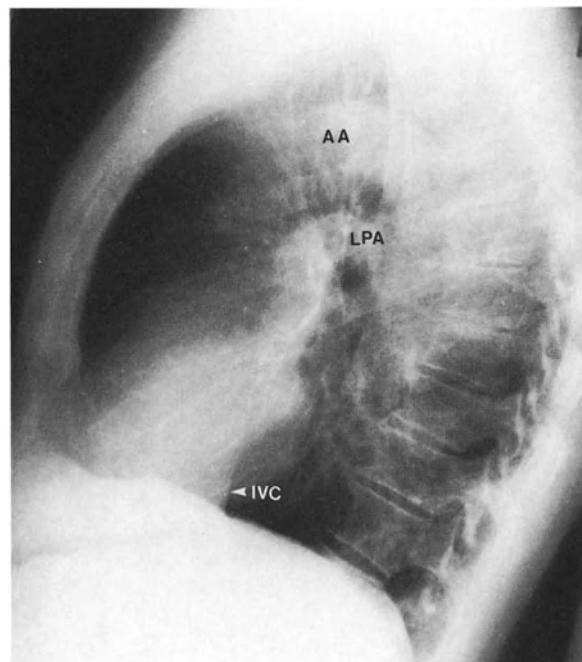


**Fig. 1.21.** Normal lateral film. AA, aortic arch; LPA, left pulmonary artery; IVC, inferior vena cava.

**Aorta.** The aortic arch is usually left-sided i.e., it arches over the left main bronchus (Fig. 1.18). It produces an indentation in the left side of the trachea. A right aortic arch may simulate a right paratracheal mass (Fig. 1.19).

**Heart.** The cardiovascular silhouette (Fig. 1.15) overlies the mid-line, usually about two thirds being to the left and one third to the right. The left and right borders should be

sharply defined. From above down, the right border comprises superior vena cava, right atrium and, sometimes, a short segment of inferior vena cava. In older patients ascending aorta may form part of the upper right cardiovascular silhouette. The left border comprises, from above down, aortic knuckle, pulmonary trunk, left atrial appendage and left ventricle.

Fat surrounding the heart may form epicardial fat pads. These may occupy the cardiophrenic angles and simulate cardiac enlargement (Fig. 1.20). Cardiac size is discussed further in Chap. 9.

**Thymus.** In infants and young children the thymus occupies a large part of the anterior mediastinum, and may obscure parts of the upper cardiovascular silhouette (Chap. 7, Fig. 7.1).

#### Analysis of the Lateral Film

The lateral film should be examined in the same methodical way as the PA film. In this view the radiodensity of the spine should decrease progressively from above down (Fig. 1.21). As in the PA view both domes of the diaphragm should be clearly visible, except where the heart is adjacent to the left dome. In adults the retrosternal and retrocardiac areas should both be occupied by aerated lung, and, therefore, appear radiolucent.

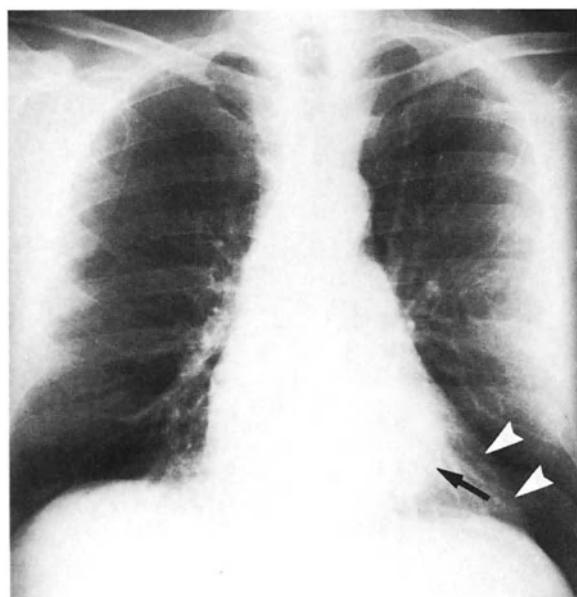


**Fig. 1.20.** An epicardial fat pad (arrowheads) overlies the cardiac apex (arrow).

#### THE ABNORMAL CHEST RADIOGRAPH

When an abnormality is encountered on a chest radiograph an attempt should be made to describe the abnormality in terms that will help the diagnosis. Try to determine if the

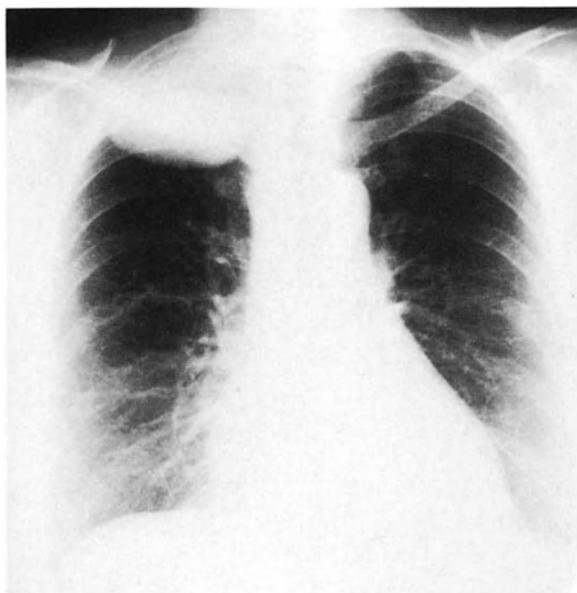


**Fig. 1.22.** Extrapleural mass. The right apical mass is sharply circumscribed, and is associated with destruction of the posterior part of the 3rd rib. Plasmacytoma.

**Table 1.4.** Extrapleural lesions

- Metastasis to ribs or soft tissues
- Rib fracture with or without hematoma
- Primary bone tumors and tumor-like conditions
- Soft tissue tumors (lipoma, fibroma etc)
- Hematoma from recent surgery or central line placement
- Plombage
- Chest wall infection

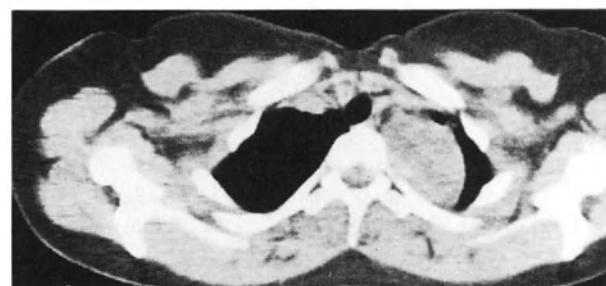
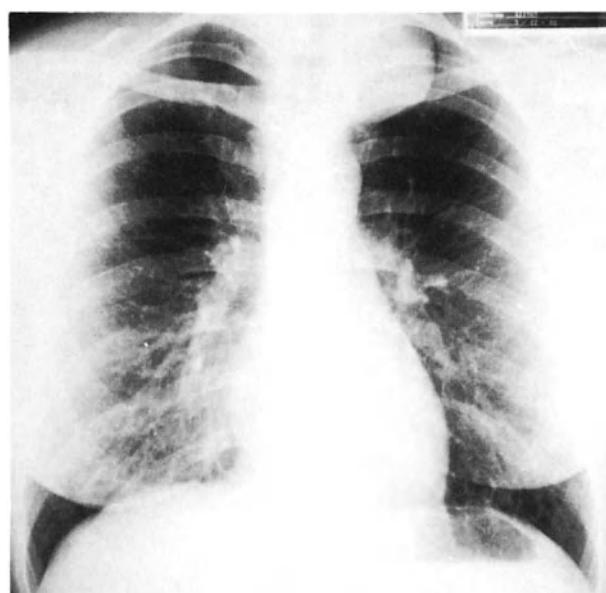


**Fig. 1.24A, B.** Posterior apical mediastinal mass. A well-margined mass in the left paraspinal recess. No bone involvement. Myxoid chondrosarcoma.

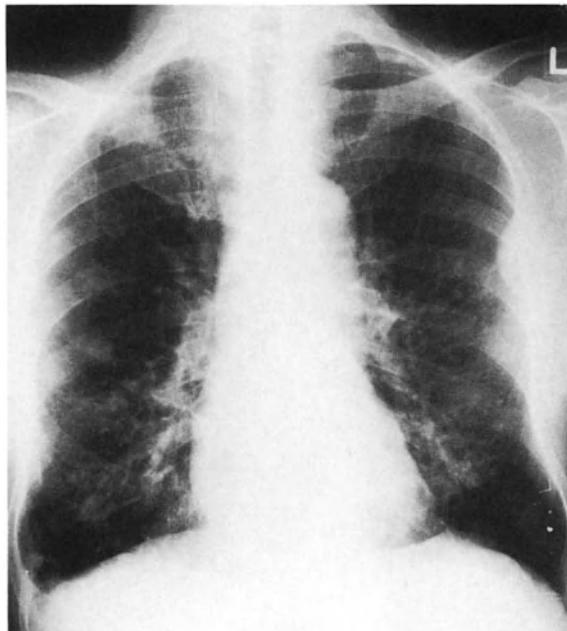


**Fig. 1.23.** Extrapleural mass in periphery of left mid-zone. Note its sharp outline and concave shape superiorly as it merges with the chest wall. Note also pulmonary nodules and small right pleural effusion. Metastatic malignant melanoma.

abnormality involves the extrapleural space, mediastinum, pleura or lung. Is the abnormality solitary, multiple or diffuse? Does the clinical background help? Last, but not least, try to obtain any previous films.

#### Extrapleural Lesions

Most extrapleural lesions arise in ribs (see Table 1.4). They are often associated with a visible bony abnormality (Fig. 1.22). The inner surface is limited by the parietal pleura, so that other than displacement of the pleura evidence of pleural disease may be absent. The edge of the lesion adjacent to the lung is remarkably sharply defined, and where seen adjacent to chest wall is usually concave (Fig. 1.23).

#### Mediastinal Lesions

Mediastinal lesions also lie outside the parietal pleura and are, therefore, usually sharply demarcated (Fig. 1.24).

#### Pleural Lesions

Pleural fluid usually collects in the costophrenic angles and has an upper concave surface (Fig. 1.25). However, 'atypical' patterns of pleural effusion are not uncommonly encountered. Fortunately even in these cases there is usually some evidence of blunting of the costophrenic angle or of fluid tracking into a fissure (Fig. 1.26). Pleural thickening and

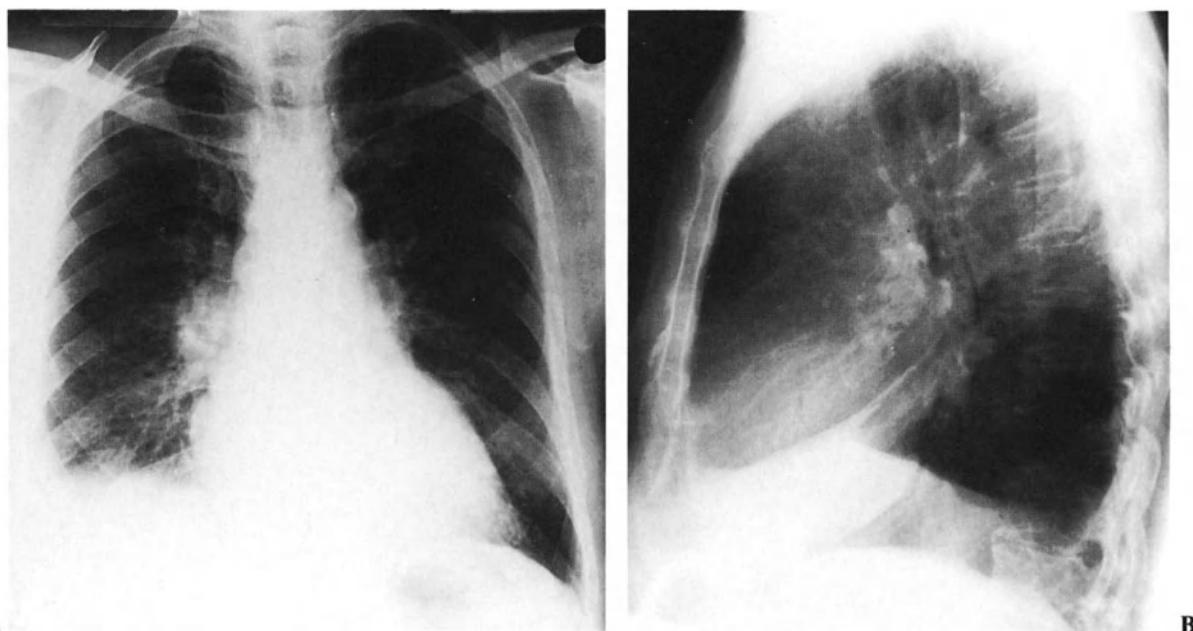


**Fig. 1.25A, B.** Pleural effusion. Homogenous density filling right costophrenic angle and extending into oblique fissure.

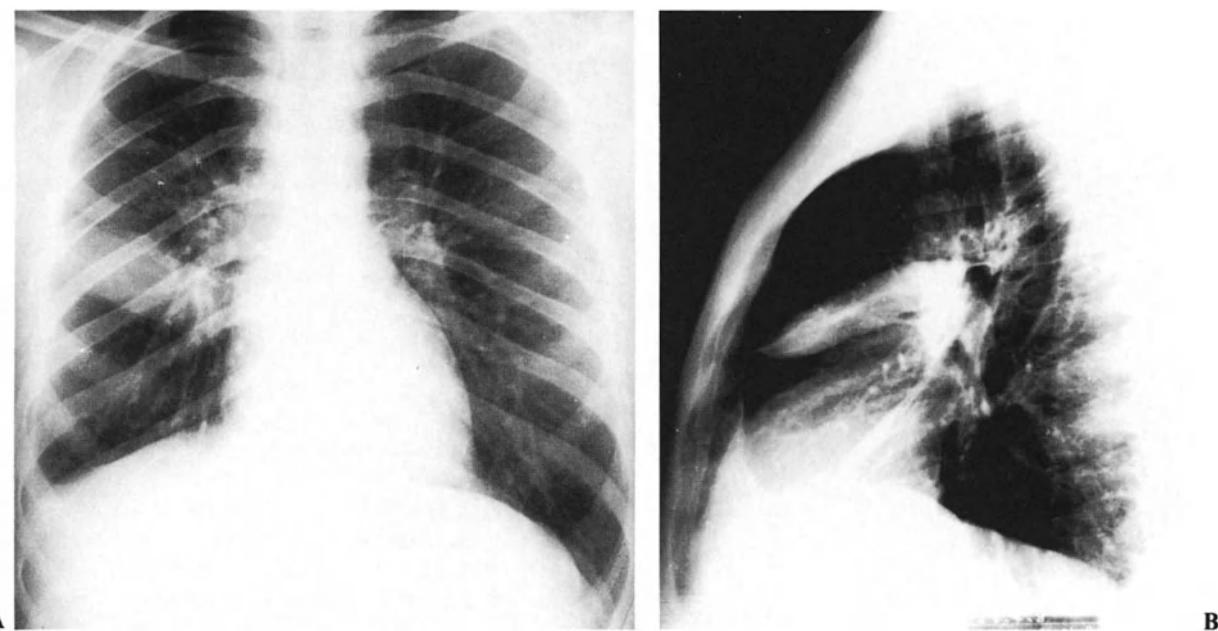
pleural masses may be difficult to distinguish from pleural fluid, but lobulation suggests a pleural tumor (Fig. 1.27). Pneumothorax allows the lung to collapse toward the hilum, and the visceral pleura becomes visible, outlined by air on both sides (Fig. 1.28).

#### Pulmonary Lesions

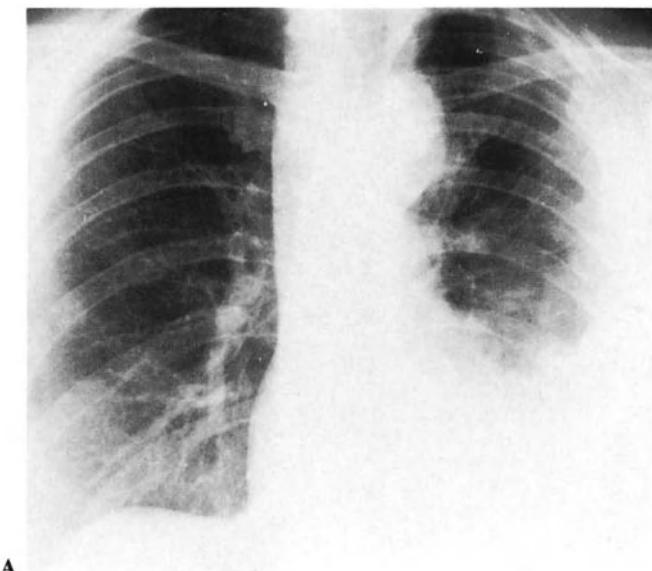
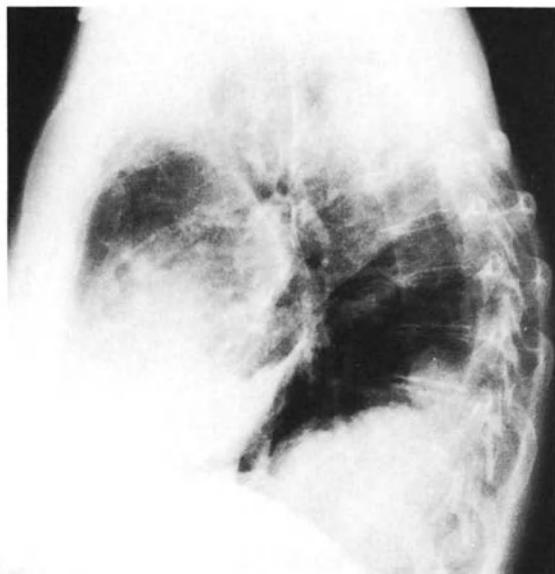
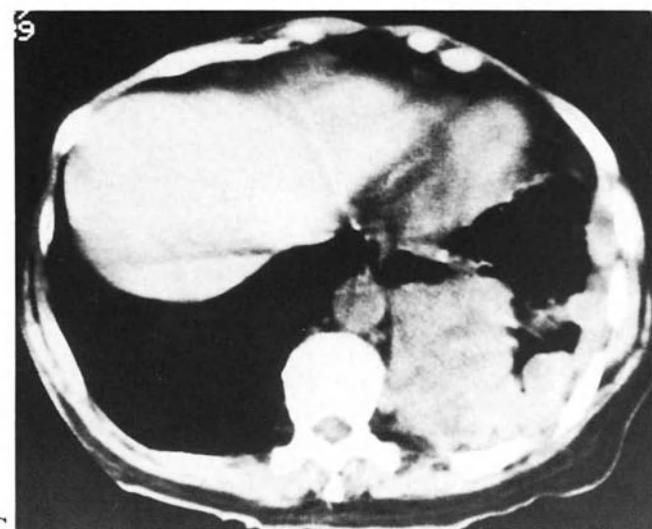
Functionally the lungs comprise blood vessels, lymphatics and airways. The trachea, bronchi and terminal bronchioles

are purely conducting airways, and the alveoli are concerned solely with gas exchange. The respiratory bronchioles, alveolar ducts and alveolar sacs are both conducting and respiratory structures. The unit of lung distal to each terminal bronchiole is an acinus. The airways and their accompanying vessels are surrounded by interstitial connective tissue.

Pulmonary abnormalities may increase or decrease the radiodensity of the lung. Conditions which cause increased



**Figure 1.26.A** Encysted pleural effusion. Poorly defined right mid-zone opacity and blunted right costophrenic angle. **B** Lateral film shows fluid is present in both the horizontal and oblique fissures.

**A****B****C**

◀ Fig. 1.27A, B. Pleural tumor. Extensive, lobulated pleural shadowing surround the left lung. C CT shows a pleural mass extending into the fissure. Malignant mesothelioma.

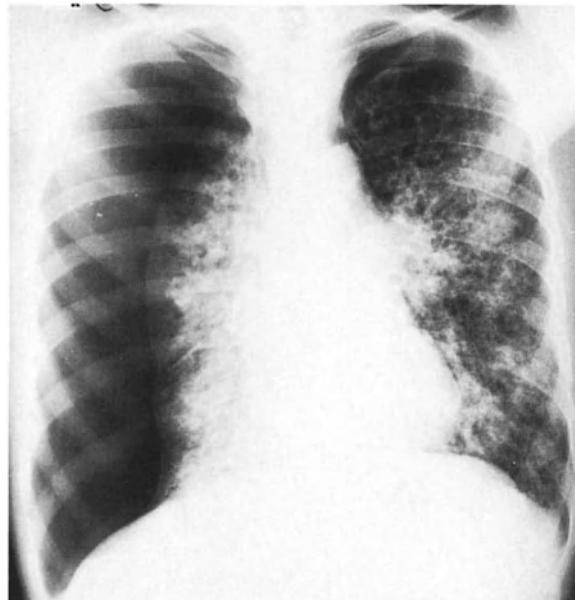


Fig. 1.28. Large right pneumothorax and small apical left pneumothorax. Note that the visceral pleura around the collapsed lung is visible. Cystic fibrosis.

density frequently have a tendency to involve predominantly either the air spaces or the interstitium, although there is often involvement of both areas. Nevertheless this distinction provides a useful basis for chest radiographic analysis.

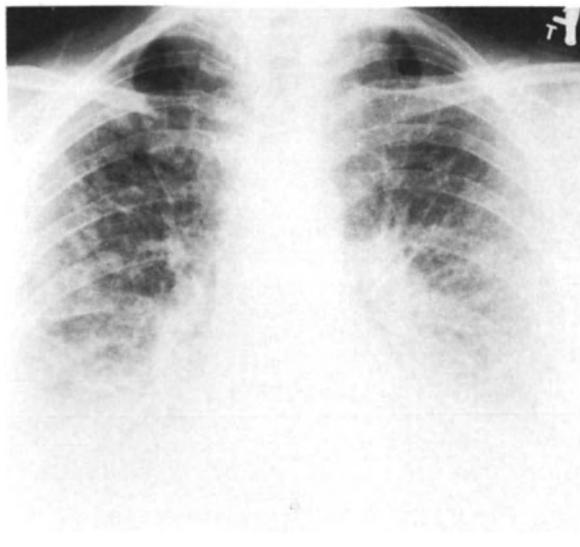
#### *Air-space Disease*

*Acinar or Alveolar Shadowing.* When an acinus becomes filled with fluid or solid it produces a round, 5–6 mm diameter nodular opacity on the chest radiograph (Fig. 1.29). Confluence of these shadows produces larger areas of homogenous shadowing with fluffy, ill-defined margins (Fig. 1.30) except where they abut a pleural surface (Fig. 1.31). The pulmonary vessels are obscured, and an air bronchogram may be visible. Causes of alveolar shadowing are listed in Table 1.5, and lobar consolidation is discussed in Chap. 3.

*Air Bronchogram.* Patent bronchi surrounded by non-aerated lung may appear as radiolucent branching structures (Fig. 1.32). This sign, termed an air bronchogram, indicates that the abnormality is intrapulmonary and that the bronchi are patent. It almost always indicates pulmonary consolidation, although it may sometimes be seen in severe pulmonary fibrosis.

*Pulmonary Collapse.* The signs of pulmonary and lobar collapse are discussed in Chap. 3.

*Silhouette Sign.* The cardiovascular silhouette and the diaphragm are normally clearly demarcated by aerated lung.



◀ Fig. 1.29. Air space disease. Poorly defined, acinar, nodular shadows are present in both lungs. Non-cardiogenic pulmonary edema – heroin overdose.

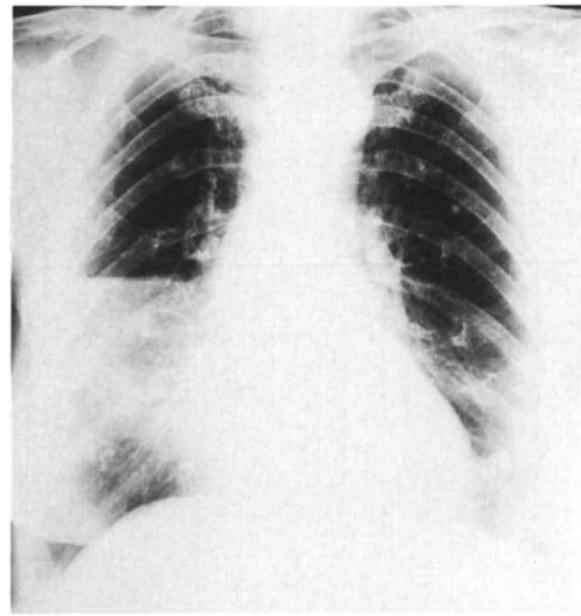


Fig. 1.31. Air space disease. Right middle-lobe consolidation obscuring the right heart border. The lower border of the consolidation is poorly defined but superiorly, where it abuts the horizontal fissure, it is sharply demarcated.

**Table 1.5. Causes of alveolar shadowing**

<b>Transudate</b>
cardiogenic pulmonary edema
non-cardiogenic pulmonary edema
<b>Exudate</b>
pneumonia
ARDS
pulmonary eosinophilia
alveolar proteinosis
<b>Hemorrhage</b>
pulmonary contusion
pulmonary infarction
pulmonary hemosiderosis
<b>Infiltration</b>
lymphoma
alveolar cell carcinoma
diffuse carcinomatosis
<b>Miscellaneous</b>
hyaline membrane disease
aspiration
sarcoidosis
radiation pneumonitis
drugs

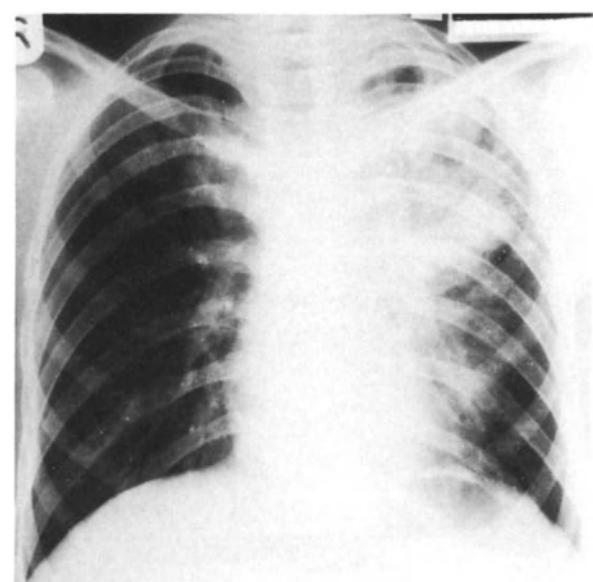
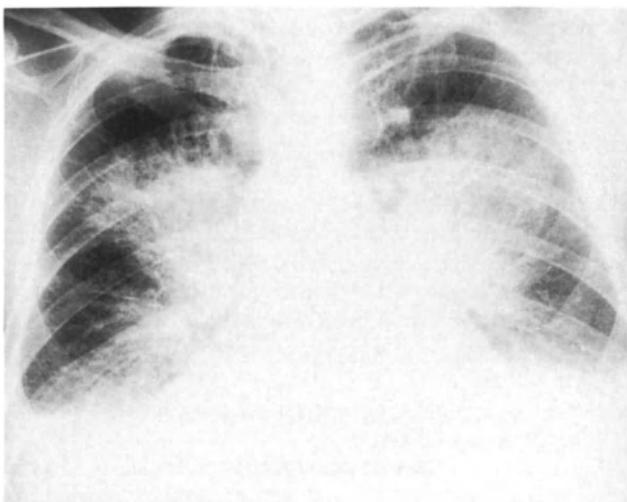
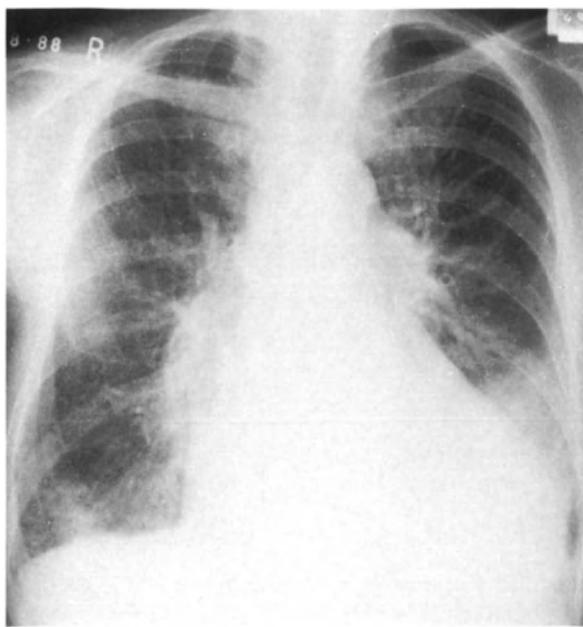


Fig. 1.32. Air bronchogram. Lucent, branching shadows are visible within the left upper lobe consolidation. There is also consolidation in the right upper zone medially. Pulmonary tuberculosis.

◀ Fig. 1.30. Air space disease. Perihilar, consolidation due to alveolar pulmonary edema. Bilateral pleural effusions are also present. Acute myocardial infarction.



**Fig. 1.33.** Silhouette sign. An area of consolidation in the left lower zone overlies, but does not obscure, the left heart border. The left hemidiaphragm, however, is obscured. The consolidation is, therefore, in the lower lobe. Pulmonary infarction.

Obscuration of part of either of these indicates that there is no longer aerated lung adjacent to it. This may be due to the lung being displaced by a pleural or mediastinal abnormality, or the lung itself may be abnormal. Conversely, if an opacity overlies a structure but does not obscure its outline, the two cannot be contiguous (Fig. 1.33). Thus if a pulmonary lesion obscures the diaphragm it is in the lower lobe, if it obscures the right heart border it is in the right middle lobe (Fig. 1.31), if it obscures the left heart border

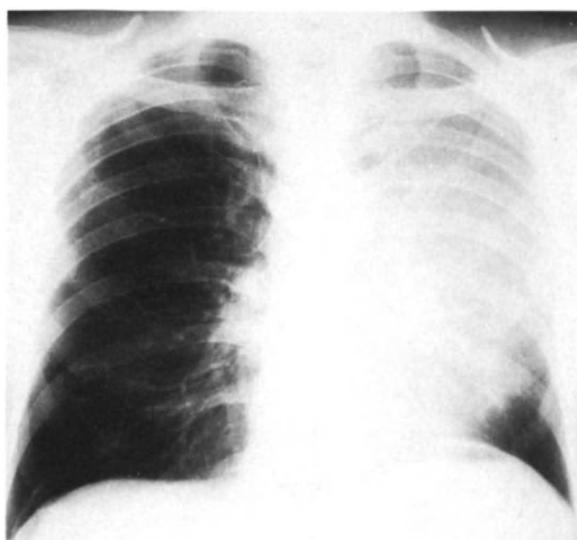


**Fig. 1.34.** Silhouette sign. Extensive opacity in left lung obscures the aortic arch and the left heart border, indicating left upper lobe and lingular abnormality. Left upper lobe collapse due to carcinoma of bronchus.

it is in the lingular and if it obscures the aortic knuckle it is in the upper lobe (Fig. 1.34).

#### *Interstitial Disease*

Thickening of the pulmonary interstitium may produce nodular, linear, reticulonodular or 'ground glass' shadowing. The shadowing may be diffuse or localized. However, certain conditions tend to have characteristic distributions e.g., sarcoidosis and most pneumoconioses usually spare the bases and asbestos tends to be basal. A wide variety of conditions may cause interstitial lung disease (see Table 1.6). A good clinical history is, therefore, essential when analysing these cases. It is important to know if there is any background of systemic disease, drug therapy or exposure to organic or inorganic dusts and whether or not the patient is ill. Yet again old films are invaluable.

**Table 1.6. Causes of interstitial lung disease**

Infections	
tuberculosis	
fungi	
viruses	
pneumocystis	
Pulmonary edema	
Neoplasms	
lymphangitis carcinomatosa	
lymphoma	
leukemia	
Connective tissue disorders	
rheumatoid disease	
scleroderma	
PAN; Wegener's granulomatosis	
SLE	
Pulmonary hemosiderosis	
Pneumoconioses	
Extrinsic allergic alveolitis	
Drugs	
Miscellaneous	
sarcoidosis	
cryptogenic fibrosing alveolitis	
histiocytosis	
tuberous sclerosis and other causes of honeycombing (see Table 1.9)	

**Table 1.7. Causes of miliary shadowing**

Tuberculosis	
Histoplasmosis	
Sarcoidosis	
Pneumoconiosis	
Metastases	
Hyaline membrane disease	
Hemosiderosis	

**Small Nodular Shadows.** Small, nodular opacities of soft tissue density and less than 5 mm in diameter may be described as miliary (Fig. 1.35). The main causes are listed in Table 1.7. Miliary tuberculosis is of particular importance since it is a treatable condition, in which a delay in diagnosis may be disastrous.

**Larger Nodular Shadows.** Multiple larger nodular opacities are frequently due to metastatic disease (Fig. 1.36), but may

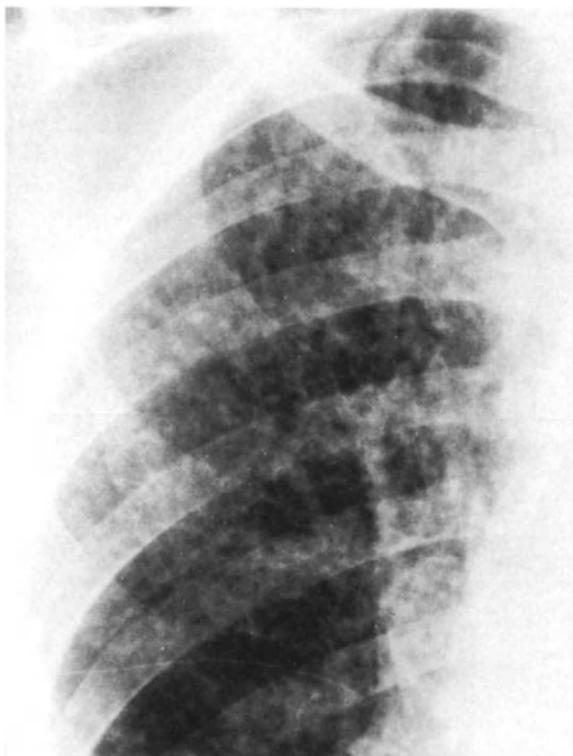


**Fig. 1.35.** Miliary shadowing. Small nodular opacities are present throughout the lung. Miliary tuberculosis.

be due to a variety of both interstitial and air-space abnormalities.

**Linear and Reticulonodular Shadowing.** The predominant pattern may be linear or there may be a combination of linear and nodular opacities, and the shadows may be fine or coarse (Figs 1.37, 1.38). If pulmonary fibrosis is present there may also be evidence of volume loss.



**Fig. 1.36.** Larger nodular shadows. Metastatic adenocarcinoma.



**Fig. 1.37.** Fine linear shadows in right lower zone and throughout left lung. In the left upper zone the linear pattern gives way to a ground glass density veiling the lung. Silico-berylliosis.

**Kerley B lines** appear as short, horizontal linear opacities in the periphery of the lower zones (Figs 1.38, 1.39). They represent fluid within or thickening of the interlobular septa (see Table 1.8 for causes).

**Honeycomb shadowing** is characterized by multiple small thin-walled ring shadows (Fig. 1.40). They represent cysts, and may be found in a number of interstitial processes (see Table 1.9). Honeycomb lung predisposes to pneumothorax. Cystic bronchiectasis may produce a similar appearance to honeycomb lung (Fig. 1.41).

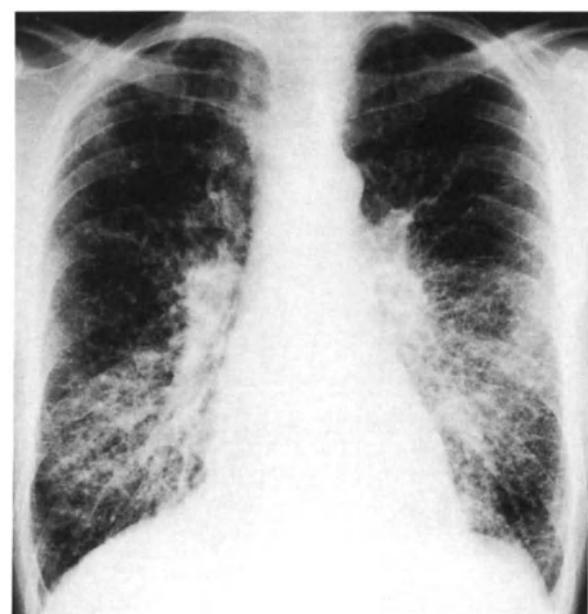


**Fig. 1.38.** Coarse linear shadows throughout both lungs, with a basal predominance. Kerley B lines are visible in both lower zones. Lymphangitis carcinomatosa.

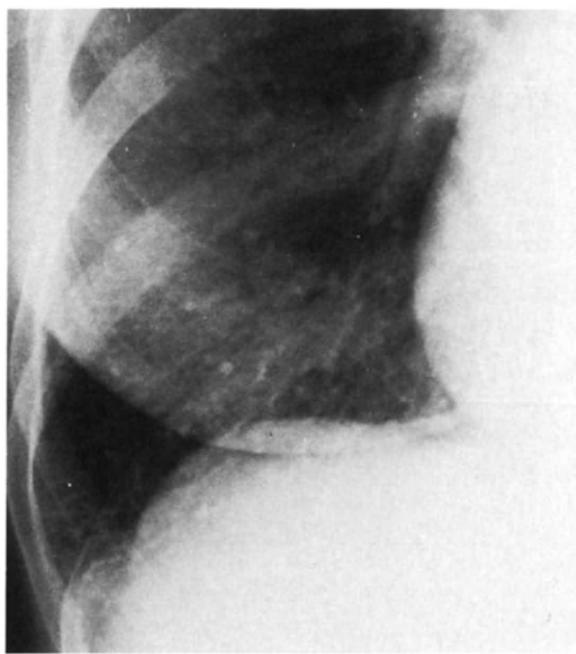


**Fig. 1.39.** Kerley B lines are visible in the costophrenic angle. Small, round, calcified nodules in the lower zone are pulmonary ossicles. Mitral valve disease.

**Table 1.8. Causes of Kerley B lines**

Cardiogenic pulmonary edema
Non-cardiogenic pulmonary edema
Lymphangitis carcinomatosa
Pneumoconiosis
Sarcoidosis
Interstitial pneumonia

**Table 1.9. Causes of honeycomb shadowing**

Common
histiocytosis
cryptogenic fibrosing alveolitis
sarcoidosis
pneumoconiosis
Uncommon
scleroderma
rheumatoid disease
tuberous sclerosis
lymphangiomyomatosis
amyloidosis
Gaucher's disease
chronic interstitial pneumonia
lipoid pneumonia
extrinsic allergic alveolitis

### Solitary Pulmonary Nodule

Most solitary pulmonary nodules are primary tumors, metastases or granulomas. Table 1.10 lists other causes. The differentiation between benign and malignant nodules is discussed in Chap. 5. The features that suggest a benign lesion

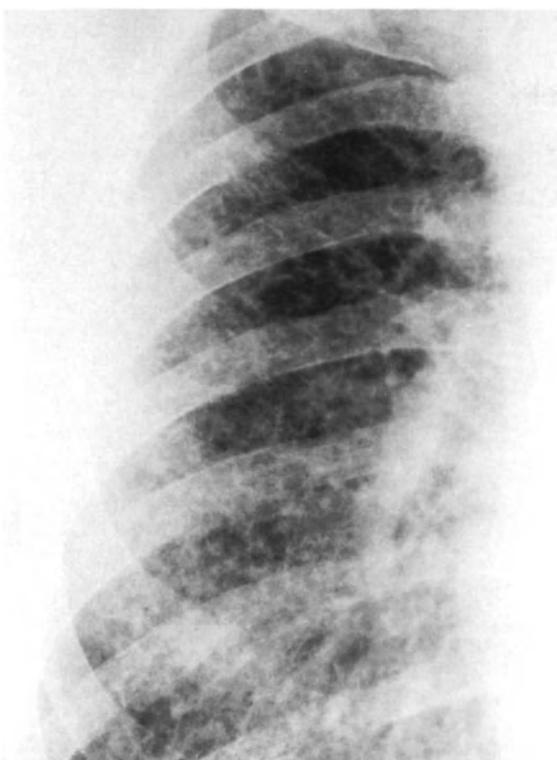


**Fig. 1.40.** Honeycomb shadowing. Multiple, small ring shadows are visible. Histiocytosis.

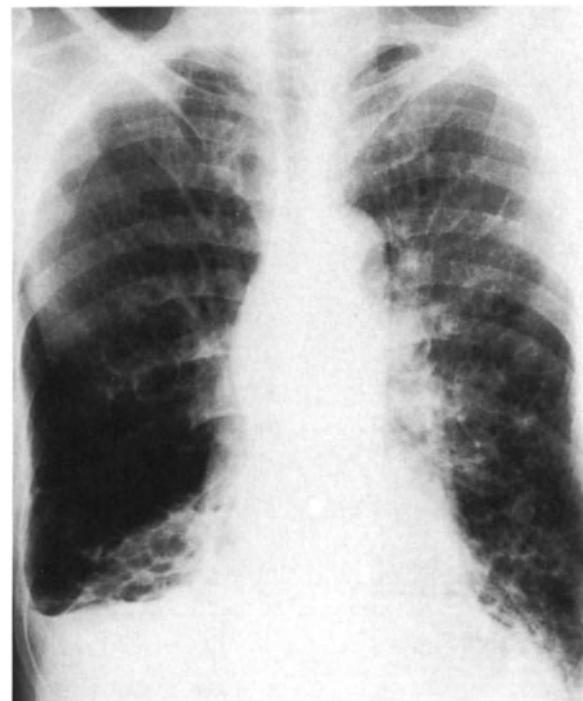


**Fig. 1.41.** Ring shadows due to cystic bronchiectasis.

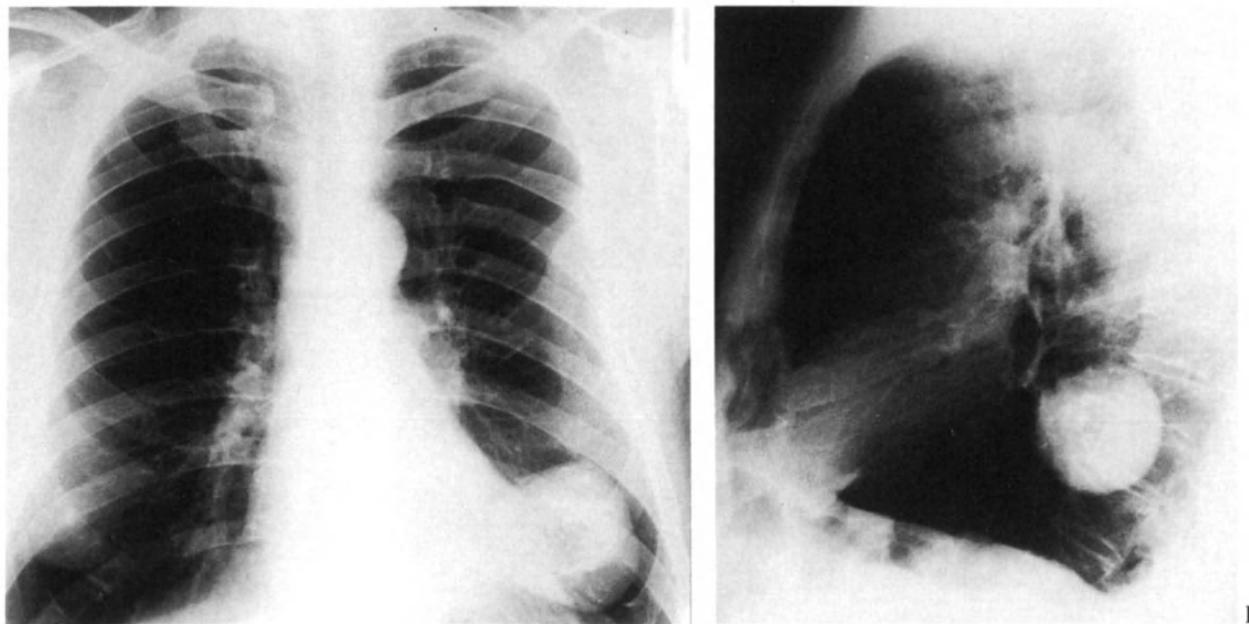


**Fig. 1.42A, B.** Benign, solitary pulmonary nodule. Sharply demarcated border and extensive, central calcification. Hamartoma. (Extrapleural density in periphery of left mid zone is due to a congenital rib anomaly.)

**Table 1.10.** Causes of a solitary pulmonary nodule

Tumors	
malignant	
primary carcinoma	
metastasis	
lymphoma	
plasmacytoma	
benign	
hamartoma	
adenoma	
AVM	
Infections	
chronic	
granuloma	
tuberculosis	
histoplasmosis and other fungi	
acute	
pneumonia	
abscess	
hydatid cyst	
Pulmonary infarct	
Pulmonary hematoma	
Collagen disease	
rheumatoid disease	
Wegener's granulomatosis	
Sarcoidosis	
Sequestered segment	
Amyloid	
Intrapulmonary lymph node	
Encysted pleural effusion	
Pleural tumor	
Skeletal and cutaneous opacities	

} May mimic a pulmonary nodule

are a well-defined edge and diffuse or central calcification (Fig. 1.42A and B), and no change in appearance over 2 years if a previous film is available. Malignant lesions tend to have an irregular or spiculated edge and may show evidence of invasion of adjacent structures (Fig. 1.43) or metastatic disease.



**Fig. 1.43.** Malignant pulmonary nodule. A right apical mass with less sharp margin than in Fig. 1.42, and associated destruction of 4th rib posteriorly. Carcinoma of bronchus.

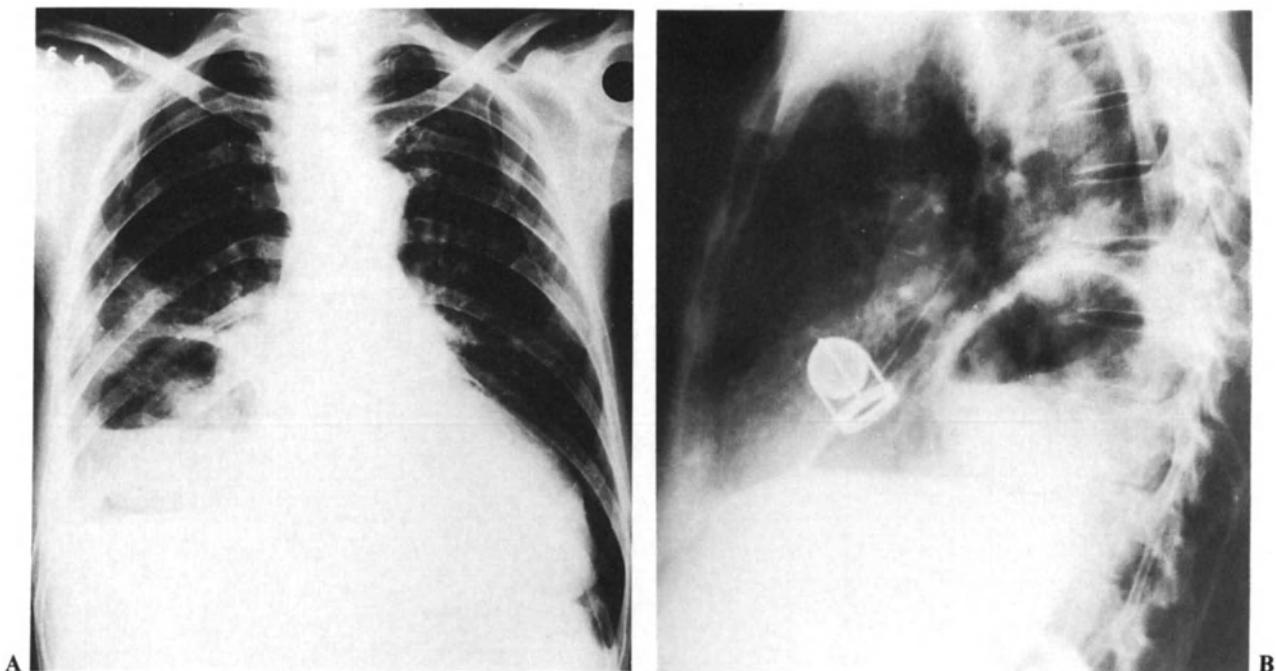


**Fig. 1.44A, B.** Lung abscess. Smooth-walled, cavitating mass in right lower lobe with fluid level and surrounding consolidation. Aortic valve replacement. *Klebsiella*.

**Table 1.11.** Causes of pulmonary cavitation

Infections	
tuberculosis	
<i>Staphylococcus*</i>	
<i>Klebsiella</i>	
histoplasmosis and other fungi	
amebic abscess	
hydatid cyst	
lung abscess*	
Tumors	
primary carcinoma	
metastasis*	
lymphoma*	
Pulmonary infarction	
Pulmonary laceration*	
Pneumoconiosis	
PMF	
Caplan's syndrome*	
Connective tissue disorders	
rheumatoid disease*	
Wegener's granulomatosis*	
Sarcoidosis	
Sequestered segment	
Cystic bronchiectasis* and bullae* may resemble thin-walled cavities	

\*These conditions may appear as multiple cavities.

### Cavities

The commonest causes of pulmonary cavitation are tuberculosis, pyogenic pneumonia and carcinoma. Other causes are listed in Table 1.11. Malignant cavities tend to have thick, irregular walls (Fig. 1.2). Abscess cavities are

often thick-walled at first, but as surrounding consolidation resolves, and necrotic material is coughed up the wall becomes smooth and thinner (Fig. 1.44). Pneumatoceles due to staphylococcal pneumonia are typically thin-walled (Fig. 1.45).

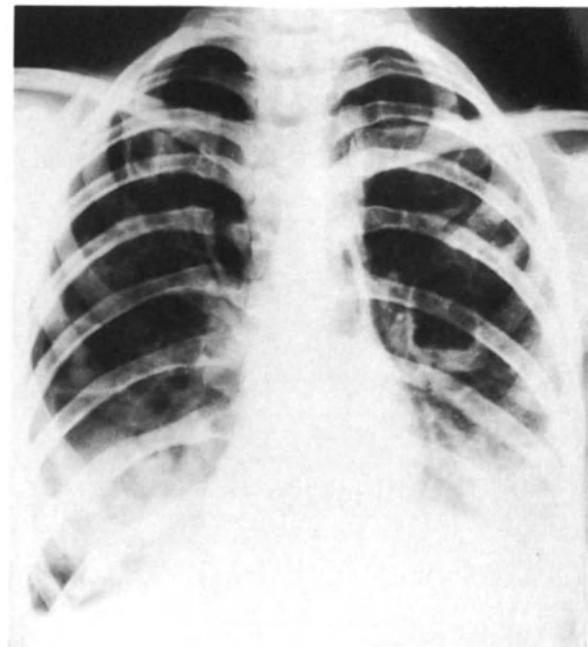


**Fig. 1.45.** Pneumatoceles. Widespread bronchopneumonia with thin-walled cavity with fluid level in left mid-zone. Staphylococcal pneumonia.

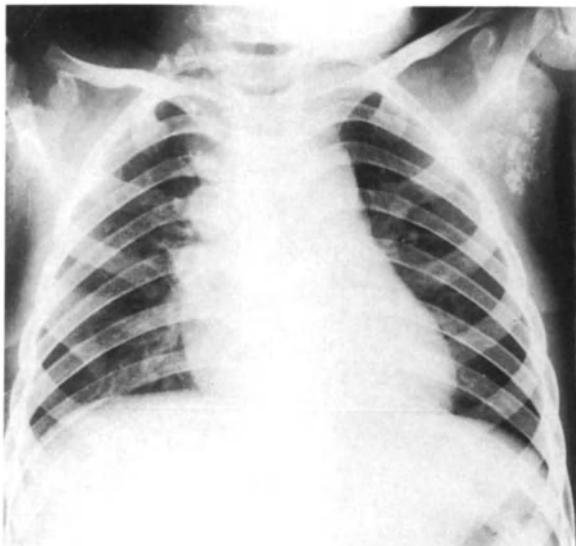


**Fig. 1.46.** Calcification in right paratracheal, right cervical and left axillary lymph nodes. Tuberculosis.



**Fig. 1.47.** Multiple, small, calcified pulmonary nodules. Healed miliary tuberculosis.

**Table 1.12.** Calcification on the chest radiograph

Chest wall	
costal cartilage	
rib fractures	
bone tumors	
Pleura	
TB	
empyema	
hemothorax	
asbestos exposure	
Pulmonary	
granulomas	
tuberculosis	
histoplasmosis and other fungi	
varicella	
tumors	
hamartoma	
carcinoid	
metastatic osteogenic sarcoma and chondrosarcoma	
AVM	
pulmonary hematoma, infarction and ossicles	
pulmonary alveolar microlithiasis	
silicosis	
Hilar nodes	
tuberculosis	
fungi	
sarcoid	
silicosis	
treated lymphoma	
Mediastinum	
cardiac	
valves	
infarcts	
aneurysms	
tumors	
pericardium	
aortic aneurysm	
mediastinal tumors	
thymic	
thyroid	
dermoid	
pulmonary arterial hypertension	

### Calcification

Abnormal calcification of the chest x-ray is most frequently due to tuberculosis (Figs 1.46, 1.47). Abnormal calcification may occur virtually anywhere in the thorax from a wide range of causes (see Table 1.12).



**Fig. 1.48.** Hyperinflated lungs with upper zone transradiancy, especially on right, and bulla adjacent to cardiac apex. Large central pulmonary arteries. Pulmonary emphysema.

**Fig. 1.50.** Hilar and mediastinal lymphadenopathy. Symmetrical enlargement of hilar and also right paratracheal and aorticopulmonary lymph nodes is due to sarcoidosis. The small right pleural effusion is an unusual manifestation. ▶

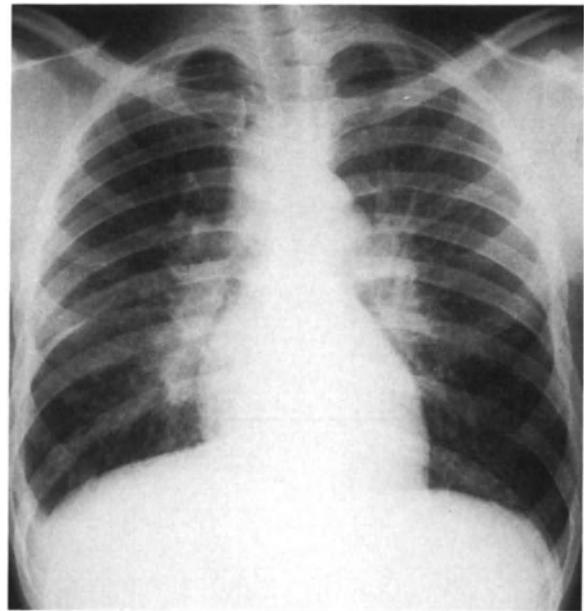


**Table 1.13.** Causes of unilateral hypertransradiancy

Apparent	
	increased density of other lung
Technical	
	rotation
Soft tissue	
	mastectomy
	absent pectoralis major
Skeletal	
	scoliosis
Compensatory hyperinflation	
	partial lung resection
	lobar collapse
Air trapping	
	bronchial obstruction
	tumor
	foreign body
	congenital lobar emphysema
	McCleod's syndrome
	chronic obstructive airways disease
Pleural	
	pneumothorax
Vascular	
	pulmonary embolism
	absent/hypoplastic pulmonary artery

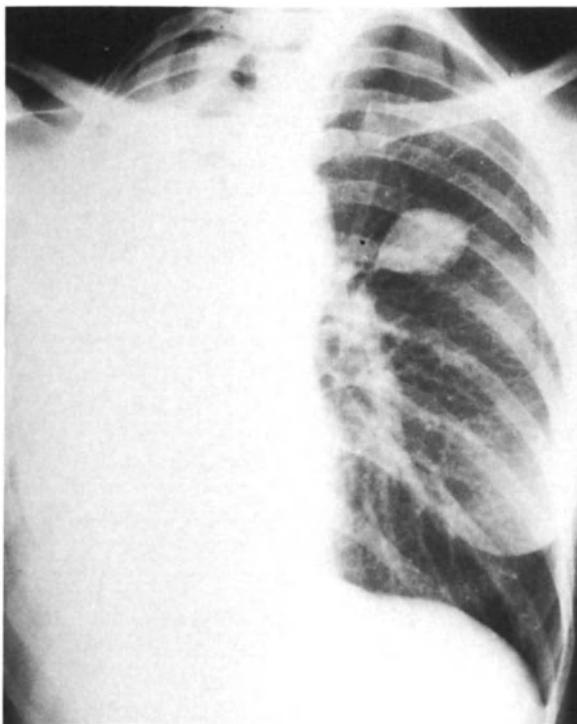


**Fig. 1.49.** Opaque right hemithorax. The mediastinum is shifted to the right indicating collapse of the right lung. A metastasis is present in the left lung. Leiomyosarcoma of right bronchus.

### Unilateral Hypertransradiancy

Hypertransradiancy of one lung may be true or apparent. The commonest causes are technical, due to rotation of the patient (Fig. 1.1) or lateral decentering, and skeletal and chest wall deformities. True hypertransradiancy is commonly due to emphysema (Fig. 1.48). Table 1.13 lists other causes.

### Opaque Hemithorax

An opaque hemithorax is usually due to complete collapse of a lung, complete consolidation of a lung or a large pleural effusion. The position of the mediastinum usually indicates

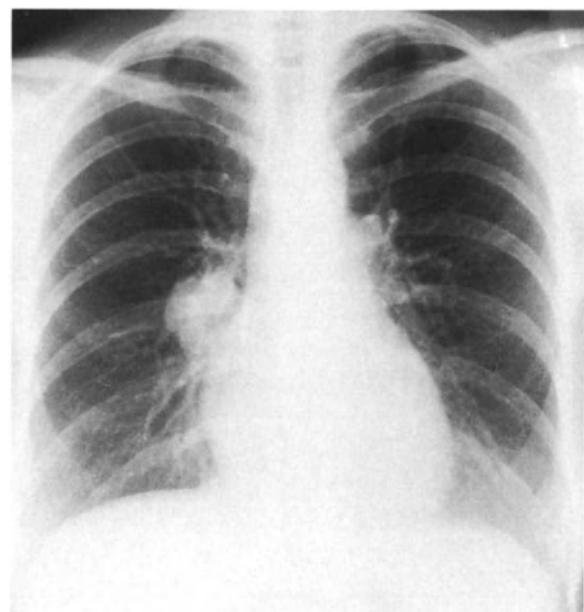


**Fig. 1.51.** Enlargement of the right hilum by a carcinoid tumor.

whether the opaque side is of normal, increased or decreased volume (Fig. 1.49).

#### Hilar Enlargement

Hilar enlargement is usually due to enlargement of the pulmonary arteries, lymphadenopathy or a mass (Figs 1.48, 1.50, 1.51). Lymphadenopathy and masses tend to be

lobulated. Of the commoner causes of lymphadenopathy, sarcoidosis tends to be bilateral and symmetrical whereas lymphoma is usually asymmetric. Pulmonary artery enlargement is most often due to pulmonary arterial hypertension secondary to chronic lung disease.

*For further reading, see p. 134.*

## CHAPTER 2

# THE CHEST WALL, DIAPHRAGM AND PLEURA

M. Rubens

---

## THE CHEST WALL

---

The soft tissues and bones of the chest wall may produce shadows that either help the observer by providing useful information, or hinder him by causing confusion.

**Artifacts.** Clothing, buttons and fasteners may produce confusing densities on the chest radiograph. Hair braids overlying the lung apices may mimic tuberculous lesions. Electrodes, tubes, lines and dressings are often seen on intensive care unit films. It is important to check whether a confusing shadow extends outside the chest, and is therefore, an artefact.

### THE SOFT TISSUES

**Breasts.** Mastectomy is a common cause of a hypertransradiant hemithorax (Fig. 2.1). Following radical resection there is alteration of the axillary folds (Fig. 2.2). Nipples may produce lower zone opacities, and it is sometimes necessary to repeat the chest film with nipple markers in order to distinguish between nipple and a pulmonary nodule. *Mammary implants* are an occasional cause of increased lower zone shadowing.

**Soft Tissue Calcification.** Adenomas in the breast, calcified cysticerci, and calcified axillary lymph nodes are uncommon causes of densities overlying the lung. Rarer causes of cutaneous calcification are dermatomyositis and phleboliths.

**Cutaneous Nodules.** Lipomas, sebaceous cysts and other cutaneous lumps may mimic pulmonary nodules. When in doubt examine the patient's skin. *Neurofibromatosis* may produce multiple soft tissue opacities (Fig. 2.3).

**Surgical Emphysema.** Following chest trauma, chest surgery or insertion of intercostal tubes air may be seen in the soft tissues producing characteristic linear lucencies (Fig. 2.4).

### THE BONES

**Sternum.** *Depressed sternum* usually has a characteristic appearance on the frontal film. The anterior ribs slope more than usual, and the heart is pushed posteriorly and to the left, making the left heart border appear straighter than usual and the right heart border indistinct (Fig. 2.5). Depressed sternum may be associated with Marfan's syndrome and atrial septal defect. Other developmental anomalies of the sternum such as agenesis, premature fusion and pigeon chest may also be associated with congenital heart disease. In Down's syndrome two manubrial ossification centers may be visible.

The sternum may be the site of myeloma, lymphoma, chondrosarcoma or metastatic carcinoma. Mediastinal tumors and ascending aortic aneurysms may erode the sternum. Fractures of the sternum may result from injuries caused by steering wheels, and osteomyelitis may be a complication of sternotomy.

**Clavicles.** *Hypoplasia* of the clavicles may be seen in various congenital syndromes including cleido-cranial dysostosis, progeria and the Holt-Oram syndrome. *Erosion of the lateral ends* is seen in rheumatoid disease and hyperparathyroidism. Neoplastic involvement is usually due to metastatic car-

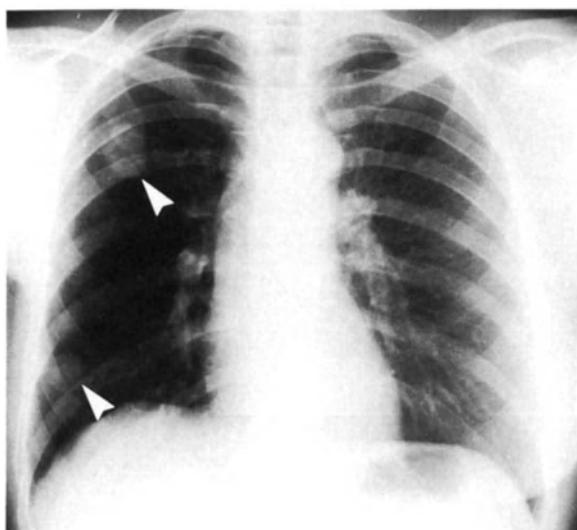


**Fig. 2.1.** Hypertransradiantral right hemithorax due to mastectomy. Note normal left breast shadow. Two metastases (arrowheads) are visible in the right lung.

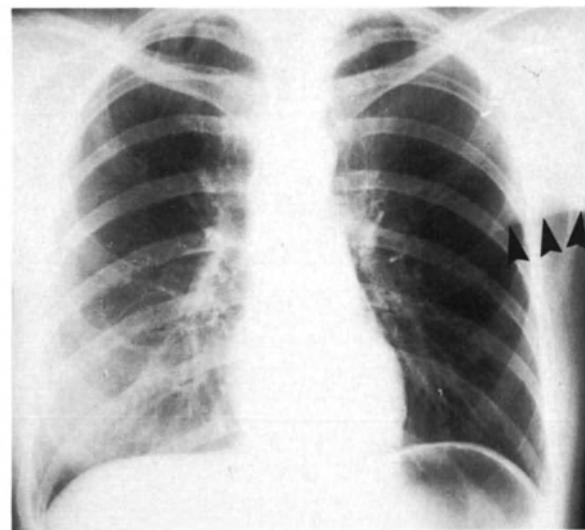


**Fig. 2.2.** Hypertransradiantral left hemithorax and abnormal left axillary fold (arrowheads) due to radical mastectomy.

cinoma, myeloma or Ewing's sarcoma. Paget's disease may occasionally involve the clavicle. Old clavicular fractures are a quite common incidental finding.

**Ribs.** Common congenital rib anomalies include cervical ribs, hypoplasia of the 1st and 2nd ribs, bifid ribs and bony bridging between adjacent ribs. In *Down's syndrome* only 11 pairs of ribs may be present.

**Rib notching** (Fig. 2.6) usually involves the inferior surface

of one or more ribs, and may be due to enlargement of intercostal arteries, veins or nerves: Table 2.1 lists the causes.

Superior notching may be seen in rheumatoid disease, hyperparathyroidism and neurofibromatosis.

Trauma and surgery may cause rib deformities. Occasionally callus of a healed fracture may mimic a pulmonary nodule (Fig. 2.7). Pseudo-fractures may be seen in osteomalacia.

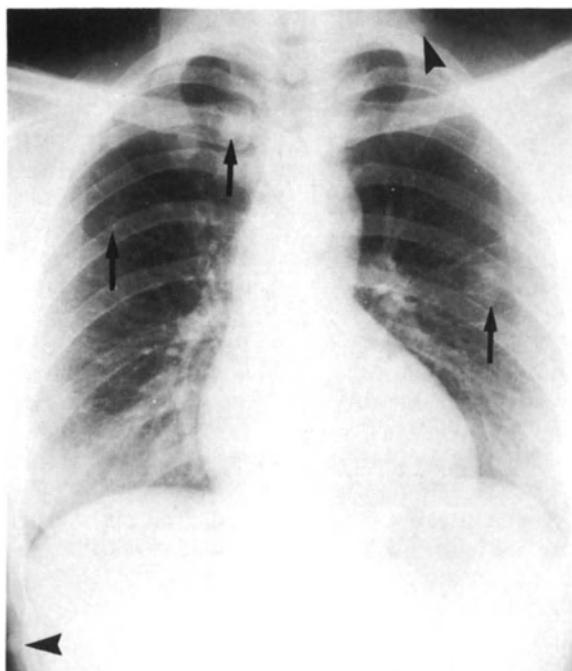


**Fig. 2.3.** Neurofibromatosis. Multiple cutaneous nodules are visible. Some are projected over the lungs (arrows) but other are obviously outside the thorax (arrowheads).

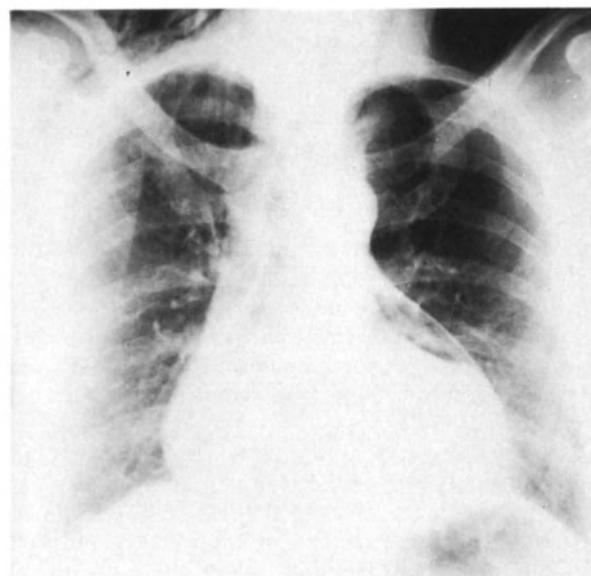


**Fig. 2.4.** Surgical emphysema is visible over the right apex, and in the right supraclavicular fossa. A pneumopericardium is also visible. Post-aortic valve replacement.

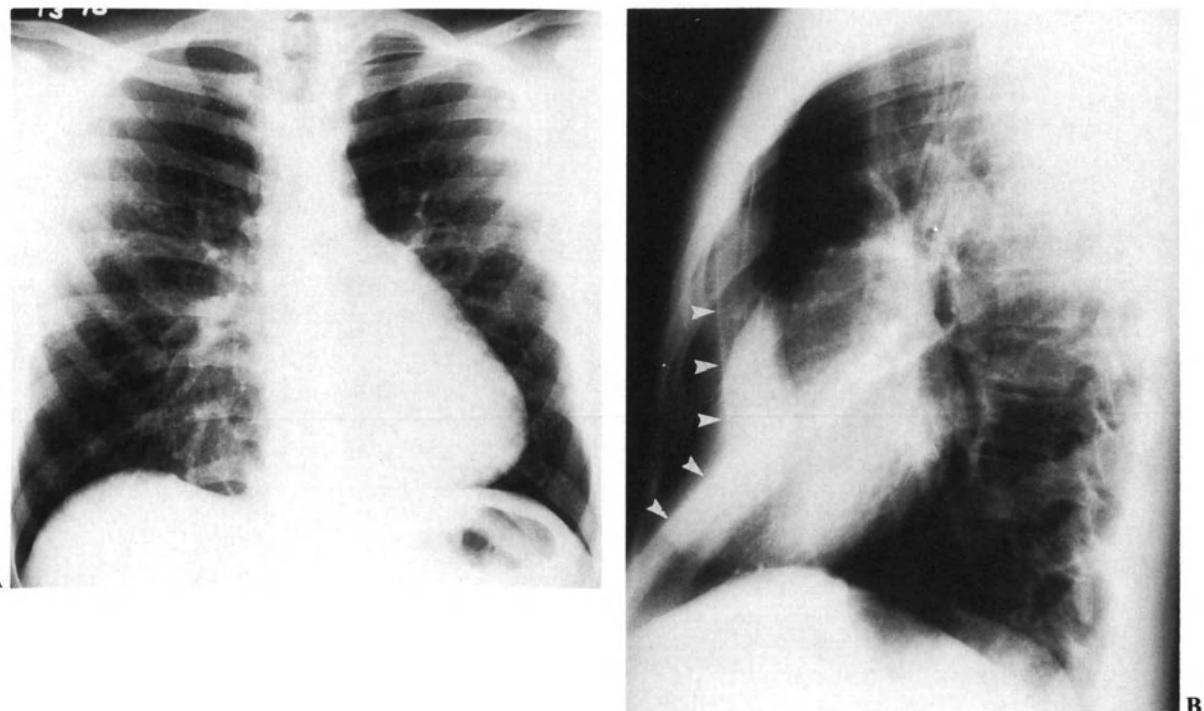


**Fig. 2.5A, B.** Depressed sternum. **A** The ribs slope steeply anteriorly, and the heart is displaced to the left. **B** The deformity of the sternum (*arrowheads*) is well demonstrated on the lateral view.

**Table 2.1.** Causes of inferior rib notching

Arterial	
aortic coarctation	
aortic obstruction	
subclavian artery obstruction (usually following Blalock–Taussig shunt)	
pulmonary atresia and severe Tetralogy of Fallot	
Venous	
SVC obstruction	
Arteriovenous	
pulmonary AVM	
chest wall AVM	
Neural	
neurogenic tumor	

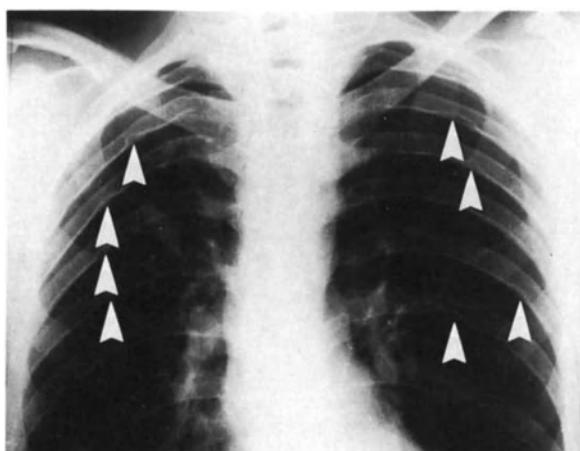


**Fig. 2.6.** Rib notching. The inferior surface of several ribs show well corticated notching posteriorly (*arrowheads*). Coarctation of the aorta.

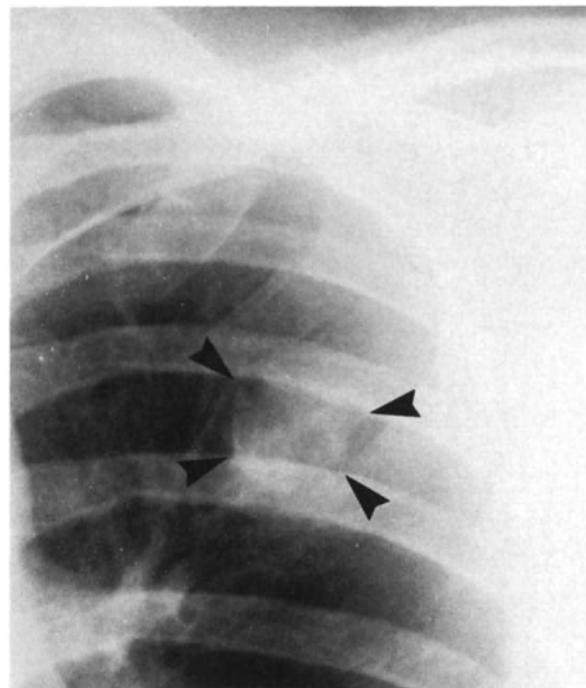


**Fig. 2.7.** Healed rib fractures. Callus (*arrowheads*) extending between two ribs might be mistaken for a pulmonary nodule.

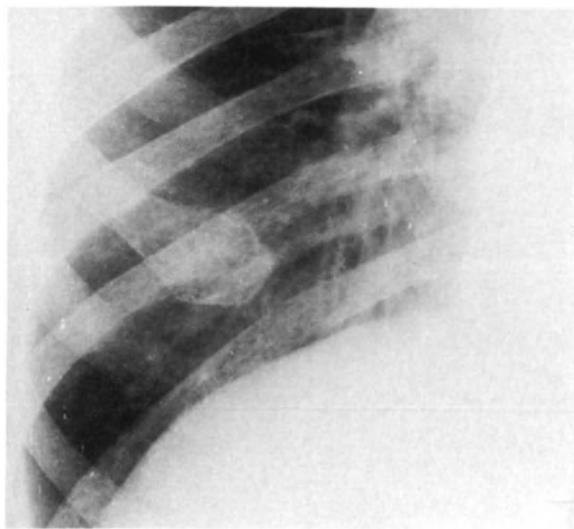


**Fig. 2.8.** Fibrous dysplasia causing expansion of the anterior end of a rib.

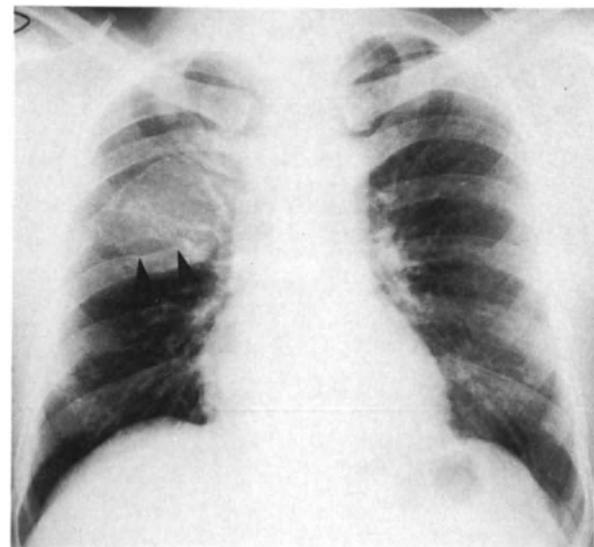


**Fig. 2.10.** Expanding rib metastasis. The posterior end of the right 6th rib is expanded by a metastasis from a thyroid carcinoma. There is pressure erosion of the superior aspect of the 7th rib (arrowheads).

Localized expansion of a rib is likely to be due to fibrous dysplasia (Fig. 2.8), plasmacytoma or a benign tumor. The commonest benign tumors of ribs are cartilaginous (Fig. 2.9). Metastases are usually destructive, but may be expansile (Fig. 2.10). Other destructive lesions are lymphoma, myeloma and infections. Destruction may also be due to invasion by tumor of the adjacent pleura, lung or soft tissues.

*Increased density of a rib may be due to Paget's disease, and diffuse sclerosis may occur in myelofibrosis, osteopetrosis, fluorosis, lymphoma and from osteosclerotic metastases.*

*Diffuse osteopenia may be seen in osteoporosis and myelomatosis. Abnormal modeling and widening of the ribs may be due to mucopolysaccharidoses and thalassemia, and*

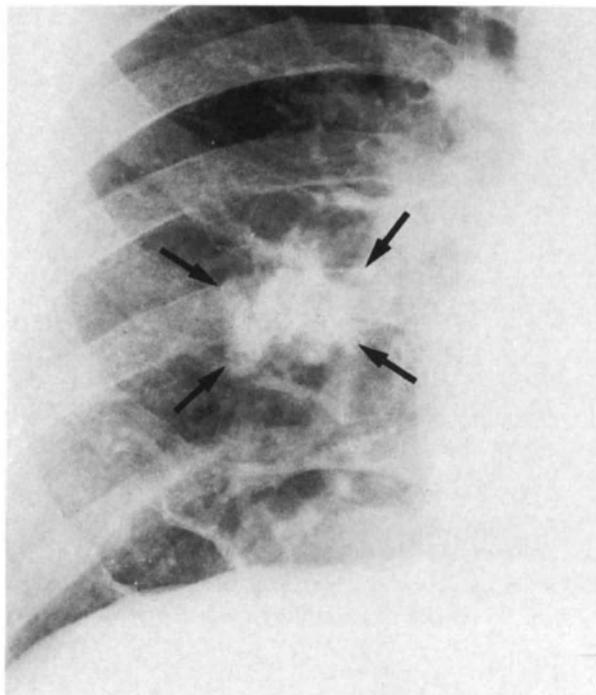
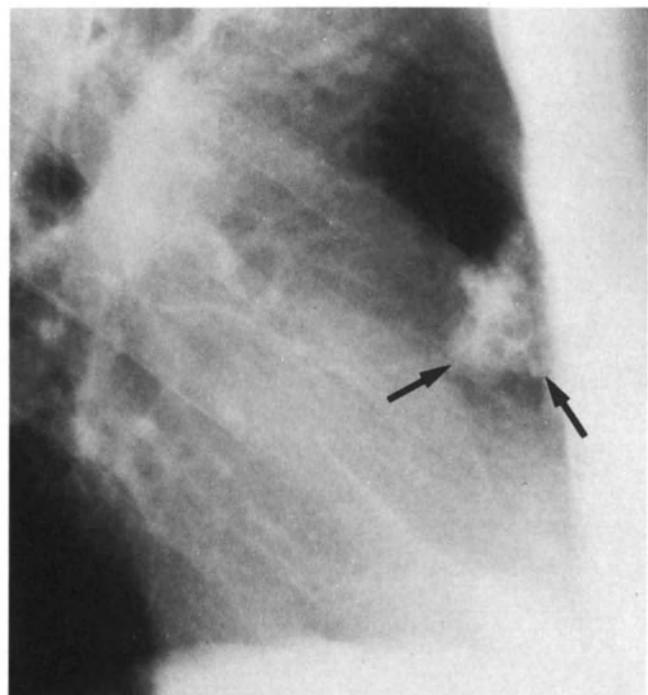


**Fig. 2.9A, B.** Osteochondroma of rib. A On the frontal view the calcified mass (arrows) might be mistaken for a pulmonary abnormality, but on the lateral view, B, it is seen to arise from the anterior end of a rib.



widening of the ribs anteriorly may be seen in scurvy and rickets.

**Spine.** Severe thoracic kyphoscoliosis not only alters the appearance of the chest radiograph but may also lead to pulmonary arterial hypertension and right heart failure. Scoliosis, block vertebra, hemivertebra and butterfly vertebra may be associated with congenital heart disease and neurenteric cysts. Reduction of the thoracic kyphosis causes a

straight back which may be associated with a floppy mitral valve.

As with the other bones of the thorax, the spine may be eroded by tumors occurring in the adjacent tissues and may also be the site of metastatic disease, myeloma, lymphoma, primary bone tumors and Paget's disease.

Osteomyelitis of the spine and acute fractures may be associated with a paraspinal mass.

## THE DIAPHRAGM

Both domes of the diaphragm should be clearly defined on both frontal and lateral films. Loss of definition of all or part of one or other dome usually indicates pathology in the adjacent pleura or lung. Normally only the superior surface of the diaphragm is visible, but *pneumoperitoneum* may make both surfaces visible (Fig. 2.11).

Although the diaphragm usually appears as a smooth convex surface, normal variants are common. They include visualization of individual muscular insertions at the costal margin, and diaphragmatic humps, which are probably due to small areas of deficient muscle.

**Diaphragmatic Movement.** Movement of both domes of the diaphragm is usually more or less symmetrical. It is best assessed by fluoroscopy, when it is usual to see excursion of between 3 cm and 6 cm. It is also possible to assess diaphragm movement with real-time ultrasound.

**Paradoxical movement** is indicated by upward movement of the diaphragm on inspiration, and is well demonstrated by sniffing. Paradoxical motion of the diaphragm may occur in normal subjects, but usually indicates phrenic nerve

paralysis. Phrenic nerve paralysis is often due to involvement by mediastinal tumor, but may be due to trauma, surgery, neuritis or neuropathy.

Decreased movement of the diaphragm may be due to lower lobe pneumonia, pleurisy and subphrenic abscess.

**Height of the Diaphragm.** The diaphragm usually appears elevated on supine and expiratory films. Decreased pulmonary compliance (e.g., due to pulmonary fibrosis and lymphangitis), obesity, ascites, distended bowel, large abdominal masses and pregnancy may also elevate the diaphragm.

Table 2.2. Causes of unilateral elevation of the diaphragm

Neuromuscular	
phrenic nerve palsy	
eventration	
Pulmonary	
lower lobe collapse	
lower lobe consolidation	
pulmonary embolism	
pulmonary hypoplasia	
Pleural/chest wall	
pleurisy	
rib fractures	
Subphrenic	
subphrenic abscess	
subphrenic mass	
distended stomach/colon	

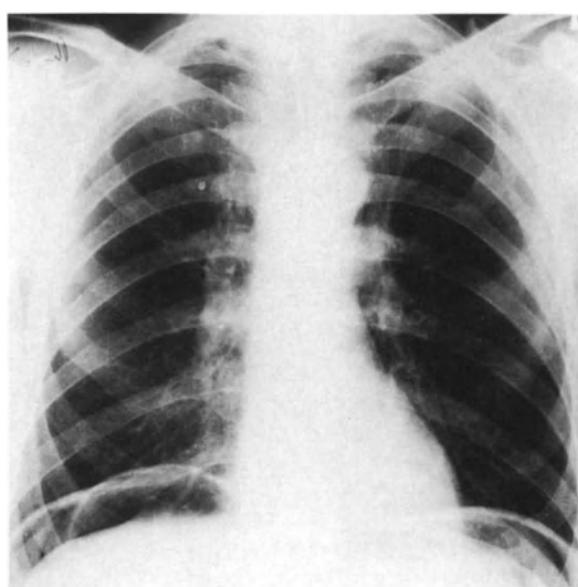


Fig. 2.11. Pneumoperitoneum due to perforated peptic ulcer. Both surfaces of the diaphragm are visible.

Unilateral elevation of the diaphragm (Table 2.2) is usually secondary to phrenic nerve palsy or paralysis, or to an abnormality of the adjacent lung, pleura or subphrenic space. Other causes include eventration, painful chest wall injuries and scoliosis. Subpulmonary pleural effusion may simulate elevation of one dome of the diaphragm (Fig. 2.12).

In chronic obstructive airways disease the diaphragm is typically low and flat. Pleural effusion may cause inversion of the diaphragm.

**Eventration.** Eventration almost always involves the left dome of diaphragm. It is due to deficiency of muscle and presents as unilateral elevation of the diaphragm (Fig. 2.13). Unlike phrenic paralysis the mediastinum is often displaced away from the eventration.

**Diaphragmatic Hernias.** *Hiatus hernia* may present as a retrocardiac mass, often with a fluid level (see Chap. 7:

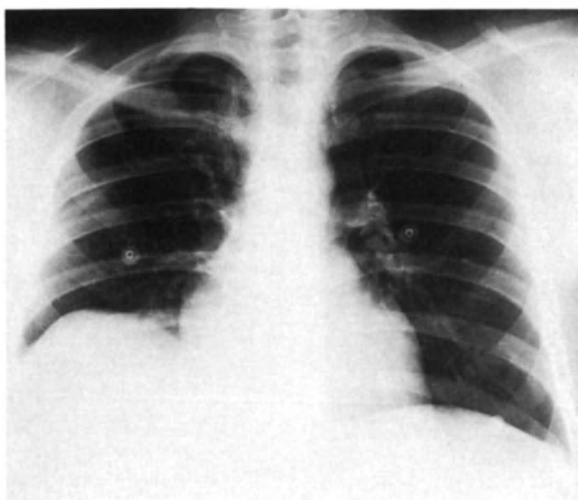


**Fig. 2.12.** Subpulmonary pleural effusion. The appearance mimics elevation of the right hemidiaphragm. However, the apex of 'right dome' is more lateral than normal.

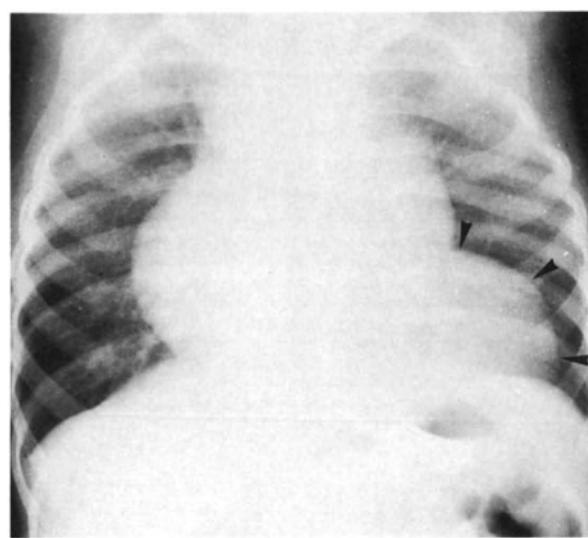


**Fig. 2.13.** Eventration of the diaphragm. A rounded density (arrowheads) is contiguous with the cardiac apex and left heart border. Ultrasound demonstrated eventration of the left hemidiaphragm anteriorly, containing part of the left lobe of the liver.

Mediastinum). Diagnosis may be confirmed by barium swallow.

*Bochdalek hernias* are due to a deficiency of the postero-lateral part of the diaphragm. They occur more frequently on the left. When small they usually present as an asymptomatic posterior paradiaphragmatic density (Fig. 2.14) containing fat, spleen or kidney. When large they may present neonatally causing respiratory distress. Loops of bowel may be visible in the thorax (Fig. 2.15).

*Morgagni hernia* is commoner on the right and usually presents as a paracardiac density. They usually contain omentum or colon (Fig. 2.16).

*Diaphragmatic rupture* is discussed in Chap. 8, with chest trauma.

**Subphrenic Abscess.** Subphrenic abscess is usually due to sepsis following abdominal surgery or a ruptured viscus. It is more frequent on the right. The chest film may show elevation of the diaphragm, a pleural effusion and basal atele-

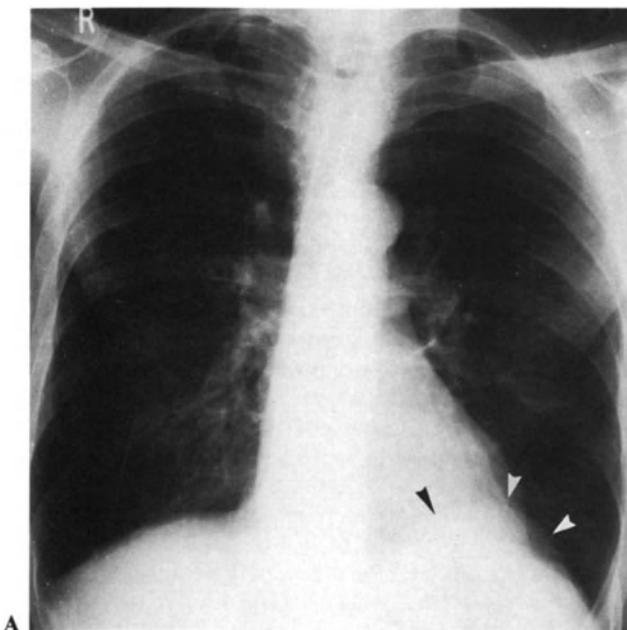


**Fig. 2.14.** Bochdalek hernia. A left-sided posterior diaphragmatic density (arrowheads) is present. On intravenous urography it was shown to contain the upper pole of the left kidney.

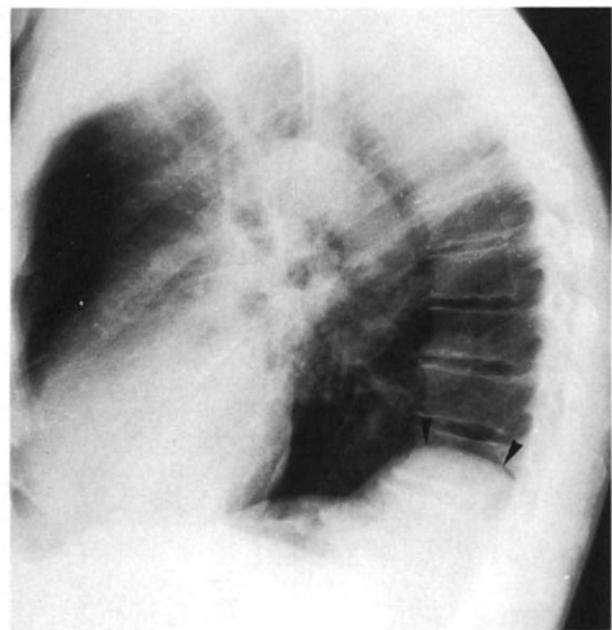


**Fig. 2.16A, B.** Morgagni hernia. A Low density gas shadows (arrowheads)► are projected over the left side of the heart. B Lateral film shows colon (arrowheads) extending into thorax anteriorly.

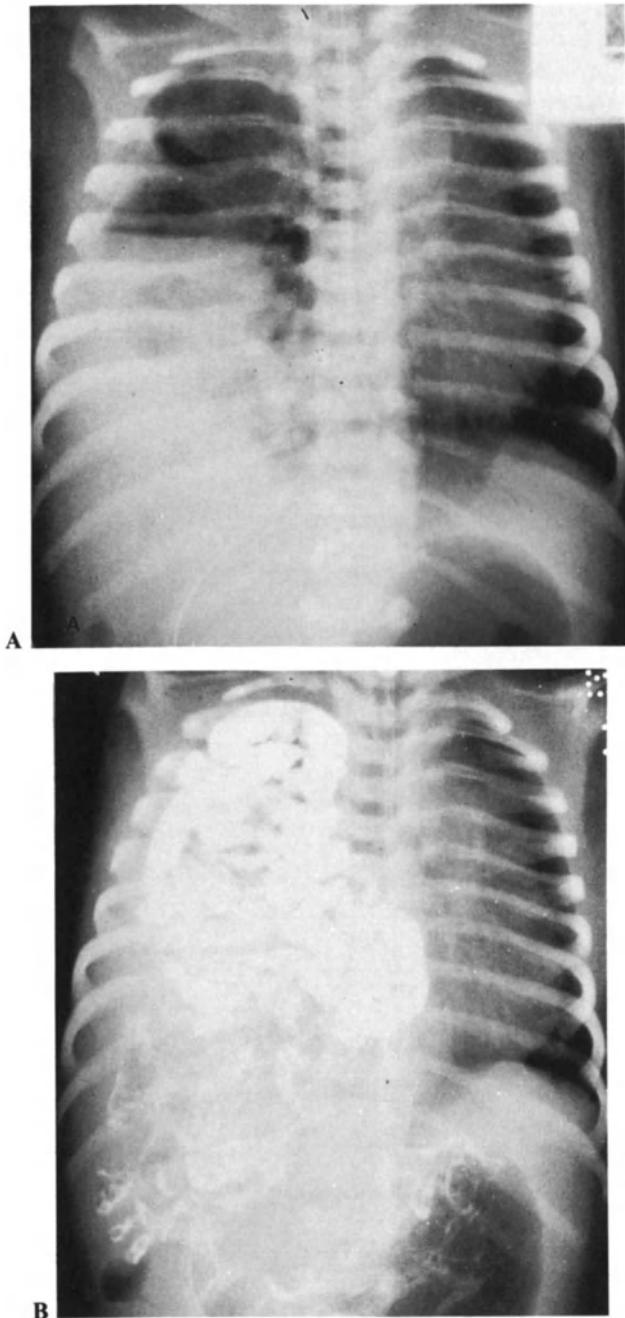


**Fig. 2.15A, B.** Congenital absence of the diaphragm. A neonate with respiratory distress. A Plain film demonstrates air-filled loops of bowel occupying the right hemithorax and displacing the mediastinum. B Barium follow-through shows several loops of small bowel in right hemithorax.

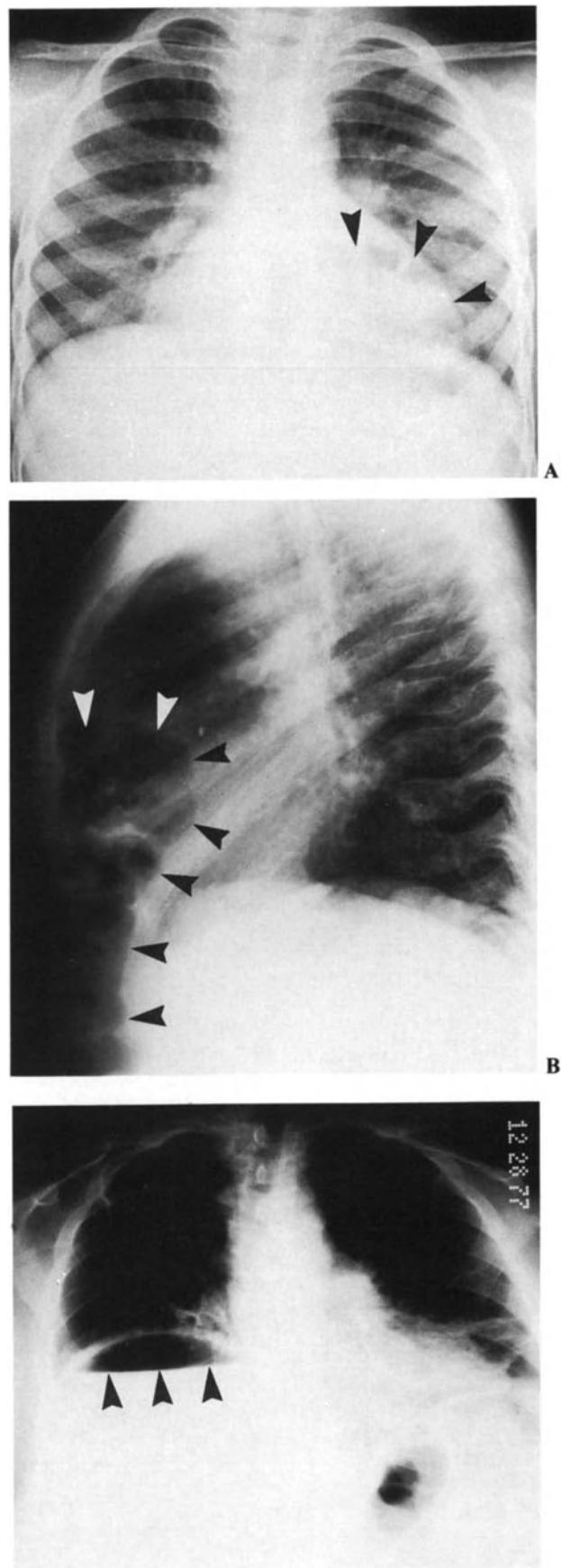


**Fig. 2.17.** Subphrenic abscess. The right hemidiaphragm is elevated, and ► gas and a fluid level (arrowheads) are visible in the right subphrenic space.

tasis. A subphrenic fluid level or a subphrenic gas collection may be visible (Fig. 2.17). The diagnosis can usually be confirmed by ultrasound.

**Diaphragmatic Tumors.** These may be benign or

malignant, and arise from fat, muscle, fibrous tissue or nerves. They are rare. They may be smooth or lobulated and may simulate evagination, a hernia or diaphragmatic elevation. Malignant tumors may cause a pleural effusion.

## THE PLEURA

The serous membranes that line the inner surface of the chest wall and cover the surface of the lungs are the parietal and visceral pleura. Under normal circumstances they are separated by a few milliliters of pleural fluid and are not visible except where the pleura extends into the lung creating the horizontal, oblique and accessory fissures.

### PLEURAL FLUID

Excess fluid in the pleural space is usually termed a pleural effusion. It may be due to transudate, exudate, pus, blood or chyle. The characteristics and causes of pleural fluids are summarized in Table 2.3. They produce similar shadows on the chest radiograph, and are, therefore, indistinguishable unless the clinical data or additional abnormality on the film point to a specific etiology. For example, there may be evidence of heart failure or trauma. However, even after pleural biopsy or thoracentesis the cause may remain obscure.

### Radiological Appearances of Pleural Fluid

The distribution of pleural fluid is influenced by the size of the effusion, the presence or absence of pleural adhesions,

the state of the underlying lung and the position of the patient.

**Free Fluid.** The posterior costophrenic angle is the most dependent recess of the pleura. Therefore, small effusions tend to collect posteriorly before blunting of the lateral costophrenic recess becomes apparent on the frontal film. Approximately 100–200 ml of pleural fluid need to be present for visualization on a frontal chest film (Fig. 2.18). Smaller amounts of fluid may be identified with horizontal beam decubitus films, ultrasound or CT (Figs 2.19–2.21). With increasing fluid a homogenous opacity extends upwards and obscures the diaphragm and lung base (Fig. 2.22). Typically the upper edge is concave and higher laterally, and fluid may be seen extending into the pleural fissures. A massive effusion may cause complete opacification of the hemithorax with contralateral displacement of the mediastinum (Fig. 2.23).

*Ultrasound* and *CT* are able to differentiate between the fluid and solid components of massive pleural shadowing (Fig. 2.41).

Atypical patterns of pleural effusion are not unusual, the commonest being lamellar and subpulmonary.

*Lamellar pleural effusions* are shallow collections adjacent

Table 2.3. Pleural fluid

	Characteristics	Causes
Transudate	Protein content – less than 3 g/dl Clear or faintly yellow fluid Often bilateral	Cardiac failure Hypoproteinemia Constrictive pericarditis Meig's syndrome Myxedema
Exudate and empyema	Protein content – more than 3 g/dl Varies from amber, slightly cloudy fluid to frank pus May clot on standing	Bacterial pneumonia Tuberculosis Carcinoma of lung Metastatic malignancy Pulmonary infarction Subphrenic infection Connective tissue disorders Non-bacterial pneumonia Post-myocardial infarction syndrome Pancreatitis Primary neoplasia of pleura
Hemothorax	Frank blood	Penetrating or non-penetrating trauma (Effusions associated with neoplasia and pulmonary infarction may be blood-stained)
Chylothorax	High neutral fat and fatty acid content Milky fluid	Trauma – usually surgical Lymphangitis Lymphangiomyomatosis

to the lateral chest wall often sparing the costophrenic angle. They are usually seen in children. Subpleural edema (i.e., fluid between the lung and visceral pleura) due to heart failure may give an identical appearance on the standard chest film.

*Subpulmonary pleural effusion* is caused by fluid accumulating between the inferior surface of the lung and the diaphragm. It may simulate elevation of the diaphragm, but the 'diaphragmatic' contour is more lateral than usual (Fig. 2.12), and the costophrenic angle may appear blunted or

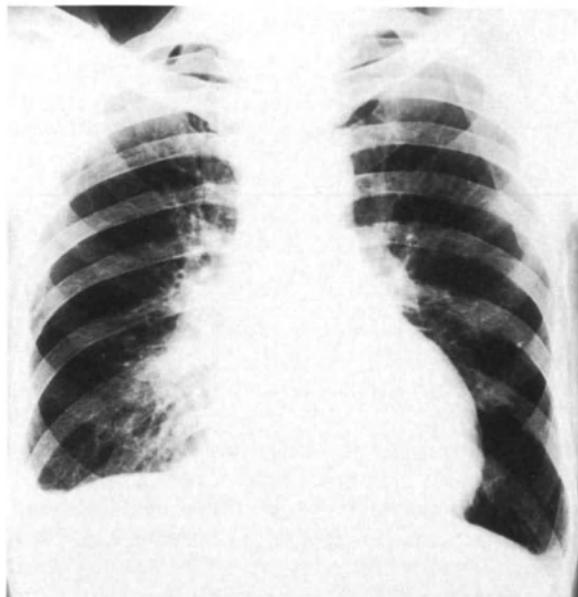


Fig. 2.18. Small pleural effusions. Both costophrenic angles are blunted.



Fig. 2.20. Ultrasound demonstration of pleural effusion. Parasagittal section through liver (Li) shows base of right lung (Lu) surrounded by echo-free effusion (Eff), diaphragm (arrows) and posterior chest wall (arrowheads).

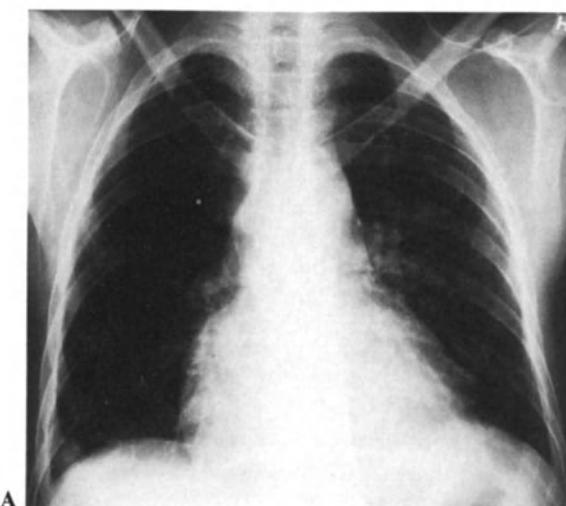
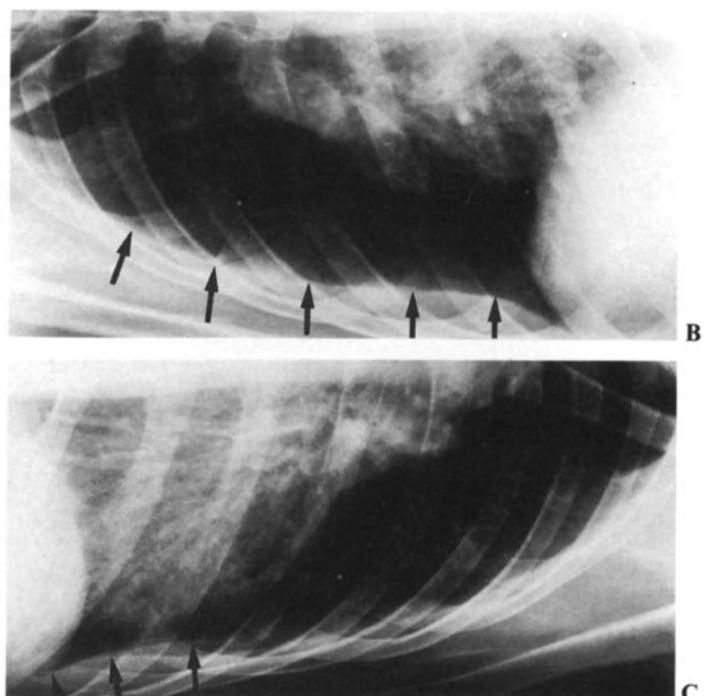
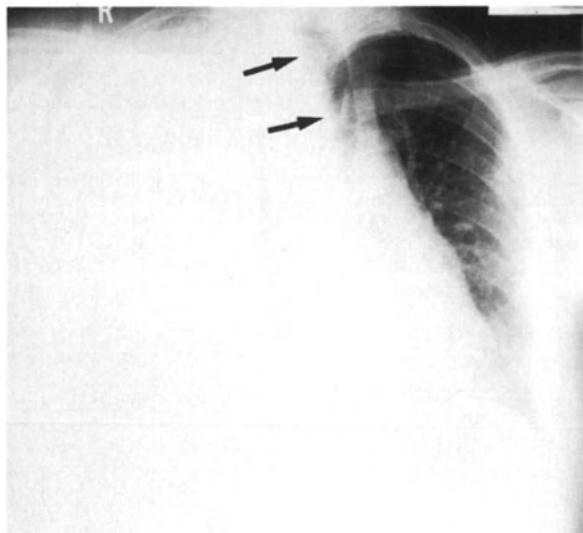


Fig. 2.19A, B, C. Small pleural effusions showing subtle blunting of costophrenic angles on PA film A, but horizontal beam decubitus films B, C show obvious pleural fluid (arrow) collecting adjacent to the dependent chest wall.





**Fig. 2.21.** CT demonstration of small pleural effusion (arrows) and small calcified pleural plaques (arrowheads) due to asbestos exposure.



**Fig. 2.23.** Massive pleural effusion displacing mediastinum. Note shift of trachea (arrows) to left.

fluid may be seen in the fissures. On the left side, increased distance between the gastric air bubble and lung base may be seen. Differentiation between subpulmonary effusion and elevated diaphragm may be made by decubitus or supine films or ultrasound (Fig. 2.24).

**Loculated Fluid.** Pleural fluid may become loculated secondary to pleural adhesions. Unlike free fluid, loculated fluid does not alter its appearance with changes of the patient's position. On the chest radiograph it may be difficult to differentiate loculated fluid from an extrapleural opacity.

parenchymal lung disease or a mediastinal mass. However, loculated effusions may be associated with free fluid or fluid extending into a fissure (Fig. 2.25). Moreover, loculated fluid tends to have much more depth in one projection but much less when seen in another view. Extrapleural lesions tend to have a sharper outline. An air bronchogram, if present, will indicate a pulmonary lesion.

*Ultrasound* will differentiate between peripheral loculated fluid and a mass, but *CT* may be necessary to distinguish between paramediastinal fluid and masses.

Loculated *interlobar effusions* are comparatively unusual. Fluid in the horizontal fissure tends to produce a lenticular, round or oval opacity in both frontal and lateral views. Fluid may be seen extending into the adjacent part of the fissure. Fluid in the oblique fissure tends to be less well-defined on the frontal view, but has a typical lenticular appearance in the lateral film (Fig. 2.26).

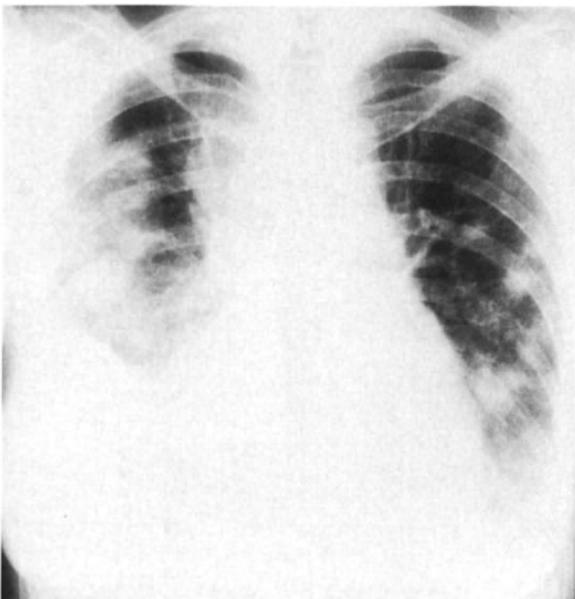


**Fig. 2.22.** Small left pleural effusion and moderate size right pleural effusion due to non-Hodgkin's lymphoma. Mediastinal lymphadenopathy and bilateral pulmonary nodules are also present.

## PNEUMOTHORAX

Air may enter the pleural space through a defect in the parietal or visceral pleura. This is often due to spontaneous rupture of an apical bleb, but may be secondary to a subpleural cavitating lesion, trauma or pneumomediastinum (see Table 2.4).

Air may enter and leave the pleural space freely in an open pneumothorax. In a closed pneumothorax there is no movement of air and, in a valvular pneumothorax, air may enter on inspiration but remain on expiration, eventually causing a *tension pneumothorax*.

### Radiological Appearances

In the absence of pleural adhesions a small pneumothorax, in the erect patient, collects at the apex. The lung retracts towards the hilum, and its visceral pleura may be visible as a sharp white line separate from the chest wall (Fig. 2.27).

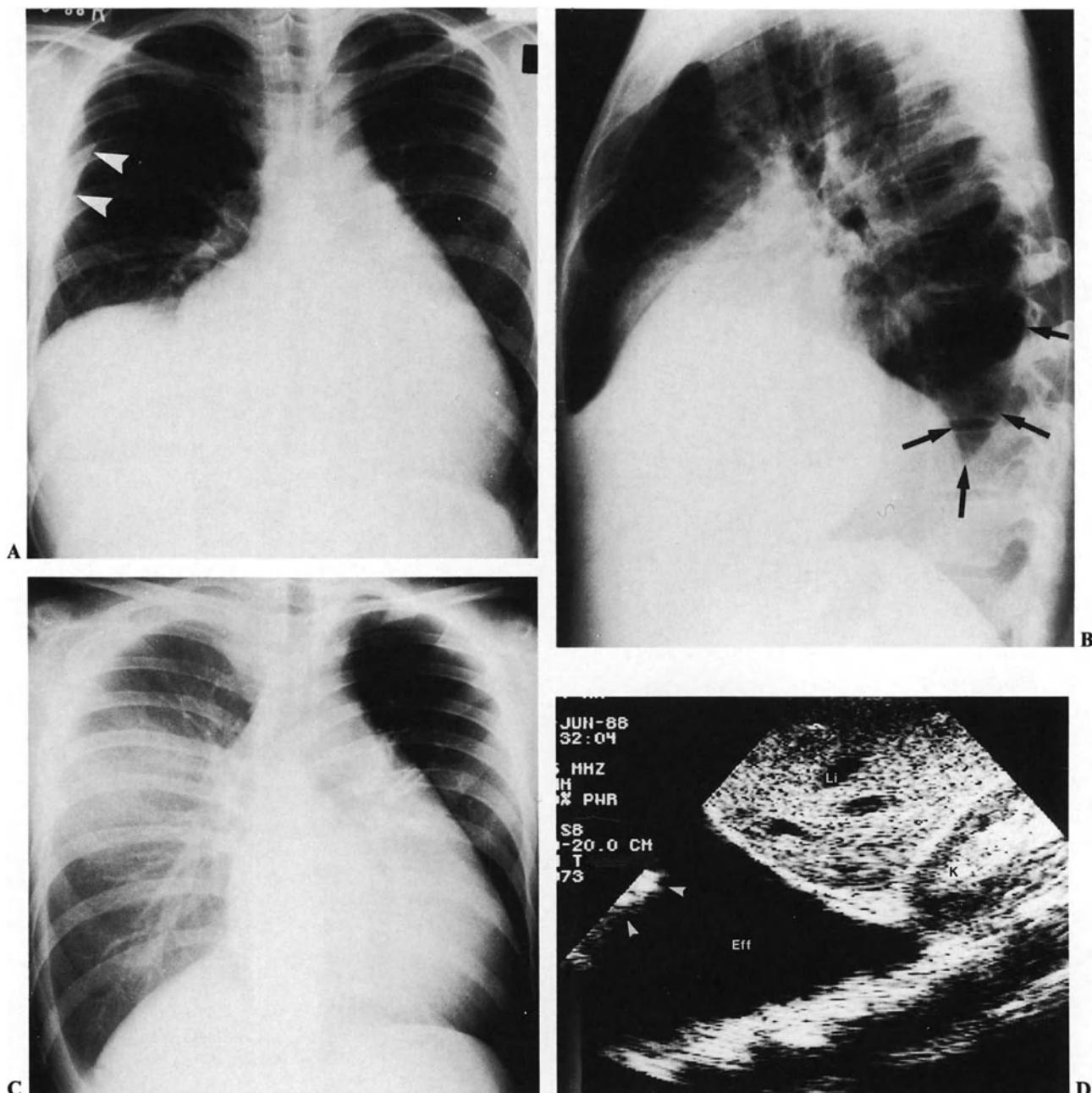


**Fig. 2.24A–D.** Subpulmonary pleural effusion. A PA film suggests elevation of right hemidiaphragm, but fluid can be seen in oblique fissure (arrowheads). B Lateral film shows fluid (arrows) in posterior costophrenic recess. C Supine film shows fluid collecting posteriorly, increasing the radiodensity of entire right hemithorax, but also revealing true level of diaphragm. D Parasagittal ultrasound scan through liver (Li) and right kidney (K) demonstrates base of left lung (arrowheads) floating in the pleural effusion (Eff).

A small pneumothorax may be seen more easily on an expiratory film (Fig. 2.28). In supine patients the air collects anteriorly, medially and basally (Fig. 2.29). In young children and infants a lateral decubitus film with the abnormal side uppermost may demonstrate a small pneumothorax adjacent to the lateral chest wall. A large pneumothorax may allow complete collapse of the lung and shift of the mediastinum to the normal side.

**Tension pneumothorax** may cause massive displacement of the mediastinum and severe circulatory and respiratory

embarrassment. The affected lung may be squashed against the mediastinum and the diaphragm may be depressed (Fig. 2.30). On fluoroscopy the mediastinal shift increases on inspiration.

#### Complications of Pneumothorax

Pleural adhesions may limit the distribution of air in a pneumothorax, causing a loculated or *encysted pneumothorax*. A ruptured adhesion may bleed causing a *hemopneumothorax*. Pneumothorax due to rupture of an

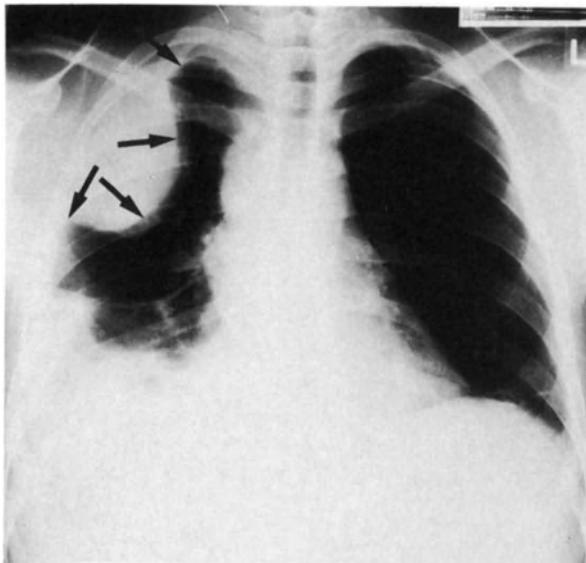
**Table 2.4.** Causes of pneumothorax

## Spontaneous

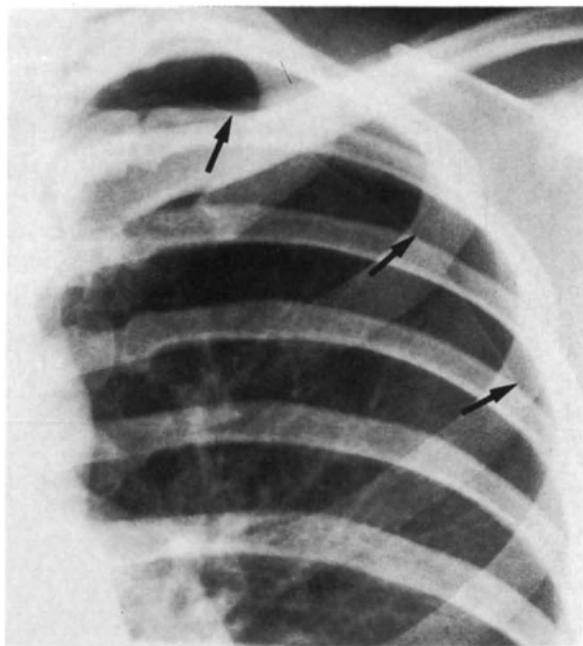
rupture of a congenital pleural bleb or bulla  
 chronic obstructive airways disease  
 asthma  
 staphylococcal pneumonia  
 tuberculosis  
 carcinoma of the bronchus  
 metastatic carcinoma  
 interstitial lung disease

## Traumatic

penetrating injury and surgery  
 pleural aspiration and biopsy  
 lung biopsy  
 closed chest trauma  
 rib fracture  
 positive pressure ventilation

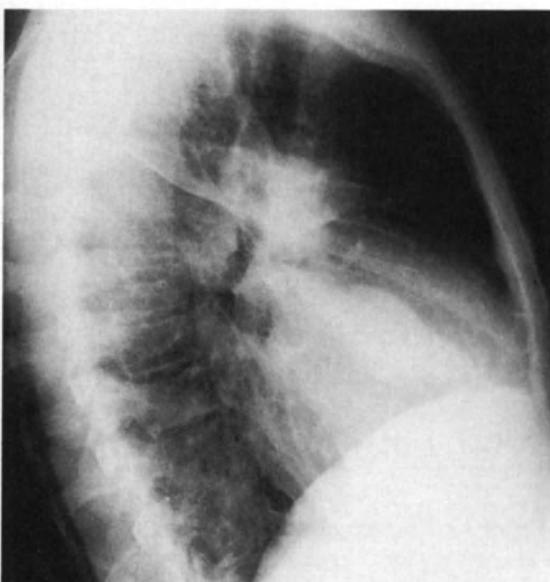
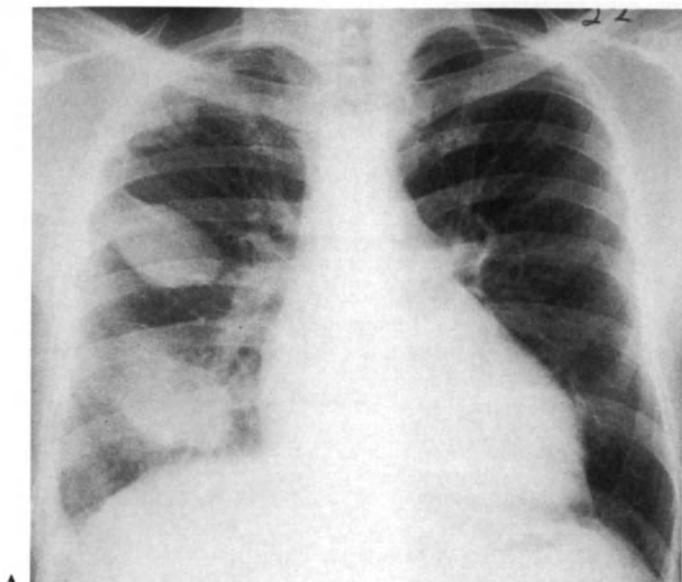


◀ Fig. 2.25. Loculated pleural effusion (arrows) in periphery of right upper zone, associated with paramediastinal fluid and lymphadenopathy and basal pleural effusion due to non-Hodgkin's lymphoma.



▲ Fig. 2.27. Apical pneumothorax. The visceral pleura (arrows) separates lung from air in the pleural space.

◀ Fig. 2.26. Loculated interlobar pleural effusions. Rounded opacities in the right mid and lower zones are caused by fluid in the horizontal and oblique fissures.



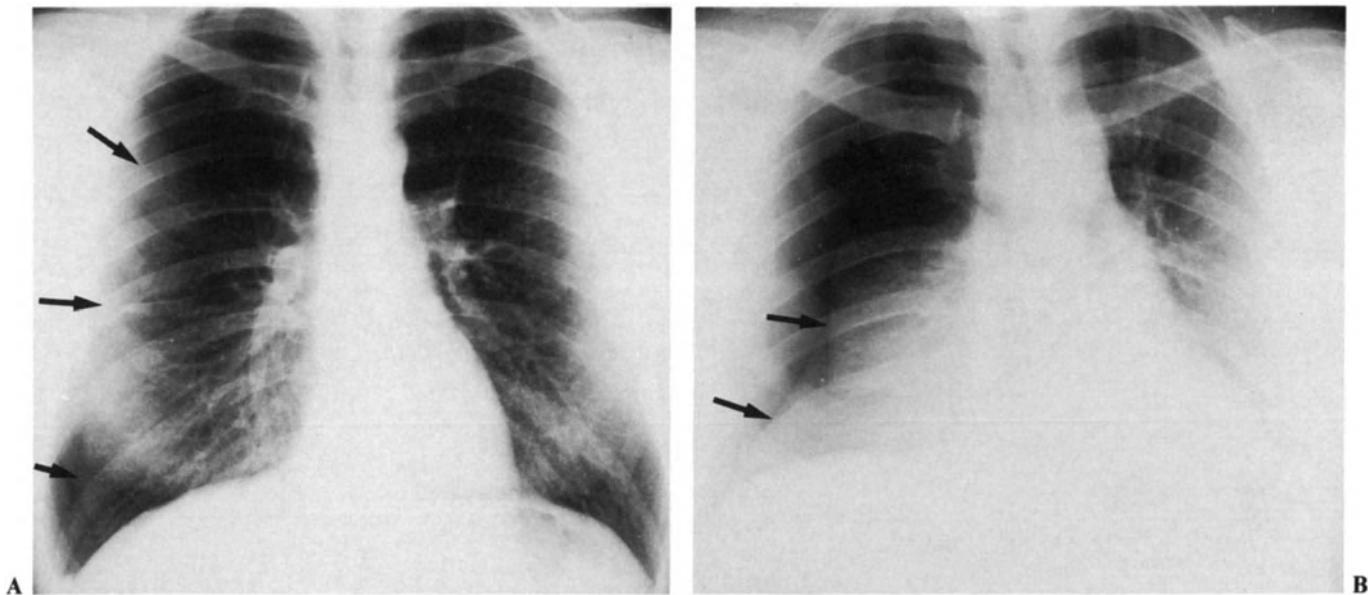


**Fig. 2.28A, B.** Pneumothorax: inspiratory and expiratory films. **A** On inspiration the pneumothorax (arrows) is difficult to see. **B** On expiration the pneumothorax appears larger, and the mediastinum has moved to the contralateral side.

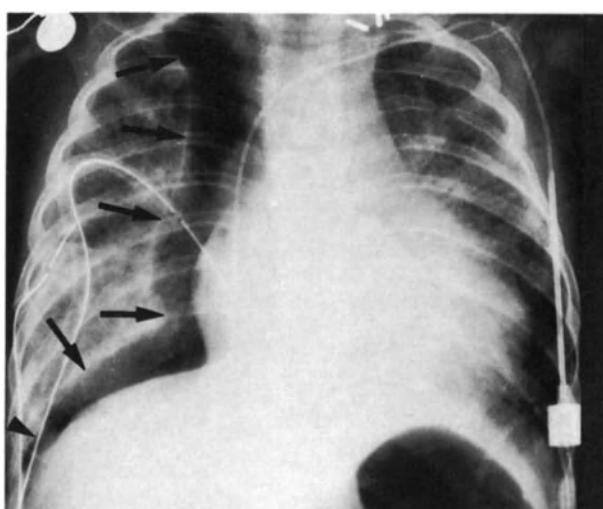
infected cavity may be complicated by infection causing *pyopneumothorax*.

It is common to see a small amount of fluid blunting the costophrenic angle in a pneumothorax (Fig. 2.31). However, a large fluid level usually indicates a complication such as hemo- or pyopneumothorax.

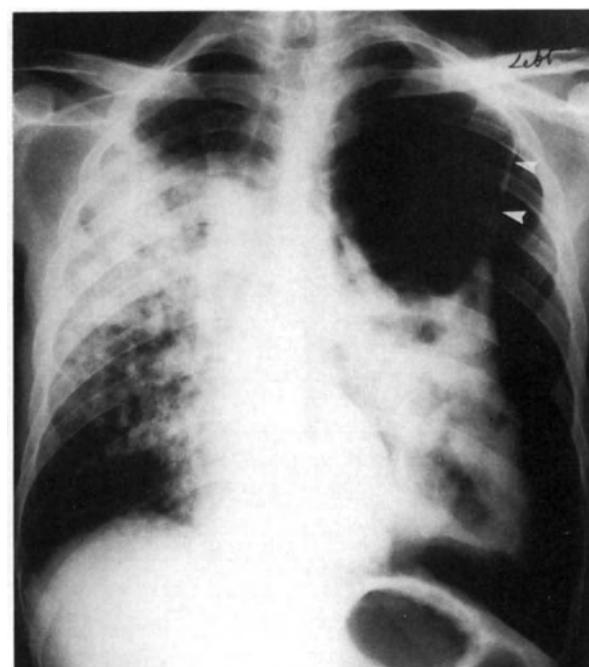
Rapid re-expansion of a pneumothorax may rarely be complicated by pulmonary edema. Collapse or consolidation of the underlying lung may delay re-expansion of a pneumothorax. Chronic pneumothorax may be complicated by pleural thickening.

#### Bronchopleural Fistula

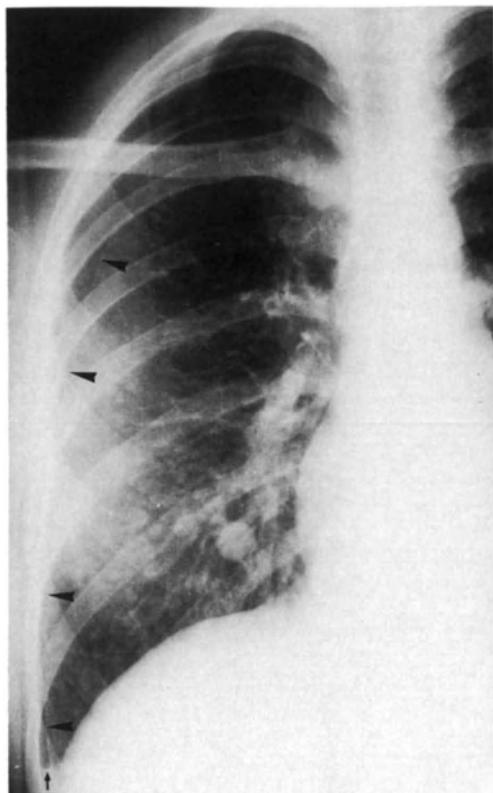
A communication between the airways and pleura is most often a complication of partial or complete *pneumonectomy*, but may be due to a *ruptured lung abscess*, *carcinoma* of the bronchus or *penetrating trauma*.



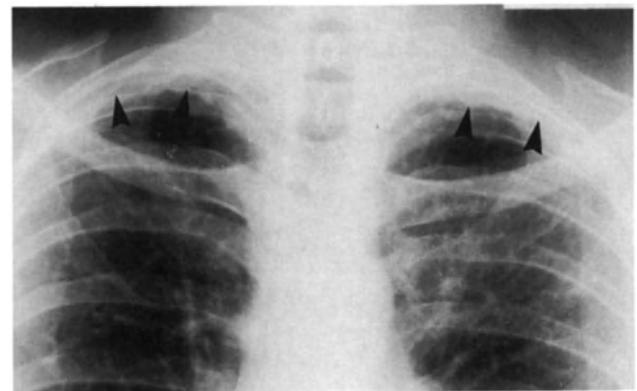
**Fig. 2.29.** Medial pneumothorax in supine patient. The pleural air has collected anteriorly outlining the medial and inferior surfaces of the lung (arrows).



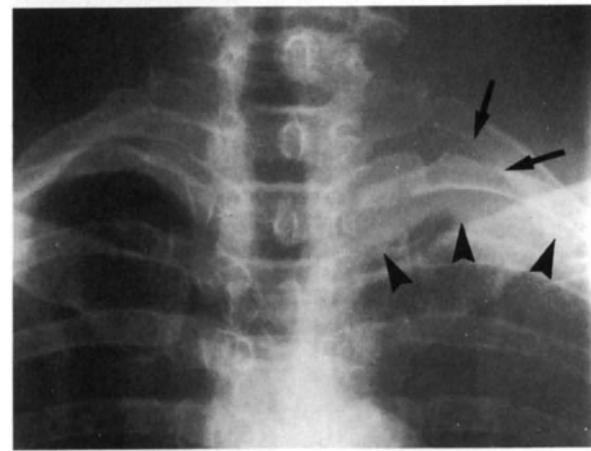
**Fig. 2.30.** Tension pneumothorax displacing mediastinum and depressing left hemidiaphragm. Extensive consolidation and cavitation in both lungs is due to tuberculosis. A pleural adhesion (arrowheads) is visible.



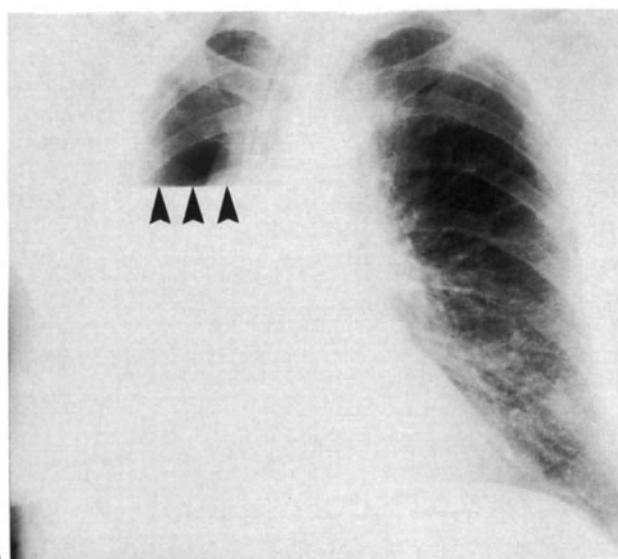
**Fig. 2.31.** Shallow hydropneumothorax. The pneumothorax (arrowheads) with a short fluid level (arrow) in the costophrenic recess is due to metastatic osteogenic sarcoma. The right scapula is missing and multiple pulmonary metastases are visible.



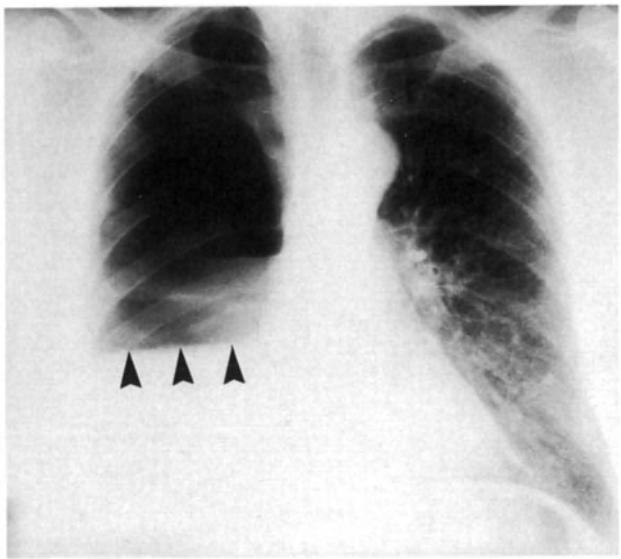
**Fig. 2.33.** Bilateral apical pleural thickening (arrowheads). Incidental finding.



**Fig. 2.34.** Unilateral apical pleural thickening (arrowheads). It is associated with invasion of the first rib (arrows) indicating an aggressive lesion. Needle biopsy confirmed carcinoma.



**Fig. 2.32A, B.** Broncho-pleural fistula. **A** Following right pneumonectomy the right pleural space is filling with fluid (arrowheads) and the mediastinum is deviated to the right. **B** Two days later the patient expectorated a large quantity of fluid. The fluid level has fallen, the amount of air in the space has increased and the mediastinum has returned to the mid-line.



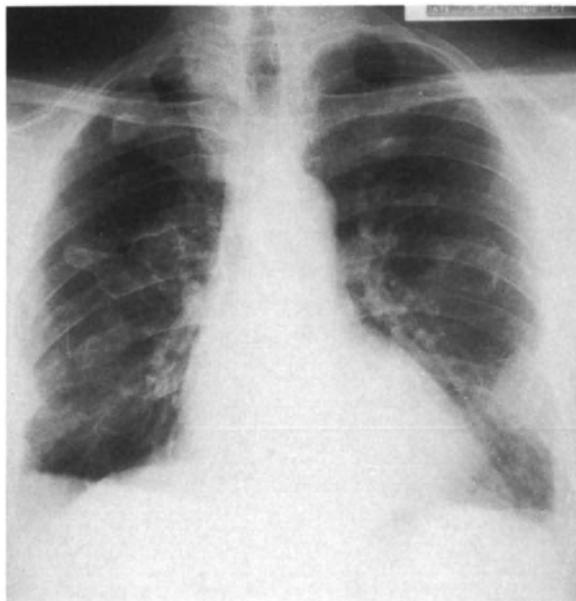
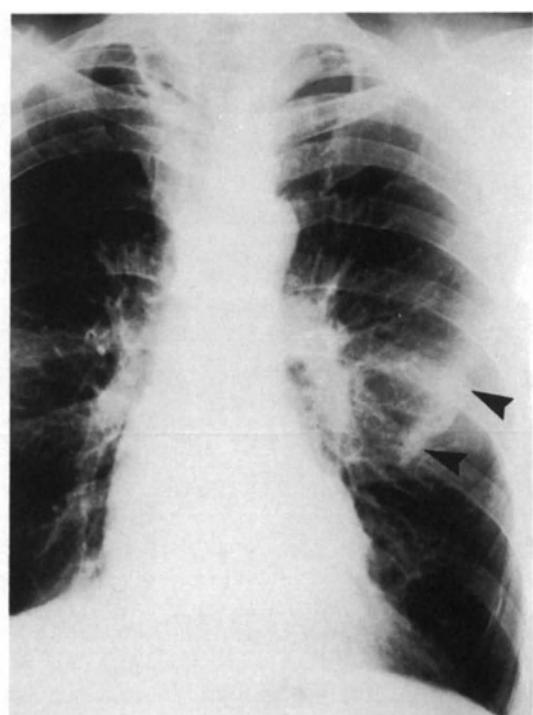


**Fig. 2.35.** Bilateral pleural plaques due to asbestos exposure. Soft tissue pleural shadows are visible adjacent to the chest wall and several calcified plaques are visible 'en face' over both lungs.



A

Following lung resection bronchopleural fistula may occur early due to faulty closure of the bronchus, or late due to infection or recurrent tumor of the bronchial stump. The patient usually expectorates fluid, and the chest radiograph shows an increase in the amount of air in the pleural space, a decrease in the amount of fluid in the space and return of the mediastinum to the mid-line (Fig. 2.32). If aspiration occurs, the contralateral lung may show areas of consolidation.

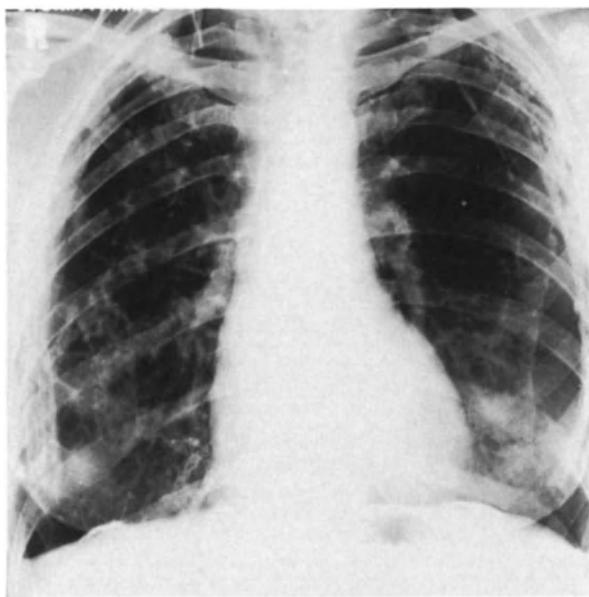
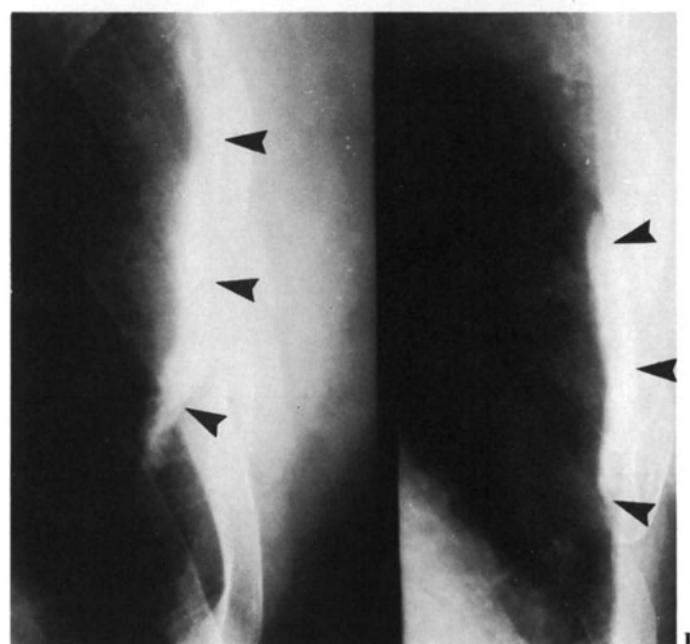


**Fig. 2.36.** Pleural calcification. Extensive pleural calcification bilaterally due to previous tuberculous pleurisy.



B

**Fig. 2.37A, B.** Calicified pleural plaque due to asbestos exposure. A The PA film shows a rather poorly defined left mid-zone opacity (arrowheads). B Oblique films aided by fluoroscopy demonstrate the pleural plaque tangentially.

#### Pleural Thickening

Symmetrical apical pleural thickening is frequently seen in middle-aged and elderly patients (Fig. 2.33). It is of no pathological significance and its etiology is uncertain.

Asymmetric or unilateral apical pleural thickening, however, may be of significance, especially if associated with

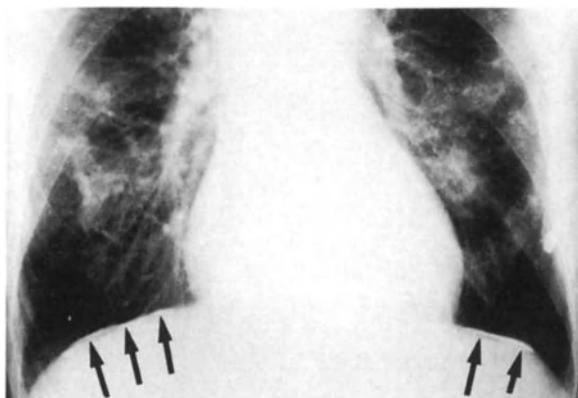


Fig. 2.38. Bilateral calcified pleural plaques (arrows) over the diaphragm, due to asbestos exposure.

pain. *Pancoast tumor* may present this way. It is important to scrutinize the ribs and spine for evidence of bone involvement (Fig. 2.34) using extra films or CT if necessary.

Blunting of a costophrenic angle and tenting of the diaphragm are common incidental findings. They probably indicate previous pleurisy, although a history of previous illness is often lacking.

More extensive unilateral pleural thickening is usually due to previous pleural effusion, hemothorax or thoracotomy. Empyema and hemothorax may cause pleural fibrosis, which, if it surrounds the entire lung, may be termed *fibrothorax*. Fibrothorax may limit ventilation of the lung to such an extent that decortication is indicated. Bilateral pleural plaques are a common manifestation of asbestos exposure (Fig. 2.35).

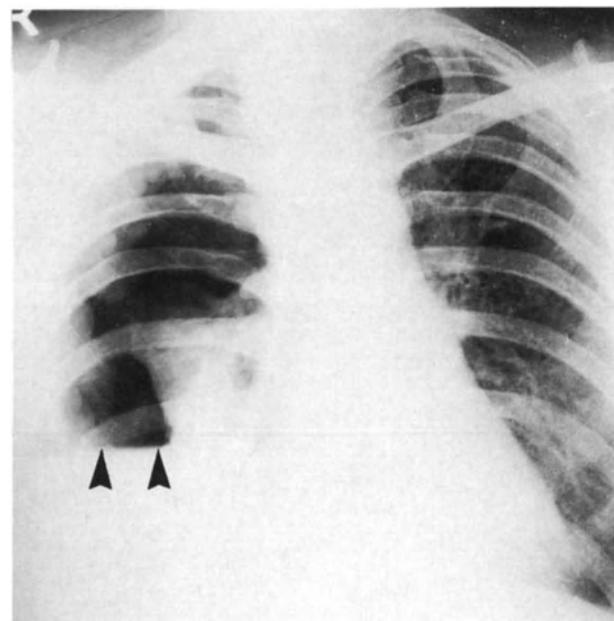


Fig. 2.39. Pleural metastases from adenocarcinoma of unknown origin. A right pneumothorax following thoracentesis revealed lobulated masses adjacent to the chest wall. Some pleural fluid (arrowheads) remains.

#### Pleural Calcification

The causes of pleural calcification are the same as those of pleural thickening. Unilateral calcification may be due to previous empyema, hemothorax or pleurisy, and bilateral cal-

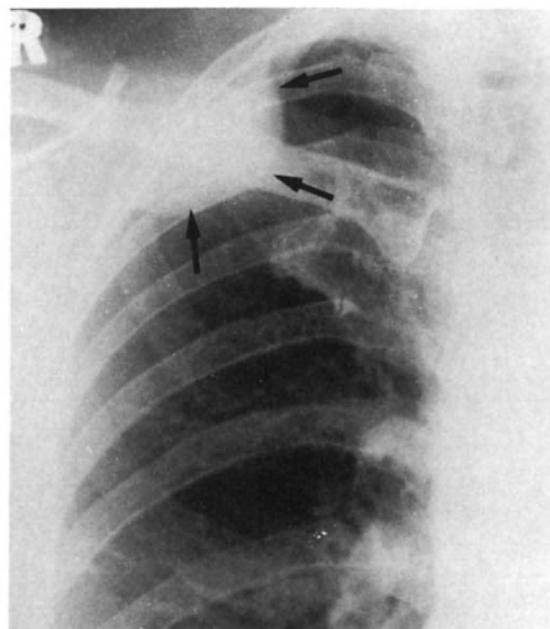
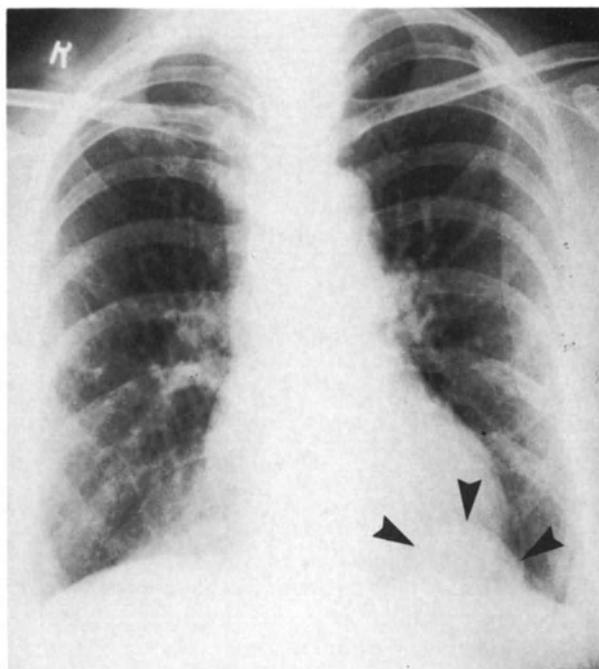
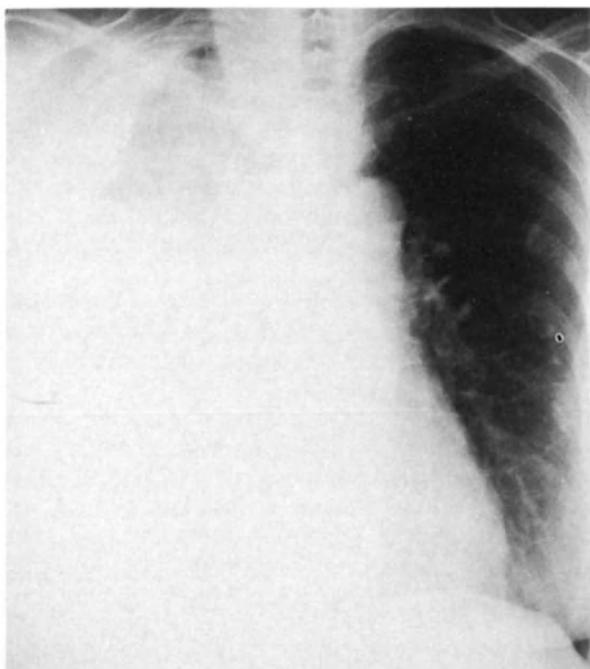
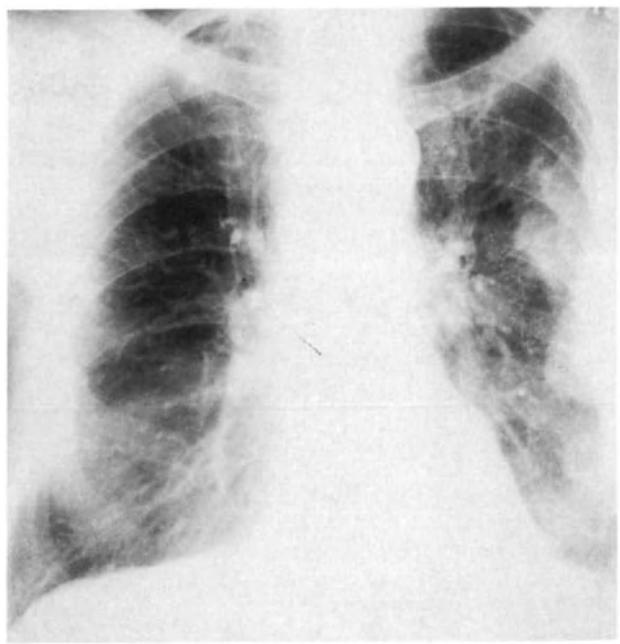


Fig. 2.40A, B. Benign pleural tumors. A Pleural lipoma (arrowheads). B Pleural fibroma (arrows).



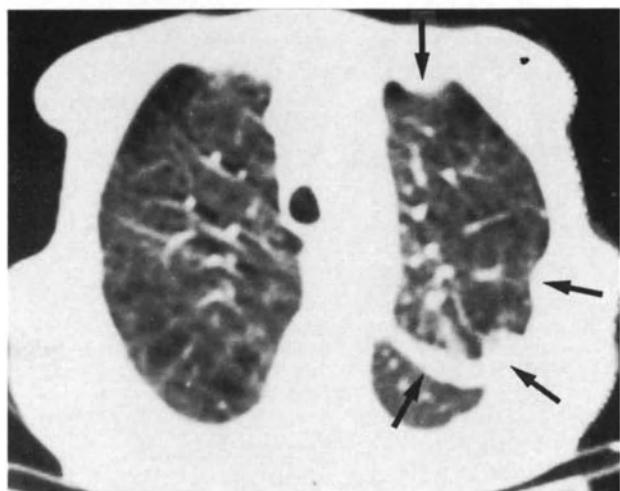
A



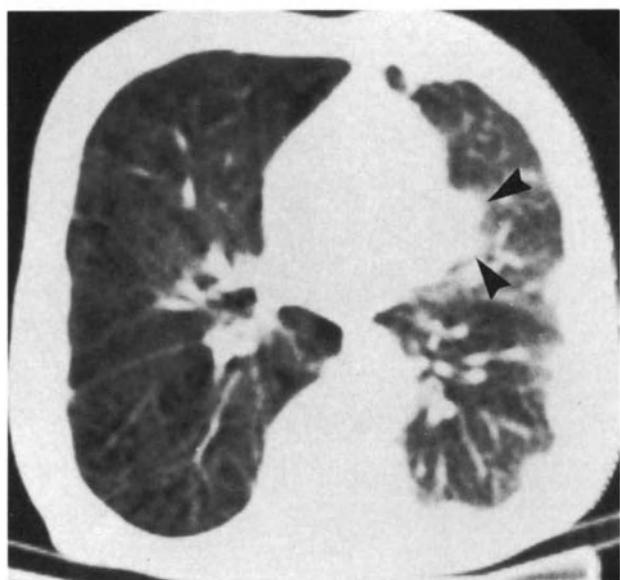
A



B



B



C

**Fig. 2.41A, B.** Malignant pleural mesothelioma. A Extensive pleural shadowing occupies most of the right hemithorax. B Ultrasound scan shows pleural fluid (Eff), nodular pleural masses over the diaphragm (arrow), liver (Li) and right kidney (K).

**Fig. 2.42A–C.** Malignant pleural mesothelioma. A Lobulated pleural thickening surrounds the left lung. B, C In addition, CT demonstrates extension of the peripheral masses (arrows) into the oblique fissure, and more nodules adjacent to the heart (arrowheads). The volume of the left lung is reduced.

cification may occur after asbestos exposure and in some other pneumoconioses, and following bilateral pleural effusions.

The calcification from previous pleurisy, infection or hemothorax is usually associated with pleural thickening, and is usually fairly dense and coarse, either in continuous sheets or discrete plaques (Fig. 2.36). If viewed 'en face' a plaque may produce a poorly defined shadow, and fluoroscopy is often the easiest method of viewing them tangentially (Fig. 2.37).

The calcification due to asbestos exposure tends to be more delicate and bilateral. It is frequently seen over the diaphragm (Fig. 2.38). CT is the most sensitive method for demonstrating pleural plaques (Fig. 2.21).

### Pleural Tumors

Primary neoplasia of the pleura is uncommon, but it is a common site for metastatic disease. *Effusion* is the usual manifestation of pleural metastatic involvement, but pleural nodules or masses may occur, although they may be obscured by fluid (Fig. 2.39).

*Benign* tumors of the pleura are mostly lipomas or fibromas. They usually present as well-defined subpleural masses (Fig. 2.40).

*Lipomas* produce a characteristic CT appearance due to their low X-ray attenuation. Pleural *fibroma*, which is also known as benign mesothelioma, often presents with finger clubbing and hypertrophic osteoarthropathy. Fibromas may be large enough to occupy most of a hemithorax.

*Malignant* pleural mesothelioma is usually due to prolonged exposure to asbestos. The chest radiograph usually shows nodular, pleural thickening and a hemorrhagic pleural effusion is often present (Fig. 2.41). In cases due to asbestos exposure the lungs may show evidence of asbestosis or pleural plaques may be visible.

The tumor may be locally invasive and involve the chest wall or abdomen. The chest film underestimates the extent of the tumor which is better assessed by CT (Fig. 2.42). Features that suggest malignancy rather than benign pleural thickening are nodular extension of tumor into fissures, pleural effusion and volume loss of the ipsilateral lung.

*For further reading, see p. 134.*

## CHAPTER 3

# DISEASES OF THE AIRWAYS: PULMONARY COLLAPSE AND CONSOLIDATION

M. Rubens

---

### THE TRACHEA

**Congenital Abnormalities.** *Tracheoesophageal fistula* may occur as an isolated anomaly. On the plain film, air may be visible in the esophagus (Fig. 3.1), but the diagnosis is usually made by a contrast study of the esophagus. Barium or low osmolarity contrast medium must be used. If a simple



**Fig. 3.1** Tracheo-esophageal fistula. Lateral chest radiograph shows fistula (arrowhead) between trachea and esophagus. The entire esophagus is air-filled.

swallow does not show the fistula, contrast medium should be injected into a nasogastric tube with the patient prone. As the tube is withdrawn the fistula is usually seen. Tracheoesophageal fistula may also be associated with esophageal atresia; in the absence of a fistula the trachea may be narrowed by pressure from a distended esophageal pouch or secondary to hypoplasia of the tracheal cartilage.

**Tracheal Narrowing.** *Laryngotracheobronchitis* or *croup* is the commonest cause of tracheal narrowing. It is usually viral and affects the upper trachea, most often in young children. Pyogenic bacteria and tuberculosis may cause a more generalized acute tracheitis.

Tuberculosis may cause fibrosis and chronic tracheal stenosis.

*Fibrosing mediastinitis*, which may be due to tuberculosis or histoplasmosis, can cause both tracheal and bronchial stenosis. Rarer chronic inflammatory causes of tracheal narrowing include *sarcoidosis*, *chronic relapsing polychondritis*, *Wegener's granulomatosis* and *rhinoscleroma*.

Primary tumors of the trachea are rare. Benign tumors present as small, well-defined intraluminal nodules. They are mostly papillomas, fibromas, chondromas or hemangiomas. Malignant tumors of the trachea tend to occur close to the carina. They are mostly carcinomas (Fig. 3.2) or cylindromas. They may cause a localized mass or a long stricture. Their extraluminal extent is best assessed by CT (Fig. 3.3).

Tracheal stenosis may also be due to *trauma*. Incomplete laceration of the trachea may heal with scarring and subsequent stenosis. Chronic strictures may also develop following tracheostomy (Fig. 3.4), or secondary to ischemia of the tracheal mucosa due to overinflation of the cuff of an endotracheal tube. Other rare causes of tracheal stenosis are

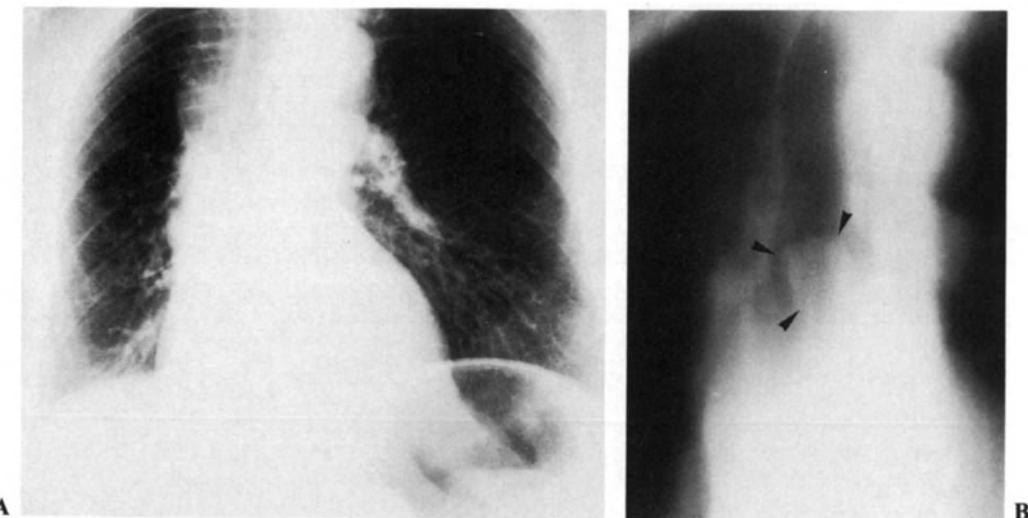


**Fig. 3.2A, B.** Carcinoma of carina. **A** The right lung volume is reduced. The trachea is difficult to assess on the standard chest radiograph. **B** Linear tomogram of trachea shows a mass (arrowheads) arising from the carina narrowing the origins of both main bronchi. The patient presented with acute dyspnea and wheeze.

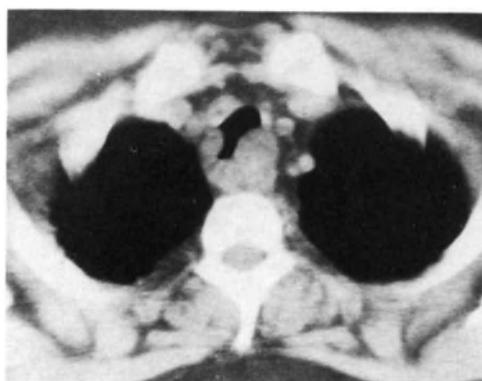
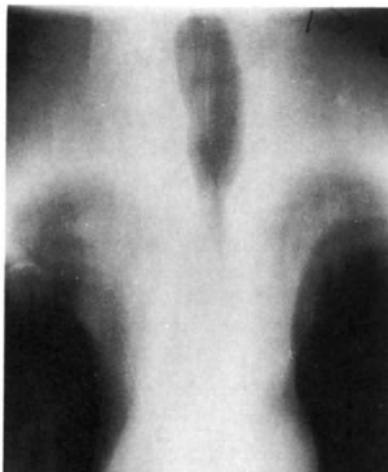


**Fig. 3.3.** Cylindroma of trachea. CT demonstrates a mass arising from the posterior tracheal wall causing narrowing of the lumen. The mass is extending into the adjacent soft tissues.



*amyloidosis, tracheopathea osteoplastica and tracheobronchiomalacia.*

Tumors of the thyroid, esophagus or lung may displace or compress the trachea, and if malignant may invade the trachea.

**Tracheal Widening.** Dilatation of the trachea is rare, and it may result from a defect of the connective tissue. It may be an isolated abnormality as in tracheobronchomegaly (Mounier-Kuhn syndrome) or associated with Ehlers Danlos syndrome or cutis laxa.

#### CHRONIC OBSTRUCTIVE AIRWAYS DISEASE

Chronic obstruction of bronchial airflow is a feature of many common chronic lung diseases. These include asthma, chronic bronchitis, pulmonary emphysema, bronchiectasis and cystic fibrosis. Clinically, patients may exhibit manifestations of more than one of these conditions, and the clinical and radiological presentations may, therefore, be mixed.

#### Asthma

Asthma is defined clinically as 'widespread narrowing of the bronchi, which is paroxysmal and reversible'. The larger airways are hyper-reactive to a variety of stimuli. *Extrinsic* asthma is usually associated with a history of allergy, and aspergillosis is an important cause. *Intrinsic* asthma may be precipitated by emotion, exercise or chest infection.

During remission the chest radiograph is usually normal. The role of the chest radiograph is to detect any complication

◀ **Fig. 3.4.** Stricture of the trachea. Linear tomogram. The patient had undergone tracheostomy 10 years earlier.

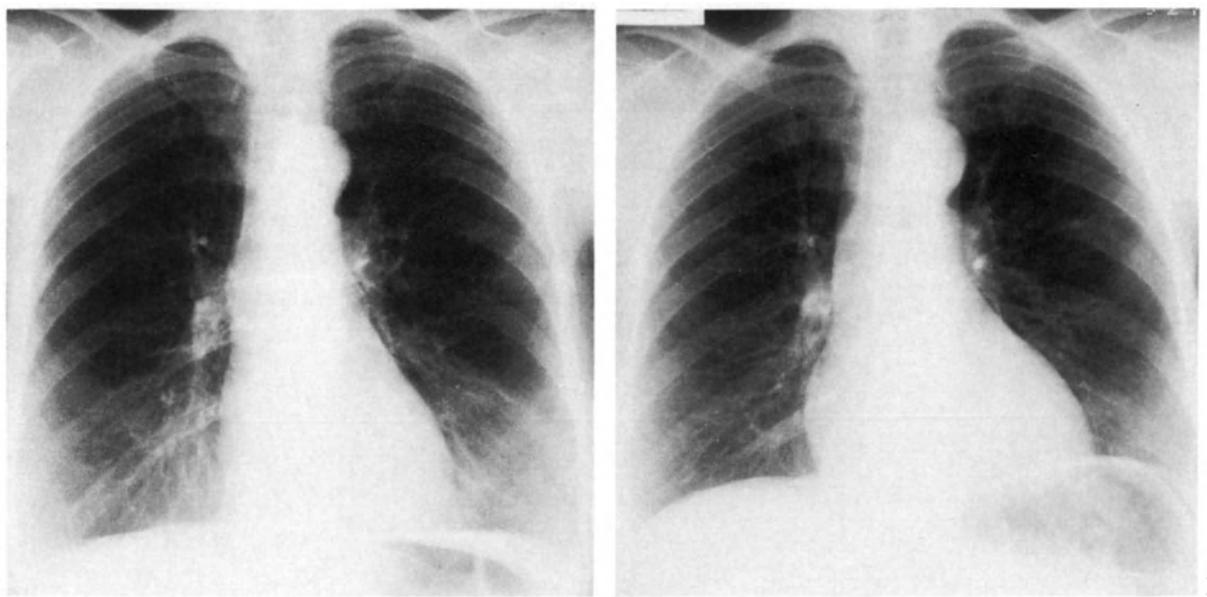


**Fig. 3.5A, B. Asthma.** A Chest radiograph during an acute exacerbation shows evidence of hyperinflation; the diaphragm is depressed and flattened. B After the acute attack has resolved the chest radiograph is normal.

during an attack, and to exclude other conditions if the diagnosis is uncertain. A *tumor* or inhaled *foreign body* in the trachea or a major bronchus may present with acute wheezing and simulate asthma (Fig. 3.2). During an asthmatic attack the chest radiograph may show evidence of hyperinflation (Fig. 3.5). Patchy infiltrates may be due to the eosinophilia of bronchopulmonary aspergillosis. Other complications that may be seen are consolidation due to infection, atelectasis due to mucus plugging, pneumomediastinum and pneumothorax.

#### Chronic Bronchitis

Chronic bronchitis is a clinical syndrome defined as 'a chronic cough without demonstrable cause, with expectoration on most days during at least three consecutive months for more than two consecutive years'. Most chronic bronchitics are smokers. Exacerbation of symptoms is often precipitated by chest infections, and *emphysema* and *cor pulmonale* are important complications.

The chest radiograph is normal in approximately 50% of patients with chronic bronchitis. Nevertheless, it may detect complications such as pneumonia or emphysema, or exclude diseases with similar symptoms such as tuberculosis and lung cancer. A few patients with chronic bronchitis have chest radiographs with generalized accentuation of the bronchovascular markings, widespread, small, poorly defined opacities or fine tramline or tubular opacities. These shadows produce what may be called the 'dirty chest'. This appearance, which is very subjective, and does not have a proven pathological basis, may suggest the diagnosis of chronic bronchitis. If emphysema and air trapping are present the diaphragm may be low and flat, and the central pulmonary arteries may be enlarged. Cardiomegaly may indicate *cor pulmonale*.

#### Emphysema

Emphysema is defined as an increase, beyond the normal, in the size of the air spaces distal to the terminal bronchioles, with dilatation and destruction of their walls.

#### Types of Emphysema and Associated Conditions

1. Pan-acinar emphysema is a non-selective process which destroys all of the lung distal to the terminal bronchiole.
2. Centriacinar emphysema selectively involves the respiratory bronchioles, sparing the more distal air spaces until a late stage.
3. Paracapillary emphysema is distension and destruction of terminal air spaces adjacent to fibrosis. It is usually secondary to tuberculosis.
4. Obstructive emphysema is better called obstructive hyperinflation. It occurs with obstruction of larger bronchi when air can enter the lung on inspiration but is trapped on expiration. The distal airways dilate, but are not necessarily destroyed.
5. Compensatory emphysema is another process that is best regarded as hyperinflation, and occurs in response to collapse, shrinkage or removal of other parts of the lung. It is discussed in the section on pulmonary collapse.
6. A bulla is an emphysematous space, 1 cm or more in diameter when distended.

#### Radiological Appearances

*Pan-acinar Emphysema.* Destruction of lung tissue, reduction of alveolar ventilation and air trapping are responsible for the main radiographic features of pan-acinar emphysema. These are (Fig. 3.6):

1. Reduction of peripheral pulmonary vascularity.
2. Pulmonary hyperinflation.

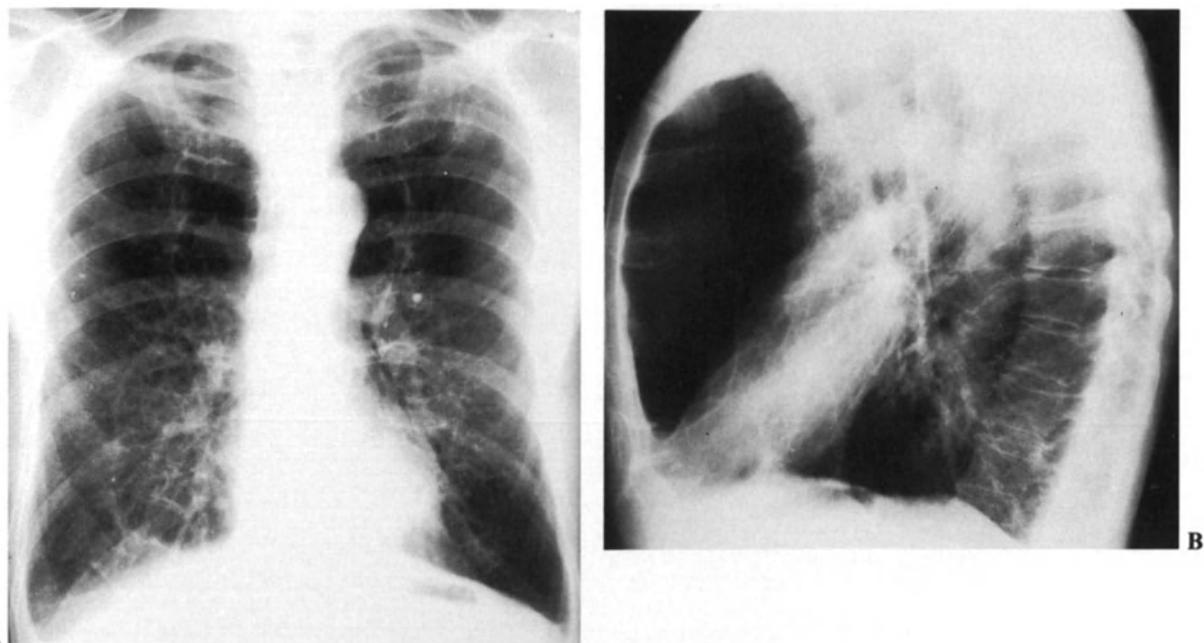


**Fig. 3.6A, B. Emphysema.** A, B The diaphragm is depressed and flattened, the retrosternal space is enlarged and the sternum is bowed anteriorly. The peripheral vascular pattern is attenuated in the right upper and left lower zones. The central pulmonary arteries are prominent.

### 3. Alteration of the central pulmonary arteries and heart.

The pulmonary vascular pattern is attenuated with fewer and smaller vessels than normal. The abnormality may be localized or generalized throughout the lung, but if widespread is usually patchy. Vessels may be seen to be displaced around emphysematous areas or bullae. In alpha-1-antitrypsin deficiency pan-acinar emphysema tends to develop basally. This may result in upper zone blood diversion, which

should not be interpreted as pulmonary venous hypertension.

Air trapping causes pulmonary hyperinflation with flattening and depression of the diaphragm. The chest may become barrel-shaped and the retrosternal air space may enlarge.

The heart may appear elongated, probably secondarily to depression of the diaphragm. If pulmonary arterial hyperten-

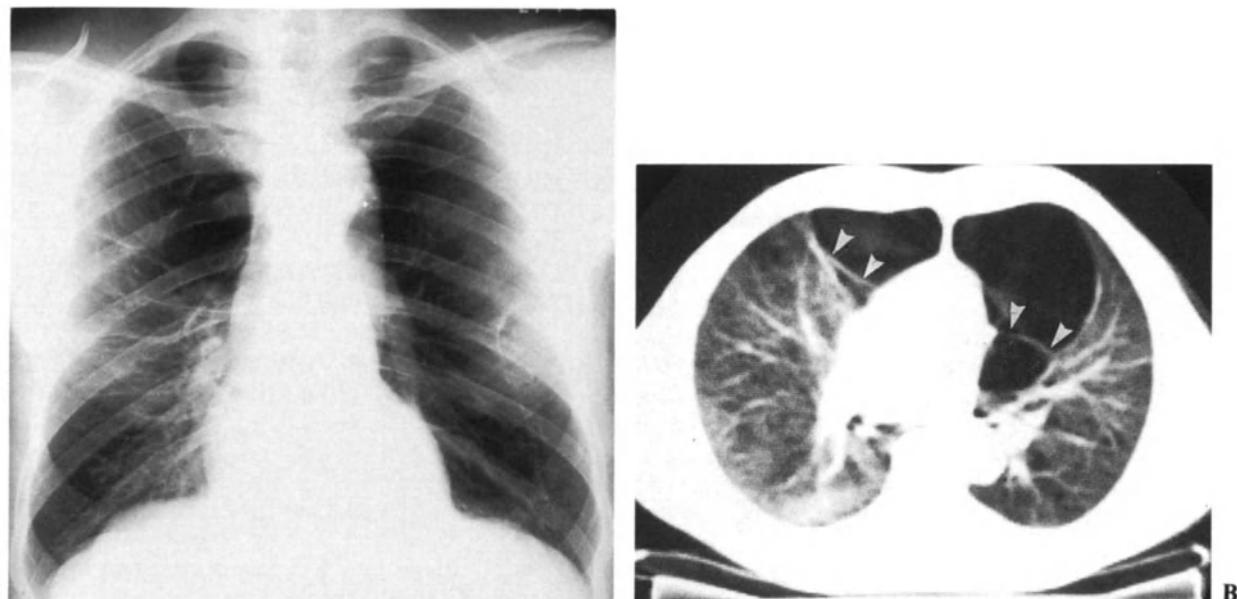


**Fig. 3.7A, B. Emphysema.** A The chest radiograph shows attenuation of the vascular pattern in both upper zones and in the periphery of the left lower zone. B CT scan demonstrates the bullae more clearly. Strands of tissue (arrowheads) can be seen crossing the bullae.

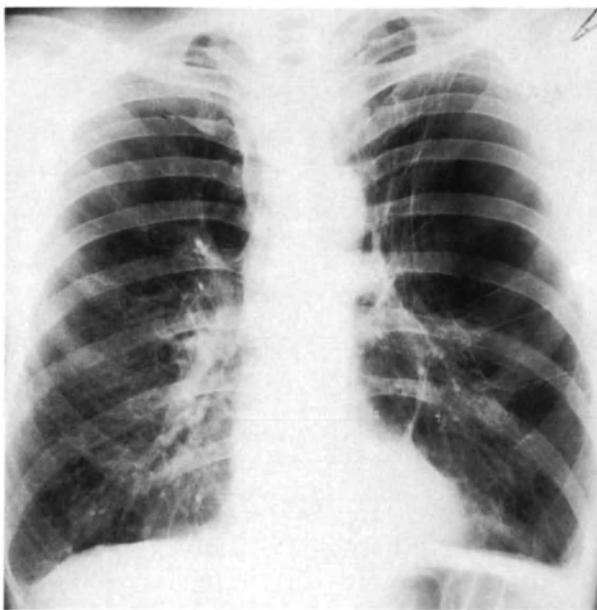


**Fig. 3.8.** Emphysema with bullae. The lungs are hyperinflated. A large bulla in the left hemithorax compresses much of the left lung.

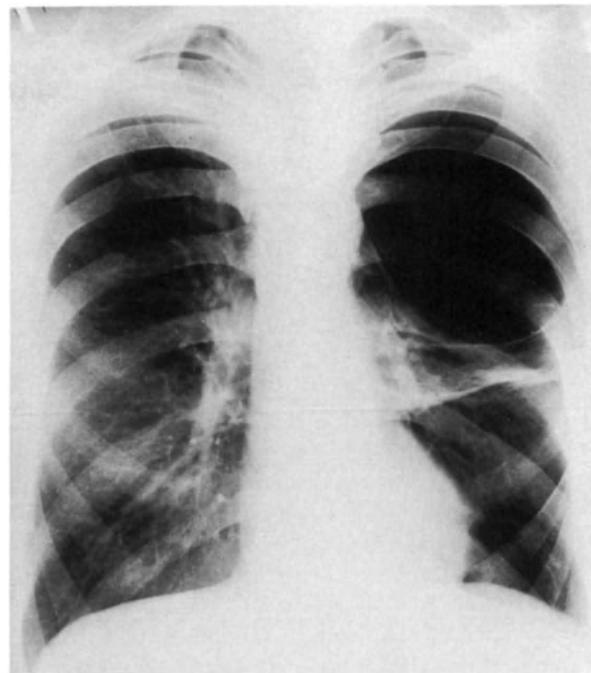


**Fig. 3.9.** Isolated bulla. A left upper zone bulla is compressing the left lung. There is no evidence of generalized emphysema or air trapping.

sion develops the central pulmonary arteries may enlarge. Enlargement of the heart may indicate cor pulmonale.

CT is more sensitive than the plain chest film in demonstrating emphysema (Fig. 3.7). Vascular attenuation may be seen earlier, and bullae are easier to identify. Moreover comparison of scans in inspiration and expiration may demonstrate areas of air trapping.

**Bullous Disease.** Bullae may be single or multiple, and vary from 1 cm in diameter to occupying an entire hemithorax. They are usually associated with emphysema (Fig. 3.8), but may occur in otherwise normal lung (Fig. 3.9). They appear as round or oval translucent areas. The wall may be seen as a fine, smooth, curved shadow, and fine strands of lung tissue may be seen crossing a bulla. Adjacent lung may be compressed by bullae and pulmonary vessels may be displaced around them. Following chest infection, bullae may fill with fluid.

**Emphysema with Chronic Bronchitis.** Emphysema and chronic bronchitis often occur together. In these cases the chest radiograph may show features of hyperinflation, pulmonary arterial hypertension and increased bronchovascular markings in varying degrees.

**Unilateral or Lobar Emphysema (Macleod's or Swyer-James' Syndrome).** This condition, which is probably a consequence of an early childhood viral bronchiolitis, is characterized by a hypertransradiant hemithorax (Fig. 3.10). The affected lung may be smaller than normal, and its blood vessels are attenuated. Moreover, there is air trapping in the involved lung, so that on expiration the mediastinum is displaced to the normal side and movement of the ipsilateral hemidiaphragm is restricted.

**Obstructive Emphysema.** Obstructive hyperinflation occurs when an endobronchial tumour or inhaled foreign body almost completely obstructs a major bronchus, and allows air to pass into the lung on inspiration but blocks it on expiration. The affected lung becomes hyperinflated and its vascular pattern is attenuated. The chest radiograph shows a hypertransradiant lung, and on an expiratory film or fluoroscopy, shift of the mediastinum to the normal side confirms air trapping (Fig. 3.11). The endobronchial abnormality may also be visible on the plain film.

**Compensatory Emphysema.** The radiological signs following collapse or removal of various parts of the lung are discussed in the section on lobar collapse.

**Congenital Lobar Emphysema.** This condition usually presents as respiratory distress in an infant. It is almost always unilateral involving an upper or middle lobe. The affected lobe is severely hyperinflated, which causes compression of the other ipsilateral lobes, and contralateral deviation of the mediastinum (Fig. 3.12).

#### *Obliterative Bronchiolitis*

Bronchiolar occlusion may result from a viral bronchiolitis in childhood or from inhalation of toxic fumes. In addition there is a cryptogenic variety which may be associated with rheumatoid disease. The chest radiograph may show evidence of pulmonary hyperinflation, and decreased vascularity in the mid and lower zones.

#### *Bronchiectasis*

Bronchiectasis is the irreversible dilatation of one or more bronchi, and is usually the result of severe, recurrent or

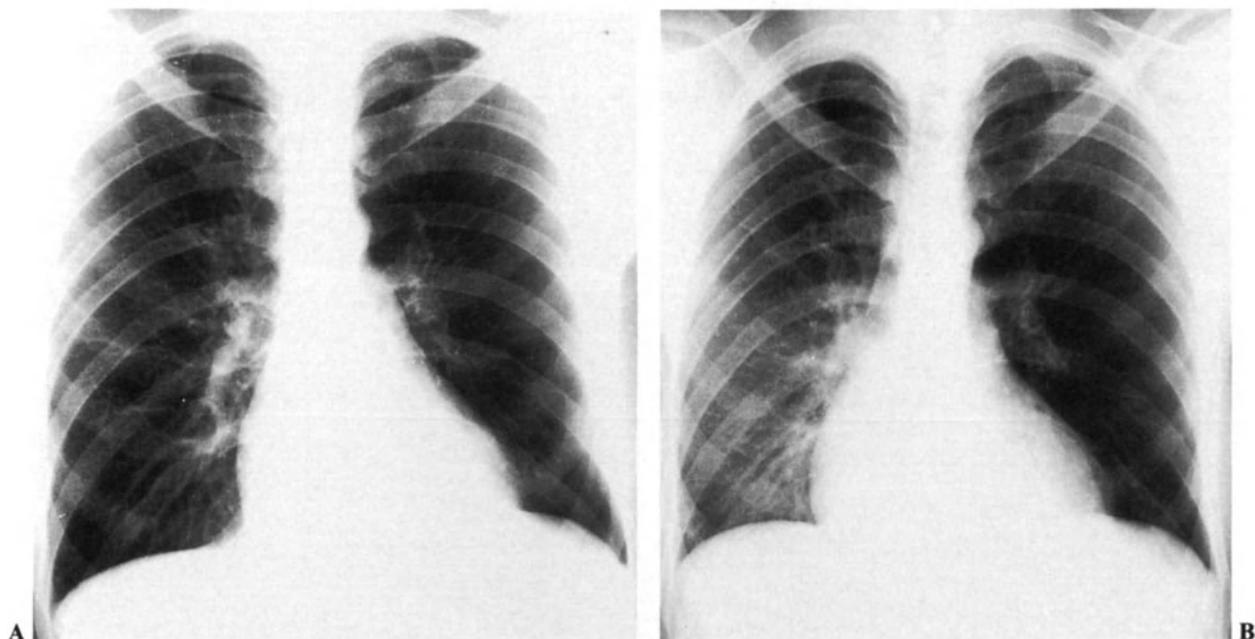


**Fig. 3.10A, B.** Unilateral emphysema. **A** The left lung is hypertranslucent and its pulmonary artery is small. **B** On expiration the height of the left hemidiaphragm is unchanged and the mediastinum has moved to the right, indicating air trapping in the left lung.

chronic infection. Childhood pneumonias, especially pertussis and measles, and tuberculosis are important causes. Other predisposing factors include chronic sinusitis, bronchial obstruction and abnormalities of the cilia, mucus and immune system (e.g., Kartagener syndrome, cystic fibrosis and agammaglobulinemia). Non-infective causes include bronchopulmonary aspergillosis and inhalation of noxious fluids or gases.

Bronchiectasis may be localized or generalized. It is frequently basal but, in tuberculosis and cystic fibrosis, it usually involves the upper zones.

On the *chest radiograph* dilated bronchi seen end-on may produce ring shadows (Fig. 3.13), dilated bronchi with thickened walls may produce tramline shadows (Fig. 3.14), and dilated, fluid-filled bronchi may cause 'gloved-finger' shadows. Accumulation of pus or secretions in ectatic bron-

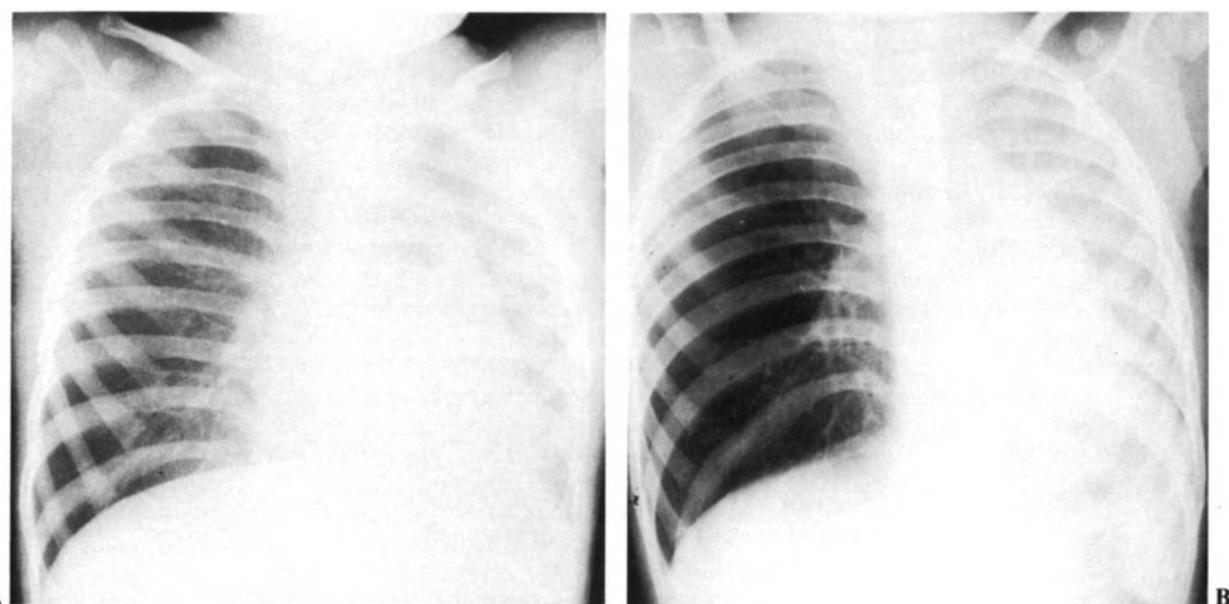


**Fig. 3.11A, B.** Obstructive emphysema. Child with inhaled foreign body in right bronchus. **A** The volume of the right lung is larger than the left. **B** On expiration, air trapping in the right lung causes further movement of the mediastinum to the left.

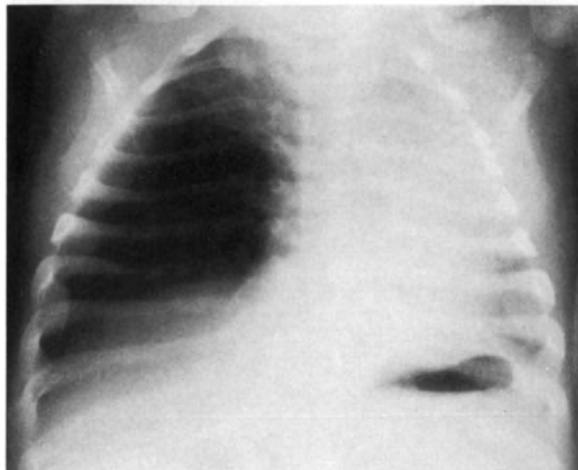


**Fig. 3.12.** Congenital lobe emphysema. The right middle lobe is severely hyperinflated displacing the mediastinum and compressing all of the other lobes.

chi may be seen as fluid levels. Chest infections frequently complicate bronchiectasis so that areas of consolidation may obscure the above signs.

*Bronchography* was the definitive method of diagnosis of bronchiectasis but is being superseded by CT. Bronchiectasis may be described as cylindrical, varicose or saccular.

*Cylindrical (or tubular) bronchiectasis* (Fig. 3.15) produces a dilated bronchus with parallel walls, in *varicose bronchiectasis* the walls are irregular and in *saccular (or cystic) bronchiectasis* (Fig. 3.16) the airways terminate as round cysts. In an individual patient it is common to see more than one pattern. Bronchiectasis usually involves the peripheral bronchi more severely than the central bronchi, but in bronchopulmonary aspergillosis this pattern may be reversed.

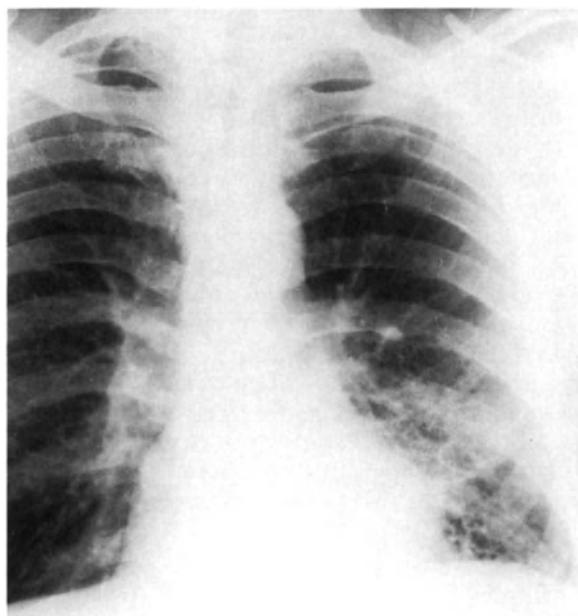


**Fig. 3.13.** Bronchiectasis. Multiple ring shadows are visible in the left lower zone.

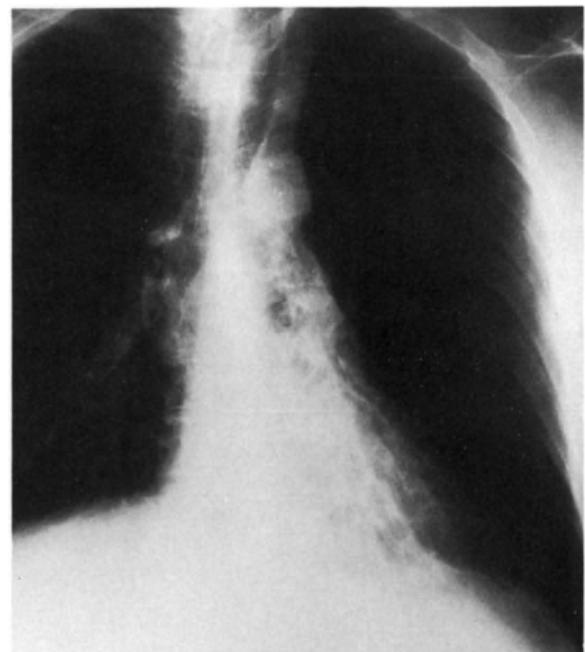


**Fig. 3.14.** Bronchiectasis. Tramline shadows are visible through the heart shadow.

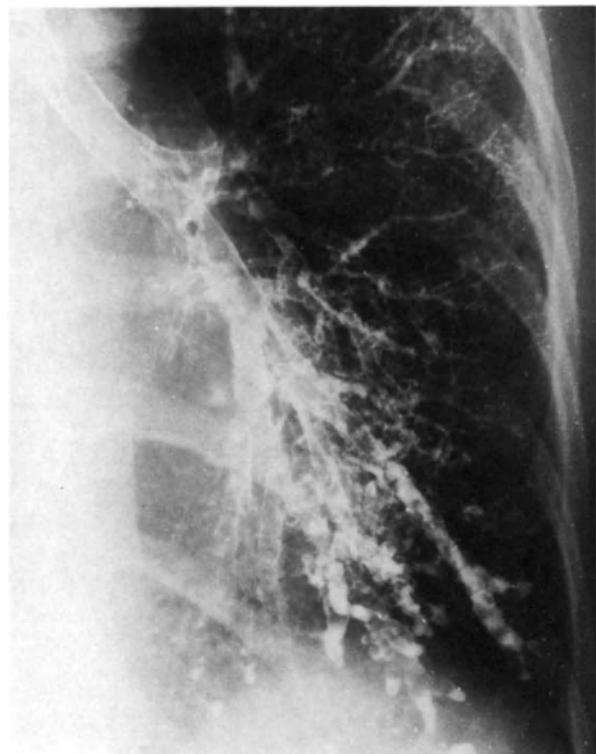


**Fig. 3.15.** Cylindrical bronchiectasis. Bronchogram shows tubular dilatation of the lower lobe bronchi.

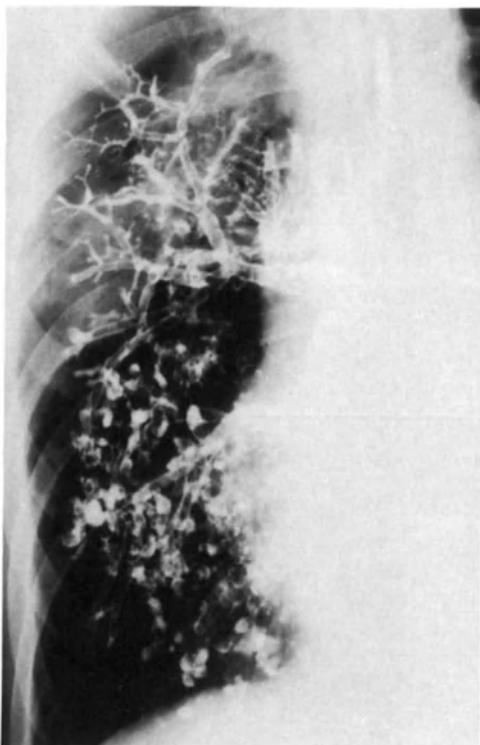


**Fig. 3.16.** Saccular bronchiectasis. Bronchogram shows cystic expansion of right middle and lower lobe bronchi.

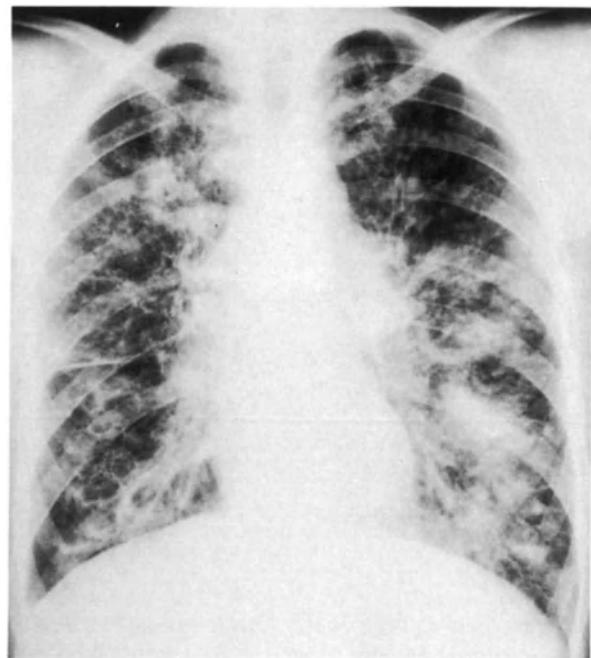


**Fig. 3.18.** Cystic fibrosis. The lungs are hyperinflated. Nodular and ring shadows are widely visible. Superimposed consolidation is present in the left mid and lower zones. The hilae are enlarged.

Bronchography is unpleasant for both patient and radiologist, so it is fortunate that narrow section CT can diagnose and assess the extent of bronchiectasis with similar accuracy (Fig. 3.17). The CT signs of bronchiectasis are those due to thickened, dilated bronchi, which may or may not contain fluid.

*Bronchial arteriography* is sometimes useful in the management of hemoptysis secondary to bronchiectasis. Severe

hemoptysis may be secondary to bronchial artery hypertrophy. If the site of bleeding can be identified, it may be treated by therapeutic embolization.

#### Cystic Fibrosis

Cystic fibrosis was formerly a condition seen only in children. However, with improved management many patients now reach adulthood.

The increased viscosity of the bronchial secretions in cystic fibrosis causes bronchial obstruction. This leads to air trapping and also predisposes to bronchiectasis. The *chest radiograph* may, therefore, show signs of air trapping with flattening of the diaphragm, bowing of the sternum and increased dorsal kyphosis, and also signs of bronchiectasis (Fig. 3.18). Peribronchial thickening, peripheral nodular opacities and ring shadows may be visible. Areas of emphysema may develop. Chest infections are common, *Staphylococci* and *Pseudomonas* being important pathogens, so that areas of consolidation may be seen. In response to chronic pulmonary infection the hilar lymph nodes may enlarge. The central pulmonary arteries may also enlarge due to pulmonary arterial hypertension. In later stages of the disease spontaneous pneumothorax may occur.



**Fig. 3.17.** Bronchiectasis. CT shows widespread dilatation of bronchi with thickened walls. Ring and tubular shadows are visible. Bronchi can be traced more peripherally than normal.

#### BRONCHOCELE AND MUCOID IMPACTION

Obstruction of a segmental bronchus may lead to accumulation of secretions and pus in the lung distally. If collateral

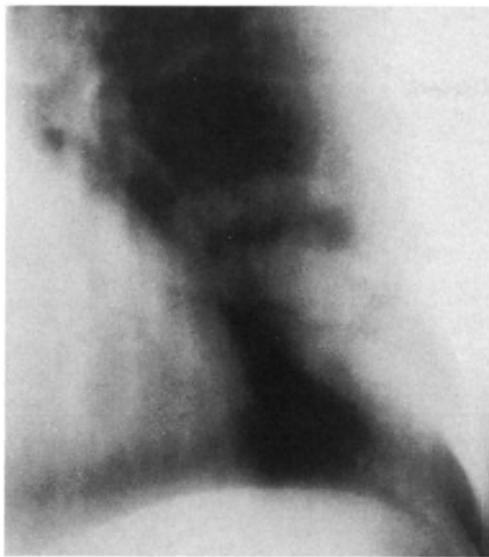


**Fig. 3.19.** Mucoid impaction. Tomogram shows dilated, fluid-filled lower lobe bronchi in patient with bronchopulmonary aspergillosis.

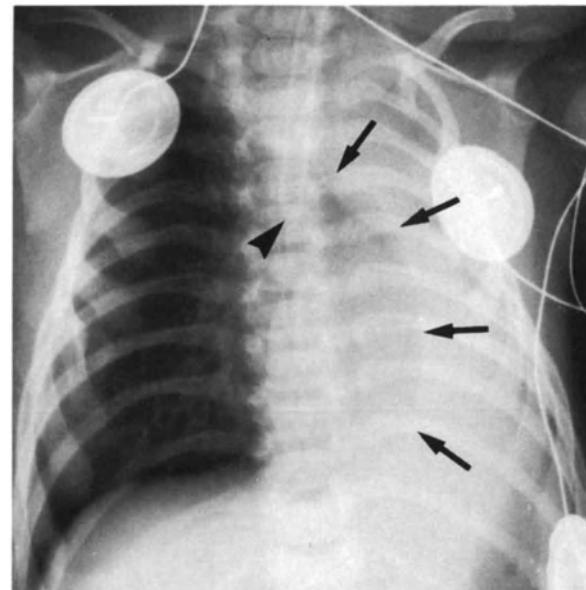


**Fig. 3.20.** Collapse of left lung. An endotracheal tube (arrowhead) has been inadvertently passed into the right bronchus. The left hemithorax is opaque. The mediastinum has moved to the left. The right lung has hyperinflated and herniated (arrows) across the mid-line.

air drift allows the affected lung to remain aerated a bronchocele or bronchial mucocele may develop. The obstruction may be congenital or due to endobronchial tumor or inhaled foreign body, or to inflammatory stricture or extrinsic compression. Mucoid impaction in asthma, allergic bronchopulmonary aspergillosis and cystic fibrosis may produce a similar obstruction. The typical appearance on the chest radiograph is a group of oval or cigar-shaped shadows, which may appear to branch (Fig. 3.19): they lie along the axis of the bronchial tree and point towards the hilum.

#### PULMONARY COLLAPSE

Loss of volume of all or part of a lung may be due to:

1. Pneumothorax or pleural effusion
2. Pulmonary fibrosis
3. Abnormality of surfactant
4. Bronchial obstruction

This section deals with collapse due to bronchial obstruction. This may be secondary to endobronchial tumor, foreign body, mucus plug, bronchial stricture or bronchial compression.

The air in alveoli distal to a bronchial obstruction is absorbed by the pulmonary capillaries causing alveolar collapse. The degree of collapse may be modified by collateral air drift, if the obstruction is distal to the main bronchus, and also by accumulation of secretions and infection.

#### Radiological Signs of Collapse

The appearance of pulmonary collapse depends upon the aetiology, the degree of collapse, the presence or absence of

consolidation, and the pre-existing state of the lung and pleura.

**Direct Signs.** *Displacement of Fissures.* This is the most reliable sign, the degree of displacement depending on the amount of collapse.

*Loss of Aeration.* Increased radiodensity of collapsed lung may not be apparent until the collapse is almost complete. However, if the involved lung is adjacent to mediastinum or diaphragm, the adjacent structures may become obscured (silhouette sign).

*Vascular and Bronchial Signs.* Vessels or bronchi in the involved lung may appear crowded.

**Indirect signs** are due to compensatory changes in response to the collapse.

*Elevation of the Hemidiaphragm.* This may be seen in lower lobe collapse but is unusual in other lobar collapse.

*Mediastinal Displacement.* The trachea may be displaced in upper lobe collapse, and the heart in lower lobe collapse.

*Hilar Displacement.* Elevation of the hilum may be seen in upper lobe collapse, and depression in lower lobe collapse.

*Compensatory Hyperinflation.* The normal lobes may become hyperinflated so that they appear hypertransradian and their vessels may be widely spaced. With major collapse the contralateral lung may herniate across the mid-line.

#### Complete Collapse of a Lung

In the absence of a pneumothorax, large pleural effusion or extensive consolidation, collapse of an entire lung causes opacification of the hemithorax with mediastinal shift to the affected side. The diaphragm rises, although this may not be apparent on the chest radiograph. The contralateral lung is hyperinflated and may herniate across the mid-line (Fig. 3.20). This herniation is usually retrosternal, but may occur behind the heart or under the aortic arch.



**Fig. 3.21.** Right upper lobe collapse. The periphery of the horizontal fissure moves upwards and towards the mediastinum and its upper surface is convex. The upper part of the oblique fissure moves anteriorly. The right upper mediastinum is obscured. The trachea moves to the right.

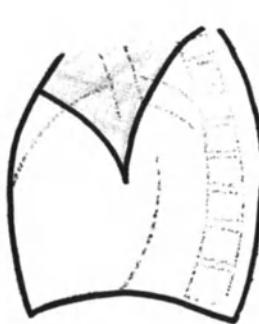


**Fig. 3.23.** Right middle lobe collapse. The horizontal is drawn downwards towards the oblique fissure. The right heart border is obscured.

### Lobar Collapse

The following descriptions of collapse of individual lobes assume that there is no pre-existing or coincidental pulmonary or pleural disease.

**Right Upper Lobe Collapse** (Figs. 3.21, 3.22). As the right upper lobe collapses the horizontal fissure pivots at the hilum. Its lateral end moves upwards and medially towards the mediastinum, and its anterior end moves upwards towards the apex. The upper half of the oblique fissure moves anteriorly. The two fissures become concave inferiorly. The right hilum rises and its lower pole may become prominent. The upper pole of the hilum and the right upper mediastinum may be obscured. The trachea may be pulled to the right, and hyperinflation of the right middle and lower lobes may be apparent.

**Right Middle Lobe Collapse** (Figs 3.23, 3.24). As the right middle lobe collapses, the horizontal fissure and lower half

of the oblique fissure move towards each other. This is best appreciated on the lateral film. The signs on the frontal film may be subtle, but there is usually loss of clarity of the right heart border. A collapsed middle lobe may be well seen on a lordotic AP film. As the right middle lobe is relatively small, indirect signs of volume loss are rarely seen.

**Lower Lobe Collapse** (Figs 3.25–3.28). In both right and left lower lobe collapse the oblique fissure moves posteriorly, but maintains its normal slope. Additionally the lower lobes collapse medially, and this may bring the oblique fissure into profile on the frontal film. Increased opacity of the collapsed lobe is usually visible on the frontal film, and adjacent parts of the diaphragm may be obscured. A completely collapsed lower lobe may be so small as to merge with the mediastinum as a thin wedge-shaped shadow. If in doubt, oblique films or fluoroscopy may demonstrate the collapse. The hilum is usually depressed and rotated medially. Hyperinflation of the

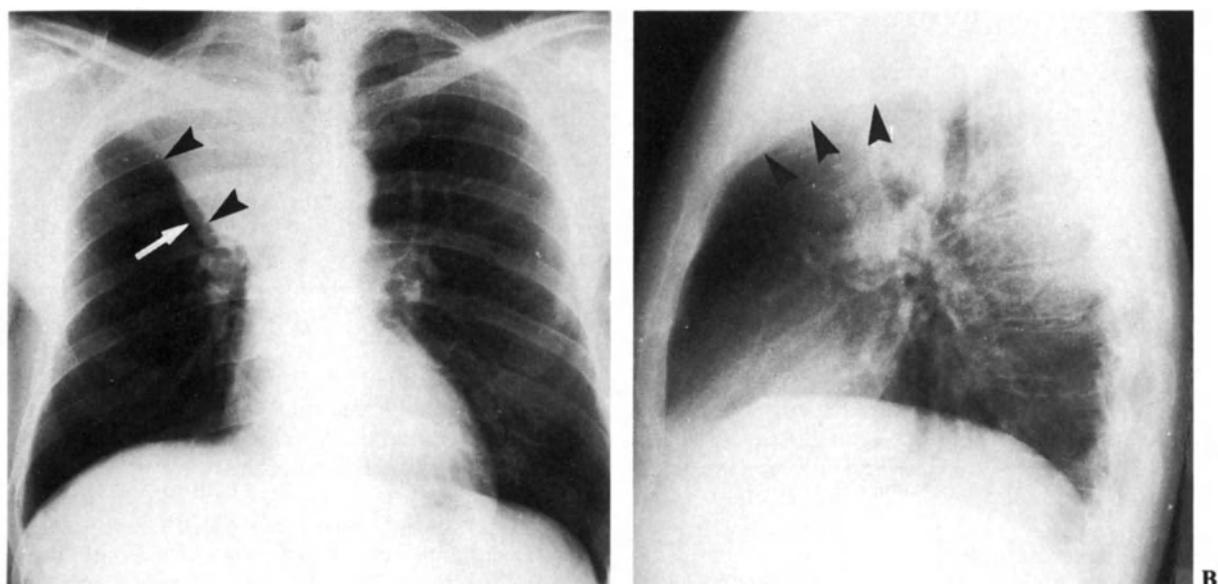
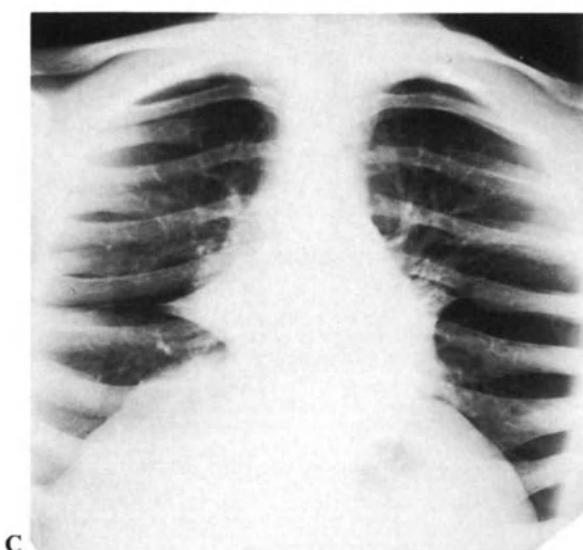
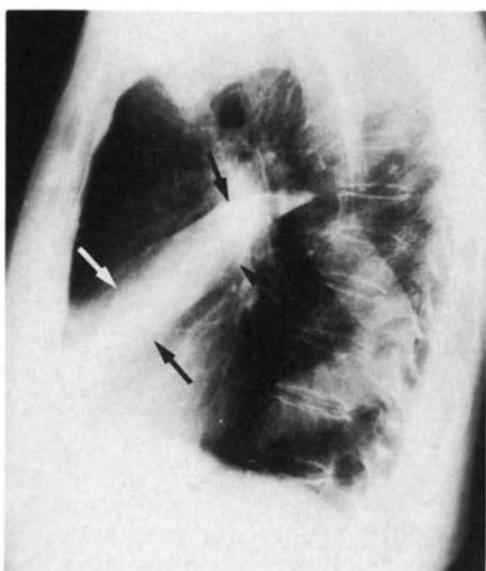
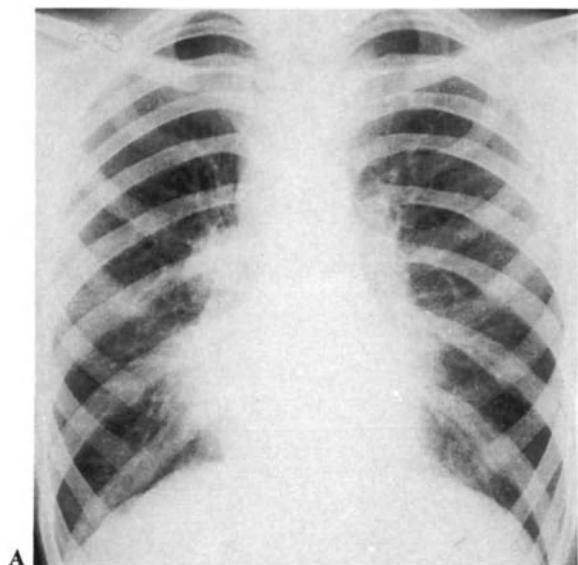


**Fig. 3.22A, B.** Right upper lobe collapse. The horizontal and oblique fissures (arrowheads) are displaced. There is a mass (arrow) at the right hilum.



◀ Fig. 3.24A, B, C. Right middle lobe collapse. A The right heart border is obscured. B The collapsed lobe is a narrow opacity (arrows) between the displaced fissures. C Lordotic film confirms the collapse.

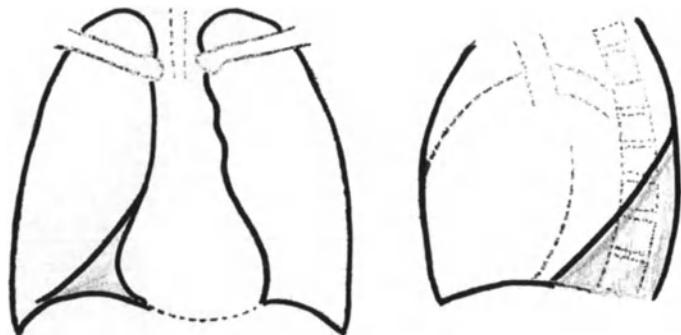


Fig. 3.25. Right lower lobe collapse. The oblique fissure and a wedge of density in the lower zone may be visible on the frontal film. The right heart border is not obscured. The oblique fissure moves posteriorly on the lateral film, and the posterior part of the right hemidiaphragm is obscured.

upper lobe is often apparent and diaphragmatic elevation sometimes occurs.

**Lingular Collapse** (Fig. 3.29). Lingular collapse is often associated with left upper lobe collapse. However, if it is an isolated occurrence it resembles right middle collapse with loss of clarity of the left heart border. On the lateral film there may be increased density anterior to the lower half of the oblique fissure, and this part of the fissure may be displaced anteriorly.

**Left Upper Lobe Collapse** (Figs 3.30, 3.31). As the left upper lobe collapses the entire oblique fissure moves anteriorly and becomes almost parallel to the anterior chest wall. The anterior part of the lobe retracts posteriorly towards the oblique fissure and eventually loses contact with the anterior chest wall. The space between the collapsed lobe and the anterior chest wall becomes occupied by either hyperinflated left lower lobe or right upper lobe which has herniated across the mid-line. Thus, on the lateral film the collapsed lobe is an elongated opacity in the anterior part of the chest, extending from the apex almost to the diaphragm. On the frontal view it presents a hazy, ill-defined opacity in the upper and sometimes lower zones. It is densest near the hilum, which may be elevated, and vessels in the hyperinflated lower lobe may be seen through the haze. The trachea is usually deviated to the left. If the lingula is also collapsed the left heart border is obscured.

**Rounded Atelectasis (Infolded Lung)**. This is an unusual form of collapse which may be misdiagnosed as a pulmonary tumor. It presents as a mass of up to 5 cm diameter, and is always pleural-based with associated pleural thickening (Fig. 3.32). Vascular shadows radiating from it may mimic a comet's tail and are often best seen on tomography. It is due to lung folding in on itself. It may be associated with asbestos exposure but is of no other pathological significance.

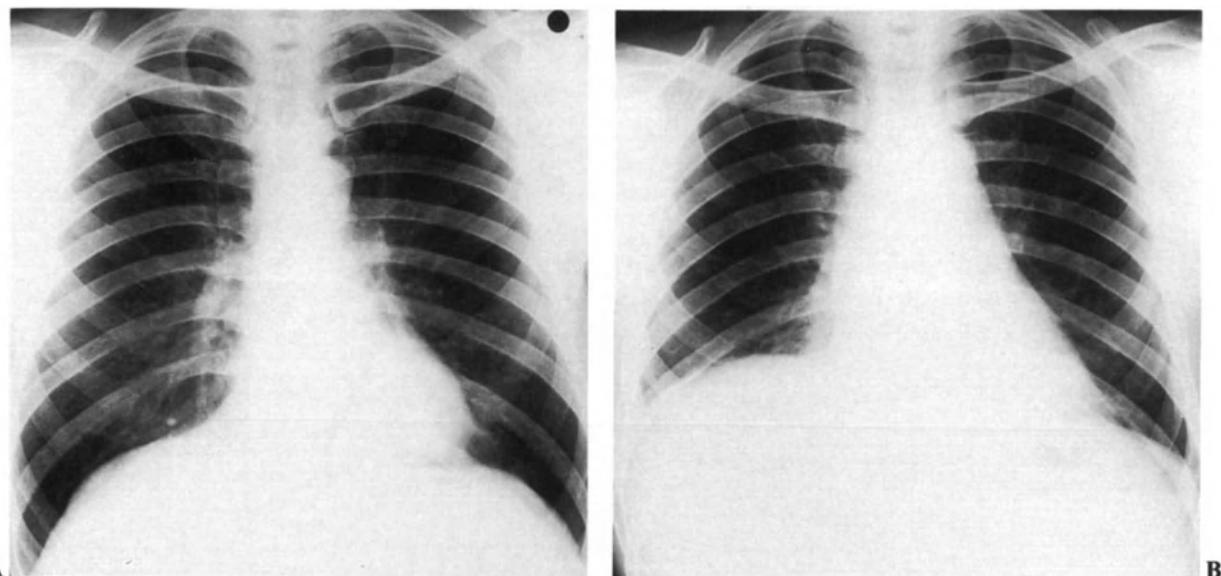


**Fig. 3.26A, B.** Right lower lobe collapse. A Normal film prior to right lower lobe collapse. B Following right lower lobe collapse, the right hilum has become depressed and has rotated medially. The right upper lobe has hyperinflated and the right hemidiaphragm has risen.



**Fig. 3.27.** Left lower lobe collapse. The oblique fissure and a wedge of density may be visible through the heart shadow. The oblique fissure moves posteriorly on the lateral film, and the posterior part of the left hemidiaphragm is obscured.

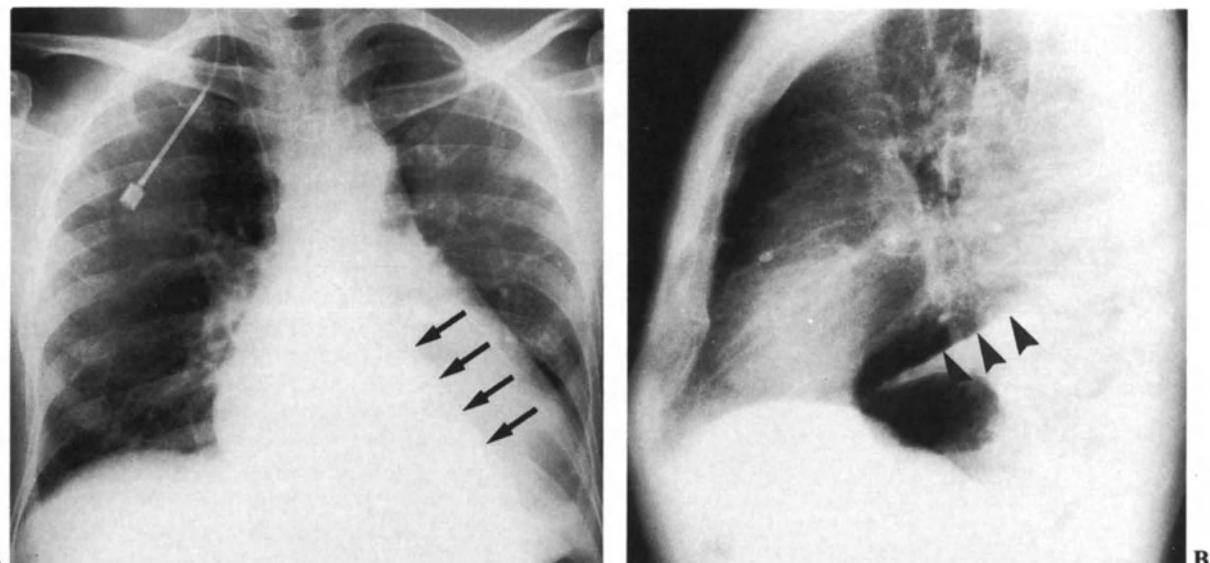


**Fig. 3.28A, B.** Left lower lobe collapse. A The collapsed left lower lobe (arrows) is visible through the heart shadow, and is obscuring the medial half of the left hemidiaphragm. B The oblique fissure (arrowheads) is displaced posteriorly, and the left hemidiaphragm is obscured.

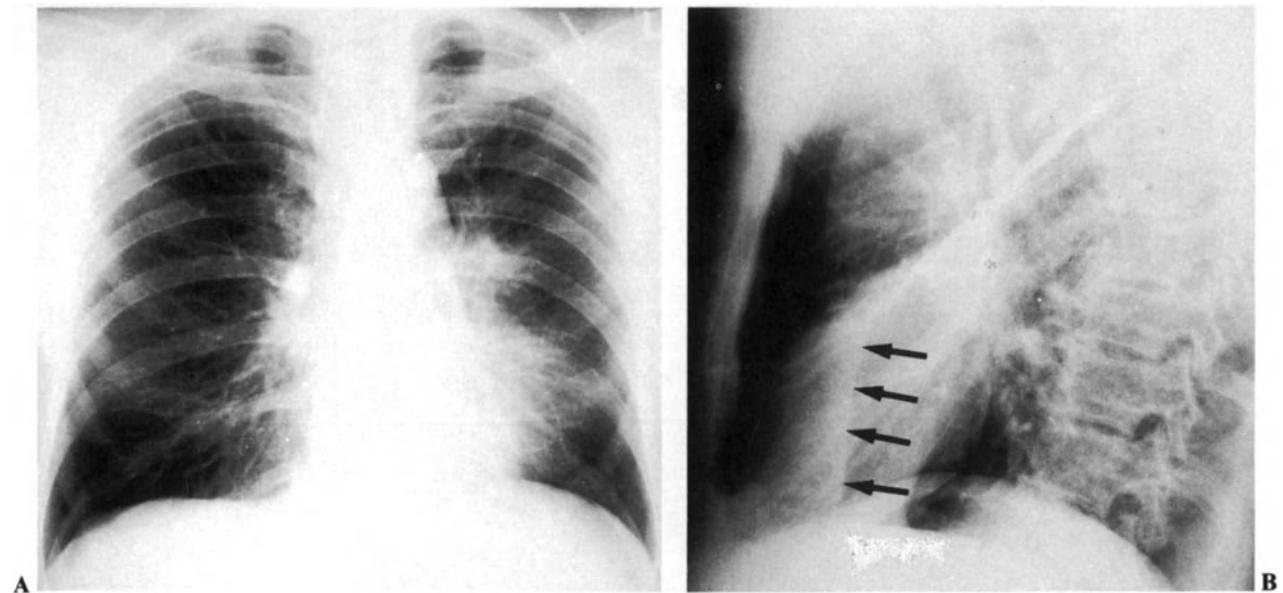
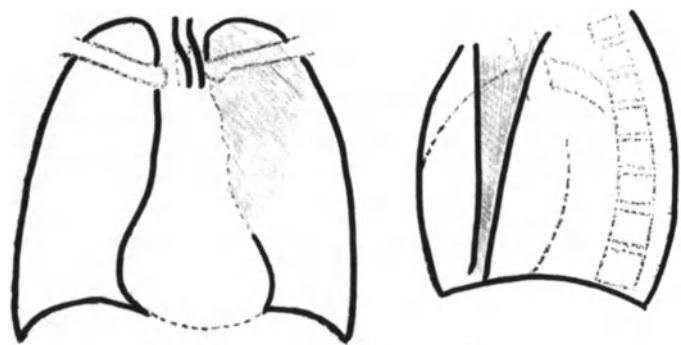
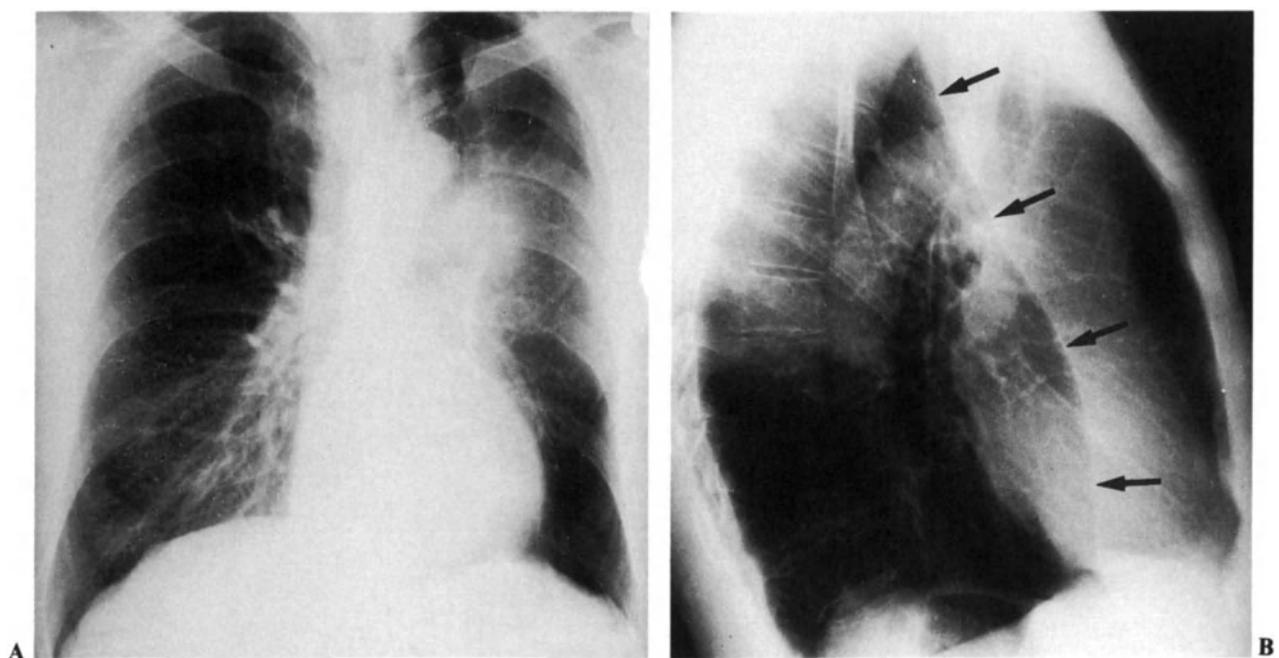


Fig. 3.29A, B. Lingular collapse. The left heart border is obscured and the lower half of the oblique fissure (arrows) is displaced anteriorly.

**Fig. 3.30.** Left upper lobe collapse. A hazy density overlies the left upper and mid zones. The oblique fissure moves anteriorly, and the anterior part of the upper lobe moves posteriorly and loses contact with the anterior chest wall. The hyperinflated lower lobe or herniated right lung fills the retrosternal area. The left upper mediastinum may be obscured and the trachea moves to the left.



**Fig. 3.31A, B.** Left upper lobe collapse. The elevated left hilum and vessels in the hyperinflated left lower lobe are visible through the left-upper and mid-zone haze. The oblique fissure (arrows) has moved anteriorly.



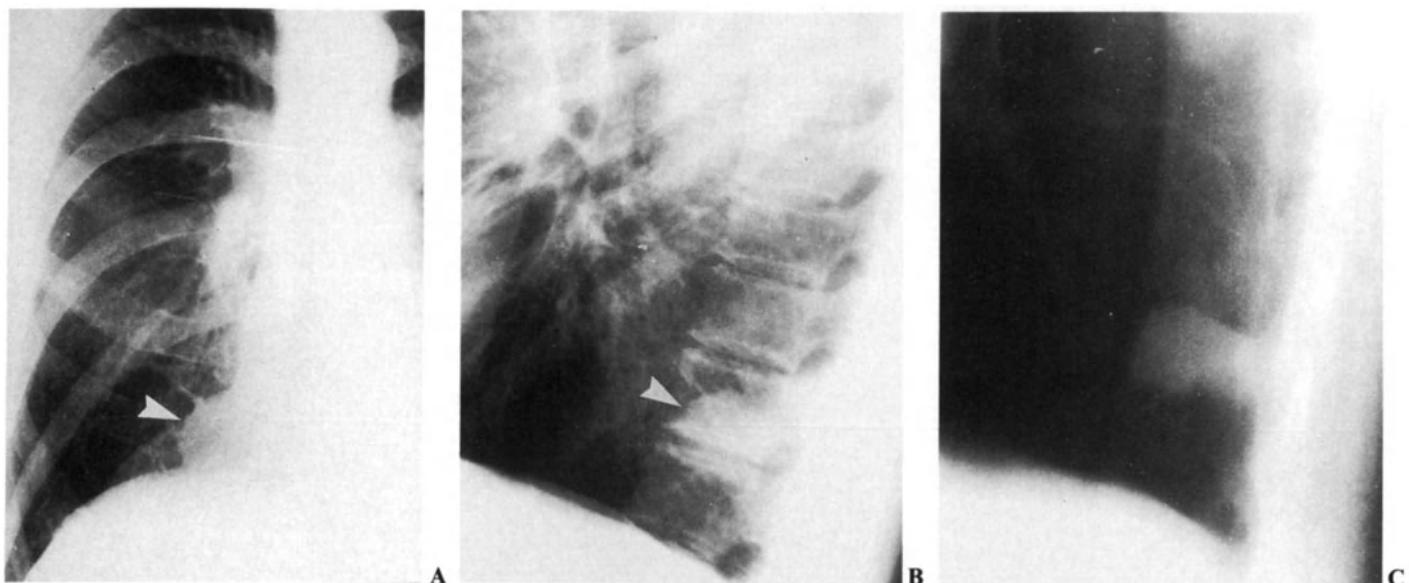


**Fig. 3.32A, B, C.** Rounded atelectasis. A, B A round, pleural-based mass (arrowheads) is present in the right lower zone posteriorly. C Tomography shows associated pleural thickening.

#### PULMONARY CONSOLIDATION

Consolidation implies replacement of air in one or more acini by fluid or solid material. This is commonly due to an acute inflammatory exudate of *pneumonia*, but other causes are *pulmonary edema*, *cardiogenic or non-cardiogenic hemorrhage*, *aspiration*, *alveolar cell carcinoma*, *lymphoma* and *alveolar proteinosis*.

Consolidation associated with a patent airway may exhibit an *air bronchogram*, due to the contrast between the air-filled airways and the opacified acini. Purely consolidated lung is similar in volume to normal lung. However, consolidation is often associated with some degree of atelectasis.

**Lobar Consolidation.** Consolidation of an entire lobe causes a homogenous density, possibly containing an air bronchogram. This density is limited by the appropriate fis-

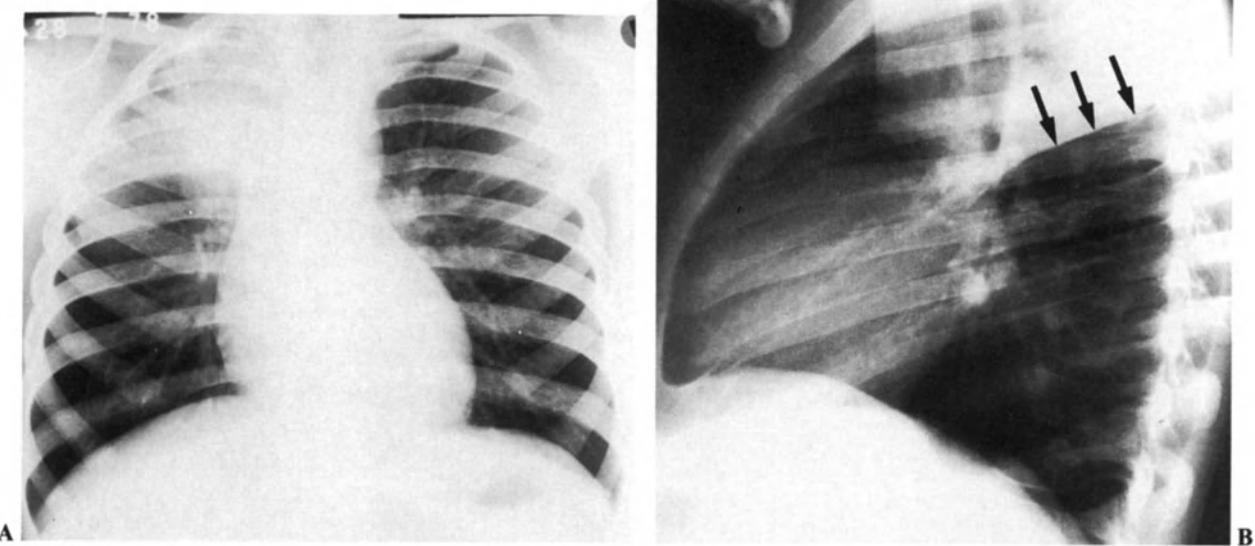


**Fig. 3.33A, B.** Right upper lobe consolidation. The right upper zone density obscures the right upper mediastinum. It is anterior to the oblique fissure (arrows).

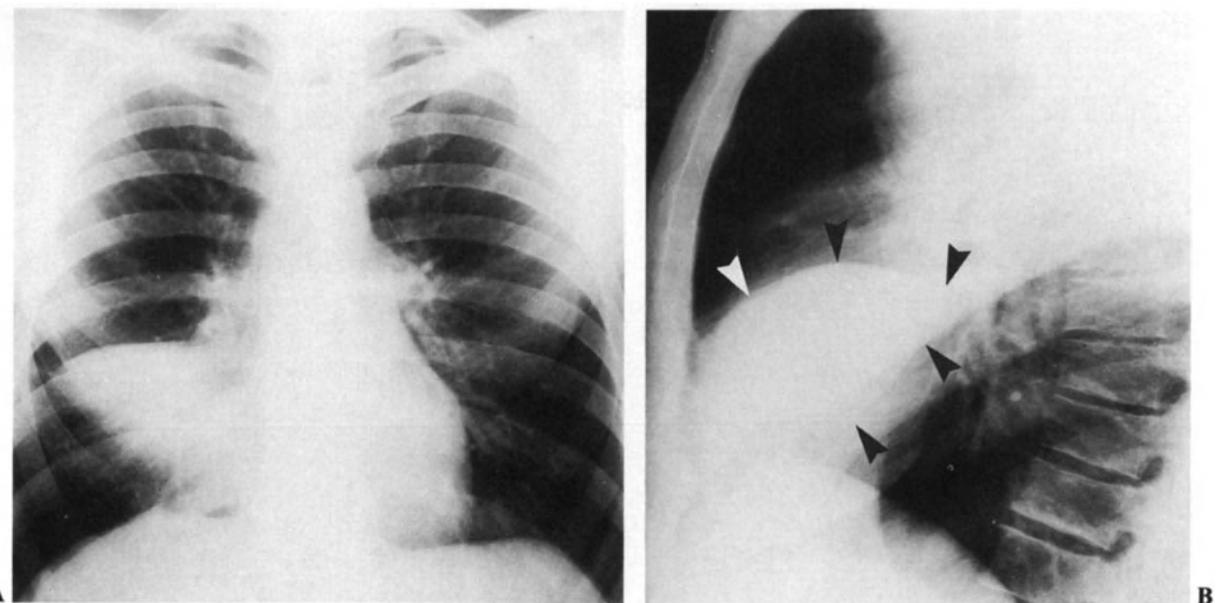


**Fig. 3.34A, B.** Right middle lobe consolidation. The right mid zone density is situated between the horizontal and oblique fissures (arrowheads) and obscures the right heart border.

sures and obscures adjacent parts of the mediastinum and diaphragm.

*Right upper lobe consolidation* (Fig. 3.33) is limited by the horizontal fissure inferiorly and the upper half of the oblique fissure posteriorly. It obscures the right side of the upper mediastinum.

*Right middle lobe consolidation* (Fig. 3.34) is limited by the horizontal fissure superiorly and the lower half of the oblique

fissure posteriorly. It obscures the right heart border.

*Lower lobe consolidation* (Fig. 3.35) is limited by the oblique fissure anteriorly. It obscures the diaphragm.

*Left upper lobe and lingular consolidation* (Figs 3.36, 3.37) are limited by the oblique fissure posteriorly. The left heart border is obscured by lingular consolidation and left upper lobe consolidation may obscure the aortic arch.

*For further reading, see p. 134.*

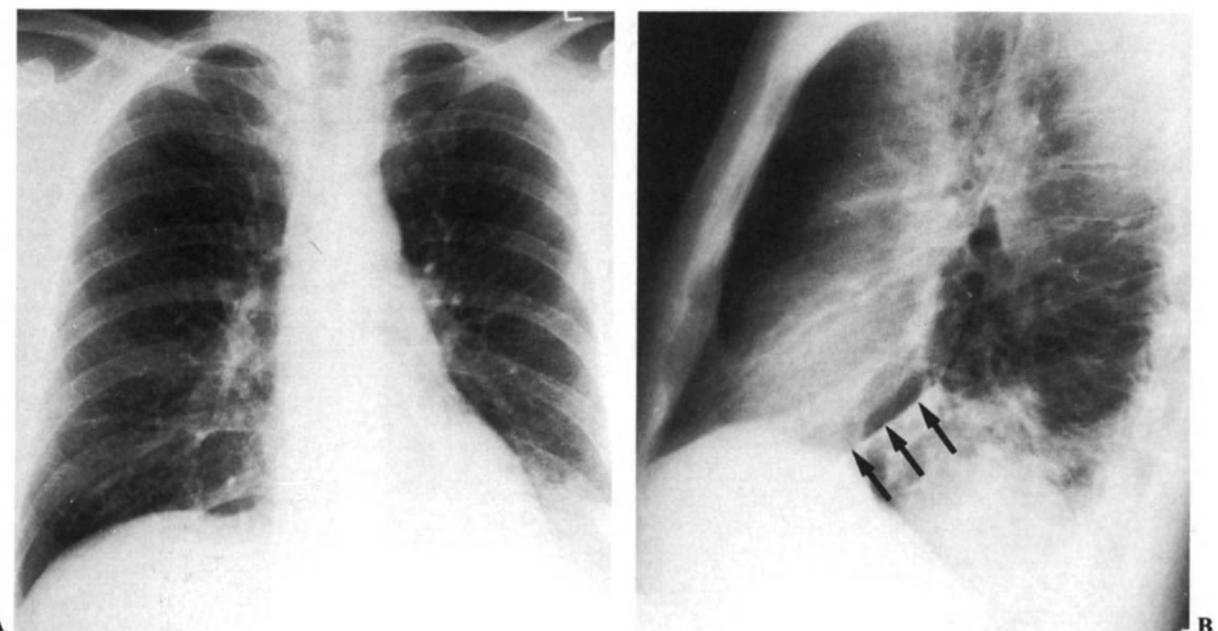


**Fig. 3.35A, B.** Left lower lobe consolidation. The left lower zone density obscures the left hemidiaphragm but not the left heart border. It is posterior to the oblique fissure (arrows).

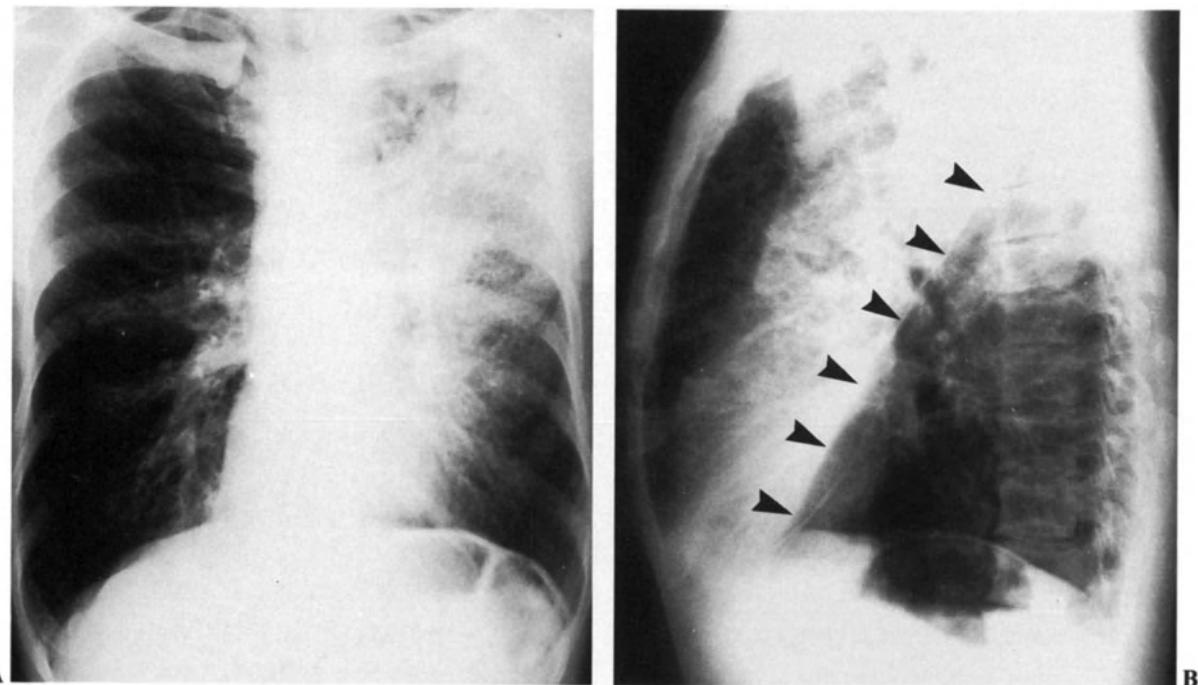


Fig. 3.36A, B. Left upper lobe and lingular consolidation. Patchy consolidation anterior to the oblique fissure (*arrowheads*) obscures the left heart border and upper mediastinum.

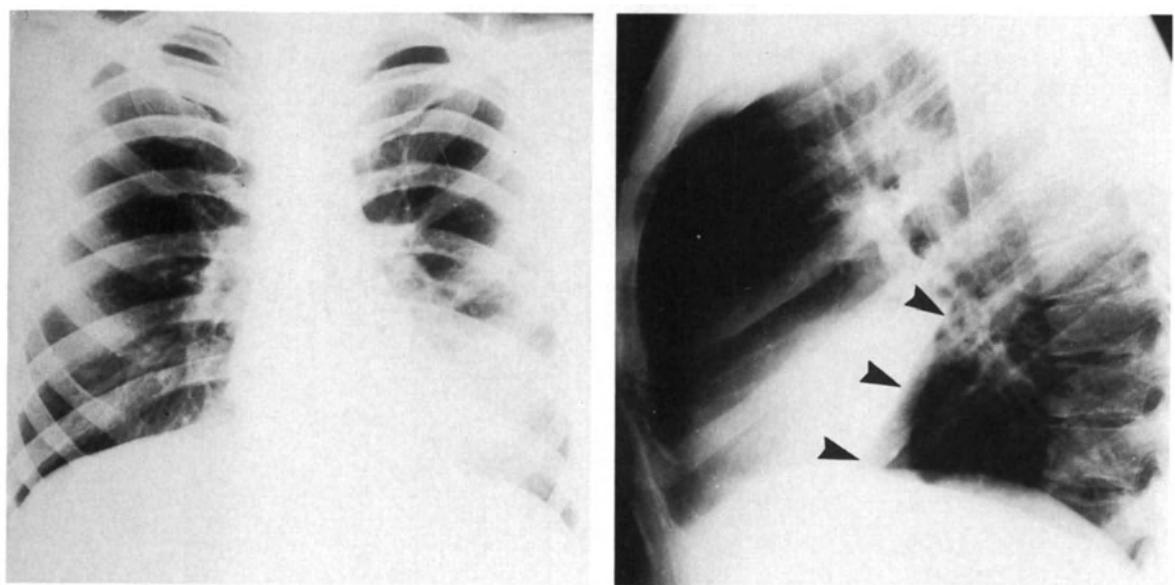


Fig. 3.37A, B. Lingular consolidation. The left lower zone density obscures the left heart border but not the diaphragm. It is anterior to the oblique fissure (*arrowheads*).

## CHAPTER 4

# PULMONARY INFECTIONS

M. Rubens

---

Inflammatory disease of the lung may be referred to as either pneumonia or pneumonitis. Although these terms are interchangeable, *pneumonia* usually implies an infective process that causes consolidation of lung, whereas *pneumonitis* tends to refer to those inflammatory processes that primarily involve the alveolar wall e.g., fibrosing alveolitis.

Pneumonias may be classified on the basis of morphology or etiology.

*Lobar pneumonia* commences as a localized infection of terminal air spaces. Inflammatory edema spreads to adjacent lung via the terminal airways and pores of Kohn, and causes uniform consolidation of all or part of a lobe. *Streptococcus pneumoniae* classically causes lobar pneumonia.

*Bronchopneumonia* is a multifocal process which commences in the terminal and respiratory bronchioles and tends to spread segmentally. It may also be called lobular pneumonia, and produces patchy consolidation. The commonest causes are *Staphylococcus aureus* and gram-negative organisms.

In clinical practice the most useful classification is according to the causative organism, since this is what influences the management and outcome of the infection. Unfortunately, it is not possible to diagnose the organism from radiology alone. However, radiology is important in confirming the presence and location of pneumonia, as well as following its course. Moreover, the chest radiograph may indicate complications of a pneumonia such as pleural effusion, empyema, pneumothorax, atelectasis, abscess formation and scarring.

## VIRAL PNEUMONIA

Viral pneumonia usually commences in distal bronchi and bronchioles as an interstitial process with destruction of the

epithelium, edema and lymphocytic infiltration. There may also be focal inflammation of the terminal bronchioles and alveoli and progression to hemorrhagic pulmonary edema.

The radiological appearances of a viral pneumonia may therefore be:

1. Peribronchial shadowing (Fig. 4.1).
2. Reticulonodular shadowing (Fig. 4.2).
3. Patchy consolidation.
4. Extensive consolidation (Fig. 4.3).

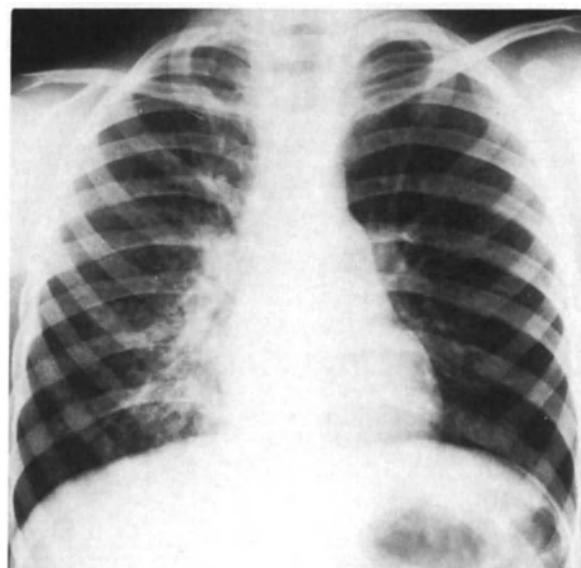
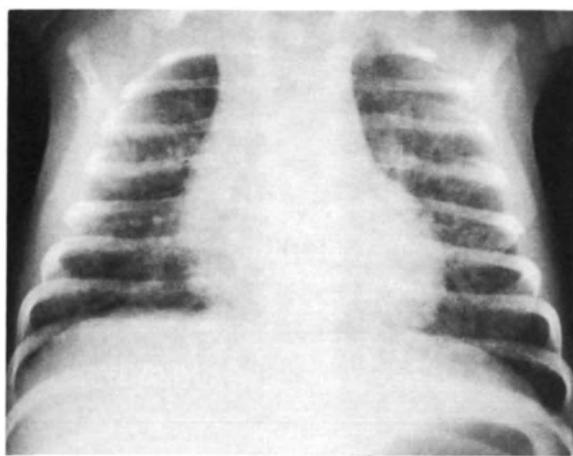


Fig. 4.1. Adenovirus infection. Perihilar shadowing is present in the right lung.



**Fig. 4.2.** Cytomegalic inclusion disease. Reticulonodular shadowing is seen throughout both lungs.

Some viral pneumonias (e.g., infectious mononucleosis) may be associated with hilar lymphadenopathy. Pleural effusion is uncommon.

Viral pneumonia is uncommon in adults, unless the patient is immunocompromised. Most pneumonias that complicate viral infections in adults are due to bacterial superinfection. However, viral pneumonias are not rare in infants and children.

#### Influenza

Pneumonia as a complication of influenza is normally due to secondary bacterial infection, often *Staphylococcus aureus*, *Streptococcus pneumoniae* or *Hemophilus*. However, the very

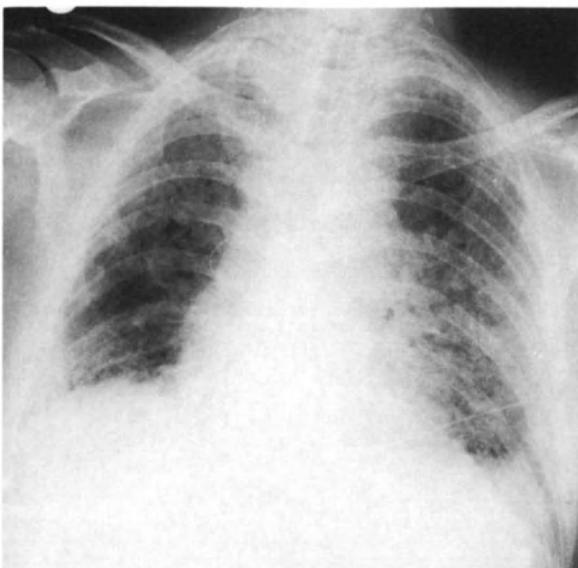


**Fig. 4.3.** Herpes simplex pneumonia. Areas of consolidation are seen in both lungs. An air bronchogram is visible in the left mid zone.

young, the elderly and debilitated patients may develop a primary viral pneumonia with patchy consolidation. Occasionally, especially during influenza epidemics, a fulminating hemorrhagic pneumonia may be seen with widespread consolidation. A patient who survives may develop extensive pulmonary fibrosis.

#### Varicella

Varicella pneumonia occurs more often in adults than in children. In the acute phase of infection the chest radiograph may show widespread nodular shadows up to 1 cm in diameter. Following recovery a small proportion of these nodules calcify, and if multiple may produce a characteristic radiographic appearance (Fig. 4.4).

### CHLAMYDIAL AND RICKETTSIAL PNEUMONIAS

*Psittacosis or ornithosis* is usually acquired by contact with sick parrots or domestic fowl and is due to *Chlamydia psittaci*. The pneumonia usually presents as patchy or lobar consolidation, although nodular shadows may be seen. There is often hilar lymphadenopathy. The radiographic changes may take several weeks to resolve.

*Q Fever* is usually acquired by contact with cattle or sheep and is due to *Coxiella burnetti*. The pneumonia typically presents as rounded areas of consolidation, up to 10 cm in diameter, in both lungs. Linear densities due to atelectasis may also be seen. The radiographic changes may take a month or more to resolve.

*Rocky Mountain spotted fever* may cause patchy consolidation, pleural effusions, and be complicated by secondary bacterial pneumonia.

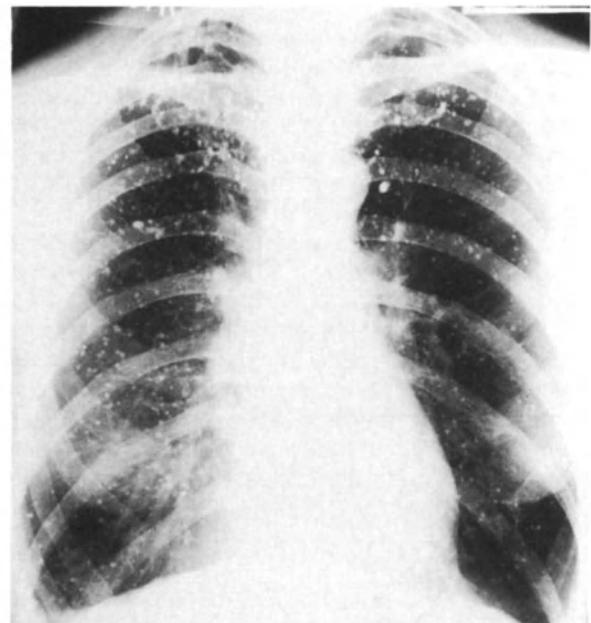


**Fig. 4.4.** Varicella. Small calcified nodules are scattered throughout both lungs following chicken pox complicated by pneumonia.

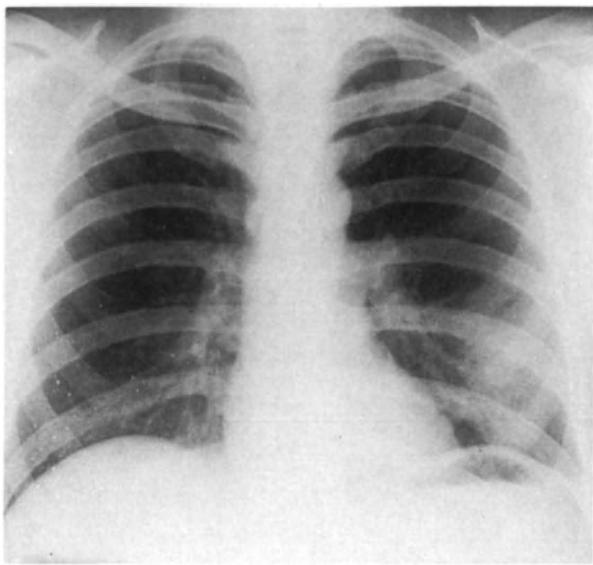


**Fig. 4.5.** Mycoplasma. Consolidation is present in the periphery of the left lower zone. The appearance is non-specific.

#### MYCOPLASMA PNEUMONIA

*Mycoplasma pneumoniae* is a common cause of pneumonia in young adults. It produces a pneumonia that typically develops and resolves more slowly than bacterial pneumonia, and causes milder symptoms than a bacterial pneumonia of similar extent.

The earliest radiographic signs are fine reticular or nodular shadows followed by the appearance of consolida-

tion, which may be segmental or lobar, and is usually unilateral (Fig. 4.5). Lymph-node enlargement and pleural effusion are uncommon and cavitation is rare.

#### BACTERIAL PNEUMONIAS

##### Pneumococcal Pneumonia

*Streptococcus pneumoniae* is a common cause of pneumonia in all age groups, and particularly in young adults. Typically it produces lobar consolidation (Fig. 4.6), which is often basal, but it may occur anywhere in the lung. The volume of the consolidated lung is normal, and an air bronchogram may be visible. Occasionally edema of the interlobular septa causes septal lines. Pleural effusion, empyema and cavitation are very unusual if the infection is treated promptly, but may be seen in debilitated patients. Resolution is usually complete.

##### Staphylococcal Pneumonia

*Staphylococcus aureus* is a common cause of pneumonia in debilitated patients. It may also cause superinfection in influenza. Hematogenous infection of the lungs may occur in septicemia, and is a common complication of intravenous drug abuse.

Infection by inhalation typically causes a bronchopneumonia with multiple, patchy areas of consolidation. Confluence of these areas may develop. Cavitation is common (Fig. 4.7), and in children pneumatoceles frequently develop. Pleural effusion, empyema and areas of atelectasis are common complications.

Hematogenous infection causes multiple round or oval nodules which have a tendency to cavitate (Fig. 4.8).

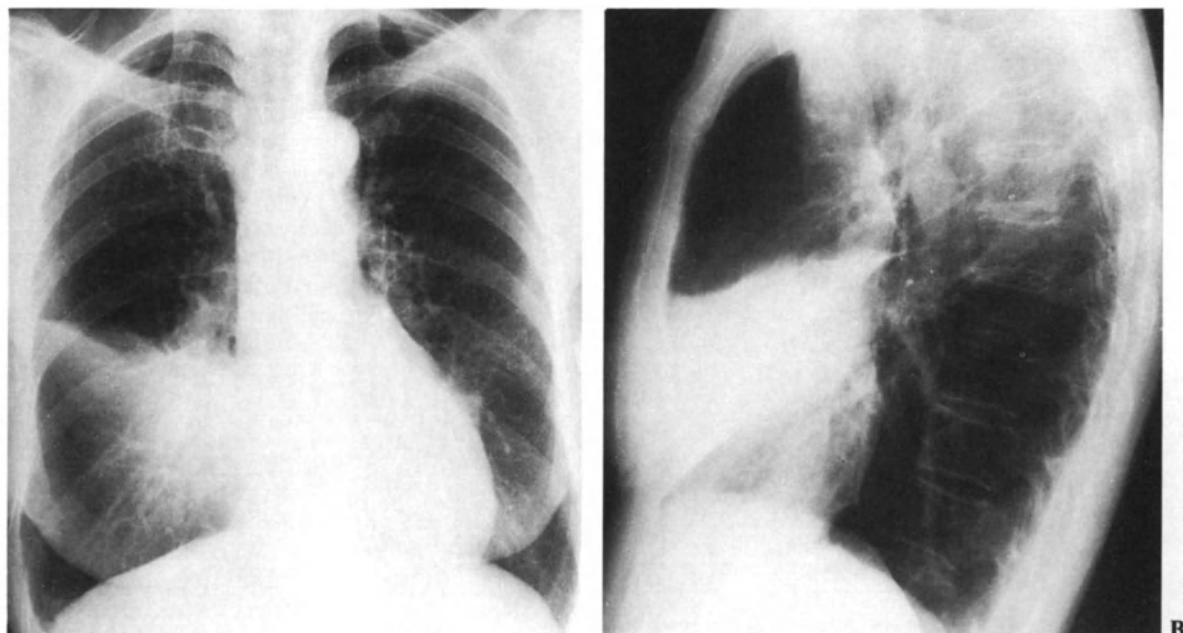


**Fig. 4.6A, B.** *Streptococcus pneumoniae*. Right middle lobe consolidation.

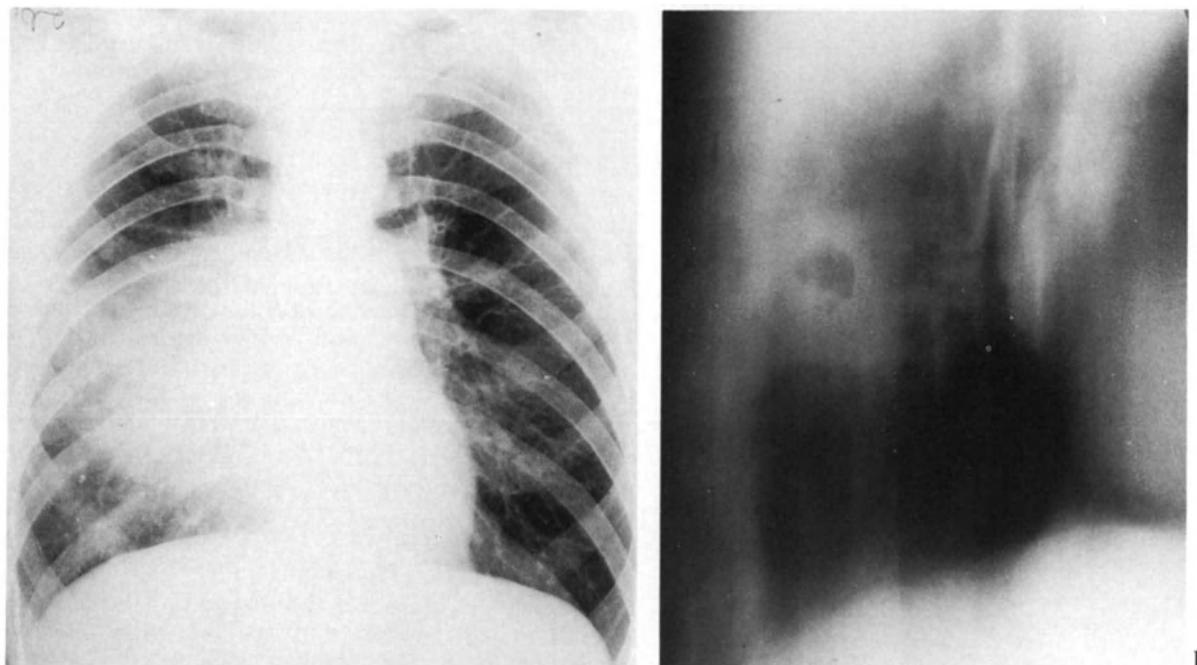


**Fig. 4.7A, B.** *Staphylococcus aureus.* A Consolidation is present in the right middle lobe and the apical segment of the right lower lobe. B Lateral tomogram demonstrates cavitation in apical segment of lower lobe.

#### Klebsiella Pneumonia

Pneumonia due to *Friedlander's bacillus* typically occurs in elderly debilitated men. There is usually lobar consolidation (Fig. 4.9), more often right-sided, and frequently upper lobe. The volume of the affected lung is maintained, or may be increased causing bulging of the fissures. Cavitation is common.

#### Legionnaires' Disease

*Legionella pneumophila* is a gram-negative bacillus that may contaminate water coolers, air-conditioning units and other

water reservoirs. It may be responsible for sporadic or epidemic outbreaks of a pneumonia which carries a 20% mortality. The pneumonia is rapidly progressive and is often associated with neurological and other systemic disturbances.

The chest radiograph typically shows local, peripheral, unilateral consolidation, which rapidly spreads to involve the other lobes and lung. Small pleural effusions are common, but cavitation is rare.

#### Other Gram-negative Pneumonias

There are many gram-negative organisms, which are normal inhabitants of the upper respiratory tract or gastrointestinal tract, that may cause pneumonia, and other infections, in debilitated patients. These include *Hemophilus influenzae*, *Pseudomonas aeruginosa* and *Escherichia coli*. They are likely to be pathogenic in patients with chronic lung disease, diabetes, following major surgery and in patients who have received longterm broad-spectrum antibiotics. Pneumonia normally results from inhalation, but may be hematogenous. The radiographic appearances are of a bronchopneumonia which is often basal (Fig. 4.10).

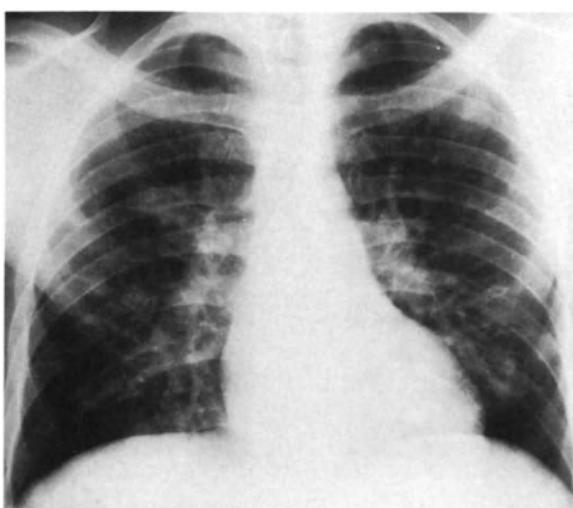


**Fig. 4.8.** *Staphylococcus aureus.* Multiple abscesses in an intravenous drug abuser. Small nodular opacities are visible in both lungs; some are cavitating.

#### LUNG ABSCESS

Suppuration and necrosis of pulmonary tissue may be due to tuberculosis, fungal infection, malignant tumor and infected cysts. However, the term lung abscess usually refers to a cavitating lesion secondary to infection by pyogenic bacteria. This is most frequently due to aspiration of infected material from the upper respiratory tract, and is often associ-

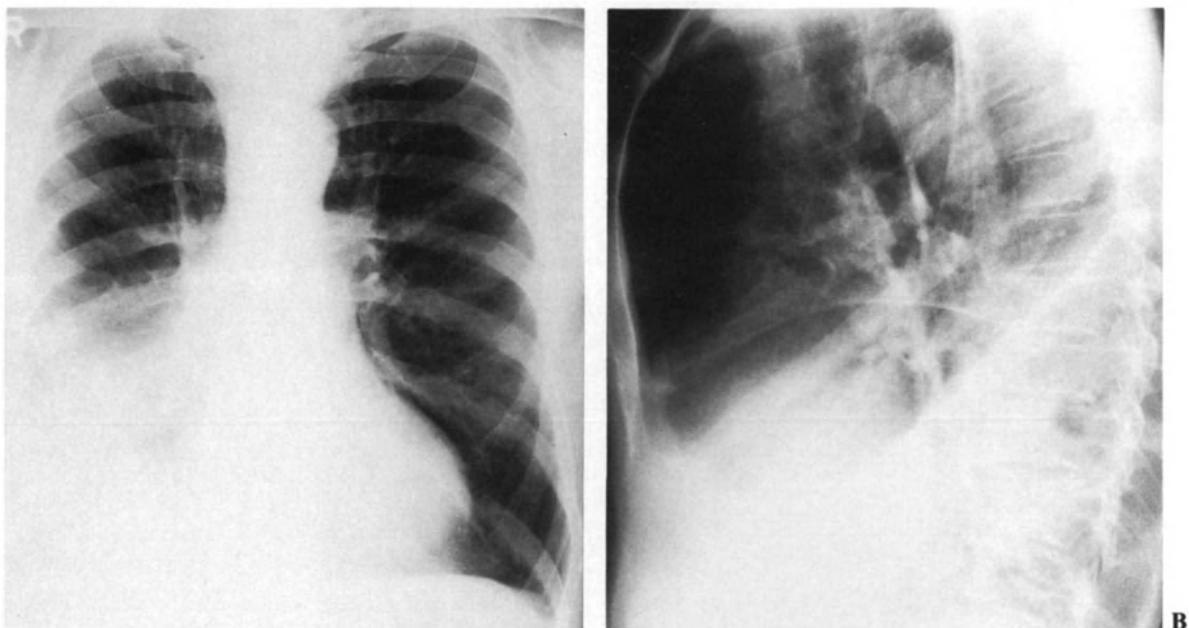


**Fig. 4.9A, B.** *Klebsiella*. The right lower lobe is consolidated.

ated with poor dentition and periodontal infection. A variety of organisms may be responsible, and anaerobic bacteria are frequently found in the sputum. Occasionally there is a history of loss of consciousness and presumed aspiration. Other causes of lung abscess include staphylococcal and *Klebsiella* pneumonia, septic pulmonary emboli and trauma.

Radiographically an abscess may or may not be surrounded by consolidation. Appearance of an air fluid level indicates that a communication with the airways has developed. The wall of the abscess may be thick at first, but with

further necrosis and coughing up of infected material it becomes thinner (Fig. 4.11).

#### PULMONARY TUBERCULOSIS

*Mycobacterium tuberculosis* is responsible for most cases of tuberculosis; fewer than 5% of cases are caused by atypical mycobacteria. Infection is usually by inhalation of organisms from open cases of the disease. Infection from milk is now rare where pasteurized milk is available.

There are racial differences in the incidence of tuberculosis, and in Britain it is 30 times more common in immigrants from the Indian subcontinent than in the indigenous population. Other factors that predispose to infection are old age, poor nutrition, alcoholism, silicosis, diabetes, pregnancy, malignant disease and immunosuppression.

Previous infection or BCG vaccination render most patients hypersensitive to tuberculin protein. Possession of such hypersensitivity influences the course of the disease, and it is traditional to classify tuberculosis as primary, if the patient is not sensitized, and post-primary if the patient is. Most cases of *post-primary* infection are due to reactivation of previous infected foci, often many years after first infection. Occasionally, a *primary* infection progresses to the *post-primary* phase without an intervening latent period.

**Pathology.** Most cases of *primary* tuberculosis are subclinical, although there may be fever, respiratory symptoms or erythema nodosum. There is an area of peripheral consolidation (the Ghon focus), and spread from this along the draining lymphatics may lead to enlargement of regional lymph nodes. Subpleural infection may cause a serous effusion. Activation of the immune system usually leads to resolution, healing and fibrosis at this stage, although if the response

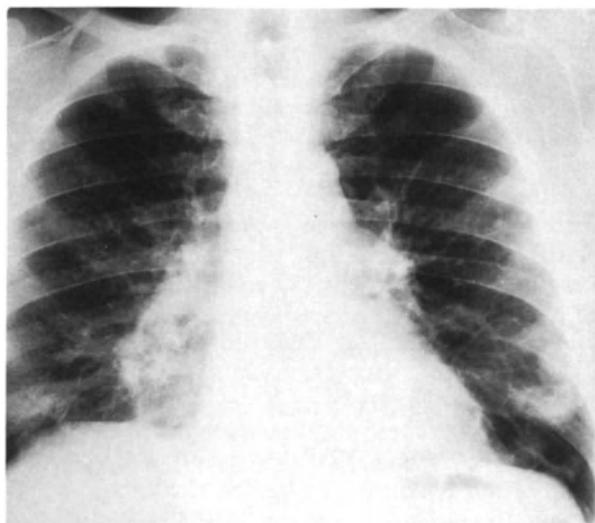


**Fig. 4.10.** Gram-negative pneumonia. Areas of consolidation are visible in both lower zones. Cavitation is seen on the left. Sputum culture grew *Pseudomonas* and *Hemophilus*.

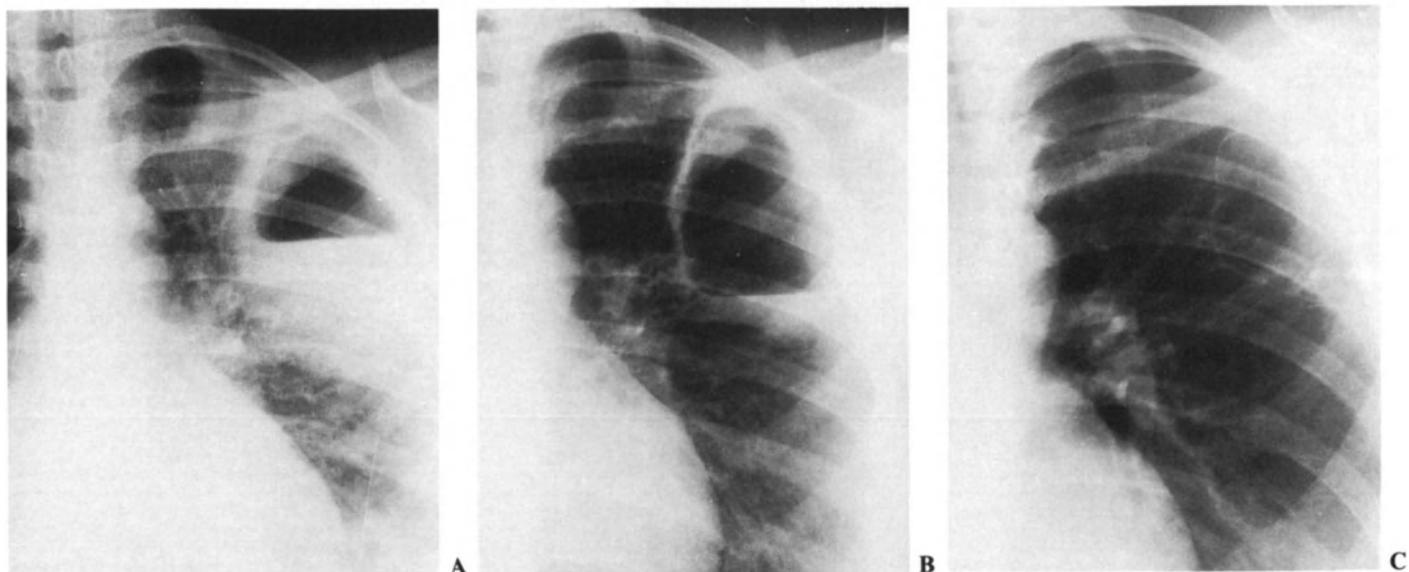


**Fig. 4.11A, B, C.** Lung abscess. **A** A thick-walled cavity in the left upper lobe contains a fluid level and is surrounded by consolidated lung. **B** 3 weeks later the consolidation has resolved, the fluid level is lower and the abscess wall is thinner. **C** 3 months later a thin-walled 'cyst' remains.

is weak the infection may progress. This may manifest as further consolidation, possibly with cavitation, and bronchogenic spread of infection. Rupture of a cavity into the pleura may cause *pneumothorax*, *pleural effusion* or *empyema*, and erosion into a pulmonary vessel may lead to hematogenous spread causing *miliary infection*.

*Lymphadenopathy* is a common feature of primary infection, but is rare in post-primary tuberculosis. Enlarged lymph nodes may press on adjacent airways and cause pulmonary collapse or air trapping with hyperinflation. Caseating nodes

may also erode into airways, causing bronchopneumonia, and into vessels causing miliary infection.

*Post-primary tuberculosis* almost always commences in the apicoposterior segment of an upper lobe or the apical segment of a lower lobe. Cavitation is common, and healing occurs with fibrosis, which usually obliterates small cavities, but large cavities may persist. As in progressive primary infection bronchopneumonia, pleural effusion, pneumothorax and miliary spread may occur. Empyema is commoner than in primary infection.

### Radiology of Tuberculosis

#### Pulmonary Changes

*Consolidation in primary infection* may involve any part of the lung, and the appearance is non-specific unless there is coincidental lymphadenopathy. The area involved may be small or affect an entire lobe, and an air bronchogram may be visible. Occasionally consolidation appears as a well-defined nodule or nodules. Healing is often complete without any sequelae on the chest radiograph although fibrosis and calcification may occur.

*Consolidation in post-primary infection* usually appears in the apex of an upper or lower lobe, and almost never in the anterior segments of the upper lobes. The consolidation is often patchy and nodular and may be bilateral (Fig. 4.12). Progressive infection is indicated by extension and coalescence of the areas of consolidation, and the development of cavities (Fig. 4.13).

Simultaneously there may be fibrosis and volume loss indicating healing (Fig. 4.14). Cavities may be single or multiple, large or small and thin- or thick-walled. Fluid levels are sometimes visible within cavities. With fibrosis there is contraction of the involved lung (Fig. 4.15) and obliteration of most cavities. However, larger cavities may persist and areas of bronchiectasis and emphysema may develop. Healed

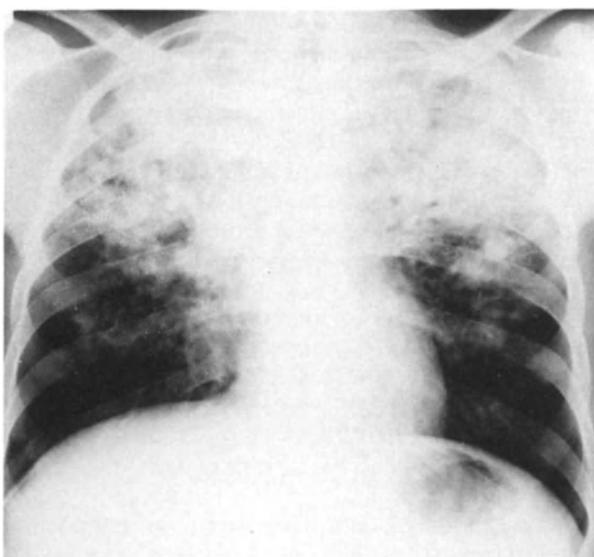


**Fig. 4.12.** Post-primary tuberculosis. Bilateral upper zone consolidation and nodular opacities.

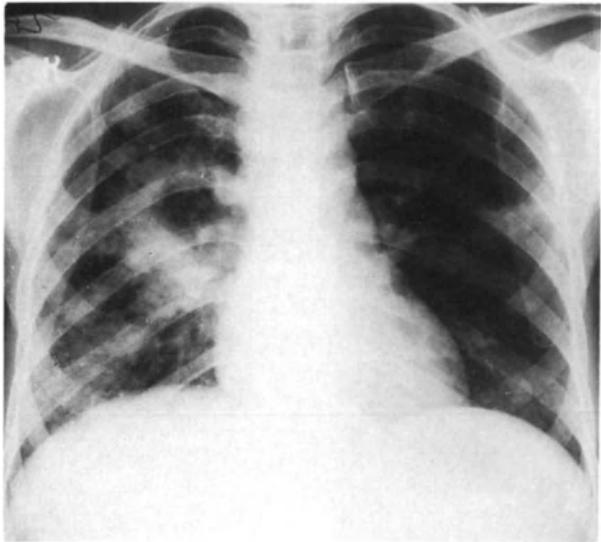


Fig. 4.13. Post-primary tuberculosis. Cavity in superior segment of right lower lobe and nodular opacities throughout right lung.

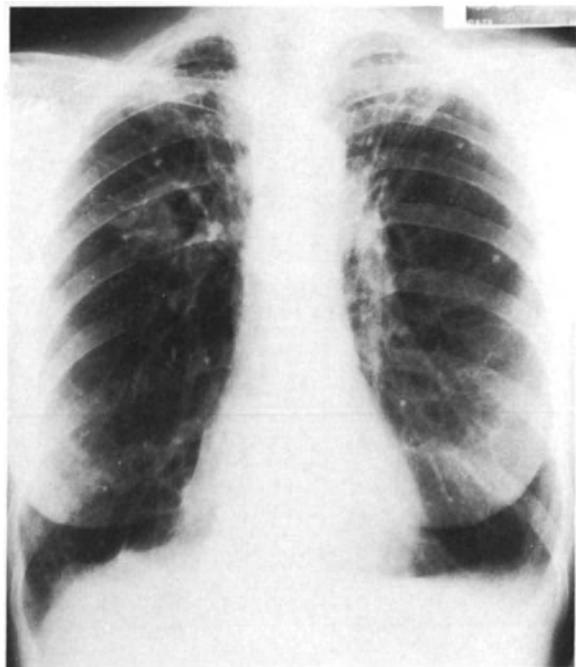


Fig. 4.15. Post-primary tuberculosis. Bilateral upper lobe fibrosis and scattered calcified nodules.

lesions often calcify. Chronic cavities are often colonized by *Aspergillus* and other fungi and mycetomas may develop.

*Tuberculous bronchopneumonia* may occur in both primary and post-primary infection, causing patchy, often nodular, areas of consolidation.

*Miliary tuberculosis* due to hematogenous spread of infection may be seen in both primary and post-primary disease. In the latter case the patients are often elderly, debilitated or immunocompromised. At first the chest radiograph may be normal, but then small, discrete nodules, 1–2 mm in

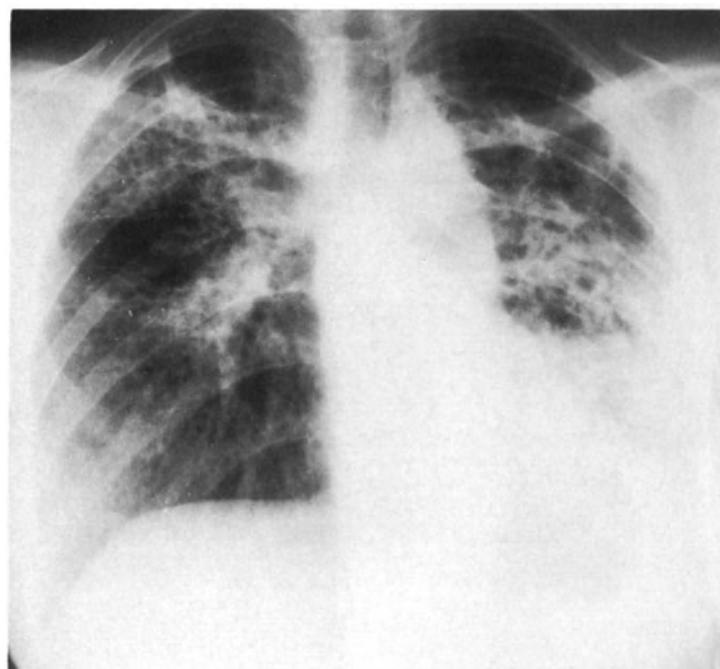
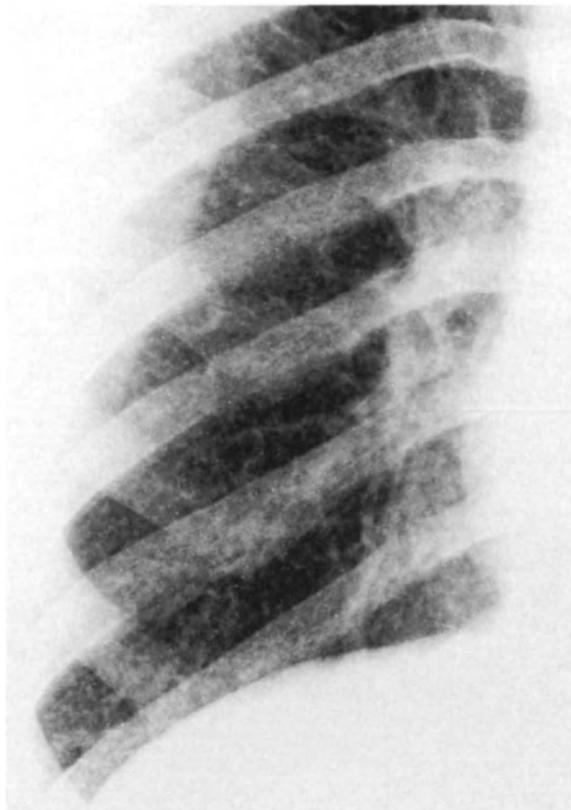
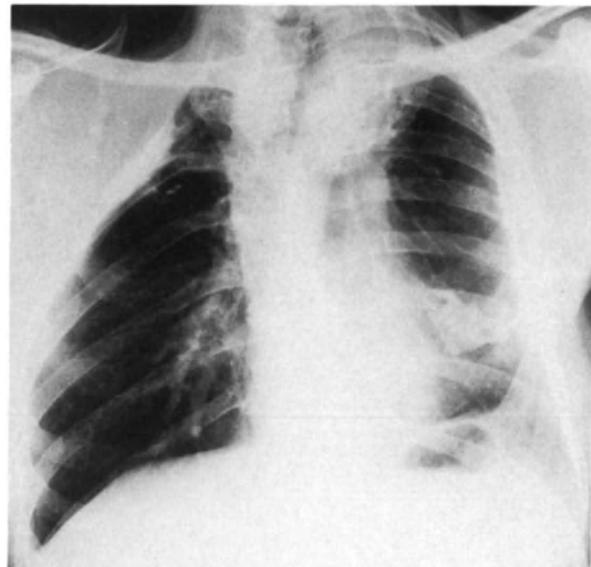


Fig. 4.14. Post-primary tuberculosis. Widespread consolidation and multiple small cavities. Elevation of horizontal fissure is due to right upper lobe fibrosis.



**Fig. 4.16.** Miliary tuberculosis. Multiple, fine, discrete nodules are distributed throughout the lung.



**Fig. 4.18.** Post-primary tuberculosis. Right thoracoplasty. Left upper lobe fibrosis. Extensive left pleural thickening and calcification.

diameter, become apparent, evenly distributed throughout both lungs (Fig. 4.16). These nodules may enlarge and coalesce, but with adequate treatment they slowly resolve. Occasionally, some may calcify.

*Tuberculoma* is a localized granuloma due to either primary or post-primary infection. It usually presents as a solitary, well-defined nodule, up to 5 cm in diameter. Calcification is common but cavitation is unusual.

#### *Lymphadenopathy*

Hilar and mediastinal lymphadenopathy is a common feature of primary infection and may be seen in the presence or absence of peripheral consolidation (Fig. 4.17). Following healing, involved nodes may calcify. Lymphadenopathy is usually unilateral, but may be bilateral.

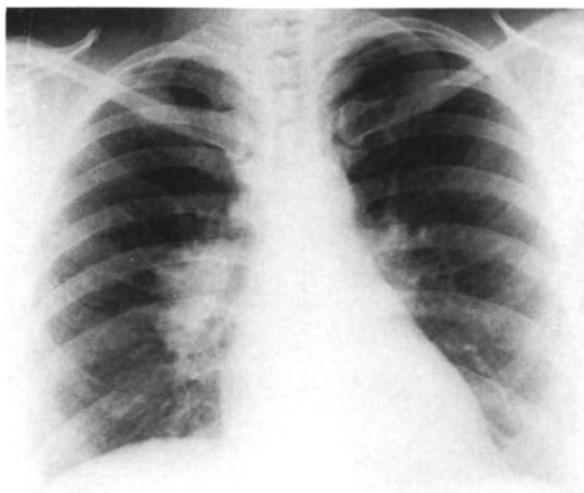


**Fig. 4.17.** Primary tuberculosis. Right hilar and right paratracheal lymphadenopathy.

#### *Pleural Changes*

*Pleural effusion* complicating primary infection is usually unilateral, and due to subpleural infection. Pulmonary consolidation and/or lymphadenopathy may or may not be apparent. At presentation the effusion may be large and relatively asymptomatic. These effusions usually resolve without complication. Pleural effusion in post-primary infection, however, often progresses to empyema. Healing is then complicated by pleural thickening and often calcification (Fig. 4.18). Uncommon complications of tuberculous empyema are bronchopleural fistula, osteitis of a rib, pleurocutaneous fistula and secondary infection.

*Pleural thickening* over the apex of the lung often accompanies the fibrosis of healing apical tuberculosis.

*Pneumothorax* may complicate subpleural cavitatory disease.

#### *Airway Involvement*

This may be secondary to lymphadenopathy (Fig. 4.19) or endobronchial infection (Fig. 4.20), and may therefore, com-

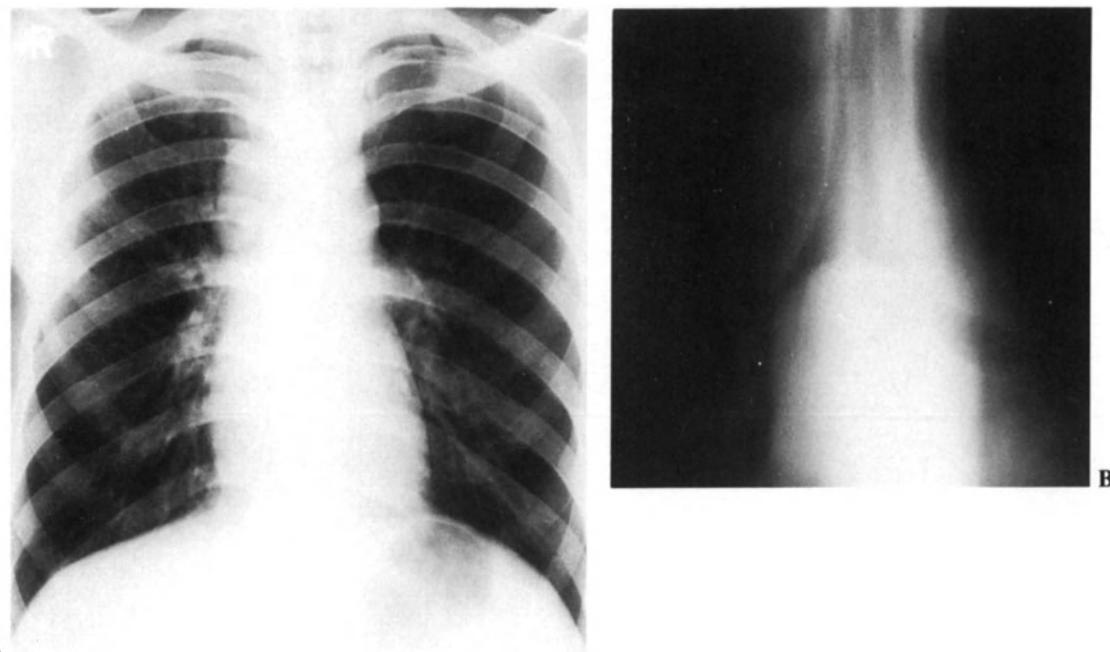


**Fig. 4.19A, B.** Primary tuberculosis. A Right paratracheal lymphadenopathy. B Linear tomogram demonstrates additional subcarinal lymphadenopathy and compression of both main bronchi.

plicate both primary and post-primary disease. Compression of central airways by enlarged nodes may cause pulmonary collapse or air trapping. Healing of endobronchial infection with fibrosis may also result in bronchostenosis. The lung distal to bronchial narrowing may develop bronchiectasis.

#### Atypical Mycobacteria

A small minority of mycobacterial infections are not caused by *Mycobacterium tuberculosis*. These atypical organisms, which include *M. xenopi* and *M. kansii*, are not particularly

pathogenic, and tend to infect debilitated individuals. Radiologically they produce changes similar to post primary tuberculosis, with a greater tendency to cavitation, but less tendency to pleural, nodal or miliary disease. They may be resistant to conventional drug therapy.

#### BRANCHING BACTERIA

*Actinomycosis*. *Actinomycosis israeli* is a commensal of the oropharynx and may rarely cause pulmonary infection by aspiration. Classically it causes abscess formation, pleural invasion, osteomyelitis of ribs and sinuses to the chest wall. However, presentation nowadays is more often a mass-like area of consolidation which may resemble lung cancer (Fig. 4.21).

*Nocardiosis*. *Nocardia asteroides* is found in soil, worldwide. Infection usually occurs in debilitated individuals. Most commonly there is non-segmental, cavitating pneumonia, often with pleural effusion or empyema. It may also present as a solitary pulmonary nodule, with or without cavitation, and occasionally with hilar lymphadenopathy.

#### FUNGAL INFECTIONS

##### Histoplasmosis

*Histoplasma capsulatum* is present in soil and bat and bird excreta in many parts of the world. It rarely causes chest infection, except in the eastern USA. Infection is usually sub-clinical and heals spontaneously, sometimes leaving a small, calcified pulmonary nodule or calcified hilar or mediastinal

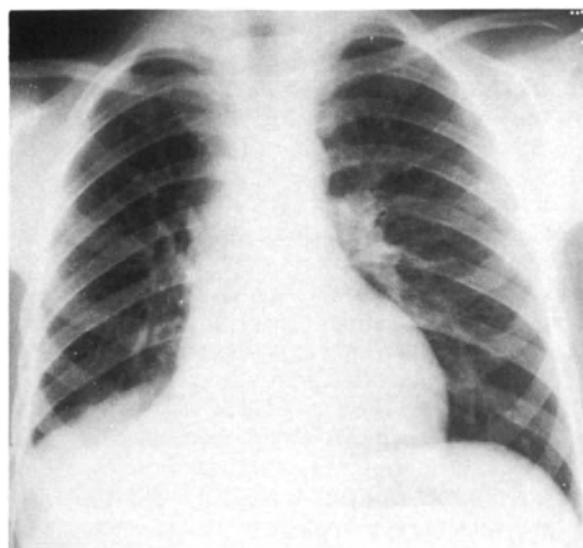


**Fig. 4.20.** Endobronchial tuberculosis. The right lower lobe is collapsed.

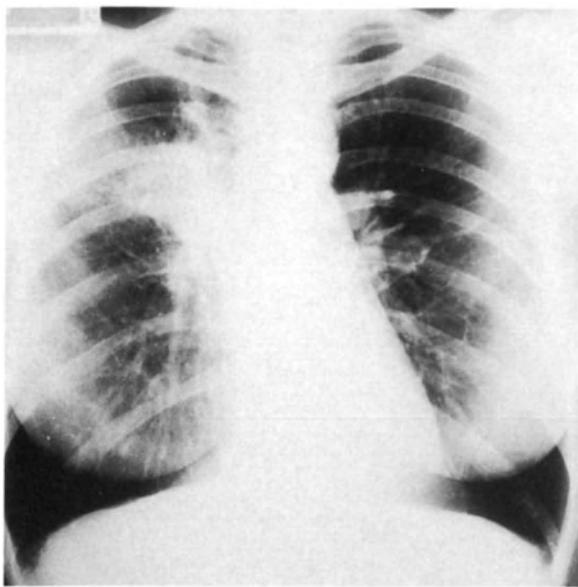


**Fig. 4.21.** Actinomycosis. A mass-like area of consolidation overlies the right hilum.

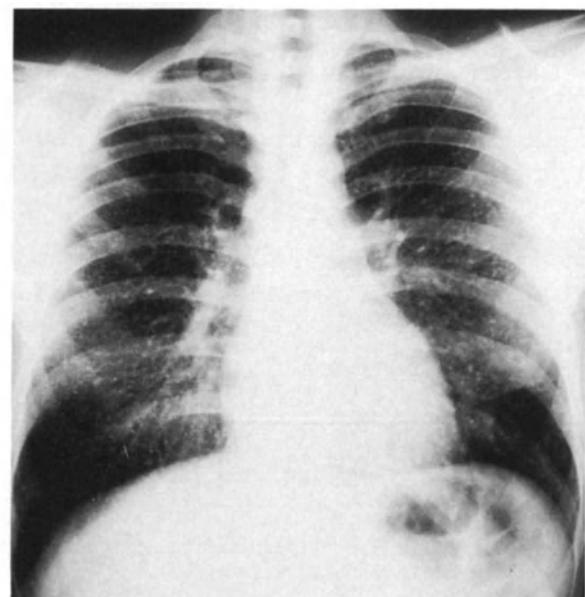


**Fig. 4.23.** Histoplasmosis. Diffuse, calcified nodules.

nodes. Rarely a calcified node may erode and obstruct a bronchus.

Massive inhalation of organisms may cause wheezing, dyspnea, a dry cough and fever. The chest radiograph shows diffuse small nodular shadows (Fig. 4.22) which, following resolution, may calcify (Fig. 4.23). Chronic infection resembles post-primary tuberculosis radiographically, and

may present as a solitary granuloma or with progressive consolidation, cavitation and fibrosis. A histoplasmoma may resemble a tuberculoma, being round, usually well circumscribed and often calcified. Pleural disease and hematogenous spread are rare.

Fibrosing mediastinitis is an uncommon complication.

#### Coccidioidomycosis

*Coccidioides immitis* causes endemic disease in parts of the southwestern USA. Most infections are subclinical but *C. immitis* may cause a pneumonic illness. The chest radiograph shows patchy consolidation, which may cavitate and be associated with pleural effusion or hilar or mediastinal adenopathy. Another presentation is single or multiple pulmonary nodules, up to 3 cm in diameter, with a tendency to form thin-walled cavities (Fig. 4.24). The fungus may also cause isolated mediastinal or hilar adenopathy. Rarer manifestations are progressive upper lobe consolidation with fibrosis and cavitation, similar to tuberculosis, and miliary disease.

#### Blastomycosis

*Blastomyces dermatitidis* is found in parts of the southeastern USA, and may cause infection similar to other fungi. It may present as a solitary nodule, patchy consolidation, lymphadenopathy, fibronodular disease or miliary disease. Cavitation is occasionally seen, but calcification is rare.

#### Cryptococcosis (Torulosis)

*Cryptococcus neoformans* is found worldwide. Infection is mostly subclinical, but may be important in debilitated patients. It may present with a pleural-based mass, possibly cavitating, that may be indistinguishable radiographically from lung cancer (Fig. 4.25). Other presentations include segmental or lobar consolidation and miliary nodules.

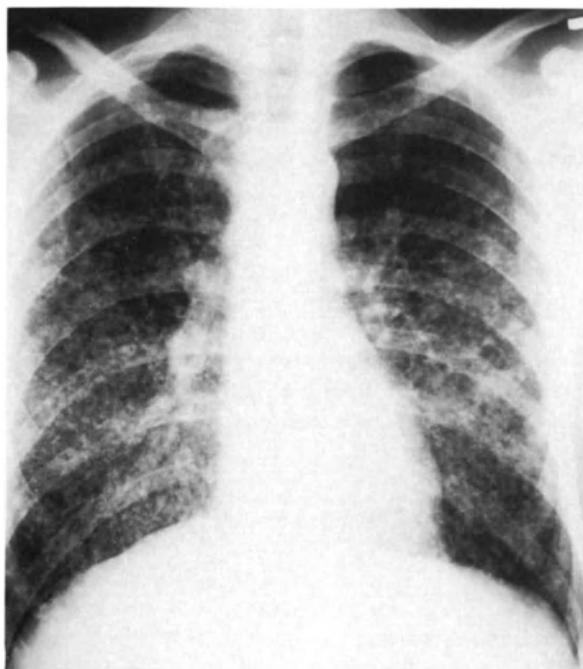


**Fig. 4.22** Histoplasmosis. Diffuse, nodular shadowing following massive inhalation of organisms.

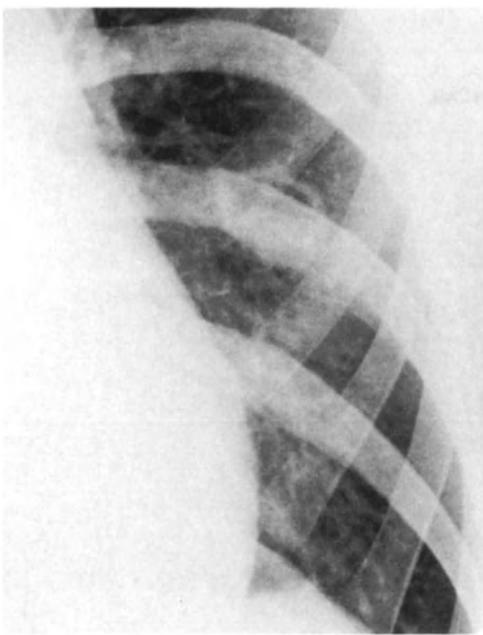


**Fig. 4.24.** Coccidioidomycosis. A thin-walled cavity is present in the left mid zone.

### ASPERGILLOSIS

*Aspergillus fumigatus* causes three fairly distinct forms of pulmonary infection.

1. *Aspergilloma*. Any chronic pulmonary cavity may be colonized by fungus. Such cavities are mostly secondary to

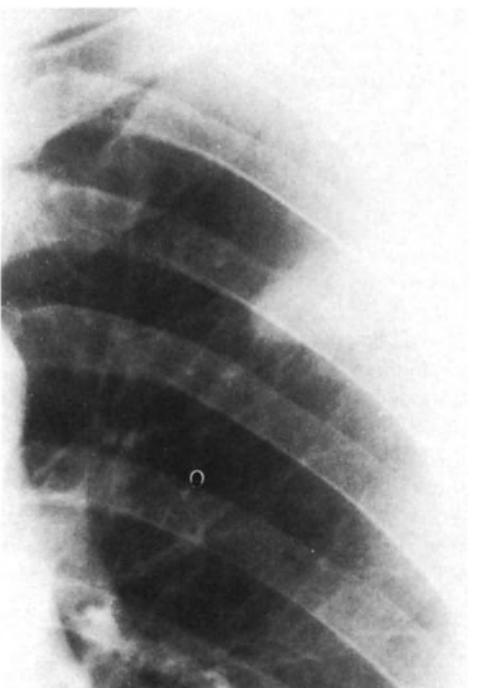


**Fig. 4.25.** *Cryptococcus*. A pleural-based mass-like area of consolidation in the left upper lobe.

tuberculosis, histoplasmosis or sarcoidosis, and are, therefore, usually in the upper lobes. The fungal hyphae form a ball or *mycetoma* which lies free in the cavity.

The *chest radiograph* may show a density surrounded by air within a cavity, but this is best shown by linear tomography or CT (Fig. 4.26). By altering the position of the patient the ball is seen to be mobile. There is almost always pleural thickening related to the mycetoma. The differential diagnosis of a mycetoma in a cavity includes *blood clot*, *cavitating tumor*, *lung abscess* and *hydatid cyst*.

Mycetomas are associated with development of vascular granulation tissue in the cavity wall, which may bleed. Life-threatening hemoptysis may be difficult to treat surgically, and may be better managed by *bronchial* or *intercostal artery embolization*.

2. *Invasive Aspergillosis*. In immunocompromised individuals *Aspergillus* may cause primary infection of the lung. This may be a bronchopneumonia, lobar consolidation or multiple nodules (Fig. 4.27). Cavitation is common, and may mimic an intracavitatory mycetoma (Fig. 4.28).

3. *Allergic Bronchopulmonary Aspergillosis*. *Aspergillus* is the commonest cause of *pulmonary eosinophilia* in the UK. It colonizes the lobar and segmental bronchi of some asthmatics where it produces a Type III reaction. Patients present with a cough and wheeze and often expectorate mucus plugs which contain fungi.

In the acute phase the chest radiograph shows patchy consolidation, often in the upper zones. Mucus plugging may cause lobar collapse (Fig. 4.29), and dilated mucus-filled bronchi may be visible as finger-like, tubular shadows (Fig. 4.30). With repeated attacks there may be pulmonary fibrosis and bronchiectasis. Fibrotic changes tend to occur in the upper zones. Bronchiectasis may produce ring shadows and tramline shadows. Unlike other causes of bronchiectasis, allergic bronchopulmonary aspergillosis produces changes that are more severe in the central airways than peripherally (Fig. 4.31).

### PROTOZOAL INFECTIONS

*Pneumocystis* is discussed under chest infections in the immunocompromised patient.

*Toxoplasmosis* rarely involves the lungs, but on occasion may be responsible for an interstitial pneumonia. The chest radiograph may show patchy consolidation and mediastinal lymphadenopathy.

*Entamoeba histolytica* involvement of the chest is usually secondary to hepatic infection and is therefore usually right-sided. A hepatic amebic abscess may erode the diaphragm and cause diaphragmatic elevation, pleural effusion, basal consolidation and lower lobe cavitation. *Ultrasound* scan may reveal liver abscesses.

### METAZOAN INFECTIONS

*Loeffler's Syndrome* may be caused by many parasitic worms, including *Ascaris*, *Taenia*, *Ankylostoma* and *Strongyloides* (see Chap. 6).

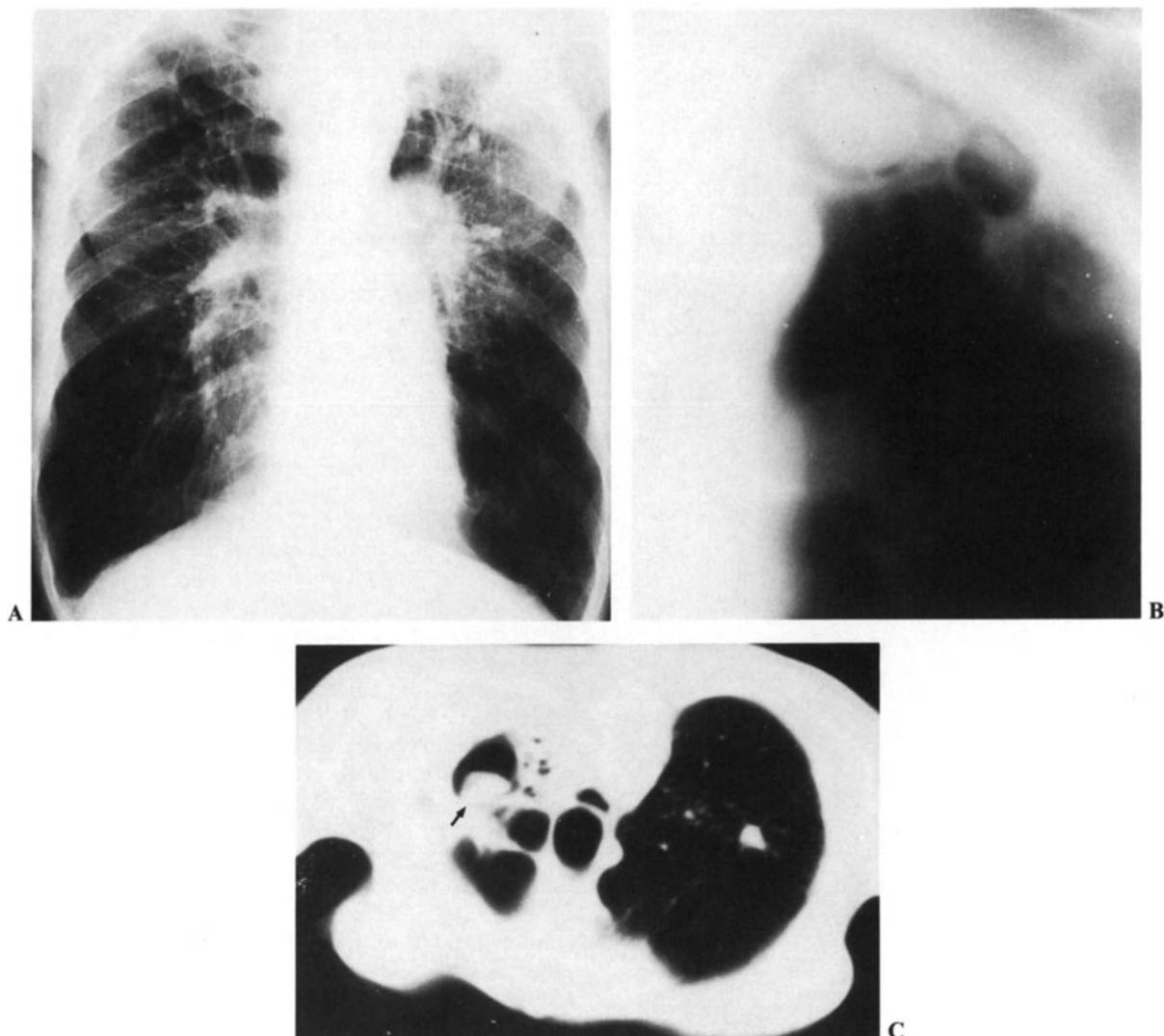


**Fig. 4.26A, B, C.** Aspergilloma. A, B Previous tuberculosis with bilateral upper lobe fibrosis. Cavities at the left apex contain fungus balls surrounded by a halo of air. C CT scan in another patient shows right upper lobe fibrosis, cavities and a fungus ball (arrow).



*Schistosomiasis* may cause pulmonary eosinophilia and also pulmonary arterial hypertension.

*Paragonimiasis* is usually acquired in the tropics from eating infected shellfish. The commonest reactions in the lung are formation of multiple 1–2 cm diameter cysts and bronchopneumonic shadowing, which may resemble tuberculosis. The dead flukes may calcify.

*Armillifer armillatus* is usually acquired by eating infected snakes. It may produce multiple thin-walled cysts on the chest radiograph. Dead larvae may calcify and be visible within the cysts.

**Fig. 4.27.** Invasive aspergillosis. Patient receiving chemotherapy for oat-cell carcinoma of lung. Bronchopneumonic changes are seen throughout left mid and upper zones.

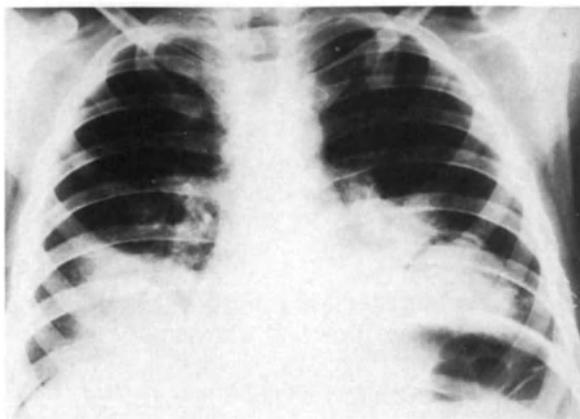


**Fig. 4.28.** Invasive aspergillosis. Patient with acute lymphoblastic leukemia. Necrotizing pneumonia in both lower zones mimics fungus balls.

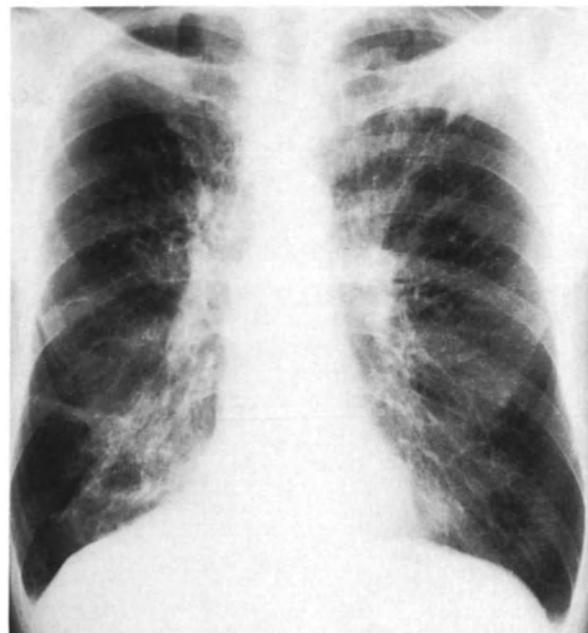


**Fig. 4.30.** Allergic bronchopulmonary aspergillosis. Finger-like opacities at ▶ left apex are due to fluid filled bronchi. Ring shadows in right upper zone indicate bronchiectasis.

*Hydatid disease* is caused by *Echinococcus granulosus*, and may cause cysts in the lungs and liver. Approximately 20% of the pulmonary cysts are bilateral, and about 10% are associated with hepatic cysts. Uncomplicated pulmonary hydatid cysts appear as well-circumscribed, round or oval, homogenous masses, which may be up to 10 cm in diameter (Fig. 4.32). Calcification is rare. Cysts may rupture into the pleura or bronchi. Following rupture into a bronchus an air fluid level may appear or the ectocyst may separate from the adventitia so that a double-walled cyst may be seen.

#### CONGENITAL ABNORMALITIES THAT PREDISPOSE TO PULMONARY INFECTION

*Cystic fibrosis* is associated with abnormally viscous mucus which impairs mucociliary function and predisposes to frequent chest infections and development of bronchiectasis. *Pseudomonas aeruginosa*, *Staph. aureus*, *Hem. influenza* and *Klebsiella* are frequent causes.

*Hypogammaglobulinemia* predisposes to bacterial infections with resultant bronchiectasis in long-term survivors.

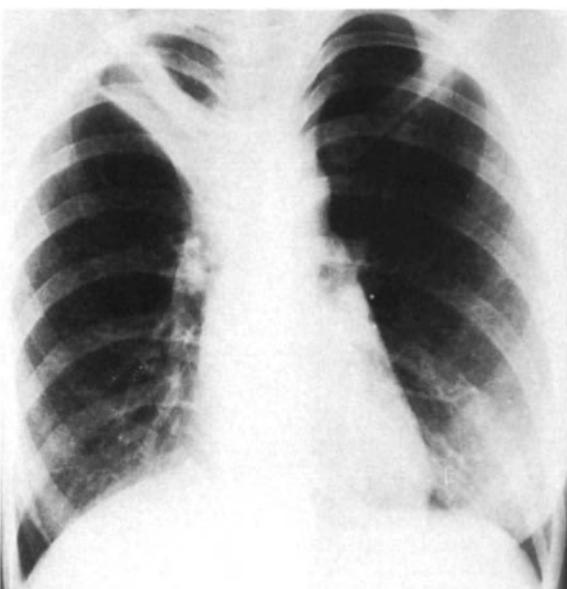


**Fig. 4.29.** Allergic bronchopulmonary aspergillosis. Right upper lobe collapse due to mucus plug.



**Fig. 4.31.** Allergic bronchopulmonary aspergillosis. CT shows bronchiectasis involving lobar and segmental bronchi, but sparing the peripheral bronchi.

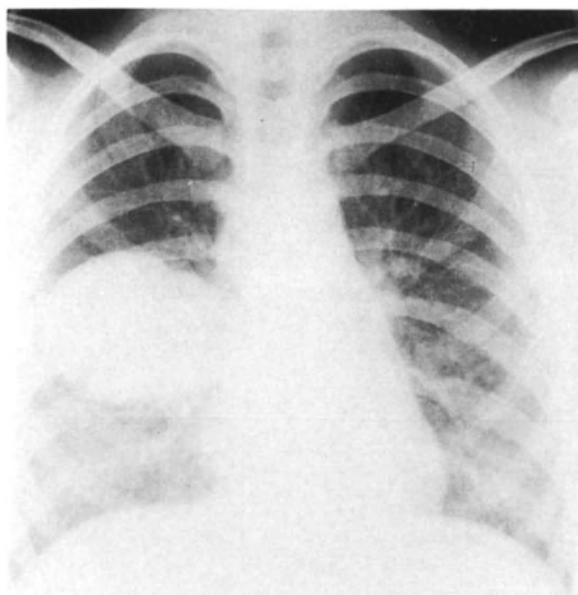


**Fig. 4.32.** Hydatid disease. A well-circumscribed, round, mass-like opacity occupying the right mid zone is a hydatid cyst.

*Abnormalities of phagocytes* as seen in chronic granulomatous disease and impaired neutrophil chemotaxis predisposes to recurrent bacterial infections.

*Congenital dyskinetic ciliary syndromes* are associated with recurrent chest infections and bronchiectasis.

*Congenital pulmonary sequestration* is an abnormality in which some lung tissue develops separated from the normal airways and pulmonary vessels. The blood supply is derived from the descending aorta. Sequestered segments are situ-

ated basally in contact with the diaphragm, and appear solid when uncomplicated. They may become infected, and develop a communication with the bronchial tree, following which they may cavitate and show a fluid level (Fig. 4.33).

#### ACQUIRED CONDITIONS THAT PREDISPOSE TO PULMONARY INFECTION

*Systemic conditions* that are associated with decreased immunity include old age, poor nutrition, diabetes, alcoholism, connective tissue disorders, many malignant diseases and AIDS.

*Pulmonary abnormalities* that predispose to chest infections include bronchiectasis and chronic bronchitis. In addition general anaesthesia, especially if prolonged, may be associated with pneumonia.

*Iatrogenic causes* include cancer chemotherapy, steroids, immunosuppression following organ transplantation and radiotherapy.

*Chronic infection of the paranasal sinuses and esophageal obstruction* may cause pneumonia or lung abscesses due to aspiration.

#### PULMONARY INFECTIONS IN IMMUNOCOMPROMISED PATIENTS

Immunocompromised patients are not only particularly susceptible to infection by normally pathogenic organisms, but may also be infected by so-called 'opportunistic' organisms which are only rarely infectious in the normal population. Table 4.1 lists the commonest causes of pneumonia in immunocompromised patients. Pneumonia in these patients

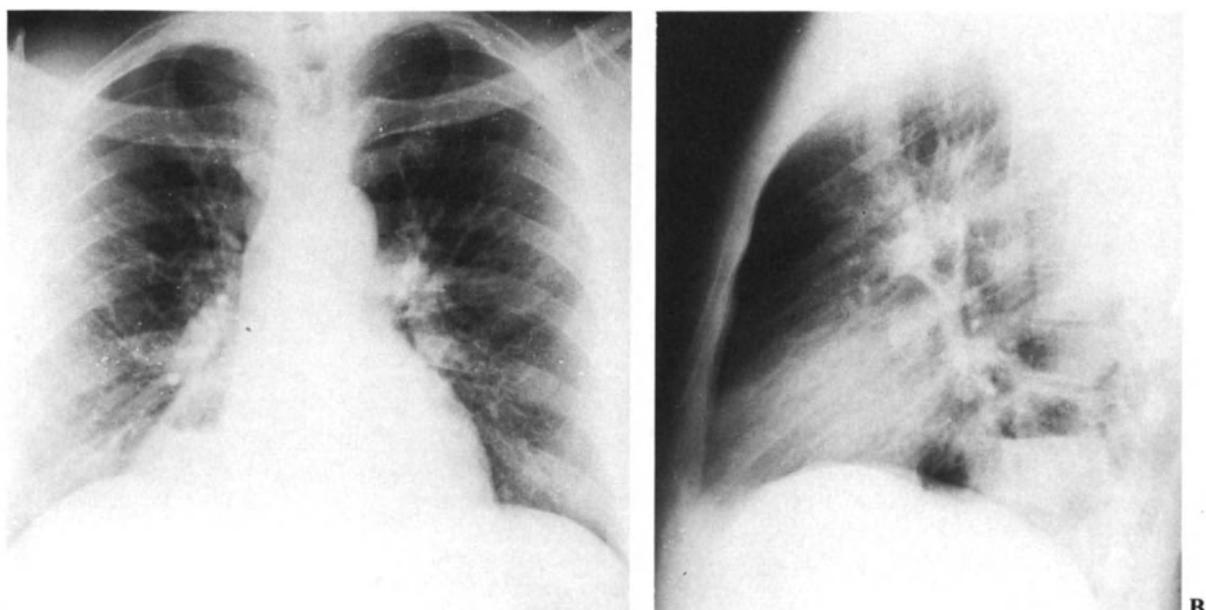


**Fig. 4.33A, B.** Congenital pulmonary sequestration. A posterior, right basal cavitating mass is visible. It represents an infected sequestered segment that has developed a communication with the bronchial tree.

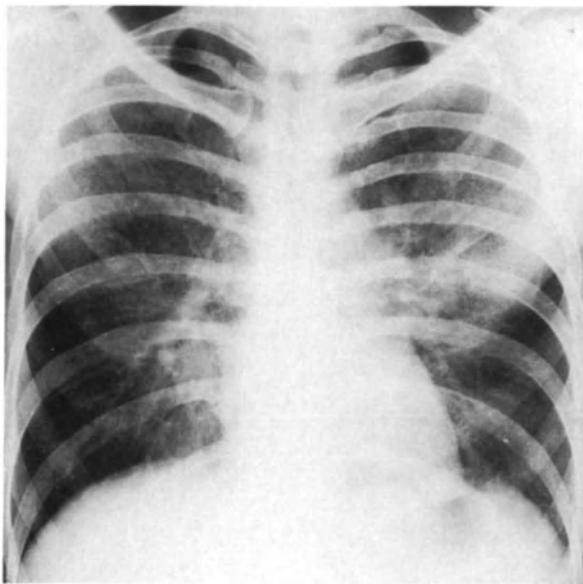


**Fig. 4.34.** Cytomegalovirus in AIDS. Multiple, nodular opacities are present in both lungs, becoming confluent in the left mid zone.

may present as diffuse pulmonary shadowing which must be differentiated from other possible causes (Table 4.2).

**Cytomegalovirus.** Cytomegalovirus is widely distributed in the normal population where infection is almost always sub-clinical. However, in the immunocompromised host it may cause a widespread interstitial pneumonia with alveolar exudation. The chest radiograph shows widespread, small nodular shadows, which may be peripheral or perihilar (Fig. 4.34).

**Table 4.1.** Causes of pneumonia in immunocompromised patients

<b>Viruses</b>
<i>Cytomegalovirus</i>
<i>Herpes</i>
<i>Varicella</i>
<b>Bacteria</b>
<i>Mycobacteria</i>
<i>Staphylococci</i>
<i>Pseudomonas</i>
<i>Legionella</i>
<i>Nocardia</i>
<b>Fungi</b>
<i>Candida</i>
<i>Aspergillus</i>
<i>Mucormycosis</i>
<i>Cryptococcus</i>
<b>Protozoa</b>
<i>Pneumocystis</i>
<i>Toxoplasma</i>

**Table 4.2.** Diffuse pulmonary shadowing in immunocompromised patients

Pneumonia
Diffuse malignancy
Pulmonary edema
Pulmonary hemorrhage
Radiation pneumonitis
Drug reaction
Transfusion reaction

**Pneumocystis.** *Pneumocystis carinii* is a widely distributed organism that is probably protozoan, although it has some fungal characteristics. Clinically apparent infection is only seen in immunocompromised patients. Pulmonary infection commences as an interstitial infiltration, which progresses

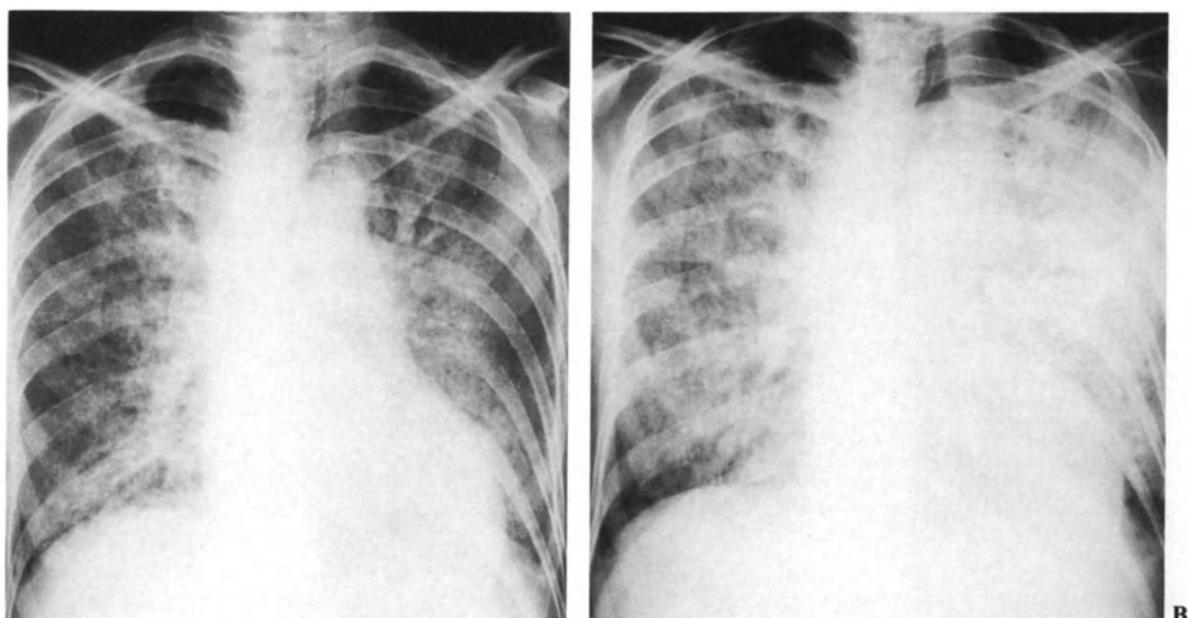


**Fig. 4.35A, B.** Pneumocystis in AIDS. A Extensive nodular shadowing progresses to, B, diffuse consolidation over 36 hours. The appearance resembles pulmonary edema.

to an alveolitis with intraalveolar exudation. Radiographically there is perihilar reticulonodular shadowing, which spreads and coalesces causing diffuse consolidation, and may resemble pulmonary edema (Fig. 4.35). Cystic areas appear, and pneumothorax is a recognized complication.

#### ACQUIRED IMMUNE DEFICIENCY SYNDROME (AIDS)

AIDS is due to infection by the human immunodeficiency virus (HIV). The syndrome comprises opportunistic infections and certain rare malignancies, and in Britain is most

often seen in homosexual males, drug addicts and hemophiliacs. Lung involvement is seen in about 40% of patients. In Britain the commonest infections are due to *pneumocystis*, *tuberculosis*, *cytomegalovirus* and *pyogenic bacteria*. In the USA, however, tuberculosis is less frequent and *atypical mycobacteria*, *cryptococcus*, *histoplasmosis* and *coccidioidomycosis* may be seen.

*Kaposi's sarcoma* and *lymphoma* occur in approximately 6% of patients. Kaposi's sarcoma may present in the chest with coarse nodular shadowing, pleural effusion and lymphadenopathy.

*For further reading, see p. 134.*

## CHAPTER 5

# PULMONARY NEOPLASMS

M. Rubens

---

A wide variety of tumors, both malignant and benign, may arise in the lungs. Since there is not unanimous agreement among pathologists in the classification of tumors in the lung, Table 5.1 lists pulmonary tumors according to frequency and behaviour, rather than by presumed tissue of origin.

### CARCINOMA OF THE BRONCHUS

Carcinoma of the bronchus is the commonest and most important primary tumor of the lung. It is also the commonest fatal malignancy in adult males in the western world. Most cases occur between the ages of 40 and 70 years. *Cigarette smoking* is the most important etiological factor. Other factors include atmospheric pollution and certain

occupations, particularly where there is exposure to asbestos.

*Squamous* (or *epidermoid*) carcinoma accounts for approximately 50% of cases of primary lung cancer. Squamous carcinomas tend to arise centrally, grow relatively slowly and often cavitate. *Adenocarcinoma* accounts for approximately 10% of cases: adenocarcinomas usually arise peripherally and are less likely to cavitate or involve the mediastinum. *Small cell undifferentiated (oat cell) carcinoma* accounts for approximately 25% of cases: these carcinomas tend to grow rapidly and are typically associated with hilar and mediastinal lymphadenopathy. Oat cell tumors rarely cavitate. The remaining 15% of cases are mostly *undifferentiated large cell carcinomas*.

Lung cancer often presents as an abnormal chest radiograph in an asymptomatic patient. Other common presen-

Table 5.1. Pulmonary neoplasms

	Malignant	Intermediate	Benign
Common	Carcinoma of the bronchus Metastases		
Uncommon	Alveolar cell carcinoma Lymphoma	Bronchial adenoma	Hamartoma
Rare and very rare	Leukemia Carcino-sarcoma Pulmonary blastoma Plasmacytoma Pulmonary sarcoma Primary melanoma of lung	Bronchial myoblastoma Papilloma of trachea/bronchus Hemangiopericytoma Pulmonary teratoma	Pseudolymphoma Benign lymph node hyperplasia Leiomyoma/fibroleiomyoma Chondroma Fibroma Lipoma Plasma cell granuloma Neurofibroma Benign clear cell tumor Chemodectoma Hemangioma Pulmonary endometriosis Intravascular and sclerosing bronchiolo-alveolar tumors (IVSBAT)

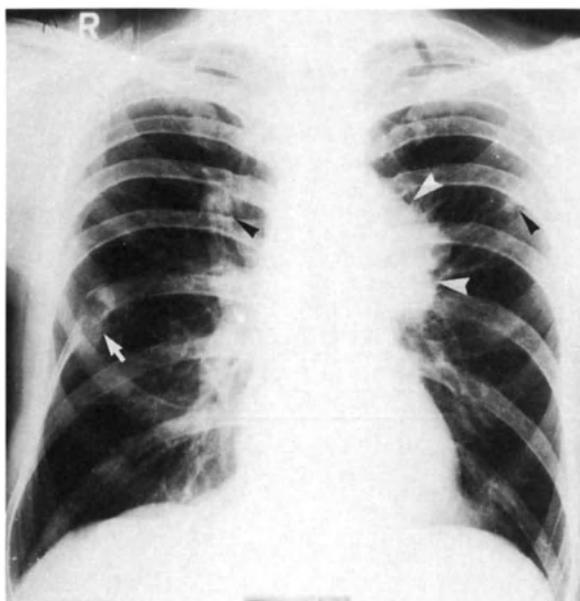


**Fig. 5.1.** Carcinoma of bronchus. The primary tumor is at the left hilum (white arrowheads). Pulmonary metastases (black arrowheads) are present in both lungs. A lytic metastasis is present in the right 8th rib (arrow).

tations are cough, breathlessness, chest pain and hemoptysis. Pneumonia, particularly if it is slow to resolve despite proper treatment, may be due to underlying lung cancer. Some patients present with symptoms of metastatic disease or of other distant effects such as hypertrophic osteoarthropathy, peripheral neuropathy or recurrent venous thrombosis.

#### RADIOLOGICAL PRESENTATIONS OF LUNG CANCER

**Hilar Enlargement.** Approximately half of primary lung carcinomas arise centrally in a proximal or segmental bronchus (Fig. 5.1). Hilar enlargement may also be due to bronchopulmonary lymph node metastases from a peripheral tumour (Fig. 5.2). Bilateral hilar lymphadenopathy may be seen with oat cell cancers (Fig. 5.3). Occasionally the hilar involvement is subtle and presents in the chest radiograph as increased density of the hilum rather than enlargement (Fig. 5.4). When in doubt, CT or conventional tomography is useful (Fig. 5.2).

**Airway Obstruction.** Carcinoma of the bronchus arises in the bronchial mucosa. Tumor may grow into the bronchial lumen and around the bronchus. As the bronchial lumen narrows, the lung distal may become consolidated and lose volume. Depending on the site of the tumor there may be

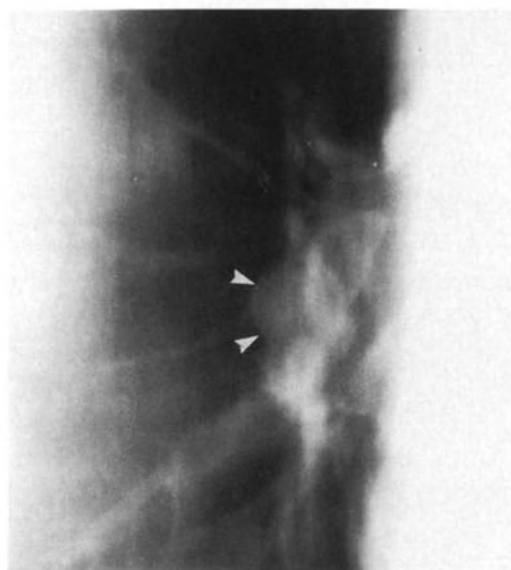
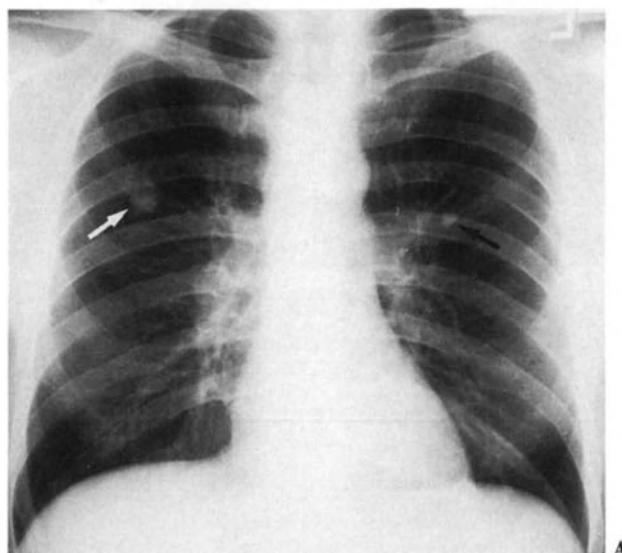


**Fig. 5.2A, B, C.** Carcinoma of bronchus. A Radiograph shows primary tumor (white arrow) in right lung, enlargement of right hilum and calcified granuloma (black arrow) in left lung. B Tomogram shows primary tumor (white arrow). It is not calcified and its edge is not sharp. C Tomogram confirms lobulated enlargement of right hilum (arrowheads) due to metastatic spread of the tumor.

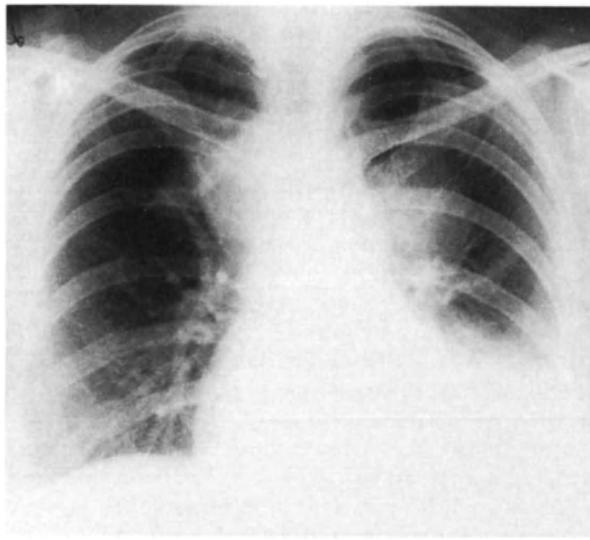


**Fig. 5.3.** Oat cell carcinoma. Bilateral hilar and mediastinal lymphadenopathy and a left pleural effusion are present.

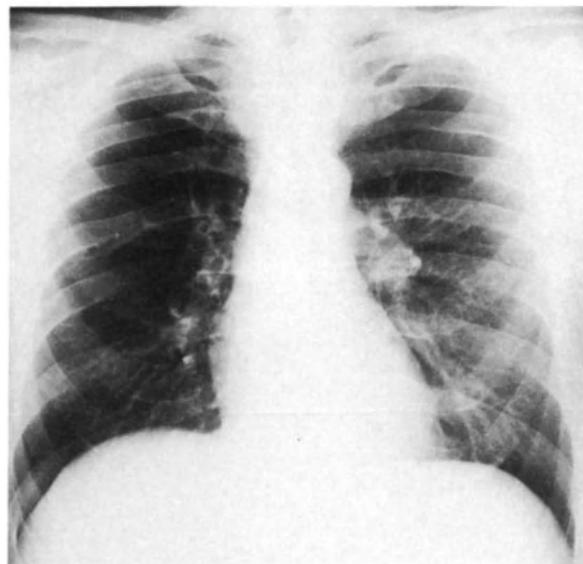
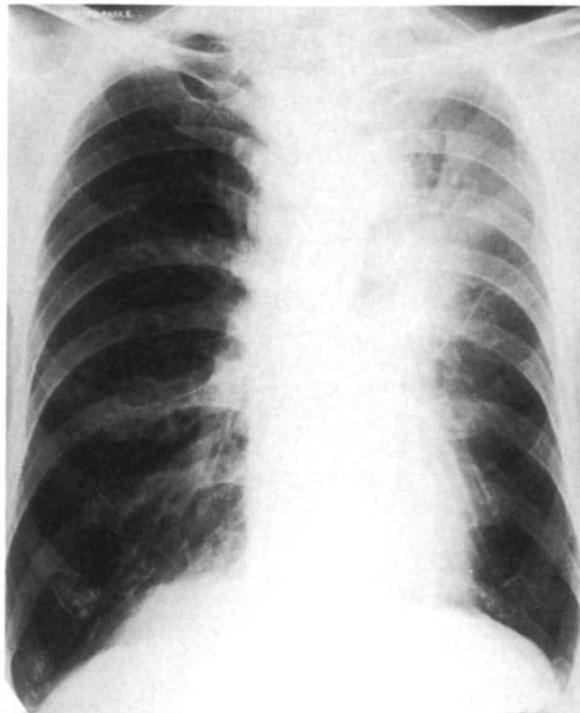


**Fig. 5.4.** Carcinoma of bronchus. The PA film shows a dense left hilum, but the lateral film was normal. A left upper lobe squamous carcinoma was found at bronchoscopy.

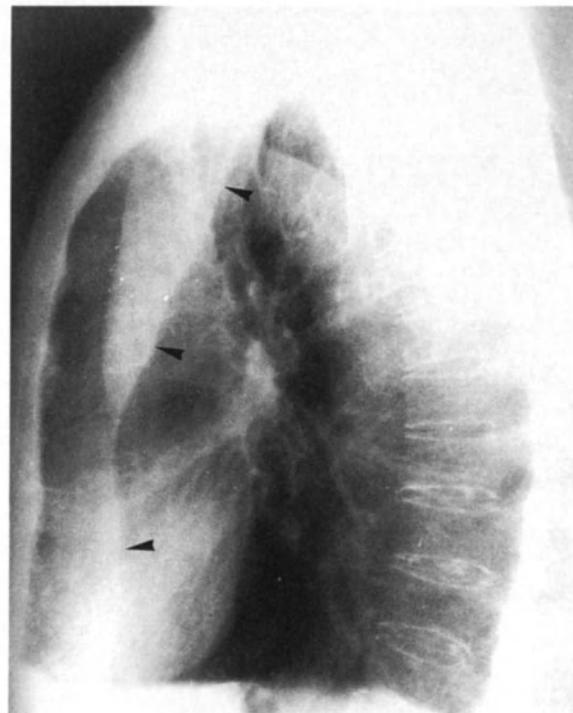
lobar or segmental collapse (Fig. 5.5), or even collapse of an entire lung.

**Peripheral Mass.** Peripheral tumors usually appear as solitary nodules or masses (Fig. 5.6). There are no features on plain films that can reliably differentiate between a benign or a malignant pulmonary nodule. However, malignant

tumors are often larger than benign lesions at the time of presentation. Moreover lung cancer tends to invade the surrounding lung so that the edge of the tumor may be poorly defined, spiculated, umbilicated or lobulated (Fig. 5.7). Satellite opacities around a mass are more commonly seen with benign lesions but may be seen with carcinomas. Masses that



**Fig. 5.5A, B.** Carcinoma of the bronchus. There is left upper lobe collapse, with increased density of the left upper zone, elevation of the left hilum, and anterior displacement of the left oblique fissure (arrowheads).



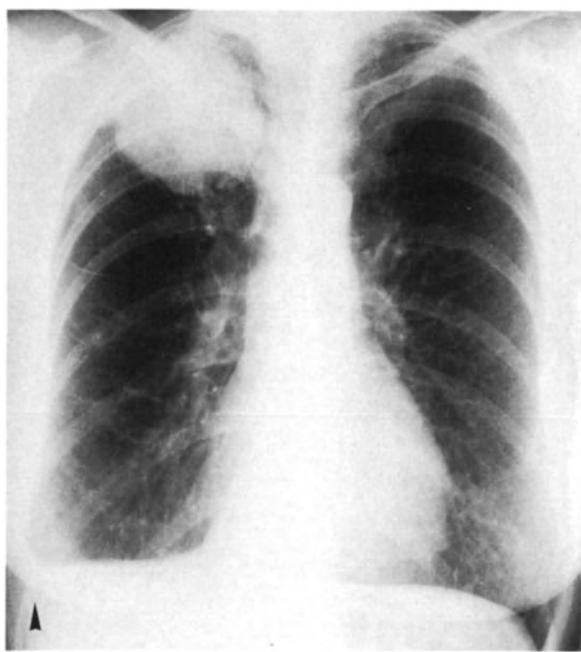


**Fig. 5.6.** Carcinoma of the bronchus. A large mass is present in the right upper zone. A small right pleural effusion (arrowhead) is present.

are diffusely calcified or that have central calcification are almost always benign. However, a bronchial carcinoma may occasionally engulf a calcified granuloma and appear eccentrically calcified (Fig. 5.8). If a previous chest radiograph is available a nodule or mass that has not changed over 2 years is almost certainly benign.

Approximately 5% of bronchial carcinomas cavitate due to central necrosis or abscess formation. Typically, malignant cavities are thick-walled with an irregular inner

margin (Fig. 5.9), but some may appear thin-walled and smooth. Cavitation is best seen with tomography or CT (Fig. 5.10).

Carcinoma of the bronchus arising at the apex of the lung is sometimes called a *Pancoast* or *superior sulcus tumor*. These tumors have a tendency to invade ribs, spine, brachial plexus and the inferior cervical sympathetic plexus. The chest radiograph may show asymmetric apical pleural thickening, but the full extent of the tumor is best seen with CT (Fig. 5.11).

**Mediastinal Involvement.** Carcinoma of the bronchus commonly metastasizes to lymph nodes in the mediastinum, and central tumors may invade the mediastinum directly. Oat cell tumors frequently cause extensive mediastinal lymphadenopathy with widening of the mediastinum (Fig. 5.3). CT is the best method of assessing the extent of mediastinal involvement (Fig. 5.12), but barium swallow will often demonstrate lymphadenopathy that is not apparent on the chest film (Fig. 5.13). Phrenic nerve involvement may cause elevation of one of the domes of the diaphragm, and fluoroscopy of the chest may be used to demonstrate paradoxical movement. Tumor in the mediastinum may cause superior vena caval obstruction, which may be confirmed by superior vena cavaography. Invasion of the pericardium may cause pericarditis and pericardial effusion (Fig. 5.14).

**Pleural Involvement.** Pleural effusion may be due to direct involvement of the pleura by peripheral tumor, or be secondary to lymphatic obstruction or obstructive pneumonitis. Rarely a peripheral, cavitating carcinoma of the bronchus will cause a spontaneous pneumothorax.

**Bone Involvement.** Peripheral tumors may invade the ribs or spine directly (Fig. 5.15). Hematogenous metastases from lung cancer are usually osteolytic (Fig. 5.1) and may be identified earliest by *isotope bone scan*. Bony metastases are often painful, but pain around the wrists and ankles may indicate *hypertrophic osteoarthropathy*.

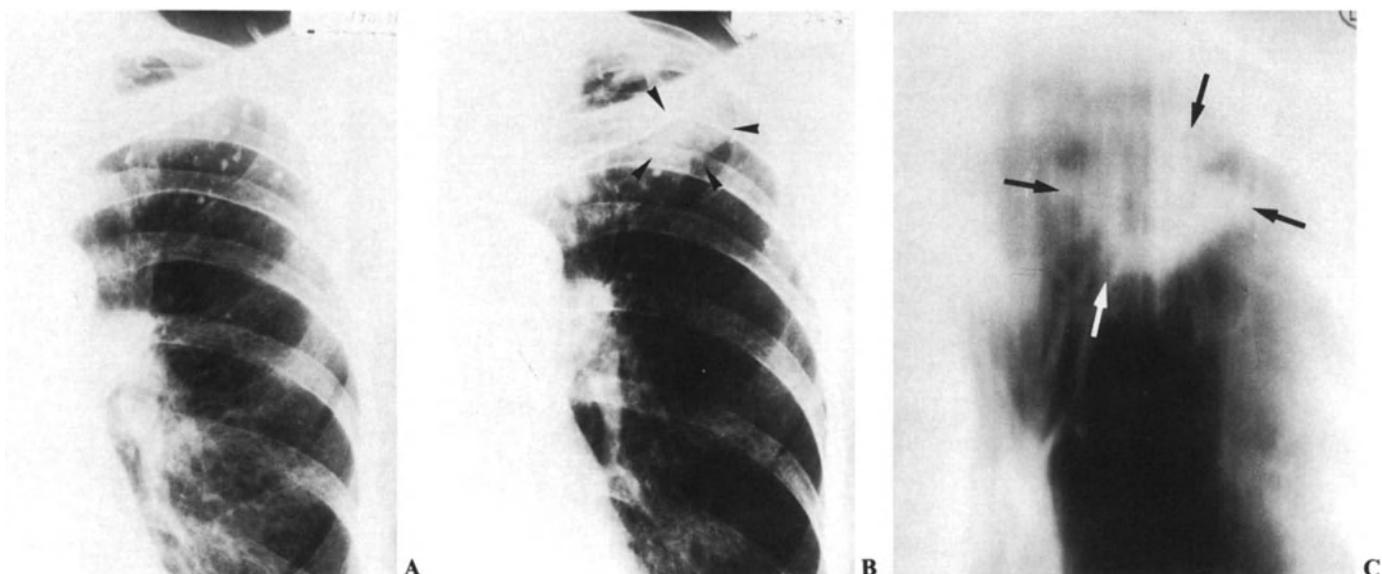


**Fig. 5.7A, B, C.** Carcinoma of the bronchus. A Calcified nodules at the left apex are due to previous TB. B Two years later further shadowing has appeared at the left apex (arrowheads). C Tomography shows a cavitating tumor with a spiculated border (arrows).

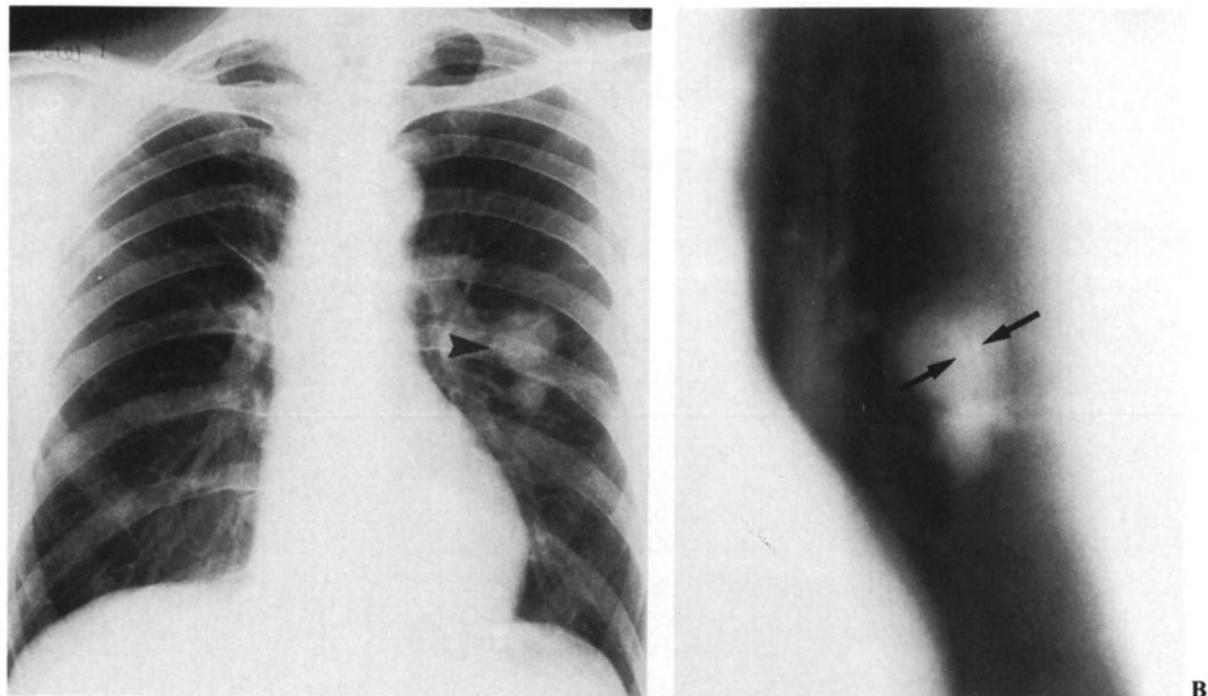


**Fig. 5.8A, B.** Carcinoma of the bronchus. A A lobulated mass (arrowhead) is present in the left mid zone. B Tomography shows eccentric calcification (arrows).

#### DIAGNOSTIC RADIOLOGY AND THE MANAGEMENT OF LUNG CANCER

The prognosis and treatment of lung cancer depends upon the general condition of the patient, the histology of the tumor and its extent at the time of presentation. Since oat

cell tumors tend to metastasize early they are often disseminated at presentation. However, they are sensitive to chemotherapy, whereas non-oat cell tumors are less so. Radiology may assist in making the histological diagnosis, staging the tumor and assessing treatment.

*Making the Histological Diagnosis.* Usually *sputum cytology*

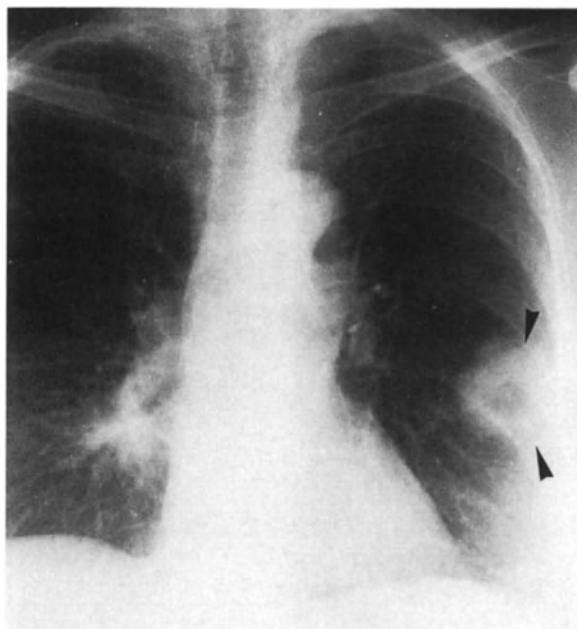


**Fig. 5.9.** Carcinoma of the bronchus. A thick-walled cavitating mass (arrowheads) is present in the periphery of the left mid zone.

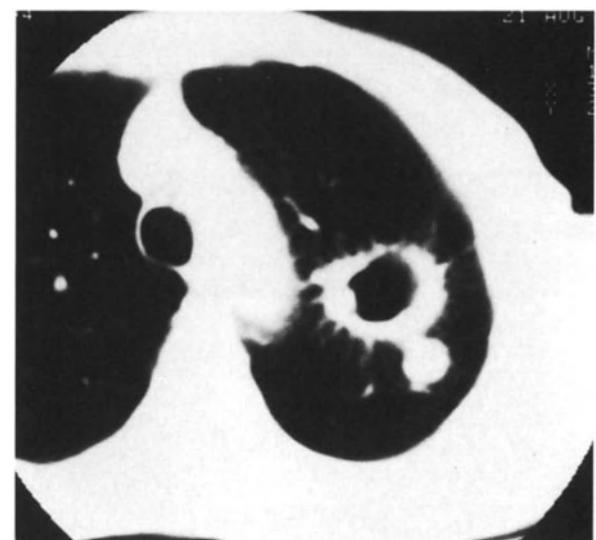


**Fig. 5.10.** Carcinoma of the bronchus. CT shows a lobulated, cavitating mass. The inner surface of the cavity is nodular. The outer surface of the mass is spiculated.

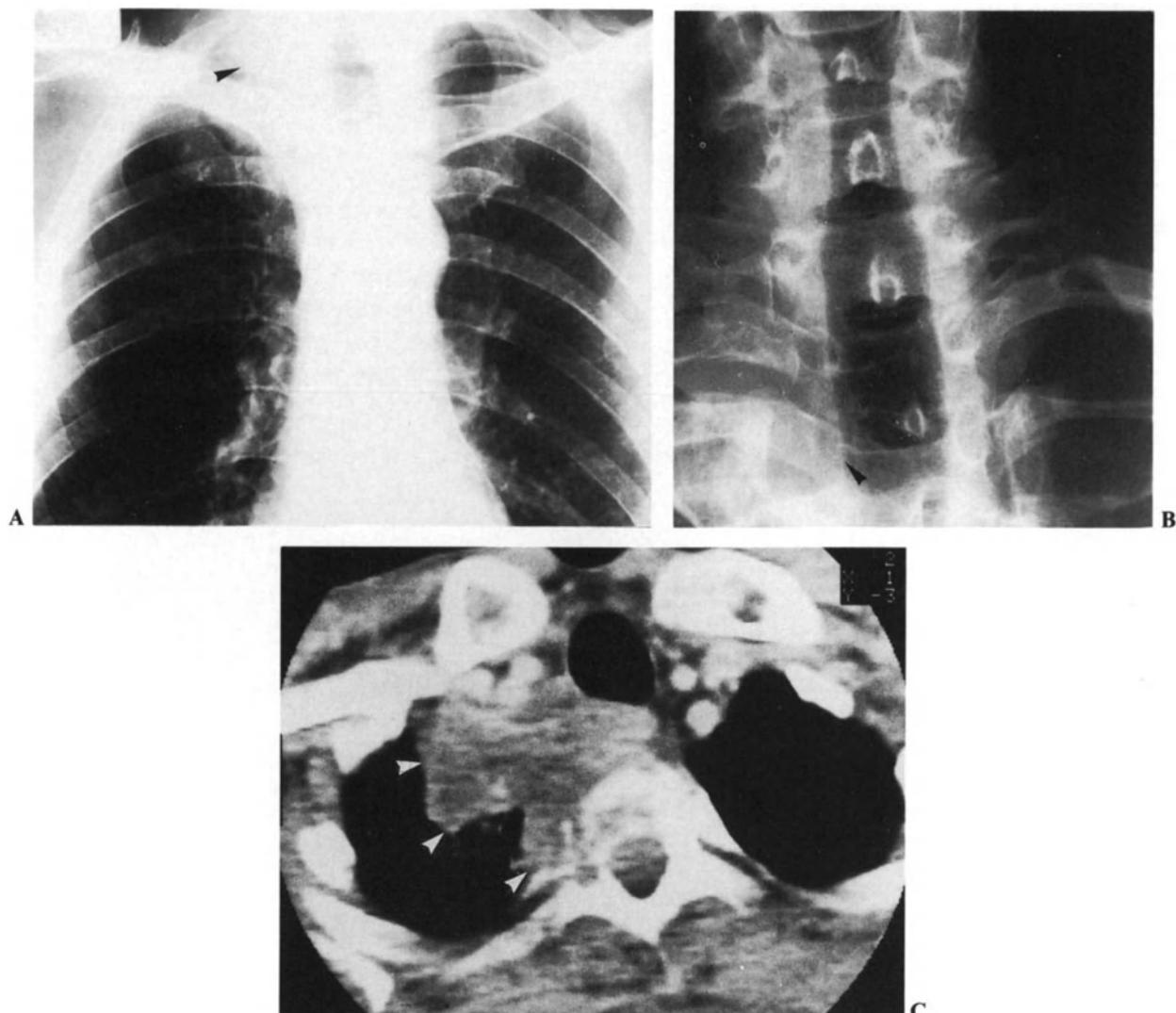


**Fig. 5.11A, B, C.** Pancoast tumor. A CXR shows asymmetric pleural thickening (arrowhead) at the right apex. B Spine film shows absence of right T-3 pedicle (arrowhead). C CT shows large right apical mass (arrowheads) infiltrating spine.



or *bronchoscopy* provide a tissue diagnosis of central tumors. Peripheral tumors, however, may require *percutaneous needle biopsy*. This may be guided by either fluoroscopy or CT. The specimen obtained may be suitable for either cytological or histological examination depending on the type of needle used. It is essential that the pathologist is skilled in examining small specimens of tissue.

*Staging the Tumor.* The main purposes of staging lung cancer are:

1. To identify patients with non-oat cell tumors who will benefit from surgery.

**Fig. 5.12.** Carcinoma of bronchus. CT shows a large right paratracheal mass (arrowheads) invading the mediastinum.

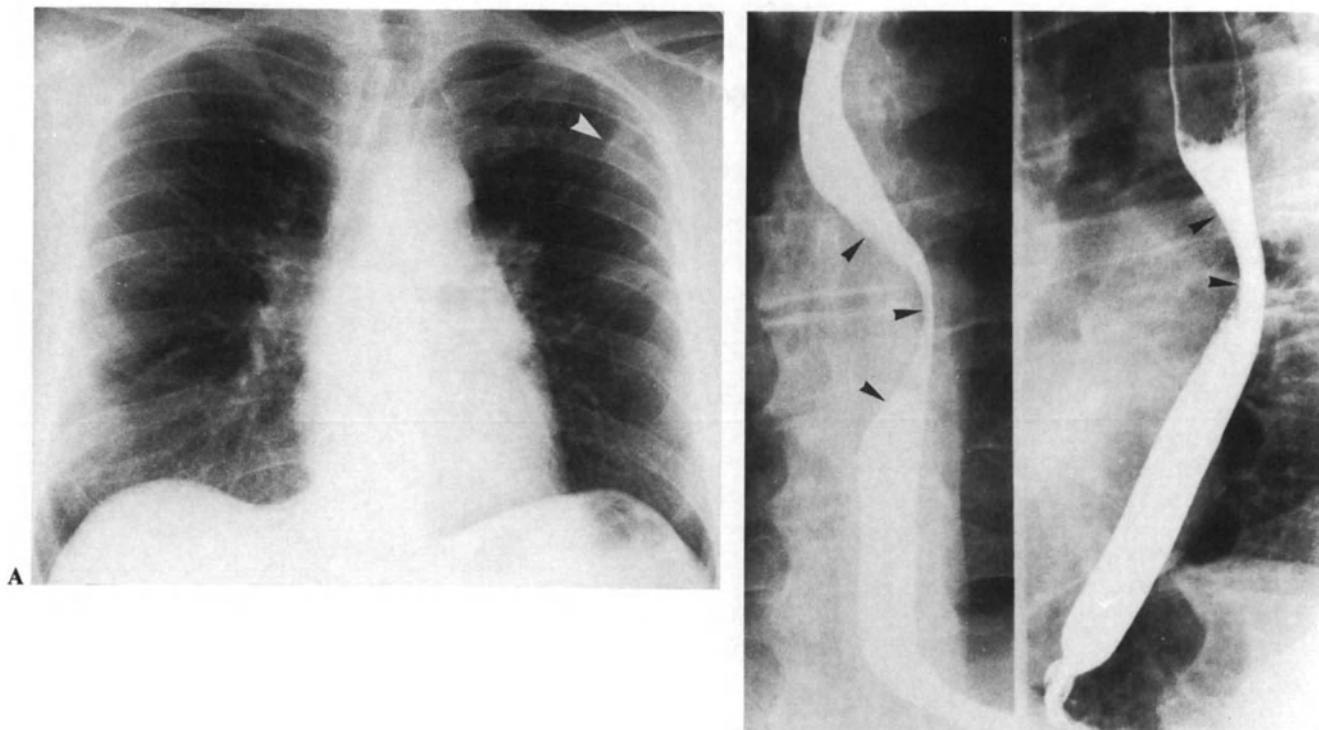


**Fig. 5.13A, B.** Carcinoma of bronchus. A CXR shows mass (arrowhead) in periphery of left upper zone and dense left hilum. B Barium swallow shows displacement of esophagus (arrowheads) by enlarged subcarinal nodes.

2. To avoid surgery in patients who will not benefit.
3. To provide data for comparing and assessing different methods of treatment.

A tumor is inoperable if it extends directly into parietal

pleura, chest wall, diaphragm or mediastinum, or is within 2.0 cm of the carina. In addition, metastasis to contralateral hilar nodes, mediastinal nodes or more distantly precludes surgical cure. The plain chest film should, therefore, be carefully scrutinized for evidence of spread of tumor. If the tumor appears localized and appears operable on bronchoscopy,

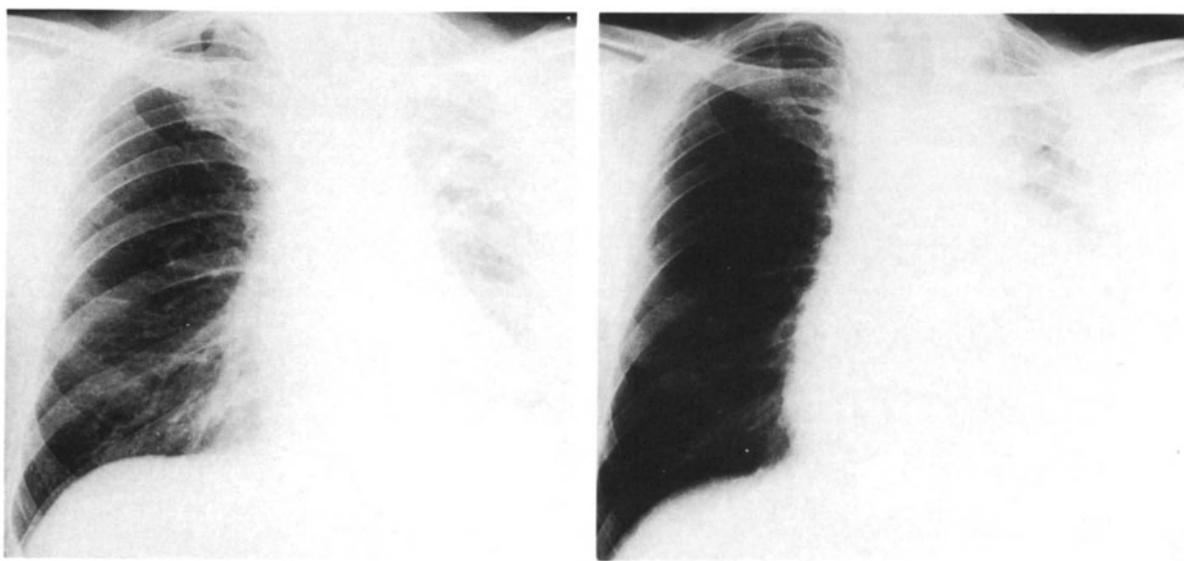
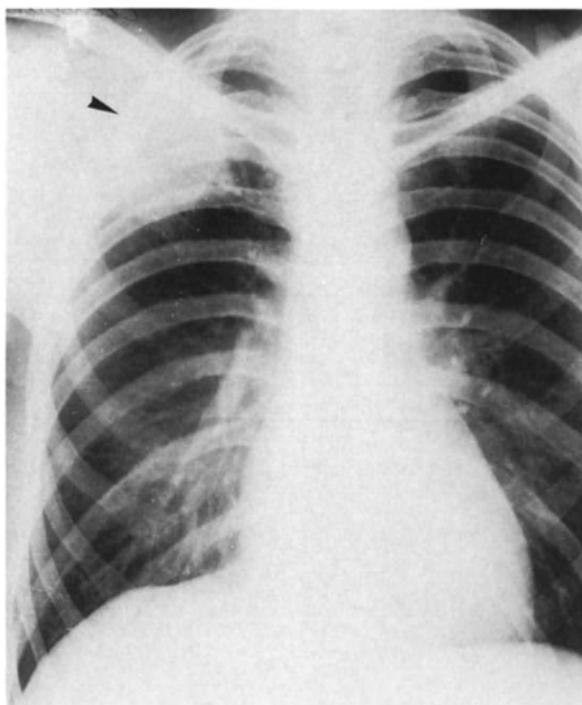


**Fig. 5.14A, B.** Malignant pericarditis. A The density of the left hemithorax is increased following radiotherapy for carcinoma of left lung. B A film 7 weeks later shows significant enlargement of the cardiovascular silhouette. Pericardial effusion was confirmed by ultrasound.



► Fig. 5.15. Carcinoma of bronchus. A peripheral right upper zone mass is invading and destroying the 3rd rib (arrowhead).



Fig. 5.16. Carcinoma of bronchus. CT shows an enlarged pretracheal node (arrow) secondary to a carcinoma of the bronchus. An aortic aneurysm is also present.

*isotope bone scan* and *liver ultrasound* should be performed and, if the tumor still appears operable, the mediastinum should be assessed by *CT*. Any node over 2 cm in diameter is likely to be involved (Fig. 5.16), and nodes of 1 cm or less are usually regarded as normal. Nodes between 1 and 2 cm present a diagnostic problem and *mediastinoscopy* may be indicated prior to thoracotomy.

**Assessing Treatment.** The post-operative patient and changes due to radiotherapy are discussed in Chap. 9. Patients with oat cell tumor may show complete regression of disease following chemotherapy, but follow-up chest radiographs are necessary to detect local recurrence. However, recurrent disease may occur extrathoracically. In addition, these patients may develop opportunistic infections.

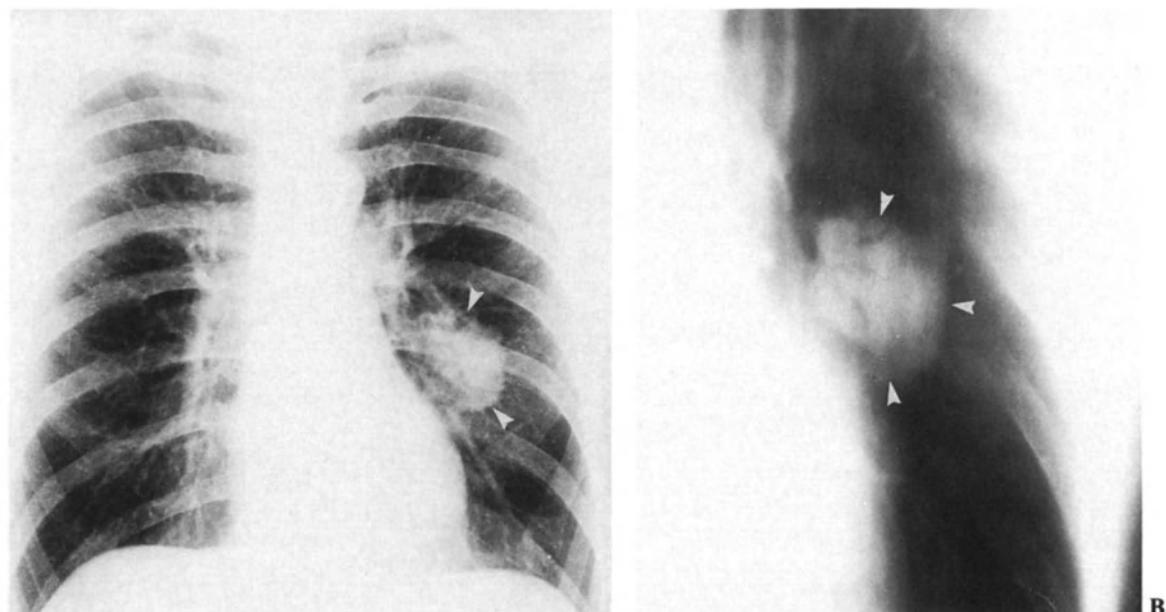
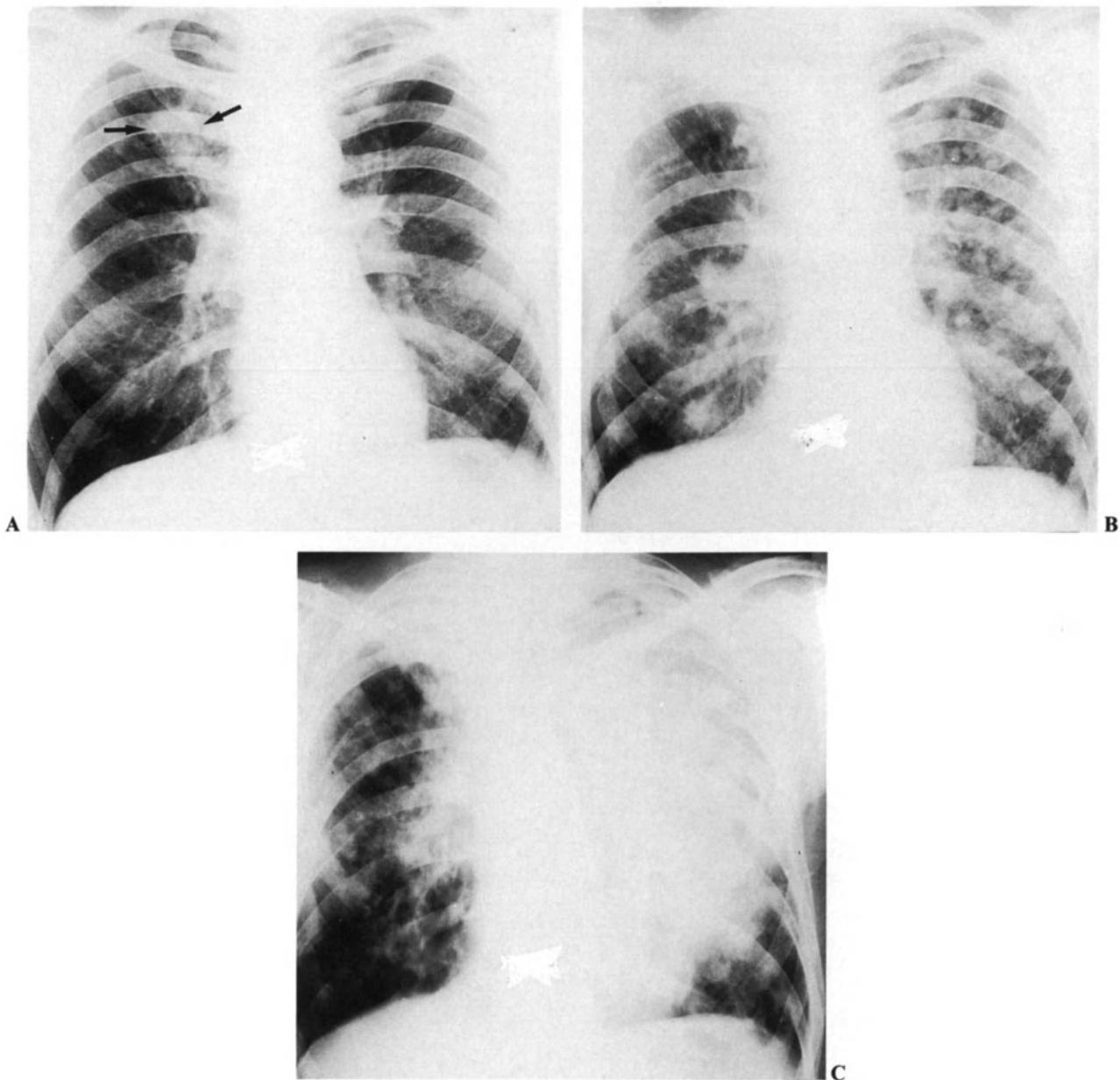


Fig. 5.17A, B. Alveolar cell carcinoma. A A solitary mass (arrowheads) is present in the left mid zone. B Tomogram demonstrates an air bronchogram within the mass (arrowheads).



**Fig. 5.18A, B, C.** Alveolar cell carcinoma. A A solitary mass (arrows) is present in the right upper zone. A right upper lobectomy was performed. B 5 months later multiple nodular opacities are present in both lungs. C 3 months later confluent areas of consolidation have developed.

#### ALVEOLAR CELL CARCINOMA

Alveolar cell, bronchiolar or bronchiolo-alveolar carcinoma accounts for 1%–2% of cases of lung cancer. These tumors arise peripherally in the alveoli and produce areas of consolidation. It is controversial whether they originate multicentrically or focally, and clinically there are two patterns. The focal form appears as a solitary mass which, unlike other types of lung cancer, may show an air bronchogram (Fig. 5.17). The diffuse form produces multiple acinar shadows throughout both lungs, often with areas of confluence. The local form may progress to the diffuse pattern by tumor spreading via the airways (Fig. 5.18).

#### METASTATIC LUNG DISEASE

The lungs are a common site of metastatic disease. Most pulmonary metastases are hematogenous, and although they may originate anywhere, 80% are from primary tumors of the breast, urogenital system and skeleton. In approximately 75% of cases pulmonary metastases are multiple. They are usually bilateral, both lungs being equally involved with a basal predominance (Fig. 5.19). They are often peripheral (Fig. 5.20). Approximately 3% of asymptomatic solitary pulmonary nodules are metastases, the commonest primary sites being carcinomas of the colon, kidney, testicle and breast, bone sarcomas and melanoma.

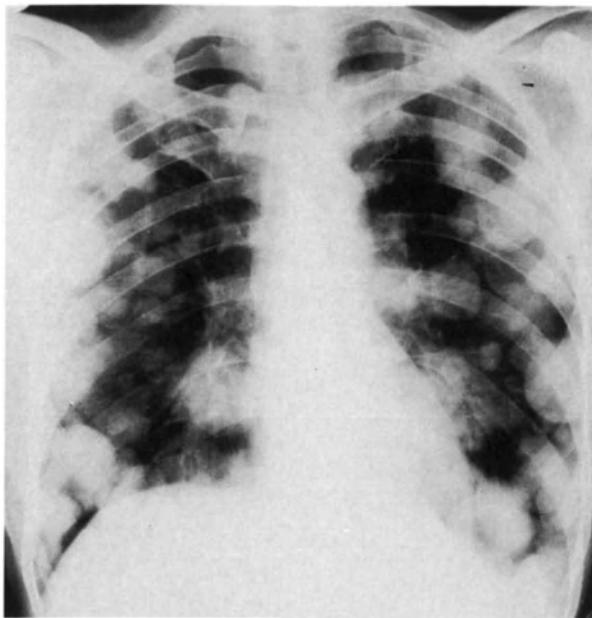


Fig. 5.19. Pulmonary metastases. Teratoma of testis. Multiple, well-defined round opacities are present throughout both lungs.

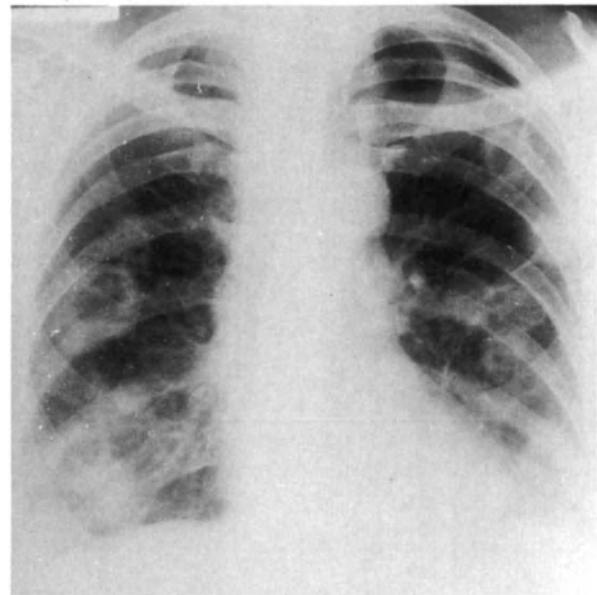
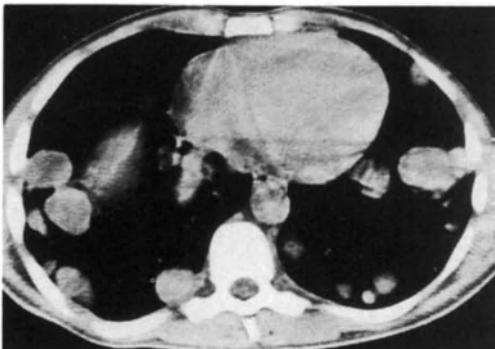
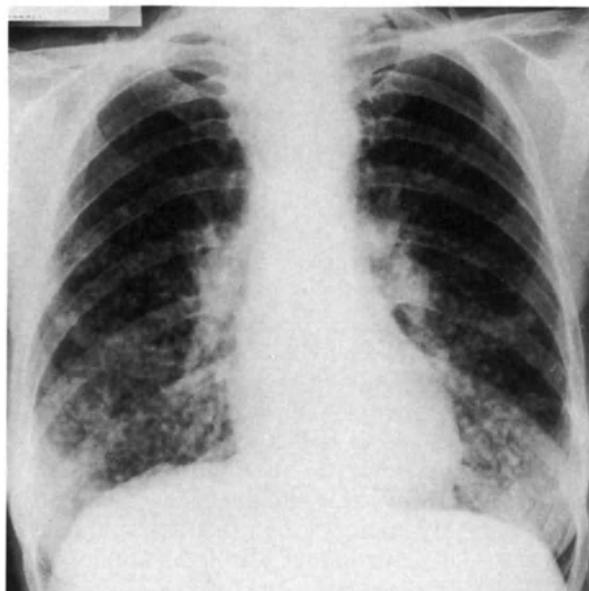


Fig. 5.22. Pulmonary metastases. Carcinoma of tongue. Several cavitating masses are present in both lungs.



◀ Fig. 5.20. Pulmonary metastases. Teratoma of testis. Several of the metastases are subpleural.



◀ Fig. 5.21. Pulmonary metastases. Adenocarcinoma. Multiple small nodules are distributed throughout both lungs.

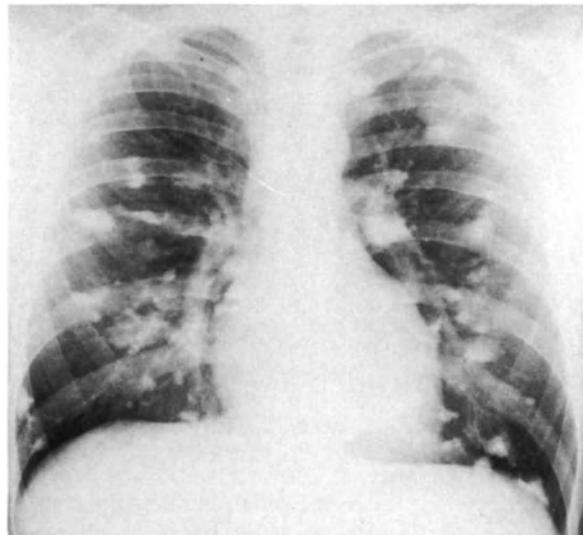
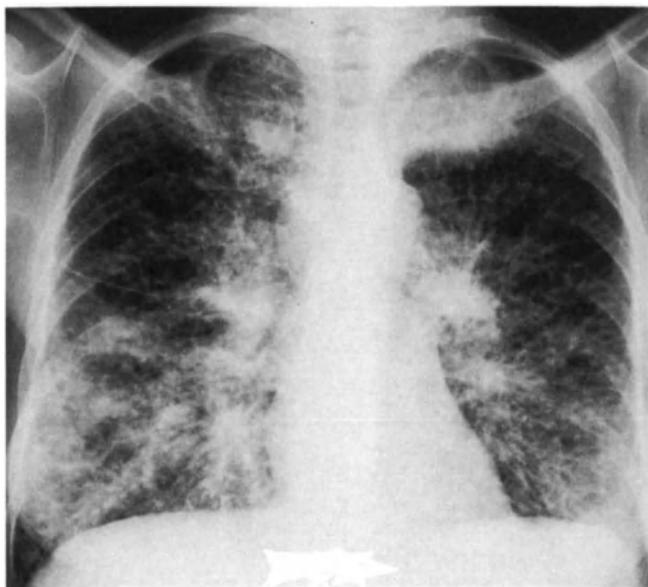
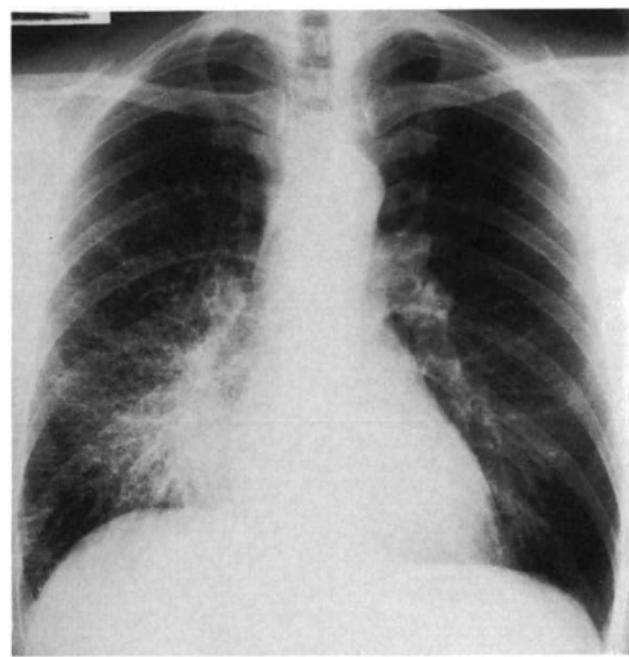


Fig. 5.23. Pulmonary metastases. Osteogenic sarcoma. Many of the metastases are ossified.



**Fig. 5.24.** Lymphangitis carcinomatosa. Carcinoma of cervix. Coarse, reticulonodular shadowing is present throughout both lungs, with a basal predominance. There is hilar lymphadenopathy.



**Fig. 5.25.** Lymphangitis carcinomatosa. Carcinoma of bronchus. Coarse reticulonodular shadowing extends from a right hilar mass into the right mid and lower zones. Interstitial lines are visible peripherally.

Pulmonary metastases tend to be spherical, with a well-defined edge and may vary from a few millimeters (Fig. 5.21) to several centimeters in diameter.

Cavitation may occur (Fig. 5.22), most often in squamous cell metastases and sarcomas, and cavitation of a subpleural metastasis is a rare cause of spontaneous pneumothorax.

Calcification is rare, usually being seen in metastatic osteo-

genic sarcoma (Fig. 5.23), and less often in chondrosarcoma and mucinous carcinomas.

Endobronchial metastases are rare, the commonest primary tumors being carcinoma of kidney, breast or large bowel. Occlusion of the airway may cause segmental or lobar collapse.

*Lymphangitis carcinomatosa* results from hematogenous

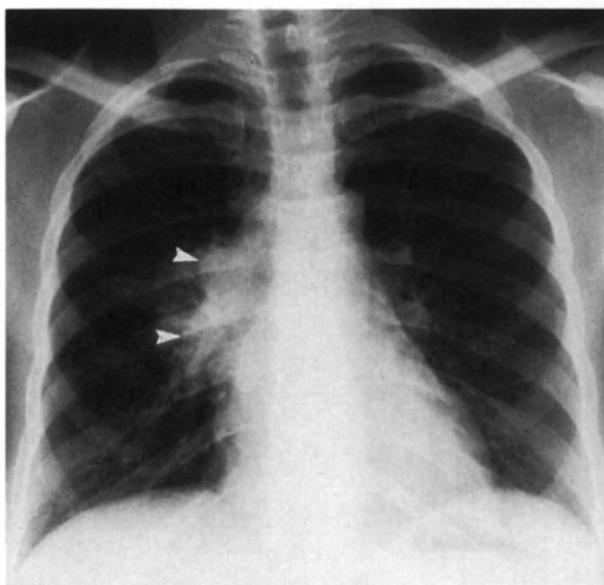
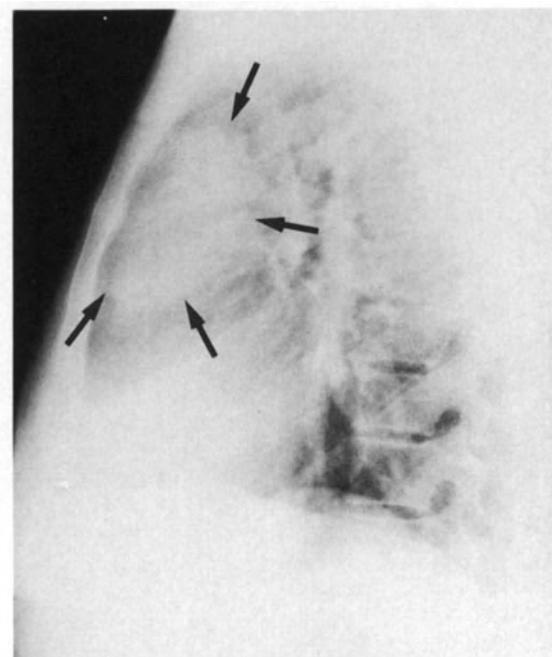


**Fig. 5.26A, B.** Hodgkin's disease. Right hilar adenopathy (arrowheads) is visible on the PA film, and a large retrosternal mass (arrows) is seen on the lateral film.



B

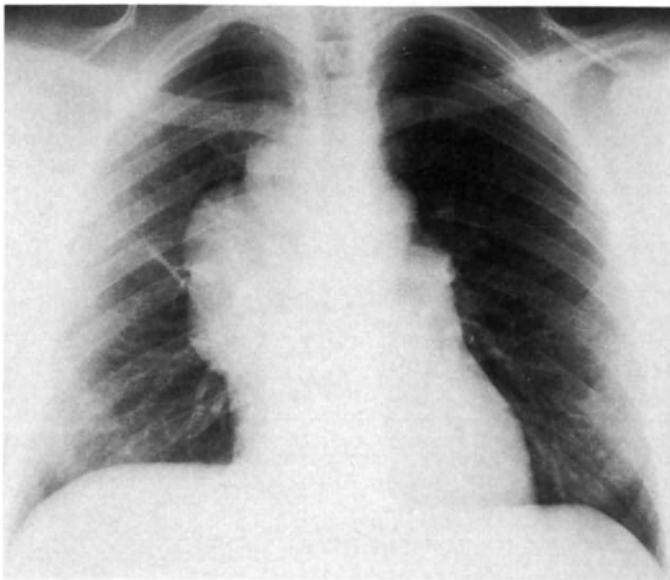


Fig. 5.27. Hodgkin's disease. There is asymmetric paratracheal and hilar lymphadenopathy.



Fig. 5.29. Histiocytic lymphoma. There are multiple pulmonary nodules and extensive mediastinal lymphadenopathy.

metastases invading and occluding peripheral pulmonary lymphatics. The commonest primary tumors are carcinoma of the lung, breast, stomach, pancreas, cervix and prostate. Lymphangitis carcinomatosa is usually bilateral (Fig. 5.24), but lung and breast tumors may cause unilateral lymphangitis (Fig. 5.25). The chest radiograph shows coarse, linear, reticular and nodular basal shadowing, often with plural effusions and hilar lymphadenopathy.

#### INTRATHORACIC LYMPHOMA AND LEUKEMIA

##### Hodgkin's Disease

Hodgkin's disease is the commonest lymphoma and the commonest malignant neoplasm of young adults. The disease usually arises in lymph nodes and hilar or mediastinal lymphadenopathy is visible on the chest film in approximately 50% of patients at first presentation (Fig. 5.26). CT may

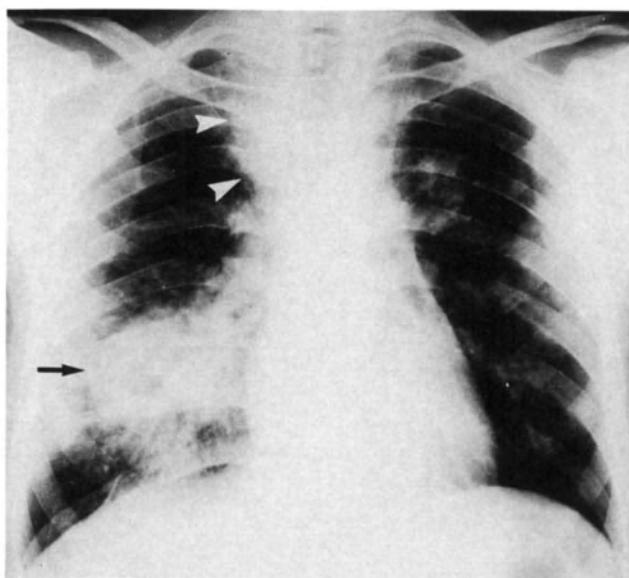
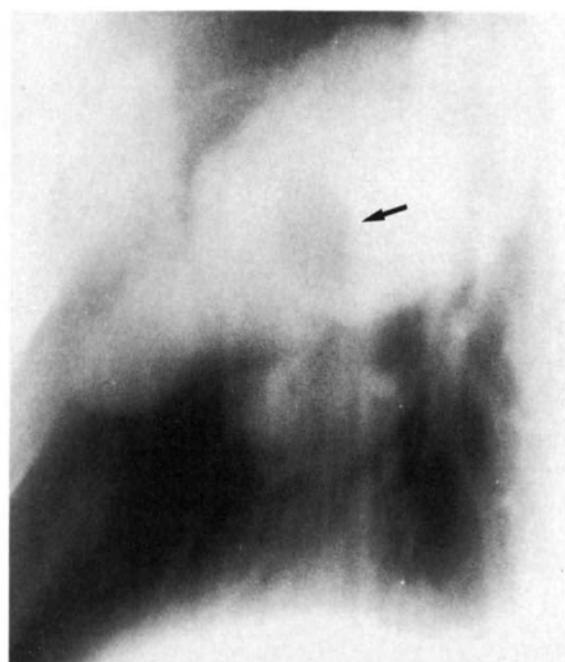
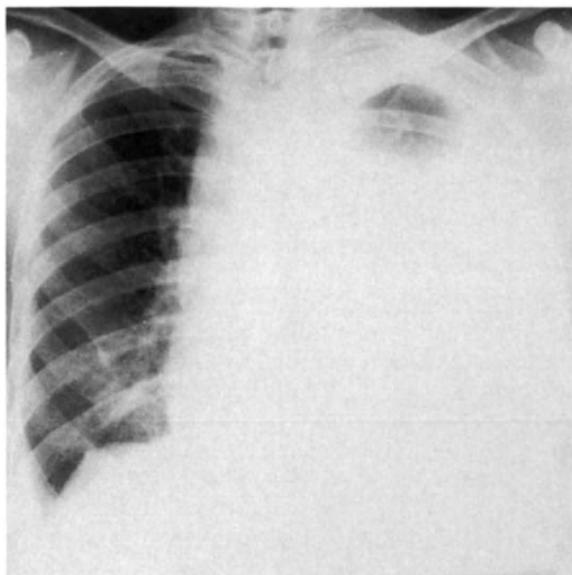


Fig. 5.28A, B. Hodgkin's disease. A Chest radiograph shows right paratracheal lymphadenopathy (arrowheads) and pulmonary consolidation (arrow). B Tomograph demonstrates cavitation (arrow) in the right lower lobe.



B



**Fig. 5.30.** Well-differentiated lymphocytic lymphoma. Small right and large left pleural effusions are present.

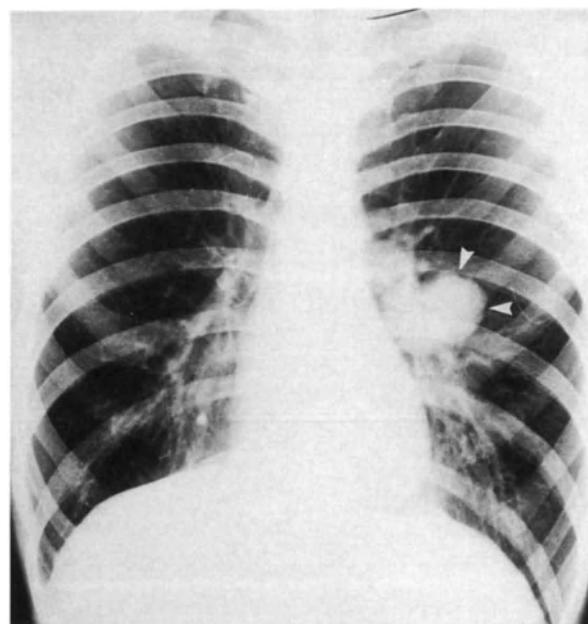


**Fig. 5.32.** Carcinoid tumor. A round mass (*arrowheads*) lies close to the left hilum.

identify lymphadenopathy not apparent on the chest film, particularly retrosternally and paraspinally. Intrathoracic nodal enlargement is typically asymmetric (Fig. 5.27) unlike that seen in sarcoidosis. The nodes sometimes calcify after chemo- or radiotherapy.

Lung involvement is seen in approximately 30% of cases, and is usually due to spread from involved lymph nodes.

Lung involvement without lymph node enlargement is rare in untreated cases. The chest radiograph may resemble that seen lymphangitis carcinomatosa, but other manifestations are solitary or multiple areas of consolidation, larger confluent areas and miliary nodules. The consolidated lung may show an air bronchogram or cavitate (Fig. 5.28). Approximately 30% of cases develop a pleural effusion and pleural plaques may be seen.

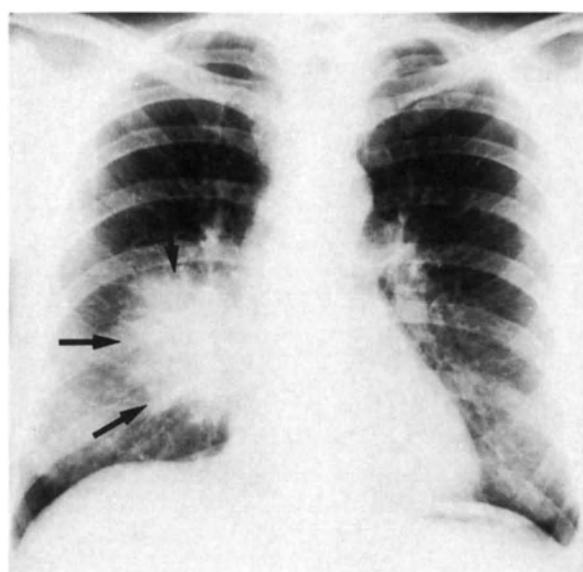


**Fig. 5.31.** Pseudolymphoma. Consolidation (*arrows*) obscures the right hilum.

#### Non-Hodgkin's Lymphoma

This group comprises nodular lymphoma, previously known as giant follicular lymphoma, and diffuse lymphoma, which includes chronic lymphocytic leukemia, lymphosarcoma and reticulum cell sarcoma or diffuse histiocytic lymphoma. The radiographic manifestations are similar to Hodgkin's disease (Fig. 5.29) although pulmonary or pleural involvement in the absence of lymph node enlargement (Fig. 5.30) is more frequently seen.

#### Leukemia

Abnormalities seen on chest films of leukemic patients are more likely to be due to a complication of leukemia, than to the disease itself. These include pneumonia, opportunistic infection, heart failure, pulmonary hemorrhage and reactions to drugs, radiotherapy or transfusion.

Mediastinal lymphadenopathy is rarely seen without evidence of lymphadenopathy elsewhere. Pleural effusions may sometimes be seen. Leukemic infiltration of the lung, which appears as bilateral streaking, reticular shadowing or patchy consolidation is usually a terminal event.

### Pseudo-lymphoma, Lymphoid Interstitial Pneumonia and Benign Lymph Node Hyperplasia

These conditions are characterized by collections of mature lymphocytes, and each may produce abnormalities on the chest film. Whether they are neoplastic or inflammatory is debatable, but they behave benignly and are not associated with extrathoracic abnormalities.

*Pseudo-lymphoma* presents as an area of localized pulmonary consolidation without adenopathy or pleural disease (Fig. 5.31).

*Lymphoid interstitial pneumonia* (LIP) causes multiple areas of consolidation and may progress to diffuse interstitial fibrosis.

*Benign lymph node hyperplasia* or *Castleman's disease* presents as an asymptomatic hilar or mediastinal mass.

### BRONCHIAL ADENOMA

Carcinoid tumors account for approximately 90% of bronchial adenomas. The remaining 10% are salivary gland type tumors.

*Bronchial Carcinoid Tumors.* 20% of bronchial carcinoid tumors are peripheral and present as well-defined round or ovoid solitary nodules (Fig. 5.32). 80% of bronchial carcinoid tumors arise centrally in lobar or segmental bronchi. They cause bronchial obstruction often leading to collapse of the lung peripheral to the tumor (Fig. 5.33). Other presentations include recurrent segmental or lobar infection, bronchiectasis, abscess formation and air trapping.

The tumor may also be locally invasive and approximately 5% of bronchial carcinoid tumors metastasize. Skeletal

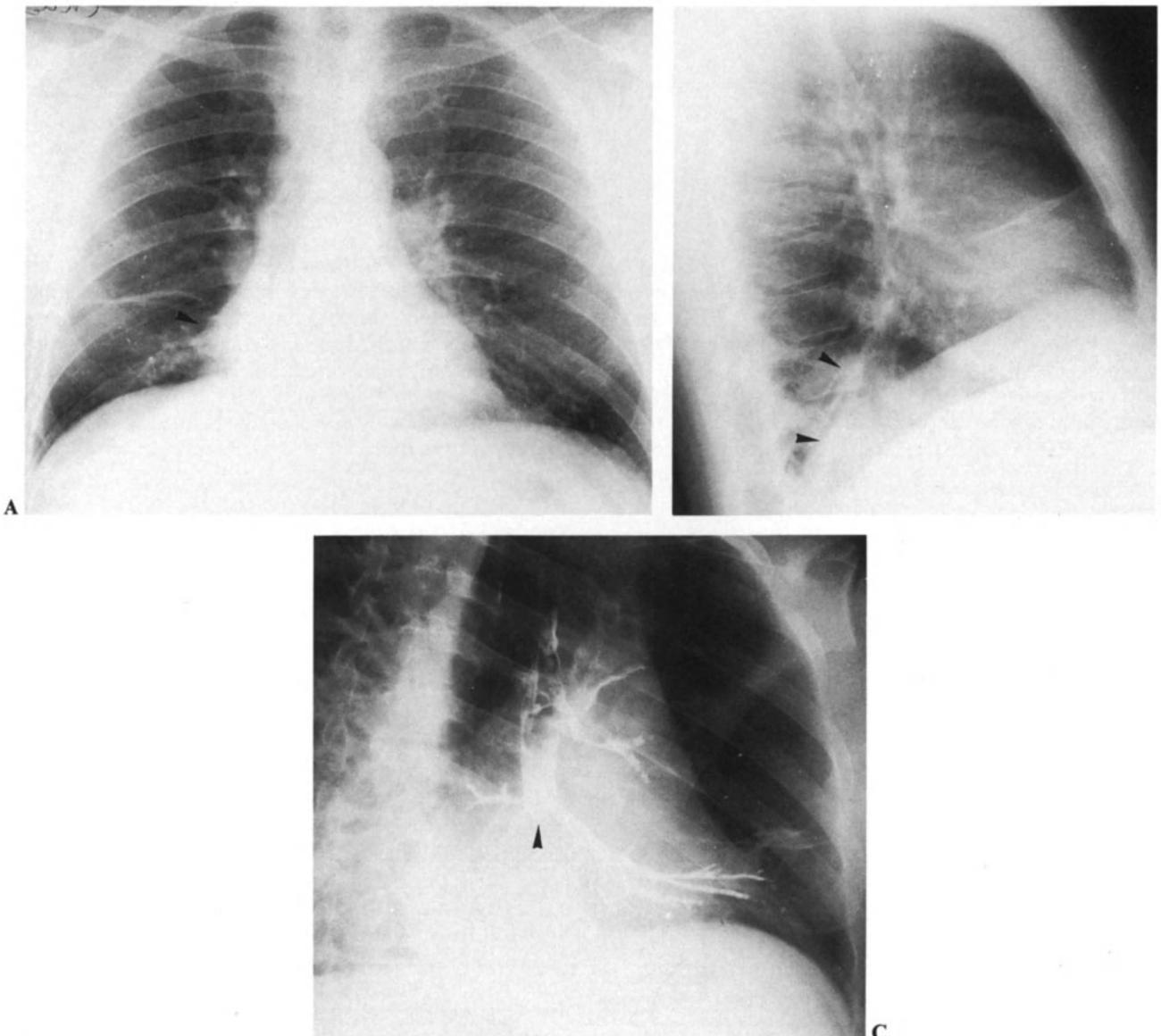
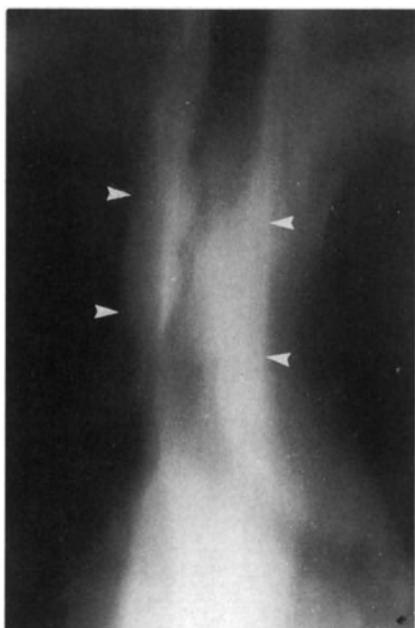


Fig. 5.33A, B, C. Carcinoid tumor. A, B Consolidation (arrowheads) is present in the posterior basal segment of the right lower lobe. C Bronchogram demonstrates occlusion (arrowhead) of right lower lobe bronchus by tumor.



**Fig. 5.34.** Cylindroma. Tomogram shows soft tissue mass (arrowheads) infiltrating and narrowing trachea.

metastases are often osteoblastic. Carcinoid tumors may produce a variety of hormones such as histamine, serotonin, kallikrein, insulin, ACTH, ADH and gastrin. Rarely, these may produce symptoms such as the carcinoid syndrome.

*Salivary Gland Type Tumors.* These are mostly cylindromas. Cylindromas usually arise in the trachea or major bronchi, and extend under the bronchial epithelium into the bronchial wall. Local invasion is common. They present radiologically as a tumor mass (Fig. 5.34) with or without airway obstruction.

#### PULMONARY HAMARTOMA

Most pulmonary hamartomas have a large cartilaginous component. They are rarely seen in childhood and most often present as a solitary pulmonary nodule in an asymptomatic adult. Unlike bronchial adenomas, most pulmonary hamartomas are peripheral. They appear as well-circumscribed nodules varying in diameter from a few millimeters to several centimeters. Approximately 30% show calcification often with a characteristic 'pop corn' appearance (Fig. 5.35). On serial films they may be seen to grow slowly.

Diffuse overgrowth of pulmonary smooth muscle may be seen in *tuberous sclerosis* producing a 'honeycomb' shadowing in the lungs, in association with hamartomas in other organs.

Localized overgrowth of smooth muscle with varying amounts of fibrous tissue causes pulmonary *leiomyomas* and *fibroleiomyomas*. They are usually peripheral, and if multiple may be difficult to distinguish both radiographically and histologically from *metastatic uterine fibroleiomyosarcoma*.

#### OTHER PULMONARY NEOPLASMS

It is not proposed to describe the individual tumors listed as rare and very rare in Table 5.1. None of them have characteristic radiographic appearances. Most may present as a solitary pulmonary nodule and some may be multiple. Many may cause bronchial occlusion and present with signs of lobar or segmental collapse or consolidation. Diagnosis of these tumors is usually made bronchoscopically or by percutaneous needle biopsy.

*For further reading, see p. 134.*

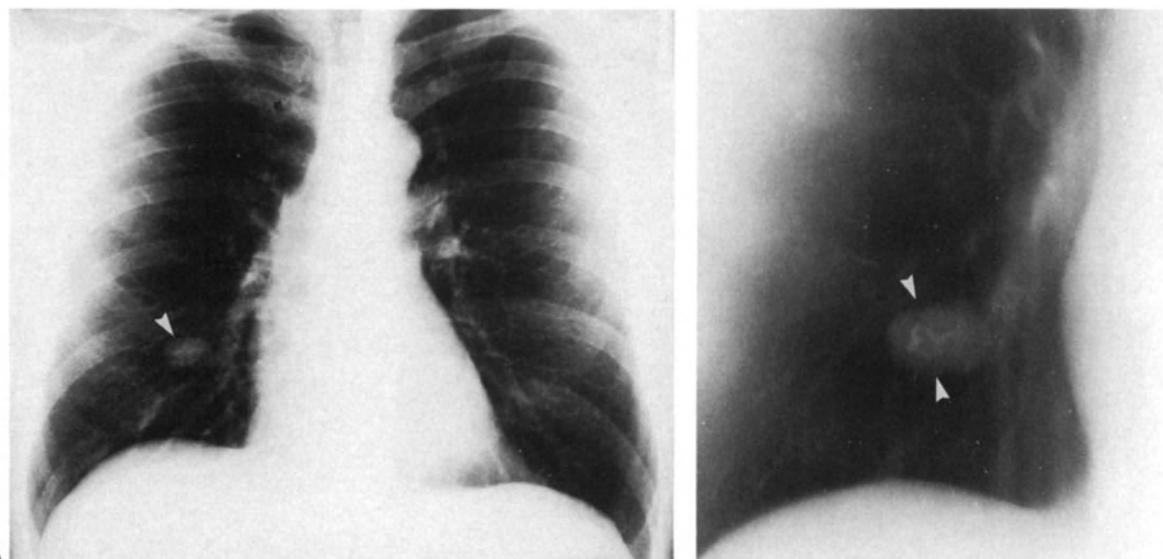


**Fig. 5.35A, B.** Pulmonary hamartoma. A A well-defined, round opacity (arrowhead) is present in the right lower zone. B Tomogram shows the mass to contain central 'pop corn' calcification (arrowheads).

## CHAPTER 6

# DIFFUSE LUNG DISEASE

M. Rubens

Diffuse abnormality of the lungs may be due to infection, neoplasia or a primary abnormality of the airways. In addition, there are many other possibilities and these are discussed in this chapter.

### SARCOIDOSIS

Sarcoidosis is a multisystem disease of unknown etiology. It is characterized by the development of non-caseating granulomas which either resolve or become fibrotic. It may occur at any age but usually presents in young adults. Blacks are 12 times more likely to develop sarcoidosis than whites, and black females are twice as susceptible as black males. Patients most commonly present with erythema nodosum, an abnormal chest radiograph or respiratory symptoms. The diagnosis is usually made by the combination of symptoms, clinical signs and histology. When the chest radiograph is abnormal transbronchial biopsy is usually diagnostic. A Kveim test is occasionally performed to confirm the diagnosis.

#### Radiological Appearances

Sarcoidosis commonly causes *thoracic lymphadenopathy* and *parenchymal lung shadows*. Adenopathy almost always precedes pulmonary shadowing, but they are often present simultaneously. The chest radiograph is abnormal at some time in 90% of patients with sarcoidosis.

Typically there is bilateral, symmetrical hilar enlargement involving both tracheobronchial and bronchopulmonary nodes (Fig. 6.1). Right paratracheal lymphadenopathy is also common, and left paratracheal adenopathy is occasionally seen. Enlargement of other mediastinal nodes is rarely appreciated on the chest radiograph but may be seen on CT. If the hilar adenopathy is very asymmetric or anterior mediastinal adenopathy is a feature, other diagnoses should

be considered. Rarely the involved lymph nodes may calcify, sometimes peripherally, causing '*eggshell*' calcification (Fig. 6.2).

Although virtually all patients with intrathoracic adenopathy due to sarcoid develop pulmonary granulomas histologically, only about half show abnormal parenchymal shadows on the chest radiograph. These shadows are usually bilateral and diffuse. *Small nodular opacities*, 1 to 3 mm in diameter, are the commonest pattern. They may create a

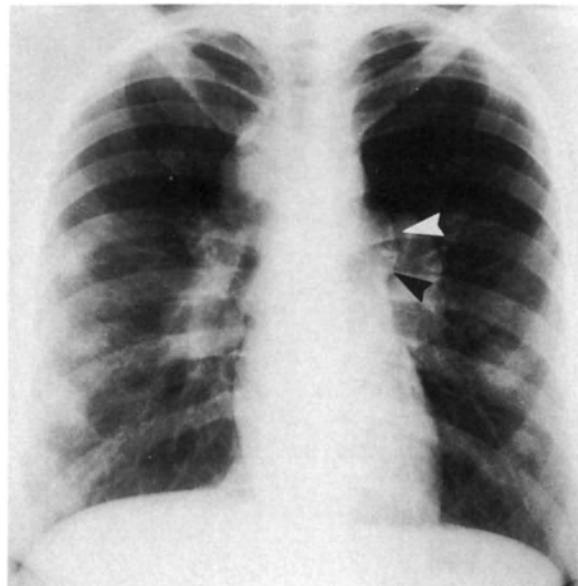
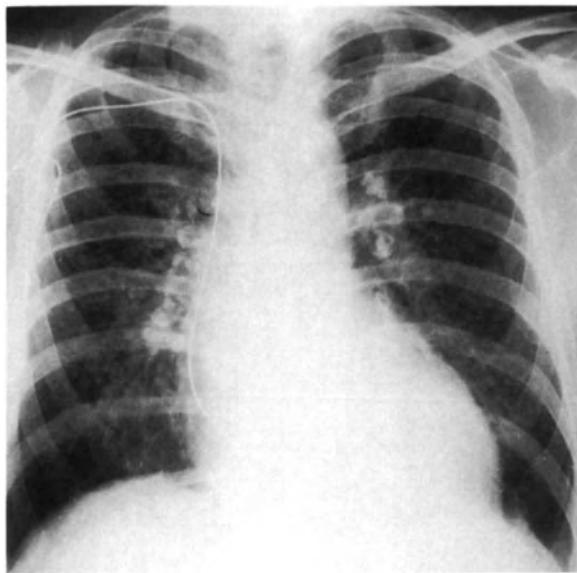
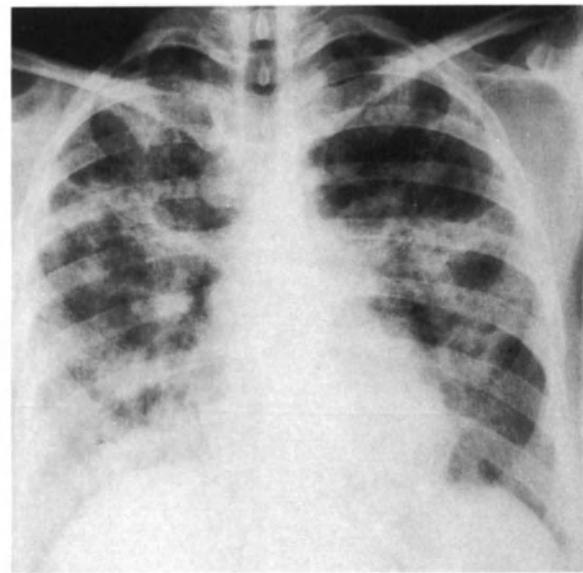


Fig. 6.1. Sarcoidosis. There is bilateral symmetrical hilar lymph node enlargement. There is also enlargement of right paratracheal nodes and nodes in the aorticopulmonary window (arrowheads). Round opacities are present in both lungs.



**Fig. 6.2.** Sarcoidosis. There is bilateral hilar lymph node calcification. Some of the nodes are calcified peripherally ('egg-shell' calcification). A pacing electrode is present. Heart block is an occasional complication of sarcoidosis.



**Fig. 6.4.** Sarcoidosis. There is diffuse pulmonary fibrosis.

fine, granular haziness or appear as miliary shadows (Fig. 6.3). Larger nodules of the order of 1 cm in diameter may be present. They may be well or poorly marginated and may coalesce to form larger opacities (Fig. 6.1). Air bronchograms may be visible, and occasionally these nodules cavitate.

Most cases of parenchymal involvement resolve completely, but approximately one third develop *pulmonary fibrosis*. This tends to involve the mid and upper zones more than the bases. Coarse, linear shadows, ring shadows and

bullae may be seen. Occasionally, confluent, fibrotic areas may develop (Fig. 6.4).

Unusual manifestations of sarcoidosis include basal septal lines, pleural effusion, spontaneous pneumothorax and bronchostenosis. *Gallium-67* is taken up by involved lymph nodes and lung, and has been used to assess the activity and extent of the disease.

#### THE PNEUMOCONIOSES

The pneumoconioses are diseases caused by inhalation of inorganic dusts. The diagnosis depends on a history of exposure to the dust, and an abnormal chest radiograph and respiratory function tests. Dusts may be termed active or inactive. Active dusts are fibrogenic in the lung, and inactive dusts are relatively inert. Inhaled dusts are often a combination of active and inactive materials. The important active dusts are asbestos and silica.

##### Silicosis

Exposure to silica may occur in granite, slate and sandstone quarrying, gold mining, sandblasting and in foundry, ceramic and pottery works. Exposure of several years may lead to pulmonary fibrosis. Fibrosis may continue after exposure has ceased.

**Radiology.** *Simple silicosis* causes multiple, nodular shadows, 2 to 5 mm in diameter (Fig. 6.5). They are most numerous in the mid and upper zones. Linear shadows and septal lines may also appear. In *complicated silicosis* the small nodules become confluent and form homogenous, non-segmental areas of shadowing. This tends to occur in the upper lobes, and the areas of fibrosis may migrate towards the hilum, creating areas of emphysema in the lung periphery. Silicosis predisposes to *pulmonary tuberculosis*. Cavitation in

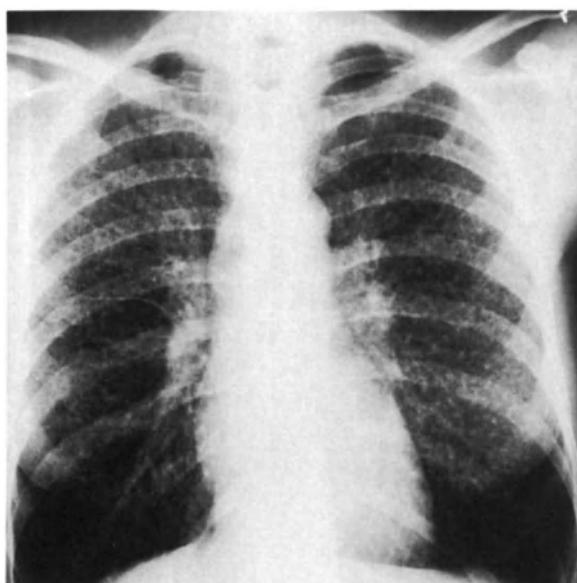


**Fig. 6.3.** Sarcoidosis. Miliary, nodular opacities are present throughout both lungs.



**Fig. 6.5.** Simple silicosis. Multiple, small nodules are present throughout both lungs.

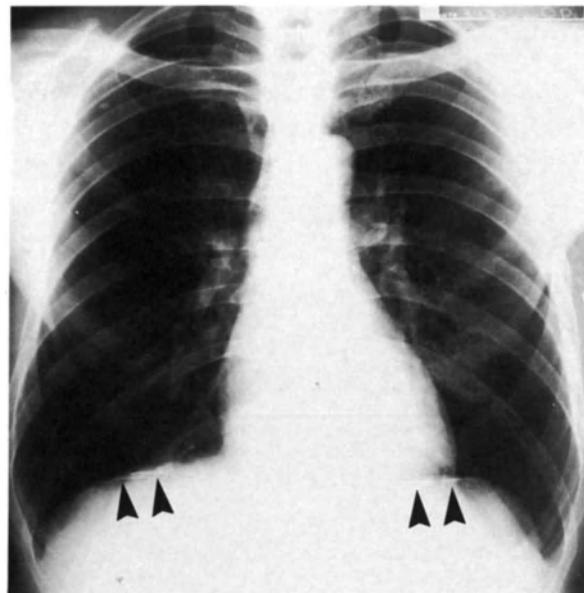


**Fig. 6.7.** Asbestos exposure. Calcified pleural plaques are visible over both domes of the diaphragm (arrowheads).

an area of massive fibrosis is usually due to ischemic necrosis or tuberculosis. Extensive fibrosis may be complicated by pulmonary arterial hypertension and cor pulmonale. Hilar lymphadenopathy is common in silicosis, and the nodes may calcify diffusely or with a peripheral 'eggshell' pattern (Fig. 6.6). Patients with silicosis and rheumatoid disease may develop *Caplan's syndrome*.

#### Asbestosis

Asbestosis exposure may occur in asbestos mining and processing, in construction and demolition work, ship building



**Fig. 6.6.** Silicosis. There is bilateral hilar lymphadenopathy. Many of the nodes are calcified, some of them peripherally. There is also basal emphysema.

and in the manufacture of some textiles. Manifestations of exposure may not become apparent for many years.

Asbestos is a mixture of silicates, which may produce pulmonary fibrosis (asbestosis) and pleural thickening and calcification. The fibrosis is probably the result of physical and chemical irritation in addition to an autoimmune mechanism. Malignant diseases which may complicate asbestosis are *adenocarcinoma* and *squamous carcinoma of the lung*, *carcinomas of the esophagus, larynx and oropharynx* and *mesothelioma of the pleura*.

Pleural plaques develop bilaterally. They tend to occur in the mid zones and over the diaphragm (Fig. 6.7). Small plaques may be difficult to see on the standard chest radiograph, but may be demonstrated with oblique views, preferably aided by *fluoroscopy*, or by *ultrasound* or *CT* (Fig. 6.8). The plaques often calcify and may produce bizarre opacities, sometimes resembling holly leaves (Fig. 6.9). Small pleural effusions may occasionally occur, unrelated to malignancy, but large effusions suggest an underlying carcinoma or mesothelioma.

Pulmonary fibrosis may be seen with or without pleural changes. In the early stages *CT* is more sensitive than the chest radiograph in identifying asbestosis (Fig. 6.8). The earliest signs are a fine reticular (Fig. 6.10) or nodular pattern in the lower zones. With progression this becomes coarser and causes loss of clarity of the diaphragm and cardiac shadow – the so-called '*shaggy heart*'. Eventually the whole lung may become involved, but the basal preponderance persists and areas of emphysema may develop.

#### Coal Worker's Pneumoconiosis

Coal dust is mostly carbon, but it may contain silica. Coal workers are prone to coal worker's pneumoconiosis, silicosis, chronic bronchitis and emphysema. As in silicosis, simple

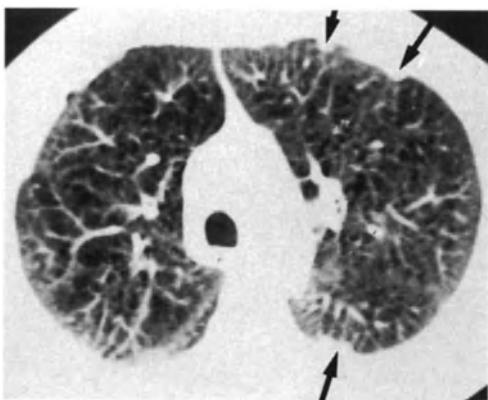


**Fig. 6.8.** Asbestosis with pleural plaques shown by CT. Small pleural plaques (arrowheads) are present. In addition, there is diffuse reticular pulmonary shadowing indicating pulmonary fibrosis. The pulmonary changes were not apparent on the chest radiograph.

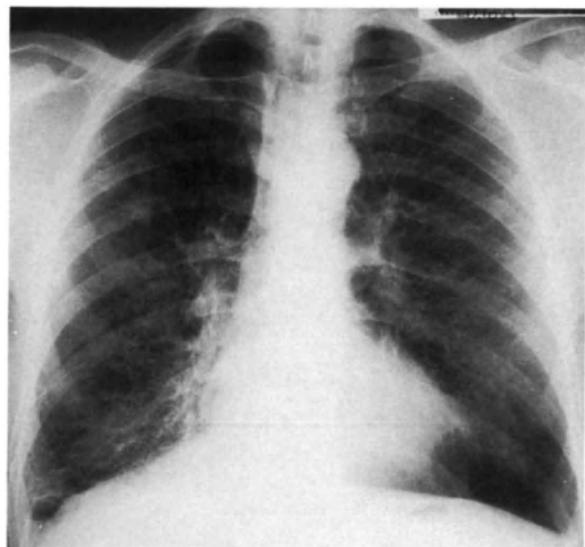


**Fig. 6.10.** Asbestosis. Fine reticulonodular shadowing in the mid and lower zones is best seen on the right. Bullous disease is present at the left base.

pneumoconiosis may progress to a complicated variety with the development of *progressive massive fibrosis* (PMF).

In the *simple pneumoconiosis*, small, faint, indistinct nodules, 1–5 mm in diameter, appear in the mid zones. Eventually nodules may be seen throughout the lungs, but remaining most numerous in the mid zones. The development of PMF is marked by coalescence of the small nodules or the appearance of larger opacities of 1 cm diameter or

more (Fig. 6.11). Areas of massive fibrosis are usually mid or upper zone and bilateral; they are round or oval and tend to migrate towards the hila creating peripheral areas of emphysema and bullae. The fibrotic masses may calcify or cavitate (Fig. 6.12).

Patients with rheumatoid disease and coal worker's pneumoconiosis may develop Caplan's syndrome. Multiple, round, well-defined opacities, 1–5 cm in diameter, may appear in the lungs. They represent fibrotic nodules, but if the underlying pneumoconiosis is not appreciated they may be misdiagnosed as metastases.

#### Other Pneumoconioses

*Chronic berylliosis* is a systemic disease characterized by widespread non-cavitating granulomas. The thoracic radiological manifestations are identical to sarcoidosis.

Iron oxide, tin oxide and barium sulphate all produce inactive dusts that may cause dense, diffuse, nodular shadowing on the chest radiograph simply by accumulating in the lungs. These conditions are known as *siderosis*, *stannosis* and *barytosis* respectively.

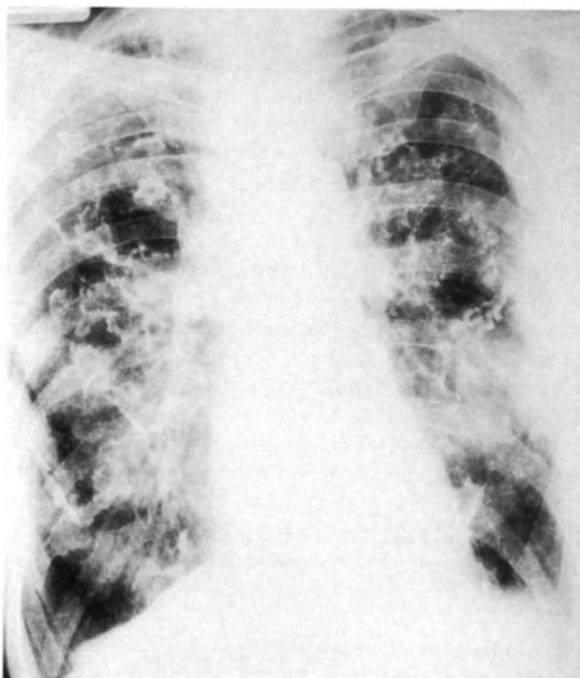


**Fig. 6.9.** Asbestos exposure. Multiple calcified pleural plaques are present bilaterally.

#### ASPIRATION AND INHALATION

Aspiration of liquid or solid material into the airways may cause mechanical obstruction, and depending on the nature of the aspirate, a variable amount of inflammation.

*Mendelson's syndrome* is due to aspiration of acid gastric contents by the anesthetized patient. Intense bronchospasm is followed by a chemical pneumonitis. The chest radiograph shows widespread pulmonary edema. Similar changes are seen in patients after near-drowning.

*Lipoid pneumonia* is due to aspiration of mineral oil, which is usually being taken for chronic constipation. Aspirated oil tends to collect in the dependent parts of the lungs where

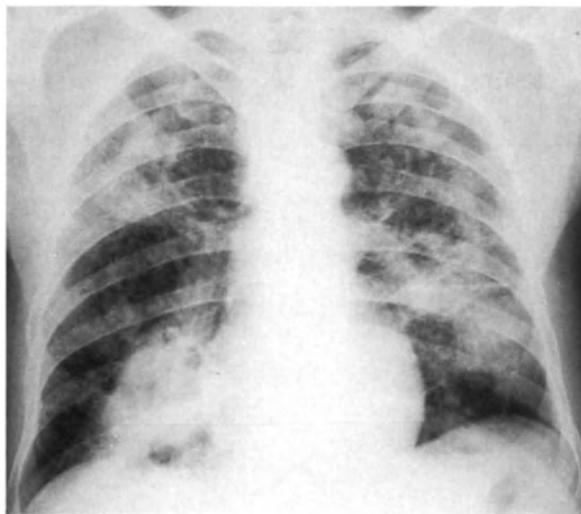


**Fig. 6.11.** Coal Worker's pneumoconiosis with PMF. Small nodular opacities in the mid and upper zones are typical of the simple pneumoconiosis, but in addition there are larger, confluent areas of shadowing indicating progressive massive fibrosis.

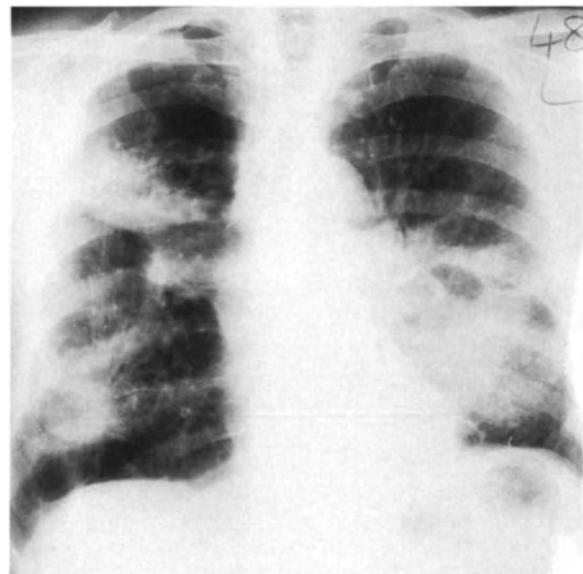


**Fig. 6.13.** Lipoid pneumonia. Large opacities are present in both lungs, representing areas of fibrosis. This patient had achalasia of the cardia, and took liquid paraffin for chronic constipation.

it causes a chronic inflammatory response. The chest radiograph usually shows large, dense, tumor-like opacities (Fig. 6.13).

*Petrol or paraffin aspiration* may cause a pneumonitis, which is usually basal. This may be followed by the development of pneumatoceles.

*Inhalation of irritant gases* such as chlorine, ammonia and oxides of nitrogen may produce pulmonary edema followed by obliterative bronchiolitis.

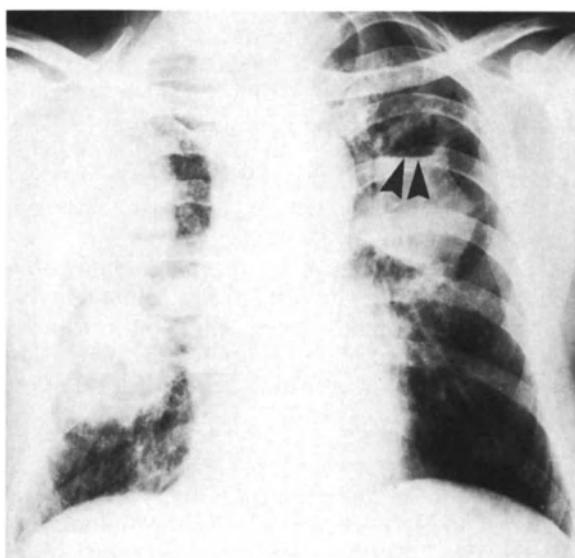


**Fig. 6.12.** Coal Worker's pneumoconiosis with PMF. Large, conglomerate masses are present in both lungs. A fluid level (arrowheads) is present in the left-sided mass which has cavitated.

*Oxygen toxicity* may occur following prolonged administration of oxygen in concentrations above 50%. Damage to the alveolar epithelium causes pulmonary edema followed by interstitial fibrosis.

#### EXTRINSIC ALLERGIC ALVEOLITIS

The inhalation of dusts containing certain organisms or proteins in particles small enough to reach the alveoli may, in sensitized individuals, produce a Type III allergic reaction. Typically the patient develops headache, fever, chills, a cough and dyspnoea 5 or 6 hours after exposure, although with smaller and more frequent exposure to the antigen there may be only progressive dyspnea. This syndrome is known as *extrinsic allergic alveolitis* or *hypersensitivity pneumonitis*.

A wide variety of dusts may be responsible. The commoner syndromes include *farmer's lung* (from mouldy hay), *bird fancier's lung* (from dried droppings or feathers), *mushroom worker's lung* (from compost), *humidifier pneumonitis* (from air-conditioning units) and *bagassosis* (from mouldy sugar cane residue).

#### Radiological Appearances

The chest radiograph may be normal, but may show diffuse fine nodular opacities or a generalized, 'ground-glass' haze (Fig. 6.14). Patchy consolidation and septal lines, similar to pulmonary edema, may also be seen in acute attacks. With repeated episodes, pulmonary fibrosis may develop. Reticulonodular shadows may progress to coarse linear opacities, typically in the mid and upper zones. Finally, severe contraction of the upper lobes with 'honeycombing', cyst formation and bronchiectasis may occur.

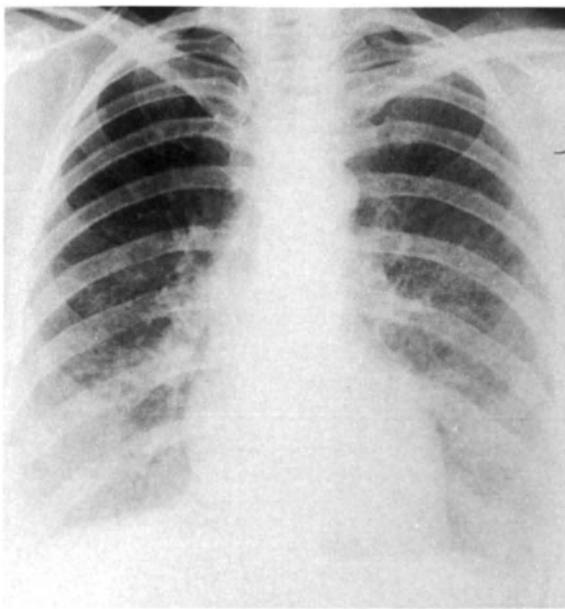


**Fig. 6.14.** Extrinsic allergic alveolitis. Fine, nodular shadowing produces a 'ground-glass' haze throughout both lungs on the chest radiograph of this bird fancier.

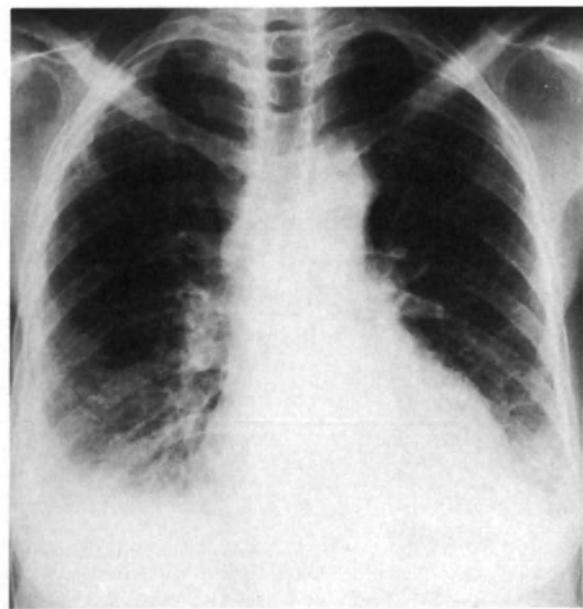


**Fig. 6.15.** Systemic lupus erythematosus. Bilateral pleural effusions are present.

## CONNECTIVE TISSUE DISEASES

This group of conditions, also known as the collagen vascular diseases, comprises a number of chronic inflammatory, autoimmune disorders. They may involve any tissue in any part of the body; joints, serous membranes and blood vessels are frequently involved, and all connective tissue diseases involve the lungs and pleura to some extent. The acute inflammatory episodes characteristically lead to fibrosis and collagen production. While many patients show clinical or radiological features that allow the diagnosis of a specific connective tissue disorder, some patients exhibit signs of more than one of the conditions. Consequently it is not always possible to make a precise diagnosis.

### Systemic Lupus Erythematosus (SLE)

SLE is typically a disease of young women, and blacks are affected more frequently than whites. The lungs or pleura are involved in approximately 50% of cases.

Pleuritic pain with a small *pleural effusion* is a common manifestation, and may occur bilaterally (Fig. 6.15). Movement of the diaphragm is decreased secondary to the pleurisy and may cause areas of *atelectasis* in the lower lobes. This may produce bilateral, horizontal basal band shadows and elevation of the diaphragm on the chest radiograph.

*Patchy consolidation*, sometimes with cavitation, may be seen, and is most often due to infection, pulmonary edema or pulmonary infarction. Lupus pneumonitis is a much less common cause. Rarely, *fibrosing alveolitis* may occur.

*Enlargement of the cardiac shadow* may be due to pericardial effusion, myocarditis or endocarditis, and should be investigated by cardiac ultrasound in the first instance.

### Rheumatoid Disease

Rheumatoid disease may cause pleural effusions, pulmonary nodules, fibrosing alveolitis and bronchiolitis obliterans. These occur more often in males than females.

*Pleural effusion*, which may be unilateral or bilateral, is usually larger than in SLE and is often asymptomatic. Rheumatoid pleural effusions often become chronic but may resolve with pleural fibrosis.

*Rheumatoid pulmonary nodules* are uncommon. These necrobiotic nodules are usually associated with subcutaneous nodules, and are similar histologically. They produce well-defined, round opacities up to 7 cm in diameter and may be single or multiple. They may appear and resolve spontaneously, and may also cavitate (Fig. 6.16).

*Fibrosing alveolitis* due to rheumatoid disease is infrequently apparent on the chest radiograph. It usually produces basal reticulonodular shadowing, but may progress to honey-combing and severe volume loss.

*Caplan's syndrome* may result from the combination of rheumatoid disease and silicosis. Crops of pulmonary nodules up to 5 cm in diameter may appear, superimposed on a background of simple silicosis. These are fibrotic nodules rather than necrobiotic nodules and may calcify (Fig. 6.17).

### Systemic Sclerosis

*Fibrosing alveolitis* commonly occurs in systemic sclerosis, although usually it is not radiologically apparent until a relatively late stage. As in other conditions with fibrosing alveolitis, the usual appearance is basal reticulonodular shadowing, with progressive pulmonary volume loss (Fig. 6.18).

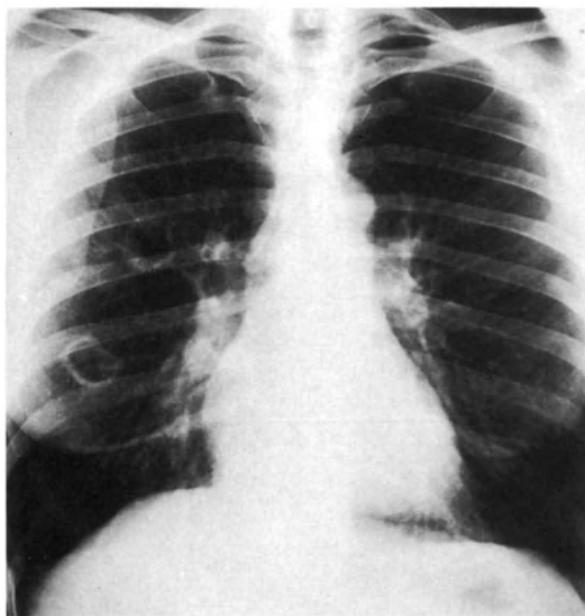


**Fig. 6.16.** Rheumatoid disease. Two cavitating necrobiotic nodules are visible in the right lung.

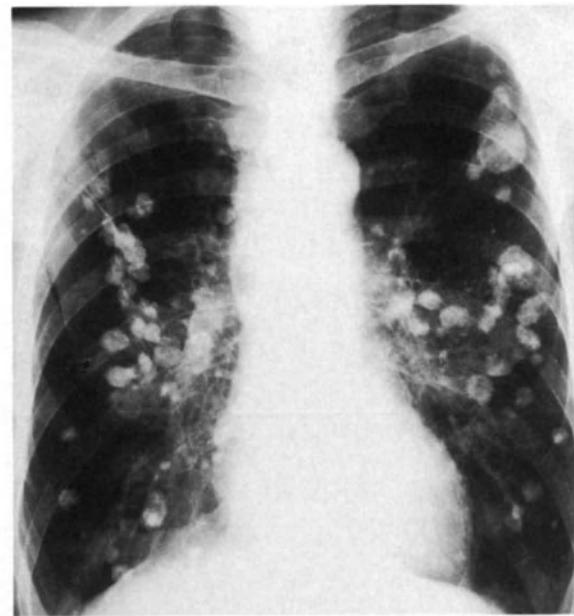


**Fig. 6.17.** Caplan's syndrome. Multiple, calcified nodules are present in both lungs.

Associated pleural disease is rare. There is a predisposition to *lung cancer*, particularly alveolar cell carcinoma.

*Esophageal involvement* may cause aspiration pneumonitis, and the dilated air-filled esophagus may be visible on the chest radiograph.

#### Systemic Vasculitides

*Wegener's Granulomatosis.* Classical Wegener's granulomatosis is a necrotizing vasculitis which involves the upper

respiratory tract, the lungs and the kidneys. There is a limited variant which is more or less confined to the thorax.

Single or multiple granulomatous masses up to several centimeters in diameter may be seen on the chest radiograph (Fig. 6.19). These masses are fairly well defined and often cavitate; they may resolve spontaneously, while new masses appear. Granulomas may also develop in the trachea or bronchi and cause pulmonary collapse. Occasionally pleural effusions develop, and reactive hilar or mediastinal lymphadenopathy may be seen.

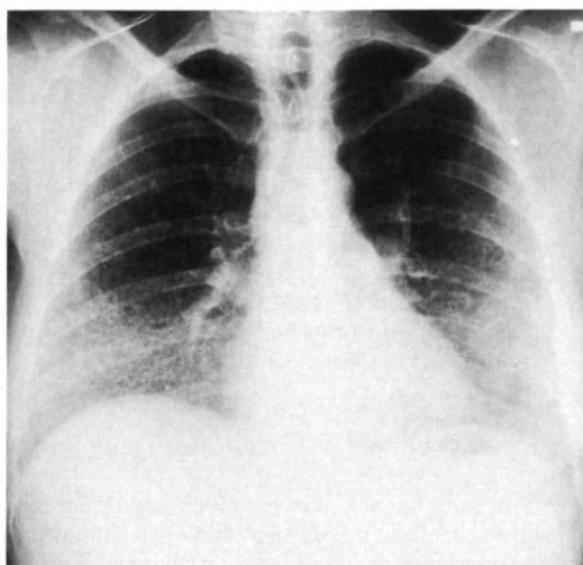


**Fig. 6.18A, B.** Systemic sclerosis. Fine reticulonodular shadowing is present in both lower zones, particularly well seen in the lateral film. Note air in the upper esophagus (arrowheads).



**Fig. 6.19.** Wegener's granulomatosis. Masses are visible in both lungs. The left upper zone mass is cavitating.

**Polyarteritis Nodosa (PAN).** Classic PAN is a vasculitis of medium sized arteries which involves the kidneys and liver more often than the lungs. PAN may be associated with eosinophilia, and may present as asthma with transient pulmonary opacities. Pulmonary edema may occur secondary to cardiac or renal failure, and areas of consolidation may be due to pulmonary hemorrhage.

**Other Vasculitides.** Churg-Strauss disease is a systemic vasculitis similar to PAN, but always involves the lungs. The patients are usually asthmatic.

Lymphomatoid granulomatosis is similar to Wegener's granulomatosis but involves the lymphoreticular tissues. Approximately 10% of cases develop lymphoma.

#### Other Connective Tissue Disorders

**Dermatomyositis and Polymyositis.** Primary lung involvement is unusual. A basal fibrosing alveolitis may occur. Involvement of the pharyngeal muscles may predispose to aspiration pneumonitis.

**Ankylosing Spondylitis.** In 1%–2% of cases of longstanding ankylosing spondylitis, upper lobe fibrosis develops. It is usually bilateral and associated with apical pleural thickening. With severe fibrosis bullae develop, which may become colonized by *Aspergillus*.

**Sjogren's Syndrome.** Sjogren's syndrome comprises dry eyes, dry mouth and one of the other connective tissue disorders. In addition to the features of that associated disease there may be pleural effusion, fibrosing alveolitis, recurrent chest infections and lymphocytic interstitial pneumonitis.

#### PULMONARY EOSINOPHILIA

A number of conditions cause transient shadows on the chest radiographs in association with an excess of eosinophils in the blood. The pulmonary shadows are due to an eosinophilic exudate. These conditions may be referred to as the PIE Syndrome (pulmonary infiltrates with eosinophilia).

**Simple Pulmonary Eosinophilia** (Löffler's syndrome). This is usually a mild, transient condition. A large number of allergens have been found responsible, but often the cause is not identified. Table 6.1 lists some of the causes. The chest radiograph shows areas of ill-defined, non-segmental consolidation which may change position over a few days, but resolve within a month.

**Table 6.1.** Pulmonary eosinophilia: types and causes

#### Simple pulmonary eosinophilia

##### Parasites

- Ascaris lumbricoides*
- Ankylostoma*
- Strongyloides*
- Taenia*
- Toxocara*

##### Drugs

- PAS
- aspirin
- penicillin
- Nitrofurantoin
- Sulphonamides

#### Chronic pulmonary eosinophilia

##### Etiology uncertain

#### Tropical pulmonary eosinophilia

##### Filariasis

#### Asthmatic pulmonary eosinophilia

##### *Aspergillus fumigatus*

#### Connective tissue disorders

- Wegener's granulomatosis
- other systemic vasculitides

**Chronic Pulmonary Eosinophilia.** This rare condition is associated with fever, malaise, cough and prolonged eosinophilia. The radiological features are similar to Löffler's syndrome, but persist for a month or more.

**Tropical Pulmonary Eosinophilia.** This is caused by filariasis, and presents with a cough, wheeze and sometimes fever. The chest radiograph shows fine, bilateral, diffuse nodular shadowing, with occasional confluent areas.

**Asthmatic Pulmonary Eosinophilia.** This is most commonly caused by *Aspergillus fumigatus* (see Chap. 4) but often no allergen is identified. Characteristically, bronchial casts may be coughed-up during attacks, and there may be fever. The chest radiograph may initially show transient shadows, but after repeated attacks there may be signs of fibrosis and bronchiectasis.

**Pulmonary Eosinophilia associated with the Systemic Vasculitides.** The radiographic features are those of the underlying connective tissue disorder.

#### DIFFUSE PULMONARY FIBROSIS

Pulmonary fibrosis may be a localized or generalized occurrence. Localized pulmonary fibrosis is commonly the result of pneumonia or radiotherapy. Diffuse pulmonary fibrosis is usually the result of a systemic condition or is due to inhalation of dusts or fumes (see Table 6.2).

**Table 6.2.** Diffuse pulmonary fibrosis: causes

Fibrosing alveolitis
cryptogenic fibrosing alveolitis
cause unknown
viral pneumonia
radiation
drugs and poisons
connective tissue diseases
systemic sclerosis
SLE
rheumatoid disease
pneumoconioses
silicosis
extrinsic allergic alveolitis
noxious gases
chronic pulmonary venous hypertension
adult respiratory distress syndrome
Infection
tuberculosis
fungi
Sarcoidosis
Histiocytosis
Neurofibromatosis
Tuberose sclerosis
Lymphangiomymomatosis

### Fibrosing Alveolitis

Fibrosing alveolitis describes a number of conditions in which there is pulmonary fibrosis associated with a chronic inflammatory reaction in the alveolar walls. It includes such conditions as diffuse idiopathic pulmonary fibrosis, diffuse interstitial fibrosis and Hamman–Rich disease. The etiology is frequently uncertain, but many cases are associated with a known cause (see Table 6.2).

### Cryptogenic Fibrosing Alveolitis

This condition may be regarded as an interstitial pneumonitis. Histologically most cases show fibrosis and cellular infiltrate confined to the alveolar walls and may be known as *usual interstitial pneumonitis* (UIP). Some cases show mononuclear cells in the alveoli and may be termed *desquamative interstitial pneumonitis* (DIP). Rarer variants are associated with bronchiolitis obliterans and diffuse alveolar damage (BIP), lymphocytic interstitial pneumonitis (LIP) or a giant cell interstitial pneumonitis (GIP).

Patients present with increasing dyspnea, a dry cough, finger clubbing, widespread basal crackles, and impaired ventilation and gas exchange. The disease may be rapidly progressive with death from respiratory or cardiac failure within a few weeks, or it may continue for many years. There is a predisposition to lung cancer.

The earliest *radiographic change* is bilateral, basal, ground-glass shadowing. This is followed by a fine nodular pattern, and then coarser, linear shadows develop, predominantly basally but spreading throughout the lungs. There is progressive pulmonary volume loss (Fig. 6.20). Ring shadows appear and may produce a honeycomb pattern (Fig. 6.21), and basal septal lines may be visible. Pleural effusion is rare.

### Histiocytosis X

The three variants of this disease, Letterer–Siwe disease, Hand–Schuller–Christian disease and eosinophilic

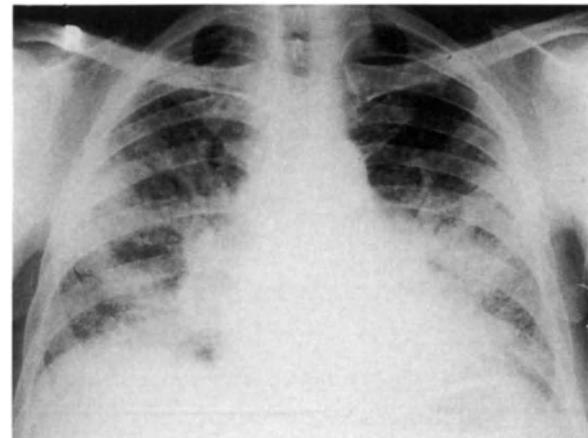


**Fig. 6.20.** Cryptogenic fibrosing alveolitis. The pulmonary volumes are reduced. Nodular shadows are present in both lungs with a basal predominance.

granuloma, involve the lung in approximately 20% of cases. Eosinophilic granuloma usually involves the skeleton, but may be confined to the lungs, when there is a male:female preponderance of 5:1.

Eosinophilic granuloma of the lung may present without symptoms, or with a dry cough, dyspnea or spontaneous pneumothorax. Histologically there is infiltration of alveolar walls by histiocytes and eosinophils, followed by fibrosis.

*Radiology.* The earliest radiological manifestation is ill-defined transient patchy consolidation, but this is rarely seen. A fine reticulonodular pattern throughout both lungs, but predominantly in the mid and upper zones, may then be seen (Fig. 6.22). As fibrosis progresses, a coarser linear pattern appears, with development of ring shadows, honeycombing and bullae (Fig. 6.23). The lung volumes are usually normal. There is a 20% incidence of spontaneous pneumothorax.

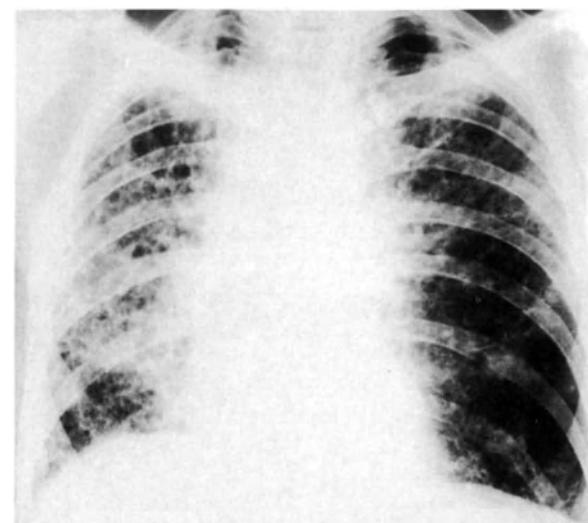


**Fig. 6.21.** Cryptogenic fibrosing alveolitis. There is diffuse reticulonodular shadowing. Ring shadows are well seen in the right upper zone.

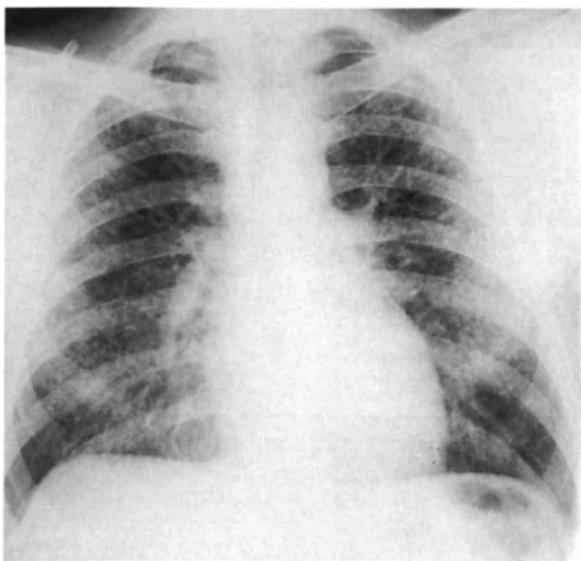
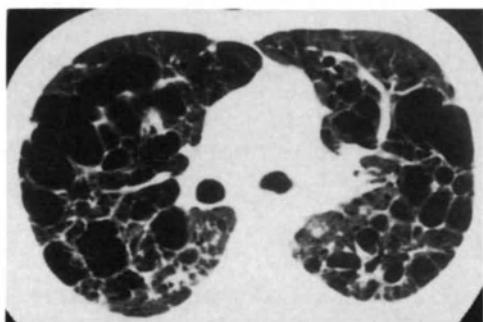


Fig. 6.22. Histiocytosis. Fine reticulonodular shadowing is present throughout both lungs, but with relative sparing of the bases.



A



B

### Tuberous Sclerosis

Approximately 1% of patients with tuberous sclerosis develop lung involvement. Diffuse hyperplasia of smooth muscle in the small airways, alveolar walls and peripheral vessels produces reticulonodular shadowing and eventually *honeycombing* on the chest radiograph. Spontaneous pneumothorax is common.

### Lymphangiomymomatosis

In this condition there is proliferation of smooth muscle and lymphatics in the alveolar walls, interlobular septa and pleura. The appearances are similar to tuberous sclerosis, with the addition of septal lines and chylous pleural effusions.

### Neurofibromatosis

Pulmonary fibrosis occurs in approximately 10% of patients with neurofibromatosis. It may produce reticular shadowing and honeycombing on the chest radiograph.

### Adult Respiratory Distress Syndrome (ARDS)

ARDS may be due to a large number of causes (Table 6.3). It presents as acute respiratory failure in patients without previous lung disease following some sort of major trauma or shock. Clinically the patient becomes hypoxic 12–24 hours after the precipitating event. There is then progressive respiratory failure over several days, usually requiring ventilatory support. During this time there may be superimposed infection, or various complications of positive pressure ventilation may develop. In excess of 50% of cases are fatal, and survivors may have chronic lung disease.

Table 6.3. Causes of ARDS

Major trauma
Septicemia
Hypovolemic shock
Fat embolism
Near-drowning
Mendelson's syndrome
Burns
Viral pneumonia
Pancreatitis
Oxygen toxicity
Disseminated intravascular coagulopathy

The corresponding pathological processes are a hemorrhagic pulmonary edema in the acute phase, followed by resolution or, more often, fibrosis.

Radiographically bilateral, patchy alveolar shadows appear in the first 24 hours. These become more extensive over the next few days (Fig. 6.24). Pleural effusions are unusual, and the heart does not enlarge. At this stage, gram-negative pneumonia frequently develops, and cavitation and pleural effusions may be seen.

Fig. 6.23A, B. Histiocytosis. A Coarser reticulonodular shadowing with ring shadows is seen. B CT demonstrates 'honeycomb' shadowing. The lung volumes are normal.

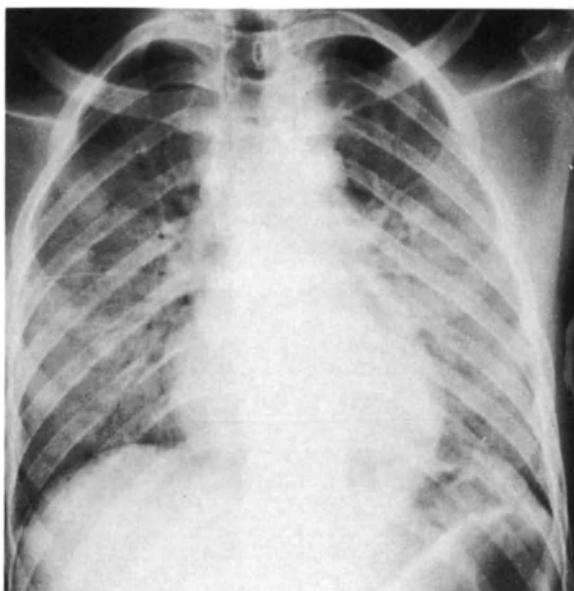


**Fig. 6.24.** Adult respiratory distress syndrome, acute phase. Overwhelming viral pneumonia. Consolidation is present throughout both lungs.

Pneumomediastinum, pneumothorax and subcutaneous emphysema may result from ventilatory support. If the patient survives, there is gradual clearing of the alveolar shadowing, which is replaced by evidence of pulmonary fibrosis. The lung volumes may be decreased and reticular shadowing may develop. A minority of patients recover fully.

#### PULMONARY HEMORRHAGE AND HEMOSIDEROSIS

*Hemorrhage* into the lungs and airways may complicate lung cancer, pneumonia, bronchiectasis, pulmonary venous hypertension, blood dyscrasias, anticoagulant therapy, disseminated intravascular coagulation and trauma. Multifocal bleeding into the alveoli not associated with any of these conditions may be referred to as pulmonary hemosiderosis.

*Pulmonary hemosiderosis* may be either *idiopathic* or associated with *renal* disease. In *Goodpasture's syndrome* pulmonary hemosiderosis occurs with a glomerulonephritis associated with circulating antiglomerular basement membrane antibodies. In other cases the nephritis may be due to *Wegener's granulomatosis*, *systemic lupus erythematosus*, *polyarteritis nodosa* or *penicillamine hypersensitivity*.

*Radiology.* During an acute episode of pulmonary hemorrhage patchy, ill-defined areas of consolidation appear on the chest radiograph (Fig. 6.25). They may become confluent and have an air bronchogram. The appearance may be indistinguishable from pulmonary edema. When bleeding stops, the shadows resolve within a few days. Following repeated episodes of bleeding, pulmonary fibrosis may develop and produce a diffuse haziness or reticular pattern.

Patients with nephritis are prone to pulmonary edema and pneumonia, and the differentiation from pulmonary hemorrhage may be difficult. Pneumonic consolidation tends to resolve more slowly than edema or hemorrhage. Cardiome-

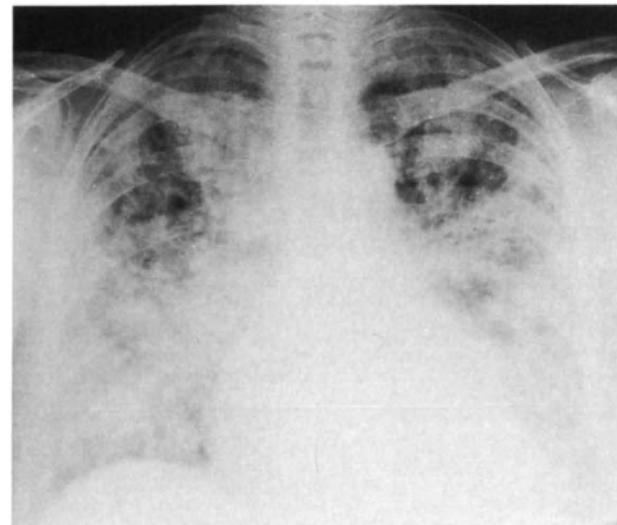


**Fig. 6.25.** Pulmonary hemosiderosis, acute phase. Patchy consolidation is present throughout both lungs.

galy, septal lines and pleural effusion suggest pulmonary edema.

The diagnosis of acute pulmonary hemorrhage may be confirmed by demonstrating increased uptake of inhaled radioactive carbon monoxide in the alveoli.

#### DRUG-INDUCED PULMONARY DISEASE

Many drugs in common use may produce diffuse pulmonary abnormalities. Consequently, when interpreting a chest radiograph with diffuse shadowing it is important to be aware of what therapy the patient has received or is undergoing. Some drugs are intrinsically toxic to the lungs (e.g., many cancer chemotherapeutic agents) and their effect on the lung may be dose-related or cumulative. Other drugs seem to cause pulmonary abnormalities in a minority of recipients who show a hypersensitivity or idiosyncratic response.

*Pulmonary Fibrosis.* Many cytotoxic drugs (e.g., azothioprine, bleomycin, busulphan, cyclophosphamide, chlorambucil) cause fibrosing alveolitis which may progress to pulmonary fibrosis. The fibrogenic effect of these drugs is enhanced by radiotherapy. The chest radiograph may show reticulonodular shadowing, often with a basal predominance. Pulmonary fibrosis may also be caused by amiodarone and oxygen toxicity.

*Pulmonary Eosinophilia.* Para-aminosalicylic acid (PAS), aspirin, penicillin, nitrofurantoin, sulphonamides and methotrexate are some substances that may produce an eosinophilia and pulmonary infiltrates. This hypersensitivity may, after prolonged drug administration, lead to pulmonary fibrosis (Fig. 6.26).

*SLE Reaction.* Some drugs, such as penicillin, procainamide, isoniazid and methyldopa may cause pleural



**Fig. 6.26.** Pulmonary fibrosis due to sulfasalazine in a patient with colitis. Coarse reticulonodular shadows are seen in both lungs.

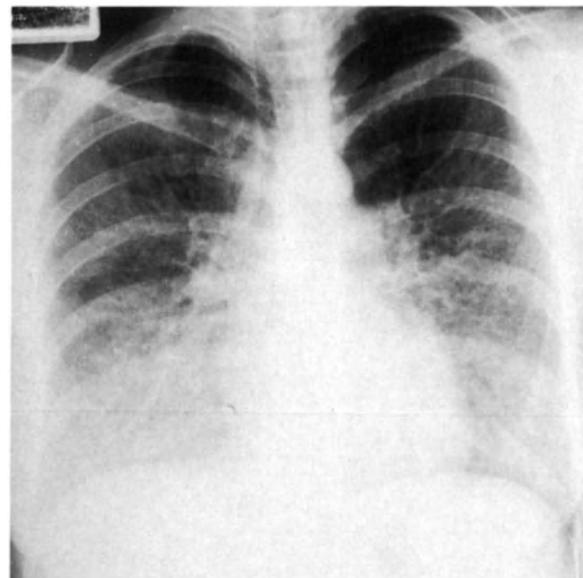


**Fig. 6.27.** Pulmonary alveolar proteinosis. Small, acinar shadows are present throughout both lungs.

effusions, pneumonitis and pulmonary fibrosis.

**Pulmonary Edema.** Pulmonary edema is a common complication of narcotic overdose. It may also be caused by overinfusion of intravenous fluids and by hypersensitivity to transfused blood or blood products.

**Pulmonary Thromboembolism.** This may arise from the use of oral contraceptives.

**Opportunistic Infection.** Drugs that suppress the immune system (e.g., cancer chemotherapeutic agents and steroids) predispose to infection. Pneumonias that are likely to be seen in this context may be due to tuberculosis, gram-negative bacteria, viruses and pneumocystis.

**Mediastinal Adenopathy.** Phenytoin may cause hilar lymph node enlargement.

### AMYLOIDOSIS

Secondary amyloidosis is rarely apparent radiographically, but primary amyloidosis may produce a variety of abnormalities in the airways and lungs.

**Tracheo-bronchial amyloid** may produce bronchial obstruction leading to atelectasis, bronchiectasis or pneumonia.

**Pulmonary amyloidosis** may produce multiple nodular opacities which may cavitate or calcify, or there may be diffuse reticulonodular shadowing or honeycombing. Hilar and mediastinal lymph node enlargement and calcification may also be seen.

### PULMONARY ALVEOLAR PROTEINOSIS

This is a rare disease of unknown etiology in which proteinaceous lipid-rich material accumulates in the alveoli.

The radiographic appearance resembles pulmonary edema.

Small, acinar, perihilar opacities are present in both lungs (Fig. 6.27). These opacities may become confluent. The disease predisposes to pulmonary infection from both common respiratory pathogens and opportunistic organisms. It may also be associated with lymphoma, leukemia and immunoglobulin deficiency. Diagnosis is made by *lung biopsy* or *bronchoalveolar lavage*. Approximately 25% of cases are fatal within 5 years.

### PULMONARY ALVEOLAR MICROLITHIASIS

This is a disease of unknown etiology which may be familial. It is characterized by the presence of multiple, fine sand-like calculi in the alveoli. The calculi are calcified and produce widespread, minute, but very dense opacities on the chest radiograph (Fig. 6.28). The strikingly abnormal radiograph contrasts with a relative lack of symptoms, although later in the disease there may be pulmonary fibrosis.

### NEONATAL PULMONARY DISTRESS

#### Hyaline Membrane Disease

Hyaline membrane disease, or idiopathic respiratory distress syndrome, is a disease of premature or physiologically immature infants. It is due to a deficiency of surfactant which predisposes to alveolar atelectasis. The earliest radiographic manifestation is a diffuse, granular pattern throughout the lungs (Fig. 6.29). With progression an air bronchogram may appear, and in severe cases the lungs may become opaque.

#### Pulmonary Interstitial Emphysema

Neonates with hyaline membrane disease may require positive pressure ventilation. Rupture of alveoli may occur and

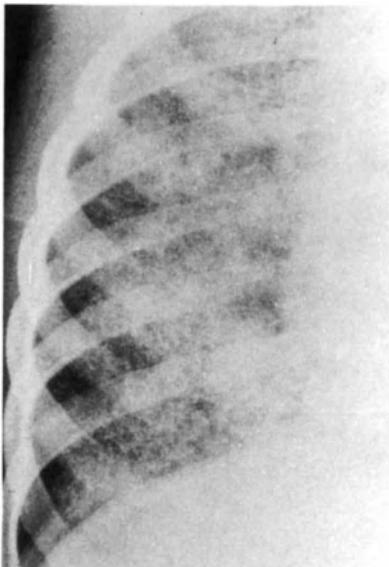


**Fig. 6.28.** Pulmonary alveolar microlithiasis. Multiple, fine dense opacities are widely visible.

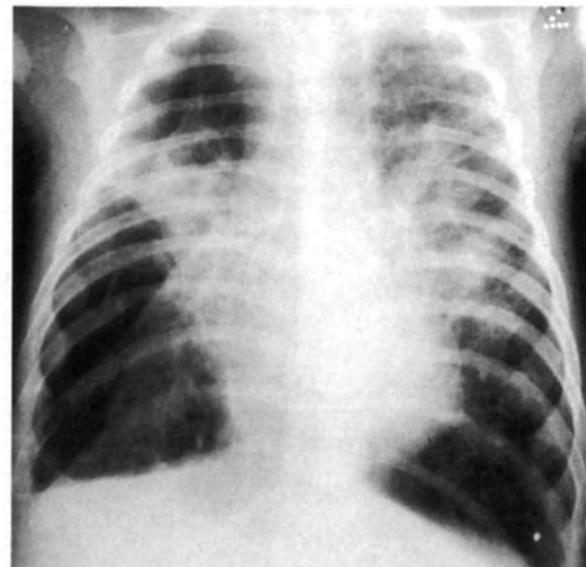


**Fig. 6.30.** Bronchopulmonary dysplasia. The lungs are generally hyperinflated. Areas of fibrosis and emphysema are visible in the right lung.

air may then dissect into the lung interstitium and lymphatics. The appearance on the chest radiograph is multiple coarse linear lucencies in the lungs, which may progress to cyst-like lucencies. If one lung only is involved, its volume is larger than the other lung. Dissection of air beyond the lung interstitium may cause pneumomediastinum, pneumothorax, and pneumoperitoneum.

#### Bronchopulmonary Dysplasia

This is another complication of artificial ventilation in the treatment of hyaline membrane disease, especially if the treatment is prolonged. Areas of fibrosis occur in parts of the lungs, while aerated alveoli develop compensatory hyperinflation and emphysema. The chest radiograph shows

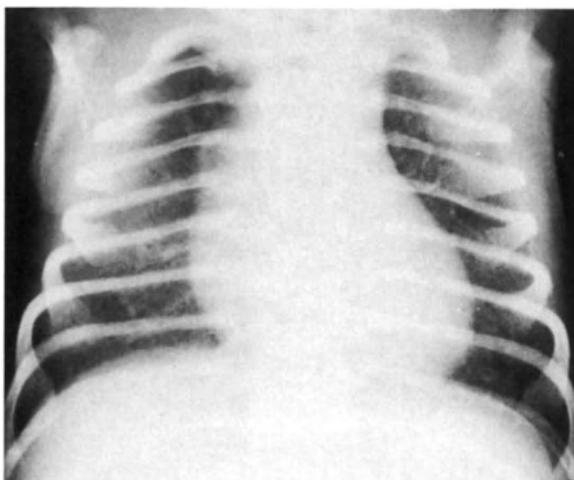


**Fig. 6.29.** Hyaline membrane disease, early changes. Diffuse, granular shadowing is seen throughout both lungs.

hyperinflated lungs, with coarse linear shadows and areas of emphysema (Fig. 6.30).

#### Wilson–Mikity Syndrome

This is a condition of unknown etiology. The patient is a neonate with respiratory distress who develops a radiological picture similar to bronchopulmonary dysplasia. However, there is no antecedent history of hyaline membrane disease or artificial ventilation.

#### Transient Tachypnea of the Newborn

This condition is also known as *wet lung disease* and tends to occur in premature babies. It is due to greater residue of fluid in the newborn lungs than usual, so that the patients are tachypneic and the chest radiograph shows variable degrees of pulmonary edema. The symptoms and signs usually show complete resolution over a few days.

#### Meconium Aspiration

Following intrauterine distress there may be neonatal distress due to aspiration of meconium. The chest radiograph shows symmetrical, bilateral streaky shadowing, with peripheral areas of atelectasis and hyperinflation. Alveolar rupture may occur and cause interstitial pulmonary emphysema, pneumomediastinum and pneumothorax.

#### Miscellaneous Conditions

Other conditions that may cause neonatal distress include pneumonia, congenital pulmonary anomalies (e.g., congenital lobar emphysema, cystic adenomatoid malformation, pulmonary hypoplasia), congenital diaphragmatic hernia, tracheo-esophageal fistula, and congenital heart disease.

*For further reading, see p. 134.*

## CHAPTER 7

# THE MEDIASTINUM

M. Rubens

---

The mediastinum is situated in the middle of the thorax between the lungs. It extends from the thoracic inlet down to the central tendon of the diaphragm. The anterior and posterior limits are the sternum and thoracic spine, and parietal pleura forms the lateral boundaries.

### MEDIASTINAL MASSES

The commonest mediastinal mass visible on the chest radiograph in *children* is the normal thymus (Fig. 7.1). Lymphadenopathy, hiatus hernia and vascular abnormalities account for most mediastinal masses seen in *adults*. Certain

masses tend to occur in particular locations so that accurate localization of a mediastinal mass aids its differential diagnosis.

Traditionally, radiologists have divided the mediastinum into anterior, middle and posterior compartments. The *anterior* compartment lies anterior to the pericardium and trachea, and the *posterior* compartment lies posterior to these structures. The *middle* compartment comprises the pericardium and its contents and the trachea. Table 7.1 summarizes the typical sites of the commoner mediastinal masses.

Table 7.1. Causes of commonly found mediastinal masses

Anterior mediastinum
thyroid mass
thymic mass
lymphadenopathy
teratodermoid tumor
ascending aortic aneurysm
Middle mediastinum
lymphadenopathy
bronchogenic cyst
aortic arch aneurysm
venous dilatation
Posterior mediastinum
neurogenic tumor/cyst
hiatus hernia
esophageal dilatation
descending aortic aneurysm

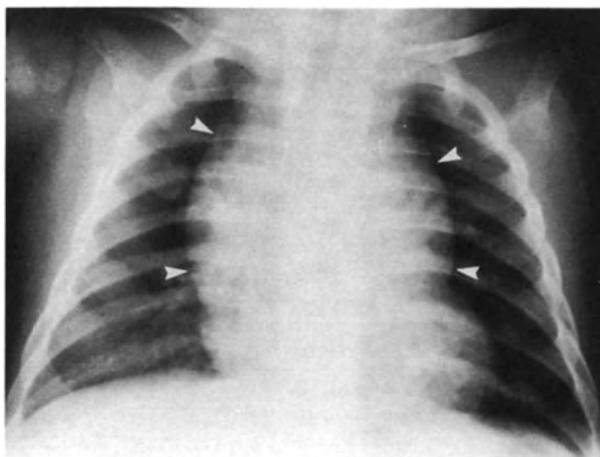
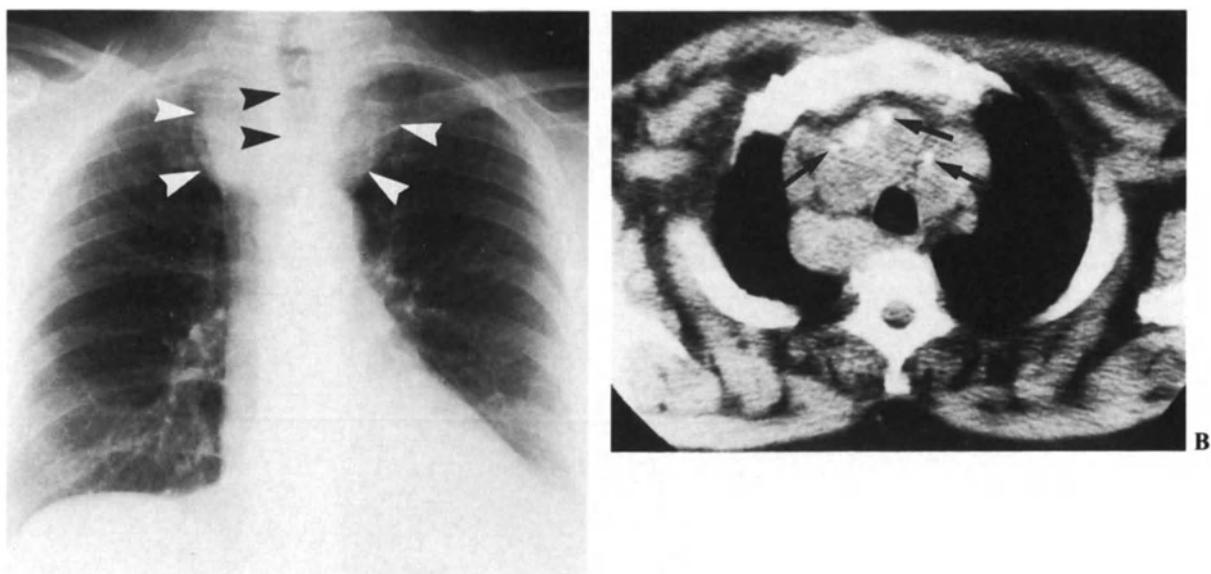


Fig. 7.1. Normal thymus. Infant with wide superior mediastinum due to normal thymus (arrowheads).

### Thyroid Masses

Thyroid masses which extend from the neck into the mediastinum produce a retrosternal goitre. These masses are usually nodular colloid goitres or thyroid carcinomas.



**Fig. 7.2A, B.** Nodular colloid goitre. **A** The superior mediastinum is widened bilaterally by a mass (white arrowheads) that extends down from the neck. The trachea (black arrowheads) is displaced to the left. **B** CT shows that the mass is mostly anterior, lobulated and partly calcified (arrows).

The usual radiographic appearance is a rounded or lobulated soft tissue mass in the superior part of the anterior mediastinum extending from the neck (Fig. 7.2). The mass may be partly calcified. Well-defined curvilinear and nodular calcification tends to occur in benign lesions (Fig. 7.3) and more amorphous calcification in malignant masses. The trachea is frequently displaced or narrowed by thyroid masses. *Ultrasound* may be used to differentiate between solid and cystic lesions, and *radionuclide scanning* with  $^{99}\text{Tc}$ -sodium

pertechnetate or  $^{123}\text{I}$ -sodium iodide will demonstrate areas of metabolically active thyroid tissue.

#### Thymic Masses

Benign and malignant thymoma are the commonest cause of enlargement of the thymus. Rarer causes include thymolipoma, lymphoma and thymic cyst. Approximately 10% of patients with a thymoma have myasthenia gravis, and approximately 15% of patients with myasthenia gravis

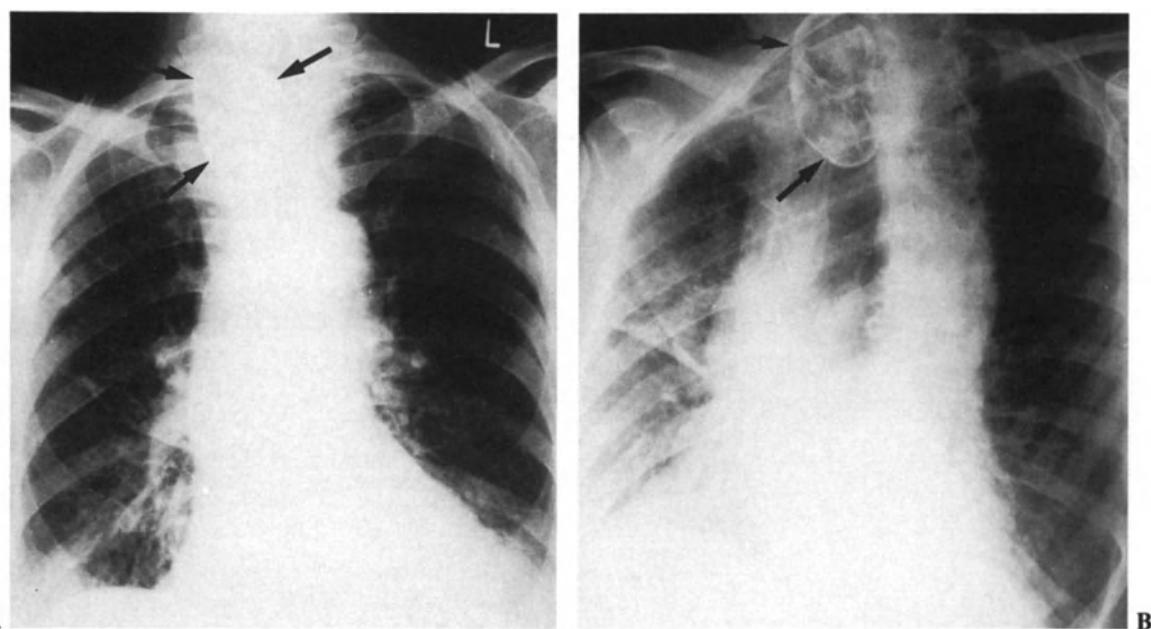


**Fig. 7.3A, B.** Calcified thyroid adenoma. **A** PA and, **B**, oblique films show an anterior mediastinal mass (arrows) with a calcified rim.

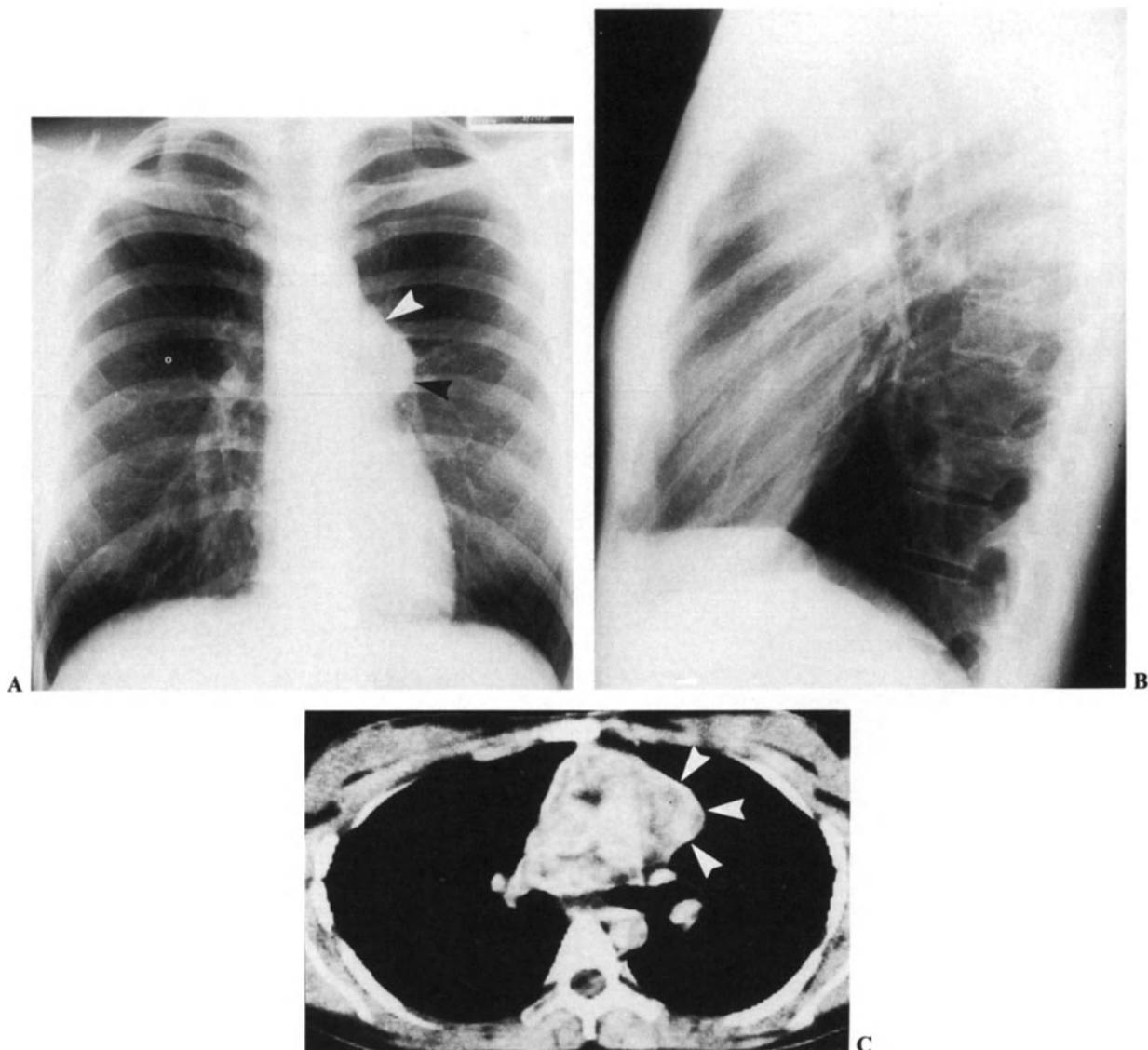


**Fig. 7.4.A, B, C. Thymoma.** Patient with myasthenia gravis. A PA film shows round mass (*arrowheads*) overlying left hilum. B Lateral film shows opacification of retrosternal space due to the anterior mediastinal mass. C CT confirms the anterior mediastinal mass. Histology : Malignant thymoma.

have a thymoma. Other associations of thymoma include Cushing's syndrome, thyrotoxicosis, Addison's disease and hypogammaglobulinemia.

At *simple radiography* thymomas appear as rounded anterior mediastinal soft tissue masses (Fig. 7.4) and peripheral, curvilinear or central nodular calcification may occasionally be visible (Fig. 7.5). Small tumors are more easily seen on *CT* than on the chest radiograph. Malignant thymomas tend to metastasize to the pleura.

#### Germ Cell Tumours

*Dermoid cysts* and benign and malignant *teratomas* account for most mediastinal germ cell tumors. They occur as anterior mediastinal masses and are usually radiographi-

cally indistinguishable from a thymoma. However, occasionally a fat-fluid level or a tooth may be seen on the *plain film* or *CT*, allowing a confident diagnosis of a teratodermoid cyst to be made. Benign teratomas tend to be cystic, and malignant teratomas are usually solid. Rarer types of germ cell tumors occurring in the mediastinum include seminoma, chorioncarcinoma and ovarian dysgerminoma, which are thought to arise from aberrant germ cells.

#### Mediastinal Lymphadenopathy

Lymph nodes are present in all compartments of the mediastinum, but are visible on the chest radiograph only when calcified or enlarged (see Tables 7.2 and 7.3 for lists of causes).

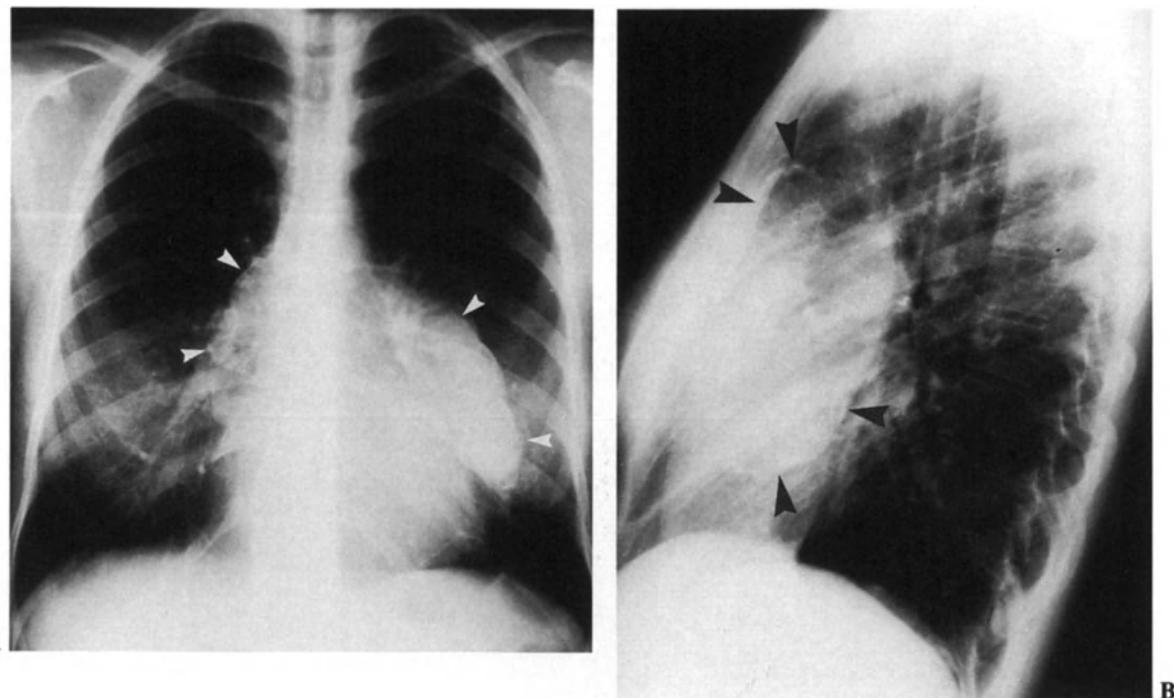


**Fig. 7.5A, B.** Calcified thymoma. Patient with myasthenia gravis. There is a large lobulated anterior mediastinal mass (*arrowheads*) with peripheral curvilinear calcification.

The *chest radiograph* is a relatively insensitive indicator of lymphadenopathy. Enlargement of right paratracheal nodes is identified more easily than left paratracheal, aorti-copulmonary or subcarinal lymphadenopathy.

*Barium swallow* is a simple method of identifying some cases of subcarinal lymphadenopathy, but *CT* is the most

accurate method of assessing mediastinal nodes. Nodes larger than 1 cm in diameter are usually abnormal, and if greater than 2 cm are most likely involved by metastatic carcinoma, lymphoma, tuberculosis, histoplasmosis or sarcoid. Mediastinal lymphadenopathy is often associated with hilar lymphadenopathy. Lymphadenopathy is a common cause of

**Table 7.2. Causes of lymph node calcification**

<b>Common</b>
tuberculosis
histoplasmosis and other fungi
<b>Rare</b>
sarcoidosis
silicosis
treated lymphoma

**Table 7.3. Causes of lymph node enlargement**

<b>Common</b>
lung cancer
metastatic carcinoma
tuberculosis
histoplasmosis and other fungi
sarcoidosis
lymphoma
<b>Rare</b>
silicosis and berylliosis
infectious mononucleosis and other viruses
brucellosis
cystic fibrosis
Castleman's disease

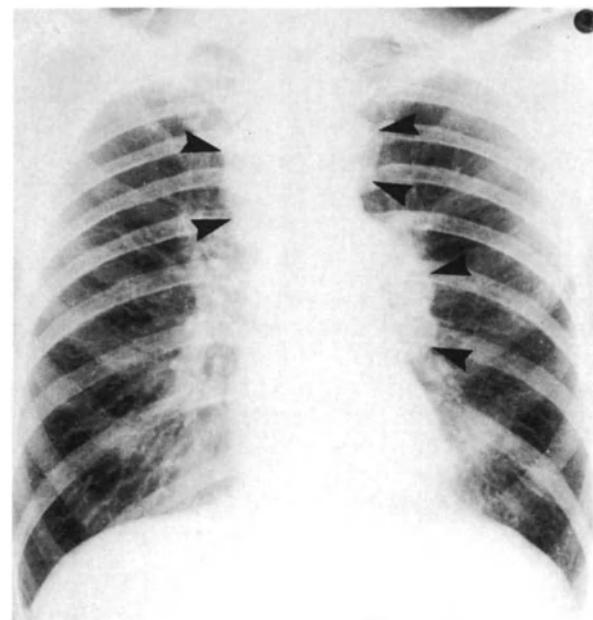


**Fig. 7.6.** Lymphadenopathy. Oat cell carcinoma. Chest radiograph shows bilateral paratracheal and left hilar lymph node enlargement (*arrowheads*).

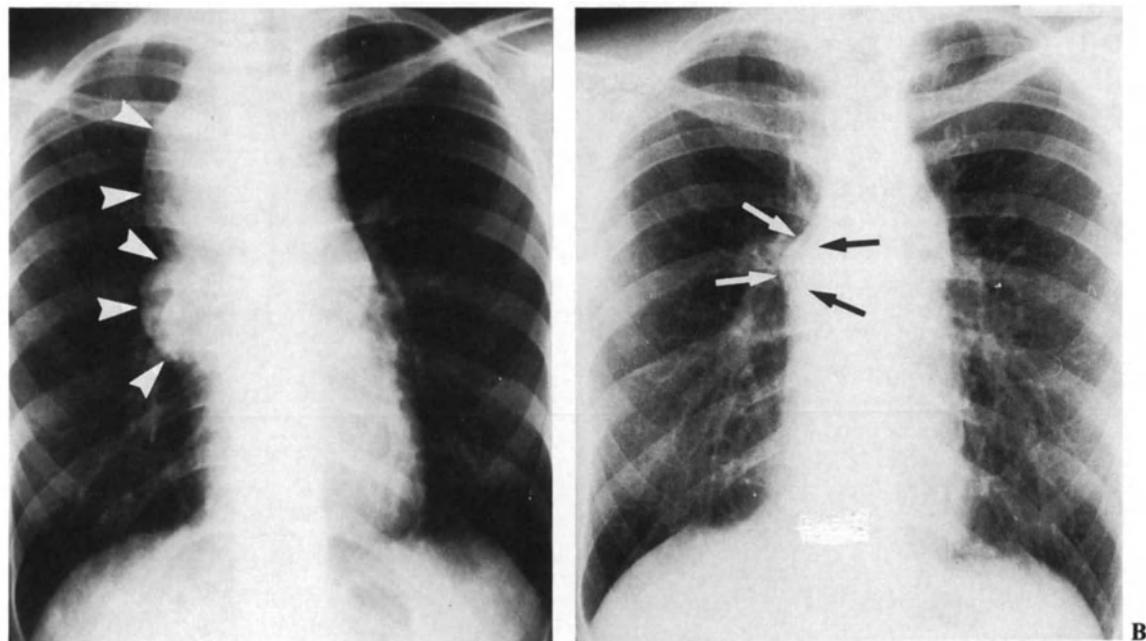


**Fig. 7.7A, B.** Lymphadenopathy. Hodgkin's disease. **A** Chest radiograph shows asymmetric right paratracheal and right anterior mediastinal lymph node enlargement (arrowheads). **B** Following radiotherapy and chemotherapy, the lymph node masses have resolved, but calcification is visible in nodes (arrows) overlying the right hilum.

an anterior or middle mediastinal mass; posterior mediastinal lymphadenopathy is less common. Lymphadenopathy usually produces lobulated shadowing on the chest radiograph.

Metastatic disease causing mediastinal node involvement is most often due to carcinoma of the *bronchus* (Fig. 7.6) or *esophagus* and may be associated with lymphangitis carcinomatosa. Extrathoracic tumors with a tendency to

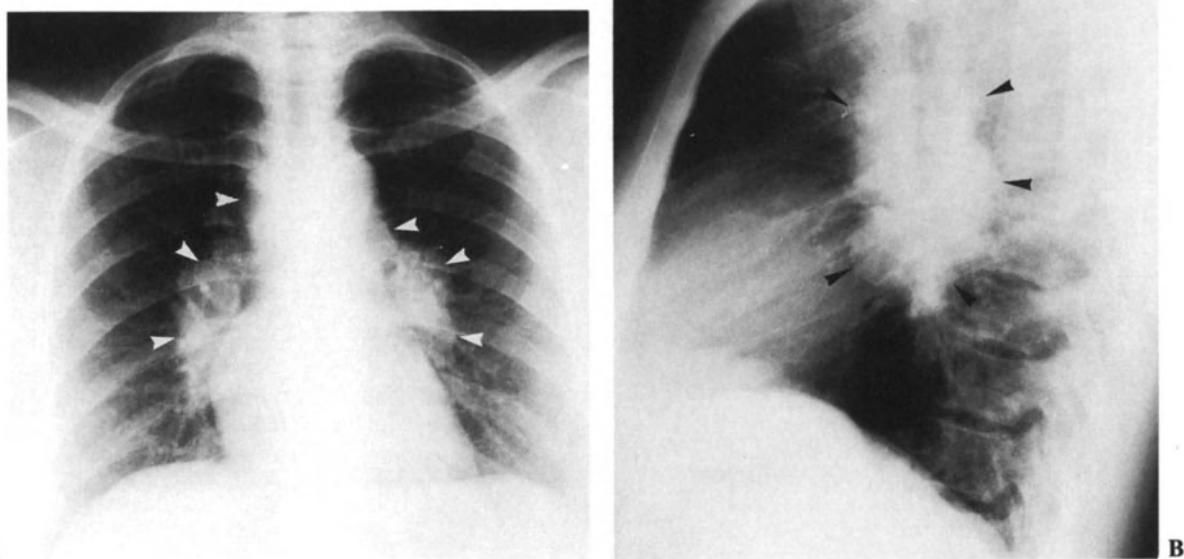


**Fig. 7.8A, B.** Lymphadenopathy. Sarcoidosis. **A** PA chest radiograph shows typical symmetrical enlargement of right paratracheal, bilateral hilar and aortopulmonary nodes (arrowheads). **B** The lateral film shows the hilar adenopathy (arrowheads) particularly well.

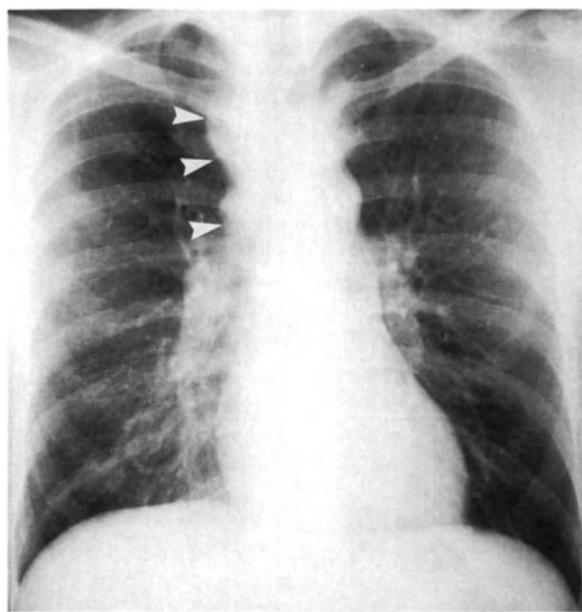


**Fig. 7.9.** Lymphadenopathy. Tuberculosis. There is extensive right paratracheal lymph node enlargement (arrowheads). The lungs are clear.

metastasize to mediastinal nodes include *breast carcinoma*, *genito-urinary tract carcinomas* and carcinoma of the *larynx* and *pharynx*.

*Hodgkin's disease* and, to a lesser extent, *non-Hodgkin's lymphoma* and *lymphatic leukemia* frequently involve the mediastinum, especially the paratracheal, tracheobronchial and anterior mediastinal nodes. Typically the lymph node enlargement is asymmetric (Fig. 7.7). Following treatment

the nodes may calcify. *Sarcoidosis* typically causes symmetrical enlargement of the bronchopulmonary nodes. Right paratracheal, tracheobronchial and aorticopulmonary nodal enlargement are also common (Fig. 7.8). Occasionally peripheral calcification may develop in involved nodes.

Primary *tuberculosis* in the chest typically causes mediastinal or hilar adenopathy with or without an area of pulmonary consolidation (Fig. 7.9). With healing, the nodes often calcify. *Histoplasmosis*, and occasionally other fungi, may produce an identical picture to tuberculosis. Other causes of mediastinal or hilar adenopathy include infectious mononucleosis, measles, whooping cough, adenoviruses and cystic fibrosis.

Benign lymph node hyperplasia or *Castleman's disease* (Fig. 7.10) is a rare cause of anterior mediastinal or hilar adenopathy in an asymptomatic patient.

#### Aneurysms of the Thoracic Aorta

The thoracic aorta arises in the middle mediastinum and then arches through the anterior, middle and posterior mediastinal compartments. Its proximal branches arise in the superior mediastinum. Dilatation or tortuosity of the aortic arch or its branches may cause widening of the mediastinal shadow. So-called 'unfolding of the aorta' is a common finding in the chest radiograph of elderly or hypertensive patients. Aneurysm of the aorta is most often due to *atherosclerosis*. Other important causes of aortic aneurysm are *cystic medial necrosis* (Marfan's syndrome), *infection* (mycotic aneurysm), *syphilitic aortitis* and *trauma*.

The presentation of an aortic aneurysm depends on its location. Many are asymptomatic and present as a mediastinal opacity on a *chest radiograph*. Often curvilinear calcification is present in the wall of the aneurysm.

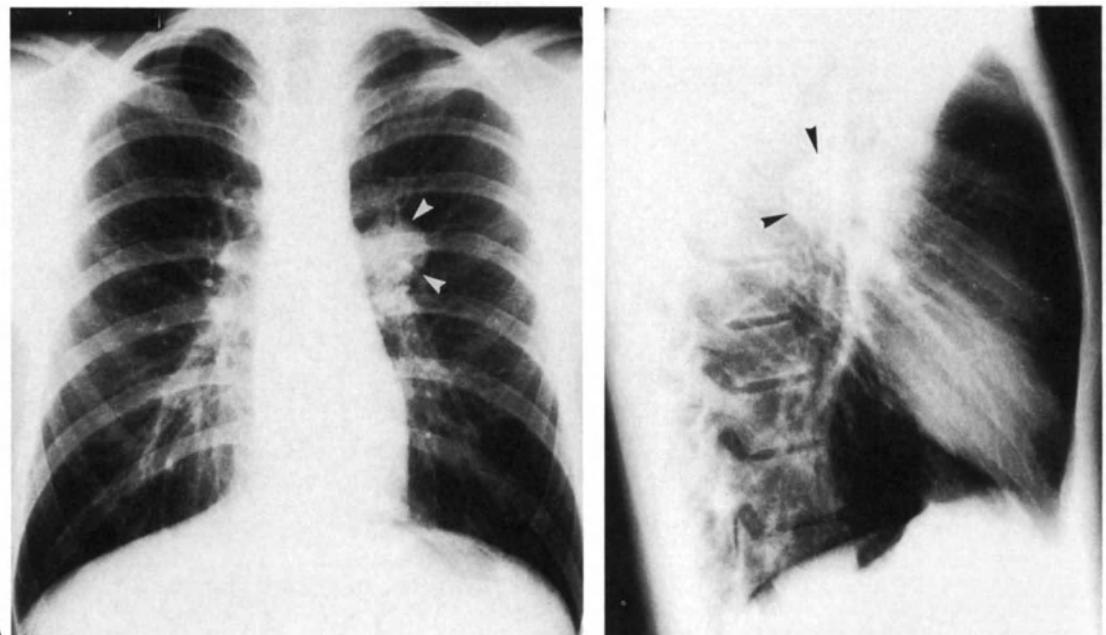


**Fig. 7.10A, B.** Lymphadenopathy. Benign lymph node hyperplasia. A left hilar mass (arrowheads) is present.

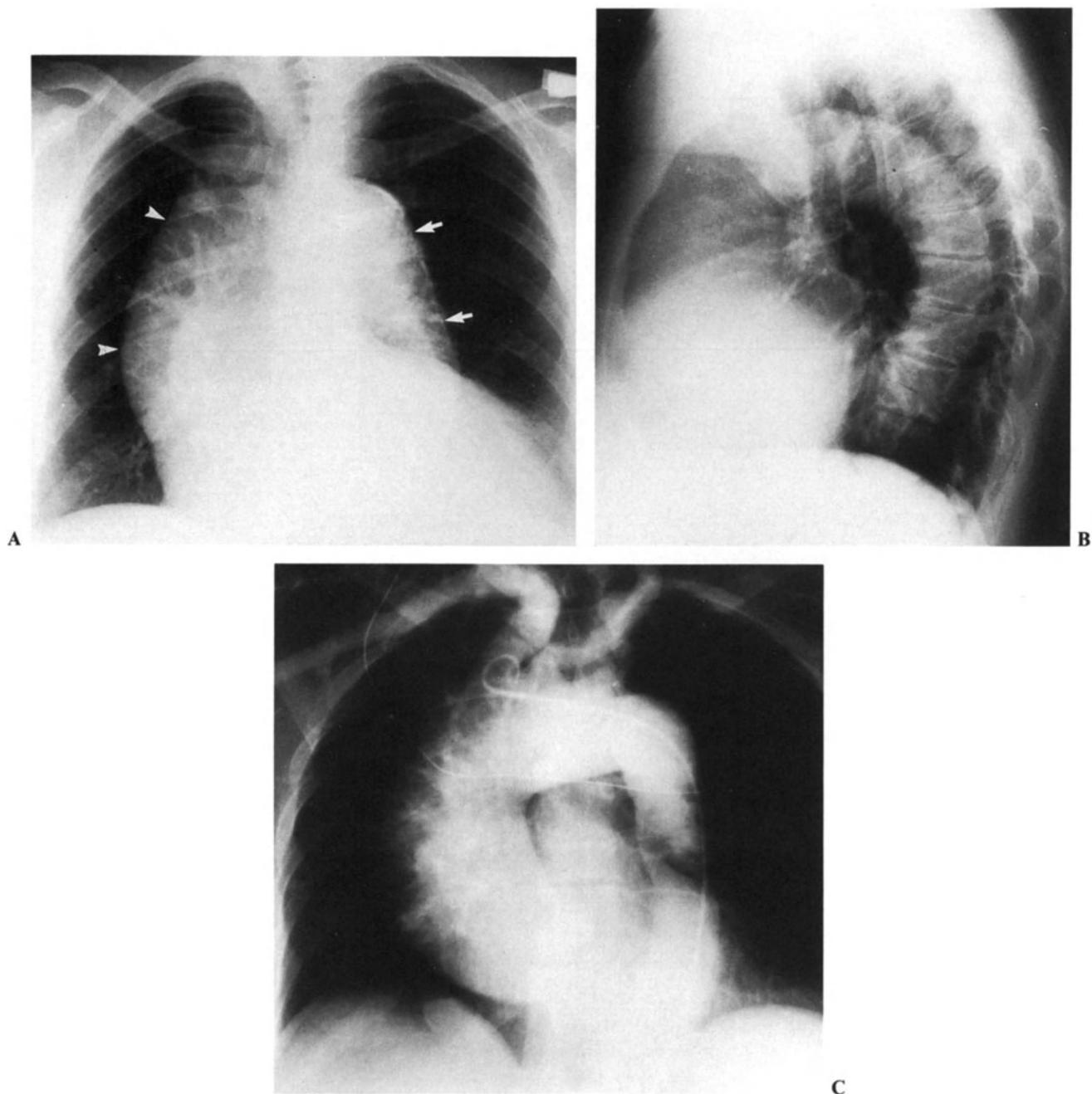


**Fig. 7.11A, B, C.** Atherosclerotic aneurysm of ascending aorta. A PA chest radiograph shows widening of mediastinum due to dilatation of ascending aorta (arrowheads) and unfolding of descending aorta (arrows). Note calcification in descending aorta. B Lateral film shows that the retrosternal space is occupied by dilated ascending aorta. C Arch aortogram confirms aneurysmal dilatation of ascending aorta.

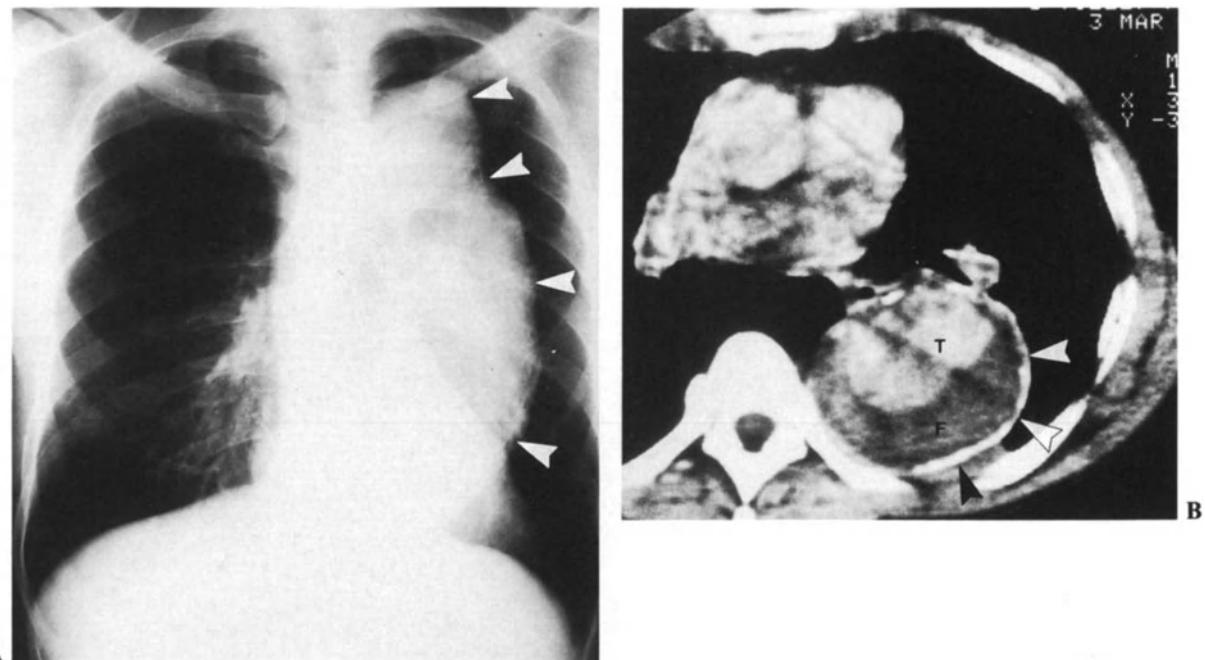


**Fig. 7.12A, B.** Dissecting aneurysm of descending aorta. A Chest radiograph shows dilatation of entire descending aorta (arrowheads). B CT with contrast enhancement shows blood in true lumen (T), clot in false lumen (F) and extensive calcification (arrowheads) in wall of aneurysm.

Aneurysms of the ascending aorta (Fig. 7.11) are usually due to atherosclerosis, cystic medial sclerosis or syphilitic aortitis. Syphilitic aneurysms are usually calcified. If aortic regurgitation is associated with the aneurysm, cardiomegaly may be present.

Aneurysms of the arch and descending aorta are usually due to atherosclerosis or dissection (Fig. 7.12). Aneurysms secondary to trauma are almost always confined to the junction of arch and descending aorta (Fig. 7.13). Aneurysm of the ascending aorta may erode the posterior surface of the sternum, and descending aortic aneurysms may cause scalloping of the spine.

The diagnosis of aortic aneurysm may be confirmed by ultrasound, angiography, CT or MRI. Both CT and MRI are excellent for demonstrating aortic dissection, and differentiating between true lumen, false lumen and clot (Figs 7.12, 7.13). In addition MRI can give information on the hemodynamics in the various channels.

Tortuosity of the innominate artery is a common cause of widening of the superior mediastinum in the elderly. Right-sided aortic arch (Fig. 7.14) and pseudo-coarctation of the aorta (Fig. 7.15) are two anomalies that may alter the appearance of the mediastinum and suggest a mass.

#### Dilatation of Mediastinal Veins

The superior vena cava and azygos veins may dilate due to increased pressure, increased flow or obstruction. Causes of increased pressure include heart failure, constrictive pericarditis, tricuspid valve disease and right atrial tumor.

Increased flow in the superior vena cava is seen in supracardiac total anomalous pulmonary venous drainage, and

in the azygos vein in congenital absence of the inferior vena cava (Fig. 7.16).

Obstruction of the superior vena cava may be due to mediastinal tumor or fibrosing mediastinitis.

#### Tracheal Abnormalities

Carcinoma of the trachea, and cylindroma are rare causes of a middle mediastinal mass. Tracheobronchomegaly and tracheomalacia are rare causes of widening of the mediastinum.

#### Bronchogenic Cyst

Bronchogenic cysts may arise anywhere along the course of the trachea, but are usually found close to the carina. Most present as asymptomatic middle mediastinal masses. On the *chest radiographs* they appear as well defined round masses (Fig. 7.17). They rarely calcify. On CT they may appear as either cystic or solid masses.

#### Pleuropericardial Cyst

On *chest films* pleuropericardial cysts appear as round, well defined opacities contiguous with the heart shadow. Most occur in the right cardiophrenic angle (Fig. 7.18). On *ultrasound* and *CT* they appear as thin-walled, fluid-filled cysts.

#### Neurogenic Tumors

Neurogenic tumors are the commonest cause of a posterior mediastinal mass. In *adults* they usually arise from intercostal nerves and are neurofibromas or neurilemmomas; in *children* they usually arise from the sympathetic ganglia and

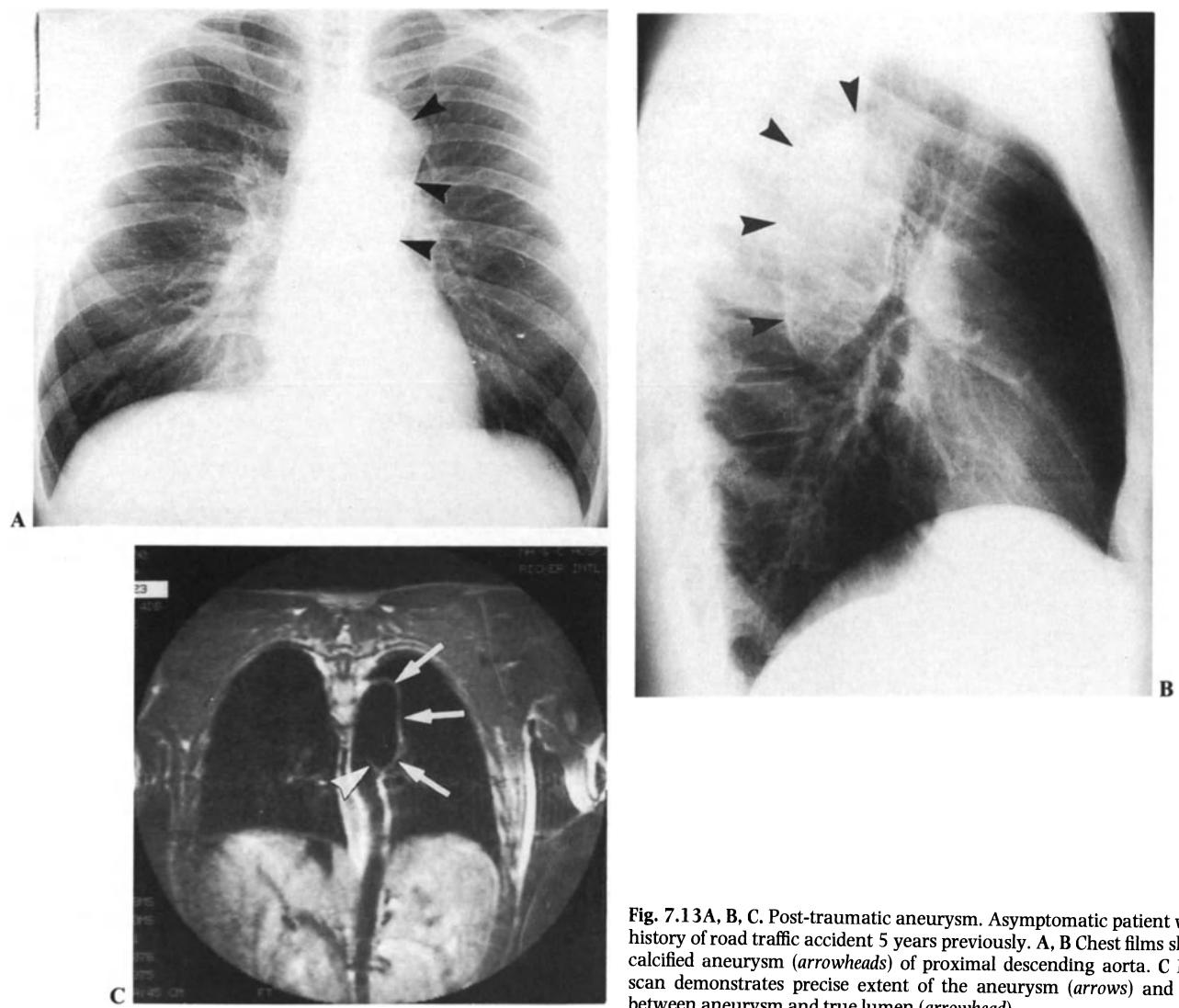


**Fig. 7.13A, B, C.** Post-traumatic aneurysm. Asymptomatic patient with history of road traffic accident 5 years previously. A, B Chest films show calcified aneurysm (arrowheads) of proximal descending aorta. C MRI scan demonstrates precise extent of the aneurysm (arrows) and flap between aneurysm and true lumen (arrowhead).

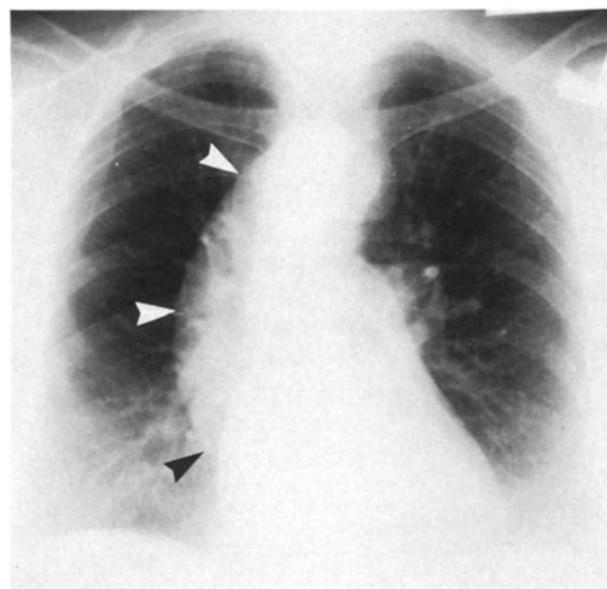


**Fig. 7.14.** Tortuous right-sided aortic arch (arrowheads) simulating a mediastinal mass.

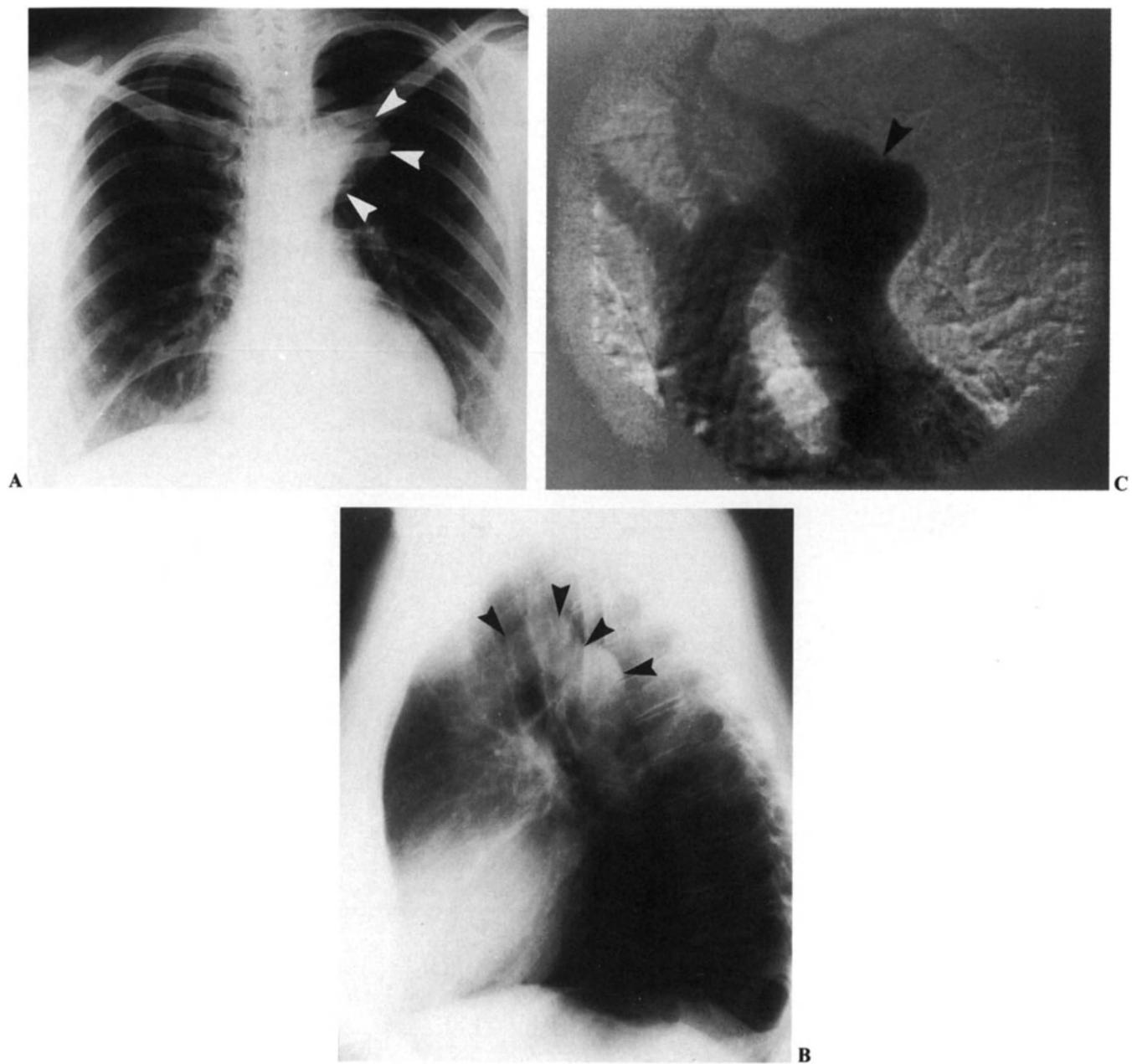
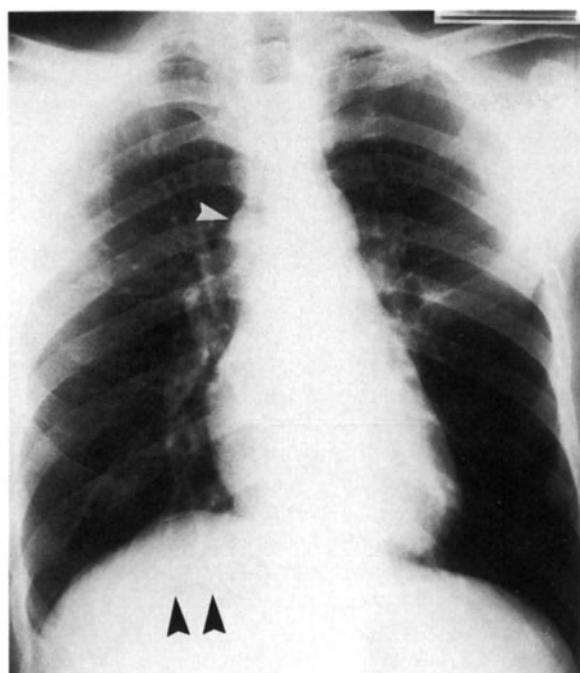
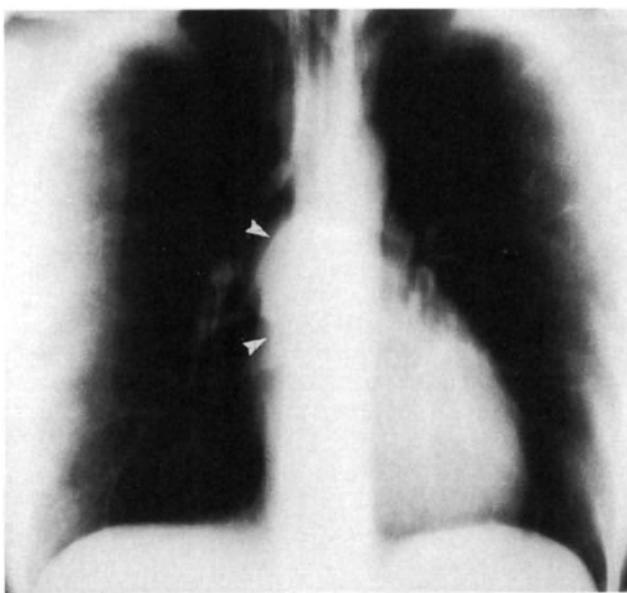


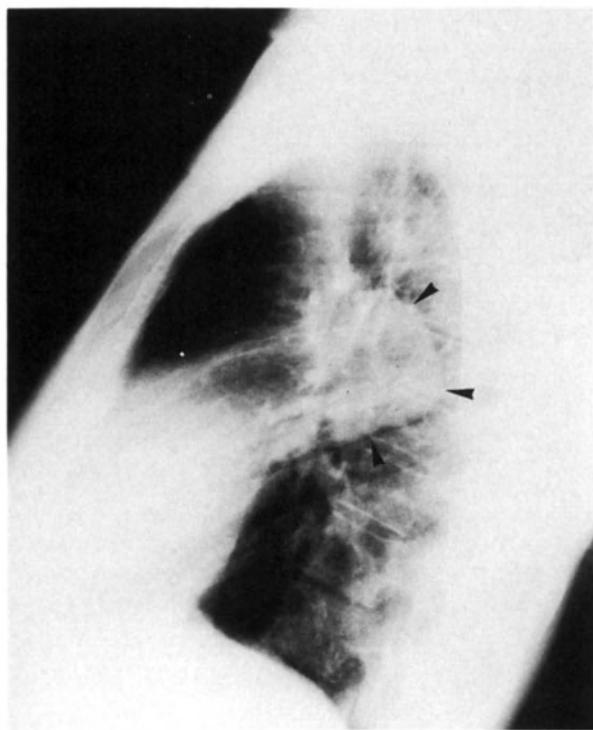
**Fig. 7.15A, B, C.** Pseudo-coarctation of aorta. **A** Chest radiograph suggests a left-sided mediastinal mass (*arrowheads*). **B** Lateral film shows typical kinking in aortic arch (*arrowheads*). **C** DSA confirms the diagnosis. The kink in the aorta is well demonstrated (*arrowhead*).



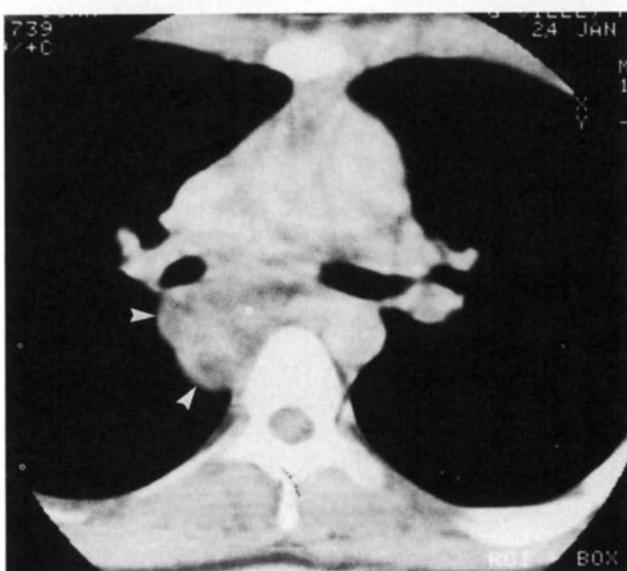
► Fig. 7.16. Dilatation of azygos vein (white arrowhead), in patient with abnormal situs. Note left-sided stomach bubble (black arrowheads).



B



A



C

Fig. 7.17A, B, C. Bronchogenic cyst. No obvious abnormality was seen on the PA film, but the lateral film, A, shows a lobulated, middle mediastinal mass (arrowheads), which on the AP tomogram, B, is seen to displace the right bronchus (arrowheads). C CT demonstrates a lobulated mass (arrowheads) in the azygo-esophageal recess.

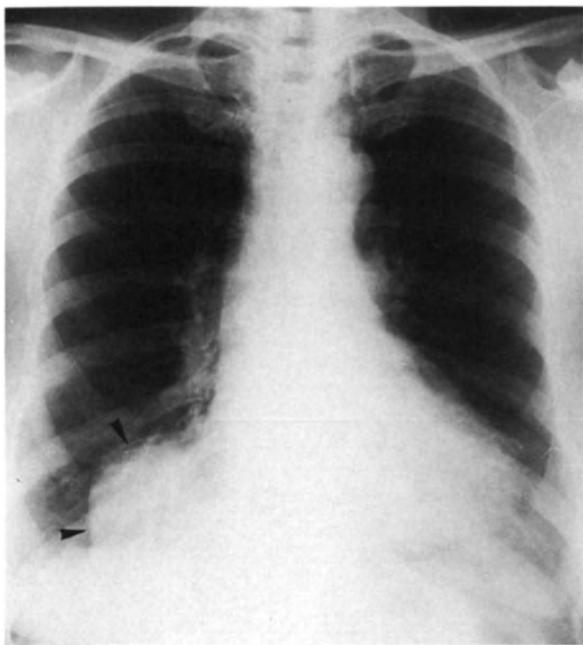


**Fig. 7.18.** Pleuropericardial cyst. A well-defined round opacity (arrowheads) occupies the right cardiophrenic angle.

are ganglioneuromas or neuroblastomas. Mediastinal neurofibromas and neurofibrosarcomas may be a part of von Recklinghausen's neurofibromatosis (Fig. 7.19). Pheochromocytomas and chemodectomas occasionally arise in the mediastinum.

**Imaging.** Most neurogenic tumors present at simple radiography as asymptomatic round, paraspinal soft tissue masses

(Fig. 7.20). They may produce symptoms by pressure on adjacent bone or on the spinal cord. Splaying of ribs posteriorly, rib notching or enlargement of neural foramina may be visible. Bone destruction usually indicates a malignant tumor. Calcification is commoner in malignant tumors. CT with water-soluble contrast medium enhancement of the CSF is the best method to assess intraspinal extent of these tumors.

*Lateral thoracic meningocele* is a rare cause of posterior mediastinal mass in von Recklinghausen's disease.

#### Neuroenteric Cysts

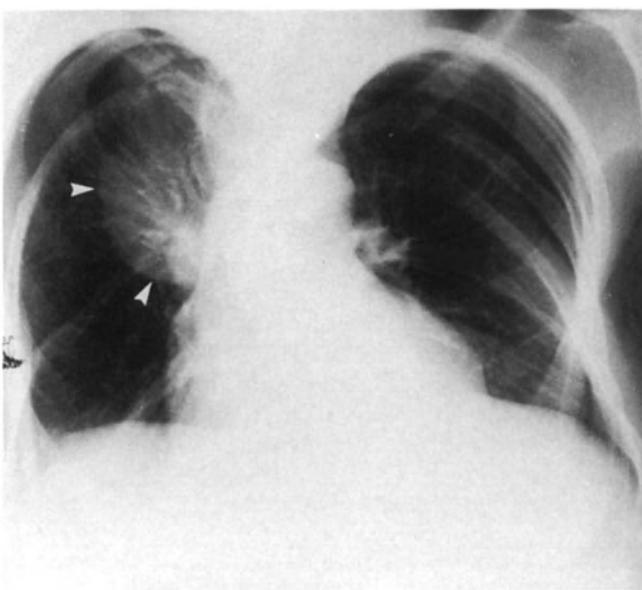
Neuroenteric cysts are rare developmental abnormalities due to persistence of elements of the neuroenteric canal. They may connect with either the foregut or the spine, and present as a round or oval soft tissue mass between the spine and esophagus. Barium swallow usually shows displacement of the esophagus and will occasionally show communication between an enteric cyst and esophagus. *Anterior meningoceles* may be associated with congenital anomalies of the spine, such as hemivertebra and block vertebra.

#### Paravertebral Lesions

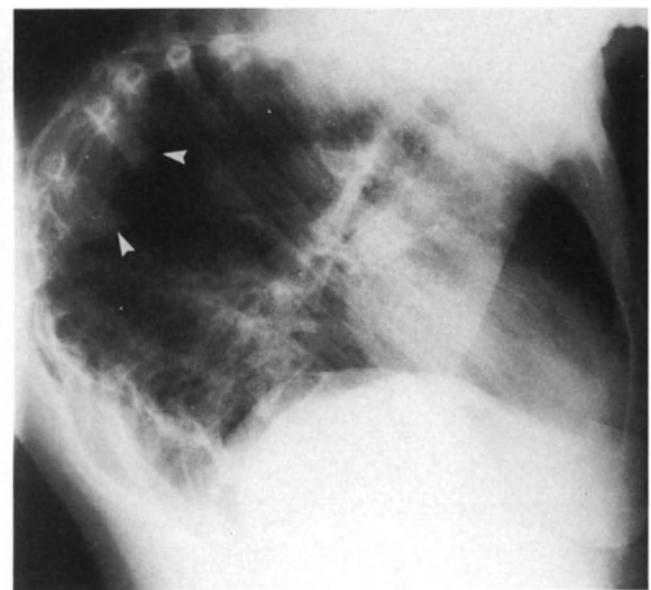
Paraspinal abscess due to pyogenic or tuberculous infection, hematoma secondary to spinal injury, metastatic cancer, myeloma, lymphoma and extramedullary hematopoiesis may all produce posterior mediastinal masses. Diagnosis is usually evident from the history and examination of dorsal spine films, but may require needle aspiration.

#### Esophageal Lesions

Zenker's diverticulum may produce a round soft tissue opacity, possibly with a fluid level, in the superior mediastinum. Dilatation of the esophagus due to achalasia, Chagas'



**Fig. 7.19A, B.** Mediastinal neurofibroma in von Recklinghausen's neurofibromatosis. A round, posterior mediastinal mass (arrowheads) is associated with thoracic kyphosis and rib deformities.



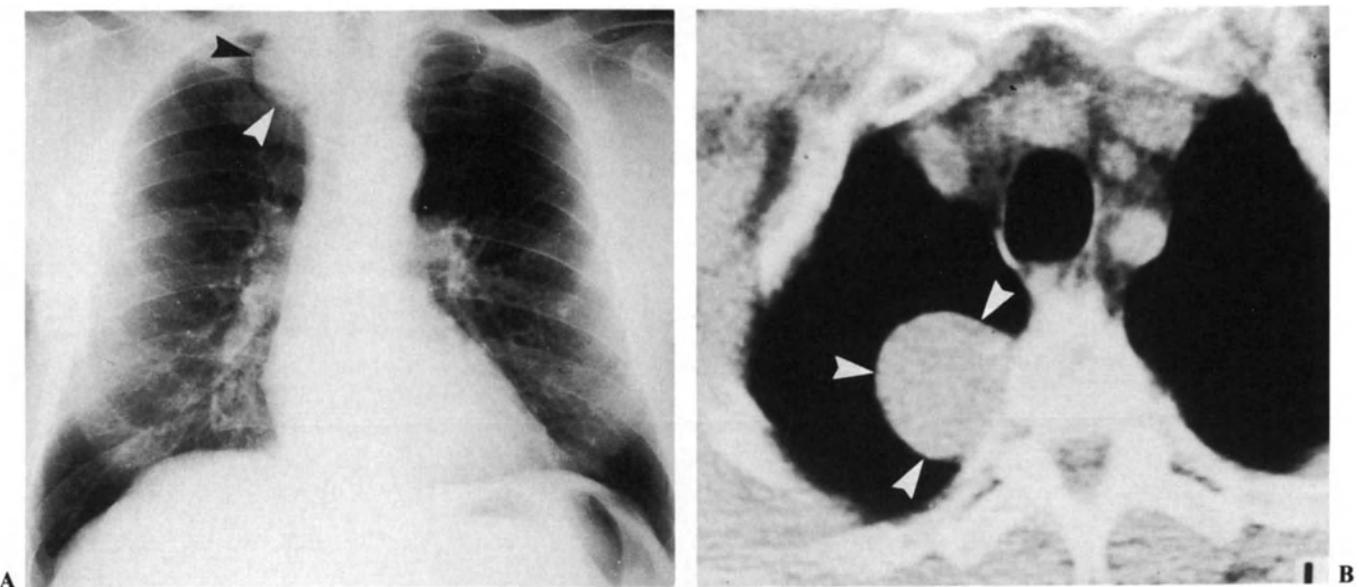


**Fig. 7.20A, B.** Mediastinal neurofibroma. A Chest radiograph in asymptomatic patient shows posterior mediastinal mass (arrowheads). B CT confirms the paraspinal location of the mass (arrowheads).

disease, scleroderma, or esophageal stricture may be visible as widening of the posterior mediastinum (Fig. 7.21). A fluid level and food may be visible in the dilated esophagus, and there may be evidence of aspiration pneumonitis.

#### Diaphragmatic Abnormalities

Hiatus hernia may present as a mid-line, retrocardiac mass. It may appear solid, air filled or show a fluid level (Fig. 7.22).

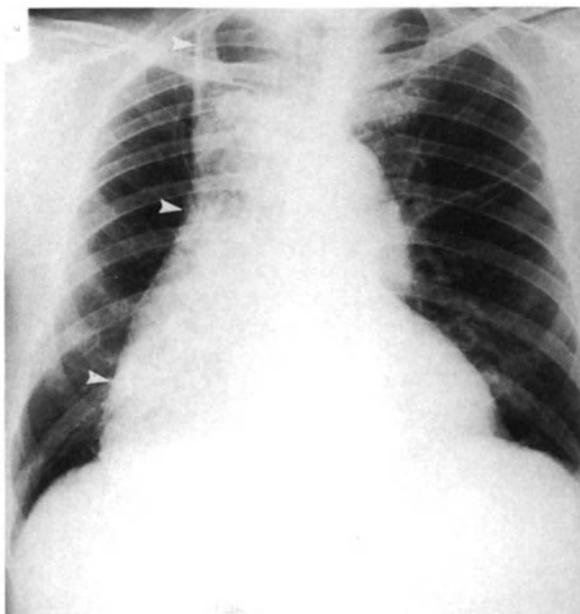


**Fig. 7.21.** Achalasia. The mediastinum is widened by the grossly dilated esophagus (arrowheads), which contains a large amount of food residue.

Morgagni hernia may present as an anterior mediastinal mass, and Bochdalek hernia as a posterior mediastinal mass.

#### Mediastinal Fat

Fat is normally present in the mediastinum. It is often easily visible in the cardiophrenic angles producing epicardial fat pads. In obesity, Cushing's syndrome and in steroid therapy excessive fat may be deposited in the mediastinum causing mediastinal widening. This can easily be differentiated from other causes of mediastinal widening by CT (Fig. 7.23).

#### Mesenchymal Tumors

Fibromas, lipomas, hemangiomas, lymphangiomas and their malignant counterparts may occur anywhere in the mediastinum.

### OTHER MEDIASTINAL ABNORMALITIES

#### Pneumomediastinum

Pneumomediastinum or mediastinal emphysema is the presence of air between the tissue planes of the mediastinum. This may occur secondary to *interstitial pulmonary emphysema*, *perforation* of the esophagus, trachea or a bronchus or from a *penetrating chest injury*.

Interstitial pulmonary emphysema results from alveolar wall rupture due to a high intra-alveolar pressure. This may occur during violent coughing, asthmatic attacks, during positive pressure ventilation or with crush injuries. Air from the ruptured alveoli may then dissect along the bronchovascular sheath and into the mediastinum.

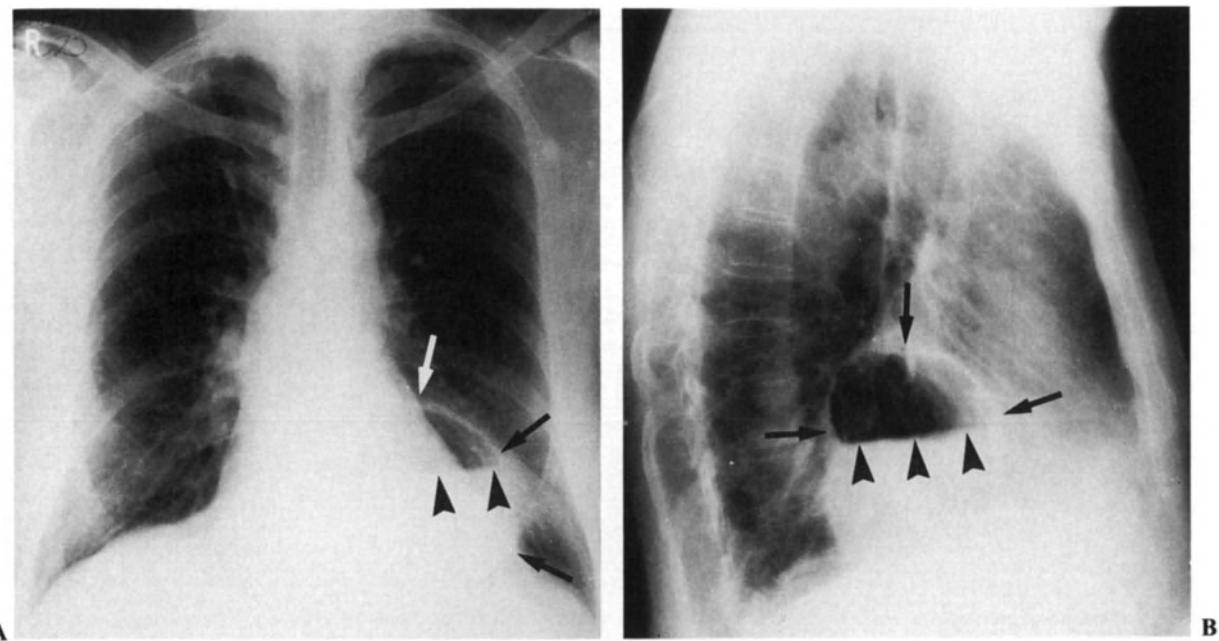


**Fig. 7.22A, B.** Hiatus hernia. A, B The hernia appears as a retrocardiac opacity (arrows) containing a fluid level (arrowheads).

The *chest radiograph* (Fig. 7.24) may show vertical, translucent streaks in the mediastinum, representing air separating the soft tissue planes. The air may extend up into the neck and over the chest wall causing subcutaneous emphysema, and also over the diaphragm. The mediastinal pleura may be displaced laterally and then be visible on the

chest radiograph. Pneumomediastinum may be complicated by a pneumothorax.

#### Acute Mediastinitis

Acute mediastinitis is usually due to perforation of the esophagus, pharynx or trachea. The chest radiograph

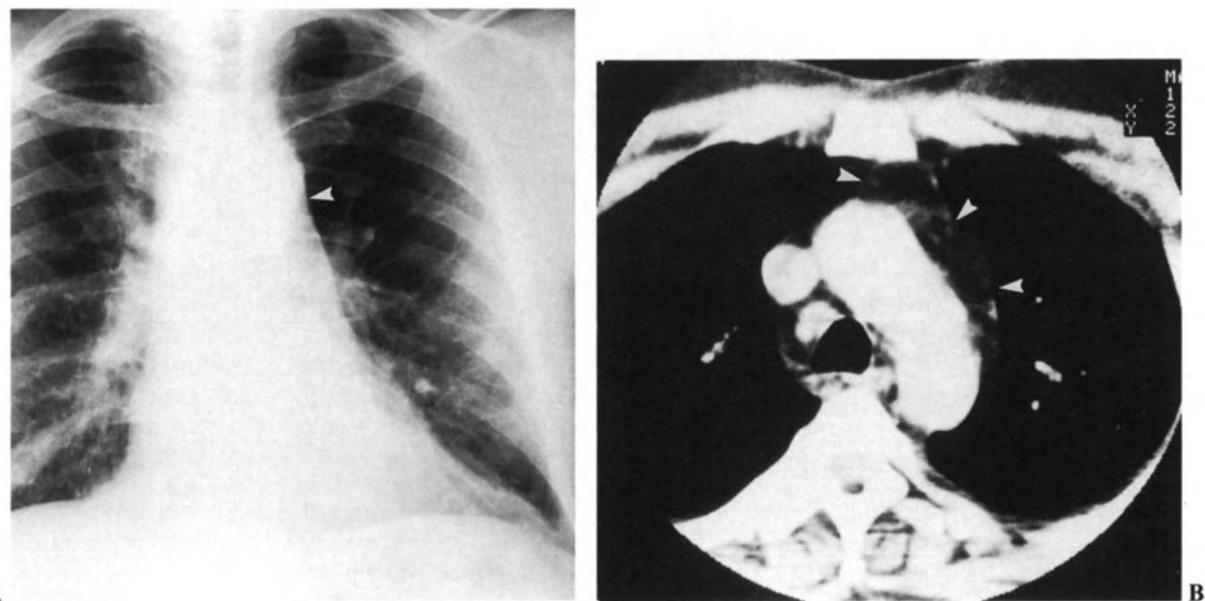


**Fig. 7.23A, B.** Mediastinal fat. A The chest radiograph was suspicious of a mass in the aorticopulmonary window (arrowhead). B CT shows this appearance is due to fat (arrowheads) adjacent to the aorta.

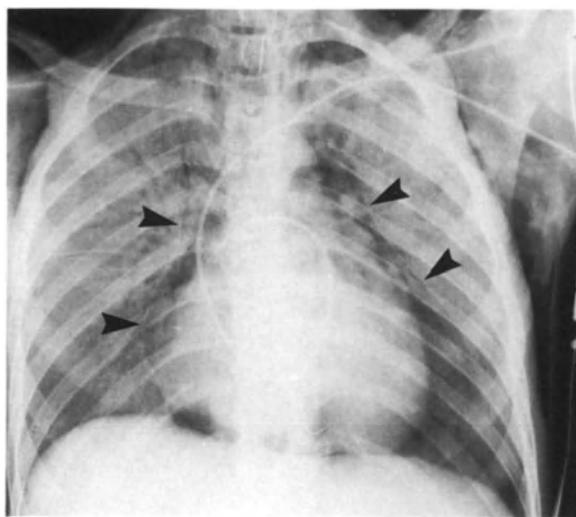


**Fig. 7.24.** Pneumomediastinum. Patient with viral pneumonia on positive pressure ventilation. Air in the mediastinum outlines the mediastinal pleura (arrowheads) and displaces it laterally, and also outlines the inferior surface of the pericardium. Streaky lucencies are visible in the upper mediastinum and soft tissue emphysema extends over the chest wall.

usually shows widening of the mediastinum. A pneumomediastinum is often apparent, and fluid levels may be visible in the mediastinum. Pleural effusions are also frequently seen.

#### Chronic Mediastinitis

Chronic or fibrosing mediastinitis usually presents as superior vena caval obstruction. The causes include *tuberculosis*, *histoplasmosis*, *radiotherapy* and *drugs* such as methysergide and practolol. It may also be *idiopathic* and associated with retroperitoneal fibrosis. The mediastinum usually appears widened (Fig. 7.25). Superior vena cavography may demonstrate occlusion of the superior vena cava and dilatation of the azygos vein and veins over the chest wall.

*Mediastinal hemorrhage* is usually due to trauma, and may occur from venous or arterial bleeding. It may also be due to a leaking aortic aneurysm or anticoagulant therapy. The mediastinum appears widened, and blood may be seen tracking over the lung apices. It is obviously imperative to identify any life-threatening cause such as aortic rupture.

*For further reading, see p. 134.*

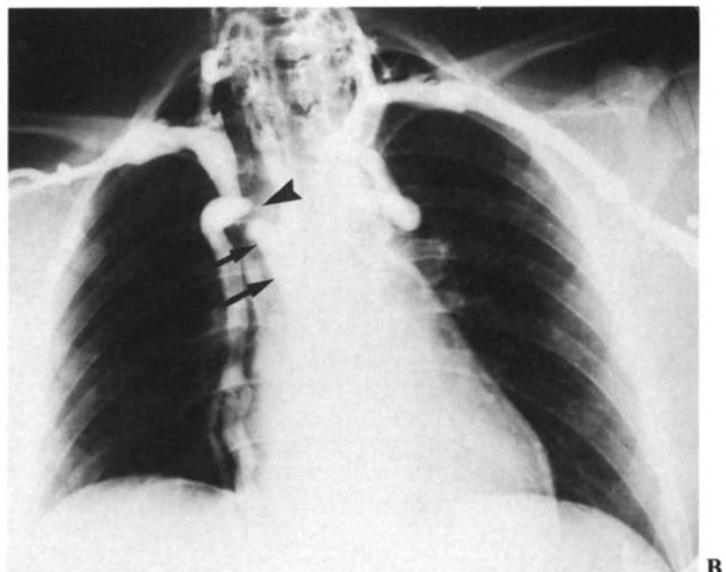
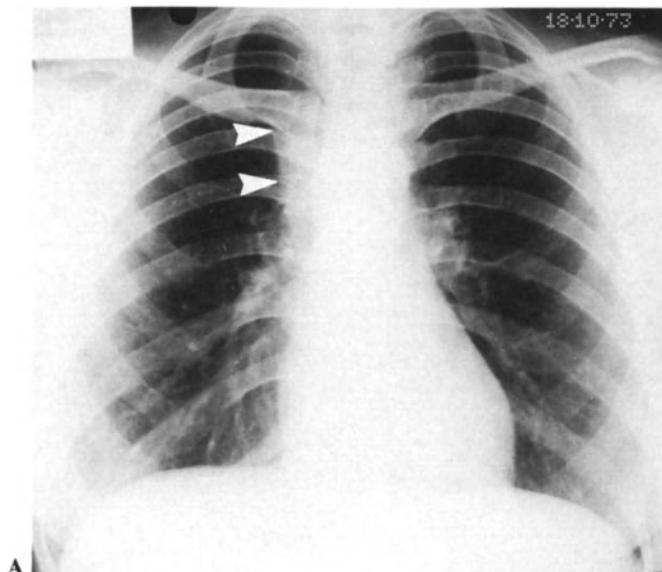


**Fig. 7.25A, B.** Fibrosing mediastinitis. A Chest radiograph shows widening of mediastinum to the right (arrowheads). B Superior vena cavogram shows occlusion of the SVC (arrowhead) dilatation of the azygos vein (arrows) and large collateral veins in the neck and thorax.

## CHAPTER 8

# CHEST TRAUMA, THE POST-OPERATIVE CHEST AND INTENSIVE CARE

*M. Rubens*

## CHEST TRAUMA

Chest trauma may result from penetrating or non-penetrating injury. The former is most often due to stabbing or shooting, and the latter to falls, blows or blasts. Major thoracic trauma is most frequently the result of a road traffic accident. Any part of the chest may be injured.

### Injuries to the Thoracic Cage

Acute rib fractures are common, but up to 15% are not visible on a standard chest radiograph. It is more important

to recognize any complication of a fracture than a fracture itself. Complications include pneumothorax (Fig. 8.1), hemothorax, subcutaneous emphysema (Fig. 8.2) and flail segment (Fig. 8.3).

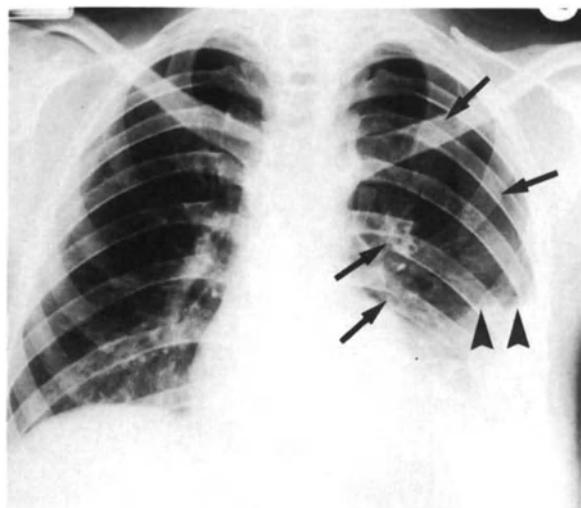


Fig. 8.1. Hemopneumothorax secondary to rib fractures. Road traffic accident. The left seventh and eighth ribs are fractured (black arrows) and a pneumothorax (white arrows) and a pleural fluid level (black arrowheads) are present.

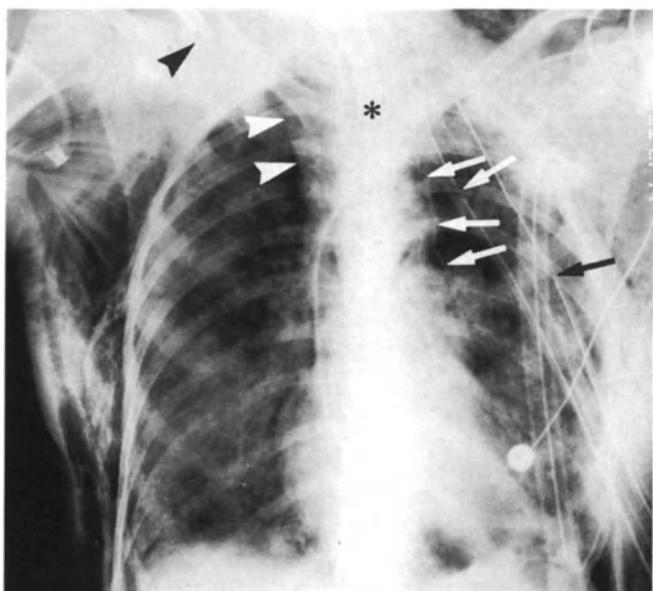
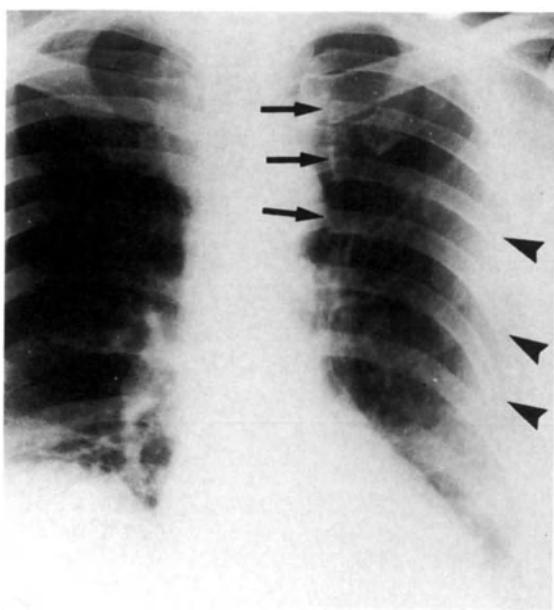
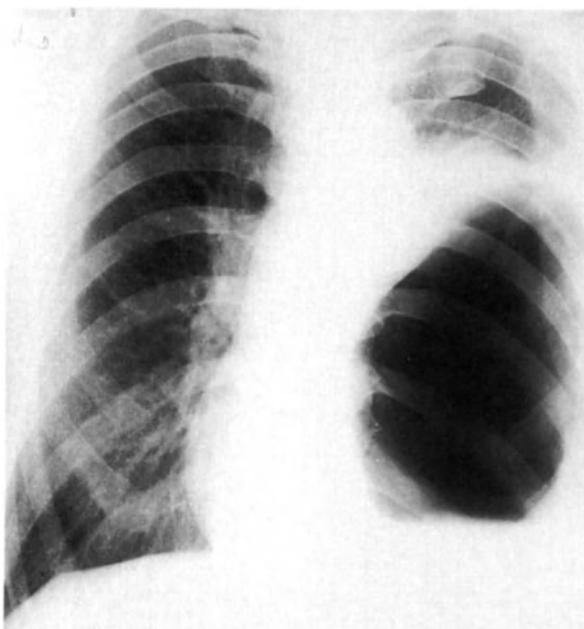


Fig. 8.2. Severe chest trauma. Road traffic accident. Several ribs were fractured (not visible on this film). Right clavicle is fractured (black arrowhead). Extensive subcutaneous emphysema extends over the chest wall separating the muscle planes. Mediastinal emphysema outlines and displaces the mediastinal pleura (white arrows). The upper mediastinum is widened by hematoma (white arrowheads). A Swan-Ganz catheter, tracheostomy tube (asterisk) and left pleural tubes (black arrows indicate side holes) are present.



**Fig. 8.3.** Flail chest. Road traffic accident. Several left ribs are fractured both posteriorly (arrows) and anteriorly (arrowheads).



**Fig. 8.4.** Laceration of the diaphragm. Patient presented with vomiting. Past history of falling from building some years earlier with multiple fractures of legs and injuring chest. The chest radiograph shows indistinct left hemidiaphragm and distended, air-filled stomach in left hemithorax. Thoracotomy showed laceration of left hemidiaphragm with herniation of stomach into left pleural space.

Fractures of the 1st and 2nd ribs are usually the result of severe trauma and may be associated with injury of the brachial plexus, subclavian vessels, aorta or major airway. Fractures of the 10th, 11th and 12th ribs may be associated with injury of abdominal viscera.

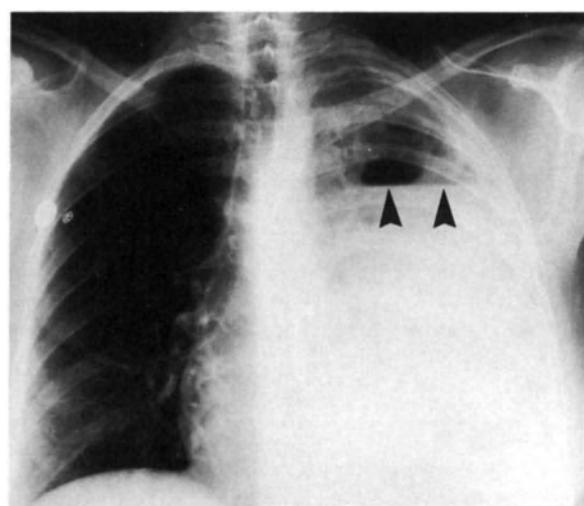
Fractures of the sternum may only be visible on a lateral film, and may be associated with injuries of the heart and aorta. Fractures of the thoracic spine may be associated with a paraspinal hematoma.

#### Injuries to the Diaphragm

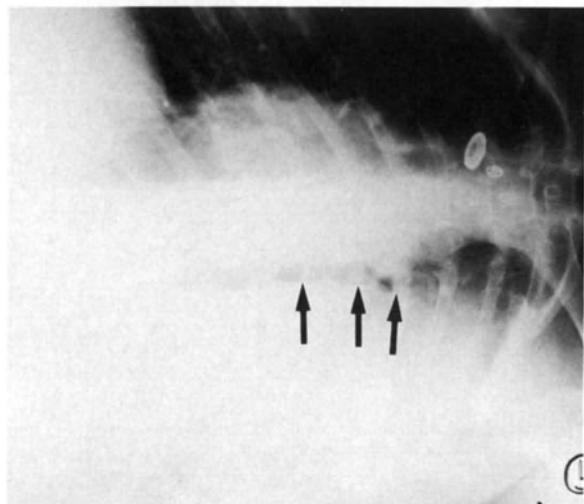
Laceration of the diaphragm occurs from both blunt and penetrating injury to the chest or abdomen. The left dome is more often involved as the liver provides some protection on the right. The involved dome is poorly defined on the chest film, and herniated abdominal viscera may be seen in the chest (Fig. 8.4).

#### Injuries to the Pleura

*Pneumothorax* and *hemothorax* may either be a complication of a rib fracture or be due to penetrating injury. If a tension pneumothorax develops it will require emergency decom-



A



B

**Fig. 8.5A, B.** Pyo-pneumothorax. Gun shot wound. A Erect chest radiograph ► shows pleural thickening over apex of left lung, and fluid level (arrowheads) in left upper zone, B Horizontal beam left lateral decubitus film shows multiple loculated fluid levels (arrows) in left pleural space.

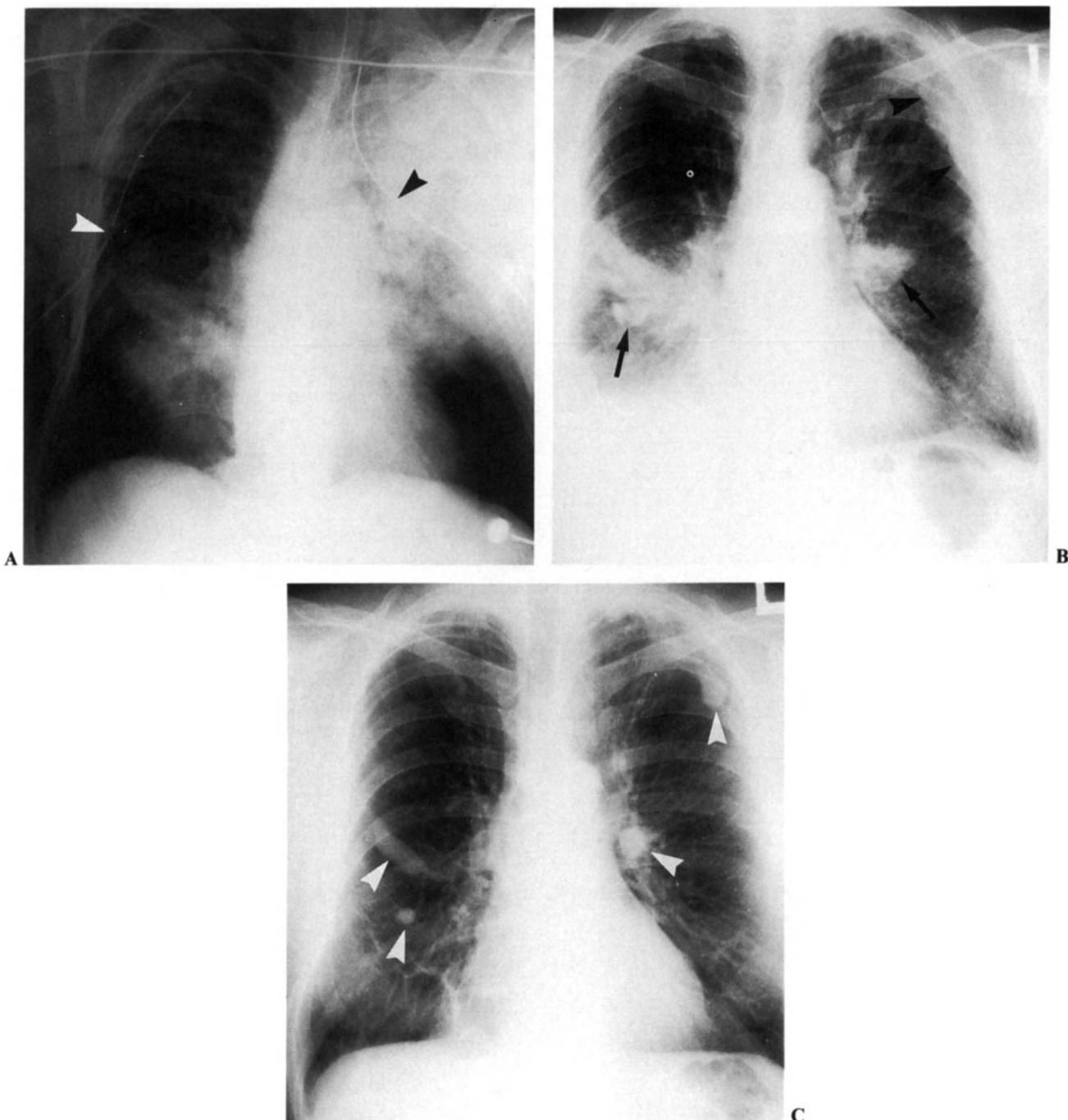


**Fig. 8.6A, B, C.** Pulmonary contusion and hematomas. Crush injury. A Consolidation is present in both lungs, particularly in the left upper and mid zones and the right lower zone. Bilateral pleural drains are present (*arrowheads indicate side holes*). B 6 days later much of the contusion has resolved revealing pulmonary hematomas (*arrows*) and extrapleural hematomas (*arrowheads*). C 30 days later the pulmonary hematomas (*arrowheads*) are still visible, but smaller.

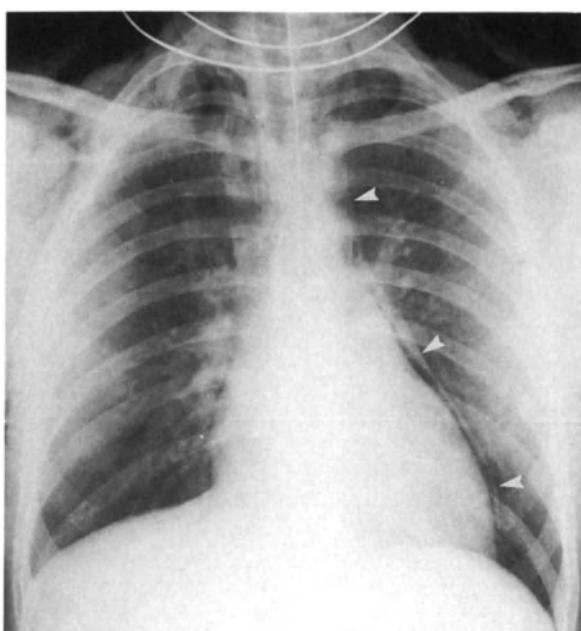


**Fig. 8.7.** Pneumomediastinum. Road traffic accident. The air in the mediastinum outlines and displaces the mediastinal pleura (arrowheads) laterally. Streaky lucencies are present in the upper mediastinum and subcutaneous emphysema is visible in the neck and supraclavicular fossa.

pression. When a hemopneumothorax is present a fluid level is seen on a horizontal beam film (Fig. 8.1). Pleural effusion secondary to open trauma may become infected and an empyema may develop (Fig. 8.5).

### Injuries to the Lung

Pulmonary contusion and laceration may occur following either penetrating or non-penetrating injury.

*Contusion* appears as patchy, non-segmental consolidation due to hemorrhagic exudation into the alveoli and interstitial spaces (Fig. 8.6). It usually resolves over 4 or 5 days.

The edges of *lacerated lung* retract to produce a cyst-like space which usually fills with blood producing a round, homogenous opacity. These pulmonary hematomas may be multiple, and may take several months to resolve (Fig. 8.6). A hematoma may be obscured by contusion in the first few days following trauma.

Other causes of patchy consolidation following trauma include *aspiration*, *adult respiratory distress syndrome* and *fat embolism*.

### Injuries to the Mediastinum

Pneumomediastinum (Fig. 8.7) or *mediastinal emphysema* may be due to penetrating or non-penetrating injury. In the latter instance it is secondary to interstitial pulmonary edema or perforation of the trachea, a bronchus or the esophagus.

*Interstitial pulmonary emphysema* develops when high intra-alveolar pressure causes alveolar rupture. This may occur in crush injuries, asthmatic attacks, during violent coughing and secondary to positive pressure ventilation.

*Laceration or rupture of the trachea* or a *bronchus* is rare. It follows severe trauma, often with fracture of the 1st rib. The injury almost always occurs within 3 cm of the carina. Mediastinal emphysema and pneumothorax are frequent (Fig. 8.8) and the diagnosis is best made by bronchoscopy.

*Esophageal rupture* is a rare complication of chest trauma. Most cases follow esophageal instrumentation or surgery,

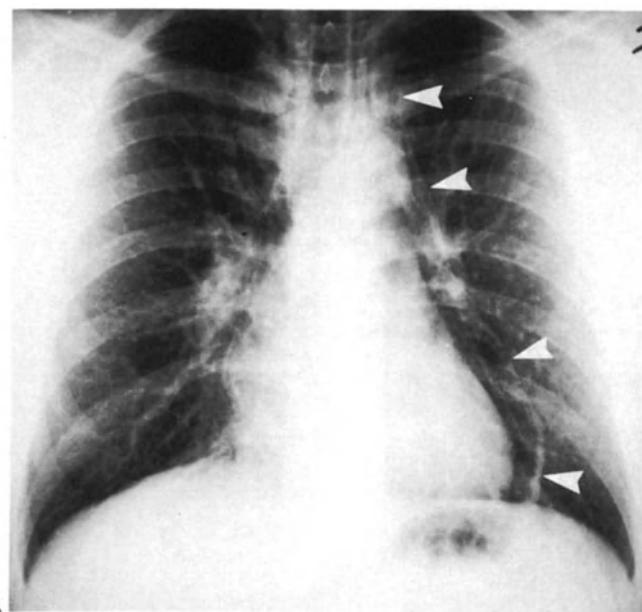


**Fig. 8.8A, B.** Lacerated trachea. Car crash victim. A Streaky lucencies in upper mediastinum, and visibility and displacement of parietal pleural (arrowheads) indicate pneumomediastinum. B One hour later a left pneumothorax has developed. Bronchoscopy showed laceration of trachea just above carina.

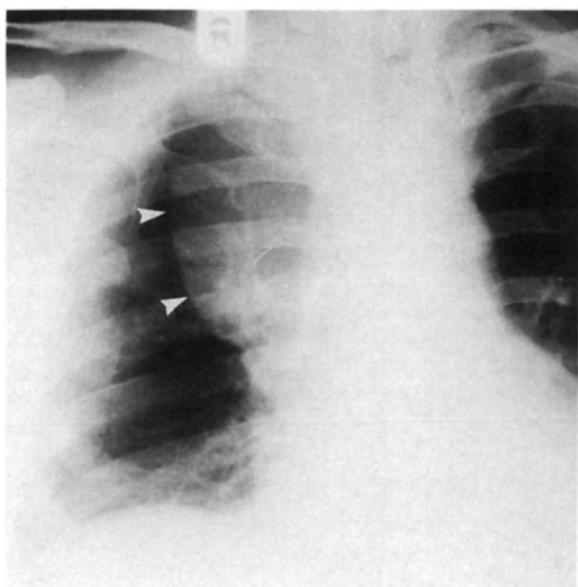


**Fig. 8.9.** Mediastinal hematoma. A large extrapleural hematoma (arrowheads) developed following attempted insertion of central venous line via right subclavian vein.

but it may occasionally occur spontaneously following sudden increase in intraesophageal pressure (Boerhaave's syndrome). The chest radiograph will usually show pneumomediastinum, pneumothorax or pleural effusion. The radiographic diagnosis may be made by a swallow with dilute barium or water-soluble contrast medium.

*Mediastinal hemorrhage* may be seen with both penetrating and non-penetrating injuries, and may be due to venous (Fig. 8.9) or arterial bleeding. The most important cause is aortic rupture. Usually there is bilateral mediastinal widening, but localized hematoma may occur.

*Aortic rupture* is usually due to a road traffic accident. Most aortic tears occur at the site of the ligamentum arteriosum. Only 10%–20% of the patients survive the injury long enough to reach hospital. The commonest abnormalities on the chest film are widening of the mediastinum and indistinctness of the aortic knuckle (Fig. 8.10). Other signs are a left apical extrapleural cap, left pleural effusion, deviation of the trachea or nasogastric tube to the right and downward displacement of the left main bronchus. The diagnosis is confirmed by aortography or CT (see Chap. 13).

#### Radiation Injuries of the Thorax

Radiotherapy for breast, lung and mediastinal tumors may damage tissues in the treatment field.

Radiation pneumonitis is characterized by two phases (Fig. 8.11). The acute or exudative phase corresponds to bronchiolar desquamation and accumulation of alveolar exudate. It appears radiographically as non-segmental consolidation often corresponding to the shape of the treatment portal. These changes develop between 1 and 6 months after treatment, and are followed by the fibrotic phase which is usually completed by 12 months after treatment. Pre-existing lung disease, previous radiotherapy and chemotherapy increase the likelihood of fibrosis.

Pleural and pericardial effusion are rare complications of radiotherapy and usually indicate progressive malignancy. Osteonecrosis of ribs or a clavicle is sometimes seen after breast radiotherapy.

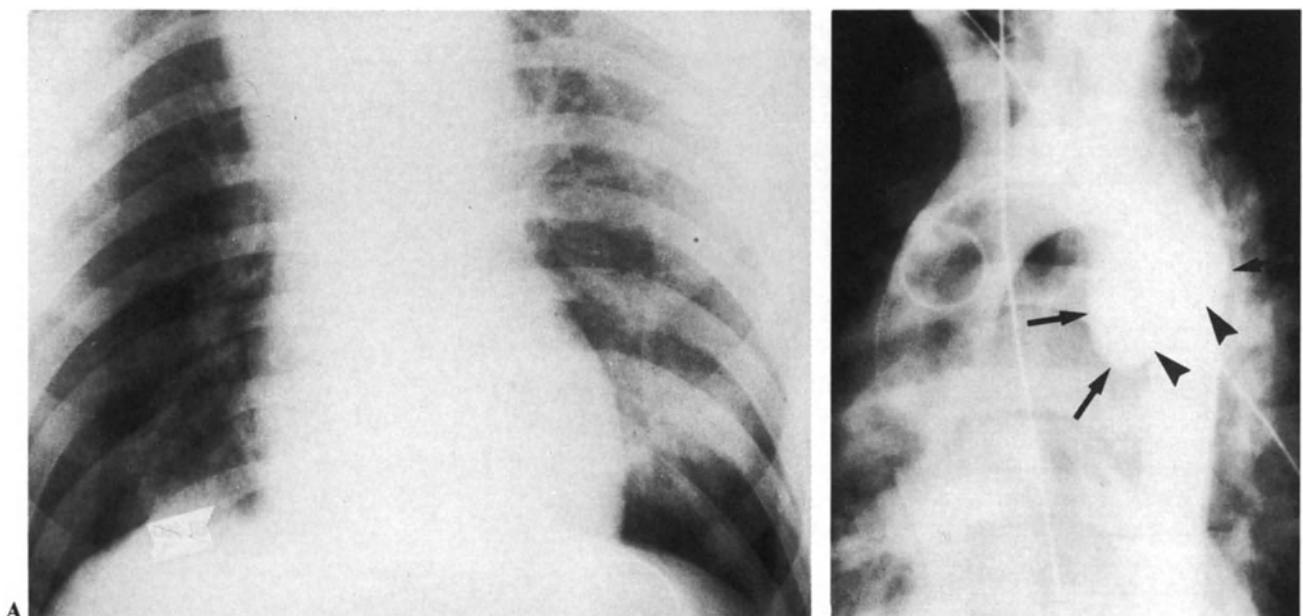


**Fig. 8.10A, B.** Mediastinal hemorrhage. Road traffic accident. A The upper mediastinum is widened bilaterally. The aortic arch is obscured. There is left pulmonary contusion. B Arch aortography shows dilatation of the aortic isthmus (arrows) and an intimal tear (arrowheads).

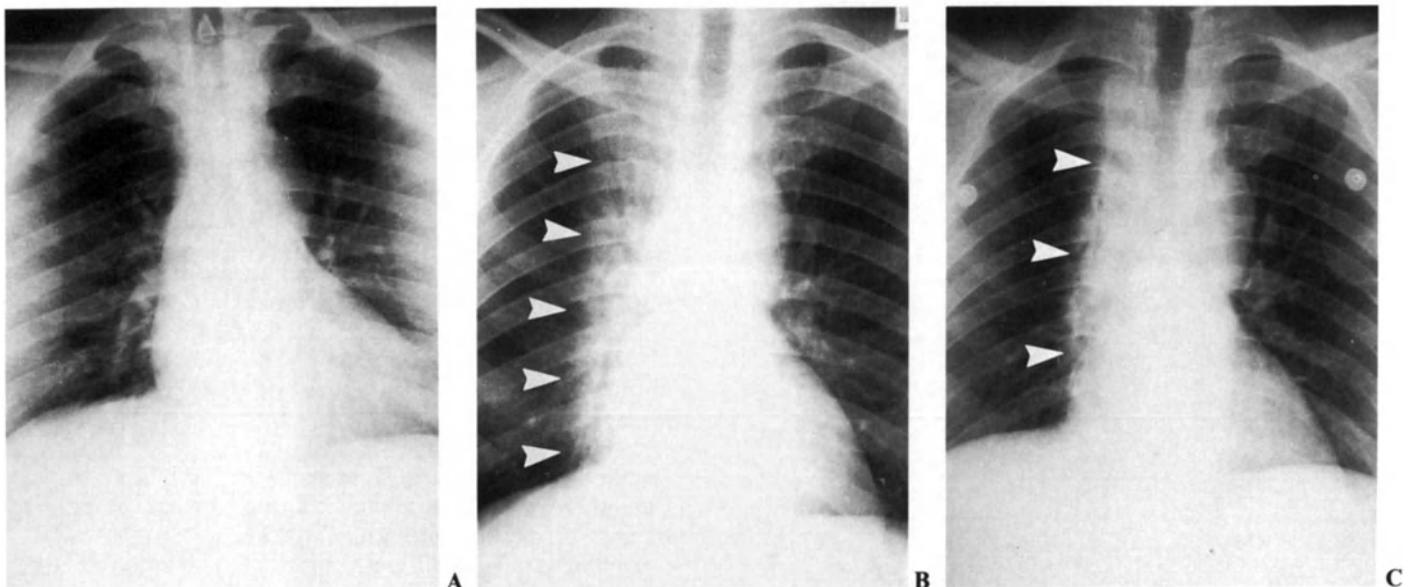


**Fig. 8.11A, B, C.** Radiation pneumonitis. Patient with upper thoracic spinal cord compression due to non-Hodgkin's lymphoma. A Prior to radiotherapy the lungs are clear. B 10 weeks after radiotherapy to whole thoracic spine there is paraspinal consolidation (arrowheads) and an air bronchogram is visible. C 14 weeks later paraspinal fibrosis (arrowheads) has developed.

## THE POST-OPERATIVE CHEST

### THORACIC COMPLICATIONS OF GENERAL SURGERY

**Atelectasis**, due to retained secretions and poor respiration, is the commonest pulmonary complication of surgery. The chest radiograph shows linear or curved band shadows, particularly in the lower zones (Fig. 8.12). They usually resolve within a day or two of surgery. **Pleural effusions** are commonly seen in the immediate post-operative period, and usually resolve within one or two weeks. Pleural effusions appearing later may be due to subphrenic infection or pulmonary embolism.

**Pneumothorax** may be a complication of positive pressure ventilation or central venous line insertion.

**Aspiration pneumonitis** is a common complication of general anesthesia. Patchy consolidation may be seen within hours of the anesthetic, and it usually resolves over 2 or 3 days. However, in major aspiration, progression to the adult respiratory distress syndrome (ARDS) may occur.

**Pneumonia** may complicate post-operative atelectasis or aspiration.

**Pulmonary edema** may occur as a result of heart failure, fluid overload or as a result of increased capillary permeability, due to ARDS, drugs or toxemia.

**Pulmonary embolism** may be associated with pulmonary shadowing, pleural effusion, elevation of the diaphragm or a normal chest radiograph. It is best diagnosed by radio-nuclide ventilation/perfusion lung scanning.

**Subphrenic abscess** usually causes elevation of the diaphragm and a pleural effusion. Subdiaphragmatic gas may be visible. The diagnosis may be confirmed by ultrasound or CT.

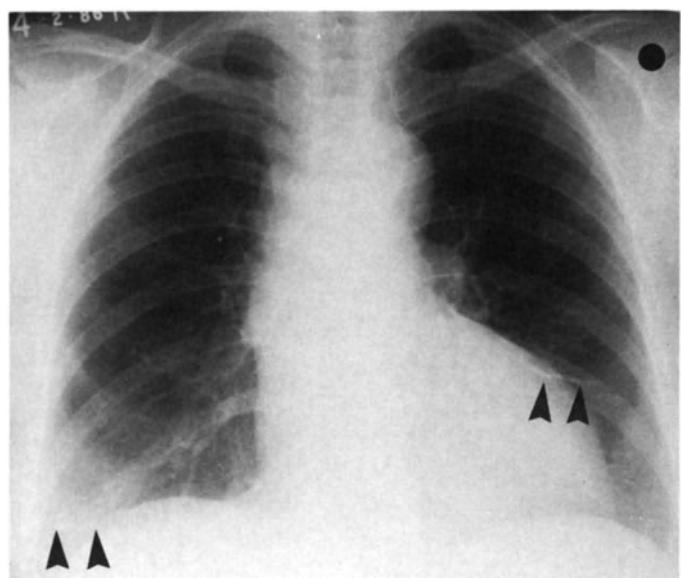


**Fig. 8.12.** Post-operative atelectasis. Horizontal band shadows (arrowheads) are visible in both lower zones.

### THORACOTOMY

Lung resections are usually performed via the 4th or 5th intercostal space.

Immediately after *pneumonectomy* the chest radiograph should show the empty pneumonectomy space, a fully inflated contralateral lung and a central mediastinum. The pneumonectomy space then obliterates slowly over the next several weeks by a combination of accumulation of fluid and gradual shift of the mediastinum to the operated side (Fig. 8.13).

Following *lobectomy* or segmental and subsegmental resec-

tions the remaining lung should hyperinflate to fill the space of the resected lung. Small air spaces, often containing fluid, are frequent and usually resolve over a few weeks.

Complications of thoracotomy include pleural effusions, empyema and bronchopleural fistula.

*Pleural effusions* are common, but if large may be due to hemorrhage or chylothorax. *Empyema* is a serious complication and may lead to bronchopleural or pleurocutaneous fistula.

*Bronchopleural fistula* occurring soon after surgery is usually due to faulty closure of the bronchus; late occurrence is usually due to infection or recurrent tumor.

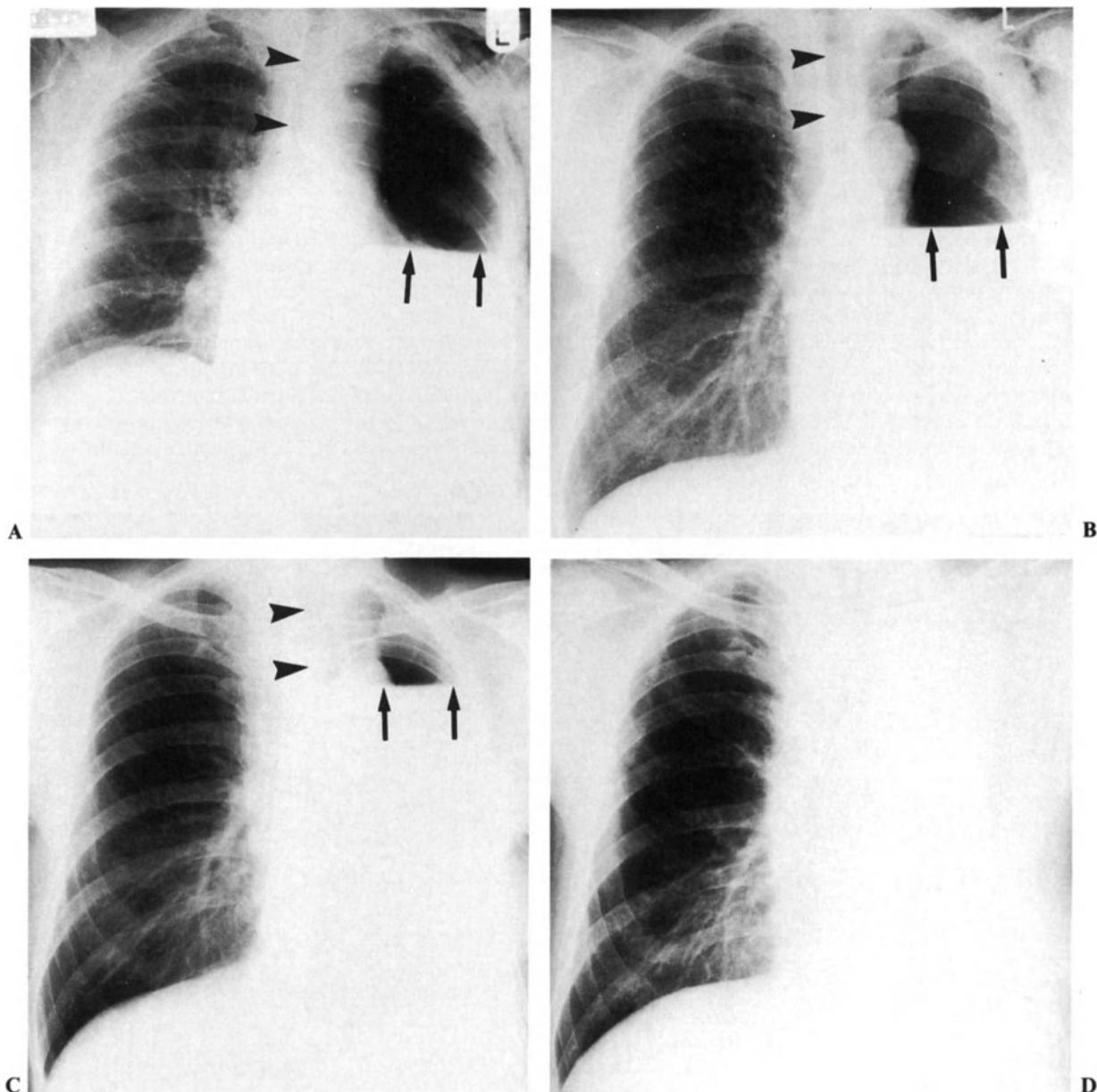
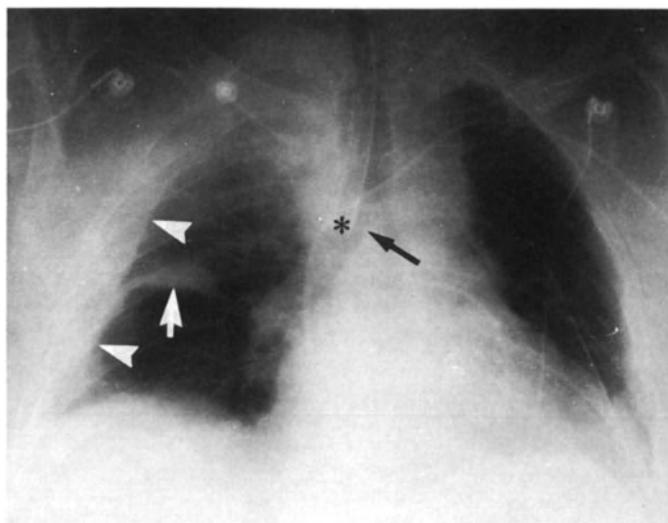
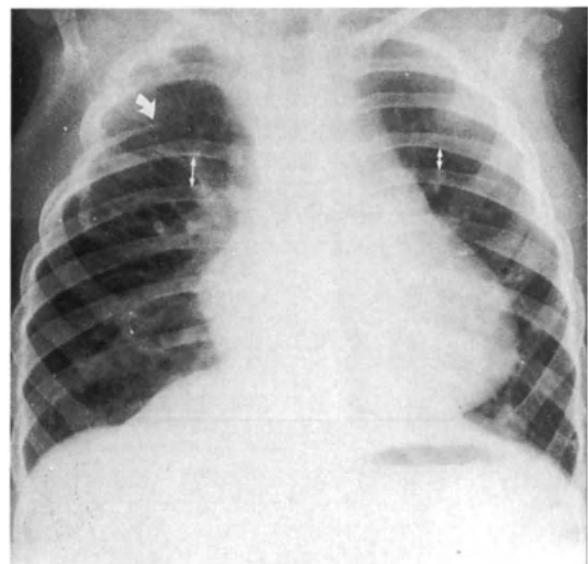


Fig. 8.13A, B, C, D. Normal post-pneumonectomy series. A One day; B 6 days; C 5 weeks; D 8 weeks after left pneumonectomy. The pneumonectomy space gradually obliterates by filling with fluid (arrows) and mediastinal shift. Note the progressive displacement of the trachea (arrowheads).



**Fig. 8.14.** Post-coronary surgery appearances. A right pleural effusion (white arrowheads) is present with fluid extending into horizontal fissure (white arrows). The endotracheal tube is inserted too far. Its tip (asterisk) passes beyond the carina (black arrow) and into the right bronchus.



**Fig. 8.15.** Thoracotomy rib changes. The right fourth rib (curved arrow) has been excised and has partly regenerated. The left fifth intercostal space is narrowed following a left thoracotomy (arrows).

### Cardiac Surgery

Most cardiac surgery is performed through a mid-line sternotomy, and *sternal wire sutures* may be visible on the chest radiograph. Mitral valve surgery is infrequently performed via a thoracotomy at present, but this route is still used in aortic coarctation, patent ductus arteriosus, pulmonary artery banding and for Blalock–Taussig shunts.

Following cardiac surgery *widening of the mediastinum* and *left basal shadowing* are almost always present, and small

*pleural effusions* are also frequent (Fig. 8.14). These changes usually resolve over several days. Sudden widening of the mediastinum soon after surgery may indicate *hemorrhage*. The pleura may be damaged at surgery causing a *pneumothorax*. *Pneumopericardium* and *pneumoperitoneum*, due to incision of the peritoneum at the lower end of the sternotomy, are of no clinical importance.

Occasionally the *phrenic nerve* may be damaged leading to paresis or paralysis of a hemidiaphragm, and rarely a major

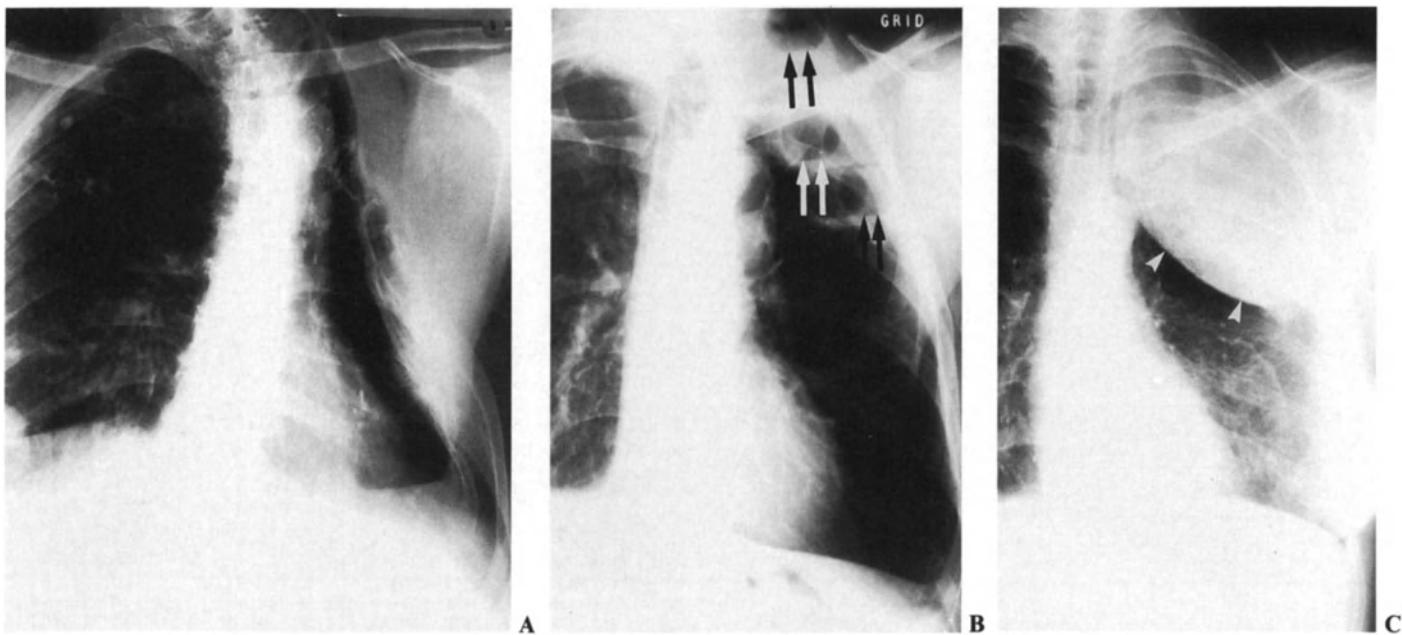


**Fig. 8.16A, B, C.** Operations for TB. A Thoracoplasty. Several of the upper left ribs have been excised. B Plombage. Hollow balls have been inserted into the extrapleural space at the left apex. The balls are permeable and several show fluid levels (arrows). C Oleothorax. Paraffin wax has been instilled extrapleurally, via a thoracotomy with partial excision of the fifth rib. The edge of the oleothorax is calcified (arrowheads).

lymphatic vessel may be damaged causing a *chylothorax*. The 1st and 2nd ribs are sometimes fractured posteriorly when the sternum is spread apart. *Sternal dehiscence*, which is usually secondary to osteomyelitis, may be seen on post-operative chest films as separation of the two sides of the sternum or as alteration in the position of the sternal sutures.

The *post-pericardotomy syndrome* may develop a month or more after surgery. It is characterized by fever, pericardial pain and pleurisy. The chest film may show enlargement of the cardiovascular silhouette due to pericardial effusion and pleural effusions.

#### Late Appearances after Chest Surgery

Following thoractomy *pleural thickening*, *resected rib* (Fig. 8.15) and *healed rib fractures* may be visible. *Rib notching* may be seen following formation of a Blalock-Taussig shunt between the subclavian and pulmonary arteries.

Following lung resection the lung tissues and hila may alter their positions. The stomach or loops of bowel may be visible in the chest following some esophageal operations. The chest film may show evidence of treatment of pulmonary tuberculosis from the pre-antibiotic area. This includes apical pleural thickening from artificial pneumothoraces, thoracoplasty and various types of plombage (Fig. 8.16).

## INTENSIVE CARE

Patients with major trauma, recent surgery or circulatory, respiratory, hepatic or renal failure may be managed with a wide variety of monitoring and life-support devices.

*Central venous pressure (CVP)* catheters are used to measure right atrial pressure. The tip should be in the superior vena cava. *Swan-Ganz catheters* (Fig. 8.14; Fig. 8.17) measure pulmonary artery and pulmonary wedge pressure. When wedge pressure measurements are not being made the catheter should be kept in the left or right pulmonary artery to prevent pulmonary infarction.

Introduction of catheters via subclavian vein puncture may be complicated by *pneumothorax* or *mediastinal hematoma* (Fig. 8.9).

*Nasogastric tubes* may not reach the stomach due to coiling

in the pharynx or esophagus, or due to insertion into the trachea (Fig. 8.18).

*Endotracheal tubes* should be placed with their tips 5–6 cm above the carina (Fig. 8.19). Tubes that are inserted too far tend to pass into the right bronchus (Fig. 8.14) causing *collapse of the left lung*. The cuff of the tube should be checked for hyperinflation, which may lead to *ischemia of the trachea*.

*Tracheostomy tubes* should be situated centrally with the tip at the T-3 level (Fig. 8.2). Their insertion may be complicated by *pneumomediastinum*, *pneumothorax* and *subcutaneous emphysema*.

*Positive pressure ventilation* may be complicated by *interstitial emphysema*, *pneumomediastinum*, *pneumothorax*, *tension pneumothorax* and *subcutaneous emphysema* (Fig. 8.20).

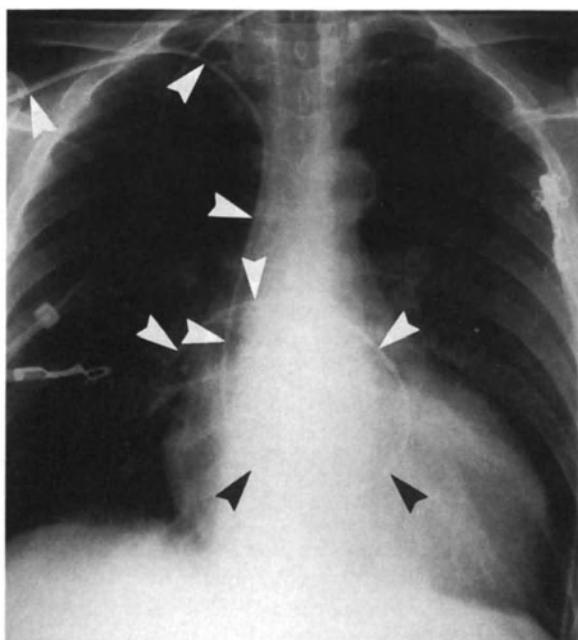


Fig. 8.17. Swan-Ganz catheter. The catheter (arrowheads) has been introduced via the right subclavian vein. Its tip is in the right basal artery.

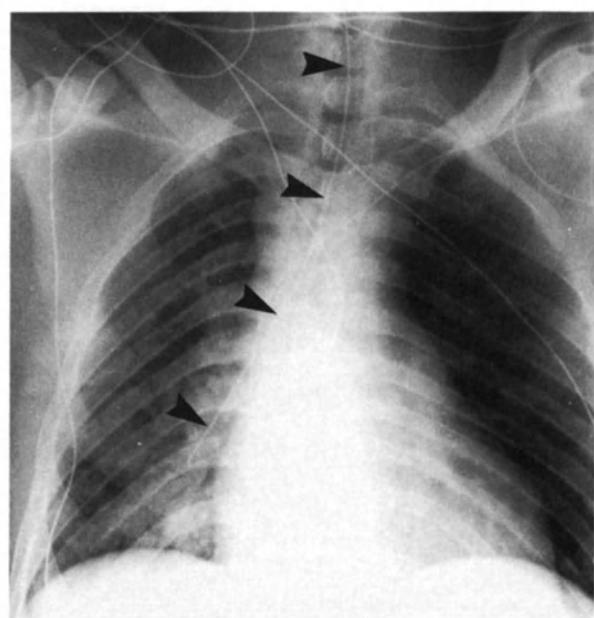
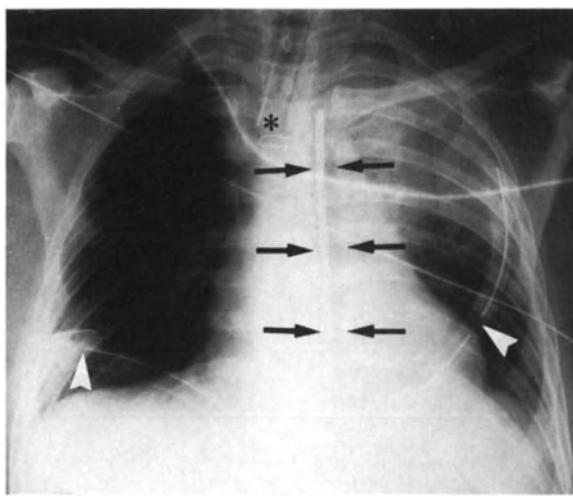
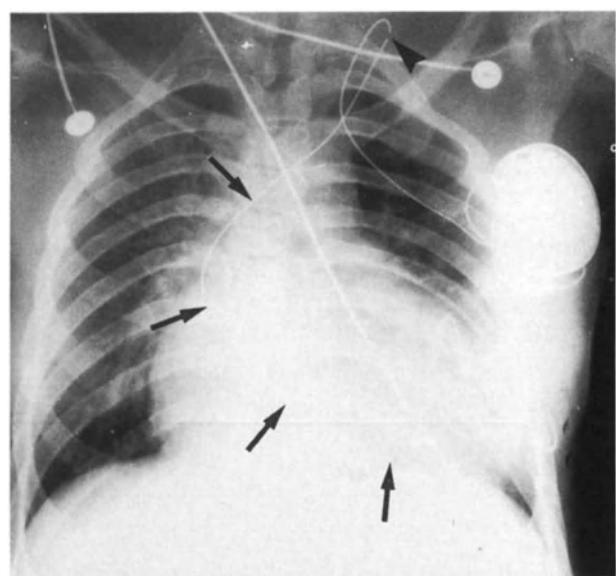


Fig. 8.18. Nasogastric tube (arrowheads) has been inserted into the right bronchus.



**Fig. 8.19.** Post-coronary artery surgery. An endotracheal tube is present with its tip (asterisk) in good position. Bilateral pleural tubes (arrowheads) and an intrathoracic aortic balloon pump (arrows) are present.



**Fig. 8.21.** Fractured pacing wire. A permanent transvenous pacing system is present. The electrode (arrows) is fractured (arrowhead).

Pleural and mediastinal drains should be checked for position (Figs 8.2, 8.6A, 8.19).

*Intra-aortic balloon pumps*, to support patients with cardiogenic shock, are introduced via the femoral artery. The balloon lies in the descending aorta, and the tip should be just distal to the origin of the subclavian artery (Fig. 8.19).

*Pacemakers* may be transvenous or epicardial. The tip of the electrode should be in stable position in the right ventricle. If a patient is not pacing properly the electrode may have slipped or fractured (Fig. 8.21).

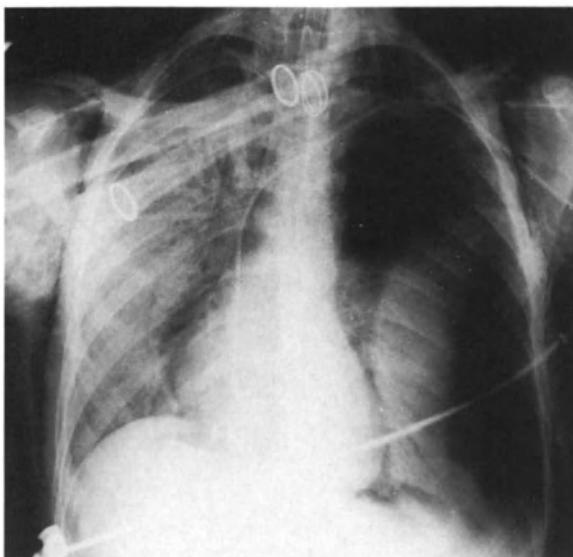


**Fig. 8.20.** Complications of positive pressure ventilation. A left tension pneumothorax is displacing the mediastinum to the right and depressing the left hemidiaphragm. Pneumomediastinum is visible and subcutaneous emphysema is present over the chest wall.

## PULMONARY EMBOLISM

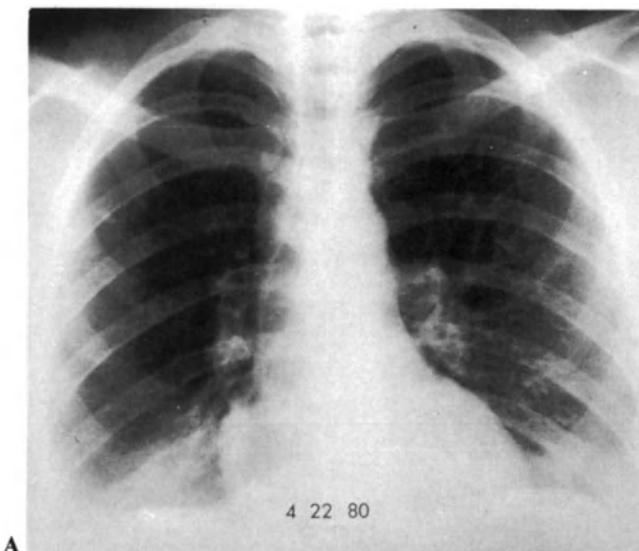
Pulmonary thromboembolism is the commonest pulmonary disease in hospitalized patients. Recent surgery, major trauma, prolonged immobilization and cardiac disease are important predisposing factors that make it a common problem in the intensive care environment. Other predisposing factors are pregnancy, oral contraceptives, malignant disease, increasing age and a history of deep venous thrombosis or previous pulmonary embolism.

Most clinically important pulmonary emboli arise in the femoral or pelvic veins. The clinical diagnosis of deep venous thrombosis (DVT) is unreliable, and the definitive diagnosis of DVT in the legs is usually made by phlebography. However, diagnosis by Doppler ultrasound is becoming widely available and will probably replace phlebography as the prime method of diagnosis. Active thrombosis may also be detected by radionuclide scanning using  $^{125}\text{I}$ -labelled fibrinogen (see Chap. 13).

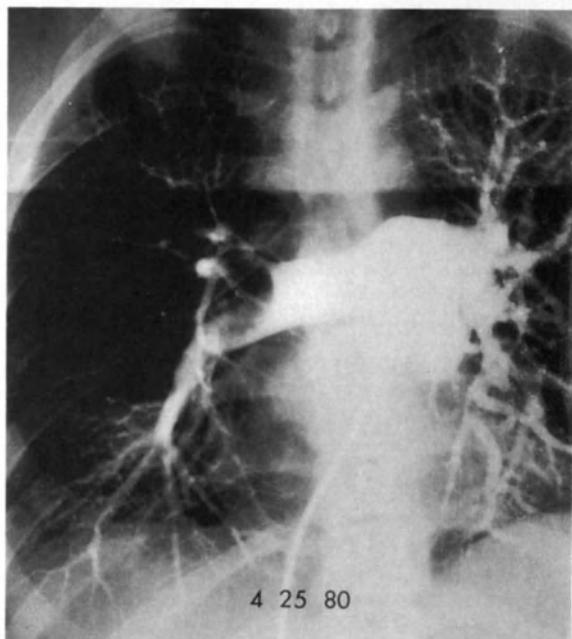
The clinical presentation of pulmonary embolism depends upon the size and number of emboli and the pre-existing cardiopulmonary state. Pulmonary infarction does not usually follow embolism unless there is already some degree of heart failure.

**Acute massive pulmonary embolism** is frequently a fatal event. However, if the patient survives, the *chest radiograph* may show areas of decreased perfusion (Fig. 8.22A). If the diagnosis is not certain on clinical grounds it may be confirmed by either ventilation-perfusion *lung scan* or *pulmonary angiography*. The diagnosis by isotope scan depends upon the demonstration of ventilation and perfusion mismatches (Fig. 8.22B). Pulmonary angiography will show occlusion of one or more central pulmonary arteries by embolus (Fig. 8.22C).

**Subacute pulmonary embolism** is usually due to fewer, smaller emboli. Areas of lung which are underperfused may



A



C

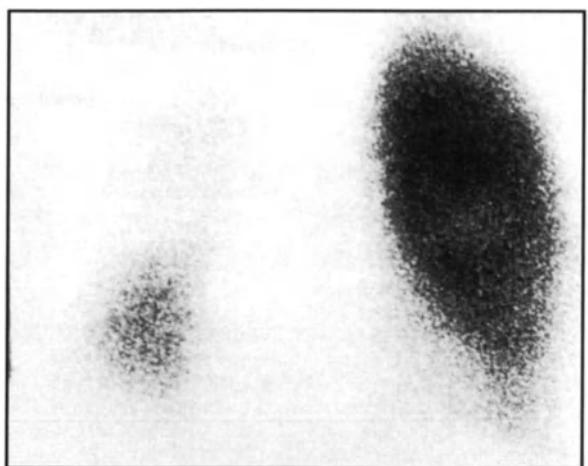


**Fig. 8.22A, B, C.** Acute massive pulmonary embolism. A Chest radiograph shows oligemic right lung. B Isotope perfusion scan. Frontal view shows non-perfused right upper lobe and poorly perfused right lower and middle lobes. The ventilation scan (not shown) was normal. C Pulmonary arteriogram shows large embolus in right pulmonary artery.

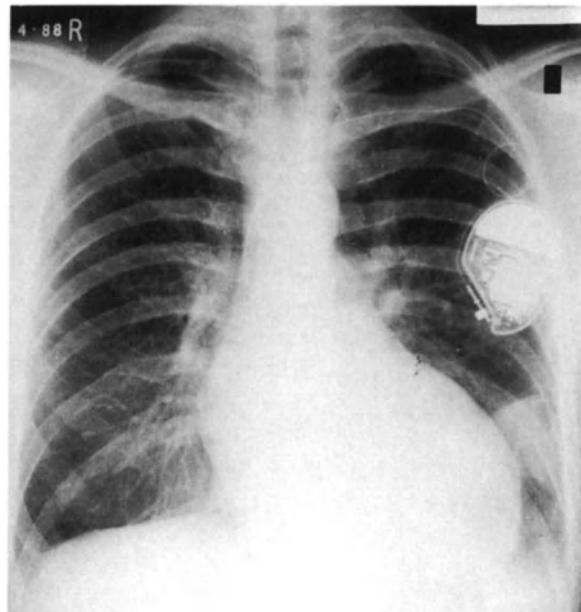


**Fig. 8.23.** Pulmonary infarcts. A pleural-based wedge-shaped area of consolidation is present in the left lower zone. Patient with congestive cardiomyopathy, heart block and pacemaker.

lose volume and appear as linear areas of subsegmental volume loss. This may be associated with elevation of the diaphragm. Pulmonary infarcts usually appear as areas of consolidation adjacent to a pleural surface (Fig. 8.23). They rarely show an air bronchogram, but may cavitate. A hemorrhagic pleural effusion may develop secondary to pulmonary infarction. An *isotope lung scan* will show areas of absent perfusion with normal ventilation and *pulmonary angiography* may demonstrate peripheral intraluminal filling defects, areas of oligemia or areas of slow flow.

**Chronic pulmonary embolism** may be due to thromboembolism, tumor emboli or bilharzia. The chest radiograph usually shows signs of pulmonary arterial hypertension with enlargement of the central pulmonary arteries and peripheral pruning.

## REFERENCES AND SUGGESTIONS FOR FURTHER READING

### GENERAL

- Crofton J, Douglas A (1981) *Respiratory Diseases*, 3rd edn. Blackwell Scientific, Oxford
- Fraser RG, Pare JAP (1977–79) *Diagnosis of Diseases of the Chest*, 2nd edn. WB Saunders Co, Philadelphia
- Heitzman ER (1973) *The Lung. Radiologic–pathologic correlations*. Mosby, St Louis
- Putman CE (1981) *Pulmonary Diagnosis. Imaging and other techniques*. Appleton–Century–Crofts, New York

### METHODS OF INVESTIGATION AND INTERPRETATION

- Felson B (1973) *Chest Roentgenology*. WB Saunders Co., Philadelphia
- Gamsu G, Webb WR, Sheldon P, Kaufman L, Crooks L, Birnberg FA, Goodman P, Hinchcliffe WA, Hedgecock M (1983) Nuclear magnetic resonance imaging of the thorax. *Radiology* 147: 473–480
- Goddard PR (1987) *Diagnostic imaging of the chest*. Churchill Livingstone, Edinburgh, London, New York
- Lavender JP (1983) Radio-isotope lung scanning and the chest radiograph in pulmonary disease. In: Steiner RE, Lodge E (eds) *Recent Advances in Radiology*, vol 6. Churchill Livingstone, Edinburgh
- Lipscomb DJ, Flower CDR, Hadfield JW (1981) Ultrasound of the pleura: an assessment of its clinical value. *Clin Radiol* 32: 289–290
- Naidich DP (1984) *Computed Tomography of the Thorax*. Raven Press, New York
- Simon G (1978) *Principles of Chest X-ray Diagnosis*. 4th edn. Butterworths, London

### THE CHEST WALL, DIAPHRAGM AND PLEURA

- Alexander G (1966) Diaphragmatic movements and the diagnosis of diaphragmatic paralysis. *Clin Radiol* 17: 79–83
- Austin JHM, Carsen GM (1977) Radiologic diagnosis of pleural effusions. In: *Current Concepts in Radiology*, vol 3. CV Mosby, St Louis, pp 261–281
- Ellis K, Wolff M (1977) Mesotheliomas and secondary tumours of the pleura. *Semin Roentgenol* 12: 303–311
- Felson B (1977) The extrapleural space. *Semin Roentgenol* 12: 327–333
- Greene R, McCloud TC, Stark P (1977) Pneumothorax. *Semin Roentgenol* 12: 313–325
- Khan A, Gould DA (1984) The primary role of ultrasound in evaluating right-sided diaphragmatic masses. *Clin Radiol* 35: 413–418
- Vix VA (1977) Roentgenographic manifestations of pleural disease. *Semin Roentgenol* 12: 277–286
- Williford ME, Hidalgo H, Putman CE, Korobkin M, Ram PC (1983) Computed tomography of pleural disease. *Am J Roentgenol* 140: 909–914

### DISEASES OF THE AIRWAYS AND PULMONARY COLLAPSE AND CONSOLIDATION

- Choplin RH, Wehunt WD, Theros EG (1983) Diffuse lesions of the trachea. *Semin Roentgenol* 18: 38–50
- Gamsu G, Webb WR (1983) Computed tomography of the trachea and mainstem bronchi. *Semin Roentgenol* 18: 51–60
- Morgan MDL, Strickland B (1984) Computed tomography in assessment of bullous lung disease. *Br J Dis Chest* 78: 10–25
- Proto AV, Tocino I (1980) Radiographic manifestations of lobar collapse. *Semin Roentgenol* 15: 117–173
- Schneider HJ, Felson B, Gonzalez LL (1980) Rounded atelectasis. *Am J Roentgenol* 134: 225–232
- Simon G (1964) Radiology and emphysema. *Clin Radiol* 15: 293–306

### PULMONARY INFECTIONS

- Berkmen YM (1980) Uncommon acute bacterial pneumonias. *Semin Roentgenol* 15: 17–24
- Berkmen YM (1980) Aspiration and inhalation pneumonias. *Semin Roentgenol* 15: 73–84
- Fanta CH, Pennington JE (1981) Fever and new lung infiltrations in the immunocompromised host. *Clin Chest Med* 2: 19–37
- Genereux GP, Stilwell GA (1980) The acute bacterial pneumonias. *Semin Roentgenol* 15: 9–16
- Janower ML, Weiss EB (1980) Mycoplasmal, viral and rickettsial pneumonias. *Semin Roentgenol* 15: 25–34
- Palmer PES (1979) Pulmonary tuberculosis – usual and unusual radiographic presentations. *Semin Roentgenol* 14: 204–243
- Reeder MM, Palmer PES (1980) Acute tropical pneumonias. *Semin Roentgenol* 15: 35–49
- Schwartz J, Baum GL (1970) Fungal diseases of the lungs. *Semin Roentgenol* 5: 13–54

### PULMONARY TUMORS

- Bateson EM (1965) An analysis of 155 solitary lung lesions illustrating the differential diagnosis of mixed tumours of the lung. *Clin Radiol* 16: 51–60
- Berkmen YM (1977) The many faces of alveolar cell carcinoma of the lung. *Semin Roentgenol* 12: 207–214
- Byrd RB, Miller WE, Carr DT, Payne WS, Woolner LB (1968) (i) The roentgenographic appearance of squamous cell carcinoma of the bronchus; (ii) The roentgenographic appearance of large cell carcinoma of the bronchus; (iii) The roentgenographic appearance of small cell carcinoma of the bronchus. *Mayo Clin Proc* 43: 327–341
- Feigin DS, Siegelman SS, Theros EG, King FB (1977) Non-malignant lymphoid disorders of the chest. *AJR* 129: 221–000
- Filly R, Blank N, Castellino RA (1976) Radiographic distribution of intrathoracic disease in previously untreated patients with Hodgkin's disease and non-Hodgkin's lymphoma. *Radiology* 120: 277–281
- Lawson RM, Ramanathan L, Hurley G, Hinson KW, Lennox SC (1976) Bronchial Adenoma: review of an 18-year experience at the Brompton hospital. *Thorax* 31: 245–000
- Spiro SG, Goldstraw P (1984) Editorial: The staging of lung cancer. *Thorax* 39: 401–407

### DIFFUSE LUNG DISEASE

- Alford BA, Kattwinkel J (1983) Neonatal respiratory distress In: Armstrong P (ed) *Critical Problems in Diagnostic Radiology*. Lippincott, Philadelphia, pp 63–99
- Fraser RG, Pare GAP (1975) Extrinsic allergic alveolitis. *Semin Roentgenol* 10: 31–41
- Freundlich IM (1979) Diffuse pulmonary disease – a radiologic approach. Saunders, Philadelphia
- Genereux GP (1975) The end-stage lung. *Radiology* 116: 279–289
- Hunninghake GW, Fauci AS (1979) Pulmonary involvement in the collagen diseases. *Ann Rev Respir Dis* 119: 471–503
- Kirks DR, Greenspan RH (1973) Sarcoid. *Radiol Clin North Am* 11: 279–294
- Parkes RW (1982) *Occupational Lung Disorders*. 2nd edn. Butterworths, London
- Turner-Warwick M, Dewar A (1982) Pulmonary haemorrhage and pulmonary haemosiderosis. *Clin Radiol* 33: 361–370

**THE MEDIASTINUM**

- Godwin JD, Herfkens RL, Skioldebrand CG, Federle MP, Lipton MJ (1980) Evaluation of dissections and aneurysms of the thoracic aorta by conventional and dynamic CT scanning. *Radiology* 136: 125–133
- Heitzman ER (1977) The Mediastinum: Radiologic Correlations with Anatomy and Pathology. Mosby, St Louis
- Heitzman ER, Goldwin RL, Proto AV (1977) Radiologic analysis of the mediastinum utilizing computed tomography. *Radiol Clin North Am* 15: 309–329
- Lyons HA, Calvy GL, Sammons BP (1959) The diagnosis and classification of mediastinal masses: a study of 782 cases. *Annal Int Med* 51: 897–932

**CHEST TRAUMA, THE POST-OPERATIVE CHEST AND INTENSIVE CARE**

- Goodman LR, Putman CE (1981) The SICU chest radiograph after massive blunt trauma. *Radiol Clin North Am* 1: 111–123
- Goodman LR, Putman CE (1983) Intensive Care Radiology: Imaging of the Critically Ill, 2nd edn. Saunders, Philadelphia
- Libshitz HI, Southard ME (1974) Complications of radiation therapy: the thorax. *Semin Roentgenol* 9: 41–49
- Moses DC, Silver TM, Bookstein JJ (1974) The complementary roles of chest radiography, lung scanning and selective pulmonary angiography in the diagnosis of pulmonary embolism. *Circulation* 49: 179–188
- Reynolds J, Davis JT (1966) Injuries of the chest wall, pleura, pericardium, lungs, bronchi and esophagus. *Radiol Clin North Am* 2: 383–414

---

**PART 2**

**Cardiovascular System**

---

## CHAPTER 9

# CARDIAC IMAGING

P. Wilde and G. G. Hartnell

The aims of imaging patients with heart disease are to make a diagnosis, to assess the severity of the disease, to detect any complicating features and to suggest the appropriate form of treatment.

To achieve these aims there should be a logical order of investigation for each clinical problem and the benefits and limitations of each imaging technique used should be fully understood (Table 9.1). Where safe, non-invasive methods are available they should be used in preference to more hazardous invasive investigations. There is today less emphasis on the older invasive investigations such as angiography, although this still has an important role, and

there is an increasing use of echocardiography, Doppler, isotopes and MRI.

The *chest radiograph* is the initial imaging investigation in most cases of heart disease, and can provide much diagnostic and functional information though there is also great scope for errors of interpretation.

### THE CHEST RADIOGRAPH

Most chest radiographs are taken in a routine way so that major variations in appearance due to differences of tech-

Table 9.1. The value of different cardiac imaging techniques

	Plain radio- graph	Echocardiography		Nuclear medicine		CT	MRI	Angiography		Catheter (non- imaging)
		2D M-Mode	Doppler	Thallium	MUGA			Digital	Cine	
Anatomical detail (chambers and valves)	+	++++	-	++	++	+++	++++	++++	+++++	
Anatomical detail (coronary arteries)	+	+	-	+	-	+	++	++++	++++	
Heart size and pulmonary vessels	+++++	++	-	++	++	+++	+++	+++	+++	
Pericardial and extracardiac detail	++++	++	-	-	-	++++	+++++	++	++	
Hemodynamics (pressures)	+	+	++++	-	-	-	+	+	+	+++++
Hemodynamics (flows)	++	++	++++	-	+++	+	+++	++	++	++++
Radiation safety	+++	+++++	+++++	++	++	++	+++++	++	+	
Non-invasiveness and patient comfort	+++++	+++++	+++++	++++	++++	++++	++++	++	+	
Economy (equipment costs)	++++	+++	++	++	++	+	+	+	+	
Simplicity to perform	+++	++	+	+++	+++	+++	+++	+	+	
Availability of technique	+++++	+++	++	++	+++	+++	+	+	+	

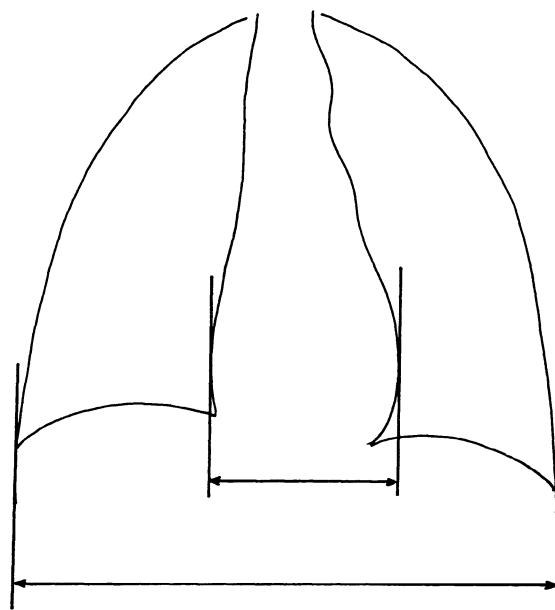


Fig. 9.1. Measurements on a PA chest radiograph used to assess cardiac size expressed as the cardiothoracic ratio.

nique are limited. This makes the chest radiograph a particularly useful method for the initial evaluation and for evaluating changes in a given patient due to disease progression or treatment. There are a number of separate aspects of the chest radiograph which should be considered in detail.

**Heart Size.** There are various normal values for the size of the heart which depend on the patient's age, gender and race. The heart size on any chest radiograph is also dependent on the technique used to take the radiograph. In the

average white male adult the *cardiac diameter* on a PA radiograph with a focus-film distance of 2 m or more is less than 13.5 cm and a diameter of over 15.5 cm indicates cardiomegaly. Alternatively the heart size can be expressed as the *cardiothoracic ratio* (Fig. 9.1) with the upper limit of normal being up to 50% in adult Europeans. These values may need to be modified for other racial groups, for different age groups, for poor inspiration and for different radiographic techniques.

The presence of cardiomegaly can make some diagnoses unlikely and others more likely, as in the differentiation of proximal pulmonary artery enlargement due to pulmonary stenosis (no increase in blood flow and therefore normal size heart) from atrial septal defect (increased blood flow and therefore cardiomegaly is usual in adults). Changes in heart size (beyond the normal interexamination variability of up to 1.5 cm), particularly if following a consistent trend, indicate deterioration or improvement of cardiac function as a result of progression or regression of disease or response to treatment (Fig. 9.2).

The size of the enlarged heart shadow reflects enlargement of one or more chambers (unless due to pericardial effusion) and is an important reflection of disease, whether it be due to ischemia, heart muscle disease, valve disease or volume overload.

Enlargement of the *left atrium* is usually reliably detectable on the chest radiograph but selective enlargement of the other chambers is often less reliably indicated. This is because, in many cases, the underlying heart disease leads to enlargement of several chambers. In cases where there is true single chamber enlargement (left atrium in mitral stenosis, right atrium in isolated tricuspid disease, left ventricle in pure aortic regurgitation) this can be more reliably diagnosed on the chest radiograph. If there is doubt, a decision on chamber enlargement should not be based on

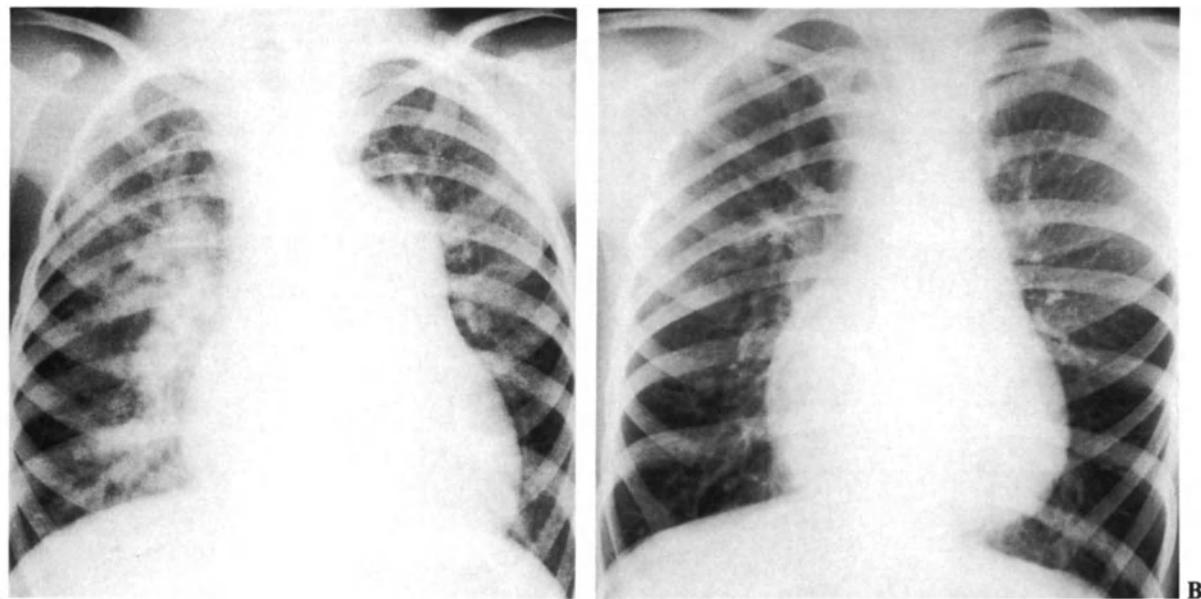
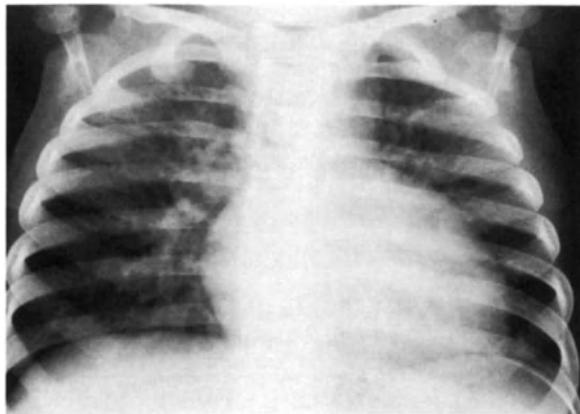


Fig. 9.2.A This patient with a large VSD has a large heart, pulmonary plethora and a large proximal pulmonary artery. B Following closure of the VSD the heart returns to normal size, the pulmonary vasculature is normal and the pulmonary artery also becomes smaller.



**Fig. 9.3.** The pulmonary plethora, narrow superior mediastinum and prominent right atrium in this patient are strongly suggestive although not diagnostic of uncorrected transposition of the great arteries.



**Fig. 9.5.** Left upper zone showing prominent upper lobe vessels and septal lines ('A' line arrowed) extending from the hilum.

chest radiograph signs, which are of varying reliability, but on the result of a more definitive non-invasive investigation, such as echocardiography.

The *cardiac configuration* may be particularly useful in making a specific diagnosis. However, whilst it may be almost pathognomonic (as in Fallot's Tetralogy) or highly suggestive (as in uncorrected transposition of the great arteries, Fig. 9.3) it can also be totally unhelpful, as in infant patients with left to right shunts (Fig. 9.4). Where there is a characteristic shape this may be very helpful but usually any diagnosis should be supported by alternative imaging methods.

**Pulmonary Vascular Pattern.** The assessment of the pulmonary circulation is one of the most important uses of

the chest radiograph in heart disease, as it provides information on cardiac function which is difficult to obtain by other non-invasive methods. There are six basic patterns of pulmonary vascularity. These are:

1. *Pulmonary venous hypertension*, which is characterized by constriction of lower lobe vessels and increasing prominence of the upper lobe vessels. With pulmonary venous pressures over 20 mmHg signs of *interstitial edema* develop, including *haziness* of hilar structures and lower lobe vessels and development of *septal lines* (Figs 9.5, 9.6). With further increases in pressure *pleural effusions* and frank *alveolar edema* are seen (Fig. 9.7).



**Fig. 9.4.** Pulmonary plethora in the presence of a non-specific heart shape as in this case is of limited diagnostic value, except to indicate that there is a shunt. In this case this was due to a VSD.

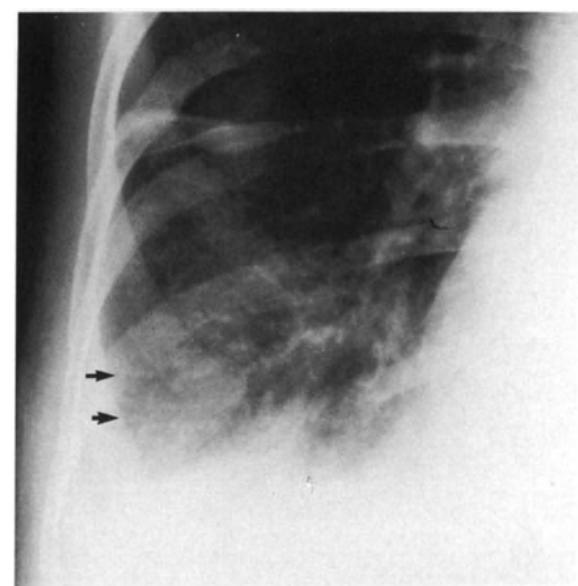


**Fig. 9.6.** Right lower zone showing a loculated pleural effusion in the transverse fissure and septal lines ('B' lines arrowed).

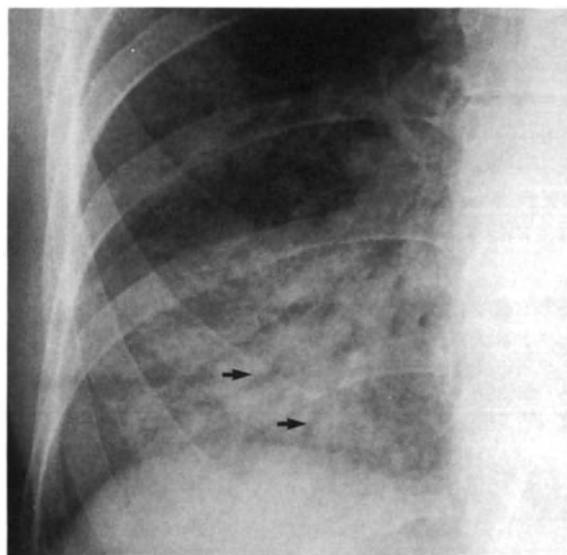


**Fig. 9.7.** Right lower zone showing alveolar shadowing (note the air bronchogram – arrows) due to pulmonary edema. Note also the absence of pleural fluid and septal lines, which may develop later.

2. *Pulmonary arterial hypertension*, due to any cause, produces dilatation of the central pulmonary arteries (which may become calcified in longstanding and severe cases, Fig. 9.8) and constriction of the peripheral pulmonary arteries. The level at which the arterial calibre changes from dilated to constricted may be related to the type of lesion causing the pulmonary hypertension but this is a difficult area for confident diagnosis.

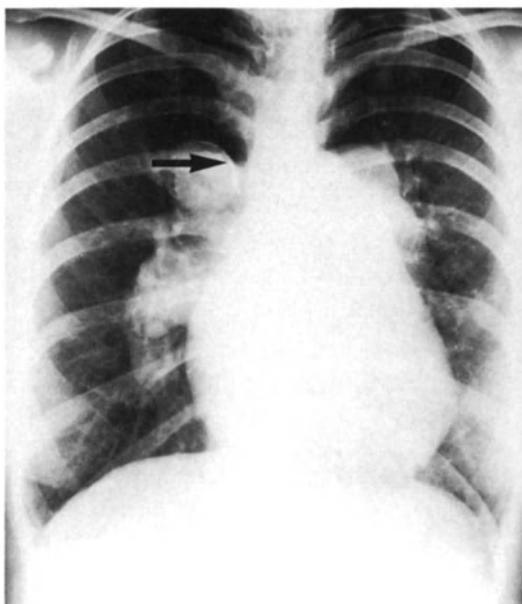


**Fig. 9.8.** Chest radiograph of a middle-aged patient with longstanding pulmonary arterial hypertension complicating a secundum ASD and leading to pulmonary artery calcification (arrow).

3. *Pulmonary overcirculation* produces large pulmonary vessels in all areas but the lower lobe vessels remain larger than the upper lobe vessels (Figs 9.2A, 9.3); radiological evidence of overcirculation usually indicates a left-to-right shunt of at least 2:1.

4. *Systemic pulmonary supply* is usually seen in association with severe cyanotic heart disease and may affect one or both lungs. It produces an irregular pulmonary vascular pattern with abnormal branching and a small or absent main pulmonary artery.

5. *Pulmonary underperfusion* indicates an obstruction to pulmonary filling (Fig. 9.9) or to filling of the right side of the heart. The central pulmonary arteries are small or not visible and the peripheral vessels are small and more widely spaced than usual.

6. *Unequal pulmonary perfusion* is most commonly the result of lung disease. However, in the context of cardiovascular disease it may be due to (1) thromboembolic disease, (2) post-operative changes (i.e., Blalock shunts) and (3) peripheral pulmonary stenoses, often in association with cyanotic heart disease, when there may also be a variable systemic supply to the lungs.

In the majority of adult patients with heart disease, changes in the pulmonary circulation are the result of changes in left atrial pressures, due either to mitral valve disease or to left ventricular dysfunction. These changes are manifested by increasing *pulmonary venous congestion* leading to pulmonary edema and, after long periods, pulmonary arterial hypertension. They are important in reflecting the functional significance of the associated cardiac lesions and the rates of deterioration and response to treatment.

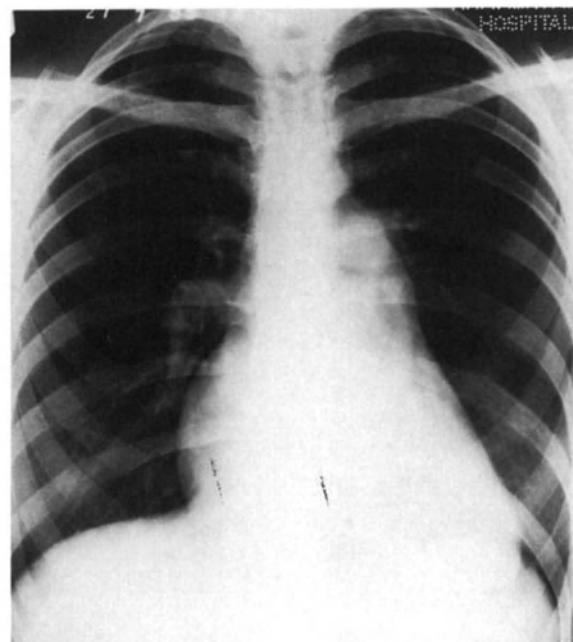


**Fig. 9.9.** Chest radiograph of a patient with severe pulmonary valve stenosis causing post-stenotic dilatation of the main pulmonary artery and underperfusion of the peripheral pulmonary arteries.

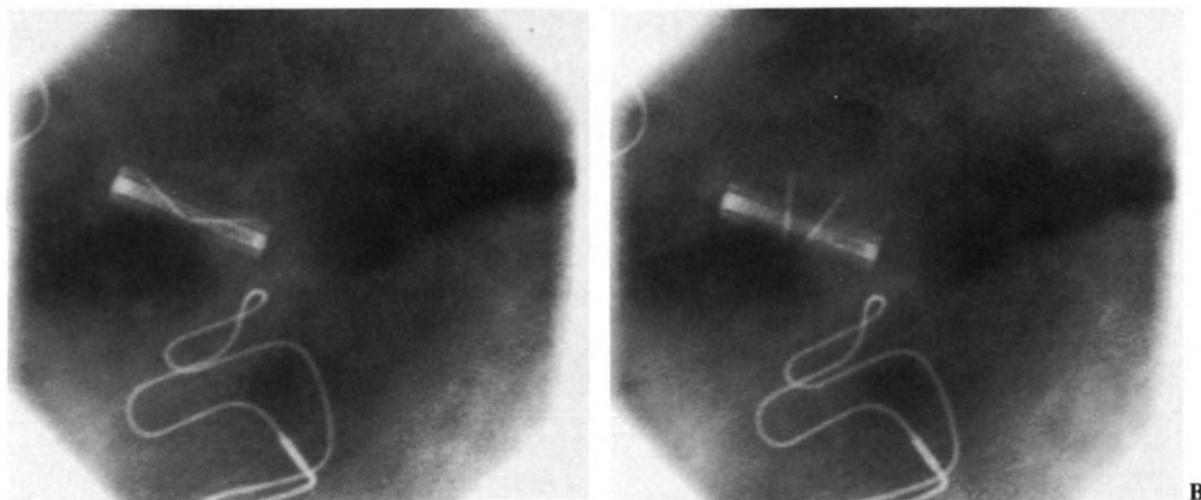


Fig. 9.10A, B. Screening of St Jude aortic valve prosthesis to show position of valve leaflets in diastole A and systole B with equal movement of both leaflets. Note also the cage of the mitral xenograft replacement.

Less commonly there is *underperfusion*, usually due to pulmonary arterial obstruction. This may be primary or secondary to cardiac disease, which is of importance in staging the severity of the associated cardiac disease and may change the available therapeutic options.

In children, the pulmonary circulation assessed on the chest radiograph is vital in the initial assessment of congenital heart disease. Together with the clinical signs, it can drastically reduce the number of possible diagnoses and it is often a guide to the severity of the lesion and the urgency of further investigation. It is also important in the assessment of the effects of surgical treatment, in particular of shunt procedures.

Signs of *previous cardiac surgery* are an important aspect of the interpretation of the chest radiograph in children and adults. As well as indicating the effects of shunts or valve replacement procedures a number of complications of surgery can be seen, and may be detected at a stage when they are clinically unexpected. This may allow further investigation at an early stage when correction is easier and safer than when the patient has become symptomatic.

There are other changes in the heart seen on the chest radiograph which are of importance in some patients. A number of conditions lead to *intracardiac calcification*. This may be visible on the chest radiograph, although a lateral or penetrated frontal radiograph may be required to show it in the denser parts of the heart shadow. Some lesions such as pericardial calcification, mitral annulus calcification and coronary calcification have diagnostic appearances but require further investigation to assess the functional importance of the diagnosis. Other causes of calcification such as mitral or aortic stenosis show fewer diagnostic appearances and confirmation by alternative methods may be required. However, the presence of calcification suggests that the valve affected is very likely to be stenosed.

*Fluoroscopy* is now seldom used but still has a limited role in detecting and assessing intracardiac calcification if alter-

native methods, such as echocardiography, are not readily available. It also has a role in the assessment of mechanical valve dysfunction (Fig. 9.10) but its other applications, such as detection of left ventricular aneurysms, have now been superseded by more reliable non-invasive methods such as echocardiography or isotope ventriculography.

## ECHOCARDIOGRAPHY

### Examination Technique

Echocardiography is perhaps the most 'operator dependent' of all cardiac imaging techniques. In most cases it takes many months of regular scanning to achieve proficiency. The reasons for this are that the ultrasonic access to the heart is limited by the lungs, ribs and other tissues that prevent good quality imaging. This means that careful positioning of both the patient and the transducer are needed to achieve the standard images.

The descriptions in this chapter on cardiac ultrasound examination will assume that a full range of examination modalities are available. Today, comprehensive cardiac ultrasound examination requires both two-dimensional examination and Doppler evaluation as well as M-mode.

### M-Mode Echocardiography

The interpretation of M-Mode traces has become highly deductive and mathematical. Much functional information about the heart had to be derived by measuring and calculating various parameters from the movement of chamber walls and valve tissues. To a large extent this highly quantitative approach to the M-Mode study has been dispensed with in favor of two-dimensional studies but it is important to retain the technique for certain valuable measurements, the most useful of which is the *dimension of the left ventricle* to assess its degree of dilatation and contractility. This is shown in Fig. 9.11A, B.

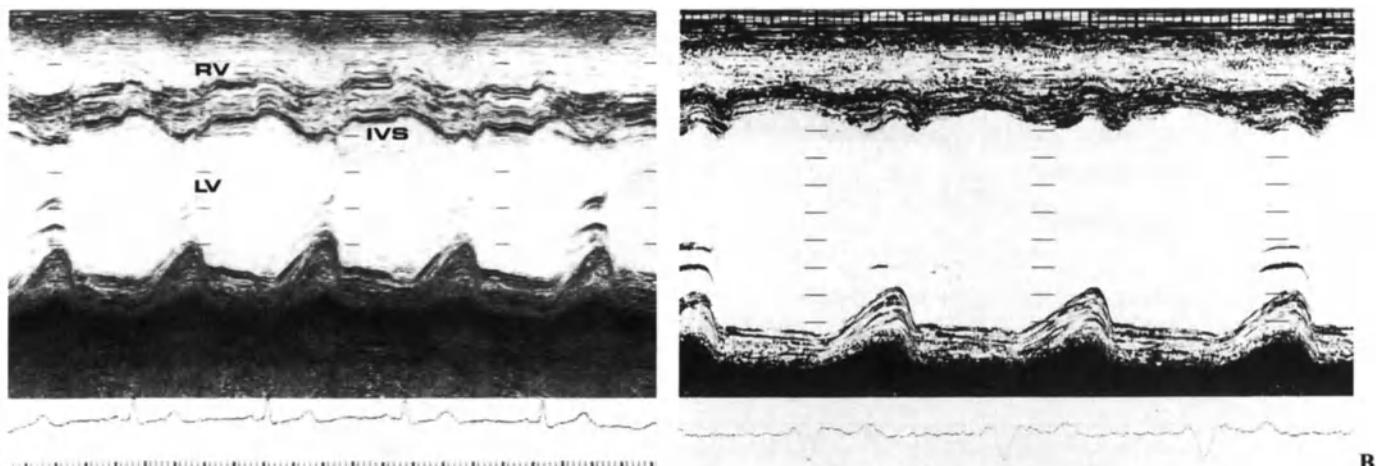


**Fig. 9.11.** A This M-Mode trace shows the left ventricular cavity (LV), the right ventricular outflow tract (RV) and the interventricular septum (IVS). Ventricular function is normal. Distance markers in the ventricle are 1 cm apart. B This M-Mode trace shows a dilated but well contracting ventricle in a case of ventricular volume overload caused by severe valvular regurgitation.

It is important to remember that the M-Mode examination is performed with a single 'pencil beam' directed through the cardiac tissues. For this reason it is open to considerable variation and misinterpretation if the positioning of this line is not constant. In addition to this the information available only relates to that single line and other abnormalities will not necessarily be evident if the structures in question are not examined. For example, an M-Mode examination through the well contracting base of the left ventricle will not reveal the presence of an apical left ventricular aneurysm.

In the original M-Mode instruments the M-Mode transducer was used 'blind', optimal positioning being identified

simply by the quality of the trace being obtained. Today the M-Mode line can be much more rapidly and accurately placed with the concomitant use of the two-dimensional image.

The M-Mode beam can most usefully record echoes returned from structures lying perpendicular to the directional beam so that for cardiac examination the left parasternal window is the optimal position for recording the left ventricle, aortic and mitral valves. Other echo windows are much less helpful as they cause the beam to be aligned parallel to valve and wall movement.

The ultrasonic pulses used to produce the M-Mode trace are repeatedly given in the same direction down the focus beam. This is quite different to the real time scanner where the beam is directed differently for each pulse to produce the two-dimensional image. This repeated firing of the pulse in the same direction produces a 'high pulse repetition frequency' which is thus particularly suitable for measuring very fast-moving structures. The fine vibrations or fluttering of a mitral leaflet struck by a regurgitant aortic jet cannot be appreciated on two-dimensional scanning but will be clearly recorded by the M-Mode examination. Fig. 9.12 shows this phenomenon.

#### *Advantages of M-Mode Study*

1. Precise linear measurements can be made off the strip chart. These can be made at a precise time within the cardiac cycle.
2. Accurate timing is possible. This can be with respect to a fixed time scale, the simultaneous electrocardiogram or comparative timing of different events within the cardiac cycle.
3. Very fast moving structures can be recorded.

#### *Disadvantages of M-Mode Technique*

1. Anatomy of the heart in adjacent regions can only be produced by comparing differently positioned M-Modes (e.g., 'sweep scan').

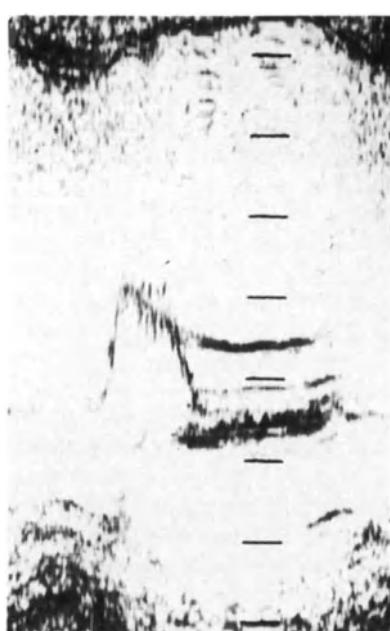


**Fig. 9.12.** This M-Mode trace shows the extremely fast vibrations of the anterior mitral leaflet recorded in a patient with aortic regurgitation. The regurgitant jet strikes the mitral leaflet and causes the 'fluttering'.

2. Measurements are subject to misinterpretation by inappropriate or incorrect recordings (e.g., an oblique measurement across the left ventricle is a common problem).
3. Limited number of echocardiographic windows are useful.
4. Probably more difficult to learn and interpret than two-dimensional imaging.

#### *Applications of M-Mode Echocardiography*

1. Assessment of left ventricular dilatation in conditions of volume overload or muscle disease.
2. Assessment of left ventricular contractility (note that regional differences may be missed).
3. Measurement of wall thickness (e.g., left or right ventricular hypertrophy).
4. Assessment of valve tissue (e.g., thickened tissue with stenotic valve).
5. Assessment of valve movement (reduced opening in stenotic valves; altered diastolic closure in mitral stenosis).
6. Confirmation of timing of abnormal events (e.g., prolapsing vegetations or valve tissue).

#### **Two-dimensional Echocardiography (2DE) (Real Time Echocardiography)**

A composite sector scan is built up by repeating the pulse of ultrasonic energy down the radial lines of a sector. A complete sweep of the sector will include information from about 100 lines which is then amalgamated by the electronic imaging processing into a two-dimensional image. The time taken to form a complete sector depends on the speed of sound in tissue (1540 m/second), the depth being studied (typically 5–15 cm) and the number of lines in the image (typically 100 lines). The next sector is commenced immediately after the first has been finished and in normal situations the sector is repeated at 20–30 times each second, which gives a smooth appearance of movement.

The main and obvious advantage of two-dimensional scanning is the appreciation of anatomy as a whole, with fine detail of structures often being visible, as shown in Fig. 9.13. This is best understood if the three planes of the heart are considered as three orthogonal views of the heart.

The long axis view can normally be obtained from the parasternal position and the left ventricular apex. It is useful for showing the left ventricle, the mitral and aortic valves and a small amount of right ventricular chamber lying anteriorly.

The short axis view can be obtained from the left parasternal position but also from the subcostal (subxiphoid) position in many individuals. This plane shows a cross sectional view of the left ventricle with the right ventricle wrapping around it. If adjusted towards the base of the heart it will show a cross-sectional view of the mitral and aortic valves with the tricuspid and pulmonary valves lying appropriately in the right ventricle as it lies anteriorly.

The four-chamber view can be obtained from the apical view quite simply in most patients and with more difficulty

from the subcostal view. This is the classical representation of the heart showing the cavities of both ventricles, both atrioventricular valves and both atria.

It is usual that in any individual patient some echo windows will be easier than others. The left parasternal and apical views are most commonly used with the subcostal view often being more difficult. In some patients, however, the parasternal view is impossible (e.g., emphysema and flattened diaphragm) but in these cases it is often surprising how good the subcostal view can be.

The suprasternal view is usually confined to assessing the great vessels lying above the heart and is particularly useful for assessing the aortic arch.

#### *Advantages of Two-dimensional Echocardiography*

1. Immediately apparent anatomy (in particular abnormal connections and anatomical features) will be obvious. Very useful in congenital heart disease.
2. Real time assessment of cardiac movement allows immediate evaluation of cardiac function.
3. Area assessments can be made (e.g., cross-sectional valve areas and area measurements of ventricle which can be used to assess volume more accurately).
4. Regional wall motion abnormalities of the left ventricle are less likely to be missed.
5. A wide range of views and echo windows can be used for full assessment.
6. Can be used to direct M-Mode or Doppler examination.

#### *Disadvantages of Two-dimensional Technique*

1. Slower frame rate than M-Mode which precludes measurement of very fast movement.
2. Less easy to measure precise distances, these having to be calculated from frozen images.
3. Less easy to measure timing (this has to be done from video tape recording or digital memory).
4. The absolute resolution is still inadequate to see fine detail of coronary arteries. This is partly due to limitation in resolution and partly due to intrinsic cardiac movement.

#### *Applications of Two-dimensional Echocardiography*

Two-dimensional studies should now form the core of all cardiac ultrasound examinations. There is no place for isolated M-Mode or Doppler examination. Thus the applications are those for echocardiography in general, which are as follows:

1. Assessment of the size, shape and movement of any of the cardiac chambers.
2. The size, shape and movement of any of the cardiac valves.
3. The functional status of cardiac valves in terms of stenosis or regurgitation.
4. The presence of additional pathological features in any cardiac chamber or on any valve (e.g., vegetations, tumors, thrombi etc).
5. The assessment of congenital heart disease.
6. The assessment of pericardial disease.
7. The assessment of thoracic aortic and aortic root disease.

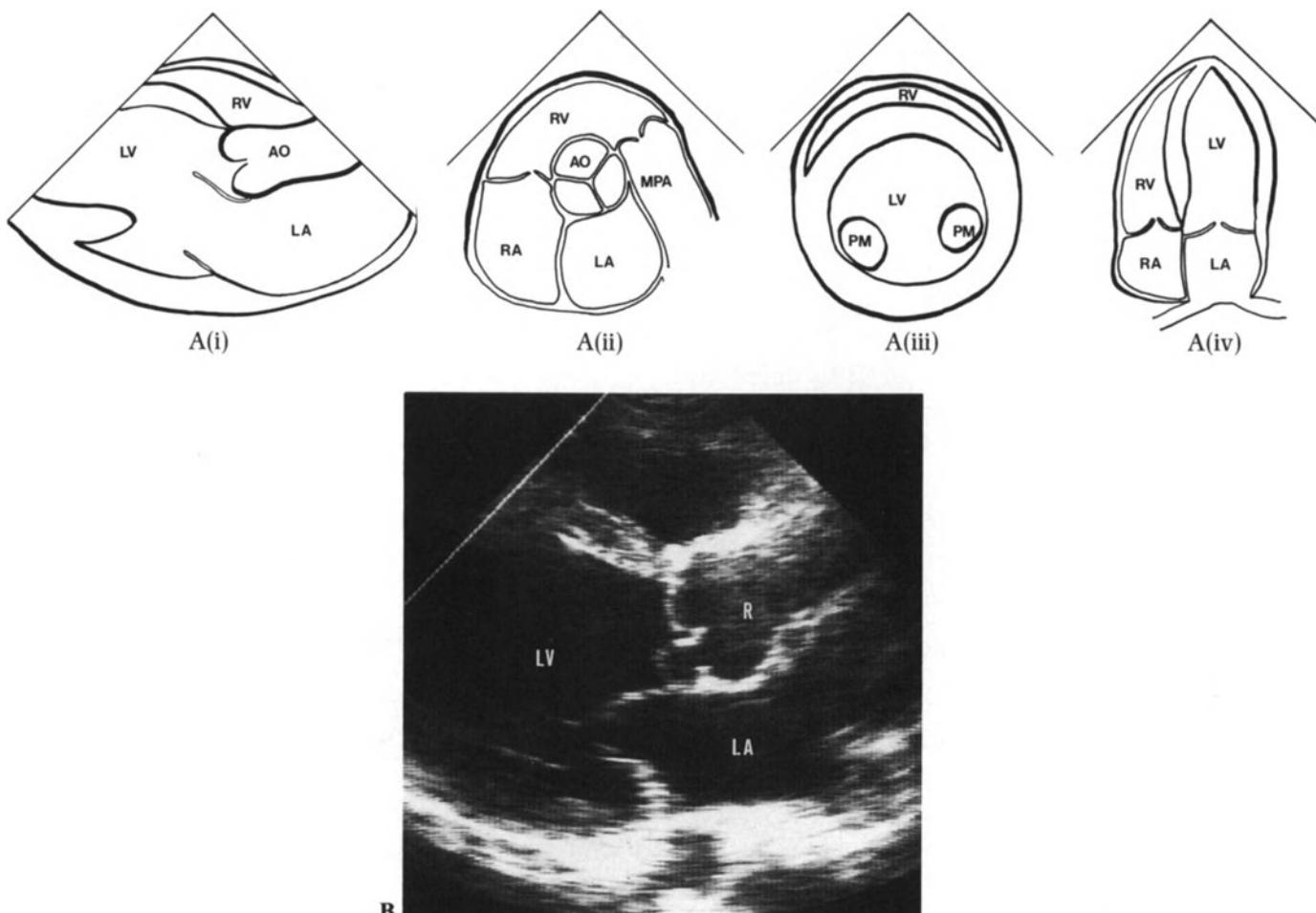


**Fig. 9.13.** A Line drawings show normal anatomical relationships seen on two-dimensional echocardiography. (i) Parasternal long axis view; (ii) Parasternal short axis view at the level of the aortic valve; (iii) Parasternal short axis view at the level of the left ventricle; (iv) Apical four-chamber view. (LV, left ventricle; RV, right ventricle; LA, left atrium; RA, right atrium; AO, aorta; MPA, main pulmonary artery; PM, papillary muscle.) B This parasternal long axis view of the left ventricle (LV), left atrium (LA) and aortic root (R) shows a thin prolapsing portion of the posterior part of the aortic valve leaflet prolapsing into the left ventricular outflow tract.

### Doppler Echocardiography

A reflected wave form returned to a source of fixed frequency will have an increased frequency if the reflector is moving towards the source. The frequency will be decreased if the reflector is moving away and it will be unchanged if the reflector is stationary. In the case of cardiac ultrasound the reflector is the blood itself.

The Doppler equation is as follows:

$$\text{Frequency shift} = 2 F V \cos\theta/C$$

where  $F$  = transducer frequency;  $V$  = velocity of moving blood;  $\theta$  = the angle between ultrasound beam and flow direction;  $C$  = the speed of sound in tissues.

Doppler studies are based on assessment of flow along the direction of the ultrasonic beam. Flow is most accurately recorded if it occurs in line with the beam and will not be recorded if it flows perpendicular to the examination beam. Intermediate angles will be recorded in accordance with a cosine function. Pure flow perpendicular to the transducer will, therefore, not be recorded in any way even if it is signifi-

cant. Turbulent flow is multi-directional (e.g., stenotic valves or regurgitant valves) and as such there will always be some component in line with the transducer beam and thus turbulent flow can often be detected from a wide range of angles.

The imaging techniques described above are all based on specular (mirror-like) reflection, whereas Doppler evaluation depends on scattered reflection by red cells which are much smaller than the wavelength of the sound itself. For this reason studies require higher energy levels than normal imaging.

Doppler evaluation can be used to measure flow through the heart, qualitatively and quantitatively. In terms of qualitative flow it is now possible to determine the site of flow, timing of flow, direction of flow and quality of flow at any point that is accessible to the ultrasonic instrument. In this way it is easy to detect such abnormalities as valve regurgitation or stenosis, with a precision that cannot be matched by clinical evaluation. The accuracy of this determination is, in many cases, equal to or even better than that produced by cardiac catheterization.

Quantitative assessment of flow can be divided into two major categories. Firstly *velocity* of flow can be measured. The velocity of flow can be used to determine pressure gradients within the heart by application of the modified Bernoulli equation. In its simplest form this is  $P = 4V^2$ , where  $P$  = pressure gradient in mm Hg and  $V$  = velocity of flow in metres/second.

This equation has been simplified considerably but even in its simplified form has been validated in most cardiological situations. The technique can be used to assess valvular gradients with accuracy. It can also be used to differentiate pressures within the heart between one chamber and another.

Secondly, *volume flow* can be assessed by use of the principle that knowledge of the cross-sectional area at a point in the circulation and the mean velocity at that area allows the calculation of flow at that point. Cross-sectional area can be determined by the imaging techniques of echocardiography and with careful application these principles can be used to measure cardiac output, left to right shunts and other aspects of cardiac flow.

The Doppler principle can be employed in three main ways: pulsed Doppler, continuous wave Doppler and colour flow Doppler.

**Pulsed Doppler.** The transducer emits a short burst of ultrasonic energy. The transducer then remains inactive for a period of time dependent on the depth of interest. After an appropriate delay (determined by the depth of interest) the transducer is activated as a receiver for a short duration. Received signals will thus correspond to those returned from the depth in question. This approach allows precise localization of flow within the heart and the depth gating together with the fixed width of the beam produced by the focusing characteristics of the transducer allow evaluation of flow from a 'sample volume'. This sample volume can be as small as 2 mm or 3 mm in diameter.

The limitation of pulsed Doppler examination is caused by the fact that repeated pulses need to be sent out. This produces a sampling rate (pulse repetition frequency) which limits the recording of high velocity flows. With unduly fast flow the pulsed Doppler recording will exhibit the artefact of aliasing which means that the peak velocity cannot be determined.

**Continuous Wave Doppler.** In this technique two transducer crystals are mounted side by side. One continuously emits ultrasonic energy and the other is activated as a continuous receiver. Their long focal pathways are superimposed. In this way return signals from any depth along the intersecting focal zones will be received. No pulsing is required in this system, and, therefore, very high velocities can be recorded. This allows some important deductions to be made about the pressure gradients producing the flows. Fig. 9.14 shows a continuous wave Doppler tracing obtained from a patient with aortic stenosis in which the peak velocity can be used to estimate the aortic pressure gradient. The major disadvantage of continuous wave Doppler is that no significant depth resolution is possible.

**Color Flow Mapping.** Recent technical advances in transducer design and electronic control have produced color flow mapping. This is based on the principle of pulsed Doppler

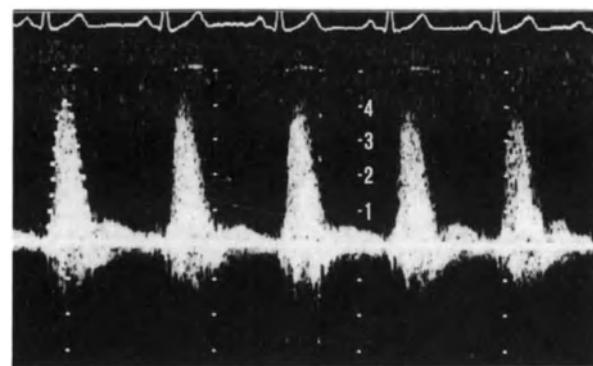


Fig. 9.14. This continuous wave Doppler trace was recorded from the suprasternal notch in a patient with severe aortic valve stenosis. The peak jet velocity is 4m/s, which can be used in the modified Bernoulli equation to give a calculated peak instantaneous valve gradient of 64 mm Hg.

examination but the system allows a pulsed Doppler evaluation across the full field of a two-dimensional image. The results of the pulsed integration are coded in color with flow towards the transducer being recorded in a different range of colors compared to flow away from the transducer. In this way there is an immediate visual appreciation of flow within the heart and many abnormal flows can be determined with very striking ease. Color flow mapping is particularly useful in complex situations of valve disease, assessment of prosthetic valves and especially in the assessment of congenital heart disease where unusual flows are often present. The color flow mapping approach, being based on pulsed Doppler, is subject to the limitations of pulsed Doppler and cannot be used for accurate quantitation of high velocity flow. It is, however, the most dramatic way in which the qualitative Doppler diagnosis can be made. Several examples of color flow mapping are shown in Fig. 9.15A-D.

#### *Applications of Doppler Echocardiography*

1. Diagnosis and quantitation of regurgitant valves.
2. Diagnosis and quantitation of stenotic valves.
3. Diagnosis of abnormal communications.
4. Determination of some intracardiac pressures (some limitations).

#### *Contrast Echocardiography*

This principle is not widely used but occasionally has considerable value. The injection of microbubbles into the venous circulation can be recorded by M-Mode or two-dimensional imaging systems as a shower of bright echoes. This can be seen entering the right atrium with normal transition to the right ventricular and right pulmonary artery. These microbubbles are absorbed in the lungs and do not normally pass to the left side of the heart. If, however, there is appearance on the left side of the heart at the same time as on the right this will indicate abnormal mixing and the presence of intracardiac communications. Contrast echocardiography is most useful in the unusual situations of right to left shunting. Microbubbles can be produced by a number of different means. Certain non-toxic dye substances can be used but

it is also quite simple to inject saline or saline mixed with blood once it has been agitated and the large bubbles have dispersed.

#### *Transesophageal Echocardiography*

This new extension of cardiac ultrasound examination offers

exceptional ultrasonic access to the heart and can be used in any of the modalities described above. The transducer is mounted on an endoscope and so the applications of the technique are somewhat restricted but there are exciting potential applications, particularly in the operating theatre and the intensive care ward.

## CARDIAC NUCLEAR MEDICINE

Nuclear medicine studies in cardiology have been consistently useful for many years, but have always had a relatively limited range of applications. The major reasons for this are the lack of precise anatomical resolution in nuclear medicine imaging and the difficulties of obtaining useful information from a constantly moving organ. The application to functional evaluation of the heart is their most important asset.

The principle of any form of nuclear medicine imaging is based on labelling a particular organ or tissue with a radionuclide tracer which can be imaged, usually by a gamma camera. A number of different radionuclides are used in

evaluation of the heart, the selection of these depending on the clinical problem and the information that is required. Radionuclide techniques are summarized in Table 9.2.

There are two main forms of cardiac nuclear medicine imaging: – imaging of the myocardium and imaging of the blood within the heart (nuclear angiography).

### MYOCARDIAL IMAGING

This type of imaging is generally performed to assess the nature of pathology in the myocardium, particularly the left

**Table 9.2.** Radionuclide techniques in cardiology

Investigation	Radiopharmaceutical
Myocardial imaging	$^{201}\text{Tl}$ $^{123}\text{I}$ -labelled free fatty acids $^{99m}\text{Tc}$ MIBI (isonitriles) Positron emitters (incorporating $^{13}\text{N}$ , $^{11}\text{C}$ , $^{18}\text{F}$ ) $^{81}\text{mKr}$ $^{133}\text{Xe}$ $^{99m}\text{Tc}$ microspheres } require aortic injection $^{99m}\text{Tc}$ -labelled pyrophosphate or diphosphonate
Infarct imaging	
Nuclear angiography	
Equilibrium technique (multiple gated acquisition, MUGA)	$^{99m}\text{Tc}$ -labelled red cells $^{99m}\text{Tc}$ -labelled albumin
First-pass technique	$^{99m}\text{Tc}$ pertechnetate $^{195}\text{Au}$ (short half-life)

**Fig. 9.15.A** This color flow Doppler image of the left ventricle (LV), mitral valve and left atrium (LA) shows a jet of mitral regurgitation (blue) entering the left atrium. **B** This color flow Doppler image is an apical long axis view showing a jet of aortic regurgitation (AR) entering the left ventricle at the same time as the normal mitral flow (MF). The fastest flowing part of the aortic regurgitant jet in the valve region shows in blue due to the color flow aliasing artefact. **C** This color flow Doppler image is a subcostal view showing flow through an atrial septal defect from the left atrium (LA) to the right atrium (RA). **D** This color flow Doppler image is an apical four chamber view showing flow across an apical muscular ventricular septal defect (arrowed) in systole from left ventricle (LV) to right ventricle (RV).

**Fig. 9.17.A** Immediate anterior view of a stress  $^{201}\text{Thallium}$  scan showing a large inferior perfusion defect. **B** Repeat image of the same patient shown in A after four hours of rest. There has been full reperfusion of the inferior defect indicating that this was a stress-induced perfusion defect caused by a severe localized coronary stenosis.

**Fig. 9.18.A** An image taken from a resting equilibrium blood pool scan (MUGA) in a normal patient. The projection is left anterior oblique with angulation of the gamma camera to give a 'four chamber' view. The left ventricle and right ventricle are seen at the bottom of the image, separated by the interventricular septum (arrow). **B** Parametric analysis has been performed on the study illustrated in A. This amplitude image shows the highest colors in areas of greatest change recorded during the accumulated cardiac cycle. The uniform high values over the left ventricle (LV) and right ventricle (RV) indicate normal function.

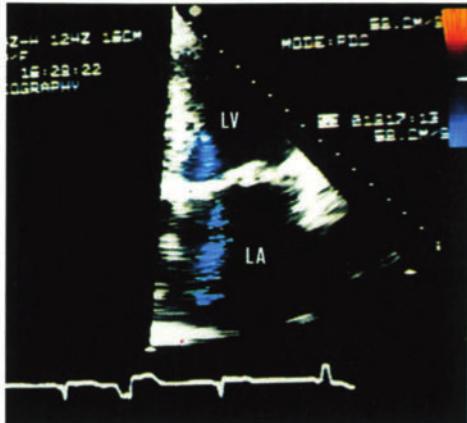


Fig. 9.15a

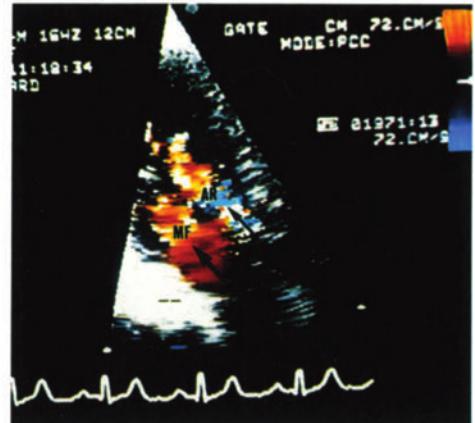


Fig. 9.15b

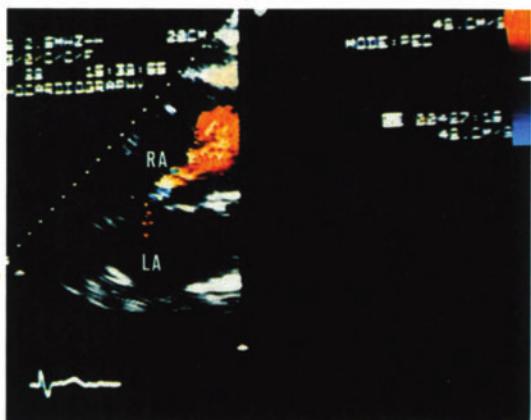


Fig.  
9.15c

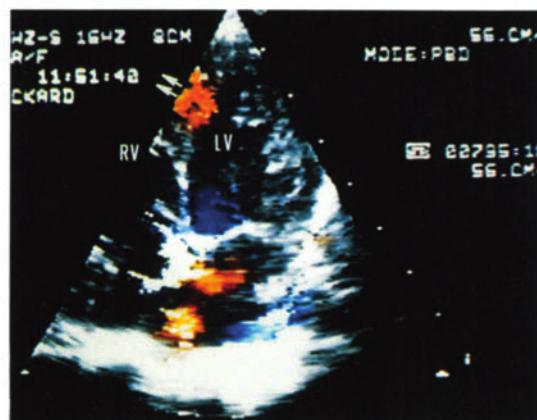


Fig.  
9.15d

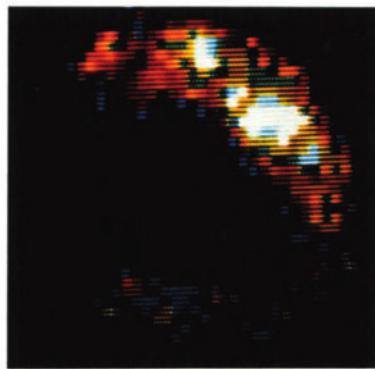


Fig. 9.17a

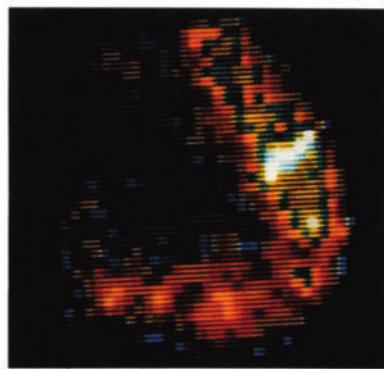


Fig. 9.17b

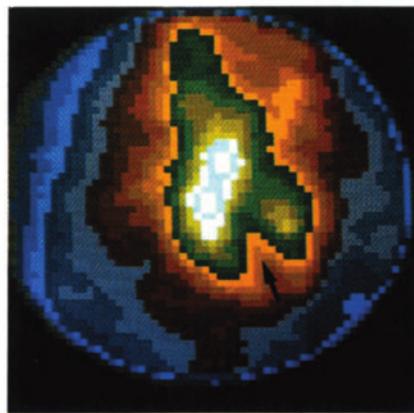


Fig. 9.18a

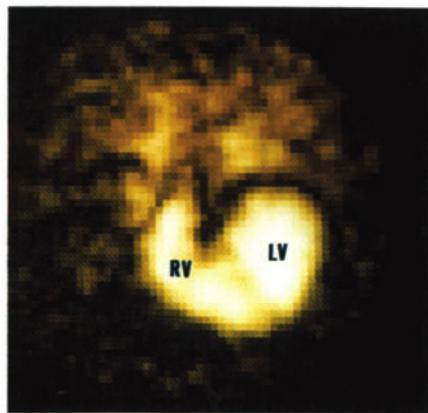


Fig. 9.18b

ventricular myocardium which constitutes the major muscle mass of the heart. In general the acquisition of information with this type of imaging is continuous and takes no account of cardiac movement. The anatomical resolution is, therefore, poor but is acceptable because only major regional differences in myocardial regions are of interest. The two main forms of conventional myocardial imaging are (i) myocardial infarction imaging and (ii) myocardial perfusion imaging.

### **Myocardial Infarct Scanning**

This technique has been available for many years and uses the common  $^{99m}\text{Tc}$  technetium pyrophosphate, an isotope that is also widely used for bone scanning. Severely damaged myocardial tissue is subject to major changes in calcium metabolism which leads to an accumulation of the radionuclide.

#### *Clinical Indications*

1. Diagnosis of recent myocardial infarction when clinical evaluation and other diagnostic tests are inconclusive. This can occur when abnormalities such as bundle branch block, cardiac hypertrophy or a permanent pacemaker produce changes in the ECG which make myocardial infarction difficult or impossible to diagnose. Right ventricular infarction is also less easy to diagnose on the electrocardiogram and from time to time serum cardiac enzyme estimations are omitted or inconclusive. In these situations it may be necessary to use a pyrophosphate scan to determine if there is a significant area of damage.

2. Determination of prognosis following myocardial infarction. It has been shown that there is good correlation between the size of abnormality seen on the scan, the size of myocardial infarction and the long term prognosis. Furthermore the persistence of the abnormality is of prognostic value, a persistently positive scan some weeks after infarction indicating a poor prognosis.

#### *Interpretation of Pyrophosphate Scans*

Simple planar images are usually satisfactory and will show the infarction as either a localized region of increased uptake in the case of a small to moderate sized infarction or a ring-shaped region in the case of a large infarction. The latter appearance is due to the fact that the extreme center of a large infarct may receive no perfusion at all and thus the radionuclide cannot be delivered to this region. Uptake will, of course, be present in bones but this can normally be easily distinguished from the myocardium on a series of views. Functioning breast tissue can also sometimes produce increased uptake.

False-positive 'infarct' scans can occasionally be produced in cases of unstable angina, cardiac inflammation, calcific valvular heart disease, pericarditis and damage due to radiation or chemotherapy or metastatic disease. These are all very rare findings. The specificity and sensitivity depend on the level at which an abnormality is graded. High sensitivity of 90% can be achieved with inclusion of all minor abnormalities but this leads to a low specificity. If only the very clear high uptake lesions are recorded there will be a very high specificity but a lower sensitivity.

### **Myocardial Perfusion Imaging**

This type of scan can be performed at rest but such scans are generally of relatively little clinical use compared to assessment of the myocardium during maximal exercise. This is because many coronary stenoses are sufficiently severe to restrict blood supply at maximal exercise when oxygen demand is greatest but they allow the passage of sufficient blood at rest to perfuse the myocardium normally. This corresponds to the well-known fact that patients with angina may have a normal resting electrocardiogram but can show severe abnormalities during exercise.

At present, the most commonly used myocardial perfusion scanning agent is thallium-201. This isotope is handled by the cell membrane in the same way as potassium and is rapidly incorporated as an intracellular ion. Thallium-201 injected into the circulation is thus rapidly incorporated into the cells of the body, most particularly into those cells which are most metabolically active and which have the best blood supply. The kidneys and the heart are particularly avid in their accumulation of the radiotracer. Any differences in regional perfusion of the myocardium which are present at the time of injection will be revealed as perfusion defects. If the patient is re-imaged 3–4 hours after exercise, equilibration of the pool of intracellular ions will have occurred and it will be possible to obtain a scan representative of the resting state. This is a very useful comparative scan which often helps in determining the significance of permanent perfusion defects which may be anatomical (i.e., related to normal features such as apical thinning) or pathological (such as are found after myocardial infarction or aneurysm) in contrast to reversible perfusion defects which are typical of those produced by stenotic coronary lesions supplying normal myocardium.

The images from thallium scanning are normally obtained by a series of planar images in the anterior, left anterior oblique and left lateral views, but with appropriate imaging equipment it is possible to obtain tomographic sections through the heart. The latter approach has some advantages because it eliminates some of the difficulties of interpretation caused by background activity and by the complex curve of the left ventricular myocardial cavity.

More recently, a new radioisotope for myocardial perfusion scanning has been introduced. This is based on technetium-99m labelling of certain isonitrile compounds (abbreviated  $^{99m}\text{Tc}$  MIBI scans) and may prove to have better characteristics for scanning and give higher quality images. Unfortunately re-distribution does not occur after exercise scans of this type and a separate resting examination has to be obtained on another day. Nevertheless it may prove to be a suitable replacement for thallium scanning which has many technical limitations.

#### *Clinical Indications for Thallium Myocardial Scanning*

1. *Detection of Acute Myocardial Infarction.* This indication is not commonly used because the condition is easy to recognize by many other diagnostic techniques. In addition to this, thallium scanning is not always available in or near the acute coronary care ward. Nevertheless a resting scan will clearly demonstrate a moderate or large-sized myocardial infarct as a perfusion defect. This can be achieved with con-

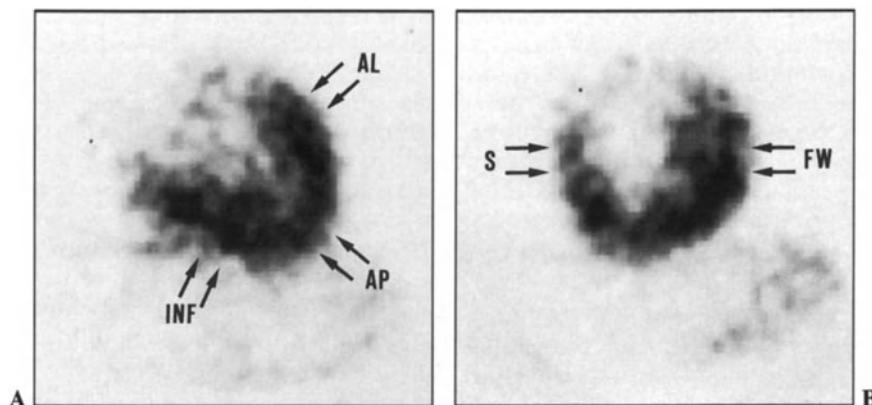


**Fig. 9.16.** A Anterior view of a normal  $^{201}\text{Thallium}$  scan showing uniform perfusion in the left ventricular myocardium. Antero-lateral (AL), apical (AP) and inferior (INF) regions of left ventricular myocardium are arrowed. B Left anterior oblique view of the same normal  $^{201}\text{Thallium}$  scan. This view shows the interventricular septum (S) and the left ventricular free wall (FW).

siderable accuracy but the technique is less sensitive for small or subendocardial infarctions.

**2. Evaluation of Patients with Suspected Myocardial Ischemia.** The published literature shows that this technique has a sensitivity of 80%–90% and a specificity of 80%–95% in the detection of significant stenoses in important coronary vessels. This technique is, however, only used in clinical practice when there is doubt about the diagnosis following other investigations. Patients with atypical chest pain, equivocal or non-diagnostic exercise electrocardiography, or asymptomatic patients with positive exercise ECGs, all present difficult clinical problems that may be aided by thallium scanning. An example of a normal thallium scan is shown in Fig. 9.16. An abnormal thallium scan is shown in Fig. 9.17.

**3. Additional Aid to Interpretation of Coronary Angiograms.** In some cases a stenosis seen on the coronary angiogram is equivocal in terms of its pathological importance. Thallium scans can sometimes be useful in determining whether a known stenosis produces significant ischemia at exercise.

**4. Sequential Follow-up of Medical or Surgically Treated Coronary Disease.** As the investigation is more easily repeatable than cardiac catheterization it can be of assistance in a number of situations such as the detection of deteriorating coronary perfusion or the occlusion of a bypass graft. Sequential assessment is simpler if an initial scan has been performed at the time of angiography.

**5. Evaluation of Less Common Myocardial Abnormalities.** Thallium scans have been reported as abnormal in a number of other conditions namely *coronary spasm*, *hypertrophic cardiomyopathy*, *mitral valve prolapse*, *cardiac tumors* and *sarcoidosis*. The usefulness of the investigation in these situations will depend on the other clinical factors.

**Contraindications.** There are no recognized complications of the administration of the thallium radionuclide but the possibility of allergy must still exist. There is a relatively high radiation dose to the patient's kidneys. For this reason the examination must be performed only as often as clinically necessary.

#### *Interpretation of Thallium Myocardial Scanning*

Thallium myocardial scans can be quite difficult to interpret because of the complex shape of the left ventricle and the anatomical variations in orientation. For this reason the scan should not be interpreted by inexperienced observers in isolation from other investigations because major pitfalls can occur. Even with experienced observers the test cannot be regarded as an absolute determinant of coronary perfusion and other clinical factors must always be kept in mind.

### RADIOMUCLIDE ANGIOCARDIOGRAPHY

#### **First Pass Technique**

This method involves the rapid intravenous injection of a simple radionuclide, the passage of which is followed through all the chambers of the heart. The study is of short duration and a fast gamma camera with computing facilities is required. The technique is quite difficult and this is not a routine examination. It is, however, useful in the study of intracardiac shunts and more recently has been useful in the sequential examination of left ventricular function during graded exercise. In the latter situation, short life radionuclides must be used to minimize the radiation dose to the patient.

#### **Multigated Equilibrium Studies (MUGA)**

This is by far the commonest type of cardiac scan performed. The examination is based on the principle of labelling red cells with  $^{99\text{m}}\text{Technetium}$ . This is most commonly done by an *in vivo* labelling method which involves an initial injection of stannous chloride followed by a second injection of sodium pertechnetate. The total patient blood pool is labelled and cardiac movement is assessed by gating the cardiac motion using the electrocardiogram. It is possible to accumulate several hundred cardiac cycles into one totalized cardiac cycle. The composite cycle is usually composed of 16–24 frames which can be replayed as a single cine loop.

### Clinical Indications for Multigated Studies (MUGA)

1. *Evaluation of Resting Abnormalities in Ventricular Function.* This is particularly useful in assessing left ventricular damage due to ischemic heart disease or cardiomyopathy. The study is simple to perform and can rapidly detect generalized or localized regional abnormalities including the presence of aneurysms with a dyskinetic movement.

2. *Monitoring of Left Ventricular Ejection Fraction.* This parameter is very important in assessing the importance of cardiac disease and its prognosis. This figure can be reliably obtained from a multigated equilibrium study and serial monitoring of left ventricular ejection fraction is often of considerable importance in assessing medical or surgical treatment. It can also be used in monitoring patients on treatment with cardiotoxic drugs.

3. *Detection of Exercise-induced Abnormality of Left Ventricular Function.* As with the electrocardiogram and the thallium scan, abnormalities caused by coronary stenoses are often revealed only on exercise. The ejection fraction will normally rise on exercise but if it fails to do this or if it falls this is an indicator of a diseased ventricle. It is sometimes possible to demonstrate a regional wall motion difference at exercise which can localize the abnormality. The technique is, of course, more complicated and time-consuming to perform as it involves scanning during dynamic exercise.

4. *Left Ventricular Assessment in Non-catheterized Pre-cardiac Surgery Patients.* In some cases this non-invasive information, often combined with echocardiographic information, is useful in planning surgery without the need for cardiac catheterization.

5. *Assessment of Right Ventricular Function.* This is relatively easy to assess, particularly in comparison with the left ventricle. Dilatation of the right ventricle can clearly be detected and the right ventricular ejection fraction can also be measured, although this is a little less accurate than the measurement of the left ventricle due to the complex shape of the right ventricle.

6. *Assessment of Regurgitant Fraction.* Careful comparison of ejected volumes from right and left ventricles can allow estimates of regurgitant fraction from the left-sided valves. This is only applicable if there is no right-sided valve regurgitation. Aortic and mitral regurgitation cannot be differentiated.

7. *Cardiac Output Estimation.* This is possible but very difficult and is not normally undertaken.

8. *Evaluation of Intracardiac Shunting in Congenital Heart Disease.* This is more suitable for first pass investigation, but equilibrium studies can be used to quantitate shunts or flow.

**Interpretation.** This is carried out on the computer and a number of manipulations can be made. The moving cine loop is the most important data to assess. The ventricular ejection fractions can be determined by comparing activity in diastole with activity in systole (after subtracting an allowance for background activity).

It is possible to perform parametric imaging which evaluates localized changes in the function pixel by pixel. The two most commonly used forms of parametric imaging are the phase and amplitude assessment which, respectively, high-

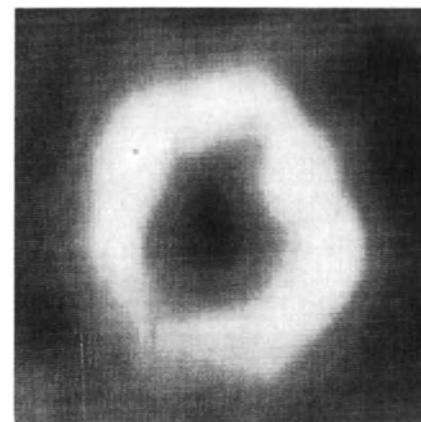


Fig. 9.19. Cross-sectional PET scan of a normal left ventricle showing even emission of activity.

light the timing of cardiac function and the amount of blood movement from each part of the image. Images from a normal gated blood pool scan are shown in Fig. 9.18.

**New Agents in Radionuclide Angiograph.** Short-lived agents, in particular  $^{195m}\text{gold}$  have become available more recently but they are still expensive. The half-life of this agent is only 30 seconds and consequently the radiation dose to the patient is very much less than with technetium. For this reason it is possible to repeat a study many times and this has mostly been used in the assessment of left ventricular function during a graded exercise test.

### Positron Emission Tomography

Positron emission tomography (PET) requires the use of a variety of substances labelled with positron-emitting radionuclides which are short-lived and therefore require a cyclotron close to the scanning apparatus to generate the radionuclides. The positrons are detected by an array of detectors and an image reconstructed in a manner similar to that used in conventional CT or isotope tomography (Fig. 9.19). Although the resolution is inferior to that of CT, the information on metabolic changes provided by PET scanning make it an important research tool. It seems unlikely that it will be in widespread clinical use for several years, although it does have the potential to be an important technique for assessing ischemia, as part of a screening program, as an adjunct to angiography or following surgery or angioplasty.

### COMPUTED TOMOGRAPHY IN CARDIAC IMAGING

Computed tomography (CT) has an important but, in its current state of development, limited role in the investigation of patients with heart disease. With the exception of some ultrafast scanners or scanners where it is possible to gate exposures to the ECG, the exposure time of CT is too long to prevent blurring of the image due to motion during the cardiac cycle. In most centres, therefore, the role of CT is confined to the assessment of structures which do not move significantly (e.g., proximal bypass grafts) or are very large (e.g., the aorta, Fig. 9.20). In addition, as blood in the heart

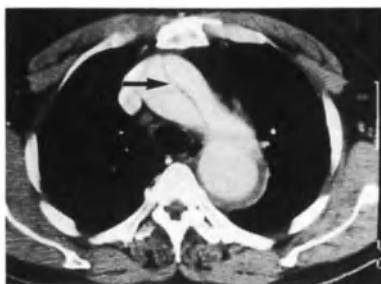


**Fig. 9.20.** Contrast-enhanced CT just below the aortic arch showing a dissection flap (arrow) in the ascending aorta.



**Fig. 9.22.** Contrast-enhanced CT in a patient with large bilateral pleural effusions and a small pericardial effusion (arrow). Left and right ventricles well shown separated by interventricular septum.

and great vessels has an attenuation similar to the surrounding tissues, it is usually necessary to give intravenous contrast medium to distinguish the cavities of the cardiac chambers from the walls. The injection of contrast medium can itself cause artefacts which can obscure or mimic abnormalities (Fig. 9.21). The use of contrast medium introduces a small risk into the examination and in many situations echocardiography, isotope studies or MRI are more appropriate. However, there are several situations when CT has a well-defined and valuable role, especially in those centres where MRI is not available. Applications of conventional cardiac CT scanning include:

1. Assessment of coronary bypass graft patency.
2. Myocardial disease causing thinning of the myocardium (e.g., left ventricular aneurysm) or thickening (e.g. hypertrophic cardiomyopathy).
3. Myocardial masses such as thrombi or tumors.
4. Pericardial effusions (Fig. 9.22), thickening or tumors, especially when arising from the adjacent mediastinum.
5. Aortic disease whether due to aneurysms, dissection or rupture.
6. Congenital aortic anomalies and vascular rings.

The development of cine-CT and gated-CT promised to be valuable in the assessment of myocardial function, perfusion and graft function. However, most of these functions can be

performed as well, if not better, by MRI without the need for irradiation or the administration of contrast media. As MRI scanners are no more expensive than cine-CT scanners it seems likely that further developments in cine-CT will be limited.

#### CARDIAC MAGNETIC RESONANCE IMAGING

There are several aspects of MR imaging which make it particularly suitable for cardiac imaging. Unlike CT or angiography, MRI is safe and does not require the use of radiation or, with the exception of some research applications, the use of potentially hazardous contrast media. This makes MRI particularly useful for studies in patients who require repeated examinations (see Fig. 11.4, Fig. 11.44): its advantages and disadvantages are summarized in Table 9.3.

**Table 9.3.** Cardiac magnetic resonance imaging: advantages and disadvantages

##### Advantages

- non-invasive (no need for contrast media)
- no irradiation
- good contrast resolution of flowing blood from surrounding tissue
- information on tissue characterization
- not affected by state of adjacent lung
- multiplanar images allow demonstration of oblique cardiac anatomy
- ECG-gating prevents motion blurring
- flow velocity and direction information
- not affected by same artefacts as echocardiography and CT

##### Disadvantages

- capital costs very high (compared with echocardiography)
- high running costs, especially cryomagnets, when compared with echocardiography and conventional CT
- contraindicated in patients with most magnetic implants (e.g., aneurysm clips) or pacemakers. This does not include the majority of valve prostheses or many orthopedic implants which do not have significant magnetism
- unsuitable for claustrophobics and many children
- anesthesia difficult (but possible)
- image degraded by motion (therefore unsuitable for restless or very sick patients)
- gated image degraded by irregular cardiac cycle
- images are sections not projections, unlike angiography, and therefore prone to misinterpretation due to partial volume effects or structures passing obliquely through scan planes



**Fig. 9.21.** Contrast-enhanced CT showing dissection flap in the ascending aorta (arrow) and descending aorta with artefact from high density SVC contrast (arrowhead) partly obscuring the ascending part of the flap.



**Fig. 9.23.** Oblique coronal gated MRI scan of a post-operative ascending aortic aneurysm showing good intrinsic contrast between flowing blood and vessel wall. (Reproduced courtesy of Trustees Bristol MRI Centre.)

The ability of MRI to be gated easily to the cardiac cycle is a further advantage over CT as is the ability to examine the heart in any plane, compared to the limited transverse scans of CT (Fig. 9.23). The use of flow-sensitive techniques allows the demonstration of flow abnormalities related to valve dysfunction and other structural defects which could previously only be visualized by Doppler or angiography. While many of the functions of cardiac MRI are fulfilled by echocardiography and Doppler, which is also considerably cheaper, not all patients are suitable cases for echocardiographic examination and some areas are poorly seen even in good patients (e.g., the pericardium and thoracic aorta). The indications where MRI is of particular value are listed in Table 9.4.

**Table 9.4.** Indications where cardiac MRI is of particular value

Thoracic aortic disease (Fig. 9.23)
Pericardial disease, especially constriction and tumors
Hypertrophic cardiomyopathy
Assessment of coronary bypass graft patency
Assessment of prosthetic valve dysfunction and periprosthetic cavities
Detection of intracardiac tumors
Congenital heart disease

In spite of its drawbacks, MRI is becoming established as an important non-invasive method in patients in whom information on structure or function cannot be obtained satisfactorily by echocardiography. Cardiac MRI should be made available to all major cardiology and cardiac surgery referral centres to allow examination of these particularly difficult cases.

#### ANGIOCARDIOGRAPHY

Although there have been major developments in non-invasive methods of cardiac imaging, such as MRI and echocardiography, there are still many diagnostic situations

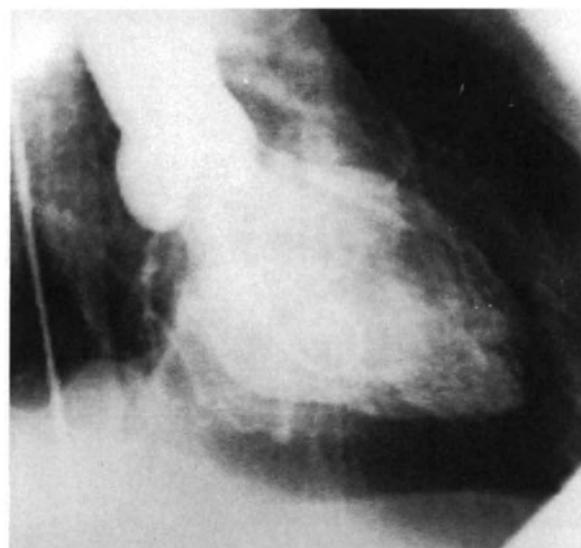


**Fig. 9.24A, B.** Normal left ventriculogram showing a projection of the whole of the left ventricle at end-diastole A and end-systole B.

where the good spatial and temporal resolution of angiography, along with its ability to provide a projection rather than a sectional image are extremely valuable (Fig. 9.24). Recent developments in digital image acquisition have allowed improvements in the ability to manipulate images, to make quantitative measurements (Fig. 9.25) and to avoid some of the problems associated with conventional angiographic techniques.

Conventional angiography has many advantages. It can demonstrate rapidly-moving structures with a clarity which is unmatched by any other imaging method and can demonstrate small structures, such as the coronary arteries, which are difficult or impossible to see in any other way. It can also show vessels not well seen by other methods due to intervening lung or complex anatomy (Fig. 9.26). At the time of angiography, pressure measurements can be taken which are accurate and provide important hemodynamic

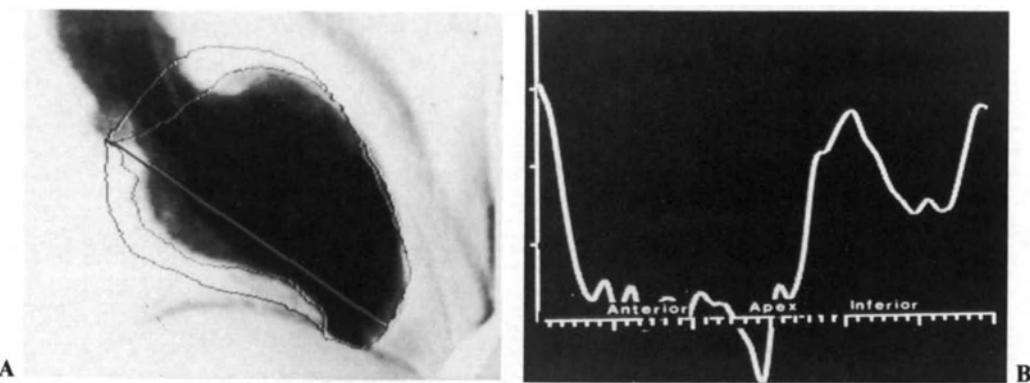


**Fig. 9.25A, B.** Digital subtraction left ventriculogram showing outline of diastolic dimension superimposed on the systolic image, A, and graphical representation of the wall motion, B, showing negligible anterior wall motion.

information which may not be readily obtained by other methods. However, there are a very large number of disadvantages in the use of conventional angiography which have prompted the development of non-invasive investigations and digital angiography (Table 9.5).

**Table 9.5. Disadvantages of conventional angiography**

**Use of radiation**

Administration of potentially hazardous contrast media  
Intracardiac manipulation of catheters with risk of serious intracardiac damage and potentially lethal arrhythmias  
Potential to cause damage to vessel used for vascular access  
Large capital costs for equipment  
Large costs of disposable equipment and contrast media  
Can be uncomfortable and unpleasant for the patient

The combined hazards of angiography lead to a significant complication rate and mortality which, although it is small, is much greater than that for alternative methods.

Because of these disadvantages, the use of angiography and cardiac catheterization in a number of situations is being replaced by less hazardous investigations:

1. Valve disease (replaced by Doppler).
2. Ventricular function (replaced by echocardiography, isotope ventriculography, MRI).
3. Hemodynamic data (partially replaced by Doppler).
4. Congenital heart disease (replaced by echocardiography, Doppler, isotopes and potentially MRI).

Cardiac catheterization remains of value in cases where non-invasive investigation is incomplete for technical reasons or where particularly small or complex structures need to be visualized. This particularly applies to the coronary arteries, coronary artery disease accounting for more than half of all cardiac catheterization procedures in many countries. It is likely that coronary arteriography will remain the investigation of choice for demonstrating the coronary arteries for many years and therefore angiography equipment and skills will be required for the foreseeable future.

#### Digital Subtraction Angiography

Digital subtraction angiography (DSA) is a method in which the angiographic images are acquired in a digital form. Images with contrast medium can be electronically subtracted from an image without contrast medium (the mask image) to produce a subtracted image of the opacified vessel being studied. The advantages and drawbacks to the use of the technique are summarized in Table 9.6.

**Intravenous DSA.** In spite of much adverse criticism there is a small but definite role for intravenous DSA (IV-DSA) in cardiac imaging. Due to the motion of the heart and overlapping of cardiac structures there is little application for intracardiac problems. There is, however, an important role in imaging the pulmonary arteries (Fig. 9.27) and veins and the thoracic aorta, particularly in congenital lesions (Fig. 9.28) and following surgery. The use of IV-DSA in these situations avoids intracardiac catheter manipulation or arterial puncture and allows outpatient examinations.

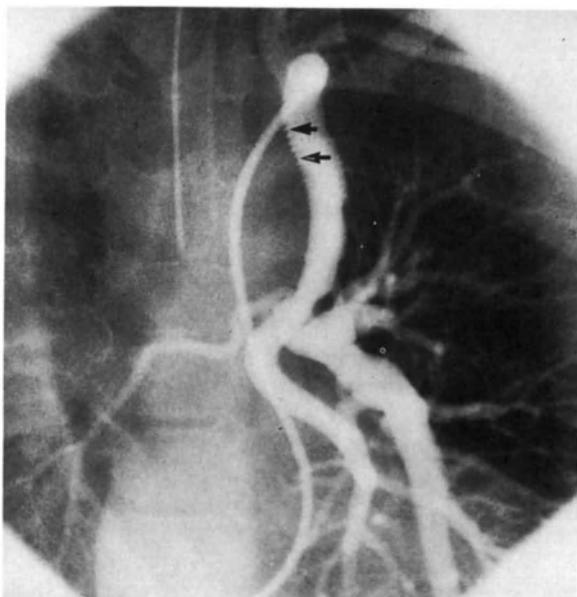


**Fig. 9.26.** Selective angiogram of left Blalock shunt showing ability to demonstrate complex structures and fine detail (note the corrugations (arrow) of the graft material).

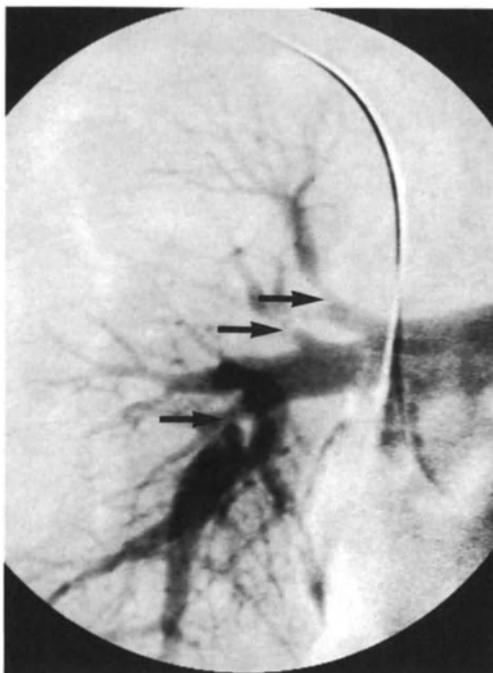


**Fig. 9.27.** Outpatient intravenous DSA showing peripheral pulmonary artery stenoses (arrow).



**Fig. 9.28.** Intravenous DSA in 8-year-old patient showing coarctation of the aorta (arrow).

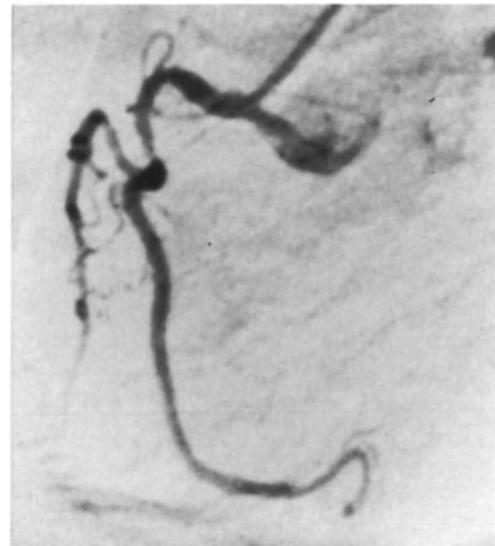


**Fig. 9.29.** DSA selective right coronary arteriogram using 2 ml contrast medium showing proximal stenosis.

**Table 9.6.** DSA in cardiac imaging

#### Advantages

- better contrast resolution than with film/screen allows use of lower doses of contrast medium
- lower film costs
- lower storage costs
- images can be manipulated to allow objective measurement of ventricular function, stenosis quantification etc.
- allows digital storage and transmission of data (with potential compatibility with other digital imaging systems)
- allows immediate replay of images which may be of value during interventional procedures
- when used for intravenous imaging procedures can be performed on outpatients

#### Disadvantages

- rapid cardiac motion makes satisfactory matching of mask and contrast image sometimes difficult or impossible
- spatial resolution inferior to cine film
- extra capital costs over and above the basic cost of conventional angiographic equipment
- intravenous studies can require use of large volumes of contrast medium

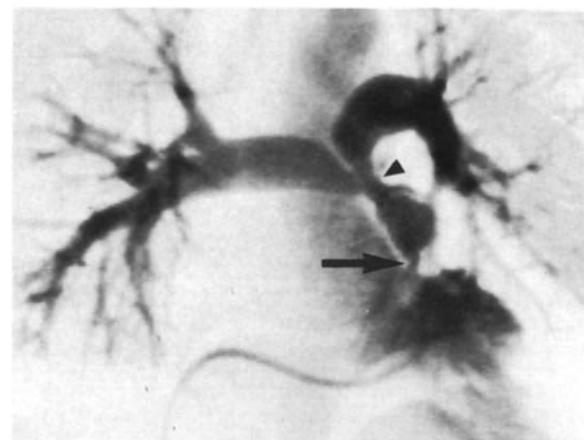


**Fig. 9.30.** DSA right ventriculogram showing subpulmonary stenosis (arrow) and main pulmonary artery hypoplasia (arrowhead) in a patient with Fallot's Tetralogy.

**Intraarterial DSA.** Some of the advantages and disadvantages of both IV-DSA and conventional angiography are seen with intraarterial DSA (IA-DSA). The better contrast resolution of DSA allows the use of smaller volumes of contrast medium per angiogram (Fig. 9.29) and the images can be manipulated after acquisition. However cardiac catheterization with the risks of intracardiac contrast injection and catheter manipulation, with arterial punctures when necessary, is still required. Add to this the poorer spatial resolution of IA-DSA compared with conventional cine film and the problems of obtaining satisfactory image subtraction, and it

is easy to understand why the use of IA-DSA in cardiac imaging is still limited, particularly in the assessment of coronary artery disease. It is more satisfactory in some pediatric cases where larger vessels in a smaller area are being examined (Fig. 9.30) and where the ability to use smaller doses of contrast medium is important. Rapid progress is being made in digital cardiac technology and this will become evident in the near future.

*For further reading, see p. 233.*

## CHAPTER 10

# ACQUIRED HEART DISEASE

*P. Wilde and G. G. Hartnell*

---

## ISCHEMIC HEART DISEASE

---

In terms of mortality and morbidity, ischemic heart disease is the most important single disease entity. In England and Wales 30% of all deaths amongst men and 22% of all deaths amongst women are the result of ischemic heart disease. This accounts for 156 000 deaths annually in England and Wales. Every year there are on average 115 000 hospital discharges with a diagnosis of ischemic heart disease.

There are marked differences in the incidence of ischemic heart disease in different countries and in some countries with a previously high incidence statistics now show a decline. This has been most marked in the USA, where the age-adjusted mortality from ischemic heart disease in men aged 35–74 years has dropped by 30% over a 15-year period to 1980. It is not, as yet, clear whether these declines are due to a true decline in incidence of disease, possibly following changes in lifestyle, or whether the decline has been due to improvements in treatment of the disease.

The likelihood of any individual suffering from ischemic heart disease of the atheromatous type depends on the interaction of many so called 'risk factors'. The important risk factors that have been clearly documented are shown in Table 10.1.

There are likely to be additional risk factors which are, as yet, not clearly identified and it is a very complex interaction of these factors that produces disease in any individual. Although the presence of many risk factors will increase the likelihood of ischemic heart disease very substantially, the presence or otherwise of significant disease cannot be determined in isolation by use of these factors. Much attention

has been given to those factors which can be changed relatively easily by the individual such as changing dietary habit, losing weight, increasing exercise and, above all, stopping smoking. Medical intervention can aid with the treatment of diabetes and hypertension but more fundamental social changes are needed to alter socioeconomic levels and stress factors.

### THE ETIOLOGY OF ISCHEMIC HEART DISEASE

In many people's minds the phrase 'ischemic heart disease' is associated with coronary artery atherosclerosis and, of course, this is the overwhelming cause of most coronary ischemia. It is important to note however that there are a

Table 10.1. Risk factors for coronary atheroma

---

Increasing age (the steepest rise in incidence occurs in the fifth and sixth decades)
Male sex
Family history of ischemic heart disease
Diet (saturated fat intake being the most important)
Abnormal lipid metabolism (raised serum cholesterol and triglyceride)
Obesity
Diabetes
Hypertension
Lack of exercise
Smoking
Stress
Low socioeconomic group

---

**Table 10.2.** Non-atheromatous causes of ischemic heart disease

Coronary spasm (often difficult to diagnose objectively)
Coronary embolism (infective, rheumatic, thrombotic)
Congenital variations (compression by major vessels, muscle bridges, fistulae)
Vasculitis (polyarteritis nodosa)
Kawasaki's disease (mucocutaneous lymph node syndrome)
Syphilis
Some tumors can compress the coronary arteries
Aortic valve stenosis (or other left ventricular outflow obstruction)
Anemia (due to the decreased oxygen carrying capacity of the blood)

number of much less common conditions which can cause myocardial ischemia. These are shown in Table 10.2.

The majority of these conditions are rather uncommon. Fig. 10.1 shows a coronary arteriogram in a patient with multiple coronary aneurysms due to vasculitis. The remainder of this chapter will be concerned with ischemic heart disease due to coronary atheroma.

#### THE CLINICAL PRESENTATION OF ISCHEMIC HEART DISEASE

The narrowing or occlusion of coronary arteries can occur at widely differing rates and in widely differing distributions and for this reason there is a very wide range of presentations of coronary artery disease. The main presentations are as follows:

1. *Myocardial Infarction.* The severity of this varies considerably. If the infarction is associated with serious ventricular arrhythmia sudden death may occur and in the early post-infarction period death may also be due to cardiogenic shock caused by massive infarction or to rupture of the heart wall, papillary muscle or interventricular septum. Less severe cases will have a spectrum of symptoms with chest pain being the predominant one. Minor infarctions can be sufficiently small to cause minimal disturbance of the patient and may be quite hard to diagnose. Pericarditis may follow myocardial infarction (Dressler's syndrome) and later developments include ventricular impairment due to myocardial damage, and left ventricular aneurysm formation.

2. *Angina Pectoris.* This is one of the commonest presentations of ischemic heart disease and is classically defined as a severe central chest pain which may radiate to the neck or arm. The pain is brought on by exertion and relieved by rest. Angina pectoris may follow myocardial infarction or may arise 'de novo'. This condition also has a wide range of severity, varying from mild angina in which patients have symptoms only on severe exercise to a level where even the most trivial exercise causes pain. Other stresses such as cold, emotion or heavy meals can also precipitate angina.

3. *Unstable Angina.* In this situation the pain of angina is present at rest or is exacerbated by the least effort. Night pain is often associated with this condition. The so-called *Prinzmetal Angina* caused by coronary spasm is different, having no clear relationship to effort.

4. *Ischemic Cardiomyopathy.* This condition follows a long course of ischemic heart disease with or without myocardial

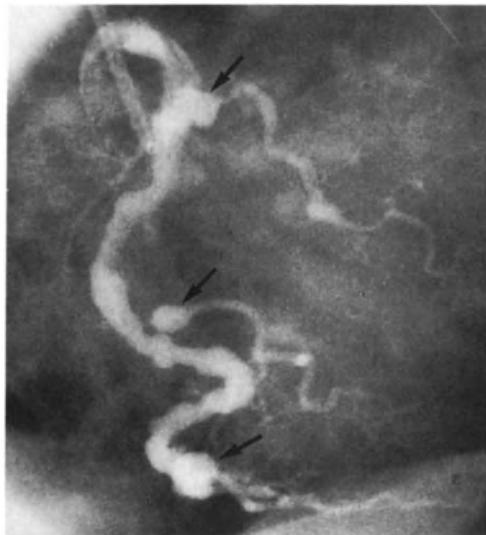


**Fig. 10.1.** Right anterior oblique view of an arteriogram of the right coronary artery. There are multiple aneurysms (arrow) on the vessels due to a vasculitis.

infarction. There is progressive fibrosis and damage to the left ventricular myocardium which ultimately impairs its overall function and leads to chronic heart failure. The condition is often associated with mitral regurgitation due to mitral annular dilatation.

#### THE TREATMENT OF ISCHEMIC HEART DISEASE

1. *Prevention.* This is very important and has been underemphasized in the past. Much money and time has been spent on treating clinically apparent coronary disease but relatively little effort has been devoted to the prevention of the disease in the first place. This is now changing and much improvement is expected in the future in the fields of dietary control, reduction of smoking, and control of plasma lipids.

2. *Angina.* The main objective in the treatment of angina is to relieve the patient of the symptoms. Initially medical therapy is employed and this is conventionally done with the use of three main agents: nitrates, calcium channel blockers and beta blockers.

If these agents are not successful in controlling anginal symptoms then further investigation of the detailed coronary pathology must be undertaken to assess the possibilities for surgery or angioplasty. These interventional procedures are carried out primarily to relieve symptoms. Present data show that coronary surgery is only valuable in prolonging life expectancy in certain specific subgroups, namely patients with severe left main coronary stenosis and those with severe widespread coronary disease. Current research is, however, suggesting that some of the less severely affected groups may be included in this category also.

3. *Myocardial Infarction and its Complications.* The primary treatment of myocardial infarction is medical and is most commonly undertaken in the coronary care unit. Recently, a more aggressive approach is being adopted in some centers,

with thrombolytic agents and even emergency coronary angioplasty being employed in some cases. Specific medical therapy in this situation will not be discussed in further detail. Radiological involvement is most useful in the diagnosis and management of complications and may lead to surgery for *myocardial rupture, mitral valve damage or left ventricular damage*. *Left ventricular aneurysm* is a late complication which is difficult to treat surgically and results are often disappointing. Nevertheless, a well-developed left ventricular aneurysm can cause cardiovascular impairment due to its paradoxical pulsation, and if a patient is in persistent heart failure due to a left ventricular aneurysm resection may be helpful. This is often performed in association with coronary artery grafting. Interventional treatment by angioplasty or surgical techniques may be necessary in post-infarction angina.

### Forms of Interventional Treatment for Ischemic Heart Disease

**Coronary Artery Bypass Grafting (CABG).** The technique is very successful in relieving symptoms of angina but, of course, involves the patient in open heart surgery with all the accompanying discomfort and inconvenience. It should be remembered also that coronary surgery involves major incisions in the patients' legs to harvest veins for grafting. This often adds significantly to the morbidity of the operation. A recent development in coronary surgery has been the reintroduction of implantation of one or both internal mammary arteries into the coronary vessels to bypass occlusions. This is often carried out in conjunction with vein grafting. Fig. 10.2 shows diagrammatically how these bypass grafts are situated.

**Percutaneous Transluminal Coronary Angioplasty (PTCA).** This technique is increasingly applied to the dilatation of cor-

onary stenoses and now is used in many patients with more than one important coronary stenosis. In general, patients are not offered coronary angioplasty unless they are suitable candidates for cardiac surgery because complications can arise which would lead to the need for emergency cardiac surgery.

**Thrombolysis.** Venous injections of thrombolytic agents have been shown to be useful in limiting or reducing the damage done at the time of myocardial infarction. Intra-coronary injection of thrombolytic agents has also been evaluated and injections may be useful in some cases in reopening a recently occluded coronary artery. This treatment may be followed by PTCA. The main limitation in this treatment is the need to act early, preferably within four hours of onset, and this is difficult to achieve in practice.

### IMAGING ISCHEMIC HEART DISEASE

Investigation will be considered under the categories of angina, myocardial infarction, angina pectoris and ischemic cardiomyopathy.

#### Angina

The oxygen demand of the heart muscle at rest is much lower than that at exercise and, therefore, it is possible for a patient to have quite severe coronary disease without producing any symptoms or myocardial ischemia at rest. It is for this reason that many investigations for the detection of coronary disease are unreliable when performed on a resting patient. It is possible to have up to 75% narrowing of a vessel before impairment of normal resting flow occurs.

The role of the radiologist in the investigation of angina is, therefore, limited to certain stress investigations and to coronary arteriography, the latter being the only definitive way of assessing the nature of coronary anatomy and pathology.

The following investigations may all be conducted under conditions of stress to compare normal and abnormal perfusion in patients with known or suspected coronary disease. All the investigations are based on the same principle of producing myocardial ischemia and it is the consequences of this ischemia that will become apparent on the test as listed below.

**Myocardial Perfusion Scanning.** Abnormal perfusion will be seen as a perfusion defect (thallium, technetium MIBI or positron agents). This defect will not be present on a resting examination in cases where the coronary stenosis affects supply to a normal region of myocardium (Fig. 9.17). If the abnormality is present on a resting examination it will suggest permanent myocardial damage such as that produced following myocardial infarction.

**Radionuclide Ventriculogram (Gated Blood Pool or First Pass)** The normal response to exercise will be to increase the left ventricular ejection fraction. In a patient with significant coronary disease the ejection fraction will not rise and may even fall. Additionally, the normal regional wall motion at rest may change to show regions of abnormal contractility at exercise.

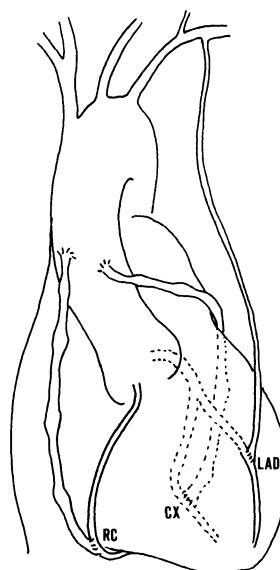


Fig. 10.2. The diagram shows a frontal view of the heart with bypass vein grafts placed from the aorta to the circumflex (CX) and right coronary (RC) arteries and a left internal mammary graft to the left anterior descending artery (LAD).



**Fig. 10.3.** A two-dimensional echocardiogram showing a short axis view of the aortic root. The right coronary artery is clearly seen but this investigation is insufficiently accurate to assess coronary stenoses.

**Echocardiography (2DE).** Normal ventricular wall motion and ejection fraction at rest may change on exercise and although exercise echocardiography is difficult to perform it can sometimes reveal abnormal segments of myocardium very clearly. Proximal coronary arteries can often be seen clearly on 2-D echocardiography but the resolution is insufficient to use for reliable clinical diagnosis of coronary stenoses (Fig. 10.3).

All the above techniques can be used in difficult cases where the diagnosis or extent of ischemic heart disease is uncertain. Their non-invasive nature allows them to be repeated following medical or surgical treatment. These tests are, however, not generally used in the routine management of a patient with coronary artery disease.

**Coronary Arteriography.** This is the definitive investigation for coronary artery disease and is the only technique which allows precise delineation of the anatomy and pathology affecting the coronary arteries to be evaluated. The examination should be performed in a center where a high volume of work is done so that the best standards are maintained. The increasing use of coronary arteriography worldwide has led to this technique becoming much safer than in previous decades and the mortality rate is now approximately 0.1%. It is, nevertheless, important to appreciate that this technique is still invasive and carries a risk of mortality as well as the risks of morbidity.

The usual indications for coronary arteriography are as follows:

1. Evaluation of known coronary disease prior to surgical or angioplasty treatment (this is the largest single group).
2. Diagnostic coronary arteriography is sometimes required in cases where chest pain is of uncertain nature. Coronary arteriography is often performed in association with catheterization for valve or myocardial disease in the absence of angina. This is done because many surgeons feel it is important to graft asymptomatic coronary disease if open heart surgery is being performed.
3. Post-operative (or angioplasty) investigation to determine the status of the coronary tree if symptoms return.

Although coronary arteriography is performed worldwide in large numbers it is still important to recognize the need for careful technique and attention to detail throughout the procedure.

The coronary anatomy varies considerably from patient to patient both in terms of the orientation of the heart as a whole and also in terms of the individual branching patterns of the coronary arteries. It is, therefore, important for the total anatomy of the coronary tree to be determined before conclusions about pathology are made.

The spectrum of coronary disease also varies considerably and does not bear a direct relationship to left ventricular function. *Left ventriculography* is always undertaken at the same time as coronary arteriography as the prognosis and treatment of a patient are heavily dependent on the functional efficiency of the left ventricle. It is quite common for a patient to have extremely severe coronary disease without any detectable damage to the left ventricle, but it is equally possible for localized coronary occlusions to cause substantial damage.

The complex nature of the coronary tree requires a three-dimensional approach to assessing coronary anatomy. It is important that every major branch and bifurcation is studied without foreshortening or overlapping so that important lesions are not missed. It is for this reason that coronary arteriography must be performed with equipment capable of cranial and caudal angulation as well as the usual oblique views. Good image qualities are required both on screening and on cine imaging. More recently some systems allow high-resolution digital recording of coronary images.

Although the general radiologist will not require detailed knowledge of coronary arterial interpretation, those performing and interpreting coronary arteriograms in the cardiac interventional centers must maintain a high level of precision when interpreting these films, because the decision with regards to coronary grafting or angioplasty is one that must be taken with extreme care.

The appearance of coronary artery disease is very variable. The segments of coronary arteries unaffected by coronary stenoses can be quite smooth in some patients and in others the vessels may be generally irregular or even dilated and ectatic (Fig. 10.4). The lesions themselves can be long or short and smooth or irregular. In some cases it is possible to identify very irregular lesions which may be ulcerated (Fig. 10.5) and in others intravascular thrombus or debris can be identified. In the latter two circumstances the threat to the distal myocardium is particularly high and this must be taken into account in planning treatment. There is no particular pattern to the development of coronary disease and all major branches must be evaluated carefully. The absence of significant disease in several major branches does not guarantee normality in any remaining vessels and, therefore, every examination must be comprehensive.

Coronary angioplasty has developed from coronary arteriography and this will be discussed elsewhere (p. 230).

#### Myocardial Infarction

The diagnosis of myocardial infarction is usually obvious clinically, with the electrocardiogram often providing rapid confirmation. The role of radiology in the management of



Fig. 10.4. A right coronary arteriogram showing marked saccular ectasia of the vessel. Right anterior oblique view.

myocardial infarction can be considered in terms of the various techniques available.

The *chest radiograph* is often considered essential for managing the patient with myocardial infarction. Whilst this is conventionally accepted, it is probably true to say that in a patient with uncomplicated myocardial infarction who is in a stable condition an immediate chest radiograph will not be essential as the management of the patient will follow a standard pattern. If there is any doubt about the nature of the diagnosis or any question of complication, particularly cardiac failure, then an immediate chest radiograph will be taken. This will show pulmonary edema which will indicate the severity of left ventricular damage. It will also show cardiac size which might indicate the presence of pre-existing

cardiac disease and it might reveal abnormalities suggesting alternative diagnoses.

Repeat chest radiographs are only required in those patients whose management will be aided by them. Once the chest film is normal there is no real gain in repeating the examination a number of times unless the patient develops new symptoms. The clinical improvement seen in a patient with myocardial infarction often precedes improvement in the findings on the chest radiograph.

In the vast majority of cases the diagnosis of myocardial infarction will be secure, but occasionally ECG and cardiac enzyme analysis will produce equivocal results. In this case pyrophosphate *myocardial infarct imaging* may be useful in determining the presence or absence of damaged left ventricular myocardium. More recently work with *anti-myosin antibody scanning* has also been shown to demonstrate myocardial infarction.

These examinations will usually reveal myocardial infarction between two and five days after the onset of symptoms. In some cases the result will be positive slightly earlier and in the cases of larger myocardial infarctions it may remain positive for longer. Nevertheless, it is important to obtain the scan at the optimal stage to ensure its reliability. Positive uptake will indicate the presence of myocardial infarction and will also indicate the size of infarction. Small infarcts will show a localized area of increased uptake, whilst large infarcts will often show a ring pattern due to a profound ischemia in the central area.

#### *Complications of Myocardial Infarction which Require Radiological Evaluation*

1. *Cardiac Failure.* The *chest radiograph* will reveal this clearly. The earliest sign of left heart failure will be relative prominence of the upper zone vessels due to early degrees of interstitial edema in the lower zones (the edema at this early stage will not be apparent but it will affect the compliance of the lower zones). More florid degrees of interstitial or alveolar edema will be obvious. The heart size will be normal in the acute phase unless there is pre-existing disease.

If detailed evaluation of left ventricular function is required then *echocardiography* is probably the most suitable approach as this can show the size of the left ventricle and will reveal any regional wall motion abnormality. It will also show any intraventricular thrombus.

2. *Ruptured Interventricular Septum.* This major complication will lead to a sudden deterioration of the patient's condition which will normally be associated with the onset of a systolic murmur. This needs to be differentiated from acute rupture of the papillary muscles which support the mitral valve.

The *chest radiograph* will usually show obvious pulmonary edema together with signs of plethora if the shunt is sufficiently large (Fig. 10.6). The appearances may be difficult to interpret as the pulmonary edema may mask the vessel outlines.

The diagnosis can be made using *echocardiography* which will reveal the defect in many cases and Doppler studies will improve the accuracy of diagnosis, as shown in Fig. 10.7. *Colour flow mapping* is particularly useful in this situation as

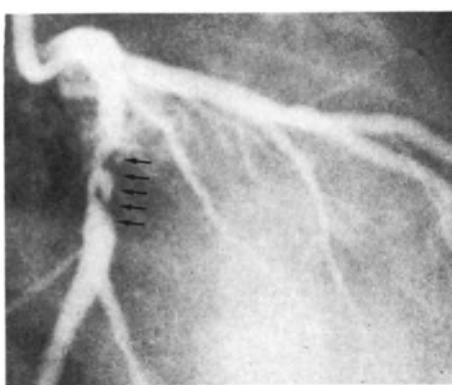
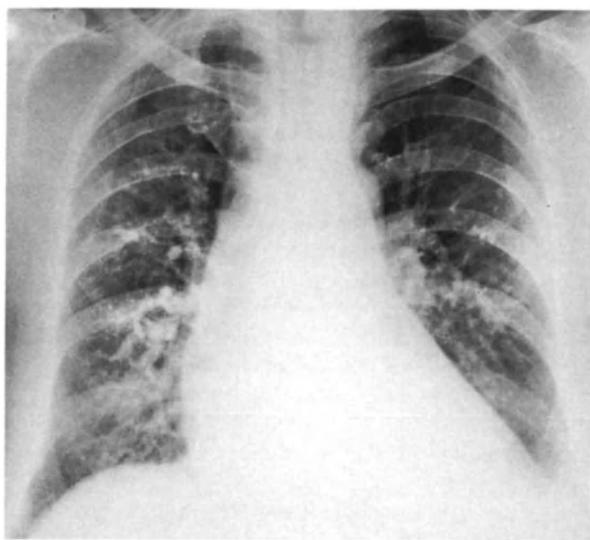
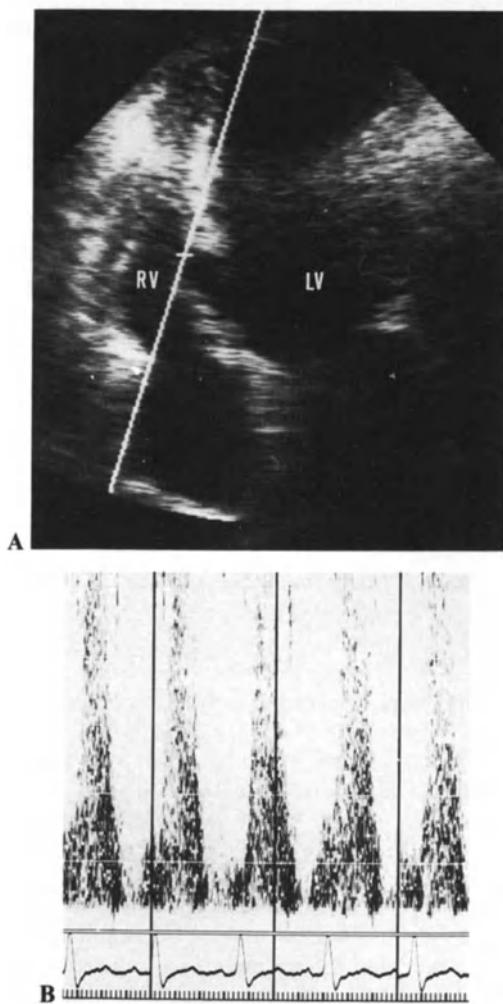


Fig. 10.5. Right anterior oblique view of a left coronary arteriogram. There is a large ulcerated atheromatous plaque in the proximal circumflex artery (arrow).



**Fig. 10.6.** The chest radiograph of a patient with an acquired ventricular septal defect complicating myocardial infarction. The pulmonary vasculature shows marked pulmonary plethora.



the patients can be quite ill and, therefore, harder than usual to examine.

*Cardiac catheterization and angiography* is very traumatic to perform in these patients and should only be reserved for those cases in whom cardiac surgery is seriously considered and in whom the surgeon specifically requires catheter-based information. In these cases, if echocardiography has revealed the nature of the abnormality in satisfactory detail, *coronary arteriography* will be the only requirement, allowing the surgeons to plan any coronary artery grafts.

**3. Ruptured Papillary Muscle.** The *chest radiograph* will show signs of heart failure, the appearances of which will depend on the severity of the regurgitation and the duration of the condition.

The condition must be distinguished from rupture of the interventricular septum and *echocardiography* and *Doppler* examination will be required to achieve this distinction with precision. Again, *ciné angiography* of the left ventricle is a hazardous procedure in this situation and must only be undertaken if non-invasive techniques are unsatisfactory.

**4. Pericardial Effusion.** This can occasionally be caused by rupture of the left ventricle (hemopericardium) but this is usually associated with sudden death and will not normally be seen on a scan. There are occasions, however, when a ventricular rupture is contained by pericardial adhesions or other limiting structures and a false aneurysm of the left ventricle can develop. It is possible to evaluate this using *echocardiography* or *MRI*, which will show that there is a break in the left ventricular wall without continuity of the myocardium around the bulge, as would be seen in a typical left ventricular aneurysm. An example of this is shown in Fig. 10.8.

More usually, pericardial effusion will develop some days after the myocardial infarction as a consequence of the 'post-infarction syndrome' of Dressler, and in this situation 2D-*echocardiography* will clearly reveal the presence of fluid. Chest radiograph appearances are very variable and depend on the size of the effusion. Effusions associated with myocardial infarction are usually quite small.

**5. Left Ventricular Aneurysm.** This abnormality develops some time after the infarction, usually only becoming apparent some weeks or months later. The aneurysm may present with cardiac failure or may simply present as an abnormality on the chest radiograph (Fig. 10.9). This may be in the classical apical position or, less commonly, posteriorly or inferiorly. In the latter situation it is hard to recognize on the chest radiograph. The *chest radiograph* cannot be regarded as a definitive guide to presence or absence of left ventricular aneurysm as the site and size of these lesions is extremely variable.

**Fig. 10.7A, B.** The two dimensional echocardiogram (A) shows a four-chamber view demonstrating a defect in the interventricular septum of a patient after a large antero-septal myocardial infarction. A pulsed Doppler sample volume has been placed in the right ventricle (RV) near the defect. The left ventricle is also labelled (LV). The spectral Doppler trace (B) shows marked systolic turbulence in this region caused by flow through the ventricular septal defect.



**Fig. 10.8.** This magnetic resonance image of the heart is taken in transverse section (S, spine; A, descending aorta; L, left ventricle). There is a large posterior false aneurysm (FA) of the left ventricle. Arrows show the edges of the myocardium of the posterior left ventricular wall.

If there is, therefore, any clinical suspicion of aneurysm formation this should be assessed with *echocardiography* or by the use of *radionuclide ventriculography* which can perform a similar function. Fig. 10.10 shows images from a radionuclide ventriculogram in a patient with a left ventricular aneurysm. It is important to know about the presence of the aneurysm because medical treatment to control potential embolus formation and cardiac failure may be considered. Surgical treatment is not commonly performed for left ventricular aneurysm, although it is occasionally necessary in cases of severe failure, cases with co-existing angina or in patients with associated intractable cardiac arrhythmias. The chest radiograph will sometimes reveal calcification in the wall of a well-established left ventricular aneurysm (Fig.

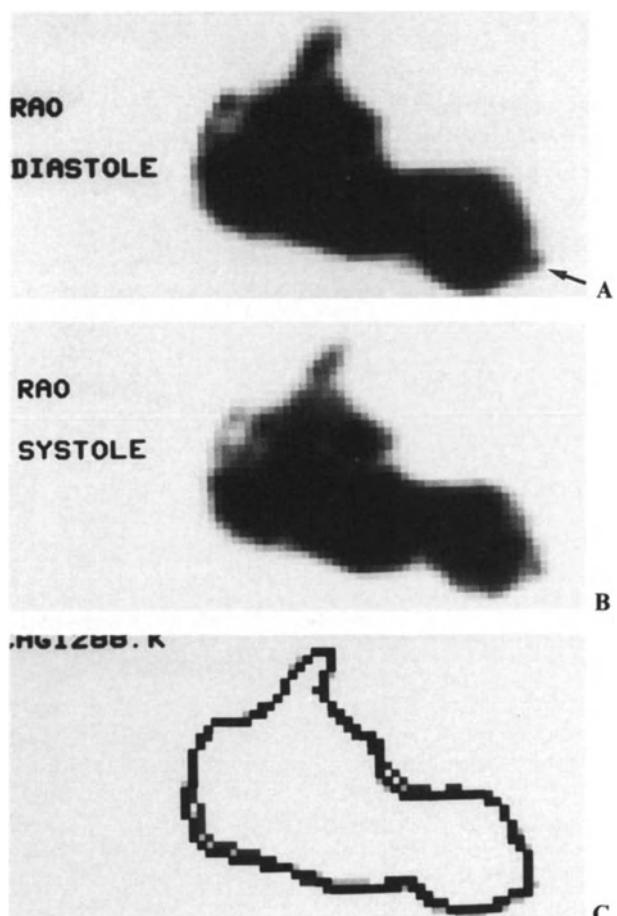


**Fig. 10.10A, B, C.** Right anterior oblique views of a resting gated equilibrium radionuclide ventriculogram (MUGA) in the same patient shown in Fig. 10.8. The patient has a severely damaged left ventricle and an apical left ventricular aneurysm. Diastolic and systolic frames from the study are shown in A and B. The apex is arrowed in the first frame. Outlines generated from the previous two frames are shown in C. The poor overall ventricular function is clearly apparent.



**Fig. 10.9.** The chest radiograph shows a considerably enlarged heart with an apical bulge due to a large apical left ventricular aneurysm.

10.11) and the calcification will also be seen on CT scanning (Fig. 10.12).

#### Angina Pectoris

The *chest radiograph* in angina pectoris is commonly normal unless there is additional cardiac disease. A few clues may be present. *Coronary artery calcification* is sometimes seen on a chest radiograph although it must be quite dense to be obviously recognizable on the standard films. The prognostic significance of this calcification varies according to the age of the patient. In patients under the age of 40 years, obvious coronary calcification is almost certainly associated with severe coronary disease whereas in the over-70 age group the presence of coronary calcification has a very much lower predictive value. Signs of aortic stenosis must be sought and the metallic clips and wires associated with previous coronary surgery will give an obvious hint. In general, however, the chest radiograph is unhelpful and other diagnostic

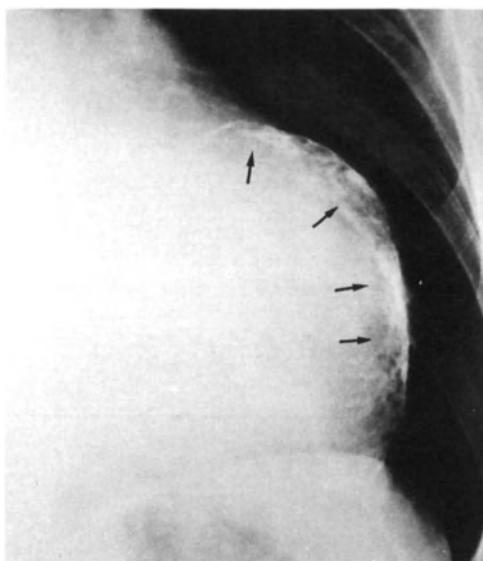


**Fig. 10.11.** Localized view from the chest radiograph of a patient with an apical left ventricular aneurysm showing calcification in the walls of the aneurysm (arrows).

approaches must be used. The clinical diagnosis of angina is of fundamental importance and the *exercise electrocardiogram* (ECG) is a powerful clinical tool for evaluating myocardial perfusion. Many patients will have a confident diagnosis of ischemic heart disease made without the need for radiological confirmation.

In some cases it will be helpful to combine the exercise ECG with a *thallium scan* to determine visually the state of left ventricular myocardial perfusion.

In spite of this, there will be a minority of patients in whom the diagnosis of ischemic heart disease remains unclear and this group will require *coronary arteriography* to determine the diagnosis. Table 10.3 demonstrates the typical diagnostic pathways used in the management of a patient with angina pectoris. In the majority of patients, coronary arteriography is used to evaluate the precise nature of the coronary arterial tree in patients who are known to have coronary disease.

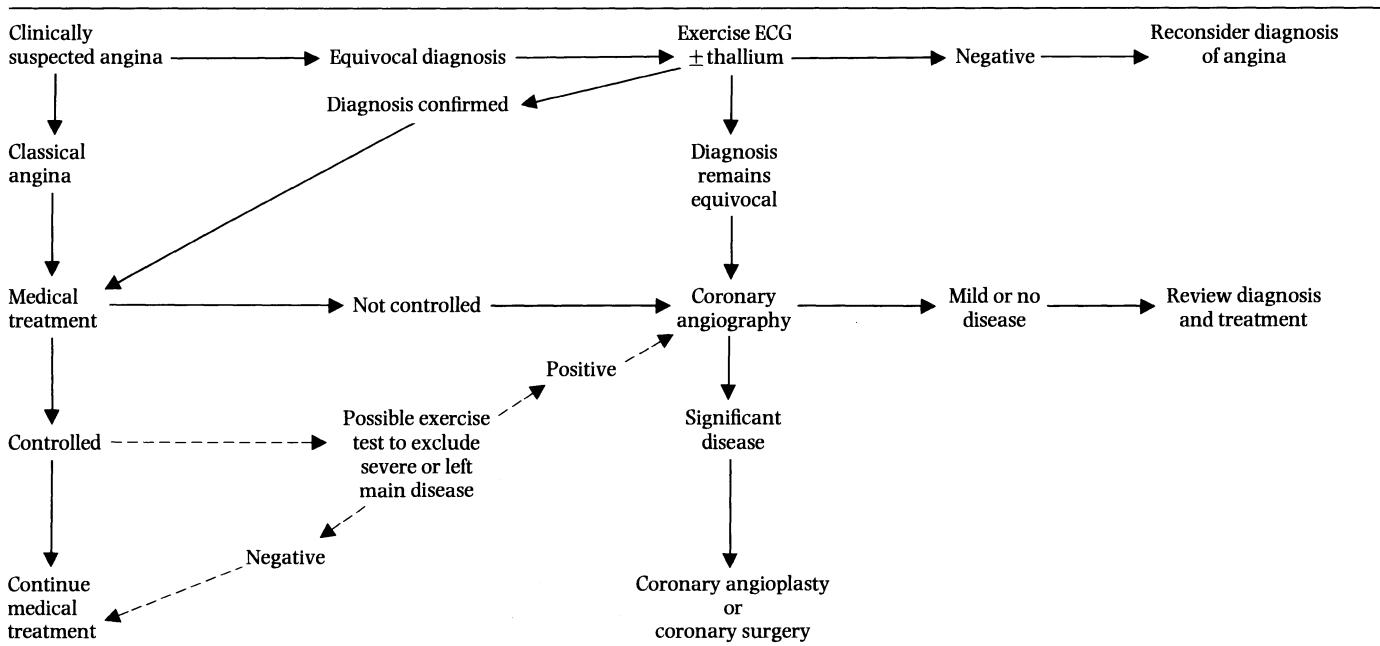
#### Ischemic Cardiomyopathy

Damage to the left ventricle caused by myocardial infarction is usually associated with obvious symptoms. It is possible, however, for the patient to have either silent myocardial infarctions or chronic myocardial ischemia, either of which can lead to a gradual deterioration in left ventricular func-



**Fig. 10.12.** The transverse CT scan shows a posterior left ventricular aneurysm with calcification clearly seen in its walls (arrows).

**Table 10.3.** Typical flow chart for the investigation and treatment of angina pectoris



tion. This is usually associated with dilatation and loss of contractility of the left ventricle caused by progressive fibrosis of the left ventricular myocardium.

The patient may be in heart failure, but often the ventricle compensates with some dilatation; the patient also modifies his lifestyle and medical therapy may be effective. All these factors can combine to give clear lung fields even with quite a severe dilated cardiomyopathy.

The deterioration of the left ventricle can be evaluated by a range of techniques including *echocardiography* and *radio-nuclide ventriculography*. It is not possible, however, to distinguish this type of myocardial damage from other causes of cardiomyopathy without the addition of positive evidence of coronary disease. This may require *coronary angiography* although this investigation may not be warranted in every case.

Dilatation and impairment of left ventricular function will often be associated with dilatation of the mitral valve annulus and this, in turn, will often produce functional mitral regurgitation. This is most easily picked up by *Doppler echocardiography* and it is probably true to say that in all cases of severe left ventricular impairment there will be some degree of mitral regurgitation.

Table 10.4 summarizes some important features of the chest radiograph in ischemic heart disease.

**Table 10.4. The chest radiograph in ischemic heart disease**

Myocardial infarction	normal heart size in acute first infarct heart failure may be present with normal heart size heart size and shape may be normal with a sizeable left ventricular aneurysm large heart indicates previous myocardial damage, valve lesion or new complication (e.g., pericardial effusion) in severe heart failure, check for pulmonary plethora due to ventricular septal rupture
Angina pectoris	the chest radiograph is often normal look for coronary calcification (PA and lateral) which is more prognostically significant in younger patients a large heart means additional ventricular or valvular disease look for signs of aortic valve disease look for calcification in the ascending aorta (hyperlipidemia or, very rarely, syphilis) look for signs of previous surgery (sternal wires, vein graft or internal mammary clips)
Ischemic cardiomyopathy	cardiac enlargement is usually present heart failure may be present but depends on the level of ventricular compensation and medical therapy lung vessels may look slightly small (differential – pericardial effusion) cannot be differentiated from other forms of dilated cardiomyopathy left atrium may be enlarged (non-compliant ventricle or mitral regurgitation)

## ACQUIRED VALVULAR HEART DISEASE

In spite of the reduction in the incidence of rheumatic heart disease in Western countries, acquired valve disease, whether due to degenerative changes, infection or other mechanisms still remains common. This is an area where non-invasive imaging methods have replaced invasive methods to a very large degree.

The imaging investigation of acquired valvular heart disease has several goals:

1. To confirm the clinical diagnosis and allow appropriate medical therapy to be given and to prevent inappropriate therapy (vasodilators for patients thought to have left ventricular failure and mitral regurgitation and, in fact, having severe aortic stenosis).
2. To determine the etiology, particularly if the underlying disease process can be treated and arrested (e.g., bacterial endocarditis).
3. To assess the results of treatment.
4. To detect the development of complications of valve disease such as left ventricular dilatation and pulmonary hypertension.
5. To assess the patient's suitability for surgery and to prevent unnecessary deterioration in myocardial function occurring before surgery.

Developments in non-invasive imaging, and in particular developments in echocardiography and Doppler have made it much easier to fulfill these goals without resorting to

invasive investigations. CT, isotope studies and MRI all have a role but these are less important than echocardiography. Angiography is often only required to provide details of the coronary artery anatomy prior to surgery.

### MITRAL STENOSIS

The majority of cases of mitral stenosis result from chronic scarring developing years after an episode of rheumatic fever, which may have been asymptomatic or undiagnosed (30% of cases or more). The mitral valve is thickened, distorted by fibrosis and shortening of the chordae tendinae, and may become calcified. Opening is further restricted by fusion of the valve commissures. The radiological features reflect changes due to the mitral valve obstruction that this produces and the secondary changes in left atrial and pulmonary hemodynamics. The appearances may be modified by the presence of other valve lesions, such as mitral regurgitation, which is found in a large proportion of cases of mitral stenosis, or aortic stenosis.

**Imaging.** The *chest radiograph* shows changes due to left atrial enlargement, pulmonary venous congestion and changes in the valve and the wall of the left atrium.

**Large Left Atrium.** There is straightening of the left heart border or prominence of the left atrial appendage below the pulmonary artery. The left atrium can be very large and may

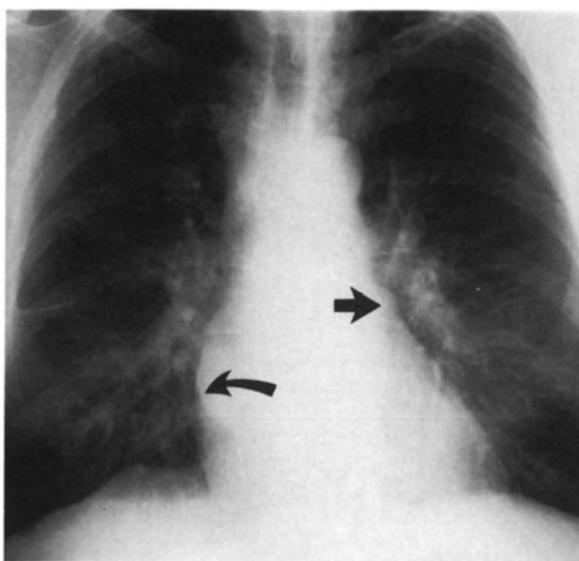


**Fig. 10.13.** Chest radiograph of a patient with severe mitral stenosis showing prominence of the left atrial appendage (straight arrow), a double right heart border due to left atrial enlargement (curved arrow) and early changes of pulmonary edema.

not initially be identifiable as such in extreme cases. An aneurysmal left atrium is more commonly seen in cases of severe mitral regurgitation. Following closed mitral valvotomy the left atrial appendage, which is usually

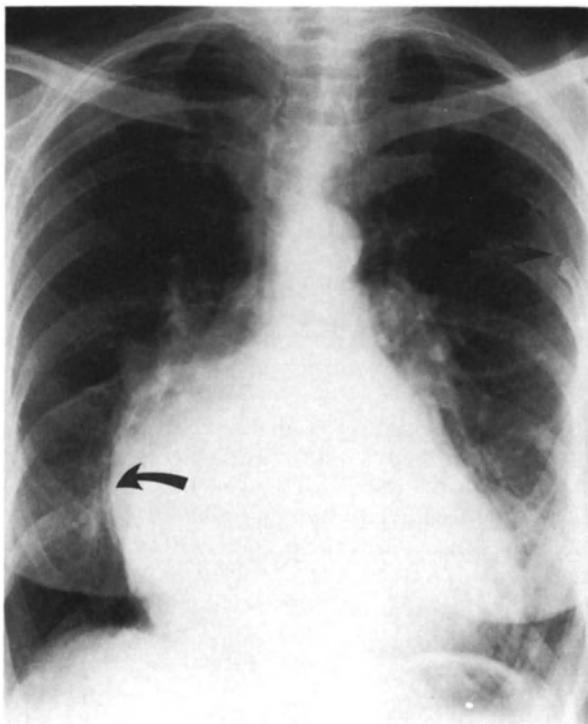


**Fig. 10.14.** Chest radiograph following closed mitral valvotomy showing rib resection at site of thoracotomy (straight arrow), large left atrium (curved arrow).

removed at surgery, is no longer visible (Fig. 10.13). Other signs seen at simple chest radiography include:

1. Double right heart border. A shadow may be visible close to the right heart border, which is the edge of the large left atrium projected behind the right atrium (Fig. 10.13), although in some severe cases the left atrial wall may be the more lateral shadow (Fig. 10.14).
2. Displacement of the esophagus posteriorly and to the left, well shown if it is outlined with barium.
3. Compression and elevation of the left main bronchus producing splaying of the carina. This, however, is one of the most frequently overdiagnosed and misinterpreted signs on the chest radiograph in patients with heart disease.

In chronic cases *calcification* develops in the valve and also in the left atrium – either in the wall of the atrium or in long-standing thrombus (Fig. 10.15). This is often best seen on the lateral chest radiograph or on fluoroscopy.

*Pulmonary venous congestion* produces the following changes:

1. Upper lobe venous distension due to raised pulmonary venous pressure; this also causes lower lobe venous constriction and therefore upper lobe blood diversion.
2. Interstitial pulmonary oedema with fluid in septal lines (Kerley's B, Fig. 9.6 and, less frequently, A lines, Fig. 9.5).
3. Alveolar pulmonary edema, particularly in the perihilar regions (Fig. 9.7).
4. In long-standing cases pulmonary hemosiderosis (multiple small opacities throughout the lungs of less than calcific density) occurs (Fig. 10.16) and it may also be seen in cases of pulmonary hypertension with pulmonary ossification (in which the opacities are denser and may be larger and more irregular). Either can occur alone.

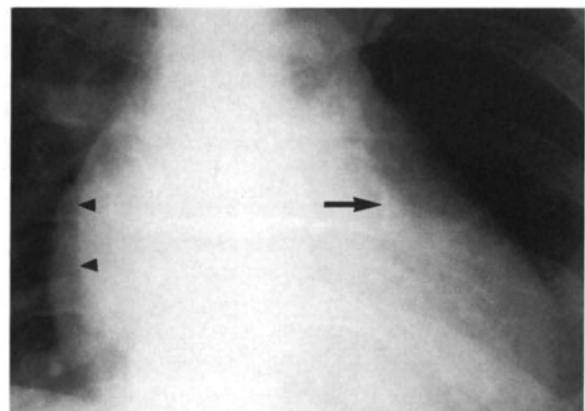


**Fig. 10.15.** Close up view from chest radiograph showing calcification in the left atrial wall (arrow) and a double right heart border due to an enlarged left atrium (arrowheads) in a patient with mitral stenosis.

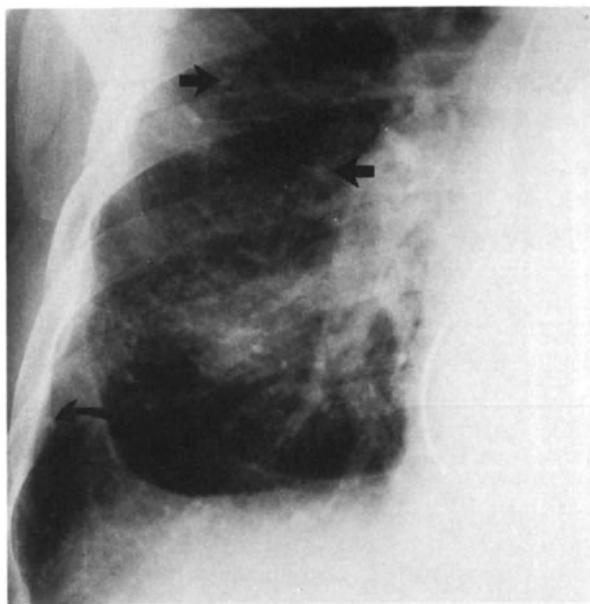


Fig. 10.16. Close up view from chest radiograph showing pulmonary hemosiderosis (straight arrows) and pulmonary ossification (curved arrows) in a patient with severe mitral valve disease.

- After a long period of pulmonary venous hypertension secondary changes develop in the pulmonary arteries leading to arterial vasoconstriction and pulmonary arterial hypertension. The main pulmonary arteries are enlarged and the peripheral arteries attenuated; there may also be evidence of right ventricular and right atrial enlargement, particularly if there is pulmonary or tricuspid regurgitation.

**Echocardiography.** Echocardiography is the most useful non-invasive method for assessing the severity of mitral stenosis and for simultaneously looking for other valve lesions. A large number of signs have been described, but the most important are those Doppler features which relate

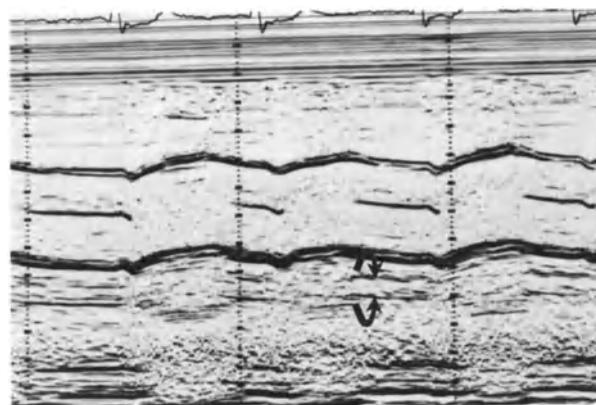


Fig. 10.18. M-Mode echocardiogram from a patient with mitral stenosis and thrombus producing mobile echoes (curved arrows) in the left atrium.

to the obstruction of the valve and allow diagnosis and accurate assessment of the severity of stenosis.

**M-Mode.** This shows thickening of the mitral valve with a reduced rate of closure of the anterior mitral leaflet (reduced diastolic closure rate, DCR); anterior motion of the mitral valve in diastole reflected by the anterior motion of the posterior leaflet; restricted opening of the valve (Fig. 10.17); and slow diastolic filling of the left ventricle. The left atrium is large and echoes from atrial thrombus may be visible (Fig. 10.18). Methods of assessing the severity of mitral stenosis on the basis of M-Mode alone have been described but are not sufficiently accurate for use in clinical practice.

**2-D Echocardiography.** As with M-Mode, the valve is thickened and has restricted opening (Fig. 10.19). This may be measurable in the short axis view, although acoustic shadowing from calcification may obscure part of the valve orifice. Some estimate of the valve area can be made from the short axis view (Fig. 10.20), but this is also liable to errors. 2-D is more reliable in showing the size of the left atrium and detecting left atrial thrombus (Fig. 10.21).

**Doppler.** Doppler can make the diagnosis of mitral stenosis and is also the most useful non-invasive method for assessing

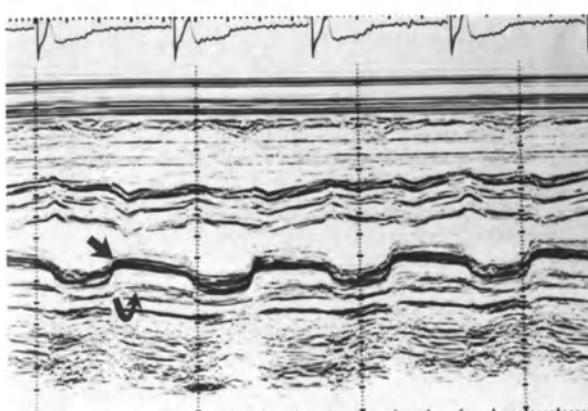


Fig. 10.17. M-Mode echocardiogram of a patient with mitral stenosis showing thickening of the mitral valve cusps (anterior cusp: straight arrow; posterior cusp: curved arrow) with poor opening and slow diastolic closure.

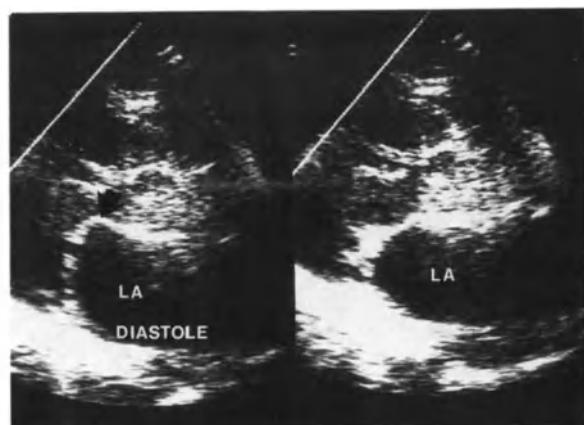


Fig. 10.19. Diastolic and end-systolic 2-D long axis images from a patient with mitral stenosis showing a large left atrium (LA) and doming of the mitral valve in diastole (arrow).



Fig. 10.20. 2-D short axis echocardiogram showing mitral valve orifice with area measured to be approximately  $2 \text{ cm}^2$ .

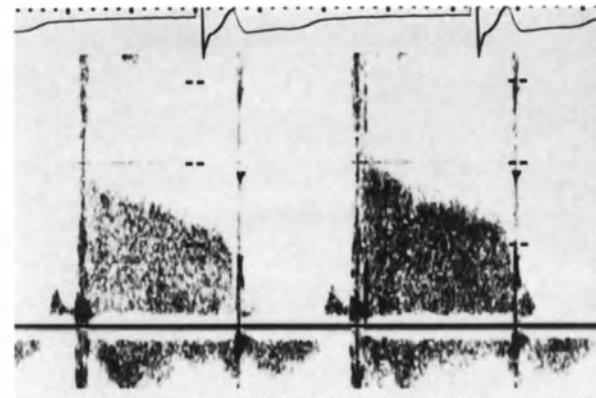


Fig. 10.22. Continuous wave Doppler of a patient with severe mitral stenosis. Pressure time is approximately 300 ms and indicates a valve area of approximately  $0.7 \text{ cm}^2$ .

the severity of mitral stenosis. Imaging by M-Mode or 2-D echo and chest radiography are often inaccurate in assessing the severity of mitral stenosis, particularly if there are other valve lesions. The chest radiograph may even be normal in some cases of severe mitral stenosis. By using the modified Bernoulli equation the peak and mean valve gradients can be estimated. Using the half-time equation (mitral valve area( $\text{cm}^2$ ) =  $220/\text{time}$  for transvalvar gradient to fall by 50% expressed in milliseconds) the size of the valve orifice can be predicted. In most cases accuracy is sufficient to allow decisions on the need for surgery, and to assess the function of prosthetic valves, especially when these become stenosed (Fig. 10.22).

**Angiography.** This has little place in the modern assessment of mitral stenosis, although coronary arteriography may be necessary to evaluate the coronary arteries before valve surgery. Mitral stenosis causes doming of the valve into the left ventricle with a negative jet of unopacified blood entering the ventricle in diastole. The left ventricle is usually of normal size unless there is other complicating valve or coronary artery disease.



Fig. 10.21. 2-D long axis image showing thrombus (arrows) in the left atrium in a patient with severe mitral stenosis.

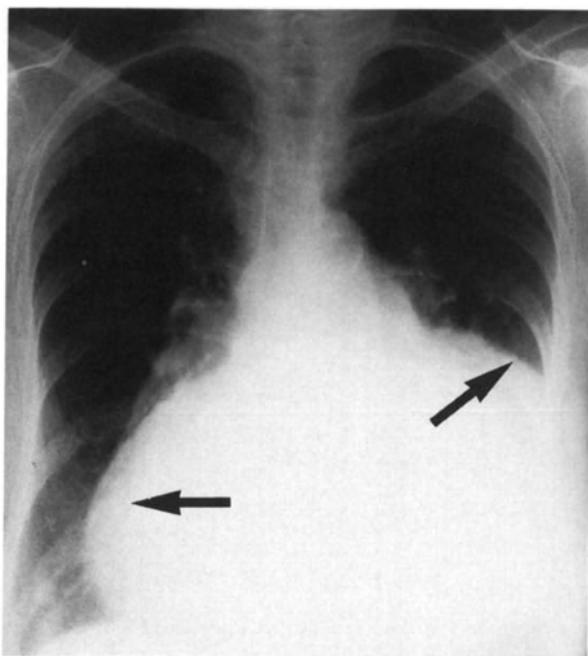
## MITRAL REGURGITATION

Mitral regurgitation is a common finding in patients with acquired heart disease and has many causes (Table 10.5). It may be due to damage of the valve cusps (as in endocarditis), of the papillary muscles (as in ischemic papillary muscle rupture), of the chordae tendinae (as in mitral prolapse), or to dilatation of the mitral valve annulus (as in many cases of left ventricular dilatation). The purpose of imaging in patients with signs of mitral regurgitation is threefold: to confirm the diagnosis of mitral regurgitation (which may be mistaken for a variety of other causes of a systolic murmur), to diagnose the underlying cause (although this may not be apparent on imaging and may be established clinically or pathologically) and to assess the hemodynamic significance of the regurgitation and its effect on cardiac performance. The methods for assessing the severity of the regurgitation apply to all cases, irrespective of the etiology.

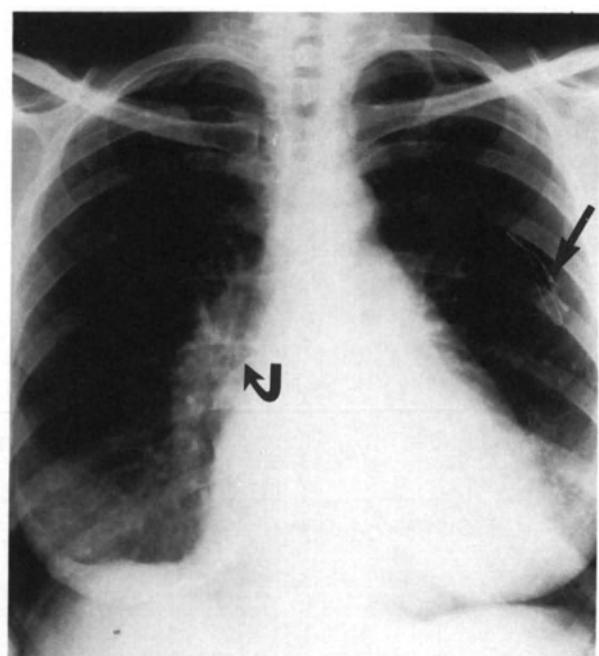
The general assessment of mitral regurgitation will be described in the context of rheumatic mitral disease. Particularly important features of imaging with other etiologies will be described individually.

Table 10.5. Important causes of mitral regurgitation

- Rheumatic heart disease
- Mitral valve prolapse
- Left ventricular dilatation (whatever the cause)
- Ischemic papillary muscle dysfunction
- Rupture of chordae tendinae
- Bacterial endocarditis
- Mitral annulus calcification
- Cardiomyopathy (often due to left ventricular dilatation but also complicating hypertrophic cardiomyopathy)
- Marfan's syndrome
- Congenital heart disease (e.g., AV canal defect)
- Rheumatic fever
- Left atrial myxoma
- Prosthetic mitral valve dysfunction
- Post-operative causes (mitral valvotomy, mitral valve repair, balloon mitral valvoplasty)
- Blunt chest trauma



**Fig. 10.23.** Chest radiograph from a patient with severe mitral regurgitation showing a very large heart with a huge aneurysmal left atrium (arrows) and a large right atrium.



**Fig. 10.24.** Chest radiograph from a patient with mitral regurgitation following closed mitral valvotomy (note suture material from thoracotomy (arrow) but no rib resection) with a large heart, large left atrium and calcification in the left atrial wall (curved arrow).

In patients with rheumatic mitral regurgitation there is often associated mitral stenosis and involvement of other valves, which should also be assessed at the same time. The initial assessment should be by chest radiography and echocardiography.

**Chest Radiograph.** The chest radiograph may show varying degrees of left atrial enlargement due to volume overload. This may lead to aneurysmal dilatation, especially in long-standing cases and those with atrial fibrillation. A very large left atrium (Fig. 10.23) suggests mitral regurgitation as the cause but with lesser degrees of left atrial dilatation it is not possible confidently to differentiate mitral stenosis from regurgitation. There may be calcification in left atrial thrombus or in the wall of the atrium (Fig. 10.24).

In rheumatic cases there may be calcification in the valve, but in most other types of mitral regurgitation the valve is not significantly calcified.

Because a variable volume of blood is ejected into the left atrium the left ventricle has to sustain an increased stroke volume. A moderate increase in stroke volume may be well tolerated, but after a variable period the left ventricle becomes dilated and the cardiac outline is enlarged. In long-standing cases, when there is pulmonary hypertension or tricuspid regurgitation, right atrial dilatation also contributes to cardiac enlargement.

The changes due to pulmonary venous congestion are similar to those described in mitral stenosis and occur with any cause of significant mitral regurgitation.

**Echocardiography.** In cases of rheumatic mitral regurgitation the echocardiogram will show thickening of the valve cusps and a variable degree of left atrial dilatation, sometimes

with left atrial thrombus. The left ventricle is often dilated with an increased ejection fraction to accommodate the increased stroke volume. There may be signs of right heart dilatation and pulmonary hypertension. Doppler is valuable to assess the severity of the regurgitation by allowing the regurgitant jet to be traced back into the left atrium (using pulsed wave or color flow). Grading of severity on the basis of the area or distance from the valve over which regurgitation can be detected correlates moderately well with the angiographic severity of the regurgitation.

**Angiography.** The severity of mitral regurgitation can be assessed at cardiac catheterization from pressure data and the degree of mitral regurgitation into the left atrium from a left ventriculogram (Fig. 10.25). Further data required for

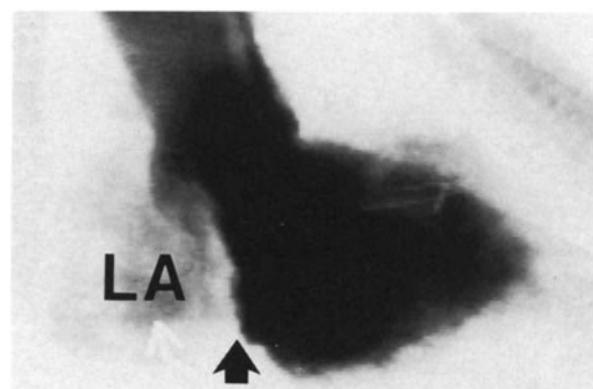


**Fig. 10.25.** DSA left ventriculogram showing contrast regurgitation through the mitral valve (arrow) into the left atrium (LA).

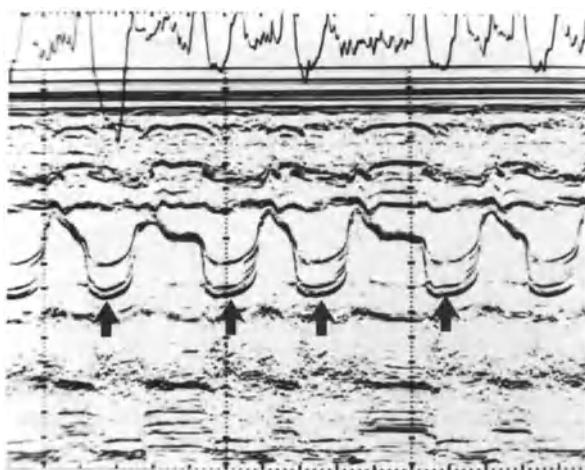


**Fig. 10.26.** M-Mode echocardiogram showing prolapse of the anterior mitral valve leaflet (arrows) throughout systole.

assessment prior to surgery about left ventricular function and coronary anatomy should be acquired at the same time.

**Magnetic Resonance Imaging.** The severity of mitral regurgitation can be assessed by MRI, although this is not yet a routine indication. In some situations when echocardiography is unsuccessful and angiography is contraindicated MRI may be a suitable alternative method for assessing the severity of mitral regurgitation.

**Mitral Valve Prolapse.** This is a common condition in which there is myxomatous degeneration of the mitral leaflets associated with stretching of the chordae tendinae. This allows the leaflets to prolapse through the mitral orifice during part of or the whole of systole (Fig. 10.26) and is associated with a variable degree of mitral regurgitation. It is a common condition, although reports of a prevalence in young women of up to 20% greatly overestimated its frequency. It may also be associated with Marfan's syndrome when it tends to have a more serious natural history. The changes on the chest radiograph reflect the severity of the mitral regurgitation; in the majority of cases the chest radiograph is normal.

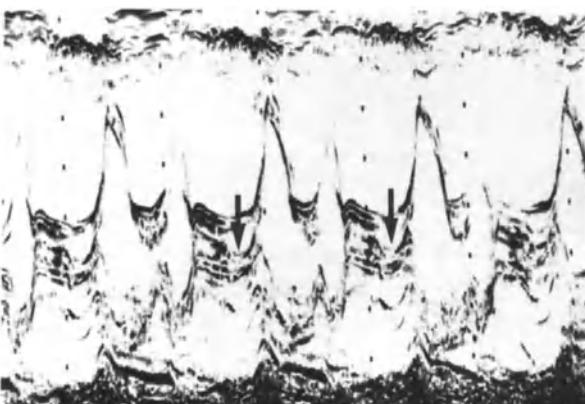


**Fig. 10.27.** M-Mode echocardiogram showing late systolic prolapse of the posterior mitral valve leaflet (arrow).

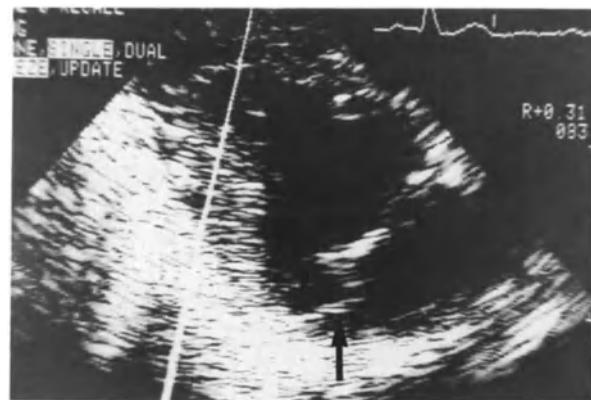


**Fig. 10.28.** 2-D echocardiogram showing prolapse of the posterior mitral valve leaflet into the left atrium (arrow).

**Echocardiography** is the key investigation for making the diagnosis. **M-Mode** will show abnormal posterior motion of the affected valve leaflet during systole (Fig. 10.27). In severe cases there is a large atrium and increased left ventricular ejection fraction. It is easy to overdiagnose mitral prolapse on M-Mode and any M-Mode diagnosis of prolapse should be confirmed by 2-D echocardiography.

**2-D echocardiography** shows normal coaptation of the tips of the leaflets but bulging of part of the leaflets into the left atrium (Fig. 10.28). The mitral valve cusps may appear thickened, an appearance which may be associated with an increase risk of systemic embolization. **Pulsed wave or color flow Doppler** should be used to assess the severity of any associated mitral regurgitation.

**Left Ventricular Dilatation.** Left ventricular dilatation, of whatever cause, is a common cause of mitral regurgitation. In practice it is usual to find at least a minor degree of mitral regurgitation in patients with significant left ventricular dilatation. The **chest radiograph** will show cardiomegaly, reflecting left ventricular and often, in generalized cardiac disease such as cardiomyopathy, right ventricular dilatation as well as atrial dilatation. Pulmonary vascular changes will reflect the degree of pulmonary venous congestion, in part due to mitral regurgitation and in part due to the raised left ventricular end-diastolic pressure found in patients with poor left ventricular function.

**Echocardiography** shows left ventricular dilatation with a reduced ejection fraction. On M-Mode the mitral valve trace appears to be abnormally suspended in the middle of the left ventricular cavity and there may be a late diastolic 'C-hump', which reflects delayed mitral closure due to the raised left ventricular filling pressure (Fig. 10.29).

**Ischemic Damage.** Mitral regurgitation in patients with ischemic heart disease may be the result of left ventricular dilatation or damage of the mitral valve apparatus by ischemia or infarction leading to papillary muscle dysfunction or chordal rupture. Papillary muscle or chordal rupture may also complicate bacterial endocarditis but ischemia is by far the commonest cause. In chronic cases the chest radio-

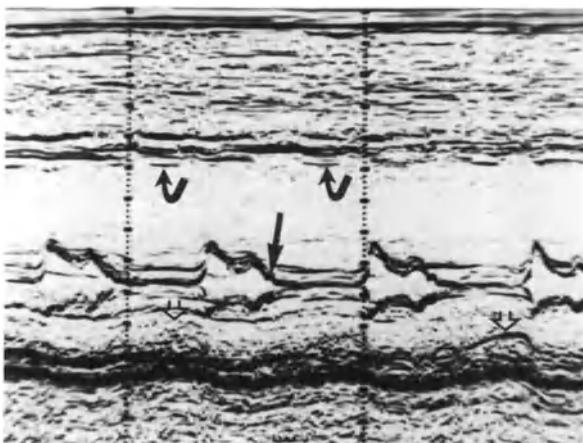


Fig. 10.29. M-Mode echocardiogram from a patient with a poorly functioning, dilated left ventricle showing a characteristic mitral valve appearance with a 'C' hump (straight arrow). Posterior wall (open arrow), interventricular septum (curved arrow).



Fig. 10.31. 2-D echocardiogram showing large vegetations on both mitral valve cusps (arrow).

graph will show a large heart with left atrial enlargement and pulmonary vascular changes which reflect the degree of left ventricular dysfunction and mitral regurgitation. In cases of acute chordal rupture or papillary muscle dysfunction, the heart may be of normal size but there is a variable degree of pulmonary venous congestion. Patients may present with severe pulmonary edema in spite of having a normal size heart (Fig. 10.30).

The diagnosis is best confirmed by echocardiography, which may show the redundant chord or papillary muscle and valve prolapse and will differentiate acute regurgitation from the important clinical differential diagnosis of a post-

infarction VSD. Doppler is used to assess the severity of the regurgitation and echocardiography will also indicate the degree of left ventricular dysfunction.

**Bacterial Endocarditis.** Bacterial endocarditis remains an important cause of acute mitral regurgitation, usually occurring on an already abnormal valve such as one affected by rheumatic heart disease or myxomatous degeneration. Therefore, the appearances may be modified by the underlying disease. Acute mitral regurgitation may cause acute pulmonary edema, but apart from this the chest radiograph reflects changes due to the pre-existing valve abnormality.

**Echocardiography** is the most useful imaging investigation in cases of endocarditis. Vegetations are often visible on both M-Mode and 2-D echocardiograph (Fig. 10.31). There may be evidence of acute left ventricular volume overload with a normal size left ventricle and an increased ejection fraction. Doppler will show the degree of regurgitation and separate jets of regurgitation through cusp perforations may be detectable, especially with color flow mapping. Echocardiography is invaluable in following the progress of patients with endocarditis, especially if there is a change in the physical signs or a deterioration in the patient's symptoms. However, it must be remembered that, unless there are vegetations and evidence of increasing valve destruction, echocardiography is not completely accurate in making the diagnosis as vegetations can persist for long periods after bacteriological cure and patients may have endocarditis, particularly in the early stages, with no echocardiographic abnormalities.

**Mitral Annulus Calcification.** Mitral annulus calcification occurs in the elderly (rarely before age 70 years) in whom there is deposition of a semicircular mass of calcification around the base of the posterior mitral leaflet. This may be visible on the PA chest radiograph (Fig. 10.32) but is usually best seen on the lateral chest radiograph as a dense C-shaped ring surrounding the position of the mitral valve. In severe cases the calcification may extend into the left ventricular wall. This condition is usually of little significance but in

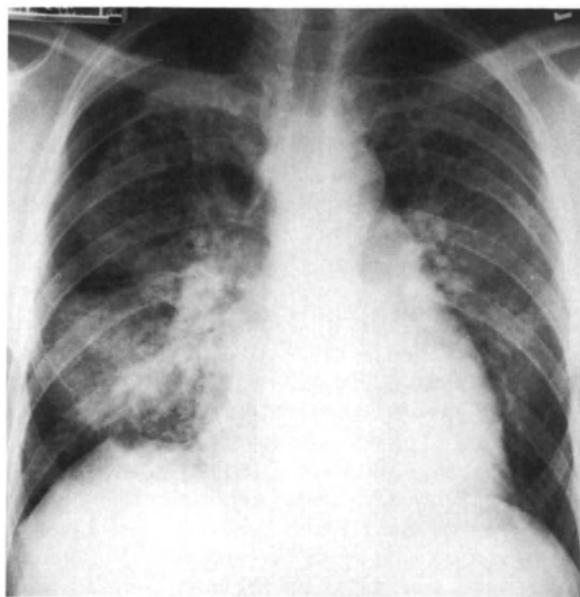
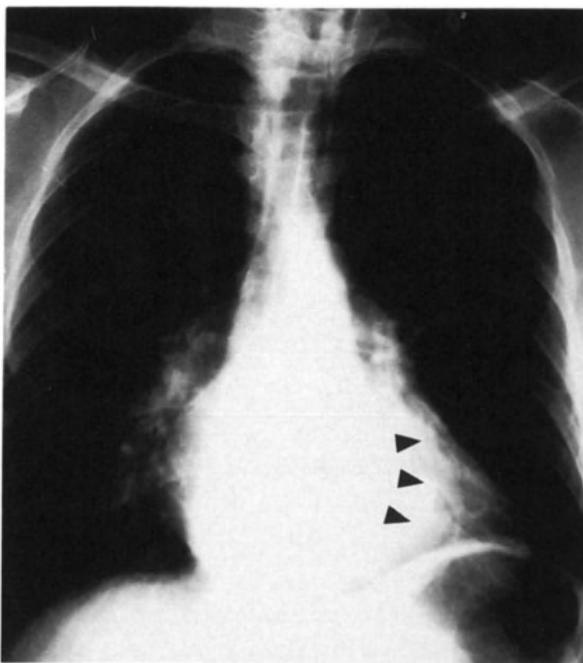
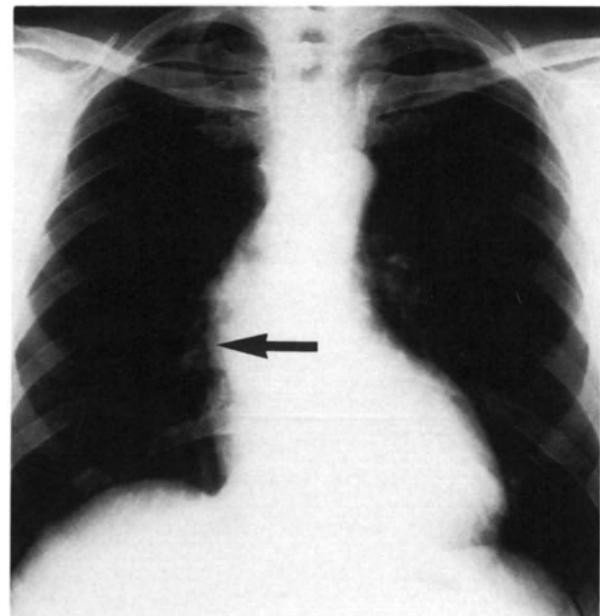


Fig. 10.30. Chest radiograph of a patient with acute mitral regurgitation showing severe pulmonary oedema ('bat's wing' distribution) in spite of a normal size heart.



**Fig. 10.32.** Chest radiograph of a patient with mitral annulus calcification (arrowheads).



**Fig. 10.33.** Chest radiograph of a patient with severe aortic stenosis and post-stenotic dilatation of the ascending aorta (arrow) but without left ventricular dilatation.

some cases it can cause mitral stenosis or regurgitation, both of which are usually mild. In some cases the calcification may involve the conducting tissues and these patients can require a pacemaker.

*Echocardiography* shows a highly echogenic mass, with acoustic shadowing beyond, around the posterior mitral leaflet and features on Doppler studies of mitral regurgitation.

**Cardiomyopathy.** Patients with a dilated cardiomyopathy, or other causes of dilating heart muscle disease, frequently have a degree of mitral regurgitation, as discussed above. In patients with hypertrophic cardiomyopathy there is distortion of the mitral valve support apparatus which leads to a variable, but usually mild degree of mitral regurgitation.

#### AORTIC VALVE STENOSIS

As the proportion of elderly patients in the population increases so the prevalence of aortic valve stenosis seems to be increasing, in spite of the reduction in the incidence of rheumatic heart valve. With the very good results of aortic valve replacement, even in very old patients, and the introduction of balloon valvoplasty, it is important that the diagnosis of aortic stenosis is made before irreversible left ventricular damage has occurred.

Acquired aortic valve stenosis may be the result of rheumatic heart disease or due to degeneration and calcification of a previously normal valve (usually in these later cases women aged over 75 years). The same appearances are produced by degenerative changes in a congenital bicuspid aortic valve which, although a congenital lesion, presents

in the same way and often the same age group as acquired aortic stenosis. These are, therefore, considered together. The clinical diagnosis is often said to be straightforward, but this is not the case in practice and a high degree of vigilance is required, particularly when reporting chest radiographs, to detect previously unsuspected aortic stenosis.

**Chest Radiograph.** The radiographic signs of aortic stenosis may be typical or may be modified by coexisting aortic regurgitation, disease involving other valves or left ventricular disease. Typically there is rounding of the cardiac apex without cardiomegaly (Fig. 10.33), unless there is left ventricular dilatation due to development of left ventricular failure (which is associated with a worse prognosis) or aortic regurgitation. There is a variable degree of post-stenotic dilatation of the ascending aorta, which may be marked in the elderly or if there is aortic regurgitation (Fig. 10.34), but which can often be missed. *Valve calcification* is often visible on the lateral chest radiograph (Fig. 10.35) but is best seen on fluoroscopy. Changes in the pulmonary vasculature associated with heart failure are the same as with other causes of heart failure. The onset of heart failure in patients with aortic valve disease indicates a worsening of the prognosis and, therefore, the chronic late changes seen in patients with chronic mitral valve disease seldom occur.

*Echocardiography.* The bulk of the diagnostic information required in patients with aortic stenosis can be obtained by echocardiography and Doppler. *M-Mode* and *2-D echocardiography* show the aortic valve as a thickened, immobile mass of dense echoes in the position of the valve (Fig. 10.36). There may be evidence of calcification extending into the surrounding tissues. Due to acoustic shadowing and poor resolution of the aortic orifice, echocardiographic imaging is a poor

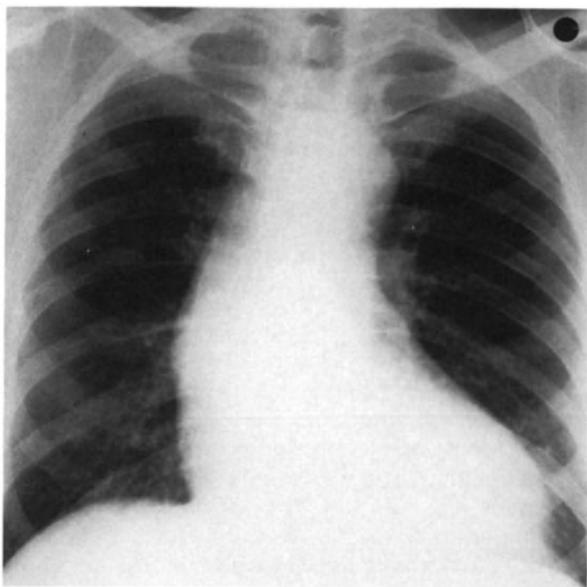


**Fig. 10.34.** Chest radiograph of a patient with aortic stenosis and regurgitation showing a large heart and marked prominence of the ascending aorta.

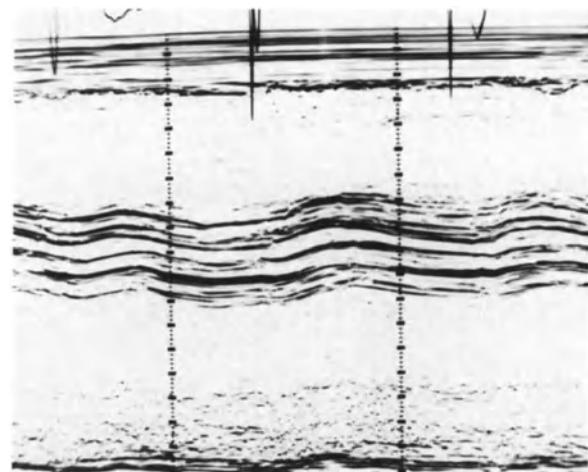


**Fig. 10.36.** M-Mode echocardiogram of stenotic aortic valve showing immobile, dense echoes within the aortic root.

method for estimating the severity of aortic stenosis and, although there is a statistical relationship between the severity of aortic stenosis and left ventricular wall thickness or left ventricular mass, this is not accurate enough to be of use in individual cases. In chronic, untreated cases the left ventricle becomes increasingly dilated and its wall becomes thinner.

*Doppler echocardiography* is crucial in the echocardiographic assessment of the severity of aortic stenosis. Using continuous wave Doppler and the modified Bernoulli equation

it is possible in most cases to obtain an accurate estimate of the peak instantaneous aortic valve gradient. Although there are some situations when the accuracy of this method is impaired, in general it provides a good estimate of the severity of aortic stenosis.

$$\text{Modified Bernoulli equation :} \\ \text{Valve gradient (mmHg)} = 4V^2$$

where  $V$  = maximum flow velocity (m/s).

Echocardiography is also required to assess left ventricular function and other valve lesions, such as aortic regurgitation (Fig. 10.37) and mitral valve disease, which are commonly associated with rheumatic aortic stenosis.

*Angiography.* Angiography is usually only required in those patients with aortic stenosis in whom there is doubt about the echocardiographic findings or as a prelude to surgery to demonstrate the state of the coronary arteries. It has been suggested that coronary angiography is not necessary in patients undergoing aortic valve replacement who do not have chest pain. Others state that significant coronary disease in this older age group is sufficiently common to justify coronary angiography in all those who have valve replacement surgery for acquired aortic stenosis. On left ventriculography, aortic stenosis is seen to cause restriction of the contrast jet passing through the valve and the valve is thickened and irregular. Usually an aortogram is performed at the same time to assess aortic regurgitation and right heart pressures and cardiac outputs may also be measured to allow calculation of the valve area. This is particularly important in patients with poor left ventricular function in whom there may be a small aortic valve gradient due to a poor cardiac output even in the presence of severe aortic stenosis.

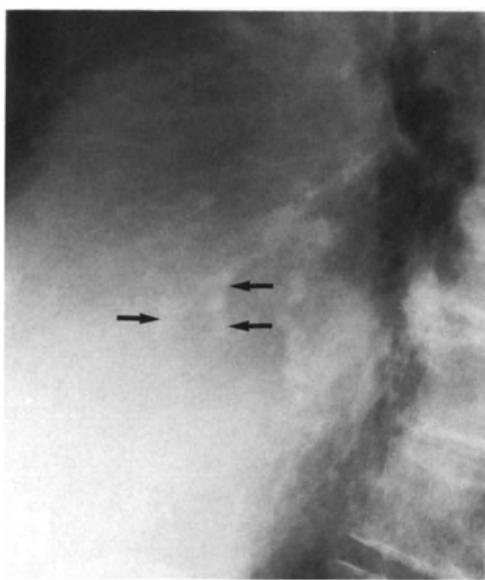


**Fig. 10.35.** Lateral chest radiograph of patient with aortic stenosis showing calcification in the aortic valve (arrow).

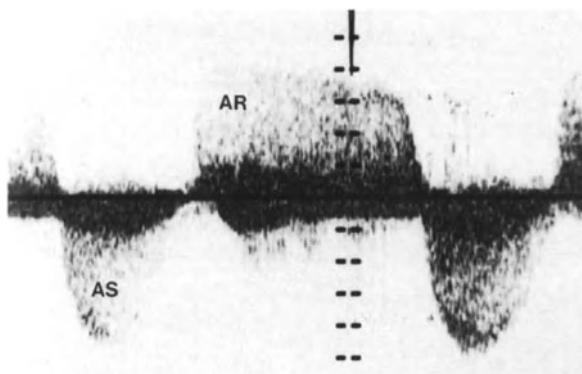


**Fig. 10.37.** Continuous wave Doppler trace from stenosed aortic valve showing high velocity systolic flow ( $4 \text{ m/s} = \text{peak gradient of } 64 \text{ mm Hg}$ ) below the baseline (AS) and aortic regurgitant flow (AR) above the baseline.

**Table 10.6.** Causes of aortic regurgitation

Degenerative (often based on a bicuspid valve)
Rheumatic
Aortic root dilatation (as in Marfan's syndrome, aortic aneurysm, aortitis syndromes)
Aortic dissection
Bacterial endocarditis
Reiter's syndrome and other related spondylitic conditions
Trauma (usually blunt chest trauma but also complicating surgical aortic valvotomy for congenital aortic stenosis and balloon valvoplasty)
Syphilitic aortitis
Rheumatoid arthritis
Degeneration of a biological valve prosthesis
Thrombosis of mechanical valve prosthesis

## AORTIC REGURGITATION

There are a larger number of causes of aortic regurgitation than stenosis. Imaging, therefore, is directed not only at making the diagnosis of regurgitation and assessing its severity but also at trying to determine the underlying pathology, although this is often also based on clinical and laboratory data. The causes of aortic regurgitation are listed in Table 10.6.

**Chest Radiography.** The radiographic changes in aortic regurgitation depend on both the severity of the regurgitation and also on the speed with which it develops. In *acute* cases, as in endocarditis or aortic dissection, the heart is of normal size or is only slightly enlarged, and this is so even in severe cases who may be in heart failure with pulmonary edema. In *chronic* cases with significant regurgitation there is, eventually, increasing cardiomegaly due to left ventricular dilatation (Fig. 10.38). The ascending aorta may be prominent due to dilatation, because of either the regurgitation or the underlying aortic disease which has led to the regurgitation.

**Echocardiography.** Echocardiography may give a clue to the etiology of the regurgitation (as in aortic dissection, endocarditis (Fig. 10.39), or aortic dilatation) by showing abnormalities of the valve cusps or the aortic root. In cases of severe regurgitation there may be premature opening of the aortic valve in late diastole due to a high left ventricular end-diastolic pressure. The left ventricle may be dilated with an increased end-systolic diameter and initially an increased stroke volume (Fig. 10.40). Sequential examinations will document the rate of deterioration of left ventricular function (Fig. 10.41). The regurgitant jet may hit the mitral valve

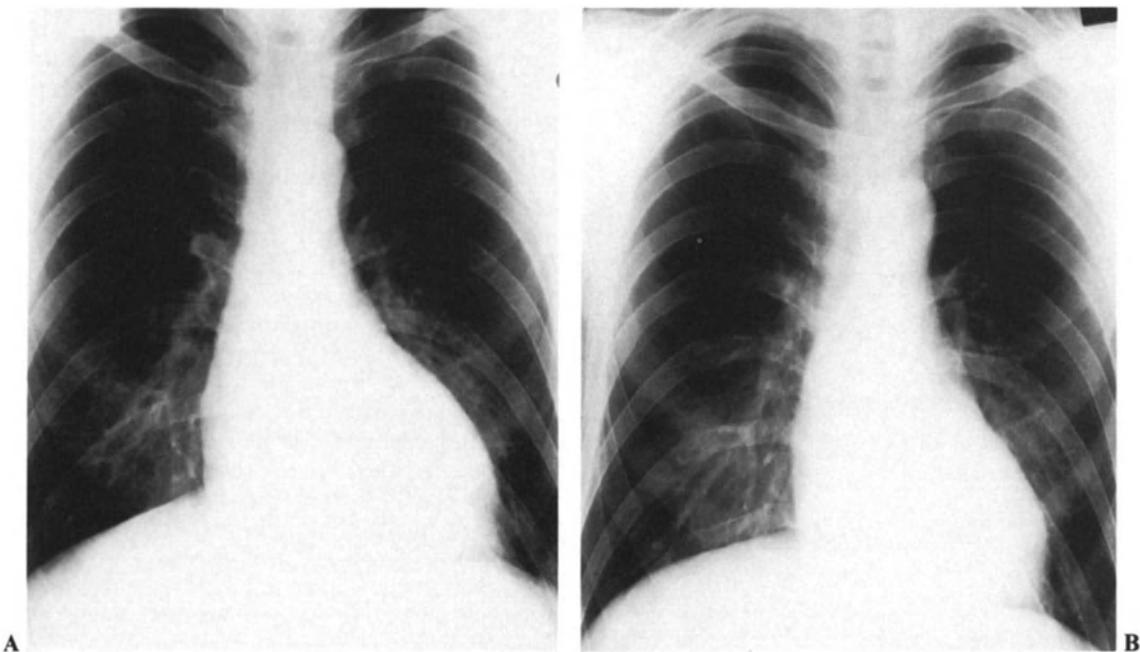


**Fig. 10.38A.** Chest radiograph of patient with Marfan's syndrome (note long thin thorax) with left ventricular dilatation due to severe aortic regurgitation.  
**B** Chest radiograph of the same patient following aortic valve replacement and return of left ventricle to normal size.

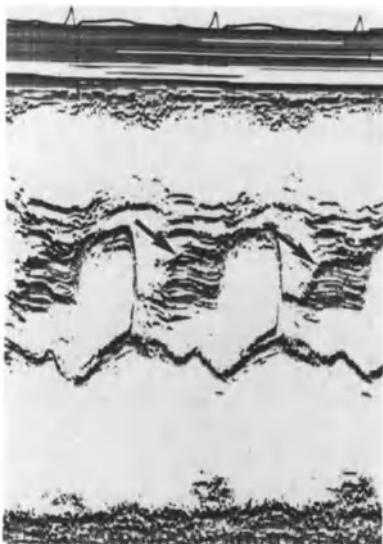


**Fig. 10.39.** M-Mode echocardiogram of vegetations (arrow) on the aortic valve of a patient with bacterial endocarditis.

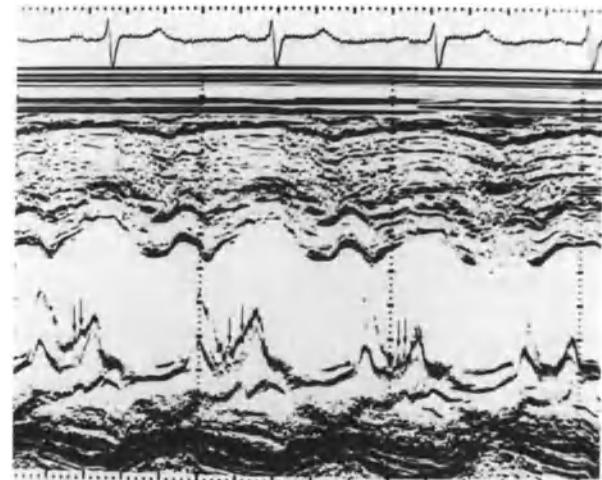


**Fig. 10.42.** M-Mode echocardiogram of mitral valve in a patient with aortic regurgitation showing flutter (arrows) of the anterior mitral valve leaflet.



**Fig. 10.40.** 2-D echocardiogram showing echogenic mass (vegetation) on aortic valve (arrow) and dilated left ventricle resulting from severe aortic regurgitation.

causing high frequency flutter of the anterior mitral leaflet (Fig. 10.42).

*Doppler* is the best non-invasive method for detecting aortic regurgitation (Fig. 10.37). Pulsed wave and color flow Doppler can be used to grade the severity of regurgitation by mapping the regurgitant jet back into the cavity of the left ventricle. The distance or area over which aortic regurgitation can be detected correlates moderately well with the degree of severity under most conditions. The shape of the continuous wave trace may also indicate the severity of regurgitation.

*Angiography.* Definition of the aortic root and valve by aortography may be required in cases who are poor echocardiography subjects. Aortography will indicate the size of the aortic root (and may, therefore, indicate the cause of the regurgitation), confirm the diagnosis and assess the severity of aortic regurgitation in cases which are difficult to assess by Doppler. Angiography can assess left ventricular function

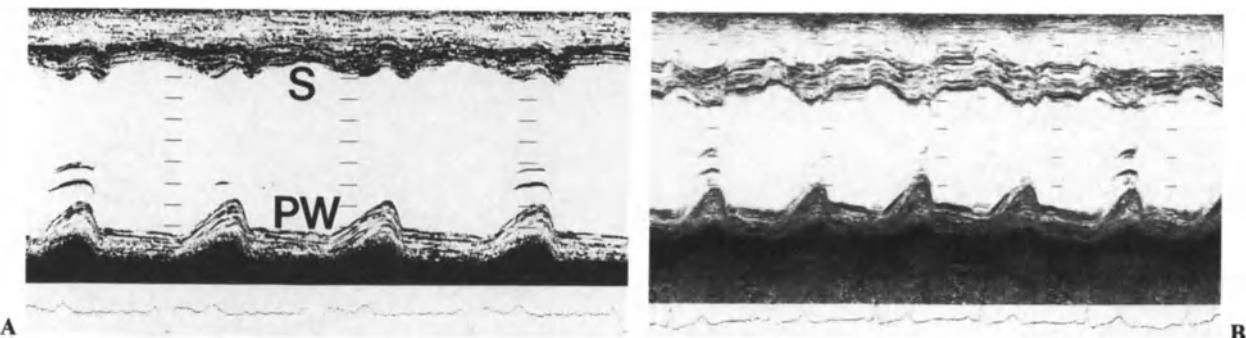


**Fig. 10.41.** A M-Mode echocardiogram in a patient with aortic regurgitation causing left ventricular dilatation (end-systolic diameter 5.8 cm, end-diastolic diameter 8 cm) in spite of continuing good contraction. Compare this with part B. A similar appearance can be seen as a result of left ventricular volume overload from other causes such as mitral regurgitation. (Posterior wall, PW; interventricular septum, S). B M-Mode echocardiogram showing a normal left ventricle.

and allows definition of coronary artery anatomy prior to surgery.

The severity of aortic regurgitation can be described in a variety of subjective semi-quantitative ways, which may be influenced by catheter position, left ventricular size and function.

#### MRI in Aortic Valve Disease

MRI is not yet so widely available as to be used in the routine assessment of aortic valve disease. However, it can be particularly useful in defining aortic root anatomy in cases of aortic regurgitation. The area of signal loss seen in the aortic root (aortic stenosis) or left ventricle (aortic regurgitation) on flow-sensitive sequences correlates well with severity. In patients with aortic regurgitation, the difference between left and right ventricular stroke volumes in patients with no right heart valve lesions is an accurate method for quantifying the degree of regurgitation.

#### TRICUSPID STENOSIS

Tricuspid stenosis is an uncommon condition, most commonly occurring in patients with *rheumatic heart disease*, and then almost always in association with mitral stenosis. Other less common causes include *pacing wires*, long-term *central venous catheters* and rarely *carcinoid syndrome*, although this usually causes tricuspid regurgitation.

The *chest radiograph* features are usually modified by the coexisting mitral valve disease. The right atrium is enlarged but this is a very non-specific finding.

*Echocardiography* shows thickening of the valve cusps and a reduced diastolic closure rate on M-Mode echocardiography. Doppler shows a prolonged half-time and higher frequencies during diastole of the type seen in mitral stenosis, although to a lesser extent.

The diagnosis can be difficult at *cardiac catheterization*, when a small gradient is found across the valve, but may be modified by the presence of a catheter across the stenosed valve. A *right atrial angiogram* may show doming of the valve into the right ventricle.

#### TRICUSPID REGURGITATION

Mild tricuspid regurgitation is commonly detected by color flow Doppler in otherwise normal patients. When tricuspid regurgitation occurs pathologically (see Table 10.7 for causes) it usually complicates right ventricular dilatation in

Table 10.7. Causes of pathological tricuspid regurgitation

Right ventricular dilatation
Pulmonary hypertension
Rheumatic heart disease
Infective endocarditis
Carcinoid syndrome
Tricuspid prolapse
Endomyocardial fibrosis
Trauma
Congenital heart disease (AV canal defect, Ebstein's anomaly etc)

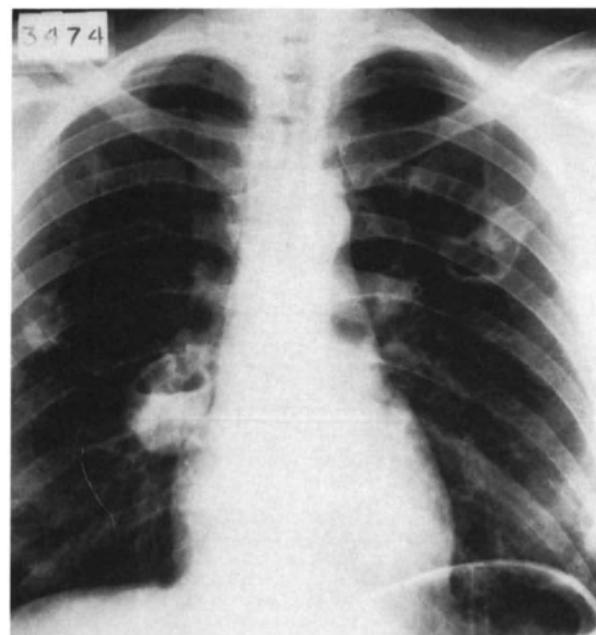


Fig. 10.43. Chest radiograph of a patient with tricuspid valve endocarditis causing multiple septic pulmonary infarcts which developed into abscesses.

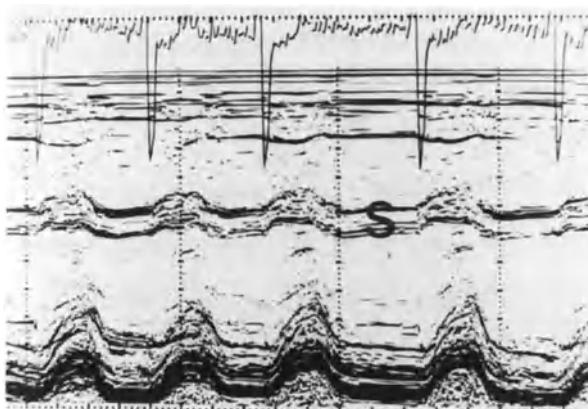
patients with congestive cardiac failure or pulmonary hypertension.

As with tricuspid stenosis, the *chest radiograph* findings are often modified by changes due to other valve diseases, ventricular dysfunction and pulmonary hypertension. The right atrium is enlarged and may be huge, almost reaching the right side of the chest wall in severe cases (Fig. 10.23). The degree of right atrial enlargement may decrease in cases of secondary tricuspid regurgitation when the underlying cause is treated. In patients with tricuspid endocarditis multiple abscesses may be seen on the chest radiograph (Fig. 10.43).

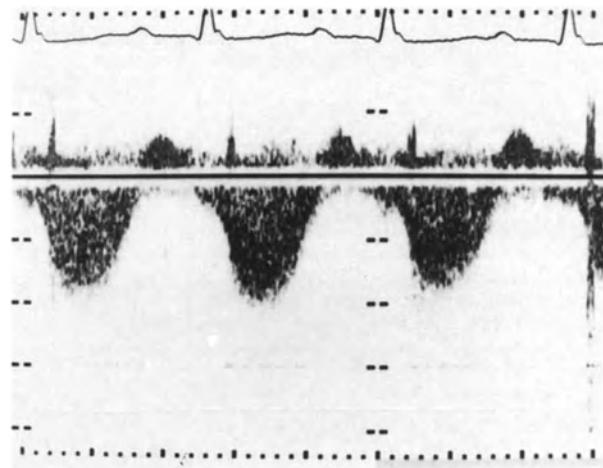
*Echocardiography* will show a large right atrium and normal thickness, mobile cusps in secondary tricuspid regurgitation (Fig. 10.44). In rheumatic or carcinoid cases the



Fig. 10.44. 2-D echocardiogram of a patient with secondary tricuspid regurgitation showing dilated right atrium (RA) with thrombus (T) on the atrial wall opposite the valve. The dilated right ventricle is not fully shown in this image.



**Fig. 10.45.** M-Mode echocardiogram showing paradoxical septal motion (i.e., the septum (*S*) moves anteriorly in systole) due to right ventricular volume overload in a patient with tricuspid regurgitation.



**Fig. 10.46.** Continuous wave Doppler recording of tricuspid regurgitation with a peak systolic velocity of 2 m/s (indicating an approximate right ventricular peak systolic pressure of 16 + central venous pressure).

valves are thickened and immobile. Volume overload of the right ventricle will cause paradoxical septal motion which is best seen on M-Mode echocardiography (Fig. 10.45). In endocarditis, vegetations may be visible on the valve cusps. In endomyocardial fibrosis the right ventricle is small, being filled by fibrosis and thrombus.

Doppler is a very accurate method for detecting tricuspid regurgitation. Pulsed wave and color flow can be used to assess the severity of regurgitation by mapping the regurgitant jet into the right atrium. Continuous wave is useful as it can give an indication of the right ventricular systolic pressure (Fig. 10.46), and, therefore, in the absence of pulmonary stenosis, also pulmonary artery pressure. In the presence of measurable tricuspid regurgitation:

$$\text{RV Pressure} = \text{Central Venous Pressure} + \text{Systolic Gradient Across TV}$$

*Cardiac catheterization* is difficult in cases of tricuspid regurgitation due to the large right atrium and systolic reverse flow across the valve, which make catheter positioning difficult.

## ACQUIRED PULMONARY VALVE DISEASE

Acquired *pulmonary stenosis* is uncommon and is radiologically similar to congenital pulmonary stenosis. The causes of acquired pulmonary stenosis include *rheumatic heart disease* and *carcinoid syndrome*, both of which are rare causes.

The radiological features are the same as for congenital pulmonary stenosis with post-stenotic dilatation of the pulmonary artery, thickening of the valve on echocardiography and a high velocity jet, detectable by Doppler, which can be used to measure the valve gradient.

Mild *pulmonary regurgitation* is a common finding in healthy patients examined with color flow Doppler. Significant pulmonary regurgitation can occur in cases of *pulmonary hypertension*, whatever the cause, *endocarditis* and *carcinoid syndrome*.

The chest radiograph usually shows the changes of the underlying condition with dilatation of the pulmonary artery. Echocardiography will show dilatation of the pulmonary artery and vegetations in cases of endocarditis or thickening in cases of carcinoid syndrome.

## HEART MUSCLE DISEASE

There are many causes of heart muscle disease (Table 10.8) but the different types usually belong to one of a few general groups. Imaging is directed at confirming the general pattern of heart muscle disease, assessing its severity and demonstrating complications.

### DILATING HEART MUSCLE DISEASE

Dilating heart muscle disease, often loosely described as congestive cardiomyopathy, is common and has many causes. Semantic arguments about what constitutes a cardio-

myopathy are largely irrelevant to imaging, which is directed at demonstrating impairment of ventricular function and its effects.

Patients with chronic volume overload of a ventricle (i.e., due to aortic regurgitation, mitral regurgitation, systemic arteriovenous shunts etc.) or pressure overload (i.e., aortic stenosis or hypertension) may also eventually develop a dilated ventricle with gradually deteriorating ventricular function. One of the aims of cardiac imaging is to identify these patients to allow surgery before there is a deterioration in left ventricular function.

**Table 10.8.** Causes of heart muscle disease

Ischemic heart disease
Hypertensive heart disease
Idiopathic (congestive cardiomyopathy)
Myocarditis (especially viral)
Endocrine (thyrotoxicosis, hypothyroidism, acromegaly)
Infiltration (e.g., hemochromatosis, glycogen storage disorders (Pompe's disease), Hurler's syndrome)
Toxins (cytotoxic drugs, alcohol, some anesthetic gases, drug hypersensitivity, heavy metals)
Puerperal disorders
Neuromuscular disorders (muscular dystrophies)
Multisystem disease (rheumatic fever, rheumatoid arthritis, SLE, scleroderma, polymyositis, sarcoidosis)
Radiation
Nutritional (beri-beri)

**Chest Radiograph.** If there is a significant degree of ventricular dysfunction the cardiac shadow is nearly always enlarged with the configuration depending on which ventricles are involved and the development of complications such as pulmonary hypertension. The changes of pulmonary arterial or venous hypertension are visible on the radiograph and reflect the severity of left ventricular dysfunction and to some extent, in the case of pulmonary arterial hypertension, its duration. Following treatment there may be an improvement in the pulmonary vascular changes and a reduction in heart size.

**Echocardiography.** Echocardiography is the most useful non-invasive investigation in patients with a large heart due to muscle disease, as it allows differentiation from other causes of cardiomegaly such as pericardial effusion and multiple valve disease. The echocardiogram shows enlargement of the involved ventricles and a reduced left ventricular

ejection fraction (Fig. 10.47). In cases of ischemic heart disease, there may be regional wall motion abnormalities which are visible on echocardiography, although these can also occur in cases with no evidence of coronary artery disease. The mitral valve appears in an abnormally central position between the septum and the posterior wall and the excursion of the anterior and posterior leaflets is almost equal (Fig. 10.48), often with a C-hump in late diastole. In some cases both ventricles are involved (Fig. 10.49). There is usually a degree of mitral regurgitation, detectable by Doppler studies, leading to left atrial enlargement. *Thrombus* may be seen in the affected ventricle (Fig. 10.50). Tricuspid and pulmonary regurgitation and signs of pulmonary arterial hypertension complicating severe cases may also be demonstrated. It is important to exclude any treatable primary valve lesion such as aortic stenosis, which can be difficult to differentiate clinically from heart muscle disease in advanced cases.

**Isotope Ventriculography.** Isotope studies can be used to document the dilated and poorly contracting ventricles and are a useful, reproducible method of assessing the progression of disease. Information is also provided on regional wall motion abnormalities.

**Cardiac Catheterization.** Cardiac catheterization and angiography are required if there is doubt about the diagnosis, to exclude ischemic heart disease and left ventricular aneurysm, although this should be demonstrable by non-invasive methods. In some cases hemodynamic data are required to monitor the effect of medical treatment or as a prelude to cardiac transplantation, where pulmonary arterial hypertension is a contraindication to orthotopic cardiac transplantation.

Pressure measurements will show that there is a high left

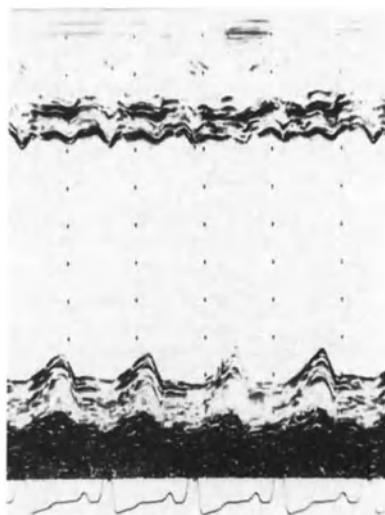


**Fig. 10.47.** M-Mode echocardiogram of a patient with alcoholic heart muscle disease with a poorly contracting, dilated left ventricle (end-diastolic diameter 6.5 cm). This appearance is non-specific and can be seen with any cause of dilating heart muscle disease (compare with normal appearance Fig. 10.41B).

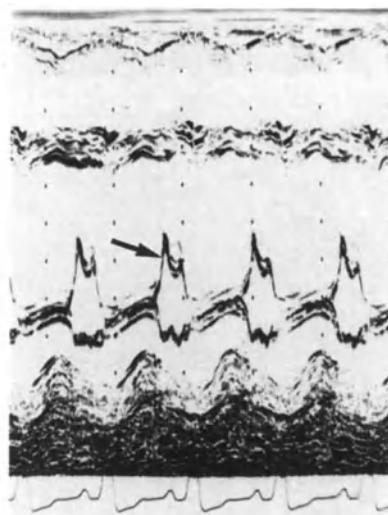


**Fig. 10.48.** M-Mode echocardiogram from the patient shown in Fig. 10.47, showing central position of the mitral valve (arrow) in the left ventricle.

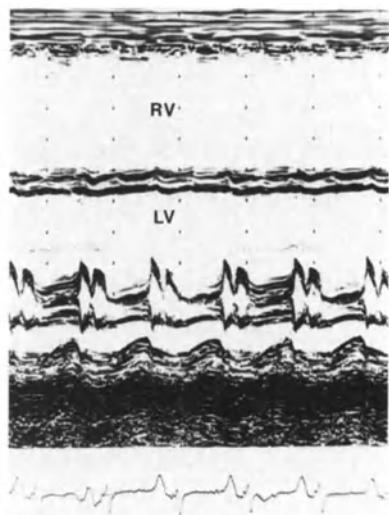


**Fig. 10.49.** M-Mode echocardiogram of a child with endocardial fibroelastosis showing dilatation and poor contractility of the left (LV) and right (RV) ventricles.



Fig. 10.50. 2-D echocardiogram of a patient with dilated cardiomyopathy and extensive thrombus filling the left ventricular apex (T).

ventricular end-diastolic pressure and as a result raised pulmonary artery and pulmonary artery wedge pressure. Valve lesions may be excluded at the same time, although these can be excluded by echocardiography which should precede angiography.

*Left ventriculography* shows a dilated, smooth walled, poorly contracting left ventricle (Fig. 10.51) with a variable degree of mitral regurgitation. Intraventricular thrombus may be visible as a filling defect in the ventricle. If there is a need to make a histological diagnosis of active myocarditis or myocardial infiltration then *endomyocardial biopsy* can be performed at the same time.

#### FEATURES OF DIFFERENT CAUSES OF DILATED HEART MUSCLE DISEASE

**Myocarditis.** Myocarditis is usually due to viral infection (most commonly Coxsackie B) which may cause a variable

amount of diffuse left ventricular damage. This may develop acutely and then resolve to a greater or lesser degree or may progress to severe left ventricular failure requiring cardiac transplantation. Changes in left ventricular function are demonstrated by echocardiography or isotope ventriculography. The diagnosis of active myocarditis is confirmed by endocardial biopsy.

**Alcohol.** Chronic alcoholism is associated with progressive dilatation of the left ventricle, demonstrable on echocardiography or isotope ventriculography, which is reversible in its early stages. Acute alcoholic intoxication may cause a picture similar to an acute myocarditis. The chest radiograph shows a large heart and may show multiple rib fractures at various stages of healing. Although this is said to be a classical appearance for alcoholic cardiomyopathy it is uncommon and of little help in making the diagnosis.

**Cytotoxic Drugs.** Some cytotoxic drugs, such as adriamycin, are cardiotoxic and produce left ventricular dilatation, which is reversible if drug use is stopped early. Regular assessment by echocardiography or isotope ventriculography of patients receiving these drugs is advisable to detect early signs of ventricular dysfunction and prevent irreversible left ventricular damage developing.

**Hypertensive Heart Disease.** In patients with hypertension there is initially a gradual increase in left ventricular wall thickness affecting both the septum and the free wall, which may become so thick that differentiation from hypertrophic cardiomyopathy can be difficult. Although the ventricle may be of normal size the heart can be enlarged on the chest radiograph due to increased ventricular wall thickness. After a variable time the left ventricle may become dilated, which can be shown on the chest radiograph as well as by echocardiography. The wall of the ventricle may remain thickened or become thin so that the overall appearance resembles a dilated cardiomyopathy. Treatment of the hypertension may allow a variable degree of reversal of these changes, although the potential for recovery is reduced once left ventricular dilatation has developed.

**Endocardial Fibroelastosis.** There are two types of endocardial fibroelastosis. The *secondary* type, in which the left ventricle is not usually dilated, occurs in cases of congenital heart disease associated with left ventricular obstruction, as in congenital aortic stenosis and coarctation. The *primary* form is characterized by dilatation of both ventricles with secondary mitral regurgitation in a manner which mimics a dilated cardiomyopathy. The chest radiograph shows a large heart with pulmonary congestion while echocardiography shows dilated, poorly contracting ventricles (Fig. 10.49), sometimes with mural thrombus.

**Amyloid.** Cardiac amyloid is a common feature of primary amyloid (up to 25% of cases) but is less common in secondary amyloid. The heart may be involved early on and there may be a familial predisposition to cardiac involvement. The heart size is usually normal on the chest radiograph but there may be a pericardial effusion which makes it appear enlarged. Pulmonary edema and pleural effusions develop with the onset of left ventricular failure.

**Echocardiography** shows a thickened left ventricular wall but normal sized ventricular cavity. The left ventricle contracts poorly, there is little thickening of the walls of the

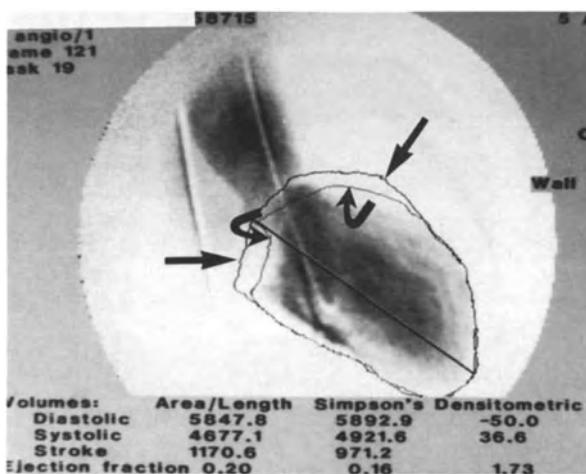


Fig. 10.51. Digital subtraction left ventriculogram of a patient with dilated cardiomyopathy showing outline of end-diastolic image (arrow) superimposed on the end-systolic image (curved arrow). The calculated ejection fractions vary from 16% to 20% depending on method of calculation.

ventricles during systole and the papillary muscles may be enlarged due to infiltration by amyloid. The diagnosis of amyloid is based on the results of biopsy of the affected organs.

*Chagas' Disease.* Chagas' disease is the late result of an insect-borne infection which affects the heart and the esophagus. Cardiac involvement is characterized by areas of fibrosis, especially around the apex of the ventricles, usually affecting the left ventricle more severely and first. Irregular involvement leads to asymmetric wall motion abnormalities, demonstrable by echocardiography or isotope ventriculography, which can mimic ischemic heart disease, even leading to the formation of left ventricular aneurysms.

*Sarcoidosis.* Cardiac sarcoidosis usually occurs in association with sarcoid elsewhere in the body, but can occur alone. Chest radiography will show evidence of pulmonary sarcoid as well as an enlarged heart. On echocardiography or angiography the left ventricle is enlarged but this is more marked around the base of the ventricle where the appearances may suggest a basal aneurysm. Abnormal signal may be detected on MRI, which can correlate with the extent of sarcoid infiltration.

#### HYPERTROPHIC CARDIOMYOPATHY

Hypertrophic cardiomyopathy (HCM) is a relatively uncommon condition where, in the absence of any predisposing cause, there is hypertrophy of a variable portion of the ventricles. The hypertrophy may involve the septum only or the whole of the left ventricle and often the right ventricle. There is often a family history, although there may be great variability in the age of onset and severity of HCM in affected families.

*Ventricular hypertrophy* may lead to a variable degree of dynamic left ventricular outflow obstruction while distortion of the support of the mitral valve apparatus may cause mitral regurgitation.

*Chest Radiography.* The chest radiograph is often normal, but in cases of severe hypertrophy the heart can be enlarged. Later on the ventricles and, more frequently, the atria may dilate and then cardiomegaly becomes more apparent. In cases with poor left ventricular function there may be changes of pulmonary venous congestion, especially in cases which develop atrial fibrillation.

*Echocardiography.* The diagnosis of hypertrophic cardiomyopathy is usually based on the echocardiographic demonstration of left ventricular hypertrophy, which may be asymmetrical involving mainly the septum (Fig. 10.52), in the absence of any predisposing cause. Various echocardiographic signs have been described but none are pathognomonic of the condition, although taken together they may strongly suggest the diagnosis. These signs include:

1. Asymmetric hypertrophy of the septum. This may also be seen in other causes of hypertrophy such as hypertension or aortic stenosis (Fig. 10.53).
2. Small left ventricular cavity with an increased ejection fraction.



Fig. 10.52. 2-D echocardiogram of the left ventricle in HCM showing septal hypertrophy (open arrows; 2.3 cm thick) but normal posterior left ventricular wall thickness (curved arrow; under 1 cm thick).

3. End-systolic obliteration of the ventricular cavity (reflecting the increased ejection fraction).
4. Systolic anterior motion (SAM) of the anterior leaflet of the mitral valve (Fig. 10.54). This may be seen in other situations where the left ventricular end-systolic volume is small.
5. Early systolic closure of the aortic valve, due to obstruction to flow developing during systole and possibly also due to the venturi effect of the high velocity jet passing through the subaortic obstruction. The continuous wave Doppler trace has a concave slope (unlike that seen in aortic stenosis) due to the variable degree of obstruction which increases during systole (Fig. 10.55).

On Doppler examination, there is an increase in flow velocity in the areas of obstruction, which allows the outflow gradient to be estimated by continuous wave Doppler. Pulse wave or color flow Doppler will show the degree of mitral regurgitation.

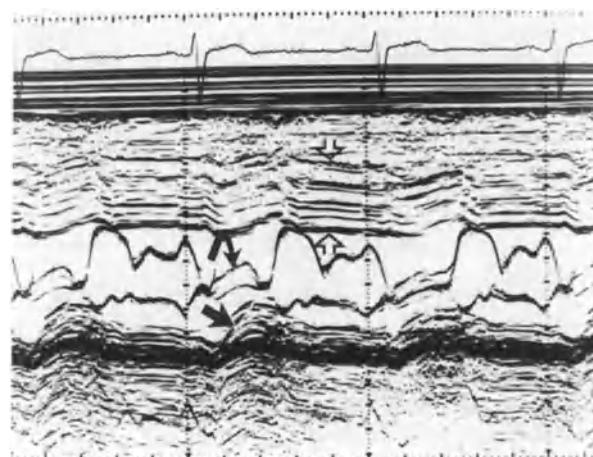
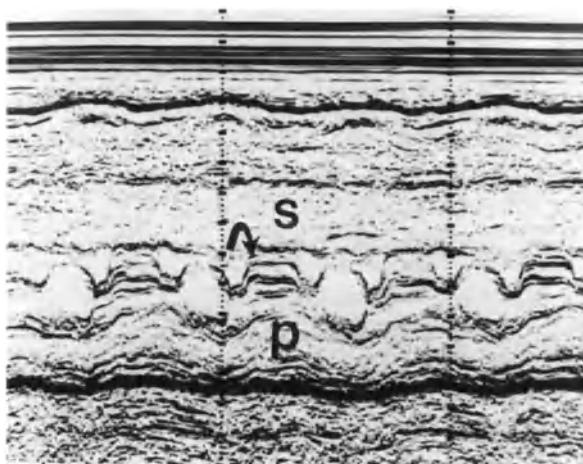
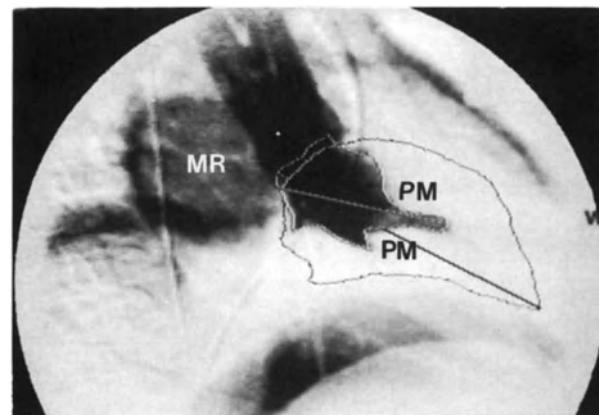


Fig. 10.53. M-Mode echocardiogram showing septal hypertrophy (open arrows), normal posterior wall thickness (straight arrow), mild systolic anterior motion of the mitral valve (curved arrow) and small left ventricular cavity in HCM.



**Fig. 10.54.** M-Mode echocardiogram showing severe hypertrophy of both the septum (S) and posterior wall (P) of the left ventricle in severe HCM. The left ventricular cavity is very small and there is very marked systolic anterior motion of the mitral valve (curved arrow).



**Fig. 10.56.** Digital subtraction left ventriculogram in patient with HCM (same patient as in Fig. 10.54) showing end-diastolic image outline superimposed on the end-systolic image. There is mitral regurgitation (MR) and prominent papillary muscles (PM) projecting into the small end-systolic cavity. The ejection fraction was calculated to be 90%.

Other non-invasive imaging methods can be used to evaluate hypertrophic cardiomyopathy and they show the same abnormalities. *Isotope ventriculography* and *MRI* show an increased ejection fraction with a small end-systolic cavity while *MRI* and *CT* will show the distribution of the ventricular hypertrophy.

**Angiocardiography.** Angiocardiography is required to diagnose hypertrophic cardiomyopathy if there is doubt about the echocardiographic diagnosis or if, in patients with angina, there might be coronary artery disease. *Pressure measurements* may show a gradient below the aortic valve, which is made worse by giving vasodilators. *Left ventriculography* shows a vigorously contracting ventricle which may be distorted by septal hypertrophy (producing the so-called 'banana shaped' ventricle) and large papillary muscles. A pool of contrast may be trapped at the apex during systole. Analysis of the ventricular wall motion shows

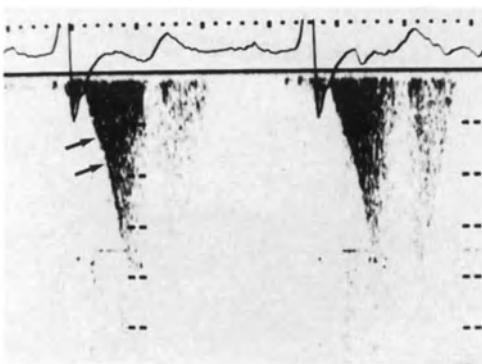


**Fig. 10.55.** Continuous-wave Doppler in HCM showing a concave early systolic slope (arrows) due to the increasing severity of the outflow gradient during systole.

vigorous contraction with an increased ejection fraction (Fig. 10.56).

#### ENDOMYOCARDIAL FIBROSIS

Endomyocardial fibrosis (EMF) is a rare condition in temperate climates but is common in tropical countries. Fibrous tissue is deposited on the endocardial surface of any of the cardiac chambers but particularly, and especially in Europeans, the left ventricular apex and there is often associated mural thrombus. In the variant known as *Loeffler's syndrome* (hypereosinophilic syndrome) there is an associated eosinophilia.

**Chest Radiograph.** The chest radiograph shows cardiac enlargement in those cases with right heart involvement but in cases of left heart involvement the heart may be of normal size. There may be an associated pericardial effusion and evidence of pulmonary congestion in cases affecting the left ventricle.

**Echocardiography.** Echocardiography shows a reduction in the size of the affected chambers, which may lead to gross distortion of the mitral and tricuspid valves with regurgitation detectable by Doppler. Thrombus may be seen separate from the mass of fibrous tissue.

**Cardiac Catheterization.** Pressure measurements will show high end-diastolic pressures reflecting the restriction of ventricular filling caused by the stiff fibrotic ventricular wall. *Ventriculography* shows mitral and tricuspid regurgitation along with obliteration of the apical portions of the ventricles, with filling defects due to thrombus. *Cardiac biopsy* at the time of cardiac catheterization can give a histological diagnosis.

For further reading, see p. 233.

## CHAPTER 11

# CONGENITAL HEART DISEASE

P. Wilde and G. G. Hartnell

---

The incidence of congenital heart disease in live births is approximately 0.5%: the incidence of the different types of diseases is noted in Table 11.1. This relatively low incidence means that many radiologists will see only a small number of congenital heart disease cases each year, particularly if they are not working in a center with special pediatric or cardiac interests. In addition to this, the term 'congenital heart disease' embraces an enormous range of abnormalities, many of which are extremely rare even in specialist units. It is, therefore, unlikely that a general radiologist or even a general pediatric radiologist will be familiar with the detailed radiology of all forms of congenital heart disease.

Over the last two decades, however, the progress in treatment of congenital heart disease has been spectacular and, in particular, operative management has led to the survival of many patients who would previously have died from their congenital malformation. In many cases surgery is able to achieve complete anatomical correction of the abnormality and in many other cases a high level of palliation can be achieved. It is, therefore, doubly important for the radiologist to have a general understanding of this subject; firstly, so that cases of congenital heart disease can be recognized as soon as possible and further investigation and treatment instituted and, secondly, because the long-term survival of many of these cases means that an increasing number of patients will return for routine radiological assessment following surgery for their congenital heart disease.

The general radiologist should understand the normal appearances of pediatric chest radiographs and should be able to assess the likely presence of certain types of congenital heart disease. The specialist radiologist will be able to offer further sophisticated investigations, particularly echocardiography and angiography. In most major pediatric cardiology units, diagnosis and management of congenital heart disease involves frequent joint consultation sessions between

pediatric cardiologists, pediatric cardiac surgeons and cardiac radiologists.

The radiologist will often be able to supply expertise in echocardiography and angiography as well as in the interpretation of changes in the plain chest radiograph both before and after surgery. More recently the radiologist has also come to have a role to play in the management of cases requiring *interventional* treatment, particularly balloon dilatation.

Table 11.1. Incidence of types of congenital heart disease in live-born infants. Data combined from several large series

---

#### *Commonest conditions*

Ventricular septal defect (30%)  
Patent ductus arteriosus (10%)

#### *Other common conditions (incidence of each is from 3% to 8%)*

Aortic stenosis (including subaortic and supravalvular stenosis, hypoplastic left heart, and interrupted aortic arch)  
Atrial septal defect  
Atrioventricular septal defect  
Coarctation  
Pulmonary stenosis  
Tetralogy of Fallot  
Transposition of the great arteries

#### *Uncommon conditions (incidence of each less than 3%)*

Anomalous pulmonary venous drainage (+ systemic venous abnormalities)  
Arteriovenous malformations  
Congenital cardiomyopathy  
Coronary fistulae and other coronary anomalies  
Double inlet ventricle ('single ventricle')  
Double outlet ventricle  
Ebstein's anomaly  
Mitral valve anomalies (including supravalvular ring and cor triatriatum)  
Pulmonary atresia  
Sinus of Valsalva aneurysm  
Tricuspid atresia  
Truncus arteriosus  
Vascular rings and other anomalies

---

tation of stenotic valves and vessels and to a lesser extent the embolization or occlusion of abnormal communications.

The radiologist must therefore deal with congenital heart disease in a series of stages.

1. Recognition that congenital heart disease is present (based on chest radiology as well as clinical and electrocardiographic findings). A preliminary diagnosis may be possible from the chest radiograph but it is rare that the plain film will give a precise and accurate result.

2. Detailed diagnosis (almost certainly by echocardiography and possibly with the addition of cardiac catheterization and angiography).

3. Detailed evaluation of investigation results (usually at a joint case conference in which the full clinical picture is assessed and management is discussed).

4. Management, which can be in the form of continued medical management, palliative surgery, corrective surgery, or interventional catheter techniques. The radiologist will have an important role in the assessment of immediate and late post-operative problems.

#### PEDIATRIC CARDIAC SURGERY

The two most obvious ways in which this method of treatment has changed in recent years are, *firstly*, the increasing number of total anatomical corrections that are possible and, *secondly*, the decreasing age of the patient at which these operations are performed. In many large units a high proportion of congenital heart abnormalities are now completely corrected before the child has reached the age of 1 year. This has a particular effect on the practise of cardiac radiology because the classical appearances of long-standing congenital heart abnormalities on chest radiography are becoming increasingly uncommon and are now rarely of practical importance.

Cardiac surgery is considered to include the heart and great vessels and can be divided into two major types; namely, closed heart surgery and open heart surgery.

In *closed heart surgery* the operation is performed whilst the heart continues to function and for this reason most closed heart operations are limited in terms of intracardiac repair. This type of procedure is most commonly carried out for abnormalities of the aorta and pulmonary artery.

*Open heart surgery* requires that the cardiac function must temporarily cease. The patient is maintained on cardiopulmonary bypass or is cooled to low temperatures to facilitate a period of cardiac standstill without detriment to him. It is vital that the cardiac surgeon has full knowledge of the nature of the abnormality or abnormalities before undertaking the operation. Many intracardiac repairs are time-consuming, but the time of repair must be kept to an absolute minimum (on bypass or profound hyperthermia) so as to reduce the chances of operative mortality or morbidity. These increase progressively with the length of bypass time.

**Preoperative Assessment.** The practice of preoperative assessment has changed considerably in recent years. Nowadays the clinical, plain radiographic and echocardiographic

data are quite adequate to make a complete diagnosis of the intracardiac abnormality. In the past, cardiac catheterization and angiography were often essential to confirm the diagnosis. Cardiac catheterization and angiography are, however, still required in a significant number of patients even with a full echocardiographic diagnosis, because certain additional details are required.

In some cases this detail is of a *hemodynamic* nature. For example, it is often necessary to measure the pulmonary vascular resistance in patients with large left to right shunts in order to exclude the possibility of irreversible pulmonary damage. Sometimes pressure gradients and absolute intracardiac pressures are needed but increasingly these are being obtained by *Doppler echocardiography*.

Secondly, it is sometimes necessary to clarify *anatomical* detail by angiography, often with a view to excluding known pitfalls that may be encountered by the surgeon. For example, coronary anatomy cannot be adequately assessed by echocardiography whilst it can be clearly assessed using cardiac cineangiography. Knowledge of the pulmonary artery anatomy is often crucial to the management and it is often not possible to visualize the left and right pulmonary arteries beyond their origins by echocardiography due to pulmonary air. Other fine details of anatomy are often obtained by cardiac catheterization and angiography. These include the assessment of small or multiple ventricular septal defects (unless high quality Doppler color flow mapping is available) and the visualization of systemic to pulmonary collaterals or shunts. In cases where the echo study has been difficult and inconclusive, the angiogram is essential.

Finally, the cardiac catheterization procedure is now sometimes accompanied by an interventional procedure. Such procedures include *Rashkind balloon septostomy* for transposition of the great arteries, *dilatation of the pulmonary valve* or of a *coarctation*, and more recently *ductal closure*, *occlusion of abnormal fistulae* and *blade septostomy*.

#### CLASSIFICATION OF CONGENITAL HEART DISEASE

The first and most important requirement is for an accurate description of what is being seen. It is, therefore, vital to recognize the morphological appearance of each cardiac chamber and each great vessel wherever possible. It is, for example, impossible to diagnose the condition of transposition of the great arteries until it can be stated with certainty which is the morphologically left ventricle, which is the morphologically right ventricle, which is the aorta and which is the pulmonary artery. It is, therefore, helpful to use the phrase 'morphologically left ventricle' to describe a ventricular chamber which has all the characteristics of the left ventricle irrespective of where it is sited and irrespective of which connections it makes. It is possible to have a morphologically left ventricle that lies on the right side of the body or to the right of the other ventricle.

The morphological features of important structures are summarized below.

1. *Left Ventricle.* This is the ventricular chamber with a more symmetrical oval shape and fine trabeculation. There

are normally two large papillary muscles in this ventricle, both of which arise from the free wall and not from the interventricular septum. The basal part of the interventricular septum is smooth without any trabeculation. The atrioventricular valve entering the left ventricle is, by definition, the mitral valve and the insertion of the mitral valve is further towards the base of the heart than the atrioventricular valve of the right ventricle, the tricuspid valve. This particular feature can be identified on echocardiography. The left ventricle usually shows fibrous continuity between the inflow and outflow valves although this is not always the case, there sometimes being a muscular outflow tube from the left ventricle, which is called a conus.

2. *The Right Ventricle.* This is rhomboid in shape and shows much more heavy *trabeculation* than the left. The trabecular patterns of the two ventricles are much easier to appreciate if both ventricles are seen. The papillary muscles arise from more than two groups in the right ventricle and there is usually some attachment of chordae to papillary muscles on the septum, which itself is heavily trabeculated. As stated above, the atrioventricular valve of the right ventricle is inserted slightly more towards the apex of the heart than on the left. There is normally an outflow muscular tube known as the conus or *infundibulum*.

3. *Left Atrium.* This chamber is usually rather smooth-walled and can most precisely be defined by its *atrial appendage* which is long and narrow, usually curling around the left side of the heart. The left atrium cannot be reliably defined by the presence of pulmonary veins, as these can often be anomalous. If the anatomy of the intra-atrial septum is clearly seen on angiogram or echocardiogram then the relationship of the ostium primum and secundum will demonstrate the morphological left side (due to the valved nature of the foramen ovale).

4. *Right Atrium.* This is a more heavily trabeculated chamber than the left particularly in its free wall and is characterized by a large triangular and broad-based atrial appendage. The *inferior vena cava* almost always enters the right atrium. This rule is not completely invariable but applies in the vast majority of cases and is a clinically useful guide.

5. *The Aorta.* This must be defined as the great artery arising from the heart which supplies the branches to the head and neck. The aorta cannot be defined in terms of connections to the heart, presence of coronary branches or absence of pulmonary arterial branches as these are all variable.

6. *The Pulmonary Artery.* This is the great artery which bifurcates into two branches after a short distance, each of which supplies one lung. If two great arteries are present then it is often easier to define the aorta first.

#### The Conventional Approach to the Description of Abnormalities

In recent years a standardized approach has been achieved in the description of congenital cardiac abnormalities. Although this is not necessarily used in the description of very simple abnormalities it is invaluable in the description

of complex abnormalities as it avoids confusion or ambiguity. The approach is one with five major steps.

1. *Body Situs.* In most people the abdominal viscera and the thoracic viscera are *asymmetrical*. For this reason normal situs can be identified and is recognized by obvious features such as the liver and inferior vena cava lying on the right side, the spleen and heart lying on the left side. The very high association with the inferior vena cava draining into the right atrium has led to the development of the term *viscero-atrial situs*. This means that the atrial situs in almost all cases conforms to the situs of the upper abdominal viscera, irrespective of the situs or position of the remainder of the heart.

It is also important to recognize the presence of *asymmetry in the lungs* which is usually apparent in the form of *bronchial situs*. The right main bronchus is shorter, wider and more vertically orientated than the left main bronchus which is normally at least 1.5 times longer than the right (from bifurcation to first major branch). The bronchial situs often corresponds to the visceral atrial situs but this is not always the case.

From time to time situs abnormalities will occur and it is important to describe them accurately.

- (a) *Situs Solitus.* This describes normal situation with normal viscero-atrial situs, normal cardiac situs and normal bronchial situs.
- (b) *Complete Situs Inversus.* In this condition there is complete reversal of all the thoracic and abdominal organs and the condition is often associated with little or no cardiac abnormality. An example of this is shown in Fig. 11.1. (It is of paramount importance that meticulous technique in the use of radiographic side markers is used in all departments. *If films are marked up after processing,*

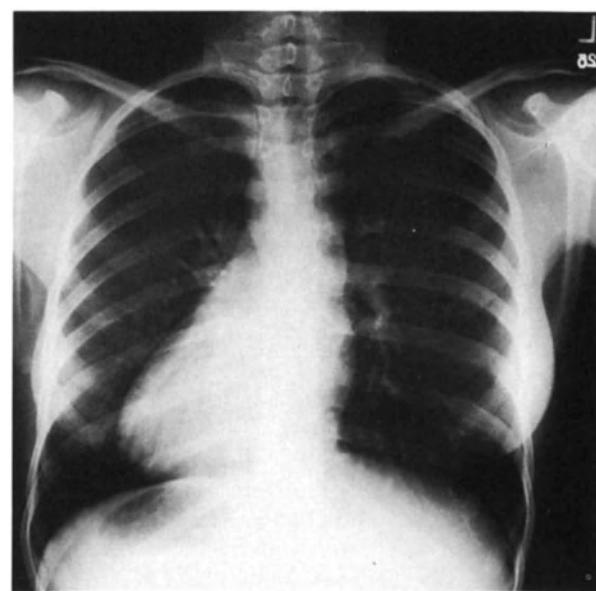
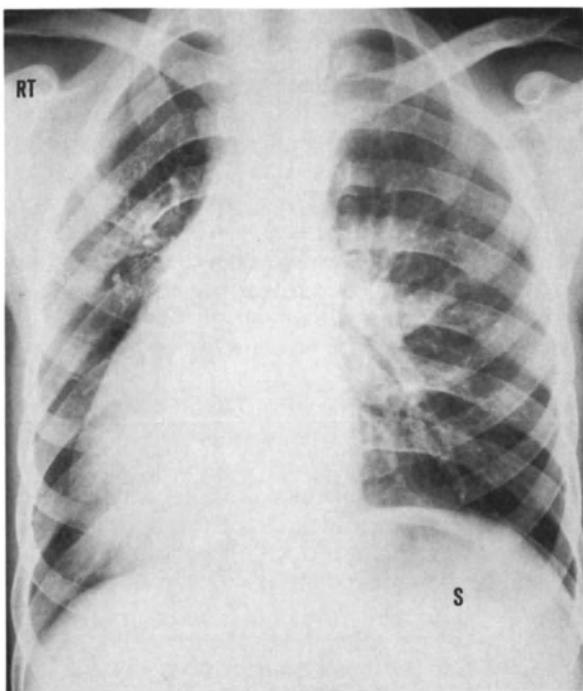


Fig. 11.1. The chest radiograph is of a patient with total situs inversus. The cardiac apex and stomach bubble are on the right side and the liver is on the left.



**Fig. 11.2.** The chest radiograph is of a patient with viscerocardiac situs solitus and dextrocardia. The stomach bubble (S) remains on the left but the cardiac apex is on the right. There were complex intracardiac abnormalities.

*the cases of total situs inversus are almost certainly going to be marked wrongly).*

- (c) *Isolated Situs Inversus of the Cardiac Mass.* In this situation there is normal viscerocardiac situs but the cardiac mass and cardiac apex are directed to the right. This is called *isolated dextrocardia* and has variable association with other cardiac anomalies. An example of this is shown in Fig. 11.2. The rarer converse of this is *viscerocardiac situs inversus* with isolated levocardia.
- (d) *Situs Ambiguus.* This difficult concept occurs when the left and right sided nature of abdominal or thoracic organs are not clearly evident. A number of variations of this can be recognized.

The first of these is most easily understood as '*bilateral right sidedness*'. In this condition there is a large *mid-line liver* running across the upper abdomen, there is an *absent spleen*, the *stomach* is usually *centrally positioned* and the *bronchial anatomy shows right-sided morphology of both major bronchi*. Both atrial chambers have *right-sided characteristics* and, not surprisingly, there is a frequent association with *abnormalities of pulmonary venous drainage*. There are often many other cardiac abnormalities also associated with this condition.

*Bilateral left sidedness* is also associated with a *mid line liver*, often smaller, but there is frequently *polysplenia*, *bilateral left atrial morphology* and the two *main bronchi both show left morphology*. Again, there is an association with major cardiac abnormality.

The final form of *situs ambiguus* is one in which the morphological characteristics of the various structures

are very hard to determine and a left or right-sided nature cannot easily be determined. In this case again many cardiac anomalies can be associated.

2. *Segmental Cardiac Connections.* Once the cardiac chambers and their connections have been identified in morphological terms then it should be possible to state which vessel or chamber is connected to which. For example, in *transposition of the great arteries* it can be stated that the aorta arises from the morphologically right ventricle and the pulmonary artery arises from the morphologically left ventricle. In this situation there is said to be *ventriculo-arterial discordance*. From time to time there will be *atrioventricular discordance* which will occur when the morphologically right atrium drains into the morphologically left ventricle and vice-versa.

*In some cases the connections will not be completely distinct* as, for example, in *Tetralogy of Fallot* where the aorta partially overrides onto the right ventricle from its position above a large ventricular septal defect. Complete overriding of great arteries can occur in the presence of a ventricular septal defect, most typically in *double outlet right ventricle*. If there is a large ventricular septal defect lying between the atrioventricular valves there can also be partial or total override. *Double inlet ventricle* is thus a recognized occurrence.

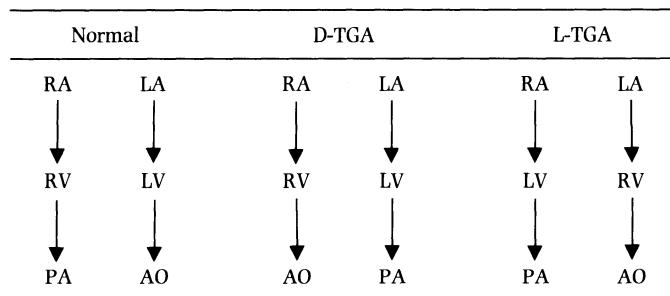
3. *Topology or Looping.* This term relates to the ventricular loop which has been formed during cardiac development. If the heart is sufficiently well developed to have two ventricles, each with an inlet and an outlet of some sort, then it will be possible to define the loop. D-loop and L-loop configurations are stereo-isomers of each other.

The normal ventricular loop is a *D-loop* which can be understood most simply using the analogy of the *right hand rule* devised by Van Praagh. In this description the right ventricle can be likened to a right hand. The inflow is represented by the thumb, the outflow is represented by the fingers and the interventricular septum will lie on the palmar side of the hand. This can be clearly recognized if one orientates one's right hand over another person's heart. If, however, the morphologically right ventricle is configured in such a way that the relationship of inflow, outflow and interventricular septum can only be represented by a left hand this infers that the ventricle is actually a *stereo-isomer (mirror image)* of a normal D-loop ventricle.

*L-looping* is most frequently seen in association with *transposition of the great arteries*. This condition is known as '*anatomically corrected transposition*' in which the cardiac apex is normally directed to the left but the morphologically left ventricle lies anterior and to the right of the posterior and leftwardly positioned ventricle which is of right morphology. Viscerocardiac situs is normal which means that there is atrioventricular discordance as well as ventriculo-arterial discordance. Thus the abnormal connections result in a physiologically corrected circulation as shown in Table 11.2.

The D-loop or L-loop nature of the ventricular chambers is absolutely fixed by the three-dimensional relationships and does not in any way relate to the actual position of the heart within the thorax.

4. *Position.* Although the position of the heart in the chest is the first thing to be seen on a chest radiograph, the absolute

**Table 11.2.** Connections in transposition of the great arteries

position is of secondary importance in describing the fundamental nature of the congenital heart abnormality. The position is, of course, of practical importance in planning surgical procedures. If the reader can imagine that the cardiac formation is constructed in the form of a model made out of extremely flexible elastic material then it is easy to see that a patient with a completely normal heart can have considerable distortion of position by twisting, stretching or turning various chambers into different positions whilst still maintaining absolutely normal situs, cardiac connections and ventricular looping.

It is important to note the position of the *aortic arch* as this is more commonly right-sided with some congenital abnormalities. The presence of a right-sided aortic arch is important for surgical planning.

**5. Malformations.** This refers to the specific deformities or abnormalities within the heart such as *stenotic or atretic valves*, *abnormal communications* and *narrowed vessels*. In many cases malformations are the only abnormality and in this situation the full description of situs, connections, looping and positions is omitted in general discussion. This applies with straightforward atrial and ventricular defects, coarctation, pulmonary stenosis and so forth. Some malformations are a little more complex, for example atrioventricular septal defects, but the remaining features are usually normal. Malformations do of course commonly occur in association with the more complex abnormalities.

#### HEMODYNAMIC PRINCIPLES

In the understanding of congenital heart disease a number of important principles should be understood.

**1. Development of Chambers and Vessels with Flow.** It is important to realize that the flow through a chamber or vessel will cause growth of that structure. Conversely, if there is no flow then the structure will be hypoplastic or absent. This is seen most dramatically in the condition of *hypoplastic left heart* in which the left ventricle fails to develop beyond a tiny size because there is mitral and/or aortic atresia which prevents flow through the chambers. Increased flow will usually lead to increase in chamber size. It is important to note that pressure load on a ventricle will cause hypertrophy but will often not change the overall size of the chamber until that chamber fails and becomes dilated.

**2. Physiological Changes at Birth.** In fetal life the right-sided cardiac pressures and the pressure in the pulmonary artery remain high because the low resistance pulmonary capillary bed has not yet opened up. At birth the first breath of the infant heralds the rapid decrease in pulmonary vascular resistance, which in turn leads to a rapid decrease in right-sided cardiac pressures. This causes the interatrial foramen to close by its valve-like action and will also stimulate closure of the patent ductus arteriosus. It is important to realize, however, that the drop in pressure can take several hours or days to be complete and this will have important consequences on the clinical and radiological presentation of certain conditions in early life.

**3. Left to Right Shunt.** In the normal situation the pressure in the right ventricle and pulmonary artery will be much lower than that on the left side because of the lower vascular resistance in the lungs. If any communication between the left and right side of the heart exists there will be a left to right shunt. If the left to right shunt is at atrial level then the pressure in the left and right ventricles will not necessarily be affected. The right ventricle can tolerate a significantly increased flow of blood by increasing its size and contractility whilst maintaining normal or slightly raised pressures. If this situation exists for many years the continuing large flow in the lungs can gradually damage the pulmonary circulation and will eventually lead to right-sided pressure increases and ultimately equalization of left and right-sided pressures. Thus *simple atrial septal defects* do not often cause trouble in childhood or early adult life, but may cause pulmonary hypertension or heart failure in middle age or later.

If there is a large *ventricular septal defect* then the left and right ventricles will immediately be at the same pressure and the lower resistance of the lungs will induce a large left to right shunt. In this situation the combination of increased flow and increased pressure in the lungs will produce progressive pulmonary vascular damage at a much earlier age than will occur with atrial mixing. Irreversible pulmonary damage will occur in this situation and ultimately the right sided pressure elevation will cause reversal of the shunt with developing cyanosis (the *Eisenmenger Syndrome*). The development of this condition is associated with a reduction in the left to right shunt with consequent reduction in heart size and pulmonary plethora. Thus the chest radiograph that is 'improving' or has returned to 'normal' may actually be showing the development of progressive irreversible damage.

A similar situation will occur with any other high pressure mixing situation such as might occur with a large *patent ductus arteriosus* or other aorto-pulmonary connection. If the ventricular septal defect is small this will increase the flow through the lungs but will not necessarily raise the pressure on the right side. Small ventricular septal defects are known to have a high probability of closure in the early years of life.

**4. Concept of a 'Single Useful Ventricle'.** There is a wide range of complex cardiac abnormalities in which there is one poorly developed and small ventricle and a second large ventricle. In this situation the large ventricle is the only functionally useful ventricle for pumping systemic and pulmon-

ary blood. Whichever form of abnormal cardiac connections exists in association with this 'single useful ventricle' there must be common mixing of both systemic and pulmonary venous blood which will lead to cyanosis, the degree of which will depend on the precise details in the individual patient.

No surgical procedure is available which can produce two useful ventricles out of one, and thus all forms of surgical treatment in this condition will make some form of compromise. In many cases palliation is carried out by *shunting additional blood to the lungs* if there is pulmonary oligemia or *banding the pulmonary artery* if there is pulmonary plethora. This is simply an attempt to produce a reasonably balanced pulmonary circulation to allow reasonable oxygenation in the systemic circulation without subjecting the lungs to damaging pressure.

The *Fontan operation* is a means of reconstructing a more normal circulation without the use of a second ventricle. This is achieved by connecting the systemic venous return through the right atrium directly to the pulmonary circulation, either through a simple anastomosis in the right atrial appendage or by the use of an additional conduit. The very low pressure of systemic venous return is a limiting factor with this operation and it can only be successfully performed in patients whose pulmonary artery anatomy is satisfactory and in whom the pulmonary arterial pressure and resistance is low.

5. *Circulation in Transposition.* If there is complete transposition of the great arteries with no other intracardiac abnormality, then life is incompatible unless there is mixing of the two circulations at some point. It is useless to have a large amount of well oxygenated blood returned to the left atrium if it is subsequently redirected to the left ventricle and then to the pulmonary artery and lungs again. It is therefore essential to ensure satisfactory mixing at an early stage in life.

In line with the principles outlined above this is best at an atrial level where the pressure is low and it is thus common practice to perform a *balloon septostomy* which ruptures

the thin septum primum that covers the foramen ovale. This facilitates increased atrial shunting which must, of course, be bidirectional. Although the total amount of shunting from left to right and right to left must be equal there is, overall, much more blood flowing in the pulmonary circuit than in the systemic circuit; the small proportion of this pulmonary flow which passes across the atrial septum will be adequate to sustain requirements. Patients with complete transposition and a large ventricular septal defect will have good mixing but will also have problems of high pressure in the lungs which may cause damage at an early stage.

6. *Pulmonary Atresia.* In many congenital cardiac abnormalities there is narrowing or atresia of the pulmonary artery or valve which may be associated with atresia or narrowing in the right ventricular outflow tract. In this situation little or no blood will enter the pulmonary circulation in the normal way and the only flow in the pulmonary circuit will be that produced by ductal flow which is present at birth. In patients in this category closure of the patent ductus arteriosus at birth can lead to rapid progressive cyanosis and it is therefore necessary to increase the blood supply to the lungs. In the short term this is done by *medical therapy* to keep the patent ductus open but as soon as practicable a *systemic to pulmonary shunt* is performed to improve the blood flow into the lungs.

The commonest type of shunt performed is a *Blalock-Taussig anastomosis* in which systemic arterial blood from the subclavian artery is directed into the pulmonary artery, either by direct anastomosis of the subclavian artery (conventional Blalock-Taussig shunt) or by means of an interposed prosthetic graft. This type of palliation will result in a mixed circulation and some degree of chronic cyanosis. Final repair of the circulation will depend on the anatomy and pathology in the individual case. It is for this reason that precise details of pulmonary artery size and anatomy must be obtained for planning of surgery and this can often prove one of the most challenging aspects of diagnosis by either echocardiography or angiography.

## IMPORTANT CONGENITAL CARDIAC ABNORMALITIES

A number of conditions will now be discussed in detail and are presented in order of frequency of occurrence in Table 11.1. There is no attempt to cover comprehensively all forms of congenital cardiac abnormality because this is beyond the scope of this chapter.

### VENTRICULAR SEPTAL DEFECT (VSD)

This abnormality is one of the commonest and can be isolated or associated with simple or complex congenital heart disease. The commonest site for a VSD is in or near the membranous septum at the base of the heart near the tricuspid valve and aortic root. It is possible, however, for single or

multiple VSDs to be present at any site throughout the large and complex shape of the interventricular septum. In diagnosis and investigation of this condition it is important not only to confirm the presence of interventricular communication but also to localize the site of the communication and to determine if there are any additional communications. The latter point is essential if corrective surgery is to be successful.

The presentation of this condition depends on the overall size of the interventricular communication. The condition does not normally present in the first few days of life unless the interventricular septal defect is very large. This is because the pulmonary vascular resistance drops steadily in the first days and weeks of life and thus prevents the development

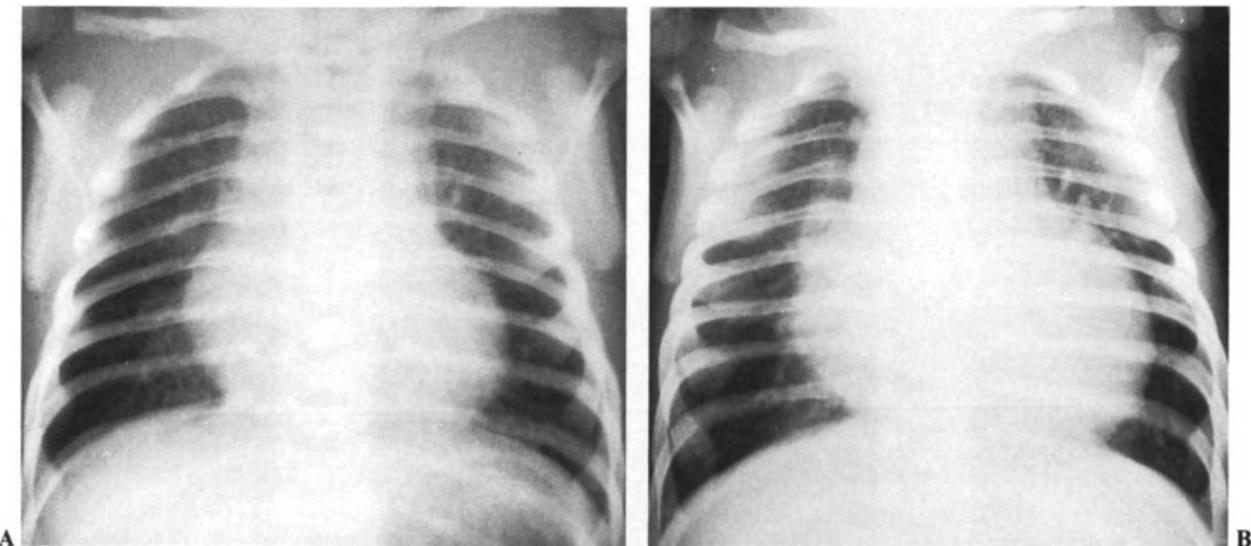


**Fig. 11.3.** A This chest radiograph was taken at the age of one day in an infant with no signs of heart disease, the film having been taken for another indication. The heart is slightly enlarged and the lung fields are normal. B The same patient at the age of one month presented with difficulty in feeding and clinical signs of heart failure. The cardiomegaly is much more obvious and the pulmonary vasculature is now plethoric. A large ventricular septal defect was present but had not presented early due to the initial high pulmonary pressures.

of pulmonary plethora to start with. Thus even with large VSDs the patient may be asymptomatic with a normal chest radiograph at birth. A large VSD will present after a few days or weeks with breathlessness and feeding difficulties and the chest radiograph will usually show moderate enlargement of the heart with prominence of the main pulmonary artery, the hilar pulmonary arteries and the peripheral pulmonary arteries. In severe cases there will be cardiac failure also. An example of this is shown in Fig. 11.3.

In the case of smaller VSDs the presentation can be much later in life and may occur with the detection of an asymptomatic murmur. In these cases the chest radiograph can range from normality, if the communication is very small, to mild or moderate cardiac enlargement with mild or moderate pulmonary plethora.

*It is not an easy matter in pediatric practice to distinguish ventricular septal defect from other left to right cardiac shunts (e.g., patient ductus arteriosus, aorto-pulmonary communication or even large atrial septal defect) on the basis of the chest radiograph alone.*

Distinction becomes easier with increasing age because the natural histories of the conditions differ, but this is obviously of little immediate value in individual infants or children. It is important to say, however, that a large VSD with a big shunt presenting early in life will inevitably lead to severe pulmonary damage and pulmonary hypertension in the first few years of life. It is thus essential to recognize the abnormality and treat the condition as soon as possible. Echocardiography is thus essential in the differential diagnosis of these conditions and must be performed as soon as possible.

The diagnosis of VSD can be confirmed on *echocardiography*. If the defect or defects are large they will be apparent on the two-dimensional image but in the case of smaller

defects it may be necessary to use *Doppler flow assessment* to evaluate their presence. In this situation the addition of *color flow mapping* (see Fig. 9.15) has been very valuable in allowing the detection of small or multiple ventricular septal defects.

*Cardiac catheterization* is often undertaken if there is any doubt about the anatomy or about the nature of the pulmonary vascular resistance. *Cardiac angiography* must be carried out to locate specifically not only the site of the known VSD but also to exclude the possibility of additional VSDs.

The most common VSD is in the *membranous* or *perimembranous* region, as shown in Fig. 11.4, and is often associated

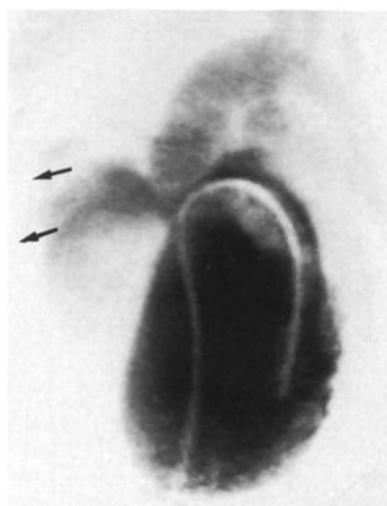


**Fig. 11.4.** A digital subtraction angiogram of a left ventricular injection taken in the left anterior oblique view. There is a moderate sized perimembranous defect with flow into the base of the right ventricle (arrowed).

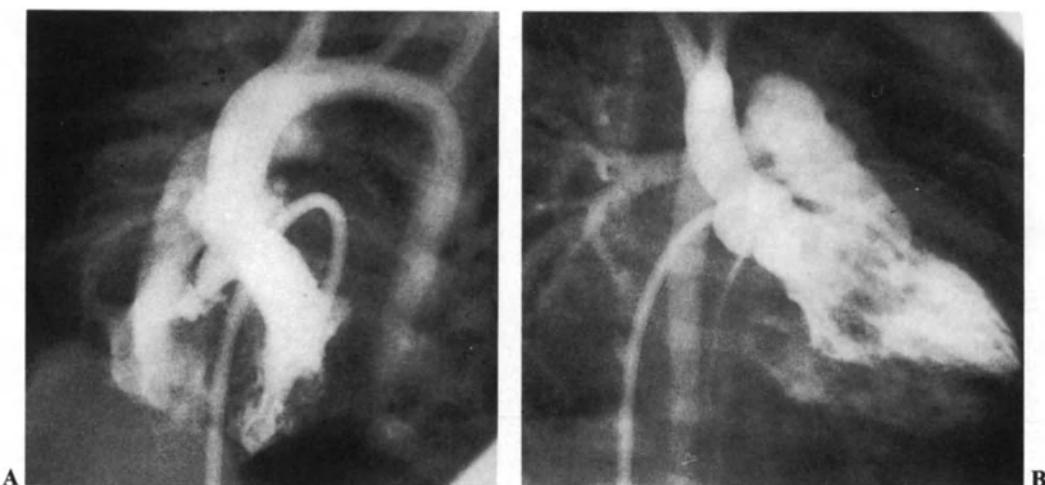


**Fig. 11.5A, B.** Left ventricular biplane ciné angiography in a patient with a perimembranous ventricular septal defect. **A** A cranially angled left anterior oblique view. There is an aneurysmal bulge in the perimembranous region with flow through it into the right ventricle. **B** The right anterior oblique view shows opacification of the right ventricle and pulmonary artery but the defect and aneurysm are not profiled.

with some form of associated fibrous tissue closely related to the tricuspid valve. In some cases the VSD is aneurysmal with a bulging structure being pushed towards the right ventricle with each systolic contraction of the left ventricle (Fig. 11.5). Often a large VSD can be virtually occluded with such a large membranous aneurysm. Large VSDs in this region can also be associated with aortic regurgitation due to prolapse of the aortic root into the defect. The presence of VSD in association with any other cardiac abnormality must also be evaluated.

*MRI* can also image VSD (Fig. 11.6), but its high cost makes it unlikely to supplant echocardiography except in special circumstances.

Treatment of a VSD is most commonly surgical. It has been common practice to place a *band* around the pulmonary artery as a palliative operation in small infants with large VSDs so that a definitive closure of the VSD can take place at a later age (often 3 or 4 years). This approach is now giving

way to earlier and earlier *primary closure* of the VSD, which is now done under the age of 1 year in many cases. Primary closure is a more complex operation in the very small infant but has the advantage that the pulmonary artery anatomy is not distorted and a second operation is not required. In patients with very small VSDs it is often best to wait for a few years to see if the defect will close spontaneously. During this period precautions must be taken against the development of infective endocarditis.

#### PATENT DUCTUS ARTERIOSUS (PDA)

The patent duct is a vital part of the fetal circulation and this communication usually closes in the first few days of life. The ductus arteriosus often remains open rather longer in premature infants, but in the majority of cases still closes spontaneously. If there is a persistent failure of closure of the duct then the consequences will depend on the size of the communication. A tiny residual patent ductus arteriosus can remain undiagnosed throughout life as it might produce minimal effect. A large patent ductus arteriosus will have similar effects to a large ventricular septal defect. In most cases patent ductus arteriosus is closed surgically both to avoid the risk of endocarditis and also for hemodynamic reasons. Patent ductus arteriosus is commonly associated with many other congenital cardiac abnormalities.

The *chest radiograph* will show pulmonary plethora if the shunt is large and there will be mild to moderate cardiac enlargement. The normally smooth outline of the aortic knuckle and descending aorta will often be interrupted by the 'bump' of the ductus but this may be difficult to detect in young infants in whom the normal descending aorta is hard to visualize. In an older child or adult it is probably true to say that the presence of a well-defined aortic knuckle leading into a straight and uninterrupted descending aorta will almost certainly exclude the presence of a patent ductus

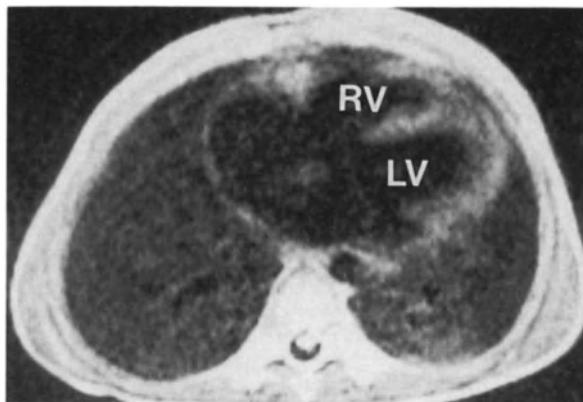


**Fig. 11.6.** Transverse MRI section (ungated spin-echo sequence) in a child with VSD (RV, Right Ventricle; LV, Left Ventricle).

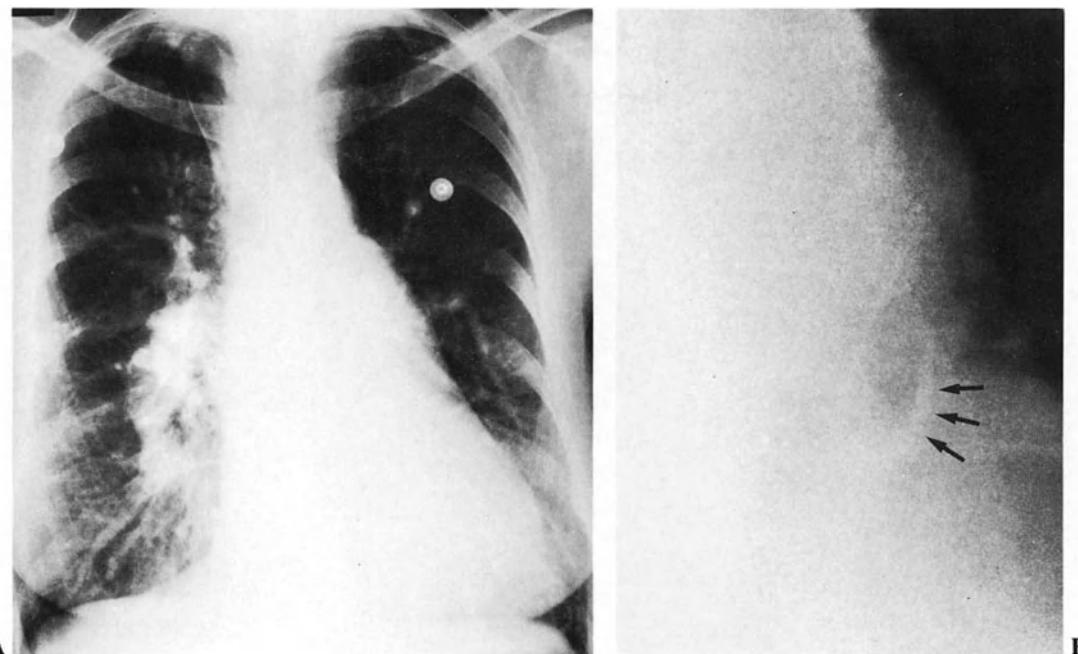


**Fig. 11.7A, B.** The chest radiograph (A) shows disproportionately large central pulmonary arteries due to lifelong pulmonary hypertension caused by a patent ductus arteriosus. B A localized view of the calcified ductus (arrow).

arteriosus. Later in life there may be some calcification present in the patent ductus as shown in Fig. 11.7. The aortic knuckle is sometimes a little larger than normal in this condition, but this cannot be regarded as a reliable sign.

*Echocardiography* will, in many cases, clearly show the persistent communication on two-dimensional scanning but as patients get older, the imaging can prove more difficult. *Doppler* evaluation is, however, highly reliable in the diagnosis of this condition.

*Angiography* is also a reliable method of diagnosing the condition and a well placed aortic injection will show the abnormality. This is sometimes achieved with an arterial catheter but frequently a venous catheter can be passed via the right heart chambers to the pulmonary artery and then to the aorta via the patent ductus itself. It is important not to overlook a PDA in the presence of other important left to right shunts. In the case of a *large VSD*, a left ventricular injection will produce almost simultaneous opacification of the aorta and pulmonary artery. In these circumstances, the PDA communication can often be hard to diagnose with certainty and a separate aortic injection is necessary to exclude the condition. *Coarctation of the aorta* is commonly associated with a patent ductus arteriosus as shown in Fig. 11.8.

*Aorto-pulmonary window* is a rare condition that can simulate a large patent ductus arteriosus. The communication is usually in the ascending aorta and may be large. Echocardiographers must be certain that the condition is not overlooked and color flow Doppler techniques will doubtless make this easier. Angiographers must also be careful not to miss the condition, as it can often be out of profile if inappropriate projections are selected.

#### AORTIC STENOSIS (CONGENITAL) AND HYPOPLASTIC LEFT HEART

Congenital aortic stenosis is a simple malformation in which the leaflets of the aortic valve remain partially fused and impair the outflow from the left ventricle. The aortic valve itself may be bicuspid or tricuspid and the obstruction may be mild, moderate or severe. Severe cases present in infancy with heart failure and possible left ventricular dilatation and impairment. Severe aortic stenosis, presenting in early infancy, carries a high mortality and early operation is required to divide the fused commissures. Milder degrees of aortic stenosis carry a better prognosis and can be operated on electively in childhood.

The condition can be recognized on *chest radiography* if there is a dilated ascending aorta due to post-stenotic dilatation, but this is usually seen in older children only. Heart failure may be recognized in infancy and in this situation there is little to distinguish the radiograph from that of severe coarctation.

*Subaortic stenosis* can be of a dynamic form (usually associated with hypertrophic cardiomyopathy) or it can be of a fixed type, either a diaphragm immediately below the aortic valve or a tunnel-like narrowing of the left ventricular outflow tract. There is a rare form of *supraaortic stenosis* affecting the aorta just above the sinuses of Valsalva. These variants can all be recognized on *echocardiography* or *angiography*.

At the most severe end of the spectrum lies *aortic atresia*. If there is no flow through the aortic valve the left ventricle itself will not develop and this abnormality is known as *hypoplastic left heart*. The abnormality may also be associated

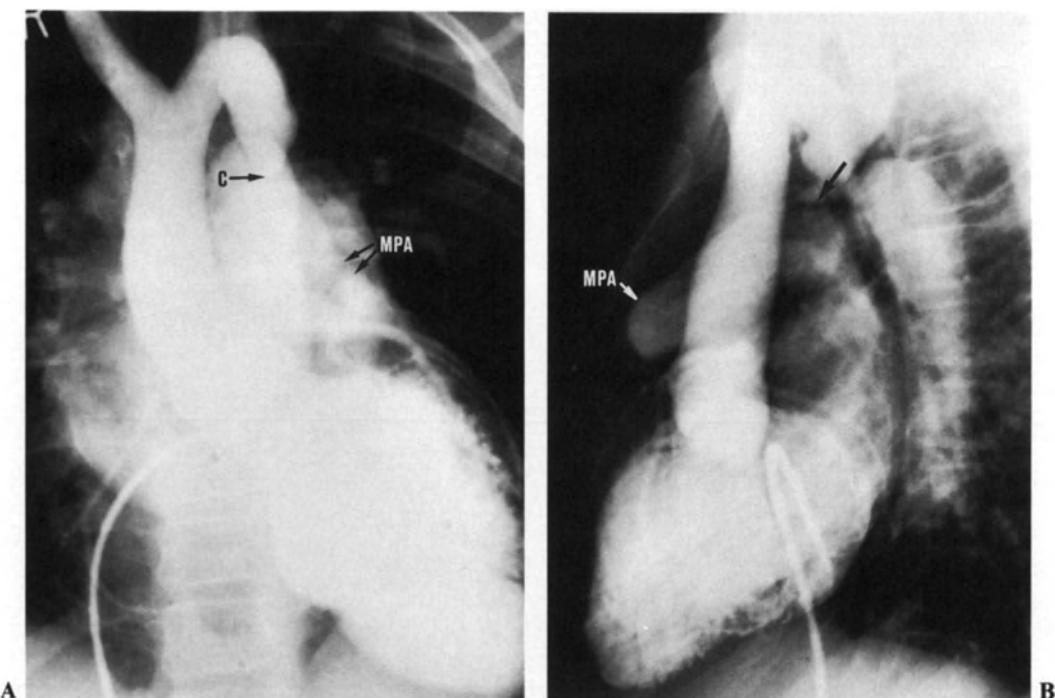


**Fig. 11.8A, B.** Frontal (A) and lateral (B) views of a biplane left ventricular angiogram. There is obvious coarctation of the aorta (C) as well as opacification of the main pulmonary artery (MPA) due to flow through the patent ductus arteriosus (arrow).

with mitral atresia. In this condition the right ventricle performs the entire systemic pumping function with the body being supplied through the ductus arteriosus. The ascending aorta is diminutive in size and carries reverse flow from the patent ductus of sufficient magnitude only to fill the coronary bed. The condition is almost uniformly fatal although some experimental approaches to surgery are now being investigated. Patients with hypoplastic left heart are often born in good condition but deteriorate very rapidly in the first few days of life.

The diagnosis of aortic stenosis or hypoplastic left heart can easily be made with *echocardiography*. The aortic valve

gradient can be measured with continuous wave Doppler and surgery can often be performed on the results of a good ultrasound study. Cardiac catheterization may precede balloon dilatation of the valve.

*Congenital bicuspid valves* (see Fig. 11.9) are not normally stenotic but they can lead to 'acquired' aortic stenosis in adult life. The abnormality can be recognized clearly on two-dimensional echocardiography. There is an association between congenital bicuspid aortic valve and coarctation of the aorta.



**Fig. 11.9.** Short axis echocardiogram showing the two leaflets of a bicuspid aortic valve.

#### ATRIAL SEPTAL DEFECT (ASD)

This abnormality can be divided into two major categories, the *ostium primum* atrial septal defect, which will be considered separately under the heading of atrioventricular septal defects, and the *ostium secundum* atrial septal defect which is the more common type. The *ostium secundum* defect is usually at the level of the foramen ovale or above and does not involve the tissues of the septum primum or the atrioventricular valves. A third form of atrial septal defect is less common and is known as the *sinus venosus* defect. This is very high in the atrial septum near the insertion of the superior vena cava. This type of defect is often associated with some form of partial anomalous pulmonary venous drainage.

Atrial septal defect must be distinguished from patent foramen ovale. The latter condition is a normal finding in small infants, because in the first few weeks or months of

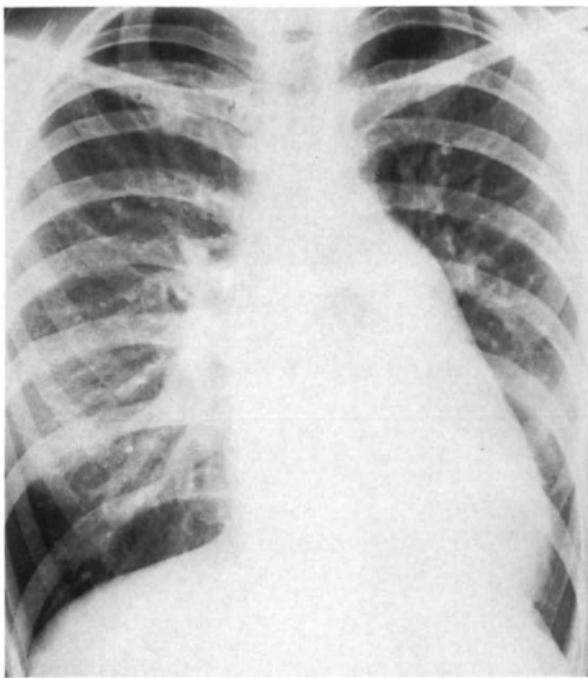


**Fig. 11.10.** The chest radiograph is from an adult with a large atrial septal defect. There is moderate cardiomegaly, a large right ventricular outflow tract and pulmonary artery and plethoric pulmonary vascularity.

life the flap valve mechanism across the foramen ovale has not finally fused shut. In abnormalities where the atrial chambers are enlarged this can cause stretching of the foramen ovale which can sometimes regress when treatment has been undertaken. For practical purposes atrial septal defect exists when there is a persisting equalization of pressure in the two atria. The low-pressure shunting that occurs with atrial septal defect is usually accommodated very well by the right ventricle and patients with an isolated ASD very rarely present in the early years of life. Presentation later in childhood or adolescence is quite common when mild abnormalities are detected on routine medical examination or chest radiography (Fig. 11.10). From time to time atrial septal defect will present in the middle-aged or elderly when heart failure or pulmonary hypertension can finally develop.

Atrial septal defect can occur in association with many other cardiac abnormalities, but does not usually present a major surgical challenge. Surgical treatment for the atrial septal defect is normally carried out even in relatively asymptomatic patients because the operation has a very low mortality and complications in later life can be avoided.

There is a theoretical risk of patients with atrial septal defect developing pulmonary hypertension and paradoxical embolus from a systemic venous thrombosis.

*Chest radiographs* with atrial septal defect can be normal if the pulmonary to systemic flow ratio is less than 2:1. With flow ratios higher than this the heart usually shows mild to moderate enlargement with concomitant enlargement of the main pulmonary artery and its branches. Pulmonary plethora is present except for the few patients who develop pulmonary arterial hypertension later in life. Two-

*dimensional echocardiography* will often demonstrate the defect and the flow across it is clearly visualized on *color flow Doppler* examination (see Fig. 9.15).

#### ATRIOVENTRICULAR (AV) SEPTAL DEFECT

This group of conditions is also known as atrioventricular canal defect. All have the same fundamental abnormality in the way that the heart is formed.

The base of the interventricular septum in the region of the membranous septum is in continuity with the atrial septum primum. This central portion of the cardiac structure is missing in both the partial and complete types of atrioventricular septal defect. The *partial* type of atrioventricular septal defect results in only an interatrial communication and leads to the so-called ostium primum atrial septal defect. The *total* atrioventricular septal defect leads to interventricular and interatrial communications with a large common atrioventricular valve. The diagrams in Fig. 11.11 and Fig. 11.12 show the difference between normals, partial AV septal defects and complete AV septal defects. There is also an intermediate type in which the interventricular communication is relatively small due to partial tethering of the common atrioventricular valve to the septal crest.

The atrioventricular valves are commonly malformed and produce regurgitation of varying degrees. This is not invariably present but it will lead to exacerbation of the symptoms produced by left to right shunting.

There is an increased incidence of this condition in patients with Down's syndrome. Presentation is variable depending on the precise nature of the abnormality, but it tends to be earlier and more severe than with conventional atrial and ventricular septal defects of similar size. There is no specific abnormality that can be detected on chest radiography to differentiate these conditions from the more usual type of atrial ventricular septal defects although the cardiac enlargement, pulmonary plethora and cardiac failure are often more prominent.

*Echocardiography* is the cornerstone of diagnosis in this range of conditions (Figs. 11.13, 11.14). The atrioventricular valve anatomy can be clearly seen and the presence of a ventricular component to the defect is usually obvious. There is usually considerable enlargement of the right-sided cardiac chambers and the right atrium may be particularly large if there is accompanying atrioventricular valve regurgitation. This regurgitation is more commonly seen through the mitral valve in ostium primum ASD and the regurgitant jet is often directed across the interatrial defect to the right atrium. The mitral valve is frequently cleft in the ostium primum condition. *Doppler* studies will clearly demonstrate the presence of atrioventricular valve regurgitation and this is particularly well seen on *color flow* studies.

*Angiocardiography* is also capable of clearly demonstrating the anatomy. The most obvious abnormality seen on angiography is the absence of the usual left ventricular outflow tract as shown diagrammatically in Fig. 11.15. The mitral valve hinges directly from beneath the aortic root and when open creates a distinct appearance that has been likened to

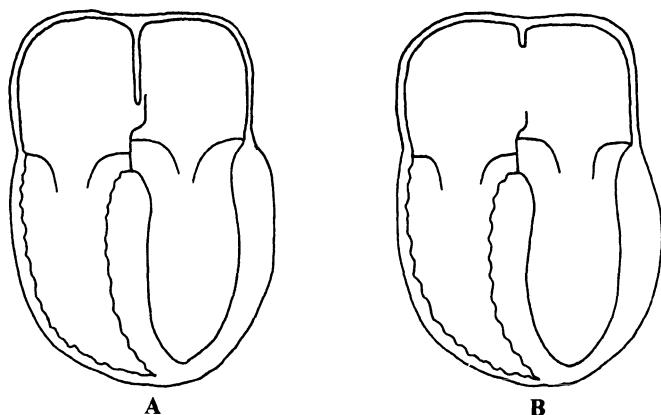


**Fig. 11.11A, B, C, D.** Diagrammatic representation of differing atrial and ventricular septal anatomy as seen from a stylized 'four chamber view'. In the normal heart the septum primum (thin line) overlaps the septum secundum to produce the normal valve of the foramen ovale (A). In ostium secundum atrial septal defect (B) the septum primum and atrioventricular valve attachments are normal and the defect is confined to the septum secundum. In the case of ostium primum atrial septal defect (partial atrioventricular septal defect) (C) the septum primum is absent and the mitral and tricuspid valves are attached to the muscular portion of the interventricular septal crest. The septum secundum is usually intact but there can be an associated secundum defect. In complete atrioventricular septal defect (D) there is no valve attachment to the septal crest because the large common valve straddles both ventricles. When the valve is open there is free communication between all four chambers of the heart.



**Fig. 11.13.** Two-dimensional echocardiogram showing a subcostal four chamber view of an ostium primum atrial septal defect (Left atrium LA and right atrium RA both labelled).

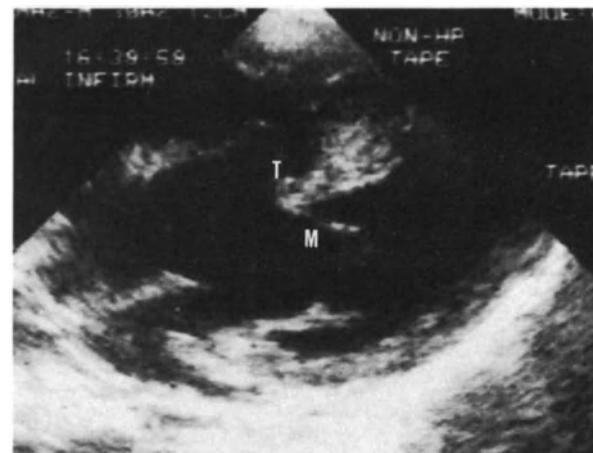
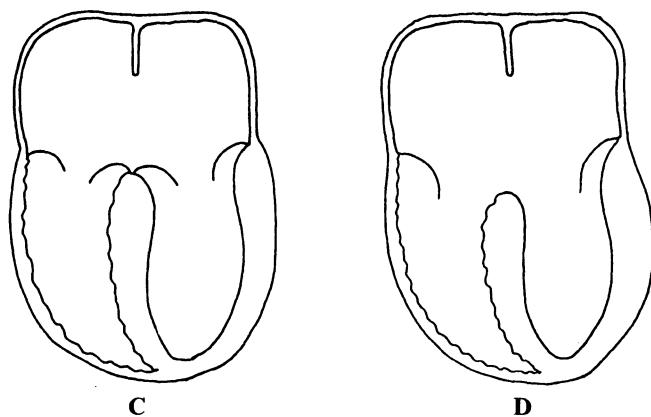


**Fig. 11.14.** Another example of an ostium primum atrial septal defect (partial atrioventricular septal defect). This clearly shows the abnormal mitral (M) and tricuspid (T) valve attachments to the crest of the interventricular septum.

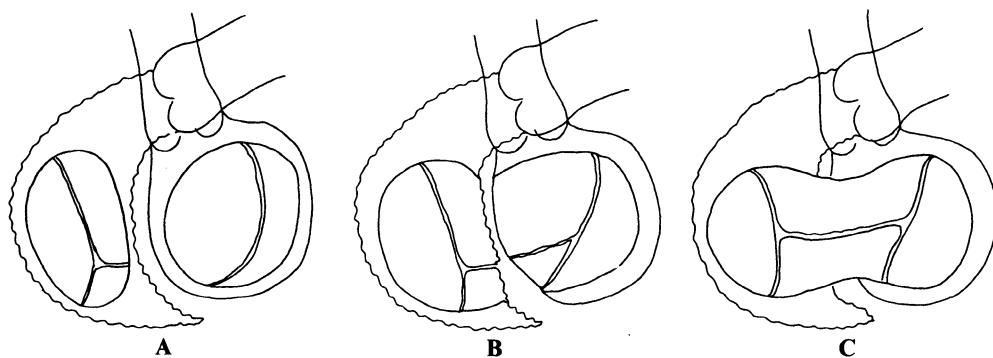


**Fig. 11.12A, B, C.** Diagrammatic representation of differing atrioventricular valve anatomy as seen viewed from the cardiac apex (left anterior oblique view). The normal heart (A) has a fully formed left ventricular outflow tract and the mitral valve has a normal round shape. In ostium primum atrial septal defect (B) the left ventricular outflow tract is absent and the (cleft) mitral valve is attached to the septum. In total atrioventricular septal defect (C) there is a single overriding atrioventricular valve with common superior and inferior leaflets.

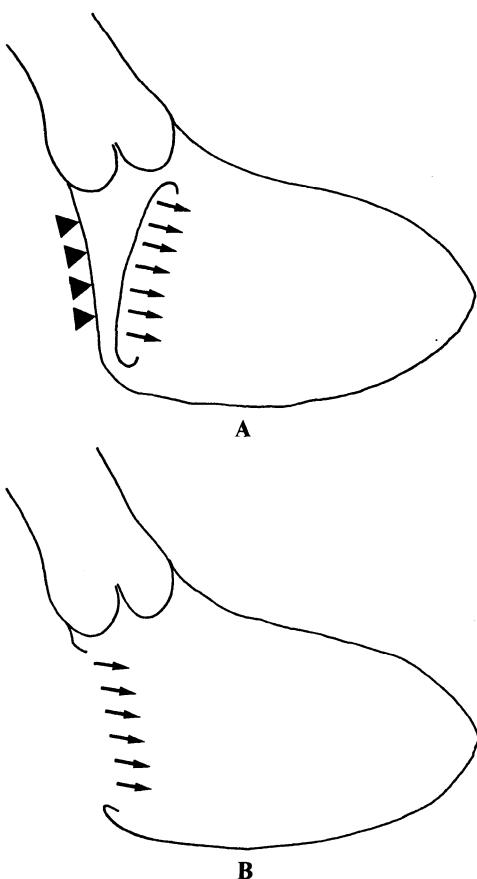


Fig. 11.15A, B. Diagrammatic representation of a left ventricular angiogram seen from the right anterior oblique view. In the normal (A) there is a fully formed left ventricular outflow tract (triangles) which is still visible when the mitral valve is open (inflow of blood, arrow). In all types of atrioventricular septal defect (B) the opening of the mitral valve is associated with loss of the contour of the left ventricular outflow tract.

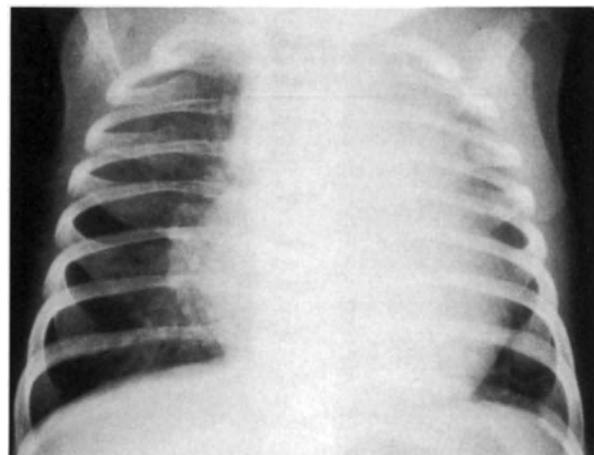


Fig. 11.16. Chest radiograph in an infant with severe coarctation of the aorta. There is cardiomegaly and heart failure due to the load placed on the heart by the aortic obstruction.

a 'goose-neck'. It is important to realize that this appearance does not indicate any narrowing of the left ventricular outflow tract as it merely reflects the distribution of contrast medium during ventricular diastole.

*Cardiac surgery* in this condition is somewhat more complex than with conventional atrial septal defects as the repair usually involves some form of reconstruction of the atrioventricular valves also. For this reason it is often performed at a slightly later age and palliative banding of the main pulmonary artery is frequently performed where clinically indicated.

#### COARCTATION OF THE AORTA

In this condition there is a characteristic shelf-like narrowing of the aorta which usually occurs just beyond the origin of the left subclavian artery. The severity of this narrowing can vary considerably and it is this severity which determines the age of presentation.

Severe coarctation or interruption of the aortic arch will present in the first few days or weeks of life with cardiac enlargement and cardiac failure (Fig. 11.16) due to the increased load on the right side of the heart which must supply blood to the lower body through the patent ductus arteriosus. Closure of the patent ductus arteriosus presents a potential hazard in severe coarctation in infancy as it may impair renal and other vital organ perfusion.

Lesser degrees of coarctation may present later in life with abnormal physical signs or abnormality on the chest radiograph. This will show a small or irregular contour of the upper descending aorta and if the condition has been present for several years rib notching may be visible (Fig. 11.17). This is caused by the prominent intercostal collateral vessels which are bypassing the narrowing.

Coarctation of the aorta varies in severity and the site of the coarctation can also vary. Occasionally, the narrowing can occur between the left common carotid and the left subclavian artery and in this situation the rib notching is likely to be unilateral, being generated only on the right side from the right subclavian distribution into the right intercostal vessels. Rib notching is notoriously variable and will, hopefully, become a less common sign as patients with coarctation are more reliably diagnosed and treated at an early age: it is rare before the age of 4 years. Interruption of the aortic arch can occur with the carotid arteries and sometimes one or both subclavian arteries arising from the ascending aorta before the interruption. The patent ductus supplies the lower half of the body which will be compromised with ductal closure.

In experienced hands *echocardiography* is reliable in the diagnosis of these conditions (Fig. 11.18) but it is increasingly difficult in older patients because of difficult ultrasonic access.

*Angiography.* Catheter access for an ascending aortic injection of contrast medium to demonstrate the aortic arch and

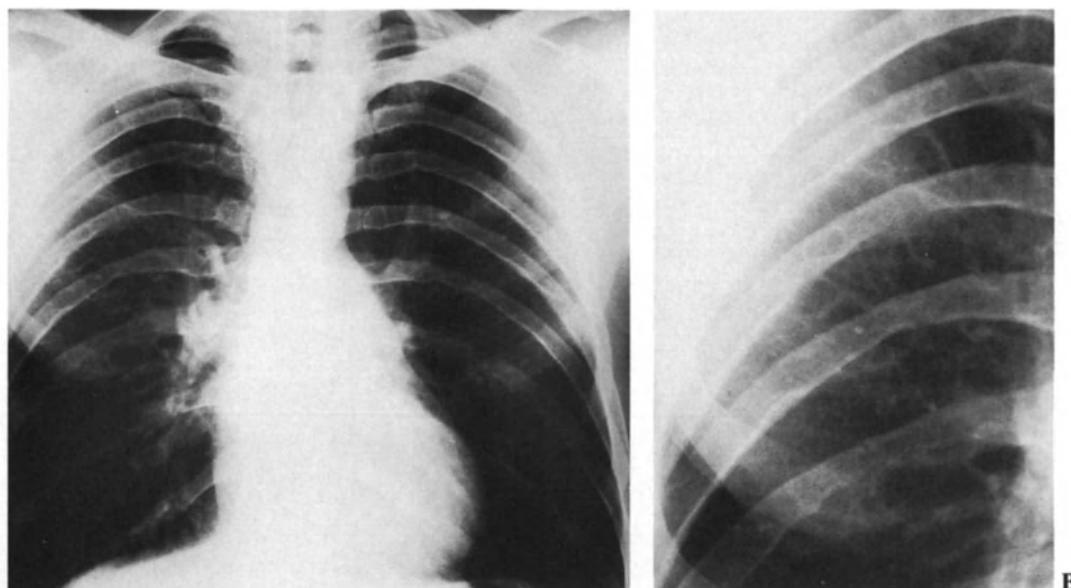


**Fig. 11.17A, B.** Chest radiograph in an adult with coarctation (A). The most definite sign is the loss of contour of the aortic knuckle which should be clearly seen in a correctly exposed film. In this film the aortic knuckle is small and irregular. Rib notching (see localized view, B) is also an important diagnostic sign but may not always be present. Rib notching does not occur in infancy.

coarctation (Fig. 11.19) can sometimes be a problem. A severe coarctation can prevent an arterial catheter from crossing from below and in older patients without a septal defect, access to the left side of the heart from the right heart chambers may not be possible due to closure of the foramen ovale. Left-sided access may be achieved by trans-septal puncture or by brachial or axillary arterial approach but these offer a higher than usual risk of complications.

Alternative angiographic approaches may be used. A pulmonary artery injection may be followed through to the left side and with good equipment excellent detail of the coarctation and collateral vessels may be achieved. Digital

subtraction angiography offers the opportunity for even better contrast enhancement in this situation as shown in Fig. 11.20. Peripheral or central venous contrast injection causes even more dilution of contrast medium and although images can be recorded these are not always of satisfactory quality (Fig. 11.21).

Coarctation of the aorta is associated with an increased incidence of hypertension and should therefore be corrected even if the patient is asymptomatic. There is also an increased association with abnormalities of the aortic valve, in particular a bicuspid aortic valve which might develop in later life to a stenotic aortic valve. Post-stenotic aneurysm is another well known complication (see p. 241).

Surgical repair is carried out by various techniques which include the incorporation of the left subclavian artery as a flap or by direct anastomosis. It should be noted, however, that surgical correction of coarctation carries a small but definite risk of paraplegia developing as an operative complication. Recent attempts at correction using balloon dilatation have been attempted but have not yet been established as a definitive technique.



**Fig. 11.18.** Two-dimensional ultrasound scan from the suprasternal approach showing the aortic arch (AA) with a coarctation (C).

#### PULMONARY STENOSIS

The most common form of pulmonary stenosis is isolated pulmonary valve stenosis in which there is residual fusion and usually thickening of the pulmonary valve leaflets. There may also be infundibular stenosis which is thought to be a response to the pulmonary valve stenosis with right ventricular hypertrophy causing increased contractility of the outflow tract.

The severity of this condition varies greatly and in *mild* cases the abnormality is of little clinical importance and may

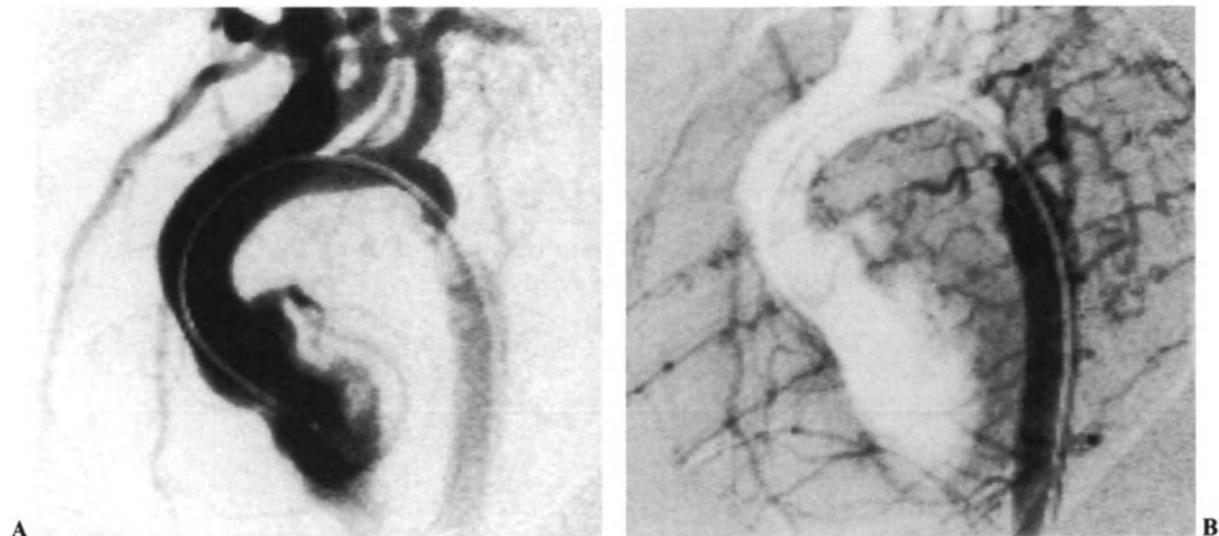


**Fig. 11.19A, B.** Digital subtraction angiogram in the left anterior oblique view (A) showing an arterial injection made into the LV and ascending aorta in a patient with severe coarctation. The catheter has traversed the coarctation and there is delay in opacification of the descending aorta due to the severity of the narrowing. Digital studies can be used to examine the timing of opacification as shown in B which is taken from the same study as A. This late frame of the study shows maximal opacification of the descending aorta and collateral vessels shown in black. The ascending aorta and left ventricle are now shown in white because a frame from the middle of the run has been used as a mask.

not present until late in life or not at all. *More severe* cases may present with breathlessness and *severe* cases may be associated with cyanosis. The most common presentation is of moderate to severe stenosis which does not interfere with cardiac output but which produces a strain on the right side of the heart.

The *chest radiograph* will often show a prominent main pulmonary artery which is caused by post-stenotic dilatation

(Fig. 11.22). The proximal left pulmonary artery is also dilated because it lies in a direct line with the main pulmonary artery. The right pulmonary artery is usually not dilated as it branches quite sharply from the main pulmonary artery. Peripheral pulmonary vascularity is normal or slightly oligemic. In cases where infundibular stenosis predominates, the main pulmonary artery may not be recognized as abnormally dilated on the chest radiography.

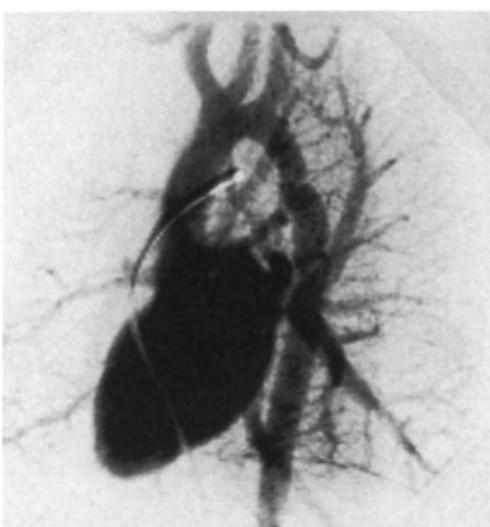


**Fig. 11.20.** Digital subtraction angiogram in the left anterior oblique view showing opacification of the left ventricle and aorta following a pulmonary artery injection. The coarctation in this case is mild.

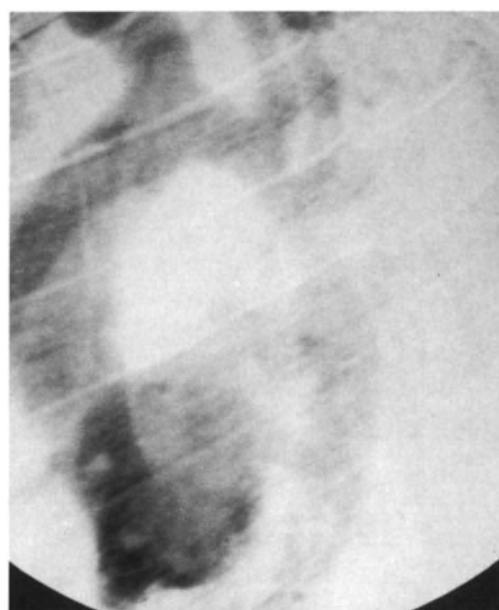


**Fig. 11.21.** This digital subtraction angiogram shows opacification of the aortic arch following peripheral venous injection of contrast medium. The coarctation can be seen but the level of contrast is poor, due to the dilution of contrast in the systemic and pulmonary circulations.

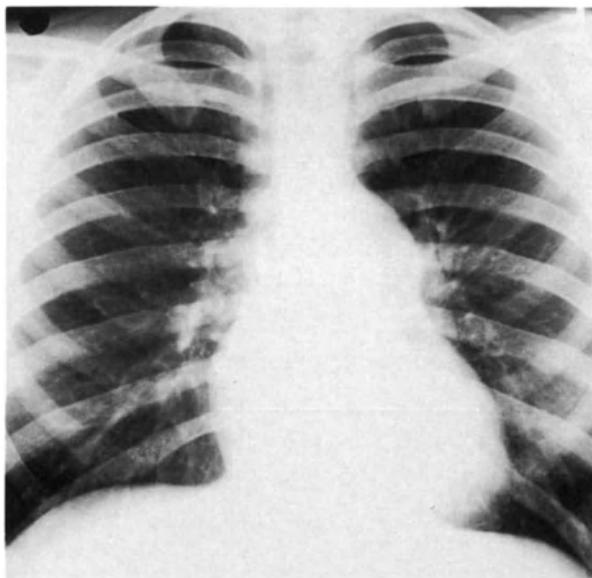


**Fig. 11.22.** Chest radiograph from a patient with pulmonary valve stenosis. The main and left pulmonary arteries are enlarged due to post-stenotic turbulence. The right pulmonary artery is not affected as it is not in direct line with the valve. The pulmonary vessels are slightly less prominent than normal.

Echocardiography will confirm the diagnosis and a Doppler examination with continuous wave techniques can be used to evaluate the valve or infundibular gradient as shown in Fig. 11.23.

Cardiac catheterization and angiography can also demonstrate this condition quite clearly (Fig. 11.24).

Treatment has changed considerably in recent years. Mild forms of pulmonary stenosis (up to a gradient of approximately 40 mmHg) do not normally require surgery. More severe cases have traditionally had pulmonary valvotomy performed surgically but recent interventional techniques

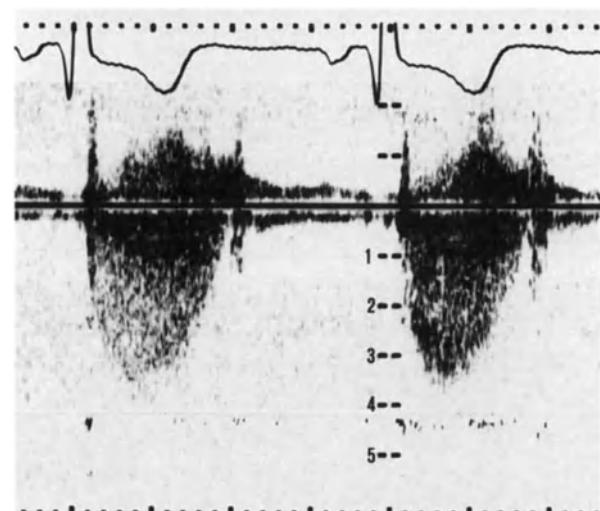


**Fig. 11.23.** Continuous wave Doppler trace obtained from a patient with pulmonary valve stenosis. The examination beam is aligned with flow through the valve. Systolic flow away from the transducer is shown below the line and the peak velocity of the flow is 3.5 m/s. The modified Bernoulli equation ( $\text{pressure gradient} = 4 \times \text{velocity}^2$ ) allows calculation of a peak gradient of 49 mmHg.

have been very successful and in straightforward cases of pulmonary valve stenosis a *balloon dilatation technique* is now the treatment of choice. Excellent results are obtained using this approach.

#### TETRALOGY OF FALLOT

This abnormality is classically composed of four abnormalities which are part of a fundamental malformation of the heart. (1). A large ventricular septal defect is associated with

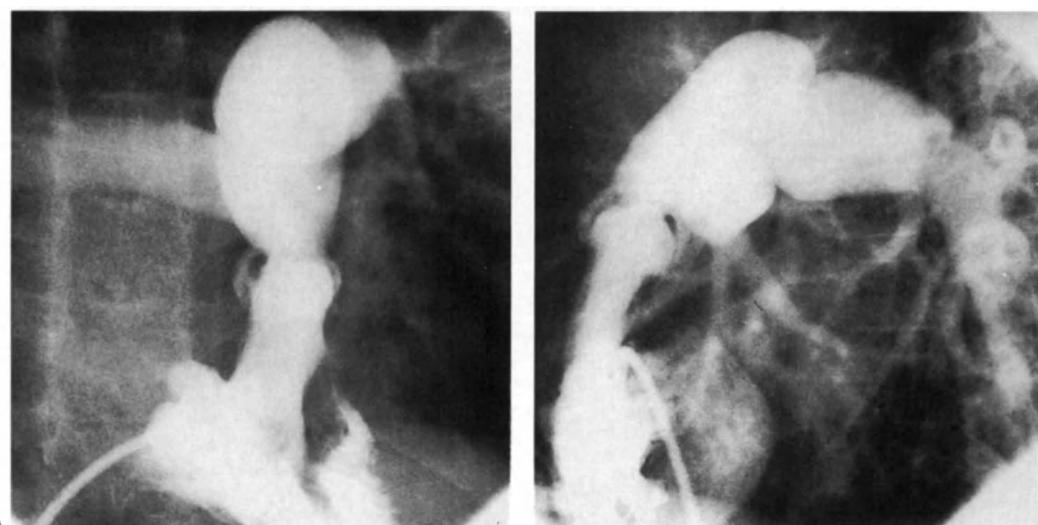


**Fig. 11.24A, B.** Biplane ciné angiogram of a right ventricular injection in a patient with pulmonary valve stenosis. The cranially tilted anterior view (A) and the lateral view (B) both show thickening and doming of the pulmonary valve leaflets and post stenotic dilatation of the main pulmonary artery.

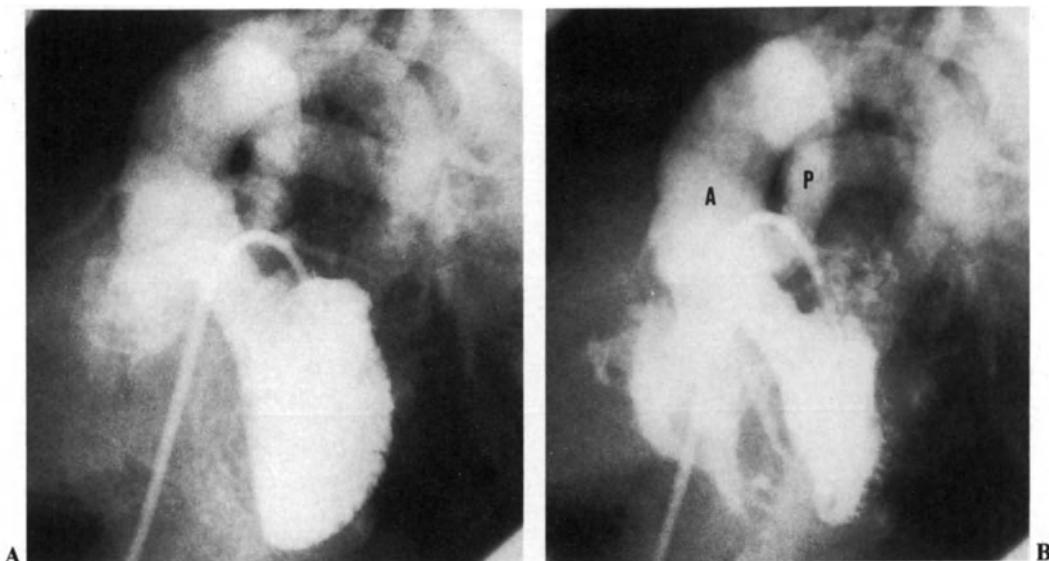


**Fig. 11.25A, B.** Cranially tilted left anterior oblique view of a ciné left ventriculogram in a patient with Tetralogy of Fallot. Early in the run (A) the left ventricle and aorta are opacified and the aortic override is clearly seen. Later in the run the right ventricle is opacified (B), showing its relationship to the aorta. Note the small size of the main pulmonary artery (P) compared to the aorta (A).

some malalignment of the great arteries leading to (2) aortic override through the ventricular septal defect onto the right ventricle (Fig. 11.25). There is (3) associated stenosis of the right ventricular outflow tract (infundibular stenosis) and pulmonary valve which is usually associated with some hypoplasia of the pulmonary annulus and main pulmonary artery. The infundibular stenosis is a dynamic obstruction, being maximal in late systole, as seen in Fig. 11.26 (4). The fourth component of the condition is right ventricular hypertrophy which develops as a response to the pulmonary stenosis (Fig. 11.27).

This abnormality has variable expression depending on the severity of the pulmonary stenosis. In mild cases of pulmonary stenosis the abnormality behaves much like a simple VSD with possible benefit caused by the restriction of blood flow into the lungs. These patients form the acyanotic end of the spectrum. More typically presenting cases are cyanosed because the pulmonary stenosis is sufficiently severe to restrict pulmonary blood flow. The most severe end of the spectrum is represented by the critical pulmonary stenosis or pulmonary atresia with no significant flow into the lungs through the pulmonary annulus. In this

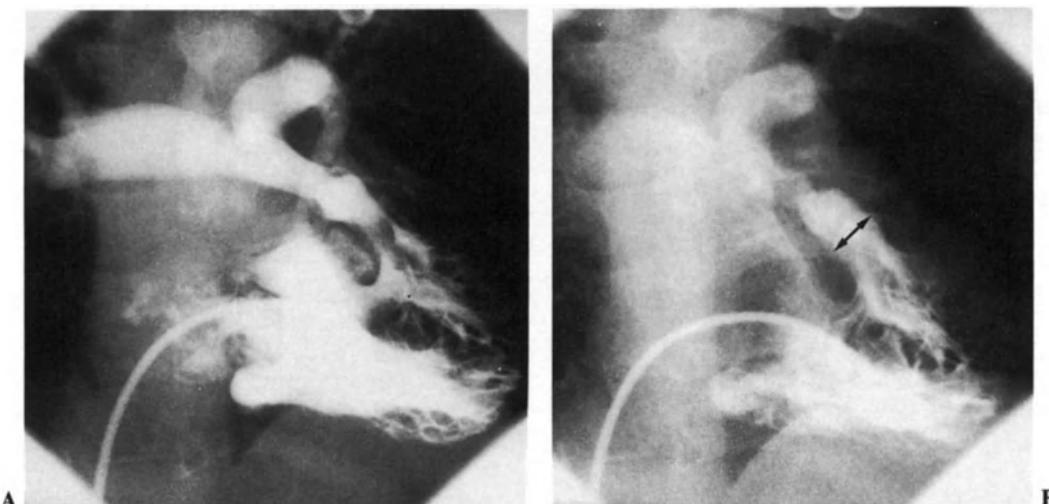


**Fig. 11.26A, B.** Cranially tilted ciné right ventriculogram of a patient with Tetralogy of Fallot. The systolic frame (A) shows the narrowing of the right ventricular outflow tract as well as the right ventricular hypertrophy, and also pulmonary valve stenosis and the hypoplastic main pulmonary artery. The diastolic frame (B) shows the larger diastolic diameter (*arrowed*) of the right ventricular outflow tract (infundibulum).

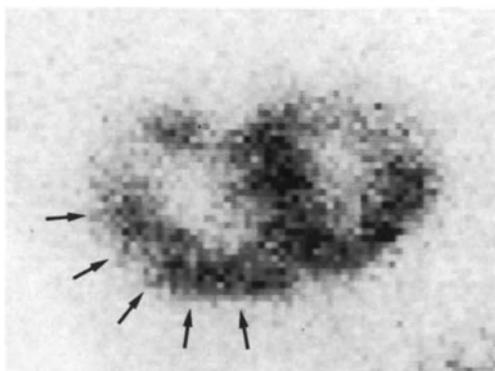


**Fig. 11.27.** Left anterior oblique view of a  $^{201}\text{Thallium}$  scan in an adult with unoperated Tetralogy of Fallot. There is gross hypertrophy of the right ventricle (arrowed). This ventricle takes up very little activity in normals.

situation life must be sustained by alternative flow into the pulmonary vascularity and this occurs by ductal flow or by aortopulmonary collaterals that develop in early life. The severe cases in this spectrum will present shortly after birth with progressive cyanosis as the ductus arteriosus closes. These patients will need urgent palliation by systemic shunting to maintain pulmonary blood flow. The less severe cases will present variably in childhood with cyanosis and fainting spells on exertion, which are usually caused by increasing infundibular obstruction to pulmonary flow with increasing cardiac work.

Approximately 25% of patients with Tetralogy of Fallot or pulmonary atresia and VSD of a similar type have a *right sided aortic arch* (Fig. 11.28). This type of right arch is usually associated with mirror imaging branching (i.e., left brachiocephalic, right common carotid, and right subclavian in order of branching).

The *chest radiograph* may not always be easy to distinguish but in the classical case there will be concavity in the left

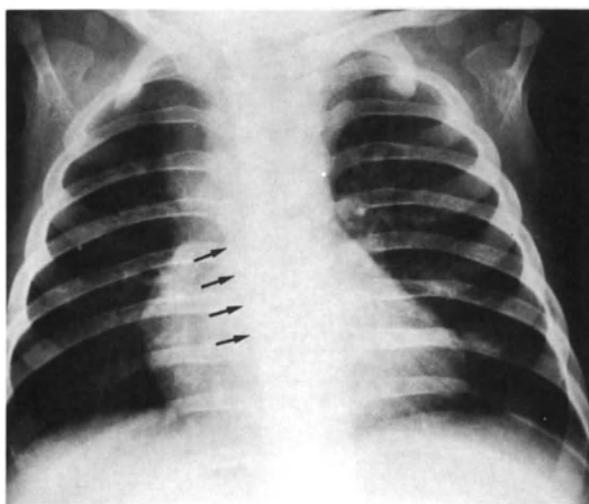


**Fig. 11.28.** Chest radiograph of an infant with Tetralogy of Fallot and a right aortic arch. The aortic knuckle is hard to see but the right sided descending aorta gives the diagnosis (arrow).

heart border in the region of the main pulmonary artery and some upward prominence of the cardiac apex due to the distortion by the large right ventricle. There will also be pulmonary oligemia and in some cases there will be a right sided aortic arch. *Echocardiography* will be useful in diagnosing the condition and Doppler studies can be used to measure the pulmonary gradients.

*Surgical treatment* depends on the severity of the condition but the long-term aim will be total correction by closure of the VSD using an oblique patch and reconstruction of the right ventricular outflow tract. In the latter situation a transannular patch may be incorporated into the repair to widen the outflow. In most cases the pulmonary valve function is destroyed by the reconstruction of the right ventricular outflow tract but the pulmonary regurgitation that follows appears to be of little clinical significance.

*Angiography* is often necessary in these cases to clarify several important details prior to surgery. Pulmonary valve annulus size as well as the size and anatomy of the more distal pulmonary arteries must be determined accurately to facilitate presurgical planning. The surgeon must decide whether to place an outflow patch from the right ventricle across the pulmonary valve annulus to the main pulmonary artery and whether or not the pulmonary arteries themselves need any enlargement or reconstruction. *Coronary anatomy* should be assessed to exclude the recognized association of the left anterior descending artery arising from the right coronary artery and running across the right ventricular outflow tract where the surgeon may place his incision for an outflow patch.

*Post-operative appearances* on the chest radiograph may be characteristic. Not only should the pulmonary oligemia revert to normal but the right ventricular outflow tract and main pulmonary artery may look unusually large due to the presence of an outflow patch. An example of this is shown in Fig. 11.29. In cases with palliation by a Blalock shunt there may be a difference in pulmonary blood flow in the two lungs, particularly if anatomical abnormalities prevent satisfactory central connection between the two pulmonary arteries. The Blalock shunt itself may cause troublesome narrowing of the pulmonary artery into which it is inserted and this can be recognized on angiography (Fig. 11.30).

#### TRANSPOSITION OF THE GREAT ARTERIES (Table 11.2)

The common form of this abnormality is *D-loop transposition* in which the atrial and ventricular anatomy is normal. There is a simple reversal of connection of the great arteries with the aorta arising from the morphologically right ventricle and the pulmonary artery arising from the morphologically left ventricle. The exact orientation of the great arteries is variable but the most common arrangement is with the aortic valve arising from a high anterior position from the right ventricle, and the pulmonary valve arising from the lower position behind the right ventricular outflow tract. The normal arrangement, where the right ventricular outflow tract and main pulmonary artery twists around the left ventricular outflow tract and the aorta, is lost and the two great arteries run upwards parallel from their respective chambers.

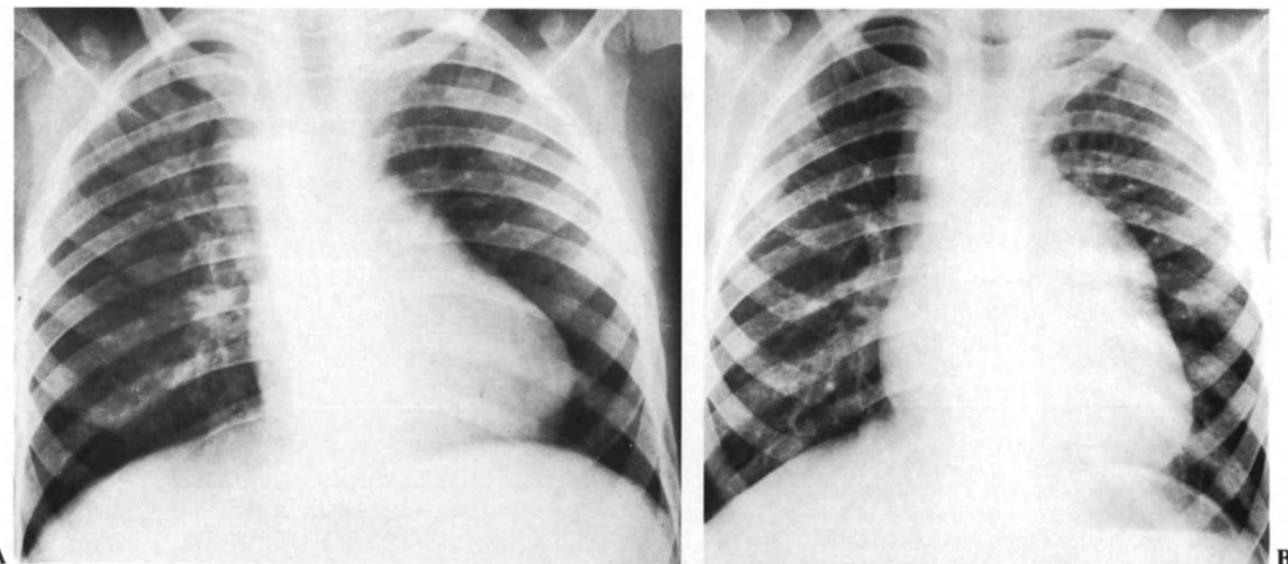


**Fig. 11.29.** A The preoperative film of a patient with Tetralogy of Fallot. As is often the case, 'typical' features are not very apparent. B The post-operative film, after successful surgery, shows a very prominent right ventricular outflow and main pulmonary artery due to the surgical placement of a prosthetic outflow patch.

This leads to the formation of a relatively narrow pedicle which can be recognized on the chest radiograph. This is shown diagrammatically in Fig. 11.31.

These infants usually present in the first few weeks of life with cyanosis and breathlessness. Cyanosis depends on the exact degree of mixing at atrial or ventricular level. Although the condition can be diagnosed simply by *echocardiography*, cardiac catheterization is commonly performed so that the *Rashkind balloon septostomy* can be performed at the same time. This technique is one where an inflated balloon is used

to rupture the thin part of the septum primum covering the foramen ovale in order to improve the atrial mixing and thus allow a higher proportion of oxygenated blood to pass from the left atrium to the right atrium and right ventricle and then to the systemic circulation.

The *chest radiograph* is often characteristic. The heart is slightly enlarged and rounded. The pedicle remains narrow because the main pulmonary artery is behind the aorta but in spite of this there is pulmonary plethora (Fig. 11.32). (The condition may give a similar appearance on the chest radio-

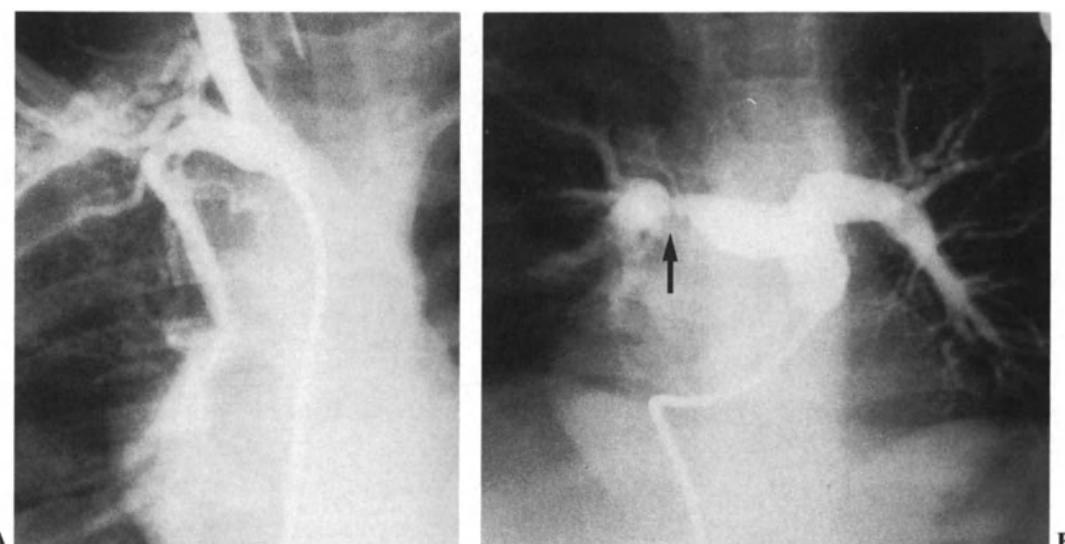


**Fig. 11.30.** A Injection into the right brachiocephalic artery in a patient with Tetralogy of Fallot. A Goretex prosthesis has been inserted to provide additional flow into the right pulmonary artery (modified Blalock shunt). B Pulmonary artery injection in the same patient shows that the surgery to the right pulmonary artery has caused some narrowing of the vessel (arrow).

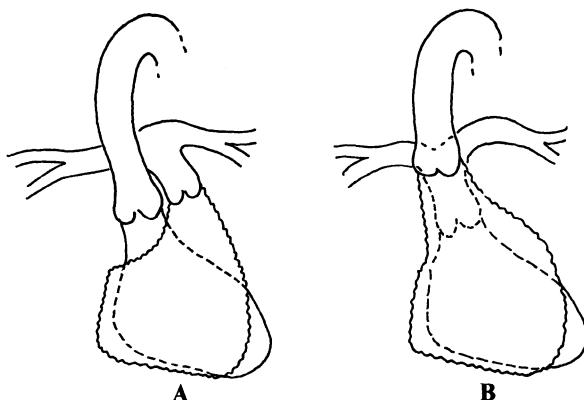


**Fig. 11.31.** A Diagrammatic representation of the typical anatomical relationships in the normal heart and, B, in the usual form of transposition of the great arteries (D-TGA). In both cases the morphological right ventricle (wavy outline) lies anterior to the morphological left ventricle. Normally the main pulmonary artery twists round the left side of the aorta to reach the posterior mediastinum and this forms a wider mediastinum than in D-TGA where the pulmonary artery arises behind the aorta and remains in that position.

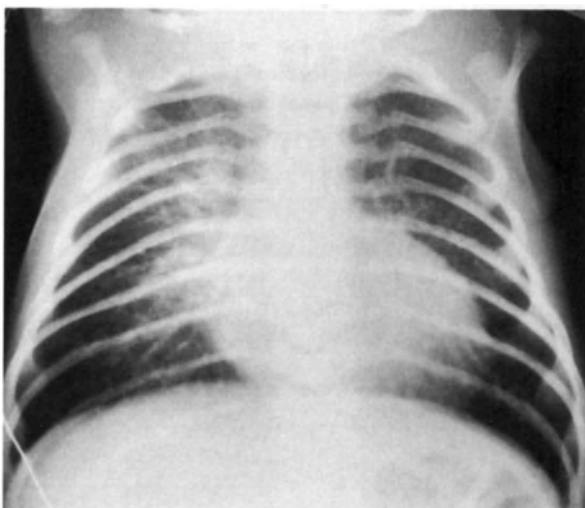


**Fig. 11.32.** Chest radiograph in an infant with D-loop transposition of the great arteries. The heart is slightly enlarged and there is pulmonary plethora but the pedicle (mediastinum) remains narrow.



graph to truncus arteriosus where there is again loss of the normal twisting arrangement of the main pulmonary artery around the aorta.)

*Echocardiographic* diagnosis is also relatively straightforward but care must be taken to correctly identify the two great arteries which usually lie in parallel (Fig. 11.33). Assumptions about which is which can be very misleading as the anatomy is somewhat variable from case to case.

*Angiography* will clearly show the abnormal connections (Fig. 11.34) and will also be useful for clarifying details of

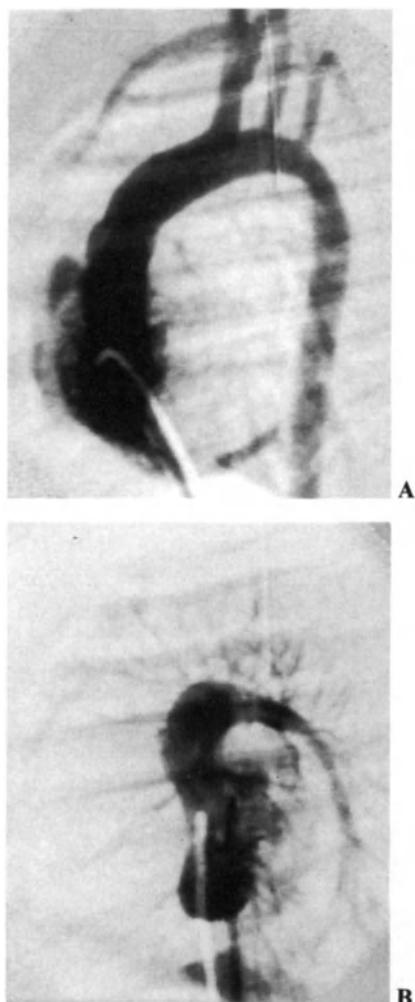


**Fig. 11.34A, B.** Two digital subtraction angiograms taken in the left anterior oblique view in a patient with D-loop transposition of the great arteries. The anteriorly positioned morphologically right ventricle gives rise to the aorta (A). The posteriorly positioned morphologically left ventricle (B) gives rise to the pulmonary artery.

◀ **Fig. 11.33.** Two-dimensional echocardiogram taken from an anterior position in the transverse plane of the chest. The aortic and pulmonary valves are both seen in cross-section. This is not normally possible in a single view and the finding indicates abnormal anatomy, with transposition of the great arteries being a strong possibility. In this case the great arteries are side by side which is a recognized variant of transposition. The definitive diagnosis of transposition requires complete tracing of the connections of both arteries.

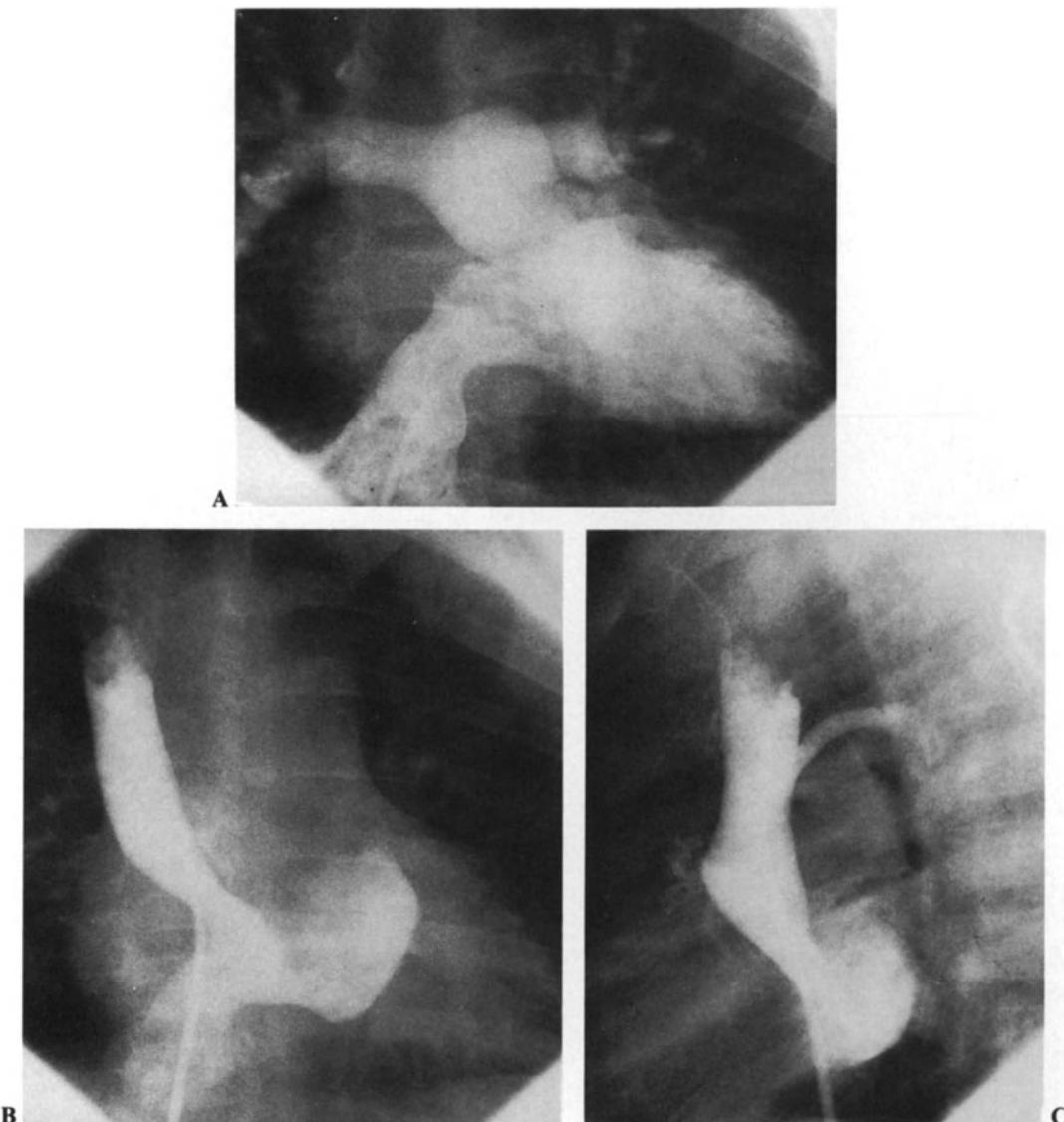


**Fig. 11.35.** A Anterior view of a ciné angiographic injection into the inferior vena cava in a patient with D-loop transposition of the great arteries who has had an atrial baffle correction performed. The inferior vena cava drains into the morphological left ventricle and then to the centrally positioned pulmonary artery. B, C. Biplane ciné angiogram performed in the superior vena cava of a patient with correction of D-loop transposition of the great arteries by an atrial baffle procedure. The newly fashioned 'systemic venous atrium' leads to the mitral valve and morphological left ventricle. The anterior view, B, shows a non-opacified indentation to the right of the 'systemic venous atrium' which is formed by the reconstructed pulmonary venous pathway that leads to the tricuspid valve. The lateral view, C, shows the posteriorly directed systemic venous drainage as well as a little reflux into the azygos vein.

anatomy concerning associated anomalies. It is again important to assess *coronary anatomy* for surgical planning.

Definitive surgical treatment is of two types.

The more traditional approach is to use an *atrial baffle* operation (Mustard or Senning) in which the venous returns are redirected at atrial level so that systemic venous return is directed to the left ventricle and pulmonary artery (Fig. 11.35A, B, C) with pulmonary venous return being directed to the right ventricle and aorta. This operation provides a satisfactory physiological circulation but it leaves the right ventricle performing the systemic pumping function and this can, from time to time, cause problems in later life. There

are also problems with stenosis developing in the surgically formed systemic venous pathways (Fig. 11.36).

The more recent approach has been to use the *great arterial switch operation*. This is complicated by the need to transpose the coronary arteries as well as the great arteries themselves. Early results of this operation have a higher mortality than the atrial baffle approach but it is thought that the longer term outlook may be better. The great arterial switch operation cannot be performed in patients where the morphologically left ventricle has become accustomed to low pressure function and thus the procedure should be performed in the first few weeks of life or later in life in patients with a large

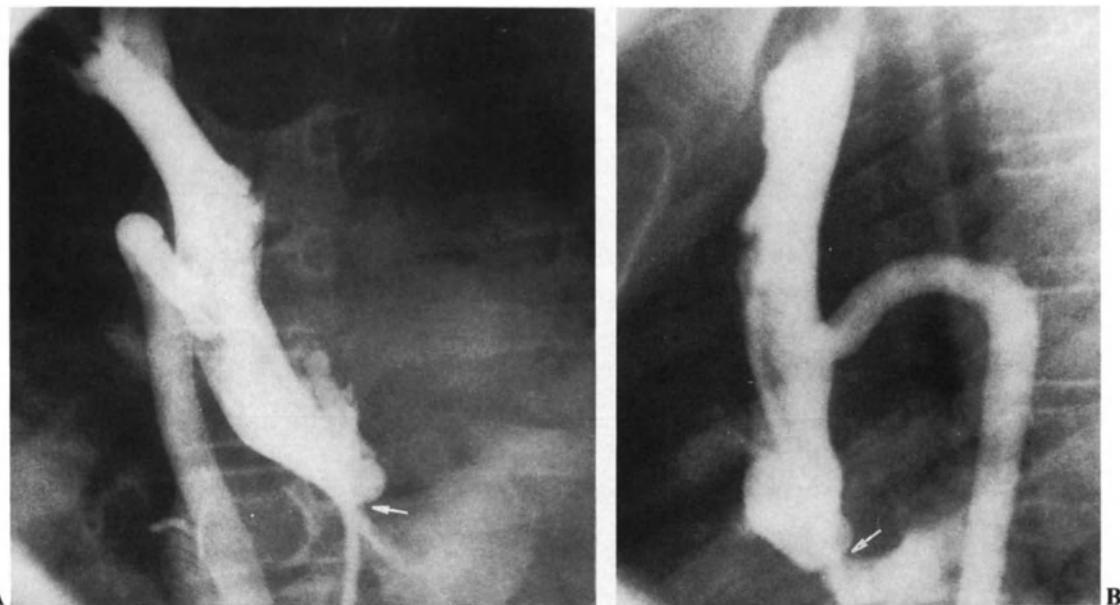


**Fig. 11.36A, B.** This patient with previous atrial baffle repair of D-loop transposition has developed stenosis of the lower end of the superior systemic conduit (arrow). The views are the same as those in Fig. 11.35 B and C. The azygous reflux is a prominent feature.

**Table 11.3. Connections in transposition of the great arteries**

Normal		D-TGA	
		Postatrial baffle	Postarterial switch
RA	LA	RA	RA
↓	↓	↓	↓
RV	LV	RV	RV
↓	↓	↓	↓
PA	AO	AO	AO
		PA	PA

VSD and equalization of the ventricular pressures. These procedures are summarized in Table 11.3.

**Associations.** Transposition of the great arteries is associated with a wide range of other conditions. Important associations are *ventricular septal defect* and *pulmonary or subpulmonary stenosis*. The latter conditions may be of various types such as subpulmonary stenosis (fixed or dynamic obstructions in the left ventricular outflow tract) or pulmonary valve stenosis. These conditions are increasingly important to diagnose because, following the great arterial switch operation, the pulmonary valve will function as the aortic valve.

Many other simple and complex conditions can be associated with transposition of the great arteries.

**L-Transposition of the Great Arteries.** The abnormalities of connection in this condition have been described above but are summarized in Table 11.2 and Fig. 11.37. Patients with this abnormality will usually have symptoms only if there is an associated abnormality. Common associations are ventricular septal defect and conduction abnormalities. The

chest radiograph may show a characteristic long curve to the left heart border but this is not reliable in all cases as the positions of the great arteries are somewhat variable. Fig. 11.38 shows a well developed example of this feature. A significant proportion of these patients have chest radiographs indistinguishable from normal.

#### ANOMALOUS PULMONARY VENOUS DRAINAGE

This abnormality of cardiac connection can take various forms.

*Partial anomalous pulmonary venous drainage* can occur when one or more individual pulmonary veins drain to the right side of the atrial septum, either into the right atrium itself or into the superior or inferior vena cavae. This abnormality is commonly associated with atrial septal defect and it is important to check pulmonary venous connections when performing echocardiographic or angiographic examination. The anomalous veins can often be redirected correctly at surgery providing the surgeon is aware of the problem.

*Total anomalous pulmonary venous drainage (TAPVD)* is a more serious condition and can take three forms, supracardiac, cardiac or infracardiac as shown diagrammatically in Fig. 11.39. In all three types the major pulmonary veins come to a confluence behind the left atrium but do not communicate directly with it.

In the case of *supracardiac TAPVD* there is a large ascending vein on the left side which is a remnant of the embryological left superior vena cava. This connects into the left brachiocephalic vein and then passes down the right sided superior vena cava into the right atrium.

The *cardiac type* of abnormality drains into the right side of the heart, usually via the enlarged coronary sinus.

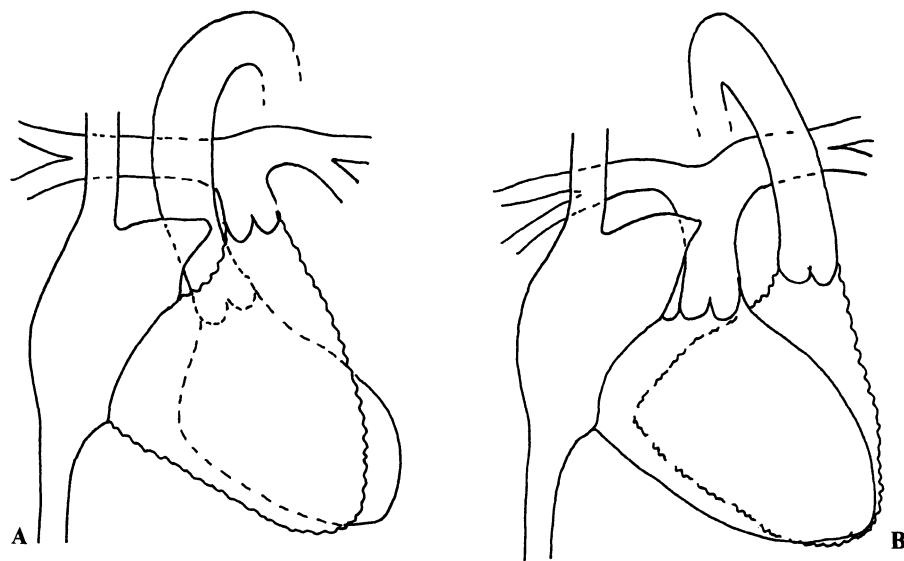


**Fig. 11.37A, B.** Diagrammatic representation of the anatomy in a normal heart and in L-loop transposition of the great arteries ('corrected transposition'). In the normal heart (A) the morphological right ventricle (wavy margin) lies anterior to the left ventricle and receives blood from the morphological right atrium. In L-transposition (B) the morphological right ventricle lies posterior and to the left of the morphological left ventricle which is anterior and right sided. The left ventricle receives blood from the morphological right atrium. Transposition of the great arteries in this situation means that the circulation has been 'physiologically corrected' but the anatomical relationships are all highly abnormal.

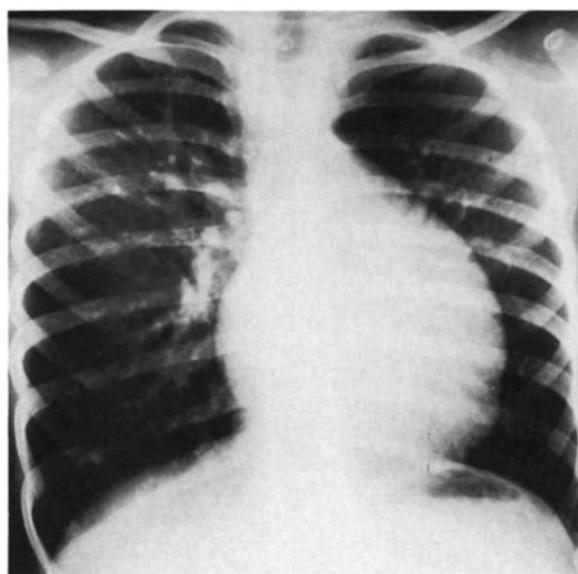


**Fig. 11.38.** Chest radiograph from a patient with L-loop transposition of the great arteries ('corrected transposition'). The left heart border has a long rounded curve formed by the abnormally positioned aorta. In some patients with this condition this feature is not obvious and the appearances may be indistinguishable from normal.

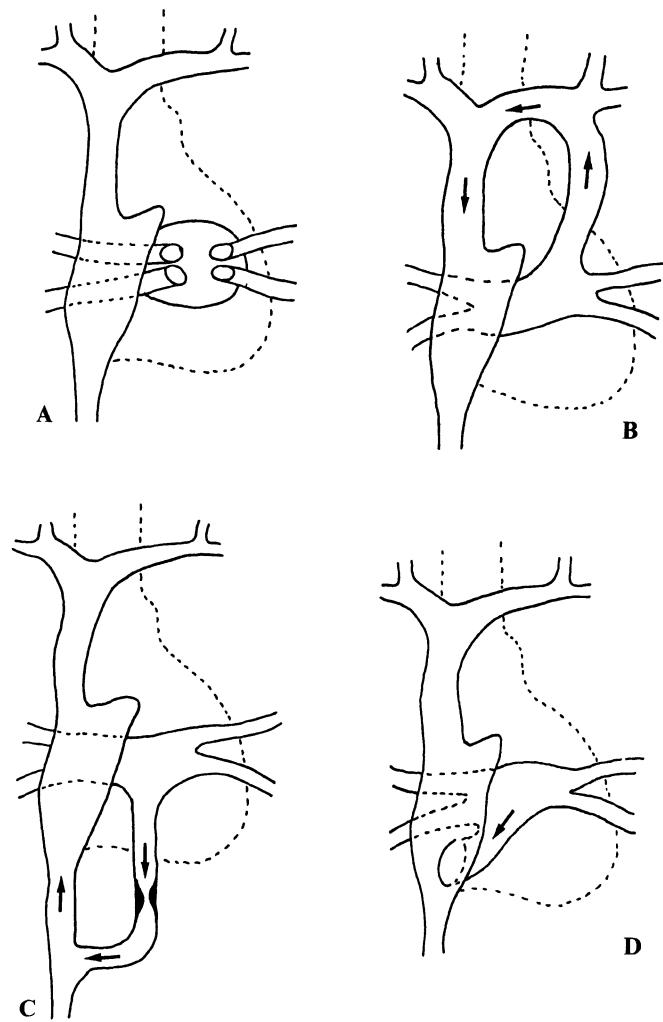


**Fig. 11.39.** A Diagrammatic illustration of normal pulmonary venous drainage and the three forms of totally anomalous pulmonary venous drainage (TAPVD). In supracardiac TAPVD, B, the pulmonary venous confluence drains into an ascending left-sided vein which then drains to the left brachiocephalic vein. In infracardiac TAPVD, C, the drainage is through a common descending vein leading through the diaphragm. There is commonly some obstruction in this route of drainage. The pulmonary venous confluence in the cardiac type of TAPVD, D, leads directly to the heart, usually via a dilated coronary sinus.

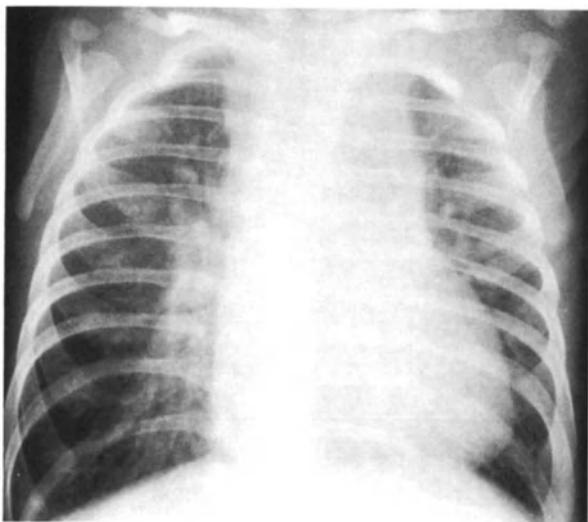


**Fig. 11.40.** The chest radiograph in this infant shows cardiomegaly with pulmonary plethora and a wide upper mediastinum. This is consistent with the known diagnosis of supracardiac totally anomalous pulmonary venous drainage but the classically described 'cottage loaf' heart is rare at this age of presentation.

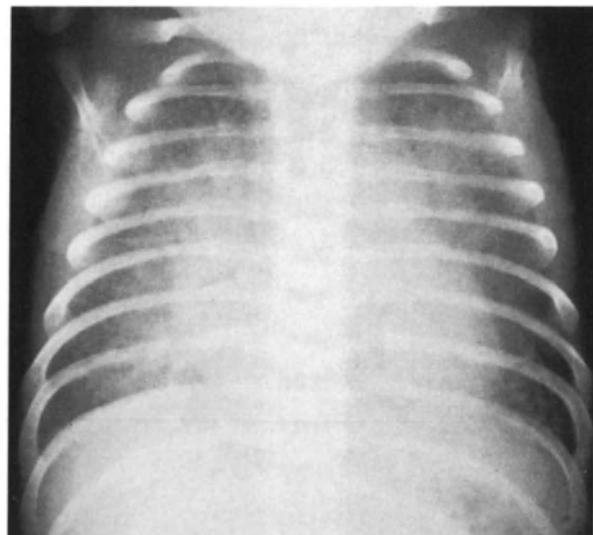


**Fig. 11.41.** The chest radiograph in this infant shows mild cardiomegaly with widespread diffuse interstitial edema. This is consistent with the known diagnosis of infradiaphragmatic totally anomalous pulmonary venous drainage with obstruction. Respiratory disease should also be considered in a patient with this type of diffuse pulmonary opacity.

In the case of *infracardiac TAPVD* the confluence of pulmonary veins drains downwards in a descending vein which passes through the diaphragm, often obstructed at this point, into either the portal venous system or the inferior vena cava. The portal venous system is usually at a higher pressure than other venous systems and this fact may also contribute to the 'obstruction' in this condition. The pulmonary venous blood then returns to the right atrium through the inferior vena cava.

In all of these conditions there is total cardiac mixing at right atrial level and the patient remains partially cyanosed.

The chest radiograph in the case of supracardiac or cardiac TAPVD shows that the heart is enlarged and there is pulmonary plethora which is obligatory, due to the need for a higher pulmonary flow in the mixed circulation. The supracardiac TAPVD will often show a wide mediastinum due to the left sided ascending vein, and in long established cases the classical *cottage loaf* heart will be evident. This will be a less well defined feature (Fig. 11.40) because these cases are now diagnosed and treated in infancy. The infracardiac type of abnormal drainage will often be associated with less cardiac enlargement and the obstruction of the pulmonary circulation will lead to interstitial edema and heart failure (Fig. 11.41). The findings of a normal or slightly enlarged heart size with severe heart failure is one that will usually signal infracardiac TAPVD.

*Echocardiography* will diagnose these conditions, the abnormal venous confluence being visible behind the left atrium. The abnormal course of drainage can usually be traced. The left atrium is usually small and there is right to left flow across the atrial septal communication.

*Angiography* will also show these features (Fig. 11.42) but is ideally avoided if the echocardiogram is adequate. Infants presenting with this condition are often quite ill and the morbidity of catheterization and angiography is significant.

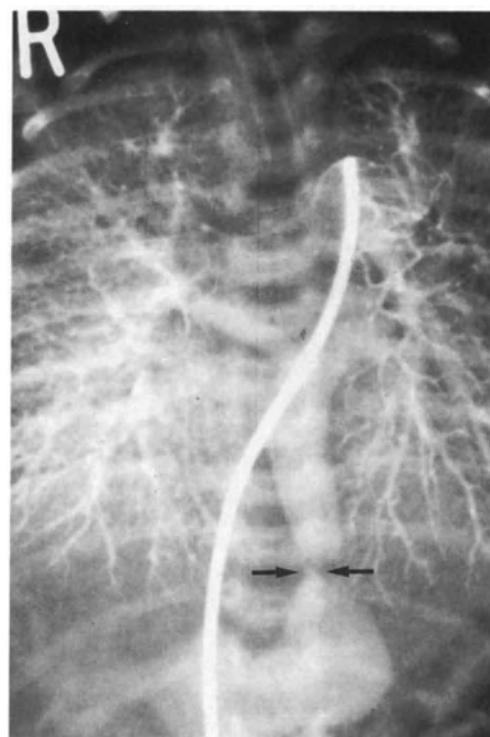


**Fig. 11.42.** The venous phase of a pulmonary arteriogram in a patient with infradiaphragmatic totally anomalous pulmonary venous drainage shows the pulmonary venous confluence draining into a descending vein that drains through a narrow point at the level of the diaphragm (arrow) and thence to a large abdominal vein.



**Fig. 11.43.** Anterior view of an angiogram with contrast medium injected into a left sided superior vena cava which drains into the coronary sinus and right atrium.

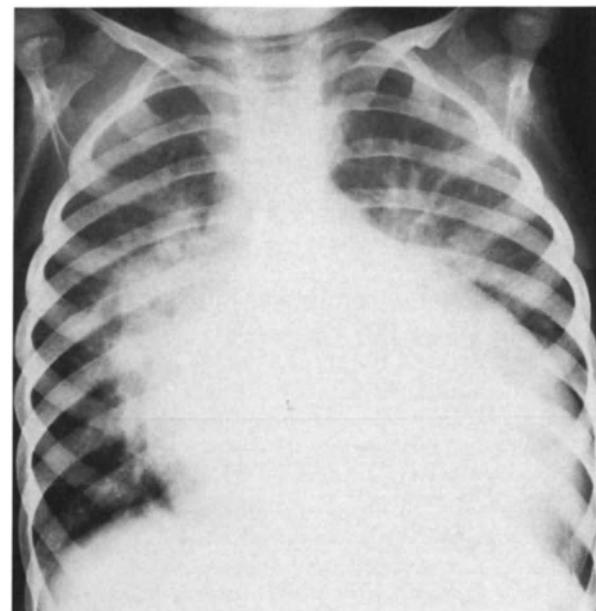


**Fig. 11.44.** Chest radiograph of an infant with a severe form of dilated cardiomyopathy. The heart is markedly enlarged and there is evidence of pulmonary edema due to heart failure.

*Surgery* is directed towards re-anastomosing the pulmonary venous confluence with the left atrium, dividing the abnormal connection and closing the atrial septal defect that is present. In spite of its apparent straightforward nature, the operation carries a high mortality.

#### BILATERAL SUPERIOR VENA CAVA

This abnormality of systemic venous drainage is quite common, being present in about 10% of patients with congenital heart disease. The left superior vena cava usually drains into the *coronary sinus* as seen in Fig. 11.43. It is not usually of clinical importance but is surgically important as the venous connections need to be correctly placed in instituting cardio-pulmonary bypass.

#### ARTERIOVENOUS MALFORMATIONS (SYSTEMIC AND PULMONARY)

*Systemic arteriovenous malformations* may cause local problems but can also produce high output cardiac failure. A shunt through an aneurysmal vein of Galen (see Chap. 41) is a possibility that must always be remembered when considering heart failure of unknown cause in infancy. An intracranial bruit is often a key sign and a left ventricular or aortic injection must be followed to the skull to exclude this condition if it is being seriously considered.

*Pulmonary arteriovenous malformations* can sometimes be obvious on the chest radiograph but this is not always the case as they may be obscured by other structures or they

may be of the complex (plexiform) type with no large vessel or aneurysm being present. These abnormalities can produce profound central cyanosis and they require *angiography* for definitive diagnosis.

In many situations, both systemic or pulmonary arteriovenous malformations are amenable to closure by trans-catheter embolization, but frequently surgical treatment is necessary.

#### CONGENITAL CARDIOMYOPATHY

Dilated cardiomyopathies occur occasionally in infancy and may be related to intrauterine infections, to inherited factors or may be secondary to valvular or coronary anomalies. The etiology of the conditions is often hard to determine. The *chest radiograph* will show a large heart with pulmonary signs of cardiac failure (Fig. 11.44) and other imaging modalities will be capable of demonstrating the poor ventricular function.

Hypertrophic cardiomyopathy with left ventricular outflow obstruction occasionally occurs in infants and children.

#### CONGENITAL CORONARY ANOMALIES

There are many variants of coronary anatomy and most cause no problems. The most common variant is the '*left dominant*' system in which the posterior descending artery arises from the circumflex artery rather than the right coronary artery. Numerous other variants in vessel course have been documented. There is one anomalous course with theoretical clinical consequences, namely the left coronary

artery which runs between the aorta and main pulmonary artery where it may be compressed.

Clinically important abnormalities include anomalous origin of one or both coronary arteries from the pulmonary artery. This clearly leads to desaturated coronary perfusion and can cause myocardial ischemia, myocardial infarction or sudden death in infancy. Surviving infants can have marked cardiomegaly due to severe ischemic cardiomyopathy.

*Coronary fistulae* to cardiac chambers or the pulmonary artery occur occasionally and often present asymptomatically with a continuous murmur. Drainage to the right side of the heart occurs in 90% of cases, most often from the right coronary artery, and function as a *left to right shunt*. The shunt itself is often less of a worry than the other potential complications such as *coronary ischemia* ('steal' phenomenon) or *endocarditis*. The fistulous communications can dilate to aneurysmal proportions with the development of unusually positioned bumps on the heart border, seen on chest radiography. The aneurysmal fistulae can theoretically rupture but this has rarely been reported.

These lesions may be diagnosed or suspected on *ultrasound* examination but *angiography* is essential for precise evaluation. The communications are commonly closed surgically to prevent complications but more recently interventional occlusion techniques have been employed to close them.

*Kawasaki's disease* is not a congenital abnormality but will be considered in this section as it mainly affects children. The disease is probably infective in origin and has systemic features which give it the alternative name of '*mucocutaneous lymph node syndrome*'. The condition arises in young children and a relatively mild illness may be followed by the development of *aneurysmal dilatation of the proximal coronary arteries*. These can often be seen on echocardiography. There is no indication for angiography because there is no specific therapy for the coronary abnormalities apart from general medical measures and observation. The coronary dilatations can resolve in many cases.

#### DOUBLE (TWO A-V VALVES) OR COMMON (SINGLE A-V VALVE) INLET VENTRICLE

There are many complex variants in this category and they must all be carefully assessed on their individual merits, but the condition is one commonly referred to as '*single ventricle*'. Multiple abnormalities are common and nothing must be taken for granted in the assessment of the cases. There is no 'typical' chest radiograph but the heart is often enlarged with the pulmonary vascularity depending on the presence of other abnormalities such as pulmonary stenosis. The inflow to a ventricular chamber usually determines its chamber size so there is usually one large functional chamber and a second chamber which often acts, with a ventricular septal defect, as an outlet chamber. *Angiography* and *ultrasound* must be used as appropriate for the circumstances.

#### DOUBLE OUTLET VENTRICLE

Double outlet right ventricle is the most usual occurrence in this category. Once again the case must be assessed on

individual merits but accurate anatomical assessment is vital. Corrective surgery is often possible but this depends on detailed knowledge of the intracardiac anatomy. There are usually two well developed ventricles with a ventricular septal defect and so the positions of the great arteries and the septal defect must all be accurately determined.

A double outlet right ventricle with a large subaortic ventricular septal defect can be corrected by closing the ventricular septal defect with an oblique patch, allowing the left ventricle to empty to the aorta. If the ventricular septal defect is subpulmonary, a similar operation will produce 'transposed great arteries' which might then have to be corrected with an atrial baffle procedure.

#### EBSTEIN'S ANOMALY

This condition is an anomaly of the tricuspid valve. It has often been described as a displacement of the tricuspid valve towards the apex of the right ventricle which produces a larger right atrium and a smaller right ventricle. This is, in effect, what is present although the more precise descriptions of cardiac morphologists are of a condition in which the tricuspid annulus is normally positioned and the valve leaflets are larger and more redundant than normal, being adherent to the right ventricular walls, particularly the septum, for some distance into the ventricular cavity (Fig. 11.45).

The result of this anomaly is a larger than normal right atrium (the so-called 'atrialized' portion of the right ventricle) and a relatively small right ventricle. The function of the tricuspid valve itself is variable, sometimes being normal, occasionally being stenotic and often showing significant regurgitation. The clinical presentation is very wide and is dependent on the tricuspid valve function. Severe cases present in infancy with right heart failure and poor forward flow to the pulmonary artery. The chest radiograph in these cases may show massive cardiomegaly (one of the few causes of 'wall to wall' heart in infancy). The mildest expression occurs in those adults who present with mild signs or symptoms and a virtually normal chest radiograph.

*Ultrasound* studies show the abnormal tricuspid valve as a very prominent feature and many of the functional aspects can be derived from Doppler studies. The need for catheterization depends on the clinical severity and the quality of the echocardiogram.

#### MITRAL VALVE ABNORMALITIES (INCLUDING SUPRAMITRAL RING AND COR TRIATRIATUM)

Obstructive lesions in or near the mitral valve include *congenital mitral stenosis*, *supramitral ring* and *cor triatriatum*. The first resembles rheumatic stenosis with fusion of the valve leaflets and doming of the valve. A supramitral ring is an obstructive diaphragm lying very close to the mitral valve on the left atrial side. Cor triatriatum is a condition in which there is an obstructive membrane in the left atrium which divides it into a high and a low pressure portion.

All these have characteristic appearances on *ultrasound* and the degree of obstruction can often be assessed using *Doppler ultrasound*.

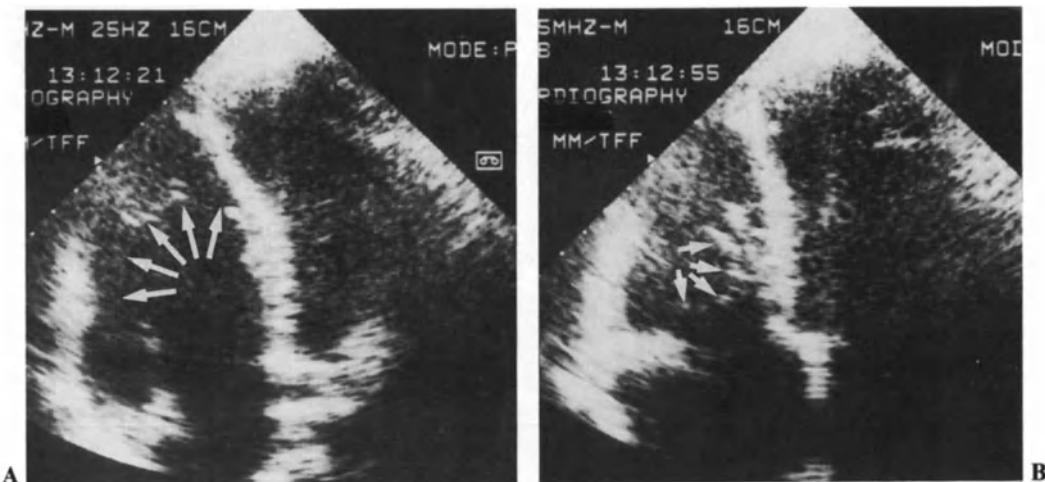


**Fig. 11.45A, B.** Two-dimensional echocardiogram showing the apical four chamber view in a patient with Ebstein's anomaly. The diastolic image, A, shows the abnormally large tricuspid valve displaced into the right ventricular cavity (arrow). In systole, B, the closed leaflets (arrow) lie close to the interventricular septum and are probably partially adherent to it.

The *chest radiograph* is similar in all cases, showing a normal sized heart with increased pulmonary vessel size due to pulmonary venous hypertension similar to that seen in the obstructed form of totally anomalous pulmonary venous drainage. There will often be pulmonary edema also.

Mitral regurgitation can form a part of a complex abnormality such as atrioventricular septal defect but can also occur alone. In the latter case there may be abnormal papillary muscle formation such as a single papillary muscle giving a 'parachute' mitral valve.

The *chest radiograph* will show signs of pulmonary venous hypertension but the heart will be larger than with obstructive mitral lesions due to the ventricular volume overload.

#### PULMONARY ATRESIA (WITH OR WITHOUT VENTRICULAR SEPTAL DEFECT)

Pulmonary atresia without a ventricular septal defect is a quite different condition to that with a ventricular septal defect. The condition should first be considered in the presence of a ventricular septal defect.

**With Ventricular Septal Defect.** In these circumstances the anomaly is essentially the same as a very severe form of Tetralogy of Fallot. The obstructed outflow of the right ventricle together with the usual override of the aorta means that the right ventricle can empty into the aorta although it must do this at the same systemic pressure as the left ventricle. Flow thus continues through the right ventricle and the chamber remains large and its walls become hypertrophied due to the systemic pressure in the chamber. The pulmonary arteries are often very small and they receive their blood supply from the patent ductus arteriosus initially and then subsequently through aortopulmonary collateral vessels of various sorts.

The *chest radiograph* shows a slightly enlarged heart, often with a slightly upturned apex due to the right ventricle being large; the pulmonary bay is small and the lung fields are oligemic. There is a right aortic arch in about 25% of cases. In older patients the multiplicity of complex aortopulmonary collaterals can give a complex vascular pattern, particularly near the hilar regions and this can sometimes be mistaken for pulmonary plethora (Fig. 11.46). Palliation with various types of shunt is often required in early life (as shown in Fig. 11.47).

*Angiography* is more often required in the diagnosis of this condition because successful definitive surgery depends on careful planning of a reconstructed outflow from the right

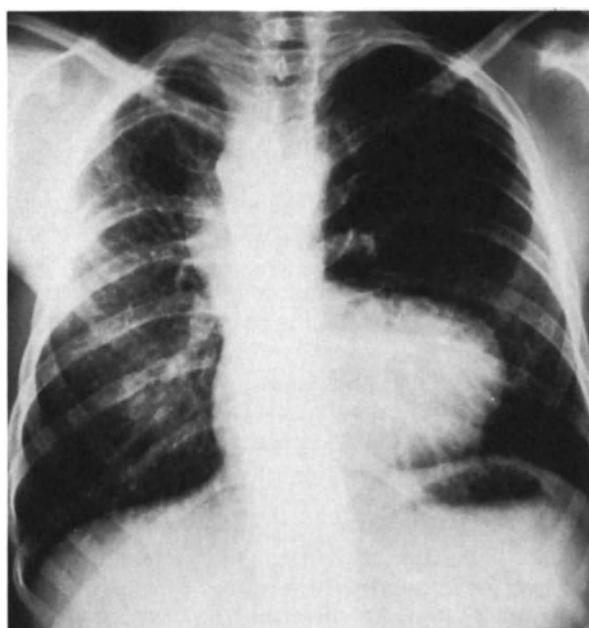


**Fig. 11.46.** Chest radiograph of an adult with pulmonary atresia and a ventricular septal defect. Note the upturned cardiac apex, the hollow pulmonary bay and the right aortic arch. The pulmonary vasculature is oligemic, but less so on the right due to a previous right-sided Blalock shunt.



**Fig. 11.47.** Digital subtraction angiogram from a patient with pulmonary atresia. The frontal view of an aortic injection shows filling of the left and right pulmonary arteries via a left sided shunt from the left subclavian artery.

ventricle to the pulmonary arteries which themselves often need reconstruction. It is usually not possible to determine all the details of the anatomy of the hypoplastic pulmonary arteries and the collaterals using *echocardiography*.

**Without Ventricular Septal Defect.** In this situation there is no outlet for the right ventricle and thus no way that it can decompress. The cavity is thus usually very small but often generates very high pressures (suprasystemic), especially if there is a small but functionally competent tricuspid

valve. Under these circumstances an unusual problem of abnormal coronary communications can occur. Blood may shunt from right to left through abnormal coronary communications and cause myocardial ischemia.

The *chest radiograph* will show a small pulmonary segment and pulmonary oligemia but the cardiac contour will show a more left ventricular contour, often similar to that seen in tricuspid atresia.

Palliative shunting may be needed in early life but a successful surgical correction is dependent on the degree of underdevelopment of the right ventricular cavity. If this is extreme then the condition must be considered as a form of 'single ventricle' but if there is some reasonable size to the right ventricular cavity a full correction might be possible although this is often a high risk procedure. Patients with very severe pulmonary valve stenosis are considered in a similar way.

Imaging techniques in this condition are, as well as other aspects, of particular importance in judging the size and function of the right ventricle.

#### SINUS OF VALSALVA ANEURYSM

In this condition there is enlargement of one of the sinuses of Valsalva in the aortic root, commonly the right sinus. This may rupture into the right ventricle with the consequent production of a *left to right shunt*. There will be continuous flow from the higher pressure aorta to the right ventricle and the murmur may be mistaken for a patent ductus arteriosus, a coronary fistula or the recognized association of ventricular septal defect with aortic regurgitation.

The *chest radiograph* may show typical features of a left to right shunt but the aneurysm itself is rarely visible on the cardiac contour. *Echocardiography*, particularly with color flow Doppler mapping will show the defect well, as will *angiography* of an aortic root injection.

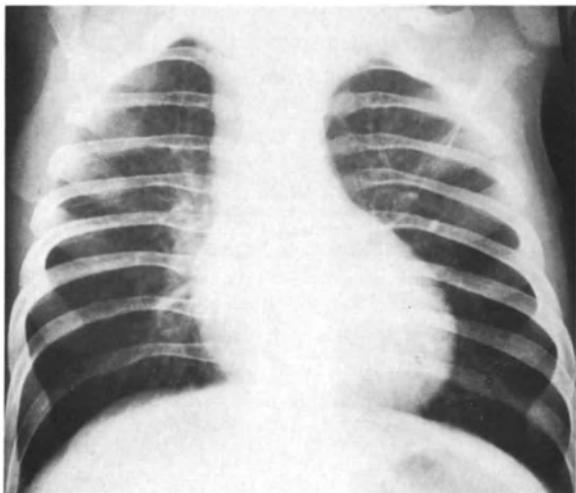


**Fig. 11.48.** Chest radiograph of a patient with tricuspid atresia showing a rounded left ventricular contour with a hollow pulmonary bay and pulmonary oligemia. The diagnosis can be suspected from these appearances but the chest radiograph will not always give a definitive diagnosis.

#### TRICUSPID ATRESIA

In this condition there is obligatory flow of the systemic venous return across an atrial septal defect to the left atrium and the left ventricle. Some blood then crosses a ventricular septal defect (VSD) to reach the right ventricle and the pulmonary artery. The VSD is often restrictive (small size with a pressure drop across it) and there may be associated pulmonary stenosis. Thus there is often relatively low pulmonary blood flow although this is not invariable, the condition having a variety of expressions. The left ventricle is thus usually large and the right ventricle is correspondingly small.

The *chest radiograph* sometimes (but not always) shows pulmonary oligemia, a small pulmonary bay and a moderately large heart with a rounded contour due to the downward and leftward enlargement of the left ventricle as seen in Fig. 11.48. MRI can be helpful in assessment before and after surgery (Fig. 11.49). The right ventricle is often so underdeveloped that the condition can frequently be considered as one of the loosely described 'single ventricle' group.

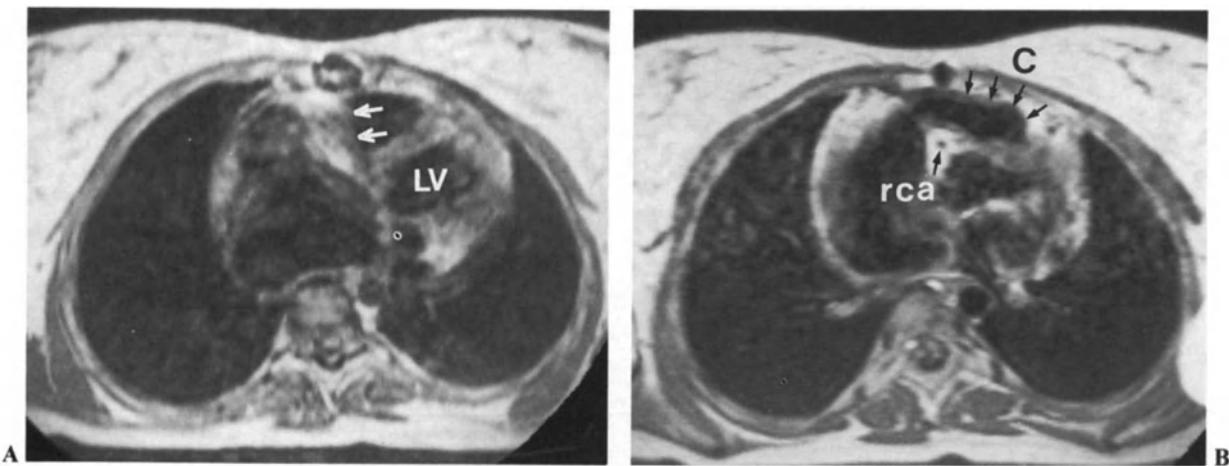


**Fig. 11.49.** A Transverse MRI section of the thorax of a young adult with tricuspid atresia. The spin-echo sequence is gated and shows good resolution. The thick tissue in the expected position of the tricuspid valve is arrowed. B A more cephalic section in the same patient as shown in A. The patient has had a Fontan procedure with a conduit (arrow) placed anteriorly between right atrium and pulmonary artery. The anterior position of the conduit is shown by the relative position of the right coronary artery (rca).

#### TRUNCUS ARTERIOSUS

In this condition a single great artery arises from the heart, because of a failure of division of the embryonic common truncus arteriosus. The common truncus arises almost always from above a large ventricular septal defect. The pattern of division of the common truncus is variable as shown diagrammatically in Fig. 11.50. A single common pulmonary artery may arise from the common truncus before it divides into left and right pulmonary arteries. In some cases the left and right pulmonary arteries arise independently from the main truncus. Various intermediate forms have also been classified.

In all cases there is common mixing across the ventricular septal defect and the flow in the pulmonary arteries is very

large because it originates directly from the common truncus which is at systemic pressure. In most cases the main pulmonary does not develop fully in its usual position and so the *chest radiograph* shows marked pulmonary plethora with a relatively narrow mediastinal shadow (as in transposition of the great vessels). There is also an increased incidence of right sided aortic arch with truncus arteriosus (Fig. 11.51). In many patients the heart is moderately enlarged and there may be cardiac failure.

*Echocardiographic* diagnosis is relatively straightforward, and this is helpful as it is difficult to perform good angiography on these patients due to the very fast blood flow through the heart with subsequent contrast dilution. The patients are often very ill and *catheterization* with *angiography* produces significant morbidity.

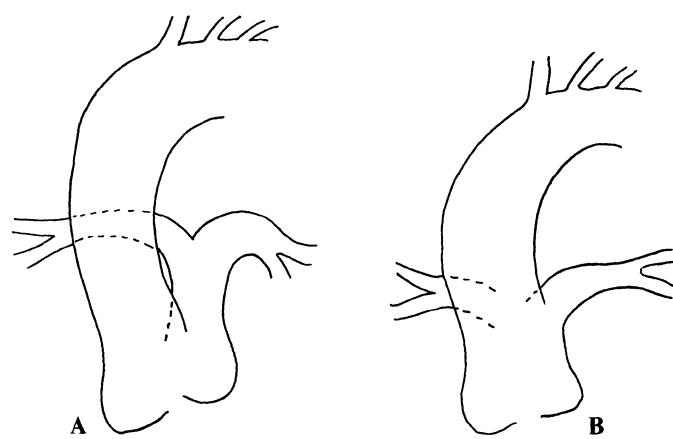


**Fig. 11.50A, B.** Diagrammatic illustration of the two main types of persistent truncus arteriosus. In the commoner type, A, there is a recognizable main pulmonary artery arising from the common trunk. In the other type, B, the two pulmonary arteries arise separately from the common trunk, causing more problems for surgical reconstruction. Intermediate varieties are also seen.

#### GREAT ARTERIAL ANOMALIES (INCLUDING VASCULAR RINGS)

The commonest major variation in the aortic arch and its branching is the *anomalous right subclavian artery* occurring with a normal left-sided arch. This vessel is the last brachiocephalic branch of the aorta, arising from the descending portion of the arch. The anomaly causes inconvenience for surgeons and those performing right brachial artery catheterization but it does not normally produce symptoms. The vessel runs obliquely behind the esophagus and its indentation can usually be recognized on the barium swallow.

There are two common forms of *right-sided aortic arch*. The first is the so-called mirror image type with the brachiocephalic branches being the mirror image of normal. This type is the most usual form of right arch to be found in association with the various types of cyanotic heart disease (25% incidence in Tetralogy of Fallot and pulmonary atresia). The second form of right arch is that with an *anomalous origin*

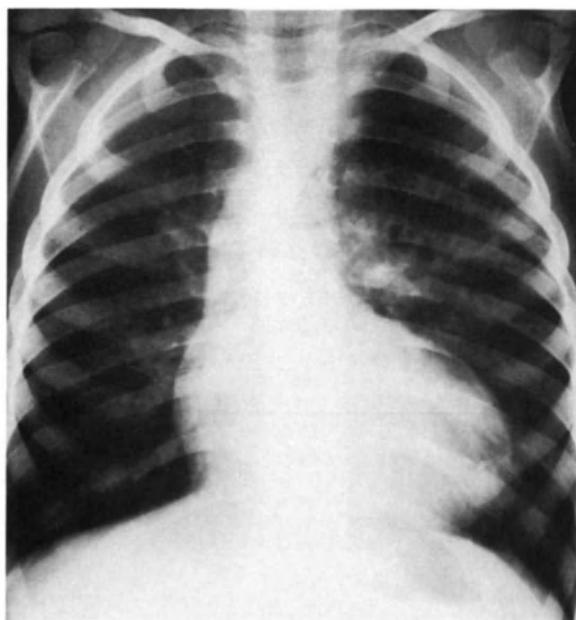


**Fig. 11.51.** Chest radiograph of a patient with persistence of the common truncus arteriosus. Note the rounded shape of the heart and the relatively narrow pedicle, exaggerated by a right aortic arch. The condition has been palliated by banding of the trunk which reduces the expected pulmonary plethora.

of the left subclavian artery. This is almost the mirror image of the anomalous right subclavian type but the anomalous vessel often arises from a prominent *diverticulum* which can make a prominent indentation in the posterior part of the esophagus. This type is the most likely to be found as an isolated anomaly (approximately 0.1% of the population). The above variations are shown in Fig. 11.52.

*Double aortic arch* is more serious as it can form a vascular ring that compresses the trachea or major bronchi and causes stridor in infancy. It can be diagnosed by *chest radiograph*, barium swallow, MRI and echocardiography, but *angiography* is usually essential for definitive confirmation.

*Anomalous origin of the left pulmonary artery (pulmonary artery sling)* is another important cause of stridor in infancy.

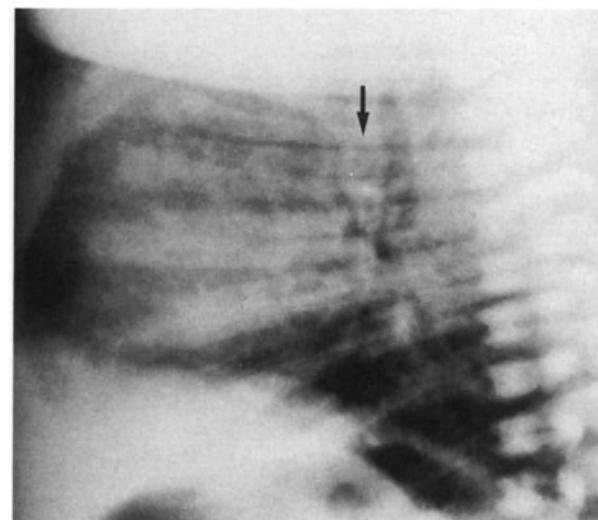
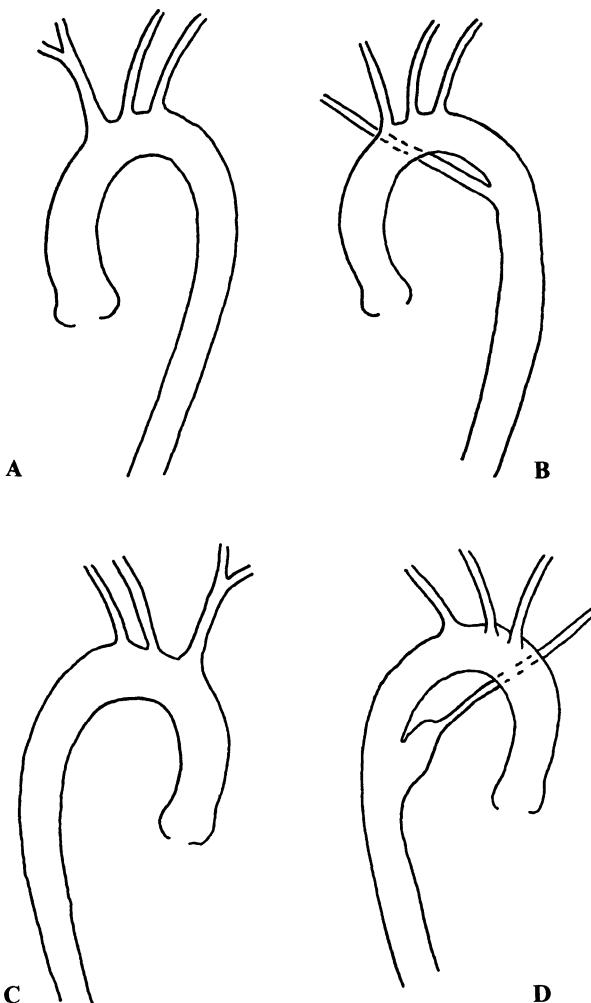


**Fig. 11.53.** Lateral chest radiograph of an infant with an anomalous origin of the left pulmonary artery from the right pulmonary artery, the so-called pulmonary artery sling. There is an abnormal soft tissue structure (the left pulmonary artery) lying between the air filled esophagus posteriorly and the trachea anteriorly (arrow).

◀ **Fig. 11.52A, B, C, D.** Diagrammatic illustration of the commonest variations in aortic arch branching. The normal arch, A, is left-sided and gives off the right brachiocephalic artery, the left common carotid artery and the left subclavian artery. The commonest important variant of the left-sided arch is the anomalous right subclavian artery shown in B. A right-sided arch with mirror image branching (C) is most commonly associated with cyanotic congenital heart disease and the branches in order are left brachiocephalic artery, right common carotid artery and right subclavian artery. A right-sided arch giving off the left common carotid artery, the right common carotid artery, the right subclavian artery and finally the anomalous left subclavian artery (D) is the commonest type of right arch found without co-existing congenital heart disease. In this type the anomalous subclavian artery often arises from a prominent posterior diverticulum.

The left pulmonary artery arises as a branch of the right pulmonary artery and runs posteriorly on the right of the trachea, reaching its destination as it passes leftwards behind the trachea. This is one of the few conditions where the abnormal vascular structure runs *anterior* to the esophagus (between esophagus and trachea). This can occasionally be recognized as an abnormal soft tissue structure on the lateral *chest radiograph* between the esophagus and trachea (Fig. 11.53). Diagnosis may involve barium swallow and bronchography but once again *arteriography* will produce the definitive diagnosis.

There are very many other vascular anomalies, some of which can cause tracheal compression. Sometimes a vascular ring is formed by rudimentary vascular bands which are not demonstrated angiographically and this possibility must always be considered. Any vascular ring has the potential to cause major airway obstruction and thus stridor in infancy is a serious problem which must always be thoroughly investigated.

#### FETAL ECHOCARDIOGRAPHY

The routine 16-to-18-week antenatal ultrasound scan has now expanded considerably to include assessment of a wide range of organs. The heart can be clearly visualized at this stage with good equipment and the examination consists of certain basic checks. At present a detailed cardiac scan is available in specialist centres only, but the technique is becoming more widely available. Important points to note are:

1. The transverse section of the fetal chest should show a four chamber view with normal orientation of the cardiac apex (Fig. 11.54).
2. The fetal heart should occupy about a third of the area of the chest on this scan.
3. Both ventricles should be of similar size.
4. Both atria should be of similar size.
5. Mitral and tricuspid valves should be seen with their normal offset relationship, the tricuspid valve being positioned slightly closer to the cardiac apex than the mitral valve.
6. The valve of the foramen ovale should be visible.
7. Adjustment of the transverse section should show normal connections of the pulmonary artery and aorta.

The technique can be extended further to show the long and short axis planes of the heart to confirm the anatomy and connections of the great arteries. The aortic arch can often be visualized (Fig. 11.55). Systemic and pulmonary venous connections can often be seen. *Doppler* studies can be used to confirm normal flow through valves and vessels and this can sometimes demonstrate pathology such as a



Fig. 11.54. Two dimensional fetal echocardiogram showing a transverse section of the fetal thorax and a normal cardiac four chamber view.



Fig. 11.55. Two dimensional fetal echocardiogram showing the fetal aortic arch.

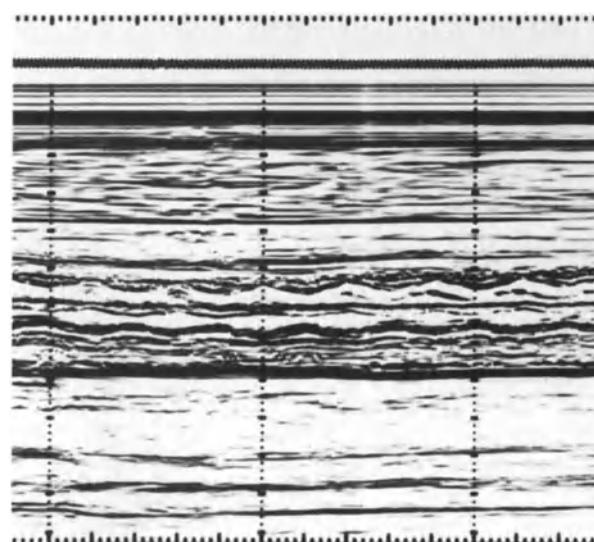


Fig. 11.56. Fetal M-Mode echocardiogram. The contractility of two equal sized ventricular free walls can be seen on either side of the interventricular septum. A regular fetal heart rate of 150/min can be calculated from the 1-second time markers.

regurgitant valve. Heart rate and rhythm as well as more detailed assessment of ventricular function can be derived from the fetal M-Mode examination (Fig. 11.56).

The schedule described above is possible in most cases and can be used to exclude virtually all major abnormalities, depending on the experience of the operator. If abnormalities are detected, decisions regarding future management can be made and these include termination of pregnancy, treatment of the mother with drugs (fetal cardiac failure) and referral to a specialist center for delivery.

Mothers who have had a previous baby with congenital heart disease are the most common referral and in this situation a normal scan is reassuring and beneficial for the mother. Referrals are also made in cases when a less experienced operator suspects an abnormality. Detailed cardiac scans may be helpful when other congenital abnormalities have been detected. Parents with congenital heart disease are now being scanned to exclude recurrence in the child. Recurrence rates in siblings or children show a slight increase on normal incidence.

### SUMMARY OF CHEST RADIOGRAPH APPEARANCES IN CONGENITAL HEART DISEASE

Fig. 11.57 and Fig. 11.58 summarize the major patterns to be seen in the majority of chest radiographs of children and infants presenting with congenital heart disease. The recognition of these patterns will not lead to a definitive diagnosis in most cases but it will usually help to classify the type of abnormality present, often allowing the radiologist to highlight key functional and anatomical features which will be of key importance in further diagnosis and management of the patient.

*For further reading, see p. 233.*

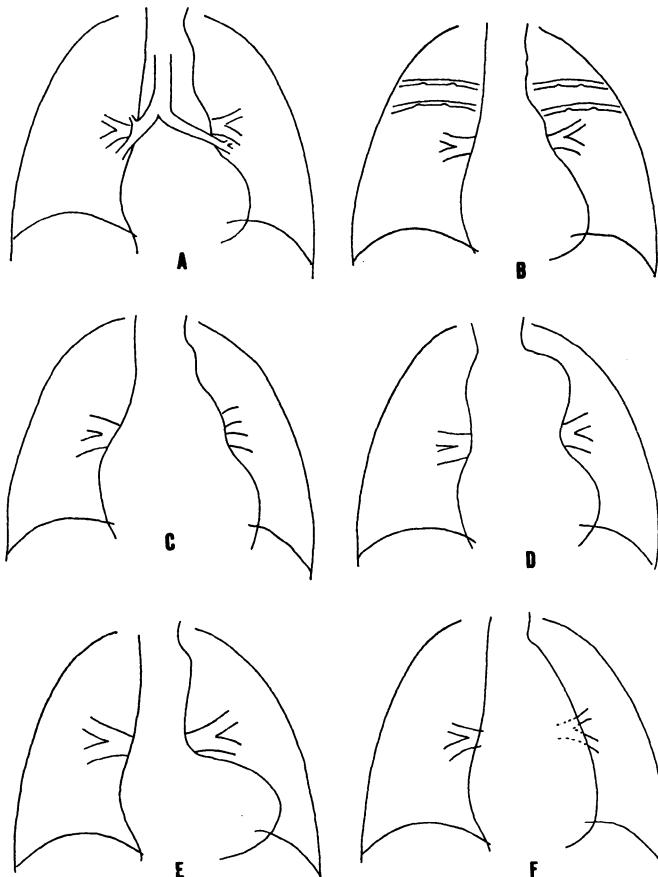
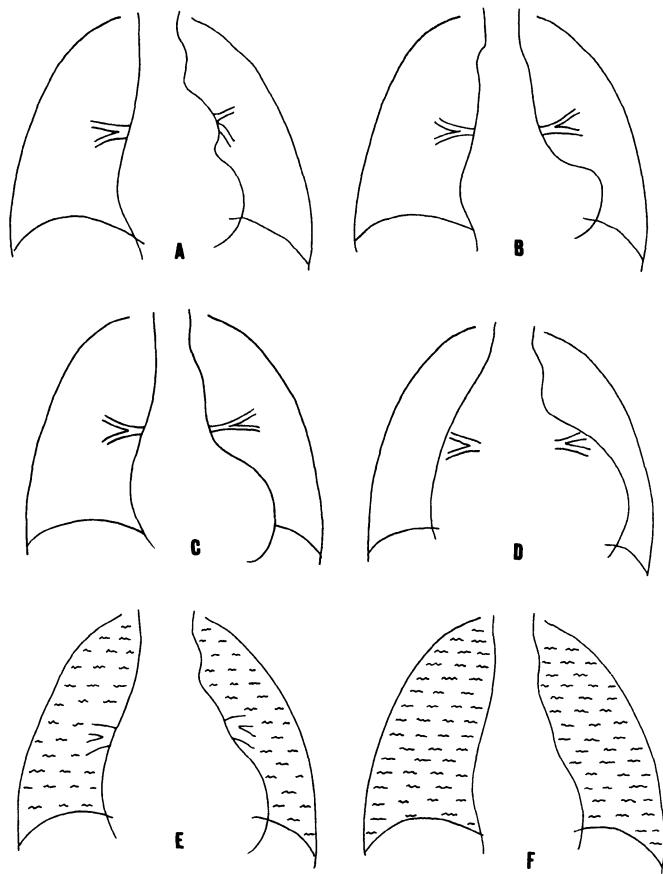


Fig. 11.57A, B, C, D, E, F. Diagrammatic illustration of some of the most important patterns to recognize in the assessment of the chest radiograph in congenital heart disease. A Normal. Remember to check viscerocardiographic situs (including bronchial situs if visible), normal size and position of the aorta and pulmonary artery (thymus may obscure these in infancy) and normal pulmonary vascularity. B Coarctation of the aorta. Note small and irregular or indistinct aortic knuckle. Rib notching in older children and adults. None of these may be visible in infancy. C Left to right shunt pattern. Note moderate cardiomegaly, large main pulmonary artery and pulmonary plethora. This is often due to ventricular septal defect, atrial septal defect or patent ductus arteriosus but is a non-specific appearance and can be seen in many more complex forms of disease. It may be impossible to determine the type of shunt from the chest radiograph alone. Marked plethora in older children or adults is more likely to be due to an atrial septal defect. D Supracardiac totally anomalous pulmonary venous drainage. Unusually wide upper mediastinum with pulmonary plethora and mild or moderate cardiomegaly. 'Cottage loaf' or 'snowman' pattern now rare and most frequently seen in older untreated patients. May be hard to distinguish from C. E D-transposition of the great arteries. Moderate cardiomegaly with rounded left heart border and pulmonary plethora but a hollow pulmonary bay (narrow pedicle). Often called 'egg on side'. Similar pattern often seen in truncus arteriosus. Right aortic arch more common with truncus arteriosus. F L-transposition of the great arteries ('corrected transposition'). Long curved left heart border due to abnormally placed aorta. Normal or plethoric lung fields depending on the co-existence of an intracardiac shunt. This cardiac contour may be seen in various other forms of complex disease including some types of 'single ventricle'.

**Fig. 11.58A, B, C, D, E, F.** Congenital heart disease chest radiograph diagrams (continued). A Pulmonary valve stenosis. Normal heart size, prominent main pulmonary artery and left pulmonary artery. Normal or oligemic pulmonary vasculature. In older patients do not confuse with pulmonary arterial hypertension in which the proximal dilatation of the arteries extends a little further out and is clearly seen in the right pulmonary artery. Some cases of pulmonary valve stenosis and most cases of infundibular stenosis do not have post-stenotic dilatation. B Tetralogy of Fallot. Note upturned apex, hollow pulmonary bay, right aortic arch (25%) and pulmonary oligemia. The spectrum of the condition is very wide and the full set of signs is present only in a minority. Pulmonary atresia with a ventricular septal defect and some forms of double outlet right ventricle are closely related. Mild or acyanotic cases may not show oligemia. C Tricuspid atresia. Rounded apex due to left ventricular enlargement, hollow pulmonary bay and pulmonary oligemia. Exact appearances will depend on the details of the individual case, for example the ventricular septal defect may not be restrictive as is usually the case. Other complex abnormalities may show this appearance. D Very large heart. This can occur in severe Ebstein's anomaly and severe congenital cardiomyopathy (including ischemic damage from anomalous coronary artery from the pulmonary artery). May also be seen in large pericardial effusions. Pulmonary vasculature can be normal or oligemic in all these conditions. E Large heart and pulmonary edema. Can be seen in severe cases of left to right shunt (including complex cases such as 'single ventricle'). Frequently seen in cases of atrioventricular septal defect with atrioventricular valve regurgitation as well as a large shunt. A very similar pattern can be seen in severe cases of congenital aortic stenosis or coarctation of the aorta. In the latter cases cardiomegaly is due to heart failure and prominent vasculature to pulmonary venous hypertension. Cardiac failure will sometimes be seen in cases of cardiomyopathy. F Small heart with pulmonary edema. Typically associated with infradiaphragmatic totally anomalous pulmonary venous drainage but can be seen with any form of obstruction to pulmonary venous return (such as congenital mitral stenosis, supramitral ring and cor triatriatum). Care is required to distinguish this from pulmonary disease.



## CHAPTER 12

# CARDIAC TUMORS: PERICARDIUM: INTERVENTIONAL TECHNIQUES

P. Wilde and G. G. Hartnell

## CARDIAC TUMORS

Cardiac tumors are common in patients with *secondary malignancy*, being found in the heart or pericardium of up to 25% of patients who die from malignant disease. Only a minority cause symptoms from hemorrhagic pericardial effusion, arrhythmias and occasionally systemic or pulmonary embolization. The majority of these present in the context of advanced, disseminated secondary malignancy and treatment and full investigation is often not necessary.

*Primary cardiac tumors* are rare but are important because they are often treatable and curable. They present with symptoms and signs which depend on the site of the tumor, most commonly systemic embolization, arrhythmias and obstruction to cardiac output or filling. Pericardial tumors are usually manifest by the development of hemorrhagic pericardial effusions and are discussed below.

### Left Atrial Myxoma

Myxomas are the commonest primary cardiac tumors and are most commonly found in the left atrium (75%), the majority of the remainder being found in the right atrium. The symptoms of atrial myxomas vary and include those due to embolization or obstruction of flow, such as shortness of breath related to body position. There may be a systemic illness which can mimic bacterial endocarditis with fever and finger clubbing. The clinical signs on examination may mimic mitral stenosis or mitral regurgitation.

The chest radiograph may show signs of mitral valve obstruction or regurgitation with left atrial enlargement and pulmonary venous congestion. Rarely, there may be enough

calcification in or on the surface of the tumor to be visible on the lateral chest radiograph or on fluoroscopy.

*Echocardiography* is usually the definitive investigation in establishing the diagnosis of atrial myxoma. *M-Mode echocardiography* shows a well-defined mass of echoes in the left atrium, which may prolapse through the mitral valve during diastole. *2-D echocardiography* shows a mass of relatively dense echoes which are often mobile on a stalk (Fig. 12.1), although sessile myxomata can also be seen on 2-D echo-



Fig. 12.1. 2-D echocardiogram showing left atrial myxoma (M) attached by a stalk (S) to the interatrial septum.



**Fig. 12.2.** 2-D echocardiogram showing left atrial myxoma (M) prolapsing through the mitral valve (arrows) in a patient who presented with episodes of syncope.



**Fig. 12.3.** 2-D echocardiogram showing the echogenic mass of a rhabdomyosarcoma (R) projecting into the right ventricle.

cardiography. Prolapse of a mobile tumor (Fig. 12.2) through the mitral valve can cause obstruction (mimicking mitral stenosis and sometimes causing syncope) or mitral regurgitation. The site of attachment is most commonly on the interatrial septum adjacent to the position of the fossa ovalis.

The commonest differential diagnosis is *atrial thrombus* and differentiation between the two can be difficult, although thrombus is often less echogenic, tends to be sessile and may be attached to other parts of the atrial wall. If the echocardiographic appearances are clear, further imaging is unnecessary and may, in the case of angiography, be hazardous. If there is doubt, as in patients who are poor echo subjects then further confirmation of the presence of a tumor can be provided by *contrast enhanced CT*, *MRI* or careful *angiography* (i.e., using the venous phase of a pulmonary arteriogram to show a left atrial myxoma).

Myxomas elsewhere in the heart have to be distinguished

from large *vegetations*, *tumor* extending along systemic veins, *clot* from peripheral veins in the right heart and *other tumors*. Other benign tumors include fibromas, hamartomas, rhabdomyomas, cysts and lipomas.

#### Malignant Primary Cardiac Tumors

Primary malignant cardiac tumors are rare and histologically are usually *rhabdomyosarcomas*. They may cause arrhythmias, obstruction to cardiac filling, hemorrhagic pericardial effusions or embolic complications.

The right atrium and then the right ventricle are the commonest sites. The chest radiograph may show a large heart or a pericardial effusion. The most useful investigation is 2-D *echocardiography*, which shows a mass of variable echogenicity projecting into and often filling the affected cardiac cavity (Fig. 12.3). Other imaging methods, as with atrial myxoma, may be required in patients who are unsuitable for echocardiography.

---

## CARDIAC IMPLANTS

---

An increasing number of devices are implanted into patients with heart disease, even into very young patients (Fig. 12.4). These vary in complexity from relatively simple *valves* and *shunts* to very complex programmable *pacemakers* and *automatic defibrillators*. When these devices malfunction there is often a tendency to use more complex and expensive investigations first without considering what information may be provided by such simple investigations as the chest radiograph.

**Imaging.** The radiological investigation of any malfunctioning implant should start with a *chest radiograph*, which may indicate a change in position of the implant, such as migration of a pacing electrode. *Fluoroscopy* has a role in some situations, as in the investigation of malfunctioning

metallic or other radiopaque valve prostheses (Fig. 9.10). *Echocardiography* is very useful in the investigation of valve prosthesis dysfunction, particularly when combined with Doppler, and in the investigation of some pacemaker complications. *CT* is helpful in a few situations but the intense artefacts produced by metal objects such as valves limit its usefulness (Fig. 12.5A). *MRI* is subject to different limitations and is *absolutely contraindicated in patients with pacemakers*. However, *MRI* is useful in the investigation of patients with valve prostheses where acoustic or radiographic artefacts limit the use of echocardiography and *CT* (Fig. 12.5B). Metallic valves are not strongly magnetic and therefore are not a contraindication to *MRI*, although local magnetic fields induced in the valves may cause artefacts.

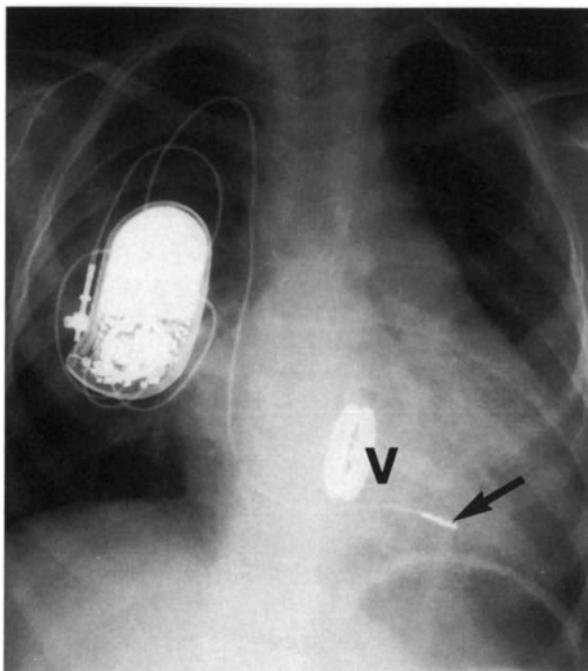


**Fig. 12.4.** Chest radiograph of a 6-year-old child with repaired A-V canal requiring the use of a Bjork-Shiley mitral valve prosthesis (V) and a permanent endocardial pacing system. Note the screw tip of the endocardial electrode (arrow) which allows positive fixation of the pacing electrode.



**Fig. 12.6.** 2-D echocardiogram of Wessex aortic valve prosthesis showing the struts which hold the prosthetic valve tissue (arrows). Radiographic appearance of this type of valve is shown in Fig. 9.10.

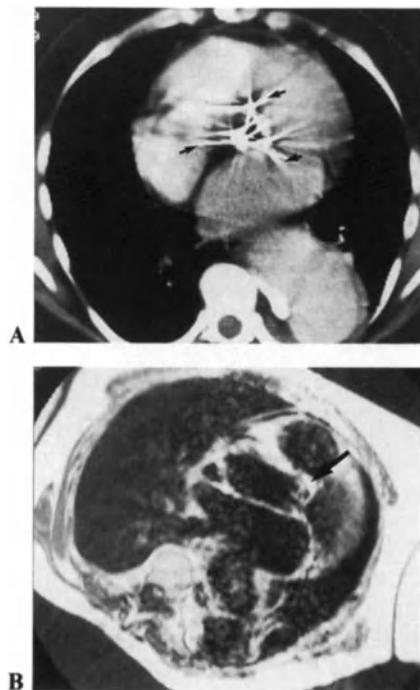


**Fig. 12.5.A** CT scan through the aortic root of a patient with a Starr-Edwards aortic valve prosthesis showing multiple linear artefacts arising from the metal valve cage (arrow). **B** MRI scan at the same level as image A, showing the aortic root at the level of the aortic valve prosthesis (arrow) without any artefact. (Fig. 12.5B reproduced by courtesy of the Trustees of the Bristol MRI Centre.)

Investigation of valve dysfunction by *cardiac catheterization* when less invasive imaging methods are available is seldom required unless information about the coronary artery anatomy is required prior to surgery. In patients with heart failure or prosthetic endocarditis cardiac catheterization is often contraindicated.

#### PROSTHETIC VALVES

There are many types of prosthetic valves in use which can be divided into a small number of groups based on their basic design.

**Homograft Valves.** This type of valve is made from antibiotic-sterilized human tissue. This valve is the nearest equivalent of a normal valve but supplies are limited and relatively few are implanted.

**Xenograft Valves.** These valves are prepared from animal tissue (usually porcine) which is used to fabricate an approximation to a three-cusped valve, producing a flow profile which is a close approximation to a natural valve. Valves of this type include the Hancock, Carpentier-Edwards, Ionescu-Shiley and Wessex valves (Fig. 12.6).

**Caged Valves.** These are made of a metal cage within which an occluding ball or disc can move to allow flow. The ball and cage types include the Starr-Edwards, DeBakey and Harken valves while the disc and cage types include the Beall and Cooley valves.

**Hinged-disc Valves.** These valves have one or two hinged discs attached to a metal cage and have the advantage of allowing a greater flow for a given size of valve ring than a caged ball or disc valve prosthesis. Examples of the single disc type include the Bjork-Shiley (Fig. 12.7) and Lillehei-Kaster valves while the commonest dual-disc valve is the St Jude valve (Fig. 9.10).

**Patterns of Valve Dysfunction.** All valves have the potential to malfunction (Table 12.1), the prevalence of each type of dysfunction depending on the type of valve. Thus ball and cage valves have a strong tendency to cause systemic embolization, unless the patient is anticoagulated, while xenografts tend to degenerate slowly and become regurgitant.

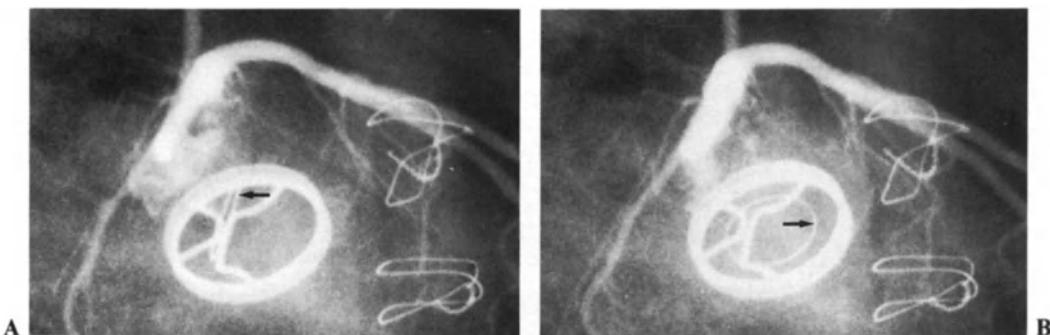


**Fig. 12.7A, B.** Position of tilting disk (arrow) of a Bjork–Shiley aortic valve prosthesis seen during systole (A) and diastole (B).

**Table 12.1.** Patterns of prosthetic valve dysfunction

- Prosthetic or paraprosthetic regurgitation
- Systemic embolization
- Endocarditis
- Strut fracture
- Valve thrombosis and stenosis
- Hemolysis

Useful information on prosthetic valve dysfunction may be obtained from the chest radiograph, fluoroscopy, echocardiography with Doppler, angiography, CT, MRI and occasionally isotope imaging.

### Prosthetic Valve Regurgitation

Prosthetic valve regurgitation is a common problem which is caused by a variety of mechanisms, some of which are predictable, such as degeneration of a xenograft, while others are unpredictable, such as fracture of a valve strut (Fig. 12.8). The aims of imaging patients with prosthetic valve regurgitation are to diagnose the cause of the regurgitation and to assess its hemodynamic importance, thereby allowing surgical replacement in appropriate cases. The radiographic features of prosthetic valve dysfunction, in terms of changes

in the pulmonary circulation and heart size are the same as in patients with equivalent dysfunction of their native valves, although these may be superimposed on post-operative changes. There are other specific features which need to be evaluated by other methods in patients with prosthetic valve dysfunction (Table 12.2).

**Table 12.2.** Causes of prosthetic valve regurgitation

- Degeneration of xenograft/homograft
- Infection (valvar or paravalvar regurgitation)
- Suture line dehiscence
- Thrombosis of prosthesis
- Changes in size of occluding ball/disc
- Strut fracture

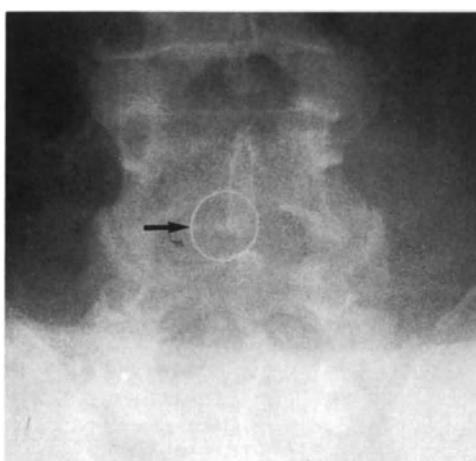


**Fig. 12.8.** View from an abdominal radiograph showing the radiopaque ring of a disk (arrow) from a Bjork–Shiley aortic valve prosthesis which lodged in the aortic bifurcation following strut fracture.

Xenograft and homograft valve prostheses have a finite life. Over a period of years the valve cusps can become thicker, less pliable and unable to close effectively. This produces an increasing degree of valve regurgitation with volume overload of the, usually, left ventricle. The severity of the regurgitation is best monitored by *2-D echocardiography*, which also assesses changes in left ventricular function and size. Initially there is an increase in ejection fraction and stroke volume to accommodate the regurgitation and this is then followed by increasing dilatation and heart failure. *Pulsed or color flow Doppler* is used to assess the severity and changes in the degree of regurgitation. *Trans-esophageal echocardiography* is often of great help in this situation.

Valve replacement should ideally occur when the regurgitation is beginning to become severe and is producing symptoms but is not producing such a significant impairment of ventricular function that it may not completely recover even after successful valve replacement.

*Isotope ventriculography* is an alternative non-invasive method for monitoring these patients. The same information on ventricular function and regurgitation can now be obtained by *MRI* (Fig. 12.9) but this is not in routine use. *Cardiac catheterization* is often requested as a prelude to valve replacement if there is doubt about the possible state of other valves and the coronary arteries.

**Infection.** Infection of prosthetic valves is a major problem which, in spite of the use of prophylactic antibiotics, occurs in 2%–3% of patients with prosthetic valves. Infection occurs particularly in patients with multiple valve prostheses and



**Fig. 12.9.** Flow-sensitive MRI image showing mitral regurgitation through the center of a mitral valve prosthesis (curved arrow) and also a paraprosthetic leak (straight arrow). Note the area of signal loss due to the presence of the metallic valve sewing ring. (Reproduced by courtesy of the Trustees of the Bristol MRI Centre.)

more commonly in the aortic position than in the mitral position. Infection can cause regurgitation by destroying the cusps of xenografts or homografts, by vegetations growing into the valve orifice, by preventing proper closure of the valve apparatus of mechanical valves or by eroding through the tissues around the valve ring.

Vegetations may obstruct the opening and closure of the valve and an indication of this can be gained from fluoroscopy. Valve ring dehiscence produces valve instability which can be seen on fluoroscopy. Normal ranges of motion have been established for different mechanical valves in different positions, although a change of valve motion from a baseline value may be more significant.

*Echocardiography* can show vegetations on the valve apparatus, particularly xenografts and homografts, although views of mechanical valves are limited by the acoustic shadowing of the valve cage. Complications of infection such as paravalvar abscesses, paravalvar sinuses and vegetations growing away from the valve may be visible. Echocardiography is important in assessing the effect of regurgitation on left ventricular function. *Pulsed or color flow Doppler* is used to identify the site of the regurgitation and can differentiate between leaks through the valve and paravalvar leaks. Using *Doppler*, the severity of the regurgitation can be estimated. In patients with endocarditis a sudden change in the Doppler findings is an important indication of progression of the valve infection which may require urgent valve replacement.

In patients where echocardiography is not clear *angiography* may show valvar and paravalvar leaks with any complicating sinuses or abscesses. However catheter manipulation near an infected valve has a risk of causing embolization and should generally be avoided.

*MRI* in difficult cases can demonstrate the sites of regurgitation and paravalvar leaks and abscesses (Fig. 12.9).

**Suture Line Dehiscence.** Suture line dehiscence may com-

plicate endocarditis but can also occur shortly after surgery at the site of inadequate suturing or later as a result of strain on the suture line. Small leaks will produce localized jets of regurgitation which are best demonstrated by *Doppler* while larger areas of dehiscence may also make the valve unstable and this can be seen as abnormal rocking of the valve on *fluoroscopy* or *echocardiography*. The assessment of the severity of the regurgitation is the same as for that in cases following endocarditis, although *angiography* is less hazardous in the absence of infection.

**Thrombosis of Prostheses.** Thrombosis of a prosthetic valve prevents proper opening and closing of the valve and can cause both *stenosis* and *regurgitation*. Thrombosis is more common in the mitral position and can extend into the left atrium.

On *fluoroscopy* or *echocardiography* a reduction in the excursion of the valve is visible and there is evidence of regurgitation or stenosis on *Doppler*. Similar appearances are produced by the ingrowth of tissue from around the valve into the valve orifice.

**Other mechanical causes of valve dysfunction**, such as ball variance (leading to the ball sticking in the cage), and ball or strut fractures are now rare. They lead to regurgitation through the valve and fractured components may cause systemic embolization (Fig. 12.8).

**Emboilic Complications.** Systemic embolization by thrombus is a major hazard in patients with mechanical valve prostheses with an incidence, even in patients who are fully anticoagulated, of 3%–5%. The greatest risk is in the first 6 months after operation. The risk from xenografts and homografts is much less and patients do not usually require anticoagulation. Embolization also complicates endocarditis and mechanical valve failure (Fig. 12.8). Further investigation of the effects of embolization depend on the site. In cerebral embolization CT will show (depending on the type of embolus) areas of infarction, hemorrhage, mycotic aneurysms or abscess formation. Elsewhere ultrasound, CT or MRI may show abscesses or areas of infarction while angiography or Doppler examination may demonstrate vessel occlusion or aneurysm formation (Fig. 12.10).

**Complications of Surgery.** There are many hemodynamic, infective and structural complications of valve surgery which occur in the immediate post-operative period. There are a number of other complications which can occur after a variable period which are not due directly to the prosthetic valve. These include:

1. *Deteriorating Left Ventricular Function.* If valve surgery for valve disease which affects left ventricular function is delayed beyond a certain time the left ventricle can be damaged, either by the volume overload of mitral or aortic regurgitation or by the pressure overload of aortic stenosis. Although the ventricle may recover to a certain extent after surgery the recovery is unpredictable and there may be permanent left ventricular impairment after valve replacement. In some cases the ventricle may continue to deteriorate, becoming increasingly dilated and poorly contracting, especially if there is prosthetic valve dysfunction. This deterioration is usually shown on serial echocardiography or isotope ventriculography. Deteriorating ventricular function in the

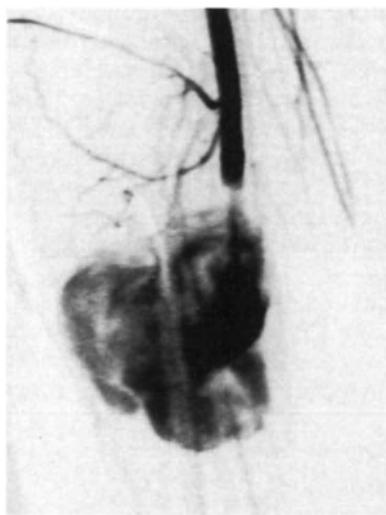


**Fig. 12.10.** Intra-arterial DSA image (lateral view) of a large mycotic aneurysm of the distal popliteal artery complicating bacterial endocarditis.

presence of significant prosthetic valve dysfunction may be an indication for further valve replacement. If the valve is working normally deteriorating left ventricular function can be monitored and may give an indication of the timing of definitive treatment by heart transplantation.

**2. Aortic Root Disease.** In some patients with conditions which affect the tissue around the valve prosthesis, such as Marfan's syndrome, there is continuing deterioration around the valve prosthesis which may lead to valve ring dehiscence, dilatation or dissection of the adjacent aorta. Although the valve may continue to function well, further replacement or reparative surgery may be required. At the time of surgery, whether for valve surgery or bypass grafting, the aortic root may be damaged and this can also lead to the development of ascending aortic aneurysms (Fig. 9.22). These are frequently associated with post-operative wound infection, which may aggravate damage to the aortic wall at the time of surgery.

#### PACEMAKERS AND COMPLICATIONS OF PACING

Indications for pacemaker insertion have increased over the last 15 years and now include symptomatic complete heart block, complete heart block with a low ventricular rate (less than 40–50 beats per minute) and symptomatic sino-atrial disease (see Table 12.3), as well as bifascicular block, carotid sinus syndrome bradycardias caused by drugs. In some patients with troublesome tachyarrhythmias pacing is required to allow the use of large doses of antiarrhythmic drugs without causing unacceptable bradycardia.

In some cases, pacing need only be temporary and can be withdrawn after a few days (e.g., following myocardial infarction when ischemia affects the tissues adjacent to the conducting tissues, or where there has been a drug overdose). In other cases permanent pacing is required.

**Table 12.3.** Causes of symptomatic A-V block

Idiopathic (the commonest cause, usually affecting the elderly)
Myocardial ischemia (usually temporary after myocardial infarction, especially with an inferior infarct)
Cardiomyopathy
Cardiac surgery (e.g., repair of A-V canal defects, aortic valve surgery, repair of Fallot's Tetralogy)
Myocarditis (usually temporary)
Drug toxicity (especially digoxin, beta-blockers, verapamil, disopyramide, tricyclic antidepressants)
Rheumatic fever
Congenital heart block

#### Pacemaker Insertion

Pacemakers are devices which produce a regular, short, small electric impulse transmitted along a wire to an electrode in contact with myocardium. The electrode may be in the *right atrium* or the *right ventricle* or there may be an electrode in *both chambers*. Sensing electrodes in the coronary sinus are now uncommon. The pacing generator can be an external device for temporary pacing or a self-contained implantable device for permanent pacing. Power is provided by chemical batteries which can have a working life in excess of 10 years. Atomic devices and devices which use an external induction coil as a power source are now obsolete.

Permanent pacing electrodes can be inserted directly into the epicardial surface of the heart, usually after cardiac surgery, or lodged on the endocardium, using electrodes inserted via a vein, usually a subclavian vein (Fig. 12.11). *Endocardial pacing* is by far the commonest method in current use. One or two electrodes may be used depending on the design of the pacemaker. An atrial electrode may be wedged in the right atrial appendage, the right atrial free wall or, rarely, the coronary sinus. The right ventricular electrode should be lodged amongst the muscle trabeculae near the apex of the ventricle unless this produces unacceptably high pacing thresholds, when another position, often on the inferior wall, is necessary.

Following pacing, especially endocardial pacing, a control penetrated *frontal and lateral chest radiograph* should be taken to document the position of the pacing electrode and the course and integrity of the pacing wire. This can be used for comparison if symptoms of pacemaker dysfunction occur at a later stage (see Table 12.4).

**Electrode and Wire Position.** *Malposition* of a pacing electrode and wire can occur at the time of insertion or

**Table 12.4.** Radiologically demonstrable complications of pacing

Electrode displacement
Myocardial perforation
Pericardial effusion
Pneumothorax
Pleural hematoma
Surgical emphysema
Systemic venous thrombosis
Pulmonary embolization
Infection
Wire fracture
Pacemaker migration
Air embolus

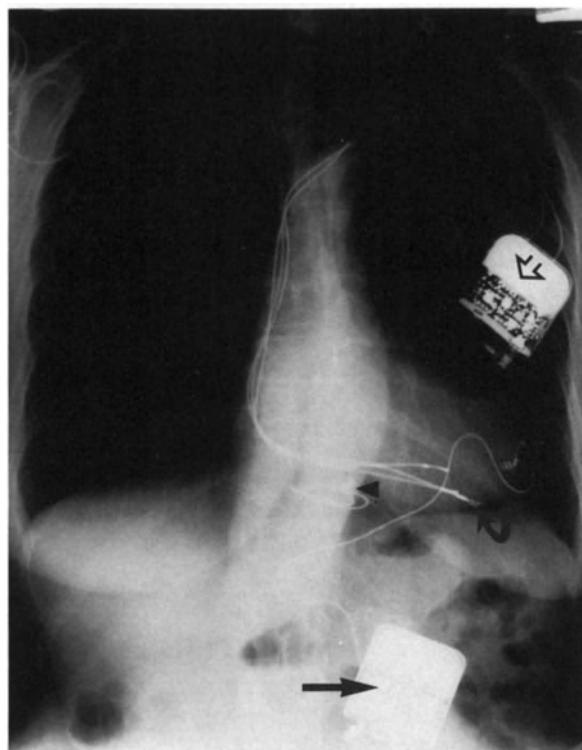


**Fig. 12.11.** Chest radiograph of a patient with rising pacing thresholds requiring repeated pacemaker insertion. There is an epicardial system (solid arrow), a redundant epicardial electrode (arrowhead), a permanent endocardial system (open arrow) with a screw tip wire (curved arrow), a redundant permanent endocardial wire and a temporary pacing wire.

develop at a variable, but usually short, time after insertion. The position of a pacing wire immediately after insertion should be in the region of the right ventricular apex, with a gentle curve of the pacing wire as it passes down the right atrium and across the tricuspid valve. There should be no excessive loop of wire in the right atrium, which can cause arrhythmias as it passes across the tricuspid valve, nor should the wire be too taut, which can cause wire displacement, arrhythmias, tricuspid regurgitation and rarely tricuspid stenosis. Occasionally the tip of the electrode can be inadvertently placed in the left ventricle, coronary sinus or one of the cardiac veins. This may not be clear on the frontal chest radiograph and a lateral view is essential to confirm a satisfactory position.

The pacing wire can become *displaced* and pass into the pulmonary artery, right atrium, coronary sinus or a cardiac vein. This should be clear when the position is compared with that on the control radiograph taken after implantation. Some patients have a compulsive desire to manipulate their pacemaker generators (*Twiddler's syndrome*) and this can lead to *withdrawal* of the pacing wire or *knotting* of the wire (Fig. 12.12) with a risk of *fracture* or *migration of the generator*.

There are a number of pacing wire designs which have a positive fixation device at their tips (such as screws (Fig. 12.6), tines or permeable electrodes) which make displacement after implantation unusual and displacement rates should be no higher than 3%–5%.

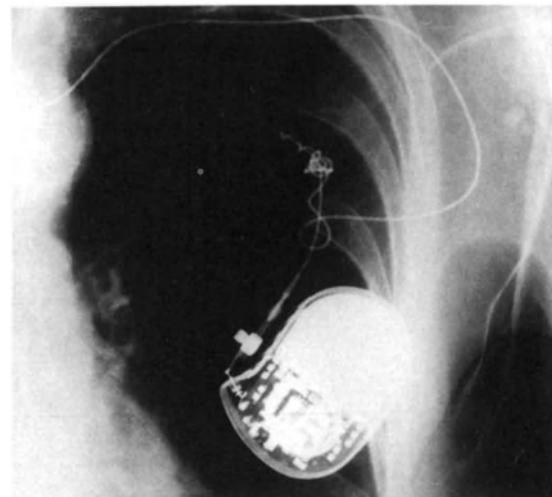


**Fig. 12.12.** Chest radiograph showing severe twisting and knotting of pacing wire due to manipulation by the patient (Twiddler's Syndrome).

**Myocardial Perforation.** Myocardial perforation occurs commonly during the insertion of endocardial pacing electrodes; the exact frequency depends on the type of electrode and the skill of the operator, but can be up to 20%. Fortunately this is only occasionally accompanied by a significant pericardial effusion and tamponade. Perforation after insertion may cause loss of pacing, diaphragmatic pacing, pericardial effusion, pain or may be asymptomatic.

The diagnosis is made on the chest radiograph which shows a change in the position of the tip of the pacemaker electrode. In an appropriate projection the pacing wire will be seen to lie within 3 mm of the epicardial surface (Fig. 12.13) and it may follow the line of the surface of the heart. Perforation can be confirmed in difficult cases by *CT* or *echocardiography*, which will also demonstrate any complicating pericardial effusion.

#### Pacing Wire Fracture

Pacing wires are now very reliable and a spontaneous fracture is rare, except with very old wires or if the wire has been damaged, either at the time of insertion or by the patient manipulating the wire under the skin. Wide separation of the ends of the wire implies that the outer plastic coat has also ruptured. In some cases only the metal wire has fractured and this causes intermittent pacing failure as the ends of the wire are held close together by the outer coat (Fig. 12.14). In this situation the diagnosis may only be made on *fluoroscopy* with the patient positioned to reproduce his symptoms. If a hairline wire fracture is suspected, magnification views without a grid may be required for confirmation. Grid lines on a conventional chest radiograph are occasionally misinterpreted as indicating a fractured wire.

#### Thromboembolic Complications

Thrombosis on the pacing wire or in the systemic veins is common following pacemaker insertion, but only causes symptoms infrequently. Thrombus on the pacing wire (Fig.

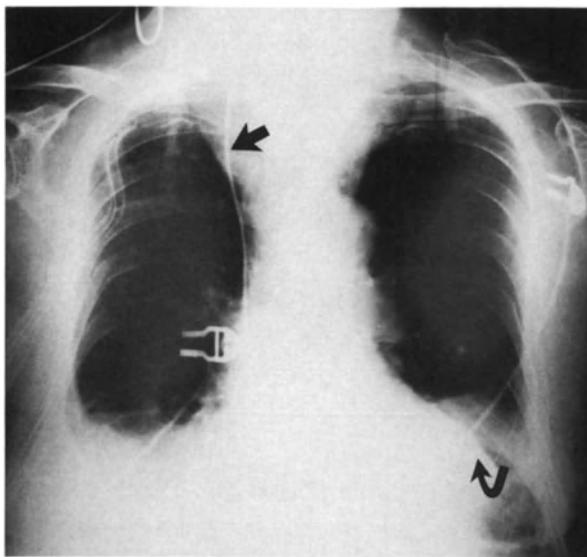


**Fig. 12.13.** Chest radiograph from a patient with a temporary pacing system showing myocardial perforation (curved arrow), chest drain introduced to drain a post-pacing pneumothorax and an apical hematoma due to puncture of the right subclavian artery (straight arrow).

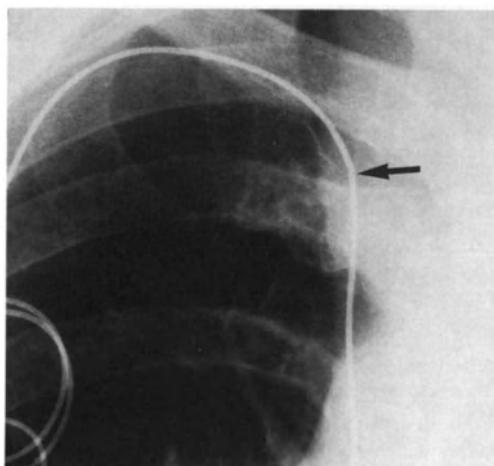


**Fig. 12.14.** Close-up view from chest radiograph showing slight angulation and a small fracture (arrow) in a permanent pacing wire.



**Fig. 12.15.** 2-D echocardiogram (parasternal oblique short axis view) showing increased echoes (arrow, 8 mm thick) on a permanent pacing wire indicating thrombus formation on the wire.

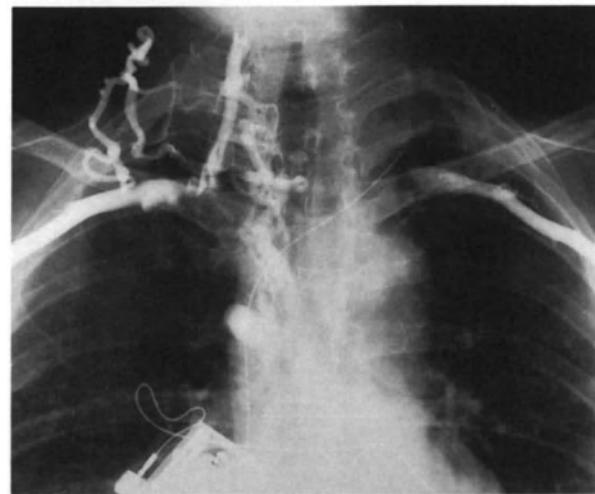


**Fig. 12.16.** Bilateral subclavian venogram showing bilateral subclavian vein thrombosis due to redundant pacing wire.

12.15) may cause pulmonary emboli (0.6%–3.5%) but these are seldom serious. The frequency of thrombosis of the subclavian veins and superior vena cava depends on the route of insertion (being commoner after cephalic vein insertion) and the size of the pacing wire (being commoner with larger diameter wires and dual wire systems). An incidence of venous thrombosis of over 20% has been reported, but with

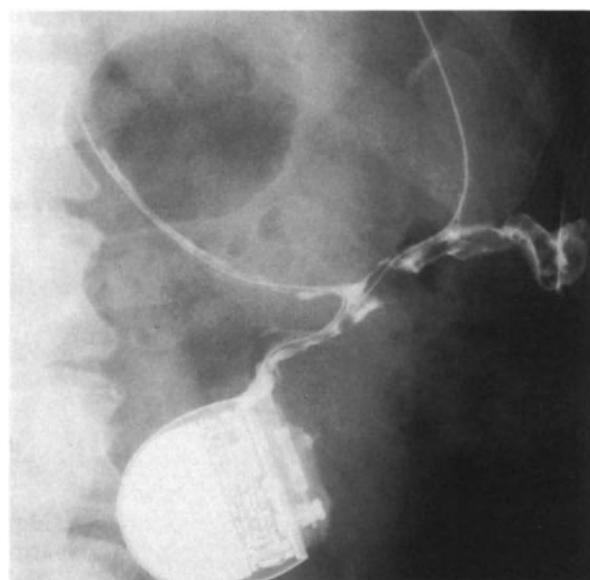


**Fig. 12.17.** Sinogram showing sterile sinus communicating with the space around a pacing system. No organisms were grown from the sinus but it failed to heal and required removal of the pacing system.

currently available wires the incidence is much less. Surprisingly, few patients develop symptomatic thrombosis though this often accompanies a complication of pacing such as infection or partial removal of the pacing system which leaves the end of the wire free in the SVC (Fig. 12.16).

### Infection

Infection may occur and complicate pacing around the pacemaker generator or spread along the pacing wire to cause septic thrombosis, endocarditis or septicemia. This is a particular hazard after emergency temporary pacing because the pacing wire provides a tract along which infection can spread from the skin, especially if the introducer sheath is left in the skin, and because these procedures are

sometimes performed under non-sterile conditions due to the urgent need to insert the pacemaker. Permanent pacemakers are inserted under better conditions and, although infection rates of up to 5% have been reported, the infection rate for new systems should be much less than this (under 1%).

*Radiological features* of infection include soft tissue swelling around the generator and, occasionally, gas in the soft tissues, although this may be present in the absence of infection (Fig. 12.17). *Isotope imaging* with labelled leucocytes may be helpful in distinguishing between sterile inflammation around the pacemaker and infection. In some cases a sinus forms between the pacing system and the skin surface, even in the absence of infection, and requires the removal of the entire system to allow healing.

## PERICARDIAL DISEASE

The normal pericardium is a thin-walled fibrous sac surrounding the heart and contains a small amount of pericardial fluid (20–30 ml). The methods available for imaging it include plain film radiography, fluoroscopy, echocardiography, CT, MRI, angiography, carbon dioxide insufflation or injection of other contrast media. Its thickness with most imaging methods is normally 2–3 mm and it is most clearly seen on CT (Fig. 12.18). Fluoroscopy, angiography and carbon dioxide insufflation are now obsolete in the investigation of pericardial disease. Injection of water-soluble contrast media may rarely have a role in demonstrating small pericardial tumors.

Normal pericardium is only visible on the chest radiograph when the pericardium is outlined by epicardial and mediastinal fat but it is sometimes more easily seen in patients with pericardial effusions. The chest radiograph may show pericardial fat pads, typically in the cardio-phrenic angles (Fig. 12.19) which may mimic cardiac enlargement or pathological masses.

**Imaging.** *Echocardiography.* This is the most useful method for investigating pericardial fluid collections, both effusions (Fig. 12.20) and cysts. It is less useful when investigating pericardial constriction or pericardial tumors, especially those which are not accessible to a suitable acoustic window.

*Computed Tomography.* CT is useful for demonstrating pericardial disease, particularly pericardial constriction, loculated effusions (Fig. 12.21) and tumors. It has the added advantage of allowing examination of the adjacent



Fig. 12.18. Normal pericardium seen on contrast enhanced CT scan and showing the pericardium as a medium attenuation line between the lower attenuation areas of surrounding fat (arrows).

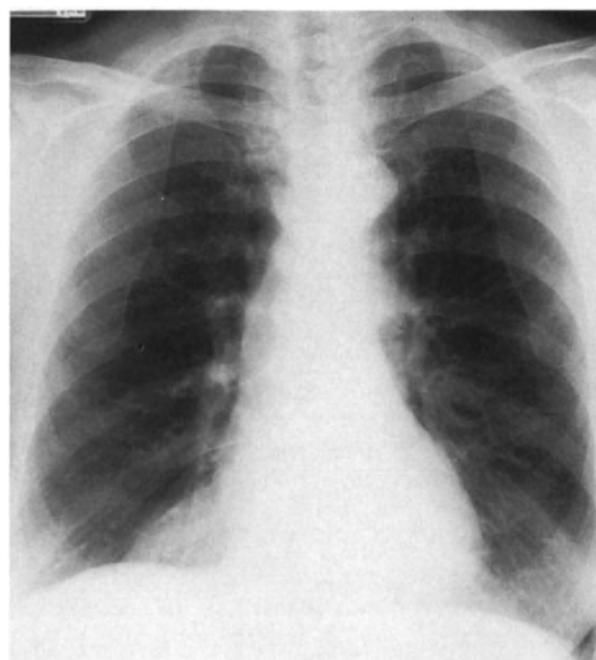
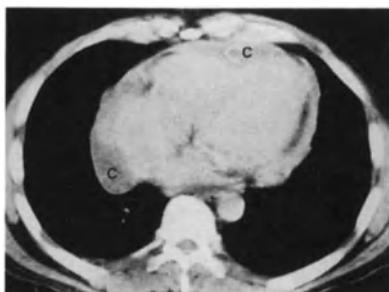


Fig. 12.19. Chest radiograph showing a pericardial fat pad in a typical position in the right cardio-phrenic angle.



**Fig. 12.20.** 2-D echocardiogram showing a fibrinous band (arrow) in a large hemorrhagic pericardial effusion (E).



**Fig. 12.21.** Contrast-enhanced CT scan showing multiple loculated pericardial fluid collections (C) in a patient with hydatid disease involving the pericardium.

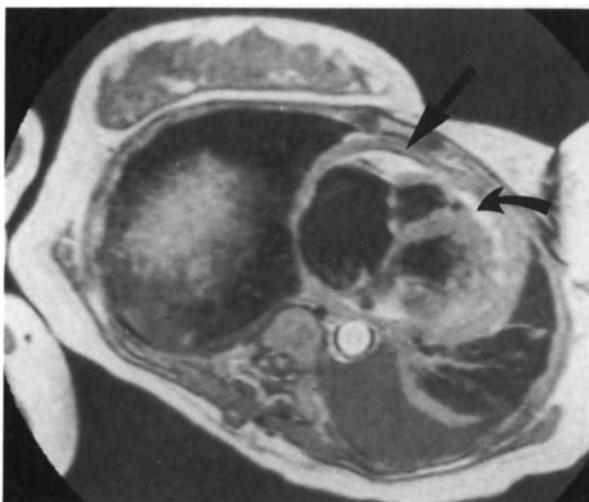


**Fig. 12.22.** Transverse gated MRI scan showing medium level signal from a purulent pericardial effusion (straight arrow) surrounding the heart and separated from it by high signal epicardial fat (curved arrow). (Reproduced by courtesy of the Trustees of the Bristol MRI Centre.)

mediastinum in patients where the pericardial disease may have spread from the mediastinum.

**Magnetic Resonance Imaging.** MRI is superior to conventional CT in demonstrating cardiac disease, as it is much easier to gate image acquisition to the patient's ECG, therefore preventing blurring due to cardiac motion which degrades the images produced by most CT scanners. This is particularly true with pericardial disease where MRI is very accurate in detecting pericardial thickening (Fig. 12.22) and tumors. The ability of MRI to show the heart in coronal and sagittal sections make it the method of choice, when available, for demonstrating pericardial disease.

## PERICARDITIS

There are many causes of pericarditis (Table 12.5) which can lead to acute pain, pericardial effusion or, eventually, pericardial constriction. The development of an effusion or progression to constriction depends on the underlying cause (viral pericarditis usually resolves while tuberculous pericarditis, especially if it is not treated or is treated late, frequently progresses to chronic constriction). A rapidly developing pericardial effusion, even when quite small, will impair cardiac filling and lead to pericardial tamponade, while a slowly developing effusion (by allowing the pericardium to stretch) may become very large without causing tamponade.

**Table 12.5. Causes of pericarditis**

Rheumatoid arthritis
Systemic lupus erythematosus
Scleroderma
Rheumatic fever
Polyarteritis nodosa
Myocardial infarction
Dressler's syndrome
Post-pericardiotomy syndrome
Drugs (including anticoagulants as well as drugs which cause a lupus-like syndrome)
Heart failure
Aortic dissection
Trauma
Infection (tubercular, viral, pyogenic, fungal, amebic)
Malignancy (metastatic, local invasion, primary, lymphoma, leukemia)
Radiation
Myxedema
Uremia

**Connective Tissue Disorders.** Pericarditis is a common feature of connective tissue disorders such as rheumatoid arthritis, systemic lupus erythematosus and scleroderma. Pericarditis is very common, but often asymptomatic, in patients with rheumatoid arthritis, pericardial effusion occurring in up to 47% cases examined at autopsy. In spite of the high prevalence in these patients progression of pericarditis to constriction is uncommon.

**Myocardial Damage.** Pericarditis is a common complication of any condition in which there is myocardial damage, such as myocardial infarction, cardiac trauma and cardiac surgery. Pericarditis can develop from one week to several

months after the damage has occurred. In Dressler's Syndrome, which occurs in 4%–14% of such cases, pericarditis can present up to 2 years after the damage to the myocardium and is characterized radiographically by pericardial and pleural effusions and pulmonary infiltrates.

**Post-radiation Pericarditis.** Pericarditis complicates radiotherapy in which the therapy field includes part of the heart and in which high doses (usually in excess of 4000 rad) are given to the pericardium. There may be a long delay before the onset of symptoms, which can be due to a pericardial effusion or constriction. There may be associated fibrosis of the adjacent myocardium.

**Drugs.** Drugs which cause pericarditis include procainamide and hydralazine, both of which can cause an SLE-like condition. Anticoagulants can cause hemopericardium, particularly in patients with poor anticoagulant control or when they are given to patients with pericarditis following myocardial infarction.

**Infective Causes.** Viral infection is thought to be one of the most common causes of pericarditis, although there is often little firm evidence to support the diagnosis. The prognosis is good, although relapses do occur and progression to cardiac tamponade and, rarely, constriction can happen. Pyogenic, fungal or amebic causes of pericarditis are all much less common but have a worse prognosis, commonly causing large effusions which may cause tamponade and frequently progress, often rapidly, to constriction. Treatment by drainage, antimicrobial therapy and often pericardectomy is required.

**Metabolic Causes.** Uremia is an increasingly important cause of pericarditis as more patients with renal failure survive and this can be complicated by tamponade and constriction. Pericarditis complicating myxedema is relatively common but is often less serious than some other causes of pericarditis, although tamponade can precede other features of myxedema.

#### DIAGNOSIS OF PERICARDIAL EFFUSIONS

**Echocardiography.** This is the imaging method of choice in the investigation of patients with a possible pericardial effusion, being safe, accurate and widely available. On both M-Mode and 2-D echocardiography pericardial effusions are visible as relatively echo-free spaces surrounding the heart with the parietal pericardium visible as a relatively immobile structure surrounding the fluid-filled space. The diagnosis is usually clear but there are some situations in which confusion may occur. In patients with purulent or hemorrhagic effusions there may be dense echoes from the fluid which make differentiation from myocardium difficult, particularly on M-Mode. Similarly, high gain levels may mask the echo-free space. Fat pads, coronary sinus and the descending aorta may all be mistaken for small effusions, especially on the basis of an M-Mode examination. M-Mode may also mistake a left pleural effusion for a pericardial effusion, but the difference should be clear on 2-D echocardiography. For this reason, unless the M-Mode shows significant anterior and posterior fluid (Fig. 12.23), the findings should be confirmed

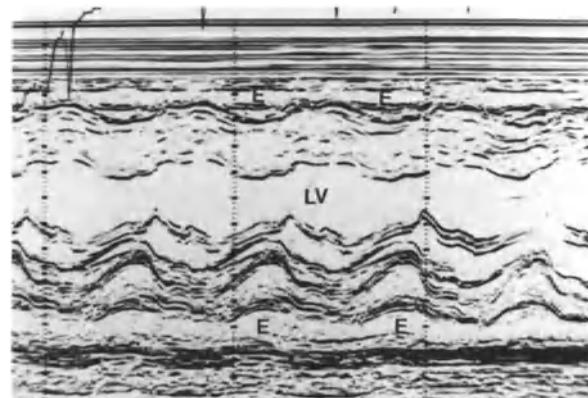


Fig. 12.23. M-Mode echocardiogram showing echo-free areas anterior and posterior to the left ventricle due to a large pericardial effusion (E).

by 2-D echocardiography, which is also useful for directing pericardial drainage procedures.

A number of echocardiographic features have been reported to indicate impending cardiac tamponade. These include reduced cardiac motion, due to poor cardiac filling, increase in right ventricular dimension on inspiration, a decrease of left ventricular dimension on inspiration and a small right ventricle. These are rather imprecise signs, but may be useful when they are present. On 2-D echocardiography, a variable concave-free wall of the right ventricle and right atrium in diastole (Fig. 12.24) is a useful sign, as is late diastolic collapse of the right ventricle which can be well seen on M-Mode and 2-D echocardiography.

**Computed Tomography.** CT has a useful role in the diagnosis of pericardial effusion, although echocardiography is usually more convenient, and it is an important method for demonstrating potential causes such as mediastinal, pleural and pericardial malignancies. Most effusions appear as low attenuation (between soft tissue and water density), non-enhancing areas surrounding the heart (Fig. 12.25) and bounded by a higher attenuation line representing the parietal pericardium. In patients with bloody or purulent



Fig. 12.24. 2-D echocardiogram showing a large pericardial effusion with collapse of the right atrial wall (arrow) in a patient with cardiac tamponade.



Fig. 12.25. Contrast-enhanced CT scan showing a large pericardial effusion as a medium attenuation area (arrow) surrounding the heart.

effusions the attenuation of the fluid may be similar to that of the myocardium, making detection difficult. In some cases of hemopericardium the fluid may be hyperdense and in chylopericardium the fat content of the chyle may make the fluid hypodense. In some cases extensive pericardial fat can mimic a pericardial effusion but is identified by having an attenuation similar to subcutaneous fat (Fig. 12.26).

CT is sometimes superior to echocardiography in detecting patients with poor acoustic windows and also with loculated effusions.

**Magnetic Resonance Imaging.** The limited availability of MRI makes it unsuitable for the initial investigation of most patients with pericardial effusion but there are a number of situations where it has a role in the investigation of pericardial effusions. This particularly applies to the investigation of echogenic effusions, which also tend to be isodense with myocardium on CT. The ability of MRI to acquire gated images of the heart in any projection (Fig. 12.27) make it particularly useful for investigating effusions which are difficult to see on CT. The ability to image the rest of the mediastinum and, to some extent, differentiate malignant masses from normal structures or fibrotic or inflammatory masses is valuable in patients in whom a cause for an effusion (particularly a hemorrhagic effusion) has not been shown by other methods.



Fig. 12.27. Coronal gated MRI scan showing a large low signal pericardial effusion (arrow) completely surrounding the heart. (Reproduced by courtesy of the Trustees of the Bristol MRI Centre.)



Fig. 12.26. CT scan (unenhanced) showing extensive epicardial and pericardial fat (arrow) which mimicked a pericardial effusion on the chest radiograph.

**Chest Radiograph.** On the chest radiograph a large cardiac shadow may be the first indication of a pericardial effusion and is useful for investigating changes in the size of the effusion.

The classical appearance of a pericardial effusion on the chest radiograph is of a large, well-defined, symmetrically enlarged cardiac shadow. There is infilling of the retrosternal space and the hila may be overlaid by the cardiac shadow. The pulmonary vasculature is usually normal, helping to differentiate this from mixed valve disease and congestive cardiomyopathy as a cause of cardiomegaly. In patients who are developing tamponade the systemic veins may be engorged and the pulmonary vasculature decreased. This can occur even with small effusions in cases where the effusion develops rapidly. The pericardial effusion may be outlined by pericardial and epicardial fat and this can give some indication of the size of the effusion.

#### PERICARDIAL THICKENING

Pericardial thickening is usually the consequence of pericarditis and can develop over a period which may vary from a few weeks to several years. Infective causes and hemopericardium are particularly common causes of thickening which can also result from invasion by tumors such as mesothelioma, metastases and lymphoma.

**Pericardial constriction** is a syndrome which develops when pericardial thickening impairs cardiac filling and leads to distension of the systemic and pulmonary veins and eventually to a reduction in cardiac output.

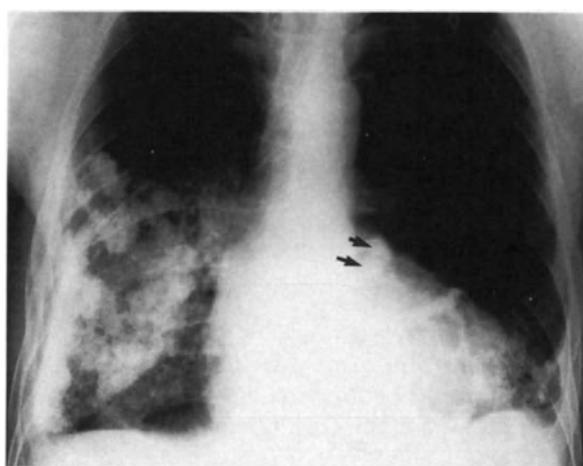


**Fig. 12.28.** Chest radiograph showing extensive pericardial calcification, particularly in the atrioventricular groove (arrow), as well as pleural calcification following tuberculous pericarditis and empyema.

In *constrictive pericarditis* there is fusion of the two layers of the pericardium, which become thickened, non-distensible and, in about 30% cases, calcified. The presence of calcification indicates that there is pericardial thickening but does not necessarily imply that there is hemodynamically important constriction.

**Imaging. Chest Radiography.** Calcification in the thickened pericardium may be widespread or localized in plaques. It particularly involves the atrioventricular groove (Fig. 12.28) and the postero-inferior surface of the left ventricle. This is often best appreciated on the lateral chest radiograph. The heart is usually of normal size, enlargement indicating that

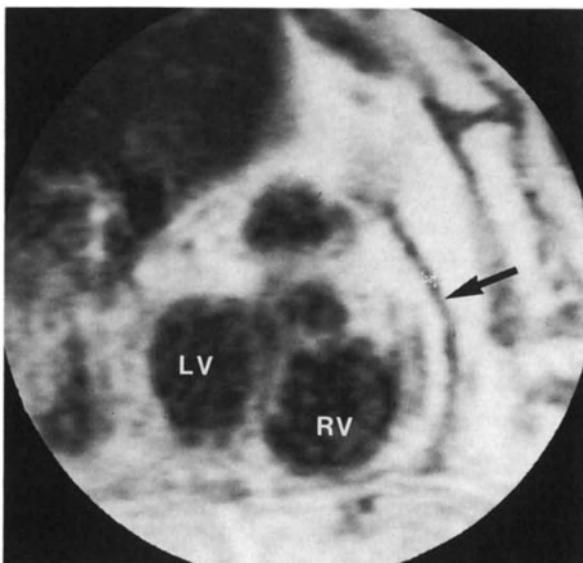


**Fig. 12.29.** Oblique sagittal gated MRI scan through the heart at the level of the base of the ventricles showing thickening of the anterior pericardium (arrow: low signal area 4.7 mm thick). (Reproduced by courtesy of the Trustees of the Bristol MRI Centre.)

there may be an effusion. In patients with hemodynamic constriction there may be pulmonary venous congestion and prominence of the superior vena cava and azygos vein. Significant thickening is implied if the pericardium outlined by fat is visible and is more than 3 mm thick.

**Echocardiography.** The thickness of the pericardium may be shown by echocardiography but this technique is less reliable than in the detection of pericardial fluid as it may be difficult to differentiate the thick pericardium from the ventricular myocardium. There are a number of abnormalities of cardiac motion seen on echocardiography which can suggest constriction (i.e., rapid early diastolic filling which comes to an abrupt halt, a steep E-F slope on the mitral valve trace and premature opening of the pulmonary valve) and reflect rapid early-diastolic filling of the heart with poor filling in late diastole and a high end-diastolic pressure. The poor overall accuracy of these findings limits their use in confirming the diagnosis of constriction.

**Computed Tomography.** CT demonstrates the thickened pericardium very well (normal pericardium is up to 2 mm thick on CT, except at its caudal insertion where it may be 3 mm thick) and may also show any coexisting loculated fluid collections. The thick pericardium appears as a high attenuation line which surrounds the heart but may be of irregular thickness and contain areas of very high attenuation due to plaques of calcification. It must be remembered that the presence of a thick pericardium does not make the diagnosis of significant constriction.

**Magnetic Resonance Imaging.** MRI is valuable for demonstrating the thickened pericardium as gated scans reduce the motion blurring produced on CT. In addition the ability of MRI to scan in a variety of planes and demonstrate all parts of the pericardium make it superior to echocardiography and conventional CT in detecting pericardial thickening (Fig. 12.29). The better definition of MRI allows, in some cases, the detection of some signs which suggest constriction (distended systemic and pulmonary veins, small right ventricle, small stroke volume).

**Cardiac Catheterization.** There are angiographic methods for demonstrating the thickness of the pericardium but these have been superseded by less invasive methods. The role of cardiac catheterization is to confirm the hemodynamic diagnosis of constriction prior to surgery and to demonstrate other coexisting cardiac disease. The features of constriction at catheterization are elevated atrial and ventricular end-diastolic pressures with equal atrial pressures and equal ventricular end-diastolic pressures.

## PERICARDIAL TUMORS

Pericardial tumors are relatively common and are best imaged by the methods used to show other types of pericardial disease. CT and MRI are particularly useful in this context.

**Benign** pericardial tumors are rare, often of mesenchymal origin and usually have a good prognosis unless they are complicated by a pericardial effusion or become very large. The types of benign tumor include teratomas, fibromas, lipomas, angiomas and neurofibromas.

*Malignant* tumors involving the pericardium are common and include metastases (especially from lung or breast), lymphomas or local tumors invading from the adjacent mediastinum (usually lung). They may present with pericardial effusions, which are often hemorrhagic and complicated by tamponade, or cause pericardial thickening with the rapid development of constriction. The features of these are the same as for other causes of effusions and thickening. CT and MRI are particularly useful for showing the extent of pericardial tumors and extension outside the pericardium.

The commonest primary pericardial tumor is *pericardial mesothelioma*, which is histologically identical to mesotheliomas elsewhere. Pleural mesotheliomas are commoner and may invade the pericardium producing effusions or constriction. Mesothelioma may produce widespread pericardial thickening or local plaques, which produce secondary features due to constriction such as pulmonary congestion and systemic venous distension. Mesotheliomas can be best visualized by CT or MRI but because there may be areas of pleural thickening uninvolved by tumor, particularly after asbestos exposure, the ability of MRI to distinguish between mesothelioma and fibrous plaque (i.e., using the STIR sequence) makes this the preferred method of imaging.

### PERICARDIAL CYSTS

Pericardial cysts are collections of fluid surrounded by tissue of pericardial origin, although the majority do not communicate with the pericardium. They occur most commonly in

the cardiophrenic recess (70% in the right recess, 20% in the left, 10% elsewhere) and are usually seen as well-defined masses on the chest radiograph in a typical position. Peripheral calcification may occur but is seldom heavy. Pericardial cysts in atypical positions have to be differentiated from other mediastinal tumors. On 2-D echocardiography they are echolucent and well-defined which allows differentiation from solid tumors, fat pads and lipomas. On CT the attenuation of the fluid in the cyst should be near that of water.

### Pericardial Diverticulum

Pericardial diverticula are congenital or acquired collections of fluid surrounded by an outpouching of the pericardium. Their size varies with the volume of pericardial fluid.

### Absence of the Pericardium

Partial absence of the pericardium is an uncommon and usually benign condition, although some patients do experience pain which may be related. There is a significant association with various congenital abnormalities which occur in up to 30% of cases. These include bronchogenic cysts, ASD, Falot's Tetralogy, hiatus hernia, lung sequestration and ectopia cordis.

On the chest radiograph the outline of the left heart border is very clearly shown, especially the main pulmonary artery, and the heart may be displaced to the left. Partial defects of the left pericardium are less common and allow herniation of part of the pericardial contents, usually of the left atrial appendage or part of the main pulmonary artery.

---

## INTERVENTIONAL TECHNIQUES IN CARDIAC RADIOLOGY

---

The use of therapeutic procedures based on angiographic catheter techniques is now well established in cardiac radiology. The greatest advance has been the development of various *balloon dilatation* applications which can be used to treat arterial and valvar stenoses (Fig. 12.30).

### CORONARY ANGIOPLASTY

Coronary angioplasty is used to treat patients who have a suitable coronary artery stenosis or occlusion. This is usually identified at earlier coronary angiography, although at some centers angioplasty may be performed immediately after the diagnostic study. Indications for coronary angioplasty are listed in Table 12.6.

Coronary angioplasty is performed by intubating the affected coronary artery with a suitable guiding catheter and passing a narrow (usually 0.012–0.014") guide wire across the lesion to be dilated. A balloon dilatation catheter is passed over the wire and across the lesion, where it is inflated several times until the pressure gradient across the lesion has been reduced, preferably to less than 20 mmHg (Fig. 12.31). The

**Table 12.6. Indications for coronary angioplasty**

---

Discrete single coronary stenosis with symptoms
Discrete multiple coronary stenoses with symptoms
Acute myocardial infarction (usually after thrombolytic treatment)
Progression of disease after bypass grafting
Bypass graft stenosis (Fig. 12.30)
Patients unsuitable for bypass grafting

---

balloon is then removed and a further angiogram performed to confirm that the lesion has been dilated. The success of coronary angioplasty is such that it is being performed for ever increasing indications and in increasing numbers of patients (see Table 12.7). In 1988, 5000 coronary angioplasties were performed in the UK, whilst over 250 000 were performed in the USA.

*Results of Coronary Angioplasty.* Between 1980 and 1984 Gruntzig's group at Atlanta achieved a success rate for coronary angioplasty of 90%, with a low complication rate (2.5% myocardial infarction rate, 0.09% mortality). Similar success rates have been achieved in many other centers. Angioplasty is much less expensive than bypass surgery

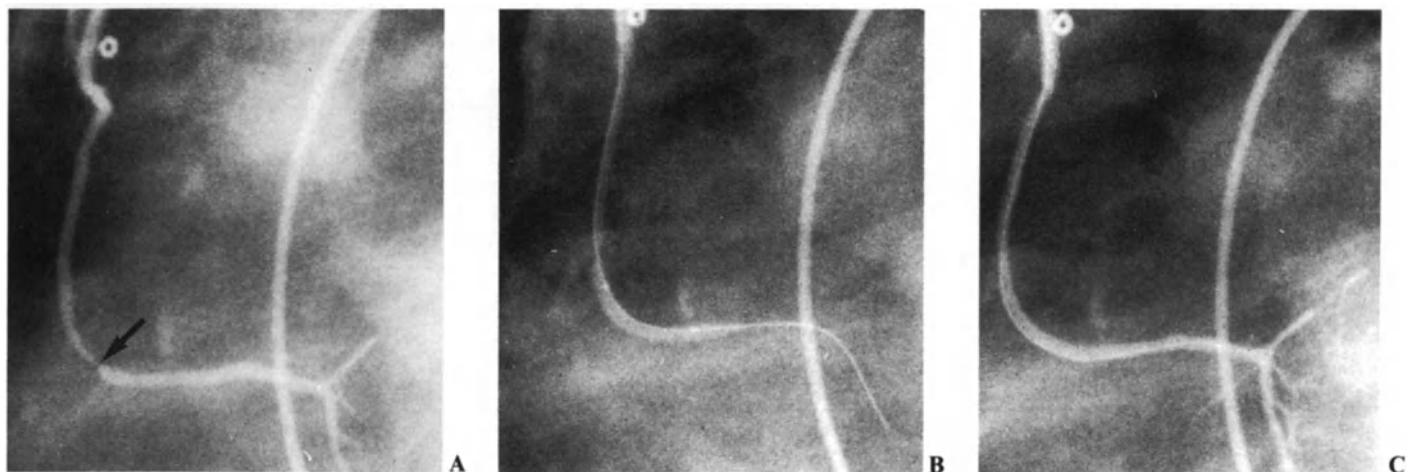


Fig. 12.30A, B, C. Coronary bypass graft stenosis (A) dilated with a 2 mm angioplasty balloon (B) with complete relief of the stenosis (C).

Table 12.7. Coronary angioplasty (PTCA) rates 1985

Country	PTCA Centers	CABG/million population	PTCA/million population	Ratio PTCA/CABG
France	90	102	91	47
Germany (FDR)	123	250	98	39
Italy	80	150	39	25
United Kingdom	54	220	27	12
USA	930	897	453	50

(usually one third to half the cost of coronary bypass grafting depending on the number of lesions treated).

Although coronary angioplasty is a very effective technique there is a definite learning curve with initially fewer successes and more complications. It is, therefore, important that angioplasty is only performed in centers with adequate experience, good angiographic equipment and surgical support.

#### BALLOON VALVOPLASTY

*Pulmonary Valvoplasty.* Pulmonary valve stenosis was the first valve lesion to be treated by balloon dilatation and this is now the treatment of choice in many patients with pulmonary valve stenosis in which the valve is narrowed but otherwise well-formed. Valvoplasty is not usually suitable for treating dysplastic pulmonary valve stenosis. The

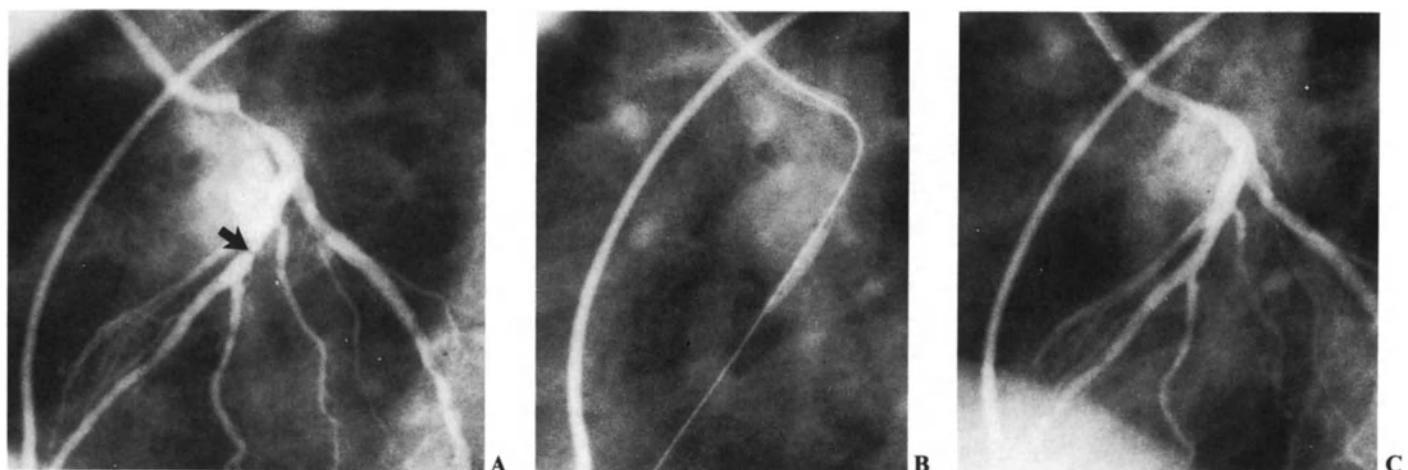
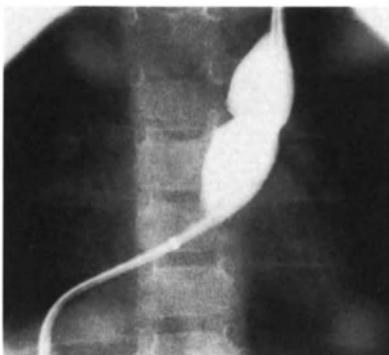
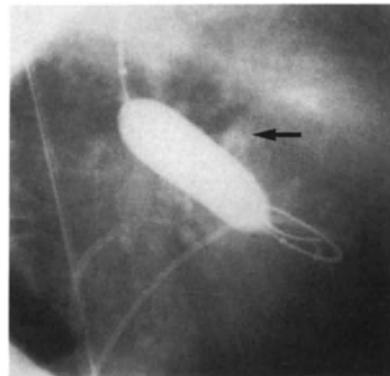


Fig. 12.31A, B, C. Proximal left anterior descending artery stenosis (arrow) (A) dilated with a 3 mm balloon (B) with relief of stenosis (C).



**Fig. 12.32.** Frontal view showing waisting of balloon catheter passed across a stenosed pulmonary valve.



**Fig. 12.34.** Retrograde aortic balloon valvoplasty with fully inflated balloon across the calcified valve (arrow) and stabilized by a stiff J-guide wire in the left ventricle.

valve is crossed with a guide wire over which an oversized balloon dilatation catheter (usually about 25%–50% larger than the valve annulus) is passed. The balloon is inflated across the valve until the waist caused by the narrow valve (Fig. 12.32) is abolished. Following the procedure a gradient at the subvalvar level may persist (due to hypertrophy of the right ventricular outflow tract) but this usually resolves in the months after relief of the valve stenosis. The results of this procedure in suitable patients are very good and are maintained for long periods.

**Aortic Valvoplasty.** Aortic valve stenosis is a common condition in elderly patients in whom the usual treatment is valve replacement. The results of this procedure, even in an older age group, are good but there are a significant number of patients in whom surgery is not possible and for whom alternative treatment was not available until the development of balloon aortic valvoplasty. This is currently advocated for the treatment of severe aortic stenosis when surgery is not possible due to advanced age, poor left ventricular

function or severe non-cardiac disease. A proportion of patients improve sufficiently after valvoplasty to have aortic valve replacement at a later stage.

Aortic valvoplasty can be performed by either the antegrade (transeptal) route (Fig. 12.33) or retrogradely from an arterial approach (Fig. 12.34). The valve is crossed with a guide wire, over which a dilatation catheter is passed; the balloon is inflated across the valve and dilated. This may be repeated several times until the gradient is reduced to a satisfactory level (ideally less than 20 mmHg). The short-term results are good but there is evidence that objective parameters of improvement are not well maintained in a large proportion of patients. In spite of this, relief of symptoms is often well maintained and justifies the procedure in a significant number of ill patients and those who would not benefit from surgery.

**Mitral Valvoplasty.** Balloon dilatation of mitral stenosis has been in use since 1984 and has been shown to be a well-tolerated procedure which can be carried out under local anesthesia, making it particularly useful in patients who are unfit for general anesthesia. Nearly all patients improve after the procedure, both in terms of symptoms and when assessed objectively. Follow-up at periods of up to 24 months shows that the improvement in symptoms and increase in valve area is well maintained.

The stenosed valve is crossed with a guide wire, usually introduced from a venous, transeptal approach, followed by a large single or double-lumen dilatation balloon catheter which is inflated across the valve. The result of the dilatation is monitored during the procedure by Doppler or pressure measurements. Inflations are repeated until a satisfactory improvement in the valve gradient has been produced.

Current opinion is that balloon mitral valvoplasty is indicated in patients with mitral stenosis where there is a relative contraindication to conventional surgery. Some patients have also been treated by balloon mitral valvoplasty where there is no contraindication to surgery and the results appear to be good. There are good reasons to expect that the long-term results of balloon mitral valvoplasty will be as good and this technique may replace surgical valvotomy.



**Fig. 12.33.** Transeptal aortic balloon valvoplasty showing waist in balloon across calcified aortic valve (short arrow). Note the loop of the balloon catheter in the left atrium (long arrow).

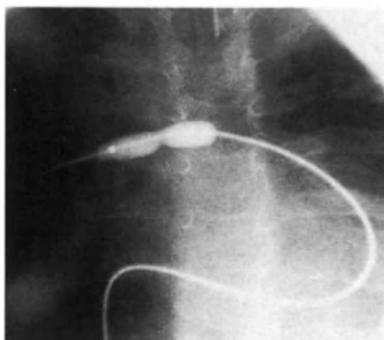


**Fig. 12.35.** Balloon dilatation of a peripheral pulmonary artery stenosis in a patient with Fallot's Tetralogy.



**Fig. 12.37.** View following pulmonary arteriogram showing contrast in a dilated pulmonary artery (arrow) feeding into a large arteriovenous fistula occluded by a balloon. A second balloon is ready for detachment to completely occlude the fistula.

#### OTHER INTERVENTIONAL TECHNIQUES

There are other interventional techniques which are occasionally used in the treatment of cardiac abnormalities. These include other balloon dilatation procedures (e.g., pulmonary artery stenosis (Fig. 12.35), re-coarctation); septostomy procedures to improve atrial mixing (using either a Fogarty catheter or a retractable blade); and various embolization techniques (Table 12.8). These are used to treat unusual conditions such as coronary artery fistulae, abnormal developmental or surgical shunts and similar vascular communications.

**Table 12.8.** Potential cardiac applications of embolization

- 
- Patent ductus arteriosus
  - Coronary artery fistulae (Fig. 12.36)
  - Surgical shunts needing closure before further corrective surgery
  - Bronchial collateral vessels in cyanotic heart disease
  - Pulmonary arteriovenous malformations (Fig. 12.37)
- 

#### REFERENCES AND SUGGESTIONS FOR FURTHER READING

Anderson RH, MacCartney FJ, Shinebourne EA, Tynan M (eds) (1987) Paediatric Cardiology. Churchill Livingstone, Edinburgh

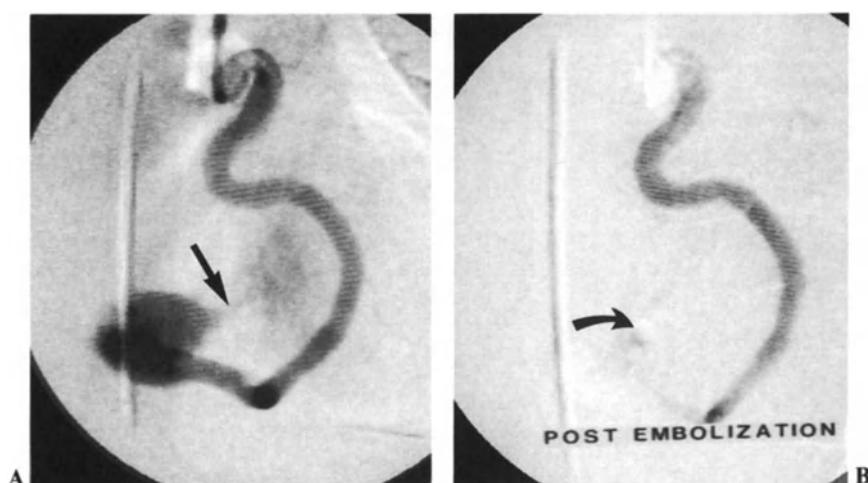


**Fig. 12.36.** A Selective DSA coronary arteriogram showing a right coronary artery to right ventricular fistula (straight arrow). B This was completely occluded by a detachable balloon (curved arrow).

- Braunwald E (ed) (1988) Heart Disease, 3rd edn. WB Saunders, Philadelphia
- Freedom RM, Culham JAG, Moes CAF (1984) Angiocardiography of Congenital Heart Disease. Macmillan, New York
- Grossman W (1986) Cardiac Catheterisation and Angiography, 3rd edn. Febiger, Philadelphia
- Hagan AD, DiSessa TG, Bloor CM, Calleja HB (1983) Two Dimensional Echocardiography. Little, Brown and Company, Philadelphia
- Seward JB, Tajik AJ, Edwards WD, Hagler DJ (1987) Two Dimensional Echocardiography Atlas, vol 1. Springer Verlag, New York
- Shuford WH, Sybers RG (1974) The Aortic Arch and its Malformations. Carles C Thomas, Springfield
- Silverman NH, Snider AR (1982) Two Dimensional Echocardiography in Congenital Heart Disease. Appleton-Century-Crofts, Norwalk
- Verrel D, Grainger RG (1978) Cardiac Catheterisation and Angiocardiography, 3rd edn. Churchill Livingstone, Edinburgh
- Wilde P (1989) Doppler Echocardiography – An Illustrated Clinical Guide. Churchill Livingstone, Edinburgh

## CHAPTER 13

# ANGIOGRAPHY

D. Sutton

---

## ARTERIOGRAPHY

---

### Techniques

It is a remarkable fact that the first arteriogram was published within a few months of Roentgen's discovery of X-rays in 1895. This was achieved by injecting radiopaque paste into the artery of a cadaver upper limb, but it demonstrates that the possibility of human angiography was realized even at that early stage of the new science. However, *in vivo* angiography was not achieved until the 1920s, and it needed the development of safer intravascular contrast media in the 1930s, and percutaneous techniques of injection in the 1940s and 1950s for percutaneous arteriography to become a routine radiological procedure.

Since then there have been many further improvements and refinements of technique. Of particular importance in recent years have been the development and expanding scope of interventional angiography, the introduction of the new and safer low osmolarity contrast media, and the development of digital subtraction angiography (DSA).

The techniques now most widely used for arteriography include:

1. Percutaneous arterial catheterization and standard cut film arteriography.
2. Percutaneous arterial needle puncture and standard cut film arteriography.
3. DSA following percutaneous i.v. injection or intra-arterial injection.

The newer imaging techniques of isotope imaging, ultrasound, CT and MRI can also be useful in the demonstra-

tion of vascular pathology, particularly where major vessels are involved.

### Contrast Media

The ideal contrast medium should be completely non-toxic and completely painless on injection. It should also be of low viscosity and easy to inject. The nearest approach to such ideal media are the new generation of low osmolarity contrast media introduced over the last 10 years. These are listed in Table 13.1.

Table 13.1. Low osmolar contrast media

Iopamidol	(Niopam)	Non-ionic
Iohexol	(Omnipaque)	Non-ionic
Iopromide	(Ultravist)	Non-ionic
Ioxaglate	(Hexabrix)	Ionic

Osmolality is related to the ratio of iodine atoms to particles in solution. The older hyperosmolar contrast media had a ratio (iodine atoms : particles in solution) of 3:2. The new non-ionic contrast media have a ratio of 3:1, whilst ioxaglate, which is ionic, has a ratio of 6:2, effectively the same 3:1.

The only major drawback to the use of these newer media is their high cost compared with the older hyperosmolar contrast media, and because of this the older media are still widely used where costs and budgets have to be considered.

*Dosage.* The dose of contrast medium and its rate of delivery is generally related to the size and blood-flow of the

vessel being injected. The highest doses are used for arch aortography where 40 ml of high concentration contrast (e.g., iopamidol 370) are injected at a speed of 20 ml per second.

Acceptable doses for selective injection in other vessels would be as in Table 13.2, with the concentrations of Iohexol (or equivalent of other contrast medium) suggested.

**Table 13.2.** Doses of contrast media and rates of delivery into vessels

Vessel	Volume injected	Medium
Abdominal aorta	30 ml in 1.5 sec	Ioxaglate 320
Femoral	20 ml in 2 sec	Iohexol 240
Subclavian	20 ml in 2 sec	Iohexol 240
Carotid	8 ml in 1 sec	Iohexol 240
Vertebral	6 ml in 1 sec	Iohexol 240
Renal artery	10 ml in 1 sec	Iohexol 240
Bronchial artery	5 ml in 1 sec	Iohexol 240
Intercostal artery	3 ml in 1 sec	Iohexol 240
Celiac axis	20 ml in 3 sec	Iohexol 300
Superior mesenteric	20 ml in 3 sec	Iohexol 300

The above doses are suggested for conventional cut film arteriography, but with intra-arterial DSA the doses can be considerably reduced and only one third or less of these amounts are necessary. The same injection volumes may be used by diluting the smaller amounts of contrast with saline. With intravenous DSA much larger amounts of contrast are necessary but the technique is, of course, simpler and can be used on an out-patient basis.

### Complications

Contrast angiography skilfully performed by experienced operators carries a relatively low morbidity. However, numerous complications have been described and there is no doubt that these are directly related to the skill and experience of the operators. Junior and inexperienced arteriographers should only practice under the direct supervision of more experienced workers.

The complications of arteriography are listed in Table 13.3. *Contrast reactions* and their prophylaxis and treatment are described in the section on Urology (Chap. 33).

*Embolus* due to catheter clot formation is one of the most common and dangerous complications. Cerebral emboli may result not only from cerebral angiography but from any type of catheterization where the catheter tip is passed proximal to the origins of the great vessels. This includes subclavian and coronary arteriography and left ventriculography. It should be guarded against by the routine use of heparinized saline for catheter flushing as well as rapid and efficient arteriography.

Cotton fibre emboli may result from wiping guide wires and catheters with gauze swabs, and air emboli can be introduced by carelessly allowing air into injection syringes for contrast or saline.

*Vagal inhibition* results in circulatory collapse with marked bradycardia and can thus be differentiated from an anaphylactoid reaction with hypotension where tachycardia is characteristic. The distinction is vital since the former is treated with atropine and the latter with epinephrine.



**Fig. 13.1.** Shortly after a percutaneous transfemoral catheterization the patient's limb became pale and pulseless. This large thrombosed clot was removed from the common femoral artery by emergency direct surgery.

*Local complications* should be carefully watched for both during and after arteriography. False aneurysm, AV fistula or local thrombosis will all require surgical intervention (Fig. 13.1). Damage to the brachial plexus is a well-recognized complication of axillary catheterization, a procedure which should only be performed by experienced angiographers.

*Damage to organs* from excess of contrast or catheter clot embolus has been recorded for many different areas including brain, spinal cord, kidneys, bowel, pancreas, testis, heart and skin.

### VASCULAR LESIONS

These form the main indication for angiography and will be discussed under the following headings: congenital lesions, aneurysms, angiomas, AV fistula, stenoses and thromboses, emboli and hemorrhage.

### Congenital Lesions

Anomalies of the arterial system are common and some are of great practical importance. Those affecting the

**Table 13.3.** Complications of contrast arteriography

General	contrast reactions (see Chap. 33)
	severe life threatening
	intermediate
	minor (coughing, sneezing, mild urticaria)
embolus	catheter clot
	cotton fibre
	air
	septicemia
	vagal inhibition
Local	puncture site
	hemorrhage and hematoma
	false aneurysm
	AV fistula
	perivasculär or subintimal contrast injection
	local thrombosis
	local infection
	damage to adjacent nerves
	damage to target or other organs due to
	excess of contrast
	catheter clot embolus
	fracture and loss of guide wire tip
	knot formation in catheters
	embolization accidents (see text)
	angioplasty accidents (see text)



**Fig. 13.2.** Abdominal aortic coarctation.



**Fig. 13.3.** Degenerative popliteal aneurysm. ►

intracranial vessels are discussed in the CNS section as are some anomalies of the aortic arch.

*Coarctation of the thoracic aorta* is described above (p. 195). *Coarctation of the abdominal aorta* (Fig. 13.2) is encountered far less commonly. A long or short segment of the abdominal aorta may be affected and the lesion may extend to the lower thoracic aorta. The origins of one or more splanchnic or renal vessels are often involved. In the latter case secondary hypertension may occur.

*Pseudocoarctation* of the thoracic aorta is due to sharp kinking of the arch at its junction with the descending aorta and can be mistaken for a mass lesion in the region of the arch on a simple PA chest film. *Buckling* of the arch can also occur in its mid portion.

*Renal arteries* are multiple in about 25% of kidneys. It is vital, therefore, that living potential kidney donors should be checked for this anomaly before being operated on. In most of these cases there are two arteries, but occasionally three are seen and very rarely four are found. Ectopic and horseshoe kidneys usually have anomalous arteries of supply from the common iliac or lower abdominal aorta and these may also be multiple.

The main *splanchnic vessels* show wide variations of pattern. The right hepatic artery or an accessory right hepatic artery, arises from the superior mesenteric in 20% of patients, and a similar proportion have a left hepatic or accessory left hepatic artery arising from the left gastric artery. The splenic and left gastric arteries sometimes arise direct from the aorta instead of from the coeliac axis.

Anomalies of the major *limb vessels* are rare, but the brachial artery occasionally divides into its terminal radial and ulnar branches in or before the axilla. In the lower limb persistence of the *primitive sciatic artery* results in the rare anomaly of the main femoral artery arising from an enlarged hypogastric artery and passing through the sciatic notch and behind the femoral neck to reach the thigh whilst the true

femoral is hypoplastic and may terminate in the profunda. The popliteal artery which normally divides into its tibial branches at the knee joint may bifurcate at a higher level.

### Aneurysms

Arterial aneurysms may arise from a variety of causes and these may be classified on an etiological basis as congenital, degenerative, traumatic, infective, dissecting, post-stenotic and necrotizing.

So-called **congenital aneurysms** arise mainly in the cerebral circulation at points of arterial bifurcation where there is a defect in the muscular coat, and are commonest in the region of the Circle of Willis where the vessels lie in the subarachnoid space CSF, unsupported by surrounding soft tissues (see Chap. 41). Although the congenital defect contributes to the development of aneurysms, these lesions are rarely seen in children and other factors such as hypertension and atheroma are considered to be major factors in their development.

**Degenerative aneurysms** are due to atherosomatous involvement of the arterial wall and are commoner in males and in specific vessels. The sites of election include the abdominal aorta, the iliac vessels, the popliteal arteries and the descending thoracic aorta, though other smaller vessels including the intracerebral and renal arteries are not immune.

Atheroma leads to weakening of the arterial wall, often followed by fusiform dilatation (ectasia). However, the dilatation may become saccular, particularly in the sites mentioned above (Fig. 13.3), and such saccular aneurysms are liable to rupture with serious or fatal results.

**Imaging.** *Simple radiographs* may show curved linear calcification in the wall of an atherosomatous aneurysm and such arc like linear calcification is diagnostic. It is frequently seen in atherosomatous aneurysms on routine abdominal films.

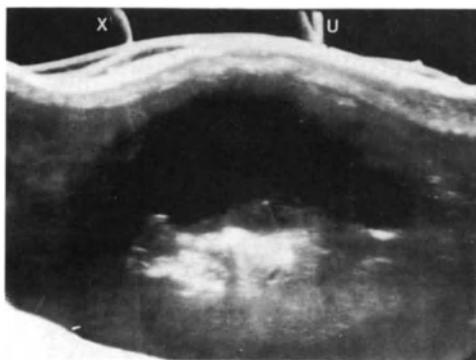


Fig. 13.4. Ultrasound sagittal section showing large abdominal aortic aneurysm.



Fig. 13.6. CT of so-called 'inflammatory' aortic aneurysm showing thickened enhancing wall.

*Angiography* is the usual prelude to surgical intervention in most symptomatic saccular aneurysms; or even when asymptomatic saccular aneurysms are found on routine examination. With abdominal aortic aneurysms it is important for the surgeon to know whether the renal artery origins are involved by the aneurysm and angiography should show this clearly. Some aneurysms can be assessed by *ultrasound* (Fig. 13.4) or by *CT* (Fig. 13.5) and such non-invasive methods are useful in serial follow-up if surgery is deferred, particularly with abdominal aneurysms.

So-called '*inflammatory aneurysms*' are an unusual variant of degenerative abdominal aortic aneurysm. The diagnosis is made by *CT* (Fig. 13.6) when the aneurysm shows an irregular thickened wall which enhances with contrast. The condition is thought to be due to periarterial fibrosis following multiple small retroperitoneal hemorrhages, and should not be confused with idiopathic retroperitoneal fibrosis (see Chap. 35).

**Traumatic aneurysms** may occur anywhere in the arterial system and are particularly common in the limbs. They may result from direct injury to vessel walls by knives or missiles, but can also follow closed injury, particularly in the thorax and abdomen.

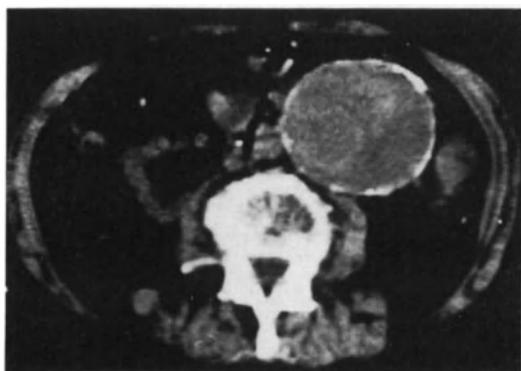


Fig. 13.5. CT of large abdominal aortic aneurysm with calcified wall.

*Traumatic aneurysm of the thoracic aorta* is now a well recognized sequel to crush injury of the chest in car accidents. The isthmus of the aorta near the ligamentum arteriosum is usually involved, the acute deceleration producing a shearing effect on the back of the arch at this point. In most cases, the rupture and associated injuries are fatal but in about 20% of cases the peri-aortic hemorrhage is contained by the peri-adventitial mediastinal tissues. Untreated, most of these cases will proceed to further hemorrhage and death within a few days and survival beyond this is rare. Urgent investigation and surgery are, therefore, fully justified.

**Imaging.** *Simple radiography* may show broadening of the mediastinum but this is difficult to evaluate in a portable film on a patient who often has multiple injuries.

*Angiography* is the definitive investigation (Fig. 13.7) and usually shows the false aneurysm. However, it is important to realize that the signs may be more subtle and may consist of slight mural irregularity or a mural flap at the affected site. The small ductus diverticulum which may occur at this site can be differentiated by its smooth wall and characteristic site, projecting downwards and medially from the lower aortic wall.

**Infective aneurysms** are most frequently seen in patients with bacterial endocarditis. In such patients mycotic aneurysms may result in any part of the vascular system and can grow rapidly in size (Fig. 13.8). In the cerebral circulation they are usually peripheral in middle cerebral territory in contrast to the commoner congenital (berry) aneurysms which are nearly always related to the Circle of Willis or the middle cerebral bifurcation.

Local bacterial abscesses may involve arterial walls and lead to infective aneurysms and we have encountered such cases in the axilla and in the groin. Tuberculous abscesses may also involve arterial walls and result in aneurysms.

Syphilis as a cause of aneurysm is now becoming rare in developed countries, though it is still encountered in underdeveloped countries. The commonest site is the ascending aorta and aortic arch (Fig. 13.9), though other vessels are not immune. Specific aortitis may produce marked dilatation of the ascending aorta with linear mural calcification.

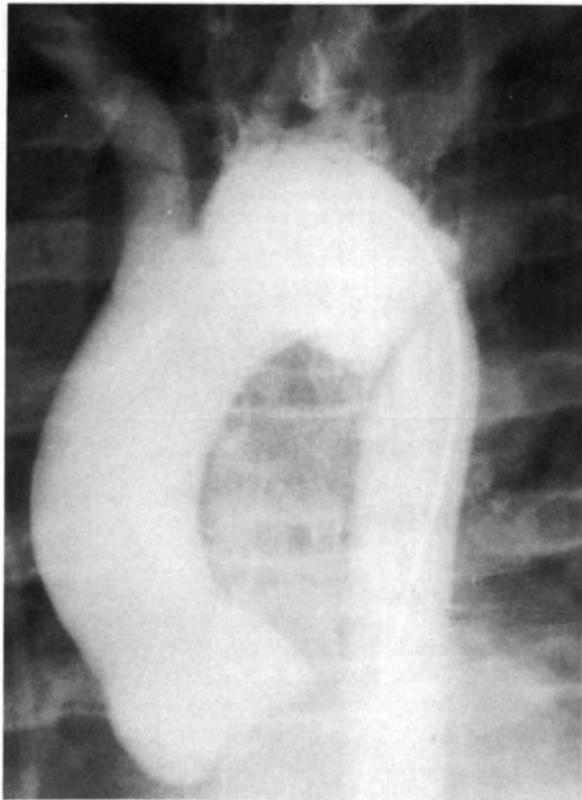


Fig. 13.7. Traumatic aneurysm of the thoracic aorta.

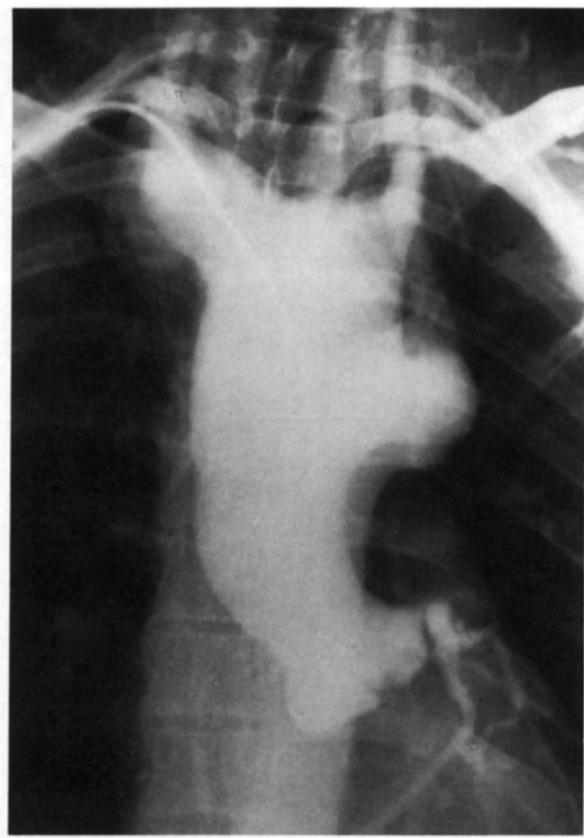


Fig. 13.9 Syphilitic aortic aneurysm involving the aortic arch and origins of the great vessels.

### Dissecting Aneurysm

Classical dissecting aneurysm involves the thoracic aorta and there is a strong association with hypertension as well as a male sex preponderance. Less commonly, local dissecting aneurysms may occur in other major vessels and we have encountered examples in the abdominal aorta and in a common iliac artery; the common carotid artery is also a well-documented site for local dissection (see Chap. 41). Most

patients with classical thoracic aortic dissections are over 50 years of age. The incidence is 5–10 cases per million population per annum.

In the rare cases which occur in younger patients there is nearly always an associated predisposing cause such as *Marfan's syndrome* or *congenital aortic lesions* such as coarctation, aortic stenosis or bicuspid valves. In younger female patients *pregnancy* is another rare precipitating cause.

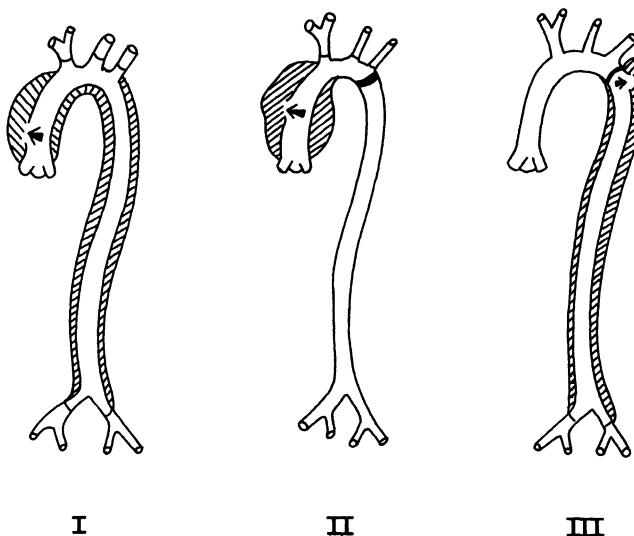
De Bakey has classified dissections into three types (Fig. 13.10). Type 1 commences in the ascending aorta and involves both it and the descending aorta (45% of cases). Type 2 involves only the ascending aorta and is the least common (10% of cases); it is usually associated with Marfan's syndrome. Type 3 commences in the arch and involves only the descending aorta (45% of cases). A more useful classification to the surgeon is type A which includes both types involving the ascending aorta and type B which is the same as type 3. This is because the prognosis in type A is much worse than in type B, and the mortality of 80% can be reduced to 35% by surgery.

The mortality rate is much lower in type B cases and is not significantly improved by surgery, so that conservative treatment is usually practiced in these cases.

**Imaging.** Simple radiography may show enlargement of the aortic knuckle; it may also show bulging of the descending aorta to the left or a left pleural effusion due to hemothorax.



Fig. 13.8. Mycotic aneurysm of the ulnar artery.



► Fig. 13.10. Diagram illustrating the different types of thoracic aortic dissecting aneurysms (after De Bakey).

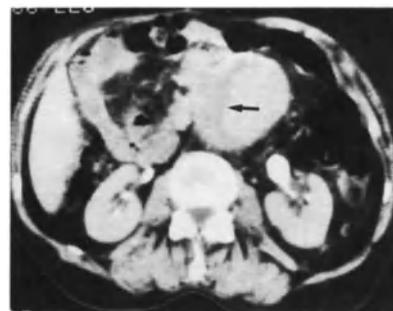


Fig. 13.12. CT of dissecting aortic aneurysm, showing intimal flap separating the two lumens.

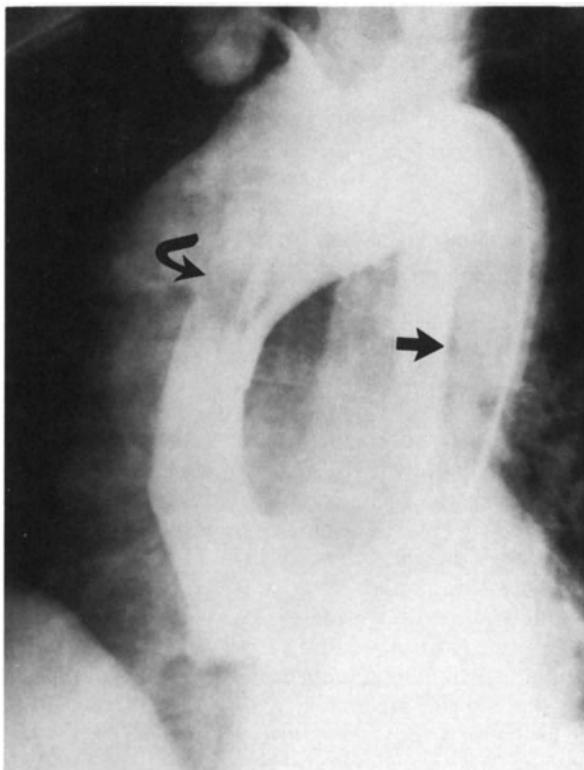
These signs are most certain and helpful if there is a recent normal film for comparison.

*Angiography* was for many years the definitive investigation, and will accurately define the type and extent of the dissection. The catheter tip should be sited in the ascending aorta for the thoracic study (Fig. 13.11), and abdominal studies are usually also necessary to define the lower limits of the lesion.

CT can also confirm the diagnosis of dissecting aneurysm in a less invasive manner (Figs 13.12, 9.20, 9.21), though intravenous contrast is necessary.

*Ultrasound* has also been used to confirm the diagnosis in a non-invasive manner by demonstrating the intimal flap, but is less reliable, particularly in the thorax.

*MRI*, if available, is a more accurate non-invasive technique for establishing the diagnosis (Fig. 13.13).



► Fig. 13.11. Dissecting aneurysm type 1 shown by angiography. Curved arrow points to site of dissection; straight arrow points to intimal flap separating true and false lumens.

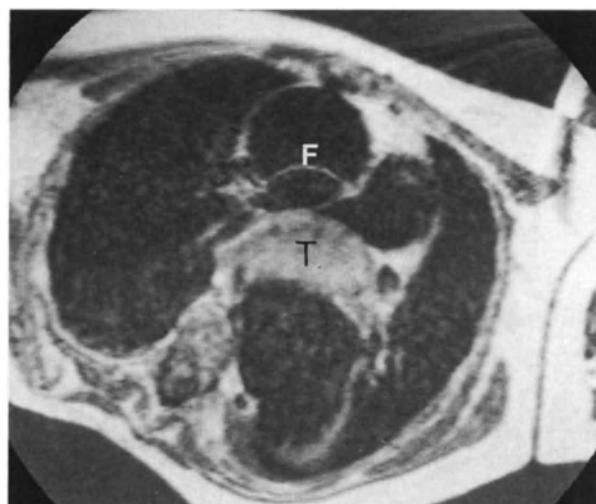
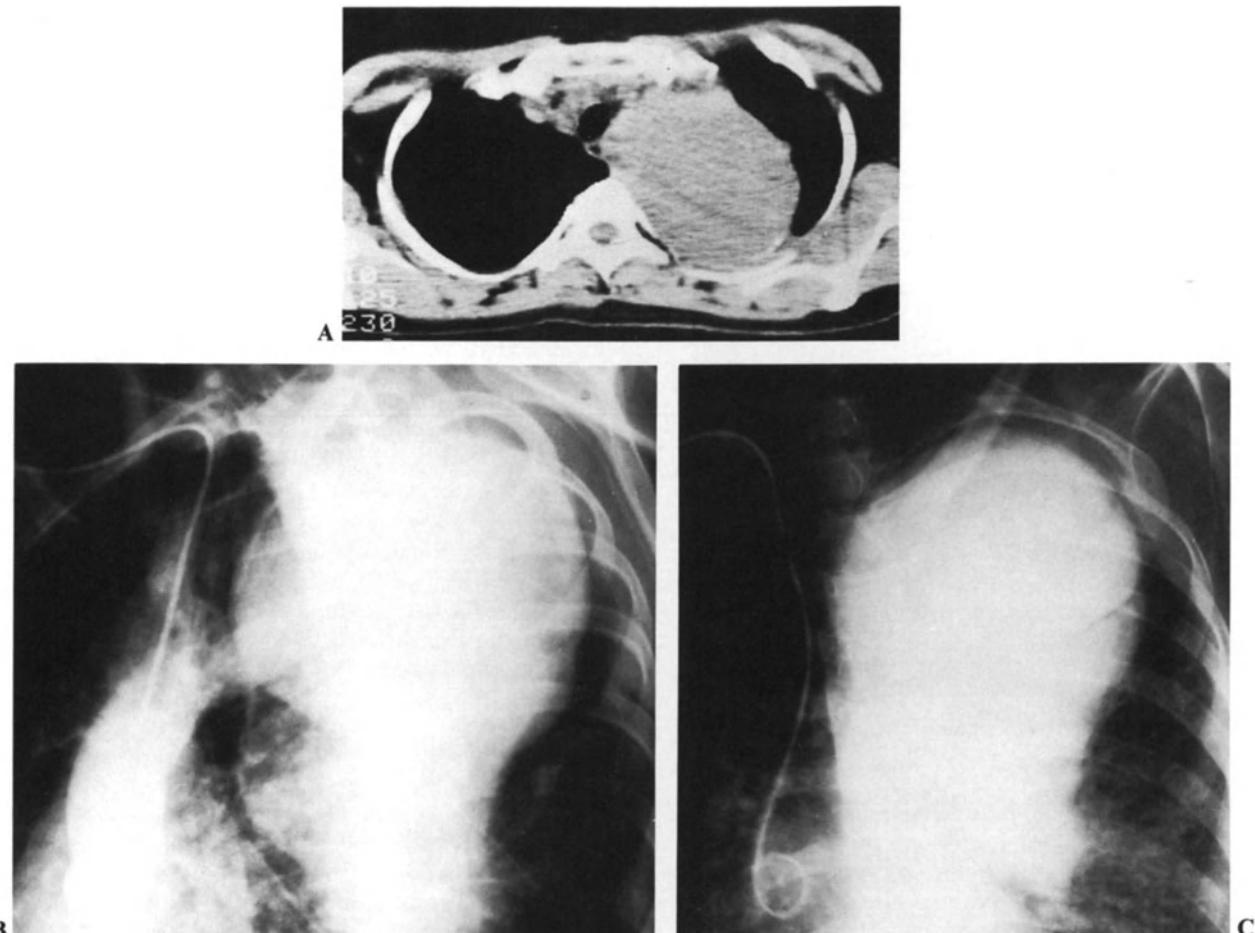


Fig. 13.13. Dissecting aortic aneurysm shown by MRI. The intimal flap and double lumen are shown in the ascending aorta (F). The false lumen contains thrombus (T) in the descending aorta. (Courtesy of Dr Peter Wilde and Bristol MRI centre.)



**Fig. 13.14A, B, C.** Giant post-stenotic aneurysm in a young female patient with unrecognized mild coarctation and presenting as a mediastinal mass. A CT shows large mass in left upper middle and posterior mediastinum. B, C Aortography confirms the huge post-stenotic aneurysm.

**Post-stenotic aneurysms** are probably due to turbulence and abnormal eddy flows affecting the vessel wall beyond the stenosis. In clinical practice such aneurysms are seen:

1. Post-coarctation in the thoracic aorta (Fig. 13.14).

2. Post-subclavian stenosis in thoracic inlet syndrome (Fig. 13.15).
3. Post-fibromuscular stenosis in the renal artery.
4. Post-atheromatous stenosis in any vessel.

**Necrotizing vasculitis** is a feature of *polyarteritis nodosa* and gives rise to multiple small aneurysms in the renal vessels and in other organs. The appearances at renal angiography are virtually diagnostic (Fig. 13.16).

Necrotizing arteritis is also seen less commonly in *systemic lupus erythematosus* and *Wegener's granulomatosis*, and is not infrequent in *drug abuse* patients, particularly with *metamphetamine*. Small vessels adjacent to the pancreas may be involved by *acute pancreatitis*, giving rise to retroperitoneal aneurysms which can rupture with disastrous consequences.



**Fig. 13.15.** Post-stenotic aneurysm in a patient with thoracic inlet syndrome due to fibrous band.

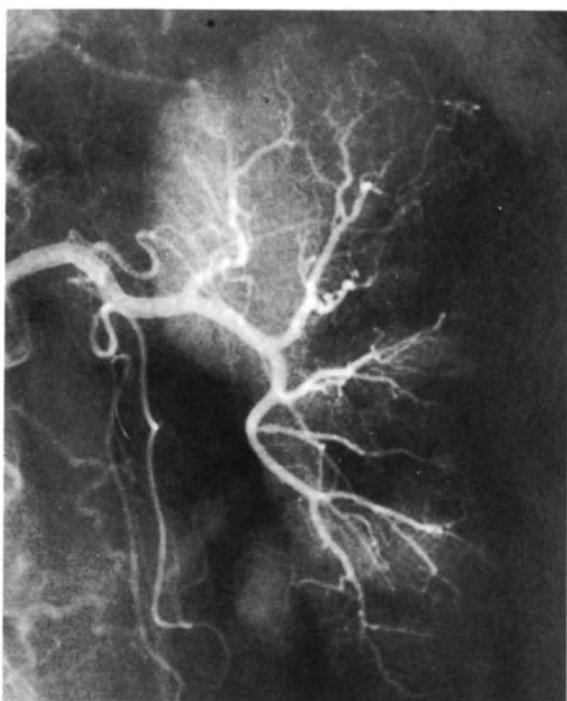


**Fig. 13.16.** Polyarteritis nodosa. Renal angiogram shows multiple small aneurysms.

progressively hypertrophy to accommodate the increased blood flow. These lesions are common in the cerebral circulation but can also occur in any part of the vascular tree and in any organ.

A typical angiomatic malformation is illustrated in Fig. 13.17. In the limbs the increased blood flow can lead to localized hypertrophy and very large angiomas can affect the heart because of the large AV shunt.

In the past these lesions could only be treated by direct surgery, but the development of interventional radiology now offers an alternative approach by percutaneous selective catheterization and embolization.

**Imaging.** These lesions can be identified by contrast-enhanced CT and by scintigraphy or even non-invasively by ultrasound and MRI, but *selective angiography* is usually required for a full anatomical demonstration of the feeding arteries and draining veins and is of course essential for treatment by embolization.

#### AV Fistula

The term is best reserved for acquired lesions, though the term congenital AV fistula has been used in the past for the congenital angiomas described above. An AV fistula is characterized by a direct communication between an artery and an adjacent vein. The majority are of traumatic origin, but a few are secondary to rupture of an aneurysm into an adjacent vein.



**Fig. 13.17A, B.** Angiomatic malformation in the pelvis. Note dilated feeding arteries and drainage vein.

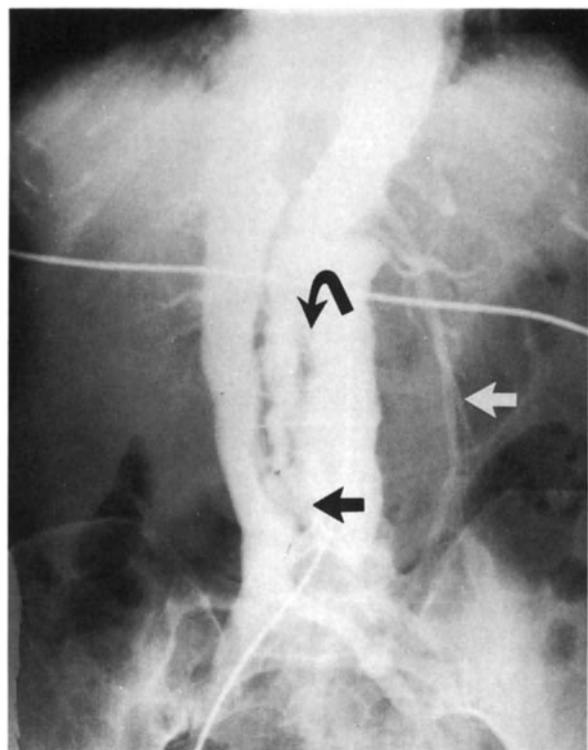


**Fig. 13.18.** Large AV fistula between the aorta and IVC and due to spontaneous rupture of an atheromatous aortic aneurysm. Black arrow points to fistula; curved arrow to apparent intimal flap; white arrow to displaced superior mesenteric outlining partly clotted part of the aneurysm, which is larger than the opacified lumen suggests. (Reproduced with permission from Gregson et al. (1983) Clinical Radiology. 34; 683.)

Penetrating wounds are the major cause but it is important to realize that AV fistulas can occasionally follow a closed or crush injury. Iatrogenic AV fistulas form an important subgroup, and are particularly common following orthopedic operations and renal biopsy.

Spontaneous AV fistula is perhaps commonest in the cavernous sinus where it follows rupture of a carotid aneurysm into the cavernous sinus (see Chap. 41). It has also been described after rupture of an aortic aneurysm into the inferior vena cava, where it can give rise to difficult diagnostic problems.

As with angiomas, there is hypertrophy of the artery involved and of the main drainage veins. A large fistula throws an extra burden on the heart because of the AV shunt and increased cardiac output and can lead to heart failure.

**Imaging.** Selective angiography is usually required for accurate localization of the fistula, and is essential for treatment by embolisation (Figs 13.18, 13.19).

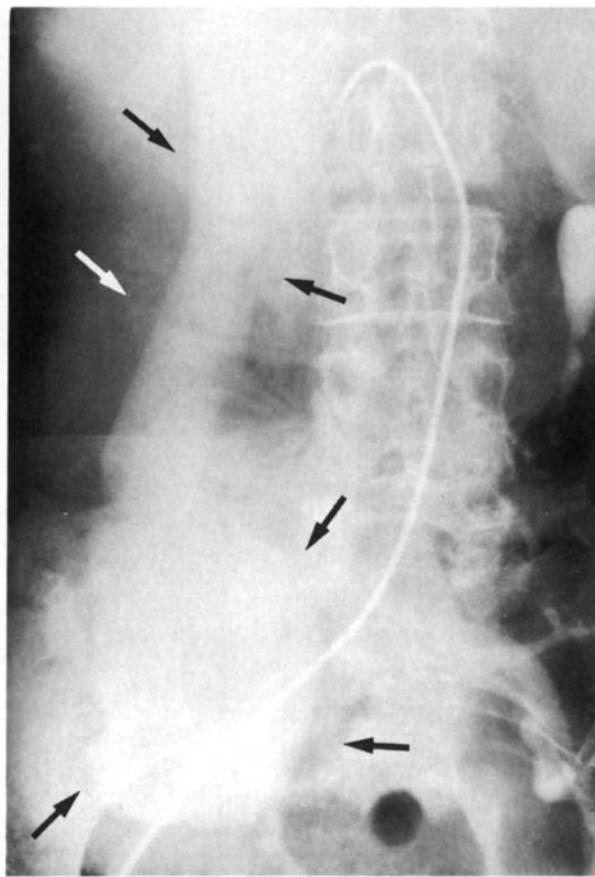
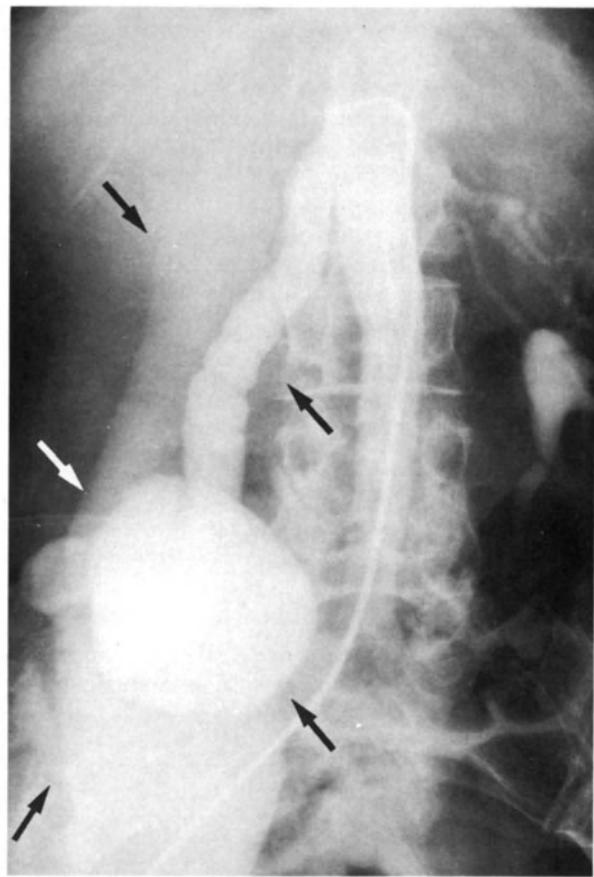


**Fig. 13.19A, B.** Large AV fistula between grossly hypertrophied right renal artery and vein from spontaneous rupture of large aneurysm secondary to fibromuscular hyperplasia.

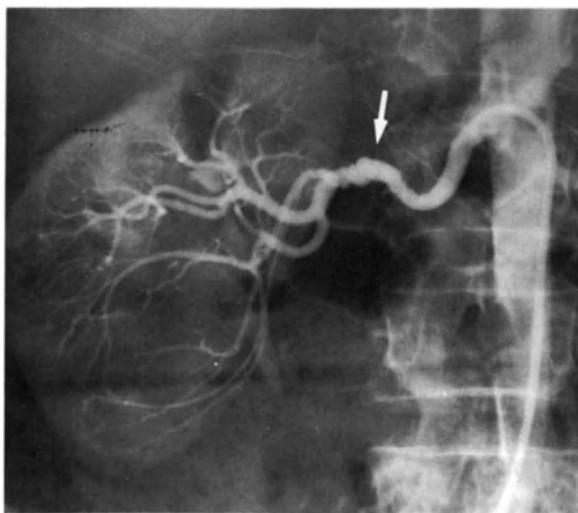


Fig. 13.20. Fibromuscular hyperplasia of the renal artery.

### Stenoses and Thromboses

Stenoses of arteries are commonly complicated by thromboses and both stenosis and thrombosis are frequent causes of morbidity. They are among the main indications for imaging of the arterial system. The causes in order of frequency include:

1. Atheroma.
2. Buerger's disease.
3. Congenital lesions.
4. Extrinsic pressure.
5. Arteritis.

*Atheromatous* arterial stenosis is a common complication of degenerative arterial disease. It may affect any of the major vessels and gives rise to a variety of clinical syndromes dependent on the particular vessel involved. Thus intermittent claudication and lower limb ischemia are seen with atheromatous stenosis and thrombosis of the femoral and iliac vessels and of the abdominal aorta; hypertension may result from renal artery stenosis; angina and cardiac ischemia occur with coronary stenosis, and transient ischemic attacks (TIAs) with internal carotid lesions.

*Buerger's disease* or 'thromboangiitis obliterans' was first described as a separate entity in 1908, and its precise nature has given rise to much controversy. Some consider it to be an unusual form of atheroma with peripheral thrombosis and sparing of the larger arteries. However, it occurs in a generally younger age group (20 to 40 years) and almost exclusively in males who are heavy smokers.

*Congenital* lesions of clinical importance include:

1. Thoracic and abdominal coarctation.
2. Fibromuscular hyperplasia.
3. Popliteal cyst.

Thoracic coarctation is described above (p. 195). *Abdominal coarctation* is also described above (see p. 237 and Fig. 13.3). It may affect a short or long segment of the aorta centered near the coeliac axis or superior mesenteric. The origins of

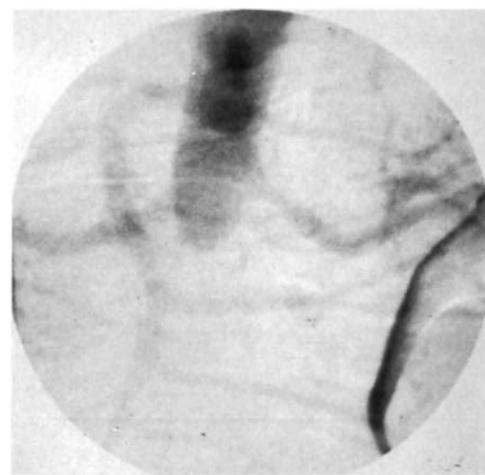


Fig. 13.21. Aortic thrombosis shown by venous DVI study.

splanchnic vessels may also be stenosed, as may the origins of the renals.

*Fibromuscular hyperplasia* is a developmental anomaly first described in the renal arteries and predominantly presenting in young adult females. It is characterized by irregular muscular hypertrophy and luminal narrowing, which often gives rise to secondary hypertension and occasionally to aneurysm formation. The disease can also occur in other vessels including the internal carotid.

*Popliteal cysts* develop in the wall of the popliteal artery in young males, leading to a smooth localized stenosis. The cyst is lined by mucin-secreting cells thought to be derived from the capsular synovial cells of the knee joint. Similar lesions have been described in other vessels including the common iliac, radial and ulnar arteries.

*Extrinsic compression* of arteries leading to stenosis may also result from congenital lesions though presenting in adolescents or adults. It occurs in:

1. *Thoracic inlet syndrome*, where the subclavian artery is compressed by a cervical rib, fibrous band or scalenus anticus muscle.
2. *Renal artery stenosis* (rarely) caused by a fibrous band or neurofibromatosis.
3. *Popliteal entrapment* by an anomalous tendon of the medial head of gastrocnemius – a rare condition presenting in adolescent or young males, often with acute thrombosis.
4. *Coeliac compression syndrome*, external compression of the coeliac origin by the median arcuate ligament of the diaphragm or by coeliac plexus fibrosis.

Stenosis of arteries can also result from pressure by a tumor mass or from invasion by a malignant tumor giving rise to 'cuffing'.

**Imaging.** *Arteriography* is usually required for the assessment of most arterial stenoses and thromboses (Figs 13.20, 13.21, 13.22) and is essential if surgery or balloon dilatation is being considered.

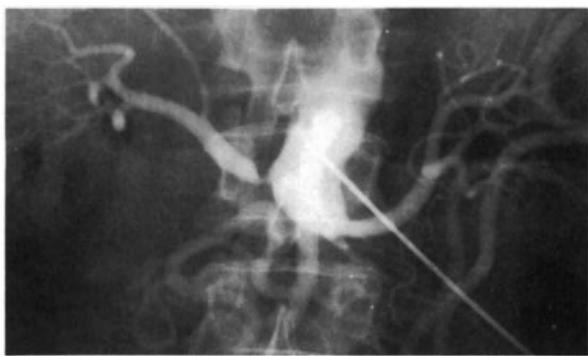


Fig. 13.22. Aortic thrombosis shown by lumbar aortography. Note the atheromatous stenosis of the renal artery.

*Duplex ultrasound* is the most widely used of the non-invasive imaging techniques and can be helpful in confirming lesions of superficial vessels such as the carotids in the neck.

### Emboli

Acute embolus may be difficult to distinguish clinically from acute thrombosis, though with most cases of embolus there

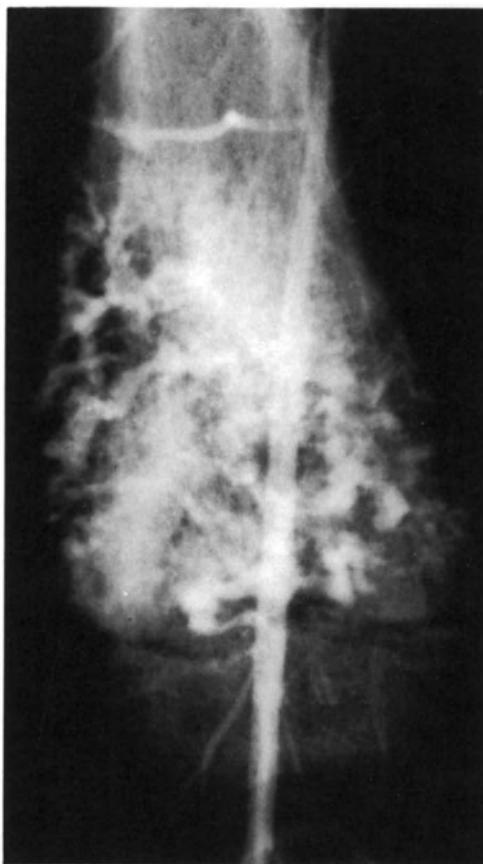


Fig. 13.23. Malignant tumor (bone sarcoma) showing pathological vessels.

is clinical evidence of the predisposing cause. These include:

1. Atrial fibrillation with left atrial clot.
2. Cardiac infarction with left ventricular clot.
3. Arterial aneurysms with mural thrombus.
4. Atheromatous plaque or ulcer with mural thrombus.
5. Paradoxical embolus from the venous system to the right auricle and then through a patent foramen ovale to the left auricle and systemic circulation. This usually requires raised right atrial pressure as in pulmonary embolus or chronic lung disease.
6. Iatrogenic – following arterial catheterization, with clot forming on the catheter tip.

Peripheral emboli in the limbs usually have quite a good prognosis, but larger emboli, such as aortic bifurcation and iliac emboli, may require urgent surgery. Cerebral emboli can also lead to grave consequences even when small because end-arteries to vital areas are frequently involved (see Chap. 41).

**Imaging.** *Arteriography*, either direct or by DSA, is required for accurate anatomical assessment.

### Hemorrhage

Internal hemorrhage may be due to many causes including trauma, malignant tumors, peptic ulceration, inflammatory lesions, ruptured aneurysms, and post-radiation. The original aim of the radiologist was to define the anatomical site and cause of the lesions, but with the increasing scope of interventional radiology he has also become increasingly involved with their treatment. This is discussed below.

## TUMORS

Neoplasms and other mass lesions were at one time widely investigated by angiography. With the advent of CT, high-resolution ultrasound and MRI the use of angiography for the diagnosis of tumors is now rarely required except to complement the non-invasive techniques in problem cases or where the surgeon requires prior information in suspected hypervascular masses. It is also used in interventional radiology for the treatment of such hypervascular tumors (see below).

Malignant tumors are, as a general rule, more vascular than the tissues in which they arise and the angiographic pattern is frequently, though not invariably, specific and diagnostic. Abnormal or 'pathological vessels' outlined by contrast may thus identify and localize the tumor. Arteriovenous shunting with early filling of drainage veins and the presence of small irregular vessels are common angiographic findings in the more malignant tumors (Fig. 13.23), as is invasion and 'cuffing' of adjacent normal vessels. Benign tumors and cysts are, by contrast, avascular or relatively hypovascular, though there are exceptions and some benign tumors can be hypervascular e.g., chromaffinomas, hemangiomas, renal angiomyolipoma and juvenile angiofibroma (Figs 13.24, 13.27).

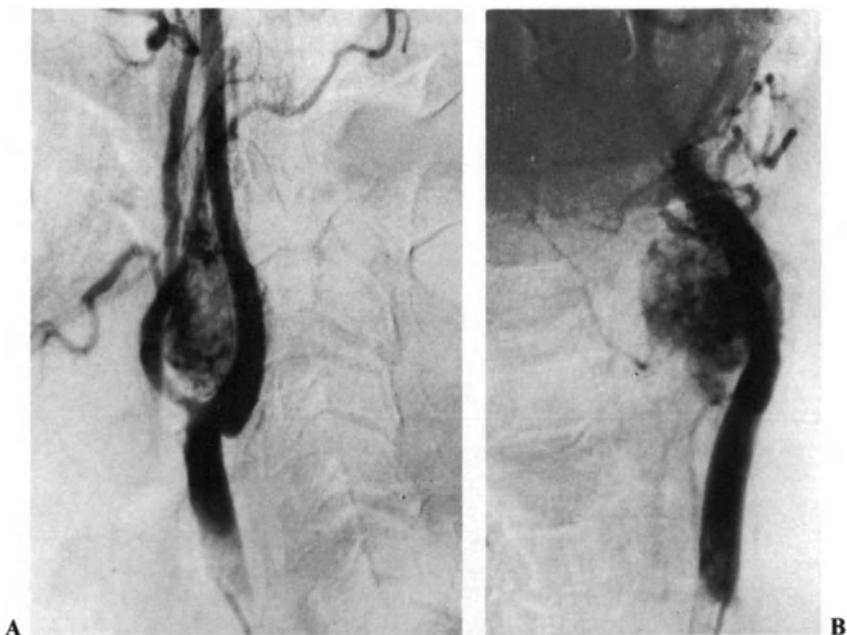


Fig. 13.24.A Carotid body tumor, lateral view. B AP view.

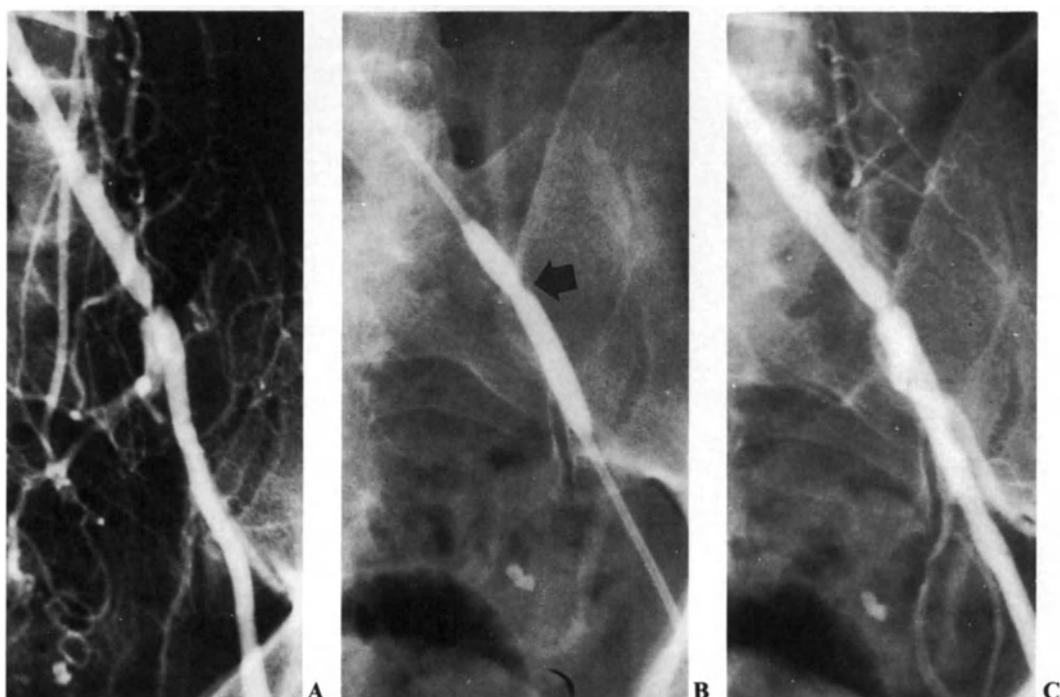


Fig. 13.25A, B, C. Angioplasty. A Severe stenosis of the left iliac artery. B The contrast-filled balloon is in position dilating the stenosis (arrow). C Immediate post-dilatation angiogram shows widening of the stenosis though some narrowing remains. However, the pressure gradient was successfully abolished with relief of symptoms.

## INTERVENTIONAL ANGIOGRAPHY

The main techniques now used in interventional angiography include percutaneous transluminal angioplasty, percutaneous catheter embolization, percutaneous catheterization for intra-arterial chemotherapy of tumors and percutaneous thrombolysis.

### Angioplasty

The major advance in this field was made by Gruntzig who first developed a double lumen dilatable balloon catheter for percutaneous dilatation of arterial stenoses (Gruntzig 1976). This led to the widespread use of percutaneous transluminal angioplasty for the treatment of arterial stenosis and thrombosis.

The femoral and iliac arteries (Fig. 13.25) were the first to be treated by this technique, which was later extended to the renals (Fig. 13.26), the coronaries and other arteries. Even abdominal aortic stenosis has been treated by using two 8-mm balloons side-by-side.

Intra-arterial pressure studies are an essential part of the technique. Pressure tracings are obtained both proximal and distal to the stenosis to confirm the presence of a pressure gradient affecting blood flow and its abolition after balloon dilatation of the stenosis.

Balloon dilatation acts by splitting the arterial intima and permitting slight dilatation of the artery and redistribution of the atheromatous plaque around the dilated artery. The results of balloon angioplasty are as good as or better than

direct surgery in most of the vessels mentioned and the mortality and morbidity are significantly lower. The duration and cost of hospitalization are also significantly reduced compared with direct surgery.

Non-ionic contrast media should be used for visualization of the stenosis before and after balloon dilatation, since they are less irritant to the traumatized intima and more comfortable to the patient. Heparin (5000 units) is injected through the catheter once its tip lies proximal to the stenosis to reduce the risk of embolus and thrombosis; for coronary dilatation 10 000 units i.v. is used. Aspirin therapy is also recommended for 24 hours before and 6 months after the procedure, and some workers also recommend long-term Warfarin therapy from the second post-operative day.

*Complications.* Apart from the complications of arteriography in general there are special hazards associated with balloon angioplasty which serve to emphasize that the procedure should only be undertaken by experienced angiographers. The complications include:

1. Local dissection due to the guide wire or catheter passing subintimally.
2. Arterial perforation by the guide wire.
3. Balloon rupture.
4. Spasm of distal leg vessels when guide wires are passed below the knee. This can be guarded against by intra-arterial Lignocaine (50 mg) injected from the catheter

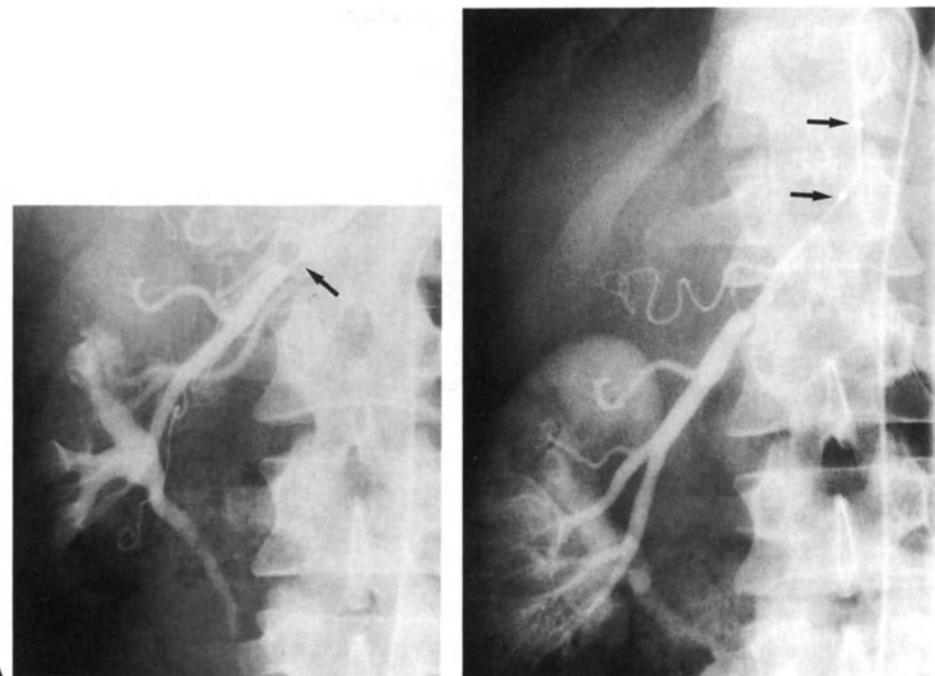


**Fig. 13.26.** A Severe localized stenosis of the right renal artery (arrow) in a young man of 25 years presenting with hypertension. Probably a variant type of fibromuscular hyperplasia. B The stenosis has just been dilated using a Gruntzig type catheter. The now deflated balloon lies between the two opaque metal clips. The BP fell to normal levels.

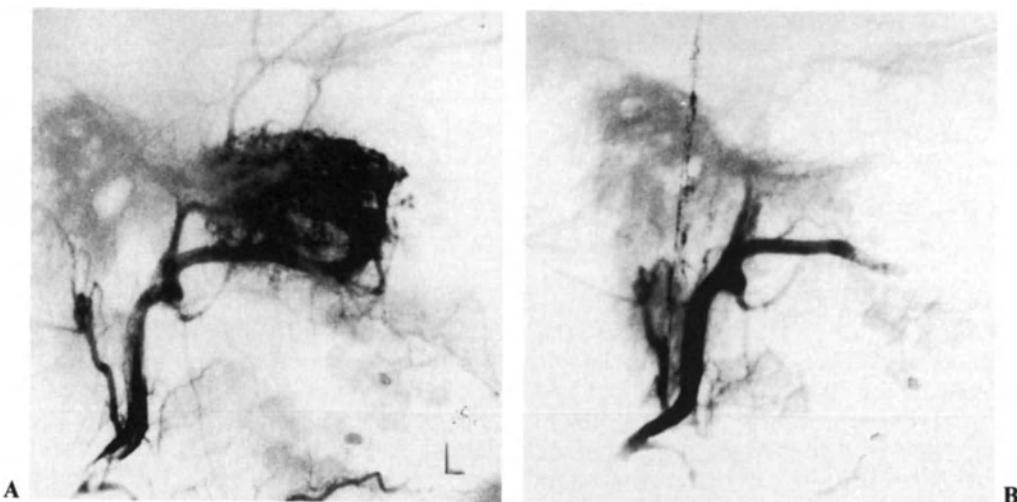


**Fig. 13.27.** A Selective internal maxillary injection shows a highly vascular juvenile angiofibroma. B Post-embolization, the vascular bed is occluded.

above the stenosis and it can be treated by intra-arterial Tolazoline (10–20 mg).

#### Embolization

Deliberate transcatheter embolization is being increasingly practiced by radiologists. The main indications include:

1. Treatment of hemorrhage.
2. Occlusion of angiomatic malformations.
3. Occlusion of AV fistula.
4. Occlusion of aneurysms.
5. Infarction of or reduction of blood flow to neoplasms (Fig. 13.27).
6. Organ infarction as an alternative to surgery (e.g., nephrectomy).
7. Testicular vein occlusion for varicocele.

**Emolic agents.** A wide variety of materials has been used for therapeutic embolization. These can be classified as follows:

1. Biological – autologous clot, muscle slips, fat, fibrous tissue and lyodura.
2. Gelatin and fibre – Gelfoam, Oxycel, and Avitene.
3. Plastic – silastic, polystyrene or acrylic spheres, Sephadex particles and polyvinyl alcohol (Ivalon).
4. Metallic – stainless steel or silastic coated metal spheres, carbon microspheres, metal filings and barium particles.
5. Steel coils with attached fibre strands.
6. Organic adhesive – Bucrylate, or ‘super glue’.
7. Sclerosing agents – alcohol, hyperosmotic contrast.
8. Detachable balloons.

The agents used depend on the specific problem and to some extent on local skills and preferences, and also on whether permanent or temporary occlusion is required. Permanent effects are produced by such agents as polyvinyl alcohol, steel coils, Bucrylate and absolute alcohol; Gelfoam

produces occlusions lasting several days or weeks but is later resorbed; autologous clot is rapidly reabsorbed and its effect lasts only hours or days.

**Hemorrhage.** At one time serious or life-threatening hemorrhage could only be dealt with by direct surgery, but in many situations percutaneous selective catheterization and embolization now offers a safer and simpler alternative. Conditions which have been successfully treated include pelvic hemorrhage (from trauma, malignant disease, or radiation), renal hemorrhage (from carcinoma or trauma), liver hemorrhage, epistaxis, bleeding from head and neck tumors, hemoptysis and gastro-intestinal hemorrhage.

**Gastro-intestinal hemorrhage** can be treated by transcatheter infusion of vasoconstrictors (vasopressin or epinephrine), and the method is very successful in controlling small vessel and capillary hemorrhage as in mucosal tears, stress ulcers and colonic diverticula. The method is less successful where larger arteries are involved, as in chronic peptic ulcers or in patients with hemocoagulation defects. In such patients embolization, if feasible, will be preferred.

**Complications of embolization.** Apart from the general complications of angiography there are special hazards associated with embolization. These include:

1. Ischemia and tissue necrosis. This can occur not only in the target area or organ, but elsewhere in the body from misplacement of the catheter tip or reflux from the injected artery. The danger of this is greatest as the capillary bed becomes increasingly blocked towards the end of the procedure.
2. Steel coils have given rise to arterial perforation or have refluxed to the aorta and distal vessels.
3. Bucrylate has given rise to internal catheter glueing.

#### Percutaneous Chemotherapy

The technique is used for inoperable tumors, particularly liver metastases and as a pre-operative measure in large tumors. Selective arterial catheterization permits maximal

doses of chemotherapeutic drugs to be delivered direct to the tumor by slow infusion.

#### Percutaneous Thrombolysis

Acute embolus or thrombosis can be treated by catheter thrombolysis as an alternative to surgery. A catheter is

inserted percutaneously with its tip in the hind end of the clot and a low dose streptokinase infusion used. The procedure is monitored by serial angiography undertaken every few hours. Successful results are usually apparent within 24 hours, and if there is no improvement after 48 hours success is unlikely.

## PHLEBOGRAPHY

**Direct Phlebography.** Imaging of the venous system is most commonly performed by direct injections of contrast into veins. In clinical practice different areas or organs are targeted according to the problem under investigation. These include:

1. The lower limb.
2. The iliac veins and inferior vena cava.
3. The upper limb and superior vena cava.
4. Hepatic, renal and adrenal veins.
5. Portal venous system.

Spinal phlebography and transosseous phlebography were once widely practiced but are now obsolete.

**Indirect Phlebography.** The venous system can also be shown by serial filming after direct injections of arteries and for obvious reasons this is the method used for studying the cerebral veins. It is also used for the portal system after injection of the celiac or superior mesenteric arteries (arteriopertigraphy). The use of DSA greatly enhances the value of this method in demonstrating the veins concerned, or those of such internal organs as the kidney.

*Duplex Doppler* ultrasound and *color flow Doppler* are now being increasingly used to assess flow in veins, particularly the larger ones, and in skilled hands can obviate the necessity for direct phlebography.

*Scintiscanning* has also been used in the assessment of venous obstruction (see below).

#### The Lower Limb

**Normal Anatomy.** It is important to understand the normal anatomy of the venous return from the lower limb. There are effectively two systems, the deep veins and the superficial veins (Fig. 13.28). These can be functionally separated but are normally connected by the communicating veins. The latter are small and paired and contain valves permitting flow from the superficial to the deep veins only. However, under pathological conditions they can hypertrophy and become incompetent, permitting reverse flow from the deep to superficial veins.

The clinical indications for phlebography of the lower limb include:

1. Suspected deep vein thrombosis.
2. Recurrent varices.

3. Swollen leg(s) of unclear etiology.
4. Venous malformations.

*Deep vein thrombosis* or suspected thrombosis is much the commonest indication, and lower limb phlebography to confirm or exclude this diagnosis is frequently requested in most imaging departments. The condition is associated with venous stasis and an increased liability to blood coagulation. Predisposing causes include malignant disease, age, obesity, trauma, surgery and prolonged immobilization. The post-surgical risk is highest after operations on the lower limb, pelvis and abdomen, particularly in patients with poor cardiac function or congestive failure.

It is claimed that at least 50% of cases are silent, and that leg symptoms are only noted when there is significant

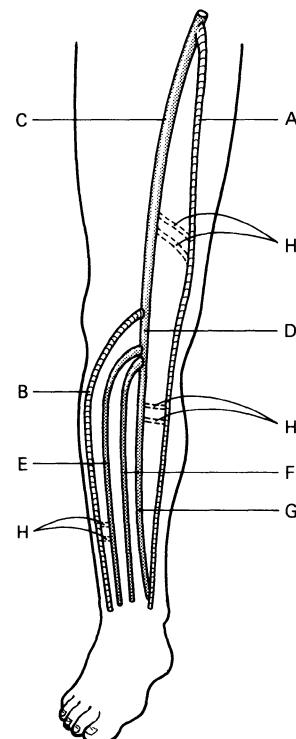


Fig. 13.28. Diagram of the superficial and deep veins of the lower limb.  
A, Long saphenous; B, Short saphenous; C, Femoral; D, Popliteal; E,F,G, Calf veins; H, Communicating Veins.



**Fig. 13.29.** Ascending phlebogram showing clot as defect in the femoral limb.

obstruction or inflammatory reaction. The main danger is that a pulmonary embolus may result, and it is estimated that there are some 600 000 cases of pulmonary embolus annually in the USA, with a mortality in different series of 10% to 30%. Post mortem evidence confirms that subclinical pulmonary emboli are extremely common. This serious problem, and the unreliability of clinical diagnosis, ensures a steady flow of requests for lower limb phlebography to imaging departments, since phlebography remains the most accurate method of confirming or excluding the diagnosis of lower limb venous thrombosis.

*Venous malformations* may occur in the form of a localized and purely venous angioma. A large varix or venous aneurysm may arise anywhere in the venous system, but particularly at the termination of the long or short saphenous veins.

*Klippel-Trenauney syndrome* is characterized by limb hypertrophy associated with a nevus and venous dysplasia. The lower limbs are most frequently affected though the upper limb can be involved. The normal venous return is replaced by a large single channel often valveless and with



**Fig. 13.30.** Inferior vena cavagram showing irregular clot.

sluggish flow. This lies laterally in the leg, and medially in the arm, and may be associated with superficial varicosities.

**Imaging.** *Phlebography* remains the most reliable method of establishing the diagnosis of lower limb venous thrombosis. Since thrombosis may be bilateral in some 30% of cases, both lower limbs should be examined. Acute thrombosis appears as a filling defect within the veins, usually with a marginal layer of contrast outlining the clot (Fig. 13.29). The clot may lie in the calf veins, the popliteal or femoral veins or in two or all of these. It may also involve the iliac veins or inferior vena cava (Fig. 13.30).

*Scintiscanning* with  $^{125}\text{I}$ -fibrinogen has also been widely used to diagnose deep vein thrombosis, but is liable to give false positive results since it is non-specific and will not differentiate it from hematomas, trauma and cellulitis. The drug is injected intravenously and is taken up by a developing thrombus. Indium-111 platelet scintigraphy, using autologous platelets extracted from a venous sample and labelled prior to reinjection, permits imaging for up to 5 days after injection, but is not widely used owing to the technical difficulties.

*Doppler ultrasound* can also be used for diagnosing deep vein thrombosis by detecting changes in flow signals over the femoral and popliteal veins and calf veins. It is more accurate in the larger veins than in the calf. However, recent work with color-coded flow Doppler has improved the accuracy of this technique and holds out very great promise for the future as a non-invasive technique that can supplant direct phlebography.

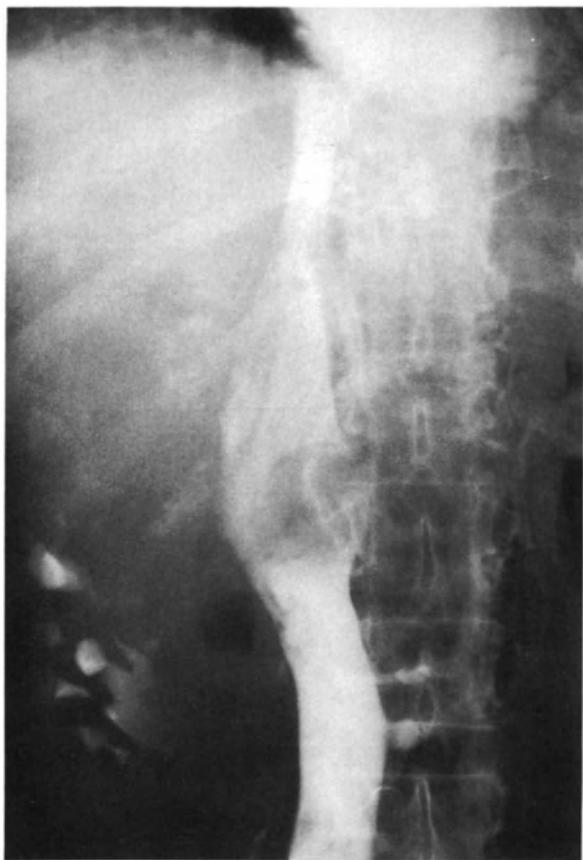


Fig. 13.31. Tumor invasion of IVC by hypernephroma extending up from the renal vein.

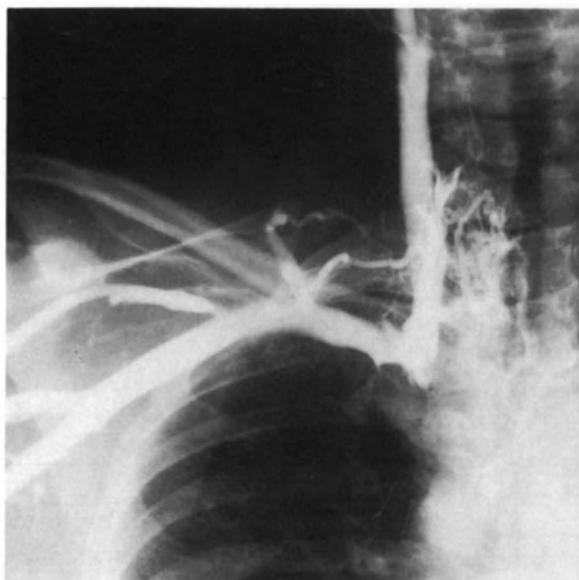


Fig. 13.32. SVC obstruction in patient with bronchial carcinoma.

### Pelvis and Abdomen

The external and common iliac veins and the inferior vena cava can be quite well shown by ascending phlebography of the lower limb and their demonstration should be part of the procedure whenever the technique is practiced. Direct injection of the femoral vein at the groin is, however, the technique of choice when the suspected lesion is intra-abdominal and the lower limb veins are not involved. The indications include:

1. Congenital anomalies.
2. Caval or iliac vein obstruction by tumor or other lesions.
3. Post-traumatic or post-radiotherapy venous damage.
4. Assisting therapeutic interruption of the IVC.

*Congenital anomalies* of the IVC are rare, the commonest being left-sided IVC, which occurs in less than 1% of patients. The anomalous vessel passes up to the left instead of to the right of the spine and usually passes back to the right at the level of the left renal hilum, where it is joined by the left renal vein. Above this level the cava is normally sited.

Other, rarer, anomalies include double inferior cava, hypoplasia and agenesis of the IVC. All of them show a higher incidence in patients with congenital heart disease.

Obstruction of the iliac veins or of the inferior vena cava may result from a wide variety of lesions. These include:

1. Malignant tumors or glandular masses compressing or invading veins (Figs 13.31, 13.32).
2. Benign tumors or other masses causing extrinsic pressure; apart from neoplasms, these include haematomas, pelvic lymphoceles, and aneurysms.
3. Retroperitoneal fibrosis.
4. Lymphedema praecox.
5. Acute thrombosis or post-thrombotic sequelae.
6. Post-traumatic or post-radiotherapy venous damage.

*Lymphedema praecox* is a term used for swelling of the left leg usually occurring in young female patients. Some cases are due to lymphatic hypoplasia (see below) but others are due to pressure of the left common iliac artery on the left common iliac vein as it crosses over it.

*Therapeutic interruption of the IVC* is practiced to prevent further and potentially fatal pulmonary emboli in high risk patients. Formerly, the procedure necessitated direct surgery or cut down on the internal jugular vein, but it can now be practiced by percutaneous passage of the filter through a catheter to the appropriate level in the IVC. This should be below the lowest renal vein as determined by prior phlebography.

*Renal phlebography* is now little practiced except for the collection of blood for renal vein renin assay in cases of renal artery stenosis. The renal veins are often double and on the left side some 7% of patients have a retro-aortic lower accessory vein forming a circum-aortic ring with the main vein.

*Adrenal phlebography* was once widely used for the demonstration of small adrenal tumors in Conn's syndrome, but has now been superseded by CT. It is still occasionally used for adrenal vein aldosterone assay in difficult cases or for adrenal ablation.

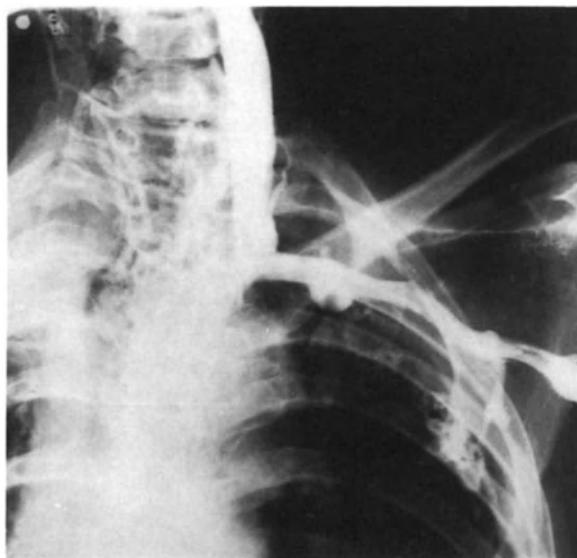


Fig. 13.33. SVC obstruction in fibrosing mediastinitis (tuberculous).

**Hepatic phlebography** is mainly performed to obtain wedged venous pressure in portal hypertension. Contrast injections will show an abnormal and irregular pattern of hepatic vein tributaries in cirrhosis and a bizarre sinusoidogram.

**Gonadal Veins.** The right ovarian (or testicular) vein drains into the inferior vena cava below the right renal vein; the left gonadal vein drains into the left renal vein. Both gonadal veins can be demonstrated by direct catheterization using the percutaneous transfemoral route.

This is occasionally done to confirm a suspected diagnosis of '*ovarian vein syndrome*', a condition in which the right

ureter is obstructed by a hypertrophied right ovarian vein crossing over it. Another indication is the so-called '*pelvic pain syndrome*' associated with varicosities of the ovarian veins, broad ligaments, and vulva. Both veins are catheterized and good results are claimed for ovarian vein ligation after the diagnosis is confirmed.

The left testicular vein is also quite frequently catheterized because its embolization has in some clinics given good results in the treatment of male infertility associated with varicocele.

#### The Upper Limb and Superior Vena Cava

The usual indications for phlebography of the upper limb include:

1. Superior vena caval or more proximal venous obstruction.
2. Demonstration of the full anatomy of venous angiomas or varices.
3. Congenital venous anomalies as in the Klippel-Trenauney syndrome.

**Superior vena caval obstruction.** This is most commonly due to malignant disease with bronchial carcinoma as the major cause (over 80% of cases), and lymphoma the cause in most of the other cases (Fig. 13.32).

Benign lesions are responsible in a minority of cases (less than 5%) and these are usually due to '*fibrosing mediastinitis*'. The etiology is either granulomatous or unknown (idiopathic). Granulomatous fibrosing mediastinitis is due to tuberculosis (Fig. 13.33) in most cases, but can also follow histoplasmosis. Ventriculo-atrial shunts are another rare cause. Non-malignant masses, such as aneurysms, can also compress the SVC.

#### Portal Phlebography

The normal anatomy of the portal vein and its major tributaries is illustrated in Fig. 13.34. The main indication for portal phlebography is the investigation of portal hypertension and its complications, particularly when surgery is being considered.

The causes of portal hypertension are discussed in Chap. 26 and are given in Table 13.4.

Table 13.4. The causes of portal hypertension

Obstruction to portal flow
prehepatic obstruction of portal vein
tumor or other extrinsic mass; thrombosis
intrahepatic obstruction
presinusoidal (schistosomiasis; periportal fibrosis)
post-sinusoidal (cirrhosis; veno-occlusive disease; infiltrative diseases)
post-hepatic obstruction
cardiac (congestive failure, constrictive pericarditis)
Increased portal flow
splenomegaly
splenic, mesenteric or hepatic AV fistula

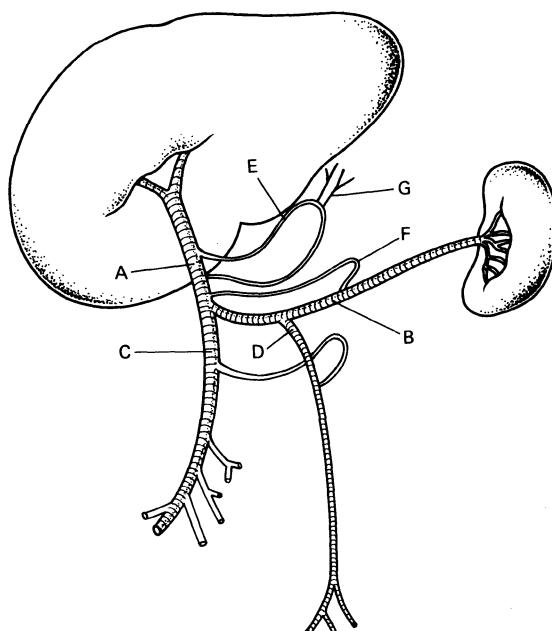
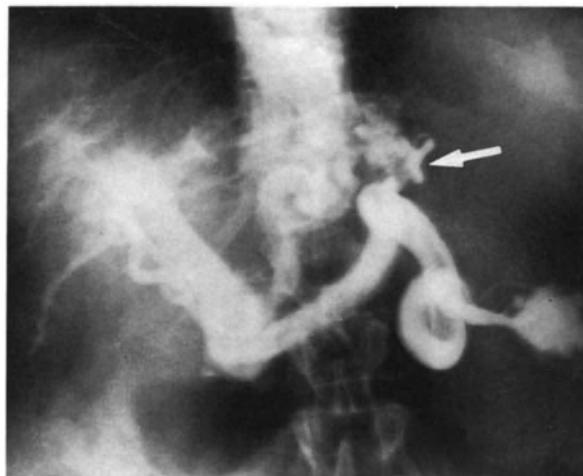


Fig. 13.34. Diagram of the normal portal system. A, Portal vein; B, Splenic vein; C, Superior mesenteric vein; D, Inferior mesenteric vein; E, Left gastric vein; F, Gastro-epiploic vein; G, Esophageal veins.

In Western countries the commonest cause in clinical practice is cirrhosis, either alcoholic or post-hepatitis; schistosomiasis is of major importance in under-developed countries.



**Fig. 13.35.** Trans-splenic portogram showing gastric and esophageal varices (arrow).



**Fig. 13.36.** Transhepatic portogram showing esophageal varices prior to embolization.

The complications of portal hypertension include splenomegaly, ascites and varices. The normally large transhepatic portal flow cannot be maintained and an ever-increasing proportion bypasses the liver and returns to the heart through normal systemic collaterals or reopened embryonic pathways.

**Imaging.** There are several different phlebographic techniques available for demonstration of the portal system:

1. Percutaneous trans-splenic portography.
2. Arterial portography.
3. Percutaneous transhepatic portography.
4. Operative portography.
5. Umbilical portography.

*Trans-splenic portography* was once widely practiced but with the development of alternative techniques is now rarely used (Fig. 13.35). *Arterial portography*, particularly with the help of DSA, can now produce excellent visualization of the portal system, and permits hepatic arteriography at the same session. *Transhepatic portography* is used when it is desired to demonstrate and embolise esophageal varices at the same session (Fig. 13.36).

*Ultrasound* can demonstrate the main portal vein and Duplex Doppler can demonstrate the presence or absence of normal flow. Ultrasound can also assess the state of the liver and the presence or absence of masses in the porta hepatis.

*CT* with contrast enhancement can supply similar information and will also clearly show ascites, splenomegaly and varices.

## LYMPHANGIOGRAPHY

Kinmonth (1952) first described a method for *in vivo* demonstration of the lymphatics using water-soluble contrast media, and this became the accepted technique for the investigation of lymphedema. The method was later extended to the investigation of nodal disease by the introduction of iodized oil as contrast medium (Wallace et al. 1962), and became widely practiced for this purpose. However the newer imaging techniques, especially *CT*, have now completely replaced lymphangiography for the study of nodal disease, being non-invasive and more accurate, particularly in the staging of tumors.

### Lymphedema

Lymphedema has been classified as primary and secondary, the distinction being the presence of a well defined cause in the latter type.

**Primary lymphedema.** This type of lymphedema is mainly due to a congenital hypoplasia of the lymph system, or less commonly, to a proliferation and hyaline degeneration of the intima of lymph vessels causing progressive narrowing. The latter type, sometimes termed lymphangiopathia obliterans, occurs mainly in young women and the etiology remains speculative but is thought to be degenerative.

Primary lymphedema has been further classified according to the age of onset as:

1. *Lymphedema congenita*, which includes Milroy's disease, and can be associated with other congenital anomalies such as Turner's syndrome (ovarian dysgenesis).
2. *Lymphedema praecox*, the commonest type encountered in clinical practice, and usually occurring in young females aged from 9 to 25 years. It is often precipitated by trauma, infection or pregnancy, which presumably affect a balanced hypoplastic system, rendering it incompetent.
3. *Lymphedema tarda*, arising after the age of 35 years.

**Imaging.** In most cases of primary lymphedema lymphangiography shows the lymphatic channels to be hypoplastic i.e., small in size and fewer in number than usual. Occasionally no lymph vessels can be found (aplasia). A small proportion (10%) show irregular beaded dilatations of the lymph channels (lymphangiectasia or lymphatic hyperplasia). These can be regarded as varicosities secondary to back pressure from flow obstruction and may be associated with dermal backflow. This is due to contrast filling of dermal lymphatics associated with incompetent valves.

*Lymphangiomatosis of bone* may also occur in lymphatic obstruction and is also probably due to incompetent lymphatic valves.

*Lymphatica porosa* is the term used for cases where contrast is seen to leak from the lymphatics causing blurring of their outlines.

**Secondary lymphedema.** Obstruction to lymphatic flow may result from many different causes, including malignant disease, surgical excision of lymph nodes, extensive traumatic skin loss, radiotherapy, filariasis, and inflammatory lesions of the lymphatic and venous systems.

*Lymphocele* may occur secondary to glandular removal, particularly following pelvic gynaecological surgery or renal transplantation. The leakage of lymph leads to a cystic collection which can present as a local pelvic mass pressing on adjacent pelvic organs. Lymphoceles fill with contrast at lymphangiography but are now diagnosed best by ultrasound; they can also be shown by CT or MRI.

*Chylous reflux* designates abnormal direction of chyle flow from the intestine. It may result from congenital dysplasia, but more commonly is secondary to trauma, malignant or inflammatory lesions. Chylous edema is the result of retrograde flow of chyle to the pelvis, genitals and lower limbs; chyluria may also occur. *Filarisis* is the commonest cause in endemic areas.

*Chylothorax* is usually traumatic in origin and may follow injury to the cisterna chyli.

## LYMPHATIC NEOPLASMS

*Lymphangiosarcoma* (Stewart-Treves Syndrome) represents a malignant degeneration in chronic primary or more commonly secondary lymphedema, and is commonest following radical mastectomy.

*Cavernous lymphangioma* consists of multiple cavities lined with endothelium and surrounded by fibrous tissue. *Cystic hygroma* contains larger cavities filled with clear or haemorrhagic fluid.

Both the above are lymphatic cavities sequestered from the normal lymphatic system, and can only be contrast filled by direct injection. They are commonest in the face, neck, axilla and mediastinum and are readily shown by ultrasound, CT, or MRI.

## REFERENCES AND SUGGESTIONS FOR FURTHER READING

### BOOKS

- Abrams HL (ed) (1983) Angiography, 3rd edn. Little Brown, Boston  
 Ansell G, Wilkins RA (1987) Complications in Diagnostic Imaging, 2nd edn. Blackwell, Oxford  
 Athanasioulis CA et al. (eds) (1982) Interventional Radiology, Saunders, Philadelphia  
 Carr DH (ed) (1988) Contrast Media. Churchill Livingstone, Edinburgh  
 Johnsruude IS, Dunnick J, Jackson DC (1987) A Practical Approach to Angiography, 2nd edn. Little Brown, Boston  
 Kinmonth JB (1982) The Lymphatics: Surgery, Lymphography and Disorders of the Chyle and Lymph Systems. Edward Arnold, London  
 Lea Thomas M (1982) Phlebography of the Lower Limb. Churchill Livingstone, Edinburgh  
 Sutton D (ed) (1987) A Textbook of Radiology and Imaging, 4th edn. Churchill Livingstone, Edinburgh

### ARTICLES

- Belli AM, Cumberland DC (1989) Percutaneous atherectomy – early experience in Sheffield. Clin Radiol 40: 122–126  
 Dawson P, Grainger RG, Pitfield J (1983) The new low osmolar contrast media. Clin Radiol 34: 221–226  
 Gregson RHS, Sutton D, Brennan J et al. (1983) Spontaneous aorto-caval fistula. Clin Radiol 34: 683–687  
 Gruntzig A (1978) Transluminal dilatation of coronary artery stenosis. Lancet i: 263  
 Gruntzig A et al. (1978) Treatment of renovascular hypertension with percutaneous transluminal dilatation of renal artery stenosis. Lancet i: 801  
 Lang EK (1981) Transcatheter embolisation of pelvic vessels for control of pelvic haemorrhage. Clin Radiol 35: 85–93  
 O'Halpin D, Legge D, McErlain DP (1984) Therapeutic arterial embolisation: Report of 5 years experience. Clin Radiol 35: 85–93

---

**PART 3**

**Skeletal System and Soft Tissues**

---

## CHAPTER 14

# CONGENITAL ABNORMALITIES OF BONE

J. W. R. Young

### FOCAL DISORDERS

Congenital abnormalities of the skeleton may be divided into two groups: focal and generalized. Focal disorders are localized and with no systemic abnormality. They are often of little clinical significance, and may be encountered as incidental findings in everyday practice. These include anomalies such as abnormalities of segmentation of the vertebrae, e.g., hemivertebra (Fig. 14.1), congenital fusion of bones, particularly in the carpus (Fig. 14.2), polydactyly (Table 14.1) (Fig. 14.3), or *Madelung's deformity* (Fig. 14.4).

Table 14.1. Some causes of polydactyly

Idiopathic sporadic congenital abnormality (in-breeding)
Ellis–van Creveld disease
Laurence–Moon–Biedl disease
Asphyxiating thoracic dystrophy
Holt–Oram syndrome
Trisomy 13
Fanconi's anemia
Cri-du-Chat syndrome

*Sprengel's shoulder*, which may be unilateral, or occasionally bilateral, consists of a 'high riding' scapula, in which there is also usually a concurrent rotation of the scapula. There may be a bony or fibrous bridge from the superior margin of the scapula to the spine.

However, whilst these anomalies usually occur in isolation, conditions such as polydactyly, Madelung's deformity and Sprengel's shoulder may be associated with other congenital anomalies, or may be part of a more widespread congenital abnormality. For example, Madelung's deformity is the hallmark of *dyschondroosteosis*. Anomalies of the distal forearm, carpus and digits, may be associated with skeletal and visceral abnormalities, (e.g., *thrombocytopenia absent radius (TAR) syndrome*) (Fig. 14.5). The heart may be abnor-

mal (e.g., *Holt Oram syndrome*). Further evaluation of these patients may then be warranted.

Various developmental conditions involve the hips. The more important are described below.

### Congenital Dislocation of the Hip

Early recognition of this is vital for correct treatment and to permit normal acetabular and femoral head development. The incidence of instability is approximately 5–10/10 000 and of overt dislocation, 1–1.5/1000. There is a female predominance (3:1), and 60% of affected children are first-



Fig. 14.1. Hemivertebra. Abnormal segmentation has occurred giving rise to a focal short segment scoliosis. Two pedicles and ribs are identified on the left arising from the vertebra, in comparison to one on the right.



**Fig. 14.2.** Fusion of the scaphoid to lunate bone is identified. This is a relatively common anomaly generally with no associated disorders.

born. There is also a greatly increased incidence in breech presentations (6:1) and approximately 25% of cases are bilateral.

Radiographically it may be difficult to diagnose congenital dislocation in the neonate, due to lack of calcification of the femoral capital epiphysis. An unusual configuration of the acetabulum with a lateral notch may be seen, and there is usually an increase in the 'acetabular angle'. If the legs are abducted to 45° with the knees extended and the femora fully internally rotated, a line drawn along the shaft of the femur should intersect the outer acetabulum and the spine at the lumbosacral junction. If dislocation is present, the line crosses the spine at a higher level.



**Fig. 14.3.** Polydactyly. Extra digits are commonly seen in communities with multiple inbreeding as in this case, but may be associated with generalized disorders.



**Fig. 14.4.** Madelung's deformity. This may occur as an isolated finding but may be seen in more generalized disorders. It is the hallmark of dyschondroosteosis.



**Fig. 14.5.** Thrombocytopenia, absent radius (TAR) syndrome. There is complete absence of the radius, with deformity at the wrist.



**Fig. 14.6.** Congenital dislocation of the hip. In this advanced case, the diagnosis was missed in infancy. There is bilateral hip dislocation, with subsequent inadequate modeling of the acetabula. A pseudo-articulation of the femoral head with the iliac bone occurs.

When the femoral capital epiphysis is calcified, the diagnosis is much easier, and this is also true when there is severe dislocation (Fig. 14.6).

After reduction, follow-up radiography is needed both to determine the success and to confirm maintenance of the reduction. Difficulty in reduction may be due to inversion of the cartilaginous rim (limbus) of the acetabulum, or to anteversion of the femoral neck, which may require corrective osteotomy. If the diagnosis of a congenital dislocation is missed, a high riding femur with a false acetabulum will develop, requiring extremely difficult corrective surgery.

*Ultrasound* shows great promise as a diagnostic technique for CDH and may supplant radiography.

*Idiopathic Coxa Varva/Proximal Femoral Focal Defect.* Proximal femoral focal defect (PFFD) and idiopathic coxa varva are regarded as being manifestations of the same disorder, but of differing severity. PFFD may present with coxa varva if the defect is subtotal. However, in severe cases, coxa varva cannot be present as the whole of the proximal femur is absent (Fig. 14.7). In coxa varva, the abnormality is usually bilateral (Fig. 14.8). The femoral head is situated low in the acetabulum, and the femoral neck is more or less horizontal with a defect in the metaphyseal region, often causing a 'wedge' of bone along the inferior aspect.

### The Lower Leg

Congenital abnormalities of the lower leg also occur. Some may be of no clinical significance (e.g., *bipartite-patella*), whilst others are associated with significant clinical problems. These occur mostly around the ankle and foot where *talipes-equino-varus* (congenital club foot), *congenital vertical talus*, and *congenital dislocation of the ankle* are of note. As in the hand and wrist, congenital fusions may occur, but in the foot and ankle these are more frequently symptomatic due to the weightbearing stresses and strains placed on this region.

### GENERALIZED DISORDERS

The second broad group of congenital abnormalities consists of conditions which are widespread, or may have generalized associated abnormalities. The remainder of this chapter will deal with this group of abnormalities.

#### Cleidocranial Dysostosis (Cleidocranial dystrophy) (Fig. 14.9).

This is inherited as an autosomal dominant. There may be absence of the clavicle, either partial (usually outer one third), or total (in 10% of cases). A small high-riding scapula and small glenoid fossa are found. The thorax is narrow with an incompletely ossified sternum. Delayed maturation of vertebral bodies and unfused neural arches are also found.

In the skull there are hypoplastic sphenoid bones and Wormian bones are present. Basilar invagination may also occur (see Chap. 39).

The pelvic bones are poorly ossified, particularly the pubic symphysis, which may be partly absent. Congenital coxa varva is also seen.

Other anomalies include abnormalities of the hands (long



Fig. 14.7. Focal femoral deficiency. This is a gross example with complete absence of the proximal femur. The acetabulum has not developed.



Fig. 14.8. Congenital coxa varva. The typical defect in the femoral neck is seen bilaterally with a characteristic 'wedge' of bone inferiorly (arrow).



Fig. 14.9. Cleidocranial dysostosis. There is marked hypoplasia of the clavicles, involving predominantly the outer portions.



**Fig. 14.10.** A Pycnodyostosis. There is acro-osteolysis of the hands and generalized increased bone density of the skeleton. B The skull shows severely hypoplastic facial bones.

metacarpals of 2nd and 5th digits), short fibulae, and pseudo-arthroses.

#### Pycnodyostosis (Fig. 14.10)

There is autosomal recessive inheritance. Generalized increased bone density of the skeleton is found. In the skull, brachycephaly with Wormian bones, and small hypoplastic facial bones are found. Acro-osteolysis occurs, and there is tapering of the lateral ends of clavicle. Unfused neural arches are also seen.

#### Osteogenesis Imperfecta

Two forms of this condition occur. *Recessive form* (Fig. 14.11). The children are usually stillborn or die soon after birth. Blue sclera are a feature and there is gross demineralization of bones with numerous fractures in many stages of healing. *Dominant form*. This has variable severity. There is demineralized bone with bowing or multiple fractures (Fig. 14.11B). Abundant callus occurs in healing. In the skull, Wormian bones are seen and basilar invagination occurs.

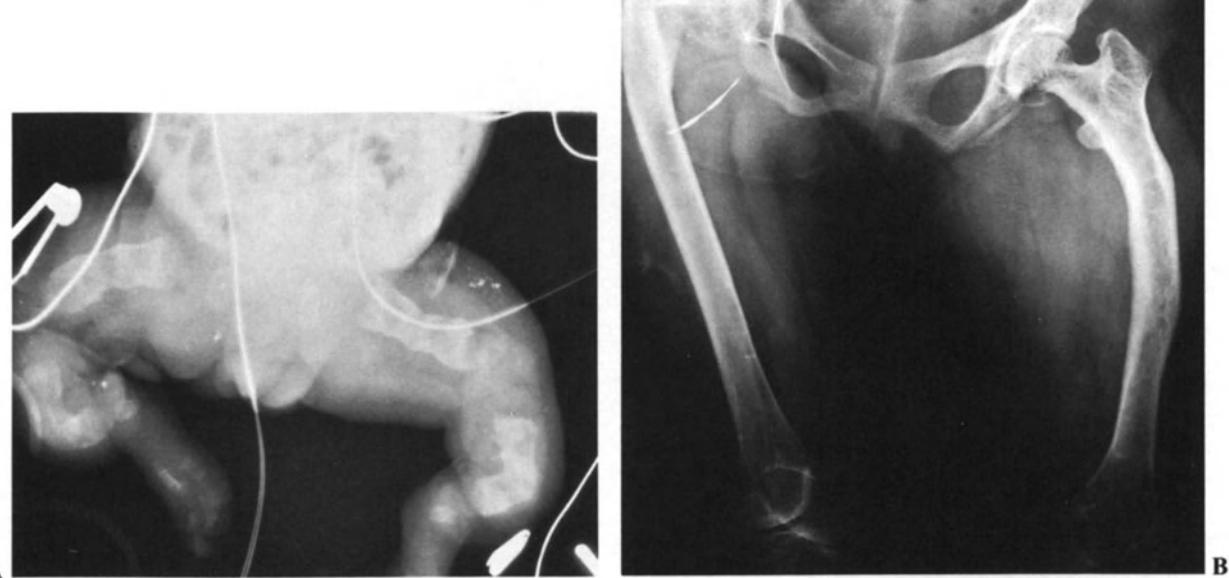


**Fig. 14.11.** A Osteogenesis imperfecta, recessive form. There is severe deformity of all of the visualized bones with abnormal trabecula and multiple fractures. B Osteogenesis imperfecta tarda : dominant form. There is marked deformity of the femurs, with bowing on the left and coxa vara on the right.



**Fig. 14.12.** Osteopetrosis, recessive form. There is marked increased density of all of the visualized bones, with evidence of a healing fracture of the distal femur.

There is flattening of the vertebrae, and in the pelvis protrusio acetabulae is sometimes seen. Sarcomatous degeneration has been reported.

#### Fibrogenesis Imperfecta Ossium (see p. 327, Chap. 17)

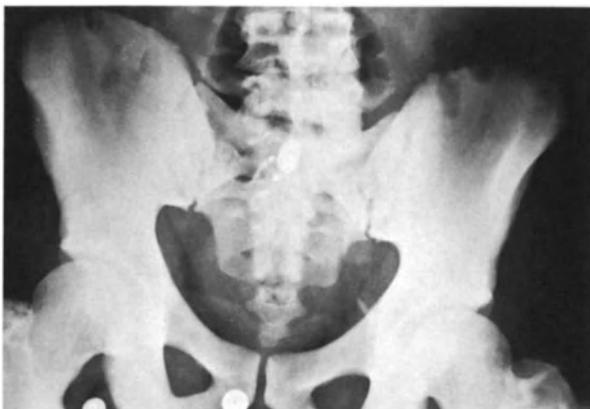


**Fig. 14.13.** Osteopetrosis. The pelvic bones and proximal femurs are seen to be extremely dense.

**Osteopetrosis** (Albers-Schonberg disease – marble bone disease). There are two forms of this condition. The *recessive* form is found in infancy and childhood (Fig. 14.12) and, in the most severe form, may be fatal. The *dominant* form presents later in life and is of varying severity (Fig. 14.13). There is increased radiodensity of abnormal bone (persistent fetal spongiosa). This may cause the appearance of a 'bone within a bone' with a 'picture frame' appearance to vertebral bodies. Modelling deformities occur especially at the metaphyses, which may give rise to *Erlenmeyer flask* deformities. Although radiographically dense, the bone is weak and multiple fractures occur. Encroachment on the medullary canal of the bones may cause extramedullary hematopoiesis.

In the skull, the base is affected more than the cranium, and there may be narrowing of the neural foramina.

**Acro-osteolysis** (Hajdu-Cheney syndrome). This disorder is inherited as an autosomal dominant. The most striking features are acro-osteolysis, Wormian bones, and spinal osteoporosis. Differentiation should be made from the many other causes of acro-osteolysis (see Table 14.2).

**Table 14.2.** Some causes of acroosteolysis

Congenital	
pycnodysostosis	
Hajdu–Cheney syndrome	
Lesch–Nyhan syndrome	
congenital indifference to pain	
Vascular/connective tissue	
scleroderma	
CSRT (CREST) syndrome	
Buerger's disease	
diabetes	
epidermolysis bullosa	
Neurological	
leprosy	
syringomyelia	
Traumatic	
electrical burns	
frost bite	
Neoplastic	
T-cell leukemia lymphoma	
Kaposi's sarcoma	
Poisons	
PVC workers	
ergot	
Metabolic	
hyperparathyroidism	

**Osteopoikilosis** (Fig. 14.14). This is a familial condition, of no clinical significance, in which multiple small dense rounded areas of bone are found, in general in close proximity to the joints, and in particular in the pelvis, hips, carpus, and tarsus. The characteristic distribution should help in differentiating the condition from metastatic disease. It is rarely associated with skin nodules.

**Osteopathia Striata** (Voorhoeve's disease) (Fig. 14.15). Dense striations occur in the long bones, especially of the lower limbs. These are of no clinical significance. However a similar condition is seen associated with cranial stenosis, enlarged skull, hypoplasia of facial sinuses, deafness, and scoliosis.



**Fig. 14.14.** Osteopoikilosis. Multiple small osteoblastic foci surround the hip joints, symphysis pubis, and sacroiliac joints.

**Melorheostosis (Leri's disease)** (Fig. 14.16). No obvious trend of inheritance is known in this condition, which affects children over the age of three years, and presents with irregular areas of increased bone density along the cortex of the bone (flowing wax). It is generally unilateral and follows a segmental distribution involving predominantly the limbs. It may be painful and there may be associated skin lesions (e.g., scleroderma) or vascular anomalies.

**Hyperostosis Corticalis Generalisata Familiaris** (Van Buchem's disease, Worth's disease). This condition also dem-



**Fig. 14.15.** Osteopathic striata. The typical pattern of longitudinal bands of increased bone density.

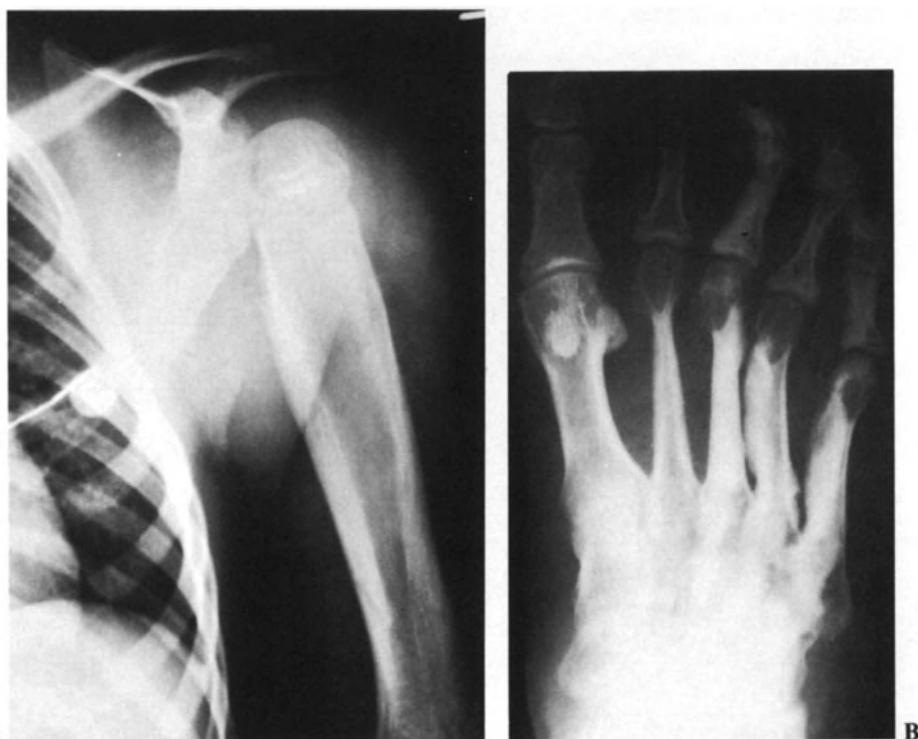


**Fig. 14.16.** **A** Melorheostosis. There is cortical thickening of the proximal humerus, and scapula. Because of the associated pain and the fact that involvement of the scapula was not initially noticed, a more malignant lesion was originally considered. **B** The more classical 'flowing candle wax' appearance of increased cortical bone in the metatarsals of the 3rd to 5th toes, and 3rd toe phalanges.

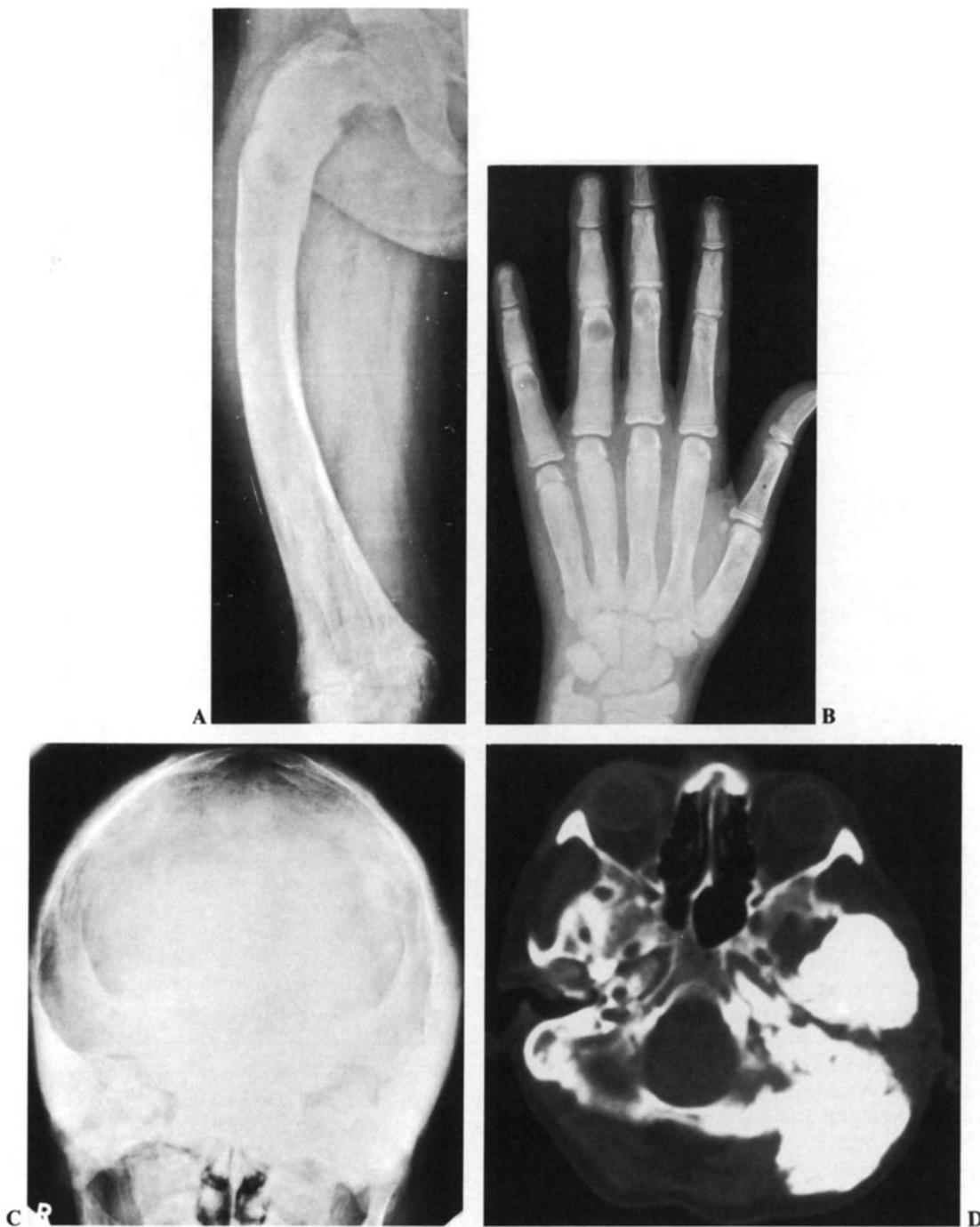


**Fig. 14.17.** A Fibrous dysplasia. Abnormal trabecular pattern of the femur, metacarpals and phalanges, B, is seen with a ground-glass appearance. The skull of the same patient reveals the characteristic sclerosis of the base, 'leontiasis ossea', C. CT scan through the skull base of a patient with fibrous dysplasia. There is massive hyperostosis of the involved basal bones on the left, D.

onstrates two forms. The *recessive* form (Van Buchem's) is more severe than the *dominant* form (Worth). Thickening and sclerosis of the skull and long bones occurs, encroaching upon the medullary cavity. The mandible may be especially large and a reverse 'Rugger jersey spine' is seen with a *central* sclerotic band.

**Fibrous Dysplasia.** Monostotic and polyostotic forms

occur. The age of onset is usually in the second and third decades. Medullary bone is replaced by fibrous tissue and cystic areas containing blood or serous fluid. Variable ossification may occur. This gives rise radiographically to lesions of either a 'ground glass' appearance, or a mixed density with well defined margins (Fig. 14.17). It may also produce a 'cotton wool' appearance, particularly in the skull (Fig. 14.18).



**Fig. 14.18.** Fibrous dysplasia. There is a bizarre cotton wool appearance to the involved skull bones. The abnormality is asymmetric and also involves the base of the skull. However it may be difficult to differentiate this from Paget's disease.



**Fig. 14.19.** Tuberous sclerosis. There is cortical thickening of many of the metatarsal bones. There is a similar cortical thickening in the tibia, B.

The lesions are usually diaphyseal and may be expansile, and are often deforming, although generally with an intact cortex. There may be massive sclerosis of the bones of the base of the skull (*leontiasis ossia*), and nerve palsies may result.

Café-au-lait skin lesions are associated and rarely (< 1%) sarcomatous degeneration may occur.

**Albright's Syndrome.** This consists of polyostotic fibrous dysplasia associated with precocious puberty. Other associations reported include Cushing's syndrome, hyperthyroidism, parathyroid hyperplasia and gynecomastia.

**Tuberous Sclerosis (Epiloia)** (Fig. 14.19). This is a dysplasia of mesodermal and ectodermal tissue. Subungual tumors, brain lesions, kidney tumors and lung lesions occur. Bone changes are seen comprising cortical cysts, periosteal thickening, and osteosclerotic lesions, particularly in hands, feet and long bones.

#### CONDITIONS INVOLVING METAPHYSES

**Familial Metaphyseal Dysplasia** (Pyle's disease). This is now regarded as a separate entity from craniometaphyseal dysplasia (see below). It is inherited as an autosomal recessive. Widening of metaphyses and adjacent diaphyses occurs, most commonly seen at the knee, wrists, medial clavicles, and anterior ribs. Thinning of the mid shafts of the bones is also a feature.

**Craniometaphyseal Dysplasia.** This occurs in two forms, autosomal recessive (severe) and dominant (mild).

There is sclerosis of the skull, particularly around the sutures and the base and there may be compression of the cranial nerves and hypertelorism. Some diaphyseal widening may occur in the long bones.

**Metaphyseal Dysplasias.** Several varieties are described of which the best recognized are:

**Jansen's.** This presents with grossly irregular metaphyses with an enlarged 'physeal line'. There are few long-term sequelae.

**Schmid's.** There are irregular metaphyses, resembling those found in rickets and leading to deformities (Fig. 14.20).

#### CONDITIONS INVOLVING EPIPHYESSES

**Multiple Epiphyseal Dysplasia** (dysplasia epiphysealis multiplex (generalisata); Fairbank's disease, Ribbing's disease) (Fig. 14.21). This autosomal dominant inherited disease is a form of short limbed dwarfism, presenting in two forms; *severe* (Fairbank's) or *mild* (Ribbing's).

It affects the epiphyses of hips, shoulders, ankles, knees, wrists and elbows, causing flattening and deformity (Fig. 14.21). 'Stubby' fingers are a feature and early degenerative arthritis may occur. A double layered patella may occur as



◀ Fig. 14.20. Metaphyseal dysplasia (Schmid). There is a mild generalized abnormality of the visualized metaphyses, with widening and mild irregularity.



Fig. 14.22. Dysplasia epiphysialis hemimelica. Abnormal development of the femoral capital epiphysis is seen on the left. There is enlargement and irregularity, predominantly involving the medial aspect.

a characteristic feature and irregular vertebral end plates with mild wedging of bodies are also seen.

**Dysplasia Epiphysealis Hemimelica** (Trevor's disease) (Fig. 14.22). In this condition there is asymmetric epiphyseal involvement (one side), with overgrowth of the affected portion, giving rise to deformity, and on occasion an appearance that may resemble an osteochondroma.

**Chondrodystrophy Calcificans Congenita** (Stippled epi-

physes, dysplasia epiphysealis punctata). Both dominant (milder) and recessive (severe) forms occur and even the milder form may be fatal. Dense 'stippling' of the epiphyses of the long bones, tarsus, carpus, spinal transverse process, and pubic symphysis occurs. This gives rise to deformity in survivors. In the recessive form, death usually occurs in the first year. Extensive stippling is seen, which may even involve the trachea.

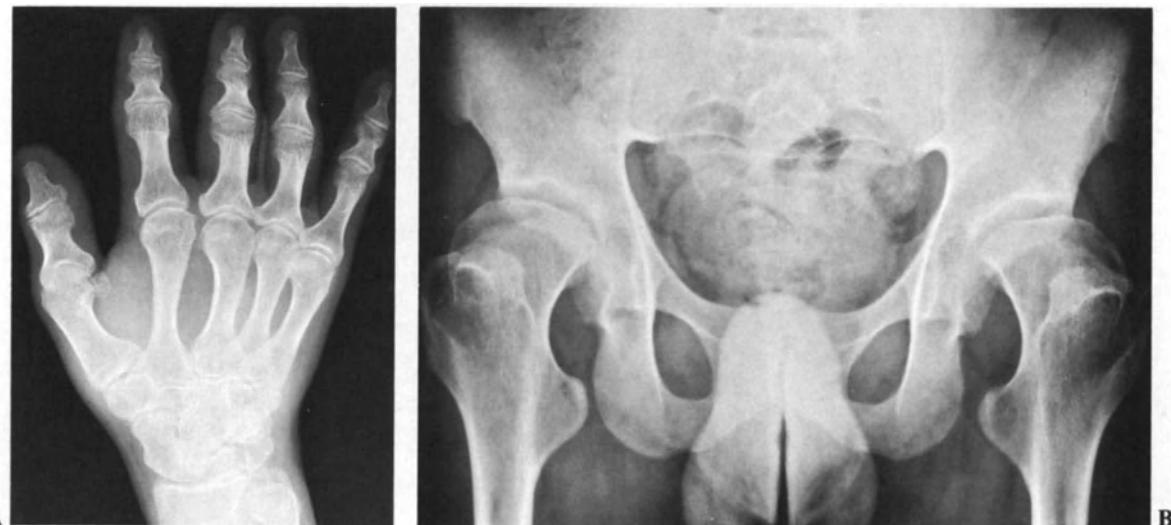


Fig. 14.21. Dysplasia epiphysialis multiplex generalisata (multiple epiphyseal dysplasia). There is deformity of the joints in the hand and wrist and, B, of the hips arising from modeling abnormalities in the epiphyses.



**Fig. 14.23.** (left) Engelman's disease. There is increased cortical thickness of the mid shaft of the tibia and fibula, with abnormal modeling.

**Fig. 14.24.** (right) Diaphyseal achalasia (multiple osteochondromatosis). The multiple exostoses are associated with modeling deformities of the bone. In this case, calcification of the cartilage caps is not seen.

#### CONDITIONS INVOLVING DIAPHYSES

**Progressive Diaphyseal Dysplasia** (Engelman's disease, Camurati's disease). There is fusiform expansion of the diaphysis of predominantly the long bones, but also rarely involving the hands and feet, due to cortical thickening of the bone (Fig. 14.23). Mild to moderate sclerosis of the skull is seen, usually involving mainly the base and mandible. The condition may be associated with decreased muscle mass, leg pain, and gait abnormalities.

**Diaphyseal Aclasia** (Multiple Exostoses) (Fig. 14.24). Multiple exostoses (osteochondroma) arising from the metaphyseal regions of long bones occur. They generally project away from the metaphysis, and are capped with cartilage, with variable calcification. The cap tends to ossify with maturity. They are also found around the shoulder and hip joint, and may give rise to nerve compression.

Degeneration to chondrosarcoma may occur in the cartilage cap particularly in the central lesions (3–10%). Increasing pain or calcification are warning signs.

This condition is associated with modeling deformities of the bones.

**Achondroplasia** (Fig. 14.25). This has an autosomal dominant inheritance, but approximately 80% of cases are the result of a spontaneous mutation.

Shortness of tubular bones occurs with prominent muscle insertions. Proximal bones are more affected than distal bones (rhizomelia) and deformed V-shaped epiphyseal/

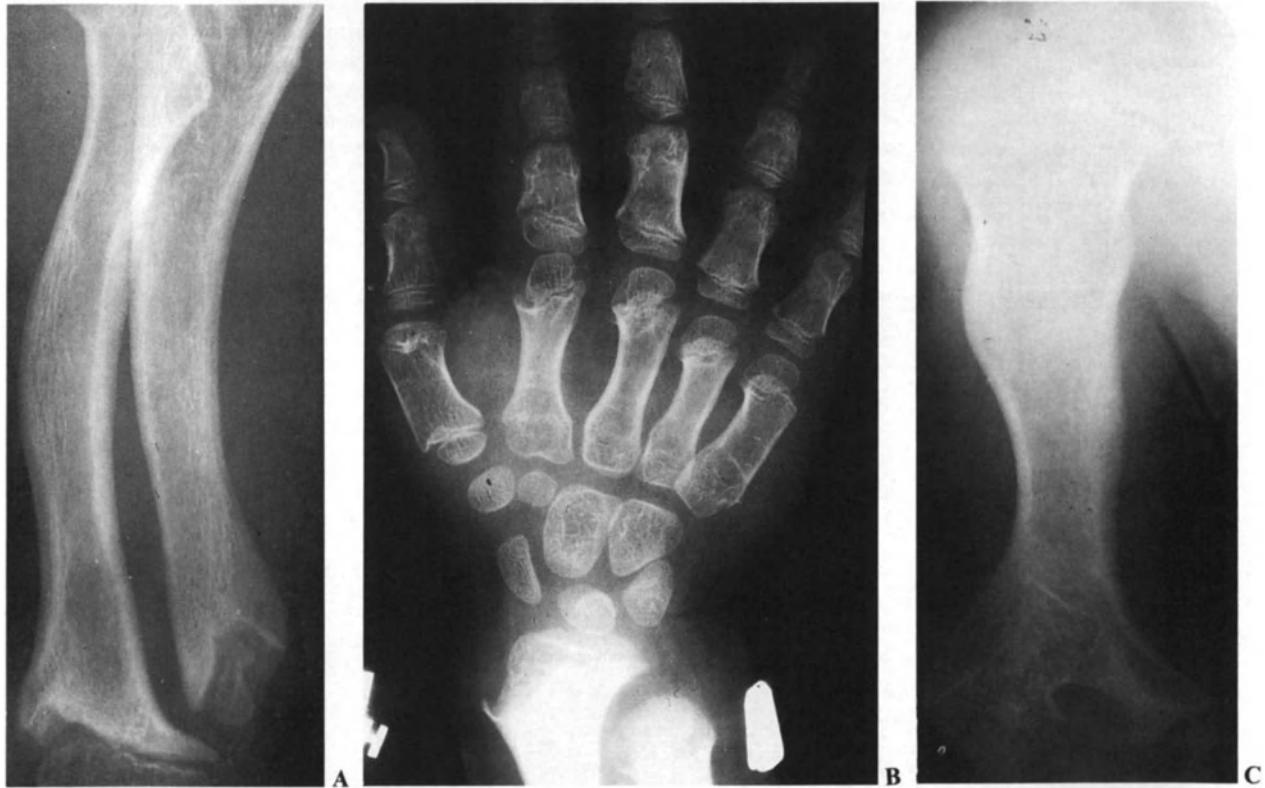


**Fig. 14.25.A** Achondroplasia. There is a characteristic V-shaped deformity of the metaphyses and growth plates of the distal radius and ulna, with modeling deformity. In the hands, **B**, the bones are short and 'stubby' with malformed epiphyseal growth plates. The humerus is short and deformed, with 'flared' metaphyseal regions, **C**.

metaphyseal junctions are seen. The 'trident' hand is a characterizing feature, and there are generally short 'stubby' digits.

The calvarium is large, with a short skull base and depressed nasal bridge. The sella is small and the foramen magnum is also small, and funnel-shaped.

There is an exaggerated lumbar lordosis, and decreased interpedicular distance of the lumbar vertebra. This may give rise to severe spinal problems in later life with spinal stenosis and disc protrusions (see Chap. 44). Occasionally wedging of thoraco-lumbar vertebrae occurs. There is also posterior scalloping of the vertebrae. A 'champagne glass' pelvis is also characteristic and squared iliac wings are found with a narrow sciatic notch.

**Hypochondroplasia.** This is similar to achondroplasia, but there is less marked shortening of the bones and no skull involvement. There is a long distal fibula relative to the tibia.

Spinal stenosis, increased lumbar lordosis, and short pedicles are also found.

**Pseudo-achondroplasia.** This presents with a variable pattern depending upon a recessive or dominant inheritance.

The skull is normal in both types, but there is flattening and 'beaking' of the vertebrae. Irregular epiphyses and broad metaphyses occur and after fusion an epiphyseal dysplasia pattern is seen. There are large iliac bones, with irregular acetabula and there may be short stubby bones in the hands. The radius and ulna are shortened with a V-shaped radio-ulnar articulation at the wrist.

**Fibrodysplasia Ossificans Progressiva (Myositis Ossificans Progressiva).** There is ossification in the soft tissues, which lies in the connective tissue within striated muscle. There is a characteristic shortening of the great toe with either fusion or hypoplasia of the proximal metacarpal occurring in 75% of cases. Similar findings may be seen in the thumb and clinodactyly of the little finger also occurs. Differentiation should be made from dermatomyositis.

**Marfan's Syndrome.** This condition has an autosomal dominant inheritance. Muscle weakness and hypermobility are associated with elongation of the tubular bones, including those of the hands and feet. Extra epiphyses are occasionally found. Depressed sternum, and a high-arched palate are also features.

Associated cardiovascular abnormalities include ASD, mitral valve lesions, and aortic dissection. Lens dislocation is also seen and spinal changes include posterior vertebrae scalloping and scoliosis.

### Metabolic Disturbances

Several inherited disorders give rise to abnormalities due to metabolic disturbances. Although mentioned below, these are discussed more fully in Chapter 17.

**Phenylketonuria.** This results from impaired conversion of phenylalanine to tyrosine. Severe mental retardation is seen and radiographically there may be cupping and beaking of the distal metaphyses of the radius and ulna with longitudinal striations.

**Hypophosphatasia** (see p. 326). There is a low or absent serum alkaline phosphatase and hypercalcemia, and patients present with the radiological appearances of rickets. There is variable severity from a fatal infantile form, to a less



**Fig. 14.26.** Hypophosphatasia. There are changes of a mild form of rickets in this patient with widening of the growth plate, and mild metaphyseal irregularity.

marked adult form, with osteoporosis and a tendency to fracture (Fig. 14.26). Phosphoethanolamine is found in the urine and plasma.

**Homocystinuria** has an autosomal recessive inheritance. Excessive urinary homocystine is found, due to the absence of the enzyme cystathione synthetase.

There is a tendency to vascular thrombosis in these patients, particularly after interventional procedures.

**Alkaptonuria/Ochronosis** (see p. 334). Inherited as an autosomal recessive, this condition results from excessive homogentisic acid due to abnormality of tyrosine metabolism. Pigment deposition in the articular cartilage leads to calcification and early degenerative arthritis. Intervertebral disc calcification is a characteristic finding.

**Wilson's Disease** (Hepatolenticular degeneration) (see p. 334).

### CHROMOSOMAL DISORDERS

#### Turner's Syndrome (Fig. 14.27)

Patients have an XO chromosomal pattern. At radiography there is generalized osteoporosis and short metacarpals are seen, particularly involving the fourth. An increased carrying angle at the elbow may be apparent, and there is a radial tilt of the trochlea. The medial tibial condyle is depressed, giving rise to a picture similar to Blount's disease (see Chap. 20). There are maldeveloped clavicles and slender ribs, and in the spine, a hypoplastic odontoid and atlas may be found. In the pelvis the sciatic notch is small and there is a narrow pubic arch.

Mental deficiency is associated, as are congenital cardiovascular abnormalities, particularly aortic coarctation.



Fig. 14.27. Turner's syndrome. A short 4th metacarpal is evident. Although not pathognomonic, this is a feature of Turner's syndrome.

#### Down's Syndrome (Mongolism)

This is due to an extra chromosome in 21–22 group. A variable radiological presentation includes hypotelorism, absent frontal sinuses, hypoplasia of maxillae, sphenoids and nasal bones, and brachycephaly. Flattening of the acetabular roof, with large iliac bones is characteristic.

Many mongoloids have only 11 pairs of ribs and extra ossification centers are found in the manubrium. Clinodactyly of the fifth digit, with hypoplasia of the middle and distal phalanges occurs. Concave anterior vertebrae are seen and the lumbar vertebrae are taller than they are wide.

Associated visceral abnormalities include congenital heart disease, aberrant right subclavian artery, duodenal stenosis or atresia, and Hirschprung's disease.

Additional chromosomal abnormalities are shown in Table 14.3.



Fig. 14.28. Basal cell nevus syndrome. Multiple cysts are present in the mandible.

#### Dwarfism

There are a variety of dwarfisms, giving rise to shortening of the long bones, spine, or both.

Some of the better known are:

1. *Diastrophic dwarfism* – short long bones: 'hitch hiker's thumb'; scoliosis.
2. *Thanatophoric dwarfism* – usually fatal. Short bones, platyspondyly with 'H'-shaped vertebrae and squared iliac bones.
3. *Metatrophic dwarfism* – initially short limbs and a normal trunk, progressing to a short trunk with severe kyphoscoliosis. Severe platyspondyly occurs giving rise to a dumb-bell appearance. The ends of the long bones are flared.

*Asphyxiating Thoracic Dystrophy.* This condition has an autosomal recessive inheritance. The characteristic finding is a bell-shaped thorax, with short 'horizontal' ribs. Polydactyly is also a common feature, and the iliac wings are flared. Death usually occurs in infancy from respiratory problems.

*Chondro-ectodermal Dysplasia* (Ellis–Van Creveld disease). In this condition the long bones are short, and usually with

Table 14.3. Chromosomal abnormalities

	Chromosome involved	Skeletal features
Down's (Mongolism)	21–22	See text
Trisomy 13–15 (Paton syndrome)	13–15	Syndactyly, polydactyly, hypertelorism marked craniofacial abnormalities
Trisomy 17–18	17–18	Short 1st metacarpal and thumb; anti-mongoloid pelvis; thin skull vault, hypoplastic maxilla and mandible, ulnar deviation of 3rd, 4th, and 5th fingers
Cri-du-Chat syndrome	4–5	Hypertelorism, microcephaly; polydactyly, syndactyly
Wolf syndrome	4–22	Polydactyly, underdeveloped pelvis, fusion defects of elbows, ribs and spine
Trisomy 9x syndrome	9	Pseudoepiphysis; clinodactyly, delayed maturation
Basal Cell Nevus syndrome	19–20	Brachydactyly, bifid ribs, mandibular cysts (Fig. 14.28)
<i>Sex linked</i>		
Turner's	XO	See text
Klinefelter's	XXY	Non-specific, clinodactyly of small finger, short 4th metacarpal



**Fig. 14.29.** Polydactyly of the ulnar side of the hand, associated with Ellis-van Creveld disease, with shortening of the tubular bones of the hand.

more severe involvement distally. Carpal coalition and polydactyly (predominantly ulnar side) may occur (Fig. 14.29). There is a narrow bell-shaped thorax. Cardiac abnormalities occur mostly as ASD and VSD. There is an ectodermal dysplasia (teeth, hair, nails).

**Dyschondrogeresis.** Inherited as autosomal dominant, this is a mesometric dwarfism with hypoplasia of the distal aspect of the ulna (Madelung's deformity, Fig. 14.4). The medial tibia may also be involved, and there may be shortening and deformity of the tibia and fibula.

#### THE MUCOPOLYSACCHARIDOSES

Several types are described

1. Hurler (Fig. 14.30).
2. Hunter.
3. Sanfilippo (Fig. 14.31).
4. Morquio Brailsford (Fig. 14.32).
5. Scheie.
6. Maroteaux-Lamy (Fig. 14.33).

They are all autosomal recessive, except the Hunter type which is X-linked. Various degrees of skeletal abnormality and mental retardation occur. Most are similar to Hurler's, but less severe.

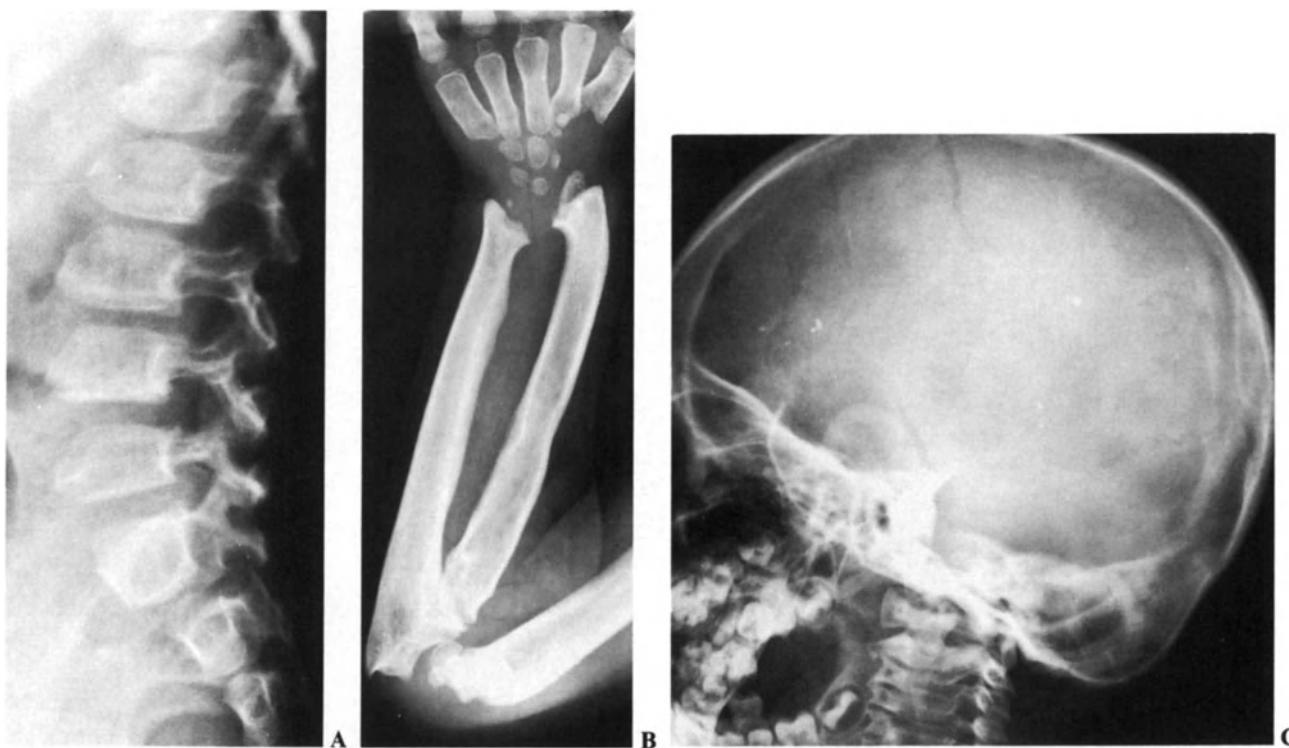


**Fig. 14.30A, B, C.** Mucopolysaccharidosis I. Hurler's syndrome. There is abnormality of the vertebrae with 'beaking' which is predominantly of the lower aspect, A. The metacarpals and forearm bones are abnormal at their ends, B. The skull demonstrates modeling deformities and an abnormal sella turcica, C.



Fig. 14.31. Mucopolysaccharidosis III (Sanfilippo). There is a characteristic 'sharpening' of the metacarpals proximal margins, with deformity of the distal radius and ulna.



Fig. 14.33. Mucopolysaccharidosis VI (Maroteaux-Lamy). There is marked irregularity of the femoral capital epiphysis, and acetabula.

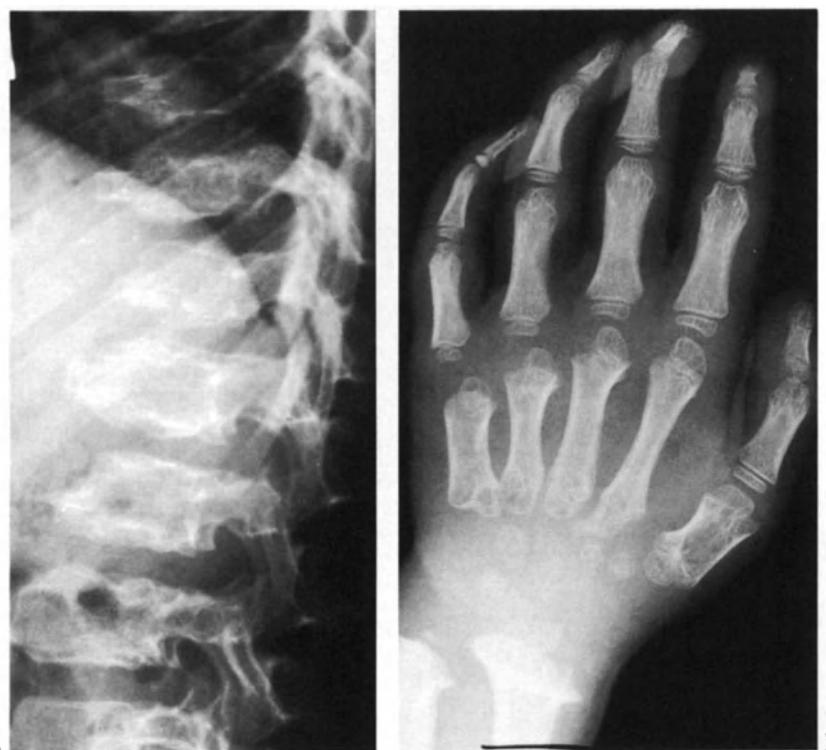


Fig. 14.32A, B. Mucopolysaccharidosis IV (Morquio's). Beaking of the vertebra involves the midportion, A. Again, abnormality of the metacarpals is seen, involving the proximal ends, and there is also irregularity of the distal radial and ulnar metaphyses, B.

*Hurler's Syndrome* (Fig. 14.30). This presents with ovoid vertebral bodies, with inferior beaking (c.f., Morquio's which has central beaking). There is variable mental retardation and coronal clouding.

Skeletal features also include stubby metacarpals with thin cortices and pointed proximal ends. Similar changes may be seen in the long bones.

In the skull there is a J-shaped sella, and poorly aerated air cells. Macrocephaly also occurs.

*Morquio's Syndrome* (Fig. 14.32). Spinal changes include kyphosis, with abnormal flattened vertebrae and beaking of the middle section anteriorly. Irregular epiphyses with fragmentation are found, especially in the femoral heads. There are also deformed acetabula. Stubby tubular bones are found in the hands and feet.

**Spondyloepiphyseal Dysplasia.** This term covers a group of conditions with platyspondyly and dysplasia of other bones. There is variation in involvement with the different varieties. These include:

*Dominant variety (congenital)* – platyspondyly mostly of thoracic spine with wedging. Early osteoarthritis occurs due to involvement of long bones.

*Recessive variety* – generalized platyspondyly, without wedging.

*X-linked variety (Tarda).* There is a characteristic appearance of mounds of bone on the posterior vertebral end plates. Mild epiphyseal abnormalities occur elsewhere. Again, early osteoarthritis may occur.

*Achondrogenesis.* This is a rare lethal infantile dysplasia

with very short limbs, and gross undermineralization, particularly of the pelvis and spine.

#### REFERENCES AND SUGGESTIONS FOR FURTHER READING

- Andrea L, Von Rosen S (1958) The diagnosis of dislocation of the hip in new borns, and the primary results of immediate treatment. *Acta Radiol [Diagn] (Stockh)* 49: 89–95
- Beighton P (1978) Inherited disorders of the skeleton. Churchill Livingstone, Edinburgh
- Dutton RV (1987) Practical radiologic approach to skeletal dysplasias in infancy. *Radiol Clin North Am* 25: 1211–1223
- Dorst JP, Scott CI, Hall JG (1972) The radiological assessment of short stature – dwarfism. *Radiol Clin North Am* 10: 343–414
- Egglei KD (1987) In: Taveras JM, Ferucci JT (eds). *Radiology. Diagnosis, Imaging, Intervention, revised edn.* Vol 5, chapter 9. JB Lippincott, London, Mexico, New York
- Freiberger RH (1987) In: Taveras JM, Ferucci JT (eds). *Radiology. Diagnosis, Imaging, Intervention, revised edn.* Vol 5, chapter 9. JB Lippincott, London, Mexico, New York
- Giedion A (1988) Genetic bone disease: Radiologic sight and insight. *AJR* 151: 651–659
- Greenfield GB (1986) *Radiology of Bone Disease*, 4th edn. JB Lippincott, Philadelphia
- McCredie J (1975) Congenital fusion of bones; radiology, embryology and pathogenesis. *Clin Radiol* 26: 47–57
- Poznanski AK (1984) The Hand in Radiologic Diagnosis, 2nd edn. WB Saunders, Philadelphia
- Poznanski AK, Gara SM, Holt JF (1971) The thumb in congenital malformation syndromes. *Radiology* 100: 115–129
- Scott ST (1989) Infant hip ultrasound. *Clin Radiol* 40: 648–650
- Spranger JW, Langer LO, Wiedermann HR (1974) *Bone Dysplasias*. WB Saunders, Philadelphia
- Sutton D (1987) *Textbook of Radiology and Imaging*, 4th edn. Churchill Livingstone, Edinburgh

## CHAPTER 15

# TRAUMA

J. W. R. Young

### GENERAL CONSIDERATIONS

A fracture occurs when there is a break, either complete or incomplete, in the continuity of bone or cartilage. When a loading force is applied to bone, it responds initially in an elastic manner, whereby cessation of the load results in return of the bone to normal. With increased force, a *plastic fracture* occurs, and the bone remains deformed after cessation of the load. Finally, failure of the bone may occur, giving rise to *complete fracture*. Furthermore, repetitive loading of a bone at 'sub-fracture' levels and muscle fatigue may play a role in the development of *stress fractures* (see below).

#### Definitions

*Open or Closed.* This refers to whether the bone fragments communicate with the outside environment, e.g. through a skin puncture (open), or remain covered with intact skin (closed).

*Incomplete or Complete.* Incomplete fractures occur most commonly in children, when bone resilience is greater and include three types.

1. *Plastic fracture* – bending of the bone without cortical disruption, or acute angulation
2. *Torus or buckle fracture* – a fracture of the cortex on the 'compressive' side of the bone with an intact cortex on the tension side (Fig. 15.1)
3. *Greenstick fracture* – a fracture only on the tension side

*Comminution.* This refers to fractures with more than two fragments.

*Apposition/Displacement.* This refers to the position of the major fragment. Fragments which are not apposed should be described according to the direction of displacement of the distal fragment relative to the proximal bone.

*Alignment.* This refers to the relationship along the axis of major fragments. There are two ways to describe alignment, but the most logical refers to the alignment of the distal fragment with respect to the proximal (Fig. 15.2). This has the additional advantage of following the same 'rules' that apply to displacement. The alternative is to describe the angulation as the direction the apex of the angle makes at the fracture site.

*Rotation.* This should always be assessed and necessitates visualization of both ends of the bone, so that the orientation of the proximal and distal joints can be assessed.

*Complications of Fracture.* In open fractures, apart from the associated soft tissue trauma, there is an increased potential for *infection* at the fracture site. Closed fractures (no skin vio-



Fig. 15.1A, B. AP and lateral view of a Torus or buckle fracture. The dorsal cortex is buckled, but the volar cortex is intact (B).



**Fig. 15.2.** There is a comminuted fracture of the mid tibia with medial displacement and medial angulation of the distal fragment.

lation), are not as susceptible to this problem. However there are other potential problems in all fractures.

1. *Delayed union.* This may occur from many causes (Table 15.1).

**Table 15.1.** Causes of delayed union and non-union

*Causes of delayed union*

- mechanical
  - poor apposition
  - inadequate stabilization
- pathological
  - age: decreased osteoblastic activity
  - dietary: vitamin deficiency (C and D)
  - pathological fracture
  - infection
  - massive initial trauma: usually goes on to non-union

*Causes of non-union*

- idiopathic (particularly tibia): probably the result of devascularization following trauma
- poor stabilization
- infection
- pathologic fracture
- massive initial trauma

2. *Non-Union.* This is the absence of bony union over a prolonged period. The radiographic appearance is usually of a persistent fracture line, with surrounding sclerosis
3. *Malunion.* This is the term given to a fracture which heals in an unsatisfactory anatomical position.

There are several pathological conditions which are or appear to be associated with trauma. These are discussed below.



**Fig. 15.3.** Post-traumatic avascular necrosis of the proximal scaphoid. The fracture through the waist has healed, leaving only minimal cortical irregularity on the radial side. The proximal scaphoid now shows increased radiodensity.

**Avascular Necrosis.** This occurs from a traumatic severance of the blood supply. Anatomically this is most likely to occur in:

1. Femoral neck fracture (femoral head)
2. Scaphoid fractures (proximal pole) (Fig. 15.3)
3. Talar fractures

The necrotic bone usually becomes denser than the surrounding bone, which may in turn become more osteopenic due to disuse. This feature may occur anywhere from 2 months to 2 years after injury.

**Sudeck's Atrophy** (post-traumatic reflex dystrophy) (Fig. 15.4). This is a rare condition in which, following injury to



**Fig. 15.4.** Sudeck's atrophy. Severe osteoporosis of the hand is seen, most marked around the ends of the bones. Courtesy of Dr James Dempsey, FRCS.



**Fig. 15.5.** A Dense new bone formation in the soft tissues of the posterior distal femur. The bone extends to the surface of the femur, mimicking a parosteal osteosarcoma. B Another case demonstrates a dense bony projection from the mid humerus. There was a history of an injury two years earlier.

a limb, intense pain and swelling occurs and severe disuse osteoporosis is seen. The initial injury may be relatively minor.

**Transient Osteoporosis.** This condition usually affects the hip, but may also be seen in the knee. Although this may represent a type of Sudeck's atrophy, a history of trauma is rare. Massive subarticular osteoporosis occurs, which is however self-limiting, with spontaneous resolution within 4–10 months. A similar appearance may be seen in the rare condition *idiopathic chondrolysis*. In this case, however, rapid progression to early degenerative disease usually occurs.

**Myositis Ossificans (Post-traumatic).** This usually occurs without overt underlying bone injury. It may be due to ossification of hematoma, or reactive periosteal elements which have been displaced into the soft tissues. The thigh is the commonest site. Hazy density in the soft tissues gives way to frank new bone formation, which may extend to the bone surface (Fig. 15.5). This may cause difficulty in distinguishing the lesion from parosteal osteosarcoma (p. 296) both radiographically and, unless adequate biopsy material is obtained, histologically (Fig. 15.5).

A similar type of calcification or ossification may occur around joints following dislocation and in cases of severe closed head injury. Ligamentous avulsions or trauma may also result in calcification, such as calcification of the medial collateral ligament of the knee in cases of chronic subclinical trauma (*Pellegrini–Stieda lesion*).

**Compartment Syndrome.** Rarely, trauma to a limb will give rise to a potentially devastating situation whereby the tissue pressure within a closed 'compartment' gives rise to progressive ischemia and ultimately necrosis. The compart-



**Fig. 15.6.** A large elbow effusion is identified by anterior and posterior fat pad elevation (arrows). This is caused by a supracondylar fracture, with mild dorsal displacement of the distal fragment. Unlike this case, the fracture line is frequently invisible on initial radiographs.

ments are created by an area surrounded by rigid osseous and fascial planes. Tissue edema or hemorrhage may be the initiating factor, either from vascular interruption or injury. The result is to raise the tissue pressure, thereby further decreasing vascular perfusion. Prompt fasciotomy is required. *Volkmann's ischemia* and contracture is probably a variety of the compartment syndrome.

**Arterial Injury.** Vascular injury may generally occur as the result of penetrating injury, although it may also be caused by bone fragments, either at the time of injury or during manipulation. The popliteal artery is the most commonly injured artery, from fractures or dislocations around the knee. Brachial artery injury may also result from supracondylar fractures of the humerus or elbow dislocations, particularly in children. Branches of the internal iliac artery, especially the superior gluteal, are at risk in pelvic ring fractures (see p. 284).

**Joint Injuries. Dislocations** occur when there is a complete loss of normal articular contact between the bones comprising the joint. *Subluxation* refers to a partial loss of articular contact. *Diastasis* refers to separation of fibrous joints, e.g. symphysis pubis; sacroiliac joint (see Figs 15.32, 15.33).

**Associated Soft Tissue Abnormalities.** Injury to a bone may be implied by associated soft tissue abnormalities, particularly if the bone is injured in the region of a joint.

**Joint effusions** may be identified either by the presence of an increased soft tissue density in the region of the bursa or by elevation of an adjacent fat pad (Fig. 15.6).

Horizontal beam radiographs may depict a 'fat fluid' level in a joint bursa, indicative of *intra-articular bone injury* (Fig. 15.7).

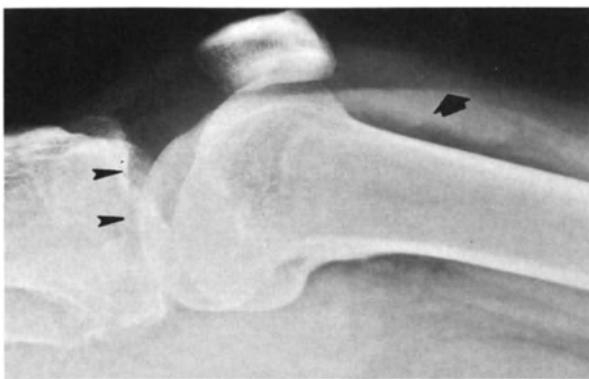


**Fig. 15.7.** Cross table lateral view of the right knee demonstrates a fat fluid level within the supra patella bursa (arrow). This indicates an intra-articular fracture – in this case, a mildly depressed fracture of the tibial plateau (arrowheads).

In the spine, *hematoma* may give rise to a paravertebral 'mass'.

A joint under stress may also exhibit a 'vacuum' phenomenon.

#### EVALUATION OF SKELETAL TRAUMA

The vast majority of injuries can be adequately visualized by *plain radiographs*. On occasion, however, *tomography* or even *computed tomography* may be helpful. This is particularly true in the evaluation of fractures of the tibial plateau, ankle joint (particularly subtalar), spine, and acetabular and pelvic fractures (see below).

In addition, *nuclear medicine* can be helpful in detecting occult fractures, such as scaphoid or femoral neck fractures, and stress fractures.

*Magnetic resonance imaging* is valuable in detecting avascular necrosis, whether as a result of direct trauma, or of more insidious trauma such as in Caisson disease, sickle cell disease, alcoholism etc. (Fig. 15.8).

#### Fractures in Childhood

Fractures in children differ from those in adults in several ways. They are often incomplete (*Torus* or *Greenstick* frac-



**Fig. 15.8.** Avascular necrosis of the femoral head on the right. There is subarticular lucency and collapse, with preservation of the joint space. MRI demonstrated a mixed signal pattern with areas of low and high signal.

tures) (Fig. 15.1), and 'plastic' fractures, without any cortical disruption, may occur. Children's bones have a greater capacity for remodeling than do adult's bones, which allows for less exact corrective angulation. However, rotational anomalies cannot be corrected by remodeling.

Finally, because of the relatively weak *epiphyseal plate*, fractures through this region are common. Damage to the epiphyseal plate may result in partial or even complete growth arrest. The Salter–Harris classification of fractures of the epiphyseal plate is the most commonly used (Figs. 15.9A, B, 15.10, 15.11). Under this system, the potential for growth arrest increases with increasing type number, Type IV and Type V having the greatest potential for growth arrest. However, it must be remembered that in a small child with an uncalcified epiphysis, it may be difficult or impossible to determine accurately damage to the epiphyseal cartilage, and what may appear to be a simple Type I or Type II fracture may indeed represent a Type IV or Type V injury, with the increased potential for growth arrest.

#### Slipped Femoral Capital Epiphysis

This occurs in adolescent children and is probably related to trauma, which may be chronic. It represents a variety of Salter–Harris Type I fracture of the epiphyseal plate. It is most commonly seen in boys approaching puberty, particularly those who are overweight and sexually immature. The incidence in girls is rising, however, possibly as the result of their increasing sporting and physical activity. It may be bilateral (30%–40%). The epiphysis is displaced from the metaphysis, usually in a posterior and slightly inferior direction reflecting an anterior and superior slip of the femoral neck with respect to the epiphysis (Fig. 15.12). 'Frog's leg' views as well as anteroposterior views may be needed to make the diagnosis and both hips should be examined because of the high incidence of bilateral involvement.

*Radiographic signs* include blurring of the epiphyseal/metaphyseal junction due to superimposition; increased width of the epiphyseal plate; so-called prolongation of the superior neck of the femur, whereby a line drawn along the superior neck fails to cut the epiphysis or cuts only a small portion (in normal patients this line usually cuts approximately one fifth to one fourth of the epiphysis); and loss of height of the epiphysis when compared to a normal contralateral hip.

#### The Battered Child

In 1946 Caffey described a syndrome of subdural hematoma, associated with multiple fractures of the long bones, often in various stages of repair. In addition, clinical inspection of such cases may demonstrate bruises, burns, evidence of malnutrition and signs of neglect. Inconsistencies in the history given by the parents or guardian are usual.

*Radiographic findings* include fractures in different stages of healing, periosteal reactions, particularly in the bones of the distal forearm or leg, multiple 'growth recovery' lines, and injuries to the skull (Fig. 15.13). Epiphyseal separations and metaphyseal infractions are particularly common. Fractures in unusual sites (e.g., femoral shaft) and from apparently minor trauma should also alert the physician to the possibility of non-accidental injury. Such findings warrant

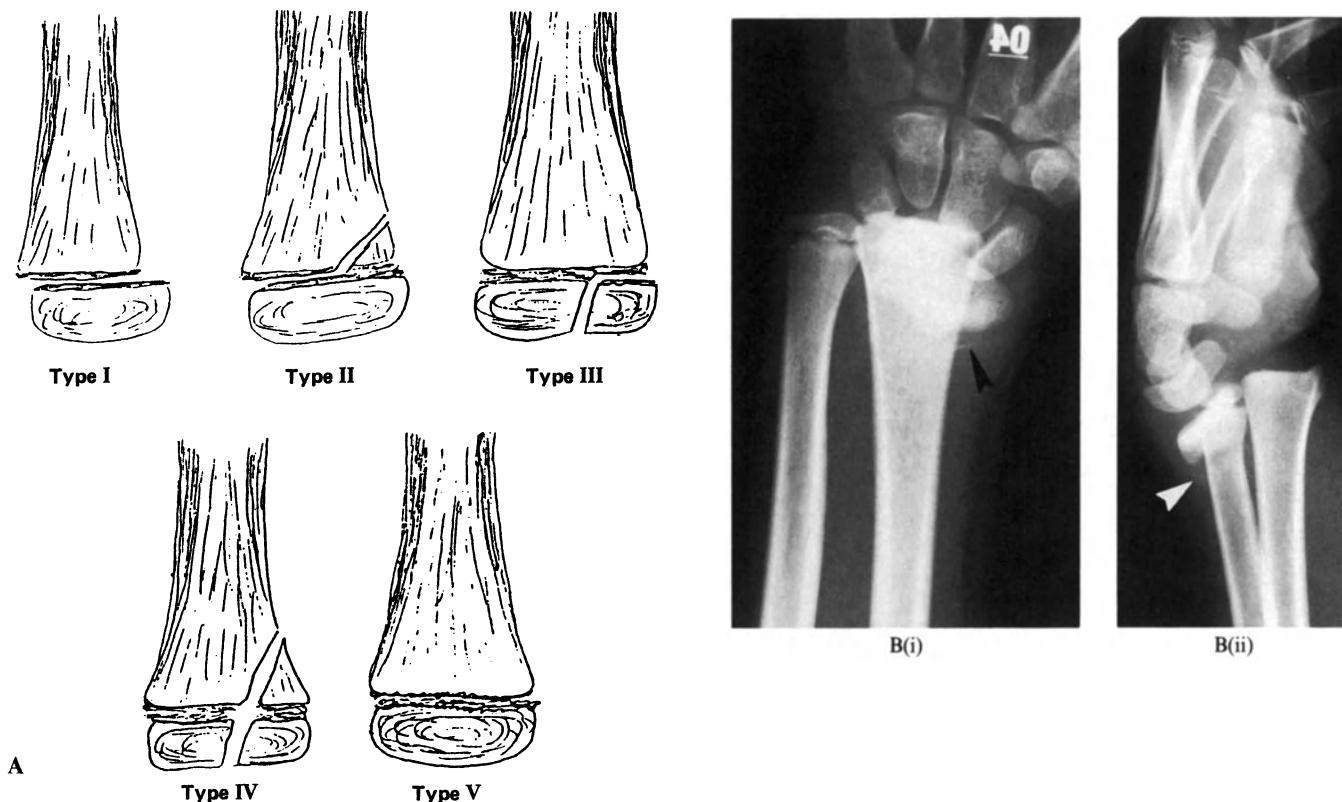


**Fig. 15.9.** A Salter/Harris classification of epiphyseal fractures. B Salter II fracture. Apparent Salter I fracture through the epiphyseal plate of the distal radius, with complete dorsal displacement of the epiphysis. In fact, a small metaphyseal fragment is seen, both on (i) the AP view and (ii) the lateral view (arrowhead), indicating a Salter II injury.



**Fig. 15.10.** (left) Salter II fracture of the distal tibia. There is mild lateral displacement of the epiphysis, and small metaphyseal fragment.

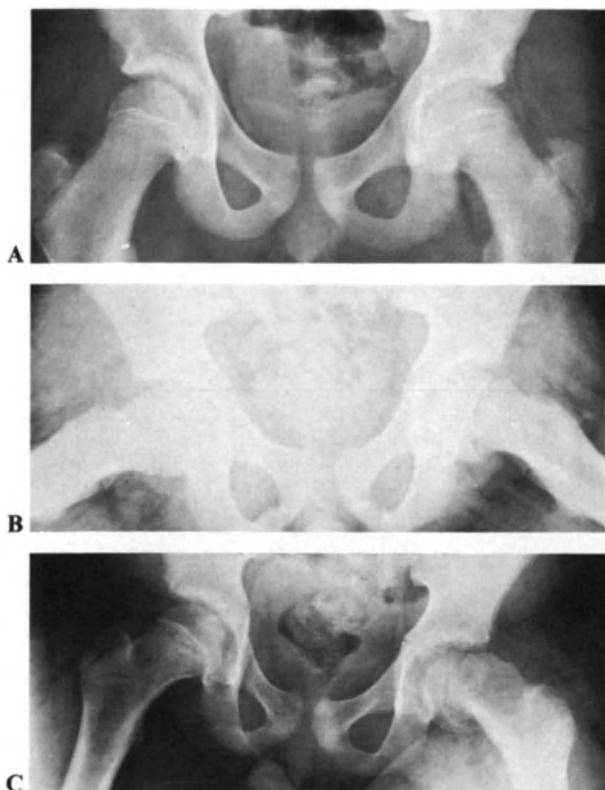
**Fig. 15.11.** (right) Salter IV fracture of the distal tibia, with fracture lines identified in the metaphysis and epiphysis.

a complete skeletal survey and communication to the referring physician immediately, as many children subjected to battering die at a subsequent assault.

#### Special Types of Trauma

**Stress (fatigue fractures).** These fractures are due to chronic repetitive forces which by themselves are insufficient to cause fracture, but over the course of time lead to the classical changes of a stress fracture. They occur in many bones, and usually at characteristic sites, often as the result of athletic activity. Examples are the 'march' fracture of the second and third metatarsal head; the stress fracture of the mid and distal tibia and fibula in long distance runners; and of these and the fifth metatarsal in ballet dancers; and fractures of the proximal fibula in paratroopers.

The earliest diagnosis can be made by *isotope scanning* where activity will be seen before radiographic signs. When radiographic signs appear, they may take several forms, depending upon the stage of healing or the chronicity of the stress factors. A hair-like lucency may be seen traversing the bone, although this may not be apparent without tomography (Fig. 15.14). New bone formation around the fracture may be the only sign, or may accompany the cortical fracture. If the patient continues the activity, a form of chronic fracture will occur, with abundant sclerotic periosteal new bone, and a persistent lucent fracture line, with surrounding sclerosis (Fig. 15.15).



◀ Fig. 15.12.A Slipped capital femoral epiphysis on the left. There is a hazy lucency identified over the growth plate (compare with the contralateral side), indicating the slippage. In addition, an imaginary line drawn along the line of the superior margin of the femoral neck will barely intersect the epiphysis. B In this frog leg view the slippage is more obvious, with clear superior displacement of the femoral neck. C A more obvious 'slippage' on the left.

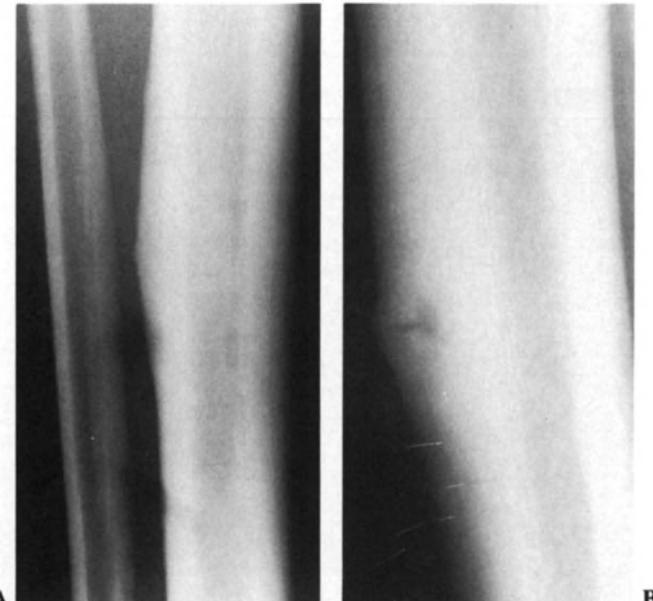


Fig. 15.14.A Stress fracture: elevated periosteal new bone is seen in the tibial diaphysis. Tomography, B, reveals the central lucency, running perpendicular to the bone surface.

A type of stress fracture is also said to account for the *pars interarticularis* defects seen in spondylolisthesis.

#### SKELETAL TRAUMA : REGIONAL

##### The Skull

The value of plain radiographic analysis of the skull continues to present a dilemma to physicians and, despite the large number of publications refuting the value of skull radiographs, they continue to be requested. The logical approach would be that if there has been sufficient injury to necessitate examination, computed tomography should be performed,

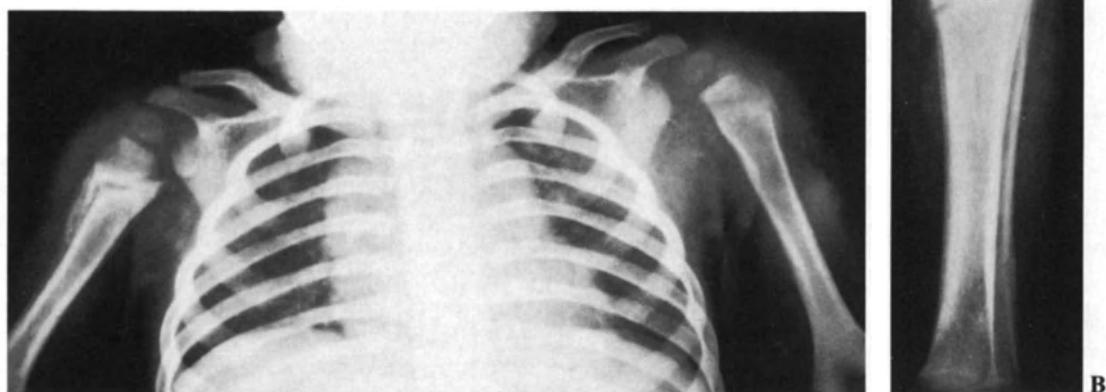


Fig. 15.13A, B. Healing fractures are identified in both proximal humeri, A, and the left tibia, B. This would be an unusual pattern for simple trauma.



**Fig. 15.15.** Stress fractures. Multiple transverse linear lucencies are seen in the tibia, with surrounding sclerosis. The patient was a runner who continued to exercise despite pain in his leg. The old fibula fracture was unrelated.

as even in the absence of a fracture, intracranial hemorrhage may occur.

The majority of skull fractures are *linear* and on occasion these may cause a diagnostic problem, simulating or being simulated by vascular grooves. In general, vascular grooves are less lucent, less sharply marginated, and are seen to branch and make curves rather than sharp angles.

Fractures which extend to the base of the skull may extend into the sphenoid sinus and an *air fluid level in the sphenoid sinus* should always be sought on a cross table lateral view. Similarly, fractures may extend into the frontal sinuses.

Depressed fractures may be readily apparent clinically, but can be missed. In general, however, they provide a typical radiographic appearance (Fig. 15.16).

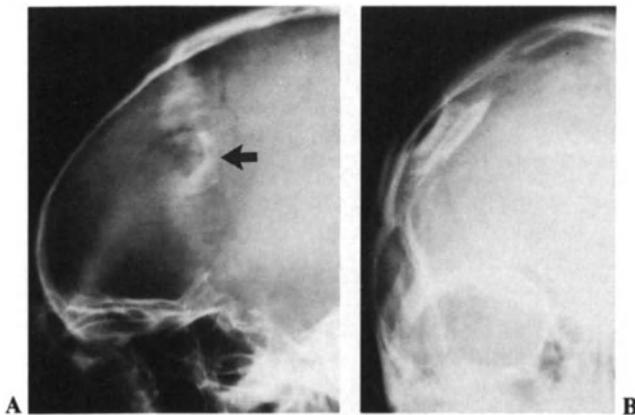


**Fig. 15.16.** A crescent of dense bone (arrow) is typical of a depressed fracture fragment. The frontal view, B, demonstrates the depressed fragment.

### The Facial Bones

Usually the result of automobile accidents, or assaults, facial bone injury comprises one of four groups; 1. mandible, 2. zygomatic arch and orbit, 3. nasal bones, and 4. complex fracture of the Le Fort varieties (Fig. 15.17).

The *Mandible* is most commonly fractured at its weak spot, adjacent to the canine tooth. However, as the mandible comprises a 'ring' structure, by virtue of its relationship to the skull, there is a strong possibility of two fractures occurring and this possibility must always be excluded.

The *nasal bones* are best identified on the lateral view, although the frontal views or occlusal film will determine lateral displacement.

The *zygomatic arch and orbital rim* are best seen on the occipitomental (Waters) view, although the submental view is good for assessing the zygoma for depression. Fluid levels or opacification of the maxillary sinus are important hints to fractures extending into the sinus and may be the only sign of '*blow out*' fractures of the orbital floor. '*Blow out*' fractures may also involve the ethmoid sinus walls, and air may penetrate the periorbital space giving rise to orbital emphysema.

**Le Fort** defined lines of weakness, leading to a classification system based on the type of fracture pattern (Fig. 15.17). In practice, pure Le Fort fractures are rare, and a combination of the injuries usually occurs.

### The Spine

**Cervical Spine.** *Normal Cervical Spine.* An understanding of the anatomy of the normal cervical spine is obligatory for correct evaluation. Various radiographic projections are suggested, but in practise, the vast majority of abnormalities can be appreciated on the *lateral view*. This should always include the body, and spinous process of C7. The anatomical features are identified in Fig. 15.18. Furthermore, high quality tomography or CT provide much better definition than oblique or pillar views, and are mandatory if spinal injury is expected or seen.

Alignment should be assessed along the anterior vertebral line, posterior vertebral line, posterior articular pillar line, spinolaminar line and spinous process. Symmetry of the disc

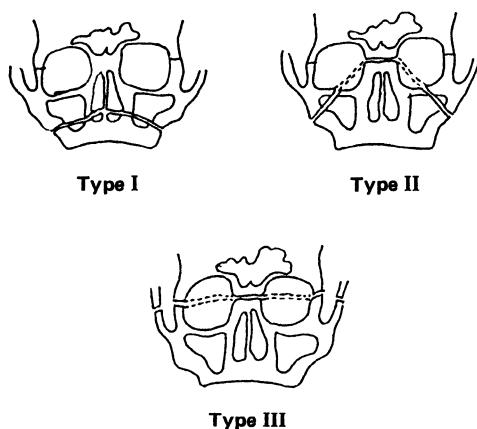


**Fig. 15.17.** Le Fort facial fracture classification.



**Fig. 15.18.** Normal lateral C-spine. Five lines should be evaluated moving from anterior to posterior: 1. The anterior vertebral line; 2. The posterior vertebral line; 3. The posterior articular pillar line; 4. The spinolaminar line; 5. The spinous process line.

spaces and the interspinous distance should be sought and the facets should also be examined for normal alignment. The laminar space should also be evaluated, as asymmetry may be the only sign of a rotational anomaly or facet fracture (Fig. 15.19). Prevertebral soft tissue measurements have been shown to be of limited value, but suggest injury when greater than 7–10 mm at the C2–C4 levels.

Spinal injury is the result of four major types of force, either alone or in combination – hyperflexion, hyperextension, rotation and axial loading.

**Hyperflexion Injuries.** These include hyperflexion sprain, flexion compression fractures, flexion teardrop fractures, bilateral facet lock and, if rotation also occurs, unilateral facet lock.

**Hyperflexion Sprain.** These injuries usually involve anterior subluxation of a vertebral body, with respect to the vertebra located inferiorly. Care must be taken in children, however, where normal subluxation of C2 on C3 can occur (pseudosubluxation). Flexion/extension views are of considerable value in problem cases although, in the acute setting, muscular spasm may prohibit movement.

Hyperflexion sprain is associated with variable *posterior ligamentous injury*. Depending upon the severity, the ligaments involved will be interspinous ligaments giving rise to widening of the interspinous distance, the ligamentum flavum and capsular ligaments, usually in association with the posterior longitudinal ligament injury, which gives rise to more severe widening of the interspinous distance, widening or subluxation of the facet joints (Fig. 15.20), or widening of the posterior disc space (Fig. 15.21). If the hyperflexion force produces enough ligamentous damage, total dislocation of the facets occurs, giving rise to *bilateral locked facets* (Fig. 15.22). This is usually associated with anterior sublux-



**Fig. 15.19.** Unilateral facet dislocation. There is abrupt narrowing of the laminar/facet space above the level of injury. This is due to variation in rotation of the spine around the injury.



**Fig. 15.20.** Hyperflexion sprain. Widening of the interspinous distance, interfacet joint (arrow), and posterior disc space. There is also a mild compression fracture of anterior aspect of C6, with a small 'teardrop' fracture of the superior anterior aspect.



**Fig. 15.21.** Hyperflexion sprain. There is widening of the interspinous distance (asterisks), interfacet joint and posterior intervertebral space, indicating severe posterior ligamentous disruption.



**Fig. 15.22.** Bilateral locked facets. There is anterior displacement of the whole of the C5 complex, with anterior dislocation of the inferior articular facets of C5 with respect to the superior facets of C6.

ation of the vertebral body above the injury of 50% or more of the AP diameter of the vertebral body. This will cause stripping or rupture of the anterior longitudinal ligament.

**Flexion Teardrop Fracture.** This occurs with flexion injuries when there is a compression fracture of the anterior aspect of the vertebral body inferior to the level of injury (Fig. 15.20), and may also be associated with a posterior displacement of the posterior portion of the affected vertebral body. It is usually a devastating injury with spinal cord compression involving the anterior columns.

**Unilateral Facet Dislocation.** When a rotational force is combined with hyperflexion, unilateral facet dislocation occurs. In such cases, the abnormal facet rotates over the normal subjacent facet. The contralateral facet acts as the fulcrum and is usually uninjured in the injury. On the abnormal side, there is either 'locking' of the inferior articulation of the facet of the rotated vertebra anterior to the superior articulation of the facet of the normally positioned subjacent vertebral body, or as occurs in approximately 30% of cases, there is a fracture through the articular facets, usually the superior facet of the lower vertebral body.

**Radiographically** the vertebral body of the rotated vertebra is normally displaced anteriorly, varying in degree up to approximately 20% of the width of the vertebral body (Figs 15.19, 15.23). Change in the laminar space is in general an accurate assessment of rotational anomaly (Fig. 15.19). There may also be a lateral 'shift' of the spinous process of the affected vertebra, identified on the frontal view.

**Wedge Fractures.** These occur when there is wedging of the anterior aspect of the vertebra, without ligamentous injury or posterior displacement of fragments. There is usually less than 30% compression of the anterior vertebra, and wedge fractures are associated predominantly with axial loading, and mild hyperflexion.

**Hyperextension Injuries.** In general, hyperextension injuries are associated with rupture of the anterior longitudinal ligament and give rise to widening of the anterior disc

space (Fig. 15.24); they may cause prevertebral soft tissue swelling. Facial injuries may be associated. It must be remembered, however, that positioning of the head in the neutral position by a well-meaning passer-by, or the placement of a cervical collar may largely restore any initial displacement, so that at the time of examination the radiograph

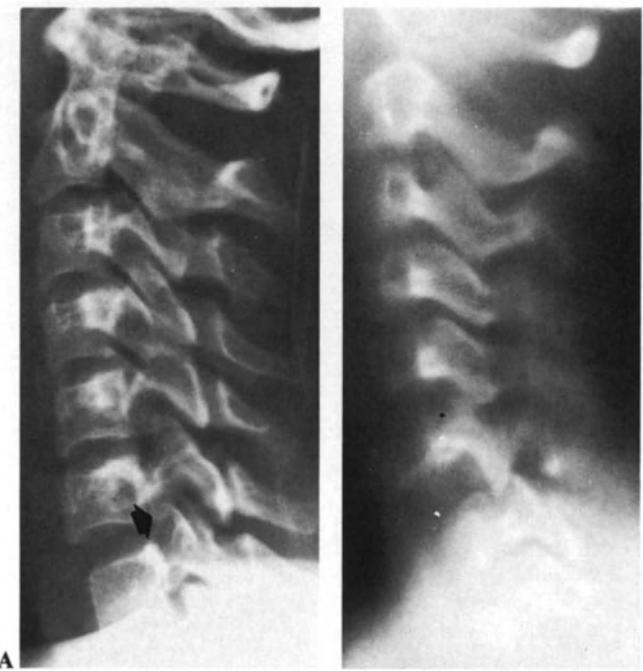


**Fig. 15.23A.** Unilateral locked facet at C6/7: There is clear obliquity of the spine at C6 and above with offsetting of the articular pillars: The pillars at C7 however, overlap, and careful inspection demonstrates one of the inferior facets of C6 to lie anterior to the corresponding superior facet of C7 (arrow). **B** Tomography confirms the findings with the inferior facets of C6 identified anterior to the superior facet of C7.



**Fig. 15.24.** Hyperextension injury. There is widening of the anterior intervertebral disc space, and at C6/7 a fracture through the lamina of C6 (arrow). The interspinous distances at C6/7 is narrow. Forestier's disease (DISH) is incidentally noted.

may not appear grossly abnormal. An additional effect of hyperextension is to cause an axial load on the posterior elements, giving rise to crush fractures of the posterior elements and narrowing of the interspinous distance (Fig. 15.24). In addition, *hyperextension tear drop fractures* usually of the anterior inferior aspect of the vertebral body involved, may occur, due to an avulsion of the anterior longitudinal ligament. Fractures through the *spinous process* may also occur, due to axial compression.

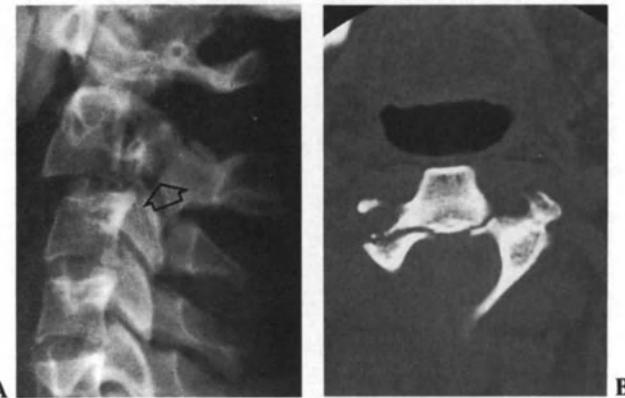


**Fig. 15.25A, B.** Hangman's fracture. A There are oblique fractures through the pedicles of C2 (arrow) with anterior displacement of the body of C2. CT scan of a different patient, B, shows extension of the fracture through the body and into the vertebral canal on the left.

**Hangman's Fracture.** This injury, misnamed because of a superficial resemblance to fractures seen in victims of hanging, occurs with hyperextension of the head and, therefore, a form of axial loading on the posterior elements of the upper cervical spine. Hyperextensive rotation of the head causes the compressing force of the occiput to be delivered in an inferior and anterior direction, causing fractures through the posterior arch of C2, which may extend into the body of C2 (Fig. 15.25). This may be an unstable injury, particularly if an oblique fracture through the body of C2 occurs, although the cord is frequently spared, due to the large AP diameter of the spinal canal at this level. The fracture may also extend into the vertebral canal, risking injury to the vertebral artery.

**Axial Loading. Jefferson Fracture: Burst fracture of C1.** In these injuries, axial loading causes compression of the lateral masses of C1 between C2 and the occipital condyles. Because of the anatomy of the region, this gives rise to a lateral displacement of the masses of C1 (Fig. 15.26), thus disrupting the bony ring. This can be appreciated on the transoral AP odontoid view. It also gives rise to anterior displacement of the anterior arch of the atlas relative to the odontoid process. Prevertebral soft tissue swelling is usual, although not inevitable. CT shows this lesion clearly.

**Burst Fractures.** These are caused by axial loading and give rise to shattering of the vertebra, often in all directions. The real importance of this injury lies in the possibility of posterior displacement of fragments into the spinal canal. *Computed tomography* is the method of choice for evaluating the position of fracture fragments, although high quality tomography may suffice if CT is not available.

**Miscellaneous Spinal Fractures. Spinous Process Fractures.** These most commonly occur at C7, and are often seen as avulsion injuries (*clay shoveler's fracture*). However, they may occur in direct trauma, or from compressive hyperextension (see above).

**Odontoid Fractures.** Fractures of the odontoid are subdivided into three types (Fig. 15.27). Ununited Type I fractures are largely accepted as the cause of the so-called *os odontoideum* (Fig. 15.28), although some authors believe this is due to an unfused ossification center. Odontoid fractures are, in general, best seen on the AP odontoid view, but should not be confused with artefacts from the posterior arch of the atlas (Mach effect) (Fig. 15.29), or overlying teeth. Type III fractures extending into the body of C2 may cause disruption of the cortical 'ring' of the lateral aspect of the body of C2, seen on the lateral view. There may also be an anterior tilt of the dens and hence anterior displacement of the posterior ring of C1.

**Rotatory Subluxation.** This is a condition where there is a rotational anomaly, usually of C1 on C2, which in children may give rise to torticollis. Although the condition may be self-limiting, occasionally it persists. It is best appreciated on open mouth odontoid views, and on both oblique projections, although tomography may be needed for full evaluation.

**Thoracolumbar Spine.** Fractures in the thoracolumbar spine are generally the result of severe axial loading (crush fractures) or acute flexion injuries, most commonly seen in seat-belt injuries in automobile accidents. Rotational forces, however, may also play a role, particularly in the upper lum-

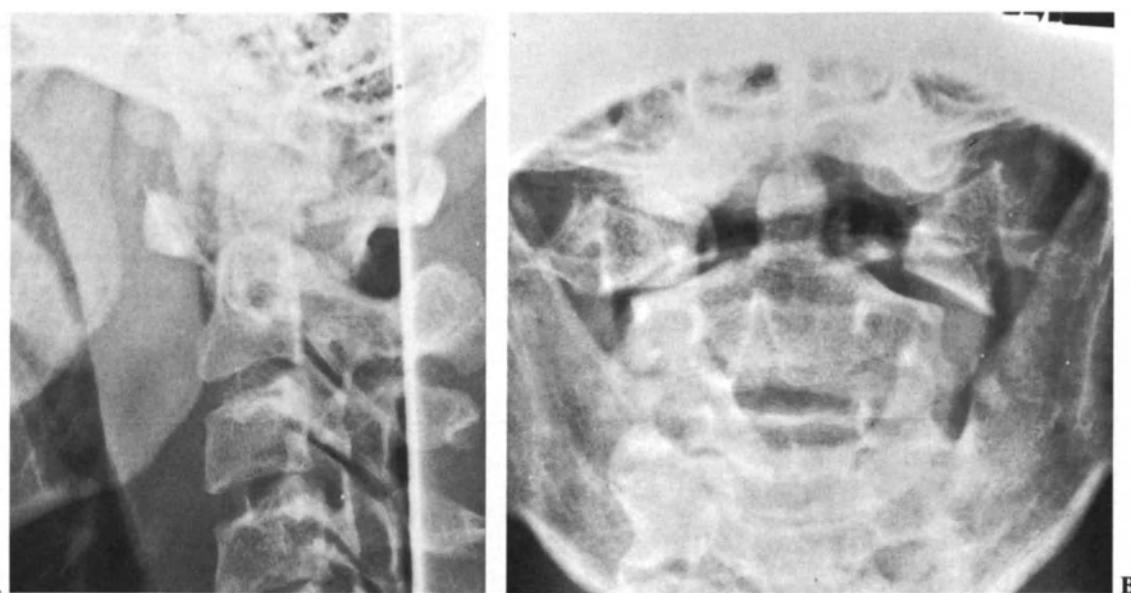


**Fig. 15.26A, B.** Jefferson burst fracture of C1. A There is anterior displacement of C1 with respect to C2, and marked pre-vertebral soft tissue swelling. B The open mouth odontoid view demonstrates lateral displacement of the lateral masses of C1.

bar region. As in the cervical spine, ligamentous injury can usually be appreciated by subluxation, either anterior or lateral. Widening of the interspinous distance, interpedicular space, or disc space are all indications of injury.

Compression injuries cause 'burst fractures' or wedge compression fractures, usually of the anterior margin, but also of the lateral aspect. Crush fractures are particularly common in the victims of falls from a height and may be

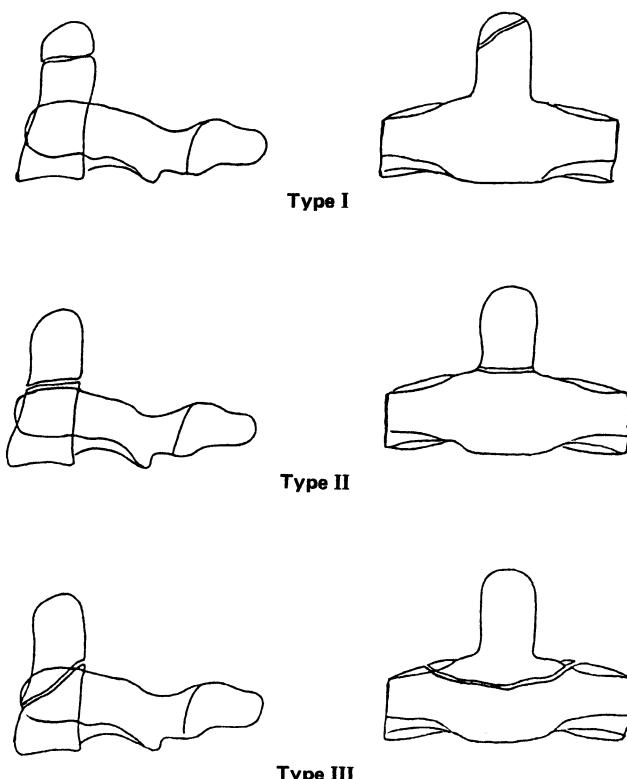


**Fig. 15.27.** Fractures of the odontoid process. Classification.

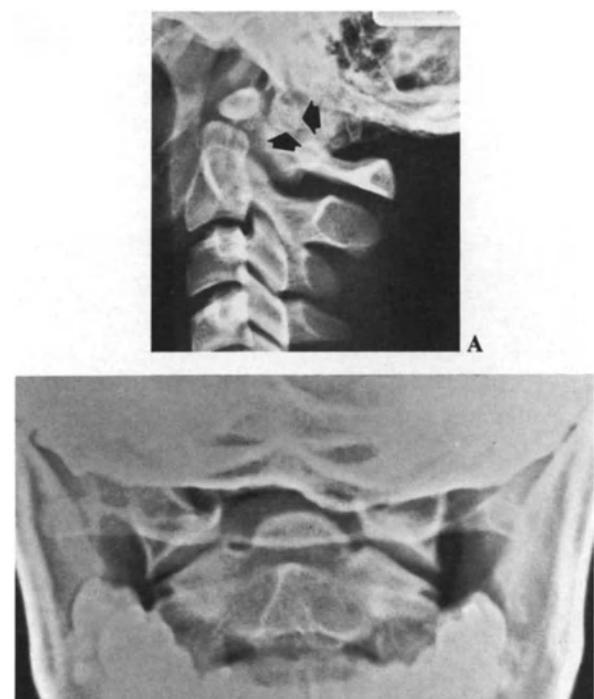


**Fig. 15.28A.** Os odontoideum, with posterior subluxation of C1 on C2. The 'Os' is well seen as a corticated rounded density (arrows) lying posterior to the anterior ring of C1. B The open mouth view demonstrates a characteristic rounded corticated margin of the stump of the odontoid.

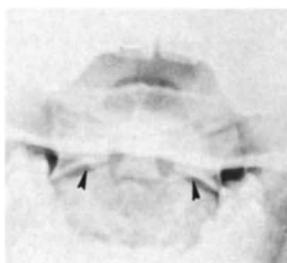


**Fig. 15.29.** Mach effect. A pseudo fracture through the base of the odontoid process, caused by the overlapping posterior ring of C1 (arrows).

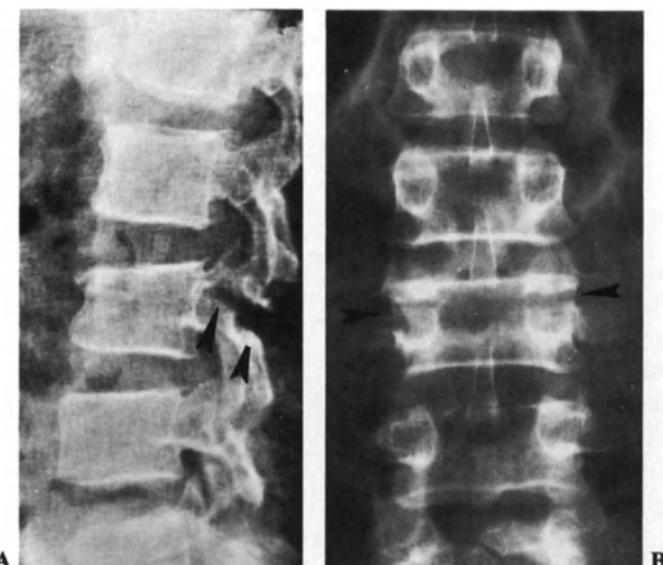


**Fig. 15.30.** A 'Smith's' fracture of L3: There is a horizontal fracture of the posterior elements of L3 well seen on the lateral view and demonstrated on, B, the frontal view by horizontal lucencies through the pedicles (arrowheads), but superior to the spinous process.



**Fig. 15.31.** Lateral compression fracture (Type I). A 'horizontal' fracture of the left symphysis is seen, with 'overlap' fractures of the inferior pubic rami and right superior pubic ramus. There is also a crush fracture of the left sacrum with disruption of the arcuate lines (arrowheads) and L. iliac fractures.

associated with calcaneal injury. All forms of compression fracture require CT to evaluate for posterior displacement of fracture fragments.

**Seat Belt Injuries.** These occur from forced hyperflexion, and are subdivided into three groups:

**Type I,** the '*Chance fracture*', occurs when the fracture extends horizontally from the spinous process into the vertebral body passing through the articular pillars and pedicles

**Type II,** the *Smith fracture*, is similar but does not involve the spinous process (Fig. 15.30)

**Type III** involves one side only, due to a rotational component

### The Pelvis and Hip

Much confusion has arisen over pelvic fractures, due to a lack of a logical and meaningful classification system. The system whereby fractures are described relative to the force of injury will be used in this text.

It has been shown that apparent single fractures of the pelvis are invariably associated with a second injury, whether bony or ligamentous. This is due to the fact that the pelvis is a bony ring, held together by ligamentous groups posteriorly and anteriorly. A search for a second site of injury should, therefore, always be made in fractures involving the pelvic ring.

**Lateral Compression Fractures.** These are subdivided into three types, depending upon the severity of the injury, and progressive involvement of the posterior pelvis. *Pubic rami fractures* are always present. Either they run 'horizontally', or in the coronal plane, or may present as a buckle or overlap fracture (Fig. 15.31). A common association is a crush fracture of the sacrum. Fracture of the medial wall of the acetabulum is also associated.

The more severe types II and III are also associated with posterior ligamentous injury, causing some instability posteriorly.

**Anterior Posterior (AP) Compression Fracture.** The damaging force in the AP (or PA) direction tends to cause 'opening' of the anterior pelvis, with splaying of the symphysis pubis, and/or fractures of the pubic rami, which are in the vertical plane.

The more severe type II and III fractures refer to increasing posterior ligamentous injury, and hence increasing instability (Figs 15.32, 15.33). Fractures of the anterior and posterior acetabular pillars are common.

**Vertical Shear Fractures.** These commonly arise from falls from a height. Fractures occur through the pubic rami and posterior pelvis, and are vertical in orientation. The large hemipelvic fracture fragment is generally displaced superiorly (Fig. 15.34).

**Mixed Fracture Pattern.** These arise from a combination of the injury force vectors and give rise to a mixed pattern of fracture. The commonest is a mixed anterolateral pattern.

**Straddle Fractures.** This term should not be used in radiology. Fractures of all four pubic rami can occur from either lateral or AP compression and clues should be sought for the likely vector, and associated injuries.

**Isolated Fractures.** Isolated fractures of the lower sacrum, iliac crest, or inferior pubic ramus may occur, and these do not violate the integrity of the pelvic ring. Such sacral frac-



**Fig. 15.32.** Type II AP compression fracture. Diastasis of the symphysis pubis and anterior left sacroiliac joint (arrowhead) is seen. There is also a fracture through the posterior pillar of the left acetabulum (arrow).



**Fig. 15.34.** Vertical shear fracture. Fractures through the left pubic rami and left sacrum are seen, with superior displacement of the left hemipelvic fracture fragment, demonstrated posteriorly by the relative positions of the inferior aspect of the iliac bones (dotted line).



**Fig. 15.33.** A Type III anteroposterior compression fracture. There is complete diastasis of the symphysis pubis and left sacroiliac joint. B CT scan of the same patient demonstrates the separation of the iliac wing from the sacrum.



**Fig. 15.35.** Avulsion of the lateral cortex of the ilium, the origin of the rectus femoris muscle.

tures are usually transverse and may be difficult to diagnose without a lateral view. Single fractures of a pubic ramus are seen, resulting from a direct blow. However, additional injury to the pelvis should always be excluded.

**Avulsion Injuries.** Avulsion injuries of the pelvis occur most commonly as the result of muscular exertion during sporting activities. The anterior superior iliac spine (sartorius), anterior inferior iliac spine (rectus femoris) and ischial tuberosity (hamstrings) are the commonest sites and muscles involved (Figs 15.35, 15.36).



**Fig. 15.36.** Avulsion fracture of the right ischium, at the insertion of adductor magnus.



**Fig. 15.37.** Fracture dislocation of the left femoral head, with a posterior dislocation. The fracture extends through the femoral head, with a large fragment retained within the acetabulum. The irregular lateral margin of the posterior acetabulum (seen through the retained femoral head fragment), indicates an acetabular injury.

### Acetabular Fractures

Acetabular fractures, in general, are regarded as involving one or more of four areas; those involving the posterior rim, the posterior pillar, the anterior pillar, or the quadrilateral plate. As expected, fractures of the *posterior rim* are usually caused by posterior dislocation of the femur (Fig. 15.37). Fractures of the *posterior pillar* may also be seen with posterior dislocations of the femur, and these varieties together with fractures of the *anterior pillar* are common in AP compression fractures of the pelvis (Fig. 15.32).

By contrast, fractures involving the *quadrilateral plate* are usually associated with lateral compression forces.

There is no question that CT provides the most detailed information about the fracture, and there is a trend towards three-dimensional imaging of these fractures. The real advantage of conventional CT over plain radiography lies in its ability to detect small bone fragments within the joint space.

Fractures of the femoral neck (see below) may be particularly difficult to diagnose on plain radiographs (Fig. 15.38). In the presence of pain, particularly in an elderly patient, a negative radiograph should not prevent additional studies, such as CT, nuclear medicine scan, or delayed radiography at 24 hours after immobilization.

### Shoulder Girdle

**The Clavicle.** Fractures of the clavicle involve the middle third in 80%, the outer third in 15%, and the medial third in 5% of cases. Over-riding of fragments and inferior displacement of the lateral fragment are common and specific views may be necessary to visualize the fracture. Fractures of the outer third may also be associated with disruption of the coracoclavicular ligaments.

**Dislocations.** Dislocations around the shoulder are relatively common and usually involve the humeral head or acromioclavicular joint.

The *humerus* is most commonly dislocated *anteriorly* (95%), or in practice, anteriorly, medially and inferiorly, coming to lie inferior to the coracoid process (Fig. 15.39). This may cause a cortical impaction both of the superior posterior aspect of the humerus (*Hill-Sachs* or '*hatchet*' deform-



**Fig. 15.38.** Subtle fracture of the right femoral neck. There is external rotation of the femur when compared to the left and 'smudging' of the trabecular pattern. Courtesy of C.S. Resnik, MD.



**Fig. 15.39.** Anterior dislocation of the right humerus. The inferior rim of the glenoid has impacted upon the superior margin of the humerus, giving rise to a Hill-Sachs, or hatchet deformity.



**Fig. 15.41.** Luxatio erecta: the humerus is held in abduction, with the superior surface wedged beneath the inferior aspect of the glenoid.

mity), and inferior aspect of the glenoid (*Bankart lesion*), or detachment of the anterior portion of the glenoid labrum. Anterior dislocations present no diagnostic difficulty.

Posterior dislocations, however, may be difficult to appreciate although they should not be missed. In general, they can be appreciated on the AP view by persistent internal rotation of the humerus and asymmetry of the gleno-humeral joint (Fig. 15.40). An axillary view may be impossible to obtain, but a transthoracic or 'swimmer's' view, or oblique (Y) view

will confirm the diagnosis.

An unusual inferior dislocation (*Luxatio erecta*) is caused by severe hyperabduction of the arm, whereby the humeral head impinges upon the acromion, which in turn acts as a fulcrum, causing an inferior displacement of the humeral head with the arm 'locked' in abduction (Fig. 15.41).

*Acromioclavicular separation* is usually the result of a fall on the outstretched arm or point of the shoulder. The importance of acromioclavicular dislocation lies in the trauma to

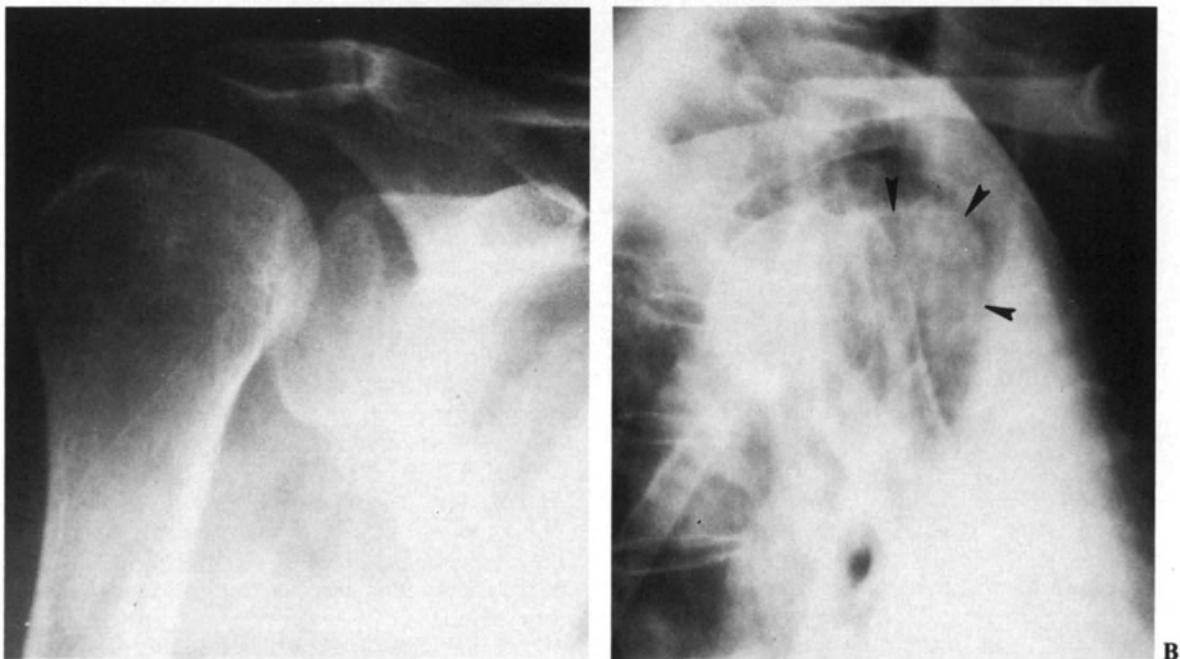


**Fig. 15.40.** A Posterior dislocation of the humerus. The humerus appears in internal rotation, giving rise to a 'light bulb' appearance. There is also asymmetry of the gleno-humeral joint space. B A swimmer's view demonstrates the articular surface of the humerus projected posteriorly and lying posterior to the glenoid (arrowheads).



**Fig. 15.42.** Contrast is seen lateral to the humeral head, in the subdeltoid bursa. This indicates a total rotation cuff tear.

the coracoclavicular ligament. This injury has been classified as sprain (Grade I), subluxation (Grade II), and dislocation (Grade III).

Grade III injuries are in general obvious on plain radiography with both acromioclavicular, and coracoclavicular separation. In Grade II injuries, stress views, with weight bearing may be needed for demonstration of the lesion. In Grade I injuries, mild widening of the acromioclavicular space, but not the coracoclavicular space may be seen on stress views.

**Rotator Cuff Injuries.** Rotator cuff is the term applied to the conjoined tendons of the supraspinatus, infraspinatus, subscapularis and teres minor muscles. The rotator cuff passes between the humeral head and acromion before inserting into the greater tuberosity of the humerus. It separates the glenohumeral joint from the subdeltoid bursa. Ruptures, either partial or complete may be diagnosed by *arthrography* (Fig. 15.42), although *ultrasound* and *MRI* are gaining popularity for diagnostic purposes. Complete rotator cuff tears are commonly associated with narrowing of the acromiohumeral joint space.

**Humerus.** Most injuries result from falls on the outstretched arm, particularly in elderly (osteopenic) females. *Fractures of the surgical neck or greater tuberosity* are the com-



**Fig. 15.44.** Anterior and posterior fat pad elevation (arrows) signifies effusion of the elbow joint. The fracture of the radial head is only identified by a minimal 'step off' of the volar cortex.

monest injuries. Spiral and oblique fractures are common, usually with displacement or angulation of the distal fragment, often requiring open fixation. Radial nerve injury occurs in up to 30% of cases.

**Supracondylar fractures** are the commonest elbow injury in children (60%), resulting from a fall on the outstretched hand. Radiographically a fracture line may not be seen initially, but hemarthrosis with elevation of the anterior and/or posterior fat pads is highly suggestive (Fig. 15.5). Volar displacement of the capitellum is also a helpful sign. These fractures, with associated vascular damage, may be of importance in the development of Volkmann's ischemia of the forearm (see p. 275).

The second most common elbow fracture in children is that of the *lateral condyle*.

**Forearm Fractures.** Fractures of the bones of the forearm are extremely common, particularly of the distal radius and ulna. The forearm effectively acts as a ring structure and an apparent single fracture may be associated with additional injury, either ligamentous or bony. Overt manifestations of this 'closed ring' concept are seen in the double forearm lesions, *Galeazzi fractures* of the radius with distal ulnar dislocation, and *Monteggia fractures* of the ulna with radial head dislocation (Fig. 15.43). It is therefore essential to examine the wrist and elbow carefully for additional injury in single bone forearm fractures.

**Fractures of the Proximal Radius and Ulna.** Fracture of the *radial head* is the commonest elbow injury in adults, usually occurring as a result of a fall on the outstretched arm. The fracture line may not be seen initially, but elbow effusion is a good warning sign, warranting immobilization and a repeat radiograph in 7 to 10 days (Fig. 15.44). Fractures of the radial head also occur with dislocations at the elbow (Fig. 15.45).

**Olecranon fractures** result from falls onto the point of the elbow, or avulsions of the triceps insertions. They must be distinguished from the unfused ossification center in children and young adults.



**Fig. 15.43.** Monteggia fracture of the ulna, with dislocation of the radial head.



**Fig. 15.45.** Complete elbow dislocation. There is also a fracture of the radial head, with small bone fragments seen overlying the ulna and radial soft tissues.

**Distal Radius and Ulna.** This is one of the commonest sites for fracture in the entire body, and most fractures are associated with eponyms.

In *Colles' fracture*, the distal radius is fractured and angled dorsally, giving rise clinically to the so-called 'dinner fork' deformity of the wrist. The ulnar styloid is also fractured in



**Fig. 15.47.** Scaphoid fracture: this was not seen on the regular views but became evident on this specific scaphoid view.

over 50% of cases, and there is almost invariably distal radio/ulnar dissociation (Fig. 15.46).

*Smith's fracture* is the reverse of the Colles' fracture, with volar angulation of the distal fragment of the radius. In *Barton's fracture*, the fracture line extends through the dorsum of the distal radius to involve the articular surface. If the volar radial rim is involved this is a reverse Barton's fracture.

*Fractures of the Carpus.* The *scaphoid* bone is the most common carpal bone to be fractured (Fig. 15.47). Once again, initial radiographic examination may be negative and follow-up radiograph in 7 to 10 days after immobilization should be performed if there is a clinical suspicion. Alternatively a *radionuclide bone scan* may be helpful. *Non-union* and *osteonecrosis* of the proximal fragment are important complications, particularly in fractures of the proximal scaphoid, as the vascular supply enters in the middle of the bone (Fig. 15.3).

Dorsal avulsion fractures of the *triquetrum* are common and may be appreciated best on the lateral view.

The other carpal bones are only rarely injured, except for the *hamate*, the hook of which may be detached acutely from blows on the proximal palm of the hand, or as the result of chronic trauma, such as from holding a tennis racquet or golf club.

*Dislocation of the Carpus.* Dislocations of the carpus are usually of the lunate or perilunate variety, the latter often being associated with a scaphoid fracture.

In *lunate dislocation*, the normal anatomy of the proximal carpal row is lost. The lunate is usually seen to overlap the capitate, hamate and triquetrum on the PA view, also taking on a triangular, rather than rectangular shape (Fig. 15.48). On the lateral projection, the lunate is seen overlying the volar aspect of the wrist, in an abnormal orientation. This injury may also occur in conjunction with a fracture dislocation of the scaphoid.

In *perilunate (± transscaphoid fracture) dislocation*, the whole



**Fig. 15.46.** A Colles' fracture of the distal radius, with dorsal angulation and, B, mild impaction of the distal fragment.

**Fig. 15.49A, B.** Trans-scaphoid/perilunate fracture dislocation. There is disruption of the carpus with disorganization of alignment between the proximal and distal carpal rows. The lunate (L) overlies the triquetrum, but still articulates with the proximal scaphoid, which is overlaid by the capitate (C) on the frontal view. The distal scaphoid fragment is in normal relationship to the capitate. Dorsal displacement of the majority of the carpal bones is identified on the lateral view, B.



**Fig. 15.48A, B.** Lunate dislocation: although easily appreciated on the lateral view, A, the lunate (L) has taken on a typical triangular configuration on the AP view, B. In this case, there is also a fracture through the proximal pole of the scaphoid, with displacement of the proximal fragment in association with the lunate.

of the carpus (minus the proximal scaphoid pole in transscaphoid injuries), is dislocated posteriorly with respect to the lunate. This is usually evident on the PA view, but again is clear on the lateral projection. Fracture/dislocation of the scaphoid is common with perilunate dislocations (Fig. 15.49).

**Scapholunate dissociation** is identified by widening of the scapholunate joint (Terry Thomas sign), often exacerbated on clenching the fist. This may be seen in rotational (rotatory) dislocation of the scaphoid.

**The Hand.** Hand injuries are common and usually present no diagnostic difficulty. Worthy of special mention is the '*Bennett's fracture*' – a fracture dislocation of the base of the first metacarpal with involvement of the articular surface (Fig. 15.50).

Another important injury in the thumb is *avulsion of the ulnar aspect of the base of the proximal phalanx*, due to forced radial or posterior hyperextension (Fig. 15.50). This injury is due either to avulsion of the ulnar collateral ligament or adductor pollicis and creates instability and loss of forceful adduction if left untreated. Although named the '*mechanical bull*' thumb, this is more common in skiing injuries, from falling into snow without releasing the ski pole.

The '*boxer's*' fracture of the 5th metacarpal is commonly seen in emergency departments (Fig. 15.51).

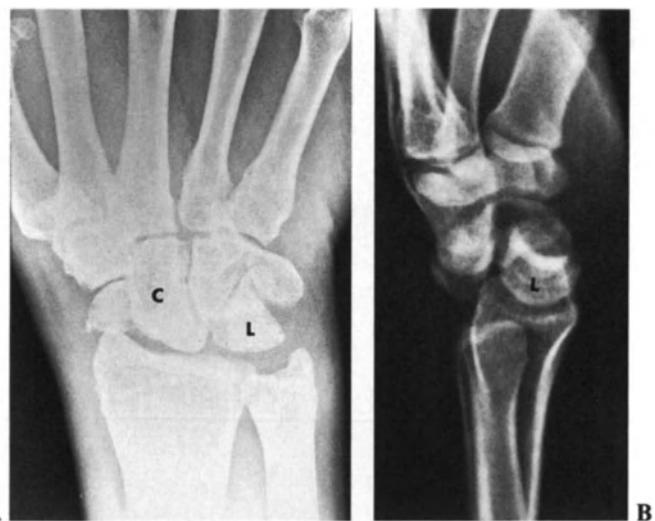


**Fig. 15.50.** Bennett's fracture of the base of the thumb metacarpal with dislocation of the major distal fragment. The minor fragment is seen in its normal relationship to the trapezium. Of note is the old undiagnosed avulsion fracture of the base of the proximal phalanx (arrow).



**Fig. 15.51.** 'Boxer's' fracture of the 5th metacarpal bone. There is moderate volar angulation of the distal fragment.

### The Lower Limb

Fracture of the *femoral neck* and *intertrochanteric fractures* are common injuries following a fall, particularly in the elderly. Nevertheless, because of the age of many of these patients, underlying pathology such as metastasis should always be excluded. These fractures may be extremely difficult to define radiographically and *radionuclide bone scan* may be necessary. A faint ill-defined linear density across the femoral neck, interruption of trabecular lines, and subtle cortical disruptions may be the only radiological signs (Fig. 15.38).

*Fractures of the femoral shaft* are almost always a sign of significant trauma, often in multitrauma victims. In trivial trauma, underlying pathology should always be suspected.

*Fractures of the distal femur* are frequently intraarticular and give rise to angulation of the distal fragments, and disruption of the joint.

*The Knee and Lower Leg.* Fractures around the knee include femoral fractures (see above), patellar fractures, or tibial plateau fractures.

The only difficulty with *patella* fractures is in differentiating them from a bipartite patella. This should be evident clinically and is usually clear radiographically although confusion may arise.

*Fractures of the tibial plateau* are generally obvious, but on occasion may not be evident as a fracture line. A cross-table lateral radiograph may demonstrate a 'fat/fluid' level in the suprapatella bursa (Fig. 15.6), indicating an intraarti-

cular fracture. Tomograms may be needed in tibial plateau fractures to determine any depression of fragments. *CT* is also gaining popularity as a method of evaluating the extent of injury.

*Injuries to the menisci* traditionally have been examined by arthrography or arthroscopy. There is growing evidence however, that *MRI* may be the method of choice for the evaluation of knee abnormalities, especially with its additional advantage of superior visualization of the internal and external ligaments and surrounding soft tissues.

Fractures of the shaft of the *tibia* are usually oblique or spiral, although transverse fractures also occur. There is invariably an associated fracture of the *fibula*, again indicating the association of double injuries with bony 'ring' structures. Complications of tibial fractures include a high incidence of open injuries and delayed union.

*Stress Fractures* are found in those who inflict chronic stress on the leg (joggers, ballet dancers, etc) (Figs. 15.14, 15.15). The proximal tibial shaft is the commonest site, but these injuries may occur at any site. Pain, with increased uptake on bone scan are the earliest signs. Periosteal reaction follows: chronic stress fractures exhibit abundant surrounding sclerosis.

*The Ankle and Foot.* Fractures of the *medial malleolus*, *lateral malleolus* and *posterior tibial margin* and disruption of the supporting ligaments may occur in a variety of combinations, depending largely upon the force of injury (Fig. 15.52). Sym-

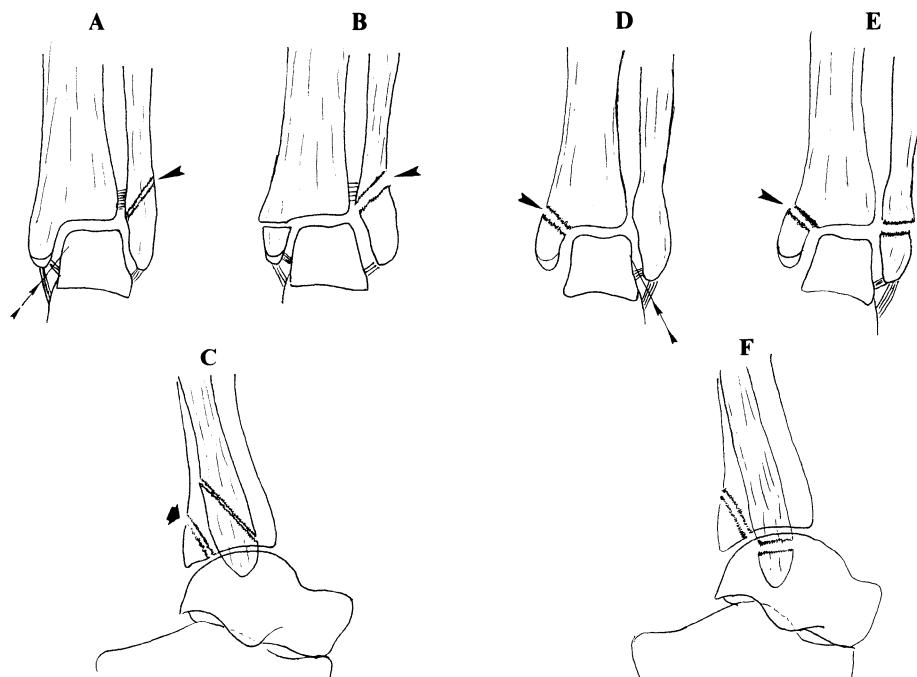


**Fig. 15.52.A, B, C Eversion Injury.** The traumatic force is transmitted in a lateral direction causing either ligamentous or bony injury or a combination. In A, there is ligamentous injury to the medial supporting ligaments (small arrowheads), and an *oblique* fracture of the distal fibula (large arrowhead). Fracture of the medial malleolus may occur, B, which are typically *transverse*. As there is frequently a rotational force (eversion/external rotation), the talus may impact upon the dorsal aspect of the tibial plafond, C, causing a fracture. **D, E, F Inversion Injury.** In inversion injuries, the pattern is reversed, with the *oblique* fracture through the medial malleolus, (D, E, large arrowhead) and either lateral ligamentous disruption, D, or a *transverse* fracture of the lateral malleolus, E. Again, if there is rotation as commonly occurs (inversion, internal rotation) the tibial plafond may be fractured, F. Of importance is the fact that when rotation occurs, the fibula fracture is often of a spiral nature, particularly with eversion injuries. The above description is a simplified version of ankle injury classifications, many of which refer to associated pronation and supination of the foot. These systems, however, seem over-complicated, and it can be argued that management is not significantly affected.



**Fig. 15.53.** Fracture dislocation of the talus. There is a comminuted fracture of the waist of the talus with posterior dislocation and rotation of the proximal fragment.



**Fig. 15.55.** Fracture of the 5th metatarsal. As in this case, this injury is often diagnosed initially on views of the ankle.

metry of the ankle mortise should be sought, as asymmetry may be the only indication of significant ligamentous injury. Stress views may be indicated to evaluate for ligamentous damage. A fracture of the posterior tibial margin may also occur at the same time; the so-called tri-malleolar fracture.

*Talar fractures* are generally avulsions or fractures through the waist, usually as a result of forced dorsiflexion. These are often associated with dislocations of the ankle or subtalar joint (Fig. 15.53). Talar dislocation may also result from forced plantar flexion injuries. Avascular necrosis is a common complication.

*Calcaneal fractures* are a frequent finding in falls from a height, and may be associated with fractures of the thoracolumbar spine (see p. 282). They may be difficult to appreciate on the lateral radiograph and axial views are mandatory. Flattening of 'Bohler's' angle is a helpful sign (Fig. 15.54).

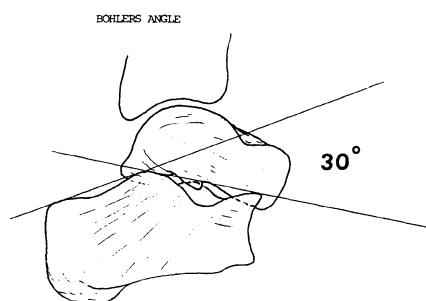


**Fig. 15.54.** Bohler's angle.

CT is particularly useful in the evaluation of calcaneal fractures.

Other notable fractures of the foot include avulsion of the *base of the fifth metatarsal* which must be distinguished from



**Fig. 15.56.** Lisfranc fracture dislocation of the base of the metatarsals.

an unfused epiphysis (Fig. 15.55), and the *Lisfranc fractures* with dislocation of the base of the metatarsals (Fig. 15.56).

#### REFERENCES AND SUGGESTIONS FOR FURTHER READING

- Acheson MB, Livingston RR, Richardson ML et al. (1987) High-resolution CT scanning in the evaluation of cervical spine fractures: comparison with plain film examinations. *AJR* 148: 1179-1185
- Daffner RH, Deeb ZL, Rothfus WE (1986) 'Fingerprints' of vertebral trauma - a unifying concept based on mechanisms. *Skeletal Radiol* 15: 518
- Daffner RH, Deeb ZL, Rothfus WE (1987) Posterior vertebral body line: Importance in the detection of burst fracture. *AJR* 148: 93
- Goldberg AL, Rothfus WE, Deeb ZL et al. (1988) Impact of magnetic resonance on the diagnostic evaluation of acute cervicothoracic spinal trauma. *Skeletal Radiol* 17: 89-95
- Greaney RB, Gerber FH, Laughlin RL, et al. (1983) Distribution and natural history of stress fractures in US marine recruits. *Radiology* 146: 339-346
- Harris JH Jr, Harris WH (1975) *The Radiology of Emergency Medicine*. Williams & Wilkins Co., Baltimore
- Keen JS, Goletz TH, Lilleas T et al. (1984) Diagnosis of vertebral fractures. A comparison of conventional radiography, conventional tomography and computed axial tomography. *J Bone Joint Surg [Am]* 64: 586-594
- Magid D, Fishman EK (1986) Computed tomography of acetabular fractures. *Semin US CT MR* 7: 351-357
- Mirvis SE, Geisler FH, Jelinck JJ, Joslyn JN, Gellad F (1988) Acute cervical spine trauma: Evaluation with 1.5 T MR imaging. *Radiology* 166: 807-816
- Mirvis SE, Young JWR, Lim C, Greenberg J (1986) Hangman's fracture: Radiologic assessment in 27 cases. *Radiology* 163: 713-717
- McArdle CB, Crofford MJ, Mirfakhraee M et al. (1986) Surface coil MR of spinal trauma: Preliminary experience. *AJNR* 7: 885-890
- Reckling FW (1982) Unstable fracture-dislocations of the forearm (Monteggia and Galeazzi lesions). *J Bone Joint Surg [Am]* 64: 857-863
- Rogers LR (1982) *Radiology of Skeletal Trauma*. Churchill Livingstone, Edinburgh
- Ryan MD, Taylor RKF (1982) Odontoid fractures. *J Bone Joint Surg [Br]* 64: 416-421
- Salter RB, Harris WR (1963) Injuries involving the epiphyseal plate. *J Bone Joint Surg [Am]* 45: 587-622
- Scott WW JR, Fishman EK, Magid D (1987) Acetabular fractures: Optimal imaging. *Radiology* 165: 537-539
- Templeton PA, Young JWR, Mirvis SE, Buddeley EU (1987) The value of retropharyngeal soft tissue measurement in trauma of the adult cervical spine. *Skeletal Radiol* 16: 98-104
- Thomason M, Young JWR (1984) Os odontoideum. *Case Report* 261. *Skeletal Radiol* 11: 144-146
- Wang SC, Grattan-Smith A (1987) Thoracolumbar burst fractures: Two 'new' plain film signs with CT correlation. *Australas Radiol* 31: 404-409
- Young JWR, Resnik CS, DeCandido P, Mirvis SE (1989) The laminar space in the diagnosis of rotational flexion injuries of the cervical spine. *AJR* 152: 103-107
- Young JWR, Burgess AR (1987) *Radiologic Management of Pelvic Ring Fractures*. Urban-Schwartzenberg, Baltimore

## CHAPTER 16

# TUMORS AND TUMOR-LIKE LESIONS OF BONE

J.W.R. Young

Bone tumors may present in a variety of radiographic patterns, varying from lytic to sclerotic, sharply defined to moth-eaten, and with or without expansion. In addition, the same tumor does not always give rise to the same radiographic pattern. This chapter will describe the common radiographic appearances that may be expected for each entity.

### TUMORS ARISING FROM THE BONE AND BONE-FORMING

#### Benign

*Osteoma*. These tumors arise predominantly from the skull, sinuses and mandible. They are slow-growing, well-defined sclerotic lesions, usually asymptomatic, but if arising from the inner table of the skull, they may give rise to symptoms. If in the sinuses they may interfere with sinus draining.

*Gardner's Syndrome* consists of hereditary polyposis and osteomatosis, with dental abnormalities (see Chaps 32, 46).

*Osteoid Osteoma*. These have a male/female predominance of 3:1. They usually occur in the second and third decades. The classical clinical presentation is of evening pain, relieved by aspirin. They are found most commonly in the *diaphysis* of long bones, particularly the femur and tibia, but have been reported in most bones in the body (Figs 16.1, 16.2, 16.3). In the spine they are usually found in the *neural arches*.

The *radiographic* appearance, is of a small rounded lucency within the cortex of the bone, the *nidus*, which may contain a central radiodensity (called the *nidus* in the UK). Surrounding sclerosis and dense periosteal reaction frequently occur though this is absent at the ends of bone beneath cartilage, where periosteum is absent (Fig. 16.3). Osteoid osteomas show intense activity on *radionuclide bone scan*. Because of the intense sclerotic reaction they may stimulate a more malignant lesion on occasion, particularly an *osteoblastic osteosarcoma* (Fig. 16.2).

*Osteoblastoma*. This has a similar histology to osteoid osteoma, but the lesion is larger (over 2 cm). There is no sex predilection; and the lesion is commonest in the second and third decade. Osteoblastomas are usually expansile, lucent lesions; generally with well-defined margins. They may have surrounding sclerosis. The majority occur in the *spine* and *flat bones* (particularly in vertebral appendages) (Figs 16.4, 16.5), although any bone may be involved. They are generally benign, but rarely may behave in an aggressive fashion.

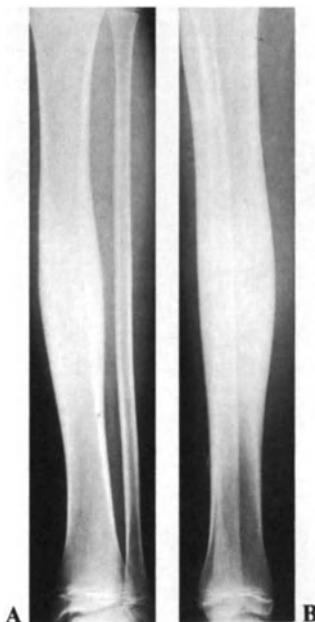
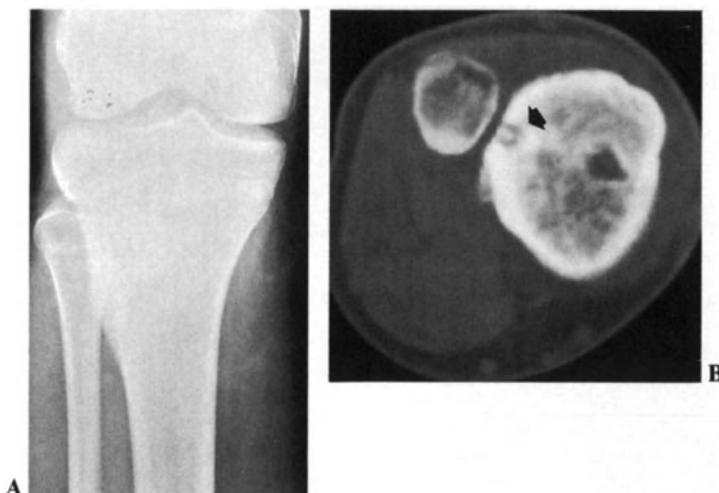


Fig. 16.1A, B. Osteoid osteoma: A AP and, B, lateral views demonstrate dense expansion of the mid-diaphysis of the tibia with abundant new bone formation. The 'nidus' cannot be seen on the plain film.



**Fig. 16.2A, B, C.** Osteoid osteoma. **A** A dense, somewhat ill-defined lesion is seen in the proximal lateral tibia, with periosteal new bone. Osteosarcoma was considered in the differential diagnosis. **B** CT scan demonstrates marked cortical density, with a characteristic nidus (arrow). The lucency more centrally was from a biopsy site.



**Fig. 16.5.** Osteoblastoma of the transverse process of L4. There is an expansive lytic lesion identified without cortical breakthrough. Courtesy of Dr WB Young, FRCR.



**Fig. 16.3.** Osteoid osteoma. There is no sclerotic reaction in this osteoid osteoma located in the subarticular portion of the talus (arrowhead). Courtesy of WB Young, FRCR.



**Fig. 16.4.** Osteoblastoma of the iliac bone. There is a large well-defined lytic process of the iliac bone. There has been collapse of the superior acetabulum with cephalad migration of the anterior hemipelvis. Courtesy of WB Young, FRCR.

### Malignant

**Osteosarcoma.** There is a slight male predominance. They are most common in the second and third decades and are the commonest primary malignant bone tumor. The most frequent site is around the knee; particularly the distal femur (Fig. 16.6). The proximal humerus and proximal tibia are also common sites (Figs 16.7, 16.8, 16.9). They generally arise in the *metaphysis*, but may cross the epiphyseal plate (Fig. 16.8). The tumor can also arise in flat bones (Fig. 16.10). There is usually a mixed pattern of bone destruction and periosteal reaction, which may be amorphous, or display a 'sun burst' spiculated appearance (Figs 16.7, 16.9). Early hematologic metastatic spread occurs, particularly to the lungs (Fig. 16.7). Lung metastases may show ossification and can cause pneumothorax. *Nuclear medicine bone scan* will show increased activity. *CT* and *MRI* are valuable in defining the extent of the lesion.

**Special Varieties of Osteosarcoma.** *Periosteal Osteosarcoma.* These arise from the periosteum with rapid extension into the soft tissues (Fig. 16.11). They occur in an older age group than osteosarcoma, peaking in the second and third decade, and have a slightly better prognosis.

*Parosteal Osteosarcoma.* These protrude from the surface of the bone and may 'surround' the bone (Figs 16.12, 16.13). They are usually dense, and well-defined with a zone of cleavage between the peripheral margins and the underlying bone cortex. They are slow-growing and occur most commonly in the third and fourth decades. They are associated with a better prognosis than are other varieties of osteosarcomas. They may be difficult to differentiate radiographically from post traumatic myositis ossificans (see Fig. 15.5).

*Diaphyseal Osteosarcoma.* Approximately 10% of osteosarcomas are diaphyseal in origin, and may cause diagnostic problems. They may resemble Ewing's tumor, and often the diagnosis is only made at biopsy.

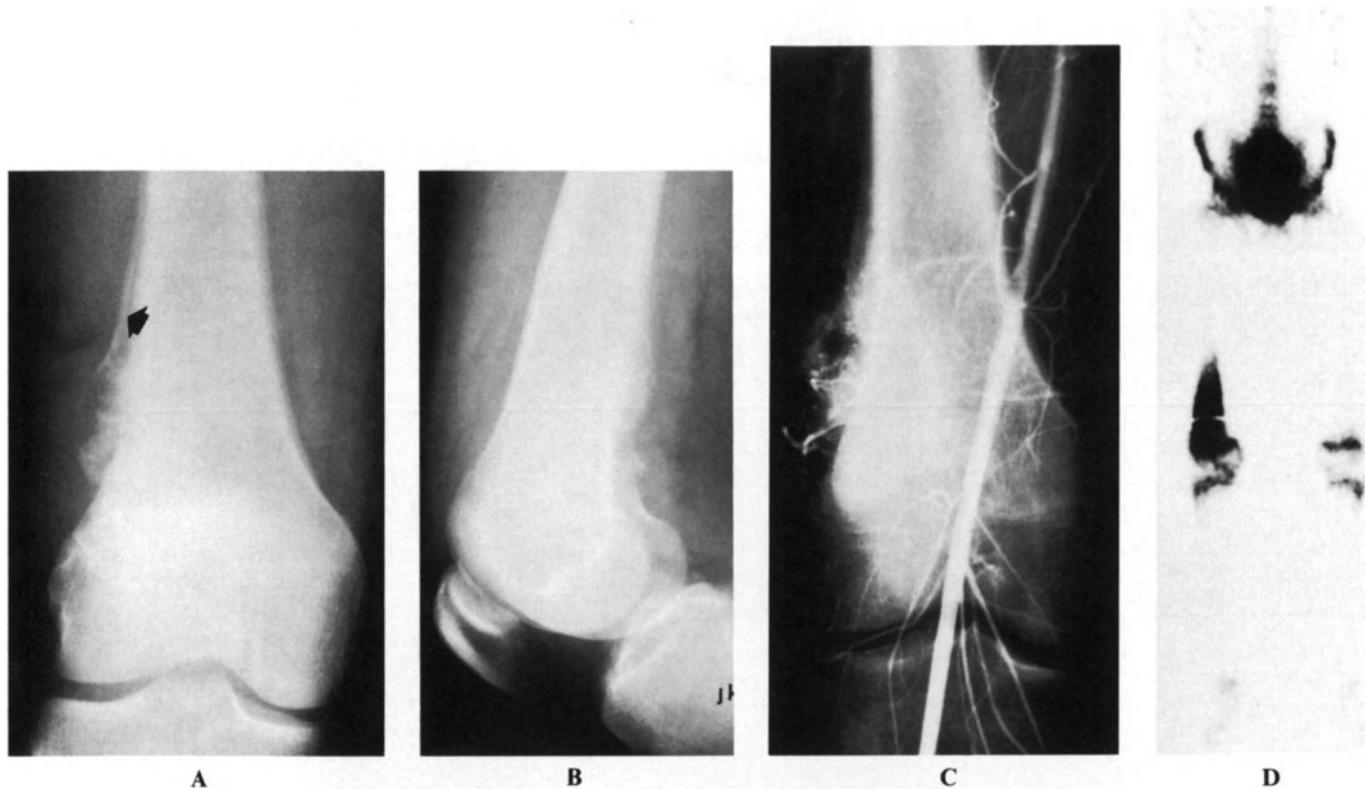


**Fig. 16.6** A, B. Osteosarcoma of the distal femur. There is increased density of the lateral aspect of the metaphysis with periosteal elevation, and a Codman's triangle identified (arrow). New tumor bone is also seen in the lateral soft tissue. C Angiography demonstrates some vascularity and D, bone scan of the patient shows intense uptake in the distal femur.

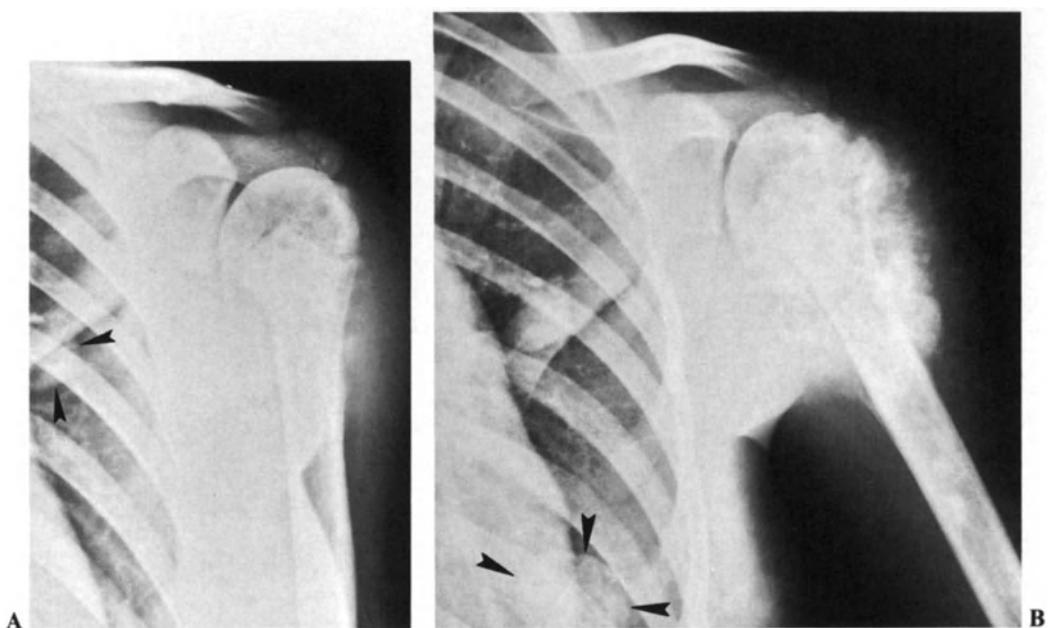


**Fig. 16.7** A Osteosarcoma of the proximal humerus. There is a poorly defined destructive process of the proximal metaphysis, with hazy spiculated periosteal reaction laterally. A lung metastasis is noted (arrowheads) B Three months later, despite treatment, the more typical periosteal reaction of osteosarcoma is seen. An additional lung deposit is now seen (arrowheads).



**Fig. 16.8.** (left) Osteolytic osteosarcoma of the proximal humerus. There is a poorly defined destructive process of the humeral head, causing periosteal elevation and 'Codman's triangle' (arrows). A soft tissue mass is also suspected.



**Fig. 16.9.** (right) Osteosarcoma. There is a poorly defined, irregularly sclerotic lesion with aggressive looking periosteal reaction.



**Fig. 16.11.** Periosteal osteosarcoma. Dense spiculated periosteal new bone arising from the periosteum and extending into the soft tissues. Courtesy of WB Young, FRCR.

**Central Osteosarcoma.** These present as lucent metadiaphyseal lesions, usually with dense sclerotic features. This may mimic a bone island, but the presence of pain should warn of a more serious problem. Radionuclide bone scan will indicate the lesion's activity.



**Fig. 16.12.** Parosteal osteosarcoma. Dense new bone is seen, which arises from the posterior aspect of the distal femur.

◀ **Fig. 16.10.** Osteosarcoma of the iliac bone. There is dense periosteal reaction with considerable sclerosis of the iliac bone.



**Fig. 16.13.** (left) Parosteal osteosarcoma of the distal femur. There is a dense mass of new bone enveloping the distal femur. Courtesy of WB Young, FRCR.



**Fig. 16.14.**

◀ **Fig. 16.14.** Multifocal osteosarcoma. Multiple sclerotic lesions are identified in the spine. Courtesy of WB Young, FRCR.

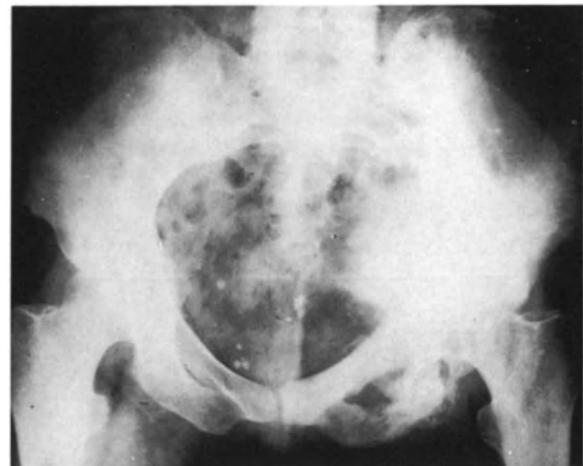


**Fig. 16.16.** Osteosarcoma developing in a patient with Paget's disease of the left pelvis. The iliac bone, ischium and superior pubic ramus show sclerosis and changes of Paget's disease. An aggressive periosteal reaction on the medial aspect of the iliac bone indicates malignant change. Courtesy of WB Young, FRCR.

**Multifocal (Multicentric) Osteosarcoma.** This occurs only in children and is rapidly fatal. It presents with multiple sclerotic lesions (Fig. 16.14).

**Soft Tissue Osteosarcoma.** This is a rare condition, usually periarticular, but is also reported in kidney and breast. A dense irregular bony lesion is identified, resembling the osteosarcoma of bone origin.

**Osteosarcoma in Abnormal Bone. Paget's Disease.** This is said to occur in approximately 1% of cases. It may be lytic, sclerotic or a mixed pattern. It occurs in older age groups (6th and 7th decade). Alteration in the clinical or radiographic findings in Paget's disease should arouse suspicion of sarcomatous degeneration (Figs 16.15, 16.16).

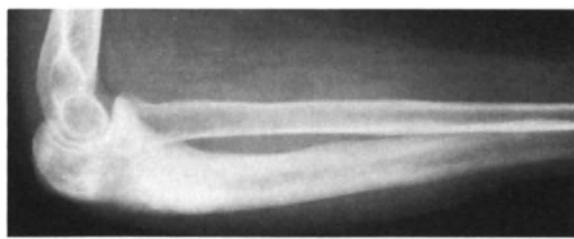


**Fig. 16.15.** Paget's sarcoma: This patient with Paget's disease began complaining of increasing pain in the proximal ulna. A focal density is identified within the area of abnormal bone.



**Fig. 16.17.** Post-irradiation osteosarcoma. This patient received irradiation following a right mastectomy 7 years previously. There is now a dense expansile sclerotic mass arising from the manubrium, which had not been evident on earlier films. There are also numerous metastatic nodules within the previously irradiated right lung.



**Fig. 16.18.** Enchondroma. Typical appearance of a peripheral lesion, with expansion and the suspicion of central flecks of calcification, suggesting a cartilaginous matrix.

**Post-radiation.** This is a rare condition occurring either from exposure to radioactive material (watch-dial workers), or therapeutic radiation, with a dose exceeding 3000 rad. There is a latent period before appearance of the tumor, usually of about 7 years (Fig. 16.17).

## TUMORS ARISING FROM CARTILAGE AND CARTILAGE-FORMING

### Benign Cartilaginous Tumors

**Enchondroma.** These are generally single tumors (see below). Approximately 10% occur in hands and feet, and 20% in long bones. The remainder are seen in flat bones, particularly the pelvis, scapula, and vertebrae. There is a small malignant potential which increases in the more central lesions (1%–5%).

Radiographically they present as lytic lesions, usually with flecks of calcific density. They may have well-defined sclerotic margins and may be expansile, particularly in the hands and feet (Fig. 16.18). In long bone, they may have poorly defined margins and be difficult to distinguish from bone infarcts or chondrosarcoma (see Fig. 16.28).

A change in symptoms (e.g., increasing pain) or in the radiographic appearance may herald a change to chondrosarcoma.

**Juxtacortical Chondroma.** This is a chondroma arising in the cortex of the long bones, usually the femur or humerus, and usually presents as a lucent, expansile cortical defect extending predominantly away from the bone. Juxtacortical chondromas may contain calcific specks and can be seen in *multiple enchondromatosis in conjunction with enchondromas*.

**Multiple Enchondromas. Ollier's Disease.** Multiple lesions occur in Ollier's disease, or multiple enchondromatosis (Fig.

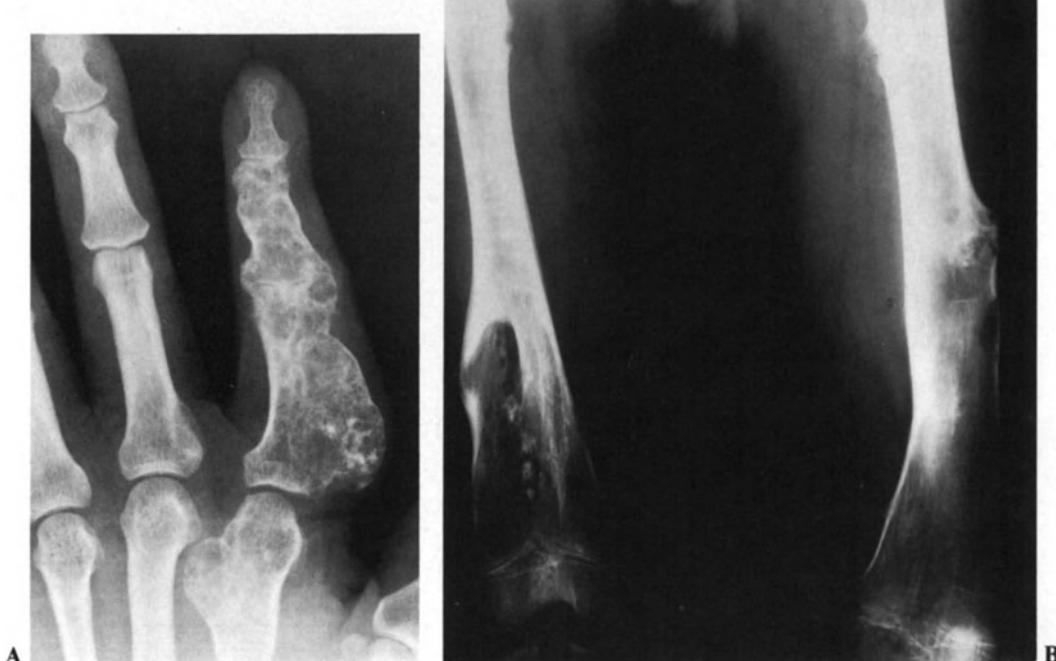


**Fig. 16.19A, B.** Multiple enchondromatosis. A Hand; B Femora. There is a deformity of the visualized bones with localized areas of abnormality. Many of these are expansile lesions containing punctate calcifications, suggestive of a cartilaginous matrix. The right femur is foreshortened.



**Fig. 16.20.** Multiple enchondromas occurring in conjunction with soft tissue hemangiomas, identified by the presence of phleboliths, is known as *Maffucci's syndrome*. Middle finger amputated.

16.19). This is a dysplastic condition which may present with marked growth and modeling deformities of the limbs. There is a reported higher incidence of sarcomatous change (5%–10%).

***Maffucci's Syndrome.*** This is the syndrome of multiple enchondromatosis in conjunction with *cavernous hemangiomas* of the soft tissues, often containing calcified phleboliths (Fig. 16.20). There is an increased incidence of sarcomatous degeneration, which has been reported as high as 20%.

***Chondroblastoma.*** Chondroblastomas generally occur in the first and second decade. They are lucent *epiphyseal* lesions which may also be seen in the *apophyses* (Fig. 16.21). They are well-defined, may have a faintly sclerotic rim and may be mildly expansile. Occasionally, speckled calcification occurs within the lesion. There is increased uptake on *isotope bone scan* due to the marked vascularity. They may extend into the metaphysis (Fig. 16.21B).

***Chondromyxoid Fibroma.*** Chondromyxoid fibromas usually occur in the second and third decade. They are in general well-defined, expansile eccentric *metaphyseal* lucent lesions, which may cross the epiphyseal plate. They are frequently found in the proximal tibia. On occasion, they may have a sclerotic rim. Histologically, they may be confused with chondrosarcoma, although sarcomatous change does not occur.

***Osteochondroma (Cartilage capped exostosis).*** These are osseous exostoses usually arising from but 'growing' away from the metaphysis of long bones. They possess a cartilaginous cap which may contain speckles of calcification and which calcifies progressively with age. They usually stop growing at skeletal maturity. They may be sessile or pedunculated.

They usually involve long bones (especially around knee and proximal humerus), although flat bones (pelvis and scapula) may also be involved (Fig. 16.22). They may cause symptoms from pressure on adjacent structures. ***Multiple exostoses*** (multiple osteochondromatosis; diaphyseal aclasia) also occur as a deforming skeletal dysplasia (see Figs 14.18, 16.23).

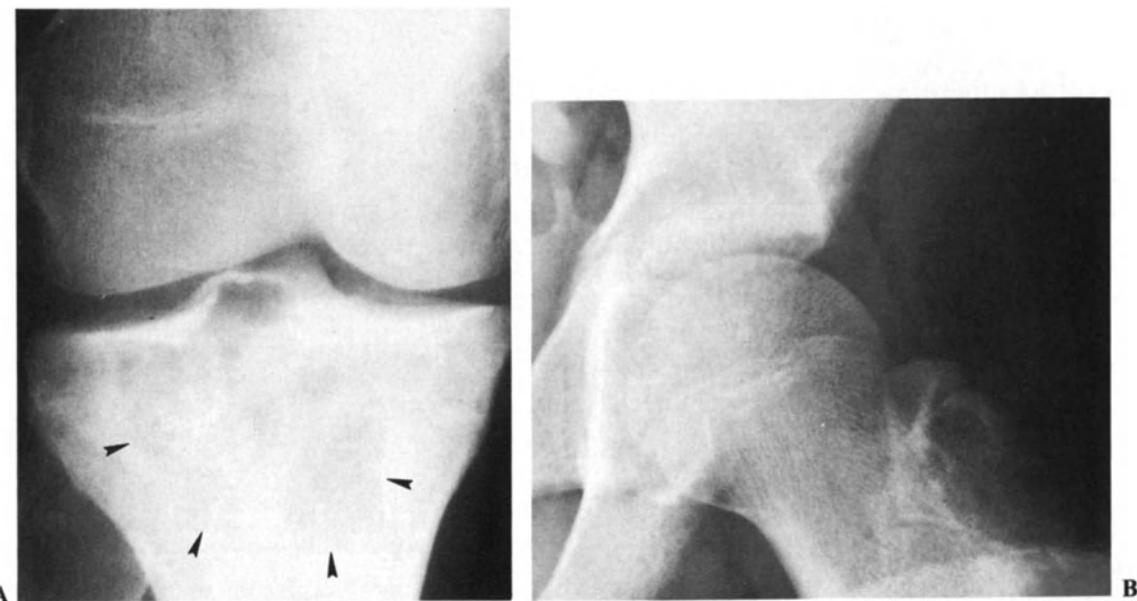


**Fig. 16.21A, B.** Chondroblastoma. A well-defined lytic lesion of the proximal tibial epiphysis which extends across the newly closed epiphyseal plate. A. Chondroblastoma may also involve an apophysis, B.



**Fig. 16.22.** Osteochondroma of the scapula. The cartilage cap is not calcified and cannot be seen.



**Fig. 16.23.** Osteochondromatosis (diaphyseal achalasia). Typical osteochondromatoma are seen arising from the distal femoral metaphysis, and 'pointing' away from the bone end. Calcification of the cartilage cap is seen on the lateral osteochondroma. The tibia also contains a cortical osteochondroma, whilst a modeling deformity of the proximal fibula is seen. ►

There is a malignant potential of the cartilaginous cap which is approximately 1% for pedunculated lesions, although multiple and more central lesions have an increased malignant potential, which may approach 10%, or for pelvic lesions, even higher. Abrupt symptomatic or radiographic change should suggest possible malignant transformation to chondrosarcoma and pelvic lesions should be regarded with extreme suspicion (Fig. 16.24).

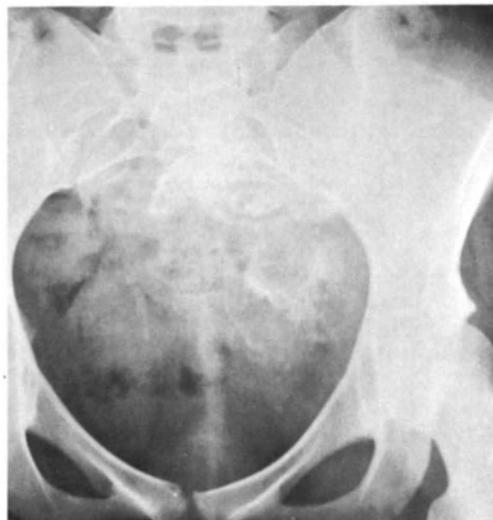
#### Malignant Cartilaginous Tumors

*Chondrosarcoma.* This is a tumor of variable malignancy and pathology from low grade (similar to enchondroma) to high grade, which may be similar to osteosarcoma. They occur in later life (30–70 years). They may be primary (approximately 90%) or arise from underlying 'benign' tumors.

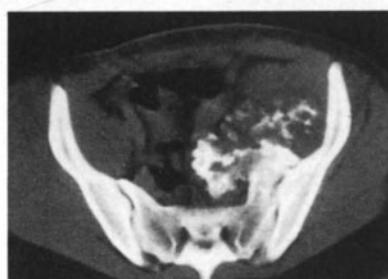
They are rare in the peripheral skeleton, the most common sites being the pelvis, ribs and proximal femur. Cartilaginous lesions of the axial skeleton, particularly the pelvis, should be regarded with suspicion due to the potential for malignancy (Fig. 16.24).

*Primary Chondrosarcoma.* These usually present radiographically as either a moderately well-defined or ill-defined area of medullary lucency with or without periosteal reaction (Figs 16.25–16.28). They may have areas of punctate calcification. They progress to cortical breakthrough with a large soft tissue mass, best seen by CT or MRI scan. Usually they are slow to metastasize via the hematogenous route, but aggressive lesions may spread more rapidly.

*Secondary Chondrosarcoma.* These arise from benign cartilage tumors, e.g., enchondroma, osteochondroma (see above). Central lesions and multiple lesions have an increased risk of malignant transformation (Fig. 16.24).



A



B

**Fig. 16.24.** A Speckled calcification is seen in the left pelvis identified by CT as a cartilaginous tumor arising from the sacrum. B. Biopsy indicated chondrosarcoma, possibly a secondary tumor arising from a previous osteochondroma.



**Fig. 16.25.** Chondrosarcoma. A moderately well-defined lytic process of the proximal humerus with central calcifications indicative of a cartilaginous tumor. There is little to suggest gross invasion on this radiography, but biopsy indicated malignancy. Courtesy WB Young, FRCR.

**Mesenchymal Chondrosarcoma.** This has been accepted as a separate entity since 1972. These tumors consist of highly undifferentiated round cells, and chondroid islands, with a well differentiated cartilaginous component. About one third arise in the soft tissues.

It is a rare tumor occurring most commonly in the second and third decade. The jaws, spine, and ribs are the commonest sites. They usually have an aggressive appearance with calcified foci, and a rapid growth.



**Fig. 16.27.** Chondrosarcoma. A more aggressive looking lytic, mildly expansile lesion, with cortical destruction in the femoral neck, and soft tissue extension.



**Fig. 16.26.** Chondrosarcoma. A well-defined, predominantly lytic lesion in the left iliac bone. Mild cortical irregularity on the lateral margin, adjacent to the femoral head, suggests breakthrough.



**Fig. 16.28.** Chondrosarcoma. There is a poorly defined area of speckled increased density in the proximal femur. Apart from the suggestion of periosteal irregularity medially, the appearance resembles benign enchondroma of the long bone. New onset of pain however led to biopsy. Chondrosarcoma was discovered.



**Fig. 16.29.** (left) Fibrous cortical defect. This is a well-defined expansile area of increased radiolucency with a lobulated outline and sclerotic margin.



**Fig. 16.30.** (right) Desmoplastic fibroma. This lesion arose from the ulnar aspect of the distal radius, extending to and involving the growth plate, giving rise to a mild partial growth plate arrest, and Madelung's deformity. There is also considerable soft tissue extension, which has caused bowing of the distal ulna.

**Dedifferentiated Chondrosarcoma.** Occasionally a low-grade malignant chondrosarcoma with abundant calcific components becomes rapidly destructive, with a lytic irregular focus of activity. Histologically, the picture may resemble osteosarcoma, fibrosarcoma or malignant fibrous histiocytoma, although areas of cartilaginous tumor will be found.

## TUMORS ARISING FROM FIBROUS TISSUE

### Benign Fibrous Tumors

**Fibrous Cortical Defect/Non-Ossifying Fibroma.** These occur most commonly in the first and second decades, and are characteristically found coincidentally in the distal femur and distal tibia. They are usually asymptomatic.

They are well-defined, mildly expansile, lobulated lucent lesions with a sclerotic rim. They are cortically situated in large bones (Fig. 16.29), but may involve the whole width of small bones. The lesions may enlarge initially with age, but eventually become 'filled in' with normal bone.

Some authors refer to fibrous cortical defects as a separate entity from non-ossifying fibroma, and found in the posteromedial aspect of the distal femur of children. They are to be distinguished from the cortical desmoids of adductor trauma (cortical avulsion syndrome), attributed to chronic low grade traction of the adductor magnus muscle.



**Fig. 16.31A, B.** Fibrosarcoma. A A moderate poorly defined destructive lesion of the fibula is identified, with marked cortical disruption. B A grossly destructive lesion of the distal femur, with a large soft tissue component.

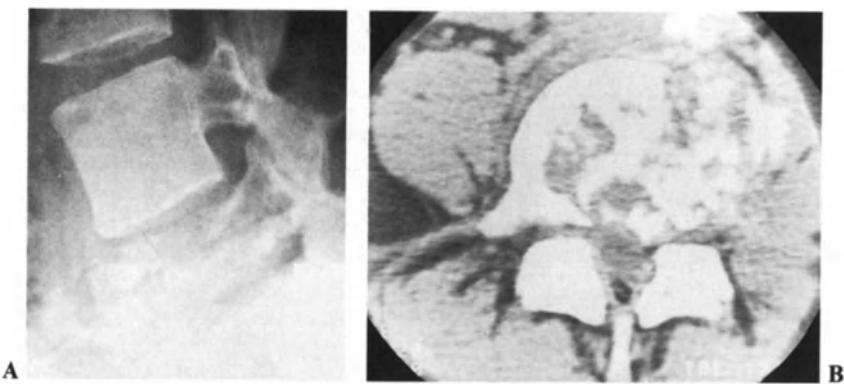


**Fig. 16.32.** A Malignant fibrous histiocytoma. This lesion is a little unusual as it is occurring in a young adult, and involves the spine; a rare site. There is extensive destruction of L5, which on CT scan is seen extending through the posterior and lateral cortex of the vertebral body. B.

**Desmoplastic Fibroma.** This is a relatively rare tumor and is histologically related to the soft tissue tumors of the abdominal wall.

Desmoplastic fibromas occur most commonly in the second and third decades, presenting as a painful swelling. They arise most commonly in the *metaphyseal* region of long bones. They are expansile osteolytic lesions with well-defined lobulated margins. The cortex may be eroded with extension of the tumor into the soft tissues (Fig. 16.30). The tumor is encapsulated, but wide resection is required to prevent recurrence.

**Congenital Generalized Fibromatosis.** This is a very rare condition, with multiple rounded cystic lesions, found in the metaphyseal regions. These generally regress with age, although if systemic involvement of the heart, lungs and muscle occurs the prognosis is poor.

#### Malignant Fibrous Tumors

**Fibrosarcoma.** These tumors with variable malignancy occur predominantly in the fourth and fifth decades with low grade pain and swelling. They may occur in the medulla, periosteum or surrounding soft tissues with bony extension. The *medullary* form is usually found in long bones with approximately 80% occurring around the knee. The *periosteal* form is common in long bones, but also affects flat bones.

They are poorly defined lytic lesions with the clarity of margins correlating with malignancy. Cortical breakthrough occurs with extra-osseous soft tissue extension (Fig. 16.31). Slow-growing varieties may cause some expansion. Soft tissue involvement is best shown by CT or MRI.

**'Secondary Fibrosarcoma'.** Sarcomatous change may occur in medullary bone infarcts and in Paget's disease, and as a result of previous radiation therapy.

**Malignant Fibrous Histiocytoma.** This has now been separated as a distinct pathological entity from fibrosarcoma. It occurs mainly in the older age group (usually over 50 years), although it is also reported in young adults (Fig. 16.32). It most commonly occurs in long bones, but is also reported in the pelvis, spine and ribs. There are destructive ill-defined lytic lesions, with a permeative pattern and cortical erosion.

#### PRIMARY MALIGNANT ROUND CELL TUMORS

**Ewing's Tumor.** This predominates in the first and second decades, although it has been reported in most age groups. The commonest presenting symptoms are pain and swelling. There is usually a raised sedimentation rate, anemia and pyrexia.

The tumors are usually found in the *diaphysis* of long bones, but on occasion may be seen in the ends of long bones (Figs 16.33, 16.34). They may also involve flat bones and



**Fig. 16.33.** A, B. Ewing's Sarcoma. A poorly defined area of sclerosis and lucency is seen. There is a laminated 'onion skin' periosteal reaction identified on the lateral view. A 'Codman's triangle' is seen on the AP projection (arrows). A, AP view; B, Lateral view. Courtesy of WB Young, FRCR.

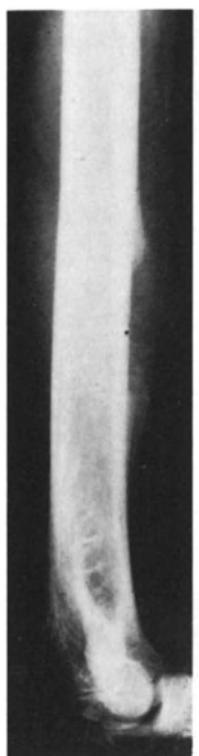


**Fig. 16.34.** (left) Ewing's tumor. There is a 'broken' periosteal reaction with 'Codman's triangle' present. Soft tissue extension and tumor bone is identified between the elevated periosteal new bone. Courtesy of WB Young, FRCR.



**Fig. 16.35** (right) A, B. Histiocytic lymphoma of bone. Poorly defined permeative lesion without gross periosteal reaction. A, AP view; B, Lateral view.



**Fig. 16.36.** Histiocytic lymphoma. A grossly destructive, permeative lesion of the humerus involving most of the bone.

the axial skeleton. Sixty per cent are found in the lower extremities and pelvis. Early metastases to bone and lungs occur.

*Radiographically* they are usually poorly defined permeative destructive lesions with cortical breakthrough, and an aggressive periosteal reaction of variable type. The classical 'onion skin' layering may be seen, but is not diagnostic of Ewing's (Fig. 16.33). *Bone scan* and *CT* or *MRI* are helpful in defining the margins.

#### MALIGNANT LYMPHOMA OF BONE

Although lymphoma is generally regarded as involving the bone secondarily, Dahlin, in his large series, discovered 43% of patients with lymphoma of bone to be free from visceral disease, indicating bone as the primary site. In addition, lymphoma of bone, whether arising primarily in bone, or involving bone secondarily, presents with a radiological picture of a tumor of the bone. It is therefore appropriate to discuss the condition in this section.

*Histiocytic Lymphoma (Reticulum Cell Sarcoma).* There is a slight male predominance (3:2). The disease can occur at any age, but is rare in the very young.

The *radiographic* appearance is usually of a permeative destructive lesion, which may be quite extensive (Figs 16.35–16.37). There may be cortical breakthrough and reactive new bone formation. Irregular sclerosis is also seen on occasion, which may simulate a chronic osteomyelitis. The lesions may be multiple, even without visceral or nodal involvement (Fig. 16.37). On occasion, sclerosis resembling



**Fig. 16.37** A, B. Histiocytic lymphoma. Lesions in the mid and distal femur are seen. The distal lesion appears particularly aggressive with cortical breakthrough and periosteal reaction. A, AP view; B, lateral view.



**Fig. 16.38A, B, C.** Adamantinoma of the long bone. An expansile 'bubbly' lesion of the tibial diaphysis is seen in this 60-year-old male, who had complained of pain and an enlarging mass for 5 years. There was cortical breakthrough at the time of presentation, with MRI scan beautifully defining the extent of the lesion, C.

Paget's disease may precede the true appearance and diagnosis of lymphoma by many years. The prognosis reportedly is the best for malignant bone tumors.

**Secondary Lymphoma.** The diagnosis of visceral lymphoma usually has been established before bone changes are seen. Lymphoma, whether of the Hodgkin's or non-Hodgkin's varieties, may involve the bone, generally giving rise to either a poorly defined, lytic (moth-eaten) lesion or a poorly defined sclerotic lesion. Hodgkin's disease involves predominantly the red marrow areas, particularly the spine and ribs. The permeative pattern of destruction may mimic other bone tumors, particularly of the round cell variety.

**Burkitt's Lymphoma.** This condition, found predominantly in African children, is usually an aggressive, rapidly fatal condition. The lesions are generally osteolytic with a particular affinity for the mandible, although the lymphoma may occur in the long bones and spine. In long bones, the lesion is more permeative, again resembling other round cell tumors.

#### TUMORS ORIGINATING FROM OTHER CELL TYPES

**Adamantinoma.** There is confusion as to whether this arises from epithelial tissue as a distinct entity, or is an unusual manifestation of another sarcoma. Histologically it resembles ameloblastoma of the jaw. It has features similar to ossifying fibroma, and may occur in association with fibrous dysplasia. It is most commonly seen in the second and third decade,

and 90% of cases occur in the tibia, mostly in the mid portion of the bone.

*Radiographically*, the lesion is a cystic, sometimes expansile, often with surrounding sclerosis. There may be cortical destruction (Fig. 16.38). Adamantinomas are generally indolent, but may metastasize rapidly.

#### GIANT CELL CONTAINING TUMORS

There are many giant cell containing tumors which are now subdivided pathologically into separate entities. These include chondroblastoma (p. 301), chondromyxoid fibroma (p. 301), aneurysmal bone cyst (p. 308), and giant cell tumor (osteoclastoma), giant cell containing osteosarcoma, giant cell reparative granuloma and hyperparathyroidism.

**Giant Cell Tumor (Osteoclastoma).** The pure giant cell tumor is a locally aggressive tumor of richly vascular tissue with spindle cells and numerous multinucleated giant cells. Osteoclastomas occur most commonly in the third and fourth decade, after epiphyseal closure. Confusion with aneurysmal bone cyst may arise in diagnosis, particularly in the spine. However, the pathologic features are usually adequate for diagnosis. In practice, giant cell tumors may be seen in association with aneurysmal bone cyst (Fig. 16.39). They are lytic expansile lesions, sometimes with a 'soap bubble' appearance and they may have sclerotic margins. They are found predominantly in the ends of long bones, but may also be seen in the vertebra, pelvis or sacrum

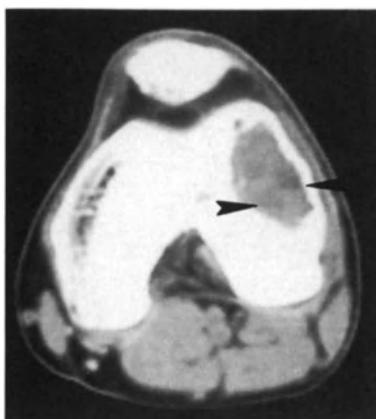


**Fig. 16.39.** Giant cell tumor associated with aneurysmal bone cyst. CT scan through the lesion in the distal femur indicates fluid/fluid levels within the lesion (arrowheads). This is compatible with the histology, where large blood filled 'lakes' were seen in the associated aneurysmal bone cyst.



**Fig. 16.41.** Giant cell tumor of the humerus. A large, expansile loculated lesion is seen, extending to the articular surface.

(Figs 16.40, 16.41, 16.42). Generally they extend to the articular surface of the bone, but may arise in an apophysis, particularly the greater trochanter. They may appear aggressive, but the radiographic appearance does not correlate well with malignancy.

Osteoclastomas are vascular tumors which show an increased activity on the blood pool phase of a *bone scan* and an increased vascularity on *angiography*. Fluid/fluid levels on CT scan have been reported, but this may be due to associated aneurysmal bone cyst (Fig. 16.39).

Frank malignancy is seen in a proportion of cases (Fig. 16.43), although this is uncommon. Diagnostic difficulties may arise between giant cell tumors and other sarcomas, particularly osteosarcoma, which may contain giant cells. 'Secondary' malignant tumors are described, occurring following treatment, usually involving radiation. Primary malignant tumors have a slightly better prognosis than 'secondary' malignant tumors.

**Aneurysmal Bone Cyst.** Although some authors claim that these lesions are not true neoplasms, most authorities agree



**Fig. 16.40A, B.** Giant cell tumor. A grossly expansile lytic lesion extends to the distal radial articular surface with some collapse and impaction of the bone.

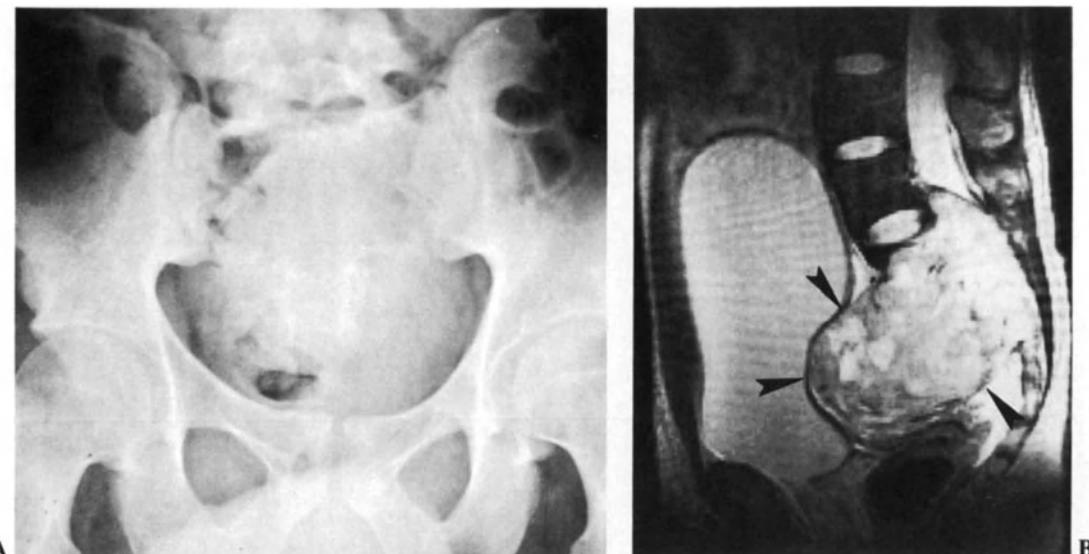


**Fig. 16.42A, B.** Giant cell tumor. **A** A hazy mass density obscures the lower sacrum, obliterating most of the sacral arcuate lines. **B** MRI scan defines the large tumor arising from the sacrum and extending into the pelvis (arrowheads). This  $T_2$ -weighted image demonstrates areas of high signal intensity, seen in giant cell tumors.

that there is sufficient evidence to support aneurysmal bone cyst as a distinct entity.

They may arise 'de novo' or may be seen in association with other lesions, particularly giant cell tumors (Fig. 16.39), chondroblastoma, chondromyxoid fibroma, or fibrous dysplasia.

They are seen in the first and second decade in the *metaphysis* of long bones, generally occurring before epiphyseal closure (Fig. 16.44). They may occur in other bones including the *spine*, *ribs* and *tarsus* (Fig. 16.45).

They are expansile lytic lesions containing cavernous blood-filled spaces and numerous giant cells. Cortical thin-



**Fig. 16.43.** Giant cell sarcoma. There is a destructive lytic process of the distal femur, destroying the medial cortex, and extending into the soft tissues. The lesion extends to the articular surface.



**Fig. 16.44.** Aneurysmal bone cyst. There is a markedly expansile lesion of the distal tibial metaphysis. Despite apparently aggressive periosteal reactions at each end, the lesion was benign.

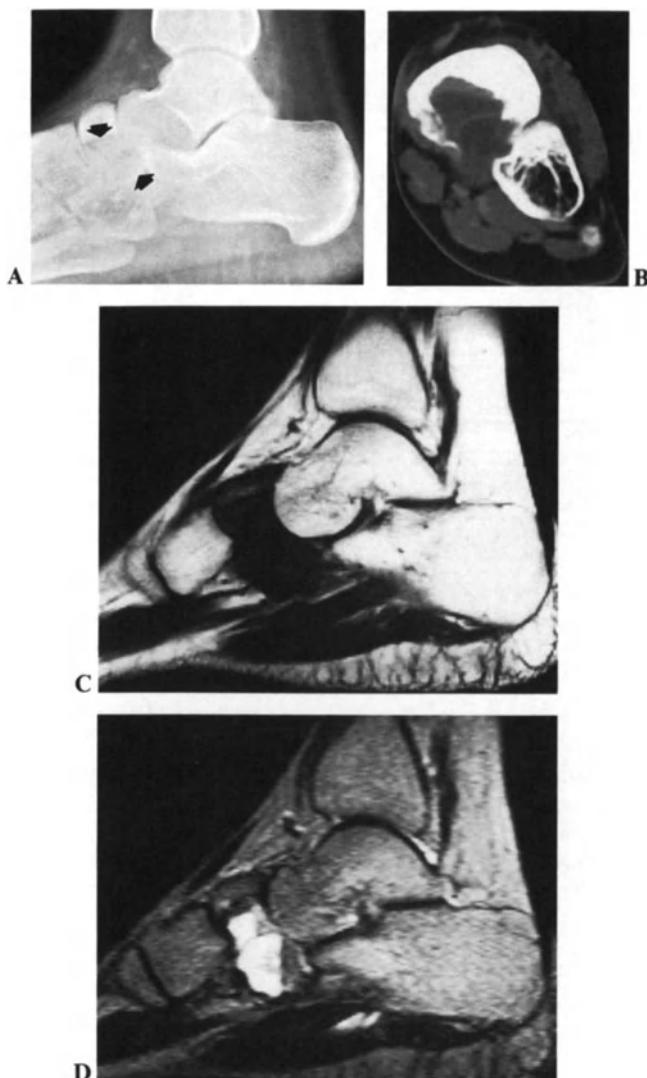


**Fig. 16.45A, B, C, D.** Aneurysmal bone cyst. A Lytic expansile lesion of the navicular bone in this 16-year-old patient (arrows). Following resection, the lesion recurred and both CT, B, and MRI, (C, T<sub>1</sub>-weighted image) demonstrated extension of the tumor beyond the margins of the bone. Fluid/fluid levels are identified on both imaging modalities, most effectively on the T<sub>2</sub>-weighted MRI image, D.

ning may be extreme. Bone scan shows increased uptake in the blood-pool phase. Treatment is by curettage and/or radiotherapy, although post-radiation sarcoma is a complication. Transcatheter embolization has also been used.

**Giant Cell Reparative Granuloma.** An unusual 'granuloma' of the jaw bones, possibly representing a reactive lesion (see Chap. 46). It must be differentiated from true giant cell tumor which, however, arises only rarely in the jaw.

Lorenzo and Dorfman have also described giant cell reparative granuloma of the hands and feet. These are a small group of lesions containing giant cells, and causing confusion with giant cell tumors, aneurysmal bone cysts, or

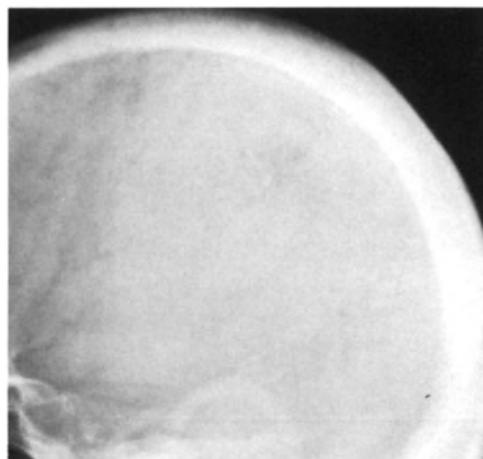


**Fig. 16.46.** Hemangioma of the skull. There is a striated radiating pattern typical for this entity.

chondroblastomas. They have also been referred to as 'giant cell lesions' and are benign.

#### TUMORS ARISING FROM VASCULAR/LYMPHATIC SYSTEMS

**Hemangiomas.** Solitary hemangiomas are benign slow-growing lesions involving predominantly the vertebrae and skull, but are also found in the long bones. They may cause pain, especially during pregnancy or when involving the vertebrae, either from vertebral collapse or soft tissue extension.

There are two types: the *capillary*, which spreads in a fine sun-burst pattern and is most commonly seen in the skull and vertebra (Figs 16.46, 16.47); and the *cavernous* type, which has large thin walled vessels, and may be indistinguishable from lymphangiomas. Indeed, the two conditions may co-exist, or may even represent different ends of a spectrum of vascular anomalies.

*Radiographic appearances* vary from a striated or sun-burst pattern, to an expansile osteolytic variety. Occasionally, there may be localized cortical thickening with spicules of bone projecting into the soft tissues, which may bear a superficial resemblance to osteosarcoma.

*Isotope bone scans* will show increased activity. In the vertebrae, this may be indistinguishable from other causes such as Paget's disease or metastases.

**Cystic Angiomatosis and Lymphangiomatosis.** These conditions present most commonly with multiple well-defined lytic lesions involving the cortex or medulla. Diffuse osteopenia of the involved bones may be seen, particularly if the vertebrae are involved. There may be an overlap between this condition and *vanishing bone disease*, both radiographically and histologically (Fig. 16.48). The histological picture may be indistinguishable between angiomatosis and lymphangiomatosis, again suggesting a spectrum of developmental vascular anomalies. There may be involvement of the

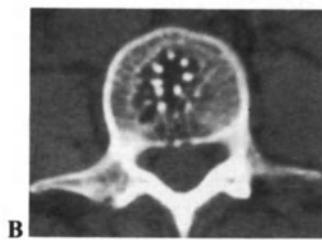


**Fig. 16.47A, B.** Hemangioma of the vertebra. A The bone is osteopenic with a pattern of coarse vertical striations. CT scan, B, demonstrates a characteristic appearance. Courtesy of Charles S. Resnik, MD.

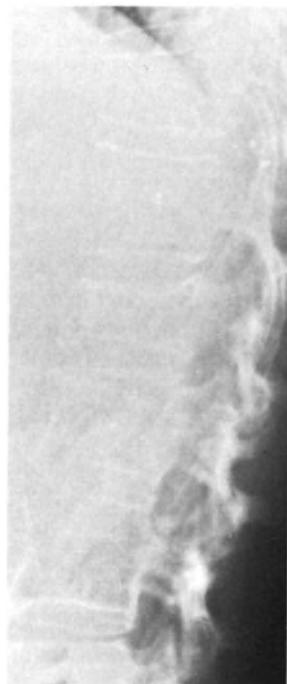


**Fig. 16.49.** Vanishing bone disease. There is destruction of the left iliac wing, extending into the posterior acetabulum (ischium) and superior pubic ramus.

viscera and soft tissues in which case the prognosis may be serious, with severe anemia or bleeding resulting.

**Vanishing Bone Disease (Gorham's Disease).** This is a rare condition in which a progressive dissolution of bone occurs, due to a destructive vascular anomaly. The lesion involves a single bone or contiguous bones, with no respect for joints (Fig. 16.49). Soft tissue involvement occurs locally and the condition may also be associated with angiomatous (vascular or lymphatic) involvement of other systems. The underlying condition may be vascular or lymphatic and it may be impossible to differentiate histologically. Although spontaneous arrest of the condition is reported progression is more common, with a poor prognosis when lesions involve the spine or viscera.

**Glomus Tumor.** This is a benign vascular tumor, usually of the soft tissues, but causing pressure erosion of the bone usually of the distal phalanx. They may occasionally arise within the bone. The radiographic picture is of a well-defined lucent lesion, often with a sclerotic rim. *Isotope bone scan* shows increased uptake in the blood pool and early phase, as the tumor is highly vascular.

**Hemangioendothelioma (angiosarcoma).** These may present a diagnostic problem, as the histological picture can be similar to vascular metastatic deposits. The condition may be unifocal or multifocal, often limited to one extremity.

**Radiologically,** the lesions are lytic with only rare reactive new bone (Fig. 16.50). They may be well or poorly defined, depending on the histological type. Prognosis also depends upon the type, the most anaplastic showing a poor survival rate.

**Hemangiopericytoma.** An extremely rare tumor, presenting with an expansile lytic lesion predominantly in ribs, mandible or vertebra. The prognosis is poor.

**Fig. 16.48.** Lymphangiomatosis of the vertebra. There is involvement of the vertebra from T11 to L3, with marked osteopenia, and collapse of T11 and L1, in this 28-year-old subject. This condition involved contiguous bones with marked soft tissue and visceral involvement.



**Fig. 16.50.** Angiosarcoma. A destructive lesion of the proximal humerus with a large soft tissue mass, but little reactive bone. Courtesy of WB Young, FRCR.

#### TUMORS ARISING FROM NERVOUS TISSUE

##### Neurofibroma and Neurofibromatosis

Neurofibromas arise from non-specific nerve cells. Neurofibromatosis presents with multiple cutaneous tumors and



**Fig. 16.51.** Neurofibromatosis. Classical tapering is seen in the fibula with pseudoarthrosis proximally. There is also marked deformity of the tibia with previous subperiosteal hemorrhage.

'café-au-lait' spots. The disease affects many organ systems, and is associated with optic nerve gliomas, meningiomas, acoustic neuromas, pheochromocytomas, aneurysms of the cerebral and renal arteries, and renal artery or aortic stenosis.

*Skeletal changes* include scoliosis, especially thoracic, *pseudoarthrosis*, particularly of the tibia, with characteristic tapering of the bones (Fig. 16.51). *Scalloping of the posterior vertebral bodies* (due to dural ectasia) occurs, as does *enlarged neural foramina* and *rib erosions* giving rise to 'ribbon ribs' (Fig. 16.52). Skull changes include abnormalities of the orbit and sphenoid wing, giving rise to the '*bare orbit*', *Harlequin orbit*, or *orbital enlargement* (Fig. 16.53). A *lytic defect in the Lambdoid suture*, usually the left, is also typical.

Malignant change to neurofibrosarcoma is said to occur in approximately 10% of cases.

*Schwannoma/Neurilemmoma.* These tumors arise from the Schwann cells of the nerve sheath and generally give rise to symptoms as a result of pressure, particularly when in an osseous canal. They occur singly, and are benign, without malignant potential. They have a predilection for the mandible.

#### TUMORS ARISING FROM FATTY TISSUE

*Lipoma.* Lipomas of bone are rare lesions, with a predilection for the calcaneus, skull, ribs, and occasionally the extremities. They produce lytic, mildly expansile lesions, often with a sclerotic rim; calcification may occur due to fat necrosis. Multiple lesions may be associated with hyperlipoproteinemia.

*Periosteal lipoma* is a rare condition which presents with characteristic strands of ossification around a lucent fatty center.

*Liposarcoma.* Most likely to be of the periosteal rather than intraosseous variety. Radiographically, the fatty lucency of the benign tumors is not seen, suggesting the more aggressive nature of the lesion.

#### TUMORS ARISING FROM NOTOCHORD

*Chordoma.* Chordoma arises from notochord remnants within the vertebrae and as such may occur from the coccyx to the buccopharyngeal membrane. In practice approximately 50% of chordomas arise in the coccyx/sacrum and the majority of the remainder in the basi-occiput and hypophyseal regions of the skull, with only 10%–15% found in the vertebrae.

They occur most commonly in males between 40 and 70 years of age. They are locally malignant destructive lesions, with a strong tendency to recur.

They present radiologically as expansile lytic lesions, often containing calcification and causing displacement of adjacent soft tissues, particularly in the pelvis. In the skull, destruction of the clivus or dorsum sella may be seen with a soft tissue mass in the nasopharynx (see Chap. 40).

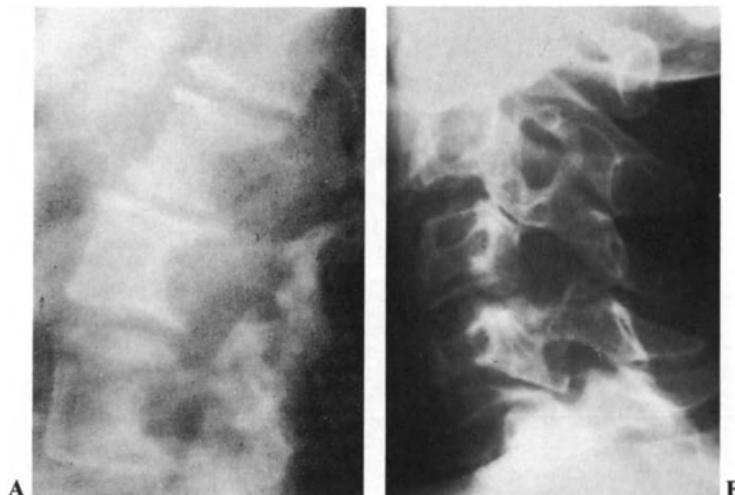


**Fig. 16.52A, B.** Neurofibromatosis. A There is marked posterior scalloping of the vertebrae due to dural ectasia. Prominence of the neural foramina of C2 and C3 is seen.

#### TUMORS ARISING FROM EPITHELIUM

**Implantation Dermoid.** These rare tumors arise following traumatic implantation of epithelial cells into the underlying bone. They usually arise in the distal phalanges of young adults as well-defined, expansile, lytic lesions. Subungual fibroma may present a diagnostic dilemma.

#### TUMORS ARISING FROM THE JOINTS

**Synovial Osteochondromatosis.** This is a condition usually occurring in young and middle aged adults, in which small areas of metaplastic cartilage are found throughout the synovium (see soft tissues). Although initially the only radio-

graphic signs may be those of increased synovial density, suggesting effusion, eventually calcification and ossification occurs (see Chap. 21).

**Pigmented Villonodular Synovitis.** Generally a disease involving a single joint, it may rarely be polyarticular. It most commonly occurs in the hip and knee, but the small joints may also be affected. Proliferation of villonodular masses of synovium occurs, with hemosiderin deposition. This gives rise to synovial thickening and sharply defined para-articular erosions, often with sclerotic margins, and usually affecting both sides of the joint (Fig. 16.54). Calcification of the synovium is extremely unusual.

**(Malignant) Synovioma.** A rapidly growing aggressive tumor, with early metastatic spread via the lymphatic system. It most commonly affects the knee, and occurs in

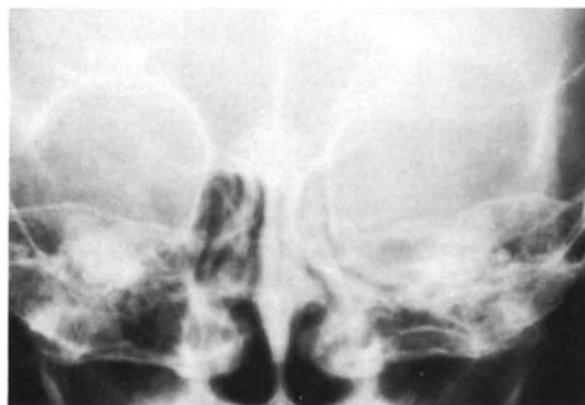


**Fig. 16.53.** Neurofibromatosis. There is enlargement of the left orbit with a bizarre appearance to the sphenoid wing, causing a type of 'Harlequin' orbit.



**Fig. 16.54.** Pigmented villonodular synovitis. Well defined lytic lesions are ► identified in the proximal tibia and distal femur (arrow).



**Fig. 16.55.** Intraosseous ganglion. The medial malleolus is a common site for this lesion. A well-defined lytic process is identified.

young adults. The tumor arises from the synovium of the joints, bursa and tendon sheaths, and calcifies in approximately 20% of cases. Irregular bone destruction occurs in about 10% of cases.

**Intraosseous Ganglion.** A relatively uncommon lesion, composed of ganglion material within a long bone, intraosseous ganglion characteristically occurs adjacent to the articular surface, usually involving the distal tibia, proximal tibia and proximal femur. The lesion is osteolytic, and may be expansile, often with a sclerotic rim (Fig. 16.55).

**Simple Bone Cyst** (Benign bone cyst; unicameral bone cyst). These fluid-filled 'cysts' with a thin wall of fibrous tissue arise on the metaphyseal side of the epiphyseal cartilage plate, although they may be found more distant from the epiphyseal plate, due to continued bony growth. They occur in the first and second decades, with a male predominance of 2:1. They are expansile, lytic lesions, with a tendency to pathological fracture (Fig. 16.56). *Isotope bone scan* is unremarkable in the blood pool phase, but delayed images show mild increased activity at the margins.

#### METASTATIC DISEASE

Post mortem studies indicate skeletal involvement in approximately 25% of deaths from malignancy, and metastatic disease is by far the commonest tumor encountered by the radiologist, particularly in patients over the age of 40 years.

The commonest bony sites for metastatic disease are the axial skeleton, followed by the proximal femur, humeri, and skull (Figs 16.57–16.60): the areas where hematopoiesis is occurring. In addition, local spread to the lumbar spine may occur from pelvic tumors. Peripheral metastases are rare, but may occur, particularly from the lung (Fig. 16.61).

Diagnostic clues to metastatic disease include *raised serum alkaline phosphatase* (normal in multiple myeloma), or *raised*



**Fig. 16.56.** Simple bone cyst. A slightly expansile lytic lesion of the proximal humerus is seen. There is a pathological fracture, with 'fallen fragments' of bone identified within the dependant portion of the lesion.

*acid phosphatase* level from prostatic carcinoma.

The commonest metastases encountered are, in men, from lung and prostatic carcinomas and, in women, from breast, although the incidence from lung carcinoma is now rising rapidly in women.

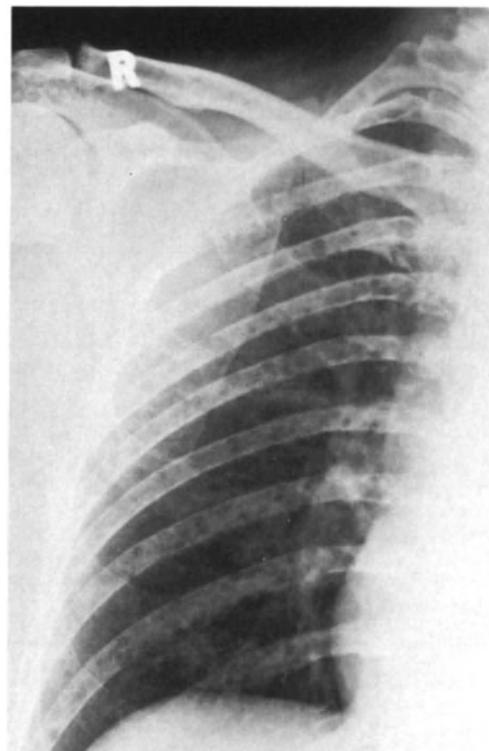


**Fig. 16.57.** Metastatic breast cancer. Multiple lytic lesions involve all the visualized bones. Spine, pelvis and proximal femur were also involved.



◀ Fig. 16.58. Metastatic disease from breast carcinoma. There are multiple lytic areas with the spine, involving the vertebral bodies, and posterior elements.



Fig. 16.59. CT scan of the patient shown in Fig. 16.58 demonstrates the destructive process involving both the vertebral body and pedicle on the left. The posterior cortex of the vertebral body and medial cortex of the left pedicle are destroyed.



Fig. 16.60. Metastatic lung carcinoma of the proximal femur, with a pathologic fracture through the neck.



Fig. 16.61. Metastases from lung carcinoma. Rarely metastases may involve the peripheries. Lytic lesions are seen in the capitate and distal ulna.



Fig. 16.62. Metastatic prostate carcinoma. Extreme density of most of the lumbar vertebrae is seen with additional foci of radiodensity in the sacrum and iliac bones.



**Fig. 16.63.** Myeloma of the hands. In general, myeloma does not involve the hands, which do not contain active marrow in this age group. Rarely, however, such involvement is seen.

Some patterns of metastatic disease are quite characteristic. For example, *lung carcinoma*, particularly of the squamous variety, destroys cortical bone, especially in the femur. *Prostatic metastases* are almost invariably osteoblastic, giving rise to multiple areas of increased hazy density, often merging together to involve the whole body (Fig. 16.62). Occasionally they may be markedly expansile.

*Renal metastases* are generally solitary, lytic lesions, particularly in the pelvis and lumbar spine. They may be highly vascular, requiring transcatheter embolization in their management.

*Breast metastases* are extremely common, and in the vast majority of cases are osteolytic, although approximately



**Fig. 16.65.** Plasmacytoma. An expansile destructive lesion of the left iliac wing is seen with cortical disruption.

10%–20% will be of a mixed pattern or even osteoblastic (Figs 16.57, 16.58). The lytic variety may be poorly defined and highly destructive or may present an almost 'pepper pot' type of destruction, again, most characteristically of the axial skeleton. Multiple small, well-defined lytic lesions may also be seen, giving a similar appearance to multiple myeloma.

**Plasma Cell Diseases.** Pathological proliferation of abnormal plasma cells may lead to either a local abnormality (plasmacytoma) or if widespread, myelomatosis.

*Plasmacytoma* presents as a solitary lesion involving predominantly the marrow-producing areas of the skeleton and hence the axial skeleton; particularly the spine, pelvis and shoulder girdle. Rarely, the peripheries may be involved (Fig. 16.63). The peak incidence is in the fifth and sixth decades. Although the single lesion may give no constitutional symptoms, eventual transformation to myelomatosis will occur, often after a latent period of many years.

**Radiography.** The lesions are usually well-defined and expansile, sometimes with a soap-bubble appearance, but often with a large associated soft tissue mass (Figs 16.64, 16.65).

*Myelomatosis* occurs in the over 40 age group, with a male to female predominance of 2:1. Abnormal protein (Bence-Jones) may be seen in the urine, resulting from excessive production of immunoglobulin light chain. Excessive urinary protein is cited as a contraindication for intravenous urography in these patients.

**Radiography.** Several patterns may be seen. A *generalized osteoporotic pattern* may be the only evidence of disease. Alternatively, these may be well-defined, 'punched out' lesions, varying in size, and usually found centrally in the bone. There may be mild expansion or *cortical scalloping* (Fig. 16.66). The skull may be diffusely involved (Fig. 16.67).

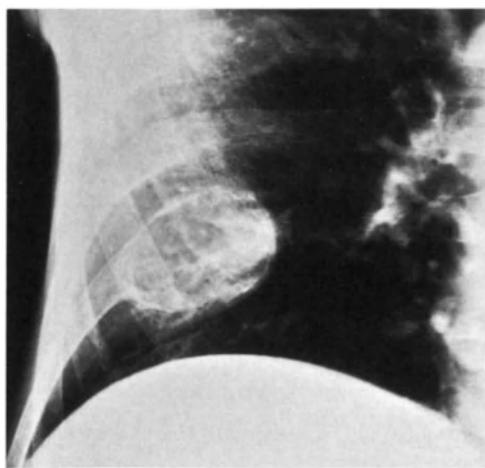


**Fig. 16.64.** Plasmacytoma. Expansile lesion of the rib with a mildly sclerotic margin.



**Fig. 16.66.** Multiple myeloma. There are typical, well defined lytic lesions of the humerus, acromion and glenoid with evidence of cortical 'scalloping'.

Osteoporosis is variable, but diffuse osteoporosis alone may be the only sign of the disease (Fig. 16.68). Rarely, a generalized osteosclerotic pattern may be seen. *Bone scan* may be negative in up to 50% of cases due to the lack of bone reaction.

#### DISORDERS THAT MAY SIMULATE NEOPLASMS OF BONE

*Hyperparathyroidism* (See Chap. 17). The brown tumor of hyperparathyroidism may cause a diagnostic problem if the



**Fig. 16.68.** Multiple myeloma. Marked osteopenia of the vertebrae is seen with the appearance of 'codfish' vertebrae, similar to that seen in osteomalacia. The aorta is calcified.

underlying disease is not appreciated. These lesions are usually lytic and may be expansile, simulating a bone neoplasm. Although they usually appear benign, age and location may raise the possibility of a malignant process such as plasmaacytoma (Figs 16.69, 16.70).

*Paget's Disease* (See p. 20) This disease of unknown etiology occurs in the older population, predominantly in the higher latitudes. Any bone may be affected. The early lesion is lytic, and may appear quite aggressive (Fig. 16.71) and destructive, particularly in the skull (*osteoporosis circumscripta*) (Fig. 16.72). The later stage shows irregular sclerosis,



**Fig. 16.67.** Gross involvement of the skull with myeloma.



**Fig. 16.69.** Brown tumor of the proximal humerus. There is a well-defined lytic lesion, without gross expansion. There is the suggestion of early distal clavicular erosion, another sign of secondary hyperparathyroidism.



**Fig. 16.70.** Brown tumor of the rib. Plasmacytoma could well be included in the differential diagnosis. (See Fig. 16.64).

usually with obvious *cortical thickening*, but the disease, if widespread may be difficult to differentiate from osteoblastic metastases (Figs 16.73, 16.74). Sarcomatous change may complicate the radiological appearance (Figs 16.15, 16.16, 16.75).

**Mastocytosis.** The skeletal manifestation of visceral masto-

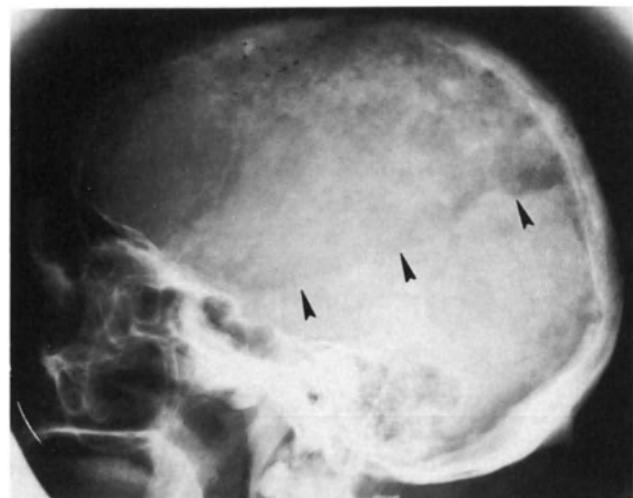


**Fig. 16.72.** Paget's disease (*osteoporosis circumspecta*). A moderately well-defined lytic process of the skull is seen involving most of the anterior aspect (arrowheads). This is quite characteristic for Paget's disease, but multiple myeloma can give a similar appearance.

cytosis, which usually presents with *urticaria pigmentosa*, is caused by infiltrates of mast cells, which cause patchy areas of increased radiodensity (Fig. 16.76).

The importance is in differentiating the lesions from disseminated metastatic disease such as from prostate carcinoma.



**Fig. 16.71.** Active Paget's disease. There is an aggressive-looking lytic process of the distal femur. There is, however, no evidence of cortical breakthroughs, and the trabeculae appear thickened.

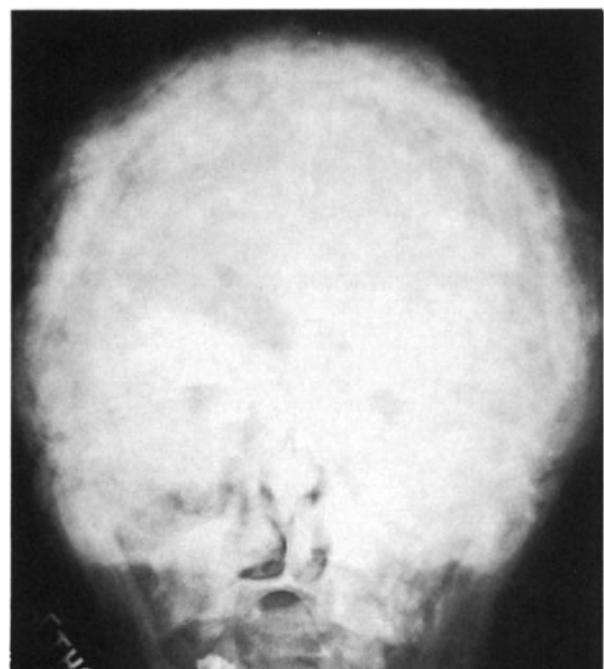


**Fig. 16.73.** The later phase of Paget's disease may show intense irregular osteosclerosis and marked thickening of the skull vault.

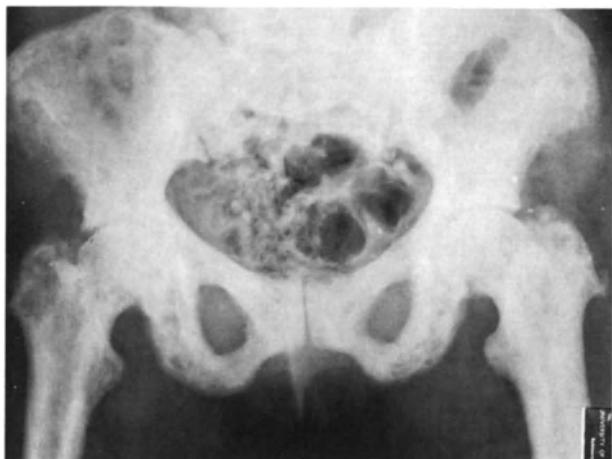


**Fig. 16.74.** Paget's disease. Most of the pelvis shows diffuse sclerosis. There is thickening of the iliopectineal line and coarsening of the trabecular pattern suggesting the diagnosis, but at times it may be difficult to distinguish between sclerotic Paget's disease and disseminated prostatic metastases. In this case, the shape of the pelvis indicates a female patient.

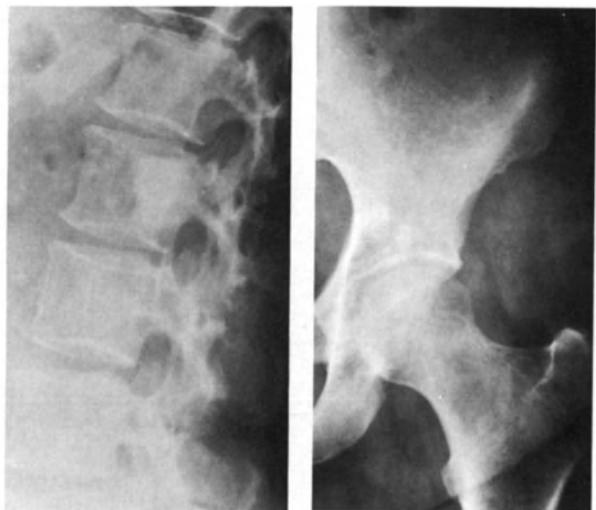


**Fig. 16.76A, B.** Mastocytosis. Moderately well-defined dense lesions are seen in the spine and supra-acetabular region of the pelvis. B. Examination of the skin will reveal urticaria pigmentosa.

**Histiocytosis.** This category includes conditions that range from the treatable *eosinophilic granuloma*, through the disseminated *Hand–Schuller Christian* disease, to the fatal *Letterer–Siwe* disease. The diseases are of the reticuloendothelial system, and usually present with well-defined

lytic lesions, which may be single, few in number (*eosinophilic granuloma*), or widespread (*Hand–Schuller Christian*, *Letterer–Siwe*). Although generally well-defined (Figs 16.77, 16.78), the lesions may appear extremely aggressive, with marked periosteal reaction (Fig. 16.79).



**Fig. 16.75.** Paget's sarcoma. There is extensive Paget's disease of the humerus and of the right 6th rib. A large destructive lytic process is also identified in the mid humerus, with a pathological fracture. Courtesy of WB Young FRCR.



**Fig. 16.77.** Eosinophilic granuloma. There is a well-defined lytic process of the proximal femur. Although the differential diagnosis is quite large, eosinophilic granuloma should always be considered.

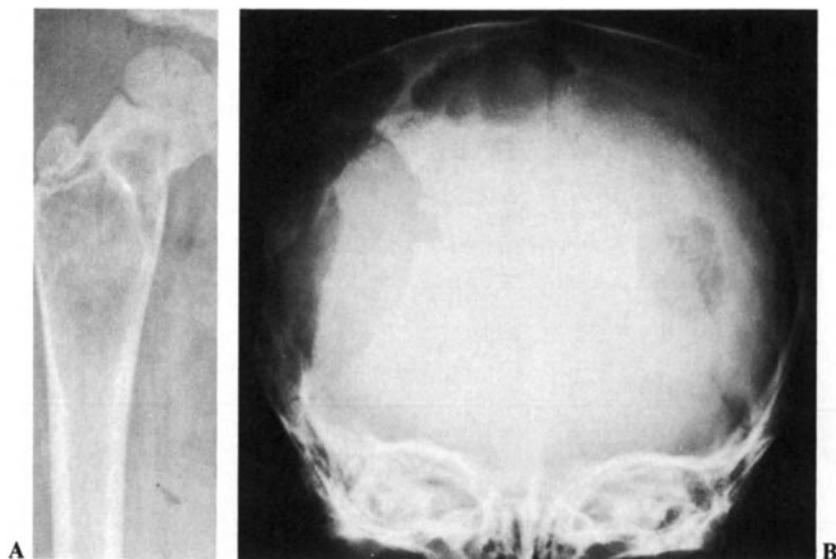


**Fig. 16.78A, B.** Eosinophilic granuloma. A moderately well-defined process of the proximal femur is seen, with the impression of a ground-glass density. Fibrous dysplasia could be considered, but views of the skull, B, demonstrate the typical appearance of eosinophilic granuloma.



**Fig. 16.79.** (left) An aggressive-looking lesion of the proximal femur is seen, with periosteal reaction and possibly early breakthrough medially. The dense nature of the periosteal reaction, however, is reassuring. Eosinophilic granuloma.



**Fig. 16.80.** Membranous lipodystrophy. Somewhat poorly defined lytic lesions are identified in the tibia and distal fibula. The fracture was coincidental.



**Fig. 16.81.** (left) Osteomyelitis. There is a poorly defined 'moth-eaten' lytic process of the distal femur with a marked soft tissue mass. In this case, osteomyelitis was found with an inflammatory mass and effusion. The appearance, however, is virtually indistinguishable from an infiltrating malignancy including lymphoma, Ewing's sarcoma, or osteosarcoma.



**Fig. 16.82.** (right) Histoplasmosis duboisii infection in a Liberian girl. The permeative destructive lesion cannot be distinguished from a malignancy.

Extension through the cortex may occur with marked soft tissue involvement. Vertebral involvement causes collapse and flattening of the vertebra (*vertebra plana*), which is reversible.

**Membranous Lipodystrophy.** A rare inherited disorder of unknown etiology, usually affecting young people, this condition is associated with mental retardation. Radiolucent lesions are identified, usually in the ends of long bones in the peripheries and showing a tendency to symmetry. The lesions may be rather irregular and poorly defined (Fig. 16.80).

**Infection (See Chap. 19).** Osteomyelitis may give a radiological appearance that is indistinguishable from involvement of a bone by tumor. This is particularly true in children, where metaphyseal involvement with osteomyelitis may mimic malignancy (Figs 16.81, 16.82). Tuberculosis may also present as a disseminated lytic process, indistinguishable from metastatic disease.

#### REFERENCES AND SUGGESTIONS FOR FURTHER READING

- Beltran J, Simon DC, Levy M, Herman LJ, Weis LD, Mueller CF (1986) Aneurysmal bone cysts: MR imaging at 1.5 T. *Radiology* 158: 689–690
- Bjorkengren AG, Resnick D, Haghghi P, et al (1986) Intraosseous glomus tumor: Report of a case and review of the literature. *AJR* 147: 739–742
- Bloem JL, Taminius AHM, Eulderink F, Hermans J, Pauwels EKJ (1988) Radiologic staging of primary bone sarcoma: CT, MR imaging, scintigraphy, and angiography correlated with pathologic examination. *Radiology* 169: 805–810
- Bonakdarpour A, Levy WM, Aegeuter E (1978) Primary and secondary aneurysmal bone cyst: A radiological study of 75 cases. *Radiology* 126: 75–83
- Dahlin DC (1986) Bone Tumors. 4th edn. CC Thomas, Springfield
- Edeiken J (1981) Roentgen Diagnosis of Diseases of Bone. 3rd edn. Williams & Wilkins, Baltimore
- Ehman RL, Berquist TH, McLeod RA (1988) MR imaging of the musculoskeletal system: A 5-year appraisal. *Radiology* 166: 313–318
- Frassica FJ, Unni KK, Beabout JW, et al. (1986) Dedifferentiated chondrosarcoma: report of clinicopathological features and treatment of seventy-eight cases. *J Bone Joint Surg [AM]* 68: 1197–1205
- Fobben ES, Dalinka MK, Schiebler et al. (1987) Magnetic resonance imaging appearance at 1.5 Tesla of cartilaginous tumors involving the epiphysis. *Skelet Radiol* 16: 647
- Glass RB, Poznanski AK, Fisher MR et al. (1986) MR imaging of osteoid osteoma. *J Comput Assist Tomogr* 10: 1065
- Hall FM, Gore SM (1987) Osteosclerotic myeloma variants. *Skelet Radiol* 17: 101–105
- Lindell MM Jr, Shirkhoda A, Raymond AK et al. (1987) Parosteal osteosarcoma: Radiologic-pathologic correlation with emphasis on CT. *AJR* 148: 323–328
- Murray RO, Jacobson HG (1982) The Radiology of Skeletal Disorders, 2nd edn. Churchill Livingstone, Edinburgh
- Nakashima Y, Unni KK, Shives TC et al. (1986) Mesenchymal chondrosarcoma of bone and soft tissue: Review of 111 cases. *Cancer* 57: 2444–2453
- Pear BL (1974) Skeletal manifestations of the lymphomas and leukaemias. *Semin Roentgen* 9: 229–240
- Pettersson H, Gillespy T III, Hamlin DJ, Enneking WF, Springfield DS, Andrew ER, Spanier S, Sloane R (1987) Primary musculoskeletal tumors: Examination with MR imaging compared with conventional modalities. *Radiology* 164: 237–241
- Resnick D, Niwayama G (1988) Diagnosis of Bone and Joint Disorders. 2nd edn. WB Saunders, Philadelphia
- Resnick D (1988) Paget disease of bone: Current status and a look back to 1943 and earlier. *AJR* 150: 249–254
- Sebes JL, Niell HB, Palmieri GMA et al. (1986) Skeletal surveys in multiple myeloma: Radiologic-clinical correlation. *Skelet Radiol* 15: 354–359
- Smith J (1982) Radiation-induced sarcoma of bone: Clinical and radiographic findings in 43 patients irradiated for soft tissue neoplasms. *Clin Radiol* 33: 205–221
- Van Lom KJ, Kellerhouse LE, Pathria MN, Moreland SI, Brown JJ, Zlatkin M, Sartoris DJ, Chevrot A, Resnick D (1988) Infection versus tumor in the spine: criteria for distinction with CT. *Radiology* 166: 851–855
- Whittaker LR (1973) Burkitt's lymphomas. *Clin Radiol* 24: 339–346
- Young JWR, Aisner SC, Levine AM, Resnik CS, Dorfman HD, Whitley NO (1989) Computed tomography and magnetic resonance of adamantinoma of long bone. *Skelet Radiol (In Press)*.
- Young JWR, Aisner SC, Levine AM, Resnik CS, Dorfman HD (1988) Computed tomography of desmoid tumors of bone: desmoplastic fibroma. *Skelet Radiol* 17: 333–337
- Young JWR, Galbraith M, Cunningham J, Roof BS, Vujic I, Gobien RP, Liebscher L, Butler WM, Fudenberg HH (1983) Progressive vertebral collapse in diffuse angiomyomatosis. Case Report. *Metab Bone Dis Rel Res* 5: 53–60
- Young JWR, Levine AM, Dorfman HD (1984) Case Report 293. *Skelet Radiol* 12: 294–297

## CHAPTER 17

# METABOLIC AND ENDOCRINE DISORDERS AFFECTING BONE

J.W.R. Young

Metabolic bone disease affects the skeleton in two ways; there is either *too much*, or more commonly, there is *too little calcified bone*. The latter state is due either to a decrease in the amount of bone formed, or to excessive resorption of bone (Table 17.1). This may be due, in turn, to a variety of causes,

Table 17.1. Causes of excessive resorption of bone

Vitamin D deficiency	
dietary	
neonatal rickets	
gastrointestinal malabsorption	
25 (OH) Vitamin D deficiency	
hepatic disease	
biliary atresia	
anticonvulsants	
25 (OH) <sub>2</sub> Vitamin D deficiency	
Renal failure	
Calcium/phosphorus imbalance	
renal tubular dysfunction (hypophosphatemic)	
tumor-related osteomalacia	

most commonly abnormalities of vitamin D and calcium metabolism, which arise from abnormality of diet or renal function, endocrine abnormalities (particularly of the parathyroid gland), drug therapy or poisoning.

Biochemical findings in metabolic and endocrine bone disease are summarized in Table 17.2.

### CHANGES DUE TO VITAMIN D ABNORMALITIES

A brief description of the actions of vitamin D is appropriate. Vitamin D is derived either from the diet, or via the action of ultraviolet light on the skin. After hydroxylation of cholecalciferol in the liver, further hydroxylation occurs in the kidney to generate the active form of vitamin D, 1,25-dihydroxycholecalciferol (1,25 DHCC). This acts in several ways.

First, absorption of calcium and phosphorus is promoted in the intestines.

Table 17.2. Metabolic findings in endocrine bone disease

	Calcium	Plasma phosphorus	Alkaline phosphatase	Urine calcium
Osteoporosis	No change	No change	No change	No change
Osteomalacia	Decreased or no change	Decreased or no change	Increased	Decreased
Primary hyperparathyroidism	Increased	Decreased or no change	Increased or no change	Increased or no change
Secondary hyperparathyroidism (renal)	No change or decreased	Increased	Increased	Decreased
Tertiary hyperparathyroidism	Increased	Variable	Increased or no change	Increased or no change
Familial hypophosphatemia	No change	Decreased	Increased or no change	No change

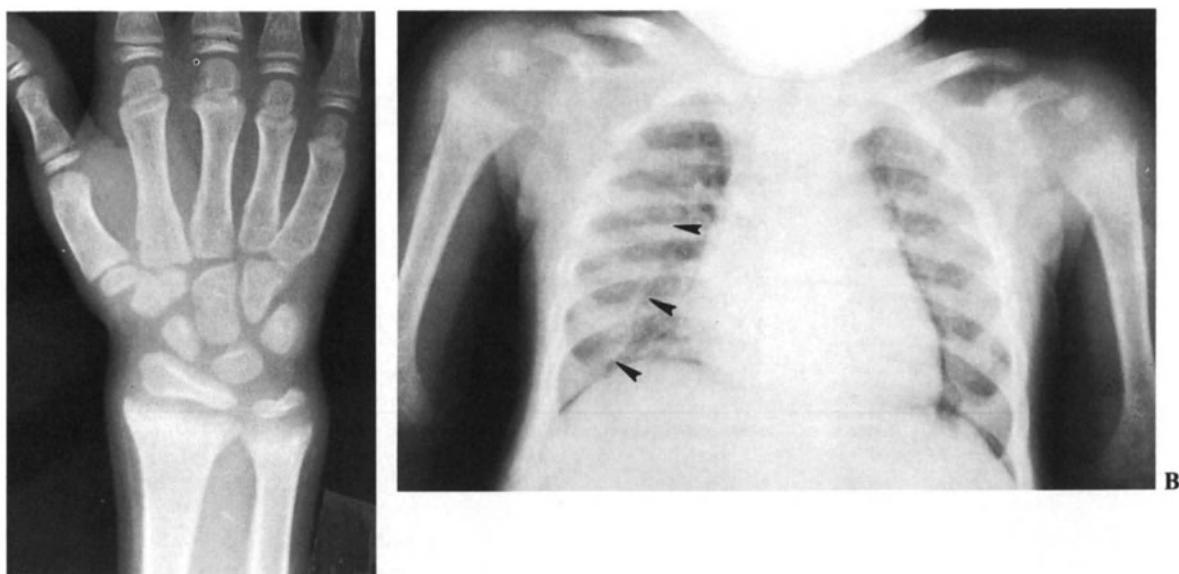


**Fig. 17.1A, B. Rickets.** A Irregularity of the metaphysis of the radius and ulna, and epiphyseal 'widening' is seen. B In the chest, there is widening of the anterior ribs (rachitic rosary, arrowheads). Metaphyseal 'fraying' of the proximal humerus is also seen.

Second, it stimulates production of relatively inert 24,25-dihydroxycholecalciferol in the kidney, which has a negative feedback effect, limiting 1,25 DHCC production.

Third, there are receptors in other organs, particularly the pituitary, placenta and breast, which are thought to reflect the increased demand for calcium, during growth, pregnancy and lactation.

#### Rickets and Osteomalacia (Vitamin D Deficiency)

Rickets and osteomalacia are identical disorders, occurring in children and adults respectively, as a result of a lack of the actions of vitamin D which in turn may be due to dietary lack, lack of production by the body, failure of absorption, or defective metabolism. In practice, nutritional deficiency only occurs when there is a dietary lack together with too little exposure to ultraviolet light. This is most commonly seen in black immigrants who make their homes in the less sunny areas of Northern Europe, although it may also occur in the neglected white elderly, particularly in larger cities in the northern latitudes.

*Malabsorption* states can result in osteomalacia due to vitamin D deficiency, as can diseases with biliary obstruction, as bile salts are necessary for vitamin D absorption. In celiac disease, the small bowel is less responsive to the action of vitamin D in calcium transport.

*Renal tubular disorders* associated with phosphorus depletion and acidosis will also cause osteomalacia, although there is argument as to whether this is a true problem of vitamin D metabolism.

*Drug therapy* may produce osteomalacia, particularly long-term anticonvulsants (dilantin) therapy. A similar effect has also been reported with rifampicin, and with glutethimide.

Finally many *toxins* have been found to cause osteomalacia by causing renal tubular damage and phosphate deficiency. These include aluminum hydroxide, magnesium

sulfate, and cadmium, the latter being associated with alkaline battery manufacture.

#### Rickets

There are many causes of rickets in childhood, and the radiological features are consistent, although varying in severity and location.

The effects are due to lack of calcification of osteoid, and are therefore most obvious at the *metaphysis*, where rapid growth is occurring. The initial abnormality is a loss of the normal 'zone of provisional calcification' adjacent to the metaphysis, although usually by the time radiographs are obtained, genuine metaphyseal abnormality is seen. This begins as an indistinctness of the metaphyseal margin, progressing to a 'frayed' appearance with a widening of the growth plate, due to lack of calcification of metaphyseal bone (Figs 17.1, 17.2, 17.3). Weight-bearing and stress on the uncalcified bone gives rise to *splaying*, and *cupping* of the metaphysis.

A similar but less marked effect occurs in the *subperiosteal* layer, which may cause lack of distinctness of the cortical margin. Eventually a generalized reduction in bone density may be seen, and in long-standing cases fractures may occur. *Looser's zones* are not seen as often as in osteomalacia (see below). In the epiphysis, there may be some haziness of the cortical margins.

With treatment, mineralization occurs giving rise to a dense white line at the zone of provisional calcification adjacent to the metaphysis, but becoming contiguous with the metaphysis in the healing process. In cases of intermittent dietary vitamin deficiency, or inadequate treatment, the metaphysis will show patchy sclerosis (Fig. 17.4).

In severe cases of rickets additional deformities of the bones occur, with *bowing of the long bones*, particularly of the lower limbs (Fig. 17.4), *thoracic kyphosis* with 'pigeon chest',



**Fig. 17.2.** Rickets. There is widening of the epiphyseal line, with mild 'fraying' of the metaphysis. The lucency in the distal femoral cortex is an incidental fibrous cortical defect.



**Fig. 17.3.** Rickets. There is irregularity of the metaphyses of the wrist and hand.

enlargement of the anterior ribs, causing the '*rickety rosary*' (Fig. 17.1), and *bossing* of the skull.

Rickets is common in premature infants and may be severe, causing spontaneous fractures and respiratory difficulty.

#### Vitamin D-resistant Rickets (Familial Hypophosphatemia)

This condition is usually inherited in a dominant sex-linked fashion, with males affected more severely than females. The disease is similar to rickets in radiographic appearance, but is refractory to vitamin D therapy, and growth retardation may be marked. In the most severe cases the bones are wide with thick cortices, and half of the patients show osteosclerosis. The condition may resemble a form of rhizomelic dwarfism, or chondrodysplasia.

#### Vitamin D-resistant Rickets Associated with Renal Tubular Disorders

A variety of renal dysfunction syndromes produce rickets and osteomalacia. These were described by Deltoni and Fanconi, and include hypercalcemia, renal phosphate loss and secondary hypophosphatemia, amino aciduria and renal tubular acidosis.

*Renal Tubular Acidosis.* Affected patients demonstrate retarded growth and short stature. The changes of osteomalacia, nephrocalcinosis and nephrolithiasis are also seen.

#### Osteomalacia

Osteomalacia refers to the changes of vitamin D deficiency in the mature skeleton. Bone pain is a frequent complaint.



**Fig. 17.4.** Incompletely treated rickets. 'Fraying' of the metaphyses is seen, with areas of sclerosis, and lucency indicative of insufficient and incomplete treatment.



**Fig. 17.5A, B, C.** Looser's zones: Cortical lucencies are identified in the proximal femur, A, ulna, B, and 2nd metacarpal, C.

Serum alkaline phosphatase is elevated, and serum phosphorus is usually low.

The *radiological* hall-mark of osteomalacia is the *pseudo-fracture* or 'Looser's zone'. This is a narrow zone of lucency, usually running perpendicular or nearly perpendicular to the bone cortex. Looser's zones are initially poorly defined, but become progressively more prominent with sclerotic margins (Fig. 17.5). They are generally accepted as occurring at sites of stress, where cortical infractions are repaired by unossified osteoid. They are frequently symmetrically bilateral, and occur at common sites such as the pubic rami, proximal femur, scapula, lower ribs, and ulna.

Osteopenia develops with 'pencilling in' of the vertebral bodies, and loss of vertebral height in a characteristic 'cod fish vertebra' pattern (see Fig. 16.68). Bowing of the long bones may occur. Compression wedge fractures of the vertebra are less common than in osteoporosis.

**Hypophosphatasia.** Inherited as an autosomal recessive trait, this disorder presents with a radiographic picture resembling a form of rickets of variable severity. This ranges from a severe and usually fatal neonatal presentation, to a milder form found in adults. There is a low serum alkaline phosphatase, and increased urinary phosphoethanolamine.

*Radiographically* the rickety changes of fraying of the metaphysis may be seen with uncalcified osteoid extending into the metaphysis (Fig. 17.6). Craniostenosis and nephrocalcinosis may occur, and in severe cases marked deformities, particularly of the distal phalanges and tibia, are seen.

**Hypophosphatemic Osteomalacia/Rickets.** There are several acquired forms of hypophosphatemia rickets. Hypophosphatemia is described in association with tumors of bone or soft tissues, often of fibrous tissue origin, or hemangioperi-

cytomas. Resolution of the osteomalacia occurs following removal of the tumor.

A similar association with neurofibromatosis and fibrous dysplasia is reported.



**Fig. 17.6.** Moderately severe splaying of the distal radial and ulnar epiphysis in this patient with hypophosphatasia.

*Fibrogenesis Imperfecta Ossium.* A rare condition affecting older patients, this presents with coarsening of the trabecular pattern of the bones, and in particular the ends of the long bones. The distinction from Paget's disease should be made. Multiple fractures are seen and the serum alkaline phosphatase is elevated.

*Axial Osteomalacia.* This rare condition is characterized by a coarsening of the bony trabeculae, similar to that seen in fibrogenesis imperfecta ossium, but only involving the vertebrae, pelvis and ribs. Histologically osteomalacia is found, but serum alkaline phosphatase levels are normal.

### Other Abnormalities of Calcium and Phosphatase

#### Metabolism

*Familial Hyperphosphatemia.* An extremely rare condition, presenting in early infancy, this is inherited as an autosomal recessive trait. Serum acid and alkaline phosphatase is elevated. The radiographic appearance is similar to Paget's disease, but occurring in infancy, and demonstrating more symmetry. The skull vault is thickened and the long bones are tubular and enlarged, but with cortical thinning.

### VITAMIN C DEFICIENCY

Vitamin C deficiency leads to a deficiency in the formation of bone matrix, as it is necessary for the formation of hydroxyproline, which is vital for collagen. In childhood, this gives rise to *scurvy*, whereas in adults *osteoporosis* occurs.

#### Scurvy

Scurvy is rare before six months of age due to a generally adequate fetal storage of vitamin C. Children present with limb pain and irritability. Radiographically four characteristic signs are seen (Fig. 17.7).

1. The epiphysis is small, and sharply marginated by a sclerotic rim (Wimberger's sign).
2. The zone of provisional calcification at the growing metaphysis is dense, giving a white line (Frankel's line).
3. Beneath this is a lucent zone, due to lack of mineralization of osteoid (Trumerfeld zone).
4. Finally, as this area is weakened, it is prone to fractures which manifest themselves at the cortical margin, giving rise to (Pelkan's) spurs.

In addition, due to capillary fragility, *subperiosteal hemorrhages* can occur, which may give rise to periosteal elevation, and subsequent new bone formation, particularly following treatment. This dense periosteal new bone should be differentiated from that found in battered infants.

Following treatment, dense bands of bone may be left, resembling growth arrest lines.

#### Osteoporosis

Osteoporosis is a decrease in bone mass, and may result from many underlying causes (Table 17.3). In general, this loss of bone mass gives rise to increased incidence of fractures, particularly in the *femoral neck*, *spine* (compression fractures), *distal radius*, and *pubic symphysis*.



Fig. 17.7. Scurvy. There are classic changes of scurvy with outlining of the epiphysis (Wimberger's sign). A dense metaphyseal line (Frankel's line) with a lucent zone (Trumerfeld zone) beneath it, and a cortical metaphyseal fracture on the medial aspect of the distal femur (Pelkan's spur).

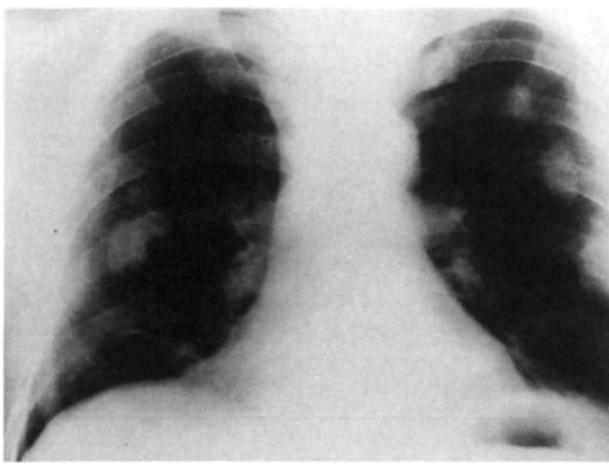
Radiographically trabecular loss in the spine causes a loss of density, which may be appreciated by 'pencilling in' of the vertebrae by the more radiographically dense end plates. So-called 'cod fish' vertebrae may occur, but this may also reflect a combination of osteoporosis and osteomalacia. In the femoral neck this condition is manifested by an apparent increase in density of the residual trabecula. It is difficult to evaluate bone loss by plain radiography and CT is now accepted as being a superior method for determining bone density. *Photon densitometry* is an alternative method with many proponents.

Table 17.3. Causes of osteoporosis

---

Immobilization
Metabolic
hypogonadal
post-menopausal
gonadal dysgenesis
senile
adrenal corticosteroid excess
thyroid hormone excess
cytotoxic drugs
miscellaneous
e.g., hepatic osteoporosis
drug-induced
idiopathic osteoporosis

---



**Fig. 17.8.** Cushing's disease. There is exuberant callus formation at the site of previous painless rib fractures.

Endosteal and intracortical resorption of bone is also prominent in osteoporosis producing cortical thinning most evident in the appendicular skeleton.

**Post-menopausal and Senile Osteoporosis (Involutional Osteoporosis).** Post-menopausal osteoporosis occurs in women typically in the 50 to 65 year age group. There is a disproportionate loss of trabecular bone, giving rise to rapid bone loss, and a proportionate increase in fractures, particularly of the vertebrae and distal radius. This has been linked to reduced estrogen levels, although additional factors such as skeletal size, level of activity, nutritional status and genetic determinants have been proposed. Blood chemistry is usually normal, although urinary hydroxyproline levels may be elevated in the acute stage.

Senile osteoporosis differs from post-menopausal osteoporosis in that there is proportionate loss of cortical and trabecular bone. Fractures occur most commonly in the femoral neck, proximal humerus, tibia and pelvis. There is no dramatic increase in bone loss in the post-menopausal stage, and patients tend to be older. The ratio of affected



**Fig. 17.9.** Avascular necrosis of the femoral head, with subcortical lucency and early collapse of the articular surface.

women to men is approximately 2:1. The etiology is uncertain, but reduced intestinal absorption, diminished adrenal function and secondary hyperparathyroidism may play a role.

**Juvenile Osteoporosis.** This rare disorder affects both sexes and occurs typically in prepubertal individuals. Patients present with bone pain, backache or limp related to fractures, characteristically of the metaphysis of the long bones (with minimal trauma) and compressions of the vertebra. The diagnosis is one of exclusion, particularly from leukemia, lymphoma and hypercorticosteroid states. Blood chemistry is normal. The condition is generally self-limiting.

**Idiopathic Male Osteoporosis.** A number of male patients present with systematic osteopenia prior to the age of 60 years, without demonstrable predisposing factors. Hypercalciuria and increased calcium absorption seem to be constant findings, and the condition may be an acquired defect in bone metabolism. Again, this is a diagnosis of exclusion.

#### Endocrine-induced Osteoporosis

Abnormality of function of the adrenal, pituitary and thyroid glands, hyperfunction of the parathyroids, hypofunction of the pancreas and gonads have all been linked with osteoporosis. As well as osteoporosis, other skeletal abnormalities are associated with particular endocrine disorders.

**Cushing's Disease.** Glucocortical excess can be due to a number of causes (see Chap. 28). If prolonged, this may lead to Cushing's disease. Exuberant callus formation at fractures is seen, particularly in long bones, ribs (Fig. 17.8) and vertebral bodies. In the latter case, a characteristic increased density of the end-plates occurs. Avascular necrosis, particularly of the femoral head may occur (Fig. 17.9). In children growth retardation may be seen.

**Hypogonadism.** In boys, this results in delayed epiphyseal plate closure. The patients have long limbs and short trunks. A similar hypogonadal disorder in girls (*Turner's syndrome*), results in increased carrying angle at the elbow, a short 4th metacarpal and changes of Blount's disease at the knee (see Chap. 20). Congenital cardiovascular anomalies also occur (see p. 267).

**Hyperthyroidism.** Osteoporosis occurs secondarily to bone remodeling and increased resorption. Increased cortical striations of the long bones are seen. *Thyroid acropachy* is a rare condition in which a characteristic periosteal thickening is found in the extremities (Fig. 17.10), and occurring following therapy for previous hyperthyroidism. Exophthalmus and pretibial myxedema are frequently present.

**Hypothyroidism.** Although not associated with osteoporosis, it is appropriate to discuss this condition at this time. In children, delayed skeletal maturation and retarded growth occur. Epiphyses are fragmented and late to appear. Wormian bones are seen in the skull, and the sella is either small and 'bowl'-like, (young children), or has a rounded and large 'cherry sella' configuration (older children). There is under-development of the paranasal sinuses. In the spine 'bullet shaped' vertebral bodies are seen, especially at the thoracolumbar junction, with a kyphosis. The long bones are short, and the incidence of slipped capital femoral epiphysis is increased.



**Fig. 17.10A, B.** Thyroid acropachy. A There is periosteal reaction identified along the first and second metatarsals. B Periosteal reaction may also be seen in the peripheral long bones, as in this case, involving the tibias.

**Pituitary Insufficiency.** Radiographic changes are confined to the child, where delayed skeletal maturation and decreased bone size is seen.

**Hyperpituitarism/Acromegaly.** It is questionable whether acromegaly is a cause for true osteoporosis. It will, however, be included in this section. Gigantism in the immature skeleton and acromegaly in the adult result from excessive growth hormone production by an adenoma of the pituitary.

The *radiographic* features of acromegaly include enlarged

mastoid air cells and sinuses, frontal bossing, and prognathism (Figs 17.11, 17.12). Pituitary fossa enlargement may be seen on the plain film, although CT or MRI are required to assess suprasellar extension (Chap. 40) (Fig. 17.13). In the spine, enlargement of the vertebral bodies with posterior scalloping is seen. The hands show bone enlargement with 'spade-like' terminal digits and 'arrowhead' distal phalanges (Fig. 17.14). Widening of the joint spaces due to overgrowth of articular cartilage may be seen (Fig. 17.14). The feet show

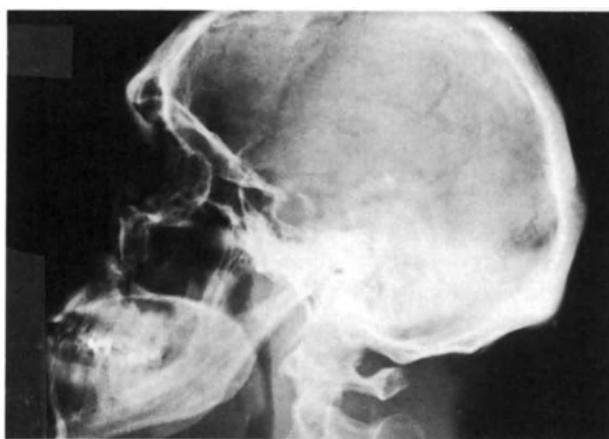


**Fig. 17.11.** Acromegaly. There is prognathism of the jaw, thickening of the skull vault, frontal 'bossing' and sella turcica enlargement.

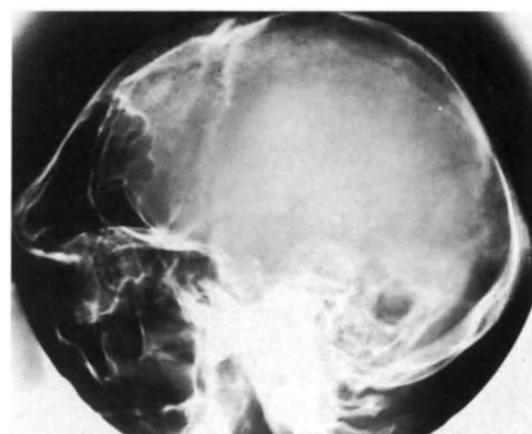


**Fig. 17.12.** Acromegaly. There is marked hyperplasia of the frontal sinuses. There is also frontal bossing. The floor of the pituitary fossa is noted to be ballooned.

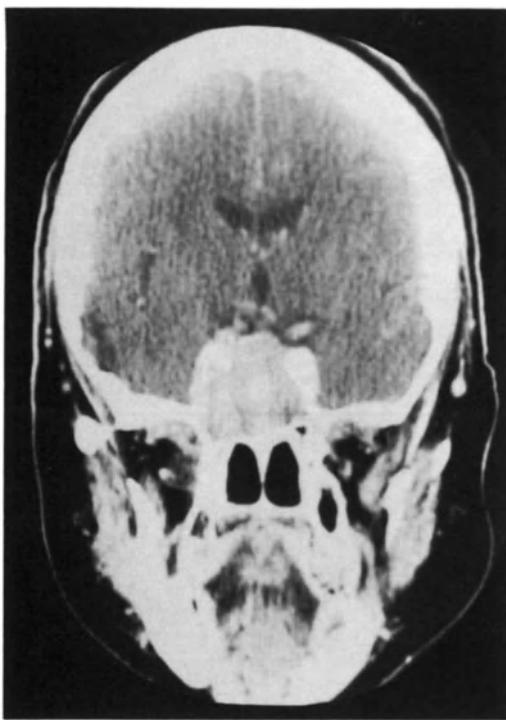


**Fig. 17.13.** Acromegaly. CT scan demonstrates a large pituitary tumor extending superiorly from the pituitary fossa.



**Fig. 17.14.** Acromegaly. The hands demonstrate large bones and soft tissues with 'arrowhead' distal phalangeal tufts. The joint spaces are also enlarged indicating prominence of the articular cartilage.

evidence of increased thickness of the heel pads (although this is not an infallible test), and elongation of the bones which, however, usually remain slender. Prominence of muscle attachments, and premature degenerative change may be seen. Calcification of the pinna of the ear occurs. Chondrocalcinosis has been reported as a rare association, although concurrent crystal arthropathy has also been proposed as an etiological factor.

**Hyperparathyroidism.** This is a common and important disorder, and will be discussed more fully below (see parathyroid glands).

**Glycogen Storage Diseases.** These comprise a group of inborn errors of metabolism and are due either to an excessive amount of normal glycogen (Types I, II, V, VI) or to abnormal glycogen (Type III, IV), the commonest being *Von Gierke's* disease, due to glucose-6-phosphatase deficiency. They are associated with hyperuricemia and gout.

They produce significant loss of bone density, most probably due to osteoporosis, with cortical thinning and widening of the tubular bones of the feet, ribs, and sternum, possibly due to marrow hyperplasia. The changes of gout may also be seen and there may be concavity of the anterior vertebral bodies, lumbar kyphosis and delayed ossification of the vertebral ring epiphysis.

**Drug and Toxin-induced Osteoporosis.** Corticosteroids, heparin, immunosuppressants, and alcohol have all been implicated in osteoporosis. In the latter case, concurrent

osteomalacia secondary to liver disease may be present.

**Localized Osteoporosis.** On occasion a localized osteoporosis may occur. The commonest cause for this is *disuse* osteoporosis, which may occur as a result of pain following trauma, severe vascular disease or enforced immobilization. A rapid, aggressive-looking resorption of bone occurs, most marked in the cortical and subarticular areas of the bones (Fig. 17.15). A similar appearance is seen in *Sudeck's Atrophy* (reflex sympathetic dystrophy), in which there is pain, swelling and limitation of movement of an extremity (Fig. 15.4). It is thought to be related to abnormal neural reflexes. Endosteal bone resorption is the most prevalent form of demineralization in this condition (see p. 274).

**Transient (Regional) Osteoporosis.** This is a rare condition of large joints where gross focal osteoporosis and pain occur. The femoral head is the commonest site. It is believed to be a form of Sudeck's atrophy (see p. 275). The condition is generally self-limiting with resolution in 4–10 months.

**Idiopathic Chondrolysis.** This is a rare disorder of unknown cause, occurring in adolescents and young adults in which chondrolysis of a joint, usually the hip, occurs. There is pain and osteoporosis. Ultimately, there is loss of joint space, early degenerative disease, and ankylosis.

**Miscellaneous Disorders Producing Osteoporosis.** *Osteogenesis imperfecta* (see p. 260) exhibits marked osteoporosis, Wormian bones, multiple fractures and exuberant callus for-

mation. Blue sclera and deafness are also seen. *Homozygous cystinuria* (p. 334) is also a cause of osteoporosis.

### THE PARATHYROID GLANDS

**Hypoparathyroidism.** This most commonly occurs after parathyroid gland removal at thyroid surgery, although rarely it can occur from excessive therapeutic radiation, hemorrhage, infection, tumor deposition in the thyroid gland, or iron deposition in iron-overload conditions.

*Idiopathic hypoparathyroidism* can occur with absence or atrophy of the glands. It is associated with a variety of endocrine and immune deficiency states including *Addison's disease*, *ovarian dysgenesis*, *hypothyroidism* and *chronic mucocutaneous candidiasis*. Circulating antibodies to the parathyroid, thyroid and adrenal glands have been found.

Radiologically, calcium deposition in the basal ganglia occurs and osteosclerosis, particularly of the pelvis, inner table of the skull, proximal femur, and vertebral bodies can be seen, as well as abnormal tooth development. Rarely osteoporosis is present. Serum calcium is low, and phosphate

diuresis follows parathormone administration.

**Pseudohypoparathyroidism.** This is an inherited disorder, characterized by hypocalcemia and hyperphosphatemia which are unresponsive to parathormone. The parathyroid glands are normal, but there is 'end-organ' resistance to parathormone. This may be due to a defect in the adenylyl cyclase-cyclic AMP system in the renal tubules and bones.

Basal ganglia calcification is more common than in idiopathic hypoparathyroidism. Short metacarpals, particularly the 4th and 5th, are seen. Abnormal dentition is also seen, and there may be calcification in the connective tissues of the skin, ligaments, tendons and fascial planes. Coxa vara, coxa valga, cone-shaped epiphyses, and bowing of long bones are also reported.

**Pseudo-pseudohypoparathyroidism.** This condition presents with the same clinical and radiographic appearances as pseudohypoparathyroidism, but with normal blood chemistry.

### Hyperparathyroidism

This condition is divided into the primary, secondary and tertiary forms. In the *primary* form, increased hormone pro-



Fig. 17.15



Fig. 17.16

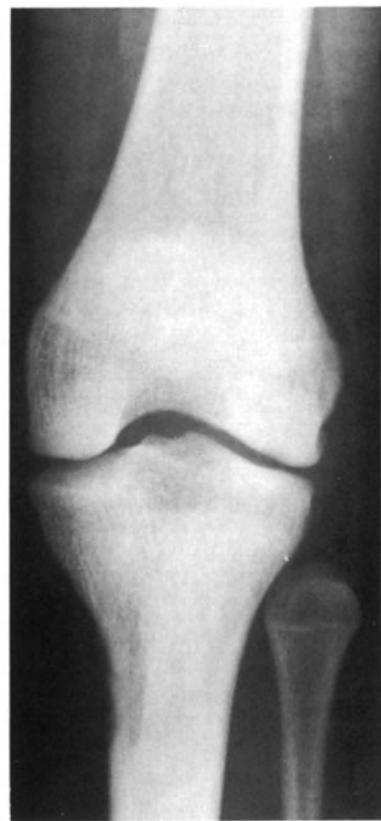
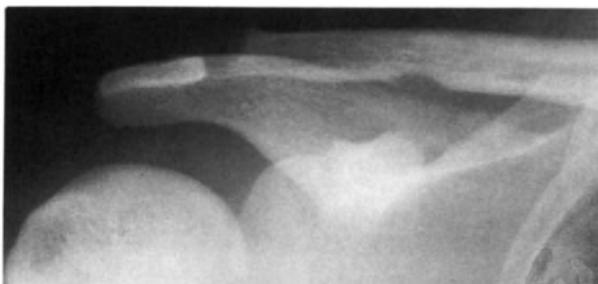


Fig. 17.17

Fig. 17.15. Disuse osteoporosis. There is lucency involving the ends of the bones and in this case patchy cortical bone loss giving rise to a ragged appearance of the bone.

Fig. 17.16. Secondary hyperparathyroidism. Subperiosteal resorption along the radial aspect of the middle metacarpals of the index, middle and ring fingers.

Fig. 17.17. Subperiosteal resorption at the medial aspect of the proximal tibia in a patient with chronic renal failure.



**Fig. 17.18.** Subligamentous resorption of the undersurface of the distal clavicle, together with subchondral resorption of the distal tip are both seen in this example of secondary hyperparathyroidism.

duction occurs, generally as a result of adenomas (75%), hyperplasia or carcinoma. It occurs most commonly in middle-aged and elderly people, and is more common in women (2:1). Symptoms include weakness, lassitude, constipation, polydypsia, polyuria, peptic ulceration, renal calculi, and psychiatric problems.

Radiographically, bone resorption is the hallmark of hyperparathyroidism although frank osteopenia is difficult to detect radiographically in early cases. Absorptiometry, however, may confirm bone mineral loss in approximately 50% of cases. More advanced cases demonstrate loss of bone density, and sometimes a ground-glass appearance. The vast majority of cases seen today are the result of *chronic renal failure*. The radiographic appearances however, are similar.

*Subperiosteal erosion* of bone, particularly along the radial aspect of the middle phalanx of the middle and index finger is virtually pathognomonic (Fig. 17.16), although fine grain film or magnification views may be required to detect it. Other sites include the medial aspect of the proximal tibia (Fig. 17.17), femur and humerus, and the ribs. *Loss of the lamina dura* around the teeth occurs, although this is not specific for hyperparathyroidism.

*Subchondral bone resorption* is another common occurrence, being found at the distal, and sometimes at the proximal end of the clavicle (Fig. 17.18), at the symphysis pubis, and the sacroiliac joints. This may also occur at the vertebral end plates, and may permit disc herniation into the vertebra (Schmorl's nodes).

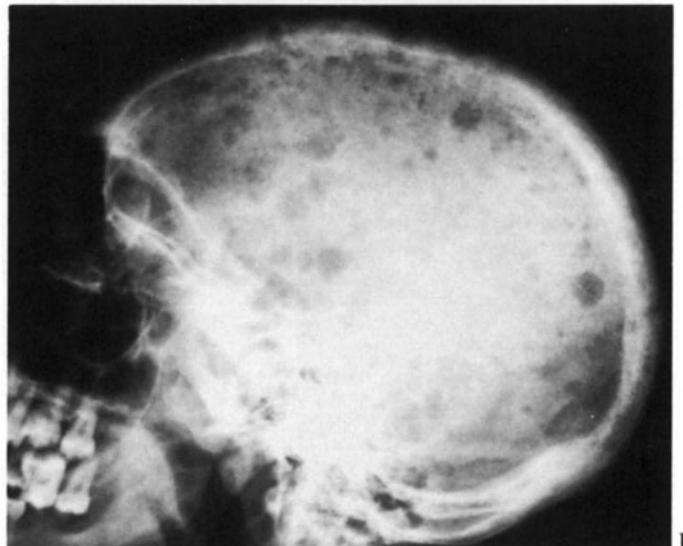
*Intracortical bone resorption* results from osteoclastic activity within the Haversian canals, giving rise to small (2–5 mm) oval or cigar-shaped lucencies within the cortex. This is a feature of rapid bone turnover, and is also seen in other conditions, such as hyperthyroidism, osteomalacia and acute (focal) osteoporosis. Loss of the cortico-medullary junction may occur with a '*basket-work*' appearance to the cortex (Fig. 17.19). In the skull, a characteristic granular or mottled appearance may occur, giving rise to the so-called '*pepper pot*' or '*salt and pepper*' (USA) skull (Fig. 17.19).

*Subligamentous resorption* occurs at sites of ligament or tendon insertions, and is seen in the ischial tuberosity, greater and lesser trochanters, inferior calcaneus and the inferior surface of the outer clavicle (Fig. 17.18).

*Brown tumors* are locally destructive areas of intense osteoclastic activity. They present as a lytic lesion which may



**A**



**B**

**Fig. 17.19A, B.** Secondary hyperparathyroidism. A Intracortical bone resorption is identified in the tibia, with loss of the corticomedullary junction and multiple cigar-shaped lucencies. B In the skull, this gives rise to a '*pepper pot*' appearance.

be expansile, and may destroy the overlying cortex (Figs 17.20, 17.21). They are generally well-defined, and may be multilocular, although they may appear aggressive (Fig. 16.69). They may resolve after treatment, but can persist for many years.

An *erosive arthropathy* may occur. This usually involves the hands, wrists and shoulders and may simulate the appearance of rheumatoid arthritis; but subperiosteal resorption is usually a concurrent feature, and the distal interphalangeal joints are often involved, unlike rheumatoid arthritis.



**Fig. 17.20.** A Brown tumors are identified in the metacarpals of the index finger bilaterally. There is also marked subperiosteal resorption of bone. B Following treatment, there is filling in of the lesions. (Courtesy of Dr James Dempsey FRCR)

*Renal calculi* have been reported in as many as 50% of patients. The majority of the calculi are calcium oxalate, although uric-acid stones may be seen. Nephrocalcinosis also occurs, but is less common.

*Secondary Hyperparathyroidism.* Parathyroid hyperplasia, involving all of the glands, occurs in response to persistent hypocalcemia. This can be seen in *rickets*, *osteomalacia* and *chronic renal failure*. The skeletal changes are similar to primary hyperparathyroidism, although brown tumors are statistically less frequently in this condition. Nevertheless, as secondary hyperparathyroidism is so much more prevalent than primary hyperparathyroidism, brown tumors are encountered quite regularly. *Calcification* of arteries and soft tissues occurs, being most common in the secondary hyperparathyroidism of renal osteodystrophy (Fig. 17.22).

*Renal Osteodystrophy.* This is of particular interest, as it

combines the findings of osteomalacia, hyperparathyroidism and bone sclerosis.

As in hyperparathyroidism, the commonest finding is subperiosteal resorption, although in severe cases all features may be present. Calcification of arteries, articular cartilage and periarticular tissues also occurs. Osteomalacia is identified predominantly by the presence of Looser's zones (Fig. 17.5). Osteosclerosis is seen in the skull, metaphyses of long bones, and adjacent to the vertebral body end plates, giving rise to the '*rugger jersey spine*' (Fig. 17.23). An aseptic erosive arthropathy, generally involving the shoulders, and a spondylitis, which may resemble a Charcot spine or infective process, are well recognized associations (Fig. 17.24).

In children, metaphyseal changes resembling rickets are seen, which together with cortical erosions can give rise to the so-called '*rotting fence post*' appearance, particularly at

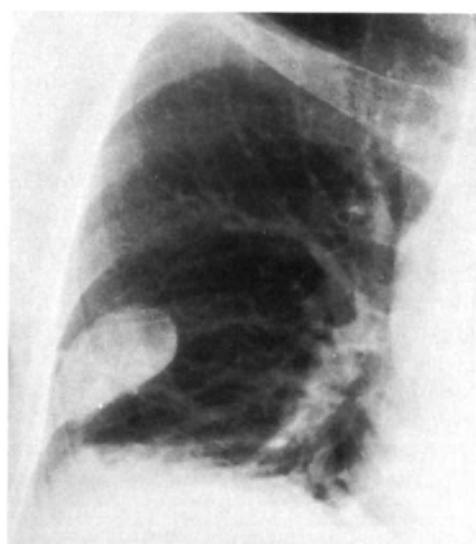


**Fig. 17.21.** Brown tumor. Primary hyperparathyroidism. An expansile lesion of the right eighth rib was identified. Hyperparathyroidism had not been diagnosed at the time of this radiograph.



**Fig. 17.22.** Massive soft tissue calcification around the shoulder in this patient with secondary hyperparathyroidism.



**Fig. 17.23.** Renal osteodystrophy. Chronic renal failure. The typical 'rugger jersey' spine is seen with dense sclerotic bands at the vertebral end plates. A non-septic arthritis of the shoulder, and spondylitis involving the upper lumbar spine are also present.



**Fig. 17.24A, B, C.** Chronic renal failure. Dialysis patient. There is an aggressive spondylitis, resembling a Charcot spine. In addition, an aseptic erosive arthropathy of the large joints, but particularly the shoulder, may be seen, C.

the femoral neck. Slipped capital epiphyses are also seen as a complication, most commonly involving the proximal femur.

**Tertiary Hyperparathyroidism.** This is the term applied in cases in which secondary hyperparathyroidism gives rise to autonomous hyperparathyroidism. Treatment of the underlying disorder fails to control the hyperparathyroidism. Surgical removal of the autonomous parathyroid tissue is necessary.

#### OTHER METABOLIC DISEASES

**Oxalosis.** Primary hyperoxaluria is inherited as an autosomal recessive trait. The main feature is recurrent urinary calculi, progressing to renal failure. Calcium oxalate deposition in bone and soft tissues is also seen.

**Ochronosis (Alkaptonuria)** (see p. 267). This rare disorder of tyrosine metabolism is inherited as an autosomal recessive trait. Due to a lack of homogentisic acid oxidase, homogentisic acid accumulates in tissues, particularly connective tissue. The urine darkens rapidly on standing. Pigment deposition in articular cartilage gives rise to calcification and early degenerative disease of the peripheral joints, and calcification of spinal disc spaces, with relatively little spondylosis. In the joints, there is considerable narrowing of the joint space, without marked osteophyte formation or sclerosis, until the later stages. In the spine, advanced changes may lead to an appearance resembling ankylosing spondylitis.

**Wilson's Disease** (hepatolenticular degeneration). This rare autosomal recessive disorder of copper metabolism produces deposition of copper in the liver, brain and other systems, with skeletal changes of osteomalacia, and a form of arthritis (of peripheral joints, with irregularity of the articular surfaces) (see Chap. 21).

Other metabolic disorders, such as *hemochromatosis* and *calcium pyrophosphate dihydrate deposition* disease also mainly produce joint disease, and will be discussed in Chap. 21.

**Homocystinuria.** This is a rare disorder inherited in an autosomal recessive fashion. There is excessive homocysteine due to a deficiency in the activity of the enzyme cystathione synthetase, which converts homocysteine to cystathione and cysteine. In one form of the disease (pyridoxine resistant), changes in the skeleton include osteoporosis, arachnodactyly, epiphyseal enlargement, scoliosis, sternal deformity, and valgus deformity of the knees and hips.



**Fig. 17.25.** Lead poisoning. Increased density of the metaphyses of the distal femur, tibia, and fibula is seen.

#### MISCELLANEOUS DISORDERS

**Toxic Effects on the Skeleton.** Many toxins and poisons may affect the skeleton. Some common conditions are discussed below.

Ingestion of lead, usually in children who ingest lead-containing paint, or water from lead-containing pipes leads to lead deposition in the growing metaphyseal regions (Fig. 17.25). This may cause modeling deformities, and increased bone density, although most of this is due to reactive change. Lead encephalopathy is a serious complication.

Bismuth intoxication (often following treatment for syphilis in the past), causes a similar appearance.

**Vinyl chloride poisoning** found in workers in PVC manufacture causes Raynaud's phenomenon, and a characteristic form of acro-osteolysis.

**Fluorosis** due to chronic fluoride poisoning is endemic in some parts of the middle and far East, but may also occur in workers in aluminum-smelting industries and, when fluorine is used as a preservative, in those who drink large quantities of wine. A generalized increased bone density is seen. Cortical thickening occurs and ossification of ligamentous and musculotendinous attachments is seen.

#### REFERENCES AND SUGGESTIONS FOR FURTHER READING

- Christie DV (1980) The spectrum of radiographic bone changes in children with fluorosis. *Radiology* 136: 85–90
- Genant HK, Block JE, Steigler P et al. (1987) Quantitative computed tomography in assessment of osteoporosis. *Semin Nucl Med* 17: 316–323
- Greenfield GB (1986) *Radiology of Bone Diseases*, 4th edn. JB Lippincott, Philadelphia
- Griffin CN (1984) Severe erosive arthritis of large joints in chronic renal failure. *Skelet Radiol* 12: 24–33
- Lewin PK, Reid M, Reilly BJ et al. (1971) Iatrogenic rickets in low birth weight infants. *J Pediatr* 78: 207–210
- Moule NJ, Golding JSR (1974) Idiopathic chondrolysis of the hip. *Clin Radiol* 25: 247–251
- Naidich JB, Massey RT, McHeffey-Atkinson B, Karmel MI, Bluestone PA, Mailoux LU, Stein HL (1988) Spondyloarthropathy from long-term hemodialysis. *Radiology* 167: 761–766
- Pitt MJ (1981) Rachitic and osteomalacia syndromes. *Radiol Clin North Am* 19: 581–599
- Rabinowitz JG (1978) *Pediatric Radiology*. JB Lippincott, Philadelphia
- Reinhold WD, Genant HK, Reiser UJ, Harris ST, Ettinger B (1986) Bone mineral content in early postmenopausal and postmenopausal women: comparison of measurement methods. *Radiology* 160: 469–475
- Resnick D, Niwayama G (1984) *Diagnosis of bone and joint disorders*. 2nd edn. WB Saunders, Philadelphia
- Steinbach HL, Young DA (1966) The roentgen appearances of pseudo-hypoparathyroidism and pseudo pseudohypoparathyroidism. *AJR* 97: 49–66
- Sutton D (1987) *A Textbook of Radiology and Imaging*, 4th edn. Churchill Livingstone, Edinburgh.
- Travers JM, Ferrucci JT (eds) (1987) *Radiology: Diagnosis, Imaging, Intervention*. vol 5, revised edn. London, Mexico City, New York

## CHAPTER 18

# HEMOPOIETIC DISORDERS

J.W.R. Young

---

### DISEASE INVOLVING RED BLOOD CELLS

**Chronic Hemolytic Anemias.** *Thalassemia* and *sickle cell disease* are the two inherited chronic anemias that are commonly associated with skeletal changes.

*Hereditary spherocytosis*, if untreated, may produce the radiographic picture of a chronic anemia. Splenectomy is effective in alleviating the problem. Other chronic anemias, such as *iron deficiency*, also may rarely produce radiographical changes if left untreated.

#### Sickle Cell Disease

This inherited disease occurs almost exclusively in the black races from Central Africa and their descendants. There are many genetic variations. The abnormal hemoglobin (HGS) may be acquired from both parents, giving rise to the homozygous state (HGSS), or it may be combined with normal hemoglobin (HGA) from one parent or with other abnormal hemoglobins; the most important of these are HGC (HGSC disease), and thalassemia (to give HGS-Thal disease). There is great variation in the clinical picture of sickle cell disease. In the severe state multiple crises may occur due to sickling episodes in the spleen, bone marrow and visceral organs. In general, the features of marrow hyperplasia are most common in patients with HGSS rather than HGSC or HGS-Thal.

The **radiographic findings** are predominantly those resulting from bone **marrow hyperplasia**, with evidence of bone and marrow infarction. Hyperplasia may give rise to secondary growth disturbance, fractures and infections. The changes of *marrow hyperplasia* begin at about 6 months, when the fetal hemoglobin (HGF), which has a protective effect, is replaced by abnormal hemoglobin.

Expansion of the medullary space produces cortical thinning, and coarsening of the trabecular pattern (Fig. 18.1), which may give rise to '*squaring*' of the small bones of the

hands and feet (Fig. 18.2). There is commonly a generalized osteoporosis and '*cod fish*' vertebrae may be found (Fig. 18.3). In the skull, there may be widening of the diploic space, and frontal bossing. A *hair on end* appearance with radially orientated striations, although not as common as in thalassemia, occurs in approximately 5% of patients with HGSS (Fig. 18.4). Rounded lytic areas, due to severe cortical thinning possibly related to narrow hyperplasia may be seen, giving rise to an appearance resembling hyperparathyroidism. These changes do not occur below the level of the internal occipital protuberance, as there is no marrow present in this region.

*Cortical thickening* and *medullary sclerosis* may occur in older patients, possibly as a result of subclinical ischemia or

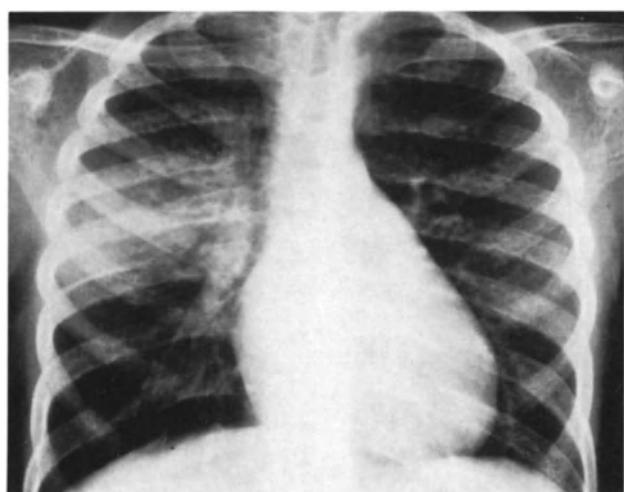


Fig. 18.1. Sickle cell disease. There is coarsening of the trabecular pattern of the ribs and clavicles, indicative of the hypercellularity of the marrow.



**Fig. 18.2.** Sickle cell disease. The tubular bones of the hand are expanded with squaring of their margins. There is also abnormal bone texture. The proximal phalanges of the ring and index finger show additional abnormality, with the impression of a lytic process in the ring finger phalanx, and cortical irregularity in the index finger phalanx. This represents bone infarction, although, radiographically, infection cannot be excluded.

infection, with revascularization, fibrosis and sclerosis. This may give rise to a '*bone within a bone*' appearance (Fig. 18.5). In addition, sclerosis of the end plates of the vertebral bodies may be seen (Fig. 18.6).



**Fig. 18.5.** Sickle cell disease. There are dense subcortical sclerotic bands in the femoral heads, acetabula and inferior pubic rami, giving rise to a '*bone within bone*' appearance.

**Bone Ischemia and Infarction.** The commonest site for infarction is the medullary cavity of the long bones, most commonly in the metadiaphyseal region. These may heal with little or no radiographic evidence, or may go on to fibrosis and calcification (Fig. 18.7). Cortical infarcts are uncommon in adults, but may occur in infants, particularly in the small bones, giving rise to a *dactylitis* in which there is pain and swelling with florid periosteal reaction (Fig. 18.2). Large metadiaphyseal infarcts also may occur in the long bones



**Fig. 18.3. (left)** Sickle cell disease. Several of the vertebral bodies show a biconcave appearance, whilst others demonstrate an appearance more suggestive of eccentric Schmorl's nodes. Both of these appearances are commonly seen in sickle cell disease.

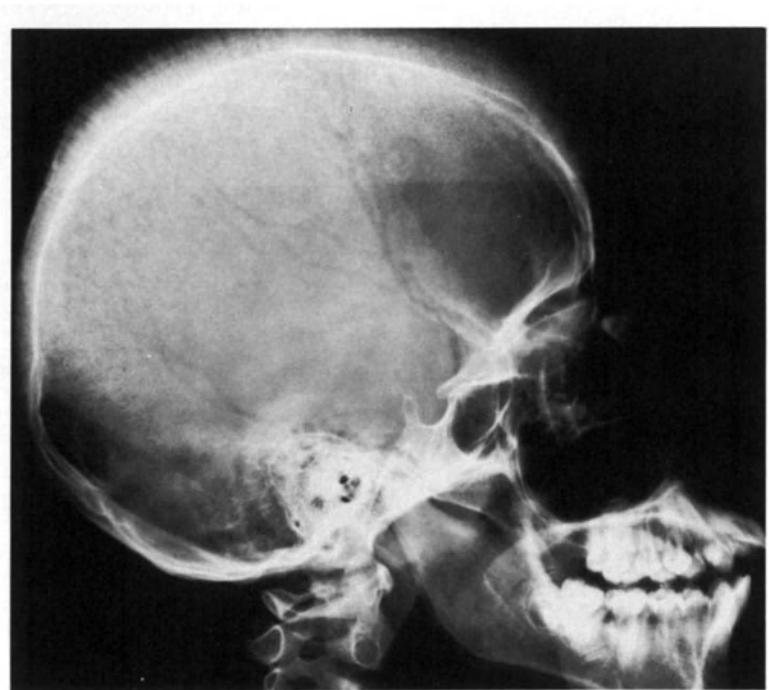


**Fig. 18.4. (right)** Sickle cell disease. There is thickening of the skull vault above the occipital protuberance, with a '*hair on end*' appearance superiorly.



**Fig. 18.6.** (left) Sickle cell disease. Sclerotic vertebral end plates may be seen.



**Fig. 18.7.** (right) Sickle cell disease. Healed infarcts are seen in the proximal radius, and distal radial epiphysis. In the proximal radius there is now fibrosis and calcification. In the distal epiphysis, the infarction has led to epiphyseal irregularity and secondary involvement of the proximal carpal row.



**Fig. 18.8.** (left) Sickle cell disease. Infarction of the 5th metacarpal, distal radius and proximal ulna is seen. The metacarpal infarct has led to an aggressive looking lesion with swelling, periosteal reaction and sclerosis. Infection could not be excluded radiographically.



**Fig. 18.9.** (right) Sickle cell disease. The classical H-shaped vertebrae are seen at several levels, with depression of the central portion of the end plate of the vertebral body.

in infants and may involve both medullary and cortical bone, giving an aggressive appearance with resorption of the cortex beneath the periosteal new bone (Fig. 18.8).

Infarction rarely may give rise to *growth disturbances*, usually in the central portion of the growth plate, the peripheries being spared by marginal metaphyseal supply. In the tubular bones, this presents as coned epiphyses, whilst in the spine a squared-off central depression may be seen in the end plate (*H vertebra*), (Fig. 18.9). A similar appearance is reported in alcoholics, women on birth-control pills, and patients with *paroxysmal nocturnal hemoglobinuria*.

*Epiphyseal avascular necrosis* occurs in 15%–30% of older patients involving most commonly the proximal femoral epiphysis, and less commonly the proximal humerus and knee. The radiographic appearance is similar to that found in Caisson disease, Gaucher's disease, etc., with initially a subarticular lucency (crescent sign), followed by collapse of the articular surface, and areas of sclerosis within the epiphysis (*snow cap sign*) (See Chap. 20).

**Osteomyelitis** due mainly to salmonella and pneumococcus occurs more frequently, especially in areas of infarction.

It may be difficult to make the diagnosis radiographically, as the appearance in both infarction and infection may be similar. The changes of infection, however, progress more rapidly.

### Thalassemia

Thalassemia is an inherited disorder of hemoglobin synthesis, with defective production of either the alpha or beta chains of the hemoglobin molecule. The most important of the thalassemia syndromes is the homozygous  $\beta$ -thalassemia major, where there is absent or decreased beta chain production, with the alpha chains deposited with the erythrocytes as insoluble bodies giving rise to increased hemolysis. When very severe, death may occur within the first 5 years of life. Treatment with multiple transfusions results in hemosiderosis. Marrow hyperplasia is marked and may result in skull and facial deformities, and in growth retardation.

Radiologically, the extreme marrow hyperplasia results in expansion of the long bones, with destruction of many trabe-



**Fig. 18.10.** Thalassemia. There is abnormal bone present in the hand and forearm, with coarsening of the trabecular pattern.

culae. The peripheral bones are often affected in the child, and show *squaring* or even *biconvexity* of the tubular bones particularly in the extremities (Fig. 18.10). A similar appearance occurs in the ribs (Fig. 18.11). There may be soft tissue densities adjacent to the posterior and sometimes anterior

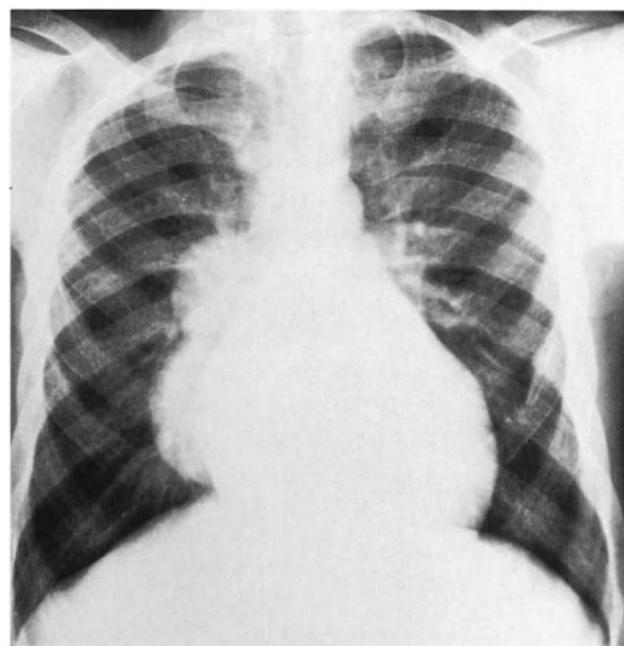


**Fig. 18.12.** Thalassemia. There is abnormality of the ribs, which are expanded with a coarse trabecular pattern. A lobulated mass lies posterior to the right heart border, representing a focus of extramedullary hematopoiesis.

ribs, and within the mediastinum, from *extramedullary hematopoiesis* (Fig. 18.12). This occurs mostly in patients with thalassemia intermedia. Interestingly, it has been shown that while extramedullary, the hyperplastic marrow remains subperiosteal. Rarely, spinal cord compression may occur.

In the skull, widening of the diploic space, hypoplasia of the paranasal sinuses due to facial bone hyperplasia (Fig. 18.13), displacement of developing teeth, and '*hair on end*' new bone formation over the skull vault may be seen (Fig. 18.14).

In the appendicular skeleton, severe osteopenia and cortical thinning may give rise to fractures. Well-defined cortical erosion may also occur, most commonly in the metaphysis.

*Premature epiphyseal fusion* is a characteristic finding, most commonly occurring in the proximal humerus, but also seen in the femur and proximal tibia.

The vertebral bodies appear striated, due to thickening of the vertical trabeculae and paucity of horizontal trabeculae (Fig. 18.15). Biconcave vertebrae, H-shaped vertebrae and compression fractures have been reported, although these are rare.

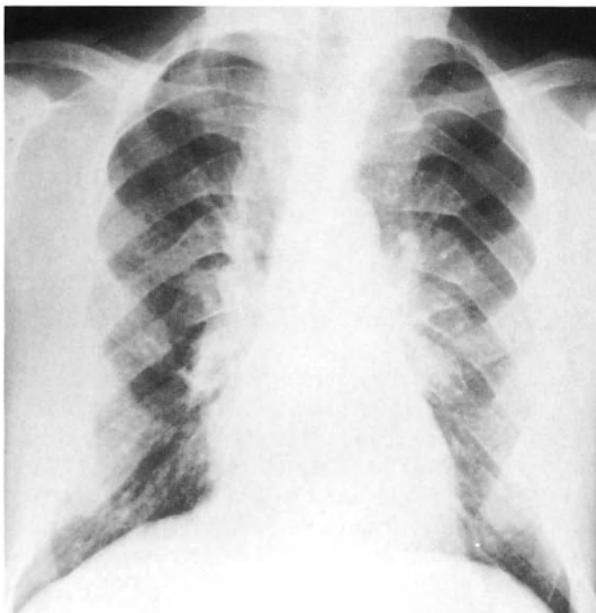


**Fig. 18.11.** Thalassemia. Expansion of the ribs is seen, particularly posteriorly due to marrow hyperplasia.

#### DISEASE INVOLVING WHITE BLOOD CELLS

##### Leukemia

The radiologic changes of leukemia are more commonly encountered in children than in adults, with approximately 50% of affected children demonstrating radiological abnormality, as compared to approximately 10% of adults. This

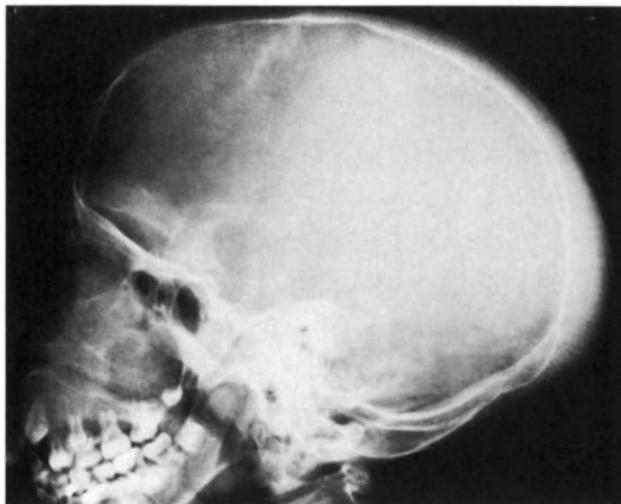


**Fig. 18.13.** Thalassemia. A moderate thickening of the posterior skull vault is seen, with expansion of many of the facial bones, causing obliteration of the frontal and maxillary sinuses. Courtesy CS Resnik, MD.



**Fig. 18.15.** Thalassemia. Abnormal bone is seen in the ribs, spine and iliac wing, with coarsening of the trabecular pattern and hence 'striations' in the vertebral bodies. Oral cholecystogram has been performed, which indicates opacified gall stones, a common finding in hemolytic anemias.

may be due to the increased red marrow areas in children. It must be stressed that whilst the clinical disease usually predates the radiological changes, in some cases (aleukemic leukemia), the converse may be true.

The radiographic changes of leukemia are characteristic and fall into several patterns.

*Metaphyseal translucency* occurs in about 90% of cases, involving the most rapidly growing and most highly

vascularized areas e.g., knees, wrists and ankles, followed by shoulders, hips and vertebra. The band of lucency may initially be narrow, and incomplete, but rapidly progresses across the whole of the metaphysis. This may resolve during remission (Figs 18.16, 18.17, 18.18).

*Metaphyseal erosions* may occur on the medial side of the proximal humerus and tibia, often as an early feature. *Osteolytic lesions* may be seen in up to 50% of cases. They



**Fig. 18.14.** Thalassemia. A marked 'hair on end' appearance of the skull vault is seen.

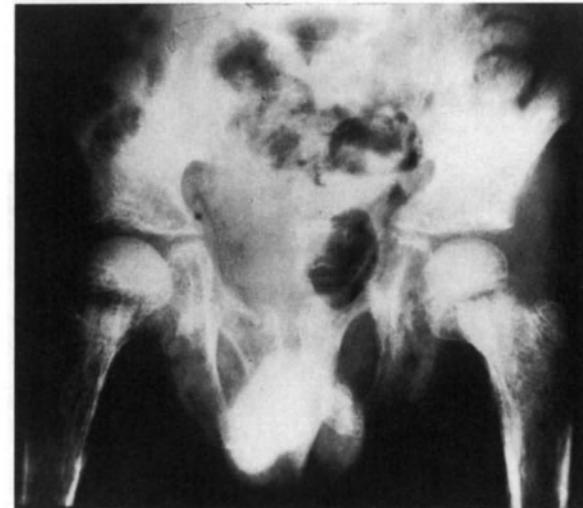


**Fig. 18.16.** Leukemia. Metaphyseal lucency is identified in the femurs bilaterally, more marked on the right.



**Fig. 18.17.** Leukemia. Large metaphyseal lucencies are noted, merging with larger areas of osteolysis.

involve predominantly the long bones, but can be seen in any part of the skeleton (Figs 18.17, 18.19). *Periosteal reaction* may occur, usually in the region of an underlying lesion (Fig. 18.20), and resulting from periosteal elevation by



**Fig. 18.18.** Leukemia. Lucency extends across the whole width of the distal radius.



**Fig. 18.19.** Leukemia. Irregular lucency is seen in the femoral neck, with a pathological fracture.

leukemic tissue. A rare manifestation is the presence of *osteosclerotic lesions* in the metaphysis. Note must be made of the similarity of the leukemic involvement to that of *metastatic neuroblastoma* (Fig. 18.21).

In the adult, the metaphyseal lesions are not usually as characteristic, and the majority of lesions are poorly defined osteolytic foci (Figs 18.19, 18.20), although rarely a generalized osteosclerotic pattern is seen in the involved red marrow area (Fig. 18.22).

An unusual variant, *B-cell leukemia/lymphoma* has recently been shown to demonstrate massive progressive acro-osteolysis (Fig. 18.23).

**Myelofibrosis (Myeloid Metaplasia).** This disease causes replacement of the hematopoietic cells by fibrous tissue resulting in a progressive anemia. The fibrous tissue may eventually be converted into bone with resulting endosteal cortical bone thickening.

*Radiographically*, the early stage of the disease is unremarkable, except for splenomegaly, which may be obvious. Later in the disease, the new endosteal bone will produce osteosclerosis, which may be patchy or generalized, giving rise to a picture of diffuse increased density of the bones (Fig. 18.24). Irregular periosteal reaction may occur, particularly in the ends of the long bones and narrowing of the medullary canal may be obvious.

When generalized sclerosis is present, differentiation should be made from other causes, including *sclerosing*



Fig. 18.20



Fig. 18.21



Fig. 18.22



Fig. 18.23. B-cell leukemia/lymphoma. Gross, rapidly progressive acroosteolysis occurred in this patient.

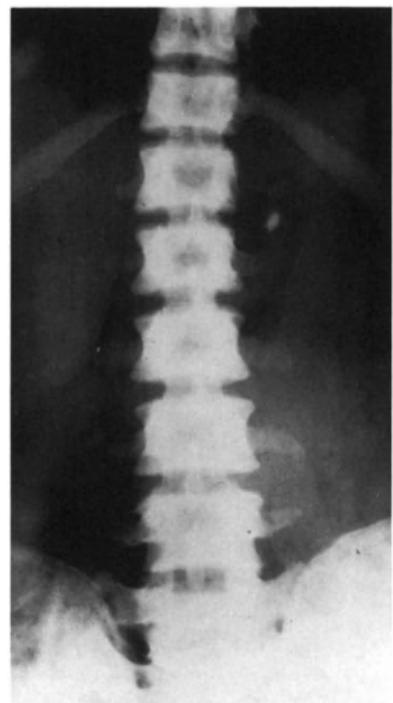


Fig. 18.24. Myelosclerosis. Dense bones are identified throughout the skeleton, but particularly in the spine.



**Fig. 18.25.** (left) Gaucher's disease. Modeling deformity of the distal femur and proximal tibia is seen. There are also areas of irregular sclerosis, suggestive of infarction, with increased metaphyseal lucency.



**Fig. 18.26.** Gaucher's disease. There are areas of lucency in the femur, with sclerosis in the femoral neck and to a mild extent in the distal diaphysis, indicating bone infarction. Subsequent pathological fracture has occurred in the femoral neck.



**Fig. 18.27.** Hemophilia. There is articular irregularity, loss of joint space and widening of the femoral canal. The distal femoral epiphysis may also be mildly enlarged, due to the associated hyperemia.

*metastases* (e.g., from prostate), *fluorosis*, particularly in endemic areas, rarely *myeloma*, and *osteopetrosis* although, in adults, this is usually an incidental finding. *Mastocytosis* may be generalized, but usually demonstrates a patchy distribution.

The *lymphomas* and *plasma cell disorders* produce changes in the skeleton which are discussed in Chap. 16.

#### STORAGE DISORDERS

A number of disorders exist, in which abnormal lipoproteins are stored in the reticuloendothelial system. The commonest of these are Gaucher's disease and Nieman-Pick disease.

**Gaucher's Disease.** A disease predominantly of Jewish females, this has variable severity from a mild chronic form to a rapidly fatal systemic disease. It is caused by a deficiency of  $\beta$ -glucuronidase. The marrow, spleen and liver are packed with histiocytes containing the abnormal lipoprotein kersin.

*Radiographically* this gives rise to localized or widespread radiolucency, and modeling deformities, particularly of the distal femur (Fig. 18.25). Localized destructive osteolytic lesions may also be seen and, in the more chronic forms, there may be a sclerotic reaction. Endosteal thickening may also develop, with appearances of a bone within a bone. If marked, these changes may mimic chronic osteomyelitis.

*Bone infarction* is common, and may be medullary or epiphyseal, involving particularly the femoral and humeral heads (Fig. 18.26).

**Nieman-Pick Disease.** A rare disorder of a type similar to Gaucher's disease, this has a predilection for Jewish female infants. Sphingomyelin is the abnormal lipoprotein found in the foam cells.

The *radiographic* changes in the skeleton are less severe than in Gaucher's disease, usually consisting of loss of bone density, coarsening of the trabecular pattern, and cortical thickening. The lungs, however, are affected with a nodular infiltrate causing a honeycomb appearance.

**Erdheim-Chester Disease.** In this disorder, abnormal cholesterol-laden foam cells are deposited in the bone marrow. There is bony sclerosis, particularly of the ends of the tubular bones of the appendicular skeleton.

**Glycogen Storage Diseases** (see Chap. 17, p. 330)

#### DISORDERS OF COAGULATION

**Hemophilia**, due to factor VIII deficiency, is the most important coagulopathy to cause skeletal abnormality.

The *radiographic* changes depend upon the severity of the disorder and reflect the effects of bleeding into the joints, most commonly the knee (Fig. 18.27), although other joints in



Fig. 18.28. Hemophilia. A moderate arthropathy of the wrist is identified.

the body may be involved (Fig. 18.28). Bleeding will present initially as radiographic evidence of effusion. Repeated episodes, however, cause synovial thickening and marginal erosions. In addition, hyperemia occurs, giving rise to osteoporosis (exacerbated by disuse), and enlargement of the epiphyses, possibly with modeling deformities and early closure of the growth plate. A coarse trabecular pattern may also be seen. Subperiosteal hemorrhage may occur in approximate 1%–2% of cases, giving rise to large osteolytic lesions (*hemophilic pseudo tumor*).

**Christmas disease**, due to factor IX deficiency and **Von Willebrand's disease**, usually give rise to soft tissue hematomas without significant joint involvement, although mild arthritic changes may occur (Fig. 18.29).



Fig. 18.29. Von Willebrand's disease. There is a mild arthropathy of the ankle.

#### REFERENCES AND SUGGESTIONS FOR FURTHER READING

- Ben-Dridi MF, Oumaga A, Gastli H et al. (1987) Radiological abnormalities of the skeleton in sickle cell anemia: study of 222 cases in Tunisia. *Pediatr Radiol* 17: 296–307
- Bohrer SP (1987) Bone changes in the extremities in sickle cell disease. *Semin Roentgen* 22: 176–183
- Colavita N, Orazi C, Danza SM, et al. (1987) Premature epiphyseal fusion and extramedullary hematopoiesis in thalassemia. *Skeletal Radiol* 16: 533–538
- Daly D (1987) 'Hair-on-end' pattern in the skull. *Semin Roentgenol* 22: 144–151
- Gaston MH (1987) Sickle cell disease – an overview. *Semin Roentgenol* 22: 150–158
- Greenfield GB (1986) *Radiology of Bone Diseases*. 4th edn. JB Lippincott, Philadelphia
- Greenfield GB (1970) Bone changes in chronic adult Gaucher's disease. *AJR* 110: 800–812
- Orzincolo C, Castaldi G, Bariani L, et al. (1988) Circumscribed lytic lesions of the thalassemic skull. *Skeletal Radiol* 17: 344–347
- Resnick D, Greenway G, Genant HK, et al. (1982) Erdheim–Chester disease. *Radiology* 142: 289–295
- Resnick D, Niwayana G (1984) *Diagnosis of Bone and Joint Disorders*. 2nd edn. WB Saunders, Philadelphia
- Sutton D (1987) *Textbook of Radiology and Imaging*. 4th edn. Churchill Livingstone, Edinburgh

## CHAPTER 19

# BONE INFECTIONS

D. Nelson

---

An infective process may involve the soft tissues, periosteum, cortex, and/or bone marrow resulting in a soft tissue abscess, infective periostitis, infective osteitis, and osteomyelitis, respectively. The most common spread of infection is by the *hematogenous* route followed by *direct* spread of infection from an adjacent soft tissue lesion. Organisms may be directly implanted into the bone as in a *penetrating injury*, either traumatic or iatrogenic. Post-operative infections, particularly following internal fixation of a fracture, disc surgery, and joint arthroplasty, are still relatively common.

**Pathology.** Initially, the infecting organism will lodge in the metaphysis of a long bone, and produce hyperemia, edema, abscess, and trabecular destruction. The pus, which is under pressure, will then enter the Haversian and Volkmann canals of the cortex, subsequently extending through the cortex and raising the periosteum to produce a subperiosteal abscess. The periosteal new bone formed around the infective foci is called the *involutum*. Cortical bone deprived of its blood supply becomes necrotic. Fragments of dead bone are called *sequestra*. Both pus and sequestra may be extruded through defects, or *cloacae*, in the involutum and extend via sinus tracts to the skin surface. When only purulent material breeches the involutum, soft tissue abscesses are formed.

**Radiographic Findings.** As early as 3 days after infection, soft tissue swelling and obliteration of fat planes may be detected, in contrast to neoplasms which tend to displace fat planes. The first bony findings may be detectable by plain films at 10 to 14 days. These consist of osteoporosis and lytic areas of destruction within the metaphysis (Figs 19.1, 19.2), although lytic areas within the cortical bone and periosteal new bone are frequently seen (Fig. 19.3). Classically the periosteal reaction is a single layer of intact new bone; however, findings such as onion-skinning and Codman's triangle may occur with more aggressive infections (Fig. 19.4). When a

soft tissue abscess forms, a soft tissue mass associated with fat plane obliteration is noted. With delay in diagnosis or treatment, inadequate treatment, or inappropriate antibiotic therapy, subacute and chronic forms of osteomyelitis are produced. Common findings are a prominent involutum, sequestra, and cloacae. Sequestra are identified as foci of increased density since the dead bone remains unchanged while the surrounding bone becomes osteoporotic (Fig. 19.5).

The difference in vascular supply and periosteal attachment results in distinctive clinical and radiologic patterns in long-bone osteomyelitis in *infants* (under 1 year old), *children* (1–16 years old or prior to closure of the growth plate), and *adults* (after closure of the growth plate). The terminal end-loop configuration of the arterial vessels supplying the metaphysis leads to a relative stasis of blood flow allowing infecting organisms to proliferate. In infants, metaphyseal vessels may perforate the physis and enter the epiphysis. The transphyseal vessels noted in infancy are no longer present in childhood and the physis serves as a relative barrier to the spread of metaphyseal infections. In

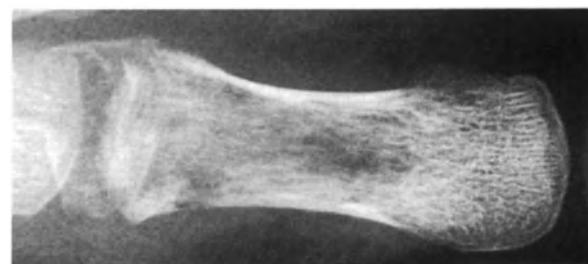
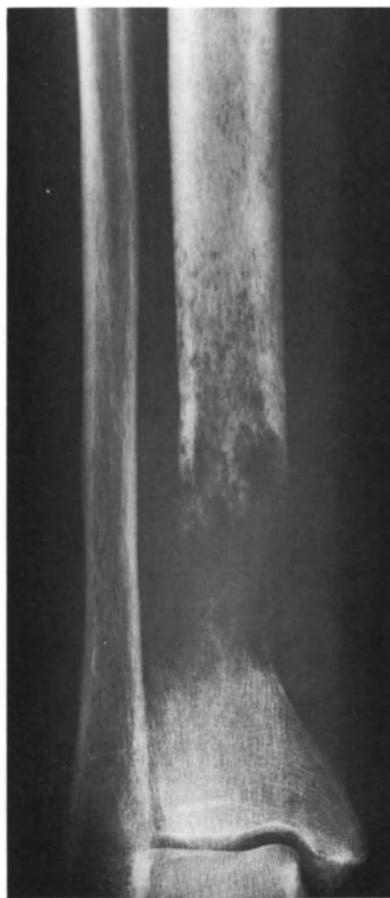


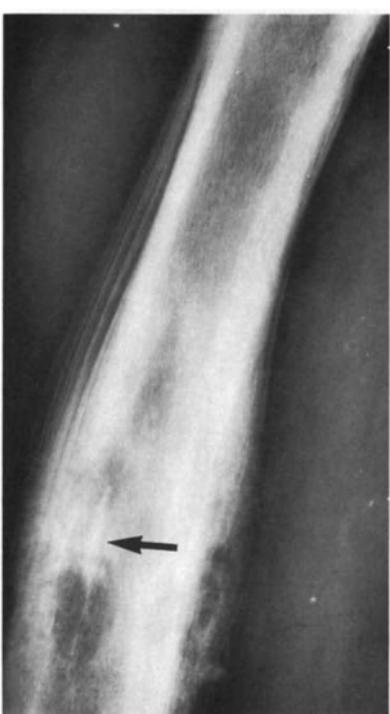
Fig. 19.1. Osteomyelitis of 1st metatarsal. Subtle lytic changes are present in the proximal metaphysis 1 week after clinical symptoms.



**Fig. 19.2.** Osteomyelitis (*S. aureus*). Aggressive, permeative and lytic destruction of the distal tibial diaphysis and metaphysis with a pathologic fracture.



**Fig. 19.3.** Osteomyelitis of fibula. Lytic metaphyseal, diaphyseal, and cortical foci are noted as well as a thick periosteal reaction. Clinically, pain, swelling, and fever were noted for only 3 days.



childhood, the epiphysis is also supplied by terminal end-loop arterial vessels. In infancy and childhood the periosteum is more loosely attached to the cortical bone and has a greater number of perforating vessels than in the adult. As a result, subperiosteal spread of infection is much more common in the infant and child.

**Infants.** Group B hemolytic *Streptococcus* and *Staphylococcus aureus* are the most frequently isolated organisms, often from infected umbilical artery catheters. The infection starts in the metaphysis, but often extends rapidly into the epiphysis (Fig. 19.6A,B). The epiphysis may show a decrease in size or be completely absent ('vanishing epiphysis'). The articular cartilage is frequently intact in these cases. Septic arthritis and multifocal infections are commonly encountered. Involucrum, sequestrum, and soft tissue abscess formation are common (Fig. 19.7).

**Fig. 19.4.** Osteomyelitis of femur. Onion-skin periosteal reaction suggests a tumor. Sequestra formation (arrow) indicates the true diagnosis of chronic osteomyelitis.



**Fig. 19.5.** Chronic osteomyelitis. Multiple, small radiodense sequestra are seen secondary to *Staphylococcus aureus* infection.

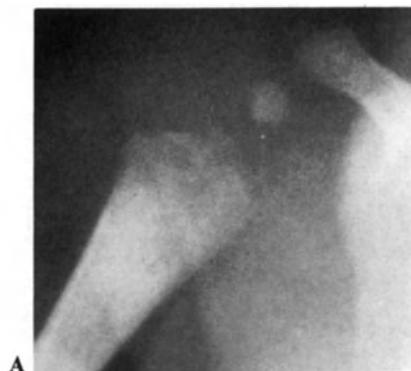


**Fig. 19.6**

**Fig. 19.6A, B. (left)** Acute osteomyelitis (infant). *E. coli* infection of the proximal humeral metaphysis, A. Increased metaphyseal destruction and disruption of the phseal plate occurred over a one week period, B.

**Fig. 19.7. (right)** Chronic osteomyelitis (infant). Prominent involucrum and sequestrum formation has occurred.



**Fig. 19.7**

**Children.** Toxic systemic signs and symptoms are frequently present as well as the local inflammatory changes. *S. aureus* is the usual infecting organism. Radiologic changes are usually found in the metaphysis or in metaphyseal equivalent sites (up to 30%) such as the ischiopubic synchondrosis in the pelvis (Fig. 19.8). Infection cannot easily spread through the growth plate and epiphyseal and joint involvement are uncommon. As in infancy, involucrum, sequestrum, and soft tissue abscess formation are common.

**Adults.** Gram-negative organisms are frequently encountered. *S. aureus* remains a common organism, especially in drug abusers. The clinical course is often insidious leading to a delay in diagnosis and treatment. Chronic forms of osteomyelitis are more common in this group. Infection is usually located in the epiphysis and may extend into the joint (Figs 19.9, 19.10). Due to the firm attachment of the periosteum, involucrum, sequestrum, and soft tissue abscess formation are uncommon in acute infections. Sinus tracts and pathologic fractures occur with chronic osteomyelitis. The frequency of non-long bone (spine, pelvis, and small bones) involvement is greatest in this group.

**Brodie's Abscess.** A well-circumscribed, eccentric lesion with a fading zone of sclerosis in a child is very suggestive of the diagnosis. Although predominantly metaphyseal, up to one third of the lesions are diaphyseal (Fig. 19.11). A sinus

tract may occur through the open growth plate into the epiphysis.

**Sclerosing Osteomyelitis of Garré.** This rare lesion occurs most often in the mandible secondary to *S. aureus* infection. If seen in the long bones, it involves the diaphysis. Marked sclerosis resulting from an intense periosteal new bone response is present. Histologically, however, no purulent exudate or necrosis is identified.

**Non-long Bone Involvement (Excluding Spine).** Non-long bone infections frequently occur secondary to contiguous spread of an adjacent soft tissue infection. Scalp and frontal



**Fig. 19.8.** Ischiopubic synchondrosis osteomyelitis. Predominately lytic changes are noted 3–4 weeks after *S. aureus* osteomyelitis of the knee.



**Fig. 19.9.** Adult osteomyelitis (diabetic). Metaphyseal lysis with extension into the joint space and involvement of the base of the proximal phalanx is seen.



**Fig. 19.10.** Diabetic osteomyelitis. Metaphyseal osteopenia with erosions of the tarso-navicular, and calcaneo-cuboid joints is seen. (Courtesy of Dr JWR Young.)



**Fig. 19.11A, B.** Brodie's abscess. Pain without fever was noted for 7 weeks. A shows an expansile lytic metaphyseal lesion with thick periosteal buttressing. The phyeal plate is not breeched. B shows almost complete healing 5 months after treatment.

**Fig. 19.12.** Osteomyelitis of the cervical spine (*S. aureus*). Endplate erosions, disc space narrowing, soft tissue swelling in the prevertebral space, and a kyphotic deformity are noted from C5 to C7. Films 1 month earlier were normal.

sinus infections are the most frequent causes of osteomyelitis in the skull. Mandibular osteomyelitis usually follows tooth extraction or trauma. Other etiologic factors include puncture wounds, bites, burns, irradiation, and surgical and interventional procedures. Early soft tissue suppuration and periosteal reaction are common.

**Diabetic Foot.** It is frequently difficult to separate the changes of osteomyelitis from those secondary to vascular insufficiency and neurologic deficit. Both will give significant soft tissue swelling and mottled lysis with sclerosis, fragmentation, and periosteal new bone formation. When the cortical margins are ill-defined, osteomyelitis should be suspected (Figs 19.9, 19.10).

**Spine.** Whereas osteomyelitis in children is usually in the appendicular skeleton, adult osteomyelitis is more frequently in the axial skeleton, particularly the spine. *S. aureus* is seen in approximately 80%–90% of patients. The remainder of cases are usually from *Streptococcus* and Gram-negative infections. Hematogenous spread via Batson's paravertebral venous plexus or through the nutrient arteries into the vertebral bodies is most common. Lesions occur with greatest frequency in the lumbar region and least commonly in the cervical spine and sacrum.

**Radiographic Findings.** Early findings (before 3 weeks) include loss of definition of the vertebral body end plate, usually the anterior aspect, and narrowing of the disc space (Fig. 19.12). Lytic foci may be seen in the vertebral body. The vast majority of patients will progress to involvement of the adjacent vertebrae at the affected disc space. Up to 25% of patients will go on to multiple disc level involvement. It is distinctly unusual for only one vertebral body and one disc to be involved. Late findings (up to 10 weeks) include sclerotic changes in the vertebrae and soft tissue extension of the infection (20%), both of which occur more frequently in *tuberculous spondylitis*.

**Discitis.** In children, infection may spread directly to the disc by the hematogenous route. *S. aureus*, the usual organism, is cultured in fewer than half of the patients. Involve-



ment is usually in the lumbar spine, followed by the thoracic and cervical spine. Radiographs demonstrate a marked narrowing of the disc space with minimal, if any, bone involvement. Later, end plate erosions and sclerosis may be seen. With healing, mild to moderate narrowing of the disc space usually persists.

**Osteitis Pubis.** Following pelvic surgery (prostate and bladder) and pregnancy, a symmetric erosive, resorptive, and sclerotic process may develop at the symphysis pubis. Most cases will heal with minimal residual changes. Occasionally, bony ankylosis of the symphysis occurs. Though the etiology is not certain, a low-grade infection, rather than trauma, is considered likely.

### Specific Organisms

**Staphylococcus** is the most commonly found organism after bone and joint surgery, in drug addicts, hemodialysis shunt infections, diabetic foot infections (Figs 19.9, 19.10), penetrating and open wounds, Brodie's abscesses, and in acute osteomyelitis in children.

**Streptococcus.** B-hemolytic *Streptococcus* is most often seen in neonatal and infantile osteomyelitis. The humerus is frequently involved when only one focus of infection is present. The lesions are lytic, occasionally with minimal sclerosis.

**Brucellosis (Undulant Fever).** This Gram-negative bacillus, endemic in the midwest of the United States, is difficult to culture, and therefore to diagnose. The reticuloendothelial system, including the bone marrow, is infected through the milk of farm animals or through contact with infected tissues or secretions.

**Radiographic findings** are a monarticular arthritis with occasional erosions and prepatellar bursitis. Characteristic spine changes are a rapidly developing lytic, destructive lesion of the vertebral body and disc, followed by the development of sclerotic changes, noncalcifying paravertebral abscesses, fusion of vertebral bodies, and rapidly developing anterolateral osteophytes. Involvement of long bones and flat bones shows changes of chronic osteomyelitis.

**Actinomycosis.** This higher bacterium, frequently misclassified as a fungus, produces a granulomatous suppurative infection usually secondary to adjacent soft tissue infection. The right side of the pelvis and spine are involved from ileocecal foci of infection. Hand infections are due to a human bite. Most lesions show a mixed sclerotic and lytic picture. Mandibular and maxillary lesions occurring after tooth extraction or trauma are predominantly lytic, whereas rib lesions are predominantly sclerotic. Rib lesions are also associated with cutaneous sinus tracts and pleuritic changes. Lytic spine lesions with surrounding sclerosis frequently involve the posterior elements, sparing the disc space.

### Fungal Infections

**Coccidioidomycosis.** Inhalation of dust contaminated with the fungus *Coccidioides immitis* leads to bone lesions in 10%–20% of people with disseminated disease. Multiple, symmetric, lytic metaphyseal lesions are found in long bones. Bony prominences, such as the tibial tuberosity, are a distinctive site of involvement. Sclerosis and sequestrum formation are unusual. Marginal rib lesions with large extrapleural masses may occur. Spine involvement frequently spares the



Fig. 19.13. *Cryptococcus* osteomyelitis. A well-defined destructive lesion is seen in the proximal humerus of this young adult. There is no obvious periosteal reaction. (Courtesy of JWR Young MD.)

disc space, occurs at multiple levels, and extends into the adjacent rib without producing a gibbus deformity.

**Cryptococcus (Torulosis).** Bony involvement occurs in 5%–10% of patients with disseminated disease. Bony prominences are commonly affected. Discrete, eccentric, cortical lytic lesions with mild surrounding sclerosis and minimal if any periosteal reaction are seen (Fig. 19.13).

**Mycetoma (Maduromycosis).** This fungus is encountered worldwide, but especially in India. The foot is usually involved by direct inoculation from contaminated soil. Localized bone destruction occurs initially, progressing to a mixed pattern with sclerosis, periosteal new bone, extensive soft tissue swelling and cutaneous sinus tracts (Fig. 19.14).

### Viral Infections

**Rubella.** 40%–45% of infants who were infected with the virus as fetuses in the first 4–5 months of pregnancy will present with symmetric vertically oriented radiolucent areas ('celery stalk' appearance) and increased density in the metaphyses. No periosteal reaction is identified. Most lesions will resolve within several weeks. *Cytomegalic inclusion disease* and *congenital syphilis* are the primary differential considerations.

**Variola (Smallpox).** Up to 5% of affected individuals develop an acute osteomyelitis and septic arthritis. Principal findings are usually a symmetric diaphyseal osteitis, periositis, or destructive epiphyseal lesion. The elbow is most commonly affected. Limb deformities and growth disturbances result from epiphyseal cartilage damage.



A

B

**Fig. 19.14.** Mycetoma (Maduramycosis). A Lysis and sclerosis of the 1st cuneiform bone are seen. A draining cutaneous sinus was also present. B There is a moderately well-defined lytic lesion, expanding and breaking through the cortex of the second metatarsal – surrounding sclerosis is present. (Courtesy of Dr WB Young.)



**Fig. 19.15.** Echinococcus. There are well-defined expansile lesions of the proximal femur, with some surrounding sclerosis. (Courtesy of Dr WB Young FRCR.)

### Miscellaneous Infections

**Echinococcus.** *E. granulosis* is found in the sheep and cattle-raising areas of South America, Africa, central Europe, the Middle East, Australia, and Canada. Humans become infected when they ingest the eggs which are found in dog feces. Expansile, lytic bone lesions of the spine, skull, pelvis, and long bones occur in 1%–2% of cases (Fig. 19.15). Eventually, the cortex is breeched and a soft tissue mass forms, which usually calcifies. Periosteal reaction is uncommon unless an associated fracture or secondary infection supervenes. Half of the cases will have spine involvement, usually sparing the disc. Spinal cord or nerve root compression may result when the posterior elements are involved.

**Ainhum (Dactylosis Spontanea).** The etiology is unclear, although an infectious origin is suspected, in this self-limiting dermatologic condition found most frequently in male black Africans in the 4th and 5th decades of life. A fibrotic band develops over the medial aspect of the 5th, and occasionally 4th toe, leading to a pressure erosion of the underlying bone and distal soft tissue swelling secondary to lymphedema. Angulation of the digit and ultimately autoamputation may result.

### Mycobacterial Infections

**Tuberculosis.** Inhalation of *Mycobacterium tuberculosis* or ingestion of *M. bovis* leads to an infection characterized by caseating granulomas sharply demarcated from the sur-



**Fig. 19.16.** Tuberculosis of the femur (acute). A predominantly lytic metaphyseal lesion with minimal surrounding sclerosis is noted.

rounding tissues. Bone involvement is usually secondary to hematogenous spread from a primary lung infection or from a post-primary site of infection. Pulmonary (50%) and urogenital (20%–45%) infections are frequently present with skeletal disease. Tuberculous infection occurs at a higher rate in patients with underlying disorders, in drug abusers, alcoholics and steroid users, and in the USA and Northern Europe in immigrant populations particularly from Asia.

**Radiographic findings.** 1. *Long bone osteomyelitis.* The initial lesion in a long bone is lytic with minimal or no surrounding sclerosis (Fig. 19.16). Periosteal reaction and sequestra are much less common than in pyogenic infections. The lesion is either epiphyseal or metaphyseal, often with extension through the growth plate. The former lesions are commonly associated with joint involvement. The radiographic findings are similar to fungal osteomyelitis.

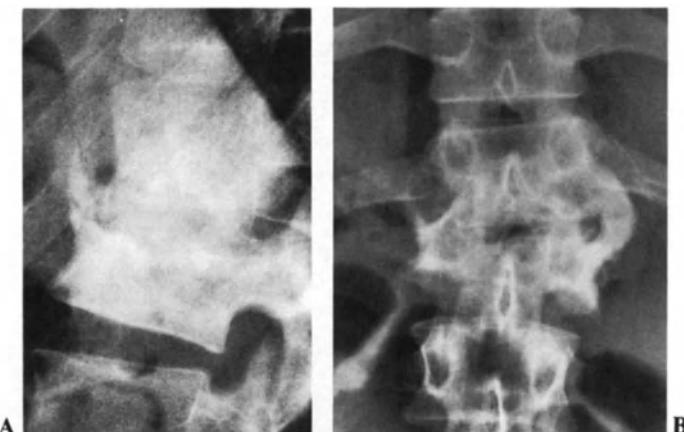


**Fig. 19.17A, B.** Tuberculosis of spine. A Destructive changes are present in the disc space and adjoining vertebral endplates. B The apparent sclerosis is due to an overlying calcified left paraspinal abscess.

2. *Dactylitis.* Painless soft tissue swelling in the digit(s) of a child less than 5 years old is usually associated with expansion of the medullary cavity of the phalanx. Variable degrees of periosteal reaction are noted. Multiple sites of involvement are seen in up to one third of the patients. An expanded, 'cystic' lesion termed *spina ventosa*, is occasionally seen. Most cases will have evidence of pulmonary tuberculosis. In contrast, the diaphyseal expansion associated with *syphilitic dactylitis* is the result of an exuberant periosteal reaction, not medullary expansion.

3. *'Cystic' lesions.* The cystic form of tuberculosis is seen in disseminated disease and may mimic disseminated metastatic disease. The peripheral skeleton is involved in children, whereas, the skull and axial skeleton are involved in adults. Although adult lesions may show marginal sclerosis, childhood lesions are purely lytic.

4. *Spondylitis.* Spine involvement, reported in 25%–60% of patients with skeletal tuberculosis, presents insidiously with back pain, stiffness, and local tenderness. There is a propensity for slow destruction of the disc and anterior aspects of the vertebral bodies (Fig. 19.17). Multiple vertebrae may be affected. Despite the slow process, only minimal sclerosis of vertebral bodies is noted. Paraspinal extension, usually anterolaterally and often calcified, occurs frequently. When the process remains subligamentous, anterior scalloping occurs. An acute kyphosis results from the anterior vertebral destruction (Fig. 19.18). Unusual findings are posterior element involvement, single vertebral involvement, bony ankylosis, and atlanto-axial destruction.

5. *Joint disease.* See discussion in Chap. 21, on joint diseases (p. 391).



**Fig. 19.18.** Tuberculosis of spine (late). Acute kyphosis with minimal sclerosis.

**Leprosy (Hansen's Disease).** *Mycobacterium leprae*, found primarily in Africa, South America, and the Orient, requires an incubation period in the human skin, mucus membranes, and peripheral nerves of 3–6 years. The two major types of the disease are the lepromatous (bone changes in 5%) and the tuberculoid (bone changes in two thirds) types. The *lepromatous* type is a more acute systemic process with lymphadenopathy and cutaneous changes. The *tuberculoid* type is less progressive and involves the nerves. Patients with leprosy have an increased incidence of lymphoma, leukemia, and squamous cell carcinoma of the skin.

The vast majority of bony findings are secondary to neurologic damage. Denervation of the motor nerves leads to bone atrophy with tapering of the bone ends, most commonly affecting the heads of the metatarsals and the proximal phalanges of the feet. In time, the findings are those of a neuropathic joint with tarsal disintegration, fragmentation, lysis and sclerosis. Progressive bone resorption is noted. Repeated trauma and secondary infections are difficult to separate from the leprosy changes. A recent report in which patients were followed for at least 5–10 years concluded that trauma and non-specific infections account for virtually all of the resorative changes observed. Infection is suspected with the following findings: florid periosteal reaction, increase in the bone destruction, and sequestration. A rare, but characteristic, finding is thin, linear soft tissue calcification in the nerve itself.

Only 3%–5% of bone findings are due to direct osseous involvement. Small bones of the hands, feet, and face are usually involved by direct extensions of an overlying soft tissue infection. Nasal destruction is the most common facial lesion. Metaphyses of the hand and feet show osteoporosis, endosteal thinning, lytic areas, and an occasional mild periostitis.

### Spirochete Infections

**Syphilis.** The radiographic manifestations of syphilis occur in the tertiary stage, which affects approximately half of infected patients, usually after a latent period of 10–30 years. Gummas, foci of caseous necrotic material resulting from degeneration of the spirochete, are formed especially in the skin and bones. In congenital syphilis the fetus is infected by transplacental passage of *T. pallidum*. The active areas of enchondral bone formation in the metaphysis are attacked, but most (75%) of affected children will be diagnosed only after 10 years of age. *Hutchinson's teeth*, *interstitial keratosis*, and *nerve deafness* make up Hutchinson's triad which is classically described, but less frequently seen.

**Radiographic findings. Congenital Syphilis.** Early bone lesions are caused by a disturbance of enchondral ossification at birth and by inflammatory granulation tissue after 1–2 months of age. Early syphilitic osteochondritis, or '*metaphysitis*', is manifested by a widening of the growth plate, metaphyseal irregularities and erosions (Fig. 19.19), and epiphyseal separation, particularly of the humerus. Usually, these early lesions will heal within weeks without deformity. Lytic diaphyseal lesions with surrounding sclerosis and overlying periosteal reaction may subsequently develop. Infiltration of the periosteum leads to a widespread, symmetric, exuberant periosteal reaction (Fig. 19.20). The



Fig. 19.19. Congenital syphilis, early. Metaphyseal irregularities and erosions of the distal femur ('metaphysitis') and periosteal new bone are present.



Fig. 19.20. Congenital syphilis. Widespread diaphyseal periosteal reaction, particularly in the tibia, is noted.



**Fig. 19.21.** Congenital syphilis, late. Thickened anterior tibial cortex with bowing ('sabre shin'). Patient is 7 years old.

diaphyseal and periosteal lesions will generally resolve after a few years. Gummas are rare at this stage. Late congenital lesions, occurring at from 5–20 years, resemble the changes of acquired syphilis. Diffuse hyperostosis of the tubular bones, anterior bowing of the tibia ('sabre shin') (Fig. 19.21) or

syphilitic dactylitis with abundant periosteal reaction, and lytic defects (gummas) are seen. Destruction of the nasal bones and mixed lytic/sclerotic calvarial lesions also occur.

**Acquired Syphilis.** *Periostitis*, most frequently seen bilaterally in the tibiae and clavicles, and an *osteitis/osteomyelitis* are the most common findings. The new bone is usually solid, but may be laminated or even perpendicular, suggesting a malignant process. The typical findings of osteomyelitis in a long bone, lysis, sequestration, and periostitis, are also seen. Skull lesions demonstrate a moth-eaten, lytic pattern of the outer table with a periosteal reaction, but without sclerosis (Fig. 19.22A,B). Later lesions, gummas, usually affect the superficial bones and are usually mixed lytic and sclerotic lesions with associated periosteal reaction. Articular changes are infrequent, usually involving the knees when present.

**Yaws.** *T. pertenue* occurs in the tropical regions of Africa, South America, the West Indies, and the South Pacific. Children acquire the infection by direct contact with open lesions. The findings are similar to those found in syphilis, and include lytic areas in the cortex and medullary cavity, often with a florid periosteal reaction (Fig. 19.23), sabre shin, and dactylitis, which may result in shortening and telescoping of the phalanges. Osteitis of the calvarium is a frequent finding, as is nasal bone destruction. The *goundou lesion* is a dense sclerotic mass arising from the maxilla. Facial ulceration with lytic destruction of the underlying bone is known as the *gangosa lesion*.

**Tropical Ulcer.** Found principally in Central and East Africa, the initial lesion ulcerates into the underlying muscles and finally into the bone, usually the mid-shaft of the tibia and occasionally the fibula. Epidermoid cancer of the skin is noted in 25% of affected individuals. The initial finding is a periosteal reaction which may be linear, onion-skin, lacework, or spiculated. Lytic and sclerotic changes and sequestra formation are then followed by the development

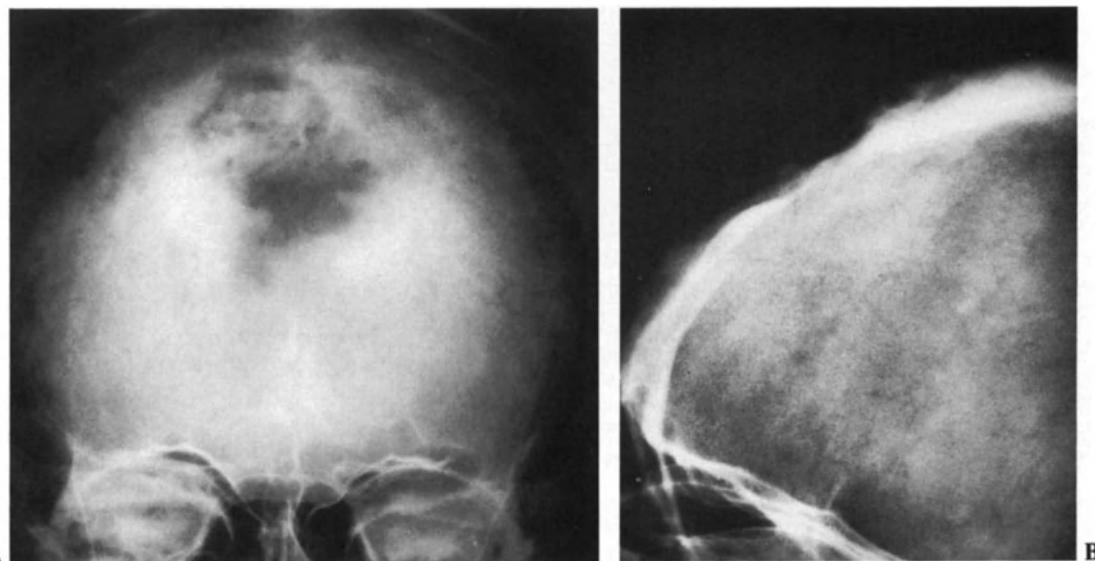


**Fig. 19.22A, B.** Acquired syphilis, skull. AP and lateral views reveal lytic destruction of the outer table of the frontal bones without sclerosis.

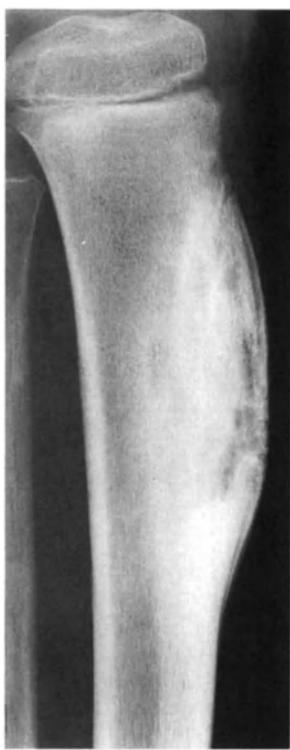


**Fig. 19.23.** Yaws of tibia. Lytic and sclerotic changes in the anterior tibial cortex with marked periosteal reaction are similar to those of syphilis.

of broad-based excrescences resembling osteomas. Elongation and bowing deformities also occur.

**Chronic Symmetric Plasma Cell Osteomyelitis.** This occurs in children between 5 and 10 years of age. An infective organism is difficult to isolate, but histologically the lesions



**Fig. 19.24.** Multifocal osteomyelitis involving both proximal femora. A subtle lytic area is noted in the right capital femoral epiphysis; however, the lateral subluxation of the femur and loss of superior joint cartilage from the pyarthrosis is obvious. On the left, a pathologic fracture through the growth plate has occurred.

demonstrate plasma cells. Pustular lesions are frequently seen in the hands and the feet. The characteristic radiographic finding is marked sclerosis with some areas of lytic change. The lesions are multiple and symmetric, primarily involving the metaphyses of long bones of the leg and the medial end of the clavicle. In the latter location the differential diagnosis would include sternoclavicular hyperostosis.

**Chronic Granulomatous Disease of Childhood** is a frequently fatal (up to 40%) X-linked recessive disorder manifested by infections in the first year of life, usually in males, and is due to the inability of leukocytes to kill phagocytosed bacteria. Purulent skin lesions, suppurative lymphadenitis, and recurrent pneumonias occur. Chronic osteomyelitis is seen in 25%–35% of patients. Due to the low virulence of the infective organism and lack of early clinical findings, patients usually present with extensive bony changes, primarily lytic areas with varying degrees of sclerosis. Sequestrum formation is unusual. The hands and feet are most frequently involved.

#### COMPLICATIONS OF OSTEOMYELITIS

The complications of osteomyelitis differ with the patient's age and the duration of the process.

1. *Premature osteoarthritis* may result if the epiphyseal contour is not restored to normal.
2. *Shortening and angulation* of a tubular bone will be seen if the cartilage of the growth plate is irreversibly damaged.
3. *Pyarthrosis* is commonly seen in infants and adults.
4. *Soft tissue abscesses* frequently complicate osteomyelitis in infants and children.
5. *Pathologic fracture* is occasionally noted in a large lytic area of destruction, most commonly in an adult (Figs 19.24, 19.25).
6. *Chronic osteomyelitis* is usually seen in adults. The diagnosis depends on the identification of sequestra, cloacae, and sinus tracts.
7. *Epidermoid carcinoma* is reported in up to 0.5% of patients with chronic draining infections of 20–30 years duration. Clinical findings are pain, increasing drainage, mass, and enlarged regional lymph nodes. The primary radiographic findings are a progressive area of lytic destruction and a soft tissue mass.

**Imaging. Plain films.** As described above, plain film diagnosis of acute osteomyelitis is usually not difficult, though bone changes are not identified for 10–14 days.

The radiographic diagnosis of osteomyelitis is most difficult when a permeative or moth-eaten pattern of destruction with or without periosteal reaction is present, which may mimic malignancy (Fig. 16.81). Tomography is rarely employed, to facilitate identification of a sequestrum.

CT is most useful in the detection of soft tissue extension of osteomyelitis and in the evaluation of chronic disease when activity is suspected. CT is superior to plain radiography and nuclear medicine scans in the detection of sequestra, cloacae, sinus tracts, foreign bodies, and gas in the soft tissues and bone marrow.



**Fig. 19.25.** Osteomyelitis with pathologic fracture. Fracture is noted in lytic areas typical of acute *S. aureus* osteomyelitis. Infection started as a soft tissue abscess which was inadequately treated.

*Nuclear medicine* bone scanning is most useful in the detection of acute osteomyelitis. When subacute and chronic disease is present, nuclear medicine scans are often equivocal due to their low specificity and poor spatial resolution.

*Technetium-99m-labeled methylene diphosphonate (MDP)* bone scanning is most frequently used and is abnormal within hours to days. Rarely, the initial lesion may appear 'cold' in the first 3 days due to lack of delivery of the radio-

nuclide secondary to vascular thrombosis or compression from the inflammatory infiltrate. *Three-phase scanning* (angiographic, blood pool, and delayed images) will demonstrate increased uptake in all 3 phases in patients with osteomyelitis, whereas cellulitis shows increased uptake in the first two phases, and tumors or fractures are usually 'hot' in only the delayed scans.

*Gallium-67 citrate.* Gallium scans are most helpful in determining the activity of chronic disease when performed in conjunction with technetium-99m MDP scans. When uptake on the gallium scan clearly exceeds that of the bone scan, active infection is nearly always present. When the uptake is equal, infection is usually present in two thirds of cases but is not invariably found. When the uptake is less than the bone scan, active infection is seen in slightly more than 10% of patients.

*Indium-111-labeled leukocytes.* Diagnostic results are best in patients with acute infections and with soft tissue abscesses.

*Magnetic Resonance Imaging (MR).* MR is superior to all other imaging modalities in the detection and localization of soft tissue infections, either primary or extending from an adjacent focus of osteomyelitis, and in the detection of active sites of infection in patients with chronic osteomyelitis or diabetic neuroarthropathy. Both inactive and active areas of infection demonstrate decreased signal intensity on the T<sub>1</sub>-weighted scans (Fig. 19.26A). Due to the increased water content in the tissues secondary to inflammation, hyperemia, and edema, the signal intensity of active lesions will markedly increase, often greater than fat, on the T<sub>2</sub>-weighted scans (Fig. 19.26B). Soft tissue abscesses are usually well demarcated and will usually demonstrate a surrounding zone of decreased signal on T<sub>2</sub>-scans. Cellulitis and edema will show a more diffuse, ill-defined pattern. A Brodie's abscess is suggested when a low signal rim, due to



**Fig. 19.26A, B.** MR of tuberculous spondylitis. A T<sub>1</sub>-images show intermediate signal material in the disc space, adjacent vertebral bodies, and both anterior and posterior to the vertebral bodies. B T<sub>2</sub>-images show all of the areas to markedly increase in signal intensity. Cord compression is noted as well.

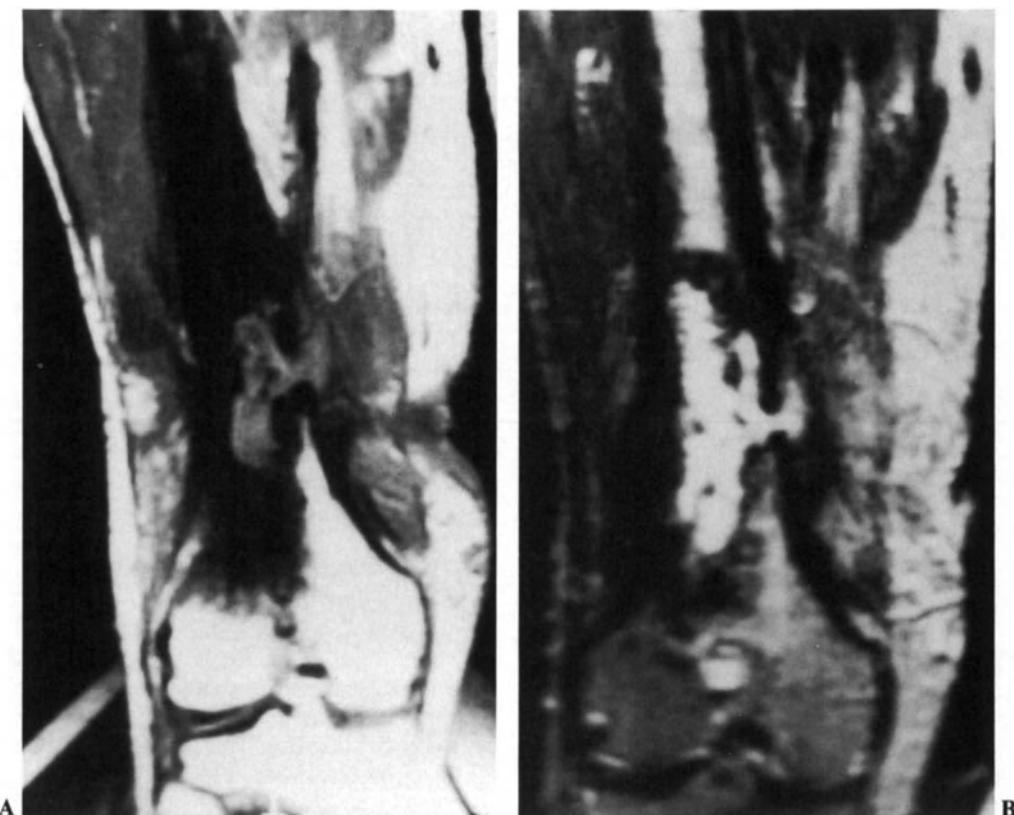


**Fig. 19.27A, B.** MR of chronic osteomyelitis of femur. A and B T<sub>2</sub> scans demonstrate typical findings of chronic osteomyelitis: low signal sequestra are seen. There is a well-defined sinus tract and soft tissue infection adjacent to the bone.

sclerotic bone, is noted around the infected zone on both T<sub>1</sub> and T<sub>2</sub>-scans. Sequestra show low signal on T<sub>1</sub> and T<sub>2</sub>-images if composed of cortical bone. If composed of cancellous bone, then the signal will be higher on both T<sub>1</sub> and T<sub>2</sub>-scans. Sinus tracts are most clearly seen on T<sub>2</sub>-scans as linear areas of high signal extending from the bone marrow into the soft tissues (Fig. 19.27A,B). However, although MR is extremely sensitive, it lacks specificity. Tumors and healing fractures, for example, may give MR findings identical to those found in osteomyelitis. Patients with ferromagnetic material in clips, pins, screws, prostheses, or fixation devices are not ideal candidates for MR because of the artefacts produced.

#### REFERENCES AND SUGGESTIONS FOR FURTHER READING

- Bonakdarpour A, Gaines VD (1983) The radiology of osteomyelitis. *Orthop Clin North Am* 14: 21
- Cremin BJ, Fisher RM (1970) Lesions of congenital syphilis. *J Radiol* 43: 333–341
- Edeiken J (1981) *Roentgen Diagnosis of Diseases of Bone*. 3rd edn. Williams and Wilkins, Baltimore
- Greenfield GB (1986) *Radiology of Bone Disease*. 4th edn. JB Lippincott, Philadelphia
- Holmes B, Quie PG, Windhorst BD, Good RA (1966) Fatal granulomatous disease of childhood: an inborn abnormality of phagocytic function. *Lancet* i: 1225
- MacMoran JW, Brand PW (1987) Bone loss in limbs with decreased or absent sensation: ten year follow-up of the hands in leprosy. *Skeletal Radiol* 16: 452–459
- Nixon GW (1978) Hematogenous osteomyelitis of metaphyseal-equivalent locations. *AJR* 130: 123
- Resnick D, Niwayama G (1988) *Diagnosis of Bone and Joint Disorders*. Second edn. WB Saunders, Philadelphia
- Tang JSH, Gold RH, Bassett LW, Seeger LL (1988) Musculoskeletal infection of the extremities: evaluation with MR imaging. *Radiology* 166: 205–209
- Tumeh SS, Aliabadi P, Weissman BN, McNeil BJ (1987) Disease activity in osteomyelitis: Role of radiography. *Radiology* 165: 781–784
- Tumeh SS, Piran A, Weissman BN, McNeil BJ. (1986) Chronic osteomyelitis: bone and gallium scan patterns associated with active disease. *Radiology* 158: 685–688
- Wing VW, Jeffrey RB Jr, Federle MP, Helms CA, Trafton P (1985) Chronic osteomyelitis examined by CT. *Radiology* 154: 171–174

## CHAPTER 20

# OSTEONECROSSES, OSTEOCHONDROSES, PAGET'S DISEASE AND MISCELLANEOUS DISORDERS

D. Nelson

### OSTEONECROSIS (Ischemic necrosis, avascular necrosis)

Ischemic death of cortical bone and marrow occurs in a progressive fashion from hematopoietic elements (6–12 hours) to bone (12–48 hours) and lastly fat cells (2–5 days). Ischemia usually results from one of the following mechanisms: vascular thrombosis/obstruction, vascular compression, intrinsic vascular damage, traumatic vascular disruption, or idiopathic causes (Table 20.1). Osteonecrosis is unusual in areas of active hematopoiesis except in patients with hemoglobinopathies or trauma.

Table 20.1. Causes of avascular necrosis

Vascular thrombosis/obstruction
hemoglobinopathies (sickle cell disease)
corticosteroid therapy; Cushing's disease; (collagen diseases)
occlusive vascular disease
Caisson disease
fat embolism (alcoholism, pancreatitis, gout)
Vascular compression
corticosteroid therapy; Cushing's disease
Gaucher's disease
pregnancy
Intrinsic vascular damage
irradiation
Traumatic vascular disruption
fracture/dislocation of the femoral head or neck, scaphoid, talus, etc.
Idiopathic
Legg-Perthes disease

*Pathologic-Radiologic Correlation (Femoral Head).* Rapid reconstitution of an adequate blood supply is critical to the process of recovery after an ischemic event. Breakdown products of the ischemic cells incite an inflammatory response

and an active hyperemia which stimulates osteoclastic activity. At this stage plain film findings are negative, although MR may indicate a variety of findings, such as edema of the medullary cavity and frank bone ischemia. Following 2–3 months of hyperemia and resorption of normal bone, a relative increase in density of the ischemic area is noted. In the hyperemic zone fibroblastic cells lay down fibre bone on existing trabeculae leading to a faint sclerotic zone between the dead bone and the area of sclerosis. Initially the subarticular bone is spared, but eventually resorption occurs in the subchondral bone, leading to a subchondral lucency ('crescent' sign) (Fig. 20.1). Articular collapse and flattening may result (Fig. 20.2). If the process continues, cartilage fibrillation and erosion occurs which may result in the formation of loose bodies within the joint and secondary degenerative changes.

**Imaging.** Plain films. The appearance of a linear radiolucent subchondral lesion, patchy sclerotic and lucent areas, articular collapse, and relative preservation of the joint/cartilage space in osteonecrosis are all late findings occurring months after the original ischemic event. A well-established plain film staging system for ischemic necrosis of the **femoral head** exists as follows:

0. High risk; normal clinical and radiographic findings
1. Positive clinical and negative radiographic findings
2. Osteopenia; areas of sclerosis and lysis
3. Subchondral fracture without articular flattening
4. Articular flattening with normal joint space
5. Joint narrowing and acetabular abnormalities

Although CT scanning is better than plain films in the diagnosis of osteonecrosis (Fig. 20.3), both nuclear medicine bone scanning and magnetic resonance (MR) imaging are

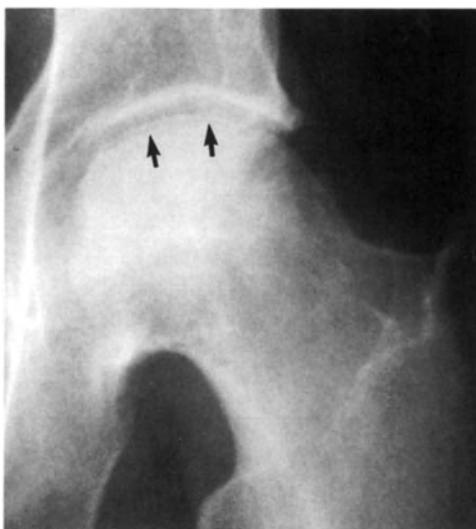


**Fig. 20.1.** Osteonecrosis of the femoral head. A subchondral lucency ('crescent' sign) is present (arrows). No articular flattening is present at this time.



**Fig. 20.2.** Osteonecrosis of the femoral head. Marked flattening, cystic changes, and secondary degenerative changes are seen in the left hip. Cystic areas (geodes) are also noted in both acetabulae. A crescent sign is seen on the right.

superior to CT in the early detection of lesions. However, CT is superior to MR in detecting subchondral and cortical fractures.

**Bone scanning.** Bone scans will be positive within days of the ischemic event (Stage 1 lesions) when plain films are normal. Since the agent requires an intact vascular supply for delivery, it is possible in the first few days to have either a 'cold' lesion or decreased uptake in the ischemic area. Thereafter, Tc-99m labeled MDP scans will demonstrate a marked increase in activity in the affected areas. The major disadvantage to bone scanning is the detection of bilateral disease. Since symmetry is important in interpreting scans, it is easy to miss osteonecrosis in the less severely affected hip.

**Magnetic Resonance Imaging** is presently the most sensitive modality for the early detection of osteonecrosis of the femoral head. Normal marrow will show high signal on both T<sub>1</sub> and T<sub>2</sub>-weighted sequences due to the short T<sub>1</sub> and long T<sub>2</sub> values of fat. Various patterns of abnormality have been described. The majority consist of focal abnormalities, which

may be linear, ring like, wedge shaped, or irregular in outline (Fig. 20.4). These usually demonstrate decreased signal on T<sub>1</sub> images, either with increasing or unchanged signal on T<sub>2</sub> images. Another pattern of diffuse low signal intensity on T<sub>1</sub> with high signal on T<sub>2</sub>, and late changes of low signal intensity on both T<sub>1</sub> and T<sub>2</sub> are also described (Fig. 20.5). Joint effusions are often seen in symptomatic early lesions. However, lack of specificity, particularly of the late pattern; inability to detect mild femoral head flattening; and difficulty diagnosing superior joint space narrowing are other limitations of MR scanning.

#### Causes of Osteonecrosis

**Traumatic disruption of the blood supply.** The most important blood supply to the femoral head is through the superior (lateral) retinacular vessels supplying primarily the anterolateral weight-bearing segment and, less important, the inferior retinacular vessels and the artery of the ligamentum teres. Rupture of the ligamentum teres and compromise of

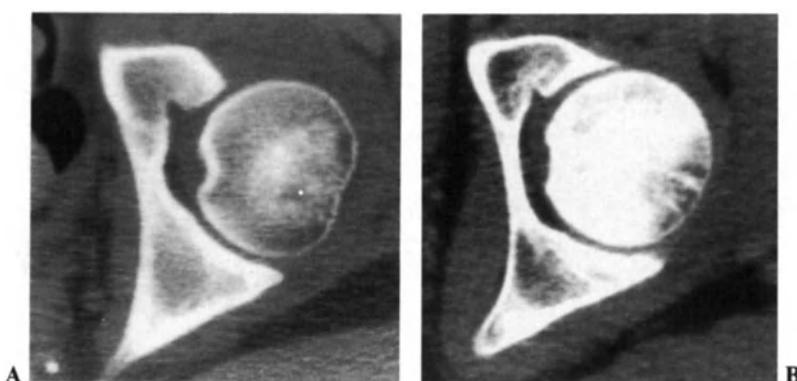


**Fig. 20.3A, B.** CT of osteonecrosis. A A normal femoral head is seen. The 'asterisk' sign, formed by primary compressive and tensile trabeculae, is disrupted in osteonecrosis. B Typically, patchy areas of sclerosis are the first CT manifestation of osteonecrosis.

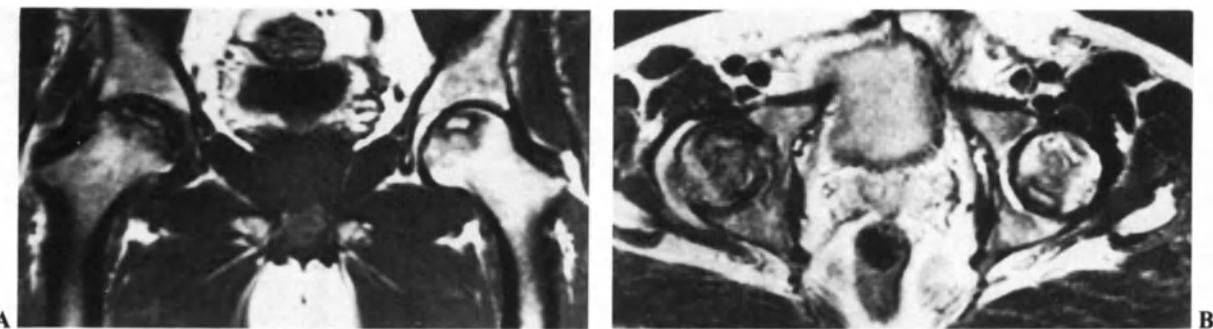


**Fig. 20.4A, B.** MR of osteonecrosis (early and intermediate). **A** T<sub>1</sub> coronal and **B** T<sub>2</sub> axial scans demonstrate bilateral disease (intermediate in the right hip and early in the left hip). Both lesions show the characteristic outer low signal ring. On the right, a joint effusion is low to intermediate signal on the T<sub>1</sub> scan and high signal on the T<sub>2</sub> scan.

the superior retinacular vessels occurs with hip dislocation. Delay in reduction increases the risk of osteonecrosis, found in up to 25% of patients. Intracapsular femoral neck fractures disrupt the retinacular vessels leaving only the artery of the ligamentum teres to supply the femoral head. Without close approximation of the fracture fragments and vascular ingrowth, bony collapse from osteonecrosis will occur, usually 9–12 months after the injury.

**Hemoglobinopathies.** Sickling of erythrocytes in sickle cell anemia leads to a functional obstruction of the vessels in the epiphyses and metadiaphyseal regions of long tubular bones. Infarction will occur if the anoxic state and sickling process are not reversed.

**Steroids.** Fat embolization of vessels and fatty infiltration of the bone marrow with vascular compression are both involved in the osteonecrosis associated with steroid use. Radiographic findings follow the onset of symptoms by 6 months. One third to one half of affected individuals will have more than one joint, usually the femoral head, humeral head, distal femur, and proximal tibia, involved (Fig. 20.6). Other radiographic findings resulting from steroid use or Cushing's disease are stress/insufficiency fractures with abundant callus and vertebral compression fractures with dense end plates, neuropathic-like arthropathy from intra-articular injections, and intra-articular and periarticular

hydroxyapatite calcification which is seen on roughly 50% of patients within 1–2 years after the injection.

The osteonecrosis seen in collagen vascular disease and renal transplant patients is probably due to steroid use.

**Dysbaric disorders** (Caisson disease). Nitrogen, released during rapid decompression, is readily absorbed by fat cells. The resultant increase in volume of the fat cells leads to increased intramedullary pressure and eventually vascular compression. Thrombosis of small vessels from undissolved bubbles of nitrogen gas is also a contributing factor. Low oxygen concentration, uncontrolled decompression, and the depth and number of dives place 10%–20% of such individuals at risk for developing radiographic changes of Caisson disease. Radiographic findings occur 4–12 months after exposure, even in the absence of decompression sickness. Juxta-articular radiodense foci may coalesce to form a 'snow-capped' appearance in the epiphysis. Ultimately, radiolucent subcortical fractures, collapse, fragmentation, and secondary degenerative changes result. Ill-defined radiodense metaphyseal and diaphyseal areas, which are, however, frequently seen in normal individuals, are also reported, as are calcified marrow infarcts.

The osteonecrosis seen in *alcoholism*, *pancreatitis*, and *gout* is probably due to fat emboli as seen in steroid induced ischemic change.

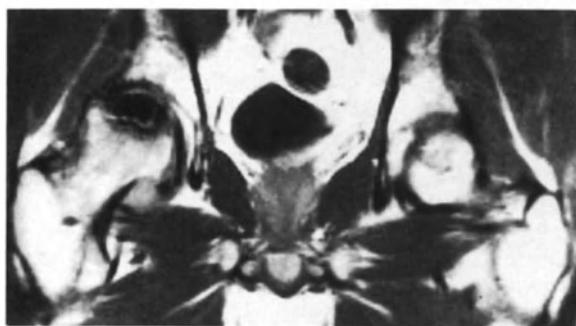


**Fig. 20.5.** MR of osteonecrosis (advanced). Relatively T<sub>1</sub> coronal scan (TR 1000 msec) shows a low signal lesion in the femoral head. There was no change in signal on the T<sub>2</sub> scans.



**Fig. 20.6.** Osteonecrosis of knees from corticosteroids. Typical changes of osteonecrosis, subchondral fracture with articular collapse, are seen in the weight-bearing aspects of the medial femoral condyles bilaterally.



**Fig. 20.7.** Osteochondritis dissecans (knee). AP view demonstrates a well-defined bone fragment separated from the underlying bone by a lucent zone along the non-weight-bearing aspect of the lateral aspect of the medial femoral condyle.

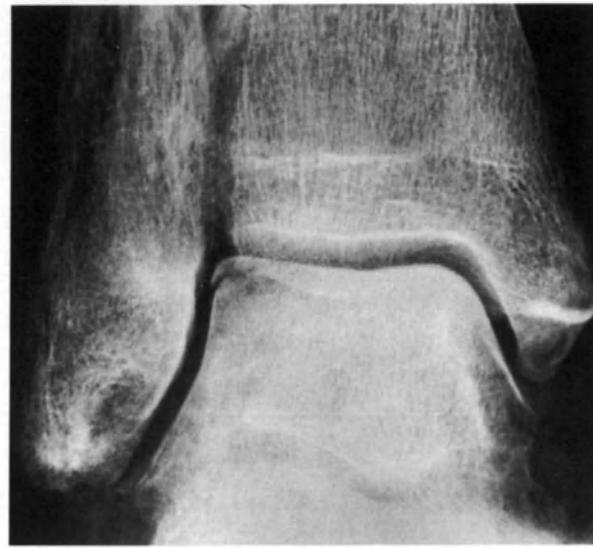


**Fig. 20.8.** Osteochondral fracture of the talus. AP view shows a 'flake' fracture of the lateral talar dome caused by inversion and shearing forces.

**Gaucher's disease.** Packing of the bone marrow with lipid-filled cells results in compression of vessels leading to ischemia and necrosis.

**Irradiation.** The most likely cause of osteonecrosis is direct injury to vessels in the radiation field.

**Pregnancy.** Symptoms develop in the third trimester probably secondary to increased intramedullary pressure from venous engorgement and slowed drainage from the enlarged uterus.

**Idiopathic causes.** In a substantial number of patients no clearly defined etiology is apparent. Four fifths of the patients in this group are males between the 4th and 7th decades. Approximately one third of patients have bilateral hip involvement. The second hip will usually manifest changes of osteonecrosis within 2–3 years.

#### Osteochondritis Dissecans

Chondral (articular cartilage only) and osteochondral (cartilage and subchondral bone) fractures resulting from shearing, tangential and especially rotary forces are most commonly seen in the knees and ankles of adolescents and young adults. Patients may be entirely asymptomatic or present with pain, limitation of motion, clicking, or locking of the joint involved. Berndt and Harty graded osteochondral lesions as follows:

1. Intact overlying cartilage
2. Non-displaceable osteochondral fragment
3. Displaceable, but attached fragment
4. Completely detached fragment, which may be loose within the joint

**Knee.** Approximately half of affected individuals report a history of trauma. Most lesions (85%) are found on the medial femoral condyle, one third being bilateral. The classic

lesion (70%) appears on the non-weight bearing aspect laterally. Larger classic lesions involving the weight-bearing articular cartilage and purely inferocentral lesions make up 15% of cases with the remainder usually found on the lateral femoral condyle. The typical lesion shows a small bony fragment separated from the underlying normal or mildly sclerotic bone by a radiolucent crescentic zone (Fig. 20.7). Slight flattening or irregularity of the articular surface often persists after healing. Occasionally, free fragments which may grow, resorb, or calcify are released into the joint. Patients ultimately may present with premature degenerative changes.

**Talus.** The radiographic findings are more subtle than those in the knee. There may only be slight irregularity of the articular surface, a shallow defect, or a thin 'flake' fracture (Fig. 20.8). Most lesions are found in the middle third of the lateral talar dome (inversion forces) or in the posterior third of the medial talar dome (inversion with plantar flexion and rotation).

**Patella.** Lesions are found in the mid to lower part of the medial facet, approximately 70% of the time.

**Imaging.** The principal factor to assess in grading osteochondral lesions (OCLs) is the status of the cartilage overlying the bony lesion. Lesions with intact cartilage are spared arthroscopy and generally treated conservatively, whereas, lesions demonstrating a breach in the cartilage usually require pinning. Plain films are less sensitive than both *bone scans* and *magnetic resonance (MR)* in the detection and grading of OCLs. MR holds the greatest potential for detecting and grading these lesions because of its ability to visualize directly the articular cartilage. Either a low signal (fibrous tissue in a grade 2 lesion) or high signal (joint fluid in a grade 3 lesion) zone will be detected between the lesion and surrounding normal bone in patients with a breach in the cartilage (Fig. 20.9). The osteochondral lesion will show

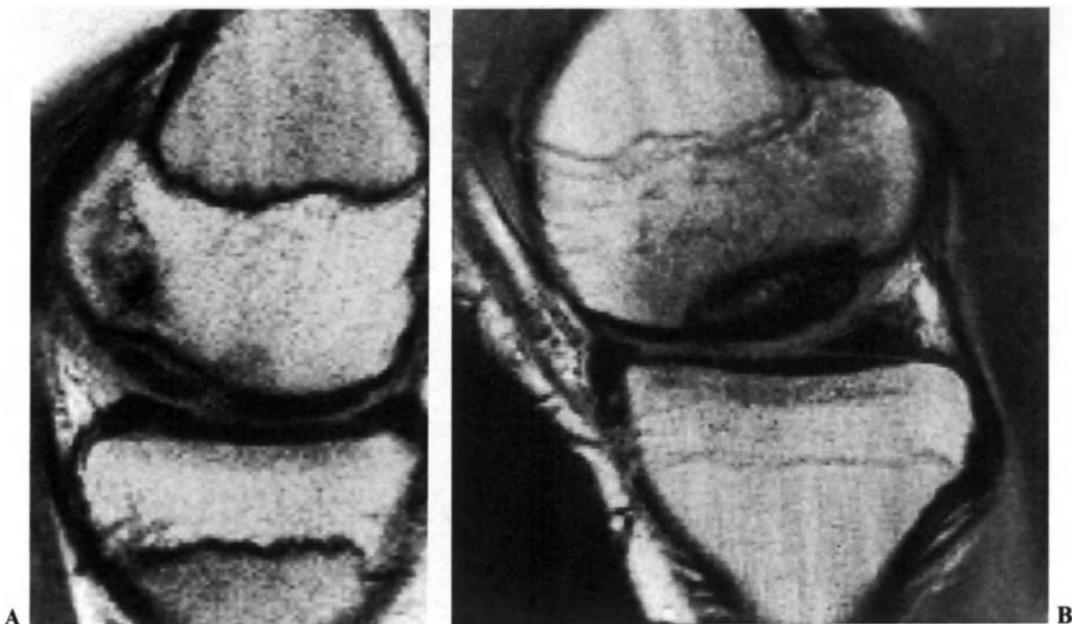


**Fig. 20.9A, B.** MR of osteochondritis dissecans. A Sagittal relatively  $T_1$  scans (TR 1000 msec) show a thin zone of high signal beneath the osteochondral lesion in a displaceable fragment. B A low signal zone posterior to a nondisplaceable fragment. The thicker zone of high signal in B is part of the lesion itself.

decreased signal intensity in the normally high signal marrow on  $T_1$  scans and a variable appearance on the  $T_2$  scans. Loose bodies may appear as high signal (marrow), low signal (calcification), or mixed signal intensity (Fig. 20.10).

*Computed tomography (CT)*, especially CT arthrography, is effective in determining the status of articular cartilage in many cases. The interventional nature of the exam and radiation exposure to the patient are drawbacks, particularly in younger patients.

**Spontaneous Osteonecrosis.** Although the lesions of spontaneous osteonecrosis and osteochondritis dissecans (OD)

occur in the medial femoral condyle of the knee, distinctive findings should allow differentiation of the two conditions. Spontaneous osteonecrosis is characterized by the abrupt onset of pain (variable or lacking in OD), tenderness, and swelling in a middle aged to elderly female (adolescent males in OD). The typical lesion occurs on the weight-bearing surface of the medial femoral condyle (non-weight bearing in OD). Involvement of the lateral femoral condyle and medial tibial plateau is less frequent. Secondary degenerative changes are more common in spontaneous osteonecrosis. Investigators favor either a vascular or traumatic insult as

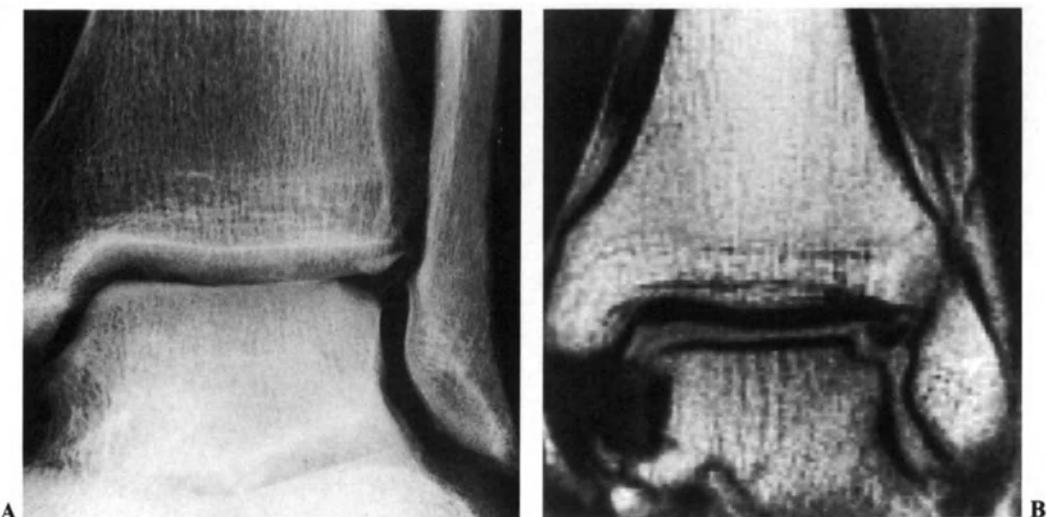


**Fig. 20.10.** A Osteochondral talar fracture with loose body. B On MR the loose body is seen as an area of low signal adjacent to a defect in the lateral talar dome.

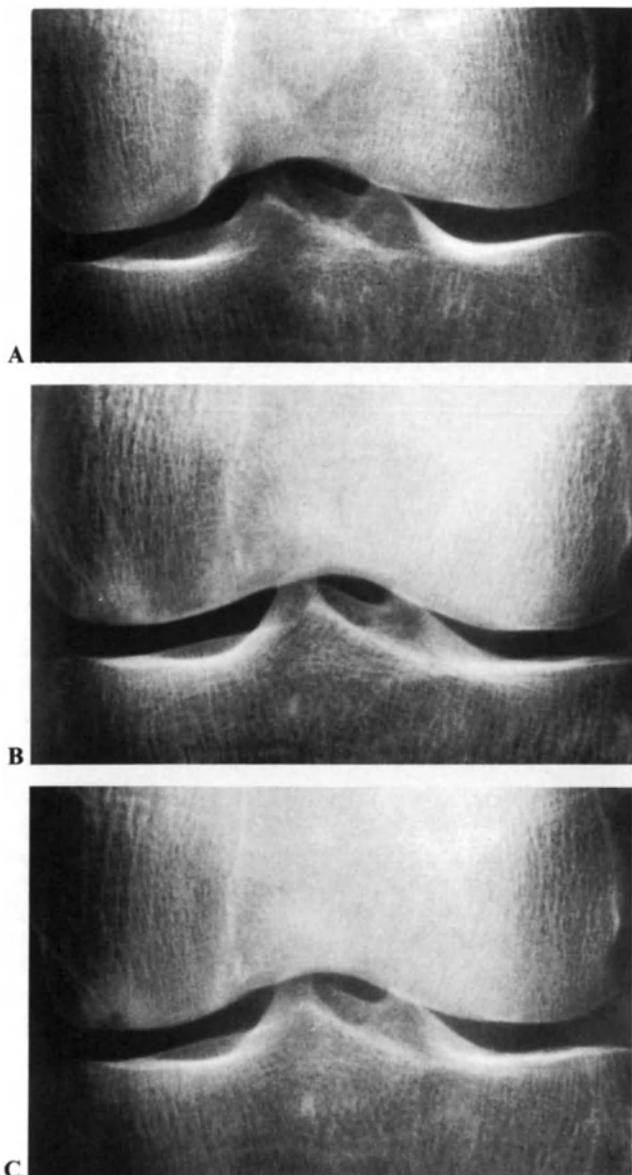


**Fig. 20.11A, B, C.** Spontaneous osteonecrosis of knee. A Initial film at time of acute pain is normal. B One month later a subtle area of sclerosis is seen beneath the weight-bearing aspect of the medial femoral condyle. C One month after B a radiolucent lesion with surrounding sclerosis has developed.

the primary process. The edema or synovial fluid that collects in the subchondral bone leads to increased intramedullary pressure which further decreases the blood supply and accentuates the ischemic process.

**Imaging.** Minimal flattening of the affected bone with an underlying zone of sclerosis is noted several weeks to months after the onset of pain (Fig. 20.11). An ill-defined, and ultimately sharply demarcated, radiolucent lesion develops weeks to months later. At this point the lesion may almost completely resolve or progress on to significant medial compartment degenerative changes with depression, sclerosis and loose bodies. Three-phase *bone scanning* (angiographic, blood pool, and delayed images) is useful for the detection



**Fig. 20.12.** Kienbock's disease (osteonecrosis of carpal lunate). Patient with chronic wrist pain and past history of trauma. Flattening and sclerosis are advanced changes of osteonecrosis of the lunate.

and staging of lesions. Acute lesions show increased activity in all three phases. Subacute and chronic lesions are usually 'hot' only in the delayed scans.

**Magnetic resonance imaging** is at least as sensitive as, and probably more sensitive than bone scanning in the detection of lesions, which demonstrate decreased signal intensity. The margins of the more acute lesion will show increased signal on  $T_2$  scans secondary to edema. MR may detect linear or stellate high signal within the medial meniscus consistent with a tear.

**Kienbock's Disease** (carpal lunate). Pain and swelling in the dominant hand of adults, usually between 20–40 years old, is noted. Most cases report a history of trauma, often repetitive and work related. The fixed position of the lunate and the vulnerable blood supply entering the dorsal and volar aspects of the lunate are felt to be predisposing factors for the fractures and subsequent osteonecrosis. Initially, subtle linear or compression fractures may only be seen on traditional or computed tomography. At this stage, however, the bone scan is likely to show increased activity and the magnetic resonance scan decreased signal in the lunate. Sclerosis, contour abnormalities, decrease in size, collapse, and fragmentation are noted later (Fig. 20.12). Complications often encountered are degenerative changes in the radiocarpal and midcarpal joints as well as scapholunate dissociation.

## OSTEOCHONDROSES

The osteochondroses are a heterogeneous group of conditions which occur primarily in the epiphyses (Legg–Perthes disease), apophyses (Osgood–Schlatter disease), or growth plates (Blount's disease) of the growing skeleton. Boys are affected more frequently than girls. In both sexes trauma plays an important role in most conditions. Histologic findings in some disorders demonstrate osteonecrosis (Legg–Perthes disease, Freiberg's infraction, Kohler's disease), while

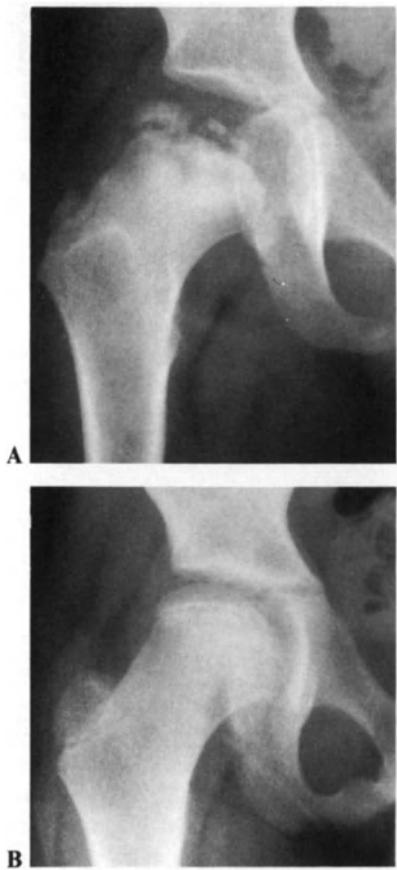


**Fig. 20.13A, B.** Legg–Calvé–Perthes disease (epiphyseal changes). A Fissuring, fragmentation, and flattening are most pronounced in the right capital femoral epiphysis. Lateral displacement of the femoral head, capsular bulging, and a widened and irregular metaphysis are also present. B Healing with only minimal residual flattening is noted several years later.

in other disorders there is no evidence of osteonecrosis (Osgood–Schlatter disease, Blount's disease, Scheuermann's disease, Sinding–Larsen disease). Regardless of the histologic findings, the typical radiographic appearance is that of fragmentation, collapse, and sclerosis followed by a gradual return to ossification of the affected bone.

**Legg–Calvé–Perthes Disease (Capital Femoral Epiphysis).** Most patients are boys and there is a peak incidence from 4 to 8 years of age. Presenting symptoms are limp, limitation of joint motion, and acute or chronic pain in the hip or referred to the inner aspect of the knee. Approximately 10% of cases are bilateral when successive, and not simultaneous, involvement occurs. If both hips are simultaneously affected, then systemic processes such as hypothyroidism and epiphyseal dysplasias should be considered. Recovery in the second hip is usually more complete. Occasionally, changes identical to Legg–Perthes disease occur after a bout of transient synovitis.

The initiating factor for the disorder is not clear. Caffey favored trauma; however, a history of trauma is noted in only 25% of patients. Between the ages of 4 and 8 years, the blood supply to the femoral head is derived almost entirely from the retinacular arteries. In this vulnerable

period perhaps lesser degrees of trauma may result in vascular injury and ischemia. Pathologically, osteonecrosis is the dominant finding. The articular cartilage is preserved or even thickened until the later stages.

**Radiographic Findings. Plain Films.** Besides the hip changes, most patients will demonstrate a generalized retardation in skeletal maturation – up to 3 years. The etiologic factor for this finding is unclear. Hip findings are as follows:

1. The earliest finding is *capsular bulging* on the lateral aspect of the joint, a non-specific finding indicating joint fluid.
2. Half of affected hips show a decrease in size of the capital femoral epiphyseal ossification center, possibly related to the generalized growth retardation present.
3. *Lateral displacement* of the femoral head (Waldenstrom's sign) is seen in 85% of patients. The medial joint space is 2–5 mm wider than the unaffected hip.
4. Fissuring and subchondral fractures, best seen in the anterior aspect of the epiphysis on the frog-leg view, are noted within the ossification center (Fig. 20.13).
5. *Flattening* and *sclerosis*, on the anterolateral superior aspect of the femoral head, subsequently develop. The sclerosis is due to new bone deposition and compression of old trabeculae.
6. *Intraepiphyseal gas*, presumably nitrogen, is an uncommon finding probably produced by the same mechanism as the vacuum phenomenon seen in normal hips on frog-leg views (Fig. 20.14).
7. *Metaphyseal changes* occur usually within 6 months of the epiphyseal findings. 'Cystic' areas, presumably representing areas of uncalcified cartilage resulting from an abnormality in enchondral bone formation, may be seen. Widening, irregularity, and finally premature closure of the growth plate, give rise to metaphyseal (femoral neck) broadening and shortening (*coxa plana*).

**Arthrography.** With the advent of magnetic resonance, arthrography is infrequently performed for the detection of intact cartilage.

**Bone Scanning.** As in other forms of osteonecrosis, bone scan findings are positive with the onset of symptoms and precede the plain film findings. Decreased uptake is seen in the first week, followed by a diffuse or segmental increased uptake in 7–10 days.

**Magnetic Resonance (MR).** Decreased signal intensity is the earliest marrow finding. MR has also demonstrated thickening of the articular cartilage in the earliest stages.

**Prognosis and Course.** In an attempt to predict the long-term prognosis, Catterall developed the following grading system at the time of presentation.

- Group 1 Anterior epiphysis involved; no collapse
- Group 2 Larger anterior segment involved; some collapse
- Group 3 Most of epiphysis involved; greater collapse
- Group 4 Total collapse of entire epiphysis

Many of the patients, usually those affected at a younger age, in Catterall's Groups 1 and 2 and a few in Groups 3

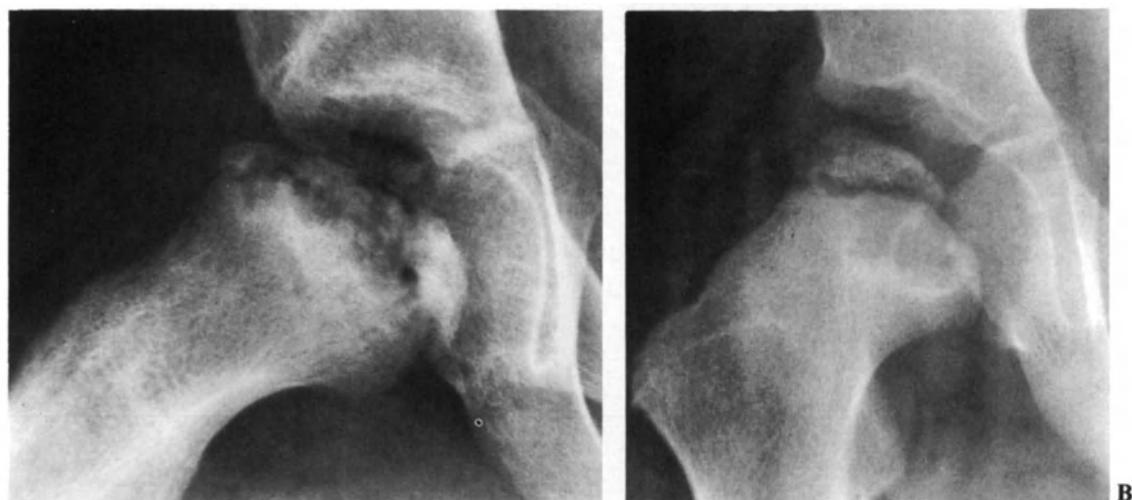


**Fig. 20.14A, B.** Legg–Calvé–Perthes disease (metaphyseal changes). **A** Early metaphyseal changes of irregularity and cystic areas are seen. Incidental note is made of intraepiphyseal gas (arrow) and a vacuum phenomenon (arrowhead). **B** Later, larger cystic areas and metaphyseal widening are present.

and 4 will heal spontaneously, and often these patients will be symptom-free 30–40 years later. However, patients with more advanced disease develop coxa plana of the femoral neck, premature degenerative changes of the hip, and osteochondral loose bodies (2%–4% of cases at least 8–10 years later). Fewer than 5% of patients, usually those with severe displacement of the epiphysis, develop a true osteochondritis dissecans.

**Differential Diagnosis.** Most of the entities to consider are usually or frequently bilateral, although changes secondary to *sickle cell disease*, *Gaucher's disease*, and *steroids* are unilateral in many cases. *Hypothyroidism* and *epiphyseal dysplasias* are bilateral and do not show a progressive fragmentation. Avascular necrosis may occur after congenital hip dislocation; metaphyseal changes are absent in these cases. *Meyer's dysplasia*, usually found in infants, shows delayed maturation, with small epiphyses and normal metaphyses. Finally, in patients with subtle irregularities of the epiphysis, the possibility of a variant of normal should be considered.

**Kohler's Disease (Tarsal Navicular).** Osteochondrosis of the tarsal navicular is a self-limited, reversible disorder occurring most frequently in males between the ages of 3 and 7 years. Patchy sclerosis, fissuring, fragmentation, flattening, and decrease in size of the tarsal navicular occur, which usually return to normal within 2–4 years (Fig. 20.15). Most cases (75%–80%) are unilateral and present with local pain, swelling and tenderness. A history of trauma is reported in one third of the cases. A recent report described a similar entity in adults with no predisposing cause of osteonecrosis. Most were females with bilateral involvement.

**Panner's Disease (Capitellum of the Humerus).** Virtually all cases are in boys from 5 to 10 years old who are involved in sports. The typical changes of osteonecrosis almost always return to normal. True osteochondritis dissecans occurs at an older age when the epiphysis is completely ossified.

**Freiberg's Infraction (Metatarsal Head).** This affects adolescents, predominantly females, and presents with local pain, tenderness, swelling, and limitation of motion in the head of the 2nd metatarsal. Occasionally the 3rd and rarely the 1st metatarsal heads are involved. Most cases are unilateral. Osteonecrosis is noted pathologically. The radiographic sign of flattening may be difficult to distinguish from a normal variant. Eventually, the metatarsophalangeal joint widens (Fig. 20.16), sclerosis and flattening increases, and cortical thickening of the metaphysis develops secondary to a periosteal reaction. Cystic changes in the head may be seen and osteochondral loose bodies may also form. Most patients will show residual flattening following healing. Secondary degenerative changes of the base of the proximal phalanx are relatively common (Fig. 20.16).

**Blount's Disease (Proximal Tibial Epiphysis).** The infantile type, occurring at 1–3 years, is up to eight times more common than the adolescent type which is detected from 8 to 15 years. The infantile type is more frequently bilateral



**Fig. 20.15.** Kohler's disease (osteochondrosis of tarsal navicular). Collapse, sclerosis, and fragmentation in the asymptomatic child are typical.



**Fig. 20.16.** A Freiberg's infraction of 2nd metatarsal head. Articular flattening occurs early. B Later changes in the same patient are residual flattening, degenerative changes on both sides of the metatarsal-phalangeal joint, and loose bodies.

(50%–75%), usually asymptomatic in obese infants, and results in more deformity, and more severe leg shortening. In both types there is no evidence histologically of osteonecrosis or inflammatory change.

Growth arrest, possibly secondary to altered mechanical forces on the medial aspect of the proximal tibial epiphysis is manifested by varus deformity of the proximal tibia, a depressed medial tibial metaphysis, and a spur projecting medially and distally from the proximal tibial metaphysis (Fig. 20.17).

**Osgood-Schlatter Disease (Anterior Tibial Tuberosity).** Traumatic disruption of the inferior patellar ligament attachment on the tibial tuberosity occurs from 11 to 15 years of



**Fig. 20.18.** Osgood-Schlatter disease. Fragmentation of the anterior tubercle with elevation of the fragments, and overlying soft tissue swelling is seen.

age, in males more frequently than in females. Bilateral involvement is reported in up to 25% of the cases. Clinically, local pain, tenderness, and most important, soft tissue swelling are noted over the tibial tuberosity, usually following a history of trauma. Calcification, frequently multiple, is seen in the avulsed cartilaginous fragment, 3–4 weeks later (Fig. 20.18). Usually, the fragments remain separated and even increase in size.

**Sinding-Larsen Disease (Patella).** Tenderness and soft tissue swelling are noted over the lower pole of the patella in active children from 10 to 14 years of age. Injury to the inferior patellar ligament leads to calcification or avulsion of the ligament. Single or multiple bony fragments may be seen. Histologically, the lesions, usually lasting 3–12 months, show no evidence of osteonecrosis or inflammatory change.

**Scheuermann's Disease (Adolescent Kyphosis).** Males and females alike, from 13 to 17 years of age, are affected. Many individuals are asymptomatic, while others show fatigue, poor posture, aching increased with activity, and tenderness in the mid to lower thoracic spine. Kyphosis is present in either the thoracic (75%) or thoracolumbar (20%–25%) spine. A purely lumbar kyphosis is rare. A less severe scoliosis at or below the level of kyphosis is frequently present. At least 3 involved vertebrae and more than 5° of anterior wedging of the vertebral bodies should be present for the diagnosis. Typical findings are undulating end plates of the vertebral bodies, radiolucent lesions with surrounding sclerosis (Schmorl's nodes presumably occurring through weakened areas in the cartilaginous end plates), anterior vertebral wedging, and narrowing of the disc space (Fig. 20.19). Limbus vertebrae are occasionally seen. Infrequently, synostosis of the anterior end plates occurs



**Fig. 20.17.** Blount's disease. Classic findings of angled and depressed medial metaphyses are noted bilaterally.



**Fig. 20.19.** Scheuermann's disease. Marked endplate irregularity of multiple lower thoracic vertebrae, disc space narrowing at multiple levels, and mild anterior wedging of multiple vertebrae are present.

with healing. The result is an increasing kyphosis with advancing age.

**Sever's Disease (Calcaneus).** Most authorities consider sclerosis and fragmentation of the posterior calcaneal epiphysis to be a variant of normal.

**Other Locations.** Osteochondroses and osteonecrosis have also been reported in the *scaphoid*, *medial clavicle*, *phalangeal bases*, *vertebral bodies*, *ischio pubic synchondrosis*, and the *medial sesamoid of the 1st toe* (Fig. 20.20).

#### PAGET'S DISEASE (Osteitis deformans)

*Paget's disease* is a relatively common disease occurring in approximately 3%–4% of people over 40 years, although rare below that age. The disease is most prevalent in high latitude



**Fig. 20.20.** Osteochondritis of the medial sesamoid of the great toe – sclerosis, flattening, and fragmentation are seen in a patient with pain. Pain relief occurred when the sesamoid was removed surgically.

areas, particularly Australia, the United Kingdom, and parts of northern Europe. Most patients are mildly symptomatic or asymptomatic. When symptomatic, clinical findings include local pain and tenderness, bowing of long bones, increased skull size, neurologic changes, and rarely congestive heart failure due to the increase in blood flow in pagetoid bone. No clear etiology is known; however, the evidence to date favors a slow viral infection of the osteoclasts. Pathologically, the disease occurs in three phases. Initially, bone is resorbed secondary to increased osteoclastic activity. Osteoblasts then form abnormal new bone. The primitive woven bone produced is disorganized, contains increased vascularity and connective tissue, and does not contain Haversian systems. These two phases are repeated until the osteoclastic activity subsides. The final, or inactive phase, is reached when there is a cessation of osteoblastic activity. Urinary hydroxyproline is a sensitive indicator of disease activity. Increase in the serum alkaline phosphatase levels results from osteoblastic activity. A sharp rise in the latter parameter may be seen in malignant degeneration.

Paget's disease usually involves more than one bone, although 10%–35% of patients have monostotic disease. The axial skeleton (skull, spine, and pelvis) and proximal femur are the most common sites (75%–80%). Any bone may be involved, but the fibula and bones of the hand and feet are rarely involved.

The three distinct radiographic phases (lytic, mixed, and sclerotic) correspond to the pathological phases. In the *lytic* phase, most commonly recognized in the skull as *osteoporosis circumscripta* (Fig. 20.21) and long bones (Fig. 20.22), a purely lucent defect is noted. As the disease progresses through the *mixed*, to the inactive *sclerotic* phase, new pagetoid bone enlarges the bone predominantly through cor-



**Fig. 20.21.** Paget's disease. Geographic lytic lesions of the frontotemporal and occipital regions are characteristic of 'osteoporosis circumscripta'.



Fig. 20.22

**Fig. 20.22.** (left) There is a lytic, mildly expansile lesion of the proximal femur, with a pointed 'flame shaped' distal margin. Coarsening of the trabeculae of the femoral neck is noted. (Courtesy of JWR Young MD.)



Fig. 20.23

**Fig. 20.23.** (right) A predominantly lytic, mildly expansile process of the distal femur is seen. Coarsening of the bony trabeculae is also seen. (Courtesy of JWR Young MD.)

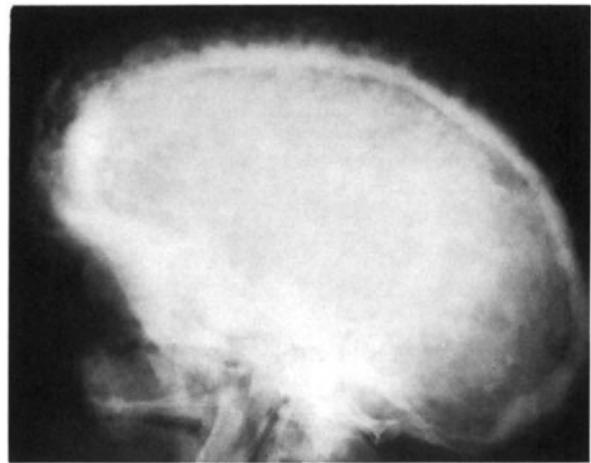


**Fig. 20.25.** Paget's disease of skull. Patchy areas of sclerosis ('cotton wool') are seen throughout the skull. Thickening of the calvarium is noted.

tical apposition. Coarsened and thickened trabeculae are also noted (Figs 20.23, 20.24) and in the skull, a 'cotton wool' appearance may be seen (Fig. 20.25). In the inactive or *sclerotic* phase a diffuse increase in bone density as well as bone enlargement is noted.

The typical findings in the spine are enlargement of the vertebral body in an AP or lateral dimension with cortical thickening (Fig. 20.26). Occasionally, the posterior elements



**Fig. 20.24.** There is expansion of most of the lower pelvis with cortical thickening, coarse trabecula, and sclerosis. (Courtesy of JWR Young MD.)

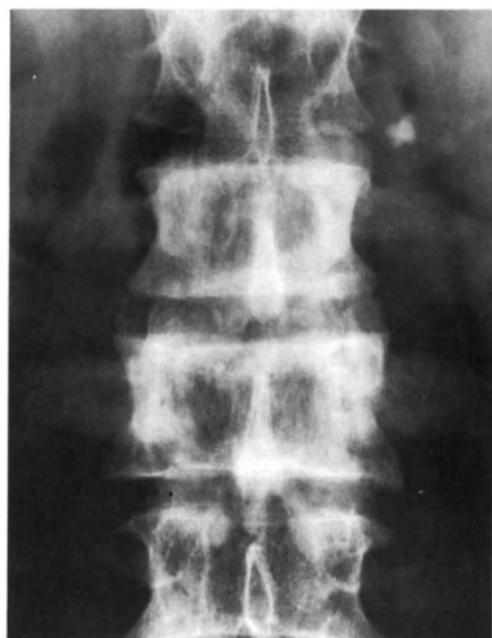


**Fig. 20.26.** Paget's disease (spine). Widening, sclerosis, and trabecular coarsening are present in the vertebral bodies of L2 and L3 and in the transverse processes of L3.

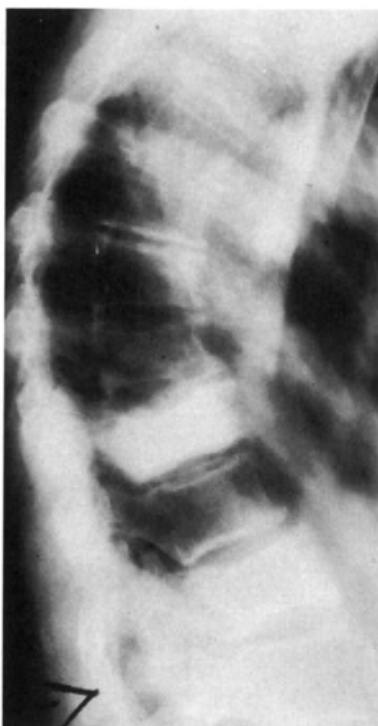


**Fig. 20.27.** Ivory vertebra of Paget's disease. A single dense vertebra is seen with mild expansion. In this case, increasing pain and irregular margins led to biopsy which indicated sarcomatous change. (Courtesy of Dr WB Young FRCR.)



**Fig. 20.28.** Paget's disease. Small, lytic insufficiency fractures are present along the convex margin of the bowed tibia.

are involved. An infrequent finding is the '*picture frame*' vertebral body caused by the lucent spongiosa surrounded by thickened cortex. Very rarely, a completely sclerotic ('ivory') vertebra is seen (Fig. 20.27).

**Pelvis.** The pelvis is commonly involved, generally demonstrating sclerosis, particularly along the iliopubic and ilioischial lines, with coarsening of the trabecular pattern (Fig. 20.24). Patchy areas of lucency and sclerosis may be seen. Protrusio acetabuli is a common late finding.

In the long bones, the initial osteolytic lesion usually starts in the subarticular region of one epiphysis (rarely both) and extends toward the diaphysis, often with a well-demarcated V-shaped zone ('blade of grass') separating the normal and abnormal bone (Fig. 20.22). Rarely, the process will arise at an apophysis, such as the tibial tubercle. With progression of the disease comes coarsening of the trabeculae, enlargement of the bone due primarily to cortical thickening, and bowing and deformity.

Complications of Paget's disease are as follows:

1. **Sarcomatous Degeneration.** Malignant degeneration is reported to be from 1%–5%, the highest incidence occurring in patients with widespread disease. The patients, usually in the 7th or 8th decade, present with increasing pain and swelling. Tumor types in decreasing order of frequency are osteosarcoma, fibrosarcoma, and chondrosarcoma. Rarely,

giant cell tumors will occur in the skull and facial bones (Fig. 20.27).

2. **Fractures.** Insufficiency or stress fractures appear as irregular, linear lucent areas along the convex margin of bowed bones. Progression to complete fracture may occur (Fig. 20.28). Complete pathologic fractures, most frequently seen in the femur, are typically oriented in the transverse plane and have a higher incidence of nonunion (Fig. 20.29).

3. **Osteoarthritis.** Articular changes in the hip and knee are most common. Clinically, the patient will present with joint pain.

4. **Bone Deformity.** Bowing of the long bones, especially the femur and tibia, is the most common manifestation (Fig. 20.28).

5. **Neurologic Findings.** Rarely, spinal cord compression may occur secondary to basilar invagination or vertebral body enlargement. Cranial nerve palsies, from foraminal narrowing, and otosclerosis have been reported.

6. **Crystal Deposition.** Hyperuricemia is present in up to 40% of patients with Paget's disease.

7. **High output cardiac failure** as a result of arteriovenous shunting has been reported but is very rare.

**Differential Diagnoses.** Most difficulty in diagnosis will occur in the mixed phase, when patchy areas of sclerosis are



**Fig. 20.29.** Paget's disease. A healing complete transverse fracture of the proximal femur and marked bowing deformity are present.



A



B

present with minimal or no bone enlargement. *Blastic metastases* from the prostate can usually be excluded by acid phosphatase measurements. When the rare ivory vertebra is encountered, metastasis and lymphoma are considerations. Involvement of the face raises the possibility of *fibrous dysplasia*. Processes causing diffuse sclerosis, such as *myelofibrosis*, *fluorosis*, *renal osteodystrophy*, and the *hemolytic anemias*, are usually easily excludable because of normal bone size. The hemolytic anemias may cause some confusion in the skull where marked diploic widening can be seen.

#### MISCELLANEOUS CONDITIONS

##### Sarcoidosis

Non-caseating granulomas in sarcoidosis involve the osseous structures in 2%–5% of patients. The disease is of unknown etiology, occurs equally in males and females, and is present much more frequently in Blacks (10:1). Most patients with osseous lesions will have pulmonary disease (80%–90%) and skin lesions (over 90%).

The most common findings are demonstrable in the hands and feet:

1. Localized cystic or lytic lesions which usually occur centrally. Eccentric lesions with endosteal scalloping may occur (Fig. 20.30).
2. Diffuse alteration in the trabecular pattern as manifest by either a lacelike or honeycomb appearance of the medullary cavity.

**Fig. 20.30.** A Sarcoidosis. Coarse 'lacelike' pattern of involvement is seen, with 'cystic' areas in the distal metaphyseal region of the affected bones. (Courtesy of JWR Young MD.) B Sarcoidosis. A single moderately well defined lytic lesion is identified in the medial malleolus. (Courtesy of JWR Young MD.)

3. Osteosclerosis of the terminal phalanges and endosteal thickening. If other osseous changes are not present, then this manifestation most likely represents a normal variant.
4. Acro-osteolysis.

**Less common findings.** Long bone lesions appear as well-circumscribed lytic lesions. Lytic areas without associated sclerosis may be seen in the skull and face, but the most common head and neck manifestation is nasal bone destruction (Fig. 20.31). Involvement of the spine usually resembles the findings in tuberculosis.

Periosteal reaction is an unusual finding in the absence of a fracture. Soft tissue calcification, usually periarticular, may occur secondary to the hypercalcemia seen in 20%–40% of patients. Both an acute and chronic polyarthritides may be seen in from 10%–35% of patients. Small and medium joints are involved; however, minimal radiographic findings are noted which usually consist of mild joint space narrowing and an occasional eccentric erosion.

### Radiation Injury

The growing skeleton is much more sensitive to radiation than the mature adult skeleton. The zone of provisional calcification in the epiphysis is the most sensitive area. Chondrocytes are damaged with doses greater than 1200 cGy. Osteoblasts are more resistant, but will be killed at doses higher than 3000 cGy.

Generalized disturbance occurs in bone growth, with the changes being dose-related and usually occurring at least 6 months after exposure. Cartilage degeneration leads to widening of the growth plate and physeal disruption (e.g., *slipped capital femoral epiphysis*). The metaphysis may become irregular and frayed. Long-term changes include iliac wing hypoplasia (Fig. 20.32), acetabular dysplasia, coxa valga and vara, sclerosis, bowing deformities, and scoliosis when asymmetric injury to the spine occurs.

With higher radiation doses, *bone necrosis* results. The usual radiographic pattern in the mandible and long bones is a permeative lytic lesion confined to the radiation field and not associated with a soft tissue mass or periosteal reaction unless a pathologic fracture occurs (Fig. 20.33). Less commonly, slowly progressing, discrete, lytic cortical lesions are found. Presence of a soft tissue mass and changes outside the radiation port indicate tumor recurrence. Osteonecrosis around the shoulder following radiation therapy for breast carcinoma may manifest itself many years after treatment (Fig. 20.34). In the skull, lesions present as a mixed lytic and sclerotic area at the center of the radiation port. In the pelvis, changes include widening, irregularity, and sclerosis of the sacroiliac joints; vertical sacral stress fractures, usually occurring in the post-menopausal group; sclerosis of the symphysis pubis; and *soft tissue calcification* not associated with a mass.

**Benign and malignant bone lesions** may occur secondarily. Benign osteochondromas and exostoses occur within 5 years. Osteosarcoma, fibrosarcoma, and malignant fibrous histiocytoma follow treatment anywhere from 4 to 42 years. A painful soft tissue mass and a new lytic or sclerotic area within a focus or radiation osteitis are the usual findings.



Fig. 20.31. Sarcoidosis. Destruction of the nasal bones has occurred. (Courtesy of JWR Young MD.)



Fig. 20.32. Radiation damage. Marked hypoplasia of the left iliac wing is noted several years after radiation therapy for a Wilms tumor.

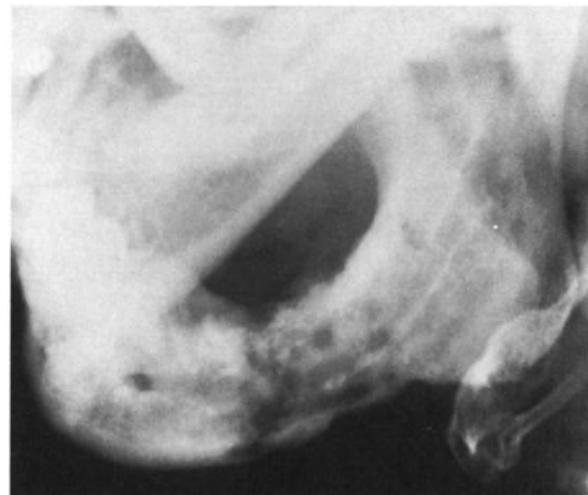


Fig. 20.33. Radiation necrosis of mandible. Irregular areas of lysis in the radiation port occurred 9 months after treatment.



**Fig. 20.34.** Radiation necrosis with pathologic fracture of humerus are seen 12 years after radiation therapy following mastectomy for breast carcinoma.

*Magnetic resonance (MR)* is much more sensitive in detecting the changes of radiation-induced bone marrow atrophy, fibrosis, and tumor formation than plain films or computed tomography. In bone marrow atrophy MR will show an increased signal in the marrow on both T<sub>1</sub> and T<sub>2</sub> sequences (Fig. 20.35). Fibrosis causes decreased signal on both the T<sub>1</sub> and T<sub>2</sub> sequences. Tumor usually shows decreased signal on the T<sub>1</sub> sequence and increased signal on the T<sub>2</sub> scans.

#### Infantile Cortical Hyperostosis (Caffey's Disease)

Caffey's disease is a disease of unknown etiology occurring in infants up to 5 months of age, and found worldwide in



**Fig. 20.36A, B.** Infantile cortical hyperostosis of mandible. A The AP view demonstrates the massive new bone formation. B The lateral view shows the marked hyperostosis of the mandible.



**Fig. 20.35.** Magnetic resonance (MR) of radiation change. MR demonstrates increased signal in the left hemipelvis and femur after radiation therapy for rhabdomyosarcoma. Marrow atrophy with fat replacement accounts for the signal change.

any race and equally in males and females. Patients present with an abrupt onset of fever, hyperirritability, and soft tissue swelling, especially over the mandible. Most cases are self-limited with resolution in several months to 1–2 years, although occasionally the disease will remain intermittently active for years. Although the acute inflammatory changes suggest an infectious origin, no organism has been isolated. Familial cases, probably transmitted as autosomal dominant with variable penetrance, are being recognized with increasing frequency. Sequential involvement of bones is characteristic.

The mandible (80%) (Fig. 20.36), long bones (Fig. 20.37) (diaphyses, especially of the ulna), clavicles, and ribs are most frequently involved. Scapular involvement may be seen in up to 10% of cases. The vertebrae and phalanges are not affected. Extensive periosteal new bone initially develops in



Fig. 20.37



Fig. 20.38

**Fig. 20.37.** (left) Infantile cortical hyperostosis of tibia. Massive periosteal new bone is noted in the left tibia.

**Fig. 20.38.** (right) Lead poisoning. Dense metaphyseal lines are seen.

the areas of soft tissue swelling, ultimately merging with the underlying cortex. The marrow cavity is narrowed at first, but expands as healing progresses. Bowing of the lower extremity, especially the tibia, occasionally occurs. Rarely, bony bridges form between the bones of the forearm, lower leg, or ribs as a late complication.

**Differential Diagnosis.** With diffuse disease hypervitaminosis A should be considered. If only a single bone is involved, then osteomyelitis, trauma, and neoplasms such as Ewing's sarcoma are possibilities.

#### Heavy Metal Poisoning

**Lead Poisoning (Plumbism).** Usually as the result of ingesting lead-based paint, children present with crampy abdominal pain, encephalopathy, peripheral neuritis, and mild anemia. Bone findings are usually evident with lead levels over 70–80 µg/dl, though a recent report suggests that the level may be as low as 40–50 µg/dl. *Radiographically*, dense transverse metaphyseal bands known as 'lead lines', are the hallmark of lead poisoning (Fig. 20.38). The increased density is due to excessive calcium deposition, with only minimal amounts of lead present in the metaphyses. With time, the bands 'migrate' toward the diaphysis, ultimately disappearing after approximately 4 years. The primary differential possibilities are poisoning from other metals, healed rickets, normal physiologic sclerosis, and transverse or stress lines sometimes

referred to as growth arrest lines. Abnormal metaphyseal modeling, similar to that seen in the storage diseases and anemias, is also noted. Widened cranial sutures secondary to increased intracranial pressure occurs. Affected adults usually present with arthritic changes related to absorption of lead into the joint cavity.

**Bismuth Poisoning.** Most cases follow treatment of syphilis. Dense metaphyseal bands similar to those seen in lead poisoning are present in children. Occasionally, the metaphyseal changes resemble syphilitic osteochondritis. Adults demonstrate changes indistinguishable from osteonecrosis.

**Aluminium Toxicity.** Found almost exclusively in patients with chronic renal failure on hemodialysis, aluminium toxicity is due to either the aluminium-containing phosphate binders or contamination of the water in the dialysate. The patients present with significant bone pain and a proximal myopathy. The most important findings are osteopenia and multiple (> 3–5), poorly-healing fractures, especially in the upper ribs, without evidence of subperiosteal erosions to suggest hyperparathyroidism. Children will present with rickets-like changes, including fraying of the metaphyses and physeal widening.

**Fluorosis** occurs in endemic areas such as India, the Persian Gulf and China or when the fluorine content is elevated in the drinking water (> 4 parts per million). Osteosclerosis is the hallmark, occurring primarily in the spine and pelvis. Increased osteoblastic activity results in cortical thickening which encroaches on the medullary space. Ligamentous calcification/ossification occurs especially in the sacrotuberous and iliolumbar ligaments and at ligamentous attachments to the ischial tuberosities and iliac crests (Fig. 20.39). Intraosseous ossification may lead to synostoses in the long bones. Thick periosteal reaction may be seen in the long bones, and in children bone deformities, especially in the lower extremity, may occur.

**Differential Diagnosis.** Ligamentous and musculotendinous calcification and ossification help to differentiate fluorosis from other entities, such as *myelofibrosis*, *hemoglobinopathies*, *osteoblastic metastases*, and *renal osteodystrophy*, which can result in diffuse bone sclerosis.

#### Tuberous Sclerosis

Tuberous sclerosis is one of the phakomatoses and is characterized by the clinical triad of adenoma sebaceum (30%–100%), mental retardation (62%), and seizure disorder (80%–93%). Hamartomatous lesions are seen most frequently in the brain, kidneys, and heart. Pulmonary manifestations are honeycomb interstitial lung disease and pneumothorax. Intracranial calcification of the brain occurs in 50%–80% of cases. Bone findings are unusual in tuberous sclerosis, but include phalangeal cysts, usually in the distal phalanx, phalangeal sclerosis, thick, undulating periosteal reaction and subperiosteal bony nodules ('periosteal warts') primarily in the metacarpals and metatarsals and subungual tumors.

Diffuse or patchy osteosclerosis of the inner table and diploic space of the skull, vertebrae, and pelvis occurs later and is usually asymptomatic.

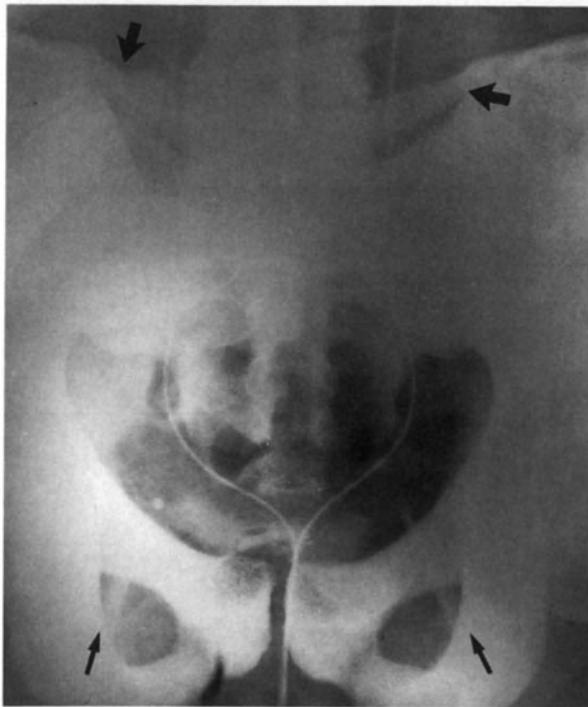


**Fig. 20.39.** Fluorosis. Typical findings of generalized increase in bone density and ligamentous calcification are noted. The iliolumbar and sacrotuberous ligaments are calcified (arrows).



**Fig. 20.40A, B.** Progeria. **A** Acro-osteolysis of the distal phalanges is present. **B** There is coxa valga of both femora in the same patient.

### Progeria

Though infants born with progeria of unknown etiology may appear normal at birth, they will manifest signs of the disease within the first year of life. Clinically, the patients present with dwarfism, alopecia, brown pigmentation of the trunk, atrophic skin with decrease in the subcutaneous fat, receding chin, and a beaked nose. The overall picture looks like premature old age. Acro-osteolysis of the distal phalanges and clavicles is a prominent finding (Fig. 20.40). Additional findings include hypoplastic facial bones and mandible, coxa valga, delayed cranial suture closure, and vascular calcification. Pathologic fractures may be noted due to thinning and constriction of the long bones and ribs.

### REFERENCES AND SUGGESTIONS FOR FURTHER READING

- Beltran J, Herman LJ, Burk JM, Zuelzer WA, Clark RN, Lucas JG, Weiss LD, Yang A (1988) Femoral head avascular necrosis: MR imaging with clinical-pathologic and radionuclide correlation. *Radiology* 166: 215–220
- Blickman JG, Wilkinson RH, Graef JW (1986) The radiologic 'lead band' revisited. *AJR* 146: 245–247
- Caffey J (1968) The early roentgenographic changes in essential coxa plana: their significance and pathogenesis. *AJR* 103: 620–634
- Caterall A (1971) The natural history of Perthes' disease. *J Bone Joint Surg [Br]* 53: 37–53
- Christie DP (1980) The spectrum of radiographic bone changes in children with fluorosis. *Pediatr Radiol* 136: 85–90
- Edeiken J (1981) Roentgen Diagnosis of Diseases of Bone. 3rd edn. Williams and Wilkins, Baltimore
- Genez BM, Wilson MR, Houk RW, Weiland FL, Unger HR Jr., Shields NN, Rugh KS (1988) Early osteonecrosis of the femoral head: detection in high-risk patients with MR imaging. *Radiology* 168: 521–524
- Greenfield GB (1986) Radiology of Bone Disease. 4th edn. JB Lippincott, Philadelphia
- Kriegshauser JS, Swee RG, McCarthy JT, Hauser MF (1987) Aluminium toxicity in patients undergoing dialysis: radiographic findings and prediction of bone biopsy results. *Radiology* 164: 399–403
- Mezgarzadeh M, Sapega AA, Bonakdarpour A, Revesz G, Moyer RA, Maurer AH, Alburger PD (1987) Osteochondritis dissecans: analysis of mechanical stability with radiography, scintigraphy, and MR imaging. *Radiology* 165: 775–780
- Mitchell DG, Rao VM, Dalinka MK, Spritzer CE, Alavi A, Steinberg ME, Fallon M, Kressel HY (1987) Femoral head avascular necrosis: correlation of MR imaging, radiographic staging, radionuclide imaging, and clinical findings. *Radiology* 162: 709–715
- Newberg AH, Tampas JP (1981) Familial infantile cortical hyperostosis: an update. *AJR* 137: 93–96
- Resnick D (1988) Paget disease of bone: current status and a look back to 1943 and earlier. *AJR* 150: 249–256
- Resnick D, Niwayama G (1988) Diagnosis of Bone and Joint Disorders. 2nd edn. WB Saunders, Philadelphia

## CHAPTER 21

# ARTICULAR DISORDERS

C.S. Resnik

Numerous disorders of varied etiology may affect the joints (Table 21.1).

Table 21.1. Classification of articular disorders

Degenerative
osteoarthritis (osteoarthritis)
diffuse idiopathic skeletal hyperostosis (DISH)
erosive (inflammatory) osteoarthritis
Synovial inflammatory
rheumatoid arthritis
psoriatic arthritis
Reiter's syndrome
ankylosing spondylitis
enteropathic arthropathy
juvenile chronic arthritis
Connective tissue
systemic lupus erythematosus (SLE)
progressive systemic sclerosis (scleroderma)
polymyositis and dermatomyositis
Crystal-induced
gouty arthritis
calcium pyrophosphate dihydrate (CPPD)
calcium hydroxyapatite
Neuroarthropathy
Septic arthritis
Miscellaneous
hemophilia
pigmented villonodular synovitis
synovial osteochondromatosis
hemochromatosis
alkaptonuria
Wilson's disease

## DEGENERATIVE DISORDERS

Degenerative disease is often thought of as a process of aging and is probably a mechanical 'wearing down' of articular cartilage and other supportive structures. Inflammation plays a minor role in the development of these changes.

### Osteoarthritis (Osteoarthrosis)

Osteoarthritis, osteoarthrosis and degenerative joint disease are synonymous terms used to describe the most common articular disorder. No joint in the body is immune from the development of osteoarthritis, although weight-bearing joints are most commonly affected. Many general diagnostic features may be present at all sites, while findings at specific articulations are often characteristic.

**General Features.** Characteristic radiographic features of osteoarthritis include localized loss of joint space, bone sclerosis, osteophyte production, and subchondral cyst formation. *Loss of joint space* is accounted for by fibrillation and denudation of articular cartilage, exposing the underlying bone. This occurs at sites of excessive pressure, producing non-uniform narrowing of the joint space. Trabecular compression and deposition of new bone causes *bone sclerosis* in the subchondral region. With *marginal osteophyte formation*, the original subchondral bone plate often remains visible radiographically (Fig. 21.1). *Subchondral cyst (geode) formation* occurs secondary to concentrated pressure on articular cartilage and subchondral bone (Fig. 21.2). This can lead either to intrusion of synovial fluid through the cartilage or insufficiency of the subchondral bone with cystic necrosis.

**Specific Sites.** The *knee* is the most common joint affected by osteoarthritis. Usually, the medial femorotibial compartment and the patellofemoral compartment are involved, although if genu valgum is present, lateral femorotibial compartment involvement may predominate (Fig. 21.2). Osteophyte formation in the knee often includes 'peaking' of the tibial spines. A common complication is the formation of osteocartilaginous debris which may be attached to the synovium or may present as 'loose bodies'.

The predominant pattern of joint space narrowing in the *hip* is superior, with superomedial or superolateral migration of the femoral head (Fig. 21.1). Osteophyte formation may be extensive along the medial surface of the femoral head, and thickening of the cortex (buttressing) along the medial femoral neck is common (Fig. 21.1).



**Fig. 21.1.** Osteoarthritis. There is complete loss of joint space superiorly with large osteophytes projecting from the lateral aspect of the acetabulum and the medial aspect of the femoral head. The original subchondral bone plate remains visible (arrows). There is also thickening of cortex along the medial femoral neck.



**Fig. 21.3.** Osteoarthritis. There is joint space narrowing, bone sclerosis, and ► osteophyte formation of all distal interphalangeal and proximal interphalangeal joints as well as the first carpometacarpal and trapezioscaphoid joints.

Osteoarthritis of the *feet* and *hands* is common in older individuals. Sites of involvement include the metatarsophalangeal joint of the great toe and the distal and proximal interphalangeal joints of the hands (Fig. 21.3). In the *wrist*, changes are usually confined to the carpometacarpal joint of the thumb and the trapezioscaphoid joint unless there is a history of predisposing occupational or accidental

trauma (Fig. 21.3).

Osteoarthritis of the *sacroiliac joints* may produce characteristic sclerosis and osteophyte formation. A similar disorder that occurs primarily in young multiparous females is *osteitis condensans ilii*, which consists of bilateral symmetrical well-defined triangular sclerosis along the inferior articular margin of the ilium (Fig. 21.4). Its etiology is unclear



◀ **Fig. 21.2.** Osteoarthritis. There is loss of joint space medially with osteophyte and subchondral cyst formation.



**Fig. 21.4.** Osteitis condensans ilii. There is well-defined sclerosis involving the ilium bilaterally along the inferior aspect of otherwise normal appearing sacroiliac joints.



**Fig. 21.5.** Degenerative disc disease. Disc space narrowing is most prominent at L4–L5 and L5–S1, with associated vacuum phenomena and osteophyte formation.

although it may be related to unusual mechanical stress. A similar appearance may occur in the symphysis pubis (*osteitis pubis*).

Degenerative disease within the *spine* occurs at numerous sites. The term *osteoarthritis* should be reserved for the synovial apophyseal joints, costovertebral joints, and perhaps the uncovertebral joints (of Luschka) in the cervical spine.

**Degenerative disc disease** can be divided into two major types: intervertebral osteochondrosis involving the nucleus pulposus, and spondylosis deformans involving the annulus



**Fig. 21.8.** DISH. There is ossification at the anterior aspect of the lower cervical disc spaces. Note the prominent ossification of the posterior longitudinal ligament at the C4–C5 level (arrows).

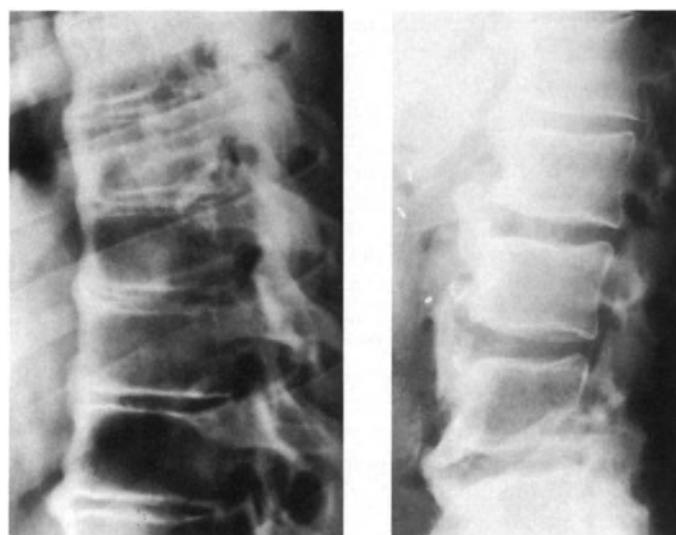


**Fig. 21.6. (left)** DISH. There is flowing ossification along the anterior surface of the entire thoracic spine.

**Fig. 21.7. (right)** DISH. There is coarse ossification bridging the vertebral bodies anteriorly.

*fibrosus*.

In *intervertebral osteochondrosis*, the stress of weight-bearing eventually leads to dehydration of the nucleus pulposus with subsequent loss of disc height (Fig. 21.5). Accumulation of nitrogen gas within discal clefts may be seen (vacuum phenomenon) (Fig. 21.5). Sclerosis of adjacent bony end plates is also common.

*Spondylosis deformans* represents breakdown in the sites of attachment of the annulus fibrosus to the vertebral rim allowing distal displacement, elevation of the anterior longitudinal ligament, and subsequent osteophyte formation at the site of ligamentous attachment to the vertebral body (Fig. 21.5). These two types of degenerative disc disease may arise separately or concurrently.

#### Diffuse Idiopathic Skeletal Hyperostosis (DISH)

Although the etiology of DISH (Forestier's disease, ankylosing hyperostosis) has not been firmly established as a degenerative process, it occurs in the same elderly population and shares many common features with spondylosis deformans. The criteria for diagnosing DISH include the presence of flowing calcification or ossification along the anterolateral aspect of at least four contiguous vertebral bodies (Fig. 21.6), preservation of intervertebral disc height, and absence of apophyseal joint bony ankylosis or evidence of sacroiliac joint inflammatory disease.

Radiographic abnormalities in DISH are most common in the *thoracic spine*. Anterolateral ossification varies considerably in thickness, producing a thin 'pseudospondylitic' pattern (Fig. 21.6) or a much coarser pattern resembling prominent osteophytes, often seen in the lumbar region (Fig. 21.7). Dysphagia may sometimes result from extensive cervical spine involvement. Neurologic symptoms may develop due to exuberant calcification or ossification of the posterior longitudinal ligament which is occasionally present encroaching on the spinal canal (Fig. 21.8).

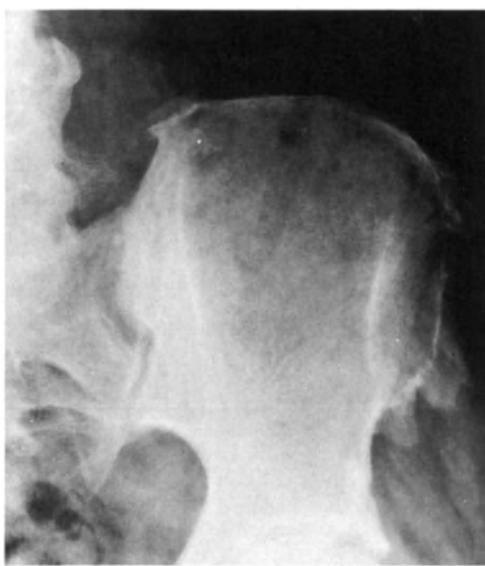


**Fig. 21.9.** DISH. There is osseous proliferation along the superior and lateral aspects of the iliac crest. There is also ossification bridging the inferior aspect of the sacroiliac joint.

Extraspinal manifestations of DISH include osseous proliferation at multiple sites of ligament and tendon attachment to bone (enthesis). These findings predominate in the pelvis, with 'whiskering' occurring along the iliac crests, ischial tuberosities, and trochanters (Fig. 21.9). Similar changes occur at the attachment of the Achilles tendon and plantar aponeurosis to the calcaneus, the quadriceps tendon to the patella, and the triceps tendon to the olecranon. These bony excrescences are generally much more prominent than in



**Fig. 21.10.** Erosive osteoarthritis. In addition to joint space narrowing and osteophyte formation of the distal interphalangeal joints, there is erosion of the central aspect of the articular surface, particularly in the index and long fingers.

simple degenerative disease. Additional features of DISH include actual ossification along the length of a ligament and para-articular osteophyte formation (Fig. 21.9).

#### Erosive (Inflammatory) Osteoarthritis

Erosive or inflammatory osteoarthritis occurs predominantly in middle aged women who present with a clinical picture of acute inflammation (although synovial biopsy does not always yield significantly inflamed tissue) and radiographic findings ranging from mild to marked erosive changes superimposed on the characteristic abnormalities of osteoarthritis (Fig. 21.10). This occurs primarily in the interphalangeal joints of the hands. Less commonly, the carpometacarpal joint of the thumb and the trapezioscapoid joint may be involved, with rare reports of involvement of larger joints. Radiographically, the erosions occur predominantly along the central portion of the articulation, possibly as a result of collapse of subchondral bone rather than synovial inflammation (Fig. 21.10). Intra-articular bony ankylosis may eventually develop.

#### SYNOVIAL INFLAMMATORY DISORDERS

Synovial inflammation and proliferation can lead to destruction of cartilage and erosion of bone. The distribution of these destructive changes often allows differentiation of *rheumatoid arthritis* from the *seronegative spondyloarthropathies* that include psoriatic arthritis, Reiter's syndrome, ankylosing spondylitis, and enteropathic arthropathy.

#### Rheumatoid Arthritis

Rheumatoid arthritis is the most commonly encountered synovial inflammatory disorder. Although abnormalities are generally found symmetrically in the hands, wrists and feet, any synovial articulation may be affected. Less commonly, cartilaginous joints, entheses, and tendons and ligaments show evidence of rheumatoid involvement radiographically.

**General Features.** Congestion and edema of the synovial membrane cause soft tissue swelling that may be the earliest radiographically-evident manifestation of rheumatoid arthritis. Associated hyperemia and disuse may lead to osteoporosis which is often periarticular.

As synovial inflammation progresses, proliferative granulation tissue (pannus) covers the cartilaginous surface leading to cartilage destruction with diffuse loss of joint space. Complete obliteration of the articular cavity may result in fibrous ankylosis; bony ankylosis is rare except in the carpal and tarsal regions. Bone erosion occurs initially along the margins of the involved joints where there is no protective layer of cartilage (Fig. 21.11). Subchondral cysts (geodes) probably represent extension of pannus into bone. More extensive destruction of bone sometimes develops.

Synovial inflammation within the lining of tendon sheaths and bursae can produce lobulated or nodular soft tissue masses, while subcutaneous rheumatoid nodules may be seen particularly over bony prominences (Fig. 21.12). Erosion of subjacent bone may be encountered. Direct involvement of tendons leads to subluxation and malalignment. Synovial cysts may occur represented by abnormal disten-



**Fig. 21.11.** Rheumatoid arthritis. There is cortical erosion along the radial aspect of the second metacarpal head with moderate loss of joint space.



**Fig. 21.12.** Rheumatoid arthritis. There is loss of joint space in all carpal compartments with erosion of the ulnar styloid process. Note also erosion and diastasis of the distal radioulnar joint as well as soft tissue nodularity along the outer aspect of the distal ulna.



**Fig. 21.13.** Rheumatoid arthritis. There is narrowing of the joint space and erosion involving the metacarpophalangeal joints as well as bony ankylosis of all of the intercarpal joints.



**Fig. 21.14.** Rheumatoid arthritis. There are multiple erosions of metatarsal heads.

sion of bursae that communicate with the adjacent articulation.

**Specific Sites.** The most common sites of involvement of rheumatoid arthritis in the hand are at the *metacarpophalangeal* (MCP) and *proximal interphalangeal* (PIP) joints, particularly of the second and third digits. Distal interphalangeal (DIP) joint involvement is much less marked. Early erosions are characteristically found along the radial aspect of the metacarpal heads, with bony destruction often progressing to involve the entire articular surface (Figs 21.11, 21.13). Bony ankylosis in the hand is only rarely encountered. *Boutonnière deformity* (flexion at the PIP joint combined with hyperextension at the DIP joint), *swan-neck deformity* (hyperextension of the PIP joint and flexion of the DIP joint), and *ulnar deviation of the digits* at the MCP joints may occur.

Early radiographic changes in the *wrist* predominate at the distal end of the ulna, although eventually all compartments may be involved (Fig. 21.12). In later stages, osseous fusion may occur between carpal bones (Fig. 21.13). Wrist deformities include dorsal subluxation of the distal ulna and ulnar migration of the proximal carpal row with resultant radial deviation of the carpus. Scapholunate and radioulnar diastasis may occur (Fig. 21.12).

In the *elbow*, soft tissue swelling may be related to a synovial cyst, olecranon bursitis, or a rheumatoid nodule. In the *shoulder*, synovial inflammation of the undersurface of the tendons adjacent to the greater tuberosity may lead to rotator cuff tear or atrophy and subsequent narrowing of the space between the humeral head and acromion. Erosions may be identified at numerous sites including the distal end of the clavicle.

The *foot* is often involved early. Metatarsophalangeal (MTP) joint erosion is common, particularly in the fifth toe (Fig. 21.14). Similar erosions are seen in the interphalangeal (IP) joint of the great toe. Lateral deviation of the digits and other toe deformities are analogous to those in the fingers. Involvement of the calcaneus and midfoot may be encoun-



**Fig. 21.15.** Rheumatoid arthritis. There is symmetric loss of joint space medially and laterally with ill-defined erosions at the margins of the tibial plateau.



**Fig. 21.17.** Rheumatoid arthritis. There is marked erosion of articular surfaces and protrusio acetabuli.

tered, with occasional intra-articular bony ankylosis in the tarsus.

In the *knee*, joint effusion and synovial cyst formation are commonly present. Joint space narrowing is uniformly distributed within the medial and lateral femorotibial compartments and often the patellofemoral compartment as well (Fig. 21.15). In the *hip*, joint space narrowing is almost always concentric with inward migration of the femoral head along the axis of the femoral neck (Fig. 21.16). Long-standing disease can lead to severe hip deformity with femoral head destruction and protrusio acetabuli (Fig. 21.17). Sacroiliac joint involvement is rare.

Rheumatoid involvement is infrequent in the thoracic and lumbar spine, but up to 70% of patients with rheumatoid arthritis will develop abnormalities in the *cervical spine*. A common finding is *atlantoaxial subluxation* with separation of the anterior arch of the atlas from the odontoid process secondary to synovial inflammation and laxity of the transverse ligament. Odontoid erosion commonly accompanies this instability. Subluxation may occur at other levels as well as erosions at discovertebral junctions, in apophyseal joints, and in the uncovertebral joints (of Luschka).

#### Psoriatic Arthritis

Psoriatic arthritis is a distinct articular disorder with synovial inflammation and abnormalities of cartilaginous joints and entheses. Although more common in patients with severe

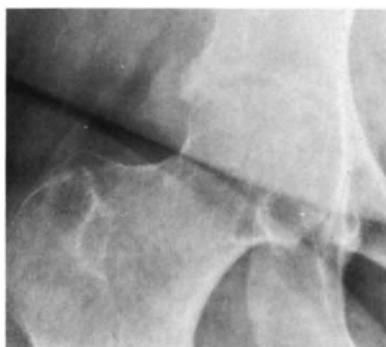


**Fig. 21.16.** Rheumatoid arthritis. There is uniform loss of cartilage with inward migration of the femoral head along the axis of the femoral neck.

cutaneous manifestations of psoriasis, radiographic changes may rarely occur before a clinical diagnosis of psoriasis can be made.

General radiographic abnormalities include soft tissue swelling, joint space narrowing, bone erosion, and bone proliferation. This latter finding is characteristic of the **seronegative spondyloarthropathies** (*psoriatic arthritis*, *Reiter's syndrome*, *ankylosing spondylitis*, *enteropathic arthropathy*) and may be observed in various forms. 'Fluffy' periosteal new bone formation can occur along metaphyses and diaphyses, particularly in the hands and feet (Fig. 21.18). Irregular spiculated excrescences are sometimes evident around psoriatic erosions. Increased radiodensity of an entire phalanx has led to the term '*ivory phalanx*'. Intra-articular bony ankylosis occurs most commonly in the hands and feet (Fig. 21.19). Finally, bony 'whiskering' can be seen at attachment sites of ligaments and tendons but is more ill-defined than that associated with DISH.

The *hands* are the most commonly involved site, usually with symmetric or asymmetric changes in distal and proximal interphalangeal joints, although metacarpophalangeal joint changes may be encountered (Figs 21.18, 21.19). Soft tissue swelling may be localized or diffuse, with 'sausage' digits being characteristic. Erosions begin at the margins of joints with eventual extension to the central portion, sometimes leading to protrusion of one eroded articular surface into an adjacent concave eroded surface (*pencil-in-cup* appearance). Resorption of distal bony tufts is occasionally seen.

In the *wrist*, psoriasis resembles rheumatoid arthritis with any or all compartments being involved (Fig. 21.19). Psoriatic changes in the remainder of the upper extremity as well as in the hip, knee, and ankle are relatively uncommon. In the *foot*, findings may be similar to those in the hands with interphalangeal and metatarsophalangeal erosion and bone proliferation. The interphalangeal joint of the great toe is a characteristic site of psoriatic involvement (Fig. 21.20). The '*pencil-in-cup*' appearance (Fig. 21.20), or an *ivory phalanx* may be seen. Ill-defined erosions of the calcaneus may occur posteriorly at the attachment of the Achilles tendon or inferiorly at the attachment of the plantar aponeurosis and again may be associated with bone proliferation.



**Fig. 21.18.** Psoriatic arthritis. Narrowing of the joint space is most prominent at the metacarpophalangeal joints with erosion most evident at the interphalangeal joint of the thumb. Note fluffy bone proliferation at multiple sites along the proximal phalanges.

The *sacroiliac joints* are frequently involved. Although usually symmetric, asymmetric or unilateral abnormalities may be encountered. Erosion of subchondral bone along the inferior aspect of the joint occurs with adjacent sclerosis.



**Fig. 21.19.** Psoriatic arthritis. There is extensive erosion of articular surfaces at distal and proximal interphalangeal joints with two sites of bony ankylosis. There are also erosions of the first through third metacarpal heads and multiple sites within the wrist.



**Fig. 21.20.** Psoriatic arthritis. There are erosions at the interphalangeal joint of the great toe as well as the second through fifth metatarsophalangeal joints. Note the 'pencil-in-cup' appearance of the fifth metatarsophalangeal joint.

More extensive changes may develop, although complete bony ankylosis is unusual.

In the *spine*, paravertebral ossification may occur, predominantly in the lower thoracic and upper lumbar regions. This ossification is usually coarse, with asymmetric bony excrescences that may vertically bridge non-marginal aspects of the vertebral bodies. In the cervical spine, changes similar to those seen in rheumatoid arthritis may be encountered.

#### Reiter's Syndrome

Reiter's syndrome is an inflammatory disorder encountered most commonly in young men and is characterized by urethritis, conjunctivitis, and arthritis. The clinical manifestations of this triad are often incomplete, making recognition of radiographic changes valuable for correct diagnosis. Typically, the *lower extremity* is most commonly affected, although hip involvement is unusual. Axial skeletal changes are also common.

As in psoriatic arthritis, radiographic findings include soft tissue swelling, joint space loss, bone erosion and bone proliferation. As discussed previously, the latter is characteristic of all of the seronegative spondyloarthropathies. Differentiation of Reiter's syndrome from psoriatic arthritis and ankylosing spondylitis is aided by observation of *asymmetric* involvement of various sites in the lower extremity. Intra-articular bony ankylosis other than in the sacroiliac joints is much less common in Reiter's syndrome. Also, unlike psoriatic arthritis, progressive and severe destruction of interphalangeal joints is unusual.

Involvement of the *great toe* is commonly encountered, although any interphalangeal or metatarsophalangeal joint may be affected. Marginal erosions often show adjacent bone proliferation (Fig. 21.21). Fluffy new bone formation may also be seen along phalanges, metatarsals, tarsal bones, and the lateral and medial malleoli at the ankle. The *calcaneus* is a characteristic site of involvement in Reiter's syndrome. Retrocalcaneal bursitis leads to soft tissue swelling that

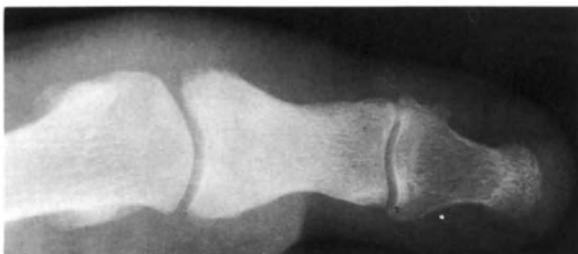


**Fig. 21.21.** Reiter's syndrome. There is erosion and bony proliferation medially at the proximal phalanx.

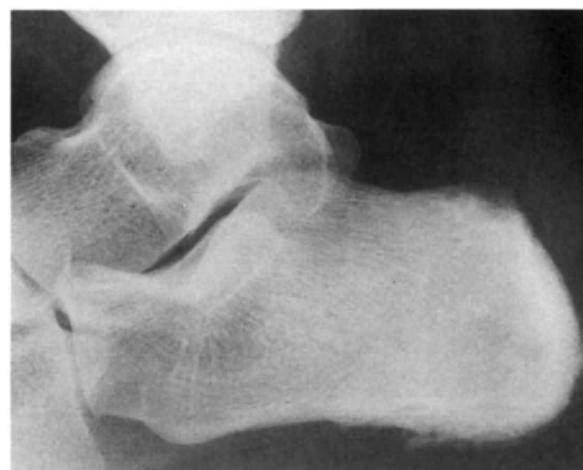


**Fig. 21.22.** Reiter's syndrome. There is swelling of soft tissue extending to the retrocalcaneal bursa, along with bony proliferation at the posterior and plantar aspects of the calcaneus.

obliterates the fat normally visualized between the top of the calcaneus and the Achilles tendon on the lateral radiography (Fig. 21.22). Ill-defined erosion of the underlying calcaneus may be seen; similar erosion as well as spur formation may be evident along the plantar surface of the calcaneus at the attachment of the plantar aponeurosis (Fig. 21.22).

**Sacroiliac joint** involvement in Reiter's syndrome is virtually identical to that in psoriatic arthritis. Most patients show bilateral and symmetric abnormalities, although asymmetric or unilateral changes may be encountered (Fig. 21.23). In the **spine**, thoracolumbar paravertebral ossification is also indistinguishable from psoriatic arthritis (Fig. 21.24). However, cervical spine involvement is infrequent in Reiter's syndrome.

### Ankylosing Spondylitis

Ankylosing spondylitis is a chronic inflammatory disorder that affects primarily the axial skeleton, most commonly in young men. Classically, radiographic abnormalities are noted at the *sacroiliac joints* followed by involvement of the thoracolumbar junction, the lumbosacral junction, the lumbar spine, the thoracic spine, and the cervical spine. This ascending pattern is characteristic although not invariable, as isolated involvement in one area or other combinations of involvement may be encountered. The combination of sacroiliac joint and cervical spine abnormalities has been reported to occur more frequently in women. Articular involvement outside the axial skeleton is often evident, particularly in the *hip* and *shoulder*.

General radiographic features include erosion, sclerosis, and osseous proliferation or bridging involving synovial articulations (sacroiliac joints), cartilaginous articulations (discovertebral junctions), and entheses (ligamentous attachments). Bony proliferation is a characteristic feature of appendicular skeletal involvement, although ankylosing spondylitis does not affect small peripheral joints as frequently as psoriatic arthritis or Reiter's syndrome.

Unlike Reiter's syndrome and psoriasis, involvement of sacroiliac joints is almost invariably bilateral and symmetric, although occasionally asymmetric involvement may appear in the early stages of the disease. Early radiographic evidence of sacroiliac joint involvement includes loss of definition of

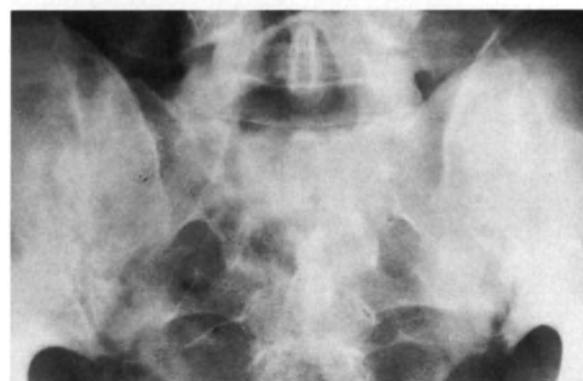


**Fig. 21.23.** Reiter's syndrome. There is ill-defined erosion of the left sacroiliac joint with sclerosis of the adjacent ilium and sacrum. There is only minimal erosion of the inferior aspect of the right sacroiliac joint.



**Fig. 21.24.** Reiter's syndrome. There is coarse paravertebral ossification, bridging vertebral bodies asymmetrically in the lower thoracic and upper lumbar regions.

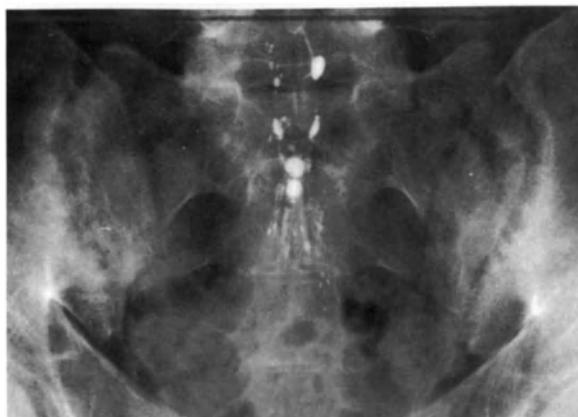


**Fig. 21.25.** Ankylosing spondylitis. There is symmetric erosion of both sacroiliac joints with sclerosis along with the iliac side bilaterally.

subchondral bone, superficial erosion, and ill-defined sclerosis at the synovial portion (lower one half to two thirds) of the articulation, particularly along the iliac side (Fig. 21.25). Progressive bony bridging may be observed both at the synovial portion of the joint and at the more superior ligamentous portion.

Early spinal changes include osteitis at the anterosuperior and anteroinferior corners of lumbar vertebral bodies, producing erosions that create '*squaring*' of these bodies (Fig. 21.26). Reactive sclerosis gives an appearance of '*shiny corners*' (Fig. 21.26). Syndesmophyte formation represents thin, vertically oriented ossification of the annulus fibrosus that bridges the corners of adjacent vertebral bodies (Fig. 21.27). This, along with ossification of the anterior longitudinal ligament and paravertebral connective tissue, creates the



**Fig. 21.27.** (left) Ankylosing spondylitis. Syndesmophytes bridge all of the disc spaces anteriorly.

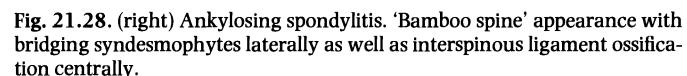


**Fig. 21.28.** (right) Ankylosing spondylitis. '*Bamboo spine*' appearance with bridging syndesmophytes laterally as well as interspinous ligament ossification centrally.

'bamboo spine' appearance (Fig. 21.28). More extensive discovertebral erosion in ankylosing spondylitis may sometimes extend to the central portion of the vertebral end plate, while central disc calcification may occasionally be observed.

Other sites of spinal abnormalities in ankylosing spondylitis include apophyseal joints, costovertebral joints, and posterior ligamentous attachments (Figs 21.28, 21.29). *Atlantoaxial erosion* and *subluxation* may occasionally be observed (Fig. 21.29). Vertebral fracture may occur, which often leads to pseudarthrosis.

Erosion, sclerosis, and ankylosis may be observed in the *symphysis pubis* and the *manubriosternal joint*, while ill-defined erosion representing enthesopathy (not as sharply defined as that seen in DISH) may be seen at the *ischial tuberosities*, *iliac crests*, and other sites of ligamentous attachment (Fig. 21.30).

In the *hip*, uniform loss of joint space leads to axial migration of the femoral head (Fig. 21.30). Characteristic osteophyte formation along the lateral aspect of the femoral head helps to distinguish ankylosing spondylitis from rheumatoid arthritis. Glenohumeral joint abnormalities are also often observed, again consisting primarily of bony erosion, particularly along the superolateral aspect of the humeral head. Asymmetric erosive arthritis in the hands and wrists may occur as well as involvement of knees, temporomandibular joints, and other articulations. Bony proliferative changes at these sites aid in differentiation from rheumatoid arthritis.

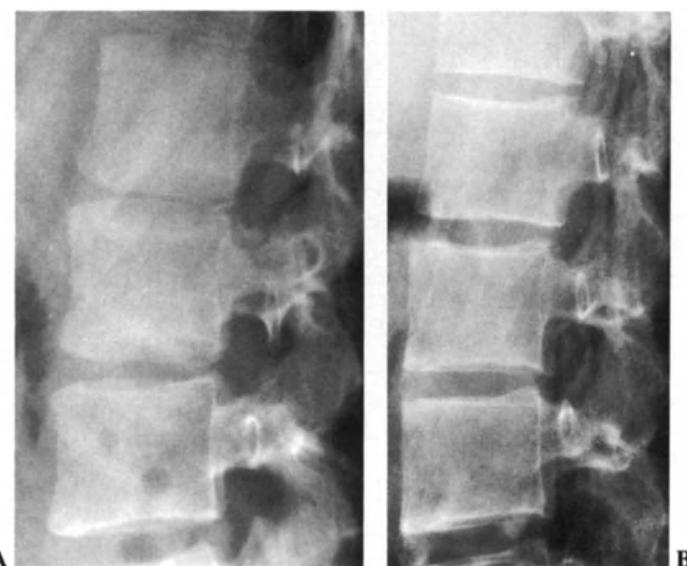


**Fig. 21.26A, B.** Ankylosing spondylitis. A A lateral radiograph of the lumbar spine before the onset of disease is normal, with slight concavity of the anterior border of the vertebral bodies. B Several years later, there is 'squaring' of the vertebral bodies due to erosion of the corners. There is also some reactive sclerosis and early syndesmophyte formation.

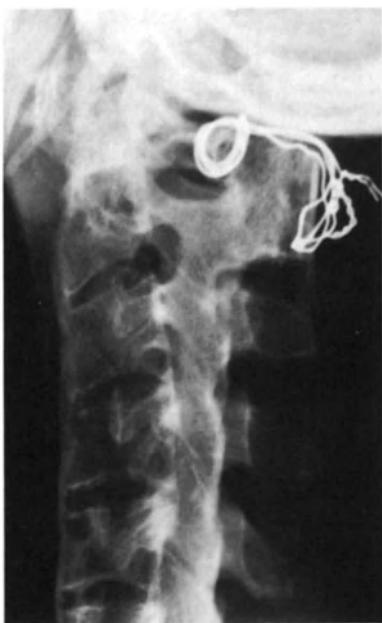


**Fig. 21.29.** Ankylosing spondylitis. There are syndesmophytes and anterior longitudinal ligament ossification as well as ankylosis of apophyseal joints. Note also separation between the anterior arch of C1 and the odontoid process with subluxation treated surgically.



**Fig. 21.31.** Juvenile chronic arthritis. There is enlargement ('ballooning') of the right distal femoral and proximal tibial epiphyses compared to the normal left side.

There is often a close temporal relationship between exacerbations of intestinal symptoms and peripheral arthralgia related to synovitis, but a similar relationship to progression of axial skeletal involvement does not generally exist.

Radiographic findings of sacroiliitis and spondylitis in enteropathic arthropathy are identical to those of ankylosing spondylitis. Bilateral symmetric sacroiliac joint involvement is characteristic, and vertebral body 'squaring', syndesmophyte formation and the 'bamboo spine' appearance may be observed. Radiographic changes in the appendicular skeleton are rare.

### Enteropathic Arthropathy

The presence of radiographically evident arthropathy has been described in numerous gastrointestinal disorders. The greatest incidence has been observed in *ulcerative colitis*, *Crohn's disease*, and, less commonly, in *Whipple's disease*. Although the exact etiology of this arthritis is not clear, the histocompatibility antigen HLA-B27 is present in the vast majority of patients who develop sacroiliitis or spondylitis.



**Fig. 21.30.** Ankylosing spondylitis. There is ill-defined bone erosion at the symphysis pubis and along the ischial tuberosities. There is also uniform loss of hip-joint space bilaterally. Note complete ankylosis of the sacroiliac joints and ligamentous ossification in the lumbosacral spine.

### Juvenile Chronic Arthritis

Chronic arthritis in children can be divided into numerous clinical subtypes including *juvenile onset adult type (seropositive) rheumatoid arthritis*, *seronegative chronic arthritis (Still's disease)*, *psoriatic arthritis*, *juvenile onset ankylosing spondylitis*, and *enteropathic arthropathy*.

Common features of juvenile chronic arthritis include soft tissue swelling and osteoporosis. Joint space narrowing and bone erosion do not occur as frequently as in rheumatoid arthritis and are usually late manifestations of disease. Eventually, however, bony ankylosis at multiple sites may develop. Periosteal bone proliferation is commonly seen as are growth disturbances. The latter may manifest as epiphyseal enlargement secondary to hyperemia (Fig. 21.31). Conversely, bony atrophy with reduction in the diameter of diaphyses may result from inhibited growth due to chronic illness. Premature epiphyseal fusion may lead to bone shortening.

A common occurrence in the wrist is erosion and eventual ankylosis of the midcarpal and common carpometacarpal articulations with sparing of the radiocarpal compartment. In the hand, any joint may be affected; periostitis is often a prominent finding. Similar abnormalities may be evident in the ankle and foot.

A characteristic knee abnormality is enlargement ('ballooning') of femoral and tibial epiphyses (Fig. 21.31) as well as 'squaring' of the patella. Widening of the intercondylar notch may also be observed. Hip abnormalities include enlargement of the femoral capital epiphysis and coxa valga deformity. *Sacroiliac joint involvement* in juvenile onset ankylosing spondylitis, psoriatic arthritis, and enteropathic



**Fig. 21.32.** Systemic lupus erythematosus. There is marked ulnar deviation of the digits at the metacarpophalangeal joints without bony erosion.



**Fig. 21.33.** Scleroderma. There is soft tissue resorption of the finger tips as well as bony resorption of the third distal phalanx. Note also small periarticular calcific deposits about multiple interphalangeal joints.

arthropathy can be difficult to evaluate radiographically since widening of this joint and indistinctness of articular surfaces are normal in children. Adjacent sclerosis and eventual bony ankylosis may occur.

*Atlanto-axial subluxation* and *erosion of the odontoid* are common findings in the cervical spine. Additional features include apophyseal joint ankylosis and growth disturbances characterized by a decreased anteroposterior diameter of vertebral bodies and decreased disc height. In the jaw, underdevelopment of the mandible and temporomandibular joint alterations may be observed.

#### CONNECTIVE TISSUE DISORDERS

A diverse group of disorders, often categorized as connective tissue diseases, includes systemic lupus erythematosus, progressive systemic sclerosis (scleroderma), polymyositis, dermatomyositis, and various combinations that can be designated as overlap syndromes.

##### Systemic Lupus Erythematosus (SLE)

SLE is a connective tissue disorder associated with alteration of the immune mechanism. It is seen most frequently in young women and involves multiple organ systems, including the musculoskeletal system. Symmetric polyarthritis is a common symptom, and mild synovial inflammation may be evident.

Soft tissue swelling and osteoporosis may be observed radiographically, but joint space narrowing and erosive arthritis are rare. More commonly, a non-erosive deforming arthropathy is present characterized by a combination of boutonnière, swan neck, and ulnar deviation deformities of

digits (Fig. 21.32). These deformities are related to capsular and ligamentous laxity and are most often completely reversible. A well-known complication of SLE is ischemic necrosis of bone which is usually but not invariably associated with steroid therapy.

##### Progressive Systemic Sclerosis (Scleroderma)

Scleroderma is a connective tissue disorder characterized by fibrosis that affects multiple organ systems. Common symptoms include Raynaud's phenomenon and skin thickening and edema of the digits. Soft tissue swelling about joints and muscle weakness are often present.

Characteristic radiographic abnormalities include resorption of soft tissue of the finger tips, amorphous calcification of soft tissues, and distal phalangeal bony erosion (Fig. 21.33). These may progress to extensive soft tissue and bone involvement (Fig. 21.34). Occasionally, osseous articular erosions may be observed, particularly at interphalangeal joints of the hand and in the first carpometacarpal joint of the wrist.

##### Polymyositis and Dermatomyositis

Polymyositis and dermatomyositis are inflammatory disorders of skeletal muscle with additional skin involvement in the latter. Gradually increasing muscle weakness may be accompanied by a diffuse erythematous skin rash. The age of onset is variable, with childhood involvement occurring in up to 20% of cases. One type of dermatomyositis in adults is associated with a high incidence of malignancy of varied origin which may occur long after initial muscular changes are observed.

Soft tissue abnormalities are often more severe in younger patients. Subcutaneous and muscular edema often leads to



**Fig. 21.34.** Scleroderma. There is extensive periarticular calcification with erosion of bone along the medial cortex of the proximal humerus.

*calcification* that may be localized, diffuse, linear, globular, or reticular (Figs 21.35, 21.36). Radiographically evident abnormalities are quite rare.

#### CRYSTAL-INDUCED ARTHROPATHIES

Deposition of various crystals in articular and periarticular structures can lead to distinctive arthropathies. These include gouty arthritis secondary to monosodium urate

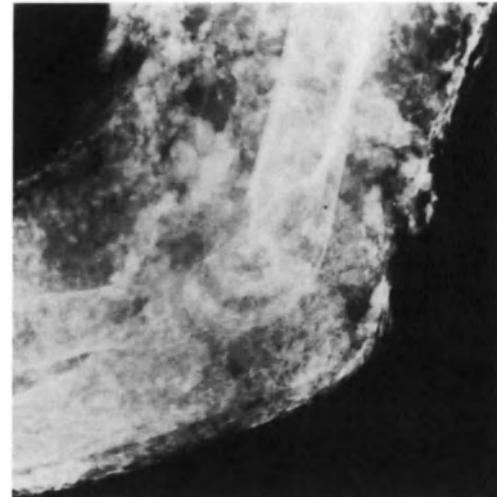


**Fig. 21.36.** Dermatomyositis. Soft tissue calcification has a reticular, 'cast-like' appearance.

crystal deposition, calcium pyrophosphate dihydrate crystal deposition disease, and calcium hydroxyapatite deposition disease.

#### Gouty Arthritis

Gout is a disease related to periarticular and intra-articular deposition of monosodium urate crystals. Men are much more commonly affected than women. Hyperuricemia is often present for a long period of time before symptoms or signs become evident. Acute gouty arthritis produces pain, tenderness and soft tissue swelling, but radiologic abnormalities generally only become apparent after a prolonged interval with the development of chronic tophaceous gout.

Asymmetric nodular prominences (*tophi*) represent crystal deposits within soft tissues (Fig. 21.37). These occur most characteristically about the olecranon and dorsum of the foot. Calcification of tophi is not commonly observed. Joint space narrowing does not generally occur until very late in the course of the disease due to non-uniform deposition of urate crystals within articular cartilage (Fig. 21.38).

*Bony erosions* may be intra-articular (asymmetric and eccentrically located along the margins of joints) or extra-articular (usually beneath soft tissue nodules). These generally have a very well-defined, often sclerotic margin unlike the erosions of rheumatoid arthritis and other inflammatory arthritides. A characteristic 'overhanging edge' is often present over gouty erosions due to periosteal new bone formation in response to slow growth of tophaceous deposits (Fig. 21.37).

The *first metatarsophalangeal joint* is the most common site of gouty arthritis with soft tissue swelling and characteristic eccentric erosions (Fig. 21.38). Extensive destruction may be seen in the tarsometatarsal joints in the foot (Fig. 21.39) as well as in the carpometacarpal joints in the hand. Interphalangeal joints and any other joint in the body may also be involved.



**Fig. 21.35.** Dermatomyositis. There is extensive soft tissue calcification that appears linear anteriorly and more globular posteriorly.



Fig. 21.37



Fig. 21.38



Fig. 21.39

**Fig. 21.37.** Gouty arthritis. There is well-defined erosion at the base of the distal phalanx of the thumb with an 'overhanging edge' of bone. Several soft tissue tophi are present.

**Fig. 21.38.** Gouty arthritis. There are relatively well-defined erosions of the articular surfaces of the first metatarsal and proximal phalanx with a normal intervening joint space.

**Fig. 21.39.** Gouty arthritis. There is extensive destruction of the tarsometatarsal joints with sharply marginated erosions at the metatarsal bases.

#### Calcium Pyrophosphate Dihydrate (CPPD) Crystal Deposition Disease

CPPD crystal deposition disease is most often an idiopathic disorder of the middle aged and elderly. The term 'pseudo-gout' has been used to describe this disorder even though only a small percentage of symptomatic patients show a clinical presentation that resembles gout. More often, those affected either are asymptomatic or have symptoms indistinguishable from osteoarthritis.

CPPD crystals may be deposited in any articular or periarticular structure. This leads to the characteristic radiologic finding of *chondrocalcinosis* which may be seen in hyaline or fibrocartilage. The former is observed as thin linear calcification that parallels the underlying subchondral bony surface (Fig. 21.40), while the latter appears as irregular radiodense collections most commonly in the menisci of the knees, the triangular fibrocartilage of the wrist, and the symphysis pubis (Figs 21.41, 21.42).



**Fig. 21.40.** Crystal deposition disease. There is thin linear calcification of the hyaline articular cartilage of the humeral head.



**Fig. 21.41.** CPPD crystal deposition disease. There is diffuse calcification of the menisci as well as some calcification of the articular cartilage of the distal femur centrally.



**Fig. 21.42.** CPPD crystal deposition disease. There is loss of joint space and bone sclerosis at the radiocarpal articulation with an osteophyte projecting from the scaphoid and a subchondral cyst in the distal radius. There is also chondrocalcinosis involving the triangular fibrocartilage (arrow).

**Pyrophosphate arthropathy** is the term used to describe the structural joint changes that develop. General features include joint space narrowing, bone sclerosis, and subchondral cyst and osteophyte formation. These resemble degenerative joint disease, although articulations other than weight bearing joints are frequently involved. Furthermore, the intra-articular distribution is often quite different from that of degenerative and other articular disorders.

The knee, the most commonly affected joint, often shows meniscal calcification (Fig. 21.41). The presence of arthropathy isolated to the patellofemoral compartment with sparing of medial and lateral femorotibial compartments is distinctive. Similarly, calcification of the triangular fibrocartilage and isolated radiocarpal compartment arthropathy are characteristic features of wrist involvement (Fig. 21.42). Scapholunate dissociation or the 'step ladder' configuration of radioscapoid and lunate-capitate joint space narrowing may also be seen.

In the hand, abnormalities predominate in the *metacarpophalangeal joints*, a location uncharacteristic of osteoarthritis (Fig. 21.43). Hip involvement may lead to narrowing



**Fig. 21.44.** Hydroxyapatite crystal deposition disease. There is cloud-like calcification in the distribution of the supraspinatus tendon.

either superolaterally or more uniformly. Rapidly progressive destruction may relate to collapse of large subchondral cysts. **Spinal abnormalities** are common with disc calcification present in addition to extensive disc space narrowing, vacuum phenomena, bony sclerosis, and osteophyte formation.

**Calcium Hydroxyapatite (HA) Crystal Deposition Disease** (HA) crystal deposition may be a primary phenomenon or may occur secondary to a number of different disorders including *collagen vascular diseases* and *renal osteodystrophy*. Primary deposition of HA crystals leads to calcific tendonitis at various sites and on occasion may be a cause of an inflammatory arthritis.

Calcific tendonitis may cause acute symptoms of pain and tenderness, but radiographic recognition of calcification in an asymptomatic patient occurs more commonly. This appears either cloudlike and poorly defined (Fig. 21.44) or dense, homogeneous, and sharply circumscribed (Fig. 21.45) and is seen most often about the shoulder, particu-



**Fig. 21.43.** CPPD crystal deposition disease. There is narrowing of the joint space, osteophyte and subchondral cyst formation, and calcification involving the second and third metacarpophalangeal joints.



**Fig. 21.45.** Hydroxyapatite crystal deposition disease. This example of calcific tendonitis is dense and sharply circumscribed.



**Fig. 21.46.** Neuroarthropathy. There is destruction of the tarsometatarsal joints with lateral dislocation of the second through fifth metatarsals as well as fracture at the base of the first metatarsal. Note extensive vascular calcification in this diabetic patient.

larly in the *supraspinatus tendon* adjacent to the greater tuberosity.

Intra-articular HA crystal deposition creates an amorphous pattern of calcification that may be associated with a destructive arthropathy including rotator cuff disruption and bony erosion. A destructive spondyloarthropathy with erosion of intervertebral discs may occur in hemodialysis patients.

#### NEUROARTHROPATHY

Numerous disorders may lead to the development of neuroarthropathy including most commonly *diabetes mellitus*, *syringomyelia*, and *tabes dorsalis*. The exact pathogenesis of neuroarthropathy is not completely understood. One theory supports a neurovascular cause with hyperemia leading to osteoclastic resorption of bone, while a second theory supports a prominent role of repetitive trauma to insensitive joints. Some combination of these factors leads to destructive and/or productive changes, often with a characteristic radiographic appearance.

Hypertrophic changes of neuroarthropathy include *osteophyte formation*, *bone sclerosis* and, most characteristically, *bone fragmentation* with intra-articular osseous debris. Soft tissue swelling may be prominent, and subluxation or dislocation is common. Multiple fractures with excessive periosteal new bone formation may be seen. Margins of the bony fragments are generally sharp unless superimposed infection is present. All of these findings are most prominent in the *foot* (Fig. 21.46) and *ankle* (Fig. 21.47) in diabetic patients and in the *spine* in *tabes dorsalis*. In the latter, sclerosis and osteophyte formation are more extreme than



**Fig. 21.47.** Neuroarthropathy. There is fragmentation of the distal tibia and fibula and the talus with loss of normal architecture of the articular surfaces. Prominent periosteal new bone formation and bone sclerosis are also evident.

in degenerative disc disease, and disc space obliteration and vertebral subluxation are more likely.

Although bone resorption can occur at any site and can be rapidly progressive, atrophic changes of neuroarthropathy are most common in the *shoulder* in *syringomyelia* (Fig. 21.48). Occasionally, resorption can be so extensive and residual bone margins so sharply defined as to resemble surgical resection. Characteristic resorption of the *foot* in *leprosy* may lead to a '*licked candy stick*' appearance (Fig. 21.49). *Congenital indifference to pain* is a rare cause of ankle and foot lesions in children.

#### INFECTIVE ARTHRITIS

*Septic arthritis* may occur secondary to hematogenous seeding, by spread from a contiguous source of infection, or by direct implantation. A hematogenous route is more common in young patients where organisms can be deposited in either synovial or epiphyseal vessels. Local clinical symptoms in a



**Fig. 21.48.** Neuroarthropathy. There is extreme resorption of bone of the proximal humerus with residual bony debris in the surrounding soft tissues in this patient with syringomyelia.



**Fig. 21.49.** Neuroarthropathy. There is extensive resorption of bone in this patient with leprosy.

mono-articular distribution predominate, although systemic signs and symptoms may be prominent.

Radiographically, joint effusion is followed by growth of inflamed synovium across cartilaginous surfaces leading to uniform joint space narrowing (Fig. 21.50). Early bone erosions often occur along the margins of the joint (Fig. 21.51) with later involvement of the more central articular surface. More extensive destruction can lead to fibrous or bony ankylosis. The most helpful signs in differentiating septic arthritis from other articular processes are the poorly defined margins of osseous erosions and the rapid progression of findings. However, with less virulent organisms such as those formed in *tuberculous* or  *fungal* infection, abnormalities may be limited to periarticular osteoporosis and marginal osseous erosions with preservation of joint space.

#### MISCELLANEOUS ARTICULAR DISORDERS

##### Hemophilia

Classic hemophilia is an X-linked recessive bleeding disorder manifest in males due to a deficiency in clotting factor VIII. Joint abnormalities begin with *hemarthrosis* that may occur spontaneously or following trauma. The lower extremity is most commonly affected, particularly the *knee* and *ankle*. Similar clinical and radiographic abnormalities may also be encountered in both males and females with bleeding disorders related to deficiency of other clotting factors.

Radiographically, intra-articular hemorrhage may produce joint effusion that eventually can appear relatively dense due to hemosiderin-laden hypertrophied synovium. As synovial inflammation progresses, hyperemia can lead to osteoporosis and, in the child, epiphyseal overgrowth and accelerated skeletal maturation. This may produce '*squaring*' of the patella and '*ballooning*' of the femoral condyles similar to that seen in juvenile chronic arthritis. Eventually, car-

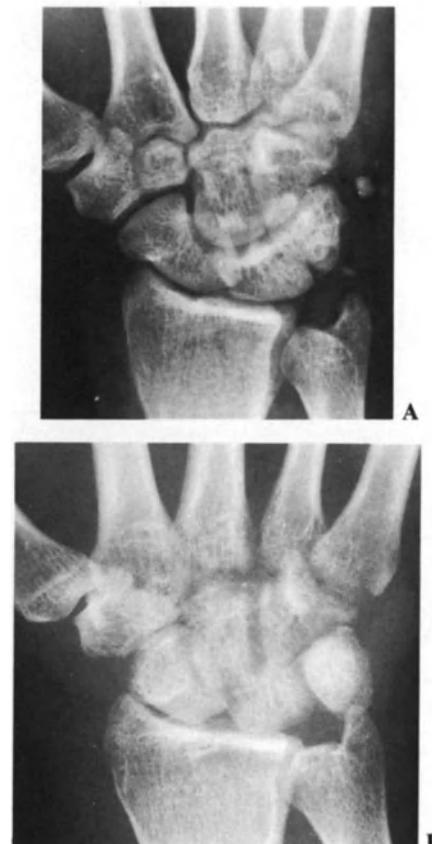


**Fig. 21.50A, B.** Septic arthritis. A Joint spaces are normal immediately after trauma. There are multiple fragments of glass in the soft tissues. B Four weeks later, there is loss of joint space at intercarpal and carpometacarpal articulations with destruction of articular cortex.

tilage destruction produces joint space narrowing, usually in a uniform distribution in involved joints. This may be followed by bony erosion with or without sclerosis and osteophyte formation (Fig. 21.52). An unusual sequel of intra-osseous hemorrhage is a *hemophilic pseudotumor* with well-defined, often multilocular and expansile lytic bone destruction.



**Fig. 21.51.** Septic arthritis. There is erosion of bone at the lateral aspect of the distal femur and the medial aspect of the proximal tibia with central articular cortex remaining intact.



**Fig. 21.52.** Hemophilia. There is complete loss of knee-joint space in a uniform distribution with sclerosis and irregular contour of bony articular surfaces as well as osteophyte formation.

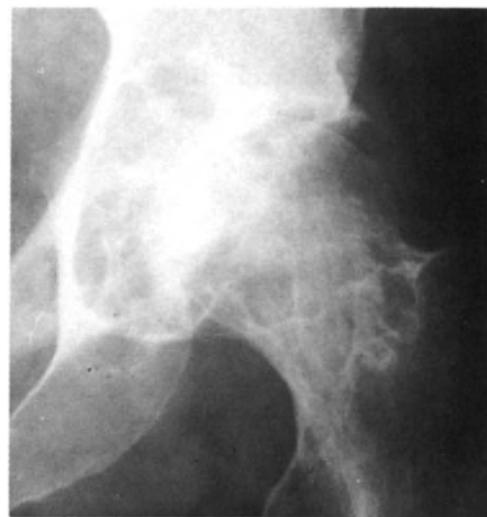


**Fig. 21.53.** Pigmented villonodular synovitis. There are multiple confluent well-defined erosions involving the femoral neck and acetabulum.

#### Pigmented Villonodular Synovitis

Pigmented villonodular synovitis is a benign condition characterized by hyperplasia of synovial villi. The *knee* and *hip* are most commonly involved in this mono-articular process. Soft tissue swelling may be localized or diffuse within the joint. Increased radiodensity may reflect chronic deposition of hemosiderin, but soft tissue calcification does not occur.

Osseous abnormalities occur secondary to pressure erosion and invasion by hypertrophied synovial tissue. Well-defined superficial cortical erosions often have thin sclerotic margins and can occur on both sides of the involved joint (Fig. 21.53). Joint space narrowing is usually absent.

#### Synovial Osteochondromatosis

Idiopathic synovial osteochondromatosis represents metaplasia of the synovial membrane leading to cartilage formation. This mono-articular disorder affects the *knee*, *hip* and *elbow*, most commonly in young adults. Symptomatology is mostly related to the development of loose bodies within the joint.

Radiographically, multiple radiodensities may be observed, usually uniform in size and no larger than a few centimeters (Fig. 21.54). They may demonstrate minimal calcification or complete ossification. Non-mineralized nodules can be observed during arthrography. Rarely, pressure erosion of adjacent bone may be seen.

#### Hemochromatosis

Hemochromatosis is a rare disorder of iron deposition that can lead to bronze pigmentation, cirrhosis, and diabetes mellitus usually recognized in older adults. Occasionally, an arthropathy can occur late in the course of this disease, which characteristically consists of non-inflammatory involvement of *metacarpophalangeal joints* with associated deposition of calcium pyrophosphate dihydrate crystals.

Radiographic abnormalities are virtually identical to those of idiopathic CPPD crystal deposition disease with chondro-

calcinosis and non-erosive articular changes resembling osteoarthritis but in a different, characteristic distribution (see earlier discussion). Additional features of hemochromatosis may include generalized osteoporosis, more prominent hyaline cartilage calcification, and distinctive hook-like osteophytes along the radial aspect of the metacarpal heads, particularly in the 4th and 5th fingers (Fig. 21.55).

#### Alkaptonuria

Alkaptonuria is an enzymatic deficiency that leads to accumulation of *homogentisic acid* in tissues. The resulting bluish-black pigmentation is termed ochronosis. An arth-



**Fig. 21.54.** Synovial osteochondromatosis. There are multiple small, uniformly size radiodensities in the suprapatellar recess of the knee joint.



**Fig. 21.55.** Hemochromatosis. There is complete loss of joint space without erosions in the metacarpophalangeal joints. Hook-like osteophytes project from the radial aspect of the metacarpal heads.



**Fig. 21.56.** Alkaptonuria. There is uniform loss of all disc spaces with sclerosis, small osteophytes, and a vacuum phenomenon.



**Fig. 21.57.** Wilson's disease. There are several small ossicles adjacent to the distal ulna and an irregular bony surface along the radial styloid process.

## OTHER IMAGING TECHNIQUES

J. W. R. Young

After plain films, the mainstay of radiological evaluation of the joints has usually been arthrography. This has been used to assess abnormalities of all of the major joints of the body, with modest effectiveness. The commonest joints examined are the knee, hip, shoulder and wrist. More recently CT, MRI and even ultrasound have been introduced into the evaluation of the joints.

**Knee.** Arthrographic examination of the knee is usually performed to evaluate the *menisci*, although it may also be used to assess for *Baker's cyst* formation or rupture, and with less success for *anterior cruciate ligament* injury. Examination of synovial abnormalities, such as *pigmented villonodular synovitis* (PVNS) or *synovial hemangioma* has also been performed, and rarely arthrography has been used to evaluate



**Fig. 21.58.** Contrast is noted tracking posteriorly from the knee joint, with an irregular inferior protrusion, due to rupture of a Baker's cyst.



**Fig. 21.60.** PVNS. Coronal MRI image (FLASH sequence) demonstrates an area of relatively high signal widening the lateral joint space, replacing the normal low signal triangular shaped meniscus. This indicates intrusion of the proliferating synovium.

for *rheumatoid arthritis*, although this is a dubious clinical indication. The double contrast technique is preferred, whereby 3–5 ml of water-soluble contrast are injected into the joint, followed by approximately 20–40 ml of air. Spot views are taken of each meniscus with the knee in varying degrees of rotation. Generally, meniscal abnormalities are identified either by intrusion of contrast into the meniscus, or by frank avulsion or absence of a portion of the meniscus. Popliteal (Baker's) cysts may also be identified if they fill with contrast or air (Fig. 21.58).

MRI evaluation appears to have many advantages over arthrography. It is non-invasive, and has the benefit of demonstrating not only the menisci, but also the cruciate ligaments, collateral ligaments, surrounding soft tissues, marrow cavities and cartilage (Figs 21.59, 21.60). The main disadvantages are cost, and hypersensitivity to early meniscal degeneration, although experience soon allows differentiation of clinically significant lesions. Meniscal injuries are indicated by increased signal within the meniscus, or clear

meniscal disruption (Fig. 21.61). Similarly ligamentous injury is indicated by interruption of the ligament (complete tear) or abnormality of signal (partial tear) (Fig. 21.62). MRI is useful in the evaluation for Baker's cysts, or meniscal cysts, although ultrasound may also be used, and is much less expensive, and less time consuming.

**Shoulder.** Double contrast arthrography of the shoulder is again the preferred technique of contrast examination. Approximately 5 ml of water-soluble iodinated contrast are injected, followed by 10–15 ml of air. Extreme pain during capsular distension with either contrast or air may be due to *adhesive capsulitis*. Following contrast injection, the arm is exercised and spot films are taken with the shoulder in various degrees of internal and external rotation, as well as abduction or adduction. Shoulder arthrography is used predominantly to diagnose ruptures of the rotator cuff (the conjoined tendons of supraspinatus, infraspinatus, and teres minor), although loose bodies, and even tears of the long

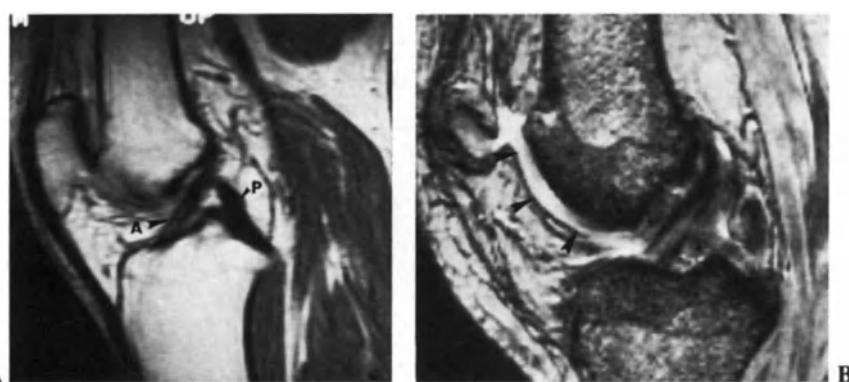


**Fig. 21.59.** **A** Normal sagittal MRI scan of the knee (T<sub>1</sub> image). The posterior (P) and anterior (A) cruciate ligaments are well seen. **B** FLASH sequence demonstrates the anterior cruciate ligament, and thick articular cartilage of the femoral condyle (arrowheads).

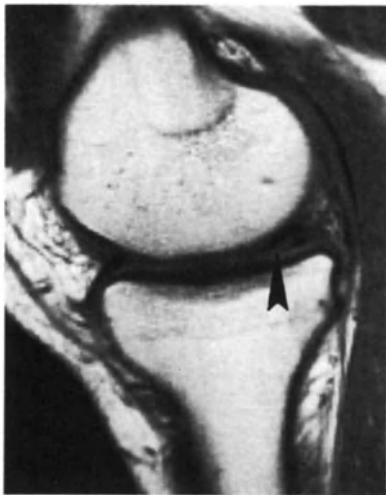


**Fig. 21.61.** MRI scan (T<sub>1</sub> image). Increased signal in the posterior horn of the medial meniscus (*arrowhead*) extending to the surface of the meniscus indicates a tear.



**Fig. 21.63.** Rotator cuff tear. Shoulder arthrography demonstrates contrast within the subdeltoid bursa (*arrowhead*), indicating a complete tear. Contrast is also seen with the superior aspect of the cuff (*small arrowheads*).

head of biceps may be visualized. Contrast or air tracking laterally into the sub-deltoid bursa, which is normally separated from the shoulder joint by the rotator cuff, indicates a tear in the cuff (Fig. 21.63). Small defects in the under surface may indicate partial tear, and may be seen by air intravasation on erect views. A combination of double contrast arthrography using a smaller quantity of contrast with computed tomography adds an additional dimension to the study, which can then be used to define the labra of the glenoid. MRI is fast becoming an acceptable alternative to arthrography, with its ability to identify ligamentous and cartilaginous abnormalities.

**Wrist.** Arthrography of the wrist is a valuable technique for the evaluation of wrist abnormalities, particularly those of chronic acute wrist instability or undiagnosed pain. The wrist joint is composed of three major compartments, the radio-carpal, the ulnar-carpal and the inter-carpal. These are



**Fig. 21.62.** Ruptured anterior cruciate ligament. Sagittal MRI (FLASH sequence). There is disruption of the normal linear appearance of the anterior cruciate with an ill defined area of mixed signal surrounding the expected position of its femoral insertion (compare with Fig. 21.59B).

separated from each other by intercarpal ligaments, and at the radio/ulnar articulation by the triangular fibrocartilage complex (TFCC). In theory, tears of the proximal carpal ligaments and TFCC should be seen following injection of the radiocarpal ligament alone, although this is not always the case, and injection of all three joint compartments is advocated by some workers. Ligament disruption is indicated by passage of contrast from the injected joint compartment into the neighboring compartment. Three compartment injections are time consuming, however, and with the revolution in design of small high definition extremity surface coils, MRI is gaining in popularity as a method of examining the wrist, with its ability to better visualize tendons, ligaments, cartilage and marrow cavities. Interosseous ligament visualization however, remains of marginal quality at this time.

**Hip.** Arthrography of the hip may be used for a variety of disorders. The commonest indication today is in the assessment of pain following total hip replacement, although hip arthrography is also used for the evaluation of hip dysplasia, inflammatory or infective processes, dislocation, or even Legg Perthes disease. Today however, ultrasound, CT and MRI have largely replaced arthrography in the evaluation of the hip joint, although arthrography is still used frequently to evaluate for hip prosthesis loosening or infection.

Plain radiographs of hip prostheses in which methyl methacrylate cement was used will indicate a narrow (approximately 1 cm) zone of lucency surrounding the cement, due to thermal osteonecrosis. An increase in this lucency, or obvious settling of the prosthesis may be seen with loosening or infection. At arthrography a spinal needle is inserted, avoiding the femoral artery and canal, until the metal implant is touched. Aspiration of fluid may be needed in multiple sites, as there is often extensive scar formation. Joint washings are also useful. Finally contrast is injected and after passive exercise, radiographs are obtained in various positions. Contrast tracking between the bone/



**Fig. 21.64.** Loose total hip prosthesis. Pre (A) and post (B) contrast injection films of the right hip show contrast tracking between the cement of the femoral component and the bone (arrowheads). (Courtesy of C.S. Resnick, M.D.)

cement interface indicates loosening (Figs 21.64A and B). Subtraction film techniques are also used, although they are time consuming.

Recently there has been a trend towards the use of non-cemented 'porous coated' prostheses. Although in theory this should prevent loosening, experience would suggest that loosening may occur, although less frequently. Long term follow-up is too limited for definitive comment at present.

Loosening or infection of a hip prosthesis may be evaluated using nuclear medicine bone scanning. Following the initial post operative increase in activity, which is relatively uniform in distribution and lasts approximately nine months to one year, any focal area of increased activity suggests loosening or infection. Although the differentiation cannot be made using  $^{99m}$ Technetium-labelled phosphate,  $^{67}$ Gallium citrate may be able to do so, due to its localization in leukocytes.

The ankle joint and elbow are rarely examined by arthrography and the indications are few. Ligamentous injuries of the ankle may be diagnosed by plain radiography with stress views following local anesthesia, and there is evidence that the modern generation of MRI scanners provide improving detail of the ligaments. Elbow arthrography is usually performed in a search for loose bodies. Contrast (approximately 2 ml) and air (4–5 ml) are injected, usually from

the lateral approach. In general, tomography is needed to evaluate the joint fully. The temporomandibular joint may also be examined by arthrography, but again high resolution CT, and MRI, are supplanting the technique.

#### REFERENCES AND SUGGESTIONS FOR FURTHER READING

- Adamson TC III, Resnick CS, Guerra J Jr, Vint V, Weisman MH, Resnick D (1983) Hand and wrist arthropathies of hemochromatosis and calcium pyrophosphate deposition disease: distinct radiographic features. *Radiology* 147: 377–381
- Bjorkengren AG, Pathria MN, Sartoris DJ, Terkeltaub R, Esdaile JM, Weisman M, Resnick D (1987) Carpal alteration in adult-onset Still disease, juvenile chronic arthritis, and adult-onset rheumatoid arthritis: Comparative study. *Radiology* 165: 545–548
- Brower AC (1988) Arthritis in Black and White. WB Saunders, Philadelphia
- Brower AC, Allman RM (1981) The neuropathic joint: A neurovascular bone disorder. *Radiol Clin North Am* 19: 571–580
- Crain DC (1961) Interphalangeal osteoarthritis. *JAMA* 175: 1049–1053
- Dorwart RH, Genant HK, Johnston WH, Morris JM (1984) Pigmented villonodular synovitis of synovial joints: clinical, pathologic, and radiologic features. *AJR* 143: 877–885
- Harrison MHM, Schajowicz F, Trueta J (1953) Osteoarthritis of the hip: a study of the nature and evolution of the disease. *J Bone Joint Surg [Br]* 35: 598–626
- Lawson JP (1982) The joint manifestations of the connective tissue diseases. *Semin Roentgenol* 17: 25–38

- Martel W, Holt JF, Cassidy JT (1962) Roentgenologic manifestations of juvenile rheumatoid arthritis. *AJR* 88: 400–423
- McEwen C, DiTata D, Lingg C, Porini A, Good A, Rankin T (1971) Ankylosing spondylitis and spondylitis accompanying ulcerative colitis, regional enteritis, psoriasis and Reiter's disease. *Arthritis Rheum* 14: 291–318
- Resnick D (1985) Degenerative diseases of the vertebral column. *Radiology* 156: 3–14
- Resnick D (1988) Common disorders of synovium-lined joints: Pathogenesis, imaging abnormalities, and complications. *AJR* 151: 1079–1093
- Resnick D, Niwayama G (1988) Diagnosis of Bone and Joint Disorders. 2nd edn. WB Saunders, Philadelphia
- Resnick CS, Resnick D (1982) Calcium pyrophosphate dihydrate crystal deposition disease. *Curr Probl Diagn Radiol* 11: 1–40
- Resnick CS, Resnick D (1985) Radiology of disorders of the sacroiliac joints. *JAMA* 253: 2863–2866
- Resnick CS, Resnick D (1985) Radiology of rheumatoid arthritis. In: Utsinger PD, Zvaifler NJ, Ehrlich GE (eds) *Rheumatoid Arthritis*. JB Lippincott, Philadelphia, pp 161–179
- Resnik CS, Resnick D (1986) Pyogenic osteomyelitis and septic arthritis. In: Taveras JM, Ferrucci JT (eds) *Radiology: Diagnosis-Imaging-Intervention* vol 5, chapter 21. JB Lippincott, Philadelphia, pp 1–11
- Resnik CS, Resnick D (1988) Crystal-induced and related arthropathies. In: Putman CE, Ravin CE (eds) *Textbook of Diagnostic Imaging*. WB Saunders, Philadelphia, pp 1520–1533
- Resnick D, Shapiro RF, Wiesner KB, Niwayama G, Utsinger PD, Shaul SR (1978) Diffuse idiopathic skeletal hyperostosis (DISH) [Ankylosing hyperostosis of Forestier and Rotes-Querol]. *Semin Arthritis Rheum* 7: 153–187
- Stoker DJ, Murray RO (1974) Skeletal changes in hemophilia and other bleeding disorders. *Semin Roentgenol* 9: 185–193
- Zimmerman C, Sayegh V (1960) Roentgen manifestations of synovial osteochondromatosis. *AJR* 83: 680–686

## CHAPTER 22

# SIMPLE RADIOGRAPHY OF THE SOFT TISSUES

F. Starer

---

The radiologist should be aware of various normal or near-normal appearances caused by the soft tissues, which can give rise to diagnostic errors at simple radiography. Perhaps the best known of these is the crescentic shadow caused by the *pinna* on a lateral radiograph of the skull. *Loose folds of skin* are commonly present on the skulls of neonates and are readily seen on radiographs. Similarly, *electrode jelly* from electroencephalograms and *sebaceous cysts* (Fig. 22.1) on the skull may produce confusing shadows. *Hair* is sometimes visible but because of its unanatomical shape should rarely cause difficulty in diagnosis (Fig. 22.2). In the chest, *nipple shadows* are a common source of confusion as may be other *skin nodules*, such as neurofibromas. These may be readily confused with intrathoracic lesions. Confusing shadows may sometimes be caused by hair overhanging a lung apex and

this may even simulate a cavity. In the abdomen, confusion may be caused by the shadow cast by a *colostomy lip* (Fig. 22.3) and in the pelvis the *penis* may cause confusion.

Another possible source of error is the appearance of a thin dark line where two soft tissue shadows overlap – the so-called '*Mach*' effect. This may sometimes simulate a fracture.

### FOREIGN BODIES

*Metals*, being radio-opaque, are easily seen. Most *glass* fragments are also radio-opaque and, unless very minute, should be readily visible. It is sometimes helpful to radiograph a fragment of the glass in question if one is available, in order to assess its radio-opacity. *Wood* and many types of *plastic* are

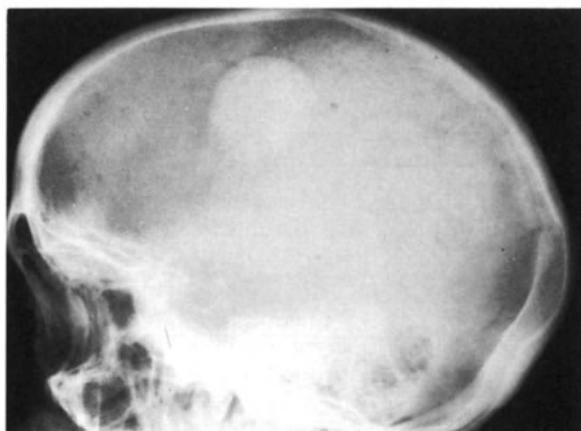


Fig. 22.1. Sebaceous cyst.



Fig. 22.2. Shadow of hair over occiput.

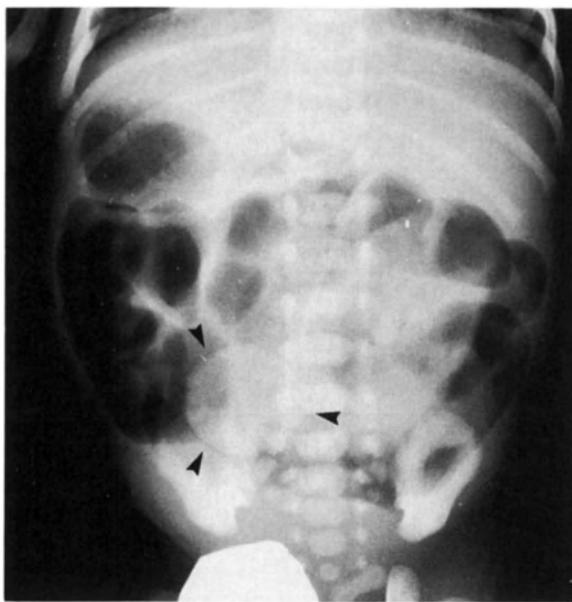


Fig. 22.3. Colostomy lip (arrows).



Fig. 22.4. Bismuth injections.

not opaque to X-rays: these may, however, be revealed by CT or ultrasound examination and these are useful means for localizing foreign bodies.

It is often helpful to mark the site of entry of a foreign body with a radio-opaque marker and obtain radiographs in two planes to enable the surgeon to find the object. It should be remembered that some foreign bodies, such as needles, can migrate either in the bloodstream or as the result of muscular action and may be found at some distance from their entry site. The position of such a foreign body should be checked shortly before its proposed removal.

Another class of foreign body, frequently seen many years ago but now becoming less common, consists of substances introduced deliberately in the course of treatment: *lipiodol* and *bismuth* (Fig. 22.4) injected into the buttocks for the treatment of rheumatoid arthritis and syphilis respectively; extravasated *Pantopaque* after attempted myelograms or *Thorotrast* after a failed angiogram. The latter is also deposited in the liver, spleen and lymph nodes and is a well-known carcinogenic agent.

#### SOFT TISSUE PATTERNS

Normally, skin can be clearly differentiated from muscle. The latter may show a faint 'herring-bone' pattern due to the structure of the muscle. In various types of *muscular dystrophies*, where normal muscle tissue is reduced and fat increased, this pattern may become more apparent. Loss of muscle mass and webbing at the elbow and knee, together with abnormally slender bones, is typical of *arthrogryposis congenita multiplex* (Fig. 22.5). Similarly, loss of muscle mass in a paralysed limb is usually obvious. Sometimes it is associated with clearly visible subcutaneous edema. This pattern is frequently seen in children with *spina bifida*. These

patients, like diabetics, also frequently develop soft tissue ulcers which may be readily seen on a radiograph (Fig. 22.6). Edema and ulceration may also be due to varicose veins and after chronic deep vein thrombosis. Varicose veins may be readily visible.

#### SOFT TISSUE MASSES

**Hematomas.** These present as a diffuse increase in soft tissue density and swelling on plain radiographs and may proceed to calcification. The diagnosis is more clearly made by CT. A history of trauma and possibly an associated fracture greatly aids in the diagnosis.

**Tumors.** These present as areas of soft tissue swelling with various degrees of demarcation from normal tissue. Usually tumors are better demonstrated by CT, preferably with enhancement. It is likely that MRI will play an increasing rôle, particularly with the use of paramagnetic 'contrast' media such as Gadolinium-DTPA. It is possible that this form of investigation may prove helpful in suggesting a tissue diagnosis. This cannot be accomplished from plain films or CT except in the case of *lipomas* which are characterized by their low density (Fig. 22.7). Some soft tissue tumors may show calcification (see below) but this does not necessarily help to distinguish benign from malignant lesions.

*Angiography* played an important part in the investigation of soft tissue tumors, though this is now largely taken over by CT and MRI. It often defines the tumor clearly and may strongly suggest that it is malignant by showing the typical vascular pattern of a malignant tumor. However, a similar vascular pattern may be found at the margins of an organizing hematoma and the angiographic findings should be treated with some reserve.

*Angiography* is particularly valuable in the investigation



Fig. 22.5. Arthrogryposis congenita multiplex. Note webbing and poor muscle development.



Fig. 22.6. Ulcer on sole of foot in diabetic.



of *angiomas* but it should be remembered that the flow in some cavernous hemangiomas is so slow that it may be difficult to fill them during angiography and this may lead to mistakes in diagnosis. On the other hand, measurement of CT values before and after enhancement may be very helpful. Angiography provides a means of treatment by embolization, either on its own or combined with surgery.

#### LESIONS OF DECREASED DENSITY

These may be due to the presence of *fat* or *gas*.

**Fat.** This is less dense than other soft tissues and, therefore, shows up well. Lipomas are usually well-defined unless they have a major fibrotic component. Lipohemarthroses are lesions consisting of fat floating on blood. They are best seen in relation to the shoulder and knee and are caused by fractures round these joints with the release of marrow fat into the joint capsule. The appearance of a fat/fluid level is diag-

Fig. 22.7. Lipoma in thigh.



Fig. 22.8. Lipohemarthrosis. Fat-fluid level marked by white markers.

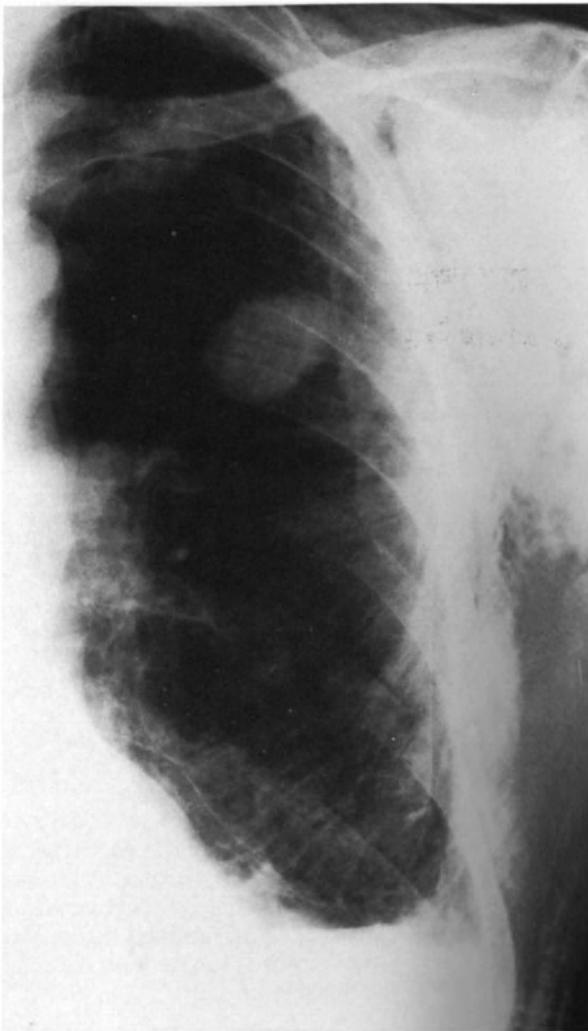


Fig. 22.9. Subcutaneous emphysema and small pneumothorax following trauma to chest. The 'mass' in the upper half of the chest resolved when the lung re-expanded.

nostic of a fracture even if this is not immediately obvious. In order to demonstrate a lipohemarthrosis it is necessary to obtain radiographs with a horizontal ray (Fig. 22.8). Similarly, displacement of the fat pad in front of the elbow joint following an injury is evidence of a fracture of the elbow joint although it is not obvious in every case. It is, nevertheless, a valuable sign, particularly in children.

**Gas.** Abnormal gas collections may occur in a number of circumstances.

1. In unusual situations, e.g., in the scrotum within gut in a hernia.

2. After surgery or penetrating injuries. Air may track extensively following fracture of a paranasal sinus or into the chest wall following a rib fracture and laceration of the lung. This produces a characteristic appearance of subcutaneous emphysema with separation of the fibres of the pectoralis major (Fig. 22.9). Air may then spread into the neck and face.

3. Following a leak into the mediastinum after  
 (a) rupture of a bronchus, usually associated with collapse of the corresponding lobe or lung  
 (b) rupture of the esophagus, spontaneous or after instrumentation  
 (c) during an asthmatic attack or during diabetic coma  
 In each case air tracks into the soft tissues of the neck and face.

4. Gas may be caused by gas-forming organisms in an abscess locally, or it may track through soft tissues from a distant abscess, e.g., into the thigh from an abscess in the pelvis such as may complicate diverticulitis. Gas formation is particularly prone to occur in diabetic patients.

A serious but fortunately rare condition is gas gangrene due to *Clostridium welchii*; the infection is often of mixed origin and there may be foreign bodies in the wound. Gas is found within the muscle bundles but may not become a prominent radiological feature for several days.

## LESIONS OF INCREASED DENSITY

### Soft Tissue Calcification

#### Vascular and Neural

1. *Arterial.* Calcification in atheroma is an almost universal concomitant of ageing. When seen in a younger age group a cause, such as hypercalcemia or hypercholesterolemia, should be sought. Ring-like calcification is found in medial sclerosis. Usually the more proximal major vessels are involved but calcification in distal vessels is common in diabetics. Plaques of calcification are frequently seen at arterial bifurcations, particularly at the carotid bifurcation. They are also found in aneurysms.

2. *Venous.* This may take the form of phleboliths, small round foci in thrombosed veins. They are particularly common in the pelvis but may be found in varicose veins and in venous angiomas (Fig. 22.10). Characteristically they are small round opacities, 3–4 mm in size and with a more trans-



Fig. 22.10. Angioma of forearm containing several phleboliths.

lucent center. Elongated calcification may occur in venous thrombus (Fig. 22.11).

3. Nerves. This is extremely rare but has been reported in leprosy and neurofibromatosis (Fig. 22.12).

#### Metabolic

Soft tissue calcification may be associated with any condition of hypercalcemia such as hyperparathyroidism,

hypervitaminosis D, idiopathic hypercalcemia and the milk-alkali syndrome. Paradoxically, it is also seen in certain metabolic conditions without hypercalcemia, such as chronic renal failure, hypoparathyroidism and pseudo-hypoparathyroidism. It occurs after renal transplants and in patients on chronic renal dialysis (Fig. 22.13). Calcification also occurs as a secondary phenomenon in the tophi of gout and in alkaptunuria.



Fig. 22.11. Calcification in venous thrombus.



Fig. 22.12. Calcification in nerves due to leprosy.



**Fig. 22.13.** Periarticular calcification in a patient in chronic renal failure and on dialysis.

#### Local Soft Tissue Injury

1. *Hematomas* may calcify, often in a circumferential manner. In children, calcification may occur very quickly, often after only a few days. A particular variety is the *cephalhematoma* in a neonate caused by a bleed during birth under the periosteum of a skull bone, usually the parietal. This causes soft tissue swelling, characterized by the fact that it is confined to the limits of one bone (Fig. 22.14A). Circumferential calcification develops within days; ultimately it may leave irregular bone density which may persist for years (Fig. 22.14B).

2. *Injections*, particularly *quinine* and *penicillin* in the buttocks.

3. *Frostbite*, particularly in the ear cartilages.

4. Areas of *chronic edema*, e.g., in the lower leg in edematous brawny skin and in relation to soft tissue ulcers (Fig. 22.15).

#### Primary Connective Tissue Disorders

1. *Congenital*. The best known instances in this group are the conditions associated with Raynaud's phenomenon, such as occurs in *systemic sclerosis*. Characteristically there is loss of soft tissues at the tips of the fingers due to ischemia with subsequent calcification in the necrotic portions. The combination of soft tissue loss and calcification is diagnostic

(Fig. 22.16). Other, less common connective tissue disorders associated with fine, scattered calcification are the *Ehlers-Danlos syndrome*, *pseudo-xanthoma elasticum* and *Weber-Christian disease*. Some of the most extensive soft tissue calcification occurs in *idiopathic dermatomyositis*. In this condition almost the entire trunk and limbs, may become encased in calcified tissue (Fig. 22.17) (see pages 387–8).

2. *Acquired*. Deposition of calcium hydroxyapatite or pyrophosphate crystals occurs around joints, producing a crystal synovitis. A form of this condition which is particularly common is calcification in the rotator cuff of the shoulder joint (Fig. 22.18). This is a painful condition in which the onset and resolution of pain do not always coincide with the period of visible calcification.

A different and unrelated form of calcification is *tumoral calcinosis*. Massive calcification in soft tissues occurs near joints, often limiting movement. The condition is benign and its cause is unknown (Fig. 22.19).

#### Tumor Calcification

Many soft tissue tumors undergo calcification, possibly due to necrosis within the lesion. Calcification is particularly common in *thyroid adenomas* (Fig. 22.20) and in *medullary carcinoma of the thyroid*. It also occurs in *hemangiopericytomas* and in some *fibrosarcomas*. Calcification cannot be taken as an indication that a tumor is benign or malignant.

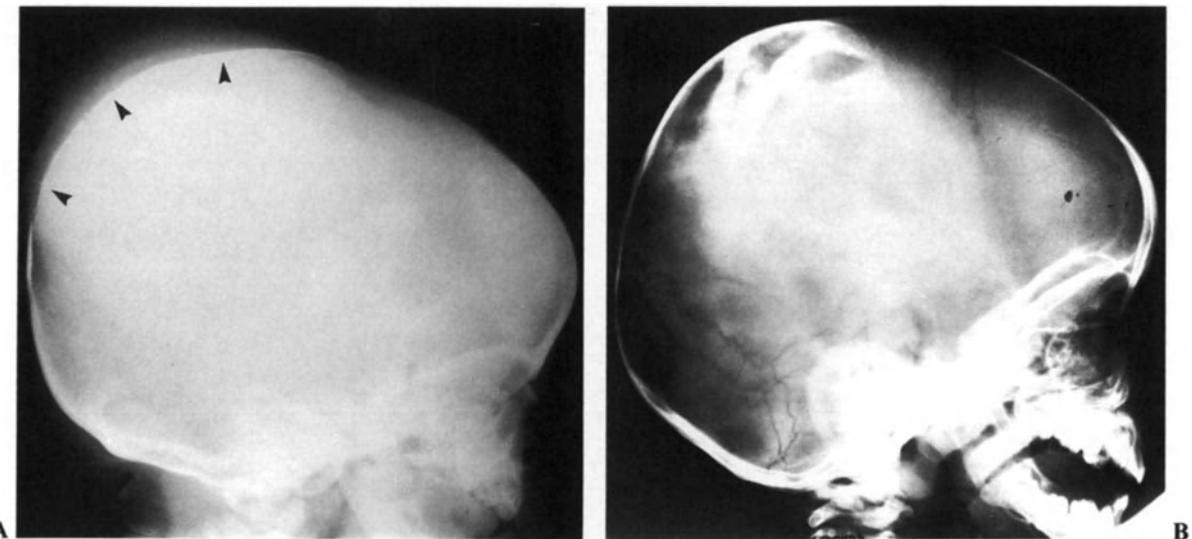


Fig. 22.14. A Cephalhematoma, acute phase. B Same patient, several years later.

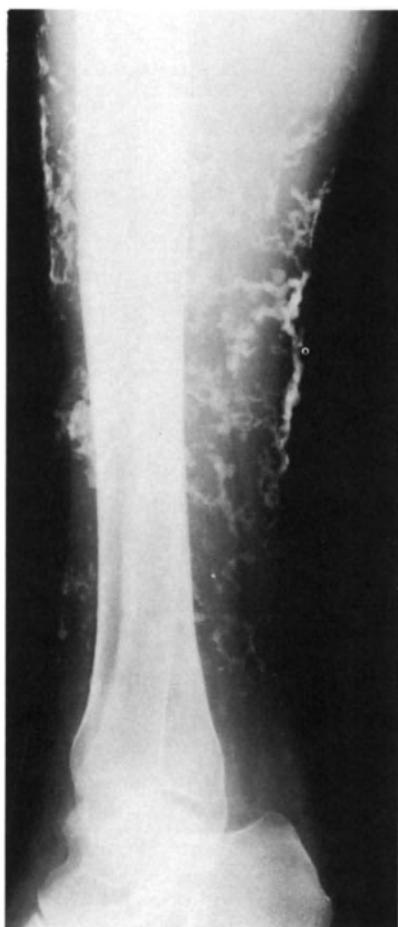


Fig. 22.15. Calcification due to brawny edema caused by varicose veins.



Fig. 22.16. Calcification and soft tissue loss in fingertips due to systemic sclerosis (scleroderma).



◀ Fig. 22.17. Dermatomyositis causing extensive calcification over almost the entire body.



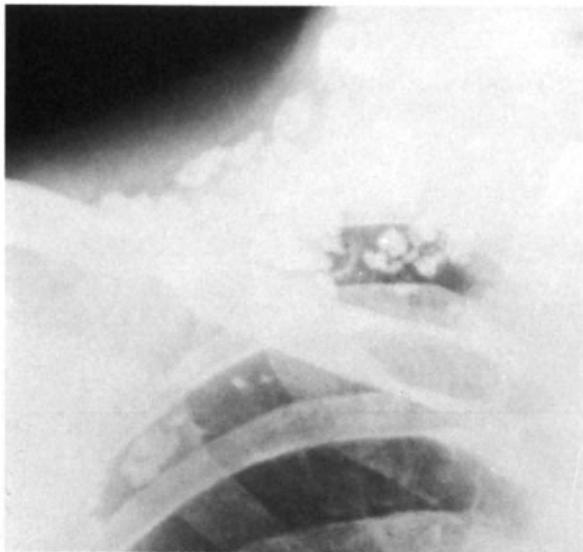
Fig. 22.19. Tumorous calcinosis in both axillae.



Fig. 22.18. Calcification in rotator cuff of shoulder.



Fig. 22.20. Calcification in large thyroid adenoma.



**Fig. 22.21.** Calcification in lymph nodes due to tuberculosis.

### Infection

1. *Granulomatous*. This is seen particularly following tuberculous infections and may occur in the regional lymph nodes (Fig. 22.21). Very rarely, chronic abscesses calcify in children with chronic granulomatous disease.

2. *Parasitic*. *Cysticercosis*. Ingestion of ova of *Tenias soleum* is followed by penetration of the embryos from the gut into the bloodstream. Some are carried to the muscles and when they die become calcified, leaving characteristic oval opacities. These tend to lie in the direction of the muscle fibres and may be present in very large numbers (Fig. 22.22).

*Loa-loa*. This occurs in West Africa and is caused by microfilaria. It is seen most commonly as tiny calcified coiled threads in the soft tissues of the hand following the death of the causative organism.

*Guinea worm* (*Drucunculus medinensis*). Again the organism calcifies after its death, producing elongated areas of calcification. These may become crushed into oval lesions by muscle action (Fig. 22.23). The disease occurs in India, the Middle East and Africa.

*Armillifer armillatus* causes characteristic comma-shaped calcification in the chest and abdomen. This, however, is not strictly within soft tissues but is situated in the pleura and peritoneum. The causative organism is an arthropod carried by snakes.

The cysts of *Trichinella spiralis* are not visible on radiographs.

### Soft Tissue Ossification

#### Congenital

*Myositis ossificans congenita* is a rare inborn abnormality. Most cases probably arise as a primary mutation but it may be heritable as an autosomal dominant. Ossification occurs primarily in the perimuscular fascia (Fig. 22.24A), causing severe disablement. The condition is associated with an



**Fig. 22.22.** Cysticercosis. Numerous calcified cysts in muscle.

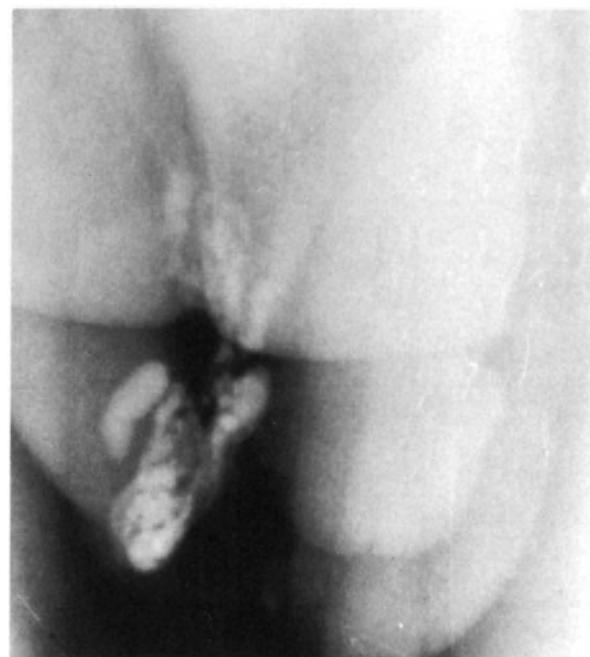


**Fig. 22.23.** Calcified guinea worm in scrotum.

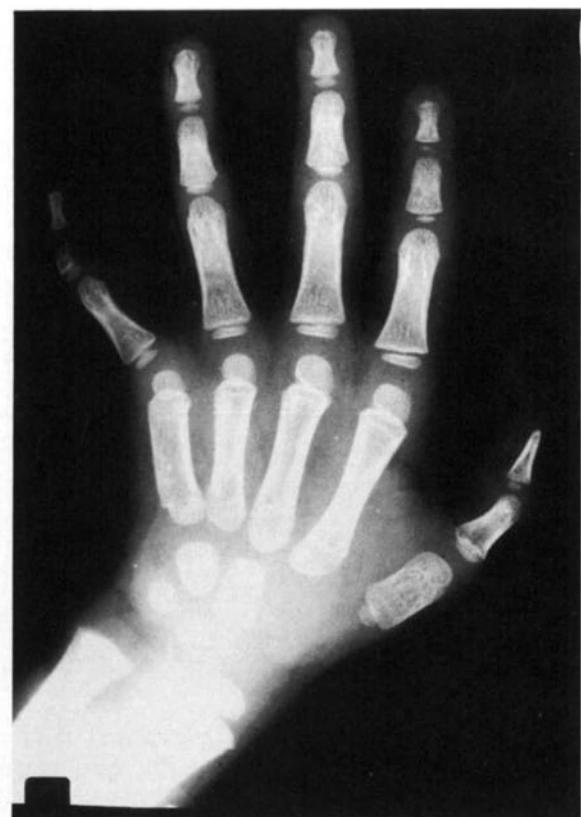


Fig. 22.24. A Myositis ossificans congenita. Note sheets of ossification in the soft tissues. B Short thumb metacarpal. C Anomalies of cervical spine.



Fig. 22.25. Ossification in traumatic myositis ossificans.

abnormally short metacarpal of the thumb and metatarsal of the big toe (Fig. 22.24B) and there may be abnormalities of vertebral bodies (Fig. 22.24C).

#### Traumatic

Ossification may occur near fractures, particularly in the brachialis and quadriceps femoris muscles (*traumatic myositis ossificans*) (Fig. 22.25). Areas of ossification may also result locally from repeated minor trauma such as the '*rider's bone*' near the acetabulum or the ossification in the medial collateral ligament of the knee (*Pellegrini-Stieda lesion*). Ossification may also occur in surgical scars; their linear nature provides the diagnosis. Certain ligaments, particularly the *ligamentum nuchae*, the *iliolumbar* and *sacrotuberous ligaments* (Fig. 22.26), are also liable to undergo ossification.

Unexplained myositis ossificans in a young child should give rise to the suspicion of non-accidental injury.

#### Paraplegic.

Very extensive soft tissue ossification, usually related to joints and most commonly round the hip, may occur in patients with paraplegia (Fig. 22.27). It is commonly found in children with spina bifida with severe neurological deficits in the lower limbs. The reason for the development of the new bone is unknown. Similar ossification has been observed around joints in patients who have suffered extensive burns (Fig. 22.28).

#### REFERENCES AND SUGGESTIONS FOR FURTHER READING

- Deithelm L (ed) (1968) Roentgen diagnosis of the soft tissues. In: Encyclopedia of Medical Radiology, vol 8. Springer Verlag, Berlin  
 Starer F (1987) The soft tissues. In: Sutton D (ed) Textbook of Radiology and Imaging 4th edn, vol 2. Churchill Livingstone, Edinburgh



Fig. 22.26. Calcification in sacrotuberous ligament (arrowheads).



Fig. 22.27. Ossification in paraplegia.



Fig. 22.28. Ossification in soft tissues following burns.

## CHAPTER 23

# MAMMOGRAPHY

*R. McLelland*

---

Mammography has assumed an increasingly important, if not the most important, role in the earlier detection of breast cancer. At present this is the only means of reducing overall mortality from this disease. It requires reproducible optimum technique and recognition and accurate interpretation of the mammographic signs of malignancy. These two points will be the major considerations of this chapter. Initially, however, some of the other factors affecting survival and mortality from this disease will be considered.

In the USA, 10% of women will develop breast cancer during their lifetime. Breast cancer is second only to carcinoma of the lung as the cause for most cancer deaths in women, and in the USA kills almost as many as the total number of people killed in motor vehicle accidents. It is a disease of ageing and is slowly increasing in incidence, though with some corresponding improvement in survival. The overall mortality rate has remained unchanged for over 60 years. It has been suggested that many, if not most, of these patients could be cured by early detection when the disease is confined to the breast. Mammography can thus improve survival and reduce mortality from breast cancer. It is much more sensitive than breast physical examination for earlier detection and is the only means of detecting non-palpable cancers. However, it is not infallible and consequently mammography and breast physical examination still remain complementary procedures, although the role and effectiveness of breast self-examination in this earlier detection effort are much less clear.

The indications for mammography are:

1. First and foremost to detect earlier breast cancer, especially when it is not palpable and when survival and mortality rates are materially improved.
2. To assist in the evaluation of symptomatic breasts for management decisions but more important to detect unsuspected cancer in the symptomatic and/or opposite breast.

3. To serve as a baseline for comparison with subsequent mammography for more accurate interpretation and earlier detection.

For those reasons the generally accepted guidelines for mammography in the USA are:

1. In symptomatic women it is an essential part of the diagnostic workup.
2. In asymptomatic women (screening):
  - a. First or baseline mammography is recommended by age 40 years.
  - b. At 1–2 year intervals at age 40–50 years based on the combined analysis of mammographic and physical findings and other risk factors, unless medically indicated sooner.
  - c. Annually after age 50 years.

Other imaging modalities such as ultrasound, light scanning, thermography, CT and MRI have all been used but lack the sensitivity to substitute for mammography in either screening or diagnosis.

The evidence is overwhelming that there is considerable breast cancer in women under 50 years of age and that the most effective way of detecting it at an earlier, more curable stage is by screening, especially by mammography. The radiation risk from modern mammography properly performed is not proven, if not non-existent, in women over age 35 years and it must be compared with the proven benefits.

## MAMMOGRAPHY IMAGING OPTIONS AND TECHNICAL CONSIDERATIONS

Optimum mammography requires proper equipment (Fig. 23.1A, B), meticulous attention to technical considerations, familiarity with the early and indirect mammographic signs of malignancy, and correlation with clinical findings.

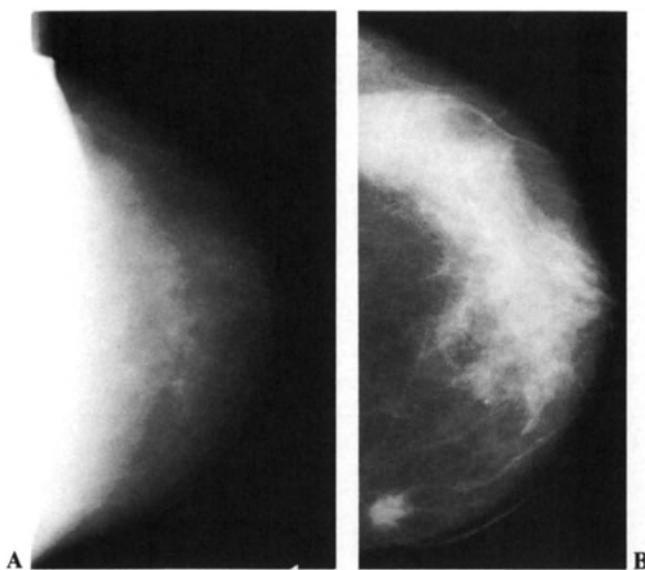


**Fig. 23.1A, B.** The necessity for dedicated mammography equipment. **A** A mammogram made with general diagnostic X-ray equipment and inadequate compression. There is a hint of some skin changes medially but the stellate cancer that is obvious in **B** is not evident and was missed. **B** The same breast imaged with dedicated mammography equipment without a grid readily demonstrates the cancer and skin changes.

Mammography is possibly the most technique-dependent procedure in all of diagnostic radiology. Reproducible optimum images are the cornerstone for accurate interpretation and best results. At present, the two most acceptable methods are film-screen and xero-mammography.

#### Film-screen Mammography

If film-screen mammography is the method of choice, it should be performed with an X-ray unit specially designed for mammography (dedicated) to include:

1. Preferably a constant potential or three-phase generator to provide shorter exposure times and reduce the possibility of motion unsharpness; and controls with a capacity for 1 kVp changes.
2. An X-ray tube with an adequate power rating (heat capacity) and current capability (mA) related to voltage (kVp), focal spot sizes, length of exposure (mAs), and source-image distance (SID).
3. An X-ray tube with a molybdenum target because of its low peak kV spectrum; an added very thin (0.03 mm) molybdenum filter to eliminate the higher and very low energy X-rays and 'clean-up' the beam; and a beryllium window to reduce filtration of this soft X-ray beam by the tube housing.

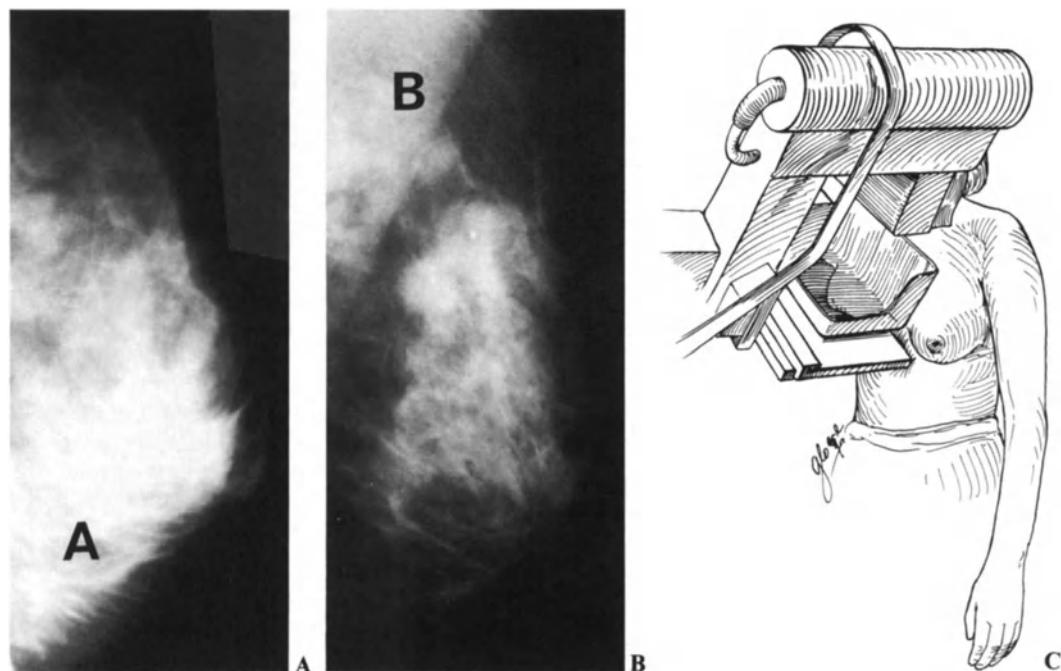


**Fig. 23.2A, B, C.** The advantages of the oblique medial-lateral view and the use of grids. **A** A straight medial-lateral view without a grid does not image the posterior margins or the structural detail of the dense fibro-glandular tissue. It does demonstrate the 1.5 cm stellate rounded cancer deep in the upper part of this breast but not nearly as well as on the oblique view. **B** An oblique medial-lateral view with a grid images the cancer and the rest of the breast much better but also enlarged metastatic axillary lymph nodes. The grid reduces scattered radiation with much better detailed resolution than on **A**. **C** Positioning for the oblique medial-lateral view (from Bassett and Gold).

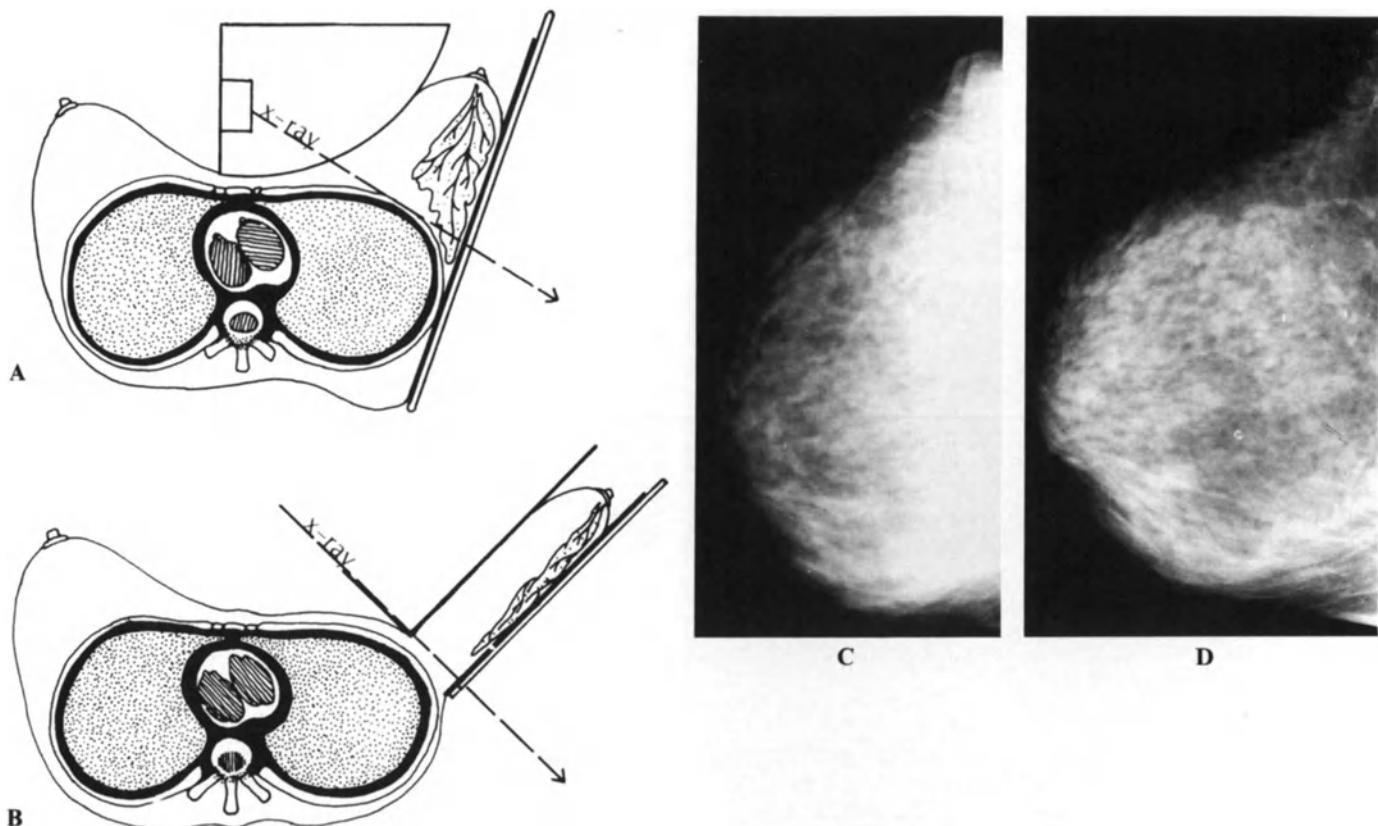


**Fig. 23.3A, B, C, D.** The virtues of proper vigorous breast compression. (From Logan WW & NCRP Report 85.) A A sloping or rounded compression device and the expected unsatisfactory results C. B A right-angled compression device uniformly flattens the breast for the straight medial-lateral view with excellent results D.

4. Preferably *measured* dual focal spots of 0.6 mm or less (0.1–0.2 mm for magnification views) for sharp, high resolution images. Magnification views are a useful adjunct to assess more precisely obscure lesions noted on one or both of the conventional views. Occasionally it will also reveal an unsuspected finding that will render a more definitive diagnosis (Fig. 23.2B).
5. Automatic exposure control with adequate density control and automatic adjustments for non-grid, and magnification techniques.
6. A source-image distance of at least 50 cm to reduce geometric unsharpness; and proper alignment of the cassette tray and the X-ray tube focal spot.
7. A single intensification screen with a small particle phosphor in contact with the single emulsion side of film with a spectral response matched to the light from the intensification screen is an excellent and the preferred image receptor combination.
8. Positioning is critical. The oblique medial-lateral view is a significant improvement over the straight lateral view especially in terms of visualizing the posterior and axillary parts of the breast (Fig. 23.2A, B, C). The cranio-caudad view usually completes the examination but mammography should be tailored to the needs of the

- individual patients and may require additional views including spot compression, magnification, and others.
9. Vigorous compression of as much of the breast as possible is essential so that it is a uniform thickness, preferably less than 5 cm. To do this, the compression device cannot have sloping or rounded edges (Fig. 23.3A–D). Compression reduces the object-film distance and thereby reduces geometric unsharpness. It also separates the internal structures of the breast for better visualization of abnormalities and reduces the likelihood of superimposed or summation densities that are a frequent cause of 'over-read' or false positive interpretations (Fig. 23.4A, B). It provides a more uniform film density by flattening the breast to a more two dimensional structure (Fig. 23.3B, D) and facilitates distinction between more compressible benign and less compressible denser malignant lesions. The amount (dose) and energy (better contrast) of radiation exposure is reduced by reducing the thickness of the breast and compression immobilizes the breast and thereby reduces motion unsharpness. Finally it improves resolution and image quality by reduction of scatter.
  10. If the breast cannot be compressed to less than 5 cm, it is probably dense or 'fibrocystic' and a special mammography grid should be used to reduce scatter and

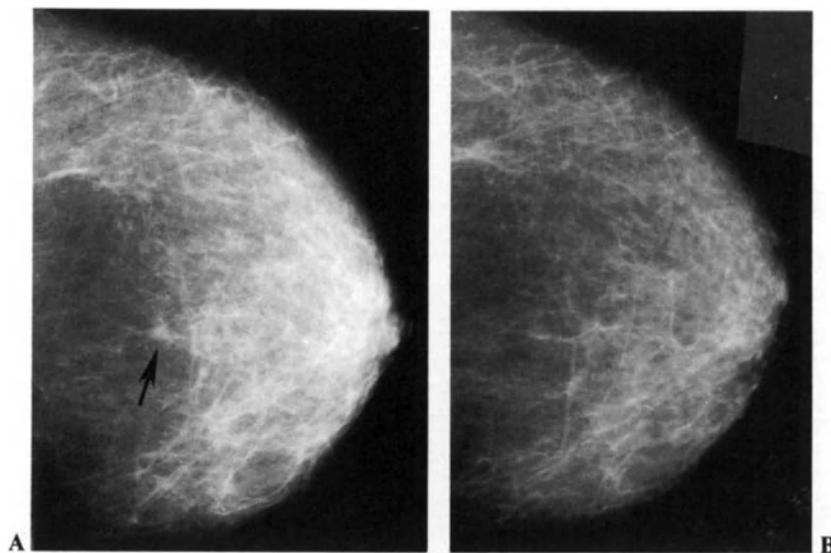


**Fig. 23.4A, B.** False positive mammography due to a summation shadow. The patient was referred to us for pre-operative mammographic localization of a small non-palpable stellate mass only seen on this crano-caudad view. A finding this far anterior in the breast and only seen on one view is very suspicious for a summation density. B Repeat examination with grid technique was negative and confirmed our impression of a false positive interpretation. The localization procedure was cancelled. Comment: localization of a non-palpable lesion necessitates its demonstration on two orthogonal views whether with mammography, ultrasound or even CT.

thereby improve resolution and image quality (Fig. 23.2A, B). This is preferably reciprocating although a stationary grid is certainly acceptable, with a 3.5 to 1 grid ratio. Most mammography is done with a grid because of the inability of clinical examination to predict breast density.

#### 11. Careful processing is essential to produce an optimum end product and is often the weakest link in the system.

Film-screen mammography should not be attempted without these equipment and technical prerequisites. It should be emphasized that conventional radiology equipment is unacceptable for film-screen mammography (Fig. 23.1A, B).

### Xero-mammography

Advantages of the xero-mammography method include:

1. *A wide recording latitude* providing good visualization of the entire breast, regardless of variations in thickness or density. However this is at the expense of differences in density (broad area contrast), such as distinguishing a mass in dense fibro-glandular tissue, although this has significantly improved with the new liquid toner system.
2. *Edge enhancement*, which facilitates the detection of calcifications and other sharply defined structures such as masses and linear spicules.

Another advantage is the ability to use a general diagnostic machine with an overhead X-ray tube with a tungsten target and 1–2 mm focal spot. However, because of the larger focal spot, this requires a long source to image distance to reduce geometric unsharpness. It also restricts the use of multiple projections, and it takes longer to do the examination. There should be added aluminum filtration to

'harden' the X-ray beam to penetrate the denser and thicker parts of the breast. The compression device is usually detached and more curved to obtain the medial-lateral view which includes part of the chest wall. It necessitates positioning of the cassette more posteriorly on the chest (Fig. 23.3A) and the interposition of a non-opaque sponge to support the breast. This displaces it away from the cassette, thereby increasing the object to image distance and, at least theoretically, geometric unsharpness. The edge enhancement of xero-radiography compensates for this and it does not seem to be a significant problem in clinical practice. However proper positioning is equally important with xero-mammography (Fig. 23.5A, B). Although, for technical

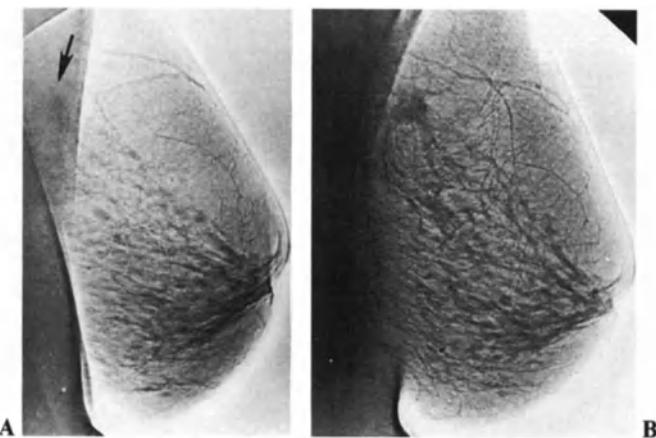


**Fig. 23.5A, B.** Good and bad positioning with xero-mammography. A Note the superimposed opposite side of the chest obscuring the posterior part of this breast and the chest wall on this medial-lateral view. A 1.5 cm stellate cancer (arrow) is obscured by the axillary fold in A, but clearly shown in B.



**Fig. 23.6A, B.** Good and bad compression with xero-mammography. **A** A medial-lateral view with excellent position and compression separating the structures within the breast. This reduces the likelihood of false positive summation shadows and enhances the chances of earlier detection of cancer. **B** Poor compression and positioning with incomplete visualization of a homogeneously dense breast which markedly limits the effectiveness of the examination.

reasons compression of the breast is less critical than with film-screen mammography, it remains very important for all of the other reasons cited with film-screen mammography but especially the separation of the internal structures of the breast and the many superimposed densities (Fig. 23.6A, B) that are a frequent cause of false positive interpretations. There is 20%–30% reduction in the X-ray dose required for imaging with the negative compared to the positive mode and even greater reduction (50%) with the new liquid toner system as well as improved broad area contrast and resolution.

#### THE MAMMOGRAPHIC SIGNS OF MALIGNANCY

There are no absolutely pathognomonic mammographic signs of malignancy. There are benign lesions that can look exactly like malignancy (Figs 23.29–23.31) but fortunately this is not common. Findings must be evaluated on the basis of probability. Correlation with the clinical history and physical and laboratory findings can be helpful in this assessment, but in the present era of earlier detection, especially of non-palpable lesions in asymptomatic women (screening), it has become increasingly important if not essential to make decisions on the basis of mammographic findings alone. This has greatly increased the responsibility of the radiologist. The untrained, inexperienced and/or insecure radiologist may

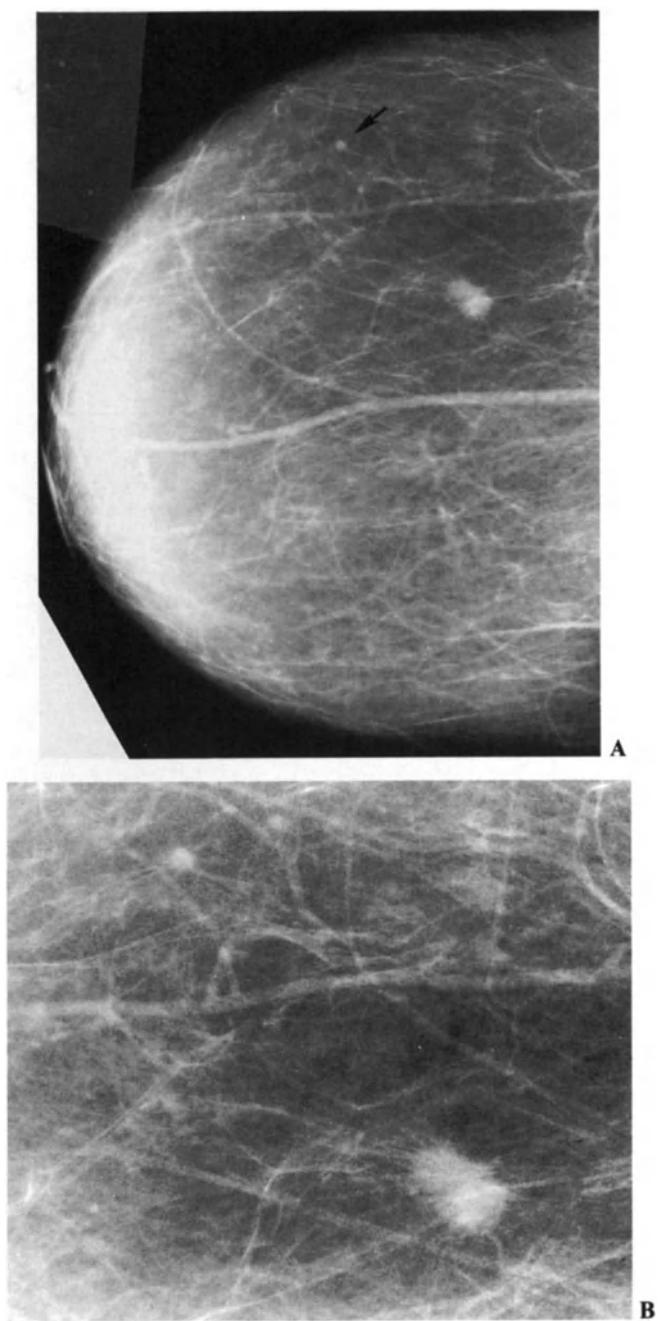


**Fig. 23.7A, B.** Multicentric stellate breast cancer. **A** The 1-cm stellate cancer is obvious but the much smaller one (arrow) is less so and would be much more difficult to see in a dense breast. **B** The numerous fine spicules radiating from both cancers are better seen with a magnifying glass.

often respond by over-reading (Fig. 23.4A, B) resulting in an increased number of false-positive mammograms. Inevitably these lead to additional tests and unnecessary biopsies.

#### The 'Classical' or Direct Mammographic Signs of Malignancy

A mass, usually stellate or spiculated (Figs 23.7–23.10) but occasionally circumscribed (less than 5%) (Figs 23.13,

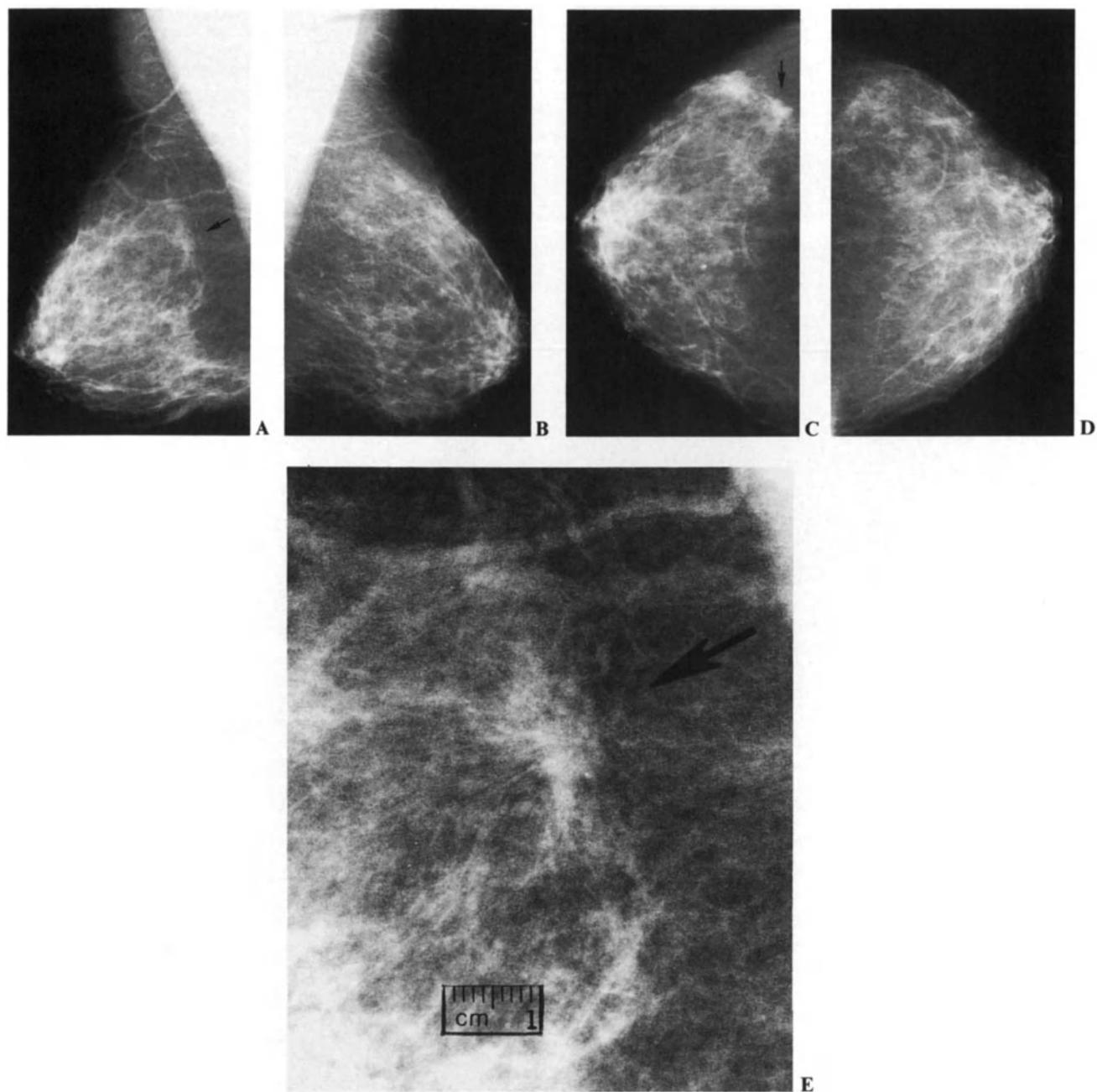


**Fig. 23.8A–E.** A less evident stellate cancer in a denser breast. Comparison of the breasts on oblique medial-lateral (A, B) and cranio-caudad (C, D) views revealed asymmetry with a small focal density in the right upper outer quadrant (arrows). Inspection with a magnifying glass (E) readily demonstrates it is stellate and contains fine calcification. This was a 6-mm infiltrating duct carcinoma.

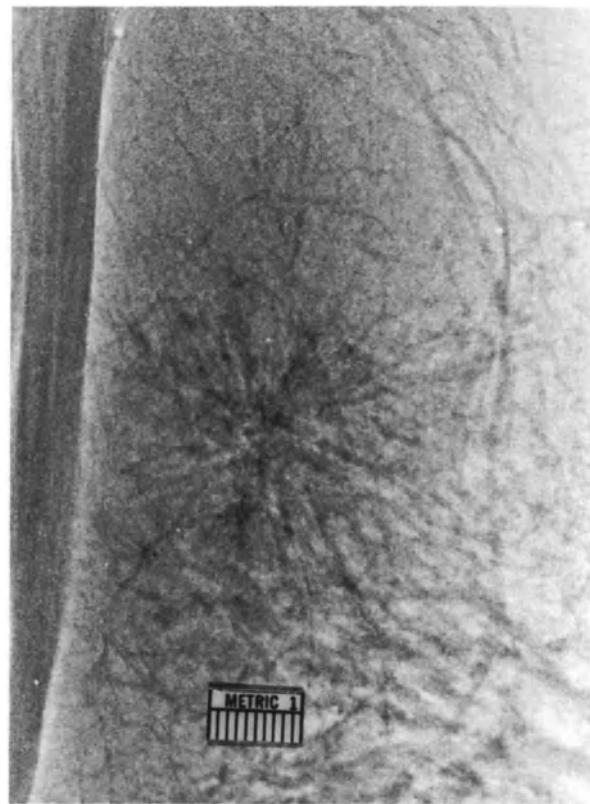
23.15), and often of mixed configuration. The border characteristics of masses are important determinants in assessing whether they are benign or malignant and at times are best demonstrated with compression spot or magnification views.

A stellate or spiculated mass is the most pathognomonic mammographic sign of malignancy (Fig. 23.11). There is controversy over the origin and character of the spicules. Theories include desmoplastic reaction provoked in the sur-

rounding breast tissue by the multiplying cancer cells and resulting in retraction of connective tissue elements with reoriented trabeculae, septa, and Cooper's ligaments, extension of the carcinoma and a combination of both. The first concept is supported by evidence that as the cancer progresses, its growth takes place mainly between and/or around the spicules which are often preserved as connective tissue bands or scaffolding between or among the proliferating

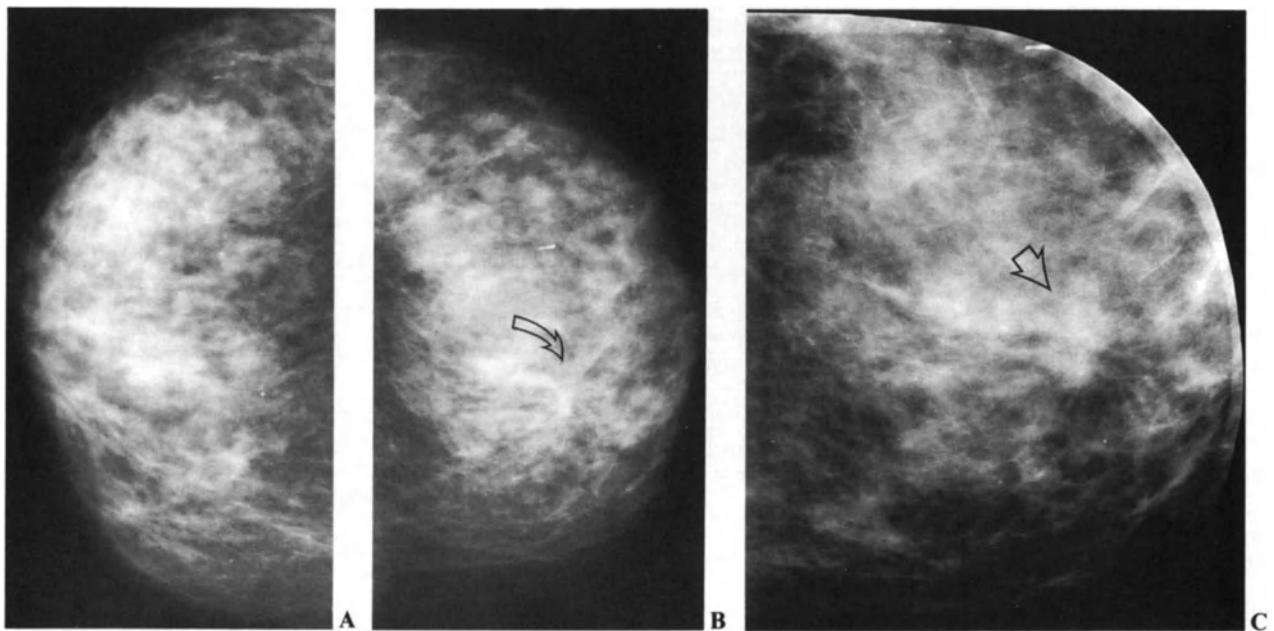
**A****B**

**Fig. 23.9A, B.** Stellate architectural distortion. Note asymmetry on the left (A) with increased density and a small area of stellate architectural distortion in the subareolar region, best seen when compared with the image of the other breast (B). This was a 6-mm infiltrating duct carcinoma.



METRIC 1  
1 2 3 4 5 6 7 8 9 10

**Fig. 23.11.** A large stellate area without a central mass. Note the central lucencies in this large stellate area which suggests a benign lesion. It was palpable and looked like cancer at surgery and on frozen section. However, it was sclerosing adenosis, a great imitator of cancer. Comment: this suggests that with optimum imaging and meticulous interpretation some of these lesions could be followed carefully rather than biopsied.

**A****B****C**

**Fig. 23.10A–C.** Additional views for the evaluation of an obscure finding. These are very dense breasts but there is asymmetry and a suggestion of a small stellate area in B (arrow) especially on comparison with the other breast (A). A coned magnification view (C) better demonstrates this 5-mm infiltrating duct carcinoma.

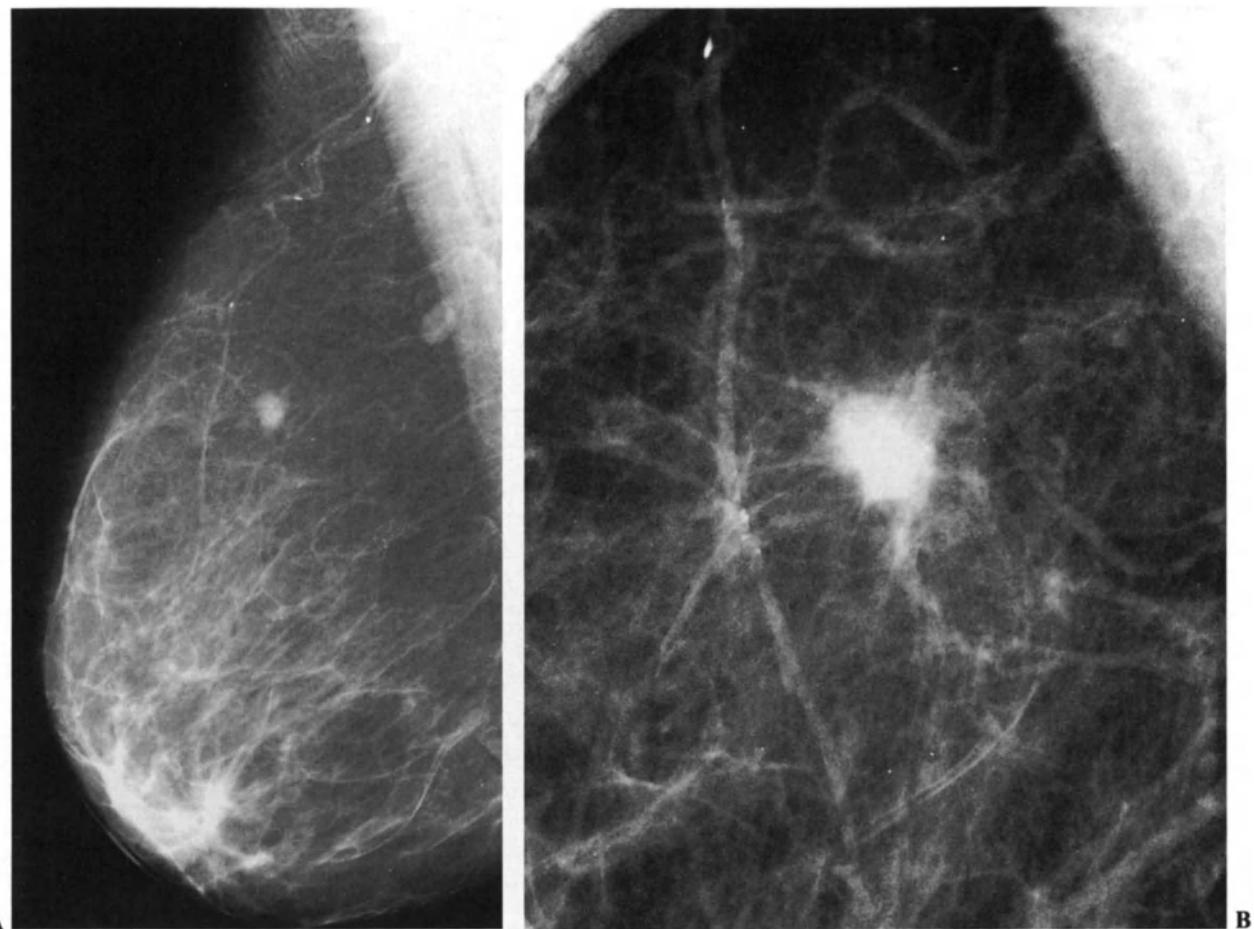


**Fig. 23.12A, B.** Magnification for better evaluation of a mass. **A** Note the small ovoid dense (much denser than the large lymph node toward the axilla) circumscribed mass. **B** A coned magnification view with more vigorous compression clearly demonstrates the increased density even with marked compression, and the numerous spicules radiating from this stellate infiltrating duct carcinoma.

cancer cells. Furthermore, these spicules are often lost after surgery, supporting the concept of more or less anchored bands of connective tissue.

Malignant masses that appear circumscribed at first glance are often spiculated on closer inspection or with coned and/or magnification views (Fig. 23.12A, B). The size of a truly circumscribed mass is often used as a determinant for management decisions with those over 1 or 1.5 cm in diameter meriting further investigation. However, the age of the patient and her estrogen status, history, and clinical findings are equally important factors. A 2-cm palpable circumscribed mass in a 35-year-old woman, even if it was not present in a previous examination, is of less significance than a new enlarging 1-cm non-palpable mass in a 60-year-old woman especially if the latter is not receiving estrogen replacement therapy (Fig. 23.15A, B). The former is usually benign (a fibroadenoma or cyst) whereas the latter has a significant possibility of being cancer. Both merit further investigation with needle aspiration or ultrasound and possibly cytology which can usually make these distinctions if not establish the diagnosis.

Malignant masses are usually less compressible and main-

tain their shape and size even with vigorous compression. They are also usually denser than the fibro-glandular tissue present whereas benign masses are usually the same density and more compressible. With palpable masses, percutaneous

---

**Fig. 23.13A–D.** A role for breast ultrasound. **A** Note the non-palpable sharply circumscribed ovoid 2-cm mass deep near the chest wall. **B–D** Ultrasound revealed it was solid (very echogenic), sharply marginated, and consistent with fibro-adenoma or medullary carcinoma. Biopsy revealed an infiltrating duct carcinoma. Comment: fine needle aspiration cytology is an increasingly useful procedure to evaluate lesions like this. It requires considerable cytology expertise and under those circumstances realizes a false negative rate of less than 10% and very rare false positives (usually fibro-adenomas). With this non-palpable mass it could have been done under ultrasound guidance.

**Fig. 23.14A–C.** Management of a non-palpable circumscribed mass. **A** There is a 3-cm round circumscribed mass in the medial part of this breast. **B** Ultrasound revealed it was cystic (good through transmission of sound with a smooth back wall and negligible internal echos). Needle aspiration under ultrasound guidance revealed sero-sanguinous fluid which raised the question of an intra-cystic carcinoma. **C** Pneumo-cystography revealed a simple cyst with no evidence of malignancy. Follow-up has been uneventful.



Fig. 23.13.

A



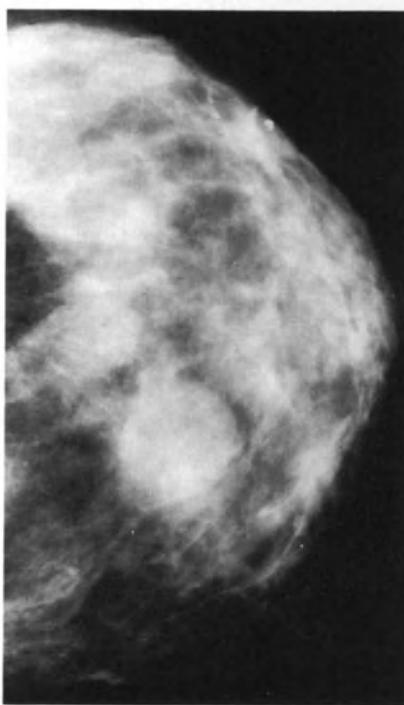
B



C



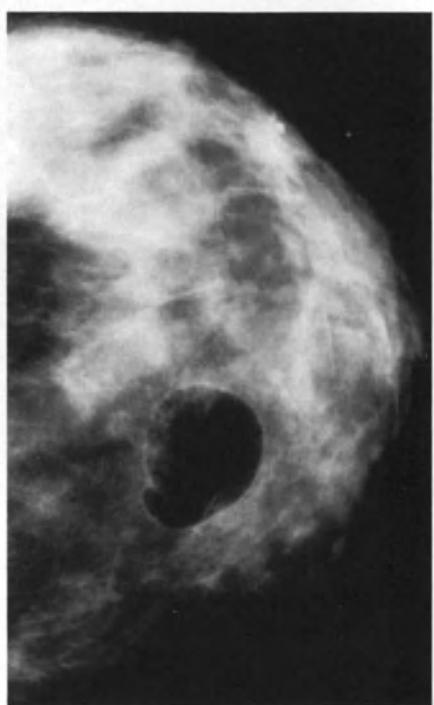
D



A



B



C

Fig. 23.14.

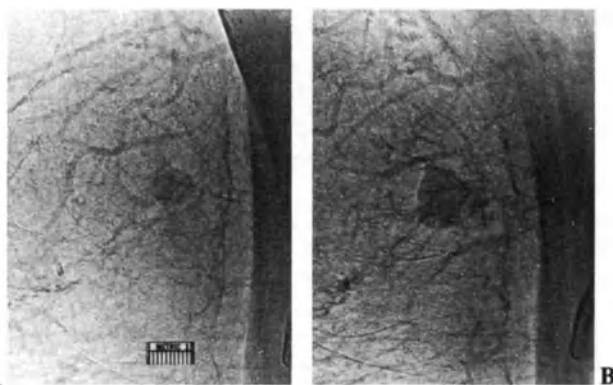


**Fig. 23.15A, B.** A small circumscribed mass. Annual screening of this asymptomatic post-menopausal woman revealed a small (A) but enlarging (B) non-palpable circumscribed mass first thought to be a lymph node. It was an intra-ductal carcinoma with a focus of invasion.

needle aspiration will usually clarify any ambiguities. Ultrasound, with or without needle aspiration, can make rather precise cyst-solid differentiations with non-palpable masses (Figs 23.13, 23.14, 23.16).

**Calcification.** *Malignant* calcifications are usually small to fine size and often difficult to see without the aid of a magnifying glass. They are clustered and/or linearly disposed within

**Fig. 23.17.** Benign calcification. The large calcification is in a palpable old degenerated fibro-adenoma (arrow). It should not distract from the detection of the non-palpable stellate cancer in the opposite side of this breast (arrowhead).

**Fig. 23.18.** Irregular benign calcification. There are extensive coarse irregular calcifications without clustering or other features of malignancy. Follow-up has revealed no change.

**Fig. 23.19.** 'Classical' malignant calcification. Clustered fine branching calcifications that are irregular in size, shape and density and are more readily and better seen with a magnifying glass. This was an intra-ductal carcinoma.

**Fig. 23.20.** Bothersome calcification. Note the similarity with Fig. 22.19 but despite the clustering and suggestive branching patterns, these calcifications are very coarse and some have lucent centers indicating benign disease.



ducts and are often irregular in size, shape and density with branching patterns (Figs 23.19, 23.21, 23.22, 23.27, 23.31). *Benign* calcifications are usually larger, more readily seen and similar in appearance with less tendency for clustering (Figs 23.17, 23.18, 23.20, 23.24, 23.26, 23.28). Thus calcifications are often obviously malignant or benign but in a significant percentage of instances the distinction is not

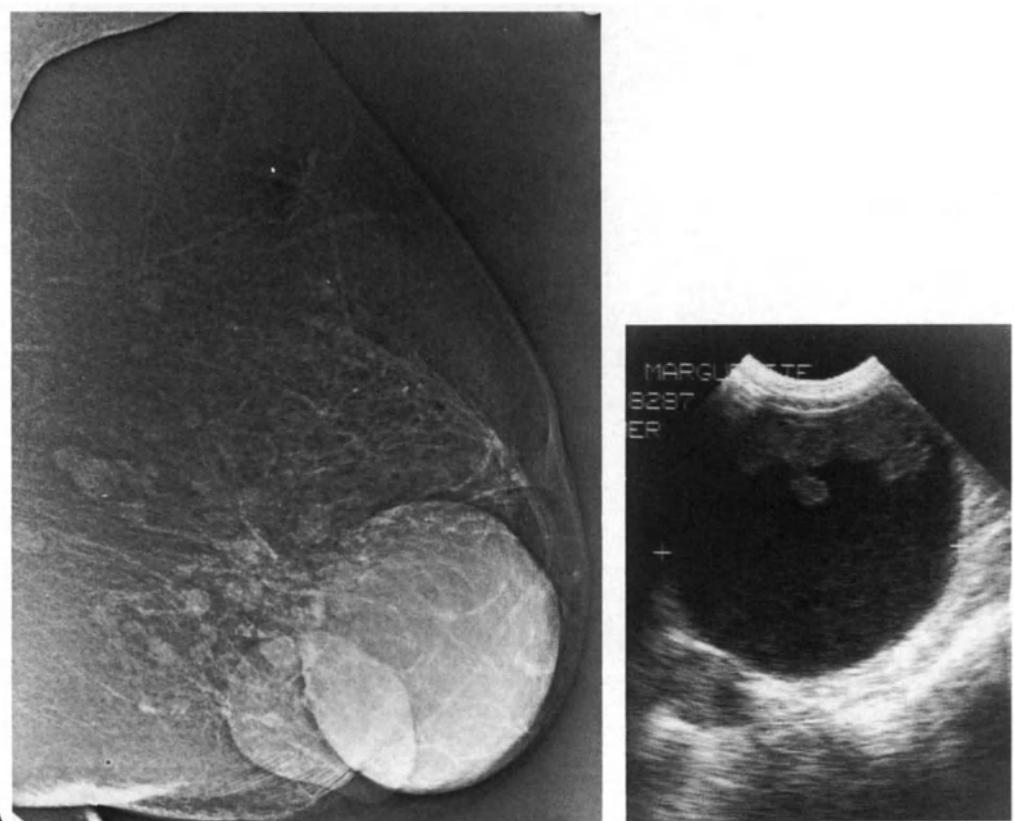


**Fig. 23.16A, B.** Ultrasound evaluation of masses. Several large well-circumscribed masses are noted (A). Ultrasound revealed multiple cysts with an irregular polypoid mass within one of them. This was an intracystic carcinoma. (From Dr Carl J. D'Orsi, University of Massachusetts Medical School.)

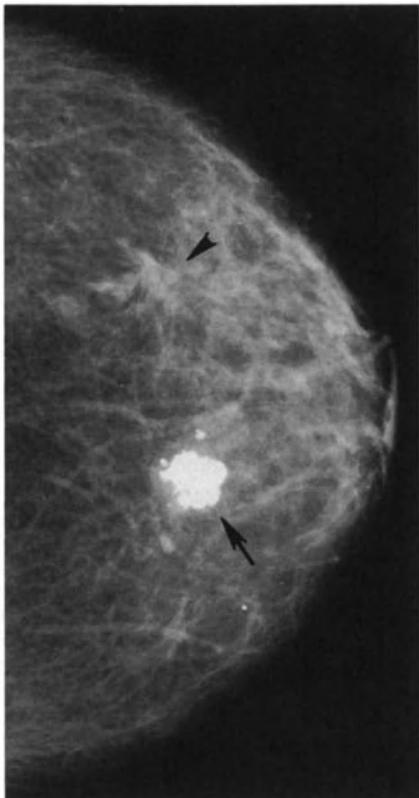


Fig. 23.17.

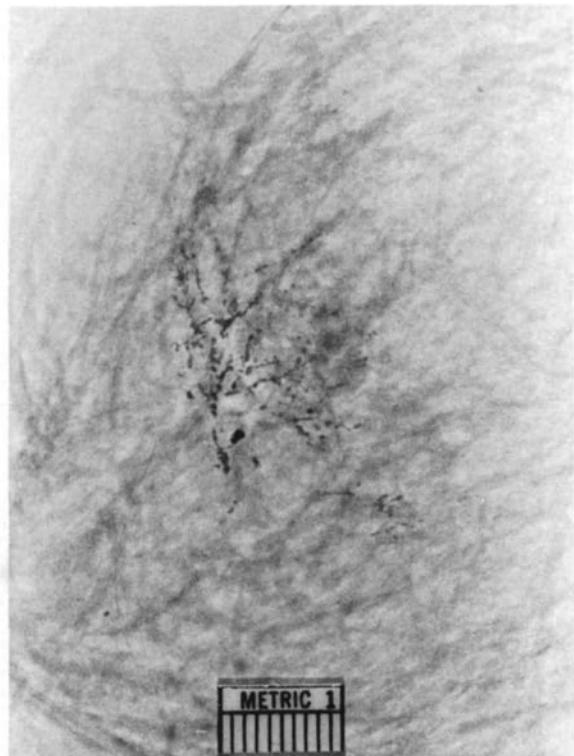


Fig. 23.19.



Fig. 23.18.

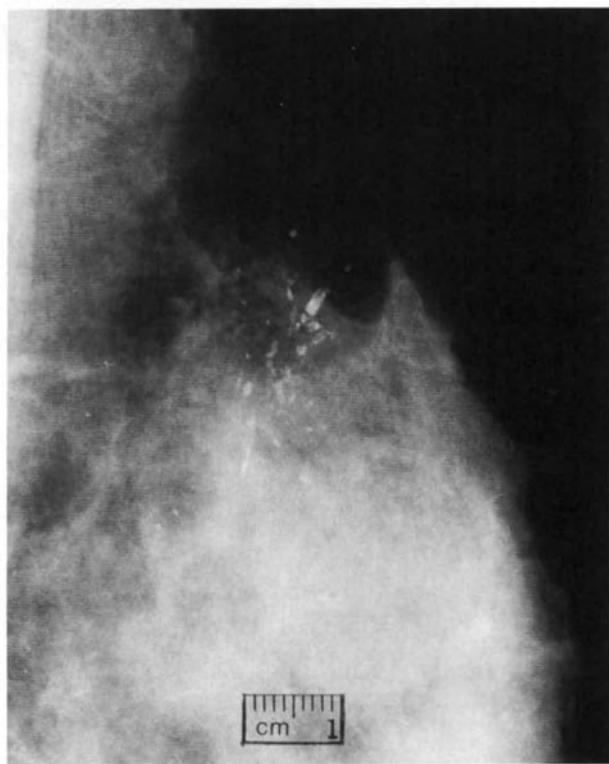
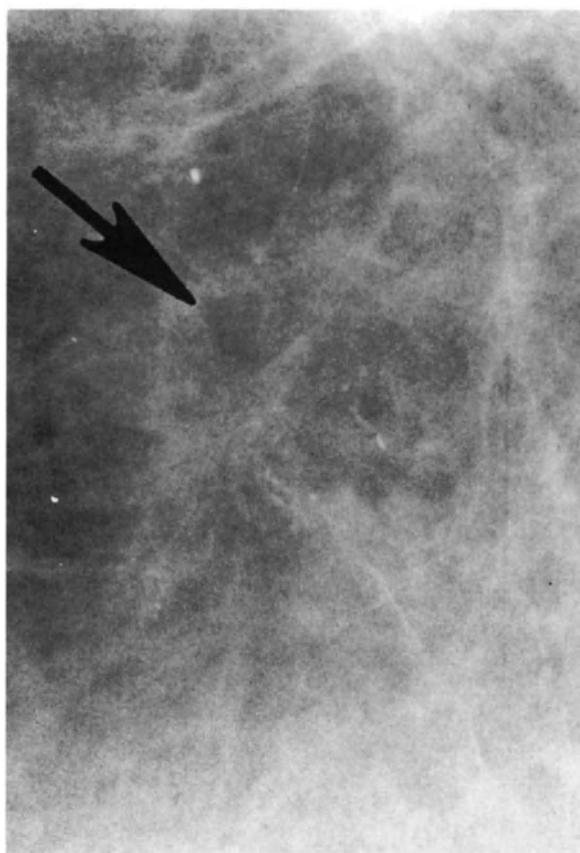


Fig. 23.20.



**Fig. 28.21.** Subtle malignant calcification. The routine mammograms suggested some calcification on the left. A magnification view better demonstrated a small cluster of fine irregular calcification better seen with a magnifying glass. This was a minimal infiltrating duct carcinoma.

clear cut (Figs 23.23, 23.25, 23.30). Compression spot and/or magnification views will often clarify this but when they do not, short-term follow-up if not biopsy is indicated.

These direct mammographic signs of malignancy can be very subtle and are more easily described than detected and recognized, especially in dense breasts. The variations and settings of both of these signs separately and in combination are numerous and require careful analysis for best results.

In addition, there are indirect mammographic signs that should alert one to the possibility of malignancy. They are often best recognized by comparison with previous studies for any change and include:

1. *A stellate area of architectural distortion without a definite mass* (Figs 23.9, 23.10) and which may represent an earlier manifestation of a stellate mass. This should be considered evidence of malignancy until proven otherwise.

2. *A less specific focal developing density* noted on comparison with previous mammograms (Fig. 23.32). The breast is an involuting structure with progressive replacement of the dense fibro-glandular tissue with lucent fat. With regular screening mammography, any new finding between examinations, regardless of how innocuous it may appear, must be viewed with suspicion and could be called a developing density whether it is a mass (stellate or circumscribed), malignant type calcification, stellate architectural distortion, or a focal density that, otherwise, defies description (Fig. 23.32). The latter is what is often meant by the developing density sign. It is a less specific but nevertheless important indirect sign of malignancy.

3. *Focal but especially isolated duct prominence* (Fig. 23.33). This is much less common, usually benign and due to simple ectasia or papillomatosis. However, it assumes greater significance if there is a spontaneous bloody discharge from this

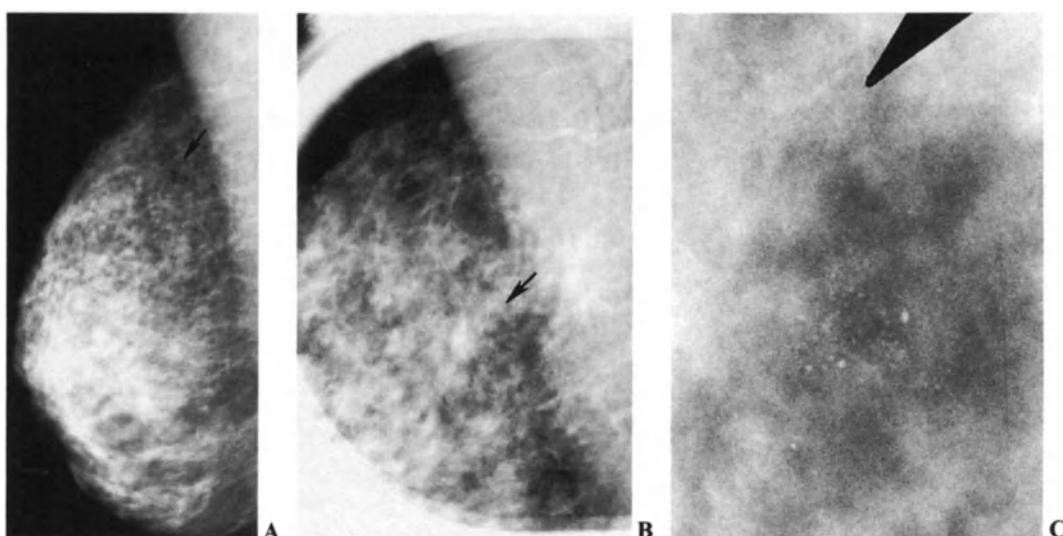


**Fig. 23.22A, B, C.** A role for magnification views. A An oblique medial-lateral mammogram reveals a dense breast with two calcifications superiorly (arrow). B A coned magnification view with vigorous compression revealed numerous clustered fine calcifications which are irregular in size, shape and density but also an unsuspected small stellate mass in the same location (arrow). This combination of findings is very suspicious if not pathognomonic for cancer, which this proved to be. C The clustered calcifications are more readily and better seen with a magnifying glass.

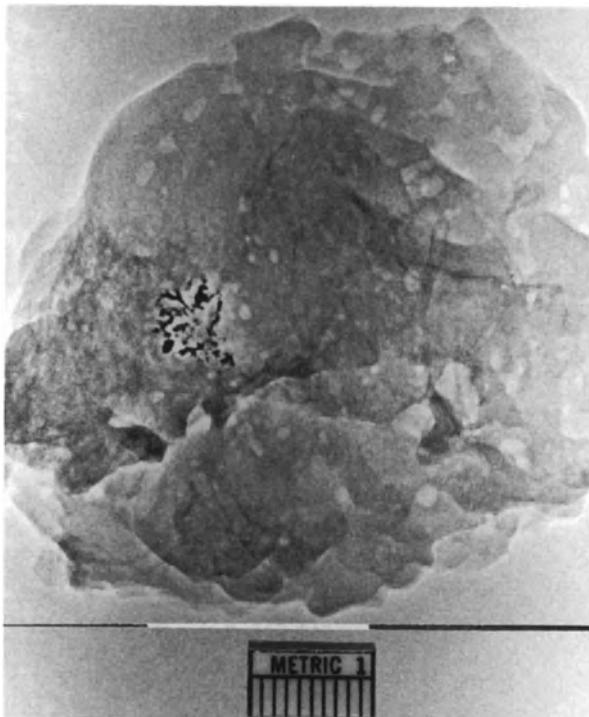


**Fig. 23.23.** Calcification simulating malignancy. Although some of these are quite coarse and they were easily seen without the aid of a magnifying glass, this is a cluster of numerous calcifications with considerable irregularity including branching patterns. This is another example of the great imitator, benign sclerosing adenosis.



**Fig. 23.24.** Benign or malignant calcification? This is a cluster of small calcifications that vary in size but they are all smooth and round or oval with a central one that is ring-shaped. Furthermore, they were only evident on one view and further examination revealed they were in the skin and obviously benign.

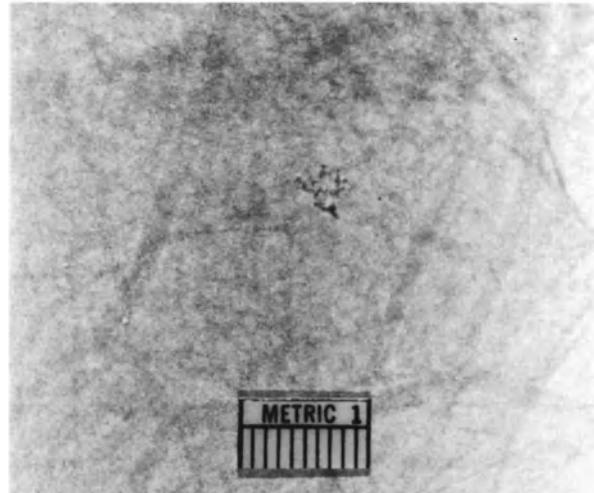


**Fig. 23.25.** Malignant-type calcification. Verified resection and histologic identification revealed benign changes with no evidence of malignancy. Long-term follow-up has been uneventful. Comment: these are suspicious for malignancy and biopsy was justified. Experience and judgement determine whether to biopsy or follow findings such as these.

duct or there are other findings to suggest malignancy (malignant type calcification and/or an associated mass).

The use of the term *asymmetry* as a separate indirect mammographic sign of malignancy seems superfluous if not harmful. All of the signs are inherently asymmetric and furthermore many normal women's breasts are variably asymmetric. To isolate this as a sign of malignancy will increase the number of over-read false-positive mammograms and the

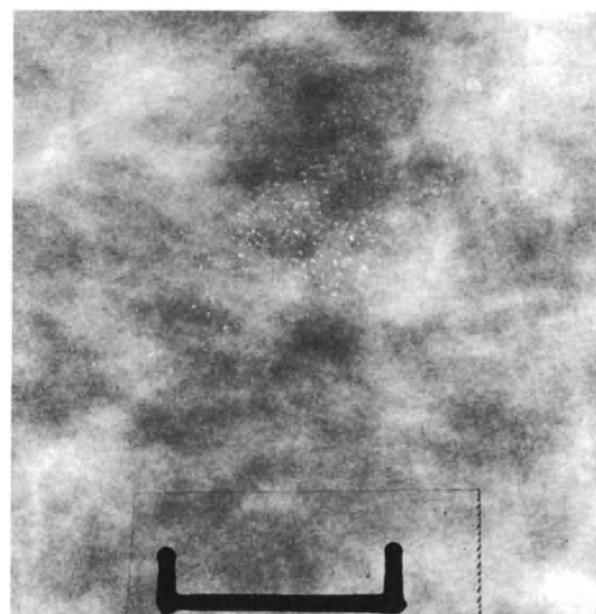


**Fig. 23.26.** Artefacts simulating fine calcification. These are finger-print artefacts caused by improper handling of the film before processing. They are usually only seen on one view and are much brighter for size than real calcification, as in this instance.

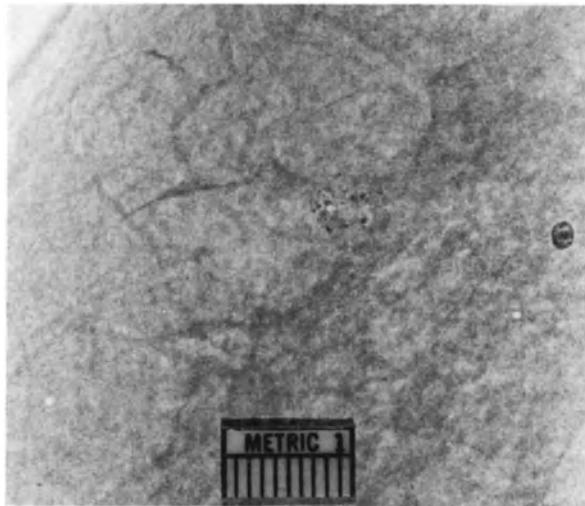


**Fig. 23.27.** Malignant calcification. They are often very difficult to see without the aid of a magnifying glass as in this instance. They are numerous, clustered, small to fine in size, and irregular in shape and density. This was an intraductal carcinoma with a small focus of invasion.

problems that may cause. Judgement is essential in evaluating these less specific asymmetric densities. When doubt remains, further investigation (compression coned, magnification and/or other views; ultrasound; and/or needle aspiration) will often provide enough additional information (including direct mammographic signs of malignancy) to recommend biopsy or not.

These indirect signs are less specific for malignancy but assume greater significance when there are physical findings

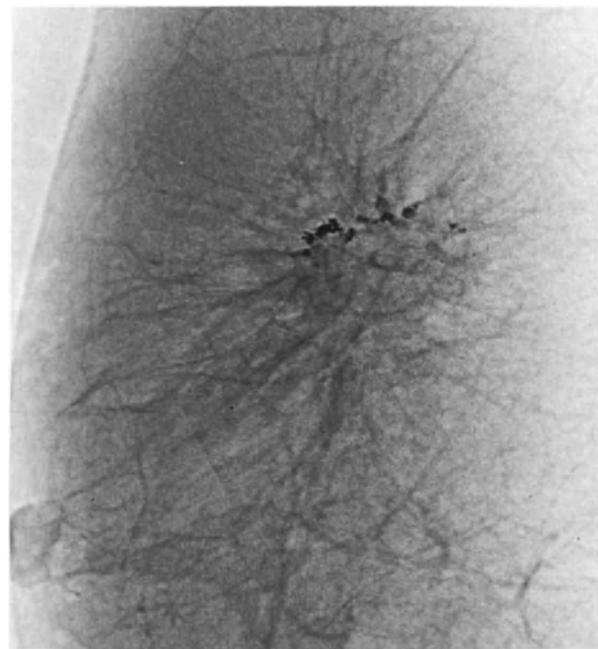


**Fig. 23.29.** An old biopsy scar simulating cancer. This asymptomatic woman with no physical findings gave a history of a previous biopsy of this breast. Mammography revealed a large stellate density with coarse amorphous calcification in a fatty breast. It is very unlikely that a stellate cancer this size would be non-palpable in a fatty breast. This was an old biopsy scar. Comment: fortunately this is uncommon but with more biopsies on the basis of mammographic findings, and lumpectomy for cancer, increased frequency of scars like this can be expected.

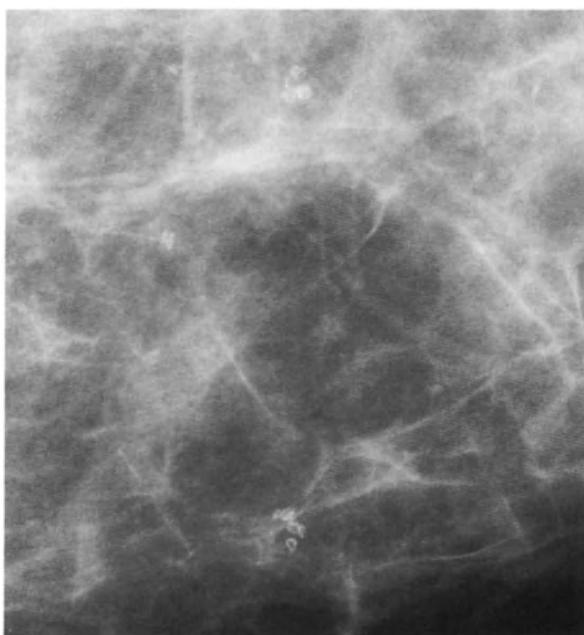


**Fig. 23.28.** Ring calcification. They are invariably benign regardless of size or location. They may be seen in the skin as in this instance and often represent calcified sebaceous glands.

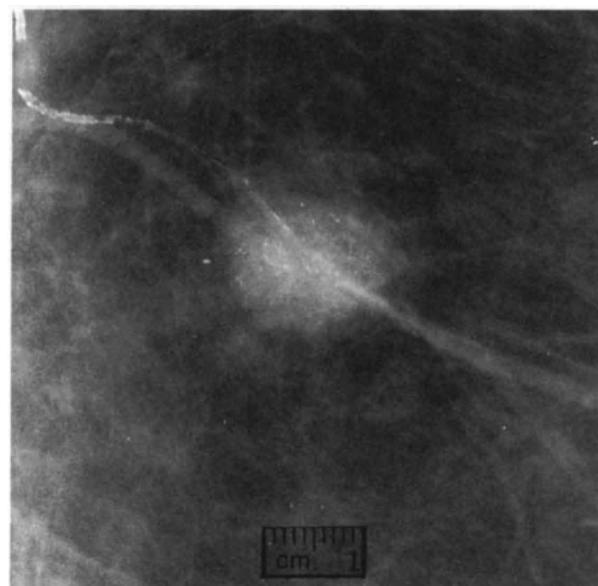


**Fig. 23.30.** A stellate mass with fine calcification. This 64-year-old woman claimed this readily palpable firm but mobile mass had been present for several years and was unchanged. Although it felt the same size as on mammography (favors benignancy), the irregular lobulated and stellate border and numerous fine calcification with linear and branching patterns within it suggest malignancy. It was a benign sclerosed fibro-adenoma.

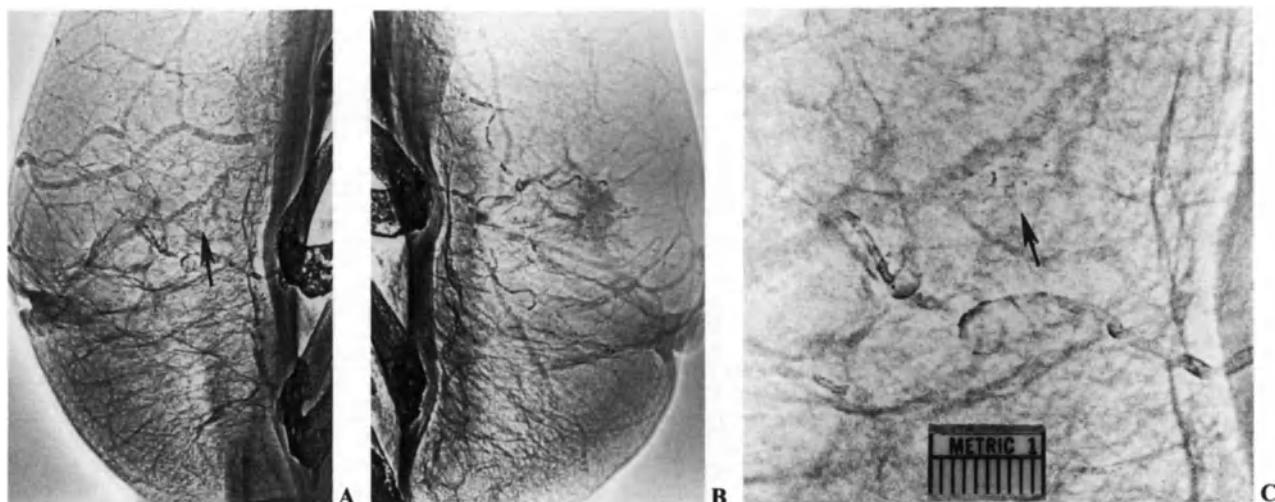


**Fig. 23.31A–C.** Don't stop looking! The non-palpable stellate density on the right (B) was much less evident on the other view (A) and was unchanged when compared with previous studies. A finding should never distract from further thorough inspection of all of the images. Note the cluster of fine irregular calcification on the left (A: arrow) and better seen with a magnifying glass (C). They were not present 1 year previously which reinforces the suspicion for malignancy. This was a 4-mm infiltrating duct carcinoma.

in the same region. At the very least, patients with these findings should be followed carefully clinically on a monthly or bi-monthly basis and with mammography within six months unless clinically indicated sooner.

#### PRE-OPERATIVE MAMMOGRAPHIC LOCALIZATION OF NON-PALPABLE LESIONS

With the mammographic detection of these small non-palpable findings it has become necessary to assist the breast surgeon in the biopsy of them to determine their origin

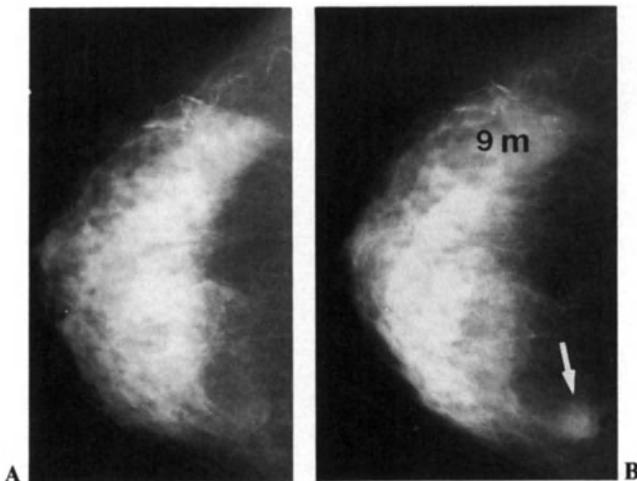


**Fig. 23.32A, B.** A developing density. A 1.5-cm ill-defined density (B) without margins, architectural distortion or calcification, developed in a post-menopausal woman 9 months after negative mammography (A). This was an infiltrating duct carcinoma.



**Fig. 23.33.** Solitary duct prominence. Note the short solitary prominent duct arching medially from the nipple with a larger rounded mass density at its proximal end. This was an intra-ductal carcinoma which cannot be distinguished from the much more common intra-ductal papilloma presenting in this fashion.

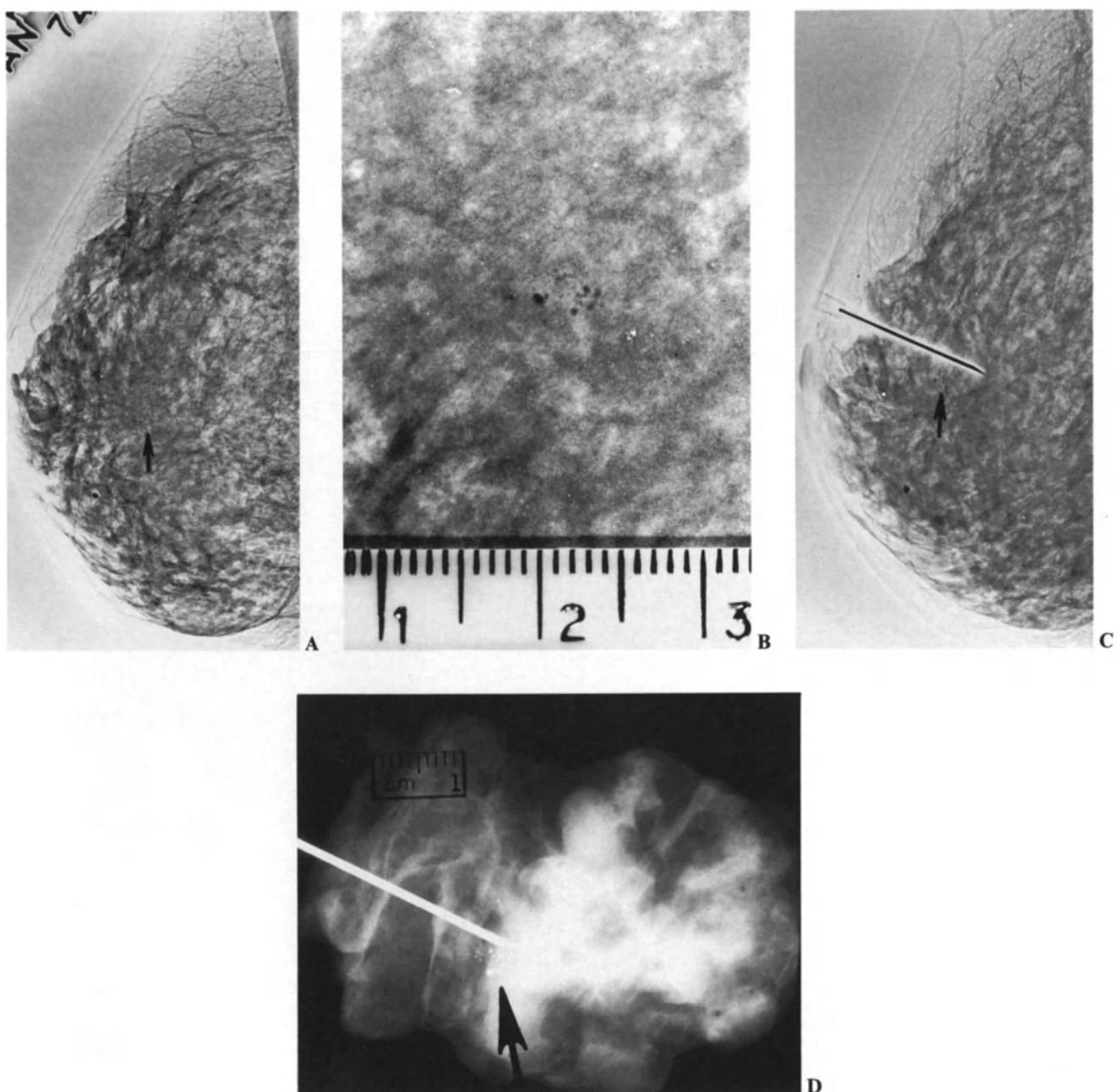


**Fig. 23.34A–D.** Mammographic localization of a nonpalpable lesion. A There is a cluster of small irregular calcification (arrow) deep in this dense breast and better seen with a magnifying glass (B). Nothing was palpable. C An inexpensive 21-gauge needle was selected with its length determined by measuring the shortest distance of the lesion from the skin surface on the orthogonal straight medial lateral and cranio-caudad views. It is inserted its entire length so that its tip is within 1 cm of the calcification and its hub can be taped at the skin surface. Mammography verifies these relationships. D Radiography with compression of the biopsy specimen is essential to verify resection of the area in question (calcification). This was a very small infiltrating duct carcinoma.

without mutilating the breast. In 1972 we used a very simple but nevertheless effective technique (Fig. 23.34A–D). Since then a variety of techniques have evolved. Accurate cytologic technology has served as the stimulus for even more precise stereotactic mammographic needle localization with

aspiration of cells for specific diagnoses which could obviate the need for excisional biopsy. Wider implementation of this technique could reduce the problem of unnecessary biopsies caused by false-positive mammography to more acceptable levels.

### MAMMOGRAPHY OF THE TREATED BREAST

Conservative treatment for breast cancer (lumpectomy and radiation therapy), and breast augmentation or reduction surgical procedures present special problems with follow-up mammography. In the breast treated for cancer, the major concerns are with residual and/or recurrent disease. Follow-up is recommended one month after the completion of therapy for any of the usual signs of malignancy (mass, calcification or stellate area of architectural distortion). If negative, the next follow-up is at six months and if this is negative, annually thereafter unless clinically indicated sooner.

With breast augmentation the opaque prosthesis can obscure breast tissue especially when it is located within the breast rather than behind the pectoral muscle. If the prosthesis can be displaced while compressing and imaging the actual breast tissue, quite satisfactory mammography can be done. With all of these surgical procedures, scarring and/or fat necrosis can mimic cancer but fortunately this is uncommon (Fig. 23.29).

### CORRELATION OF MAMMOGRAPHY AND BREAST PHYSICAL EXAMINATION

Mammography and breast examination by the physician are the only proven effective procedures in the detection of breast cancer. Under optimum conditions, modern mammography is much more sensitive than physical breast examinations and the only means of detecting non-palpable carcinomas when they are more curable. However, they remain complementary procedures with a much smaller percentage of carcinomas detected by physical breast examination alone. Positive results with either examination should be the overriding consideration for biopsy, and a negative result with the other modality should not deter that course of action. Equivocal results necessitate careful short-term follow-up observation.

Clinical-mammographic-surgical-pathology correlations are not only invaluable means of self-instruction, learning, and improving one's interpretive skills but also of assessing results and accuracy. They should be encouraged and regularly performed.

### SUMMARY

Optimum screening mammography and physical breast examination are very effective in the earlier detection of breast cancer (Fig. 23.35). There is evidence that this could reduce overall mortality from this disease though debate on this issue still continues. Reproducible optimum mammography requires well-trained and experienced radiologists and technologists; proper equipment, technique and methods of

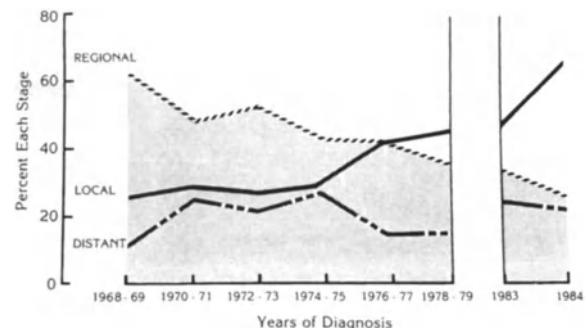


Fig. 23.35. 20 years ago only 25% of the breast cancers seen at North Carolina Memorial Hospital were confined to the breast with no evidence of axillary lymph nodes and/or distant metastases. 60+ % of the patients had metastases to axillary nodes. With screening and earlier detection, we have reversed those data and now in over 65% of our patients the cancer is confined to the breast. Extrapolate that experience world-wide and we can anticipate significant reduction in mortality from this disease.

quality assurance; and meticulous accurate interpretation of the images. The end results are only as good as the weakest link in this chain of events. Challenges are to obtain sufficient competent personnel and facilities to make optimum screening widely available at the lowest possible cost.

Note: Except where indicated otherwise, all of the illustrations are from Robert McLelland, MD and are part of the American College of Radiology Home-study Course and Learning File on Breast Imaging.

### REFERENCES AND SUGGESTIONS FOR FURTHER READING

- Andersson I (1986) Mammography in clinical practice. Medical Radiography and Photography (Eastman Kodak, Rochester, NY) 62: 1-40
- Feig SA, (ed.) (1988) Breast Imaging. Categorical Course Syllabus, American Roentgen Ray Society, Reston VA
- Feig SA (ed.) (1988) Diseases of the Breast (Test and Syllabus). American College of Radiology, Reston VA
- Feig SA, McLelland R (eds) (1983) Breast Carcinoma: Current Diagnosis and Treatment. American College of Radiology & Masson USA
- Lanyi M (1987) Diagnosis and Differential Diagnosis of Breast Calcifications. Springer-Verlag, New York
- Martin JE (1986) Atlas of Mammography. Williams & Wilkins, Baltimore
- Moskowitz M (ed.) (1986) Breast Imaging. Categorical Course Syllabus, Radiological Society of North America, Oak Brook, Illinois
- Sickles EA (ed.) (1987) Breast Imaging. Radiologic Clinics of North America. WB Saunders, Philadelphia
- Tabar L, Dean PB (1985) Teaching Atlas of Mammography. Thieme-Stratton, New York
- Wolfe JN (1983) Xero-radiography of the Breast. Charles C Thomas, Springfield, Illinois
- Wolfe JN (ed.) (1983) Mammography. Radiologic Clinics of North America. WB Saunders, Philadelphia

---

**PART 4**  
**Abdomen**

---

## CHAPTER 24

# THE ACUTE ABDOMEN

Janet Murfitt

### IMAGING INVESTIGATION

*Plain films* are the initial, and frequently only, radiological investigation of the acute abdomen. At least a *supine* and a *horizontal beam film*, such as an erect chest film, should be obtained. Positive findings are present in 50% of cases, although frequently they are non-specific or misleading. Films for investigating the acute abdomen are listed in Table 24.1. Normal features on the plain film are listed in Table 24.2.

Table 24.1. Films for the acute abdomen

Supine
Horizontal beam
erect abdomen
erect chest
decubitus
supine
prone
left lateral

Table 24.2. Normal features on the plain film

Small bowel
lies centrally
short fluid levels: maximum 3
maximum diameter 2.5 cm
small amounts of gas only
valvulae conniventes seen in jejunum
Large bowel
lies peripherally
longer fluid levels especially cecum
maximum 5 fluid levels
maximum diameter variable
hastra
feces
Normal calcification
arterial – especially splenic artery in elderly
phleboliths – in pelvis
mesenteric nodes
costal cartilage

The *supine* film must include the inguinal regions and the diaphragm. For *horizontal beam films* the patient should be left in position for at least 10 minutes to allow any free intraperitoneal gas to rise prior to the film being taken. The *erect chest film* will demonstrate lung changes such as pneumonia and a pleural effusion as well as free gas under the diaphragm (Fig. 24.1A, B). Young children with lobar pneumonia may present with signs suggesting an acute abdomen, and a chest film should always be obtained in addition to the abdominal film.

In the elderly, the very sick, young children and neonates a *supine* or *decubitus* film may be preferred to an *erect* film. The *left decubitus* (right side up) will demonstrate small amounts of free gas which collects between the liver and the chest wall. *Prone* films are indicated for the neonate in whom an anorectal atresia is suspected. The *left lateral* film will demonstrate a calcified aortic aneurysm.

Gas and fluid levels are frequently seen in the stomach and duodenum. Only small amounts of gas are normally present in the adult small bowel. A loop which is completely filled with gas should be considered abnormal.

The normal bowel wall is less than 2 mm thick. The thickness may be assessed when there are adjacent gas-filled loops so that the thickness of the two adjacent bowel walls can be measured. In the elderly the colon is often very distended, up to 15 cm in diameter, in the absence of significant bowel symptoms. However a diameter exceeding 5.5 cm in patients with colitis is consistent with toxic megacolon.

The large bowel is identified by its peripheral position and by the presence of haustra, although in the descending and sigmoid colon haustra are often absent.

The *properitoneal fat line* lies in the flank and outlines the peritoneum. In addition fat outlines the liver, spleen, kidneys, and psoas muscles. These structures are identified on over half of films. Non-visualization is common in normal patients and absence of these outlines should be interpreted cautiously.

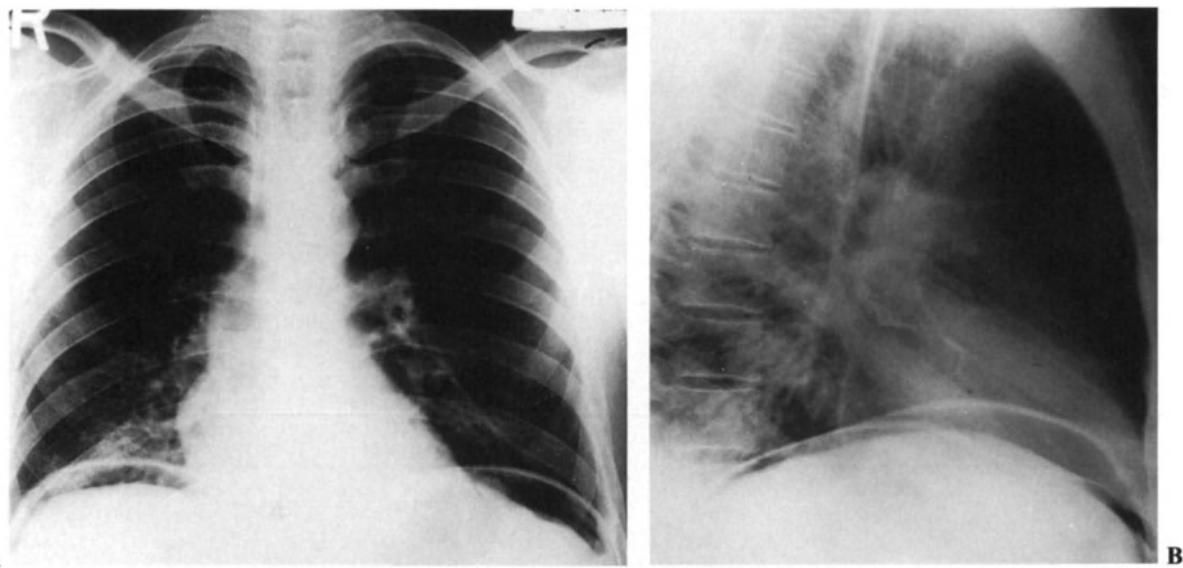


**Fig. 24.1A, B. Pneumoperitoneum. A Erect AP chest. B Erect lateral. Consolidation is present in the posterior basal segment of the right lower lobe.**

**Table 24.3. Abnormal features on the plain film**

Fluid levels
Dilated loops
gas or fluid containing
Displacement of bowel by masses
Abnormal gas shadows
free gas
retroperitoneal gas
gas in biliary tree, portal vein, bowel wall, abscess, hernia
Abnormal calcification
Fat lines
displacement, blurring, effacement
Free fluid
Chest
elevated diaphragm, pleural effusion, atelectasis
Bones
metastases
congenital abnormalities

Abnormal features to look for on the plain film are listed in Table 24.3 and should be carefully sought.

*Ultrasound* and *CT* can both provide helpful information in the acute abdomen by demonstrating free intra-peritoneal fluid, by identifying abdominal abscesses and providing guidance for their percutaneous drainage, and by elucidating abdominal trauma.

At *CT* ascitic fluid (density 0–15 HU) is easily seen. A higher density suggests infection, blood or fluid with a high protein content. Small amounts of intraperitoneal gas are identifiable even when plain films are negative, and hemorrhage following trauma or organ lacerations is easily seen.

*Ultrasound* also shows ascitic fluid well and small amounts lying in Morrison's pouch or in the pelvis can be shown. Bowel loops float and are separated by the ascites. Debris identified within the ascitic fluid is seen with malignant ascites, blood and infection.

The use of ultrasound in acute appendicitis is described below.

#### BOWEL OBSTRUCTION

Bowel obstruction is frequently responsible for the acute abdomen. The causes are listed in Table 24.4.

The characteristic plain film features of obstruction are dilatation of the bowel down to the site of obstruction with fluid levels and absence of gas in the distal bowel. Incomplete or intermittent obstruction results in a confusing pattern with the distal bowel containing gas, although not distended. It takes 5–6 hours for bowel loops to distend and up to 12 hours for gas in the large bowel beyond an obstruction to absorb. A high obstruction causes vomiting so that fluid levels do not develop.

Obstruction must be differentiated from *meteorism* when the bowel is extensively gas filled but only slightly distended. This is associated with respiratory problems and renal colic.

**Table 24.4. Causes of bowel obstruction**

Congenital
atresia, stenosis, webs, bands
duplication
internal hernia
external hernia
inguinal, femoral, umbilical
malrotation
meconium ileus
Hirschsprung's disease
Infections
tuberculosis
parasites
lymphogranuloma venereum
actinomycosis
Tumors – intrinsic and extrinsic
Intussusception
Volvulus
Diverticulitis
Crohn's disease
Gallstone ileus
Fecal impaction
Drug-related strictures

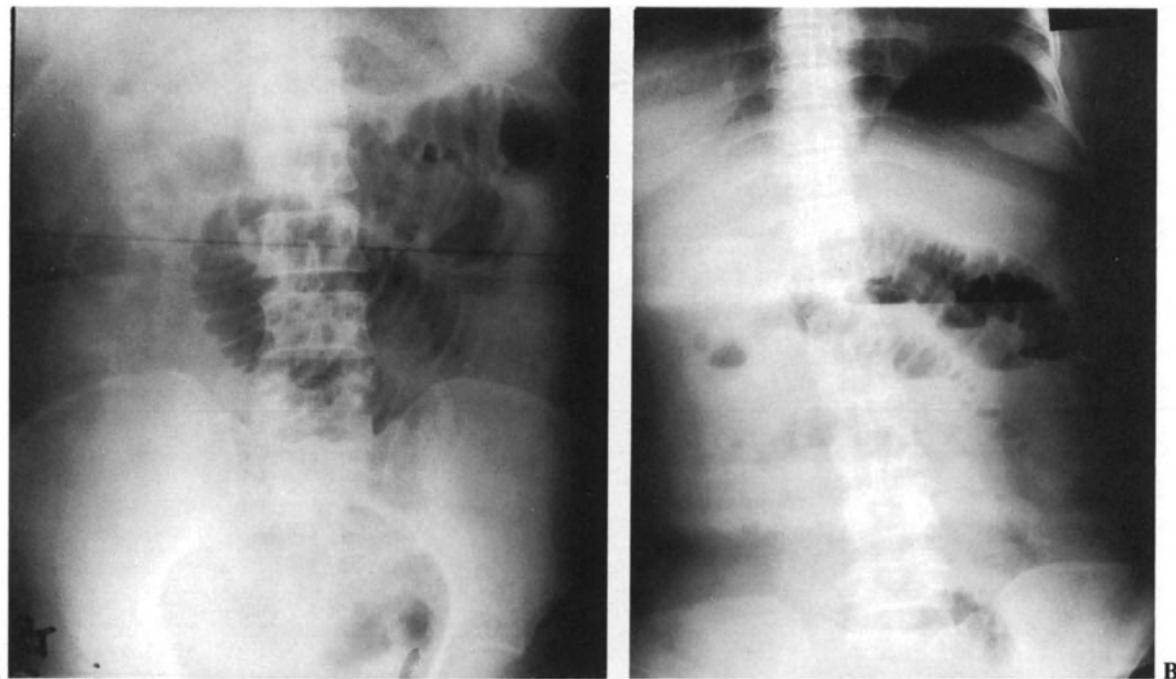


**Fig. 24.2A, B.** Small bowel obstruction. **A** Supine. **B** Erect. Multiple dilated small bowel loops with little gas in the distal bowel. Elderly patient with history of previous abdominal surgery. Adhesions found at laparotomy.

In children it is difficult to differentiate small from large bowel. In the neonate it takes up to 9 hours for gas to reach the sigmoid colon.

Apart from examining the pattern of dilated loops, the bowel wall should be assessed for evidence of *intramural gas*, *ulceration* or *thickening*. In addition *abnormal gas collections* (biliary tree, portal vein, abscess, free gas) may be found.

Fluid levels may be present in a number of conditions:

- Normal
- Gastroenteritis
- Following washout enemas
- Jejunal diverticulosis
- Celiac disease
- Obstruction
- Paralytic ileus
- Infarction
- Pseudo-obstruction

#### Small Bowel Obstruction

In the UK and USA *adhesions* account for around 80% of cases of small bowel obstruction, *strangulated hernias* 10% and *gallstone ileus* 1% to 2%. In Africa, by contrast, 80% of cases are the result of a strangulated hernia.

Characteristically there are centrally lying dilated small bowel loops with multiple fluid levels at different heights. Dilated jejunum has a 'coiled spring' appearance due to the *valvulae conniventes* (Fig. 24.2A, B) whilst ileal loops are featureless. Small bowel loops have a smaller arc (maximum 5 cm) than large bowel loops. The inguinal regions should be checked for gas lying within a hernia.

A fluid-filled loop may appear as a sausage-shaped soft tissue mass. If a small amount of gas is present within this loop it becomes trapped between the *valvulae conniventes* resulting in a 'string of beads' pattern. When a strangulated loop of small bowel contains only gas it resembles a coffee bean in shape.

*Gas in the bowel wall* is a serious prognostic sign and may indicate infarction following mesenteric occlusion or bowel strangulation.

*Gas in the biliary tree* has numerous causes. The most likely diagnosis in the presence of an acute abdomen is a gallstone ileus.

To demonstrate the site of an obstruction in the small bowel barium is used in preference to water-soluble contrast media which are hypertonic and become diluted so that the site of the obstruction is difficult to identify, particularly if distal. Barium should not be used in the presence of a large bowel obstruction because it forms concretions in the colon.

#### Large Bowel Obstruction

Common causes of large bowel obstruction include *malignancy*, *diverticulitis*, *volvulus* and *extrinsic masses*. Obstruction of the large bowel results in gaseous distension and fluid levels with collapse of the distal colon and absence of gas in the rectum. Haustra are seen as thick incomplete bands in the ascending and transverse colon but their presence is variable in the distal colon. In chronic obstruction a large amount of feces builds up in the proximal bowel. The large bowel often becomes very distended without obstruction in the elderly. However, in colitis a diameter of 5.5 cm is considered critical.

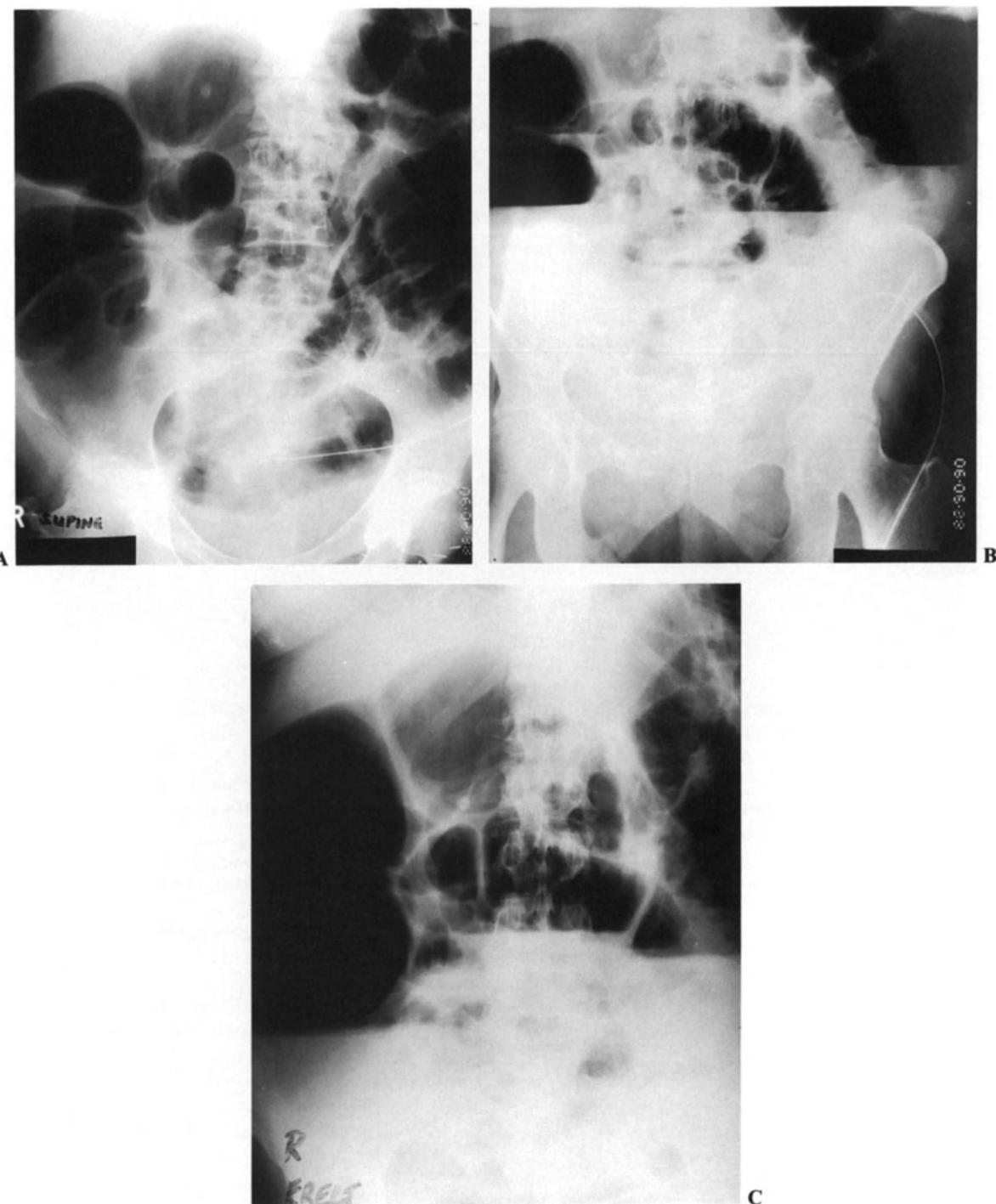


**Fig. 24.3A, B, C.** Large bowel obstruction due to adhesions developed in the post-operative period. **A** Supine film: distended large bowel with some small bowel distension. **B** Erect film. **C** Erect film two days later. Gross distension of the cecum. Cecostomy was performed to prevent cecal rupture.

When the large bowel dilates, the ileocecal valve may be competent or incompetent. An incompetent valve is associated with a relatively non-dilated cecum and dilated small bowel. This appearance is similar to an ileus, although in the case of an obstruction the rectum does not contain gas. A competent ileocecal valve results in cecal distension. When the cecal diameter exceeds 9 cm there is a high risk of perfor-

ation and a cecostomy should be performed (Fig. 24.3A, B, C). The closed ileocecal valve obstructs the small bowel which becomes dilated.

#### Colonic Pseudo-obstruction (Ogilvie's Syndrome)

Colonic pseudo-obstruction has the clinical and radiological features of obstruction without an actual obstructing lesion.

Bowel perforation may occur and the condition is particularly common in the bed-ridden elderly. Barium studies show a non-obstructed megacolon. Causes of pseudo-obstruction are given in Table 24.5.

**Table 24.5. Causes of pseudo-obstruction**

Primary	
Secondary	
idiopathic	
acute illness	renal failure, pneumonia
myocardial infarction	
cardiac failure	
abdominal infection	
drugs	tricyclics, phenothiazine
neurological	
diabetes mellitus	
spinal cord lesions	
Parkinson's disease	
collagen diseases	
amyloid	
endocrine	
adrenal failure, myxedema, hyperparathyroidism	
cathartic colon	

## VOLVULUS

A volvulus develops when gut twists on its mesentery. This results in gross distension of the affected bowel, with proximal dilatation and distal collapse. The blood supply becomes impaired.

The stomach, small bowel, omentum, cecum, sigmoid colon, colonic flexures and transverse colon are recognized sites for a volvulus.

Presentation is acute or intermittent. In the neonate, intermittent small bowel volvulus may present with malabsorption and failure to thrive.

**Gastric Volvulus.** With a gastric volvulus there is torsion around the longitudinal and transverse or mesenteric axis. Obstruction occurs at the cardia or the pylorus or both. Characteristically on the plain film there is moderate gastric dilatation with a large fluid level in the left upper quadrant extending across the midline, and elevation of the left hemidiaphragm. The small bowel contains little or no gas.

*Causes of gastric dilatation* include:

Paralytic ileus

Obstruction – pyloric (ulceration, malignant), small bowel and duodenal obstruction

Volvulus

Intubation, air swallowing

Drugs

Diabetes mellitus

**Small Bowel Volvulus.** This develops due to malrotation or adhesions. The small bowel is dilated with fluid levels and some loops may be very distended. In the presence of malrotation, the dilated small bowel lies on the right side of the abdomen. When the blood supply becomes compromised,



**Fig. 24.4. Cecal volvulus.** The distended cecum with a single haustrum lies in the right lower quadrant. There is some small bowel dilatation. The volvulus developed 48 hours after a hysterectomy.

thumbprinting of the bowel wall and intramural gas may be seen on the plain film.

**Cecal Volvulus.** The cecum is mobile in 10% of the population. Characteristically the cecum inverts to lie in the left upper quadrant, resulting in an empty right iliac fossa. However in a similar number of cases the cecum twists on its axial plane and lies centrally or on the right side in the lower abdomen (Fig. 24.4). One or two haustra and a single fluid level may be seen in the dilated cecum, and a dilated appendix assists in making the diagnosis. Small bowel obstruction may develop early. The distal colon becomes collapsed and the cecum may perforate.

**Sigmoid Volvulus.** This is particularly common in the elderly, and must be distinguished from simple gaseous distension. The grossly dilated sigmoid appears as an inverted 'U' extending from the pelvis to the left hemidiaphragm, overlapping the liver and the descending colon (left flank overlap sign) (Fig. 24.5).

On the supine film, the sigmoid loop has three dense lines, two lateral walls and a central denser line which is formed by the two adjacent inner walls. These lines converge towards the left side of the pelvis. Generally the sigmoid loop contains a large amount of gas, two fluid levels and is ahastral. The proximal colon becomes distended.

A barium enema demonstrates obstruction with the characteristic 'bird of prey' sign at the head of the column of barium in the rectosigmoid region.



**Fig. 24.5.** Sigmoid volvulus. Supine film. The grossly dilated ahastral sigmoid loop converges to the left side of the pelvis.

Plain film signs of a sigmoid volvulus can be summarized thus (Young et al. 1978):

Gas distended loop  
inverted 'U'  
extends to left hemidiaphragm  
converges to left side of pelvis  
overlaps liver, descending colon  
two fluid levels  
ahastral

Colonic distension

**Ileosigmoid Knot.** An ileosigmoid knot develops when the small bowel becomes looped around the base of the pelvic colon. There is distension of the colonic loop, as well as small bowel obstruction. Feces become trapped in the proximal colon.

#### GALLSTONE ILEUS

Gallstone ileus is usually caused by a single large cholesterol stone eroding through an inflamed gall bladder wall into the duodenum and impacting in the distal ileum to give rise to a small bowel obstruction. Occasionally the stone impacts in the proximal small bowel, duodenum or colon. Erosion through the gall bladder wall allows air to enter the biliary tract in one third of cases (Fig. 24.6A, B).

The plain film signs of gallstone ileus include:

Small bowel obstruction – complete, incomplete  
Gas in biliary tree and/or gall bladder (33%)  
Abnormally positioned gallstone



**Fig. 24.6A, B.** Gallstone ileus. **A** Supine. Multiple dilated small bowel loops. Large calcified stone (arrowheads) to the left of L4. **B** Erect. Gas in biliary tree (arrowheads). Note 'string of beads' sign (arrows) due to fluid-filled small bowel loop.

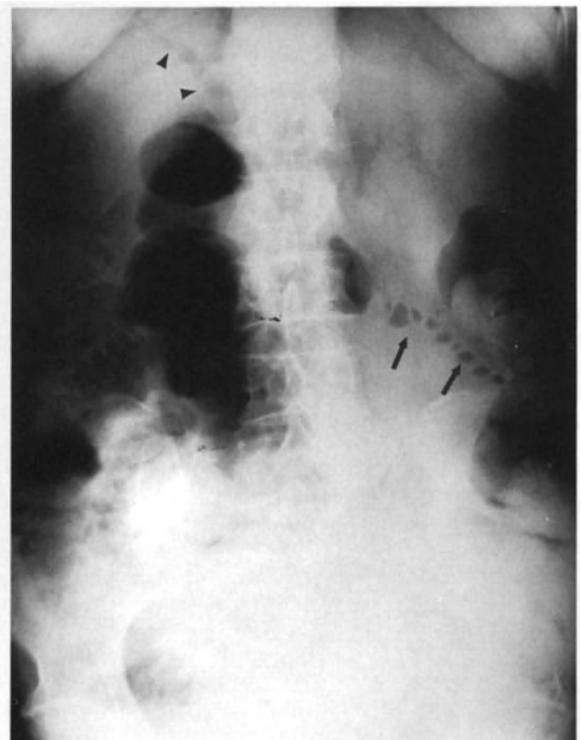




Fig. 24.7. Intussusception. Supine film. Large soft tissue mass in right upper quadrant (arrow) with slight dilatation of the proximal small bowel.

The stone may be identified in the pelvis provided that it has a calcified rim and is not obscured by dilated loops.

#### INTUSSUSCEPTION

Intussusception (Fig. 24.7) occurs when bowel invaginates distally into adjacent bowel. Commonly it presents in young

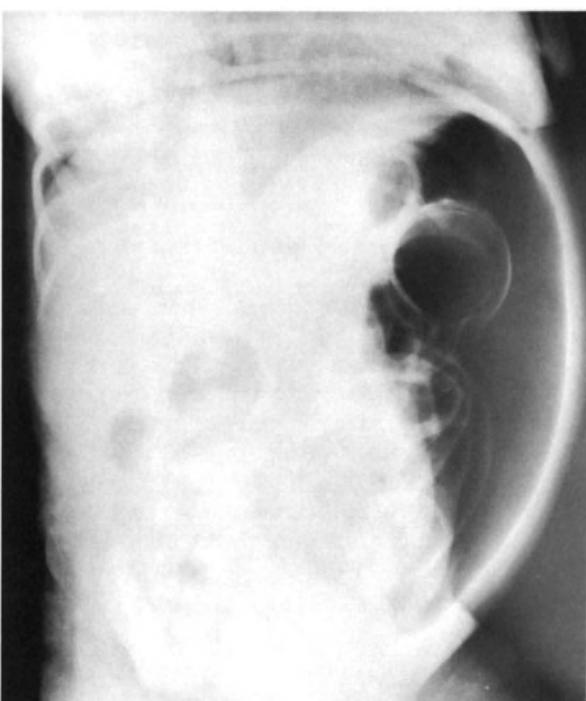


Fig. 24.8. Pneumoperitoneum. Supine horizontal beam film. Perforated Meckel's diverticulum. Both the inside and outside walls of the bowel loops (Rigler's sign) are seen.

children, usually males of 6–12 months as a result of *mesenteric adenitis*. Other causes include *ectopic pancreatic tissue*, *polyps*, *Meckel's diverticulum*, *ileal duplication* and *tumor*. Characteristically the child has an acute onset of severe pain which occurs at frequent intervals and passes 'redcurrant jelly' stools. Frequently a sausage-shaped abdominal mass is palpable on examination.

Imaging with plain films may show the following:

Small bowel obstruction – distension, fluid levels

Absence of gas and feces in the right iliac fossa

Soft tissue mass – may have a crescent of gas

The cecum is pulled up by the intussusception which usually lies in the right upper quadrant. This results in an empty right iliac fossa.

A *barium enema* demonstrates a concave defect in the head of the column of barium, and often the characteristic 'coiled spring' sign of barium passing around the invaginating bowel. The intussusception may be reduced during the enema using hydrostatic pressure, provided there are no clinical contraindications. Air or oxygen with pressure monitoring have been used instead of barium to reduce an intussusception.

#### PNEUMOPERITONEUM

Free intraperitoneal gas following perforation of a peptic ulcer is demonstrated on the erect film in some 75% of cases and on the supine film in some 50% of cases (Fig. 24.8). Gas collects under the diaphragm in the erect position. Small amounts of gas can be shown in the left lateral decubitus film between the liver and chest wall. A perforated ulcer is occasionally outlined by gas. In difficult cases CT is helpful for confirming a suspected perforation when the plain films are normal. There are many causes of pneumoperitoneum, some of which are not associated with peritonitis (Table 24.6).

Table 24.6. Causes of pneumoperitoneum

Perforated viscus
ulcer, tumor, ischemia, diverticulitis, toxic megacolon
Necrotizing enterocolitis
Pneumatosis coli, jejunal diverticulosis
Post-operative, peritoneal dialysis, endoscopy
Pneumomediastinum
Female water skiers (gas enters via Fallopian tubes)

Post-operatively, free gas takes up to 24 days to absorb. Signs of pneumoperitoneum on the supine film may be obvious, but can be subtle and should be carefully looked for. They include:

Double wall sign (Rigler's sign)

Gas in Morrison's pouch

Outlined falciform, umbilical ligament (Fig. 24.9)

Gas between bowel loops

Round collection overlaying liver

Gas in lesser sac

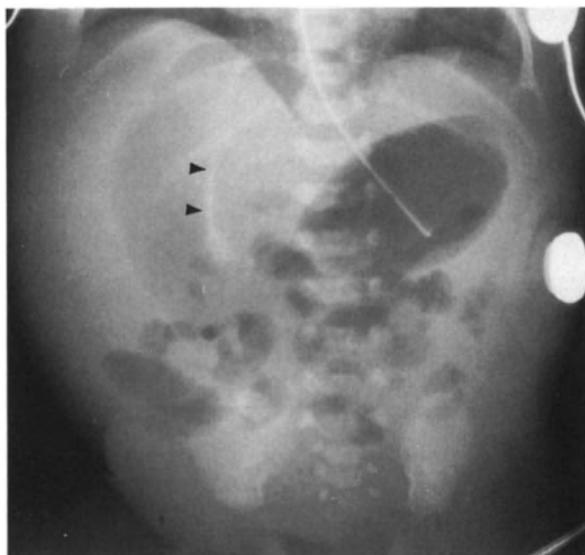


**Fig. 24.9.** Pneumoperitoneum. Supine film of neonate. Free gas outlines the falciform ligament (arrows).

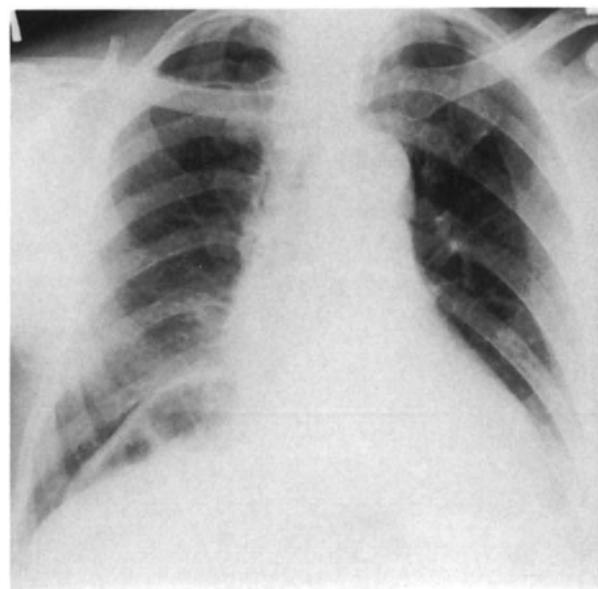


**Fig. 24.11.** Chilaiditi's syndrome. Erect chest. Gas under the right hemidiaphragm lies within the large bowel.

#### Gas in subhepatic space

Associated paralytic ileus, free fluid

In the presence of free intraperitoneal gas, the bowel wall of a gas-filled loop is outlined by the gas on either side of its wall. This sign of perforation on a supine film was described by Rigler (Fig. 24.10). A similar appearance may be seen in the absence of free gas when there are two adjacent gas-filled loops. In this situation it is the two adjacent bowel walls which are outlined.

Gas within Morrison's pouch appears as a triangular lucency beneath the liver edge. A subhepatic gas collection is linear. When gas becomes trapped between bowel loops triangular lucencies may be seen. On the erect film a gas collection within the lesser sac results in a second gastric fluid level.



**Fig. 24.10.** Pneumoperitoneum. Supine. Rigler's sign. Visualization of both sides of the bowel wall (arrows).

There are several conditions which may mimic a pneumoperitoneum but which are distinguishable with care. These are Chilaiditi's syndrome, subdiaphragmatic fat, extraperitoneal gas, subphrenic abscess, atelectasis of the lower lobes and pneumatoxisis coli.

*Chilaiditi's syndrome* is common in the elderly and in those with obstructive airways disease. Bowel, usually colon, becomes interposed between the liver and diaphragm. The bowel pattern is easy to identify and there should be no difficulty in differentiating this syndrome from a perforation (Fig. 24.11). The bowel interposition is usually intermittent.

Occasionally, in the obese, the fat deposited beneath the diaphragm appears as a linear lucency. In contrast to a perforation this fatty lucency lies lateral to the apex of the hemidiaphragm.

#### RETROPERITONEAL GAS

Retroperitoneal gas has a mottled appearance and may outline the psoas, kidney and adrenal (Fig. 24.12). When the gas extends to the hemidiaphragm it does not lie at the apex of the diaphragm, in contrast with a perforation. Causes include *acute pancreatitis* and *perforation of the rectum and sigmoid colon*. Endoscopic procedures, particularly sphincterotomy, may be complicated by retroperitoneal perforation. Free intraperitoneal gas is rare following perforation of the colon as a result of diverticular disease, when an abnormal collection of gas often accumulates in the region of the left hip.

#### INTRAMURAL GAS

Common causes of intramural gas are necrotizing enterocolitis, *pneumatosis cystoides intestinalis*, bowel necrosis and gangrene.

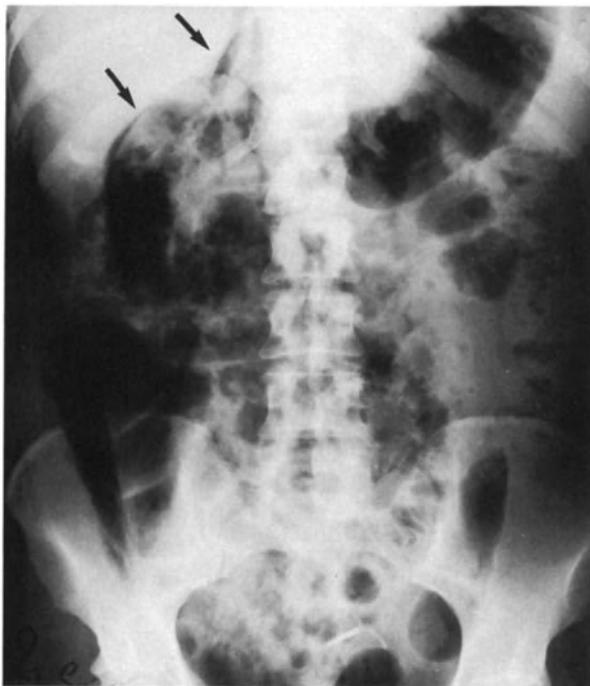


**Fig. 24.12.** Retroperitoneal gas outlining right kidney and adrenal (arrows) following endoscopic sphincterotomy.

Rare causes are after endoscopy, toxic megacolon, intramural perforation of a peptic ulcer, diabetes, infection and corrosive gastritis.

Interstitial gas appears as linear gas shadows in the bowel wall.

*Pneumatosis cystoides intestinalis* is a condition of unknown etiology, possibly associated with obstructive airways disease. Patients may have pain and excessive mucus with diarrhea. There are multiple cysts up to 3 cm diameter in

**Table 24.7.** Causes of paralytic ileus

Post-operative
Inflammatory
peritonitis
acute pancreatitis, cholecystitis, appendicitis, salpingitis
abscess
septicemia
chest infections
Metabolic
hypokalemia, hypochloremia
abnormal magnesium, calcium levels
renal failure
ketotic diabetic coma
adrenal failure
Drugs
morphine, atropine
Trauma
spinal, rib injuries
leaking aneurysm
retroperitoneal bleeding
Vascular
occlusion
sickle-cell disease
heart failure
Renal colic



**Fig. 24.13.** Pneumatosis coli. Supine film. The typical cysts of pneumatosis are well seen in the transverse colon.

the bowel wall, particularly the descending colon (Fig. 24.13). Asymptomatic perforation can occur (Fig. 24.14).

#### PARALYTIC ILEUS

The numerous causes may be classified as shown in Table 24.7.

A paralytic ileus may be generalized or localized. On the plain film there are small and large bowel fluid levels with dilated loops. Similar findings are seen with a distal large bowel obstruction or an incomplete small bowel obstruction. Radiologically it may be impossible to differentiate these conditions although they are often quite apparent on clinical examination.

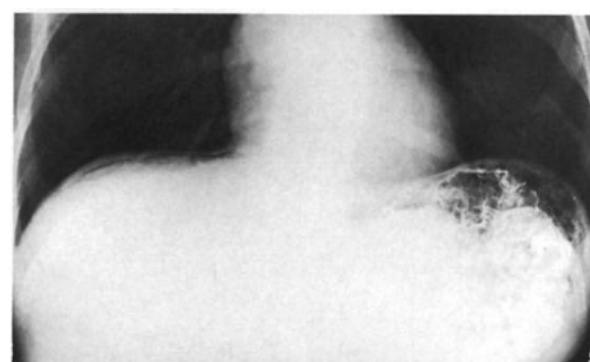


**Fig. 24.14.** Pneumoperitoneum and pneumatosis coli. Erect film. Free gas under right hemidiaphragm. Asymptomatic perforation.



Fig. 24.15. Acute appendicitis. Supine film. Dilated small bowel loops.

Adhesions can develop within a few days post-operatively and colonic function may not return for 72 hours. To distinguish obstruction from an ileus serial films are helpful. Increasing bowel distension suggests obstruction. Increasing amounts of free gas on serial films suggests that a post-operative fistula has developed. Post laparotomy free gas may take 24 days to absorb although this normally occurs in about 10 days. Meteorism is another cause of dilated loops post-operatively.

#### INFECTIONS

**Acute Appendicitis.** Frequently radiological examination is unnecessary, the diagnosis being apparent clinically. However when plain films are obtained appearances are invariably non-specific (Table 24.8). Acute appendicitis often



Fig. 24.16. Appendicolith (arrow). Supine film. Asymptomatic patient.

Table 24.8. Signs of acute appendicitis

Fluid levels and dilatation
RIF
cecum
generalized small bowel
Appendicolith
Fluid right lower quadrant with separation of loops
Peritoneal fat line
blurred or widened
Psoas line
blurred or absent
Scoliosis
concave to right
On ultrasound
non-compressible appendix
thick wall, diameter exceeds 6 mm
'target' appearance cross-section
appendicolith
fluid in paracolic gutter suggests peritonitis
echogenic mass (abscess)

causes a *localized ileus* (Fig. 24.15). An *appendicolith* is present in some 15% of cases and appears as an oval opacity in the right lower quadrant (Fig. 24.16). Gas in the appendix is a non-specific and frequently a normal finding.

Abscess formation and peritonitis with a paralytic ileus are possible sequelae. An appendix *abscess* may be seen as a soft tissue mass indenting the cecum. On occasions it causes bowel obstruction.

At *ultrasound* there are positive findings in three quarters of patients with acute appendicitis, although sensitivity is reduced following perforation of the appendix. The normal appendix is not visualized. The acute appendix is seen to be thickened and non-compressible. An appendicolith with acoustic shadowing may be identified and fluid within the paracolic gutter may suggest pancreatitis.

**Acute Cholecystitis.** (See Chap. 25)

**Acute Pancreatitis.** (See Chap. 27)

**Pelvic Inflammation.** An acute abdomen may develop as a result of many gynaecological lesions including acute salpingitis, tubo-ovarian abscess, ectopic pregnancy and endometriosis. *Ultrasound* is the investigation of choice.

*Plain film* signs which may be seen include:

Localized ileus of pelvic ileal loops; slight dilatation with fluid levels

Pelvic mass

Free fluid in the pelvis

**Intra-abdominal Abscess.** Intra-abdominal abscesses usually develop post-operatively after gastric, biliary or pancreatic surgery or following gut perforation with peritonitis. Common sites include the *pelvis*, *subphrenic* and *subhepatic* spaces, *lesser sac*, *paracolic* and *infracolic* areas. The pelvis is the most frequent site for abscess formation. Such collections are relatively asymptomatic and often very large at presentation. Ten to twenty per cent of patients have multiple abscesses. Abscesses within the lesser sac may form with pancreatitis or following peptic ulcer perforation.

Investigation includes supine, horizontal beam and lateral films, ultrasound, CT and fine needle aspiration. CT has been

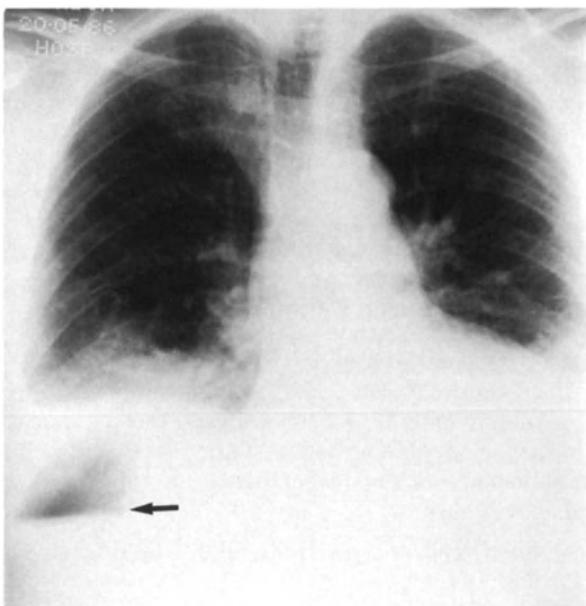


Fig. 24.17. Large right subphrenic abscess with fluid level (arrow). Erect film. Small bilateral pleural effusions and basal consolidation.

reported as the most sensitive investigation for the detection of abscesses. Gallium scanning may be helpful in patients with no localizing signs. Drainage may be undertaken with CT or ultrasound control.

**Plain film findings of abdominal sepsis include:**

- A soft tissue mass displacing stomach, gut
- Gas and/or fluid level within abscess
- Localized ileus
- Free intraperitoneal fluid
- Effacement of normal fat lines
- Pleural effusions, basal atelectasis

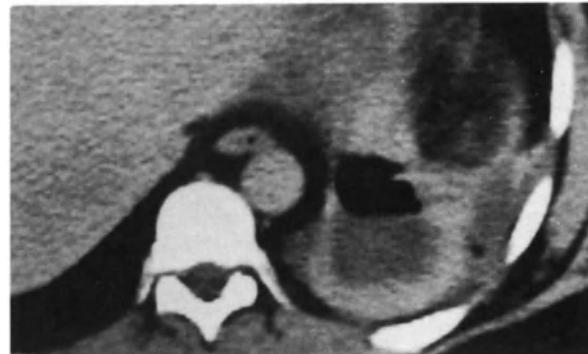


Fig. 24.19. CT scan. Left subphrenic abscess with air fluid level.

Free intraperitoneal fluid causes separation of the bowel loops and thinning of the fat lines with a generalized hazy shadowing. In the pelvis, fluid collects in the pouch of Douglas and is seen on either side of the rectum displacing the sigmoid colon upwards. Subhepatic fluid results in indistinctness or absence of the inferior liver edge outline. There may be separation of the liver and lateral abdominal wall by the fluid with a resultant lucency seen on the plain film. Fluid displaces the colon medially from the properitoneal fat line.

**Subphrenic Abscess.** The majority of subphrenic abscesses develop post-operatively. The right subphrenic space communicates with the right paracolic gutter and pelvis whereas the left does not. As a result of this subphrenic abscesses are more commonly found on the right side.

*Plain film signs* include a pleural effusion and basal lung changes with elevation and reduced excursion of the hemidiaphragm. There is downward displacement of the liver or spleen, stomach and colonic flexures. Gas within the abscess is seen beneath the hemidiaphragm (Fig. 24.17).

At *ultrasound* there is a fluid collection, often with posterior acoustic enhancement and internal echoes of blood, pus or gas (Fig. 24.18). The outline may be irregular with a thick wall. Septa are often present. A large amount of gas or debris can result in a solid-looking mass.

At *CT* there is a low-density mass which contains gas in 50% of cases (Fig. 24.19) a feature which is virtually diagnostic. Frequently there is contrast enhancement of the edge of the abscess. Sometimes the mass appears solid. It can be difficult to differentiate subphrenic from pleural fluid at CT. The position of the fluid with respect to the crus of the diaphragm should be determined. Intra-abdominal fluid lies in front of the crus.

Percutaneous drainage may be undertaken and aspiration will confirm the diagnosis.

A *paracolic abscess* will displace the colon medially (Fig. 24.20).

**Peritonitis.** A local or generalized peritonitis may develop due to bacterial infection following perforation and penetrating trauma or post-operatively, or due to extension from a localized infection such as appendicitis or from a septicemia.

Complications include acute obstruction due to adhesions, paralytic ileus and abscess formation. Free fluid may be present.



Fig. 24.18. Ultrasound. Right subphrenic abscess.

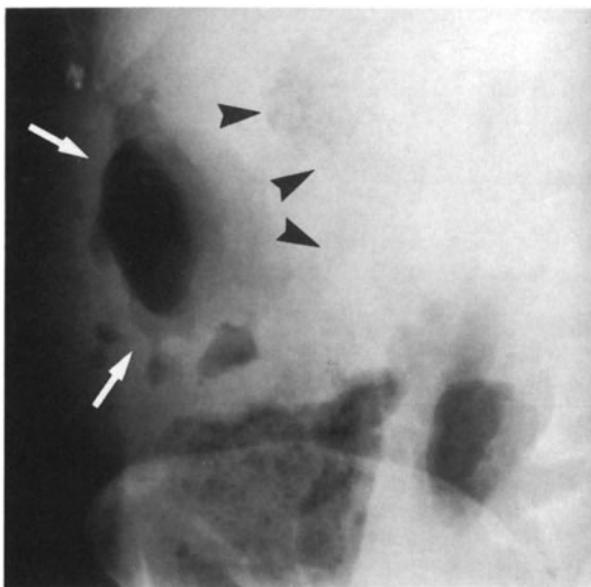


Fig. 24.20. Right paracolic abscess (arrows) following perforation of carcinoma of the colon. The colon (arrowheads) is displaced medially.

#### ACUTE COLITIS

In *severe ulcerative colitis* the colon may be completely gas free. In less severe cases the extent of fecal residue gives an indication of the extent of the colitis.

*Acute toxic dilatation of the colon* is usually due to ulcerative colitis. Patients are severely ill and there is a high risk of bowel perforation. The colon is paralyzed and distended.



Fig. 24.21. Toxic megacolon with perforation. The colon is dilated with a nodular thickened wall. Rigler's sign of perforation is present (arrowheads). There is residual barium from a recent barium enema.

Dilatation is in excess of 5.5 cm. In addition there is nodular irregularity of the bowel wall due to mucosal islands and loss of haustration (Fig. 24.21). Gas in the bowel wall indicates necrosis and perforation with peritonitis may follow.

*Pseudomembranous colitis* may develop as a result of antibiotic therapy or colonic obstruction and must be differentiated from ulcerative colitis. The entire large bowel is affected with mucosal thickening and lack of haustration.

#### VASCULAR LESIONS

**Superior Mesenteric Artery Occlusion.** Occlusion of the superior mesenteric artery results in ischemia of the entire small bowel, usually leading to necrosis. Branch occlusions will cause segmental ischemia. Patients present with an acute abdomen and bloody diarrhea.

*Plain film signs are:*

Dilated small bowel loops with multiple fluid levels which develop within 4 hours

Bowel and mucosal thickening with increased loop separation

Free gas (perforation)

Gas in the bowel wall and portal vein (gangrene)

Ileus

**Inferior Mesenteric Artery Occlusion.** Occlusion of the inferior mesenteric artery results in ischemia of the splenic flexure and distal colon sparing the rectum. The descending colon is dilated with thickening and mucosal irregularity or 'thumbprinting' of the bowel wall. The proximal bowel may become distended.

**Aortic Aneurysm.** Aortic dissection or rupture of an abdominal aneurysm results in retroperitoneal bleeding and hematoma formation which is demonstrable by CT or ultrasound. Frequently there is meteorism so that plain film signs become obscured by bowel gas.

*Plain film signs include:*

Loss of the left psoas outline

A calcified aneurysm with soft tissue mass extending beyond the calcification (a lateral film is most helpful)

Ileus

**Bleeding Diathesis.** The duodenum is a common site for an *intramural hematoma* because of its fixed position overlying the spine. Children with Henoch-Schonlein purpura and adults on anticoagulants are recognized groups which are liable to develop a bowel hematoma. This may obstruct the bowel lumen or produce mucosal 'thumbprinting'.

#### ABDOMINAL TRAUMA

Trauma may be blunt (closed) or penetrating. Blunt trauma is often associated with seat belt or steering wheel injuries.

*Plain film investigation* should include supine and horizontal beam abdominal films and a chest film as associated chest injuries are common. Both gut and solid organs may be damaged.

Injury of the liver, spleen and kidneys is often accompanied by *fractures of the ribs and transverse processes*. Bleeding following trauma may be retroperitoneal, intraperitoneal, parenchymal or subcapsular.

Being in a fixed position the duodenum is the commonest site of bowel injury. Perforation may be intraperitoneal or extraperitoneal and an intramural hematoma may develop.

Rupture of the diaphragm is nearly always left-sided. This may be complicated by strangulation if the bowel herniates.

*Features to look for on a plain film* include free gas, retroperitoneal gas, free fluid, retroperitoneal bleeding, intramural hematoma, liver, spleen or kidney enlargement (hematoma) and associated fractures of the pelvis, ribs and transverse processes.

*CT* of the abdomen and pelvis is the investigation of choice for patients who have undergone significant abdominal trauma. *Intraperitoneal bleeding* should be looked for in Morrison's pouch, the paracolic gutters and in the pelvis, in the pouch of Douglas and paravesical fossae. Fresh blood has a high density (50–70 HU) but within a few days density decreases with clot lysis. In addition CT is excellent for assessing damage to abdominal organs.

## THE NEONATAL ABDOMEN

After birth gas reaches the small gut within 3 to 4 hours and the rectum at 6 to 9 hours. It is normal for there to be extensive gas filling of the bowel and fluid levels are common.

Differentiation between small and large bowel loops is difficult. It is a good policy to handle sick neonates as little as possible and to keep them warm. Therefore the minimum number of films should be undertaken with minimal disturbance. Using horizontal ray decubitus films rather than erect films creates less disturbance.

### OBSTRUCTION

Clinical signs include abdominal distension and vomiting. However there are numerous other causes for both these symptoms. Non-obstructive causes of distension include an abdominal mass, excessive air swallowing, ascites, ileus and pneumoperitoneum. Excessive air swallowing can occur during mechanical ventilation or with respiratory distress, and is also a feature of certain forms of tracheoesophageal fistula.

*Causes of neonatal obstruction* include atresia, stenosis, malrotation, volvulus, duplication cyst, hernia, meconium ileus, meconium plug and Hirschsprung's disease (see Chap. 32).

**Pyloric Stenosis.** Classically this develops after 4 to 6 weeks in first-born males, resulting in projectile vomiting. *Plain film* findings include gastric distension with a fluid level. Increased peristalsis may result in a 'caterpillar' outline to the stomach. There is a paucity of gas in the small bowel.



Fig. 24.22. Duodenal atresia. Supine film. Gas in stomach and duodenum. Distal bowel is gas free. Multiple vertebral and rib anomalies.

Imaging investigations which may be undertaken include *ultrasound* and *barium studies* (see Chap. 30).

**Duodenal Obstruction.** Causes of neonatal duodenal obstruction include atresia (Fig. 24.22), stenosis, webs, annular pancreas, malrotation and volvulus and peritoneal bands.

On the erect film there is the characteristic 'double bubble' appearance of fluid levels in the stomach and duodenal cap. This may be diagnosed *in utero* on ultrasound. Partial obstruction allows gas to enter the distal bowel. There is an increased incidence of duodenal obstruction in Down's syndrome.

**Small Bowel Atresia.** This is thought to result from intrauterine ischemia of the bowel. Plain film findings are of a proximal obstruction with bowel distension and fluid levels. Features of peritonitis may be present. In spite of the atresia, meconium may be passed from the distal bowel beyond the obstruction. However, it does not contain bile and, therefore, is a lighter color than normal meconium.

It should be noted that a functional ileus is not uncommon in premature babies during the initial 48 hours. There is delayed passage of meconium and bowel distension before normal peristalsis becomes established.

A **duplication cyst** is the most frequent gastrointestinal mass found in the neonate. Vertebral anomalies may be present. A duplication cyst usually occurs in the distal small bowel and may cause obstruction. A soft tissue mass may



Fig. 24.23. Necrotizing enterocolitis. Erect film. Dilated bowel loops with gas in the wall of the stomach (arrows) and bowel.

be evident on the plain film. *Ultrasound* may demonstrate a cystic mass.

**Malrotation** results in the cecum being left-sided and volvulus is a common complication. In addition, associated peritoneal bands obstruct the small bowel which may become ischemic with resulting necrosis, perforation and ascites.

**Meconium ileus** presents in 10%–20% of patients with cystic fibrosis. Meconium inspissates within the large bowel and terminal ileum resulting in small bowel obstruction with dilated loops. On *plain films* the meconium has a granular or speckled appearance and this is seen predominantly in the right iliac fossa. Fluid levels are few because of the viscous nature of the meconium. There is a high risk of perforation and peritonitis.

Prenatal perforation results in a chemical peritonitis with adhesions. **Calcification** of the peritoneum and bowel wall

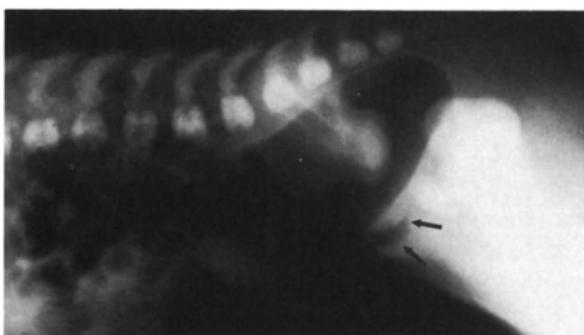


Fig. 24.24. Rectal atresia. Prone film. Gas is present in the bladder (arrows) indicating a fistula.

may occur. The colon is underdeveloped (a microcolon). An enema with a hyperosmolar water soluble contrast medium may be used to soften the meconium and to relieve the obstruction, but possible complications include dehydration and hypovolemia, and colonic mucosal necrosis.

**Hirschsprung's disease** is due to absence of the myenteric plexus from a segment of colon. In 80% of cases the plexus is absent in the rectosigmoid region but the whole of the large bowel may be affected. There is an increased incidence in males and in Down's syndrome.

In the neonate there is delayed passage of meconium. The proximal bowel is dilated and enterocolitis may develop.

**Necrotizing enterocolitis** is predominantly a complication of *prematurity*, developing after 48 hours and associated with umbilical catheters and respiratory problems. In the full-term child it is usually due to obstruction, often as a result of Hirschsprung's disease. The baby has severe diarrhea, abdominal distension with vomiting and a severe systemic upset. Rectal bleeding is common. Contrast studies should be avoided because of the risk of perforation. Following recovery ileal or colonic strictures may develop, often within a few weeks.

*Plain film* signs of necrotizing enterocolitis (Fig. 24.23) include:

Gas in the bowel wall – a linear or cystic pattern

Bowel dilatation

Gas in the portal vein

Pneumoperitoneum

**Anorectal Abnormalities.** *Rectal atresia* is classified as being high, intermediate or low referring to the level of the distal patent bowel with respect to the puborectalis sling. A normal sling is necessary for fecal continence. A high atresia is associated with an inefficient puborectalis and surgery is indicated. Absence of the 3rd and 4th sacral segments is an indication of poor development of puborectalis. Long segment atresias (A) are commonly associated with vertebral (V), tracheal (T), esophageal (E) and renal (R) abnormalities (the 'Vater' acronym).

The shoot-through lateral film in the prone position has been advocated to define the level of the atresia. However, the apparent level of obstruction seen on the film may be misleading because the inspissated meconium prevents bowel gas rising freely. Gas lying within the bladder (Fig. 24.24) or vagina indicates the presence of a *fistula*, usually rectourethral in boys and rectovaginal in girls; occasionally there may be a rectovesical or rectoperineal fistula.

#### REFERENCES AND SUGGESTIONS FOR FURTHER READING

- Anderson JR, Mills JOM (1984) Caecal volvulus; a frequently missed diagnosis? *Clin Radiol* 35: 65–69
- Benson MD (1985) Adult survival with intrahepatic portal venous gas secondary to acute gastric dilatation, with a review of portal venous gas. *Clin Radiol* 36: 441–443
- Brooke Jeffrey R, Laing FC, Lewis FR (1987) Acute appendicitis: High-resolution real-time ultrasound findings. *Radiology* 163: 11–14
- Clark RA, Towbin R (1983) Abscess drainage with CT and ultrasound guidance. *Radiol Clin North Am* 21: 445–459
- Colquhoun J (1965) Intramural gas in hollow viscera. *Clin Radiol* 16: 71–85

- Federle MP (1983) Computed tomography of blunt abdominal trauma. *Radiol Clin North Am* 21: 461–475
- Felson B, Wiot JF (1973) Another look at pneumoperitoneum. *Semin Roentgenol* 8: 437–443
- Field S (1984) Plain films: The acute abdomen. *Clin Gastroenterol* 13: 3–40
- Johnson CD, Rice RP, Kelvin FM, Foster WL, Williford ME (1985) The radiologic evaluation of gross caecal distension: Emphasis on caecal ileus. *AJR* 145: 1211–1217
- Love L (1973) Large bowel obstruction. *Semin Roentgenol* 8: 299–322
- Love L (1960) The role of the ileocaecal valve in large bowel obstruction: a preliminary report. *Radiology* 75: 391–398
- Miller RE (1973) The technical approach to the acute abdomen. *Semin Roentgenol* 8: 267–269
- Mueller PR, Simeone JF (1983) Intra-abdominal abscesses: diagnosis by sonography and computed tomography. *Radiol Clin North Am* 21: 425–443
- Puylaert JBCM (1986) Acute appendicitis: ultrasound evaluation using graded compression. *Radiology* 158: 355–360
- Vessal K, Borhanmanesh F (1976) Hepatodiaphragmatic interposition of the intestine (Chilaiditi's syndrome). *Clin Radiol* 27: 113–116
- Williams JL (1962) Fluid filled loops in intestinal obstruction. *AJR* 88: 667–686
- Young WS, Englebrecht HE, Stoker A (1978) Plain film analysis of sigmoid volvulus. *Clin Radiol* 29: 553–560
- Young WS, White A, Grave GF (1978) The radiology of ileosigmoid knot. *Clin Radiol* 29: 211–216

## CHAPTER 25

# THE BILIARY TRACT

*Janet Murfitt*

---

### INVESTIGATION

Imaging of the biliary tract can utilize a wide variety of different techniques: plain film, oral cholecystogram, ultrasound, percutaneous transhepatic cholangiogram – PTC, endoscopic retrograde cholangiography – ERCP(see Chap. 27), CT, radioisotope imaging, operative cholangio-



Fig. 25.1. Normal oral cholecystogram. Post-fat film demonstrating the cystic duct and CBD.

gram, T-tube cholangiogram, intravenous cholangiogram – IVC, MRI, biopsy and therapeutic procedures.

**Plain films** should always be taken before any contrast examination of the biliary tract, to demonstrate calcification and stones which may become obscured by the contrast.

**Oral cholecystography** has an accuracy of around 90% in the diagnosis of gallstones provided a low kV technique is used including multiple coned views, with tomography and screening when necessary. The cystic and common ducts are often seen on the post-fat film which may also demonstrate Rokitansky–Aschoff sinuses and small filling defects not seen on the pre-fat film (Fig. 25.1). Non-filling of the gallbladder is not necessarily due to pathology (Table 25.1).

Table 25.1. Causes of non-opacification of the gallbladder

Incorrect procedure
Failed absorption
esophageal, gastric obstruction
diarrhea and vomiting
small bowel malabsorption
intestinal resection
Obstructed cystic duct
Abnormal gallbladder
cholecystitis, ectopic, absent
Reduced liver function
Cholestasis
Acute pancreatitis

**Ultrasound** has a similar degree of accuracy to oral cholecystography in the diagnosis of gallstones. The patient is kept fasting for 6 hours. Multiple scans are obtained in various positions including supine and lateral. In addition the liver, bile ducts and pancreas are assessed.

Ultrasound is the investigation of choice for distinguishing obstructive from non-obstructive jaundice.

The normal common bile duct is smaller than the portal vein and measures less than 7 mm in diameter. Size increases in the elderly when the normal duct may exceed 7 mm;



Fig. 25.2. Ultrasound scan. Dilated intrahepatic bile ducts.

post cholecystectomy up to 10 mm is accepted as normal. The gallbladder wall thickness should not exceed 3 mm. A normal gallbladder measures less than 5 cm by 10 cm.

The *valves of Heister* in the cystic duct may cast acoustic shadows which may be difficult to differentiate from a stone in the cystic duct. Acoustic shadowing from the gallbladder may be simulated by adjacent bowel gas, but can be overcome by scanning in the lateral position.

Dilated intrahepatic bile ducts appear as fluid-filled channels with irregular walls, characteristic stellate radiation and posterior acoustic enhancement (Fig. 25.2). A dilated common bile duct must be scanned throughout its length to assess the level of obstruction (Fig. 25.3). With a low obstruction duct, dilatation may take several days to develop, so that the ultrasound result may be misleading. Frequently the level of obstruction in the common duct cannot be identified because of overlying bowel gas. *Intraoperative ultrasound* is useful for demonstrating stones in the common duct at cholecystectomy.

**PTC.** In the presence of dilated ducts a successful puncture is achieved in over 90% of patients. Normal-sized ducts can be punctured in 80% of cases. Clotting factors must be normal. Ascites is a contraindication because of the increased risks of *bleeding* and *bile leakage*. Other complications include *pneumothorax*, *hemobilia*, *septicemia* and *cholangitis*, which may be precipitated by overfilling of the ducts with contrast. The normal common bile duct measures less than 8 mm. The type and level of the bile duct obstruction is well shown. PTC may be followed by catheter drainage of an obstructed



Fig. 25.3. Ultrasound scan. Dilated CBD (1.9 cm). The CBD (arrow) is dilated throughout its length and is obstructed by a carcinoma of the head of the pancreas. Pv = Portal vein.

system. This is advisable, unless immediate surgery is planned, to prevent bile leakage and biliary peritonitis.

**CT.** Normal intrahepatic ducts are not visualized, and the gallbladder is better shown at ultrasound. Bile has a density measurement of -5 to +15 HU. Dilated ducts are well shown as linear branching structures of water density converging on the porta. The level of obstruction is usually easily detected and an accuracy of over 90% has been reported. Gallstones are of variable density depending on the degree of calcification. Stones in the common duct are frequently not demonstrated.

**Radioisotope imaging.**  $^{99m}\text{Tc}$ -IDA (Fig. 25.4) is very accurate in the diagnosis of *acute cholecystitis*. It is useful for demonstrating the patency of biliary-enteric anastomoses, showing biliary fistula and leaks and for assessing emptying of the post-operative dilated CBD and of an afferent loop following surgery. In the neonate these scans may differentiate biliary atresia (no excretion) from neonatal hepatitis (poor hepatic uptake).

Normal findings are: hepatocyte uptake, 5–20 minutes; common duct filling, 10–30 minutes; gallbladder filling, 20–60 minutes; bowel activity within 20–60 minutes.

Renal excretion is increased in the presence of hepatocellular disease. There is no gallbladder filling in acute chole-

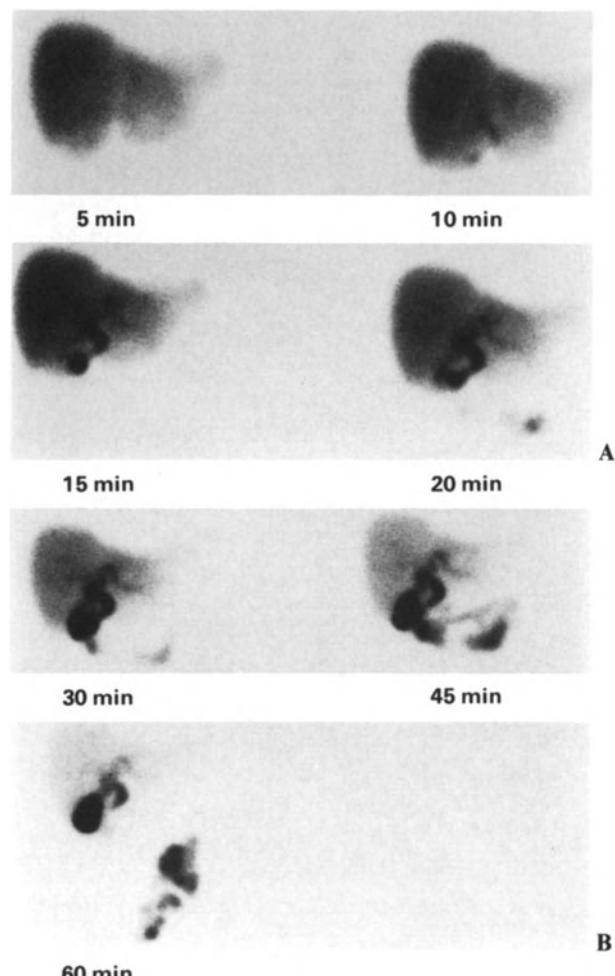


Fig. 25.4A, B. Normal  $^{99m}\text{Tc}$ -IDA.

Fig. 25.6. T-tube cholangiogram. Large stone in lower CBD.

cystitis and filling is delayed beyond one hour in chronic cholecystitis.

**Operative cholangiography.** Only two thirds of stones in the common duct are palpable at surgery. After contrast injection there should be free flow into the duodenum. Filling defects present may be *stones*, *bloodclot* or *air bubbles*. Bubbles are spherical and move up when the patient is tilted feet down.

**T-tube cholangiography** is performed 7 to 10 days post-operatively using low-density contrast media (Fig. 25.5). If stones are demonstrated (Fig. 25.6) and endoscopic sphincterotomy and manipulation fails, the T-tube may be left in situ for a further 5 weeks to allow a track to become established. Steerable catheters and baskets, or dissolution compounds may be put down the track to disintegrate or remove a stone. *Lithotripsy* may be used in conjunction with these techniques.

**Intravenous cholangiography** (Fig. 25.7) has a high toxicity and has been superseded by other imaging techniques. Occasionally it is useful for demonstrating duct anatomy



Fig. 25.5. Normal T-tube cholangiogram.



Fig. 25.7. Intravenous cholangiogram. Normal common duct. Stones in ▶ gallbladder.

**Table 25.2.** Therapeutic procedures

Procedure	Method	Indication
External drainage	Percutaneous	Obstructed common duct
External-internal drainage	Percutaneous	Obstructed common duct
Stent insertion	Percutaneous or Endoscopic	Malignant strictures Benign strictures Duct fistula
Stone removal	Endoscopic Sphincterotomy Percutaneous Insert T-tube Direct gallbladder puncture Dissolution therapy Endoscopic	Cholesterol stones Bile duct dyskinesis Sphincter spasm
Manometry		Cholangiocarcinoma
Sphincter of Oddi		Cholangiocarcinoma
Laser therapy	Percutaneous	Benign stricture
Iridium wires	Percutaneous	Biliary anastomosis
Balloon angioplasty	Percutaneous	

prior to surgery. Gallbladder opacification is poor. Opacification of the ducts fails in the presence of jaundice and the examination is contraindicated in *renal failure* and *myelomatosis*. The normal duct opacifies at 20 minutes and has a diameter of less than 1 cm on the film.

**Fine needle biopsy** using a fine cutting or aspiration needle is performed under CT, ultrasound or screening control.

Three passes are made. A disadvantage is that there is a high false negative rate.

**MRI.** As with CT, the normal intrahepatic bile ducts are not visualized. T<sub>1</sub>-weighted images are best for demonstrating the extrahepatic biliary tree, whilst T<sub>2</sub>-weighted images are better for showing dilated intrahepatic ducts. These images usually have poor signal to noise characteristics. At present CT and ultrasound must be considered superior.

Recent interest has focused on the MR characteristics of bile within the gallbladder. A different (higher) signal intensity has been reported from bile accumulating in a normal as opposed to a diseased gallbladder. The clinical usefulness of this observation remains to be determined.

**Therapeutic procedures.** Many therapeutic procedures involving the biliary tracts are now carried out with the use of imaging (Table 25.2).

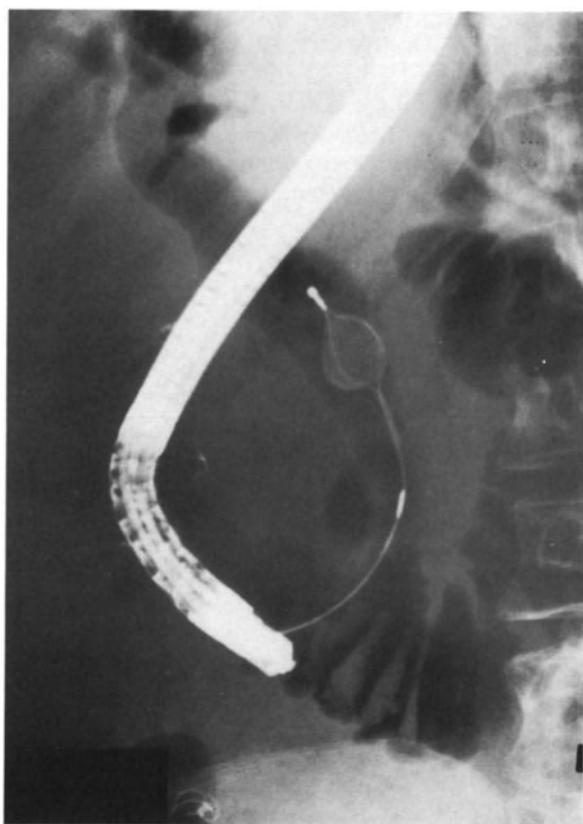
**External-internal biliary drainage** is achieved with a percutaneous catheter having side holes positioned above and below the obstructing lesion. Aspiration of duodenal contents may result in cholangitis and this is prevented by clamping the catheter externally. Stent insertion has the advantage that the patient is free of external tubes but has the disadvantage that there is no percutaneous access to the ducts if the stent becomes occluded or displaced.

**Endoscopic stent insertion** has the major complication of cholangitis. Bleeding and perforation may follow the sphincterotomy. **Percutaneous stent insertion** (Fig. 25.8). is associated with a higher morbidity and mortality. Serious complications occur in 5% and include bleeding, biliary peritonitis and pneumothorax. In view of this, difficult duct lesions not crossed by endoscopy may be attempted with a combined approach. First a percutaneous guide wire is passed through the lesion and then an endoscopic stent is passed, using it as guide. All stents may migrate and perforate the duodenum particularly if there is extensive malignant invasion. Stent occlusion is frequent after a few months.

**Gallstone removal.** **Endoscopic sphincterotomy** permits the removal of stones using baskets or catheters (Fig. 25.9), and percutaneous removal is possible through a T-tube tract or a percutaneous tract into the gallbladder, although larger stones must be crushed by mechanical means or by ESWL.

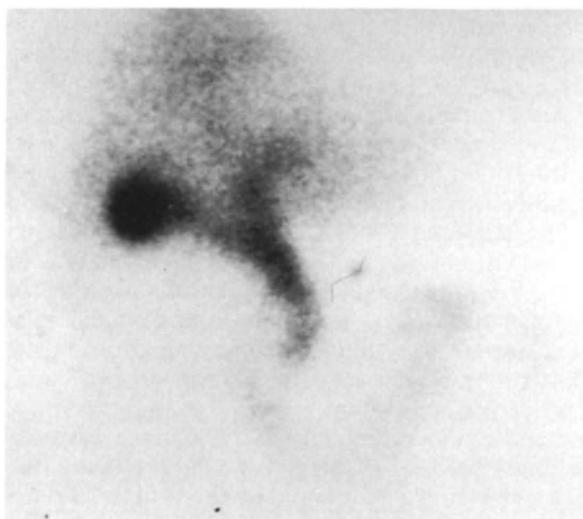


Fig. 25.8. Percutaneous stent insertion through malignant obstruction of common duct due to carcinoma of the pancreas. Temporary external drainage catheter in-situ.



**Fig. 25.9.** Endoscopic removal of gallstone with Dormia basket.

*Extracorporeal shock wave lithotripsy (ESWL)* is suitable for cholesterol stones less than 3 cm in diameter with no calcification evident on a plain film and little visible even at CT. A maximum of 3 stones is considered feasible for treatment, but the gallbladder should be functioning with a patent cystic duct and normal common bile duct. Up to one third of patients have biliary colic after the procedure but up to two thirds eventually become asymptomatic.



**Fig. 25.10.**  $^{99\text{m}}\text{Tc}$ -IDA scan. Intrahepatic gallbladder.

*Methyl-tert-butyl-ether* (MTBE) can be used to dissolve cholesterol stones via a percutaneous cholecystotomy. This procedure may take many hours. MTBE has anesthetic properties and only small aliquots are inserted into the gallbladder to prevent spillage into the duodenum or peritoneum. Other complications include hemolysis and nausea.

#### CONGENITAL ABNORMALITIES

Congenital abnormalities of the gallbladder and bile ducts are listed in Table 25.3.

**Table 25.3.** Congenital abnormalities

<i>Gallbladder</i>	
Agenesis	rare
	associations include biliary atresia, imperforate anus, bone abnormalities, polysplenia
Hypoplasia	
Left sided gallbladder	
Intrahepatic (Fig. 25.10)	
Floating	has a mesentery; may infarct
Double	two cystic ducts: rare (Fig. 25.11)
	Phrygian cap 3%–6%. Folding back or kinking of fundus (Fig. 25.12)
Septate	
	Single (hourglass) or multiple increased incidence of stones
Diverticula	increased incidence of stones
Cystic fibrosis	small irregular gallbladder
<i>Bile ducts</i>	
Accessory bile ducts	
Atresia	
Choledochal cyst: Type 1	
Choledochal diverticulum: Type 2	
Choledochocele: Type 3	
Caroli's disease	

Normally the cystic duct is short. It may be long with a low insertion, or enter the right or left hepatic ducts.

Accessory or anomalous hepatic ducts are present in nearly half of the population.

**Biliary Atresia.** There is failure of canalization or complete absence of the intrahepatic and extrahepatic ducts. The gallbladder may be absent. Presentation is in the neonatal period with persistent jaundice which must be differentiated from neonatal hepatitis and other conditions such as infections, metabolic and storage diseases, hemolytic abnormalities, gut atresia and choledochal cyst.

**Choledochal cyst** has an increased incidence in the Chinese population. There is a smooth fusiform dilatation of the common duct and the hepatic ducts may be dilated. Initial presentation is usually in childhood, characteristically with an upper abdominal mass, pain and jaundice. Adults complain of recurrent cholangitis. There is a high incidence of malignant change within the cyst. Occasionally the cyst ruptures resulting in biliary peritonitis. At ultrasound there is a fluid-filled mass.



**Fig. 25.11.** Oral cholecystogram. Duplication of the gallbladder.

**Choledochal Diverticulum.** The diverticulum arises from the lateral side of the distal common duct.

**Choledochocele.** There is dilatation of the intramural common bile duct with protrusion into the duodenum. These patients usually present in adult life with pancreatitis, biliary

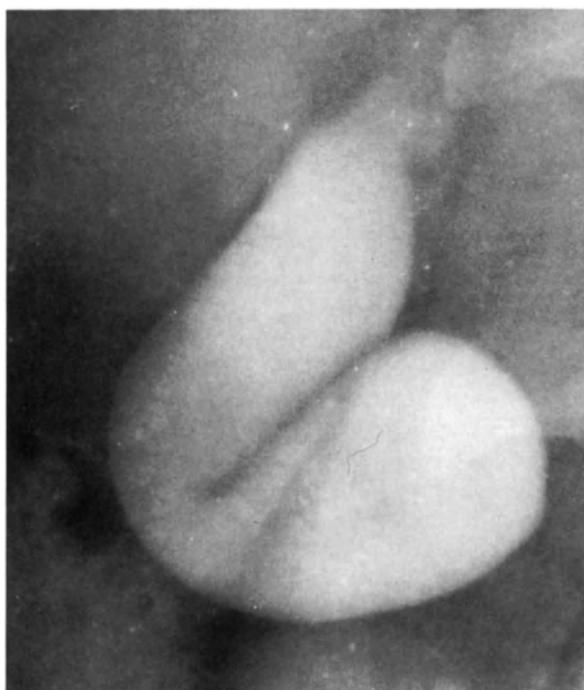


**Fig. 25.12.** Oral cholecystogram. Phrygian cap.

colic or jaundice, or they may be asymptomatic, though gallstones are often present.

**Caroli's Disease.** This is the intraphepatic form of choledochal cyst and presents with cholangitis. In addition there is an increased incidence of gallstones which are rarely calcified and of cholangiocarcinoma. The peripheral ducts are predominantly affected, with multiple saccular dilatations.

### GALLSTONES

Gallstones are present in 10% of the population, predominantly the middle-aged and elderly with a female to male ratio of 3:1. In the elderly the sex incidence is almost equal. In childhood, stones usually consist of pigment and are associated with a hemolytic disorders, such as hereditary spherocytosis and thalassemia.

There is an increased incidence of gallstones associated with liver failure, Crohn's disease and ileal resection.

Most stones are asymptomatic but there are several possible complications (Table 25.4).

**Table 25.4.** Complications of gallstones

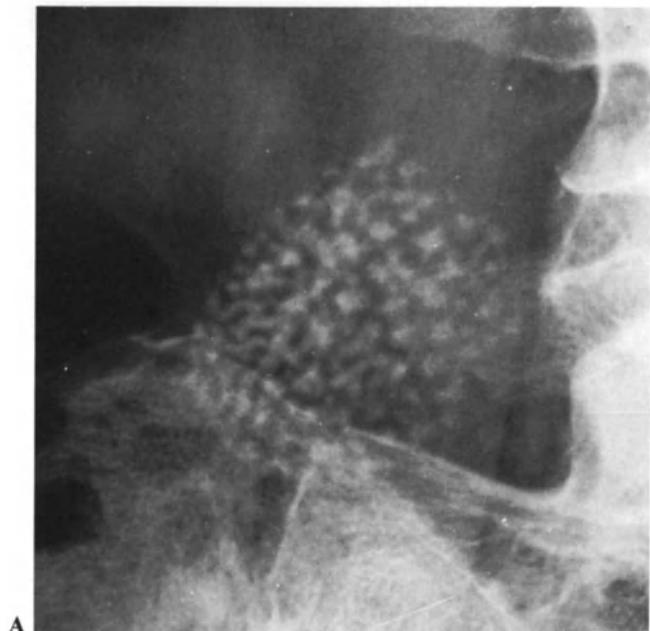
Acute cholecystitis
Chronic cholecystitis
Obstructed cystic duct
mucocele
empyema
limy bile
porcelain gallbladder
Obstructed common duct
jaundice
Mirizzi's syndrome
Acute pancreatitis
Gallstone ileus
Gallbladder malignancy

The radiodensity of gallstones correlates with calcium content and some 10%–20% are opaque on plain films (Fig. 25.13A, B). Occasionally stones develop within the ducts but these are rarely calcified. Biliary sludge consists of pigment and cholesterol crystals and is rarely radio-opaque.

The majority of stones contain cholesterol although only 10% are *pure cholesterol* stones. *Mixed* stones have a high cholesterol content in most cases and also contain calcium salts. Cholesterol stones are often solitary and large but may be multiple and float in the bile. Calcium deposition gives a laminated appearance. Stones with a high calcium content are often mulberry-shaped. Precipitation of calcium carbonate results in *limy bile*. Of all stones, 20% are mainly *pigment* and these are usually multiple, small and faceted.

Rarely, non-opaque stones are identified on plain films by linear gas shadows within the stone thought to be caused by gas-forming organisms. This is the so called Mercedes-Benz sign. Such stones float.

**Oral Cholecystography** (Fig. 25.14). There is an accuracy exceeding 90% for the diagnosis of gallstones although opaque stones may be obscured by the contrast. Erect films will show small floating stones (Fig. 25.15) which are often not readily apparent on supine films and are usually

**A****B**

**Fig. 25.13A, B.** Plain films. A Multiple small gallstones. B Mixed laminated stones.

cholesterol. Occasionally pigment stones have a dense rim formed by contrast adhering to the outer surface of the stone.

**Ultrasound.** The typical appearance is of a highly echogenic mobile stone within the gallbladder with distal acoustic shadowing which is related to the size of the stone (Fig. 25.16). Multiple scans in various positions are needed to demonstrate stone mobility and shadowing. Small stones may not have a detectable shadow and in such cases other lesions must be considered and rescanning is indicated at a later date.

Mobile echogenic lesions in the gallbladder, without acoustic shadowing, may be seen with small stones, blood



**Fig. 25.14.** Oral cholecystogram. Multiple laminated and faceted stones.



**Fig. 25.15.** Erect film oral cholecystogram. Multiple small floating stones, probably cholesterol, and single large stone.



**Fig. 25.16.** Ultrasound scan. Gallbladder contains large stone with associated acoustic shadow.



Fig. 25.17. Ultrasound scan. Biliary sludge and gallstone.

clot, parasites and sludge balls. Stones are immobile if impacted in the cystic duct or adherent to the gallbladder wall.

A small contracted gallbladder containing multiple stones may be difficult to differentiate from bowel gas. Such a gallbladder gives a persistent collection of high-level echoes in the region of the gallbladder bed with marked acoustic shadowing. Sometimes the anterior gallbladder wall is seen as an outer highly reflective line with an underlying echo-free layer anterior to the highly reflective stones and acoustic shadowing; the 'double-rim' sign.

**Biliary sludge** is often present in patients being fasted or intravenously fed, with acute or chronic cholecystitis and with biliary obstruction. At ultrasound sludge is mobile and moderately echogenic but without acoustic shadowing. It often forms a fluid-fluid level (Fig. 25.17).

**Limy Bile**. Limy bile is very viscous with a high calcium carbonate content giving diffuse opacification on a plain film which resembles cholecystography (Fig. 25.18). A fluid level is often present on an erect film. Usually the cystic duct is

obstructed by a stone and the gallbladder non-functioning. At ultrasound the bile is echogenic with distal shadowing.

**Porcelain Gallbladder**. The porcelain gallbladder is non-functioning with obstruction of the cystic duct. Malignancy is reported in 10%–20% and there is an increased incidence of gallstones. Calcification of the gallbladder wall is focal or generalized. On plain films there is curvilinear or granular calcification of the wall (Fig. 25.19).

At ultrasound the gallbladder wall is highly echogenic with acoustic shadowing. A similar appearance occurs with emphysematous cholecystitis and with a contracted gallbladder containing stones. CT appearances are characteristic.

#### HYPERPLASTIC CHOLECYSTOSIS

Hyperplastic cholecystoses include cholesterosis and adenomyomatosis. Both conditions occur predominantly in females.

**Cholesterosis (Strawberry Gallbladder)**. This condition is often asymptomatic, although the incidence at post mortem is 10%. Small cholesterol deposits are adherent to the gallbladder mucosa. Occasionally small mural nodules are seen at oral cholecystography and the gallbladder outline is ill-defined. However appearances are usually normal.

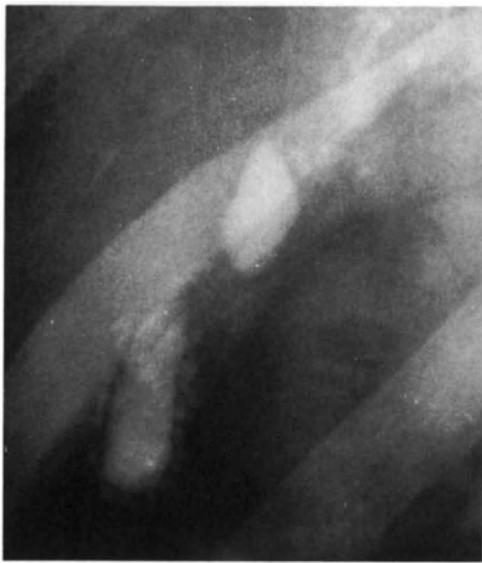
**Adenomyomatosis (Cholecystitis Glandularis Proliferans)** There is focal or generalized muscle hypertrophy with invagination of mucosa forming Rokitansky–Aschoff sinuses. The sinuses are seen most often on the post-fat cholecystogram film (Fig. 25.20). Other features include a fundal nodule, often umbilicated, and a stricture producing an hour-glass deformity, which is also better seen on the post-fat film. At ultrasound the gallbladder wall is thickened. The separate compartments and the sinuses may be seen. Slow



Fig. 25.18. Plain film. Limy bile.



Fig. 25.19. Plain film. Porcelain gallbladder.



**Fig. 25.20.** Oral cholecystogram post-fat film. Adenomyomatosis with a stricture and filling of the Rokitansky-Aschoff sinuses.



**Fig. 25.21.** Plain film. Emphysematous cholecystitis.

filling of the distal compartment of the gallbladder may be seen on radionuclide imaging.

### ACUTE CHOLECYSTITIS

Acute cholecystitis is a common cause of severe acute right upper quadrant pain but must be distinguished from other causes such as a perforated peptic ulcer, acute appendicitis and acute pancreatitis. The causes are listed in Table 25.5. In 90% of adult cases there are gallstones with cystic duct obstruction, and 10% of cases are acalculous. Initially the bile is sterile, but within three days 80% of gallbladders are infected. In children the incidence of acalculous cholecystitis is much greater, being at least 50%.

**Table 25.5.** Causes of acute cholecystitis

Gallstones (90%)
Acalculous (10%)
severe illness, starvation
infections – tuberculosis, salmonella,
cholera, parasites
extrinsic cystic duct compression
myocardial infarction

Acute cholecystitis is a grave condition which may resolve spontaneously or proceed to resolution, empyema, gangrene, perforation and its associated complications (peritonitis, abscess formation, choledocho-enteric fistula) and to chronic cholecystitis.

*Emphysematous cholecystitis* has a high incidence in patients with diabetes mellitus. It is commoner in males and is often acalculous. The mortality is 10%. Infection occurs with gas-forming organisms. Gangrene and perforation are frequent.

**Imaging.** Plain film findings may include radio-opaque gallstones, localized ileus of the duodenum and hepatic flexure, a right upper quadrant mass depressing the adjacent gut, an ill-defined liver edge inferiorly and gas in the gallbladder lumen, wall and biliary tree.

Gas in the gallbladder wall appears as linear streaks or small bubbles (Fig. 25.21). An air-fluid level indicates gas in the lumen.

At oral cholecystography there is no function.

Ultrasound findings include gallstones, positive sonographic Murphy's sign (pain caused by scanning directly over the gallbladder), a large globular gallbladder (exceeding 5 cm diameter), a thickened gallbladder wall, a pericholecystic fluid collection (perforation with abscess), echogenic bile and sludge, intraluminal strands and gas in the lumen.

Thickening of the gallbladder wall beyond 3 mm is abnormal (Fig. 25.22A, B, C). Frequently the wall has a sandwich appearance with an echo-free layer surrounded by two highly reflective layers. There are however, other causes of a thickened gallbladder wall (Table 25.6).

**Table 25.6.** Causes of a thick gallbladder wall

Acute cholecystitis (50%–70%)
Chronic cholecystitis (25%)
Contracted gallbladder after emptying
Ascites
Low albumen states
Congestive cardiac failure
Carcinoma of the gallbladder

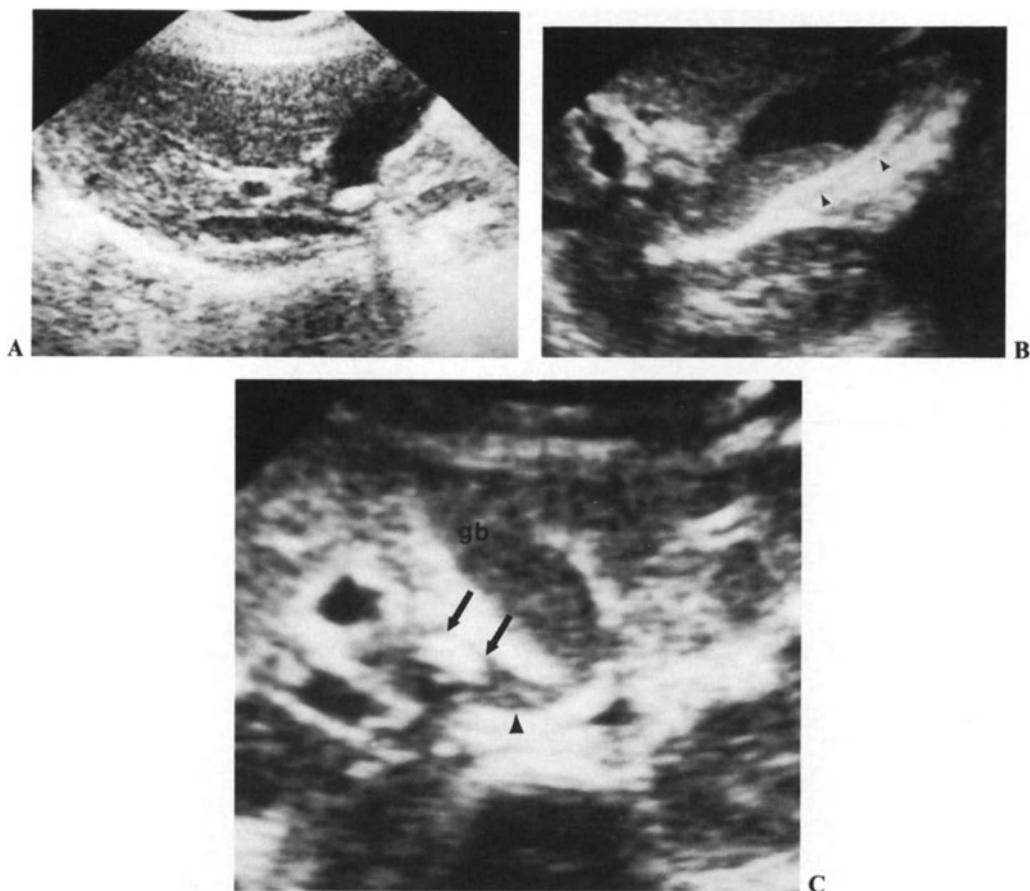


**Fig. 25.22A, B, C.** Acute cholecystitis. A Ultrasound scan. 3 months previously. Stone in gallbladder. B Ultrasound scan. Thickened gallbladder wall (arrowheads). Biliary sludge. Enlarged gallbladder. C Ultrasound scan. Stone (arrow) impacted in cystic duct (arrowhead).

Irregularity of the wall suggests ulceration and gangrenous cholecystitis. In addition there may be intraluminal strands of fibrous exudate and coarse echoes from pus within the bile. Gas in the wall and lumen is highly reflective with marked acoustic shadowing and may be easily confused with large stones or a porcelain gallbladder.

**Radionuclide Imaging.** A normal  $^{99m}\text{Tc}$ -IDA scan virtually excludes the diagnosis of acute cholecystitis. Typically the gallbladder fails to fill in acute cholecystitis but the common bile duct is seen and there is normal bowel activity within 60 minutes. False positive results can occur in the very ill and with those having parenteral nutrition.

**CT.** Possible findings include gallstones, increased bile density, a thickened wall with or without irregularity, pericholecystic fluid, thickening and streaking of tissues around the gallbladder due to spreading inflammation and gas within an abscess.

#### Gall Bladder Perforation

Causes of gallbladder perforation include gallstones, acute cholecystitis, gangrene, malignancy, trauma and steroids.

A pericholecystic abscess often forms following perfor-

ation. Peritonitis and fistula formation are less common. Occasionally a gallstone can be seen outside the gallbladder.

#### Fistulae

*Choledochoenteric fistula* may develop after gallbladder perforation by a stone or a duodenal ulcer, and in the presence



**Fig. 25.23.** Barium meal. Biliary fistula following gallbladder perforation by a stone. Barium in gallbladder and bile ducts.



Fig. 25.24. Gas in the biliary tree.

of gallbladder and biliary malignancy, chronic cholecystitis, inflammatory bowel disease, diverticulitis and hydatid disease. Gas enters the biliary tract and a fistula may develop between the gallbladder and bowel, the skin surface and occasionally the kidney. Barium studies may demonstrate the fistula with barium refluxing into the ducts and gallbladder (Fig. 25.23). IDA scanning is only helpful if the cystic duct is patent or if the fistula involves the main ducts.



Fig. 25.25. Ultrasound scan. Gas in the biliary tree. Highly echogenic branching structures (arrows).

### Gas in the Biliary Tree

**Plain films.** When the gallbladder contains gas it is seen lying lateral to the duodenal cap and above the hepatic flexure. Causes of gas in the biliary tree are given in Table 25.7: the gas results in a branching pattern of translucency lying centrally around the porta hepatis (Fig. 25.24). This must be distinguished from gas in the portal venous system, which may develop from a portal pyemia. Portal vein gas is best demonstrated by a horizontal beam film with the patient lying on his left side. The venous gas extends to the periphery of the liver, unlike biliary gas which is more central. Gas in the main portal vein appears as a transverse lucency in the right upper quadrant.

Table 25.7. Causes of gas in the biliary tree

Iatrogenic – surgical fistulae, endoscopy, sphincterotomy
Recent passage of a stone
Fistula – gallstone ileus; malignancy e.g. duodenum, colon; perforated ulcer
Infections with gas-forming organisms, parasites
Incompetent sphincter in the elderly

At *ultrasound* gas in the biliary tree is highly echogenic with posterior acoustic reverberation (Fig. 25.25). Biliary gas is easily identified at *CT* (Fig. 25.26).

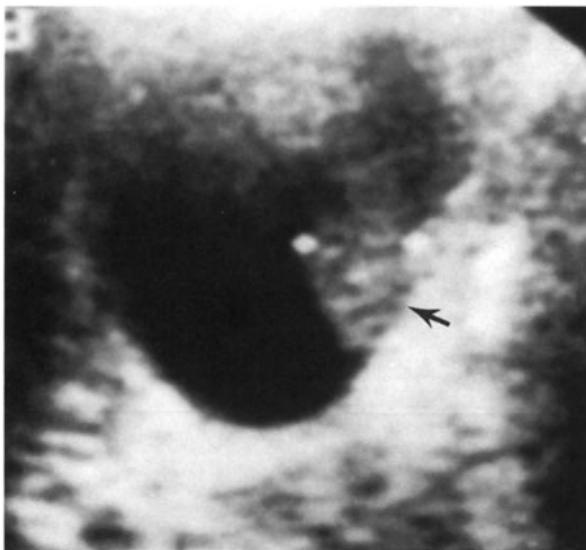
### CHRONIC CHOLECYSTITIS

Over 90% of cases of chronic cholecystitis are associated with gallstones. The gallbladder wall is thickened and fibrotic. A *procoplain* gallbladder may develop. At *oral cholecystography* there is non-function. *Ultrasound* demonstrates stones, and biliary sludge is often present. There is smooth thickening of the gallbladder wall; areas of irregular thickening suggest malignancy. With  $^{99m}\text{TC}-\text{IDA}$  scanning gallbladder filling is typically delayed beyond 1 hour; occasionally uptake is normal or there is non-filling.

**Mucocele of the Gallbladder.** The gallbladder is chronically obstructed and non-functioning. *Ultrasound* shows a large gallbladder which may contain stones.



Fig. 25.26. CT scan. Gas in the biliary tree.



◀ Fig. 25.27. Ultrasound scan gallbladder. Small mucosal polyp (arrow).

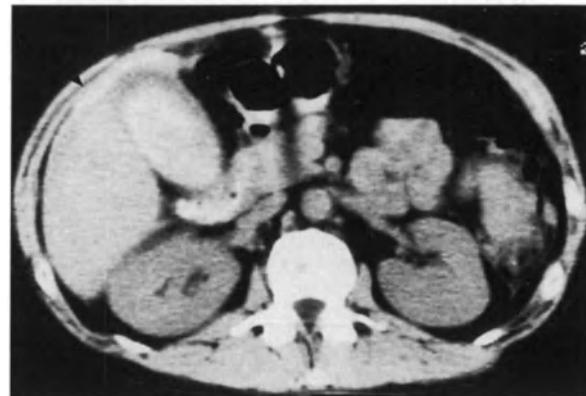


Fig. 25.28. CT scan unenhanced. Stab wound to liver. High density fresh blood in gallbladder and subcapsular hematoma of liver (arrow).

**Mirizzi Syndrome.** This complication of chronic cholecystitis is often associated with a low insertion of the cystic duct. Jaundice is a feature. A stone becomes impacted in the cystic duct and subsequently an inflammatory mass developed obstructing the common duct. Subsequently a fistula and ascending cholangitis may develop.

*Ultrasound* demonstrates the dilated common duct and intrahepatic ducts but may fail to show the inflammatory mass.

*Percutaneous transhepatic cholangiography* shows non-specific extrinsic compression of the common duct which must be distinguished from other masses such as lymph nodes, pancreatic cysts and tumors.

### GALLBLADDER TUMORS

**Benign.** At cholecystectomy polyps are present in 5% of gallbladders. They are sessile or pedunculated and there are several histological types including cholesterol, inflammatory, hyperplastic and adenoma. Lesions exceeding 1 cm are considered premalignant. Multiple polyps may occur with Gardner's syndrome and Peutz-Jegher's syndrome.

At *ultrasound* there is a fixed mass (Fig. 25.27) which may be difficult to differentiate from an adherent stone, malignancy, folds in the gallbladder, cholesterosis and adenomyomatosis.

**Malignant.** *Carcinoma of the gallbladder* is a rare malignancy which occurs in the elderly and is associated with gallstones. In addition malignancy is a frequent complication of the porcelain gallbladder. Presentation is late and features include jaundice, pain and weight loss. The prognosis is very poor.

Usually the gallbladder fails to opacify at *oral cholecystography*. PTC will show malignant invasion of the bile duct.

At *ultrasound* there is a polypoid mass within the gallbladder lumen with distortion of the outline and thickening of the gallbladder wall, or an extensive tumor forming a large complex mass in the gallbladder bed, with dilated bile ducts and liver metastases. Similar appearances are found at *CT*.

**Metastases.** These are predominantly from gastrointestinal tumors and melanoma and produce filling defects within the lumen.

### GALLBLADDER TRAUMA

Bleeding into bile results in increased reflectivity at *ultrasound*. At *CT* fresh blood is initially high density (Fig. 25.28) but the density decreases after a few hours. There may be laceration or avulsion with resulting biliary peritonitis.

### BILE DUCT TUMORS

Bile duct tumors (Table 25.8) present with jaundice. Benign tumors are very rare. *Sarcoma botryoides* and choledochal cyst are the common causes of jaundice in childhood.

Table 25.8. Bile duct tumors

Benign	
adenoma: polypoid	
mesenchymal: single or multiple	
papilloma: rare	
Malignant	
cholangiocarcinoma	
sarcoma botryoides	
children	
grapelike with cystic masses	
poor prognosis	
metastases	

**Cholangiocarcinoma.** This is usually an adenocarcinoma. The prognosis is better than for pancreatic adenocarcinoma because of a slower growth rate but long-term survival rates are very low. An increased incidence is reported in association with inflammatory bowel disease, sclerosing cholangitis, gallstones, Caroli's disease and *Clonorchis sinensis* infection.

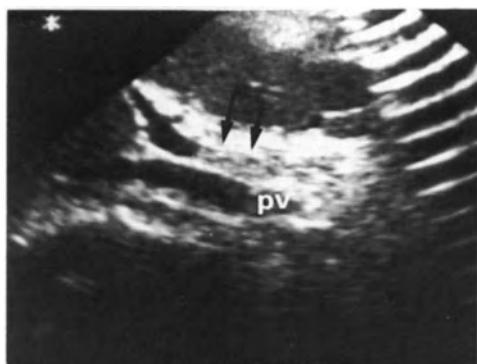


**Fig. 25.29.** Ultrasound scan. Cholangiocarcinoma (arrows) of common duct with proximal duct dilatation. Pv = Portal vein.

The tumor produces solitary or multiple strictures. The majority arise within the common duct (60%) or at the porta (20%) (the Klatskin tumor) but the intrahepatic ducts may be affected as well. A single tumor affecting the duct of one lobe may be asymptomatic. The chronic obstruction results in lobar atrophy.

At *ultrasound* there is proximal duct dilatation with sudden cut-off at the site of the tumor (Fig. 25.29). Occasionally the tumor is seen as a small periductal non-shadowing mass. Similar appearances are seen at *CT*, the mass being low density.

At *PTC* and *ERCP* the strictures are usually short with proximal duct dilatation (Fig. 25.30). Intraluminal filling



**Fig. 25.30.** PTC. Cholangiocarcinoma of common duct.

defects may be seen. Lobar atrophy is suggested by crowding of the ducts. At *isotope scanning* lobar uptake is reduced.

Possible treatments include surgical drainage, achieved by anastomosing gut to the proximal duct, an hepatoenterostomy, or gut to gallbladder, choledochoenterostomy, for a distal common duct lesion. If surgery is not possible stents may be inserted transhepatically or endoscopically. Both right and left hepatic duct systems may need to be drained with separate stents if dilated (Fig. 25.31). Draining only one set of dilated ducts increases the risk of cholangitis on the other side.

$^{192}\text{Iridium}$  wires may be positioned through a percutaneous catheter at the level of the tumor. Increased survival times have been reported.

#### BILE DUCT STRICTURES

Bile duct strictures may be classified as malignant or benign (Table 25.9) and may develop at the site of a previous T-tube after several years.

A misplaced suture is immediately apparent on contrast examination resulting in a stricture or occlusion and causing jaundice. These strictures are difficult to treat and may require long-term stenting or a surgical anastomosis to bypass the lesion.

Typically, benign strictures are smooth: malignant lesions are irregular, have a rat's tail appearance or result in a sudden cut off with a convex edge (Figs 25.32, 25.33). Classically gallstones have the meniscus sign (Fig. 25.34). The stone indents the contrast column and some contrast passes around the edge of the stone. Chronic pancreatitis rarely obstructs the bile duct but causes a long smooth stricture (Fig. 25.35); pancreatic calcification suggests the diagnosis.

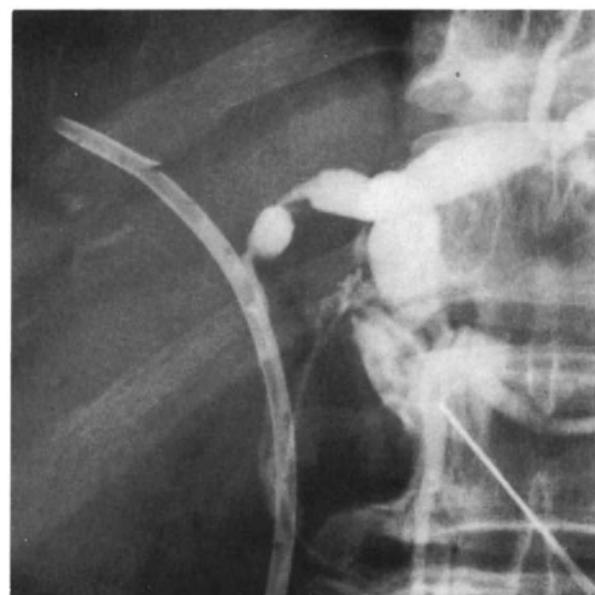


**Fig. 25.31.** PTC. Cholangiocarcinoma with dilated left duct system. Endoscopically inserted stent draining right duct system.



◀ Fig. 25.32. PTC. Portal mass of malignant lymph nodes with dilated intra-hepatic ducts. Previous gastric carcinoma.

**Table 25.9. Bile duct strictures**

Malignant	
cholangiocarcinoma	
carcinoma pancreas	
carcinoma ampulla	
portal lymphadenopathy (Fig. 25.32)	
malignancy: stomach, duodenum, liver, gallbladder	
Benign	
surgery (80%)	
inflammatory	
chronic pancreatitis	
penetrating duodenal ulcer	
recurrent cholangitis	
Mirizzi's syndrome	
passage of a stone	
sclerosing cholangitis	
congenital	
tumors	
tuberculous	

Obstruction of both the pancreatic and bile ducts usually indicates pancreatic malignancy rather than an inflammatory cause.

#### BILE DUCT STONES

Duct stones are often asymptomatic with no duct dilatation. Around one fifth of cholecystectomy patients have duct



Fig. 25.33. PTC. Carcinoma of the head of the pancreas obstructing the common duct.

stones. They rarely calcify and are easily missed on CT and ultrasound. In addition acoustic shadowing is not a constant feature.

At ERCP and PTC (Fig. 25.36) the stone may be floating or impacted in the duct.

#### PRIMARY SCLEROSING CHOLANGITIS

Associated diseases are ulcerative colitis, Crohn's disease, retroperitoneal and mediastinal fibrosis and Riedl's thyroiditis.

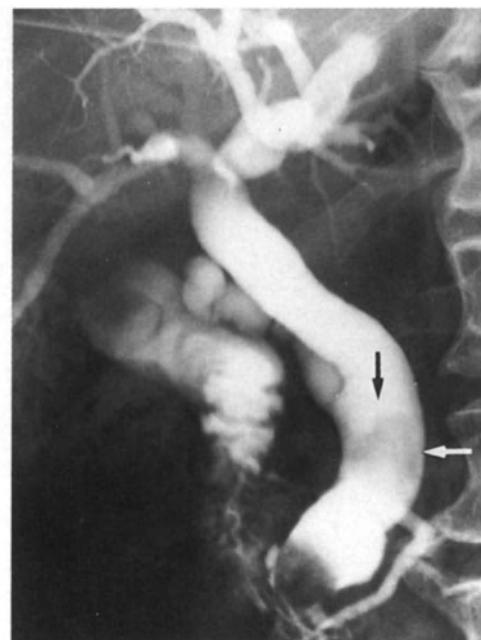


Fig. 25.34. PTC. Gallstone impacted at lower end of CBD. A second stone (arrow) is present in the dilated duct and there is a stone in the gallbladder.

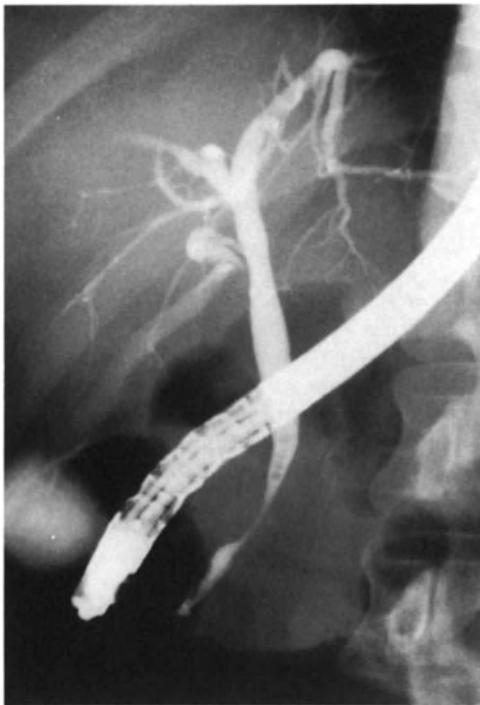


Fig. 25.35. ERCP. Chronic pancreatitis. Long smooth stricture of the common duct.

There is diffuse fibrosis of the ducts with short multiple strictures of both the intra and extrahepatic ducts but with only slight dilatation of the normal duct segments (Fig. 25.37). Beading and saccular outpouchings of the duct system are characteristic. The disease is commoner in males. It progresses to occlusion of the ducts, biliary cirrhosis and hepatic failure and there is an increased incidence of cholangiocarcinoma. The ducts may be demonstrated by ERCP or PTC. At ultrasound and CT the ducts have thick walls

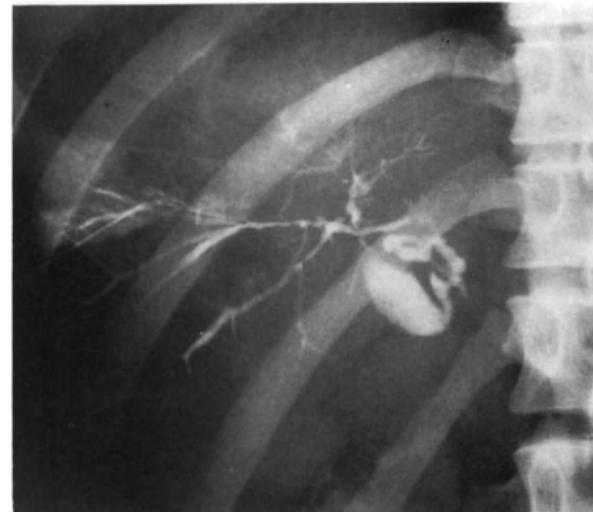


Fig. 25.37. PTC. Sclerosing cholangitis. 18-year-old male with Crohn's disease and jaundice.

and may contain debris. It may be difficult to differentiate sclerosing cholangitis from diffuse cholangiocarcinoma.

Although the gallbladder is said to be normal there have been recent reports of an increased incidence of gallbladder stones, tumors and involvement of the gallbladder by the primary process.

Inflammatory bowel disease is associated with a number of liver and biliary abnormalities: sclerosing cholangitis, chronic active hepatitis, cirrhosis, cholangiocarcinoma, fatty liver, gallstones (Crohn's), and amyloid.

*Secondary sclerosing cholangitis* may develop following chronic biliary obstruction.

## INFECTIONS

**Suppurative Cholangitis.** Suppurative cholangitis usually develops in obstructed ducts associated with an impacted stone, and is uncommon in the presence of malignancy unless there has been instrumentation (Fig. 25.38). In addition cholangitis may complicate surgical biliary enteric anastomoses.

Cholangiography demonstrates multiple intrahepatic abscesses with filling defects consisting of pus in the ducts.

Treatment is by percutaneous or endoscopic drainage and appropriate antibacterial therapy.

Recurrent cholangitis results in cirrhosis. The ducts become fibrosed and featureless with reduced side branch filling. Strictures may develop.

**Liver Fluke (*Clinorchis sinensis*).** The liver fluke is common in eastern Asia and may cause oriental cholangiohepatitis. The worm is found in the duct, and stones and debris form multiple filling defects in the intrahepatic ducts. Biliary colic, cholangitis, jaundice and hepatitis may develop.

***Ascaris lumbricoides*.** The roundworm is common in Africa, Asia and central America. It migrates from the small bowel through the ampulla into the common bile duct and

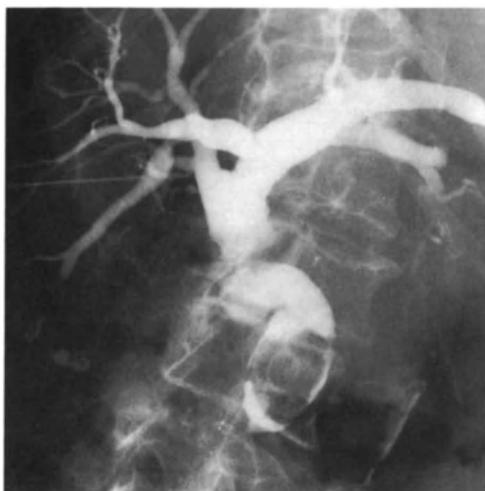


Fig. 25.36. PTC. Very large stone in dilated common duct. The intrahepatic ducts are dilated.

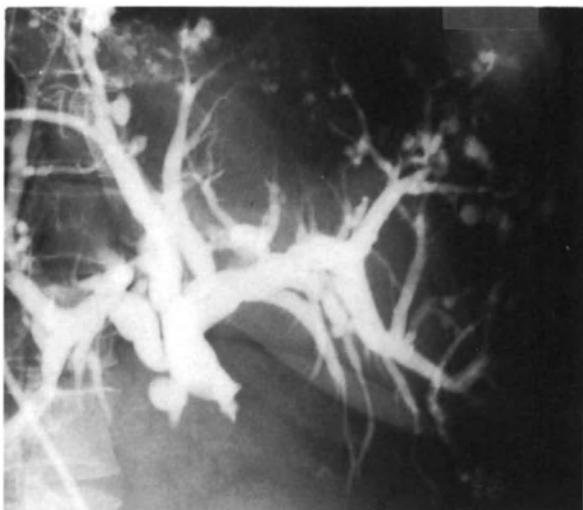


Fig. 25.38. PTC. Suppurative cholangitis with multiple abscesses following failed endoscopic stent insertion for malignant stricture.

may cause biliary colic. Ascending cholangitis and abscesses may develop.

At ultrasound the worm is seen as a single highly reflective line, or as double parallel reflective lines with a central echo-



Fig. 25.39. PTC. Biliary-enteric fistula and external fistula to skin surface. Jaundice developed following gastric surgery. Gas in the left duct system.

free region. A bull's-eye appearance is seen on cross-section. Multiple stones may be present. The diagnosis is often made on the plain film.

**Hydatid Disease.** Hepatic cysts compress and displace intrahepatic ducts and occasionally may communicate with the duct.

#### BILE DUCT TRAUMA

The majority of cases of trauma to the bile ducts occur during cholecystectomy or gastric surgery. Possible problems are stricture formation, complete obstruction by a misplaced suture, tearing or transection of the duct resulting in fistula formation with gut or occasionally the skin surface (Fig. 25.39), and an abnormal collection of bile due to leakage. A *biloma* may be demonstrated by ultrasound, CT and radioisotope imaging.

#### REFERENCES AND SUGGESTIONS FOR FURTHER READING

- Ferrucci JT, Mueller PR, Harbin WP (1980) Percutaneous transhepatic biliary drainage. *Radiology* 135: 1-13
- Fowler RC, Reid WA (1988) Ultrasound diagnosis of adenomyomatosis of the gallbladder: ultrasonic and pathological correlation. *Clin Radiol* 39: 402-406
- Friedman AC (1987) *Radiology of the Liver, Biliary Tract, Pancreas and Spleen*. Williams and Wilkins, pp 305-615
- Gibson RN et al. (1986) Bile duct obstruction: radiologic evaluation of level, cause and tumor resectability. *Radiology* 160: 43-47
- Hamlin JA, Friedman M, Stein MG, Bray JF (1986) Percutaneous biliary drainage: complications of 118 consecutive catheterisations. *Radiology* 158: 199-202
- Haskin PH, Teplick SK, Sammon JK, Gambescia RA, Zitomer N and Pavlides CA (1987) Monoctanoin infusion and stone removal through the transparenchymal tract: use in 17 patients. *AJR* 148: 185-188
- Hofman AF (1986) Walter B Cannon Lecture - Bile, bile acids and gallstones: will new knowledge bring new power? *AJR* 151: 5-12
- Laing FC et al. (1986) Biliary dilatation: defining the level and causes by realtime ultrasound. *Radiology* 160: 39-42
- Lees WR, Kellett MR (1989) Gallbladder stones: New role for the radiologist. *Clin Radiol* 40: 501-503
- Mason RR (1985) Percutaneous extraction of retained gallstones. *Clin Gastroenterol* 14: 403-419
- Reiman TH, Balfe DM, Weyman PJ (1987) Suprapancreatic biliary obstruction: CT evaluation. *Radiology* 163: 49-56
- Sauerbruch T, Delius M, Paumgartner G et al. (1986) Fragmentation of gallstones by extracorporeal shock waves. *N Engl J Med* 314: 818-822
- Van Sonnenberg E, Wittich GR et al. (1986) Diagnostic and therapeutic gallbladder procedures. *Radiology* 160: 23-26
- Weiner SN, Koenigsberg M, Morehouse H, Hoffman J (1984) Sonography and computed tomography in the diagnosis of carcinoma of the gallbladder. *AJR* 142: 735-739
- Williams SM, Harvey RK (1987) Hepatobiliary complications of inflammatory bowel disease. *Radiol Clin North Am* 25: 175-188

## CHAPTER 26

# LIVER AND SPLEEN

Janet Murfitt

---

## LIVER

---

### INVESTIGATION OF THE LIVER

All the following imaging techniques can provide useful information in the investigation or therapy of liver disease: abdominal film, chest film, barium studies, ultrasound, CT, radionuclide imaging, angiography, fine needle biopsy, therapeutic procedures and MRI.

#### The Plain Abdomen Film

Relevant features to note on the plain film are liver size, calcification, abnormal gas shadows in the region of the liver, ascites and splenomegaly.

**Hepatomegaly.** The inferior edge of the liver is outlined by extraperitoneal fat and by adjacent gas filled gut. Marked hepatomegaly is usually easily detected on the plain film (Fig. 26.1).

Plain film signs of hepatomegaly are depression of the hepatic flexure and right kidney, displacement inferolaterally of the stomach, displacement inferomedially of the duodenal loop, depression of the splenic flexure (left lobe), elevation of the right hemidiaphragm with decreased excursion, bulging of the right lateral properitoneal fat line and splaying of the right lower ribs.

Some masses may be seen as a localized bulge to the liver or diaphragm outline.

On occasions a normal-sized liver appears to be enlarged because it is being pushed downwards by a subphrenic collection or by a depressed diaphragm, secondary to emphysema or a sub-pulmonary effusion. Renal and other



Fig. 26.1. Hepatomegaly. Large calcified hepatoma with elevation of right hemidiaphragm and depressed hepatic flexure of colon (arrow).

**Table 26.1.** Causes of hepatomegaly

Increased venous pressure
congestive cardiac failure
constrictive pericarditis
tricuspid valve disease
hepatic vein occlusion
Tumors
metastases
primary malignant
benign
lymphoma
Polycystic disease
Early cirrhosis
Infiltration
fatty liver
amyloidosis
histiocytosis
hemochromatosis
Gaucher's disease
glycogen storage disease
sarcoidosis
Wilson's disease
Nieman-Pick's disease
Hematological disorders
Obstructive jaundice
Infections
abscesses – pyogenic, amebic, hydatid
hepatitis, glandular fever
tuberculosis, syphilis, Weil's disease
malaria, toxoplasmosis, Kala-azar
histoplasmosis
Riedl's lobe
Trauma, hematoma

retroperitoneal masses may be difficult to distinguish from hepatomegaly on plain films. The causes of hepatomegaly are summarized in Table 26.1.

Calcification within the liver is uncommon, but may have characteristic appearances (Table 26.2).

Increased liver density, not due to calcification, may be seen in hemochromatosis. Thorotrust, which was used as an intravascular contrast medium many years ago, also gave rise to increased liver density.

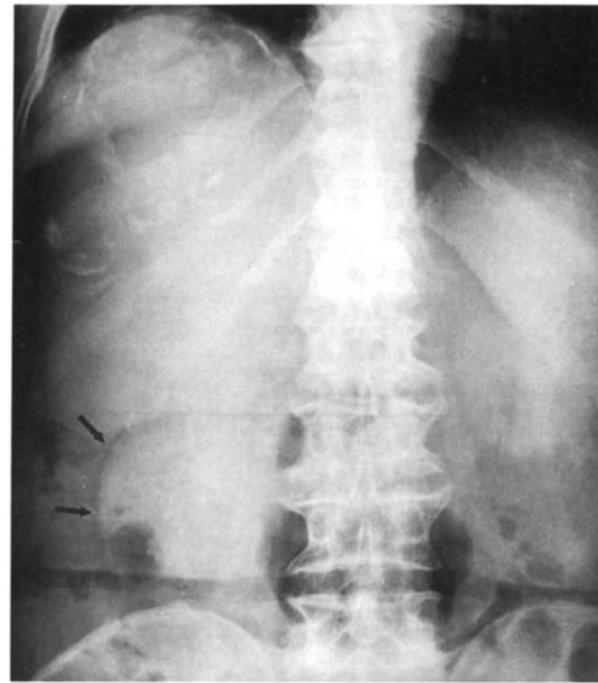


**Fig. 26.2** Calcification in hydatid cyst. Hepatomegaly with elevated hemidiaphragm and depressed right kidney (arrows).

**Abnormal Gas Shadows.** Abnormal gas shadows within the liver may also be seen on the plain film, and these may be localized to different sites: parenchymal, subphrenic or subhepatic (see Chap. 24) portal vein (see below), biliary tract (see p. 457).

Gas within the liver **parenchyma** may lie within an *abscess* or follow *penetrating trauma*. Infection with gas-forming organisms can complicate embolization of hepatic tumors. The volume of gas within an abscess is usually small and

**Table 26.2.** Causes of plain film calcification

Lesion	Appearance
Neoplasms	
hepatoma	stippled, sunray
hepatoblastoma	stippled, sunray
metastases	granular, punctate, amorphous, spiculated
mucus-secreting adenocarcinoma	
medullary cell carcinoma thyroid	
neuroblastoma	
osteogenic sarcoma	
hemangioma	spiculated, phleboliths (rare)
Infections	
old abscess	amorphous
hydatid cyst	curvilinear, crumpled eggshell (Fig. 26.2)
granulomata	multiple nodules
Miscellaneous	
cysts	curvilinear (rare)
duct stones	very rarely calcified
hepatic artery aneurysm	curvilinear
hematoma	amorphous
portal vein thrombosis	linear



Fig. 26.3. Gas in the peripheral branches of the portal vein. Premature neonate with necrotizing enterocolitis.

is commonly seen as multiple small bubbles rather than a single large fluid level.

**Portal venous gas** (Fig. 26.3) forms a pattern of multiple linear translucencies extending to the periphery of the liver, in contrast to the centralized pattern of **biliary gas**. Occasionally gas is identified within the portal and mesenteric veins as well. Portal venous gas is a highly significant finding and is associated with a grave prognosis. The causes are listed in Table 26.3.

Table 26.3. Causes of portal vein gas

<b>Neonatal</b>
necrotizing enterocolitis
umbilical vein catheterization
<b>Adults</b>
bowel ischemia
septicemia
abdominal sepsis
hemorrhagic pancreatitis
small bowel obstruction
disseminated intravascular coagulation
ulcerative colitis

### Chest Film

Diaphragm elevation, pleural effusions and basal atelectasis or shadowing frequently accompany inflammatory processes within the liver or subphrenic space.

The normal *azygos vein* lies in the right tracheobronchial angle. Enlargement occurs with *obstructive portal hypertension* as well as with heart failure and superior and inferior vena caval obstruction.

Increased blood flow through the *hemiazygos vein* results in enlargement of the left paravertebral shadow. Occasionally there is aneurysmal dilatation producing a wavy left paravertebral shadow.

### Barium Studies

Hepatic enlargement, particularly of the left lobe, may result in elongation of the intra-abdominal esophagus as well as widening of the lesser curve of the stomach and posterior displacement of the stomach.

Portal hypertension is associated with an increased incidence of peptic ulceration. Varices may be shown in the esophagus, gastric fundus and duodenum. Isolated gastric varices are found with splenic vein occlusion.

### Ultrasound

The normal liver has a smooth outline and an homogenous echo pattern which is slightly more echogenic than the kidney and spleen, but of slightly lower echogenicity than the pancreas. The portal veins are tubular anechoic structures with echogenic walls. Ultrasound has a high degree of accuracy in the detection of focal liver lesions but is of limited assistance in the diagnosis of diffuse liver disease. The extreme lateral sections of both the right and left lobes are often difficult to visualize satisfactorily and are areas where mass lesions may be missed.

*Endoscopic transesophageal ultrasound* can be used to identify gastro-esophageal varices. Doppler studies demonstrate the direction of blood flow within the vessels and this is helpful in assessing patients with portal hypertension or those who have undergone shunt procedures. Thrombus within vessels can also be shown.

### Computed Tomography

The normal liver has a density measurement of 40 to 70 HU. Normal bile ducts are seen centrally around the porta and are non-enhancing. The portal veins appear as low density, branching structures which enhance with contrast.

Contrast enhancement is frequently undertaken to demonstrate focal lesions and blood vessels. Most masses are hypodense. Enhancement may be obtained with a bolus of contrast or by rapid venous infusion or via a selective arterial injection. Dynamic scans can assist in diagnosing certain lesions such as hemangiomas. An accuracy exceeding 90% is reported for the detection of mass lesions.

### Radionuclide Imaging

<sup>99m</sup>Technetium Sulphur Colloid. This isotope is taken up by the Kupffer cells of the reticulo-endothelial system, which constitute some 20% of the liver cell volume. 80%–90% of the isotope is taken up by the liver, 5%–10% by the spleen and a small percentage by the bone marrow.

Sulphur colloid scans are predominantly used for detecting focal lesions. Masses smaller than 2 cm are not usually seen. Emission computed tomography improves the pick-up rate but not to the level attained by CT. Sensitivity for metastases is around 85% but specificity is low. Metastases (Fig. 26.4), hepatoma, lymphoma, abscesses, hydatid cysts and many other lesions appear as cold areas. In addition there are a number of normal areas of decreased uptake including the porta hepatis, falciform ligament, hepatic veins and IVC, renal and gallbladder fossae. Adjacent lesions such as renal masses, subphrenic abscess and colonic barium will cause areas of decreased uptake as well.

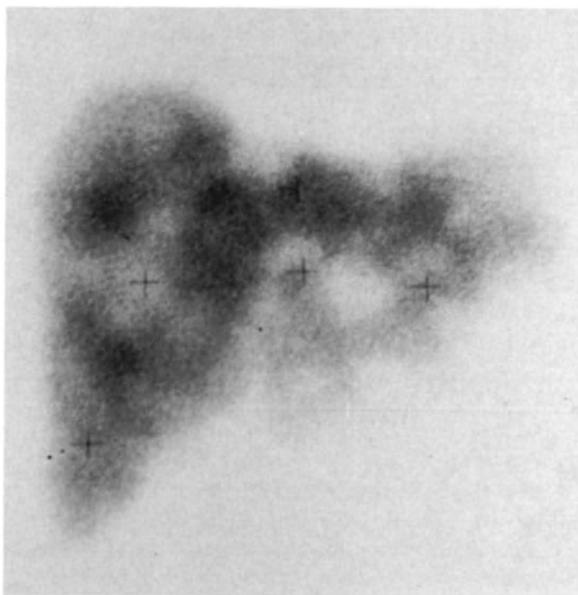


**Fig. 26.4.** Liver metastases from bronchogenic carcinoma.  $^{99m}\text{Tc}$  sulphur-colloid scan. Anterior projection.

Splenic uptake exceeds liver uptake when there is liver failure, (in which case skeletal uptake is also increased), or with splenic pathology.

**$^{67}\text{Gallium-citrate}$  and  $^{75}\text{Selenomethionine}$ .** Increased uptake occurs within an abscess or its wall and within a hepatoma. These isotopes are useful for differentiating a hepatoma from a pseudotumor.

#### Angiography

**Arteriography.** Both the superior mesenteric artery and celiac axis should be injected to ensure that all branches of the hepatic artery are shown. In 60% of cases the hepatic artery arises solely from the celiac axis. Common variations include the left hepatic artery arising from the left gastric artery, the hepatic artery or a branch arising from the superior mesenteric artery (Fig. 26.5) or hepatic branches arising directly from the aorta.

Predominantly arteriography is used for assessing tumor resectability or for demonstrating bleeding points. Nowadays it is rarely used to assist in the diagnosis of liver masses.

The capillary phase (hepatogram) is often uneven and spotty whereas on recirculation the portogram is even and homogenous. Most tumors are supplied by the hepatic arteries and appear hypovascular on the portogram.

**Portography.** There are several angiographic techniques for demonstrating the portal venous system.

1. Recirculation after splenic or superior mesenteric artery injection.
2. Direct splenic puncture (see p. 253).
3. Transhepatic.
4. Other: transumbilical, transjugular.

The portal venous system is shown on delayed films following splenic or superior mesenteric injection of large volumes of contrast (70–80 ml at 6–10 ml/second).

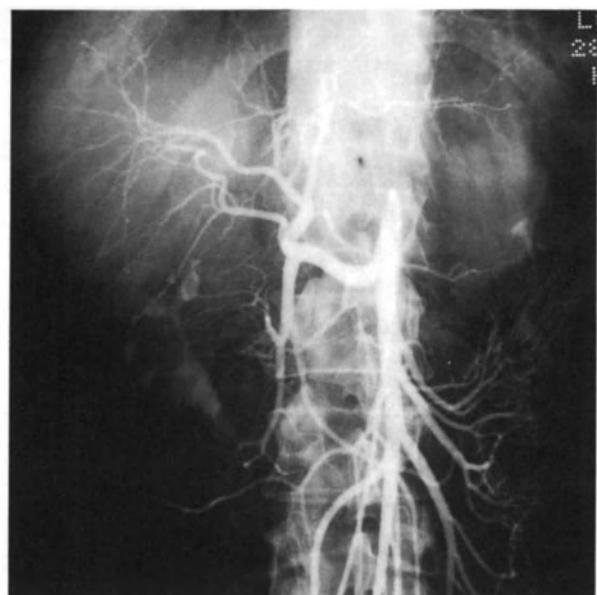


**Fig. 26.5.** Selective superior mesenteric angiogram. Hepatic artery arising from the superior mesenteric artery.

Transhepatic phlebography (Fig. 26.6) is performed using a similar technique to percutaneous transhepatic biliary drainage. Normal clotting factors are mandatory. The hepatic track may be embolized on removing the catheter.

This route is used for presurgical demonstration of varices, for variceal embolization and for venous sampling. Embolization of varices is successful in stopping bleeding only for a few weeks and should be followed by surgery before recanalization occurs.

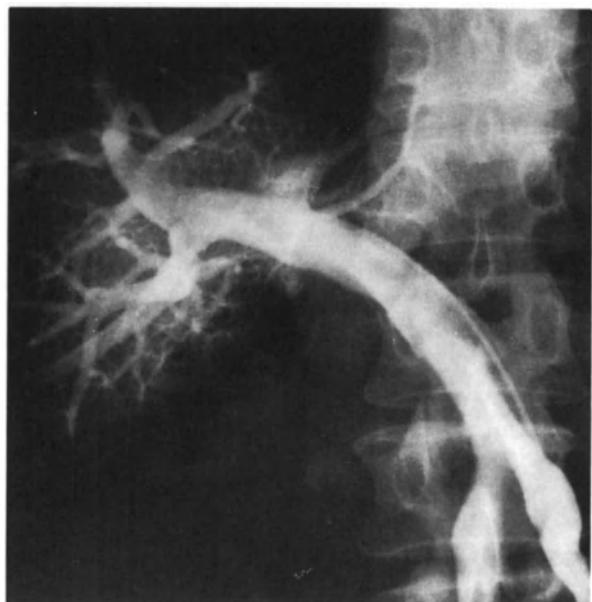


**Fig. 26.6.** Normal transhepatic portal venogram.

**Hepatic Phlebography.** The hepatic veins are catheterized via the IVC using an occlusal balloon catheter. Contrast may be injected and the wedge pressure measured to distinguish prehepatic from post-hepatic portal hypertension.

#### Fine Needle Biopsy

Fine needle biopsy of liver masses with a small gauge needle is undertaken using CT (Fig. 26.7) or ultrasound (Fig. 26.8). In addition larger core biopsies may be performed percutaneously or using the transjugular route for investigation of diffuse liver disease. Clotting studies must be normal for the percutaneous approach.

#### Therapeutic Procedures

**Hepatic Embolization.** Embolization of primary and secondary tumors is performed via the hepatic artery to palliate symptoms or for devascularization prior to surgery. Occasionally embolization is used to treat aneurysms or hemobilia. The portal vein must be patent or liver necrosis will occur on embolizing the hepatic artery. The main complication is abscess formation. The *post-embolization syndrome* consists of nausea, vomiting, pyrexia and neutrophilia and develops between one and 5 days after the procedure.

**Chemotherapy Infusion.** A catheter is left in situ within the hepatic artery to allow infusion of cytotoxic drugs to treat certain liver tumors, particularly metastases. Daily follow-up films are necessary to ensure that the catheter does not become dislodged.

#### MRI of the Liver

The liver remains a tempting organ for MR studies (Fig. 26.9). At present MR in expert hands is similar to CT in the detection of focal liver lesions and is often useful in recognizing and characterizing *hemangiomas* (very long T<sub>2</sub>). MR is also useful in demonstrating the spread of tumor and has become a routine investigation in those few patients in whom hemi-hepatectomy is being considered.

MR is less successful in characterizing diffuse liver disease, although the accumulation of iron in *hemosiderosis* and *hemochromatosis* is recognized by a marked reduction in liver signal intensities.

#### CONGENITAL LIVER LESIONS

*Congenital lobar agenesis* is extremely rare. Acquired agenesis may follow vascular or biliary obstruction. Occasionally ectopic nodules of liver occur intra-abdominally.

A *Riedl's lobe* is a frequent finding, commoner in females. There is downward extension of the right lobe of the liver laterally, easily visualized on the plain film (Fig. 26.10).

#### FOCAL LIVER DISEASE

Focal liver lesions are classified in Table 26.4.

#### Cysts

The majority of simple liver cysts are *congenital* and asymptomatic. Occasionally a cyst presents as an abdominal mass, with jaundice or with pain following an intracystic bleed,



Fig. 26.7. CT scan showing guided biopsy in prone position of an ill-defined low density mass. A hepatoma.



Fig. 26.8. Ultrasound guided biopsy of hepatoma (same patient as Fig. 26.7). Bright echo (arrow) indicates needle tip.

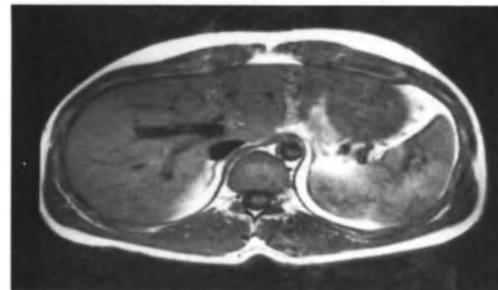


Fig. 26.9. MRI of normal liver. T<sub>1</sub>-weighted image, 1.5 Tesla. (Courtesy of Dr G Cherryman, CRC Radiology Research Group, Royal Marsden Hospital, UK.)



Fig. 26.10. Riedl's lobe extending into right iliac fossa. Two gallstones present.

Table 26.4. Classification of focal liver lesions

Simple cysts
Tumors
benign
hemangioma, adenoma
focal nodular hyperplasia
mesenchymal hamartoma
infantile hemangioendothelioma
hemangioblastoma
malignant
hepatoma, fibrolamellar hepatoma
metastases
sarcoma, lymphoma, leukemia
intrahepatic cholangiocarcinoma
hepatoblastoma
Infections
pyogenic abscess
amebic abscess
hydatid cyst
candidiasis

rupture or torsion. Congenital cysts do not communicate with the biliary tree. Polycystic liver disease has an autosomal dominant inheritance and is associated with renal cysts in half of the cases. Hepatic fibrosis and portal hypertension may develop.

At *ultrasound* cysts are well defined, unilocular, and anechoic with marked posterior acoustic enhancement. Blood within the cyst produces some echoes. At *CT* they are well defined non-enhancing lesions of low density (0–20 HU). Wall calcification is unusual.



Fig. 26.11. Ultrasound scan hemangioma in right lobe of liver. Incidental finding in patient with subphrenic abscess (arrows).

### Hemangioma

This is the commonest benign liver tumor. Although usually less than 2 cm in size, they may be large necrotic masses with symptoms from bleeding or rupture. Some are pedunculated. Calcification occurs in a spiculated pattern but is unusual and is only found in the larger masses. Typically at *ultrasound* there is a well defined echogenic mass in a subcapsular position and with posterior acoustic enhancement (Fig. 26.11). Larger tumors are complex with cystic areas.

The main differential diagnosis is from metastases. Fine needle biopsy is usually thought to be safe but is not often necessary as *CT* and isotope studies may be characteristic.

At *CT* there is a well-defined low-density lesion. Dynamic scans after a bolus of intravenous contrast show dense peripheral enhancement at 15 seconds with gradual infilling so that the lesion becomes isodense. *Isotope* blood pool images with  $^{99m}\text{Tc}$ -labelled red blood cells characteristically demonstrate increased activity with decreased activity on flow studies. At *angiography* lakes of contrast appear early with staining of the tumor (Fig. 26.12). There is delayed filling with contrast of the center of larger tumors.

### Adenoma

Adenomas are more common in females. There is an association with usage of the contraceptive pill. In addition there is an increased incidence in Von Gierke's disease and with androgen therapy. They are highly vascular lesions often presenting with symptoms of bleeding. At *ultrasound* there is usually an echogenic mass which contains some areas of low-level echoes due to blood or necrosis. At *CT* there is typically a well-defined low-density mass which enhances moderately with contrast. An adenoma may be difficult to distinguish from a hepatoma and focal nodular hyperplasia.

### Focal Nodular Hyperplasia

Focal nodular hyperplasia is thought to be either a hamartoma or an area of regeneration following an ischemic



**Fig. 26.12.** Hepatic angiogram. Large cavernous hemangioma. A highly vascular mass with vessel displacement. (Courtesy of Dr R Travis, Auckland, New Zealand.)

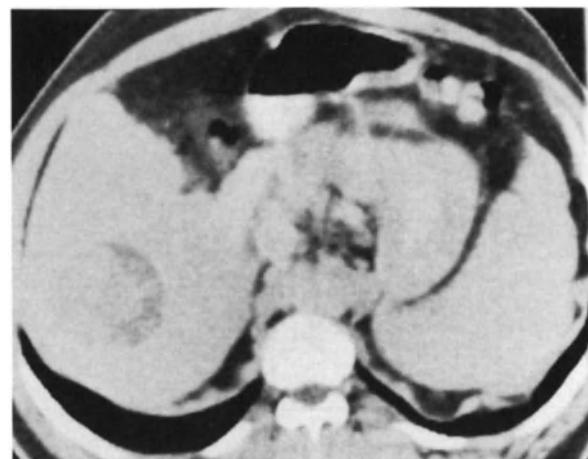


**Fig. 26.13.** CT scan hepatoma. Enhanced scan. Solitary lesion in right lobe of liver.

episode. It is commoner in females and may result in vague abdominal pain though usually asymptomatic. Frequently there is a central spiculated area of fibrotic tissue within a subcapsular mass which is seen at ultrasound and CT. At *ultrasound* focal nodular hyperplasia has a variable appearance but usually there is a central collection of high-level echoes within a well-defined mass. At *CT* there is a well-defined low-density mass (20–40 HU) with a central lucency. After contrast enhancement the mass becomes isodense and the lucent area may disappear. *Angiography* demonstrates a hypervascular mass. The majority of *sulphur-colloid scans* are normal due to uptake of the isotope by the mass. Occasionally there is no uptake or there is increased uptake producing a hot spot.

### Hepatoma

Hepatoma or hepatocellular carcinoma is the commonest primary liver tumor and has a very poor prognosis. In Europe and the USA most cases occur in elderly men with alcoholic cirrhosis. However, in parts of Africa and Asia this tumor presents in a younger age group (20–30 years). The causes are listed in Table 26.5. The tumor may be solitary, multifocal or diffuse. In 90% of cases there is a raised alpha fetoprotein level.

**Imaging.** At *simple radiography* calcification is uncommon and more often found with fibrolamellar hepatoma (see below). The liver may be enlarged or there may be a localized bulge to its outline formed by the tumor.

At *ultrasound* the appearances are variable. Small tumors tend to be well-defined masses of low echogenicity whereas larger tumors are more echogenic than the liver and may be complex masses. There may be a surrounding halo of decreased echogenicity. Diffuse tumors produce an irregular pattern similar to metastases.

At *CT* there is a well-defined low-density mass which may

contain necrotic areas or calcification. Contrast enhancement occurs to a lesser degree than in the normal liver (Fig. 26.13). Multiple masses or diffuse involvement also occur. Signs of IVC and portal vein obstruction include tumor or thrombus within the vessels, ascites and splenomegaly.

There is no uptake by the tumor on a *sulphur-colloid scan* but prominent uptake with <sup>67</sup>Gallium-citrate and <sup>75</sup>Selenomethionine (Fig. 26.14A, B).

*Angiography* reveals a highly vascular tumor with tumor vessels, a-v shunting, vessel encasement and early venous filling (Fig. 26.15). Some 10% are hypovascular. Embolization may be undertaken for palliation of symptoms.

**Fibrolamellar Hepatoma.** This hepatoma variant has a better prognosis. It occurs in a younger age group (5–35 years), is not associated with cirrhosis and  $\alpha$ -fetoprotein levels are normal. Typically there is a large solitary mass with a central fibrotic scar which calcifies in a stellate pattern in half of cases. At *CT* there is a well-defined low-density mass with calcification. At *angiography* the mass is avascular.

**Table 26.5.** Causes of hepatoma

Cirrhosis
Hemochromatosis
Alpha-1-antitrypsin deficiency
Chronic hepatitis B infection
Toxins
aflatoxin (found on mouldy peanuts)
siderosis
androgens
Thorotrust
Childhood
biliary atresia
neonatal hepatitis
glycogen storage disease Type 1
galactosemia
tyrosinosis

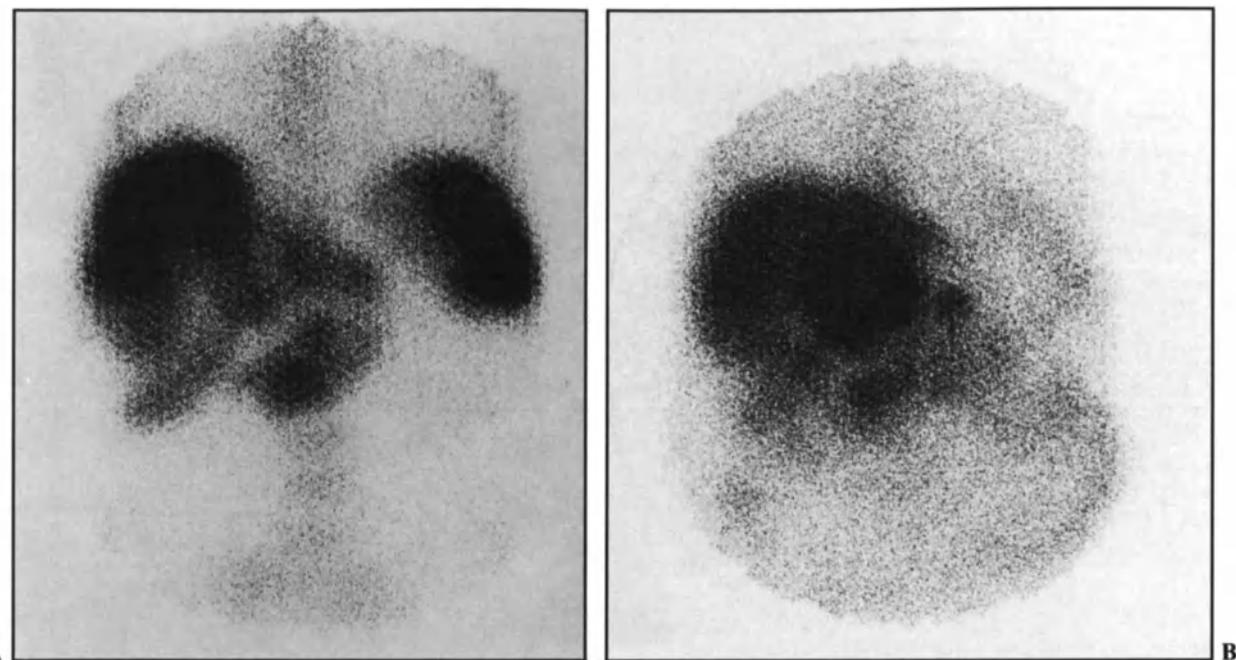


**Fig. 26.14.** A  $^{99m}\text{Tc}$  sulphur-colloid scan. Hepatoma. Decreased and irregular isotope uptake centrally and in left lobe of liver. B  $^{75}\text{Se}$ -methionine scan. Hepatoma (same patient). Increased uptake by tumor.

### Metastases

Liver metastases are often asymptomatic. Symptoms may arise from hepatomegaly, liver failure and ascites, and from blood vessel and bile duct obstruction.

**Imaging.** Plain films may show hepatomegaly but calcification is very uncommon and when present usually has a fine stippled pattern. Causes of calcified metastases are listed in Table 26.6.

At ultrasound lesions as small as 5 mm may be demonstrated. Appearances are variable. Metastases may be echogenic,

**Table 26.6.** Causes of calcified metastases

Colloid carcinoma of colon and ovary
Thyroid carcinoma
Osteogenic sarcoma
Neuroblastoma
Renal cell carcinoma

echopoor, cystic or necrotic or have a target appearance with an echopoor halo (Fig. 26.16). Confluent metastases produce an irregular moth-eaten pattern (Fig. 26.17) whereas diffuse miliary metastases may result in a bright liver. Gastrointestinal and pancreatic metastases are usually echogenic. Colloidal tumors may have cystic metastases.

CT will reveal the majority of metastases greater than 1 cm. Most are low density and non-enhancing (Fig. 26.18). Isodense lesions will show up within an enhanced liver. Enhancing metastases include those from renal cell carcinoma and islet cell tumors. Diffuse lesions may not be detected.

**Isotopes.** 80% of metastases are demonstrated on sulphur-colloid scans, appearing as cold areas.

Most metastases are supplied by the hepatic artery and at angiography are avascular. Vascular metastases are associated with renal carcinoma, melanoma, choriocarcinoma, islet cell tumors, pheochromocytoma and carcinoid tumors (Fig. 26.19). Arterial chemotherapy infusion and embolization of the hepatic artery for palliation may be undertaken (Fig. 26.20).

### Lymphoma and Leukemia

Hepatic lymphoma is usually secondary disease and more commonly diffuse rather than nodular. Focal lesions are well-defined by ultrasound and hypoechoic. Diffuse disease



**Fig. 26.15.** Selective hepatic angiogram. Multifocal hepatoma. Multiple hypervascular masses with neovascularity and hepatomegaly.



**Fig. 26.16.** Ultrasound scan. Metastasis with a 'target' appearance. Primary lesion in breast.



**Fig. 26.19.** Hepatic angiogram. Multiple vascular metastases from a carcinoid tumor.



**Fig. 26.17.** Ultrasound scan. Multiple metastases producing an irregular moth-eaten echo pattern. Primary lesion in stomach.



**Fig. 26.18.** CT scan. Metastases from teratoma of testis. Multiple low density masses.

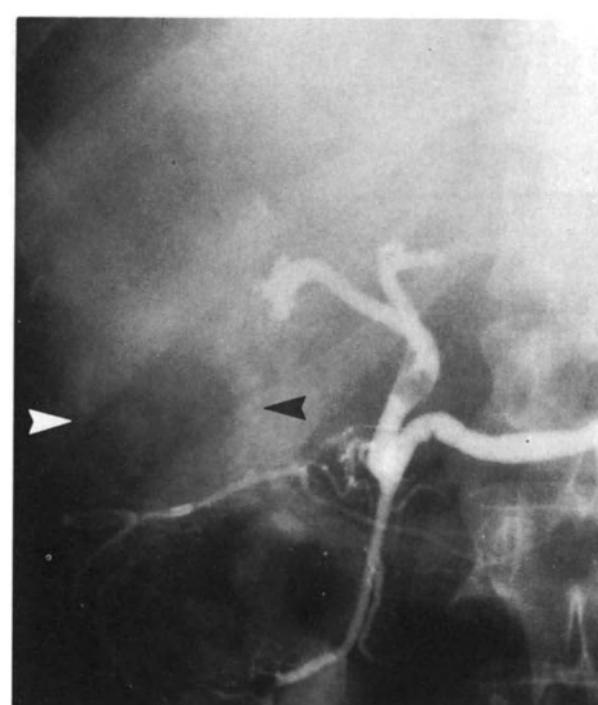


**Fig. 26.20.** Hepatic artery embolization to palliate symptoms of carcinoid metastases: same patient as Fig. 26.19. The metastases are seen as lucencies (arrows).

produces an irregular liver pattern. At CT there are non-enhancing low-density lesions which cannot be distinguished from metastases. Frequently diffuse involvement is difficult to detect at both ultrasound and CT.

#### Intrahepatic Cholangiocarcinoma

This is a cholangiocarcinoma arising in the peripheral bile ducts, producing a liver mass.

A small amount of irregular or punctate calcification may be seen on a plain film.

Echogenicity at *ultrasound* is variable but there are usually associated dilated ducts. At *CT* there is a hypodense mass with an enhancing central area.

### **Angiosarcoma**

This tumor develops in people who work with polyvinyl chloride and is the commonest malignancy following Thorotrast exposure. Usually there is a multinodular mass seen as a complex lesion of mixed echogenicity at *ultrasound*. At *CT* there are multiple low-density lesions with enhancement peripherally after contrast.

### **Infantile Hemangioendothelioma (Hemangioblastoma, Hemangioma)**

These benign tumors are associated with skin hemangiomas in half of the cases and mostly present in infants under 6 months. Cardiac failure, platelet sequestration with thrombocytopenia and bleeding are possible features. Spontaneous regression can occur. Occasionally, speckled calcification is detected on *plain films*. *Ultrasound* appearances are variable but at *CT* there is a calcified low-density mass. Sometimes the tumor is multifocal. At *angiography* the lesions are vascular.

### **Mesenchymal Hamartoma**

This is a multicystic mass which presents in infancy as an abdominal swelling.

### **Hepatoblastoma**

Hepatoblastoma is the commonest primary liver tumor found in young children (up to 3 years). Hemihypertrophy is a recognized associated feature. The prognosis is poor with metastatic spread to the lungs, bones and lymph nodes. Amorphous speckled calcification is frequently present in an enlarged liver on a *plain film*. A large mass with a mixed echo pattern, possibly septate, is seen at *ultrasound*. At *CT* the tumor is a low density mass.

### **Pyogenic Abscess**

Pyogenic liver abscesses are commoner in the *immunosuppressed* and in patients with *chronic granulomatous disease* and *sickle cell disease*. The infection may be derived from a septicemia, portal sepsis secondary to an abdominal infection, cholangitis, an adjacent pus collection such as a subphrenic abscess, or from penetrating trauma and surgery. Abscesses are commoner in the right lobe of the liver and are often multiple, in which case the mortality rate is higher.

**Imaging.** In the majority of cases *plain films* are not helpful. Possible findings include hepatomegaly, gas in the liver, an elevated hemidiaphragm, basal atelectasis and pleural effusion.

Calcification may develop within healed abscesses.

At *ultrasound* findings vary depending upon the maturity of the abscess. In the early stages there is an ill-defined lesion of slightly increased echogenicity compared with the surrounding area. Later there is an area of decreased echogenicity or an anechoic lesion with distal acoustic enhancement and a well-defined irregular echogenic wall. Echogenic debris



Fig. 26.21. Ultrasound scan. Large well-defined amebic abscess.

and highly echogenic gas with acoustic reverberation may be present.

At *CT* there is a low-density or cystic mass with contrast enhancement of the wall. A surrounding low-density halo (the double target sign) is present in one quarter of the cases undergoing dynamic *CT*.

**Isotopes.** There is no uptake on a *sulphur-colloid* scan but marked uptake of  $^{67}\text{Gallium-citrate}$ .

At *angiography*, now superseded in this condition, there was increased vascularity of the abscess wall.

### **Amebic Abscess**

An amebic abscess is usually solitary, often large and typically lies beneath the diaphragm in the right lobe of the liver. Lesions are multiple in 25% of cases. The main symptoms are pain and fever. Some cases are associated with a recent symptomatic gastrointestinal infection. Rupture can occur into the pericardial, pleural and peritoneal cavities, bronchial tree, mediastinum and gastrointestinal tract.

**Imaging.** On *simple radiography* there may be elevation of the hemidiaphragm with a pleural effusion and basal pulmonary atelectasis or shadowing. Gas within the abscess suggests that rupture has occurred.

Appearances at *ultrasound* are variable but often there is a well-defined cystic or hypoechoic mass with acoustic enhancement and containing some debris (Fig. 26.21).

*CT* shows a well-defined low-density mass often septate with some contrast enhancement of the wall.

**Isotopes.** There is no uptake on sulphur-colloid scans but  $^{67}\text{Gallium-citrate}$  is taken up by the wall of the abscess.

### **Hydatid Cyst**

Most hydatid cysts are due to infection with *Echinococcus granulosus*. The liver is involved in three quarters of patients, usually the right lobe. Frequently the hydatid cysts are asymptomatic but rupture can occur into the biliary tree, abdomen or thorax and may be accompanied by anaphylaxis.

The cysts are often very large, compressing the bile ducts, portal vein or hepatic veins causing jaundice, splenomegaly and Budd-Chiari syndrome. Characteristically daughter cysts lie peripherally within the main cyst.



Fig. 26.22. Ultrasound scan. Two hydatid cysts.

**Imaging.** On a plain film calcification is a common finding with a curvilinear or 'crushed eggshell' pattern. The right hemidiaphragm is often elevated. Gas may be present within the cyst forming an air-fluid level.

A large simple or multiloculated cystic mass is seen at ultrasound (Fig. 26.22). Very occasionally there is a solid mass. The wall is thick with echogenic foci of calcification (Fig. 26.23). Daughter cysts are seen around the edge of the main cyst. A floating membrane is characteristic. Biliary rupture produces echogenic sludge within the ducts.

At CT there is well-defined cystic mass with calcification (Fig. 26.24). Septa may be present. Both the cyst wall and septa enhance with contrast.

Fine needle aspiration has a theoretical risk of anaphylaxis and peritoneal spillage, although many centres consider it to be a safe procedure.

*Echinococcus multilocularis* infection produces diffuse hepatic changes with multiple very small cysts. Appearances are difficult to differentiate from metastases.

#### Candidiasis

*Candida* infection develops in the immunosuppressed and those with chronic granulomatous disease.

At ultrasound there are multiple lesions with one of the following characteristics (Pastakia et al. 1988):

1. A characteristic bull's-eye appearance of an echogenic centre surrounded by a hypoechoic area.
2. A similar lesion with an additional central nidus of low echogenicity, described as a 'wheel within a wheel'.
3. A lesion of low echogenicity.
4. A small echogenic focus which is usually seen late in the disease.

CT shows multiple low-density areas which may have a 'target' appearance. Calcified lesions develop later.

*Isotopes* studies are unhelpful as there is no uptake of  $^{99m}\text{Tc}$  sulphur-colloid or  $^{67}\text{Gallium}$ -citrate.



Fig. 26.23. Ultrasound scan. Hydatid cysts. Extensive calcification of the wall with acoustic shadowing.

#### The Fatty Liver

Within the fatty liver there is an excess of triglycerides. Although usually a diffuse process, a focal pattern may occasionally occur. The condition is often asymptomatic, but presentation may be acute with liver failure or non-acute with pain and hepatomegaly. Common causes of fatty liver are listed in Table 26.7.

Table 26.7. Common causes of fatty liver

Toxic	
alcohol	
halothane	
steroids	
chlorinated hydrocarbons	
cytotoxics	
Nutritional	
obesity	
diabetes mellitus	
parenteral nutrition	
starvation	
intestinal bypass surgery	
Chronic tuberculosis	
Congestive cardiac failure	
Pregnancy	
Familial hyperlipemia	
Reye's syndrome	
Hepatitis	



Fig. 26.24. CT scan contrast enhanced. Large hydatid cyst in right lobe.

#### DIFFUSE LIVER DISEASE

Diffuse liver disease is often difficult to detect at an early stage using either ultrasound or CT.



**Fig. 26.25.** CT scan unenhanced. Fatty liver. Note the prominent portal vessels.

**Table 26.8. Causes of the echogenic liver**

Fatty infiltration
Cirrhosis
Chronic hepatitis
Diffuse metastases
Congestive cardiac failure
Hemochromatosis

**Imaging.** Very occasionally, a relatively translucent liver is seen on a *plain film*. The fatty liver is highly echogenic at *ultrasound* with a fine echo pattern, reduced visualization of the ducts and vessels and reduced beam penetration but the appearances are non-specific (Table 26.8).

At *CT* appearances are characteristic with the liver density reduced and prominent portal vessels (Fig. 26.25). Comparison of the density of the liver and spleen is helpful, the spleen normally being slightly less dense than the liver.

#### Acute Viral Hepatitis

The liver is enlarged, with rounded contours. Echogenicity is decreased, with strong echoes arising from the portal vessel walls. Frequently the gallbladder wall is edematous.

**Table 26.9. Some causes of cirrhosis**

Alcohol
Post-viral hepatitis
Chronic cardiac failure
Budd-Chiari syndrome
Hereditary: e.g., Wilson's disease, hemochromatosis, fibrocystic disease, glycogen storage disease
Intestinal bypass surgery
Biliary obstruction
Primary biliary cirrhosis
Drugs: e.g. methotrexate, nitrofurantoin
Neonatal hepatitis
biliary atresia

#### CIRRHOSIS AND PORTAL HYPERTENSION

There are numerous causes of liver cirrhosis, of which the commonest is alcoholic liver disease. Cirrhosis may progress to portal hypertension and liver failure. Hepatoma develops in 5% of cases. The causes of cirrhosis are listed in Table 26.9 and the causes of portal hypertension in Table 26.10.

**Cirrhosis.** Initially the liver is normal in size or slightly enlarged, but later it becomes small. Ascites and splenomegaly may develop. Barium studies will demonstrate esophageal, gastric and duodenal varices, peptic ulcers and erosions.

At *ultrasound*, in the early stages, the liver is often slightly enlarged with a generalized increase in echogenicity and a fine speckled pattern with indistinct vessels due to fatty infiltration. Later the liver, particularly the right lobe, becomes small with a coarse echo pattern and an irregular nodular outline. Regenerating nodules have a similar echo pattern to the adjacent parenchyma.

Ascites is easily demonstrated as echo-free fluid around the liver and in Morrison's pouch (Fig. 26.26A, B). Bowel loops are seen floating within the ascites. Echogenic debris within the ascites suggests infection, bleeding or malignancy. Ascitic and pleural fluid are distinguished by identifying the diaphragm; ascites lies beneath the diaphragm and pleural fluid above.

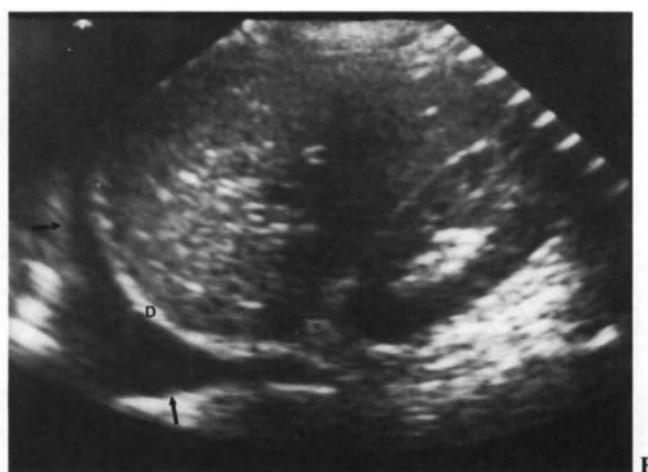


**Fig. 26.26.** A Ultrasound scan. Ascites surrounding liver (L) and bowel (B). B Ultrasound scan. Pleural effusion (arrows) above diaphragm (D).

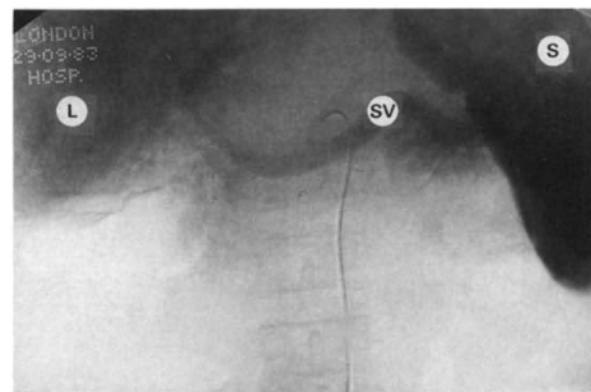
**Table 26.10.** Classification and causes of portal hypertension

Extrahepatic presinusoidal
Portal vein thrombosis
extrinsic mass (Fig. 26.28)
sepsis: umbilical vein catheter, pancreatitis, abdominal sepsis
trauma
abnormal blood clotting
pre-eclampsia of pregnancy
Arterial-portal venous fistula – surgery, trauma
Intrahepatic
cirrhosis
veno-occlusive disease
congenital hepatic fibrosis
schistosomiasis
sarcoidosis
lymphoma
vinyl chloride workers
Extrahepatic post-sinusoidal
congestive cardiac failure
constrictive pericarditis
veno-occlusive – Budd-Chiari syndrome

There is splenomegaly and enlargement of the portal and mesenteric veins. Collateral vessels appear as circular or tubular translucencies and can be seen at many sites including the cardia, lesser curve of the stomach and splenic hilum. In portal hypertension the portal vein size increases and a diameter in excess of 14 mm is significant. The normal change in size with inspiration is lost. If the portal vein is occluded a diamond-shaped area of increased echogenicity is seen at the porta. *Doppler studies* are helpful in determining portal vein patency and direction of blood flow.

In early cirrhosis, fatty infiltration results in a low density liver at CT with relatively high attenuation portal vessels. Later, isodense regenerating nodules appear. The liver outline becomes irregular and the fissures more prominent as the liver gets smaller, whilst the caudate lobe becomes relatively large. The main vessels and the collaterals, including the umbilical vein in the *ligamentum teres*, are assessed using contrast. Ascites is well demonstrated (Fig. 26.27).

*Angiography* shows intrahepatic corkscrew vessels with displacement around regenerating nodules. At *portography* there is splenomegaly with a dilated splenic artery, splenic vein and portal vein. Collaterals will fill if the portal flow is

**Fig. 26.27.** CT scan. Ascites.**Fig. 26.28.** Portal venogram. Recirculation film from selective splenic arteriogram. A large mass of malignant lymph nodes at the porta compresses the portal vein. Note splenomegaly (S).

reversed (Fig. 26.28). A percutaneous transhepatic approach allows the demonstration and embolization of gastroesophageal collaterals.

On *isotope* studies sulphur-colloid liver uptake is reduced and patchy, with increased bone marrow uptake.

Bony changes which may be detected on *plain films* include hypertrophic osteoarthropathy, a reduced bone density due to osteoporosis or osteomalacia, infarction and avascular necrosis, thought to be due to fat emboli from the liver.

### Schistosomiasis

Schistosomiasis is the commonest cause of portal hypertension throughout the world. Infection is with *Schistosoma japonicum* or *Schistosoma mansoni* causing periportal fibrosis.

At *ultrasound* this appears as echogenic bands extending into the liver from the porta. In the presence of portal vein thrombosis the vein cannot be identified at ultrasound, but there is a diamond-shaped band of high-level echoes at the porta with dilated splenic and superior mesenteric veins.

The periportal fibrosis is dense at CT, and in the presence of portal vein thrombosis, dense thrombus can also be identified. Calcification is rarely seen but, if present, suggests portal vein occlusion. Enhancement of the thrombus is highly suggestive that malignancy is the cause for the thrombosis. Cavernous transformation of the portal vein is not easily identified at CT.

*Cardiac Failure.* Dilated hepatic veins and dilatation of the IVC are present with congestive cardiac failure (Fig. 26.29).

### Wilson's Disease

There is impaired excretion of copper resulting in accumulation throughout the body, particularly the liver. Patients may present with features of liver failure or with neurological and psychiatric disorders. Other findings include gallstones, amino-aciduria, osteoarthritis, osteochondritis dissecans, bone demineralization and the characteristic corneal Kayser-Fleischer ring. Inheritance is autosomal recessive.

CT may show a dense liver but coexistent fatty change often results in non-specific appearances.



**Fig. 26.29.** Ultrasound scan. Dilated hepatic veins. Elderly patient with congestive cardiac failure.

### Hemochromatosis

Causes of hemochromatosis are given in Table 26.11; hemochromatosis may be classified as *primary* or *secondary*. Clinical features include heart failure, diabetes mellitus, portal hypertension, chondrocalcinosis, subchondral metacarpal cysts with joint narrowing and an increased incidence of hepatoma.

**Table 26.11. Causes of hemochromatosis**

Primary
Secondary
excess iron in the diet
repeated blood transfusion
cirrhosis
portacaval shunts

**Imaging.** Characteristically, the liver is very dense at CT (75–130 HU) with prominent portal vessels. Occasionally increased liver density is noted on plain films. *Ultrasound* appearances are not helpful.

### Budd–Chiari Syndrome

The causes are listed in Table 26.12.

In over 50% of cases of Budd–Chiari syndrome no causal factors can be identified. The liver venous drainage is obstructed. The caudate lobe has a separate venous system from the remainder of the liver and is usually spared, undergoing compensatory hypertrophy. In the acute phase the liver is enlarged with associated ascites and pain. Later sub-

**Table 26.12. Causes of Budd–Chiari syndrome**

Idiopathic (primary veno-occlusive)
IVC thrombosis
congenital IVC web (common in Japan)
extrinsic compression (masses)
polycythemia
contraceptive pill
pregnancy
trauma

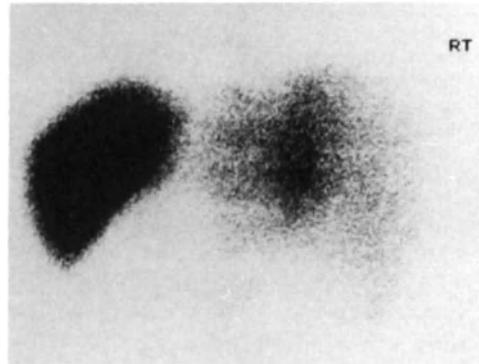


**Fig. 26.30.**  $^{99\text{m}}\text{Tc}$  sulphur-colloid posterior scan. Budd–Chiari syndrome. Increased uptake in the caudate lobe with decreased uptake in the other lobes.

capsular collaterals develop and there is progression to cirrhosis and portal hypertension.

**Imaging.** Liver infarcts are hypodense and non-enhancing at CT and are well shown with sulphur-colloid isotope studies. In addition isotope uptake is increased centrally corresponding to the caudate lobe, and decreased peripherally (Fig. 26.30). Splenic and bone marrow uptake is increased. An enlarged caudate lobe is seen at CT and *ultrasound*. There is marked contrast enhancement of the caudate lobe with decreased enhancement of the rest of the liver. Non-visualization of the hepatic veins, collaterals and thrombosis or narrowing of the IVC can be seen at CT and ultrasound and Doppler studies are valuable in assessing flow.

**Hepatic phlebography** demonstrates a spider's web network of collateral veins. IVC webs are thin and concave with a central channel; dilatation can be achieved with an angioplasty balloon. There is an incidence approaching 50% of hepatoma in patients with congenital webs.

### LIVER TRAUMA

Liver trauma is associated with a significant mortality. Other intra-abdominal organs are frequently damaged and in 50% of cases there are rib fractures. The liver may be completely fragmented or lacerated or have a subcapsular (Fig. 26.31) or intrahepatic hematoma (Fig. 26.32). Intraperitoneal bleeding, hemidiaphragm elevation and basal lung changes often develop.

**Imaging.** On *plain films* there may be loss of definition or irregularity of the liver edge. Free peritoneal fluid can be identified with CT and *ultrasound*. Intrahepatic haematomas and lacerations are better shown by CT than by ultrasound.

CT is the investigation of choice and should precede peritoneal lavage, which can cause intraperitoneal bleeding (Table 26.13).

**Therapeutic embolization** can be undertaken for arterio-venous fistulae, hemobilia and aneurysms.

Other causes of hepatic artery aneurysm include arteriosclerosis, local infection, or septicemia and polyarteritis nodosa.

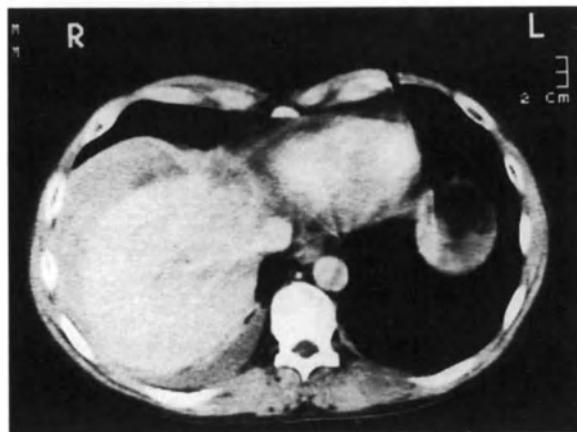


Fig. 26.31. CT scan enhanced. Stab wound. Large subcapsular hematoma.

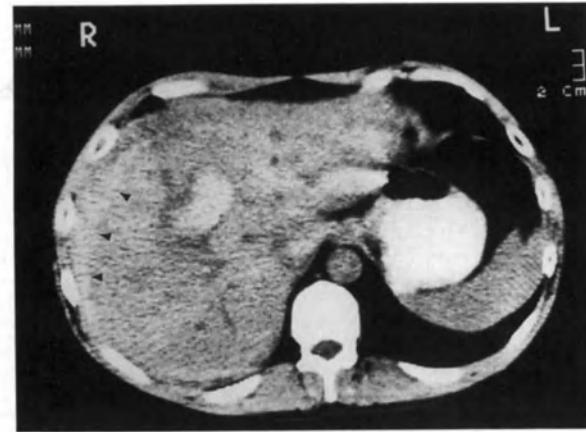


Fig. 26.32. CT scan unenhanced. High density intrahepatic hematoma and subcapsular hematoma (arrows). Recent stab wound: same patient as Fig. 26.31.

Table 26.13. Ultrasound and CT features of liver trauma

Lesion	Ultrasound	CT
Hematoma	Early echogenic	Early isodense or hyperdense non-enhancing
Subcapsular hematoma	Later anechoic $\pm$ internal echoes $\pm$ septa Anechoic, hypoechoic Curvilinear	Later hypodense Well-defined low density Curvilinear Density decreases with age
Laceration	Not always well seen	Linear, branching low density

## SPLEEN

The spleen is the largest collection of lymphoid tissue present in the body. Splenic size is variable but the normal adult spleen does not exceed 15 cm in length. In the elderly there is a decrease in splenic size by as much as 50%. Usually the spleen has a semilunar shape. Fetal notching or lobulation may be present.

Lying in the left upper quadrant along the line of the 10th rib, the spleen is closely related to the base of the left lung and to the posterior costophrenic sulcus. Medially lie the fundus of the stomach and the splenic flexure of the colon. The kidney is posteroinferior. The pancreatic tail and adrenal gland are related to the splenic hilum.

The *splenic artery* usually arises from the celiac axis but occasionally arises from the aorta or superior mesenteric artery. It passes along the upper border of the pancreas, where it is often involved by pancreatic tumors or pancreatitis. It divides into several branches in the splenic hilum. Tortuosity increases with age and extensive calcification often develops. The splenic vein runs in the lienorenal ligament anterior to the aorta and kidney and behind the pancreas.

The following imaging techniques can all provide useful

information in disorders of the spleen: plain film, ultrasound, CT, radionuclide imaging, angiography and MRI.

### THE PLAIN FILM

The normal spleen is outlined by fat and is often seen on the plain film; it should not extend below the costal margin and its length should not exceed 15 cm.

Clinically the adult spleen must be doubled or trebled in size before it becomes palpable whereas *moderate splenomegaly can be identified on a plain film*. In children the normal spleen is often palpable.

Features to note on a plain film are:

1. Splenic size (see Table 26.14).
2. Calcification (see Table 26.15).
3. Increased splenic density (rare).
4. Gas within the spleen.
5. Gas within the subphrenic space.
6. Elevated hemidiaphragm; abnormal lung base.

**Table 26.14.** Causes of splenomegaly

Circulatory disorders
congestive cardiac failure
portal hypertension
portal or splenic vein thrombosis
Banti's syndrome
Infections
Viral and bacterial infections, e.g., subacute bacterial endocarditis, glandular fever, typhoid
Tuberculosis, histoplasmosis
brucellosis
malaria*
leishmaniasis*
congenital syphilis*
schistosomiasis
hydatid disease
Connective tissue disorders
SLE
rheumatoid arthritis
Felty's syndrome
polyarteritis nodosa
Blood disorders
hemolytic anemia, e.g., thalassemia,* hereditary spherocytosis
polycythemia
sickle cell disease
osteopetrosis
myelofibrosis
Lipid storage disease
Gaucher's disease*
Niemann–Pick disease*
Infiltration
amyloid
mucopolysaccharidoses
hemochromatosis
histiocytosis
Tumors
benign e.g., hematoma, cysts – congenital, acquired
malignant
metastases
leukemia*
lymphoma
Trauma
rupture, hematoma
Sarcoidosis

\*Gross splenomegaly may develop.

**Table 26.15.** Causes of splenic calcification

Vascular
arterial
phleboliths
aneurysm of the splenic artery
Granuloma
tuberculosis
histoplasmosis
Cyst
Abscess
Hematoma, infarct
Sickle cell disease
[Increased density (not calcification)]
Thorotrust hemochromatosis]

On the plain abdominal film splenomegaly is identified by downward displacement of the splenic flexure and displacement of the gastric gas shadow medially and downwards.

This leads to a paucity of gas shadows in the left upper quadrant (Fig. 26.33). The left kidney is also displaced downwards and elevation of the left hemidiaphragm is often present.

*Splenic artery calcification* is often seen in the elderly and may be extensive. The artery becomes very tortuous and when seen end on appears as a ring of calcification. This must be differentiated from a splenic or a renal artery aneurysm. Curvilinear calcification is also seen in *cysts*, *hydatid cysts*, *sickle cell disease* and old *hematomas* (Fig. 26.34). Amorphous calcification may develop within an old *abscess* or *infarct*. Punctate calcification occurs as a result of *tuberculosis* (Fig. 26.35), *histoplasmosis* and *sickle cell disease* and may be seen within *vascular tumors*.

In children with homozygous *sickle cell disease* the spleen is enlarged. Recurrent infarcts result in a reduction in splenic size so that in the adult the spleen is shrunken. Splenic opacification is seen in one third of affected patients. A punctate pattern is often seen in the earlier stages. Later the pattern

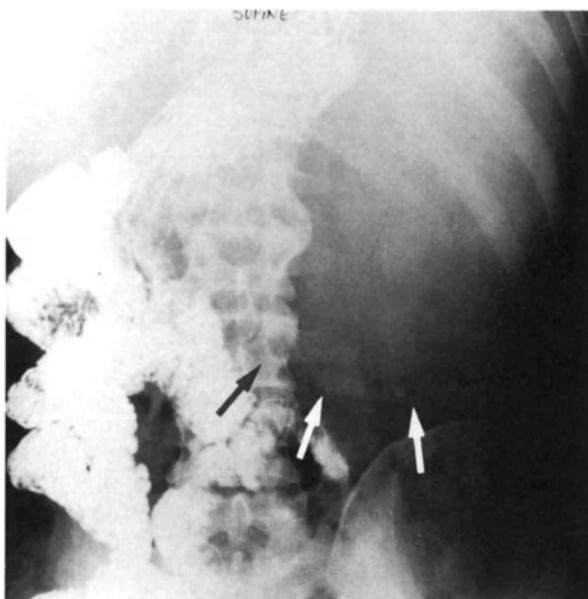


**Fig. 26.33.** Splenomegaly. The large spleen (*arrows*) extends across the midline, displacing stomach and small bowel.

becomes amorphous and the spleen may be completely calcified. In addition a curvilinear pattern of calcification has been described.

*Thorotrust*, or thorium dioxide, was a contrast medium used for angiography in the 1930s and 1940s (Fig. 26.36). It was radioactive with a very long half life and was taken



**Fig. 26.34.** Calcified splenic hematoma. Middle-aged man with past history of abdominal injury 25 years previously.

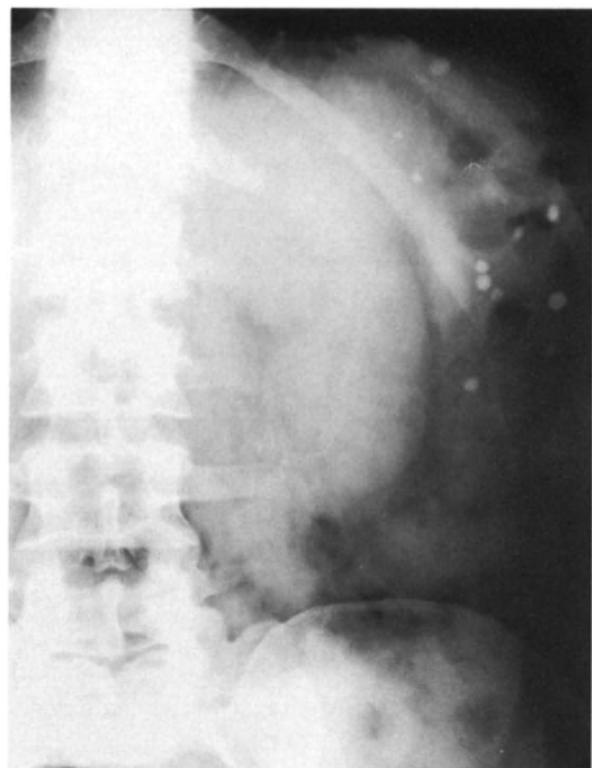


**Fig. 26.35.** Calcified tuberculous foci in spleen.

up by the reticulo-endothelial cells of the spleen, liver and bone marrow. Hepatic tumors such as angiosarcoma, hepatoma and cholangiocarcinoma, were frequent complications. The spleen becomes shrunken but splenic tumors rarely develop. Punctate opacities resembling calcification are seen in the liver, spleen and peripancreatic nodes. Less dense areas which subsequently develop on serial films

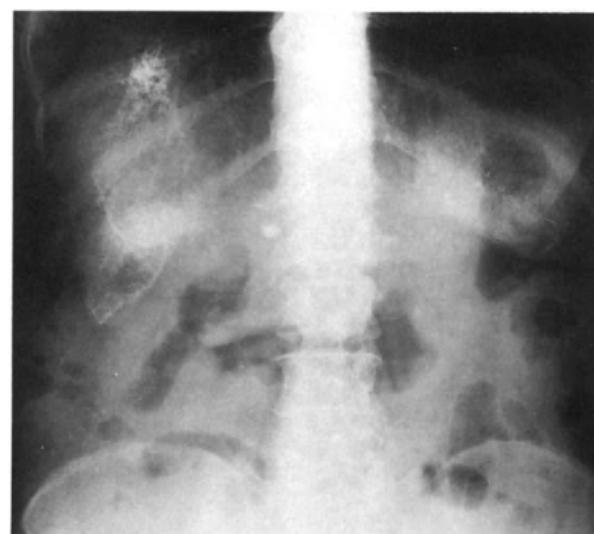


**Fig. 26.36.** Thorotrust in liver and spleen.

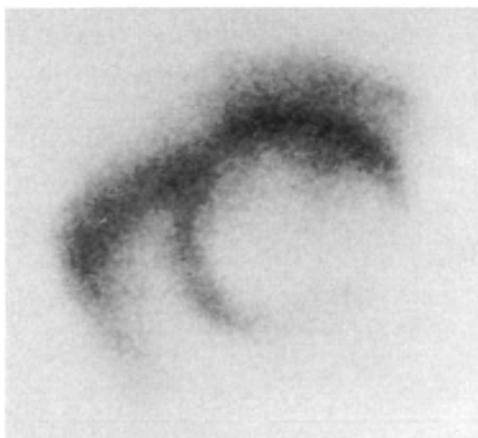


**Fig. 26.37.**  $^{99m}\text{Tc}$  sulphur-colloid scan. Large lymphomatous deposit in spleen.

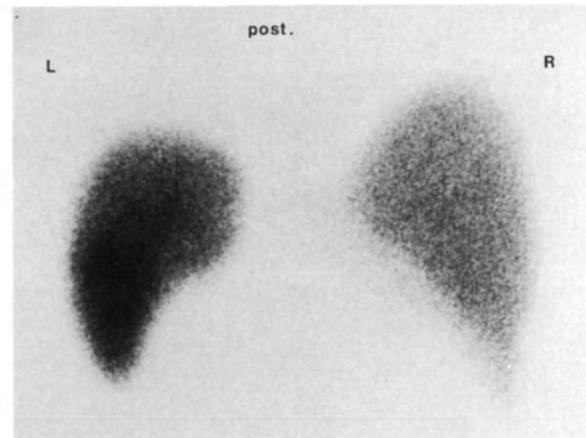


**Fig. 26.38.**  $^{99m}\text{Tc}$  sulphur-colloid scan. Posterior projection. Splenomegaly with increased uptake.

within the liver and spleen suggest tumor formation. A dense spleen may also develop in *hemochromatosis*. This is rarely evident on a plain film but is detectable at CT.

Occasionally *gas* is seen in a splenic abscess. This is a poor prognostic sign. However it must be differentiated from bowel gas.

### ULTRASOUND

Visualization is often restricted by adjacent gas-filled bowel and overlying ribs and lung. The normal-sized spleen is demonstrated on scanning through the lower intercostal spaces in a left anterior oblique or decubitus position with the left side up. A large spleen can be assessed subcostally.

The spleen has an homogenous echo pattern which is slightly less echogenic than the liver. A few blood vessels are seen within the spleen.

Ultrasound is useful for demonstrating splenomegaly but rarely assists in distinguishing the cause.

Focal splenic lesions may be seen and ultrasound is particularly useful in the follow up of lesions such as an abscess or a hematoma.

Patency of the splenic and portal veins may be assessed with Doppler studies. The normal splenic vein has a width of less than 1 cm.

### COMPUTED TOMOGRAPHY

At CT splenic density approaches that of the liver. An increased density occurs with *hemochromatosis* and *thalassemia* and is easily demonstrated. There is marked contrast enhancement of the spleen and this assists in demonstrating focal lesions.

At CT difficulty may be experienced in distinguishing pleural fluid from ascites. There are two helpful signs that have been described.

1. The *Interface Sign* assesses the interface between the fluid and the spleen or liver. A sharp interface is seen with

ascites whereas pleural fluid forms a hazy or indistinct margin.

2. The position of the fluid is assessed with respect to the crus of the diaphragm. Pleural fluid lies between the crus and vertebral column displacing the crus laterally. However sometimes the crus is difficult to identify.

### RADIONUCLIDE IMAGING

**$^{99m}\text{Technetium Sulphur Colloid}$ .** This isotope is taken up predominantly by the reticuloendothelial cells of the liver and spleen, with a small amount of uptake by the bone marrow. Splenic size can be assessed and focal lesions such as an abscess, infarct, lymphomatous deposit (Fig. 26.37) or hematoma can be demonstrated. A focal defect may be seen in the presence of a normal spleen if there is splenic lobulation, an enlarged left lobe of the liver or barium in the splenic flexure of the colon.

Increased splenic uptake occurs with liver cirrhosis and chronic infective states where there is increased blood flow through the spleen (Fig. 26.38). Infiltration without an increased blood flow results in decreased uptake by the spleen.

**Functional Studies.** Blood pool studies of the spleen use heat damaged autologous red cells labeled with  $^{99m}\text{Technetium}$ . This technique is used to identify asplenia, polysplenia, residual splenic tissue after splenectomy and ectopic peritoneal splenic tissue which occurs after rupture.

**Functional asplenia** is seen with many conditions including splenic infiltrations, the hemoglobinopathies, nutritional deficiencies and splenic artery occlusion.

### ANGIOGRAPHY

The splenic artery may be demonstrated by catheterization of the celiac axis or by selective catheterization. The splenic and portal veins are demonstrated on recirculation from arterial catheterization by using a larger volume of contrast

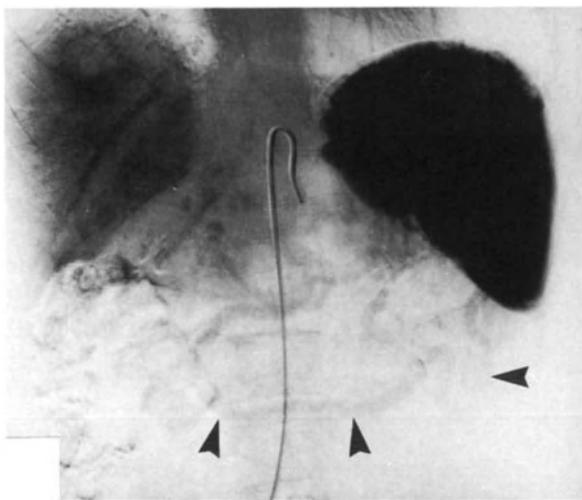


**Fig. 26.39.** Splenic arteriogram venous phase. Subtraction film. Occluded splenic vein. Splenomegaly. Multiple collateral veins (arrows). Elderly patient with inoperable pancreatic carcinoma.

(50–70 ml at 5–10 ml/second) and obtaining delayed films up to 30 seconds after the end of the injection. Normal venous filling occurs after 7–10 seconds but filling may be delayed if there is splenomegaly or splenic or portal vein compression or occlusion. The splenic and portal veins can also be demonstrated by direct splenic puncture with a cannula though this technique is no longer widely used. For this technique clotting factors must be normal. Gross ascites or a small spleen are contraindications. Splenic rupture may occur. The risk of bleeding after the procedure may be reduced by embolization of the tract.

If DSA is used smaller volumes of contrast are necessary.

The normal splenogram is homogenous or slightly patchy. Indications for angiography include:

1. Trauma.
2. Splenic artery aneurysm.
3. To assess malignant infiltration (Fig. 26.39).
4. To assess splenorenal shunts.

*Therapeutic procedures* which may be performed include:

1. Infusion of cytotoxic agents via a catheter.
2. Embolization for hypersplenism, trauma, splenic artery aneurysm and prior to surgery for splenectomy when clotting is abnormal.

A major complication of embolization is *abscess* formation. This occurs more frequently with particulate embolization and occlusion of the splenic artery with a coil or balloon is thought to be preferable.

#### MAGNETIC RESONANCE IMAGING

The spleen has a high blood content and for this reason the normal spleen has relatively prolonged T<sub>1</sub> and T<sub>2</sub> values. Splenic vessels and *varices* are well seen, as are splenic *cysts*. Splenic *hemangiomas* (although the spleen is a less common

site) have a characteristic MR appearance. On spin echo images the lesions appear very dark on T<sub>1</sub> and very white on T<sub>2</sub>-weighted sequences due to the very long T<sub>1</sub> and T<sub>2</sub> relaxation times.

Unfortunately *metastatic disease* and *lymphomatous infiltration* have similar MR imaging characteristics to normal spleen. *Hematomas* have complex appearances depending on size and age; typically they are hyperintense on T<sub>1</sub>-weighted sequences obtained soon after the injury.

*Splenomegaly* typically has normal splenic MR imaging characteristics. With congestion of splenic tissue the T<sub>2</sub> values may increase. The accumulation of iron within the spleen will dramatically reduce signal intensity.

The role of MR in the investigation of splenic pathology has yet to be established. Preliminary studies have not shown any great advantage in the technique and its role may well remain complementary to ultrasound and CT especially in lesion characterization.

#### CONGENITAL ABNORMALITIES

**Asplenia** is associated with multiple cardiac, renal and gastrointestinal abnormalities including *situs ambiguus*, intracardiac shunts, malrotation, annular pancreas and agenesis of the gallbladder. Frequently both lungs have 3 lobes. The cardiac lesions are often fatal.

**Polysplenia** is commoner in females and has a lower mortality than asplenia. Frequently *situs* is indeterminate and the lungs are bilobed. Multiple small collections of splenic tissue are found throughout the abdomen. There may be associated abnormalities of the cardiovascular and gastrointestinal tracts.

**Splenunculi**, or accessory spleens, occur in up to 25% of the population. They are usually small, being less than 3 cm, and found at the splenic hilum although they have been reported in multiple abdominal sites including the testis. The splenunculus may undergo torsion. Hypertrophy of splenunculi occurs after splenectomy. A large splenunculus presenting as a parasplenic mass may cause diagnostic problems. *Radionuclide* studies are usually diagnostic.

The **wandering spleen** is commoner in females and presents as a mass or with symptoms of torsion. *Sulphur colloid scans* are diagnostic.

**Splenic-gonadal fusion** is very rare and usually presents as a left scrotal mass. *Sulphur colloid scans* are diagnostic.

#### INFECTIONS

**Abscess.** Splenic abscesses are rare and usually multiple. Their incidence is increased in the *immunosuppressed* and in patients with a *septicemia* such as subacute bacterial endocarditis and drug addicts. Infection may follow surgery, trauma, therapeutic embolization or spread from an adjacent focus of infection. Occasionally a cyst or hematoma becomes infected.

*Plain film* signs which may be seen are:

1. Splenomegaly.
2. Elevated hemidiaphragm.



Fig. 26.40. Ultrasound scan. Splenic abscess.

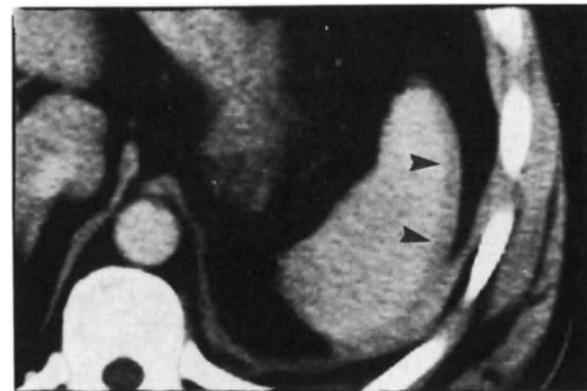


Fig. 26.41. CT scan. Enhanced. Subcapsular hematoma of spleen (arrows) following stab wound.

3. A left pleural effusion, basal atelectasis.
4. A localized ileus.
5. Intrasplenic gas.
6. Calcification of a chronic abscess.

Initially at *ultrasound* there is an ill-defined lesion of mixed echogenicity which becomes better defined and anechoic with time. Internal echoes of debris, gas or septa may be present (Fig. 26.40). Perisplenic fluid may be seen.

At *CT* there is a low-density area which may contain a fluid level or gas. Gas may also be seen within the splenic and portal veins. Perisplenic fluid is demonstrated when present. The mass may compress the splenic vessels. Aspiration biopsy and drainage may be performed with *CT* or ultrasound guidance.

**Hydatid Cyst.** Appearances are as described for the liver (see above).

**Candidiasis.** Appearances are as described for the liver (see above).

#### TRAUMA AND RUPTURE OF THE SPLEEN

Blunt or penetrating injuries may be incurred in road traffic accidents, at surgery or following invasive diagnostic procedures such as renal biopsy.

Spontaneous *rupture* of the spleen is associated with infective processes such as glandular fever, malaria and subacute bacterial endocarditis, blood disorders and splenic tumors. After rupture *splenosis* may occur; splenic tissue is transplanted on to the mesentery resulting in adhesions and obstructions.

Splenic injury may result in an intrasplenic hematoma, a subcapsular hematoma, laceration of the spleen and rupture of the spleen with a hemoperitoneum. Occasional complications include *splenosis* and *abscess formation*.

Plain film signs to look for are:

1. Splenomegaly.
2. An increase in splenic size on serial films.
3. An ill-defined outline to the spleen.

4. Rib fractures.
5. An elevated hemidiaphragm, pleural effusion.
6. Gastric dilatation.
7. Intraperitoneal fluid.
8. Extraperitoneal fluid with loss of renal and psoas outlines.

**Imaging.** *CT* is the investigation of choice having a diagnostic accuracy exceeding 90%. In addition it allows assessment of other organs and demonstrates intraperitoneal bleeding. Peritoneal lavage may be associated with some bleeding and should not precede *CT*, otherwise interpretation may be difficult.

In its early stages a *hematoma* is higher density or isodense but later becomes hypodense; in addition the contour of the spleen may be abnormal. A subcapsular bleed appears as a well-defined peripheral low-density, non-enhancing area with associated flattening of the lateral border of the spleen (Fig. 26.41). A *laceration* is seen as irregular low-density branching areas.

At *ultrasound* there may be an enlarged spleen with an irregular outline. A *hematoma*, a subcapsular *hematoma*, perisplenic blood and free intraperitoneal blood may be demonstrated as well as a pleural effusion. Serial ultrasound examinations are useful for detecting an increase in splenic size suggesting further bleeding.

**Angiography** is rarely performed as a primary investigation for splenic trauma unless therapeutic embolization is being considered. Possible findings include:

1. Non-opacification of the spleen.
2. Contrast leakage from the spleen.
3. Ruptured splenic artery.
4. Focal areas of reduced or non-filling with contrast.
5. A mottled parenchymal pattern.
6. Displacement of vessels by a *hematoma* or subcapsular *hematoma*.
7. Linear or wedge defects.
8. An arteriovenous fistula (which may lead to portal hypertension).

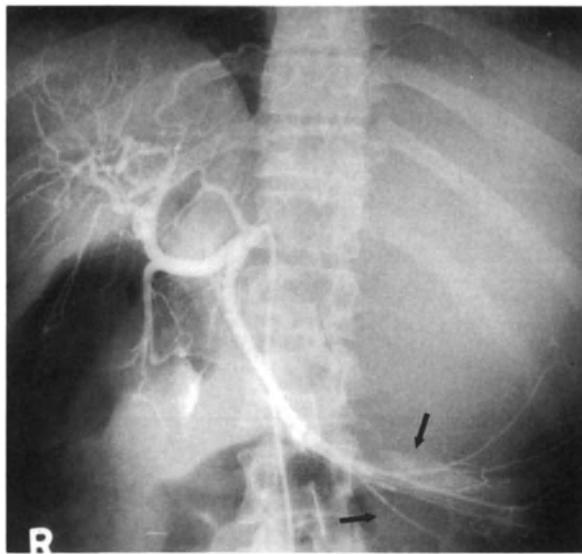


Fig. 26.42. Celiac angiogram. Large splenic cyst. An avascular mass displacing the normal vessels. Elevated left hemidiaphragm. Depressed left kidney (arrows).

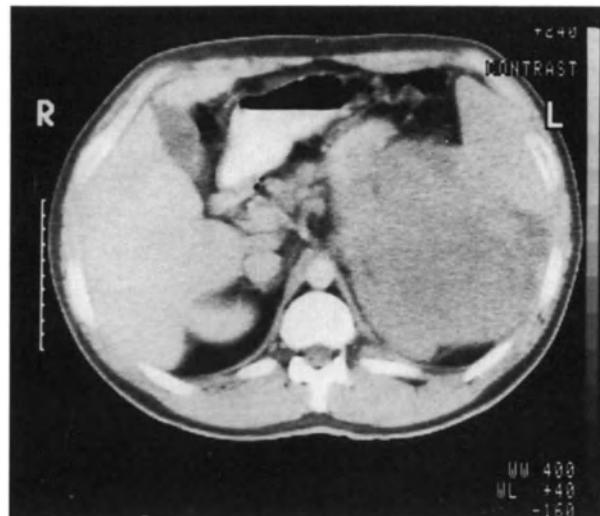


Fig. 26.44. CT scan enhanced. Large lymphomatous deposit of relatively low density in the spleen. Young man with T-cell lymphoma.

#### FOCAL LESIONS

**Cysts.** The majority (80%) of splenic cysts are solitary and are *pseudocysts* developing within a hematoma or infarct. *Congenital cysts* (20%) may be solitary or associated with polycystic renal disease. 2% of patients with polycystic kidneys have splenic cysts. Other cystic lesions include *cystic tumors* and *hydatid cyst*.

Cysts are usually asymptomatic unless very large or if there is intracystic bleeding or rupture.

A large cyst may result in splenomegaly (Fig. 26.42) visible on a plain film. Curvilinear calcification may be present.

**Ultrasound** and **CT** are the investigations of choice and help to differentiate a simple cyst from hydatid disease, an abscess, hematoma and pancreatic pseudocyst.



Fig. 26.43. Ultrasound scan. Lymphomatous deposit in spleen. Large mass of low echogenicity (arrows) above left kidney (K).

At ultrasound the cyst is transonic with posterior acoustic enhancement. Intracystic bleeding produces internal echoes which may form an echogenic level.

**Hemangioma.** This is the commonest benign tumor of the spleen and is usually asymptomatic. Occasionally rupture occurs and multiple tumors may cause hypersplenism with anemia and thrombocytopenia. Radiological findings are the same as with an hemangioma of the liver (see p. 468).

**Lymphoma.** At presentation the spleen is involved in 30%–40% of patients. Splenic involvement with a normal liver is often a feature of Hodgkin's lymphoma. There may be multiple masses, a solitary mass or miliary infiltration. The spleen may also be enlarged due to reactive hyperplasia rather than infiltration.

At **ultrasound** focal lesions are well defined and of low echogenicity or even anechoic (Fig. 26.43); diffuse infiltration is difficult to identify. Enlarged lymph nodes may be seen at the splenic hilum.

At **CT** appearances are non-specific with low-density masses in the spleen (Fig. 26.44).

**Metastases.** Splenic metastases are usually associated with liver involvement and are frequently found at post mortem. Common primary sites include the breast, lung, ovary, stomach and melanoma. Radiological features are the same as for liver metastases (see p. 470).

**Infarction.** Splenic infarcts may occur due to sickle cell disease, leukemia, subacute bacterial endocarditis, pancreatitis, malignancy of the tail of the pancreas, sarcoidosis, torsion and arterial disease. Infarction may be asymptomatic or cause pain.

At **ultrasound** there are hypoechoic foci which may be wedge shaped; with massive infarction the spleen is enlarged and of decreased echogenicity. Old infarcts appear as echogenic streaks. Infarcts seen at **CT** appear as low-density areas.

**Radionuclide studies** are also useful for demonstrating the presence of infarcts.

**Splenic Artery Aneurysm.** The splenic artery is the commonest site of aneurysm formation of the visceral vessels. There is an increased incidence of aneurysm formation associated with arteriosclerosis, pancreatitis, trauma and Ehlers-Danlos syndrome. A large aneurysm may be painful and on examination there may be a palpable mass with a bruit. There is an increased risk of rupture in pregnancy.

Frequently curvilinear calcification is present.

Embolization via selective catheterization may be undertaken.

**Lymphangiomatosis.** This is a benign malformation consisting of multiple lymph-containing cysts diffusely involving the spleen. Other organs such as the liver, kidneys and lungs may be affected.

Curvilinear calcification may be present. Well-defined cystic areas are seen at both ultrasound and CT.

#### REFERENCES AND SUGGESTIONS FOR FURTHER READING

##### LIVER

- Beggs I (1985) The radiology of hydatid disease. *AJR* 145: 639–648  
 Boechat MI, Kangaroo H, Gilsanz V (1988) Hepatic masses in children. *Semin Roentgenol* 13: 185–193  
 Brandt DJ, Johnson CD, Stephens DH, Weiland LH (1988) Imaging of fibrolamellar hepatocellular carcinoma. *AJR* 151: 295–299  
 Edmonson HA, Peters RL (1983) Tumours of the liver: pathologic features. *Semin Roentgenol* 18: 75–83  
 Glazer GM (1988) MR imaging of the liver, kidneys and adrenal glands. *Radiology* 166: 303–312  
 Gosink BB (1981) Intrahepatic gas: differential diagnosis. *AJR* 137: 763–767  
 Itai Y, Furni S, Araki T, Yashiro N, Tasaka A (1980) Computed tomography

of cavernous haemangioma of the liver. *Radiology* 137: 149–155  
 Martino C, Haaga JR, Bryan PJ et al. (1984) CT guided liver biopsies: eight years experience. *Radiology* 152: 755–757

Moss AA, Goldberg HI, Stark DB et al. (1984) Hepatic tumours: magnetic resonance and CT appearance. *Radiology* 150: 141–147

Murphy FB, Steinbergh HV, Shires GT, Martin LG, Bernardino ME (1986) The Budd-Chiari syndrome: a review. *AJR* 147: 9–15

Pastakia B, Shawker TH, Thaler M et al. (1988) Hepato-splenic candidiasis: wheels within wheels. *Radiology* 166: 417–424

Radin DR, Ralls PW, Colletti PM, Halls JM (1988) CT of amoebic liver abscess. *AJR* 150: 1297–1301

Snow JH (Jnr), Goldstein HM, Wallace S (1979) Comparison of scintigraphy, sonography, and computed tomography in the evaluation of hepatic neoplasms. *AJR* 132: 915–918

Teeffey SA, Stephens DH, James EM, Charboneau JE, Sheedy PF (1986) Computed tomography and ultrasonography of hepatoma. *Clin Radiol* 37: 339–345

Wing VW, Federle MP, Morris JA et al. (1985) The clinical impact of CT for blunt abdominal trauma. *AJR* 145: 1191–1194

##### SPLEEN

- Dwyer A (1978) The displaced crus: a sign for distinguishing between pleural fluid and ascites on computed tomography. *J Comput Assist Tomog* 2: 598–599  
 Jeffrey RB, Laing FC, Federle MP, Goodman PC (1981) Computed tomography of splenic trauma. *Radiology* 141: 729–732  
 King DJ, Dawson AA, Bayliss AE (1985) The value of ultrasonic scanning of the spleen in lymphoma. *Clin Radiol* 36: 473–474  
 Mittlestaedt CA, Portain CL (1980) Ultrasonic pathologic classification of splenic abnormalities: grey scale patterns. *Radiology* 134: 697–705  
 Pierarski J, Federle MP, Moss AA, London SS (1980) Computed tomography of the spleen. *Radiology* 135: 683–689  
 Randall PA, Moller JH, Amplatz K (1973) The spleen and congenital heart disease. *AJR* 119: 551–559  
 Teplick JG, Teplick SK, Goodman L, Haskin ME (1982) A computed tomographic sign for distinguishing pleural and intra-abdominal fluid. *Radiology* 144: 359–362

## CHAPTER 27

# THE PANCREAS

Janet Murfitt

---

The pancreas lies transversely in the upper abdomen at the L1–2 level. The head and body are retroperitoneal whereas the pancreatic tail lying in the splenorenal ligament is intraperitoneal. Pancreatic size is quite variable.

Normal adult AP measurements are 3 cm for the head, body and tail and 2.5 cm maximum for the neck. In the majority of cases the pancreas has a horizontal lie or an oblique lie with the tail higher than the body.

### DEVELOPMENT

The pancreas develops from two buds, dorsal and ventral, which arise from the duodenum. In the sixth week of life the ventral bud with the common bile duct rotates behind the duodenum to fuse with the dorsal bud. The head and uncinate process are derived from the ventral bud and the remaining pancreas from the dorsal bud. The ventral duct and the distal dorsal duct fuse to form the *duct of Wirsung* which drains into the ampulla. In some 45% of cases the duodenal end of the dorsal duct persists as the *accessory duct of Santorini*, draining into the minor papilla which enters the duodenum just above and anterior to the ampulla. In a similar number the accessory duct is not patent. In 9% the ventral and dorsal ducts fail to fuse (*pancreas divisum*). Usu-

ally the pancreatic and bile ducts form a common duct but in a small percentage of cases there are separate orifices.

### IMAGING

The following investigations are used: abdominal film, chest film, ultrasound, CT, ERCP, barium studies, angiography, fine needle biopsy, transhepatic venous sampling, MRI and radionuclide imaging.

**Plain Films.** *Pancreatic calcification* (Fig. 27.1A, B) is present on the plain film in 20%–40% of cases of alcoholic pancreatitis and 60% of cases of hereditary pancreatitis. Tumors which may calcify include cystic tumors, hemangioma and cavernous lymphangioma, in which phleboliths develop and very rarely islet cell tumors. Other causes of pancreatic calcification include hyperparathyroidism, cystic fibrosis and kwashiorkor. Some cases are idiopathic.

**Ultrasound.** Bowel gas frequently obscures some or all of the pancreas at ultrasound examination. Methods suggested to improve visualization include using the liver as an acoustic window in the erect position, filling the stomach with water, and using the spleen as an acoustic window in the lateral position to show the pancreatic tail. Fluid-filled loops may be mistaken for tumors or cysts and rescanning

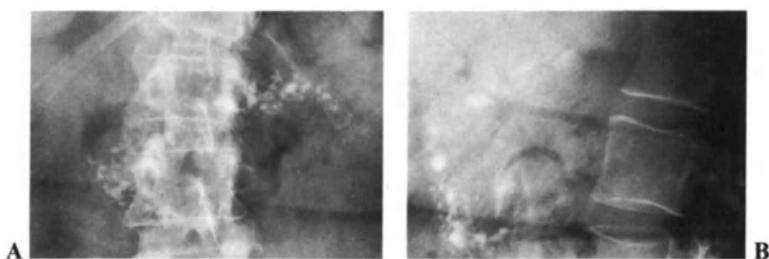


Fig. 27.1A, B. Plain abdomen. A AP. B Lateral. Extensive pancreatic calcification.



Fig. 27.2. ERCP. Opacification of the biliary tree. Multiple gallstones in the gallbladder. Stone in the distal CBD (arrow).

in a different position or after oral fluid is helpful if there is any doubt.

The normal pancreas has a homogenous echo pattern of slightly higher echogenicity than the liver. In childhood the pancreas is relatively larger and of lower reflectivity. With age, fat content rises with a resultant generalized increase in pancreatic reflectivity. Fatty infiltration also occurs in the obese, in diabetics and with steroid therapy. Focal areas of increased echogenicity are a feature of chronic pancreatitis. The normal *pancreatic duct* is less than 2 mm in diameter and is identified in the majority of patients. Its size increases with age. The common bile duct runs posteriorly in the pancreatic head and its diameter here should be less than 4 mm.

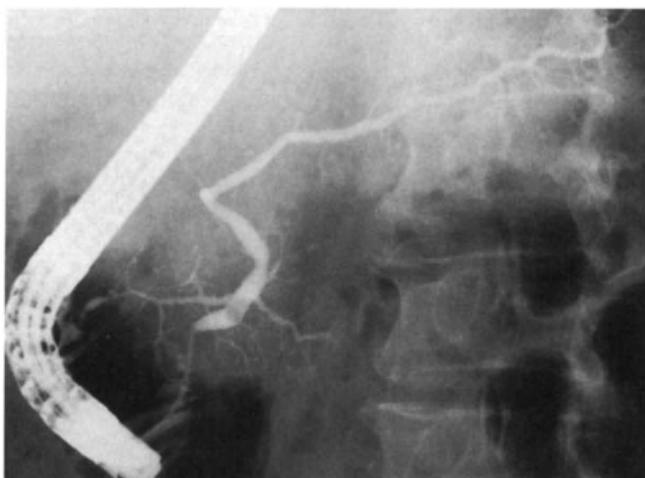


Fig. 27.3. ERCP. Normal pancreatic duct with complete filling of the main duct and side branches.

*Intraoperative ultrasound scanning* is a very accurate method for localizing small pancreatic endocrine tumors. Ultrasound guided *percutaneous pancreatography* has been used as another route for demonstrating the pancreatic duct.

CT is more helpful than ultrasound for assessing the pancreatic outline, tail, peripancreatic tissues and blood vessels. Oral and intravenous contrast help to differentiate gut and tortuous blood vessels from pancreatic masses. The outline of the pancreas is variable in appearance from smooth to lobulated. Abnormal findings include a *focal bulge* to the outline, *loss of homogeneity*, *cystic areas*, *calcification* and a *dilated pancreatic duct*.

ERCP allows endoscopic assessment of the upper gastrointestinal tract and ampulla as well as contrast assessment of the pancreatic and bile ducts (Fig. 27.2). It is considered to be the most effective method of imaging the pancreatic duct. Duct cannulation however may fail if there has been gastric surgery, if the duodenum is extensively infiltrated with tumor or in the presence of a duodenal diverticulum. A disadvantage is that a normal examination does not exclude a peripheral mass or chronic pancreatitis.

Certain therapeutic and diagnostic procedures may be undertaken at ERCP. These include:

1. Sphincterotomy
2. Stone extraction from bile duct and/or pancreatic duct
3. Biopsy of gut or ampulla
4. Cytology of pancreatic juice and brushings
5. Balloon dilatation of benign strictures
6. Stent insertion
7. Pancreatic cyst drainage

Complications develop in 1%–2% of cases and include *cholangitis* and *pancreatitis*, which is related to overfilling of the pancreas with contrast and parenchymal opacification. Amylase levels often rise after the procedure and many patients have reflux of duodenal contents into the ducts. ERCP is contraindicated in acute pancreatitis.

The normal pancreatic duct should fill throughout its length (Fig. 27.3). In the tail of the pancreas the duct may be bifid. The side ducts should fill and be smoothly tapered. Normal tapering of the main duct occurs at the junction of the head and neck and in addition some narrowing is present in the intrapapillary duct. The examination is performed in the prone oblique position which often results in underfilling of the right hepatic ducts.

*Barium studies and hypotonic duodenography* are no longer first line investigations for pancreatic disease. Findings associated with pancreatic masses are described later.

**Angiography.** With the development of other imaging techniques angiography is used predominantly for assessing resectability of a malignancy, looking for encasement or occlusion of major arteries and veins. The veins are assessed on the venous phase with films taken up to 30 seconds after the end of selective superior mesenteric and splenic artery injections of large volumes of contrast (40–70 ml at 6–8 ml/second). Abnormal vessels occur both with malignancy and chronic pancreatitis.

Islet cell tumors are small and may have a marked capillary blush, although superselective pancreatic angiography is often necessary for their demonstration.

**Transhepatic Portal Venous Catheterization and Venous Sampling.** Transhepatic catheterization should be undertaken only if clotting studies are normal; the track may be embolized at the end of the procedure on withdrawing the catheter to reduce the risk of bleeding. Pancreatic venous sampling has a high degree of accuracy for diagnosing insulinomas. Multiple samples are taken from the splanchnic veins including the splenic, superior mesenteric, inferior mesenteric and portal veins.

**Radioisotope Studies.**  $^{75}\text{Seleno-methionine}$  is taken up by the pancreas, liver and spleen. However, there is a high false positive rate for pancreatic disease and this procedure is no longer favored.

**MRI.** The normal pancreas is shown on MRI, in Fig. 27.4. The pancreas is a difficult organ to image adequately with MR and images are frequently degraded by respiratory motion. CT and ultrasound remain the methods of choice for demonstrating the smaller pancreatic lesions. Mass lesions on MRI are still identified by morphological criteria and are usually greater than 2 cm in diameter before they become visible. Short  $T_1$  inversion recovery (STIR) sequences have been successfully used to differentiate pancreatic carcinoma from exuberances of pancreatic tissue. Interestingly islet cell tumors are often easier to see with MR as they tend to have prolonged  $T_1$  and  $T_2$  times.

MRI is relatively successful at demonstrating peripancreatic tissue spread of disease. Blood vessel neoplastic invasion is particularly well seen.

**Fine needle biopsy** is performed under ultrasound, CT or fluoroscopy control. This procedure can be very painful and requires analgesia. Two or three passes are made with a small gauge needle. The centre of a mass is often necrotic, so that a biopsy of the periphery of a lesion is more likely to produce a positive result. True positive rates up to 95% have been reported and complication rates are very low though acute pancreatitis has been described following biopsy.

#### CONGENITAL ABNORMALITIES

Pancreatic agenesis, hypoplasia and duct atresia are extremely rare. The more common congenital lesions are described below.

**Ectopic Pancreas.** Ectopic nodules of pancreatic tissue are present in the bowel wall in 2% of cases at post mortem. These nodules are usually small and are commonly found in the stomach and duodenum, but also occur in the small bowel and Meckel's diverticulum. On barium examination they appear as smooth filling defects which may be ulcerated. Occasionally there is a short duct which fills with barium.

**Annular Pancreas.** The duodenum is encircled by the pancreas following failure of the ventral bud to rotate normally. Associated anomalies include Down's syndrome, esophageal and duodenal atresia, tracheoesophageal fistulae, imperforate anus, gut malrotation and congenital heart lesions. In 85% of cases the second part of the duodenum is affected. 50% of cases present in the neonate with clinical signs of

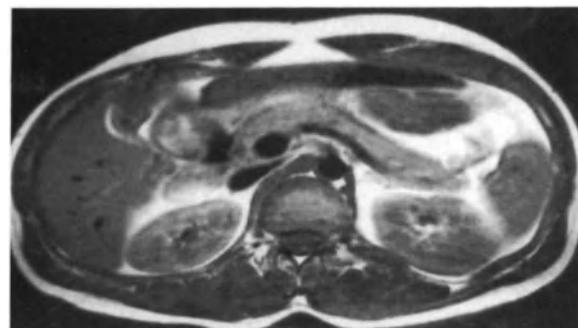


Fig. 27.4. MRI. Normal pancreas. T<sub>1</sub>-weighted image. 1.5 Tesla. The splenic vein is clearly visualized. Courtesy of Dr G. Cherryman, CRC Radiology Research Group, Royal Marsden Hospital, Sutton, UK.

duodenal obstruction and the characteristic 'double bubble' on plain films of fluid levels in the stomach and duodenum with no gas in the distal bowel. Adults may be asymptomatic or have pain, nausea, vomiting and chronic pancreatitis.

**Ultrasound** demonstrates an enlarged pancreatic head. ERCP is diagnostic in most cases but is unhelpful in the 15% of cases when the annular segment does not drain into the duct of Wirsung.

**Ventral Pancreas – Pancreas Divisum.** This abnormality has an incidence of around 9%. The ventral bud of the pancreas rotates normally but there is no fusion of the dorsal and ventral ducts. The larger dorsal segment drains into the accessory papilla via the duct of Santorini. Drainage may be impaired with resulting duct dilatation and chronic pancreatitis. This can be relieved by endoscopic papillotomy, balloon dilatation of the duct or surgery.

The ventral segment drains via the main papilla and is small with early parenchymal filling with contrast at ERP (Fig. 27.5).

**Cystic Fibrosis.** One of the many manifestations of cystic fibrosis is pancreatic insufficiency with steatorrhea. The pancreas is replaced by fatty and fibrous tissue making it highly

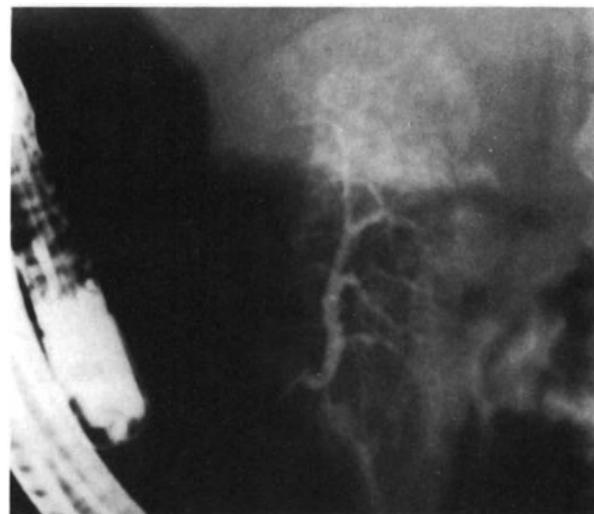


Fig. 27.5. ERP. Pancreas divisum. 53-year-old female complaining of right upper quadrant pain which persisted after cholecystectomy.

reflective at *ultrasound*. Pancreatic calcification on the plain film is unusual. Associated pancreatico-biliary disease includes pancreatitis, a small gall bladder, gallstones and biliary cirrhosis.

Other causes of fatty pancreas include old age, steroid treatment, Cushing's syndrome, obesity, cystic fibrosis, Schwachmann-Diamond syndrome and pancreatic duct obstruction. In the *Schwachmann-Diamond syndrome* the exocrine pancreatic tissue is replaced by fat. There are associated skeletal and bone marrow abnormalities.

**Hemochromatosis.** Iron deposition within the liver, pancreas and spleen results in an increased density at CT.

### ACUTE PANCREATITIS

In acute pancreatitis there is edema of the pancreas. This may progress to necrosis of the pancreas, blood vessels and fat. The pancreas does not have a capsule and inflammation may spread to involve the lesser sac, retroperitoneum and anterior pararenal spaces.

Most cases are due to alcohol abuse or gallstones but no cause is identified in some 20% of cases. Causes of acute pancreatitis are listed in Table 27.1.

Table 27.1. Causes of acute pancreatitis

Gallstones
Alcohol
Viruses: mumps, typhoid, glandular fever
Drugs: steroids, contraceptive pill
Penetrating peptic ulcer
Surgery, trauma
Pancreas divisum
Pancreatic neoplasm
Hyperparathyroidism
Hyperlipidemia
Polyarteritis nodosa

**Complications** are seen in up to 20% of patients. Some patients die, whilst others develop acute relapsing pancreatitis. Severe cases develop a solid inflammatory pancreatic mass or *phlegmon*. *Abscess* formation may develop within 10–14 days and can form within the phlegmon or a fluid collection. It is associated with a high mortality (about 50%). Needle aspiration assists in the diagnosis and helps to distinguish an abscess from a cyst and from phlegmon.

Rupture of an obstructed pancreatic duct results in *pseudocyst* formation. Encapsulation develops by six weeks and this is a suitable time for drainage. However spontaneous decompression occurs in one third of cases. Predominantly the cysts develop in the lesser sac, displacing the stomach anteriorly, but many other sites have been described including the posterior mediastinum, pelvis, mesocolon and the root of the small bowel mesentery. Hemorrhage into a cyst may occur whilst calcification of the cyst wall is very unusual.

Necrosis may involve the blood vessels with *bleeding* into the gut, a pseudocyst or retroperitoneally. *Pseudoaneurysm* formation may occur. There may be *venous thrombosis* of mesenteric vessels.

*Fistulae* may develop between pseudocysts and the colon; occasionally they involve the pleura, pelvis or bronchi.

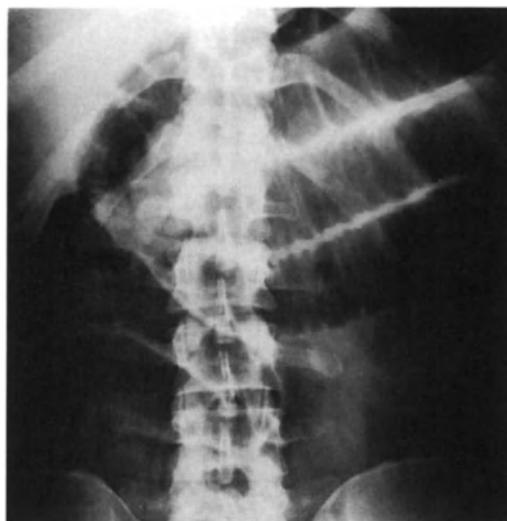


Fig. 27.6. Plain abdomen. Acute pancreatitis. Ileus of jejunum and upper ileum.

*Biliary obstruction* as a result of edema compressing the bile duct has been described and *ascites* is frequently present. Plain film changes of acute pancreatitis are listed in Table 27.2.

Table 27.2. Plain film changes of acute pancreatitis

Chest
left pleural effusion
basal shadows, atelectasis
elevated diaphragm
pulmonary edema
wide mediastinum (pseudocyst)
Gallstones
Colon cut-off sign
Sentinel loop
Ileus of duodenum
Ileus of small bowel (Fig. 27.6)
Gasless abdomen
Gastrocolic separation
Left renal halo sign
Obliterated left psoas outline
Ascites
Gas in pancreas
Fat necrosis
Bone changes

**Radiography.** A *left pleural effusion* frequently develops with severe pancreatitis, the pleural fluid having a very high amylase content. Of the many abdominal film signs listed the most specific is duodenal ileus; the *colon cut off sign* where the transverse colon is dilated but cuts off abruptly at the splenic flexure is less specific. Persistent vomiting results in a *gasless abdomen*. *Intrapancreatic gas* is usually seen as multiple small bubbles and occurs within an abscess or following fistula formation. *Fat necrosis* results in mottled shadowing seen in the left upper quadrant (Fig. 27.7) but which can become generalized.

Bone changes described include *avascular necrosis*, *bone infarcts* and *lytic lesions*.

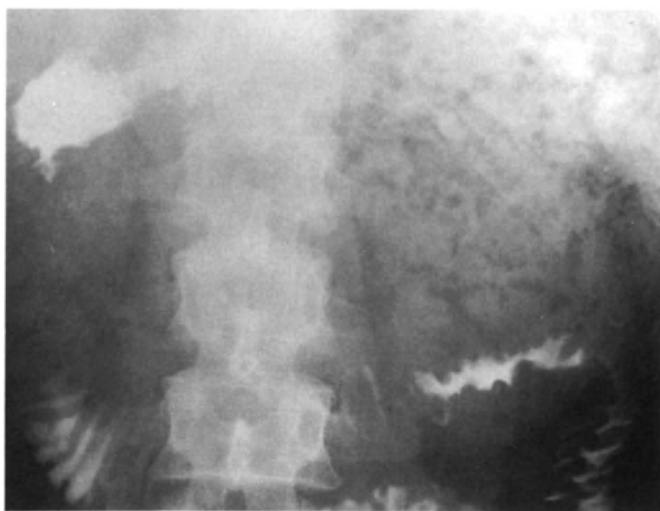


Fig. 27.7. Plain abdomen. Acute pancreatitis with fat necrosis.

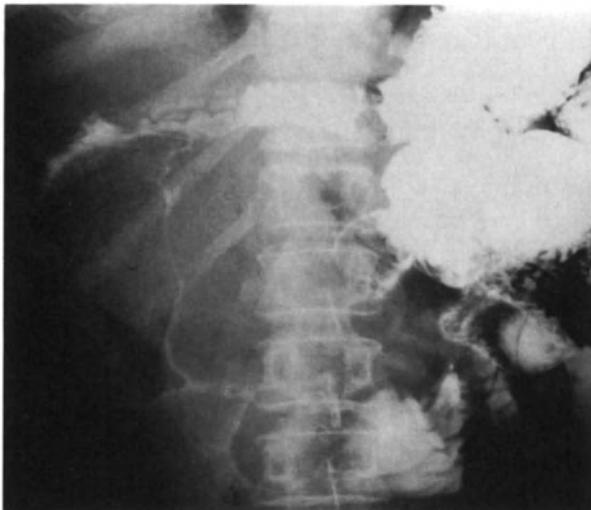


Fig. 27.8. Barium meal. Large pancreatic cyst. Compression and widening of the duodenal loop with upward displacement of the pyloric antrum.



Fig. 27.9. Ultrasound scan. Large pancreatic pseudocyst in the region of the body and tail of the pancreas (P).

**Barium Studies.** The edematous pancreas or a cyst widens the duodenal loop and compresses its medial border (Fig. 27.8). There is ampullary edema and thickening of the gastric and duodenal folds. Barium may enter a cyst in the presence of a fistula.

**Ultrasound.** Appearances are normal in 30% of cases of acute pancreatitis. Changes take 12 to 24 hours to develop. An associated gut ileus may completely obscure the pancreas.

Pancreatitis may be focal or generalized. A proximal neoplasm frequently causes focal pancreatitis in the distal pancreas. The pancreas is enlarged and reflectivity is lower than normal. Some duct dilatation may be present. Phlegmon, which is solid, appears as a mass of low reflectivity and needle aspiration may be necessary to distinguish it from an abscess or cyst.

Other masses which may develop include hemorrhage, pseudoaneurysms, abscess formation, fluid collections and pseudocysts. Initially hemorrhage is echogenic but it becomes virtually anechoic within a few days. In the early stages pseudocysts are ill-defined with irregular edges, but later become well-defined and echofree (Fig. 27.9). Septa are rare and may develop following infection or bleeding. Serial examinations are useful for assessing progress and cyst formation.

**CT.** Computed tomography is considered to be the best imaging technique for demonstrating the pancreas and peripancreatic tissues (Fig. 27.10A, B) in acute pancreatitis and its complications. Appearances are normal in one third of cases of acute pancreatitis.

Positive findings include:

1. Pancreatic enlargement: diffuse, focal
2. Decreased attenuation of the pancreas
3. Indistinct outline of the pancreas
4. Phlegmon: low-density mass (5–20 HU)
5. Hemorrhage: high-density areas
6. Fluid collections: pancreatic or peripancreatic
7. Inflammation of the peripancreatic tissues
8. Abscess, may be gas-containing

Hemorrhage may occur within the phlegmon or fluid collections and has a high-density measurement for the initial 48 hours (50–80 HU). Spread of inflammation into the peripancreatic tissues is identified by thickening of Gerota's fascia and the bowel mesentery and an increased density of the peripancreatic fat. Fluid collections (Fig. 27.11) form within the pancreas or in the peripancreatic tissue and are common in the lesser sac. I.v. contrast enhances inflamed pancreatic tissue so that fluid collections are better seen. Needle aspiration under CT control will enable an abscess to be differentiated from a cyst or phlegmon, although there are the risks of bleeding or infection of a sterile cyst. An infected cyst requires immediate drainage.

**ERP.** ERP is contraindicated in acute pancreatitis because of the risk of introducing infection into pancreatic cysts. There is early parenchymal filling with compression of the ducts by the pancreatic edema.

**Angiography** will demonstrate pseudoaneurysms or hemorrhage from the splenic and gastroduodenal arteries. Embolization may be performed if necessary.

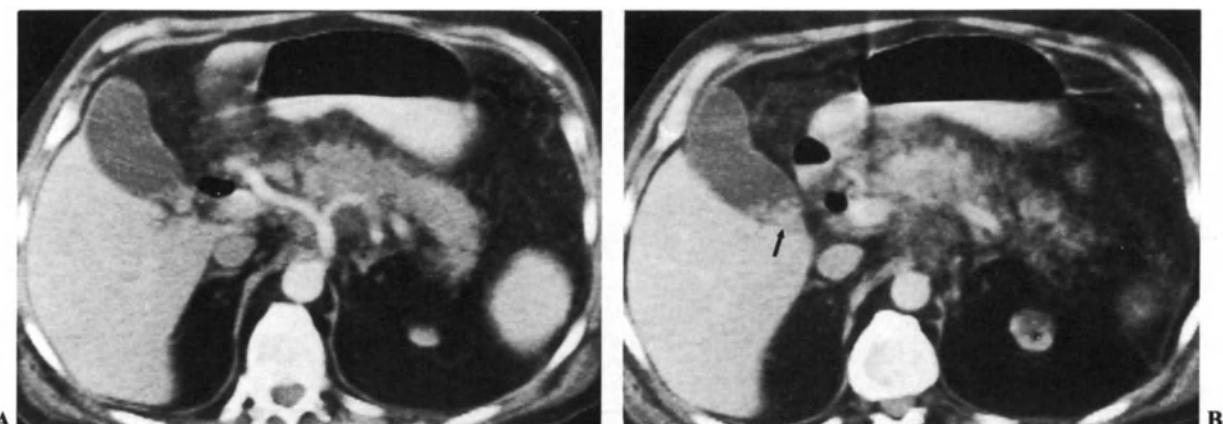


**Fig. 27.10A, B.** CT scan; enhanced contiguous slices. Acute pancreatitis. Swelling of the pancreas with ill-defined borders. Streaky shadows in peripancreatic tissues. Gallstones in gallbladder (arrow).

### CHRONIC PANCREATITIS

The clinical presentation of chronic pancreatitis includes recurrent abdominal pain, steatorrhea, diabetes mellitus which is characteristically difficult to control, and obstructive jaundice.

The pancreas atrophies. There is calcification of the protein plugs within the ducts to form calculi. The duct becomes dilated, strictures develop and there may be duct obstruction. Pseudocysts form in 20% of cases and pseudoaneurysms may develop. Bile duct obstruction develops in 10% of cases but complete obstruction is unusual and is commonly seen in

pancreatic malignancy. Characteristically there is smooth tapering of the CBD in the pancreatic head.

Causes of chronic pancreatitis are listed in Table 27.3.

*Heredity pancreatitis* is an autosomal dominant abnormality presenting as chronic calcific pancreatitis in children, and with a high incidence of pancreatic malignancy.

**Imaging.** *Plain films.* Pancreatic calcification is predominantly a feature of alcoholic pancreatitis. The calcified foci are multiple, and variable in both size and outline and the majority arise in the head of the pancreas. Foci which exceed 5 mm in diameter are usually associated with obstruction of the pancreatic duct. *Bone infarcts* and *avascular necrosis* occur in both acute and chronic pancreatitis.

*Barium studies.* The duodenal loop becomes abnormal with a double contour, reversed 3 or epsilon sign, effacement or spiculation of the duodenal folds and ampullary edema. Duodenal obstruction may develop. Mucosal changes in the posterior wall of the stomach can occur.

*Ultrasound and CT findings.* The pancreas is enlarged or may be smaller than normal. Changes can be focal or diffuse with an irregular outline and loss of definition of the fascial plains. Frequently both the pancreatic and common bile ducts are dilated (Fig. 27.12). Dilatation of the pancreatic ducts may be smooth or irregular (Fig. 27.13) and significant dilatation is a valuable confirmatory sign of chronic pancreatitis. Irregular dilatation results in a 'chain of lakes' appearance. Extensive calcification may be present (Fig. 27.14). Findings are summarized in Table 27.4.

Side-duct ectasia appears as small cysts less than 5 mm in diameter. Pseudocysts are common but are usually smaller than in acute pancreatitis and may be multiple. Splenic vein thrombosis and splenomegaly may be demonstrated.

*ERP.* Duct changes are well demonstrated and can be classified (after Jones, Lees & Frost, 1988) as minimal (Fig. 27.15), moderate and advanced (Table 27.5, Fig. 27.16A, B, C).

Cysts (Fig. 27.17) and cavities (Fig. 27.18) will fill with contrast if they are communicating with the duct.

Pancreatic duct occlusion does not commonly occur in chronic pancreatitis and raises the possibility of malignancy.

Endoscopic drainage of the pancreatic duct and cysts, and stone extraction from the duct may be undertaken.



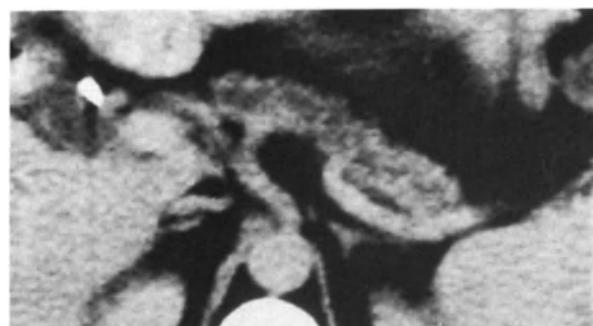
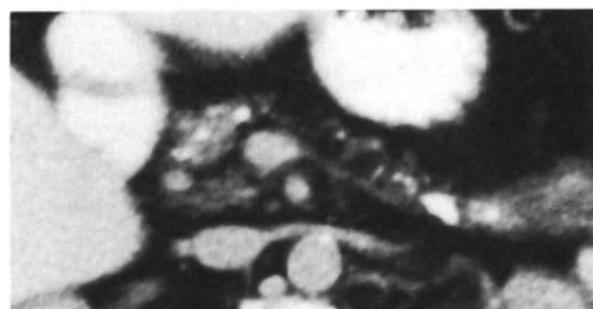
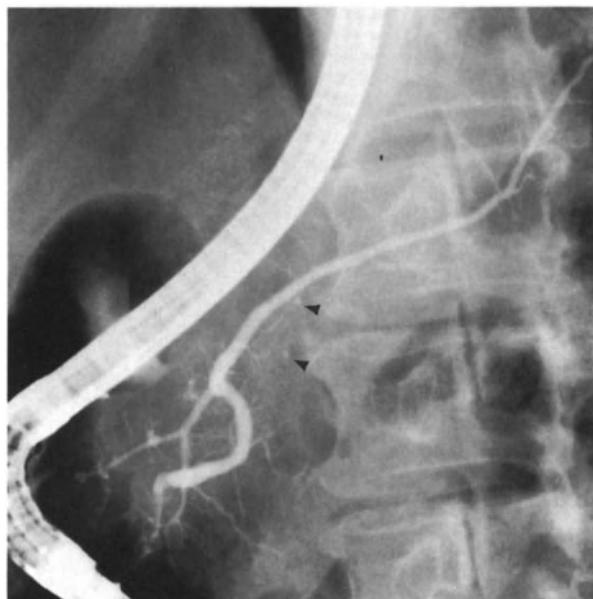
**Fig. 27.11.** CT scan. Acute pancreatitis with a large low density pseudocyst.

**Table 27.4.** Ultrasound and CT findings in chronic pancreatitis

	Ultrasound	CT
Pattern	Uneven echoes	Irregular density
Calcification	Echogenic foci with acoustic shadows	Multiple dense foci
Outline	Irregular, ill-defined	Irregular, loss of fascial plains
Pancreatic duct	Dilated	'Chain of lakes'
CBD	Wall echoes increased Dilated	Dilated

**Table 27.5.** Duct changes in chronic pancreatitis

Minimal change	
main duct	
normal or slight irregularity	
side branches	
more than 3 abnormal ducts	
slight dilatation, irregularity	
narrowed origins: 'nipping'	
decreased filling	
Moderate	
main duct	
irregular, dilated	
side branches	
irregular filling,	
cystic dilatation,	
obstructed	
CBD	
slight narrowing	
Marked	
main duct	
gross dilatation, obstruction	
stenoses and beading 'chain of lakes'	
calculi (filling defects)	
cysts, cavities	
delayed emptying	
side branches	
stenosed, occluded	
CBD	
smooth stricture with angulation	
occluded	

**Fig. 27.13.** CT scan. Dilated pancreatic duct.**Fig. 27.14.** CT scan. Chronic calcific pancreatitis.**Fig. 27.12.** Ultrasound scan, transverse. Chronic pancreatitis. Calculus (arrows) in the pancreatic duct (PD) with distal dilatation. SV = splenic vein.**Fig. 27.15.** ERP. Minimal change chronic pancreatitis. The main pancreatic duct is normal. There is early dilatation of side branches (arrows).

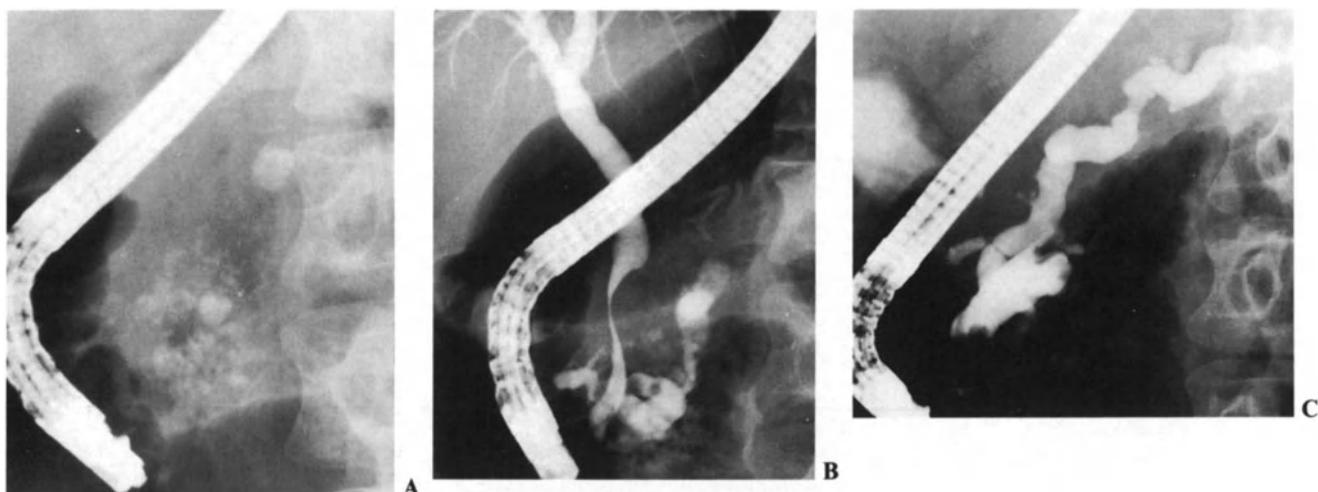


**Fig. 27.16A, B, C.** Chronic pancreatitis. **A** Plain film. Calcific pancreatitis. **B** ERCP. Smooth angulated stricture of CBD. **C** Grossly dilated, irregular pancreatic duct. The side branches are dilated.

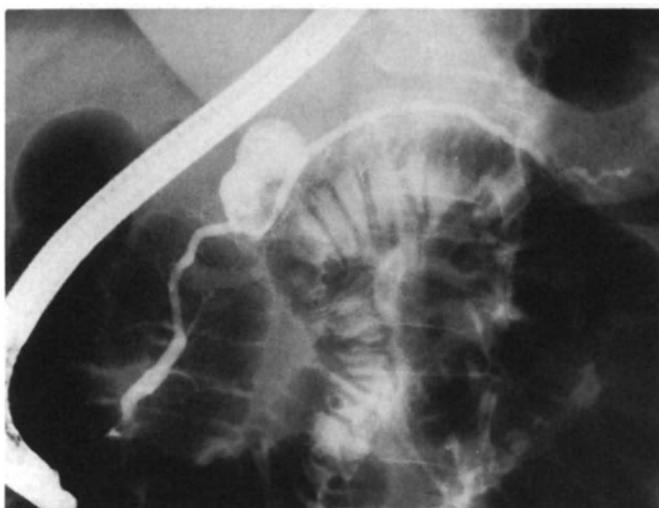


**Fig. 27.17.** ERCP. Chronic pancreatitis with pseudocyst filled with contrast.

Other causes of pancreatic duct occlusion include carcinoma of the pancreas, pseudocyst, calculus, abscess, carcinoma of the ampulla and surgery and trauma.

At *angiography* there may be pseudoaneurysms and splenic vein thrombosis. The pancreatic vessels are irregular and beaded but occlusion is unusual.

#### TRAUMA

Trauma may be penetrating or closed. In road traffic accidents the pancreas is damaged when compressed between the steering wheel and the spine. There may be transection of the pancreas or rupture of the duct with pseudocyst formation (Fig. 27.19). CT will demonstrate the features of

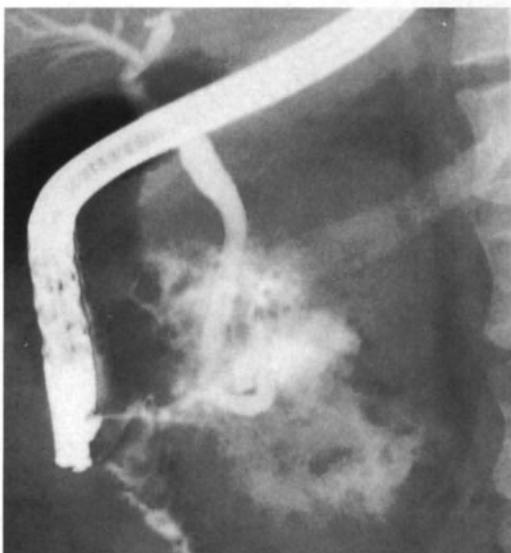


**Fig. 27.18.** ERCP. Large pancreatic pseudocyst with duct obstruction.



**Fig. 27.19.** CT scan. Traumatic pancreatic pseudocyst (arrow) following road traffic accident. Courtesy of Dr R. Travis, Auckland, New Zealand.

intraperitoneal and retroperitoneal fluid, but transection of the gland may be difficult to confirm and require ERCP for a definite diagnosis.

### PANCREATIC CYSTS

Pancreatic cysts may be classified as in Table 27.6. Single cysts are rare, often large and do not communicate with the duct system. The pancreas is involved in 10% of patients with polycystic kidneys.

Multiple tumors develop in patients with Von Hippel-Lindau disease including pancreatic cysts (in over half of cases), pancreatic cystadenoma, cerebellar hemangioblastoma, retinal angioma, pheochromocytoma and tumors of the kidney, viscera, lungs and bones.

**Table 27.6. Classification of pancreatic cysts**

Type I True
congenital
single
polycystic disease
von Hippel-Lindau disease
retention
malignant
Type II Pseudocysts
Type III Hydatid infection

### PANCREATIC TUMORS

Common pancreatic tumors are listed in Table 27.7.

**Table 27.7. Pancreatic tumors**

Ductal
adenocarcinoma (plus variants)
serous cystadenomas (microcystic adenoma, glycogen-rich adenoma)
mucinous cystadenoma
Pancreaticoblastoma
Ampullary carcinoma
Islet cell
Others
mesenchymal
metastases
lymphoma
sarcoma

### ADENOCARCINOMA OF THE PANCREAS

Adenocarcinoma constitutes three quarters of all pancreatic neoplasms. Clinical presentation is late with early metastatic spread and local invasion of vital structures. Consequently the prognosis is very poor. The majority of lesions are in the head of the pancreas (60%) presenting primarily with jaundice. Lesions in the body (25%) and tail (15%) present very late with weight loss and pain as a result of invasion of retroperitoneal tissues and the spine. 20% of tumors are diffuse or multifocal.



**Fig. 27.20. Barium meal. Large pancreatic carcinoma involving the posterior wall of the stomach (arrows).**

Additional presentations include focal pancreatitis in one third of patients and late onset diabetes mellitus in 25%. An occasional feature is superficial thrombophlebitis. Duodenal obstruction is a late complication.

**Imaging.** *Plain films.* These tumors do not calcify. Metastases, lymphangitis carcinomatosis and malignant effusions may develop in the chest. Splenic enlargement follows splenic vein obstruction by the tumor which may also obstruct the duodenum. Occasionally there is direct invasion of the lumbar spine. Bony metastases are commonly lytic.

*Barium studies. Hypotonic duodenography.* Positive findings are present in over half of patients. Signs of malignant invasion are commonly seen in the posterior wall of the stomach (Fig. 27.20) and duodenum but have been reported in the esophagus and colon. Large masses result in widening of the retrogastric space.

Duodenal abnormalities described include a widened loop, a fixed loop, anterior displacement of the loop, spiculated mucosal folds medially, nodular filling defects, double contour to the wall due to tumor, inverted 3 sign of Frostberg, and a dilated gallbladder indenting the cap.

*Ultrasound.* Positive findings have been reported in 80–90% of cases. Lesions in the tail of the pancreas are particularly difficult to demonstrate because of overlying gas, and are frequently missed. This area is better demonstrated at CT. The recent development of endoscopic ultrasound using a 10 MHz probe and scanning through the posterior wall of the stomach and in the region of the DJ flexure allows the identification of very small tumors.

Ultrasound findings of pancreatic tumors include:

1. Focal bulge to pancreas outline
2. Low or mixed echogenicity mass
3. Distal chronic pancreatitis
4. Dilated CBD



**Fig. 27.21.** CT scan. Carcinoma of the head of the pancreas. Grossly dilated CBD (arrows).

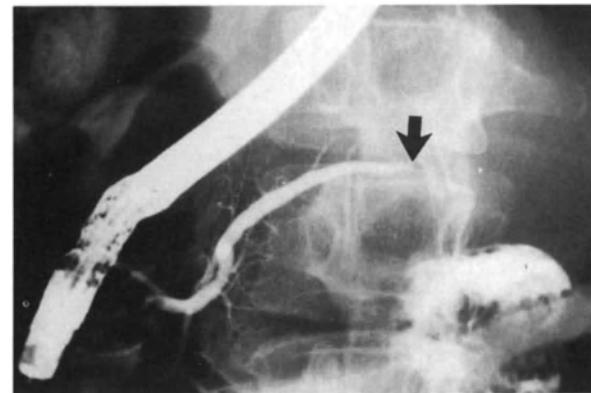


**Fig. 27.22.** ERCP. Carcinoma of the body of the pancreas occluding the pancreatic duct (arrow).

5. Dilated pancreatic duct distally
6. Signs of spread – hypoechoic liver metastases, portal and peripancreatic nodes, loss of definition of adjacent tissues, and occlusion of the splenic vein

CT. The pick-up rate for tumors is slightly superior to ultrasound. Intravenous contrast helps to delineate the mass and assess invasion of the major vessels and peripancreatic tissues.

CT findings of pancreatic tumors include:

1. An irregular mass
2. An abnormal pancreatic contour
3. A mixed-density mass (usually less dense than pancreas); with occasional cystic areas
4. Non-enhancement
5. Dilated pancreatic duct and CBD (Fig. 27.21)
6. Atrophy of the distal gland beyond the tumor
7. Signs of spread – liver metastases, peripancreatic nodes, ascites, thickened Gerota's fascia, displaced stomach, duodenal loop, streaky shadows in the peripancreatic fat, loss of tissue planes of the aorta and IVC
8. Vessel occlusion or encasement – splenic vein, portal vein, celiac axis and superior mesenteric artery
9. Varices, splenomegaly

ERCP. Tumors are demonstrated in 95% of cases although small and very peripheral tumors may be missed. ERCP has the additional advantages of endoscopic stent insertion into the common bile duct to relieve jaundice, and endoscopic assessment of the upper gastrointestinal tract for invasion and varices. Classically malignant duct occlusion is described as being 'rat's tail' or 'cut off'. However appearances are extremely variable.

ERCP findings include:

1. Occluded or narrowed pancreatic duct with distal dilatation (Fig. 27.22)
2. Occluded or narrowed CBD (Fig. 27.23)
3. Necrotic cavity containing contrast – the 'scrambled egg' appearance

4. Side branches, displaced or non-filling
5. Normal

*Fine needle biopsy* may be performed under CT or ultrasound control to confirm the diagnosis (Fig. 27.24).

Occasionally differentiation of carcinoma from pancreatitis may be difficult. Features which favor pancreatitis are:

1. Normal CBD
2. A patent pancreatic duct within the mass
3. Pancreatic calcification
4. No evidence of retroperitoneal invasion at CT
5. Abnormal side branches

*Angiography.* Predominantly angiography is performed to assess resectability of a pancreatic carcinoma prior to



**Fig. 27.23.** Percutaneous transhepatic cholangiogram. Grossly dilated CBD and intrahepatic ducts. Carcinoma head of the pancreas.

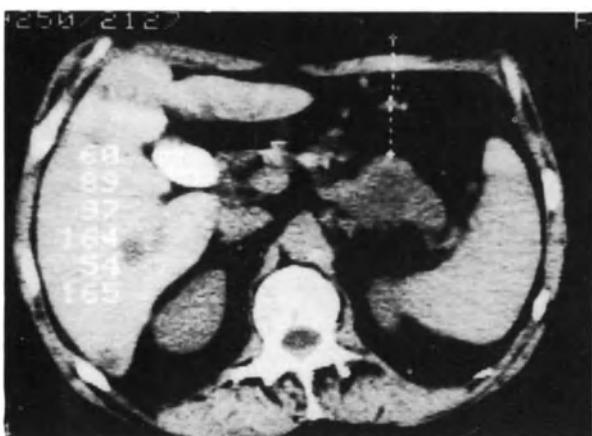


Fig. 27.24. CT guided needle biopsy of small adenocarcinoma in the tail of the pancreas. Low density liver metastases. (Courtesy of Dr D. Sutton.)

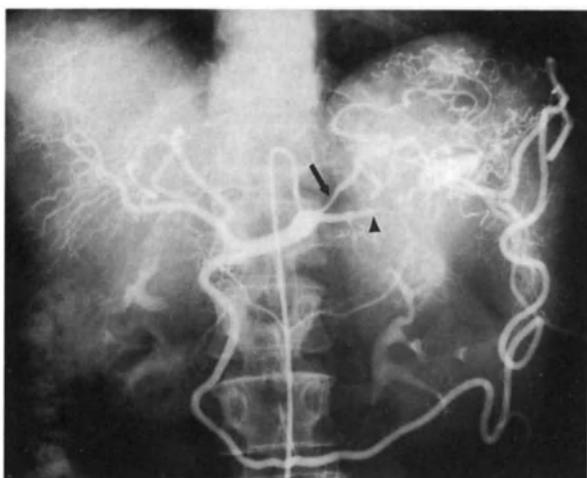


Fig. 27.25. Celiac angiogram. Inoperable carcinoma of the body of the pancreas with occlusion of the splenic artery (arrowhead). The left gastric artery is encased by tumor (arrow).

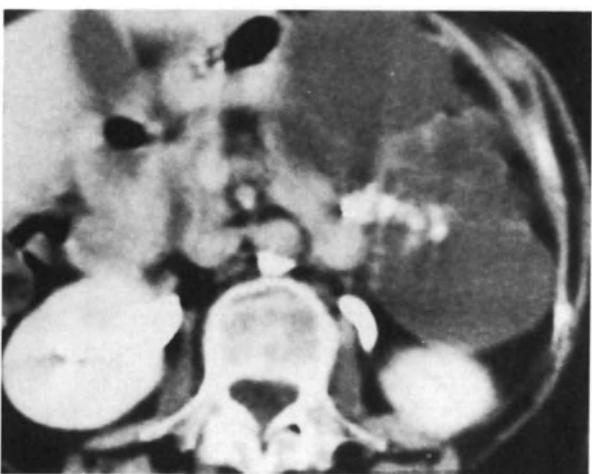


Fig. 27.26. CT scan enhanced. Calcification in mucinous cystadenoma arising in the tail of the pancreas.

surgery, though CT with contrast enhancement is considered to be equally accurate. Selective celiac and superior mesenteric angiography with delayed films to show venous filling are obtained. Encasement or occlusion of major vessels implies non-resectability (Fig. 27.25). The tumors are relatively non-vascular.

*Cystic neoplasms (serous cystadenoma, mucinous cystadenoma).* The mucinous cystadenoma is frequently malignant. Predominantly it arises in the body and tail of the pancreas so that jaundice is rarely a presenting feature. Dystrophic calcification is common. Characteristically these tumors are highly vascular at angiography and enhance well with contrast at CT. They are often large tumors consisting of cystic and solid elements with a thick wall. Septa may be present. These features are well demonstrated on ultrasound and CT (Fig. 27.26).

The microcystic adenoma is benign, consisting of small cysts which are not always apparent at CT and ultrasound. Calcification is present in 35%, and increased vascularity is characteristic. These tumors are often large at presentation.

#### PANCREATICOBLASTOMA

This is a large tumor occurring in very young children and fortunately very rare. Cystic degeneration and necrosis are common.

#### AMPULLARY CARCINOMA

Ampullary carcinoma has a relatively good prognosis particularly if the tumor is small (less than 2 cm) and amenable to surgery. Obstruction of the pancreatic and common bile ducts results in jaundice, which may be intermittent, pancreatitis and pain. The diagnosis is usually made at endoscopy. The tumor is rarely seen at CT or ultrasound unless very large. Quite small tumors can be shown at duodenography (Fig. 27.27); occasionally barium enters the ampulla.

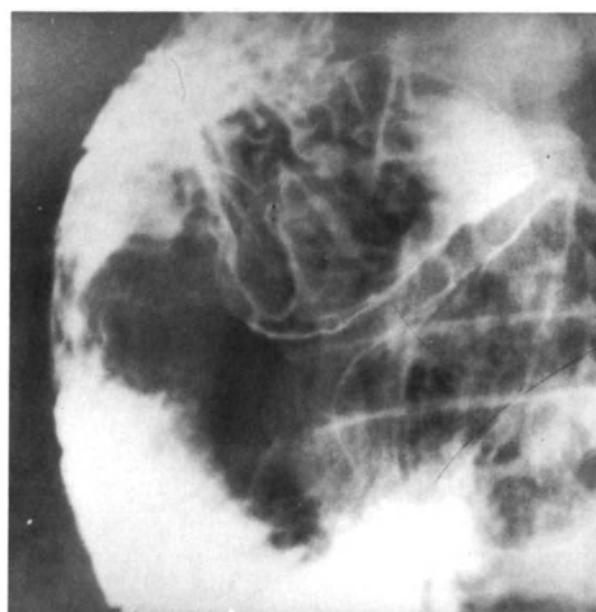


Fig. 27.27. Barium meal. Ampullary carcinoma. ►

**Table 27.8.** Islet cell tumors

Cell	Hormone	Clinical syndrome	Malignancy (%)
Alpha	Glucagon	Diabetes mellitus Skin rashes Anemia	50
Beta	Insulin	Hypoglycemia Obesity	10
Non-beta	Gastrin	Zollinger-Ellison syndrome	60
Delta	Somatostatin	Variable: diabetes mellitus, achlorhydria, steatorrhea	60
Delta-VIP	Vasoactive intestinal polypeptide	Watery diarrhea Hypokalemia, achlorhydria Large gallbladder (WDHA or Verner-Morrison syndrome)	60
PP	Pancreatic polypeptide		

There is an increased incidence of ampullary carcinoma in Gardner's syndrome.

### ISLET CELL TUMORS

The endocrine cells form only 4% of the pancreatic mass. Islet cell tumors are listed in Table 27.8. They are often termed APUDomas after the system introduced by Pearse, who emphasized their cell origin from neuroectoderm and their shared features of amine metabolism (Amine Precursor Uptake and Decarboxylation).

Islet cell tumors may be a single adenoma, multiple adenomas, microadenomas or adenocarcinoma or there may be islet cell hyperplasia. They occur anywhere in the pancreas although insulinomas tend to arise in the head of the pancreas. Hormones are actively secreted by 80% of tumors and metastases are usually active as well; 10% of insulinomas and 20% of gastrinomas are multiple. The tumors tend to be very small (less than 2 cm) so that ultrasound is rarely helpful. However *intraoperative ultrasound* will show masses of 5 mm or even smaller. Large masses are usually malignant and the presence of coarse calcification is highly suggestive of malignancy. Insulinomas and their metastases tend to be very vascular producing a characteristic blush on *angiography* and enhancing with contrast on *dynamic CT scanning*. Other islet cell tumors are less vascular so that percutaneous transhepatic venous sampling is necessary to locate the tumors. Therapeutic embolization is helpful in treating endocrine active hepatic metastases.

Multiple peptic ulcers and diarrhea are the characteristic findings of the Zollinger-Ellison syndrome, although 60% of patients have only a single duodenal ulcer. Ulceration in the jejunum and third part of the duodenum is pathognomonic.

The folds of the duodenum, stomach and proximal jejunum are thickened with duodenal and jejunal dilatation and increased gastric resting juice.

Around one quarter of patients with islet cell tumors have multiple endocrine neoplasia (MEN) Type 1 or Werner's syndrome. These tumors are usually gastrinomas and extrapancreatic.

### REFERENCES AND SUGGESTIONS FOR FURTHER READING

- Freeny PC (ed) (1989) Radiology of the pancreas. Radiol Clin North Am 27: 1
- Freeny PC, Lawson TL (1982) Radiology of the Pancreas. Springer-Verlag, New York
- Frieson SR (1982) Tumours of the endocrine pancreas. N Engl J Med 306: 580-590
- Galiber AK, Reading CC et al. (1988) Localisation of pancreatic insulinoma: comparison of pre- and intra-operative ultrasound with CT and angiography. Radiology 166: 405-408
- Gilinsky NH, Leung JWC, Heron C, Cotton PB (1984) Calcific pancreatitis: calcification patterns and pancreatogram correlations. Clin Radiol 35: 401-404
- Hill MC, Barkin J, Isikoff MB et al. (1982) Acute pancreatitis: clinic versus CT findings. AJR 139: 263-269
- Jones SN, Lees WR, Frost RA (1988) Diagnosis and grading of chronic pancreatitis by morphological criteria derived by ultrasound and pancreatography. Clin Radiol 39: 43-48
- Millward SF, Breathnach E, Simpkins KC, Mahon MJ (1983) Do plain films of the chest and abdomen have a role in the diagnosis of acute pancreatitis? Clin Radiol 34: 133-137
- Ring EJ, Boyd-Eaton S, Ferrucci JT, Welland F, Short MD (1973) Differential diagnosis of pancreatic calcification. AJR 17: 446-452
- Sarner M, Cotton PB (1984) Classification of pancreatitis. Gut 25: 756-759
- Siegelman SS, Copeland BE, Saba GP et al. (1980) CT of fluid collections associated with pancreatitis. AJR 134: 1121-1132
- Wolfman NT, Ramquist NA, Karstaedt N et al. (1982) Cystic neoplasms of the pancreas: CT and sonography. AJR 138: 37-41

## CHAPTER 28

# THE ADRENAL GLANDS

Janet Murfitt

The adrenal glands consist of an outer cortex and inner medulla. Each gland weighs in the region of 3–6 g of which the medulla constitutes 10%. Average size is 3–5 cm long, 2–3 cm wide by 0.5 cm thick.

Developmentally and histologically the cortex and medulla differ. The cortex is of mesodermal origin arising from the urogenital ridge. The medulla is derived from the neuroectoderm. Both cortex and medulla secrete hormones as listed in Table 28.1.

Table 28.1. Adrenal hormones

Zone	Hormone secretions
Cortex	
Zona glomerulosa	Mineralocorticoids aldosterone
Zona fasciculata	Glucocorticoids cortisol
Zona reticularis	Androgens testosterone dehydroepiandrosterone androsterone estrogen
Medulla	Catecholamines adrenaline noradrenaline

The catecholamines secreted are adrenaline and noradrenaline in the ratio of 4:1. The cortical sex hormones make no significant contribution to normal sex hormone activity but do have a role in protein synthesis. Only small amounts of estrogen are produced by the adrenals.

**Anatomy.** The right adrenal is usually triangular in shape, lying adjacent to the upper pole of the kidney behind the IVC and between the liver and the right crus of the diaphragm.

The left adrenal is semilunar in shape. It lies anteromedial to the upper pole of the kidney, with the tail of the pancreas and splenic vessels anteriorly, the esophago-gastric junction

cephalad, the crus of the diaphragm and the spleen superolaterally.

**Vascular Anatomy.** The arterial supply is variable. Commonly there are three arteries which divide prior to entering the gland (Fig. 28.1).

1. The superior adrenal artery arising from the inferior phrenic artery.

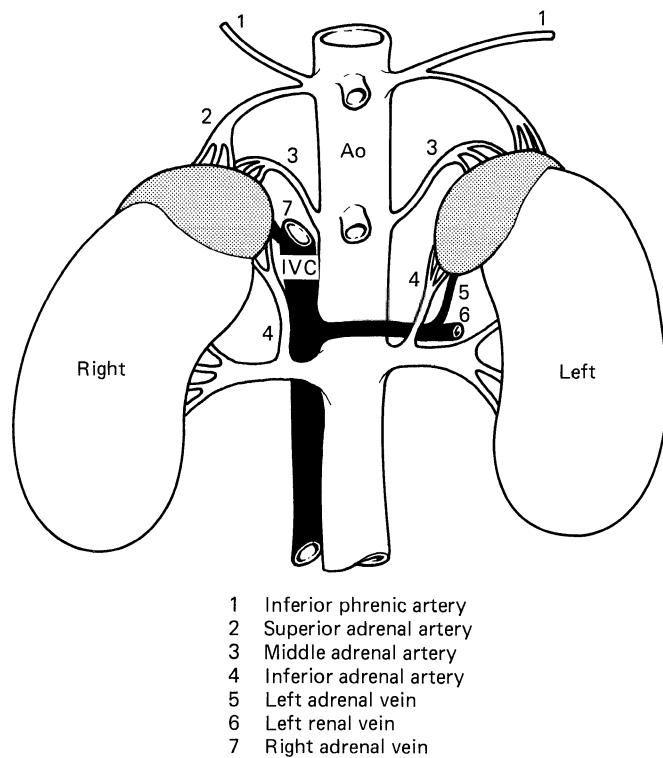


Fig. 28.1. Adrenal arterial supply and venous drainage.

2. The middle adrenal artery arising directly from the aorta.
3. The inferior adrenal artery arising from the renal artery.

Venous drainage normally occurs through single veins. The right adrenal vein is short, entering the IVC post-erolaterally above the upper pole of the kidney. Occasionally it drains into an hepatic vein. On the left side the vein enters the renal vein just lateral to the vertebrae, passing medial to the upper pole of the kidney.

### IMAGING OF THE ADRENAL

All the following methods are or have been used in the investigation of the adrenals.

1. Plain films and tomography
2. Ultrasound
3. CT
4. Radionuclide imaging
5. Arteriography
6. Phlebography
7. Venous and arterial sampling
8. Needle biopsy
9. MRI
10. IVU with nephrotomography
11. Therapeutic adrenal ablation
12. Retroperitoneal pneumography (obsolete)

CT is now considered the first-line investigation of the adrenal glands if available, although ultrasound is preferred in children and neonates.

#### Plain Films and Tomography

Occasionally a large *soft tissue mass* may be identified with associated downward displacement of the kidney. However, appearances are rarely diagnostic and differentiation from renal, splenic, pancreatic, gastric and retroperitoneal tumors requires further investigation.

*Calcification* may be demonstrated (Fig. 28.2), and the causes are listed in Table 28.2.

*Wolman's disease*, or familial cholesterosis, is a rare lipoid storage disease which presents in the first few months of life



Fig. 28.2. Bilateral adrenal calcification. Asymptomatic young woman.

Table 28.2. Causes of adrenal calcifications

Idiopathic	
Neonatal	infarction, hemorrhage, infection in infancy, maternal infection and maternal diabetes mellitus
Tuberculosis, histoplasmosis	
Cyst	
Tumor	<ul style="list-style-type: none"> <li>neuroblastoma 30%–50%</li> <li>pheochromocytoma</li> <li>carcinoma 33%</li> <li>adenoma</li> <li>dermoid</li> </ul>
Addison's disease	
Wolman's disease	

with hepatosplenomegaly, diarrhea, vomiting and failure to thrive. The adrenals are enlarged and often heavily calcified.

In Cushing's disease *abnormalities of the skeleton* may be present and include an increased incidence of fractures with abundant callus formation, a diffuse osteoporosis, avascular necrosis and retarded skeletal development in children.

#### Ultrasound

Visualization of the normal adrenal by ultrasound in the adult is difficult, although an accuracy of 70% has been described in diagnosing adrenal masses using ultrasound by experienced operators. The right gland is more easily seen. Ultrasound is considered to be the investigation of choice in the neonate and young children when the relatively small amounts of retroperitoneal fat make CT a less satisfactory technique. Lesions as small as 12 mm may be detected. Ultrasound, however, is more likely than CT to produce a false positive result.

The adult adrenal gland is slightly more echogenic than the kidney. The neonatal adrenal gland is relatively large and the medulla appears as a thin echogenic line surrounded by a thicker less echogenic cortex. When a neonatal adrenal mass is identified the two most likely causes are *neuroblastoma* and *adrenal hemorrhage*.

The left adrenal lies in a triangle formed by the spleen, left crus of the diaphragm and the upper pole of the kidney. A left adrenal mass must be distinguished from normal splenic vessels, splenic lobulation, the esophagogastric junction and masses arising from the kidney, spleen and pancreas.

A mass within the right adrenal must be differentiated from retrocaval lymphadenopathy, the right crus of the diaphragm and masses arising from the liver and kidney.

#### Computed Tomography

With 5 mm contiguous slices the adrenals are identified in nearly all patients at CT. CT has a reported accuracy of more than 90% in the diagnosis of adrenal masses. Tumors of less than 1 cm are often demonstrated and ectopic adrenal lesions may be identified. On routine abdominal scanning up to 1% of patients will have a non-functioning adrenal mass such as a metastasis, cyst, adenoma, myelolipoma or carcinoma. Characteristic appearances are seen at CT with adrenal cysts, which are of fluid density, and *myelolipomas*, which are of fatty density.

The normal adrenal glands have a variable appearance at CT. Usually the right gland is linear or V-shaped, its body lying anteriorly and the medial and lateral limbs posteriorly. The medial limb is more caudal and is larger, measuring up to 4 cm in length.

The left adrenal gland is V-shaped, triangular or has a Y-configuration with its apex anteromedial and its limbs posteriorly. The lateral limb is longer than the medial.

Absolute criteria for enlargement of the adrenals at CT do not exist. Convexity of the adrenal outline is significant and should be considered abnormal. Comparison of the medial limb of the right adrenal gland with the right crus of the diaphragm is helpful; a normal gland should not be thicker than the crus. Hyperplasia cannot be detected by CT in 50% of cases.

On occasions adjacent structures such as the splenic vessels are misinterpreted as an adrenal mass. Therefore, contrast studies should be undertaken when necessary.

### Radiionuclide Imaging

$^{131}\text{I-MIBG}$  (*-metaiodobenzyl guanide*) and  $^{123}\text{I-MIBG}$ . This isotope concentrates in the adrenergic neurotransmitter vesicles and is used for demonstrating *pheochromocytomas*. It has a high sensitivity for primary and secondary tumors, although false positive and negative scans occur. Certain drugs must be discontinued prior to scanning including reserpine, cimetidine, and tricyclic antidepressants. Scanning takes place over a three-day period after blocking thyroid uptake with potassium iodide. The bladder should be empty so that a pelvic lesion is not obscured.

Other tumors such as neuroblastoma, paraganglioma, carcinoid and thyroid medullary carcinoma may concentrate MIBG. High activity labeled MIBG is used therapeutically for malignant and disseminated tumors.

$^{75}\text{Selenium-6-selenomethyl cholesterol}$  and  $^{131}\text{I-6-Iodomethyl-19 norcholesterol}$  (NP-59). Increased bilateral uptake indicates *hyperplasia*. In addition there is increased uptake by an *adenoma*, although accuracy is below 50% for Conn's tumors. Using dexamethasone suppression of the normal adrenal tissue to reduce its uptake of the isotope, results in relatively enhanced uptake by the adenoma and increased accuracy. However, the degree of accuracy achieved with isotope scanning is lower than with CT.

Masses such as carcinoma, cysts, metastases and pheochromocytomas do not take up the isotope and appear as cold areas.

### Arteriography

Arteriography was used predominantly for demonstrating a pheochromocytoma when CT has failed. Alpha and Beta blockade prior to this investigation is mandatory, and the patient should be carefully monitored throughout the procedure by his physician. Initially flush aortography is performed, followed by selective injections if necessary although selective adrenal arteriography is technically difficult.

### Phlebography

Phlebography is technically difficult, particularly on the right side, although there is a 90% success rate in experienced hands. The adrenals should not be over-filled and

unintentional infarction occurs in 2%–4% of cases. A maximum of 5 ml of contrast is used on the left side and 2 ml on the right side.

Phlebography is highly accurate for demonstrating small avascular tumors, particularly in Conn's syndrome, but has now been superseded by CT.

Occasionally *therapeutic ablation* by phlebography is performed in cases of malignancy or endstage Cushing's syndrome.

### Venous and Arterial Sampling

In suspected cases of ectopic pheochromocytoma, venous samples are taken from the SVC, innominate and internal jugular veins, right atrium, the high and low IVC, renal veins and iliac veins. In addition arterial samples are taken. This method may help to localize an area for imaging by CT or MRI.

Adrenal vein samples are taken, if necessary, to help in the differentiation of bilateral hyperplasia from an adenoma causing Conn's syndrome. Hyperplasia is associated with abnormal levels on both sides, whereas an adenoma results in ipsilateral hormone elevation.

### Fine Needle Biopsy

This is performed under ultrasound or CT control. Biopsy is often necessary when a non-functioning adrenal mass is picked up on routine scanning. If the mass has a diameter in excess of 3 cm, biopsy should be undertaken to exclude malignancy, the incidence of which increases with the size of the tumor.

### Magnetic Resonance Imaging

As with CT, the presence of retroperitoneal fat is crucial to the demonstration of the normal adrenal glands. The normal adrenals are best seen on T<sub>1</sub>-weighted sequences (Fig. 28.3) where exceptionally cortex may be differentiated from medulla. T<sub>2</sub>-weighted sequences are less satisfactory. *Adrenal hyperplasia* is recognized by enlargement with normal configuration and signal intensity.

*Adenomas* are often incidental findings and typically have T<sub>1</sub> and T<sub>2</sub> relaxation times similar to normal adrenal tissue. *Carcinomas* usually have a more varied appearance dependent on tumor size, vascularity and the presence or absence of hemorrhage and/or necrosis. Calcification occasionally

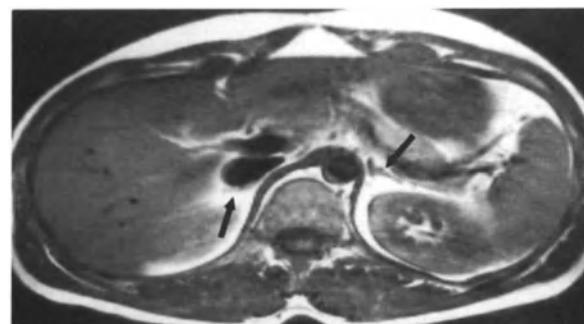


Fig. 28.3. MRI. T<sub>1</sub>-weighted image. 1.5 Tesla. Normal adrenal glands (arrows). Courtesy of Dr G. Cherryman CRC Radiology Research Group, Royal Marsden Hospital, Sutton, UK.



**Fig. 28.4.** IVU with nephrotomography. Large right adrenal mass (arrows).

differentiated from carcinomas and benign and malignant lesions may appear similar.

#### IVU and Nephrotomography

These procedures are rarely performed when CT is available. Routine intravenous urography is of little value although occasionally renal displacement is demonstrated with a large adrenal mass such as a neuroblastoma.

Nephrotomography with contrast infusion is considerably more helpful and at least 50% of adrenal masses may be demonstrated or implied by displacement of the kidney or separation of the spleen and left kidney (Fig. 28.4).

### ADRENAL SYNDROMES

Several clinical syndromes result from adrenal disease or dysfunction. These together with the underlying adrenal pathology are listed in Table 28.3.

**Table 28.3.** Adrenal syndromes

Syndrome	Aetiology
Acute adrenal insufficiency	Adrenal Addison's congenital adrenal virilizing syndrome post-adrenalectomy trauma, hemorrhage
Chronic adrenal insufficiency (Addison's syndrome)	Hypopituitarism Atrophy 60%–70% autoimmune disease with associated thyroiditis, hypoparathyroidism, pernicious anemia Tb 30%–35% Others 8%–10% metastases amyloid leukemia hemochromatosis adrenalectomy ACTH deficiency prolonged cortisol treatment blastomycosis infarction histoplasmosis
Adrenal cortical hyperfunction (Cushing's syndrome)	Hyperplasia 70%–75% pituitary dependent Adenoma 10%–20% Carcinoma 5%–10% Micronodular dysplasia (rare)
Primary	Ectopic ACTH 8%–10% oat cell carcinoma pancreatic carcinoma bronchial carcinoid thymoma pheochromocytoma ganglioneuroma
Secondary	Adenoma 60%–90% Bilateral micronodular hyperplasia 20%–40% Carcinoma (rare)
Primary aldosteronism (Conn's syndrome)	Cortical hyperplasia Adenoma Carcinoma
Adrenogenital syndromes	

**Table 28.4.** Adrenal masses

Neoplasms	
Cortex	Carcinoma Adenoma
Medulla	Pheochromocytoma Ganglioneuroma Ganglioneuroblastoma Neuroblastoma
Stromal	Metastases Sarcoma Lipoma Fibroma Myelolipoma Neurofibroma Hemangioma Melanoma
Other	Granuloma Tuberculosis Histoplasmosis Blastomycosis Hyperplasia Cysts Pseudocyst 39% Endothelial 45% Infective Epithelial Hematoma

### ADRENAL MASSES

Adrenal masses (Table 28.4) are often asymptomatic, small and non-functioning. However adrenal tumors may present with a wide variety of syndromes and symptoms. Frequently unsuspected adrenal masses are shown on routine CT scanning of the abdomen. A mass which exceeds 3–4 cm is more likely to be malignant than a smaller mass and should be biopsied. Smaller masses can be followed up by CT every three months or so if there is no evidence biochemically of a functioning mass. Those lesions which are typically cysts or myelolipomata at CT need not be biopsied even if large but should be followed up.

#### ADRENAL CARCINOMA

In up to 50% of cases there is an associated endocrinopathy including Cushing's disease, Conn's syndrome and the



**Fig. 28.6.** Ultrasound scan. Right adrenal carcinoma (arrows). Same patient as Fig. 28.5. K=kidney.

adrenogenital syndrome. However a carcinoma is a relatively uncommon adrenal tumor. Usually the mass is large and 10% are bilateral.

Irregular *calcification* seen on the *plain film* is present in one third of cases. *CT* is the investigation of choice. Typical appearances are of a large irregular mass with central low-density areas of necrosis and hemorrhage (Fig. 28.5). There is irregular enhancement with a thin peripheral rim of enhancement after intravenous contrast. Local invasion and liver metastases can be assessed.

At *ultrasound* there is a mass of mixed echogenicity (Fig. 28.6). Usually the mass is highly vascular at *angiography*.

#### ADENOMA

The vast majority of adenomas are non-functioning. There is a reported incidence of 5% at post mortem. Functioning adenomas may be associated with Cushing's syndrome, hyperaldosteronism or virilizing syndromes. A very small number, 1 or 2%, are bilateral.

At *CT* there is a well-defined oval or round mass with a smooth outline and usually measuring less than 5 cm (Fig. 28.7). Calcification is occasionally present. Density measurements range from –15 HU to +60 HU. Central low-density

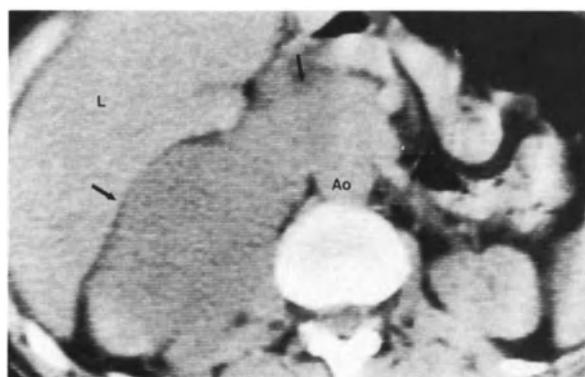


**Fig. 28.5.** CT scan. Large carcinoma of the right adrenal (arrows) invading adjacent structures. L=liver, Ao=aorta.

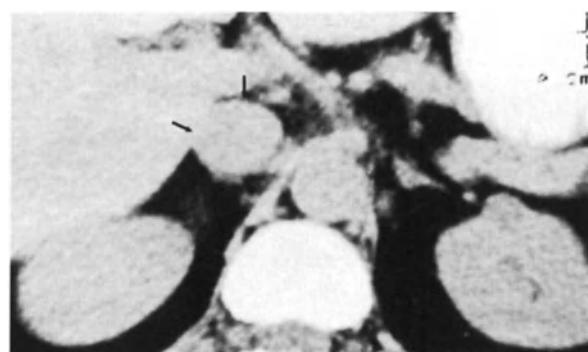


**Fig. 28.7.** CT scan. Adenoma right adrenal (arrows).

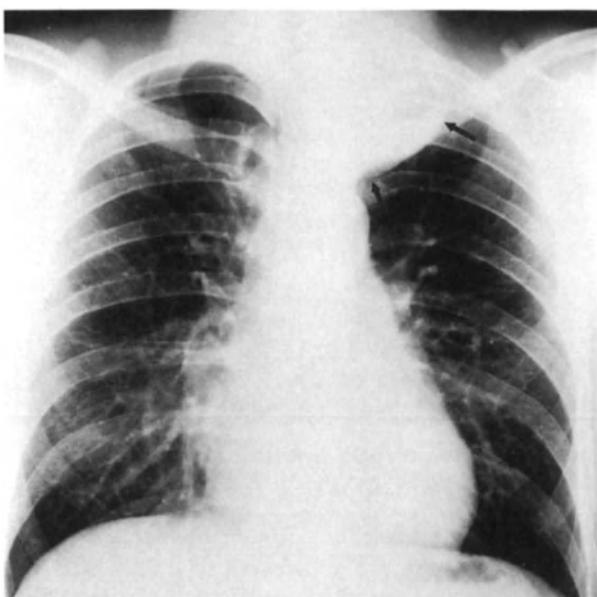


Fig. 28.8. Pheochromocytoma in anterior mediastinum (arrows). Young male student. Hypertension noted when admitted to hospital following a road traffic accident.

areas of fat are seen with Conn's syndrome. Contrast enhancement is more pronounced in Cushing's syndrome.

#### PHEOCHROMOCYTOMA

A pheochromocytoma arises from the adrenal medulla and secretes adrenaline or noradrenaline. Presenting clinical features include sustained or paroxysmal hypertension, anxiety attacks, tremor, palpitation and sweating. Urinary catecholamines are elevated.

10% of tumors are extraadrenal arising from the sympathetic chain. Most are para-aortic or paracaval but

they have been reported to occur in many sites including the bladder wall and thorax (Fig. 28.8). Occasionally ectopic tumors compress the renal artery. 10% of these tumors are malignant and 10% are multiple. In children 30% of these tumors are extraadrenal and 30% are multiple and the rate of malignancy is reported to be as high as 50%. There is an increased incidence of pheochromocytoma in von Hippel-Lindau disease and tuberous sclerosis and 5% of patients have neurofibromatosis.

Metastases occur in the lymph nodes, bones, liver and lungs.

In *Multiple Endocrine Neoplasia (MEN) Type 2* or Sipple's syndrome a pheochromocytoma is present in 50% of cases and is associated with medullary carcinoma of the thyroid and mild hyperparathyroidism due to parathyroid adenomas. The pheochromocytomas are often bilateral and small with atypical presenting symptoms. Inheritance is autosomal dominant for all the three types of MEN.

Pheochromocytomas may also occur in *MEN Type 3*. These patients have multiple mucosal neuromas of the face and a Marfanoid habitus. Occasionally parathyroid adenomas and medullary carcinoma of the thyroid develop.

*MEN Type 1* or *Werner's syndrome* is the commonest form of MEN. Pheochromocytomas do not occur. There is hyperplasia of the parathyroids, islet cells, pituitary or thyroid. Two thirds of patients have two endocrine glands affected, the most common being the parathyroids. Presentation is usually with features of hypercalcemia.

**Imaging.** A pheochromocytoma is rarely large enough to be seen on a plain film. Calcification is very uncommon.

At ultrasound the smaller tumors have an homogenous echo pattern. Large tumors are often complex masses with cystic areas of necrosis and hemorrhage.

CT demonstrates a well-defined mass (Fig. 28.9). In rare cases there is punctate or rim calcification. There are multiple low-density areas within the tumors. Contrast enhancement is marked (Fig. 28.10) but should only be undertaken after alpha and beta blockade. If the adrenals

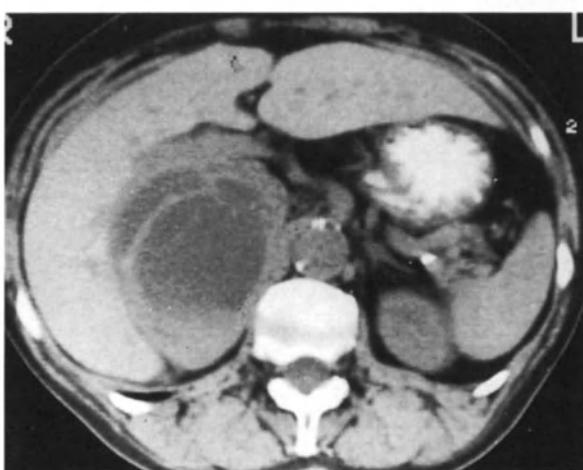


Fig. 28.9. CT scan unenhanced. Large right pheochromocytoma with cystic areas. The mass is displacing liver.

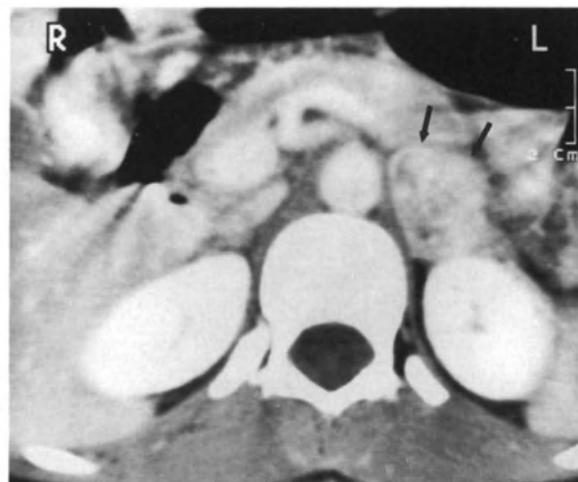
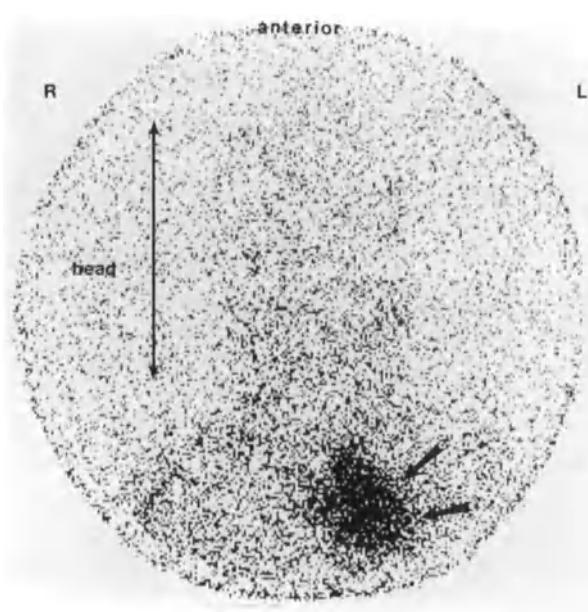


Fig. 28.10. CT scan contrast enhanced. Small enhancing left adrenal pheochromocytoma (arrows), lying anterior to upper pole of left kidney.



**Fig. 28.11.**  $^{131}\text{I}$ -MIBG scan head and neck. Ectopic pheochromocytoma in left anterior mediastinum (arrows). Same patient as Fig. 28.8.

are normal further scans should be obtained of the abdomen, pelvis and chest.

**Radionuclide imaging** using  $^{131}\text{I}$ -MIBG is particularly useful for identifying the extra-adrenal tumors (Fig. 28.11) and metastases. Accuracy is high although false positive and negative results do occur.

**Angiography** (Fig. 28.12) was performed with alpha and beta blockade but is now replaced by CT. Tumors are highly vascular with a dense capillary blush in 80% of cases and are often shown with flush aortography. In those cases when the tumor is avascular, adrenal phlebography may be more helpful.

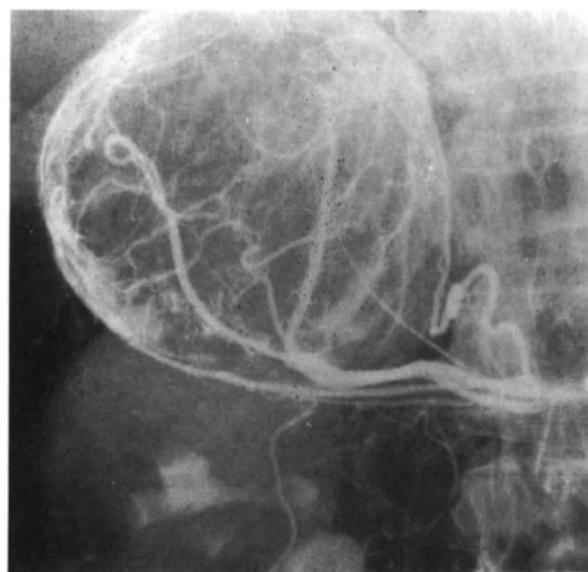


**Fig. 28.12.** Right suprarenal arteriogram. Highly vascular adrenal pheochromocytoma. Selective injection of right inferior adrenal artery.

If other imaging techniques fail *venous sampling* is performed taking samples at multiple sites include the internal jugular and innominate veins, SVC, right atrium, both renal veins and iliac veins and high and low IVC with concomitant arterial samples.

At *MRI* a pheochromocytoma is hyperintense on  $T_2$ -weighted images and of lower intensity on  $T_1$ -weighted images.

*Fine needle biopsy* may cause bleeding or precipitate a hypertensive crisis in a small number of cases.

### NEUROBLASTOMA

These highly malignant tumors occur predominantly in young children. One third of cases occur in the first year of life and only 10% arise in children over 8 years. A neuroblastoma is the commonest solid childhood tumor. At presentation two thirds of patients have distant spread, usually to the bones but also the liver, orbits and subcutaneously.

50% of tumors arise in the adrenal. The remainder may occur anywhere within the sympathetic chain including the chest and abdomen.

**Imaging.** The tumors are often large and a calcified mass is frequently identified on the *plain film*. Punctate calcification is seen in 40%–50% of cases. Typically the ipsilateral kidney is displaced inferiorly and the upper pole rotated medially with extrinsic calyceal distortion.

At *ultrasound* appearances are variable. Often a neuroblastoma is echogenic with cystic areas of necrosis and hemorrhage; a similar appearance is seen with adrenal hemorrhage in the neonate. Local invasion, liver metastases and spread to para-aortic nodes may be present.

Calcification is present in 80% of tumors at *CT*. It has a punctate, globular or edge pattern. The tumor is of variable density with areas of necrosis and hemorrhage. Contrast enhancement is usual and is often peripheral. Tumor encasement of splanchnic vessels is a common finding and is helpful in differentiating a neuroblastoma from a Wilms' tumor.

At *MRI* the tumor is hyperintense on  $T_2$ -weighted images. Calcification is not well demonstrated.

**Radionuclide imaging.** Both the primary tumor and metastases take up  $^{131}\text{I}$ -MIBG.

### GANGLIONEUROMA

These neurogenic tumors are more benign than neuroblastomas and 60% occur in children. Only 10% arise in the adrenal and these may involve the spinal canal and present with associated cord compression. Calcification is frequently present.

### METASTASES

Involvement of the adrenals by metastases is common and in half of cases both adrenals are affected. Common primary sites are breast, bronchus, melanoma, stomach, kidney,



Fig. 28.13. CT scan enhanced. Right adrenal metastasis (arrow) from esophageal carcinoma. Liver metastases (arrowheads).

colon and pancreas. Usually adrenal metastases are asymptomatic. The majority arise within the adrenal medulla and they are more common on the left side. They may be very large and necrotic. Calcification is unusual.

At *ultrasound* appearances are non-specific. There is no isotope uptake with *radionuclide imaging*. At *CT* metastases are soft tissue density masses which may be necrotic (Fig. 28.13). Some contrast enhancement occurs. MRI also shows

metastases well particularly on *T<sub>2</sub>*-weighted images (Fig. 28.14).

#### MYELOLIPOMA

A myelolipoma is a rare tumor which is usually small and asymptomatic. Occasionally there is pain following bleeding or necrosis.

At *CT* there are characteristic appearances. The high fat content results in a low attenuation mass of -50 to -80 HU. Central necrosis and edge calcification may be present. The tumor is highly echogenic at *ultrasound*.

#### CYSTS

An adrenal cyst may be congenital or infective, usually as a result of hydatid or amebic infection, or a pseudocyst which forms following hemorrhage or infarction into a gland or tumor. Although usually asymptomatic, pain may result from bleeding into a cyst.

Approximately 20% of cysts have a thin rim of calcification on a *plain film*. Occasionally the cyst contains a milky calcium suspension. *CT* appearances are usually characteristic; the cyst is thin walled and of fluid density. A pseudocyst has a thicker wall. Equivocal appearances may be clarified by needle biopsy.

#### NEONATAL ADRENAL HEMORRHAGE

Common causes include birth trauma and coagulation disorders. Neonatal adrenal hemorrhage may be unilateral or bilateral although more commonly right sided. It may be asymptomatic or present with neonatal distress, an abdominal mass, anemia and jaundice.

The other common cause of a large adrenal in the neonate is a neuroblastoma.

In the early stages at *ultrasound* the adrenal is anechoic; later there is a solid or complex mass which becomes cystic and eventually forms a small echogenic area of calcification. If the adrenal capsule ruptures there will be a perirenal hematoma. Initially at *CT* the adrenals are enlarged and of high density (50 HU to 75 HU) with streaky shadowing in the periadrenal fat. Calcification may develop. Later the gland becomes smaller and less dense. Occasionally calcification is seen in the newborn indicating that the hemorrhage occurred in utero.

In adults adrenal hemorrhage occurs in association with bleeding diatheses, severe stress and trauma.

#### ADDISON'S SYNDROME

Over 90% of the total adrenal cortex must be destroyed before hypoadrenalinism becomes apparent. Clinical features include muscle weakness, weight loss, pigmentation, hypotension, hypoglycemia, nausea and vomiting. The commonest cause of Addison's syndrome is autoimmune disease, and the next



Fig. 28.14. Coronal MRI scan (T<sub>2</sub>-W) shows bilateral adrenal masses (arrows) due to secondaries from lung carcinoma, which is also well shown with collapse of right upper lobe. (Courtesy of Trustees of Bristol MRI centre).

commonest tuberculosis. In 25% of patients adrenal *calcification* is seen on the *plain film* and frequently it is gross. However bilateral adrenal calcification may occur with normal adrenal function.

At *CT* and *ultrasound* calcification can be identified. Some adrenal enlargement may be evident at *CT*. Cystic changes may be seen at *ultrasound*.

### CUSHING'S SYNDROME

As many as 70% of cases arise as a result of bilateral adrenal hyperplasia secondary to raised ACTH levels from a pituitary lesion such as a basophil adenoma. Ectopic ACTH production accounts for up to 10% of cases and is associated with tumors of the bronchus, parotid, pancreas and thymus, while 30% of patients have an adrenal tumor with an adenoma being twice as common as a carcinoma.

Characteristically these patients have truncal obesity with a buffalo hump and moon face, hirsutism, abdominal striae, psychoses, hypertension, diabetes mellitus, decreased bone density and hypercalciuria.

**Imaging.** *Plain films* may show extensive bony changes. These include osteoporosis, vertebral collapse, rib fractures and avascular necrosis. Occasionally there is mediastinal fat deposition which is seen as mediastinal widening on the plain film.

In most cases *ultrasound* is unhelpful because of the patient's obesity.

*CT* is highly accurate in detecting mass lesions but is less helpful in diagnosing hyperplasia. It has been reported that only 50% of cases of hyperplasia are definitely diagnosed at *CT*, although the pickup rate is increased with contrast enhancement. A large mass (5–10 cm) is more likely to be a carcinoma and calcification is present in one third of cases. In addition Cushing's disease is one of the many causes of fatty liver and this should be looked for at *CT*.

*Radionuclide imaging* is useful for distinguishing adrenal hyperplasia from an adenoma and for detecting residual adrenal tissue after surgery. There is bilateral uptake with hyperplasia but only unilateral uptake in the presence of an adenoma, the contralateral normal gland being suppressed (Fig. 28.15).

Some cases of adrenal hyperplasia are the macronodular form which results in enlarged nodular glands and is associated with pituitary lesions. This may be difficult to differentiate from an adenoma.

Adrenal hyperplasia may be associated with other adrenal disorders, hyperthyroidism and acromegaly.

### CONN'S SYNDROME

In Conn's syndrome there is hyperaldosteronism with resulting hypertension, hypokalemia and low plasma renin levels. The majority of cases are due to an adenoma, hyperplasia is present in 10%–20% and rarely this syndrome results from a carcinoma.

The tumors are usually small, 0.5 to 3 cm (Fig. 28.16), and 20% cannot be identified at *CT* even when using conti-

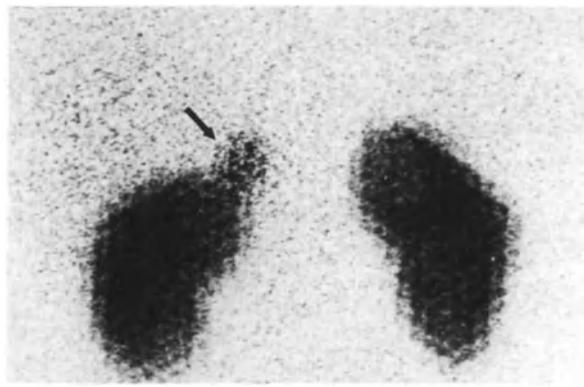


Fig. 28.15.  $^{75}\text{S}$ econo-cholesterol scan. Functioning right adrenal adenoma (arrow). Young female with Cushing's syndrome.

guous 5 mm cuts. The tumors have a high cholesterol content which results in low attenuation (20 HU). Occasionally *ultrasound* demonstrates a small mass of low echogenicity.

*Adrenal phlebography* had an accuracy of 70% in experienced hands, but is now superseded by *CT*. *Adrenal vein sampling* assists in distinguishing adenoma from hyperplasia. Aldosterone levels are elevated bilaterally with hyperplasia but on the abnormal side only in the presence of an adenoma.

*Radionuclide imaging* with  $^{75}\text{S}$ elenium-6-selenomethyl cholesterol has an accuracy of some 80%. The pickup rate is increased using dexamethasone which suppresses normal adrenal tissue.

### ADRENOGENITAL SYNDROME

The majority of cases are due to a congenital enzyme deficiency of autosomal recessive inheritance. A few cases are associated with an adrenal adenoma or carcinoma. Several enzymes may be affected. The enzyme defect results in a lack of cortisol which precipitates increased excretion of ACTH resulting in adrenal hyperplasia and an excess of cortisol precursors including androgen.

There are several possible clinical presentations most of which are seen in the neonate. At birth there is female

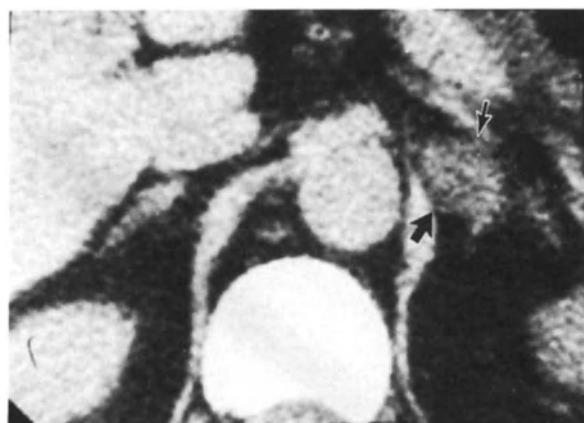


Fig. 28.16. CT scan. Conn's tumor left adrenal (arrows).

masculinization or female pseudohermaphroditism and there may be associated hypertension or acute adrenal insufficiency. In boys precocious sexual development may occur at 2–4 years; the testes remain small.

Acute adrenal insufficiency occurs in nearly one third of affected neonates. There is salt and water depletion with vomiting. Dehydration manifests itself on the chest film as a small heart, thin soft tissues and increased transradiancy of the lungs. Vomiting may produce a gasless abdomen.

Multiple associated abnormalities have been described including congenital hypothyroidism, syndactyly and a webbed neck. Very rarely adrenal feminization develops due to a carcinoma of the cortex.

At CT the adrenals are symmetrically enlarged or nodular. Adrenal density is increased due to a decrease in the adrenal fat content. Thickening may be seen at ultrasound.

#### REFERENCES AND SUGGESTIONS FOR FURTHER READING

- Adams HL, Siegelman SS, Adams DF et al. (1982) Computed tomography versus ultrasound of the adrenal gland: a prospective study. *Radiology* 143: 121–127
- Adams JE, Johnson RJ, Rickards D, Isherwood I (1983) Computed tomography in adrenal disease. *Clin Radiol* 34: 39–49
- Bernardino ME, Walther MM, Phillips VM et al. (1985) CT-guided adrenal biopsy: accuracy, safety and indications. *AJR* 144: 67–69
- Dunnick NR, Heaston D, Halvorsen R, Moore AV, Korobkin M (1982) CT appearance of adrenal cortical carcinoma. *J Comput Assist Tomog* 6: 878–982
- Eghari M, McLoughlin MJ, Rosen IE et al. (1986) The role of computed tomography of the adrenal glands. *J Comput Assist Tomog* 4: 71–77
- Felson B (ed) (1988) The adrenals. *Semin Roentgenol* 23: 4
- Fishman EK, Deutch BM, Hartman DS, Goldman SM, Zerhouni EA, Siegelman SS (1987) Primary adrenocortical carcinoma: CT evaluation with clinical correlation. *AJR* 148: 531–535
- Francis IR, Glazer GM, Shapiro B, Sisson JC, Gross BH (1983) Complementary roles of CT and  $^{131}\text{I}$ -MIBG scintigraphy in diagnosing phaeochromocytoma. *AJR* 141: 719–725
- Geisinger MA, Zelch MG, Bravo EL, Risius BF, O'Donovan PB, Borkowski GP (1983) Primary hyperaldosteronism: comparison of CT, adrenal venography and venous sampling. *AJR* 141: 299–302
- Glazer HS, Weyman PJ, Sagel SS, Levitt RG, McClellan BL (1982) Nonfunctioning adrenal masses: incidental discovery on CT. *AJR* 139: 81–85
- Hattery RR, Sheedy PF, Stephens DH, van Heerden JA (1981) Computed tomography of the adrenal gland. *Semin Roentgenol* 16: 290–300
- Huebener KH, Treugott H (1984) Adrenal cortex dysfunction. CT findings. *Radiology* 150: 195–199
- Hussain S, Belldegrun A, Seltzer SE, Richie JP, Gittes RF, Abrams HL (1985) Differentiation of malignant from benign adrenal masses: predictive indices on CT. *AJR* 144: 61–65
- Older RA, Van Moore A, Glenn JF, Hidalgo HJ (1984) Diagnosis of adrenal disorders. *Radiol Clin North Am* 22: 433–455
- Schultz CL, Haaga JR, Fletcher BD et al. (1984) Magnetic resonance imaging of the adrenal glands: a comparison with computed tomography. *AJR* 143: 1235–1240
- Stark DD, Moss AA, Brasch RC, et al. (1983). Neuroblastoma: diagnostic imaging and staging. *Radiology* 148: 101–105
- Sample WF (1978) Adrenal ultrasonography. *Radiology* 127: 461–466
- Sutton D (1976) Diagnosis of Conn's and other adrenal tumors by left adrenal phlebography. *Lancet* i: 453–455

## CHAPTER 29

# SALIVARY GLANDS, OROPHARYNX AND ESOPHAGUS

D.J. Ott

---

## SALIVARY GLANDS

---

The paired parotid and submandibular glands may be affected by stones, inflammations, neoplasms, and rare autoimmune processes, such as Sjögren's syndrome. This section discusses techniques of examination, emphasizing contrast sialography, normal radiographic anatomy, and the more common pathologic abnormalities of the salivary glands.

Conventional radiographic techniques using *plain films* and *contrast sialography* have been used traditionally for examining the salivary glands (Fig. 29.1). More recently, *computed tomography* and *ultrasound* have been employed, especially for evaluating masses and suspected neoplasms.

### Normal Radiographic Anatomy

The parotid gland is located behind the mandible and consists of a superficial and deep portion (Fig. 29.2). The main parotid duct (Stenson) runs anteriorly to pierce the buccinator muscle opening on a papilla on the buccal mucosa opposite the second upper molar tooth. Accessory ducts

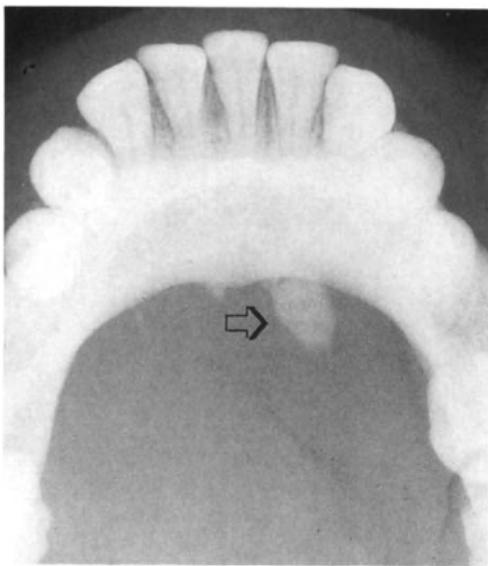


Fig. 29.1. Intraoral view showing opaque stone (arrow) near orifice of left submandibular duct.

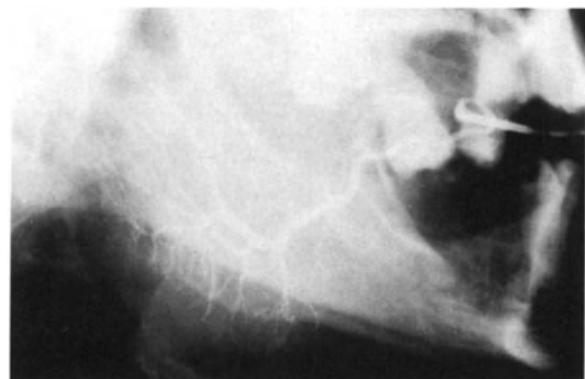
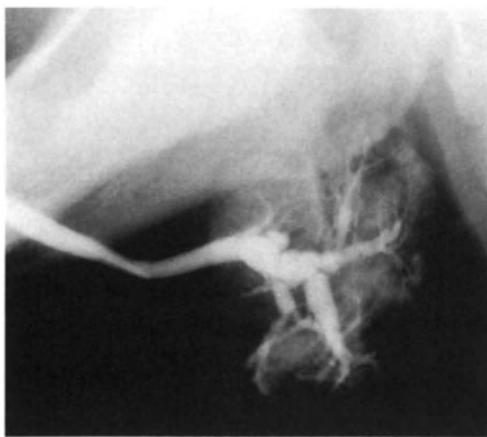


Fig. 29.2. Parotid sialogram; lateral view of normal parotid gland.



**Fig. 29.3.** Lateral view of normal submandibular gland.

anterior to the main body of the parotid gland are commonly seen.

The submandibular gland is smaller than the parotid gland and lies in the submaxillary triangle just below the mandible (Fig. 29.3). The main duct (Wharton) passes forward and medial to open on a papilla lateral to the frenulum at the base of the tongue. The orifice of Wharton's duct is much smaller than that of Stenson's duct making cannulation more difficult.

#### Salivary Gland Disease

Salivary gland diseases may be divided into stones, inflammations and neoplasms. Plain films and contrast sialography are more useful in evaluating for stones and inflammatory processes although the latter is contraindicated in acute inflammation or infection. Focal masses suggesting

neoplasms may be evaluated by sialography, but computed tomography often combined with ductal injection of contrast material is now preferred.

**Stones.** The majority of salivary stones (sialolithiasis) are opaque, stressing the importance of preliminary plain films (Fig. 29.1). Multiple stones occur in 25% of patients. The submandibular gland is most often involved (80%). Stones are usually found in the main salivary duct but may be located anywhere from the orifice to the hilum of the gland. Sialography can identify and localize both opaque and non-opaque stones and also assess for their complications. These include obstruction, sialodochitis, sialoadenitis, ductal stricture or pseudodiverticulum, abscess or atrophy of the gland, and fistula formation.

**Inflammations.** A heterogeneous group of disorders may produce unilateral or bilateral enlargement of the salivary glands. *Sialosis* refers to non-inflammatory swelling of the parotid glands due to a variety of systemic causes, some of which are drug induced. Radiographically, the parotid gland is enlarged and the ductal structures stretched but otherwise normal. Clinical correlation is needed for proper diagnosis.

Several chronic and non-specific inflammatory diseases cause distortion of the main or terminal ductal structures of the salivary gland. *Sialodochitis* is inflammation of larger ducts causing segmental areas of narrowing and dilatation (*sialectasia*) with normal terminal ducts (Fig. 29.4A). Delayed emptying is often present and complications of *abscess* and *fistula* may occur. *Sialoadenitis* is acinar inflammation causing punctate or globular sialectasis of the terminal ducts with the main duct appearing normal (Fig. 29.4B). Delayed emptying is typically present. Sialodochitis and sialoadenitis may occur in the same gland and can be associated with sialolithiasis.

*Autoimmune sialosis* is seen most commonly as part of *Sjögren's syndrome*. Parotid gland enlargement is present in up to half of patients. Sialographic abnormalities are usually

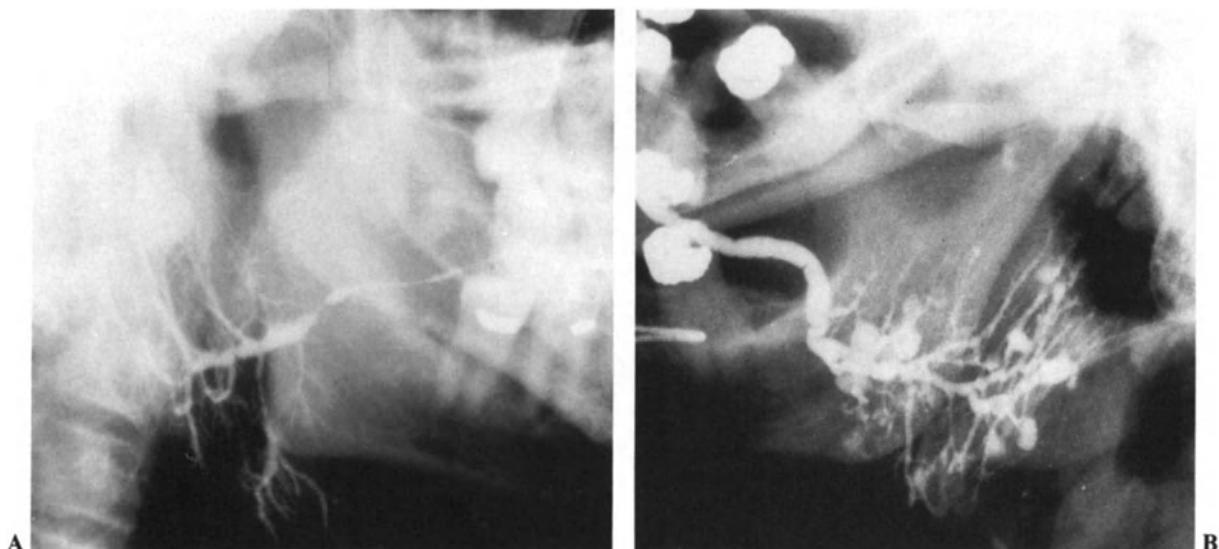


**Fig. 29.4.A** Sialodochitis causing diffuse and segmental narrowing of Stenson's duct and several of its main branches. **B** Sialoadenitis with globular collections arising from smaller salivary ducts.

bilateral and usually consist of spherical collections of contrast material distributed throughout the gland. These punctate collections may subsequently coalesce to form larger cavities. Delayed emptying is typical.

**Neoplasms.** Salivary tumors are uncommon with 80% affecting the parotid gland. The majority are benign and the most common is the *pleomorphic adenoma* or *mixed tumor*. Benign neoplasms are generally encapsulated and appear as a focal parenchymal defect with draping and displacement of the adjacent ducts.

**Malignant neoplasms** have a variety of radiographic appearances. Some may be encapsulated and resemble a benign tumor. Many infiltrate the gland producing an irregular filling defect with ductal distortion and destruction. Cavitation and fistula formation may also be seen.

**Congenital absence of the major salivary glands**, either partial or total, is a rare but well documented condition which can present in young adults with dry mouth and dental decay. Absence of normal duct papillae followed by CT will confirm the diagnosis.

## OROPHARYNX AND HYPOPHARYNX

The oropharynx is usually examined radiographically as part of a more general evaluation of the esophagus or upper gastrointestinal tract. In patients with major swallowing difficulty at substantial risk of aspiration, a more limited examination of the oropharynx and cervical esophagus using small amounts of various materials may be needed. Barium examination should combine static filming with motion recording techniques such as videotaping or cineradiography to evaluate properly structural and functional abnormalities of the oropharynx and cervical esophagus.

### Radiographic Anatomy

The pharynx consists of the nasopharynx, oropharynx, and hypopharynx. The *hypopharynx* extends from the epiglottis

to the esophageal inlet. Hypopharyngeal anatomy is best appreciated on the frontal view (Fig. 29.5). The epiglottis is seen as a barium-coated smooth arcuate shadow projecting just above the paired valleculae. The hypopharynx extends inferiorly as the piriform sinuses, which surround the laryngeal vestibule laterally and posteriorly. The lateral view of the hypopharynx is complicated by superimposition of structures (Fig. 29.5). The epiglottis is seen in profile just posterior to the valleculae at the level of the hyoid bone. The aryepiglottic folds slant posteriorly downward to the arytenoid cartilages. The piriform sinuses are also superimposed. The posterior pharyngeal wall is well shown. The valleculae often contain small filling defects representing lymphoid tissue of the lingual tonsil (Fig. 29.5). The *crico-*

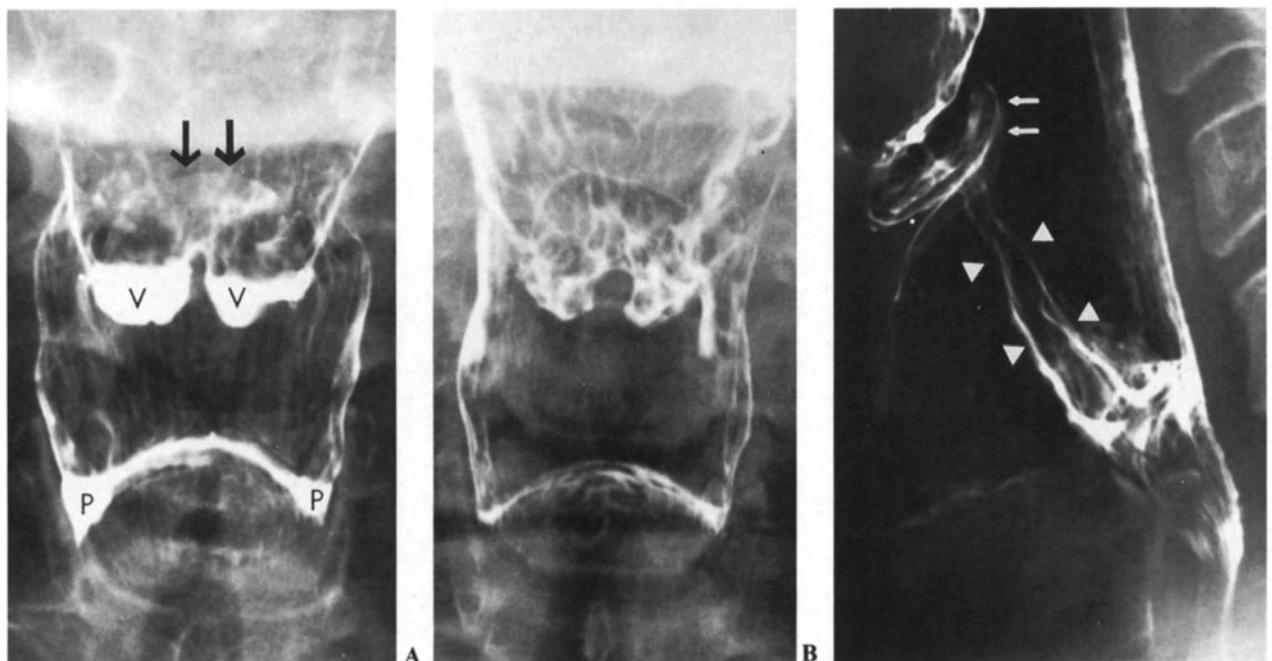


**Fig. 29.5.** A Frontal appearance of normal hypopharynx. Epiglottis is seen as a curvilinear structure (arrows) just above the paired valleculae (V). P = piriform sinuses. B Multiple small filling defects in the valleculae representing lymphoid tissue. C Lateral appearance of normal hypopharynx. Epiglottis seen in profile (arrows). Superimposed aryepiglottic folds (arrowheads) slant posteriorly. (All with permission Gelfand DW, Ott DJ (1981) Anatomy and technique in evaluating the esophagus. Semin Roentgenol 16: 168–182.)

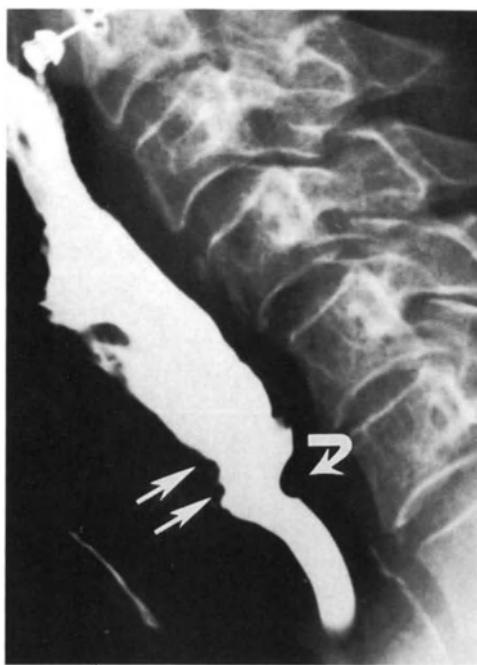


**Fig. 29.6.** The cricopharyngeus muscle causes a posterior indentation (curved arrow) at the pharyngesophageal junction. Anteriorly, a normal postcricoid impression (arrows) is also seen at this level. (With permission, Ott DJ (1983) Radiologic evaluation of the esophagus. In: Castell DO, Johnson LF, (eds). Esophageal Function in Health and Disease. Elsevier Biomedical; New York, pp 210–235.)

*pharyngeal muscle* may cause a posterior indentation at the pharyngoesophageal level, just anterior to the sixth cervical vertebra. The cartilages of the larynx and their membranous attachments may produce smooth, extrinsic compressions on the hypopharynx. Just below the cricoid cartilage impression, a small indentation ascribed to redundant mucosa may be seen (Fig. 29.6). This normal variant is called the *postcricoid impression* and has a variety of appearances, some of which may mimic a web or neoplasm.

#### Structural Abnormalities

**Congenital Anomalies.** Anomalies of the hypopharynx are rare. Congenital diverticula may occur laterally from remnants of the third or fourth pharyngeal pouches. Communicating branchial cleft cysts or sinuses opening on the neck also occur.

**Webs.** Hypopharyngeal webs arise from the anterior wall, often extending laterally and occasionally circumferentially. Most webs appear as thin smooth structures and must be distinguished from the posterior indentation of the cricopharyngeal muscle or the normal anteriorly located postcricoid impression (Fig. 29.7). Webs are best demonstrated with motion recording techniques. They have been reported in 1%–5% of asymptomatic individuals and in up to 15% of patients with dysphagia. The relationship between esophageal webs and iron deficiency anemia, the so-called Plummer–Vinson syndrome, remains controversial.

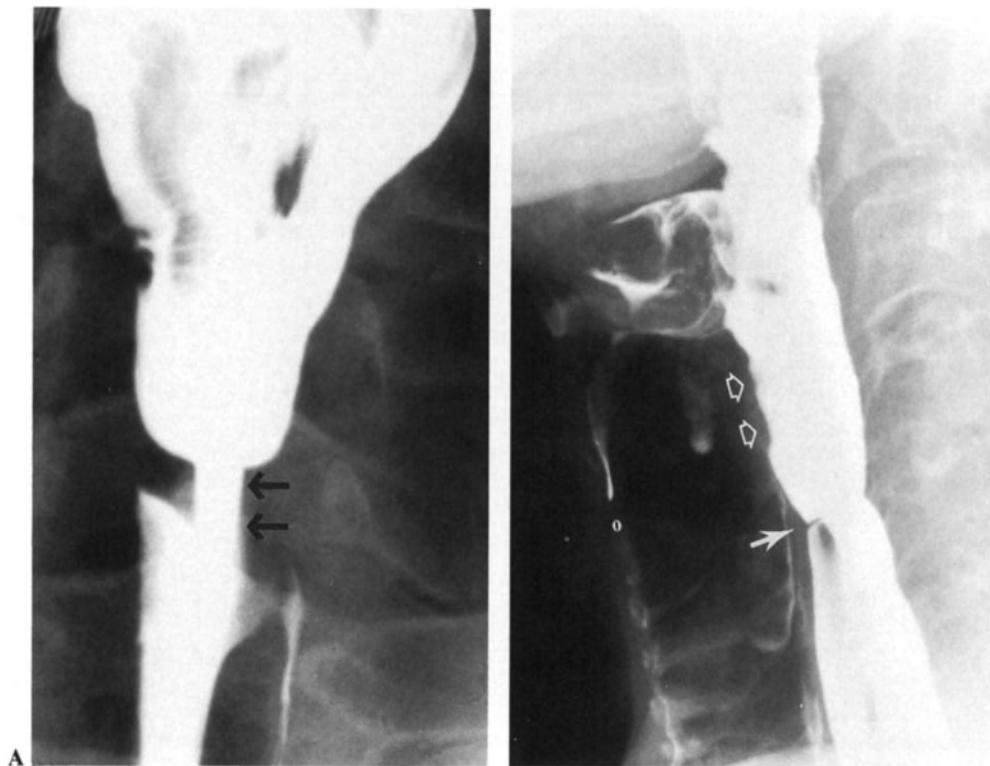


**Fig. 29.7.** A Circumferential web (arrows) in the lower hypopharynx producing a ‘jet’ phenomenon. B Thin cervical esophageal web (closed arrow) arising anteriorly below a broad postcricoid impression (open arrows). (With permission, Ott DJ (1988) Radiologic evaluation of esophageal dysphagia. Curr Prob Diagn Radiol 17: 1–33.)

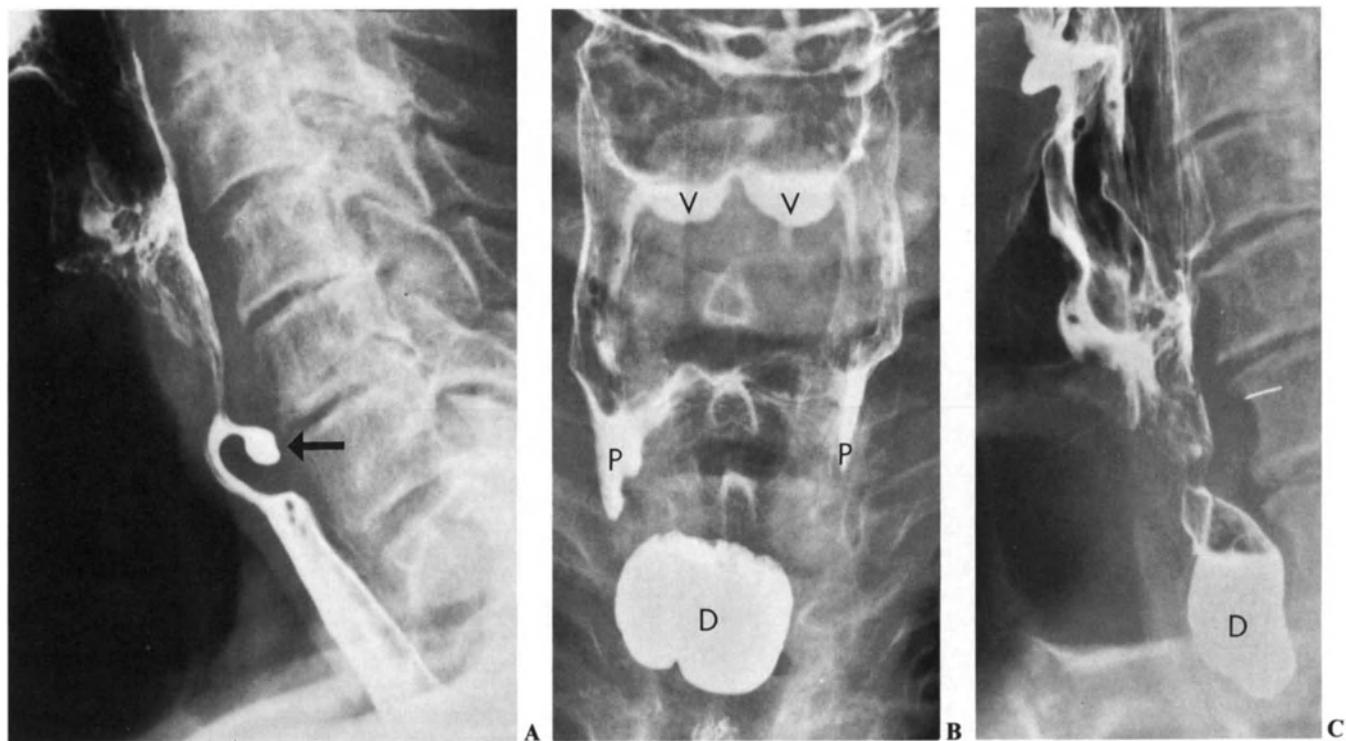


**Fig. 29.8.** A Small Zenker's diverticulum (arrow) protrudes posteriorly just above the impression of the cricopharyngeal muscle. (With permission, Ott DJ (1983) Radiologic evaluation of the esophagus. In: Castell DO, Johnson LF (eds). *Esophageal Function in Health and Disease*. Elsevier Biomedical, New York, pp 210–235.) B, C Frontal B and lateral C views of a 3.5-cm saccular Zenker's diverticulum D. V = valleculae; P = piriform sinuses.

**Diverticular Disease.** Pharyngeal diverticula may be classified by origin as congenital or acquired or by location as anterior, lateral, or posterior. The most common is the acquired pouch arising posteriorly known as the *Zenker's diverticulum*. Lateral pharyngeal diverticula are rare and terminology has been confusing. Lateral bulging of the pharynx due to anatomic weakness at the level of the thyrohyoid membrane is often seen on frontal views of the well-distended hypopharynx. These pouches are more frequent in older patients and have been called *hypopharyngeal pouches* or *ears*, and *pharyngoceles*. Lateral bulges may also occur in the tonsillar fossae.

The Zenker's diverticulum originates in the midline on the posterior wall of the hypopharynx in a triangular area of muscular weakness called *Killian's dehiscence*, resulting from the divergence of the oblique fibers of the inferior pharyngeal constrictor superiorly and laterally and the cricopharyngeus muscle inferiorly. The Zenker's pouch is an acquired pulsion diverticulum of debatable etiology. Although cricopharyngeal dysfunction has been previously postulated as a cause of Zenker's diverticulum, more recent studies have questioned this association.

Zenker's diverticula show a variety of radiographic appearances (Fig. 29.8). Small diverticula may have a spiculated shape and appear transiently shortly after swallowing barium. Larger diverticula have a more permanent clubbed appearance. They arise in the midline posteriorly just above the cricopharyngeus muscle. Much larger diverticula are saccular and extend inferiorly and even laterally,

often compressing the esophagus. Retention of food, secretions and barium is seen in these larger pouches.

**Neoplasms.** Nearly all tumors arising from the pharynx are epithelial malignancies. Evaluation of the esophagus is important since squamous cell carcinomas in the oropharynx and esophagus may be multiple. Malignant neoplasms of the pharynx present as an intraluminal mass or deformity due to tumor infiltration causing focal loss of pharyngeal distensibility (Fig. 29.9). Small malignant tumors may produce minimal mucosal irregularity and are occasionally difficult to demonstrate or differentiate from normal anatomic variants.

**Post-operative Appearances.** Surgery on the pharynx or larynx for a malignant neoplasm is the usual explanation for post-operative changes in the pharynx. Structural changes include absence of portions of the normal pharyngeal recesses, such as the piriform sinuses, pharyngeal deformity, and focal or diffuse narrowing. The latter may be caused by scarring with stenosis, radiation or tumor recurrence. More recent surgical advances, including placement of voice prostheses and jejunal grafts, have their own unique radiographic appearances.

**Extrinsic Effects.** Diseases in a variety of juxtaposed structures may secondarily involve the hypopharynx causing extrinsic deformity. The larynx, thyroid and parathyroid glands, cervical lymph nodes and the cervical spine are the major considerations. *Spondylosis* of the cervical spine may encroach posteriorly on the hypopharynx and be a rare cause of dysphagia. Severe degenerative changes of the cervi-



**Fig. 29.9.** Polypoid squamous cell carcinoma (arrows) of hypopharynx. Hypopharyngeal pouch (P) projects from the right side.

cal spine are common in older patients and other reasons for dysphagia, such as oropharyngeal dysfunction, must be carefully excluded.

#### Functional Abnormalities

Swallowing difficulty is the major reason for radiographic examination of the oropharynx. Functional disorders are an important cause of oropharyngeal dysphagia, and the area is best evaluated by combining motion recording techniques with static filming. Normal swallowing is divided into oral, pharyngeal and esophageal stages, which involve rapid and complex events beginning as a voluntary act and ending with an involuntary initiation of esophageal peristalsis.

**General Abnormalities.** A variety of disorders can alter the function of the oropharynx. *Oral transport difficulty* manifests as poor control of the bolus in the oral cavity, disordinated movement of the material posteriorly, and misdirection into the nasopharynx or out of the mouth instead of into the oropharynx.

The pharyngeal stage may be disrupted by a delayed or absent swallowing reflex with spillover of material and early aspiration.

*Pharyngeal paresis* reduces laryngeal movement and may cause aspiration with swallowing and stasis in the hypopharyngeal recesses after swallowing, the so-called val-

lecular sign (Fig. 29.10A). A persistent cricopharyngeal impression, especially associated with other signs of oropharyngeal dysmotility, may indicate upper esophageal sphincter dysfunction.

**Specific Disorders.** Functional oropharyngeal dysphagia may result from a wide variety of neuromuscular causes (Table 29.1). Many of these disorders produce similar functional disturbances in the oropharynx and clinical correlation is needed. The major role of radiographic evaluation in these patients is to identify the types and severity of functional disturbance and risk of aspiration, particularly with different types of liquids and non-liquid materials. Also, structural diseases of the oropharynx may mimic functional abnormalities and must be excluded. Unilateral pharyngeal paresis, for example, can cause asymmetry of the hypopharynx and be confused with neoplastic involvement.

**Table 29.1.** Neuromuscular disorders causing functional abnormalities of the oropharynx

Central nervous system
Cerebrovascular accident
Parkinson's disease
Huntington's chorea
Demyelinating disease
Amyotrophic lateral sclerosis
Tumors (primary/metastatic)
Congenital disorders
Miscellaneous degenerations
Peripheral nervous system
Bulbar poliomyelitis
Peripheral neuropathies
Myoneural junction
Myasthenia gravis
Skeletal muscle
Polymyositis
Dermatomyositis
Muscular dystrophies
Metabolic myopathy

Since the radiographic findings in many of these neuromuscular disorders are similar, only a few specific comments follow.

*Cerebral vascular accidents*, probably the most common cause of swallowing difficulty, can present as unilateral pharyngeal paresis although several other disorders may have similar findings.

*Myasthenia gravis* typically shows general and diffuse functional abnormalities with progressive worsening with repeated attempts at swallowing, but improvement following parenteral injection of neostigmine.

*Myotonic dystrophy* characteristically appears as a continuous column of barium extending from the pharynx into the cervical esophagus with a wide-open cricopharyngeal segment and marked esophageal-pharyngeal regurgitation (Fig. 29.10B).

*Cricopharyngeal Dysfunction.* Possible functional abnormalities of the cricopharyngeus muscle include:

Elevated or low resting pressure, the latter typically seen in *myotonic dystrophy*

Delayed opening, as in *familial dysautonomia*

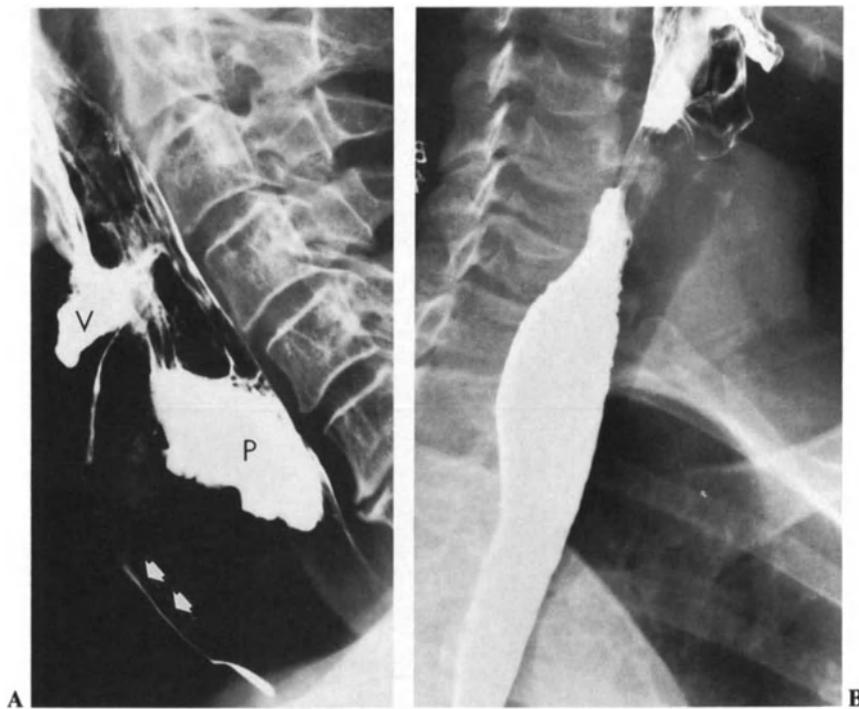


**Fig. 29.10.** A Lateral view of hypopharynx (*V* = valleculae, *P* = piriform sinuses) showing barium stasis and aspiration (arrows) in amyotrophic lateral sclerosis. Repetitive swallowing failed to clear barium from the pharyngeal recesses – called the *vallecular sign*. (With permission, Ott DJ (1983) Radiologic evaluation of the esophagus. In: Castell DO, Johnson LF (eds) Esophageal Function in Health and Disease. Elsevier Biomedical, New York, pp 210–235.) B Myotonic dystrophy with stasis of barium seen as a continuous column extending from pharynx into cervical esophagus.

Premature closure, possible but debatable cause of *Zenker's diverticula*

Failure of relaxation, so-called *cricopharyngeal achalasia*.

*Cricopharyngeal achalasia* was originally described radiographically as a persistent or transient posterior indentation (or cricopharyngeal bar) at the pharyngoesophageal junction seen during swallowing (Fig. 29.6). However, the clinical significance of this indentation has been controversial, about 5% of individuals without oropharyngeal dysphagia showing a minor cricopharyngeal impression. Normal relaxation of the upper esophageal sphincter manometrically

occurs in many of these asymptomatic patients with persistent cricopharyngeal impressions, questioning the validity of the term *achalasia*. Thus, in asymptomatic individuals showing minimal cricopharyngeal impression and no other oropharyngeal abnormalities, the importance of this finding is debatable. Approximately 20% of patients with oropharyngeal dysphagia will show a cricopharyngeal impression, which may also be found in a variety of neuromuscular disorders and be associated with other functional abnormalities. Consequently *cricopharyngeal dysfunction* is the preferred term for these upper esophageal sphincter abnormalities.

## ESOPHAGUS

Radiographic examination of the esophagus may be performed separately, often combined with evaluation of the oropharynx, depending on the clinical indications. Effective radiology of the esophagus, requires a thorough understanding and selected use of a variety of radiographic techniques.

### TECHNIQUES OF EXAMINATION

The multiphasic examination of the esophagus combining different examining techniques is the most effective means of radiographic evaluation of the esophagus (Table 29.2).

Each technique has its advantages and limitations and no single method provides optimal examination of the esophagus. In addition to the standard techniques, supplemental techniques may be occasionally needed. The following methods are used for the routine multiphasic examination of the esophagus (Fig. 29.11A):

Double contrast technique

Full column technique

Mucosal relief technique

Fluoroscopic observation and motion recording techniques

**Table 29.2.** Radiographic examination of the oropharynx and esophagus

Oropharynx and cervical esophagus
patient upright in frontal position
motion recording of swallow(s)
spot-film taken after swallow
sequence repeated lateral position
Thoracic esophagus and esophagogastric region
double-contrast examination
patient upright turned left
gas producing agent taken
barium drunk rapidly
multiple spot-films obtained
full-column examination
patient prone oblique position
bolster may be used
single swallows for peristalsis
rapid swallowing for distension
mucosal relief examination
barium-coated collapsed esophagus
spot-film(s) obtained
Supplemental examining techniques
iced barium method
four ounces crushed ice
add to dense barium
do full-column technique
solid bolus methods
barium tablets
12.5 mm size
use water
marshmallow
half regular size
dilute barium
full-column exam
other materials available
esophageal intubation
small bore tube
double-contrast examination
pharmacologic aids
glucagon (food impaction)
anticholinergics (varices)
amyl nitrite (achalasia)
other drugs available

Small neoplasms and various types of esophagitis are well shown on double-contrast films. In about a third of patients, however, the esophagogastric region is not adequately distended and small hiatal hernias, lower esophageal mucosal rings and occasional peptic strictures may not be detected. Esophageal motility is best assessed fluoroscopically in the prone position using a single swallow of barium. Hiatal hernias, lower esophageal mucosal rings and peptic strictures are best shown by full column technique.

Small neoplasms, various types of esophagitis and esophageal varices can be detected by mucosal relief films. Indeed, varices are best shown by mucosal relief technique, particularly if the patient is prohibited from swallowing and parenteral anticholinergics are used to further relax the esophagus.

Motion recording techniques aid in evaluation of functional disorders of the oropharynx and esophagus. The rapidity of events, especially in the oropharynx, makes appreciation and static filming of transient abnormalities difficult.

**Supplemental Techniques.** Inadequate distention of the esophagus may be a problem if the patient cannot ingest

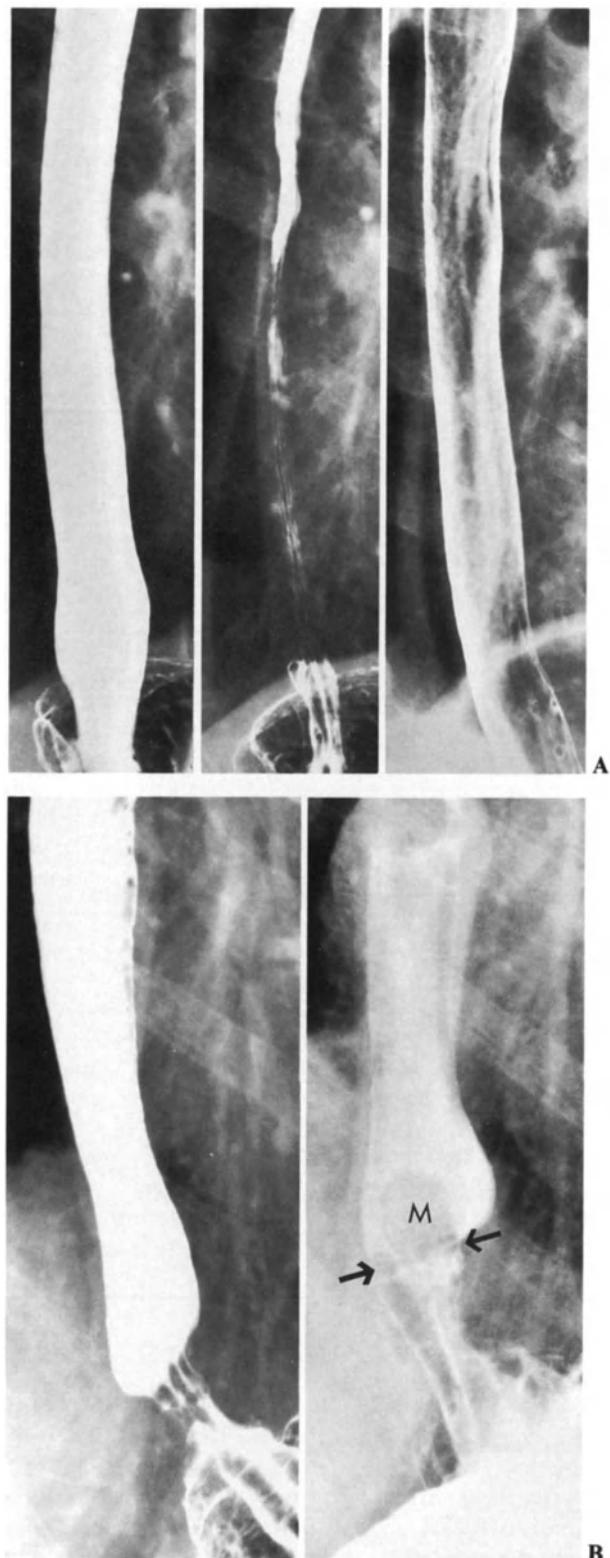


**Fig. 29.11.** A Normal full-column (left), mucosal relief (middle) and double-contrast (right) techniques from a multiphasic esophogram. B Patient with intermittent dysphagia to solid food. Full-column examination (left) with liquid barium is normal. Repeat evaluation (right) with dilute barium and marshmallow (M) shows impaction of the solid by a 13-mm mucosal ring (arrows). (With permission, Ott DJ, Gelfand DW, Wu WC, Chen YM (1986) Radiological evaluation of dysphagia. JAMA 256: 2718–2721.)

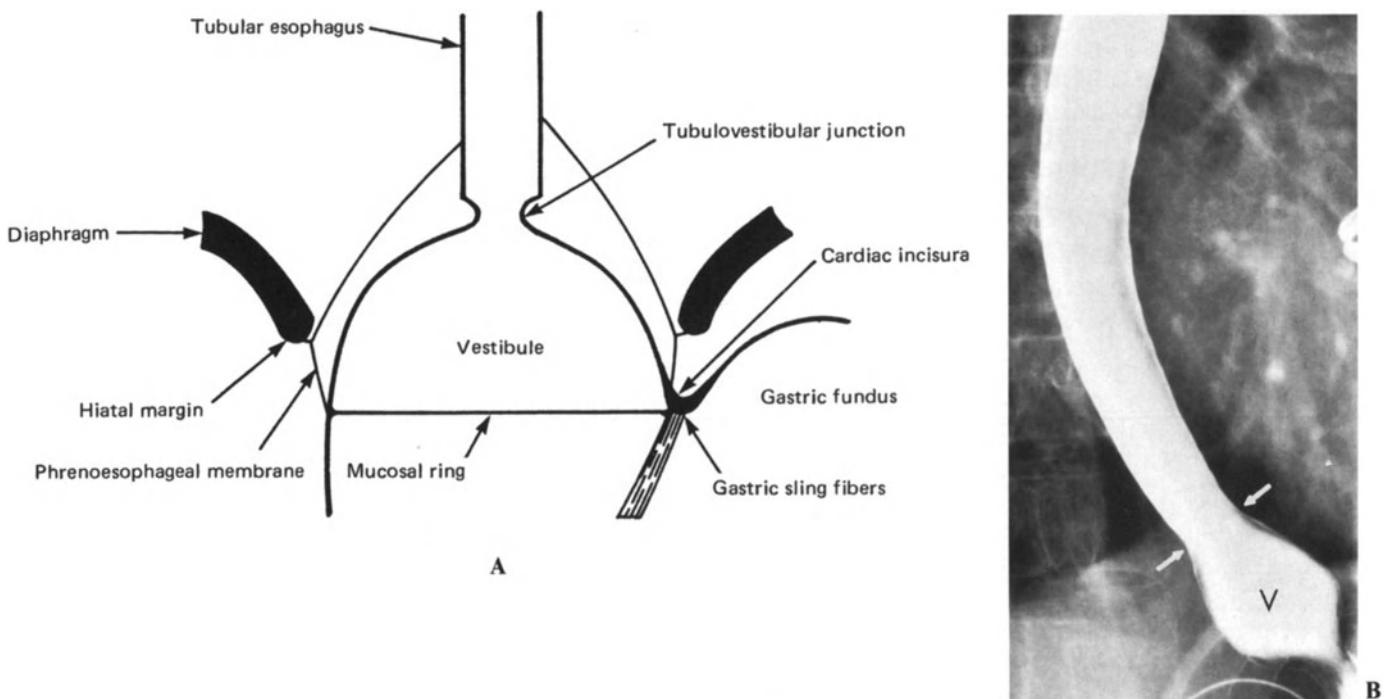


**Fig. 29.12.** A Diagram of lower esophageal anatomy with simplification of terminology. Esophageal vestibule is defined by the tubulovestibular junction superiorly and upper margin of gastric sling fibers inferiorly. When present, mucosal ring lies at lower level of esophageal vestibule. (Modified from Zboralske FF, Friedland GW (1970) Disease of the esophagus-present concepts. West J Med 112: 33–51.) B Tubulovestibular junction (arrows) demarcates the upper tubular esophagus from the esophageal vestibule (V).

barium rapidly. The relaxant effect of iced barium is useful on the esophagogastric region. The use of solid boluses, such as marshmallows, are important in patients with dysphagia for better demonstration of abnormalities or reproduction of symptoms (Fig. 29.11B). Occasionally, a solid bolus will even bring out a lesion not shown on the examination with liquid barium. Esophageal intubation and pharmacologic aids are used for specific indications.

#### RADIOLOGIC ANATOMY

**Normal Anatomy.** The cervical and thoracic portions together are called the tubular esophagus. Several smooth, longitudinal folds course the entire length of the normal cervical and thoracic esophagus in their collapsed state (Fig. 29.11A). Many important structures lie adjacent to the esophagus and may normally impress upon the organ. The major impressions occur at the level of the aortic arch, the left main stem bronchus and the heart.

The anatomic transition between the lower end of the thoracic esophagus and the stomach is complex (Fig. 29.12). The tubular esophagus unites with the vestibule at the tubulovestibular junction or A level. Under normal resting conditions, a portion of the esophageal vestibule lies within the abdomen. The esophagogastric junction represents the point of union of the vestibule with the stomach. The mucosal transitional level, often called the B level, between the esophagus and stomach lies at the lower margin of the vestibule. The lower esophageal sphincter is a manometric

high-pressure zone coinciding in position to the esophageal vestibule although a discrete anatomic structure representing the sphincter has not been clearly identified.

**Anatomic Variants.** Normally, a potential space exists between the aortic arch and the left main stem bronchus called the aorticobronchial triangle. The esophagus may focally protrude into this space and resemble a diverticulum. A fine nodular appearance of the esophageal mucosa due to *glycogen acanthosis* is occasionally seen on double-contrast films, particularly in older individuals. These glycogen deposits are typically under 5 mm in size and are of no clinical significance except for confusion with disease, such as infectious esophagitis. Transient esophageal motility phenomena, such as *tertiary contractions*, must be distinguished from a fixed deformity due to neoplasm or esophagitis. Fleeting transverse folds often called *esophageal rimping* may be seen. These are probably due to muscularis mucosae contractions and may be more prevalent in patients with gastroesophageal reflux disease.

**Congenital Anomalies.** Congenital anomalies of the esophagus include esophageal atresia, stenosis and webs, and duplications.

*Esophageal atresia* usually accompanied by a tracheoesophageal atresia usually includes five types with about 85% being associated with a fistula to the lower esophageal segment. Isolated atresia and the H-type fistula account for most of the rest.

*Congenital stenosis and webs* are rare. In general, focal esophageal constriction in a child is usually caused by a peptic stricture rather than a congenital anomaly.

The esophagus is a common site for *duplication* in the gastrointestinal tract. Duplications resemble cysts, compress the esophagus, but rarely communicate with the lumen.

### HIATAL HERNIA AND RINGS

**Hiatal Hernia.** Hiatal hernia is the most common diaphragmatic hernia and is classified into three types:

1. Sliding or axial hernias
2. Paraesophageal hernia
3. Mixed hernia.

The vast majority of hiatal hernias are of the sliding type, in which the esophagogastric junction forms the most orad portion of the herniated stomach. Axial hernias are usually small and generally slide relative to the esophageal hiatus, but may be fixed. Radiographic signs of hiatal hernia depend on showing landmarks of the esophagogastric junction extending above the esophageal hiatus (Fig. 29.13). The most important landmarks include the lower esophageal mucosal ring, notch from the gastric sling fibers, and the orad level of the area gastricae of the stomach.

A direct causal relationship between hiatal hernia and gastroesophageal reflux disease has not been established. Lower esophageal sphincter dysfunction is felt to be the primary cause of abnormal gastroesophageal reflux. Hiatal hernia is found radiographically in 40%–60% of adults, but only a minority will have reflux esophagitis endoscopically. Conversely, about 90% of those with reflux disease have hiatal hernias if appropriate radiographic techniques are used. Patients without hiatal hernia are furthermore unlikely to have the more severe forms of endoscopic esophagitis. Thus, hiatal hernia is unlikely to be the primary cause of abnormal gastroesophageal reflux, but may play a permissive role by enhancing the likelihood of lower esophageal dysfunction in some individuals.

Paraesophageal hernias account for less than 5% of hiatal hernias. The esophagogastric junction remains fixed below the hiatus but a portion of gastric fundus herniates alongside the lower esophagus into the chest. The herniated stomach may be small or large and also undergoes varying degrees of twisting. Mechanical complications, such as volvulus and strangulation, can occur necessitating surgical repair.

The mixed hernia is a combination of sliding and paraesophageal hernias and is often large with much of the stomach lying within the chest (so-called intrathoracic stomach). The herniated stomach may rotate and even become inverted. Patients are often asymptomatic, but mechanical complications can occur.

**Esophageal Rings.** Ring-like constrictions have been described at locations throughout the length of the esophagus. *Web* and *ring* are the most common terms used for these constrictions. For descriptive purposes, web will be used to describe esophageal constrictions totally covered by squamous epithelium and located above the level of the tubulovestibular junction. *Esophageal webs* are not common and occur most often in the cervical region (Fig. 29.7B). They may rarely involve the thoracic esophagus or be multiple. Webs appear as thin transverse folds and may be easily

missed if full distention of the esophagus is not achieved.

The term *ring* will be limited to narrowing in the esophagogastric region occurring predominantly at the upper and lower borders of the esophageal vestibule. These are most commonly classified as muscular or mucosal rings.

The *muscular ring* occurs at the tubulovestibular junction and appears as a broad smooth narrowing. The caliber of the muscular ring varies during the examination and it may be associated with hiatal hernia and esophageal motility disorders (Fig. 29.13B).

The *lower esophageal mucosal ring*, or *Schatzki's ring*, marks the lower border of the vestibule and appears as a thin, transverse structure encircling the esophagogastric junction (Fig. 29.13C). The margins of the mucosal ring are typically smooth and symmetric and its caliber is fixed (Fig. 29.13A). Occasionally, use of a solid bolus will show a mucosal ring not seen on the examination with liquid barium and often reproduces the patient's symptoms (Fig. 29.11B). The radiologic method is more sensitive than endoscopy in detecting mucosal rings, especially if the diameter of the ring is above the caliber of the endoscope used. The lower esophageal mucosal ring is an important cause of solid food dysphagia. The prevalence of dysphagia is related to the caliber of the ring and is rarely present in rings above 20 mm. Conversely, rings less than 13 mm nearly always cause dysphagia, while 13–20 mm rings may be symptomatic depending on their size and probably on the eating habits of the patient.

### REFLUX ESOPHAGITIS

Reflux esophagitis is the most common inflammation of the esophagus (Table 29.3). Patients with symptomatic gastroesophageal reflux may have a normal appearing esophageal mucosa, histologic abnormalities only, or gross morphologic changes of reflux esophagitis. The term *gastroesophageal reflux disease* has been used to include all of these patients. About 60% of patients suffering from

Table 29.3. Causes of esophagitis

Common causes
reflux esophagitis
infectious esophagitis
<i>Candida</i> esophagitis
herpetic esophagitis
cytomegalic virus
other infections
caustic esophagitis
radiation esophagitis
medication-induced injury
Rarer causes
Crohn's disease
pemphigoid
epidermolysis bullosa
ulcerative colitis
Behcet's syndrome
graft vs. host disease
Zollinger-Ellison syndrome
eosinophilic esophagitis
thermal injury
traumatic cause

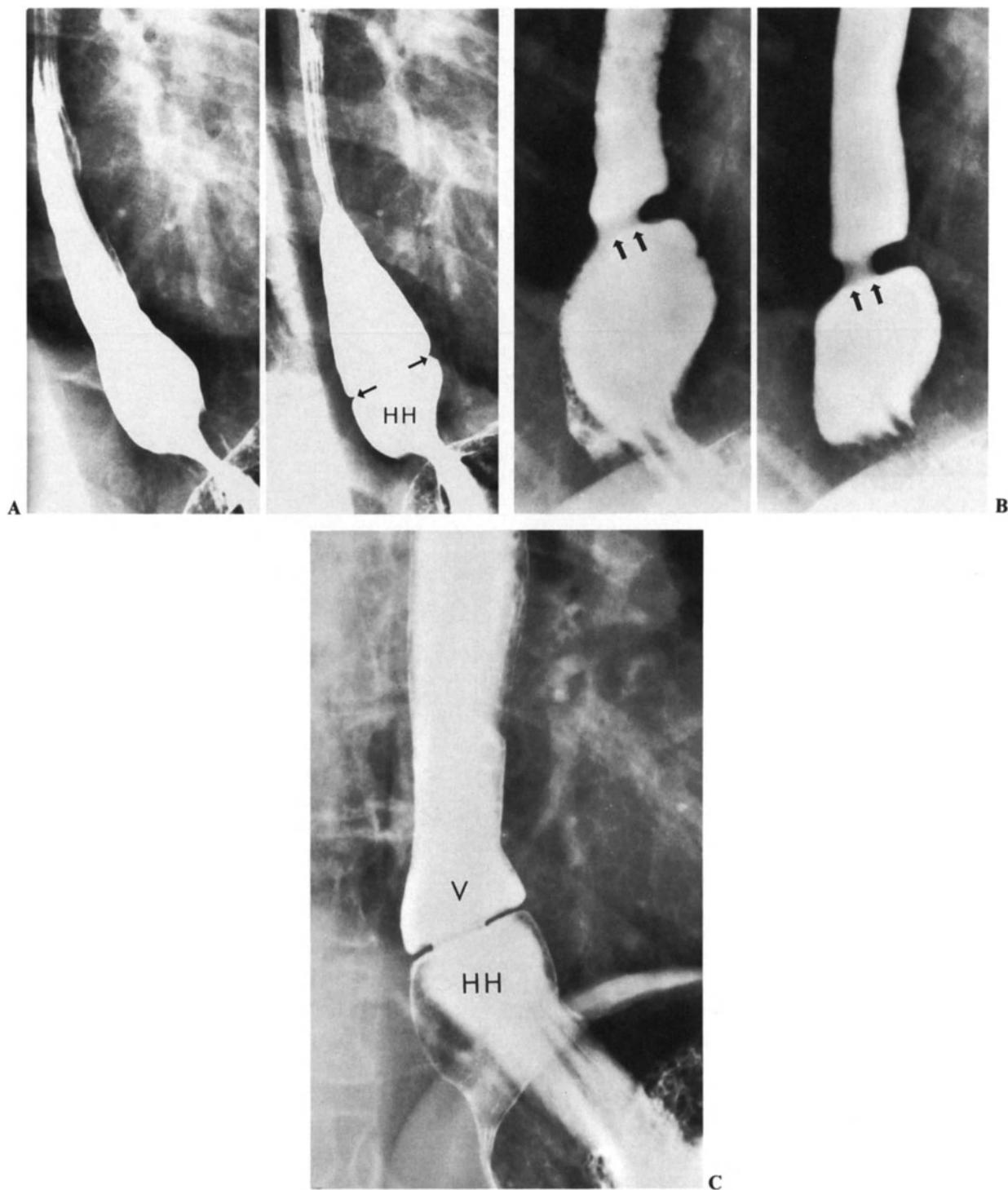


**Fig. 29.13.** A Two-full-column views of the esophagogastric region during the same examination. Hiatal hernia (HH) and mucosal ring (arrows) are shown with better distention (right). (With permission Ott DJ (1983) Radiologic evaluation of the esophagus. In: Castell DO, Johnson LF (eds) Esophageal Function in Health and Disease. Elsevier Biomedical, New York, pp 210–235.) B Two views of a broad, smooth muscular ring at tubulovestibular junction (arrows). Caliber of ring changes from 12 mm (left) to 6 mm (right) during the examination. (With permission Ott DJ, Gelfand DW, Wu WC, Castell DO (1984) Esophagogastric region and its rings. AJR 142: 281–287.) C Lower esophageal mucosal ring demarcating esophageal vestibule (V) and hiatal hernia (HH).

gastroesophageal reflux disease show abnormalities endoscopically. In the remaining 40% of symptomatic patients, biopsy and histologic examination may show mild epithelial

erosions or other inflammatory changes of the mucosa. Using endoscopic criteria, the severity of reflux esophagitis has been classified variously, usually dividing the disease into

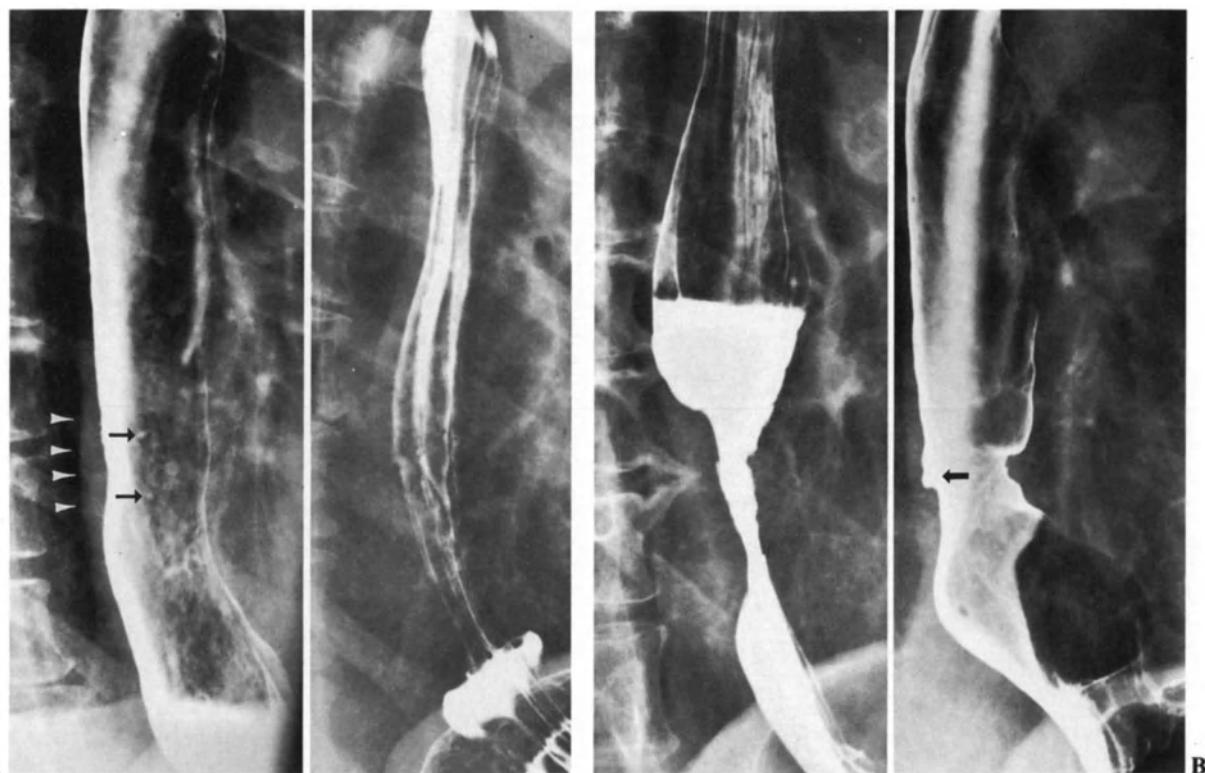


**Fig. 29.14.** A Severe endoscopic esophagitis with erosions (arrows), mild narrowing and wall thickening (arrowheads) on double-contrast film (left). Marked fold thickening and irregularity on mucosal relief film (right). B Irregular peptic stricture (left) due to associated active esophagitis. Smooth, eccentric peptic stricture (right) with wall thickening and pseudodiverticulum (arrow). (Both with permission Ott DJ (1985) Barium esophagram. In: Castell DO, Wu WC, Ott DJ (eds) Gastroesophageal Reflux Disease. Futura Publishing Co., Mount Kisco, pp. 109–128.)

three categories:

- Mild – erythema with exudation or friability
- Moderate – erosions or ulcerations
- Severe – marked ulceration or stricture.

Radiographic detection of reflux esophagitis depends on the severity of disease.

**Radiologic Findings.** Currently, the major role of the barium esophagram in evaluating gastroesophageal reflux disease appears to be the detection of reflux esophagitis and its complications. Abnormalities of esophageal motility and volume clearance are common in patients with reflux disease and may be also assessed by radiologic imaging. Barium reflux may occur spontaneously (free reflux) or during various provocative tests (stress reflux), such as the Valsalva maneuver or the water siphon test. Reflux of barium is observed in only about 33% of symptomatic patients. Despite initial enthusiasm, the radionuclide reflux study has shown about a 60% average detection rate of gastroesophageal reflux.

The more common structural abnormalities that may be seen radiographically in reflux esophagitis include mucosal and contour irregularity, fold thickening, erosions and ulceration, wall thickening, and segmental narrowing, particularly from stricture formation (Fig. 29.14). *Intramural pseudodiverticula*, inflammatory polyps and pseudomasses, and esophagogastric fistula are less often seen. In mild esophagitis, radiographic detection is generally poor. How-

ever, the combined sensitivity for diagnosing moderate and severe reflux esophagitis has averaged 90% with 95% detection of peptic stricture. Endoscopic detection of peptic stricture is also excellent, but may well decrease as smaller caliber endoscopes are more widely used.

**Barrett Esophagus.** Barrett esophagus is characterized by progressive columnar metaplasia of the lower esophagus caused by chronic reflux esophagitis. In patients with reflux disease, the overall prevalence of Barrett esophagus is about 10%. Barrett esophagus is a premalignant condition with an increased risk of adenocarcinoma, which occurs on the average in 15% of those with columnar metaplasia. Barrett esophagus is suggested radiographically when focal esophagitis, ulcer or stricture is separated from an accompanying hiatal hernia by a normal segment of esophagus (Fig. 29.15). More recently a reticular mucosal pattern has been described as a more specific sign of the columnar-lined esophagus, although the specificity of the finding has been debated.

#### NON-REFLUX ESOPHAGITIS

Non-reflux esophagitis results from numerous causes, and the more common types will be emphasized (Table 29.3). The rarer causes require clinical correlation since the radiographic findings often overlap the appearances seen in other forms of esophagitis.

**Infectious Esophagitis.** Infectious esophagitis can be pro-

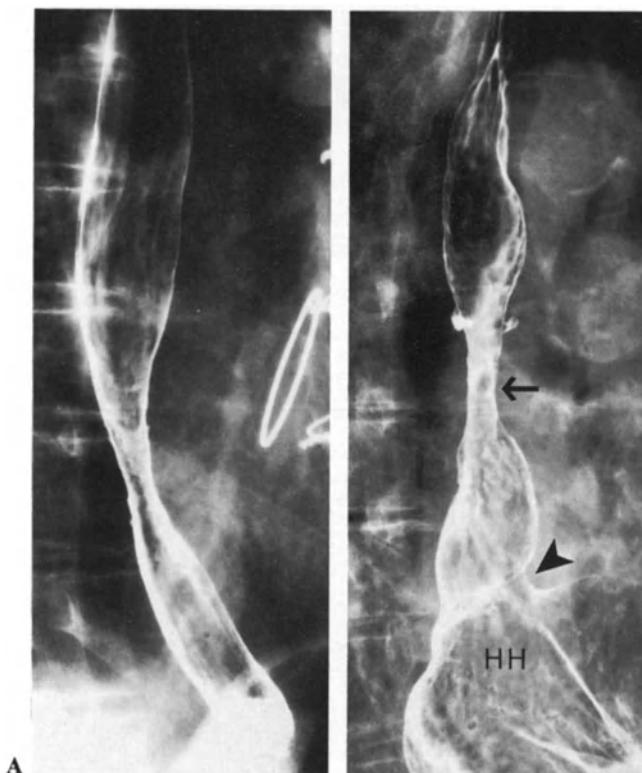


**Fig. 29.15.** A Double-contrast view in Barrett esophagus showing a mid-esophageal stricture. (With permission, Ott DJ (1985) Barium esophagram. In: Castell DO, Wu WC, Ott DJ. Gastroesophageal Reflux Disease. Futura Publishing Co., Mount Kisco, pp 109–128.) B Large hiatal hernia (HH) with peptic stricture (arrow) well above esophagogastric junction (arrowhead) in Barrett esophagus. Several pseudodiverticula are seen at top margin of stricture. (With permission Ott DJ (1988) Radiologic evaluation of esophageal dysphagia. Curr Probl Diagn Radiol 17: 1–33.)

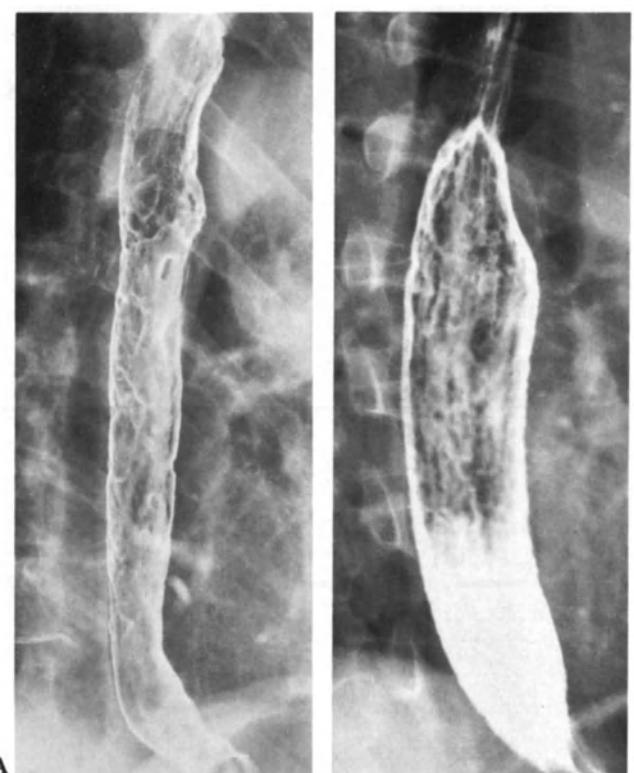


**Fig. 29.16.** A Diffuse *Candida* esophagitis in patient with dysphagia on immunosuppressants. B Diffuse herpetic esophagitis. (Both with permission Ott DJ (1988) Radiologic evaluation of esophageal dysphagia. Curr Probl Diagn Radiol 17: 1–33.)

duced by a wide variety of fungal, viral, or bacterial agents. *Candida albicans* is the most common infectious esophagitis and usually presents as an opportunistic infection. Oral lesions are absent in about 50% of patients. Radiologic feature of *Candida* esophagitis vary according to the severity and length of esophagus involved (Fig. 29.16A). Fine ulcerations and a cobblestone pattern are early findings best shown on double-contrast or mucosal relief films. Abnormal motility, severe ulceration and pseudomembrane formation are later features. Rarer manifestations include stricture, fungal masses and fistula with abscess.

*Herpes simplex* and *cytomegalic virus* most commonly cause *viral esophagitis*. These are usually opportunistic infections causing symptoms similar to *Candida* esophagitis, although herpetic infection has occurred in otherwise healthy individuals. Although discrete ulceration may be an early and suggestive finding, histologic examination is needed for definitive diagnosis. More advanced disease causes an ulcerated and cobblestone appearance indistinguishable from fungal esophagitis (Fig. 29.16B). Rarely, combined fungal and viral esophagitis may occur.

**Caustic Esophagitis.** Most caustic injuries of the esophagus are due to accidental ingestion by children or suicide attempts in adults. Early functional disturbances include

esophageal dilatation and atony or poor distensibility with segmental contractions. Radiographic findings in the severer forms include exudative plaques, pseudomembrane formation, erosions and ulceration. Intramural dissection and even perforation with mediastinitis can occur acutely. Strictures may result and usually develop several weeks or later after the initial caustic insult (Fig. 29.17).

**Radiation Esophagitis.** Radiation injury to the esophagus is seen mainly in patients treated for esophageal carcinoma but can occur following radiation to the mediastinum for other malignancies. The combination of chemotherapy and radiation greatly enhances the chance of esophageal damage. Acute and chronic radiation effects to the esophagus generally occur after 4500–6000 rads given over 6–8 weeks. Radiologic abnormalities include abnormal esophageal motility, mucosal irregularity, ulceration, stricture, pseudodiverticula and fistula. Motility disturbances usually occur within 1–3 months following radiotherapy and stricture generally at 6–8 months.

**Medication-induced Injury.** In recent years, a wide variety of medications have been implicated as a cause of focal esophagitis. The most common drugs reported have been *emepronium*, *tetracycline* and slow-releasing *potassium chloride*. Slow clearance of the medication from the esophagus

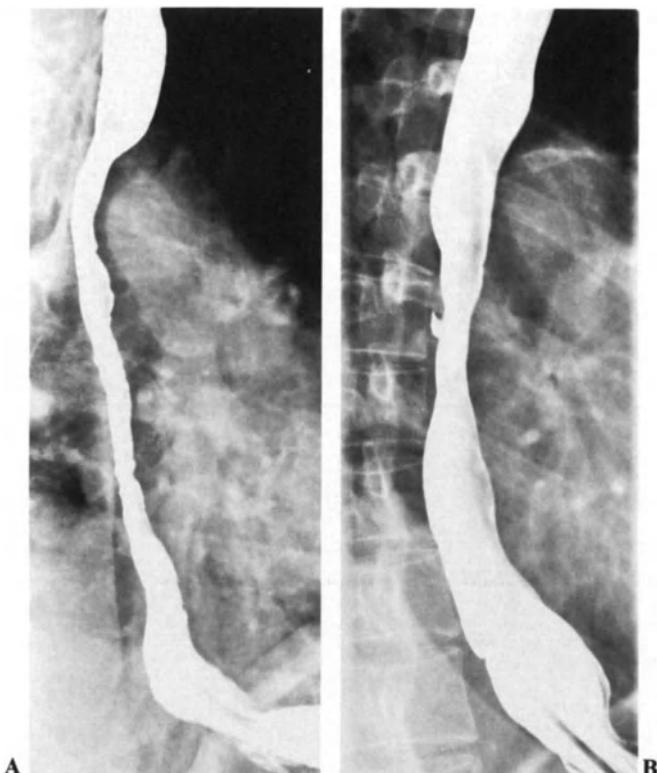


**Fig. 29.17.** A Mildly irregular long stricture due to lye ingestion. B Shorter mid-esophageal caustic stricture with pseudodiverticulum 20 years after lye ingestion.

gus or abnormal motility may be causative. The usual site of involvement has been the midesophagus in the proximity of the aortic arch with superficial erosions and ulcerations (Fig. 29.18). Focal esophageal narrowing, often caused by spasm, edema, or rarely stricture, may be present. The findings usually resolve quickly upon withdrawal of the medication.

#### NEOPLASTIC DISEASE

A diversity of neoplasms and tumor-like lesions may involve the esophagus (Table 29.4). Benign and malignant primary neoplasms, secondary neoplasms and a variety of unrelated non-neoplastic conditions have been described. Only the more common types of these lesions will be discussed.

#### Benign Neoplasms

Although *leiomyoma* is the most common benign tumor of the esophagus, comprising over half of such lesions, they are relatively rare with only one seen for about every 50 esophageal carcinomas. Many patients are asymptomatic and the smooth muscle neoplasm is found incidentally (Fig. 29.19A). Leiomyomas generally occur as solitary lesions most often located in the lower two thirds of the esophagus. They are usually 2–6 cm in size and typically present as a smooth, eccentric filling defect due to their intramural location. Ulceration and calcification are rare. Larger leio-



**Fig. 29.18.** Young woman on tetracycline with acute onset of odynophagia. Focal erosions and ulceration in mid-esophagus. Symptoms quickly subsided after cessation of the medication.

**Table 29.4. Neoplasms and tumor-like lesions of the esophagus**

Benign neoplasms
leiomyoma
squamous papilloma*
myoblastoma*
vascular tumors*
adenoma*
lipoma*
Malignant neoplasms
squamous cell carcinoma
adenocarcinoma
carcinosarcoma*
lymphoma*
leiomyosarcoma*
Secondary neoplasms
contiguous spread
lymph nodal metastases
hematogenous metastases*
Tumor-like lesions
inflammatory reflux polyp
inflammatory fibroid polyp*
fibrovascular polyp*
congenital/acquired cysts*
intramural hematoma*

\*Extremely rare.

myomas show an adjacent mass effect and may be apparent on plain films of the chest (Fig. 29.19B). Multiple leiomyomas are even rarer and may cause considerable distortion of the esophageal lumen.

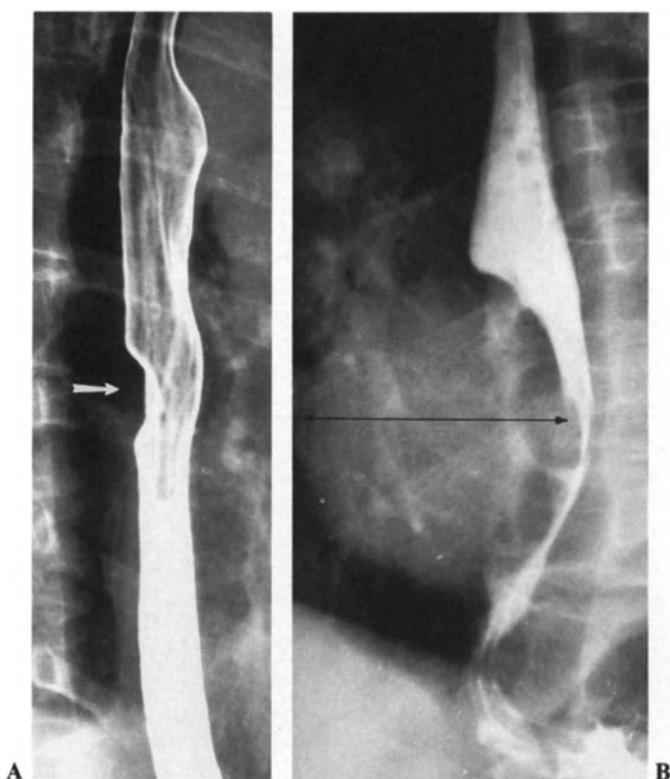


**Fig. 29.19.** A 1.5-cm leiomyoma (arrow) found incidentally in a patient without esophageal symptoms. B Large ( $6.5 \times 7.5$  cm) leiomyoma (connected arrow) with adjacent mass effect in patient with dysphagia. (Both with permission Ott DJ (1988) Radiologic evaluation of esophageal dysphagia. Curr Probl Diagn Radiol 17: 1–33.)

### Malignant Neoplasms

Squamous cell carcinoma and adenocarcinoma are the most common primary esophageal neoplasms.

*Squamous cell carcinomas* may be superficial, polypoid, fungating, ulcerative and/or infiltrative. Thus, a wide variety of radiologic appearances are seen. Small, superficial carcinomas may appear as focal mucosal irregularity or nodular protrusion best seen with double-contrast or mucosal relief technique (Fig. 29.20A). Polypoid malignancies vary from small, eccentric defects to large, bulky intraluminal tumors. Ulceration may accompany the other morphologic types or be a predominant form associated with surrounding tumor mass. Infiltrative carcinoma often causes eccentric or annular constriction with a typically irregular, ulcerated contour (Fig. 29.20B). Malignant infiltration with a smooth contour is rare, except following radiation therapy, but may mimic a benign stricture. Early detection of esophageal carcinoma portends a better prognosis, and *computed tomography* has become important in evaluating patients with

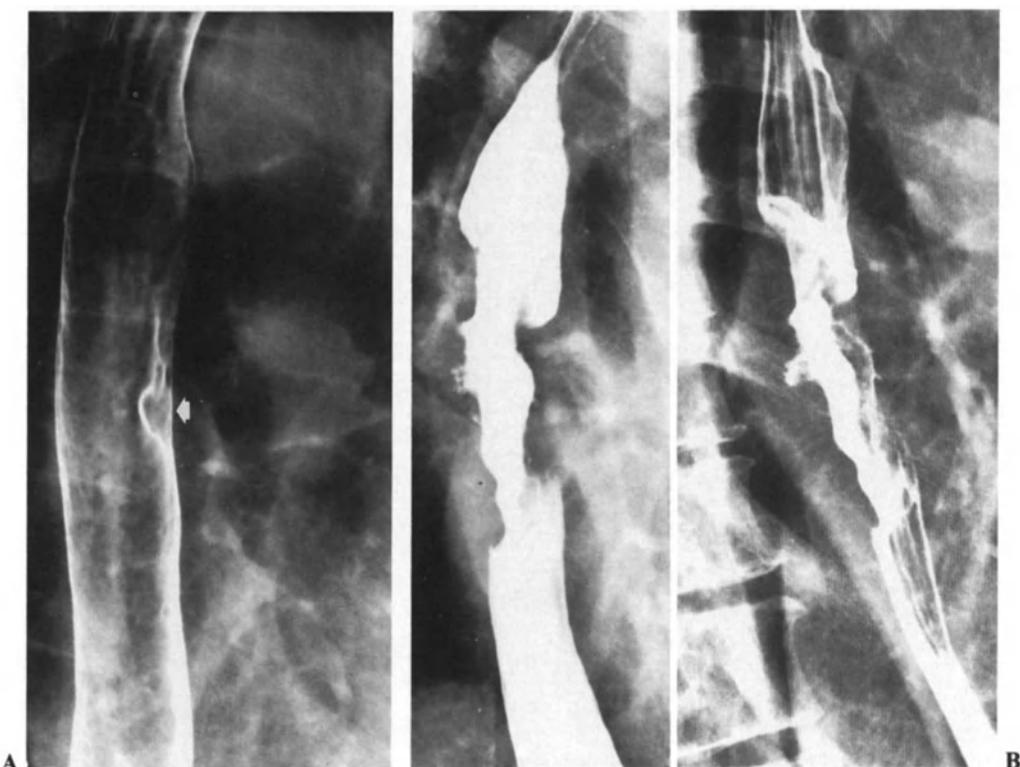


**Fig. 29.20.** A  $6 \times 8$  mm small esophageal carcinoma (arrow) best shown on double-contrast examination. (With permission Ott DJ (1988) Radiologic evaluation of esophageal dysphagia. Curr Probl Diagn Radiol 17: 1–33.) B Full-column (left) and double-contrast (right) views of an ulcerated annular carcinoma of the mid-esophagus. (With permission Ott DJ (1983) Radiologic evaluation of the esophagus. In: Castell DO, Johnson LF (eds) Esophageal Function in Health Disease. Elsevier Biomedical, New York pp 210–235.)

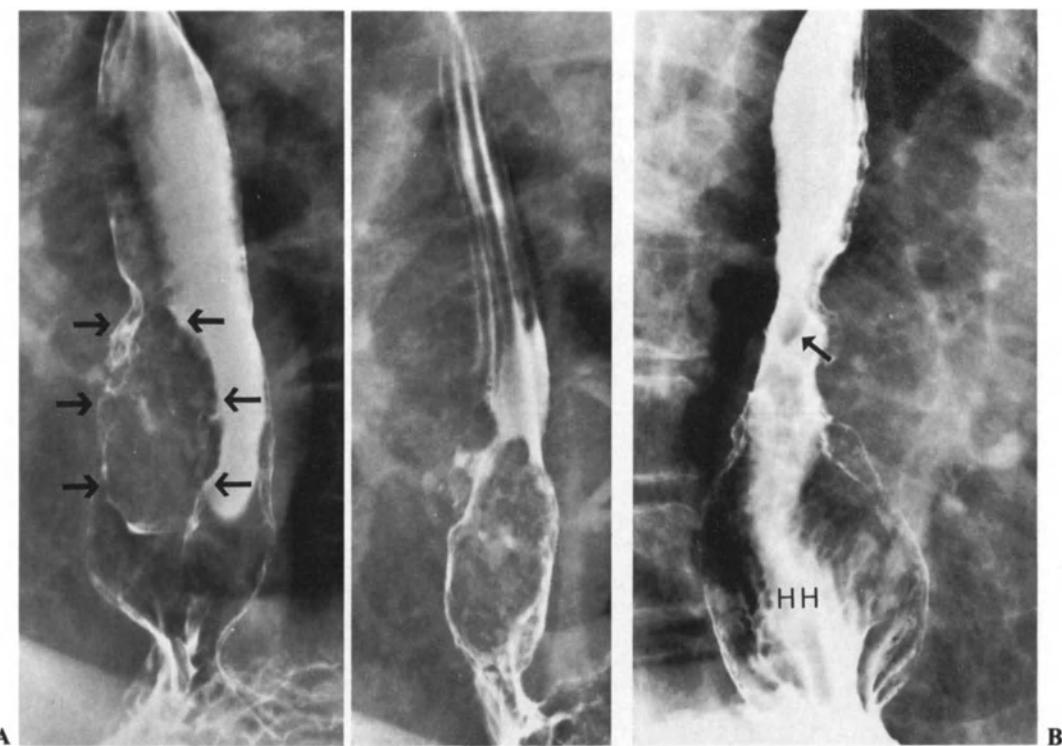


**Fig. 29.21.** A Double-contrast (left) and mucosal relief (right) views of a polypoid adenocarcinoma (arrows) of the lower esophagus. B Adenocarcinoma from Barrett epithelium. Nodularity and ulceration (arrow) within an irregular peptic stricture located well above a hiatal hernia (HH).

esophageal carcinoma for assessing the extra-luminal extent of disease and staging of malignancy.

Adenocarcinoma accounts for about 10% of primary esophageal malignancies and originates mainly in the lower esophagus. Adenocarcinoma may arise from the esophageal glands, or heterotopic remnants of gastric mucosa, but the most common origin of primary adenocarcinoma of the esophagus is felt to be from dysplastic Barrett epithelium.

Radiologic appearances of Barrett carcinoma overlap features of squamous cell carcinoma and secondarily invading gastric carcinoma. Patterns of involvement include infiltrative, varicoid, polypoid, ulcerative and mixed forms (Fig. 29.21).

#### Secondary Neoplasms

Neoplasms may involve the esophagus secondarily by contiguous spread, mediastinal lymph nodal metastases, or hematogenous metastases.

Hematogenous metastasis is the least common route, but occurs particularly from melanoma and carcinomas of the breast and lung.

Metastases to *mediastinal lymph nodes* is the second most common source of esophageal involvement by secondary neoplasms, particularly from lung and breast, although any metastatic mediastinal tumor may invade the esophagus.

Direct tumor extension by *contiguous spread* from carcinomas of adjacent organs is the most frequent route (Fig. 29.22). Malignancies of the pharynx, larynx, thyroid, lung and gastric cardia predominate. Contiguous spread of carcinoma of the stomach into the lower esophagus is well known and may mimic achalasia and produce secondary esophageal motility disturbances.

#### Tumor-like Lesions

Most non-neoplastic lesions that may simulate esophageal neoplasms are quite rare, and only the inflammatory reflux polyp will be discussed. An uncommon endoscopic finding

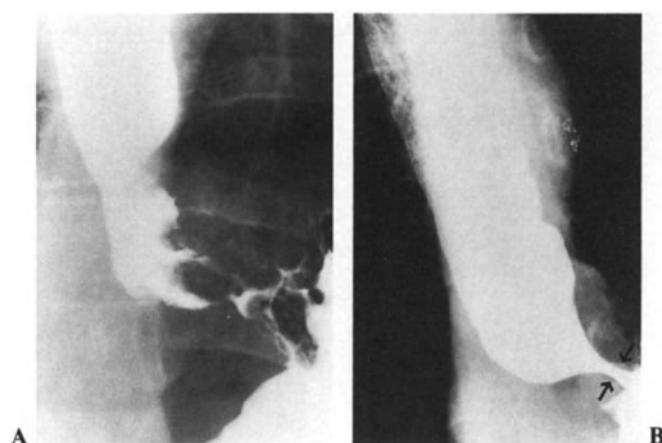


**Fig. 29.22.** A Nodular adenocarcinoma of gastric cardia invading the lower esophagus. B Adenocarcinoma of stomach invading esophagus causing smooth, tapered narrowing (arrows) simulating achalasia. Esophageal dilation with aperistalsis also present.

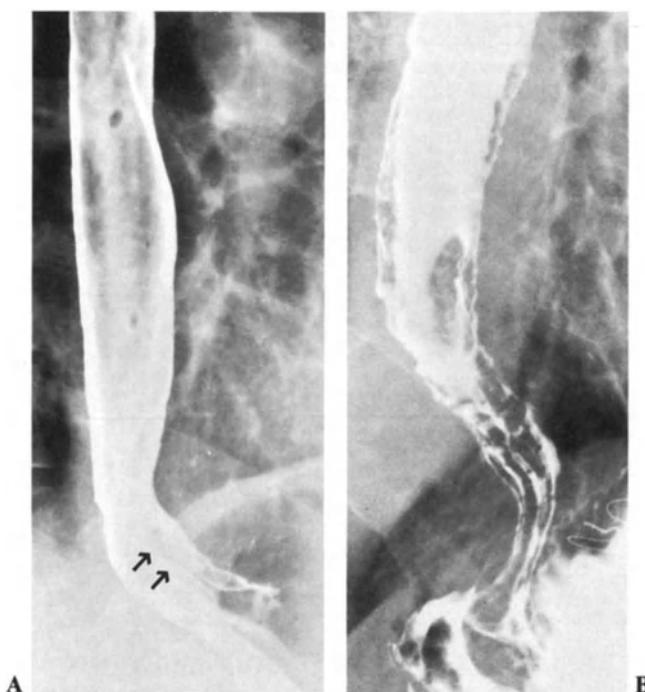


**Fig. 29.23.** A Thickened fold (arrows) at esophagogastric junction shown to be an inflammatory reflux polyp at endoscopy. B Gastric and esophageal varices simulating esophagitis with reflux polyp.

in reflux esophagitis is the presence of an enlarged, inflamed gastric fold near the squamo-columnar mucosal transition. This has been named the *sentinel fold* and is seen radiographically as a polypoid defect at the esophagogastric junction (Fig. 29.23A). The inflammatory reflux polyp must be dif-

ferentiated from a true neoplasm (Fig. 29.22A), or may appear compressible and resemble an esophageal varix (Fig. 29.23B). Endoscopic examination is needed for differentiation.

#### DIVERTICULAR DISEASE

Diverticula of the esophagus are acquired abnormalities usually of the pulsion variety. They may be classified by cause, location or appearance. The prevalence of diverticula increases with age and many are found incidentally. *Pulsion diverticula*, representing mucosal herniations through the muscular wall of the esophagus, may be related to esophageal motility disorders, mechanical obstruction or chronic wear-and-tear forces. The latter is likely the predominant mechanism in the production of the Zenker's diverticulum, and along with motility disturbances the underlying cause of most esophageal diverticula.

*Midesophageal Diverticula.* Diverticula in the midesophagus are most often of the pulsion types with their appearance and cause similar to that of the epiphrenic diverticulum (Fig. 29.24A). However, *traction diverticula* due to extrinsic inflammatory involvement of the esophagus also occur in this location. Fibrotic healing of tuberculous or fungal infection of adjacent lymph nodes exert traction and initiate a focal outpouching of the esophageal wall. Local pulsion forces within the esophagus may also be contributory. Traction diverticula are generally small and have a conical or triangular shape (Fig. 29.24A). They often show changeable deformity during esophageal peristalsis due to longitudinal shortening of the esophagus and mediastinal fixation of the diverticulum.

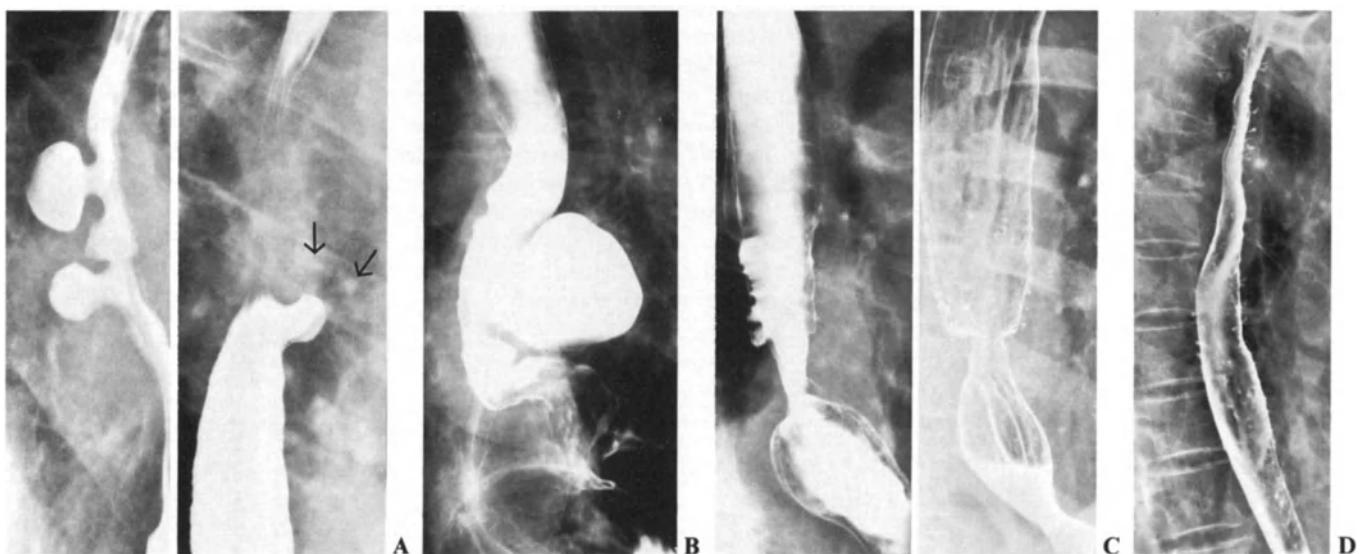


**Fig. 29.24.** A Mid-esophageal diverticula. Two oval pulsion diverticula (left) associated with non-specific esophageal motility disorder. Traction diverticulum (right) with conical deformity and adjacent calcification (arrow). B Epiphrenic diverticulum with large hiatal hernia. Non-specific esophageal motility disorder present fluoroscopically and manometrically. (With permission Ott DJ (1988) Radiologic evaluation of esophageal dysphagia. Curr Probl Diagn Radiol 17: 1–33.) C Two different patients with peptic stricture associated with focal pseudodiverticulosis. (Both with permission Ott DJ (1985) Barium Esophagram. In: Castell DO, Wu WC, Ott DJ (eds) Gastroesophageal reflux disease. Futura Publishing Co, Mount Kisco, pp 109–128.) D Diffuse pseudodiverticulosis of the esophagus.

**Epiphrenic Diverticula.** Epiphrenic diverticula occur in the lower third of the esophagus just above the diaphragm and are usually associated with hiatal hernia. Nearly all are pulsion diverticula. Most are larger than similar diverticula in the midesophagus and vary in size from 1–7 cm. Typical small pulsion diverticula have a smooth, rounded appearance and may be seen to expand concentrically and collapse (Fig. 29.24B). Larger diverticula tend to project to the right and have well-defined necks with a dependent portion acting as a passive reservoir. Retention of food and secretions occur in these large structures and the adjacent esophageal wall may be compressed. A large esophageal diverticulum may be seen on chest films as a soft tissue mass, often containing an air-fluid level.

**Intramural Pseudodiverticulosis.** Intramural pseudodiverticulosis is a rare disease, in which multiple, small outpouchings are seen in the wall of the esophagus. They are thought to represent dilated submucosal glands. Their cause is not clear but most likely relates to chronic mucosal inflammation, usually as a result of reflux esophagitis (Fig. 29.24C). Diffuse pseudodiverticulosis may be associated with stricture, *Candida* esophagitis, herpes esophagitis and even carcinoma of the esophagus (Fig. 29.24D).

## ESOPHAGEAL MOTILITY DISORDER

Esophageal motility disorders are an important cause of esophageal complaints and must be considered when symptoms are not readily explained by a structural abnormality. This section discusses radiographic evaluation of esophageal motility and its abnormalities, with the more common primary motility disorders emphasized.

### General Principles

Following ingestion of barium, a normal primary peristaltic sequence is seen as an aboral contraction wave that obliterates the esophageal lumen, progressively stripping barium from the esophagus (Fig. 29.25). Occasionally, some proximal escape or retrograde flow of barium occurs at the level of the aortic arch because of the lower amplitude pressure normally present at the striated-smooth muscle transition of the esophagus. Proximal escape becomes more frequent with age and may be misinterpreted as abnormal peristalsis.

Esophageal motility disorders are usually classified as primary or secondary (Table 29.5). Primary motility disorders

**Table 29.5. Esophageal motility disorders**

Primary motility disorders
achalasia and variants
diffuse esophageal spasm
non-specific motility disorder
nutcracker esophagus
presbyesophagus?
intestinal pseudo-obstruction
Secondary motility disorders
collagen vascular disease
chemical or physical agents
reflux esophagitis
caustic esophagitis
radiation injury
medication-induced injury
infectious esophagitis
metabolic/endocrine disease
alcoholism
diabetes mellitus
thyroid disease
neuromuscular disorders*
miscellaneous causes

\*See Table 29.2 (similar causes).

involve the esophagus predominantly, while secondary motility disorders affect the esophagus as a consequence of local disease, such as esophagitis, or as the result of a diverse variety of systemic, neurologic and other types of disorders. The classification of primary esophageal motility disorders is still evolving with new disorders, such as the 'nutcracker esophagus', added in recent years.

### Primary Motility Disorders

**Achalasia** is characterized by aperistalsis of the esophagus and dysfunction of the lower esophageal sphincter. Primary peristalsis is absent radiographically on all single swallows, and the lower end of the esophagogastric region shows a smooth tapering that reflects failure of the barium bolus to distend the non-relaxing sphincter (Fig. 29.26A). Repetitive, non-peristaltic contractions may occasionally be seen, a variant called 'vigorous achalasia'. In more severe disease of long duration, the esophagus shows marked dilatation with retention of food, secretions, and barium during the radiographic evaluation (Fig. 29.26B, C).

Achalasia may be mimicked by other causes of lower esophageal narrowing and dysfunction, such as intrinsic and extrinsic neoplasms, peptic stricture, and complicated scleroderma.

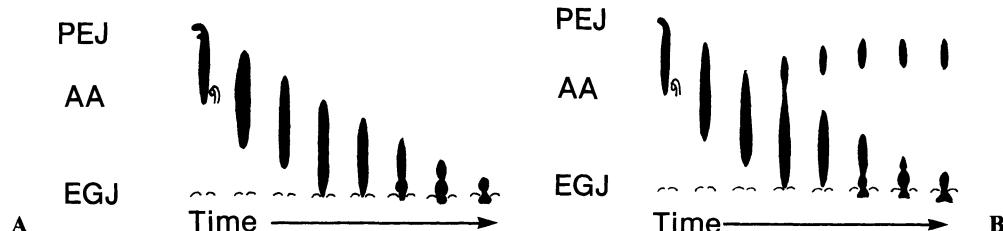


**Fig. 29.25.** A Schematic representation of normal primary peristalsis with lumen-obliterating contraction wave stripping all of the barium from the esophagus. PEJ, pharyngoesophageal junction; AA, aortic arch, EGJ, esophagogastric junction. B Normal primary peristalsis with proximal escape because contraction wave fails to obliterate the esophageal lumen completely at the level of the aortic arch. Peristaltic sequence continues aborally. (Both with permission Ott DJ (1988) Radiologic evaluation of esophageal dysphagia. Curr Probl Diagn Radiol 17: 1–33.)

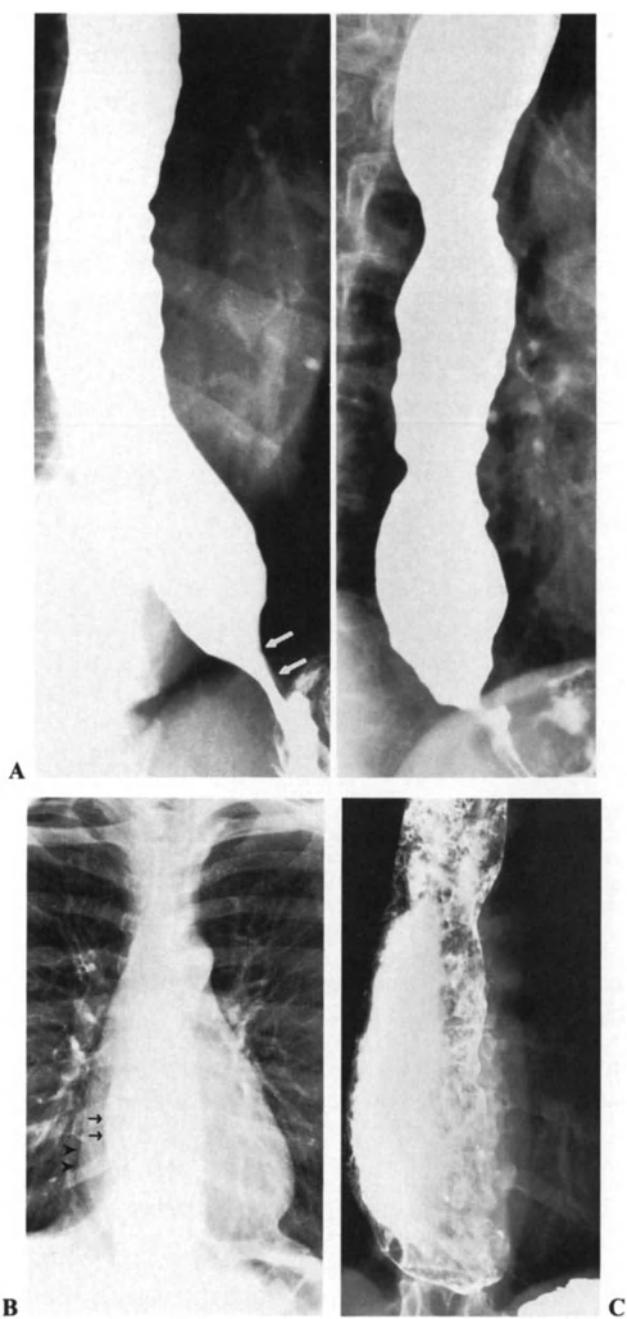


**Fig. 29.26.** A Two different individuals with achalasia. Esophageal dilatation and aperistalsis fluoroscopically in both patients. Smooth beaking (arrows) representing dysfunctional lower esophageal sphincter (left). Repetitive contractions (right) in 'vigorous achalasia'. B Frontal chest film showing right heart border medially (arrows) and markedly dilated achalasic esophagus (arrowheads) laterally. C Esophagram of same patient as in Fig. 29.26B with retention of large amount of food within the dilated esophagus.

Uncommonly, *carcinoma of the gastric cardia* or extrinsic neoplasms involving the esophagogastric region may cause smooth tapering with associated peristaltic abnormalities that resemble achalasia (Fig. 29.22B). Hiatal hernia is seen in most patients with *peptic stricture*, but is uncommon with achalasia. *Scleroderma* typically shows a widened

esophagogastric region, but may be complicated by peptic stricture.

*Diffuse esophageal spasm* is an uncommon esophageal motility disorder. Manometric diagnosis shows intermittently normal peristalsis with simultaneous contractions and usually normal lower esophageal sphincter function. Radiographically, peristalsis is disrupted on some swallows in the smooth muscle segment of the esophagus where non-peristaltic contractions replaced the disrupted primary wave (Fig. 29.27A, B). Spontaneous, obliterating contractions may compartmentalize the esophageal lumen, causing the typical 'corkscrew' or 'rosary-bead' appearance.

*Non-specific esophageal motility disorder* has become a catch-all term used to describe symptomatic patients with motility disorders that defy specific classification. The natural history and clinical significance of this disorder is not fully understood. Manometric abnormalities include intermittent absence of peristalsis, low amplitude peristalsis, occasional repetitive contractions, or incomplete lower esophageal sphincter relaxation. Radiographically, patients may show primary peristaltic disturbance and 'tertiary' contractions that suggest an esophageal motility disorder (Fig. 29.27C, D). However, only minor manometric abnormalities are often seen and the radiographic examination is normal.

*Nutcracker esophagus* is a newly described esophageal motility disorder diagnosed in some patients with chest pain. Manometrically, primary peristalsis is intact, but peristaltic contractions in the lower esophagus have abnormally high amplitude and prolonged duration. In most patients with nutcracker esophagus, the radiographic examination is normal, although non-specific tertiary contractions of uncertain significance may be present.

*Presbyesophagus* has been a controversial entity in recent years. As described originally, presbyesophagus referred to esophageal motility dysfunction associated with aging. The major manometric criteria included decreased incidence of normal peristalsis, increased frequency of tertiary contractions, and occasional lower esophageal sphincter dysfunction. Radiographic abnormalities reflected the manometric changes. However, many patients studied in earlier reports of this entity had neurologic disorders or diabetes mellitus, which may have produced esophageal dysmotility. Recent manometric investigations in healthy older individuals have shown relatively minor changes in esophageal function associated with age. Since many of the manometric criteria of presbyesophagus overlap those used for non-specific esophageal motility disorder, the latter has become the preferred term.

#### Secondary Motility Disorders

Radiographic diagnosis of secondary motility disorders is often based on demonstration of non-specific functional disturbances combined with clinical correlation. *Scleroderma* and several of the other collagen diseases are the most important considerations. Scleroderma is characterized by peristaltic abnormalities in the smooth muscle segment of the esophagus and lower esophageal sphincter hypotension, which predisposes to reflux esophagitis. Radiographically, primary peristalsis is disordered or absent in the lower two thirds of the oesophagus, the organ is often dilated, and hiatal

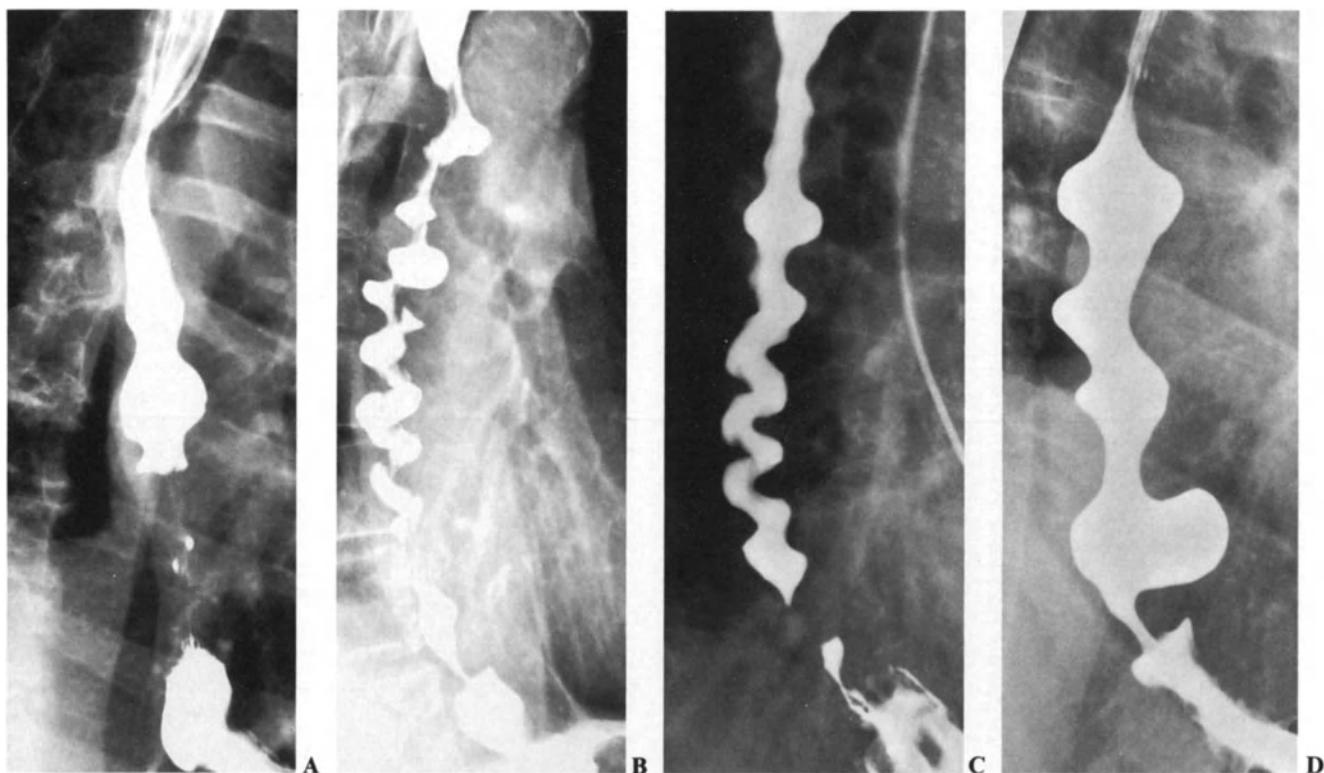
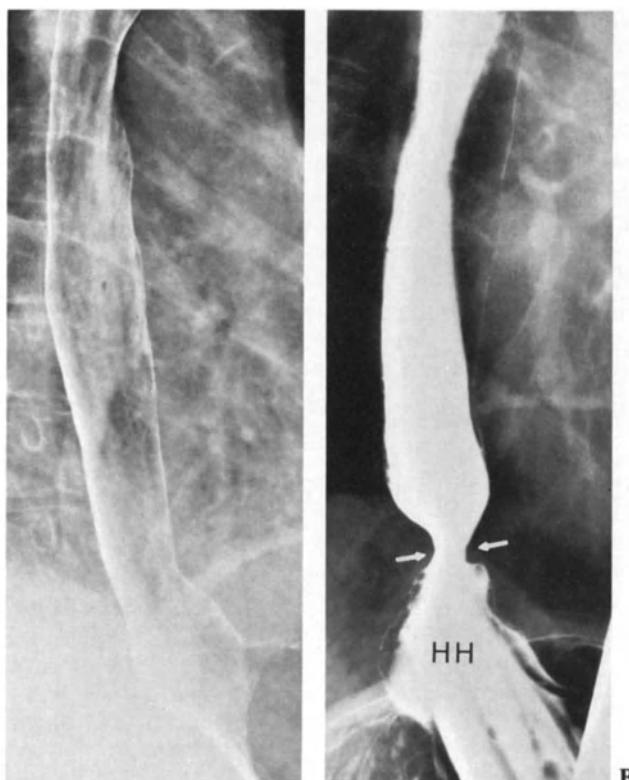


**Fig. 29.27.** A Diffuse esophageal spasm with intermittent disruption of primary peristalsis associated with focally obliterative simultaneous contraction. B Typical 'corkscrew' or 'rosary-bead' appearance in diffuse esophageal spasm. C 89-year-old man without chest pain. Diffuse 'curling' of esophagus seen. Non-specific esophageal motility disorder manometrically. Clinical and manometric correlation important for specific diagnosis. D Elderly man with no esophageal symptoms showing simultaneous tertiary contractions. (All with permission Ott DJ (1988) Radiologic evaluation of esophageal dysphagia. *Curr Probl Diagn Radiol* 17: 1–33.)



hernia is typically present (Fig. 29.28A). Peptic stricture may complicate scleroderma and then more closely mimic achalasia (Fig. 29.28B). Other gastrointestinal abnormalities that may be seen in scleroderma include *megaduodenum*, *small bowel dilatation*, and *eccentric sacculations* involving the *small bowel or colon*.

#### MISCELLANEOUS ESOPHAGEAL DISORDERS

**Esophageal Varices.** Esophageal varices are most commonly of the 'uphill' variety due to portal hypertension from cirrhosis of the liver. Other causes include thrombosis of the splenic, portal or hepatic veins, and compression by tumors or congenital stenosis of the same venous structures. Varices appear as changeable fold thickening or as serpiginous and polypoid defects in the lower esophagus. They are best shown by mucosal relief technique (Fig. 29.29A). The patient is examined in the horizontal oblique position and a small amount of dense barium suspension or paste is given. Swallowing is suspended to avoid squeezing the blood from the distending varices (Fig. 29.29B). Various respiratory

**Fig. 29.28.** A Scleroderma with hiatal hernia and absence of peristalsis fluoroscopically in smooth muscle segment of esophagus. Note changes at the lung bases. B Scleroderma with hiatal hernia (HH) and peptic stricture (arrows).

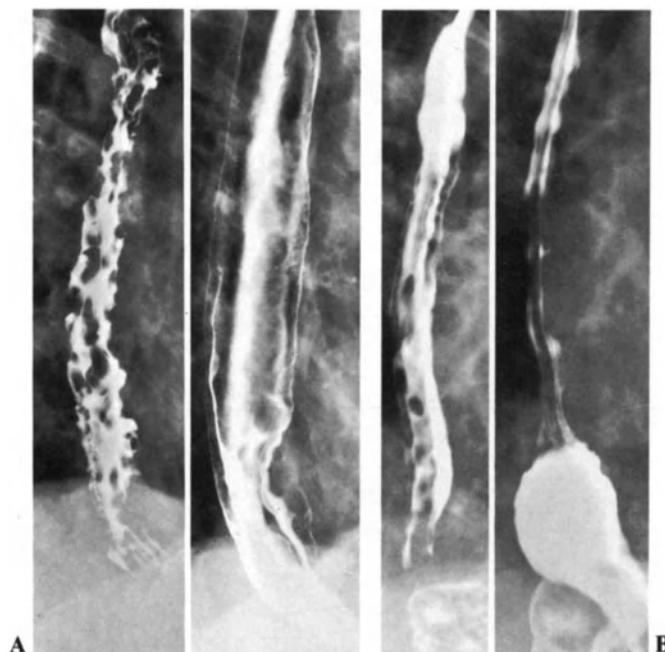


**Fig. 29.29.** A Esophageal varices shown extensively on mucosal relief view (left) but less prominent on double-contrast examination (right) B Varices well shown on mucosal relief film (left) but emptying with a peristaltic stripping wave (right).

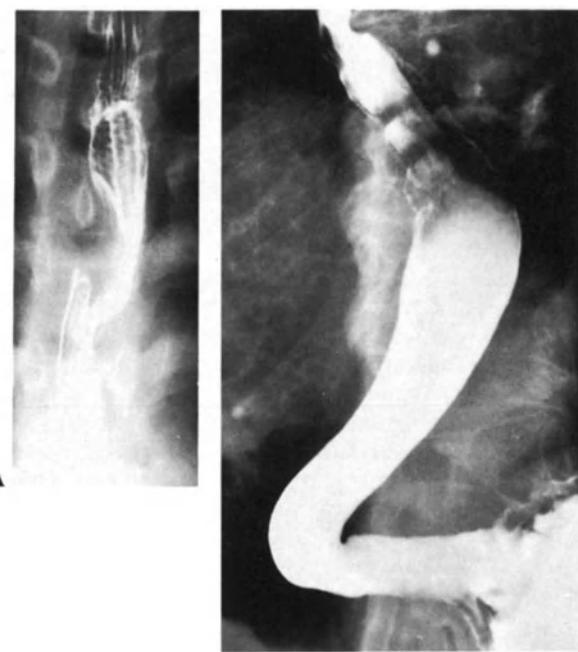


**Fig. 29.30.** A Aberrant right subclavian artery causing an oblique defect on the esophagus in a patient with dysphagia. B Elderly patient with dysphagia showing acute angulation of the lower esophagus due to aortic tortuosity. (With permission Gelfand DW, Ott DJ (1981) Anatomy and technique in evaluating the esophagus. Semin Roentgenol 16: 168–182.)

maneuvers and parenteral anticholinergics may also be used.

**Traumatic Effects.** Esophageal trauma may result from foreign body, surgery, endoscopic and therapeutic procedures, blunt or penetrating injury, and post-emetic trauma. *Esophageal perforation* is the most serious consequence and is often iatrogenic from endoscopy, dilation procedures, or surgery. Postemetic trauma related to severe vomiting shows a spectrum of injury which includes the *Mallory–Weiss tear*, intramural hematoma, and spontaneous *Boerhaave rupture*. Water-soluble contrast material should be used for initial examination of the esophagus for suspected trauma. If perforation is not present, examination with barium should follow for detection of more subtle abnormalities.

**Foreign Bodies.** A wide variety of foreign objects may be purposely swallowed by infants, children or psychiatric patients and by adults unintentionally. The most common foreign body found in adults is a *meat bolus* that lodges at an area of anatomic or pathologic narrowing. A lower esophageal mucosal ring or peptic stricture is the usual pathologic cause of narrowing. An impacted meat bolus may be dislodged by the use of glucagon and a gas-producing agent or it may be removed endoscopically. Proteolytic enzyme digestion of a food impaction is no longer recommended due to the risk of esophageal perforation.

**Post-procedural Effects.** Surgery or therapeutic endoscopy on the esophagus is done for various reasons (Table 29.6). Many of these procedures produce characteristic changes, such as the Nissen fundoplication, or may be associated with a variety of complications. An understanding of the procedure performed, its typical radiographic normal appear-

**Table 29.6.** Surgical and therapeutic endoscopic procedures performed for esophageal disease

Antireflux surgery
Nissen fundoplication
Belsey Mark IV procedure
Angelchik device
peptic stricture repairs
intrathoracic fundoplication
Collis gastroplasty
Motility disorders
cricopharyngeal myotomy
Heller myotomy (achalasia)
long myotomy (diffuse spasm)
diverticular surgery
Carcinoma surgery
esophagogastrectomy
jejunal/colon interposition
Miscellaneous surgical procedures
congenital anomalies
esophageal varices
trauma/foreign bodies
non-peptic stricture
Therapeutic endoscopy
foreign body removal
endoscopic pneumatic dilatation
peptic stricture dilatation
sclerotherapy (varices)
endoprostheses placement

ances, and the possible complications are required properly to evaluate these patients.

**Extrinsic Effects.** Extrinsic structural lesions are easily detected on films of the distended esophagus if the abnormality encroaches on the esophageal lumen.

In the neck, thyroid enlargement from benign or malignant disease can compress and displace the cervical esophagus, often affecting the trachea as well. Neoplastic or inflammatory disease of the mediastinum and enlargement of the heart are additional causes of extrinsic involvement. Symptomatic compression of the esophagus by the thoracic aorta or by aberrant vessels can also occur.

*Dysphagia lusoria* results from a symptomatic impression on the upper thoracic esophagus from an aberrant right subclavian artery, which usually passes behind the esophagus producing an oblique defect (Fig. 29.30A). Most patients with this anomaly, however, do not have dysphagia. *Dysphagia aortica* describes symptomatic compression of the lower esophagus by a tortuous descending thoracic aorta (Fig. 29.30B). Although displacement and compression of the lower esophagus by an atherosclerotic aorta is frequently seen in the elderly, most patients will not have dysphagia. Cardiac enlargement and kyphosis of the thoracic spine associated with aortic tortuosity may aggravate the symptoms.

#### REFERENCES AND SUGGESTIONS FOR FURTHER READING

- SALIVARY GLANDS
- Lowman RM, Cheng GK (1976) Diagnostic roentgenology. In : Rankow RM, Polages IM (eds) Diseases of the Salivary Glands. WB Saunders, Philadelphia, pp 54–88
- Som PM, Shugar JMA, Train JS, Biller HF (1981) Manifestations of parotid gland enlargement: radiographic, pathologic, and clinical correlations. Radiology 141: 415–426
- Whyte AM, Hayward MWJ (1989) Agenesis of the salivary glands. Br J Radiol 62: 1023–1025
- OROPHARYNX
- Curtis DJ, Cruess DF, Berg T (1984) The cricopharyngeal muscle: a videorecording review. AJR 142: 497–500
- Ekberg O, Nylander G (1985) Double-contrast examination of the pharynx. Gastrointest Radiol 10: 263–271
- Jones B, Kramer SS, Donner MW (1985) Dynamic imaging of the pharynx. Gastrointest Radiol 10: 213–224
- Knuff TE, Benjamin SB, Castell DO (1982) Pharyngoesophageal (Zenker's) diverticulum: a reappraisal. Gastroenterology 82: 734–736
- Seaman WB (1983) Pharynx-radiology. In: Margulis AR, Burhenne HJ (eds). Alimentary Tract Radiology, vol 1, 3rd edn. C.V. Mosby, St. Louis, pp 491–518
- ESOPHAGUS
- Agha FP (1987) Secondary neoplasms of the esophagus. Gastrointest Radiol 12: 187–193
- Agha FP, Wilson JAP, Nostrand TT (1986) Medication-induced esophagitis. Gastrointest Radiol 11: 7–11
- Boyle JT (1982) Congenital disorders of the esophagus. In: Cohen S, Soloway RD (eds) Diseases of the Esophagus. Churchill Livingstone, New York, pp 97–120
- Dodds WJ (1983) Esophagus-radiology. In: Margulis AR, Burhenne HJ (eds) Alimentary Tract Radiology, vol 1, 3rd edn. C.V. Mosby, St. Louis, pp 529–603
- Dodds WJ (1988) The pathogenesis of gastroesophageal reflux disease. AJR 151: 49–56
- Gelfand DW (1984) Gastrointestinal Radiology. Churchill Livingstone, New York
- Hupscher DN (1986) Technique of examination of the esophagus. Diagn Imag Clin Med 55: 241–253
- Katz PO, Castell DO (1985) Esophageal motility disorders. Am J Med Sci 290: 61–69
- Levine MS (1988) Barrett's esophagus: a radiologic diagnosis? AJR 151: 433–438
- Levine MS, Dillon EC, Saul SH, Laufer I (1986) Early esophageal cancer. AJR 146: 507–512
- Levine MS, Moolten DN, Herlinger H, Laufer I (1986) Esophageal intramural pseudodiverticulosis: a reevaluation. AJR 147: 1165–1170
- Ott DJ (1983) Radiologic evaluation of the esophagus. In: Castell DO, Johnson LF (eds) Esophageal function in health and disease. Elsevier Biomedical, New York, pp 211–235
- Ott DJ (1988) Radiologic evaluation of esophageal dysphagia. Curr Probl Diagn Radiol 17: 1–33
- Ott DJ, Gelfand DW, Wu WC, Castell DO (1984) Esophagogastric region and its rings. AJR 142: 281–287
- Ott DJ, Kelly RJ, Gelfand DW (1981) Radiographic effects of cold barium suspensions on esophageal motility. Radiology 140: 830–833
- Ott DJ, Richter JE, Wu WC, Chen YM, Gelfand DW, Castell DO (1986) Radiologic and manometric correlation in 'nutcracker esophagus'. AJR 147: 692–695
- Rivkin L, Bremner CG, Bremner CH (1984) Pathophysiology of mid-esophageal and epiphrenic diverticula of the oesophagus. S Afr Med J 66: 127–129
- Vahey TN, Maglente DDT, Chernish SM (1986) State-of-the-art barium examination in opportunistic esophagitis. Dig Dis Sci 31: 1192–1195
- Yamada A (1979) Radiologic assessment of resectability and prognosis in esophageal carcinoma. Gastrointest Radiol 4: 213–218

## CHAPTER 30

# THE STOMACH AND DUODENUM

D.W. Gelfand

---

The barium examination of the stomach and duodenum is often the primary method of evaluation of these organs. Although the upper gastrointestinal series (barium meal) has been partially replaced by endoscopy, it still remains a mainstay of general clinical practice.

### EQUIPMENT

Two types of fluoroscopic equipment are employed for the upper gastrointestinal study. The *conventional fluoroscope*, with an under-table tube and a spot-film device cantilevered above the table, constitutes the majority of machines in current use. However, the *remote control fluoroscopic table*, with an overhead tube and under-table spot-film device, is being increasingly utilized. To a modest extent, the filming sequence during an upper gastrointestinal series is determined by the type of equipment employed.

The singular advantage of the conventional fluoroscope is the examiner's proximity to the patient and the ability manually to compress the stomach and duodenum. Its disadvantages are the short tube-film distance and the inability to angle the beam during fluoroscopy for the purpose of acquiring unobstructed images of the stomach or duodenum if overlapped by other structures.

The remote control fluoroscope has the advantages of superior radiographic geometry, ability to angle the beam during fluoroscopy and filming, and complete radiation protection for personnel. It also provides the convenience of working while sitting down and without wearing a leaded apron or gloves. Also, all films are taken under fluoroscopic control, which increases the accuracy of positioning. However, the proximity of the examiner to the patient is lost, which makes handling the patient more difficult and precludes manual palpation.

In most institutions, radiographs are obtained on individual cassettes using conventional film-screen technology.

This procedure has the advantages of simplicity and reliability, and produces images of maximum possible sharpness. To reduce motion unsharpness, rare earth screens should be employed. Rare earth screens also have the advantage of partial rejection of scattered radiation due to their decreasing sensitivity at lower energies.

Alternatively, photofluorography with a 100-mm spot-film camera may be used for spot-filming. The spot-film camera has the advantage of convenience, speed and less exposure to radiation. However, the images are of lower resolution than those acquired with standard cassettes. Electronic digital spot-filming has recently become available, but existing devices using  $1024 \times 1024$  matrices produce images of resolution lower than either conventional cassettes or photo-spot cameras. In Europe and Japan examinations are often conducted entirely with spot-films, while in North America, most examinations combine spot-films with radiographs obtained using an overhead tube and table Bucky device.

The *kilovoltage* employed for barium radiography should be in the range of 90–125 kV. If lower kilovoltages are employed, motion unsharpness becomes a problem in many patients and the barium may be poorly penetrated radiographically. Kilovoltages higher than 125 kV encounter the problems of increased scattered radiation and decreased contrast between the barium suspension and soft tissues.

### MATERIALS

Single and double-contrast studies require barium sulfate suspensions with differing characteristics. *Single-contrast* examinations are performed using suspensions of 60%–100% weight/volume (w/v) density while double-contrast examinations employ suspensions of 200%–250% w/v. The best available materials for single-contrast examinations are of moderate or high viscosity to maximize suspension

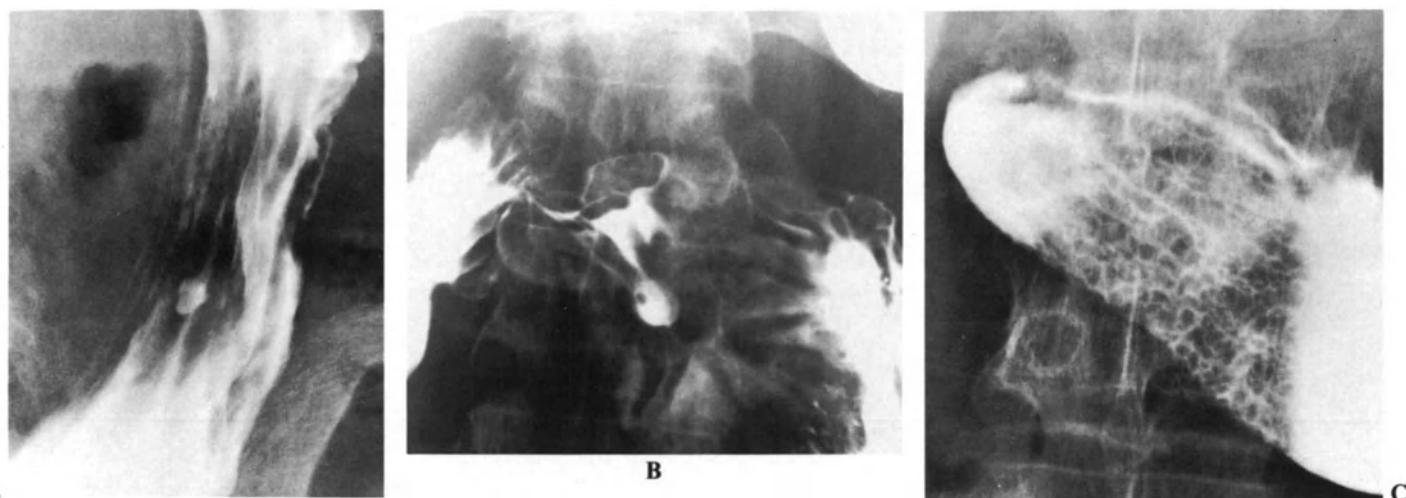


**Fig. 30.1.** A Compression during a single-contrast study showing a small benign gastric ulcer surrounded by edema. B Compression during a double-contrast examination demonstrating a small antral ulcer. C Compression film obtained during a double-contrast study using high-density barium and showing the areae gastricae.

stability. Barium suspensions for *double-contrast* examinations are of low viscosity to improve delineation of small surface features such as the area gastricae. In performing double-contrast studies, many radiologists employ a lower density suspension during the compression or mucosal relief phases of the examination, while using a high-density suspension during the actual double-contrast filming.

The double-contrast examination also requires use of gas-producing granules or tablets. These universally incorporate sodium bicarbonate, citric or tartaric acid, and an antifoaming agent. The products are formulated to dissolve rapidly and release 300–450 ml of carbon dioxide.

*Pharmacologic aids* may be used during the double-contrast examination to paralyze the stomach and to prevent rapid progress of the barium suspension into the small bowel where it might obscure the distal half of the stomach. In Europe and Japan, 10–20 mg of *Buscopan* (hyoscine-n-butylbromide) intravenously is most often employed. In the United States, 0.1–0.25 mg of intravenous *glucagon* is used, since *Buscopan* is unavailable.

#### EXAMINATION TECHNIQUES

Radiologic examinations of the stomach and duodenum use a combination of the following techniques: *compression*, *mucosal relief*, *distension with barium suspension*, and *double-contrast*. The *single-contrast* examination employs the first three techniques mentioned. The '*double-contrast*' examination should ideally incorporate all four techniques when possible. This latter, *multiphasic examination* provides the highest possible accuracy and is the examination employed in Japan for detection and evaluation of gastric carcinoma. Somewhat lesser accuracy is achieved by *single-contrast* examinations or by simple examinations employing only *double-contrast* technique. The *multiphasic* examination should be employed for all patients sufficiently cooperative to allow a satisfactory study to be obtained. Recent investiga-

tion suggests that simple single and double-contrast studies fail to diagnose approximately 20% of lesions visible on multiphasic examinations.

*Compression* is the most important single-contrast method of examining the stomach and duodenum. The application of compression brings the front and back walls of the stomach or duodenum into apposition, thinning the barium column and making small ulcers (Fig. 30.1) and filling defects easily visible. Compression is most useful in the distal two thirds of the stomach and in the duodenum. However, obese or unusually muscular individuals may be difficult to examine. Compression technique is capable of showing lesions and structural details of all sizes down to and including gastric erosions and the area gastricae. A major disadvantage is its limited ability to examine the proximal stomach and those stomachs that are in a high transverse position beneath the ribs.

*Mucosal relief* films are obtained by radiographing the stomach prone and supine with a small amount of barium (Fig. 30.2). The technique is specifically useful in demonstrating the character of the gastric rugae. Mucosal relief films also serve as a partial substitute for compression films in patients whose physique or physical condition does not allow an adequate compression examination.

*Distension with barium suspension* provides an outline of the barium-filled organ and of any mucosal abnormality traversed tangentially by the beam (Fig. 30.3). To insure tangential views of most of the gastric mucosal surface, 3–5 films are taken in varying positions. Distended views of the duodenum are relatively more productive than those of the stomach because of the smaller diameter of the duodenum. The major disadvantage of the barium-distended view is that small lesions are easily obscured by the overlying mass of barium suspension, particularly gastric lesions.

*Double-contrast* films (Fig. 30.4) provide the greatest mucosal detail of any available examination technique. The best visualization of a lesion occurs when it lies on the dependent wall of the stomach or duodenum, since barium suspen-

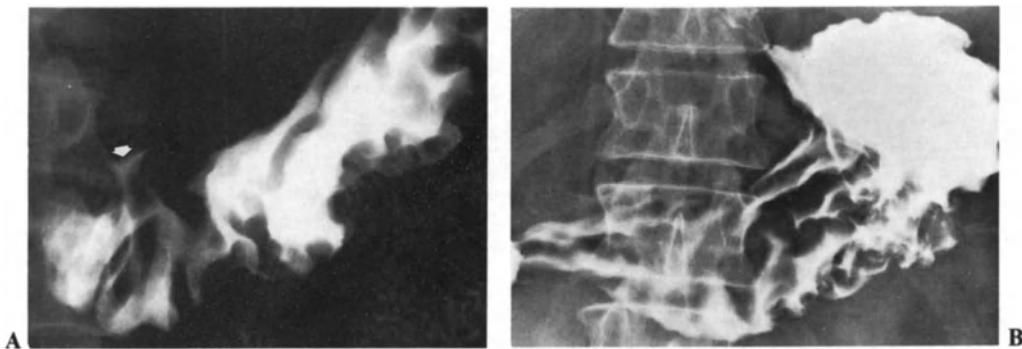


Fig. 30.2. A Prone mucosal relief film obtained with a small amount of barium demonstrating a lesser curve ulcer (arrow). B Thickening of folds in a patient with gastric lymphoma demonstrated on a supine mucosal relief film.

sion collected on the dependent wall delineates small ulcers and filling defects with exquisite detail. However, lesions on the non-dependent surface are not reliably demonstrated. To ensure that most of the mucosal surface of the stomach is demonstrated in double-contrast while in a dependent position, multiple projections are utilized. Nevertheless, most of the anterior wall of the stomach and duodenum is never well demonstrated during routine double-contrast examinations. For this reason, double-contrast filming of the stomach and duodenum must be combined with compression and/or prone mucosal relief filming, since the latter technique demonstrate lesions on the anterior wall of the stomach and duodenum with greater accuracy.

#### THE EXAMINATIONS

**Single-contrast examination.** The examination begins with the table upright and with the patient's back to the table. The patient ingests 2–4 swallows of barium suspension and its passage through the esophagus is observed. A careful compression/palpation examination of the stomach is performed (Fig. 30.1). The table is lowered to the horizontal

position and supine and prone mucosal relief films are obtained (Fig. 30.2). The patient is then placed in the right prone oblique position and distended views of the esophagus are acquired. Single swallows are used to assess esophageal motility if indicated. A mucosal relief view of the esophagus is also obtained, preferably utilizing a swallow or two of dense, 250% w/v barium suspension. With the stomach now distended, the following views are taken of the stomach and duodenum: prone, right-prone oblique, and right lateral (these may alternatively be obtained at the conclusion of the study using the overhead tube). Barium-distended views of the duodenum also are obtained at this point. The patient is then turned to the supine position and double-contrast films of the distal stomach (Fig. 30.4C) and duodenal bulb are taken. Finally, the patient is returned to the erect position and a compression examination of the duodenal bulb is performed. Alternatively, the compression examination of the bulb may be performed using an inflatable paddle under the abdomen with the patient in the prone position.

The major limitation of the single-contrast examination is its lesser ability to demonstrate gastric erosions, gastric polyps, and small lesions of the proximal third of the stomach. Also, the examination may be difficult to perform

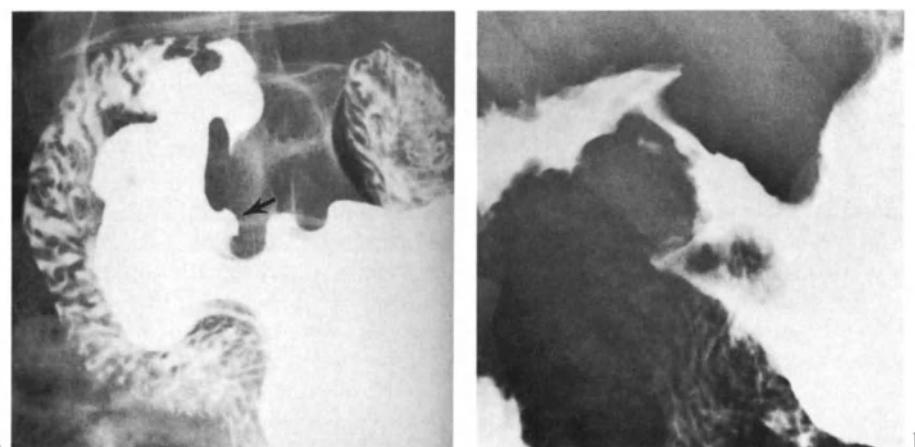
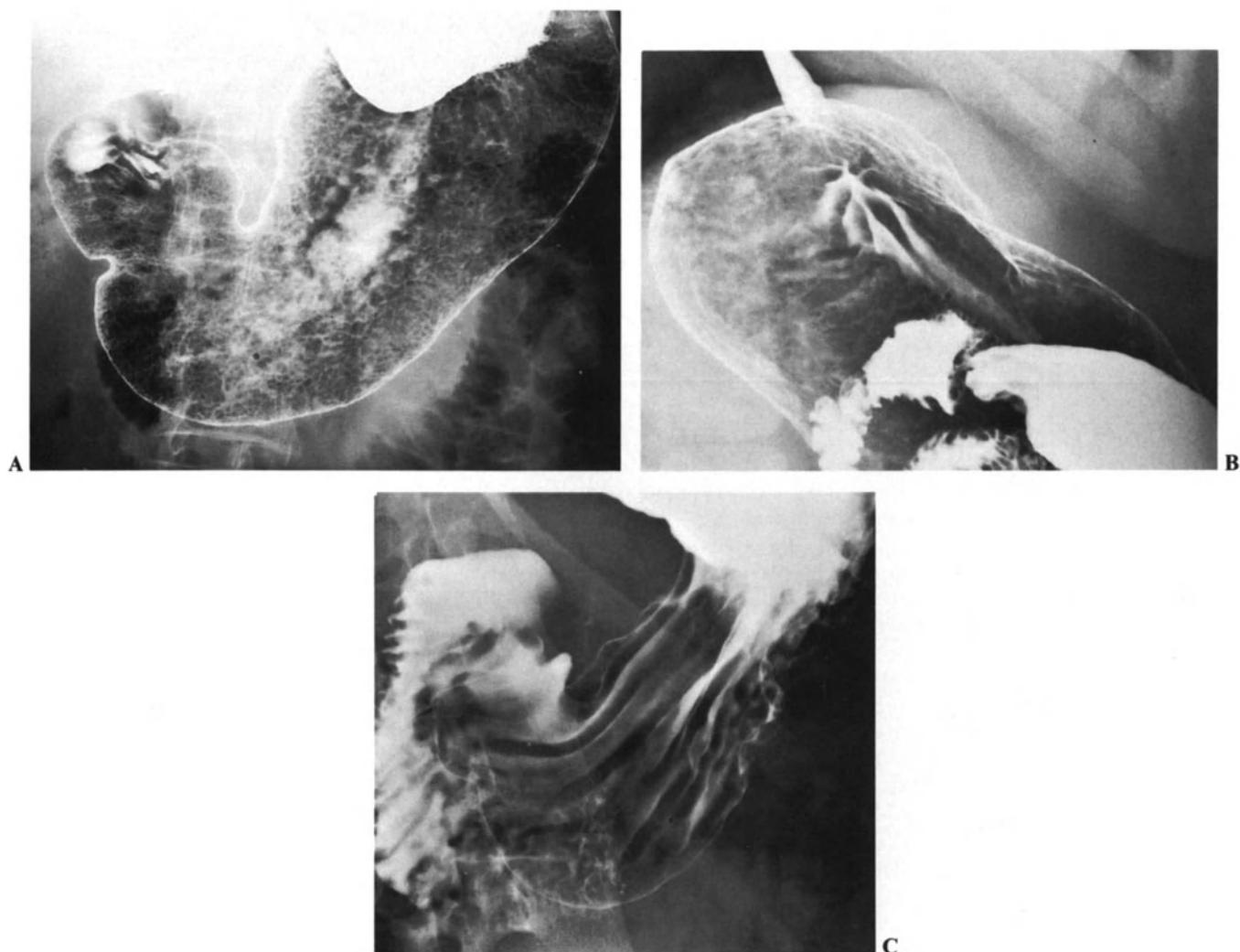


Fig. 30.3. A Barium-filled view demonstrating a lesser curve ulcer (arrow), which is viewed tangentially. B Barium-filled view demonstrating a constricting, circumferential carcinoma of the gastric antrum.



**Fig. 30.4.** A Supine double-contrast view demonstrating the areae gastricae. (Reproduced with permission from Gelfand DW (1986) *The stomach*. In: Grainger, Allison (eds) *Diagnostic Radiology*. Churchill Livingstone, Edinburgh.) B Right lateral double-contrast view demonstrating normal converging folds at the esophagogastric junction. (Reproduced with permission from Gelfand DW (1984) *Gastrointestinal Radiology*. Churchill Livingstone, New York.) C Left posterior oblique double-contrast film of the gastric antrum taken during a single-contrast study and showing the normal rugae. (Reproduced with permission from Gelfand DW (1984) *Gastrointestinal Radiology*. Churchill Livingstone, New York.)

optimally on patients who are obese or muscular. In such individuals, a double-contrast or multiphasic examination should be performed if possible.

**Multiphasic examination.** The multiphasic examination incorporating double-contrast filming begins in an identical fashion. First, however, the patient receives an injection of glucagon or Buscopan to induce gastroparesis. A small amount of barium suspension is ingested by the patient and compression and mucosal relief filming of the stomach are performed as described above. The table is returned to the upright position and the double-contrast filming commences. With the patient facing away from the table and turned 45° to the left, gas-producing granules are ingested with 15 cc of water. As rapidly as possible, the patient drinks 4–5 oz of the 250% w/v barium suspension, providing double-contrast views of the esophagus. The esophagus is distended by carbon dioxide while the ingested barium suspension flows down and coats the esophageal mucosa. Tim-

ing of these films is critical for success.

Following the above, the table is lowered to the horizontal position and the patient is rolled 360° twice. This coats all surfaces of the stomach and breaks up residual bubbles. The following films of the stomach are obtained: supine (Fig. 30.4A), left-supine oblique, right-supine oblique with the table elevated 45°, right lateral (Fig. 30.4B), right prone oblique and prone. When the double-contrast examination of the stomach is completed, the remainder of the examination is pursued in a manner identical to that of the single-contrast study described above. Distended and mucosal relief views of the esophagus are obtained in the right prone oblique position. Filled and double-contrast views of the duodenum are also obtained. Finally, a compression examination of the duodenal bulb is performed.

The above examination closely parallels the Japanese-type examination originated by Ichikawa and Shirakabi in its use of all four available examination techniques.

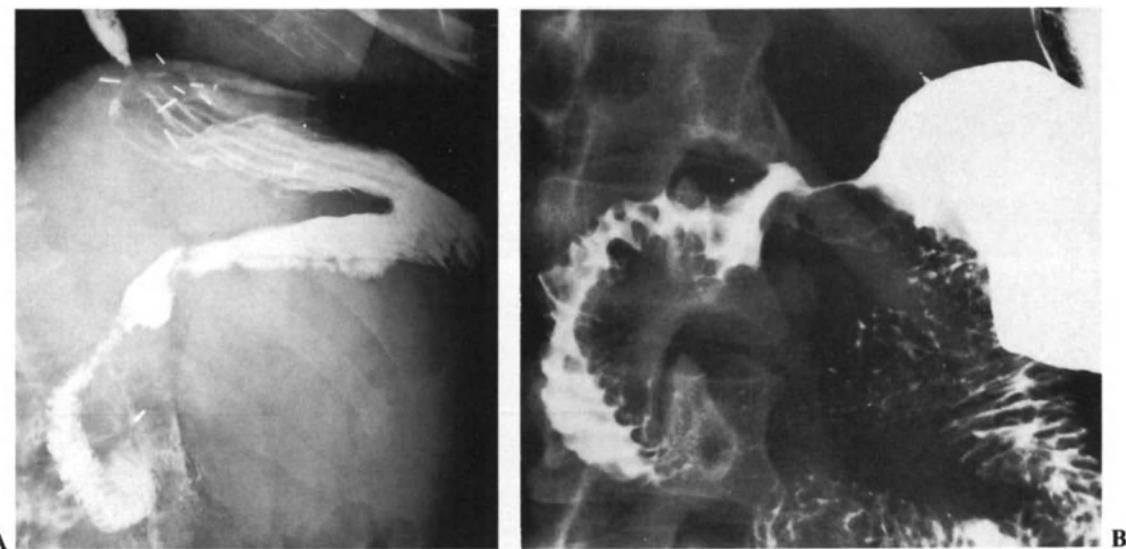


**Fig. 30.5.A** Upward displacement of the entire stomach by a large lymphomatous mass in the region of the pancreas. (Reproduced with permission from Gelfand DW (1984) Gastrointestinal Radiology. Churchill Livingstone, New York.) **B** Displacement of the duodenal loop and gastric antrum by carcinoma of the pancreas. (Reproduced with permission from Gelfand DW (1984) Gastrointestinal Radiology. Churchill Livingstone, New York.)

#### NORMAL STOMACH AND DUODENUM

The stomach is anatomically divided into three parts: fundus, body and antrum. The *gastric fundus* lies above a transverse line drawn through the esophagogastric junction. The *body of the stomach* is that portion lying between the gastric fundus and a line transecting the stomach at the *incisura angularis*. The *gastric antrum* extends from the *incisura angularis* to the pyloric canal. In slender individuals, the stomach is dependent and roughly J-shaped. In stout patients, the stomach extends transversely across the upper abdomen and may lie almost totally beneath the costal cartilages.

The mucosal surface of the stomach incorporates two features that are visible radiographically. The *rugae*, or longitudinal folds, tend to parallel the long axis of the stomach (Fig. 30.4C) although there may be one or two circular folds present in the antrum. The rugae are easily visible on mucosal relief films obtained when the stomach contains a small amount of barium suspension. However, with sufficient distension the folds may disappear entirely. The *areae gastricae* are small tufts of gastric mucosa measuring 1–3 mm in size (Fig. 30.4A) and representing the distribution of a single arteriole. The *areae gastricae* can be seen on approximately 75% of well performed double-contrast studies.

A unique pattern of folds is seen at the esophagogastric junction. When viewed *en face* on double-contrast studies, radiating folds are visible extending from the orifice of the junction (Fig. 30.4B). Additionally, the superior aspect of the orifice may be hooded by a single curved fold.

The duodenum describes a C-shaped curve extending from the pyloric canal to the junction of the duodenum and jejunum at the ligament of Treitz. The duodenal loop is conventionally divided into four segments: the duodenal cap, the descending limb containing the papillae, the transverse

limb extending behind the superior mesenteric artery, and the limb ascending to the ligament of Treitz. Together, these segments roughly encircle the head of the pancreas.

The duodenal bulb (or cap) is usually devoid of mucosal folds. However, circular folds typical of the small intestine are present throughout the remainder of the duodenum. These are normally no more than 2 mm in thickness and are straight and smooth in contour when the duodenum is distended. The *papilla of Vater* (major papilla) is visible as an ovoid filling defect on the medial aspect of the second portion of the duodenum. Extending inferiorly from the papilla of Vater is a consistently present longitudinal fold. The smaller *minor papilla* is located proximal to the major papilla on the anterior wall of the duodenum and may be seen on prone double-contrast views of the duodenum.

#### EXTRINSIC MASSES

The stomach is loosely suspended by the lesser omentum and is easily displaced by a perigastric mass or an enlarged adjacent organ. The left lobe of the liver lies anterior to the stomach and its enlargement displaces the stomach posteriorly. Splenic enlargement results in anteromedial displacement. Left renal enlargement displaces the body of the stomach anteriorly. Pancreatic enlargement or enlargement of adjacent retroperitoneal lymph nodes displaces the distal stomach superiorly (Fig. 30.5A).

The duodenum, being retroperitoneal in location, is somewhat less sensitive to displacement by intra-abdominal masses. However, displacement of the duodenal loop is an excellent indicator of enlargement of the head of the pancreas (Fig. 30.5B) or adjacent retroperitoneal lymph nodes. Enlargement of the right kidney medially displaces the descending limb of the duodenum. Occasionally, the superior mesenteric artery may obstruct the third portion of the

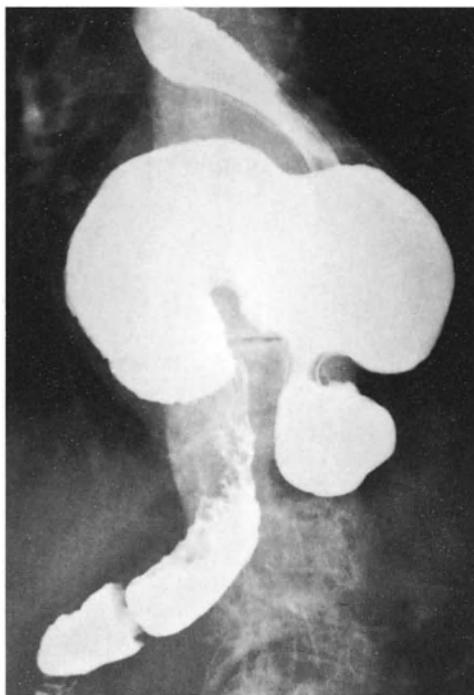


**Fig. 30.6.** Partial gastric volvulus within a large hiatus hernia.

duodenum, causing *superior mesenteric artery syndrome*. Such patients demonstrate dilation of the proximal duodenum and little progress of barium beyond the crossing of the superior mesenteric artery. The syndrome is most frequently associated with prolonged bed rest (body cast syndrome), severe weight loss, and massive burns.

#### GASTRIC VOLVULUS

*Gastric volvulus* is most frequently encountered in patients with a very large hiatal hernia or traumatic rupture of the left diaphragm following blunt abdominal trauma. Two varieties of gastric volvulus have been described.

*Organo-axial volvulus* describes a twist of the stomach occurring through the esophagogastric junction and pyloric region, with rotation of the stomach around a line joining the two regions.

*Mesentero-axial volvulus* is a less frequent type in which the stomach rotates on its own mesentery.

Partial volvulus occurs in association with large hiatal hernias, but is usually asymptomatic (Fig. 30.6). Volvulus causing gastric obstruction or compromise of the gastric circulation is most often found in association with a post-traumatic tear of the left hemidiaphragm.

#### CONGENITAL AND DEVELOPMENTAL ABNORMALITIES

The most frequently encountered congenital anomaly of the stomach is the presence of a *gastric diverticulum* (Fig. 30.7) located near the esophagogastric junction. These are true diverticula containing all layers of the gastric wall and are mildly contractile when observed fluoroscopically.

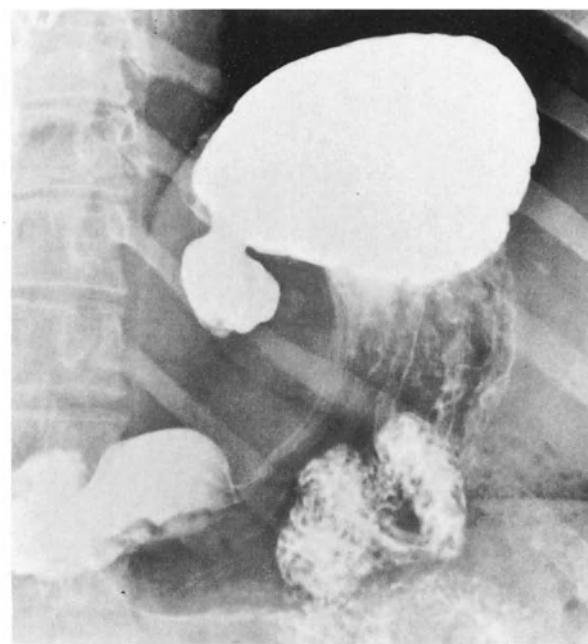


**Fig. 30.7.** Gastric diverticulum in its most common location adjacent to the esophagogastric junction.

*Antral web* is a diaphragm composed of mucosal and submucosal tissues found several centimeters proximal to the pyloric canal. It demarcates a chamber that lies between the main portion of the stomach and duodenal bulb. The opening through the diaphragm may be small enough to cause symptoms of gastric outlet obstruction.

*Hypertrophic pyloric stenosis* may persist from childhood into adult life, exhibiting the classic signs of an elongated, narrowed pyloric canal surrounded by a muscle mass that impinges on the base of the distal gastric antrum and duodenal bulb. A similar radiographic appearance is produced by the adult variety of hypertrophic pyloric stenosis, which may be retained from childhood or may be associated with chronic antral inflammatory processes.

*Duodenal diverticula* are developmental rather than congenital and increase in prevalence with age. They most often occur on the medial aspect of the second portion of the duodenum in proximity to the papilla of Vater. The papilla is usually located within the neck of the diverticulum or within the diverticulum itself. Although partially digested food may be retained in the diverticulum, they are regarded as asymptomatic. Their main importance lies in the difficulty they present for endoscopic cannulation of the major papilla and in performance of endoscopic papillotomy.

#### GASTRITIS

The radiologic diagnosis of *gastritis* is often unreliable and is complicated by poor correlation between radiologic, endoscopic, histologic, and clinical findings. Several reasonably well-defined types of gastritis do exist, however, and are amenable to radiologic detection.

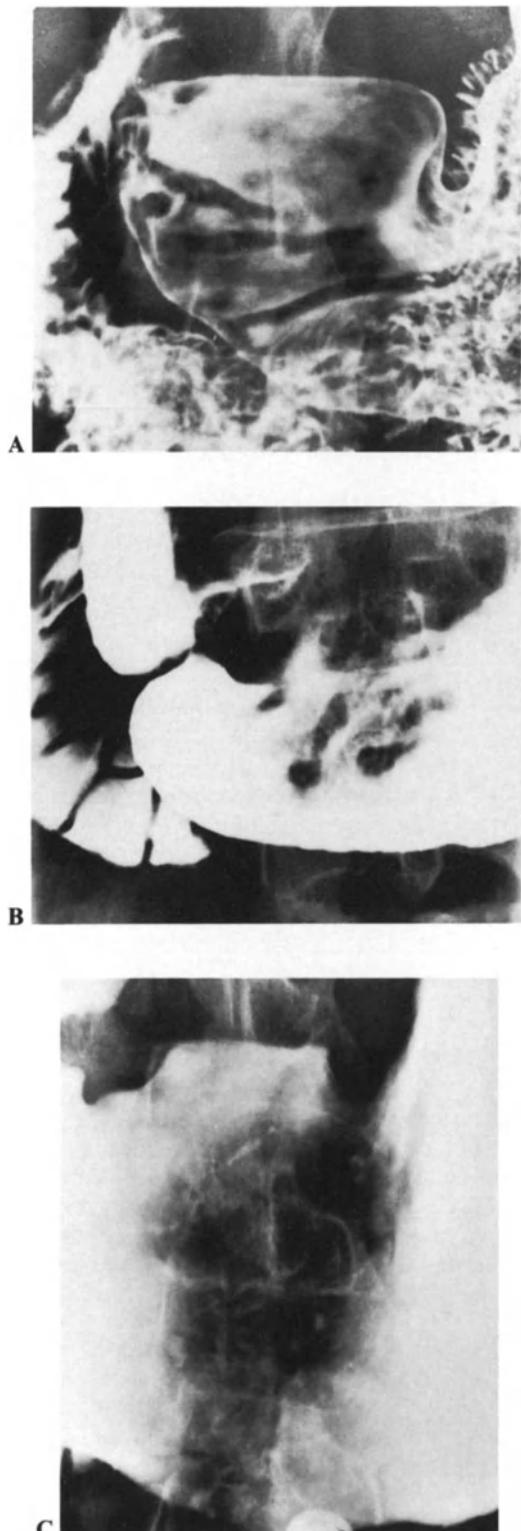


**Fig. 30.8.** A Complete gastric erosions seen as small collections of barium surrounded by a radiolucent rim. (Reproduced with permission from Gelfand DW (1986) The stomach. In: Grainger, Allison (eds). Diagnostic Radiology. Churchill Livingstone, Edinburgh.) B Gastric erosions seen only as small nodules during compression filming. C Incomplete gastric erosion visible during compression as small barium collections with a surrounding radiolucency. (Reproduced with permission from Gelfand DW (1984) Gastrointestinal Radiology. Churchill Livingstone, New York.)

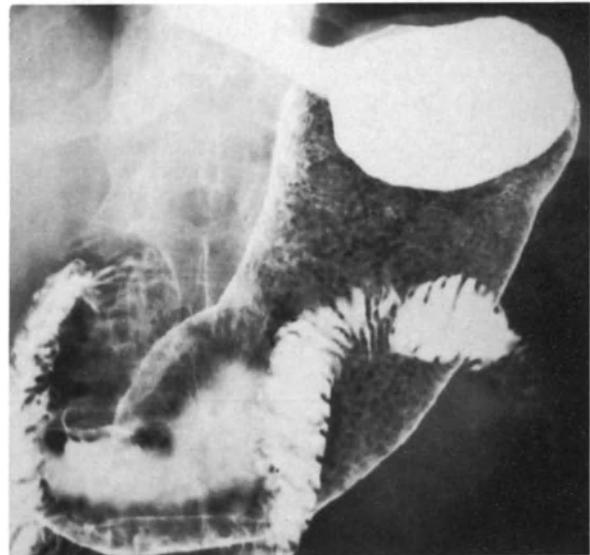


**Fig. 30.9.** Total absence of folds and a small but prominent pattern of areae gastricae in a patient with atrophic gastritis.

*Erosive gastritis* may be chronic or acute, and is often a response to insult by alcohol, aspirin or other gastric irritants. Radiographically, erosions are seen as tiny collections of barium which may be visible at fluoroscopy and are consistent from film to film. Erosions are usually surrounded by a tiny mound of edema that causes an accompanying ring of radiolucency. These are often described as complete or varioliform erosions (Fig. 30.8A). In many cases, however, the small mound of edema will be detected radiologically as a subtle nodule but the erosion itself may be too shallow to retain barium and will not be visible (Fig. 30.8B). Erosions located in the antrum are often aligned on the longitudinal folds, producing a string of beads appearance. When erosions are not accompanied by edema, they are termed incomplete erosions and are more difficult to detect radiographically (Fig. 30.8C).

*Chronic antral gastritis* should be suggested by the presence of thickened, nodular folds with or without visible erosions, and by narrowing of the gastric antrum. However, care must be taken to rule out the presence of an antral ulcer or carcinoma, both of which may similarly narrow the antrum. Additional causes of antral narrowing include *Crohn's disease*, *syphilis*, *tuberculosis*, and *eosinophilic gastritis*.

*Atrophic gastritis* and *gastric atrophy* are associated with achlorhydria and increased risk of gastric carcinoma. Biopsies show a variable spectrum of inflammation and atrophy. The prevalence of atrophic gastritis and gastric atrophy increase with age, with a 70%–80% incidence reported in elderly females. The radiologic findings include a loss of distensibility that produces a tubular appearance and decreased prominence of folds throughout the stomach (Fig. 30.9), the folds being obliterated with only modest distension.

*Hypertrophic gastritis* is characterized by increased thickening and tortuosity of the gastric rugae. The areae gastricae, as seen on double-contrast films, may similarly be enlarged and prominent (Fig. 30.10). This condition is often associ-

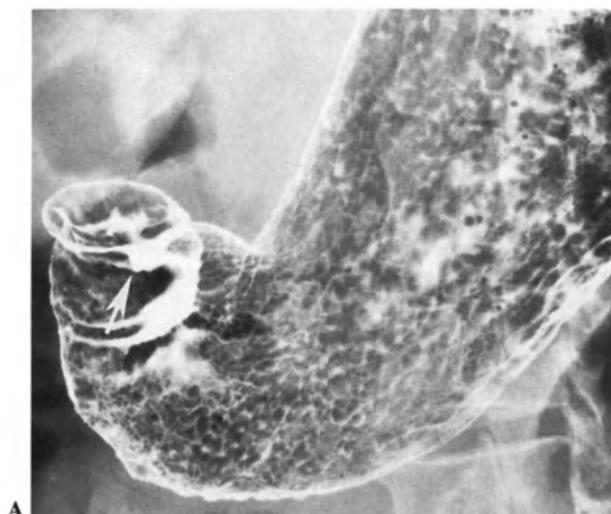


**Fig. 30.10.A** Prominent areae gastricae in a patient with an antral ulcer (arrow). **B** Prominent areae gastricae associated with a duodenal ulcer.

ated with gastric hypersecretion and should prompt a careful examination for the presence of peptic ulcer and reflux esophagitis. Infrequently, hyperrugosity may be associated with *Zollinger-Ellison syndrome*, which is associated with gastrin producing, non-beta islet cell tumors of the pancreas. In such cases, there will be marked hypersecretion, visible as fluid in the stomach, as well as the presence of large and/or multiple peptic ulcers.

*Ménétrier's disease* is characterized by a massive increase in the thickness of the folds in the proximal stomach and along the greater curvature. Ménétrier's disease may be associated with gastrointestinal protein loss. Although the distribution of gastric fold thickening is characteristic, it must be differentiated from *infiltrating carcinoma*, *lymphoma* and *gastric varices*.



**Fig. 30.11.** Severe scarring and shrinking of the stomach following ingestion of household bleach.

*Corrosive gastritis* results from the ingestion of strong acids and alkalis, particularly the former. In the acute phase, these patients should be examined with a water-soluble contrast medium because of the possibility of gastric necrosis and perforation. The radiographic findings are extremely variable and, depending upon severity and the interval since injury, may include swelling of folds, absence of folds, extensive ulceration, and undermining of the mucosa. Eventually, most patients develop a greatly diminished gastric volume due to scarring (Fig. 30.11).

## DUODENITIS

*Non-specific duodenitis* occurs with several times the frequency of duodenal ulcer. Symptoms mimic peptic ulcer and the entity may cause duodenal hemorrhage. Most cases are unaccompanied by peptic ulcer. Duodenitis often accompanies antral gastritis and may be associated with use of alcohol or non-steroidal analgesics. Endoscopic examination reveals mucosal erythema, friability, punctate hemorrhages, fold-thickening, and nodularity.

The radiologic signs of duodenitis similarly include *fold-thickening*, *nodularity* and *erosions* (Fig. 30.12). The combination of fold-thickening and nodularity is most common. Florid cases are easily diagnosed, while mild changes may escape radiologic detection. The nodularity of duodenitis may be indistinguishable from *Brunner's gland hypertrophy*, which is usually present in duodenitis.

Specific disease entities also causing duodenitis include *Crohn's disease* (Fig. 30.13), *eosinophilic gastroenteritis* and *tuberculosis*. These result in variable combinations of ulceration, fold-thickening, and constrictive deformation. Further causes of fold-thickening in the duodenum include *Zollinger-Ellison syndrome*, *gastric hypersecretion*, *pancreatitis*, *parasitic infestations*, *hypoalbuminemia* and *renal failure*.

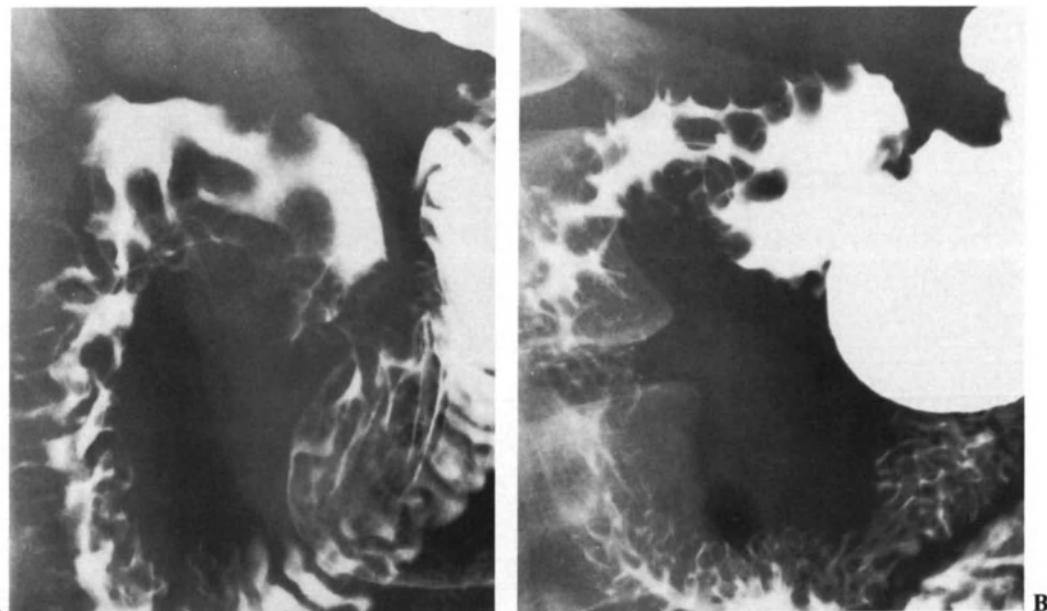


**Fig. 30.12A, B.** Non-specific duodenitis demonstrated as thickening of folds, A, and nodularity, B, in the proximal duodenum. (Reproduced with permission from Gelfand DW (1984) Gastrointestinal Radiology. Churchill Livingstone, New York.)

At least three entities may cause fine nodularity of the proximal duodenum, namely nodular lymphoid hyperplasia, heterotopic gastric mucosa and non-tropical sprue.

*Nodular lymphoid hyperplasia* is an enlargement of the normally present lymphoid follicles of the small bowel and is seen radiologically as 1–2-mm nodules scattered throughout the small intestine including the duodenum. It is usually associated with gamma globulin deficiencies or diffuse intestinal lymphoma.

*Heterotopic gastric mucosa* presents as 1–5 mm nodules

clustered in the proximal half of the duodenal bulb and is of no known clinical significance.

*Non-tropical sprue* may occasionally cause a fine nodular pattern in the duodenum.

#### BENIGN GASTRIC ULCER

Factors contributing to the development of peptic ulcer disease include *alcohol* consumption, *smoking*, *psychological stress*, and use of non-steroidal *analgesics*. *Renal failure* and *emphysema* are also associated with an increased incidence of peptic ulcer.

The *radiologic finding* specifically indicating the presence of a gastric ulcer is the detection of an *ulcer crater* or *niche*. When seen *en face*, the most characteristic finding is the presence of a dense, ovoid collection of barium within the crater itself (Fig. 30.14). Compression and double-contrast techniques enhance the visibility of this barium collection. On double-contrast films, anterior wall ulcer craters may be seen as complete or incomplete ring shadows (Fig. 30.15). Gastric ulcers also may be seen in profile as barium-filled projections extending from the lumen of the stomach.

In North America and Europe, the vast majority of gastric ulcers seen radiologically are benign. However, all ulcerating lesions must be carefully examined for the possibility of carcinoma. Careful compression and double-contrast views of the mucosa surrounding the ulcer should be obtained and a vigorous attempt to film the ulcer in profile also should be made.

Differentiation of benign versus malignant gastric ulcers is based on the following criteria:

1. Benign ulcers project beyond the lumen of the stomach, while malignant ulcers rest upon a mass that extends into the lumen of the stomach



**Fig. 30.13.** Gastroduodenal Crohn's disease visible as constriction of the distal antrum, pyloric canal, and duodenal bulb.

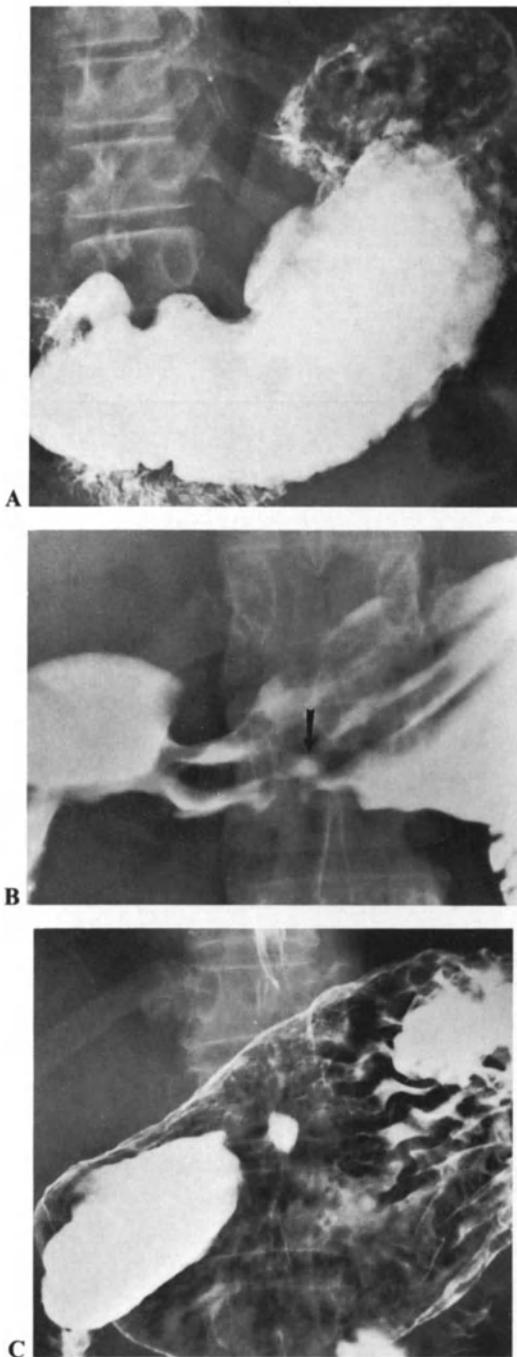


**Fig. 30.14.** A Large benign gastric ulcer projecting from the lesser curve of the body of the stomach. B Small antral ulcer visible during compression (arrow). C Double-contrast view of a posterior wall, barium-filled ulcer crater. (Reproduced with permission from Gelfand DW (1984) Gastrointestinal Radiology. Churchill Livingstone, New York.)

2. Benign ulcers are more likely to be deep, while malignant ulcers are more likely to be shallow
3. The mucosal surface surrounding a benign gastric ulcer is smooth, while the mucosa surrounding a malignant ulcer has a nodular or irregular component

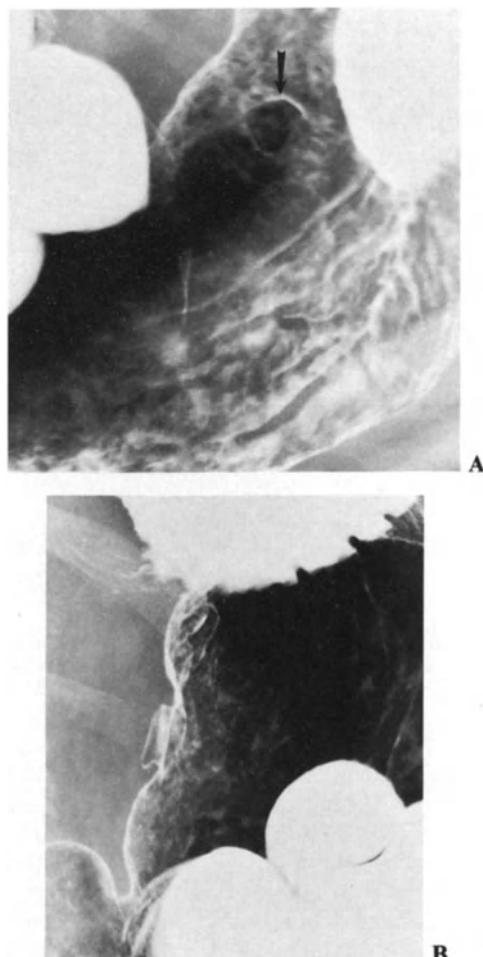


**Fig. 30.15.** A, B. Anterior wall benign ulcer visible as a ring-shadow (arrow, A) and in profile (B).

4. The edematous mound surrounding a benign gastric ulcer is symmetrical and smooth in outline, while the infiltrating tumor surrounding a malignant ulcer is usually asymmetrical and may be distinctly mass-like
5. Folds entering the margin of a benign gastric ulcer are smooth and distinct from each other, while folds converging toward a malignant ulcer may be irregular, nodular and variable in thickness, and may merge as they reach the margin of the ulcer

In differentiating benign from malignant gastric ulcers, the lesions should be characterized as falling into one of three categories: obviously benign, obviously malignant, or indeterminate. Because of the possibility of gastric cancer, ulcers in the latter two categories should be endoscopically biopsied to rule out or confirm the presence of malignancy. However, carefully radiographed ulcers that are typically benign in appearance have a negligible probability of malignancy and can safely be treated medically and followed to healing without endoscopic intervention. Two recent investigations have shown that the incidence of malignancy among radiographically benign gastric ulcers is essentially zero. When



**Fig. 30.16A, B, C.** Active duodenal ulcer craters visible on barium-filled view, A, compression film, B, and double-contrast film, C. (Reproduced with permission from Gelfand DW (1984) Gastrointestinal Radiology. Churchill Livingstone, New York.)

complete healing of a gastric ulcer is observed radiologically, the possibility of carcinoma is infinitely small. Ulcer healing is in fact a more accurate indication of a benign lesion than the results of endoscopic biopsy.

#### DUODENAL ULCER

The radiographic diagnosis of duodenal ulcer depends upon demonstration of an *ulcer crater* (Fig. 30.16). Compression is the most useful single technique for demonstrating duodenal ulcers, since graded compression can be used to express the barium suspension away from the ulcer, leaving the collection of barium in the ulcer crater clearly visible. Double-contrast technique may occasionally demonstrate a duodenal ulcer when other techniques have failed, but most anterior wall ulcers will not be demonstrated.

*Duodenal deformity* may be employed as an indirect sign of duodenal ulcer disease, but cannot be used to indicate ulcer activity. The typical cloverleaf deformity associated with duodenal ulcer disease often results in several recesses that collect barium and may simulate an ulcer. However,

the ulcer that has produced the cloverleaf deformity is most often found at its center (Fig. 30.16B). The peripheral recesses of a cloverleaf deformity are usually pseudodiverticula produced by scarring.

Although most duodenal ulcers are found in the bulb, *post-bulbar ulcers* occasionally occur in the descending limb of the duodenum. Detection of a post-bulbar ulcer is often aided by secondary signs accompanying the ulcer. Thickening of adjacent folds is usually present and an edematous mound, or 'pad sign', may be produced by an ulcer penetrating into adjacent tissues. Also, local irritability or scarring may cause an *incisura* to form on the wall opposite a post-bulbar ulcer (Fig. 30.17).

**Giant duodenal ulcers** are a large, penetrating form of peptic ulcer of the duodenal bulb. The diagnosis of 'giant ulcer' is made when the size of the ulcer exceeds 2 cm or approaches the size of the duodenal bulb. A giant ulcer may closely mimic the outline of the bulb, and in such instances the ulcer may be undetected because the fluoroscopist believes he is observing the duodenal bulb itself. Failure of the ulcer to undergo peristaltic contractions should alert the fluoroscopist to its presence.

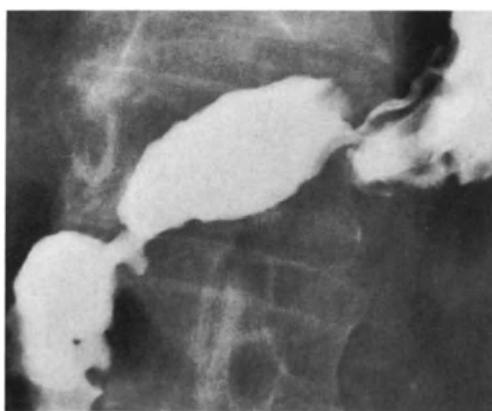


**Fig. 30.17.** Post-bulbar ulcer situated at the junction of the first and second segments of the duodenum, and accompanied by an *incisura* on the opposite wall. (Reproduced with permission from Gelfand DW (1984) Gastrointestinal Radiology. Churchill Livingstone, New York.)

#### CARCINOMA OF THE STOMACH

Most of the recent advances in the radiologic diagnosis of early gastric cancer have originated in Japan. In particular, the technique of double-contrast gastric radiography was perfected by Shirakabi, Ichikawa, Kawai and others for accurate detection of gastric cancer.

*Early gastric cancer* (Fig. 30.18) is by definition limited to the mucosa or submucosa without invasion of the muscularis propria, lymph node involvement or distant metastases. Early gastric cancer is associated with an 80%–95% five-year survival rate versus a dismal prognosis for advanced lesions. Unfortunately, the predominance of benign gastric lesions in Western countries has produced a tolerance of gastric symptoms that results in most carcinomas being in an advanced stage when detected.

The Japanese classification of early gastric cancer on the basis of macroscopic appearances is presented in Fig. 30.19.

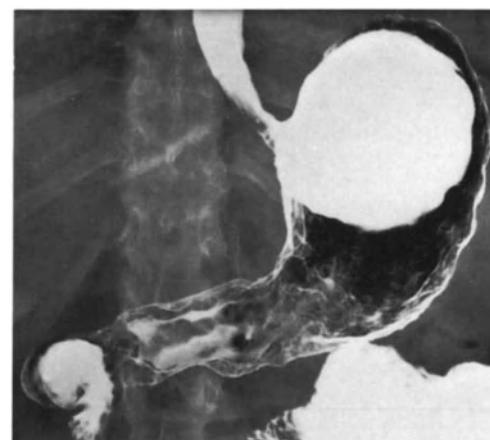


**Fig. 30.18.** Early gastric cancer visible as a depressed area accompanied by converging folds of varying thickness.

The most difficult early gastric cancer to detect radiologically is type II, in which there is only minimal elevation or depression of the lesion. Because of the paucity of early gastric cancers in Europe or the Western hemisphere, Western radiologists infrequently encounter such lesions.

*Advanced gastric cancer* takes many forms (Fig. 30.20) and can be described by the following adjectives: *circumferential, infiltrative, ulcerating, mass-like and fungating*.

The most common presentation of advanced gastric carcinoma is a lesion that has infiltrated a significant fraction of the stomach wall and has become partially or completely



**A**



**B**



**C**

**Fig. 30.20.** A Infiltrating gastric carcinoma (linitis plastica) involving the distal half of the stomach. B Mass-like advanced gastric carcinoma adjacent to the esophagogastric junction. C Advanced gastric carcinoma demonstrating a small, deep ulceration and irregular infiltration of the surrounding region.

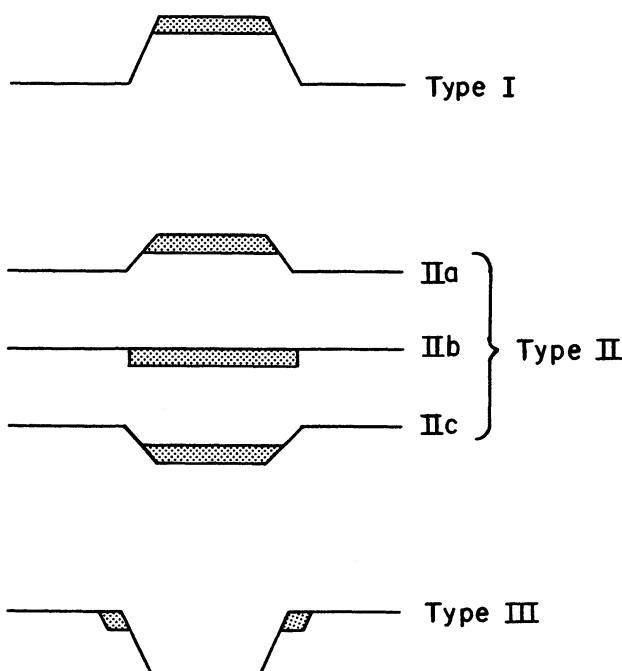


**Fig. 30.19.** Japanese classification of early gastric cancer as projecting (Type I), flat (Type II), and ulcerating (Type III).



Fig. 30.21. Several hyperplastic polyps visible in the gastric antrum.

circumferential. Unless the esophagogastric junction is involved, lesions of the body of the stomach usually do not obstruct the gastric lumen. On the other hand, antral carcinomas may produce gastric outlet obstruction. Large, ulcerating masses are a second common presentation of gastric carcinoma and may be located anywhere in the stomach. Although a localized, sizeable ulceration may be present, the accompanying neoplastic mass is usually obvious. *Scirrhous carcinoma* may infiltrate much or all of the stomach submucosally without producing an obvious localized mass or ulceration, and thus may be subtle in appearance and difficult to detect. This form of gastric cancer is also known as *limitis plastica*.

Because gastric carcinoma is pleomorphic and presents a variety of macroscopic appearances, it must be differentiated from *benign gastric ulcer*, *Menetrier's disease*, *Crohn's disease*, *syphilis*, *tuberculosis*, *eosinophilic gastroenteritis* and *amyloidosis*. All of the above can produce thickening of folds, ulcerations or narrowing of the gastric lumen capable of mimicking gastric carcinoma.



Fig. 30.22. Multilobular adenomatous polyp of the gastric antrum shown during compression filming.

**Gastric lymphoma** has become almost as common as gastric carcinoma in the United States because of the considerable decline in the incidence of the latter disease. Typically, gastric lymphoma produces bulkier lesions than gastric carcinoma. The usual presentation is diffuse infiltration of the wall of the stomach with enlargement of folds (Fig. 30.2B) and ulcerations. A less common presentation of lymphoma is that of a discrete mass. On the whole, gastric lymphoma should be included in the differential diagnosis of any malignant appearing gastric lesion.

### BENIGN GASTRIC NEOPLASMS

*Benign polyps* of the stomach are encountered considerably more often than gastric malignancies and histologically fall into two categories: *hyperplastic* and *adenomatous*.

The majority of polyps observed in the stomach during radiographic examinations are hyperplastic (Fig. 30.21). These are usually small and multiple, with most lesions being under 1 cm in size.

Adenomatous polyps (Fig. 30.22) are generally larger and fewer in number, and are considered to have a malignant potential. The probability of malignancy is related to the number and sizes of the lesions, with lesions larger than 2 cm carrying a significant risk. Because carcinoma may be present in a radiologically benign appearing polypoid lesion, endoscopy with biopsy of suspicious lesions is advisable.

The stomach is affected in at least three polyposis syndromes. In *familial polyposis coli*, the stomach may contain numerous small adenomas. Like their colonic counterparts, there is a potential risk of malignant degeneration. In *Peutz-Jegher's syndrome*, benign hamartomatous polyps are found throughout the gastrointestinal tract, including the stomach. In the *Cronkhite-Canada syndrome*, consisting of gastrointestinal polyposis with nail and hair changes, the stomach and duodenum are paved by innumerable benign sessile polyps with a histological appearance similar to that of juvenile polyps.

Benign tumors of mesothelial origin occurring in the stomach include *leiomyomas*, *lipomas*, *fibromas*, and those associated with neural support tissues such as *neurofibromas* and *Schwannomas*. Most common of these is the *leiomyoma*, which usually projects into the gastric lumen as a hemispherical filling defect smoothly covered with mucosa (Fig. 30.23). These neoplasms may ulcerate, causing significant bleeding, and ulcer is often identifiable radiographically. *Leiomyosarcomas* present similarly, but are usually considerably larger than the typical benign leiomyoma. These bulky malignancies often outgrow their blood supply, producing a large, necrotic ulcer.

### DUODENAL NEOPLASMS

*Primary carcinoma of the duodenum* is a relatively rare lesion. Duodenal carcinoma may occasionally be detected as a small polypoid lesion, but most encountered radiologically are large and circumferential.

*Carcinoma of the head of the pancreas* may invade and encircle the duodenum, producing a lesion that is indis-



**Fig. 30.23.** Leiomyoma of the gastric fundus visible as a smooth, hemispherical lesion.

tinguishable from primary carcinoma. Since both lesions are adenocarcinomas, it may be impossible to determine which organ is the site of the primary tumor.

*Lymphoma, leiomyosarcoma,* and the full spectrum of benign gastrointestinal lesions also occur in the duodenum.

#### GASTRIC SURGERY

A variety of surgical procedures have been performed for the reduction of hiatal hernia and the amelioration of peptic ulcer disease. The following is a description of those pro-

cedures most likely to be encountered in current radiologic practice.

The *Nissen fundoplication* is performed for reduction of hiatal hernia, and consists of wrapping the gastric fundus around the esophagogastric junction as a means of constricting the lumen and preventing gastroesophageal reflux. The resulting wrap of tissue causes a mass-like filling defect in the fundus at the esophageal orifice (Fig. 30.24A). If successful, the procedure results in a lumen through the esophagogastric junction of a few millimeters diameter as seen on barium swallow. If unsuccessful, there may be an unwrapping of the fundoplication (Fig. 30.24B), herniation of the stomach within the wrap, enlargement of the lumen through the wrap, or too constrictive a lumen through the region (Fig. 30.24C).

The *Angelchik procedure* is a more recent operation in which a donut shaped silicon rubber prosthesis is wrapped around the esophagogastric junction to secure the stomach in the abdomen and constrict the lumen sufficiently to prevent gastroesophageal reflux (Fig. 30.25). Complications of the Angelchik procedure include herniation of the proximal stomach through the prosthesis, loosening of the tie that secures the prosthesis with its subsequent migration within the abdomen, herniation of the prosthesis into the chest, and erosion of the prosthesis into the lumen of the stomach.

Several varieties of *partial gastric resection* have been performed over the decades for peptic ulcer disease. Their nomenclature and description are as follows:

1. Billroth I. Subtotal gastric resection is combined with an end-to-end gastroduodenostomy (Fig. 30.26A).
2. Antrectomy. A variation of the Billroth I procedure in which only the gastric antrum is resected, usually combined with vagotomy.
3. Billroth II. Subtotal gastric resection is combined with a gastrojejunostomy in which the end of the remaining gastric pouch is joined to the side of the first loop of

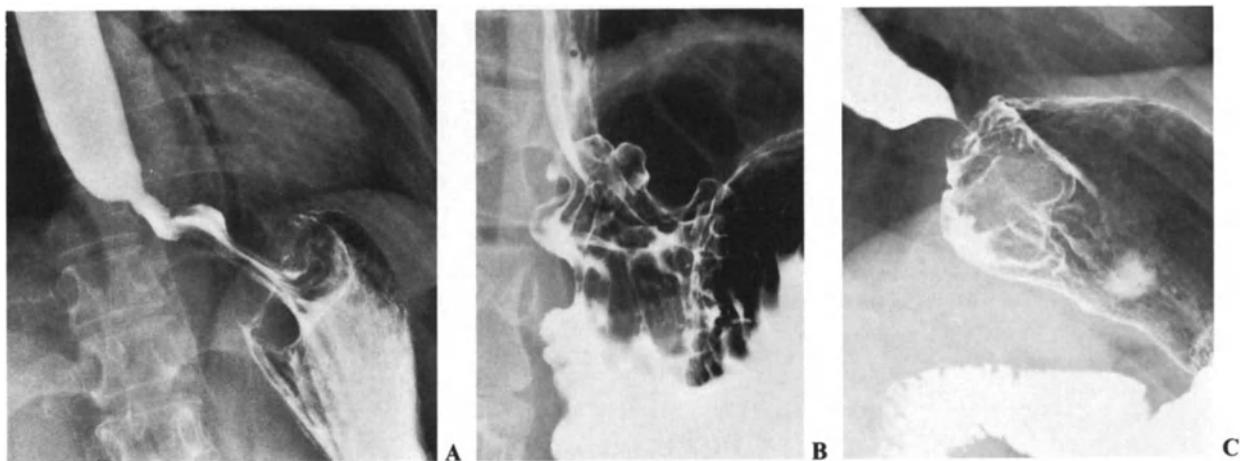


**Fig. 30.24.** A Intact Nissen fundoplication forming a mass in the gastric fundus, with an accompanying distal esophageal stricture. (Reproduced with permission from Gelfand DW (1984) Gastrointestinal Radiology. Churchill Livingstone, New York.) B Nissen fundoplication which has become unwrapped, with a recurrent hiatal hernia. (Reproduced with permission from Gelfand DW (1989) Radiologic diagnostic studies in the evaluation of the esophagus. In: Orringer MB (ed) Surgery of the Alimentary Tract – the Esophagus. W.B. Saunders, Philadelphia.) C Partial obstruction within a Nissen fundoplication causing dysphagia and esophageal dilatation. (Reproduced with permission from Gelfand DW (1989) Radiologic diagnostic studies in the evaluation of the esophagus. In: Orringer MB (ed) Surgery of the Alimentary Tract – the Esophagus. W.B. Saunders, Philadelphia.)

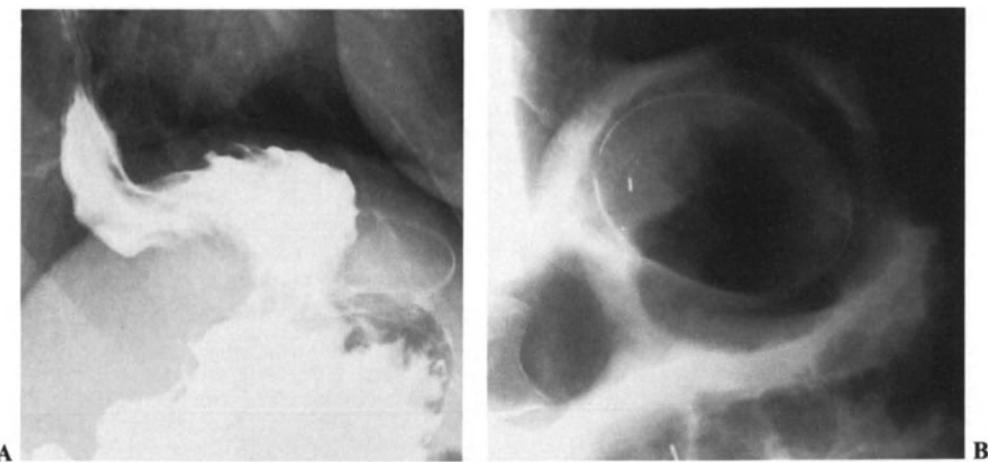


**Fig. 30.25.** A Angelchik procedure with the gastric fundus herniated through the prosthetic ring. (Reproduced with permission from Gelfand DW (1989) Radiologic diagnostic studies in the evaluation of the esophagus. In: Orringer MB (ed) Surgery of the Alimentary Tract – the Esophagus. W.B. Saunders, Philadelphia.) B Angelchik prosthesis that has eroded into the gastric lumen. (Reproduced with permission from Gelfand DW (1989) Radiologic diagnostic studies in the evaluation of the esophagus. In: Orringer MB (ed) Surgery of the Alimentary Tract – the Esophagus. W.B. Saunders, Philadelphia.)

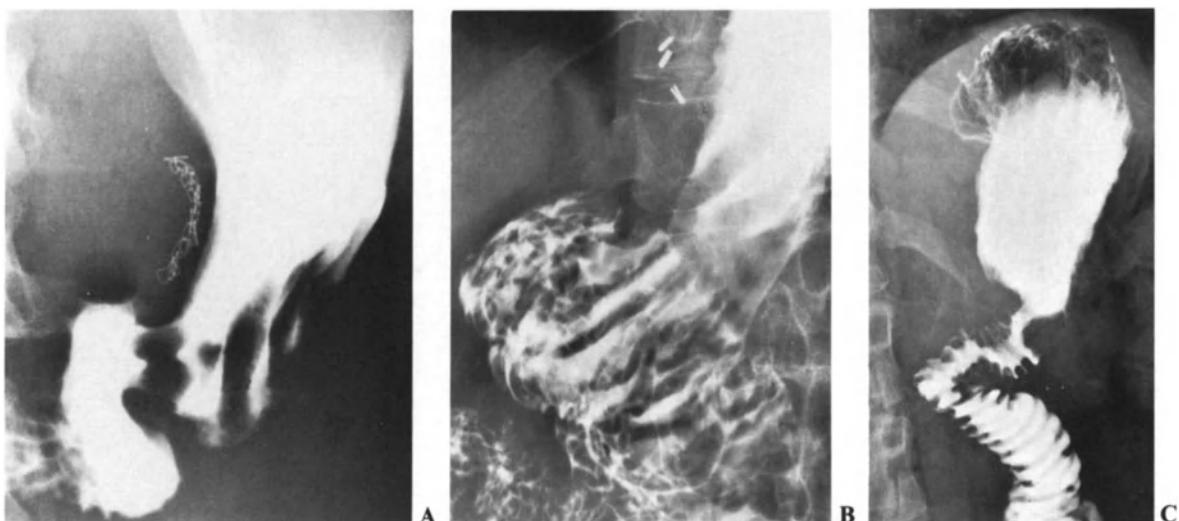


**Fig. 30.26A, B, C.** Common varieties of subtotal gastrectomy. A Billroth I procedure with gastroduodenostomy. B Anastomotic region following a Billroth II procedure. C Subtotal gastric resection with gastroenterostomy to a jejunal Roux-en-Y.

jejunum. The older Polya variation creates a full opening between stomach and jejunum. The more recent Hofmeister variation creates a restricted opening to prevent dumping syndrome (Fig. 30.26B).

- Subtotal gastrectomy with gastroenterostomy to a jejunal Roux-en-Y (Fig. 30.26C) is the most recent form of subtotal resection. It is designed to prevent reflux of alkaline bile into the gastric pouch and esophagus, thus minimizing the incidence of post-operative bile reflux gastritis and esophagitis.

#### REFERENCES AND SUGGESTIONS FOR FURTHER READING

Balikian YP, Yenikomshian SM, Jedjian YD (1967) Tuberculosis of the pyloro-duodenal area. AJR 101: 414–420

- Burhenne HJ, Carbone JV (1966) Eosinophilic (allergic) gastroenteritis. AJR 96: 332–338  
 Cho KY (1976) Gastric antral diaphragm. Radiology 1: 37  
 Cohen WC (1967) Gastric involvement in Crohn's disease. AJR 101: 425–430  
 Craig O, Gregson R (1981) Primary lymphoma of the gastrointestinal tract. Clin Radiol 32: 63–71  
 Eisenberg RL, Margulis AR, Moss AA (1978) Giant duodenal ulcers. Gastrointest Radiol 2: 347–353  
 Fraser GM, Earnshaw PM (1983) The double contrast barium meal: a correlation with endoscopy. Clin Radiol 341: 121–131  
 Gelfand DW, Dale WJ, Ott DJ, Wu WC, Kerr RM, Munitz HA, Chen YM (1985) Duodenitis: endoscopic-radiologic correlation in 272 patients. Radiology 157: 577–581  
 Gelfand DW, Chen YM, Ott DJ (1987) Multiphasic examinations of the stomach: efficacy of the individual techniques and combinations of techniques in detecting 153 lesions. Radiology 162: 829–834  
 Gelfand DW (1987) Radiologists look at primary panendoscopy. Gastrointest Endosc 33: 48–49

- Gelfand DW, Ott DJ, Chen YM (1987) Primary panendoscopy: a radiologist's response. *AJR* 149: 519–520
- Gelfand DW (1984) Gastrointestinal Radiology. Churchill Livingstone, Edinburgh
- Gelfand DW, Ott DJ (1981) Single-contrast vs. double-contrast studies: a critical review of reported statistics. *AJR* 137: 523–528
- Gelzayd EA, Gelfand DW, Rinaldo JA (1973) Non-specific duodenitis. *Gastrointest Endosc* 19: 131–133
- Gordon R, Laufer I, Kressel HY (1980) Gastric polyps found on routine double-contrast examination of the stomach. *Radiology* 134: 27–30
- Horikoshi H (1971) Characteristics of x-ray examination of the stomach. In: Murakami T (ed) Early Gastric Cancer. GANN monograph on cancer research II. University of Tokyo Press, Tokyo, pp 93–103
- Kawai K, Tanaka H (1978) Differential diagnosis of gastric diseases. Yearbook Publishers, Chicago, pp 11–53.
- Kressel HY, Laufer I (1979) Principles of double-contrast diagnosis. In: Laufer I (ed) Double Contrast Gastrointestinal Radiology. W.B. Saunders, Philadelphia, pp 21–44
- Langkemper R, Hoek AC, Dekker W, Op den Orth JO (1980) Elevated lesions in the duodenal bulb caused by heterotopic gastric mucosa. *Radiology* 137: 621–624
- Laufer I, Hamilton J, Mullens JE (1975) Demonstration of superficial gastric erosions by double contrast radiography. *Gastroenterology* 68: 387–391
- Legge DA, Carlson HC, Judd ES (1970) Roentgenologic features of regional enteritis of the upper gastrointestinal tract. *AJR* 110: 355–360
- Menuck LS (1976) Gastric lymphoma, a radiologic diagnosis. *Gastrointest Radiol* 1: 157–161
- Ming SC (1976) The adenoma-carcinoma sequence in the stomach and colon. II. Malignant potential of gastric polyps. *Gastrointest Radiol* 1: 121–125
- Montesi A, Graziani L, Pesaresi A, et al. (1982) Radiologic diagnosis of early gastric cancer by routine double-contrast examination. *Gastrointest Radiol* 7: 205–215
- Op den Orth JO (1979) The Standard Biphasic-contrast Examination of the Stomach and Duodenum. Martinus Nijhoff, The Hague, pp 1–21
- Ott DJ, Chen YM, Gelfand DW, Wu WC (1986) Radiographic efficacy in gastric ulcer: comparison of single-contrast and multiphasic examinations. *AJR* 147: 697–700
- Ott DJ, Gelfand DW, Wu WC, Kerr RM (1982) Sensitivity of single- vs. double-contrast radiology in erosive gastritis. *AJR* 138: 263–266
- Ott DJ, Gelfand DW (1982) Detection of gastric ulcer: comparison of single- and double-contrast examination. *AJR* 139: 93–97
- Press AJ (1975) Practical significance of gastric rugal folds. *AJR* 125: 172–183
- Reese DF, Hodgson JR, Dockerty MD (1962) Giant hypertrophy of the gastric mucosa (Ménétrier's disease): a correlation of roentgenographic, pathologic, and clinical findings. *AJR* 88: 619–624
- Shandalakis JE, Gray SW (1962) Smooth muscle tumors of the alimentary tract: leiomyomas and leiomyosarcomas – a review of 2525 cases. Charles C. Thomas, Springfield, IL

## CHAPTER 31

# THE SMALL INTESTINE

Dina F. Caroline and D.D.T. Maglinte

---

Barium imaging remains the primary method for depiction of intrinsic small bowel pathology. *Enteroclysis* or the small bowel enema represents a significant improvement in the method of small bowel examination, both for the diagnosis of subtle pathology and for the demonstration of small bowel normality. Meticulously conducted oral small bowel examinations can be high-yield diagnostic procedures, particularly if the clinical reasons for referral genuinely suggest small bowel disease.

Although the small bowel is one of the largest organs in the body, small bowel pathology is uncommon. This, combined with difficulty in demonstrating small bowel abnormalities due to the multiple coils of superimposed bowel in a limited space, contributes to the uncertainty that many radiologists feel when trying to analyze small bowel changes. The small bowel also reacts to many systemic processes in addition to the pathologic processes affecting the small bowel alone. Thus, there may be a wide range of diagnostic possibilities to consider when a patient presents with *colic*, *diarrhea*, *malabsorption* and *bleeding*, which are the primary clinical clues to the existence of small bowel pathology. In some instances, the radiologic findings are suggestive of a specific disease; in many, however, the diagnosis will still be uncertain and a biopsy may be required for the final diagnosis. This need does not reflect imaging failure, but the limited way that the small intestine reacts to various insults.

### RADIOLOGIC ANATOMY

The small intestine courses from the duodenojejunal junction (ligament of Treitz) to the ileocecal valve. The small bowel lies within the greater peritoneal sac and is attached to the posterior abdominal wall by a mesentery which runs in a diagonal course from the left upper to the right lower quadrants of the abdomen. The mesentery is a wide, fan-shaped, double layer of peritoneum which allows a great deal

of mobility to the loops of small bowel especially in its midportion. Normally, the jejunum lies in the left upper abdomen and the ileum in the lower right portion of the abdomen. The small bowel is supplied by jejunal and ileal branches of the superior mesenteric artery.

The small bowel measures approximately 19–22 feet in length. The lumen diameter decreases gradually from proximal to distal small bowel. Normally, the small intestine is partially collapsed. Measurements of lumen diameter vary depending on the examination technique. On enteroclysis, the lumen diameter is considered abnormal if it is more than 4.5 cm in the proximal jejunum, 4 cm in the mid small bowel and 3 cm in the ileum. On follow-through examinations, the lumen should not exceed 3.5 cm in the jejunum and 3 cm in the ileum. The wall of the small intestine consists of the mucosa, submucosa, muscularis propria and serosa. On contrast radiography, the normal distance space between two adjacent loops is 2–3 mm, which represents the thickness of the apposing intestinal walls.

The characteristic radiographic appearance of the small bowel is produced by the *valvulae conniventes* which are crescentic folds of the mucosa and submucosa. These appear as a criss-crossing, feathered pattern in collapsed small bowel and as circular or spiral bands in distended small bowel. Typically, the folds are more prominent and more numerous in the jejunum and gradually becomes less numerous in the ileum (Fig. 31.1).

### METHODS OF EXAMINATION

#### Plain Film Radiography

Plain film evaluation is perhaps the most difficult area of radiologic interpretation in the GI tract. It is immensely aided by clinical information which should be supplied to the radiologist. This is the least expensive imaging method and should

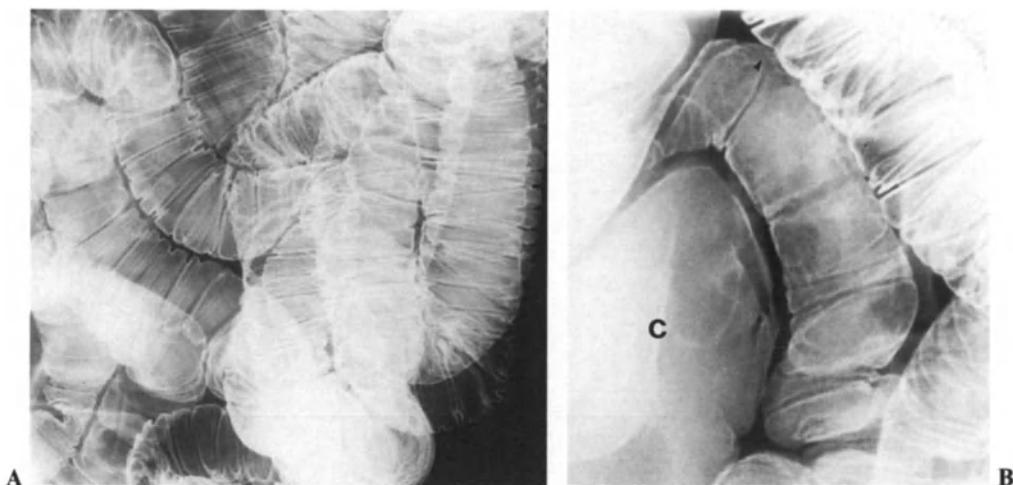


**Fig. 31.1A, B.** Normal appearance of small bowel by double contrast enteroclysis. **A** Overview of jejunum and proximal ileum shows gradually decreasing number of folds from jejunum to terminal ileum. There are approximately 4–7 folds per inch in the jejunum and 3–5 folds per inch in the ileum. **B** In younger patients, aggregate lymph nodes are frequently seen in the terminal ileum manifested in the radiograph as small uniform nodular elevations (arrowhead points to one). Jejunal folds are not obliterated with distension; however, even mild distension may obliterate ileal folds. **C**, cecum.

lead to the next appropriate modality if the clinical questions relevant to patient management are unanswered. In approximately 30%–40% of patients with *small bowel obstruction* the plain film is unconvincing or ‘normal’ and contrast examination then becomes necessary.

#### Barium Contrast Examination

There is controversy concerning the relative accuracy of the *oral* methods of examination and the *intubation infusion* (enteroclysis or the small bowel enema) techniques. A prospective study has confirmed that the intubation infusion method of examining the small bowel obviates most of the inherent limitations of the oral methods and is superior to the follow-through even when the latter is done carefully.

In order for a barium study of the small bowel to be considered diagnostic, the *mucosal surface*, *fold pattern*, *distensibility* and *mobility* of each bowel loop must be demonstrated. Overlapping loops of bowel must be separated from adjacent loops by using a double contrast technique to create a translucent effect or by adequate compression to separate adjacent loops. The older concept of assessing the presence of malabsorption or abnormal transit by the presence of *flocculation* or *segmentation* of barium is no longer considered to be of significant diagnostic value. It has been demonstrated that this effect is dependent on the type of barium suspension used as well as exposure to intestinal secretions and prolonged transit time. There is a very wide normal variation in transit time and this feature is therefore considered to be of little diagnostic value.

Thus, diagnostic small bowel examinations must be performed with adequate volume and rate of barium infusion as well as with close fluoroscopic monitoring in order to be sure that each loop of bowel is adequately examined.

**Conventional Small Bowel Series.** This type of small bowel examination is performed as an adjunct to an upper GI study. If double contrast upper GI examinations are performed utilizing high density barium, the contrast given to evaluate small bowel after the GI examination must be considerably

more dilute than if a single contrast upper GI study is performed. Evaluation of the small bowel is generally performed by obtaining overhead radiographs at approximately 20 min to half-hour intervals and then examining the terminal ileum when it has been filled with contrast. Even with interval fluoroscopy, this type of examination frequently fails to provide a diagnostic examination of the small bowel since evaluation of normality or early pathologic change is compromised by the overlap of loops, variability in normal appearance, unpredictability of transit time, and difficulties in returning patients to a fluoroscopy suite at optimal times to examine various portions of the small bowel.

**Dedicated Small Bowel Meal.** This examination is designed specifically to examine the small bowel without a complete upper GI examination. The patient is given a large volume of barium (about 600 ml) of density for optimizing visualization of small bowel loops with fluoroscopic compression technique. Drinking a large volume of barium at one sitting stimulates pyloric relaxation and helps produce a continuous column of barium leaving the stomach and reaching the cecum reasonably quickly. Use of pro-kinetic agents such as *metoclopramide* and additional barium ingested at intervals during the procedure also encourages motility and tends to shorten the time of the examination. Intermittent fluoroscopy and compression films are taken at intervals in addition to overhead films. This procedure may be augmented by using effervescent granules to produce at least a partial double contrast effect (the *oral double contrast small bowel follow-through*) or with a peroral pneumocolon.

The *peroral pneumocolon* provides detailed examination of the terminal ileum and ileocecal area. In this technique, air is insufflated per rectum after barium has reached the cecum. Intravenous *glucagon* (1 mg) is given to facilitate ileocecal reflux of air and to induce bowel hypotonia. This type of examination usually provides the most diagnostic evaluation of the terminal ileum and ileocecal region.

**Enteroclysis (Small Bowel Enema).** This procedure is performed by infusion of contrast material directly into the small

bowel through a catheter which is positioned either orally or nasally. With this technique, the volume and rate of barium can be controlled to permit efficient examination of the entire small bowel with adequate bowel distension and compression when necessary. The technique may be performed as a single contrast examination or as a double contrast examination using methylcellulose, or occasionally air or water, to provide double contrast. Double contrast enteroclysis permits the most detailed examination of the small bowel mucosal and fold pattern. It also provides specific information regarding the level and cause of obstructions. In cases of partial small bowel obstructions, the bowel distension provided by the technique exaggerates the change in caliber proximal and distal to the point of obstruction and permits identification of lesions that are not readily apparent on other techniques.

### Radionuclide Scintigraphy

Nuclear medicine offers several advantages in the investigation of patients with some small bowel disorders. It is non-invasive, reproducible and moderate in cost. It is of value in the detection of gastric mucosa within Meckel's diverticulum, particularly in children and values of 85% to 95% for sensitivity, specificity and accuracy have been reported using a high resolution gamma camera.

Radionuclide scintigraphy is the technique of choice for the initial investigation of severe acute lower gastrointestinal bleeding. <sup>99m</sup>Technetium sulfur colloid and <sup>99m</sup>Technetium red cell methods have both been used. These studies assist the angiographer in excluding patients not actively bleeding and in limiting studies to vessels likely to be involved. <sup>111</sup>Indium labeled leucocytes have been used to define activity (detection of inflammation) in inflammatory bowel disease. Radionuclide studies have also been of value in protein-losing enteropathy and malabsorption.

### Ultrasound

Ultrasonography has been of little clinical value in the primary investigation of small bowel diseases. However, since sonography is commonly utilized in the initial evaluation of patients suspected of having abscesses or fluid collection, it may be the first study to detect disorders of the small bowel. Sonography has an additional role in the evaluation of patients with equivocal findings on plain film examination when small bowel obstruction is suspected. Dilated fluid-filled loops are readily demonstrated by ultrasound. Like computed tomography, it is of value in evaluating the bypassed small bowel when contrast cannot be introduced.

### Computed Tomography

Barium studies and endoscopy provide detailed information about mucosal abnormalities. Though CT can demonstrate the bowel lumen, its unique and complementary value lies in its ability to demonstrate anatomic detail of the bowel wall itself and of surrounding organs and tissues. CT may provide important correlative and additional information about the extraluminal component of diagnosed small bowel disease. CT is increasingly utilized in the investigation of Crohn's disease complications, extent of tumor recurrence, mesenteric ischemia and the diagnosis of small bowel obstruction

in patients with a history of abdominal malignancy. It is a relatively expensive imaging procedure and should be reserved to answer precise clinical queries not possible with contrast studies. Additionally, it is used by the radiologist to guide percutaneous interventional procedures (percutaneous biopsy of tumor masses or drainage of abscesses).

### Angiography

In the small bowel, superior mesenteric arteriography is predominantly employed in severe active bleeding. It is generally performed only if a preceding scintigram is positive, since angiography is less sensitive and more invasive than radioisotope studies. Tumors may also be diagnosed by visceral arteriography. Angiography may also be used to arrest bleeding sites by intra-arterial infusion of vasopressin or by embolotherapy.

### Enteroscopy

Reports of small bowel endoscopy have appeared since the mid 1970s. It is still an underutilized technique in the United States due to the limited availability of enteroscopes and technical difficulty in performing the examination. Enteroscopy appears to have more complications than upper gastrointestinal panendoscopy or colonoscopy. The diagnostic application of enteroscopy has not been widely reported. It appears that enteroscopy is more sensitive in the detection of pathology than the conventional barium follow-through. It may have its role in the preoperative histologic confirmation as well as preoperative planning (biopsy) of lesions demonstrated by enteroclysis.

### Magnetic Resonance Imaging

There is little experience to date with magnetic resonance imaging and it is not yet possible to predict its future role in the small bowel.

## EMBRYOLOGY

The small bowel arises from the embryologic midgut. During the sixth gestational week, the midgut herniates into the umbilical cord as a U-shaped loop. The extra-abdominal intestine then begins to rotate around an axis formed by the superior mesenteric artery. Growth of the pre-arterial limb of bowel ultimately gives rise to the jejunum and most of the ileum, while the post-arterial (ceccocolic) limb gives rise to the distal ileum and proximal half of the colon. The complex rotation continues after the bowel returns to the abdomen during the tenth week of gestation. The prearterial and post-arterial segments rotate independently. The prearterial (duodenjejunal) limb rotates 180° counterclockwise about the superior mesenteric artery while it is extracelomic. It continues an additional 90° arch during the tenth week with a return of the mid-intestine to the left upper quadrant of the abdomen. The cecocolic limb follows into the abdomen with the cecum returning last. The cecocolic limb completes its rotation after it is within the abdominal cavity until the cecum lies in the right upper quadrant near the right lobe of the liver. The process is completed when the cecum



**Fig. 31.2.** Omphalocele. Maternal ultrasound (transverse section) shows liver contained in an omphalocele. Note thin membrane (peritoneal lining) covering liver extending to left. Linear fluid containing structure is portal vein. Rounded fluid-filled structure to right represents fetal urinary bladder. (Courtesy of P. Radecki MD)

descends to the right iliac fossa and becomes fixed to the posterior peritoneum.

#### CONGENITAL AND DEVELOPMENTAL ABNORMALITIES

##### Errors of Rotation

**Omphalocele.** Omphalocele results from the complete arrest of rotation and failure of the midgut to return from the umbilical cord. The abdominal wall musculature is developed which distinguishes it from the condition known as *gastroschisis*. Various degrees of small intestine, proximal

colon as well as other midgut derivatives such as liver and pancreas may be found within an omphalocele (Fig. 31.2).

When the midgut returns to the abdomen with rotation arrested after the initial 90° rotation counterclockwise, the small bowel lies entirely on the right and the colon on the left. This is complete *nonrotation* (Fig. 31.3) and may be associated with a complete *situs inversus*. Varying degrees of partial rotation also occur, as do reversed rotation and anomalous fixation of the mesenteries. Rotational abnormalities sometimes result in *internal hernias* into the paraduodenal fossae, and less commonly into other defects in the peritoneum or mesenteries. Internal hernias are recognized by fixation of one or more loops of small bowel within a defined sac and may cause bowel obstruction (Fig. 31.4).

Incomplete rotation of the bowel is frequently associated with remnants of peritoneal bands (*Ladd's bands*) that course from the malpositioned cecum across the duodenum and attach to the liver or abdominal wall. This may result in complete or partial small bowel obstruction. Shortening of the small bowel mesentery also predisposes to *midgut volvulus* or twisting of a segment of small bowel around its vascular pedicle. This occurs most frequently in neonates with incomplete rotation, and if not detected speedily, may have a catastrophic outcome. Midgut volvulus may be suggested by the finding of small bowel obstruction on plain abdominal radiographs. Urgently performed contrast examination of the small bowel may show abnormal fixation of the ligament of Treitz, spiral torsion of the duodenum, proximal jejunum in the right upper quadrant and abnormal position of the cecum.

##### Atresia and Stenosis

Congenital atresias and stenoses are the results of intestinal ischemia in utero. They are evenly distributed between the

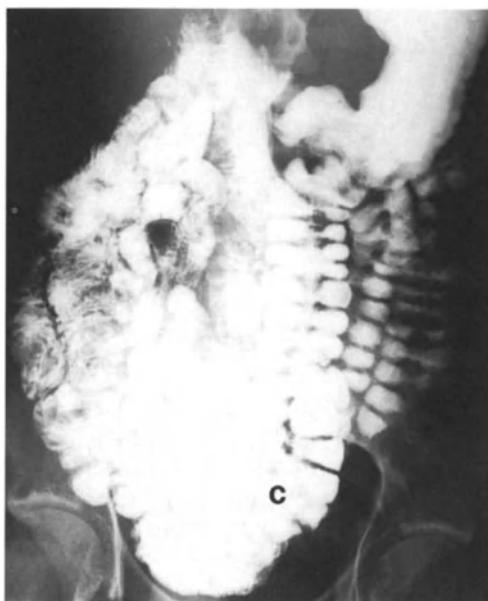


**Fig. 31.3.** Overview of small bowel follow-through showing non-rotation of midgut. All loops of mesenteric small intestine lie in the right hemi-abdomen and the colon in the left hemi-abdomen. The terminal ileum crosses the midline to enter the ileocecal valve which faces medially. C, cecum.



**Fig. 31.4.** Left paraduodenal hernia. Loops of jejunum are confined in a sac in the left hemiabdomen. Only the efferent loop (arrow) passes through the hernial orifice where a slight change in caliber is seen. The afferent loop (obscured by the barium-filled stomach) enters the sac posteriorly at the point where the duodenum emerges from the retroperitoneum. (Courtesy of A. Friedman MD)

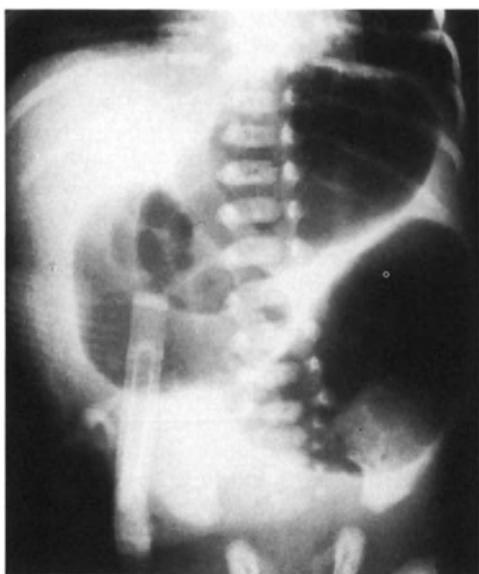
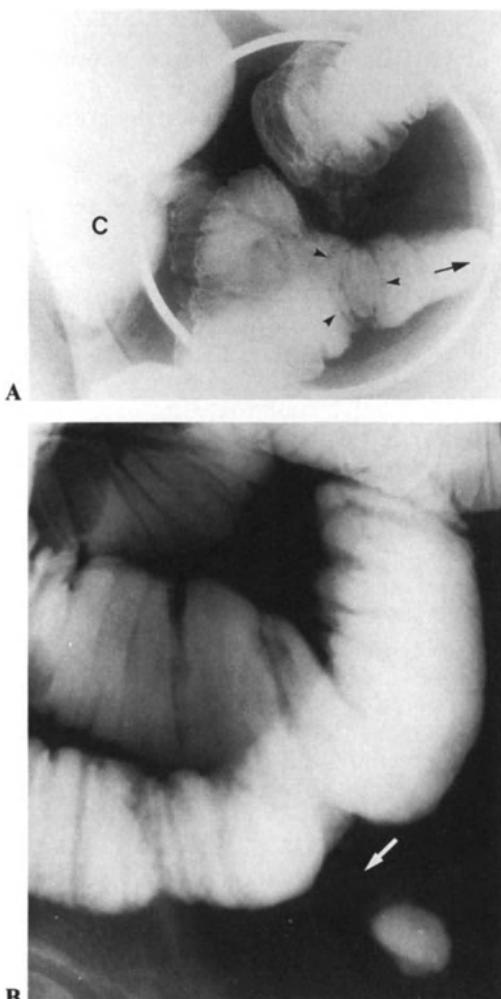


**Fig. 31.5.** Jejunal atresia. Plain radiograph shows gaseous distension of stomach, duodenum and proximal small bowel.



jejunum and ileum. Associated anomalies including malrotation, volvulus, meconium ileus, or omphalocele occur in about 25%. Extragastrointestinal anomalies are uncommon. Obstruction develops in the immediate newborn period. The level of obstruction is frequently easy to determine on plain abdominal films. Few dilated loops of small bowel in the upper mid abdomen are found in jejunal atresia while in ileal obstructions there are numerous dilated loops of bowel present (Fig. 31.5).

#### Meckel's Diverticulum

Meckel's diverticulum represents partial persistence of the omphalo-mesenteric duct at its junction with the ileum resulting from failure of the yolk stalk to close completely. It is considered the most common anomaly of the GI tract. Important features may be remembered by the 'rule of two', which is very helpful if not highly accurate. Meckel's diverticulum occurs in approximately 2% of the population, is found about 2 feet proximal to the ileocecal junction and is generally about 2 inches long. It is found on the antimesenteric border of the ileum.

Meckel's diverticulum is usually asymptomatic but may be complicated by *gastrointestinal hemorrhage* due to ulceration of the ectopic gastric mucosa which is present in about 25% of cases. Radionuclide scanning as noted above frequently detects the ectopic gastric mucosa. Other complications which occur unusually in Meckel's diverticulum include *acute inflammation, obstruction and stone formation*.

Barium examination of the small bowel demonstrates the Meckel's diverticulum as a blind sac protruding from the antimesenteric border of the ileum. Mucosal folds in a triangular arrangement at the base of the diverticulum are characteristic (Fig. 31.6).

#### Diverticulosis

Jejuno-ileal diverticula are acquired herniations of mucosa and submucosa through the muscular layer of the mesenteric surface of the bowel wall. Like colonic diverticula, herniation occurs at a weak point of the muscle caused by the penetration of mesenteric vessels. Diverticula are commonly multiple and occur most frequently in the jejunum, followed by the terminal ileum. They increase in frequency with age. In contrast to Meckel's diverticulum, these idiopathic small bowel diverticula do not contain a complete muscle wall; they occur on the mesenteric border of the bowel, are commonly multiple and may be found throughout the small bowel.

On barium study, large outpouchings from the small bowel, occasionally obliterating most of the normal mucosal

**Fig. 31.6A, B.** Meckel's diverticulum. A The characteristic junction (arrowheads) of the diverticulum (arrow) with the ileum allows for a confident diagnosis. No other abnormality produces this appearance. C, cecum. B Small Meckel's diverticulum with a narrow neck (arrow) which barely filled with contrast during enteroclysis. One of the reasons for the poor sensitivity of the small bowel meal is non-filling of the diverticulum because of the narrow opening. A prior small bowel meal done on this patient failed to show the anomaly.

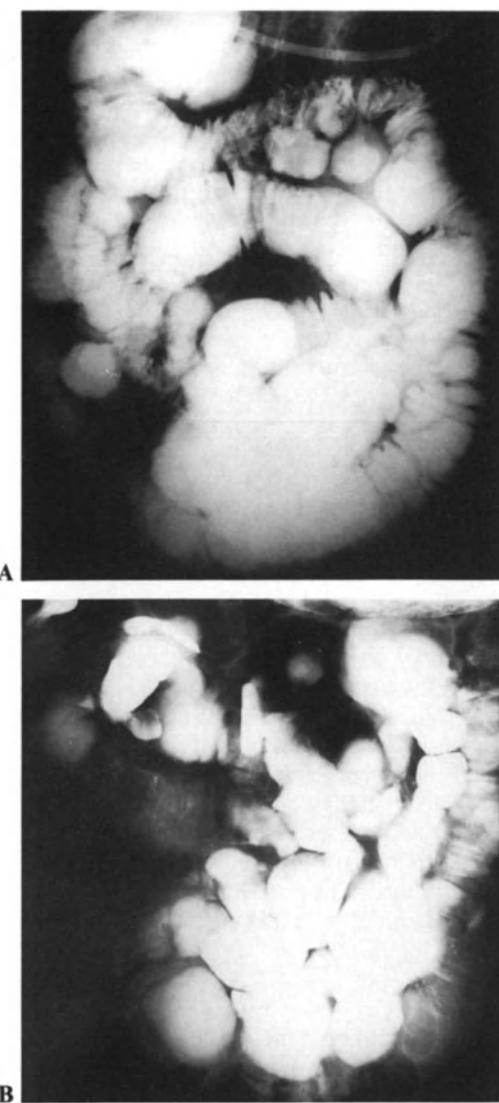


**Fig. 31.7A, B.** Jejunoileal diverticulosis. A Multiple outpouchings devoid of folds are shown by enteroclysis scattered throughout the small bowel. Small diverticula were also present in the terminal ileum. Plain films may show rounded featureless gas collections and air fluid levels on upright or decubitus radiographs. B Bacterial overgrowth syndrome secondary to acquired jejunoileal diverticulosis. Stasis and increased fluid in small bowel is suggested by dilution of contrast and prolonged transit. The diverticula are denser than the main lumen because of contrast retention.

pattern, may be seen (Fig. 31.7A). An upright film of the abdomen will demonstrate multiple air fluid levels within the diverticula. Sacculations, or pseudodiverticula, which are seen in patients with Crohn's disease, scleroderma, celiac disease or resulting from previous surgery, may mimic intestinal diverticula.

The most common complication of small bowel diverticula is caused by the metabolic abnormality from bacterial overgrowth. This is due to the lack of normal peristalsis resulting in stasis of intestinal contents (Fig. 31.7B). It may be associated with *malabsorption* and *megaloblastic anemia*. *Hemorrhage*, *diverticulitis* with abscess or fistula formation, and *intestinal obstruction* are other rare complications which may occur.

### Duplications

Small bowel duplications are congenital malformations of the small bowel which usually develop within the layers of the mesentery and are adherent to the intestinal tract. Most occur in the ileum. They are lined by intestinal epithelium and contain a muscular layer. Ectopic gastric mucosa is found in approximately 15%. Communication with the true bowel lumen occurs in *tubular* type duplication but rarely occurs with the more common *spherical* duplications.

Clinically significant duplications are usually diagnosed in infancy and present as a complete or partial small bowel obstruction, volvulus, intussusception or with an associated atresia. Ischemia may result secondary to compression of the normal lumen by a distended duplication. Duplications may also present as soft tissue masses in the right lower quadrant. A sonolucent or echogenic mass may then be detected by ultrasound. Contrast examinations generally demonstrate effacement of an adjacent bowel loop by extrinsic compression by the duplication.

### INFLAMMATORY DISEASES

#### Crohn's Disease

Crohn's disease, or *regional enteritis* is an idiopathic inflammatory disease of the bowel. Although it may affect all areas of the gastrointestinal tract from the mouth to the anus, the small bowel is the major site of involvement. Crohn's disease is a chronic, usually progressive disease which presents most commonly in young adults. It occasionally presents in children as young as 2 years of age and a late peak of onset also occurs between ages 50 and 60 years. In some cases, the tendency to develop inflammatory bowel disease appears to be familial. The most common symptoms include diarrhea, abdominal pain, weight loss and fever. Significant ileocolic Crohn's disease is frequently accompanied by a palpable right lower quadrant mass.

The terminal ileum is the most common site of involvement. Small bowel involvement occurs in 80% of patients with Crohn's disease. It is confined to the small bowel in 30%, whereas 50% have colonic as well as small bowel disease. Isolated involvement of the colon occurs in 15%–20% and isolated perianal disease in 2%–3% of patients. Disease occurring in the upper GI tract including the esophagus, stomach and duodenum is being recognized with increasing frequency, but invariably occurs in conjunction with small bowel and/or colonic disease.

Pathologically, Crohn's disease is a transmural process and noncaseating granulomas are frequently identified in the submucosa and serosa accompanied by lymphoid proliferation and a non-specific chronic inflammatory reaction. Lymphoid proliferation occurs early and may cause a superficial *granular* or *slightly nodular* appearance on barium study. The lymphatic obstruction results in slight thickening of the mucosal folds. The characteristic early mucosal change is the small superficial aphthous ulcer, which is the result of degeneration of the mucosa overlying hyperplastic lymphoid follicles.

As disease progresses, ulceration increases with formation of *linear* and *criss-crossing* ulcers. Multiple intersecting ulcers



**Fig. 31.8.** Early radiographic manifestations of Crohn's disease. Aphthae are manifested as punctate or sometimes stellate barium collections surrounded by a halo (arrow). Minimal fold thickening is also present. Note coarse granular surface pattern (compare to adjacent loop). Coarse granularity is a reflection of villous abnormality, usually blunted or fused villi.

form a characteristic cobblestone appearance. Deep discrete ulcers or fissures tracking through the submucosal and muscular layers also occur frequently. Grossly, the inflamed bowel and adjacent mesentery are thickened. Typically, the disease process is segmental and *skip lesions* with normal intervening segments of bowel are characteristic. The bowel circumference is typically involved eccentrically, with ulceration and bowel wall thickening more prominent on

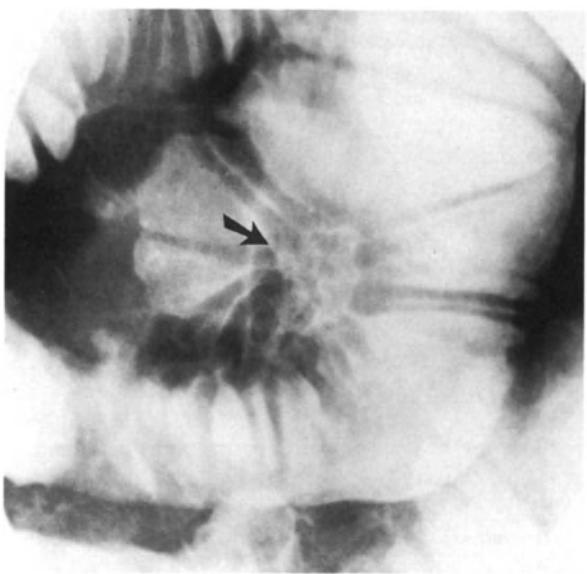


**Fig. 31.9.** Large irregular discrete ulcer crater in jejunum (arrow). Radiating folds indicate chronicity. Note fold thickening of adjacent segments.

the mesenteric surface. Pseudosacculations consequently develop on the relatively unininvolved antimesenteric surface. Significant complications of Crohn's disease include formation of *inflammatory masses, fistulas, abscesses* and *strictures*.

Mucosal changes of Crohn's disease are best evaluated radiographically by high quality barium examinations. Early changes consist of slight thickening and distortion of folds due to primarily submucosal inflammation. Coarse granularity or a nodular pattern is occasionally seen. The earliest characteristic radiographic finding of Crohn's disease is the *aphthous ulcer* (Fig. 31.8). These are small varioliform erosions with tiny superficial collections of barium surrounded by a radiolucent halo representing surrounding edema. These are well demonstrated by enteroclysis or by peroral pneumocolon when they are present in the terminal ileum. Aphthous ulcers may be the only finding of Crohn's disease, or may be found at the periphery of more seriously involved bowel segments, or may occur separate from more actively involved areas. With progressive disease, larger ulcers are seen (Fig. 31.9). These may be *linear* with barium streaks parallel to the long axis of the bowel or deep fissures penetrating deeply into, and sometimes through, the diseased bowel wall. The *cobblestone* pattern which is classically associated with Crohn's disease usually results from multiple intersecting longitudinal and transverse ulcers with small intervening patches of non-ulcerated mucosa (Fig. 31.10). Occasionally, this pattern may result from bulging edematous folds or from pseudopolyp formation with barium trapping in the interstices. Regeneration of mucosa may result in a smooth featureless bowel segment or, occasionally, pseudopolyps may form.

*Luminal narrowing* is common in Crohn's disease resulting from spasm, edema and/or fibrosis. Early in the course of the disease there is often a mild lack of distensibility due to spasm and edema. Later in the course of the disease there are fixed stenoses and strictures with significant loss of bowel pliability (Fig. 31.11). The strictures may be single or multiple, long or short. The bowel loops become straightened and rigid and are separated from each other because of inflammatory thickening of the bowel wall and the associated mesentery. Partial bowel obstruction with prestenotic dilatation of unininvolved bowel proximal to the obstructed level is common. Fibrosis often occurs in an asymmetric fashion with pseudosacculations forming on the antimesenteric borders of affected segments. The '*string sign*' (marked narrowing of a long segment of usually terminal ileum) is a well-described feature of Crohn's disease and may result primarily from spasm or a fixed long stenosis. This can readily be differentiated by enteroclysis.

Clinically, the most important complications of Crohn's disease include *small bowel obstruction, fistula* and *abscess* formation. Complete small bowel obstruction is unusual even with severe Crohn's disease; however, partial small bowel obstruction due to distal strictures and stenoses are common and sometimes require surgical intervention. Chronically obstructed loops between areas of small bowel affected with severe Crohn's disease may become markedly dilated. Fistulas and abscesses result from transmural penetration of ulcers. Fistulas may involve adjacent loops of small bowel, including colon and stomach. These areas are usually not

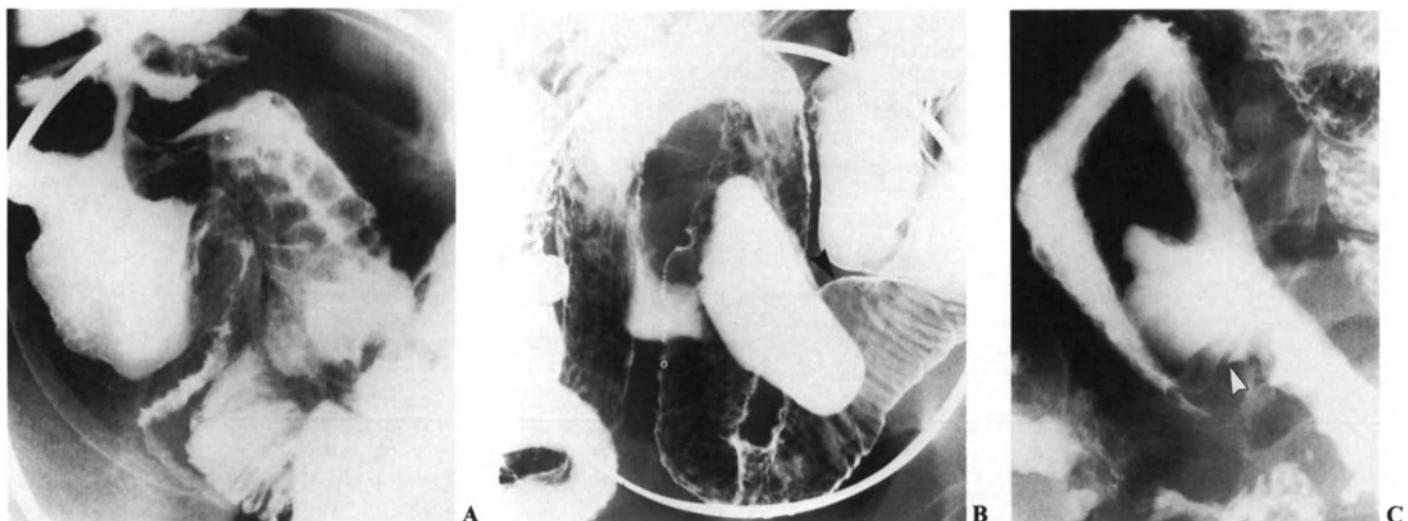


**Fig. 31.10A, B, C.** Cobblestone pattern in Crohn's disease. **A** Multiple intersecting linear transverse or longitudinal ulcers produce the cobblestone appearance. Appendiceal involvement is apparent. **B** Barium between bulging edematous folds also produces a cobblestone pattern. Villous abnormality (coarse granular surface) and aphthae are present in a less involved proximal segment (arrowhead). **C** Severe ulcerations producing cobblestone pattern. Note pseudosacculation (arrowhead) on antimesenteric side secondary to deep ulcers on the mesenteric border.

themselves diseased and may be considered to be *proximity lesions* (Fig. 31.11). If the primarily involved area is resected, proximity lesions heal. Fistulas outside the GI tract usually involve the urinary bladder, vagina, perineum and abdominal wall. Abscesses arise from cavitation and infection of extraluminal spread of Crohn's disease through complex fistulas or into the mesentery.

Bowel wall thickening, fistulas and abscesses are best evaluated by CT and, occasionally, by *ultrasound*. Abscesses are well-defined masses with fluid density frequently containing air. Presence of contrast media within the cavity is diagnostic of fistulous communication with the bowel. Abscesses and fistulas which may require surgical intervention should be differentiated from the inflammatory mass representing thickened bowel wall and associated infiltrated mesentery separating thickened bowel loops (Fig. 31.12).

*Adenocarcinoma* of the small bowel occurs with increased frequency in long-standing Crohn's disease. The radiographic findings are non-specific and diagnosis is difficult.

Recurrence of Crohn's disease occurs commonly after surgical resection, characteristically in the region of surgical anastomosis (Fig. 31.11). Surgery is, therefore, usually reserved for complications including significant obstruction, abscess, and complex fistula formation.

#### Infectious Enteritis

**Tuberculosis.** Enteric tuberculosis is rare in Western countries but still occurs with some frequency in the Third World. Primary infection occurs from ingestion of *Mycobacterium bovis* and secondary infection results from ingested sputum or hematogenous spread of pulmonary tuberculosis. The *distal small bowel* including the ileocecal region, is the most common site of involvement. Radiographic manifestations are varied and may mimic findings in Crohn's disease, carcinoma, and other small bowel disorders. The features may include either a predominantly ulcerative or a hypertrophic form. The terminal ileum and cecum are characteristically narrow, thick and rigid, with the cecum contracted into a conical shape. The ileocecal valve is hypertrophied. In the *ulcerative* form of the disease, multiple transverse ulcers overlie the submucosal nodules formed by tubercle formation. This is also associated with increased spasm, nodularity and thickening of folds and altered motility. Strictures may be

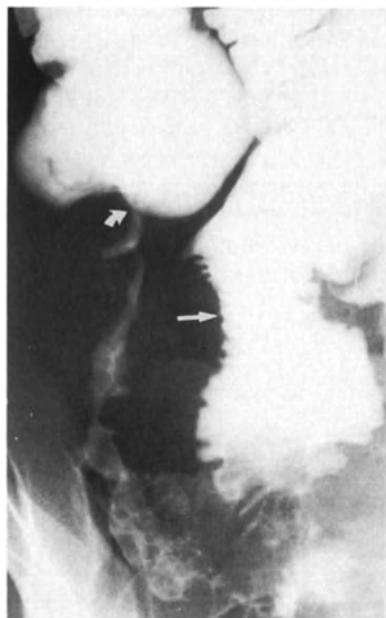


**Fig. 31.11.** Stricture formation in Crohn's disease. Progression of disease proximal to the ileocolic anastomosis (curved arrow) is manifested by diffuse narrowing, multiple deep ulcers and increased distance to adjacent loop indicating mesenteric extension of disease. Note unilateral wall flattening and fold thickening of adjacent medial loop suggesting a 'proximity' lesion (straight arrow).

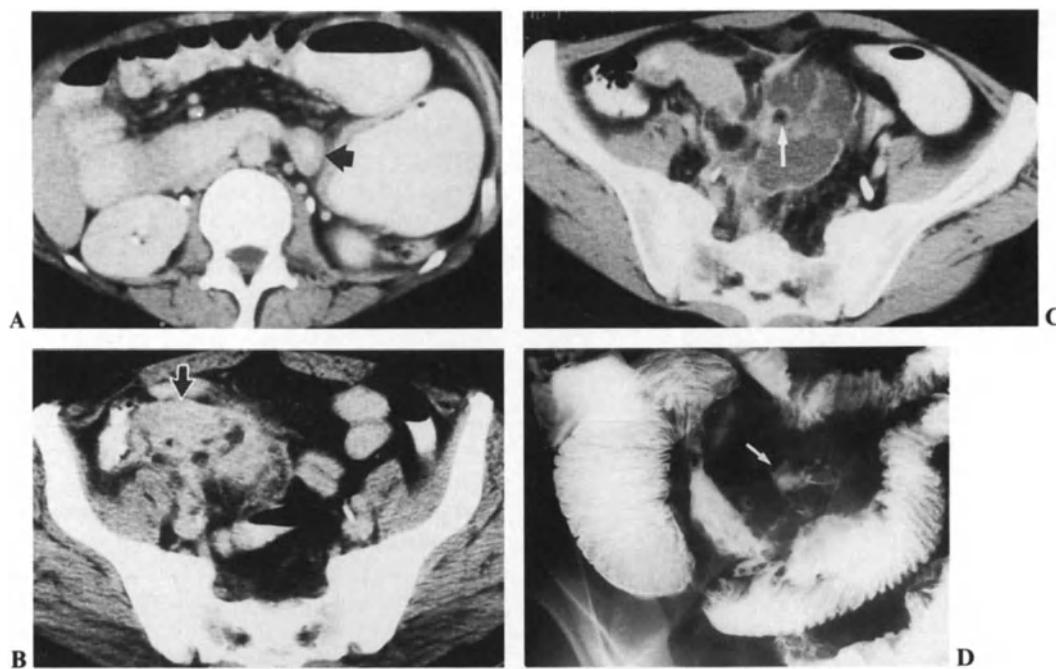


**Fig. 31.12A, B, C, D.** CT of Crohn's disease. A Circumferential wall thickening (arrow) secondary to Crohn's disease. Note dilatation proximal to lesion indicating obstruction. The thickness of the wall is well shown by CT. A 'double halo sign' reflecting the attenuation differences of the different layers of the inflamed bowel has been described but is not unique to Crohn's disease. Ischemia and radiation produce a similar appearance. B Inflammatory mass (matted inflamed loops of bowel) in right lower quadrant (arrow) secondary to distal small bowel Crohn's disease. Note absence of fluid collection. C Crohn's disease with abscess. CT shows well-defined fluid collection with adjacent inflammatory reaction. Small pocket of air (arrow) in fluid collection indicates fistula. D Enteroclysis of patient shown in part C shows enter-enteric fistulae, sinus tracts and extraluminal barium collection. Demonstration of extraluminal barium (arrow) secondary to deep ulcers and the increased distance between adjacent segments indicate abscess formation.

single or multiple and proximal obstruction may occur. Fistula formation also occurs with some frequency (Fig. 31.13).

The small bowel may be affected by tuberculous peritonitis and mesenteric disease. Small bowel dilatation and/or distortion secondary to retraction from infiltration of the mesentery may be seen in addition to the high density ascites, peritoneal thickening and lymphadenopathy characteristics

of tuberculous peritonitis.

*South American blastomycosis, histoplasmosis and actinomycosis* may affect the ileocecal region in a manner similar to tuberculosis.

**Yersinia Ileitis.** Infection with species of *Yersinia*, a gram-negative bacillus, may cause acute inflammation of the terminal ileum. The diagnosis is often made incidentally at laparotomy in patients with a clinical presentation of acute appendicitis. The terminal ileum is characteristically inflamed and edematous with associated lymph node enlargement. Many cases previously diagnosed as acute Crohn's disease which showed clinical resolution were probably secondary to *Yersinia* infection. The radiographic findings may be similar to those seen in ileal tuberculosis (Fig. 31.13).

**Giardiasis.** Giardiasis lamblia is a flagellated protozoan parasite which infests the upper portion of the small intestine. Infestation is via the oral-fecal route and it is usually contracted by drinking contaminated water. Infestations occur in non-compromised hosts traveling endemic areas and are more common in children. There is increased incidence of infection in association with various congenital immune deficiency states as well as in patients with AIDS and other immunocompromised hosts. Patients may present with abdominal pain and diarrhea and heavy infestation may cause malabsorption. Diagnosis may be made from identification of the parasite in the stool or by duodenal aspiration.

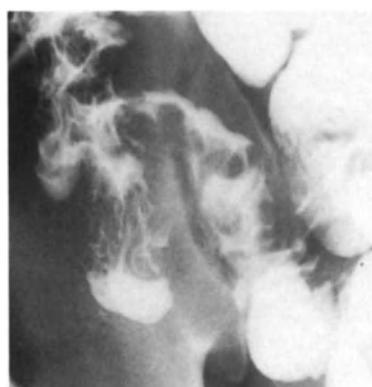


**Fig. 31.13.** Ileocecal tuberculosis. Fold thickening and multiple nodules are present in the terminal ileum. The appearance is mimicked by the other enteropathies involving the distal ileum. Tuberculosis should be considered with this appearance in a patient (an immigrant) from a third-world country or in immunosuppressed individuals.

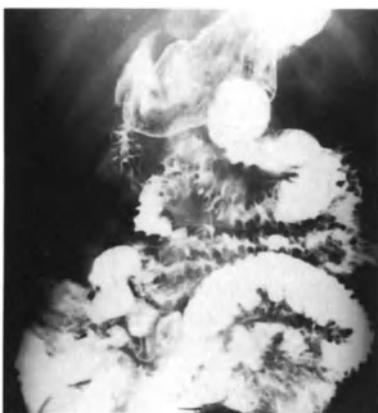


**Fig. 31.14.** Mixed small bowel infections (giardiasis and cryptosporidiosis) in an acquired immune deficiency patient. Thickened nodular folds and increase fluid in proximal small bowel is seen.

Radiographic features include distortion and thickening of the mucosal folds primarily in the duodenum and proximal jejunum. Increased fluid in the small bowel as well as spasm of the small bowel loops may also be seen (Fig. 31.14). In patients with associated dysgammaglobulinemia, associated nodular filling defects due to lymphoid hyperplasia may be seen associated with the changes of giardiasis (Fig. 31.15).

**Strongyloidiasis.** Strongyloidiasis is caused by a round-worm infestation, widespread in the tropics, and causing intestinal and pulmonary manifestations. Primary infection occurs from larval penetration of the skin. The larvae pass through the lungs whence developing worms are then swallowed and subsequently invade the small bowel mucosa. Patients present with abdominal pain, vomiting, diarrhea or weight loss. Diagnosis is made by examination of stool, sputum or duodenal aspirate.

Radiologic examination may demonstrate focal fold thickening and spasm in the proximal small bowel. Mucosal ulceration and stricture formation occur in more serious cases. Late findings include long areas of strictures with a



**Fig. 31.15.** Nodular lymphoid hyperplasia in a patient with hypogammaglobulinemia. Diffuse small uniform nodules are seen throughout the distal small bowel.

'pipistem' appearance secondary to thickening of the wall with loss of normal mucosal fold pattern. Significant dilatation of bowel proximal to strictures may occur.

**Ascariasis.** *Ascaris lumbricoides* is a common tropical infection acquired from ingestion of food or water contaminated with the ova. The worms hatch in the small bowel, migrate through the respiratory tract during their developmental cycle and are finally swallowed. The adult worm lives in the small bowel. The most common problem is from intestinal obstruction developing in children with a large worm burden. Plain films of the abdomen may demonstrate the presence of masses of coiled worms. Their appearance on a barium examination is unique as the long, smooth worm may be identified with a thin linear track of barium centrally outlining the worm's digestive tract.

**Other Parasites.** Hookworm infestation (*Ankylostomiasis*) is a common disease in tropical areas and also occurs in temperate zones. Two species of roundworms (*Ankylostoma duodenale* and *Necator americanus*) cause the disease. The adult worms live attached to the small bowel mucosa and cause chronic blood loss. Radiographic findings are non-specific. *Anisakiasis* is another parasitic infestation which is acquired from the ingestion of raw fish. Infection is caused by the worms burrowing through the intestinal wall, causing granuloma formation and rarely ulceration or perforation. Radiographic findings are non-specific. *Tapeworms* also inhabit the small bowel and may cause significant symptoms: however, radiographic demonstration is unusual.

**Bacterial Enteritis.** Infection with *Salmonella typhosa* (typhoid fever) and *Campylobacter* sp. may result in acute inflammatory changes of the ileocecal region. Though rarely examined radiographically, changes with these infections resemble acute Crohn's disease.

Non-typhoidal strains of salmonella may also invade the small bowel mucosa and cause inflammatory changes, most prominently edema and ileus. Again, these are rarely studied radiographically.

#### Non-infectious Enteritis

**Eosinophilic Enteritis.** In eosinophilic enteritis or gastroenteritis, eosinophilic infiltration of the bowel is found most commonly associated with an atopic response. The eosinophilic reaction may be confined to the mucosa, mural or transmural and accompanied by eosinophilic ascites. The jejunum is most prominently involved, but the duodenum, ileum and gastric antrum are also commonly affected. Radiographic findings include regular symmetric thickening of the valvulae conniventes (Fig. 31.16). In transmural disease the folds may be more irregular and angulated.

**Radiation Enteritis.** The most common cause of radiation enteritis is radiation therapy for treatment of carcinoma of gynecological and other pelvic malignancies, though current radiation dosages minimize the possibility of acute radiation syndromes. Most patients develop a chronic radiation syndrome at least a year after radiotherapy.

Radiation enteritis results from ischemia caused by an obliterative endoenteritis of small vessels. Early radiographic changes are due to edema, which causes uniform thickening of the mucosal folds with a consequent spiked appearance



**Fig. 31.16.** Eosinophilic enteritis. There is diffuse decreased distensibility and fold thickening of the distal small bowel. No ulcers, fistulas or increase of fluid are seen. The increase of fluid reported in follow through examinations is likely to be a reflection of poor coating.

of the barium filling the intrafold spaces. Bowel wall edema may cause a nodular pattern of filling defects ('thumbprinting'), and separation of the involved loops. In the rare event of severe acute radiation damage, there may be ulceration and bowel necrosis with complications including perforation, fistulas or abscess formation. Progressive fibrosis with chronic radiation damage results in chronic thickening of the bowel wall with loss of normal fold pattern and stricture formation. Chronic radiation damage is often accompanied by adhesion formation in the same area and changes in the mesentery which may lead to fixation and angulation of bowel loops as well (Fig. 31.17). Extensive radiation enteritis may be indistinguishable from recurrent neoplastic disease.

**Ulcerative Enteritis.** This is a somewhat obscure condition in which multiple ulcers occur in a focal area of ileum or



**Fig. 31.17.** Radiation enteritis. Diffuse fold thickening and fixation of loops confined to the external radiation portal suggests the diagnosis. The patient had radiation for carcinoma of the cervix.

jejunum. Ulcerative enteritis represents a complication of *celiac disease* in some patients. In another group, ulcerative enteritis occurs in patients with clinical symptoms similar to those of celiac disease and with villous atrophy; however, unlike celiac disease, these patients do not respond to gluten withdrawal. In a third group, the condition appears to be *idiopathic*. Ulcerative enteritis may predispose to or be a precursor to lymphoma.

The radiologic findings of ulcerative enteritis show a focally thickened and rigid segment of bowel with abnormal folds. Ulceration may be demonstrated. If the condition becomes chronic, strictures may develop. The radiographic findings are often indistinguishable from bowel lymphoma.

**Lymphoid Hyperplasia.** Lymphoid hyperplasia may be loosely considered within the designation of enteritis as it is most commonly a non-specific inflammatory response. In children and adolescents, lymphoid follicles in the distal ileum are normally quite prominent. In fact, prominent lymphoid follicles are believed to be the lead points of so-called 'idiopathic' ileocolic intussusceptions in children up to 2 years of age. Diffuse nodular lymphoid hyperplasia is associated with immunodeficiencies or lymphoma (Fig. 31.15). The condition is demonstrated as the presence of numerous small (2–3 mm) uniformly sized filling defects which correspond to the hyperplastic lymphoid follicles. In patients with immunodeficiencies, giardiasis is a common super-infection (Fig. 31.14). In adults, lymphoid hyperplasia in the distal ileum may occur as a response to a bacterial or viral infection. In addition, some investigators believe that a prominent lymphoid pattern may be the first radiographically demonstrable finding in early Crohn's disease.

#### Small Bowel Involvement in AIDS

Gastrointestinal symptoms are common in AIDS, with diarrhea being a frequent problem. Unlike most patients, AIDS patients frequently have multiple pathologic processes simultaneously. Multiple infections involving small bowel are common. **Infections** found in small bowel in these patients include *Giardia*, *Cryptosporidium*, *Isopora*, *cytomegalovirus*, *herpes*, and *Candida*. For the most part radiographic findings are non-specific. The small bowel folds are thickened, and there is often increased small bowel fluid. Deep ulceration is usually associated with cytomegalovirus infection. Infections tend to affect jejunum more than ileum (Fig. 31.14).

*Mycobacterium avium intracellulare* is an acid-fast organism related to tuberculosis which causes systemic disease in AIDS patients. It affects the small bowel in a manner similar to Whipple's disease with engorgement of the villi by macrophages which stain positive for PAS. Examination of the small bowel may demonstrate fold thickening, nodularity of folds secondary to villous engorgement and increased secretions. Mesenteric involvement and lymphadenopathy may cause mass effect and separation of bowel loops.

The **neoplasms** most commonly associated with AIDS include *Kaposi's sarcoma* and *lymphoma*. The nodular lesions associated with Kaposi's sarcoma are rarely demonstrated in the small bowel. Mesenteric or retroperitoneal lymphadenopathy which may be present usually causes non-specific mass effect or separation of small bowel loops. AIDS-related lymphoma is very aggressive and extranodal involve-

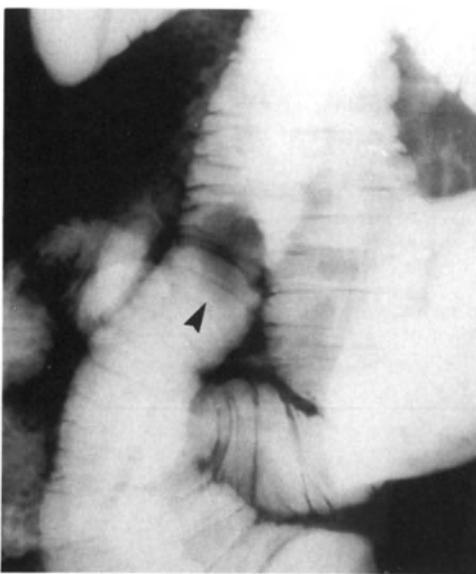


**Fig. 31.18.** Lipoma demonstrated by enteroclysis. A rounded intramural submucosal defect is seen in the mid small bowel (arrowhead) which at surgery proved to be an ulcerated lipoma. Other benign small bowel tumors look similar. Lipomas, however, appear to be more compressible. Attenuation of larger lipomas can be accurately depicted by CT.

ment is common. Primary involvement of the gastrointestinal tract, including the small bowel, is more common than in the normal population. Lesions may involve the small bowel and/or mesenteric and retroperitoneal nodes.

### NEOPLASMS

By far the most common neoplastic involvement of small bowel is that due to *metastatic disease*. *Primary small bowel*

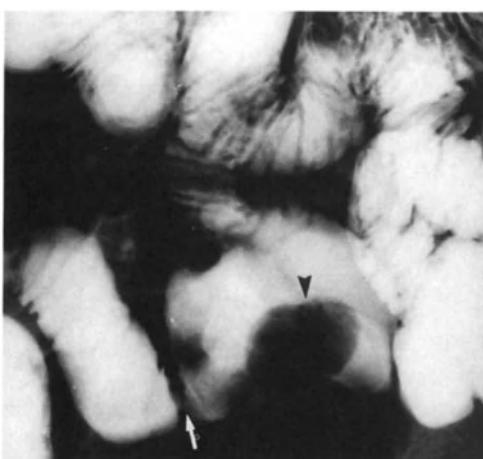


**Fig. 31.19.** Leiomyoma in a 'blind pouch'. The patient, an elderly female who had a history of surgery at birth for atresia, now presents with unexplained GI bleeding. Enteroclysis demonstrated a pouch proximal to an anastomosis (arrow). An intramural extramucosal mass (arrowhead) is seen inside the pouch. At surgery, an ulcerated leiomyoma in a dilated segment of ileum proximal to an end to side anastomosis.

tumors are rare, comprising only 5% of all gastrointestinal tract neoplasms. Benign and malignant tumors occur with approximately equal frequency and, in spite of their rarity, a wide variety of neoplasms may be found in the small bowel. The reason for the low neoplastic incidence in the small bowel is poorly understood. Symptoms and signs caused by small bowel neoplasms are non-specific and consideration of a small bowel neoplasm is generally a diagnosis of exclusion after normal examinations of the upper and lower GI tracts are obtained. All of these factors, compounded by the relative inaccessibility of the small bowel to examination, combine to make radiographic diagnosis a significant challenge even for experienced radiologists. Enteroclysis represents the most sensitive radiographic method for the detection of early focal small bowel lesions.

### Benign Tumors

Considering the infrequency with which small bowel tumors occur, there is a wide spectrum of tissue types which may develop into tumors. *Adenomatous polyps* and *leiomyomas* occur with equal frequency as the most common primary tumors seen. Other benign tumors include *neurofibromas* (especially in patients with neurofibromatosis), *lipomas*, *hemangiomas* and less usual *mesenchymal* lesions.

Most benign small bowel tumors are identified incidentally or found at autopsy. Relatively few benign tumors of the small bowel are symptomatic. Those that are, present with abdominal pain usually resulting from partial obstruction, or bleeding. Most benign tumors have similar radiographic appearance but some features may aid in pinpointing the diagnosis (Fig. 31.18).

**Adenoma.** Adenomas occur most frequently in the duodenum and their incidence decreases in the most distal small bowel. Adenomas arise in the mucosa and appear as intraluminal filling defects which tend to be lobulated or pedunculated.

**Leiomyoma.** Leiomyomas are the most common tumor of mesenchymal origin found in the small bowel. They may originate in submucosa or subserosal layers of the bowel wall. When detected on barium studies, they will present as smooth filling defects which usually form an angle of 90° or greater with the bowel wall (Fig. 31.19). Leiomyomas may occasionally be pedunculated or intraluminal and present with intussusception. Leiomyomas are frequently hypervascular and present with bleeding. In the appropriate clinical situation, angiography may be warranted as it frequently demonstrates the hypervascular mass and may also show contrast extravasation into bowel lumen (Fig. 31.20).

**Other Benign Tumors.** *Lipomas* are most common in the ileocecal region and the duodenum. Like leiomyomas, they are of mesenchymal origin and are demonstrated on contrast examination as smooth ovoid masses protruding into the bowel lumen (Fig. 31.18). Lipomas are characteristically soft lesions and, if they are large enough, change in their contour with compression or change in patient position is a characteristic finding. *Intestinal hemangiomas* are rarely detected by barium studies unless they attain sufficient size to cause an intraluminal or intramural mass on barium study. When present, they are usually found in association with other findings suggesting a specific syndrome complex. Most com-

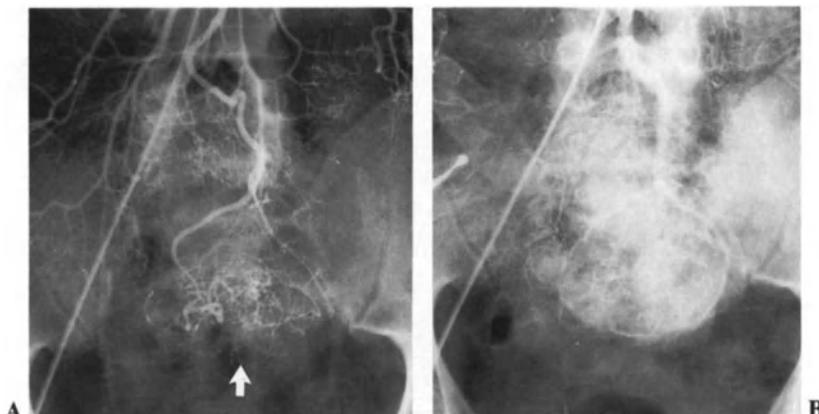


**Fig. 31.20A, B.** Superior mesenteric arteriogram of a leiomyoma. **A** The arterial phase shows a vascular mass in the upper pelvis (arrow). **B** The venous phase shows a rounded vascular mass with a prominent draining vein.

mon of these is Osler–Weber–Rendu disease (hereditary hemorrhagic telangiectasia). Hemangiomas may also be found in patients with tuberous sclerosis and Turner's syndrome. *Neurofibromas* are more likely to be multiple than other mesenchymal tumors and are found in patients with GI tract involvement in neurofibromatosis.

**Polyposis Syndromes.** Small bowel *hamartomas* are characteristic of *Peutz–Jegher's syndrome*. This hereditary polyposis is transmitted as an autosomal dominant and consists of the association of intestinal hamartomas with mucocutaneous pigmented lesions seen about the mouth, hands and feet. The small bowel hamartomas are benign and show no malignant potential. They appear as intraluminal filling defects and are commonly multiple (Fig. 31.21). The polyps have a propensity to bleed and cause intussusception. In patients with Peutz–Jegher's syndrome, polyps may also be found in the colon and stomach. Polyps in the colon may be hamartomas or adenomas. While there is no specific increased risk of malignancy in the small bowel, there is a somewhat increased risk of malignancy in the stomach, duodenum and colon.

Other polyposis syndromes are not characterized by small bowel involvement although small bowel polyps may occur in some cases. These syndromes are discussed in other chapters.

#### Carcinoid Tumors

It is difficult to classify carcinoid tumors as either benign or malignant since they may be benign, indeterminate, or frankly malignant. Of all neoplasms found in the small bowel, carcinoids are most uniquely associated with the small bowel, especially the distal ileum. Carcinoids represent the most common *primary* small bowel tumor (one third of all small bowel neoplasms). Furthermore, one third of all gastrointestinal tract carcinoids arise in the small bowel.

Carcinoids arise from enterochromaffin cells (APUD) which produce serotonin, kinin and other active hormones and peptides. The *appendix* is the most common site of carcinoid tumor where virtually all are benign and are found incidentally. Carcinoids generally arise in the submucosa but frequently erode into the mucosa. They may be single or multiple. Malignancy is determined by behavior of the tumor, regarding presence of mural invasion or distant metastases, rather than by histology which is usually quite bland. Malignant features are more common in larger lesions. Tumors larger than 2 cm are considered malignant. A desmoplastic reaction is common in carcinoid tumors and probably is an effect of hormonal stimulation.

The carcinoid syndrome consisting of skin flushing, tachycardia, diarrhea, wheezing and right heart disease is also mediated by the systemic effects of *serotonin* and *bradykinin*. Presence of the carcinoid syndrome almost always signifies the presence of liver and lymph node metastases. Most patients with carcinoid tumors are *asymptomatic* or present with *abdominal pain* or *obstructive* type symptoms. Presentation with the carcinoid syndrome is unusual.

Radiographically, most carcinoids are depicted as single or multiple submucosal or intramural nodules in the distal ileum (Fig. 31.22). Small lesions which are easily missed on routine studies are better demonstrated by enteroclysis. In later stages, the radiographic appearance is quite variable. Muscular hypertrophy and desmoplastic reaction in the



**Fig. 31.21.** Peutz–Jegher's syndrome. There are multiple polyps (arrowheads) in distal small bowel representing hamartomas.

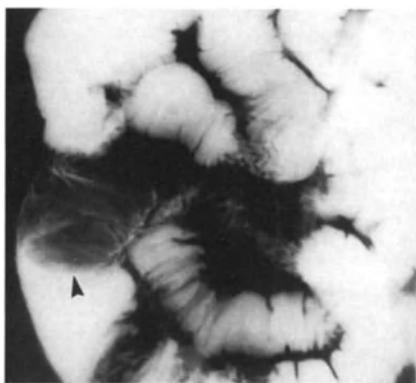


**Fig. 31.22.** Partially intussuscepting carcinoid (arrowhead) in distal ileum.

mesentery causes narrowing, rigidity and separation of bowel loops (Fig. 31.23). Retraction of the mesentery may cause fixation and angulation of affected loops. Intraluminal filling defects and short annular lesions may occur (Fig. 31.24). Presence of extraluminal tumor and serosal invasion may cause spiculation of the small bowel folds. Because of the wide range of radiographic appearances, carcinoid should be considered as part of the differential diagnosis of all of the above radiographic appearances. The radiographic differential diagnosis of carcinoid includes Crohn's disease, metastatic disease, inflammatory mass and lymphoma. Ultrasound and/or CT are useful adjuncts for demonstrating thickening of the bowel wall and mesenteric abnormalities, and play an indispensable role for the demonstration of liver metastases and retroperitoneal adenopathy.

#### Malignant Neoplasms

**Primary malignant tumors** of the small bowel are exceedingly rare, accounting for only 1%–2% of primary gastrointestinal tract malignancies. Adenocarcinoma, lymphoma, and sarcomas (especially leiomyosarcoma) are the important tumors to consider.

*Adenocarcinoma* primarily occurs in the duodenum and jejunum. This contrasts to carcinoid tumor which predominates in the distal ileum. Why adenocarcinoma of the small



**Fig. 31.23.** Desmoplastic reaction in carcinoid. There is fixation, narrowing and separation of loops with tethering of folds.



A



B



C

**Fig. 31.24.** A Carcinoid in jejunum. The large almost annular mass (arrow) just distal to the balloon (arrowhead) of the Maglinte Enteroclysis Catheter is indistinguishable from an adenocarcinoma which is more frequent in this location. B Diffuse nodularity and fixation of distal small bowel from carcinoid. The nodularity is secondary to lymphatic obstruction. C CT of bowel in part B shows tumor in terminal ileum (asterisk) with adjacent thickened loops retracted toward terminal ileum.

intestine is so uncommon is unknown, although theories abound. Patients with Crohn's disease have an increased risk for development of intestinal adenocarcinoma, as do patients with celiac disease. Patients with familial polyposis and Gardner's syndrome also have some increased risk of carcinoma in the duodenum, especially in the periampullary region. Most patients with adenocarcinoma are symptomatic,

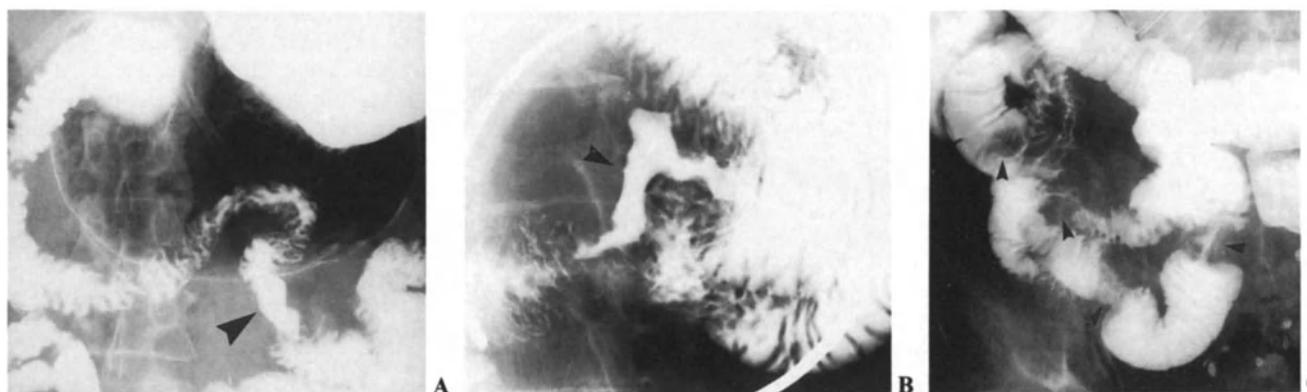


**Fig. 31.25.** A Jejunal adenocarcinoma. A large ulcerating mass (arrowhead) is seen just distal to the ligament of Treitz. Since most adenocarcinomas are close to the duodeno-jejunal segments, a carefully performed upper GI study should diagnose the abnormality. B Adenocarcinoma in a patient with celiac disease. The ulcerating infiltrative mass (arrowhead) has produced obstruction. C Multiple primary adenocarcinomas (arrowheads) demonstrated by enteroclysis. This may be difficult to differentiate from metastasis. In the absence of a known primary tumor, a multifocal carcinoma should be considered.

presenting with obstruction, pain, bleeding or anemia. A palpable mass may be present. Metastases to regional nodes and the porta hepatis are often present at the time of diagnosis.

Radiographically, most adenocarcinomas are short annular lesions, similar in appearance to those found in the colon. Abrupt, shelf-like margins define the area of abnormality which has a narrow lumen with loss of normal mucosal pattern. Polypoid or ulcerative lesions may also occur (Fig. 31.25).

Primary intestinal lymphoma is a rare tumor, although intestinal involvement with diffuse lymphoma occurs with much greater frequency. Non-Hodgkin's lymphoma predominates. Primary bowel lymphoma is the most common small bowel malignancy in the pediatric population and is being seen with increased frequency in AIDS patients.

Lymphomas have a wide spectrum of radiologic manifestations. Lesions may be single or multiple (Fig. 31.26). In the nodular form, multiple nodules are usually depicted as submucosal filling defects. They are larger and more variable in size than the nodules seen in lymphoid hyperplasia or diseases in which villous engorgement is a prominent feature. In the polypoid form of lymphoma, a discrete intraluminal mass, which may achieve considerable size, may be demonstrated. Such lesions often cause *intussusception* and are an important consideration in the differential diagnosis of intussusception in children over 2 years of age.

In the *infiltrative* form of lymphoma, the affected portion of the bowel becomes thickened with irregular thickening or complete loss of mucosal folds. Intramural infiltration by tumor with destruction of the myenteric plexus causes loss of muscular tone and is depicted as 'aneurysmal' dilatation of the affected segment. When the tumor develops as a large mass which extends beyond the bowel wall, it is described

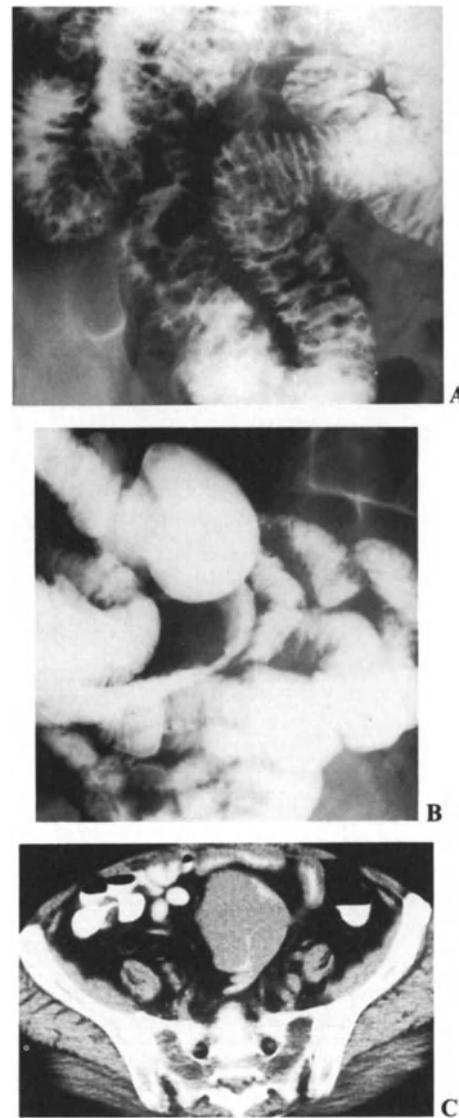


**Fig. 31.26.** A, B, C. Small bowel lymphoma. A Multiple nodules of variable sizes are seen throughout distal small bowel. B A large mass has caused displacement, narrowing and effacement of folds of a focal segment of bowel. C CT of bowel in part B shows the full extent of mass.

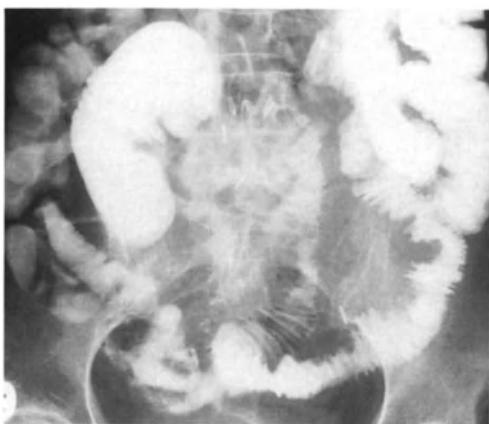


**Fig. 31.27.** Seeded metastasis from ovarian carcinomatosis. Note fixation, tethering and nodular mural defects along mesenteric margins.

as an *exo-enteric lymphoma*. These tumors tend to ulcerate and are predisposed to excavate and develop fistulas within the mass and communicating to adjacent bowel. Lymphoma may also develop considerable mesenteric invasion. In such cases, there may be large extraluminal masses displacing the bowel loops and other abdominal organs and causing the bowel folds to appear distorted. Differential diagnosis for this type of appearance includes primarily metastatic disease and primary mesenteric lesions such as retractile mesenteritis (*mesenteric lipodystrophy*). With lymphoma, there is less desmoplastic reaction and fixation than with the other described entities and the bowel loops generally remain more pliable.

CT is indispensable for staging intra-abdominal lymphomas, assessing adenopathy, the extent of extraluminal invasion and distant metastases.

*Leiomyosarcoma* is the most common sarcoma to involve the small bowel. These lesions are demonstrated as extrinsic or mural masses with displacement of adjacent bowel loops. Predominantly, leiomyosarcoma spreads by direct extension into the mesentery and portal system, rather than by intraperitoneal seeding, lymphangitic or hematogenous spread. The lesions tend to ulcerate into the bowel. On



**Fig. 31.28.** Serosal implants with invasion into the bowel wall. The mucosal folds are tethered and the involved bowel demonstrates a focus of eccentric nondistractability (arrows).

barium examination the necrotic tumor mass may be demonstrated as an irregular extraluminal collection of barium.

**Metastatic Tumor.** Metastases to the small bowel represent the most common type of neoplastic involvement of the small bowel. Small bowel metastases usually develop either from intraperitoneal seeding or from hematogenous dissemination of tumor. Direct extension from adjacent primaries may also be considered with metastases. In patients with diffuse abdominal carcinomatosis, CT should be the primary imaging modality performed. When involvement of the small bowel itself predominates, a barium examination may provide invaluable clinical information.

*Intraperitoneal seeding* occurs most often from gastrointestinal or gynecologic malignancies. The bowel is seeded along the routes of flow of ascitic fluid and deposits accumulate in dependent areas of the abdomen such as the pelvic cul-de-sac, ileocecal region and along the route of the small bowel mesentery (Fig. 31.27).

Serosal implants may be demonstrated as nodular protrusions into the lumen causing a distortion of the normal contour. The mucosal folds covering the lesion appear flattened and hazy (Fig. 31.28). Invasion of the mucosa is a late feature of seeded metastases. Seeded metastatic deposits are most often multiple and, if they are large enough, their detection and radiographic diagnosis is usually clear. If the tumor produces a desmoplastic response, there may be fixation and angulation of bowel loops with luminal narrowing and obstruction. Normal bowel fold pattern is lost or obscured. In such cases, the appearance must often be differentiated from extensive adhesions, radiation changes and inflammatory changes.

*Hematogenous* metastases to the small bowel are uncommon. When they are found, the primary tumors most involved are metastatic melanoma, breast and lung cancer. These generally develop as submucosal nodules which ulcerate into the lumen early (Fig. 31.29). These may appear as 'target' lesions, or intraluminal polypoid masses. Occasionally, they may form large ulcerating masses or annular constricting lesions. Direct invasion from a locally aggressive tumor usually demonstrates considerable mass effect. Small bowel may be displaced, show narrowing and fixation within the tumor or be completely encased by surrounding tumor.

## SMALL BOWEL OBSTRUCTION

Mechanical small bowel obstruction occurs when the lumen of the bowel is completely or partially occluded by an intrinsic or extrinsic process. The initial evaluation for small bowel obstruction is the acute abdominal plain film series. This is discussed in detail in Chap. 24. In cases of complete or high grade obstruction or when free air is detected on the abdominal series, the patient is taken immediately to surgery and no further radiographic imaging is usually necessary. The role of barium evaluation of small bowel in obstructions is most relevant in cases of intermittent, chronic or partial small bowel obstruction. In such cases, delay in clinical diagnosis and definitive treatment is common and small bowel studies, especially enteroclysis, may play an important role

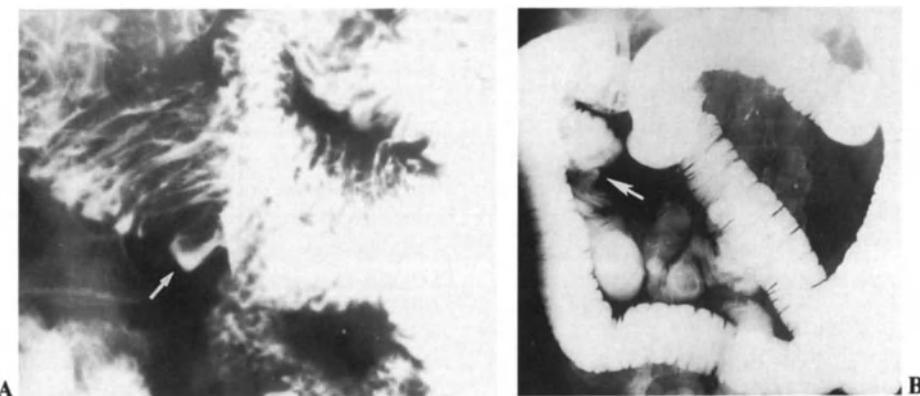


**Fig. 31.29.** A Ulcerating nodule (arrow) from metastatic lung carcinoma. B Ulcerating stricture in distal ileum with partial obstruction. Surgery showed metastatic lesion from colon carcinoma.

in patient management. The availability of decompression/enteroclysis catheters (Maglente Decompression Tube, Cook Inc., Bloomington, IN) allows for immediate performance of enteroclysis following initial decompression in those patients in whom medical management is elected. This allows diagnosis of unsuspected closed loop obstruction, a frequently misdiagnosed condition which leads to strangulation. In many cases small bowel studies can define the level and cause of obstruction.

Small bowel obstruction is the most common surgical condition to affect the small bowel. The most important differential diagnosis is between a *mechanical* small bowel obstruction and an *adynamic ileus*. Ileus represents a disorder of intestinal motility secondary to a wide range of causes both directly related to bowel problems and secondary to multiple systemic disorders. Presenting symptoms may be similar to those of a small bowel obstruction and, as with a mechanical obstruction, the small bowel is dilated and fluid-filled. This important radiographic distinction is usually made on plain films of the abdomen. Adynamic ileus usually affects the large and small bowel. Air fluid levels are seen on horizontal beam films throughout the small bowel and colon. The bowel

is diffusely dilated and there is no disproportionate distension of more proximal loops. These features tend to distinguish the adynamic ileus from mechanical small bowel obstruction.

**Adhesions.** Adhesions are the most common cause of small bowel obstruction occurring in up to 75% of affected patients. Most adhesions are the result of prior surgery. Approximately half of the patients presenting with symptoms related to adhesions have partial or intermittent small bowel obstructions and respond to conservative management. Barium studies, especially enteroclysis, are useful when the diagnosis of obstruction is in doubt, the etiology of obstruction is unclear or when a clinical decision of surgery versus decompression tube management needs to be made. The study may be performed with the patients drinking the barium or through a decompression tube which was previously inserted for management of obstruction.

Obstructions due to adhesions may be caused by a single band completely crossing the bowel lumen or adherent to one wall. Radiographic features observed in such cases include *abrupt luminal narrowing* which demarcates the level of the adhesion. Bowel proximal to the obstruction is dilated; however, the normal mucosal pattern is preserved right up to the level of the obstruction. Bowel distal to the obstruction is collapsed or of normal caliber (Fig. 31.30).

Obstruction by multiple adhesions or bands surprisingly causes a lower grade obstruction than a single band (Fig. 31.31). Radiographic features include the presence of several short constrictions of the lumen over a limited length of bowel, normal fold patterns throughout, and often adherence to the anterior abdominal wall. Multiple adhesions are more common in the *pelvis* than in the proximal small bowel. Occasionally, extensive small bowel adhesions occur (Fig. 31.32). Sometimes these are more difficult to distinguish radiographically from changes due to an extrinsic mass, or radiation changes when that is a clinical consideration. Several radiographic features do help distinguish these etiologies. With extensive adhesions, a flattened loop of small bowel may be closely apposed to an adjacent structure to which it is adherent. The deformity caused by adhesions tends to be more two-dimensional than that which would be caused by a bulky tumor mass, which would be respon-



**Fig. 31.30.** Partial obstruction from an adhesive band. The point of obstruction (arrow) is indicated by the change in caliber of bowel.

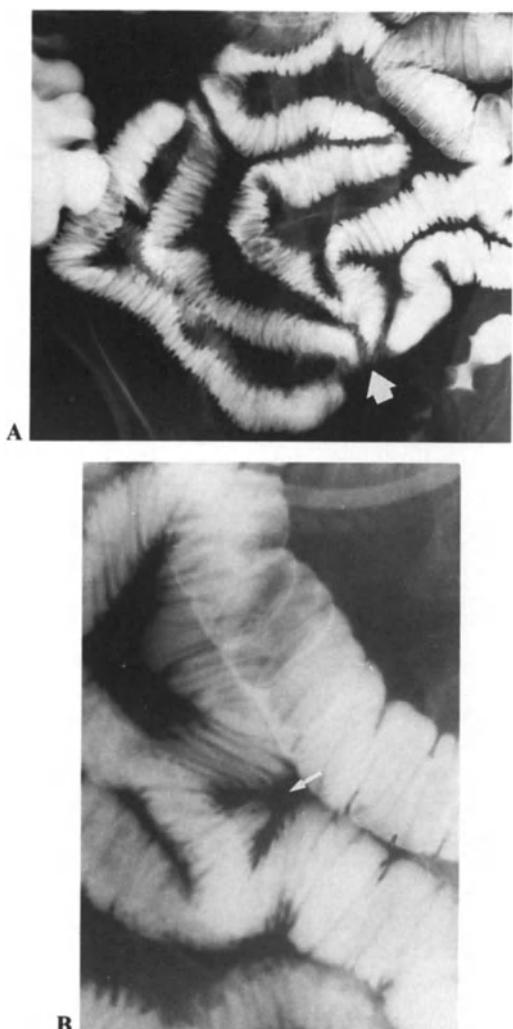


**Fig. 31.31.** A Adhesions fixing multiple segments of small bowel to a focal point (arrow). The degree of stasis is very minimal. B Peritoneal adhesions fixing adjacent walls of bowel producing tenting of focal bulges (arrow). No obstruction is seen during forced infusion.



**Fig. 31.32.** Extensive adhesions fixing loops of bowel to parietal peritoneum. Note long areas of narrowing and fixation with proximal dilatation.

sible for the same degree of deformity of small bowel. In addition, in cases of adhesions, bowel wall folds which are not fixed may be demonstrated fluoroscopically to be separable and of normal caliber.

**Hernias.** Abdominal hernias occur when the bowel protrudes through defects in the mesentery or peritoneum. These are most commonly through a normal peritoneal fossa resulting in inguinal, femoral or umbilical hernias. Internal hernias also may occur through gaps in the mesentery created by developmental variant of mesenteric fusion related to intestinal rotation. Included in this category are paraduodenal and pericecal hernias as well as hernias through other mesenteric defects. Hernias also occur following abdominal surgery in iatrogenically produced defects. Ventral incisional hernias are the most common in this category.

When a hernia becomes incarcerated, or non-reducible, obstructive symptoms may occur. If a herniated segment of bowel becomes strangulated, its blood supply is compromised and patients may present acutely with peritonitis or perforation due to the bowel ischemia. Radiographic findings in these cases are often apparent on plain abdominal films. Barium evaluation is generally performed in patients with non-specific or mild obstructive symptoms (Fig. 31.33A). Diagnosis of hernias is confirmed by the depiction of bowel protruding through a normal peritoneal fossa or through an abnormal orifice in the abdomen. The involved segment of bowel may sometimes be demonstrated contained within a well-circumscribed pouch representing the hernia sac. Fluoroscopy with the patient performing a Valsalva maneuver may demonstrate an elusive hernia or one in which only one wall of bowel is involved (Richter type hernia (Fig. 31.33B)). CT may be useful in demonstrating abdominal wall hernias or pelvic hernias.

**Volvulus.** Small bowel volvulus, though more usually associated with the life-threatening midgut volvulus found in neonates, may also present later in life. In this condition, the small bowel twists on its mesentery and may become fixed by the presence of congenital bands or acquired adhesions. Patients present with *small bowel obstruction*. Occasionally, coiled, gas-filled loops may be seen on plain abdominal films. On contrast examination, the point of torsion is identified by a beak-like configuration of the obstructed loop. The non-contrast-filled dilated closed loop may be seen distal to the beak-like obstruction on the films. *Ischemia* is an important consideration in the presence of a volvulus and its presence is suggested by the presence of thickening of the mucosal fold pattern secondary to submucosal edema or by focal hyperperistalsis proximal to the area of involvement. Clinical and radiologic findings are unreliable in the preoperative diagnosis of volvulus and other causes of closed loop obstruction. The prompt performance of enteroclysis in patients with mechanical obstruction where a trial of medical management is elected will uncover unsuspected closed loop obstruction (Fig. 31.34).

**Intussusception.** Ileocolic intussusceptions are the most frequent. They are not uncommon in infants from 6 months to 2 years old and in these cases are most often caused by a *lymphoid hyperplasia* in the terminal ileum. After 2 years of age, a lead point causing the intussusception should

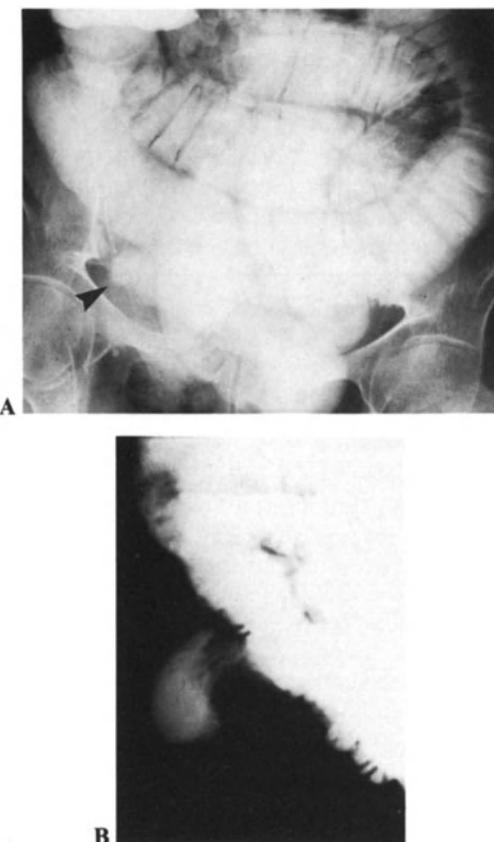


**Fig. 31.33.** A Tight mechanical obstruction secondary to obstruction of afferent loop at neck of a femoral hernia (arrowhead). Although external abdominal hernias may be clinically reducible, the obstruction of a segment of the afferent loop at the neck may not preclude clinical reduction of the loops contained in the hernial sac. B Radiograph in lateral position after cessation of enteroclysis infusion in an obese patient with unexplained recurrent abdominal pain and distension. A small ventral hernia (arrow) is apparent during straining but reduces during quiet respiration. An abdominal CT showed adherence of bowel at incision site but the hernia was not shown with the patient in the supine position in suspended respiration.

always be sought. Etiologies include *tumor* and *Meckel's diverticulum*. Less common causes include *cystic fibrosis*, *celiac sprue* and *Henoch-Schönlein purpura*. These intussusceptions are frequently intermittent and reducible during a study. Thus, they must be sought when the patient is symptomatic. Contrast evaluation may demonstrate the classic coiled-spring appearance around the intussusceptum. Sometimes the intussusception may appear as a partially or completely obstructing mass (Fig. 31.22).

**Obturation.** The small bowel may be completely obstructed by objects which completely clog the small bowel lumen. Gallstone ileus is the classic cause and occurs in elderly patients when a large gallstone erodes into the small bowel and impacts in the ileum (Fig. 31.35). Foreign bodies and bezoars are other causes of obturation type obstructions of small bowel.

**Meconium Ileus.** Meconium ileus is a condition associated with bowel obstruction in neonates with cystic fibrosis. The meconium in these infants is abnormally thick and viscous

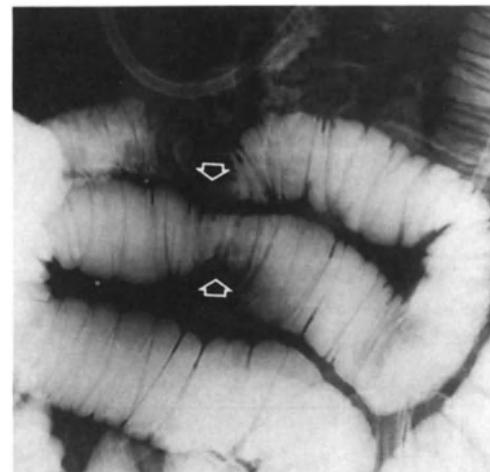


**Fig. 31.34.** Dense adhesive band fixing two adjacent segments of bowel (arrows) demonstrated by enteroclysis. Although no twist has occurred, a closed loop effect is produced. Partial volvulus around a band, an ileostomy opening or a mesenteric opening can be diagnosed by enteroclysis prior to strangulation.

and may obstruct the ileum. This may be complicated by *in utero* ischemia or necrosis and result in atresias, calcification of bowel wall or meconium peritonitis which may also calcify. Volvulus may also complicate meconium ileus.

On plain abdominal radiographs the meconium appears as a mottled mass. There is usually a paucity of air-fluid levels



**Fig. 31.35.** Gallstone ileus. A large non-opaque gallbladder calculus is demonstrated by the barium study. Note deformity of proximal duodenum and contrast in gallbladder indicating site of cholecystoduodenal communication

in spite of the obstruction. Diagnosis is generally made by a retrograde contrast examination with demonstration of a microcolon, and an intraluminal mass in the terminal ileum.

*Other Causes of Obstruction.* Metastatic disease, radiation injury, and vascular compromise as well as inflammatory conditions especially Crohn's disease may present with small bowel obstruction. These disorders are discussed in other sections.

### MALABSORPTION AND IMMUNE DEFICIENCY

The physiologic processes involved in normal digestion and absorption of nutrients are extremely complex. The normal process may be interrupted at multiple levels ranging from deficiencies in the secretion of digestive enzymes to abnormalities in uptake and transport of nutrients through the small bowel mucosa or in their delivery to the appropriate organs. An abnormality at any point in this sequence may lead to symptoms and signs which are considered in the malabsorptive stage. The narrower definition of malabsorption requires the presence of *steatorrhea* (the passage of bulky greasy stools), as determined by fecal fat analysis or D-xylose absorption, which are clinical markers of malabsorption. *Villous atrophy*, demonstrated by small bowel biopsy, is the histologic marker. Celiac disease is the accepted prototype for malabsorption.

Most generalized small bowel diseases are accompanied by some degree of malabsorption as are several systemic diseases which may affect the bowel. Gastric and intestinal surgery and other conditions leading to a shortened effective length of bowel or bypassed conditions leading to bacterial overgrowth also produce malabsorption type disorders.

Malabsorption is a clinical diagnosis. The role of radiology is to demonstrate specific small bowel abnormalities that may present as malabsorption, to exclude conditions that may produce villous atrophy, and to demonstrate complications of clinically established malabsorption states, for example the presence of lymphoma complicating celiac disease.

Disease processes included in this section include those in which symptoms of malabsorption predominate. Malabsorption may also be found in many other conditions affecting the small bowel, for example in Crohn's disease, especially when extensive, and in many of the infectious processes.

#### Celiac Disease

Celiac disease is a congenital or acquired sensitivity to gluten, a protein found in certain grains especially wheat. Celiac disease, or sprue, is most prevalent in Northwestern Europe and presents with diarrhea, steatorrhea, weakness, weight loss and abdominal discomfort. There is malabsorption of all nutrients. Symptoms resolve promptly when gluten is withdrawn from the diet.

The mucosa of the proximal small bowel is the primary site of involvement. Diagnosis is made by small bowel biopsy which shows characteristic blunting or complete absence of the villi. This is usually associated with lymphocytic infiltration and thickening of the lamina propria.

Although the diagnosis of celiac disease is a clinical one, there are specific radiologic findings which are associated with this condition. The classic description of barium flocculation within the small bowel is related to a combination of increased bowel secretion, delayed transit and the barium suspension used, a reflection of a suboptimal examination method. This is a very nonspecific finding and its presence is significantly reduced with modern barium suspensions and with increased use of enteroclysis and other dedicated small bowel examinations. Most often, patients with celiac sprue will have a small bowel of normal appearance. When radiographic changes are present, the most common finding is that of *mildly dilated bowel*. This is a non-specific finding which is also seen in bowel obstruction, scleroderma, hypoalbuminemia and as a result of vagotomy and gastric resection.

There is a strong association of celiac disease with an absolute decrease in the number of folds in the jejunum as demonstrated by enteroclysis (Fig. 31.36). Normally, there are five or more folds of jejunum per inch; patients with celiac disease have three or fewer. The reason for this is unclear. Conversely, there is an increased number of folds in the ileum. This is sometimes referred to as 'jejunization' of the ileum. Thickening of the small bowel folds may also occur when malabsorption in sprue results in hypoalbuminemia. Mucosal changes may also be depicted in the duodenum with thickening of the folds, a 'bubbly' mucosal pattern or small punctate collections of barium due to erosions. A fine mozaic pattern of 1–2 mm grooves in the jejunum is also described. A variety of motility disorders, ranging from accelerated transit to marked hypomotility, which may cause pseudo-obstruction may occur in celiac disease. Transient enteroenteric intussusceptions are occasionally seen during a small bowel follow-through examination. Lumen distension and the more rapid transit with enteroclysis appear to prevent the formation of this asymptomatic entity.

Imaging studies play an important role in evaluating complications of celiac disease especially when symptoms recur or are exacerbated in spite of a gluten-free diet. Complications associated with celiac disease include development of small bowel *lymphoma*, *carcinoma* and *ulcerative enteritis*. These are entities which are discussed elsewhere. Mesenteric and retroperitoneal *adenopathy* sometimes occur without evidence of malignancy. Rarely there may be diffuse cavitation of the massively enlarged lymph nodes. *Hyposplenism* is also associated with celiac disease.

#### Tropical Sprue

Tropical sprue is unrelated to celiac disease but symptoms are very similar. It is not known whether this is caused by a specific infection. Tropical sprue responds to folate and tetracycline.

#### Whipple's Disease

Whipple's disease is a rare disorder in which periodic acid-Schiff (PAS) positive macrophages are found in the lamina propria of the small bowel, as well as in other tissues. The disease is caused by a bacterium which has eluded attempts at culture or transmission. The disease is most common in

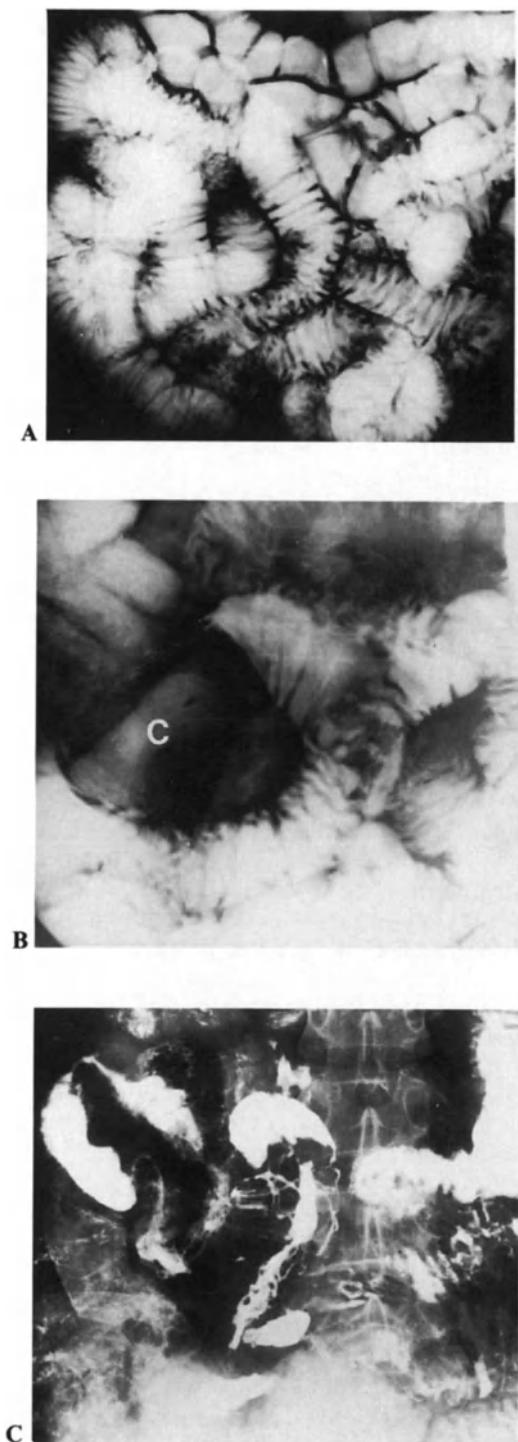


**Fig. 31.36A, B, C.** Relevance of enteroclysis in the evaluation of malabsorption. A Defermant of flocculation because of a more rapid transit and the ability of the infusate to push fluid in small bowel allows better fold depiction. A reduced number of folds per inch of jejunum is apparent. B An increase in the number of folds per inch of distal small bowel is shown in this compression radiograph of distal ileum of same patient. Note fluid in the right side of colon pushed by infused contrast in this patient with sprue. C, cecum. C Transient intussusceptions in sprue using the small bowel meal: more likely a reflection of inability to demonstrate the fold pattern and luminal surface than an actual morphologic alteration, in essence a flow/coating artefact popularized in the older radiology literature. There are no clinical or histological counterparts to this radiologic 'non-entity'.

middle-aged white males. In addition to the small bowel, Whipple's disease may affect the heart valves, central nervous system and joints. Radiographic findings are somewhat variable and non-specific. The bowel may be slightly dilated and the folds irregularly thickened. In other cases, a diffuse pattern of tiny, 1-mm nodules may be superimposed on the thickened folds. This is caused by the engorged villi. There is usually increased bowel fluid. Whipple's disease is usually considered with malabsorption rather than with infection since malabsorption is a major component of the presentation and its infectious nature was not understood until recently.

#### Lymphangiectasia

Lymphangiectasia occurs as a primary disease or may be secondary to lymphatic obstruction. The *primary* form affects children or young adults and is the result of a developmental abnormality of the lymphatic system. The lymphatics in the intestinal mucosa and submucosa are markedly dilated. Patients present with edema, diarrhea and steatorrhea. Intestinal loss of protein and vitamins may result in hypoalbuminemia, rickets and loss of intestinal lymphocytes, which predisposes patients to a variety of infections. *Secondary* lymphangiectasia may be associated with any condition which causes lymphatic obstruction including retroperitoneal and mesenteric nodal involvement by lymphoma, tumors (Fig. 31.24B) or infections. Lymphangiectasia may also be caused by congestive heart failure, retroperitoneal fibrosis and radiation damage.

Barium examination of the small bowel generally shows diffusely mildly dilated bowel lumen with increased intraluminal fluid. The folds are thickened. The thickened folds in lymphangiectasia are sometimes likened to a 'cog-wheel'. High-quality examinations may demonstrate multiple clusters of tiny nodules representing the distended villi. The radiographic appearance is very similar to that seen in Whipple's disease but the fold pattern in lymphangiectasia is usually more uniform and sand-like than the irregular thickening described with Whipple's disease (Fig. 31.37).

#### Scleroderma

Scleroderma, or progressive systemic sclerosis (PSS), is a systemic autoimmune disorder in which there is replacement of normal body tissues by collagen. The disease affects the skin, lungs, kidneys, bones and heart as well as the digestive organs. Within the GI tract, the *esophagus* and *small bowel* are most often affected. Intestinal symptoms include functional small bowel obstruction (pseudo-obstruction) due to loss of normal peristalsis; malabsorption sometimes develops due to subsequent stasis and bacterial overgrowth.

Two different radiographic findings in small bowel are characteristic of the disease. The first is called the 'hidebound' bowel. In this case, the small bowel folds are straight, or normal width, and are crowded together. The bowel itself is somewhat dilated. This appearance is characteristic because the folds are crowded rather than being somewhat separated, as would be the case in bowel obstruction or paralytic ileus. Crowding of the folds is believed to result from replacement of the muscularis propria by collagen (Fig. 31.38).



**Fig. 31.37.** Coned view of a segment of jejunum in a patient with primary intestinal lymphangiectasia. A distinct granular or sand-like surface pattern with diffuse fold thickening is seen.

The second finding characteristic of small bowel in scleroderma is that of *sacculations* or wide-mouthed diverticula on the antimesenteric border. Rare associations with scleroderma include transient intussusception and *pneumatosis intestinalis* which may lead to a benign pneumoperitoneum.

#### Amyloidosis

Amyloidosis may mimic many other entities and should be considered in the differential diagnosis of many radiographic

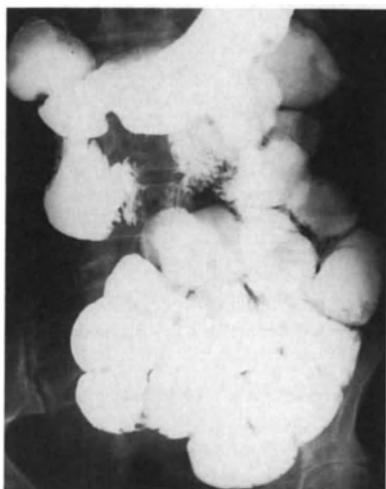


**Fig. 31.38.** Scleroderma. Small-bowel meal showing dilated flacid loops of jejunum with suggestion of crowding of folds per inch. Pseudosacculations are probably present on antimesenteric margin but are not clearly shown by study.



**Fig. 31.39.** Zollinger-Ellison syndrome. Dilated fluid-filled small bowel is seen. Note changes in distal stomach and fold thickening of folds in descending duodenum.

patterns. The bowel may appear entirely normal in some cases but there may be diffusely thickened folds and large smooth nodules may occur. The bowel may also be dilated with thin folds causing a pseudo-obstruction if the innervation of the bowel wall is disrupted or muscle is replaced by amyloid.

#### Zollinger-Ellison Syndrome

Zollinger-Ellison syndrome is caused by a functioning islet cell tumor of the pancreas which secretes gastrin. This tumor of variable malignancy results in constant secretion of gastric acid. Thus, the primary manifestation of this condition is its effect on the gastrointestinal tract, often presenting with *severe diarrhea* and *multiple peptic ulcers*. Multiple ulcers are characteristically found in the duodenum. Ulcers are also common in the stomach and jejunum, and are recognized with increasing frequency in the esophagus. The small bowel is dilated with thickened folds and a significant increase in luminal fluid (Fig. 31.39). The combination of multiple duodenal antral and jejunal ulcers with dilated, fluid-filled small bowel is characteristic of Zollinger-Ellison syndrome. The symptoms may respond dramatically to high doses of H<sub>2</sub> blockers. If the primary tumor can be identified, cure is sometimes achieved by resection. Total gastrectomy is another method used to control the symptoms of the disease.

#### Systemic Mastocytosis

This is a primarily dermatologic disorder presenting with urticaria pigmentosa. In the rare systemic form of mastocytosis, there is mast-cell proliferation throughout the body including the GI tract. Histamine release causes symptoms of flushing, tachycardia, headache and secretory diarrhea.

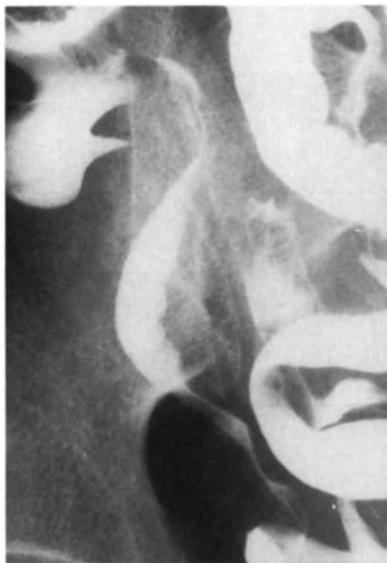


**Fig. 31.40.** Graft versus host disease (GVHD). Compression view of distal ileum shows diffuse fold effacement and decreased distensibility. GVHD is a differential diagnosis of the tubular or ribbon-like small bowel. The clinical background is diagnostic. (Courtesy of S. Somers MD)

On radiologic examination, mastocytosis may be identified by the association of changes in the bowel with sclerotic bony lesions. The wall of the small bowel may be thickened and demonstrate a diffuse nodular pattern. These nodules are somewhat larger than those found in Whipple's disease and lymphangiectasia and may represent urticaria. Fold thickening and nodules may also be seen in the gastric antrum. There is an increased association with peptic ulcers and hepatosplenomegaly.

#### Graft versus Host Disease

Bone marrow transplants are becoming more common for the treatment of acute leukemia, aplastic anemia and lymphoma. Graft versus host disease develops when the host is unable to reject the antigenically foreign graft. Acute graft versus host disease occurs within one to three weeks after transplant. Profuse diarrhea is characteristic. Radiographic changes at this stage include diffuse thickening of the bowel wall with narrowing of the bowel lumen and obliteration of the folds. The ileum tends to be affected more than the jejunum (Fig. 31.40). Ulceration may also occur. In the subacute phase of the disease, changes become more segmental with areas of stenosis developing. Thickening of the bowel wall and narrowing of the lumen are still present. In the chronic stage of the disease the underlying changes in the small bowel are complicated by infections such as cytomegalovirus.

#### Other Malabsorption or Maldigestive States

**Bacterial overgrowth** within the small bowel may cause frank malabsorption or non-specific symptoms including weight loss, diarrhea and anemia. This may be associated with *bowel stasis* due to a number of conditions many of which can be included in a chronic pseudo-obstruction syndrome. This may occur as a primary muscular or neurologic

disorder. It is also associated with many other conditions, including scleroderma and other collagen disorders. Any systemic disorder leading to a chronic ileus including diabetes, hypothyroidism, use of narcotics or ganglionic blockers, electrolyte disorders, cathartic abuse and chronic ischemia may ultimately permit bacterial overgrowth. Specific anatomic abnormalities associated with bowel stasis and bacterial overgrowth include multiple small bowel diverticula, blind loops or pouches (from previous surgery), enteric fistulas, and strictures from any cause.

In patients with continued bacterial seeding of the small bowel, similar symptoms occur. This includes patients who have undergone gastrectomy, patients with decreased gastric acid, fistulas between small bowel and colon or stomach and chronically infected bile.

The wide variety of primary and secondary immune deficiencies is also associated with diarrhea and/or malabsorption. Radiographic findings in these cases are non-specific, usually associated with thick bowel folds and increased fluid. *Nodular lymphoid hyperplasia* causing numerous small filling defects within the small bowel is sometimes seen. Selective *IgA deficiency* is the most common primary immune defect and there is an established association with lymphoid hyperplasia and giardiasis.

In another group of diseases, *lack of digestive enzymes* is the primary cause of impaired digestion. This includes patients with *cystic fibrosis*, *chronic pancreatitis* and other disorders of pancreatic origin. Defective delivery of bile into the duodenum secondary to *biliary obstruction* or *hepatocellular disease* may also cause steatorrhea. In cystic fibrosis, the small bowel folds may appear thickened and distorted. This is primarily due to the presence of inspissated secretions coating the bowel mucosa rather than a primary abnormality of the small bowel. In the other disorders in this category, the small bowel is normal radiographically.

A common clinical cause of maldigestion is due to *lactase* or other *disaccharidase deficiency*. Radiographic studies used to be performed commonly but are now rarely done. Lactose added to barium causes increase in bowel secretion resulting in some bowel dilatation and an indistinct mucosal pattern. Examination of the same patients without lactose added to the barium shows completely normal small bowel.

## VASCULAR DISORDERS

#### Ischemic Bowel Disease

Impaired blood flow through the mesenteric vessels results in intestinal ischemia. In most cases, diminished arterial perfusion is non-occlusive and is secondary to *low flow states*, usually a result of primary cardiac abnormalities including congestive failure, arrhythmias and myocardial infarction. Renal dialysis patients as well as those with any condition leading to volume depletion, or decreased cardiac stroke volume are also prone to develop *non-occlusive mesenteric ischemia*. The clinical presentation is generally non-specific. Patients may have abdominal pain and mild intestinal bleeding.

Abdominal plain films play an important role in these patients since symptoms are so frequently vague and non-

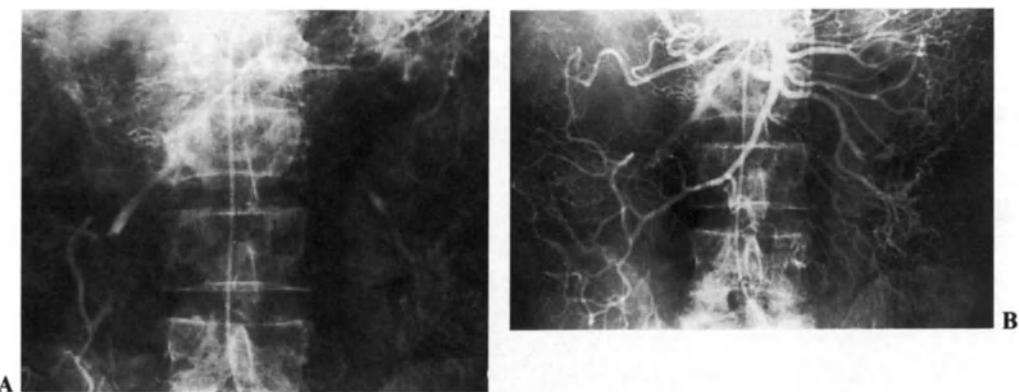


**Fig. 31.41.** A Superior mesenteric arteriogram of acute occlusive ischemia. Branches of SMA show sharp cut-offs indicative of arterial emboli. B Intra-arterial infusion of papaverine shows reversal of changes in part. Circulation has been restored.

specific. A mild ileus pattern may be the first radiographic indication of non-occlusive ischemia and should be suggested in high risk patients. Evidence of bowel wall thickening with 'thumbprinting' indicating edematous bowel loops as well as separation of narrow loops or a totally gasless abdomen may be seen on plain films.

CT performed in this group of patients for a variety of unrelated clinical disorders may suggest the diagnosis if thickening of bowel wall segments and/or presence of intramural gas are identified. *Angiography* performed in patients with non-occlusive low flow ischemia demonstrates the presence of vasoconstriction of mesenteric vessels with slow filling of peripheral branches and apparent avascularity of the intestinal wall. The changes of low flow perfusion may be approached therapeutically by angiography with intra-arterial perfusion of vasodilators such as papaverine or tolazoline.

**Acute occlusive ischemia** is most often caused by acute *thrombosis* or *embolism*. Acute thrombosis secondary to atherosclerosis usually involves the proximal segment of the superior mesenteric artery and may result in extensive, often catastrophic infarction of most of the small bowel. Emboli into the branches of the mesenteric arteries result in acute segmental ischemia but this is less acute in presentation. Acute segmental ischemia may also result from strangulated hernias or volvulus and occasionally from an acute vasculitis. Acute rapid vascular occlusion usually results in massive tissue necrosis with subsequent bowel perforation.



**Fig. 31.42.** CT of mesenteric ischemia. Acute gangrene of bowel is diagnosed when air lies within the mesenteric vessels. These are premorbid findings.

peritonitis and shock, and is often fatal. Therapeutic angiographic procedures with infusion of low dose *streptokinase* or *urokinase* may promote clot lysis when diagnosed early (Fig. 31.41). Patients with gangrenous bowel require immediate surgery (Fig. 31.42).

**Mesenteric venous thrombosis** is an unusual cause of intestinal ischemia. The condition is associated with hypercoagulable states, portal hypertension and malignancy. It is characterized by a gradual onset of edema, hemorrhage and mucosal necrosis with congestion of the mesentery. Angiography is again the diagnostic study of choice and demonstrates the presence of arterial vasoconstriction with prolonged staining of the bowel wall. Thrombosed veins fail to opacify. CT may demonstrate thickening of bowel wall and occasionally large thrombosed veins.

Barium examination of the small bowel is useful in patients in whom the diagnosis of ischemic bowel is equivocal or unsuspected. Segmental injury involving mid or distal small bowel is most common. Submucosal hemorrhage and edema occur in the ischemic segments. This may cause thickening and scalloping or 'thumbprinting' of the bowel wall, or the mucosal folds may appear rigid or spiked similar to a 'picket fence'. Alternatively, the folds may be completely blurred or completely effaced. Spasm and hypermotility are also frequently seen in ischemic segments. The findings of ischemic bowel may reverse spontaneously or with treatment of the underlying cause. Occasionally, progressive fibrosis results, with formation of bowel strictures which may be smooth and symmetric or asymmetric with eccentric sacculations.

#### Intramural Hemorrhage

Intramural intestinal bleeding occurs from a variety of causes including abdominal *trauma* and *coagulation abnormalities* which may be primary or iatrogenic, induced by anticoagulants, oral contraceptives or other medications. Diseases such as hemophilia, leukemia, polycythemia vera, myeloma and lymphoma are also known causes of intramural hemorrhage. Symptoms may be mild and non-specific or may produce a clinical picture of intestinal obstruction.

The radiographic appearance of submucosal hemorrhage is often characteristic. There is discrete segmental involve-



**Fig. 31.43.** Ischemic small bowel with submucosal hemorrhage. There is diffuse thickening of folds with small 'thumbprints' in some segments. Coalescence of continuous segments where submucosal deposition of substances has occurred, produces the thumbprint.

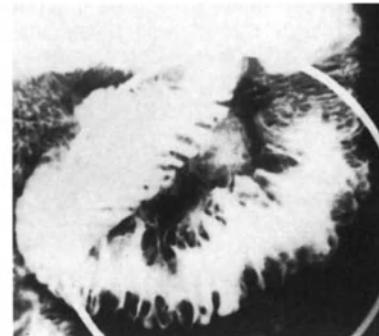


**Fig. 31.45.** Adult Henoch-Schönlein vasculitis. There is diffuse thickening of folds of a segment of jejunum. The findings are similar to any disease resulting in fluid deposition primarily in the submucosa and mucosa.

ment with uniform symmetric thickening of the bowel folds. Analogies are often made to a 'stack of coins' or 'picket fence' (Fig. 31.43). Rigidity and separation of bowel loops occurs in a varying degree depending on the length of bowel involved. Narrowing of the bowel lumen is frequently an accompanying feature. With intramural bleeding, CT demonstrates nonspecific thickening of the bowel wall. Extension of bleeding into the mesentery is more definitively depicted by CT than by barium examination (Fig. 31.44). Mesenteric hematomas may be demonstrated as masses causing separation of adjacent bowel loops and causing extrinsic compression along their mesenteric borders.

#### Vasculitis

*Polyarteritis nodosa* is a necrotizing vasculitis affecting multiple systems including the gastrointestinal tract. It may cause focal areas of bowel wall infarction and mucosal ulcers. Angiographic demonstration of multiple small aneurysms of medium size arteries is characteristic.

*Henoch–Schönlein syndrome* is an acute arteritis characterized by purpura, nephritis, abdominal and joint pains. The disease tends to be self-limited often developing several weeks after a streptococcal infection. At times, it evolves into a syndrome that is indistinguishable from polyarteritis nodosa or glomerulonephritis (Fig. 31.45).

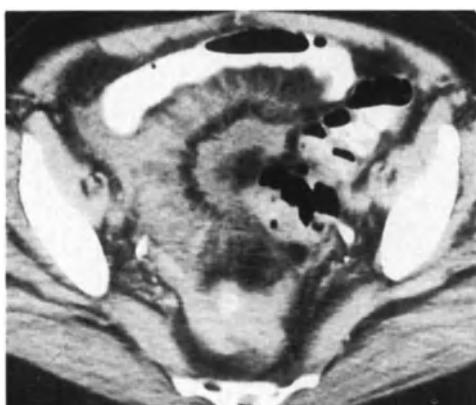


**Fig. 31.44.** CT of mesenteric bleed. There is diffuse thickening of bowel wall with spike-like margins extending into mesentery.

*Behçet's syndrome* is another vasculitis affecting small vessels in multiple organ systems. The disease was originally described as consisting of the triad of ulcerations in the mouth, eye and genitalia associated with large joint arthritis. Peripheral thrombophlebitis and ulceration of the gastrointestinal tract also occur with some frequency. Barium studies may demonstrate enteritis and colitis which may simulate ulcerative colitis or Crohn's disease. There may be diffuse superficial ulceration or shallow aphthoid ulcers. The presence of deep penetrating ulcers is more common than with idiopathic inflammatory bowel disease and bowel perforations are not uncommon. The ileocecal region is most commonly affected.

*Focal lesions of the small bowel* are an infrequent cause of **gastrointestinal hemorrhage**. Diagnosis is frequently difficult and delayed while causes of upper GI or colorectal bleeding are sought. Small bowel lesions which may cause intestinal hemorrhage include Meckel's diverticulum, Crohn's disease, leiomyoma, primary or metastatic tumor and primary metastatic tumor. Arteriovenous malformations, a well-known cause of elusive gastrointestinal hemorrhage from the colon, also occur in the jejunum.

In cases of rapid bleeding, localization of the hemorrhage to the small bowel may occasionally be made by *radionuclide scanning* as described above. *Angiography* may demonstrate focal areas of bleeding from arteriovenous malformations or from hypervascular lesions such as leiomyomas or certain metastases. *Barium contrast* studies play a role in cases of low grade or intermittent bleeding. Structural abnormalities including small tumors, ulcers, and Meckel's diverticulum may then be demonstrated.

#### Radiation Enteritis

The pathophysiology of radiation damage is primarily due to damage to the radiosensitive endothelial cells of arterioles. Thus, the changes of radiation enteritis are due to ischemic damage to the bowel wall. Radiographic appearances are discussed in the previous section on inflammatory disorders.

#### Trauma

Traumatic injury to the small bowel is usually the result of blunt abdominal trauma. Although the transverse portion

**Table 31.1.** Fold patterns, Type I: thin, straight folds. This category is caused by situations which cause the small bowel to distend with resultant straightening, stretching and thinning of the folds (1–2 mm thickness). The folds can be either close together or far apart

Mechanical obstruction	Post vagotomy (surgical or chemical)
Lactose deficiency	
Adynamic ileus	Diabetes with hypokalemia
Amyloidosis	
Scleroderma	Chronic idiopathic intestinal pseudo-obstruction
Sprue	

**Table 31.2.** Fold patterns, Type II: thick, straight fold. The folds are thicker (more than 3 mm), fairly straight or only slightly undulating and usually close together. The diseases which cause these thickened folds do not usually result in the degree of distension encountered in Type I

<i>Edema</i>	<i>Intramural hemorrhage</i>	<i>Submucosal infiltrates (cellular)</i>
Inflammation	Anticoagulant therapy	Infectious mononucleosis
Crohn's disease	Ischemia (both arterial and venous)	Whipple's disease
Zollinger-Ellison syndrome	Trauma	Amyloidosis
corrosive ingestion	Vasculitis	Eosinophilic enteropathy
Hypoproteinemia (serum albumin level below 2 g)	connective tissue diseases	
cirrhosis	Henoch-Schonlein syndrome	
nephrotic syndrome	Buerger's disease	
protein-losing enteropathy	Hemophilia	
Lymphatic blockage	Idiopathic thrombocytopenic purpura	
tumor infiltration	Coagulation defects secondary to other diseases	
lymphangiitis,	hypoprothrombinemia	
post-irradiation	leukemia	
mesenteric fibrosis	multiple myeloma	
Venous congestion (congestive heart failure)	lymphoma	
Proximal to mechanical obstruction	metastatic carcinoma	
	hypofibrinogenemia	

of the duodenum is most commonly affected, other areas of small bowel may be injured as well. Usually the injury causes intramural bleeding or hematomas which are reflected in the radiographic findings. Penetration injury may cause small bowel perforations.

#### RADIOGRAPHIC APPROACH TO DIFFERENTIAL DIAGNOSIS

A pattern approach is the most practical way of approaching radiographic diagnosis of small bowel disease, especially diffuse diseases. Achieving high quality studies so that the appropriate findings are made is essential. Correlating with radiographic clues outside the small bowel (for example, identification of sclerotic bone lesions in a patient with mastocytosis) and understanding the given clinical setting provides the background for being able to make an intelligent radiographic differential diagnosis.

Valuable radiographic features used for the differential diagnosis of small bowel disease are as follows:

1. Extent and location of abnormality (focal versus diffuse, proximal versus distal).
2. Caliber of the bowel (normal versus dilated).
3. Mucosal fold pattern (thickness, shape and distribution).
4. Presence and size of nodules.

5. Separation of bowel loops.
6. Associated involvement of the stomach.
7. Contour distortions due to abnormalities extrinsic to the bowel.
8. Presence of increased intestinal secretions.

The simultaneous use of many criteria may result in confusion to the average radiologist who does not see enough diffuse small bowel disease in practice. The approach to differential diagnosis of diffuse small bowel abnormalities presented below is based primarily on the fold pattern (Tables 31.1–31.5). Only after the fold category is identified should other features be used to identify the most likely possibilities.

**Table 31.3.** Fold patterns, Type III: nodular folds. This category is characterized by nodular changes which may be associated with otherwise normal folds or thickened folds. The nodules may be seen on the mucosal folds or between them. Nodules are often caused by neoplastic entities but may also be associated with inflammatory conditions

Crohn's enteritis
Lymphoma
Lymphoid hyperplasia
Whipple's disease
Leukemias
Congenital lymphangiectasia
Canada-Cronkhite syndrome
Primary and secondary neoplasia
Parasitic infestation

**Table 31.4.** Fold patterns, Type IV : abnormal folds, plus increased intraluminal fluid. Diseases associated with abnormal amounts of fluid with any pattern of small bowel folds characterize this category

Proximal to mechanical obstruction

Crohn's disease

Infectious enteritis

Zollinger-Ellison syndrome

Acute caustic ingestion

Celiac disease

Disaccharidase deficiency

Parasitic infestation

Whipple's disease

Lymphangiectasia

**Table 31.5.** Fold patterns, Type V : the tubular or ribbon-like bowel. Diseases that produce severe mucosal edema in addition to submucosal thickening efface the folds. Except for celiac disease, the lumen is usually narrowed

Radiation

Graft versus host disease (GVHD)

Viral enteritis

Strongyloidiasis

Floxuridine toxicity

Celiac disease (primarily decreased number folds proximally)

If one takes into account the patient's clinical background, the correct diagnosis or the more likely possibilities will usually be arrived at.

A gamut-like approach to focal abnormalities of the small bowel is usually unnecessary but can be helpful. The interested reader is referred to Chapter 30 of Herlinger H, Maglinte DDT (1989).

#### REFERENCES AND SUGGESTIONS FOR FURTHER READING

- Bartram CI (1980) The radiological demonstration of adhesions following surgery for inflammatory bowel disease. *Br J Radiol* 53: 650-653
- Caroline DF, Herlinger H, Laufer I et al. (1984) Small bowel enema in the diagnosis of adhesive obstructions. *AJR* 142: 1133-1139
- Federle MP, Goldberg HI (1983) Conventional radiography of the alimentary tract. In: Sleisenger MH, Fordtran JS (eds) *Gastrointestinal Disease*, 3rd edn. W.B. Saunders Co., Philadelphia, pp 1634-1667
- Herlinger H, Maglinte DDT (eds) (1989) *Clinical radiology of the small intestine*. W.B. Saunders Co., Philadelphia
- James S, Balfé DM, Lee JKT, Picus D (1987) Small bowel disease: categorization by CT examination. *AJR* 148: 863-868
- Maglinte DDT, Lappas JC, Kelvin FM, Rex D, Chernish SM (1987) Small bowel radiography: how, when, and why? *Radiology* 163: 297-305
- Maglinte DDT, Peterson LA, Vahey TN et al. (1989) Enteroclysis in partial small bowel obstruction. *Am J Surg* 147: 325-329
- Merine D, Fishman EK, Jones B. CT of the small bowel and mesentery. *Radiol Clin North Am* 27: 707-715
- Price J, Nolan DJ (1989) Closed loop obstruction: diagnosis by enteroclysis. *Gastrointest Radiol* 14: 251-254
- Sellink JL, Miller RE (1982) *Radiology of the small bowel*. Martinus Nijhoff Publ, The Hague

## CHAPTER 32

# THE COLON

Dina F. Caroline

---

### METHODS OF INVESTIGATION

The primary methods of radiologic evaluation of the colon are *plain films* of the abdomen and the *barium enema*. The value of plain films is discussed in Chap. 24.

#### Barium Enema

Evaluation of the colonic mucosa requires adequate cleansing regardless of the barium enema technique used. Cleansing is accomplished by a combination of hydration, low-residue diet, laxatives and cleansing enemas. The exact combination used to achieve optimal results varies from practice to practice.

Barium enemas are performed using double contrast (DCBE) (high density, high viscosity barium sulfate suspension with air insufflated to produce the double contrast effect) or single contrast (SCBE) (low density, low viscosity barium sulfate suspension with compression and technique adequate to penetrate the barium).

The DCBE is the method of choice for the radiographic demonstration of polyps, particularly those smaller than 1 cm. Detection of premalignant neoplasms and of carcinoma at an early stage is believed to afford an improved prognosis. The DCBE is also the superior method for depicting mucosal abnormalities such as the superficial ulcerations of inflammatory diseases.

The SCBE is the method of choice in emergency situations, and for aged or debilitated patients. It should be used when there is a suspicion of large bowel obstruction, acute diverticulitis, fistula formation or acute appendicitis. It may also be used to salvage a failed DCBE.

Barium is contraindicated when there is concern for colonic perforation. If a contrast study is necessary in such a situation, a water-soluble agent should be used.

#### Other Techniques

*Water-Soluble Contrast Enema.* This technique is reserved for evaluation of possible colonic perforation or anastomotic

leak. In neonates hyperosmolar water soluble contrast enemas may be used therapeutically for fecal or meconium impaction.

*Angiography.* Angiography is used primarily to localize and treat the site of acute lower gastrointestinal bleeding. Electively it is sometimes used to identify elusive vascular lesions.

*Computed Tomography.* CT is superior to barium examination for the evaluation of colonic wall thickness. It is the method of choice for the detection of extraluminal spread of primary colon tumors. CT is valuable for the detection and drainage of perirectal and pericolic abscesses in Crohn's disease, diverticulitis and appendicitis.

*Ultrasound.* Sonography plays a limited role in the evaluation of the colon. Normal bowel is generally not recognized due to the intraluminal air and fluid. Complications of inflammatory or neoplastic disease such as abscesses or other fluid collections may be identified, followed and sometimes treated with sonographic guidance. Ultrasound has recently become an important tool in the diagnosis of acute appendicitis.

*Radionuclide Scintigraphy.* Red blood cells or sulfur colloid labeled with *technetium 99m* are used to determine the presence of active lower GI bleeding. These methods are more sensitive but less specific than angiography. *Technetium 99m pyrophosphate* is used for bowel transit studies in patients with motility disorders. *Indium 111*-labeled white blood cells are sometimes used to assess the extent of disease in patients with severe inflammatory bowel disease.

*Magnetic Resonance Imaging.* At the present time, MR is not used in the routine evaluation of the colon.

### RADIOLOGIC ANATOMY

The colon or large intestine is about 1.5 m long and extends from the ileocecal valve and cecum to the anus. It is divided into the cecum, ascending, transverse, descending and sigmoid colon and terminates with the rectum and anus. The



**Fig. 32.1.** Normal colon. DCBE (left lateral decubitus), shows a normal haustral pattern, sharp mucosal outline and featureless mucosa.

cecum with the veriform appendix extending from its base, is a blind pouch proximal to the ileocecal valve at the base of the small bowel mesentery. The ascending colon progresses to the hepatic flexure along the right lateral colic gutter. Variable persistence of the mesentery frequently occurs and permits mobility of the right colon. At the hepatic flexure, the colon turns anteriorly to become the intraperitoneal



**Fig. 32.3.** Lymphofollicular pattern. DCBE. Left lateral decubitus view of the hepatic flexure. Tiny uniform nodules are seen, formed by lymph follicles.

transverse colon. At the phrenicocolic ligament (splenic flexure), the colon returns to a retroperitoneal location as the descending colon. Near the pelvic brim, the colon is again attached to a mesentery at which point it becomes the sigmoid colon which extends to the subperitoneal rectum.

Three strips of longitudinal muscle, the teniae coli, give the colon its haustrated appearance. They originate at the base of the cecum and continue to the rectum where they form a continuous layer. Contractions of the teniae form the haustral sacculation characteristic of the colon.

With DCBE, the normal colon generally has a featureless mucosa (Fig. 32.1). Occasionally, very fine transverse folds called innominate lines or grooves may be seen (Fig. 32.2). Another feature which may be seen are tiny (1–2 mm) nodules of uniform size seen segmentally or throughout the colon (Fig. 32.3). This is the lymphofollicular pattern and is considered to be a normal appearance, especially in young people.

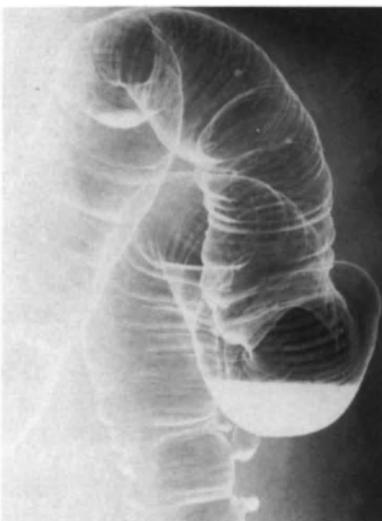


**Fig. 32.2.** Innominate lines. DCBE. Erect view of the splenic flexure. Scattered diverticula are seen.

## PATHOLOGY

### Congenital and Developmental Anomalies

**Rotational Abnormalities.** The bowel undergoes a complex process of rotation during organogenesis (or fetal development). This results in the jejunum being located in the left upper quadrant of the abdomen and the cecum fixed in the right lower quadrant at the base of the small bowel mesentery.

If the bowel fails to rotate (*non-rotation*), the entire small bowel will be located on the left side of the abdomen, and the entire colon will be right-sided. Incomplete rotation indicates early termination of the process resulting in a *malrotation*. **Abnormal fixation** or mobility of a segment of colon occurs when a portion of the mesentery which under normal circumstances is absorbed, persists.

**Anorectal Abnormalities.** This category of abnormalities is almost always diagnosed in the neonatal period presenting as colonic or small bowel obstruction. *Imperforate anus* may be caused by a thin obstructing membrane or by a relatively



**Fig. 32.4.** Microcolon. Small unused colon in neonate with duodenal atresia. There is a dilated air-filled stomach and duodenal bulb forming the 'double bubble' sign.



**Fig. 32.5.** Hirschsprung's disease. Transition zone separates the dilated normal colon, from the distal, small calibre, aganglionic bowel.

long atretic segment. This anomaly is classified as low, intermediate, or high, depending on its relationship to the levator sling. Intermediate and high lesions are more often associated with other congenital abnormalities such as fistulas to the genitourinary system or the VATER Syndrome (vertebral, anal, tracheoesophageal, renal and radial anomalies). An *ectopic anus* fails to reach the anal dimple on the perineum and may open more anteriorly on the perineum or into the vagina, urethra or bladder.

**Stenosis or Atresia of the Colon.** These rare abnormalities are believed to occur secondary to ischemia *in utero*. Stenoses may also occur as a complication of necrotizing enterocolitis.

**Microcolon.** Microcolon is the result of an unused colon. This may occur with proximal small bowel atresia or obstructions as with meconium ileus in cystic fibrosis (Fig. 32.4). The *small left colon* (hypoplastic) syndrome is believed to be due to delayed neurogenic development in infants of diabetic mothers.

**Hirschsprung's Disease.** This condition, also known as *aganglionosis* or *congenital megacolon*, results from a failure of complete migration of the myenteric plexus, resulting in a non-distensible segment of colon. It is much more prevalent in males. Usually, only the distal rectum is affected (Fig. 32.5) but it may extend more proximally. Total colonic aganglionosis occurs rarely and is almost always fatal.

On barium examination, the abnormal distal segment is normal in caliber and free of feces. Paradoxically, the normally innervated proximal colon is dilated and feces-filled. There is an abrupt transition between the normal and abnormal segments.

#### Polypoid Lesions

**Radiographic Appearances.** Polypoid lesions are protrusions into the lumen of the bowel. They are caused by a wide range of benign and malignant neoplasms as well as non-neoplastic lesions. On both single and double contrast barium enemas,

polyps may be recognized as fixed filling defects with the barium pool.

On double contrast examination polyps have several characteristic appearances depending on barium coating, angle of the radiograph tube and the shape of the polyp itself. Since polyps are solid structures, when they are seen *en face* and coated with a thin layer of barium, the barium forms a ring shadow. It has a sharp inner border and an ill-defined outer border. When seen obliquely, the appearance of barium coating the surface of a polyp merging with the meniscus forms the 'bowler hat' sign (Fig. 32.6).

**Pedunculated polyps** (Fig. 32.7) have stalks of variable thickness and length, and are frequently mobile. The stalk is depicted as two parallel lines of barium. If the head of the polyp is lying in the barium pool, lines formed by the stalk coursing in a direction inconsistent with the normal haustral pattern, may be the only clue that a polyp is present. When the head of a polyp and its stalk are superimposed *en face*, one may see a target or 'Mexican hat' sign.

**Villous adenomas** tend to be large sessile polyps with frond-like projections. Barium trapped in the folds creates the typical appearance of a carpet-like lesion or bunch of grapes (Fig. 32.8A).

Polyps are evaluated for radiographic features which indicate an increased incidence of malignant degeneration. Features suggestive of malignancy include large size, irregular contour, and distortion of the underlying bowel wall. Patients with multiple polyps are also at increased risk of malignancy. Benign polyps tend to be small smooth lesions. Stalks, if present, are long and slender and there is no retraction of the underlying bowel wall.

**Classification (Histology).** *Hyperplastic (Metaplastic) Polyps.* These are by far the most common type of colonic polyp. Not truly neoplastic, they represent mucosal proliferation of normal tissue. Hyperplastic polyps are usually small, smooth, sessile lesions and are most common in the rectum. These

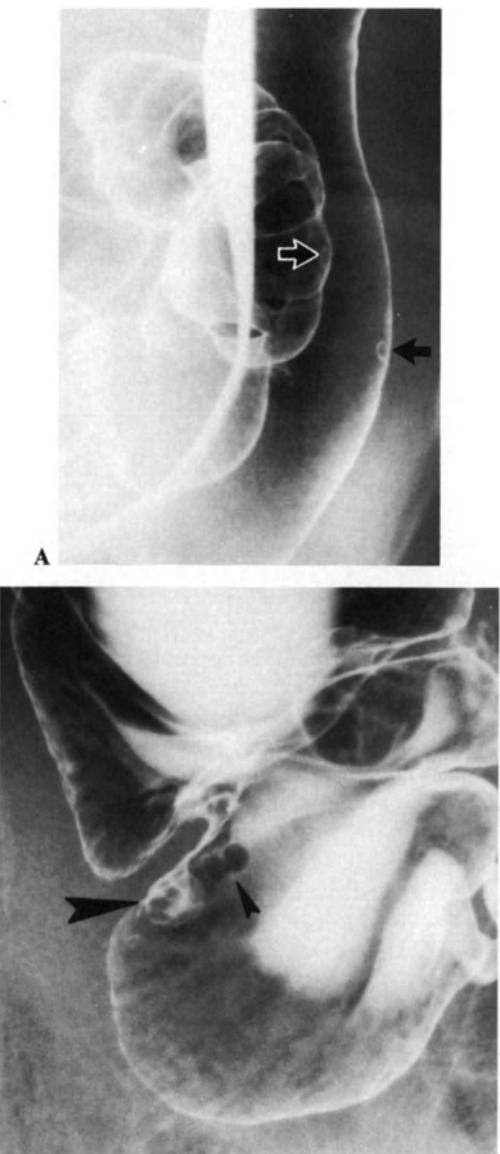


**Fig. 32.6.A** Small smooth polyps are demonstrated by ring shadows. **B** Bowler hat sign of a cecal polyp (large arrowhead). There are two additional polyps causing a filling defect in the barium pool (small arrowhead). (Courtesy of Dr J.W.R. Young.)

polyps have no malignant potential, but are important to identify because small adenomas may have a similar appearance.

**Hamartomas.** Hamartomas are collections of normal tissue in abnormal locations. Hamartomas of the colon are an unusual type of polyp and are associated with several disorders including *Peutz-Jegher*, *Cowden*, and *Turcot syndromes* and *basal cell nevus syndrome*. *Juvenile polyps* which are usually solitary, stalked, lobulated rectal polyps found in children are generally classified as hamartomas.

**Inflammatory Polyps.** These lesions are associated with inflammatory bowel disease and represent regenerating mucosa. Polyps found in *Canada-Cronkhite syndrome* and

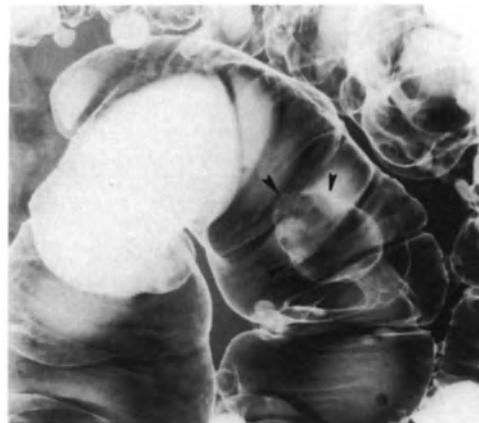


**Fig. 32.7.** Pedunculated polyp of the sigmoid colon (arrowheads).

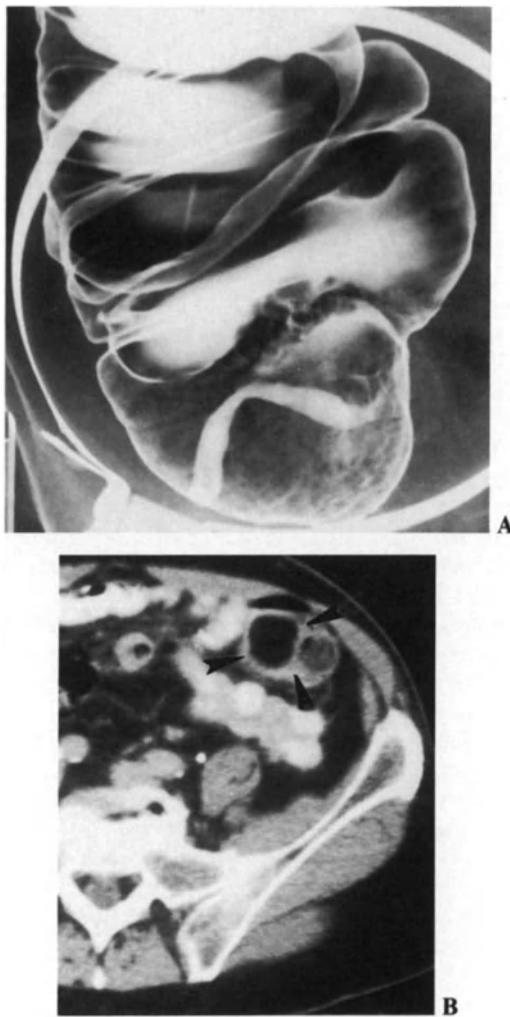


**Fig. 32.8.A** A villous polyp in the cecum demonstrates a lacy pattern of fronds projecting into the lumen, outlined by barium in the interstices. **B** Lipoma. CT depicts a fat-density mural mass (arrowheads) in the descending colon.

**Table 32.1.** Evaluation of polyps for risk of malignancy. Modified from Caroline D, Maglinte DDT (1987) Radiology of the Colon. In : Geddaudas-McClees R, Kristina (ed) *Gastrointestinal Imaging*. Churchill Livingstone, New York

	Benign	Malignant
Size	< 2.0 cm	> 2.0 cm (50%) malignant)
Contour	Smooth	Multilobulated or irregular
Stalk	Present (pedunculated, long and thin)	Absent (sessile, short and thick)
Underlying colon wall	Smooth	Retracted
Number of polyps	Single	Multiple

juvenile polyps are also sometimes classified as inflammatory.

**Adenomas.** Adenomas are the most common neoplastic polyp of the colon. They are important to identify because of the risk of malignant degeneration. Histologically, there is proliferation of glandular elements into tubules or fronds (villi). This is reflected in their gross appearance with tubular adenomas being lobular pedunculated polyps and villous adenomas sessile lesions with a frond-like surface. Villous adenomas are more likely to contain malignant elements than tubular or tubulovillous adenomas. Morphologic features associated with increased risk of malignancy are reviewed in Table 32.1.

**Lipomas and Other Mesenchymal Tumors.** These are benign neoplasms which arise in the submucosal or muscular layers of the bowel. Lipomas are the most common tumor in this

group, and are found mostly in the region of the ileocecal valve. They are smooth, soft lesions which change shape with position or compression (Fig. 32.8B). Other mesenchymal tumors, including leiomyomas are rare in the colon.

**Lymphoid Hyperplasia.** Enlarged lymphoid follicles secondary to a local or systemic inflammatory or neoplastic process cause the condition known as reactive lymphoid hyperplasia. The nodules are somewhat larger and more variable in size than that seen in the normal lymphofollicular pattern. The appearance may mimic neoplastic polyps. The findings should prompt careful scrutiny for an underlying cause.

#### Polyposis Syndromes

Polyposis syndromes include a variety of conditions both inherited and sporadic with intestinal polyps as part of their spectrum.

**Familial polyposis** is a genetic disorder inherited as an autosomal dominant trait. The presence of innumerable polyps, often completely carpeting the colon, is characteristic. These polyps have an extremely high malignant potential (Fig. 32.9). The condition may be recognized after puberty and, if untreated, carcinoma is likely to be present by age 30; prophylactic proctocolectomy is usually recommended prior to that age.

**Gardner's syndrome** manifests in the colon in the same manner as familial polyposis. Extraintestinal features present in Gardner's syndrome include osteomas and other soft tissue tumors, especially desmoid tumors with a large amount of associated fibrosis. Hyperpigmentation and a variety of dental abnormalities may be present. Familial polyposis and Gardner's syndrome may represent a spectrum of the same genetic mutation.

**Turcot syndrome** is a rare familial disease with an association of gliomas of the brain or spinal cord and colonic adenomas.

The **Peutz-Jegher syndrome** is characterized by hamartomas of the intestine, especially the small bowel. Hamartomas or adenomas may also be found in the colon (Fig. 32.10). Pigmented mucocutaneous lesions are also characteristic.

In **Cowden's disease** or multiple hamartoma syndrome, hamartomas may be found throughout the GI tract. Circumoral papillomas, nodular gingivitis and benign and malignant lesions of the breast and thyroid are also found in this rare inherited disease.

Unlike the other syndromes described, **Canada-Cronkhite syndrome** is a sporadic (non-inherited) polyposis which

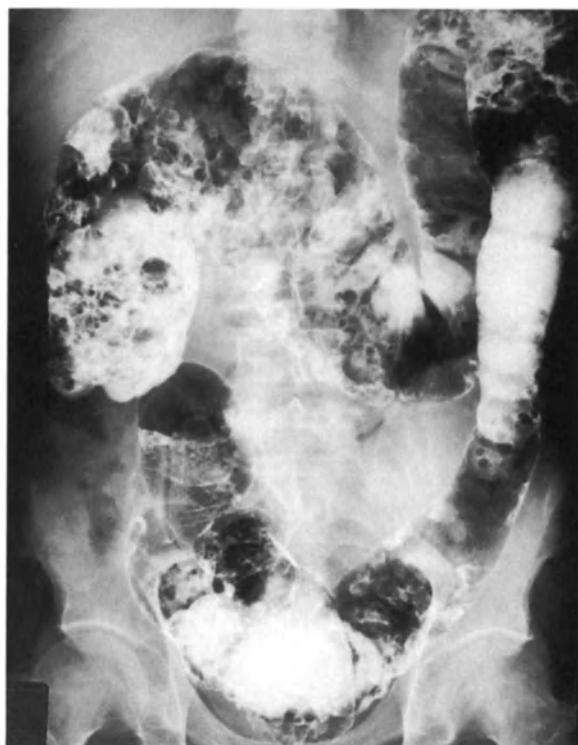


**Fig. 32.9.** Familial polyposis with carcinoma. Numerous polyps of varying size are present throughout the colon. Four synchronous carcinomas, one of which obstructs the cecum were present.

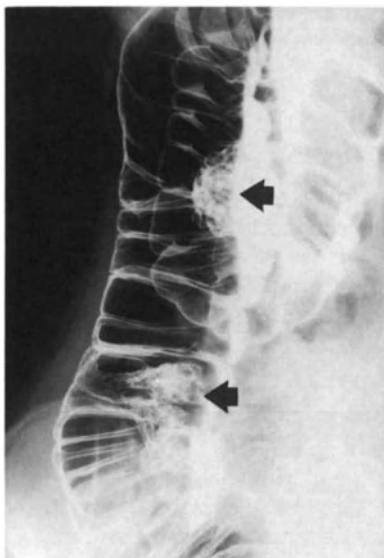


**Fig. 32.10.** Peutz–Jegher's syndrome. Two large colonic hamartomas are seen in a patient with small bowel polyps and mucocutaneous lesions. These polyps are radiographically indistinguishable from villous adenomas.

affects older people. Alopecia, dystrophic nail changes and hyperpigmentation are present. Hamartomas or inflammatory polyps which have no known malignant potential, are most common in the colon and stomach. The condition is very debilitating due to diarrhea and electrolyte imbalance.

#### Carcinoma

Colorectal carcinoma is the second most common malignancy in the United States and 100,000 new cases are diagnosed yearly. The vast majority of the tumors are *adenocarcinomas* which are believed to develop in preexisting adenomatous polyps. Most carcinomas are found in the rectum and sigmoid, however some studies indicate an increasing incidence of right-sided lesions. Patients with colon cancer are at risk for synchronous or metachronous colon cancers. About 25% have additional adenomatous polyps.



**Fig. 32.11.** Polypoid carcinomas, sigmoid (arrowheads). Also, note the prominent lymphoid pattern in recto-sigmoid.

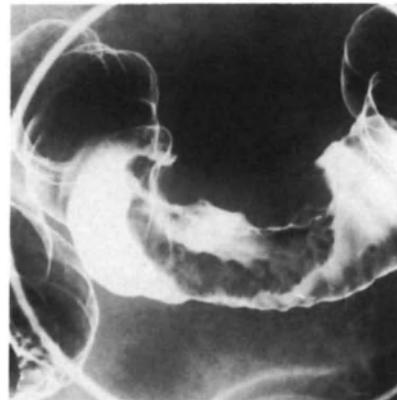


**Fig. 32.12.** Ulcerated carcinoma of the sigmoid colon.

Patients with ulcerative colitis and to a lesser degree Crohn's disease are at increased risk of developing colon cancer. Other risk factors include other malignancies, family history and adenomatous polyposis syndromes. The low fiber Western diet also appears to be a significant risk factor.

**Radiographic Appearance.** Colon cancers are *polypoid*, *ulcerated* or *annular* lesions (Figs. 32.11–32.13). Infiltrating (scirrhouss) carcinoma is rare in the colon. Most early lesions are polypoid. Some lesions appear as relatively flat plaques which are recognized by irregularities in the mucosal surface or by barium-etched lines coursing in abnormal directions (Fig. 32.14).

Tumor development may occur as part of an adenoma–carcinoma sequence. Dysplastic changes occur in the head of a benign adenoma which then degenerates into frank malignancy. As this occurs the tumor invades the polyp stalk and then invades the colon wall. As the tumor infiltrates the wall of the colon and grows circumferentially, it may assume a *saddle-like* and later an *annular* or *apple-core* configuration.

On barium enema annular or partially circumferential tumors are usually less than 4 cm long. The margins are sharp with overhanging edges. A polypoid component may protrude into the lumen at the margins.



**Fig. 32.13.** Annular carcinoma near the anatomic splenic flexure. There is a classical apple-core configuration.

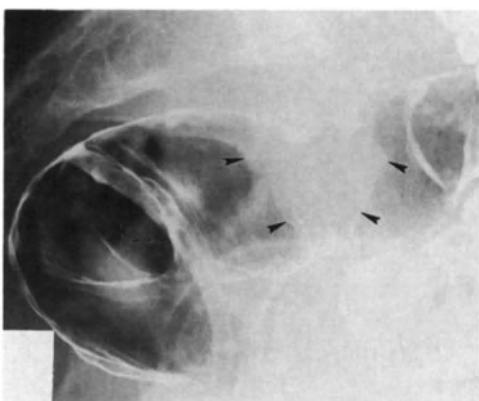


Fig. 32.14. Flat plaque-like recto-sigmoid carcinoma (arrowheads).



Fig. 32.15. Sigmoid carcinoma with contained perforation. Sharp, overhanging margins and absence of normal mucosa may help distinguish perforated carcinoma from diverticular abscess.



Fig. 32.16. Normal post-operative appearance after right hemicolectomy with side-to-side ileocolic anastomosis.

Polypoid lesions may cause *obstruction* or *intussusception*. Annular lesions usually present with symptoms of chronic obstruction. Ischemic colitis or colonic urticaria are rare complications of chronic obstruction. Focal perforation of carcinomas may result in pericolic abscess (Fig. 32.15). In such cases, the radiographic appearance may be indistinguishable from acute diverticulitis. CT is generally superior to barium enema for the demonstration of extra-luminal masses, while barium examination provides a superior evaluation of the lumen and the mucosal surface. Free intraperitoneal perforation of colon cancer is unusual.

Post-operative evaluation after resection of colorectal carcinoma involves assessment of the anastomotic sites and tumor bed, as well as looking for distant metastases (Fig. 32.16). Since metachronous carcinomas develop in about 5% of patients, and new adenomas develop in 20%–25%, routine surveillance of the colon should also be performed. At the anastomosis, recurrent tumor is recognized on barium enema by the presence of *nodularity*, *eccentricity*, *mass effect* or *narrowing*. Pelvic recurrence, especially after resection of the rectum, and recurrence in the tumor bed are best defined by CT. Metastatic spread of colon cancer is to the liver, peritoneal cavity, lungs, and less frequently to other organs.

#### Other Colorectal Malignancies

**Lymphoma.** Lymphoma rarely involves the colon and when it does it is usually secondary to systemic disease. It may present with a variety of radiographic appearances including bulky polypoid masses, multiple submucosal nodules of varying sizes, or diffusely thickened folds (Fig. 32.17). Depending on its appearance, colonic lymphoma may be confused with primary carcinoma, Crohn's disease, familial polyposis, and lymphoid hyperplasia amongst other conditions.



Fig. 32.17. Colonic lymphoma with large submucosal nodules.

Other unusual malignancies may occur in the colon. *Scirrhous carcinoma*, which is similar to *linitis plastica* or infiltrating carcinoma of the stomach usually affects the rectosigmoid. Similar appearances may be seen with ischemic, inflammatory, or metastatic disease, especially from breast cancer. *Mucinous carcinomas* produce large amounts of mucus and multiple hazy calcification may be demonstrated radiographically. When colon cancer appears in people younger than 40 years, it is likely to be of this type.

*Cloacogenic carcinoma* is a rare, aggressive tumor arising from transitional cells in the anorectal junction and affecting elderly patients. *Squamous cell carcinoma* is another aggressive tumor arising from the anal mucosa and affecting elderly patients. *Carcinoid tumors* may be found in the colon, particularly in the rectum. For the most part, these arise in the submucosa and are clinically benign. About 10% of rectal carcinoids are aggressive and may invade locally and metastasize. Malignant mesenchymal tumors, such as *leiomyosarcoma* or *liposarcoma* are rare in the colon.

#### Diverticular Disease

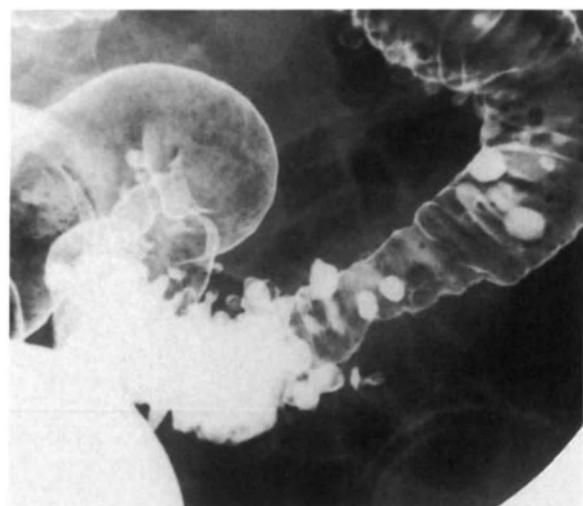
Diverticular disease commonly affects people over the age of 40 in Western countries. The presence of this condition increases with age and half of the population over 60 is affected. A diet high in refined carbohydrates and low in fruit is widely regarded as the etiology of diverticular disease.

Diverticular disease encompasses a spectrum of abnormalities. Changes in the ultrastructural array of collagen and elastin are believed to be at least partially responsible for the development of diverticulosis. Hypertrophy of the circular muscle layer of the colon may play a role. Thickening of the colonic wall, especially in the sigmoid may or may not be associated with the presence of diverticula (*diverticulosis*). Conversely, diverticula may also be found without apparent muscular hypertrophy. Diverticula are small saccules formed by herniation of the mucosa and muscularis mucosa through areas of diminished resistance in the bowel wall. *Diverticulitis* is the term used when there is evidence of active inflammation arising from diverticula.

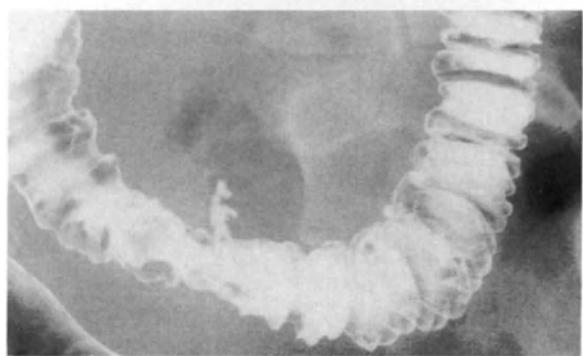
The sigmoid colon is involved in over 90% of cases of diverticulosis. When more proximal colon is involved, it is usually in addition to sigmoid involvement. Diverticulosis is confined to the cecum and ascending colon in fewer than 10% of cases.

*Diverticulitis* is the most common complication of diverticulosis. The most common clinical presentation is left lower quadrant pain, fever and leukocytosis. This results from acute inflammation extending beyond the lumen into the pericolic tissue. In more severe cases, symptoms may result from abscess formation, obstruction, fistula, and peritonitis. Rectal bleeding is another complication of diverticular disease. This occurs most often without acute diverticulitis and results from erosion into a vessel present in a diverticulum.

Radiographically, diverticular disease is usually evaluated by *barium enema* examination. The muscular abnormality is demonstrated as thickening of the bowel wall with lack of distensibility. An analogy to the pleats of an accordion or concertina or the term 'sawtooth' is often used to describe this finding on barium enema. Diverticula are seen as smooth



A



B

Fig. 32.18A, B. Acute diverticulitis. A There is pericolic inflammation with microperforation. Note the deformity of the inferior wall of adjacent bowel. Multiple diverticula are seen in the adjacent sigmoid. B Large gas-containing abscess partially filled with barium.

round projections from the bowel wall containing air and/or barium. When viewed *en face*, diverticula may sometimes appear as filling defects and be confused with polyps demonstrating a 'bowler hat' or 'Mexican hat' configuration. The entities can usually be separated by altering patient position so that the lesion in question is viewed in profile, and by demonstrating barium collecting within a diverticulum, which cannot occur with solid polyps.

The radiographic diagnosis of diverticulitis should be reserved for those cases in which extravasation of contrast from the diverticulum can be demonstrated. This may involve a very small amount of contrast (microperforation), or may fill large abscess cavities (Fig. 32.18). Several contiguous diverticula may be involved with linear tracking of barium seen on radiographs. The presence of a *pericolic abscess* demonstrated by an extraluminal mass impressing the bowel is a more common, but less specific finding with diverticulitis. A pericolic abscess may be depicted much better by CT than by barium enema, especially if there is no significant mass effect on the colon (Fig. 32.19). Other less specific radiographic findings include spasm, stenosis or deformity of the bowel, diffuse or focal ileus, and small or large bowel obstruction. Free extra- or intraperitoneal perforation is unusual; however, that possibility should be excluded prior to proceeding with a contrast study.

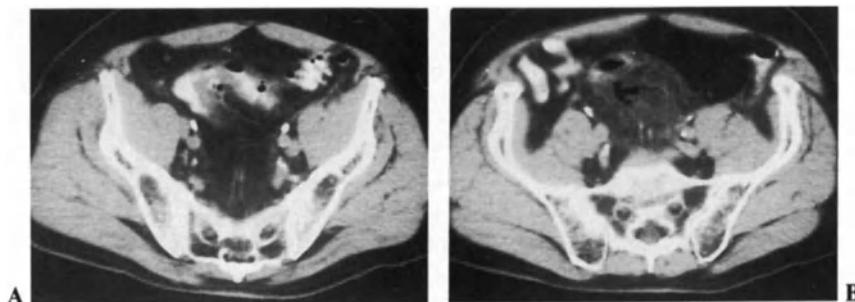


**Fig. 32.19A, B.** Acute diverticulitis with abscess. CT. A There is thickening of the wall of sigmoid colon with a small focal extraluminal collection of contrast and air at the site of perforation. B The bulk of the large gas-containing abscess is superior to the sigmoid and causes no significant mass effect on the colon.

**Fistula formation** is another complication of diverticulitis. This occurs by dissection of an abscess through tissue planes to adjacent organs. The urinary bladder, vagina, small bowel and skin may be affected.

Rarely, giant diverticula may be found. These are almost always found in association with diverticulosis and are believed to be a sequel to previous diverticulitis (Fig. 32.20).

The most important consideration in the differential diagnosis of diverticulitis is primary *carcinoma*. If there is focal perforation of the carcinoma, the two entities may be impossible to differentiate at initial presentation. Ability to demonstrate normal mucosa in diverticulitis and an abnormal mucosa in carcinoma is the key. Other entities which should be considered in the differential diagnosis of diverticulitis include *metastatic disease*, *Crohn's disease*, *radiation* or *ischemic colitis*, and diverticulosis without diverticulitis.

#### Ulcerative Colitis

Ulcerative colitis (UC) is an idiopathic inflammatory disease of the colon. The radiographic appearance of UC serves as a descriptive prototype for the colitides in which mucosal changes predominate.

The incidence of UC in the USA is 5–6 per 100 000 population and the peak time of presentation is in the third decade of life. A second smaller peak occurs in the 5th decade,

although some patients included in this group probably have ischemic rather than ulcerative colitis. UC may be associated with other systemic disorders. Arthralgia or arthritis, especially ankylosing spondylitis and its variants, occur in about one 4th of UC patients. Liver abnormalities, most notably sclerosing cholangitis, occur in 10%. Other associations include the ocular disorders uveitis and episcleritis, and the dermatologic disorders pyoderma gangrenosum and erythema nodosum as well as renal and hematologic disorders. The classic pathophysiologic abnormality is the crypt abscess.

Characteristic of UC is bowel involvement essentially confined to the superficial layers of the colon. The disease nearly always affects the rectum. Within the affected region mucosal involvement is contiguous, without intervening areas of normal mucosa. When pancolitis is present, the ileocecal valve is widely patent. Rare involvement of the terminal ileum, called *backwash ileitis*, is the only extracolonic bowel involvement in UC.

Rectal bleeding, diarrhea and fever are common presenting features of UC. Onset may be acute or insidious. With very severe or unrelenting attacks large areas of mucosa may be sloughed and inflammation may penetrate into the muscular layers. This subgroup of patients is at risk for developing *toxic megacolon* which most often requires total proctocolectomy.

*Radiographic studies*, especially the double contrast barium enema correlate well with endoscopic findings. The earliest change is that of fine mucosal granularity with blurring of the normally sharp mucosal line. These changes correspond to the endoscopic findings of hyperemic, edematous mucosa. These changes involve the rectum in over 90% of cases. Colon proximal to the affected area is completely normal.

As the disease progresses, the mucosa becomes friable with shallow ulcerations. Barium enema demonstrates a corresponding pattern with stippling of the mucosal pattern, sometimes compared to a 'grain of sand' or granular appearance (Fig. 32.21). Ulceration is a more prominent feature as the disease becomes more severe with the degree of ulceration correlating with severity of disease. Ulcers become deeper and often assume the shape of a flask, 'T', or collar button (Figs 32.22, 32.23). This configuration is caused by linear undermining of the submucosa. Although the ulcers may appear quite deep, they are usually confined to the



**Fig. 32.20.** Giant sigmoid diverticulum (arrowheads). (Courtesy of Anna S. Lev-Toaff, MD.)



**Fig. 32.21.** Ulcerative colitis. There are diffuse superficial ulcerations with a granular mucosal pattern. Chronic changes including loss of haustral folds and abnormality of the colonic contour are present.

edematous mucosa and submucosa and rarely penetrate into the muscular layers.

With chronic or inactive ulcerative colitis, the mucosa appears coarsely granular without ulceration. The entire colon may be foreshortened and appear narrow and straightened with loss of haustration. The rectum also becomes narrowed with widening of the presacral space. The appearance of the colon with chronic ulcerative colitis is often compared to a 'lead pipe' (Fig. 32.24).

Polypoid changes may occur at any stage of inflammatory bowel disease. The radiographic findings are non-specific although the pathogenesis differs depending on the etiology. With diffuse ulceration, residual patches of mucosa may appear nodular or polypoid. During the inactive phase of the disease, regenerating mucosa may also form polypoid lesions, sometimes thin linear or branching 'filiform' polyps (Fig. 32.25). The terms pseudopolyp, inflammatory and post-



**Fig. 32.23.** Acute and chronic pancolitis. Deep symmetric ulcers are present from the rectum to the cecum. Loss of the haustral pattern, and small calibre and foreshortening of the colon are signs of chronic ulcerative colitis. (Courtesy of Anna S. Lev-Toaff, MD.)

inflammatory polyp are interchangeable when describing radiographic findings.

Complications of ulcerative colitis include predisposition to development of *colon cancer*, *toxic megacolon*, and *stricture*

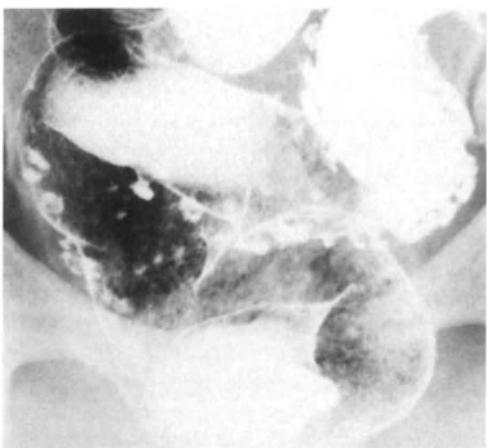


**Fig. 32.22.** Acute ulcerative colitis. 'Collar-button' ulcers are seen in the rectum. A diffuse superficial ulceration with stippled pattern covers the entire mucosal surface.



**Fig. 32.24.** Chronic ulcerative colitis. There is foreshortening of the colon and the flexures are depressed. There is severe narrowing of the rectum, sigmoid and descending colon ('lead-pipe' configuration).



**Fig. 32.25.** Filiform polyps. Fine elongated polyps are found during the quiescent phase of colitis. Filiform polyps may also be branched or form mucosal bridges.

formation. Development of a malignancy becomes a significant risk in patients who have had UC for 10 years or more. That risk is 5 to 30 times greater than in the general population, and is highest in patients with pancolitis and long duration of disease. Multiple synchronous cancers are common and carcinoma often develops in severely dysplastic epithelium. While most often diagnosed by random biopsies, dysplastic epithelium may be recognized on gross inspection and on double contrast barium enema. Radiographically dysplasia is suggested by an angular or polygonal pattern

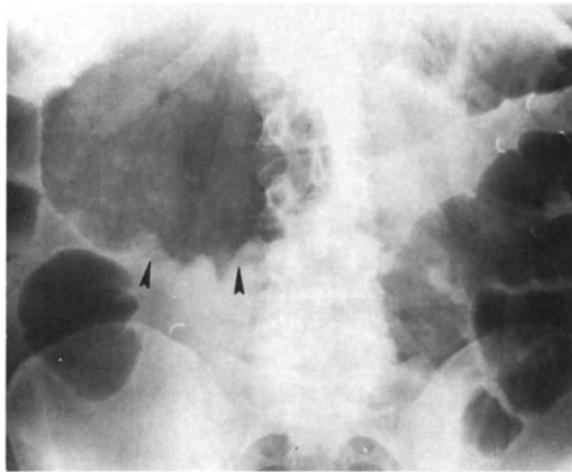


**Fig. 32.26.** Toxic megacolon. The transverse colon is markedly dilated. There is thickening of the bowel wall with nodular impressions ('thumbprinting') caused by edema (arrowheads). Pseudopolyps may sometimes cause similar soft tissue impressions. (Courtesy of Richard L. Baron, MD.)

on a slightly elevated or nodular mucosa. Most carcinomas associated with UC are infiltrative and difficult to distinguish from benign strictures.

*Toxic megacolon* occurs in about 2% of UC cases, either at initial presentation or during exacerbations. The etiology is unknown but probably is the result of a combination of factors including extension of ulceration into the muscular layers and reflex neuromuscular changes. Evaluation is usually confined to serial plain radiographs (Fig. 32.26). Initially, the bowel wall may appear thickened with nodular areas of somewhat increased density called 'thumbprinting'. This represents thick edematous bowel and is identical to the appearance in ischemic bowel disease. Neuromuscular changes cause the colon to become distended and thin-walled. The risk of perforation is particularly great at this stage.

Surgery for UC may be performed urgently in the case of toxic megacolon or severe intractable disease. More often, it is performed electively in patients with long-standing pancolitis, strictures or severe dysplasia. The standard procedure is a total proctocolectomy with ileostomy. Newer surgical procedures also considered curative for UC, include formation of a continent ileostomy or a mucosal proctectomy and total colectomy with an ileoanal anastomosis.

#### Crohn's Disease

Crohn's disease (CD) or granulomatous colitis, like ulcerative colitis, is an idiopathic inflammatory bowel disease. CD, however, is characterized by transmural inflammation. In contrast to the diffuse, continuous pattern of distribution seen in UC, CD typically has a patchy distribution with 'skip' lesions. CD may involve any portion of the gastrointestinal tract from the mouth to the anus while UC is confined to the colon.

The colon is the sole organ involved in about 20% of CD cases. Colon and small bowel are affected in another 50% and small bowel involvement occurs alone in 30%. CD of the terminal ileum and cecum is the commonest combination. The rectum is affected in 50% of cases in contrast to UC. Anal and perianal disease is common and is the sole site of involvement in 1%–2%. When other areas of the GI tract are involved, colon and/or small bowel are also affected. The peak age of onset of CD is between 15 and 30 years.

In involved areas, the bowel wall and mesentery are thick and rigid with increased fat and fibrous tissue 'creeping' over the bowel wall. Retraction of the bowel wall along the mesenteric surface, contributes to the typical asymmetry of the lesions. Sacculation, caused by asymmetric fibrosis and retraction along the mesenteric surface, angulation, stenosis, and fixation of bowel are characteristic features. Development of fissures, fistulas, strictures, inflammatory masses and abscesses are complications associated with CD. Histologically, CD is characterized by transmural inflammation with monocytes, histiocytes and discrete non-caseating granulomas.

Radiologic studies play an indispensable role in the evaluation of CD. In fact, establishment of the diagnosis may rely heavily on the radiographic depiction of features characteristic of CD. Superficial mucosal abnormalities are best demonstrated on high quality double contrast barium



**Fig. 32.27.** Crohn's disease. Aphthous ulcers. There are discrete erosions with a lucent halo on a background of normal mucosa.

enema. Single contrast barium enema may be more valuable for the demonstration of sinus tracts and fistulas. Computed tomography (CT) has proven to be an invaluable adjunct for the demonstration of inflammatory masses, abscesses, and bowel wall thickening.

The earliest lesions identified in CD are *aphthous ulcers*. These are discrete superficial erosions penetrating no deeper than the submucosa and surrounded by a lucent halo on

a background of normal looking mucosa (Fig. 32.27). They are formed by necrosis of foci of lymphoid hyperplasia with surrounding edema. The mucosa separating aphthous ulcers is entirely normal. Aphthous ulcers are associated with early or mild CD in a newly involved area, or on the margins of more severely affected areas. The differential diagnosis of aphthous ulcers includes *amebiasis*, *yersinia enterocolitis*, *gonorrhea*, and *Behcet's syndrome*. Aphthous ulcers are not a characteristic feature of UC.

*Deep, large ulcers* are found in more severe CD. They may be discrete or form serpiginous fissures which crisscross longitudinally and transversely across the mucosal surface. The residual patches of relatively preserved mucosa between the crisscrossing ulcer form the '*cobblestone*' appearance characteristic of CD (Fig. 32.28). Ulcers may be indistinguishable from those seen in UC and called by such descriptive names as '*collar-button*', '*rose-thorn*', or '*flasks*'. However, normal intervening mucosa is generally identifiable in CD. Lesions also tend to be distributed asymmetrically (Fig. 32.29). In the unusual case when CD occurs as pancolitis without disease elsewhere, its appearance may be indistinguishable from severe UC by radiologic examination as well as by endoscopic and even pathologic evaluation.

*Polyoid lesions* are non-specific and may be found at any stage of CD (Fig. 32.30). They may be called pseudopolyps, inflammatory or post-inflammatory polyps and do not have malignant potential. They may occasionally form a large obstructing mass.

Separation and rigidity of bowel loops occur as a result of the transmural nature of the disease with development of inflammatory masses consisting of thickened bowel with the associated mesentery. These features as well as strictures and stenotic segments are also less common in colonic CD than in small bowel disease. Compared to strictures found in UC, those in CD tend to be more eccentric and irregular (Fig. 32.31).



**Fig. 32.28.** Acute Crohn's disease with cobblestone pattern. Some discrete deep ulcers are also present.



**Fig. 32.29.** Crohn's disease. The colon is asymmetrically affected with eccentric ulcerations. Small pseudopolyps are also seen. The colon is normal on either side of this area.

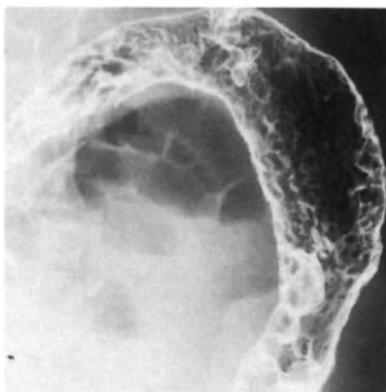


Fig. 32.30. Extensive polypoid changes (in subacute Crohn's colitis).

Serious complications of CD include the development of *fistulas* and *abscesses*. These complications occur in up to 50% of CD patients. *Fissures* and *sinuses* develop from the ulcers as do *intramural tracks* which are characteristic of active CD. As these extend beyond the wall and mesentery of the primary loop of diseased bowel, they may penetrate into other viscera, skin, genitourinary tract (especially the bladder), and muscle (Fig. 32.32). Perirectal and perianal fissures and fistulas are common and are frequently the presenting abnormality.

*Toxic megacolon* and development of colon *carcinoma* are complications that occur in CD but less frequently than in UC. The spectrum of systemic disorders associated with CD is similar to that of UC.

Surgery in CD is generally limited to treating complications since the disease tends to recur, particularly in proximity to operative sites. A summary of important distinguishing features of CD and UC is given in Table 32.2.

The radiographic differential diagnosis for CD varies depending on the stage of disease and the features present. Important considerations include UC and infectious colitides. Ischemic colitis, diverticulitis, malignancy, and other entities must also be considered in some cases.

#### Infectious Colitis

Infection with a wide variety of agents, including viruses, bacteria, fungi, protozoa, and worms may cause inflammatory changes in the colon. Infectious colitis is most common in tropical climates. In the industrialized world, it occurs most commonly in patients who are immunocompromised on the basis of tumor, chemotherapy, organ transplant or acquired immunodeficiency syndrome (AIDS).

*Radiographic findings* cover the spectrum described above for ulcerative colitis and Crohn's disease. Some organisms are likely to cause superficial inflammatory reactions simulating ulcerative colitis. Others instigate transmural reactions, simulating Crohn's disease. Some organisms have a predilection for specific areas in the bowel.

#### Amebiasis

Amebic dysentery caused by *Entameba histolytica*, is found worldwide and is endemic in many areas. It is a common cause of infectious colitis and may present with a wide range of radiographic and pathologic manifestations.



Fig. 32.31. Segmental stricture in Crohn's disease. There is a short asymmetric stricture with cobblestoned mucosal pattern in the splenic flexure. This was the sole site of colonic involvement (skip lesion).

*Radiologic features* include *colitis* which may be diffuse or segmental. *Amebiasis*, or mass lesions caused by a combination of infection and fibrosis are found primarily in the cecum, rectum and the flexures. Occasionally they may cause bowel obstruction. At times, these may be difficult to distinguish from carcinoma or acute diverticulitis. Toxic

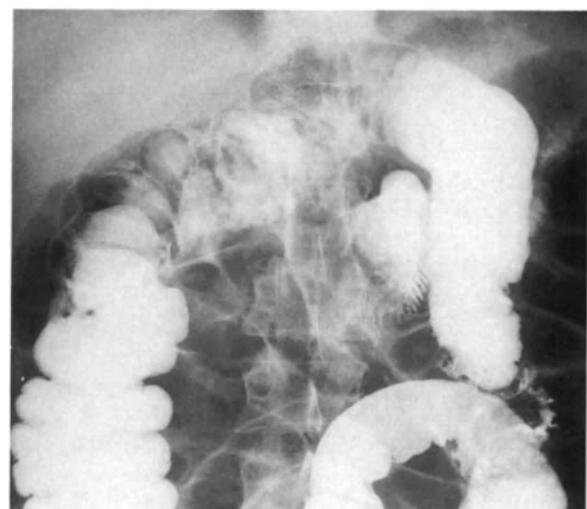


Fig. 32.32. Crohn's disease with extensive fistula formation. The small bowel has been filled on a barium enema from a fistula involving the jejunum sigmoid, and transverse colon.

**Table 32.2.** Features useful in distinguishing ulcerative colitis from Crohn's disease. Modified from Caroline D, Maglinte DDT (1987) Radiology of the Colon. In: Gedgaudas-McClees R, Kristina (ed). *Gastrointestinal Imaging*. Churchill Livingstone, New York

	Ulcerative Colitis	Crohn's Disease
Distribution	Confined to colon	May involve any area of GI tract Skip lesions
Rectal involvement	Contiguous involvement from rectum proximally 95%–100%	25%–50%
Perirectal space	Yes	Rare
Anal involvement	No	Rare Frequent fistulas and abscesses
Ileocecal valve	Gaping or normal	Narrow
Symmetry	Circumferential	Eccentric
Ulceration	Superficial	Transmural Deep or aphthoid
Background mucosa	Abnormal	Normal
Fistula	No	Frequent
Toxic megacolon	Infrequent	Rare
Pseudopolyps	Yes	Yes
Coexisting diverticula	Rare	May be present
Colon cancer	Significant increase after 8–10 years	Probably higher than general population
Strictures	Yes	Yes
Surgery	Curative	May exacerbate disease

megacolon and colonic perforation may also occur in severe cases of amebiasis.

During the acute phase of infestation, there may be a diffuse colitis with superficial ulceration similar to ulcerative colitis. Alternatively, deep ulcers with discontinuous and eccentric lesions which may simulate Crohn's disease may be seen. Unlike Crohn's disease, the small bowel, including the terminal ileum, is rarely affected.

Chronic manifestations of colonic amebiasis include stricture formation, which most commonly involves the cecum and causes a characteristic cone-shaped cecum. Mucosal inflammatory polyps and localized abscesses may also occur. The most serious systemic complication is caused by migration of amebae to the liver which occurs in about 15% of cases.

### Tuberculosis

Primary intestinal tuberculosis is caused by ingestion of milk infected with *M. bovis*. Intestinal tuberculosis may also be caused by hematogenous and lymphatic spread from primary pulmonary disease. Only about 50% of patients with intestinal tuberculosis have radiographically evident pulmonary disease.

Intestinal tuberculosis causes hypertrophic, ulcerative, or mixed type lesions. Involvement of the ileocecal region occurs in 80%–90% of patients but radiographic changes of tuberculous infection may be seen in any part of the GI tract. The clinical and radiologic features may be indistinguishable from Crohn's disease. In the ileocecal region there may be edema causing nodular change and ulceration early in the disease. In the chronic state, the cecum may be contracted and cone-shaped. The terminal ileum is frequently involved and may be strictured or fixed open in a gaping position. This

is characteristically distinguishable from amebiasis in which the terminal ileum is not involved.

The presence of intra-abdominal masses, and bowel strictures are characteristic of the hypertrophic form of tuberculosis. The small bowel mesentery is usually involved, and fistula formation is common. Involvement of an isolated segment of the colon is unusual with the exception of the ileocecal region. The differential diagnosis includes *lymphoma*, *Crohn's disease*, *actinomycosis* and *blastomycosis* when there is fistula formation.

### Schistosomiasis (Bilharziasis)

Infection with the blood flukes, most often *Schistosoma mansoni*, affects the GI tract especially the colon. An inflammatory reaction is caused by the presence of ova in the bowel wall. The tendency for the eggs of the parasite to be deposited in the inferior mesenteric vein explains the predisposition of radiographic changes in the rectum, sigmoid and descending colon.

Early infection is demonstrated on double contrast barium enema by the presence of a granular mucosal pattern reflecting fine, superficial ulcerations. A proliferative granulomatous reaction leads to the formation of large polyps which are most often seen in the sigmoid colon in chronic schistosomiasis. The polyps may occasionally be large enough to cause colonic obstruction.

### Other Parasitic Infestations

*Strongyloides stercoralis* is similar to hookworm. Superficial ulceration, mimicking ulcerative colitis, and occasionally strictures may be found.

*Anisakisis* is a nematode related to *Ascaris*, acquired by the ingestion of raw fish. Infection results in thickening of the

bowel wall of the cecum and terminal ileum.

*Esophagostomum* is another nematode which may cause colitis. This typically causes transmural nodular lesions with fibrosis and inflammation which extends into the pericolonic tissue.

Lesions may ulcerate and form abscesses with whipworm infection by *Trichuris trichiura*. The small coiled worms may be demonstrated on a barium study associated with an edematous mucosa.

*Chagas' disease* is caused by the protozoan *Trypanosoma cruzi*. Destruction of ganglion cells in the colon and esophagus occurs, causing megacolon and megaesophagus. The colonic findings are identical to Hirschsprung's disease, while those in the esophagus are identical to achalasia.

### Bacterial Dysentery

*Shigella* infection causes a common form of bacterial dysentery. Radiographic manifestations demonstrate a superficial ulceration similar to ulcerative colitis and most severe in the rectosigmoid.

*Salmonella* infection usually results from food poisoning and causes an acute self-limiting colitis. Radiographic findings are generally confined to the colon. The mucosa is inflamed and edematous with the right side of colon more commonly involved. Wall thickening of the colon, with submucosal edema, may also be appreciated on CT.

*E. coli* infection also causes self-limiting dysentery and is rarely evaluated radiographically.

*Campylobacter* colitis causes changes which are indistinguishable from acute ulcerative colitis. This disease also is generally self limited and heals completely.

*Yersinia enterocolitis* most commonly affects the terminal ileum but may extend into the right side of the colon. Most prevalent are nodular lesions secondary to lymphoid hyperplasia. Ulcers simulating Crohn's disease may occur.

*Gonococcus* infection causes superficial ulcerations which are usually confined to the rectum. Radiographically, the appearance is indistinguishable from idiopathic ulcerative proctitis.

### Viral Colitis

Most viral colitides are opportunistic infections which occur in immunocompromised hosts. Herpes and cytomegalovirus are the most common infections in this category (see below).

### Sexually Transmitted Colon Infection

Several organisms are associated with venereal infections. *Lymphogranuloma venereum* is a venereal disease caused by chlamydia infection. In the acute phase there is an ulcerative proctitis. This may progress to cause pelvic, perineal, and ano-rectal abscesses and fistulas. Inguinal adenopathy is a prominent feature. The healing phase is manifested by considerable fibrosis with strictures and stenoses present. The strictures begin just above the anus and continue proximally for a varying length. The differential diagnosis includes *Crohn's disease*, *radiation*, *scirrhous carcinoma*, *syphilis* and *metastases*.

Many organisms have recently been associated with colitis in the homosexual population and are collectively sometimes referred as causing the '**gay bowel**' syndrome. These organ-



Fig. 32.33. CMV colitis. Two irregular ulcers in descending colon (arrows).

isms include, *Ameba*, *Gonococcus*, *Shigella*, *Salmonella*, and *Campylobacter*. *Non-specific proctitis* and *traumatic proctitis* are also common. Several colitides, especially those of *viral* etiology, are found predominantly in acquired immune deficiency syndrome (AIDS) patients. Other severely immunocompromised patients may also be affected.

**Cytomegalovirus** (CMV) colitis may be diagnosed radiographically; this is clinically important since CMV infection of the bowel causes deep ulcerations which frequently lead to fatal perforation and hemorrhage (Fig. 32.33). In CMV colitis, barium examination of the colon shows features which suggest either ulcerative colitis or Crohn's disease. The mucosa may be granular, with superficial ulcerations, thickened folds and spasticity. Aphthous ulcers have also been described. The abnormalities may be distributed in a diffuse or segmental manner. Deep ulcerations in a segmental distribution suggestive of Crohn's disease may also occur. Unlike Crohn's disease however, perforation and severe hemorrhage are frequent complications. The pathogenesis of deep ulceration in CMV infection is believed to be a result of ischemic necrosis secondary to vascular involvement. In addition to the deep ulceration, submucosal hemorrhage and toxic megacolon may occur.

**CT scanning** of the abdomen and pelvis is frequently the primary imaging modality performed in AIDS patients with suspicion of abdominal pathology. The most common CT finding in CMV colitis is *thickening* and *edema* of the colon wall. The 'target sign', which is a linear low-density line in the submucosal region adjacent to the thicker soft tissue density of the remaining colon wall is a non-specific finding due to submucosal edema which is usually present in these cases.

This is useful in distinguishing inflammatory from neoplastic thickening of the colon wall. In CMV colitis right-sided involvement is almost always present with pancolitis present frequently and left-sided colitis less common. The distal ileum is also frequently affected. The constellation of these findings in an AIDS patient is highly suggestive of CMV.

*Cryptosporidium* and *Mycobacterium avium intracellular* (MAI) are found in the colon of AIDS patients but do not produce specific radiographic findings. *Herpes* and *Candida* infection have also been described.

*Typhlitis* is a severe inflammation of the cecum and ascending colon which has been described in severely neutropenic patients, especially leukemics. This condition may also be found in AIDS patients. CT examination when this condition is suspected is safer than a barium examination and equally diagnostic. There is marked thickening of the wall of the cecum with infiltration of the surrounding fat and tissue planes due to infection, neoplastic infiltration, non-neoplastic inflammation, hemorrhage and/or ischemia. Ulceration and perforation may occur.

#### Neoplastic Involvement in AIDS Patients

Two major neoplasms are associated with colonic involvement in AIDS patients. These are Kaposi's sarcoma and lymphoma.

Kaposi's sarcoma presents radiographically with either submucosal nodules, target lesions or evidence of submucosal infiltration.

AIDS related lymphoma more commonly involves the colon than is found in the general population. The radiographic appearance is wide-ranging. Bulky polypoid lesions with intussusception may occur. The rectum is much more commonly involved than in non-AIDS patients. Colonic lymphoma in AIDS, as with small bowel lymphoma, is frequently a primary site; that is without discernible diffuse nodal involvement.

#### Antibiotic-associated Colitis (pseudomembranous colitis)

Many broad spectrum antibiotics, most prominently *clindamycin* and *lincomycin* are associated with antibiotic induced colitis. This most likely results from an overgrowth of *Clostridium difficile* in the colon which releases cytotoxin and enterotoxin. Pseudomembranous colitis may present with symptoms ranging from mild to fulminant diarrhea which may resolve spontaneously or may be treated effectively with *vancomycin*.

Plain radiographs may show dilated colon with thickened wall and thumbprinting. In severe cases, toxic megacolon with perforation may occur.

Diagnosis is usually made endoscopically but may also be made on *barium enema*. Pseudomembranes representing areas of sloughed mucosa are seen as nodular defects or as a shaggy mucosal pattern. This is caused by a combination of elevated plaques, ulcers and edema.

Diagnosis may also be made by CT in either clinically unsuspected cases or as an incidental finding (Fig. 32.34). CT findings include colonic dilatation and bowel wall thickening. Linear lucencies in the submucosal region of bowel wall secondary to edema may also be identified; when seen in cross section this produces a 'target sign'. Ascites may also



Fig. 32.34. Pseudomembranous colitis. CT. There is circumferential thickening of colon wall with a lucent submucosal line due to edema (arrowheads). In cross-section this forms the 'target' sign. Discrete pseudomembranes are not seen.

be present. Differential diagnosis of these findings most commonly includes ischemic colitis, inflammatory colitis and idiopathic inflammatory bowel disease as well as diverticulitis.

#### Ischemic Colitis

Many underlying factors may cause impaired blood flow to the colon and result in ischemic insult, as the colon has a relatively poor blood supply. Ischemic changes may occur with venous obstruction, arterial occlusion by thrombus or emboli, and with low flow states resulting in hypoperfusion. The changes caused by radiation colitis, systemic lupus erythematosus, polyarteritis nodosa and other vasculitides also reflect inadequate perfusion. Patients at high risk for ischemic bowel disease include patients over 50 years of age especially those with a history of cardiovascular disease, and patients with hypercoagulation.

The *splenic flexure*, representing the watershed area between the area supplied by the superior and inferior mesenteric arteries, is the classic site of involvement. However, there is considerable variation in the collateral blood supply and ischemic colitis may occur anywhere in the colon including the rectum.

Radiographic changes reflect the severity of the process including the degree and duration of the ischemia and the underlying collateral circulation.

On plain films, early changes may be manifested by mild diffuse bowel dilatation or a gasless abdomen. In acute severe ischemia, submucosal edema and/or hemorrhage cause bowel wall thickening resulting in the radiographic findings of *thumbprinting* (Fig. 32.35). Toxic megacolon may occur in cases of severe ischemia with bowel necrosis. *Pneumatosis*, manifested by linear collections of intramural air also suggests the presence of bowel necrosis. Ischemia may develop proximal to a mechanical obstruction or within a closed loop.

Acute ischemia, associated with a clinical presentation with acute abdominal pain, tenderness, rectal bleeding (cranberry stool) and diarrhea suggests emboli to the mesenteric circulation. In such cases, *angiography* is the most useful imaging modality. Emboli may be diagnosed, and in some cases treated with *thrombolytic therapy* or *angioplasty*.

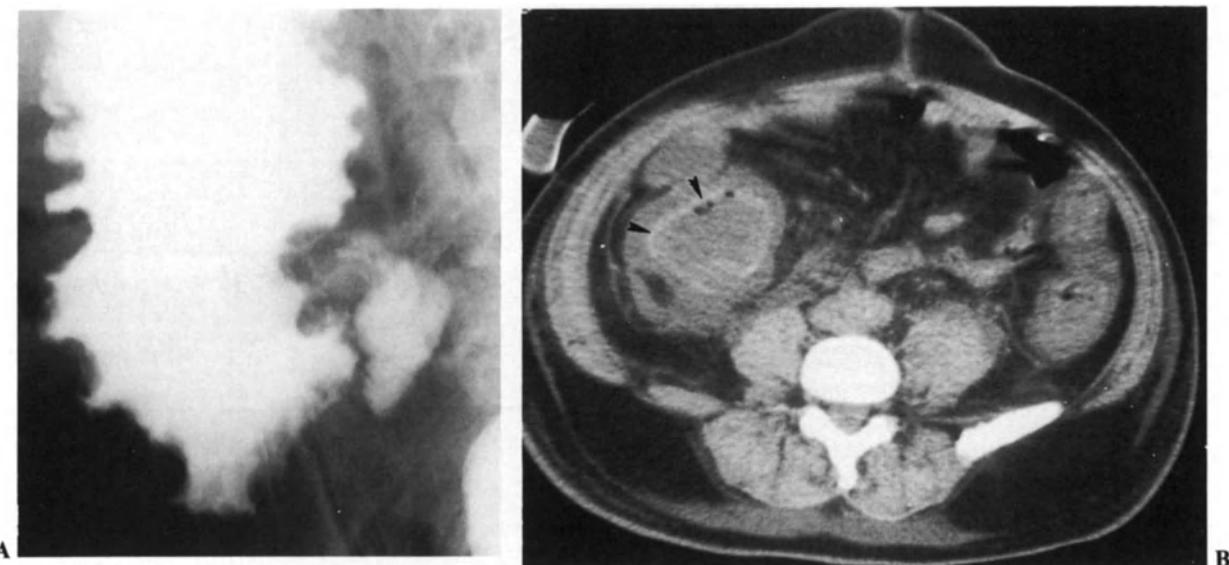


**Fig. 32.35A, B.** Acute ischemic colitis. **A** There is 'thumbprinting' of the cecum. **B** CT of same patient shows thick walls in the descending colon and cecum. With no intraluminal contrast the mucosal line is higher attenuation (arrowheads) than the edematous bowel wall.

Thrombi, atherosclerotic plaques, and narrowing and spasm associated with low flow states may also be diagnosed and treated angiographically. Intra-arterial papaverine has been demonstrated to be an effective treatment for spasm of the mesenteric vessels.

*Barium studies* are most useful in the subacute and chronic stages of ischemic colitis. The earliest changes demonstrated include thickening of the bowel wall associated with narrowing and spasm. This is reflected as scalloping or *thumbprinting* of the bowel wall. Thumbprinting may also cause multiple nodular filling defects mimicking polyps. *Ulceration* may occur and may be superficial or deep, segmental or

generalized. These findings may be completely reversible. If significant fibrosis occurs with healing, stricture formation ensues. *Strictures* may be long, smooth and tapered or asymmetric with eccentric sacculation (Fig. 32.36), and tend to be shorter than the area initially involved with ischemia.

#### Radiation Colitis

The pathogenesis of radiation colitis is similar to that of ischemia, although the two are frequently distinguishable radiographically. The effects of radiation are confined to the treatment fields and in the colon are most often found in the rectum and sigmoid from the treatment of pelvic

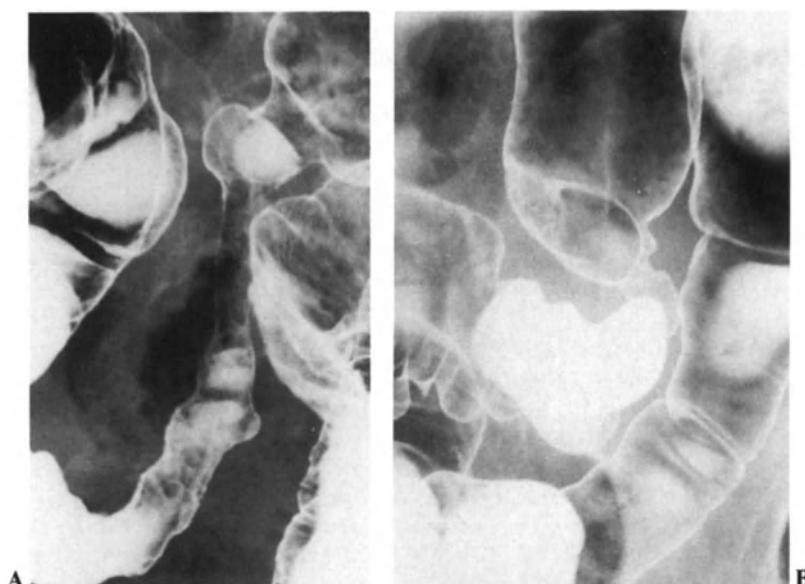


**Fig. 32.36A, B.** Partially reversible ischemic colitis. **A** There is a long stricture in the subacute period due to a combination of edema and fibrosis. **B** Several months later the stricture is shorter.

malignancies. *Acute radiation colitis* which is not a frequent occurrence with current dosage regimens, has a radiographic appearance indistinguishable from ulcerative proctitis or proctosigmoiditis.

*Chronic radiation changes* usually begin to manifest about a year after therapy although presentation may be delayed for many years. Acute radiation colitis is not a necessary precursor for chronic radiation damage. Radiographic changes include demonstration of a narrow, rigid, and featureless bowel segment, usually the rectosigmoid. These findings are caused by *fibrosis* within the bowel wall and within the radiation field outside the bowel wall. Other findings include widening of the presacral space, findings usually associated with chronic ulcerative colitis, and elevation of the rectosigmoid colon out of the pelvis. Pelvic adhesions may cause extrinsic impressions on the bowel wall. On occasion, this may be prominent enough to mimic recurrent tumor. *Ulceration and fistula formation* (rectovaginal fistulas in gynecologic malignancies) may occur. Pseudopolyps, caused by inflammation and subsequent healing of the mucosa, may also be seen in radiation colitis.

### Necrotizing Enterocolitis

Necrotizing enterocolitis (NEC) is found in premature neonates. It preferentially involves the small bowel, although the colon may also be affected. Presenting with bloody diarrhea, NEC is of unknown etiology. Breast milk appears to be protective. Patients are followed with plain films and contrast studies are rarely performed.

*Radiographic findings* demonstrate the spectrum associated with ischemic colitis in the adult, from early subtle bowel distension, to bowel loops separated with the development of edema and the bowel wall appearing scalloped with hazy margins. The development of pneumatosis intestinalis is a characteristic of severe disease (Fig. 32.37). NEC may be complicated by development of portal venous gas and bowel perforation.

### Cathartic Colon

Chronic laxative abuse causes irritation of the colonic epithelium which may lead to an alteration in the appearance and the function of the colon. Typically, the patient is a middle-aged or elderly female with a long history of constipation and chronic laxative use.

On barium examination, the colon is somewhat dilated with loss of haustral markings. Changes are typically more marked on the right side of the colon. The ileocecal valve is patent and there may be secondary inflammatory changes in the terminal ileum similar to those seen in backwash ileitis. Ulcerative colitis is the most important radiographic differential diagnosis to be made. In cathartic colon unlike ulcerative colitis, the bowel remains distensible and pliable although there may be transient pseudostriatures. The flexures also remain in a normal, rather than depressed position. Another distinguishing feature is that the rectum and sigmoid are relatively spared.

### Behçet's Syndrome

Behçet's syndrome is a chronic condition of unknown etiology which is frequently considered part of the autoimmune

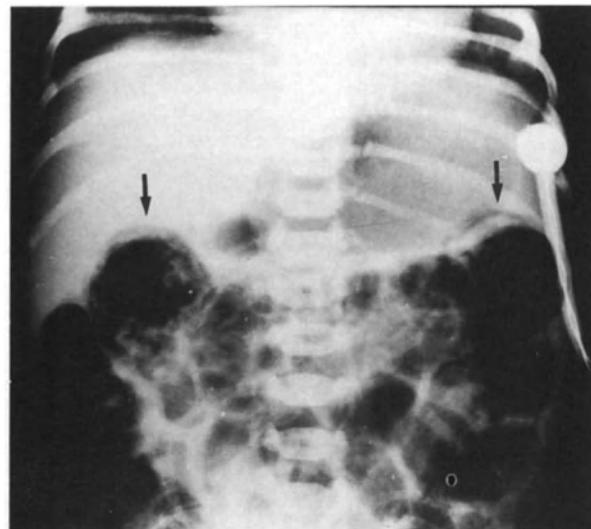


Fig. 32.37. Necrotizing enterocolitis. Linear pneumatosis is seen in the hepatic and splenic flexures (arrows).

disorders which includes inflammatory bowel disease, various arthritides and vasculitides. The classic description of the syndrome described the triad of *oral and genital ulcers* with *ocular inflammation*. *Arthritis* is commonly present and *colitis* is reported in about a third of the cases. The colitis most closely resembles Crohn's disease with aphthous ulcers or deep, discrete ulceration with normal surrounding mucosa. The lesions are more commonly found on the right side of the colon. Hemorrhage and free perforation may occur more commonly than in Crohn's disease while significant bowel wall thickening and stricture formation are less dominant features.

### Colonic Obstruction

Most intestinal obstructions occur in the small bowel. About 20% of intestinal obstructions are colonic. *Carcinoma*, predominantly sigmoid, accounts for about 65% of colonic obstructions and *diverticulitis* for another 20%.

*Volvulus*. A volvulus may occur when a segment of bowel twists around a long mobile mesentery.

*Sigmoid volvulus* is more common since the sigmoid colon is normally on a mesentery. An elongated or redundant sigmoid may twist on its mesentery and cause an obstructed blind loop. This leads to characteristic findings on abdominal plain films. The obstructed sigmoid loop undergoes massive dilatation and projects up from the pelvis and towards the right upper quadrant. A linear soft tissue density projecting up from the midpelvis which represents the apposed walls of the twisted segment is often seen. With erect or decubitus (horizontal beam) films two separate air fluid levels are seen. In cases of suspected sigmoid volvulus an emergency single contrast barium enema is often confirmatory. Barium is introduced under fluoroscopic control to the point that the obstruction is identified only. With a sigmoid volvulus the contrast column ends abruptly in a 'beak' representing the point where the bowel twists on the mesentery (Fig. 32.38).

*Cecal Volvulus*. The cecum and ascending colon may retain a variable amount of mesentery. When a volvulus of the

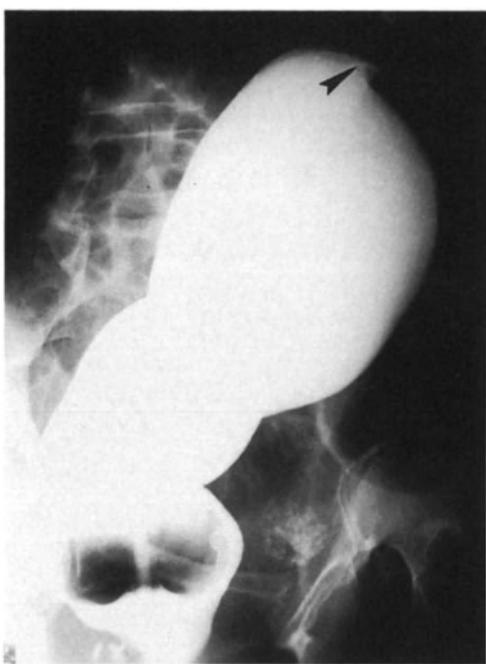


Fig. 32.38. Sigmoid volvulus. Contrast terminates in a 'beak' at the point where the bowel twists on its mesentery (arrowheads).

cecum occurs the dilated cecum rotates from the right iliac fossa toward the midabdomen or left upper quadrant (Fig. 32.39). If the ileocecal valve is patent, a considerable amount of small bowel distension may also occur. On erect or decubitus radiographs, there is typically a single air-fluid



Fig. 32.39. Cecal volvulus. A supine radiograph shows the massively dilated cecum crossing to the left side of the abdomen, with the central 'fold' pointing to the right iliac fossa.

level present within the obstructed cecum. Cecal distension may also occur in the condition known as *cecal bascule*. In this condition a mobile cecum, which is on a retained mesentery, folds without twisting across the more distal bowel. This is usually an asymptomatic condition and the distension is relieved by positional variation.

The *transverse colon* which is also normally on a mesentery is rarely affected by a volvulus which occurs when two separate loops of bowel twist around each other to form an *intestinal knot* or *compound volvulus*. An *ileosigmoid knot* occurs more commonly in developing countries and chronic parasitic infestations may be a predisposing factor.

### Intussusception

Intussusception is caused by the invagination of a bowel segment (the *intussusceptum*) through the surrounding bowel (the *intussuscipiens*). Most are *ileocolic* intussusceptions and occur in children between the ages of one month and 2 years. They are probably caused more commonly by enlarged or inflamed lymphatic patches in the ileum which serve as lead points. Carefully performed barium enemas in these cases may often establish the diagnosis and are frequently performed as therapeutic maneuvers in order to reduce the intussusception.

In adults and older children, the lead point of an intussusception is virtually always a mass lesion. *Colo-colic* intussusceptions are more common in adults. Intussusceptions have a characteristic coiled spring appearance which may be identified on CT as well as barium examination (Fig. 32.40).

*Other Causes of Colonic Obstruction.* Other less frequent causes of colonic obstruction include *incarcerated hernias*, *abscess*, *metastatic disease*, and *foreign bodies*.

*Pseudo-obstruction.* Colonic pseudo-obstruction, also known as colonic ileus or *Ogilvie syndrome*, refers to colonic dilatation without evidence of mechanical obstruction and with relative lack of small bowel distension. Pseudo-obstructions usually occur in elderly patients who have



Fig. 32.40. Colonic intussusception. On CT, the intussuscepting carcinoma in the ascending colon presents as a mass with multiple layers representing the cross section of the invaginated intussusceptum with contrast and mass in the lumen (arrowheads), its wall and low-density mesenteric fat surrounded by the intussuscipiens.

undergone recent surgery or with major systemic diseases. *Perforation*, most often of the cecum, may occur.

Contrast examinations are indicated if it is necessary to rule out a mechanical obstruction. Colonic pseudo-obstruction may be more pronounced in the cecum than in the remainder of the colon. It may be relieved by positional variation or reduced colonoscopically; occasionally surgical intervention is required to prevent perforation and a cecostomy is performed.

### Megacolon

**Megacolon** is a descriptive term for abnormal dilatation of the colon. The condition may be acute or chronic, and may represent an incidental clinical finding or may be life threatening. Chronic megacolon may result from chronic constipation which may be idiopathic, related to drug use, or psychogenic causes. It may also result from neuromuscular damage to the colon. *Congenital megacolon* or *Hirschprung's disease* is caused by deficient development of the myenteric plexus in the colon. In *Chagas' disease*, the myenteric plexus is destroyed secondary to infection with the trypanosome.

**Toxic megacolon** occurs as a complication of inflammatory conditions. This is a life-threatening condition and predisposes to hemorrhage and bowel perforation. It is associated with *ulcerative colitis*, *ischemic colitis*, *Crohn's disease*, *amebiasis*, and *shigellosis*. If toxic megacolon is suspected, contrast examination is contraindicated. These patients should be followed with plain films of the abdomen.

On abdominal radiographs, changes of toxic megacolon are usually most visible in the transverse colon since this is the most anterior portion of the colon and is the least dependent portion in supine patients. The colon may be dilated and thin walled. Alternatively, the bowel wall may be thickened secondary to edema and demonstrate nodular soft tissue impressions (thumbprinting).

### Endometriosis

Endometriosis is a condition in which endometrial tissue is found outside the uterus. The condition usually affects reproductive organs in contiguity with the uterus, but occasionally may involve organs other than those of the female reproductive tract. The *rectosigmoid*, pelvic *small bowel*, and *urinary bladder* are most often involved. Occasionally, remote implants may be found e.g. on the pleura. Intestinal involvement occurs in 10%–20% of patients with endometriosis and the rectosigmoid is involved in at least 25% of these cases. The appendix, cecum and ileum are other potential sites of involvement.

Findings on *barium enema* examination generally mimic those of a serosal implant and include stretching or spiculation of the mucosal folds. *En face* these lesions appear crinkled or crenellated. Pelvic masses caused by endometriosis may also cause smooth extrinsic impressions on the involved colon (Fig. 32.41). Occasionally, intraluminal polypoid lesions or endometriomas may form, which may be indistinguishable from neoplastic polyps. Short annular lesions, difficult to distinguish from carcinoma or long tapered strictures, may also occur. In some cases, there is a considerable

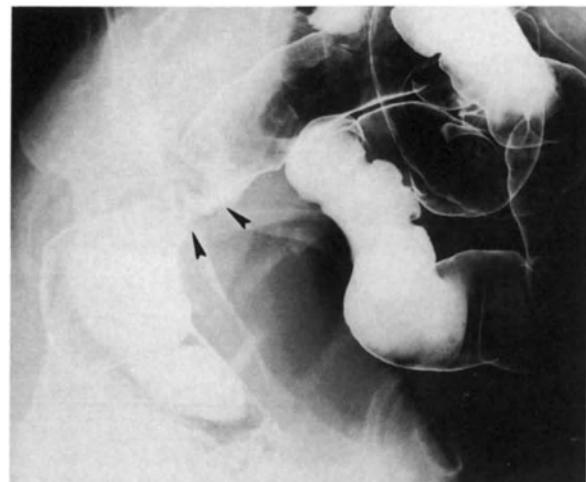


**Fig. 32.41.** Endometriosis. A pelvic 'mass' is causing extrinsic impression on the anterior wall of the rectum and inferior wall of the sigmoid. The rectosigmoid colon is narrowed with spiculated folds from circumferential mural involvement (arrowheads).

fibrotic reaction which may cause kinking and angulation of the bowel which may resemble findings of a carcinoid tumor.

### Pneumatosis Coli

The presence of air within the wall of the colon is called *pneumatosis coli*. The collections may be linear or ovoid and may extend into the mesentery, small intestine (*pneumatosis intestinalis*) or into adjacent structures.

The etiology of pneumatosis is not well understood and is probably multi-factorial. The condition may represent an incidental finding, for example, in patients with *obstructive lung disease*, *connective tissue disorders* or *jejuno-ileal bypass*. Benign gas cysts in the bowel wall may originate from small mucosal tears which trap air and subsequently seal. Pneumatosis may also result from *ischemic insult*, *bowel necrosis*, *obstruction* or *infection*. In such cases, it may be life threatening.

Linear or oval lucencies around the colonic wall may be seen on plain abdominal radiographs, or during a barium enema (Fig. 32.42). Occasionally, a mottled appearance similar to that seen with retained stool or abscesses may be seen. If there is a suspicion of bowel necrosis or perforation, barium examination should not be performed. Pneumatosis may sometimes be demonstrated as an incidental finding on barium enema. The bowel wall appears scalloped in the case of cystic pneumatosis and may mimic ischemia, lymphoma, or polyps. However, gas density cysts, usually on the left side of the colon and about 1–2 cm in diameter, should be identified originating from the bowel wall.

### Colitis Cystica Profunda

This is a rare condition in which multiple small cysts are demonstrated in the submucosa of the rectosigmoid. These are mucous retention cysts which are believed to be a complication of bacillary dysentery or other chronic inflammation.

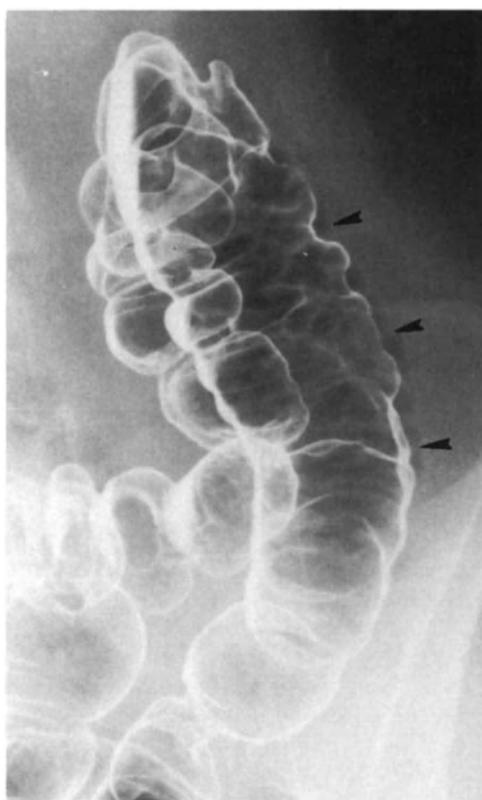


**Fig. 32.42.** Pneumatosis coli. Oval lucencies representing gas cysts are an incidental finding in the patient (arrowheads). The round air density collections identified in the bowel wall may be mistaken for intraluminal polyps.

### Vascular Abnormalities

**Hemorrhoids**, caused by enlargement of the internal hemorrhoid veins at the anorectal junction, are the most common vascular abnormality of the colon. They may be appreciated on double contrast barium enema examinations after the enema tip is removed. They appear as submucosal serpiginous or nodular filling defects extending for several centimeters from the anorectal junction. More extensive *varices* may rarely be found more proximally in the rectum or elsewhere, usually as a result of portal hypertension and mesenteric venous obstruction.

**Hemangiomas** are another unusual vascular disorder which may be found in the colon, usually the rectum. Multiple hemangiomas may be found in patients with a systemic angiomyomatosis. Small hemangiomas are imperceptible on barium examination. Larger lesions may produce mass lesions which are usually pliable submucosal nodules. Large lesions may contain phleboliths, which suggest the definitive diagnosis.

**Angiodysplasia** is a relatively common disorder which causes chronic or acute GI bleeding in elderly people. Prosthetic aortic valves may predispose patients to this condition. These are usually undetected on barium examination, and are diagnosed, and frequently treated by colonoscopy. **Angiography** is the definitive imaging procedure for the depiction of vascular abnormalities.

### Amyloid

Amyloidosis is a rare systemic disorder caused by the deposition of abnormal protein-polysaccharide with specific (histologic staining) characteristics, around blood vessels, muscles and mucous membranes. The disorder may be secondary to a wide variety of chronic conditions or may be idiopathic, or primary. Tissue damage occurs both by infiltration and by ischemia.

There is a wide spectrum of *radiographic manifestations* of amyloidosis which is known to mimic many other conditions. *Infiltration* of the bowel wall may lead to thickening of the muscular or mucosal layers and cause thickening of mucosal folds or multiple polypoid lesions. Infiltration may also lead to the formation of a narrow rigid bowel with loss of haustral markings. Neuromuscular involvement may cause diffusely dilated, thin walled colon (megacolon). Occasionally, mucosal ulceration may occur.

### Scleroderma

Scleroderma (progressive systemic sclerosis) is a systemic autoimmune disease in which muscle is replaced by collagen and other connective tissues. Gastrointestinal tract involvement occurs most frequently in the esophagus and small bowel. The colon is involved less frequently.

*Radiographic findings* include *diffusely dilated bowel* in association with a functional pseudo-obstruction. The demonstration of large asymmetric sacculations or wide-mouthed diverticula, is considered characteristic of scleroderma. These represent haustra distorted by loss of normal musculature. *Pneumoperitoneum* may also be found.

### Colonic Complications of Renal Disease

With the large, and increasing, population of patients on dialysis or with renal transplants, there has been growing awareness of colonic complications in these patients occurring with higher frequency than in the general population. Complications include *diverticulitis* with a high incidence of intraperitoneal perforation. *Ischemic colitis*, sometimes referred to as *uremic colitis*, *pseudomembranous colitis*, *hemorrhagic proctitis*, and *appendicitis* have also been reported with some frequency.

### Irritable Bowel Syndrome

The irritable bowel syndrome is a common condition usually presenting with chronic pain, constipation and/or mucous diarrhea. The traditional role of radiology in this condition has been to exclude other pathology. Abnormal colonic motility may be a factor in at least some of these patients. This may be evaluated by *scintigraphy* by following the transit of radiopaque markers on abdominal radiographs.

### Solitary Rectal Ulcer Syndrome

Solitary rectal ulcer syndrome (SRUS) is believed to be caused by muscular discoordination during defecation. The term is somewhat misleading because the syndrome may manifest with mucosal edema of the rectum, either without any ulceration, or with single or multiple ulcers.

*Barium enema* may demonstrate a variety of findings including thickening of the valves of Houston, edema, manifested by shallow nodularity of the mucosa, ulcers, usu-

ally on the anterior wall, or stricture. The syndrome occurs most often in young adults.

There is increasing interest in evaluating symptoms related specifically to the rectum by defecography or dynamic proctography. For this procedure, evacuation of a thick barium paste from the rectum is monitored fluoroscopically.

### Appendix and Ileocecal Region

The cecum is the blind proximal pouch of ascending colon formed by the convergence of the three bands of tenia coli. It extends distally to the level of the first prominent haustral fold. The ileocecal valve is situated on its medial or posterior medial aspect. The appendix is usually found in the right lower quadrant; however it is retrocecal in 15% of patients and may be found in more unusual locations such as deep in the pelvis or even in the left upper quadrant. The appendix arises as an outpouching from the tip of the cecum and opens onto the same wall as the ileocecal valve. The terminal ileum enters the colon between the lips of the ileocecal valve and is often seen as a beak-like configuration. *En face* the appearance of the valve may appear as a rosette or ovoid lucency.

The entire spectrum of colonic pathology may be found in the ileocecal region. In addition, there are several conditions unique to this area.

### Neoplasms involving the Ileocecal Region

The ileocecal valve itself is occasionally diffusely enlarged secondary to *lipomatous infiltration*. The appearance is similar to the normal ileocecal valve with a smooth or lobulated surface but is larger than 3 cm. This is of no clinical significance; however, it may be mistaken for a true neoplasm. True *lipomas* are encapsulated benign neoplasms and have a propensity for the ileocecal region. They are second in incidence to *adenomas* in the colon. Lipomas are submucosal lesions but may form pseudopodicles and appear stalked. They are soft and pliable and characteristically change configuration with change in position or compression. CT is often confirmatory.

*Carcinoid* tumors may arise in the valve but are much less frequent than in the appendix or the terminal ileum. Lipomas

involving the valve are usually associated with involvement of the terminal ileum as well. *Adenomatous polyps* and *carcinomas* rarely arise in the valve but may be found in the cecum and involve the ileocecal valve.

*Colonic urticaria* is an unusual condition which has been found most often in the cecum. It is usually secondary to submucosal edema or chronic ischemia secondary to distal obstruction. Rare cases of true colonic urticaria due to an allergic response have been documented. In all of these cases, the radiologic findings is that of multiple, contiguous small smooth, nodular or angular filling defects.

### Acute Appendicitis

Acute appendicitis secondary to inflammation is the most common lesion in the appendix and is the most common cause of emergency abdominal surgery. Pathogenesis is believed to be related to obstruction of the lumen of the appendix caused by fecal residue that may occasionally form a calcified appendicolith (Fig. 32.43). Foreign bodies, tumors, and parasites may also obstruct the appendix.

Plain film findings include the presence of a *calculus* in the right lower quadrant, *partial small bowel obstruction* or *focal ileus* on the right. The presence of an air-fluid level in the cecum or distal ileum in a symptomatic patient is considered suggestive. A soft tissue mass may also be present.

Single contrast barium enemas may be useful in some uncertain cases. If the appendix fills completely, the likelihood of acute appendicitis is negligible. Incomplete or non-filling of the appendix however, is considered suggestive but not diagnostic.

Recently, *ultrasound* examination has been proposed for the diagnosis of acute appendicitis. A dilated, fluid-filled thick-walled appendix fixed in position is highly suggestive of appendicitis (Fig. 32.44).

Complications of appendicitis are secondary to necrosis and perforation with subsequent inflammation and *abscess* formation. A soft tissue mass with displacement of bowel and a mottled air pattern on plain abdominal radiograph suggests the presence of an abscess. Periappendiceal inflammation is frequently complicated by *small bowel obstruction*. *Ultrasound* and especially *CT* examination are the imaging

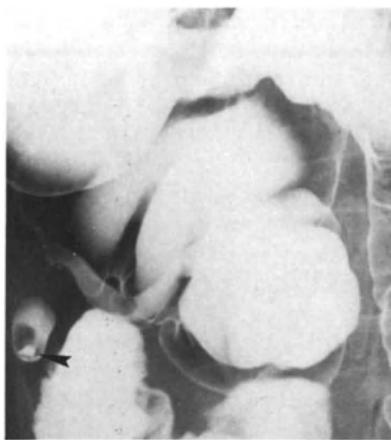


Fig. 32.43. Appendicolith. A calcified appendicolith (arrowhead) at the base of the appendix is depicted on barium enema.

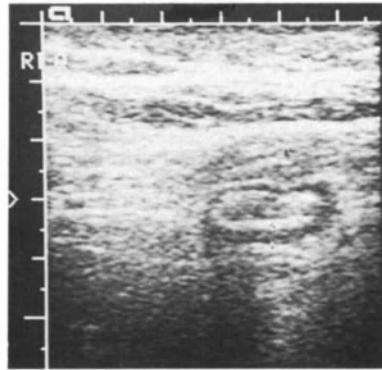


Fig. 32.44. Ultrasound demonstration of acute appendicitis. Cross-section of a fixed dilated appendix with thick wall (measuring cursors).



**Fig. 32.45.** CT periappendiceal abscess. A pelvic abscess with encapsulated fluid is seen (arrowhead).

modalities of choice in suspected appendiceal abscess (Fig. 32.45). In some cases, percutaneous drainage of a periappendiceal abscess may prove therapeutic or may be used to defer surgery.

Patients who have undergone appendectomy often show a typical defect at the base of the cecum caused by inversion of the appendiceal stump. This usually causes a small deformity of the wall of the cecum sometimes with a polypoid filling defect.

Mucoceles may arise due to obstruction of the base of the appendix with subsequent filling of the lumen with mucus. Alternatively, they may arise as a primary process due to excess mucus secretion. This may also occur secondary to a cystadenoma or cystadenocarcinoma. *Myxoglobulosis* of the appendix is a condition caused by calcification of globules of mucus within the lumen of the appendix. Rarely a mucocele may rupture leading to a rare complication known as *pseudomyxoma peritonei*. In this condition there are multiple peritoneal implants of mucoid material and ascites occurs. This condition often exhibits aggressive behavior with extension of the implants, ascites and recurrent small bowel obstructions.

The appendix is frequently involved in patients who have *Crohn's disease*, *intestinal tuberculosis* or *actinomycosis* of the ileocecal region. Fistula formation may involve the appendix in these conditions.

A variety of **neoplasms** may involve the appendix, including benign and malignant tumors. These include *mucoceles*, *cystadenomas*, and *cystadenocarcinomas* as well as *adenomas* and *adenocarcinomas*. *Carcinoid* tumors are the most common neoplasm of the appendix; they are almost always small and found incidentally at surgery and almost never malignant. On barium enema, neoplasms of the appendix usually cause a smooth defect at the base of the cecum. This is a non-specific appearance also found with periappendiceal abscesses (Fig. 32.46).

### Trauma

Colonic trauma is relatively uncommon, rarely occurring alone, but found in patients with multiple abdominal trauma. Penetrating trauma may result in bowel perforation. Blunt trauma may lead to mural hemorrhage or contusions with complicating ischemic changes. Contrast studies are rarely necessary in the acute stage of colonic trauma. Abnormality such as mural thickening may be depicted by CT examination.

Ingested foreign bodies may cause bowel obstructions or perforations. These are most frequent in terminal ileum and appendix.

### Extrinsic Deformities of the Colon

Any mass, be it inflammatory, neoplastic or even normal structures adjacent to the colon, may cause extrinsic impression upon it. Smooth obtuse impressions may be caused by contiguous normal structures such as the right lobe of the liver, gallbladder, kidney or uterus. A mass lesion within the organ causes a more prominent impression (Fig. 32.47) and occasionally even partially obstructs the lumen.



**Fig. 32.46.** Periappendiceal abscess. There is a smooth impression on the base of the cecum. An identical appearance could be caused by mucoceles and other appendiceal lesions.



**Fig. 32.47.** Extrinsic impression. There is a smooth mass effect on hepatic flexure from a renal mass. Note the normal caliber smooth folds stretched over mass.



**Fig. 32.48.** Metastasis. A discrete mass causing spiculation of the bowel wall from a metastatic implant on the superior surface of the transverse colon.

*Pelvic lipomatosis* is an asymptomatic condition in which there is a large amount of non-neoplastic fatty tissue in the pelvis. Contour abnormalities consisting of elevation and elongation of the rectosigmoid, but more often of the urinary bladder (pear-shaped bladder) are typical. CT will confirm the diagnosis.

Inflammatory processes contiguous to the colon may cause spasm, edema and thickening of the wall, and spiculation of folds. Generally, discrete masses are not as prominent a finding as with metastatic disease. *Pancreatitis* is the most common inflammatory condition to involve the colon in a secondary fashion. Most of the pancreas is connected to the transverse colon by the transverse mesocolon which extends to the splenic hilum. Pancreatitis may cause distension of the transverse colon with abrupt narrowing distal to the splenocolic ligament resulting in the 'colon cut off' sign. Pancreatic pseudocysts, which vary widely in size and location, may cause extrinsic impression on the colon.

Intra-abdominal *metastatic disease* or direct extension of tumor often involves the colon. With most types of secondary involvement by malignancy the colonic wall is involved first and the mucosa is spared until very late. Metastatic lesions tend to be found as multiple discrete lesions. A mass effect is usually more prominent than with inflammatory disease. In metastatic disease the bowel wall folds tend to be thickened and fixed and appear distorted and hazy (Fig. 32.48). Whilst there is some overlap with the findings in an inflammatory process, the presence of multiple lesions, a discrete mass effect, and distorted thickened bowel folds all favor malignancy. Occasionally metastatic involvement may be circumferential and be indistinguishable from primary colonic malignancy. Hematogenously spread metastases may be found with primary melanoma, lung and breast cancer. These lesions are primarily mucosal.

Intraperitoneal seeding of metastatic disease is found most often from pelvic or other GI tract malignancies. Dependent areas of the abdomen are most commonly affected. These include in descending order of frequency, the cul-de-sac, medial wall of the cecum and terminal ileum, superior aspect of the sigmoid and right paracolic gutter (Fig. 32.49).

*Endometriosis* may cause implants on the colon, most commonly in the cul-de-sac along the anterior rectosigmoid wall. The appearance of endometrial implants is identical to that seen in metastatic disease. Findings are distinguished on the basis of age and clinical history.

#### REFERENCES AND SUGGESTIONS FOR FURTHER READING

- Balthazar EJ, Megibow AJ, Fazzini E, et al. (1985) Cytomegalovirus colitis: radiographic findings in 11 patients. Radiology 155: 585–589
- Caroline DF, Evers K (1987) Colitis: radiographic features and differentiation of idiopathic inflammatory bowel disease. Radiol Clin North Am 25: 47–66
- Caroline DF, Hilpert PL, Russin V (1987) CMV colitis mimicking Crohn's disease in a patient with acquired immune deficiency syndrome (AIDS). J Can Assoc Radiol 38: 227–228

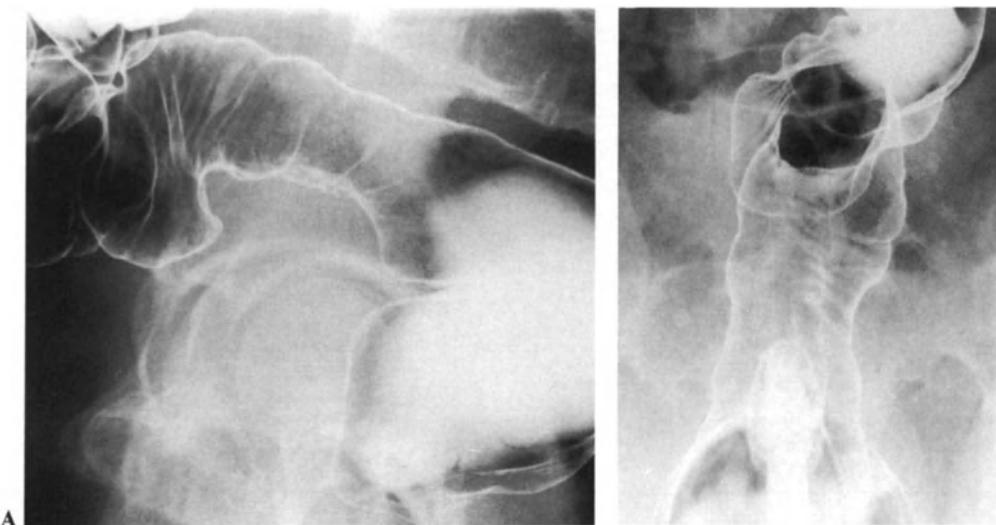


**Fig. 32.49A, B.** Metastatic disease. A Lateral view of the rectum shows narrowing and straightening and distortion of the anterior wall of the rectosigmoid. B Prone angle view of the rectosigmoid in the same patient shows enface view of the affected area with 'crinkling' or 'striped' appearance.

- Finlay IG (1988) Proctography symposium. *Int J Colorectal Dis* 33: 67–89
- Frager DH, Fragher JD, Brandt LJ, Wolf EL, Rand LG, Klein RS, Beneventano TC (1986) Gastrointestinal complications of AIDS: radiographic features. *Radiology* 158: 597–603
- Gardiner R, Smith C (1987) Infective enterocolitis. *Radiol Clin North Am* 25: 67–68
- Halpert RD (1987) Toxic dilatation of the colon. *Radiol Clin North Am* 25: 147–155
- Iida M, Iwashita A, Yao T, Kitagawa S, Sakamoto K, Tanaka K, Fujishima M (1988) Villous tumor of the colon: correlation of histologic macroscopic and radiographic features. *Radiology* 167: 673–677
- Kohda E, Fujioka M, Ikawa H, Yokoyama J (1986) Congenital anorectal anomaly in CT evaluation. *Radiology* 157: 349–352
- Letourneau JG, Day DL, Steely JW, Goldberg ME (1987) CT appearance of antibiotic-induced colitis. *Gastrointest Radiol* 12: 257–261
- Maglinte DDT, Keller KJ, Miller RE, Chernish SM (1983) Colon and rectal carcinoma: spatial distribution and detection. *Radiology* 147: 669
- Margulis AR, Thoeni RF (1988) The present status of the radiologic evaluation of the colon. *Radiology* 167: 1–5
- Merine D, Fishman EK, Jones B (1987) Pseudomembranous colitis: CT evaluation. *J Comput Assist Tomogr* 11: 1017–1020
- Wall DS, Ominsky S, Altman DF, Perkins CL, Sollitto S, Goldberg HI, Margulis AR (1986) Multifocal abnormalities of the gastrointestinal tract in AIDS. *AJR* 146: 1–5
- Young JWR (1982) The double contrast barium enema: why bother? *Southern Med J* 75: 46–52

---

**PART 5**  
**Genitourinary System**

---

## CHAPTER 33

# RENAL IMAGING: CONGENITAL LESIONS

Nancy S. Curry

---

## RENAL IMAGING

---

### EXCRETORY UROGRAPHY

**Indications.** Excretory urography (commonly termed 'IVP' or intravenous pyelography) is utilized to evaluate a wide variety of urologic disorders including hematuria, trauma, suspected congenital anomalies, neoplasm, obstruction, infection, post-surgical complications, and neurogenic bladder.

**Contrast Media.** The contrast media traditionally used for excretory urography are water-soluble, benzoic acid derivatives which contain three iodine atoms. These agents ionize in solution into two basic particles, the benzoate *anion* carrying the iodine responsible for the radio-opacity of the compound and the *cation* which is usually sodium or N-methylglucamine. The diatrizoate and iothalamate contrast agents are referred to as ratio 1.5:1 compounds because there are three iodine atoms to two particles in solution. They are high in osmolality when compared to plasma (around 1500 mOsm/kg compared to 300 mOsm/kg) which probably accounts for many of the adverse effects associated with them.

Newer contrast agents have been developed which have considerably lower osmolality than the conventional agents. They are referred to as ratio 3:1 agents because they contain three iodine atoms per single, non-ionizing particle in solution. Iopamidol and iohexol are 3:1 agents. Ioxaglate, which is an ionizing dimer, has this same ratio advantage because there are six iodine atoms to two particles in solution. These materials, although more expensive, appear to represent a significant advance in safety and efficacy.

**Physiology.** The small, fully substituted molecules of contrast material are not bound by plasma proteins and are therefore freely excreted by glomerular filtration. Less than

1% is excreted by the liver, small intestine, stomach, salivary, lacrimal and sweat glands. Extrarenal hepatic excretion of contrast can be seen as gallbladder opacification 24 h after excretory urography. This 'vicarious' excretion becomes an important alternative pathway of excretion in the patient with decreased renal function. The accepted standard dose for urography in an adult is approximately 15–25 g iodine (300 mg I/kg body weight). The plasma concentration of intravenously injected contrast media is dependent on the dose delivered, the rate of injection and the body size. A rapid, bolus injection produces a significantly higher peak plasma iodine concentration than slow infusion.

The amount of contrast excreted is determined by the product of the plasma concentration and the glomerular filtration rate. After contrast has passed into the glomerular filtrate, obligatory water resorption in the proximal convoluted tubule increases the contrast concentration 5–10 times, independent of the state of hydration. Under the influence of antidiuretic hormone (ADH), water is further reabsorbed in the distal tubules and collecting ducts producing a concentration of contrast 30–50 times the plasma level. Urinary iodine concentration is somewhat higher with agents which contain sodium as the cation rather than meglumine because the salt is reabsorbed with water in the tubule, whereas meglumine is excreted as an osmotically active particle.

### CONTRAST REACTIONS

The mechanism of contrast reactions is unknown but a number of factors have been suggested including blood–brain barrier interruption, anxiety, activation of the complement and

coagulation systems, histamine and serotonin release, and antigen-antibody formation. Direct chemotoxicity and the marked hyperosmolality of contrast material have been shown to produce physiological changes which affect the cardiovascular, pulmonary, and central nervous systems.

Contrast reactions are generally classified as mild, intermediate, and severe. *Mild* reactions are self-limiting and related to physiological effects, causing nausea, vomiting, heat or cold sensation, sneezing, tachycardia or bradycardia, arm pain and mild urticaria. *Intermediate* reactions include extensive urticaria, angioneurotic edema, bronchospasm, laryngospasm and hypotension; they require treatment but show a rapid response. *Severe*, life-threatening reactions are manifested as cardiopulmonary collapse, pulmonary edema or refractory bronchospasm, laryngospasm and hypotension. Fatalities occur in approximately 1 in 40,000 cases.

**Iodism.** If there is free iodine present in contrast material it will interfere with the performance of radioactive iodine tests of thyroid function. Hyperthyroidism may be induced and salivary gland enlargement ('iodide mumps') may occur several days after the study.

**Risk Factors.** Major risk factors associated with contrast media reactions include:

1. Extremes of age (patients over the age of 60 and under 1 year of age)
2. Previous contrast material reaction
3. Allergy or asthma
4. Cardiovascular disease

Minor risk factors include:

1. Azotemia
2. Diabetes mellitus
3. Dehydration
4. Hemoglobinopathy
5. Dysproteinemia
6. Anxiety

**Pretesting.** Pretesting with small amounts of intravenous contrast material has largely been abandoned because it is not a reliable predictor of reaction. Deaths have been recorded after a negative pretest and have been associated with the pretest itself.

**Pretreatment.** Known prior contrast reactors have a repeat reaction rate of from 15% to 60%. A combination of oral prednisone 50 mg, given every 8 hours for three doses along with ephedrine 25 mg, and diphenhydramine 50 mg, an hour before the study may decrease the repeat reaction rate to 5%. Steroids in conjunction with standard contrast media reduce the mild reaction rate to a level comparable to that attained by using the new contrast agents. There is no proof, however, that steroids reduce the incidence of severe or fatal reactions.

If a previous contrast reaction required intensive treatment and hospitalization, alternate methods of examination such as ultrasound or nuclear imaging may be necessary subsequently. If the prior reaction was not severe and the indications for the contrast study are strong, the pretreatment regimens described above coupled with the use of a low osmolar agent are recommended.

**Nephrotoxicity.** High-dose urography (600 mg I/kg body weight), tomography and delayed filming will result in faint pelvocalyceal opacification despite marked renal failure. Ultrasound has replaced excretory urography in renal insufficiency, however, because contrast materials are nephrotoxic themselves. Slightly less than 1% of hospitalized patients without pre-existing renal disease and 5% of patients with chronic renal insufficiency develop acute renal failure due to contrast toxicity. The effect ranges in severity from asymptomatic, non-oliguric renal dysfunction to oliguric, severe renal failure requiring dialysis, although the latter rarely occurs.

The pathogenesis of contrast material-induced nephrotoxicity is unknown but may be due to a combination of factors including renal vasoconstriction, direct toxic effect on tubular cells, intratubular cast formation and intrarenal obstruction. Risk factors associated with nephrotoxicity of contrast media are *large dose, dehydration, pre-existing renal insufficiency, multiple myeloma and diabetes mellitus*.

Three fourths of diabetic patients with serum creatinine levels between 2 and 5 mg/dl develop acute renal failure after exposure to intravenous contrast. The more severe the level of pre-existing renal insufficiency, the greater the likelihood that contrast-induced changes in renal function will be irreversible. It is important to avoid dehydration in the diabetic patient with compromised renal function if contrast exposure is necessary. Caution is also advised in administering contrast to the patient with multiple myeloma and Bence Jones proteinuria. Renal failure may occur due to deposition of protein casts within the tubules leading to intrarenal obstruction. Again, dehydration must be avoided and contrast studies conducted for only very compelling clinical reasons.

Because contrast agents are uricosuric, patients with hyperuricemia are at risk for the development of acute gouty nephropathy. Alkalizing the urine, increasing fluid intake and administering allopurinol may be helpful in diminishing the potential for induced renal failure.

**Treatment of Contrast Reactions.** The first signs of an impending major reaction may be non-specific such as nausea and vomiting, restlessness, apprehension and agitation. The patient's vital signs should be monitored. *Hypotension*, which usually accompanies intermediate and severe reactions should be treated by supportive measures such as release of compression, elevation of the legs, rapid intravenous fluid administration and oxygen administration. A *rapid* pulse rate suggests that the hypotension is on the basis of an anaphylactoid reaction while a *slow* rate suggests it is due to a vasovagal reaction. This is a vital distinction since a vasovagal reaction requires treatment with *atropine* while the anaphylactoid reaction is more appropriately treated with *epinephrine*. The necessary drugs and equipment should be immediately available because a rapid response is critical in successful resuscitation.

#### EXCRETORY UROGRAPHIC TECHNIQUE

Urographic studies should be tailored to meet the needs of the specific clinical situation. While there is no universal

agreement on the exact timing and sequence of filming, urographic studies should consist of preliminary ('scout') radiographs to include the abdomen and pelvis, serial radiographs up to 15 minutes post-injection of contrast material and post-void and sometimes delayed films.

**Preliminary Film.** A 14" × 17" initial radiograph of the abdomen is obtained centered low enough to include the entire bony pelvis. One purpose of the scout films is to delineate calculi and calcifications in the urinary system which might subsequently be obscured by contrast. When there are suspected renal calculi, an oblique view of the kidney is obtained to verify intrarenal location. Size and position of the kidneys can be assessed and contraindication to compression may be discovered (e.g., calcified abdominal aortic aneurysm).

**Post-contrast Radiography.** Immediately after the intravenous administration of contrast material the concentrating function of the proximal tubules renders the renal parenchyma radiodense resulting in the *nephrogram* phase of the study. This provides the optimum opportunity to evaluate renal size, contour and axis. Tomography is often performed routinely at this time as part of the examination of older individuals to improve anatomic definition (Fig. 33.1). The next radiograph exposed is a 5-minute coned view of the kidneys, when the nephrogram has begun to fade and a *pyelogram* appears. This is evaluated for symmetry and promptness of excretion. At this time if the collecting system is not well seen, a compression device may be applied to provide better distension of the collecting system, provided that there is no contraindication (abdominal aortic aneurysm or recent abdominal surgery). Also oblique views collimated to the kidneys may be helpful. A film of the entire abdomen is made after the compression is removed. Often, because of peristalsis, segments of the ureters are not visualized and additional films with the patient in the prone or upright position may be helpful. When ureteral obstruction is present, upright or prone positioning will cause the contrast material pooling in the dilated pelvis and ureter to 'sink' to the level of obstruction because it has a higher specific gravity than urine. This may eliminate the need for multiple delayed films.

Generally, if the bladder has been adequately included on the abdominal film only a post-void film is necessary to complete the evaluation of the lower urinary tract. Occasionally oblique views of the pelvis are utilized to better image the bladder base and confirm prostatic enlargement in men.

## UROGRAPHIC ANATOMY

**Kidneys.** The size, contour and axis are noted on the immediate films in the nephographic phase. Normal kidneys vary considerably in length from 10 cm to 15 cm depending on age, sex and body habitus. The adult kidney measures between three and four lumbar vertebral bodies in height (inclusive of disk spaces). There should not be a size discrepancy between the kidneys of more than 1.5 cm, although the left kidney has a tendency to be longer by about 0.5 cm. The right kidney is usually situated more caudally than the left because of the presence of the bulk of the liver



Fig. 33.1. Tomogram of nephrogram phase.

cephalad to it. In about 10% of patients the right kidney is positioned higher than the left.

Clefts on the surface of the fetal kidney correspond to separate renal lobes. Developmental fusion of the lobes obliterates the surface markings, but retained fetal lobation often persists in portions of one or both kidneys. These sharp, smooth notches can usually be distinguished from renal scars by their position between calyces (Fig. 33.2). The axis of the kidneys parallels that of the psoas muscles. Shifts in this axis can be secondary to intra- or extrarenal masses, hydronephrosis, malrotation or fusion anomalies.

Renal parenchyma consists of the renal cortex and medulla arranged in a series of lobes. The glomeruli are found in the cortex while the medulla is composed of tubules. Each lobe is a pyramidal structure with the cortex surrounding the medulla except at the tip which projects itself into the calyx. The portion of the calyx surrounding the papilla is the fornix which appears cup-shaped when viewed tangen-



Fig. 33.2. Retained fetal lobation. Note sharp clefts at regular intervals along the lateral surface of the kidney. The capillary phase of a renal angiogram is shown to demonstrate this finding most clearly.

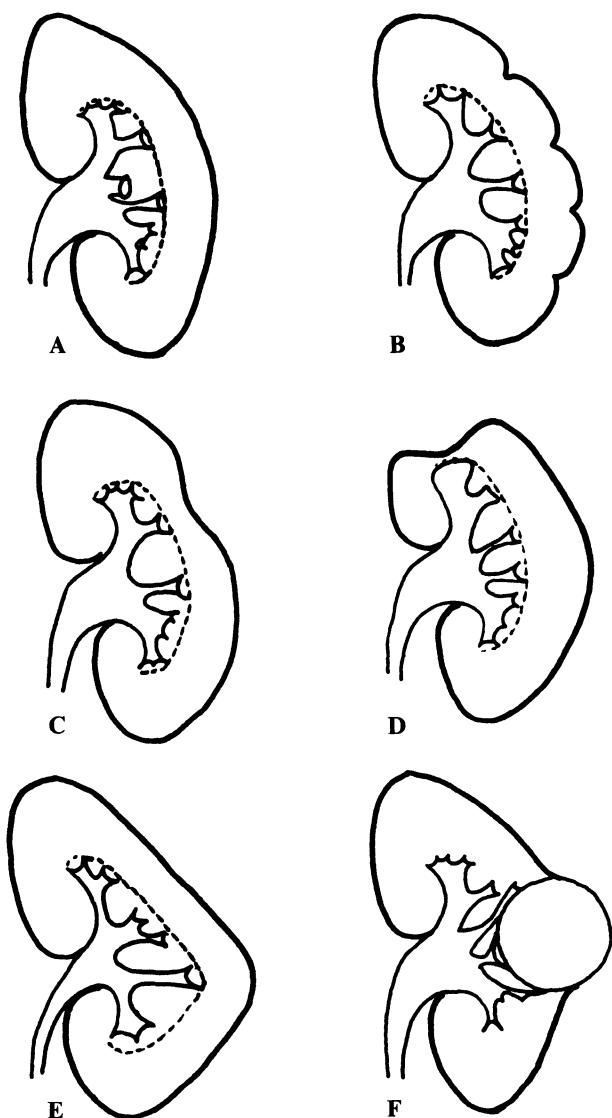


**Fig. 33.3.** Diagram of alterations in renal contour, normal and abnormal. Contour defects due to scar or tumor are identified as focal increase or decrease of parenchymal thickness between the interpapillary line and the outer border of the kidney. **A** Normal kidney. **B** Retained fetal lobation. **C** Focal infarct. **D** Chronic pyelonephritis (reflux nephropathy). **E** Dromedary hump. **F** Renal mass.

tially. Renal parenchyma is thickest at the poles due to lobar fusion. The fused cortical tissue between two adjacent lobes is termed the *septum of Bertin* and the fused papillae of adjacent lobes are called compound papillae.

Parenchymal thickness can be assessed on the urogram by drawing a line connecting the most lateral-projecting papillary tips and comparing it with a line drawn along the cortical margin. The distance between these two lines should be uniform with a slight increase at the poles. Any scars or masses will be readily apparent while normal variants such as a dromedary hump will not be mistaken for a mass (Fig. 33.3).

**Pelvicalyceal System.** The number of calyces may range from one ('unipapillary' kidney) to forty four. Multiple calyces drain into zero to four infundibula which in turn drain

into the renal pelvis. The renal pelvis may be small and intrarenal or large and extrarenal. There are frequently vascular impressions on parts of the collecting systems, particularly on the upper pole infundibulum.

**Ureter.** The ureter originates at the pelvic-ureteric junction lying within Gerota's fascia until it reaches the lumbarosacral region where it enters the anterior pararenal space. It then follows a posterolateral course into the pelvis. Well-developed psoas musculature may displace the upper ureters laterally and the lower ureters medially. There may be a slight medial and anterior deviation of the ureter where it crosses over the iliac vessels, particularly in elderly patients.

**Bladder.** On AP projection the bladder has a round or oval configuration dependent on the degree of filling. There may be smooth mass impressions on the superior surface of the bladder by contiguous bowel or by the uterus in the female. The bladder wall is smooth and its base lies immediately above the symphysis pubis. Overlying gas shadows may mimic filling defects within the bladder; however, this should not be a problem if the film is scrutinized carefully and oblique views will project the gas away from the bladder. Transitory anterolateral protrusions of the bladder into the inguinal rings may be seen normally in infants and in some older female patients. These have been termed 'bladder ears'.

On early filling films of the bladder the *ureteric ridge* may be seen as a thin, uniform radiolucent zone on either side of the contrast-filled intramural ureter. Pathologic processes such as ureteral calculus or tumour may cause this ridge to become swollen or irregular.

## RETROGRADE PYELOGRAPHY

With excellent urographic technique and other imaging methods now routinely available, a retrograde pyelogram is now rarely indicated. Insufficient visualization of the pyeloureteral systems in a patient with unexplained hematuria is one indication. Others include the assessment of the ureter distal to a point of obstruction, investigation of urinary fistulae, and evaluation of the collecting systems and ureters in a patient who cannot undergo intravenous administration of contrast material. Retrograde pyelography is usually performed in the operating room as a follow-up to cystoscopy (Fig. 33.4).

## RETROGRADE LOOPOGRAPHY

After cystectomy, the urinary system may be diverted into a loop of isolated small bowel or colon which is brought out to the skin surface as a stoma. A retrograde study is easily accomplished by catheterizing the loop and infusing contrast. The retrograde route is preferable to excretory urography for the detection of recurrent urothelial carcinoma or leakage. Deteriorating renal function may be due to obstruction, which is readily excluded if the loopogram demonstrates free reflux and prompt drainage of the pyeloureteral systems. Not all loops reflux, however, so that a retrograde obstruction does not necessarily indicate that an antegrade obstruction is present. Excessive infusion pres-



**Fig. 33.4.** Left retrograde pyelogram; normal study.

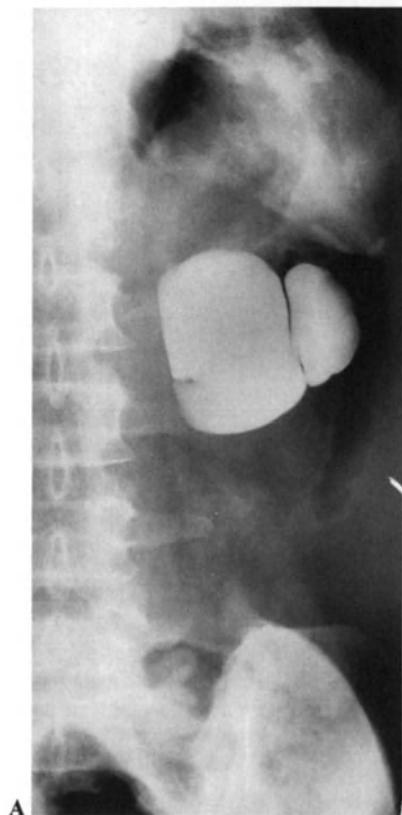
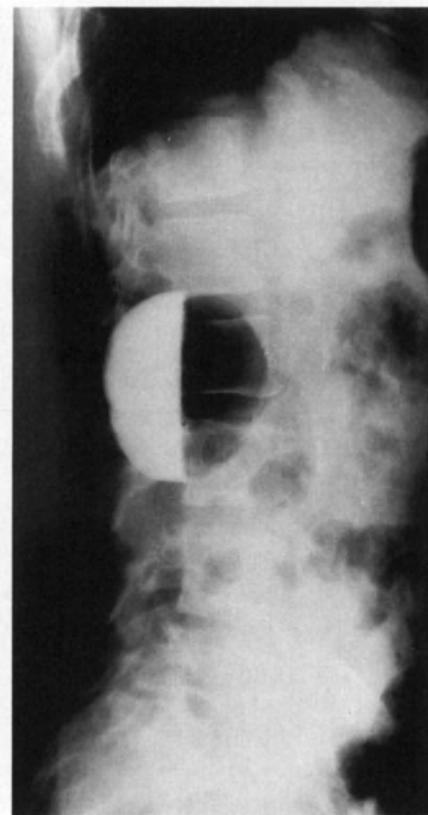


**Fig. 33.5A, B.** Double contrast study of a benign cortical cyst. A AP supine and B cross-table lateral supine views show thin, incomplete septations. These and additional projections not shown (cross-table lateral prone, upright and decubitus views) revealed no mass.



sure and introduced air should be avoided. Glucagon (1 mg i.v.) can be given to inhibit peristalsis in a vigorously hyperactive loop. A post-drainage film is essential.

#### ANTEGRADE PYELOGRAPHY AND PERCUTANEOUS NEPHROSTOMY

**Antegrade pyelography** is performed by the insertion of a small gauge needle into the renal collecting system with aspiration of urine and injection of contrast material. It may be valuable in detecting a level of obstruction or in renal transplant patients. Percutaneous puncture is either fluoroscopically or ultrasonically guided with the patient in the prone position. After pelvic puncture is accomplished, the urine obtained can be sent for appropriate cytologic, bacteriologic and chemical analysis. Contrast material is infused by low-gravity drip to outline the site of suspected obstruction. Upright spot filming may be necessary to achieve this purpose. A *Whitaker test* of ureteral perfusion pressure can be obtained by measuring differential intrarenal/bladder pressures during a steady infusion of fluid through the needle. The normal pyeloureteral system will accept a flow rate of 10 ml/min without exceeding a differential pressure of 13 cm of water with the bladder empty.

**Percutaneous Nephrostomy.** Percutaneous catheterization of the renal pelvis provides temporary drainage of upper

tract obstruction. Assessment of renal function recovery, renal calculus therapy (dissolution, extraction, or disintegration), and creation of access for ureteral stenting, dilation, ablation, or foreign body retrieval are all indications for percutaneous nephrostomy.

The complication rate of percutaneous nephrostomy is low, ranging from 0.7%–4%. *Infection* (superinfection or exacerbation of existing infection) accounts for the largest number of complications. Others include *hemorrhage*, *urinary leakage*, *catheter dislodgement*, and *persistent hematuria*.

#### RENAL MASS PUNCTURE

Unequivocally cystic or solid renal masses rarely require further clarification by needle puncture. Mass puncture is indicated when there are conflicting or indeterminate results from two good-quality imaging studies; when fever or unexplained hematuria are present; and when lymphoma or a primary neoplasm is present elsewhere in the body.

The mass may be punctured using fluoroscopy, ultrasound or CT for guidance. Ultrasound localization is independent of renal function and avoids exposure to radiation and contrast, although it is of limited value in the obese patient, in very small lesions and in masses inaccessible to the ultrasound beam. In the latter cases, more expensive and time-consuming puncture under CT may be necessary.

A small-gauge needle is used to puncture the lesion from a posterior approach to avoid the peritoneum and bowel. Care must be taken in upper pole masses to avoid transgression of the posterior pleural space which may cause a pneumothorax.

If present, aspirated fluid can be sent for microbiologic stains and cultures, chemistry studies (LDH\*, fat and glucose), and cytopathologic evaluation. To ensure that the cyst aspirated corresponds to the whole space-occupying lesion and that there are no filling defects within, contrast infusion is performed. Approximately half of the fluid should be removed and this volume replaced by equal amounts of dilute contrast and air (Fig. 33.5). Over-injection of the cyst is to be avoided because the extravasated contrast may cause pain, fever and perirenal fibrosis.

A clear aspirate with negative cytology and chemistries is indicative of a benign cyst. The presence of *turbid or hemorrhagic fluid* in a non-traumatic puncture suggests the possibility of malignancy. A lesion that yields *no fluid* is usually a neoplasm that will require surgery for definitive diagnosis. Biopsy may be performed when lymphoma or a metastasis from a known primary of other than adenocarcinoma cell type is suspected.

The incidence of major complication associated with mass puncture is 1.4%, including perirenal hemorrhage, pneumothorax, infection, arteriovenous fistula, urinoma formation, and massive hematuria. The theoretical risk of seeding malignant cells along a needle tract has not proved to be significant with the use of small-gauge needles in the kidney.

### ULTRASOUND

Ultrasound of the kidney is used to evaluate renal masses, suspected polycystic kidney disease, hydronephrosis, renal transplants and neonatal kidneys. A 3.5 MHz transducer is used for a large patient while a 5 MHz transducer provides excellent images in the small patient or superficially located transplant.

Transverse and longitudinal scans should be obtained utilizing the liver as an acoustic window on the right (Fig. 33.6). The spleen can be used as an acoustic window to the left kidney, although this is often more difficult to image. The renal cortex has an echo intensity slightly less than that of normal hepatic parenchyma at a similar depth. The medullary pyramids are relatively sonolucent, especially in neonates, and arcuate vessels can sometimes be identified as dense echoes at the corticomedullary junction. The renal sinus generates a very dense, compact echo pattern. Normal renal length in the adult is 9–12 cm. These figures are lower than those derived from urographic measurements because there is no swelling from contrast-induced osmotic diuresis and no artificial enlargement due to geometric magnification.



Fig. 33.6. Normal sagittal ultrasound scan of the right kidney seen through liver.

### COMPUTED TOMOGRAPHY

Axial images of the urinary system obtained by CT are not degraded by overlying tissues as in excretory urography and there is much better contrast resolution. Parenchymal masses which may escape detection on the urogram are readily identified on CT. These include small lesions located on the anterior or posterior surface of the kidney. Spatial resolution is not comparable, however, so that the urogram can be more sensitive in the detection of collecting system abnormalities.

The kidneys are enveloped in fat which is surrounded by the anterior and posterior leaves of Gerota's fascia (Fig. 33.7). The perirenal fat and fascia are clearly evident on CT. Fat lying outside Gerota's fascia is contained in the anterior and posterior pararenal spaces. Without contrast enhancement, the kidneys measure between 30 and 60 Hounsfield units (HU). There is marked increase in attenuation with intravenous contrast and, when it is delivered in a rapid bolus fashion with serial dynamic scans, corticomedullary differentiation is possible.

CT indications include the evaluation of renal masses, obstructive hydronephrosis, retroperitoneal trauma, staging of neoplasms, guidance for biopsy procedures or placement of abscess drainage catheters. CT can also be of great value in the investigation of congenital, inflammatory, and vascular disorders.

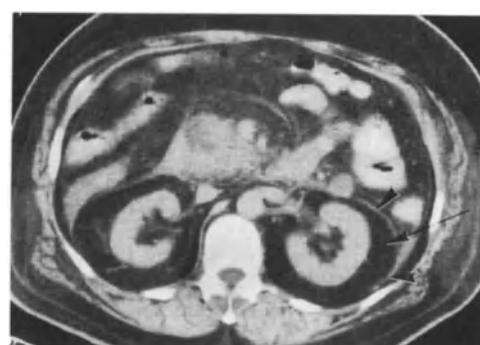
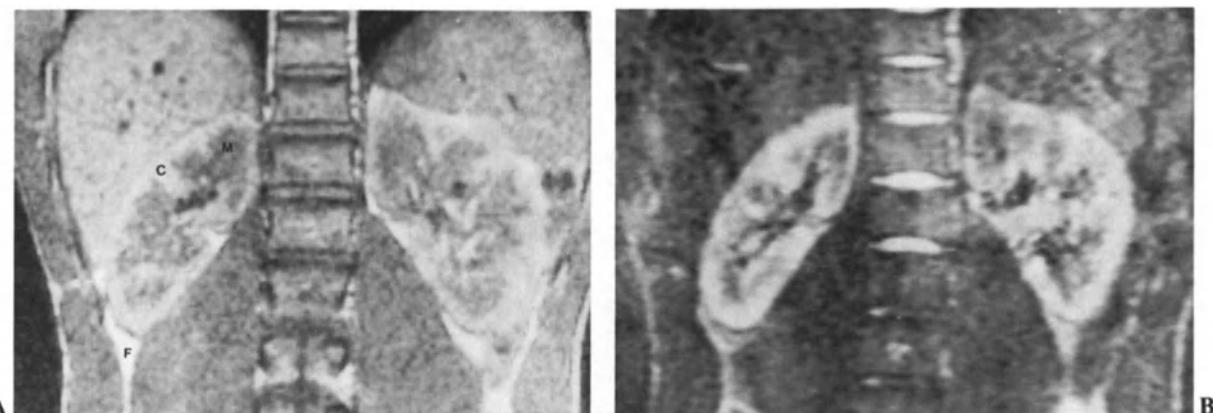


Fig. 33.7. CT scan at the level of the kidneys without intravenous contrast material in a patient with an inflammatory pancreatic mass. Retroperitoneal edema accentuates Gerota's fascia (arrowheads) enclosing the fat in the perirenal space (arrow) in an obese patient.

\*Lactic dehydrogenase



**Fig. 33.8A, B.** Magnetic resonance image of normal kidneys, coronal section, spin echo technique. A T<sub>1</sub>-weighted image (600/20 ms, 1.5T) demonstrates low intensity signal from the medulla (M) relative to the cortex (C). Perinephric fat (F) has high signal intensity. B T<sub>2</sub>-weighted image (2000/80 ms, 1.5T). Corticomedullary differentiation is not seen.

### MAGNETIC RESONANCE IMAGING

The appearance of the renal parenchyma varies according to the imaging technique and pulse parameters utilized. On T<sub>1</sub>-weighted images the cortex and medulla can be differentiated because the medulla has a lower signal intensity (Fig. 33.8). Vascular structures are seen as areas of signal void. The renal pelvis may be detectable as an area of low signal intensity while perirenal fat shows high signal intensity. At present MRI is not utilized as a primary imaging modality because of limitations in spatial resolution and high cost.

### SCINTIGRAPHIC IMAGING

*Cortical imaging* is performed by technetium-99m DMSA (dimercaptosuccinate) or technetium-99m glucoheptonate. These agents are selectively taken up by the renal tubular cells. Only the renal parenchyma is imaged since very little

tracer is excreted into the urine. Cortical scintigrams are useful in the evaluation of renal scars and pseudotumors.

*Radionuclide angiography* is part of a <sup>99m</sup>Tc-DTPA (diethylene-triamine pentaacetic acid) study. The abdominal aorta and renal parenchyma are imaged in rapid sequence on the gamma camera providing assessment of renal perfusion. Subsequent excretory studies provide images analogous to excretory urography since <sup>99m</sup>Tc-DTPA, like contrast material, is handled primarily by glomerular filtration. Spatial resolution, however, is poor compared to excretory urography. A *renogram* of time-activity curves can be plotted for each kidney providing quantitative differential function assessment.

<sup>131</sup>I-Hippuran renal scans are useful in the evaluation of *tubular function* since this agent is almost entirely extracted by the renal tubules with little glomerular filtration.

<sup>99m</sup>Tc-DTPA and <sup>131</sup>I-Hippuran scans are utilized in the evaluation of *renal transplants, children, and patients with contraindication to contrast materials*.

---

## CONGENITAL ANOMALIES

---

### KIDNEYS

*Embryology.* Development of the fetal kidney starts with generation of a ureteral bud from the mesonephric duct at approximately four weeks. It grows cephalad into undifferentiated mesenchyme inducing the renal anlage. The kidneys ascend from their initial pelvic position to reach the upper abdomen, eventually rotating to bring the anterior renal pelvis into an anteromedial position. During ascent, the kidneys derive their blood supply from the iliac vessels and abdominal aorta, successively adding more cranial vessels and dropping the more caudal supply as upward migration proceeds.

**Renal Agenesis.** Failure of both kidneys to develop is a rare event which is not compatible with life. Lack of urine produc-

tion in utero results in oligohydramnios and pulmonary hypoplasia. These infants have the characteristic Potter's syndrome facies with prominent medial canthal fold, flattened nose, low-set ears, hypertelorism and micrognathia.

Renal agenesis may occur as a result of failed development of the ureteral bud, the Wolffian duct, or the nephrogenic mesenchyme, or from lack of induction of nephrogenic blastema by the ureteral bud. Unilateral agenesis has a radiographically detected incidence of approximately 1:1800. The ipsilateral adrenal gland develops normally most of the time but in 10% of cases there is adrenal agenesis as well. Associated genital tract anomalies occur in 25%–50% of females who may have a unicornuate or bicornuate uterus, absent or hypoplastic vagina, ovaries or fallopian tubes. In males with unilateral agenesis, ipsilateral hypoplasia of the

seminal tract or testis may be found. Additional associated anomalies include imperforate anus, tracheoesophageal fistula, esophageal atresia, rectovaginal fistula, omphalocele, Meckel's diverticulum, skeletal anomalies, and pancreatic agenesis.

**Radiographically**, the empty renal fossa is occupied by neighboring organs such as liver, spleen, pancreas, and large and small bowel. The solitary kidney demonstrates compensatory hypertrophy. On **ultrasonography**, the adrenal gland appears enlarged and has a characteristic oblong shape with an echogenic medulla and anechoic cortex. On **cystoscopy**, a hemitrigone with only one ureteral orifice is noted in one half of cases. When the trigone does develop normally, the ureteric orifice is absent or blind.

**Supernumerary Kidney.** Very rarely, more than two separate renal units may develop. As many as five kidneys in one individual have been reported. The supernumerary kidney may be hypoplastic or dysplastic and there are frequently other urogenital abnormalities.

**Renal Hypoplasia.** True congenital renal hypoplasia is rare. There is a reduced number of nephrons, lobes and calyces. More often, a hypoplastic appearing kidney reflects an acquired condition such as reflux nephropathy, post-obstructive atrophy, or ischemia. The true hypoplastic kidney may be ectopic, will have five or fewer calyces, and possesses a uniformly small renal artery. The contralateral kidney exhibits compensatory hypertrophy. Bilateral hypoplasia will result in renal failure in childhood and may be very hard to distinguish from acquired renal disease.

**Renal Dysplasia.** Dysplasia is a maldevelopment of the kidney which can affect the whole kidney or only a portion of it. The parenchyma contains primitive nephrons, cartilage and cysts. The condition may be related to congenital obstruction or ureteral bud anomalies.

**Multicystic Dysplastic Kidney.** This extreme, classic form of renal dysplasia is thought to be due to collecting system atresia occurring early in fetal development, usually before 8 to 10 weeks. Enlarged collecting tubules form cysts with intervening undifferentiated mesenchyme and fibrovascular tissue but no recognizable renal tissue. The cysts do not communicate, there is no renal function, and the ureter is either absent or atretic. The incidence of multicystic dysplastic kidney is approximately 1:4300 live births.

If the intrarenal obstruction occurs later in fetal life, between week 10 and 36, a hydronephrotic form of multicystic dysplastic kidney (MCDK) results. There is cyst formation, pelvic and calyceal dilatation and a lesser degree of renal dysplasia. After 36 weeks of gestation, a hydronephrosis without dysplasia results from obstruction.

Prior to the availability of prenatal ultrasound, multicystic dysplastic kidney usually presented as an abdominal mass in the neonatal period. On **plain films** the mass displaces loops of bowel medially and anteriorly. **Ultrasound** demonstrates the disorganized arrangement of cysts of varying size with no definable renal pelvis, sinus or parenchymal tissue (Fig. 33.9). The hydronephrotic form of the disorder can produce an appearance difficult to distinguish from simple hydronephrosis. **Excretory urography** will not demonstrate function although there may be faint opacification of the cyst walls. In the hydronephrotic form of MCDK some function



Fig. 33.9. Multicystic dysplastic kidney, ultrasound examination. Distinguished from hydronephrosis by non-communication of cysts, no visible parenchyma and lack of a dilated central pelvis. (Courtesy of R. MacPherson.)

remains and a parenchymal rim may be observable. **Radioisotope scanning** provides useful information on the degree of renal function present.

When detected in adulthood, MCDK may be associated with calcification in the cyst walls (Fig. 33.10). The fate of multicystic kidneys left *in situ* is not well-documented. Some investigators believe that the natural history involves cyst shrinkage and involution. Some cases of unilateral renal agenesis in adults may in fact represent the end result of spontaneous involution of a multicystic kidney.

Multicystic dysplastic kidney is associated with abnormalities of the contralateral kidney in almost one third of cases. Most often the abnormality is a *pelvi-ureteric junction obstruction*.

**Congenital Megacalyces.** In this condition, the renal parenchyma appears thinned while the calyces appear widened and polygonal in contour. This appearance is due to congenital underdevelopment of the medulla in which the medullary tips are flattened rather than conical. The renal pelvis is normal. Parenchymal thinning is due to reduced mass of medullary tissue with the cortex remaining normal. There may be an increase in number of calyces (polycalyces)

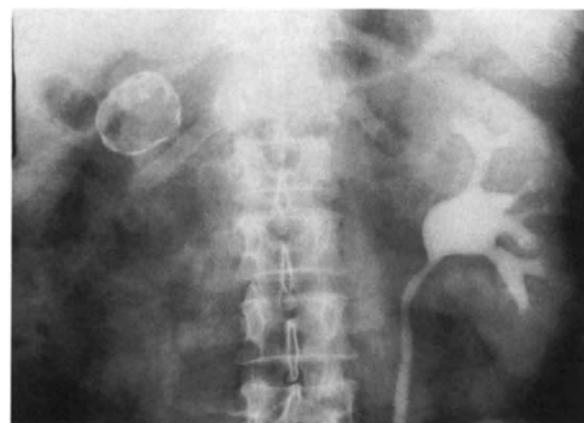


Fig. 33.10. Multicystic dysplastic kidney, adult. Calcified cyst walls in a non-functioning right kidney. Retrograde pyelography showed atretic right ureter (not shown). Note compensatory hypertrophy on the left.



**Fig. 33.11.** Pelvic kidney. The collecting structures of the left kidney project over the sacrum.



**Fig. 33.12.** Crossed ectopia without fusion. Fusion of the kidneys at the adjacent poles is the more usual situation.

as well. The condition may be unilateral or bilateral. The diagnosis is one of exclusion because post-obstructive atrophy or reflux nephropathy could lead to similar findings.

Patients with congenital megacalyces have normal renal function, although some patients demonstrate a concentrating defect. The dilated calyces predispose to the development of stasis, infection and calculus formation.

**Renal Ectopia.** In its embryonic ascent from the pelvis, the kidney may become arrested at an abnormal location. Usually only one kidney is affected although there may be bilateral failure of ascent. The *pelvic kidney* derives its blood supply from the lower abdominal aorta or iliac vessels. It may be distinguished from a ptotic kidney by the presence of a shortened ureter and malrotation. A pelvic kidney may be difficult to visualize on urography (Fig. 33.11). Because of its position, the pelvic kidney may be mistaken for a gynecologic mass. Obstruction or infection of a pelvic kidney may result in a confusing clinical presentation causing mistaken diagnosis of *appendicitis* or *salpingitis*. Preoperative urography or ultrasonography will identify the anomalous renal position.

The kidney also may continue upward migration to become a *thoracic kidney*. Nearly always, however, the thoracic kidney occurs as a result of herniation through a defect in the diaphragm, either through a Bochdalek hernia or a traumatic rupture of the diaphragm.

**Crossed ectopia** occurs when the kidney migrates to the opposite side of the abdomen while the ureteral orifice remains on the ipsilateral side. In 90% of cases the crossing kidney fuses to the lower pole of the opposite kidney, termed *crossed fused ectopia*. Crossed ectopia without fusion is rare (Fig. 33.12) and crossed ectopia with a solitary kidney is extremely rare. The embryogenesis of this anomaly is uncertain but may be due to the ureteral bud crossing with induced formation of the kidney from the contralateral nephrogenic blastema. Alternatively, the kidneys may fuse during ascent into the abdomen and both migrate cephalad to one side.

**Malrotation.** The kidney may underrotate, overrotate or reverse rotate in the normal or ectopic kidney. The most common abnormality is underrotation where the renal pelvis maintains its *anterior* location.

**Fusion Anomalies.** The most common fusion anomaly is the *horseshoe kidney* which is found in the general population with an incidence of 1:400 to 1:750. In this anomaly, the lower poles of the kidneys are fused by bridging parenchyma or occasionally by a fibrous band. The individual is likely to be otherwise normal, although there is an increased incidence of Wilms' tumor. The kidneys are often low in position with the renal pelvis lying anteriorly and lower pole calyces pointing medially (Fig. 33.13). The vascular supply is anomalous with multiple vessels supplying the parenchyma from multiple aortic or iliac sites. *Radionuclide studies* and



**Fig. 33.13.** Horseshoe kidney, excretory urogram. Note abnormal axis of the kidneys with lower pole calyces pointing medially.



**Fig. 33.14.** Complete right ureteral duplication.

computed tomography can demonstrate whether the bridging tissue is parenchyma or not. This may be of importance if division is contemplated at surgery for complications of the condition. *Hydronephrosis, stasis, infection and stone formation* may all occur because the ureters have to course over the fused tissue.

#### URETER

**Duplication.** Occurring in approximately 2% of the population, duplication is the most common anomaly of the upper urinary tract. It occurs when two ureteral buds arise from the mesonephric duct. Complete duplication refers to the presence of two ureters which enter the bladder through separate orifices (Fig. 33.14). The ureter draining the upper pole segment opens medially and inferior to the orifice of the lower pole segment (*Meyer–Weigert rule*). The shorter, more perpendicular intramural course of the lower pole ureter predisposes it to reflux while the upper pole ureter may become obstructed if associated with a ureterocele.

The duplicated or partially duplicated kidney is significantly larger than a normally developed kidney. Because lobar fusion is not uniform where the two portions of the duplex kidney join, the septal cortex lying between the two systems may appear prominent enough to cause a mass effect. This normal variant has been termed **renal pseudotumor**, heterotopic cortex, hypertrophied septum of Bertin or lobar dysmorphism. If necessary, a *radionuclide scan* or *CT* will demonstrate the presence of normal functioning renal tissue.

Incomplete duplication occurs when ureters from two separate pelvises join somewhere along their course with only one ureteral orifice. With a high ureteral junction, peristalsis initiated from one pelvis may be propagated in a retrograde

fashion up into the other pelvis. The alternative filling and emptying of each system into the other is visualized fluoroscopically as the so-called 'yo-yo' phenomenon.

**Ectopic Ureter.** Malpositioning of the ureteral bud off the mesonephric duct ultimately results in ureteral ectopia. Most cases occur in females with completely duplicated systems but a single ureter may be ectopic as well. In females the ureteral orifice may be found in the urethra, vagina, vestibule, cervix, uterus, fallopian tubes or bladder neck with consequent continuous *urinary incontinence* (Fig. 33.15). In males, the ectopic ureter is always found above the external sphincter so that incontinence is not a feature. The ureter may open into the prostatic urethra, ejaculatory duct, seminal vesicle, or vas deferens.

*Reflux, obstruction and dysplasia* of the ipsilateral kidney is associated with ectopic ureters which will be reflected in imaging studies obtained on these individuals. When the upper pole system is obstructed and dilated, there is displacement of the lower pole structures laterally and inferiorly. This has been referred to as the '*drooping lily*' appearance (Fig. 33.16). Too few calyces, absence of calyces serving the upper pole, and lateral displacement of the upper ureter are additional signs suggesting upper pole obstruction.

**Ureterocele.** A *simple, adult-type ureterocele* is a congenital cystic dilation of the distal ureter with prolapse into the bladder. The condition is found in females more frequently than males. Unlike the ectopic ureterocele of infancy (see below),

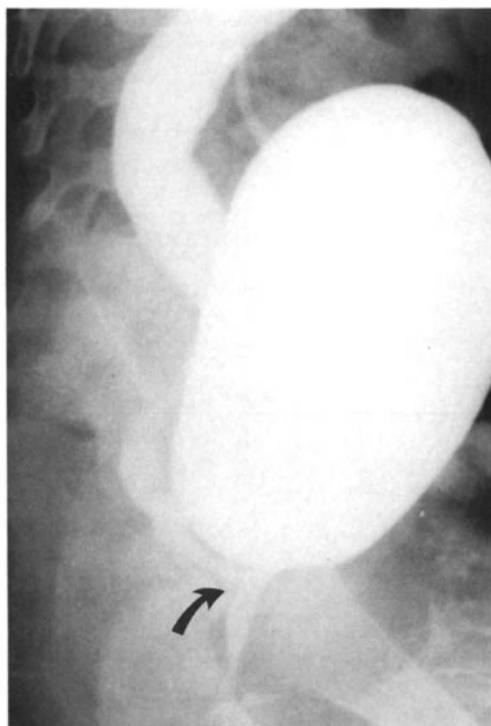


**Fig. 33.15.** Ectopic ureter. Voiding cystourethrogram demonstrates reflux into the right ureter which opens ectopically into the urethra (arrow). (Courtesy of R. MacPherson.)

the ureter is usually not duplicated and the orifice is normally located. On *excretory urography* the walls of the dilated ureter are seen as a thin, uniform lucency outlined on the outside by contrast material in the bladder and on the inside by contrast material in the dilated distal ureter. A 'spring onion' or 'cobra head' appearance results (Fig. 33.17). If the ureter is not filled with contrast, the collapsed ureterocele will appear as an ovoid filling defect. Although usually asymptomatic, ureteroceles may be associated with *calculi* and *obstruction*.



**Fig. 33.16.** Obstructed, duplicated left upper pole system. Excretory urogram shows 'drooping lily' configuration of the left lower pole pelvis and calyces.

**Pseudoureteroceles** are created by tumor, inflammation or edema associated with distal ureteral calculi at the ureteroovesical junction. They can be distinguished from true ureteroceles because the wall is thick and irregular.

An **ectopic ureterocele** is almost always associated with the upper pole of a completely duplicated collecting system. Urographic findings are summarized in Table 33.1. The condition may be bilateral in 10% of cases. The ureterocele can be characterized as a cystic ballooning of the lower end of the ureter which lies between the bladder mucosa and the detrusor musculature. Its orifice is located distal to the trigone, at the bladder neck or in the urethra. It may be visualized on urography or cystography as a radiolucent filling defect in the bladder and may be large enough to obstruct the contralateral ureteral orifice (Fig. 33.18). A filling defect will not be seen, however, when intravesical pressure is sufficient to collapse or evert the ureterocele, in which case it may sometimes resemble a bladder diverticulum.

**Table 33.1.** Urographic findings in ectopic ureterocele

Contralateral duplication in 50%
Rotation of renal axis
Displacement of lower pole system ('drooping lily' configuration)
Reduced number of calyces
Lateral displacement of the proximal lower pole ureter by the dilated upper ureter
Radiolucent bladder filling defect

The upper pole frequently demonstrates dysplasia or post-obstructive atrophy with little or no function. In these cases, the kidney appears normal in size and only subtle changes will be evident in the urogram.

*Ultrasound* will demonstrate hydronephrotic collecting structures, if present. The lower pole ureter has a normally positioned orifice; however distortion and displacement by the ureterocele can shorten the intramural course of the ureter, which predisposes it to reflux.

Various types of ectopic ureteroceles have been described. The *stenotic* type have a narrowed orifice, the *sphincteric* type terminate in the internal sphincter and the *sphincterostenotic*



**Fig. 33.17.** Bilateral simple, adult-type ureteroceles. Note lucent halo around the distal ureters and bilateral 'jets' of contrast squirting from each orifice into the less opacified bladder urine.



► Fig. 33.18. Ectopic ureterocele associated with an obstructed, duplicated right upper pole system. The ureterocele is visualized as a large filling defect in the bladder. (Courtesy of R. MacPherson.)



Fig. 33.20. Retrograde pyelogram in congenital PUJ obstruction. The ureter is normal in caliber with massive dilation of the renal pelvis.

type have a stenosed orifice with prolapse into the proximal urethra. Embryologically, these conditions occur either due to persistence of a sheet of epithelium (Chwalle's membrane) covering the ureteral orifice or due to failure of the ureteral orifice to expand.

**Primary Megareter.** *Hydroureter* is the term used to describe ureteral dilatation with a known cause, such as obstruction, reflux, pregnancy or excess fluid processing (diabetes insipidus). The term **megareter** should be used in instances of congenital dilatation of the ureter without such a cause. The ureteral dilatation may be unilateral or bilateral and is usually segmental, frequently involving the *distal one-third* of the ureter. Although the cause is unknown, it is

thought to be related to abnormal ureteral wall musculature. The abnormal portion of the ureter is aperistaltic, creating a functional obstruction.

**Congenital Hydronephrosis.** Congenital obstruction at the pelvi-ureteric junction (PUJ) is usually detected in childhood although it occasionally is seen in the adult. The etiology is unknown and although congenital bands, adhesions, and aberrant vessels have all been suggested, the abnormality is functional rather than anatomic. Ineffective peristalsis in an extrarenal pelvis may lead to incomplete pelvic emptying and hydronephrosis which can progress to severe obstructive atrophy.

The *imaging* findings are variable, with the most severe cases demonstrating marked hydronephrosis with severe parenchymal atrophy, readily identified by *ultrasound* or *CT* (Fig. 33.19). An *excretory urogram* will show non-function and a mass on the affected side with compensatory hypertrophy of the normal kidney. A *retrograde pyelogram* will show a normal caliber ureter abruptly filling a massively dilated renal pelvis (Fig. 33.20). In lesser degrees of obstruction, glomerular filtration continues as a result of increased lymphatic uptake, tubular water resorption and fornecal micro-tears with urine leakage into interstitial and vascular spaces. On *urography*, there is renal enlargement and a negative pyelogram as the residual thin parenchyma enhances around the unopacified, dilated pyelocalyceal system. Calyceal 'crescent' may be seen, representing opacifying dilated tubules stretched over the rounded calyces (Fig. 33.21).

With collecting system dilation, *ultrasound* demonstrates a central dilated pelvis extending into uniformly arrayed,

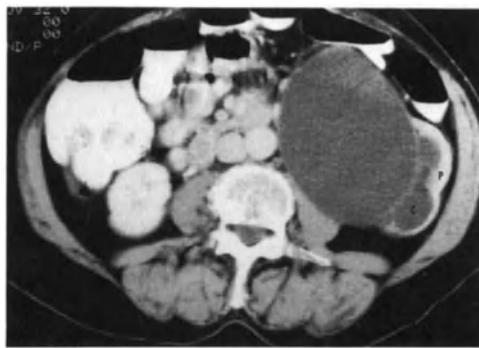
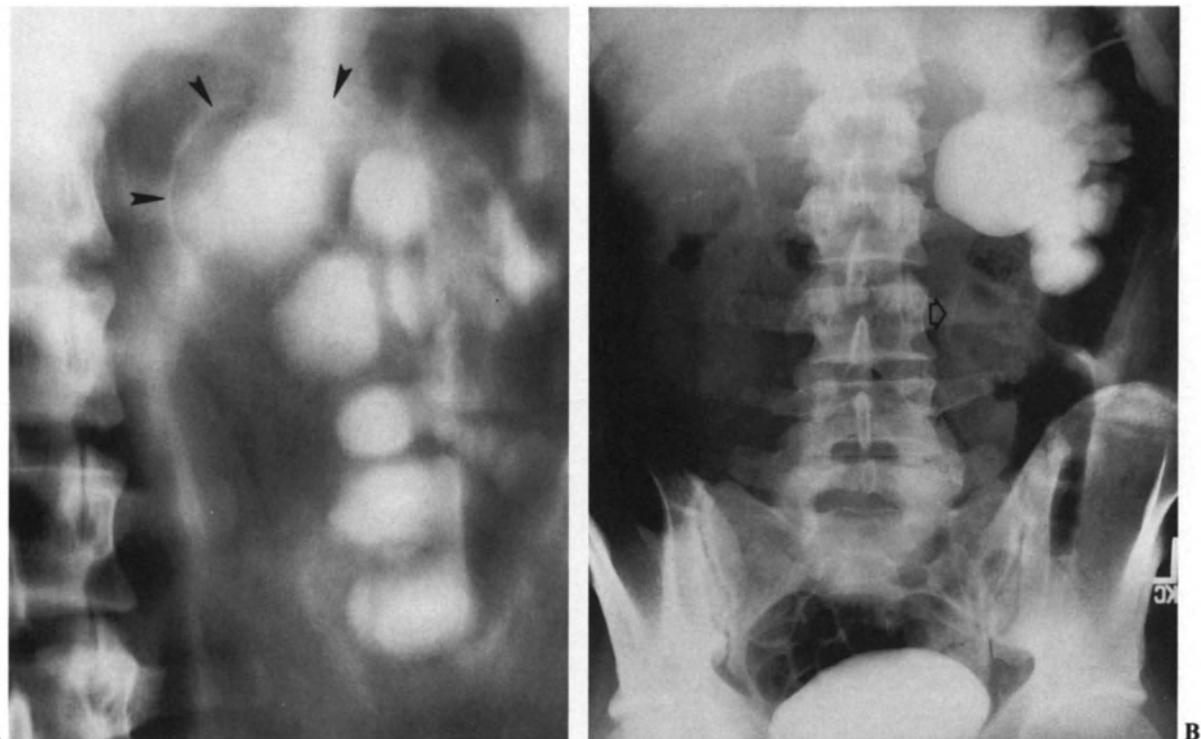


Fig. 33.19. CT scan of a patient with severe post-obstructive atrophy of the left kidney due to congenital PUJ obstruction. Parenchyma is reduced to a thin rim of non-functioning tissue. (P, parenchymal rim; c, dilated calyx.)



**Fig. 33.21A, B.** Excretory urogram in congenital PUJ obstruction. A Tomogram demonstrates calyceal crescents (arrows) and beginning opacification of markedly dilated calyces. B Later film shows hydronephrosis.

peripheral dilated calyces. While these ultrasound characteristics exclude tumor, they can also be seen in reflux nephropathy, congenital megacalycosis, diuresis, and diabetes insipidus. The hydronephrotic form of multicystic dysplastic kidney may also mimic PUJ obstruction. In equivocal cases *diuresis radionuclide studies* and *percutaneous Whitaker testing* may be helpful in evaluation.

**Retrocaval Ureter.** In the normal situation, the ureter lies anterior to the vena cava. During the complex development of the cava, anomalous persistence of the subcardinal portion of the vena cava results in an abnormal course of the right ureter. It passes posteriorly behind the cava taking an abruptly medial course at the level of L3, passing between the vena cava and aorta (Fig. 33.22). The ureter then assumes its normal position distally. Hydronephrosis may result from this anomaly. Vascular maldevelopment may also result in a retroiliac ureter.

**Rudimentary Branched Ureter.** Probably representing an abortive attempt at complete ureteral duplication, the rudimentary branched ureter is an unusual finding. The proximal portion is blind-ending (Fig. 33.23). Solitary ureteral diverticula probably represent dilated, blind-ending rudimentary ureters. In this setting urinary stasis can result in infection or calculus formation.



#### BLADDER AND URETHRA

**Duplication of the Bladder and Urethra.** Complete, side by side, bladder and urethral duplication is a rare anomaly associated with other abnormalities, especially of the lower

◀  
**Fig. 33.22.** Retrocaval ureter. The looped catheter lies within the inferior vena cava. The ureter courses medially and posteriorly to it. (Courtesy of W. Goodwin.)



**Fig. 33.23.** Rudimentary branched ureter on left with blind ending.  
(Courtesy of C. Griffin.)

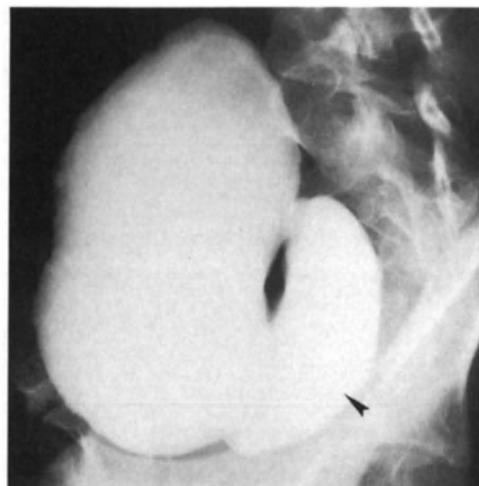


**Fig. 33.25.** Bladder diverticulum (arrow). Cystogram in right posterior oblique position.

gastrointestinal tract. Each bladder receives the ureter of the ipsilateral kidney. When incomplete duplication occurs, the bladders share the same bladder neck and urethra. A complete or incomplete sagittal septum, consisting of a muscular or mucosal membrane, may also divide the bladder into chambers of equal or unequal size.



**Fig. 33.24.** Extrophy of the bladder. Note widened symphysis pubis (arrows), solitary left kidney with hydroureteronephrosis.

An '*hourglass*' bladder results when the bladder is divided into upper and lower chambers by a fibromuscular ring with the ureters opening into the lower segment. It may be distinguished from a vesical diverticulum or urachal diverticulum because both chambers contract during voiding while the diverticula, having no muscular wall, will distend with bladder contraction.

A *double urethra* in the male refers to complete duplication in a single penis. The accessory urethra usually lies dorsal to the normal ventral urethra. Complete duplication of the female urethra with a single bladder is extremely rare.

**Extrophy-Epispadias Complex.** Extrophy of the bladder is a very rare congenital anomaly with a 2:1 male predominance. The complex varies in severity from epispadias to the full-blown extrophy complex in which the bladder lies open on the anterior abdominal wall with associated anomalous development of the pelvis. There are varying degrees of outward rotation of the iliac bones, and outward rotation and widening of the pubic bones (Fig. 33.24). Generally, only symphysis pubis diastasis is seen in epispadias. The upper urinary tracts may be normal. There is a significant incidence of bladder carcinoma in the surgically inverted bladder extrophy. In some cases, the patient must undergo urinary diversion.

**Bladder Diverticula.** Most bladder diverticula occur at the ureteroovesical junctions (Hutch diverticula) and represent herniation of the bladder mucosa through defects in the detrusor musculature (Fig. 33.25). These congenital areas of weakness become apparent in situations resulting in high intravesical pressures such as bladder outlet obstruction, posterior urethral valves, or neurogenic dysfunction.

Bladder diverticula assume clinical importance when they become the setting of *infection*, *calculus formation* or *tumor*. Large bladder diverticula sometimes cause medial deviation of the distal ureters. A ureter may enter directly into a diverticulum or adjacent to it with resultant vesicoureteral reflux. During voiding, as the bladder wall contracts, urine distends the diverticulum since it has no muscular wall of its own.

A striking degree of residual urine can be seen within a diverticulum on a post-void radiograph.

**Urethral Diverticula.** Most urethral diverticula are acquired rather than congenital as a result of strictures, abscess or instrumentation. Saccular or diffuse diverticula can occur congenitally in the male with compression and obstruction of the urethra.

**Prune Belly Syndrome (Eagle Barrett Syndrome).** Nearly always affecting males, the classic prune belly syndrome consists of deficient anterior abdominal wall musculature, undescended testes, and urinary tract abnormalities which usually involve dilatation. The condition is rare, occurring in approximately 1:29,000 live births. Cases of hypoplastic abdominal musculature have occurred in female infants but they do not have the associated genitourinary tract abnormalities. Theories of etiology include in utero urinary tract obstruction, massive temporary fetal ascites, and aberrant mesenchymal development but none satisfactorily explains all elements of the syndrome. Other anomalies frequently associated with prune belly syndrome include abnormalities of the gastrointestinal tract, musculoskeletal system and cardiovascular system.

The newborn infant with prune belly syndrome presents with wrinkled, prune-like appearance of the abdominal wall. The accompanying urinary tract abnormalities vary in extent and severity. Bilateral cryptorchidism and infertility are consistently present. Of affected newborns, 20% are stillborn or die in the neonatal period due to renal dysfunction or pulmonary hypoplasia secondary to oligohydramnios. Another 30% die within two years of renal failure or urosepsis. Long-term survivors with less severe renal involvement have been reported.

The kidneys show various degrees of dysplasia. The ureters are tortuous and demonstrate dilatation ranging from minimal to extreme with peristalsis which is poor to non-existent. Ureteral dilatation is more pronounced in the distal portions of the ureters. Obstruction is usually not a feature but vesicoureteral reflux is present in 70% of cases (Fig. 33.26). The bladder is large and irregular and frequently has coexistent urachal abnormalities. Urodynamic studies have not shown obstruction at the bladder outlet in the majority of cases. The prostatic urethra is characteristically widened and elongated at the bladder neck. Enlargement of the urethra (megalourethra) may occur.

**Urachal Abnormalities.** The primitive connection between the bladder and the allantois is the *urachus*. Failure of the urachus to regress results in four distinct abnormalities.

A *patent urachus* is an open, draining communication from the bladder to the umbilicus. This communication can be demonstrated on voiding cystography.

Closure of the communication at both ends of the tract entraps fluid within a *urachal cyst* which may become infected.

When the vesical end of the tract is closed, the persistent tract to the umbilicus is a *urachal sinus*.

Closure at the umbilical end results in a *urachal diverticulum*. The latter abnormality is frequently found in the prune belly syndrome.

**Posterior Urethral Valves.** Posterior urethral valves are usually discovered on prenatal ultrasonography, in the

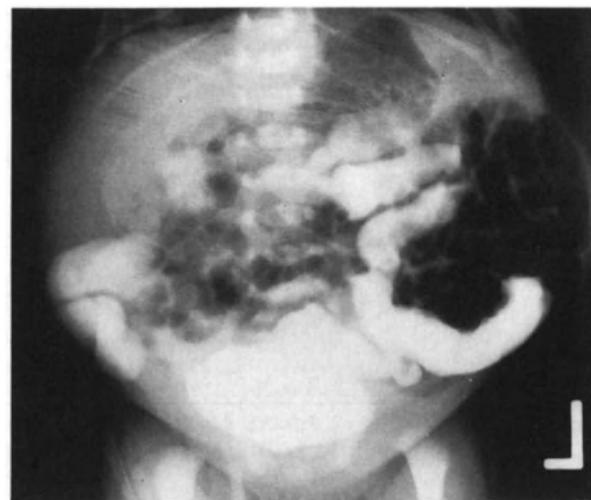


Fig. 33.26. Prune belly syndrome. Note bulging flanks due to abdominal muscle deficiency and marked, bilateral hydronephrosis due to reflux. (Courtesy of R. MacPherson.)

neonate or during the first year of life. The vast majority (Type 1), are *mucosal folds* that extend anteriorly and inferiorly from the lowermost aspect of the verumontanum. The folds fuse from dorsal to ventral, leaving a ventral aperture. Variable degrees of obstruction result. A narrow opening obstructs the outflow of urine from the bladder with resulting detrusor hypertrophy.

The bladder becomes trabeculated with saccule and diverticula formation and the posterior urethra becomes dilated to the level of the valves (Fig. 33.27). A pronounced posterior ridge of tissue at the bladder neck due to hypertrophy (described as Type 2 valves in older literature) is probably the result of obstruction rather than the cause of it. Detrusor hypertrophy from valves is associated with vesicoureteral reflux or bilateral ureteral obstruction.

The sometimes massive hydronephrosis may lead to leakage of urine into the perirenal space (perinephric

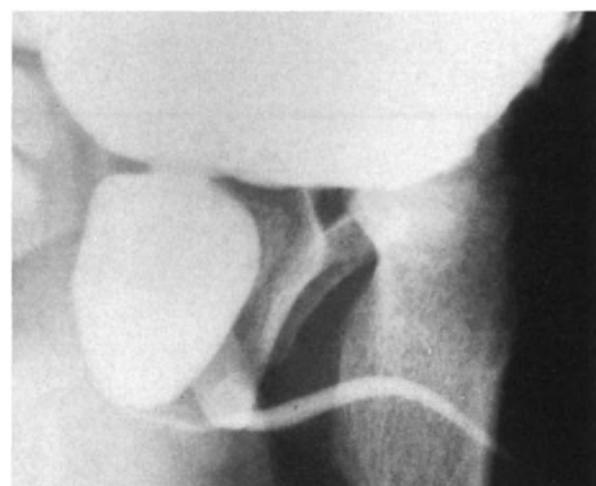


Fig. 33.27. Posterior urethral valves in a male infant. Note the marked dilation of the prostatic urethra.

urinoma) or peritoneal cavity (urine ascites). If the reflux occurs in utero, varying degrees of renal dysplasia may result. The combination of dysplasia, reflux, obstruction, and infection may ultimately lead to renal failure if measures to correct these abnormalities are not instituted.

*Ultrasonography* is a valuable diagnostic tool before or after birth. *Voiding cystourethrography* definitively demonstrates the valves ballooning on micturition with abrupt change in caliber of the urethral stream. *Excretory urography* demonstrates the severity of hydroureteronephrosis when renal function is normal. *Renal radionuclide studies* provide functional information and diuretic radionuclide renography may help distinguish between obstructive and non-obstructive hydroureteronephrosis.

**Anterior Urethral Valves.** Anterior urethral valves are rare congenital urethral obstructions frequently associated with urethral diverticula. They may be due to abortive urethral duplications and occur just proximal to the penoscrotal junction.

#### REFERENCES AND SUGGESTIONS FOR FURTHER READING

##### RENAL IMAGING

- Berkseth RO, Kjellstrand CM (1984) Radiologic contrast-induced nephrotoxicity. *Med Clin North Am* 68: 351–356
- Cohen RH, Dunnick NR, Bashore TM (1988) Treatment of reactions to radiographic contrast material. *Radiology* 151: 263–268
- Davidson AJ (ed) (1985) *Radiology of the Kidney*. W.B. Saunders Co., Philadelphia
- Dyer RB, Munitz HA, Bechtold R, Choplin RH (1986) Abnormal nephrogram. *Radiographics* 6: 1039–1046
- Fischer HW, Doust VL (1972) An evaluation of pretesting in the problem of serious and fatal reactions to excretory urography. *Radiology* 102: 497–502
- Friedland GW, Filly R, Goris ML, Gross D, Kempson RL, Korobkin M, et al. (eds) (1983) *Uroradiology: An Integrated Approach*. Churchill Livingstone, Edinburgh
- Glazer GM (1988) MR imaging of the liver, kidneys, and adrenal glands. *Radiology* 166: 303–308
- Hattery RR, Williamson B Jr, Hartman GW, et al. (1988) Intravenous urographic technique. *Radiology* 167: 593–599
- McClellan BL (1987) Low-osmolality contrast media: premises and promises. *Radiology* 162: 1–8
- McClellan BL, Lee JKT, Peterson RR (1986) Anatomy of the perirenal area. *Radiology* 158: 555–561
- McClellan BL, Rabin DN (1989) Kidney. In: Lee JKT, Sagel SS, Stanley RJ (eds) *Computed Body Tomography*, 2nd edn. Raven Press, pp 755–826
- Newhouse JH, Pfister RC (1979) The nephrogram. *Radiol Clin North Am* 17: 213–217
- Pfister RC, Papanicolaou N, Yoder IC (1986) Diagnostic, morphologic and urodynamic antegrade pyelography. *Radiol Clin North Am* 24: 561
- Spataro RF (1984) Newer contrast agents for urography. *Radiol Clin North Am* 22: 365–369
- Witten DM, Myers GH, Utz DC (1977) *Clinical Urography*. W.B. Saunders Co., Philadelphia

##### CONGENITAL ANOMALIES

- Abrahamson J (1961) Double bladder and related anomalies: clinical and embryological aspects. *Br J Urol* 33: 195–199
- Felson B, Cussen LJ (1975) The hydronephrotic type of unilateral congenital multicystic disease of the kidney. *Semin Roentgenol* 10: 113–118
- Friedland GW, Cunningham J (1972) Elusive ectopic ureterocele. *AJR* 116: 792–797
- Greskovich FJ, Nyberg LM (1988) The Prune Belly Syndrome: a review of its etiology, defects, treatment and prognosis. *J Urol* 140: 707–711
- Haber K (1973) Bifid ureter with a blind-ending branch diagnosed by excretory urography: report of a case. *J Urol* 110: 38–41
- Hayden CK, Swischuk LE, Smith TS, Armstrong EA (1986) Renal cystic disease in childhood. *Radiographics* 6: 97–104
- MacPherson RI, Leithiser RE, Gordon L, Turner WR (1986) Posterior urethral valves: an update and review. *Radiographics* 6: 753–759
- Marshall FF, Freedman MT (1978) Cross renal ectopia. *J Urol* 119: 188–192
- Risdon RA, Young LW, Chrispin AR (1975) Renal hypoplasia and dysplasia: a radiological and pathological correlation. *Pediatr Radiol* 3: 213–218
- Sanders RC, Hartman DS (1984) The sonographic distinction between neonatal multicystic kidney and hydronephrosis. *Radiology* 151: 621–627
- Stuck KJ, Koff SA, Silver TM (1982) Ultrasonic features of multicystic dysplastic kidney: expanded diagnostic criteria. *Radiology* 143: 217–223
- Talner LB, Gittes RF (1974) Megacalyces: further observations and differentiation from obstructive renal disease. *AJR* 121: 473–479
- White D, Lebowitz RL (1977) Extrophy of the bladder. *Radiol Clin North Am* 15: 93–98

## CHAPTER 34

# CYSTS AND NEOPLASMS

Nancy S. Curry

---

## CYSTIC DISORDERS OF THE KIDNEY

---

### CORTICAL DISORDERS

The commonest cystic disorder of the kidney is the **simple renal cortical cyst**. These cysts may be solitary or multiple, unilateral or bilateral, and range in size from a few millimeters to larger than the kidney itself. They are lined with a low cuboidal epithelium, contain a serous fluid, and are usually unilocular although they may have an incomplete septum. Although probably acquired, cysts become increasingly frequent with age, so that 50% of the population develop one or more cysts by the age of 50 years. At autopsy, 2%–6% of children are found to have cortical cysts but these are rarely recognized clinically. Cysts are incidental and usually asymptomatic even when they achieve remarkable size. Rarely, when large, they may cause pain, obstruction, polycythemia or hypertension. Simple cysts do not impair renal function but they may become symptomatic when infection, hemorrhage or rupture into the collecting system occurs. The etiology of simple cysts is unknown but theories have included an origin in embryonic rests or tubular obstruction accompanying ischemia.

**Imaging.** *Excretory urography* with tomography will detect renal cysts larger than 2 cm in size. They demonstrate a smooth, lucent, round defect in the nephrogram phase of the examination with a 'claw' or 'beak' sign at the interface of the cyst and the margin of the kidney (Fig. 34.1), although this sign is not specific for cysts and may be seen in other mass lesions of the kidney. The periphery of the cyst should not have a wall thickness greater than 1 mm. Exophytic

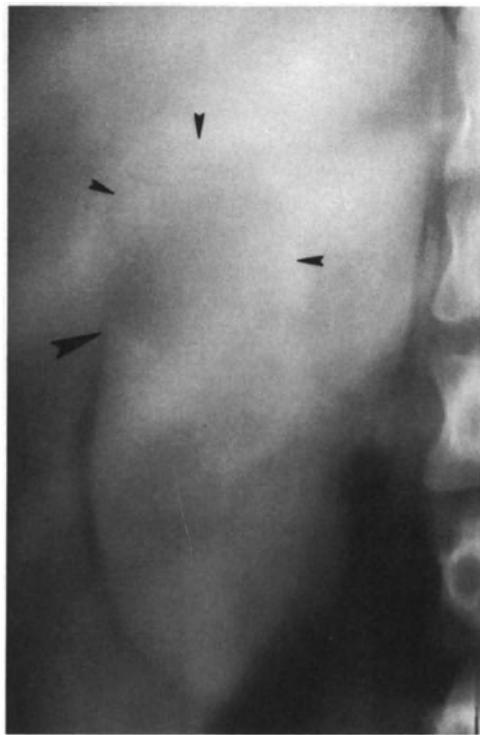


**Fig. 34.1.** Renal cyst. Nephrogram phase of excretory urogram demonstrates round, lucent mass in the upper pole of the right kidney (small arrowheads). Note 'beak effect' (large arrowhead) at the interface of the cyst with the renal parenchyma.



**Fig. 34.2.** Ultrasound of a simple renal cyst. Note absence of internal echoes and good through-transmission of the sound beam.

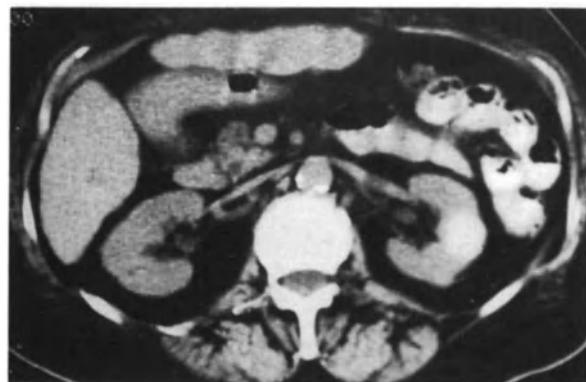


**Fig. 34.4.** Hyperdense cyst, left kidney. Non-contrast CT scan.

lesions protrude from the cortical surface without producing displacement or distortion of the collecting system. Larger or more centrally located cysts distort and splay adjacent collecting structures, and in some cases, the infundibulae and pelvis are compressed enough to cause obstruction. Larger cysts may also cause renal axis deviation or displacement of the kidney.

**Calcification** occurs in the walls of benign cysts in approximately 2% of cases, usually in those which have been complicated by hemorrhage or infection. It is seen as a delicate, thin rim of continuous calcification. Peripheral calcification which is thick, irregular and interrupted should raise the suspicion of carcinoma since 20% of peripherally calcified lesions may harbor malignancy.

Because abscesses and hypovascular hypernephromas may resemble cysts on urography, the presence of a suspected simple cyst should be verified by *ultrasound*. Using this imaging modality, simple cysts are usually round and uniformly anechoic with a well-defined back wall and strong through-transmission of the ultrasonic beam (Fig. 34.2). One or more thin, usually incomplete septations may be present. Deviation from these characteristics indicates further evalua-



**Fig. 34.3.** CT of multiple bilateral simple renal cysts. Note two very large left cortical cysts, one showing a fleck of calcium in its wall (arrowhead). Note also the right parapelvic cyst. The patient was asymptomatic with normal renal function.

tion is necessary. If interpreted with these criteria in mind, ultrasonography is highly accurate in distinguishing simple cysts from other, more significant lesions.

*Computed tomography* identifies more cysts than excretory urography. CT may be necessary to further define a cystic lesion, particularly those which are small or in locations difficult to examine by ultrasonography. The CT characteristics of simple cysts are:

1. Homogeneity
2. Low attenuation content (Hounsfield numbers less than 20)
3. Sharp cyst–parenchyma interface
4. No enhancement with contrast
5. No definable wall.

When incidentally found in the asymptomatic patient, a lesion with all these characteristics is safely considered a simple renal cyst and no further imaging investigation is necessary (Fig. 34.3).

Although CT is regarded to be nearly 100% accurate in the identification of cysts, there are several potential pitfalls. Partial volume effects at the margins of the lesion may be responsible for indistinct outlines or artificially elevated attenuation coefficients. Normal parenchyma ringing the outer margin of a cyst can mimic a thick wall.

In addition to artefacts which can cause interpretation error, benign cysts which have become complicated by superimposed infection or hemorrhage may not have the characteristics expected of uncomplicated cysts. Comprising approximately 5% of masses, these lesions are termed '*indeterminate*' or '*complex*' and will require further evaluation. Many will have calcification in their walls or high attenuation numbers. While uncomplicated cysts are lower density on non-contrasted CT scans than the surrounding parenchyma, '*hyperdense*' cysts appear much denser than the adjacent renal tissue (Fig. 34.4). This phenomenon has been ascribed to contrast enhancement related to prior intravenous or retrograde study, high-protein content within the cyst fluid, hemorrhage, or a paste-like calcium content. These lesions may be assumed to be benign when they are: round, smooth, sharply marginated and homogeneous, non-enhancing, and definitely cystic on

ultrasound. A negative needle puncture is not definitive for a benign lesion, because of the hemorrhagic content of the lesion, whether it is in fact benign or is malignant.

On *magnetic resonance imaging* a simple retention cyst shows a homogeneous, low-intensity signal on T<sub>1</sub>-weighted images and an intermediate to high intensity signal on T<sub>2</sub>-weighted images. MR can differentiate uncomplicated cysts from solid masses with accuracy comparable to CT and ultrasound. Hemorrhagic and infected cysts, however, have variable signal intensities rendering MR ineffective in establishing the nature of these indeterminate lesions.

*Angiography* has been supplanted by ultrasound and CT in the evaluation of cysts. A simple cyst appears as an avascular mass with stretching of otherwise normal vessels around the margins. Superimposed infection or hemorrhage into the cyst, however, may induce abnormal vessels at the border of the lesion making it difficult to distinguish from neoplasm.

*Cyst puncture* is rarely necessary because of the accuracy of ultrasound and CT in determining the presence of simple renal cysts. Indications for cyst puncture include conflicting or indeterminate results on CT or ultrasound, the presence of fever or unexplained hematuria and the presence of a large renal cyst causing pain, hypertension or obstruction.

Aspiration of a simple cyst yields translucent fluid which is low in fat and lactic dehydrogenase (LDH) and has negative cytology. Turbid or hemorrhagic fluid in a non-traumatic tap suggests the possibility of malignancy even if the aspirate does not demonstrate malignant cells. A radiographic study of the cyst wall may be performed as outlined in Fig. 33.5. The filled cyst should correspond to the known size of the lesion. The fluid volume removed should be replaced by an equal volume of contrast since underfilling may result in wrinkling and redundancy of the cyst wall, mimicking mural tumor.

**Multiple Simple Cysts.** In many older patients there are multiple simple cortical cysts which should be evaluated in the same manner as single lesions. Since cysts and tumor may coexist in the same individual or in the same kidney, each lesion should fulfill the criteria for cyst. In some cases the number of cysts is striking enough to resemble polycystic kidney disease. Overall renal size is not enlarged, however, and there are areas of intervening normal renal parenchyma, unlike polycystic kidney disease.

#### SYNDROMES ASSOCIATED WITH RENAL CYSTS

**Tuberous Sclerosis.** In addition to the multiple renal angiomyolipomas associated with tuberous sclerosis, there is also an increased incidence of cysts. The histopathology of these cysts differs from cortical cysts associated with aging in being lined with hyperplastic columnar cells similar to proximal tubular epithelial cells. These cysts usually are small (3 cm in size) although they can become large enough and numerous enough to cause renal insufficiency. In this situation, the radiologic manifestations are indistinguishable from adult polycystic kidney disease.

**Von Hippel-Lindau Syndrome.** This autosomal dominant disease is noted for central nervous system tumors (retinal

angiomas and cerebellar hemangioblastomas), abdominal tumors and renal cysts and carcinoma. The renal cysts are histologically similar to ordinary simple cysts. The presence of numerous cysts and pancreatic cysts may make the condition indistinguishable from adult polycystic kidney disease.

**Other Miscellaneous Syndromes.** Other conditions which have been reported to be associated with renal cysts include *Turner's syndrome*, *Conradi's disease*, *Zellweger syndrome* (cerebrohepatorenal syndrome) and some of the trisomy states.

#### EXTRAPARENCHYMAL RENAL CYSTS

**Parapelvic Cysts.** Cysts which occur in the renal hilum are called parapelvic cysts. Their origin is unknown but they may derive from obstructed renal lymphatics. Like simple cortical cysts, parapelvic cysts are incidental findings which only rarely cause significant problem.

On *urography* they impress upon the neighboring pelvis and infundibula and in some cases cause obstruction of the surrounding collecting structures. They may simulate renal sinus fibrolipomatosis, aneurysm, cortical cyst or tumor. On *ultrasonography*, multiple parapelvic cysts may mimic hydronephrosis. They are most easily diagnosed on CT where their water density surrounds contrast in displaced collecting structures (Fig. 34.3).

**Pyelogenic Cysts (Calyceal Diverticula).** Pyelogenic cysts are diverticula of the collecting system which may be congenital in origin or possibly acquired from rupture of a cyst or abscess into a calyx. These cysts are identified at urography as smoothly rounded collections of contrast extending beyond the interpapillary line and connected to the fornix of a calyx by a narrow neck. Those which originate off an infundibulum are more centrally located. Pyelogenic cysts are usually small and asymptomatic, but they may not drain well and become complicated by infection, obstruction or calculi (Figs 34.4, 34.5). Clusters of calculi or milk of calcium may be found in them.

**Perinephric Pseudocyst (Urinoma).** Urine may extravasate from the kidney due to trauma, surgery or obstruction with spontaneous leakage into the perinephric tissue. On *urography* or *antegrade pyelography* communication with a portion of the collecting system can usually be demonstrated. Usually this leakage is absorbed, but when there is continued extravasation an inflammatory response may occur. Weeks to months after the injury the urine becomes encysted in a fibrous capsule which lacks an epithelial lining. This collection may be subcapsular or extracapsular in location and may exhibit calcification (Fig. 34.6). Depending on its size and locations a mass effect on the neighboring renal parenchyma, pelvis or ureter is seen.

#### POLYCYSTIC KIDNEY DISEASE

Polycystic kidney disease occurs in childhood and adult forms which, although superficially similar, are, in fact, very different diseases. They differ in incidence, inheritance pattern, clinical course and histopathology.



**Fig. 34.5A, B.** Pyelogenic cysts. **A** Calyceal diverticulum, right upper pole. Note extension beyond the interpapillary line. **B** Large cyst originating from the lower pole infundibulum, obstructing several lower pole calyces.

**Childhood Polycystic Kidney Disease.** Cystic dilatation of the renal tubules and hepatic periportal fibrosis are hallmarks of this rare condition which has an incidence of 1 in 6000 to 1 in 14 000. It is inherited by autosomal recessive transmission and although the etiology is unknown, it is thought to be due to hyperplasia of the interstitial portions of the collecting tubules that develop from the ureteral bud. Polycystic kidney disease of childhood can be divided into four main subgroups which reflect the spectrum of renal and hepatic involvement. The more severe degrees of renal disease are accompanied by less severe liver disease and vice versa.

The shortest survival occurs with the *perinatal form* of childhood polycystic kidney disease which is associated with

90% involvement of the renal tubules and minimal hepatic fibrosis. Most infants are stillborn having oligohydramnios in utero with accompanying pulmonary hypoplasia. The diagnosis may be made on *obstetric ultrasound* examination. The kidneys are massively enlarged with parenchymal replacement by innumerable tiny cysts. Because of the small size of the cysts and their uniform distribution, the reniform shape of the kidney is preserved and there is little distortion of the renal pelvis and calyces.

The *neonatal form* of the condition is associated with 60% renal involvement and mild hepatic fibrosis allowing somewhat longer survival. Those children affected by the *infantile form* of the disease have 25% renal involvement and moderate periportal fibrosis. With only 10% renal involvement, the *juvenile form* is associated with little compromise of renal function. The marked degree of bile duct proliferation and periportal hepatic fibrosis, however, leads to portal hypertension, gastrointestinal hemorrhage and liver failure.

**Radiographic findings** include soft tissue flank masses corresponding to the massively enlarged kidneys with displacement of adjacent bowel. When there is sufficient renal function, the *excretory urogram* demonstrates smoothly enlarged kidneys with radially arrayed streaks in the nephrogram (Fig. 34.7). In the infantile forms, the pyelocalyceal systems are poorly opacified. The forms of disease with less severe renal involvement will show fewer cysts and the dilated distal collecting tubules may simulate the appearance of medullary sponge kidney.

**Ultrasonography** will demonstrate the kidneys to be smoothly enlarged. Individual cysts are not identified due to their small size but they impart a marked increase in echogenicity to the kidneys related to the multitude of acoustic

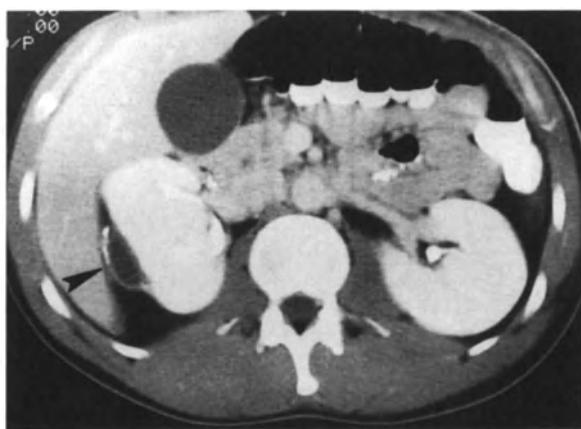


**Fig. 34.6.** Contrast enhanced CT. Perinephric pseudocyst secondary to remote trauma. The outer wall of the lesion is partially calcified (arrowhead).



**Fig. 34.7.** Infantile polycystic kidney disease, excretory urogram. Initial radiographs showed no excretion but this 24-hour delayed film demonstrates hugely enlarged kidneys with a striated, dense nephrogram. (Courtesy of R. Macpherson MD).

interfaces produced by the ectatic tubules. Corticomedullary differentiation is lost and, characteristically, a prominent central echolucency and a sonolucent rim are seen (Fig. 34.8).

**Adult Polycystic Kidney Disease.** Adult polycystic kidney is a more common condition than the childhood disorder, with an incidence of 1 in 200 to 1 in 1000. Occasionally this disorder presents in infants or children. The inheritance pattern is autosomal dominant with varying degrees of penetrance. Approximately one third of patients in pathologic studies have associated cysts in the liver, although CT data suggest an even higher incidence of associated polycystic liver disease. The pancreas has cysts in 10% of cases and the spleen in 5%. Occasionally, other organs such as the lung, thyroid, or ovary may have cysts as well. The renal cysts are of varying sizes and develop from any part of the nephron, involving both cortex and medulla. Their gradual increase in size leads to compromise of the normal nephrons with subsequent renal failure. Patients may become symptomatic due to rupture and hemorrhage of cysts or from obstructing ureteral calculi which develop in as many as 20% of cases. Most often, the patients become symptomatic



A



B

**Fig. 34.9A, B.** Adult polycystic kidney disease. A Nephrogram phase of excretory urogram demonstrates multiple lucent cysts and enlarged kidneys. B Pyelographic phase demonstrates poor concentration of contrast, and splaying and distortion of the calyces.



**Fig. 34.8.** Infantile polycystic kidney disease. Sagittal ultrasound scan through the right kidney shows renal enlargement, increased echogenicity, loss of corticomedullary differentiation and a prominent central lucency.

with hypertension and azotemia in the third decade. Cerebral aneurysms are associated with this condition and subarachnoid hemorrhage is a cause of death in approximately 10% of patients.

The *excretory urogram* is characterized by enlarged kidneys with poorly defined, nodular contours, a 'Swiss cheese' nephrogram of multiple lucencies, and splaying and distortion of the collecting systems (Fig. 34.9). Occasionally, calcium is present in the walls of the cysts. The degree of severity of these findings varies from patient to patient just as the severity of involvement of one kidney over the other in the same patient may vary. At urography, the main differential diagnosis would include multiple simple renal cortical cysts and tuberous sclerosis.

On *ultrasonography* not only are the multiple renal cysts demonstrated but hepatic cysts can be imaged as well (Fig. 34.10). Screening of family members for genetic counseling should be accomplished.

CT examination may be helpful in the assessment of a patient with a complication of polycystic disease. Cyst hemorrhage or ureteral obstruction may be more easily determined in the face of compromised renal function (Fig. 34.11).



**Fig. 34.10.** Adult polycystic kidney disease. Ultrasonogram of the right kidney demonstrate multiple, variably-sized cysts.



**Fig. 34.12.** Renal tubular ectasia. Ten-minute IVP film shows linear striations radiating from the papillae.

**MEDULLARY SPONGE KIDNEY**

A non-familial, non-progressive developmental abnormality, medullary sponge kidney is probably present at birth but is asymptomatic unless a complication intervenes in adulthood. It has been associated with *congenital hemihypertrophy*, *congenital hepatic fibrosis* and *Caroli's disease*. The condition is characterized by ectatic collecting ducts in the renal pyramids with cysts which may or may not communicate with the collecting ducts. The incidence of the condition is 0.5% on urography; however, with the use of low osmolality contrast agents, the incidence of observed ectatic tubules has increased.

Renal tubular ectasia is the least severe form of this condition. On *urography*, one papilla, several papillae or all papillae are affected, the process being bilateral in 75% of cases. Discrete, radiodense, linear striations which radiate from the papillary tips are characteristic (Fig. 34.12). This must be

distinguished from the intense, homogeneous pyelotubular 'blush' sometimes seen in normal young individuals with excellent renal function. Features suggesting medullary sponge kidney rather than pyelotubular blush include widened calyces and persistence of the linear striations beyond the first few minutes of the study.

In more advanced cases, there are ovoid, 1–6-mm cystic collections of contrast in the medullary regions. *Calcifications* occurring within the cystic dilatations due to stasis and precipitation develop in about one half of cases. The passage of these calculi and infection are responsible for the development of symptomatology which bring these patients to atten-

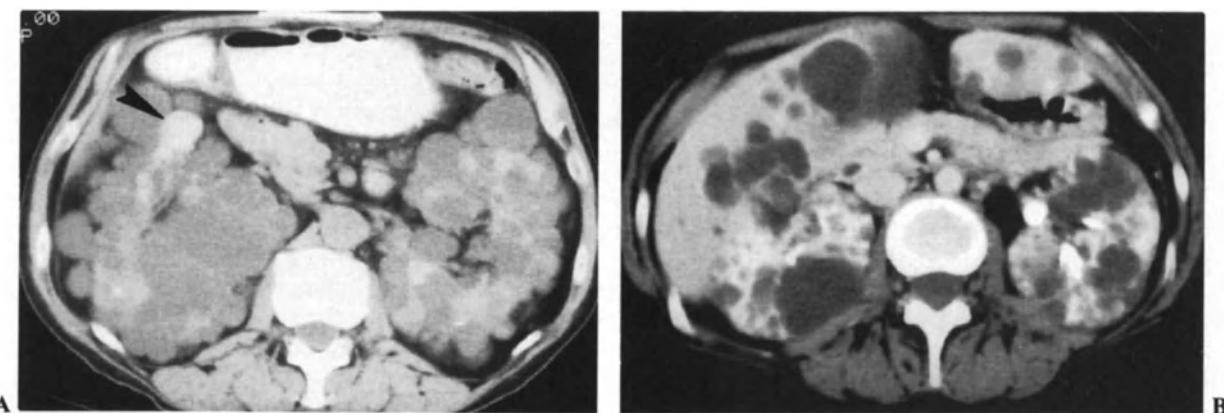


**Fig. 34.11.A** Adult polycystic kidney disease. CT scan demonstrates massive renal enlargement with innumerable cysts, some of which are hyperdense due to recent hemorrhage (arrowhead). **B** Multiple cysts in liver and both kidneys in polycystic disease.

tion, for the condition by itself does not cause renal dysfunction. Small, grouped calculi distributed in the medulla become obscured by contrast during the pyelographic phase of an excretory urogram. On *sonography*, the medullary pyramids appear highly echogenic due to the multiple small cysts.

### MEDULLARY CYSTIC DISEASE

Also known as *juvenile nephronophthisis*, medullary cystic disease is a rare, familial disorder characterized by numerous medullary cysts. Clinically, patients present in adolescence with salt-losing nephropathy and severe uremia.

At *urography* the kidneys are small and granular and demonstrate little if any excretion of contrast. The cysts vary in size but are usually not large enough to distort the contours of the kidney or cause significant displacement of the pyelocalveal structures. *Ultrasonography* demonstrates small kidneys with smooth contours, loss of corticomedullary differentiation, increased parenchymal echogenicity and cysts in the medulla and corticomedullary region.

### ACQUIRED CYSTIC DISEASE OF THE KIDNEY

Patients on *long-term hemodialysis* and *peritoneal dialysis* have been found to develop cysts in their kidneys with a frequency depending on the duration of dialysis. Approximately 64% of patients on dialysis for three years or longer develop acquired cystic disease of the kidney (ACDK). Regression of the condition may occur after renal transplantation. The etiology of ACDK is unknown but theories include intratubular obstruction due to interstitial fibrosis or oxalate crystals, a cystogenic nephrotoxin, and vascular degeneration. Hemorrhage is a complication of the disorder due in part to platelet dysfunction of uremia and the use of anticoagulants during hemodialysis, bleeding into the cyst wall vessels or neoplasms arising in the cyst wall. Bleeding may also occur into the pyelocalveal system or retroperitoneum.

As many as 10% to 45% of patients having ACDK develop neoplasms which may be benign or malignant. The tumors appear to arise from the hyperplastic lining epithelium of the

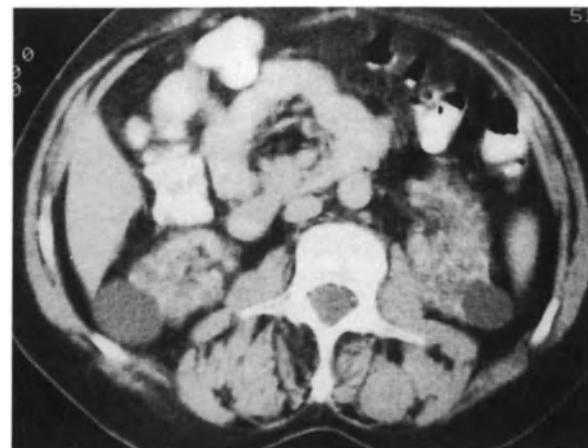


**Fig. 34.13.** Acquired cystic disease of the kidney. The kidneys are filled with innumerable, mostly tiny, cysts. The patient had undergone hemodialysis for 4 years. A previous CT scan (not shown) demonstrated atrophic, non-functioning kidneys with no cysts.

cysts or from non-cystic tubules. The tumors are usually small, bilateral and multifocal. While they are usually asymptomatic metastases may occur.

While either *CT* or *ultrasound* may be used to make the diagnosis of ACDK, *CT* is the most effective method for identifying the solid tumors which may coexist with the numerous cysts. The condition may be distinguished from congenital adult polycystic kidney disease by the evolution during dialysis, small renal size and small cyst size (Fig. 34.13). It should be noted, however, that there is a tendency for the kidneys in ACDK to become increased in size, especially if hemorrhage occurs.

### OTHER CYSTIC DISORDERS

*Multicystic dysplastic kidney* due to fetal renal obstruction has already been discussed in the preceding chapter. Neoplasms such as *cystic renal cell carcinoma* and *multilocular cystic nephroma* are discussed in the following section.

---

## RENAL NEOPLASMS

---

### BENIGN NEOPLASMS

#### Renal Adenoma

The commonest benign lesion of the renal parenchyma is the renal adenoma which arises from the proximal convoluted tubule. Because of their small size and lack of symptomatology, these tumors are rarely discovered in life, despite an autopsy incidence of from 15%–20%. Microscopi-

cally they are indistinguishable from well-differentiated renal cell carcinomas. Whilst masses over 3 cm in size are likely to be carcinomas and those under 3 cm are often adenomas, size is not regarded as a reliable predictor of malignant potential. Clinically, a small lesion may demonstrate aggressive behaviour or a very large tumor behave in a benign fashion. There are no imaging characteristics which can distinguish benign adenoma from renal cell carcinoma. In fact, many

investigators believe that a renal adenoma is the precursor of renal cell carcinoma before it exhibits malignant features of invasion and metastasis.

### **Renal Oncocytoma**

Another benign type of adenoma arising from the proximal convoluted tubule is the renal oncocytoma. The distinguishing feature of the oncocyte is its eosinophilic cytoplasm which microscopically demonstrates a large number of mitochondria. It does not exhibit cellular pleomorphism or mitotic figures. Neoplasms made up of this cell type have also been found in the thyroid, parathyroid, adrenal and salivary glands. Oncocytomas account for only 1%–2% of resected renal parenchymal tumors. Well-differentiated tumors (Grade 1) are composed only of oncocytes and behave in a non-malignant fashion. Higher-grade tumors may exhibit cellular characteristics of malignancy and capsular or venous invasion.

**Imaging.** Oncocytomas are solid tumors indistinguishable from renal cell carcinoma on *excretory urography*. They appear to be well-defined and homogeneously solid on CT examination, sometimes exhibiting a stellate central scar. *Sonography* is non-specific although a central scar may suggest the diagnosis. On *angiography* the lesions are hypervascular with a 'spoke-wheel' configuration of vessels, a homogenous capillary phase, and a sharp, smooth margin.

They lack clearly malignant vasculature and do not demonstrate arterio-venous shunting typical of renal cell carcinoma.

Although the diagnosis might be suggested preoperatively, the imaging features are not reliably specific as the lesion may be indistinguishable from renal cell carcinoma. Needle aspiration biopsy is not sufficient to diagnose an oncocytoma because renal cell carcinoma can exhibit internal areas with cellular oncocytic features. Nephrectomy therefore remains the treatment of choice except in unusual clinical situations such as solitary kidney, bilateral disease or chronic renal disease where tumorectomy or partial nephrectomy might be considered.

### **Mesenchymal Tumors**

Typically very small and asymptomatic in life, there are a variety of mesenchymal (non-epithelial) tumors which usually are discovered incidentally at autopsy in about 10% of patients. They include *leiomyomas*, *fibromas*, *lipomas*, and *hemangiomas*. They generally are under 1 cm in size and are of no clinical importance. Occasionally these lesions can become large enough to be detected.

### **Reninoma**

A reninoma is a very rare benign tumor affecting young adults, predominantly females. It arises from the juxtaglomerular cells and elaborates renin, producing hypertension. The lesions tend to be *small* and *subcapsular* in location and removal results in cure of the hypertension. The tumor is usually hyperechoic on *sonography*, hypovascular at *angiography* and does not enhance after contrast administration during CT.

### **Angiomyolipoma**

Angiomyolipoma is a type of benign mesenchymal tumor which is clinically important. Also termed hamartomas, these lesions are composed of three main tissue types: fat, smooth muscle and blood vessels. The tumor occurs in two distinct clinical situations. Patients with *tuberous sclerosis* in 80% of cases have angiomyolipomas which are likely to be bilateral and multifocal. Only 40% of patients with angiomyolipomas, however, have *tuberous sclerosis*. The remainder occur in middle-aged females, usually as a single tumor. At autopsy, 10% of kidneys may harbor hamartomas less than a centimeter in size.

**Imaging.** Angiomyolipoma can be identified in almost all cases. The imaging appearance of these tumors will vary depending on the differing proportions of the tissue groups composing it and by the presence of tumor necrosis or hemorrhage. Tumors with large amounts of fat can be identified on plain films and *excretory urography* by the recognition of radiolucency within the mass.

*Ultrasound* studies classically show a highly echogenic mass because of the fat content of the tumor (Fig. 34.14A). Since some renal cell carcinomas are hyperechoic, however, suspected angiomyolipoma should be confirmed by CT. The finding of fat (reproducible attenuation number less than  $-10 \text{ HU}$ ) even in small amounts is considered a reliable indicator of angiomyolipoma (Fig. 34.14B). Rarely, CT may demonstrate regional lymph node involvement which is thought

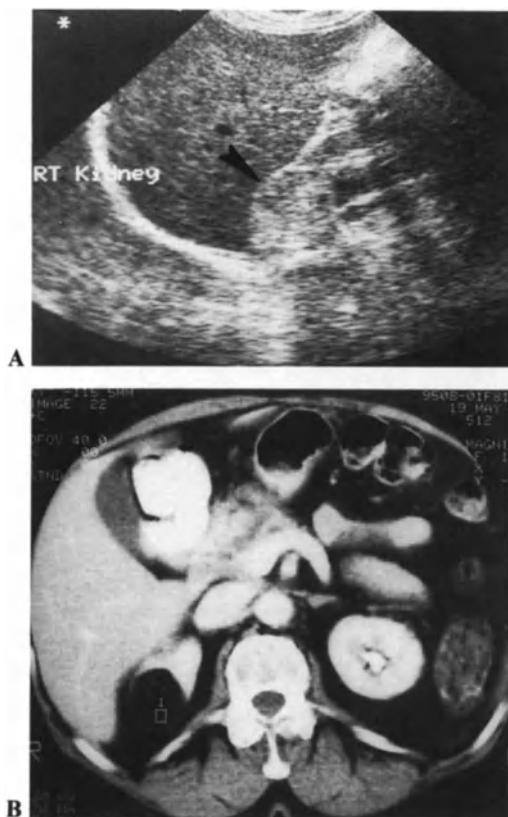


Fig. 34.14A, B. Angiomyolipoma. A Ultrasound scan, sagittal section, right kidney, shows echogenic mass in the upper pole (arrowhead). B CT scan, with contrast, shows the lesion containing tissue similar to retroperitoneal fat. The cursor measured an attenuation coefficient of  $-70 \text{ HU}$ .

to be a second hamartomatous focus rather than a metastasis. Extension of the tumor into the vena cava can occur although this, too, is quite unusual.

*MR imaging* of angiomyolipoma reveals high-intensity on T<sub>1</sub>-weighted images similar to perinephric fat.

The *angiographic* appearance of these tumors is dependent on the amount of angiomatic tissue present. When abundant, the tumor is fed by large, tortuous, aneurysmally dilated vessels. The distinction between angiomyolipoma and renal cell carcinoma is not possible by angiography. *Angiography embolization* has proved extremely helpful, however, in the management of life-threatening hemorrhage associated with these tumors.

### Multilocular Cystic Nephroma

This unusual benign, cystic renal tumor is usually seen in two clinical settings: *male children* aged 3 months to 4 years and in *female adults* in the 4th to 8th decade. It is characterized by multiple, non-communicating cysts surrounded by a dense fibrous capsule. Undifferentiated mesenchymal and primitive nephronic elements are found in the connective tissue septa, between the cysts. These tumors do have malignant potential as foci of Wilms' tumor in children and sarcoma in adults have been discovered in the septations.

*Imaging.* Excretory urography demonstrates a normally functioning kidney containing a well-defined mass whose septations may be evident. Calcifications may be detectable. One feature of multilocular cystic nephroma (MLCN) is the tendency toward herniation of the tumor into the renal pelvis resulting in a filling defect or obstruction. The mass is a complex cystic structure with highly echogenic septae on *ultrasound*.

*CT* demonstrates a well-margined rounded or polycystic mass with thick, enhancing septations between cysts of varying size and attenuation (Fig. 34.15). *Angiography* may reveal irregular vessels in the septa indistinguishable from malignant vascularity. *Needle puncture* yields fluid which may be clear, turbid, viscous or bloody and the cystic locules do not communicate.

*Differential Diagnosis.* Other lesions with a multilocular configuration which resemble MLCN include focal aggre-

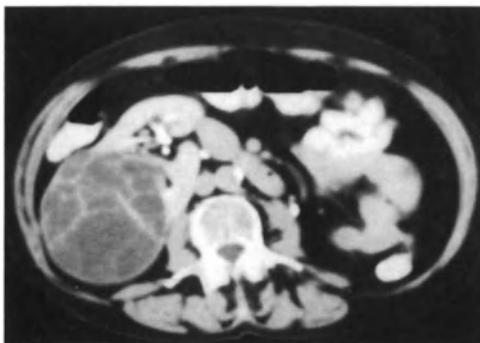


Fig. 34.15. Benign multilocular cystic nephroma. Contrast CT scan shows an encapsulated right renal mass containing numerous septations and cystic locules of differing sizes. (Courtesy of R. Dyer and J. Caldemeyer, reprinted with permission from Grune and Stratton, Inc. publishers of Benign space-occupying conditions of the kidneys, Semin Roentgenol 1987; 22: 275-283, Fig. 5, p 281.)

gates of *simple cysts*, *segmental multicystic dysplastic kidney*, *mesoblastic nephroma* and *multiloculated renal cell carcinoma*.

### Mesoblastic Nephroma

An uncommon benign renal neoplasm, the mesoblastic nephroma is a solid lesion which develops in *neonates*. Occasionally the tumor exhibits multilocular features due to cystic degeneration.

*Imaging.* Abdominal radiographs show a large soft-tissue mass which only rarely calcifies. Excretory urography reveals mass effect on the pelvocalyeal system with displacement, distortion and sometimes obstruction. The tumor is vascular at angiography and CT examination reveals a solid or multilocular mass.

*Differential Diagnosis.* *Multilocular cystic nephroma* and *cystic nephroblastoma* (cystic Wilms' tumor) occur in the older infant. *Multicystic dysplastic kidney* usually involves the whole kidney although segmental forms of this condition are described. They are usually associated with ureteral duplication which is not a feature associated with mesoblastic nephroma.

## MALIGNANT RENAL NEOPLASMS

### Renal Adenocarcinoma (Hypernephroma)

Renal adenocarcinoma accounts for 85% of all malignancies affecting the adult kidney. It is not a common disease, representing only 3% of cancers. There is a 2:1 male predominance with a peak incidence in the sixth decade. The classic symptom triad of flank pain, mass and hematuria is present in less than a third of cases. Some cases are found incidentally and as many as 30% of patients will already have metastases at the time of diagnosis. Hypernephromas are usually unilateral with only a 2% incidence of bilaterality. Bilateral or multiple tumors may be seen in *von Hippel-Lindau syndrome* and *acquired cystic disease* of the kidney associated with long-term dialysis.

*Imaging.* *Excretory Urography.* The excretory urogram remains the screening modality of choice when a patient presents with hematuria. If a mass is present, it will be detected from some or many of the following features: a defect in the nephrogram; focal parenchymal contour bulge with thick-walled or irregular margin; renal axis abnormality; calcification; calyceal splaying, distortion, amputation, invasion or clubbing (Fig. 34.16). Renal non-function can be due to renal vein thrombosis, obstructive uropathy or parenchymal replacement.

*Ultrasound.* If a mass is discovered on urography, ultrasound examination can confirm the finding. A lesion is solid and most likely a renal carcinoma (Fig. 34.17). A lesion which appears hypoechoic but has irregular or thick walls, or focal high-intensity echoes (suggesting mural calcification) is not a simple cyst and deserves further investigation with CT examination or needle puncture and cystography (Fig. 34.18). It has been found that 45% are renal parenchyma, 20% are hyperechoic, and 35% are hypoechoic lesions which can resemble cysts although acoustic shadowing is absent or disproportionate to the size

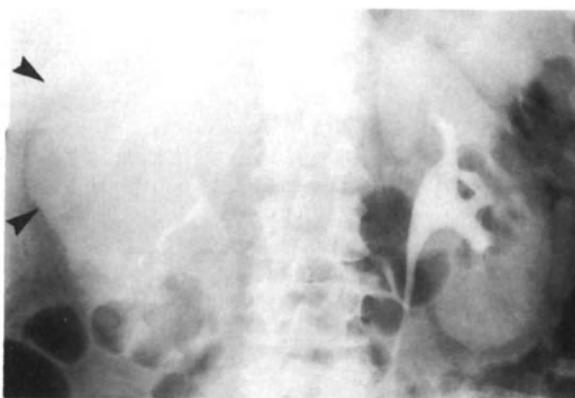


**Fig. 34.16.** Renal cell carcinoma. Excretory urogram shows focal enlargement of the right upper pole (*arrowheads*) with attenuation and irregularity of the renal pelvis from tumor invasion.

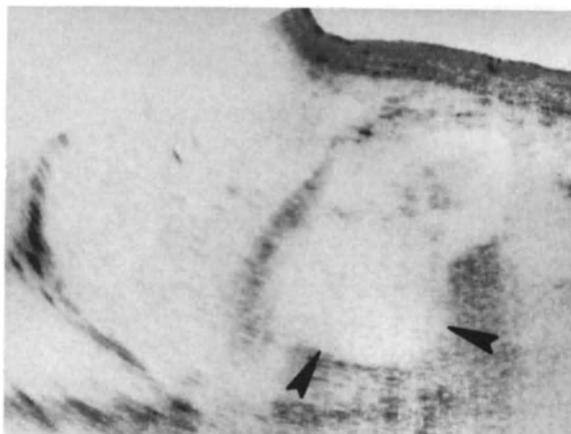


**Fig. 34.17.** Renal cell carcinoma. Static sagittal ultrasound, right kidney, shows an echogenic mass occupying the posterior upper pole (*arrowheads*).

of the lesion. Renal vein and inferior vena caval extension of tumor can also be identified.

**CT.** If no mass is detected on a urogram which has excluded other reasons for hematuria and there remains suspicion of neoplasm, a CT examination is indicated. Malignancies under 3 cm in size, especially in an anterior or posterior position, may not be detectable at urography. CT is also utilized in *staging* malignancy if it is discovered (Table 34.1). The tumor is usually less dense than the surrounding normal parenchyma on non-contrasted scans.

**Table 34.1.** Staging of renal cell carcinoma

Stage	Extent of involvement
Stage 1	Tumor confined to renal parenchyma
Stage 2	Tumor penetrating renal capsule but confined within Gerota's fascia
Stage 3A	Renal vein or IVC extension
Stage 3B	Regional lymph node involvement
Stage 3C	Local vessels and lymph nodes
Stage 4A	Adjacent organs invaded (excluding adrenal gland)
Stage 4B	Distant metastases

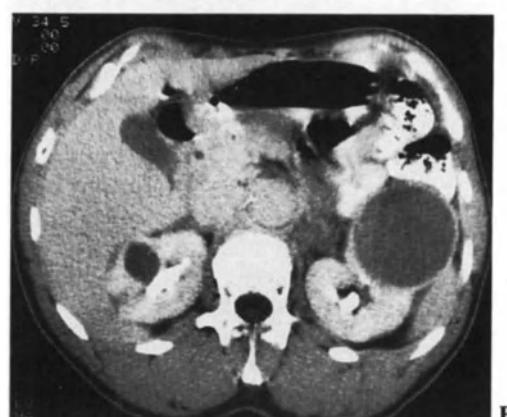


**Fig. 34.18A, B, C.** Renal cell carcinoma with cystic degeneration. A Ultrasound examination shows a relatively sonolucent mass, but with a thick wall, some internal echoes and poor through-transmission of the acoustic beam. B Contrast CT scan, demonstrates a large left renal lesion with a thick wall, slightly increased attenuation (22 HU), and slight inhomogeneity. Compare with the simple renal cyst in the right kidney. C Needle puncture with contrast injection shows irregular lesion contours and nodular filling defects (*arrowheads*). Aspirated fluid was brown and turbid.



**Fig. 34.19.** Renal cell carcinoma. CT scan demonstrates a large inhomogeneous right renal tumor with central areas of necrosis.

After contrast is injected there is inhomogeneous enhancement although the degree of enhancement is less than that of the normal parenchyma. Other CT characteristics of malignancy include indistinct lesion-parenchymal interface, calcification, high attenuation number, and tumor spread to the venous structures or retroperitoneal lymph nodes (Fig. 34.19). Caval or renal venous tumor thrombus can present as a filling defect or enlargement of the vessel. Venous occlusion may also be suggested by renal edema, non-function and dilated venous collateral vessels.

*Phlebography* of the inferior vena cava is still sometimes required when the results of ultrasound or CT are equivocal (Fig. 34.20). Approximately 10%–15% of renal carcinomas calcify with the calcification being central or peripheral (Fig. 34.21). When peripheral, the calcification tends to be thick

**A****B**

**Fig. 34.21A, B.** Bilateral renal cell carcinoma. A Excretory urogram shows a calcified mass in the right upper pole (arrow) and a large non-calcified mass in the upper pole of the left kidney causing downward displacement of the collecting structures. B CT scan through the right upper pole shows a mass of high attenuation with thick, irregular, calcified margins.

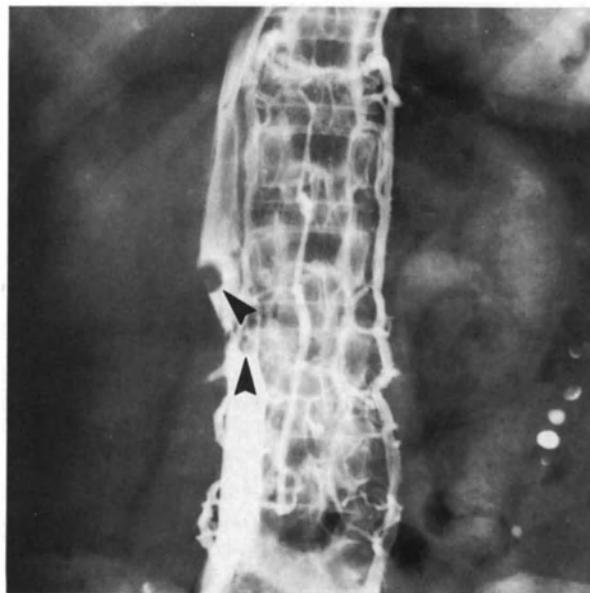


**Fig. 34.20.** Renal cell carcinoma. Tumor extension into the inferior vena cava is demonstrated (arrowheads) on a cavogram. Multiple collaterals ascending lumbar vessels are opacified as well. The right kidney is enlarged and non-functioning due to the tumor thrombus.

and interrupted and often associated with a soft tissue mass. While the majority of peripherally calcified masses are complicated cysts, 20% prove to be carcinomas.

*Renal Angiography.* Renal angiography is no longer primarily used in the diagnosis of renal tumors, having been supplanted by ultrasound and CT. The study still provides information which may be useful to the surgeon, that is, the extent of neovascularity and the presence of parasitized vessels. Renal cell carcinomas are hypervascular in 75% of cases, demonstrating vessel irregularity, tumor encasement, puddling of contrast, arteriovenous fistulae, early draining veins and large capsular vessels (Fig. 34.22). Hypernephromas are in 20% of cases hypovascular and in 5% avascular. Occasionally renal *embolization* is utilized to decrease the vascularity of the tumor prior to surgery. It has been proposed that infarction of the tumor with a delay of a week until surgery may boost the patient's immune competence toward that tumor. Enthusiasm for this approach has been tempered by uncertain results and by the unpleasant post-infarction syndrome which the patient must suffer.

*Aspiration and Percutaneous Biopsy.* Cyst puncture and fine needle aspiration biopsy can be utilized in the evaluation of



**Fig. 34.22.** Renal cell carcinoma. Abdominal aortogram demonstrates an intensely hypervascular right tumor with enlarged feeding vessels and puddling of contrast.



**Fig. 34.23.** Renal cell carcinoma. MR scan, coronal section, T<sub>2</sub>-weighted image demonstrates a well-encapsulated left renal mass with both high and low signal intensity. Large collateral vessels are present. Hemorrhage into the mass and perirenal space was found at operation.



**Fig. 34.24.** von Hippel-Lindau disease. Contrast CT scan shows multiple cysts and masses in the kidneys. Note also the cysts and calcifications in the pancreas. (Courtesy of R. Dyer.)

indeterminate cystic lesions or to determine whether a renal lesion in a patient with a known primary malignancy elsewhere has a metastasis or a second primary tumor. Otherwise, it is not necessary to biopsy clearly solid lesions which should be treated surgically. Needle tract seeding of the puncture site is unlikely to occur when small gauge needles are used.

**MR.** Renal cell carcinomas vary in their MR characteristic although these masses usually show an intensity intermediate between the renal cortex and medulla on T<sub>1</sub>-weighted images and appear hyperintense on T<sub>2</sub>-weighted images (Fig. 34.23). Magnetic resonance imaging has not superseded CT in the detection of renal masses. Small solid renal tumors which do not alter renal contours can be difficult to detect due to isointensity with the surrounding normal renal tissue. The use of paramagnetic contrast agents may improve MR capability in the future. MR can readily identify tumor within the renal vein or vena cava since the usual signal void created by flowing blood is replaced by a tissue signal similar to the intrarenal malignancy.

There is little difference in the accuracy of MR versus CT in the staging of renal cell carcinoma. Neither method is reliable in distinguishing Stage 1 from Stage 2 lesions.

#### The Relationship of Cysts to Renal Cell Carcinoma

The relationship of cysts to renal tumors is complex and can take one of the following forms:

1. Coincidental cyst and tumor in the same kidney with no other relationship
2. Simple cyst immediately adjacent to a tumor. It is possible that the tumor is responsible for the development of the cyst.
3. Multiple cysts and multiple tumors in patients with *von Hippel-Lindau syndrome* or *chronic renal dialysis* (Fig. 34.24)
4. Cystic degeneration of a renal tumor due to necrosis (Fig. 34.18)
5. Cystic growth pattern in a renal tumor
6. Cyst containing a mural nodule of tumor

#### Wilms' Tumor

Wilms' tumor (nephroblastoma) is the most common renal tumor in children, usually occurring between ages 1 and 4 years and rarely seen after the age of 7 years. It usually presents with an abdominal mass, and there may be hematuria and hypertension. The tumor is bilateral in 5%–13%. Associations with congenital hemihypertrophy, aniridia and other genitourinary abnormalities (cryptorchidism, horseshoe kidney, hypospadias) are known. Wilms' tumor metastasizes most commonly to the lungs.

*Excretory urography* demonstrates a mass which is more frequently found in the upper pole of the kidney (Fig. 34.25). Calyceal distortion instead of displacement helps distinguish this lesion from obstructed upper pole duplications and adrenal neuroblastomas. *Calcification* is present in the tumor in 10% of cases.

*Ultrasound* demonstrates a solid lesion which may be somewhat heterogeneous due to tumor necrosis or hemor-



**Fig. 34.25.** Wilms' tumor. Excretory urogram in a child shows distortion and splaying of the calyces of the left kidney by a large tumor.

rhage. This modality is useful in detection of tumor spread into the inferior vena cava although large tumors may compress venous structures to the extent that they cannot be identified.

CT is not as satisfactory in the child as in the adult because of the relative paucity of retroperitoneal fat. CT will confirm the presence of a mass and aid in tumor staging and evaluation of the contralateral kidney. MR is valuable in the determination of the origin of the mass and in detecting intravascular extension.

#### Renal Lymphoma

Primary renal lymphoma is very rare since there is no lymphoid tissue in the kidney. Instead, renal lymphoma results from hematogenous metastases or from contiguous extension from retroperitoneal lymphoma. Usually, hematogenous dissemination results in multiple bilateral



**Fig. 34.26.** Lymphoma. CT shows bilateral renal parenchymal masses and enlarged retroaortic and left perihilar lymph nodes.

parenchymal nodules. Less frequently a single lesion will be found. Direct invasion from a retroperitoneal source can occur through the capsule into the cortex or ascend the ureteral wall and pelvis into the renal sinus. Interstitial growth in the kidney preserves internal renal architecture.

*Excretory urography* may show multiple nodules with a nephrogram resembling polycystic kidneys, a solitary lesion mimicking renal cell carcinoma, or renal enlargement with attenuation and compression of the collecting structures. If sufficient renal parenchyma is infiltrated and destroyed, non-function may be present. Obstructive uropathy from uric acid calculi can occur during the course of the disease.

On *ultrasound* examination lymphomatous masses are homogeneous and hypoechoic. They can be identified in the perirenal lymph nodes as well as in the renal parenchyma.

CT is the most useful modality in the evaluation and follow-up to the lymphoma patient with accurate depiction of renal parenchymal masses, perirenal extension and retroperitoneal lymphadenopathy. Splenomegaly and thickening of Gerota's fascia may be present. Renal masses are usually isodense with the unenhanced renal parenchyma. With contrast, they enhance slightly and become hypodense to the renal parenchyma (Fig. 34.26).

MR of lymphoma presents as low-intensity, homogeneous masses on T<sub>1</sub>-weighted images with a similar appearance to the accompanying lymphadenopathy.

#### Leukemia

The kidney is frequently involved in leukemia, especially chronic lymphocytic leukemia. The disease causes a diffuse infiltration with bilateral smooth renal enlargement and attenuated collecting systems. Obstructive uropathy may occur as a result either of blood clots from intrarenal hemorrhage or uric acid calculi from increased cell turnover associated with the disease.

#### Renal Metastases

Renal metastases are usually clinically silent. The most frequent source is from *squamous cell carcinoma of the lung*. When advanced metastatic disease is present elsewhere in the body, the finding of a new renal mass is likely to represent a metastasis to kidney. These lesions are indistinguishable from primary renal cell carcinoma. The imaging modality most sensitive to the detection of metastases is *contrast-enhanced CT*. Features which suggest metastasis over primary tumor include multiplicity, bilaterality, and association with metastatic deposits in other organs. The lesions tend to be small in size (Fig. 34.27). When the distinction between a metastasis and a primary renal cell carcinoma is clinically important, *percutaneous needle biopsy* may be performed.

*Differential Diagnosis.* Multiple renal masses can occur with *lymphoma*, *multifocal renal cell carcinoma*, *von Hippel-Lindau disease*, and *multifocal bacterial nephritis*. Clinical features are usually helpful in make the diagnosis.

#### Tumors of the Renal Pelvis and Ureter

*Transitional cell carcinoma*, which accounts for 10% of all primary malignant renal tumors, is the most common tumor of the renal collecting system. There is a 2:1 male to female ratio and the tumor occurs most during the 6th and 8th



**Fig. 34.27.** Multiple, bilateral low density renal masses due to metastases from small cell carcinoma of the lung, proven by CT-guided percutaneous biopsy.

decades. Etiologic factors may include tobacco smoking, exposure to chemical agents, and phenacetin. Patients with analgesic or Balkan nephropathy or a past history of bladder transitional cell carcinoma are at particular risk.

**Imaging.** On *excretory urography*, radiographically detectable transitional cell carcinoma is usually papillary in nature, presenting as a radiolucent filling defect projecting into the lumen (Fig. 34.28). It must be distinguished from non-opaque calculus, blood clot, aberrant renal papilla, sloughed papilla, cholesteatoma, fungal ball, pyeloureteritis cystica, or vascular impression. Large invasive tumors or small, strategically located tumors can cause hydronephrosis. Rarely, calcification appearing stippled or granular is seen in these tumors. When the growth pattern is infiltrating, transitional cell carcinoma presents at urography as infundibular narrowing, an amputated calyx, parenchymal mass or renal non-function. When *excretory urography* is suspicious for transitional cell carcinoma, *retrograde pyelography* can be utilized to show mucosal surfaces in greater detail and provide access for brush biopsy.

If the tumor lies in the ureter, the ureter expands to accommodate the lesion. This creates a 'wine-goblet' appearance to the ureter distal to the tumor (Fig. 34.29). Less commonly, an infiltrating growth pattern in the ureter can result in the appearance of a smooth ureteral stricture. If the distinction cannot be made at urography, *CT* is able to distinguish between a calculus and tumor. Tumor is identified as a soft tissue mass which enhances with contrast (Fig. 34.30).



◀ **Fig. 34.28.** Transitional cell carcinoma. Excretory urogram shows a large, lobulated filling defect occupying the entire left renal pelvis.

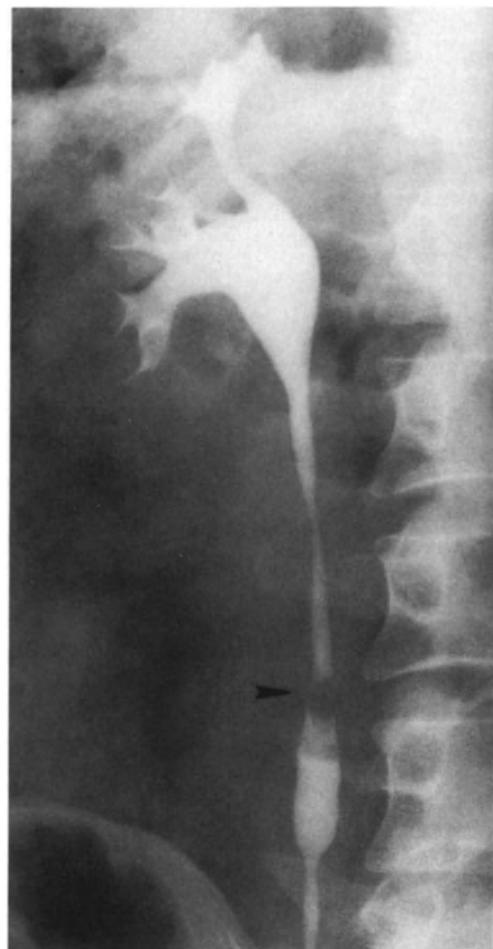


**Fig. 34.29.** Transitional cell carcinoma. Retrograde pyelogram demonstrated an irregular filling defect of the upper ureter.



**Fig. 34.30.** Transitional cell carcinoma. Contrast CT scan reveals a soft tissue opacity (cursor reading 68 HU) within the lateral aspect of the right renal pelvis.

Although CT is inferior to excretory urography and retrograde pyelography in the detection of transitional cell carcinoma, it is useful in *staging* the tumor.

*Angiography* is rarely utilized in this condition but the tumor is hypovascular in nature.

**Squamous Cell Carcinoma** is much less commonly seen than transitional cell carcinoma, affects an older age group and is usually associated with chronic infection, calculus disease and leukoplakia (a premalignant form of squamous metaplasia of the urothelium). The tumor cannot be distinguished radiographically from an infiltrating transitional cell carcinoma.

#### REFERENCES AND SUGGESTIONS FOR FURTHER READING

##### CYSTIC DISORDERS OF THE KIDNEYS

- Amis ES, Cronan JJ (1988) The renal sinus: An imaging review and proposed nomenclature for sinus cysts. *J Urol* 139: 1151-1155
- Basile JJ, McCullough DL, Harrison LH, Dyer RB (1988) End stage renal disease associated with acquired cystic disease and neoplasia. *J Urol* 140: 938-943
- Becker JA, Schneider M (1975) Simple cyst of the kidney. *Semin Roentgenol* 10: 103-108
- Bosniak MA (1986) The current radiological approach to renal cysts. *Radiology* 158: 1-6
- Bosniak MA, Ambos MA (1975) Polycystic kidney disease. *Semin Roentgenol* 10: 133-138
- Elkin M, Bernstein J (1969) Cystic disease of the kidney - radiologic and pathologic considerations. *Clin Radiol* 20: 65-71
- Garel LA, Habib R, Tariante D, Broyer M, Sauvegrain J (1984) Juvenile nephronophthisis: Sonographic appearance in children with severe anemia. *Radiology* 151: 93-99
- Gordon RL, Pollack HM, Popky GL, Duckett JW (1979) Simple serous cyst of the kidney in children. *Radiology* 131: 357-362
- Jabour BA, Ralls PW, Tang WW et al. (1987) Acquired cystic disease of the kidneys. Computed tomography and ultrasonography appraisal in patients on peritoneal and hemodialysis. *Invest Radiol* 22: 728-732
- Mitnick JS, Bosniak MA, Hilton S, Raghadendra BN, Subramanyam BR, Geneiser NB (1983) Cystic renal disease in tuberous sclerosis. *Radiology* 147: 85-91
- Pulubinskas AJ (1961) Medullary sponge kidney. *Radiology* 76: 911-915
- Rosenfield AT, Siegel NJ, Kappelman NB, Taylor KJW (1977) Gray scale ultrasonography in medullary cystic disease of the kidney and congenital hepatic fibrosis with tubular ectasia. *AJR* 129: 297-301
- Rosenberg ER, Korobkin M, Foster W, Silverman PM, Bowie KD, Dunnick NR (1985) The significance of septations in a renal cyst. *AJR* 144: 593-597
- Sussman S, Cochran ST, Pagani JJ et al. (1984) Hyperdense renal masses: A CT manifestation of hemorrhagic renal cysts. *Radiology* 150: 207-212
- Zirinsky K, Yong HA, Rubenstein WA et al. (1984) CT of the hyperdense renal cyst: sonographic correlation. *AJR* 143: 151-158
- RENAL NEOPLASMS**
- Balfe DM, McClellan BL, Stanley RJ et al. (1982) Evaluation of renal masses considered indeterminate on computed tomography. *Radiology* 142: 421-428
- Baltarowich OH, Kurtz AB (1987) Sonographic evaluation of renal masses. *Urol Radiol* 9: 79-83
- Bennington JL, Beckwith JB (eds) (1975) Tumors of the kidney, renal pelvis and ureter. Atlas of tumor pathology, ser. 2, fasc. 12 Washington, DC: Armed Forces Institute of Pathology, 243-311
- Bosniak MA, Megibow AJ, Hulnick DH et al. (1988) CT diagnosis of renal angiomyolipoma: the importance of detecting small amounts of fat. *AJR* 151: 497-501
- Bruneton N, Ballanger P, Ballanger R et al. (1979) Renal adenomas. *Clin Radiol* 30: 343-348
- Choyke PL, White EM, Zeman RK et al. (1987) Renal metastases: clinicopathologic and radiologic correlation. *Radiology* 162: 359-363
- Curry NS, Schabel SI, Betsill WL Jr (1986) Small renal neoplasms: diagnostic imaging pathologic features and clinical course. *Radiology* 158: 113-117
- Dunnick NR, Hartman DS, Ford KK et al. (1983) The radiology of juxtaglomerular tumors. *Radiology* 147: 321-328
- Fein AB, Lee JKT, Balfe DM et al. (1987) Renal cell carcinoma: MRI and CT staging. *AJR* 148: 749-753
- Hartman DS, David CJ, Goldman SM, Friedman AC, Fritzsche P (1982) Renal lymphoma: radiologic pathologic correlation of 21 cases. *Radiology* 144: 759-763
- Hricak H, Thoeni R, Carroll PR et al. (1988) Detection and staging of renal neoplasms: a reassessment of MR imaging. *Radiology* 166: 643-648
- Madwell JE, Goldman SM, David CJ, Hartman DS et al. (1983) Multilocular cystic nephroma: a radiographic-pathologic correlation of 58 patients. *Radiology* 146: 30-34
- Levine E, Grantham JJ, Slusher SL (1984) CT of acquired cystic kidney disease and renal tumors in long-term dialysis patients. *AJR* 142: 125-129
- Mulhern CB, Arger PH, Coleman BG (1982) Wilms' tumor: diagnostic and therapeutic implications. *Urol Radiol* 4: 193-198
- Parienty RA, Pradel J, Parienty I (1985) Cystic renal cancers: CT characteristics. *Radiology* 157: 741-746
- Pollack HM, Banner MP, Arger PH et al. (1982) The accuracy of gray-scale renal ultrasonography in differentiating cystic neoplasms from benign cysts. *Radiology* 143: 741-747
- Quinn MJ, Hartman DS, Friedman AC et al. (1984) Renal oncocyotoma: new observations. *Radiology* 153: 49-53
- Warshauer DM, McCarthy SM, Street L et al. (1988) Detection of renal masses: sensitivities and specificities of excretory urography/linear tomography, US and CT. *Radiology* 169: 363-368

## CHAPTER 35

# CALCULI: INFECTION: MISCELLANEOUS

Nancy S. Curry

---

## URINARY TRACT CALCULI (UROLITHIASIS)

---

Approximately 90% of calculi affecting the urinary tract are *radiopaque*. These calculi consist of a mucoprotein matrix with various, frequently mixed crystalline aggregates of calcium oxalate, calcium phosphate, calcium carbonate, magnesium ammonium phosphate and urates. In pure form, cystine stones are *poorly opaque* and have a 'ground glass' appearance while pure uric acid, xanthine, and matrix calculi are *radiolucent*.

Urolithiasis is most commonly **idiopathic**, but it may also occur **secondary to metabolic disorders or anatomic defects**. The usual type of stone formed is calcium oxalate or calcium phosphate with no identified etiology. Formation of these calculi may possibly be related to such factors as hypercalciuria, lack of inhibiting substance in the urine, or inability to acidify the urine.

**Metabolic disorder** calculus formation occurs in hyperoxaluria, xanthinuria, cystinuria, abnormal uric acid metabolism and conditions that result in hypercalcemia.

*Xanthinuria* results from a rare inherited abnormality in the oxidation of purines. *Cystinuria* is an inherited disorder of amino acid transport.

*Primary hyperoxaluria* is a rare inherited disease which is responsible for urolithiasis and nephrocalcinosis. *Secondary hyperoxaluria* occurs in the setting of distal small bowel disease such as Crohn's disease, ulcerative colitis, jejuno-ileal bypass or small bowel resection with interruption of normal bile acid metabolism. Excess resorption of oxalates leads to hyperoxaluria and calcium oxalate stone formation. There is also an increased incidence of *uric acid* calculi in these patients because of dehydration and bicarbonate loss.

Patients with *hypercalcemia* usually form calcium phosphate calculi. Disease states associated with hypercalcemia

include hyperparathyroidism, milk-alkali syndrome, hypervitaminosis D, prolonged immobilization, sarcoidosis, Cushing's disease, and hyperthyroidism.

Accounting for approximately 10% of calculi in the USA, *uric acid* calculi usually occur in middle-aged men with elevated uric acid levels in the urine. These stones also occur in conditions of hyperuricemia such as gout, myeloproliferative disease, or malabsorptive disorders. In pure form these calculi are radiolucent, but they are frequently mixed with opaque components.

Any **anatomic** congenital or acquired abnormality which leads to *urinary stasis* is a predisposing factor in calculus formation. Congenital ureteropelvic junction obstruction, pyelogenic cysts, horseshoe kidney, vesical diverticula and bladder outlet obstruction may all become complicated by calculi.

The radiologist's role in calculous disease is to determine the size, number, position and interval change in stones. 'Metabolically active' stones demonstrate increase in size and number over a period of time, and 'surgically active' stones shift from unobstructing, asymptomatic location to a position of potential or actual obstruction.

The radiologist also plays an important role in therapeutic management of nephroureterolithiasis. *Extra-corporeal shock wave lithotripsy* (ESWL) has become standard management of small intrarenal calculi in most large centers. A lithotripsy device generates repetitive shock waves which are focused on the stone within the kidney, pulverizing it into fragments. The fragments are usually passed without difficulty. Large calculi may be treated by a combination of percutaneous extraction, percutaneous ultrasonic lithotripsy, ESWL, or dissolution by chemical irrigation. These calculi usually



**Fig. 35.1.** Staghorn calculus outlining the collecting system of the left kidney.

require the placement of one or more percutaneous nephrostomy catheters and tube tract dilation which requires the skills of the interventional radiologist.

**Imaging. Radiographic Features.** Calcium oxalate calculi are usually quite dense with a stippled appearance. In the urinary bladder they can become quite large with a stellate, 'jackstone' appearance.

**Triple phosphate** calculi (magnesium-ammonium-calcium phosphate) are usually the components of a branched, 'staghorn' calculus (Fig. 35.1). These calculi are frequently laminated. They occur as the result of infection with urea-splitting organisms (commonly *Proteus mirabilis*) which raise urinary pH and predispose to their formation. Other, less common staghorn calculi are formed by uric acid or cystine stones.

**Milk of calcium** stones are tiny calculi which are too small to be visualized radiographically as discrete entities. They appear as milky opacities which will layer out dependently on upright or decubitus views.

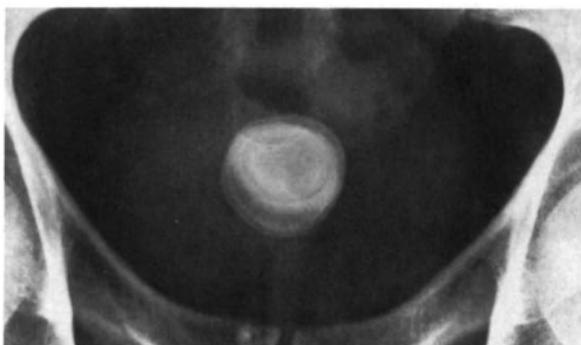


**Fig. 35.2.** Bladder calculus. Note the laminations.

Ureteral calculi are usually single unless the patient has undergone a lithotripsy procedure where a cascade of small stone fragments line up along the path of the ureter ('steinstrasse'). Bladder calculi lie in the middle of the bladder unless trapped in a vesical diverticulum or displaced by a large prostate (Fig. 35.2).

**Excretory Urography.** Oblique views are important prior to contrast radiography to locate the origin of opacities overlying the kidneys. Inspiratory films or tomography may also be helpful. Obstructing ureteral calculi frequently tend to lodge at the ureteropelvic junction or at the level of the common iliac vessels. These areas should be inspected carefully on the preliminary radiograph. Pelvic and lumbar phleboliths may mimic calculi.

A patient with acute ureteral colic may demonstrate splinting of the lumbar spine (curvature convex to the opposite side). The affected kidney becomes smoothly enlarged and demonstrates an increasingly dense, persistent nephrogram with time. Excretion into the pyelocalyceal system is delayed, often for many hours. The examination should be carried out until the pyelocalyceal system and ureter are sufficiently opacified to define the site and source of obstruction. Maintaining the patient in the prone or upright position between radiographs will allow the contrast material to 'settle' distally and reduce the number of films necessary to complete the study. When visualized, the ureter appears mildly dilated with a standing column of contrast to the level of obstruction (Fig. 35.3). Edema at the ureterovesical junction from impaction of a calculus can cause mass effect in the bladder at that point.

**Ultrasound** is not used as a primary methodology for detection of intra-renal calculi although calculi can be identified as bright echoes with sharply marginated acoustic shadows (Fig. 35.4).

**CT** can differentiate between a tumor of soft tissue density and a non-opaque calculus which shows high attenuation (Fig. 35.5).

## NEPHROCALCINOSIS

While nephrolithiasis is a term describing the presence of calculi in the pelvicalyceal system, nephrocalcinosis refers to parenchymal calcification. Focal calcifications associated with tumor, cysts, infarcts or inflammatory masses are not included in this classification. Nephrocalcinosis may occur in either the cortex or the medulla. Table 35.1 lists some of the more common etiologies associated with each.

**Cortical Nephrocalcinosis.** Infrequently encountered, cortical nephrocalcinosis usually occurs as a result of *acute cortical necrosis* or *chronic glomerulonephritis*. Occasionally a *rejected renal transplant* will show cortical calcification. Cortical necrosis develops as the result of near-fatal hemorrhage or other condition leading to severe hypotension and cortical non-perfusion. Chronic glomerulonephritis in *Alport's syndrome* (hereditary nephropathy and nerve deafness) is also associated with cortical nephrocalcinosis.

**Radiographically** the condition is recognized as peripheral, diffuse cortical calcifications in kidneys with preserved con-

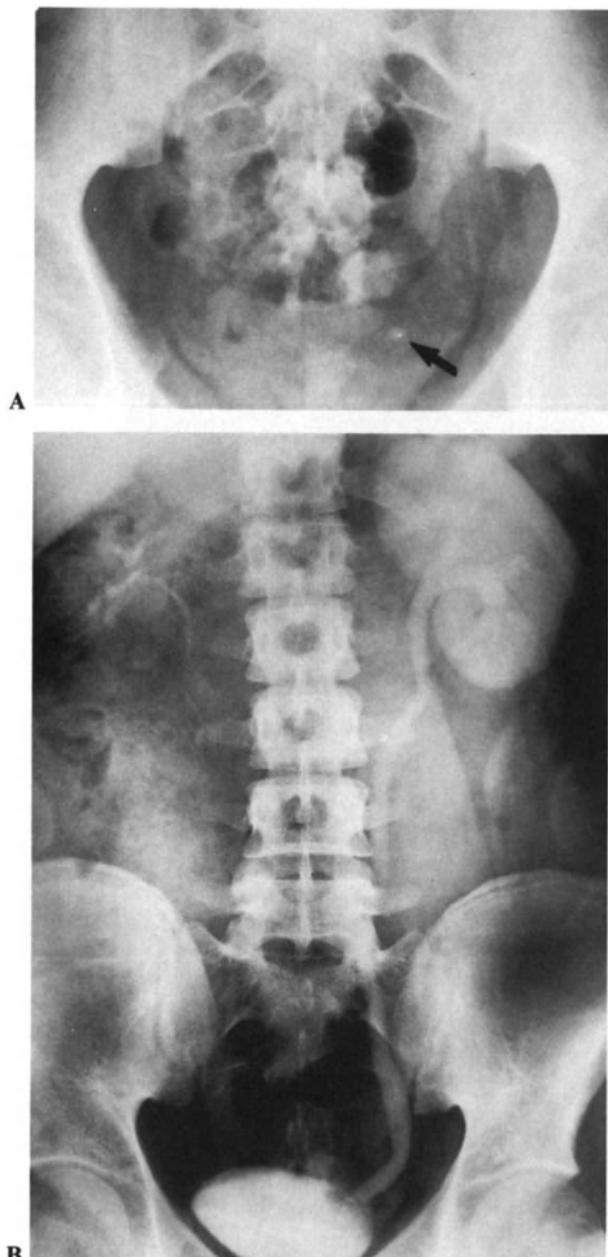


**Fig. 35.3A, B.** Left ureteral calculus with acute obstruction. A Preliminary radiograph demonstrates a small, opaque calculus at the left ureterovesical junction. B Delayed film shows a persistent, dense nephrogram and mild dilation of the ureter to the level of the calculus. Note vesical edema at the UVJ.

tours but with marked atrophy (Fig. 35.6). Sometimes two 'tramline' parallel tracks of calcification are seen.

**Medullary Nephrocalcinosis.** Clustered aggregates of calcification in the medullary pyramids are seen in many conditions associated with hypercalciuria and hypercalcemia. The most common conditions associated with medullary nephrocalcinosis are *primary hyperparathyroidism*, *renal tubular acidosis* and *medullary sponge kidney*. Other conditions are listed in Table 35.1.

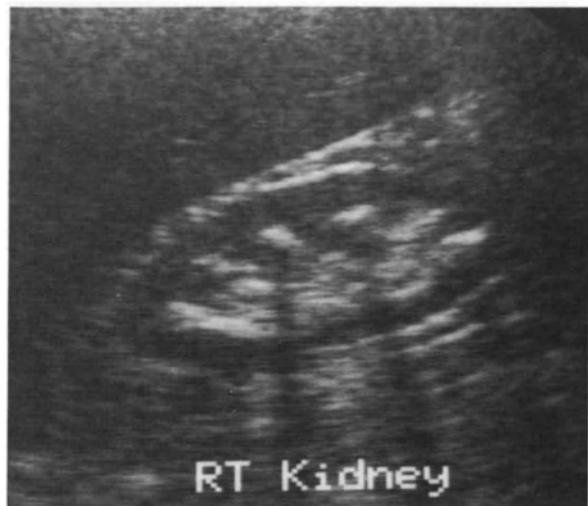


**Fig. 35.4.** Ultrasound in a patient with multiple small intrarenal calculi due to medullary sponge kidney. The calculi appear as bright echoes with strong acoustic shadows.

**Table 35.1. Nephrocalcinosis**

Cortical	acute cortical necrosis chronic glomerulonephritis rejected renal transplants
Medullary	
	primary hyperparathyroidism renal tubular acidosis medullary sponge kidney primary hyperoxaluria sarcoidosis milk-alkali syndrome hypervitaminosis D nephrotoxic drugs multiple myeloma Paget's disease hyperthyroidism bone metastases prolonged immobilization



**Fig. 35.5.** Non-contrasted CT scan shows high attenuation right renal pelvic calculus adjacent to a ureteral stent (arrow) placed for hydronephrosis. The calculus was not visible on plain radiographs.



**Fig. 35.6.** Cortical nephrocalcinosis. This 13-year-old boy developed proliferative glomerulonephritis at 18 months of age. The renal cortex has calcified and both kidneys are small.

Dense and extensive calcification often occurs in renal tubular acidosis (Fig. 35.7). Type 1 RTA is a type of distal tubular dysfunction in which there is inability to excrete an acid urine due to disordered hydrogen ion exchange. This results in systemic acidosis, persistently alkaline urine, and calculi and medullary nephrocalcinosis in the majority of patients with the abnormality. Type 2 RTA which is a proximal tubular dysfunction is not associated with calculi.

Distinction between the various causes of medullary nephrocalcinosis can be difficult. The calculi associated with medullary sponge kidney (Fig. 35.8) appear to 'grow' as contrast surrounds them in the cystic spaces in which they lie. Cysts and dilated tubules not containing calculi also opacify helping to identify this condition.

#### LOWER URINARY TRACT UROLITHIASIS

##### Bladder Calculi

Primary calculi of the bladder are rare and occur in undeveloped countries where dietary deficiencies may be the cause of non-opaque or poorly opaque bladder calculi in



**Fig. 35.7.** Medullary nephrocalcinosis. Renal tubular acidosis has resulted in dense, grouped calculi in the medullary regions of both kidneys.

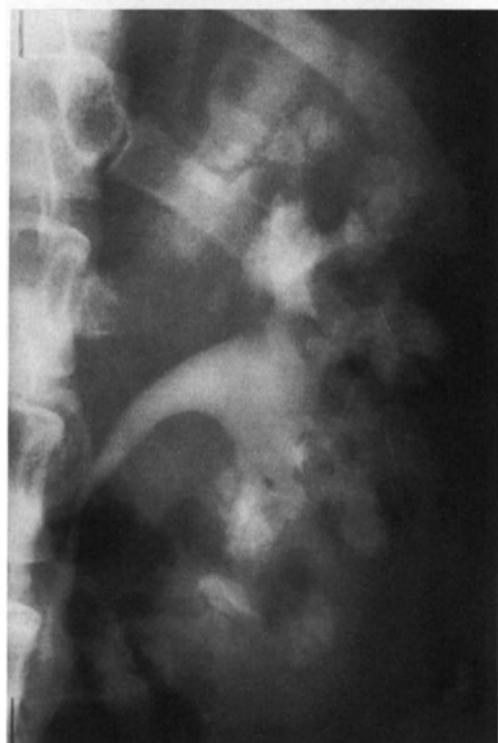
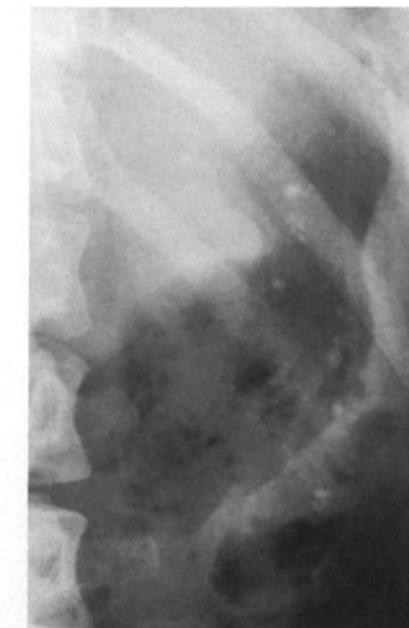


**Fig. 35.8A, B.** Medullary nephrocalcinosis in a patient with medullary sponge kidney. **A** Preliminary radiograph demonstrates small clusters of calculi over the medullary portions of the left kidney. **B** Following intravenous contrast injection, a close-up image of the left kidney demonstrates the classic, striated appearance of medullary sponge kidney, with the calculi lying within the dilated collecting tubules.

patients without other reason to have calculi. Usually children, particularly young boys, are affected.

Secondary bladder calculi occur in adults due to some anatomic abnormality which is associated with urinary

stasis. These include *neurogenic bladder*, *bladder outlet obstruction* from prostatism or urethral strictures, *bladder diverticula*, and large *cystoceles*. The calculi formed may be single or multiple, very dense or poorly opaque depending on their composition. The calculi may be laminated when associated with an alkaline urine and chronic infection. The position of the calculi is dependent on the associated bladder pathology. Free stones will lie centrally in the lower pelvis, while calculi entrapped in diverticula will lie eccentrically. Calculi associated with cystoceles may have a position well below the pelvis (Fig. 35.9).

Another etiology for bladder calculi is the presence of a *foreign body* which serves as the nidus for stone formation. Foley catheter balloon fragments, suture material, self-inserted objects all may become encrusted.

Migrant calculi in transit from an upper urinary tract origin are another source of bladder calculi.

### Prostate Calculi

Small grouped calcifications can be seen overlying the expected region of the prostate in older men. They originate in the prostatic ducts and while extensive calcifications may be associated with chronic prostatitis, they may be idiopathic and not associated with clinical symptomatology.

### Urethral Calculi

Calculi in the urethra occur during passage from an upper urinary tract origin or from native formation within a diverticulum or proximal to a stricture.



**Fig. 35.9.** Huge calculi which have formed in the markedly prolapsed bladder in an elderly female.

---

## INFECTION

---

### Acute Pyelonephritis

Acute pyelonephritis is usually the result of an ascending gram-negative bacterial infection acquired from contamination of the urethra by colonic flora. Except in intravenous drug abusers, hematogenous seeding of the kidney from a staphylococcal or streptococcal focus rarely occurs in the modern era of antibiotics. Acute pyelonephritis presents with the symptom complex of fever, flank pain, bacteriuria and pyuria usually in an adult female. These infections which first appear in adulthood are distinctly different from urinary tract infections which occur in childhood in association with vesicoureteral reflux. The childhood disorder leads to structural damage to the kidney (reflux nephropathy) while scarring does not occur in the adult.

**Imaging.** The *urogram* in acute pyelonephritis is most frequently normal; however, the affected kidney may show smooth enlargement and calyceal attenuation due to edema, and decreased pyelographic density due to impairment of concentration (Fig. 35.10). There may be pelviectasis and ureterectasis due to endotoxic inhibition of ureteral peristalsis. The prime reason for urography in this illness is to exclude a predisposing anatomical abnormality.

**Ultrasound** examination will demonstrate renal enlargement and diminished echogenicity. The lack of significant

dilatation of the collecting system or debris in the fluid make pyohydronephrosis unlikely. Intrarenal or perirenal abscesses can also be excluded.

**CT** shows diffuse, somewhat streaky decreased attenuation in the affected kidney (Fig. 35.11). It is primarily of use in



**Fig. 35.10.** Acute pyelonephritis. Excretory urogram shows an enlarged right kidney with attenuated pelvicalyceal structures.



**Fig. 35.11.** Acute pyelonephritis. CT scan demonstrates streaky areas of decreased attenuation in the swollen left kidney.

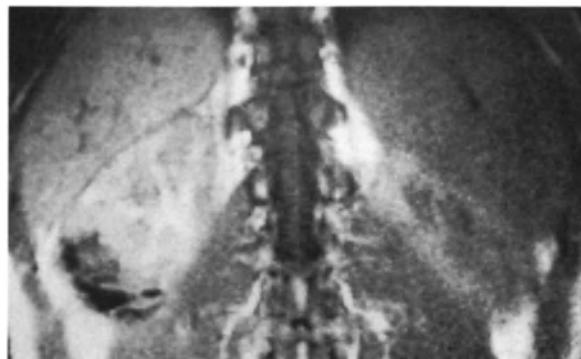


**Fig. 35.14.** Emphysematous pyelonephritis. MR scan, coronal plane, T<sub>1</sub>-weighted image shows a collection of gas in the lower pole of the right kidney.

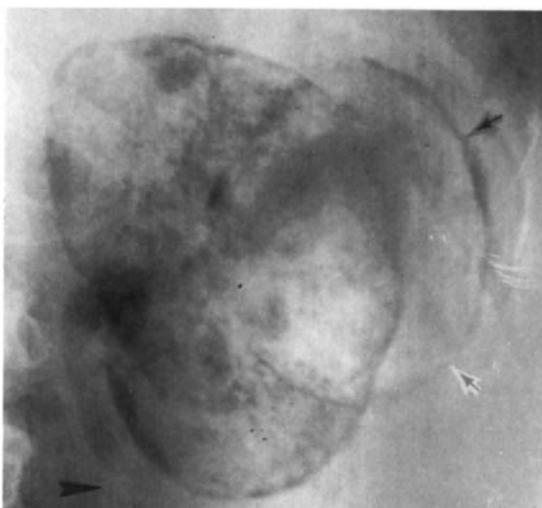


**Fig. 35.12.** Emphysematous pyelonephritis. Plain radiograph shows extensive gas lucencies in and around the left renal kidney. A renal cyst is outlined by the perirenal gas (arrows). Gas is also present in the renal pelvis and upper ureter which are obstructed by a calculus (arrowhead). (Courtesy Dr. S. Schabel.)

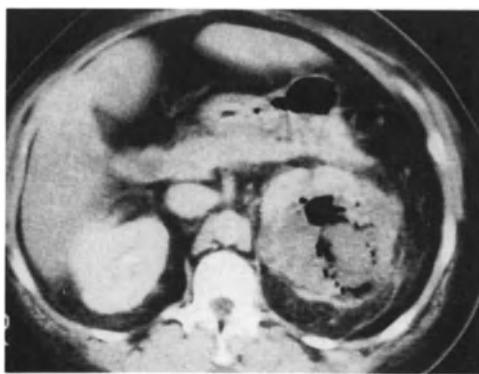


**Fig. 35.13.** Emphysematous pyelonephritis. CT scan demonstrates gas lucencies in the substance of the left kidney. Note thickening of Gerota's fascia posteriorly.

the exclusion of renal abscess when the patient is not responding to appropriate antibiotic therapy.

#### Emphysematous Pyelonephritis

Emphysematous pyelonephritis is a severe type of renal infection afflicting diabetics and patients with altered immune status. In non-diabetic patients the process is nearly always associated with obstruction. This life-threatening necrotizing infection is caused by gas-forming organisms, most frequently *E. coli*, which produce a characteristic radiographic appearance. The kidney is enlarged and non-functioning with gas radiolucencies dispersed throughout the renal substance and perirenal space (Fig. 35.12). The presence of gas interferes with sound transmission which causes a confusing image on ultrasound exam. CT and MR readily display intrarenal gas (Figs. 35.13, 35.14).

#### Focal Bacterial Nephritis

Localized renal parenchymal infection is known by a variety of terms such as focal pyelonephritis, acute focal bacterial nephritis and lobar nephronia. They indicate the presence of a focal inflammatory mass without liquefaction. The condition is usually regarded as the midpoint between a spectrum of infection ranging from acute, uncomplicated pyelonephritis to frank abscess formation in one lobe of the kidney.

*Urography* will show a non-specific mass effect while *ultrasonography* reveals a hypoechoic mass. *CT* demonstrates a wedge-shaped or rounded, non-enhancing mass of decreased attenuation with numbers higher than water density. The borders of the lesion are less well-defined than a renal abscess. *Needle aspirate* yields positive cultures of the infecting organism but no fluid. Multifocal acute bacterial nephritis may be seen in drug addicts as multiple areas of low density in enlarged kidneys (Fig. 35.15).

#### Renal and Perirenal Abscess

Renal abscesses develop in the same manner as acute pyelonephritis and may result from tissue necrosis in an area of focal pyelonephritis. On *urography* a mass is identified. *Ultrasonically* the lesion resembles a simple cyst but may con-



**Fig. 35.15.** Multifocal bacterial nephritis. Multiple, bilateral low-density areas are seen in both kidneys. The patient was an intravenous drug user.



**Fig. 35.17.** Perinephric abscess. CT of a large renal and perirenal abscess being drained by a percutaneous catheter. There is inflammatory reaction in the tissues of the flank.

tain a few internal echoes or demonstrate thick, irregular walls. *Radionuclide imaging* with gallium-67 or indium labelled white blood cells are not specific since they may be positive with masses due to either infection or tumor. On CT a well-defined, fluid density mass sometimes demonstrating an enhancing rim will be seen (Fig. 35.16). Small amounts of gas may be present in the lesion and there is often thickening of the renal fascia. Renal abscesses appear as inhomogeneous, low-intensity masses on MR and appear indistinguishable from neoplasm.

*Needle aspiration* or *catheter drainage* combined with antibiotic therapy may render surgical intervention unnecessary.

Perinephric abscesses usually initiate from an intrarenal infection although direct extension from bowel or pancreas may occur. *Urography* may demonstrate obliteration of the psoas contour, perirenal gas, lumbar splinting, and fixation of the kidney. Frequently, a non-functioning kidney with calculi is present. CT demonstrates thickening of Gerota's fascia and increased attenuation frequently in the dependent posterior pararenal space (Fig. 35.17). Extension into the flank occurs.

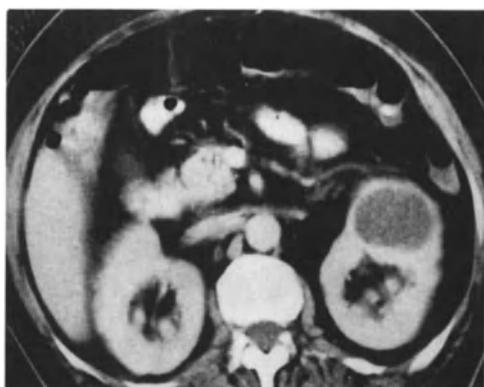


**Fig. 35.16.** Renal abscess. CT scan shows a well-defined mass in the left kidney with a thick wall and central fluid density.

### Pyonephrosis

Pyonephrosis is the term used to describe an infected hydronephrosis. The dilated collecting system is readily identified by US and CT and debris can sometimes be recognized within it.

### Xanthogranulomatous Pyelonephritis

Xanthogranulomatous pyelonephritis (XGP) is a chronic renal infection characterized by the diffuse or focal infiltration of the renal parenchyma with masses of lipid-laden histiocytes (foam cells). It develops as a complication of long-standing obstructive uropathy and is associated with calculi in 75% of cases, often staghorn in type. Female diabetics are most frequently affected and the infecting organism is usually *Proteus mirabilis*.

The commonest form of XGP is the diffuse variety with the *urographic* finding of an enlarged, non-functioning kidney with a staghorn calculus (Fig. 35.18). *Ultrasound* shows an enlarged kidney containing echogenic calculi and anechoic areas corresponding to dilated calyces and collections of pus. CT demonstrates dilated collecting structures with enhancing walls containing fluid density and highly attenuating calculi (Fig. 35.19). Extension into the perinephric and posterior pararenal spaces may occur.

With focal XGP only a portion of the intrarenal collecting structures are obstructed by calculi so that renal function is preserved. The focal (tumefactive) form of the disease can mimic an abscess, tuberculosis or neoplasm.

### Malakoplakia

Malakoplakia is closely related to XGP in that it is a granulomatous inflammatory condition of histiocytic proliferation probably related to abnormal handling of bacteria by the macrophage system. Microscopically, Michaelis-Gutman bodies are seen in the histiocytes which likely represent calcification of incompletely digested bacteria. The condition is most common in diabetics and immunocompromised patients and the infecting organism is usually *E. coli*. This condition may represent a mild form of chronic granulomatous disease of childhood.

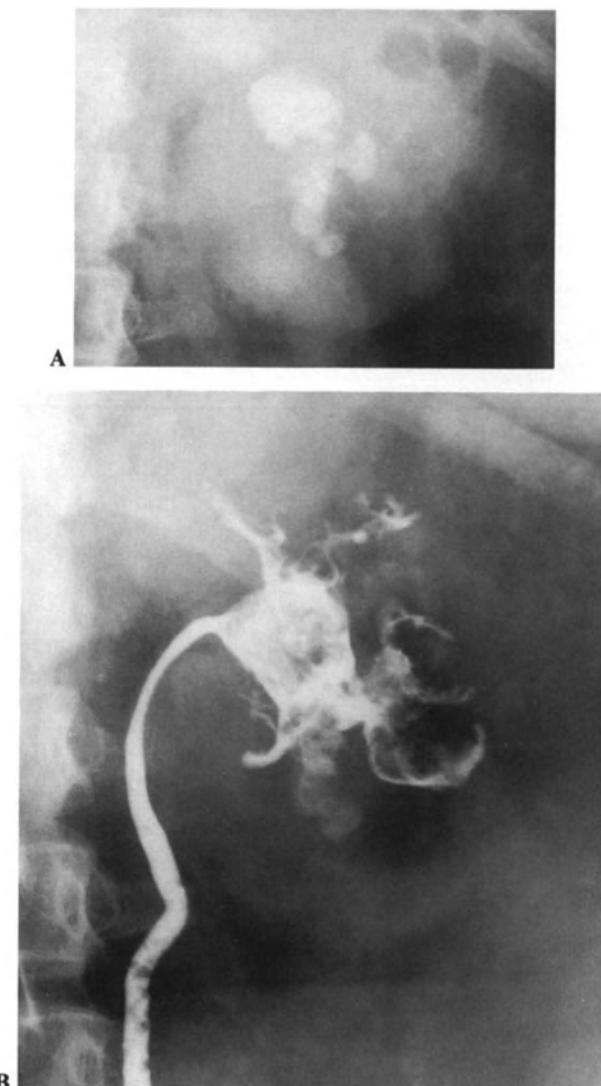


**Fig. 35.18A, B.** Xanthogranulomatous pyelonephritis. A Scout radiograph shows partial staghorn calculus overlying the pelvis and lower pole of a kidney which was non-functional on IVP. B Retrograde pyelogram demonstrates the pelvis and calyces to be filled with calculi and debris. Ureteritis cystica is present in the ureter at the level of L3–L4.

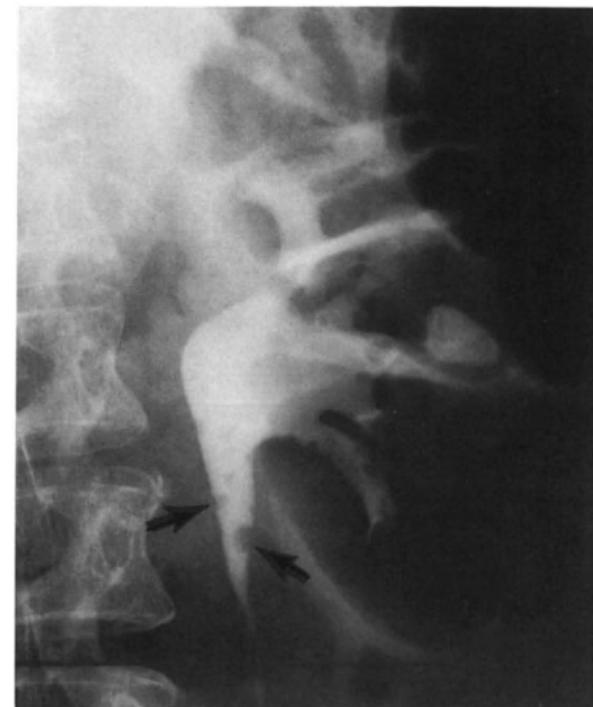
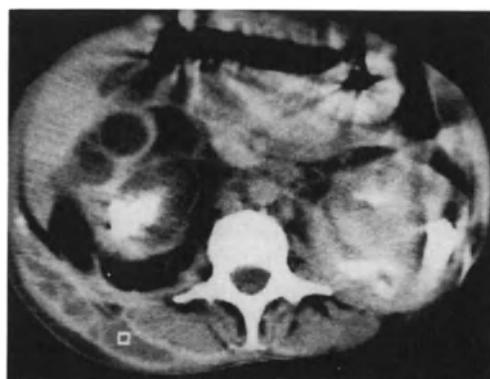


**Fig. 35.20.** Pyeloureteritis cystica. Excretory urogram in a patient with a calyceal diverticulum containing a calculus in the interpolar region. There are multiple, small cystic blebs in the pelvis and in the ureter (arrows).

The bladder and ureters are most commonly affected by this condition with rare involvement of the renal pelvis and parenchyma. Most cases of bladder malakoplakia are not radiographically detectable because the granulomatous masses are too small. Larger masses mimic bladder carcinoma. When the ureter or pelvis is involved, multiple filling defects causing hydronephrosis may be seen. With renal parenchymal involvement there may be a solitary tumefaction or multifocal masses.

#### Leukoplakia

Squamous metaplasia of the urothelium may occur as a response to chronic urinary tract infection. This condition is associated with calculi in 50% of patients and is considered premalignant. Radiographically, local or diffuse irregularities of the pelvicalyceal walls are seen. Leukoplakia and cholesteatoma are probably similar disorders although cholesteatoma is not regarded as a premalignant condition. Similar radiographic findings are present in both.

#### Pyeloureteritis Cystica

As a response to chronic urinary tract infection or stone disease, small fluid-filled cysts develop in the wall of the renal pelvis and ureter. These appear radiographically as multiple, small (1–5 mm), discrete filling defects (Figs 35.18B, 35.20).

**Fig. 35.19.** Xanthogranulomatous pyelonephritis. CT shows an enlarged, hydronephrotic, non-functioning right kidney containing an opaque calculus. Inflammatory changes are present in the soft tissues of the adjacent flank.



**Fig. 35.21.** Chronic atrophic pyelonephritis. Excretory urogram shows a small left kidney with focal scars over clubbed calyces (arrows).

The lucent filling defects produce a characteristic scalloping appearance when seen in profile. This benign condition must be distinguished from multifocal transitional cell carcinoma.

#### Chronic Pyelonephritis (Reflux Nephropathy)

Chronic pyelonephritis is the result of infection and reflux occurring in childhood. Bacteria originating in the bowel gain access to the urethra and bladder and then reach the kidney by vesicoureteral reflux. Intrarenal reflux of infected urine results in lobar infection with ultimate scar formation. Compound, refluxing papillae have rounded rather than slit-like openings which allow intrarenal reflux. These com-

pound papillae most commonly occur at the polar regions of the kidneys explaining the frequency of scarring at the poles.

*Excretory urography* demonstrates one or more areas of focal parenchymal loss directly over calyces which are clubbed due to inflammatory retraction (Fig. 35.21). Intervening areas of normal tissue show compensatory hypertrophy. Overall renal size is usually reduced and the scarring may be unilateral or bilateral. When there is reflux associated with ureteral duplication and ectopia, scarring is usually associated with the lower pole. Focal parenchymal loss is detectable on *CT* where anterior or posterior scars invisible to urography may be seen. *Radionuclide studies* can be of benefit to determine the degree of residual renal function in an affected kidney.

*Differential Diagnosis.* The scars associated with lobar infarction are not associated with the calyceal clubbing seen in chronic atrophic pyelonephritis/reflux nephropathy. Retained fetal lobation results in smooth, sharp indentations between calyces. Loss of parenchyma in chronic post-obstructive atrophy is uniform and diffuse with dilation of all calyceal groups.

#### Vesicoureteral Reflux

Backward flow of urine from the bladder to the ureter and kidney is prevented by the normal ureterovesical junction. The distal ureter enters the bladder through a relatively long, oblique intramural tunnel and has a cone-like orifice. *Primary reflux* occurs when there is a congenital abnormality of the UVJ in which the ureteral orifice is more laterally placed, has a shorter, less oblique submucosal tunnel and has a wider opening.

There are various grading systems to describe the severity of reflux and one is illustrated in Fig. 35.22. Most reflux tends to resolve spontaneously in later childhood. High grade reflux and infection results in chronic scarring which can lead to severe renal atrophy (Figs 35.23, 35.24). Progression

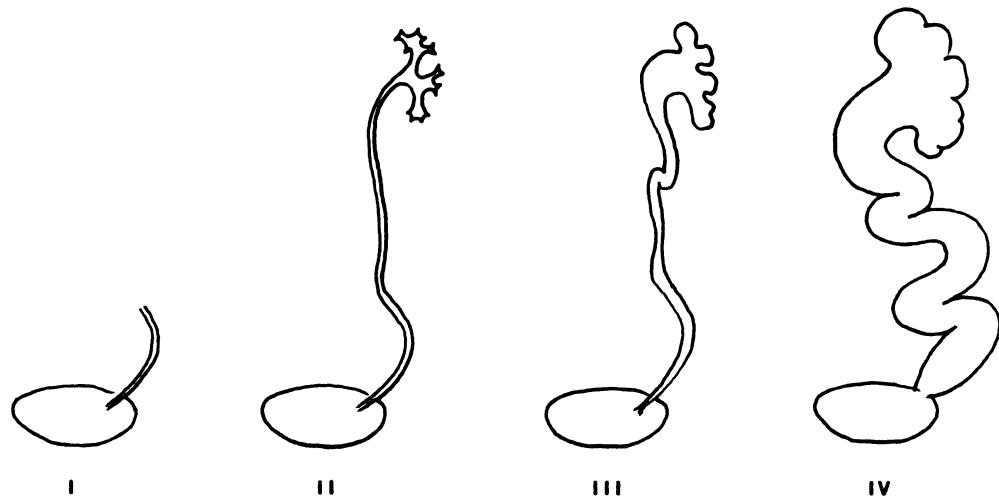


**Fig. 35.22.** Grading of vesicoureteral reflux. Grade I, lower ureteral filling; Grade II, ureteral and pelvicalyceal filling without other abnormality; Grade III, ureteral and pelvicalyceal filling with calyceal clubbing, pelvic dilatation and slight ureteral tortuosity; Grade IV, massive hydroureteronephrosis.



**Fig. 35.23.** Grade IV vesicoureteral reflux in a male child with posterior urethral valves and a trabeculated bladder.

of reflux nephropathy can be prevented by suppression of urinary tract infection or surgical reimplantation of the ureter when necessary.

Pathologic conditions which can cause reflux include *congenital anomalies* such as ureteral duplication and ectopia, vesical diverticula and *acquired disorders* such as cystitis, bladder carcinoma, neurologic dysfunction, and lower urinary tract obstruction.

#### Renal Tuberculosis

Renal tuberculosis arises primarily from hematogenous spread from a pulmonary infection although only 10%–15%

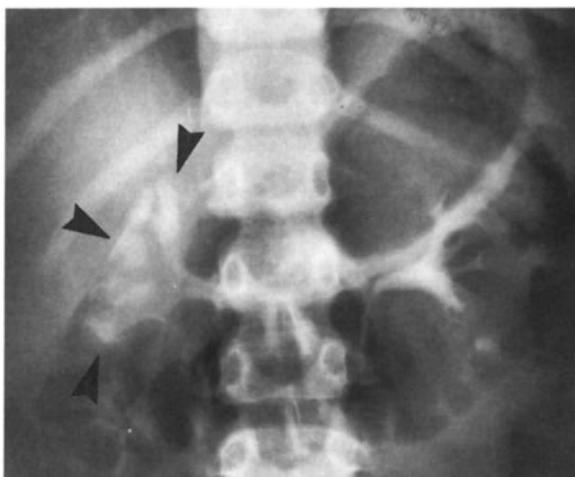


**Fig. 35.24.** Reflux nephropathy. Excretory urogram shows severe atrophy secondary to high-grade vesicoureteral reflux and infection. Note compensatory hypertrophy on the left.



**Fig. 35.25.** Renal tuberculosis. Retrograde pyelogram demonstrates moth-eaten calyces in the upper pole.

of patients have active pulmonary tuberculosis at the time of renal involvement. Urinary frequency and sterile pyuria are commonly seen. Tubercle bacilli enter the kidney through the glomerular and peritubular capillaries and although both kidneys are diffusely involved, most initial lesions heal. The surviving foci ulcerate into the tubules causing a papillitis. Further extension into the pelvicalyceal system involves the lower urinary system with reactive fibrosis and strictures.

*Imaging.* Tuberculosis of the kidney may take many forms reflecting the stage of involvement. Early in the disease there is no radiographic abnormality. When findings are present, in more than 70% of cases a single kidney is involved. The earliest radiographic manifestation on *urography* is irregularity of the calyces which appear 'moth-eaten' (Fig. 35.25). As granulomas grow and coalesce, focal masses, sometimes with calcification are seen. When they caseate and rupture into the collecting system, irregular cavities form which can mimic papillary necrosis. Parenchymal loss and scarring accompanied by calyceal dilation and distortion may resemble non-tuberculous pyelonephritis. Stricturing of the calyces and infundibula lead to one or more areas of focal hydronephrosis with a bizarre appearance on urography (Figs 35.26, 35.27). In very advanced disease the kidney is grossly destroyed and calcifies, resulting in *autonephrectomy* (Fig. 35.28).

Strictures of the ureter in tuberculosis are unifocal or multifocal. The ureter can demonstrate a rigid, shortened 'pipistem' appearance, beading due to multiple strictures or discontinuous calcification. Tuberculous cystitis leads to a small capacity, contracted bladder with mucosal irregularity due to granulomas and edema. Gross vesicoureteral reflux develops in advanced disease.

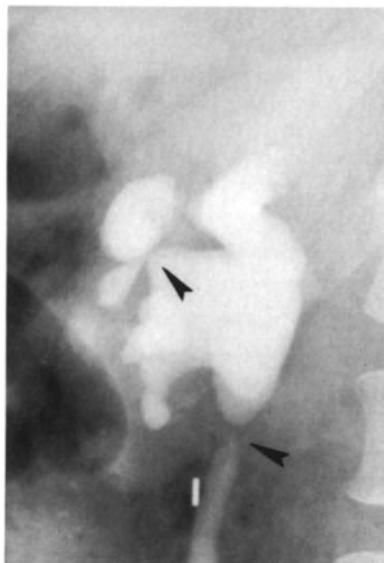


**Fig. 35.26.** Renal tuberculosis. Excretory urogram shows focal parenchymal loss and focal infundibular strictures causing clubbed, pinched-off calyces (arrowhead). Another stricture is seen in the upper ureter (lower arrowhead). Overall renal size is reduced.



**Fig. 35.27.** Renal tuberculosis. Multifocal, severe stricturing of the pelvi-calyceal system.

Tuberculosis leads to calcification of the prostate, seminal vesicals, vas deferens and epididymitis. Other findings seen in tuberculosis are psoas or paravertebral abscess.

#### Schistosomiasis

Schistosomiasis is a parasitic disease endemic to parts of Africa and the Middle East. When eggs of *Schistosoma hematobium* are voided into water, they rupture and liberate a larval form (miracidium) which enters an intermediate snail host. Within the snail, free-swimming cercaria develop which are excreted back into the water where they penetrate human skin or mucous membranes. After reaching the portal vein, adult flukes develop and migrate to the bladder where eggs are laid in submucosal veins. Penetration into the bladder lumen completes the life cycle.

In the bladder the ova produce necrosis of tissue, fibrosis and granulomas.

*Radiographically* the most distinctive finding is that of bladder wall calcification which is symmetric. Bladder capacity is normal despite calcification until late in the disease when contraction occurs. Filling defects in the bladder may be due to papillomatous granulomas or carcinoma which is a well-known complication. The malignancies that develop are squamous cell carcinoma or adenocarcinoma rather than transitional cell carcinoma which affects the normal bladder.

The ureter may demonstrate distal strictures, reflux, calcification, and filling defects due to ureteritis cystica or polyps.

#### Candidiasis

*Renal candidiasis* may be due to ascending infection or to systemic disease and occurs in the setting of immunosuppression and chronic debilitating diseases. Diabetics, neonates and patients on antibiotic or steroid therapy are at risk. The

kidney is usually not the only organ involved.

The *radiographic* manifestations are varied and can include hydronephrosis, features consistent with acute pyelonephritis, multiple abscesses, or papillary necrosis. Fungus ball formation may be identified on ultrasonography



**Fig. 35.28.** Renal tuberculosis. Autonephrectomy. The left kidney has been replaced by masses of amorphous calcified debris which also extends into the upper ureter.

as echogenic foci without acoustic shadowing. Plain radiographs or CT may demonstrate gas in the collecting structures or bladder liberated by *C. albicans* fermentation.

#### Echinococcus

Infection with the *Echinococcus* larval tapeworm usually affects the liver and lungs with renal involvement occurring in only 3% of cases. Peripheral calcification in one or more hydatid cysts may be seen on plain film. Calcified daughter

cysts may be present within the calcified parent cyst. CT reveals solitary unilocular or multilocular cortical cysts which may contain calcification. Unless similar cysts are present in the liver or daughter cysts are recognized within the parent renal cyst, the condition may be indistinguishable from other multilocular cystic disorders of the kidney. Since anaphylactic reaction can occur from spillage of cyst contents, needle puncture should not be performed if echinococcal infection is suspected.

---

### MISCELLANEOUS RENAL LESIONS (RENAL VASCULAR DISEASE: RENAL INJURY: RENAL TRANSPLANT: URETERAL DEVIATION)

---

#### Hypertension and Renal Artery Stenosis

The majority of patients with hypertension have *essential hypertension* of unknown etiology. A small percentage of patients are found to have *secondary hypertension* due to *adrenal tumor*, *aortic coarctation* or a *renal cause* for the disorder such as renal artery stenosis, renal microvascular disease, or chronic parenchymal disease. *Wilms' tumor*, occasionally *renal cell carcinoma*, or extremely rarely, a *renin-secreting juxtaglomerular tumor* may also cause hypertension.

The common pathway to hypertension among these varied conditions is the presence of *ischemia* which stimulates renin production, aldosterone release, and vasoconstrictor activity. Decrease in arterial pressure, extracellular fluid depletion, and changes in sodium concentration sensed at the macula densa, all stimulate renin production from the juxtaglomerular cells. Renin acts on angiotensinogen to produce angiotensin I which is not vasoactive. In the presence of a converting enzyme, angiotensin I is converted to angiotensin II, a potent vasoconstrictor which also stimulates aldosterone release from the adrenal gland. The resultant increased sodium absorption expands the blood volume and helps maintain perfusion pressure.

#### Renal Artery Stenosis

Renovascular hypertension caused by renal artery stenosis accounts for only about 1% of all hypertensive patients, estimated to number over thirty million in the USA. Excretory urography and radionuclide renography are not regarded as reliable screening examinations because the false-negative and false-positive rates are unacceptably high. Sensitivity is limited because the patient may have bilateral stenoses or segmental lesions. On the other hand, it should be noted that many elderly patients have renal vascular stenoses which are not hemodynamically significant and not responsible for hypertension.

**Imaging.** Imaging examinations performed to identify surgically-correctable hypertension should be restricted to patients who have the following characteristics:

1. Age under forty.
2. Worsening hypertension in the elderly.
3. Poorly-controlled hypertension.

4. Rapid onset, malignant hypertension.

5. The presence of an abdominal bruit.

*Excretory urography* demonstrates one or more of several findings in the kidney with a positive study for renal artery stenosis (Table 35.2). CT will show many of these changes in cross-sectional manifestation. Global reduction of renal size reflects decreased blood flow or ischemic atrophy of the kidney (Fig. 35.29). Focal renal infarcts from occlusion of small vessels leads to shallow scars without underlying calyceal deformity.

Table 35.2. Urographic changes in renal artery stenosis

---

Global decrease in renal size
Delayed pyelogram
Hyperconcentration of contrast
Reduced pelvocalyeal volume
Ureteral notching (collaterals)

---

Delayed excretion reflects decrease in glomerular filtration rate and results in a slower appearance of the pyelogram on the affected side. Films obtained at one-minute intervals will show this pyelographic delay.

Renal artery stenosis causes slowed transit time through the kidney which results in greater tubular reabsorption of salt and water. The excreted urine on the affected side is, therefore, hyperconcentrated and of lower volume than the normal side. Late effects of ischemia will interfere with the tubular concentrating ability which may prevent the appearance of hyperconcentration.

Collateral circulation to the ischemic kidneys derives from capsular, lumbar and periureteric branches which become enlarged and tortuous and make an impression on the pelvis and ureter. The indentations appear as multiple areas of notching.

*Radionuclide renography* is a safe and easily performed examination but has a 10% false-positive and false-negative rate. Captopril renography shows some promise of reducing the false-positive rate of the nuclear medicine study. Captopril blocks the production of angiotensin II resulting in a significant drop in glomerular filtration rate which is detected on the renogram.

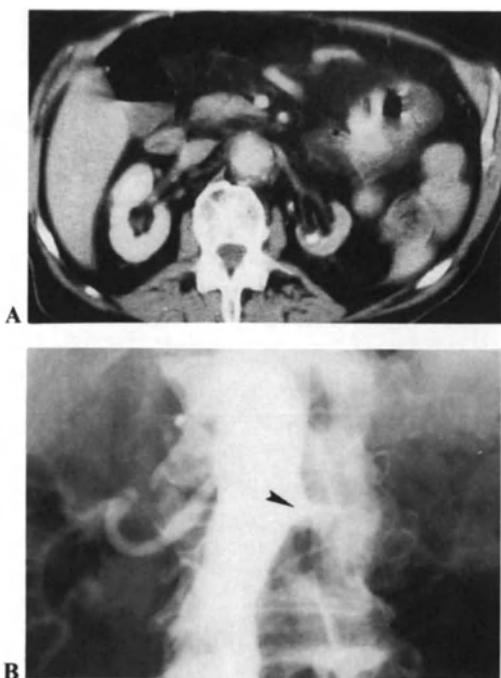


**Fig. 35.29A, B.** Ischemic atrophy of the left kidney due to renal artery stenosis caused by atherosclerotic disease. A CT scan demonstrates small left kidney with absent nephrogram. Several calculi are present. B Abdominal aortography shows near complete occlusion of the left renal artery at its origin (arrowhead).

**Digital Subtraction Angiography.** Intravenous and intra-arterial digital subtraction angiography (IV-DSA and IA-DSA, respectively) have been advocated as a more reliable screening examination for renovascular hypertension. Image quality in IV-DSA is compromised by the presence of superimposed vessels and spatial resolution is inferior to that

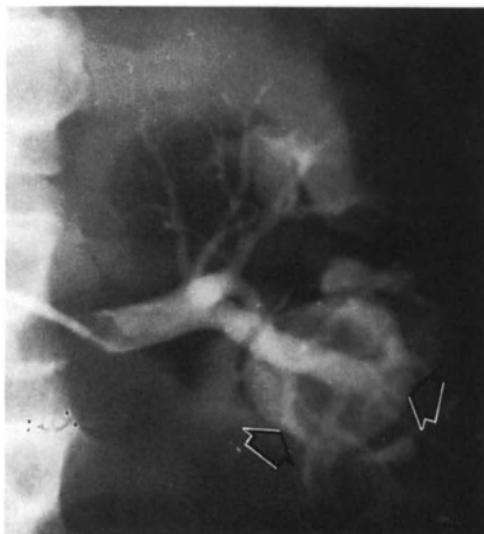


**Fig. 35.30.** Large left renal artery false aneurysm (arrows) due to percutaneous core biopsy.

obtained by formal angiography. IA-DSA represents an improvement over conventional angiography in that the catheter size and volume of contrast used can be significantly smaller. The examination time is also shorter but, again, the spatial resolution is not as good.

**Renal Angiography.** Renal angiography is undertaken in patients who are candidates for surgical revascularization or renal artery angioplasty. In most adults the vascular abnormality is a major vessel stenosis, two thirds of which occur due to *atherosclerotic plaque*. These lesions occur at the origin of the renal artery from the aorta or within the proximal third of the vessel. Post-stenotic dilatation caused by turbulent flow is often associated. Spontaneous dissection and thrombosis can lead to total occlusion.

Most of the remainder of renovascular lesions are due to stenoses caused by various types of *fibrodysplasia* which affect some portion of the arterial wall. These lesions of unknown etiology occur in younger individuals, usually female, and involve the middle and distal thirds of the main renal artery and branch vessels. The commonest of this group is *medial fibroplasia* (fibromuscular hyperplasia) which appears angiographically as a 'string of pearls' pattern on angiography because of multiple, serial stenoses with intervening aneurysms (Fig. 13.20). In children, *intimal fibroplasia* is the most common form of stenosis.

Selective *renal vein renin sampling* with simultaneous peripheral vein sampling is utilized to predict the likelihood of cure of hypertension when a stenosis is relieved either by surgery or percutaneous angioplasty. A renal vein renin ratio greater than 1.5 to 1 indicates that a lesion is likely to be significant.

#### **Microvascular Disease (Arteritides)**

Hypertension can also occur on the basis of small renal vessel disease from the same mechanism of renin elaboration. The diseases that affect the small vessels of the kidney include *polyarteritis nodosa*, *drug-induced arteritis*, *Wegener's granulomatosis*, *lupus erythematosus*, *scleroderma*, and *radiation nephritis*.

**Imaging.** *Excretory urography* will show uniform bilaterally small kidneys and the peripelvic sinus fat may become abundant. Renal function may be impaired with poor opacification.

**Ultrasonography** demonstrates increased echogenicity which is not specific to any disease state but reflects the degree of sclerosis pathologically present in the kidney.

**Renal Angiography.** These arteritides affect the interlobular arteries and afferent arterioles. The affected vessels become irregular and thrombosed and, in the case of the necrotizing disorders like polyarteritis nodosa and drug-abuse angiitis, there are multiple small aneurysms (Fig. 13.16, p. 242). The capillary phase is inhomogeneous and there may be areas of infarction.

#### **Other Renal Arterial Disorders**

**Renal Artery Aneurysms.** Renal artery aneurysms can be congenital, post-traumatic (false aneurysm) (Fig. 35.30), or associated with stenoses (either fibromuscular or atherosclerotic). Microaneurysms are present in polyarteritis

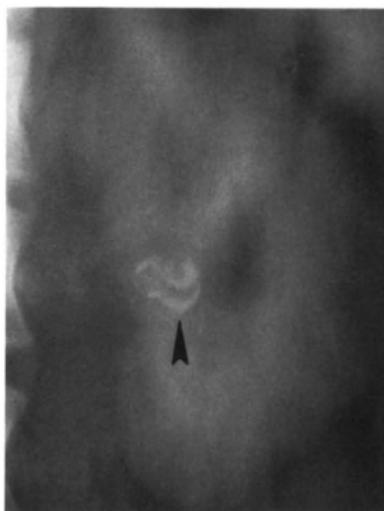


**Fig. 35.31.** Small, calcified left renal artery aneurysm is seen in the hilum of the left kidney during nephrotomography (arrowhead).

nodosa. Branch points of the vessel are commonly affected and there may be associated calcification (Fig. 35.31). Complications of renal aneurysms include rupture and infarction (Fig. 35.32).

**Arteriovenous Malformations and Fistulae.** Arteriovenous malformations are rare congenital lesions which may be responsible for hematuria or hypertension. They are variable in size and may be too small to be detected on angiography. Arteriovenous fistulae are acquired communications between the renal arterial and venous systems that occur due to penetrating trauma, percutaneous renal core biopsy, neoplasm and sometimes post-nephrectomy (Fig. 35.33).

#### Renal Infarction and Ischemia

**Renal Embolization.** Acute renal infarction is usually due to emboli originating in the heart. The source is mural thrombi from the ventricle due to myocardial infarction or from atrial thrombi due to mitral valvular disease with atrial fibrillation. Occasionally the emboli derive from cholesterol plaques in the aorta. Clinically, the patient usually presents with acute onset of flank pain and there is accompanying hematuria and fever.

**Imaging.** *Excretory urography* demonstrates non-function in a normal-sized or somewhat enlarged kidney when infarction is total. *Ultrasound* and *retrograde pyelography* demonstrate no evidence of hydronephrosis. *Angiography* will show the occluding thrombus as an intraluminal filling defect (Fig. 35.34). *CT* shows an absent nephrogram with an enhancing cortical rim due to perfusion by capsular collateral arteries.

If the embolus involves vessels more peripheral than the main renal artery, a pattern of *lobar infarction* is seen. The excretory urogram will demonstrate function with a normal appearing pelvocalceal system and a wedge-shaped defect in the nephrogram with focal loss of parenchyma. The parenchymal loss is also readily displayed by CT. Abrupt cut-off of vessels in the infarcted area and absent nephrogram are seen on selective renal angiography.

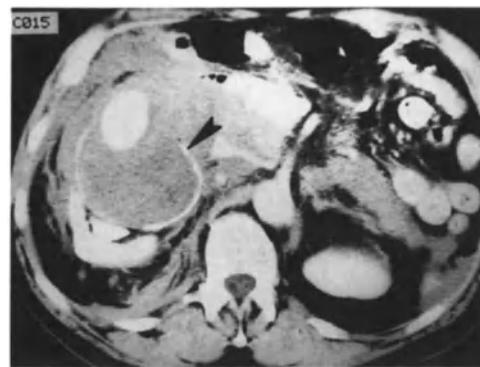


**Fig. 35.32.** CT of a patient who developed acute right flank pain and hypotension. A huge, ruptured renal artery aneurysm can be seen anterior to the right kidney. The arrowhead points to the calcified rim of the aneurysm. The intensely enhancing lumen of the vessel can be seen at the twelve o'clock position. Blood fills the perirenal space and surrounds and compresses the inferior vena cava. (Courtesy L. Liebscher, M.D.)

#### Renal Vein Thrombosis

Renal vein thrombosis is most commonly seen in infants with severe dehydration. In adults, renal venous thrombosis is usually secondary to a primary renal disease process which reduces renal blood flow such as membranous glomerulonephritis, amyloidosis, or pyelonephritis. Associated coagulopathy may also be contributory. Nephrotic syndrome which is often seen with renal vein thrombosis appears to be the consequence of the primary renal process rather than the renal venous occlusion. Propagation of tumor thrombus occurring with renal cell carcinoma and trauma are other etiologies.



**Fig. 35.33.** Acquired arteriovenous fistula due to penetrating trauma. There is early communication of the renal artery (A) with the renal vein (V) in the lower pole of the kidney. Note early filling of the inferior vena cava (arrow).

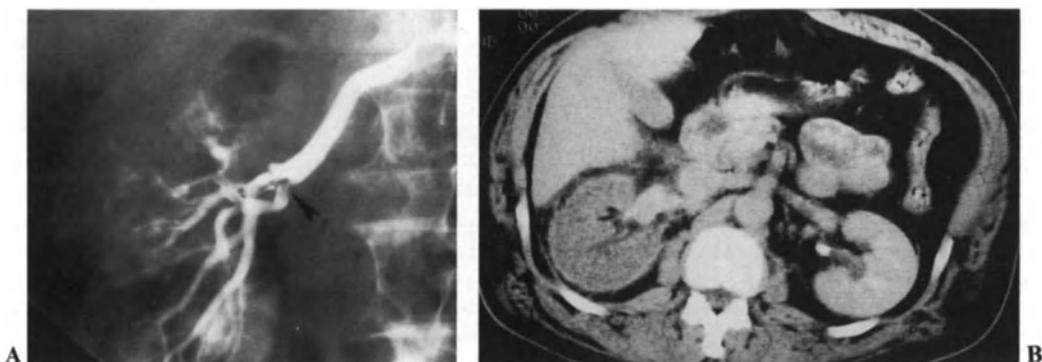


**Fig. 35.34A, B.** An elderly female with rheumatic heart disease and chronic atrial fibrillation developed acute onset of right flank pain and hematuria. The excretory urogram showed non-function on the right and an ultrasound revealed no evidence of hydronephrosis. A A selective right renal angiogram three days after the onset of symptoms demonstrates thrombus at the renal artery bifurcation (arrowhead) and in several intrarenal branches. B CT demonstrates acute infarction with swelling and absent nephrogram except for faint rim of opacification due to capsular blood supply.

Clinical and radiographic presentation depend on the rapidity and completeness of occlusion. Radiographic findings may be normal if the occlusion is incomplete or gradual enough to allow collateral vessels to compensate. Symptoms similar to acute arterial infarction are present when renal vein thrombosis is acute and total. *Excretory urography* demonstrates a swollen, non-functioning kidney and *retrograde pyelography* reveals attenuation of the pelvicalyceal system.

With subacute occlusion, collateral blood flow from the subcapsular veins into the adrenal, lumbar, ureteric and

gonadal veins develops. Renal function is preserved at *urography* although the kidney is enlarged and the collecting systems compressed due to edema. The nephrogram may become increasingly dense over time and may develop a striated appearance. The collateral venous circulation may cause ureteral notching.

*Ultrasound* shows renal enlargement and sonolucent medullary pyramids. Thrombus in the inferior vena cava may be identified on real-time examination.

*CT* will demonstrate renal enlargement, perirenal venous

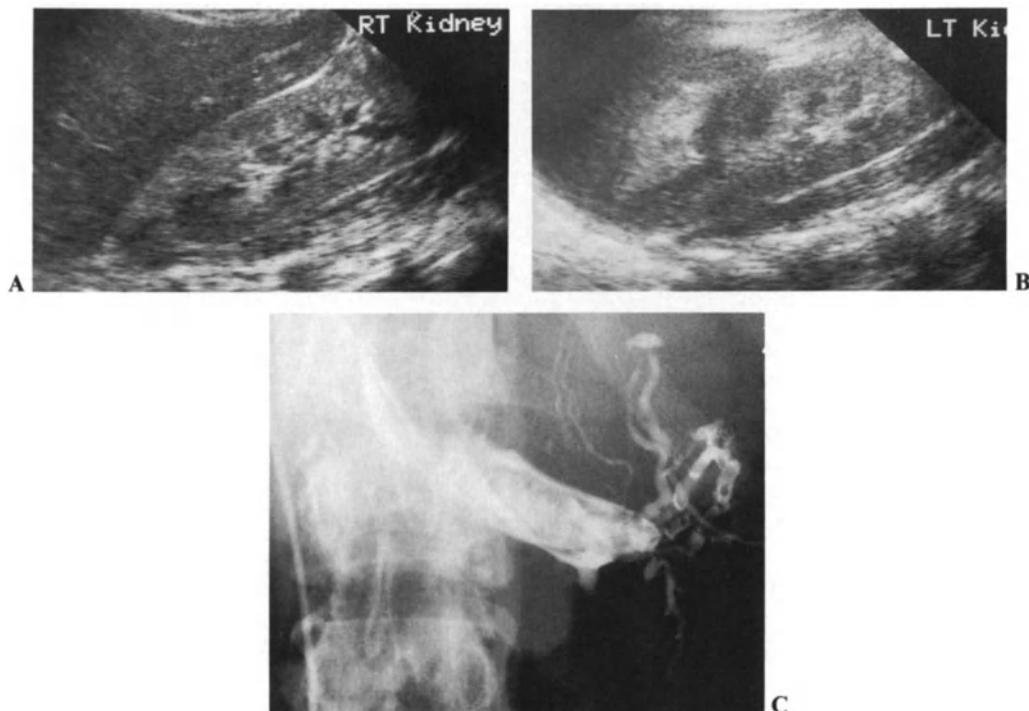


**Fig. 35.35A, B, C.** Renal vein thrombosis associated with Goodpasture's syndrome. A Right sagittal ultrasound scan demonstrates a slightly enlarged, echogenic kidney due to glomerulonephritis. B Sonography of the left kidney demonstrates enlargement and a more echoluent pattern. C Venography demonstrates a large thrombus within the left renal vein.

collateral vessels and may directly demonstrate the occluding thrombus in the vein. Prolongation of corticomedullary differential opacification may occur on the affected side. Retroperitoneal hemorrhage may also be present.

*Phlebography* is the most direct way to demonstrate the occluding renal vein thrombus if CT or US fail to identify it (Fig. 35.35). A lower venacavogram should be performed first to exclude the possibility of thrombus occurring secondary to an ascending pelvic or lumbar thrombophlebitis. Direct renal vein catheterization without taking this precaution could result in dislodgement of clot with embolization to the pulmonary circulation.

### Renal Papillary Necrosis

Ischemic necrosis of the papillary tips occurs when the blood supply to the medulla (the vasa recta) is occluded or damaged. Disease processes frequently associated with papillary necrosis include *diabetes mellitus* and infection, *sickle hemoglobinopathy*, and *analgesic abuse*. Less commonly, *sterile*

*obstruction, cirrhosis, renal vein thrombosis or trauma* may be causative. Papillary necrosis is usually bilateral and affects more than one papilla. The necrotic papilla may separate and slough off causing ureteral colic.

Papillary necrosis can present as an acute, fulminating disease with smoothly enlarged, non-functioning kidneys indistinguishable from other conditions associated with acute renal failure such as acute tubular necrosis, acute cortical necrosis, and acute gouty nephropathy.

*Imaging.* On *excretory urography* the kidney in chronic papillary necrosis remains normal in size, except in analgesic nephropathy where renal size diminishes and the contour becomes somewhat irregular. Cavities which communicate with the calyx may be central or appear as linear extensions from the fornices into the medulla (Fig. 35.36). With complete separation of the papilla, the sloughed tissue can be seen as a radiolucent triangular-shaped filling defect in the opacified calyx. Once the necrotic tissue has been passed, the margins of the cavity smooth over leaving a rounded-

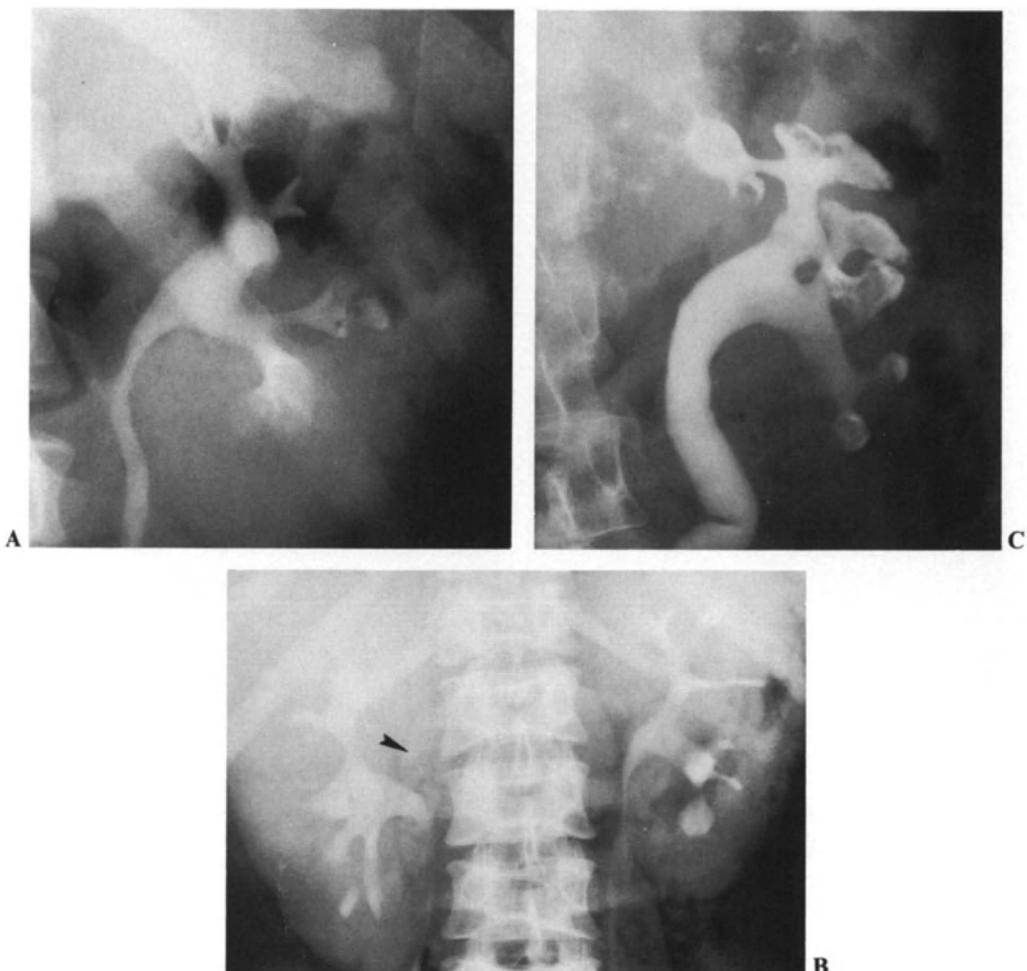
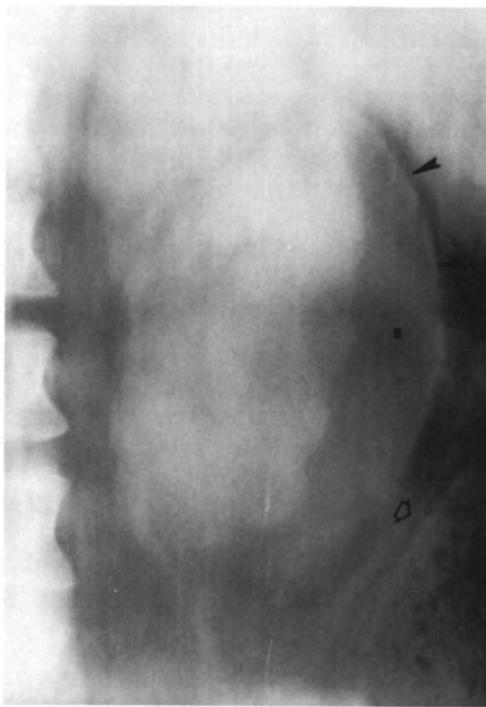


Fig. 35.36A, B, C. Renal papillary necrosis. A A patient with SA hemoglobinopathy demonstrates large cavity in the center of a calyx in the interpolar region. B Virtually all the calyces are blunted and distorted in this patient with hemoglobin SS disease. Note cholelithiasis (arrowhead) and typical changes in the vertebral bodies of trabecular coarsening and depressed central end plates. C Retrograde pyelogram in a diabetic patient demonstrates extensive papillary necrosis with sequestered papillae creating multiple 'ring' shadows. Diabetes was secondary to chronic calcific pancreatitis (note pancreatic calcifications across upper pole). (Courtesy of R. Dyer, M.D.)



**Fig. 35.37.** Large subcapsular hematoma. Tomogram in the nephrographic phase demonstrates subcapsular hemorrhage (s) and some compression of the renal parenchyma. Arrowheads outline the displaced capsule and the open arrow points to Gerota's fascia outlined by fat in the perirenal and anterior pararenal spaces.

appearing calyx indistinguishable from post-obstructive changes. Necrotic papillae which are not passed (*necrosis in situ*) may calcify and appear as an opaque rim around an uncalcified nidus. Papillae which are sloughed may cause ureteral obstruction with a radiographic appearance similar to that caused by calculi. Chronic, extensive disease may lead ultimately to renal failure.



**Fig. 35.38.** Nephrographic phase of an angiogram demonstrates wedge-shaped defect in the lower pole of the left kidney due to parenchmal laceration. The less intense nephrogram of an excretory urogram would show similar findings.

**Differential Diagnosis.** The smudged appearance of the calyx in early *tuberculous erosion* of the papilla can mimic papillary necrosis. Unless features of more advanced tuberculosis are seen, it may not be possible to distinguish these two diseases. *Chronic pyelonephritis* with calyceal clubbing is usually identifiable due to the associated deep overlying parenchymal scars. *Pyelogenic cysts* are smooth and connected to the fornix by a narrow neck while the calyceal structures are otherwise totally normal. *Medullary sponge kidney* is characterized by multiple opacities in the papilla while in papillary necrosis the cavity is usually single.

## RENAL TRAUMA

### Renal and Ureteral Injuries

The kidney may be subject to blunt or penetrating injury.

Usually *penetrating* abdominal wounds are explored without extensive imaging studies which are time-consuming. An emergency 'one-shot' urogram on the operating table will demonstrate the presence of two excreting kidneys. Although one kidney may be damaged, the decision to do a nephrectomy depends on the presence of a healthy contralateral kidney.

In *blunt* trauma, if the trauma is thought to be confined only to the kidney, an emergency urogram is a satisfactory screening examination. Where available, CT scan is probably preferable to the IVP because it provides the same functional information and additionally discloses significant abnormalities in other viscera.

*Excretory urography* is performed with tomography, if possible, but compression is not used. The plain film may show fractures of the lower ribs or transverse processes of the spine. Intrarenal hematoma presents as a rounded area of decreased density in the nephrogram phase with calyceal displacement. Subcapsular hematomas produce compression of the underlying parenchyma with displacement of the renal capsule (Fig. 35.37). Lacerations in the parenchyma may be seen as linear defects in the nephrogram (Fig. 35.38) and, if the tear involves the collecting system, extravasation of contrast material is seen (Fig. 35.39). Unresolved leaks may become encapsulated as a *urinoma*. Lacerations which extend through the capsule will produce a perinephric hematoma which may displace the kidney, rotate its axis or cause obstruction. The late sequel to a perinephric or subcapsular hematoma is the development of a fibrinous pseudocapsule with resultant hypertension (*Page kidney*).

Non-function on urography may be secondary to obstruction due to blood clot or to a vascular pedicle injury. Pre-existing abnormality such as congenital solitary kidney, pelvic kidney or severe PUJ obstruction may be responsible for the demonstration of only one excreting kidney.

*Ultrasound* examination is of little use in the evaluation of the acutely traumatized kidney, because function cannot be assessed and the coexistence of rib fractures makes examination difficult. This modality is of use, however, in the investigation of suspected injury due to needle biopsy. Intrarenal hematomas, subcapsular and perinephric fluid accumulations are readily identified. Large pseudoaneurysms may also be recognized.

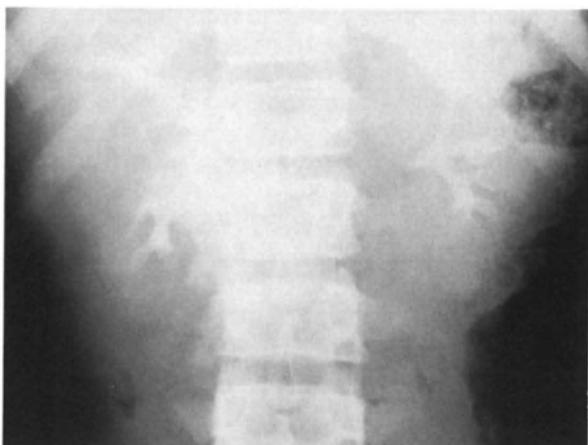


**Fig. 35.39.** Laceration of the collecting system, excretory urogram. Blunt trauma to the right flank in a 9-year-old boy. Extravasation of contrast material around the right pelvis and ureter is apparent on this 10-min film.



**Fig. 35.40.** Focal, acute right renal infarction due to trauma. CT shows a wedge-shaped defect in the nephrogram anteriorly (large arrowhead) with a rim of preserved capsular blood supply. Small arrowhead points to areas of laceration in the spleen.



**Fig. 35.41.** Blunt trauma to the right flank resulted in laceration of the renal parenchyma, capsule and collecting system. Extravasation of contrast material (arrowheads) and hemorrhage into the perirenal and anterior pararenal spaces is seen.

CT is a very useful tool in the evaluation of blunt abdominal trauma. The integrity of the major vascular structures can be assessed indirectly by the intensity, symmetry and regularity of parenchymal enhancement (Fig. 35.40). Large pseudoaneurysms can be seen. Lacerations will appear as wedge-shaped or linear defects in the nephrogram while intrarenal hematomas will be more poorly defined and hyperdense on non-contrasted CT. Perirenal hematomas conform to the perirenal space while subcapsular hematomas are crescent-shaped with compression of the renal parenchyma. Extravasation of contrast material is readily seen (Fig. 35.41).

**Renal Angiography.** The most direct information about the status of the renal pedicle is obtained from angiographic studies. Because the kidney does not tolerate ischemia for very long, pedicle injuries must be recognized and treated immediately if the kidney is to remain salvageable. A flush aortogram will demonstrate abrupt cessation of the renal artery somewhat distal to its origin (Fig. 35.42). Occlusion may be secondary to laceration, transection or thrombosis. Other injuries include traumatic dissection, pseudoaneurysm or arteriovenous fistulae.

#### RENAL TRANSPLANTATION

A potential renal donor undergoes clinical and radiologic evaluation to determine suitability. *Excretory urography* is performed to establish that the patient has two functioning kidneys free of diseases and conditions which would exclude them as potential donor organs. Such abnormalities include congenital anomalies (horseshoe kidney, crossed fused ectopia), chronic pyelonephritis, neoplasms, large calculi or pap-

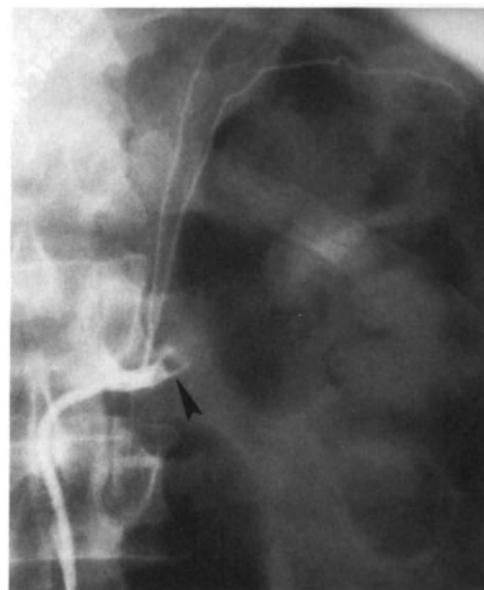


**Fig. 35.42.** Selective left renal angiography after blunt trauma shows abrupt cessation of the main renal artery just distal to the inferior adrenal and superior capsular branches. The arrowhead points to the intraluminal thrombus.

illary necrosis. Cysts, duplication or ectopia without fusion are not conditions which would prevent use of kidney for transplantation. When the urogram is normal, the patient is further evaluated by *arteriography* to determine the number of renal arteries. The presence of multiple renal arteries which are known to occur in some 25% of kidneys may render the kidney unsuitable for transplantation.

The **transplant recipient** undergoes *voiding cystourethrography* to determine bladder capacity, function, and emptying as well as to exclude urethral strictures and vesico-ureteral reflux. Occasionally this study induces mucosal tears in a small-capacity, unused bladder resulting in extravasation. There are no clinical consequences of this extravasation.

### Complications of Renal Transplantation

A renal transplant may fail because of *parenchymal abnormalities* such as acute tubular necrosis, rejection, recurrence of primary renal disease or cyclosporin toxicity. *Surgical complications* such as bladder or ureteral leak, ureteral obstruction, and renal artery stenosis may also be the source of failure. Baseline ultrasound and radionuclide scans are usually obtained in the early post-transplantation period and are extremely useful in serial evaluation when correlated with clinical data.

*Acute tubular necrosis* usually occurs in the early post-operative period. Perfusion is normal or somewhat reduced on DTPA radionuclide scans while the  $^{131}\text{I}$ -hippuran scan indicates depressed tubular function. Renal ultrasound and MR imaging show no change over baseline.

*Rejection* presents with decreased renal perfusion on DTPA scanning. MR imaging demonstrates poor corticomedullary differentiation on  $T_1$ -weighted images, which appears to be a non-specific sign, however. Renal ultrasound may show decreased echogenicity of the renal pyramids. In chronic rejection the parenchyma becomes hyperechoic. Doppler ultrasound can identify decreased blood flow in the renal transplant but has not yet proved capable of distinguishing acute rejection and the other causes of graft dysfunction associated with decreased perfusion.

*Ureteral obstruction* can be due to calculus, ureteral necrosis and stricture, or due to external compression caused by a urinoma or lymphocele. Ultrasound will identify the hydronephrosis although care should be taken to examine the patient with an empty bladder since vesical distension can cause some degree of hydronephrosis.  $^{99\text{m}}\text{Tc}$ -DTPA scan will show dilated upper tracts with delayed excretion that does not respond to a furosemide challenge. If necessary, antegrade pyelography can demonstrate a point of obstruction.

*Peritransplant fluid collections* include those due to *hematoma, abscess, lymphocele or urinoma*. Ultrasonography can readily demonstrate these collections although their appearance is non-specific. Radionuclide scans will specifically indicate a urinoma as an area of activity outside the expected confines of the urinary tract, although the exact site of the leak cannot be determined. A cystogram will then identify a bladder leak, if present (Fig. 35.43). If the cystogram is negative, an excretory urogram or antegrade pyelogram is indicated to find the point of extravasation (Fig. 35.44).

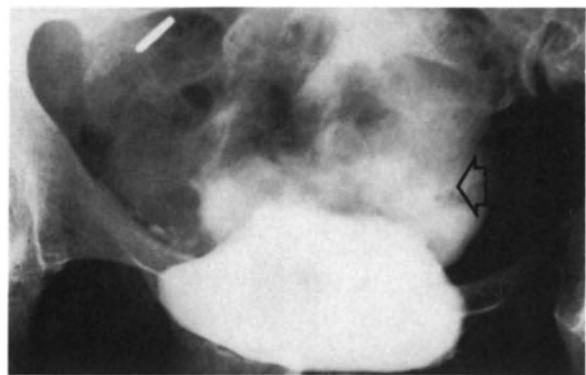


Fig. 35.43. Renal transplant ultrasound demonstrated a pelvic fluid collection which was identified as urinary extravasation by radionuclide studies. Subsequent cystogram shows extravasation of contrast material from the bladder (arrowhead) at the ureterocystostomy site.

Lymphoceles or other fluid collections which cause obstruction can be aspirated for diagnostic and therapeutic reasons. Hematomas can be identified on CT by their high-attenuation value. Perirenal abscesses and hematomas can be distinguished from lymphoceles and seromas at MR imaging because of their higher signal intensity on  $T_1$ -weighted images.

*Vascular complications* of renal transplantation include renal artery thrombosis, renal artery stenosis, pseudoaneurysm, renal vein thrombosis and arteriovenous fistula.  $^{99\text{m}}\text{Tc}$ -DTPA scans demonstrate non-specific reduced perfusion and are not effective in identifying this group of disorders from rejection. *Angiography* is the most direct way to determine if a vascular disorder is present. Digital vascular

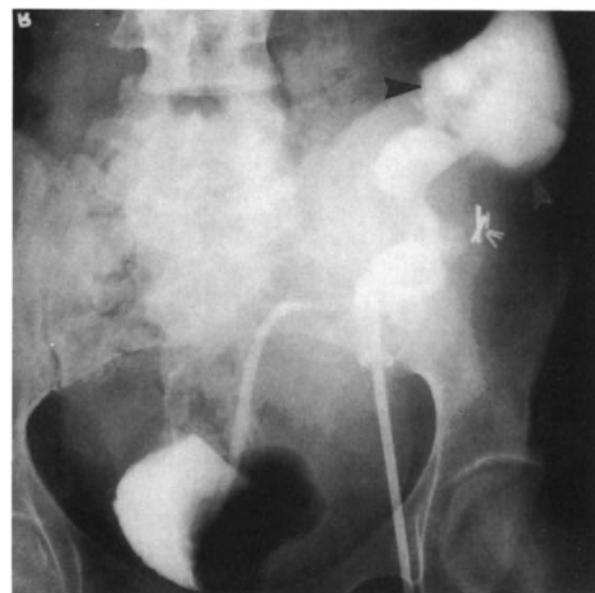
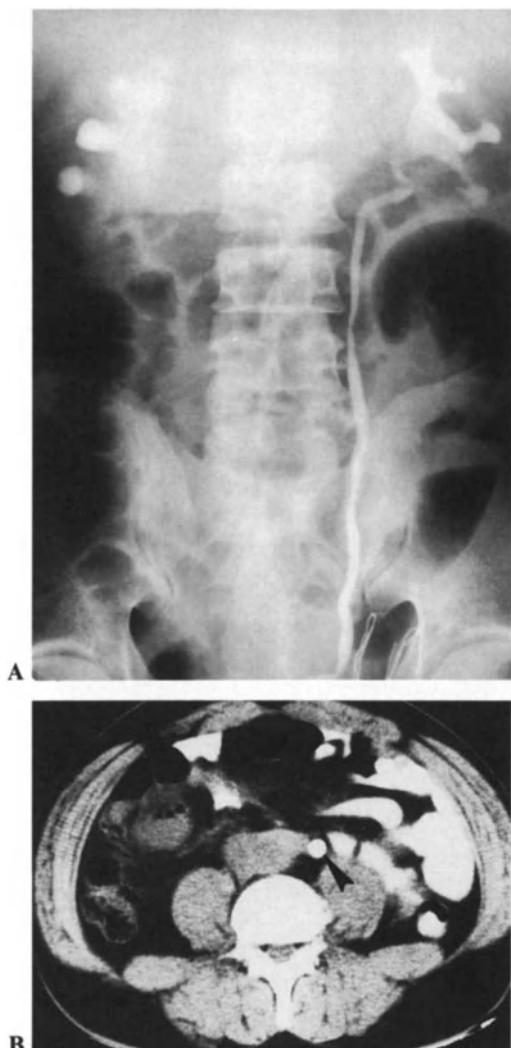


Fig. 35.44. Antegrade pyelogram via nephrostomy catheter in a renal transplant demonstrates upper pole encapsulated extravasation. The urinoma was caused by sacrifice of an accessory upper pole artery at the time of transplantation with subsequent necrosis of a portion of the upper pole.



**Fig. 35.45A, B.** Retroperitoneal fibrosis. A Left retrograde pyelogram demonstrates mild hydronephrosis and some straightening and medial deviation of the distal left ureter. Previous injection on the right demonstrated similar findings. B CT scan shows soft tissue mass surrounding the aorta and vena cava. The ectatic left ureter (arrowhead) is filled by contrast infused via a percutaneous nephrostomy catheter. The ureter was encased in fibrosis on more caudal sections.

angiography shows promise because it is less invasive than formal angiography and involves less contrast exposure.

#### RETROPERITONEAL CONDITIONS LEADING TO URETERAL DEVIATION

Many conditions occur in the retroperitoneum which will cause deviation of the ureters. These include congenital variants (retrocaval ureter, discussed separately in the chapter on congenital anomalies), normal variants (psoas hypertrophy), benign and malignant masses, aneurysms, and retroperitoneal fibrosis.

#### Retroperitoneal Fibrosis

An uncommon condition, retroperitoneal fibrosis results in proliferation of fibrous tissue around the ureters causing obstruction. The etiology is usually idiopathic although the underlying cause may be metastatic malignancy, lymphoma, leaking or repair of an aortic aneurysm, radiation therapy, drugs (methysergide, ergotamine, LSD, or methyldopa) or inflammatory bowel disease. Clinically, the patient is usually a male aged 40–60 years who presents with back or abdominal pain and impaired renal function.

**Imaging.** *Excretory urography* demonstrates bilateral hydronephrosis, although the condition may be asymmetric, affecting one ureter more than the other. The mid-ureters at the level of L4–L5 are most commonly affected although the process can extend proximally to the renal hilum and distally along the iliac vessels into the pelvis. The mid-ureters become tapered and deviate medially in an abrupt, step-like fashion while the distal ureter takes a vertical course instead of curving laterally in the pelvis. Typically, despite evidence of obstructive nephropathy with compromised renal function, retrograde catheterization can readily be accomplished. Interference with ureteral peristalsis may be responsible.

On CT, retroperitoneal fibrosis is seen as a mass of soft tissue obliterating the fat planes around the aorta and vena cava with lateral extension involving the ureters (Fig. 35.45). The distinction between benign and malignant etiology cannot be made. Percutaneous needle biopsy is not always diagnostic since it may not identify sparse cancer cells within the extensive desmoplastic reaction. Diagnosis may require numerous deep, intraoperative biopsies.

#### Abdominal Aortic and Iliac Aneurysms

The presence of an aneurysm of the abdominal aorta or iliac artery can cause renal or ureteral displacement. An aortic aneurysm usually causes lateral and anterior displacement of the left ureter while there is a traction medial displacement of the right ureter. An iliac artery aneurysm can cause medial or lateral deviation of the mid-ureter depending on whether the mass effect is greatest above the crossing point of the ureter over the iliac vessels or caudal to it. In either case, there is usually significant hydronephrosis (Fig. 35.46).

#### Normal Variant

Patients with bulky iliopsoas musculature and a small bony pelvis may show evidence of medial deviation of the distal ureters due to crowding (Fig. 35.47). As many as 20% of normal excretory urograms show the right ureter medial to the pedicles of the L4 and L5 vertebral bodies, particularly in young, muscular males.

#### Retroperitoneal Masses

*Retroperitoneal lymphadenopathy* is a common cause of ureteral deviation. Para-aortic and paracaval lymph node enlargement from lymphoma or metastatic disease causes lateral bowing of one or both mid-ureters. Lymphadenopathy in the pelvis causes medial displacement of the distal ureters.

Primary *retroperitoneal tumors* which can cause ureteral deviation include liposarcoma, leiomyosarcoma, fibro-

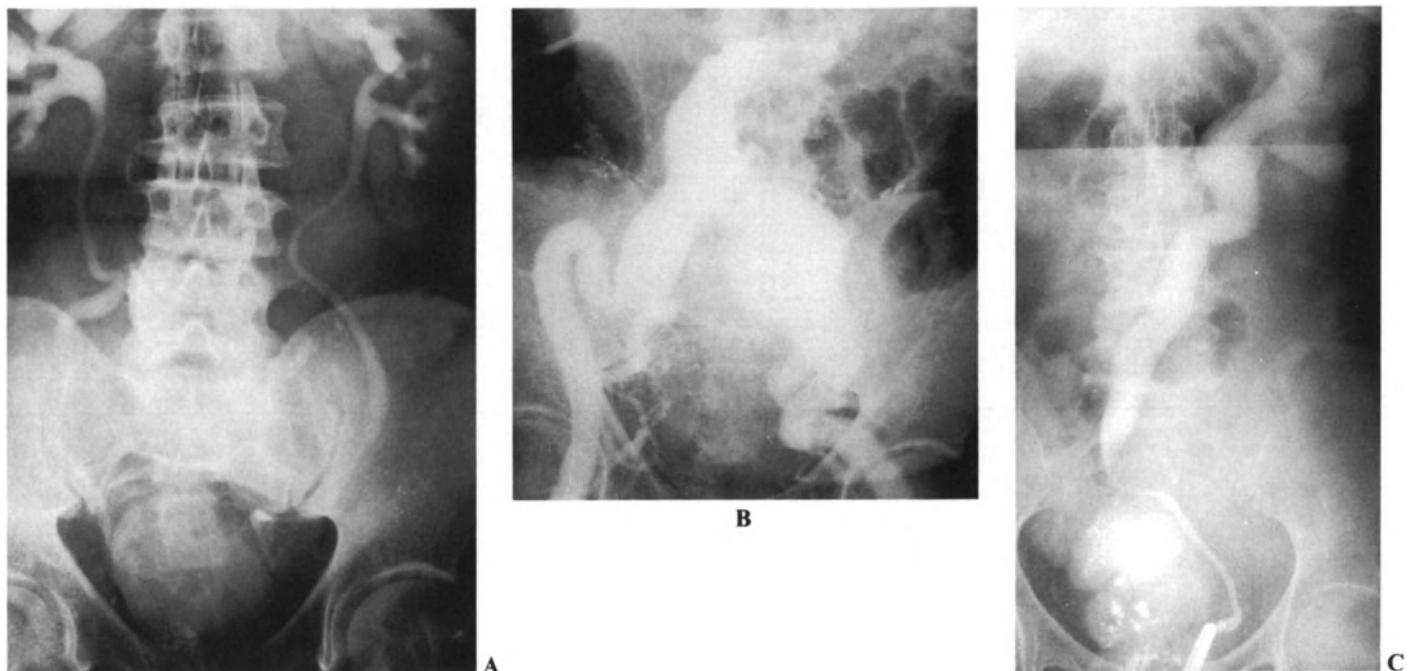


**Fig. 35.46A, B, C.** Ureteral deviation secondary to iliac artery aneurysm. **A** Excretory urogram in an elderly male demonstrates mild bilateral hydroureronephrosis with lateral bowing of the middle thirds of both ureters. **B** Aortogram shows large aneurysms of both common iliac arteries causing the ureteral deviation. **C** Retrograde pyelogram in a different patient reveals moderate hydroureronephrosis with abrupt, marked medial deviation at the site of a leaking iliac artery aneurysm.

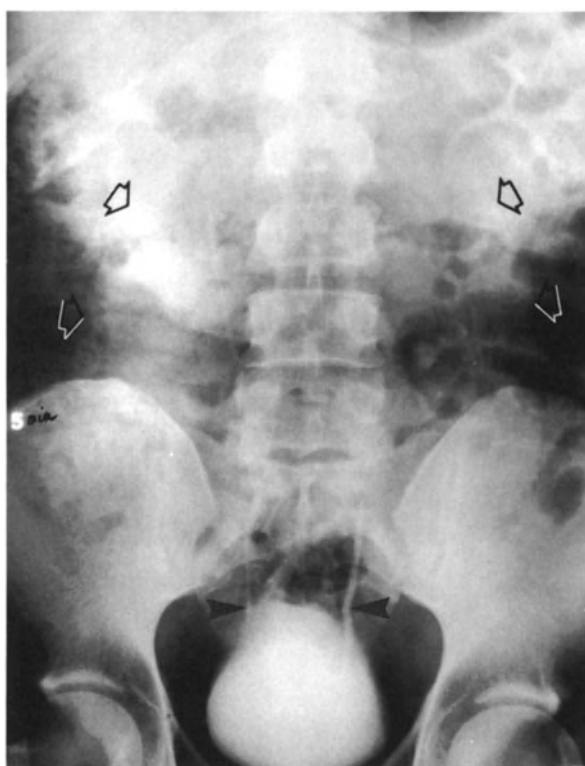


**Fig. 35.47.** Ureteral deviation due to iliopsoas hypertrophy. Excretory urogram in a young male demonstrates symmetric medial deviation of the lower ureters (arrowheads) due to hypertrophy of the iliopsoas musculature (upper margins outlined by open arrows).

sarcoma, malignant teratoma, rhabdomyosarcoma, hemangiopericytoma and chondrosarcoma. These are usually large, inhomogeneous tumors which can distort, invade and displace the kidneys and ureters (Fig. 35.48).

*Pelvic lipomatosis* is a benign condition in which there is overgrowth of normal fatty tissue in the bony pelvis. The masses of fat in the perirectal and perivesical spaces cause compression of the bladder which appears narrowed and elevated. The fat can be visualized on plain film as hyperlucency in the pelvis. The distal ureters are displaced medially and there is often hydronephrosis.

#### Post-surgical or Post-traumatic Conditions

Patients who have undergone abdomino-perineal resection of the colon for carcinoma characteristically demonstrate medial positioning of the distal ureters (Fig. 35.49). Radical pelvic surgery with transection of lymphatic vessels can result in the formation of lymphoceles, large collections of lymph which can deviate and displace the pelvic ureters and bladder. Post-operative or post-traumatic abscesses may also cause similar effects. Hematoma due to blunt or penetrating trauma is a common cause of ureteral deviation (Fig. 35.50).

#### Bladder Diverticulum

Large bladder diverticula may occur adjacent to the ureteral orifice, in which case the distal ureter is characteristically deviated medially (Fig. 35.51).

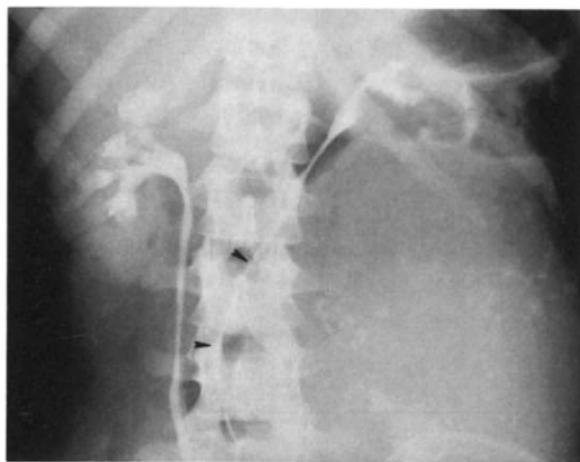


**Fig. 35.48.** Ureteral deviation due to chondrosarcoma. Excretory urogram in a 23-year-old female reveals huge mass containing calcifications which has displaced the upper and mid-ureter across the mid-line (arrowheads).

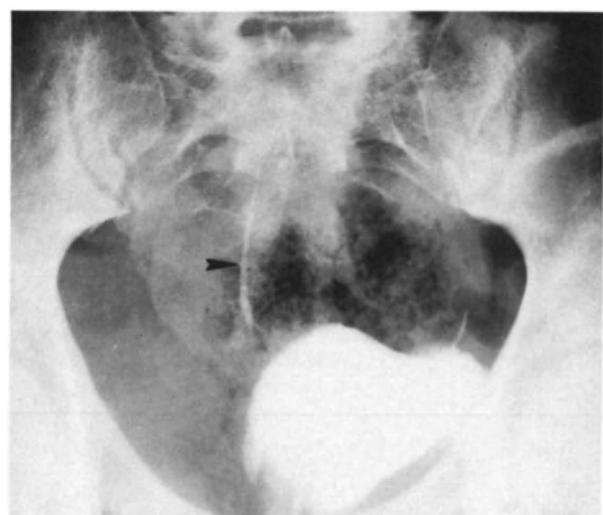


**Fig. 35.50.** Medial deviation of the distal ureter due to hematoma. A gunshot wound to the abdomen caused a large hematoma with resultant medial deviation of the distal right ureter (arrowhead) and displacement of the bladder toward the left.



**Fig. 35.49.** Medial displacement of the distal ureters due to abdomino-perineal resection.

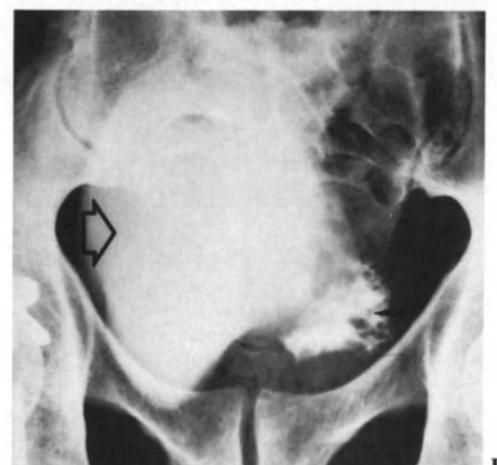


**Fig. 35.51A, B.** Medial deviation of the distal ureter due to bladder diverticulum. A Excretory urogram reveals a large mass in the right true pelvis with deviation of the distal ureter medially (arrowheads). B Post-void radiograph shows contrast material filling a huge bladder diverticulum (open arrow). The contracted bladder is displaced toward the left (arrowhead).

## REFERENCES AND SUGGESTIONS FOR FURTHER READING

## CALCULI AND NEPHROCALCINOSIS

- Banner MP, Pollack HM (1982) Urolithiasis in the lower urinary tract. *Semin Roentgenol* 17: 140
- Pollack HM (ed) (1984) Newer aspects of urolithiasis management. *Urol Radiol* 6
- Pollack HM, Arger PH, Banner MP et al. (1981) Computed tomography of renal pelvic filling defects. *Radiology* 138: 645
- Pollack HM, Arger PH, Goldberg BB et al. (1978) Ultrasonic detection of non-opaque renal calculi. *Radiology* 127: 233
- Schwartz G, Lipschitz XX, Becker JA (1984) Detection of renal calculi: the value of tomography. *AJR* 143: 143
- Singh EO, Malek RS (1982) Calculus disease in the upper urinary tract. *Semin Roentgenol* 17: 113
- Thornbury JR, Parker TW (1982) Ureteral calculi. *Semin Roentgenol* 17: 133
- Wolfman MG, Thornbury JR, Braunstein EM (1979) Non-obstructing radio-opaque ureteral calculi. *Urol Radiol* 1: 97

## INFECTION AND REFLUX

- Becker JA (1988) Renal tuberculosis. *Urol Radiol* 10: 25-35
- Goldman SM (1988) Acute and chronic urinary infection: present concepts and controversies. *Urol Radiol* 10: 17-23
- Goldman SM, Hartman DS, Fishman EK et al. (1984) CT of xanthogranulomatous pyelonephritis: radiologic-pathologic correlation. *AJR* 141: 963-968
- Hartman DS, Davis CJ, Lichtenstein JE et al. (1980) Renal parenchymal malacoplakia. *Radiology* 136: 33-38
- Hertz M, Zissin R, Dresnik Z et al. (1984) Echinococcus of the urinary tract: radiologic findings. *Urol Radiol* 6: 175-181
- Hodson CJ, Smith PK (eds) (1979) Reflux Nephropathy. Masson, New York
- Hoffman EP, Mindelzun RE, Anderson RU (1980) Computed tomography in acute pyelonephritis associated with diabetes. *Radiology* 135: 691-696
- Kintanar C, Cramer BC, Reid WD et al. (1986) Neonatal renal candidiasis:

sonographic diagnosis. *AJR* 147: 801-807

- Morehouse HT, Weiner SN, Hoffman-Tretin JC (1986) Inflammatory disease of the kidney. *Semin US CT MR* 7: 256-263
- Rauschkolb EN, Sandler CM, Patel S et al. (1982) Computed tomography of renal inflammatory disease. *JCAT* 6: 502-507
- Rosenfield AT, Glickman MG, Taylor KJW et al. (1979) Acute focal bacterial nephritis (acute lobular nephronia). *Radiology* 132: 553-560
- Young SW, Khalid KH, Farid Z (1974) Urinary tract lesions of Schistosoma haematobium. *Radiology* 111: 81-88

## MISCELLANEOUS

- Becker JA (ed) (1985) Special issue-GU Trauma. *Urol Radiol* 7
- Blafox MD, Freeman LM (1988) Renewed role of nuclear medicine in renovascular hypertension. *Urol Radiol* 10: 35-37
- Brun B, Laursen K, Sorenson IN et al. (1981) CT in retroperitoneal fibrosis. *AJR* 137: 535-540
- Hillman BJ (1984) Digital imaging of the kidney. *Radiol Clin North Am* 22: 341-364
- Hillman BJ (1988) Renal hypertension. *Urol Radiol* 10: 31
- Hollifield JW, Page DL, Smith C et al. (1975) Renin-secreting clear cell carcinoma of the kidney. *Arch Int Med* 135: 859-865
- Hricak H, Terrier F, Marotti M et al. (1987) Post-transplant renal rejection: comparison of quantitative scintigraphy, US and MR imaging. *Radiology* 162: 685-688
- Kay CJ, Rosenfield AT, Armm M (1980) Gray-scale ultrasonography in the evaluation of renal trauma. *Radiology* 134: 461-466
- Lang EK (1985) Imaging examinations in the management of renal trauma. *Semin US CT MR* 6: 100-104
- Pistolesi GF, Procacci C, Candana R et al. (1984) CT criteria of the differential diagnosis in primary retroperitoneal masses. *Eur J Radiol* 4: 127-132
- Thornbury JR, Stanley JC, Fryback DG (1984) Optimizing work-up of adult hypertensive patients for renal vascular stenosis. Observations about hypertensive urography, digital subtraction angiography, and patient selection. *Radiol Clin North Am* 22: 333-339
- von Knorring J, Fyhrquist F, Ahonen J (1981) Varying course of hypertension following renal trauma. *J Urol* 126: 798-883
- Winsett MZ, Amparo EG, Fawcett HD et al. (1988) Renal transplant dysfunction: MR evaluation. *AJR* 150: 319-323

## CHAPTER 36

# THE LOWER URINARY TRACT

D. Rickards and S. Jones

### Congenital Lesions

Congenital lesions of the lower urinary tract have already been described in Chap. 33. They include bladder extrophy and epispadias, bladder duplication, urachal abnormalities and prune-belly syndrome.

### Bladder Tumors

*Transitional cell carcinomas* (Fig. 36.1) account for 92% of bladder tumors and occasionally show surface calcification due to encrusted salt deposits (Fig. 36.2). Predisposing factors include smoking, exposure to aniline dye rubber and leather products. Bladder tumors reflect a dysplasia of the urothelium and therefore synchronous and metasynchronous lesions may occur.

The remainder of bladder tumors are *squamous cell* or *adenocarcinomas*. The former are associated with chronic uri-

nary tract infection, specifically schistosomiasis and bladder calculi. *Secondary tumors* involving the urothelium are usually either lymphoma or melanoma deposits. *Sarcomas* occur in childhood, are rare and carry a very poor prognosis.

Clinically tumors present with hematuria and diagnosis is by cystoscopy. Imaging has little to add. Once diagnosed, the lesion has to be staged by intravesical ultrasound (Fig. 36.3), computed tomography (Fig. 36.4) or magnetic resonance (Fig. 36.5) if cystoscopy fails to stage. Staging depends upon invasion of the tumor into perivesical fat and adjacent viscera together with involvement of the medial obturator and iliac nodes. In the presence of such invasion and spread, the lesion is inoperable. Synchronous upper tract urothelial lesions must be excluded by excretory urography. Inoperable tumors that are associated with uncontrolled hematuria can be treated by embolizing the internal iliac vessels that supply the tumor (Fig. 36.6).

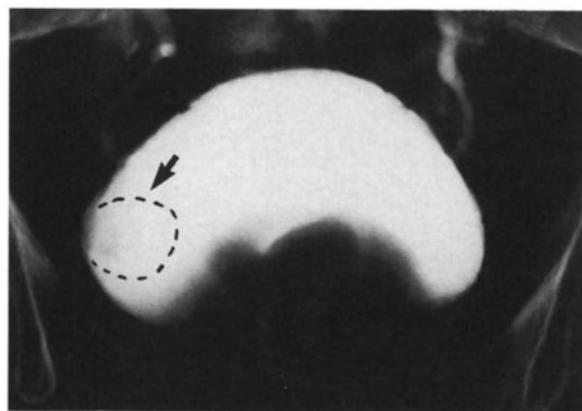


Fig. 36.1. Bladder film of an excretory urogram. There is elevation of the bladder base due to an enlarged prostate and there is a filling defect in the right lateral aspect of the bladder (arrow) which is a transitional cell tumor.

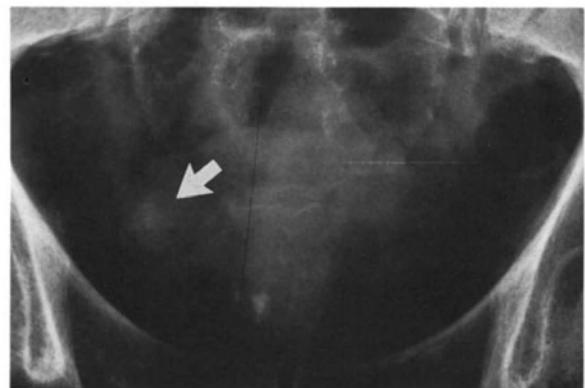


Fig. 36.2. Plain film. There is a little calcification above the symphysis pubis, prostatic in nature, and there is faint calcification of the transitional cell bladder tumor (arrow).



**Fig. 36.3.** Intravesical ultrasound of a bladder tumor. The ultrasound probe (arrow) has been inserted urethrally. A transverse section of the bladder is obtained. The tumor (curved arrow) is extending through the bladder wall.



**Fig. 36.5.** A coronal MRI section of a bladder tumor (arrow).

### Bladder Inflammatory Disease

*Schistosomiasis* is extremely common, being endemic in the tropics. The inflammatory process is a granulomatous reaction produced by ova deposited by the female of the *Schistosoma hematobium* worm. A fresh-water snail acts as an intermediate host and the cercaria enter man by penetrating the skin, usually of the foot.

*Calcification* of the bladder wall is a characteristic radiological feature (Fig. 36.7) which can extend to involve the ureters, but never the urothelium of the pelvicalyceal system. Other sites of involvement include the urethra and prostate in the male, and vagina, cervix and uterus in the female. Complications include strictures, vesicoureteric reflux and the development of squamous cell carcinoma as well as urodynamic abnormalities related to decreased bladder capacity.

*Emphysematous cystitis* is characterized by gas in the bladder or bladder wall and is seen in diabetics or immunosuppressed patients. *Malakoplakia* is a chronic granulomatous infection with *E. coli*, which usually affects the bladder rather than the rest of the urothelium. Multiple filling defects on cystoscopy are typical. *Tuberculous cystitis* leads to a small contracted bladder which is irregular in outline and is always associated with upper tract involvement (Fig. 36.8).

### Bladder Diverticula

Diverticula can be *congenital* or *acquired*. Acquired diverticula are a result of a pathological rise in intravesical pressure either due to obstruction or a neurogenic bladder. They are usually small and multiple. Complications include *urinary infection*, *calculus formation* and *neoplasia*. Large diverticula (Fig. 36.9) can hold considerably greater volumes of urine than the bladder itself and cause a large post-micturition residue. Bladder function is further compromised because diverticula prevent adequate bladder pressures being generated. They are best seen at *cystography*, where folds of bladder mucosa enter them. Tumors within diverticula may not be seen at cystoscopy because the isthmus is too narrow. Both *ultrasound* and *CT* are diagnostic (Fig. 36.10).

### Neuropathic Bladder

Neurological control of micturition may be compromised by a variety of upper and lower motor neuron disorders. These usually result in a low capacity, high pressure bladder that contracts involuntarily (*detrusor instability*) and results in urge incontinence. Conditions that may lead to this include trauma, spina bifida (Fig. 36.11, Fig. 36.12), Parkinson's disease, multiple sclerosis and diabetes mellitus. The bladder is assessed by urodynamics.

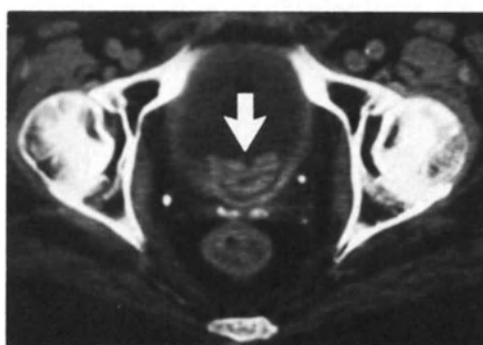


**Fig. 36.4.** CT scan of the bladder. There is a filling defect due to a soft tissue mass in the posterior aspect of the bladder which is a transitional cell tumor (arrow). There is no evidence of spread beyond the bladder wall.

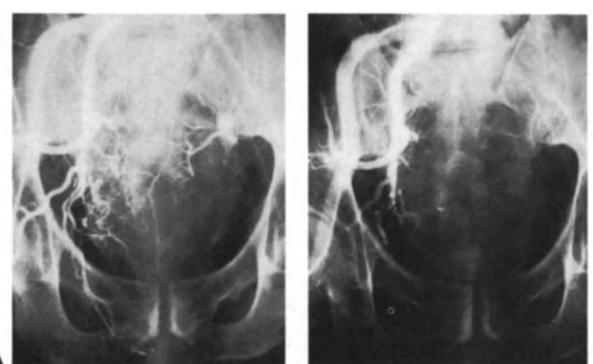


**Fig. 36.6.** A Selective internal iliac angiogram of a bladder tumor that was responsible for considerable hematuria. The tumor was inoperable. B To minimize the hematuria, the internal iliac artery has been embolized.

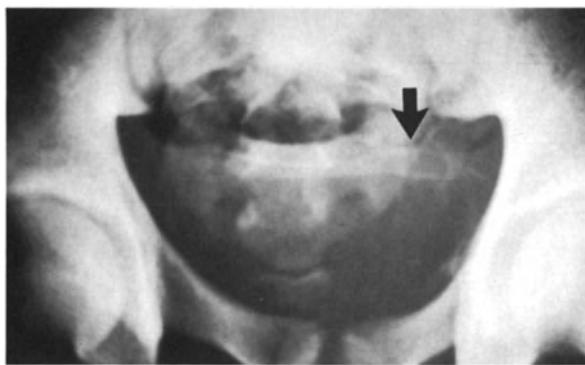


**Fig. 36.7.** Plain film of the pelvis. There is faint calcification of the bladder wall (arrow), characteristic of Schistosomiasis.



**Fig. 36.9.** A post-bladder drainage film via a catheter. The bladder has emptied, but there is residual contrast in a huge diverticulum which has a narrow connection with the bladder (arrow).

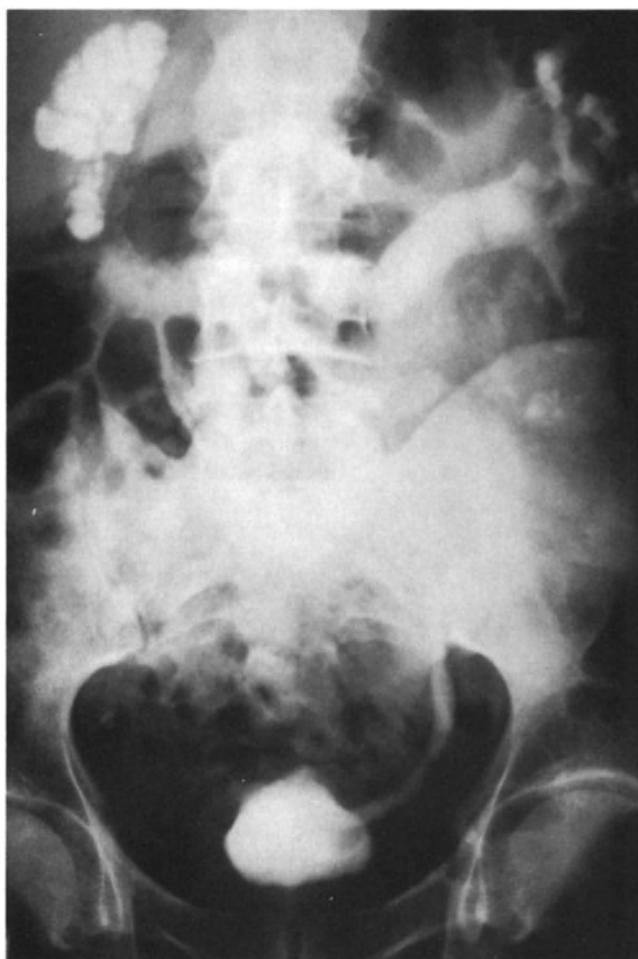


**Fig. 36.8.** Full length excretory urogram film. There is a small contracted bladder due to tuberculous cystitis. Note the autonephrectomy of the right kidney (calcified), also due to tuberculosis.



**Fig. 36.10.** CT scan of the pelvis. There is a large bladder diverticulum in which a small soft tissue mass is seen (arrow). This was not seen at cystoscopy in a patient with hematuria. The mass was confirmed at surgery to be a bladder tumor.



**Fig. 36.11.** Plain film of the pelvis showing spina bifida of the sacrum ► (arrow).



**Fig. 36.12.** Excretory urogram of the same patient as in Fig. 36.11. The bladder outline is trabeculated due to a neuropathic bladder.

Typical *radiological features* include a trabeculated, thick-walled bladder with saccules and diverticula and often an open bladder neck due to sphincter dyssynergia. If high-pressure reflux occurs, upper tract dilatation will ensue and subsequent renal failure will develop. Often, these patients are best treated by urinary diversion into a low pressure ileal loop to preserve renal function (Fig. 36.13).

#### Bladder Trauma

Trauma causes bladder rupture which can be intra- or extra-peritoneal. Imaging is performed to differentiate the two.

*Intrapерitoneal* rupture is characterized by extravasation of contrast at cystography into the peritoneum, usually through the dome of the bladder, and is treated by surgical repair (Fig. 36.14).

*Extraperitoneal* rupture can be at any site and is frequently associated with a pelvic fracture. Contrast extravasates into the perivesical spaces and management is primarily conservative by draining the bladder. Associated injuries to the

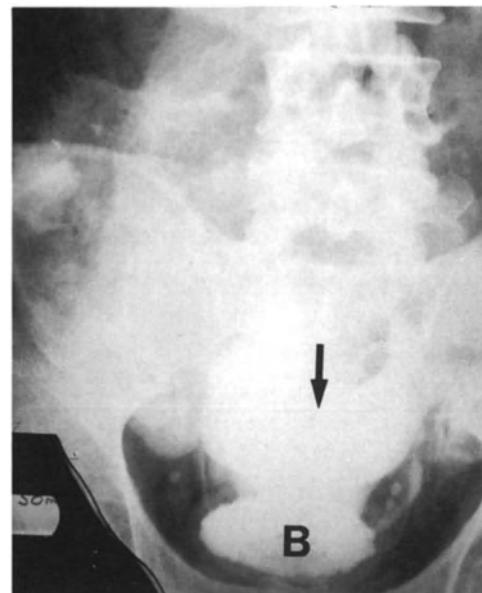


**Fig. 36.14.** Cystogram showing extravasation of contrast above the bladder (arrow) secondary to an intraperitoneal bladder rupture. *B*, bladder.

kidneys, distal ureters and urethra must be sought by excretory urography and urethrography. A post-micturition film of the bladder will prevent a small localized rupture being missed.

#### Pelvic Lipomatosis

This can be a normal variant often seen in black males. It may also occur pathologically in those patients on steroids or with Cushing's disease.

*Radiologically*, a characteristic perivesical lucency is present together with elongation of the bladder. It never causes ureteric obstruction and rarely interferes with bladder function. The differential diagnosis includes hematoma following pelvic trauma, lymphadenopathy, obstruction of the inferior vena cava and psoas muscle hypertrophy. CT confirms the diagnosis by characterizing the pelvic fat distribution.

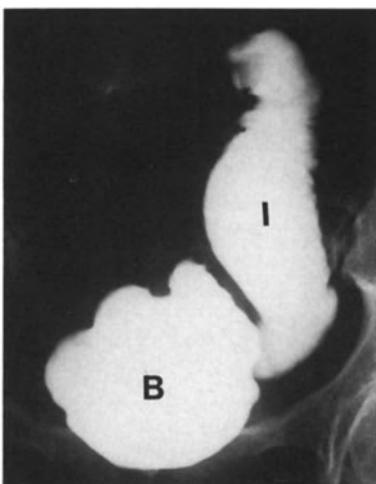


**Fig. 36.13.** Bladder augmentation. A cystogram of a patient in whom a loop of ileum (arrow) has been attached to the bladder. *B*, bladder; *I*, ileum.

## THE PROSTATE

#### Prostatic Tumor

The normal gland weighs 20 g with external dimensions of  $4 \times 3 \times 3.8$  cm. There are two zones to the gland, peripheral and central (Fig. 36.15).

*Benign hypertrophy* originates in the periurethral central zone. It is the inevitable consequence of ageing. Typically, benign hypertrophy is due to adenoma formation and causes urodynamic problems of bladder outlet obstruction.

*Imaging.* *Transrectal ultrasound* is the modality of choice and demonstrates a well-defined nodule or diffuse enlargement of the gland (Fig. 36.16). The capsule is preserved and glandular volume can be calculated.

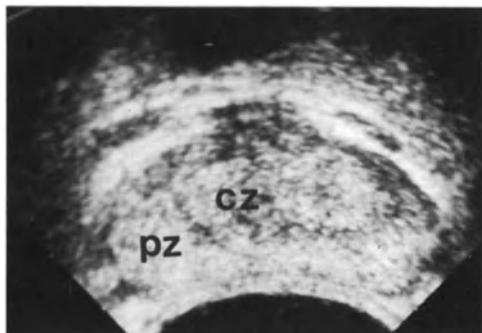


**Fig. 36.15.** Transrectal ultrasound of normal prostate. The gland is well-defined and the peripheral zone (*pz*) has a different echo pattern from the central zone (*cz*).



**Fig. 36.18.** Transrectal transverse axial ultrasound of the prostate. There is such marked calcification in the corpora amylacea (*arrows*) that none of the central zone of the gland can be identified.

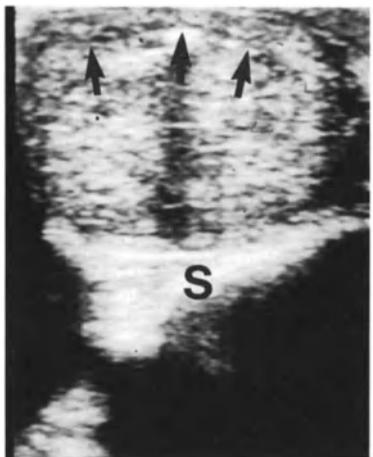


**Fig. 36.16.** A linear array sagittal ultrasound section of the prostate. The prostate is enlarged due to benign hypertrophy. The peripheral zone of the gland is normal (*arrows*). *S*, symphysis.

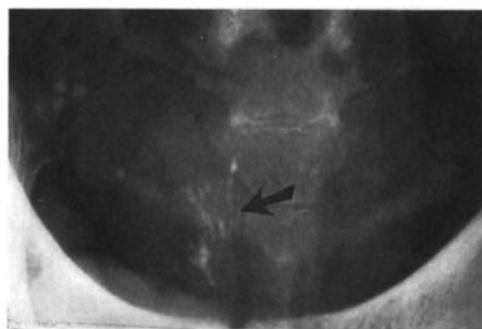


**Fig. 36.17.** Plain film of the pelvis showing calcification of the corpora amylacea (*arrow*).

*Urography* may show a basal bladder defect due to the enlarged prostate or a residue on the post-micturition film, and the bladder may be trabeculated.

Calcification is a non-specific finding in benign hypertrophy and is also seen in prostatic inflammatory disease and rarely in malignancy. It is usually around the ejaculatory ducts as they run in the corpora amylacea (Figs 36.17, 36.18).

*Prostate cancer* originates in the peripheral zone of the gland in the majority of cases. Small tumors appear as echo-poor lesions (Fig. 36.19), although isoechoic and hyperechoic lesions can occur. The findings are not pathognomonic and abnormal areas must be biopsied under ultrasound control (Fig. 36.20). If the capsule of the gland is breached, the tumor is advanced (Fig. 36.21). Nodal involvement is assessed with *CT* (Fig. 36.22) or *magnetic resonance*. Lymphangiography now has no place in assessment. *Bone scintigraphy* is the most sensitive method of detecting bone deposits, which can become widespread and are usually sclerotic at *simple radiography*.

#### Prostatic Cysts

These are congenital or acquired. Acquired cysts are either obstructive due to ejaculatory duct obstruction (Fig. 36.23)

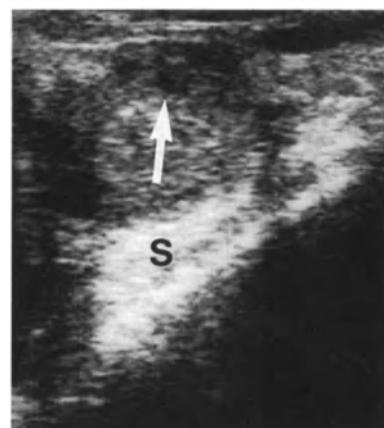


**Fig. 36.19.** Transrectal sagittal ultrasound of the prostate. There is an irregular echo-poor lesion in the peripheral zone of the gland (*arrow*). *S*, symphysis.



**Fig. 36.20.** Transrectal guided biopsy of the lesion illustrated in Fig. 36.19. An 18-gauge Trucut biopsy needle is within the echo-poor lesion (arrow). Histology confirmed prostatic malignancy.



**Fig. 36.23.** Transverse transrectal ultrasound of the prostate. There is a well-defined echo-free lesion in the posterior aspect of the gland (arrow). This is due to a blocked ejaculatory duct.

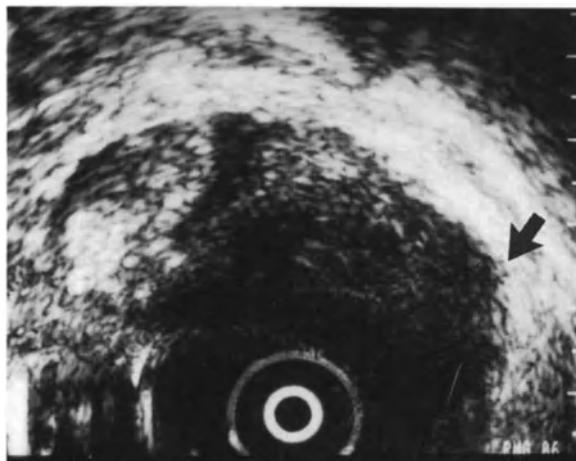


**Fig. 36.21.** Transrectal ultrasound of the prostate. Transverse section. The prostate is enlarged, predominantly echo-poor and the capsule of the gland is no longer well defined (arrow). This represents an advanced malignancy.

by calculi or urethral surgery, or represent cystic change within a neoplasm.

#### Prostatic Inflammation

Prostatitis can be acute or chronic. This can be bacterial, usually due to *E. coli*, or non-bacterial. At ultrasound the gland is abnormal with increased or decreased echoes throughout. Prominence of the peri-prostatic venous plexus is suggestive and the finding of an irregular, predominantly echo-poor area is indicative of a prostate abscess (Fig. 36.24) which can be aspirated under ultrasound control. Inflammation of the seminal vesicles is usually secondary to prostatitis.

#### Post-prostatectomy Appearances

Following transurethral resection or retropubic prostatectomy, there is excision of the bladder neck and proximal prostatic urethra up to the level of the distal sphincter mechanism. This produces a cavity on *cystography* and *transrectal ultrasound* (Fig. 36.25). Measurement of the size of the cavity bears little relation to the resultant flow rate.

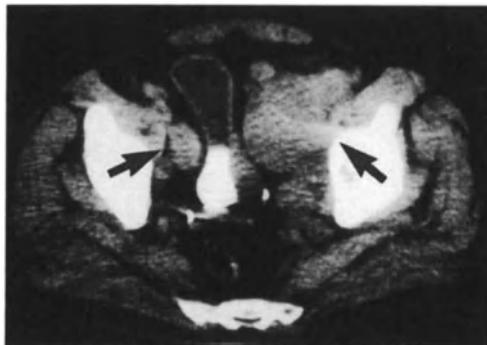


**Fig. 36.22.** Pelvic CT scan of a patient with prostate cancer. There is a mass of nodes compressing the bladder (arrows).



**Fig. 36.24.** Transrectal prostate ultrasound. There is a complex, predominantly echo-poor lesion (arrow) which on aspiration was found to be a prosthetic abscess.



**Fig. 36.25.** Transrectal ultrasound of the prostate showing a TUR cavity (arrow), leading into the bladder. P, residual prostate.

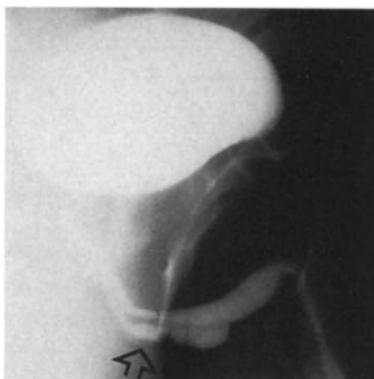


**Fig. 36.26.** Micturating cystogram showing duplication of the urethra (arrow).



**Fig. 36.27.** The dividing membrane between the true urethral lumen and the duplication has been divided. A urethrogram shows a large caliber urethra.

## THE URETHRA

### Congenital Lesions

*Congenital narrowing* of the urethra can vary from mild stenosis of part of the urethra to complete atresia of the urethral canal. *Atresia* usually results in fetal death in the fourth month of gestation when urine is produced. Survival depends upon a fistula, either via the urachus to the umbilicus or with the rectum. *Duplication* of the urethra is rare and usually partial (Fig. 36.26). Stasis precipitates infection. Duplication is usually treated by excision of the dividing membrane (Fig. 36.27).

### Urethral Stricture

Acquired strictures are due to infection or trauma.

*Infective* causes are gonorrhoea and non-specific urethritis, tuberculosis and schistosomiasis. The usual site of stricture is in the anterior urethra. Strictures rarely involve the distal sphincter mechanism (Fig. 36.28). *Gonococcal* strictures tend to involve several centimeters of the urethra and because the whole of the anterior urethral columnar lining is affected, there is no sharp transition between healthy and abnormal urethra. Not all patients with gonorrhoea will develop a stricture. Adequate early treatment prevents urethral damage. Those patients with mild symptoms or where treatment is delayed are more likely to develop strictures.

*Tuberculous* strictures are due to spread of the bacillus from a renal focus. Primary urethral tuberculosis is rare. Strictures are often secondary to periurethral abscess formation.

Urethral strictures in *schistosomiasis* are either due to a granulomatous prostatitis, abscess or fistula formation.

*Traumatic* strictures are due to :

1. Instrumentation e.g., cystoscopy, transurethral resection of the prostate, catheter insertion
2. Chemical instillation
3. Foreign bodies
4. Straddle injuries
5. Pelvic fractures

The urethra is a sensitive structure and very liable to injury during *instrumentation*, especially the male urethra which has a tortuous proximal course. Damage to the urethra can produce stricture formation which may become symptomatic many years after the initial instrumentation. Strictures tend to be short and the transition to normal tissue sharply defined. Stricture can occur in any part of the



**Fig. 36.28.** There is a short anterior urethral stricture (arrow), due to gonorrhoea.

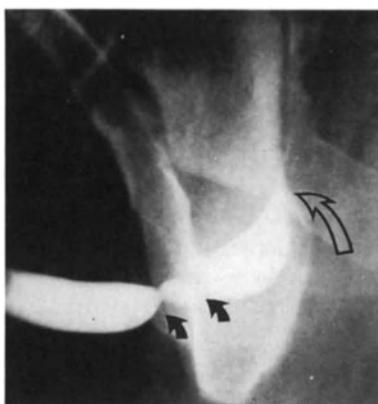


**Fig. 36.29.** A subprostatic stricture (arrows) in the part of the urethra a little distal to the distal sphincter mechanism (open arrow).

urethra, but the subprostatic urethra is particularly prone to trauma because it is the point where the urethra runs anteriorly after coursing through the prostate from the bladder (Fig. 36.29). Strictures here are liable to involve the distal sphincter mechanism. In those patients who have undergone transurethral resection of the bladder neck and prostate, continence depends upon the distal sphincter mechanism alone. The treatment of these sphincter strictures must maintain continence. Ascending urethrography must detail the exact site and length of the stricture as well as defining its relationship to the sphincter mechanism. This may require additional descending urethrography to define the anatomy (Fig. 36.30).

*Catheter* strictures can also involve the subprostatic urethra. Long strictures occur when there is an allergic reaction to the catheter used or if the dimensions of the catheter are too large (Fig. 36.31). At urethrography, long segments of the anterior urethra will be irregular with possibly multiple stenotic segments.

*Chemical* strictures are now uncommon. They have been associated with potassium permanganate irrigation solutions used to treat gonococcal urethritis and more recently with podophylline, 5-fluorouracil and silver nitrate solutions in the treatment of urethral warts.

Any *foreign body* inserted into the urethra is likely to cause stricture. The site of stricture is variable depending on how bizarre the object is.

*Straddle injuries* are due to compression of the proximal anterior urethra against the inferior aspect of the pubic symphysis. The resultant stricture is usually localized, but the extent of the lesion can vary from a mild contusion to complete transection of the urethra. An ascending urethrograph must be done to assess the injury before any attempt at catheterization.

*Pelvic fractures* involve the urethra in 12% of cases. The extent of injury varies greatly, from compression of the urethra caused by pelvic hematoma to complete transection. In the acute stage, these patients require urethrography, and if urethral injury is present a suprapubic catheter is necessary. Often, there is a long defect which classically involves the subprostatic urethra and distal sphincter mechanism. The bladder neck is frequently incompetent, because resolving pelvic hematoma results in fibrosis and contraction, holding the bladder neck open (Fig. 36.32).

If there is associated spinal injury, bladder function has to be assessed. Two weeks after urethral reconstruction, urethrography is performed to assess the anastomotic site and sphincter function. Continence usually depends upon excision of the fibrosis from around the bladder neck.

Urethral strictures are treated by *urethrotomy* or *dilatation*. If the stricture recurs, it can be stented following urethrotomy (Fig. 36.33).

*Urethroplasty* is reserved for the problem case.

*Complications* of strictures include periurethral abscess, sinus and fistula, and urethral diverticulum which can be very large (Fig. 36.34), but often has a narrow neck.

*False passages* are usually iatrogenic, short and run roughly parallel to the true passage. False bladder necks can be fashioned and cystography may be crucial to define the true bladder neck (Fig. 36.35).

A secondary group of complications result from stasis and include stone formation and renal tract inflammation.

#### Urethral Carcinoma

Squamous cell carcinoma of the urethra is rare and is associated with a stricture. It usually presents with obstruction,

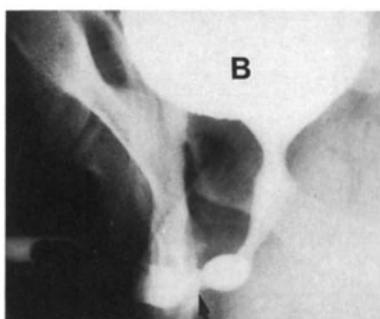


**Fig. 36.30.** A descending urethrogram showing the exact relationship of a stricture (arrow) to the posterior urethra. *B*, bladder.



**Fig. 36.31.** Urethrogram showing multiple anterior urethral strictures following catheter insertion 8 years before.

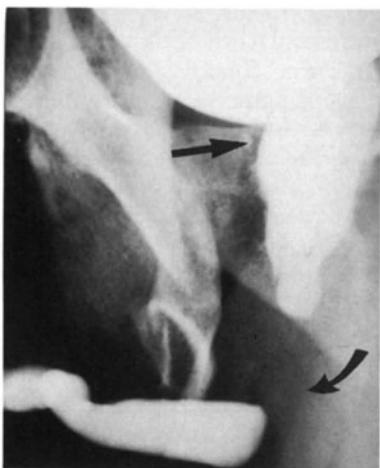


**Fig. 36.32.** A suprapubic cystogram combined with an ascending urethrogram following pelvic fracture stricture. The bladder neck is open (arrow) and there is a long defect in the urethra (curved arrow).

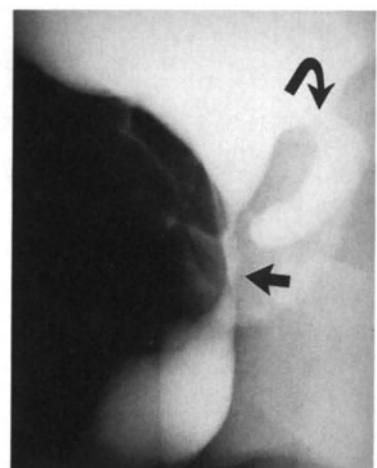


**Fig. 36.35.** A descending urethrogram following multiple dilatations for a urethral stricture. A false passage (arrow) now communicates the urethra and the bladder. The true bladder neck and posterior urethra is seen posteriorly (curved arrow).

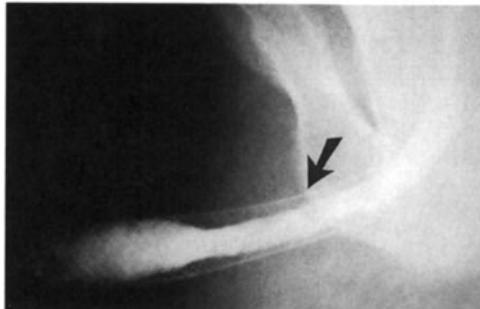


**Fig. 36.33.** A urethrogram showing a wire mesh stent (Wallstent) (arrow) maintaining a good caliber to the urethra following multiple failed urethrotomies for a stricture.



**Fig. 36.34.** A micturating cystogram showing a large urethral diverticulum, the result of surgery.

a palpable mass and urethral bleeding. Urethrography shows an irregular mass lesion communicating with the urethral lumen (Fig. 36.36).

#### The Post-operative Urethra

There are devices for maintaining continence in patients whose sphincter mechanisms no longer work.

The *Kaufman prosthesis* is a silastic capsule placed over the urethra and stapled to the pubic arch. The capsule is filled with contrast medium and acts by continuously obstructing the urethra (Fig. 36.37). Failure of the device can be due to leakage from the capsule resulting in deflation. Under these circumstances, the capsule needs topping up under fluoroscopic control.

The *Brantley Scott prosthesis* aims to be more physiological (Fig. 36.38). An inflatable cuff is placed around the urethra. The pressure within the cuff can be altered by activating a



**Fig. 36.36.** A urethrogram showing an irregular urethral mass lesion (curved arrow) and extravasation of contrast (arrow) due to urethral carcinoma.

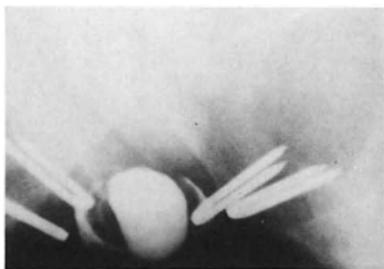


Fig. 36.37. The Kaufman prosthesis. A contrast-filled silastic capsule is stapled to the pubic bones.

pump mechanism placed in the scrotum or labium. The cuff is deflated during micturition and then reinflated to maintain continence. The device is filled with contrast and leakage from the cuff results in radiologically visible deflation.

## URODYNAMICS

Urodynamic assessment of the urinary tract involves separate studies of the upper and lower systems.

The upper system continuously produces urine and functions as a distensible conduit with intrinsic peristalsis to transport urine from the nephrons down the ureters and through a uni-directional valve at the vesico-ureteric junction. The latter mechanism protects the nephrons from damage by back pressure.

The bladder fulfils two functions: the collection and low pressure storage of urine and its subsequent high-pressure expulsion at an appropriate time and place. The pathophysiology of the male and female urethra differ. Although both sexes have two sphincter mechanisms, the proximal sphincter in the male (bladder neck mechanism) provides a powerful block to the retrograde passage of semen during ejaculation and serves both a genital and urinary role. In the female there is no significant anatomical or functional mechanism at this site. In the male, either the bladder neck or the distal sphincter mechanism can be responsible for continence. Anything that compromises the normal func-

tion of the distal sphincter mechanism in the female will result in incontinence. As a consequence, male patients run a risk of developing obstruction, whereas females are prone to incontinence. Cystography provides anatomical information and contributes little to the understanding of function. Current techniques aimed at assessing function are encompassed by the term 'urodynamics'.

Urodynamic assessment includes:

1. Uroflowmetry
2. Ultrasound urodynamogram (USUD)
3. Intravenous urodynamogram (IVUD)
4. Cystometry (CMG)
5. Videocystometry (VCMG)

### Flow Rate

The simplest and most widely applicable investigation is the urinary flow rate. Uroflowmetry is by itself an adequate investigation for uncomplicated prostate outflow obstruction in nearly 50% of patients. The flow rate is only of value if more than 200 ml are voided. Investigation of flow rate can be combined with both ultrasound and excretory urography.

Despite the presence of symptoms suggestive of outflow obstruction the measured flow rate may appear normal, particularly in the early stages of obstruction. This is due to an increase in the voiding pressure sufficient to compensate for the increased outflow resistance. Observed flow pattern is more important than individual values such as the maximum flow rate.

### Ultrasound Cystodynamogram (USUD)

Ultrasound can be combined with the flow rate to provide more detailed information on bladder function. The pre- and post-micturition bladder volume is calculated and a flow rate measured (Fig. 36.39). This is of value in post-surgical patients and in those with compromised bladder function e.g., detrusor failure and sphincter dysfunction.

### Intravenous Urodynamogram (IVUD)

After the 20-minute full length film of an excretory urogram, 20 mg of intravenous frusemide is given. When naturally full, the patient voids, in private, into a flow meter and a post-micturition film is taken. This study provides reliable evidence of the presence or absence of residual urine.

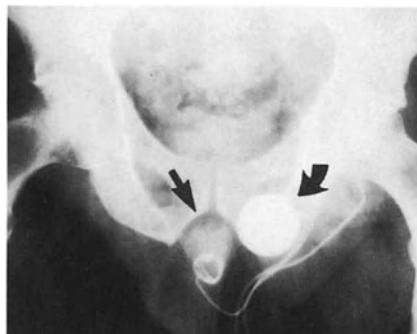
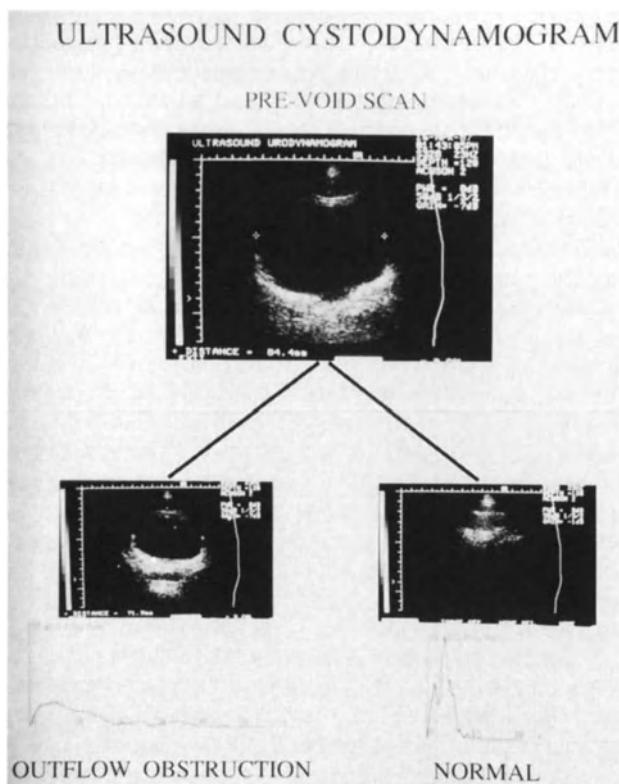


Fig. 36.38. Brantley Scott prosthesis. There is an inflatable cuff around the urethra (arrow). The cuff can be inflated with contrast from the reservoir (curved arrow) via a pump which is inserted within the scrotum.

### Cystometry (CMG) and Videocystometry (VCMG)

If more detailed urodynamic investigation is necessary, measurement of *detrusor pressure* during controlled bladder filling and subsequent voiding with measurement of *flow rate* (filling and voiding CMG) is performed. The detrusor pressure is estimated by the automatic subtraction of *rectal pressure* (as an index of intra-abdominal pressure) from the *total bladder pressure*, thus removing the influence of artefacts produced by abdominal straining or posture. In addition to pressure and flow measurements, the initial bladder residual, the bladder volume at the time of the patient's first sensation of filling, the tolerated bladder volume and the residual volume after voiding are measured.

The VCMG combines pressure studies with *imaging* of the lower urinary tract. The appearances of the bladder, the



**Fig. 36.39.** An ultrasound cystodynamogram. On the left, the flow rate is reduced and there is still urine within the bladder. This is seen in patients with prostatic outflow obstruction. On the right, there has been complete emptying of the bladder at normal flow rates, the normal cystodynamogram.

presence of *ureteric reflux*, the level of any outflow obstruction in the urethra, and sphincter competence are documented (Fig. 36.40).

The normal adult bladder can tolerate 500 ml of fluid. During filling, the subtracted detrusor pressure should not exceed 15 cm of water. Any rise in pressure above this whether in the supine or erect position is diagnostic of *detrusor instability* (Fig. 36.41). This must be differentiated from *poor bladder compliance* where there is a gradual linear rise in pressure during filling. This occurs when the bladder wall has been infiltrated with collagen, e.g., in interstitial cystitis, thus restricting its volume.

If detrusor instability occurs in the presence of documented coexisting neurological abnormality then the condition is defined as '*detrusor hyperreflexia*'. Conversely, if the bladder is able to accommodate an increased volume, e.g., 900 ml, due to peripheral denervation, then a slow rise in pressure will be noted due to passive visco-elastic effects and this is termed the '*plastic bag effect*'.

The normal adult's first sensation of filling is experienced at 150 to 250 ml. *Sensory urgency* occurs if there is increased afferent stimulation during bladder filling and therefore first sensation will be experienced at lower volumes. *Schistosomiasis* and *tuberculosis* are two causes of sensory urgency, although it is important to exclude an intravesical *foreign body* or intravesical *neoplasia*, especially carcinoma in situ. The latter is usually manifest by non-specific reddening of the mucosa and its name belittles its sinister potential for rapidly progressing to highly malignant neoplasia in up to 50% of cases. Having excluded all of these various causes of exaggerated afferent input and associated reduced bladder capacity the diagnosis of a sensory disorder can be made.

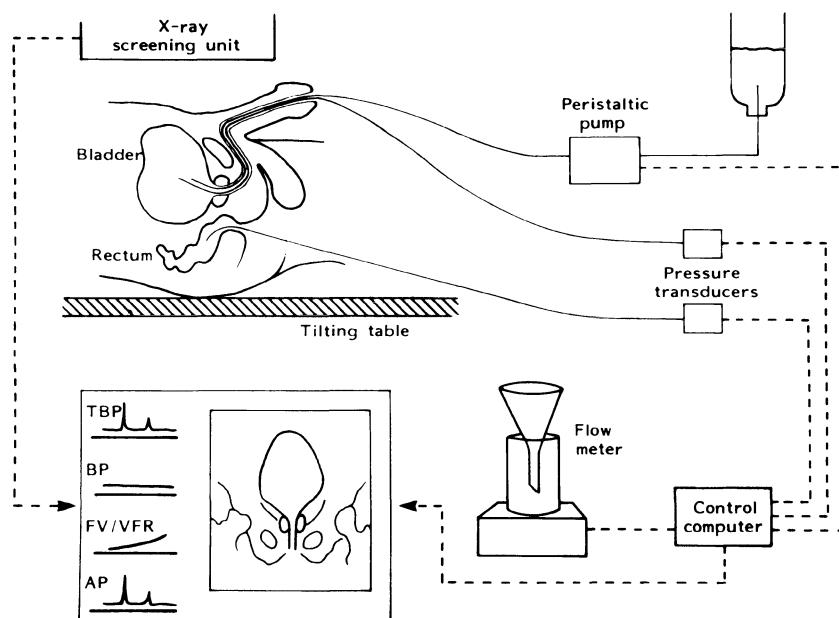


**Fig. 36.40.** Schematic diagram of the VCMG. During bladder filling and voiding, total bladder pressure (TBP) and abdominal pressure (AP) are measured. The true bladder pressure (BP) is calculated by subtracting the abdominal pressure from the total bladder pressure. Simultaneous images of the bladder are recorded. The rate at which the bladder is filled (FR) and the voiding flow rate (VFR) are also recorded.

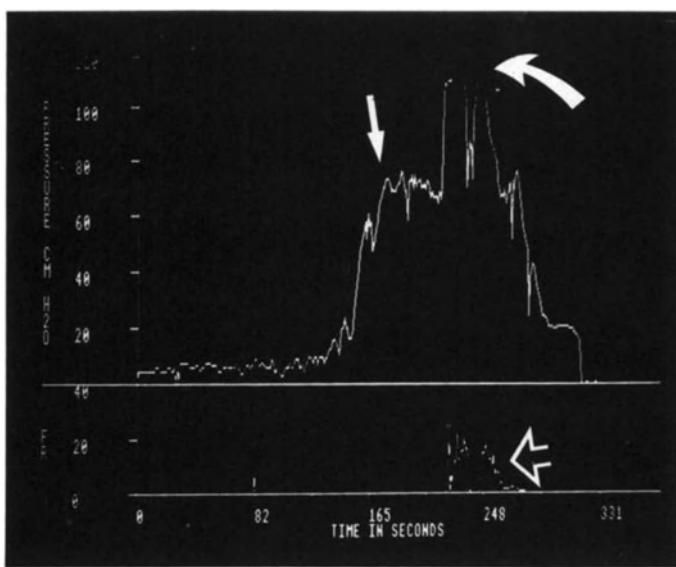


Fig. 36.41. A pressure tracing in a man with unstable outflow obstruction. The detrusor pressure has risen to 60 cm of water during filling (arrow). When asked to void, the patient has done so with a high bladder pressure (curved arrow) and with poor flow rates (open arrow).

During the voiding phase, the patient's bladder should empty completely with a maximum detrusor pressure of 40–50 cm of water in men and 20–30 cm of water in women. Maximum flow rates are 30–40 ml/s with an average of 15–18 ml/s. Voiding is the result of a balance between detrusor pressure and outflow resistance. If there is increased outflow resistance, increased voiding detrusor pressures are needed to achieve a normal flow rate.

The commonest cause of outflow obstruction in men is prostatic enlargement. When the condition becomes symptomatic the typical picture is of a low flow rate with normal or increased voiding pressure. Low flow rates may, however,

also be due to low detrusor pressures. This latter group of patients is not obstructed and will not respond to prostate surgery. CMG or VCMG must be performed on these patients.

Additional indications for CMG and VCMG are for persistent symptoms despite previous surgery, for defining the recovery of function in a patient who fails to void following prostatectomy and for chronic retention despite prolonged suprapubic catheter drainage.

Obstructive symptoms in patients with prostatic outflow obstruction are 'irritative', namely urgency, nocturia and urge incontinence. Urodynamics has demonstrated that these symptoms are largely related to *detrusor instability* which occurs in up to two thirds of these patients and which resolves in a similar percentage following surgery. Residual detrusor instability is the most important cause of post-prostatectomy incontinence in patients with an intact distal sphincter mechanism and its documentation has therapeutic and medico-legal consequences.

Bladder outlet obstruction which occurs in a younger age group (third or fourth decade) is due to a *congenital dyssynergia* of the bladder neck mechanism. Unless recognized and treated appropriately, there is a significant risk of severe bladder dysfunction and chronic retention in later years. The appearances during VCMG are characteristic. When asked to interrupt micturition, the normal patient will milk contrast back from the distal sphincter mechanism through the bladder neck into the bladder; this is termed the 'stop test'. If there is obstruction at the level of the bladder neck, contrast will be trapped within the prostatic urethra and is referred to as a 'positive Whiteside trapping sign' (Fig. 36.42).

Voiding difficulty in females is usually due to a *neuropathic* disorder affecting the bladder, e.g., denervation following vaginal hysterectomy. There is a small, but distinct, group of middle-aged or elderly patients who present with acute retention and often vigorously deny any previous history of voiding difficulty. Urodynamic assessment demonstrates that the bladder has a large capacity with reduced sensation and further questioning usually reveals a life-long history of infrequent voiding.

*Acute retention* can occur in young women and in recent years a specific group of patients has been recognized where there is failure of relaxation of the urethral sphincter mechanism. The pathogenesis of this condition is unknown, but characteristic electromyographic appearances are evident and there appears to be an association with polycystic ovary disease.

*Urinary incontinence* is the commonest cause for the referral of women for urodynamics. The pathogenesis can be broadly classified into urethral and extra urethral.

*Extra-urethral pathology* is rare but includes conditions such as ectopic ureter and vesico-vaginal fistula.

Sphincter weakness is the commonest *urethral* cause of incontinence which is often precipitated by obstetric trauma. If stress incontinence is demonstrable on clinical examination in the absence of any symptoms suggestive of detrusor instability, then urodynamic investigation is not indicated. Even if there are mild 'irritative' symptoms associated with gross stress incontinence, it is likely that surgical correction of the stress incontinence will be indicated whether or not there is co-existent detrusor instability. In

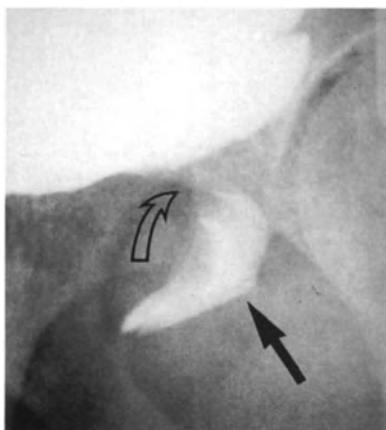


Fig. 36.42. Cystogram. The male patient has been asked to stop micturating. Instead of the contrast milking back into the bladder (the normal situation), there is trapping of contrast in the posterior urethra (arrow) due to obstruction at the bladder neck (open curved arrow). This is called a positive Whiteside sign.



Fig. 36.43. Ultrasound of a testicle invaded by seminoma. There are echo-poor lesions within the testicle (arrow).

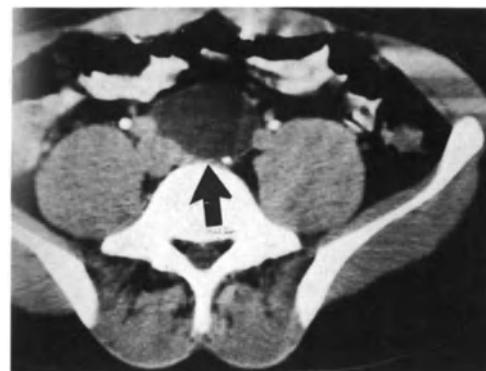


Fig. 36.45. CT scan of the pelvis. The patient has a teratoma and has had treatment. A previously solid node has become cystic (arrow).

the absence of significant stress incontinence the possibility of idiopathic 'detrusor instability' has to be considered.

## THE TESTES

### Testicular Tumor

The origins of 95% of tumors are *germ cells*. The remainder of testicular tumors arise either from mesenchymal tissue, Sertoli or Leydig cells. They are most common in the 25–35 year age group and usually present as a painless enlargement: 10% are bilateral and there is an increased incidence of tumor in undescended testes.

*Seminoma* account for the majority of tumors. On *ultrasound*, they are usually uniformly echo-poor, sometimes containing areas of necrosis (Fig. 36.43). *Teratoma* occurs in a slightly younger age group and in contrast tends to have a mixed, often bizarre echo pattern, often with cystic changes together with echogenic areas (Fig. 36.44). Calcification is a feature. Both tumor types are commonly associated with a hydrocele. *Embryonal cell* and *choriocarcinoma* are the other two types of germ cell tumor and tend to be highly aggressive



Fig. 36.44. Teratoma of the testicle. There is a lesion within the testicle that has a cystic component (arrow).

malignancies. Occasionally, these tumors may undergo spontaneous regression, resulting in a fibrous scar.

It is not possible on ultrasound alone to distinguish with confidence between tumor types. Metastatic disease preferentially involves the para-aortic and paracaval nodes at the level of the renal hilum. These are imaged by *CT*. Extranodal disease involves the lungs, liver, kidney and bone. Following treatment, solid nodes may become cystic and this is strong evidence that no residual tumor persists (Fig. 36.45).

*Secondary deposits* in the testes are more common in the older age group. The kidney and prostate are common primary sites. *Leukemia* and *lymphoma* may also involve the testis and are usually diffusely echo-poor.

### Extratesticular Tumor

These involve the epididymis and are rare. The majority are adenomatoid tumors which are usually well-defined and have an echo pattern similar to or greater than the testis.

### Scrotal Inflammatory Disease

*Epididymo-orchitis* is usually a sequel to urinary tract pathogens of which *Chlamydia*, *E. coli* and *Neisseria gonorrhoeae* are the most common, although the mumps virus, tuberculosis and syphilis should also be considered. On ultrasound, the epididymis is enlarged and echopoor and 20% of patients will have associated changes in the testis. There may be an associated hydrocele.

In *chronic epididymitis*, the epididymis appears echogenic and the tunica albuginea is thickened. Inflammatory disease can be complicated by abscess formation in either the testis or epididymis.

### Miscellaneous Lesions

*Varicocele*. The vast majority of these are left-sided and they occur in 12% of healthy males. They are associated with infertility. The ultrasound appearances are characteristic (Fig. 36.46), but small varicoceles may be missed unless the patient is scanned whilst standing. Doppler studies confirm the vascular nature of the abnormality.

*Hydrocele*. These are either congenital or acquired. The former usually resolve spontaneously. The latter may result from trauma, although an underlying neoplasm must



**Fig. 36.46.** Scrotal ultrasound of a varicocele. There are multiple linear echo-free structures around the testicle (arrow) characteristic of a varicocele.

always be excluded. On ultrasound, hydroceles are transonic. Internal echoes will be seen in *haematoceles* and *pyoceles*.

**Epididymal Cysts and Spermatoceles.** These are small cystic areas related to the epididymis. They present as palpable scrotal nodules and ultrasound confirms their benign nature.

**Torsion.** This acute and painful condition needs to be distinguished from epididymo-orchitis and is a clinical diagnosis

as the ultrasound appearances are very similar. Doppler may be of value in this distinction, as may isotope scanning with  $^{99m}\text{Tc}$ , which shows reduced activity in torsion and increased activity in orchitis.

**Undescended Testicle.** This can affect one or both testicles. The normal descent of the testis from the abdomen to the scrotum is interrupted and it is commonly sited in the inguinal canal. If it cannot be palpated, both *ultrasound* and *CT* may locate it. If these fail, testicular venography is performed. There is an increased incidence of infertility and malignant change.

Unilateral or bilateral anorchia and an ectopic position of the testes must also be considered in the differential diagnosis of an empty scrotum.

#### REFERENCES AND SUGGESTIONS FOR FURTHER READING

- Bright TC, Peter PC (1979) Injuries to the bladder and urethra. In: Campbell's Urology. Saunders, Philadelphia
- Chisholm GD (1985) Carcinoma of the Prostate. In: Whitfield HN, Hendry EF (eds) Textbook of Genitourinary Surgery. Churchill-Livingstone, Edinburgh, pp 1001–1018
- Christmas TJ, Chapple CR, Rickards D (1989) Urodynamics. Current Imaging 1: 187–191
- Crispin AR, Gordon I, Hall C, Metreweli C (1980) Diagnostic Imaging of the Kidney and Urinary Tract in Children. Springer-Verlag, Berlin
- Kellett MJ, Oliver RT, Husband JE, Fry KI (1980) CT as an adjunct to bimanual examination in the staging of bladder cancer. Br J Urol 52: 101–191
- Rickards D (1989) Imaging the prostate. Clin Radiol 40: 335–336
- Turner Warwick RT, Whiteside GC (1979) Symposium on clinical urodynamics. Urol Clin North Am 6: 1

## CHAPTER 37

# GYNECOLOGY

Kathryn Grumbach

---

### TECHNIQUE OF ULTRASOUND EXAMINATION

There are now several available methods for examination of the pelvis utilizing ultrasound.

**Transabdominal sonography** is best performed through a distended urinary bladder. The urine-filled bladder acts as a sonographic window permitting clear visualization of pelvic viscera, displaces small bowel loops out of the pelvis and away from the uterus and adnexa, and, by compression, it places the uterus in a more horizontal position relative to the ultrasound beam, resulting in better quality images. **Real-time sonography** using a variety of high-frequency, small diameter, focused transducers is the most widely accepted and most versatile method of scanning the female pelvis. A 3.5 mHz transducer has the appropriate focal length and is generally used. Transducers with medium or long internal focus permit optimal penetration and image resolution in most adult patients. **Sector transducers** (mechanical or annular) are better suited to the female pelvis than are linear transducers, as they allow the operator to angle the transducer caudally behind the pubic symphysis and laterally along the pelvic side walls. In modern practice, static scanning plays a very limited role, although it can be used to obtain global views of very large masses which cannot be encompassed within the realtime sector.

A complete transabdominal examination of the female pelvis involves both *transverse* (axial) and *parasagittal* images. Typically scans are obtained in the transverse plane from the umbilicus to the symphysis pubis at 1–2 cm intervals. Similarly, parasagittal images are obtained scanning from one side of the true pelvis to the other at 1–2 cm intervals. Oblique planes may be necessary to demonstrate organs lying at oblique angles within the pelvis, which is often the case with the uterus and ovaries.

More recently, **endovaginal scanning** has become a popular method of examining the female pelvis. As most endova-

ginal transducers are of high frequency (usually 5.0, 6.5 or 7.5 mHz) and have a relatively short focal length, an empty urinary bladder is preferred in order to bring the uterus and adnexa closer to the face of the transducer. An endovaginal ultrasound examination is performed by placing a protective condom over the transducer and inserting the probe 6–10 cm into the vagina. **Sagittal** views of the uterus and adnexa are obtained by fanning the ultrasound beam from one side of the pelvis to the other. It should be noted that on sagittal views the fundus of the uterus lies just under the abdominal wall which is displayed toward the left side of the screen. **Coronal** images of the uterus and adnexa are obtained by rotating the transducer 90° in a counterclockwise direction. These coronal images are equivalent to the axial or transverse images obtained on transabdominal sonography.

### NORMAL ULTRASOUND ANATOMY OF THE FEMALE PELVIS

On transabdominal sonography the **vagina** appears as a hypoechoic collapsed tubular structure, with a central high amplitude linear reflection at its center, caused by the apposed surfaces of the vaginal mucosa. The vagina is approximately 7–10 cm in length and is located between the bladder and rectum. When the urinary bladder is fully distended the axis of the vagina points posteriorly toward the sacrum. On sonography the vaginal wall thickness should not exceed 1–2 cm in the normal adult female (Fig. 37.1).

The **uterus** is divided anatomically into three segments: the **fundus** lies superior to the entrance of the Fallopian tubes. The **corpus** of the uterus lies inferior to the uterine fundus and superior to the **endocervix**. The lowest portion of the uterine corpus, the **isthmus**, is transitional between the smooth muscle of the uterine corpus and the fibrous tissue of the uterine cervix.

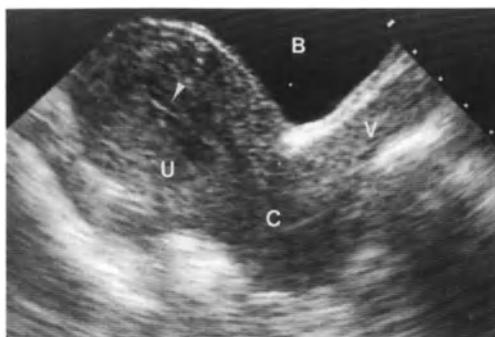


**Fig. 37.1.** Normal uterus. The normal premenopausal uterus is demonstrated on this sagittal transabdominal scan. The vagina appears as an echoic tube (V) and the cervix (C) is tissue of homogeneous echo texture connecting the vagina to the uterine corpus (U). The endometrial stripe is clearly identified (arrowhead). *B*, urinary bladder.

The *cervix* is also subdivided into the *endocervical* and *ectocervical* portions, and is a cylindrical structure 2–4 cm in length through which the cervical canal passes. The proximal portion of the cervical canal, continuous with the uterine corpus, is the *internal cervical os* and the distal portion of the cervical canal is continuous with the vagina and is called the *external cervical os* (Figs 37.1, 37.2).

The size of the uterus varies with the age and parity of the patient as well as the stage of the menstrual cycle. The *prepubertal* uterus measures 1–3.5 cm in length and 0.5–1 cm in width, and the cervix and isthmus may comprise up to two thirds of the organ size. The maximal *postmenarchal* uterine size is 7–8 cm in length and 4–5 cm in anterior–posterior diameter and width, and the uterus attains a characteristic pear shape, with a thicker fundus and corpus and a more tapered, shorter cervix. *Postmenopausally*, the uterus atrophies due to lack of hormonal stimulation and is less than 6.5 cm in length and 2.0 cm in anterior–posterior diameter or width. *Multiparity* affects uterine size causing an overall increase in uterine size of 1–2 cm in all dimensions.

The uterus displays three prominent regions of differing echogenicity on sonography. The *myometrium* is represented by a thick homogeneous band of low-to-medium echogenicity, and forms the outer smooth muscle layer of the uterus. The *endometrial cavity* is represented by a moderate-to-high amplitude, thin echogenic line (the *endometrial stripe*),

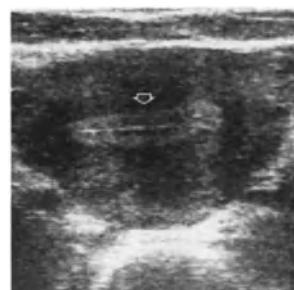


**Fig. 37.3.** Normal uterus. A more detailed image of the endometrial echo complex is seen on this transverse scan of the uterus in another premenopausal female in the secretory phase of her menstrual cycle. The internal echogenic line (arrowhead) surrounded by successive hypoechoic, hyperechoic and hypoechoic regions of the endometrium is seen.

which is slightly less bright than the midline vaginal echo. Surrounding the endometrial cavity is the slightly hypoechoic *endometrium* which measures 2–4 mm in thickness in the proliferative phase of the menstrual cycle and approximately 5–6 mm in thickness in the secretory phase of the menstrual cycle. An echo-poor halo may be seen surrounding the endometrial stripe in some premenopausal women, probably representing a network of capillaries and veins in the innermost layer of the myometrium, and most obvious in the post-ovulatory and premenstrual portions of the menstrual cycle (Fig. 37.3).

The uterus is normally in the midline and anteverted 45–90° relative to the vagina. With maximal bladder distension, on transabdominal sonography the uterus assumes a more horizontal and less anteverted position in the pelvis and may be deviated laterally to the right or the left.

Retroposition of the uterus occurs when the entire uterus is tilted posteriorly from the level of the cervix (*retroversion*) or when the body and fundus of the uterus are flexed posteriorly relative to the uterine cervix (*retroflexion*). Retroflexed and retroverted uteri tend to have a globular fundal contour and may be difficult to image with transabdominal sonography due to the angle of the uterus relative to the ultrasound beam. As a result it may be difficult to distinguish a normal retroverted uterine fundus from a myoma (Fig. 37.4) and therefore, the retroverted uterus is best examined using an endovaginal technique.

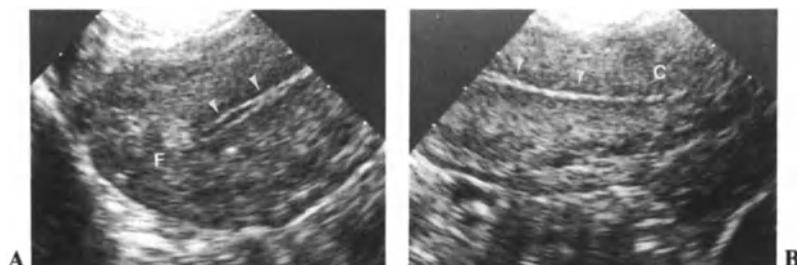


**Fig. 37.2A, B.** Normal uterus. Two sagittal scans A and B through the uterus of a 23-year-old, non-gravid female from an endovaginal examination reveal superior detail of the endometrium (arrowheads) and myometrium. On sagittal scans the cervix (C) is displayed on the right side of the screen and the uterine fundus (F) on the left.



**Fig. 37.4.** Retroposition of the uterus. A sagittal sonogram through a normal retroverted uterus demonstrates poor definition of the endometrial stripe (arrowhead). It is difficult to distinguish the normal uterine fundus from a fundal myoma (large arrow) on this transabdominal scan. An endovaginal examination revealed no evidence of myomas.



**Fig. 37.5.** Normal ovary. The normal ovary in a 26-year-old female is seen in this transverse scan from a transabdominal sonogram (arrow). Small follicles (< 1 cm in size) are noted within the cortex. U, uterus.

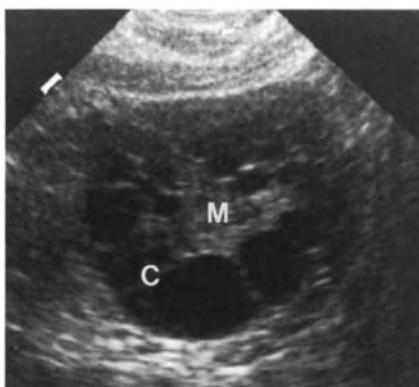


**Fig. 37.6.** Ovarian anatomy. On endovaginal sonography, the cortex (C) and medulla (M) of the ovary in a premenopausal female are more easily identified. Follicular structure and size are beautifully demonstrated making endovaginal sonography ideally suited for imaging in infertility. The follicles in this ovary are large and densely packed, due to hyperstimulation by human menopausal gonadotropin.

The uterus is covered superiorly by peritoneum, and this is reflected posteriorly into the cervical area forming the rectouterine pouch of Douglas.

The **broad ligaments** extend from the lateral aspect of the uterus to the pelvic sidewalls and contain the Fallopian tubes in their free borders. The broad ligaments are usually only identified when they are surrounded by free intraperitoneal fluid and occasionally when the uterus is retroverted. In addition, the uterus is supported by the cardinal and uterosacral ligaments inferiorly and the round ligaments superiorly.

The **Fallopian tubes** are fibromembranous structures which take a serpiginous course from the uterine cornua to the region of the ovary. The distal ends of the Fallopian tubes are suspended from the pelvic brim by a band of peritoneum, the infundibulopelvic ligaments. Anatomically, the Fallopian tubes are divided into the interstitial, isthmic and ampullary portions. The *interstitial* portions course obliquely from the apex of the uterine cornua through the myometrium. The *isthmic* portion is slightly wider and connects the tortuous *ampullary* segment to the fimbriated end of the tube. The ostium of the infundibular portions opens into the peritoneal cavity and the fimbria abut on the lateral aspect of the ovary. Unless the Fallopian tube is distended it is not commonly visualized on transabdominal sonography. However, it may be identified as a thin hypoechoic tubular structure no greater than 5 mm in diameter on endovaginal scanning.

The **ovaries** are ovoid in shape with their long axes lying parallel to the internal iliac artery and vein. Ovarian location is variable but in most nulliparous females each ovary is situated in the ovarian fossa, which is located along the lateral pelvic sidewall and is bounded *posteriorly* by the ureter and internal iliac artery, *superiorly* by the external iliac vessels, and *anteriorly* by the broad ligament. The fimbriated portions of the Fallopian tube and the suspensory ligament of the ovary or mesovarium are located along its superior surface. The suspensory ligament of the ovary connects the medial pole of the ovary with the uterine cornua.

On transabdominal ultrasound, the normal ovary demonstrates a homogeneous echotexture which is hypoechoic to the surrounding pelvic fat. In post-pubertal females, multiple *follicles* may be seen as tiny hypoechoic cystic structures arranged around the periphery of the ovary (Fig. 37.5). On endovaginal scanning it may be possible to differentiate the central more echogenic ovarian medulla from the surrounding less echogenic cortex containing multiple follicles (Fig. 37.6). The ovaries change in size with age. In the young child, ovarian volume is usually less than 1 ml, whereas in post-pubertal adults ovarian volume is usually greater than 6 ml and may be as high as 14 ml in the normal individual. During the post-menopausal period the ovary atrophies and should be less than 2.5 ml in volume.

#### CONGENITAL ANOMALIES OF THE FEMALE GENITAL TRACT

The Fallopian tubes, uterus and cervix arise from the paired Mullerian ducts which descend from a lateral position in the fetal abdomen and fuse medially during the first month of

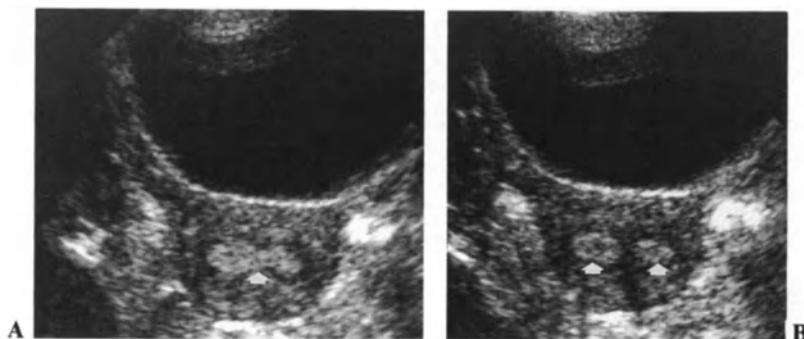


**Fig. 37.7A, B.** Bicornuate uterus. **A** A transverse sonogram through the uterus shows a bilobed uterine contour and dumbbell shaped endometrial echo complex (arrowhead) typical of a bicornuate uterus. **B** A transverse scan at a slightly more cephalad level reveals divergence of the two endometrial echo complexes (arrowheads).

embryogenesis. The fused portion then recanalizes to form the uterus and cervix which unites with the sinovaginal bulbs (primitive vagina) by the 9th week of fetal development. Full canalization of the Fallopian tubes, uterus and vagina is completed by the 18th week of fetal development. Failure of any developmental step may lead to a genital tract anomaly ranging from complete agenesis to more subtle anomalies of fusion.

1. Anomalies which result from arrested Mullerian duct development include **uterine aplasia** if the process is bilateral and **unicornuate uterus** if the process is unilateral. Total absence of the uterus is identifiable on both transabdominal and endovaginal ultrasound, but unicornuate uterus may be difficult to classify on sonography alone. The loss of the normal pear shape of the uterus and tapering of the fundus with a lateral deviation of the uterus may be difficult to distinguish from uterine hypoplasia or a normal uterus.

Malformations resulting from failure of Mullerian duct fusions include **uterus didelphys** (two vaginas, two cervixes, two uterine corpora), **bicornuate uterus** (one vagina, one cervix, two uterine horns), and **arcuate uterus** (failure of fusion of the fundal region only).

On sonography *uterus didelphys* appears as two widely spaced uterine corpora and two distinct endometrial stripes

and cervixes. This appearance may be identical to bicornuate uterus and the diagnosis of *uterus didelphys* depends upon the pelvic examination findings of a double vagina and/or double cervix. **Bicornuate uterus** is by far the most common anomaly of the uterus and presents on transabdominal and endovaginal ultrasound as a bilobed external uterine cervix (Fig. 37.7). During the first trimester of pregnancy a bicornuate uterus is more easily identified on sonography; the eccentric location of the gestational sac and echogenic debris or decidua reaction in the non-gravid horn make the diagnosis more obvious (Fig. 37.8). However, in advanced pregnancy the fetus often effaces the non-gravid horn making the correct diagnosis of bicornuate uterus impossible. The findings in **arcuate uterus**, characterized by a saddle-shaped uterine fundus and increased transverse diameter of the uterine cavity, are too subtle to be diagnosed on ultrasound.

2. The second major class of anomalies of the uterus involve total or partial non-resorption of the sagittal uterine septum. These include **septate uterus** (total non-resorption) and **uterus subseptus** (partial non-resorption). The normal external uterine contour seen in both forms of septate uterus can be confirmed on ultrasound.

**Septate uterus** is the most common uterine congenital anomaly associated with reproductive failure and therefore it is important to distinguish this anomaly from bicornuate uterus. However, as both transabdominal and endovaginal ultrasound usually fail to demonstrate the vaginal septum in the non-gravid patient, additional imaging modalities may be necessary such as magnetic resonance imaging or hysterosalpingography, and diagnostic laparoscopy may even be required to confirm this clinically important diagnosis.

3. The third important class of anomalies of the uterus result from decrease in or lack of a hormonal stimulation during fetal development. These include **infantile uterus**, **uterine hypoplasia**, and a variety of malformations of uterine shape such as **T-shaped uterus**. This latter abnormality is seen in approximately 16% of women exposed to diethylstilbestrol (DES) in utero. Both transabdominal and endovaginal ultrasound are useful in identifying small uterine size and volume but they may be limited in their ability to identify abnormal cavity shapes.



**Fig. 37.8.** Gravid bicornuate uterus. The presence of an early intrauterine pregnancy makes the identification of a uterine anomaly easier. The gestational sac of the 7-week gestation is clearly seen (arrowheads) and a small amount of fluid is noted in the non-gravid uterine horn (arrow).

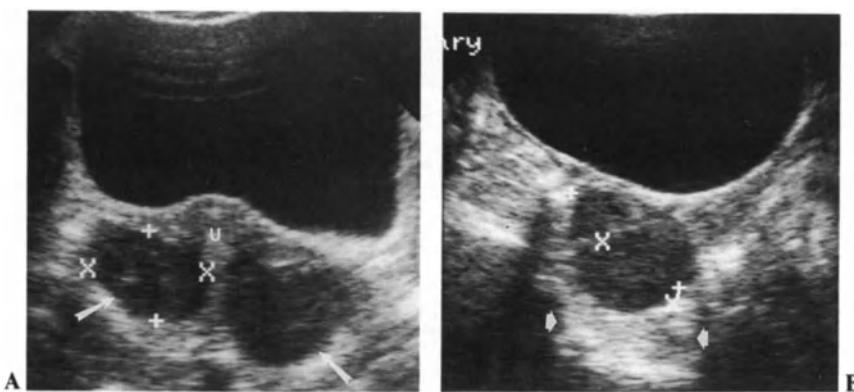


**Fig. 37.9A, B.** Bilateral adnexal endometriomas. **A** A transverse sonogram through the pelvis of a 29-year-old female presenting with dysmenorrhea reveals bilateral hypoechoic masses representing 'chocolate' cysts (arrows). **U**, uterus. **B** On sagittal scan through the mass on the left, the enhanced sound transmission behind the mass is seen (arrowheads) and is due to the fluid nature of the cyst contents.

Approximately 20%–25% of women with genital tract anomalies will have coexistent urinary tract anomalies including *unilateral renal agenesis* and *renal ectopia*. It is therefore necessary to examine the kidneys and bladder when a female genital tract anomaly is suspected.

#### INFLAMMATORY DISEASES

##### Endometriosis

Endometriosis is defined as the presence of ectopic endometrial tissue located at extrauterine sites such as ovaries, broad ligament, bowel, bladder or ureter. During menses hypertrophy and bleeding occurs in these endometrial aggregates, causing dysmenorrhea. It is the major contributing factor to infertility in 15% of infertile women and may be found in as many as 8%–30% of premenopausal women at surgery.

The most popular theories as to its etiology are transformation of peritoneal epithelium into functional endometrium, or peritoneal seeding by a retrograde transport of endometrial cells during menses. It is commonly felt that sonography is neither sensitive nor specific for endometriosis and plays only a minor role in the diagnosis and treatment of patients who have no palpable mass on examination. In one series of 37 patients with laparoscopic proof of endometriosis, transabdominal ultrasound was capable of detecting endometriosis in only 4 patients (10.8%). Large masses located in the ovary or parametrial tissues known as 'chocolate cysts' are visible by transabdominal or endovaginal technique and are usually characterized by predominantly cystic masses with irregular walls containing low-level echoes (Fig. 37.9A, B). In addition, these masses may be septated and may contain fluid–fluid or fluid–debris levels internally.

**Adenomyosis** refers to the presence of endometrial aggregates within the myometrium. This most commonly results in diffuse uterine enlargement with a normal endometrial stripe and normal myometrial echotexture and uterine contour. Rarely, focal aggregates of endometrial tissue occur and present as a focal uterine mass, usually fundal, which is isoechoic with normal myometrium. This form may be indis-

tinguishable from leiomyomas and where the two coexist, they cannot be distinguished from one another (Fig. 37.10).

##### Pelvic Inflammatory Disease

The term pelvic inflammatory disease (PID) is defined as infection of the uterus, Fallopian tubes, ovaries and peritoneal cavity. In the pathogenesis of venereal infection bacteria ascend through the uterine cervix to involve the endometrium (endometritis), Fallopian tubes (salpingitis), ovaries (oophoritis), and peritoneal cavity with abscess formation (tubo-ovarian abscess). Organisms most commonly causing PID secondary to venereal infection are *N. gonorrhoeae* and *Chlamydia trachomatis*. Factors which predispose to pelvic infection include uterine manipulation at surgery, puerperal or post-abortal complications or the use of the intrauterine contraceptive device (IUD).

Acute infection of the *endometrium* usually presents as an enlarged uterus with indistinct margins, hypoechoic myometrium and echolucent or absent endometrial echoes on transabdominal or endovaginal ultrasound. In addition, small amounts of fluid within the endometrial cavity or in



**Fig. 37.10.** Uterine adenomyoma. A sagittal sonogram through the uterus of a 33-year-old female reveals a focal fundal mass of inhomogenous echotexture (arrow). Although sonographically indistinguishable from a leiomyoma this proved to be an adenomyoma (localized adenomyosis) at surgery.

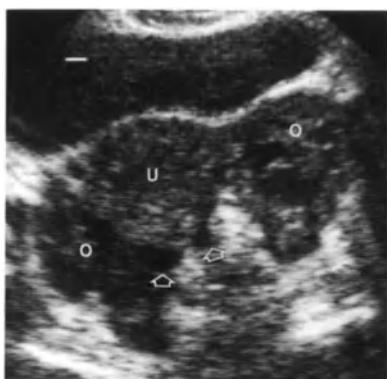


**Fig. 37.11.** Pelvic inflammatory disease. A transverse sonogram through the pelvis in this 24-year-old female reveals indistinct, enlarged adnexa. Small amounts of fluid are noted surrounding the ovaries (O) and in the cul-de-sac (arrowheads). U, uterus.

the cul-de-sac may also be identified. When *salpingitis* and *oophoritis* ensue, enlarged ovaries, hypoechoic poorly defined parametrial tissues, and cul-de-sac fluid are usually present (Fig. 37.11).

**Pyosalpinx**, resulting from accumulation of purulent material within a non-patent Fallopian tube, is characterized by an ovoid or serpiginous, cystic structure in the location of the Fallopian tube containing low-level echoes.

**Acute tubo-ovarian abscess** results from loculation of pus in the region of the ovary and Fallopian tube and presents as a multilocular, hypoechoic mass, containing echoes, fluid-

debris levels, or septa surrounding the ovary or within the cul-de-sac. Most have thick walls, indistinct margins and show good sound transmission (Figs 37.12A, B). Bilateral tubo-ovarian abscesses are more common in venereally acquired PID, whereas unilateral abscess is most commonly due to IUD, previous tubal infection with adhesions, or prior tubal surgery. *Ruptured tubo-ovarian abscess* presents with free fluid in the cul-de-sac or elsewhere in the peritoneal cavity.

Ultrasound is highly sensitive in detecting the presence of tubo-ovarian abscess and should also be used in assessing response to antibiotic therapy. The abscess should decrease in size within 2–5 days of initiating appropriate antibiotic therapy and if this does not occur, percutaneous or surgical drainage may be necessary.

The findings in **chronic pelvic inflammatory disease** include dense pelvic adhesions which may obliterate the margins of the uterus and ovaries on ultrasound. *Hydrosalpinx*, resulting from adhesions in the region of the Fallopian tubes leading to obstruction and accumulation of fluid within the tubal lumen, presents as an anechoic, tubular or ovoid structure in the parametria between the uterus and ovary (Fig 37.13A, B). It may be confused with ovarian or parovarian cyst and definite diagnosis may require laparoscopy or hysterosalpingography.

#### Intrauterine Fluid Collections

Intrauterine fluid collections in non-pregnant patients are relatively common findings on ultrasound and the differential diagnosis includes *endometritis*, *hematometra*, and fluid

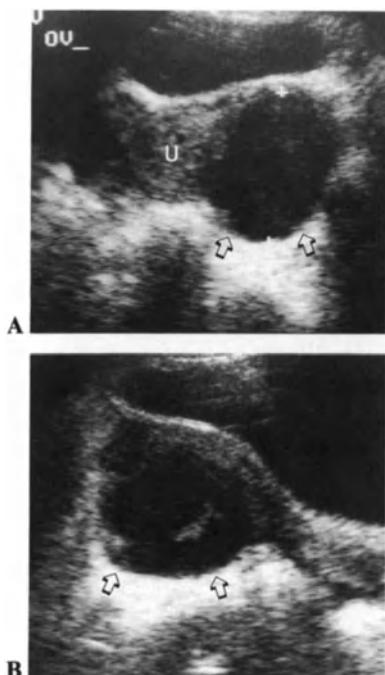


**Fig. 37.12A, B.** Tubo-ovarian abscess. Transverse A and sagittal B transabdominal sonograms demonstrate a large hypoechoic mass containing debris and septa (arrowheads) in the left adnexa. This proved to be a tubo-ovarian abscess at surgery complicating pelvic inflammatory disease due to *N. gonorrhoea*. U, uterus.

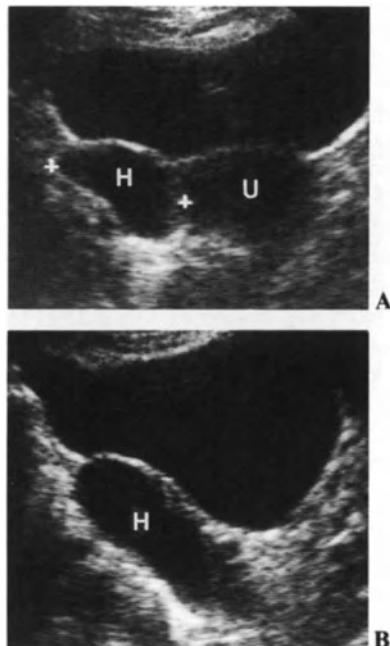


**Fig. 37.13A, B.** Hydrosalpinx. A right hydrosalpinx presents as a tubular anechoic structure (h) adjacent to the uterus in transverse, A, and right sagittal sonograms B. This 28-year-old female had a prior history of pelvic inflammatory disease. U, uterus.



**Fig. 37.14A, B, C.** Intrauterine fluid collections. A A sagittal scan through the uterus (*U*) and vagina (*V*) reveals echogenic material in a distended vagina and uterus. This represents accumulated menstrual blood and secretions in an 18-year-old female with imperforate hymen and primary amenorrhea. B A complex fluid collection composed of residual amniotic fluid and fetal parts (*arrows*) is noted on this sagittal sonogram of the uterus. This represents a missed abortion in the 33-year-old gravid patient with heavy vaginal bleeding. C Fluid is noted within the uterine cavity in a patient with cervical stenosis secondary to radiation therapy for cervical carcinoma. The uterus is filled with hypoechoic, serous fluid (*F*) which represents a hydrometrium developing proximal to an obstructed cervix (*C*).

collection associated with *endometrial* or *cervical neoplasms* or *gestational trophoblastic disease*.

In young patients, *imperforate hymen*, *intact vaginal membrane* or *vaginal atresia* may lead to accumulation of the menstrual secretions in the vagina and uterus and may result in *hydrometrocolpos* (Fig. 37.14A). Also, retained products of conception after delivery of spontaneous or therapeutic abortion may lead to accumulation of echogenic material within the uterus, which may mimic a *hematometra* (Fig. 37.14B).

In *post-menopausal* patients the differential diagnosis of intrauterine fluid collections is different. The majority of these patients will have associated *uterine* or *cervical neoplasms* causing cervical stenosis. This leads to accumulation of blood and uterine secretions proximal to the obstruction (Fig. 37.14C). Recent reports, however, have associated benign disease including *endometrial polyp*, *chronic inflammation* or *endometrial atrophy* with intrauterine fluid collection in post-menopausal patients. On sonography it may be difficult to distinguish *pyometrium* (pus in the endometrial cavity) from *hydrometrium* and *hematometrium*. The presence of gas within the uterus indicates a pyogenic infection with gas-forming organisms, but this is the only distinguishing feature.

Early *intruterine pregnancy* and its complications can also cause intrauterine fluid collections. The differential diagnosis includes *very early intruterine pregnancy*, *blighted ovum*, *missed* or *incomplete abortion*, *ectopic pregnancy* or *gestational trophoblastic disease*. It may be impossible to distinguish between these different etiologies using transabdominal and endovaginal ultrasound and correlation with quantitative HCG levels is often necessary to arrive at a correct diagnosis.

#### NEOPLASTIC DISEASE

##### Leiomyomas

Leiomyomas are the most commonly encountered neoplasms of the uterus, occurring in approximately 40% of all women beyond 35 years of age. They are the most common cause of uterine enlargement in the non-pregnant

population. They are composed of smooth muscle and connective tissue and are hormone dependent, changing in size and echotexture during pregnancy and after the menopause.

The clinical presentation of patients with uterine leiomyomas includes a pelvic mass on physical examination, menorrhagia, pelvic pain and less commonly, infertility, habitual abortion or obstructed labor. These tumors may range in size from microscopic aggregates of smooth muscle to huge masses. They may be submucosal in location (lying just deep to the endometrium), intramural (within the myometrium) or subserosal (located just below the outer uterine surface). Most arise in the fundus and corpus of the uterus with only 3% of lesions located in the cervical region. They may become extruded from a subserosal location and may be pedunculated with a tendency to torsion, infarction and infection. Degenerative changes within leiomyomas account for the large spectrum of gross pathologic and sonographic findings. Central necrosis and infarction often occur in large neoplasms which have outgrown their vascular supply. Sarcomatous degeneration of preexisting uterine leiomyomas gives rise to *leiomyosarcoma*, the most common mesenchymal malignancy of the uterus.

The sonographic features of uterine leiomyomas are diverse. In one series of 41 cases examined with transabdominal ultrasound 76% manifested a bulbous uterine fundus, focal uterine mass, anterior contour irregularity or lobulated contour (Fig. 37.15).

Alterations in uterine echotexture are common, with approximately equal numbers showing *hypoechoic* and *hyperechoic* masses. Hyaline degeneration is usually manifested by hypoechoic or anechoic areas within a mass without distal wall enhancement, whereas cystic degeneration presents as irregular sonolucent areas within a solid mass with distal acoustic enhancement.

*Calcification* may occur in up to 25% of leiomyomas and usually presents as high amplitude echoes clustered within the mass with acoustic shadowing. Calcification may also be located around the rim of the tumor. There are limitations to the diagnosis of leiomyomas with ultrasound. Tumors less than 1–1.5 cm in size may be entirely missed, although endovaginal sonography may be useful in locating small



**Fig. 37.15.** Uterine leiomyomas. A sagittal scan through the uterus of a 45-year-old post-menopausal female reveals an enlarged uterus with lobulated contour. Anterior and posterior leiomyomas distort the uterine contour (arrows) but the endometrial echo complex is partially preserved (arrowhead). The myomas appear slightly hypoechoic relative to the surrounding normal myometrium.

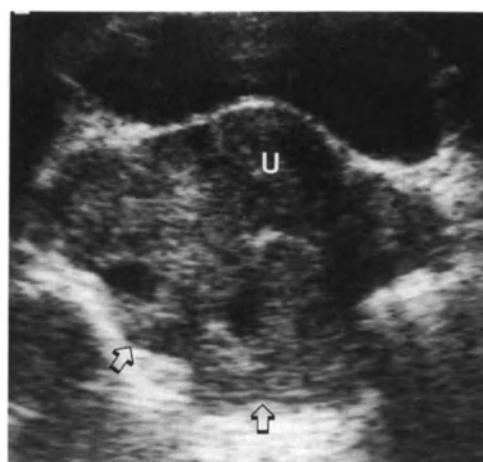


**Fig. 37.16.** Invasive endometrial carcinoma. A large, lobulated mass of heterogeneous echo texture is noted posterior to the uterus (arrows) on this sagittal scan. Although this mass cannot be distinguished sonographically from leiomyoma, it represented parametrial extension of endometrial carcinoma at surgery. *U*, uterus.

aggregates of smooth muscle tumor. Pedunculated lesions connected to the uterus by only a narrow pedicle may be confused with solid ovarian masses. Submucous fibroids may be difficult to distinguish from endometrial polyp or endometrial carcinoma.

#### Endometrial Carcinoma

Adenocarcinoma of the endometrium is the fourth most common malignancy in women and most patients present with watery or bloody vaginal discharge. The diagnosis is established by means of an *endometrial biopsy*. The clinical staging system for endometrial carcinoma has been established by the International Federation of Gynecology and Obstetrics (FIGO) and is shown in Table 37.1.

**Table 37.1.** FIGO staging criteria for endometrial carcinoma

Stage	Criterion
I	Carcinoma confined to the uterine corpus
IA	Length of uterine cavity $\leq$ 8 cm
IB	Length of uterine cavity $>$ 8 cm
II	Carcinoma involves uterine corpus and cervix but does not extend beyond uterus
III	Carcinoma extends outside uterus but is confined to true pelvis
IV	Carcinoma extends outside the true pelvis or involves the mucosa of the bladder or rectum
IVA	Carcinoma involves adjacent organs
IVB	Distant metastases

Accurate preoperative staging is necessary since the different clinical stages are treated with different regimens of radiation, chemotherapy and surgery. Ultrasound can easily distinguish disease confined to the uterus (Stages 1 and 2) from disease outside the uterus (Stages 3 and 4) on the basis of size, contour and echo pattern of the uterus. In one report,

ultrasound had a sensitivity of 94% in detecting disease confined to the uterus and cervix. These patients had a normally shaped or bulbous uterine contour with normal or hypoechoic echo pattern. Patients with tumor extending outside the uterus tended to have a lobulated uterine contour with a mixed hyper- and hypoechoic echo pattern arising from the endometrium (Fig. 37.16). In these patients it may be difficult to distinguish Stages 3 and 4 disease from leiomyomas. Ultrasound, however, is limited in its ability to detect lymph node metastases, direct invasion into adjacent organs such as bladder and rectum, pelvic sidewall involvement and peritoneal metastases and *CT* and *MRI* are more sensitive in assessing widespread metastases in this particular type of tumor.

Recent reports indicate that ultrasound may be useful in distinguishing Stage 1 and Stage 2 disease and assessing the depth of myometrial invasion by endometrial carcinoma. In one study, depth of myometrial involvement was correctly predicted in 70% of 20 cases. Superficially invasive tumors (involving less than 50% of myometrial thickness) were manifest by complete or partial preservation of the subendometrial halo on sonography, whereas deeply invasive tumors showed subendometrial halo disruption in most cases.

#### Endometrial Polyps

Endometrial polyps are composed of hyperplastic or adenomatous endometrial tissue and commonly present with vaginal bleeding. They are more common in the perimenopausal or post-menopausal period. On sonography, they usually present as prominent endometrial echoes or as a discrete mass within the endometrial cavity. When they attain a large size they may cause enlargement of the uterus. Difficulty arises in distinguishing these masses from submucous leiomyomas or endometrial carcinoma and a definitive diagnosis may be made only on biopsy.

### Cervical Carcinoma

Cervical malignancies usually have a squamous histology and present in women of reproductive age. Staging criteria for cervical carcinoma are shown in Table 37.2. With appropriate therapy all patients with Stage 0 disease and 80% of patients with Stage 1 disease are curable, contrasted with approximately a 40% cure rate for women with Stage 3 disease.

**Table 37.2. FIGO staging criteria for cervical carcinoma**

Stage	Criterion
O	Carcinoma <i>in situ</i>
I	Carcinoma confined to cervix
IA	Microinvasive
IB	Invasive
IC	Carcinoma confined to cervix but clinically detectable
II	Carcinoma extends beyond cervix but does <i>not</i> involve pelvic sidewalls or lower one third of vagina
IIA	Medial parametrial extension with vaginal involvement
IIB	Lateral parametrial extension
III	Carcinoma extends to pelvic side wall and/or lower one third of vagina
IIIA	Lower one third of vagina involved
IIIB	Extension to pelvic side wall, hydronephrosis
IV	Carcinoma extends beyond true pelvis <i>or</i> involves bladder or rectal mucosal
IVA	Biopsy-proven bladder or rectal mucosal involvement
IVB	Distant metastases beyond true pelvis

Ultrasound is limited in its ability to detect Stage 0 and Stage 1 disease and diagnosis depends largely on screening tests such as the Pap smear. In more advanced lesions (Stage 2 or greater), the most common ultrasound finding is an enlarged cervix with an irregular contour, which is hypoechoic relative to normal myometrium. The endometrial canal usually appears normal but may become distorted with very large masses. Extension into contiguous structures such as vagina or parametria may also be seen. Pelvic sidewall invasion, pelvic lymphadenopathy and distant metastases are best detected on alternate imaging modalities, such as CT or MRI. Ultrasound evaluation of the cervix itself may be optimized by use of a water enema or a fluid-soaked tampon in the vagina with transabdominal ultrasound or by utilization of the endovaginal technique.

Overall, CT and ultrasound are about equally sensitive in detecting primary malignancies in the female pelvis, with a sensitivity of about 90%. However, up to a third of cases of cervical carcinoma may be understaged utilizing either CT or ultrasound alone and, therefore, other imaging modalities have been sought for accurate staging. Techniques which hold promise for the future include endovaginal or endorectal sonography and magnetic resonance imaging.

### Other Uterine Malignancies

**Carcinosarcomas** are rare uterine tumors composed of mixed stromal and Mullerian elements, and commonly present as very large hypoechoic uterine masses. They are usually indistinguishable from large leiomyomas.

**Leiomyosarcoma** may arise *de novo* within the uterus or secondary to sarcomatous degeneration of a preexisting leiomyoma. Again, sonographically these tumors may be indistinguishable from benign leiomyomas, but sarcomatous change should be suggested if a preexisting leiomyoma expands rapidly in size in a post-menopausal patient.

**Lymphoma** may infiltrate the uterine cervix or corpus, usually as a sequel of disseminated disease, and may cause a focal uterine or cervical mass which is more hypoechoic than the surrounding myometrium. Finally, **rhabdomyosarcoma** presents in the pediatric age group, usually involving the uterus, cervix or vagina. The 'botryoid' or bunch-of-grapes appearance is the most common ultrasound presentation, with multiple polypoid hypoechoic masses extending from the cervix into the vagina.

### Gestational Trophoblastic Disease

The spectrum of gestational trophoblastic disease includes complete or partial **hydatidiform mole** and hydatidiform mole with a coexistent fetus.

**Complete hydatidiform mole** results from the fertilization of an egg with an absent or inactivated nucleus resulting in a 46XX aggregate of proliferative trophoblast and hydropic villi; fetal parts are absent. This results in a diploid karyotype. In 15%–30% of cases, patients with complete mole will develop persistent gestational trophoblastic disease or metastases. Patients with hydatidiform mole present clinically with first trimester vaginal bleeding, pre-eclampsia prior to 24 weeks gestation, large uterine size for gestational age, or hyperemesis gravidarum. Very high maternal serum HCG levels are suggestive of the diagnosis, although multiple gestations may also present with this finding. On ultrasound, complete mole presenting during the first trimester appears as a homogeneous echogenic mass of tissue within the uterine cavity and the sonolucencies of hydropic villi are not prominent due to their small size (less than 2 mm). In patients presenting in the second and third trimesters numerous small, cystic, fluid-containing spaces may be noted scattered throughout a moderately echogenic mass within the uterine cavity. This is the classical ultrasound picture of hydatidiform mole (Fig. 37.17).

**Partial hydatidiform mole** is associated with fetal structures, and normal placental tissue and membranes. It is composed largely of edematous villi and little trophoblastic degeneration. The fetus in this case has a triploid karyotype and displays multiple congenital anomalies. Partial mole is associated with persistent trophoblastic disease or metastases in only 2%–4% of cases. When fetal parts are seen associated with numerous cystic spaces within the placenta on ultrasound this diagnosis should be suggested (Fig. 37.18A, B).

Another variation of molar pregnancy is a **complete mole coexistent with a normal fetus**. This results from the development of a complete mole in one sac and a normal fetus and placenta in the other sac of a twin gestation. On ultrasound this cannot be distinguished from a partial mole with coexistent fetus, and chorionic villous sampling or amniocentesis may be necessary to distinguish between the two. It should be noted that hydropic degeneration of the placenta is seen in up to 20%–40% of placentas from abortuses. It is not



**Fig. 37.17.** Complete hydatidiform mole. An endovaginal scan in the sagittal plane through the uterus of a 32-year-old gravid female with vaginal bleeding reveals marked uterine enlargement. The uterus contains an echogenic mass with scattered sonolucencies (M), typical of a second-trimester complete mole.

associated histologically with trophoblastic degeneration and has no malignant potential.

With complete hydatidiform mole, *invasive mole* develops in approximately 15%–20% of patients and *metastatic choriocarcinoma* occurs in 5%–8% of patients. On ultrasound it may be very difficult to distinguish invasive from non-invasive mole. However, disease extending into parametrial areas should suggest the diagnosis of invasive mole. In *choriocarcinoma*, the most malignant form of trophoblastic disease, the villous pattern is no longer visualized pathologically. There is no typical sonographic pattern in this disease and both hypo- and hyperechoic masses have been detected.

Adnexal pathology is a common feature in complete hydatidiform mole and malignant trophoblastic disease, in the form of *ovarian theca lutein cysts*. These commonly present on ultrasound as multiple cystic masses in both ovaries and are seen in association with 10%–35% of complete moles. They result from ovarian stimulation due to very high levels of HCG.

## OVARIAN NEOPLASMS

### Epithelial Tumor

**Serous cystadenoma** and **cystadenocarcinoma** account for 30% of all ovarian tumors. The *benign* form of serous cystadenoma presents as a well-margined anechoic mass, usually unilocular, which may contain septations. In the *malignant* form, solid, echoic masses of neoplastic tissue commonly project into the interior of the mass (Fig. 37.19A, B). Both the benign and malignant forms of serous tumor may attain a very large size, exceeding 15 cm in 56% of patients in one series.

**Table 37.3.** FIGO staging criteria for ovarian carcinoma

Stage	Criterion
I	Carcinoma confined to ovaries
IA	One ovary involved; no ascites
IB	Both ovaries involved; no ascites
IC	One or both ovaries involved; ascites
II	Carcinoma of ovary with pelvic extension
IIA	Extension to uterus and/or tubes only
IIB	Extension to other pelvic tissue
IIC	Pelvic extension; ascites
III	One or both ovaries involved; intraperitoneal metastases and/or positive retroperitoneal nodes
IV	One or both ovaries involved; distant metastases outside peritoneal cavity

**Mucinous cystadenoma** and **cystadenocarcinoma** account for approximately 20% of all ovarian tumors. The benign form is more common than the malignant form and either type of tumor may also attain very large size. On ultrasound, septations, papillary excrescences and low-level echoes in the dependent portions are commonly seen particularly in the malignant form of the tumor. This tumor is bilateral in approximately 25% of cases. The FIGO staging system for carcinoma of the ovary is shown in Table 37.3. Ultrasound is not currently the examination of choice for the staging of this tumor and CT continues to be the primary method of choice.

Other epithelial tumors of the ovary include *endometrioid carcinoma*, *clear cell carcinoma* and *Brenner tumor* of the ovary, which account for approximately 20% of all ovarian cancers.



**Fig. 37.18A, B.** Partial hydatidiform mole and coexistent fetus. A A sagittal, static scan through the right side of the gravid uterus reveals a fetal head (arrow) and relatively normal placenta (P). B A sagittal scan further to the left shows an echoic mass, contiguous with normal placenta containing multiple hypoechoic areas representing hydropic villi (M). The fetus resulting from this gestation was triploid on chromosomal analysis.

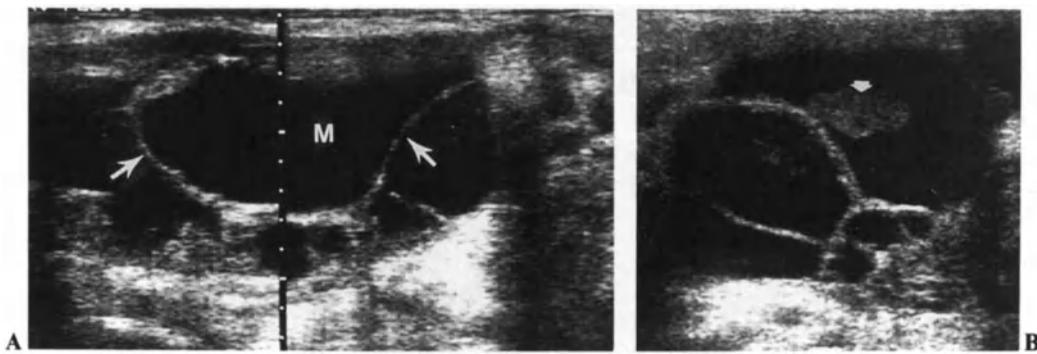


**Fig. 37.19A, B.** Serous cystadenocarcinoma of the ovary. Sagittal, and transverse, B, scans through a large pelvic mass (M) using a linear transducer reveal a predominantly cystic mass with multiple internal septa (arrows). A nodule of solid tissue (arrowhead) is noted projecting into the interior of the fluid-filled mass suggesting malignancy. Note the acoustic enhancement distal to the mass reflecting its cystic nature.

Endometrioid carcinoma and clear cell carcinoma present as complex masses with cystic portions which may contain areas of necrosis or hemorrhage. Brenner tumor usually presents as a solid mass which may be very large in size and is benign.

#### Teratomas and Dermoids

These tumors of the ovary are relatively common, particularly in their benign form (dermoid cysts). Dermoids are teratomas which are composed largely of ectodermal elements. Sonographically, a dermoid usually presents as anechoic mass containing an echogenic mural focus (the so-called dermoid plug) (Fig. 37.20A). Alternatively, the entire mass may appear echogenic with poor visibility of the back wall due to the presence of hair, fatty material, and calcific elements, such as bone or teeth (Fig. 37.20B). Typically, these lesions may be confused with bowel gas and endovaginal sonography or plain film of the abdomen may be useful in further delineating these lesions. *Malignant teratomas*, *dysgerminomas* and *endodermal sinus tumors* are all malignancies which are usually found in young individuals. They appear sonographically as echogenic masses which may contain hypoechoic areas of hemorrhage or necrosis.

#### Other Ovarian Tumors

There are a variety of other less common tumors of the ovary including *granulosa cell tumors*, *thecomas*, *fibromas* and *Sertoli-Leydig cell tumors*. These tumors usually present sonographically as echoic masses with or without acoustic shadowing and are of varying malignant potential. Ovarian fibromas are usually hypoechoic with posterior acoustic shadowing and may be associated with ascites and pleural effusions in *Meig's syndrome*.

It should also be noted that the ovary is often the site of metastatic tumor and may be involved in disseminated lymphoma or metastatic carcinoma. The term '*Krukenberg tumor*' has been applied to bilateral ovarian metastases from gastrointestinal origin such as carcinoma of the stomach, colon, or pancreas. Sonographically, these tumors are identical to cystadenocarcinoma of the ovary.

#### NON-NEOPLASTIC OVARIAN MASSES

A wide variety of non-neoplastic entities may lead to solid, cystic or complex masses of the ovary. Those which present as predominantly cystic masses include functional or physio-

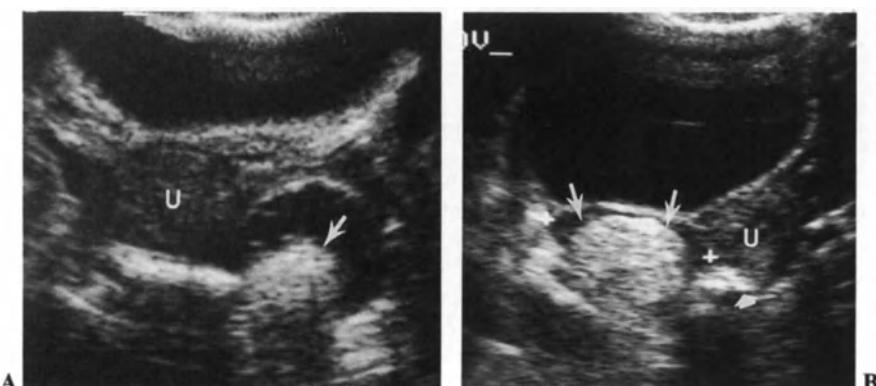


**Fig. 37.20A, B.** Ovarian dermoids. A A typical cystic dermoid of the ovary is seen in the left adnexa on this transverse scan through the pelvis of an 18-year-old female with pelvic pain. The echogenic focus in the dependent portion of the cyst (arrow) is the characteristic 'dermoid plug'. U, uterus. B A transverse scan through the pelvis of another young female reveals a markedly echogenic mass in the right adnexa (arrows) with an adjacent calcification with acoustic shadowing (arrowhead). At surgery this was a large cystic dermoid containing fat, hair and teeth. U, uterus.

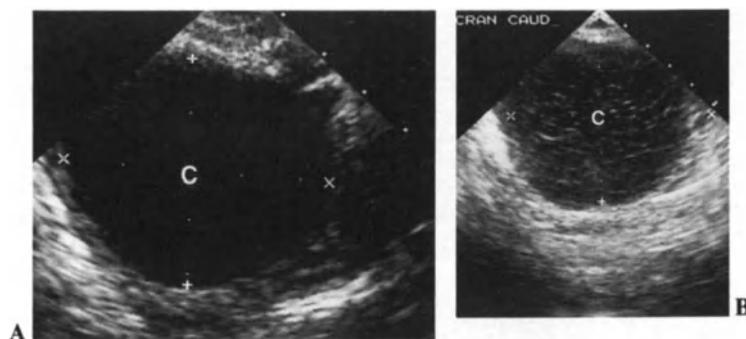


**Fig. 37.21A, B.** Benign ovarian cysts. **A** An anechoic, unilocular cystic mass (C) is demonstrated in the right ovary of a non-gravid female on endovaginal sonography. This represented a follicular cyst at surgery. **B** Another endovaginal scan through the right ovary of another patient reveals an echogenic mass (C) with good distal sound transmission. At surgery this was a hemorrhagic follicular cyst.

logic cysts of the ovary (*follicular cysts, corpus luteum cysts, or theca-lutein cysts*), *ovarian remnant syndrome, parovarian cysts* and *endometriomas*.

**Follicular cysts** are diagnosed when a follicle exceeds 2.5 cm in diameter and appears sonographically as a well-margined, thin-walled unilocular anechoic structure (Fig. 37.21A). These functional cysts may undergo hemorrhage and sonographically may contain low-level echoes and septations (Fig. 37.21B). A corpus luteum cyst may persist after the discharge of the oocyte and fail to involute within 14 days. These may achieve large size and are prone to hemorrhage. The corpus luteum cyst of pregnancy attains its largest size by 8–10 weeks of gestation and usually does not exceed 6 cm in diameter. By 16–18 weeks the corpus luteum cyst of pregnancy has involuted in most individuals.

**Theca-lutein cysts** are the result of excessive stimulation of the ovary by high levels of HCG and may be found in association with gestational trophoblastic disease, ovarian hyperstimulation syndrome and rarely with normal pregnancy. Sonographically, these appear as multilocular bilateral large anechoic structures within the ovaries. The *ovarian remnant syndrome* is a predominantly cystic mass

arising from the vestige of an ovary left at incomplete oophorectomy. Sonographically, this may present as a hypoechoic mass in the pelvis post-oophorectomy.

**Parovarian cysts** are Wolffian duct remnants arising within the mesovarium and may range in size from very small lesions to up to 20 cm in diameter. Sonographically, these are usually anechoic and unilocular although they may undergo hemorrhage. They are usually impossible to differentiate from cystic masses arising from ovary (Fig. 37.22A).

**Endometriomas**, as has already been mentioned, may appear as predominantly cystic masses although they usually contain low-level echoes or fluid-debris levels within. They result from the accumulation of blood within a peritoneal endometrial implant (Fig. 37.22B).

**Torsion of the ovary** may occur secondary to ovarian cyst or neoplasm, pregnancy, or the hyperstimulation syndrome. Sonographically, torsion of the ovary presents as a unilaterally enlarged ovary surrounded by multiple hypoechoic structures representing dilated uterine vessels or Fallopian tube. This is commonly associated with free fluid in the cul-de-sac.

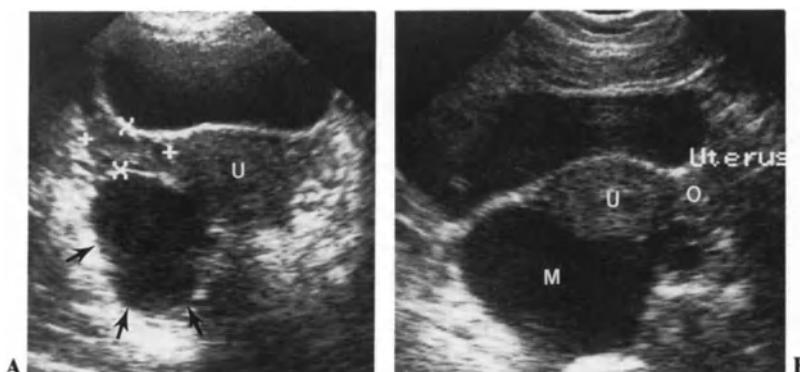


**Fig. 37.22A, B.** Non-ovarian pelvic masses. **A** A large hypoechoic mass, posterior to the right ovary is demonstrated on this transverse scan through the pelvis of a 26-year-old female (arrows). This mass is separate from the ovary (outlined with cursors) and contains some internal echoes. Good sound transmission distal to the mass indicates that it is fluid-filled and at surgery it proved to be a parovarian cyst. **B** A similar transverse scan through the pelvis of non-gravid female reveals a fluid-filled mass (M) containing internal echoes which is clearly separate from the ovary (O). When examined pathologically this mass was an endometrioma.

### INTRAUTERINE CONTRACEPTIVE DEVICES

Ultrasound, both transabdominal and endovaginal, plays a key role in the evaluation of intrauterine contraceptive devices (IUD). Due to their widespread use and possible association with secondary infertility it is important to recognize the morphologic differences of these devices on ultrasound.

The *Lippes loop* is a continuous polyethylene rod shaped into five transverse segments connected by four curves. The *Progestasert* is a T-shaped plastic device with a solid cross arm and hollow long arm containing a reservoir of progesterone and barium. The *Tatum-T* and *Copper-7* are similar devices with polyethylene short arms and a fine copper wire wound around the long limb. Occasionally, one may encounter long-discontinued IUD types such as the *Saf-T-coil* or the *Dalkon Shield*. The *Saf-T-coil* is identified by its double coil shape extending from a central long limb. The *Dalkon Shield* is spider-shaped with multiple projections.

On sonography, an IUD presents as an intrauterine high-amplitude reflector with entrance-exit echoes reflecting the shape of the device. Posterior acoustic shadowing is usually only seen in the long axis view where the sonic beam is perpendicular to the short limbs of the device (Fig. 37.23A, B). It is usually simple to identify that the device is properly located as an anechoic halo of tissue representing the endometrium should surround the IUD on either side indicating that it lies within the uterine cavity. Pitfalls to the localization of IUDs include retroversion or retroflexion of the uterus, fibroid uterus, or the presence of fetal parts in an intrauterine pregnancy or incomplete abortion. All of these entities may make the localization of the IUD within the uterine canal difficult. Also, ultrasound cannot be relied upon as a good predictor of uterine perforation by an IUD. An IUD deeply and symmetrically embedded in the myometrium or only superficially perforating may be missed on transabdominal and transvaginal ultrasound.

### PELVIC ULTRASOUND IN INFERTILITY

Ultrasound is now widely used to monitor ovarian function in infertile females and to confirm and follow the ovarian response to ovulation induction regimens. In the normal ovary, follicles are first identified when they are 4–5 mm in diameter. In the normal cycle, the follicle grows approximately 2–3 mm per day from day 9–10 until ovulation. The average size of the follicle at ovulation ranges from 17–24 mm. The mature ovum surrounded by granulosa cells comprises the *cumulus oophorus* and this may be seen sonographically in 15%–80% of cases. When this process fails to occur spontaneously, ovulation induction agents such as clomiphene citrate and human menopausal gonadotropin may be used in combination with HCG to stimulate ovulation.

Transabdominal and transvaginal ultrasound have been used to monitor follicle size and number particularly in preparation for *in vitro* fertilization and embryo transfer. Many sonographic features have been proposed to signal follicular maturity including follicular size, fluid in the cul-de-

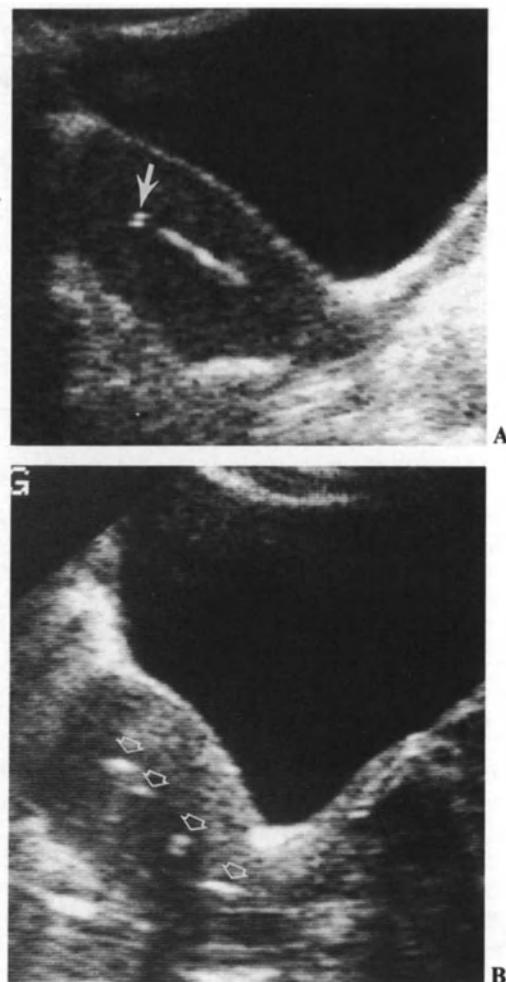


**Fig. 37.23A, B.** Intrauterine contraceptive devices. **A** A Copper-7 IUD is located within the endometrial canal on this sagittal scan through the uterus. The cross-bar of the IUD is seen as an echogenic dot with entrance-exit echoes (arrow). **B** The 4 rungs of a Lippes loop IUD are well visualized as high-amplitude echoes with distal acoustic shadowing (arrowheads). Note the lowest rung is situated in the uterine cervix indicating that the IUD is seated too low in the uterine cavity and may be extruded.

sac, the presence of a cumulus oophorus, internal echogenicity and septations or wall irregularity (Fig. 37.24). None of these signs is 100% reliable as to imminent ovulation and a combination of these is necessary for accurate prediction of ovulation and follicular maturity. Ultrasound is also useful in guiding oocyte harvest for *in vitro* fertilization and embryo transfer. This is most commonly achieved by the endovaginal technique.

### OTHER IMAGING METHODS (D. Sutton)

#### Gynecological Radiology

Ultrasound is now the most important method of imaging in gynecology, but simple radiography can sometimes provide valuable information, particularly with calcified lesions.

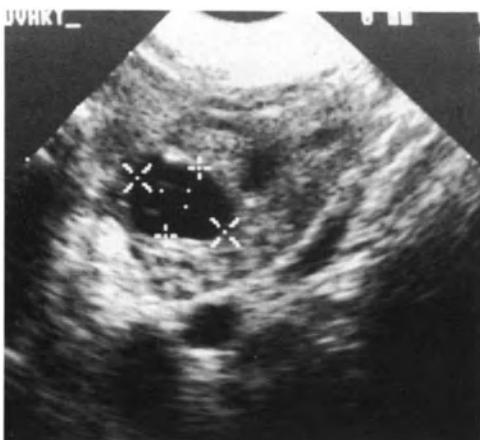
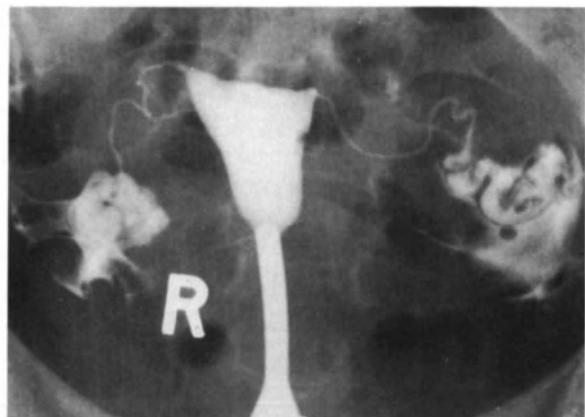


**Fig. 37.24.** Ovarian follicle in a stimulated ovary. A dominant follicle with internal echoes is demonstrated on an endovaginal scan of the left ovary in an infertility patient undergoing stimulation with human menopausal gonadotropin. The internal septations indicate follicular maturity and follicular size is about 20 mm.



A



B

**Fig. 37.25.** A Normal hysterosalpingogram. Both tubes are outlined and there is free spill into the peritoneum on both sides. (B) Hysterosalpingogram with venous intravasation

A plain film of the pelvis may show evidence of a pelvic mass as an abnormal soft tissue density, which may be displacing gas-filled bowel, and such lesions should be carefully looked for on routine abdominal or urinary films. Some lesions may show calcification, and this is often of a characteristic nature.

Uterine *fibroids* are common gynecological tumors and frequently contain speckled or patchy calcification which is diagnostic.

Ovarian *dermoids*, though much rarer, sometimes show diagnostic features at simple radiography. Thus the presence of rudimentary or fully-formed teeth, or of a radiolucent area of fat, in the pelvic mass are both characteristic.

Ovarian *fibromas* are also rare tumors, but are sometimes densely calcified. They can give rise to ascites and pleural effusion (Meig's syndrome).

Tuberculous pyosalpinx can give rise to hazy amorphous calcification, sometimes bilateral.

Intrauterine contraceptive devices are usually checked by ultrasound if there is clinical doubt as to whether they are still properly sited, but they are radiopaque and can be seen on plain films of the pelvis.

The student should be aware of the appearance of intravaginal tampons on pelvic films, where they appear as a rectangular lucency superimposed on the bladder area.

### Hysterosalpingography

This procedure was once widely practiced for a variety of gynecological problems but its use is now largely restricted to the investigation of infertility and the confirmation of tubal patency or the monitoring of tubal patency or occlusion after surgical procedures. It is also still used for the demonstration of congenital abnormalities or other lesions in patients with recurrent abortion.

The investigation is usually performed about the middle of the menstrual cycle and is contraindicated during menstruation or pregnancy. Other contraindications include

pelvic sepsis, a recent dilatation and curettage, severe cardiac or renal disease, and sensitivity to contrast media.

Hysterosalpingography is usually performed under image intensifier fluoroscopic control so that appropriate films may be obtained showing the distended uterine cavity and opacified tubes and confirming spill into the peritoneal cavity (Fig. 37.25A). Any water-soluble contrast medium of the type used for urography is suitable for the procedure.

Complications include exacerbation of previous pelvic infection and venous intravasation of contrast medium. This results from excessive injection pressure or trauma to the endometrium from the tip of the cannula. The contrast is taken up by the interstitial veins in the wall of the uterus and drains into the ovarian and iliac veins. Apart from providing a rather dramatic and unexpected picture the accident is fortunately harmless to the patient (Fig. 37.25B).

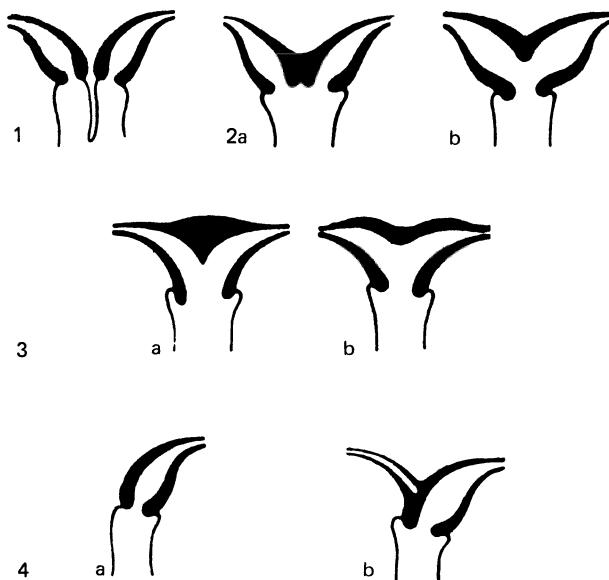


Fig. 37.26. Diagram of uterine congenital abnormalities. (See text).

### Abnormalities of the Uterus

Congenital abnormalities are due to varying degrees of failure of fusion of the Mullerian ducts giving rise to the abnormalities listed below and illustrated in Fig. 37.26.

1. Uterus didelphys
2. Uterus bicornis bicollis and Uterus bicornis unicollis
3. Septate uterus and Arcuate uterus
4. Uterus unicornis unicollis, with and without rudimentary opposite horn

The uterus is normally visualized in AP projection at salpingography but when anteflexed or retroverted is seen in an almost axial projection. Uterine fibroids may cause deformity of the uterine cavity depending on their position. Submucous fibroids may even appear as polypoid projections into the uterine cavity, but the commoner interstitial fibroids merely distort the uterine cavity.

**The Fallopian Tubes.** As noted above active salpingitis or other pelvic infections are contraindications to salpingography, but old healed infection may lead to tubal or fimbrial adhesions and blockage or to hydrosalpinx. These are common findings at the investigation of infertile women by hysterosalpingography. Blocked tubes with no free spill into the peritoneum are usually found but occasionally the contrast will enter and outline a distended hydrosalpinx. In some cases the contrast will pass through the tube but remain loculated near the fimbrial end due to peritoneal adhesions.

*Salpingitis isthmica nodosa* is the term used for a rare condition where small blobs of contrast are seen outside the tubal lumen in the isthmus region, presumably representing small diverticula. The etiology is not clear but there appears to be a relationship to endometriosis.

### CT in Gynecology

Ultrasound is the imaging technique of choice in most gynecological lesions since it can provide diagnostic information



Fig. 37.27. Sagittal MRI section ( $T_2$ -weighted) shows mixed high and low signal from rounded uterine fibroid lying behind the bladder (high signal). Vagina and cervix lie between the bladder base and the rectum.

about pathological conditions much more cheaply than CT. The latter may be used where technical considerations such as obesity or an unstable bladder render ultrasound examination more difficult. CT is also invaluable in the staging of malignant tumors in the female pelvis.

### Magnetic Resonance Imaging

MRI can also provide valuable information, but like CT is too expensive to compete with ultrasound for routine use. It can provide excellent anatomical detail of the bladder, uterus, vagina and cervix in sagittal (Fig. 37.27), axial or coronal planes. Like CT it can help with the staging of gynecological tumors.

### REFERENCES AND SUGGESTIONS FOR FURTHER READING

#### TECHNIQUE OF EXAMINATION AND NORMAL ANATOMY

- Deutsch AL, Gosink BB (1982) Normal female pelvic anatomy. Semin Roentgenol 17: 241–250  
 Kurtz AB, Rifkin MD (1985) Normal Anatomy of the Female Pelvis: Ultrasound with Computed Tomography Correlation. In: Sanders RC, James AD (eds) Principles and Practice of Ultrasonography in Obstetrics and Gynecology. Appleton-Century-Crofts, Norwalk, CT pp 99–121  
 Leopold GR (1987) Pelvic Ultrasonography. In: Sarti DA (ed) Diagnostic Ultrasound: Text and Cases. Year Book Medical Publishers, Chicago, IL pp 684–690

#### CONGENITAL ANOMALIES

- Mintz X, Grumbach K (1988) Imaging of congenital uterine anomalies. Semin. US, CT and MR. 9: 167–174

#### INFLAMMATORY DISEASE: ENDOMETRIOSIS AND ADENOMYOSIS

- Bohlman ME, Ensor RE, Sanders RC (1987) Sonographic findings in adenomyosis of the uterus. AJR 148: 765–766  
 Friedman H, Vogelzang RL, Mendelson EB, Neiman HL, Cohen M (1985) Endometriosis detection by US with laparoscopic correlation. Radiology 157: 217–220

**PELVIC INFLAMMATORY DISEASE**

- Berland LL, Lawson TL, Foley WD, Albarelli JN (1982) Ultrasound evaluation of pelvic infections. *Radiol Clin North Am* 20: 367-382  
 Swayne LC, Love MB, Karasick SR (1984) Pelvic inflammatory disease: sonographic-pathologic correlation. *Radiology* 151: 751-755

**INTRAUTERINE FLUID COLLECTIONS**

- McCarthy KA, Hall DA, Kopans DB, Swann CA (1986) Postmenopausal endometrial fluid collections: always an indicator of malignancy? *J Ultrasound Med* 5: 647-649

**NEOPLASTIC DISEASE: LEIOMYOMAS**

- Fleischer AC, Entman SS, Porrath SA, James AE (1985) Sonographic evaluation of uterine malformations and disorders. In: Sanders RC, James AE (eds) *The Principle and Practice of Ultrasonography in Obstetrics and Gynecology*. Appleton-Century-Crofts, Norwalk, CT pp 531-568  
 Lev-Toaff AS, Coleman BG, Arger PH, Mintz MC, Arenson RL, Toaff ME (1987) Leiomyomas in pregnancy: sonography study. *Radiology* 164: 375-380

**ENDOMETRIAL CARCINOMA**

- Fleischer AC, Dudley BS, Entman SS, Baxter JW, Kalemeris GC, James AE (1987) Myometrial invasion by endometrial carcinoma; sonographic assessment. *Radiology* 162: 307-310  
 Regnard CK, Wicks JD, Mettler FA (1981) Ultrasonography in the staging of endometrial carcinoma. *Radiology* 140: 781-785

**CERVICAL CARCINOMA**

- Sanders RC, McNeil BJ, Fineberg HJ, Hessel SJ, Siegelman SS, Adams DF, Alderson PO, Abrams HL (1983) A prospective study of computed

tomography and ultrasound in the detection and staging of pelvic masses. *Radiology* 146: 439-442

**GESTATIONAL TROPHOBlastic DISEASE**

- Callen PW (1988) Ultrasound evaluation of gestational trophoblastic disease. In: Callen PW (ed) *Ultrasonography in Obstetrics and Gynecology*. Saunders, Philadelphia, PA pp 412-422  
 Reid MH, McGahan JP, Oi R (1983) Sonographic evaluation of hydatidiform mole and its look-alikes. *AJR* 140: 307-311

**OVARIAN NEOPLASMS**

- Moyle JW, Rochester D, Siderh et al. (1983) Sonography of ovarian tumors: predictability of tumor type. *AJR* 141: 985-991  
 Williams AG, Mettler, FA, Wicks JD (1983) Cystic and solid ovarian neoplasms. *Semin Ultrasound* 4: 166-183

**NON-NEOPLASTIC OVARIAN MASSES**

- Hall DA (1983) Sonographic appearance of the normal ovary, of polycystic ovarian disease and of functional ovarian cysts. *Semin Ultrasound* 4: 149-165

**INTRAUTERINE CONTRACEPTIVE DEVICES**

- Najarian KE, Kurtz AB (1986) New observations in the sonographic evaluation of intrauterine contraceptive devices. *J Ultrasound Med* 5: 205-210

**ULTRASOUND IN FERTILITY**

- Mendelson EB, Friedman H, Neiman HL et al. (1985) The role of imaging in infertility management. *AJR* 144: 415-422

## CHAPTER 38

# OBSTETRIC ULTRASOUND

Kathryn Grumbach

---

### TECHNIQUE OF EXAMINATION: FIRST TRIMESTER

The major goals of the first trimester ultrasound examination are to determine fetal viability and to establish if the gestation is intrauterine in location. The **transabdominal** examination is performed through an optimally distended urinary bladder, usually achieved by maternal ingestion of 4–6 glasses of water, 30–40 minutes prior to the examination. Sagittal, transverse and oblique scans are obtained through the uterus and adnexa with an internally focused 3.5 or 5.0 mHz transducer. Real-time sector transducers, either mechanical or annular, are best suited to imaging early gestations transabdominally, as they can be angled to allow for variation in uterine and adnexal position. Occasionally, a linear transducer may give superior anatomic detail of fetal structures during the first trimester.

The recent introduction of **endovaginal scanning** has enhanced our ability to image early gestations and has radically improved our diagnostic confidence in evaluation of early pregnancy failure. Most endovaginal transducers are of high frequency (usually 5.0, 6.5 or 7.5 mHz) and have a short focal length. As a result an empty urinary bladder is preferred, in order to bring the transducer as close to the uterus and adnexa as possible. In addition, the empty urinary bladder minimizes compression of the gestational sac, allowing for excellent visualization of sac contents and accurate measurements. The method of performing an endovaginal scan has been described in the previous chapter and need not be modified significantly for the pregnant patient in the first trimester. This examination can be safely performed in the pregnant patient presenting with bleeding and pain in the first trimester and is a particularly valuable tool for differentiating between viable intrauterine gestation, missed or incomplete abortion and ectopic pregnancy.

### NORMAL ANATOMY: FIRST TRIMESTER

The earliest finding in an intrauterine gestation is a **gestational sac** which appears as a round or oval anechoic structure surrounded by a highly echogenic rim. The smallest gestational sac identifiable on endovaginal sonography is about 2–3 mm in *mean sac diameter* (MSD) and on transabdominal scan is about 5 mm MSD. The normal early sac is surrounded by two concentric, echogenic rings of decidua (the double decidua sign); the *decidua parietalis* lines the endometrial cavity and the *decidua capsularis* surrounds the gestational sac (Fig. 38.1A, B). This sign can be seen as early as 4 weeks menstrual age and is a valuable sign of a normal early intrauterine gestation.

*Embryonic structures* can be seen within the sac by 5–6 weeks menstrual age or when the sac reaches a size of 10–15 mm MSD. The yolk sac–amniotic sac complex consists of the early pulsating embryo, only 2–3 mm long, surrounded on one side by amnion and on the other by yolk sac. By 6.5–7 menstrual weeks the *fetus* is clearly visualized lying within the amniotic sac and the secondary yolk sac now extends into the chorionic cavity outside the amnion (Fig. 38.1C, D). The yolk sac regresses entirely by 9–10 gestational weeks, and the amnion and chorion fuse by 13–15 gestational weeks.

By 8–9 menstrual weeks, *fetal anatomic parts* become visible, especially with the endovaginal technique. The head and rump of the fetus can be distinguished, as well as limbs, spine, heart bulge and umbilical cord; even urinary bladder and stomach may be detected (Fig. 38.2). Structures of the head, particularly the developing ventricular system and choroid plexus, may be seen. By the end of the first trimester an entire anatomic survey can be accomplished and gross congenital anomalies may be identified.

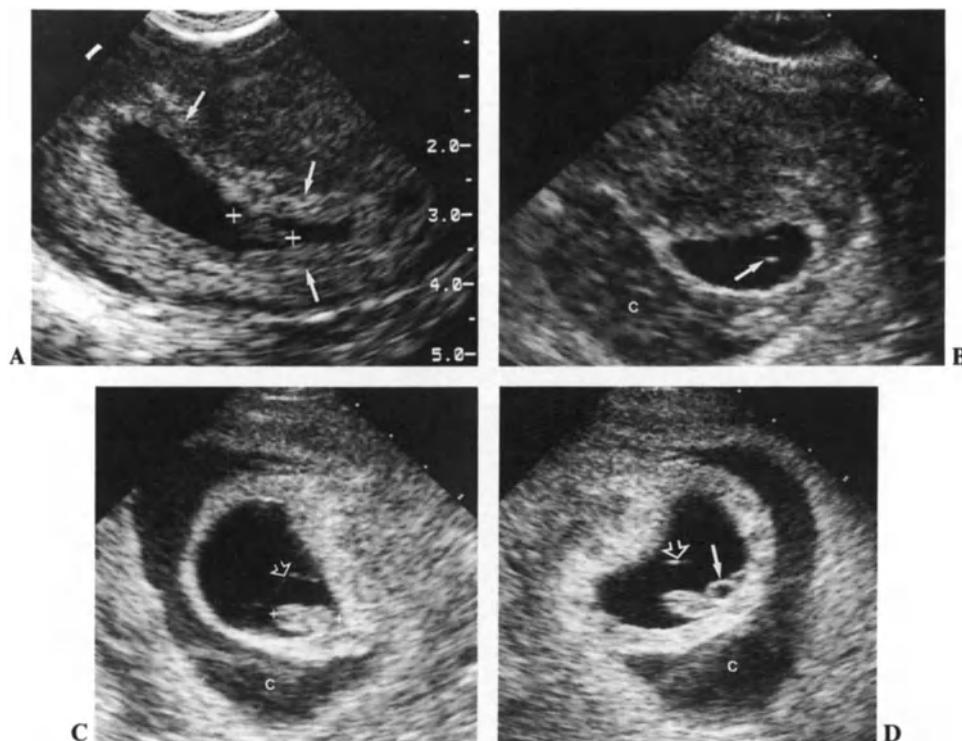


**Fig. 38.1A–D.** Early intrauterine gestations: first trimester. **A** A sagittal image from an endovaginal scan reveals a single viable intrauterine gestation at 7 menstrual weeks. The double decidual ring is easily identified (arrows) and the fetal pole is demarcated by cross marks for measurement of crown-rump length. **B** A coronal endovaginal sonogram through another gravid uterus at about 6 menstrual weeks shows a yolk sac (arrow). The double decidual ring is separated by fluid (probably blood) in the uterine cavity (C) surrounding the conceptus. **C, D** Coronal endovaginal scans through another gestational sac at about 7 menstrual weeks reveals the fetal pole (demarcated by cross-marks) surrounded by amnion (arrowhead). The gestational sac is rendered more visible by a fluid collection in the uterine cavity (C).

The **corpus luteum cyst** of pregnancy develops from the ovarian follicle and helps to support the developing early gestation (Fig. 38.3). It may attain large size, up to 6–10 cm, and with internal hemorrhage may develop internal echoes and septae. A corpus luteum cyst should regress by 14–16 gestational weeks, whereas ovarian tumors occurring during pregnancy will not.

Prior to about 6.5 menstrual weeks the most reliable

estimation of **gestational age** is made by measurement of MSD. Long axis and AP measurements are obtained from a sagittal image and sac width must be obtained on a transverse or coronal image. These values are added together and divided by three to arrive at an MSD measurement which is plotted on a standard table (Table 38.1). Between 6.5 and 10–11 menstrual weeks the *crown–rump length* of the fetus provides the best estimation of gestational age and is accu-



**Fig. 38.2.** Early intrauterine gestation: 9–10 weeks. A transabdominal sonogram through the gravid uterus at 9–10 weeks shows fetal features such as head (arrow), lower extremity (arrowhead) and spine (black arrows).

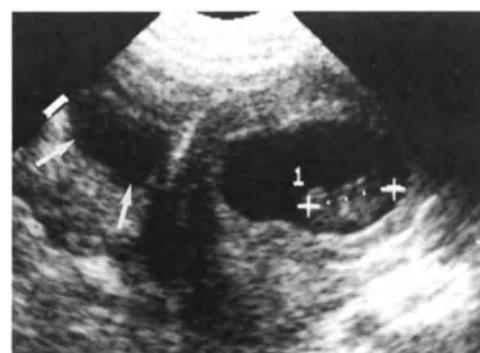


**Fig. 38.3.** Corpus luteum cyst. A transverse transabdominal sonogram through the pelvis reveals an intrauterine gestation with the fetal pole delineated with cross-marks. The corpus luteum cyst (arrows) is visible in the right ovary and appears as a simple cyst, 3–4 cm in diameter.

**Table 38.1.** Gestational sac measurement table

Mean predicted gestational sac (cm)	Gestational age (weeks)	Mean predicted gestational sac (cm)	Gestational age (weeks)
1.0	5.0	3.6	8.8
1.1	5.2	3.7	8.9
1.2	5.3	3.8	9.0
1.3	5.5	3.9	9.2
1.4	5.6	4.0	9.3
1.5	5.8	4.1	9.5
1.6	5.9	4.2	9.6
1.7	6.0	4.3	9.7
1.8	6.2	4.4	9.9
1.9	6.3	4.5	10.0
2.0	6.5	4.6	10.2
2.1	6.6	4.7	10.3
2.2	6.8	4.8	10.5
2.3	6.9	4.9	10.6
2.4	7.0	5.0	10.7
2.5	7.2	5.1	10.9
2.6	7.3	5.2	11.0
2.7	7.5	5.3	11.2
2.8	7.6	5.4	11.3
2.9	7.8	5.5	11.5
3.0	7.9	5.6	11.6
3.1	8.0	5.7	11.7
3.2	8.2	5.8	11.9
3.3	8.3	5.9	12.0
3.4	8.5	6.0	12.2
3.5	8.6		

$$\text{Gestational Age (weeks)} = \frac{\text{Gestational Sac (cm)} + 2.543}{0.702}$$

From Hellman LM, Kobayashi M, Fillisti L, et al. (1969) Growth and development of the human fetus prior to the twentieth week of gestation. Am J Obstet Gynecol 103: 784

rate to  $\pm 5\text{--}7$  days. The distance from the top of the head to the end of the body, exclusive of limbs (Fig. 38.1A, C), is measured and plotted on a curve (Table 38.2). By 12–13 menstrual weeks the crown–rump measurements become inaccurate and biparietal diameter (BPD) and femur length (FL) can now be used to predict gestational age.

#### EARLY PREGNANCY FAILURE

**Threatened abortion** or bleeding and pain during the first trimester of pregnancy occurs in about 25% of pregnancies, although only 50% of these will go on to abort spontaneously. Factors which increase the risk of spontaneous abortion include advanced maternal age, numerous or submucous myomas, uterine anomalies and DES exposure. The spontaneous abortion rate is highest early in the first trimester; the rate of loss was 5% between 7 and 9 menstrual weeks dropping to 1%–2% between 10 and 12 menstrual weeks in one series.

**Complete spontaneous abortion** is an abortion in which all the products of conception have been expelled from the uterus and for this reason it cannot be distinguished from a non-gravid uterus on ultrasound. An **inevitable abortion** is defined as an abortion in progress with heavy bleeding, dilated cervix and progressive extrusion of the conceptus. This is rarely witnessed at ultrasound examination, although

**Table 38.2.** Crown-rump length measurement table

Mean predicted crown-rump length (mm) 'Regression Analysis'	Gestational age (weeks)	Mean predicted crown-rump length (mm) 'Regression Analysis'	Gestational age (weeks)
6.7	6.3	34.0	10.1
7.4	6.4	35.5	10.3
8.0	6.6	36.9	10.4
8.7	6.7	38.4	10.6
9.5	6.9	39.9	10.7
10.2	7.0	41.4	10.9
11.0	7.1	43.0	11.0
11.8	7.3	44.6	11.1
12.6	7.4	46.2	11.3
13.5	7.6	47.8	11.4
14.4	7.7	49.5	11.6
15.3	7.9	51.2	11.7
16.3	8.0	52.9	11.9
17.3	8.1	54.7	12.0
18.3	8.3	56.5	12.1
19.3	8.4	58.3	12.3
20.4	8.6	60.1	12.4
21.5	8.7	62.0	12.6
22.6	8.9	63.9	12.7
23.8	9.0	65.9	12.9
25.0	9.1	67.8	13.0
26.2	9.3	69.3	13.1
27.4	9.4	71.8	13.3
28.7	9.6	73.9	13.4
30.0	9.7	76.0	13.6
31.3	9.9	78.1	13.7
32.7	10.0	80.2	13.9
		82.4	14.0

From Robinson HP, Fleming JEE (1975) a critical evaluation of sonar 'crown-rump length' measurements. Br J Obstet Gynaecol 82: 702

the dilated cervix and extruded sac may be seen. A **missed abortion** involves retention of a dead fetus for at least 2 months. Certainly, death of the fetus can be documented on ultrasound when the embryo is noted to lack cardiac motion. This needs to be carefully documented, often with an endovaginal transducer, as lack of fetal heart motion will prompt evacuation of the non-viable conceptus. Other sonographic features suggesting non-viability include an irregularly shaped gestational sac, incomplete or poor decidual reaction, lack of the double decidual sac sign and low position of the gestational sac (Fig. 38.4A, B). An even more important prognostic sign as to favorable outcomes is the presence of a *fetal pole* and *yolk sac*. A non-viable pregnancy can be reliably predicted if a gestational sac greater than 25 mm MSD lacks a fetal pole or if a sac greater than 20 mm MSD lacks a yolk sac.

The absence of a visible fetal pole has been termed a *blighted ovum* or *anembryonic pregnancy* and is detected sonographically when the empty gestation sac is too small for menstrual dates or no fetus or yolk sac is identified on serial scans at an interval of 7–10 days. In addition, the presence and size of a gestational sac can be correlated with the maternal serum HCG level. A normal gestational sac is consistently identified on transabdominal sonography at HCG levels greater than 1800 mIU/ml (2nd International Standard) and on endovaginal scans at HCG levels greater

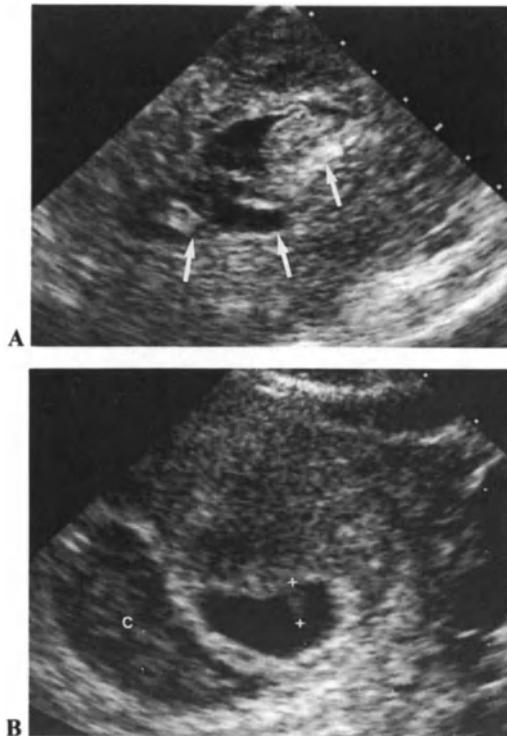


**Fig. 38.4A, B.** Early pregnancy failure. A Incomplete abortion. A sagittal endovaginal ultrasound reveals retained products of conception, blood clots and fluid within the endometrial cavity (arrows) in an incomplete abortion. B Implantation hemorrhage. A large fluid collection (C) is noted adjacent to the gestational sac containing a fetal pole (demarcated by cross-marks). Fetal heart motion could not be detected in the 6-week gestation indicating fetal death.

than 1000 mIU/ml. A normal gestational sac grows 1.1 mm/day and serum HCG levels normally double every 2–3 days to reach a maximum level at about 8 menstrual weeks. Failure of normal increase in serum HCG levels coupled with poor gestational sac growth is also evidence of poor pregnancy outcome.

**Ectopic pregnancy** results from implantation of a gestation outside the uterine cavity, 97% of which are tubal in location. Patients at risk for ectopic pregnancy are those with a previous history of pelvic inflammatory disease, an IUD in place, or previous tubal surgery, tubal ligation or conception by in vitro fertilization. The importance of recognizing this clinical entity cannot be overemphasized in that it carries a mortality rate of 1 in 1000 cases. In addition, it is associated with subsequent infertility; there is a conception rate of only 60% in women who have had a previous ectopic pregnancy and 10% of these conceptuses are recurrent ectopics.

The most valuable finding on ultrasound which excludes the diagnosis of ectopic pregnancy, is a *viable intrauterine gestation* with a fetal pole and yolk sac. As the reported incidence of simultaneous intra- and extra-uterine gestation is no less than 1 in 7000 gestations and may be as infrequent as 1 in 30 000 pregnancies, the identification of a normal intrauterine gestation effectively excludes an ectopic pregnancy. However, the critical period for identification of ectopic pregnancy comes before the appearance of the

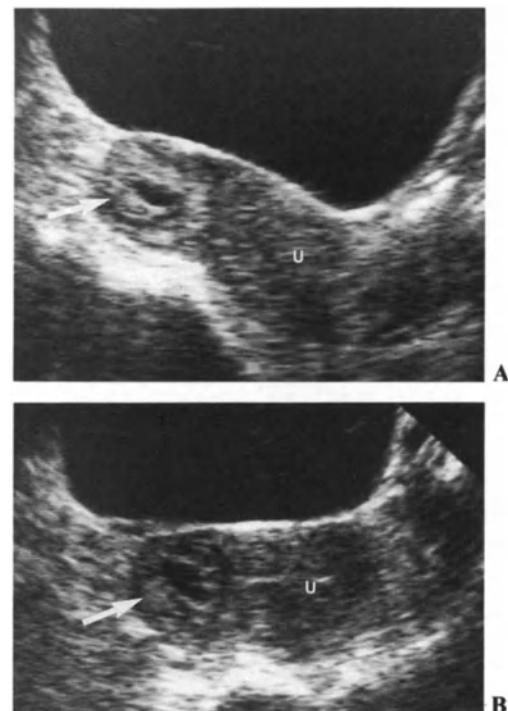


**Fig. 38.5A, B.** Ectopic pregnancy. Sagittal (A) and transverse (B) transabdominal sonograms reveal a uterus (U) without evidence of an intrauterine gestation in the patient with a quantitative hCG of 4500 mIU. A thick walled mass with hypoechoic center is noted superior and to the right of the uterus (arrow). This was an ectopic pregnancy in the cornual portion of the Fallopian tube.

embryo or yolk sac at 5–6.5 menstrual weeks or earlier. During this period it may be very difficult to distinguish the decidual reaction and intrauterine fluid associated with ectopic pregnancy (*pseudogestational sac*) from a very early intrauterine gestation. The presence of a double decidual sac sign is not reliable in all cases and a follow-up ultrasound examination and serial HCG determinations may be necessary to distinguish ectopic gestations. The absence of a normal intrauterine gestation coupled with the ultrasound findings of cul-de-sac fluid and a complex adnexal mass raises the diagnostic specificity to greater than 70% (Fig. 38.5A, B). However, only the diagnosis of an adnexal gestational sac containing a living embryo or yolk sac is 100% specific and demonstration of such adnexal pathology is facilitated by utilizing the endovaginal probe (Fig. 38.6). Clearly, ultrasound alone cannot be depended upon to make this important diagnosis and correlation with serum HCG levels and often diagnostic laparoscopy is still necessary in many cases of suspected ectopic gestation.

#### TECHNIQUE OF EXAMINATION: SECOND AND THIRD TRIMESTERS

The assessment of the gravid uterus during the second and third trimesters is a detailed examination requiring organiza-

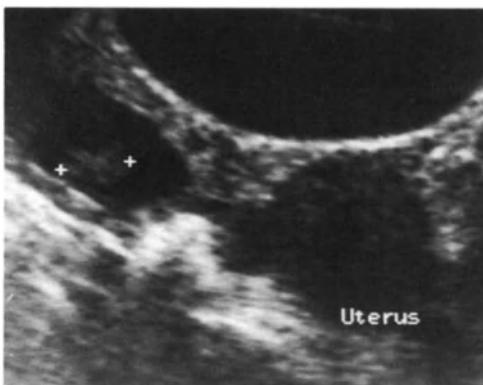


**Fig. 38.6.** Ectopic pregnancy. A transverse, magnified image through the uterus and right adnexa in another pregnant patient also shows a thick-walled cystic structure but this contains a fetal pole (demarcated by cross-marks) in which heart motion was detected on real time. This represented a living ectopic gestation in the ampillary portion of the Fallopian tube.

tion, perseverance and strict attention to detail on the part of the examiner. With the development of high resolution real-time equipment, highly detailed anatomic evaluation of the fetus is now possible; indeed the fetus may now be treated as a 'patient' in its own right. Not only can gross features of a pregnancy such as placental position, fetal lie and viability, number of fetuses and amount of amniotic fluid be assessed, but accurate anatomic diagnosis of subtle fetal congenital anomalies can be achieved.

The examination should be performed with an internally focused 3.5 or 5.0 mHz transducer for optimal transabdominal images. The frequency of the transducer utilized should be dictated by the gestational age of the fetus, maternal body habitus and the structure being imaged. Both sector (either annular or mechanical) and linear transducers are useful for evaluating fetal anatomy, but fetal measurements should be made with a *linear transducer* whenever possible, to minimize inaccuracies introduced across a sector transducer.

Early in the second trimester, when the fetus is still quite small in size, an endovaginal transducer (with a frequency of 5.0 or 6.5 mHz) may be useful in detailed assessment of fetal anatomy or in evaluation of maternal adnexal masses. However, by 14–16 menstrual weeks the size of the fetus has exceeded the focal length of most endovaginal transducers and the transabdominal technique is preferred.

For evaluating *placental position* and imaging of the *cervical os* a full maternal urinary bladder is necessary, and this is achieved in the same manner as for routine pelvic ultrasound.

The examination usually begins with determination of **fetal position** and **viability**. The fetal lie and right and left sides in relation to maternal right and left must be established. Also, a rapid identification of *fetal heart motion* and *fetal motion* determines viability. Once these basics have been noted, the uterus and fetal environment are examined. *Placental location* and state of *maturity* are determined and the presence of *uterine* or *adnexal masses* is assessed. *Amniotic fluid volume* is estimated; this determination is difficult to quantitate and largest fluid pocket size or total uterine volume has proved unreliable in diagnosing polyhydramnios

or oligohydramnios. Probably the most accurate method of determining abnormalities of amniotic fluid volume is rapid realtime scanning of the entire uterus by an experienced operator. Also, at this time the *number of vessels in the umbilical cord* is determined and the insertion of the cord into the placenta and the fetal abdomen is evaluated.

The **fetal anatomic survey** should follow a predictable pattern on every examination so that no fetal organ system is excluded. My systematic approach is simple, beginning with the head, face and spine, followed by the organs of the chest and abdomen, ending with a brief examination of the limbs. If a specific anomaly is suspected clinically, then special attention is given to that particular organ system. Also, an evaluation of fetal well-being should be performed by noting fetal limb and body motion and episodes of respiratory activity, even if a formal biophysical profile is not clinically indicated.

The final important portion of the obstetrical ultrasound examination involves the fetal measurement for assessment of **gestational age** and **fetal growth**. The particular measurements made depend on the gestational age of the fetus. Between 12 and 20 gestational weeks *biparietal diameter* (BPD), *femur length* (FL), and *abdominal circumference* (AC) are routinely measured and after 20 weeks *head circumference* (HC) is also obtained in order to calculate HC/AC ratio. After 25 gestational weeks *estimated fetal weight* (EFW) is routinely calculated from either BPD and AC or AC and FL.

BPD is always obtained in the transaxial plane at the widest portion of the skull; the *thalamic level* has been chosen as the standard level for this measurement. On modern equipment this measurement is usually obtained with electronic calipers and is measured from the outer edge of the calvarial table in the near field to the inner edge of the far calvarial table (Fig. 38.7A). The femur is the easiest fetal long bone to image and is measured on the long axis of the diaphysis, not including the proximal and distal epiphyseal cartilages, also using electronic calipers (Fig. 38.7B). The HC and AC measurements are usually made with an electronic digitizer to trace the perimeter of the head or abdomen. The AC is drawn around an axial image of the fetal abdomen at the level of the liver, specifically at the level of the umbilical portion of the left portal vein (Fig. 38.7C). The HC is measured on an axial section of the head at the level of the thalami, the same level which is utilized for BPD measurements (Fig. 38.7A). Using electronic calipers or digitizers, with a linear transducer the error in these measurements is approximately 2 mm.

## NORMAL FETAL ANATOMY

### Neural Axis

The *calvarium* begins to ossify by the beginning of the second trimester, and as a result of the high mineral content of the cranial bones, the tables of the *skull* appear as brightly echogenic curved structures (Fig. 38.8A). On ultrasound when the *skull base* is viewed in axial section it appears as an echogenic X-shaped structure formed by the petrous pyramids posteriorly and the sphenoid wings anteriorly. Another brightly echogenic linear structure which bisects the head



**Fig. 38.7A, B, C.** Fetal measurements. **A** BPD. An axial sonogram through the fetal head at 30 gestational weeks is obtained at the thalamic level and the BPD is measured from the outer edge of the calvarial table in the near field to the inner edge of the far calvarial table (arrows) using electronic calipers. **B** FL. The FL is measured along the diaphysis of the long bone (arrows) using electronic calipers as shown in this image of a femur in a 33 week gestation. **C** AC. The AC is drawn electronically around the perimeter of the fetal abdomen at the level of the stomach (*S*) and umbilical portion of the left portal vein (arrow).

is the *falk* which is visible throughout gestation (Fig. 38.8A). Early in the second trimester the *cerebral cortex* appears hypoechoic and smooth in contour and gyri and sulci do not become visible until the latter part of the third trimester. The *thalami* appear as oval or arrow-shaped structures on either side of the midline, split by the tiny parallel echoes demarcating the *third ventricle* (Fig. 38.8A). These structures are best visualized on axial sections. The thalami merge inferiorly to form the cerebral peduncles and midbrain around which are seen the pulsating vessels of the circle of Willis.

The *cerebellum*, surrounded by the echoic tentorium, is best imaged on sagittal or coronal scans, with the characteristically echogenic cerebellar vermis. The *cisterna magna* is consistently demonstrated as a fluid-containing space posterior to the cerebellum, and should not exceed 11 mm in size during the third trimester. The *lateral ventricles* are easily identified by the echogenic *choroid plexus* filling the trigone and are most obvious at about 12 gestational weeks (Fig. 38.8B). With increasing gestational age the ventricles occupy less and less of the intracranial volume as the brain develops around them. At 15 weeks, the ratio of lateral ventricular

width to hemispheric width (LV/HW) is 56%; however, this value decreases to 30% by 30 menstrual weeks and remains at this level until term (Fig. 38.8B).

The *fetal spine* is clearly seen from the start of the second trimester, but it is not until 18–20 menstrual weeks that optimal visualization is achieved making reliable diagnosis of *neural tube defect* (NTD) possible. By this time the three major ossification centers composed of the anterior vertebral body and the two posterolateral ossification centers of the neural arch are visible. On axial scans, these appear as echo-geneic linear foci grouped in a U or C configuration. The laminae forming the posterior portions of the neural arch normally have an inward angulation, and if they are splayed outward, *spina bifida* is suspected (Fig. 38.9A). On sagittal views, the fetal spine shows a normal thoracic kyphosis, with lordotic curves in the cervical and lumbar regions (Fig. 38.9A, B). Also on sagittal views, the anterior and posterior ossification centers form parallel echogenic structures flaring in the cervical region and tapering in the sacral region. The *dura* may be seen as a linear bright reflector within the spinal canal (Fig. 38.9B). Also, the skin and subcutaneous tissues

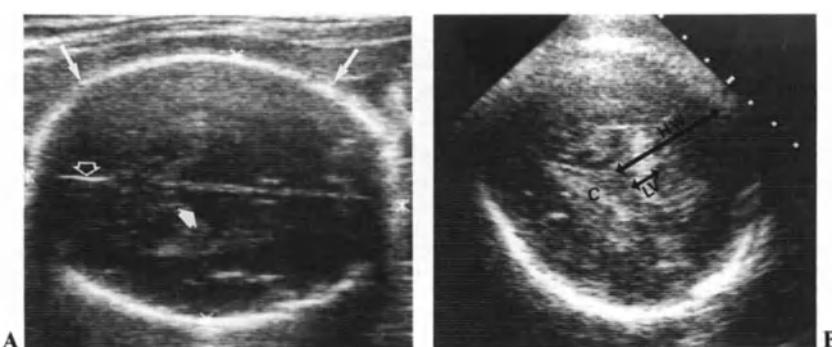


**Fig. 38.8A, B.** Fetal head anatomy. **A** Axial scan through the level of the thalami (arrowhead) reveals the echogenic calvarium (arrows) and falx (open arrow). Note the cerebral cortex appears smooth in contour on this second trimester scan. **B** Echogenic choroid plexus fills the atria of the lateral ventricles (C) on this axial scan through the head during the second trimester. The LV/HW ratio can be measured at this level.

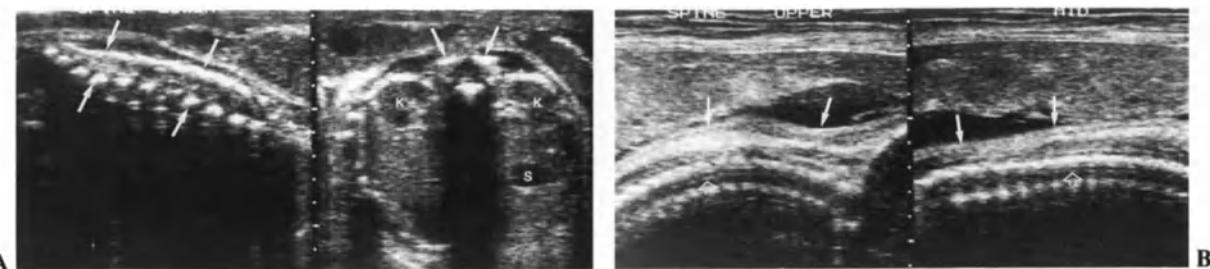


**Fig. 38.9A, B.** Fetal spinal anatomy. **A** The left-hand image shows a transverse view through the lumbar spine in a third trimester fetus. The echogenic posterior ossification centers (arrows) slant toward the midline. The kidneys (K) and stomach (S) are also identified on this image. The right-hand scan shows a longitudinal view of the lumbosacral spine with echogenic posterior and anterior ossification centers (arrows). **B** The spinal curvature is well demonstrated on these sagittal images of the thoracic (right-hand image) and cervical (left-hand image) spine in the same fetus. Note the echogenic line of the dura (arrowheads) and that the skin and subcutaneous tissue lie flat over the posterior spinal elements (arrows).

should lie flat over the posterior spinal elements, a feature which is helpful in identification of *myelomeningocele*.

The structures of the **face**, particularly bony structures such as *orbit*, *maxilla* and *mandible* can be distinguished as early as 12–14 weeks (Fig. 38.10). By the third trimester fine facial features such as the lips, palate, nares and ears are visible and diagnosis of common congenital anomalies of the face is possible. Also, it is commonly possible to distinguish movements of the fetal mouth, tongue, pharynx and eyelids during the third trimester.

#### Heart and Thorax

In the early part of the second trimester the **fetal thorax** can be identified as a dome-shaped body cavity framed by the echogenic ribs on coronal or sagittal ultrasound sections. The **lungs** are homogeneously echogenic and are separated from the similarly echoic liver by an echolucent curved band representing the *diaphragm*. It is impossible to judge fetal lung maturity based upon pulmonary echogenicity on ultrasound and biochemical tests such as amniotic fluid lecithin/sphingomyelin ratios are much more reliable. This becomes extremely important in the timing of premature deliveries to coincide with fetal lung maturity to avoid neonatal respiratory distress syndrome. By 16–20 menstrual weeks

fetal respiratory motion can be observed in short episodes lasting 60 seconds or longer. Other thoracic structures visible by the third trimester include the *great vessels* of the mediastinum and the *thymus*.

With high-resolution real-time equipment it is now possible to study the **fetal heart** in the same detail as the neonatal or adult heart. By 16–18 gestational weeks the four cardiac chambers can be discerned and chamber shape and size, valve motion and cardiac rate and rhythm can be assessed. The two *ventricles* are about the same size and are separated by a thick intraventricular septum; whereas, the *atria* are spherical, thin-walled and are separated by an incomplete septum, perforated by the foramen ovale (Fig. 38.11A). The **heart rate** should be regular at 135–155 beats/minute although transient episodes of bradycardia down to 60 beats/minute are normal. Cardiac rhythm and rate, valve motion, and chamber size can be assessed in greater detail with M-Mode (time-motion mode) ultrasound (Fig. 38.11B) and with more modern equipment direction and volume of blood flow can be evaluated using duplex or color-flow Doppler ultrasound.

As the technology has become more advanced, the amount of anatomic detail visible on ultrasound has steadily increased, and an in-depth discussion of fetal cardiac anatomy is outside the scope of this chapter.

#### Abdomen

The **abdominal wall** is well visualized prior to the beginning of the second trimester and it maintains a rounded or oval shape throughout the remainder of gestation (Fig. 38.12A). As the fetus enlarges, echogenic fat is deposited in the *abdominal wall* and this is separated from underlying organs such as liver by the hypoechoic abdominal wall muscles, which may be mistaken for fetal ascites. The anterior abdominal wall is perforated by the **umbilical cord**, containing the umbilical vein which enters the liver to join the left portal vein, and two umbilical arteries which arise from the iliac vessels (Fig. 38.12B).

Gastrointestinal organs are visible from early in gestation. The **stomach** appears as a rounded, anechoic structure in the left upper quadrant at about 12 menstrual weeks. If it is not visualized the patient should be re-examined in 30 minutes to 1 hour to document gastric filling. The **small bowel** is usually quite echogenic and individual loops cannot



**Fig. 38.10.** Facial bones. The orbits (O), maxilla (M) and mandible (arrows) are easily seen on this coronal view of the fetal face of a second trimester fetus.

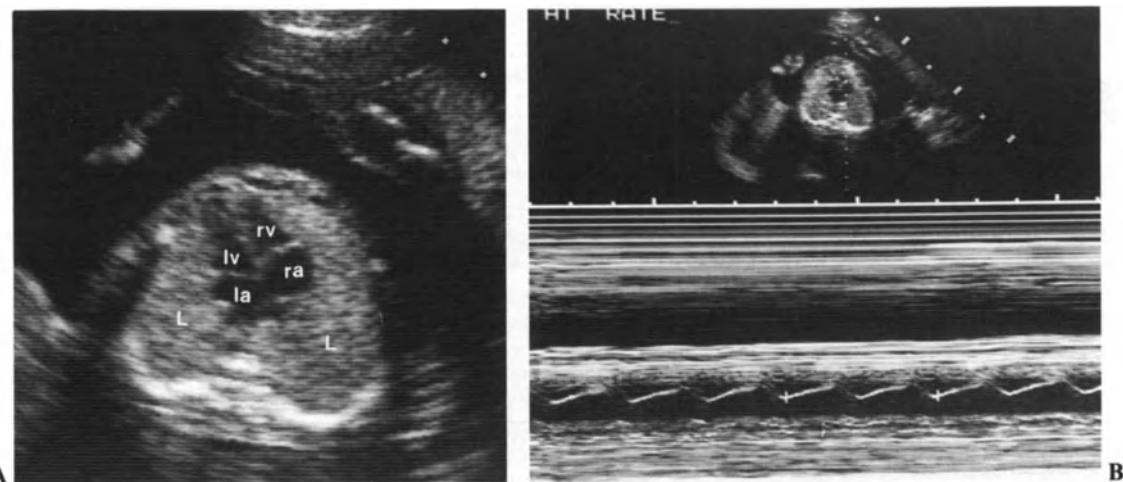


**Fig. 38.11A, B.** Fetal cardiac anatomy. A The four-chamber view. The cardiac ventricles (*lv* and *rv*) and atria (*la* and *ra*) are depicted on this axial section through the fetal chest during the third trimester. The intraventricular septum and foramen ovale can be located. The lungs (*L*) appear of homogeneous echo-texture. B Time-motion mode tracing through an A-V valve is a valuable method of assessing rate and rhythm. Also, quantitative measurement of valve motion and chamber size can be achieved using this method.

be delineated. However, in the third trimester the normal colon may appear more hypoechoic, filled with meconium, and can be identified by its peripheral position in the abdominal cavity.

The liver is of homogeneous echogenicity and *portal veins*, *hepatic veins*, *inferior vena cava* and *gallbladder* are easily identified in the third trimester fetus. The *spleen*, *adrenal glands* and *pancreas* are also homogeneous in echo texture and are often visualized with careful scanning.

The first organ of the fetal urinary tract to become visible on ultrasound is the **urinary bladder** and it is consistently identified after 12 menstrual weeks (Fig. 38.13A). As with

the stomach, re-examination may be necessary to demonstrate a fluid-filled bladder. By 15 menstrual weeks the kidneys become visible as rounded, hypoechoic structures on either side of the spine. The echogenic renal capsule and renal sinus fat does not become clearly visible until 20 weeks, and by term the hypoechoic medullary pyramids can be distinguished from the more echoic renal cortex (Fig. 38.13B). Normally the renal pelvis may contain anechoic urine but should measure less than 5 mm in AP diameter; 5–10 mm renal pelvic size is equivocal for fetal hydronephrosis and a greater than 10 mm AP diameter of the renal pelvis suggests **hydronephrosis**. Female internal genitalia are rarely seen on

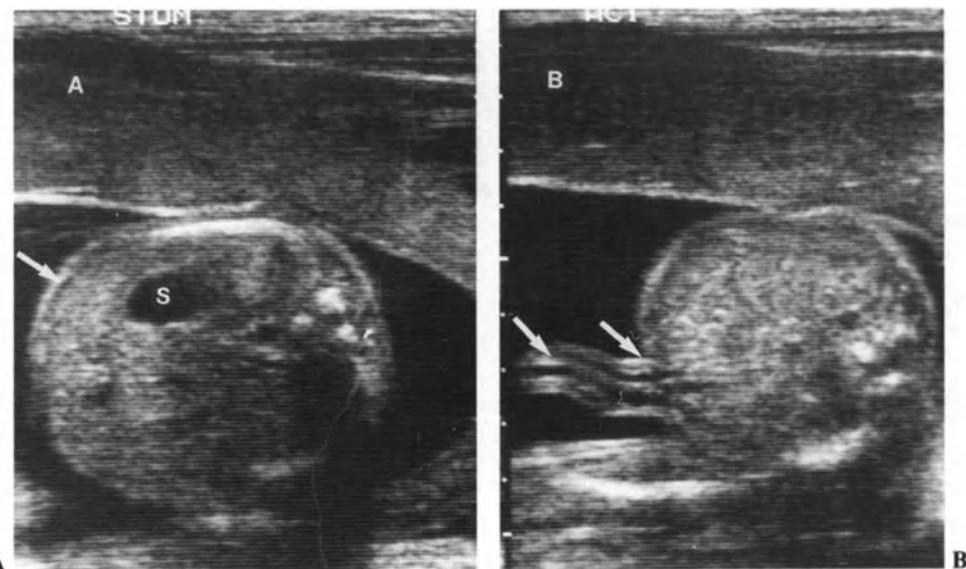


**Fig. 38.12A, B.** Fetal abdominal anatomy. A Transverse section through the fetal abdomen during the third trimester reveals the fluid-filled stomach (*S*) and the rounded configuration of the abdominal wall. The thin hypoluent line (arrow) just beneath the skin is caused by abdominal muscles (not ascites). B The insertion of the umbilical cord into the anterior abdominal wall (arrows) is depicted on this transverse image of the abdomen in the same fetus.

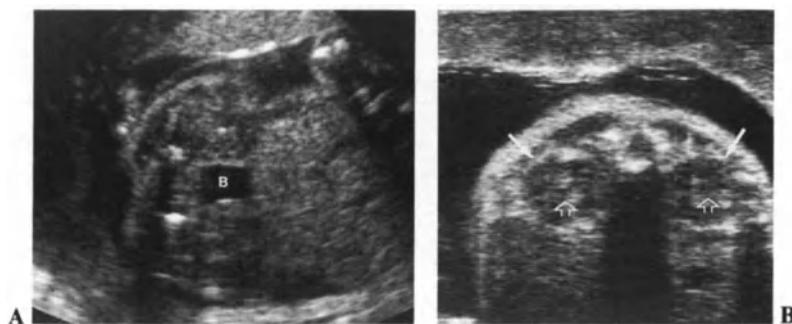


**Fig. 38.13A, B.** Fetal urinary tract anatomy. **A** Coronal image of the lower abdomen in a third trimester fetus reveals the urinary bladder (**B**) within the pelvis. **B** Transverse section through the fetal kidneys during the third trimester shows echogenic renal capsule (**arrows**) and renal collecting systems (**arrowheads**).

ultrasound unless abnormally distended with fluid, but **external genitalia** may be visible as early as 15 weeks in males and 20 weeks in females.

#### Skeleton

The fetal **long bones** begin to ossify by 9 menstrual weeks and by the mid-second trimester the phalanges and metatarsals are visible, allowing detailed morphologic study of the

fetal limbs. Not only is the length of the long bones important for the diagnosis of skeletal dysplasias, but the degree and quality of ossification as well as the shape of long bones should be assessed.

Epiphyseal ossification centers are also visualized, the most consistently identified is the **distal femoral epiphysis**, seen at 33–34 gestational weeks. A complete evaluation of the fetal skeleton also includes evaluation of the skull, spine, and ribs, and the normal appearances of these have been discussed previously.

#### Placenta and Umbilical Cord

Although not a portion of the fetus itself, the **placenta** is an extremely important organ for exchange of oxygen, nutrients and waste. The fetal portion forms from the chorion frondosum and the maternal portion from the decidua basalis. As early as 7–8 menstrual weeks it may be identified as an echogenic crescent surrounding a portion of the gestational sac and in the 10–12 week gestation is easily localized for transabdominal or transcervical chorionic villous sampling (CVS). The placenta maintains an homogeneous echo-texture throughout the second trimester (Grade 0) (Fig. 38.14A) but during the third trimester *calcifications* develop first at the base (Grade 1) and later along the chorionic plate and into the substance of the placenta along septae dividing the cotyledons (Grade 2 and 3) (Fig. 38.14B). Anechoic spaces may also be seen within the placenta, representing *venous lakes*, which may increase in size with increasing gestational age. Swirling blood flow can be visualized within these spaces, and flow within them may be documented using Doppler ultrasound. The normal placental thickness should not exceed 3 cm in AP diameter. The position of the placenta is of great importance to the obstetrician and the exact relationship of the placenta to the cervical os needs to be carefully evaluated to exclude *placenta previa*.

The normal **umbilical cord** consists of a single umbilical vein (the largest vessel) and two umbilical arteries (the small vessels). On transverse section the 'Mickey Mouse' appearance of the large umbilical vein flanked by two small arteries is routinely noted (Fig. 38.15). The number of vessels contained within the cord is important as a *single umbilical artery* is associated with a 10–40 times greater risk of congenital anomalies than is a normal cord. Also, the position of the

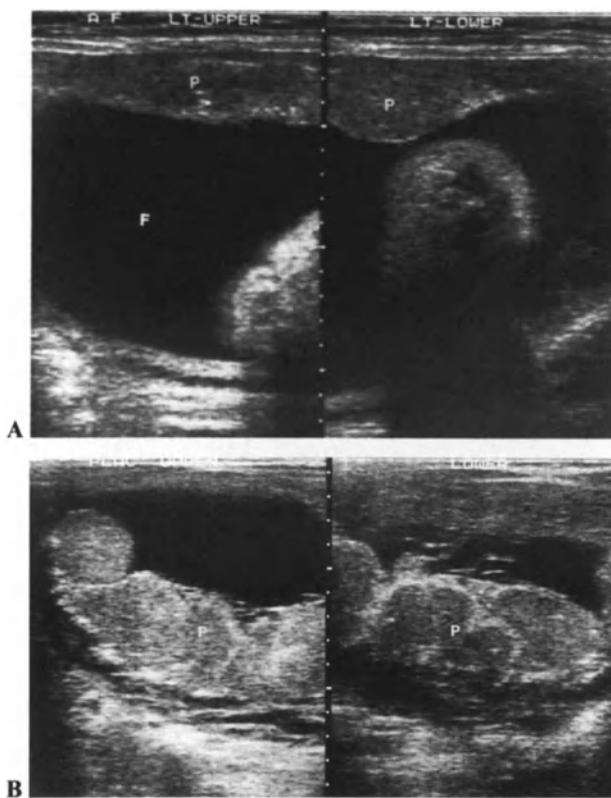


**Fig. 38.14A, B.** Placental anatomy. **A** A homogeneous, grade 0 placenta (**P**) is noted along the anterior uterine wall. In this late second trimester gestation there is polyhydramnios (**F**, amniotic fluid). **B** A calcified, grade 3 placenta (**P**) is shown in a third trimester, growth-retarded gestation. Note the echogenic material at the base of the placenta and along the chorionic plate.



**Fig. 38.15.** Umbilical cord anatomy. A transverse view through the umbilical cord reveals the central umbilical vein (*v*) flanked by the smaller umbilical arteries (*a*).

cord needs to be determined, as it may be wrapped around the fetal neck (*nuchal cord*) or *prolapsed* through the dilated cervix.

#### ASSESSMENT OF GESTATIONAL AGE: SECOND AND THIRD TRIMESTER

The **gestational age** of the fetus in the latter two trimesters of pregnancy can be estimated using a wide variety of sono-

graphic measurements. Historically, BPD has been most widely utilized and has proven quite reliable. The method of making this measurement has been discussed previously, and once a BPD value is obtained it is plotted on a standard table (Table 38.3) to determine gestational age. Up to 24 gestational weeks BPD is accurate to  $\pm$  5–7 days; greater than 30 weeks its accuracy decreases to  $\pm$  2 weeks. At term, BPD measurements may be as inaccurate as  $\pm$  3.5–4 weeks.

As a result of these inaccuracies near term, other anatomic structures are usually measured. Since the *femur* is the easiest long bone to image on sonography, it is commonly measured and plotted on established tables for gestational age (Table 38.4). The accuracy of FL measurements equals that of BPD before 30 weeks and probably exceeds that of BPD near term. Although AC measurements are no more accurate than BPD in establishing gestational age (Table 38.6), AC is generally considered to be the most sensitive predictor of **intrauterine growth retardation** (IUGR). In addition, HC/AC ratio can detect asymmetric head and body growth (Table 38.5) and may be used to determine the presence of asymmetric IUGR (abdomen size lags behind the head size). In addition, an **estimation of fetal weight** (EFW) may be achieved with either BPD and AC or FL and AC using a specific equation for either two parameters, providing very useful information about fetal size to the obstetrician.

**Table 38.3.** Composite biparietal diameter table

Biparietal diameter (cm)	Gestational age (weeks)		Biparietal diameter (cm)	Gestational age (weeks)		Biparietal diameter (cm)	Gestational age (weeks)	
	Mean*	Range 90% variation <sup>+</sup>		Mean*	Range 90% variation <sup>+</sup>		Mean*	Range 90% variation <sup>+</sup>
2.0	12.0	12.0	4.7	19.7	17.8 to 21.6	7.3	28.7	27.6 to 29.8
2.1	12.0	12.0	4.8	20.0	18.2 to 21.8	7.4	29.1	28.1 to 30.1
2.2	12.7	12.2 to 13.2	4.9	20.3	18.6 to 22.0	7.5	29.5	28.5 to 30.5
2.3	13.0	12.4 to 13.6	5.0	20.6	19.0 to 22.2	7.6	30.0	29.0 to 31.0
2.4	13.2	12.6 to 13.8	5.1	20.9	19.3 to 22.5	7.7	30.3	29.2 to 31.4
2.5	13.5	12.9 to 14.1	5.2	21.2	19.5 to 22.9	7.8	30.8	29.6 to 32.0
2.6	13.7	13.1 to 14.3	5.3	21.5	19.8 to 23.2	7.9	31.1	29.9 to 32.5
2.7	14.0	13.4 to 14.6	5.4	21.9	20.1 to 23.7	8.0	31.6	30.2 to 33.0
2.8	14.3	13.6 to 15.0	5.5	22.2	20.4 to 24.0	8.1	32.1	30.7 to 33.5
2.9	14.5	13.9 to 15.2	5.6	22.5	20.7 to 24.3	8.2	32.6	31.2 to 34.0
3.0	14.8	14.1 to 15.5	5.7	22.8	21.1 to 24.5	8.3	33.0	31.5 to 34.5
3.1	15.1	14.3 to 15.9	5.8	23.2	21.5 to 24.9	8.4	33.4	31.9 to 35.1
3.2	15.3	14.5 to 16.1	5.9	23.5	21.9 to 25.1	8.5	34.0	32.3 to 35.7
3.3	15.6	14.7 to 16.5	6.0	23.8	22.3 to 25.5	8.6	34.3	32.8 to 36.2
3.4	15.9	15.0 to 16.8	6.1	24.2	22.6 to 25.8	8.7	35.0	33.4 to 36.6
3.5	16.2	15.2 to 17.2	6.2	24.6	23.1 to 26.1	8.8	35.4	33.9 to 37.1
3.6	16.4	15.4 to 17.4	6.3	24.9	23.4 to 26.4	8.9	36.1	34.6 to 37.6
3.7	16.7	15.6 to 17.8	6.4	25.3	23.8 to 26.8	9.0	36.6	35.1 to 38.1
3.8	17.0	15.9 to 18.1	6.5	25.6	24.1 to 27.1	9.1	37.2	35.9 to 38.5
3.9	17.3	16.1 to 18.5	6.6	26.0	24.5 to 27.5	9.2	37.8	36.7 to 38.9
4.0	17.6	16.4 to 18.8	6.7	26.4	25.0 to 27.8	9.3	38.8	37.3 to 39.3
4.1	17.9	16.5 to 19.3	6.8	26.7	25.3 to 28.1	9.4	39.0	37.9 to 40.1
4.2	18.1	16.6 to 19.8	6.9	27.1	25.8 to 28.4	9.5	39.7	38.5 to 40.9
4.3	18.4	16.8 to 20.2	7.0	27.5	26.3 to 28.7	9.6	40.6	39.1 to 41.5
4.4	18.8	16.9 to 20.7	7.1	27.5	26.7 to 29.1	9.7	41.0	39.9 to 42.1
4.5	19.1	17.0 to 21.2	7.2	28.3	27.2 to 29.4	9.8	41.8	40.5 to 43.1
4.6	19.4	17.4 to 21.4						

From Kurtz AB, Wapner RJ, et al. (1980) Analysis of biparietal diameter as an accurate indicator of gestational age. J Clin Ultrasound 8: 319.

© 1980, John Wiley & Sons.

\*From weighted least mean square fit equation:  $Y = -3.45701 + 0.50157x - 0.00441x^2$

<sup>+</sup>For each biparietal diameter, 90% of gestational age data points fell within this range.

**Table 38.4.** Femur measurement table

Bone length (mm)	Gestational age (weeks)			Bone length (mm)	Gestational age (weeks)		
	5th percentile	Predicted mean value	95th percentile		5th percentile	Predicted mean value	95th percentile
10	10.4	12.6	14.9	46	23.1	25.4	27.6
11	10.7	12.9	15.1	47	23.6	25.9	28.0
12	11.1	13.3	15.6	48	24.0	26.1	28.4
13	11.4	13.6	15.9	49	24.4	26.6	28.9
14	11.7	13.9	16.1	50	24.9	27.0	29.1
15	12.0	14.1	16.4	51	25.1	27.4	29.6
16	12.4	14.6	16.9	52	25.6	27.9	30.0
17	12.7	14.9	17.1	53	26.0	28.1	30.4
18	13.0	15.1	17.4	54	26.4	28.6	30.9
19	13.4	15.6	17.9	55	26.9	29.1	31.3
20	13.7	15.9	18.1	56	27.2	29.6	31.7
21	14.1	16.3	18.6	57	27.7	29.9	32.1
22	14.4	16.6	18.9	58	28.1	30.3	32.6
23	14.7	16.9	19.1	59	28.6	30.7	32.9
24	15.1	17.3	19.6	60	28.9	31.1	33.3
25	15.4	17.6	19.9	61	29.4	31.6	33.9
26	15.9	18.0	20.1	62	29.9	32.0	34.1
27	16.1	18.3	20.6	63	30.1	32.4	34.6
28	16.6	18.7	20.9	64	30.7	32.9	35.1
29	16.9	19.0	21.1	65	31.1	33.4	35.6
30	17.1	19.4	21.6	66	31.6	33.7	35.9
31	17.6	19.9	22.0	67	32.0	34.1	36.4
32	17.9	20.1	22.3	68	32.4	34.6	36.9
33	18.3	20.6	22.7	69	32.6	35.0	37.1
34	18.7	20.9	23.1	70	33.3	35.6	37.7
35	19.0	21.1	23.4	71	33.7	35.9	38.1
36	19.4	21.6	23.9	72	34.1	36.4	38.6
37	19.9	22.0	24.1	73	34.6	36.9	39.0
38	20.1	22.4	24.6	74	35.1	37.3	39.6
39	20.6	22.7	24.9	75	35.6	37.7	39.9
40	20.9	23.1	25.3	76	36.0	38.1	40.4
41	21.3	23.6	25.7	77	36.4	38.6	40.9
42	21.7	23.9	26.1	78	36.9	39.1	41.3
43	22.1	24.3	26.6	79	37.3	39.6	41.7
44	22.6	24.7	26.9	80	37.9	40.0	42.1
45	22.9	25.0	27.1				

From Jeanty P, Rodesch F, Delbeke D, Dumont JE (1984) Estimation of gestational age from measurements of fetal long bones. *J Ultrasound Med* 3: 75

**Table 38.5.** Head to abdomen circumference ratio table

Gestational age (weeks)	5th percentile	Mean	95th percentile
13 to 14 weeks	1.14	1.23	1.31
15 to 16	1.05	1.22	1.39
17 to 18	1.07	1.18	1.29
19 to 20	1.09	1.18	1.29
21 to 22	1.06	1.15	1.25
23 to 24	1.05	1.13	1.21
25 to 26	1.04	1.13	1.22
27 to 28	1.05	1.13	1.22
29 to 30	0.99	1.10	1.21
31 to 32	0.96	1.07	1.17
33 to 34	0.96	1.04	1.11
35 to 36	0.93	1.02	1.11
37 to 38	0.92	0.98	1.05
39 to 40	0.87	0.97	1.06
41 to 42	0.93	0.96	1.00

From Campbell S, Thomas A (1977) Ultrasound measurement of the fetal head to abdomen circumference in the assessment of growth retardation. *Br J Obstet Gynaecol* 84: 165

The early identification of IUGR is mandatory in order to improve the high perinatal morbidity and mortality rates among these small-for-gestational-age infants (less than 10th percentile for weight). Also, when IUGR is suspected, early delivery improves the neonatal outcome, as most fetuses do better in the nursery than in a hostile intrauterine environment. In order to make this diagnosis using sonographic measurements, a knowledge of gestational age either from reliable menstrual dates or a first trimester ultrasound measurement is necessary. The optimal time for screening for IUGR is between 32 and 34 gestational weeks. An AC measurement below the 15th percentile at 28–34 weeks and below the 10th percentile after 36 weeks has a sensitivity of about 75% and a positive predictive value of 70%. Also, an EFW of less than the 5th percentile for gestational age has a sensitivity of 75% and a positive predictive value of 40%. Abnormal HC/AC ratio is not as sensitive, as it only detects asymmetric forms of growth where the head is spared at the expense of the abdomen. A FL/AC ratio of greater than 23.5 has a sensitivity of only 60% for IUGR with a low posi-

**Table 38.6.** Abdominal circumference measurement table

Abdominal circumference (cm)	Gestational age (weeks): predicted mean values	Abdominal circumference (cm)	Gestational age (weeks): predicted mean values
10.0	15.6	24.0	28.2
10.5	16.1	24.5	28.7
11.0	16.5	25.0	29.2
11.5	16.9	25.5	29.7
12.0	17.3	26.0	30.1
12.5	17.8	26.5	30.6
13.0	18.2	27.0	31.1
13.5	18.6	27.5	31.6
14.0	19.1	28.0	32.1
14.5	19.5	28.5	32.6
15.0	20.0	29.0	33.1
15.5	20.4	29.5	33.6
16.0	20.8	30.0	34.1
16.5	21.3	30.5	34.6
17.0	21.7	31.0	35.1
17.5	22.2	31.5	35.6
18.0	22.6	32.0	36.1
18.5	23.1	32.5	36.6
19.0	23.6	33.0	37.1
19.5	24.0	33.5	37.6
20.0	24.5	34.0	38.1
20.5	24.9	34.5	38.7
21.0	25.4	35.0	39.2
21.5	25.9	35.5	39.7
22.5	26.8	36.0	40.2
23.0	27.3	36.5	40.8
23.5	27.7		

From Hadlock FP, Deter RL, Harrist RB, Park SK: Fetal abdominal circumference as a predictor of menstrual age. AJR 139: 367, 1982. Copyright by The American Roentgen Ray Society, 1982

tive predictive value of 20%; however, this ratio may be useful in predicting IUGR when the gestational age is unknown. The presence of oligohydramnios is a poor predictor of IUGR with a positive predictive value of only 40%. Overall, the most sensitive predictors of IUGR are AC and EFW and should be obtained on every third trimester gestation.

**Macrosomic infants** are greater than the 90–95th percentile for weight at birth, are at risk for obstetrical accidents such as dystocia, and are frequently the fetuses of diabetic mothers. The following criteria have been established for determining macrosomia using ultrasound measurements during the third trimester:

1. An AC greater than 2 standard deviations (SD) above the mean for gestational age
2. EFW greater than the 90th percentile for gestational age
3. FL/AC ratio less than 20.5
4. Polyhydramnios

If all of these criteria are met a diagnosis of macrosomia can be suggested.

#### FETAL CONGENITAL ANOMALIES

##### Neural Axis

**Hydrocephalus** or increased intracranial content of cerebrospinal fluid is one of the most common CNS anomalies. It may be caused by *aqueduct stenosis*, *neural tube defect*

(*NTD*), *chromosomal abnormalities*, *infections*, *Dandy-Walker malformation*, *agenesis of the corpus callosum*, or *communicating hydrocephalus*. It occurs quite frequently, with an incidence of 0.3–0.8 cases per 1000 live births. Associated anomalies are quite common, with other intracranial anomalies in 37% and extracranial malformations in 63% of cases. In the early second trimester the most common ultrasound finding is an increase in lateral ventricular size with displacement of the choroid plexus away from one wall of the ventricle (Fig. 38.16A). The choroid plexus may appear small and may fall to the dependent portion of the ventricle. Later in gestation the ratio of lateral ventricular width relative to the hemispheric width may increase markedly. In advanced cases the cortical mantle may become thinned, but is still present, and a dilated third ventricle may be seen, especially in aqueduct stenosis (Fig. 38.16B).

**Holoprosencephaly** results from failed cleavage of the rostral cerebral vesicle and is a complex anomaly involving fusion of the lateral ventricles and a variety of cerebral and facial malformations. In its most severe form (*alobar*) a single, large lateral ventricle, absent interhemispheric fissure, falx, and third ventricle, fused thalamus and severe facial malformations such as proboscis and cyclopia are seen (Figs 38.17A, B). In the partial forms of this anomaly (*semilobar* or *lobar*) a sickle-shaped single lateral ventricle is seen, but cortical mantle and divided midline structures such as thalamus are present. The facial defects associated with these anomalies are less severe and include hypotelorism and facial clefts.

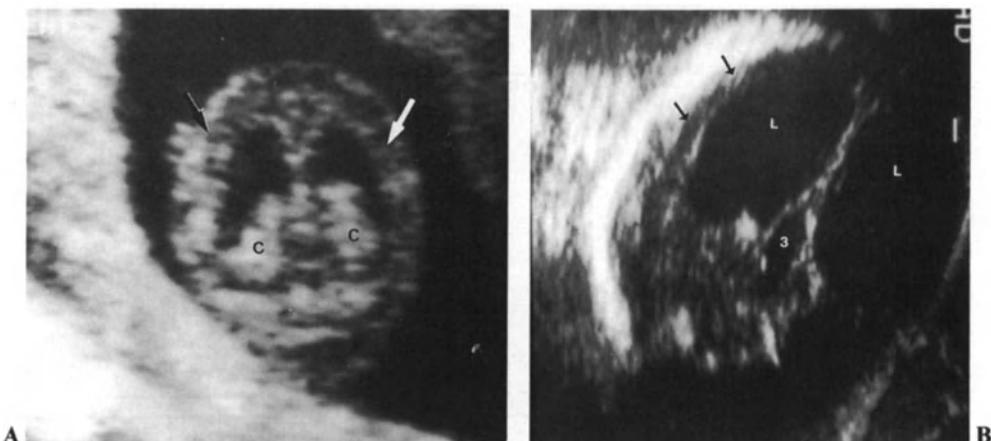


**Fig. 38.16A, B.** Hydrocephalus. **A** Enlarged lateral ventricles with an abnormally increased LV/HW ratio for a gestational age of 16 weeks are shown. The choroid plexus (*C*) is displaced away from the lateral wall of the lateral ventricle indicating ventriculomegaly. The cortical mantle (*arrows*) is maintained. **B** On a coronal scan through the head of a third trimester fetus shows dilated lateral ventricles (*L*) and third ventricle (*3*). The cortical mantle is thinned (*arrows*). The cause of the hydrocephalus in this case was aqueductal stenosis.

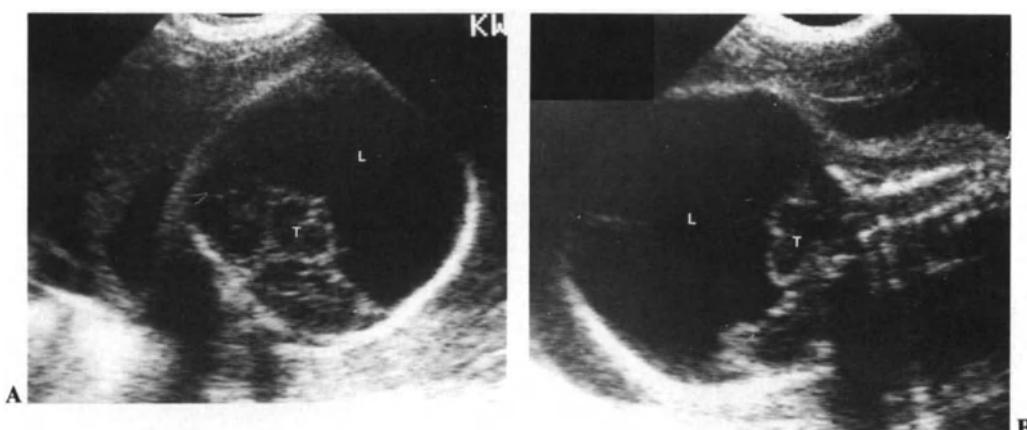


**Fig. 38.17.A, B.** Holoprosencephaly. Coronal, **A**, and sagittal, **B**, scans through the head of a third trimester fetus with alobar holoprosencephaly reveal a single large lateral ventricle (*L*), absent falx and cortical mantle and fused thalamus (*T*). The face of this fetus demonstrated cyclopia and proboscis (not shown).



**Fig. 38.18.** Hydrencephaly. Single axial view of the head shows fluid surrounding the falx and midbrain structures (*arrows*). No definite cortical mantle is identified in this third trimester fetus.

**Hydrencephaly** is caused by vascular occlusion leading to failure of development of the cerebral hemispheres. On ultrasound, midline structures such as falx, thalamus and brainstem appear normal but the remainder of the cranium is fluid-filled and the cortical mantle is lacking (Fig. 38.18).

A variety of cystic masses may arise in the fetal cranial cavity including **Dandy–Walker cyst**, **arachnoid cyst**, **porencephalic cyst**, and **choroid plexus cyst**.

The **Dandy–Walker malformation** consists of a cystic dilatation of the fourth ventricle leading to a posterior fossa cyst associated with hypoplasia of the cerebellar vermis. Varying degrees of lateral and third ventricular dilatation may result from the presence of the cystic mass (Fig. 38.19).

**Porencephaly** results from localized vascular, traumatic or infectious insult to the cerebral cortex leading to a CSF-containing cyst usually communicating with the ventricular system (Fig. 38.20). These may be difficult to distinguish from *arachnoid cysts* which arise on the surface of the brain and do not communicate with the cerebral ventricles.



**Fig. 38.19.** Dandy-Walker malformation. A coronal image through the posterior fossa reveals the trefoil-shaped posterior fossa cyst (C) and mildly dilated lateral and third ventricles (arrows). The defect in the cerebellar vermis is noted at the superior aspect of the cyst (arrowheads).



**Fig. 38.20.** Porencephaly. Coronal scan through the head of a third trimester fetus demonstrate a cyst (C) in the parieto-occipital region, communicating with the lateral ventricle (arrows) on the right. The cortex surrounding the cyst is markedly thinned.

**Choroid plexus cysts** are very common, and appear as small cystic structures arising in the choroid of the atria of the lateral ventricles. They usually resolve by 20–24 weeks and those that persist may be associated with chromosomal abnormalities such as trisomies.

**Anencephaly** is the most severe form of neural tube defect resulting in absent cerebral hemispheres and cranial vault. On ultrasound the cervical spine terminates at the craniocervical junction with wide splaying of posterior and anterior elements on sagittal scans. No cranial vault is seen above very prominent orbits and maxilla (Fig. 38.21A, B). There may be associated polyhydramnios.

**Encephalocele** results from a defect in the calvarium causing herniation of meninges or brain outside the cranial cavity. When it occurs in the midline, especially in the occipital region, it is usually the result of failure of closure of the neural tube. Off-axis encephaloceles are caused by the *amniotic band syndrome*. The cranial defect and herniated brain or cystic structure not surrounded by bone are easily identified on ultrasound (Fig. 38.22A, B). Confusion may occur with *cystic hygromas* or *cervical meningoceles*, although in these anomalies careful examination of the skull reveals an intact cranium. This anomaly may also be associated with polyhydramnios.

**Acrania** results from total lack of formation of the calvarium and on ultrasound disorganized cerebral tissue is noted floating freely above the level of the termination of the cervical spine.

Other cerebral abnormalities which may be identified in utero include tumors, such as **dermoids** or **teratomas** which may be solid or cystic, or vascular malformations, such as **vein of Galen aneurysm**. In this latter abnormality a cystic mass may be noted in the region of the vein of Galen associated with hydrocephalus and fetal hydrops (due to high output cardiac failure). **Intracranial hemorrhage** may also be seen on ultrasound as an echogenic intraventricular or parenchymal mass and may lead to communicating hydrocephalus.

**Neural tube defects (NTD)** involving the spine are the most common CNS anomaly, with an incidence of 0.2–4.1 per

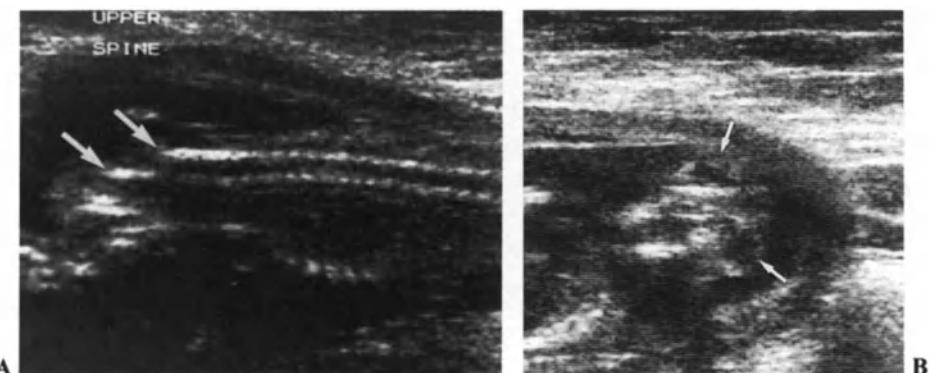


**Fig. 38.21A, B.** Anencephaly. **A** A sagittal scan through the thoracic and cervical spine shows splaying of anterior and posterior spinal elements at the abrupt termination of the cervical spine (arrows). No calvarium is identified in this anencephalic fetus at 20 gestational weeks. **B** A coronal image through the face of the same fetus reveals very prominent orbits (arrows) with no calvarium or brain noted above them. This is characteristic of the facies of an anencephalic.

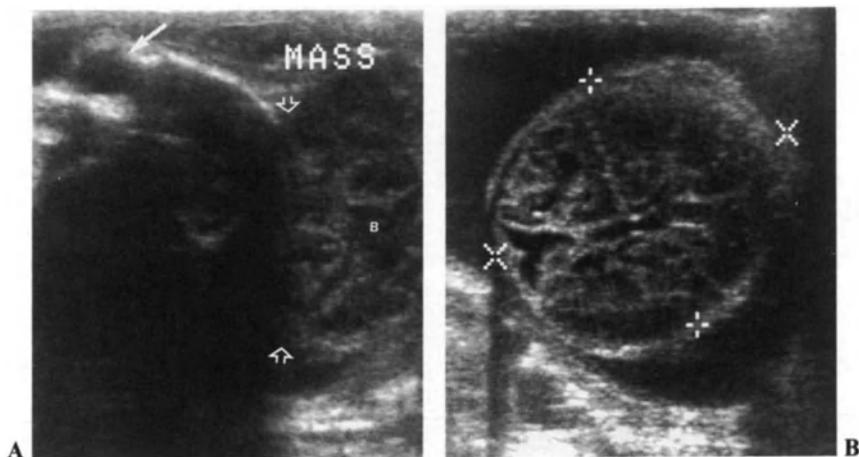


**Fig. 38.22A, B.** Encephalocele. **A** An axial scan through the calvarium and orbits (arrow) reveals a large defect in the skull in the parieto-occipital region (open arrows) with extrusion of brain (B), in a term fetus. **B** An axial scan through the extruded brain shows gyri and sulci of cerebral cortex not surrounded by calvarium.

1000 live births. An elevated maternal serum *alpha-fetoprotein* (AFP) may indicate this anomaly, *encephalocele* or *anencephaly*. Among women with an elevated AFP, 42%–74% harbour a fetus with NTD. The midline spinal defect may be occult (bony involvement only in 15%) or may lead to exposure of meninges (*meningocele*) or meninges and neural tissue (*myelomeningocele*) in 85% of cases.

Most spinal NTD with myelomeningocele occur in the lumbosacral region. Ultrasound findings include a widened neural canal on coronal images, and loss of posterior neural arch and laminae on sagittal and axial scans (Figs 38.23A, B). The meningocele or myelomeningocele may be noted projecting posteriorly as a fluid-filled sac or solid mass (Fig.

38.23A). Up to 90% of spinal NTDs are associated with an *Arnold-Chiari II malformation* characterized by downward herniation of portions of the cerebellum leading to a crescentic-shaped cerebellum ('banana' sign), obliteration of the cisterna magna and varying degrees of hydrocephalus. Also, the frontal bones may be abnormally scalloped leading to a lemon-shaped head ('lemon' sign) (Fig. 38.24).

The most important anomaly to distinguish from lumbosacral NTD is a *sacrococcygeal teratoma*. This is the most common tumor diagnosed prenatally and it presents on ultrasound as a large, cystic or mixed solid and cystic mass usually projecting posteriorly from the sacrum. The lumbosacral spine may or may not be intact (Fig. 38.25A, B).

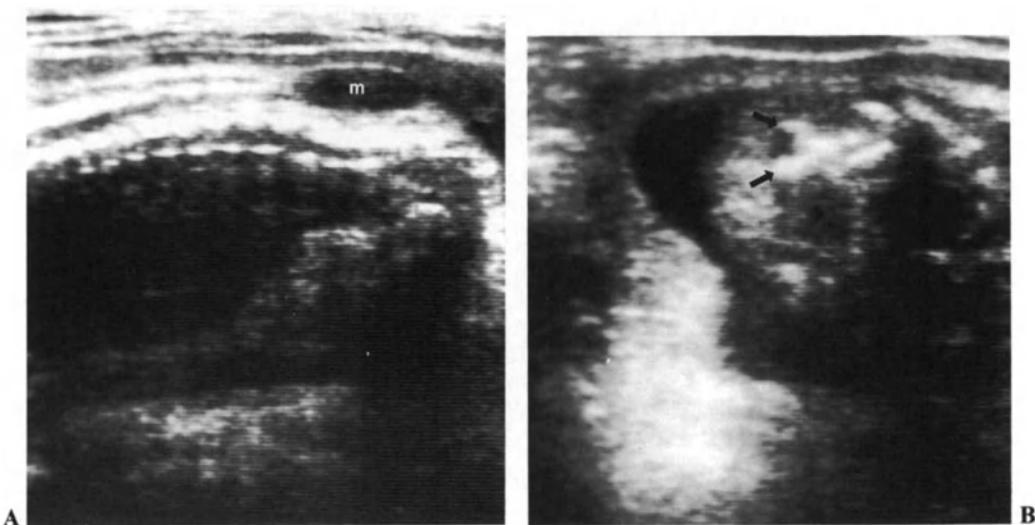


**Fig. 38.23A, B.** Neural tube defects. **A** Lumbosacral meningocele. A sagittal scan through the lumbosacral spine demonstrates a cystic mass (m) protruding from the spinal canal. Note loss of posterior spinal ossification centers in region of meningocele. This meningocele contained no neural tissue. **B** Spina bifida without meningocele. Splaying of the posterior spinal elements (arrows) is visible without definite meningocele on transverse scan. This proved to be a spina bifida occulta at birth.

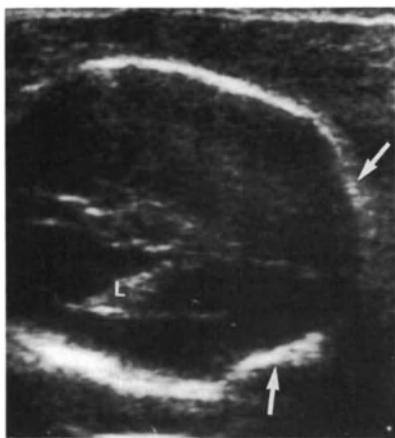


**Fig. 38.24.** 'Lemon sign' and hydrocephalus in NTD. Scalloping of the frontal bones (arrows), referred to as the 'lemon sign', and enlarged lateral ventricle (L) in a fetus with Arnold–Chiari II malformation and lumbosacral myelomeningocele.

As these lesions are often resectable in the neonatal period and are only rarely malignant prenatal diagnosis is helpful to choose the safest mode of delivery.

#### Face and Neck

The most commonly encountered facial anomalies are **cleft lip and palate**, which are best demonstrated on coronal or axial views of the face. The successful ultrasound diagnosis is dependent upon a favorable fetal head position during scanning to obtain these views. The defect demonstrated in the lip or palate may be midline or eccentric. Other facial anomalies which may be detected on ultrasound in the second and third trimester include **hypotelorism** (closely-set eyes), **hypsotelorism** (widely-set eyes), **cyclopia** (single orbit), **arhinia** (absent nose), **proboscis** (midline protrusion) or **micrognathia** (hypoplastic mandible). Facial anomalies are frequently associated with more severe cerebral anomalies such as **holoprosencephaly**.

The most common cystic mass arising from the neck or thorax of a fetus is a **cystic hygroma** caused by lymphatic obstruction early in development. It may resolve in utero leaving a residual webbed neck only, or it may progress to fetal hydrops. Approximately 50% of fetuses with cystic hygroma have *Turner's syndrome* (45XO) and amniocentesis is indicated in all cases of cystic hygroma to exclude this syndrome. The sonographic features of cystic hygroma include:

1. A septate, predominantly cystic mass of the posterior neck or thorax
2. Fetal hydrops
3. Oligohydramnios (Fig. 38.26A, B)

Other neck masses which need to be distinguished from cystic hygroma include **cervical meningocele**, **low encephalocele**, **cystic teratoma**, **thyroglossal duct** or **branchial cleft cysts** and **marked nuchal skin edema**. Thickening of edema of the nuchal skin may be seen as a feature of *Turner's syndrome* or *Trisomies 21 or 18*. Solid masses which may occur in the fetal neck are less common and may be caused by **goiters**, **solid teratomas** or **hemangiomas**.

#### Thorax

**Congenital diaphragmatic hernia** (CHD) occurs secondary to protrusion of abdominal organs through a defect in the diaphragm. Most diaphragmatic hernias are left-sided, occurring through the foramen of Bochdalek (80%–90%), while the minority are right-sided and parasternal through the foramen of Morgagni (1%–2%).

Ultrasound findings include fluid-filled bowel or stomach at the level of the heart with peristalsis, absent intraabdominal stomach, mediastinal and cardiac shift away from the side of the hernia and decreased abdominal circumference (Fig. 38.27). Occasionally the defect in the diaphragm may be visible. The major cause of morbidity and mortality from this anomaly is **pulmonary hypoplasia** secondary to pulmonary compression by hernia contents, resulting in a high neonatal death rate (35%).

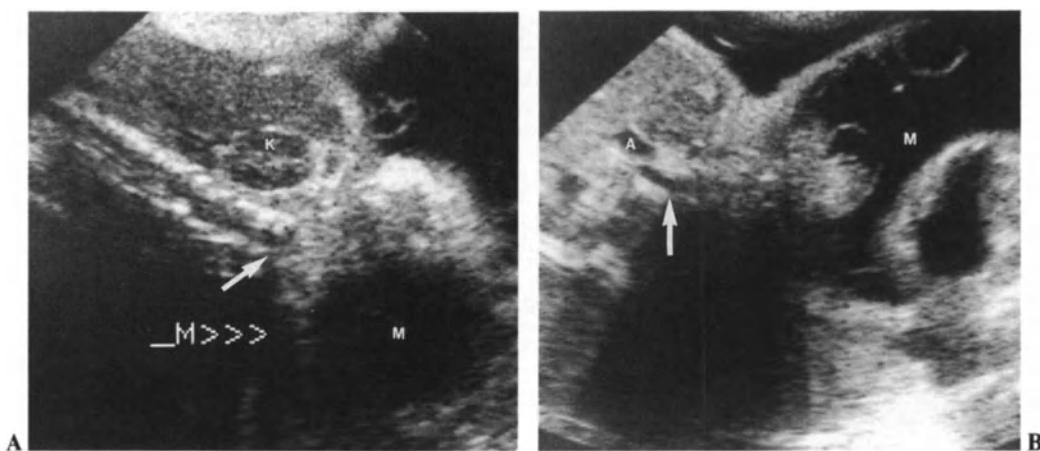


**Fig. 38.25A, B.** Sacrococcygeal teratoma. Coronal, A, and axial, B, images through the lumbosacral spine reveal abrupt termination of the sacral spine (arrow) with a mass protruding posteriorly (M). The mass has both solid and cystic elements and this proved to be a well differentiated teratoma at surgery. K, kidney; A, aorta.

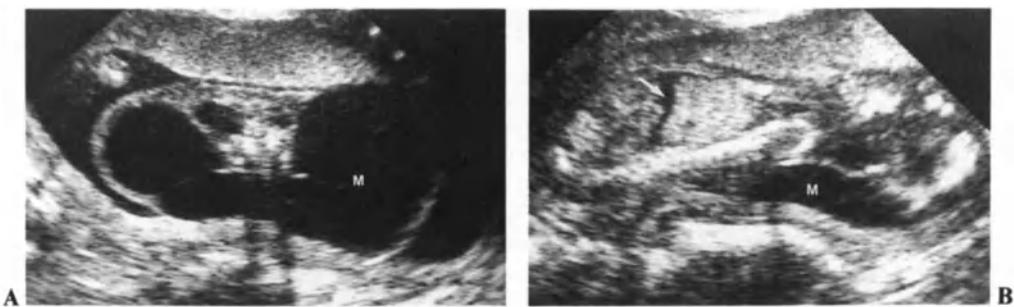


**Fig. 38.26A, B.** Cervical cystic hygroma. Transverse, A, and sagittal, B, sections of the neck of a second trimester fetus with Turner's syndrome (45XO) shows a large cystic mass (M) projecting from the posterior aspect of the neck. The posterior spinal elements are intact differentiating this cystic hygroma from a cervical meningocele. In addition, there is fetal hydrops evidenced by pleural effusions (arrow).

**Cystic adenomatoid malformation (CAM)** also causes an intrathoracic mass and is defined as a congenital hamartoma of the lung. It is caused by arrested connection between the primitive airways and lung parenchyma with overgrowth of terminal bronchioles. The cysts within these masses may be large (up to 10 cm) and thick-walled (Type I); intermediate in size, less than 1.5 cm (Type II); or microcystic with cysts less than 0.5 cm in size (Type III). On ultrasound, Types I and II lesions appear as cystic or solid and cystic masses causing mediastinal shift. Type III lesions present sonographically as large, echogenic, solid masses and the cysts are too small to be resolved. Due to esophageal and caval compression *polyhydramnios* and *fetal hydrops* may develop if the mass is very large. Other intrathoracic masses which may also be detected on prenatal sonography include **bronchogenic cyst**, **neureteric cyst**, **teratoma** (Fig. 38.28), **thoracic meningocele** and **extralobar pulmonary sequestration**. In some cases it may be difficult to distinguish these anomalies from CHD and CAM on the basis of ultrasound alone.

#### Heart

Congenital heart disease is one of the most common fetal congenital anomalies, occurring with a frequency of 8–9

cases per 1000 live births. Every effort is now being made to utilize ultrasound to evaluate the fetal heart in the most detailed manner possible. Not every fetus is a suitable candidate for this time-consuming and expensive study, but the general indications for fetal cardiac ultrasound include *polyhydramnios*, *fetal hydrops*, *cardiac dysrhythmias*, *intra-and extra-cardiac anomalies* picked up on routine scanning, *chromosomal abnormalities* and *symmetric IUGR*. A family history of congenital heart disease or a maternal history of drug or alcohol abuse, viral infection or diabetes should also prompt an in-depth cardiac evaluation. Almost every cardiac anomaly, including complex combinations of several anomalies, can now be reliably diagnosed and a list of anomalies diagnosed in utero is shown in Table 38.7. A complete discussion of each anomaly and the findings on ultrasound is beyond the scope of this chapter, but a few important points should be made.

Fetal **arrhythmias** are commonly noted on routine scanning, and most, such as premature atrial contractions, are usually benign. Other arrhythmias that may be detected include second and third degree A–V block, paroxysmal atrial tachycardia, atrial flutter or fibrillation. Supraventricular tachycardia has a poorer prognosis in utero and may necessitate pharmacological therapy. Any arrhythmia

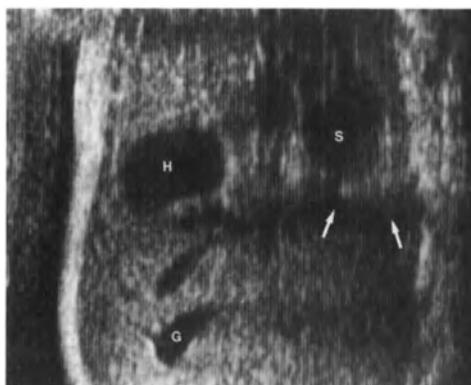


**Fig. 38.27.** Congenital diaphragmatic hernia. Fluid-filled stomach (S) is noted above the diaphragm (arrows) at the same level as the heart (H) on this coronal image. The heart is shifted to the right in this term fetus with a foramen of Bochdalek hernia on the left. The fluid-filled structure below the diaphragm is the gallbladder (G).



**Fig. 38.28.** Mediastinal teratoma. An echogenic mass (M) is interposed between the aorta and the heart (H) on this axial view of the chest of a third trimester fetus. Surgery at birth revealed a mediastinal teratoma.

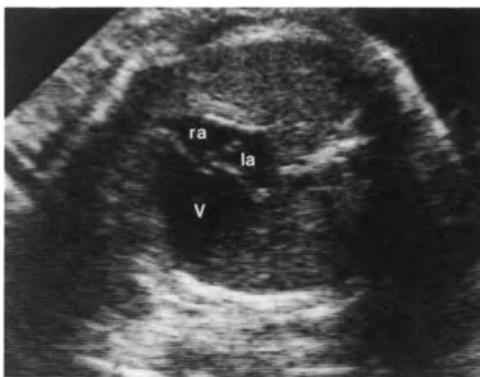


**Fig. 38.29.** Single ventricle. An axial image through the fetal chest reveals a single ventricle (v) without an intraventricular septum and two normal atria (la and ra). This cardiac anomaly was easily identified on routine prenatal scan.

**Table 38.7.** Cardiac anomalies routinely diagnosed on ultrasound

VSD/ASD
Hypoplastic left heart syndrome
Truncus arteriosus
Tetralogy of Fallot
Ebstein's anomaly
Cardiac tumors
Transposition of the great vessels
Valvular atresias/stenoses
Single ventricle/single atrium
Endocardial cushion defects
Endocardial fibroelastosis
Double outlet right ventricle
Hypoplastic right ventricle
Coarctation of the aorta
Dextrocardia
Acardiac
Ectopia cordis

associated with signs of fetal hydrops warrants careful examination for structural cardiac anomalies.

Most of the major cardiac anomalies listed in Table 38.7 can be picked up on routine scanning by distortion of the normal anatomy of the four-chamber view (VSD, endocardial cushion defect, tetralogy of Fallot, truncus, double-outlet right ventricle, single ventricle (Fig. 38.29), cardiac tumors) or marked disproportion of chamber size (hypoplastic left heart syndrome, hypoplastic right ventricle, coarctation of the aorta, aortic stenosis, Ebstein's anomaly (Fig. 38.30)). Also, the relationship of the aorta and pulmonary artery to each ventricle should be noted to allow diagnosis of anomalies such as truncus or transposition. Any fetus in whom an abnormality is suspected on routine scanning should be referred immediately for detailed consultative cardiac examination.

#### Abdomen

Abdominal wall defects which can be diagnosed in utero include omphalocele, gastroschisis, limb-body wall complex and amniotic band syndrome.

Omphalocele results from herniation of abdominal contents into the base of the umbilical cord and is covered by a thin peritoneal membrane (Fig. 38.31).

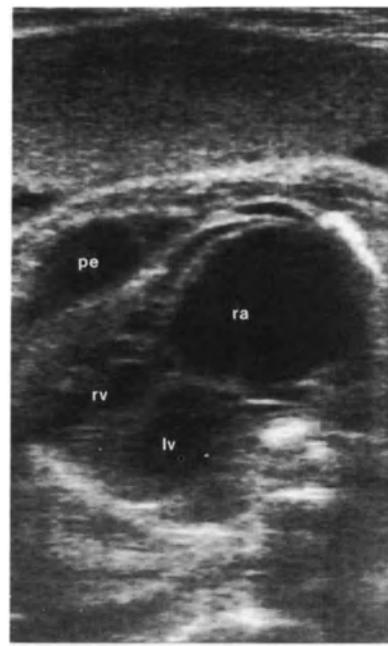


**Fig. 38.30.** Ebstein's anomaly. A magnified axial section of the fetal heart demonstrates a markedly enlarged right atrium (ra) dwarfing the left (lv) and right (rv) ventricles in a third trimester fetus with Ebstein's anomaly. There is a pleural effusion (PE) indicative of fetal congestive heart failure and hydrops.

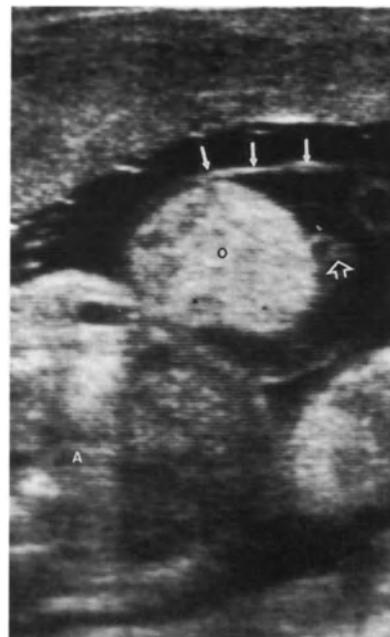


**Fig. 38.31.** Omphalocele. An omphalocele (O) containing homogeneously echogenic liver is surrounded by peritoneal membrane (arrows) on this axial image. The omphalocele contains umbilical vessels (arrowhead) which pass through it. A, abdominal cavity.

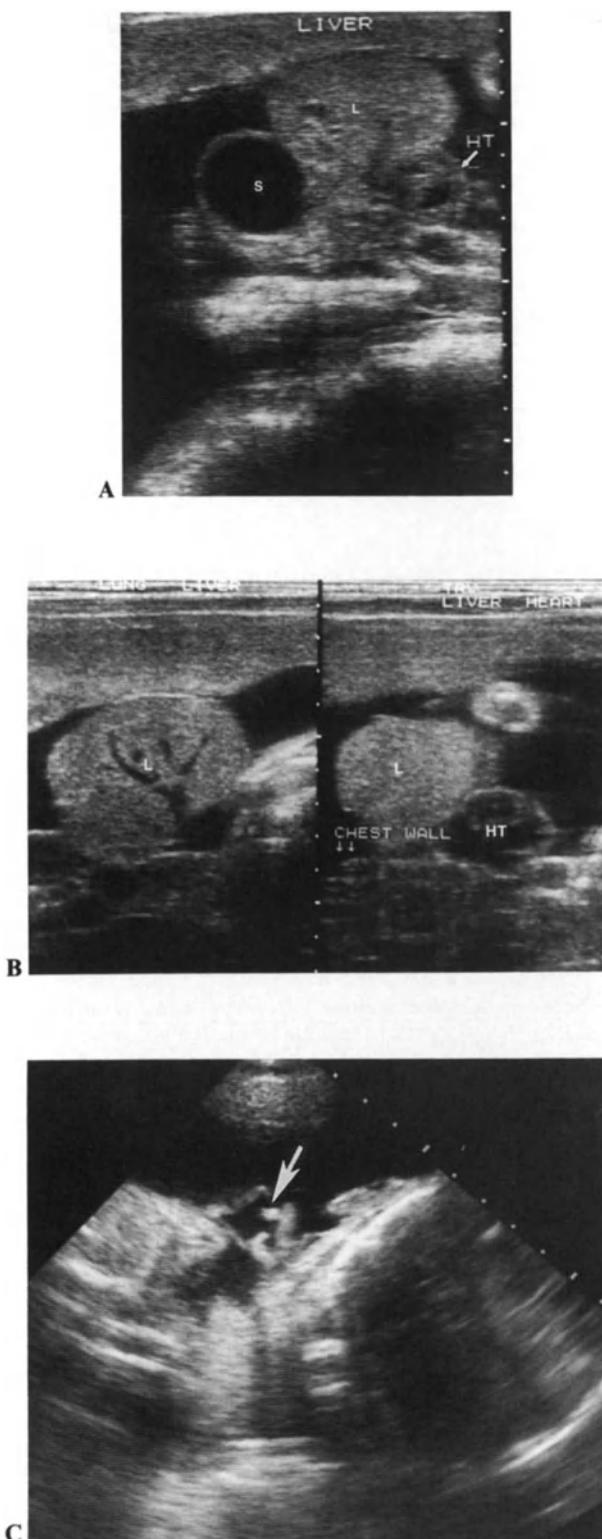


**Fig. 38.32A, B, C.** Amniotic band syndrome. A, B Sagittal scans through the fetal chest and abdominal wall reveal a large defect through which heart (HT), liver (L) and stomach (S) have herniated. No membrane covers the eviscerated organs. C A coronal image through the head and neck of the same fetus reveals a thin membrane around the fetal neck consistent with an amniotic band (arrow). At autopsy, there were numerous amniotic bands adherent to the fetus with evisceration of the heart, liver, stomach and bowel.

**Gastroschisis** results in evisceration of abdominal organs through a defect in the abdominal wall to the right of the cord. The loops of bowel and, rarely, liver in a gastroschisis lie free in the amniotic fluid and are not covered by a membrane; also, the insertion of the umbilical cord into the abdominal wall is normal in gastroschisis. It is important to distinguish between these two anomalies, as omphalocele is associated with other congenital anomalies in 35%–58% of cases, whereas gastroschisis is usually an isolated abnormality.

A lethal constellation of anomalies, called the **limb-body wall complex**, includes a lateral body wall defect with evisceration similar to gastroschisis, NTD, scoliosis and limb anomalies.

Another syndrome which may give rise to abdominal wall defects is the **amniotic band syndrome**. It is caused by rupture of the amnion leading to entanglement and adherence of fetal parts onto the 'sticky' chorion (Fig. 38.32A–C). The site of abnormalities is random and follows no embryological pattern. *Visceral defects* include evisceration of bowel, liver, heart or lungs; *limb defects* involve rings, constrictions or amputations of any part of the limb; and *craniofacial anomalies* include off-axis encephalocele, anencephaly, facial clefts and acrania.

Obstruction of the gastrointestinal tract is one of the major causes of **polyhydramnios** since swallowed amniotic fluid cannot reach the small bowel to be reabsorbed; polyhydramnios is most severe when the obstruction is in the proximal portions of the gastrointestinal tract such as the esophagus or duodenum. **Esophageal atresia** may be suggested on sonography when no stomach can be identified on serial examinations and there is marked polyhydramnios. However, this anomaly is commonly associated with tracheoesophageal fistula, and if the distal esophageal limb communicates with the trachea, a small fluid-filled stomach will be identified. It is rare to see a fluid-distended proximal esophageal pouch on prenatal scanning.

**Intestinal atresias** may be caused by a transverse diaphragm, blind-ending loops with a fibrous band connecting the two-loops, blind-ending loops which are completely separated, or an apple-peel atresia leading to absence of large portions of small bowel. On sonography **duodenal atresia** presents as a 'double bubble sign' which is a fluid-distended stomach and proximal duodenum in the left upper quadrant (Fig. 38.33). Polyhydramnios is a constant feature of the anomaly. Thirty per cent of cases of duodenal atresia occur in *Trisomy 21* and amniocentesis is indicated if this abnormality is suspected. Other causes of prenatal duodenal obstruction may lead to similar sonographic findings and these include *duodenal web*, *Ladd's bands* or *annular pancreas* (Fig. 38.34). When the intestinal atresia occurs in the jejunum or ileum, multiple fluid-filled, dilated small bowel loops will be detected on sonography and cannot be distinguished from other causes of small bowel obstruction in utero, such as *midgut volvulus* (Fig. 38.35).

**Meconium peritonitis** results from the leakage of bowel contents (meconium) into the peritoneal cavity secondary to a bowel perforation. The extruded meconium causes a chemical peritonitis and sonographic findings include *ascites*, *intra-abdominal calcifications* usually on peritoneal surfaces,



Fig. 38.33



Fig. 38.34

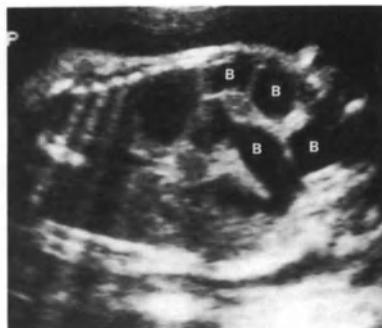


Fig. 38.35

**Fig. 38.33.** Duodenal atresia. An axial scan through the fetal abdomen demonstrates a dilated stomach (*S*) and proximal duodenum (*D*) in a third trimester fetus with duodenal atresia. There is polyhydramnios.

**Fig. 38.34.** Annular pancreas. An axial scan through the abdomen of another fetus shows gastric dilatation (*S*) without duodenal distention. This fetus had an annular pancreas constricting the proximal duodenum without evidence of atresia at surgery.

**Fig. 38.35.** Jejunal atresia. A coronal scan through the abdomen shows multiple loops of dilated, fluid-filled small bowel (*B*) in a third trimester fetus. This bowel obstruction was secondary to an atresia of the distal jejunum.

or persistent *cystic masses* within the peritoneal cavity (Fig. 38.36A, B). Among cases of meconium peritonitis, 25%–40% are associated with meconium ileus in the setting of cystic fibrosis, but the remainder are due to distal small intestinal or colonic obstruction with perforation which may become sealed by adhesions.

#### Urinary Tract

A wide range of urinary tract anomalies can be identified on prenatal ultrasound. The most severe anomaly of the urinary tract is **bilateral renal agenesis**. On the sonography no kidneys are identified in the renal fossae and no urinary bladder is visible on serial examinations. Severe *oligohydramnios* is present after 16 weeks and causes *Potter's sequence* of pulmonary hypoplasia, typical facies and limb anomalies. This is a uniformly fatal anomaly due to absent renal function and pulmonary hypoplasia. **Unilateral renal agenesis** and abnormalities of fusion such as **horseshoe kidney** or **crossed fused ectopia** can also be diagnosed in utero but are

associated with normal renal function and normal amniotic fluid volumes.

**Multicystic dysplastic kidney** may be bilateral, unilateral or segmental and usually results in a cystic kidney with an atretic ureter. The cysts vary in size and little or no normal renal parenchyma is visible on sonography; the cysts usually do not communicate with the renal pelvis (unlike the dilated calyces of a hydronephrotic kidney) (Fig. 38.37). When the process is bilateral, the bladder will not be visualized and oligohydramnios with *Potter's sequence* is the usual result.

**Infantile polycystic kidney disease** causes symmetrically enlarged echogenic kidneys without visible cysts and the bladder is usually poorly visualized. The renal cysts are too small to resolve on ultrasound and therefore the kidneys appear echogenic due to multiple interfaces caused by tiny cysts (less than 1–2 cm in size). In its most severe form, this disease is associated with oligohydramnios and *Potter's sequence*, although in the neonatal and juvenile forms survival into childhood is possible.

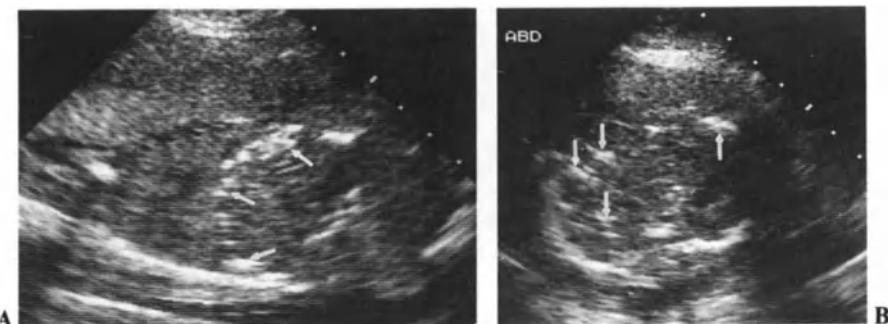


**Fig. 38.36A, B.** Meconium peritonitis. Echogenic calcifications (arrows) are noted along the peritoneal surface of the liver and on loops of bowel on sagittal, A, and axial, B, scans through the fetal abdomen. These are characteristic of meconium peritonitis, although no site of bowel perforation was identified.



**Fig. 38.37.** Multicystic dysplastic kidney. A unilateral multicystic dysplastic kidney (K) is shown on this axial scan through the fetal abdomen. Note that cysts are disorganized and do not radiate from a recognizable renal pelvis, nor is there any visible renal cortex. The contralateral kidney (not shown on this image) was normal.

**Obstructive uropathy** in the fetal period may be caused by *ureteropelvic junction obstruction*, *ureterovesical junction obstruction*, *primary megaureter*, *ectopic ureterocele with hydronephrosis*, *posterior urethral valves*, *massive vesicoureteral reflux* and the *prune-belly syndrome*. The ultrasound appearances of hydronephrosis regardless of the cause include:

1. A dilated renal pelvis, greater than 10 mm in AP diameter

2. Dilated calyces communicating with the renal pelvis
3. Visible rind of renal parenchyma (Fig. 38.38A–C)

In cases of distal obstruction, the dilated ureter may also be identified as a tortuous, fluid-filled, sausage-shaped structure in the fetal abdomen. When bladder outlet obstruction occurs, as in posterior urethral valves, a large, fluid-filled bladder is seen in addition to bilateral hydronephrosis and hydroureter. When oligohydramnios ensues (as in any bilateral renal process) the post-natal prognosis is poor due to the development of Potter's sequence (Fig. 38.39A, B).

Congenital anomalies of the urinary bladder are rare, although **urachal cysts** and **patent urachus** may be identified in utero. When these extend into the base of the umbilical cord they are called **allantoic cysts** (Fig. 38.40). Urachal anomalies are a feature of the **prune-belly syndrome** which includes bilateral hydronephrosis and hydroureter, dilated urinary bladder and protruding abdomen with absent abdominal wall musculature. Other genitourinary anomalies which can be diagnosed on prenatal sonography include **hydrometrocolpos** or **cystic adnexal mass** in females and **hydroceles** (which may be a normal finding) in males.

#### Skeleton

The number and range of severity of **skeletal dysplasias** which can be diagnosed by prenatal ultrasound is enormous

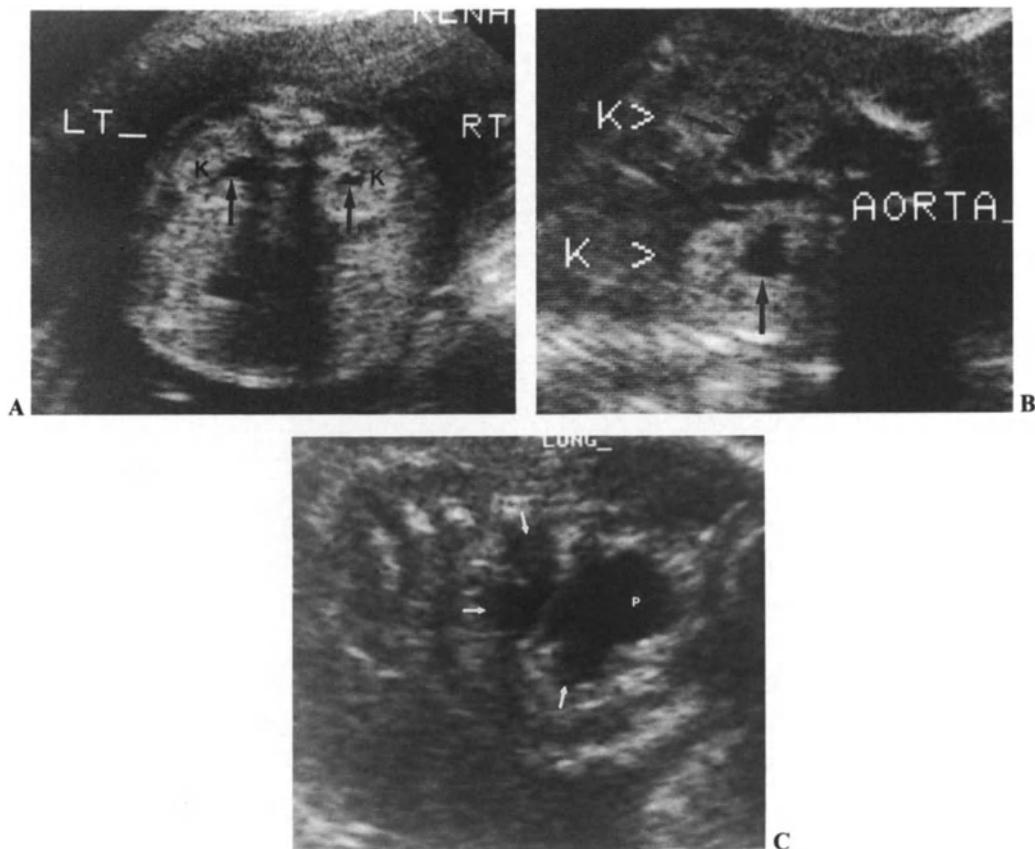


**Fig. 38.38A, B, C.** Hydronephrosis. Bilateral renal pelvic dilatation (greater than 5 mm AP diameter) is demonstrated on axial, A, and coronal, B, scans through the kidney (K) in a third trimester fetus. On prenatal scans only dilated renal pelves were noted, without evidence of dilated calyces. However, on post-natal scan there was bilateral hydronephrosis secondary to bilateral ureteropelvic junction obstruction. A magnified sagittal image, C, through the kidney of another fetus reveals a typical hydronephrosis with fluid-filled renal pelvis (P) and communicating dilated calyces (arrows).

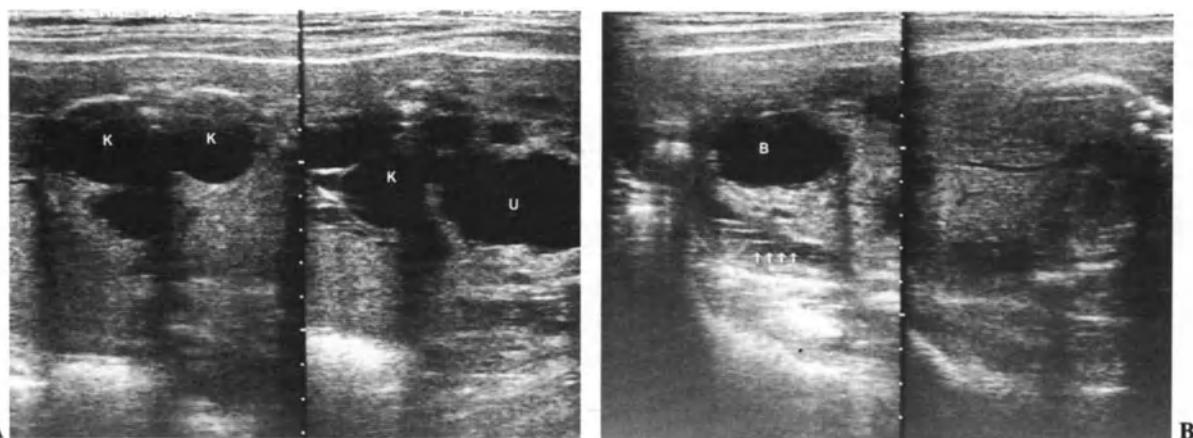


**Fig. 38.39A, B.** Posterior urethral valves. Severe bilateral hydronephrosis (K) and dilated ureters (U) and urinary bladder (B) are demonstrated on axial, A, and coronal, B, images of the abdomen and pelvis in this third trimester male fetus. There is severe oligohydramnios and the fetus died at birth from pulmonary hypoplasia (Potter's sequence).

and a detailed discussion of each disease entity is beyond the scope of this chapter. However, a brief classification of the more commonly encountered skeletal abnormalities will be undertaken.

**Lethal skeletal dysplasias** (those incompatible with extrauterine survival) include *achondrogenesis*, *thanatophoric dwarfism*, *homozygous achondroplasia* and the perinatal types of *osteogenesis imperfecta* and *hypophosphatasia*. **Achondrogenesis** is characterized by severe short limb dwarfism, lack of vertebral ossification and large head with normal calvarium. **Thanatophoric dwarfism**, however, features very short limbs, hypoplastic thorax and associated 'clover leaf' skull.

Another group of skeletal dysplasias is characterized by a small thorax and includes *asphyxiating thoracic dysplasia*, *short-rib polydactyl syndromes*, *campomelic dwarfism* and

*chondroectodermal dysplasia*. The decreased thoracic volume is easily appreciated on prenatal ultrasound in these disorders.

Skeletal dysplasias that are primarily due to impaired bone mineralization include *osteogenesis imperfecta* and *hypophosphatasia*. Both these disorders are characterized by decreased echogenicity of the skull and long bones due to lack of mineralization, multiple fractures and deformities of the long bones, and bell-shaped thorax due to multiple rib fractures.

**Heterozygous achondroplasia** is characterized by short limbs, particularly short femur, although this may not be detectable on ultrasound until the latter part of the second trimester (Fig. 38.41A, B).

**Limb reduction abnormalities** refer to the absence of an entire limb or segment of a limb, and with careful scanning may be picked-up on ultrasound. These include *amelia*

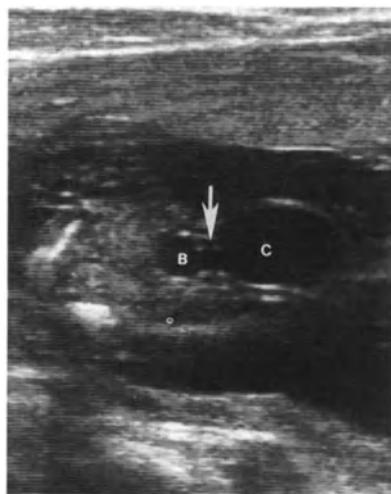


**Fig. 38.40.** Allantoic cyst. A single axial scan through the fetal pelvis reveals a large cyst (C) at the base of the umbilical cord representing an allantoic cyst. It communicates with the urinary bladder (B) by a patent urachus (arrow).

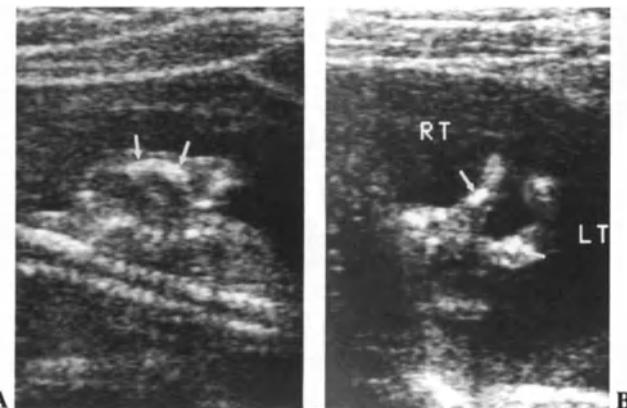


**Fig. 38.41A, B.** Heterozygous achondroplasia. A Severely shortened limbs are noted in this second trimester fetus with heterozygous achondroplasia. A sagittal scan of the humerus (arrow) demonstrates long-bone shortening with curvature but normal mineralization. B Other long bones of the same fetus, such as the femurs (arrows), are extremely short in length.

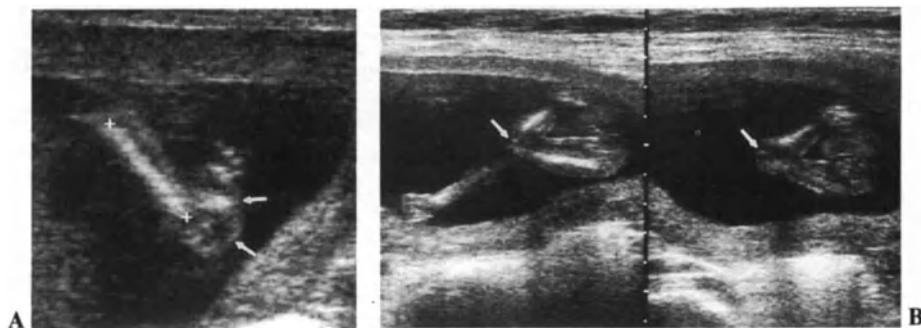


**Fig. 38.42A, B.** Limb deformities. A Sagittal scan through the lower leg reveals an inverted foot (*arrows*) and the metatarsals are visible in the same plane as the tibia (outlined by cursors). This is the typical configuration of clubfoot. B Limb contractures of the lower extremity are noted in this fetus. The knee was consistently flexed (*arrow*) during real-time scanning. This fetus had a syndrome which included multiple flexion contractures.

(absence of a limb or limbs), *hemimelia* (absence of one segment of a limb, i.e., the radius), *phocomelia* (hypoplastic limb), *acheira* (absence of the hands), and *apodia* (absence of the feet).

Subtle anomalies of the limbs can also be diagnosed on prenatal sonography; *clubfoot* (Fig. 38.42A), *congenital limb contractures* (Fig. 38.42B) and *polydactyly* may be detected with careful scanning techniques.

#### Other Fetal Abnormalities

**Hydrops fetalis** results from accumulation of fluid in fetal tissues (anasarca) and serous cavities due to excess total body water. The sonographic features of fetal hydrops include subcutaneous edema (skin thickness greater than 5 mm), ascites, pleural and pericardial effusions, polyhydramnios and thickened placenta (Fig. 38.43A–C). **Immune hydrops**, due to Rh or other blood group incompatibility, is much less common today than is **non-immune hydrops**. The causes of non-immune hydrops are summarized in Table 38.8. It should be noted, however, that 40% of cases are *idiopathic* (no cause is found at autopsy or birth) and another 40% are

due to cardiac congenital anomalies. Only 20% are due to all other causes summarized in Table 38.8.

The fetus that dies during the second or third trimester may also develop hydrops. But if the **fetal death** goes undetected for up to 2 weeks, the fetus will appear macerated with loss of anatomic details. The cranial sutures overlap (Spalding's sign) and the spine and limbs may collapse and become poorly defined. Oligohydramnios may also ensue and the placenta decreases in size.

With modern real-time equipment and careful scanning technique, **multiple gestations** are easily identified on sonography.

Fraternal or *dizygotic twins* are by definition dichorionic, diamniotic and have two separate placentas and a thick intervening membrane on ultrasound. **Monozygotic twins** (identical twins) may be dichorionic, diamniotic (30%), but the majority are monochorionic, diamniotic with a solitary placenta and thin intervening membrane (less than 2 mm in thickness) (Fig. 38.44). Only a small percentage of monozygotic twins are monochorionic, monoamniotic with a solitary placenta and no membrane between the fetuses;

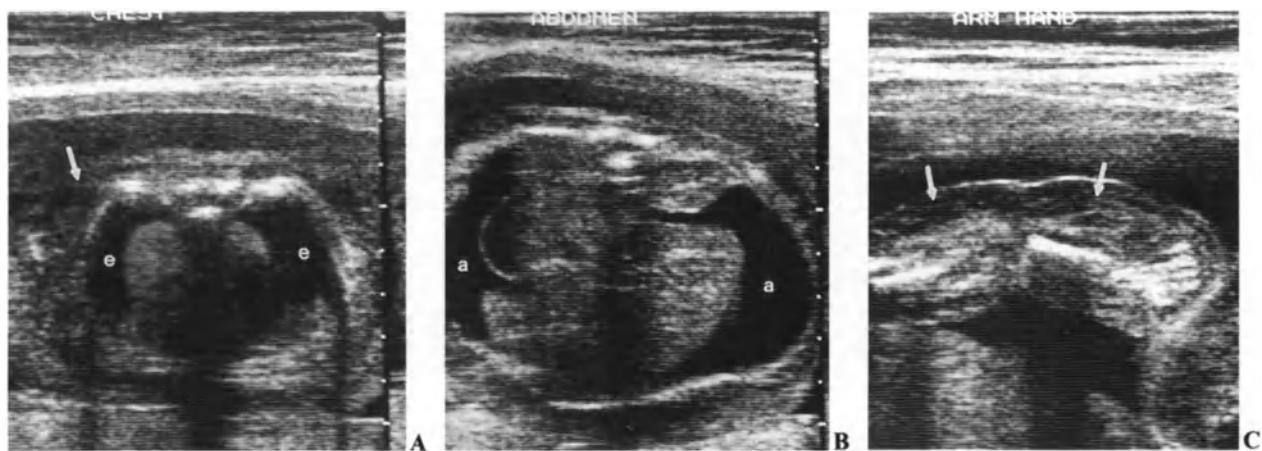


**Fig. 38.43A, B, C.** Non-immune fetal hydrops. A Transverse scans through the fetal chest reveal bilateral pleural effusions (*e*) and skin edema (*arrows*) in the third trimester fetus. B Transverse scans through the abdomen demonstrate ascites (*a*) and skin edema as well in the same hydropic fetus. C Sagittal scans through an upper extremity show marked skin edema (*arrows*). There is polyhydramnios. This fetus had non-immune hydrops secondary to a congenital heart defect and congestive heart failure.

**Table 38.8.** Causes of non-immune fetal hydrops

Hematologic
hemoglobinopathies
fetal blood loss
twin-twin transfusion syndrome
Infections
syphilis
CMV
toxoplasmosis
Cardiovascular
cardiac anomalies
cardiac arrhythmias
A-V malformations
umbilical vein thrombosis
Tumors
hepatic hemangiendothelioma
chorioangioma
congenital neuroblastoma
Pulmonary
lymphangiectasia
cystic hygroma
cystic adenomatoid malformation
Renal
congenital nephrotic syndrome
renal vein thrombosis
Hepatic
hepatic failure
hepatitis
Metabolic
maternal diabetes
Gaucher's disease
achondroplasia
osteogenesis imperfecta
Multiple severe congenital anomalies

this form of twinning has a very high prenatal mortality rate (50%) due to high incidence of cord and fetal entanglement.

*Multiple gestations* with more than two fetuses are also easily identified on sonography, but fetal evaluation during the third trimester may become difficult due to overlap of fetal parts.

Congenital anomalies singular to twin gestations include conjoined twins and twin-twin transfusion syndrome. Con-

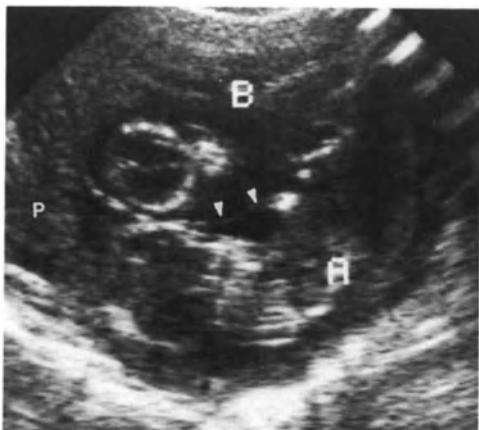


**Fig. 38.44.** Twins. A 12-week monochorionic, diamniotic twin gestation is shown with a solitary placenta (P) and thin intervening membrane (arrowheads). The fetuses are designated A and B.

*joined twins* can be identified on ultrasound when no point of separation can be seen between conjoined parts and the fetuses are in unusual positions (usually facing one another) at all times during scanning. The *twin-twin transfusion syndrome* results from sizable shunts within a monochorionic placenta causing one fetus to 'donate' blood to the other. The 'donor' fetus becomes small and growth-retarded and oligohydramnios develops within its sac. The recipient twin becomes large and may go into high output cardiac failure resulting in fetal hydrops. Also, polyhydramnios develops in the recipient's sac. These features can now be detected on ultrasound and appropriate obstetrical intervention planned depending on the severity of sonographic findings.

### Uterine and Placental Abnormalities

**Placenta previa** occurs when the placenta inserts covering the cervical os. This may lead to placental rupture when the fetal head enters the cervical canal during labor resulting in fatal or near-fatal maternal hemorrhage. It is, therefore, extremely important to make this diagnosis on ultrasound so that Cesarean delivery may be planned. As the uterus enlarges, the placenta commonly moves away from the cervix, so that a placenta previa diagnosed in the first or second trimester should be followed with a third trimester scan to establish persistence of this abnormality. Also a full maternal urinary bladder may appose the walls of the lower uterine segment making the cervix look longer than it really is and giving a false sonographic diagnosis of previa (Fig. 38.45A, B). In this case partial emptying of the bladder or examination with an endovaginal transducer may exclude a false-positive diagnosis.

**Placental abruption** is caused by premature separation of the placenta from the uterine wall, resulting in hemorrhage. The bleeding may occur behind the placenta (retroplacental hematoma), but more commonly occurs between the chorion and the uterine wall (subchorionic hematoma) (Fig. 38.46). Acute hemorrhage appears echogenic or isoechoic with normal placenta but over time the hematoma develops hypoechoic areas due to liquefaction and breakdown of clot.

Rarely, the placenta implants into regions of the uterus deficient in decidua (**placenta accreta**) or may penetrate into the myometrium (**placenta increta**). When the placenta completely penetrates the myometrium, **placenta percreta** results. These anomalies may be suggested on sonography when there is thin or deficient myometrium covering the placenta. Obviously, they pose the threat of maternal hemorrhage at delivery of the placenta.

**Chorioangioma** is the most common placental tumor and it usually arises on the surface of the placenta near the cord insertion. On ultrasound it appears heterogeneous in echo texture and lobulated in contour. If it attains sufficient size fetal circulation may be compromised leading to fetal cardiac failure, hydrops and polyhydramnios.

**Premature dilatation of the cervix** prior to term may lead to spontaneous abortion or premature delivery. A short cervix with protrusion of fetal membranes into the cervical os on transabdominal or endovaginal scan suggests this diagnosis; however, ultrasound is not uniformly reliable in detecting this abnormality due to variability in cervical visualization (Fig. 38.47).

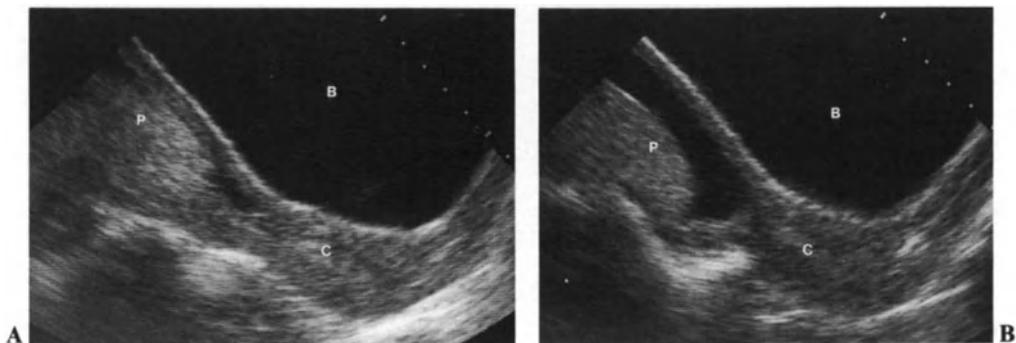


**Fig. 38.45A, B.** False-positive placenta previa. **A** Pre-void sagittal scan through the cervical region (**C**) reveals a placenta (**P**) which covers the cervical os. **B**, bladder. **B** After partial voiding the cervical os (**C**) is now free of placenta (**P**). The very full maternal urinary bladder causes apposition of the walls of the lower uterine segment making the cervix look longer than it actually is. Post-void the lower uterus relaxes allowing an accurate view of the cervix. **B**, bladder.

Other abnormalities of the uterus which may be diagnosed during pregnancy include uterine myomas, congenital anomalies of the uterus and the presence of an intrauterine device.

**Uterine myomas** are usually hypoechoic or heterogeneous in echotexture and they may enlarge during pregnancy (Fig. 38.48). By position they may obstruct labor if they occupy the lower uterine segment and obstruct the cervical os.

**Congenital uterine anomalies** such as bicornuate or septate uterus may be difficult to identify on ultrasound late in gestation, due to compression of the non-gravid horn or uterine septum by the large fetus.

The presence of an **IUD** during pregnancy is easy to locate on sonography in the first trimester, but as the fetus and uterus become larger, the IUD may be pushed to the peripheral portions of the uterus and may be difficult to find in the third trimester. Sonography can also be used to assist in IUD removal in the pregnant patient.

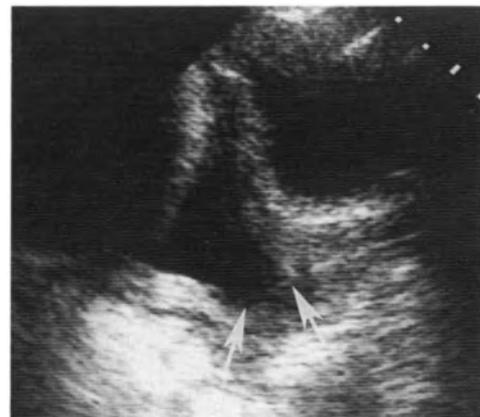


**Fig. 38.47.** Incompetent cervix. A dilated cervix (arrows) with membranes and amniotic sac bulging through it is shown on sagittal scans. This resulted in premature rupture of the membranes and premature delivery.



**Fig. 38.46.** Subchorionic hemorrhage. Sagittal image through the gravid uterus in the second trimester reveal a hypoechoic collection (**H**) representing a subchorionic hemorrhage in a patient presenting with vaginal bleeding. The hemorrhage is separate from the placenta (**P**) and lies just deep to the echoic chorionic membrane (arrows). The hemorrhage resolved spontaneously with a good obstetrical outcome.

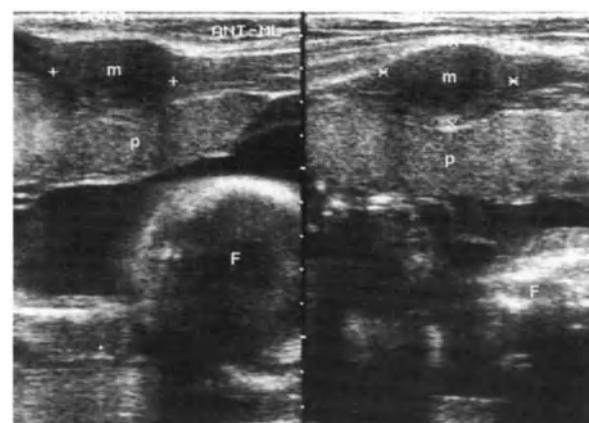


**Fig. 38.48.** Retroplacental myoma. A myoma (**M**) is noted posterior to the placenta (**P**) in this second trimester gestation. Note that the myoma is hypoechoic and heterogeneous, a typical picture of a fibroid during pregnancy. **F**, fetal parts.

## REFERENCES AND SUGGESTIONS FOR FURTHER READING

- Benson CB, Jones TB, Lavery MJ, Platt LD (1988) *Atlas of Obstetrical Ultrasound*. JB Lippincott, Philadelphia
- Callen PW (ed) (1988) *Ultrasonography in Obstetrics and Gynecology*. WB Saunders, Philadelphia
- Chadleigh P, Pearce JM (1986) *Obstetric Ultrasound*. Churchill Livingstone, Edinburgh
- Fleischer AC, James AF (1989) *Diagnostic Sonography, Principles and Clinical Application*. WB Saunders, Philadelphia
- Hansmann M, Hackeloer B-J, Staudach A (1986) *Ultrasound Diagnosis in Obstetrics and Gynecology*. Springer-Verlag, Berlin
- Hobbins JC, Winsberg F, Berkowitz RL (1983) *Ultrasonography in Obstetrics and Gynecology*. Williams & Wilkins, Baltimore
- Romero R, Pilu G, Jeanty P, Ghidini A, Hobbins JC (1988) *Prenatal Diagnosis of Congenital Anomalies*. Appleton and Lange, Norwalk, Connecticut
- Saunders RC, James AE (eds) (1985) *The Principles and Practice of Ultrasonography in Obstetrics and Gynecology*. Appleton and Lange, Norwalk, Connecticut
- Sarti DA (ed) (1987) *Diagnostic Ultrasound, Text and Cases*. Year Book, Chicago

---

**PART 6**  
**CNS and Skull**

---

## CHAPTER 39

# THE CENTRAL NERVOUS SYSTEM: METHODS, CONGENITAL LESIONS

*D. Sutton*

---

### METHODS OF EXAMINATION

The following imaging methods are currently used to examine the CNS.

1. Simple radiographs and tomography
2. CT
3. MRI
4. Arteriography
5. Myelography
6. Ultrasound

**Choice of technique.** Where CT and MRI are available they are now the imaging methods of choice for investigation of most neurological lesions. Pneumography and radioisotopes, once widely used by neuroradiologists are now obsolete and the use of simple radiographs has declined.

Angiography and myelography are also less widely used since the development of CT and MRI though their use in

interventional neuroradiology and in computed myelography (CM) has grown in recent years.

Ultrasound is extremely valuable for the investigation of the brain through the fontanel (Fig. 39.1) but is little use in older patients except in an open operative technique or for duplex imaging of neck vessels.

Disorders of the skull and brain will be considered sequentially under the following headings: congenital lesions, neoplasms, vascular lesions, infections and infestations, trauma, white matter diseases, degenerative disorders and metabolic disorders.

### CONGENITAL LESIONS

#### Lesions Affecting the Skull

These are listed below and are readily shown by simple radiography.

- Craniosynostosis
- Lacunar skull
- Meningocele and encephalocele
- Congenital dermal sinus
- Platybasia
- Basilar invagination (basilar impression)
- Cleidocranial dysostosis
- Fragilitas ossium
- Congenital parietal foramina
- Sinus pericranii
- Hypophosphatasia

**Premature Craniosynostosis.** The cranial sutures normally remain open into adult life. Partial closure begins about the age of 22 years and proceeds into later decades, though there is considerable individual variation. Premature cranio-



Fig. 39.1. Coronal ultrasound showing congenital hydrocephalus. (Courtesy of Dr Keith Dewbury.)



Fig. 39.2. Scaphocephaly. Lateral skull film.

synostosis usually occurs *in utero* and is present at birth; less commonly it develops in infancy or in early childhood. All forms are commoner in males than in females.

The suture primarily involved determines the resultant shape of the head. Using Greek terminology the different shapes have been labeled as follows.

1. *Microcephaly* results from generalized fusion of the sutures and is normally associated with mental defect.

2. *Scaphocephaly* ('boat shaped' from the resemblance of the vault to the long narrow keel of a boat) is the commonest form of premature craniostenosis and involves the sagittal suture. Apart from the odd shape of the skull it is usually asymptomatic (Fig. 39.2).

3. *Turricephaly*, *oxycephaly* or *acrocephaly* are all descriptive terms for the 'tower' or 'turret' shaped brachycephalic skull (Fig. 39.3A) resulting from premature fusion of the coronal and lambdoid sutures. Proptosis occurs because of the shortened anterior fossa and raised intracranial pressure with papilledema and optic atrophy may also occur.

Several rare syndromes may be associated with acrocephaly. *Apert's syndrome* (acrocephalosyndactyly) is characterized by the presence of syndactyly (Fig. 39.3B) and maxillary hypoplasia, whilst *Carpenter's syndrome* (acrocephalopolysyndactyly) includes polydactyly and clinodactyly with syndactyly, as well as obesity and mental retardation. Other variant forms of acrocephalopolysyndactyly have also been described.

*Crouzon's craniofacial dysostosis* in an autosomal dominant disease with acrocephaly, hypertelorism, maxillary hypoplasia, parrot beak nose and prognathism leading to a characteristic facies.

4. *Plagiocephaly* or asymmetrical skull results from asymmetrical fusion of sutures with a varying degree of resultant deformity.

5. *Trigonocephaly* ('triangular skull') results from intrauterine fusion of the metopic suture leading to a pointed forehead.

**Lacunar Skull.** This condition is found in infant skulls and develops *in utero* in the membranous part of the skull vault. It is characterized by multiple oval pit-like depressions of the inner table separated by ridges of thicker bone. These markings begin to fade in the perinatal period and disappear by 4 to 6 months. There are usually associated anomalies of the central nervous system, most commonly myelomeningocele or encephalocele. These may occur with hydrocephalus due to aqueduct stenosis or the Chiari Type 2 malformation (see below). Because of the associated anomalies there is a high mortality.

**Meningocele and Encephalocele.** These present in infancy usually as midline herniations in the parieto-occipital or frontal regions. Less commonly they may be seen in the mid-parietal region, and very rarely lateral to the midline. There is an abnormal defect in the skull vault beneath the lesion and diagnosis is usually clinically obvious.

Rarely the lesion may be found in the *frontonasal* region, and can protrude into the nasal cavity presenting with nasal

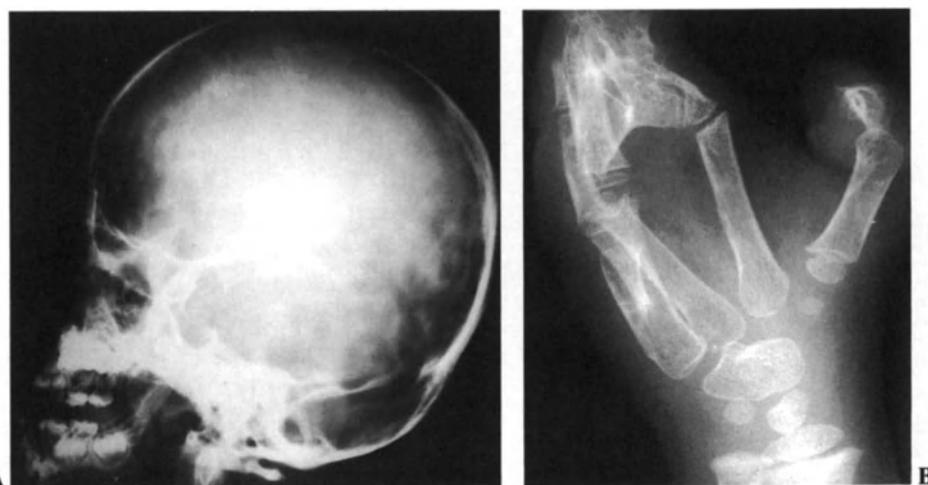


Fig. 39.3. A Turricephaly. Lateral skull film in child with Apert's syndrome. B Syndactyly in Apert's syndrome.

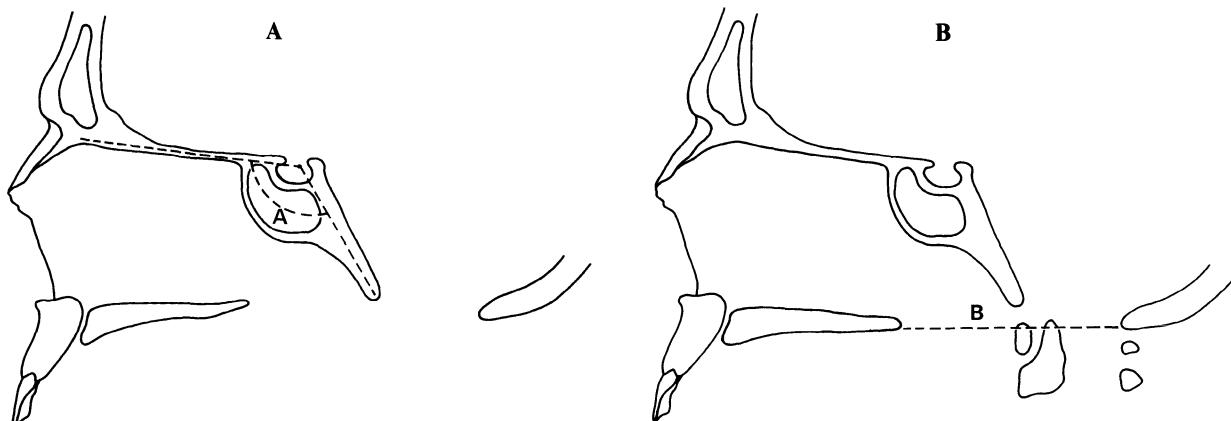


Fig. 39.4A, B. Diagram to show A Basal angle, B McGregor's line (see text).

obstruction. The latter lesion can also be associated with a cleft palate or with hypertelorism. A basal view of the skull may show a central defect in the sphenoid or sphenoethmoid region, and a lateral view will show a soft tissue mass in the nasopharynx. CT or MRI will confirm the true nature of the mass, and prevent an uninformed and potentially catastrophic surgical intervention.

An unusual form of meningocele may occur in *neurofibromatosis* associated with a congenital defect in the greater wing of the sphenoid. This permits herniation into the orbit resulting in proptosis (see Fig. 39.22).

With lesions of the skull vault the bony defect shows tapering of the bone affecting mainly the inner table, and curving out to meet the outer table. Problems in differential diagnosis can arise with small untreated lesions presenting in older children or adults. This is particularly so with the lateral parietal type, where small encephaloceles have been surgically excised as 'sebaceous cysts' with disastrous results. Sebaceous cysts involving the skull vault usually have no underlying defect or affect the outer table by pressure. Other lesions which enter into the radiological differential diagnosis usually affect both tables of the vault, and can be readily distinguished on clinical grounds.

**Congenital Dermal Sinus.** These may be found in the occipital region, and point downwards. They produce a midline tubular elongated defect in the bone with a corticated margin, an appearance suggestive of the diagnosis. The track may lead down to or through the meninges into the brain and terminate in a posterior fossa dermoid (see Figs 40.37, 40.39, p. 744).

**Platybasia.** This term is used to denote flattening of the base of the skull. The '*basal angle*' is defined as the angle between the plane of the clivus and the plane of the midline of the base of the anterior fossa measured from the nasion to the *tuberculum sellae* (Fig. 39.4A). The measurement, widely used by anthropologists and comparative anatomists, is easily obtained from a lateral skull film.

In man the skull has a basal angle between 115° and 143°, whilst in other primates it measures over 150°, and in most other mammals it is near 180°. Platybasia is therefore defined as a skull with a basal angle greater than 143°.

Isolated platybasia may be symptomless and of no clinical importance. However it may be associated with *mongolism* and has also been described following suboccipital craniotomy in childhood.

The term is sometimes wrongly used to include *basilar invagination* (*basilar impression*), a condition with which it is commonly but not always associated.

*Basilar impression* may be *congenital* as when it occurs together with anomalies of the craniocervical junction such as atlanto-occipital fusion or with Klippel-Feil syndrome. The *foramen magnum* may be abnormal in shape and size. Such cases may also be associated with congenital CNS malformations, particularly the Chiari Type 2 anomaly.

*Basilar invagination* also occurs with *diseases causing softening of bone*. The commonest of these is *Paget's disease*, but the condition is also seen with *rickets*, *scurvy*, *fragilitas ossium* (Fig. 39.5), *cleidocranial dysostosis* (Fig. 39.7) and rarely with *hyperparathyroidism*. *Basilar invagination* may result in neurological symptoms from pressure of the dens or tight dura on the medulla or upper cervical cord, and hydrocephalus can also result.

As already noted platybasia may be symptomless, but neurological symptoms due to the associated lesions mentioned above are frequently seen with basilar impression. The associated CNS abnormalities are best characterized with sagittal MRI sections (see Fig. 39.7), but can also be well shown by CT (Figs 39.5, 39.6).

Many measurements have been used in the past to define platybasia and basilar invagination. The basal angle has been described above. Chamberlain's line, Bull's line, and McGregor's line have all been used to decide whether the relationship of the dens or *foramen magnum* to the base of the skull are normal. McGregor's line is illustrated in Fig. 39.4B. AP tomograms through the plane of the atlanto-occipital joints will also help decide whether there is invagination of the *foramen magnum*.

**Congenital Parietal Foramina.** Large posterior parietal parasagittal bone defects, nearly always bilateral and symmetrical, are occasionally seen on a routine skull radiograph. They can be up to 2 cm or more in diameter but are of no pathological significance though they may be familial.



**Fig. 39.5.** Computed myelography in a patient with fragilitas ossium and basilar invagination. Coronal and sagittal reformat sections showing bony relationships to brainstem.



**Fig. 39.7.** Basilar invagination in a patient with cleidocranial dysostosis. Sagittal MRI section, T<sub>1</sub>-weighted, clearly shows upward displacement of anterior arch of atlas and dens impinging on and deforming brainstem. (Courtesy of Dr Gordon Thomson and Bristol MRI centre.)

More frequently a tiny foramen is found in the same position, and is the site where a small emissary vein passes through the skull vault.

**Sinus Pericranii.** A small midline defect is sometimes seen in the frontal bone where a small emissary vein passes through.

**Cleidocranial Dysostosis.** The bone lesions of this disorder have been described in detail in Chap. 14. The skull lesions consist of persistence of the metopic suture and anterior fontanel, wide sutures with delayed closure, multiple Wormian bones, small facial bones and delayed dentition, and basilar invagination (Fig. 39.7).

**Osteogenesis Imperfecta.** This condition is described in Chap. 14. There is poor mineralization of the skull vault with wide sutures and multiple Wormian bones along the sutures. As already noted basilar invagination may result.

**Hypophosphatasia.** This is due to an inborn error of metabolism and is also described in Chap. 14. Some 50% die in

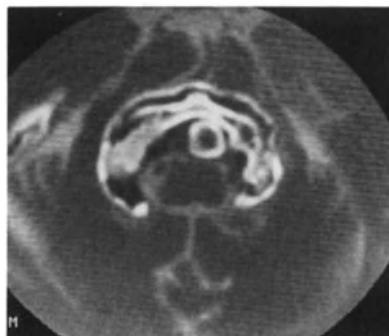


**Fig. 39.6.** Axial section showing relationship of atlas and dens to intracranial structures in same patient shown in Fig. 39.5.

early infancy, but others survive and present in later infancy or childhood. The young infant skull is poorly mineralized and the sutures seem abnormally wide with irregular margins. Later premature fusion of the sutures and craniosynostosis with brachycephaly may be seen. Cases seen in adult life show features of osteomalacia.

#### Lesions Affecting the Brain

Congenital lesions affecting the brain are listed below (Table 39.1). Most are well demonstrated by CT or MRI.

**Meningocele and Encephalomeningocele.** These lesions are usually obvious clinically though, as noted above, small

**Table 39.1.** Congenital lesions affecting the brain

Meningocele and encephalomeningocele
Macrocephaly
Hemimegalencephaly
Chiari malformations
Aqueduct stenosis
Dandy–Walker syndrome
Arachnoid cyst
Ependymal cyst
Septal agenesis
Septo-optic dysplasia
Cyst of the septum pellucidum
Cyst of the cavum vergae
Agenesis of the corpus callosum
Lipoma of the corpus callosum
Coarctation of the frontal horn
Porencephaly
Schizencephaly
Hydranencephaly
Holoprosencephaly
Lissencephaly
Heterotopic grey matter
Phakomatoses

lesions of the vault or larger lesions involving the skull base and nasopharynx can be misdiagnosed with potentially disastrous results.

The skull defects visible at simple radiography have been described above. The nature and extent of the cerebral deformity, particularly with basal meningocele, can be clearly defined by CT or MRI before surgical intervention.

**Macrocephaly (Megalencephaly).** Pathologically this is defined as a brain weighing more than 1800 g. Such brains may be structurally normal, but more frequently there is a diffuse glial proliferation or a pathological process. The latter include *cerebral lipidoses*, *spongy degeneration of the white matter* and *Alexander's disease*. The condition may also be seen in *tuberous sclerosis*.

In infants or children presenting with large heads the primary differentiation is from hydrocephalus. Ultrasound in infants will readily confirm hydrocephalus and in older children CT or MRI will differentiate and elucidate other pathological processes.

**Hemimegalencephaly.** In this condition enlargement of the skull is unilateral and confined to the vault. The asymmetrical skull is secondary to a congenital unilateral enlargement of the brain, and is associated with fits, hemiplegia and hemianopia. Pathologically there is thickening of the grey matter and increase of the white matter with abnormal shallow sulci on the affected side. The ventricle on this side is also enlarged.

The brain lesions are well shown by CT or by MRI.

**Chiari Malformations.** These were originally described by Chiari in 1891 and 1896, and were labeled Types 1 to 4 in degrees of deformity. Types 3 and 4 have the major deformities with cerebellar hypoplasia and downward displacement of the brainstem and a high cervical or occipital encephalocele.

Type 2 also presents in neonates or infants usually with a dorsilumber myelomeningocele. The associated brain deformities consist of caudal herniation of the medulla and vermis with a caudally displaced and elongated 4th ventricle. A backward kink may be seen at the caudally displaced junction of cervical cord and medulla.

There are also various other malformations of the brain. These include hypoplasia or absence of the falx and tentorium with interdigititation of the cerebral hemispheres; absence of the corpus callosum with forward pointing of the frontal horns; deformity of the midbrain (*dorsal beaking*); enlargement of the cerebellar vermis and forward protrusion of the cerebellar hemispheres as pointed projections around the brainstem; gyral malformations, and other lesions.

Many of these brain deformities can be identified by CT or MRI, and some by neonatal ultrasound. Simple radiography may show a lacunar skull and forward bowing of the petrous bones and clivus.

Type 1 is the least obvious clinically and may not be diagnosed till adult life. It consists merely of tonsillar herniation through the foramen magnum with or without varying degrees of cerebellar ectopia and usually with a normal 4th ventricle. Slight downward herniation of the tonsils (up to 3 mm) can be regarded as a normal variant, but greater degrees (usually 10–15 mm) are seen with this malformation.



Fig. 39.8. Tonsillar ectopia clearly shown by sagittal MRI section, T<sub>1</sub>-weighted. There is an associated syringomyelia extending up to C2. (Courtesy of Dr Gordon Thomson and Bristol MRI centre.)

**Syringohydromyelia** (see p. 808) is associated with the condition in up to 70% of cases. The patients do not present clinically till adult life when the symptoms and signs of syringomyelia develop; less typically symptoms suggesting involvement of the lower cranial or cervical nerves are seen and very rarely patients present with hydrocephalus. Bony anomalies of the craniocervical junction are present in some 5% of cases, particularly assimilation of the atlas.

**Imaging.** The diagnosis is best confirmed by MRI which also shows the syrinx non-invasively (Fig. 39.8). CT will show the tonsillar ectopia well, but computed myelography with delayed films is necessary to show the syrinx (Fig. 44.19).

**Aqueduct Stenosis.** In this condition there is a congenital stenosis or obstruction of the aqueduct which results in hydrocephalus involving the third and lateral ventricles. Whilst this usually presents in infancy or childhood, the condition is occasionally diagnosed in adults. In all cases it is necessary to exclude obstructive hydrocephalus due to a local tumor or ependymitis. There is also a recognized association with neurofibromatosis.

**Imaging.** The diagnosis can be made by CT but is more elegantly shown by sagittal MRI sections through the aqueduct (Figs 39.9, 39.10). Hydrocephalus is present involving the lateral and third ventricles and the mouth of the aqueduct is dilated in a bell-like or trumpet-like manner, while the lower aqueduct and 4th ventricle appear normal. There is no evidence of a mass lesion in the brainstem or posterior fossa.

**Dandy-Walker Syndrome.** In this condition there is a more-or-less complete membranous obstruction to the foramina of Magendie and Luschka which causes cystic dilatation of the 4th ventricle. The lesion may occur on its own or in association with other congenital anomalies such as

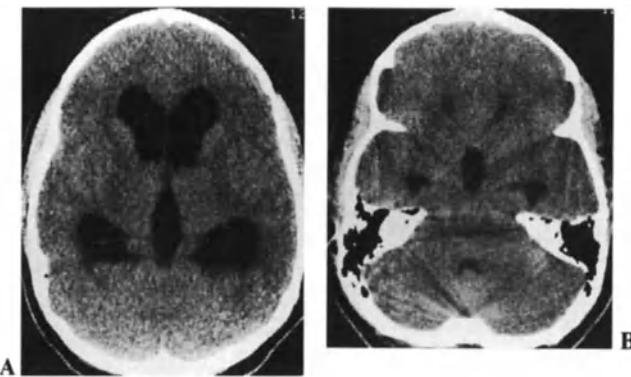


**Fig. 39.9A, B.** Aqueduct stenosis shown by CT. A Section showing grossly dilated lateral and third ventricles. B Section showing dilated third and normal sized fourth ventricles.

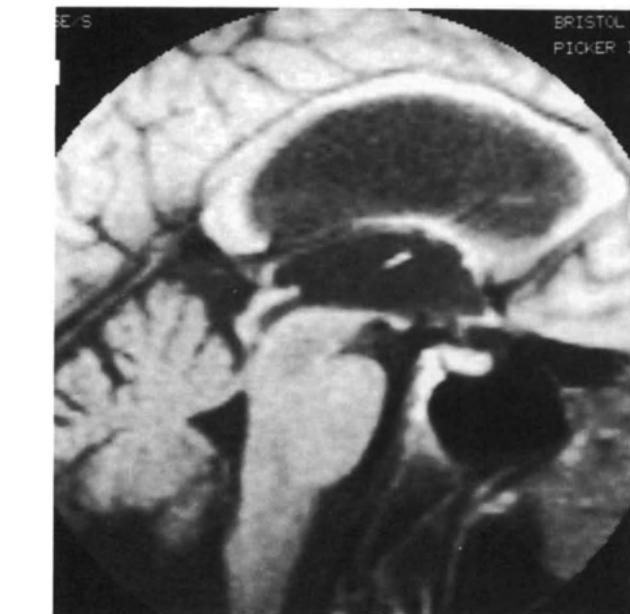
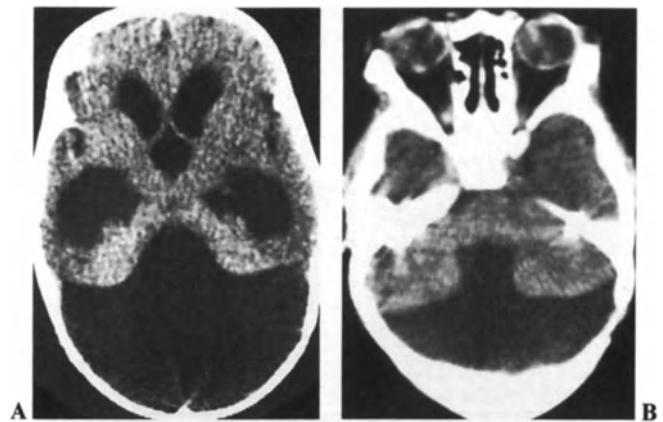


**Fig. 39.10.** Aqueduct stenosis. Midline sagittal MRI section ( $T_1$ -weighted) shows upper part of aqueduct and third ventricle dilated with normal sized lower aqueduct and fourth ventricle. The stenosis is lower in the aqueduct than is usual in these cases. (Courtesy of Dr Gordon Thomson and Bristol MRI centre.)

**Fig. 39.11.A, B** Dandy-Walker syndrome shown by CT. Hydrocephalus with giant cystic fourth ventricle and cerebellar hypoplasia. **C** Coronal ultrasound study in an infant shows the posterior fossa below the tentorium occupied by a giant Dandy-Walker cyst which has been shunted. (Courtesy of Dr Keith Dewbury.)

meningocele or defects in the corpus callosum. The cerebellum may be dysplastic and in severe cases its hemispheres are vestigial and the grossly dilated 4th ventricle extends up to and above the tentorium and thins the occipital bone. There is also hydrocephalus with dilatation of the ventricles above the 4th.

**Imaging.** CT or MRI shows the anatomical features described and permits an immediate diagnosis, (Fig. 39.11A, B). Differential diagnosis from an arachnoid cyst, a giant cisterna magna or a gliomatous cyst is normally easy with

the presence of a normal or small 4th ventricle as a key distinguishing feature. The dysplastic cerebellum in Dandy-Walker syndrome also helps to distinguish the condition. In infants the diagnosis may be made by ultrasound (Fig. 39.11C).

**Arachnoid Cyst.** Arachnoid cysts are intracranial but extracerebral. They may be found anywhere around the brain, but are seen particularly in the middle and posterior cranial fossae, in the suprasellar region and behind the 3rd ventricle. They contain clear fluid indistinguishable from cerebrospinal fluid and are lined by arachnoid tissue. This helps to distinguish them from post-traumatic lesions such as subdural hygromas and from post-inflammatory loculations.

They usually present in children, particularly if large enough to produce a mass effect, or hydrocephalus. There

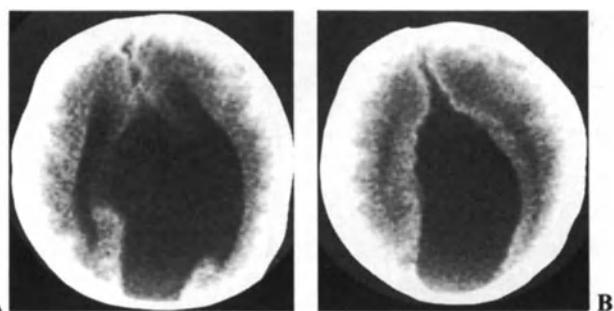


Fig. 39.12A, B. Large interhemispheric arachnoid cyst displacing both hemispheres and lateral ventricles.

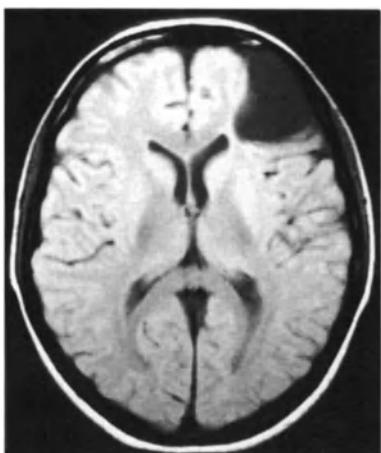


Fig. 39.13. Arachnoid cyst shown by MRI (proton density). (Courtesy of Dr Gordon Thomson and Bristol MRI centre.)

may be hypoplasia of underlying cerebral tissue such as the temporal pole, considered by some to represent a coexistent congenital malformation and by others to be secondary to the mass effect. Symptomless cases are sometimes found coincidentally at CT or MRI examination of adults for other lesions. In neonates or small infants the cysts may be diagnosed by ultrasound, but in older children or adults they are diagnosed by CT or MRI. They usually lie in one of the classical sites mentioned above, are of CSF density, and have no enhancing capsule or adjacent calcification (Figs 39.12, 39.13, 39.14).

**Ependymal Cyst.** These very rare cysts are lined by a thin wall of ependyma and can be intra- or paraventricular. The latter can resemble a hydatid cyst at CT and show no marginal enhancement. The former if large can resemble unilateral hydrocephalus since they usually occur in the lateral ventricle and the wall is difficult to define at CT. Intrathecal or intraventricular contrast has been used to establish a diagnosis, by outlining the cyst within the opacified ventricle.

**Septal Agenesis.** This can occur as an isolated lesion giving rise to a single ventricle communicating across the midline. A similar situation can arise in severe hydrocephalus following rupture of the septum. Both conditions are readily identified at CT or MRI.

**Septo-optic Dysplasia (*De-Morsier's disease*).** This is characterized at CT by absence of the septum pellucidum with squaring of the frontal horns and with a large chiasmatic cistern. The child has poor vision because of the hypoplastic chiasm and optic nerves, and retarded development.

**Cyst of the Septum Pellucidum.** The double septum or 5th ventricle is due to the abnormal persistence of the fetal cavum septi pellucidi. This can be demonstrated by ultrasound to be present in over one third of neonates,

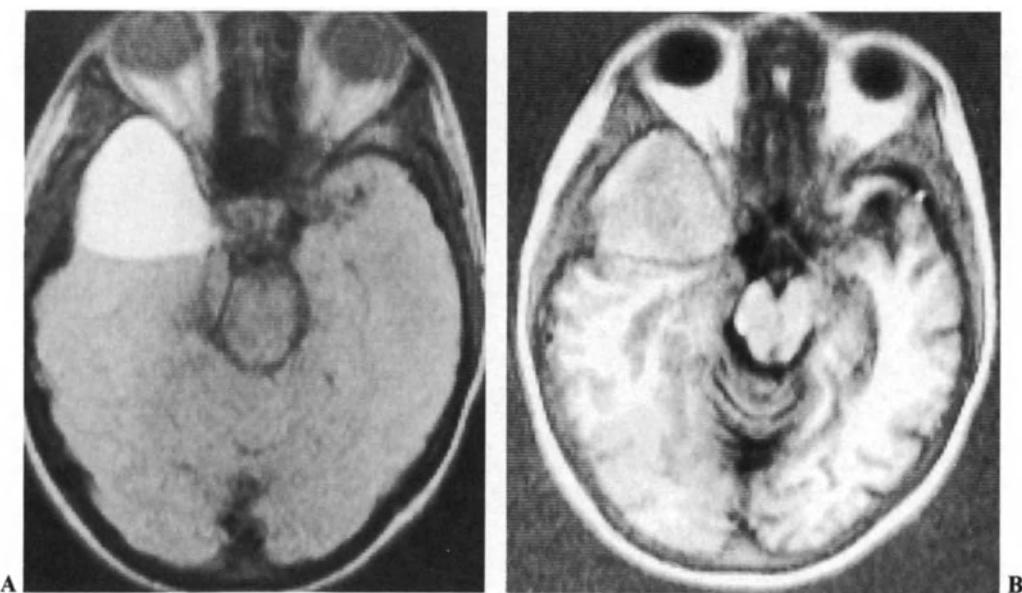
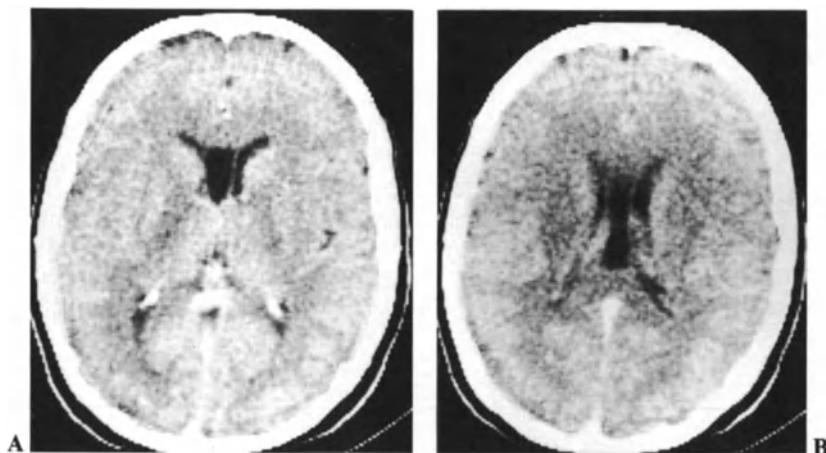


Fig. 39.14A, B. Anterior temporal arachnoid cyst shown by MRI. A High signal on T<sub>2</sub>-weighted study. B Moderately high signal on T<sub>2</sub>-weighted study suggests hemorrhage into cyst.



**Fig. 39.15.** A Cyst of septum pellucidum shown by CT. B Cyst of cavum vergae in same patient extending backwards and upwards between the ventricular bodies and continuous with the septal cyst.

though the incidence falls rapidly through childhood. Nevertheless the condition persists in a small percentage of adults, and is frequently seen as a chance finding at imaging (Fig. 39.15A).

**Cyst of the Cavum Vergae.** This represents the so-called 6th ventricle and is a backward extension of the septal cyst, though much less commonly seen. Anatomically it lies beneath the posterior part of the corpus callosum above and the velum interpositum below. On axial CT sections the cavum vergae appears as a rectangular structure continuous with a septal cyst anteriorly, both being of CSF density (Fig. 39.15B). It should not be confused with the normal velum interpositum which is also of CSF density and lies above the third ventricle. The latter is frequently seen at CT, but is tri-

angular in shape with the apex lying anteriorly, and contains the enhancing internal cerebral veins.

**Agenesis of the Corpus Callosum.** This may be partial or, less often, complete. It may occur as an isolated finding, or in association with other malformations.

At CT complete agenesis is characterized by wide separation of the medial borders of the lateral ventricles with a high third ventricle extending up between them and also enlargement of the occipital horns. Partial agenesis usually involves the posterior part and the anterior part may remain normal.

MRI shows similar feature on axial or coronal sections but a midline sagittal section (Fig. 39.16) shows the lesion more clearly with the high 3rd ventricle extending up into and above the position of the absent corpus callosum. A lipoma may sometimes be found at the site of the absent corpus callosum (see below).

**Lipoma of the Corpus Callosum.** Intracranial lipomas are rare tumors which occur mainly in relation to the corpus callosum, but can also occur in the suprasellar and pineal areas. They may lie above a normal corpus callosum but can be associated with partial or complete agenesis. There is often marginal calcification where they merge with adjacent cortical tissue; this can be of a characteristic 'brackets' type which occasionally permits diagnosis from a simple PA radiograph. A large lesion may also produce an area of increased radiolucency between the brackets.

Their typical situation together with their fatty density makes these lipomas readily identifiable at CT or MRI. Adjacent calcification is best seen at CT (Fig. 39.17), but this may be minimal or absent with small lesions.

**Ventricular Coarctation.** In this rare condition the frontal horns fail to develop normally and the lateral and medial walls appear adherent or apposed due to ependymal fusion. The rest of the ventricular system is normal. Its importance lies in recognizing its congenital nature when seen as a chance finding at imaging, and in not mistaking the deformity for the effects of compression by a local tumor.

**Porencephaly.** Porencephaly has been classified as congenital or acquired. The *congenital* form is due to localized agenesis of the cortical mantle resulting in the formation of



**Fig. 39.16.** Partial agenesis of the corpus callosum shown by MRI midline sagittal section ( $T_1$ -weighted).

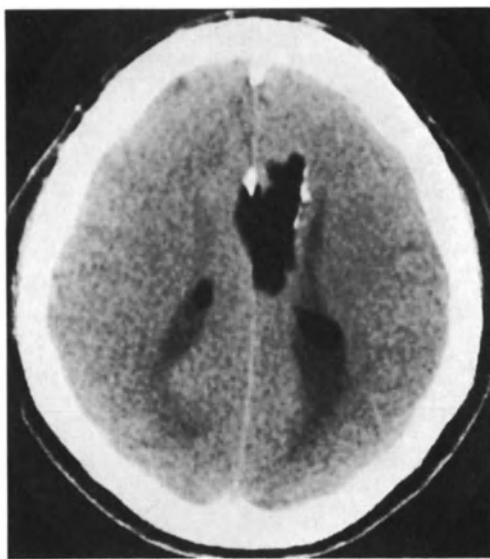


**Fig. 39.17.** Lipoma of the corpus callosum. The CT study shows the lesion to be of fatty density and with marginal calcification.

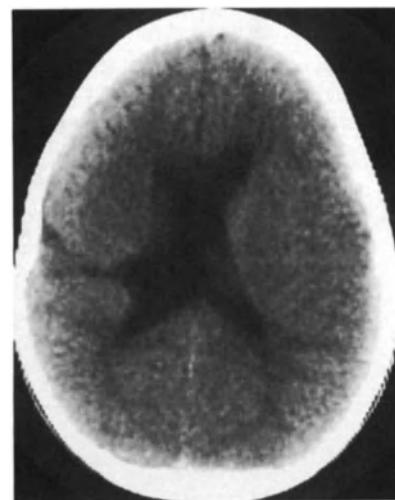


**Fig. 39.18.** Schizencephaly. CT shows lateral cleft extending from ventricular body to brain surface.

a cavity or a lateral slit through which the lateral ventricle communicates with the convexity of the brain. The cavity is lined by ependyma and laterally by a thin pia-ependymal layer which may rupture into the subarachnoid space.

The so called *acquired* type, is secondary to any type of cerebral destructive process, ranging from trauma to infarction. Sometimes called false porencephaly, they are better labeled by their etiological cause, if this is known, e.g., post-traumatic or post-infarction cerebral cavities.

Porencephalic cavities or clefts can be identified or suspected by ultrasound in the neonate or infant. In children or adults they are demonstrated by CT or MRI.

**Schizencephaly.** This term is used for a bilateral form of porencephaly in which two cavities or clefts extend from the ventricles to the convexity in the operculo-insular regions. The lesion is usually symmetrical but can be unilateral and it may be associated with a single ventricle and other malformations especially heterotopias. CT or MRI in the axial plane will demonstrate the lesions well (Fig. 39.18).

**Hydranencephaly.** This condition is generally the result of a major destructive process, often in the prenatal or perinatal period, and results in massive intracerebral cavitation which can resemble gross ventricular dilatation. It tends to affect the anterior parts of the hemispheres suggesting major involvement of the areas supplied by the internal carotids.

The falx is present (a distinguishing feature from severe holoprosencephaly), and the posterior fossa and basal ganglia appear normal. The ventricular dilatation resembles gross hydrocephalus, but the infant's head is not enlarged.

The diagnosis in the neonate can be suggested by ultrasound, and the anatomical feature can be delineated by CT or MRI.

**Holoprosencephaly.** This comprises a complex cranio-cerebral and facial anomaly classified in grades of severity from *alobar* through *semilobar* to *lobar*, which is the least

severe. It results from a failure of normal development of the forebrain (prosencephalon). The severe *alobar* form is incompatible with survival beyond infancy. The child has multiple craniofacial anomalies (cleft lip and palate, hypotelorism, anophthalmia or cyclopia). Intracranially the midline structures (falx, corpus callosum, septum pellucidum and olfactory bulbs) are absent and the two hemispheres are replaced by a single large ventricle with a thin rim of cortical mantle. The thalamus are fused.

*Semilobar* holoprosencephaly, the intermediate form, shows less severe facial deformity and the brain has a thicker mantle with recognizable occipital horns (Fig. 39.19). In the mildest (*lobar*) type there are well-formed lateral ventricles and a recognizable 3rd ventricle though the septum and Sylvian fissures are usually absent.

The grosser forms may be suspected from the clinical appearance of the infant, but imaging will be required in all varieties to delineate the intracranial anomalies (Fig. 39.19).

**Lissencephaly (Agyria).** This is characterized by the absence of sulci and convolutions in the cortex, and is the normal appearance before the 7th month of fetal life. Its persistence to term may be total or involve only part of the hemispheres. It is associated with severe mental retardation, fits and decerebrate rigidity. There is often a characteristic nodule of calcification in the septum pellucidum near the foramen of Monro, which can be seen at simple radiography or CT examination. The latter, like MRI, will identify the agyria.

**Pachygryria.** In this condition the convolutions and cortex are abnormally wide and thick. The condition can occur together with agyria and other anomalies such as heterotopic grey matter.

**Heterotopia.** These may be observed as an isolated phenomenon in the form of small masses of grey matter in the centrum ovale near the caudate nuclei, in the cerebellar white matter and in the brainstem. There are usually associ-

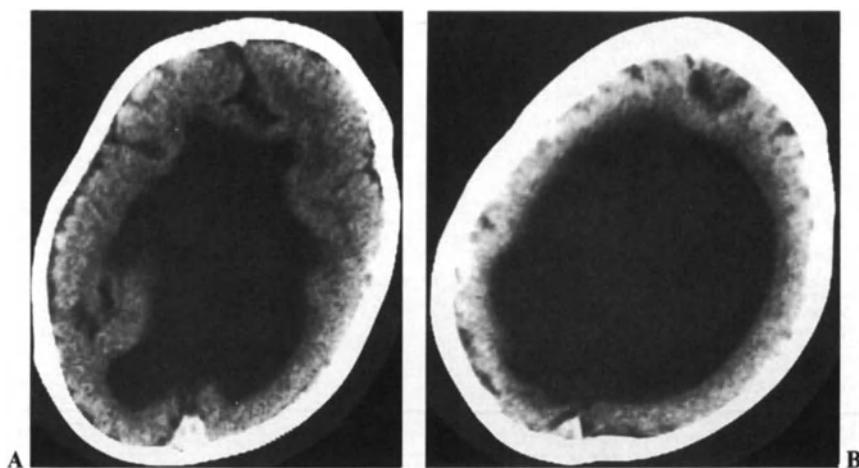


**Fig. 39.19.** Holoprosencephaly – semilobar type shown by CT.

ated congenital anomalies, but isolated lesions have been mistaken for neoplastic areas at CT.

**Phakomatoses.** Phakos was the Greek word for a lentil and the term phakoma was used for a lentil-shaped object such as a spot on the body or in the retina. The term phakomatoses is used to refer to a group of diseases of different etiologies but having in common lesions of the skin, retina and nervous system and the fact that they are developmental. They are also referred to as neuro-ectodermal dysplasias, and include tuberous sclerosis, neurofibromatosis, Sturge–Weber syndrome and Von Hippel–Lindau's disease.

**Tuberous Sclerosis (*syn. Epiloia, Bourneville's Disease*).** The lesions of this condition can affect not only the skin and nervous system but many other systems including the bones (see p. 264), respiratory system (p. 102), kidneys (p. 619), heart and skeletal muscle. There are multiple areas of dysplasia in the brain containing abnormal and giant glial cells. These often contain calcification which can be recognized

on a simple radiograph. Typically they are widely scattered, small, rounded, discrete calcifications, though they can be irregular, sinuous or densely nodular. The multiple scattered nature should suggest the diagnosis at simple X-ray.

At CT a diagnostic feature is the presence of small nodular protrusions into the ventricles, often with calcified foci. The latter are of course much easier to see at CT (Fig. 39.20) than at simple radiography. MRI shows the areas of dysplasia well but has the disadvantage of not imaging the calcification (Fig. 39.21).

**Neurofibromatosis (*syn. Von Recklinghausen's Disease*).** This is a common familial disorder and can involve the skull, spine and central nervous system. The skull lesions include hemihypertrophy or hemiatrophy of the cranium and macrocranium. Absence of the greater wing of the sphenoid is one of the causes of the 'bare orbit' giving rise to unilateral exophthalmos (Fig. 39.22). Other skull lesions include lytic defects in the calvarium usually in or near the lambdoid

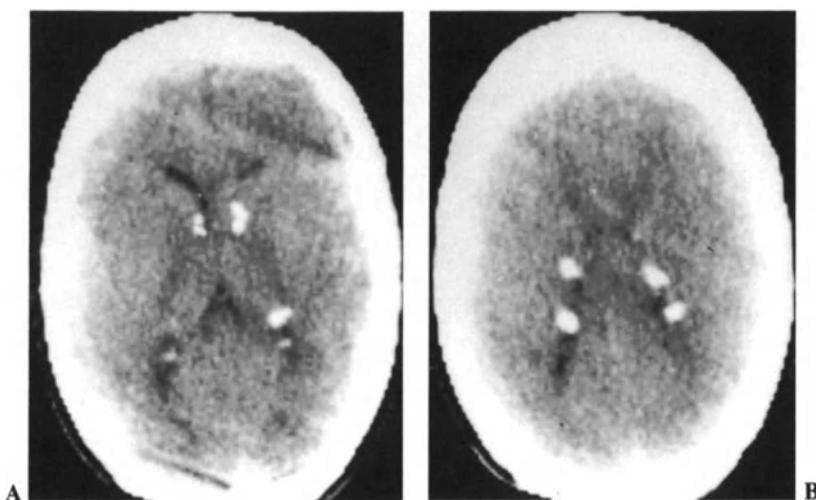
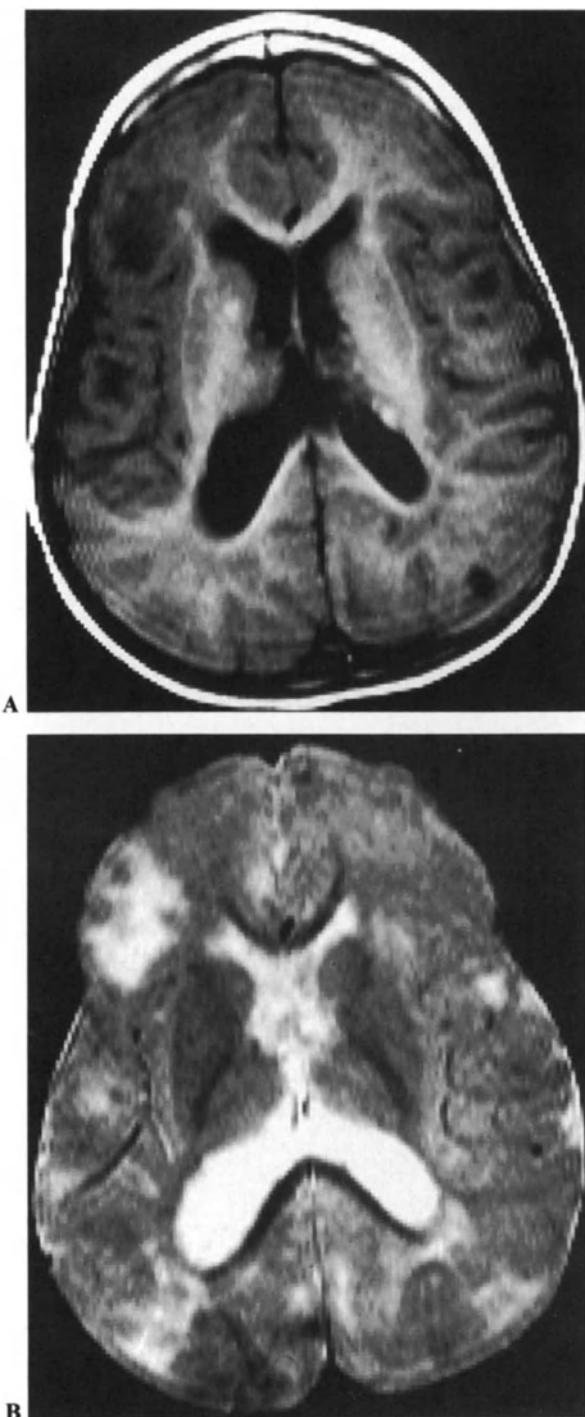


**Fig. 39.20A, B.** Tuberous sclerosis. CT shows calcified nodules protruding into lateral ventricles.



◀ Fig. 39.21A, B. Tuberous sclerosis shown by MRI. A T<sub>1</sub>-weighted study shows irregular nodules protruding into lateral ventricles and subcortical tubers as low signal areas. B T<sub>2</sub>-weighted study shows subcortical tubers as high signal areas and intraventricular nodules as relatively low signal, possibly due to calcification which is not specifically recognized by MRI.



Fig. 39.22. Proptosis in a patient with neurofibromatosis due to 'bare orbit' caused by defect of greater wing of sphenoid. The CT study shows absence of the greater sphenoid wing behind the orbit.

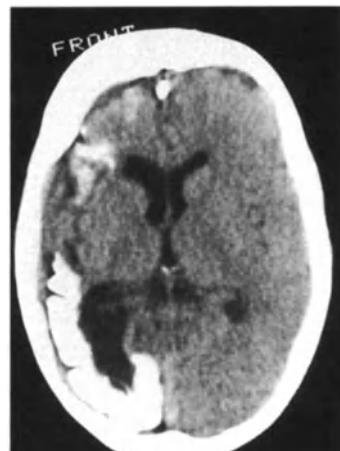


Fig. 39.23. Sturge-Weber syndrome. The CT examination shows heavy cortical calcification, predominantly occipital, with some atrophy.

suture. Also recognizable on simple radiography are unusually extensive calcifications in the choroid plexuses.

The lesions involving the CNS include meningiomas and neuromas, especially acoustic neuromas. The presence of bilateral acoustic neuromas is virtually pathognomonic. Optic nerve gliomas also occur in this condition as do, less commonly, optic nerve meningiomas. Gliomas of the brain-stem have also been described. The intracranial lesions can be characterized by CT or MRI.

Other features of neurofibromatosis are described elsewhere and include skeletal deformities (p. 312), and rare associations with renal artery stenosis or aneurysm and with pheochromocytoma.

*Sturge-Weber Disease (Encephalo-trigeminal Angiomatosis).* This condition involves a flat and often extensive unilateral angioma of the 'port wine' stain type in the facial and scalp distribution area of the trigeminal nerve. It is accompanied by a leptomeningeal angiomatosis in the parieto-occipital

area, which is associated with underlying cortical gliosis and calcification. The latter gives rise to the characteristic 'tramline' calcification seen on simple radiographs. This represents the margins of sulci where the calcification is seen end on. The occipital calcification is also well shown by CT, but the classical tram line appearance is obscured since CT shows all the extensive calcification and not just that end-on at the sulcal margins (Fig. 39.23).

*Von Hippel–Lindau's Disease (Retino-cerebellar Angiomatosis).* This rare familial disease is characterized by the occurrence of multiple hemangioblastomas in the retina and cerebellum. They may also be found in the spinal cord and rarely in the cerebrum. There is also an association with

visceral tumors and cysts, particularly renal and pancreatic tumors.

*Imaging.* The intracranial lesions can be demonstrated by CT or MRI but angiography is more specific. It is important to realise that hemangioblastomas occur much more commonly as isolated lesions, single or multiple in the cerebellum, and without the retinal lesions of Von Hippel–Lindau's disease. They can also occur as isolated lesions in the spine. Their diagnosis is discussed below in the chapters on cerebral tumors (p. 746) and spinal tumors (p. 808).

*For further reading, see p. 790.*

## CHAPTER 40

# NEOPLASMS

D. Sutton

---

## NEOPLASMS INVOLVING THE SKULL

---

Changes in the simple skull radiograph due to neoplasms can be specific or non-specific. The *non-specific* changes are those resulting from raised intracranial pressure and will be dealt with first.



Fig. 40.1. Suture diastasis involving mainly the coronal suture in a child.

### RAISED INTRACRANIAL PRESSURE

It is important to differentiate between the changes due to raised intracranial pressure seen in infants and children and those seen in adults.

In an **infant** or small child (up to 10 years of age) the cardinal sign is *suture diastasis*, mainly involving the coronal and sagittal sutures (Fig. 40.1). In a neonate the maximum normal width is up to 1 cm but this is reduced to 2 mm by 3 years of age. If the hydrocephalus is long standing the suture diastasis may be accompanied by excessive interdigitations. Craniolacuna can sometimes be seen in the neonate (see p. 716). So called *increased convolutional markings* may be seen in older infants and children, but this is an unreliable sign, since it may be a normal finding, particularly between the age of 4 and 10.

*Sellar changes*, which are the cardinal sign in adults, are usually absent in children. When present they indicate long-standing raised pressure and always appear after suture diastasis.

In **adults** *sellars changes* are the main sign since the sutures are now fused and cannot respond to raised pressure (Fig. 40.2). The changes commence with cortical porosis first affecting the so-called *lamina dura* at the base of the dorsum and progressing to destruction of the dorsum in long-standing chronic raised pressure (Fig. 40.3). Before diagnos-

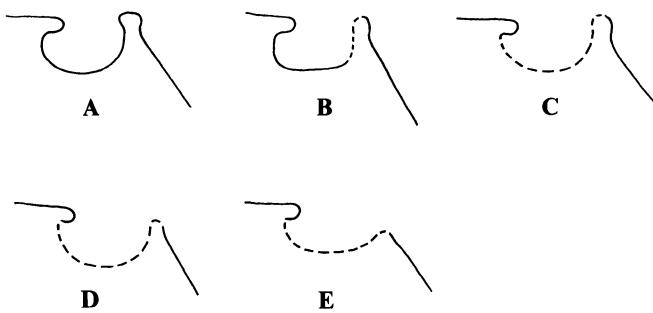


Fig. 40.2. Diagram showing progressive sellar changes with raised intracranial pressure.

Table 40.1. Neoplasms affecting the skull radiograph

Primary skull neoplasms
osteoma
dermoid and epidermoid
hemangioma
ossifying fibroma
osteogenic sarcoma
plasmacytoma
rodent ulcer and epithelioma
nasopharyngeal carcinoma
sphenoid carcinoma
chordoma
glomus jugulare tumor
Secondary neoplasms
carcinoma
neuroblastoma
multiple myeloma
lymphoma
lymphosarcoma
leukemia
histiocytosis
Intracranial neoplasms
pituitary tumors
acoustic neurinoma
fifth nerve neurinoma
optic nerve glioma
meningioma
Intracranial tumors with calcification (see Table 40.2)



Fig. 40.3. The sella in a patient with longstanding raised intracranial pressure. Note destruction of dorsum and posterior part of sellar floor and thinning of anterior clinoids.

ing raised intracranial pressure from the appearance of the sella it is important to exclude other conditions which can produce a similar appearance. These are severe or chronic *hypertension* and the generalized *osteoporosis* so commonly seen in the elderly.

Another sign seen in adults and which has some localizing value is lateral *displacement of the calcified pineal*. On normal PA or Towne's films this lies within 3 mm of the midline and displacement beyond this provides good evidence of the presence of a mass lesion in one hemisphere (Fig. 40.4).

**Specific Skull Changes.** The changes just described provide general evidence of the presence of an intracranial tumor. However changes of a more specific nature also occur with tumors affecting the skull and brain. Neoplasms involving the skull and brain and in which abnormalities have been identified at simple radiography are listed in Table 40.1.

#### PRIMARY TUMORS OF THE SKULL

**Osteomas** may involve the skull vault when they present as small flat very dense lesions projecting from the outer table. More commonly they are encountered in a frontal sinus as a chance finding at a routine examination. Very rarely these lesions can become very large and perforate through the frontal sinus into the cranium giving rise to *pneumocephalus*.

**Dermoids** involving the skull occur most commonly just above the outer angle of the orbit. They produce a rounded defect with a sclerotic margin (Fig. 45.6, p. 815) and there is local soft-tissue swelling. **Epidermoids** (cholesteatomas) can also occur in the skull vault and produce a clear-cut area of bone destruction with expansion of the bone and a corticated and lobulated margin.

**Hemangioma** of the skull vault usually presents as a circular translucency with stippled or slightly spiculated bony contents, giving a very characteristic appearance (Fig. 16.46, p. 310). Some, however, can resemble epidermoids with a fine rim of peripheral bone condensation or slightly sclerotic margin. They can be differentiated by their internal spicular trabeculation (strands) or reticulation.



Fig. 40.4. Towne's view showing calcified pineal (arrow) displaced 1 cm to the left by a right hemisphere tumor. Midline is marked by open arrow with square tail.



◀ Fig. 40.5. Densely calcified tumor invading sella and nasopharynx from the sphenoid sinus. Histology: ossifying fibroma.

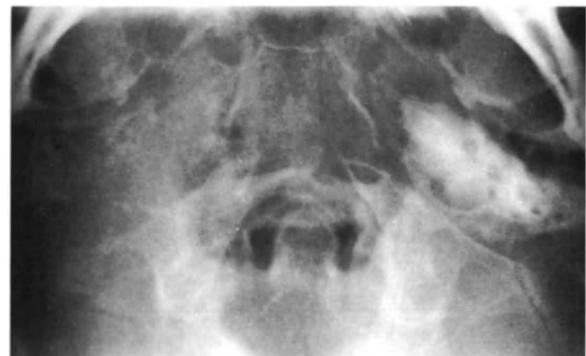


Fig. 40.6. Basal view of skull showing destruction of right petrous bone and jugular foramen region by extensive glomus tumor.

**Osteogenic sarcoma** involving the skull vault is rare, but can be seen as a complication of Paget's disease. The affected bone may show local hyperostosis with extension into the overlying soft tissues and sun-ray spiculation.

**Ossifying fibroma** is also rare, though there appears to be an unusually high incidence in East Africa, commencing in childhood. It usually begins in the antrum or an adjacent paranasal sinus and can give rise to considerable facial swelling. It is regarded by some as a localized form of fibrous dysplasia. The expanded sinus may be largely of soft tissue density, but usually contains calcified areas. Occasionally the whole lesion is densely calcified. Sphenoid involvement can expand into the pituitary fossa (Fig. 40.5).

So-called **solitary plasmacytoma** can give rise to a swelling over the skull vault associated with a large lytic lesion expanding the bone. This is usually in the occipital or occipito-parietal region and may contain internal bony septa. The expanded bone can also press on the underlying intracranial structures. Tangential views may show apparent spiculation extending into the soft tissues and has led to erroneous diagnoses of sarcoma or meningioma. Although such lesions can remain solitary for years they will eventually progress to generalized multiple myeloma (see Chap. 16).

**Rodent ulcers** or **epitheliomas** affecting the scalp and forehead can invade and erode the underlying bone, producing irregular defects.

**Carcinoma of the nasopharynx** can extend up into the cranium. This is usually by infiltration through the basal foramina, but sometimes it will invade bone and produce irregular basal defects involving the floor of the middle fossa. Carcinoma of the sphenoid sinus can also invade and erode the skull base in the region of the overlying pituitary fossa.

**Chordomas**, though rare tumors, are relatively frequent in the region of the clivus. Typically they expand both upwards and backwards into the prepontine space and forwards and downwards into the nasopharynx. Calcification is identified at simple radiography in less than one third of cases, usually behind the clivus. More commonly the tumors present a soft tissue mass projecting into the

nasopharynx and well seen in a lateral skull radiograph. They may also produce erosion of the skull base involving the clivus, sella or petrous apex, and have even been recorded extending forward into the orbit. They can also be eccentric and mainly on one side, raising problems in differential diagnosis. Occasionally affected bone shows irregular sclerotic changes. Some cases also involve the anterior part of the foramen magnum and upper cervical vertebrae. Intracranial extension is discussed below (p. 750).

**Glomus jugulare tumors** produce erosion of the margins of the jugular foramen which is best identified on a half axial view of the skull base. Larger tumors will erode the under surface of the petrous bone, and large long-standing tumors can produce very widespread erosion (Fig. 40.6).

## SECONDARY TUMORS

**Metastases** to the skull vault from carcinoma are very common once the tumor is disseminated. Most of these deposits are lytic in type though occasional sclerotic secondaries are seen. The defects may have a characteristic 'moth-eaten' margin, particularly when large (Fig. 40.7), or present as more clear-cut defects. Metastases to the skull base may also be seen.

**Neuroblastoma** in children frequently metastasizes to the skull. Here it frequently involves the sutures, particularly the

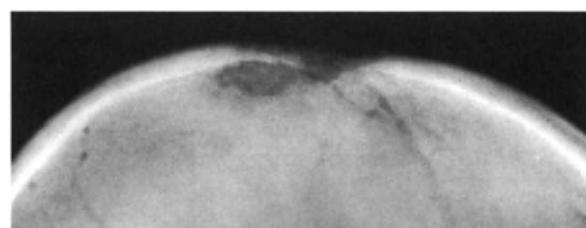


Fig. 40.7. Irregular erosion of skull vault by secondary carcinoma from breast.

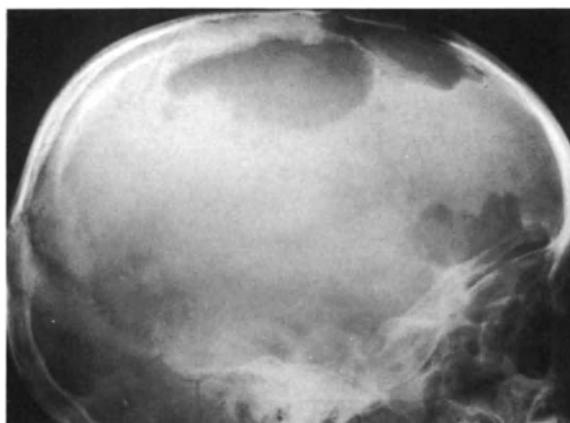


Fig. 40.8. Geographical skull defects in histiocytosis.

coronal, and produces a characteristic widening and irregularity. The appearance may be accentuated by true suture diastasis from intracranial masses. These may be extradural and continuous with the bony lesions. Orbital deposits producing proptosis are also common in this condition. Lesions of the bony vault can produce large lucencies and can also raise the periosteum giving rise to sunray spiculation extending into the soft tissues.

*Multiple myeloma* usually involves the skull vault when widespread, and produces a characteristic appearance of multiple small holes in the bone (Fig. 16.67, p. 317). The occasional presentation as a solitary plasmacytoma has been mentioned above.

*Lymphoma* and *lymphosarcoma* rarely affect the skull. When they do they usually produce multiple small erosions, but these can become confluent and appear larger.

*Leukemia* affecting the meninges and CNS can produce hydrocephalus and sutural widening, but hardly ever seems to affect the bony skull.

*Histiocytosis* commonly involves the skull vault, particularly in *Letterer-Siwe* and *Hand-Schuller-Christian* disease, where it gives rise to the classical 'geographical' skull defects (Fig. 40.8). The more benign *eosinophil granuloma* (Fig.

16.78B, p. 320) can also give rise to similar lesions but may also occur as an isolated lesion in the skull vault, when it can show a sclerotic margin. Such an isolated granuloma will be difficult to distinguish from similar lesions such as localized fibrous dysplasia or epidermoids. So-called 'button' sequestration is claimed to be characteristic.

#### INTRACRANIAL TUMORS INVOLVING THE SKULL

**Pituitary tumors** characteristically produce ballooning or enlargement of the pituitary fossa (Fig. 40.9). The typical appearance is of a generalized enlargement with backward bowing of the dorsum. Occasionally when the dorsum is completely destroyed it may be difficult to differentiate from the result of chronic raised intracranial pressure, though the clinical features are usually diagnostic. Confusion can also arise in the so-called 'empty sella', where there may also be expansion of the sella. In this condition the sella shows no bony erosion.

Small pituitary adenomas (*microadenomas*) are not normally diagnosable from the simple radiograph, though it has been claimed that local asymmetry of the sellar floor can suggest the diagnosis. However this is a sign to be treated with caution since it can occur in the normal, as can the so-called double floor to the sella seen in some of the larger tumors.

**Acoustic tumors** can expand and erode the mouth of the internal auditory canal, a feature best seen in the Towne's or transorbital projections or on tomography (Fig. 40.10).

**Neuromas of the 5th nerve** usually lie near the petrous apex which they may straddle. They can produce erosion of the petrous apex or of the floor of the middle fossa just anterior to the apex.

**Optic nerve glioma** which is predominantly seen in children can give rise to local expansion of the optic foramen. This is best identified by comparing the two sides.

**Meningiomas** frequently involve the skull where they usually produce a hyperostotic reaction. This first involves the inner table, but can extend through the diploe to the outer table. Rarely this will result in a palpable or even visible bony swelling and sunray spicules on the radiograph. The parasa-

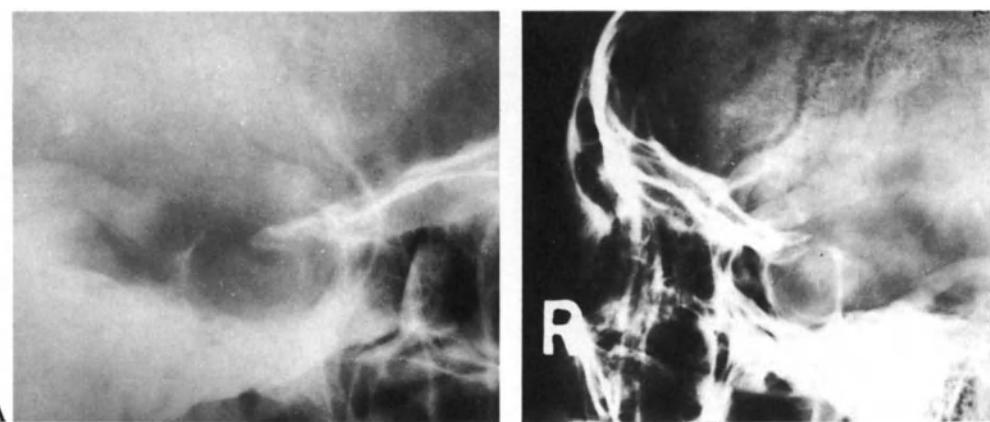


Fig. 40.9A, B. Pituitary tumors producing enlargement of the sella with undercutting of the anterior clinoids and ballooning of the floor and dorsum.



Fig. 40.10. Enlargement of the left internal auditory meatus due to local bony erosion. Acoustic neurinoma.

gittal region and the sphenoidal ridge are classical sites for meningioma hyperostosis. At the sphenoidal ridge where they produce marked thickening of the lesser or greater wings or both (Fig. 40.11) proptosis frequently results. Meningiomas arising at the anterior clinoid or jugum sometimes produce an unusual localized bone enlargement with pneumatization ('blistering'). At the superomedial wall of the orbit they can produce so-called '*pneumosinus dilatans*', an abnormal dilatation of the normal air sinuses (see p. 814).

Increased vascular markings may also be seen in the region of bony involvement or adjacent to it, mainly due to enlarged meningeal vessels.

**Gliomas** have been recorded which have grown through the dura and produced bone erosion, but this is extremely rare. However, superficial gliomas in children will occasionally impinge on and locally bulge the skull.

#### INTRACRANIAL TUMORS WITH CALCIFICATION

Calcification is commonly found in many intracranial tumors, and is most readily identified by CT rather than by simple radiography. Nevertheless, despite the overlying bony



Fig. 40.11. Hyperostosis of the left lesser and greater sphenoid wings due to meningioma.

skull vault, a significant number of calcified tumors are identified on the simple radiograph. Depending on the type of tumor the proportion may be high or low, ranging from 80% in craniopharyngiomas to less than 1% in pituitary tumors. Whilst CT will identify a much higher percentage of calcified lesions, MRI, in contrast, is unable to image calcification at all, and this remains one of its major drawbacks.

The calcification in tumors has to be differentiated from the intracranial calcification due to other causes and from physiological calcification with no clinical significance. The causes of intracranial calcification are listed in Table 40.2.

Table 40.2. Intracranial calcification

Normal or physiological	
pineal and habenula	
choroid plexus	
dural (falx, tentorium, vault)	
ligamentous (petroclinoids, interclinoid)	
Pachionian bodies	
basal ganglia and dentate nuclei	
pituitary	
lens	
Neoplasms	
craniopharyngioma	
glioma	
meningioma	
ependymoma	
papilloma of the choroid plexus	
pinealoma	
chordoma	
dermoid, epidermoid and teratoma	
hamartoma	
lipoma	
pituitary adenoma (rarely)	
metastasis (rarely)	
Vascular	
atheroma	
aneurysm	
angioma	
subdural hematoma	
intracranial hematoma	
Infections and infestations	
toxoplasmosis	
cytomegalic inclusion body disease	
herpes	
rubella	
tuberculosis	
pyogenic abscess	
cysticercosis	
hydatid cyst	
paragonimus abscesses	
trichinosis	
torulosis	
coccidioides	
Metabolic and miscellaneous	
idiopathic basal ganglia calcification	
hypoparathyroidism	
pseudohypoparathyroidism	
tuberous sclerosis	
Sturge–Weber syndrome	
neurofibromatosis	
lissencephaly	
Fahr's syndrome	
Cockayne's syndrome	
X-radiation and methotrexate	
hemodialysis	
lead poisoning	
carbon monoxide poisoning	

The table includes both very common and very rare conditions, and does not differentiate between those causes where visible calcification is frequently found and those where it is relatively rare.

Calcification in specific tumors and visible on simple radiography is described in the following section on brain tumors. The other causes of pathological calcification are dealt with and illustrated in later chapters.

## CEREBRAL NEOPLASMS

Cerebral neoplasms will be discussed under the following headings:

Epidemiology and age incidence

Imaging – general considerations

Glioma

Tumors of ependymal origin (ependymoma, choroid plexus papilloma, colloid cyst)

Medulloblastoma

Ganglioglioma

Meningioma

Pituitary tumors (suprasellar masses, empty sella syndrome)

Craniopharyngioma

Rathke's cleft cyst

Inclusion tumors (epidermoid, dermoid, teratoma)

Pineal tumors

Acoustic tumors

Glomus jugulare tumors

Hemangioblastoma

Metastases

Primary lymphoma

Congenital tumors	2.0%
Granulomas	6.4%
Lymphomas	3.2%
Miscellaneous	9.5%

**Age Incidence.** Cerebral tumors are predominantly tumors of adult life with a peak incidence of 13 cases per 100 000 population at age 55 to 65 years. They are relatively uncommon in infants and children at 2 cases per 100 000.

Whilst examples of most *primary* intracranial tumors can occur at any age, it is helpful in differential diagnosis to know that certain tumors occur mainly in certain age groups. These include:

1. 0–5 yr: brainstem glioma, optic nerve glioma
2. 5–15 yr: medulloblastoma, cerebellar astrocytoma, papilloma choroid plexus, pinealoma, craniopharyngioma
3. 15–30 yr: ependymoma
4. 30–65 yr: glioma, meningioma, acoustic neuroma, pituitary tumor, hemangioblastoma
5. Above 65 yr: meningioma, acoustic tumor, glioblastoma

*Secondary* tumors of the brain affect mainly the middle-aged and elderly groups with the exception of secondary neuroblastoma which occurs mainly in children.

In adults supratentorial tumors outnumber posterior fossa tumors by a ratio of 7 to 3, but in children this ratio is reversed, and posterior fossa tumors are the most common.

The four main infratentorial tumors of childhood are cerebellar glioma, pontine glioma, medulloblastoma and choroid plexus papilloma.

## IMAGING – GENERAL CONSIDERATIONS

The localization and characterization of a suspected intracranial tumor depends today on CT and MRI. Other methods of imaging localization are now obsolete or of ancillary importance.

*Simple skull radiography* can provide helpful information very cheaply but since its specificity is low (less than 50% compared with the 99% of the newer imaging techniques), many workers now dispense with its use.

The more invasive techniques of *pneumography* and *scintigraphy*, once so important in neuroradiology, are no longer used except where there is no access to modern imaging.

Gliomas	31.4%
Metastases	20.3%
Meningiomas	15.4%
Angiomas	5.9%
Pituitary adenomas	4.4%
Acoustic tumors	1.5%

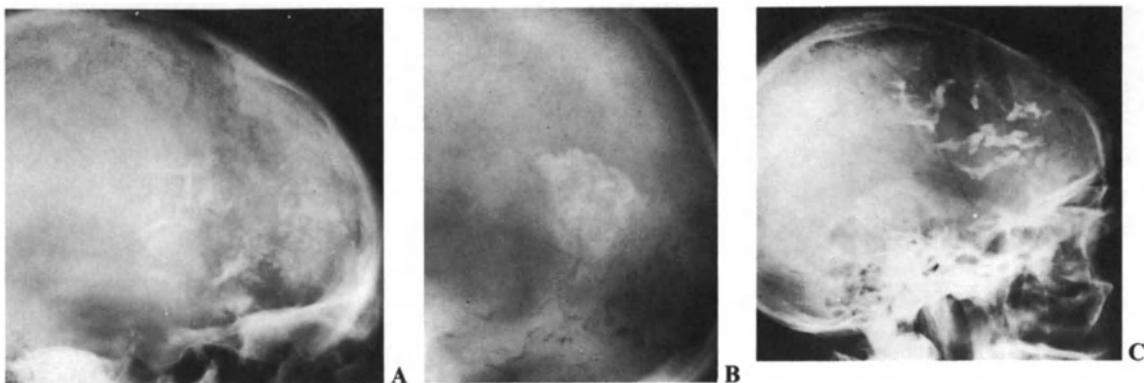


Fig. 40.12. A Calcification in a frontal glioma. B Calcification in an occipital glioma. C Serpiginous calcification in a large frontal glioma (oligodendrogloma).

*Angiography* was, before the advent of CT, the most widely used technique for cerebral tumor localization and characterization, but is now only used in special circumstances, e.g., to provide more information about the vascularity or vascular relationships of large meningiomas involving major sinuses, or in the assessment of suspected multiple hemangioblastomas. Angiography has also been used for the preoperative *embolization* of vessels which do not supply nervous tissue, but do form part of the supply to large vascular meningiomas.

*Ultrasound* is of great value in the investigation of infants but is of no use in the primary diagnosis of intracranial tumors in adults. It is however proving more useful as an *intraoperative* technique for the assessment of the nature and extent of cerebral tumors.

### GLIOMAS

These common intracranial tumors vary greatly in malignancy. This has led to specific names being used based on the histological appearances, e.g., astrocytoma and oligodendrogloma for well-differentiated slow-growing tumors, and glioblastoma and spongioblastoma multiforme for highly malignant ones. Most workers, however, favour grading by degree of malignancy, ranging from Grade 1, which is relatively benign, through Grade 2 to Grades 3 and 4 which are highly malignant (Kernohan). Some 50% of gliomas belong to Groups 3 and 4, and about 25% to Grade 1.

Gliomas can occur at any site in both children and adults, but gliomas of the optic chiasm and of the brainstem are particularly common in children, where they have a peak incidence at 1 to 6 years and 1 to 4 years respectively. Cerebellar astrocytoma is also commoner in children, with a peak incidence at 5 to 10 years.

**Imaging.** *Simple radiography* of the skull will show calcification in only a small proportion of gliomas (5%) (Fig. 40.12), but the proportion is higher in specific slow-growing tumors such as oligodendroglomas (50%) and cerebellar astrocytoma (20%). General signs of raised intracranial pressure may be present, as described above (p. 727), as may lateral displacement of the calcified pineal (Fig. 40.4).

CT. Modern high resolution CT will localize and characterize the vast majority of cerebral gliomas and the same is true of MRI.

At unenhanced CT the classical appearance is an area of low density confined almost exclusively to the white matter and often containing patchy areas of mixed density. Sometimes there is a well-defined circular area of low density suggesting a cystic tumor. There is usually a mass effect with displacement and deformity of the ventricles. Edema is frequently present around the tumor, particularly with the more malignant gliomas and this may be difficult to differentiate from tumor on the unenhanced scan. Calcification, if present, is much more easily identified than at simple radiography. As already noted, it is relatively common in the rare oligodendrogloma and in the cerebellar astrocytoma of children.

Post-enhancement there is uptake of contrast in all but the slowest growing Grade 1 tumors and this may be patchy, circumferential, or less commonly homogeneous (Fig. 40.13). Marginal or circumferential enhancement does not necessarily imply a necrotic or cystic center; in these cases a delayed scan will sometimes show central enhancement also.

The most difficult tumors to demonstrate are slow-growing gliomas with no enhancement and only minor or equivocal reduced attenuation. CT cisternography may be helpful in these cases if the lesion is adjacent to the basal cisterns as with brainstem or hypothalamic tumors.

**MRI.** Most intracerebral gliomas have long T<sub>1</sub> and T<sub>2</sub> values and appear therefore as low signal on T<sub>1</sub>-weighted sequences and as high signal on T<sub>2</sub>-weighted sequences (Fig. 40.14A, B, C, D). Mass effect is well shown and the facility for direct coronal cuts is an advantage in assessment. Inability to image calcification remains a disadvantage compared to CT, as does frequent inability to separate tumor from edema. Some T<sub>2</sub>-weighted studies may, however, show the tumor margin as a low-density ring and thus separate tumor from surrounding edema. Studies with contrast enhanced MRI using i.v. Gadolinium-DTPA suggest that differentiation can also be achieved with this technique.

*Angiography* is now rarely used in the diagnosis of gliomas. The more benign tumors are relatively avascular but can be

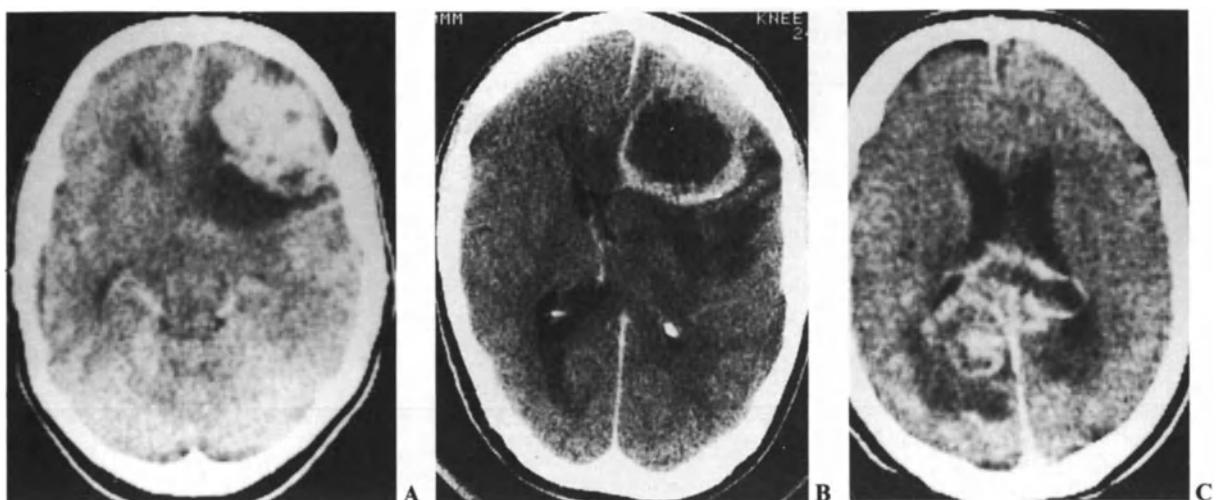


Fig. 40.13A, B, C. Post-enhancement CT in malignant gliomas. A Largely homogeneous enhancement with surrounding edema. B Marginal enhancement with posterior edema showing digital pattern. C Serpiginous enhancement pattern extending bilaterally through corpus callosum with surrounding edema.

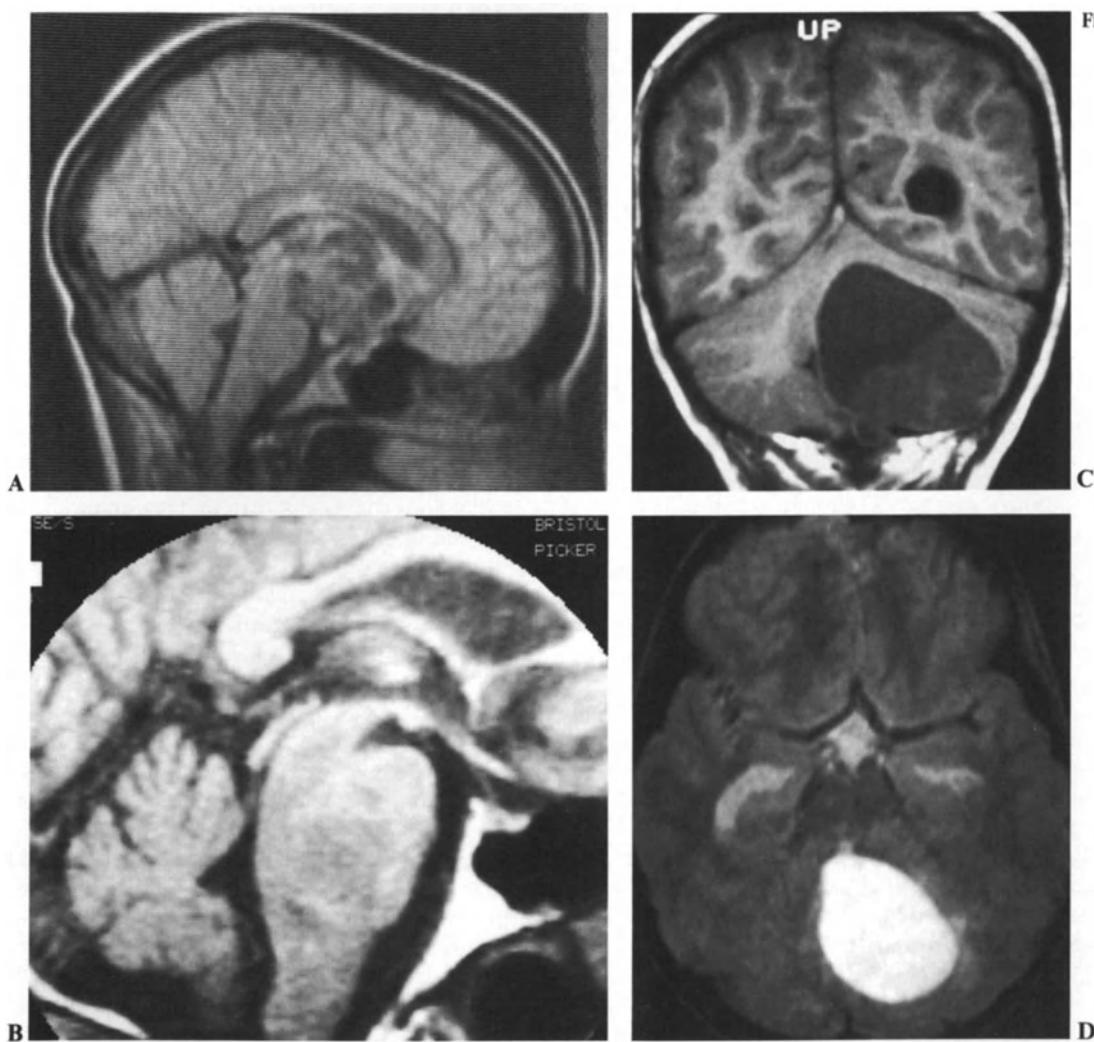
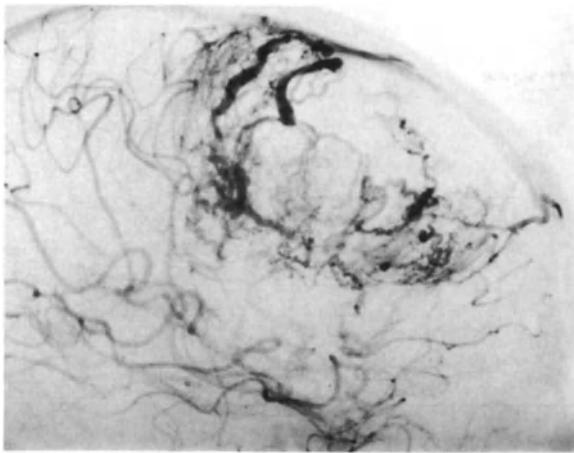
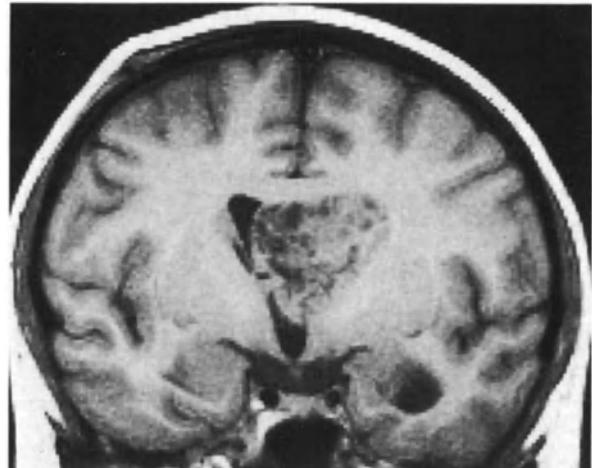


Fig. 40.14



**Fig. 40.15.** Angiogram of fronto-parietal malignant glioma. Note pathological vessels and rapid arterio-venous shunting.



**Fig. 40.18.** Coronal MRI section ( $T_1$ -weighted) shows tumor of mixed but mainly low signal filling body of left lateral ventricle and extending through Foramen of Monro into third ventricle. Histology: ependymoma.



**Fig. 40.16.** CT demonstrates irregular tumor invading and obstructing fourth ventricle and showing moderate contrast enhancement. Histology: ependymoma.



**Fig. 40.17.** Contrast enhancing tumor extending from lateral recess of fourth ventricle into CP angle. Ependymoma.

◀ **Fig. 40.14A, B, C, D.** MRI of malignant gliomas. A Hypothalamic glioma invading third ventricle. The tumor is mainly low signal ( $T_1$ -weighted). B Brainstem glioma of mixed but mainly low signal ( $T_1$ ). The brainstem is swollen and bulging back the aqueduct and fourth ventricular floor. Midline sagittal section. (Courtesy of Dr Gordon Thomson and Bristol MRI centre.) C Cystic cerebellar astrocytoma.  $T_1$ -weighted coronal section shows the tumor as mainly low signal area with the darker cyst above. D Axial section of same case as C ( $T_2$ -weighted) shows the tumor and cyst as high signal.

localized by the vascular displacements. The more malignant tumors can be highly vascular and show typical malignant vasculature, with abnormal or pathological vessels (Fig. 40.15).

#### TUMORS DERIVED FROM EPENDYMAL CELLS

The ependymocytes are of glial origin and the following tumors derived from them are classified by some as gliomas. However, most authors treat them separately. They include ependymomas, choroid plexus papillomas and colloid cysts.

**Ependymomas.** These tumors are seen mainly in the posterior fossa in children, but can be seen in the supratentorial compartment, particularly in older patients. They are not uncommon and would form about 3% of a pathological series of brain tumors.

CT shows a mass of slightly higher density than normal brain, which enhances uniformly or patchily. It may occupy and expand the 4th ventricle, producing obstructive hydrocephalus and is then difficult to distinguish from a medulloblastoma (Fig. 40.16). Calcification, if present, will favour ependymoma. Another characteristic feature is downward spread through the foramina of Luschka into the cerebello-pontine angle or through the foramen of Magendie into the cisterna magna, features which render surgical removal more difficult (Fig. 40.17).

Some of these tumors behave aggressively and can seed through the ventricles or by meningeal spread.

MRI will also readily localize these tumors (Fig. 40.18).

**Choroid Plexus Papilloma.** These rare tumors occur mainly in children, though they are occasionally seen in adults. They form less than 1% of a pathological series. The 4th ventricle and the lateral ventricle seem to be the sites of election.

CT shows a mass of increased density which enhances strongly and uniformly after contrast. If in the 4th ventricle it will be difficult to differentiate from a medulloblastoma or

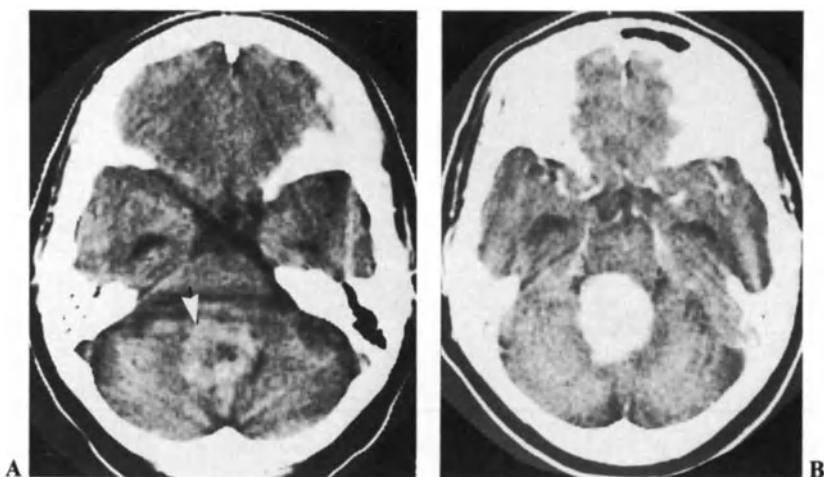


**Fig. 40.19.** A CT shows rounded mass of increased attenuation with low density center occupying fourth ventricle. B After contrast, a slightly higher CT section shows strong enhancement of the tumor. Histology: choroid plexus papilloma.

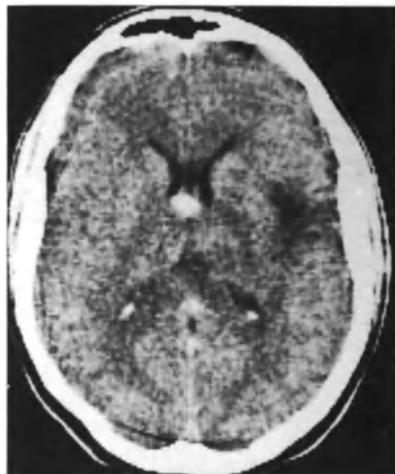


**Fig. 40.20.** CT of high density colloid cyst of the third ventricle. There is a coincidental low density cyst of the septum pellucidum.

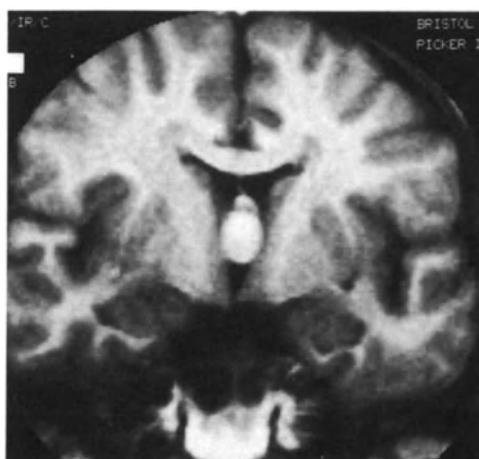


**Fig. 40.21.** MRI (T<sub>1</sub>-weighted) showing colloid cyst as high signal lesion in third ventricle. Coronal section. (Courtesy of Dr Gordon Thomson and Bristol MRI centre.)

ependymoma (Fig. 40.19). In the lateral ventricle (more commonly the left) it lies in the region of the atrium, which is dilated. The ventricles may also be generally dilated from overproduction of CSF.

**Colloid Cyst.** These tumors are, according to one theory, derived from the parapysis and have been termed parapysial cysts. The parapysis is a gland normally found in the human fetus at one stage of development but which later disappears; it is present in some lower vertebrates, but its function is unknown. Other workers are sceptical of this theory and prefer to use the non-committal term 'neuroepithelial' cyst.

The cyst lies in the roof of the 3rd ventricle directly behind the foramen of Monro, and contains amorphous gelatinous material (colloid). Because of its position it can give rise to intermittent obstruction of the foramen of Monro when quite small. The tumors usually present in adults at any age, but have been described in children.

**CT.** The appearances are usually diagnostic on the unenhanced scan. Symmetrical hydrocephalus of the lateral ventricles is present with a high-density spherical cyst at the base of the septum pellucidum in the region of the foramen of Monro (Fig. 40.20). The appearances are normally unchanged after contrast enhancement, except in the case of the rare isodense cyst. Marginal enhancement may be seen in these latter cases following high-dose contrast either from the opacified capsule or from stretched veins around it.

**MRI** will also characterize the cyst and shows it well in the coronal plane as in the IR 1500/500 sequence illustrated (Fig. 40.21). These tumors are also described as of variable signal on T<sub>1</sub>-weighted images, but of high signal on T<sub>2</sub>-weighted images.

#### MEDULLOBLASTOMA

These tumors are classified by some with the gliomas, but as they derive from neuronal rather than glial cell precursors, they are best considered separately. They are predominantly tumors of childhood and form about 3% of

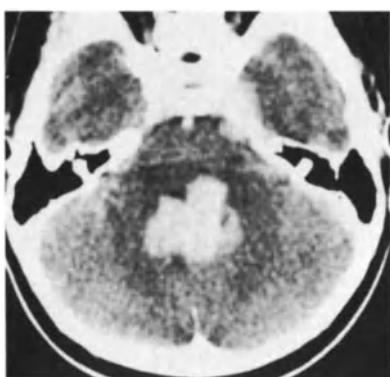


**Fig. 40.22.** CT showing strongly enhancing tumor in fourth ventricle. Medulloblastoma.

large pathological series. Their site of election is the cerebellar vermis, particularly the lower end. From here they involve the cerebellar hemispheres and invade the 4th ventricle. Seeding to the spinal canal and brain occurs via the cerebro-spinal fluid pathways.

**CT.** This shows a slightly hyperdense mass lying centrally and growing into the 4th ventricle from behind, and producing hydrocephalus. It shows homogeneous or less commonly patchy enhancement after contrast (Fig. 40.22).

Calcification is absent and if noted would favour a diagnosis of ependymoma or astrocytoma. Small seedings may be seen at sites remote from the primary or invading the ventricles.

**MRI** will show similar features to those already described for CT, and can readily show the tumor in sagittal or coronal planes.

#### GANGLIOGLIOMA (GANGLIOCYTOMA)

This is a very rare tumor of children and young adults which arises in the floor of the 3rd ventricle, where it has been referred to as hamartoma of the tuber cinereum. It has also

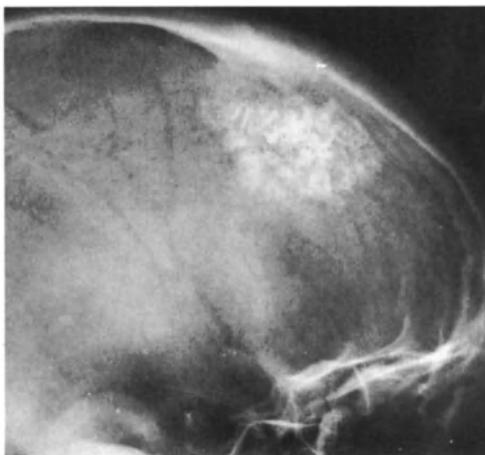


**Fig. 40.23.** Calcified tumor adjacent to the skull vault and parasagittal in the PA film. Meningioma.

been described in the temporal lobe. The tumor is small and well-circumscribed and is relatively benign with no tendency to recurrence after surgical removal.

**CT** shows a small mass in the floor of the 3rd ventricle which protrudes down into the suprasellar cistern. The mass is isodense or slightly hyperdense and enhances a little with contrast.

**MRI** will demonstrate the lesion well in midline sagittal section.

#### MENINGIOMAS

These tumors are particularly gratifying to diagnose since they are the commonest benign intracranial tumors. However, a small proportion can become malignant and these are the vascular angioblastic type. Recurrence after surgery is also not uncommon, particularly with tumors in difficult sites where complete extirpation is difficult. Meningiomas can arise anywhere over or under the brain from arachnoid cell rests, but have several sites of election shown in Table 40.3, a consecutive series of 100 cases examined by the author.

**Table 40.3.** Sites of origin of meningiomas (100 cases)

Parasagittal	26
Convexity	32
Tuberculum sellae (suprasellar)	13
Sphenoidal ridge and pterion	12
Cerebello-pontine angle	8
Subfrontal	3
Cerebellar convexity	3
Tentorium	2
Intraventricular	1

Other well-documented sites not represented in this series include the optic nerve sheath and the olfactory groove. The falx is also a common site of origin, though most of these are listed as parasagittal. The latter can invade the sinus, as can tumors adjacent to the lateral, sigmoid and cavernous sinuses.

*Multiple meningiomas* occur in about 5% of cases and are usually parasagittal. There is also an association with neurofibromatosis.

**Imaging** Simple skull radiography may show evidence of an intracerebral tumor in some two thirds of cases, and diagnostic evidence of the presence of a meningioma in about one third, either from bone changes or from calcification. The specific bone changes have been described above (p. 710). Calcification in these tumors is sufficient to be radioopaque in some 15% and is often specific. Thus homogeneous ball-like calcification at a typical site is virtually diagnostic as is less regular or dense calcification adjacent to typical bony changes (Fig. 40.23).

**CT.** On the unenhanced scan meningiomas usually appear as homogeneous high-density masses with rounded well-defined margins, the attenuation values being slightly higher than normal brain if uncalcified and considerably higher when uniformly calcified. Calcification which is found in

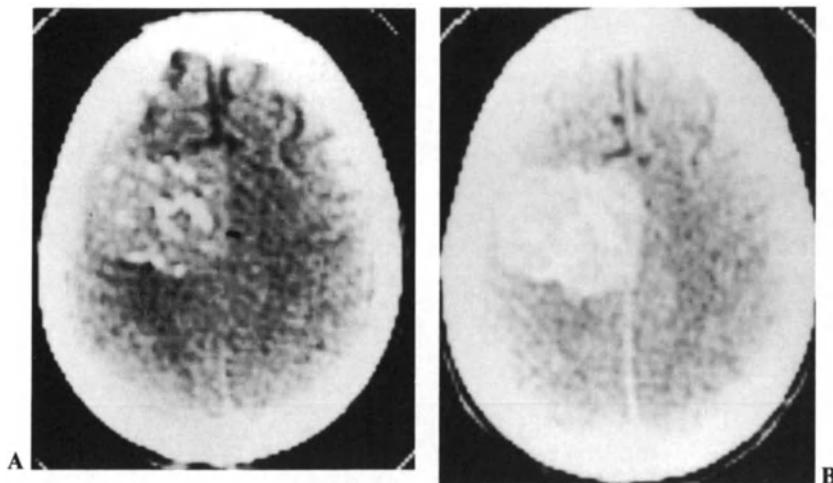


**Fig. 40.24.** A Unenhanced CT shows high density parasagittal tumor with irregular calcification. B The tumor enhances strongly after contrast. Meningioma.

16%–20% of cases can also be present in an irregular pattern (Fig. 40.24). The 'en plaque' type of tumor may be more difficult to identify, particularly adjacent to the cavernous sinus or sphenoid ridge. However the bony involvement often seen in these tumors may be more obvious at bone window.

Post-enhancement meningiomas nearly always show marked opacification and increase uniformly in density (Fig. 40.25). Edema surrounding the tumor tends to be absent or minimal and circumscribed; only very occasionally is it extensive and with the characteristic digital elongation of more malignant tumors. Cystic components to meningiomas are uncommon, but in a few cases (4% in our series) they can be a major feature.

Mass effect is moderate or minimal in most cases, though it can be marked in some 10%.

The appearances just described are sufficient together with the characteristic sites to permit a specific diagnosis in all but exceptional cases. The occasional false negative diagnoses reported in past series should not occur with modern high resolution apparatus, provided the appropriate area is

adequately covered. An occasional false positive diagnosis may still occur in the differential diagnosis from a superficial intracerebral tumor, which is usually a metastasis. The rare intraventricular meningioma has to be differentiated from an intraventricular papilloma or ependymoma.

**MRI.** In the imaging of meningiomas most early studies suggested that the method was less accurate than contrast-enhanced CT. This was due to lack of intrinsic contrast between the tumor and the adjacent brain irrespective of the pulse sequences used, and to the inability of MRI to detect calcification. However more recent studies with more modern techniques suggest that MRI is now equal to CT or superior in the diagnosis of these tumors. The inversion-recovery sequence may be more sensitive than spin-echo in detecting some meningiomas and is also highly sensitive to enhancement with Gd-DTPA. MRI can also demonstrate dural sinus involvement.

The tumors manifest by mass effect and displacement of surrounding brain and white matter, and the low intrinsic contrast may help to differentiate from most other intra-

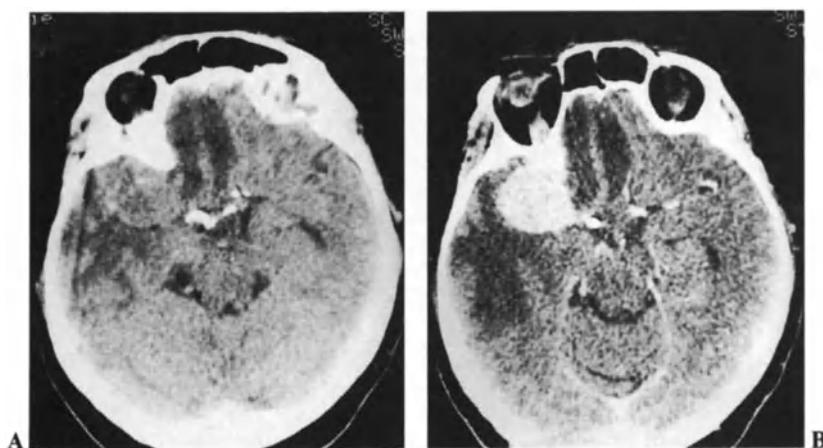


**Fig. 40.25.** A Unenhanced CT shows rounded isodense mass with few flecks of calcification in anterior temporal region. B The tumor shows strong uniform enhancement. Note low density due to edema in adjacent temporal lobe. Sphenoidal ridge meningioma.

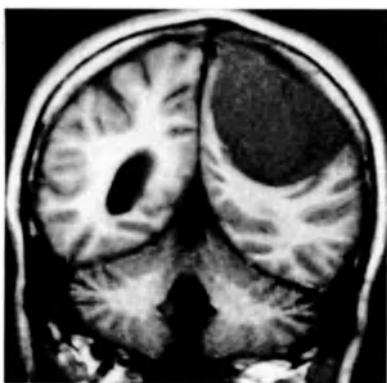


**Fig. 40.26.** Coronal MRI section  $T_1$ -weighted shows uniformly low signal and clearly extracerebral tumor. Its upper medial margin extends to the sagittal sinus. Large parasagittal meningioma. (Courtesy of Dr Gordon Thomson and Bristol MRI centre.)

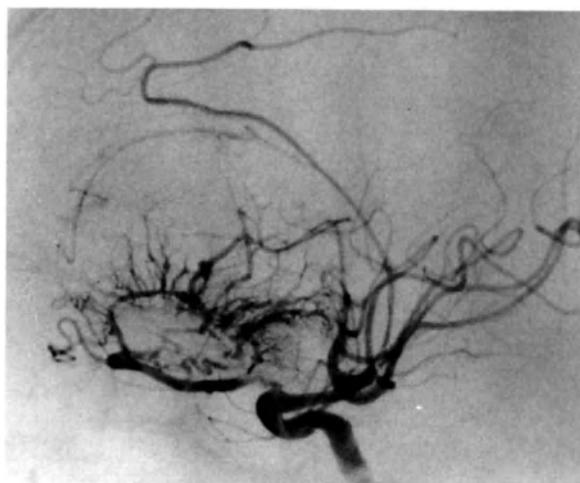


**Fig. 40.27.** Angiogram (arterial phase) showing hypertrophied ophthalmic artery and ethmoidal branches supplying olfactory groove meningioma.

cerebral tumors. A low signal rim due to vascular structures may be imaged in some cases, and in others a high signal rim due to edema in adjacent brain may outline the tumor (Fig. 40.26).

**Angiography.** Although angiography is now little used in tumor diagnosis, it still has a place in the assessment of some meningiomas. This is particularly so where the tumor is adjacent to the sagittal or other major sinus and may be involving or occluding the sinus. The major sinuses are well shown by intravenous DSA which can be performed on an outpatient basis without the risks of arterial puncture. Some neurosurgeons still require arterial studies of the blood supply and vascular relationships before surgery in highly vascular or potentially more malignant meningiomas. Some tumors of this type have been treated prior to surgery by embolization from the external carotid of meningeal feeding vessels not supplying cerebral tissue.

The blood supply of most meningiomas is mainly from the meningeal branches of the external carotid, but there is often a major supply from the internal carotid (Figs 40.27, 40.28).

#### PITUITARY TUMORS

Pituitary adenomas can be classified as endocrine-active or endocrine-inactive. The former can manifest clinically when still quite small but the latter are not diagnosed until large enough to produce chiasmal pressure and visual impairment. So-called *microadenomas* are less than 10 mm in diameter and lie within the pituitary gland.

*Endocrine-active* tumors now form about 80% of those encountered and *non-secreting* tumors about 20%, as shown in Table 40.4.

*Prolactinomas* manifest with gonadal dysfunction in both sexes and with galactorrhea in a proportion. Symptoms can be associated with large tumors, but many are microadenomas when they first present. Since hyperprolactinemia can also be produced by a variety of different drugs,

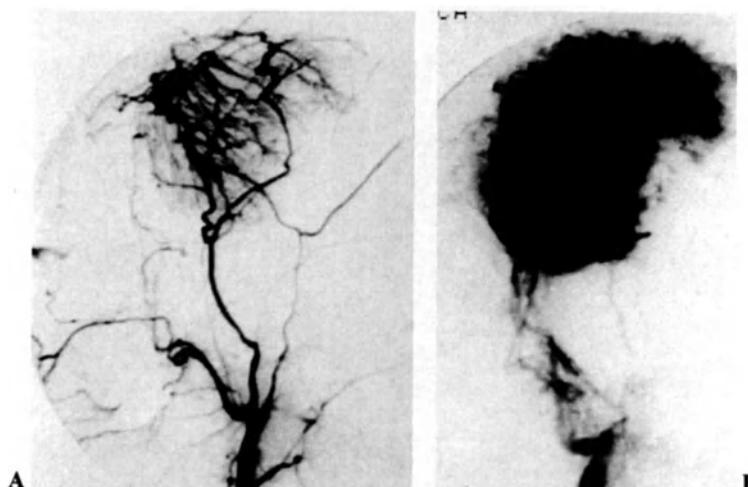


**Fig. 40.28.** **A** External carotid angiogram by arterial DSA showing blood supply to parasagittal meningioma. **B** Internal carotid arterial DSA (slightly later phase) shows dense tumor smear or 'blush'.



**Fig. 40.29A, B.** Axial CT sections showing two different pituitary adenomas extending upwards into the suprasellar cistern and laterally. The tumors were of slightly increased density and enhance well with contrast. The tumor in B also extends behind the sella. **C** Coronal reformat (post enhancement) in another patient showing upward extension into hypothalamus and third ventricle.

**Table 40.4. Pituitary tumors**

Endocrine active	
prolactinomas	35%
somatotrophic (acromegaly and gigantism)	25%
corticotropic (Cushing's and Nelson's syndrome)	5%
miscellaneous and mixed (STH-PRL, ACTH-PRL, PRL-STH, thyrotropic, gonadotropic)	15%
Non-secretory	20%

it is important to exclude this cause before imaging investigation is begun.

**Imaging.** *Simple radiography* has been discussed above (p. 710), and the diagnostic appearances produced by large adenomas described. The characteristic skull changes seen in acromegaly and gigantism have also been described (Ch. 17, Figs 17.11 and 17.12).

The diagnosis of microadenomas by simple radiographs or tomography of the sella, showing local bulging or asymmetry, is of dubious value since there is a wide range of normal variation.

CT will demonstrate adenomas large enough to produce chiasmal compression and will show the extent and relationships of the suprasellar component. The tumor first extends into the normal suprasellar cistern and then into the anterior end of the third ventricle. Eventually it can extend as high as the foramen of Monro, but is often quite asymmetrical. The tumor can also extend laterally into the cavernous sinuses and temporal lobe or downwards into the sphenoid sinus; large tumors may extend subfrontally or above and behind the sella (Fig. 40.29A, B, C).

Pituitary adenomas normally show homogeneous density similar to or slightly denser than normal brain tissue and enhance moderately well and uniformly after contrast. Some cases however contain cystic or necrotic areas which stand out more clearly after contrast.

The CT diagnosis of *microadenomas* requires high-resolution CT and direct coronal sections are preferable to reformats. Contiguous 1.5 mm sections should be obtained post-enhancement. The typical microadenoma can be recognized as a small low-density area within the opacified gland (Fig. 40.31). Other features which may be seen are deviation

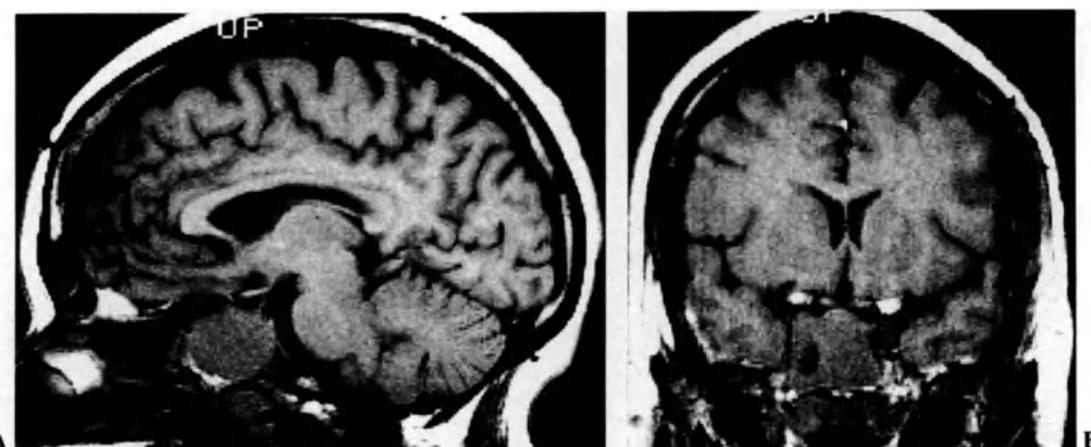


**Fig. 40.30.** **A** Sagittal midline MRI section ( $T_1$ -weighted) shows large globular pituitary adenoma. **B** Coronal section ( $T_1$ -weighted) shows relationship of tumor to the internal carotids which appear black because of flow defects.

of the infundibulum and upward bulging of the upper surface of the gland, but these are not diagnostic and can have other causes, as can local bulging of the sellar floor.

**MRI.** Large adenomas and their relationships to the adjacent brain are well shown by MRI which compares favourably with CT in this respect because of the ease with which direct sagittal and coronal sections can be obtained. The normal optic chiasm, carotid vessels and sphenoid sinus are also highly conspicuous at MRI (Fig. 40.30) and their relationships to the tumor well shown. The clivus, because of its fatty marrow appears as high signal, whilst the sphenoid air sinus appears as low signal antero-inferior to the sella.

Microadenomas were thought at one time to be beyond the resolving ability of MRI, but with up-to-date techniques and machines they too can now be imaged (Fig. 40.32) appearing as small areas of increased signal on T<sub>2</sub>-weighted images.

**Angiography.** Some neurosurgeons require angiography prior to surgery on pituitary adenomas, particularly with the subfrontal approach, so that the relationships of the adjacent vessels which may be involved can be assessed (Fig. 40.33). They also wish to be forewarned of possible aneurysms which are said to be slightly more common in these patients.

**Differential Diagnosis.** There are a wide variety of mass lesions which can occur in the suprasellar region. Many of these can be indistinguishable clinically from pituitary adenomas, and some can resemble them at imaging (Table 40.5).

Table 40.5. Suprasellar lesions

Common	<ul style="list-style-type: none"> <li>pituitary adenoma</li> <li>craniopharyngioma</li> <li>aneurysm</li> <li>suprasellar meningioma</li> </ul>
Rare	<ul style="list-style-type: none"> <li>optic chiasm glioma</li> <li>hypothalamic glioma</li> <li>germinoma</li> <li>hamartoma of the tuber cinereum</li> <li>ganglioglioma</li> <li>metastasis</li> <li>arachnoid cyst</li> <li>epidermoid</li> <li>Rathke's cleft cyst</li> </ul>

Many of the lesions listed have features which readily differentiate them from pituitary adenomas, and these are described under the individual lesions. In cases where there is more difficulty in differentiation the appearance of the sella at simple radiography is often very helpful. It nearly always shows diagnostic appearances with pituitary adenomas large enough to produce suprasellar masses, but remains relatively normal with most of the other lesions listed.

Calcification, if present, suggests a craniopharyngioma; if arc or ring-like, aneurysm or craniopharyngioma are possible. Suprasellar meningiomas can also calcify but present in an older age group, and calcification, if present, is homogeneous or nodular and never arc like.

Arachnoid cysts are easily identified by their CSF density and thin capsule at CT.

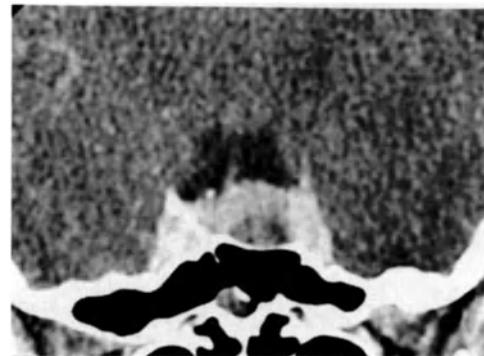


Fig. 40.31. Pituitary microadenoma shown by CT. The low density microadenoma is also bulging the floor of the sella.

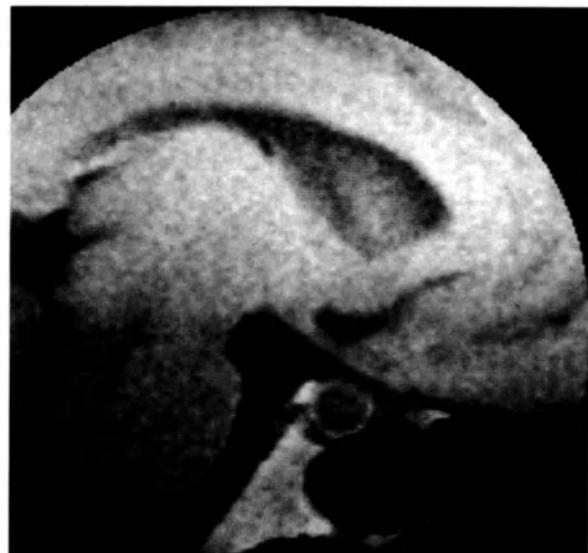


Fig. 40.32. Pituitary microadenoma shown by MRI (proton density).

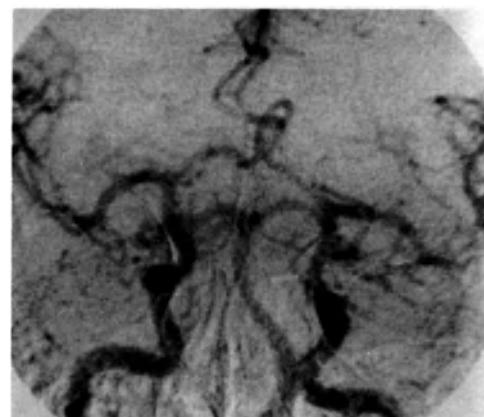
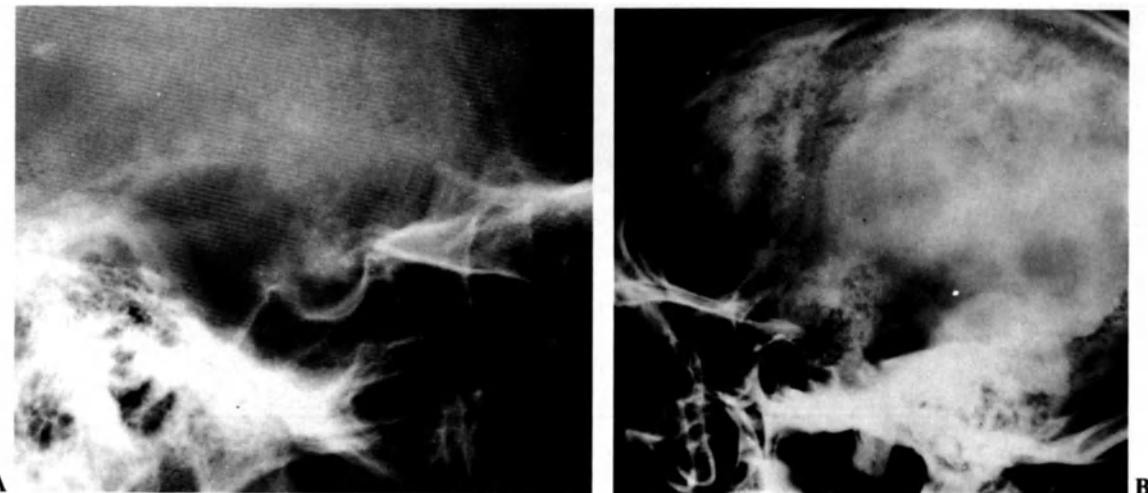


Fig. 40.33. I.v. angiogram (DSA). Shows both carotid syphons displaced laterally and slight upward bowing of the anterior cerebrals by a large pituitary adenoma.



**Fig. 40.34A, B.** Suprasellar calcification and erosion of the dorsum due to craniopharyngiomas. Two different cases.

**Empty Sella.** The 'empty sella syndrome' is discussed here because it sometimes enters into the differential diagnosis both clinically and radiologically of pituitary tumors. An empty sella may be classified as primary or secondary:

1. Primary (idiopathic) empty sella
2. Secondary empty sella: post-hypophysectomy or post-tumor removal, post-radiation therapy of sellar contents, post-infarction of pituitary (normal or tumor)

*Primary* empty sella is due to a congenital defect in the diaphragma sellae permitting suprasellar arachnoid and CSF to herniate into the sella. The pituitary gland is compressed against the back and floor of the sella and much or most of the sella is occupied by CSF. The condition may be entirely symptom free and only discovered as a chance finding at imaging or autopsy for other causes. Symptomatic cases are commoner in females and there may be an association with raised intracranial pressure, since they are often obese, multiparous and hypertensive. Visual field defects can occur due to prolapse of optic nerve or chiasmal tissue into the empty sella. The sella itself may become enlarged presumably from pulsating CSF, and this with the clinical findings can lead to an erroneous diagnosis of pituitary tumor.

*Secondary* empty sella may be due to any of the causes listed above and can also, give rise to symptoms suggesting tumor recurrence.

**Imaging.** *Simple radiography.* The sella may appear normal, but can be enlarged in a globular manner. As already noted this can be mistaken for enlargement by a pituitary adenoma.

CT or MRI will show the pituitary fossa to be occupied largely by fluid of CSF or water density rather than a normal gland.

#### CRANIOPHARYNGIOMA

Most of these tumors present in childhood or adolescence, though they can also occur in adults. Calcification is present in over 80% of the childhood cases, but is often absent in

the less common adult cases. The tumors usually grow above the sella and are intimately adherent to the floor of the 3rd ventricle and infundibulum, which makes surgical extirpation difficult or impossible.

A small proportion (15%) grow into the pituitary fossa and can produce enlargement and deformity of the sella.

**Imaging.** *Simple radiography* is often diagnostic in children, where the presence of suprasellar midline calcification should immediately suggest the diagnosis. This can vary from a few flecks to dense nodular calcification (Fig. 40.34A, B). Arc like calcification can also occur in the margin of tumor cysts.

In most cases the sella is normal but in some there is enlargement. The intrasellar cases can produce enlargement resembling that of pituitary adenomas but the presence of calcification should indicate the true pathology. Forward bowing of the dorsum as if pressed on from above is also seen in some cases with apparent flattening of the sella and this is very suggestive of the cause.

CT. Suprasellar calcification is more readily identified than at simple radiography and always suggests the diagnosis (Fig. 40.35). The tumors are often cystic or partly cystic, and the cysts may be multiple or single. Whilst the solid non-calified parts can enhance well after contrast the cystic components do not. The latter may be of low or high density before contrast depending on their content. Thus there is a wide spectrum of appearances ranging from a homogeneous mass which enhances moderately well, to a cystic mass which shows only marginal enhancement, or a mass showing mixed enhancement.

Some of these tumors may appear slightly ectopic and to lie in the third ventricle or behind the sella.

MRI. Apart from its poor visualization of calcification, MRI shows most of the features of a craniopharyngioma as well as CT and shows the relationships with brain and adjacent tissues to best advantage, particularly in sagittal and coronal sections (Fig. 40.36).

**Rathke's cleft cyst.** It is important to differentiate these rare lesions from craniopharyngiomas since they are much easier

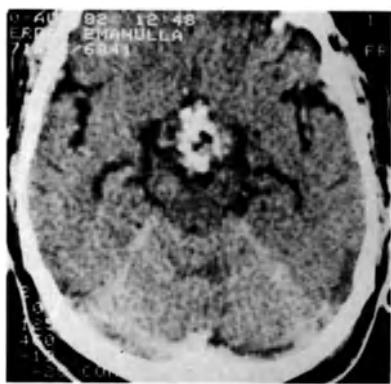


**Fig. 40.35.** CT shows calcified and partly enhancing suprasellar mass (craniopharyngioma).

to treat surgically. They are benign thin-walled unilocular cysts, which do not recur even after simple evacuation. They have no solid components and do not calcify. They are lined with cuboidal epithelium and contain mucinous cyst fluid.

CT shows a round mass in the suprasellar cisterns with no calcification. The density varies from CSF like (in which case it cannot be differentiated from an arachnoid cyst before histological examination of the cyst wall) to more solid looking when the contents are viscous and pus like. The capsule may then enhance slightly resembling a cystic craniopharyngioma.

MRI shows similar features to those just described for CT.

### INCLUSION TUMORS

Epidermoid tumors, dermoid tumors and teratoma have been classified together as inclusion tumors. They are all rare and together form less than 2% of intracranial tumors, though

epidermoids are twice as common as the other two. Epidermoids can occur at any age, but dermoids and teratomas are seen mainly in children. Teratomas are commoner in males, but the other two inclusion tumors occur equally in the two sexes.

**Epidermoid.** Histologically epidermoids are tumors with a thin capsule of epidermis (squamous keratinized epithelium); they contain desquamated epithelial debris and cholesterin, which gives rise to their characteristic metallic or 'pearly' sheen.

They usually present in adults and are commonest in the CP angle or suprasellar region in the subarachnoid space. Other sites are in the Sylvian fissure and in the ventricles.

The exact site of origin is often difficult to determine since the tumors can infiltrate widely around vessels and nerves as they extend in the subarachnoid space.

**Imaging.** CT. The tumors are usually of very low (fatty) density, but density can be as high as CSF, depending on the content. The margins may be ill defined and they do not enhance with contrast. Calcification is unusual but has occasionally been noted at the capsule in a fleck-like manner.

**MRI** can show these tumors well and characterizes their fatty contents. The appearances depend on the relative proportions of cholesterol (short  $T_1$ ) and keratin (long  $T_1$ ) within the tumor.

**Dermoids** are more complex tumors. Their wall contains a full width of dermis which may contain hair and sebaceous glands and an outer layer of connective tissue as well as a connective tissue capsule. The cyst may contain matted hair and glandular secretions as well as desquamated keratinized epithelium. They normally present in children, and may lie in the midline at the base of the brain or near the 4th ventricle. The latter may show an occipital skin dimple with a stalk leading through the bone to the lesion. Such dermoids can become infected.

**Imaging.** *Simple radiography.* As noted above (p. 717) posterior fossa dermoids in children may be suggested by an occipital bone defect. Wherever sited, calcification of an arc like type resembling that seen in aneurysms may occur in the capsule and is seen in 20% (Fig. 40.37).

**CT.** The cysts are usually of fatty or low density and more rounded than epidermoids. They are seen in the posterior fossa near the midline, or above the floor of the anterior fossa but they can occur over the convexity or elsewhere. Capsular calcification occurs more commonly than with epidermoids (Fig. 40.38). Rupture of a cyst may occur with escape of the fatty contents into the CSF followed by arachnoid scarring and hydrocephalus; rupture into a ventricle has also been reported and this has been recognized at CT by a fat-fluid level.

**MRI** should show most of the features seen at CT but will fail to show calcification (Fig. 40.39).

**Teratomas** present mainly in children (average age 12 years), and can be seen even in infants below one year of age. About 50% lie in the pineal region, and other common sites are the floor of the 3rd ventricle and the suprasellar area.

Their macroscopic appearance is variable as they can be cystic, multicystic or solid. The solid tumors may contain all primitive tissue elements including teeth.



**Fig. 40.36.** Sagittal midline MRI section (proton density; 1500/30) shows large cystic craniopharyngioma as high signal mass occupying suprasellar region and occluding the third ventricle. (Courtesy of Dr Gordon Thomson and Bristol MRI centre.)



**Fig. 40.37.** Lateral skull film shows marginal calcification (arrow) in a midline posterior fossa dermoid.

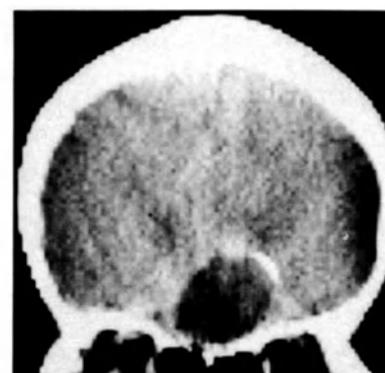


**Fig. 40.38.** CT shows marginal calcification in a midline cyst lying subfrontally above the ethmoids and olfactory groove. Dermoid.

**Imaging.** *Simple Radiography.* Calcification is present in 50% of mature teratomas, and may suggest the diagnosis, though the very rare presence of recognizable dental elements is the only truly diagnostic feature. The typical site (pineal or 3rd ventricle) may also suggest the diagnosis.

**CT.** Cystic or multicystic tumors will be recognized at CT, and the age of the patient and classical site may suggest the diagnosis. However, the specific diagnosis of teratoma will depend on the recognition of multiple tissues (such as fat together with more solid or calcified elements) or of dental elements.

**MRI** suffers from not characterizing calcification, but will show and differentiate the soft tissue and cystic components.

#### PINEAL TUMORS

The terms pineal tumor or pinealoma are conventionally used for any tumor occurring in the pineal area. In fact, a variety of different tumors can arise in this region. They are listed in Table 40.6 with (in parentheses) figures showing the relative incidence of different types in a large series of 54 verified cases (Ganti et al. 1986). It should be noted that teratomas are classified in Table 40.6 with germ cell tumors to which they are related, though they can be classified with the inclusion tumors as above.

**Table 40.6.** Pineal tumors

Pineal cell tumors (13)
pineoblastoma (8)
pineocytoma (5)
Glial tumors (16)
astrocytoma
glioblastoma
Germ cell tumors (25)
germinoma (16)
teratoma (5)
embryonal cell carcinoma (1)
choriocarcinoma (1)
Inclusion tumors (0)
epidermoid
dermoid
Metastases (0)

The commoner tumors are listed in the upper half of the table; tumors below teratoma are all very rare in the pineal region, though all have been recorded.

Another mass lesion which can occur here in children is the *arachnoid cyst*. Differential diagnosis also includes adjacent tumors such as *meningioma* of the tentorial apex and *aneurysm of the vein of Galen*.

**Imaging.** The *simple radiograph* may show abnormal calcification in the pineal area which raises the possibility of a tumor here, and this is most likely to be a germ cell tumor. There may also be general evidence of raised intracranial pressure.

**CT.** A soft tissue mass is shown in the pineal area. This can be recognized even if quite small and uncalcified by the characteristic indentation of the back end of the 3rd ventricle. The mass may be solid or cystic or mixed solid and cystic. Obstruction to the mouth of the aqueduct results in symmetrical hydrocephalus.

Calcification can be localized and nodular or very extensive and is seen mainly with germ cell tumors (Fig. 40.40).



**Fig. 40.39.** Midline sagittal MRI study (T<sub>1</sub>-weighted) showing low signal mass with high signal lower part in the lower vermis. Posterior fossa dermoid.



**Fig. 40.40.** CT shows gross hydrocephalus of lateral and third ventricles due to large calcified mass in pineal region.

It is usually absent in gliomas and pineal cell tumors. A recognizable area of fat content may be seen in teratomas or inclusion tumors, whilst the presence of a dental element is diagnostic of teratoma.

The solid part of a pineal tumor usually enhances strongly after contrast.

**MRI.** The pineal tumors are readily shown by MRI since they are so well shown in sagittal section. Cystic and solid areas are well differentiated but calcification is not identified.

solitary tumors but in von Recklinghausen's neurofibromatosis bilateral acoustic tumors may be seen.

**Imaging.** *Simple radiography* either alone or with tomography will show expansion of the internal auditory meatus in a significant proportion of these tumors, usually the larger ones (Fig. 40.10). There may also be generalized evidence of raised intracranial pressure with sellar erosion.

**CT.** Large and medium-sized acoustic tumors are generally isodense and difficult to visualize on the unenhanced scan. Rotational deformity of the 4th ventricle however may suggest their presence as may symmetrical hydrocephalus. Most of these tumors, however, will manifest clearly after contrast by enhancing strongly (Fig. 40.41).

The rare cystic tumors are of low density and may simulate an arachnoid cyst or epidermoid in the cerebello-pontine angle. Only the solid part of the tumor will enhance.

Small acoustic tumors (less than 10 mm in diameter), or tumors lying in or just protruding from the internal auditory meatus, are more difficult or impossible to demonstrate on conventional CT. They can however be readily shown by the special technique of *CT with air meatography* (Fig. 40.42).

**MRI.** Acoustic tumors are very well demonstrated by MRI (Fig. 40.43A, B), with or without Gadolinium-DTPA enhancement. Direct coronal cuts can image both sides at the same time and since there is no interference from bone even small tumors can be identified in the meatus or extending into it (Fig. 40.43B). Many workers believe that this is already the method of choice for imaging small acoustic tumors, and being non-invasive is preferable to CT with air meatography.

#### ACOUSTIC NEUROMA

Acoustic neuromas occur mainly in the middle-aged and elderly. They are, in fact, Schwannomas or tumors of the Schwann cells which form the nerve sheath. They are firm encapsulated tumors which vary greatly in size at presentation. The larger tumors may become irregular and lobulated and can become cystic. As a rule they are single

#### GLOMUS JUGULARE TUMORS

These tumors originate in the jugular body situated in the wall of the jugular bulb. They proliferate into the middle ear and can present at the drum as a 'cherry red' polyp. They can also extend into the posterior fossa, and down into the neck. They are commoner in females.

**Imaging.** *Simple Radiography.* The characteristic appearances have been described above (p. 729).



**Fig. 40.41.** CT shows acoustic neuroma as large lobulated enhancing mass in CP angle.

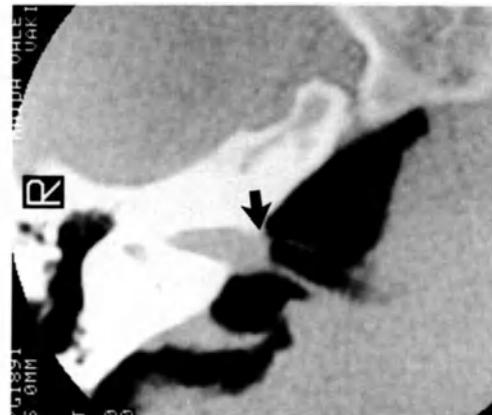


**Fig. 40.42.** CT of air meatogram shows small acoustic neuroma protruding from meatus.

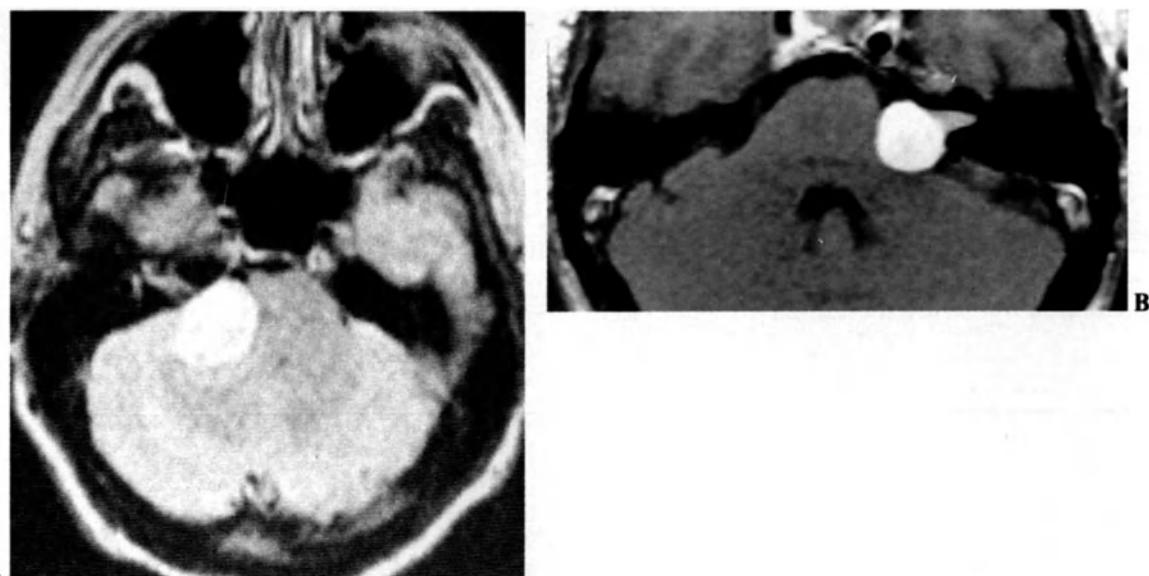


**Fig. 40.43A, B.** A. Axial MRI study ( $T_2$ -weighted) shows large rounded acoustic as high signal lesion in right CP angle. B. Axial MRI study ( $T_1$ -weighted) shows a medium-sized acoustic tumor in the left CP angle. Gadolinium enhancement highlights the tumor and its extension into the IAM. (Courtesy of Dr Peter Phelps.)

CT. This will show the bone destruction well and post-enhancement any associated intracranial extension and downward extension into the neck.

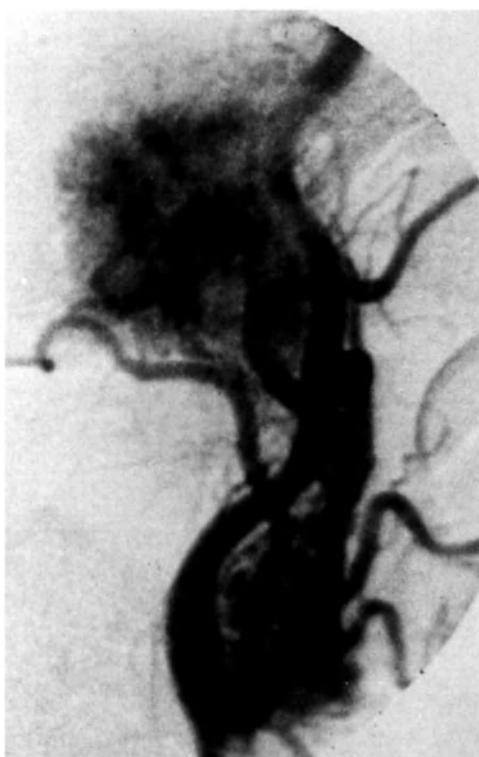


**Fig. 40.44.** Carotid angiography shows both a large glomus jugulare tumor at the skull base and a concomitant carotid body tumor at the carotid bifurcation.

**MRI.** The ability to obtain direct coronal sections is helpful in assessing the full extent of the tumor, and is particularly useful in showing involvement of the internal jugular vein.

**Angiography.** These tumors like most chemodectomas are highly vascular (Fig. 40.44) and are well demonstrated by angiography. Selective external carotid angiography with subselective catheterization of the occipital and ascending pharyngeal arteries has been used both for diagnosis and for therapeutic embolization.

#### HEMANGIOBLASTOMA

These tumors may be solitary or multiple and are most commonly found in the posterior fossa. Less frequently they may be seen in the spinal cord (see Chap. 44). The association with von Hippel–Lindau syndrome is well known but most cases occur without this. Supratentorial tumors are very rare and appear to occur only with the von Hippel–Lindau syndrome.

Hamangioblastomas are seen in adult patients with a peak incidence from 35 to 45 years. They are vascular tumors but may develop large cysts which can mask the underlying vascular nodule.

**Imaging.** CT. The appearances vary with the presence or absence of a large cystic component. A solitary nodule with a large cyst can easily be mistaken for a low-density glioma or gliomatous cyst (Fig. 40.45) unless the mural nodule is identified in the post-enhancement scan. The tumor nodule is isodense or slightly hyperdense, and enhances strongly after contrast (Fig. 40.46). Multiple tumors are often small and can measure only a few mm in diameter. Thus they are easily missed even on high-quality scans if not included in the section.

**MRI.** The cysts and nodules can be well demonstrated and

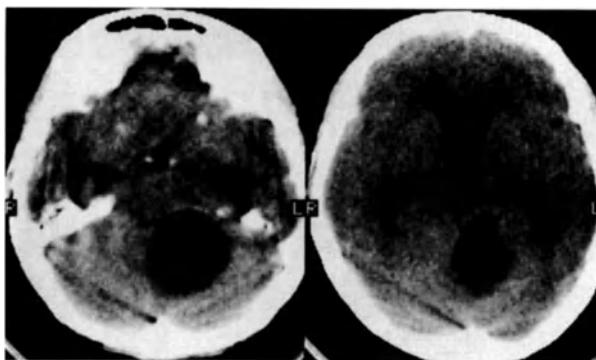


Fig. 40.45. CT of cystic hemangioblastoma. The vascular tumor nodule can easily be missed in these cases.

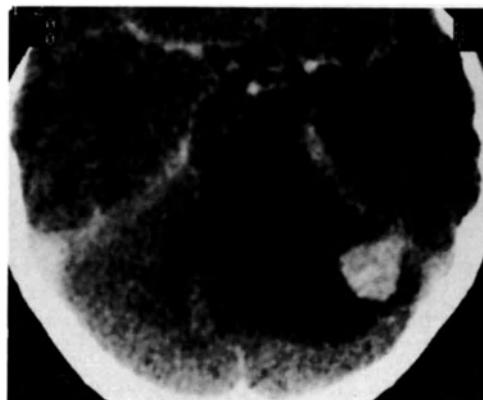


Fig. 40.46. CT shows both the tumor cyst and the vascular hemangioblastoma nodule. Post enhancement scan.

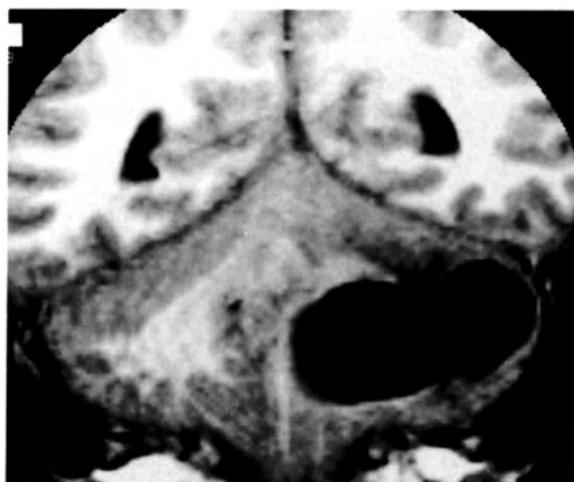


Fig. 40.47. Coronal MRI study (T<sub>1</sub>-weighted). A large hemangioblastomatous cyst is well shown. (Courtesy of Dr Gordon Thomson and Bristol MRI centre.)

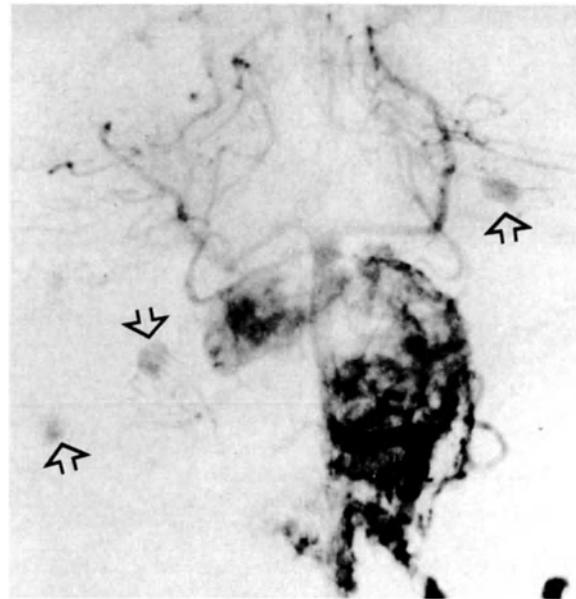


Fig. 40.48. Vertebral angiogram shows two large vascular hemangioblastomas near the midline as well as several smaller tumor nodules (arrows). Subtraction print.

characterized by MRI, but as with CT small nodules are easily overlooked (Fig. 40.47).

**Angiography.** Hemangioblastomas are highly vascular tumors and show a characteristic appearance at angiography. There is a dense blush of contrast commencing in the arterial phase and continuing through into the venous phase. The large nodules can be 1 to 2 cm in diameter and can resemble angiomas or even aneurysms. They may show arteriovenous shunting with one or more large drainage veins visible in the arterial phase. Smaller nodules appear as smears of contrast in the arterial phase (Fig. 40.48).

Vertebral angiography is indicated in most cases of suspected hemangioblastoma, even after CT or MRI, since it is the most accurate method of identifying multiple small lesions. Many of the smaller lesions are easily missed at CT or MRI.

## METASTASES

Metastasis to the brain, skull or meninges can occur in most forms of systemic cancer.

Skull metastases have been described above (p. 729). Rather surprisingly most have little effect on the brain, but occasionally a large deposit will grow inwards and involve the meninges and underlying brain.

Intracerebral deposits are seen most frequently from the following three primary tumors:

Lung (commonest in males)

Breast (commonest in females)

Melanoma

Primary melanoma is of course less common than the other two tumors, but metastasizes to brain more often and

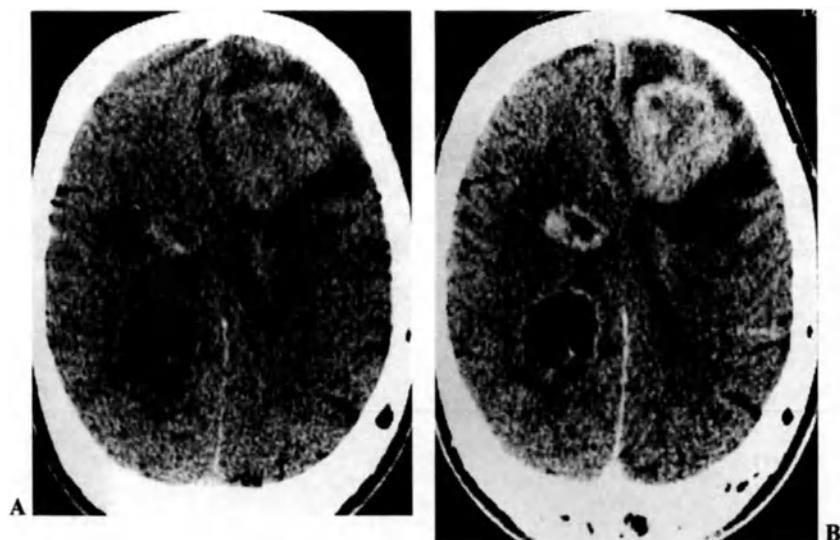
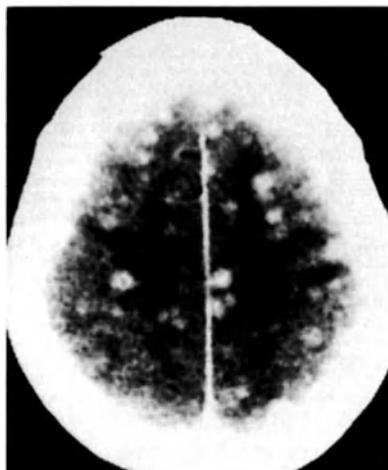


**Fig. 40.49A, B.** CT of multiple cerebral metastases from lung carcinoma showing different patterns of enhancement. A Before and B after contrast.



thus is able to rival them in importance (40% of melanomas metastasized to brain as against 20% for lung and 10% for breast in one large series).

Other primary tumors which metastasize to brain and figure prominently in most major series include:

Kidney  
Gastrointestinal tract  
Testis

Primary testicular tumors, though less common than the others, again show a higher incidence of cerebral metastasis

◀  
**Fig. 40.50.** CT of multiple nodular enhancing deposits from breast carcinoma.

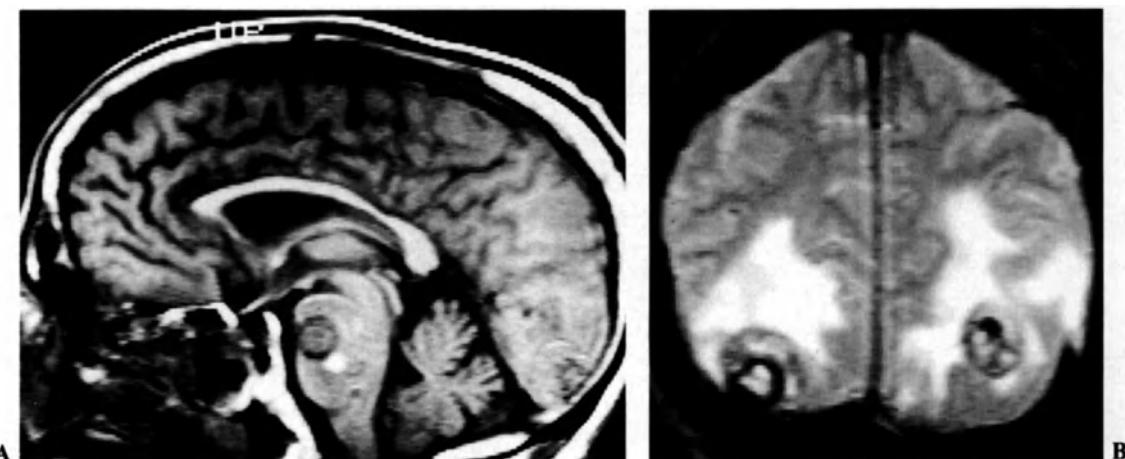


**Fig. 40.51.A** Sagittal MRI study (T<sub>1</sub>-weighted) shows metastases in the pons and in the occipital pole. **B** Coronal MRI study (T<sub>2</sub>-weighted) shows symmetrical deposits in both occipital poles with surrounding edema as high signal. High signal within the secondaries probably due to recent hemorrhage.



**Fig. 40.52.** CT shows chordoma as calcified mass protruding up from clivus and deforming brainstem.

(45% as against 20% for kidney and 3% for gastrointestinal tumors).

Lymphoma can metastasize to brain but this is very uncommon. In one large series it occurred in only 1% of cases, all of these being non-Hodgkin's lymphoma. The question of primary lymphoma of the brain (so called microglioma) is dealt with below.

Metastatic disease of the brain in children is less common than in adults and arises from different tumors. The most common are neuroblastoma, Wilms' tumor, rhabdomyosarcoma and osteogenic sarcoma.

**Imaging.** Simple radiography has been discussed above (see p. 729) and the appearances described. There is rarely

generalized evidence of raised intracranial pressure as the symptoms usually evolve rapidly.

**CT.** Multiple small deposits tend to seed peripherally in the brain with a predilection for the grey-white matter interface. However deposits can occur anywhere including brainstem, cerebellum, basal ganglia, and white or grey matter. One helpful feature with solitary deposits is disproportionate edema of the white matter which may be seen even with a small superficial lesion.

Most deposits are isodense but melanoma secondaries are characteristically hyperdense, sometimes from hemorrhage. Hemorrhagic secondaries have less commonly been described from other tumors (breast, hypernephroma, choriocarcinoma and sarcoma).

**Calcification** is very rare and is a point against the diagnosis of metastasis. However it can occur and has been described from bone sarcoma and colonic carcinoma. It may also be seen post-radiation treatment.

Large metastases tend to become necrotic centrally and may appear cystic.

Contrast enhancement, often very marked, is an almost universal feature of metastases. This may be seen as a well-defined nodule within an area of surrounding edema, or if the centre is necrotic or cystic as a marginal or ring enhancement (Figs. 40.49, 40.50). Superficial nodules easily missed on the pre-enhancement scan may be more easily recognized after contrast.

**Differential Diagnosis.** The presence of multiple discrete lesions within the brain should always suggest the diagnosis of metastases. Similar appearances may be seen with multiple small abscesses or granulomas, though the clinical features will often help to differentiate. In the posterior fossa multiple hemangioblastomas may have to be considered.

Unfortunately a high proportion of patients (50% or more in some series) present with a solitary metastasis, and unless there is a known primary this can raise a difficult problem

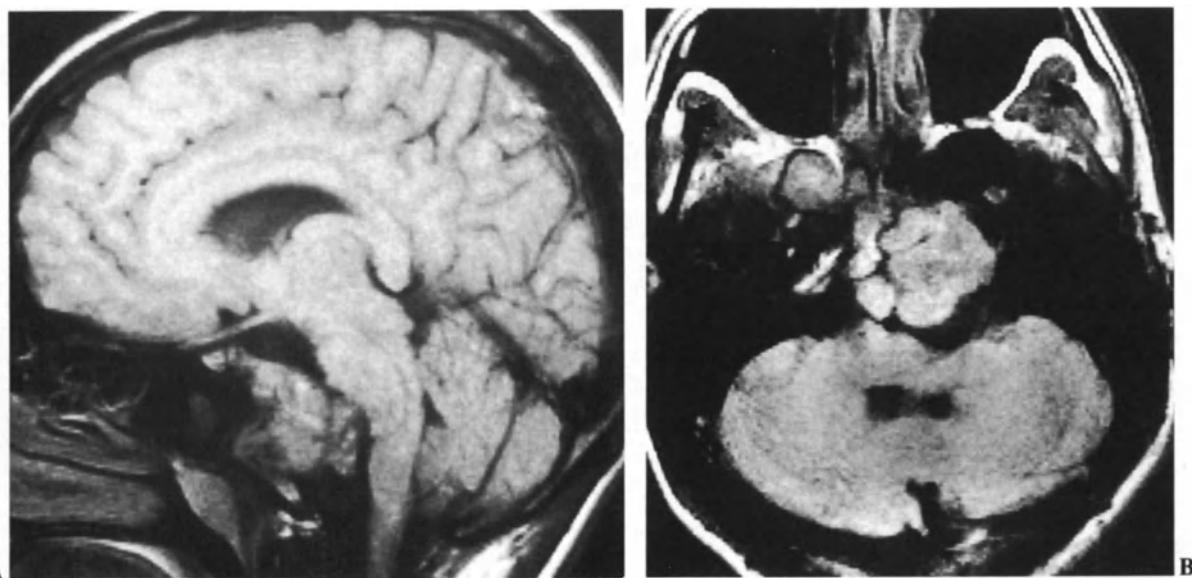


**Fig. 40.53.** A Sagittal midline MRI study ( $T_1$ -weighted). Chordoma of the clivus protruding backwards into the brainstem and forwards into the nasopharynx. B Axial section through the tumor.

of differentiation from a primary brain tumor or cerebral abscess. In some cases this may only be resolved by biopsy.

*MRI.* As with CT multifocal lesions always raises the possibility of metastases (Fig. 40.51) though multiple abscesses or granulomas can produce similar appearances. The solitary lesion raises similar problems to those just described for CT.

**Primary Lymphoma (microglioma).** As noted above secondary lymphoma of the brain is rare, though it can occur. More usually however, lymphoma of the brain is found without any systemic involvement, especially in immunocompromised patients. These tumors were once referred to as microgliomas, but are now called primary lymphomas. The prognosis is poor and median survival is about twelve months even with active treatment.

*CT.* Their general appearance and enhancement resembles that seen in metastases i.e., they are hyperdense and enhance homogeneously with contrast, and can be unifocal or multifocal. However they show less or no edema and central necrosis is not a feature. They also tend to lie more

deeply, in the basal ganglia or paraventricular region and subependymal spread may occur.

### CHORDOMA

These tumors have been described above (p. 729 and p. 312, Chap. 16). Intracranial extension is often a feature of those arising from the clivus and they may present with symptoms and signs suggesting an intracranial tumor arising in the region of the brainstem or cerebello-pontine angle.

The intracranial extension and its relationship to the brain are best shown by CT or MRI (Figs 40.52, 40.53). *CT* clearly demonstrates the calcification which is often present in these tumors and should suggest the diagnosis. However *MRI* has the advantage of more easily obtaining sagittal and coronal as well as axial images and gives a better demonstration of the full extent and morphology of the lesion.

*For further reading, see p. 790.*

## CHAPTER 41

# VASCULAR LESIONS

D. Sutton

Vascular lesions involving the brain will be considered under the headings of congenital, fibromuscular hyperplasia, dissection, stenosis and thrombosis, embolus, infarcts, aneurysm, angiomatic malformation, AV fistula and hemorrhage.

### CONGENITAL LESIONS

The *Circle of Willis* is theoretically a perfect collateral system. If one carotid is blocked it permits easy flow from the other side or from the posterior circulation; similarly there should be free flow between the anterior and posterior circulations if either is obstructed. In practise a high proportion of patients have inadequacy of the Circle of Willis because the anterior communicating or posterior communicating artery is hypoplastic (Fig. 41.1A).

*Anomalies of the great vessels* are also frequent (Fig. 41.1B) and these are important to the neuroradiologist performing transfemoral catheterization for cerebral angiography. The innominate and left common carotid arteries arise in common in some 20% of white people and in 36% of black; much less commonly the left common carotid arises from the innominate. An anomalous right subclavian arises from the distal arch in 1%-2% of patients, and the left vertebral arises directly from the arch in 5%. There are many other much rarer anomalies, often associated with congenital heart lesions.

The common carotid normally bifurcates opposite C3 or C4 but can bifurcate as low as C7 or as high as C2. Rarely there may be aplasia of the internal or external carotid arteries.

*Anomalous carotid basilar anastomoses* are described and named trigeminal, acoustic and hypoglossal arteries after the cranial nerves they accompany (Fig. 41.2). The commonest is the trigeminal which connects the internal carotid as it enters the cavernous sinus with the termination of the

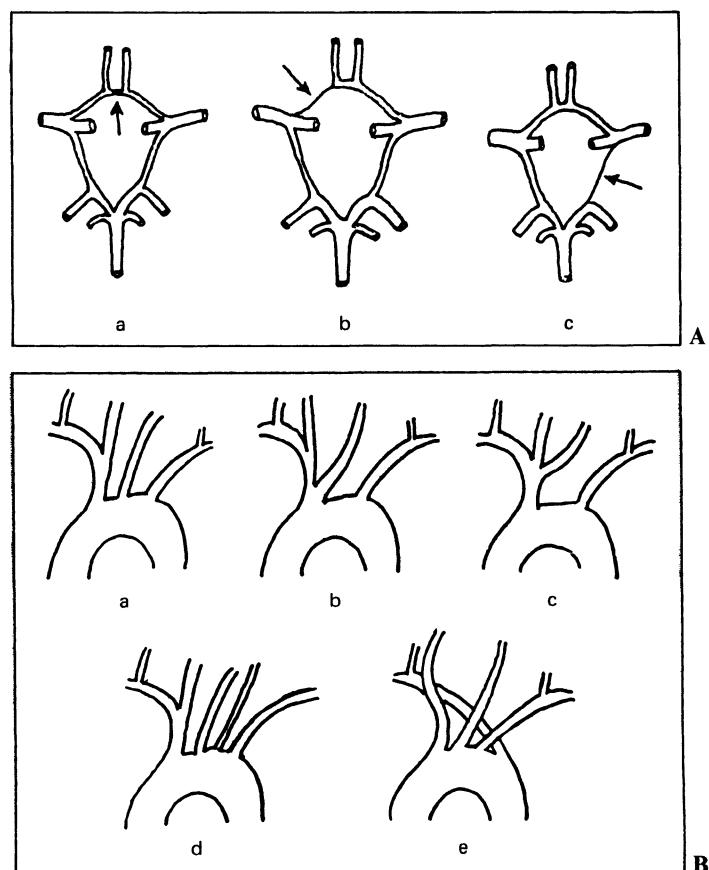
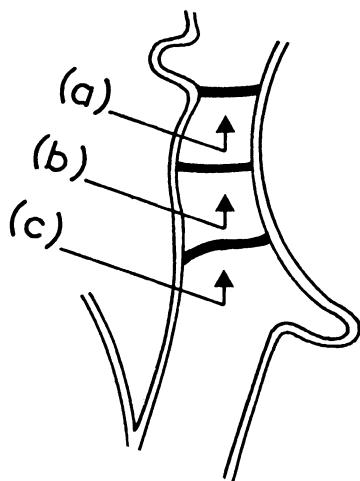


Fig. 41.1.A Anomalies of the Circle of Willis. a, hypoplastic anterior communicating artery; b, hypoplastic proximal segment of anterior communicating artery; c, hypoplastic posterior communicating artery. B Diagram illustrating common anomalies of the great vessels. a, normal; b, joint origin of innominate and left common carotid; c, left common carotid arises from innominate; d, left vertebral arises directly from the arch; e, anomalous right subclavian arises distally from the arch and passes behind the esophagus.



**Fig. 41.2.** Diagram illustrating anomalous communications between carotid and vertebro-basilar systems. a, trigeminal artery; b, acoustic artery; c, hypoglossal artery.

basilar and is seen in one patient in 500. The hypoglossal artery which passes through the anterior condyloid foramen is less common, whilst the acoustic artery which passes through the internal auditory meatus is very rare indeed.

The *proatlantal intersegmental artery* arises from the internal carotid in the neck and supplies the vertebral as it passes backwards on the arch of the atlas.

Hypoplasia of the terminal segment of the vertebral artery beyond the origin of the posterior inferior cerebellar artery is not uncommon and fenestration of this segment is also seen. Fenestration of the basilar artery is also described.

*Anomalous origin of the middle meningeal artery* or its anterior branch from the ophthalmic artery is occasionally seen. The converse anomaly, origin of the ophthalmic from the middle meningeal, can also occur and it is important for the interventional neuroradiologist to exclude this anomaly before embolizing the internal maxillary. The middle meningeal can also arise from the stapedial artery, an intrapetrosal branch of the internal carotid.

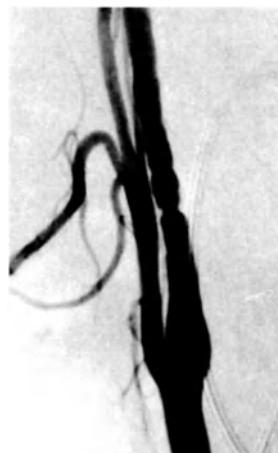


**Fig. 41.3.** Fibromuscular hyperplasia of the internal carotid artery.

Another rare but clinically important anomaly is *lateral kinking of the internal carotid* in its intrapetrosal course with the apex of the kink lying in the internal ear behind the drum. This can give rise to pulsating tinnitus and be mistaken for a vascular tumor with disastrous consequences. The anomaly is well shown by angiography in the AP view where the affected segment protrudes laterally and appears narrowed. It has also been diagnosed by contrast enhanced CT.

*Azygos anterior cerebral artery* is the name given to the large single anterior cerebral artery which can rarely replace the normal paired anterior cerebrals. It can be associated with agenesis or lipoma of the corpus callosum.

*Imaging.* Most of the anomalies described above are diagnosed or encountered as chance findings at angiography. Lesions of the larger vessels may also be recognized at CT or MRI.

#### FIBROMUSCULAR HYPERPLASIA

This disorder is a congenital anomaly of the muscular wall of arteries first described in the renal, but later shown to involve many other vessels including the internal carotid and vertebral. The patients are usually middle-aged females and the internal carotid is found at angiography to show the irregular beading characteristic of the anomaly (Fig. 41.3).

**Dissection of the internal carotid** may be spontaneous or traumatic and is described below (see Chap. 42, p. 780).

#### STENOSIS AND THROMBOSIS

**Atheromatous stenosis** of the major vessels supplying the brain is common, the sites of election being the origins of the internal carotid and vertebral arteries. Stenosis of the internal carotid may be suspected by the presence of a bruit or the occurrence of transient ischemic attacks (TIAs). The latter are due to small emboli arising from the atheromatous plaques, particularly if ulcerated (Fig. 41.4).

Stenosis of the internal carotid origin is widely treated by endarterectomy as a prophylactic measure against the thrombosis which may eventually ensue. However the result of thrombosis of the internal carotid is unpredictable and depends on the adequacy of the collateral circulation, especially the Circle of Willis. In some patients it may give rise to grave symptoms including a dense hemiplegia. Other patients with carotid thrombosis may show no symptoms at all, and occasionally thrombosis, by removing the source of emboli, may even improve the patient by curing TIAs previously present.

The symptoms resulting from carotid thrombosis (Fig. 41.5) depend on the pattern of ischemic brain damage. This is variable depending on collateral circulation and general circulatory efficiency. It is discussed in more detail below under 'infarcts'.

Multiple lesions may be present affecting the origins of all four vessels supplying the brain and including mixed thrombosis and stenosis (Fig. 41.6). Atheromatous stenosis may also be present in the carotid siphon as it passes through the cavernous sinus. Though less common than stenosis of



**Fig. 41.4.** Stenosis of the internal carotid origin showing ulcerated atheromatous plaque.



**Fig. 41.6.** Intravenous DSA study showing stenosis of the left internal carotid origin (box arrow) and also of the left vertebral origin (curved arrow).

the internal carotid origin, this is frequent enough to be significant and the area should always be checked at angiography.

Localized stenosis and thrombosis of the smaller intracranial vessels is less common, but does occur and may require careful examination of serial angiographic films for diagnosis. Atheromatous stenosis and thrombosis can also involve the great vessels arising from the aortic arch and affect cerebral blood flow. Atheromatous irregularity and plaques are also common in the aortic arch and may be a source of emboli.

*Subclavian steal* is the term used for thrombosis of the proximal segment of the left subclavian artery with the left vertebral artery acting as a major collateral and supplying

the blood flow to the arm by retrograde flow. The unfortunate title was coined in the belief that blood was being 'stolen' from the brain to supply the arm. However, the situation rarely produces any symptoms in humans and the right vertebral seems to cope easily with the increased flow. We have often encountered the lesion as a chance finding in patients being investigated for other lesions. Right sided subclavian steal may also be encountered but is less common.

Atheromatous stenosis of the vertebral artery is commonest at its origin but can occur at higher levels. Compression by osteophytes is also quite common.

Atheroma of the basilar artery may lead to thrombosis with fatal effects. However patients can survive quadriplegic and comatose or with a 'locked in' syndrome, i.e. conscious but mute and paralysed.

*Arteritis* can accompany a large number of disorders of differing etiology. They include:

1. *Takayasu's arteritis* (pulseless disease) which affects the aortic arch and great vessels. Originally described in young Japanese women the disease is now known to be widespread in other races and can also affect men. The etiology remains obscure.
2. *Infective*. Bacterial (pyogenic, tuberculous and syphilitic), fungal and other inflammatory basal meningitis.
3. *Collagen disorders*. Systemic lupus, polyarteritis nodosa and temporal arteritis can all involve smaller arteries.



**Fig. 41.5.** Thrombosis of the internal carotid.

*Moyamoya disease* is a vascular occlusive disease first described in young Japanese women, but now known to be widely distributed. The Japanese name meaning 'puff of smoke' refers to the appearance at angiography of the large number of tiny collaterals at the base of the brain. These arise to compensate for severe congenital or acquired stenosis of the terminal internal carotid and origins of the anterior and middle cerebral arteries.



► Fig. 41.7. Arch aortogram showing atherosomatous stenosis of the left internal carotid origin.

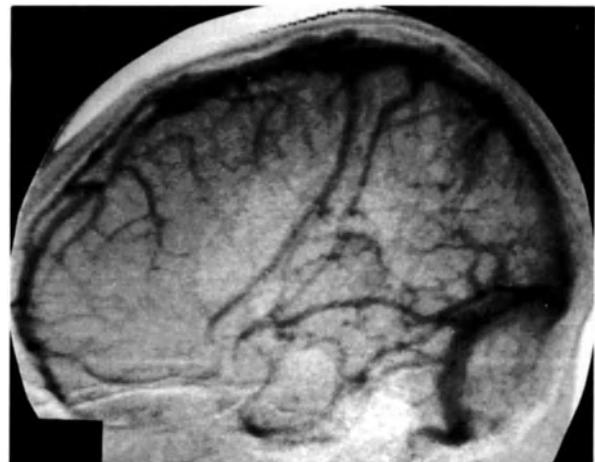


Fig. 41.8. DSA study of the superficial cerebral veins and major sinuses which appear normal.

**Venous Thrombosis.** Thrombosis of the sagittal, cavernous or lateral sinuses may occur secondary to infection of frontal sinuses, facial soft tissues, mastoid or middle ear. It may also follow dehydration, congestive heart disease, pregnancy, post-operative states and blood disorders. Cortical veins can also be involved either primarily or by extension from thrombosed sinuses. Depending on the site and extent of the thrombosis there may be little effect or extensive venous infarction with congested swollen and hemorrhagic brain.

**Imaging.** *Angiography* is required for the definitive diagnosis of most of the lesions described above (Figs 41.4–41.7). However CT or MRI will show clearly the resulting brain lesions and these are discussed below under *infarcts*.

Stenosis and thrombosis of the internal carotid origin may also be demonstrated by *ultrasound*, but most surgeons will require full vascular studies by angiography if surgery is to be undertaken.

A full vascular investigation will require demonstration of the aortic arch and great vessels, the origins of both internal carotids and vertebrals, the carotid syphons and the intracranial vessels. This is impractical in most cases but the minimum investigation should be aimed at showing both internal carotid bifurcations and the carotid syphons. This can be achieved by bilateral common carotid angiography using transfemoral catheterization with small catheters and low osmolarity contrast. Other workers prefer arch aortography and oblique projections of the neck to show all four vessels supplying the brain (Fig. 41.7). Four-vessel studies are also practiced using either venous or arterial DSA (Fig. 41.6).

Study of the intracranial vessels requires selective angiography preferably with low osmolar contrast media. In cases of carotid thrombosis angiographic studies may demonstrate excellent crossflow from the other side with filling of the contralateral anterior and middle cerebral arteries through the anterior communicating artery. Other methods of collateral

flow which have been demonstrated by selective angiography are:

1. From the posterior circulation via the posterior communicating artery.
2. From the external carotid to the maxillary to the ophthalmic artery and then retrogradely to the carotid siphon and terminal carotid (the carotid siphon represents the upper limit of the thrombosis).
3. From pial anastomoses between the terminal branches of the anterior, middle and posterior cerebral arteries.

The sinuses and cortical veins are best studied by DSA (Fig. 41.8), though occlusion of the sagittal sinus can be demonstrated by CT as a filling defect in the sinus, the so-called 'Delta sign' (Fig. 41.9).

**Pseudo-thrombosis of the Internal Carotid.** Thrombosis of the internal carotid may be falsely diagnosed at angiography in the following circumstances:

1. The catheter tip is near the carotid bifurcation and most or all of the injected contrast has been directed up the external carotid. In all suspected cases of carotid stenosis or thrombosis the catheter tip should be well below the carotid bifurcation which must be clearly visible.
2. Grossly raised intracranial pressure. The patient is usually deeply comatose and respiration assisted. *Angiography* shows only sluggish and delayed flow up the internal carotid with contrast layering on the posterior wall and failing to progress beyond the siphon even on delayed films. Intracranial pressure is higher than systolic pressure and effectively prevents flow. In these circumstances the prognosis is hopeless since brain death from hypoxia is inevitable or already present.

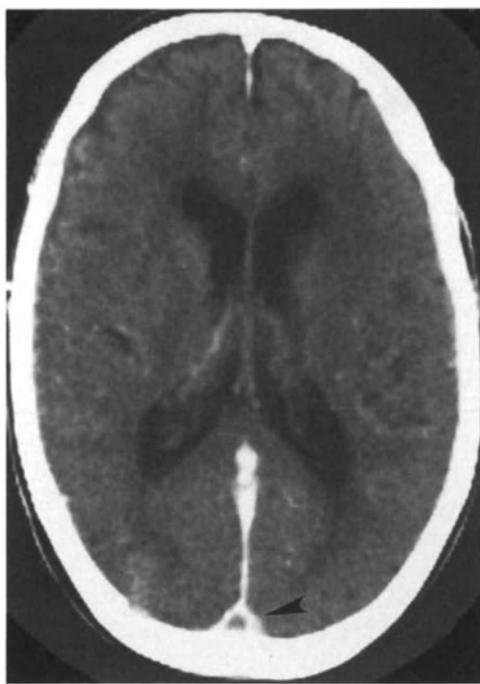


**Fig. 41.9.** The 'Delta sign' (arrowhead). The sagittal sinus is largely occluded by clot – post-enhancement study.

### EMBOLUS

Cerebral embolus usually involves the intracranial circulation rather than the neck vessels so frequently affected by thrombosis. The middle cerebral artery or its branches are most frequently involved, reflecting the fact that it receives the major part of cerebral blood flow. The causes of cerebral embolus are given in Table 41.1.

**Imaging.** The clinical effects of a cerebral embolus are

**Table 41.1.** Causes of cerebral embolus

Cardiac	clot from a fibrillating auricle secondary to mitral stenosis or other cause clot from the left ventricle following myocardial infarction
SBE	with detachment of infected emboli. These may also give rise to aneurysms
	paradoxical embolus from the systemic circulation reaching the brain through a congenital cardiac septal defect, usually with raised right auricular pressure from right heart failure
Aneurysms	involving the aortic arch or great vessels with detachment of contained clot
Atheromatous plaques	in the arch or great vessels with formation and detachment of clots
Atherosomatous plaques	in the internal carotid with small emboli giving rise to TIAs
Iatrogenic.	Clot forming on the tips of catheters during left heart and coronary catheterization or during arch aortography or transfemoral cerebral or upper limb angiography
Air embolism.	Fatal air embolism is probably due to a mixture of resulting pulmonary and cardiac dysfunction though some air can enter the systemic and cerebral circulation
Fat embolus	following fracture. These fat globules reach the brain after passing through the pulmonary circulation, usually from a limb fracture releasing large amounts of fat

generally indistinguishable from those due to acute thrombosis or hemorrhage although the etiology may sometimes be suspected from the clinical context. The effect on the brain is to produce hypoxia and infarction in the area supplied by the embolized artery.

CT or MRI are the usual primary investigations. Either technique will demonstrate cerebral infarcts and suggest which vessel is mainly involved. They will exclude hemorrhage but will not distinguish between embolus and acute thrombosis or other causes of cerebral hypoxia. The relevant appearances are described below under 'infarcts'.

*Angiography* will demonstrate the occluded vessel readily when a major artery is involved, but careful examination of high quality serial arteriograms may be necessary to identify emboli in small peripheral arteries. If a small artery involving the internal capsule is involved it may not be identified despite severe clinical deficit. The appearance of occluded arteries is not diagnostic and cannot be differentiated from the occlusions produced by acute thrombosis. Some workers avoid angiography in suspected infarcts, unless it is likely to contribute to management, in the belief that intravascular contrast can further damage ischemic brain.

### INFARCTS

Cerebral infarcts are the end result of cerebral ischemia whether due to arterial thrombosis, embolus, spasm or hypotension. They are restricted to the vascular territory of the vessel involved. Thus occlusion of anterior, middle or posterior cerebral artery will lead to infarcts of more or less of the area supplied by them depending on the efficiency of pial collaterals and general circulation.

Occlusion of a major vessel like the internal carotid can as already noted produce effects varying from none at all to infarction of much of the hemisphere. A wide spectrum of changes in between these extremes may also occur. These depend on the interaction of two variables – adequacy of the Circle of Willis and efficiency of the general circulation.

In some cases the infarcted area may be middle cerebral territory only. In others the boundary areas between the three major arteries of supply – anterior, middle and posterior cerebral – are involved. The latter are referred to as 'watershed' or boundary zone infarcts, and arise because they are in the areas most peripheral to an occluded major vessel such as the internal carotid. The reduced blood flow supplied through the Circle of Willis may be adequate for the proximal vessels but is inadequate for the most peripheral. These are also among the areas most likely to suffer from prolonged hypotension or other cause of hypoxia (Fig. 41.10).

Equally at high risk are the small penetrating vessels arising from the proximal middle cerebral trunk and supplying the basal ganglia and internal capsule. This is because they are *end arteries* with no collaterals at their terminations. Small infarcts involving the basal ganglia are therefore quite common, both as isolated findings and in association with larger infarcts.

**Imaging.** Most infarcts present clinically as 'strokes' and it may not be clear clinically whether they are due to thrombosis, hemorrhage or embolus.



**Fig. 41.10.** Watershed infarcts at boundaries between middle and anterior cerebral territory (arrow), and between middle and posterior cerebral territory (curved arrow).

CT is the usual primary investigation. The earliest CT changes with infarcts are often visible within a few hours but can be delayed for a day or more. They consist of reduced density in the affected area with ill-defined margins but affecting both white and grey matter. Some infarcts are more clearly marginated and some show more patchy loss of density (Fig. 41.11).

Over the ensuing two weeks the density shows little change but at 2 to 3 weeks corresponding to the resolution of edema and macrocytic and vascular infiltration the lesion may become isodense for a short period and can easily be missed on the unenhanced scan. After the third week low density reappears and continues to progress until at 2 to 3

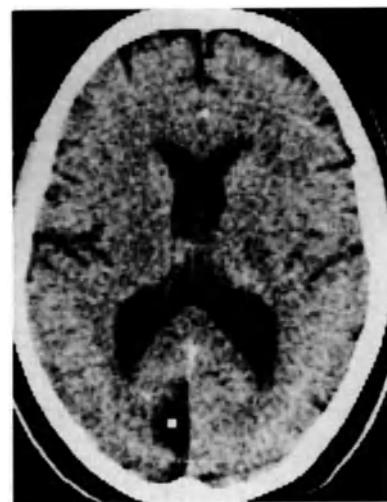


**Fig. 41.12.** Mature occipital infarct (white dot).

months the lesion reaches the CSF density of the mature infarct (Figs 41.12, 41.13).

*Contrast enhancement* of infarcts was widely practiced at one time but is now generally regarded as undesirable since it could compromise the viability of damaged but recoverable neurones. Most acute infarcts will enhance to some degree but the pattern is variable ranging from homogeneous enhancement of the whole infarct through the more common patchy enhancement to marginal ring enhancement. Enhancement continues for 6 weeks or longer but ceases as the infarct matures.

There is usually mass effect with the larger infarcts in the acute stage but this becomes less and disappears after the

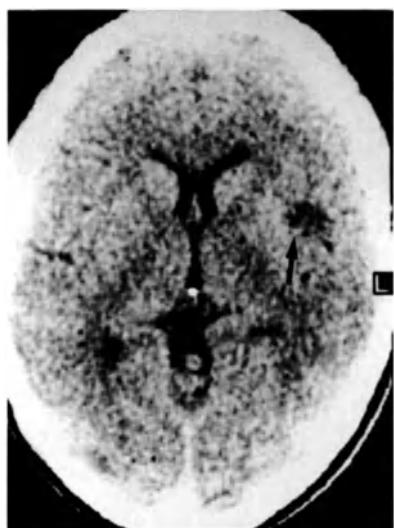


**Fig. 41.11.** Middle cerebral embolus complicating catheter angiogram. Low density area near insula (arrow) shown 3 days after incident. CT immediately following incident was negative. (Courtesy of Dr J. Stevens.)

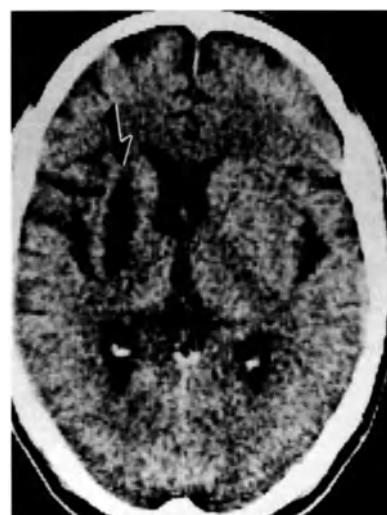


**Fig. 41.13.** Large established infarct in right capsular region (arrow), and medial to the insula.

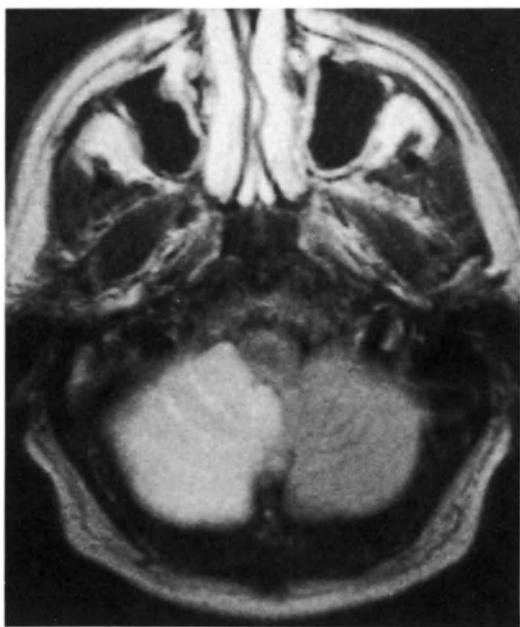


Fig. 41.14. Axial MRI study ( $T_2$ -weighted) shows high signal from right cerebellar infarct (PICA).

first week or two. With the mature infarct there is local atrophy.

*Hemorrhagic infarcts* are mainly seen with venous infarction and congestion of the affected area. They may be bilateral in the case of sagittal sinus thrombosis. The affected brain is swollen and of low density but may contain high-density areas due to small hemorrhages. Hemorrhagic infarcts are also sometimes seen with ischemic infarction. In the past this was thought to suggest an embolic cause, but this is no longer generally accepted.

It has already been noted that small infarcts can occur involving the internal capsule and basal ganglia and these are easily missed in the acute stage. In the later stages when mature they are more easily recognized as small 'lacunar infarcts'. Larger infarcts may also be seen in this area (Fig. 41.13).

*MRI.* Acute ischemic infarction is well shown by MRI (Fig. 41.14) but can resemble early hemorrhage and be difficult to differentiate. Older infarcts have a long  $T_1$  and  $T_2$  and established infarcts resemble CSF. More lesions can usually be identified by MRI than by CT particularly in difficult areas like the brainstem.

Periventricular small areas of high signal may be seen in the elderly on spin-echo ( $T_2$ )-weighted images, and these probably represent small areas of subclinical infarction. They are also seen in Binswanger's disease (see Chap. 43, p. 785).

## ANEURYSMS

Cerebral aneurysms may be classified as

1. Congenital (saccular, berry) aneurysms
2. Atherosclerotic (fusiform) aneurysms
3. Dissecting aneurysms (see Chap. 42, p. 780)

4. Traumatic aneurysms
5. Mycotic aneurysms
6. Venous aneurysms

Most saccular cerebral aneurysms are congenital in origin and arise at points of arterial bifurcation where there is a defect in the muscular coat. However other factors such as age, hypertension and atheroma appear to contribute to their clinical development. The vast majority of these congenital cerebral aneurysms are located on or near the Circle of Willis. The sites of election in order of frequency are:

1. Anterior communicating: 30%
2. Posterior communicating: 25%
3. Middle cerebral artery at bifurcation of main trunk: 20%
4. Terminal internal carotid artery: 10%
5. Posterior circulation (vertebral and basilar arteries): 10%
6. Peripheral and other sites: 5%

Cerebral aneurysms present clinically in three different ways.

*Subarachnoid hemorrhage* is far the commonest mode of presentation and is discussed in detail below. A smaller number of patients will present with *oculomotor pareses*. The 3rd, 4th and 6th nerves can all be involved in or proximal to the cavernous sinus by pressure from an aneurysm. Finally a few cases will present as *apparent cerebral tumors* since aneurysms at the base of the brain may rarely reach a very large size without rupture. Such aneurysms can press on the adjacent cerebral tissue and simulate a tumor. *Venous aneurysms* are found in patients with large cerebral arteriovenous shunts and are not uncommon with angiomatic malformations (see below).

*Imaging.* *Simple radiography* is rarely helpful in the diagnosis of symptomatic aneurysms. A long-standing congenital aneurysm may occasionally calcify but unless large these calcified congenital aneurysms are usually chance findings. The appearances are however characteristic presenting as small ring or arc-like shadows near the sella or anterior communicating artery region. Very rarely these thin ring shadows may be quite large and suspicion of tumor may have been raised clinically (Fig. 41.15). Calcification is also sometimes seen in the walls of the much rarer arteriectatic atheromatous aneurysms affecting the basilar artery or terminal carotid.

Bone erosion is a rare manifestation of a large aneurysm adjacent or anterolateral to the sella (Fig. 41.17). Erosion of the inferolateral margin of the optic foramen (the optic strut) and the inferomedial aspect of the anterior clinoid on the affected side are typical.

*CT.* CT is more sensitive than simple radiography and shows asymptomatic calcified saccular aneurysms even more readily (Fig. 41.16). It will also show clearly large arteriectatic aneurysms, particularly with atheromatous calcification in their walls, and large basal aneurysms simulating tumors.

Such aneurysms may be recognized before enhancement, being slightly denser than adjacent brain tissue, but are more clearly shown as vascular by their strong enhancement immediately after contrast is administered (Fig. 41.17B, C).

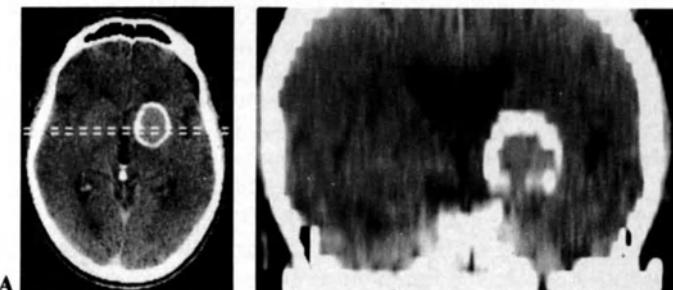
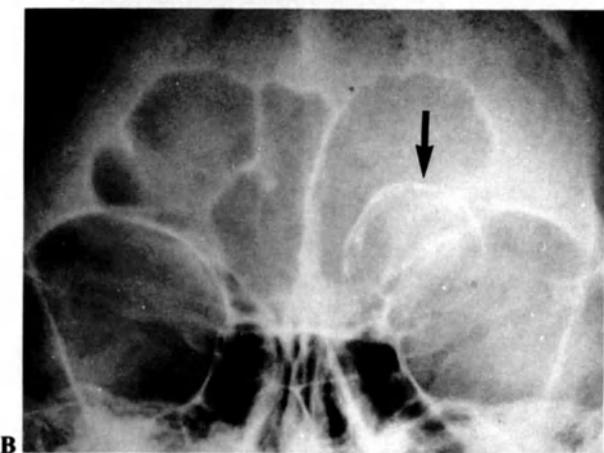


**Fig. 41.15A, B.** Large calcified aneurysm showing marginal calcification on simple films. A Lateral view, B PA view.

Small berry aneurysms however will only occasionally be identified even with high-quality scans.

**MRI.** MRI will also image and characterize large arteriovenous or saccular aneurysms, but not the smaller lesions.

**Angiography.** This is the most definitive examination and will clearly demonstrate the size, shape and site of origin of both large and small aneurysms including, with the use of magnification techniques, those beyond the resolving power of other imaging techniques. However, it will only be indicated if the aneurysm is symptomatic and neurosurgery is being considered. It is discussed in detail under 'subarachnoid hemorrhage' below.

#### ANGIOMATOUS MALFORMATIONS (Syn. Arteriovenous malformation; Angioma)

Angiomatous malformations are direct shunts from arterioles to venules without the interposition of a capillary bed. They are quite common in the cerebral circulation, and although they usually present in young adults (20 to 40 years of age), they are considered to be congenital in origin. They probably increase in size with age, particularly after adult blood pressure is established. They may be quite small, with only one or two hypertrophied feeding vessels and drainage veins, or quite large with multiple feeding arteries and drainage veins. They then appear as a tangled mass of vessels on the surface of the brain. Larger angiomas extend down into the brain in the manner of an inverted cone.

In silent areas of the brain the lesions may be asymptomatic, but in sensitive areas like the motor or occipital cortex even small lesions can produce such effects as Jacksonian

**Fig. 41.16A, B.** CT of large aneurysm with calcified wall. A Axial view. B Coronal reformat.



**Fig. 41.17A, B, C.** CT of large suprasellar aneurysm. A There is evidence of bone erosion medial to the left anterior clinoid. B A rounded isodense mass is shown in the suprasellar cistern. C After contrast the aneurysm enhances strongly.

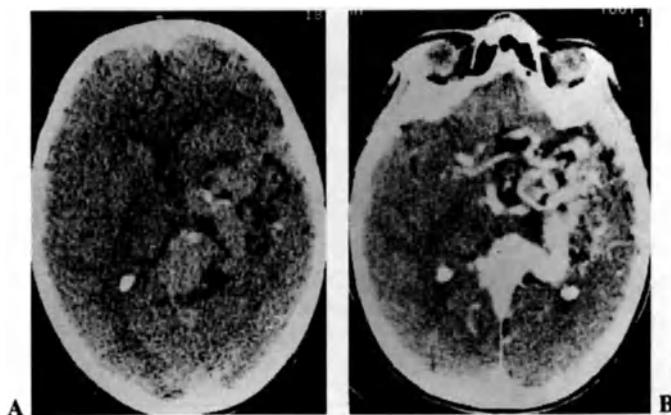


**Fig. 41.18.** A Unenhanced CT showing mottled area of low and high density, and a few flecks of calcification. B Post-enhancement CT confirms serpiginous vessels of angioma draining into aneurysmal Vein of Galen.

epilepsy or field defects. Headache of a migrainous character may also occur and a significant number will present with subarachnoid or intracerebral hemorrhage.

In addition to the relatively common arteriovenous malformation other types of angioma are occasionally seen. These include **cavernous** and **venous angiomas** and **capillary telangiectasia**. The cavernous type can give rise to focal epilepsy and both it and the venous type occasionally give rise to cerebral hemorrhage.

**Imaging.** *Simple radiography* is usually non-contributory in the diagnosis of these lesions but with large angiomas diagnostic changes are occasionally seen. The most important of these is a fairly typical *calcification* consisting of a few scattered flecks of the type seen in atheromatous vessels; sometimes there are associated arc-like calcifications of the type seen in aneurysms. The latter lie in venous aneurysms in the dilated drainage veins.

Another diagnostic sign but one less frequently seen is the presence of grossly *hypertrophied meningeal vascular markings* of a generalized type and unlike the more common unilateral localized type seen with meningiomas.



**Fig. 41.19.** MRI (T<sub>2</sub>-weighted) shows flow defects in dilated vessels of large central angioma. (Courtesy of Dr Gordon Thomson and Bristol MRI centre.)

**CT.** Arteriovenous malformations are well shown by CT, but the appearances will vary with the mode of presentation. In those with subarachnoid or cerebral hemorrhage the latter may be the most prominent feature on the unenhanced scan (see below). In other cases the large angiomas will show on the unenhanced scan as serpiginous or rounded shadows (depending on the angle of section) of slightly increased density relative to brain, and flecks or small arcs of calcification may also be noted. Small low-density areas may also be seen in and around the malformation and these represent post-hemorrhagic cysts or ischemic brain. The mixture of higher and lower density shadows may give rise to a mottled appearance which is fairly characteristic (Fig. 41.18A).

Post-enhancement the vascular nature of the shadows is clearly shown (Fig. 41.18B).

**Venous angiomas** are rarely diagnosed at CT but are occasionally suggested by a small rounded hyperdense area without mass effect, but which shows linear vessels after enhancement. **Cavernous hemangiomas** are also rounded, often subcortical lesions, which are slightly hyperdense and show slight homogeneous enhancement after contrast. There is no edema or mass effect but calcification is present in about 30% of cases. This and their subcortical position may cause difficulty in differentiation from meningioma.

**MRI.** Large angiomas can be identified by MRI due to the low signal intensity from flowing blood (Fig. 41.19), but smaller angiomas are less well seen. Intracerebral hemorrhage leads to a high signal (short T<sub>1</sub>) which persists for several months but this is not shown in the acute phase during the first week.

**Angiography.** Although the definitive diagnosis of angioma can be made by less invasive methods, angiography will be required if curative surgery or embolization is being considered in order to demonstrate the precise anatomy of the feeding arteries and drainage veins. The major arteries of supply and the major drainage veins are hypertrophied in direct proportion to the degree of shunt. They also become lengthened and more tortuous (Fig. 41.20).

Large shunts will be supplied not only by their ipsilateral major arteries but may attract blood from the contralateral internal carotid and the posterior circulation. They may also be supplied from the external carotid circulation via hypertrophied meningeal vessels. Venous aneurysms may develop in the proximal drainage veins because of the high flow and their walls can become calcified.

**Cavernous angiomas** are not identified at angiography because of their low bloodflow, but **venous angiomas** are readily defined.

**Aneurysm of the Vein of Galen.** This is a special example of venous aneurysm seen mainly in infants and young children, though it can present at a later age.

The Vein of Galen undergoes aneurysmal dilatation because of a massive shunt through a malformation or AV fistula fed by the posterior cerebral or sometimes middle cerebral vessels. The infant may present with heart failure or hydrocephalus. Imaging by ultrasound is possible in the infant and CT or MRI will diagnose the lesion non-invasively in the older child or adult. However angiography will be required to define the anatomy of the major feeding vessels (Fig. 41.21).

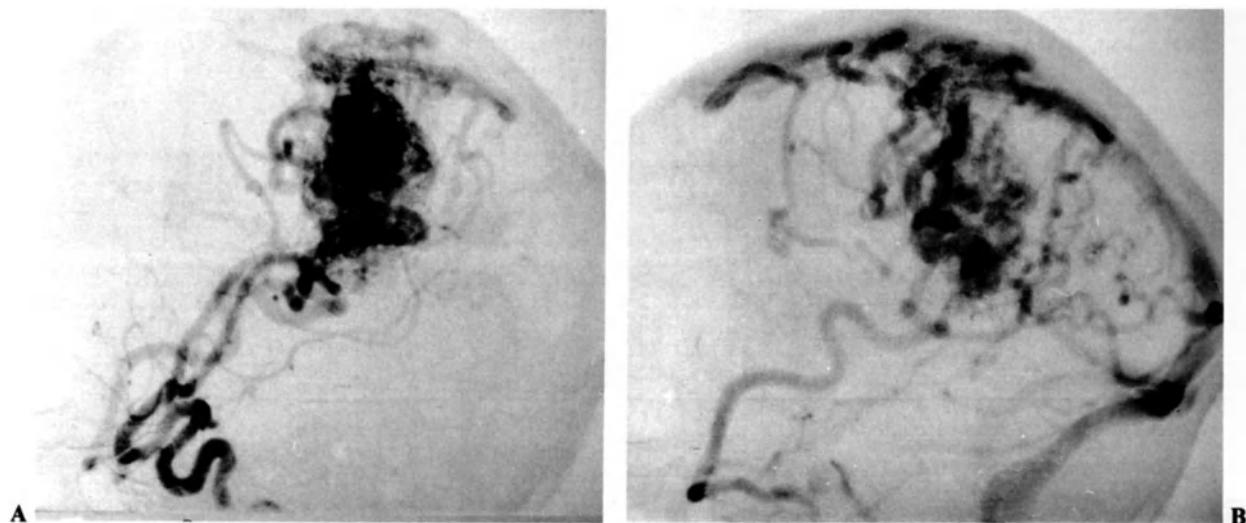


**Fig. 41.20A, B.** Internal carotid angiography of large parietal angioma fed by hypertrophied middle cerebral branches and with dilated veins draining to the sagittal sinus.



#### DURAL AV FISTULA (Syn. Dural AV malformation)

Abnormal connections between meningeal vessels and dural veins may be found close to major sinuses such as the cavernous or lateral sinuses. They can present with *proptosis* if connected to the cavernous sinus, a *bruit* troublesome to the patient near the lateral sinus, and occasionally with *subarachnoid hemorrhage* if connected to cerebral veins. The majority involve the cavernous sinus or the occipito-mastoid region (lateral sinus). The cavernous sinus lesions can resemble clinically the larger traumatic AV fistulas described below but the proptosis and symptoms are usually much milder.

**Imaging.** CT or MRI may demonstrate hypertrophied drainage veins as in Fig. 41.22A but is often negative, and high quality *selective angiography* of the feeding vessels is essential to identify the shunt and determine whether

◀  
**Fig. 41.21.** Vertebral angiography in an infant shows a large aneurysm of the Vein of Galen supplied by hypertrophied posterior cerebral arteries.

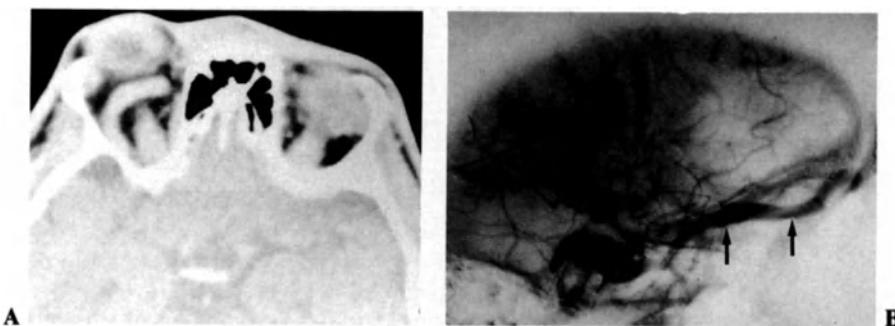


**Fig. 41.22.A** Proptosis due to a dural AV fistula. Enhanced CT shows a grossly dilated superior ophthalmic vein. **B** Carotid angiogram shows carotico-cavernous fistula opacifying cavernous sinus and draining into superior ophthalmic vein (arrows).

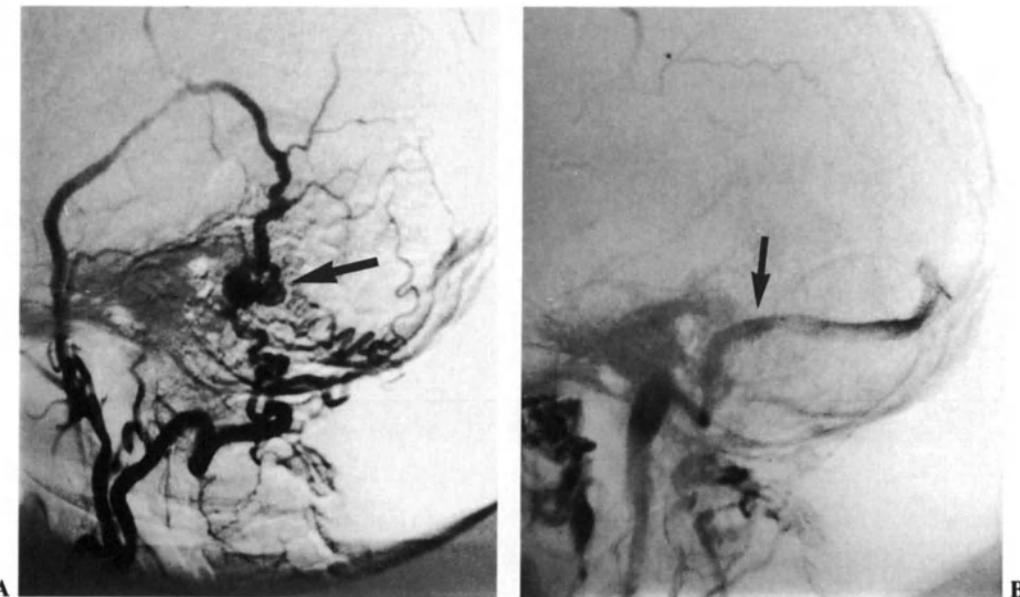


**Fig. 41.23A, B.** A mastoid dural AV fistula (arrows) is supplied by a hypertrophied occipital artery and the posterior branch of the superficial temporal artery. Drainage is into the lateral sinus with some retrograde flow.

embolization, which is often carried out at the same session, is feasible (Fig. 41.23).

Cavernous sinus lesions may be supplied by branches of the meningo-hypophyseal artery arising from the internal carotids on one or both sides as well as by meningeal branches from the external carotids. Occipito-mastoid lesions can receive vessels from the vertebral as well as the occipital artery. Full investigation may require extensive bilateral selective angiography.

#### AV FISTULA

An arterio-venous (AV) fistula is an acquired direct communication between an artery and a vein, usually of traumatic origin. They may also arise from rupture of an aneurysm into an adjacent or adherent sinus or vein. Traumatic carotico-cavernous and meningeal AV fistula are discussed in Chap. 42.

*Carotico-cavernous fistula* is usually traumatic but spontaneous rupture of an intracavernous aneurysm also occurs; the latter is seen mainly in females. The shunts are usually much larger than with the dural AV fistula involving the cavernous sinus and described above.

**Imaging.** CT and MRI are of little value though dilated drainage veins may be demonstrated by CT, particularly in the orbit (Fig. 41.22A).

*Angiography* is essential to demonstrate the exact site of the fistula and the pattern of drainage (Fig. 41.22B). With a large carotico-cavernous fistula the drainage outflow pattern from the cavernous sinus varies and may include alone or in combination:

1. Superior ophthalmic vein to facial veins.
2. Inferior ophthalmic vein to pterygoid plexus.

3. Superior petrosal to sigmoid sinus.
4. Basal vein to straight sinus.
5. Convexity veins to various sinuses.
6. Crossflow to the contralateral cavernous sinus and its drainage veins.

These lesions are now being frequently treated by balloon embolization.

#### HEMORRHAGE

Intracranial hemorrhage can be classified as traumatic or spontaneous.

*Traumatic hemorrhage* is dealt with below (Chap. 42, p. 777). It can, as noted, be purely extradural, subdural or intracerebral in type, or mixed. Traumatic subarachnoid hemorrhage may also be associated.

*Spontaneous hemorrhage* is usually primarily intracerebral or primarily subarachnoid or a mixture of both. It can be classified on an etiological basis as follows:

1. Hypertensive.
2. Ruptured aneurysm.
3. Ruptured angioma.
4. Blood dyscrasia and anticoagulation.
5. Tumor hemorrhage.
6. Infantile.

Hypertension, blood disorders and tumors give rise to mainly intracerebral hemorrhage, but large hemorrhages can rupture into the ventricles or subarachnoid space as well. Aneurysms and angiomas rupture into the subarachnoid space, but can also rupture into the brain and ventricles.

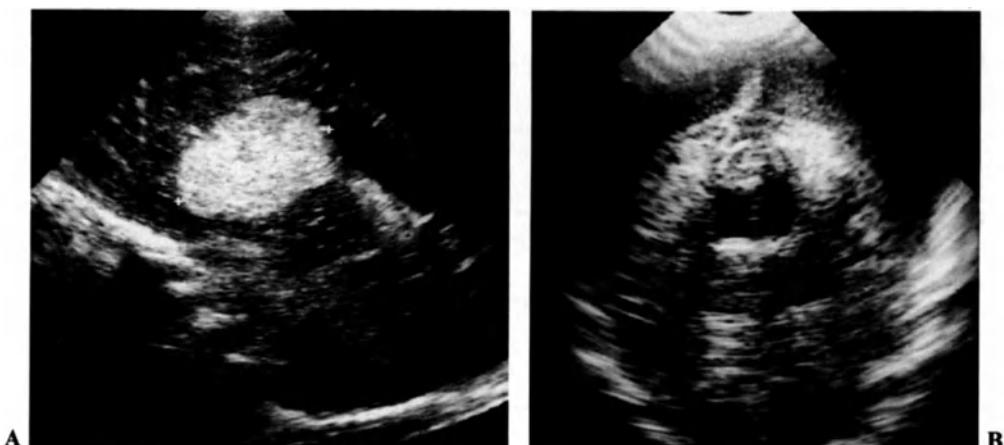


**Fig. 41.24.** A Left parasagittal ultrasound section shows high signal from large paraventricular hemorrhage. B Coronal ultrasound study shows bilateral subdurals compressing brain and ventricles. (Courtesy of Dr Keith Dewbury.)

**Infantile intracranial hemorrhage** is seen particularly in premature infants where it is the most common CNS abnormality. The *germinal matrix*, situated subependymally, is particularly vascular and normally involutes by term. Hemorrhage may occur here (Fig. 41.24A) or from the vascular choroid plexus as a result of a hypoxic episode and venous stasis. Intraventricular and sometimes subarachnoid hemorrhage may also result as may subdural hemorrhage.

Subarachnoid and subdural hemorrhage (Fig. 41.24B) resulting from perinatal trauma can also occur in the full-term infant.

White matter hemorrhage occurs both in premature and full-term infants following hypotension affecting the underperfused boundary areas between different vascular territories. In the premature infant it may be associated with *periventricular leukomalacia*.

Hemorrhage from vascular **tumors** is less frequent and is mainly intracerebral. Metastases are the commonest source, particularly from *melanoma*, *choriocarcinoma* and *bronchial carcinoma*.

**Imaging.** CT is the best method for demonstrating acute intracerebral hemorrhage since clotted blood increases in density to as much as 90 H compared with the near isodensity with brain of normal intravascular blood. Thus the hematoma appears as an area of increased attenuation ranging from 50 to 90 H. It is surrounded by a thin low-density ring resulting from clot retraction and edema.

The high attenuation of intracerebral hematomas is visible immediately from the time of hemorrhage (Fig. 41.25) and decreases slowly over the subsequent weeks. Contrast enhancement is unnecessary and is contraindicated since it can mask the underlying density and lead to erroneous diag-

#### INTRACEREBRAL HEMATOMA

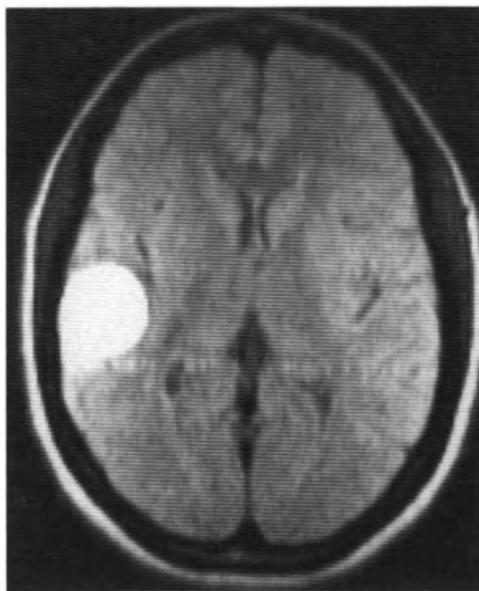
**Hypertensive hemorrhage** is the commonest cause of spontaneous intracerebral hematoma. The majority (80%) occur in the cerebral hemispheres, whilst the remainder occur equally in the brainstem or cerebellum. The site of election is the basal ganglia and 80% of the cerebral hemisphere hemorrhages occur here; the rest involve the cerebral white matter in the frontal, parietal, occipital or temporal lobes.

Hypertensive hemorrhages are due to the formation and rupture of microaneurysms, first described by Charcot and Bouchard, on small intracerebral arteries (50 to 200 µm in diameter). They are most numerous in the basal ganglia perforating arteries arising direct from the middle cerebral trunk, which explains why cerebral hemorrhage is commonest from these vessels.

**Blood disorders** can cause cerebral hemorrhage and this is said to occur in 20% of patients with acute myeloblastic or chronic myeloid leukemia and is often multifocal. Subarachnoid and subdural hemorrhage can also result. **Anticoagulant therapy** can give rise to similar complications.



**Fig. 41.25.** Unenhanced CT scan shows a large parietal hematoma following spontaneous hemorrhage in a hypertensive patient.



► Fig. 41.26. Ten days after an ictus MRI (mildly T<sub>2</sub>-weighted) shows hematoma as high signal area.

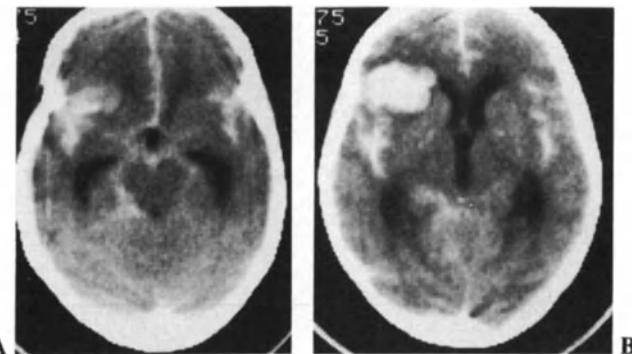


Fig. 41.27A, B. Unenhanced CT 8 hours after a subarachnoid hemorrhage. A The basal and ambient cisterns and insulae contain clotted blood giving high signal instead of the normal low signal of CSF. B There is a large hematoma at the anterior end of the right insula indicating rupture of a right middle cerebral aneurysm.

noses if not preceded by an unenhanced scan. Mass effect depends on the size of the hematoma but is less than with comparably sized tumors, and edema is rarely very marked. Resolution takes place from the periphery of the clot inwards and goes through an isodense phase before reaching a low-density residue. The end result is a CSF density lesion, smaller and well defined, and with some local atrophy.

Blood frequently enters the ventricles and large amounts may form casts. Small amounts usually gravitate to the posterior tips of the occipital horns, since these are the most dependent parts in the supine patient. With superficial clots blood may also enter the subarachnoid space. Hydrocephalus may result from obstruction to CSF flow.

*MRI* is inferior to CT in the diagnosis of acute hemorrhage, but shows older hemorrhage and *surrounding vasogenic edema* well (after 2 to 7 days) as markedly increased signal intensity on T<sub>2</sub>-weighted images and this remains for several months (Fig. 41.26).

*Angiography* is not usually indicated in hypertensive intracerebral hemorrhage but may be requested if there is doubt whether the hemorrhage has originated from a ruptured aneurysm or angioma. This can occur if there is blood in the subarachnoid space at the CT scan.

#### SUBARACHNOID HEMORRHAGE

The vast majority of patients presenting with spontaneous subarachnoid hemorrhage are proved to be suffering from a ruptured *aneurysm*. A smaller number (some 10%) arise from rupture of an *angioma* and a similar number are shown to have intracerebral *hematomas*. Most of these are presumed to arise from hypertensive hemorrhage, though some may be from angiomas or small aneurysms which have been destroyed in the hemorrhage and fail to show either at angiography or autopsy. Other uncommon causes are *blood dyscrasia* or *anticoagulation* and finally hemorrhage from

superficial *tumors*. The latter is responsible in only 1% of cases.

**Imaging.** CT is the primary investigation of choice. This will confirm the diagnosis of recent subarachnoid hemorrhage in over 80% of cases by showing the presence of clotted blood in the basal cisterns and/or cortical sulci. The normal low-density CSF is replaced by the high density of blood clots (Figs 41.27A, B).

In some cases an intracerebral hematoma may also be shown and provide valuable localizing evidence as to the site of the ruptured aneurysm (Figs 41.27B, 41.28). This may be of great practical value if, as happens in 15% of patients, subsequent angiography prior to surgery shows multiple aneurysms, and the surgeon has to decide which to clip. It will also obviate the need for four-vessel or other extensive angiographic studies.

The sites of election for saccular aneurysms have been described above. Anterior communicating aneurysms can bleed upwards into the septum pellucidum (Fig. 41.28) or third ventricle and clot can extend into one or both frontal lobes. Middle cerebral aneurysms bleed into the insula and temporal lobe (Fig. 41.27B), and terminal internal carotid aneurysms can rupture upwards into the basal ganglia. Posterior communicating aneurysms however rarely rupture into cerebral tissue.

Intraventricular hemorrhage may also be seen in some cases of subarachnoid hemorrhage (Fig. 41.28), often in association with intracerebral hematoma.

The aneurysms giving rise to subarachnoid hemorrhage are usually too small to be directly identified at CT but occasionally a larger aneurysm can be directly shown (Fig. 41.17).

*Vascular spasm* is often associated with subarachnoid hemorrhage and this can give rise to ischemic changes in the territory most affected. Infarcts may be recognizable at CT and complicate the diagnostic picture. Hydrocephalus from obstruction of the CSF pathways is another complication which may arise quite rapidly and require treatment.



**Fig. 41.28.** Unenhanced CT following rupture of an anterior communicating aneurysm. Blood clot is present in a cyst of the septum and the right frontal and occipital horns as well as between the frontal lobes.

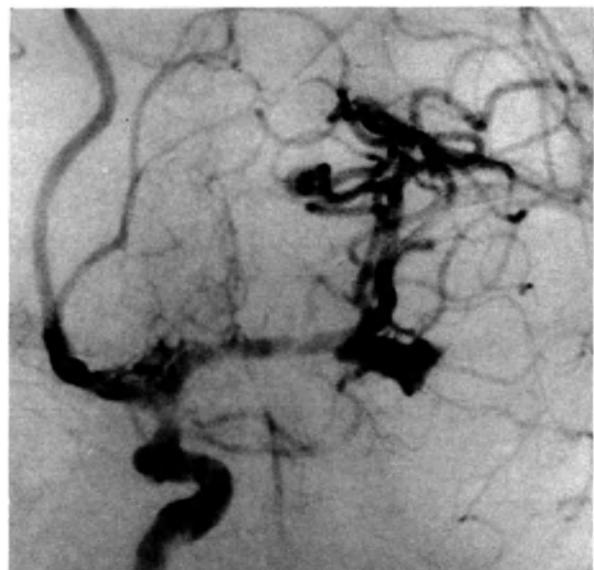


**Fig. 41.30.** Oblique AP view of large irregular aneurysm with broad neck arising from middle cerebral bifurcation.



**Fig. 41.29.** Right carotid arteriogram following SAH. An oblique view shows a saccular aneurysm of the middle cerebral bifurcation filling despite intense spasm of all vessels distal to the internal carotid terminal segment.

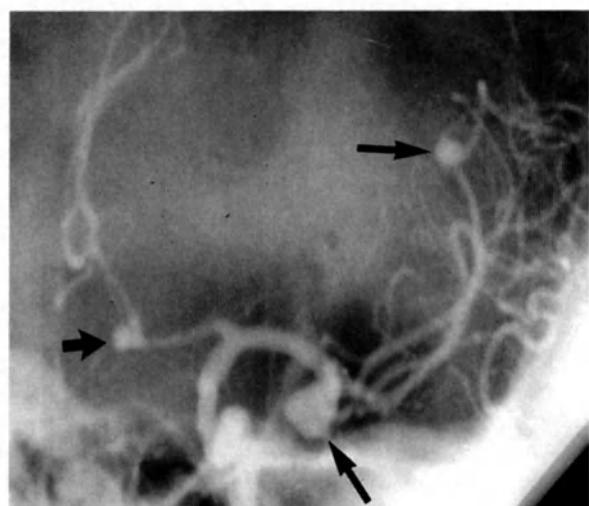


**Fig. 41.31.** Oblique AP view of left carotid angiogram showing three aneurysms arising from the anterior communicating, middle cerebral bifurcation and distal middle cerebral respectively (arrows).

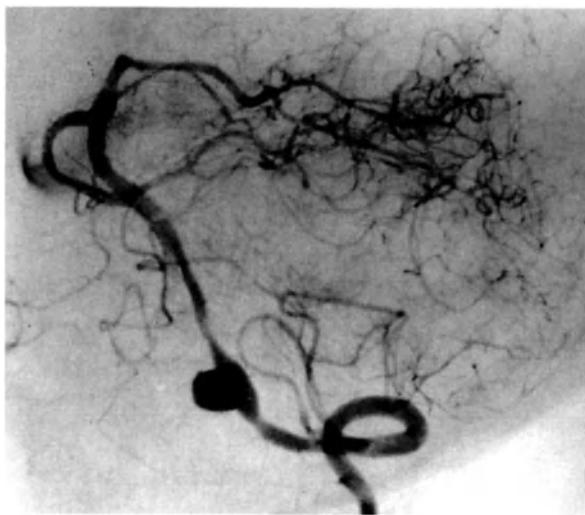


Fig. 41.32. Vertebral angiogram showing a saccular aneurysm arising at the vertebrobasilar junction.

However the CT findings may be negative in up to 20% of the patients with subarachnoid hemorrhage, usually when this is minor in degree.

MRI is of little value in the acute stage but will show clot in the cisterns and sulci after a few days when it appears as a high signal (short  $T_1$ ).

**Angiography.** This is mandatory if neurosurgery is to be undertaken and will require high-quality selective angiography to demonstrate clearly the anatomy of aneurysms or angiomas and their feeding vessels and drainage veins (Figs 41.29–41.32).

In the investigation of aneurysms internal carotid angiography may require oblique and oblique transorbital views as well as the standard AP and lateral views in order clearly to define the site of origin and neck of the aneurysm (Figs 41.30, 41.31). As noted above severe spasm may be seen (Fig. 41.29) and multiple aneurysms may be found in 15% of cases (Fig. 41.31). If CT gives no clue as to which has bled then it is likely to be the one which appears largest at angiography.

*For further reading, see p. 790.*

## CHAPTER 42

# INFECTION: TRAUMA

D. Sutton

---

## INFECTIONS AND INFESTATIONS

---

### INFECTIONS INVOLVING THE SKULL

**Bacterial Infections.** Acute and subacute osteomyelitis involving the skull is now seen mainly as a result of compound fracture or other severe injury or in spread from an infected frontal sinus. The major manifestations with gross bone destruction and sequestrations are now rare but subacute infection with patchy sclerosis and some bone destruction are not uncommon. Post-operative infection of bone flaps may also occur and is characterized by erosion of the bone margin and scattered lytic areas within the flap. It should be remembered that a similar appearance may result from bone necrosis due to radiotherapy.

**Tuberculosis** of the skull is now rare except in immigrants from underdeveloped countries. It produces a small rounded area of bone destruction associated with a soft tissue swelling due to a cold abscess.

**Syphilis** of the skull vault (Fig. 19.22A, p. 355) is no longer seen in developed countries, but it could produce widespread irregular erosions, the so called 'moth-eaten appearance'.

**Hydatid disease** of bone is rare and skull involvement very rare, though it can occur. It gives rise to a multilocular cystic mass expanding the bone and bulging it outwards.

### INFECTIONS OF THE BRAIN AND MENINGES

Infections of the brain will be discussed under the causative organism classified as bacterial, viral, fungal and parasitic.

#### Bacterial Infections

**Meningitis.** Acute bacterial meningitis is diagnosed clinically and is of little importance to the radiologist. Chronic

granulomatous meningitis may occur with treated tuberculous meningitis and with some fungal infections such as *Cryptococcus* or *Coccidioidomycosis*. It may also occur with sarcoidosis.

**Imaging.** Simple radiography of the skull in patients cured of tuberculous meningitis often shows characteristic flecks of calcification in the healed exudate at the base of the brain and situated just above or behind the sella (Fig. 42.1).

CT shows increased density in the basal cisterns and sulci and around the brainstem instead of the normal low-density CSF. There is some enhancement after intravenous contrast (Fig. 42.2) and there is usually evidence of communicating hydrocephalus. Calcification may be noted in old healed tuberculous basal meningitis.

**Extradural and Subdural Empyema.** These are usually due to direct spread, either from an infected sinus or from a compound fracture with cranial osteomyelitis. The causative lesion is usually obvious on a simple radiograph, but CT or MRI will be required to identify the abscess.

CT shows an *epidural abscess* as a crescentic collection over the convexity with density higher than CSF but less than blood and with enhancement of the capsule. Small and shallow collections may be difficult or impossible to separate from overlying bone and the outer capsule is obscured by it.

*Subdural abscesses* also lie over the vault, but can loculate in a parafalcine or interhemispheric position. Their appearances at CT are similar to epidural abscesses except for the interhemispheric abscess where the whole of the capsule may be seen after contrast.

**Brain Abscess.** Brain abscesses are caused by pyogenic bacteria (usually *Streptococcus*, *Staphylococcus* or *Pneumococcus*) that reach the brain by direct spread from an open skull fracture or penetrating wound or from an adjacent focus of

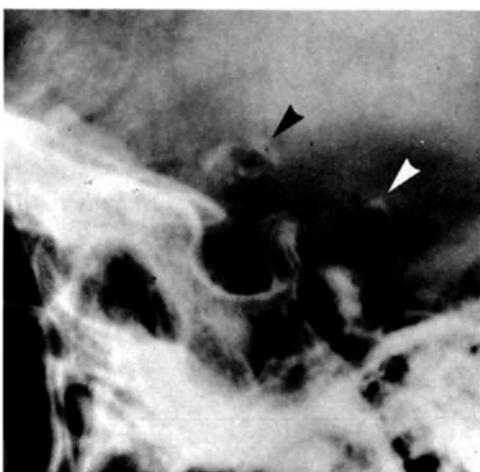


Fig. 42.1. Calcification in healed tuberculous exudate in the basal cisterns (arrowheads).

infection (sinusitis or mastoiditis), or by hematogenous spread from a distant focus (lung sepsis, bacterial endocarditis, skin or genitourinary infection).

Abscesses due to direct spread are sited adjacent to the cause; in the frontal lobe from an infected frontal sinus; in the temporal lobe or cerebellum from otitis media or mastoiditis; in situ from penetrating wounds or post-neurosurgical intervention. Hematogenous metastatic abscesses may occur anywhere but are often multiple and deeply sited. They are commonest in the frontal and parietal areas reflecting major blood flow via the middle cerebral artery. The commonest sources are lung sepsis (bronchiectasis and lung abscess) and SBE in congenital cyanotic heart disease.

**Imaging.** Simple radiography is helpful in demonstrating an infected frontal sinus or mastoid or a skull fracture in cases

due to direct spread. A very rare direct sign of an intracerebral abscess is a gas-fluid level within the abscess; the gas enters from the infected sinus or mastoid in direct spread cases, or in blood borne cases is due to gas forming organisms. With hematogenous abscesses a simple chest radiograph may show evidence of lung infection or of congenital heart disease.

**CT.** In the earliest stage of cerebritis there may be an area of decreased attenuation in the affected white matter (Fig. 42.3). As the capsule forms this may be evident on the unenhanced scan as a marginal ring of slightly higher density accentuated by surrounding low-density edema, and there is considerable mass effect.

Following intravenous contrast the capsule enhances strongly in a ring-like manner. Usually there is a single ring shadow but abscesses can become loculated or multicystic with two or more adjacent or superimposed ring shadows (Fig. 42.4).

As already noted gas within an untapped abscess is a very rare but pathognomonic sign.

Whilst the diagnosis in most cases is clear cut on clinical and imaging evidence, the CT evidence is not specific and similar appearances can be seen with malignant tumors and sometimes with infarcts or resolving hematomas.

**MRI.** Cerebritis and edema are better shown and picked up earlier by MRI but the appearance are non-specific.

**Tuberculoma.** These are now encountered mainly in immigrants from underdeveloped countries where tuberculosis is still widespread. Some 20% of intracranial tumors in India are tuberculomas and more than half occur in children. Indeed, in one study 50% of posterior fossa tumors in Indian children were tuberculomas. Although the cerebellum is a common site the lesions occur also in the cerebral hemispheres and brainstem, and are often multiple.

**Imaging. Simple Radiography.** Calcification was at one time thought to be common in tuberculomas of the brain, but it



Fig. 42.2. CT post-contrast shows enhancing exudate in the sulci and cisterns. Tuberculous meningitis.

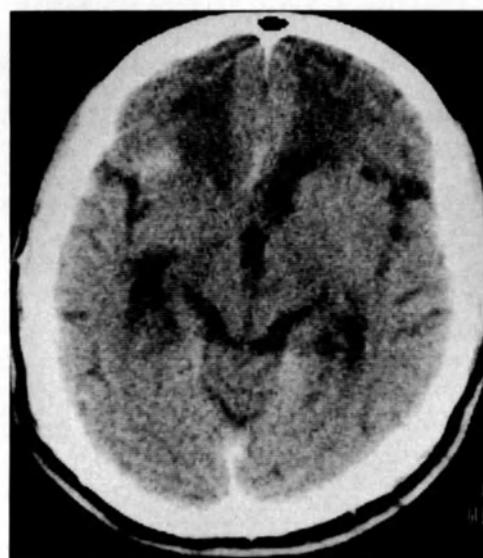


Fig. 42.3. Bifrontal areas of low density due to cerebritis and before capsule formation. The patient later developed bilateral abscesses.

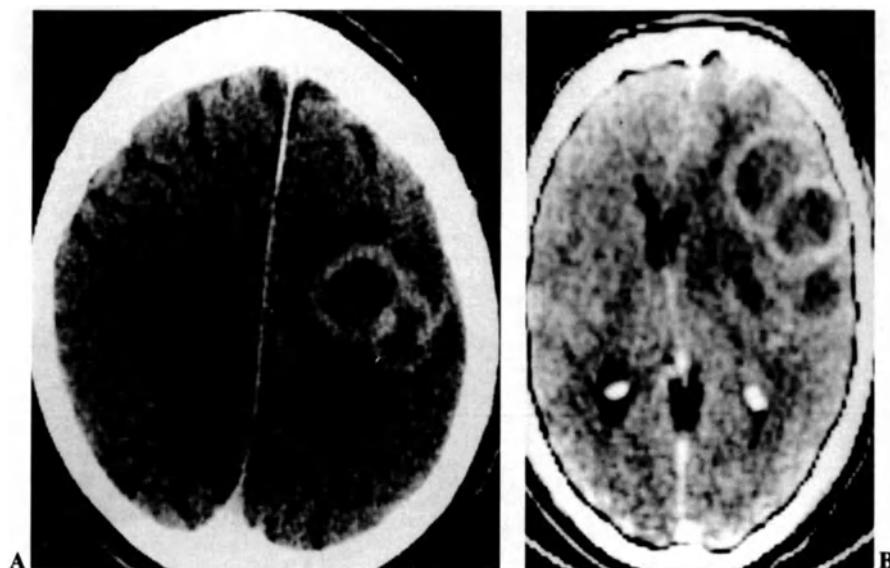


Fig. 42.4A, B. Multiloculated abscesses. Two different cases.

is in fact rare for a patient with proven intracerebral tuberculoma to show recognizable calcification on a simple radiograph. This is in contrast to the calcification which occurs in the basal exudate of healed tuberculous meningitis, and which has been described above (Fig. 42.1). The chest radiograph may show evidence of pulmonary tuberculosis.

**CT.** Tuberculomas form small rounded masses which are often isodense and difficult to define on an unenhanced scan since there is little or no edema. They enhance well with contrast except for the necrotic center and appear as solid or ring-shaped nodules, depending on the angle of cut. They are usually small (1 to 2 cm) in diameter, though sometimes larger. The ring shadows may be thick-walled ('target sign'), though they can also be thin-walled (Figs 42.5, 42.6). Calcification is rarely seen.

The lesions can resemble metastases though the absence of edema or significant mass effect favours granuloma.

**MRI.** This will identify the lesions but has no particular advantages over CT.

#### Viral Infections

These may be classified into non-specific and specific infections.

**Non-specific virus infection** of the CNS is variously described as *post-infectious encephalitis*, *post-infectious perivenous encephalitis*, *acute disseminated encephalomyelitis* and *acute disseminated leukoencephalitis*. The condition may complicate many viral diseases but in particular the exanthemata such as measles, chickenpox, rubella and smallpox or it may follow smallpox vaccination. The basic mechanism is thought

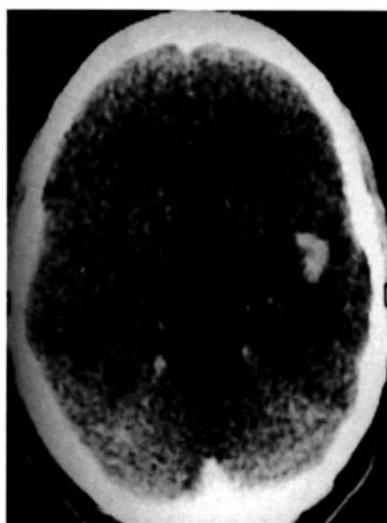


Fig. 42.5. Enhancing tuberculoma in the left Sylvian fissure in patient being treated for tuberculous meningitis.

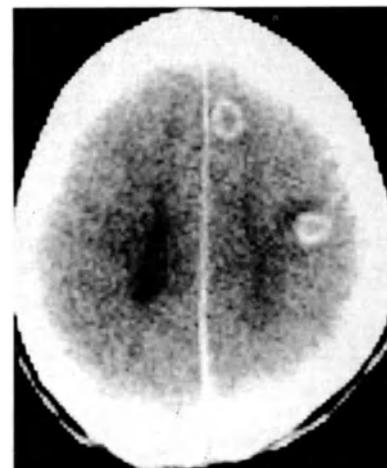
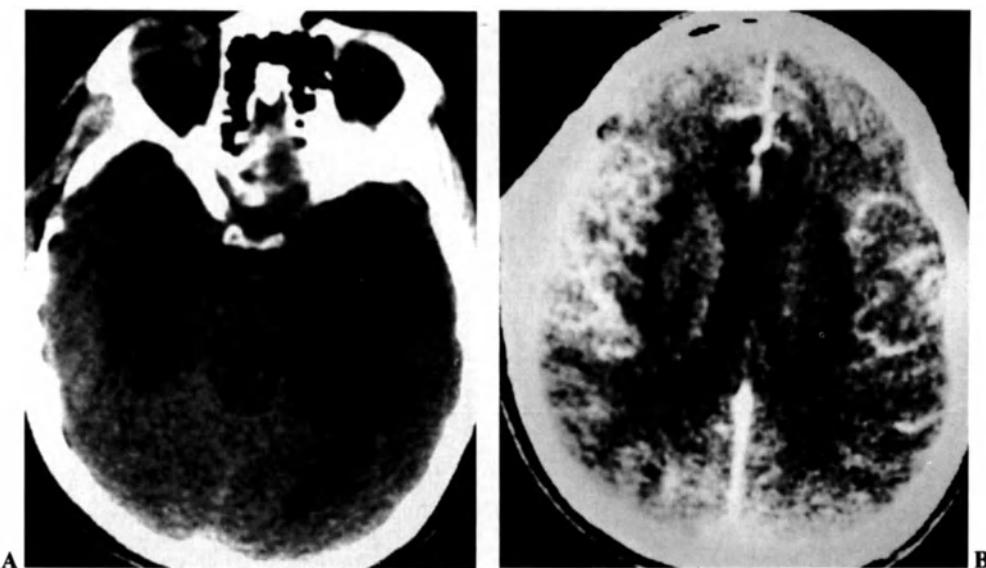


Fig. 42.6. Tuberculomas. Two small lesions with thick ring enhancement.



**Fig. 42.7A, B.** Herpes encephalitis. **A** Extensive low-density areas in both temporal lobes. Burr hole for brain biopsy on right side. **B** Marked gyral enhancement after contrast.

to be immunoallergic and the histological features are characteristic, consisting of lymphocytic and plasma cell infiltrates around the venules of the neural parenchyma with perivenous foci of demyelination.

**Imaging.** CT may show no changes, but in the more severe cases there may be areas of patchily reduced density reflecting vasogenic edema in the white matter.

MRI is more sensitive than CT in demonstrating areas of edema and demyelination in the white matter and may show changes more extensive than suggested by CT, or even when CT is negative.

**Reye's Syndrome.** This condition, as originally described, predominantly affected children below the age of 16 years, but is now known to affect adults as well. The patients are recovering from an illness of viral or presumed viral etiology when they develop both hepatitis and encephalitis. About one third of the patients die within a few days from raised intracranial pressure.

Liver function is severely affected and half the patients have enlarged livers. Toxic agents, particularly salicylates, have been associated with the syndrome and the interaction of toxin and virus has been postulated as the cause.

**Imaging.** CT or MRI in the acute phase shows widespread cerebral edema with compression of the ventricles. Patients who recover may show enlargement of the ventricles and sulci and diminished attenuation of the cerebral white matter.

**Specific virus infection** is usually referred to as viral encephalitis or acute infective encephalitis and may be due to many different viruses. These can be classified as shown in Table 42.1.

The best known of the enteroviruses is the poliovirus responsible for acute anterior poliomyelitis. The arthropod-borne viruses spread by mosquitoes are responsible for the St. Louis, Eastern and Western equine, Japanese B and Murray Valley encephalitides; those spread by ticks result in Russian spring-summer and Central European encephalitis.

**Table 42.1.** Causative agents for viral encephalitis

RNA viruses
enteroviruses
arboviruses (arthropod borne)
rabies
paramyxoviruses
DNA viruses
herpes simplex viruses
cytomegalovirus
herpes zoster
papovaviruses
unidentified viruses (Encephalitis lethargica; Uveomeningoencephalitis; Behcet's disease)

Among the paramyxoviruses measles can cause subacute sclerosing panencephalitis as well as the quite different acute post-infectious encephalitis already described.

**Subacute sclerosing panencephalitis (SSPE)** occurs in children or young adults several years after a known episode of measles. The precise mechanism of this delayed or prolonged viral infection is still poorly understood but is presumably related to immunological factors. The disease runs a protracted course ending in death or severe disablement.

**Imaging.** CT and MRI may show low attenuation in the white matter similar to that already described for non-specific encephalitis with MRI being the more sensitive.

**Herpes simplex Type 1 encephalitis** involves predominantly the temporal lobes and is a grave illness with a mortality of 55%. The severity of the infection can lead to hemorrhagic necrosis and considerable mass effect. The changes are bilateral but may appear predominantly unilateral in the acute phase, and this may lead to a false diagnosis of tumor at imaging.

CT shows reduced density in the affected temporal lobe(s) (Fig. 42.7A) and the adjacent posterior frontal region usually with mass effect. The changes may be minimal in the first 2 or 3 days despite severe neurological impairment and should be carefully sought.



**Fig. 42.8.** Herpes encephalitis. Low-density area in right temporal lobe with slight mass effect.

Hemorrhage rarely shows a clear hematoma but may give rise to patchy areas of slightly increased density. After contrast, enhancement is seen in most cases and may be patchy, peripheral or gyral (Fig. 42.7B). As already noted mainly unilateral cases can give rise to diagnostic error (Fig. 42.8).

In the chronic stage there may be large low-density areas with associated local atrophy in the affected regions.

*MRI* which is more sensitive to white matter changes may show the lesions to be more extensive than appears at *CT* and will identify them at an earlier stage.

*Herpes simplex virus Type 2* may affect neonates and infants acquired either transplacentally or at birth. Intrauterine infection of the fetal brain may give rise to microcephaly and intracranial calcification, both periventricular and in white and grey matter. This may be recognized both at simple radiography and *CT*.

**Cytomegalovirus (CMV) infection** is widespread but does not normally involve the CNS except in patients with compromised immunity, as in AIDS, or with undeveloped immunity as in the fetus. The latter is infected from a carrier

mother across the placental barrier. It is estimated that some 1200 infants a year are born in the UK with congenital CMV infection and that 200 a year suffer major defects.

**Imaging.** *Simple radiography.* The skull radiograph of an affected infant may show microcephaly and in some cases calcification which is characteristic. The calcification is stippled in type, bilateral and symmetrical and mainly subependymal and periventricular.

*CT* or *MRI* will show dilated ventricles due to atrophy with paraventricular and cortical calcifications.

**Progressive multifocal leukoencephalopathy (PML)** is due to a papovavirus and occurs only in special pathological circumstances. It particularly affects patients with compromised immunity such as patients with chronic lymphatic leukemia and Hodgkin's disease or patients receiving immunosuppressive therapy.

Multifocal demyelinating lesions occur and spread in the hemispheres, often asymmetrically. They are accompanied by neurological defects and dementia leading to death.

*CT* and *MRI* will both show the white matter lesions well; in the case of *CT* as spreading areas of low density (Fig. 42.9).

#### Fungal Infections

Fungal infection of the CNS is only rarely seen in healthy people. In these cases it is usually spread by the bloodstream from a primary focus in the lungs or elsewhere in the body.

Most cases occur in patients whose resistance to infection is lowered by conditions such as leukemias, lymphomas, malignant disease or AIDS, or by prolonged use of antibiotics, steroids, cytotoxic drugs or immunosuppressive agents.

The infecting fungus may be one of the usual human pathogens such as the fungi of aspergillosis or actinomycosis or a saprophytic fungus (opportunist infections).

The following list, which is by no means exhaustive, contains many of the reported fungus infections to involve the CNS:

actinomycosis	coccidioidomycosis
aspergillosis	cryptococcosis
blastomycosis	histoplasmosis
candidosis	nocardiosis
cladosporioses	mucormycosis

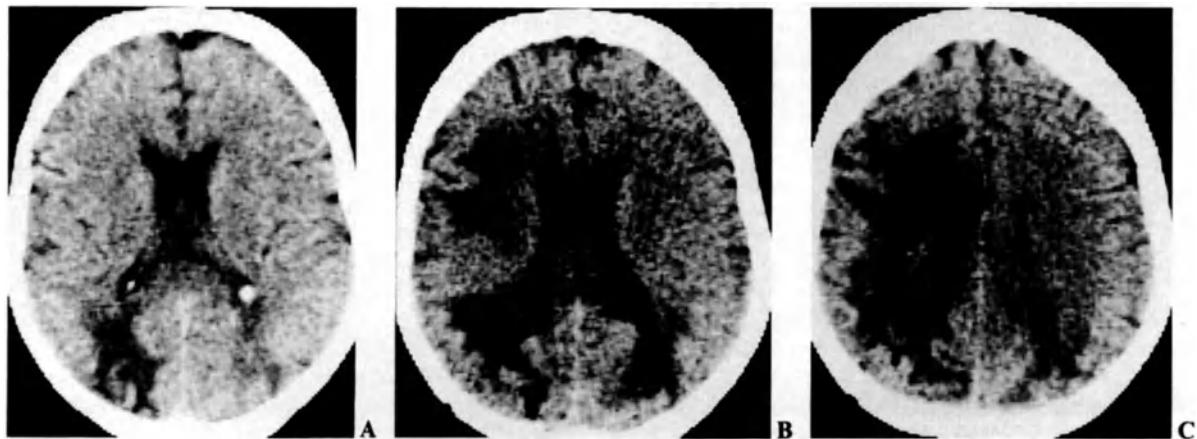


**Fig. 42.9A, B, C.** Progressive multifocal leukoencephalopathy (PML). A Occipital lesions more marked on the right. B, C Several weeks later there has been marked extension through both hemispheres.

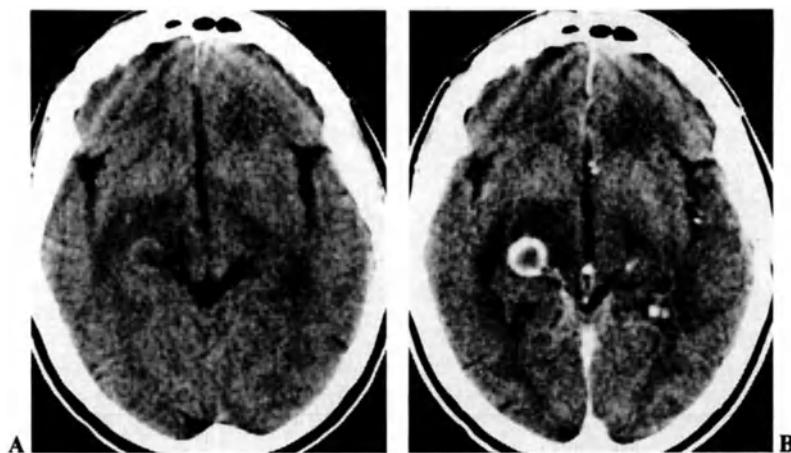


Fig. 42.10A, B. Cryptococcal abscess before and after enhancement.

Candidosis and cryptococcosis (torulosis), like coccidioidomycosis, can give rise to a chronic granulomatous meningitis as well as to granulomas or parenchymatous abscesses. Mucormycosis may complicate uncontrolled diabetes or acute leukemia.

**Imaging.** *Simple Radiography.* A chest radiograph may show evidence of a primary fungal infection or of an opportunistic infection.

**CT.** The abscesses produced by fungal infections are often small and multiple but larger single abscesses can occur. The

appearances are non-specific. Homogeneous enhancement as well as ring enhancement may be seen in smaller lesions.

Chronic granulomatous meningitis, if present, resembles that already described in tuberculous meningitis (p. 767). MRI is more sensitive than CT in detecting early lesions (Fig. 42.10, Fig. 42.11).

#### Parasitic Infections

Table 42.2 gives a list of the different parasitic infections which can involve the brain.

Table 42.2. Parasitic infections which can involve the brain

Protozoal
toxoplasmosis
amebiasis
malaria
trypanosomiasis
Chagas' disease
Metazoal
tapeworm (cestodiasis)
fluke (trematode)
roundworm (nematode)

The incidence of parasitic infections of the nervous system varies greatly in different geographical regions. They may involve the brain producing cysts, granulomas or abscesses, and they can also involve the meninges.

**Toxoplasmosis.** The causative organism (*Toxoplasma gondii*) is an obligatory intracellular parasite. The definitive hosts are the cat family in whom the entire life cycle can be completed. Other mammals and birds can become infected as can humans either from cats or from eating meat from chronically infected animals.

Two types of brain infection are seen in humans, the *congenital* and the *adult*. This is because the CNS is only involved in humans with an immature system as in the fetus or with compromised immunity (as in AIDS or immunosuppression).

The congenital type results in a child with more or less extensive brain damage at birth and with bilateral choroidoretinitis. The lesions remain apparently healed and the condition does not progress. The adult type attacks

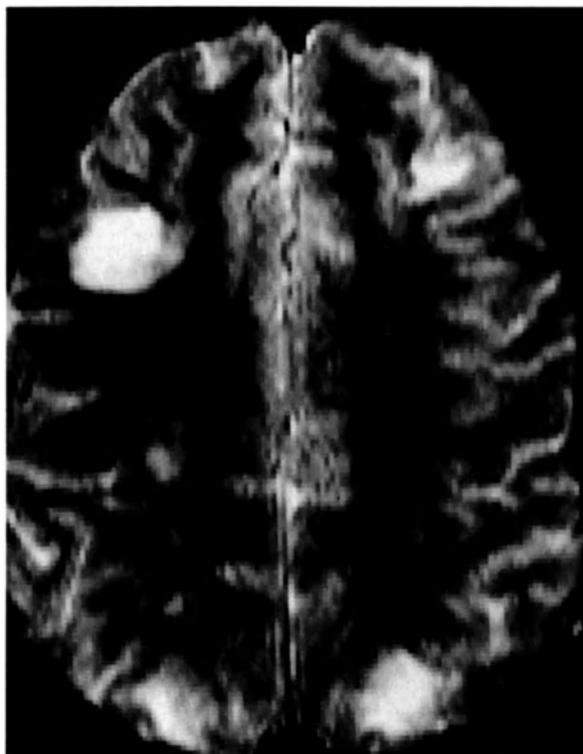


Fig. 42.11. Areas of cryptococcal cerebritis shown as high signal by MRI (T<sub>2</sub>-weighted). These were not identified on a CT scan taken at the same time.

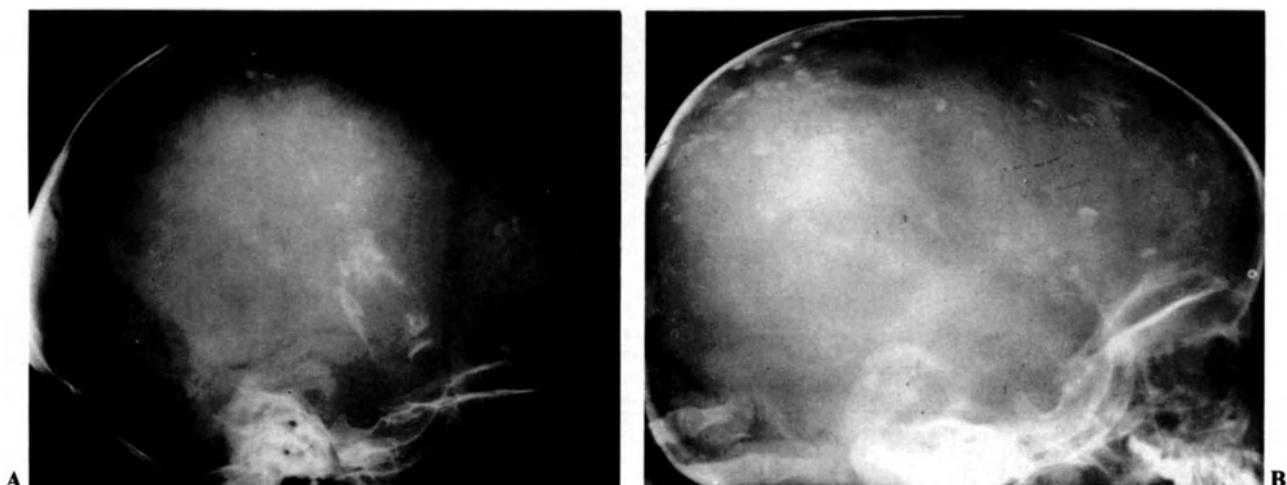


Fig. 42.12A,B. Calcification in congenital toxoplasmosis granulomas. Two different cases.

patients with impaired immune systems and produces multiple brain lesions involving the basal ganglia and subcortical regions. There is clinical evidence of encephalitis and the disease is usually fatal without appropriate antibiotic therapy.

**Imaging.** *Simple Radiography* is helpful in the congenital type and may show characteristic intracranial calcification. This consists of linear streaks in the basal ganglia region and multiple subcortical flecks of calcification (Fig. 42.12).

*CT.* In the congenital type there is a more or less gross degree of ventricular dilatation depending on the degree of brain destruction caused by the infection. There is also extensive calcification in the basal ganglia and subcortical regions (Fig. 42.13).

The adult type usually shows multiple lesions of slightly reduced density in the thalamus and basal ganglia or subcortically. They are best identified after high dose contrast enhancement when most will show ring or nodular enhancement, though some will not (Fig. 42.14). There is usually mass effect and some local edema. In the appropriate

context the appearances are suggestive but not specific, since other inflammatory lesions can produce similar appearances as can neoplastic lesions.

*MRI.* This appears to be more sensitive than CT in detecting the intracerebral lesion and is thus claimed to permit earlier biopsy and appropriate treatment.

**Amebiasis.** Amoebic abscess of the brain is rare and is usually a late and fatal hematogenous complication of intestinal, hepatic or pulmonary infection with *Entameba histolytica*. There is usually a single abscess in the subcortical or basal ganglia region.

Infection of the CNS with other types of amoeba (*Negleria fowleri*; *Hartmanella acanthameba* group), have also been described.

*Negleria fowleri* produces a primary amoebic meningoencephalitis. It is acquired by previously healthy children and young adults swimming in contaminated water and is usually fatal within a few days.

*Hartmanella acanthameba* by contrast affects debilitated or immunocompromised individuals and produces a

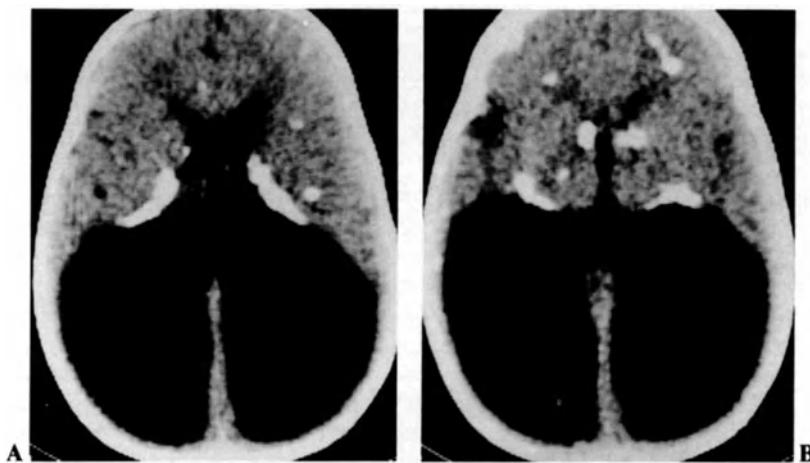
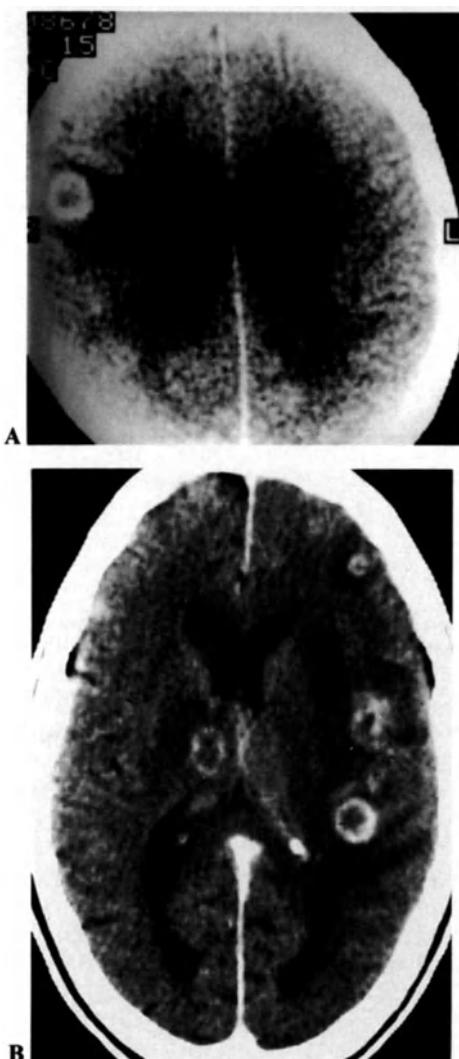


Fig. 42.13A, B. CT shows gross cerebral atrophy due to congenital toxoplasmosis. Note calcification in cerebral and basal ganglia granulomas.



**Fig. 42.14A, B.** Enhancing toxoplasmosis abscesses in patients with AIDS. Two different cases.

granulomatous amebic encephalitis which is also fatal though the course is more prolonged.

**Malaria.** Cerebral malaria occurs only in malignant tertian malaria due to *Plasmodium falciparum*. There is a high mortality and the main macroscopic abnormalities in the brain are edema, vascular congestion and petechial hemorrhages.

**Tapeworms (Cestodes).** The tapeworm infections which can involve the brain include cysticercosis, hydatid disease and coenurosis.

**Cysticercosis.** *Cysticercus cellulosae* is the larval stage of *Tenia solium*, a tapeworm whose permanent host is man. Animals including the pig are intermediate hosts and harbor the cysts after ingesting eggs excreted in human feces. The eggs release the embryos in the intestine of the animal and they penetrate the intestinal wall and are carried to all organs including brain and muscles. Here the larvae develop a cystic wall.

Humans can become intermediate hosts either from self-infection with eggs or by eating infected pork. The disease is widespread in India and Latin America, where it accounts for a high proportion of brain tumors.

**Imaging. Simple Radiography.** Calcification is commonest in the muscle cysts and shows a pathognomonic appearance already described (see Fig. 22.22). Calcification can also occur in the cerebral cysts. It is also characteristic but is far less common and is different in appearance. It consists of small 2–3 mm rounded nodules (Fig. 42.15A) instead of the larger oat-shaped calcifications seen in the muscles. Since any patient with cerebral cysticercosis is likely also to have muscle cysts and they are more commonly calcified, radiography of the muscles will establish the diagnosis more certainly than skull radiography.

**CT.** The appearances depend on the number, size and distribution of the cysts as well as on their stage of evolution. Their number can vary from just one to over a hundred. They are commonest in the brain but can involve the meninges and the ventricles.

In the acute stage parenchymatous cysts appear as small rounded low-density lesions which enhance strongly with contrast (Fig. 42.15B). In the chronic stage they do not enhance but may develop punctate calcification. Obstructive hydrocephalus may develop from cysts obstructing the ventricles or basal cisterns, where they may form racemose groups.

**MRI.** This will demonstrate the lesions well, particularly in the acute stages, but it will not show the calcifications.

**Hydatid Disease (Echinococcosis).** This is produced by the larval stage of the dog tapeworm. The eggs are ingested by sheep who form the usual intermediate host. Man can become the intermediate host through contact with infected dogs or by ingesting contaminated food. The embryos pass via the portal system to the liver and thence to the lungs and general circulation. Hydatid cysts of the brain are usually solitary cystic and unilocular. They commonly lie in middle cerebral territory in the parietal region and can reach a large size, often being more than 6 cm in diameter.

**Imaging. CT.** Typical cases show a large cystic lesion lying subcortically in the parietal lesion. There is some mass effect but there is no enhancement after contrast and no surrounding edema or adjacent calcification. In rare cases there may be more than one cyst or the cyst may be deeply sited adjacent to the ventricle.

**MRI.** This also shows the lesions well but has no particular advantage over CT.

**Coenurosis.** This is an infection due to another dog tapeworm, *Taenia multiceps*, which has occasionally infected humans. The cysts are similar to hydatid cysts but not as large. In the brain they are usually single but multiple racemose groups have been described in the ventricles or basal cisterns.

**Trematodes (flukes).** **Paragonimiasis.** This infection is caused by the lung fluke, *Paragonimus westermanii*, and may affect other organs notably the brain. Human infection is caused by eating poorly cooked crustaceans infected by the larval stage of the parasite. The disease is endemic in the Far East where most recorded cases have been encountered and in South Korea it is one of the commonest causes of brain

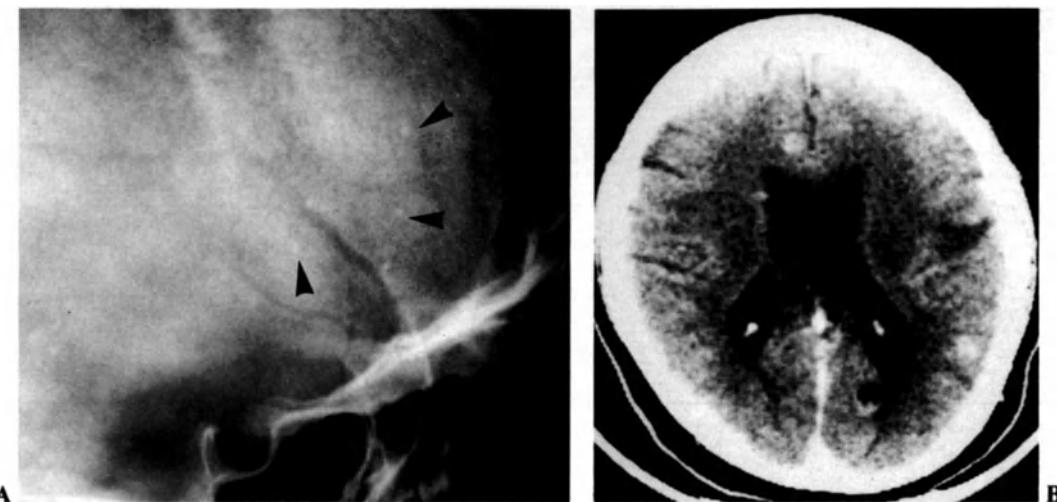


**Fig. 42.15.** A Small punctate calcifications in chronic stage of cerebral cysticercosis. B CT shows small rounded enhancing lesions in acute stage of cerebral cysticercosis.

tumor. The organism gives rise to a large granuloma usually in the temporal or parieto-occipital regions which may later heal with marginal calcification.

**Imaging.** Simple Radiography in the chronic healed stage may demonstrate characteristic 'soap bubble' calcification outlining the margins of the large granuloma.

CT. In the acute stage there is a large irregular low-density area in the affected area and there is some mass effect. Marginal enhancement occurs after intravenous contrast suggesting an abscess or tumor. Later in the chronic stage the characteristic marginal calcification may be demonstrated.

**Schistosomiasis (Bilharzia).** Although human infection is common, involvement of the brain is very rarely seen and is always secondary to infection elsewhere in the body. When it occurs it gives rise to multiple small granulomas which can involve the brain, spinal cord or meninges.

**Nematodes (roundworms).** *Loa loa*, a filarial worm, is prevalent in West Africa and can cause multiple small cerebral granulomas. Similar lesions may occur in *trichinosis*, due to *Trichinella spiralis* which has a worldwide distribution.

#### AIDS

CNS infections are a common complication of AIDS, and manifest clinically as meningitis, focal lesions or generalized abnormalities.

Meningitis is most commonly due to *Cryptococcus neoformans*, but can arise from *Mycobacteria* or *herpes simplex*.

Focal lesions are mainly due to infections giving rise to abscesses and granulomas. The commonest organism responsible is *Toxoplasma gondii*. Other organisms seen are *Mycobacteria* and the fungi *Cryptococcus*, *Aspergillus fumigatus* and *Candida albicans*.

Focal brain lesions in patients with AIDS can be neoplastic as well as inflammatory. In particular lymphoma and rarely Kaposi's sarcoma are found in the brain.

More generalized changes are seen with viruses, in particular *cytomegalovirus*, *herpes simplex* and the JC papovavirus responsible for PML. The HIV virus itself has been found in the brain of AIDS patients at autopsy, and is considered by some workers to be responsible for a direct cytopathic effect leading to the encephalopathy, dementia and atrophy frequently encountered.

**Imaging.** CT and MRI may both show non-specific changes such as atrophy or ventricular dilatation, and will identify focal lesions such as abscesses due to *Toxoplasma* or *Cryptococcus* (Figs 42.10, 42.11, 42.14). The appearances seen in PML and involvement by lymphoma have also been described above. In some case brain biopsy may be necessary to distinguish between abscess and neoplasm. However toxoplasmosis is the commonest cause of focal lesions in AIDS patients and anti-infective treatment with pyrimethamine and sulphadiazine may be given a trial of treatment before brain biopsy is resorted to.

---

## TRAUMA

---

### SKULL FRACTURES

**Simple Fractures.** Simple linear fractures of the skull vault appear as dark lines on the radiograph which in most cases are readily distinguished from vascular markings (Figs

42.16, 42.18). The inner suture line which lies directly beneath the outer serrated suture is linear but its characteristic position and non-branching nature should serve to differentiate it.

Occasionally, where the margins of a fracture minimally



**Fig. 42.16.** Skull fracture (arrows). The vertical fracture shows as a linear density due to overlapping bone margins.

overlap, the double density gives rise to a linear shadow which appears whiter than the adjacent bone (Fig. 42.16).

Provided there is no associated brain injury, simple fractures will eventually heal without problems. However healing is slow and the fracture may still be visible for several years.

*Cephalhematoma* is a birth injury characterized by localized swelling in the parietal region on one or both sides (Fig. 22.14). The hematoma lies under the pericranium and its margin rapidly become calcified giving rise to a characteristic picture on simple radiography of the infant's skull. As the infant grows the swelling becomes less prominent and the calcification merges with the underlying skull vault.

#### COMPLICATED FRACTURES

These include

1. Compound fracture. Here the main danger, as with compound fracture elsewhere, is of infection

2. Fracture with meningeal tear or penetration. At the skull base this may give rise to CSF rhinorrhea or otorrhea. It may also lead to infection from the sinuses or ear and meningitis, or to air entering the meninges and brain (pneumocephalus) and secondary brain damage

Over the skull vault in children it can give rise to a leptomeningeal cyst with overlying bone defect

3. Fracture with vascular injury involving a middle meningeal branch, cortical veins or a dural sinus. Extracranial or subdural hematoma may result and these are discussed below

4. Fracture with brain injury. These are either depressed fractures (Fig. 15.17, p. 279) with resulting direct brain trauma (Fig. 42.17) or more commonly *contre-coup* injuries. These and the more serious brain shearing injuries are also discussed below.

*Bone infection* gives rise to radiological appearances which have already been described.

*CSF rhinorrhea* is an important complication of fracture involving the floor of the anterior fossa or the sphenoid. Surgical intervention is usually required to prevent intracranial infection. The exact site of the fracture is often difficult to localize. If simple tomography fails, it may be necessary to proceed to CT with contrast cisternography, or to isotope cisternography to localize the site of the leak.

*CSF otorrhea* may complicate fractures of the petrous bone and require similar measures to localize the lesion.

*Pneumocephalus* can be diagnosed at an early stage, and before too much damage results, by obtaining lateral skull films of good quality with a horizontal radiograph beam. These will clearly show an air-fluid level or air in the subdural or subarachnoid space that could be missed with the conventional vertical beam (Fig. 42.18). If air enters the cerebral substance an expanding pneumocele may develop which can cause progressive brain damage.

Lateral shoot-through films will also show a fluid level in the *sphenoid sinus*, if one is present. This is an important sign which usually means that a basal fracture has allowed CSF to enter the sinus. The horizontal ray films should be taken with the patient supine and the head brow up since the

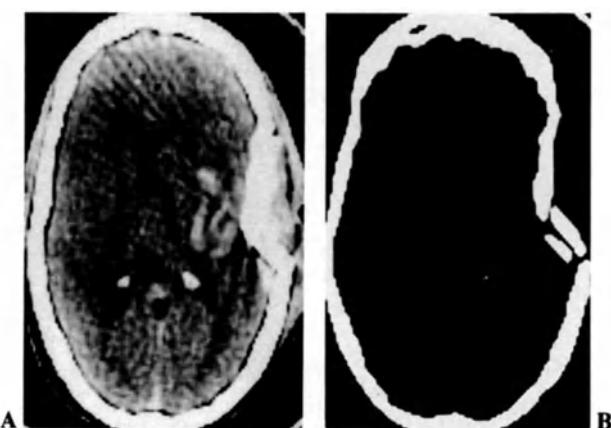


**Fig. 42.17.** A CT shows depressed fracture with hemorrhagic brain damage and contusions. B CT at bone window shows the depressed fragments.



Fig. 42.18. Skull film taken with horizontal beam and patient brow up shows frontal fractures and subdural air-fluid level.

superimposed zygomatic arch can easily be mistaken for a fluid level in the sphenoid sinus if the patient is examined erect.

CT will show intracranial air readily and will identify small amounts more easily than plain films (Figs 42.19, 42.20). It may also be helpful in defining basal fractures.

*Post-traumatic cyst* (lepto-meningeal cyst) may follow a childhood fracture of the vault. There is local cyst formation



Fig. 42.19. CT shows subarachnoid air in the suprasellar and anterior temporal regions following fracture involving air sinuses.

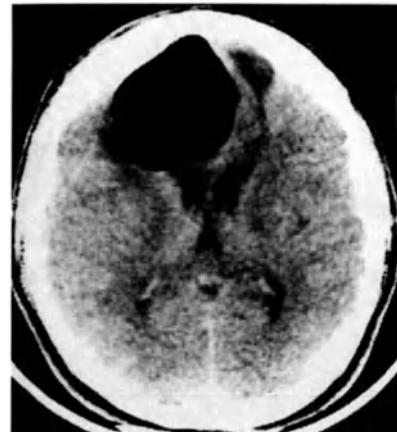


Fig. 42.20. CT demonstrates right frontal aerocele following frontal fracture involving the frontal sinus.

under the fracture which erodes the bone margin and can produce quite large bony defects, usually elongated. Most cases present in young children in the parietal or parieto-occipital region often with local swelling long after the original trauma has been forgotten. The appearances of the simple radiograph are characteristic and should immediately suggest the true diagnosis.

#### THE BRAIN AND MENINGES

Cranial trauma is a major problem in hospital accident and emergency departments and is responsible for 150 000 hospital admissions a year in the UK. It is also responsible for 9 deaths per 100 000 population per annum and for even higher figures in the USA. There is also a high incidence of patients with severe residual neurological handicap – 150 per 100 000 population in the UK.

*Imaging.* Where intracranial hematoma or brain damage is suspected CT is the best and cheapest method of rapid assessment. MRI will also show hematomas well and may have advantages with small contusions and with edema and subtle lesions of the white matter, particularly in difficult areas for CT such as the brain stem and posterior fossa.

Head trauma in infants can be assessed by *ultrasound*, and this is particularly useful in the investigation of suspected perinatal trauma (Fig. 41.24, p. 762).

#### Extradural Hematoma

These are most frequent in the fronto-parietal region but can occur elsewhere including the posterior fossa. There is usually evidence of skull fracture in the appropriate area and involving a meningeal vessel.

CT shows a pathognomonic high-density biconvex lesion immediately subjacent to the skull vault (Fig. 42.21A, B). There is usually considerable mass effect with displacement of the ventricles to the contralateral side. The displacement may be disproportionate to the size of the hematoma indicating swelling of the ipsilateral hemisphere.

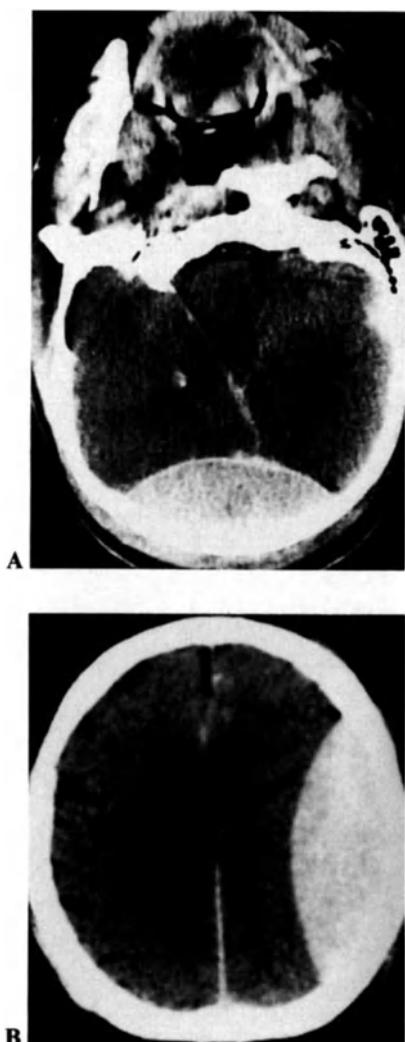


**Fig. 42.21A, B.** CT showing extradural hematomas in two different patients.  
A Occipital. B Parietal.

*MRI* shows extradural hematomas as well or better than CT as high-signal lesions (short T<sub>1</sub>, long T<sub>2</sub>), and without interference from adjacent bone.

#### Subdural Hematoma

There is usually a history of head trauma, but this may be relatively minor and ignored at the time. It should also be remembered that demented or alcoholic patients are particularly liable to suffer head injuries and that such patients are unlikely to provide a correct history.

*CT.* An acute subdural hematoma contains freshly extravasated blood and is of the same high density as an acute extradural hematoma. It also lies peripherally, most commonly in the parietal region. The shape, however, is crescentic rather than biconvex (Fig. 42.22); this is because the blood can spread more easily in the subdural space and is under less pressure.

The density of the lesion gradually diminishes over the first 2 weeks until it becomes isodense with subjacent brain, and after 3 weeks or so it is of lower density than the subjacent brain. A chronic subdural hematoma may be of the same low density as CSF (Fig. 42.24).

During the isodense stage a subdural hematoma may be easily missed unless the scan is carefully examined. The absence of visible peripheral sulci on the unenhanced scan and the enhancement of the underlying brain after contrast are signs which should draw attention to the lesion (Fig. 42.23).

There is usually mass effect with displacement of the ventricles. However this sign will not be seen with bilateral subdurals, though squeezing together of the frontal horns may be noted.

*MRI* will also show subdurals as well as or better than CT (Fig. 42.25) and is particularly useful at the CT isodense stage.

*Subarachnoid hemorrhage* frequently accompanies severe head injuries and may be associated with extra- or intra-cerebral hemorrhage.



**Fig. 42.22.** Acute subdural hematoma (arrows).

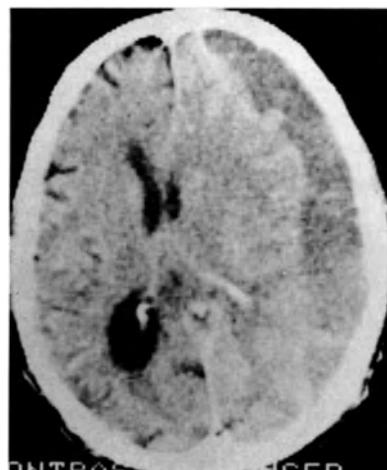


**Fig. 42.23.** Subacute subdural. The high density at the lower part is due to clotted blood.



◀ Fig. 42.24. Bilateral chronic subdurals.



Fig. 42.26. Contre-coup brain injury affecting both frontal poles, where there are small hemorrhages, contusions and edema.

CT shows subarachnoid hemorrhage best on the unenhanced scan where it opacifies the CSF containing basal cisterns or cortical sulci.

#### Intracerebral Hemorrhage

An isolated large hematoma is more likely to be seen in spontaneous hemorrhage than following trauma. Multiple small hemorrhages or contusions are more typical and these may

be due to 'contre-coup' injury affecting the tip of the temporal lobe or the frontal or occipital poles (Fig. 42.26).

CT shows scattered high-density lesions in the affected area often subcortical in position (Figs 42.17A, 42.26) and there may be associated low-density lesions due to edema. Contusions appear as patchy areas of mixed density lying superficially and involving the cortex; they can however spread into the adjacent white matter as hemorrhage increases.

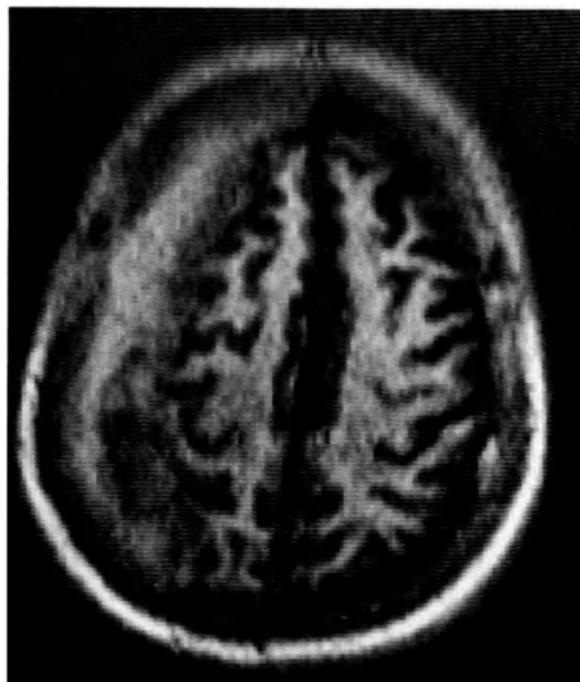


Fig. 42.25. MRI study ( $T_1$ -weighted) shows right subdural as high signal.

#### DIFFUSE BRAIN DAMAGE

A surprisingly high proportion (almost 50%) of patients who suffer immediate prolonged unconsciousness following a head injury have no obvious mass or focal lesions of the types just described and this is true of 35% of fatal cases. In these patients the lesions present have been classified into four types:

1. Multiple petechial hemorrhages
2. Diffuse axonal injury
3. Brain swelling
4. Hypoxic brain damage

*Multiple Petechial Hemorrhages.* This type of injury is seen throughout the white matter and brainstem and is rapidly fatal. It is therefore more likely to be seen in a post-mortem room than in the imaging department.

*Diffuse Axonal Injury* (white matter shearing). This severe injury may show virtually no macroscopic change in the affected brain. There is disruption of axons in the subcortical parasagittal white matter and in various other sites including the internal and external capsules, fornix and cerebellum. It is claimed to result from acute lateral acceleration of the head and can occur without anything actually striking the head.



**Fig. 42.27.** Contusions and small hemorrhages, mainly subcortical following shearing injury.

The patient is unconscious from the moment of impact and remains unconscious, vegetative or severely disabled until death.

**CT.** Despite the severe brain damage and the very grave state of the patient it should be understood that this is a condition where there may be little or nothing shown at CT.

Small focal hemorrhages have been described in the corpus callosum and in the dorsolateral quadrant of the rostral brainstem and such lesions could theoretically be demonstrated, as can small subcortical hemorrhages (Fig. 42.27).

**Brain Swelling.** Diffuse swelling of the entire brain occurs mainly in children and adolescents. The pathogenesis is debated and it is thought to be due to vasodilatation and increased cerebral blood volume in the first place. This is recoverable, but if it persists for any length of time, true edema may follow.

Diffuse swelling of the ipsilateral hemisphere can also occur with focal and mass lesions described above, including acute subdural hematoma and extensive unilateral contusions. Focal edema may also occur with hemorrhages and contusions.

**CT.** With diffuse bilateral swelling the ventricles are compressed and appear small and slit like; the basal cisterns may be occluded. The white matter shows no reduction in density and appears normal, though evidence of edema may be seen in cases with prolonged coma (Fig. 42.28).

**Hypoxic Damage.** This is due either to a prolonged drop in systolic blood pressure or to arterial spasm or to both. Evidence of hypoxic damage is seen in the first place at major arterial boundary zones (see Chap. 41), and frank infarction may ensue.

Infarction may also result from brain swelling and tentorial herniation compromising the posterior cerebral circulation, or from trauma to major vessels.

**CT.** The appearances of cerebral infarcts are discussed in Chap. 41. On the unenhanced scan the earliest evidence is a low-density area, but this is non-specific and may be associated with contusions or edema, so that differentiation in the acute stage is not possible.

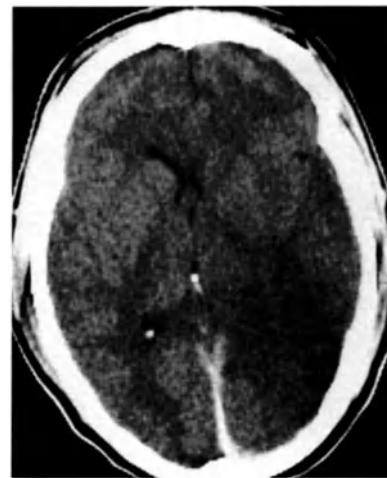


**Fig. 42.28.** Head injury in a child. There is cerebral edema mainly on the left with compression of the ventricles and some shift to the right.

**MRI.** This appears more sensitive than CT at defining cerebral infarcts. The lesions have a long T<sub>1</sub> and T<sub>2</sub> and are seen earlier from onset. They also appear more extensive and are detectable for a longer period compared with CT.

#### VASCULAR TRAUMA

Injury to the head and neck can affect major vessels supplying the brain as well as intracranial vessels. The major lesions resulting include:

- Traumatic thrombosis
- Traumatic dissection
- Arterio-venous fistula
- Traumatic aneurysm
- Ruptured veins

**Traumatic thrombosis** of the internal carotid artery may follow a direct blow to the neck. The occlusion extends down to the origin of the vessel and the appearance at angiography resembles that seen in the far commoner atheromatous thrombosis. The clinical effects are also similar but are complicated by any associated traumatic lesion to the affected hemisphere.

In a young patient with a good Circle of Willis and an adequate collateral circulation there may be no cerebral damage at all. However, in a patient with an inadequate collateral circulation plus a head injury with cerebral spasm or other lesion affecting normal circulation the result can be infarction of most of the hemisphere. Intermediate cases may show less extensive infarcts affecting only boundary zones.

**Dissection of the internal carotid artery** may result from trauma to the neck and usually involves the high cervical segment. At angiography the diagnosis is readily made if the false channel fills with contrast. Most commonly it does not but the diagnosis should still be suspected if there is a long narrowed arterial segment.

Thrombosis and dissection of the vertebral artery have both been described following neck trauma with damage to cervical vertebrae. The lesions are usually asymptomatic because of the excellent anastomotic circulation from the other vertebral artery.

*Traumatic aneurysms* are usually false aneurysms. They can affect the major cerebral vessels in the neck or intracranial arteries and are readily demonstrated by angiography.

*Traumatic AV fistula* may also affect major or minor vessels, but certain types deserve special mention.

*Carotico-cavernous fistula* gives rise to exophthalmos which may be pulsating. The diagnosis may be clinically obvious but can also be suggested at early CT following a head injury, where the proptosis and hugely dilated superior ophthalmic vein may be noted (Fig. 42.22).

Definitive diagnosis and also treatment by balloon embolization depend on arteriography and are discussed elsewhere (p. 761).

*Meningeal AV fistula* can produce hypertrophy of the meningeal vascular markings shown at simple radiography.

#### LATE EFFECTS OF BRAIN TRAUMA

These include cerebral atrophy, porencephalic cyst, hydrocephalus, infections and CSF leaks.

*Post-traumatic atrophy* may be focal or generalized. *Focal* atrophy occurs in any area of brain damage whether due to contusions, hemorrhage or infarction. It is characterized by local enlargement of sulci and fissures and local dilatation of the adjacent ventricle. *Generalized* atrophy may follow any severe trauma and may also be associated with focal lesions. It may also result from the cumulative effects of repeated trauma as in the 'punch drunk' boxer syndrome.

*Porencephalic cysts* have been described above (p. 722). They may follow large hemorrhages or infarcts and can communicate with the ventricles. Smaller cysts may also be seen in areas of previous brain hemorrhage or infarction.

*Hydrocephalus* following head injury may result from obstruction to the CSF flow from subarachnoid hemorrhage leading to communicating hydrocephalus.

*For further reading, see p. 790.*

## CHAPTER 43

# WHITE MATTER, DEGENERATIVE AND METABOLIC DISORDERS

D. Sutton

---

## WHITE MATTER DISEASES

---

Leukoencephalopathy is the term used for a miscellaneous group of conditions of differing etiologies which have in common involvement of the white matter. Included among these are multiple sclerosis, Schilder's disease, acute disseminated encephalomyelitis (see p. 769), disseminated necrotizing leukoencephalopathy (see p. 789), progressive multifocal encephalopathy (see p. 771), Reye's syndrome (see p. 770), central pontine myelinolysis, Marchiafava-Bignani disease, leukodystrophies and Binswanger's disease.

Changes in the white matter are well shown by CT, but there is no doubt that MRI is even more sensitive in demonstrating white matter lesions. The changes in specific pathological conditions are described below, but it should be realized that there are also many physiological causes of changes in white matter density.

*Neonates*, particularly premature infants, normally show low attenuation white matter at CT. This is due to incomplete myelination and improves as myelination progresses usually resolving by 2 months of age. Low attenuation white matter is also seen in the *elderly* usually in association with generalized senile atrophic changes.

Other causes of generalized low attenuation of the white matter at CT include *uremic* and *hepatic coma* and *hypertensive crises*. The *lipidoses* and *mucopolysaccharidoses* are also associated with low attenuation white matter, whilst *malignant disease* and *muscular dystrophy* are other rare causes.

## MULTIPLE SCLEROSIS

This is one of the commonest of neurological disorders and is characterized by disseminated plaques of demyelination and gliosis throughout the neuraxis. The sites of election are:

1. Periventricular
2. Optic pathways
3. Brainstem
4. Cerebellar white matter and peduncles
5. Spinal cord

Most authorities consider the etiology to be immunopathological, and there is an increased incidence of certain tissue-type antigens in the affected patients. There is also raised gamma globulin in the CSF. Young adults are primarily affected with an increased incidence in the colder wet temperate zones of the Northern hemisphere.

*Imaging.* CT may show no abnormality even in the acute stages. In about one third of patients small low-density areas are seen in the white matter, particularly adjacent to the atria or in other periventricular sites (Fig. 43.1). In the acute stage these may show marked enhancement (Fig. 43.2), but chronic lesions fail to enhance. Occasionally, enhancing small lesions are seen which were isodense before contrast. Classical cases show no mass effect or surrounding edema,

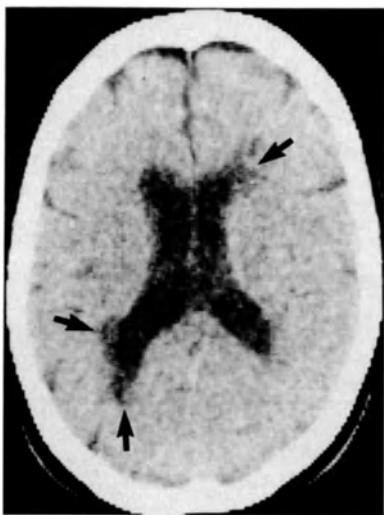


**Fig. 43.1.** Unenhanced CT shows small periventricular lucencies due to multiple sclerosis plaques.

but very rarely mass effect and edema are encountered which can simulate tumor, particularly with a single large lesion.

*MRI* is far more sensitive than CT in the demonstration of MS plaques, and it has been claimed that an accuracy approaching 100% can be obtained with modern machines (Fig. 43.3). MRI has the further advantage that it can even image lesions in the spinal cord. T<sub>2</sub>-weighted sequences are more sensitive than T<sub>1</sub>-weighted sequences in defining the white matter lesions. Plaques are well shown in the periventricular regions and at the grey white matter interfaces.

It should, however, be remembered that MRI is so sensitive that it shows similar periventricular lesions in some 25% of elderly patients. These may represent ischemic lesions since



**Fig. 43.2.** Post-enhancement CT showing enhancing plaques (arrowheads) in a patient with multiple sclerosis.



**Fig. 43.3.** MRI study (T<sub>2</sub>-weighted) shows multiple sclerosis plaques as areas of high signal in the white matter.

they are particularly noted in patients with multi-infarct dementia. Similar lesions have also been noted following radiotherapy.

#### SCHILDER'S DISEASE (EP. DIFFUSE SCLEROSIS)

This condition affects children as well as young adults. Histopathologically the lesions are similar to those of MS but are more extensive and clinically the course is continuous and progressive, even fulminant, rather than intermittent and relapsing. The main lesions extend through the corpus callosum into both parieto-occipital regions.

*Imaging.* CT shows bilateral low attenuation regions in the parieto-occipital regions which enlarge progressively but not symmetrically. Contrast enhancement is uncommon.

*MRI* shows the white matter lesions better than CT and their true extent is more clearly reflected.

#### CENTRAL PONTINE MYELINOLYSIS

This rare condition primarily affecting the pontine white matter was originally thought to be due to chronic alcoholism and malnutrition, but was later shown to be associated with many other chronic illnesses including neoplasia, liver and kidney diseases. The underlying cause may be an abnormality of plasma sodium and in most cases hyponatremia has been observed, though the relationship is not a simple one.

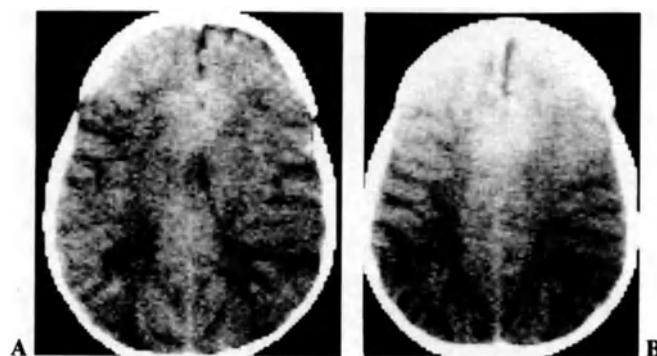


Fig. 43.4A, B. Leukodystrophy showing extensive white matter attenuation.

### MARCHIAFAVA-BIGNANI DISEASE

This is another rare condition with a peculiar white matter localization. The corpus callosum is mainly affected though other central pathways may also be involved. There is an association with *chronic alcoholism*, but this is not invariable and chronic *cyanide* intoxication can produce similar lesions.

### LEUKODYSTROPHIES

Leukodystrophy is a term commonly used to refer to dysmyelination disorders. They are mainly due to genetic defects in the formation and maintenance of myelin and usually present in infants and children. They include the following which, like most disorders of lipid metabolism, are inherited as autosomal recessives and are associated with lysosomal enzyme deficiencies:

*Metachromatic leukodystrophy*

*Globoid leukodystrophy (Krabbe's disease)*

*Spongiform degeneration (Canavan's disease)*

X-linked leukodystrophies are less frequent, but two important ones are adrenoleukodystrophy and Pelizaeus-Merzbacher disease.

*Metachromatic leukodystrophy* is one of the commoner hereditary leukodystrophies and clinical symptoms usually commence in infancy, though they can be delayed into adolescence or later. It is due to a deficiency of the enzyme aryl-sulfatase A. There is a mental retardation or regression and other neurological signs which progress to a fatal outcome.

*Globoid leukodystrophy (Krabbe's disease)* is characterized by a lack of the enzyme beta galactocerebrosidase. It presents in infancy as a failure to thrive and is usually fatal by the second year.

*Spongiform degeneration* is so called because of the characteristic spongy degeneration produced in the white matter of the affected infant. It is one of the few leukodystrophies that produce enlargement of the head, others being Alexander's disease and GM2 gangliosidosis (Tay-Sach's disease).

*Alexander's disease* is also one of the few leukodystrophies which occurs sporadically and is characterized histopatholo-

gically by the abundant presence of Rosenthal fibres in the affected brain.

*Batten's disease* (neuronal ceroid lipofuscinosis) was also referred to as amaurotic family idiocy and cerebromacular degeneration and in contrast to the above the brain is atrophic, often markedly so.

*Adrenoleukodystrophy* is an X-linked genetic disease which was at one time confused with Schilder's disease. It affects boys aged 4 to 6 years and occasionally a little older. The victims develop adrenal insufficiency resembling Addison's disease together with dementia, cortical blindness, ataxia and spasticity.

*Pelizaeus-Merzbacher disease* is also X-linked. It presents mainly in infancy, but can begin later. There is progressive dementia, ataxia and nystagmus often with extrapyramidal features such as dystonic postures and torsion spasms. The metabolic basis remains obscure.

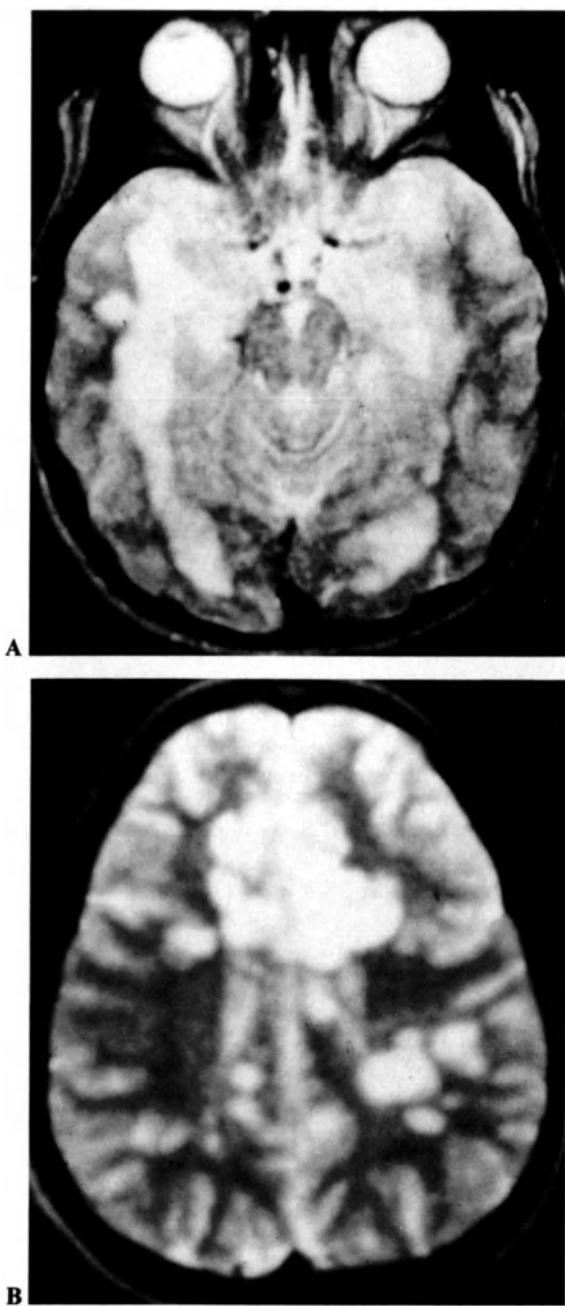
**Imaging.** CT in the leukodystrophies shows low-density areas in the white matter which are bilateral but not necessarily symmetrical and become more extensive as the disease process progresses (Fig. 43.4).

In Alexander's disease the parieto-occipital regions are involved and a thin curvilinear or serrated rim of contrast enhancement may be seen representing perivascular inflammation at the margins of the extending process. Such enhancement is not seen in the other leukodystrophies described above.

**MRI** is more sensitive than CT in the demonstration of white matter disease. Changes can be diagnosed earlier, are shown more clearly, and appear more extensive. T<sub>2</sub>-weighted sequences produce a high signal from affected white matter (Fig. 43.5). However, because of their rarity, the leukodystrophies have not yet been fully characterized by MRI.

### BINSWANGER'S DISEASE (SUBCORTICAL ARTERIOSCLEROTIC ENCEPHALOPATHY)

There is a frequent association between hypertension, arteriosclerosis and dementia or other neuropsychiatric manifestations. The deep penetrating arteries of the brain are affected leading to ischemic changes in the deep white matter associated with generalized atrophy. Some authorities con-



◀ Fig. 43.5A, B. MRI study (T<sub>2</sub>-weighted) in a child showing extensive white matter lesions as areas of high signal.



Fig. 43.6. MRI study (T<sub>2</sub>-weighted) showing deep cerebral ischemic changes as periventricular high signal in a patient with Binswanger's disease. (Courtesy of Dr Gordon Thomson and Bristol MRI centre.)

sider this to be a form of multi-infarct dementia, but others regard them as non-specific senile changes.

*Imaging.* CT shows generalized atrophy with multifocal or generalized low attenuation of the white matter particularly around the ventricles. There is no enhancement after contrast. However similar low attenuation changes may be seen in the brains of many elderly people who are normotensive and without dementia or other neurological signs.

MRI will demonstrate the white matter changes more sensitively than CT and will also show the generalized atrophy. Periventricular lesions are well shown (Fig. 43.6) but it should be realized that these are not specific and similar lesions may be seen in symptomless elderly patients.

## DEGENERATIVE AND METABOLIC DISORDERS

In this section we consider a miscellaneous group of conditions of varying etiology, listed in Table 43.1.

### CEREBRAL ATROPHY

Cerebral atrophy may be focal or generalized.

*Focal* atrophy may be vascular, infective or traumatic in origin and has been discussed in the previous chapters. It

may also be degenerative as in olivopontocerebellar atrophy which is discussed below.

*Generalized* atrophy is more commonly degenerative or idiopathic though vascular, inflammatory, toxic and traumatic types also occur or may be associated. Toxic atrophy may follow alcohol or drug abuse.

Generalized atrophy of the brain is a routine concomitant of the ageing process and is a normal finding in the elderly, becoming more marked in those of advanced age. The loss

**Table 43.1.** Degenerative and metabolic disorders

Cerebral atrophy
Senile and presenile dementias
normal or low pressure hydrocephalus
Alzheimer's disease
Pick's disease
Creutzfeldt-Jacob disease
Huntington's chorea
Olivopontocerebellar atrophy
Parkinsonism
Wilson's disease
Basal ganglia calcification

of neural tissue in the senile brain occurs in a cranium of unchanged size and is, therefore, compensated by an increased volume of CSF which occupies the resulting enlarged ventricles, sulci and subarachnoid space.

So called *senile dementia* shows similar changes but most patients with generalized atrophy show no evidence of dementia and the findings are therefore non-specific.

*Multi-infarct dementia* has been mentioned above in association with Binswanger's disease, but again the findings are non-specific.

**Imaging.** CT or MRI of patients with cerebral atrophy shows:

1. Ventricular dilatation with rounding of the ventricular angles.
2. Enlargement of the cerebral and cerebellar sulci.
3. Increased width of the subarachnoid space and basal cisterns with increased prominence of the interhemispheric and Sylvian fissures.

**Differential Diagnosis.** The most important differentiation is from *hydrocephalus*. This is usually obvious on clinical grounds, but can occasionally be more difficult in patients with communicating hydrocephalus, particularly in the elderly patient with so called normal-pressure or low-pressure hydrocephalus.

With hydrocephalus the ventricular bodies and frontal horns are often more rounded and the temporal horns more dilated than with atrophy. In addition the sulci are less prominent rather than dilated. *Periventricular lucencies*, usually most marked around the frontal horns are also a feature of hydrocephalus, and are due to seepage of CSF through the ependyma. Nevertheless cases do arise where imaging remains equivocal and in these cases further investigation may be required.

The problem is usually to decide whether a patient with dementia is suffering from low-pressure hydrocephalus or merely atrophy since the former may benefit from a shunting operation. *Isotope cisternography* or *CT cisternography* may help to decide. With both methods the ventricles of hydrocephalus patients may be outlined at 12 to 24 hours and remain so for 48 to 72 hours; normal patients or those with atrophy show little isotope or contrast within the ventricles but much over the cortex, and this disperses within 24 hours.

**Pseudoatrophy.** Fluid shift from the brain may result from high dose steroids and from antidiuretics. It is also described in anorexia, protein starvation and severe dehydration. The resulting pseudoatrophy may simulate the CT appearances of true atrophy, but is reversible with appropriate treatment.

## SPECIFIC DEMENTIAS

*Alzheimer's disease* and *Pick's disease* are both associated with well-marked brain atrophy, and in Pick's disease this is said to be mainly frontal and temporal.

The atrophy is well shown by imaging with CT or MRI but in neither case are there any reliable specific features to differentiate from senile or physiological atrophy and definitive diagnosis is made on clinical and pathological grounds rather than by imaging.

*Huntington's chorea* is also associated with brain atrophy but there is selective and more marked atrophy of the corpus striatum. In the most typical cases the head of the caudate nucleus, instead of bulging into the floor of the lateral ventricle, shrinks to a narrow ribbon, and the inferolateral floor of the ventricle becomes rounded outwards. These characteristic appearances may be recognized at CT or MRI, but are not entirely specific since similar changes are seen in some cases of Pick's disease.

*Creutzfeldt-Jacob disease* is a rare form of presenile dementia presenting with a subacute or chronic course and proven to be transmissible, though the agent responsible has not yet been identified. The more chronic cases show evidence of brain atrophy but there are no specific features at imaging. The definitive diagnosis is made by histopathology.

## PARKINSON'S DISEASE

This is often associated with generalized brain atrophy but there are no specific imaging features and the appearances are usually within normal limits for the age of the patient.

## OLIVOPONTOCEREBELLAR ATROPHY

This is a complex group of disorders with a focal or more diffuse atrophic pattern. The etiology may be degenerative (both sporadic and familial types are described), toxic (mainly alcoholic), or paraneoplastic. It is characterized by atrophy of the inferior olives, pons and cerebellum, and the basal ganglia and spinal cord can also be involved.

CT or MRI will demonstrate the lesions well. The cerebellum appears shrunken with enlarged sulci and prominent folia and the brainstem and medulla are small and surrounded by enlarged cisterns (Figs 43.7, 43.8).

## WILSON'S DISEASE (HEPATO-LENTICULAR DEGENERATION)

Hepato-lenticular degeneration is a familial metabolic disease due to an abnormality of copper metabolism in which cirrhosis of the liver is associated with degeneration of the corpus striatum. It usually commences in the second decade. Clinically there is progressive rigidity and tremor, dysarthria and dysphagia, and in the terminal stages some degree of dementia. A characteristic feature is a ring of brown pigmentation in the cornea (Kayser-Fleischer ring).

Imaging of the brain may show no significant changes, but low-density lesions may be seen at CT in the basal ganglia of more advanced cases.

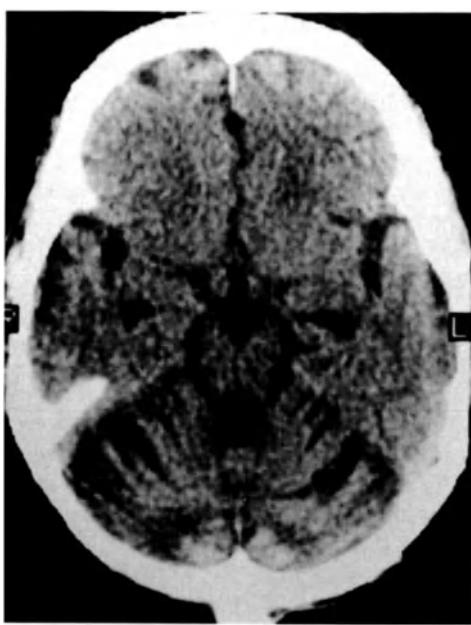


Fig. 43.7A, B. CT showing focal atrophy of brainstem and cerebellum.

#### CALCIFICATION OF THE BASAL GANGLIA

Bilateral symmetrical calcification of the basal ganglia is not uncommon. Pathologically the heaviest calcifications are found in the *globus pallidus*, caudate nucleus, putamen and lateral part of the thalamus. The dentate nuclei of the cerebellum and the internal capsule may also be involved. Smaller collections, which are only rarely visible at imaging, occur at the junction of cortex and white matter and in the cerebellar cortex. Histopathologically the calcifications are due to deposits of tiny pericapillary calcospherites plus calcification in the medial walls of tiny arteries and veins.

The causes may be listed as idiopathic, familial, hypoparathyroidism, pseudohypoparathyroidism, Fahr's syndrome and Cockayne's syndrome.

*Idiopathic* calcification is far and away the commonest cause and is seen mainly in the elderly, where it may be regarded as a normal variant of little pathological significance.

*Familial* calcification is very rare but when it occurs affects young as well as elderly members of the same family.

*Hypoparathyroidism*, either idiopathic or following thyroidectomy, is the most important etiological cause since it is potentially treatable.

*Pseudohypoparathyroidism* (Albright's syndrome) may also be associated with similar calcification. This rare condition is described in the bone section (p. 264).

*Fahr's syndrome* (idiopathic familial cerebrovascular ferrocalcinosis) is a rare familial condition commencing in childhood and characterized by the deposition of iron and calcium in the basal ganglia, dentate nuclei and subcortical regions. It presents with spasticity and choreoathetoid movements proceeding to progressive mental deterioration.

*Cockayne's syndrome*, which is inherited as an autosomal recessive, is characterized by dwarfism and progeria. There is microcephaly and a thick cranial vault as well as the intracranial calcification.

There are several other conditions in which calcification of a less typical type may be found in the basal ganglia. They include carbon monoxide poisoning, lead poisoning, toxoplasmosis, mineralizing microangiopathy and secondary hyperparathyroidism.

The calcification in *toxoplasmosis* is linear rather than amorphous (Fig. 42.12, p. 771) and in the other conditions the diagnosis is usually clear from the history and clinical findings.

**Imaging.** The condition is usually encountered as a chance finding either at simple radiography of the skull or more frequently at CT.

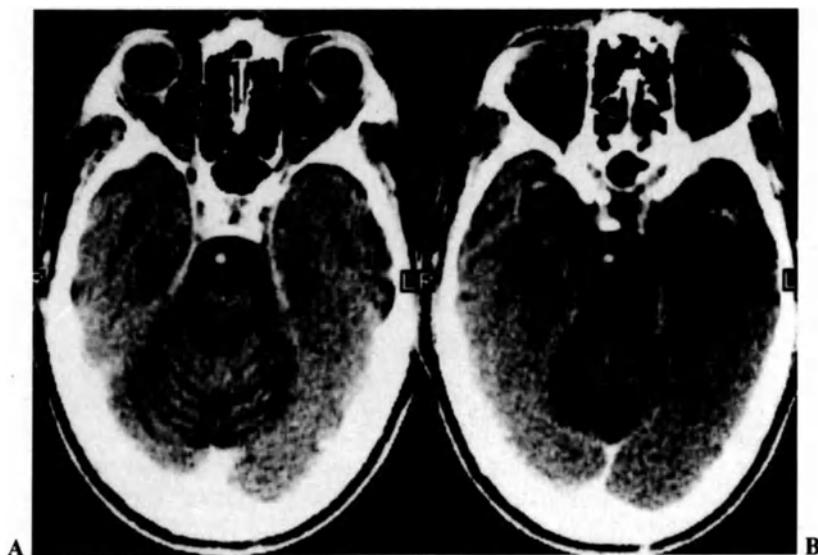


Fig. 43.8A, B. CT showing focal atrophy of cerebellum and brainstem.

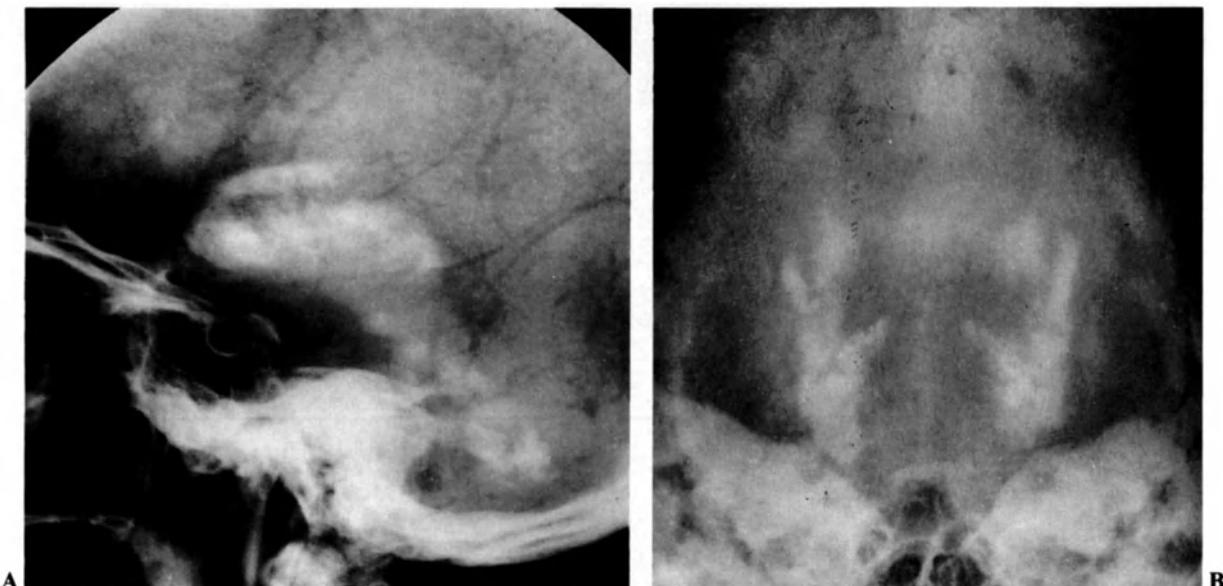


Fig. 43.9A, B. Calcification of the basal ganglia.

Simple radiography shows amorphous calcification involving the head of the caudate nucleus and sometimes extending more widely in the basal ganglia (Fig. 43.9). The calcification is bilateral and symmetrical and the dentate nuclei in the posterior fossa may also be involved. Cortical calcification described above is hardly ever identified.

CT is more sensitive than simple radiography and has shown the condition to be more common than previously thought (Fig. 43.10A, B). In one large series of 7000 consecutive CT examinations 42 examples were discovered (0.6%).

*Carbon monoxide poisoning* is usually due to attempted suicide. In classical cases there is necrosis of the globus pallidus giving rise to bilaterally symmetrical small lucent areas in

this characteristic site. Calcification is unusual but has been described.

*Mineralizing microangiopathy* is also referred to as disseminated necrotizing leukoencephalopathy (p. 783). It is a rare condition seen mainly in patients with leukemia treated with cerebral radiotherapy followed by intrathecal methotrexate. In the acute phase there is bilateral leukoencephalopathy and CT may show bifrontal low density in the white matter, but atrophy later follows.

Mineralizing microangiopathy shows low attenuation in the white matter mainly near the corticomedullary junction and with relative sparing of the deeper white matter. Thin reticular or serrated linear calcification is also present at the corticomedullary junction as well as in the basal ganglia and

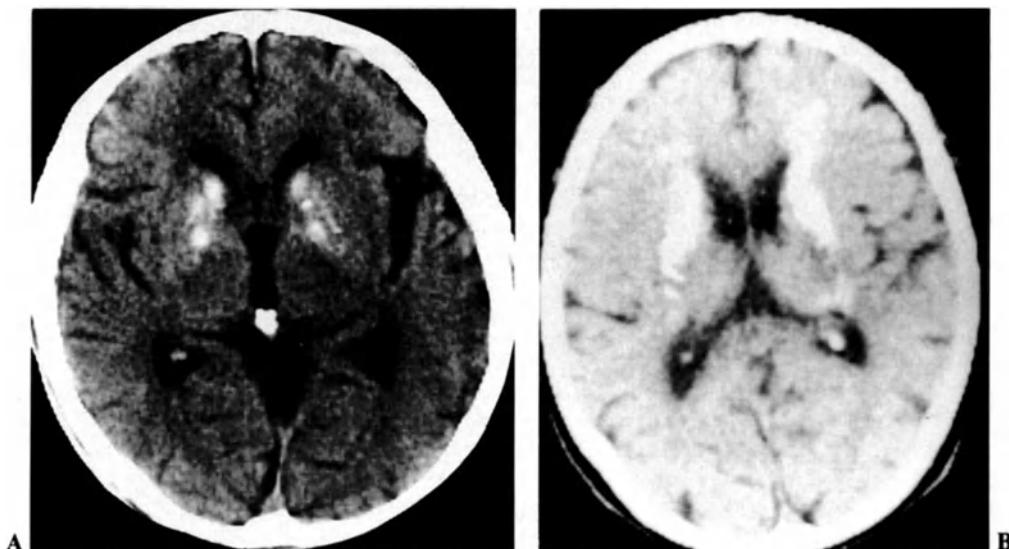
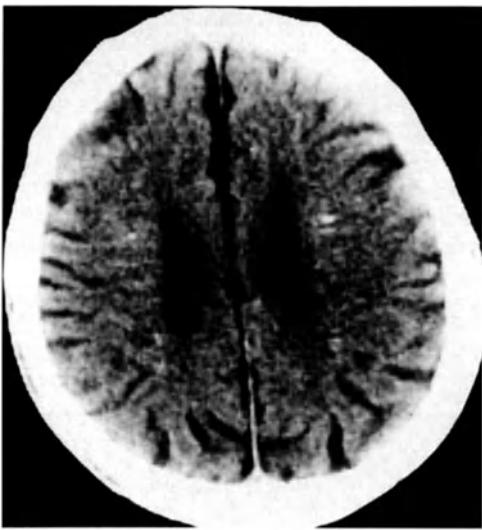


Fig. 43.10A, B. CT showing idiopathic calcification in the basal ganglia in two different patients.



**Fig. 43.11.** Calcification in the white matter due to secondary hyperparathyroidism in a patient in chronic renal failure.

posterior fossa, giving rise to a very characteristic appearance.

*Secondary hyperparathyroidism* is often associated with extensive calcification in the falx and tentorium, and this is evident at simple radiography of the skull. Rarely intracerebral calcification is identified at CT and occurs in the basal ganglia and also in the white matter (Fig. 43.11).

#### REFERENCES AND SUGGESTIONS FOR FURTHER READING

##### BOOKS

- Brant-Zawadski M, Norman D (1986) Magnetic Resonance Imaging of the CNS. Raven Press, New York
- Daniels DL, Haughton VM, Naidich TP (1987) Cranial and Spinal MRI. Atlas and Guide. Raven Press, New York
- Du Boulay GH (1980) Principles of X-ray Diagnosis of the Skull. Butterworth, London
- Hume Adams J, Corsellis JAN, Duchen LW (eds) (1984) Greenfield's Neuropathology, 2nd edn. Arnold, London

- Haughton, VM, Williams AL (1985) *Cranial Computed Tomography*. Mosby, St Louis
- Lee SH, Rao KCVG (1987) *Cranial CT and MRI*. McGraw Hill, New York
- Osborn AG (1980) *Introduction to Angiography*. Harper and Row, Hagerstown
- Post MJ Donovan (1984) *Computed Tomography of the Spine*. Williams and Wilkins, Baltimore
- Ramsey R (1987) *Neuroradiology*, 2nd edn. Saunders, Philadelphia
- Russell DS, Rubinstein IJ (1989) *Pathology of Tumours of the Nervous System*, 4th edn. Arnold, London
- Sutton D (1987) *Textbook of Radiology and Imaging*, 4th edn. Churchill Livingstone, Edinburgh

##### JOURNALS

- Berkovich AJ, Norman D (1988) MRI of schizencephaly. *AJNR* 9: 297–302
- Bories J, Derhy S, Chiras J (1985) CT in hemispheric ischaemic attacks. *Neuroradiology* 27: 468–483
- Brant-Zawadski M, Fein G, Van Dyke C et al. (1985) *AJNR* 6: 675–682
- Davidson HD, Abraham R, Steiner RE (1985) MRI of agenesis of the corpus callosum. *Radiology* 155: 371–373
- Ganti SR et al. (1986) CT of pineal tumors. *AJNR* 7: 97–104
- Gerard E, Healy ME, Hesselink JR (1987) MR demonstration of mesencephalic lesions in central pontine myelinolysis. *Neuroradiology* 29: 582–584
- Illum I, Dupont E (1985) Calcification in the basal ganglia in idiopathic hypoparathyroidism. *Neuroradiology* 27: 32–37
- Jack CR, Reese DF, Scheithauer BW (1985) Radiographic findings in 35 primary cases of CNS lymphoma. *AJNR* 6: 899–904
- Kalifa GL et al. (1987) Hemimegalencephaly: MRI imaging in 5 children. *Radiology* 165: 29–33
- Kendall B, Cavanagh N (1988) Intracranial calcification in pediatric CT. *Neuroradiology* 28: 324–330
- Kucharczyk W et al. (1987) Rathke cleft cysts. MRI and pathological features. *Radiology* 165: 491–495
- Martin N, de Brooker T, Cambier J et al. (1987) MRI evaluation of tuberous sclerosis. *Neuroradiology* 29: 427–433
- Post JD et al. (1985) Cranial CT in AIDS. *AJNR* 6: 743–754
- Post JD et al. (1988) CT, MRI and pathology in HIV encephalitis and meningitis. *AJNR* 9: 469–476
- Press GA, Messelenk JR (1988) MRI of CP angle and IAM lesions. *AJNR* 9: 241–251
- Raybaud CA, Strother CM, Hald JK (1989) Aneurysms of the Vein of Galen. *Neuroradiology* 31: 109–128
- Roosen N, Gahlen D, Stark W et al. (1987) MRI of colloid cyst of the 3rd ventricle. *Neuroradiology* 29: 10–14
- Som PM, Shapiro MD (eds) (1989) *MRI of the head and neck*. Radiol Clin North Am 27
- Swartz JD et al. (1985) Aberrant internal carotid artery lying within the middle ear. *Neuroradiology* 27: 322–326
- Zimmerman HM (1971) The ten most common types of brain tumour. *Semin Roentgenol* 6: 48–58

## CHAPTER 44

# THE SPINE AND SPINAL CORD

J.M. Stevens

---

This chapter is concerned with diagnosis of lesions of the spinal cord and nerve roots, and the skeletal disorders which may involve these structures. It is convenient to classify abnormalities as either *extradural* or *intradural* and to further subdivide the latter into *extramedullary* and *intramedullary*.

**Methods of Investigation.** Methods now in regular use in modern neuroradiology departments are:

1. Plain radiography
2. Scintigraphy
3. Water soluble myelography
4. Computed tomography (CT)
5. Computed myelography (CTM)

6. Magnetic resonance imaging (MRI)
7. Spinal angiography

*Simple tomography* is obsolete where high definition CT is available. *Epidural phlebography* was developed to diagnose the presence of epidural masses not shown by myelography, but CT and MRI have also made this obsolete. *Facetography* and *epidural myelography* may still be used as a preliminary to therapeutic epidural or facet joint injections, and *discography* is usually performed prior to chemonucleolysis. However, these procedures no longer have a significant role to play in diagnosis, except by therapeutic trial or in the case of discography, by evoking specific pain.

---

## EXTRADURAL LESIONS

---

### CONGENITAL LESIONS

These are virtually all skeletal, and involve the spinal cord and nerve roots by producing either basilar invagination, vertebral instability or spinal canal stenosis. Minor degrees of instability predispose to spondylosis and intervertebral disc herniation.

The conditions to be considered are sacralization of L5, cranial assimilation of the atlas, Klippel–Feil anomaly and other fusions, *os odontoideum* and other dysplasias of the dens, generalized skeletal dysplasias and miscellaneous conditions.

**Sacralization of L5** is very common and rarely complete. It results in immobility at L5–S1, and may predispose to back pain and L4–5 disk degeneration. It is a frequent source of confusion when defining levels in the lumbar spine. In this context it is useful when viewing plain radiographs to recall

that there are normally 4 anterior sacral foramina and a sacralized L5 creates a 5th. At myelography the S1 root sheaths are the longest and the abrupt transition to the far smaller S2 sheaths is a helpful distinguishing feature.

**Cranial assimilation of the atlas** (occipitalization), is usually asymmetrical and incomplete. On imaging it results in immobility of the atlantoaxial joint at one extreme, through close application of C1 to the occiput, to invisibility of the atlas as a separate structure at the other. It may be associated with instability at the craniocervical junction due to insufficiency of the transverse ligament, stenosis of the foramen magnum, congenital basilar invagination, or Chiari malformations; usually it is of no significance.

**Klippel–Feil anomaly** specifies intercorporeal fusions of one or more cervical vertebrae, resulting in block vertebrae. In extreme forms, the individual vertebrae may be indistinguishable and the patient may have a short neck. The

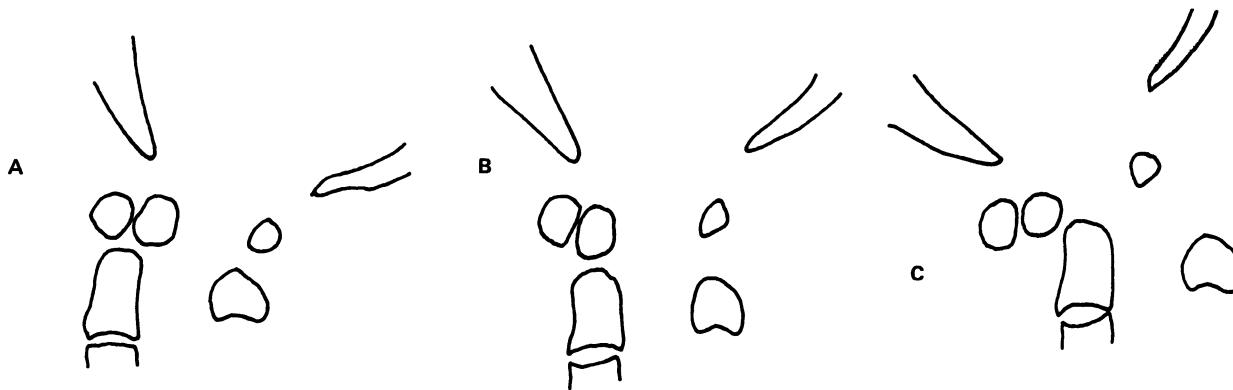


**Fig. 44.1A, B, C.** Diagrams showing the types of instability which may result from os odontoideum (mobile) A posterior atlantoaxial subluxation; B reduced; C anterior atlantoaxial subluxation.

spinal canal is usually focally widened at the site of the fusion, mainly at the expense of the sagittal diameter of the vertebral bodies, which is narrowed. It predisposes to abnormal mobility and degeneration of the intervertebral discs above and below the fusion and rarely it is found with Chiari malformations and syringomyelia.

**Os odontoideum** is a form of segmentation anomaly of the odontoid process of the axis. Anomalies may involve the apical, middle or basal 3rds of that structure; the *os odontoideum*

is an ossicle representing the middle 3rd, the *os terminale*, an ossicle representing the distal 3rd, and persistence of the C1–2 intervertebral disk reveals the basal third. *Hypoplasia* or *agenesis* of the dens represents absence of one or all parts, and *dens tripartitus*, persistence of all 3 as separate ossicles. Instability of the atlantoaxial joint is frequently present. Os odontoideum is often associated with posterior atlantoaxial subluxation and hypoplasia or agenesis with anterior atlantoaxial subluxation (Fig. 44.1).

**Table 44.1.** Skeletal dysplasias

Dysplasia	Abnormalities which involve neural structure	Approximate frequency	Dural ectasia	Scoliosis
<b>Dwarfing dysplasias</b>				
Achondroplasia	Lumbar spinal canal stenosis but clinical onset is usually determined by degenerative spondylosis angular kyphosis in thoracolumbar area	20% (cauda equina syndrome) 15% (spinal cord syndrome)	No	No
Morquio's syndrome	Atlantoaxial subluxation (anterior or posterior) Narrow canal and/or spinal subarachnoid space below C1 Vertebral retrolisthesis, usually at thoracolumbar junction, including the cervical region	90% 60%	No	Mild
Spondyloepiphyseal dysplasias (X-linked)	Hypoplasia of dens (anterior atlantoaxial subluxation)	16%	No	Often by adulthood
Diastrophic dwarfism	Cervical kyphosis (severe progression)	50%	No	Usually
Chondrodystrophy calcificans congenita (Conradi)	Lumbar spinal canal stenosis Cervical kyphosis	60% ?	No	Yes
Metaphyseal dysostosis	Atlantoaxial subluxation	?10%	No	Yes
	Cervical kyphosis	50%	No	Yes
	Atlantoaxial instability	?50%	No	Yes
<b>Non-dwarfing dysplasias</b>				
Down's syndrome (trisomy 21)	Atlantoaxial subluxation (usually due to dysplasias of the dens and ligament laxity, the latter diminishing with increasing age. It is often irreducible)	30%	No	No
Marfan's syndrome	Subaxial subluxations	rare		
Homocystinuria	Severe spondylolisthesis (L5–S1)	rare	Yes	Yes
Ehlers–Danlos	Thrombotic vasculopathy		Yes	Yes
	Early degenerative spondylolisthesis		Yes	Yes
Osteopetrosis pycnodysostosis	Fractures	Uncommon	No	No

**Skeletal dysplasias** of various types involve the spinal column. Some are associated with neurological complications, and most of these are dwarfing dysplasias. Some are listed in Table 44.1. Plain radiographs often suggest the diagnosis, but the nature and extent of neurological involvement is usually only shown by myelography, computed myelography or MRI. New conceptions about the mechanisms of neural compression are emerging as increasing numbers of patients with these rare disorders are examined by modern imaging techniques. Abbreviated results of some of these are included in the table. Dural ectasia is the most common cause of expansion of the spinal canal and sometimes also of the neural foramina in these disorders.

**Miscellaneous anomalies** of the spinal column include many lesions most of which are insignificant, or important only in that they may be confused with other disease processes. *Dysraphisms* involving dura and intradural structures will be considered below. Minor *spina bifida occulta* of S1 or L5 occurs in 22% of the normal population. *Non-fusion of the posterior arch of C1* occurs in about 6% of normals and non-fusion of the anterior arch in a somewhat smaller proportion.

*Hypoplasia of a pedicle*, and occasionally *aplasia*, are uncommon anomalies found most often in the cervical or thoracic regions. Other elements of the neural arch and lateral masses may also be absent, and sclerosis is frequently present in the contralateral pedicle. Associated laminar dysplasia and fusions have resulted in focal cervical canal stenosis and myelopathy.

*Butterfly vertebra* contains a midsagittal cleft towards which the superior and inferior surfaces are depressed, and which progressively widens. The notochord is divided and neurenteric cysts and other anomalies are occasionally associated.

*Hemivertebra* is a wedge-shaped unilateral element of a vertebral body. Sometimes the posterior half of the absent hemivertebra is present. Scoliosis and kyphoscoliosis result.

*Scoliosis*, or lateral curvature of the spine, is defined in terms of the side to which the convexity is directed. Most scolioses are *idiopathic*. Infantile, juvenile and adolescent forms are recognized. The latter is by far the most common, occurring in about 5% of the general population and more frequently in girls.

*Congenital scoliosis*, on the other hand, is caused by vertebral anomalies of which the most important are hemivertebra (especially when multiple and unilateral) and unilateral unsegmented bar (hemivertebral corporeal or appendage fusions). About 20% are associated with malformations of the spinal cord.

*Neuromuscular scoliosis* is associated with syringomyelia, tumors and destructive processes of the spinal cord, especially gliomas and poliomyelitis.

A scoliosis developing after the age of skeletal maturity is unlikely to be of the common idiopathic variety, especially if there is no family history of spinal curvature, the patient is a man and the scoliosis is to the left. Many patients with severe scoliosis are investigated by myelography prior to straightening procedures because of the frequency of occult neural abnormalities. Planar imaging techniques such as CT and MRI can be difficult both to perform and interpret;

indeed, it may be impossible to fit the patient into the aperture of the CT or MRI scanner.

Finally, some scolioses are due to a painful unilateral spinal or paraspinal lesion, which should be sought on the concave side of the maximum curvature.

## INFLAMMATORY AND INFECTIOUS DISORDERS

### Spondylitis

The conditions to be considered are:

1. Rheumatoid arthritis
2. Other inflammatory arthritides

Still's disease  
ankylosing spondylitis  
psoriatic arthropathy  
Reiter's syndrome  
intestinal arthropathy (ulcerative colitis and Crohn's disease)  
connective tissue diseases (lupus, scleroderma, mixed connective tissue disease)

The region of the spine most often involved in the seropositive spondylitides (mainly rheumatoid arthritis) is the atlantoaxial joint, and in the HLA-B27 associated arthritides (mainly ankylosing spondylitis), the sacroiliac joints.

**Rheumatoid Arthritis.** This disease causes erosions, subluxations and inflammatory hypertrophy of synovial structures. About 30% of rheumatoid patients have spinal involvement and in over 80% the atlantoaxial joints are affected. Neurological disability results from subluxations, and rarely from soft tissue masses which compress the cord. Clinical assessment is complicated by the generalized arthropathy and frequent presence of neuropathies and myopathy.

**Subluxations** are the most salient feature and horizontal atlantoaxial subluxation is the most common. It is nearly always anterior resulting in widening of the atlantodental interval (ADI) on flexion beyond the normal limit of 2.5 mm in adults and 4 mm in young children (Fig. 44.2). Ligamentous laxity due to inflammation, especially of the transverse ligament, is the principal cause and widening of the ADI beyond 10–12 mm indicates rupture of that ligament. Posterior atlantoaxial subluxation occurs on head extension (Fig. 44.1) and requires fracture of the dens or erosion of its anterior surface.

Vertical atlantoaxial subluxation (translocation of the dens, craniovertebral settling), is present when the body of C2 enters the C1 ring and the apex of the dens enters the cranial cavity. However the latter may not occur when the dens is markedly eroded. Lateral and rotatory subluxations are also common accompaniments (Fig. 44.3). The subluxations are not completely reducible in over 50%, and in up to 30% little reduction can be achieved.

Involvement of the spinal cord is variable, and cannot be predicted from plain radiographs unless the sagittal diameter of the spinal canal is reduced below 10 mm by the subluxation. The degree of clinical disability correlates poorly with the degree of subluxation, but fairly well with the degree of compressive deformity of the spinal cord and size of the avail-



**Fig. 44.2.** Lateral view of a myelogram, patient supine, head flexed. There is pathological widening of the atlantodental interval (short curved arrow) and compression of the spinal cord (open arrow). Anterior atlantoaxial subluxation in rheumatoid arthritis.



**Fig. 44.3.** Lateral atlantoaxial subluxation shown by computed tomography. Coronal reformatted image. Rheumatoid arthritis.

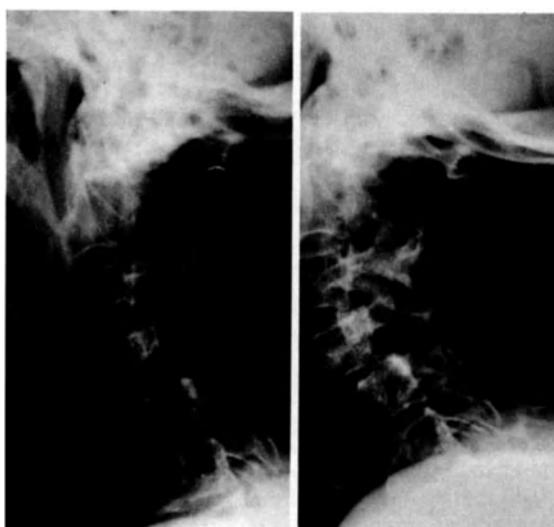


**Fig. 44.4.** Lateral radiographs of the spine. Multiple subaxial subluxations in rheumatoid arthritis.

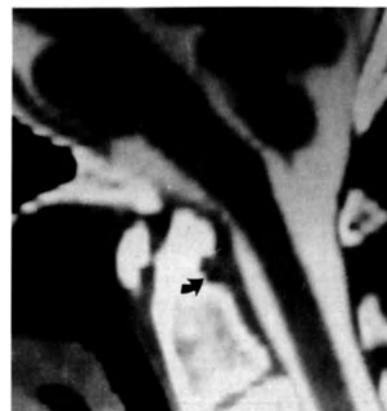


**Fig. 44.5.** Sagittal reformatted image of a computed cisternogram, showing a hook erosion of the base of the dens (arrow) but no subluxation. The neural axis is not compressed.

able subarachnoid space. Subaxial subluxations are an uncommon cause of neurological disability (Fig. 44.4).

Erosions of the odontoid and lateral atlantoaxial and atlantooccipital joints are common, though they are severe in only 15% of cases. Occasionally they occur without subluxation. The most common erosion is the posterior surface of the base of the dens opposite the transverse ligament (Fig. 44.5). Translocation of the dens occurs when erosion of the lateral masses of C2 results in disintegration of those structures; this happens in less than 10% of patients with atlantoaxial involvement.

Inflammatory soft tissue masses are found near erosions and continuity with synovium can usually be established. They may contribute to compression of the spinal cord and sometimes extensive intracranial soft tissue masses are found. Rheumatoid nodules occur in the dura but usually they are small or plaque-like and not identified radiologically.

**Imaging.** Horizontal cervical subluxations are accurately evaluated by plain lateral radiographs of the cervical spine in flexion and extension. Erosions of the dens may also be visible but tomography or high definition CT will reveal more. Cases with suspected neurological involvement require some form of myelography, the most appropriate being computed myelography and MRI.

**The Other Inflammatory Arthropathies.** Syndesmophytes are the radiological hallmark of the spondylitides. They are symmetrical and most extensive in ankylosing spondylitis, but are usually asymmetrical or incomplete in the other conditions where spinal involvement is less common. Neurological complications can occur, especially in ankylosing spondylitis. There are three mechanisms:

1. Atlantoaxial subluxation
2. Discovertebral fractures and pseudoarthroses through ankylosed regions of the spine, especially the cervical region and thoracolumbar junction
3. Dural ectasia, with diverticula and cysts compressing the cauda equina (rare)

Discovertebral microfractures resulting in pseudoarthroses, which may also involve the neural arches, can be diffi-

cult to distinguish from inflammatory erosive spondylopathy and infective spondylitis. Such discovertebral destructive processes have been called *Andersson* or *Romanus* lesions. Lesions of similar appearance, though presumed to be of non-inflammatory origin, have been described in calcium pyrophosphate dihydrate deposition disease (*pseudogout*), neuropathic spondylopathy (*Charcot spine*), and in patients on long-term hemodialysis.

### Infective Spondylitis

There are 3 types of osteomyelitis of the spine: discovertebral, central and subligamentous.

In over 90% of cases the source of infection is hematogenous, but occasionally it results from local trauma (especially iatrogenic) or from paraspinal sepsis. Lymphatic dissemination may play a role in tuberculous spondylitis. It is more common in adults than children, and is also commoner in drug addicts and the immunosuppressed.

The causative organisms are usually classified as pyogenic or non-pyogenic, the former being the most common, especially *Staphylococcus aureus*. Each organism may produce any of the three types of spondylitis, but usually one type predominates (see Table 44.2).

**Imaging.** *Discovertebral Osteomyelitis.* On simple radiography the anterior part of one of the vertebral end-plates first appears demineralized, and this spreads rapidly to involve the full extent of both end plates. The disc space is narrowed. In pyogenic infections, simple radiographic changes usually become visible 8–12 weeks after symptoms, and in tuberculosis after 1 year or longer.

CT reveals textural changes in subchondral bone resulting in a moth-eaten appearance of the vertebral end plate and this may occur weeks or months before changes on plain

radiographs; the paraspinal soft tissue involvement is also much better shown.

Abnormalities are recognizable even earlier on MRI. On T<sub>2</sub>-weighted images, signal from disc substance increases (loss of the internal horizontal lamina may be the earliest detectable sign), and there is increased signal from the vertebral bodies adjacent to the disc (Fig. 44.6). On T<sub>1</sub> and proton density weighted images signal from the disc and adjacent parts of the vertebrae is reduced.

*Radionuclide bone scanning* usually shows increased uptake long before changes appear on plain radiography and even CT, but probably does not detect lesions any earlier than MRI.

As the disease progresses, osteophytes form and structural collapse of the vertebrae may occur, often resulting in kyphotic deformities of the spine.

**Central Type.** On plain radiographs and CT punched out or ill defined destructive lesions are shown. These involve mainly the vertebral bodies but often extend into the appendages. Simple radiography usually greatly underestimates the extent of bone destruction. Vertebral collapse and subluxations occur, and disc spaces are preserved.

**Subligamentous Type.** Plain radiographs and CT show destruction of the anterior surfaces of adjacent vertebral bodies and the lesions are often multiple. Disc height may be preserved, but discovertebral lesions are often identifiable at one or more levels.

**Neurological Involvement.** This may complicate the course of all types of infective spondylitis. The cause is usually spinal cord compression, due to vertebral collapse, kyphosis, or intraspinal (epidural) abscess, granuloma or pachymeningitis. Secondary vasculitis may occur. Paraplegia develops in about 0.5% of cases of pyogenic spondylitis and in up to 40% of patients with tuberculous spondylitis;

Table 44.2. Infective spondylitis

Agent	Type of spondylitis	Other features
<b>Pyogenic</b>		
<i>S. aureus</i>	Discovertebral	Paravertebral abscess 20% (usually small and not calcified)
<i>E. coli</i>		Usually one level only
<i>Pseudomonas</i>		
<i>Salmonella</i>		
<i>Klebsiella</i>		
<i>Brucella</i>		
<b>Non-pyogenic</b>		
Tuberculosis	Discovertebral (80%) Central Subligamentous	Paravertebral abscess 80% (large, often calcified) Multiple levels 10%–20%
Actinomycosis	Central	Paravertebral sepsis 100% Destroyed adjacent ribs Periosteal reactions
Aspergillosis	Central	
Blastomycosis	Discovertebral Central Subligamentous (often all three)	Multiple levels 50% Destroyed adjacent ribs
Coccidiomycosis	Central	Paravertebral mass common Multiple levels frequent
Cryptococcosis	Central	Paraspinal mass occasional Multiple lesions
Hydatidosis	Central but crosses disc spaces	Paraspinal mass common, often eccentric
Histoplasmosis	Central	Multiple levels Paraspinal masses



**Fig. 44.6.** Discovertebral osteomyelitis on a T<sub>2</sub>-weighted sagittal MRI image (2000/80). The long arrow indicates the destroyed C5-6 intervertebral disk, and the short arrow an associated prevertebral abscess tracking down from the source of infection.

it is also more common with the other non-pyogenic agents. Other factors which increase the chance of paraplegia are increasing age and cervical involvement.

**Epidural Abscess.** Infection of the epidural space can occur primarily by hematogenous dissemination from a remote focus, or by extension from vertebral osteomyelitis. Children and adults may be affected. Infection characteristically spreads over many vertebral segments, and may involve the entire spinal epidural space especially in children. The thoracic region is most often involved, and paraplegia is common. Local pain and tenderness are usual.

**Imaging.** Plain radiographs are usually normal. Myelography demonstrates an extensive epidural mass usually lying dorsal to the compressed subarachnoid space. Computed myelography shows the anatomy even better. MRI demonstrates compression of the theca by material of variable signal which may or may not be homogeneous, and often reveals the source of infection in a vertebra or disc.

**Epidural granulomas** occur with tuberculosis and fungal infections. Sometimes this results in diffuse epidural fibrosis and dural thickening which may constrict the cord and radiculomedullary vessels.

## NEOPLASMS

Both primary and secondary neoplasms involve the osseous spine.

### Primary Neoplasms

The conditions to be considered are vertebral hemangioma, osteochondroma, osteoblastoma and osteoid osteoma, giant cell tumor, aneurysmal bone cyst, chordoma and sarcomas.

**Vertebral hemangioma** consists of dilated capillaries and venules, and involves one or more vertebrae in up to 10% of adults. The lesions are usually symptomless, but very rarely the spinal cord becomes compressed, particularly when the neural arch is involved. Soft tissue paraspinal and intraspinal masses can also occur.

**Imaging.** On plain radiographs the vertebra has a translucent appearance and shows vertical striations. On axial CT these striations give the vertebra a stippled appearance. Spinal angiography shows uniform opacification of the entire vertebra from a unilateral injection (in normals only ipsilateral hemivertebral opacification occurs) and may opacify associated soft tissue masses. Embolization of osseous arteries may result in relief of spinal cord compression. Hemangiomas contain fat and may yield signal of high intensity on MR images.

**Osteochondroma.** Even in patients with diaphyseal aclasis only 7% of such lesions involve the spine. The neural arch and costovertebral junction are affected, and the cervical and upper thoracic vertebrae are most frequently involved. Spinal cord compression has often been present in reported examples.

**Imaging.** Osteochondromas have the typical appearance of exostoses on plain radiographs, and are especially well shown by CT.

**Osteoblastoma** is a benign neoplasm of osteoid tissue. About 50% involve the spine, and 97% occur in patients under 30 years. The neural arch is slightly more often involved than the body. Rapid growth over months sometimes occurs, and about 20% cause extensive bone destruction and resemble malignancy. About 30% produce symptomatic spinal cord compression.

**Imaging.** On plain radiographs about 70% appear as purely lytic, often expansile lesions, but on CT ossification of the matrix is more often evident and extension into surrounding soft tissues is better shown.

**Osteoid Osteoma.** Only about 5% of these lesions involve the spine. This is a self-limiting benign growth, less than 2 cm in size, sclerotic and usually painful, but it is not a cause of neural compression.

**Giant Cell Tumor (Osteoclastoma).** About 70% occur in patients between 20 and 40 years, and 12% involve the spine. The sacrum is most frequently involved; most of the remaining spinal cases occur near the thoracocervical junction, and almost exclusively in young women. About 70% involve mainly the vertebral body. Spinal cord compression is usual in thoracocervical lesions.

**Imaging.** They are usually lytic, expansile lesions on plain radiographs, and their full extent into skeletal elements and soft tissue is better shown by CT. Recurrences after attempted excision show extensive bone destruction and enlarging soft tissue masses.

**Aneurysmal bone cysts** are a tumor-like reaction in bone. About 25% of cases involve the spine. About 80% occur in patients under 20 years. Vertebral appendages are most often involved. Spread to contiguous vertebrae may occur.

**Imaging.** On plain radiographs there is an expansile lytic process, usually showing no internal septation. On CT large lesions sometimes have a highly characteristic appearance, consisting of multiple cysts of different density with some showing gravitational layering. This appearance has been seen also on MRI. It reflects the variable state of the blood contained in the large blood-filled intraosseous cavities which constitute the lesion.

**Chordomas** are tumors of the notochord, 50% affecting the lower sacrum (S4, S5), 30% the clivus, and 15% the rest of the spine. C2 involvement predominates in some spinal series. They usually occur in patients between 50 and 70 years of age. The tumor arises from notochordal remnants, and 90% produce bone destruction usually centered on a vertebral body. They may involve adjacent vertebrae across a disc space and 10%–40% metastasize.

**Imaging.** On plain radiographs and CT, bone destruction is shown, with marginal sclerosis in 40% and extensive sclerosis in 10%. Rare appearances are ivory vertebra, a paravertebral mass without bone destruction, and widening of an intravertebral foramen. Matrix calcification is seen in 20% on plain radiographs and 40% on CT. About 40% of cases show circumscribed areas of low attenuation within the matrix on CT, and such areas return relatively higher signal on MRI.

**Sarcomas.** In this group are chondrosarcoma, Ewing's sarcoma, osteosarcoma and reticulum cell sarcoma.

**Chondrosarcomas** arise from irradiation, Paget's disease or osteochondromas and 10% affect the spine. Pain is an important clinical feature. Calcifications in the matrix, shown by CT and plain radiographs is usual.

**Ewing's sarcoma** occurs in the spine in about 5% of cases, and of these over half are in the sacrum.

**Osteosarcoma** involves the spine in only about 1% of cases, usually in older patients than osteosarcomas elsewhere. Large soft tissue masses are characteristic as in all sarcomas. They nearly all arise from irradiation, Paget's disease and other bone tumors or dysplasias. A spinal lesion may be a metastasis, especially if multiple levels are involved.

**Reticulum cell sarcoma** (histiocytic lymphoma) may involve the spine primarily in 10% of cases, but usually it is metastatic.

### Secondary Neoplasms

In this group are metastases, myeloma and lymphoma.

**Metastases** are the most common bone tumors of the spine in both children and adults. Only 10%–30% are solitary. The anterior margins of the body and pedicles are most frequently involved early. Plain radiographs only detect lesions which destroy over half the structure involved; CT is more sensitive.

Spinal cord compression may arise from circumferential, mainly anterior or mainly posterior intraspinal spread. Myelography and computed myelography or MRI are needed to determine these features.

**Myeloma** involves the vertebral body rather than pedicles, and is nearly always lytic. Diffuse permeative and localized expansile bone lesions may occur. Diffuse osteoporosis is common. Paravertebral and intraspinal masses are frequent (Fig. 44.7).

**Lymphoma** eventually involves the osseous spine radiolo-

gically, in about 20% of cases.

**Imaging.** Anterior body erosions, permeative or focally destructive lesions or vertebral sclerosis may be found on plain radiographs and CT; paravertebral soft tissue masses are frequent. MRI shows involvement of the marrow cavities in a far higher proportion of cases. Scintigraphy shows increased uptake with metastases but not with myeloma.

### TRAUMA

The vertebrae may be considered to consist of 3 structural columns:

1. Anterior column or the anterior half of the vertebral body
2. Middle column or the posterior half of the vertebral body
3. Posterior column or the neural arch and articulations

Fractures or major ligamentous tears involving two or more columns are unstable. Major ligament or joint injuries causing instability are rare without fractures.

There are three types of vertebral fracture:

1. Anterior compression fracture
2. Fracture dislocation
3. Burst fracture

**Anterior compression fractures** involve only the anterior column. The spine is stable, and neurological complications do not occur.

**Fracture dislocations** often involve all three columns and are usually unstable; neurological complications are frequent.

**Burst fractures** involve the anterior and middle columns, and may be unstable on weight bearing due to increased retropulsion of bone fragments into the spinal canal (Fig. 44.8).

Many fractures represent a combination of one or more of these types.

**Imaging.** CT demonstrates the injury better than any other modality. However, plain radiographs are usually important to localize where to scan, and are the most frequently employed method for excluding spinal column injuries. Signs of injury on plain radiographs are therefore still of crucial importance.

**Fracture dislocations** usually disturb vertebral alignment on the lateral view, and an anterolisthesis of more than 3 mm is pathological. When this is 25% or more of the vertebral body width, it indicates unilateral facet dislocation (*locked facet*), and when 50% or more bilateral facet dislocation. Rotation of the spinous process away from the side of a unilateral locked facet may be shown on an anterior view, and distortion of the intervertebral canal on an oblique view.

Focal widening of an interspinous distance on a lateral view may be the only sign of a reduced subluxation but with extensive and mainly ligamentous damage. Delayed dislocation may occur when muscle spasm and pain subside, even months after the injury. Hence flexion and extension views should be cautiously obtained when pain and muscle spasm have subsided. High resolution, thin section CT is particularly helpful to assess the actual extent of injury and unsuspected fractures are frequently found.

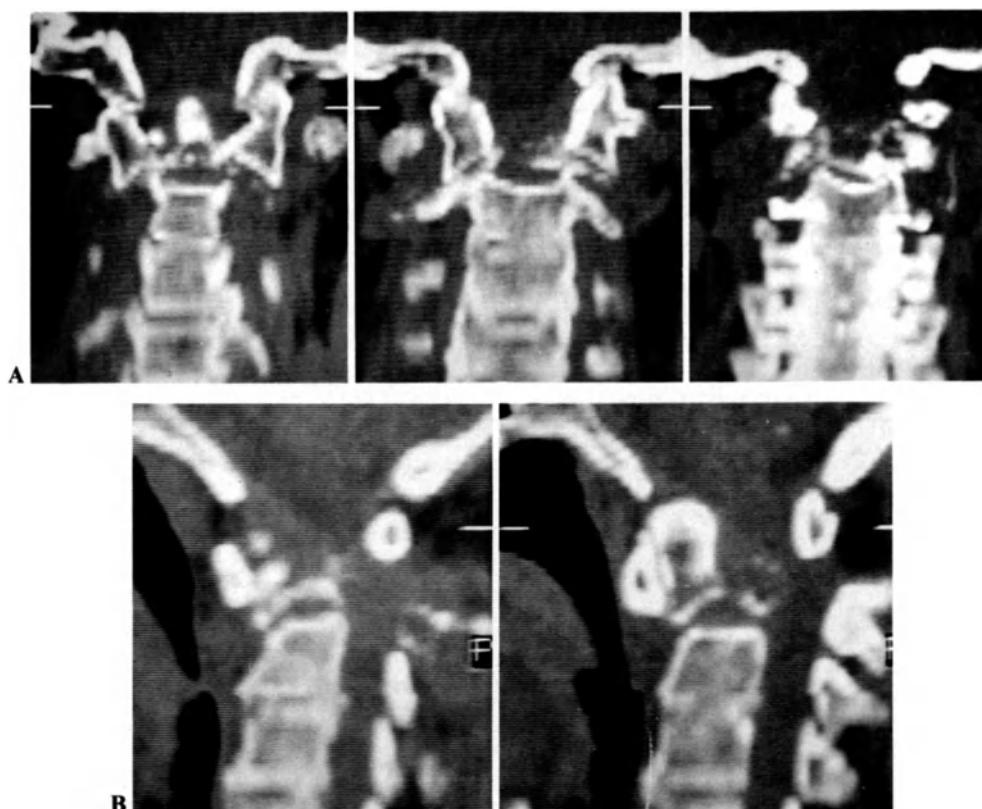


**Fig. 44.7A, B.** A series of coronal, A, and sagittal, B, reformatted CT images of the upper cervical spine. Myeloma involving the body of C2 with pathological fracture and atlantoaxial subluxation.

**Burst fractures** cause loss of vertical height of a vertebra, and transverse expansion with widening of the interpedicular distance. Retropulsed fragments may be visible in the spinal canal in the simple lateral view but frequently they are not. In the cervical region, a midsagittal fracture line is visible on the anterior view and quadriplegia is usual; in the lateral view a large anteriorly displaced fragment resembling

a 'tear drop' is often seen and neural arch damage is common.

#### Other Types of Fracture.

- These include:
1. *Fracture of the dens* – this may occur through the apex, base or body of C2 and instability results.
  2. *Bilateral pedicle fractures of C2* – Hangman's fracture – over half are stable. About 25% also have a major head injury. Oblique radiographs are often necessary to show the fractures; CT is best if in doubt.
  3. *Jefferson fracture* – bilateral fractures of the junctions of the anterior and posterior arches of the atlas. Plain radiographs show bilateral lateral subluxation of the lateral atlantoaxial joints on the anterior view, but CT shows these fractures best. Severe distraction of the lateral masses of C1 indicates rupture of the transverse ligament.
  4. *Chance fracture* (seat belt injury) is a hyperflexion injury to the upper lumbar spine. There are horizontal fractures of neural arches and of pedicles involving the vertebral body. In the Smith fracture the ligaments rather than the bones are mainly involved. On the anterior view the interspinous distance and height of the neural foramina on each side are increased.

**Myelography in Spinal Trauma.** Myelography is rarely indicated in acute spinal trauma. The attitude to myelography varies in different centers; those centers which are most



**Fig. 44.8.** Axial CT image of L2. Burst fracture.

inclined to perform surgical procedures usually require myelography more than those which adopt a conservative approach. However the following is a list of possible indications:

1. Spinal cord syndrome but no fracture shown on plain radiography
2. Spinal cord syndrome disproportionate to the extent and type of fractures shown on plain radiography
3. Unexplained radiculopathy
4. Mild or moderate spinal instability with neck pain, possibly indicating intermittent compression of the spinal cord (especially instability at the craniocervical junction, where occipital pain and Lhermitte's sign may be features)
5. Delayed onset of neurological disability

MRI, if available, is a satisfactory and often preferable method of examination, accommodating all the indications for myelography.

#### MISCELLANEOUS SPINAL CONDITIONS

##### **Paget's Disease**

Paget's disease commonly affects the spine, especially the sacrum, lumbar and lower thoracic vertebrae. More than one bone is affected in 80% of cases. About 20% of involved vertebrae are enlarged, with resultant spinal canal stenosis. *Spinal cord compression* may develop in the thoracic region, and occurs in 25% of cases involving the cervical spine. Non-ossified paraspinal Paget masses may occur, and in a few cases an osteogenic or other sarcoma may develop in later life.

**Imaging.** Plain radiographs and CT show the various stages of the disease, CT indicating the details more sensitively and more clearly.

##### **Hyperparathyroidism**

Hyperparathyroidism causes osteopenia or sclerosis in the spine, and vertebral end-plate infractions are common. Brown tumors are very rare in the spine, but if they occur in the cervical or thoracic spine they can cause cord compression. *Chronic hemodialysis* patients can develop an erosive spondylosis the cause of which is unclear; the cervical spine is commonly involved.

##### **Crystal Deposit Diseases**

Gout rarely involves the spine, but when it does the cervical region is usually affected. Subluxations may result, especially at the craniocervical junction.

*Pseudogout* may involve the lumbar or cervical spine. Disc space calcification and severe degenerative changes are the principal features. Instability may develop, and may affect the craniocervical junction. Ligaments may calcify, including the posterior longitudinal ligament and transverse ligament of the atlas.

**Intraspinal ligament ossification.** The posterior longitudinal or other ligaments may ossify in disseminated skeletal

hyperostosis (DISH), hypophosphatemic rickets or as a primary disorder, especially in the Japanese and other Oriental races. Cord compression may result, especially when nodular masses develop. The cervical region is often implicated.

#### INTERVERTEBRAL DISC DISEASE

##### **Traumatic and Degenerative Disc Disease**

*Acute trauma* to a healthy disk may cause rupture of an annulus fibrosus and herniation of material from the nuclear matrix.

*Degenerative changes* in the substance of the disc are a normal part of ageing with progressive dehydration and reduction in discal volume. Instability ensues causing fissuring of the annulus fibrosus predisposing to nuclear herniation and the osteoarthritic changes in the synovial and syndesmial joints of the spine known as spondylosis. The pathological and radiological features of disc disease vary in each region.

**Cervical Lesions.** Acute nuclear herniations may occur due to trauma, and are a cause of traumatic myelopathy or radiculopathy in which there is no spinal fracture.

More common in the cervical spine are osteophytes, which result from instability and form ridges or more focal excrescences which encroach upon the spinal or neural canals. They constitute the most common forms of spinal cord or root compression, and the resulting syndromes are termed 'cervical spondylotic myelopathy' or 'radiculopathy', or both. Factors of importance in the genesis of the syndrome are:

1. Narrow sagittal diameter of the spinal canal
2. Abnormal mobility at the affected levels
3. Increasing patient age

It is worth noting that soft discal herniations are a more common cause of root pain than osteophytic narrowing of the root canals, and that over 80% of clinically significant lesions are large enough also to compress the spinal cord.

**Imaging.** Plain radiographs of the cervical spine show narrowing of the sagittal diameter of the canal. The significant levels are the most narrowed levels. Diameters below 10 mm on a standard lateral view result in distortion of the spinal cord. However, correlation with clinical disability is poor.

*Myelography* demonstrates cord compression and narrowing of the subarachnoid space. Correlation with clinical disability is poor unless there is severe compression and a complete or partial myelographic block.

*Computed myelography* provides accurate images of the degree of compression, its nature, and the state of the subarachnoid space. Clinical correlation is poor with mild to moderate degrees of cord compression unless:

1. The subarachnoid space is almost obliterated
2. Abnormal mobility is demonstrated at the level of maximum compression; this is most easily determined from plain radiographs or at the time of myelography

Regardless of these factors, if the sagittal diameter of the cord is reduced to less than 50% of normal (under 4 mm)



**Fig. 44.9.** A Sagittal reformatted image of a computed myelogram at T8–9. Large curved arrow, huge calcified extruded disc fragment; small arrows, spinal cord within the subarachnoid space. Large disc protrusion causing severe compression of the subarachnoid space and spinal cord. B Large dorsal disc compressing cord is well shown by MRI ( $T_2$ -weighted). (Courtesy of Dr Gordon Thomson, Bristol MRI centre.)

or the measured cross-sectional area is less than  $50\text{ mm}^2$ , over 80% of patients will have clinical myelopathy.

Plain CT of the cervical spine does not permit evaluation of the spinal cord, and is rarely useful in assessing these syndromes.

*MRI* is at least as accurate as computed myelography. Sagittal images may underestimate the degree of cord compression, and axial images are usually essential. It may be impossible to distinguish soft disc material from osteophyte.

**Thoracic Lesions.** Small thoracic disc herniations are relatively common, and since the spinal cord is closely applied to them because of the kyphosis, mild flattening of its anterior surface is usual. However, because the subarachnoid space posterior to the cord is usually wide, these lesions are of little clinical significance. Larger lesions however, may deeply indent the anterior surface of the cord causing over 50% reduction in sagittal diameter, and very large ones may completely obliterate the spinal canal (Fig. 44.9).

**Imaging.** Thoracic disc herniations are often calcified and may be visible on plain radiographs. Plain CT shows them well, but myelography and computed myelography are usu-

ally necessary to evaluate the cord (Fig. 44.9A). Clinical disability correlates only with severe compression associated with larger lesions. MRI shows the range of abnormalities well and without contrast injection (Fig. 44.9B).

**Lumbosacral Lesions.** The following types of discal lesion should be distinguished

1. Bulging annulus fibrosus
2. Eccentric bulging of the annulus (subligamentous nuclear herniations)
3. Herniation of the nuclear matrix
  - central
  - posteriorolateral
  - sequestered

Annular bulges, whether symmetrical or asymmetrical, are an uncommon cause of entrapment neuropathy; the usual cause is nuclear herniation. L4–5 and L5–S1 are the levels involved in over 90% of cases, and the L5 or S1 roots those most commonly entrapped. Over 80% of patients with mainly unilateral leg pain have demonstrable root entrapment, but less than 50% of those with mainly back or bilateral leg pain. L5–S1 herniations usually entrap the S1 root, L4–5 herniations the L5 root. Occasionally the herniated fragment lies more laterally and involves the intervertebral canal, and if large this may compress the root exiting below the pedicle of the vertebra above (e.g., L4 root compression may result from a large lateral L4–5 nuclear herniation). Herniations or bulges more lateral than the intervertebral canals are unlikely to be significant.

**Imaging.** Plain radiography demonstrates degenerative changes in the vertebrae, reduced disc height and sometimes intradiscal, or even intraosseous subchondral gas due to the vacuum phenomenon.

Myelography remains a good test for demonstrating root entrapment, but lesions need to be large enough or medial enough to indent the thecal sac or spinal root sheaths. Lateral disc herniations may compress at the level of the dorsal root ganglia, lateral to both theca and root sheath.

CT of the lumbar spine is a sensitive test for diagnosing the various forms of disc disease. It also detects lateral herniation which may not be visible on the myelogram. Contrast medium in the theca is usually unnecessary, but can be helpful in difficult cases and after previous surgery. Intravenous contrast can also be helpful in delineating the theca and distinguishing non-enhancing recurrent herniation from enhancing post-operative scar tissue. The theca is drawn towards scar tissue, and indents and moulds the scar; the theca is displaced away from and indented by recurrent disk herniations.

Disc material sometimes needs to be distinguished from other extradural masses, such as metastases and neurofibromas. A sequestered disc fragment can resemble an extradural neurofibroma, but the nerves should be identifiable as separate structures. With other types of herniation, continuity with an intervertebral disc should be demonstrable.

*MRI* also shows lumbar disc disease well. Sagittal images should be supplemented by axial images to include areas above and below the disc.  $T_2$ -weighted images demonstrate hydration changes in discs at a very early stage, but clinical



Fig. 44.10. Axial MRI of the L4–5 disc. There is central posterior bulging of the annulus fibrosis, compressing the thecal sac (arrow).

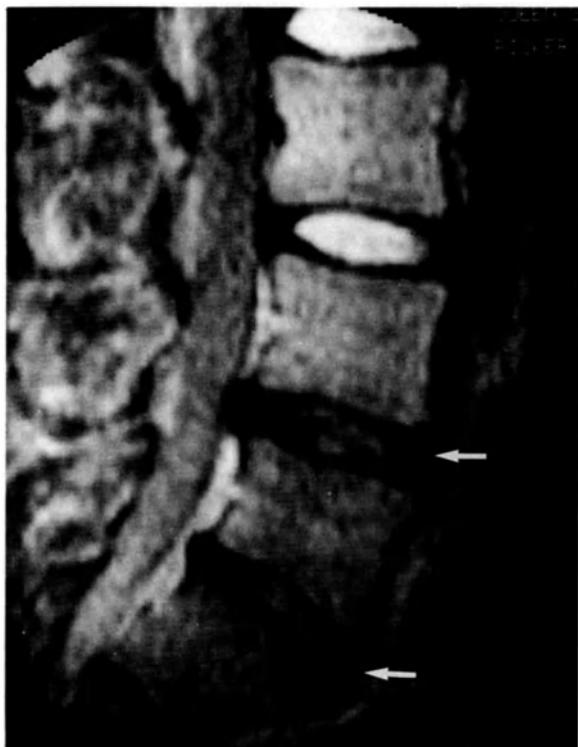


Fig. 44.11. Sagittal MRI, T<sub>2</sub>-weighted image (2000/80). The L4–5 and L5–S1 intervertebral discs show disruption of the horizontal lamina and markedly reduced signal. The annulus fibrosis of each bulges into the spinal canal, and that of L4–5 causes minimal indentation of the spinal theca.

application of such sensitivity has not yet been demonstrated (Figs 44.10, 44.11).

**Discitis.** This term is reserved for a syndrome of focal disc space narrowing associated with back pain in children aged between 1 and 14 years (mean 5 years). A similar syndrome has been observed in young adults. Appearances on plain radiographs of the spine resemble mild discovertebral osteomyelitis but only about 12% progress to interbody fusion. Resolution usually occurs. The etiology is unclear but is likely to be infectious. No consistent organism has been identified.

### SPINAL STENOSIS

There are two types of spinal stenosis: developmental and degenerative. The onset of symptoms of cord or cauda equina compression is unusual before adult life and is usually dependent, in both types, upon the development of disk degeneration. The bones or the soft tissues or both may be involved.

Spinal stenosis may also be classified in the following morphological way:

1. *Diffuse*: this is usually developmental (e.g., achondroplasia, or non-specific congenitally narrow spinal canal); less commonly it is acquired as in acromegaly (often mainly soft tissue), and in extensive Paget's disease.
2. *Focal*: this is usually degenerative, but can be congenital due to local anomalies of pedicles or laminae
  - a Central – narrowing of the midsagittal diameter
  - b Lateral – narrowing of the subarticular lateral part of the canal with preservation of the midsagittal diameter
  - c A combination of central and lateral

An important form of focal spinal stenosis is associated with an irreducible degenerative type of L4–5 spondylolisthesis, and occurs almost exclusively in middle-aged and elderly women. The forward slip of L4 is caused by osteoarthritic collapse or disintegration of the articular surfaces of the posterior joints. Stenosis is caused by hypertrophy of the articular facets and related ligaments, with or without symmetrical bulging of the annulus fibrosus (Fig. 44.12).

*Imaging.* Plain radiographs identify reduction in midsagittal and interpedicular distances in the spinal canal. Sagittal measurements below 12 mm in the cervical region and 17 mm in the lumbar region indicate diameters below the 90th percentile in the normal population. Hypertrophy of apophyseal joints, medially converging facet joints, and thickening of laminae and pedicles may suggest stenosis despite normal sagittal and transverse measurements.

CT provides a far more accurate indication of the axial dimensions of the spinal canal. Lateral stenosis is well shown, but the actual dimensions of the lateral recesses, in which the subarticular parts of the root canals lie, are difficult to measure and the clinical significance of a morphological narrowing can be difficult to judge. The nerve roots are seldom visible because extradural fat is usually absent at stenotic levels, and this in itself suggests a significant stenosis.

*Myelography* shows the stenosis and its effects upon cord and nerve roots. The demonstration of wavy, tortuous roots of the *cauda equina* above a level of stenosis suggests root



**Fig. 44.12.** Axial image of the L4–5 disk level in a computed myelogram. The thecal sac (arrow) is compressed by a mildly bulging annulus fibrosus anteriorly, and slightly thickened yellow ligaments and articular processes posterolaterally. Focal spinal canal stenosis at L4–5.

entrapment at the stenosis, resulting in redundant lengthening of the roots themselves. (Roots can increase in length, relatively inelastically, by almost 20% before axonal stretching occurs.)

*MRI* also shows the effects on theca and cord, but not the roots within the lumbar theca.

### SPONDYLOLISTHESIS

We have already considered irreducible *degenerative spondylolisthesis* at L4–5. Another type is due to an oblique defect in the interarticular part of the neural arch (pars interarticularis). Some of these are *congenital* and associated with a smaller lamina and deviation of the spinous process to the side of the defect. Others seem to represent *stress fractures*, and are often bilateral. The defect is referred to as spondylolysis, and the anterior slip of the vertebra above as spondylolisthesis. The malalignment is rarely reducible. Spinal canal stenosis and root entrapment are rare, but back pain is usual. The L5–S1 level is most commonly involved, and men are more often affected than women.

**Imaging.** Plain radiographs show the alignment abnormality and the pars defects, the latter especially on oblique views. However many pseudodefects are seen due to a Mach effect from hypertrophied facet joints.

Axial CT usually shows the pars defect at pedicle level, but it can be difficult to distinguish from the apophyseal joint. Reformatting images in oblique coronal planes through the laminae, or in parasagittal planes through the apophyseal joints, usually clarifies the situation.

*Myelography* is seldom indicated. MRI shows displaced articular facets, but an undisplaced spondylolysis will usually pass unnoticed.

---

## DURAL AND INTRADURAL EXTRAMEDULLARY LESIONS

---

### CONGENITAL LESIONS

In this section the following conditions will be considered: lipo-myelo-meningo-dysplasia, meningocele (dorsal, ventral, lateral, caudal (sacral)) and arachnoid cysts (extradural, intradural, perineurial).

#### Lipo-myelo-meningo-dysplasias

This composite term describes a variety of dysplasias which have many features in common. Spina bifida is present, and there is usually a fatty subcutaneous mass though this may not be detectable clinically. The fat, often referred to as a *lipoma*, extends through a skeletal neural arch defect and the dura mater and usually involves the terminal segments of an abnormally low spinal cord. The theca is usually expanded into a diffuse intraspinal sac and the bony spinal canal is considerably enlarged in the vicinity. The lumbosacral region is most often involved.

**Imaging.** Plain radiographs show spina bifida in the lower lumbar or sacral region, or a large sacral hiatus. The defects in the neural arches are usually more than 3 mm wide, and the spinal canal is expanded.

*Myelography* shows an enlarged lumbosacral theca, and the low spinal cord merging with the posterior aspect of the

dura. Intradural and extradural masses are usually recognizable.

Plain CT shows the intradural lipoma in continuity with the subcutaneous adipose tissue which is usually increased in amount, as well as the neural arch defects and expanded spinal canal.

Computed myelography and MRI provide more exact delineation of fat, dura and cord, as well as the extent of cord involvement. Any associated abnormalities such as dermoids or ependymal cysts are also identified though some of these may also be shown by myelography (Fig. 44.13).

#### Meningoceles

These are focal expansions of the thecal sac involving both arachnoid and dura. They may be associated with generalized expansion of the theca, usually referred to as *dural ectasia*, or with other defects such as spina bifida or sacral agenesis. The spinal canal is expanded and the meninges protrude through defects in the spinal canal. Dorsal meningoceles extend into a wide posterior spina bifida, ventral meningoceles into deficiencies in the vertebral bodies (usually the various forms of sacral agenesis), lateral meningoceles through enlarged intervertebral foramina or sacral canals.

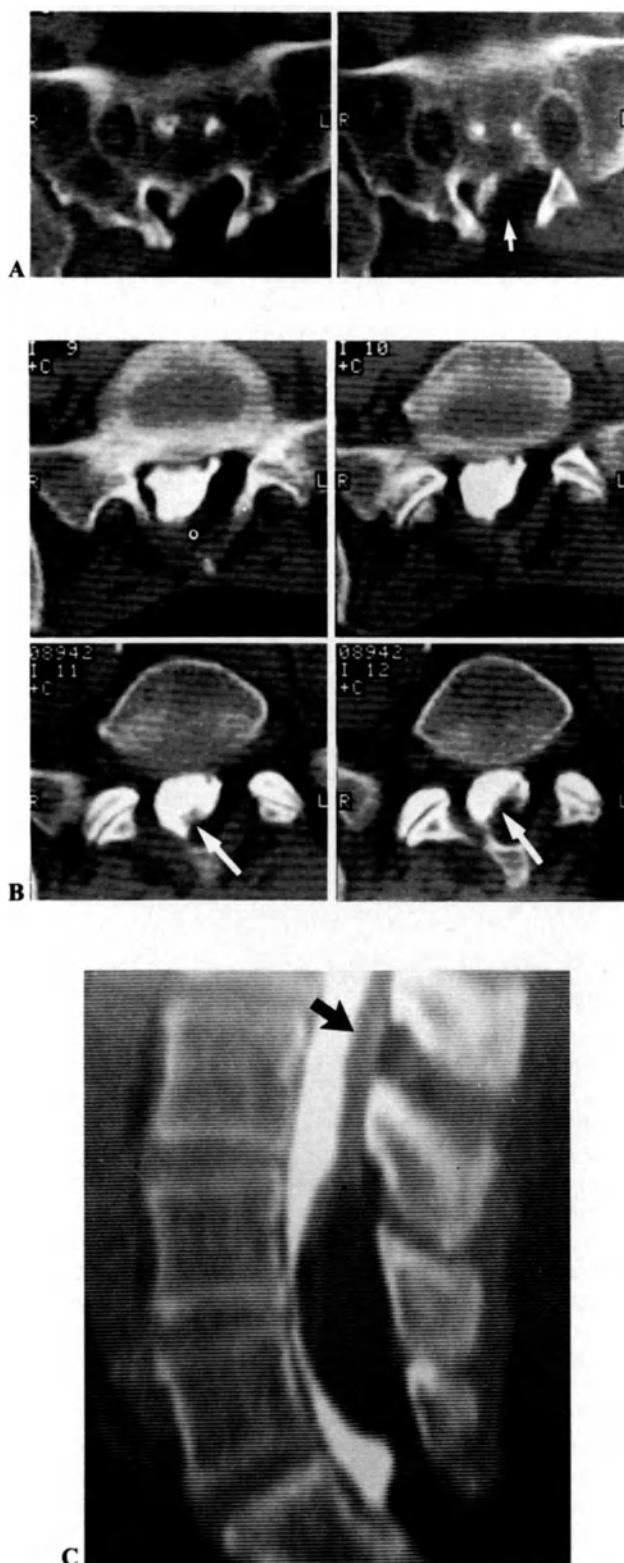


**Fig. 44.13A, B, C.** Computed myelogram of a typical example of lipomyelomeningocele. **A** Axial images in the sacral region. Large sacral hiatus through which subcutaneous fat blends with the dural sac (arrow). **B** Further axial images through L5 and S1. Fat involving dura (upper images) blends with fat in the very low spinal cord (arrow). **C** Sagittal reformatted image of the same case showing the low spinal cord (arrow) and the extent of the lipoma.

A *sacral, intrasacral or caudal cyst* is a midline meningocele of the sacral canal, caudal to the normal level of termination of the dura. There is usually a constricted channel between the cyst and the normal thecal space above. The sacral canal is expanded.

*Dural ectasia*, when severe, may result in lateral thoracic or lateral sacral meningoceles, often multiple. The causes of such severe ectasia include neurofibromatosis, ankylosing spondylitis and Ehlers–Danlos syndrome; some cases are idiopathic.

**Imaging.** Plain radiographs may show the soft tissue masses, expanded spinal and neural canals or osseous defects. Lateral thoracic meningocele is an important cause of a paraspinal mass, and anterior or anterolateral sacral meningocele, of a presacral mass.

**Myelography** shows opacification of the cyst or cysts, but dilution of water soluble contrast medium in the voluminous subarachnoid space may cause difficulty in defining the extent of the abnormality.

CT reveals the fluid-filled masses distinct from other soft tissue, and suggests that the content is CSF. CT performed after myelography, provides the most accurate definition of the abnormalities.

MRI indicates fluid-filled cavities in continuity with the subarachnoid space. Signal from the cyst fluid may be greater than in the general subarachnoid space due to reduced car-diosynchronous pulsation of fluid in the cyst.

#### Arachnoid Cysts

Arachnoid cysts are lined by arachnoid and do not involve the dural envelope.

*Extradural* arachnoid cysts probably represent herniation of arachnoid through a defect in the dura; many of these are acquired by surgical or accidental trauma and are not congenital lesions. The spinal canal is expanded due to pressure erosion in most cases.

*Intradural* arachnoid cysts represent duplications of the arachnoid or aberrant septation of the subarachnoid space. The spinal canal is rarely expanded by intradural cysts. The thoracic region is most often involved, and most cysts are dorsal to the theca or cord. Loculation of the subarachnoid space posterior to the cord is common in the thoracic region, and does not always warrant being termed an arachnoid cyst.

*Perineural* cysts are arachnoidal cysts which form in relation to the dural ostia for the spinal nerves. They are most commonly found on the S2 or S3 roots. When large, they cause erosion of the related neural canals.

**Imaging.** Plain radiography and CT may show widening of the spinal or neural canals.

**Myelography** shows an intradural or extradural mass usually involving several vertebral segments, and cord compression may be evident. The mass usually opacifies with water soluble contrast, but this may be delayed, and late films may show contrast in the cyst long after it has cleared from the rest of the subarachnoid space. Cysts which opacify early may be invisible as a separate structure.

**Computed myelography** usually reveals opacification of the cyst, even if it was not evident on myelography, and delayed CT usually shows retention of contrast medium. A cyst may

be invisible if opacification of cyst and subarachnoid space is equal, but usually the membranous wall of the cyst is visible. The critical observation to make is whether the spinal cord is compressed. Fortunately, cord substance is relatively easy to deform and is relatively inelastic. Its cross-sectional shape therefore, should show flattening or concavity opposite the cyst. However, the latter may vary in size and may not be compressing the cord at the time of imaging.

### ARACHNOIDITIS

The arachnoid mater is devoid of blood vessels and therefore does not become inflamed. However, inflammatory processes involve the subarachnoid space and pia mater, to which the arachnoid may become adherent via organization of exudate. Sometimes, the arachnoid undergoes necrosis allowing access to the subdural space. Nerve roots of the cauda equina become matted together, and adherent to the theca. The spinal cord becomes incompletely tethered to the theca which sometimes causes marked distortion of the cross-sectional shape of the cord. The dura and extradural tissues may be involved and become thickened, contributing to the narrowing of the subarachnoid space.

Clinical syndromes associated with arachnoiditis are *radiculopathies*, which are often multiple, and various types of *myelopathy* including syringomyelia. Major causes include:

1. Myodil (Pantopaque) myelography
2. Operative procedures
3. Spinal meningitis
  - tuberculosis
  - other bacterial and fungal agents
  - HIV1 (tropical neuromyelopathy)
  - sarcoidosis
  - cysticercosis

**Imaging.** Plain radiographs are usually irrelevant.

*Myelography* shows several appearances, many of which may coexist:

1. Complete block, with an irregular configuration
2. A smooth, featureless lumbar thecal sac in which no roots or root sleeves are visible
3. Irregular opacification of the thoracic or cervical subarachnoid space in which the spinal cord is difficult to discern
4. Thickened roots of the cauda equina, few in number, and one or more showing unusual angulations or straightened segments. Non-filling of root sleeves is normally associated

*Computed myelography* also shows these features. The spinal cord may be irregular in shape. Delayed images may demonstrate syringomyelia. Partial loculations and true cysts of the subarachnoid space may be shown. *MRI* has proven insensitive in the evaluation of the subarachnoid space; it may indicate that the subarachnoid space is abnormal if the arachnoiditis is severe but milder forms may cause no abnormality.

### ANGIOMAS

Over 80% of spinal arteriovenous malformations represent small dural arteriovenous fistulae, variously termed '*dural arteriovenous malformation*' or '*radiculo-meningeal arteriovenous fistula*'. The latter term best describes the nature of the abnormality. The fistula is usually located near a mid or lower thoracic root sheath, and is fed by one or two spinal arteries. It drains, often via a single vein, into the intrathecal veins, especially those surrounding the spinal cord. An important feature of many cases is extremely slow flow in the draining veins. Patients often present clinically with a 'stuttering' myelopathy in which pain and sphincter disturbance are prominent features.

**Imaging.** *Myelography* nearly always shows enlargement of the intrathecal veins, especially those of the dorsal venous plexus of the spinal cord. The cord is normal in size or only minimally enlarged. *Computed myelography* is usually non-contributory. The definitive investigation is *spinal angiography*. Although most fistulae are found in the thoracic region, they can occur anywhere from the base of the skull to the sacrum. Embolization of the feeding arteries is an effective form of treatment.

*MRI* does not provide precise diagnostic information. The spinal cord may show diffuse signal changes presumably reflecting the consequences of stagnant hypoxia. This is thought to be the usual mechanism of the myelopathy. These signal changes have been shown to resolve after embolization.

### NEOPLASMS AND OTHER TUMORS AND CYSTS

The following conditions will be considered in this section: neurofibroma, meningioma, metastases, cysts (dermoid, epidermoid, entodermal, neuroectodermal, parasitic (cysticercosis)) and other intradural masses.

#### Neurofibroma

Most solitary spinal nerve root tumors are *neurilemmomas*; most multiple lesions are *neurofibromas*. Any spinal level may be involved from C1 to the coccyx. Many lesions have an extradural component as well as the intradural. Some are elongated masses which extend over several segments within the thecal sac and alongside the spinal cord; others appear as diffuse neural thickening.

**Imaging.** Plain radiographs show erosion of one or more pedicles, and focal expansion of the spinal canal, or both. These are seen in 50% of cases (Fig. 44.14A, B). A paraspinal mass may also be visible with large thoracic lesions.

*Plain CT* shows the bony erosions and extradural or extra-spinal components, but usually not the intradural portion (Fig. 44.14C).

*Myelography* detects even small lesions, and diffuse neural thickenings. Intradural masses have a characteristic appearance (Fig. 44.15). *Computed myelography* adds greater precision (Fig. 44.14C). Continuity with a specific nerve root can rarely be established.

*MRI* usually shows the larger lesions well, and discloses their full extent (Fig. 44.16B) both inside and outside the the-

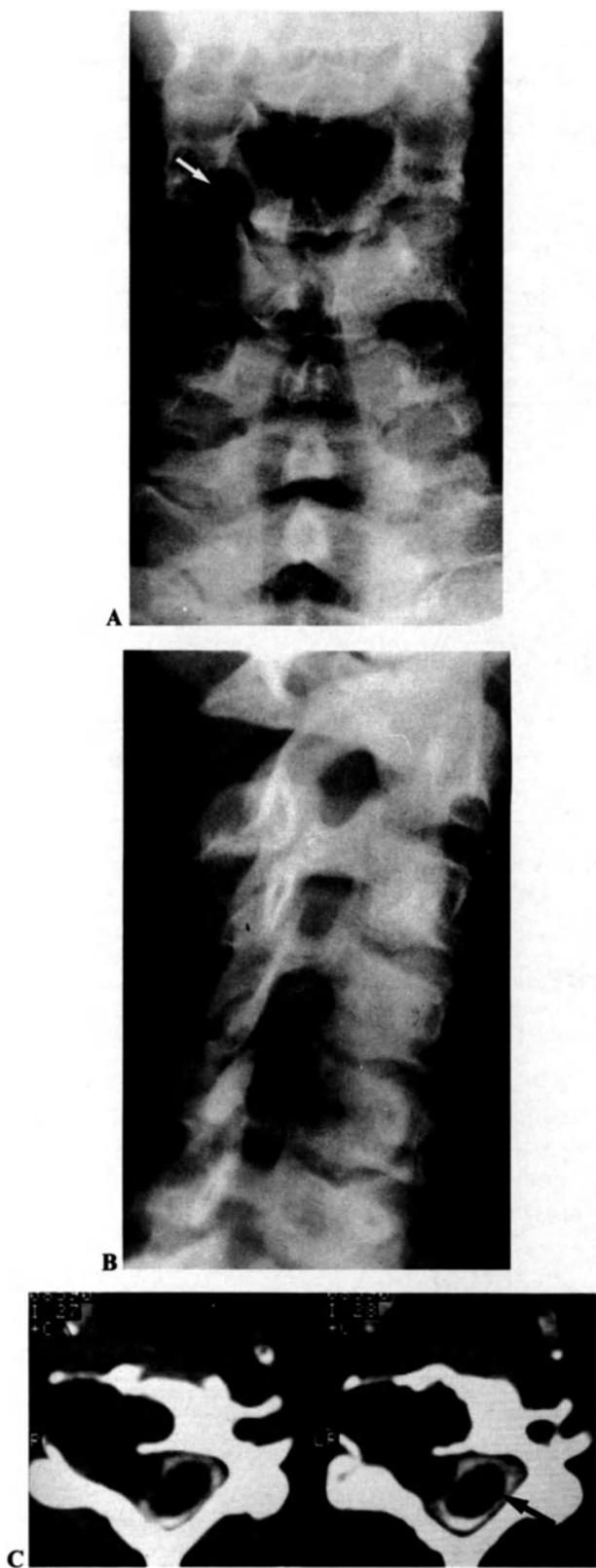


**Fig. 44.14A, B, C.** Large but typical cervical neurinoma. A, B are frontal and oblique plain radiographs of the cervical spine showing extensive pedicular and vertebral body erosion (arrow); C shows two axial images from the computed myelogram of the same case. The spinal cord (arrow) is also compressed.



**Fig. 44.15.** Another cervical neurinoma. Cervical myelogram, showing typical appearances of an intradural mass.

cal sac. Small lesions in the subarachnoid space are detected with greater sensitivity by myelography. The administration of intravenous Gadolinium-DTPA increases the sensitivity of MRI in this context.

#### Meningioma

Over 80% occur in the thoracic region, in middle-aged women and mainly dorsal to the spinal cord. About 17% occur in the cervical region, where men and women are equally affected, and where most lesions lie ventral to the cord. The majority are entirely intradural masses, but transdural forms are known.

**Imaging.** Plain radiography is abnormal in less than 20% of cases. Calcification is visible on CT in only about 10%, and hyperostosis may rarely be present. Appearances on myelography (Fig. 44.16B) and computed myelography are usually indistinguishable from intradural neurofibroma. MRI usually shows the lesions well, with or without Gadolinium enhancement. Again they may be indistinguishable from neurofibromas (Fig. 44.16A).

#### Metastases

Intradural metastases may arise from the following: carcinoma (bronchus, breast), melanoma, lymphoma, medulloblastoma, ependymoma and chordoma (usually only after attempts at removal).

**Imaging.** On myelography and computed myelography metastases appear as nodules on the cord or cauda equina, or sometimes as diffuse thickening of many roots. MRI is not

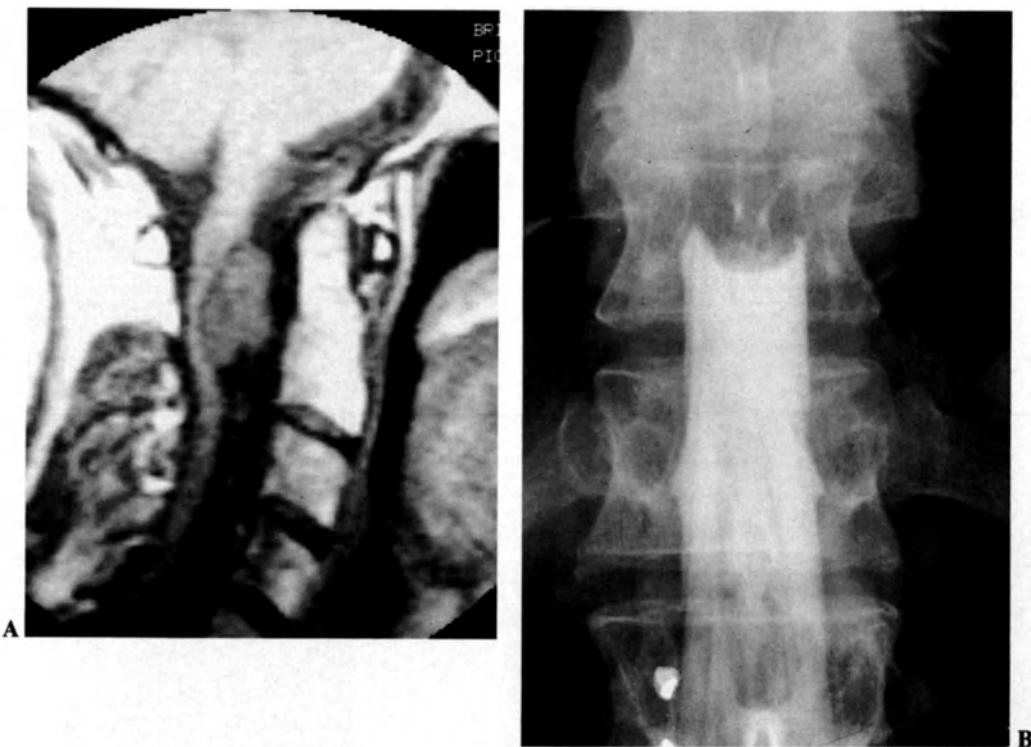


**Fig. 44.16.** A T<sub>1</sub>-weighted sagittal MRI shows neurofibroma compressing cord at C2. (Courtesy of Dr JR Bradshaw and Bristol Medico-Chirurgical Journal.) B Myelography showing a spinal block due to an intradural meningioma at T11.

a sensitive tool in this context, but will show large lesions, and Gadolinium enhancement increases sensitivity.

#### Cysts

*Congenital cysts* may be extramedullary or intramedullary. They are most frequent in the thoracic and lumbar regions.

*Dermoid* and *neuroectodermal (entodermal)* cysts are usually associated with some form of dysraphism, especially dorsal dermal sinus or butterfly vertebra respectively.

Some epidermoid cysts represent epidermal inclusions following lumbar puncture. Other acquired cysts are *parasitic*; of which the only common one is *Cysticercus cellulosae*.

**Imaging.** On myelography and computed myelography,

delayed penetration of contrast into all forms of cyst may occur. *Cysticerci* may be mobile within the subarachnoid space.

#### Other Intradural Masses

The following is a short list of other rare causes of intradural extramedullary masses:

- Primary intraspinal melanoma
- Hemangioblastoma
- Aneurysms and varicose veins
- Granulomas (tuberculomas, sarcoid)
- Hemangiopericytoma

## INTRADURAL INTRAMEDULLARY LESIONS

### CONGENITAL LESIONS

The lesions to be considered are myelomeningocele, intramedullary lipoma and diastematomyelia.

#### Myelomeningocele

In this condition part of the neuroectoderm has failed to separate from the surface ectoderm, and the neural tube has failed to form in this region. The result is a flat plate (or placode) of nervous tissue on the surface of the skin, usually

in the lumbar or lumbosacral region, though it can occur elsewhere. Nerve roots arise from its ventral surface and traverse an underlying meningocele. The spinal cord fuses with its cranial end, and the central canal opens onto its surface. The neural arches of the underlying vertebrae fail to develop, and widely separated and everted arch remnants are all that remain. The vertebral bodies are relatively narrow in sagittal diameter.

The condition is clinically obvious but radiology helps to delineate the underlying abnormal anatomy and identify

associated lesions such as lipomas and dermoids and especially the Chiari Type 2 malformation and hydrocephalus.

#### Intramedullary Lipoma

Separation of neuroectoderm from surface ectoderm is termed *disjunction*, and formation of the neural tube *neurulation*. If disjunction occurs before neurulation is completed at any spinal level, mesenchyme in contact with the dorsal surface of the neural plate develops into adipose tissue. The result is a lipoma attached to the posterior aspect of the spinal cord, commonly in the thoracocervical junction region. The posterior columns are separated by the fat which often extends along the central canal for a variable distance. Angiomatous elements may also be present.

**Imaging.** The spinal canal shows focal expansion on *plain radiography*, and a fatty mass is readily diagnosed on plain CT. *Myelography* usually shows abrupt expansion of the posterior aspect of the cord, and *computed myelography* shows the distribution of fatty and non-fatty tissue within the cord. MRI shows all these features exceptionally well.

#### Diastematomyelia

In this condition the spinal cord is split for a variable distance into two unequal hemicords, each containing only ipsilateral tracts and grey columns. Many remain entirely asymptomatic. The split involves the cord only in 50%, but in the other 50% the dural tube and sometimes the spinal canal are also divided to a variable extent. Vertebral anomalies are usual and rather characteristic. They consist of a widened spinal canal, narrow disk spaces and fused laminae; sometimes a central spicule of bone traverses the spinal canal between the hemicords. The hemicords reunite caudally in most cases.

**Imaging.** Plain radiographs often suggest the presence of diastematomyelia. Sometimes this is an incidental finding, and unless neurological abnormalities are present, further investigation is not warranted. The anatomy is usually clearly shown by *myelography*, *computed myelography* and *MRI*.

## TUMORS

In this section the following conditions will be considered: gliomas, hemangioblastoma and miscellaneous tumors.

#### Gliomas of the Spinal Cord

The histological types commonly found in the spinal cord are astrocytoma and ependymoma. Rarer types include glioblastoma, oligodendrogloma and subependymoma.

Nearly 50% of spinal gliomas involve the lumbar region (Fig. 44.17B), and in this site the lesion is almost always an ependymoma, usually of myxopapillary type. Astrocytomas and ependymomas are about equally frequent in the thoracic and cervical regions.

Gliomas in the spinal cord are nearly always well circumscribed lesions. About 70% are associated with *cysts*, of which at least 40% involve cord substance cranial or caudal to the tumor and are indistinguishable from syringomyelia; the others are intratumoral.



Fig. 44.17. A T<sub>2</sub>-weighted sagittal MRI shows cervical glioma as mixed high and low signal. (Courtesy of Dr Gordon Thomson and Bristol MRI centre.) B Sagittal MRI of the lumbar spine, T<sub>2</sub>-weighted image (2000/80). Ependymoma of the filum terminale. The lower structure yielding a very high signal was a tumoral cyst (arrow).

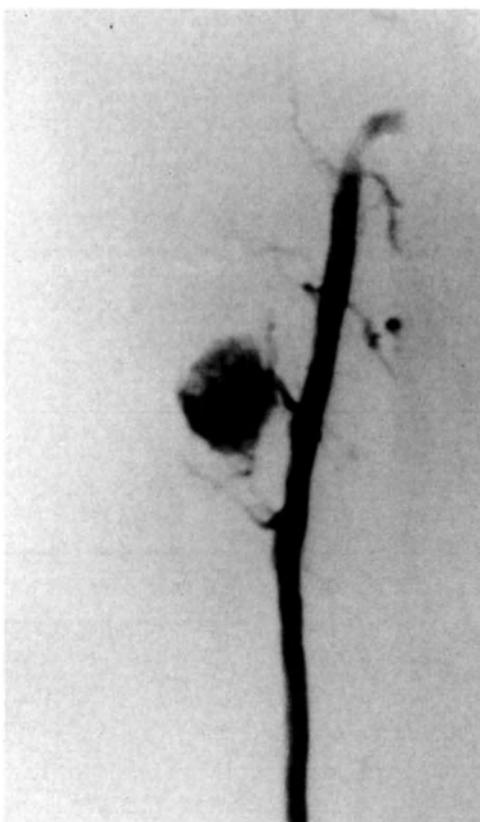


**Fig. 44.18.** Digital vertebral arteriogram, showing a typical intramedullary hemangioblastoma at C6.

**Imaging.** Plain radiographs show widening of the spinal canal in only about 12% of spinal cord gliomas, but in as many as 80% of ependymomas of the filum terminale; these are often giant tumors by the time of diagnosis. Plain radiograph changes are twice as common in children as in adults.

**Myelography** and **computed myelography** show fusiform smooth or lobulated expansion of the cord, or a lobulated or rounded mass or masses in the lumbar thecal sac. Expansion may be focal or diffuse. **Delayed CT** images often show contrast penetration into intratumoral and syringomyelic cysts (Fig. 44.19).

**MRI** shows the expanded cord, and often circumscribed areas of signal change (Fig. 44.17). This altered signal often, but not always, indicates cyst. If the signal is low on T<sub>2</sub>-weighted images, the region is very likely to represent a cyst. A reliable method of distinguishing solid from cystic components is *intraoperative spinal sonography*.

**Endomyelography** in which the spinal cord is needled percutaneously was occasionally performed in the past. Fluid was aspirated from any cysts and sent for cytology. A small amount of contrast was injected into the cavity to outline its extent. It is rarely indicated nowadays.

#### Hemangioblastoma

Hemangioblastoma is a circumscribed neoplasm usually presenting in patients 20–40 years of age. Patients who present under 20 years are more likely to have multiple

lesions, especially in the cerebellum and retina, and may also have visceral abnormalities. Inheritance can be via an autosomal dominant gene (von Hippel-Lindau syndrome). Lesions may be cystic or solid, and up to 80% are associated with cord cavitation. About 7% are extramedullary, and related to spinal nerve roots.

**Imaging.** *Myelography* shows either focal fusiform expansion of the cord, or extensive enlargement due to associated syringomyelia. In about 80% of cases, enlarged vessels are visible on the surface of the cord.

Localization of the actual tumor, and definitive diagnosis is usually provided by *spinal angiography*, where a well circumscribed dense capillary blush (Fig. 44.18) is characteristic.

**MRI** does not always indicate the site of the tumor, although sometimes it is evident on T<sub>2</sub>-weighted images. Gadolinium enhancement would be expected consistently to localize the tumor, even in the presence of extensive cystic enlargement of the cord.

#### Miscellaneous Tumors

Rare causes of intramedullary neoplastic swellings are metastases, primary melanoma, intramedullary neurofibroma, ganglioglioma, entodermal, dermal and epidermal cysts and teratoma (germinoma). Any of these may be associated with syringomyelia (Fig. 44.19).

#### SYRINGOMYELIA

Syringomyelia is a degenerative disease of the spinal cord characterized by the presence of one or more elongated, glial-lined central or eccentric cavities. The fluid within the cavities is usually indistinguishable from CSF, though occasionally protein is raised and a few mainly histiocytic cells are present. Several types of syringomyelia are distinguishable by their etiological associations. In each the clinical picture of suspended, dissociated sensory loss and patchy loss of myotonic reflexes generally correlates well with radiological evidence of the disease. In the usual forms of syringomyelia, the spinal cord is enlarged in about 80%, normal in size in 12% and small in about 8% of cases. In some cases, the process also involves the brain stem.

**Chiari malformation Type 1** is associated with syringomyelia in about 50% of cases overall (Fig. 44.20) but when the tonsils lie at a level between the neural arches of C1 and C2, the incidence rises to over 70%. Less than 20% of cases with minimal cerebellar ectopia have a syrinx, and in about 20% of cases of syringomyelia no etiological associations of any kind are found.

**Post-traumatic syringomyelia** is a relatively common consequence of major spinal cord injury. It is usually confined to a few cord segments near the level of injury, and either does not extend or is asymptomatic. A small proportion produce an ascending central myopathy which is sometimes associated with severe pain (Fig. 44.21).

**Tumor-associated syringomyelia** (Fig. 44.19) has been discussed above.

**Arachnoiditis associated syringomyelia** occurs in some cases of chronic spinal meningitis, most frequently

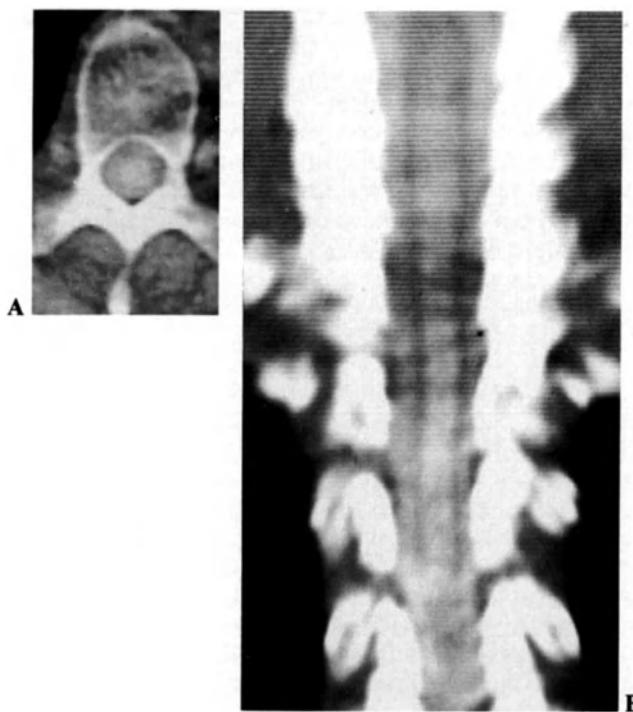


**Fig. 44.19.** A Axial image (T6) and B coronal reformatted image of a computed myelogram made about 7 hours after introduction of intrathecal contrast. At autopsy a solitary metastasis from carcinoma of the lung was found in the cord at T2. This is not visible on the CT study, but an extensive central syrinx is well shown presumably caused by the presence of the intramedullary tumor.



**Fig. 44.21.** Mid-sagittal MRI, T<sub>1</sub>-weighted image (1000/40). Post-traumatic syringomyelia due to a burst fracture of C5. Two types of cyst are present: (1) low signal cysts (open arrow) near the site of trauma, which, on myelography, filled immediately with contrast from the subarachnoid space, (2) more extensive cysts of higher signal (arrow) in which contrast was only shown 12 hours after myelography.



tuberculous. It has also been reported with arachnoid cysts of uncertain etiology.

In addition to these forms of syringomyelia, central cord cavitation has been observed in several other conditions, which include *cervical spondylosis* (Fig. 44.22), *multiple sclerosis* and other forms of *myelitis*, and in *cysticercosis*.

**Imaging.** The spinal canal may be expanded on plain radiographs, usually in the cervical region. This is seen in less than 10% of cases overall but in over 20% of children with the disease. *Myelography* usually shows diffuse or smooth fusiform enlargement of the cord, commonly ending rather abruptly at the level of C2; occasionally the cord is small or normal. Sometimes contrast medium is visible within the syrinx. *Computed myelography* shows the enlarged cord, and contrast in the syrinx especially on images made 6–12 hours, or up to 24 hours post-myelography (Figs 44.19, 44.22).

**Fig. 44.20.** Mid-sagittal MRI, showing a distended cord due to syringomyelia, and cerebellar ectopia with the cerebellar tonsils lying at the level of C1 arch (see text). T<sub>1</sub>-weighted image (500/20).

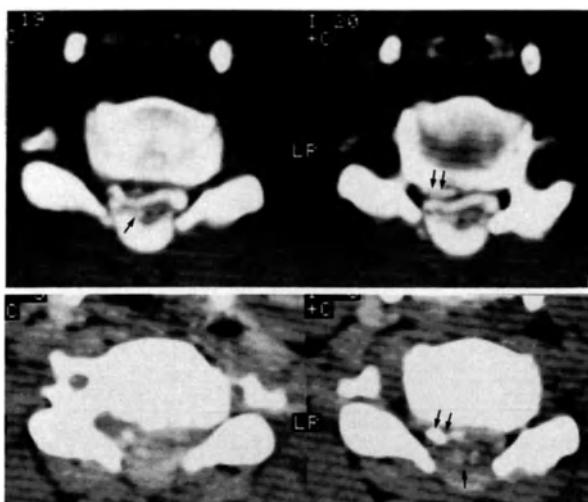


**Fig. 44.22.** Axial images from a computed myelogram through C5. The upper images were made 1 hour after myelography, the lower images 7 hours later. There has been a laminectomy, but the cord is deformed by anterior osteophytes and disc material (double arrows). Contrast has accumulated in each lateral funiculus of the spinal cord (single arrow) giving rise to what has been termed a 'cat's eyes' appearance. This is probably not true syringomyelia, but represents necrosis affecting mainly the central grey matter and immediately adjacent tracts.



MRI (Figs 44.20, 44.21) usually shows a circumscribed central region of low signal on T<sub>1</sub>-weighted images. On T<sub>2</sub>-weighted images the signal from the syrinx may be high or low depending on the mobility of the fluid within it. Occasionally a diffuse increase in signal is seen in cord substance around and cranial to the syrinx, the mechanism of which remains uncertain (Fig. 44.23). After successful shunting, at least part of the syrinx collapses, and movement of fluid within it diminishes.

### CORD TRAUMA

The spine is usually fractured when the cord is injured, but not always. Occasionally a *hematomyelia* occurs, in which the spinal cord is distended by a blood clot. There is evidence that MRI can distinguish clot from contusion and edema even in early stages, but this will not always be the case. *Post-traumatic syringomyelia* has been considered above.

Another cause of delayed or ascending post-traumatic myelopathy is *post-traumatic arachnoid cyst*. This lesion arises when the dura is torn. Often the cyst is lined not by arachnoid but by fibrous tissue, and is termed a *pseudomeningocele*. The latter occurs most frequently in the cervical region as a result of *cervical root avulsion*, and such cysts are often partly or entirely extraspinal in location. Myelopathy from pseudomeningoceles is rare, although some cord compression from the intraspinal component is commonly demonstrated.

Plain radiographs often show pedicular erosion, and *myelography* and *computed myelography* show the anatomy well.

### INFLAMMATION

*Abscesses* and *granulomas* are occasionally reported in the spinal cord, due to similar agents to those affecting the brain. They result in expansion of the spinal cord which is often subtle and diffuse, but is usually detectable on myelography and computed myelography.

*Myelitis* is more frequently encountered. This can be caused by viruses and some bacteria such as spirochetes (especially *Borreliae*). It can also occur as an infection-related hypersensitivity phenomenon in association with diseases such as tuberculous meningitis, and in post-infection encephalomyelitis. Multiple sclerosis also commonly involves the spinal cord.

*Irradiation myelitis* is actually a vasculopathy but is conveniently considered with this group of conditions.

*Imaging.* The cord shows varying degrees of fusiform swelling on myelography and MRI, but only in the acute phase.

**Fig. 44.23.** T<sub>2</sub>-weighted MRI (2000/80). Sagittal image of the case of post-traumatic syringomyelia shown in Fig. 44.21. There is diffuse high signal in cord substance around the cysts and throughout the medulla oblongata including the dorsal column nuclei (arrow). This has been attributed to gliosis, but is more likely to represent alterations in the extracellular fluid compartment due to the presence of the cyst, or perhaps the original trauma or both. The high signal is more marked than usual in these cases.

The cord signal is increased on MRI. Chronic lesions cause cord atrophy, and very occasionally syringomyelia. In multiple sclerosis, about 50% of patients with clinically isolated cord lesions have disseminated cerebral lesions.

### SPINAL CORD ANGIOMAS

Angiomas involving the spinal cord are rare. They resemble intracerebral arteriovenous malformations and may be localized or extensive. They are supplied by radiculomedullary arteries.

*Imaging.* The cord is often swollen on *myelography*, especially at the site of the malformation, and enlarged vessels on the surface of the cord are visible. Definitive evaluation is provided only by *spinal angiography*, and successful embolization is feasible in some cases. *MRI* may localize the lesion, and can be of assistance in evaluating the effects of treatment.

### SPINAL CORD ATROPHY

In a patient with myelopathy, a rather thin spinal cord is sometimes all that is shown on MRI, myelography or computed myelography. It is well to be aware of the possible causes of an atrophic cord, and the following is a short check-list:

1. Syringomyelia
2. Multiple sclerosis

3. Motor neurone disease
4. Post-irradiation myelopathy
5. Cord infarction
6. Others
  - subacute combined degeneration
  - tabes dorsalis
  - Friedreich's ataxia
  - some of the spinal muscular atrophies and other motor and sensory neuropathies

### REFERENCES AND SUGGESTIONS FOR FURTHER READING

- Bethem D, Winter RB, Lutter L et al. (1981) Spinal Disorders of Dwarfism. *J Bone Jt Surg [Am]* 63 : 1412-1425
- Du Boulay GH, (ed) (1984) A Textbook of X-ray Diagnosis by British Authors. Neuroradiology. Lewis, London
- Kricun ME (ed) (1988) Imaging Modalities in Spinal Disorders. WB Saunders Co., Philadelphia, London, Toronto
- Moseley I (1986) Diagnostic Imaging in Neurological Disease. Churchill Livingstone, Edinburgh
- Newton TH, Potts DG (1983) Modern Neuroradiology vol 1 : CT of the Spine. Clavadel Press, San Anselmo, San Francisco
- Seibert CE, Barnes JE, Dreisbach SN et al. (1981) Accurate measurement of the spinal cord using metrizamide: physical factors. *AJNR* 2 : 75
- Stevens JM, Kendall BE, Crockard AA (1986) The spinal cord in rheumatoid arthritis with clinical myelopathy: a computed tomographic study. *J Neurol Neurosurg Psychiatry* 49 : 140
- Stevens JM, Olney JS, Kendall BE (1985) Post-traumatic cystic and non-cystic myelopathy. *Neuroradiology* 27 : 48
- Stevens JM, Valentine AR (1987) Review Article: magnetic resonance imaging in neurosurgery. *Br J Neurosurg* 1 : 405-426
- Stevens JM, Valentine AR, Kendall BE (1988) Computed Cranial and Spinal Imaging. A Practical Introduction. William Heinemann Medical Books, London, pp 189-227

## CHAPTER 45

# ORBITAL IMAGING

G. Lloyd

---

The imaging techniques that may be used for examination of the orbit can be divided into those for the demonstration of bone (plain radiograph and CT), those for the demonstration of the soft tissues (CT and MRI), and those for the demonstration of the vasculature (carotid angiography and orbital phlebography).

In practice, the majority of patients with exophthalmos and suspected orbital disease are diagnosed by a combination of plain radiograph, CT and/or MRI.

Although CT is the dominant investigation, plain radiograph should never be neglected: in a series of 1070 patients with unilateral exophthalmos investigated by the author approximately one third showed plain film changes, and these were totally diagnostic in 21% of cases. Most of the ENT lesions causing proptosis can be diagnosed on straight films as can a significant proportion of the intracranial causes, since over 50% of the latter are due to meningiomas. Arteriography is now reserved for the small minority of patients with arterio-venous malformations in the orbit, requiring embolization. Although orbital phlebography remains the best method of demonstrating a venous malformation, it is now seldom required in the management of these patients.

### EXOPHTHALMOS

Exophthalmos, either bilateral or unilateral, is a common presenting symptom of orbital disease either primary or secondary. In a small proportion of patients, the exophthalmos may be due to an *intracranial* cause, the commonest of which is a sphenoid ridge meningioma. More frequently the cause of the condition is to be found in the *sinuses* or *nasopharynx*. The final group of patients are those in which the proptosis arises primarily *within the orbit*. These include

*dysthyroid disease, tumors, vascular anomalies and inflammatory processes.*

### Dysthyroid Exophthalmos

The enlargement of the extraocular muscles which occurs in this condition may be clearly demonstrated by computed tomography (CT) or magnetic resonance (MR). In dysthyroid patients multiple rectus muscle enlargement is usually present bilaterally or less commonly unilaterally. Single muscle enlargement may also occur in a minority of patients. The muscle enlargement tends to affect the belly of the muscle rather than its origin or insertion, and this may help to differentiate from other inflammatory processes such as pseudotumor affecting muscle. This typical enlargement predominantly affects the medial recti and produces a characteristic indentation on the medial orbital wall (Fig. 45.1). This will persist after regression of muscle enlargement and



Fig. 45.1. Typical dysthyroid disease showing extraocular muscle enlargement and indentation on the medial orbital wall by the medial recti.



**Fig. 45.2.** Axial CT scan showing the second type of dysthyroid change, in which there is a generalized increase in the fat content of the orbit with little or no enlargement of the extraocular muscles.

remains as evidence that the muscles have been enlarged in the past.

In some dysthyroid patients the fat content of the orbit may increase and this may be the primary cause of the exophthalmos with little or no muscle enlargement. This produces a different appearance on imaging, with forward displacement of the eyeball, an increase in the fat in the intraconal space, and sometimes a characteristic angulation of the lateral rectus muscles at the point where they are held by the lateral check ligaments (Fig. 45.2). This type of change is less common than muscle enlargement, but in some patients elements of both may coexist.

#### TUMORS OF THE ORBIT

##### Orbital Meningioma

Meningioma in the orbit may occur as a primary tumor or it may present as the secondary extension of a growth originating in the anterior or middle fossa of the skull.

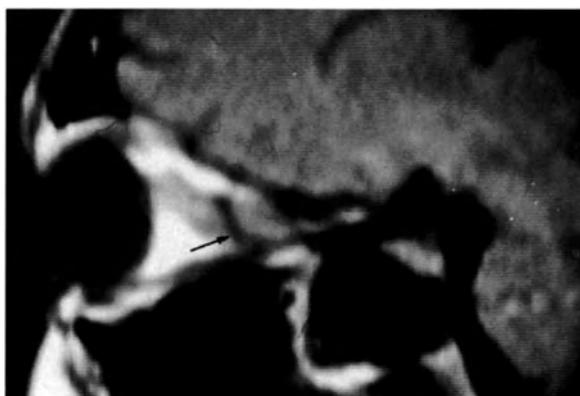


**Fig. 45.3.** Oblique sagittal magnetic resonance scan showing enlargement of the optic nerve due to an optic nerve meningioma. The ophthalmic artery is visible passing around the enlarged nerve (arrow).



**Fig. 45.4.** Axial CT showing 'tramline' calcification in an optic nerve meningioma.

##### *Primary intraorbital meningioma* may be:

1. Extradural: arising within the orbit remote from the optic nerve
2. Sheath meningioma: arising from clusters of arachnoid cap cells found in the meningeal sheath covering the optic nerve.

The retrobulbar sheath meningiomas occur predominantly in middle-aged women.

**Imaging.** Characteristically they give little sign of their presence on plain radiography, but a minority may show calcification and some may show minor change in the size of the optic canal – either enlargement or narrowing. Diagnosis is based upon the CT or MR findings. Visual deterioration in the middle-aged or elderly patient with obvious optic-nerve enlargement on imaging (Fig. 45.3) and minimal or no change in the size of the optic canal is characteristic of sheath meningioma. A diagnostic feature is the so-called 'tramline' enhancement of the enlarged optic nerve after intravenous contrast, or shown as calcification. (Fig. 45.4).

Primary extradural meningiomas in the orbit usually present with proptosis before compressing the optic nerve. Characteristic of these tumors are concomitant changes in the adjacent orbital wall or paranasal sinuses – either invasion, hyperostosis or the change referred to as pneumosinus dilatans; i.e., an abnormal dilatation of the paranasal sinus cavity, containing air only and provoked by the adjacent meningioma (Fig. 45.5). The importance of recognizing this condition is to alert the radiologist to the possible presence of an occult meningioma requiring MR or CT imaging.

**Secondary Meningiomas.** These occur as the extension of a meningioma arising in the middle fossa of the skull or less commonly in the anterior fossa. Meningioma en plaque, affecting the greater and lesser wings of the sphenoid and taking origin in the region of the pterion is the most common variety to affect the orbit secondarily.

##### Dermoids, Epidermoids and Cholesterol Granuloma

Dermoids and epidermoids result from sequestration of the primitive ectoderm in the region of the orbit. *Epidermoids*

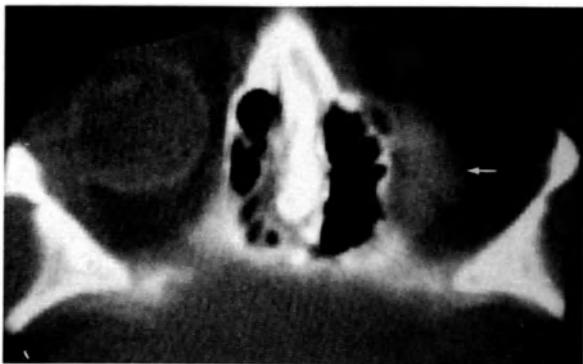


Fig. 45.5. Pneumosinus dilatans. The ethmoid cells are expanded due to an adjacent extradural meningioma (arrow).



Fig. 45.7. Coronal CT scan. Typical dermoid showing well-defined area of negative attenuation due to oil or fat.

occur when epidermal elements are solely concerned and a dermoid when the deeper dermal layer is also involved. Dermoids are cystic and may contain oil, sebum and hair while the epidermoid is a solid tumor consisting of a mass of desquamated cells containing keratohyaline encased in a capsule of stratified squamous epithelium. Both may arise in the diploe of the skull and in the bones forming the orbit, and occur most commonly in the superolateral quadrant. They may also occur more posteriorly involving the greater wing of the sphenoid and lateral orbital wall, where they produce a very characteristic cyst-like appearance in the bone (Fig. 45.6).

Dermoids in the superotemporal orbit also produce an indentation on the frontal bone and need to be differentiated from a *cholesterol granuloma*, which is also found in the same location. Both produce well-defined defects in the frontal bone on plain radiograph. A differentiating feature is the sclerotic margin often shown by dermoids and not present in cholesterol granuloma, while a diagnostic feature of the latter is extension of the defect in the diploe of the frontal bone down to the frontomalar suture. The two conditions can now be totally differentiated by CT and MR. Dermoids

may give a characteristic appearance on CT; the presence of oil or fat produces a localized area of low attenuation in the negative range of the Hounsfield scale (Fig. 45.7). While cholesterol granuloma is now readily diagnosed by MR, the presence of cholesterol has the effect of shortening the  $T_1$  and  $T_2$ -relaxation times, producing a strong signal on both  $T_1$  and  $T_2$ -weighted images. The diagnostic feature is the very strong signal on inversion recovery (Fig. 45.8), shown without the presence of negative attenuation in the lesion on CT.

#### Neurofibromatosis

The changes in the orbit and in the adjacent parts of the skull which can occur in this condition are striking and characteristic. Typically the orbit is enlarged, the sphenoid ridge elevated and there may be a large defect in the greater wing of the sphenoid, forming the posterior boundary of the orbit, producing an encephalocele (Fig. 45.9). This allows the pulsation of the brain to be transmitted to the eye and orbital contents thus producing a pulsating exophthalmos. The bone defect and soft tissue herniation is best demonstrated by CT (Fig. 45.10). These changes may be associated with

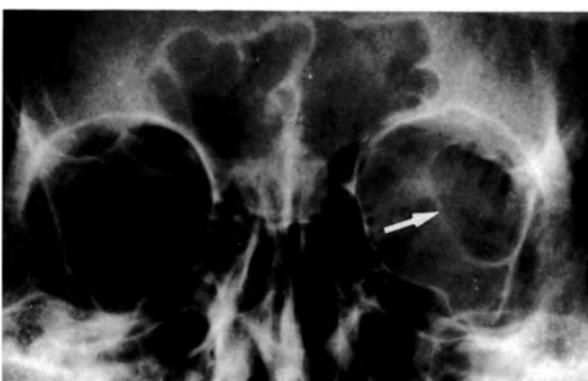


Fig. 45.6. Typical area of rarefaction produced by a dermoid. The edges of the defect are sharply defined and sclerotic (arrow).

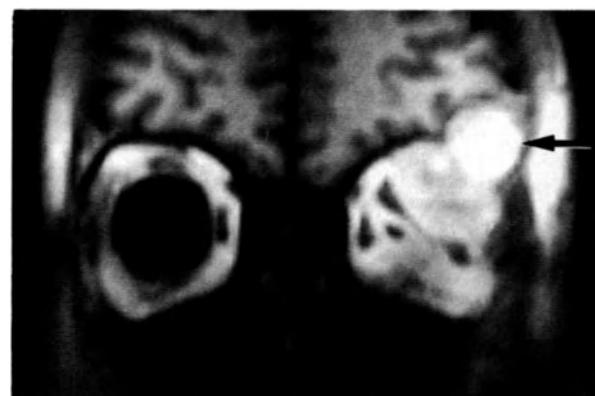


Fig. 45.8. Inversion recovery magnetic resonance sequence showing a cholesterol granuloma of the orbit and frontal bone (arrow). There is high signal, due to the presence of cholesterol shortening the  $T_1$ -relaxation time.



**Fig. 45.9.** Neurofibromatosis showing enlargement of the right orbit with a posterior encephalocele.



**Fig. 45.11.** Coronal CT showing orbital neurofibromatosis with involvement of the infraorbital nerve (arrow).

an infraorbital neurofibroma, which may also be seen as a solitary lesion: in either case it shows as a soft tissue mass in the roof of the antrum and floor of the orbit (Fig. 45.11).

#### Rhabdomyosarcoma

This is the most common cause of orbital malignancy in children and the majority of these tumors occur in the first decade of life. Clinically the condition presents with proptosis of rapid progression accompanied by swelling in the eyelids, canthi, or fornices. Radiologically these tumors cause progressive enlargement of the orbit and later they may cause bone erosion with extension to extraorbital structures including the temporal fossa and cranial cavity. CT shows a bulky tumor which usually enhances after contrast and frequently occupies an anterior location in the orbit extending both inside and outside the muscle cone.

#### Lymphoma

Both *benign* and *malignant* lymphoma occur in the orbit. The so-called benign lymphoma is, however, better termed *benign reactive lymphocytic hyperplasia* and should really be classified

as a variety of pseudotumor. However the histopathology of these tumors gives little indication of the ultimate outcome: a tumor diagnosed as benign may later disseminate and conversely a histologically malignant tumor may not.

Lymphomas in the orbit occur most frequently in the sixth and seventh decades and have an equal sex distribution. Typically they give rise to a painless swelling around the eye, and tend to arise outside the muscle cone in the anterior orbit. On CT it is not always possible to distinguish a lymphoma from other infiltrating processes, notably *pseudotumor* or *metastasis*. However some clue to the diagnosis can be obtained from the position of the mass in the orbit. Approximately two thirds of lymphomas are anterior and extraconal in location which gives rise to the characteristic pattern of these tumors: an anterior, palpable mass enveloping the globe in an elderly patient (Fig. 45.12). Lymphomas arising in the orbit do not as a rule involve bone.

#### Metastases

In contradistinction to lymphoma in the orbit metastases commonly involve bone.



**Fig. 45.10.** Axial CT showing a posterior encephalocele in neurofibromatosis.



**Fig. 45.12.** Coronal CT showing typical location of a lymphoma in the anterior orbit surrounding and displacing the left globe laterally.

On plain radiography the typical appearance is that of an ill-defined osteolysis, often difficult to appreciate but frequently accompanied by loss of the innominate line on the PA projection. Osteoplastic secondaries occur in the orbit, usually from a breast or prostate primary, and produce an increased bone density often indistinguishable from the hyperostosis of meningioma.

These changes can also be demonstrated by CT, and are usually accompanied by soft tissue infiltration, most often extraconal in location.

Involvement of an extraocular muscle is also a feature of some metastases, and a single rectus muscle may be involved without infiltration of other structures. In five examples of this presentation seen by the author three, surprisingly, were from primary carcinoid tumors.

### Lacrimal Gland Tumors

These comprise:

1. Benign pleomorphic adenoma
2. Carcinomas (including adenocarcinoma, adenoid cystic carcinoma, and undifferentiated types)
3. Lymphomas

Recognition of the type of tumor present is important in the surgical management of the epithelial tumors, and good correlation of the radiological and clinical findings in most instances will give an accurate forecast of the likely histology. Clinically the length of history and presence or absence of pain will help determine if the lesion is likely to be benign or malignant, and the diagnosis and pathological type may also be suggested by a combination of plain radiography, CT and MR. Signs of malignancy include invasion and sclerosis of the bone of the lacrimal fossa, calcification in the tumor (Fig. 45.13) and extension of the mass outside the lacrimal gland area as shown on the CT or MR scan.

### Neurilemmoma

These are benign tumors of the peripheral nerves which have their origin in the sheath of Schwann and usually occur either in the roof of the orbit extraconally or within the muscle cone. The intraconal variety closely mimics a hemangioma both clinically and radiologically, and presents on CT or MR as a clearly defined rounded and encapsulated mass. At surgery some of these tumors have been shown to have connexions passing through the superior orbital fissure, which may be slightly enlarged. Preoperative distinction from cavernous hemangioma is unnecessary since the treatment is the same in both tumors.

## VASCULAR ANOMALIES

### Arteriovenous Malformation

The orbit is a relatively uncommon site for an arteriovenous malformation, which may occur as a congenital anomaly or may follow trauma to the anterior orbit. Clinically the condition presents either as a pulsating exophthalmos, sometimes associated with an audible bruit, or as a simple



Fig. 45.13. Axial CT showing a nidus of calcification in a lacrimal gland carcinoma (arrow).

proptosis. Carotid angiography is the essential investigation both to show the nature of the lesion and its blood supply.

### Hemangioma

The orbital hemangiomas are divided into capillary and cavernous types.

*Capillary hemangioma* is a lesion which occurs in infants and may give rise to unilateral proptosis. It is often associated with a superficial capillary nevus and may be demonstrated as a fine vascular network on carotid angiography or in some patients an extensive pathological circulation.

*Cavernous hemangioma*, on the other hand, is a disease of adult patients and is a benign encapsulated neoplasm or hamartoma typically found within the muscle cone. They are well demonstrated prior to orbitotomy by CT or MR. The lesion consists of a sharply demarcated tumor mass with a rounded contour. They are indistinguishable from neurilemmoma but are more common and represent approximately 60% of lesions which present as a discrete rounded mass within the rectus muscle cone (Fig. 45.14).

### Orbital Varices

These may be primary or secondary. Primary varices are classified as a congenital venous malformation; while

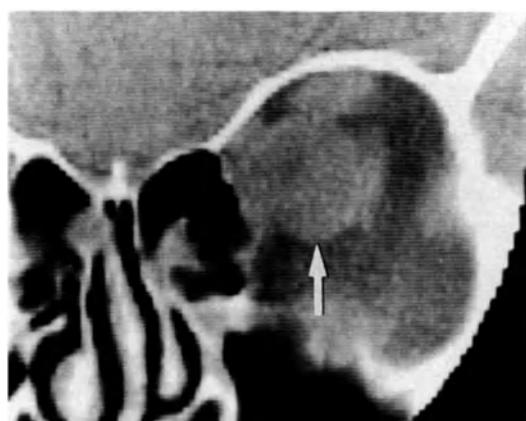


Fig. 45.14. Coronal CT scan. Cavernous hemangioma. Typical rounded, well-defined mass within the muscle cone (arrow).



**Fig. 45.15.** Enlargement of the orbit with multiple phleboliths: diagnostic of a venous malformation.

secondary varices represent a dilatation of otherwise normal veins as a result of an arteriovenous malformation or carotico-cavernous fistula.

#### Congenital Venous Malformation

These patients usually give a history of proptosis dating from birth or early childhood and characteristically the proptosis is provoked or made worse by an increase in venous pressure in the head. Orbital varices are sometimes accompanied by similar malformations in other parts of the head and neck and may be seen in the Klippel-Trenaunay-Weber syndrome. The plain radiograph features may be totally diagnostic and consist of enlargement of the orbit, the presence of phleboliths in the orbit or adjacent structures (Fig. 45.15) and prominent vascular markings and venous 'lakes' in the frontal bone above the affected orbit.

Venous malformations are best demonstrated by orbital phlebography but this is now seldom required since the diagnosis is readily confirmed by CT and MRI. A varix may present as a rounded mass either intra- or extraconally, or show on CT as a more diffuse soft tissue mass extending outside or inside the rectus muscle cone, often associated with phleboliths. The clearly defined rounded varix may present a problem in differential diagnosis since it may be indistinguishable from the commoner intraconal tumors such as

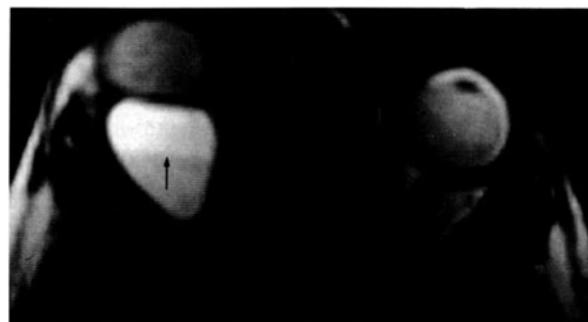


**Fig. 45.17.** Blood cyst in the orbit. MR scan showing the characteristic layering phenomenon (arrow).

hemangioma or neurilemmoma. However, the CT image of the varix can be shown to enlarge with increase in the venous pressure. A simple way to do this is to repeat the scan with the patient prone instead of the usual supine position.

A venous malformation may also show characteristic features on T<sub>1</sub>-weighted magnetic resonance sequences. The changes are particularly well shown on inversion recovery, when the varix presents a signal of mixed intensity with areas of high signal and signal void interspersed (Fig. 45.16). This is probably the result of mixed blood flow rates, the presence of altered blood, and the formation of thrombi and phleboliths.

#### Hematomas and Blood Cysts

*Retrobulbar hemorrhage* may occur in adult patients and the cause (usually a small varix) may be revealed by orbital phlebography. It may be possible to show extravasation of contrast leaking from the varix. In children retrobulbar bleeding and sudden proptosis may be accompanied by vomiting and sometimes loss of visual acuity due to optic nerve compression. The onset may mimic that of a tumor such as rhabdomyosarcoma. The collection of blood is usually found at surgery to be within the intraconal space but extraconal locations are also encountered. The hematoma can be shown on CT but the changes are non-specific. The condition is also readily diagnosed by MRI, and layering, due to red-cell sedimentation, may be demonstrated (Fig. 45.17).



**Fig. 45.16.** Inversion recovery MR sequence showing a venous malformation in the left orbit: there is a mixed signal pattern with areas of high signal and of signal void.

## INFLAMMATORY CONDITIONS IN THE ORBIT

#### Acute Infection

*Orbital cellulitis* results from an acute bacterial infection which in most patients is secondary to sinus infection, usually an ethmoiditis or maxillary antritis. A dental abscess may be the initial cause in some instances. Evidence of the sinus infection is usually present on plain radiography as a clouding of the sinus affected, and rarely, *abscess* formation may be evident as a small gas-fluid level in the orbital soft tissues. *CT* is the definitive investigation to show both the sinus infection and adjacent abscess formation within the

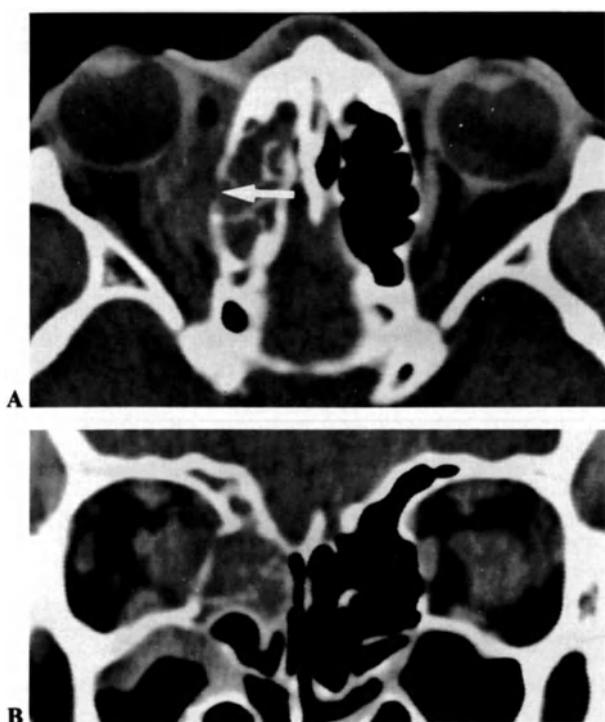


**Fig. 45.18A, B.** Axial and coronal CT scans showing infection in the ethmoid cells with orbital cellulitis and abscess formation. Note the bone destruction in the medial orbital wall (arrow) at the site of the abscess.

orbit (Fig. 45.18A, B). Unequivocal evidence is provided when there is gas in the soft tissues with or without a fluid level. Ring enhancement after intravenous contrast will also suggest abscess formation.

#### Chronic Infection: Orbital Pseudotumor

The name pseudotumor has been given to a group of cases which are difficult to differentiate clinically from orbital tumors but which on pathological investigation have proved to be of chronic inflammatory origin; they are in fact a spectrum of different conditions rather than a single entity. They

occur throughout the orbit from the region of the lacrimal gland to the orbital apex

**Imaging.** Plain radiography is negative except for the presence of sinus infection or nasal polyposis, which is sometimes associated with pseudotumor. On *orbital phlebography* pseudotumor characteristically causes a block in the second or third part of the superior ophthalmic vein. Positive evidence of the lesion within the orbit is best obtained by CT. The appearance is that of an infiltrative lesion, with an irregular ill-defined edge and variable density. The changes occur with equal frequency in an anterior or posterior location in the orbit and may be associated with enlargement of one or more rectus muscles. Although a similar appearance can be seen in some patients with *metastases* or a *lymphoma*, a mass filling the orbital apex with local muscle enlargement is very suggestive of this condition. In some patients the whole of the muscle cone may be infiltrated by the inflammatory process (Fig. 45.19).

#### Tolosa–Hunt Syndrome

A similar non-specific inflammatory process occurs in the retro-orbital tissues with the presence of granulation tissue in the superior orbital fissure or cavernous sinus. The condition presents as a painful ophthalmoplegia and, as in the case of pseudotumor in the orbit, usually responds dramatically to steroid therapy.

### DACRYOCYSTOGRAPHY

#### Technique

The technique is based upon an injection method using a nylon catheter. The radiographic exposure is made during the injection of the contrast medium so that optimal filling of the ducts can be obtained: in most instances this produces an image of the contrast continuous throughout the lacrimal drainage system.

Before catheterization of the inferior canaliculus, a drop of amethocaine is instilled into the conjunctival sac. A non-viscous contrast medium is used (ultrafluid Lipiodol). The punctum is first dilated with a Nettleship dilator and the tip of the catheter introduced into the canaliculus. The catheter is held in place by sticking plaster applied to the cheek at the outer canthus. Slight pressure is applied to the loop of the catheter so that it is under tension and thereby held in position during the injection (Fig. 45.20). An initial control film is taken for subtraction studies and two exposures are made during the injection. Macrography is used to enlarge the image.

In summary the method employs:

1. Intubation to produce distension of the duct system and better contrast filling
2. Macroradiography to produce better radiographic definition
3. Subtraction to produce bone-free visualization of the ducts

#### Demonstration of the Site of Stenosis

Blocks in the upper and lower canaliculi are indicated when contrast regurgitates through the punctum injected, and on



**Fig. 45.19.** Axial MR. T<sub>1</sub>-weighted image showing a diffuse mass in the right orbit due to a pseudotumor.



Fig. 45.20. Method of securing the nylon catheter. Both inferior canaliculi are intubated and the catheters are kept under slight tension by securing them to the cheek with sticking plaster.

the radiograph the injected canalculus is outlined as far as the stenosis. Common canalculus blocks are characterized by regurgitation of contrast from the upper punctum, with outlining of both upper and lower canalici on the radiograph, without filling of the lacrimal sac if the obstruction is complete, or with partial filling of the sac if incomplete. Subtraction studies are particularly useful for the complete demonstration of the common canalculus. Partial filling of the common canalculus usually denotes an obstruction at its medial end at the level of the lacrimal sac mucosa. Non-filling of the lumen of the common canalculus suggests a block involving its whole length.

The most frequent site of obstruction in the lacrimal passages is at the neck of the sac, and this may result in a lacrimal sac *mukocele* (Fig. 45.21). Blocks in the nasolacrimal duct itself are commonly located at the entrance of the bony canal

or at the lower ostium (Fig. 45.21). They are characterized by a dilatation of the duct proximal to the obstruction and failure of the contrast to enter the nasal cavity.

#### LOCALIZATION OF FOREIGN BODIES IN THE EYE

The radiologist should have some knowledge of the methods used by the ophthalmic surgeon to remove foreign bodies from the eye. There are two surgical approaches to the problem.

In the anterior extraction the foreign body is removed through an incision in the cornea, the foreign body being brought to the site of incision by an electromagnet. Foreign bodies in both anterior and posterior chambers may be removed by this method. The disadvantage of this technique of extraction is that it is possible to damage the lens or for impaction of the foreign body to occur in the iris, when it is brought from the posterior to the anterior chamber by the magnet.

For this reason the posterior route of extraction is preferred. In this approach an incision is made in the sclera immediately at the site of the foreign body, which is then removed by forceps or by the magnet. Exact localization is required for this technique so that the incision can be placed accurately. In order to site the incision, the surgeon needs to know the meridian of the globe in which the foreign body lies, and the distance the foreign body lies along that meridian using the limbus as a reference point. The surgeon then takes a pair of dividers and separates them to a distance corresponding to this measurement. The dividers are placed in the line of the correct meridian with the forward point on the limbus; the other point indicates the spot on the sclera at which the incision should be made (Fig. 45.22).

The radiologist, therefore, needs first to establish that there is an intraocular foreign body present, and then to provide the ophthalmic surgeon with the essential data for its extraction: namely the exact meridian of the globe in which the foreign body lies, and its distance from the limbus by caliper measurement.

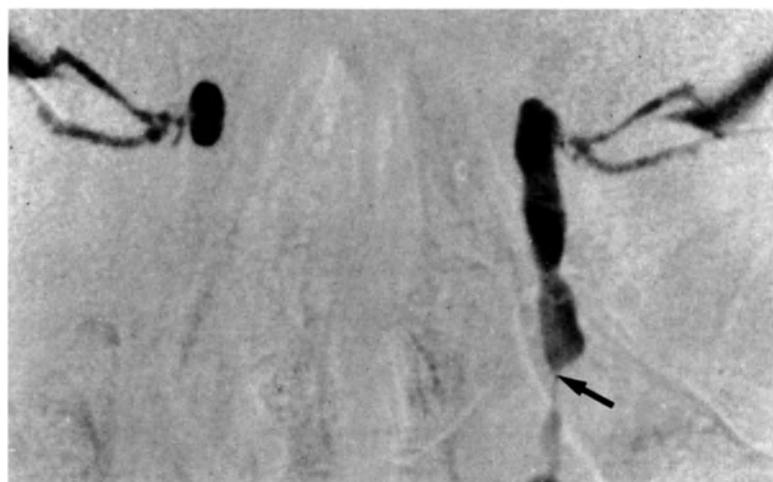


Fig. 45.21. Subtraction macrodacryocystogram showing a lacrimal sac mucocele on the right side, and dilatation of the left lacrimal duct due to an incomplete obstruction at the lower ostium (arrow).



**Fig. 45.22.** Method used for the site of incision for removal of a foreign body. The calipers have been placed along the meridian of the eye in which the foreign body lies, and are separated to a distance corresponding to the measurement of the foreign body from the limbus. One point of the dividers is placed on the limbus; the other then indicates the correct site of incision in the sclera.



**Fig. 45.23.** Eye-moving lateral film. The film has been taken with a double exposure with the eye looking up and down. The foreign body shows the typical image shift of an intraocular foreign body; i.e., around the arc of a circle.



The localization procedure can be considered under the following headings:

1. Preliminary radiographs to determine if an intraocular foreign body is present, and localization based on these films
2. Tomographic localization: either by CT or conventional tomography
3. Charting the foreign body
4. Localization by radiopaque marker: this may be needed for non-magnetic foreign bodies

#### Preliminary Films and Localization

The initial film is a straight lateral, using non-screen film to determine if there is a foreign body in the region of the globe. If this film gives positive evidence of a foreign body in the orbit, two further views are taken to decide whether it is intra- or extraocular. These are a PA projection taken in the nose-chin position (orbitomeatal line tilted cranially 35°), and an eye-moving lateral view using two exposures, the eye first looking upward and then downward, while the head remains still. From these views it will be possible to establish that there is an intraocular foreign body if there is an opacity within the outline of the orbit, and if on the eye-moving lateral it moves in the manner of an intraocular foreign body: namely a movement of the foreign body in the arc of a circle around the central axis of rotation of the globe (Fig. 45.23).

Once the presence of an intraocular foreign body is established it is often possible to make an accurate localization from the preliminary films. Provided the PA view is correctly positioned, it is possible to place the foreign body in its correct meridian with respect to the eyeball by relating it to the outer rim of the orbit as a simulated clock face (Fig. 45.24).

This provides half the information required by the ophthalmologist for the recovery of the foreign body; the remainder may be obtained from the lateral film. Provided this is accurately centered it is possible in most patients to visualize the anterior surface of the cornea. The distance back from the anterior surface of the cornea to the foreign body can then be measured directly, allowance being made for radiographic magnification. This completes the data required for localization. Fig. 45.25 shows a plan view of the eye in which the various meridians are plotted as seen from above. It is apparent that the position of the foreign body will be placed at the point where the plot, representing the known meridian in which the foreign body lies, intersects the line representing the distance back from the cornea as measured on the lateral film. This method of localization assumes that the foreign body lies either within or attached to the coats of the globe, and while this is true for the vast majority of foreign bodies in the eye there is a small minority in which this is not so. The location of these is, however, in most cases easily diagnosed from the standard films. The data obtained from the

**Fig. 45.24.** PA view showing position of the foreign body. If the intraocular location of the foreign body has been confirmed by an eye-moving film, it is apparent that the foreign body lies in the 6 o'clock meridian.

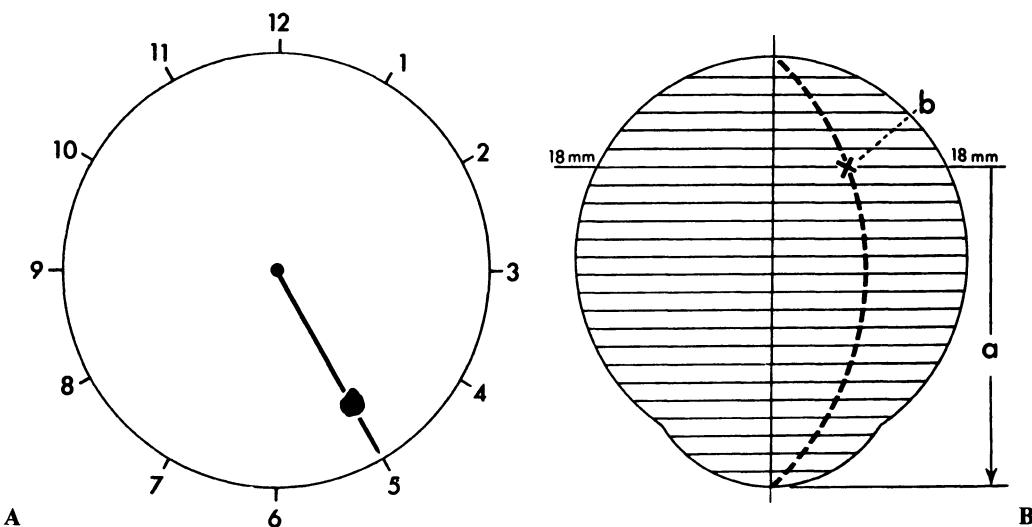


**Fig. 45.25A, B.** Method of foreign body localization from plain radiographs. The foreign body is placed in its correct meridian (in this case 5 o'clock) by examination of the postero-anterior film, A. The line of the 5 o'clock meridian is then plotted on the plan view of the eye, B. The distance (*a*) i.e., anterior surface of the cornea to the foreign body is measured from the lateral film. The foreign body must then lie at the position where the 18-mm line intersects the line of the 5 o'clock meridian (*b*).

preliminary films thus allows an accurate plot to be made of the position of the foreign body, and the limbus to foreign body measurement can then be obtained (see below, Charting the Foreign Body).

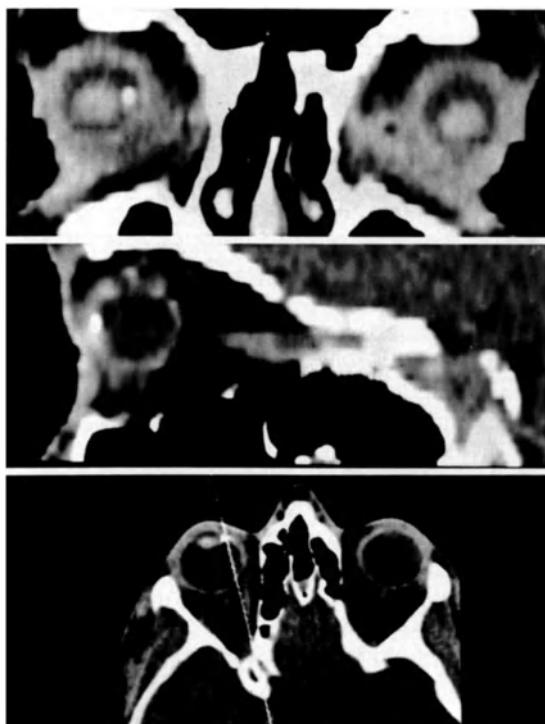


**Fig. 45.26.** CT localization of an intraocular foreign body. The foreign body is demonstrated on axial section and on reformatted coronal and sagittal projections. It is apparent that the foreign body lies in the ciliary body in the 2.45 meridian.

#### Tomographic Localization

Multisection linear tomography can be used for accurate localization of a foreign body if the preliminary localization needs verification or if, for any reason, satisfactory radiographs cannot be obtained. CT is, however, an easier technique and has the advantage of showing the relationship of the coats of the globe to the foreign body (Fig. 45.26). The main drawback of computerized tomography is the relatively high dose of radiation received by the eye, when a large number of thin CT sections are made to cover the whole area of the globe. These should be made in the axial plane and be of 1-mm thickness so that if necessary they can be reformatted to the coronal and sagittal planes. The three coordinates necessary for an exact localization can be measured directly from the scans or from the reformats.

1. The distance deep to the plane tangential to the center of the anterior surface of the cornea
2. The distance of the foreign body above or below the horizontal corneal axis
3. The distance to the temporal or nasal side of the vertical corneal axis

#### Charting the Foreign Body

The final stage in the process of localization is to plot the position of the foreign body on a suitable localization chart. This is needed whatever the method of localization used, in order to get a true measurement of the distance of the foreign body from the limbus, which can only be obtained from the charts. To get an accurate measurement, the foreign body should be plotted in three planes and the limbus to foreign body distance taken from the appropriate projection of the globe depending upon the position of the foreign body. For instance, this measurement is best obtained from the plan view of the eye if the foreign body lies at 2, 3, and 4 o'clock or at 8, 9, and 10 o'clock. For foreign bodies at other loca-

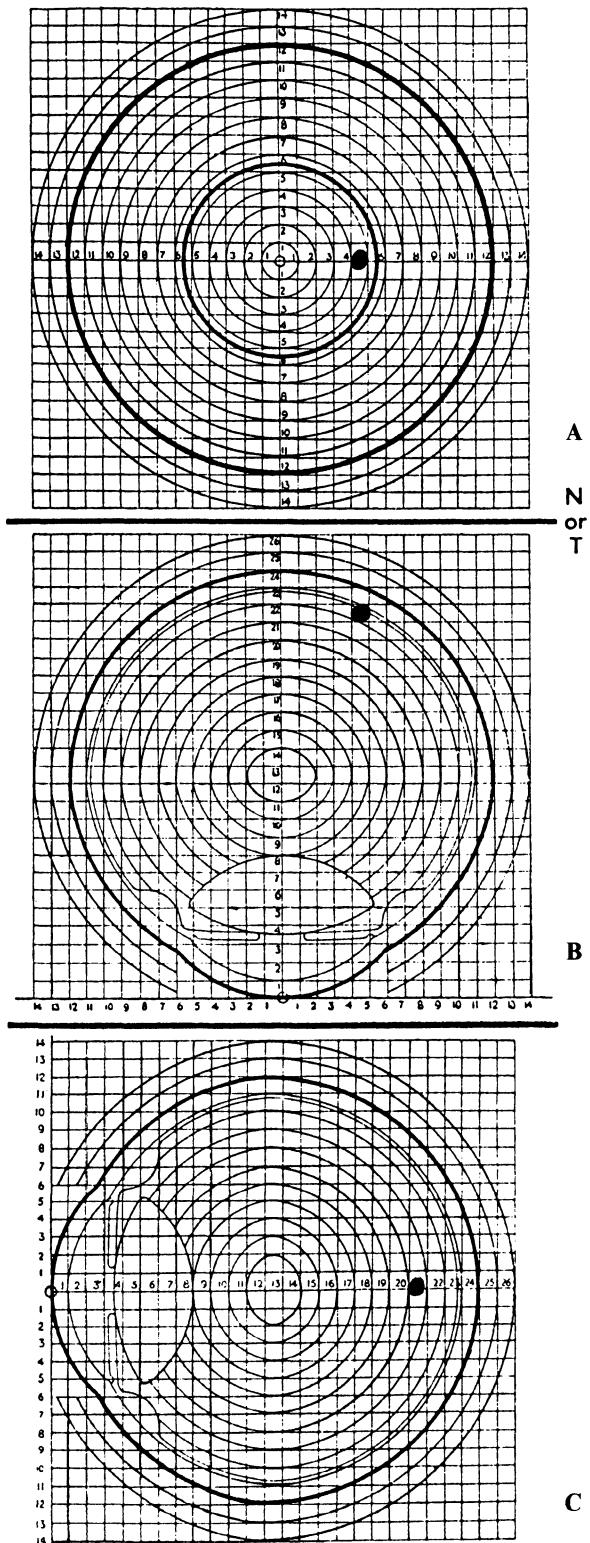


**Fig. 45.27.** Specimen localization report. The report states that the foreign body is present in the left orbit, A, 4.5 mm to the temporal side of the vertical corneal axis, B, 21.5 mm deep to the plane tangential to the center of the anterior surface of the cornea and, C, 0 mm above/below the horizontal corneal axis. It is intraglobular. The foreign body lies in the coats of the globe in the 3 o'clock meridian, 20 mm back from the limbus by caliper measurement.

tions the distance should be measured from the lateral projection of the globe (Fig. 45.27).

#### Localization by Radiopaque Marker

There is an additional method which may be needed if the foreign body is non-magnetic. Since it will need to be removed by forceps rather than the electromagnet, the scleral incision for removal must be sited with pinpoint accuracy. To do this the foreign body is first localized by the methods described, and the surgeon attaches a small radiopaque marker such as a wire suture, at the calculated point of scleral incision. Standard lateral and postero-anterior views are then taken in the operating theatre, and the position of the foreign body related to the opaque marker. This allows any error in the original localization to be corrected before the scleral incision is made. It can be appreciated that this technique will correct for the other possible sources of error: for anatomical variation in the size of the eye, and for any possible surgical error in determining the correct meridian.

#### REFERENCES AND SUGGESTIONS FOR FURTHER READING

- Enzmann DR, Donaldson SS, Kriss JP (1979) Appearance of Grave's disease on orbital computed tomography. *J Comput Tomogr* 3: 815–819
- Keast-Butler J, Lloyd GAS, Welham RN (1973) Analysis of intubation macrodacryocystography with surgical correlations. *Trans Ophthalmol Soc UK* 80: 343–351
- Krohel GB, Wright JE (1979) Orbital haemorrhage. *J Ophthalmol* 88: 254–258
- Krohel GB, Krauss HR, Winnick J (1982) Orbital abscess. *Ophthalmology* 89: 492–501
- Lloyd GAS (1981) Lacrimal gland tumours: the role of CT and conventional radiology. *Br J Radiol* 54: 1034–1041
- Lloyd GAS (1982) Vascular anomalies in the orbit: CT and angiographic diagnosis. *Br J Radiol Orbit* 1: 45–51
- Lloyd GAS (1986) Cholesterol granuloma of the facial skeleton. *Br J Radiol* 59: 481–485
- Lloyd GAS (1987) The Orbit and Eye. In: Sutton D (ed) *Textbook of Radiology and Imaging*. Churchill Livingstone, Edinburgh, London.
- Travis RC, Murray PI, Moseley IF, Wright JE (1989) Orbital intraconal haematoxytic cysts in young people: computed tomography and magnetic resonance imaging. *Br J Radiol* 62: 521–525
- Trokell SL, Hilal SK (1979) Recognition and differential diagnosis of enlarged extraocular muscles in computed tomography. *Am J Ophthalmol* 87: 503–512

## CHAPTER 46

# RADIOLOGY OF THE TEETH AND JAWS

P. Renton

### DENTAL ANATOMY

The tooth consists of the visible crown and neck as well as the root embedded in bone (Fig. 46.1). The crown is capped by radiodense enamel, which is insensitive but is the site of caries. The bulk of the tooth consists of dentine, which is homogeneous and is slightly less dense than enamel. The central pulp chamber contains blood vessels and nerves. It tapers towards the apex of the root. The apex itself gradually closes off during development. The root lies within a radiolucent space, the periodontal membrane space, surrounded by the bony cortex of the socket – the lamina dura – seen as a thin white line. The root itself is surrounded by cementum, but this is not seen on radiography unless it has undergone hypertrophy.

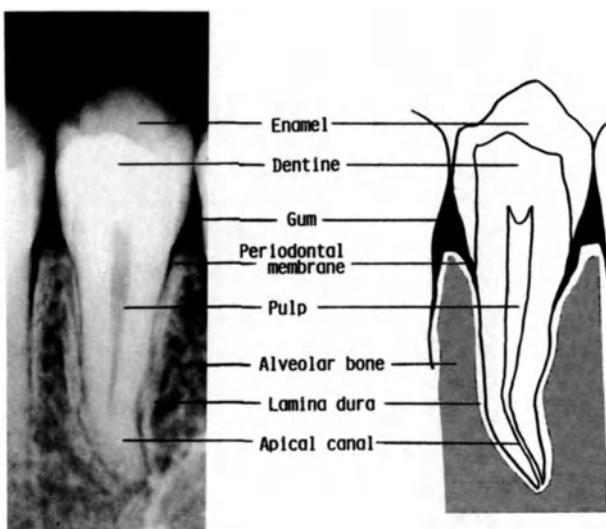


Fig. 46.1. Normal anatomy of a tooth.

The surrounding alveolar bone beyond the lamina dura may be heavily or sparsely trabeculated, or a 'stepladder' pattern of bone may be present. Alveolar bone between teeth peaks to a 'crest'.

Nutrient canals carrying the blood vessels and nerves to the roots are seen as radio-opaque lines extending to the apices, often more prominent in the elderly or demineralized mandible. Interdental nutrient canals extending to the alveolar margins are wider and are also more prominent in edentulous patients.

The *maxillary antra* lie above the roots of the premolar and molar teeth and the antral floor often dips down between the roots, giving a lobular or septate appearance, especially on intraoral and panoramic views (Fig. 46.2). This change is accentuated after local dental loss, when the antrum expands and the alveolus recedes. Bony trabeculae are however superimposed on the antral lucency on the intraoral radiograph, from the overlying buccal and lingual antral walls. These trabeculae are destroyed by periodontal



Fig. 46.2. Supernumerary distodens.

pathology. Locally arising dental cysts or tumors are therefore truly more radiolucent. Radicular cysts are usually unicellular and are situated on the dental apices rather than dipping down between the teeth (Figs 46.20B and 46.21).

Bone density may vary greatly in the normal jaw and areas of radiolucency may be mistaken for pathology. Comparison with the other side is helpful in excluding or confirming disease. An intact lamina dura virtually excludes periapical disease.

### DENTAL DEVELOPMENT

The chronology of dental development is listed in Table 46.1), and it should be noted that teeth develop earlier in females.

**Table 46.1. Chronology of tooth development.** (Teeth in females appear earlier than in males)

Tooth	Formation of crown complete	Appearance in mouth cavity
<i>Deciduous</i>		
Incisors	2–3 months	6–9 months
Canines	9 months	16–18 months
1st molars	6 months	12–14 months
2nd molars	12 months	20–30 months
<i>Permanent</i>		
Incisors	4–5 years	Lower: 6–8 years Upper: 7–9 years
Canines	6–7 years	Lower: 9–10 years Upper: 11–12 years
Premolars	5–7 years	10–12 years
1st molars	2½–3 years	6–7 years
2nd molars	7–8 years	11–13 years
3rd molars	12–16 years	17–21 years

*Tooth charting.* Teeth are labeled thus in the primary dentition:

e d c b a : a b c d e

— — — — —

e d c b a : a b c d e

and thus in the secondary dentition:

8 7 6 5 4 3 2 1 : 1 2 3 4 5 6 7 8

— — — — —

8 7 6 5 4 3 2 1 : 1 2 3 4 5 6 7 8

### DEVELOPMENTAL ANOMALIES

#### Absence of Teeth

This is often isolated and hereditary. The third molar and the upper lateral incisor are most commonly absent. These changes also occur in Down's syndrome. Hypodontia- or total anodontia may also be seen in *Ellis-van Creveld syndrome* and may follow local infection, tumor and the administration of cytotoxic drugs or radiotherapy in childhood, while the tooth germ is forming. Preservation of the deciduous teeth may



**Fig. 46.3. Cleidocranial dysostosis.** Preservation of the primary dentition together with failure of eruption of the secondary dentition and numerous supernumerary teeth are characteristic of this condition. On occasion, there may be a midline mandibular cleft.

be the result of absence of the underlying permanent dentition.

#### Supernumerary Teeth

Duplication is often familial, but can be associated with skeletal dysplasia. Supernumerary teeth occur more commonly in the maxilla, in permanent teeth and in males. Most do not erupt and thus are seen only at radiography (Fig. 46.2). They usually resemble the adjacent teeth in shape but are often smaller and may be bilateral. They may cause physical inhibition of eruption of adjacent teeth and they may also be surrounded by cysts of their follicles.

Common supernumerary teeth include the midline maxillary *mesiodens* and the fourth molar *distodens* (Fig. 46.2). Supernumerary teeth are found in *cleidocranial dysostosis* (Fig. 46.3), *Gardner's syndrome* and accompanying *cleft palate*.

#### Dens-in-dente

The maxillary incisors are most commonly affected. The crown invaginates into a broadened pulp canal, giving what looks truly like a tooth within a tooth. Communication between the exterior and the apical bone can exist, predisposing to infection (Fig. 46.4).

Other dental anomalies include *microdontia* and *fusion*. Microdontia may be *congenital* or may follow *irradiation*, or



**Fig. 46.4. Dens-in-dente associated with a globulomaxillary cyst.**



Fig. 46.5. Multiple non-eruption.

may be associated with *mandibular atrophy*. Fusion may involve either the crowns or the roots, or both. Often a broad tooth with a single large canal results. Local *macrodontia* may be seen with *facial hemihypertrophy* and generalized macrodontia may be present in *gigantism*.

#### Dental Malalignment and Non-eruption

Children are often examined radiologically because of failure of dental eruption. Non-eruption is usually due to a lack of space following *early loss of a deciduous tooth*, allowing drift of adjacent permanent teeth into the available space. Obstruction can also be due to *cysts*, *odontomes*, *supernumerary teeth* and *bone thickening* following infection or trauma. The non-erupted tooth may end up abnormally aligned, so that eruption eventually becomes impossible. The third molar and maxillary canine teeth are most frequently affected (Fig. 46.5) (Table 46.2). Partially erupted mandibular third molar teeth often impact distally against the ascending ramus. Local resorption of bone occurs, often complicated by local infection.

#### Dental Caries

Dental caries is the end result of bacterial infection by plaque, a gelatinous layer adherent to teeth containing bacteria. The pH drops locally, resulting in local enamel destruction by acid, eventually causing a cavity which may penetrate through to the pulp. Because of the more widespread admin-



Fig. 46.6. Caries shown by a bitewing examination, seen as a radiolucent area destroying both enamel and dentine, but not yet invading the pulp.

Table 46.2. Delayed or non-eruption of teeth

Congenital	
	cleidocranial dysostosis
	Down's syndrome
	osteopetrosis; progeria; pyknodysostosis
	Goltz-Gorlin basal cell naevus syndrome
	Ellis-van Creveld's syndrome
	Apert's syndrome
Endocrine	
	hypothyroidism, hypopituitarism, hypoparathyroidism
Familial tendency	
Local disease	<p>lack of space, retained deciduous teeth, ectopic eruption, cleft palate</p> <p>inflammation and reactive bone sclerosis</p> <p>ankylosis</p> <p>local tumors</p> <p>odontogenic cysts etc., fibrous dysplasia, cherubism</p>

istration of *fluoride*, the incidence of caries is rapidly diminishing.

Caries on the crown can usually be seen clinically. Radiographs are however necessary to show interdental lesions, that is, those on the vertical contact points and these are best demonstrated, especially at molar and premolar teeth, by bitewing radiographs (Fig. 46.6).

Radiographs tend to underestimate the extent of demineralization by caries, which is seen as an area of rarefaction, initially of the enamel, extending into dentine, then into the pulp. The lesions progress more quickly in the primary dentition but can take up to two years to enter the pulp. The usual appearance is of a lucent triangle based at the surface of the tooth. Chewing causes collapse of an undermined surface, leaving a large cavity.

*Root caries* involves both cement and dentine at the neck of the tooth following alveolar recession in elderly patients.

**Periodontal disease** is also the result of local infection by plaque spreading between root and gum causing 'pocketing', local destruction of bone, and gingivitis. Calculus and exuberant prominent fillings accentuate the process. Bitewing and periapical views using a long cone technique are essential to show normal bone-tooth relationships. Blunting of the alveolar crests is followed by horizontal bone loss, especially involving interdental bone. Bone loss also occurs adjacent to the crowns of impacted wisdom teeth. Finally, bifurcation bone loss isolates molar roots (Fig. 46.7).

#### INFECTION

Changes may be periapical or more widespread in surrounding bone (*osteomyelitis*). Deep caries kills the pulp by tamponade within the confined canal. Younger patients with wider canals are less susceptible to canal necrosis. Infection can then spread to the periapical region.

The clinical signs of pain and swelling occur before radiological change. The earliest radiographic change is that of widening of the periodontal membrane space due to local edema. This is followed by loss of definition of the *lamina dura* (Table 46.3).

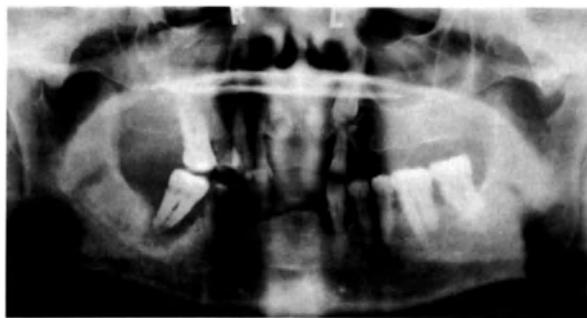


**Fig. 46.7.** Periodontal disease. There is marked alveolar bone loss associated with calculus. The disease has caused pocketing and extends to the apical region at the right lower 6. Apical bone loss has caused reactive sclerosis.

**Table 46.3. Loss of lamina dura**

<b>Infective</b>	local infections, including granulomas and apical cysts
<b>Endocrine</b>	senile osteoporosis, Cushing's disease, hyperparathyroidism
<b>Metabolic</b>	osteomalacia, hyperphosphatasia
<b>Neoplastic</b>	benign fibrous dysplasia, cementoma malignant leukemia, metastatic disease, myeloma
<b>Diseases of unknown origin</b>	Paget's disease, eosinophilic granuloma
<b>Following orthodontic treatment</b>	

Loss of the lamina dura is followed by periapical demineralization and trabecular bone loss (Fig. 46.8). If the patient is placed on antibiotics at the onset of symptoms, this change need never be seen. With healing some or all of the trabecular bone may reappear.

Less frequently, a permanent, poorly marginated area of periapical bone destruction due to a chronic abscess may result. A chronic abscess may communicate via a sinus to the mouth or skin resulting in a purulent discharge. Should a maxillary molar tooth be affected, sinusitis can follow.

A **granuloma** is rather better defined than a chronic abscess but is less well-defined than a periapical cyst. Granulomas have a fairly thick zone of reactive sclerosis and



**Fig. 46.9.** Osteomyelitis following dental extraction. The socket for the right lower 8 is irregular and sequestration of bone is seen within it. The abnormal area is larger than the original socket.

a rather patchy texture, are not typically apical, and are small (1.5 cm). The local tooth is not vital. Granulomas may result from healing of an abscess or may appear *ab initio*.

A similar appearance, of well-defined apical bone loss to the apex or pulp canal may be seen after surgery. Granulomas are often asymptomatic until secondarily infected.

**Osteomyelitis** of the jaws may cause widespread bone destruction and may follow apical infection. Precipitating factors include immune suppression, local radiotherapy, chemotherapy, abnormal bone (as in osteopetrosis), trauma and dental extraction (Fig. 46.9) or major injury. Fungal infection by actinomycosis is rarely described. Bone changes are similar to those of infection elsewhere. The mandible is most commonly affected because of the prevalent spongiosa. Sequestration occurs (Fig. 46.10) but a florid periostitis is unusual in the mandible. Tunnelling – a finger-like process of extension – is pathognomonic of the disease (Fig. 46.11). Infection also takes place around surgical plates or prostheses, as at the hip. Bone repair is often associated with sclerosis.

On occasion, mandibular osteomyelitis comes from a distant source via the bloodstream, but this is rare. Mandibular infections can metastasize distally.



**Fig. 46.8.** Loss of the lamina dura is associated with widening of the periodontal membrane space. There is bifurcation and apical bone loss. The apical loss is poorly defined in this patient with early infective change.



**Fig. 46.10.** Florid osteomyelitis of the left mandible in this infant has caused a periosteal reaction with expansion of the bone and sequestration associated with bone destruction. The surviving dental follicles are misplaced.



Fig. 46.11. Tunnelling in osteomyelitis. A finger-like process of bone destruction extends from a socket into the body of the mandible (arrow).

### Eosinophilic Granuloma

Both tunnelling and marked surrounding reactive sclerosis are absent in *eosinophilic granuloma* (Fig. 46.12). Here, single or multiple lytic lesions occur at alveolar margins or around teeth, and the patients are younger than is the rule in osteomyelitis. Teeth may be exfoliated, but the lesions respond well to radiotherapy.

### SCLEROSIS OF THE JAWS

Sclerosis of the jaws may be generalized or localized (Table 46.4).

Table 46.4. Lesions causing osteosclerosis

Congenital dysplasias	
osteopetrosis	
pyknodysostosis	
Infective	
chronic sclerosing osteomyelitis	
Garré's osteomyelitis	
condensing osteitis	
reparative osteosclerosis	
Neoplastic	
benign fibrous dysplasia	
ossifying fibroma	
cementoma	
osteoma (e.g., Gardner's syndrome)	
malignant	
osteosarcoma	
sclerosing metastasis	
Diseases of unknown origin	
Paget's disease	
Caffey's disease	
Following radiotherapy treatment	
radio-osteonecrosis	



Fig. 46.12. Eosinophilic granuloma. Multiple lytic lesions are present (arrows). They are well-defined, extend in places to the alveolar margins and resorb the lamina dura.

*Generalized* sclerosis occurs in osteopetrosis and fibrous dysplasia in the young, and in Paget's disease and metastatic disease in the elderly. It may also follow widespread dental sepsis.

*Localized* areas of sclerosis are common and are usually benign.

### Chronic Osteomyelitis

Chronic infection around the apices resulting in bone destruction may become modified in time by a surrounding reactive increase in density. This is described as *condensing osteitis*, and is localized to the periapical region, often in continuity around multiple affected teeth. The change is usually confined to the alveolar region. Bone density may revert to normal if the foci of infection are treated.

Occasionally, the entire mandible is involved in the sclerosing process. The medulla has cortical density and corticomедullary differentiation is lost. The inferior dental canal stands out in sharp relief. Only the condylar and coronoid processes are spared (Fig. 46.13).

*Chronic sclerosing osteomyelitis* results from a balanced reaction between infection and host, and is seen in the body of the bone rather than in the periapical regions. Osteolysis progresses to sclerosis as with chronic infections elsewhere. Sequestra and periostitis occur and lucent areas remain.

*Garré's sclerosing osteomyelitis* is rare and probably results from overgrowth of periosteum and cortex following infection in children and young adults.

*Reparative Osteosclerosis*. In this condition well-defined localized areas of very dense bone blend intimately with normal bone, usually around the apices of teeth and continuous with the underlying lamina dura. Changes often extend to the alveolus. The lesions are usually less than 2 cm in size (Fig. 46.14). The cause of this change is not always clear. It may follow infection, trauma or dental extraction, resulting in a dense socket. This may resemble a retained root. This change may also be seen beneath a bridge due to stress. It is not infective and does not generally resolve. The change is often associated with a vital tooth and should be ignored by the surgeon.

*Hypercementosis* is shown radiologically as an increase in width of the root *within* the periodontal membrane space and lamina dura which are consequently laterally displaced. The excess cementum is shown as a local increase in root density as well as width but maybe less dense than the under-



Fig. 46.13. Condensing osteitis. In this patient, the entire mandible is involved with reactive sclerosis secondary to periodontal disease. The inferior dental canal stands out in relief against the dense bone.

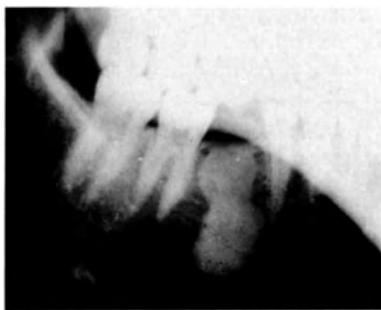


**Fig. 46.14.** Benign osteosclerosis. An area of very dense bone extends to the alveolar margin. There is no surrounding radiolucency.

lying dentine of the root. The change may be secondary to inflammation or is often idiopathic. The teeth are normally vital but may be difficult to extract (Fig. 46.15).

**Cementoma** is another cause of periapical sclerosis but is, in fact, a form of bone dysplasia resembling fibrous dysplasia but limited in extent. The lesions are most commonly situated at and around the mandibular incisors and result from proliferation of fibrous tissue at the apices of usually multiple contiguous teeth. Poorly defined radiolucencies at the apices result in loss of bone and lamina dura. With time, a progressive, rather fluffy ossification of the fibrous tissue occurs centrally (Fig. 46.16) and eventually the areas totally ossify and may vanish. Teeth normally remain vital unless infection supervenes. The lesion can usually thus be ignored.

#### Complex and Compound Odontome

These are two further lesions which are radiologically similar. A dense periapical or alveolar mass is surrounded by a thin zone of lucency contained within a zone of reactive sclerosis.

The *complex odontome* is a totally irregular dense mass containing all the dental elements – enamel, dentine, cementum and fibrous tissue – and is usually found in the young, especially in the molar region. The mass may replace a normal tooth or prevent eruption of an adjacent tooth.

In the *compound odontome*, multiple small denticles aggregated together arise distinct from the adjacent normal dentition. Often up to 50 separate cusps may be present, bound

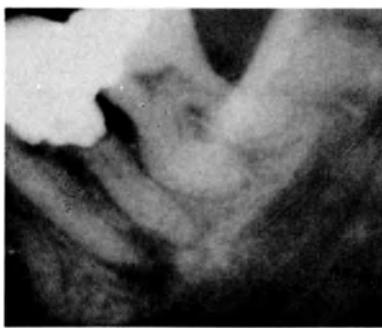


**Fig. 46.15.** Hypercementosis. Affected roots are expanded and displace the surrounding lamina dura. The bone beyond the lamina dura is normal. A granuloma or area of chronic infection is shown at the apex of lower 4.



**Fig. 46.16.** Cementoma, shown as a large well-defined ossifying radiolucency.

together in one dense mass surrounded by a thin lucent zone. The mass prevents eruption of adjacent teeth and usually arises in the canine region. They are thus discovered when a cause of non-eruption is sought (Fig. 46.17).

#### Radionecrosis and Other Radiation Changes

Radiation to bone causes cell death both directly by the radiation and secondarily by vascular occlusion. Such bone is susceptible to infection and trauma (Fig. 46.18). Oral hygiene should therefore be immaculate before therapeutic irradiation. The mandible is the more susceptible as the maxilla has a relatively better blood supply and, statistically, the mandible receives more irradiation. The changes resemble those seen in infections with mixed areas of osteolysis and sclerosis, complicated by superadded infection from which it often cannot be distinguished. Sequestra may be present but periostitis, as always, is not prominent on the mandible.

Radiation given in childhood also affects dental and mandibular growth, both of which are inhibited.

*Mandibular sclerosis* may also be generalized in *osteopetrosis (Albers-Schönberg's disease)*, in which bone expansion may be associated with a 'bone within a bone' appearance, dis-



**Fig. 46.17.** Compound odontome. Multiple small recognizable dental elements prevent the eruption of an underlying tooth.

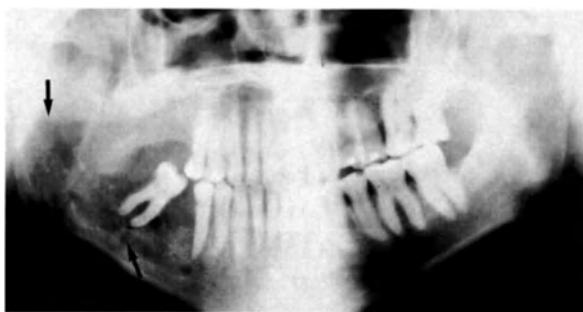


Fig. 46.18. Radionecrosis following irradiation for squamous cell carcinoma. Osteomyelitic resorption of the angle of the mandible is occurring (arrows).

ordered dentition and pathological fractures. The dense bone is very susceptible to periapical and generalized infection. *Pyknodysostosis* is a rare form of sclerosing dysplasia associated with severe dwarfism. The facial skeleton is hypoplastic and the mandibular angle is lost. The skull fontanelles remain open.

### CYSTS OF THE JAWS

Intraosseous cysts can be classified as in Table 46.5. From this table it can be seen that cysts may be:

1. *Fissural*, resulting from the inclusion of epithelial remnants between the fusing processes that go to make up the facial skeleton

Table 46.5. Cysts of the oral tissues (after Lucas)

Non-odontogenic developmental (fissural) cysts
nasopalatine
median palatal
median mandibular
Odontogenic cysts
developmental
primordial
dentigerous
inflammatory
radicular
globulomaxillary
residual
Non-epithelialized bone cysts
solitary bone cyst
aneurysmal bone cyst
Inclusion cysts
salivary (Stafne)



Fig. 46.19. Nasopalatine cyst. This occurs in the midline close to the incisor apices.

2. Similar to cysts arising in any other bone (e.g., aneurysmal or simple bone cysts)
3. Derived from the dental elements, either at the apex or crown of a tooth, or replacing it all together

These lesions have many radiological features in common. They commence as round, well-defined bone defects at characteristic sites. They have a thin outer white line of reactive sclerosis and are surrounded by entirely normal bone. They grow very slowly and radially by cell proliferation and hyperosmolar drawing in of fluid until a dense structure such as another tooth or the cortex is reached. Growth is then modified and the lesions become elliptiform, causing only slight further expansion of bone. These changes can be seen on both panoramic and occlusal radiography. Maxillary cysts can encroach upon the antrum and cause local radio-opacity, resembling polyps, but surrounded by dense cortical bone.

Midline cysts are usually *fissural* and large. The local dentition is normal and, in the mandible, the cysts are situated in part below the inferior dental canal. In the maxilla, a large central cyst is likely to be a *median palatal cyst*, while two smaller cysts on either side of the midline, heart-shaped and medial to the incisors are likely to lie in remnants of the obliterated *nasopalatine ducts*. Midline cysts are well-demonstrated on occlusal views (Fig. 46.19).

*Aneurysmal* and *simple bone cysts* are not related to the teeth, may be beneath the inferior dental canal, but are uncommon and otherwise unremarkable. Some non-dental cysts may have a *traumatic* aetiology (Fig. 46.20A).

**Cysts of dental origin** are those most commonly seen and the most common of these by far is the *apical* or *radicular cyst* (Figs 46.20B, 46.21).

Extension of caries into the pulp canal results in ascending inflammation causing a granuloma to form at the apex of the tooth. Local epithelial cell rests proliferate and invade the granuloma, which then undergoes cystic degeneration. A sterile, epithelial-lined sac at the dental apex remains.

Radiologically, these lesions are very sharply defined and come to lie at the apex of a tooth, which is usually carious. The lesions are often multiple but are rarely more than 1.5 cm in size. They present because of reinfection or fracture. Should the offending tooth be removed and the socket heal over, a *residual cyst* may remain (Fig. 46.22). The *globulomaxillary cyst* is an 'apical' cyst lying between the maxillary canine and lateral incisor, shaped like an inverted pear extending to the alveolar margin and separating the adjacent roots (Fig. 46.4).

The lamina dura is inevitably deficient at the cyst, but commences beyond the cyst margins unless infection supervenes.

### Developmental Odontogenic Cysts

The relatively common *dentigerous* or *follicular* cyst results from cystic degeneration of the enamel organ after the tooth has formed but before it erupts. The follicle expands in size, above its usual 2–3 mm in width, and soon a large cyst, always related to the crown, begins to displace the tooth, preventing its eruption. The cysts may be up to 3–4 cm in

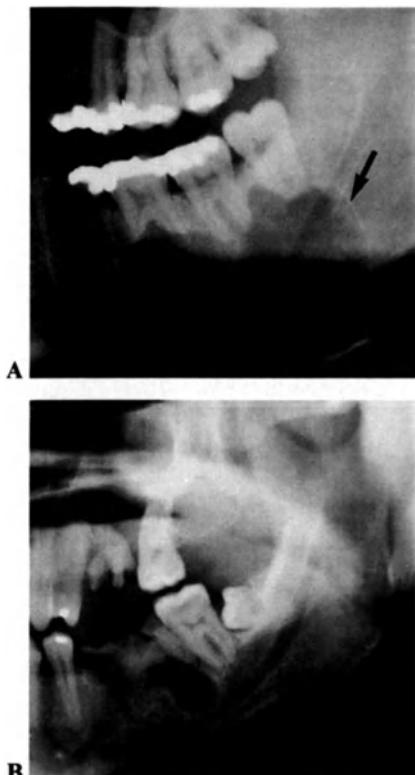


**Fig. 46.20.** A Traumatic hemorrhagic cyst of the mandible. A very large osteolytic lesion is seen, expanding the bone in the axial view (arrow). B Radicular cyst. A well-defined cystic lesion is seen at the apex of the carious left lower 6. The appearances are typical.

size. Canine and wisdom teeth are commonly affected (Fig. 46.23). The cysts are occasionally bilocular.

The primordial or *odontogenic keratocyst* is lined with keratinized epithelium and has a propensity for recurrence. After surgery, therefore, these lesions are followed for up to 20 years. They are the least common and the largest of the cysts of dental origin, caused by cystic degeneration of the enamel organ before the enamel has begun to form, the cyst

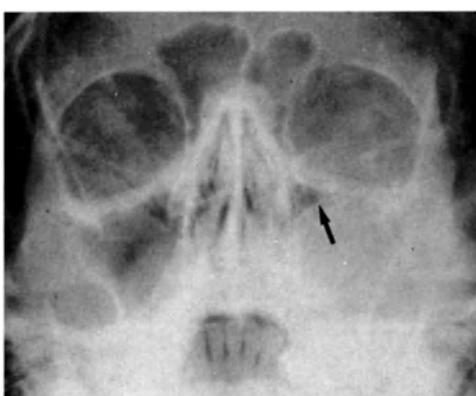


**Fig. 46.21.** Cyst of the antrum. When a radicular cyst arises in relation to a tooth situated beneath the antrum, the cyst displaces the antral floor upwards. A soft tissue mass is seen in the antrum, resembling a polyp from which it is distinguished by a superficial hard thin dense white line of cortical bone (arrow). The cyst is extra-antral.



**Fig. 46.22.** Residual cyst. A cyst of the angle of the mandible is separated from the alveolar margin by a sclerotic zone of reparative new bone.

replacing the tooth. The lesion is often situated at the mandibular angle extending up to the condyle and expanding the ascending ramus. It can incorporate a tooth by virtue of its growth, so simulating a dentigerous cyst, but the true diagnosis can usually be inferred from the large size and the position of lesion (Fig. 46.24).

The *salivary inclusion cyst of Stafne* is an uncommon but characteristic cyst-like lesion situated below the inferior dental canal just anterior to the angle of the mandible. The tissue is derived from the submandibular gland and a communication with it may be demonstrated at sialography (Fig. 46.25).

#### ENDOCRINE DISORDERS

##### Gigantism

Excess of growth hormone before skeletal fusion results in a long, thin skull with a grossly elongated mandible. The dental age is advanced. Teeth show hypercementosis.

##### Acromegaly

After skeletal maturity an excess of growth hormone broadens the face and increases the mandibular size, spreading the teeth. This process is associated with macroglossia. Prognathism is present. The mandibular angle is rounded and low in relation to the cervical spine.



**Fig. 46.23.** Follicular cysts. They lie in relation to the crowns of unerupted wisdom teeth.



**Fig. 46.24.** Odontogenic keratocyst. A large, apparently multilocular cyst occupies much of the mandible, extending up the ascending ramus to the coronoid process. The size alone is indicative of a keratocyst.



**Fig. 46.25.** Inclusion cyst of Stafne. This lesion is situated at the angle of the mandible below the inferior dental canal.

**Cretinism** results in a delay in dental maturity (Fig. 46.26), as does **hypopituitarism**. Conversely **thyrotoxicosis** accelerates maturity.

In **hyperparathyroidism**, the cortical lamina dura is resorbed and brown tumors are present (Fig. 46.27). In **hypoparathyroidism**, the crowns of the teeth are irregular,



**Fig. 46.26.** Cretinism. There is delay in the dental age in this 17-year-old patient.

the **lamina dura** is thickened and the roots are hypoplastic. Monilia is often present.

**Cushing's syndrome** results in loss of the **lamina dura**.

## TUMORS

**Benign tumors** arising from any of the elements of bone may occur in the jaw, but are rare.

**Osteomas** may be solitary, or multiple in **Gardner's syndrome** (associated with polyposis coli) (Fig. 46.28). Large osseous excrescences deform the face. Radiologically, medullary sclerosis is also present.

**Giant-cell tumors** or **osteoclastomas** may present in patients with hyperparathyroidism associated with loss of the lamina dura (Fig. 46.27). True giant-cell tumors, such as occur around the knee, are uncommon in the mandible but can occur in the 20–40 age group. The **giant-cell granuloma** occurs in a younger age group, mainly in females. The appearance is of a well-defined unilocular lucency. The distinction between it and the true giant-cell tumor is mainly histological. The lesion is entirely benign.

**Fibrous lesions** are relatively common in the jaws.

**Fibrous Dysplasia.** This exists in non-hereditary monostotic or polyostotic forms and in an inherited form



**Fig. 46.27.** Hyperparathyroidism. This condition is associated classically with loss of the lamina dura and osteoclastomas of the jaw.



**Fig. 46.28.** Gardner's syndrome. Multiple osteomas are shown on the mandible and maxilla and within the antra. There is also osteosclerosis of the mandible, with dense areas of bone lying within the medulla.



**Fig. 46.29.** Fibrous dysplasia. The left maxillary antrum is expanded and its cavity obliterated by dense new bone. Abnormal texture is also shown in the left frontal bone and around the left orbit. Sclerosis and expansion are typical of maxillary lesions in this disease. Tomography of the left antrum in fibrous dysplasia shows sclerosis and expansion.



**Fig. 46.30.** Fibrous dysplasia. More generalized involvement of the mandible and the maxilla with expansion and sclerosis. The right side of the mandible is not affected.



**Fig. 46.31.** Cherubism. Widespread expansion of maxilla and mandible. Bone is replaced by a multilocular cystic form of fibrous dysplasia localised to the jaws.

**Fig. 46.32.** Ossifying fibroma. Another form of a localized fibrous tumor in which dense abnormally calcified bone is surrounded by a zone of radiolucency, similar to the previously shown cementoma.

localized to the jaws – *cherubism*. The major clinical features of fibrous dysplasia are bone enlargement and deformity and these are the major radiological features. Expansion of the maxilla is associated with obliteration of facial sinuses, especially the maxillary, and encroachment upon the orbit (Fig. 46.29). The dental arch is displaced. The monostotic form may affect one antrum or part of the mandible. Polyostotic disease may affect both antra and the mandible as well as other parts of the skeleton (Fig. 46.30). Distribution may be assessed by radioisotope bone scans.

The fibrous tissue lesion results in bone which may be lucent, ‘ground glass’ or sclerotic in density, or a mixture of all three, depending on the degree of abnormal ossification present in the fibrous lesions. The lucent areas may be truly fibrous or cystic in nature. Facial sclerosis and expansion is very typical.

*Cherubism* is localized to the face, presents in children and affects the maxilla and mandible diffusely. Expansion is associated with a grossly cystic pattern in the jaws (Fig. 46.31). Teeth either fail to arise or erupt abnormally. The change is said to involute with growth. Fibrosarcomatous degeneration occurs rarely in fibrous dysplasia.

**Ossifying fibroma** resembles fibrous dysplasia clinically presenting in children, with a localized painless swelling of the jaw. Radiologically, the lesions tend to resemble the focal lesion of fibrous dysplasia seen in the femoral neck, that is, a localized well circumscribed lesion with a sclerotic rim and an ossifying central matrix (Fig. 46.32). Fibrous dysplasia is generally not circumscribed in the jaws.

The *cementoma* (noted above) is another fibro-osseous dysplasia of the jaws.

**Cartilage** tumors are unusual in the jaws, though they have been described in the maxillary alveolar region. There is some doubt as to whether cartilaginous tumors can occur in bones arising in membrane and it may be that these lesions arise from ‘rests’ or by migration of cartilage from the nasal septum.

#### Malignant Lesions

Most oral malignant tumors are **squamous cell carcinomas**; these make up around 5% of all malignant lesions in the Western world, but they are more common in Asia (up to 50% of cancers). They occur in patients with poor oral hygiene, in tobacco and alcohol abusers and in betel nut chewers in India. Lesions are adherent to the underlying





**Fig. 46.33.** Squamous cell carcinoma. In this untreated patient invasion of the mandible has occurred, resulting in quite marked destruction with expansion of the underlying bone.

bone which is not, however, inevitably invaded. When it is a diffuse permeative destruction lesion is seen on radiography (Fig. 46.33).

**Metastases** occur more commonly in the mandible than in the maxilla, and in the expected age group (45+). Involvement of the inferior dental nerve causes paresthesia. Pathological fractures may occur or teeth may be exfoliated and malignant debris discharged from the socket. Lesions may be shown coincidentally at skeletal scintigraphy. Primary lesions in breast, lung and kidney metastasize most frequently to the jaws, but as the marrow is relatively sparse in the mandible, metastases are not particularly common (Fig. 46.34).

**Myeloma** is much more commonly seen in the jaws. Some 30% of patients with myeloma are said to be affected; this however is not as frequent as is skull involvement in myelomatosis (50%). Lesions may be characteristically 'raindrop' or larger and are often well defined. Myeloma is usually not demonstrated on scintigraphy by an increase in uptake, but may present as a defect on the scan.

**Osteosarcoma** and **Ewing's tumor** are both rare in the jaws but are similar in appearance to those seen elsewhere. Soft tissue masses are associated with bone destruction, periostitis and new bone formation in osteosarcoma (Fig. 46.35).

Ewing's tumor occurs at the same age in the jaw as elsewhere, but osteogenic sarcoma has a later peak in the jaw

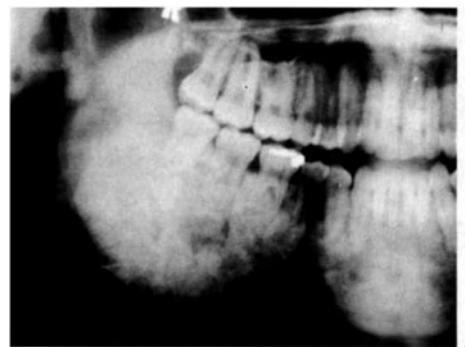


**Fig. 46.35A, B.** Osteogenic sarcoma. A In this 30-year-old male, the right hemimandible is the site of an aggressive expansile bone-forming tumor. B CT scan of the same lesion. Following radiotherapy the patient remains alive and well ten years later.

(30–40 years). Prognosis is often better than lesions elsewhere.

**Burkitt's lymphoma** occurs throughout the world, but in central Africa it accounts for up to 50% of all children's malignancies. Lesions are multifocal but the jaws are greatly expanded by destructive lesions associated with large soft tissue masses and new bone formation (Fig. 46.36).

**Ameloblastoma** is another lesion which is much more common in Africa. There it accounts for 0.3 per cent of all tumors and occurs in younger patients and in a more aggressive form involving the midline of the jaws. In Europe, a more lateral location of lesions is the more common. The tumor arises more frequently in the mandible.

Occasionally the tumor is unilocular, at the alveolar margin, vaguely resembling an apical cyst, but most commonly a characteristic 'soap bubble' multilocular tumor is seen, with small satellite lesions (Fig. 46.37). As in fibrous dysplasia, some of the lytic lesions are cystic and some cellular. This tumor is one of the few that destroys adjacent dental roots. Occlusal views show bone expansion and cortical thinning as well as the septate nature of the lesion. Occasionally they can be seen to arise in dentigerous cysts. Treatment involves complete excision, since curettage may cause the tumor to metastasize to the lungs by aspiration. Follow-up is essential.



**Fig. 46.34.** Metastatic disease from carcinoma of the breast. Widespread permeation and destruction of the body and ascending ramus of the mandible are shown.

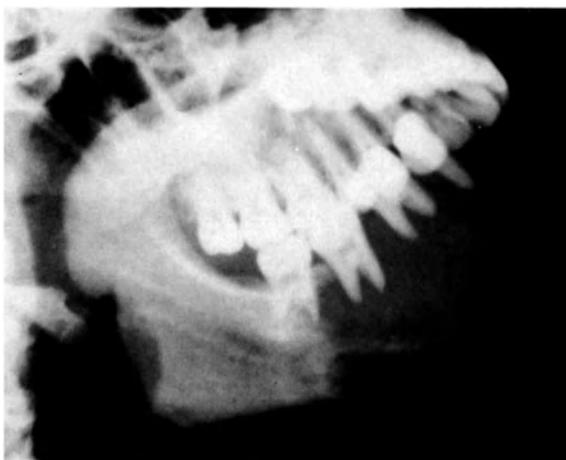


**Fig. 46.36.** Burkitt's lymphoma. A large expansile lytic destructive lesion is shown involving much of the mandible.

#### MISCELLANEOUS LESIONS

**Paget's Disease (*Osteitis deformans*).** This is characterized by bone expansion and alteration of texture. The lesions are initially lucent, as in osteoporosis circumscripta, but the more advanced lesions become first patchily, then totally, sclerotic. The disease is common in the skull vault but is relatively rare in the maxilla or mandible. Its distribution may be monostotic or polyostotic and may be assessed by skeletal scintigraphy. Unlike fibrous dysplasia, Paget's disease is a disease of the elderly and thus often affects edentulous patients. Examination of other bone lesions is always helpful in coming to a diagnosis. In Paget's disease, the mandible is enlarged and either totally or patchily sclerotic.

**Thalassemia.** Marrow hypertrophy causes expansion of the mandible with cortical thinning and trabecular loss. The maxillary marrow expands to occupy the paranasal air sinuses, with the exception of the ethmoids, which remain aerated (Fig. 18.13, p. 341).



**Fig. 46.37.** Ameloblastoma. A characteristic soap-bubble or honeycomb appearance is shown. Multiple satellite lesions are present at the periphery of the lesion.



**Fig. 46.38.** Osteoarthritis. A large osteophyte is shown on the eroded and sclerotic condyle, demonstrated by hypocycloidal tomography.

#### THE TEMPOROMANDIBULAR JOINTS

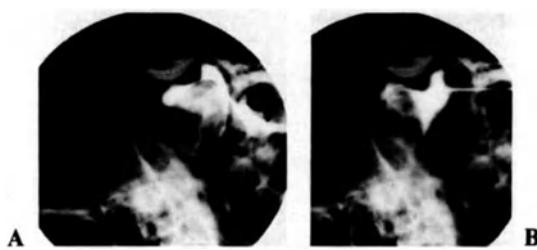
The obliquely directed and olive-shaped condylar head sits upon the mandibular neck and articulates in a synovial-lined joint with the reciprocally shaped condylar fossa and the anterior articular eminence of the temporal bone. The joint is divided into two by an intra-articular meniscus attached anteriorly and divided into two parts posteriorly at a bilaminar zone for superior and inferior attachments to the skull and condylar neck. The lax attachment of the meniscus permits both it and the condyle to move during articulation. The condyle sits symmetrically within the fossa at rest and moves forwards within the lax synovium-lined capsule to lie at the apex of the articular eminence when the mouth is opened. Excess forward movement is as abnormal as restricted movement. Radiological orientation of the joint on transcervical views and arthrography is facilitated if it is noted that the temporomandibular joint lies anterior to the external auditory meatus.

**Osteoarthritis** is characterized by preserved bone density, joint space narrowing and osteophytosis, often associated with partial loss of the articular mass of the head. Joint narrowing often involves meniscal loss or perforation (Fig. 46.38).

**Seronegative and Seropositive Arthritides.** At least 30%–40% of patients with chronic rheumatoid arthritis complain of temporomandibular joint pain and may have the joint changes of osteoporosis, joint narrowing and erosion (Fig. 46.39). Similar changes occur in the seronegative arthritides.



**Fig. 46.39.** Rheumatoid arthritis. Large erosions are shown on the condylar head.



◀ Fig. 46.40. Injection of the inferior compartment of the temporomandibular joint shows a soft tissue mass related to the undersurface of the meniscus (arrow). Passage of the head over this mass results in an audible 'clunk'.

*Tumors of synovium*, including pigmented villonodular synovitis and synovioma, can destroy both articular surfaces.

*Hyperparathyroidism* causes changes at the condyle similar to those seen in the phalanges, with osteoporosis, cortical resorption and marginal erosions.

**Temporomandibular Joint Dysfunction Syndrome.** Young patients, often female, present with a syndrome-complex of joint pain, restricted opening, clicking, crepitus or locking in the open-mouth position. Response to antidepressants may be dramatic, but often meniscal derangement needs to be confirmed by arthrotomography and magnetic resonance imaging. The meniscus usually becomes bunched anteriorly, resulting in a physical obstruction to condylar movement, and may be stretched or perforated posteriorly. Surgical intervention may then be needed (Fig. 46.40).

Abnormal condylar morphology may also be present in the mucopolysaccharidoses. Irregular, hypoplastic condyles are inevitably present in MPS I–H and MPS IV, the most common types.

#### MANDIBULAR TRAUMA

The mandible is a semicircle but, by virtue of its attachments to the skull base, functions as a ring and usually fractures in two places (Fig. 46.41).

A fracture on one side of the mandible, at the site of direct trauma, is often associated with a fracture of the opposite side (Fig. 46.42), in the region of the neck of the condyle (Fig. 46.43). Similarly, a blow to the chin causing a fracture at the symphysis mentis may be associated with bilateral condylar neck (guardsman's) fractures.

*Condylar fractures* may be intra- or extracapsular. The condyle is usually pulled medially by the lateral pterygoid and dislocates internally. This change is best assessed on postero-anterior or Towne's views. Fractures of the ascending ramus and body are adequately shown on panoramic views. Views of the ascending ramus at right-angles are obtained on postero-anterior radiographs. As the radiograph beam does not usually pass directly through a mandibular fracture but is obliquely incident, each fracture is often demonstrated anteriorly and posteriorly at both the lingual and buccal cortices. Displacement is usually minimal and periostitis is not marked during healing, especially after wiring. Isolated fractures of the coronoid process are of no significance. Fractures involving the body are often compound and may involve the inferior dental nerve and the teeth, as may isolated fractures of the alveolus.

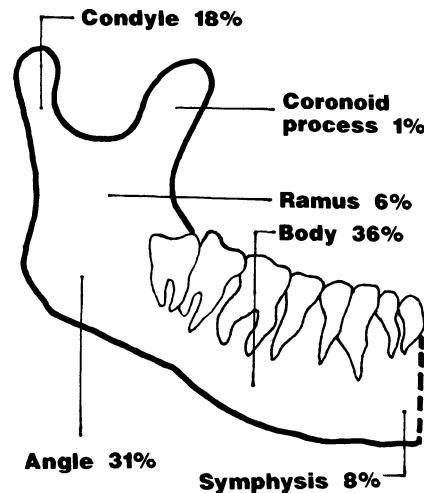


Fig. 46.41. Sites of mandibular fracture.



Fig. 46.42. Mandibular fractures. These are seen on both sides of the midline (arrows). That through the angle of the mandible has fractured the root of the left lower 8. The fracture on the opposing side of the mandible is seen to have caused loosening of the right lower 2. The fracture line is seen on both ingual and buccal sides of the mandibular cortex because of the obliquity of the panoramic beam. The sharper edge is that nearer the film.



Fig. 46.43. A lateral oblique view of the jaws demonstrates a fracture of the condylar neck (arrow). Note also the long styloid process in this patient.

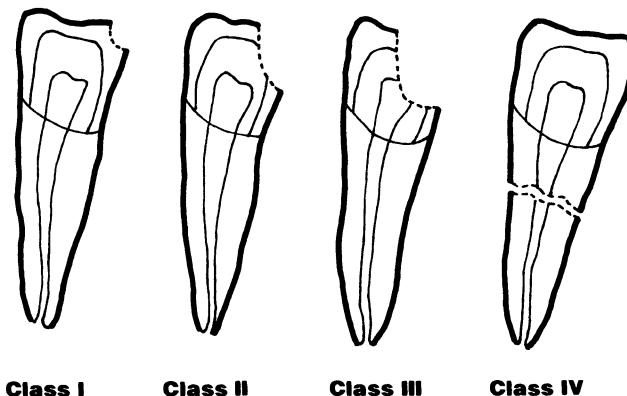


Fig. 46.44. Classification of dental fractures.



Fig. 46.45. Dental fractures involving pulp canal.



Fig. 46.46. Alveolar fractures associated with dental loosening, as shown by widening of the periodontal membrane space.



Fig. 46.47. Oro-antral fistula. The left maxillary antrum was opaque. The film shows the defect of the socket in continuity with the antrum.

### DENTAL TRAUMA

Damage to a tooth may have no visible radiographic effect but the blood supply to the pulp may still be disrupted. Pulp necrosis may lead to apical infection and granuloma formation or the canal may be slowly obliterated by the laying down of reparative secondary dentine. Pulpless teeth do not seem to develop apical abscesses but are not vital and rapidly become discolored.

Injuries to the teeth have been classified (Fig. 46.44). Dental fractures occur most commonly in children around ten years of age and the maxillary incisors are most often involved. Of great importance is the assessment of dental loosening and involvement of the pulp canal (Fig. 46.45).

Intraoral views are the most useful as detail is optimal. The alveolar margin at the neck of a tooth should not be mistaken for a fracture line. A tooth is not always fractured in isolation and evidence of trauma to adjacent teeth or the alveolar bone should be sought (Fig. 46.46). Root resorption

may follow fracture of a tooth.

Removal of a tooth intimately related to the maxillary antrum may result in a fracture of the antral floor, giving an *oro-antral fistula* (Fig. 46.47), or part of the root may be displaced up into the antrum. This acts as a nidus for calculus deposition, resulting in an *antrolith*.

### REFERENCES AND SUGGESTIONS FOR FURTHER READING

- Goaz PW, White SC (1987) Oral Radiology. Principles and Interpretation. CV Mosby, St Louis
- McIvor J (1986) Dental and Maxillofacial Radiology. Churchill Livingstone, Edinburgh
- Manson-Hing LR (1980) Panoramic Dental Radiography. CC Thomas, Springfield, Ill
- Mason RA (1988) A Guide to Dental Radiography. Wright, London
- Smith NJD (1980) Dental Radiography. Blackwell, Oxford
- Stafne EC (1985) Stafne's Radiographic Diagnosis, 5th edn. WB Saunders, Philadelphia

## CHAPTER 47

# THE PARANASAL SINUSES

S.I. Schabel

---

While the gas-filled cavities of the face, the paranasal sinuses, are one of the most complex bony areas of the body, their exact function remains unknown. Many pathologic conditions affect the sinuses and imaging is central to their diagnosis. *Plain radiographs* (Caldwell, Waters, lateral and submentovertex projections performed with a horizontal beam when possible) have been the primary imaging modality. Even today plain films remain the major screening examination and are often the only test needed in cases of uncomplicated infection, allergy and minor trauma.

Because of the complexity of the bony structures of the paranasal sinuses, *tomography* (plain, pluridirectional, CT and MRI) is also very useful. Unfortunately, all tomographic techniques have resolution limited to the plane of the slice so that multiple tomographic projections are often necessary. CT and MRI are both excellent imagers of soft tissue, but because of its superior resolution in bone, thin section (5 mm or less) CT has become the imaging technique of choice in the sinuses. Complicated infection, trauma, tumors and preoperative patients are all best evaluated by CT. Three dimensional computed tomography while in its infancy and still somewhat limited in resolution, offers great potential for imaging of the paranasal sinuses in the future.

All of the paranasal sinuses undergo major growth in childhood. The *ethmoid* cells, paired on either side of the nasal cavity, usually ten in number are the first to develop and are present in young children. The *maxillary* sinuses, the largest in adults have usually begun to aerate by three and are well formed by ten years of age. The *frontal* sinuses are an outgrowth of the anterior ethmoid cells and are usually well formed by eight. Like most anatomic structures there is much symmetry in the paranasal sinuses though minor variations are common, particularly in the size, shape and number of the frontal cells.

*Hypoplasia* of the maxillary sinuses, the most commonly affected by pathologic conditions, is fortunately rare. The affected sinus is usually thick-walled, and the nasal septum

and orbital floor bow toward the hypoplastic sinus. The turbinates are enlarged.

The bony walls of the paranasal sinuses are separated from the lumen by a thin layer of mucosa usually less than 3 mm thick. While a tiny amount of fluid is always present it is not detectable by standard images. The mucosa is very responsive and is usually the first detectable abnormality when the sinus is affected by toxins, allergens or infection. There is swelling, increased mucus production and often a focal mucosal thickening.

## INFECTION AND ALLERGY

**Sinusitis** is the commonest sinus pathology, but separation of *infectious* and *allergic* etiologies is often difficult both clinically and radiographically. Unfortunately, there is overlap in the imaging findings (Table 47.1) and the two conditions frequently coexist. Unilateral sinus disease, particularly with an air-fluid level is most often infectious (Fig. 47.1) whereas medial wall maxillary sinus disease and undulating mucosal thickening particularly when affecting both maxillary sinuses is usually allergic in nature. The turbinates are often markedly swollen in allergic sinusitis and the radiographic findings may change rapidly. Pansinusitis even when infectious usually has an allergic background (Fig. 47.2).

Table 47.1. Mucosal changes in sinusitis

Infectious	Allergic
Often unilateral	Diffuse
Asymmetric	Symmetric
Whole sinus affected	Medial wall maxillary sinuses
Straight mucosa	Undulating mucosa
Air-fluid level common	Air-fluid level uncommon
Normal turbinates	Turbinates swollen
Polyps common	changing pattern



**Fig. 47.1.** Waters view of face demonstrates an air-fluid level (arrow) in the left maxillary sinus and smooth mucosal thickening of the entire sinus typical of acute sinus infection. The nasal cavity and right maxillary sinus are normal.

The commonest bacterial pathogens in sinusitis are *Strep. pneumoniae*, *H. influenzae*, *Staph. aureus* and  $\beta$ -hemolytic streptococci. Anaerobic infections may occur in chronic sinusitis. Of all sinus infections, 10% are due to spread from adjacent dental disease. Suggestion of a causative agent of infectious sinusitis is usually not possible with radiographic findings alone. *Viral sinusitis* can produce radiographic changes identical to bacterial disease, even with an air-fluid level, but when radiographic findings of sinusitis are present

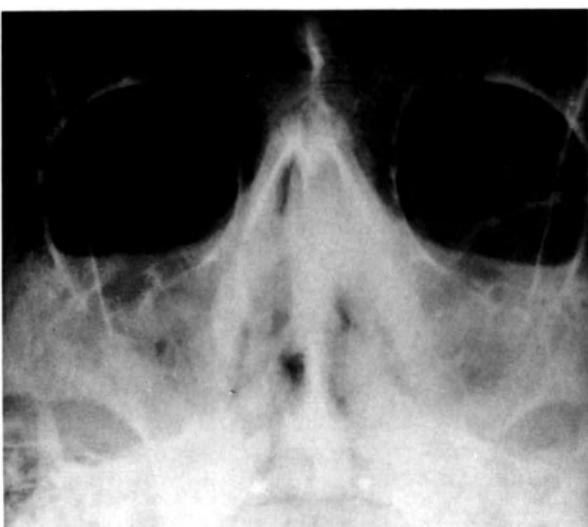


**Fig. 47.2.** Waters view of the face demonstrates typical findings of allergic sinusitis. There is symmetrical involvement of both maxillary and ethmoid sinuses with almost complete opacification of the air spaces. The nasal cavity is filled with polypoid soft tissue density. No air-fluid level is present.

in a patient with viral illness, a mixed infection, bacterial and viral is usually present.

**Fungal sinusitis** usually with *aspergillosis* or *mucormycosis* is a disease of debilitated or diabetic patients. Radiographically the changes are of marked mucosal thickening, bony sclerosis and focal bony destruction usually of an ethmoid or maxillary sinus. The organisms when invasive have a tendency to spread along vascular channels and CNS complications are common.

Complications of sinusitis are infrequent. If the infection spreads through the mucosa *bony infection* can occur. The earliest radiographic change is the disappearance of the sharp sinus cortical bone, the mucoperosteal line, followed by frank destruction of bone. *Orbital cellulitis* may develop, particularly in young children following ethmoid sinusitis. A more dangerous complication of sinusitis is infection of the *central nervous system* with subdural empyema (Fig. 47.3A, B), meningitis, brain abscess and cavernous sinus thrombosis. Since their walls are thin, these complications usually occur secondary to acute infections of the frontal and less often of the sphenoid sinuses either through direct or perineural spread, septic thrombophlebitis or sepsis. Since its ostium is naturally dependent, the presence of an air-fluid level in the frontal sinus indicates obstruction and in the presence of signs of infection should prompt urgent treatment.

*Recurrent or chronic bacterial sinusitis* may lead to bony changes. The walls of the sinuses, particularly the maxillary antra, may thicken and increase in density and the entire lumen may become obliterated by new bone.

**Mucocele.** When a sinus route of drainage becomes obstructed, either from a scar, from trauma, surgery or infection, or from a polyp or other tumor, its mucosal cells continue to secrete fluid and eventually the sinus will fill completely producing a mucocele. The sinus will increase in density and eventually it will begin to expand in size, first by bowing and thinning its internal septation and then its outer margin. Adjacent structures, the orbit and nasal cavity are displaced and eroded. Rarely the edges of a mucocele may calcify. Mucoceles are rare in children and when seen in patients under age 10 years should suggest *cystic fibrosis*. Since its drainage route is the longest, the frontal sinus is the most often affected by mucocele, followed by the ethmoids usually in the anterior cells, sphenoid and maxillary sinuses.

Frontal and sphenoid sinus mucoceles may expand into the subarachnoid space causing cerebral spinal fluid leaks and meningitis and those of the maxillary sinus may cause loosening of the teeth. CT is the imaging technique of choice to evaluate mucocele allowing evaluation of the extent and affect on adjacent structures and planning of surgical drainage. Intravenous contrast material does not cause significant enhancement of a mucocele, but when infected, a *pyocele* often shows edge enhancement.

**Polyps.** As a sequela of chronic inflammation, infection or allergy, polyps often develop in the sinuses or nose. The radiographic appearance is similar regardless of the cause. *Secretory polyps* (retention cysts) are local mucoceles due to obstruction of the ducts of a single mucous gland and typically produce smooth mucosal masses in the floor and lateral

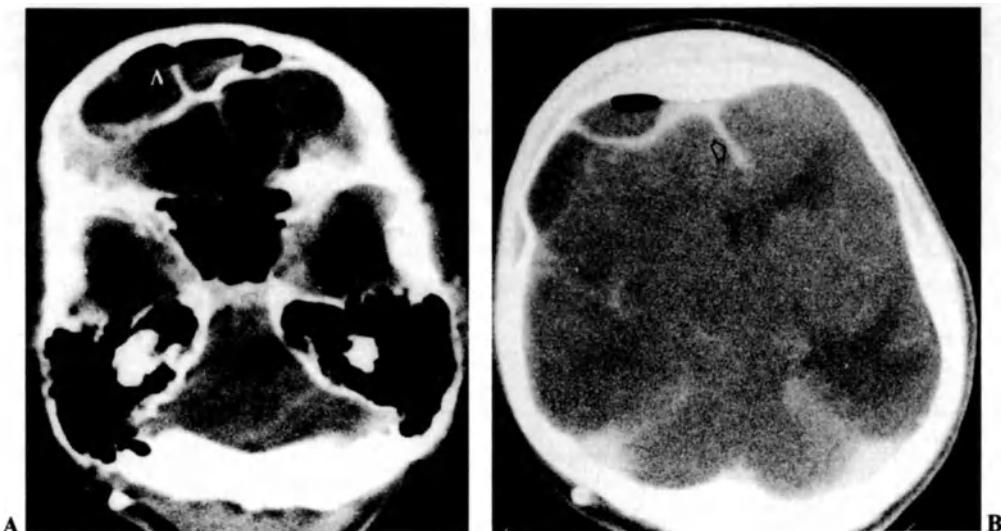


**Fig. 47.3.** A Enhanced axial CT scan through the frontal sinus reveals a long air fluid level in the sinus (arrow). B A slice 3 cm higher reveals another air-fluid level in the subdural space with an enhancing rim due to the subdural empyema. Note mass effect with falx displaced toward the left (arrow).

walls of the maxillary sinuses. They are very commonly seen in asymptomatic patients and are present in 13% of autopsies. *Non-secretory polyps*, usually due to allergy or inflammatory disease, are a collection of fluid in the submucosal space. They are also most commonly seen in the maxillary antrum inferiorly. *Hyperplastic mucosal polyps* can occur in any sinus usually in the maxillary (Fig. 47.4) and ethmoid cells. They often extend into the nasal cavity and may be massive and erode the orbits. A special type of hyperplastic polyp, the *antrochoanal polyp*, arises in the maxillary sinus and grows through its ostium into the nose and then into the nasopharynx. The polyp usually produces ipsilateral

maxillary sinus opacity secondary to obstruction and one third of patients have bilateral maxillary sinus opacity.

**Granulomatous diseases** may affect the sinuses. *Sarcoidosis* affects the respiratory mucosa at all levels. Nodular mucosa particularly in the nasal passages, polypoid masses and cloudiness of the sinuses are frequently seen in patients with sarcoidosis. *Wegener's granulomatosis*, a necrotizing granulomatous vasculitis, typically affects the sinuses. The maxillary antra and ethmoid cells become opaque. There is often sclerosis of the sinus walls, nasal septum perforation, necrosis of turbinates and polypoid masses. Bony necrosis and destruction is unusual. *Lethal midline granuloma* (malignant granuloma) is a progressive destructive ulceration of the nose, sinuses, and occasionally pharynx, localized to the midline. This leads to mutilating midline facial destruction.

#### NEOPLASMS

True neoplasms of the sinuses are rare compared with sinus infection. Masses which expand the sinuses with smooth walls can generally be assumed to be benign, such as mucocele or benign tumors. Malignant tumors usually erode the sinus wall rather than expand it. The commonest benign tumor of the sinuses is the *osteoma*. These typically present as well defined ossified density masses occasionally with a central lucency (Fig. 47.5). They range in size from a few millimeters to several centimeters and grow slowly with time. Osteomas occur most commonly in the frontal sinuses and are usually asymptomatic until they obstruct the outflow of the sinus. They are often multiple in patients with *Gardner's syndrome*.

Another common benign tumor of the sinuses is the *inverting papilloma*. This tumor has benign clusters of squamous mucosa but it frequently recurs locally when inadequately resected and may progress to frank squamous cell carcinoma. Its radiographic appearance is identical to other



**Fig. 47.4.** Polyp of maxillary sinus on left is easily seen on this Waters view as a smooth sessile mass in the inferior recess of the sinus.



**Fig. 47.5.** This AP tomogram demonstrates typical findings in this case of a right maxillary sinus osteoma. The tumor arises from the lateral wall of the sinus and bows the medial wall into the nasal cavity. Note the slightly lucent center.

benign polyps producing opacity of the affected nasal cavity. Sinus opacification often occurs due to obstruction. There is frequently expansion of the affected space often with adjacent bony sclerosis.

Another benign sinus tumor is the *angiomatous polyp*, usually seen in young men. They usually occur near the maxillary ostium and present with epistaxis. *Cysts of dental origin* may extend into the maxillary sinus and mimic mucosal tumors. Occasionally, a bony margin will be seen around the tumor correctly indicating its site of origin (Fig. 47.6).

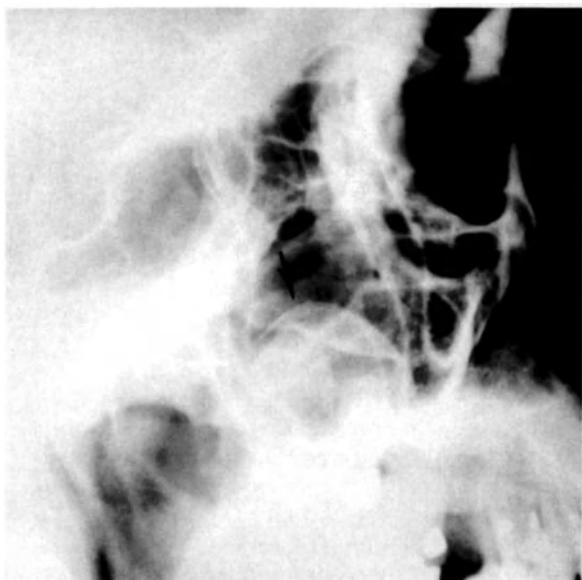
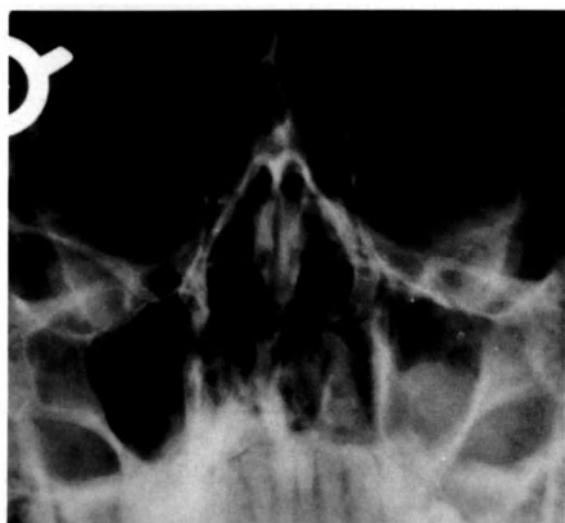
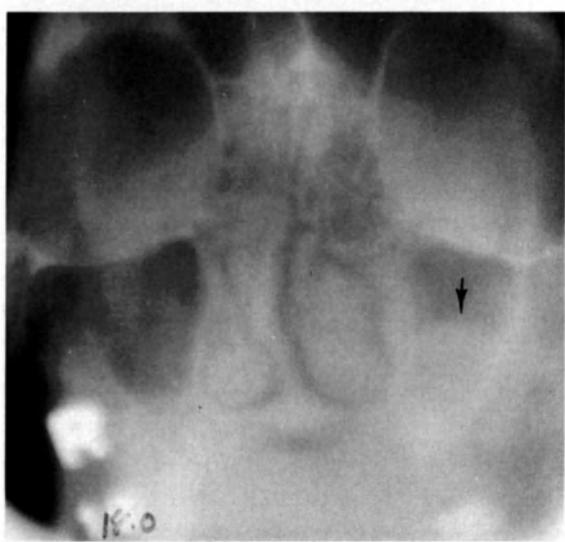


**Fig. 47.6.** Lateral view of the sinuses reveals a soft tissue mass in the inferior aspect of the maxillary sinus posteriorly. The thin bony rim (arrow) indicates the bony site of origin of this dentigerous cyst of the maxilla.



A



B

**Fig. 47.7.A** Waters view reveals a smooth soft tissue mass in the inferior aspect of the left maxillary sinus. **B** AP tomogram shows the mass (arrow) and demonstrates no evidence of bone destruction. Because of symptoms of chronic dull pain a biopsy was performed and revealed an adenocarcinoma.

**Malignant tumors** of the sinuses are uncommon. The vast majority occur from the maxillary or ethmoid sinuses with tumors of sphenoid and frontal sinuses being very unusual. Most patients with malignant sinus tumors present with symptoms which mimic infectious disease and the radiographs are often non-specific early in their course (Fig. 47.7A, B). Chronic unilateral sinus disease which is unexplained particularly with a history of local dull pain, unilateral nasal obstruction or epistaxis should raise the suspicion of neoplasm. Unfortunately, most tumors when diagnosed are not confined to a single sinus and have often broken through into the adjacent soft tissues.

**Squamous cell carcinomas** are the most frequent, comprising three fourths of malignant sinus tumors. **Adenocarcinomas** are the second most frequent and over a third have metastatic deposits in lymph nodes at the time of diagnosis.

*Radiographically* the tumors generally show the same findings with a bony erosion most often of the medial wall of the maxillary sinus and sinus opacification.

*Computed tomography* is the major diagnostic tool for evaluation of malignant sinus tumors. It elegantly demonstrates bony erosions and the extent of tumor into the adjacent soft tissue planes allowing accurate staging for planning of surgery and/or radiation therapy (Fig. 47.8). Lymph node metastases when present are often detectable. Occasionally very vascular tumors will demonstrate enhancement following intravenous contrast injection.

Metastatic deposits to the sinuses are infrequent and most often occur from primary tumors of kidney, testis, breast, and lung.

*Hematopoietic tumors* are uncommon. Of the various cell types the most frequently seen is plasma cell tumor, a solitary, extramedullary **plasmacytoma**. This lesion usually presents as a single mucosal mass in the maxillary sinus, or nasal cavity. Most will develop dissemination into multiple myeloma if the primary tumor is inadequately treated. Nueral cells from the ophthalmic tract may serve as a site for malignant **esthesioneuroblastoma** in the anterior and middle ethmoid cells. While relatively indolent, 20% develop widespread metastases.

## TRAUMA

In our modern society trauma to the facial bones and sinuses is becoming more frequent. Because of its ability to demonstrate thin bony structures and to assess injury to soft tissues of the face, orbit, and brain, thin section *computed tomography* is the mainstay of diagnoses, particularly in complex facial fractures. Its only major limitation is the difficulty in imaging in the plane of the slice often requiring multiple planes of view. *Plain radiographs* are often performed in patients with trauma as initial screening tests and to localize sites needing further imaging. Many fractures will be demonstrated on plain film, and particularly with local injuries such as nasal fractures, isolated fractures of the zygoma, etc., plain radiographs are often all that is required. Soft tissue swelling, opacification of sinuses and gas in soft tissues, subarachnoid space, and orbits may all be demonstrated on plain films.

The commonest fracture type accounting for almost half of all facial injuries is the *tripod* or *trimaleolar* fracture. This fracture usually occurs due to a direct blow on the cheek with resulting separation of the lateral wall and floor of the orbit from the rest of the face (Fig. 47.9). The frontal zygomatic suture, zygomatic arch, and lateral and superior maxillary sinus walls are fractured. The infraorbital nerve is often injured producing facial numbness. The fracture fragments may be displaced inferiorly and posteriorly interfering with the coronoid process of the mandible and limiting opening of the mouth.

Another common type of local facial injury, the *blow-out* fracture, results from a direct blow to the eye. Since the globe itself is quite strong, the orbital contents transmit the force to the walls of the bony orbit. Fractures often occur in the orbital floor or medial ethmoid wall or both and occasionally to the orbital roof. Very few complications arise from isolated



Fig. 47.8. Direct coronal CT slice through the mid face demonstrates the extent of the squamous cell carcinoma arising in the right maxillary sinus. The tumor has extended into the right nasal cavity destroying the medial wall of the sinus and the right ethmoid cells. It has also grown through the orbital floor and is invading the inferior extraocular muscles. The floor of the frontal fossa is destroyed on the right (arrow).

medial wall fractures and the radiographic search is usually directed at inferior orbital fractures. Of blow-out fractures 97% are visible on *plain films* seen as a fracture of the orbital floor, an opaque sinus or air-fluid level, herniated contents at the orbital floor and gas in the orbit. *CT* is the ideal diagnostic tool for evaluation of blow-out fractures as it allows

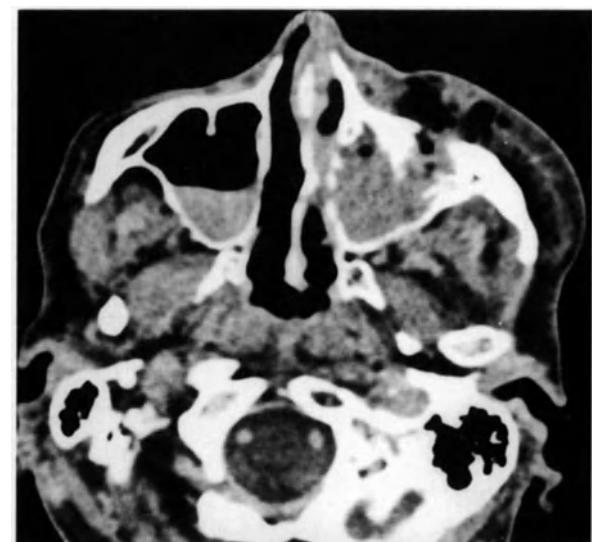


Fig. 47.9. Axial CT slice through the mid face reveals findings of a tripod fracture with almost complete opacification of the left maxillary sinus, soft tissue swelling and subcutaneous emphysema. Fractures through the orbital rim and floor and lateral wall of the maxillary sinus are visible. A zygomatic arch fracture was visible on a cut 1 cm lower. No bony fracture to explain the air-fluid level in the right maxillary sinus was detected.

determination of the fracture site, and the nature of any herniated material, whether fat or extraocular muscles. Almost two thirds of patients with blow-out fractures also suffer an injury to the eye and CT offers the added benefit of imaging of the globe itself. Occasionally, an isolated fracture of the floor of the orbit will produce a *hematoma* which displaces the mucosa of the maxillary sinus inferiorly mimicking a blow-out fracture when none is present. In such cases CT allows the correct diagnosis to be made.

Other isolated fractures can occur in the sinuses. *Frontal bone injuries* are uncommon and when they involve only the anterior cortex of the frontal sinus generally have few complications. If the posterior wall of the sinus has been fractured, the risk of cerebral spinal fluid leak and meningitis is significant. CT again offers the ideal diagnostic tool of evaluation.

Similarly, fractures of the *skull base* often affect the sphenoid sinus. When a gas fluid level is present in the sphenoid sinus after trauma, a basal skull fracture should be suspected.

The most complex facial injuries are the *mid-face fractures*. In many high-speed facial injuries the fractures are difficult to classify and have been termed 'total craniofacial smash'. Recognizable patterns of facial injury have been described

as falling into three major categories: LeFort one, two, and three fractures, grouped by the plane of the fracture (see Fig. 15.17, p. 279).

The *LeFort one* fracture is through the inferior aspect of the maxilla separating the teeth and hard palate from the remainder of the face. The *LeFort two* or paramital fracture separates the nose maxilla, and hard palate from the orbital floor's zygoma and skull. The *LeFort three* has fracture planes extending from the base of the nose posteriorly and separating the entire face below the globes including the zygomas from the rest of the skull. Since many of the fracture planes extend in the anteroposterior dimension they may be difficult to demonstrate by axial CT alone and are best shown by direct coronal imaging.

Three dimensional computed tomography offers exciting potential particularly for imaging of facial fractures.

#### REFERENCES AND SUGGESTIONS FOR FURTHER READING

- Manchus AA, Hanafee WN (1985) Computed Tomography and Magnetic Resonance Imaging of the Head and Neck, 2nd edn. Williams & Wilkins, Baltimore  
The Otolaryngologic Clinics of North America (August 1988) Volume 21(2)  
Diagnostic Imaging in Otolaryngology

# SUBJECT INDEX

---

Abortion  
complete spontaneous 689  
inevitable 689  
missed 689  
threatened 689  
Abscess  
Brodie's 349  
intra-abdominal 440  
lung 64  
paracolic 441  
paraspinal 118  
subphrenic 32, 128, 441  
Achalasia 119  
Achondrogenesis 271  
Achondroplasia 266  
Acoustic tumor 730, 745  
Acromegaly 329  
Acro-osteolysis 335  
progeria 376  
sarcoïd 372  
Actinomycosis  
bone 351  
Acute abdomen 431  
plain films 431  
Acute appendicitis 440  
Acute colitis 442  
Acute toxic dilatation of the colon 442  
Adamantinoma 307  
Adhesions 433  
Adrenal  
Addison's syndrome 504  
adrenogenital syndrome 504  
adenoma 501  
anatomy 497  
vascular 497  
calcification 498, 501  
carcinoma 501  
Conn's syndrome 504  
Cushing's syndrome 504  
cysts 504  
ganglioneuroma 503  
hormones 497  
hyperplasia 505  
imaging 497–500  
metastases in 503  
myelolipoma 504  
neonatal hemorrhage 504  
neuroblastoma 503  
pheochromocytoma 502  
in MEN types 1 and 2 502  
syndromes 500  
tumors (masses) 501  
Adrenoleukodystrophy 785  
Adult Respiratory Distress Syndrome (ARDS) 102  
causes (Table 6.3) 102  
Atherosomatous stenosis and thrombosis 254  
cerebral vessels 752

AIDS  
cerebral 775  
lung infections 76  
lung tumors 76  
small bowel 553, 555, 558, 559  
colon 585, 587, 588  
Ainhum 351  
Albers-Schonberg disease 261  
Albright's syndrome 264, 788  
Alexander's disease 785  
Alzheimer's disease 787  
Alkaptonuria 267, 334, 393  
Aluminum toxicity 374  
Amebiasis  
brain 773  
liver 472  
pulmonary 71  
colon 585  
Amyloid  
lungs 104  
colon 593  
small bowel 565  
Aneurysm  
abdominal aortic 442  
rupture 442  
displacing ureter 652  
dissection 442  
cerebral 757  
congenital 237  
classification 237  
degenerative 237  
dissecting 239  
hepatic artery 476  
iliac 652  
infective 238  
inflammatory 238  
left ventricle 159, 162  
post stenotic 196, 241  
renal artery 645  
splenic artery 484  
Sinus of Valsalva 210  
syphilitic 238  
traumatic 238, 781  
Vein of Galen 207, 744, 759  
Aneurysmal bone cyst 308  
Angina  
pectoris 158, 159  
unstable 158, 163  
Angiocardiography 152  
radionuclide 150  
first pass technique 150  
multigated equilibrium (MUGA) 150  
Angiomatous malformation (angioma) 207, 242  
Angioplasty  
complications 247  
coronary 159, 230  
systemic 247

Ankylosing spondylitis 384  
bamboo spine 385  
juvenile onset 386  
lungs 100  
ulcerative colitis 581  
Anomalous origin of the L. pulmonary artery (pulmonary artery sling) 212  
Anomalous pulmonary venous drainage 204  
Anomalous R. subclavian artery 211  
Anorectal abnormalities 444  
Anti-myosin antibody scanning 161  
Anus  
ectopic 575  
imperforate 574  
VATER syndrome 575  
Aort-a(-ic)  
abdominal aneurysm  
dissection 442  
rupture 442  
arch  
double 212  
R. sided 200  
coarctation 195, 237, 267  
intra-aortic balloon pumps 131  
rupture 127  
pseudocoarctation 237  
traumatic aneurysm 238  
Aortic atresia 191  
Aortic regurgitation 174  
angiography 175  
causes (Table 10.6) 174  
chest X-ray 174  
echocardiography 174  
MRI 176  
Aortic valve stenosis, congenital 191  
Aortic valve stenosis 172  
chest X-ray 172  
echocardiography 172  
MRI 176  
Aortography  
in chest trauma 5  
in pulmonary sequestration 5  
Aorto-pulmonary window 191  
Apert's syndrome 716  
Appendix 594  
acute appendicitis 594  
appendicolith 440  
carcinoïd 594  
mucocele 594  
APUDomas 496  
Arachnoid cyst 744, 803, 808  
Armillifer armillatus 72, 407  
Arnold-Chiari see Chiari  
Arteriography  
pulmonary 5  
bronchial 6, 52  
complications 236

- Arteriography—cont.**  
 systemic 235  
 techniques 235  
 vascular lesions 236  
 tumors and cysts 245
- Arteriovenous fistula (AV fistula)** 242  
 cerebral 761  
 traumatic 781
- Arteriovenous malformation** *see* angiomas 242
- Arteritis** 753
- Artery**  
 azygos anterior cerebral 752  
 internal carotid  
   dissection 780  
   lateral kinking 752  
   pseudothrombosis 754  
   thrombosis  
     atheromatous 752  
     traumatic 780
- pro-atlantal intersegmental 752
- anomalous middle meningeal 752
- vertebral trauma 781
- Arthritis**  
 septic 391  
 tuberculous 392
- Arthrography double contrast** 395
- Arthrogryposis congenita multiplex** 400
- Asbestosis** 95  
 malignant disease 95  
 mesothelioma 44, 95  
 pleural plaques and calcification 95  
 shaggy heart 95
- Aspergillosis** 71, 100
- Aspirin therapy** 247
- Asthma** 46
- Atlanto-axial dislocation 352, 387, 793, 794
- Atlanto-axial fusion 717
- Atrial septal defect 187, 192
- Atrioventricular (AV) septal defect 195
- Atrium(-al)**  
 enlargement of left 140  
 myxoma left 217  
 thrombus 218
- Avascular necrosis** 274, 276, 359  
 causes 359, 360
- Cushing's disease** 361
- dysbaric disorders** 361
- Gaucher's disease** 362
- hemoglobinopathy** 361
- imaging 359
- in pancreatitis 488, 490
- steroids 361
- Axial osteomalacia** 327
- B-cell leukemia/lymphoma** 342
- Bacterial endocarditis** 171  
 echocardiography 171
- Baker's cyst** 394, 395
- Balloon valvoplasty** 231
- Balloon septostomy** 188
- Bankart lesion** 287
- Barium sulfate contrast** 529
- Barium swallow, in chest studies** 5
- Barytosis** 96
- Batten's disease** 785
- Battered child** 276
- Behcet's syndrome** 569
- Benign lymph node hyperplasia** 90
- Bernoulli equation** 172
- Berylliosis** 96
- Bicuspid valves congenital** 192, 196
- Bilateral left sidedness** 186
- Bilateral right sidedness** 186
- Bilateral superior vena cava** 207
- Biliary tract** (*see also gallbladder*) 447  
*Ascaris lumbricoides* infection 461  
 bile duct stones 460  
 bile duct strictures 459  
 bile duct tumors 458  
 biliary atresia 451
- Caroli's disease** 452, 458
- Chlonorchis sinensis** infection 458, 461
- cholangiocarcinoma** 458, 471
- cholangitis**  
 primary sclerosing 460  
 secondary sclerosing 461, 581  
 suppurative 461
- choledochal cyst** 451
- choledochal diverticulum** 452
- common bile duct** 447
- CT** 448
- cystic duct anomalies** 451
- fine needle biopsy** 450
- gas in** 457
- hydatid disease** 462
- i.v. cholangiography** 449
- Klatskin tumor** 459
- MRI** 450
- operative cholangiography** 449
- percutaneous transhepatic cholangiography (PTC)** 448
- radioisotope imaging (IDA)** 448
- stent insertion** 450
- therapeutic procedures** 450
- Binswanger's disease** 785
- Biopsy, percutaneous**  
 mammographic 426  
 in chest disease 11
- Bipartite patella** 259
- Bismuth**  
 injection 400  
 poisoning 335, 374
- Bladder** 604, 613, 657  
 acute retention 666  
 calcification 643, 658  
 calculi 636  
 carcinoma 643, 657  
 cystometry (CMG) 666  
 detrusor instability 667  
 diverticula 614, 653, 658  
 duplication 613  
 emphysematous cystitis 658  
 epispadias 614  
 extrophy 614  
 hourglass 614  
 incontinence 666  
 malakoplakia 658  
 neuropathic 658  
 outlet obstruction 666  
 pelvic lipomatosis compression 653, 660  
 prune belly syndrome 615  
 schistosomiasis 643, 658  
 trauma 660  
 tuberculosis 642, 658  
 tumors 647  
 vesico-ureteric reflux 641  
 videocystometrography (VCMG) 666
- Blalock-Taussig anastomosis** 188
- Blastomycosis** 70
- Blount's disease** 366
- Bochdalek hernia** 32
- Body situs** 185
- Bohler's angle** 292
- Bone**  
 metastases 314  
 primary tumors 295  
 syphilis 354
- Boorhaave's syndrome** 127
- Bowel obstruction** 412
- Brain**  
 abscess 767  
 agenesis of the corpus callosum 722  
 aneurysms 757  
 angiomas 758  
 aqueduct stenosis 719  
 arachnoid cysts 720  
 arterio-venous fistula 761  
 arteritis 753  
 atrophy 786  
   post traumatic 781
- Chiari malformations** 719
- congenital anomalies** 718
- cyst of the cavum Vergae** 722
- cyst of the septum pellucidum** 721
- Dandy-Walker syndrome** 719
- dural AV fistula** 760
- ependymal cysts** 720
- fungal infections** 771
- hemimegalencephaly** 719
- hemorrhage** 761  
 intracerebral 762  
 extradural 777  
 subdural 778  
 subarachnoid 763
- heterotopia** 723
- holoprosencephaly** 699, 723
- hydranencephaly** 669, 723
- hypoxic damage** 780
- infarcts** 755–757
- lipoma of the corpus callosum** 722
- lissencephaly** 723
- macrocephaly (megalencephaly)** 719
- meningitis** 767
- neurofibromatosis** 723
- porenephaly** 722
- pachygryria** 723
- parasitic infections** 772
- schizencephaly** 723
- septal agenesis** 721
- septo-optic dysplasia** 721
- Sturge-Weber disease** 725
- swelling** 780
- tuberculoma** 768
- tuberous sclerosis** 723
- tumors** (*see also under specific types*)  
 epidemiology 732  
 imaging 732  
 metastases 747
- venous thrombosis** 754  
 Delta sign 754
- ventricular coarctation** 722
- viral infections** 769
- Von Hippel-Lindau disease** 726, 746
- Brodie's abscess** 349
- Bronchi(al)** 13  
 adenoma 90  
 air bronchogram 17  
 bronchiectasis 49  
 bronchocele 52  
 bronchopleural fistula 39  
 carcinoid tumor 90  
 carcinoma 77  
   bone involvement 80  
   cavitating 80  
   histological types 77  
   mediastinal involvement 80  
 Pancoast 80  
 percutaneous needle biopsy 82  
 pleural involvement 80  
 radiology 78  
 staging 82
- chronic bronchitis** 47
- cylindroma** 91
- mucoid impaction** 52
- neoplasms (Table 5.1)** 77
- obliterative bronchiolitis** 49
- rupture** 126
- salivary gland tumor** 91
- situs** 185
- Bronchiectasis** 49
- Bronchogenic cyst** 112
- Bronchography** 5, 51
- Bronchopulmonary dysplasia** 104
- Brown tumors** 332
- Brucellosis** 351
- Buerger's disease** 244
- Burkitt's lymphoma** 307
- Buscopan** 532
- Caffey's disease** 373
- Caisson disease** 361
- Calcific tendonitis** 389

- Calcification, soft tissues 402  
acquired 404  
basal ganglia 788  
breast 420  
congenital diseases 404  
dermatomyositis 388  
frostbite 404  
gouty tophi 403  
hypercalcemia 403  
intracranial 731  
metabolic causes 403  
parasitic 405  
penicillin injection 404  
quinine injection 404  
tissue injury 404  
tumor 404  
tumoral calcinosis 404
- Calcium hydroxyapatite (HA) crystal deposition disease 389
- Calcium pyrophosphate dihydrate (CPPD) crystal deposition disease 389
- Caplan's syndrome 96
- Carbon monoxide poisoning 789
- Carcinoma, *see* specific organs and tumors
- Carcinoid 557, 580, 594
- Cardiac (*see under* Heart)
- Cardiomegaly 140
- Cardiomyopathy  
congenital 207  
hypertrophic 180, 207  
ischemic 158, 164  
mitral regurgitation 172
- Carotid-basilar anastomosis 751
- Carotico-cavernous fistula 781
- Carpenter's syndrome 716
- Castleman's disease 90, 112
- Cavernous angioma of brain 759
- Cavernous lymphangioma 254
- Central pontine myelinolysis 784
- Cephalhematoma 404, 776
- Cerebral *see* Brain
- Chagas' disease  
cardiac 180  
colon 586, 592  
esophageal 118
- Chest  
aortic arch 14  
extrapleural lesions (Table 1.4) 15  
calcification 24  
heart shadow 14  
mediastinum 13  
opaque hemithorax 25  
post operative complications 128, 130  
radiation injury 127  
radiograph, analysis (Table 1.1) 11  
thymus 14  
trauma 123  
diaphragm 124  
hemothorax 124  
flail chest 123  
lung 126  
pneumothorax 124  
radiation 127  
subcutaneous emphysema 123  
sternal fracture 124  
unilateral hypertransradiancy 25  
wall 27  
artefacts 27  
breasts 27  
bones 27  
neurofibromatosis 27  
soft tissues 27
- Chemodectoma, mediastinal 118
- Chiari malformations 717, 719, 808
- Chilaiditi's syndrome 438
- Chondroblastoma 301
- Chondrodystrophy calcificans congenita 264
- Chondroectodermal dysplasia 268
- Chondromyxoid fibroma 301
- Chondrosarcoma 302–304
- Chordoma 312, 750
- Choriocarcinoma, mediastinal 109
- Choroid plexus papilloma 735
- Christmas disease 345
- Crohn's disease 386, 583, 585
- Chromosomal abnormalities 268
- Chronic bronchitis 47
- Chronic granulomatous disease 74, 356
- Chronic obstructive airways disease 46  
asthma 46  
bronchitis 47
- Chronic symmetric plasma cell osteomyelitis 356
- Churg-Strauss disease 100
- Chylothorax 254  
post operative 131
- Chylous reflux 254
- Ciliary syndromes, congenital dyskinetic 74
- Circle of Willis 751
- Cleidocranial Dysostosis 259, 718
- Coarctation of the aorta  
thoracic 195  
balloon dilatation 196  
bicuspid aortic valves 196  
cardiac failure 195  
post stenotic aneurysm 196  
rib notching 195  
Turner's syndrome 267  
abdominal 237, 244
- Coccidiomycosis 70, 351
- Cockayne syndrome 788
- Codman's triangle 347
- Coeliac compression syndrome 244
- Coenurosis, cerebral 774
- Colloid cyst 736
- Colon(-ic)  
adenoma 577  
AIDS 586, 587, 588  
"gay bowel" syndrome 587  
lymphoma 588  
Kaposi's sarcoma 588
- amebiasis 586
- amyloid 593
- angiodyplasia 593
- atresia 595
- bacterial dysentery
- basal cell nevus syndrome 576
- Canada-Cronkhite syndrome 576, 577
- carcinoid 580, 594
- carcinoma 578, 585  
cloacogenic 580  
mucinous 580  
scirrhous 580
- cathartic 590
- cecal bascule 591
- Chaga's disease 587, 592
- colitis cystica profunda 592
- Cowden's disease 576, 577
- Crohn's disease 583  
complications 585
- cut off sign (pancreatitis) 585
- Cytomegalovirus colitis 587
- diverticulitis 580
- diverticulosis 580
- endometriosis 592
- extrinsic deformities 595
- familial polyposis 577
- fistula 581, 585
- Gardner's syndrome 577
- hamartomas 576
- hemangioma 593
- Hirschsprung's disease 575, 592
- ileocecal neoplasms 594
- imperforate anus 574
- infections 586
- irritable bowel syndrome 593
- ischemic colitis 588
- intussusception 578, 591
- lipoma 577
- lymphogranuloma venereum 587
- lymphoid hyperplasia 577
- lymphoma 578, 588
- megacolon 592
- microcolon 575
- necrotising enterocolitis 575, 589
- non rotation 574
- obstruction 590
- pericolic abscess 578, 580
- parasitic infestations 586
- Peutz-Jeger syndrome 576
- polyposis syndromes 576, 577
- polyps 575  
inflammatory 576
- pneumatosis coli 588, 589, 592
- pseudomembranous colitis (antibiotic associated colitis) 588
- pseudo-obstruction (Ogilvie syndrome) 434, 591  
causes 435
- radiation colitis 588
- radiologic anatomy 573
- renal disease complications 593
- schistosomiasis 586
- scleroderma 593
- small left colon (hypoplastic) syndrome 575
- solitary rectal ulcer syndrome 593
- stenosis 575
- toxic megacolon 581, 583, 585, 588, 592
- trauma 595
- tuberculosis 586
- Turcot syndrome 576, 577
- typhlitis 588
- ulcerative colitis 581  
complications 582
- villous adenoma 575
- viral colitis 587
- volvulus, cecal 590  
compound (ileosigmoid) 591  
sigmoid 590
- Colostomy lip shadow 399
- Complete situs inversus 185
- Computerised tomography *see* CT
- Congenital bicuspid valves 192
- Congenital dislocation of the ankle 259
- Congenital dislocation of the hip 257
- Congenital generalised fibromatosis of bone 305
- Congenital heart disease  
classification 184  
incidence 183
- Congenital vertical talus 259
- Contrast media 235, 601  
iodism 602
- Coronary arteriography 160, 164
- Coronary artery  
angioplasty, percutaneous transluminal (PTCA) 159, 230  
indications 230  
results 230
- by-pass grafting (CABG) 159
- calcification 163
- congenital anomalies 207
- Kawasaki's disease 208
- thrombolysis 159
- Craniometaphyseal dysplasia 264
- Cranioopharyngioma 742
- Creutzfeldt-Jacob disease 787
- Crohn's disease 550
- Cronkhite-Canada syndrome 541
- Crouzon's craniofacial dysostosis 716
- Cryptococcosis 70, 351
- Crystal induced arthropathies 388
- CSF otorrhea 776
- CSF rhinorrhea 776
- CT  
cardiac 151  
chest disease 6
- Cushing's disease 505  
avascular necrosis 361  
fatty liver 473, 505  
mediastinal fat 119, 505
- Cylindroma 91, 112
- Cystic angiomatosis of bone 310
- Cystic fibrosis 52, 73
- Cysticercosis 407, 774
- Cytomegalovirus  
bone 351  
colon 587
- encephalitis 771

- Cytomegalovirus—*cont.*  
 pulmonary infection 75
- Cystometry (CMG) 666
- Dacrocystography 819  
 Dactylitis 351  
 Dermatomyositis 387  
 lungs 100  
 Dermoid  
 cerebral 743  
 mediastinal 109  
 Desmoplastic fibroma 305  
 Diaphyseal aclasia 266, 301  
 Diabetic  
 foot 350  
 neuroarthropathy 391  
 Diaphragm(atic) 31  
 evagination 31  
 hernia 31, 119  
 Bochdalek 32, 119  
 Morgagni 32, 119  
 subphrenic abscess 32  
 tumors 34  
 unilateral elevation (Table 2.2) 31  
 Diffuse idiopathic skeletal hyperostosis (DISH) 379  
 Diffuse pulmonary fibrosis 100  
 causes (Table 6.2) 101  
 Digital Chest Radiography 4  
 Digital subtraction angiography (DSA) 154  
 Disc disease  
 cervical 799  
 thoracic 800  
 lumbosacral 800  
 Discitis 350, 801  
 Dissecting aneurysm 239  
 Dissection, internal carotid 780  
 Double aortic arch 212  
 Double inlet ventricle 208  
 Double outlet ventricle 208  
 Down's syndrome 268  
 annular pancreas 487  
 AV septal defect 193  
 Hirschsprung's disease 444  
 ribs 28  
 Drug abuse and necrotising vasculitis 241  
 Duodenum(al)  
 carcinoma 541  
 diverticula 534  
 duodenitis 536  
 heterotopic gastric mucosa 537  
 hypotonic duodenography 493  
 neoplasms 541  
 nodular lymphoid hyperplasia 537  
 non tropical sprue 537  
 normal radiological anatomy 533  
 obstruction 443  
 superior mesenteric artery syndrome 534  
 ulcer 539  
 Dwarfism 268  
 Dyschondrogenesis 269  
 Dyschondroosteosis 257  
 Dysplasia epiphysealis hemimelica 264
- Ebstein's anomaly 208  
*Echinococcus* see Hydatid  
 Echocardiography 143  
 amyloid myocardial disease 179  
 atrial myxoma 217  
 bacterial endocarditis 171  
 color flow 147, 180, 193  
 continuous wave 147  
 contrast 147  
 Doppler 146, 198, 200  
 Doppler equation 146  
 flow assessment 147  
 pulsed 147  
 fetal 213  
 hypertrophic cardiomyopathy 180  
 mitral annulus calcification 172  
 mitral stenosis 167
- mitral regurgitation 169  
 M-mode 143  
 transesophageal 148  
 two-dimensional (2DE) 145, 160, 193
- Ehlers–Danlos syndrome  
 dural ectasia 803  
 splenic artery, aneurysm 484  
 trachea 46  
 Eisenmenger syndrome 187  
 Electrode jelly artefacts 399  
 Embolus(-i) 245  
 cerebral 755  
 pulmonary 132
- Embolisation  
 agents 248  
 cardiac applications 233  
 complications 248  
 indications 248  
 therapeutic 52, 248
- Emphysema 47  
 bullous 49  
 compensatory 49  
 congenital lobar 49  
 obstructive 49  
 unilateral 49
- Enchondroma 300  
 Encephalomeningocele 716, 718  
 Endometriosis 675  
 chocolate cysts 675  
 Endomyocardial fibrosis 181  
 Engelmann's disease 266  
 Enteropathia arthropathy 386  
 Eosinophil granuloma 319, 730  
 Ependymoma 730  
 Epidermoid 743  
 Epidermoid carcinoma 356  
 Erdheim–Chester disease 344  
 Erlenmeyer flask deformity 261  
 Erosive (inflammatory) osteoarthritis 380  
 Esophagus(-eal)  
 achalasia 524, 118  
 atresia 515  
 Barrett esophagus 518  
 Boerhaave rupture 527  
 congenital stenosis 515  
 diffuse esophageal spasm 525  
 diverticula 523  
 duplication 516  
 dysphagia aortica 528  
 dysphagia lusoria 528  
 foreign bodies 527  
 glycogen acanthosis 515  
 hiatal hernia 516  
 intramural diverticulosis 524  
 Mallory–Weiss tear 527  
 motility disorders 524  
 neoplasms  
 adenocarcinoma 518, 522  
 inflammatory reflux polyp 522  
 leiomyoma 520  
 secondary 522  
 squamous cell carcinoma 521  
 non reflux esophagitis  
 caustic 519  
 infectious 519  
 medication induced 519  
 radiation 519  
 nutcracker esophagus 525  
 presbyesophagus 525  
 pseudodiverticula 518  
 radiological anatomy 515  
 reflux esophagitis 516  
 rimping 515  
 rings 516  
 Schatzki's 516  
 rupture 126  
 scleroderma 118, 525  
 stricture 119  
 techniques of examination 513  
 tertiary contractions 515  
 trauma 527  
 varices 526
- Zenker's diverticulum 118, 511  
 Ewing's tumor 305  
 Exercise ECG 164  
 Exophthalmos, dysthyroid 813  
 Extra-corporeal shock wave lithotripsy (ESWL) 451, 633  
 Extradural hematoma 777  
 Extraventricular empyema 767  
 Extramedullary hematopoiesis 118  
 Extrinsic Allergic Alveolitis 97  
 Eye, foreign body localisation 820–823
- Facets, dislocation and locked 279, 280  
 Fahr's syndrome 788  
 Fallopian tubes  
 anatomy 673  
 blocked 685  
 hydrosalpinx 676, 685  
 pyosalpinx 676  
 tuberculous 684  
 salpingitis 675  
 isthmica nodosa 685  
 tubo-ovarian abscess 675, 676  
 Fallot's tetralogy 198  
 Familial hyperphosphatemia 327  
 Familial hypophosphatemia 325  
 Familial metaphyseal dysplasia 264  
 Familial polyposis coli 541  
 Fetus(-al)  
 abdomen 693  
 abdominal circumference 691, 696  
 brain 692  
 biparietal diameter 689, 691, 696  
 congenital anomalies  
 abdomen 704  
 neural axis 688–702  
 face and neck 702  
 Turner's syndrome 702  
 heart 703–4  
 skeleton 707–9  
 thorax 702  
 urinary tract 706–7  
 Potter's sequence 706, 707  
 crown rump length 688  
 death 709  
 face 693  
 femoral length 689, 691, 696  
 genitalia 694  
 gestational age assessment 696  
 gestation sac (MSD) 688  
 head circumference 691  
 HC/AC ratio 696, 697  
 heart 693  
 hydrops 709  
 intra-uterine growth rate (IUGR) 697  
 macrosomic 698  
 multiple 709  
 pole 689  
 skeleton 694  
 skull 691  
 spine 692  
 spina bifida 692  
 thorax 693  
 twin 709  
 conjoined 710  
 twin-twin transfusion syndrome 710  
 urogenital tract 694  
 weight, estimated (EFW) 691, 696, 697
- Fibrodysplasia ossificans progressiva 267  
 Fibrogenesis imperfecta ossium 261, 327  
 Fibroleiomyosarcoma of uterus  
 lung metastases 91
- Fibroma  
 pleural 44  
 Fibromuscular hyperplasia 244, 752  
 Fibrosarcoma of bone 305  
 Fibrosing alveolitis 101  
 cryptogenic 101  
 Fibrosing mediastinitis 112, 252  
 Fibrous dysplasia 263  
 Fistula(e) rectal 444

- Fluoroscopy 5  
 Fluorosis 335, 374  
 Fontan operation 188  
 Foreign bodies 399  
 Forestier's disease 379  
 Fractures and fracture dislocations  
     acetabular 286  
     avascular necrosis 274  
     buckle 273  
     childhood 276  
     comminuted 273  
     complications 273  
     delayed union 274  
     facial bones 279  
     greenstick 273  
     isotope scanning 277  
     lower limb 291  
     malunion 274  
     non-union 274  
     pelvic 284  
     plastic 273  
     Salter-Harris classification 276  
     shoulder girdle 286  
     skull 278  
     sphenoid sinus 279  
     spine 279  
         burst 282  
         hangman's 282  
         Jefferson 282  
         odontoid 282  
         seat belt 284  
     stress 277, 291  
     Sudeck's atrophy 274  
     upper limb 288  
         Barton's 289  
         Bennett's 290  
         Colles 289  
         Galeazzi 288  
         Monteggia 288  
         Smith's 289  
 Frankel's lines 327  
 Freiberg's infraction 366  
 Fungal brain infections 771
- Gadolinium DTPA 400  
 Gallbladder (*see also* Biliary tract) 447  
     acute cholecystitis 455  
         radionuclide imaging 456  
     adenomyomatosis 454  
     biliary sludge 454  
     carcinoma 458  
     cholesterosis (strawberry gallbladder) 454  
     chronic cholecystitis 457  
     emphysematous cholecystitis 455  
     fistulae 456  
     gas in 457  
     limy bile 454  
     lithotripsy 449  
     metastases in 458  
     Mirizzi syndrome 458  
     mucocele 457  
     oral cholecystogram 447  
     perforation 456  
     polyps 458  
     porcelain 454  
     Rokitansky-Aschoff sinuses 447  
     trauma 458  
     ultrasound 447, 454  
     valves of Heister 448
- Gallstones 452  
     complications 452  
     gallstone ileus 433, 436, 563  
     extracorporeal shockwave lithotripsy (ESWL) 451  
 Methyl-tert-butyl-ether (MTBE) dissolution 451  
 oral cholecystography 452  
     ultrasound 453  
 Gallium scanning  
     bone infection 357  
     in chest 7  
     sarcoidosis 94  
 Ganglioglioma 737
- Gangosa lesion 355  
 Gardner's syndrome 295, 458, 577, 826, 833, 841  
 Garre's sclerosing osteomyelitis 349  
 Gas in soft tissues 401  
     intramural (bowel wall) 433, 437  
     in biliary tract 433, 436, 457  
     portal vein 444, 457, 490  
     retroperitoneal 438  
 Gas gangrene 402  
 Gaucher's disease 344, 362  
 Germ cell tumors  
     mediastinal 109  
     pineal 744  
 Geode formation 377  
 Giant cell reparative granuloma 310  
 Giant cell tumor 307  
 Giardiasis 554  
 Glialoma 731, 733, 744  
     optic nerve 730  
 Globoid leukodystrophy 785  
 Glomus jugulare tumor 745  
 Glomus tumor 311  
 Glucagon 532  
 Glycogen storage diseases 330  
 Gold radionuclide ( $^{195m}$ gold) 151  
 Goodpasture's syndrome 103  
 "Goose-neck" appearance 195  
 Gorham's disease 311  
 Gouland lesion 355  
 Gout 388  
 Great vessel anomalies 751  
 Guinea worm 407
- Hand Schuller-Christian disease 101, 319, 730  
 Hansen's disease *see* Leprosy  
 Hemangioblastoma 746  
 Hamartoma  
     pulmonary 91  
 Heart (cardiac)  
     aneurysm (left ventricle) 159  
     angiocardigraphy 153  
     balloon valvoplasty 231  
     calcification 143, 163, 171  
     cardiomegaly 140  
     CT 151  
     DSA 154  
     embolisation procedures 233  
     failure 161  
     fluoroscopy 143  
     hemodynamic principles 187  
     implants 218  
     interventional techniques 217  
     ischemic disease 157  
         chest X-ray (Table 10.4) 165  
         clinical presentation 158  
         non-atheromatous causes 158  
         risk factors (Table 10.1) 157  
         treatment 158  
     malformations 187  
     MRI 152  
     muscle disease 177  
         causes 178  
         imaging 178  
         features of different types 179  
     nuclear medicine 148  
         techniques (Table 9.2) 148  
         myocardial imaging 148, 159  
         radionuclide angiography 150  
         radionuclide ventriculogram 159  
     position 186  
     prosthetic valves 219  
     septostomy 233  
     size 140  
     tumors 217  
     ultrasound *see* Echocardiography
- Hemangiopericytoma 311  
 Hemangioma of bone 310  
 Hemangiopericytoma 311  
 Hematoma, soft tissue 400  
 Hemivertebra 257  
 Hemochromatosis 393, 467, 476
- Hemodialysis spondyloarthropathy 391  
 Hemophilia 344, 392  
     hemophilic pseudotumor 392  
 Hemorrhage 245, 248  
     gastro-intestinal 248  
 Hemosiderosis 166, 467  
 Henoch-Schonlein purpura 442, 563, 569  
 Hepatic, hepato- *see* liver  
 Hereditary spherocytosis 337  
 Herpes simplex encephalitis 770  
 Herpes simplex type 2 encephalitis 771  
 Hiatus hernia 119  
 Hirschsprung's disease 444, 575, 592  
 Histiocytic lymphoma of bone 306
- Histiocytosis X  
     bones 319  
     lungs 101  
     skull 710  
 Histoplasmosis 69  
 Hodgkin's disease 88  
 Holt-Oram syndrome 257  
 Homocystinuria 267, 331, 334  
 Huntington's chorea 787  
 Hurler's mucopolysaccharidosis 269, 271  
 Hyaline membrane disease 104  
 Hydatid disease  
     bone 351  
     pulmonary 73  
 Hydrocephalus  
     communicating 781  
     low pressure 787  
 Hyperostosis corticalis generalisata familiaris 262  
 Hyperparathyroidism 331, 790  
 Hyperthyroidism 328  
 Hypertrophic cardiomyopathy (HCM)  
     imaging 180  
 Hypervitaminosis A 374  
 Hypochondroplasia 267  
 Hypogammaglobulinemia 73  
 Hypogonadism 328  
 Hypoparathyroidism 331, 788  
 Hypopharynx  
     anatomy 509  
     crico-pharyngeal dysfunction 512  
     malignant neoplasms 511  
     myasthenia gravis 512  
     myotonic dystrophy 512  
     pharyngeal diverticular 511  
         pharyngeal pouch 511  
         Zenker's 511  
     pharyngeal paresis 512  
     Plummer-Vinson syndrome 510  
     post-cricoid impression 510  
     webs 510  
 Hypophosphatasia 267, 326, 718  
 Hypophosphatemic osteomalacia/rickets 326  
 Hypoplastic left heart 187, 191
- Idiopathic chondrolysis 275, 330  
 Idiopathic coxa vara 259  
 Idiopathic hypoparathyroidism 331  
 Iliopsoas muscles displacing ureters 652  
 Ileal duplication 437  
 Ileosigmoid knot 436  
 Implantation dermoid 313  
 Indium 111 labelled leukocytes 357  
 Infantile cortical hyperostosis 373  
 Inferior vena cava  
     anomalies 251  
     therapeutic interruption 251  
 Insulinoma 496  
 Intensive care  
     catheters 131  
     tubes 131  
 Intervertebral osteochondrosis 379  
 Interventional angiography 247  
 Intracerebral hemorrhage 762, 779  
     multiple petechial 779  
 Intramural hematoma 442  
 Intraosseous ganglion 314  
 Intussusception 437, 570, 591

- Iodism 602  
 Isolated dextrocardia 186  
 Isolated levocardia 186  
 Isotope scanning  
     bone infection 357  
     three phase 357
- Jaws *see* Teeth and jaws  
 Juvenile chronic arthritis 386  
 Juxtacortical chondroma 300
- Kaposi's sarcoma  
     lung in AIDS 76  
 Kartagener syndrome 50  
 Kawasaki's disease 208  
 Kerley's A and B lines 89, 166  
 Kidney (renal)  
     abscess 638  
     acquired cystic disease 623  
         neoplasms in 623  
     adenoma 623  
     anatomy 603  
     angiomyolipoma 624  
     antegrade pyelography 605  
     candidiasis 643  
     calculi 633  
     congenital hydronephrosis 612  
     congenital megacalyses 608  
     cortical cyst 617  
         calcification 618  
         multiple simple 619  
 CT 606  
 embryology 607  
 extra-corporeal shock wave lithotripsy (ESWL) 633  
 fetal lobulation 603  
 focal bacterial nephritis 638  
 horseshoe 609  
 hydatid 643  
 hypernephroma 625  
     calcification 627  
     cysts and 628  
     staging 626  
 hypertension and renal artery stenosis 644  
     renal angiography 645  
     renal vein renin sampling 645  
 leukemia 629  
 leukoplakia 631, 640  
 lymphoma 629  
 malakoplakia 639  
 malrotation 609  
 mass puncture 605  
 medullary cystic disease 623  
 medullary sponge 622  
 mesenchymal tumors 624  
 mesoblastic nephroma 625  
 metastases in 629  
 MRI 607  
 multicystic dysplastic 608, 623  
 multilocular cystic nephroma 625  
 nephrocalcinosis 634  
     cortical 634  
     medullary 635  
 oncocyrtoma 624  
 papillary necrosis 646  
 parapelvic cysts 619  
 pelvi-calyceal system 604  
 percutaneous nephrostomy 605  
 perinephric abscess 639  
 perinephric pseudocyst 619  
 polycystic disease 619  
     childhood types 620  
     adult 621  
 pyelogenic cysts 619  
 pyelonephritis  
     acute 637  
     chronic 641  
     emphysematous 638  
         xanthogranulomatous 639  
 pyeloureteritis cystica 640  
 pyonephrosis 639
- radioisotope scintigraphy 607  
 reflux nephropathy 641  
 renal agenesis 607  
 renal dysplasia 608  
 renal ectopia 609  
 renal hypoplasia 608  
 renal tubular acidosis 636  
 renal tubular ectasia 622  
 reninoma 624  
 retrograde loopography 604  
 retrograde pyelography 604  
 squamous cell carcinoma 631  
 supernumerary 608  
 transitional cell carcinoma 629  
 trauma 649  
 transplantation 650  
     complications 651  
 tuberculosis 642  
 tuberous sclerosis 619, 624  
 urinoma 619  
 ultrasound 606  
 Von Hippel-Lindau syndrome 619, 625  
 Wilms' tumor 628
- Kienbock's disease 364  
 Klatskin tumor 459  
 Klippel-Feil syndrome 717, 791  
 Klippel-Trenauney syndrome 250  
 Kohler's disease 366  
 Kyphoscoliosis 31
- Large bowel obstruction 433  
 Lead poisoning 335, 374  
 Left atrium, morphology 185  
 Left ventricle(-ular)  
     aneurysm 159, 162  
     dilatation 170  
     morphology 184  
 Legg-Calvé-Perthes disease 365  
 Leprosy 354, 391, 403  
 Leptomeningeal cyst (post traumatic) 777  
 Letterer-Siwe disease  
     bones 319  
     lungs 101  
     skull 730  
 Leukemia  
     bone 340  
     liver 470  
     lung 89  
     skull 730  
 Leukodystrophies 785  
 Leukoencephalopathy 783  
 Lipiodol 400  
 Lipoma  
     bone 312  
     pleural 44  
     soft tissue 400  
 Lipohemarthrosis 401  
 Liposarcoma of bone 312  
 Liver (hepatic, hepato-)- 463  
     abscess  
         amebic 472  
         pyogenic 472  
     adenoma 468  
     angiography 466  
     angiosarcoma 473  
     biopsy, fine needle 467  
     Budd-Chiari syndrome 472, 476  
     calcification 464  
     candidiasis 473  
     chemotherapy infusion 467  
     cholangiocarcinoma 471  
     cirrhosis 474  
     CT 465  
     cysts 467  
         hydatid 472  
         polycystic disease 468  
     embolisation 467  
     fatty 473  
     focal nodular hyperplasia 468  
     gas shadows in 464  
     hemangioblastoma 473
- hemangioma 468  
 hemochromatosis 467, 476  
 hemosiderosis 467  
 hepatoblastoma 472  
 hepatoma 469  
     fibrolamellar 469  
 hepatomegaly 463  
 leukemia 470  
 lobar agenesis 467  
 lymphoma 470  
 mesenchymal hamartoma 472  
 metastases 470  
 MRI 467  
 phlebography 467  
 radionuclide imaging 465  
 Reid's lobe 467  
 schistosomiasis 475  
 trauma 476  
 ultrasound 465  
 viral hepatitis 474  
 Wilson's disease 475  
 Loa-loa 407, 775  
 Loeffler's syndrome 71, 100  
 Looping  
     D-loop 186  
     L-loop 186  
 Looser's zones 324, 326  
 Lung  
     abscess 64  
     aspiration 96  
         meconium 105  
         post operative pneumonitis 128  
     air bronchogram 17  
     alveolar cell carcinoma 85  
     alveolar edema 141  
     alveolar shadowing 17  
         causes (Table 1.5) 18  
     amyloidosis 104  
     atelectasis, post-operative 128  
     carcinoma *see* bronchial carcinoma  
     cavity 23  
     collapse 53  
         lobar 54  
     consolidation 58  
         lobar 58  
     diffuse pulmonary shadowing in immunocompromised causes (Table 4.2) 75  
     drug reactions 103  
     edema 104, 128  
         interstitial 141  
     empyema 129  
     eosinophilia 100, 103  
     fibrosis due to cytotoxic drugs 103  
     hamartoma 91  
     hemorrhage 103  
     hemosiderosis 103  
     hila(r) 13  
         enlargement 26  
     Hodgkin's disease 88  
     honeycomb shadowing 21  
     infection (*see also under* pneumonia) 61  
         in immunocompromised 74  
             causes (Table 4.1) 75  
             post operative 128  
             predisposing causes 74  
     interlobar fissure 13  
     interstitial disease  
         causes (Table 1.6) 19  
     interstitial pulmonary emphysema 119  
 Kerley B lines 20, 21, 141  
 leukemia 89  
 metastases 85  
     calcification 87  
     cavitated 87  
     uterine fibroleiomyosarcoma 91  
     lymphangitis carcinomatosa 87  
 miliary shadowing causes 19  
 non-Hodgkin's lymphoma 89  
 oxygen toxicity 97  
 post-operative complications 128  
 radiation pneumonitis 127  
 rounded atelectasis 55

- septal lines 141  
 sequestration 74  
 silhouette sign 17  
 solitary nodule 20, 21  
 trauma 126  
   radiation 127  
   tuberculosis 65  
 Lymphangiography 253  
 Lymphangiomatosis  
   bone 254, 310  
   spleen 484  
 Lymphangiomyomatosis 102  
 Lymphangiosarcoma 254  
 Lymphangitis carcinomatosa 87, 493  
 Lymphedema 253  
 Lymphedema praecox 251  
 Lymphocoele 253, 651  
 Lymphoid interstitial pneumonia 90  
 Lymphoma  
   bone 306  
   cerebral 750  
   intrathoracic 88  
   liver 470  
   lung in AIDS 76  
   skull 730  
 Lymphomatoid granulomatosis 100  
 Lymphsarcoma, skull 730
- Mach effect 399  
 Machiafava–Bignani disease 785  
 Macleod's syndrome 49  
 Madelung's deformity 257, 269  
 Maduromycosis *see* Mycetoma  
 Maffucci's syndrome 301  
 Magnetic Resonance Imaging (MRI)  
   aortic valve disease 176  
   avascular necrosis 360  
   bone infection 357  
     radiation injury 373  
   cardiac 152  
   chest disease 7  
   joints 395  
   soft tissue masses 400  
 Malabsorption 324  
 Malaria cerebral 774  
 Malignant fibrous histiocytoma of bone 305  
 Malrotation 444  
 Mammography 411  
   calcification 420  
   indications 411  
   preoperative localisation 425  
   signs of malignancy 415  
 Mandible *see also* Teeth and jaws  
   fractures 837  
 Marfan's syndrome 112, 239, 267  
 Mastocytosis 318, 566  
 Meconium aspiration 105  
 Meconium ileus 444, 563  
 Meconium peritonitis 563  
 Meckel's diverticulum 437, 549, 563  
 Mediastinum(al) 107  
   aneurysm of thoracic aorta 112  
   acute mediastinitis 120  
   bronchogenic cyst 112  
   chronic (fibrosing) mediastinitis 121  
   emphysema 119, 126  
   fat 119  
   germ cell tumors 109  
   hemorrhage 121, 127  
 Lymph nodes  
   Castleman's disease 112  
   calcification causes (Table 7.2) 110  
   enlargement causes (Table 7.3) 110  
   Hodgkin's disease 112  
   lymphadenopathy 109  
   lymphatic leukemia 112  
   non-Hodgkin's lymphoma 112  
   sarcoidosis 112  
   tuberculosis 112  
   histoplasmosis 112  
 masses (Table 7.1) 107
- mesenchymal tumors 119  
 neurogenic tumors 112  
 pleuroperitoneal cyst 112  
 retrosternal goitre 107  
 thymic 108  
 trauma 126  
 veins dilated 112  
 Medulloblastoma 736  
 Melorheostosis 262  
 Ménétrier's disease 536  
 Membranous lipodystrophy 321  
 Mendelson's syndrome 96  
 Meningocele 716, 718  
   lateral thoracic 118  
 Mesenteric adenitis 437  
 Mesenteric artery occlusion 442  
 Mesothelioma, pleural 44  
 Metachromatic leukodystrophy 785  
 Metaphyseal dysplasias 264  
 Meteorism 412  
 Meyer's dysplasia 366  
 Mineralising microangiopathy 785  
 Mitral annulus calcification 171  
 Mitral regurgitation 168  
   angiography 169  
   bacterial endocarditis 171  
   causes (Table 10.5) 168  
   chest X-ray 169  
   echocardiography 169  
   ischemic damage 170  
   left ventricular dilatation 170  
 Mitral stenosis 165  
   angiography 168  
   chest X-ray 165  
     pulmonary venous congestion 166  
     Kerley's A and B lines 166  
   congenital 208  
   echocardiography 167  
 Mitral valve abnormalities  
   congenital mitral stenosis 208  
   cor triatriatum 208  
   supravalvular ring 208  
 Mongolism *see* Down's syndrome  
 Morgagni hernia 32  
 Morquio–Brailsford mucopolysaccharidosis 269, 271  
 Mounier–Kuhn syndrome 46  
 Moyamoya disease 753  
 Mucopolysaccharidoses 269  
 Multiple enchondromas 300  
 Multiple endocrine neoplasia (MEN)  
   type 1 (Werner's syndrome) 496, 502  
   type 2 (Sipple's syndrome) 502  
   type 3 502  
 Multiple exostoses 266, 301  
 Multiple myeloma 316, 730  
 Multiple metaphyseal dysplasia 264  
 Multiple sclerosis 783  
 Muscular dystrophy 400  
 Myasthenia gravis 108  
 Mycetoma 351  
 Myelofibrosis 342  
 Myelomatosis 316, 730  
 Myocardial disease, dilating  
   myocarditis 179  
   alcoholic 179  
   amyloid 179  
   Chagas' disease 180  
   cytotoxic drug 179  
   hypertensive 179  
   endocardial fibroelastosis 179  
   sarcoidosis 180  
 Myocardial infarction  
   chest X-ray 161  
     pulmonary edema 161  
   complications 158, 161  
   scanning 149  
     <sup>99m</sup>Tc pyrophosphate 149, 161  
 Myocardial perfusion imaging 149, 159  
   <sup>99m</sup>Tc MIBI 149  
   Thallium-201 149  
 Myodil (Pantopaque) 400  
 Myositis ossificans 275, 410
- Myositis ossificans congenita (progressiva) 267, 407
- Necrotising enterocolitis 444  
 Neonatal intestinal obstruction 443  
 Neonatal pulmonary distress 104  
 Neurilemmoma *see* Schwannoma  
 Neuroarthropathy 391  
 Neurofibroma  
   bone 312  
   skin nodules 399  
 Neurofibromatosis  
   bone 312  
   calcification 403  
   chest wall 28  
   lungs 102  
   mediastinal 118  
   orbit 717, 815  
   pheochromocytoma in 502  
   skull 724  
 Neurogenic tumors, mediastinal 112  
 Neuroenteric cyst 118  
 Nieman–Pick disease 344  
 Nipple shadows 399  
 Non-Hodgkin's lymphoma 89
- Occipitalisation of the atlas 791  
 Obliterative bronchiolitis 49  
 Obstetric ultrasound 687  
 Ochronosis *see* alkaptonuria  
 Odontoid anomalies 792  
 Odontoid erosion 382, 387  
 Ogilvie's syndrome 434  
 Olivopontocerebellar atrophy 787  
 Ollier's disease 300  
 Orbit(-al)  
   inflammatory conditions  
     abscess 818  
     cellulitis 818  
     pseudotumour 819  
 tumors  
   AV malformation 817  
   blood cysts 818  
   cholesterol granuloma 815  
   dermoid 815  
   epidermoid 814  
   hemangioma 817  
   hematoma 818  
   lacrimal gland 817  
   lymphocytic hyperplasia, benign reactive 816  
   lymphoma 816  
   meningioma 814  
   metastases 816  
   carcinoïd 817  
   neurilemmoma 817  
   neurofibromatosis 815  
   rhabdomyosarcoma 817  
   varices 817  
   venous malformation 818  
 Oropharynx 509  
 Os odontoideum 792  
 Osgood–Schlatter disease 367  
 Ossification  
   soft tissues 409  
     paraplegic 410  
 Osteitis condensans ilii 378  
 Osteitis pubis 351, 379  
 Osteoarthritis 377  
 Osteochondritis dissecans 362  
 Osteogenesis imperfecta 260, 330, 718  
 Osteoid osteoma 295  
 Osteoma 295  
 Osteoblastoma 295  
 Osteochondritis dissecans 362  
 Osteochondroma 301  
 Osteochondroses 364  
 Osteoclastoma 307  
 Osteomalacia 324, 325  
 Osteomyelitis 347  
   complications 356  
   diabetic of foot 350

- Osteomyelitis—*cont.*  
 mandibular 350  
 sclerosing (Garré) 349  
 spine 350  
 Osteonecrosis *see* avascular necrosis  
 Osteopathia striata 261  
 Osteopetrosis 261  
 Osteopoikilosis 261  
 Osteoporosis 327–331  
   endocrine 328  
   idiopathic male 328  
   juvenile 328  
   localised 330  
   postmenopausal 328  
   senile 328  
     transient (regional) 330  
 Osteosarcoma 296–300  
 Ostium primum defect 192  
 Ostium secundum defect 192  
 Ovar-ies(-ian)  
   Brenner tumor 681  
   clear cell carcinoma 681  
   corpus luteum cyst of pregnancy 688  
   cumulus oophorus 683  
   dermoid cyst 681, 684  
   endometriod carcinoma 681  
   endometriomas 682  
   fibromas 681, 684  
     Meig's syndrome 681, 684  
   follicles 673, 680  
   follicular cysts 682  
   function monitoring 683  
   metastases in 681  
     Krukenberg tumor 681  
   mucinous cystadenoma 680  
   mucinous cystadenocarcinoma 680  
   oophoritis 675  
   parovarian cysts 682  
   remnant syndrome 682  
   serous cystadenocarcinoma 680  
   serous cystadenoma 680  
   size 673  
   teratoma 681  
   theca lutein cysts 680, 682  
   torsion 682  
   tubo-ovarian abscess 676  
 Ovarian dysgerminoma, mediastinal 109  
 Ovarian vein syndrome 252  
 Oxalosis 334
- Pacemakers 132, 222  
 complications 222  
 infection 225  
 insertion 222  
 thromboembolic complications 223  
 Twiddler's syndrome 223  
 Paget's disease 317, 368  
 complications 370  
 osteoporosis circumscripta 317, 368  
 osteosarcoma 299, 317, 370  
 Pancoast tumor 42, 80  
 Pancreas(-eatic) 485  
 abscess 488  
 acute pancreatitis 488  
   barium studies 489  
   complications 488  
   CT 489  
   necrotising vasculitis 241, 488  
   ultrasound 489  
 adenocarcinoma 493  
 ampullary carcinoma 495  
 angiography 486, 494  
 annular 487  
 biopsy, fine needle 487, 494  
 calcification 485, 490  
 chronic pancreatitis 490  
 CT 486  
 cysts 493  
   Von Hippel–Lindau disease 493  
 cystic fibrosis 487  
 development 485
- divsum 487  
 ectopic 487  
 endoscopic retrograde cholangiopancreatography (ERCP) 486  
 fatty 487–8  
 hemochromatosis 488  
 hereditary pancreatitis 490  
 islet cell tumors 496  
 microcystic adenoma 495  
 mucinous cystadenoma 495  
 pancreaticoblastoma 495  
 pseudocyst 488, 490, 492  
 Schwanachmann–Diamond syndrome 488  
 trauma 492  
 ultrasound 485
- Panner's disease 366  
 Pantopaque (Myodil) 400  
 Paragonomiasis  
   cerebral 774  
   pulmonary 72  
 Paralytic ileus 439  
 Parasitic brain infections 772  
 Parkinson's disease 787  
 Parotid *see* Salivary glands  
 Patella, bipartite 259  
 Patent ductus arteriosus 187, 190  
 Patent foramen ovale 192  
 Pediatric cardiac surgery 184  
 Pelizaeus–Merzbacher disease 785  
 Pelikan's spurs 327  
 Pellegrini–Stieda lesion 275, 410  
 Pelvic inflammatory disease (PID) 675  
 Pelvic lipomatosis 653, 660  
 Pelvic pain syndrome 252  
 Percutaneous biopsy *see* biopsy  
 Percutaneous chemotherapy 248  
 Percutaneous thrombolysis 248  
 Pericardium(-al)  
   absent 230  
   constrictive pericarditis 229  
   cysts 230  
   disease 225  
   diverticulum 230  
   effusion 162, 227  
     imaging 227  
     imaging 225  
   post pericardotomy syndrome 131  
   pericarditis 226  
   thickening 228  
   tumors 229  
 Peritonitis 441  
 Peutz–Jegher syndrome 458, 541, 576  
 Pharynx *see* hypopharynx and oropharynx  
 Phenylketonuria 267  
 Pheochromocytoma 502  
   mediastinal 118  
 Phlebography 249  
   lower limb 249  
 Phrenic nerve operative damage 130  
 Pick's disease 787  
 Pigmented villonodular synovitis (PVNS) 313, 393, 394  
 Pineal tumors 744  
 Pinna shadow 399  
 Pituitary insufficiency 329  
   empty sella 742  
   tumors 730, 739  
 Placenta(-l)  
   abruption 710  
   accreta 710  
   calcification 695  
   chorioangioma 710  
   chorionic villous sampling 695  
   increta 710  
   percreta 710  
   previa 695, 710  
   site 691  
 Plasmacytoma 316  
 Pleura(l)  
   calcification 42  
   empyema 129  
   fluid (effusion) 15, 34, 141
- causes (Table 2.3) 34  
 lamellar effusions 34  
 loculated 36  
 post thoracotomy 129, 130  
 rheumatoid disease 98  
 subpulmonary pleural effusions 35  
 thickening 41  
 fibrothorax 42  
 tumors 44  
 Pleuropericardial cyst 114  
 Plummer–Vinson syndrome 510  
 Pneumatocele 23  
 Pneumatoctes cystoides intestinalis 439  
 Pneumocephalus 776  
 Pneumoconioses 94  
   asbestosis 95  
   barytosis 96  
   berylliosis 96  
   coal worker's 95  
   progressive massive fibrosis (PMF) 96  
   Caplan's syndrome 96  
   siderosis 96  
   silicosis 94  
   stannosis 96  
 Pneumocystis carinii 75  
 Pneumonia and pneumonitis  
   aspiration  
     gastric fluid (Mendelson's syndrome) 96  
     paraffin 97  
     petrol 97  
     operative 128  
   branching bacteria  
     Actinomycosis, Nocardiosis 69  
   bronchopneumonia 61  
   chlamydial 62  
   fungal  
     aspergillosis 71  
     histoplasmosis 69  
     coccidioidomycosis 70  
     blastomycosis 70  
     cryptococcosis (torulosis) 70  
   Gram-negative 64  
   hypersensitivity  
     bagassosis 97  
     bird fancier's lung 97  
     farmer's lung 97  
     humidifier (air conditioning) 97  
     mushroom worker's lung 97  
 influenza 62  
 irritant gas 97  
 Klebsiella 64  
 Legionnaires' disease 64  
 lipoid 96  
 lobar 61  
 lymphoid interstitial 90  
 mycoplasma 63  
 pneumococcal 63  
 post operative 128  
 protozoal  
   Entamoeba histolytica 71  
   Pneumocystis  
     Toxoplasmosis 71  
   rickettsial 62  
   staphylococcal 63  
   varicella 62  
   viral 61  
 Pneumopericardium, post operative 130  
 Pneumoperitoneum 437, 444  
   causes 437  
   post operative 130  
 Pneumothorax 36  
   causes (Table 2.4) 38  
   complications 37  
   hemopneumothorax 38  
   postoperative 128, 130  
   pyopneumothorax 39  
   tension 37  
   Histioticosis X 101  
 Polyarteritis nodosa (PAN),  
   arterial aneurysms 241  
   chest 100  
   small bowel 569

- Polydactyly 257  
 Polymyositis 387  
   lungs 100  
 Popliteal cyst 244  
 Popliteal entrapment 244  
 Porencephalic cyst 781  
 Portal hypertension 252, 475  
 Portal vein  
   arterial portography 252  
   gas in 444, 457, 465  
   percutaneous transhepatic portography 253  
   phlebography 252, 466  
   schistosomiasis 475  
 Positron emission tomography (PET) 151  
 Post infectious encephalitis 769  
 Pregnancy  
   anembryonic 689  
   early failure 689  
   ectopic 690  
   first trimester 687  
 Primitive sciatric artery 237  
 Progeria 375  
 Progressive diaphyseal dysplasia 266  
 Progressive massive fibrosis (PMF) 96  
 Progressive multifocal leukoencephalopathy (PML)  
   771  
 Prostate(-ic)  
   benign hypertrophy 660  
     outflow obstruction 668  
   calculi 637  
   carcinoma 661  
   cysts 661  
   inflammation 662  
   post prostatectomy appearances 662  
 Prosthetic cardiac valves 219  
   dysfunction 219  
   imaging 220  
   regurgitation 220  
 Proximalfemoral focal defect (PFFD) 259  
 Prune belly syndrome 615  
 Pseudo-achondroplasia 267  
 Pseudocoarctation of the thoracic aorta 237  
 Pseudohypoparathyroidism 331  
 Pseudolymphoma 90  
 Pseudomembranous colitis 442  
 Pseudo-pseudohypoparathyroidism 331  
 Pseudothrombosis of the internal carotid 754  
 Psittacosis 62  
 Psoriatic arthritis 382, 386  
 Pulmonary see Lung for most lesions  
   alveolar microlithiasis 104  
   alveolar proteinosis 104  
   angiomatic malformation 207  
   arterial hypertension 141, 167  
   artery sling 212  
   edema 104, 161  
     interstitial 141, 142  
     post operative 128  
   eosinophilia 100  
   embolism 132  
     chronic 133  
     post operative 128  
     predisposing factors 132  
   emphysema  
     interstitial 126  
     neonatal 104  
   hemosiderosis 166  
   overcirculation 142  
   systemic supply 142  
   underperfusion 142, 143  
   unequal perfusion 142  
   venous congestion 142, 166  
   venous hypertension 141  
 Pulmonary atresia 188, 209  
   with VSD 209  
   without VSD 210  
 Pulmonary stenosis 196  
   acquired 177  
   infundibular 196  
 Pulmonary valve regurgitation 177  
 Pyarthrosis 356  
 Pycnodynostosis 260
- Pyloric stenosis 443  
 Q-Fever 62
- Radiation injury bone 372  
 Radionuclide scanning, heart *see under* Heart and angiography  
 Radionuclide scanning lung 7  
 Rathke's cleft cyst 742  
 Rectal atresia 444  
 Rectourethral fistula 444  
 Rectovaginal fistula 444  
 Rectovesical fistula 444  
 Reiter's syndrome 383  
 Renal *see also* Kidney  
 Renal artery(-ies)  
   aneurysm 645  
   AV fistula 646  
   AVM 646  
   congenital multiple 217  
   embolisation 646  
   microvascular disease 645  
   stenosis 244, 644  
 Renal calculi  
   hyperparathyroidism 332  
 Renal osteodystrophy 332  
 Renal tubular acidosis 325  
 Renal tubular disorders 324  
 Renal vein thrombosis 646  
 Reticulum cell sarcoma 306  
 Retroperitoneal fibrosis 652  
 Retroperitoneal gas 437  
 Retrosternal goitre 107  
 Reye's syndrome 770  
 Rhabdomyosarcoma, cardiac 218  
 Rheumatoid arthritis 380  
   atlanto-axial subluxation 382, 386  
   juvenile onset 386  
   odontoid erosion 382, 386  
 Rheumatoid disease  
   lung 98  
   and pneumoconiosis (Caplan's syndrome) 96, 98  
 Rib(s)  
   expansion 30  
   fractures 124  
   increased density 30  
   notching 28, 29, 131, 195  
 Rickets 324  
 Right atrium, morphology 185  
 Right sided aortic arch 200, 211  
 Right ventricle, morphology 185  
 Rigler's sign 437  
 Rocky Mountain spotted fever 62  
 Rotator cuff injury 288  
 Rubella 351  
 Ruptured intraventricular septum 161  
 Ruptured papillary muscle 162
- Sacralisation of L5 791  
 Salivary gland(s)  
   anatomy 507  
   calculi 508  
   congenital absence 509  
   ductal stricture 508  
   inflammation  
     sialadenitis 508  
     sialosis 508  
   Sjogren's syndrome 508  
   tumor  
     mixed tumor 509  
     malignant 509  
     pulmonary 91  
 Sarcoidosis  
   bone 371  
   cardiac 180  
   pulmonary 93  
   egg-shell calcification 93  
 Scheuermann's disease 367  
 Schilder's disease 784
- Schistosomiasis  
   bladder and ureter 643  
   cerebral 775  
   colon 586  
   portal 475  
   pulmonary 72  
 Schwannoma  
   bone 312  
 Scleroderma 119, 387, 565, 593  
 Scurvy 327  
 Segmental cardiac connections 186  
 Seminoma, mediastinal 109  
 Seronegative chronic arthritis 386  
 Seronegative spondyloarthropathies 382  
 Sever's disease 368  
 Sickle cell disease 337, 361  
 Siderosis 96  
 Silicosis 94  
   Caplan's syndrome 95  
   egg-shell calcification in nodes 95  
 Simple bone cyst 314  
 Sinding-Larsen disease 367  
 Single inlet ventricle 208  
 Sinus of Valsalva aneurysm 210  
 Sinus venosus defect 192  
 Sinuses  
   angiomatic polyp 842  
   carcinoma 842  
   esthesioneuroblastoma 843  
   lethal midline granuloma 841  
   maxillary sinus hypoplasia 839  
   metastases 843  
   mucocele 840  
   osteoma 841  
   plasmacytoma 843  
   polyps 840  
   sarcoidosis 841  
   sinusitis 839  
     complications 840  
     fungal 840  
 trauma 843  
   blow-out fracture 843  
   mid face fractures  
     Le Fort types 844  
     sphenoid sinus and skull base 844  
     tripod fracture 843  
 Wegener's granulomatosis 841  
 Situs ambiguus 186  
 Situs solitus 185  
 Sjogren's syndrome 100, 508  
 Skull  
   basal angle 717  
   basilar impression 717  
   basilar invagination 717  
   congenital parietal foramina 717  
   congenital dermal sinus 717  
   craniosynostosis 715  
   encephalocele 716  
   fractures 775  
   histiocytosis 730  
   intracranial tumors involving 730  
   lacunar 716  
   meningocele 716  
     sphenoid in neurofibromatosis 717  
   platybasia 717  
   raised intracranial pressure 727  
   sinus pericranii 718  
   suprasellar lesions 741  
   tumors  
     primary  
       carcinoma of the nasopharynx 729  
       carcinoma of the sphenoid 729  
       chordoma 729  
       dermoid 728  
       epidermoid 728  
       glomus jugulare 729  
       hemangioma 728  
       ossifying fibroma 728  
       osteoma 728  
       osteogenic sarcoma 728  
       solitary plasmacytoma 729  
       secondary 729

- Slipped femoral capital epiphysis 276  
 Small bowel  
   actinomycosis 553  
   adenocarcinoma 552, 558  
   AIDS 553, 555, 559  
   amyloidosis 565  
   angiography 547  
   anisakiasis 554  
   ascariasis 554  
   atresia 443, 548  
   barium examinations 546  
   Behcet's syndrome 569  
   blastomycosis 553  
   Campylobacter infection 554  
   carcinoid syndrome 557  
   celiac disease 564  
   Crohn's disease 550  
     complications 551  
   CT 547  
   cystic fibrosis 563, 567  
   disaccharidase deficiency 567  
   diverticulosis 549  
   duplications 550  
   embryology 547  
   enteroclysis 546  
   enteroscopy 547  
   eosinophilic enteritis 554  
   gallstone ileus 563  
   Giardiasis 553  
   graft versus host disease 567  
   hemorrhage 547, 569  
     intramural 568  
   Henoch-Schonlein purpura 563, 569  
   hernia 562  
     Richter 562  
   histoplasmosis 553  
   hookworm infestation 544  
   internal hernias 548  
   lactase deficiency 567  
   lower g.i. bleeding and radionuclides 547  
   lymphangiectasis 565  
   lymphoid hyperplasia 555, 562, 567  
   ileocolic intussusception 555, 562  
   lymphoma 559  
   malabsorption 564  
     bacterial overgrowth 567  
     immune deficiency 567  
   Meckel's diverticulum 549, 563  
   mesenteric artery occlusion and ischemia 567  
   mesenteric venous thrombosis 568  
   midgut volvulus 548  
   neoplasms 556  
     benign 556  
       carcinoïd 557  
       malignant 558  
       polyposis 557  
     metastatic 560  
   nonrotation 548  
   obstruction 433, 560  
     adhesions 561  
     gallstone ileus 563  
     hernias 562  
     intussusception 562  
     Ladd's bands 548  
     meconium ileus 563  
     volvulus 562  
   omphalocele 548  
   polyarteritis nodosa 569  
   pseudodiverticula 549  
   radiation enteritis 554, 569  
   radiological anatomy 545  
   radionuclide scintigraphy 547  
   scleroderma 565  
   stenosis 548  
   strongyloidiasis 554  
   systemic Mastocytosis 566  
   trauma 569  
   tropical sprue 564  
   tuberculosis 552  
   typhoid 554  
   ulcerative enteritis 555  
   ultrasound 547  
   vasculitis 569  
   Whipple's disease 564  
   Yersinia ileitis 553  
   Zollinger-Ellison syndrome 566  
 Spinal cord  
   dural and intradural extramedullary lesions 802  
     arachnoid cysts 803  
     arachnoiditis 804  
     cysts 806  
     dermoid 802  
     dural AV fistula 804  
     dural ectasia 794, 802, 802, 803  
     lipo-myelo-meningo-dysplasia 802  
     meningioma 804  
     meningocele 802  
     metastases 804  
     neurofibroma 804  
     sacral cysts 803  
   intradural intramedullary lesions 806  
     angioma 811  
     atrophy 811  
     ependymoma 807  
     glioma 807  
     hemangioblastoma 808  
     inflammation 810  
     irradiation 810  
     lipoma 807  
       diastematomyelia 807  
       myelomeningocele 806  
       syringomyelia 808  
     trauma 810  
 Spine  
   ankylosing spondylitis 794  
   congenital anomalies 791  
   crystal deposit diseases 799  
   DISH 799  
   epidural abscess 795  
   epidural granuloma 795  
   hyperparathyroidism 799  
   osteomyelitis 795  
   scoliosis 791  
   inflammatory diseases 791  
   neoplasms 796–7  
   Paget's disease 799  
   rheumatoid arthritis 791  
     atlanto-axial subluxation 791  
     erosions 792  
     inflammatory soft tissue masses 792  
   sacral agenesis 802  
   spondylolisthesis 802  
   stenosis 810  
   trauma 796–9  
 Spleen (splenic) 477  
   abscess 480, 481  
   angiography 480  
   asplenia 481  
   calcification 478, 483  
   candidiasis 482  
   CT 480  
   cysts 483  
   hemangioma 483  
   hydatid 482  
   infarct 483  
   lymphangiomatosis 484  
   lymphoma 483  
   metastases 483  
   MRI 481  
   polysplenia 481  
   radionuclide imaging 480  
   sickle cell disease 478  
   spleno-gonadal fusion 481  
   splenomegaly 478  
   splenuculi 481  
   Thorotrust 479  
   trauma 482  
   ultrasound 480  
   wandering 481  
 Smallpox *see* Variola  
 Spondyloepiphyseal dysplasia 271  
 Spondylosis deformans 379  
 Spongiform degeneration 785  
 Spontaneous osteonecrosis 363  
 Sprengel's shoulder 257  
 Stannosis 96  
 Sternum(-al)  
   dehiscence 131  
   depressed 27  
 Still's disease 386  
 Stomach (gastric)  
   antral web 534  
   barium examination techniques 530  
     multiphasic examination 532  
   benign neoplasms 541  
     leiomyoma 541  
     polyps 541  
   benign ulcer 537  
   carcinoma 539  
     diverticulum 534  
     limitis plastica 541  
   extrinsic masses 533  
   gastritis 534  
     atrophic 535  
     chronic antral 535  
     corrosive 536  
     erosive 535  
     hypertrophic 535  
     Menetrier's disease 536  
     Zollinger-Ellison syndrome 536  
   hypertrophic pyloric stenosis 534  
   lymphoma 541  
   normal radiological anatomy 533  
   surgery 542  
   volvulus 534  
 Strangulated hernia 433  
 Subacute sclerosing panencephalitis 770  
 Subaortic stenosis 191  
 Subarachnoid hemorrhage 757, 763, 778  
 Subclavian steal 753  
 Subdural hematoma 778  
 Subdural abscess 767  
 Syringomyelia 719, 808  
 Sudeck's atrophy 274, 330  
 Superior vena cava  
   phlebography 252  
   obstruction 252  
 Supraspinatus tendonitis 389  
 Surgical emphysema 27  
 Swyer-James syndrome 49  
 Synovial osteochondromatosis 313, 393  
 Synovioma, malignant 313  
 Syphilis  
   bone 354  
 Syringomyelia  
   neuroarthropathy 391  
 Systemic Lupus Erythematosus (SLE)  
   avascular necrosis 387  
   lung 98  
   necrotising arteritis 241  
   polyarthritis 387  
 Systemic sclerosis  
   bones and joints 387  
   lungs  
     aspiration pneumonia 99  
     carcinoma 99  
     fibrosing alveolitis 98  
 Tabes dorsalis neuroarthropathy 391  
 Talipes equino varus 259  
 Takayasu's arteritis 753  
 Teeth and jaws  
   acromegaly 832  
   caries 825, 827  
   cementoma 830  
   complex odontome 830  
   compound odontome 830  
   cretinism 833  
   Cushing's syndrome 833  
   cysts of the jaws  
     aneurysmal bone 831  
     fissural 831  
     inclusion (Stafne) 832  
     odontogenic  
       developmental 831

- inflammatory 831  
 simple bone 831  
 development 825  
 developmental anomalies  
   anodontia 826  
   dens in dente 826  
   macrodontia 827  
   microdontia 826  
   supernumerary teeth 826  
 eosinophil granuloma 829  
 gigantism 832  
 hypercementosis 829  
 hyperparathyroidism 833  
   brown tumors 833  
 infection  
   granuloma 828  
   periapical 827  
   loss of lamina dura 828  
   osteomyelitis 827, 828  
 malalignment 827  
 non eruption 827  
 normal anatomy 825  
 Paget's disease 836  
 periodontal disease 827  
 radionecrosis 830  
 sclerosis of jaws  
   chronic osteomyelitis 828  
   chronic sclerosing osteomyelitis 829  
   Garre's sclerosing osteomyelitis 829  
   osteopetrosis 830  
   pyknodysostosis 831  
   reparative osteosclerosis 829  
 Thalassemia 836  
 trauma and fractures 838  
 tumors  
   ameloblastoma 835  
   Burkitt's lymphoma 835  
   Gardner's syndrome 833  
   Ewing's 835  
   fibrous dysplasia 833  
     cherubism 834  
   giant cell 833  
   metastases 835  
   myeloma 835  
   ossifying fibroma 834  
   osteoma 833  
   osteosarcoma 835  
   squamous cell carcinoma 834  
 Technetium  
   <sup>99m</sup>Tc MIBI scans 149  
   <sup>99m</sup>Tc pyrophosphate 149  
 Temporo-mandibular joints  
   dysfunction syndrome 837  
   hyperparathyroidism 837  
   mucopolysaccharidoses 837  
   osteoarthritis 836  
   rheumatoid arthritis 836  
   sero-negative arthritides 836  
 Teratoma  
   cerebral 743  
   mediastinal 109  
 Tertiary hyperparathyroidism 334  
 Testis(-icular)  
   anorchia 670  
   ectopic 670  
   epididymo-orchitis 669  
   epididymal cysts 670  
   hydrocele 669  
   spermatocele 670  
   torsion 670  
   tumors 669  
   undescended 670  
   varicocele 669  
 Thalassemia 339  
 Thallium-201 149  
 Thoracotomy, complications 128  
 Thoracic inlet syndrome 244  
 Thorotrust 400  
 Thrombocytopenia absent radius (TAR) syndrome 257  
 Thrombolysis 159, 249  
 Thrombosis
- arterial 244  
 venous 249  
 Thymus(ic) 14  
   masses 108  
   thymoma 108  
 Thyroid acropachy 328  
 Tomography, linear chest 4  
 Topology *see* Looping  
 Torulosis *see* cryptococcosis  
 Toxoplasmosis  
   cerebral 772  
   pulmonary 71  
 Tracheal(l) 45, 13  
   abnormalities 114  
   amyloid 104  
   carcinoma 114  
   cylindroma 114  
   narrowing 45  
   rupture 126  
   tracheomalacia 114  
   tracheosophageal fistula 45  
   tumors 45  
   widening (tracheobronchomegaly) 46, 114  
 Transient osteoporosis 275  
 Transient tachypnea of the newborn 105  
 Transposition 188  
 Transposition of the great arteries 200  
   atrial baffle operation 203  
   great arterial switch operation 203  
   L-transposition 204  
   Rashkind balloon septostomy 201  
 Trichinosis 775  
 Tricuspid atresia 210  
 Tricuspid regurgitation 176  
 Tricuspid stenosis 176  
 Tropical ulcer 355  
 Trumerfeld zone 327  
 Truncus arteriosus 211  
 Tuberculosis  
   bone 352  
   pulmonary 65  
     lymphadenopathy 65, 68  
     miliary 67  
     pleural 68  
     silicosis and 94  
     tuberculoma 68  
 Tuberous sclerosis  
   bones 264, 374  
   kidneys 619  
   lungs 91, 102  
   pheochromocytoma 502  
 Turner's syndrome 276, 328  
 Ulcerative colitis 386  
 Ultrasound, in chest disease 7  
 Umbilical cord 695  
   single artery 695  
   nuchal 696  
   prolapsed 696  
 Urachus(-al)  
   cyst 615  
   diverticulum 615  
   patent 615  
   sinus 615  
 Urethra(-l)  
   atresia 663  
   anterior urethral valves 616  
   calculi 637  
   carcinoma 664  
   congenital narrowing 663  
   diverticula 615  
   duplication 613, 614, 663  
   infections and strictures 663  
   periurethral abscess 664  
   posterior urethral valves 615  
   post operative 665  
   prune belly syndrome 615  
   stricture 663  
   trauma 663  
 Ureter(-al) 664, 610  
   calculi 633
- deviation by retroperitoneal lesions 642  
 duplication 610  
 ectopic 610  
 hydronephrosis 612  
 post transplant obstruction 651  
 primary megaureter 612  
 pyeloureteritis cystica 640  
 retrocaval 613  
 rudimentary branched 613  
 schistosomiasis 643  
 transitional cell carcinoma 629  
 vesico-ureteric reflux 641  
 Ureterocele 610  
   ectopic 611  
   pseudoureterocele 611  
 Urodynamics 666  
 Urodynamogram  
   ultrasound (USUD) 666  
   intravenous (IVUD) 666  
 Uroflowmetry 666  
 Urticaria pigmentosa 318  
 Uter-us(-ine)  
   adenomyosis 675  
   carcinosarcoma 679  
   cervical carcinoma 679  
    staging 679  
   choriocarcinoma 680  
   congenital anomalies 674, 685, 711  
    associated renal anomalies 675  
 CT 685  
 endometrial carcinoma 678  
   staging 678  
 endometrial cavity 672  
 endometrial polyp 678  
 endometritis 675  
 fibroid 677, 684, 685  
 hysterosalpingography 684  
 hydatidiform mole 679  
 hydrometrocolpos 677  
 intrauterine contraceptive devices (IUD) 675, 683,  
   684  
 intrauterine fluid collections 676  
 MRI 685  
 leiomyoma 677, 684  
 leiomyosarcoma 677, 679  
 lymphoma 679  
 pregnancy abnormalities  
   congenital anomalies 711  
   premature dilatation of cervix 710  
   myomata 711  
   IUD 711  
 pyometrium 677  
 rhabdomyosarcoma 679  
 retained products 677  
 retroversion 672  
 retroflexion 672  
 size 672  
 ultrasound 671  
 Vacuum disc phenomenon 379  
 Vagina(-al)  
   endovaginal ultrasound scanning 671, 687  
   ultrasound anatomy 671  
   tampon 684  
 Vanishing bone disease 311  
 Varicella 62  
 Variola 351  
 Vascular rings 211  
 Vasoconstrictors in GI hemorrhage 248  
 VATER acronym 444  
 Vein(s)(-enous)  
   azygos 13, 465  
   hemiazygos 465  
   imaging 250  
   lower limb 249  
   malformations 250  
   pelvis 251  
   thrombosis 249  
     splenic 492  
     upper limb 252  
 Venous angioma of brain 759

- Ventilation, positive pressure, complications 131  
Ventricular septal defect 187, 188  
Verner–Morrison (WDHA) syndrome 497  
Videocystometrygraphy (VCMG) 666  
Vinyl-chloride poisoning 335  
Viscero-atrial situs inversus (isolated levocardia) 186  
Vitamin C deficiency 327  
Vitamin D abnormalities 323  
Vitamin D deficiency 324  
Vitamin D resistant rickets 325  
Volkmann's ischaemic contracture 275  
Volvulus 435  
Von Gierke's disease 330
- Von Hippel–Lindau disease 493, 502, 619, 746, 808  
Von Recklinghausen's disease, see neurofibromatosis  
Von Willebrand's disease 345
- Waldenstrom's sign 365  
Wegener's granulomatosis  
  chest 99  
  arteritis 241  
Wet lung disease 105  
Whipple's disease 386, 564  
White matter diseases 783  
White matter shearing (diffuse azonal injury) 779
- Wilson's disease 334, 394, 475, 787  
Wilson–Mikity syndrome 105  
Wimberger's sign 327
- Xero-mammography 414
- Yaws 355
- Zenker's diverticulum 118  
Zollinger–Ellison syndrome 496, 536, 566